

# HANDBOOK OF ELECTRIC MOTORS

**ELECTRICAL AND COMPUTER ENGINEERING**  
*A Series of Reference Books and Textbooks*

FOUNDING EDITOR

***Martin O. Thurston***

Department of Electrical Engineering  
The Ohio State University  
Columbus, Ohio

1. Rational Fault Analysis, *edited by Richard Saeks and S.R. Liberty*
2. Nonparametric Methods in Communications, *edited by P.Papantoni-Kazakos and Dimitri Kazakos*
3. Interactive Pattern Recognition, *Yi-tzuu Chien*
4. Solid-State Electronics, *Lawrence E. Murr*
5. Electronic, Magnetic, and Thermal Properties of Solid Materials, *Klaus Schroder*
6. Magnetic-Bubble Memory Technology, *Hsu Chang*
7. Transformer and Inductor Design Handbook, *Colonel Wm. T. McLyman*
8. Electromagnetics: Classical and Modern Theory and Applications, *Samuel Seely and Alexander D. Poularikas*
9. One-Dimensional Digital Signal Processing, *Chi-Tsong Chen*
10. Interconnected Dynamical Systems, *Raymond A. DeCarlo and Richard Saeks*
11. Modern Digital Control Systems, *Raymond G. Jacquot*
12. Hybrid Circuit Design and Manufacture, *Roydn D. Jones*
13. Magnetic Core Selection for Transformers and Inductors: A User's Guide to Practice and Specification, *Colonel Wm. T. McLyman*
14. Static and Rotating Electromagnetic Devices, *Richard H. Engelmann*
15. Energy-Efficient Electric Motors: Selection and Application, *John C. Andreas*
16. Electromagnetic Compossibility, *Heinz M. Schlicke*
17. Electronics: Models, Analysis, and Systems, *James G. Gottling*
18. Digital Filter Design Handbook, *Fred J. Taylor*
19. Multivariable Control: An Introduction, *P.K. Sinha*
20. Flexible Circuits: Design and Applications, *Steve Gurley, with contributions by Carl A. Edstrom, Jr., Ray D. Greenway, and William P. Kelly*
21. Circuit Interruption: Theory and Techniques, *Thomas E. Browne, Jr.*
22. Switch Mode Power Conversion: Basic Theory and Design, *K. Kit Sum*
23. Pattern Recognition: Applications to Large Data-Set Problems, *Sing-Tze Bow*
24. Custom-Specific Integrated Circuits: Design and Fabrication, *Stanley L. Hurst*
25. Digital Circuits: Logic and Design, *Ronald C. Emery*
26. Large-Scale Control Systems: Theories and Techniques, *Magdi S. Mahmoud, Mohamed F. Hassan, and Mohamed G. Darwish*
27. Microprocessor Software Project Management, *Eli T. Fathi and Cedric V.W. Armstrong (Sponsored by Ontario Centre for Microelectronics)*
28. Low Frequency Electromagnetic Design, *Michael P. Perry*
29. Multidimensional Systems: Techniques and Applications, *edited by Spyros G. Tzafestas*
30. AC Motors for High-Performance Applications: Analysis and Control, *Sakae Yamamura*
31. Ceramic Motors for Electronics: Processing, Properties, and Applications, *edited by Relva C. Buchanan*
32. Microcomputer Bus Structures and Bus Interface Design, *Arthur L. Dexter*
33. End User's Guide to Innovative Flexible Circuit Packaging, *Jay J. Miniet*
34. Reliability Engineering for Electronic Design, *Norman B. Fuqua*
35. Design Fundamentals for Low-Voltage Distribution and Control, *Frank W. Kussy and Jack L. Warren*
36. Encapsulation of Electronic Devices and Components, *Edward R. Salmon*
37. Protective Relaying: Principles and Applications, *J. Lewis Blackburn*
38. Testing Active and Passive Electronic Components, *Richard F. Powell*
39. Adaptive Control Systems: Techniques and Applications, *V.V. Chalam*
40. Computer-Aided Analysis of Power Electronic Systems, *Venkatachari Rajagopalan*

41. Integrated Circuit Quality and Reliability, *Eugene R.Hnatek*
42. Systolic Signal Processing Systems, *edited by Earl E.Swartzlander, Jr.*
43. Adaptive Digital Filters and Signal Analysis, *Maurice G.Bellanger*
44. Electronic Ceramics: Properties, Configuration, and Applications, *edited by Lionel M.Levinson*
45. Computer Systems Engineering Management, *Robert S.Alford*
46. Systems Modeling and Computer Simulation, *edited by Naim A.Kheir*
47. Rigid-Flex Printed Wiring Design for Production Readiness, *Walter S.Rigling*
48. Analog Methods for Computer-Aided Circuit Analysis and Diagnosis, *edited by Takao Ozawa*
49. Transformer and Inductor Design Handbook: Second Edition, Revised and Expanded, *Colonel Wm. T.McLyman*
50. Power System Grounding and Transients: An Introduction, *A.P.Sakis Meliopoulos*
51. Signal Processing Handbook, *edited by C.H.Chen*
52. Electronic Product Design for Automated Manufacturing, *H.Richard Stillwell*
53. Dynamic Models and Discrete Event Simulation, *William Delaney and Erminia Vaccari*
54. FET Technology and Application: An Introduction, *Edwin S.Oxner*
55. Digital Speech Processing, Synthesis, and Recognition, *Sadaoki Furui*
56. VLSI RISC Architecture and Organization, *Stephen B.Furber*
57. Surface Mount and Related Technologies, *Gerald Ginsberg*
58. Uninterruptible Power Supplies: Power Conditioners for Critical Equipment, *David C.Griffith*
59. Polyphase Induction Motors: Analysis, Design, and Application, *Paul L.Cochran*
60. Battery Technology Handbook, *edited by H.A.Kiehne*
61. Network Modeling, Simulation, and Analysis, *edited by Ricardo F.Garzia and Mario R.Garzia*
62. Linear Circuits, Systems, and Signal Processing: Advanced Theory and Applications, *edited by Nobuo Nagai*
63. High-Voltage Engineering: Theory and Practice, *edited by M.Khalifa*
64. Large-Scale Systems Control and Decision Making, *edited by Hiroyuki Tamura and Tsuneo Yoshikawa*
65. Industrial Power Distribution and Illuminating Systems, *Kao Chen*
66. Distributed Computer Control for Industrial Automation, *Dobrivoje Popovic and Vijay P.Bhatkar*
67. Computer-Aided Analysis of Active Circuits, *Adrian Ioinovici*
68. Designing with Analog Switches, *Steve Moore*
69. Contamination Effects on Electronic Products, *Cari J.Tautscher*
70. Computer-Operated Systems Control, *Magdi S.Mahmoud*
71. Integrated Microwave Circuits, *edited by Yoshihiro Konishi*
72. Ceramic Materials for Electronics: Processing, Properties, and Applications, Second Edition, Revised and Expanded, *edited by Relva C.Buchanan*
73. Electromagnetic Compatibility: Principles and Applications, *David A.Weston*
74. Intelligent Robotic Systems, *edited by Spyros G.Tzafestas*
75. Switching Phenomena in High-Voltage Circuit Breakers, *edited by Kunio Nakanishi*
76. Advances in Speech Signal Processing, *edited by Sadaoki Furui and M.Mohan Sondhi*
77. Pattern Recognition and Image Preprocessing, *Sing-Tze Bow*
78. Energy-Efficient Electric Motors: Selection and Application, Second Edition, *John C.Andreas*
79. Stochastic Large-Scale Engineering Systems, *edited by Spyros G.Tzafestas and Keigo Watanabe*
80. Two-Dimensional Digital Filters, *Wu-Sheng Lu and Andreas Antoniou*
81. Computer-Aided Analysis and Design of Switch-Mode Power Supplies, *Yim-Shu Lee*
82. Placement and Routing of Electronic Modules, *edited by Michael Pecht*
83. Applied Control: Current Trends and Modern Methodologies, *edited by Spyros G.Tzafestas*
84. Algorithms for Computer-Aided Design of Multivariable Control Systems, *Stanoje Bingulac and Hugh F.VanLandingham*
85. Symmetrical Components for Power Systems Engineering, *J.Lewis Blackburn*
86. Advanced Digital Signal Processing: Theory and Applications, *Glenn Zelniker and Fred J.Taylor*
87. Neural Networks and Simulation Methods, *Jian-Kang Wu*
88. Power Distribution Engineering: Fundamentals and Applications, *James J.Burke*
89. Modern Digital Control Systems: Second Edition, *Raymond G.Jacquot*
90. Adaptive IIR Filtering in Signal Processing and Control, *Phillip A.Regalia*
91. Integrated Circuit Quality and Reliability: Second Edition, Revised and Expanded, *Eugene R.Hnatek*
92. Handbook of Electric Motors, *edited by Richard H.Engelmann and William H.Middendorf*
93. Power-Switching Converters, *Simon S.Ang*
94. Systems Modeling and Computer Simulation: Second Edition, *Naim A.Kheir*
95. EMI Filter Design, *Richard Lee Ozenbaugh*

96. Power Hybrid Circuit Design and Manufacture, *Haim Taraseiskey*
97. Robust Control System Design: Advanced State Space Techniques, *Chia-Chi Tsui*
98. Spatial Electric Load Forecasting, *H.Lee Willis*
99. Permanent Magnet Motor Technology: Design and Applications, *Jacek F.Gieras and Mitchell Wing*
100. High Voltage Circuit Breakers: Design and Applications, *Ruben D.Garzon*
101. Integrating Electrical Heating Elements in Appliance Design, *Thor Hegbom*
102. Magnetic Core Selection for Transformers and Inductors: A User's Guide to Practice and Specification, Second Edition, *Colonel Wm. T.McLyman*
103. Statistical Methods in Control and Signal Processing, *edited by Tohru Katayama and Sueo Sugimoto*
104. Radio Receiver Design, *Robert C.Dixon*
105. Electrical Contacts: Principles and Applications, *edited by Paul G.Slade*
106. Handbook of Electrical Engineering Calculations, *edited by Arun G.Phadke*
107. Reliability Control for Electronic Systems, *Donald J.LaCombe*
108. Embedded Systems Design with 8051 Microcontrollers: Hardware and Software, *Zdravko Karakehayov, Knud Smed Christensen, and Ole Winther*
109. Pilot Protective Relaying, *edited by Walter A.Elmore*
110. High-Voltage Engineering: Theory and Practice, Second Edition, Revised and Expanded, *Mazen Abdel-Salam, Hussein Anis, Ahdab El-Morshedy, and Roshdy Radwan*
111. EMI Filter Design: Second Edition, Revised and Expanded, *Richard Lee Ozenbaugh*
112. Electromagnetic Compatibility: Principles and Applications, Second Edition, Revised and Expanded, *David Weston*
113. Permanent Magnet Motor Technology: Design and Applications, Second Edition, Revised and Expanded, *Jacek F.Gieras and Mitchell Wing*
114. High Voltage Circuit Breakers: Design and Applications, Second Edition, Revised and Expanded, *Ruben D.Garzon*
115. High Reliability Magnetic Devices: Design and Fabrication, *Colonel Wm. T.McLyman*
116. Practical Reliability of Electronic Equipment and Products, *Eugene R.Hnatek*
117. Electromagnetic Modeling by Finite Element Methods, *João Pedro A.Bastos and Nelson Sadowski*
118. Battery Technology Handbook: Second Edition, *edited by H.A.Kiehne*
119. Power Converter Circuits, *William Shepherd and Li Zhang*
120. Handbook of Electric Motors: Second Edition, Revised and Expanded, *edited by Hamid A.Toliat and Gerald B.Kliman*

*Additional Volumes in Preparation*

Transformer and Inductor Design Handbook, *Colonel Wm. T.McLyman*

Energy-Efficient Electric Motors: Third Edition, Revised and Expanded, *Ali Emadi*

# HANDBOOK OF ELECTRIC MOTORS

*Second Edition, Revised and Expanded*

*edited by*  
HAMID A.TOLIYAT  
*Texas A&M University*  
*College Station, Texas, U.S.A.*

GERALD B.KLIMAN  
*Rensselaer Polytechnic Institute*  
*Troy, New York, U.S.A.*

Published in 2004 by  
CRC Press  
Taylor & Francis Group  
6000 Broken Sound Parkway NW, Suite 300  
Boca Raton, FL 33487-2742

© 2004 by Taylor & Francis Group, LLC  
CRC Press is an imprint of Taylor & Francis Group

International Standard Book Number-10:0-8247-4105-6 (Hardcover)  
International Standard Book Number-13:978-0-8247-4105-1 (Hardcover)

This book contains information obtained from authentic and highly regarded sources. Reprinted material is quoted with permission, and sources are indicated. A wide variety of references are listed. Reasonable efforts have been made to publish reliable data and information, but the author and the publisher cannot assume responsibility for the validity of all materials or for the consequences of their use.

No part of this book may be reprinted, reproduced, transmitted, or utilized in any form by any electronic, mechanical, or other means, now known or hereafter invented, including photocopying, microfilming, and recording, or in any information storage or retrieval system, without written permission from the publishers.

For permission to photocopy or use material electronically from this work, please access [www.copyright.com](http://www.copyright.com) (<http://www.copyright.com/>) or contact the Copyright Clearance Center, Inc. (CCC) 222 Rosewood Drive, Danvers, MA 01923, 978-750-8400. CCC is a not-for-profit organization that provides licenses and registration for a variety of users. For organizations that have been granted a photocopy license by the CCC, a separate system of payment has been arranged.

**Trademark Notice:** Product or corporate names may be trademarks or registered trademarks, and are used only for identification and explanation without intent to infringe.

---

**Library of Congress Cataloging-in-Publication Data**

---

Catalog record is available from the Library of Congress

---



Taylor & Francis Group is the Academic Division of T&F Informa pic.

Visit the Taylor & Francis Web site at  
<http://www.taylorandfrancis.com>  
and the CRC Press Web site at  
<http://www.crcpress.com>

# In Memoriam

While this book was in production, Dr. Gerald B. Kliman was killed in a tragic auto accident. Dr. Kliman was a Research Professor in the Department of Electrical, Computer & Systems Engineering at Rensselaer Polytechnic Institute, Troy, New York, following his retirement from General Electric. He received the B.S. (1955), S.M. (1959), and Sc.D. (1965) from the Massachusetts Institute of Technology, Cambridge. Following graduation, he was Assistant Professor of Electrical Engineering at Rensselaer Polytechnic Institute. Later, he joined the General Electric Transportation Systems Division, where he worked on the design, performance prediction, and testing of induction motors in inverter-fed adjustable-speed drives; development of analysis techniques for high-speed linear induction motors; and design of ac and dc motors for various conventional and unconventional adjustable-speed traction drives. He also worked on system engineering and inverter design for advanced systems. Dr. Kliman joined the General Electric Nuclear Energy Division Large Electromagnet Pump Development Program where he developed analysis techniques for large electromagnetic

pumps and was responsible for the electromagnetic design of the GE/ERDA 14,500 gpm, 200 psi, 1000°F, sodium pump (the world's largest and most powerful electromagnetic pump at that time). He also worked on electromagnetic flowmeter design and the development of new concepts for both nuclear and commercial applications of electromagnetic pumping and electromagnetic techniques. He was a Life Fellow of the IEEE and a senior member of the AIP, Sigma Xi, and Eta Kappa Nu. He served on the Rotating Machinery Theory Committee of PAS and the Electric Machines and Land Transportation Committees of IAS. Dr. Kliman was an associate editor of the journal *Electric Power Components and Systems*. He had 86 patents granted in his name with 25 pending and numerous professional publications. He is listed in the current edition of *Who's Who in America*. He will be cherished by his family, friends, colleagues, and students for the richness of his life, his humanity, and honesty. His contributions were many and this book is dedicated to his memory.

*Hamid A. Toliyat*

# Preface to the Second Edition

We recognize the monumental and successful work of Professors Richard H.Englemann and William H.Middendorf in preparing the first edition of the *Handbook of Electric Motors*. We have retained the organization of the previous edition and the text has been updated and revised to reflect the most recent advances and technology.

Although it is sometimes assumed that electric motor technology is mature, with only incremental changes to be expected, that is not the case. In the few years since the publication of the first edition there have been many advances and innovations in materials, electronics, controls, and motor geometries or concepts. Some of those developments primarily interest academics, but many have made a major impact on motor manufacturing and application and other advances are emerging commercially. The size of this work has been expanded by more than 30% in order to deal with the new developments, without slighting the established technologies.

A number of new machine concepts have been investigated in academic laboratories. The switched reluctance motor (Section 15.2) has been adopted in some applications for small industrial and appliance applications. Research on superconducting generators has been in progress for some years, but recently attention has turned to high-horsepower motor applications and large machines have been demonstrated for marine propulsion (2.5.8).

Other special-purpose motors have been added to the volume due to their increasing potential importance and to broaden coverage of major market segments. These include: doubly fed induction motors (2.2.9), universal motors (2.5.9), synchronous reluctance motors (2.5.6), aerospace motors (2.5.7), linear synchronous motors (5.6), and “line start” (uncontrolled) permanent magnet and reluctance ac motors (2.5.10). The sections on brushless dc (15.3) and ironless motors (2.3.9) have been expanded, as well as the section on 400 Hz motors (2.5.2).

Remarkable advances in the tools for motor analysis and design have taken place. In particular, the capabilities of finite element electromagnetic analysis tools have exploded, taking advantage of the rapidly increasing computational capability of widely available, low-cost computers. These advances have mandated a complete revision of the finite element overview and applications (1.5, 4.10, 5.8 and 6.9). Also capitalizing on advanced computing and graphic interfaces, a revolution in and motor CAD tools has taken place (4.9).

Another area of rapid progress has been in electronic controls. Power devices and circuits (9.3–9.6) have grown in power-handling capability, and reduced costs have expanded low-power market penetration. Real time computational capability and new control methods have been equally revolutionary with the advent of vector controls (15.1). The control of the traditional dc motor has also been impacted (3.8.2 and 6.7). Section 15.1, on controls for ac motors, reviews the most advanced techniques; however, more basic discussions are included in earlier chapters where appropriate.

Along with the many benefits of electronic motor controls there have also been negative effects. Because electronic controls can damage motor insulation and bearings, the means to deal with those effects must be addressed (13.5, 8.4). The interaction of motors and electronic controls also impact the power quality of the power systems feeding the drives (12.8).

Electronics has greatly enhanced reliability and protection with the increasing application of microprocessor-based relays and circuit breaker controls (10.2.5). Computing capability has also led to new ways to detect failure and incipient failure in motors (13.4) and the use of core monitoring previously restricted to generators (14.6.5).

*Gerald B.Kliman  
Hamid A.Toliyat*



# Preface to the First Edition

The earliest recorded demonstration of rotation produced by electromagnetic means was by Michael Faraday at the Royal Institution in London in 1821. The nearly simultaneous solution in 1832 of the commutation problem in dc machines by Pixii in Paris and Ritchie in London led to the first industrial use of dc motors in 1837 by Davenport in Rutland, Vermont. Alternating current generator development began with Werner Siemens in 1856; other contributors to alternator development were Henry Wilde in England and Zenobe Gramme in France (Gramme's alternator being installed in Paris for street lighting service in 1878). With the 1888 announcement of induction motors by Nikola Tesla, the family of generic electric motors was complete.

Since that time there have been many refinements to the generic machines, but a new era of motor development began in the early 1960s with the appearance of solid-state electronic devices with ever-increasing voltage and current capabilities. The brushless dc motor, the stepper motor, and a variety of inverters are only a few examples of the innovations that have made possible a broad and still expanding selection of motor drive systems.

This book provides comprehensive coverage of electric motors and relevant associated topics, such as controls, protection, environmental considerations, mechanical considerations, and reliability. Its focus is not simply on motors in the generic forms of direct current, induction, and synchronous machines—the reader will also find coverage of series, shunt, compound, and permanent magnet direct current motors; stepper motors; traction motors; brushless dc motors; linear motors (both induction and synchronous); 400-Hz machines; hermetically sealed refrigeration motors; deep-well and submersible motors; and solid rotor induction motors.

The engineer who is concerned with any aspect of the design of motors, their selection, specifications, purchasing, testing methods, installation, maintenance, or repair will find this book to be a valuable reference. In addition to fundamental design equations, the designer will also find information on finite element analysis, computer-aided design, motor insulation systems, performance and dimensional standards, and other topics relevant to the design

process. The application engineer will find some of these same topics to be of value, but in addition will benefit from discussions of motor control and protection, testing, reliability, and similar topics. Maintenance is an important consideration for all motors. In addition to one specific chapter on this subject, material will be found in other chapters on insulation and on bearings and lubrication. Generous use has been made of figures, tables, and references throughout, and examples have been included in those sections where the reader will find them most useful. Of special note are the references to standards, such as those issued by IEEE, NEMA, and UL. Sources for these standards are listed in [Appendix B](#).

The *Handbook of Electric Motors* is organized so that fundamentals are presented first, followed by information on applications, design, testing, and motor insulation, ending with practical information on installation and use.

[Chapter 1](#), “Principles of Energy Conversion,” includes discussion of magnetic materials, the basic mathematical functions related to electromagnetic fields, magnetic circuits and their solution (including finite element methods), and stored energy, forces, and torques in magnetic systems.

The first three sections of [Chapter 2](#), concerning types of motors and their characteristics, are on the three generic forms of electric machines. The first section is devoted to synchronous motors. Both three-phase and single-phase motors are discussed in the induction motor section, which also includes information on mounting, enclosures, design classes, standard-efficiency and high-efficiency motors, performance on variable frequency sources, and linear induction motors. The third section in this chapter, on dc motors, not only covers the conventional classifications (series, shunt, and compound), but also includes permanent magnet motors, brushless dc motors, and ironless armature motors. These sections on the generic forms of electric motors are followed by a section on traction motors which covers the entire range of traction applications, from golf carts to mine haul vehicles to mass transit. A section on special applications completes the chapter, using stepper motors, 400-Hz motors, deep-well pump motors, submersible motors, solid rotor induction motors, and watt-hour meters as examples of the wide variety of machines that are possible.

**Chapter 3**, “Motor Selection,” begins with a discussion of standards (both NEMA and IEC) on enclosures, dimensions, and performance, typical mechanical loads, motor efficiency, energy usage, payback analysis, life-cycle costing, and safety considerations. The section on how to specify a motor will help the application engineer eliminate most misunderstandings and uncertainties between the purchaser and the vendor. A section illustrating some unusual considerations in motor selection completes the chapter.

**Chapter 4**, on induction motor analysis and design, includes computer-aided design and finite element analysis techniques for both polyphase and single-phase motors, as well as full discussions of rotating fields and their harmonics; average and harmonic torques; radial forces; stator windings; rotor construction; leakage reactances; and equivalent circuits for steady-state, transient, and variable frequency conditions. This chapter also includes sections on mechanical and thermal design considerations.

“Synchronous Motor Analysis and Design” and “Direct-Current Motor Analysis and Design” (**Chapters 5 and 6**) include similar design information, although with less detail.

**Chapter 7**, “Testing for Performance,” introduces test standards and types of performance tests for polyphase and single-phase induction motors, synchronous motors, and dc motors as well as test methods for hermetically sealed refrigeration motors. Special test procedures for induction motors and permanent magnet motors are explained, and selection, specification, and purchasing considerations for motor loading and data recording equipment are discussed.

**Chapter 8**, concerning motor insulation systems, contains a wealth of information on motor insulation for both random-wound and form-wound motors, with sections on insulation testing methods.

**Chapter 9**, “Motor Control,” begins with ac supply system considerations and induction motor control, including bus transfer and reclosing. A few examples are given of dc motor control using relays and contactors. A brief exposition of the characteristics of the most used power electronic devices serves

to introduce the reader to solid-state converter circuits and controllers. A section on open- and closed-loop control of permanent magnet stepper motors illustrates advanced control methods.

**Chapter 10**, on motor protection, discusses protection against overloads, unbalanced voltages, and internal failures and includes selection of switching devices, mechanical protection, and various accessories. Fuses and protection coordination are considered, as are thermal protectors and their testing standards and requirements.

**Chapter 11**, “Mechanical Considerations,” includes noise, standards relative to noise levels, experimental means for noise investigation, and means for reduction of noise. The chapter also contains information on vibration measurement and evaluation, rotor balancing, sleeve and antifriction bearings, brushes, and motor mounting.

**Chapter 12**, “Environmental Considerations,” discusses heat transfer, ventilation, cooling, enclosures, and the thermal circuits used for analysis. Both RMS loading analysis and time-constant analysis are considered. Altitude effects, chemicals, seismic activity, and nuclear plant safety are part of the information on ambient and environmental effects.

**Chapter 13**, on reliability, considers the reliability of large motors, antifriction bearings, and brushes and discusses modern means of monitoring for signs of wearout.

**Chapter 14**, on maintenance, emphasizes the importance of good lubrication practice, the significance of various vibration signatures, maintenance and repair of commutators, brush replacement, repair of windings, and core testing methods.

The book was written by 47 authors, each of whom chose the subject area of his expertise. The biographical sketches at the end of the book illustrate the breadth of the experience of the contributors. Extensive interaction with the authors by the editors ensured clarity and consistency of exposition.

*Richard H.Engelmann*  
*William H.Middendorf*

# Acknowledgments

We thank the many individuals and companies who contributed their expertise, materials, and time to make this work as complete and up-to-date as possible. We also acknowledge the advice and guidance given to us by Richard Johnson and Rita Lazzararo at Marcel Dekker, Inc. We

especially thank our wives for their patience and support in spite of the piles of paper in our dining rooms and the hours we spent at our computers. Special thanks to Mina Rahimian (Toliyat) for assisting Hamid Toliyat with the preparation of the texts for publication.

# Contents

<i>Preface to the Second Edition</i>	v	1.5.6 Parameters from Fields	19
<i>Preface to the First Edition</i>	vii	1.5.7 Applications in Two and Three Dimensions	19
<i>Acknowledgments</i>	ix	1.5.8 Finite Elements Compute Equivalent Circuit Parameters	19
<i>Contributors</i>	xix	1.5.9 Finite Elements Directly Compute Motor Performance	20
<b>1. PRINCIPLES OF ENERGY CONVERSION</b>	<b>1</b>	<b>1.6 ENERGY STORED IN MAGNETICALLY COUPLED MULTIPLE-LOOP SYSTEMS</b>	<b>21</b>
1.1 GENERAL BACKGROUND	2	1.7 FORCES AND TORQUES IN THE SYSTEM	21
1.2 MAGNETIC MATERIALS	4	References	23
1.2.1 Properties of Ferromagnetic Materials	5	<b>2. TYPES OF MOTORS AND THEIR CHARACTERISTICS</b>	<b>25</b>
1.2.2 Boundary Conditions for $\vec{B}$ and $\vec{H}$	6	2.0 INTRODUCTION	26
1.3 SOME BASIC FUNCTIONS RELATED TO ELECTROMAGNETIC FIELDS	6	2.1 POLYPHASE SYNCHRONOUS MOTORS	28
1.3.1 Scalar Potential	7	2.1.1 Synchronous Machine Performance Considerations	32
1.3.2 Vector Potential	7	2.2 INDUCTION MOTORS—POLYPHASE AND SINGLE-PHASE	35
1.3.3 Electromagnetic Induction	8	2.2.1 General Theory and Definition of Terms Used	35
1.3.4 Energy in an Electromagnetic Field	8	2.2.2 Classification of Motors According to Size	38
1.3.5 Self-Inductance and Mutual Inductance	8	2.2.3 Power Requirements, Mechanical, and Thermal Design Considerations	38
1.3.6 Energy Stored in Current-Carrying Coil	9	2.2.4 Standard-Efficiency Motors vs. High-Efficiency Motors	41
1.4 MAGNETIC CIRCUITS	9	2.2.5 Electrical Design Options—Polyphase	41
1.4.1 Concept of a Magnetic Circuit	9	2.2.6 Electrical Design Options—Single-Phase	42
1.4.2 Two-Dimensional Field Problems	12		
1.5 FINITE ELEMENT ANALYSIS OF MAGNETIC FIELDS	15		
1.5.1 Motivation	15		
1.5.2 Energy Functionals	15		
1.5.3 Finite Element Formulation	16		
1.5.4 Boundary Conditions	17		
1.5.5 Solution Techniques	17		

2.2.7 Performance on Variable-Frequency Sources	43	3.3 INITIAL MOTOR SELECTION	184
2.2.8 Linear Induction Motors	46	3.3.1 Steady-State Solutions	184
2.2.9 Doubly Fed Induction Motors	54	3.3.2 Dynamic Analysis	184
<b>2.3 DIRECT-CURRENT MOTORS</b>	<b>58</b>	<b>3.4 MOTOR EFFICIENCY AND ENERGY CONSIDERATIONS</b>	<b>185</b>
2.3.1 Introduction	58	3.4.1 Efficiency Considerations	185
2.3.2 General Description	58	3.4.2 Energy Considerations	188
2.3.3 Tests	62	<b>3.5 PAYBACK ANALYSIS AND LIFE-CYCLE COSTING OF MOTORS AND CONTROLS</b>	<b>188</b>
2.3.4 Shunt Motors	64	3.5.1 General-Purpose vs. Special Machines	189
2.3.5 Series Motors	66	<b>3.6 SAFETY CONSIDERATIONS</b>	<b>190</b>
2.3.6 Compound-Wound DC Motors	68	3.6.1 Application Information	190
2.3.7 Permanent Magnet Motors	68	3.6.2 Installation	190
2.3.8 Brushless DC Motors	70	<b>3.7 HOW TO SPECIFY A MOTOR</b>	<b>190</b>
2.3.9 Ironless Armature DC Motors	71	3.7.1 Scope	191
<b>2.4 ELECTRIC TRACTION</b>	<b>77</b>	3.7.2 Codes and Standards	191
2.4.1 Externally Powered Vehicles	78	3.7.3 Service Conditions	191
2.4.2 Internal Combustion Powered Vehicles	87	3.7.4 Starting Requirements	191
2.4.3 Battery Powered Vehicles	94	3.7.5 Rating	192
2.4.4 Design Considerations	98	3.7.6 Construction Features	193
<b>2.5 MOTORS FOR SPECIAL APPLICATIONS</b>	<b>109</b>	3.7.7 Accessories	197
2.5.1 Stepper Motors	109	3.7.8 Balance and Vibration	198
2.5.2 400-Hz Motors	123	3.7.9 Sound Levels	198
2.5.3 Deep Well Turbine Pump Motors	126	3.7.10 Paint	198
2.5.4 Submersible Motors	133	3.7.11 Nameplates	198
2.5.5 Solid-Rotor Induction Motors	134	3.7.12 Performance Tests	199
2.5.6 Synchronous Reluctance Motors	142	3.7.13 Quality Assurance	199
2.5.7 Aerospace Motors	153	3.7.14 Preparation for Shipment and Storage	199
2.5.8 Superconducting Synchronous Motor	153	3.7.15 Data and Drawings	200
2.5.9 Universal Motors	156	<b>3.8 SPECIAL APPLICATIONS</b>	<b>200</b>
2.5.10 Line-Start Synchronous Reluctance and Permanent Magnet Motors	159	3.8.1 Hermetically Sealed Refrigeration Motors	200
2.5.11 Watthour Meters	160	3.8.2 Selection of DC Motors with Chopper Drives for Battery Powered Vehicles	209
References	162	References	214
<b>3. MOTOR SELECTION</b>	<b>167</b>	<b>4. INDUCTION MOTOR ANALYSIS AND DESIGN</b>	<b>215</b>
3.1 STANDARDS	168	4.0 INTRODUCTION	216
3.1.1 Enclosures	168	4.1 INDUCTION MOTOR FIELD ANALYSIS	219
3.1.2 Dimensions	175	4.1.1 Generation of the Rotating Field	219
3.1.3 Performance	176	4.1.2 Winding of the Stator	223
<b>3.2 CHARACTERISTICS OF DRIVEN EQUIPMENT</b>	<b>181</b>	4.1.3 Spatial Harmonics in the Field Curve	237
3.2.1 Inertial Torques	182	4.1.4 Reactances of the Induction Motor	241
3.2.2 Viscous Friction Torque	182	4.1.5 Radial Force Waves	245
3.2.3 Sticking Friction	182		
3.2.4 Coulomb Friction	183		
3.2.5 Fluid Loads	183		
3.2.6 Unusual Load Situations	183		

4.1.6	Homopolar Flux and Unbalanced Magnetic Pull in the Two-Pole Induction Motor	247	4.10	FINITE ELEMENT ANALYSIS OF INDUCTION MOTORS	293
4.1.7	Tangential Forces Caused by Harmonics	249	4.10.1	Motivation for Induction Motor Finite Element Analysis	293
4.1.8	Components of Air Gap Flux Caused by Inverter Supplies	251	4.10.2	Three-Phase Induction Motor Finite Element Analysis	293
4.1.9	Switching Transients	252	4.10.3	Single-Phase Induction Motor Finite Element Analysis	296
4.2	ROTOR CONSTRUCTION	256	References		297
4.2.1	Introduction	256	<b>5. SYNCHRONOUS MOTOR ANALYSIS AND DESIGN</b>		<b>299</b>
4.2.2	Squirrel-Cage Design	257	5.0	INTRODUCTION	300
4.2.3	Wound-Rotor Design	257	5.1	FLUX AND FLUX DISTRIBUTION	300
4.3	INDUCTION MOTOR EQUIVALENT CIRCUITS	258	5.2	ARMATURE WINDINGS	300
4.3.1	Introduction	258	5.2.1	Armature Inductance	301
4.3.2	Steady-State Equivalent Circuit	258	5.2.2	Slot Leakage	301
4.3.3	Transient or Dynamic Equivalent Circuit	260	5.2.3	Harmonics in the Flux Distribution	302
4.4	EQUIVALENT CIRCUITS FOR VARIABLE FREQUENCY	261	5.2.4	Effects of Inverters	302
4.4.1	Introduction	261	5.3	FIELD WINDINGS	302
4.4.2	Rotor Deep-Bar Effect	262	5.3.1	Leakage Flux	302
4.4.3	Solution of Equivalent Circuits	263	5.3.2	Field Winding Ampere-Turns	302
4.5	IMPORTANT DESIGN EQUATIONS	263	5.4	DAMPER WINDINGS	303
4.5.1	Output Equation and Main Dimensions	263	5.4.1	Leakage Flux	303
4.5.2	Design of Stator Winding	264	5.5	EQUIVALENT CIRCUITS	303
4.5.3	Fractional Slot Winding	265	5.5.1	Steady-State Operation	303
4.5.4	Squirrel-Cage Rotor Design	265	5.5.2	V-Curves	304
4.6	SPECIAL INDUCTION MOTOR DESIGNS	271	5.5.3	Equivalent Circuits During Transients	304
4.6.1	Linear Induction Motor Design	271	5.5.4	Starting Equivalent Circuits	305
4.6.2	Solid-Rotor Induction Motor Design	273	5.6	LINEAR SYNCHRONOUS MOTORS	305
4.7	MECHANICAL DESIGN	277	5.6.1	Definitions, Geometries, and Principle of Operation	305
4.7.1	Crawling and Cogging	277	5.6.2	Topologies	306
4.7.2	Vibration and Noise	278	5.6.3	Performance Calculation	313
4.7.3	Lamination Fatigue Mechanisms	279	5.6.4	Applications	317
4.8	THERMAL DESIGN	282	5.7	DESIGN EQUATIONS FOR A SYNCHRONOUS MACHINE	318
4.8.1	Methods of Cooling	283	5.7.1	Magnetic and Electric Loading	318
4.8.2	Design of the Ventilation Circuit	284	5.7.2	Main Dimensions and Stator Windings	318
4.9	COMPUTER-AIDED DESIGN OF ELECTRIC MACHINES	284	5.7.3	Cylindrical Rotor Design	319
4.9.1	Why We Need Computers in the Design of Electric Machines	284	5.7.4	Salient-Pole Rotors	320
4.9.2	The Nature of the Design Process	285	5.7.5	Field Winding Design	320
4.9.3	Steps Needed to Design an Electric Machine	286	5.7.6	Full-Load Field Ampere-Turns	320
4.9.4	Examples of Specialized Computer Analysis	290	5.7.7	Machine Oscillations and the Damper Winding	321
4.9.5	Automation of the Design Process	292	5.8	FINITE ELEMENT ANALYSIS OF SYNCHRONOUS MOTORS	321
			5.8.1	Advantages of Finite Element Analysis of Synchronous Motors	321

5.8.2	Motors with Permanent Magnet Rotors	321	6.9.1	Advantages of FEA of DC Motors	354
5.8.3	Variable-Reluctance Stepper Motors	323	6.9.2	Permanent Magnet Brush DC Motors	355
5.8.4	Axial Flux Machines	323	6.9.3	Magnetization of Permanent Magnets	355
References		325	6.9.4	Wound-Field Brush DC Motors	356
			6.9.5	Universal Motors	356
			References		364
<b>6. DIRECT-CURRENT MOTOR ANALYSIS AND DESIGN</b>		<b>327</b>	<b>7. TESTING FOR PERFORMANCE</b>		<b>365</b>
6.0	INTRODUCTION	328	7.0	INTRODUCTION	366
6.1	ARMATURE WINDINGS	328	7.1	POLYPHASE INDUCTION MOTOR TESTING	366
6.1.1	Wave Windings	328	7.1.1	Electrical Test Standards	366
6.1.2	Equalizers	328	7.1.2	Types of Tests	366
6.1.3	Lap Windings	329	7.1.3	Sample Calculations	369
6.1.4	Machines with Reduced Numbers of Slots	330	7.1.4	Variation in Testing	369
6.2	COMMUTATORS	331	7.1.5	Miscellaneous Tests	371
6.2.1	Commutator Construction	331	7.2	SINGLE-PHASE INDUCTION MOTORS	371
6.2.2	Brushes and Holders	331	7.2.1	Electrical Test Standards	371
6.3	FIELD POLES AND WINDINGS	332	7.2.2	Types of Tests	371
6.3.1	Pole Laminations	332	7.2.3	Choices of Tests	371
6.3.2	Main Field Windings	332	7.2.4	Variations Due to Uncontrolled Factors	372
6.3.3	Commutating Poles and Windings	332	7.2.5	Curve Fitting of Performance Data	373
6.3.4	Pole Face Windings	333	7.2.6	Miscellaneous Tests	373
6.4	EQUIVALENT CIRCUIT	334	7.3	SYNCHRONOUS MOTOR TESTS	374
6.4.1	Steady-State Analysis	334	7.3.1	Electrical Test Standards	374
6.4.2	Transient Analysis	334	7.3.2	Types of Tests	374
6.5	DESIGN EQUATIONS	334	7.3.3	Choices of Tests	388
6.5.1	Magnetic Circuit	335	7.3.4	Variations Due to Uncontrolled Factors	388
6.5.2	Saturation	335	7.3.5	Curve Fitting of Performance Data	388
6.5.3	Detailed Magnetic Circuit Calculations	335	7.3.6	Miscellaneous Tests	390
6.6	DC MOTORS IN CONTROL SYSTEMS	338	7.4	DC MOTOR TESTS	391
6.6.1	Basic Motor Equations	338	7.4.1	Electrical Test Standards	391
6.6.2	Basic Mechanical Equation	339	7.4.2	Preparation for Tests	391
6.6.3	Block Diagrams	340	7.4.3	Performance Tests	392
6.6.4	Typical Motor Characteristics and Stability Considerations	341	7.4.4	Special Tests	393
6.6.5	Field Control	341	7.5	HERMETICALLY SEALED REFRIGERATION MOTORS	394
6.7	DC MOTORS SUPPLIED BY RECTIFIER OR CHOPPER SOURCES	343	7.5.1	Electrical Test Standards	394
6.7.1	List of Symbols	343	7.5.2	Types of Tests	394
6.7.2	Analysis	343	7.5.3	Choices of Tests	394
6.7.3	Rectifier Sources	344	7.5.4	Variations Due to Uncontrolled Factors	396
6.7.4	Chopper Sources	347	7.5.5	Curve Fitting of Performance Data	397
6.8	PERMANENT MAGNET DC MOTORS	349	7.5.6	Miscellaneous Tests	397
6.8.1	Magnetic Materials	349	7.6	SPECIALTY TESTING	397
6.8.2	Design Features	351	7.6.1	Induction Motor Stators	397
6.8.3	Servo and Control Motors	354	7.6.2	Induction Motor Rotors	398
6.9	FINITE ELEMENT ANALYSIS OF DC MOTORS	354			

7.6.3	Permanent Magnet Motors	400	9.1.5	Accelerating Torque and Multispeed Applications	456
7.7	SELECTION AND APPLICATION OF TEST EQUIPMENT	400	9.1.6	Starting Duty Thermal Limitations	461
7.7.1	Reasons for Testing	400	9.1.7	Miscellaneous Induction Motor Starting Topics	464
7.7.2	Functional Specifications of Test Equipment	400	9.1.8	Bus Transfer and Reclosing of Induction Machines	467
7.7.3	Recommended Steps in Purchasing Test Equipment	401	9.1.9	Induction Motor Speed Control	473
7.7.4	Types of Tests	401	9.1.10	Induction Motor Braking	474
7.7.5	Types of Data Recording Devices	401	9.2	DIRECT-CURRENT MOTORS	475
7.7.6	Mechanical and Electrical Loading Devices	402	9.2.1	DC Motor Starting	475
7.7.7	Instrumentation	403	9.2.2	DC Motor Speed Control	477
References		404	9.2.3	Braking of Direct-Current Motors	480
<b>8. MOTOR INSULATION SYSTEMS</b>		<b>407</b>	9.3	GENERAL CONSIDERATIONS CONCERNING SOLID-STATE CONVERTERS AND CONTROLLERS	482
8.1	INTRODUCTION	407	9.3.1	Converters	482
8.1.1	Insulation and Ratings	408	9.3.2	Controllers	483
8.1.2	Influence of Insulation on Motor Efficiency	408	9.4	POWER ELECTRONIC DEVICES	483
8.1.3	Influence of Insulation on Motor Life	408	9.4.1	Diodes	484
8.1.4	Random- and Form-Wound Motors	409	9.4.2	Thyristors	484
8.2	RANDOM-WOUND MOTORS	410	9.4.3	Gate Turn-Off Thyristors	485
8.2.1	Insulation System of Random- Wound Motors	410	9.4.4	Bipolar Transistors	486
8.2.2	Insulation Testing of Random- Wound Motors	412	9.4.5	Metal Oxide Semiconductor Field-Effect Transistors	487
8.2.3	Causes of Insulation Failure	415	9.4.6	Insulated-Gate Bipolar Transistors	488
8.3	FORM-WOUND MOTORS	416	9.4.7	Integrated Gate-Commutated Thyristor	488
8.3.1	Insulation Systems	416	9.5	CONVERTER CIRCUITS	488
8.3.2	Factors Affecting Insulation System Design	419	9.5.1	Rectifier Circuits	489
8.3.3	Insulation Testing	422	9.5.2	Cycloconverters	492
8.4	EFFECT OF INVERTER DRIVES ON STATOR INSULATION	427	9.5.3	Chopper Circuits	493
8.4.1	Surge Voltage Environment	427	9.5.4	Six-Step Inverters	493
8.4.2	Distribution of Voltage Surges within Stator Windings	428	9.5.5	Pulse-Width Modulation Inverters	495
8.4.3	Mechanisms of Insulation Deterioration	429	9.5.6	Multilevel Converters	498
References		429	9.6	CONTROLLERS	498
General References		430	9.7	OPEN- AND CLOSED-LOOP CONTROL OF A PERMANENT MAGNET STEPPER MOTOR	500
<b>9. MOTOR CONTROL</b>		<b>431</b>	9.7.1	Open-Loop Operation of the Stepper Motor	501
9.0	INTRODUCTION	432	9.7.2	Closed-Loop Control of a Stepper Motor	503
9.1	INDUCTION MOTORS	432	9.7.3	Experimental Results	509
9.1.1	Electrical Voltage Surges	432	References		511
9.1.2	Voltage Drop During Start-up	437	<b>10. MOTOR PROTECTION</b>		<b>515</b>
9.1.3	Starting Torque Characteristics	447	Part A Overview		
9.1.4	Reduced Starting Duty Schemes	451	10.1	INTRODUCTION	516
			10.2	PROTECTION AGAINST OVERLOADS	516



10.2.1 Fuses	517	10.9.4 Selection of Bimetallic Thermal Protectors for Shaded-Pole, Permanent-Split Capacitor, and Other Slow Heat Rise Single-Phase Motors	536
10.2.2 Thermal Overload Relays	517	10.9.5 Selection of Bimetallic Thermal Protectors for Single-Voltage Split-Phase, Capacitor-Start, Capacitor-Start/Capacitor-Run, and Other Single-Phase Motors	537
10.2.3 Switchgear-Type Thermal Relays	517	10.9.6 Selection of Bimetallic Thermal Protectors for Dual-Voltage Split-Phase, Capacitor-Start, Capacitor-Start/Capacitor-Run Single-Phase Motors	540
10.2.4 Imbedded Temperature Detectors	517	10.9.7 Selection of Bimetallic Thermal Protectors for Three-Phase Motors	541
10.2.5 Microprocessor Motor Protection Relays	518	10.10 TESTING AGENCY REQUIREMENTS FOR MOTOR THERMAL PROTECTORS	542
10.2.6 Damper Bar Protection	520	10.10.1 General	542
10.2.7 Special Current Detection	520	10.10.2 Protection Types	542
10.2.8 Pull-Out Protection	520	10.10.3 Test Voltages and Frequencies	542
10.3 UNBALANCED VOLTAGE PROTECTION	520	10.10.4 Protector Calibration Ranges	543
10.3.1 Phase Loss Relays	521	10.10.5 Temperature Measurements	543
10.3.2 Negative-Sequence Voltage Relays	521	10.10.6 Ambient Temperature	543
10.3.3 Current Unbalance Relays	521	10.10.7 Multispeed Motors	543
10.3.4 Microprocessor Devices	521	10.10.8 Motor Mountings	543
10.4 PROTECTION FOR INTERNAL ELECTRICAL FAILURES	521	10.11 PERFORMANCE REQUIREMENTS AND TESTS	543
10.4.1 Stator Insulation Failure Protection	521	10.11.1 Running Heating Tests	543
10.4.2 Microprocessor Protection for Internal Faults	522	10.11.2 Running Overload Tests	543
10.5 SELECTION OF SWITCHING DEVICES	522	10.11.3 Locked-Rotor Tests	544
10.5.1 Contactors	522	10.11.4 Locked-Rotor Endurance Test	544
10.5.2 Electrically Operated Circuit Breakers	522	10.11.5 Dielectric Tests	544
10.6 MECHANICAL PROTECTION	523	10.11.6 Limited Short-Circuit Tests	544
10.6.1 Vibration Detectors	523	References	545
10.6.2 Bearing Temperature Monitors	523	<b>11. MECHANICAL CONSIDERATIONS</b>	<b>547</b>
10.6.3 Microprocessor Protection	524	11.1 NOISE	548
10.7 ACCESSORIES	524	11.1.1 Noises of Electromagnetic Origin	551
10.7.1 Filters	524	11.1.2 Influence of Motor Configuration and Design	554
10.7.2 Ventilation Opening Guards	524	11.1.3 Regulation of Noise: Typical Levels	555
10.7.3 Space Heaters	524	11.1.4 Reduction of Noise Levels: Special Treatment	560
Part B Fuses and Protection Coordination		11.1.5 Experimental Investigation of Noise	561
10.8 INTRODUCTION	524	11.2 VIBRATION	566
10.8.1 Single-Element Fuses	525	11.2.1 Vibration Measurement and Evaluation	568
10.8.2 Protection Coordination with Single-Element Fuses	525		
10.8.3 Dual-Element Fuses	527		
10.8.4 Protection Coordination with Dual-Element Fuses	528		
10.8.5 Single-Phasing Protection	529		
Part C Bimetallic Thermal Protectors			
10.9 INTRODUCTION	532		
10.9.1 Definitions	532		
10.9.2 Typical Devices	533		
10.9.3 Considerations in Device Selection	535		

11.2.2	Housing and Shaft Vibration	571	12.7.1	Ambient Temperature	640
11.2.3	Mounting	572	12.7.2	Altitude	640
11.2.4	Variable-Speed Motors	572	12.7.3	Moisture	641
11.2.5	Standards	573	12.7.4	Solid Contaminants	641
11.3	BALANCING THE ROTOR	575	12.7.5	Chemicals	642
11.3.1	Rigid Rotors	575	12.7.6	Hazardous Locations	642
11.3.2	Flexible Rotors	575	12.7.7	Seismic Activity	643
11.3.3	Unbalance Quality	576	12.7.8	Nuclear Plant Safety	643
11.4	BEARINGS	576	12.8	POWER SYSTEM QUALITY	644
11.4.1	Sleeve Bearings	576	12.8.1	Parameters of Power System Quality	644
11.4.2	Antifriction Bearings	591	12.8.2	Adjustable Speed Drives	650
11.5	BRUSHES	596	References		653
11.5.1	Introduction	596	<b>13. RELIABILITY</b>		<b>655</b>
11.5.2	Grade Characteristic Definitions	597	13.1	RELIABILITY OF LARGE MOTORS	656
11.5.3	Specialty Brushes	601	13.1.1	Introduction	656
11.5.4	Summary	602	13.1.2	IEEE 1983–1985 Survey	656
11.6	MOTOR HANDLING, MOUNTING, AND MECHANICAL CONNECTION	602	13.1.3	Failure Rate and Downtime Data	656
11.6.1	Motor Handling	602	13.1.4	Data on Failed Components	657
11.6.2	Motor Mounting Dimensions	603	13.1.5	Causes of Failure	658
11.6.3	Shaft Connections—Belts	610	13.1.6	Comparison: 1973–1974 and 1983–1985 IEEE Surveys	659
11.6.4	Shaft Connections—Chain and Sprocket Drives and Flat Belt Drives	613	13.1.7	Comparison: AIEE 1962 and 1983–1985 IEEE Surveys	659
11.6.5	Shaft Connections—Couplings	613	13.1.8	Comparison: 1983 EPRI and 1983–1985 IEEE Surveys	660
11.6.6	Shaft Connections—Splines	614	13.2	RELIABILITY OF ANTIFRICTION BEARINGS	660
11.6.7	Initial Operation	614	13.2.1	Failure Modes of Rolling Bearings	660
References		614	13.2.2	Damage Progression to Failure	662
<b>12. ENVIRONMENTAL CONSIDERATIONS</b>		<b>617</b>	13.2.3	Statistical Variation of Bearing Life	663
12.1	INTRODUCTION	618	13.3	GUIDELINES FOR SUCCESSFUL COMMUTATION AND BRUSH OPERATION	663
12.2	HEAT TRANSFER	619	13.3.1	Summary	663
12.2.1	Modes of Heat Transfer	620	13.3.2	Introduction	663
12.2.2	Ventilation	623	13.3.3	Acceptable Commutator Conditions	663
12.3	COOLING OF BASIC MOTOR TYPES	626	13.3.4	Destructive Commutator Conditions	664
12.3.1	Induction Motors	626	13.3.5	Conclusion	669
12.3.2	Synchronous Motors	627	13.3.6	Reference Note	669
12.3.3	DC Motors	627	13.4	MONITORING FOR SIGNS OF WEAROUT	669
12.3.4	Special Cooling	627	13.4.1	Introduction	669
12.4	ENCLOSURES	628	13.4.2	On-Line Tests	669
12.4.1	IEC Enclosures	628	13.4.3	Off-Line Tests	670
12.4.2	NEMA Enclosures	628	13.4.4	Continuous (On-Line) or Periodic (Off-Line)?	672
12.5	THERMAL CIRCUITS	629			
12.5.1	Steady-State Circuits	630			
12.5.2	Time-Varying Circuits	632			
12.5.3	Simplified Circuits	633			
12.6	DUTY CYCLES	636			
12.6.1	RMS Loading Analysis	636			
12.6.2	Time-Constant Analysis	638			
12.7	AMBIENT AND ENVIRONMENTAL EFFECTS	639			

13.5	RELIABILITY IMPACT OF ADJUSTABLE SPEED DRIVES (ASDs) ON BEARINGS	672	14.6	CORE TESTING	719
	13.5.1 Introduction	672	14.6.1	Loop Test Physical Arrangement	719
	13.5.2 Bearing Current Induced by Supply Voltage	673	14.6.2	Thermovision Monitoring During the Loop Test	720
	13.5.3 An Equivalent Circuit for Bearing Displacement and EDM Currents	677	14.6.3	Other Core Test Factors	721
	13.5.4 Methods to Mitigate Bearing Currents and Their Cost	688	14.6.4	Core Hot Spot Repairs	721
13.6	RELIABILITY IMPACT OF ADJUSTABLE SPEED DRIVES (ASDs) ON INSULATION	690	14.6.5	EL CID Test	721
	References	690		References	727
<b>14.</b>	<b>MAINTENANCE</b>	<b>693</b>	<b>15.</b>	<b>ELECTRONIC MOTORS</b>	<b>731</b>
14.1	LUBRICATION	694	15.1	ALTERNATING CURRENT MOTOR SPEED CONTROL	732
	14.1.1 Lubrication and Maintenance of Sleeve Bearings	694	15.1.1	Introduction	732
	14.1.2 Lubrication and Maintenance of Antifriction Bearings	694	15.1.2	Thyristor-Based Voltage- Controlled Drives	733
14.2	IMPLEMENTATION OF A RELIABILITY BASED MAINTENANCE PROGRAM	698	15.1.3	Thyristor-B ased Load- Commutated Inverter Synchronous Motor Drives	736
14.3	MAINTENANCE AND REPAIR OF COMMUTATORS	700	15.1.4	Transistor-Based Variable- Frequency Induction Motor Drives	740
	14.3.1 Causes of Poor Commutation	701	15.1.5	Field Orientation	746
	14.3.2 Ordering New Parts	702	15.1.6	Induction Motor Observer	752
14.4	BRUSH REPLACEMENT	702	15.1.7	Permanent Magnet Alternating Current Machine Control	754
	14.4.1 Introduction	702	15.2	WITCHED-RELUCTANCE MACHINES	759
	14.4.2 When to Replace Brushes	702	15.2.1	Definition, History, and Properties	759
	14.4.3 Installation of Brushes	702	15.2.2	Theory of Operation	760
	14.4.4 Summary	704	15.2.3	Controller Architecture	763
14.5	MAINTENANCE AND REPAIR OF WINDINGS	704	15.2.4	Applications	763
	14.5.1 Installation of New Equipment	704	15.3	BRUSHLESS DC MOTORS	763
	14.5.2 Establishing a Maintenance Schedule	705	15.3.1	Introduction	763
	14.5.3 Choosing Test Equipment	705	15.3.2	Rotor Construction	764
	14.5.4 Performing Preventative Maintenance	707	15.3.3	Magnets and the Magnetic Circuit	765
	14.5.5 Evaluating Winding Failures	711	15.3.4	Armature Windings	768
	14.5.6 Choosing Repair Facilities	715	15.3.5	Torque Analysis	769
	14.5.7 Selecting Repair Methods	716	15.3.6	Voltage Analysis	770
	14.5.8 Testing Repaired Windings	718	15.3.7	Equivalent Circuit	770
	14.5.9 Evaluating Repaired Equipment	718	15.3.8	Motor Drive Circuit	770
	14.5.10 General References on Maintenance and Repair of Windings	719	15.3.9	Performance	771
				References	772
				<i>Appendixes</i>	
				<i>A Equivalent Units</i>	775
				<i>B Association and Institute Addresses</i>	777

# Contributors

**Robert G.Bartheld\*** Consultant, Siemens Energy and Automation, Inc., Roswell, Georgia, U.S.A.

**Richard K.Barton\*** Consultant, General Electric Company, Erie, Pennsylvania, U.S.A.

**David Bertenshaw** Adwel International, Ltd., Watford, Herts, England

**Marc Bodson** University of Utah, Salt Lake City, Utah, U.S.A.

**Stewart V.Bowers** Emerson Computational Systems, Inc., Knoxville, Tennessee, U.S.A.

**L.Edward Braswell III** Life Cycle Engineering, Charleston, South Carolina, U.S.A.

**John R.Brauer** Milwaukee School of Engineering, Fish Creek, Wisconsin, U.S.A.

**Robert N.Brigham<sup>†</sup>** Octagon Engineering, Monroe, Connecticut, U.S.A.

**Kenneth A.Bruni\*** National Electrical Carbon, Downingtown, Pennsylvania, U.S.A.

**Lloyd W.Buchanan\*** Consultant, Lima, Ohio, U.S.A.

**Kao Chen<sup>†</sup>** Carlson's Consulting Engineers, Inc., San Diego, California, U.S.A.

**John N.Chiasson** University of Tennessee, Knoxville, Tennessee, U.S.A.

**Paul L.Cochran\*** Consultant, General Electric Company, Schenectady, New York, U.S.A.

**Frank DeWolf<sup>†</sup>** General Electric Company, Erie, Pennsylvania, U.S.A.

**Richard E.Dippery, Jr.** Kettering University, Flint, Michigan, U.S.A.

**Gopal K.Dubey** Indian Institute of Technology, Kanpur, India

**James H.Dymond** General Electric Company, Peterborough, Ontario, Canada

**Richard H.Engelmann\*** University of Cincinnati, Cincinnati, Ohio, U.S.A.

**Edwin Fisher** General Electric Company, Fort Wayne, Indiana, U.S.A.

**Jacek F.Gieras** United Technologies Research Center, Hartford, Connecticut, U.S.A.

**Glenn Goebel\*** Kirwood Commutator Company, Lakewood, Ohio, U.S.A.

**Richard D.Hall** National Electrical Carbon, Greenville, South Carolina, U.S.A.

**Howard B.Hamilton<sup>†</sup>** University of Pittsburgh, Pittsburgh, Pennsylvania, U.S.A.

**Charles R.Heising** Industrial Reliability, Wynnewood, Pennsylvania, U.S.A.

**Howard F.Hendricks, Sr.\*** Consultant, Penn Engineering and Manufacturing Corporation, Prescott, Arizona, U.S.A.

**George E.Herzog\*** Consultant, Troy, Ohio, U.S.A.

**William R.Hoffmeyer\*** General Electric Company, Holland, Michigan, U.S.A.

**Paul R.Hokanson** General Electric Company, Erie, Pennsylvania, U.S.A.

- J.Edward Jenkins, Jr.** Jenkins Electric Company, Charlotte, North Carolina, U.S.A.
- Karel Jezernik** University of Maribor, Maribor, Slovenia
- J.Herbert Johnson\*** Consultant, A.O. Smith Electrical Products Company, Tipp City, Ohio, U.S.A.
- George D.Kalinovich** Woodward FST, Greenville, South Carolina, U.S.A.
- Swarn S.Kalsi** American Superconductor Corporation, Westborough, Massachusetts, U.S.A.
- Shailesh Kapadia\*** Welco Industries, Inc., Houston, Texas, U.S.A.
- Haran C.Karmaker** General Electric Company, Peterborough, Ontario, Canada
- Russell J.Kerkman** Allen-Bradley, Milwaukee, Wisconsin, U.S.A.
- Gerald B.Kliman<sup>†</sup>** Rensselaer Polytechnic Institute, Troy, New York, U.S.A.
- Eugene A.Klingshirn\*** Cleveland State University, Cleveland, Ohio, U.S.A.
- Norman L.Kopp** Windings, Inc., New Ulm, Minnesota, U.S.A.
- Thomas A.Lipo** University of Wisconsin, Madison, Wisconsin, U.S.A.
- Walter E.Littmann\*** Metal Failure Investigations, Inc., West Chester, Ohio, U.S.A.
- Joseph C.Liu\*** Oil Dynamics, Inc., Tulsa, Oklahoma, U.S.A.
- Jerry D.Lloyd** Emerson Motor Technology, St. Louis, Missouri, U.S.A.
- Walter J.Martiny\*** Consultant, General Electric Company, Fort Wayne, Indiana, U.S.A.
- Jeffrey Mazereeuw** General Electric Company, Multilin, Markham, Ontario, Canada
- Robert M.McCoy\*** Consultant, General Electric Company, Orleans, Massachusetts, U.S.A.
- Edgar F.Merrill\*** Consultant, Westinghouse, Austin, Texas, U.S.A.
- William H.Middendorf<sup>†</sup>** University of Cincinnati, Cincinnati, Ohio, U.S.A.
- T.J.E.Miller** University of Glasgow, Glasgow, Scotland
- David M.Mullen\*** Siemens Energy and Automation, Covington, Kentucky, U.S.A.
- Richard L.Nailen\*** Consultant, Hales Corners, Wisconsin, U.S.A.
- Vilas D.Nene** The MITRE Corporation, McLean, Virginia, U.S.A.
- Chauncey Jackson Newell\*** Consultant, Erie, Pennsylvania, U.S.A.
- Neil Nichols** KSG Consulting Engineers, Inc, Glendale, California, U.S.A.
- Nils E.Nilsson** Ohio Edison Company, Akron, Ohio, U.S.A.
- Robert Oesterli\*** Consultant, Magnetek Inc., St. Louis, Missouri, U.S.A.
- Thomas H.Ortmeyer** Clarkson University, Potsdam, New York, U.S.A.
- Edward L.Owen** General Electric Company, Schenectady, New York, U.S.A.
- Philip Packard** General Electric Company, Fort Wayne, Indiana, U.S.A.
- Derek Paley** Adwel International, Ltd., Watford, Herts, England
- Edward P.Priebe\*** Consultant, General Electric Company, Erie, Pennsylvania, U.S.A.
- Eike Richter\*** Consultant, General Electric Company, Vancouver, Washington, U.S.A.
- Dennis L.Rimmel** Sloan Electric Company, San Diego, California, U.S.A.
- Roland Roberge** National Electrical Carbon, Greenville, South Carolina, U.S.A.
- Vincent I.Saporita** Cooper Industries, St. Louis, Missouri, U.S.A.
- Mulukutla S.Sarma** Northeastern University, Boston, Massachusetts, U.S.A.
- Mladen Sasik** Adwel International, Ltd., Toronto, Ontario, Canada
- R.Gene Smiley** MTS Systems, Milford, Ohio, U.S.A.

**Robert L. Steigerwald** General Electric Company, Niskayuna, New York, U.S.A.

**Lewis E. Unnewehr\*** Ford Motor Company, Ormond Beach, Florida, U.S.A.

**Gregory C. Stone** Iris Engineering, Toronto, Ontario, Canada

**Alfredo Vagati** Politecnico di Torino, Turin, Italy

**Peregrin L. Timár** Royal Melbourne Institute of Technology, Melbourne, Victoria, Australia

**Sheo P. Verma\*** University of Saskatchewan, Saskatoon, Saskatchewan, Canada

**Colin E. Tindall\*** Queen's University, Ballinahinch, Northern Ireland

**Edward J. Woods\*** Consultant, Boeing Company, Poulso, Washington, U.S.A.

**Hamid A. Toliyat** Texas A&M University, College Station, Texas, U.S.A.

---

\*Retired

†Deceased

# 1

## Principles of Energy Conversion

Vilas D.Nene and Hamid A.Toliyat (Sections 1.1–1.4, 1.6, and 1.7)/John R.Brauer (Section 1.5)

<b>1.1 GENERAL BACKGROUND</b>	<b>2</b>
<b>1.2 MAGNETIC MATERIALS</b>	<b>4</b>
1.2.1 Properties of Ferromagnetic Materials	5
1.2.2 Boundary Conditions for $\vec{B}$ and $\vec{H}$	6
<b>1.3 SOME BASIC FUNCTIONS RELATED TO ELECTROMAGNETIC FIELDS</b>	<b>6</b>
1.3.1 Scalar Potential	7
1.3.2 Vector Potential	7
1.3.3 Electromagnetic Induction	8
1.3.4 Energy in an Electromagnetic Field	8
1.3.5 Self-Inductance and Mutual Inductance	8
1.3.6 Energy Stored in a Current-Carrying Coil	9
<b>1.4 MAGNETIC CIRCUITS</b>	<b>9</b>
1.4.1 Concept of a Magnetic Circuit	9
1.4.2 Two-Dimensional Field Problems	12
<b>1.5 FINITE ELEMENT ANALYSIS OF MAGNETIC FIELDS</b>	<b>15</b>
1.5.1 Motivation	15
1.5.2 Energy Functional	15
1.5.3 Finite Element Formulation	16
1.5.4 Boundary Conditions	17
1.5.5 Solution Techniques	17
1.5.6 Parameters from Fields	19
1.5.7 Applications in Two and Three Dimensions	19
1.5.8 Finite Elements Compute Equivalent Circuit Parameters	19
1.5.9 Finite Elements Directly Compute Motor Performance	20
<b>1.6 ENERGY STORED IN MAGNETICALLY COUPLED MULTIPLE-LOOP SYSTEMS</b>	<b>21</b>
<b>1.7 FORCES AND TORQUES IN THE SYSTEM</b>	<b>21</b>
<b>REFERENCES</b>	<b>23</b>
<b>SUGGESTED READING</b>	<b>24</b>

## 1.1 GENERAL BACKGROUND

The study of electromagnetic devices involves interactions between elemental electric charges at a *macroscopic* level. Consequently, a crude atomic model, consisting of a heavy positively charged nucleus with a number of light negatively charged electrons orbiting around it, is sufficient for developing the concepts of electromagnetics. An electron is then the elemental negative electric charge; a proton is the elemental positive charge. A *charged body* has a surplus of either positive or negative elemental charges. Charged bodies may be considered as *point charges* when the distances between them are very large in comparison to their dimensions.

The electric force, called the *Coulomb force*, between two static point charges is given by Coulomb's equation:

$$\bar{F}_{12} = \frac{1}{4\pi\epsilon} \frac{q_1 q_2}{r^2} \bar{u}_{12} \quad (1.1)$$

where

- $\bar{F}_{12}$  = the force in newtons (N) on the point charge  $q_2$  due to the point charge  $q_1$
- $q_1, q_2$  = the magnitudes in coulombs (C) of the two point charges
- $r$  = the distance in meters (m) between the two charges
- $\bar{u}_{12}$  = a unit vector directed from  $q_1$  to  $q_2$
- $\epsilon$  = the permittivity in Farads per meter (F/m) of the medium in which charges are placed

The two charges will repel each other if they are of the same sign; they will attract each other if they are of opposite signs.

Equation 1.1 may be written as:

$$\begin{aligned} \bar{F}_{12} &= \left( \frac{q_1}{4\pi\epsilon r^2} \bar{u}_{12} \right) q_2 \\ &= q_2 \bar{E}_{12} \end{aligned} \quad (1.2)$$

The vector function  $\bar{E}_{12}$ , called the *electric field* caused by the charge  $q_1$ , is the force exerted by  $q_1$  on a unit charge placed at a distance  $r$  in the direction of  $\bar{u}_{12}$ . This function may be defined for all points in space surrounding the charge  $q_1$ .

If there are several charges  $q_1, q_2, \dots, q_N$  present in space, the resulting electric field  $\bar{E}$  at any point in space may be obtained by vectorially adding the electric fields  $\bar{E}_1, \bar{E}_2, \dots, \bar{E}_N$  caused by these charges; that is, by using the principle of superposition of electric fields.

The Coulomb force on a charge  $q$  placed in an electric field  $\bar{E}$  can then be written as:

$$\bar{F} = q \bar{E} \quad (1.3)$$

If the two point charges  $q_1$  and  $q_2$  are in motion with respect to the observer, the force between them differs from the Coulomb force of Eq. 1.1, and is given by:

$$\bar{F}_{12} = \frac{1}{4\pi\epsilon} \frac{q_1 q_2}{r^2} \bar{u}_{12} + \frac{\mu}{4\pi} \frac{q_1 q_2}{r^2} \bar{v}_2 \times (\bar{v}_1 \times \bar{u}_{12}) \quad (1.4)$$

where:

- $\bar{v}_1, \bar{v}_2$  = the velocities of motion of the two point charges in meters per second (m/s)
- $\mu$  = the permeability of the medium in henrys per meter (H/m)

The second term in the force law of Eq. 1.4 is referred to as the *magnetic force* between the charges.

The ratio of the maximum value of the magnetic force and the Coulomb (electric) force is:

$$\left. \frac{F_{\text{magnetic}}}{F_{\text{electric max}}} \right|_{\text{max}} = \epsilon \mu \bar{v}_1 \bar{v}_2 \quad (1.5)$$

If the medium is free space, with permittivity of  $\epsilon_0$  ( $8.854 \times 10^{-12}$ ) and permeability of  $\mu_0$  ( $4\pi \times 10^{-7}$ ), this ratio becomes:

$$\left. \frac{F_{\text{magnetic}}}{F_{\text{electric}}} \right|_{\text{max}} = \frac{\bar{v}_1 \bar{v}_2}{c_0^2} \quad (1.6)$$

where  $c_0$  is the velocity of light in free space. The magnitude of the magnetic force compared to the electric force is thus quite small for velocities much smaller than the speed of light. When the charges are associated with moving electrons, however, the magnitude of the magnetic forces are quite significant.

The magnetic force between two moving charges as given in Eq. 1.4 can alternatively be written as:

$$\bar{F}_{m12} = q_2 \bar{v}_2 \times \left( \frac{\mu}{4\pi} \frac{q_1 \bar{v}_1 \times \bar{u}_{12}}{r^2} \right) \quad (1.7)$$

The term in parentheses depends only on the properties of the point charge  $q_1$ , and can be considered to represent a certain vector function existing around the charge  $q_1$  whenever it moves with respect to the observer; if the charge is stationary, the function is zero. This vector function, termed the *magnetic flux density* produced by a single moving charge, is thus defined as:

$$\bar{B}_1 = \frac{\mu}{4\pi} \frac{q_1 \bar{v}_1}{r^2} \times \bar{u}_{12} \quad (1.8)$$

The magnetic force on charge  $q_2$  moving with a velocity  $v_2$  can now be written in terms of the magnetic flux density produced by the moving charge  $q_1$  as:

$$\bar{F}_{m12} = q_2 \bar{v}_2 \times \bar{B}_1 \quad (1.9)$$

From Eq. 1.9, the unit of measurement  $\bar{B}$  of is newton-second per coulomb-meter (N-s/C-m), which is referred to as the *tesla* (T), also equivalent to one weber per square meter (Wb/m<sup>2</sup>).

The portion of the space in which moving charge experiences a magnetic force described by Eq. 1.9 is called a *magnetic field*. If there are several charges moving with respect to the observer with velocities much smaller than the speed of light, the total force on any charge may be obtained by vectorially adding forces exerted on it by each charge individually; that is, by using the principle of superposition of magnetic forces. For the several moving charges  $q_1, q_2, \dots$ ,



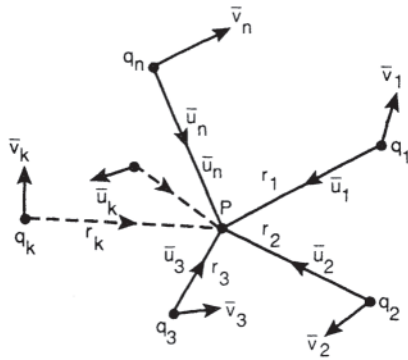


**Figure 1.1** A number of moving charges in space.

$q_N$ , as shown in Fig. 1.1, the resulting flux density  $\bar{B}$  at the point  $P$  in space can be written as:

$$\begin{aligned}\bar{B} &= \sum_{k=1}^N \bar{B}_k \\ &= \frac{\mu}{4\pi} \sum_{k=1}^N \frac{q_k \bar{v}_k}{r_k^2} \times \bar{u}_k\end{aligned}\quad (1.10)$$

If there is now a charge  $q$  at  $P$  moving with a velocity  $\bar{v}$ , the total magnetic force on the charge  $q$  is given by:

$$\bar{F}_m = q\bar{v} \times \bar{B}\quad (1.11)$$

The sum of the Coulomb force and the magnetic force on a moving charge  $q$  can now be written as:

$$\bar{F} = q(\bar{E} + \bar{v} \times \bar{B})\quad (1.12)$$

This is the classic Lorentz force on a charge.

Equation 1.12 can be applied to obtain the force experienced by a current-carrying conductor placed in a magnetic field. Considering an elemental volume  $\delta V$  of conductor with  $N$  free charges per unit volume, the force  $\delta\bar{F}$  on it is given as:

$$\delta\bar{F} = (Nq\delta V)\bar{v} \times \bar{B}\quad (1.13)$$

The quantity  $Nq\bar{v}$ , with the units of coulombs per meter squared-second ( $C/m^2\cdot s$ ), is commonly referred to as the current density  $\bar{J}$  in amperes per square meter ( $A/m^2$ ). The force on the elemental volume can then be written as:

$$\delta\bar{F} = \bar{J} \times \bar{B} \delta V\quad (1.14)$$

and the total force on a given volume is then:

$$\bar{F} = \int_V \bar{J} \times \bar{B} \delta V\quad (1.15)$$

If the current is flowing through a thin wire, the above equation can be rewritten in conventional terms as follows. Taking the elemental volume as a small length of the conductor in Fig. 1.2, the current flow is along the length of the wire with:

$$\bar{J} dV = I d\bar{l}\quad (1.16)$$

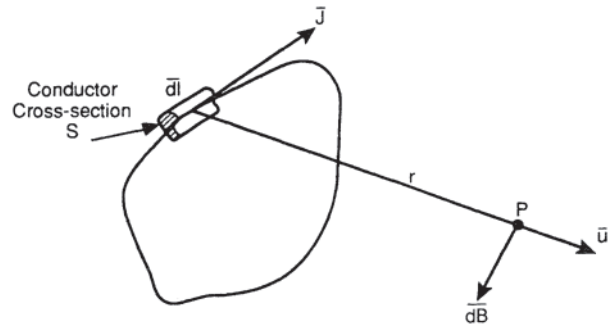


**Figure 1.2** Magnetic field of a current-carrying coil.

For a closed-current-carrying loop, the force is then:

$$\bar{F} = I \oint d\bar{l} \times \bar{B}\quad (1.17)$$

In a similar manner, Eq. 1.10 can be applied to obtain the magnetic field resulting from a steady current. Again consider a small volume  $\delta V$  containing  $N$  free charges per unit volume, with  $q$  being the magnitude of each charge. If the volume  $\delta V$  is sufficiently small, all the charges can be considered to move with the same velocity  $\bar{v}$ . The magnetic flux density at a distance  $r$  resulting from these charges can then be written as:

$$\begin{aligned}\delta\bar{B} &= \frac{\mu}{4\pi} \frac{Nq\bar{v}}{r^2} \times \bar{u} \delta V \\ &= \frac{\mu}{4\pi} \frac{\bar{J} \times \bar{u}}{r^2} \delta V\end{aligned}\quad (1.18)$$

The flux density produced by a given volume is then:

$$\bar{B} = \frac{\mu}{4\pi} \int_V \frac{\bar{J} \times \bar{u}}{r^2} dV\quad (1.19)$$

For the current-carrying coil of Fig. 1.2, this expression can be rewritten as:

$$\bar{B} = \frac{\mu I}{4\pi} \oint_c \frac{d\bar{l} \times \bar{u}}{r^2}\quad (1.20)$$

A steady electric current  $I$  thus produces a static magnetic field at a macroscopic level.

For any surface within a magnetic field, a scalar function denoted as  $\phi$  defines the *magnetic flux* flowing across the surface as:

$$\phi = \int_S \bar{B} \cdot d\bar{S}\quad (1.21)$$

The unit of magnetic flux is the weber (Wb). To help visualize the magnetic field, magnetic flux lines and magnetic flux tubes are used. A *magnetic flux line* is drawn tangential to  $\bar{B}$  at all points. A *magnetic flux tube* is tubular surface formed by magnetic flux lines. Because  $\bar{B}$  by this definition is tangential to the surface of a magnetic flux tube, the magnetic flux in any cross section along the length of a tube is constant. It is customary to draw magnetic flux lines representing tubes of equal flux; the density of the flux lines is then a measure of the magnitude of the flux density vector  $\bar{B}$ .

It also follows that the magnetic flux through any closed surface is zero, i.e.:

$$\oint \vec{B} \cdot d\vec{S} = 0 \tag{1.22}$$

This is also expressed in differential form as:

$$\text{div } \vec{B} = 0 \tag{1.23}$$

It must be noted here that two distinctly different approaches have been introduced in analyzing the performance of electromagnetic devices. These are a *field approach*, which attempts to solve for the electromagnetic field in and around the device, and a *circuit approach*, which considers different devices to be a system of magnetically coupled current-carrying coils. An attempt is made here to develop the basic concepts that will be useful to both these approaches.

For any current loop placed in a steady magnetic field, as shown in Fig. 1.3, the field can be resolved into two components in relation to the loop, the normal component  $\vec{B}_N$  and the parallel component  $\vec{B}_p$ . Using the results of Eq. 1.17, the normal component  $\vec{B}_N$  will exert deforming forces  $\vec{F}_2$  on the loop that will tend to increase or decrease the size of the loop. The parallel component  $\vec{B}_p$ , however, will produce  $\vec{F}_1$  forces that create a torque on the loop, tending to turn the loop so that the magnetic field generated by the current loop will coincide with the direction of  $\vec{B}$ .

The torque  $\vec{T}$  on the loop is given by:

$$\vec{T} = I\vec{S} \times \vec{B} \tag{1.24}$$

where  $\vec{S}$  is the area of the loop, with the vector directed toward the magnetic flux density caused by the current in the loop; that is, if a right-hand screw is turned in the direction of the current in the loop,  $\vec{S}$  will point to the direction of the longitudinal screw motion. The product  $I\vec{S}$  is usually called the *magnetic moment*  $\vec{m}$  of the loop, and then:

$$\vec{T} = \vec{m} \times \vec{B} \tag{1.25}$$

### 1.2 MAGNETIC MATERIALS

The concepts just developed may be used to study the magnetic behavior of materials. From a macroscopic point of view, and on the basis of the crude atomic model described earlier, electrons moving in circular orbits around the nucleus may be considered as tiny current loops. A magnetic moment can be associated with each atom because of the current loops represented by the moving electrons. In the absence of an external magnetic field, the magnetic moment vectors associated with individual atoms are randomly oriented in space, and consequently result in a net zero magnetic field at a macroscopic level. When placed in an external magnetic field, each atom experiences a torque that tends to align the individual moments in the direction of the field. Because of the intra-atomic and interatomic forces and dynamics, the individual moments of atoms within the material do not all orient themselves with the external magnetic field. The net magnetic field generated by this realignment within the material is denoted as  $\vec{M}$ . For most substances, the magnetization  $\vec{M}$  is given by:

$$\vec{M} = \frac{1}{\mu_0} \frac{\chi_m}{1 + \chi_m} \vec{B} \tag{1.26}$$

The constant  $\chi_m$  is referred to as the *magnetic susceptibility* of the material.

The *magnetic field intensity*  $\vec{H}$  is defined as:

$$\vec{H} = \frac{\vec{B}}{\mu_0} - \vec{M} \tag{1.27}$$

The magnetic field intensity is measured in terms of amperes per meter (A/m).

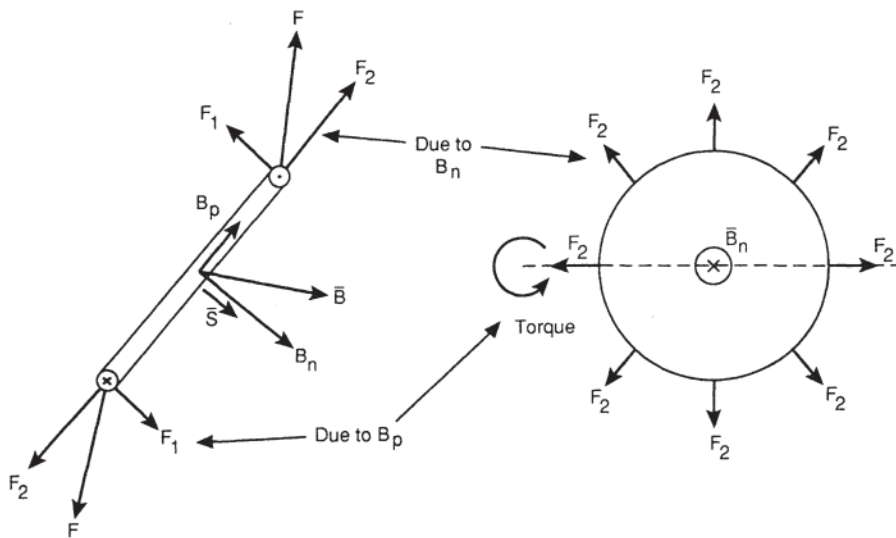


Figure 1.3 Forces and torques on a current-carrying coil placed in a magnetic field.

Using Eq. 1.26, one can write:

$$\begin{aligned}\bar{H} &= \frac{\bar{B}}{\mu_0} \left( 1 - \frac{\chi_m}{1 + \chi_m} \right) = \frac{\bar{B}}{\mu_0 (1 + \chi_m)} \\ &= \frac{\bar{B}}{\mu_0 \mu_r} = \frac{\bar{B}}{\mu}\end{aligned}\quad (1.28)$$

where  $\mu$  is the permeability and  $\mu_r$  is the relative permeability of the material.

Materials with  $\mu_r < 1$ , such as copper and silver, are known as *diamagnetic* materials, and those with  $\mu_r > 1$  but almost equal to unity, such as aluminum are known as *paramagnetic* materials. For most practical applications, the relative permeability of these materials is considered to be equal to unity. Some materials such as iron, cobalt, nickel, and others exhibit  $\mu_r \gg 1$  and these materials are known as *ferromagnetic*.

### 1.2.1 Properties of Ferromagnetic Materials

All ferromagnetic materials exhibit two important characteristics, magnetic saturation and hysteresis. For these materials, a unique value of  $\mu$  cannot be defined so that  $\bar{B} = \mu \bar{H}$  can be satisfied at all values of  $\bar{H}$ . If the permeability of these materials is defined on an incremental basis as  $\mu = \delta B / \delta H$ , the value of  $\mu$  decreases with increasing  $H$ . Beyond some value of  $H$ , the incremental  $\delta B$  decreases continually as  $H$  increases. This is *magnetic saturation*. Also, the  $B$ - $H$  relationship depends on the magnetic history of the material; that is, for a given value of  $H$ , the resulting  $B$  depends on how the material is magnetized. This is *hysteresis*. These properties can be illustrated with the help of Fig. 1.4.

Consider a piece of a material that has never been magnetized but is now magnetized in successive cycles between  $\pm H_m$ . As  $H$  increases between 0 and  $+H_m$  for the first time, the  $B$ - $H$  relationship is plotted by a curve such as 0-1 in Fig. 1.4.

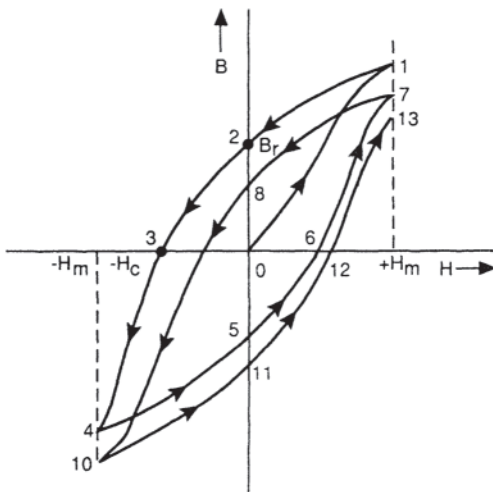


Figure 1.4 Magnetization of a ferromagnetic material.

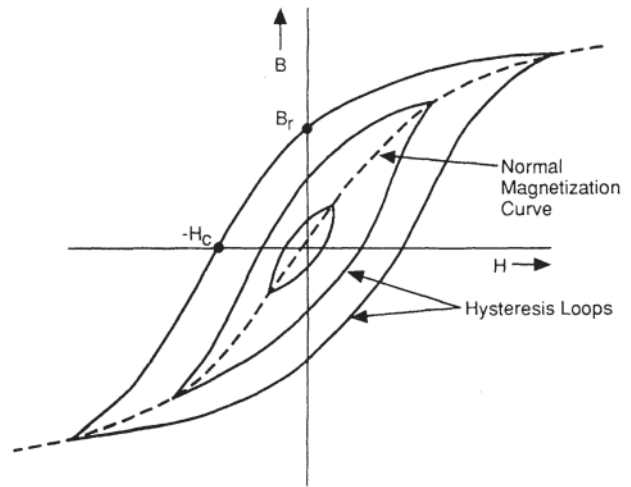


Figure 1.5 Hysteresis loops.

Now if  $H$  is reduced to  $-H_m$  the  $B$ - $H$  relationship traces a different curve, such as 1-2-3-4. At point 2,  $H$  is zero but  $B$  has a finite value  $B_r$ , referred to as the *residual flux density*.  $H$  has to be reversed to a value  $-H_c$ , called the *coercive field intensity*, to bring the flux density  $B$  to zero at point 3. Starting at point 4, if  $H$  is increased from  $-H_m$  to  $+H_m$  the  $B$ - $H$  relationship traces a curve 4-5-6-7, and the flux density for  $H = H_m$  is different from that at point 1. If the magnetization cycles are repeated several times, the  $B$ - $H$  relationship will stabilize and trace a closed curve known as the *hysteresis loop*. For different values of  $+H_m$ , the hysteresis loop will be different, as shown in Fig. 1.5. The locus of the tip of the hysteresis loop is called the *normal magnetization curve*. At high values of  $H$ , the relative permeability is reduced to unity, and the material is said to be *magnetically saturated*. In saturation, all the individual magnetic moment vectors representing the atoms are totally aligned with the external field.

When a magnetic material is subjected to alternating field intensity, the  $B$ - $H$  relationship traces the hysteresis loop once every cycle of field intensity variation. The magnetic moment vectors are continually moving, trying to orient themselves along the external field. These atomic movements are accompanied by friction, and a certain amount of energy is lost as heat in the material during each magnetization cycle. This lost energy is the *hysteresis loss*, and the loss per unit volume of material per magnetization cycle is proportional to the area of the hysteresis loop.

The ferromagnetic material can be considered to be made up of small permanently magnetized *domains*. These domains are of equal magnetic moment and they all tend to align themselves with the field. There is, however, a class of materials where these magnetized domains are of unequal magnitude. Under the influence of an external magnetic field, domains with larger moment align with the field, whereas the domains with smaller moment align in opposition to the field. These materials are called *ferrimagnetic* materials. *Ferrites* are ferrimagnetic substances having a very low electrical conductivity.

Every ferromagnetic material loses its ferromagnetic properties and behaves as a paramagnetic material above a certain temperature known as its *Curie temperature*.

### 1.2.2 Boundary Conditions for $\vec{B}$ and $\vec{H}$

The vector  $\vec{H}$  exhibits the important property (Ampère’s law) that for any closed contour  $C$ :

$$\oint_C \vec{H} \cdot d\vec{l} = \int_S \vec{J} \cdot d\vec{S} = \text{sum of all currents through } C \quad (1.29)$$

The differential form of Ampère’s law is usually written as:

$$\text{curl } \vec{H} = \nabla \times \vec{H} = \vec{J} \quad (1.30)$$

or

$$\text{curl } \vec{B} = \nabla \times \vec{B} = \mu \vec{J} \quad (1.31)$$

The relationships between the components of vector  $\vec{B}$  (and also of vector  $\vec{H}$ ) at adjacent points on the opposite sides of a boundary between two magnetic media are generally referred to as the *boundary conditions*. One such boundary is illustrated in Fig. 1.6. Considering small areas on surfaces on either side of the boundary around points  $P_1$  and  $P_2$ , one can use Eq. 1.21 to write an equation for the flux through  $\delta S$ , namely:

$$B_{1n} \cdot \delta S = B_{2n} \cdot \delta S$$

and hence:

$$B_{1n} = B_{2n} \quad (1.32)$$

and for linear magnetic media:

$$\mu_1 H_{1n} = \mu_2 H_{2n} \quad (1.33)$$

The relationship between the tangential components is obtained by applying Ampère’s law of Eq. 1.29 to the contour shown in Fig. 1.6.

$$\oint_C \vec{H} \cdot d\vec{l} = H_{1t} \delta x - H_{2t} \delta x = \text{current enclosed} = J_s \delta x$$

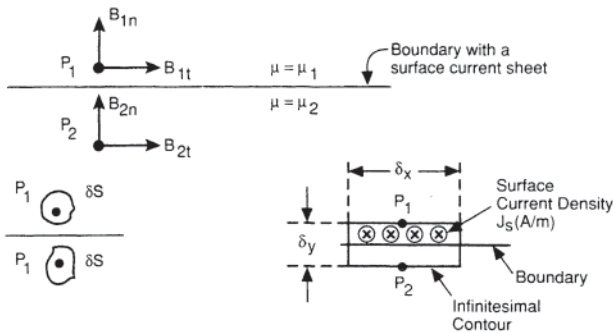


Figure 1.6 Boundary between two magnetic media.

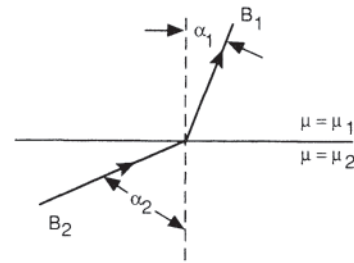


Figure 1.7 Magnetic refraction at a boundary.

that is:

$$H_{1t} - H_{2t} = J_s \quad (1.34)$$

In the absence of a surface current sheet at the boundary,

$$H_{1t} = H_{2t} \quad (1.35)$$

and for linear magnetic media:

$$\frac{B_{1t}}{\mu_1} = \frac{B_{2t}}{\mu_2} \quad (1.36)$$

The relationship between  $B_1$  and  $B_2$  can now be seen as illustrated in Fig. 1.7. For any angle  $\alpha_2$ , the angle  $\alpha_1$  is obtained from

$$\tan \alpha_1 = \frac{\mu_1}{\mu_2} \tan \alpha_2 + \frac{\mu_1 J_s}{B_{2t}} \quad (1.37)$$

The magnetic flux lines are thus bent at any boundary similarly to light rays being bent at optical boundaries. This is called *magnetic refraction*.

Boundaries between ferromagnetic materials ( $\mu_r \gg 1$ ) and nonmagnetic materials such as air, copper, and aluminium ( $\mu_r = 1$ ) are very commonly found in electromagnetic devices. In such a case, in the absence of any current at the boundary:

$$\tan \alpha_1 = \frac{\mu_{r1}}{\mu_{r2}} \tan \alpha_2 \approx 0 \quad (1.38)$$

That is, magnetic flux lines are practically normal to ferromagnetic surfaces, as shown in Fig. 1.8.

### 1.3 SOME BASIC FUNCTIONS RELATED TO ELECTROMAGNETIC FIELDS

In developing the theory of electromagnetic fields and its applications to solving problems related to electrical machines, some basic functions must be defined as follows.

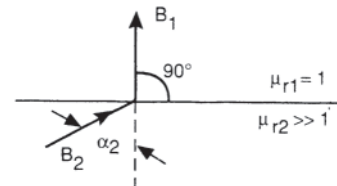


Figure 1.8 Magnetic refraction at a ferromagnetic surface.

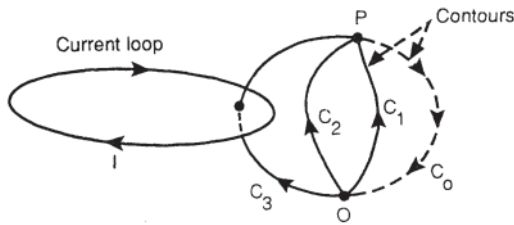


Figure 1.9 Definition of scalar potential.

### 1.3.1 Scalar Potential

The *magnetic scalar potential*  $\mathcal{F}_m$  at a point  $P$  with respect to a reference point  $O$  is defined as:

$$\mathcal{F}_m = - \int_0^P \bar{\mathbf{H}} \cdot d\bar{\mathbf{l}} \quad (1.39)$$

The negative sign is introduced so that the magnetic flux will always flow from higher potential to lower potential. We have, however, seen earlier that according to Ampère's circuital law:

$$\oint_C \bar{\mathbf{H}} \cdot d\bar{\mathbf{l}} = \text{sum of all currents through } C \quad (1.40)$$

Referring to Fig. 1.9, therefore, one can write:

$$\oint_{C_1} \bar{\mathbf{H}} \cdot d\bar{\mathbf{l}} + \oint_{C_0} \bar{\mathbf{H}} \cdot d\bar{\mathbf{l}} = 0 \quad (1.41)$$

whereas:

$$\oint_{C_3} \bar{\mathbf{H}} \cdot d\bar{\mathbf{l}} + \oint_{C_0} \bar{\mathbf{H}} \cdot d\bar{\mathbf{l}} = -I \quad (1.42)$$

hence:

$$\left( -\oint_{C_3} \bar{\mathbf{H}} \cdot d\bar{\mathbf{l}} \right) - \left( -\oint_{C_1} \bar{\mathbf{H}} \cdot d\bar{\mathbf{l}} \right) = I \quad (1.43)$$

It will now at once be clear that the scalar potential defined by Eq. 1.39 cannot be a single-valued function unless certain constraints are established for contours. For this, consider a current loop as shown in Fig. 1.10. The point  $P$  is in the plane of the loop;  $P_1$  is just above the plane, and  $P_2$  is just under it. From Ampère's law:

$$\int_b \bar{\mathbf{H}} \cdot d\bar{\mathbf{l}} + \int_a \bar{\mathbf{H}} \cdot d\bar{\mathbf{l}} = -I \quad (1.44)$$

and the first term is almost zero because  $d^*$  is almost equal to zero. Hence, one may write:

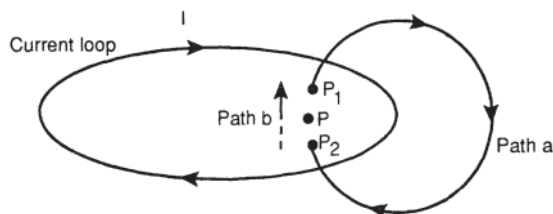


Figure 1.10 Single-valued definition of scalar potential.

$$\int_a \bar{\mathbf{H}} \cdot d\bar{\mathbf{l}} = -I \quad (1.45)$$

The scalar magnetic potential of  $P_1$  with respect to  $P_2$  is:

$$\mathcal{F}_{mP_1,P_2} = - \int_{P_2}^{P_1} \bar{\mathbf{H}} \cdot d\bar{\mathbf{l}} = \int_a \bar{\mathbf{H}} \cdot d\bar{\mathbf{l}} = -I \quad (1.46)$$

and conversely:

$$\mathcal{F}_{mP_2,P_1} = - \int_{P_1}^{P_2} \bar{\mathbf{H}} \cdot d\bar{\mathbf{l}} = - \int_a \bar{\mathbf{H}} \cdot d\bar{\mathbf{l}} = +I \quad (1.47)$$

Thus any two points on either side of a current loop have a magnetic scalar potential difference equal to the current in the loop. The side with higher potential is given by the classic right-hand screw rule.

The scalar potential can now be uniquely defined as follows. The potential of  $P$  with reference to  $O$  is given by:

$$\mathcal{F}_m = - \int_C \bar{\mathbf{H}} \cdot d\bar{\mathbf{l}} \quad (1.48)$$

where  $C$  is any contour from  $O$  to  $P$ ; every time the contour  $C$  goes through a current loop, add a term  $I$  if the loop is crossed in the direction of travel of a right-hand screw turned in the direction of the current in the loop; subtract  $I$  if the loop is crossed in the opposite direction. The magnetic scalar potential thus defined is now a single-valued function. Referring back to Fig. 1.9,

$$\begin{aligned} \mathcal{F}_{mP,O} &= - \int_{C_1} \bar{\mathbf{H}} \cdot d\bar{\mathbf{l}} = - \int_{C_2} \bar{\mathbf{H}} \cdot d\bar{\mathbf{l}} \\ &= - \int_{C_3} \bar{\mathbf{H}} \cdot d\bar{\mathbf{l}} - I \end{aligned} \quad (1.49)$$

From the basic definition of the scalar potential, it can be shown that:

$$\bar{\mathbf{H}} = - \nabla \mathcal{F}_m \quad (1.50)$$

and then:

$$\bar{\mathbf{B}} = - \mu \nabla \mathcal{F}_m \quad (1.51)$$

Also, since  $\nabla \cdot \bar{\mathbf{B}} = 0$ :

$$\nabla^2 \mathcal{F}_m = 0 \quad (1.52)$$

### 1.3.2 Vector Potential

The *vector potential function*  $\bar{\mathbf{A}}$  is defined such that it satisfies the following conditions:

$$\bar{\mathbf{B}} = \nabla \times \bar{\mathbf{A}} \quad (1.53)$$

and:

$$\nabla \cdot \bar{\mathbf{A}} = 0 \quad (1.54)$$

Because any vector function such as  $\bar{\mathbf{A}}$  can be completely specified in terms of its curl ( $\nabla \times \bar{\mathbf{A}}$ ) and its divergence ( $\nabla \cdot \bar{\mathbf{A}}$ ),  $\bar{\mathbf{A}}$  is thus uniquely defined.

Using Ampère's law in differential form:

$$\nabla \times \bar{\mathbf{B}} = \nabla \times \nabla \times \bar{\mathbf{A}} = \nabla(\nabla \cdot \bar{\mathbf{A}}) - \nabla^2 \bar{\mathbf{A}} = - \nabla^2 \bar{\mathbf{A}} = \mu \bar{\mathbf{J}}$$

that is:

$$\nabla^2 \bar{A} = -\mu \bar{J} \quad (1.55)$$

A general solution of the above equation has the form:

$$\bar{A} = \frac{\mu}{4\pi} \int_v \bar{J} \frac{dV}{r} \quad (1.56)$$

and the vector potential  $d\bar{A}$  due to elemental current  $\bar{J}dV$  is in the same direction as  $\bar{J}$ .

This solution can be used to obtain, for example, the vector potential resulting from a current-carrying loop. Referring back to Fig. 1.2, if the current in the loop is  $I$ :

$$\bar{J} dV = \bar{J} dS dl = I d\bar{l} \quad (1.57)$$

and

$$\bar{A} = \frac{\mu I}{4\pi} \oint_c \frac{d\bar{l}}{r} \quad (1.58)$$

### 1.3.3 Electromagnetic Induction

Let us now consider currents and charges that are functions of time. If the variation in time is slow enough, the electric and the magnetic field at any time will be almost identical to the field caused by a constant current equal to the value of the time-varying current at that instant in time; such a system is generally referred to as a *quasi-stationary system*. For such a system, Maxwell's law (a generalization of Faraday's law) of electromagnetic induction can be expressed in two different forms:

$$\oint_c \bar{E} \cdot d\bar{l} = \int_s \nabla \times \bar{E} \cdot d\bar{S} = - \int_s \frac{\partial \bar{B}}{\partial t} \cdot d\bar{S} \quad (1.59)$$

(integral form)

$$\nabla \times \bar{E} = - \frac{\partial \bar{B}}{\partial t} \quad (\text{differential form}) \quad (1.60)$$

If, for example, a closed thin loop with contour  $C$  is placed in a time-varying field  $\bar{B}$ , the voltage induced in the loop can be obtained by Eq. 1.59 as:

$$e = \oint_c \bar{E} \cdot d\bar{l} = - \frac{\partial}{\partial t} \left[ \int_s \bar{B} \cdot d\bar{S} \right] = - \frac{\partial \phi}{\partial t} \quad (1.61)$$

where  $\phi$  is the flux through the loop—also known as the flux linkage of the loop.

### 1.3.4 Energy in an Electromagnetic Field

Since  $\bar{B} = \nabla \times \bar{A}$ , using Eq. 1.60, one may write:

$$\nabla \times \bar{E} = - \frac{\partial}{\partial t} (\nabla \times \bar{A}) \quad (1.62)$$

and hence:

$$\bar{E} = - \frac{\partial \bar{A}}{\partial t} \quad (1.63)$$

The power necessary to maintain this field is then given by:

$$p = - \int_v \bar{E} \cdot \bar{J} dV = \int_v \bar{J} \cdot \frac{\partial \bar{A}}{\partial t} dV = \frac{\partial}{\partial t} \left[ \int_v \int_o^A \bar{J} \cdot d\bar{A} dV \right] \quad (1.64)$$

For a quasi-stationary system with a magnetically linear medium,  $\bar{J}$  and  $\bar{A}$  are similar functions of time, and then:

$$p = \int_v \bar{J} \cdot \frac{\partial \bar{A}}{\partial t} dV = \frac{\partial}{\partial t} \int_v \frac{1}{2} \bar{J} \cdot \bar{A} dV \quad (1.65)$$

The energy stored in the magnetic field can then be defined as:

$$W_m = \int_v \frac{1}{2} \bar{J} \cdot \bar{A} dV \quad (1.66)$$

and this can also be shown to be:

$$W_m = \int_v \frac{1}{2} \bar{B} \cdot \bar{H} dV \quad (1.67)$$

### 1.3.5 Self-Inductance and Mutual Inductance

Consider two closed thin loops of conducting material as shown in Fig. 1.11. If the loop 1 carries a time-varying current  $i_1$ , it will cause a time-varying magnetic field  $\bar{B}_1$  in the space surrounding the loop. This magnetic field will induce an electromagnetic force (emf)  $e_2$  in loop 2 given by:

$$e_2 = - \frac{\partial}{\partial t} \left[ \oint_{s_2} \bar{B}_1 \cdot d\bar{S}_2 \right] = - \frac{\partial \phi_{12}}{\partial t} \quad (1.68)$$

where:

$$\phi_{12} = \oint_{s_2} \bar{B}_1 \cdot d\bar{S}_2 \quad (1.69)$$

is the flux linkage of loop 2 due to a current in loop 1. The flux density  $\bar{B}_1$  and the flux linkages  $\phi_{12}$  are both proportional to the current  $i_1$  if the medium between the two loops exhibits linear magnetic behavior. Hence a constant  $L_{12}$  can be defined such that:

$$\phi_{12} = L_{12} i_1 \quad (1.70)$$

It will be apparent that the unit of the constant  $L_{12}$ , known as the *mutual inductance* of loop 2 with respect to loop 1, is weber pre ampere. This unit is also known as the *henry*.

The flux linkage  $\phi_{12}$  can be written as:

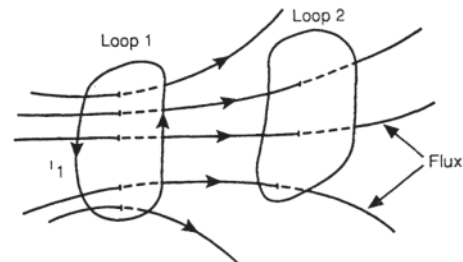


Figure 1.11 Inductances of current loops.

$$\begin{aligned}\phi_{12} &= \int_{s_2} \bar{\mathbf{B}}_1 \cdot d\bar{\mathbf{S}}_2 = \int_{s_2} \nabla \times \bar{\mathbf{A}}_1 \cdot d\bar{\mathbf{S}}_2 \\ &= \oint_{c_2} \bar{\mathbf{A}}_1 \cdot d\bar{\mathbf{I}}_2\end{aligned}\quad (1.71)$$

Hence, referring back to Eq. 1.58:

$$\phi_{12} = \oint_{c_2} \left[ \frac{\mu I_1}{4\pi} \oint_{c_1} \frac{d\bar{\mathbf{I}}_1}{r} \right] \cdot d\bar{\mathbf{I}}_2 \quad (1.72)$$

That is:

$$L_{12} = \frac{\phi_{12}}{I_1} = \frac{\mu}{4\pi} \oint_{c_2} \oint_{c_1} \frac{d\bar{\mathbf{I}}_1 \cdot d\bar{\mathbf{I}}_2}{r} \quad (1.73)$$

Because the value of the integral is unchanged when the subscripts 1 and 2 are interchanged, it is possible to write:

$$L_{12} = \frac{\phi_{12}}{I_1} = \frac{\phi_{21}}{I_2} = L_{21} \quad (1.74)$$

The *self-inductances*  $L_{11}$  and  $L_{22}$  can similarly be defined in terms of the flux linkages of loops 1 and 2 resulting from the currents in them:

$$L_{11} = \frac{\phi_{11}}{I_1} \quad \text{and} \quad L_{22} = \frac{\phi_{22}}{I_2} \quad (1.75)$$

If only loop 1 carries a current, the flux linkage  $\phi_{11}$  of loop 1 will be larger than the flux linkage  $\phi_{12}$  of loop 2. This is because some of the flux lines will close on themselves without passing through the surface of loop 2; the difference ( $\phi_{11} - \phi_{12}$ ) is the leakage flux  $\phi_{e1}$  of loop 1. Similarly,  $\phi_{22} > \phi_{21}$ , and the difference ( $\phi_{22} - \phi_{21}$ ), is the leakage flux  $\phi_{e2}$  of loop 2. It is therefore possible to write:

$$L_{11}L_{22} = \frac{\phi_{11}}{I_1} \frac{\phi_{22}}{I_2} > \frac{\phi_{12}}{I_1} \frac{\phi_{21}}{I_2} = L_{12}^2 \quad (1.76)$$

That is:

$$L_{11}L_{22} > L_{12}^2 \quad (1.77)$$

The ratio  $k = L_{12}/\sqrt{L_{11}L_{22}}$  is, therefore, always less than 1. The constant  $k$  is generally referred to as the *coupling coefficient*. A higher value of  $k$  means less leakage flux and signifies better coupling between the loops 1 and 2.

### 1.3.6 Energy Stored in a Current-Carrying Coil

Referring back to Fig. 1.2, the energy  $W_m$  stored in the coil can be obtained as:

$$W_m = \int_V \frac{1}{2} \bar{\mathbf{J}} \cdot \bar{\mathbf{A}} dV \quad (1.78)$$

However,  $\bar{\mathbf{J}} dV = I d\bar{\mathbf{I}}$ , and then:

$$W_m = \int_V \frac{1}{2} \bar{\mathbf{J}} \cdot \bar{\mathbf{A}} dV = \oint_c \frac{1}{2} I \bar{\mathbf{A}} \cdot d\bar{\mathbf{I}} \quad (1.79)$$

Also:

$$\oint_c \bar{\mathbf{E}} \cdot d\bar{\mathbf{I}} = - \oint_c \frac{\partial \bar{\mathbf{A}}}{\partial t} \cdot d\bar{\mathbf{I}} = - \frac{\partial \phi}{\partial t} \quad (1.80)$$

Hence:

$$\phi = \oint_c \bar{\mathbf{A}} \cdot d\bar{\mathbf{I}} \quad (1.81)$$

and then:

$$W_m = \oint_c \frac{1}{2} I \bar{\mathbf{A}} \cdot d\bar{\mathbf{I}} = \frac{1}{2} I \phi \quad (1.82)$$

If there are no other current-carrying coils in the vicinity of the coil and the self-inductance of the coil is equal to  $L$ , then  $\phi = iL$ , and Eq. 1.82 can then be written in the familiar form:

$$W_m = \frac{1}{2} Li^2 \quad (1.83)$$

## 1.4 MAGNETIC CIRCUITS

Electromagnetic devices usually have current-carrying conductors embedded in magnetic cores. If these magnetic cores are made of thin laminations, currents flowing in them, known as eddy currents, can usually be ignored as a first approximation. With solid cores, however, effect of these eddy currents must be considered in studying the characteristics of electromagnetic devices. Study of magnetic fields resulting from conductors embedded in iron cores is therefore very important. Several techniques have been developed over the years for analyzing such problems.

### 1.4.1 Concept of a Magnetic Circuit

Let us consider an elemental length of a narrow tube of flux as shown in Fig. 1.12, thus permitting use of scalar rather than vector notation. If the cross section of the tube  $\delta S$  is sufficiently small, the flux density  $\bar{\mathbf{B}}$  can be considered to be uniform, and the flux  $\delta\phi$  is then equal to  $B\delta S$ . Since:

$$\oint H dl = \text{total current enclosed} = NI$$

one may write:

$$H \delta l = \delta(NI)$$

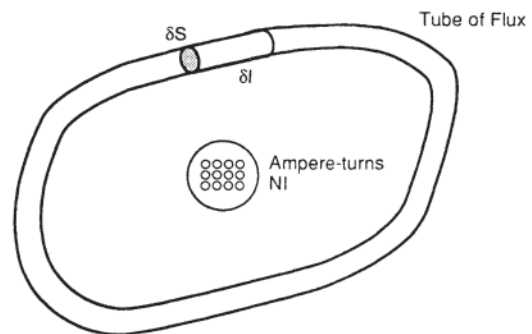


Figure 1.12 Concept of a magnetic circuit.

that is:

$$\frac{B}{\mu} \delta l = \delta(NI)$$

or

$$\delta\phi \left( \frac{\delta l}{\mu\delta S} \right) = \delta(NI) \tag{1.84}$$

The quantity  $NI$  is referred to as the *magneto-motive force* (mmf) because that is what causes the flux  $\phi$ . Comparing the relationship between electric current (analogous to magnetic flux) and emf (analogous to mmf), the quantity  $\delta l/\delta S$  is usually referred to as magnetic resistance or *reluctance* of the medium in which the flux is caused.

For any length of a flux tube, the reluctance  $R_m$  is given by:

$$R_m = \int_c \frac{dl}{\mu\delta S} \tag{1.85}$$

In magnetic fields involving ferromagnetic materials, with or without small air gaps, the magnetic flux is usually confined to ferromagnetic cores, although some leakage flux is present outside the cores. The performance of these devices can be analyzed approximately by constructing equivalent magnetic circuits (analogous to electric circuits) with nodes and branches. The mmf and the flux in the branches can then be obtained by calculating the reluctance of various branches and solving circuit equations similar to those for electric circuits.

1.4.1.1 Linear Magnetic Circuits

Consider the simple electromagnet of Fig. 1.13. If the magnetic material has a constant relative permeability  $\mu_r$  that is independent of the flux density, the device is considered to have a *linear magnetic circuit*. The electromagnet can then be represented by the equivalent circuit of Fig. 1.14, where all the  $R$ 's are reluctances of parts of the magnetic circuit. The reluctances  $R_{FA}$  and  $R_{CD}$  are given by the following equations:

$$R_{FA} = \frac{l_{AF}}{\mu_r\mu_0 S_{AF}} \text{ (for magnetic material)} \tag{1.86}$$

$$R_{CD} = \frac{l_{CD}}{\mu_0 S_{CD}} \text{ (for air)} \tag{1.87}$$

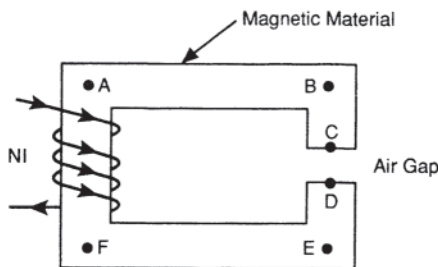


Figure 1.13 A simple electromagnet.

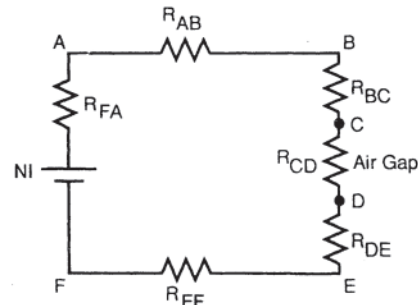


Figure 1.14 An equivalent electrical network.

Other reluctances can be written similarly.

The flux  $\phi$  in the circuit is then given by:

$$\begin{aligned} \phi &= \frac{\text{mmf}}{\text{Total reluctance}} \\ &= \frac{NI}{R_{FA} + R_{AB} + R_{BC} + R_{CD} + R_{DE} + R_{EF}} \end{aligned} \tag{1.88}$$

Another magnetic device is shown in Fig. 1.15. It is a doubly excited device with two air gaps. If the magnetic material is linear, the device can be represented by the equivalent circuit of Fig. 1.16. This can then be analyzed as an electric circuit by solving the related equations.

1.4.1.2 Nonlinear Magnetic Circuits

If the relative permeability of any magnetic material is a function of the flux density, the material is said to be nonlinear. Magnetic devices with such materials exhibit nonlinear characteristics, and cannot be analyzed with the help of equivalent linear magnetic circuits. Simple circuit topologies can be analyzed with graphical techniques, although complex circuits can be analyzed only by trial-and-error methods.

Consider again the circuit of Fig. 1.13. Let  $B=f(H)$  represent the nonlinear magnetization characteristics of the core material. For the air gap across CD the mmf-flux relationship is obtained as:

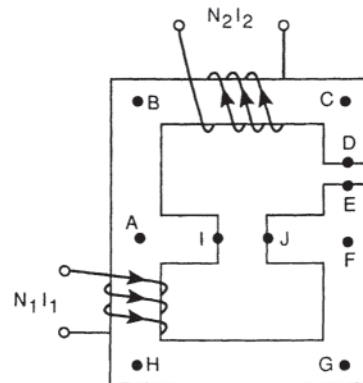


Figure 1.15 An electromagnet with multiple excitation.



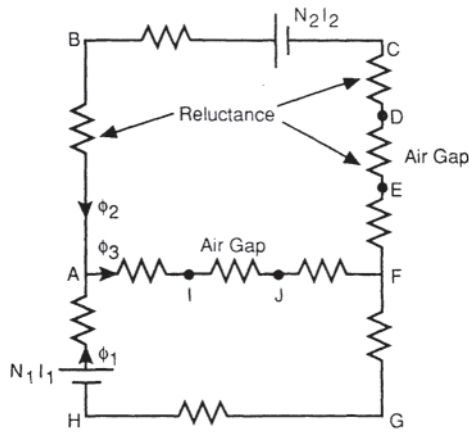


Figure 1.16 Equivalent electrical network.

$$B_{CD} = \frac{\phi}{S_{CD}}$$

$$mmf = F_{CD} = H_{CD}l_{CD} = \frac{B_{CD}}{\mu_0} l_{CD}$$

$$= \frac{\phi l_{CD}}{\mu_0 S_{CD}} = R_{CD}\phi \tag{1.89}$$

For the ferromagnetic portion of the magnetic circuit, this relationship is obtained as follows. For the path BC:

$$F_{BC} = l_{BC}H_{BC} = l_{BC}f^{-1}\left(\frac{\phi}{S_{BC}}\right) \tag{1.90}$$

Hence, for the entire ferromagnetic path, the total  $F_T$  is given by:

$$F_T = F_{FA} + F_{AB} + F_{BC} + F_{DE} + F_{EF} = f_l(\phi) \tag{1.91}$$

Also:

$$F_T + F_{CD} = NI \tag{1.92}$$

This equation can be solved graphically as shown in Fig. 1.17 by plotting both  $F_T$  and  $F_{CD}$  as functions of  $\phi$ . The intersection of these curves gives the solution of the above equation.

If the circuit is a little more complex as in Fig. 1.15, even a graphical solution is not very easy. For this circuit, there are

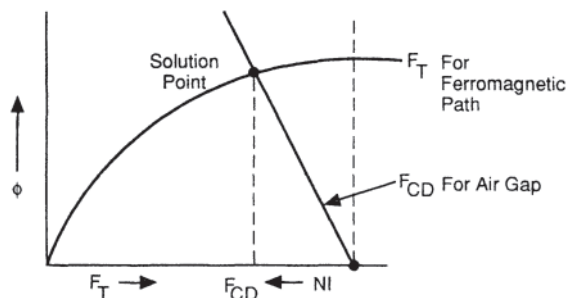


Figure 1.17 Graphical solution to problem of Fig. 1.13.

principally three branches: path FGHA with flux  $\phi_1$ , path ABCDEF with flux  $\phi_2$ , and path AIJF with flux  $\phi_3 = (\phi_1 + \phi_2)$ . For the first path:

$$F_{FA} = N_1I_1 - F_{AH} - F_{HG} - F_{GF}$$

$$= N_1I_1 - f_1(\phi_1) \tag{1.93}$$

Similarly, for the second path:

$$F_{FA} = N_2I_2 - f_2(\phi_2) \tag{1.94}$$

and for the third path one can write:

$$F_{FA} = f_3(\phi_3) \tag{1.95}$$

If the first two relationships are plotted as shown in Fig. 1.18(a), at any point  $Q_2$  one can find  $F_{FA}$  and:

$$\phi_3 = \phi_1 + \phi_2 = Q_2Q_3 + Q_2Q_1 = Q_1Q_3 \tag{1.96}$$

where  $Q_2Q_3$  and  $Q_2Q_1$  are the values of  $\phi_1$  and  $\phi_2$  from the figure and  $Q_1Q_3$  is the value of  $\phi_3$ .

By taking a series of points  $Q_2$  one can thus generate a relationship:

$$F_{FA} = f_4(\phi_3) \tag{1.97}$$

The solution of the three equations Eqs. 1.93–1.95 is then obtained by plotting the functions  $f_3(\phi_3)$  and  $f_4(\phi_3)$  as shown in Fig. 1.18(b).

It should be realized here that the above analyses of electromagnetic devices based on their equivalent magnetic circuits are approximations of their actual behavior. This is because the magnetic flux was assumed to be constrained to the magnetic core, and was simply assumed to be crossing over any air gaps; leakage flux was assumed to be zero everywhere.

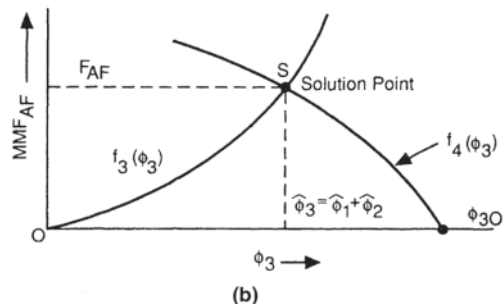
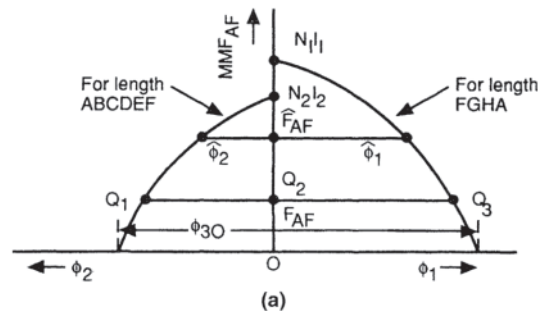


Figure 1.18 Graphical solution to problem of Fig. 1.15.

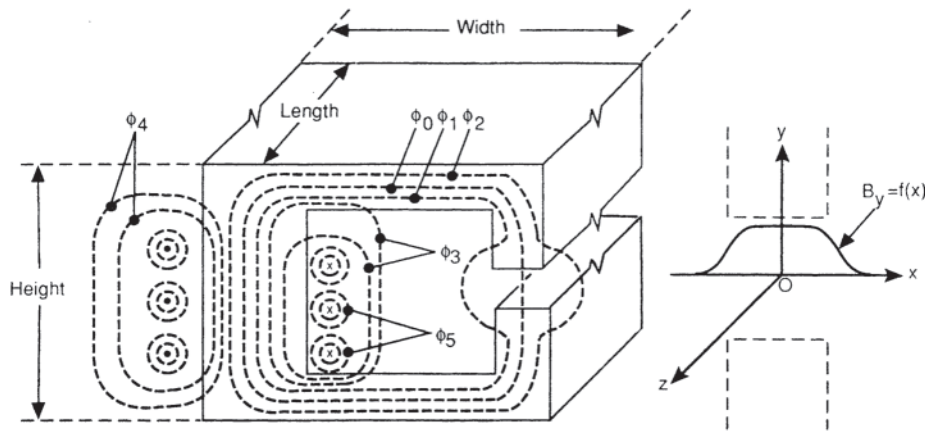


Figure 1.19 Two-dimensional field problem.

### 1.4.2 Two-Dimensional Field Problems

Let us now reconsider a magnetic device such as that shown in Fig. 1.13. In analyzing the circuit based on equivalent magnetic reluctances, the entire magnetic flux was considered to be constrained within the magnetic core, and all this flux was assumed to cross the air gap only across the two surfaces facing each other. If the magnetic core is not saturated, and the air gap is small compared to the other dimensions of the device, such approximation can usually be justified without sacrificing much in accuracy. Otherwise, however, several types of magnetic flux lines can be defined as shown in Fig. 1.19. These include:

- $\phi_0$  = Main flux: going through the core and crossing the air gap directly from face to face
- $\phi_1, \phi_2$  = Leakage flux: going through most of the core but fringing around the air gap
- $\phi_3, \phi_4$  = Leakage flux: crossing largely through the air, but still linking the whole winding
- $\phi_5$  = Leakage flux: all in the air, linking only part of the winding

In general, the flux density  $\bar{B}$  at any point in space in and around the device is a function of all three spatial variables. For many devices, however, the general three-dimensional field problem can be simplified. In the electromagnet of Fig. 1.19, if the length is large compared to other dimensions, variation of  $\bar{B}$  with respect to  $z$  may be ignored; the flux density  $\bar{B}$  and the magnetic scalar potential  $\mathcal{F}_m$  are then functions of only two variables,  $x$  and  $y$ . The function  $\mathcal{F}_m(x, y)$  can then be obtained as the solution to the equation:

$$\nabla^2 \mathcal{F}_m = 0 \tag{1.98}$$

with appropriate boundary conditions. Furthermore, if the ferromagnetic cores are unsaturated, the two-dimensional field problem can be simplified further by assuming core permeability to be infinite; any finite flux density  $\bar{B}$  is then possible in the core with  $H=0$ . The iron surfaces can then be assumed to be equipotentials, except when current sheets are present. For example, referring back to Fig. 1.19, the equivalent

two-dimensional field problem can be formulated as illustrated in Fig. 1.20. The core on one side of the exciting coil is assumed to be at  $\mathcal{F}_m = +1$ ; the core on the other side of the coil is assumed to be at  $\mathcal{F}_m = -1$ ; along the height of the coil, the potential  $\mathcal{F}_m$  is assumed to vary linearly between  $-1$  and  $+1$ . The line of symmetry can be assumed to represent the equipotential  $\mathcal{F}_{bc} = 0$ .

Several techniques have been developed to solve two-dimensional field problems, such as conformal mapping [1], and Fourier series method.

#### 1.4.2.1 Fourier Series Solutions

The two-dimensional Laplace equation for  $\mathcal{F}_m$  is:

$$\frac{\partial^2 \mathcal{F}_m}{\partial x^2} + \frac{\partial^2 \mathcal{F}_m}{\partial y^2} = 0 \tag{1.99}$$

If a general solution is assumed to have a form:

$$\mathcal{F}_m = \exp(\alpha x \pm \beta y) \tag{1.100}$$

then satisfying the Laplace equation requires:

$$\alpha^2 + \beta^2 = 0, \text{ that is } \alpha = \pm j\beta \tag{1.101}$$

Using all possible combinations of signs, and all possible values of  $\alpha$ , a most general solution can be written as:

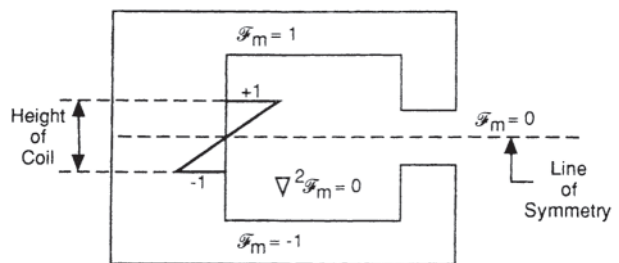


Figure 1.20 Formulation of the field problem.

$$\begin{aligned} \mathcal{F}_m = & \sum_n [A_n \cosh(\alpha_n y) \cos(\alpha_n x) + B_n \sinh(\alpha_n y) \cos(\alpha_n x) \\ & + C_n \cosh(\alpha_n y) \sin(\alpha_n x) + D_n \sinh(\alpha_n y) \sin(\alpha_n x)] \end{aligned} \quad (1.102)$$

The constants  $A_n$ ,  $B_n$ ,  $C_n$ ,  $D_n$  and  $\alpha_n$  can be determined by imposing appropriate boundary conditions.

For the rectangular region of Fig. 1.21 (a), the general solution becomes:

$$\begin{aligned} \mathcal{F}_m = & \sum_n F_n \frac{\sinh [(2n - 1) \pi (h - y)/2b]}{\sinh [(2n - 1) \pi h/2b]} \\ & \times \sin \left[ (2n - 1) \frac{\pi x}{b} \right] \end{aligned} \quad (1.103)$$

It satisfies the boundary conditions:

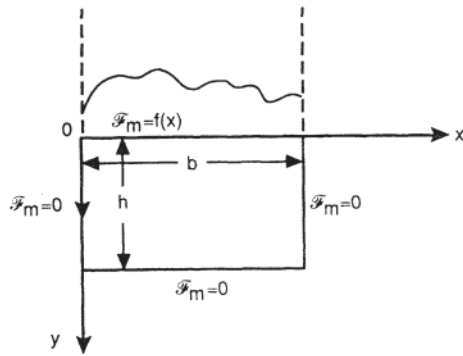
$$\mathcal{F}_m = 0 \text{ at } x=0 \text{ and } x=b$$

and:

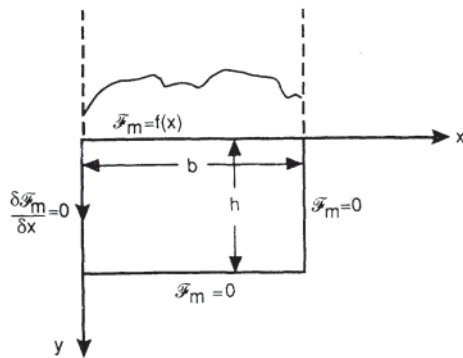
$$\mathcal{F}_m = 0 \text{ at } y=h$$

Furthermore,  $F_n$  can be determined such that:

$$f(x) = \sum_n F_n \sin \left[ (2n - 1) \frac{\pi x}{b} \right] \quad 0 \leq x \leq b \quad (1.104)$$



(a)



(b)

Figure 1.21 Certain basic two-dimensional field problems.

so that:

$$\mathcal{F}_m = f(x) \text{ at } y=0$$

For the rectangular region of Fig. 1.21(b), however, the general solution has the form:

$$\begin{aligned} \mathcal{F}_m = & \sum_n G_n \frac{\sinh [(2n - 1) \pi (h - y)/2b]}{\sinh [(2n - 1) \pi h/2b]} \\ & \times \cos \left[ (2n - 1) \frac{\pi x}{2b} \right] \end{aligned} \quad (1.105)$$

This function satisfies all the boundary conditions.

If there are known potential distributions on more than one boundary, the solution can be obtained by applying the superposition theorem, by defining several simpler problems.

With interconnected regions, the problem becomes increasingly difficult, although the technique is quite straightforward, as can be seen from the problem of double-slotting in Fig. 1.22(a) [2]. In this figure, the dimensions of the structure are:

- $S$  = slot width
- $t$  = tooth width
- $\lambda$  = tooth pitch= $s+t$
- $g$  = length of the air gap
- $h$  = depth of the slot

the dimensions of the slots and the teeth being identical on the two surfaces. If the teeth on both surfaces face each other, the corresponding field problem can be defined as presented in Fig. 1.22(b). The two regions I and II in this figure have a common boundary ED; the magnetic scalar potential and its spatial derivatives must be continuous across this boundary. The problem is, therefore, solved in two steps:

1. Assume an arbitrary potential distribution along ED in terms of some unknown Fourier coefficients. Solve the field equations in regions I and II.
2. Obtain the unknown coefficients by matching the normal derivative of the potential function along ED.

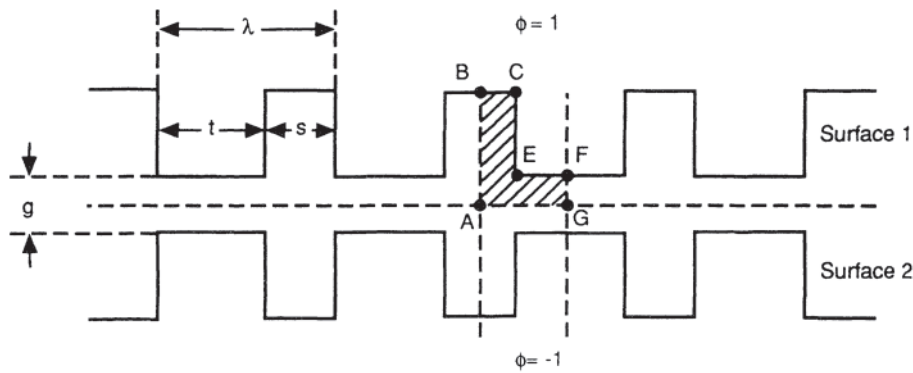
Step 1: Solution of  $\nabla^2 \mathcal{F}_m = 0$  in regions I and II. With the  $x$ - $y$  coordinates fixed at B as shown, let the potential across ED be assumed to be given by:

$$\begin{aligned} \mathcal{F}_{ED} = & \sum_{q=1} B_q \sin \left( \frac{2q\pi}{g} (y - h) \right) \\ \text{for } & h \leq y \leq h + \frac{g}{2} \end{aligned} \quad (1.106)$$

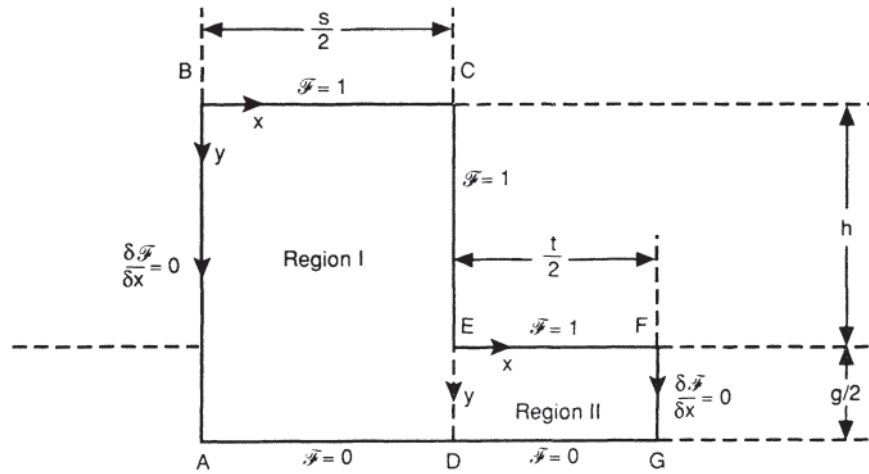
The constants  $B_q$  are the unknown Fourier coefficients.

The potential  $\mathcal{F}_I$  in region I is then given by:

$$\mathcal{F}_I = \sum_{n=0} \frac{4(-1)^n}{(2n+1)\pi} \frac{\sinh \left[ \frac{(2n+1)\pi}{s} \left( h + \frac{g}{2} - y \right) \right]}{\sinh \left[ \frac{(2n+1)\pi}{s} \left( h + \frac{g}{2} \right) \right]}$$



(a)



(b)

Figure 1.22 (a) An identical double-slotted placed tooth opposite tooth, (b) The corresponding field problem.

$$\times \cos\left(\frac{(2n + 1)\pi x}{s}\right) \quad \alpha = \frac{2h}{2h + g} \quad (1.109)$$

$$+ \sum_{m=1} C_m \frac{\cosh\left(\frac{m\pi x}{h+g/2}\right)}{\cosh\left(\frac{m\pi s/2}{h+g/2}\right)} \sin\left(\frac{m\pi y}{h+g/2}\right) \quad (1.107)$$

where:

$$C_m = \frac{2}{m\pi} [1 - \cos(m\pi\alpha)] + \frac{2(1-\alpha)}{\pi} \sin(m\pi\alpha) \\ \times \sum_{q=1} \frac{q(1-\delta_{q,m(1-\alpha)})}{q^2 - m^2(1-\alpha)^2} B_q \\ + \sum_{q=1} (1-\alpha) B_q \delta_{q,m(1-\alpha)} \cos\left(\frac{2q\pi h}{g}\right) \quad (1.108)$$

With x-y coordinates fixed at E as shown in Fig. 1.22(b), the potential  $\mathcal{F}_{II}$  is:

$$\mathcal{F}_{II} = \sum_{n=0} \frac{4}{(2n + 1)\pi} \frac{\sinh\left[\frac{(2n + 1)\pi\left(\frac{g}{2} - y\right)}{t}\right]}{\sinh\left(\frac{(2n + 1)\pi g}{2t}\right)} \\ \times \sin\left(\frac{(2n + 1)\pi x}{t}\right) \\ + \sum_{q=1} B_q \frac{\cosh\left[\frac{2q\pi\left(\frac{t}{2} - x\right)}{g}\right]}{\cosh\left(\frac{2q\pi t}{g}\right)} \sin\left(\frac{2q\pi y}{g}\right) \quad (1.110)$$

and:

*Step 2:* Equations for the Fourier coefficients. A set of simultaneous equations in the  $B_q$  coefficients can now be written by equating  $d\mathcal{F}_I/dx$  and  $d\mathcal{F}_{II}/dx$  on ED as:

$$\begin{aligned}
& \sum_{q=1} \left\{ 2q\pi \tanh [q\pi\mu(1-\beta)] \sin \left( 2q\pi \frac{y}{g} \right) \right. \\
& + \sum_{m=1} \left[ 2m(1-\alpha)^2 \delta_{q,m(1-\alpha)} \cos \left( \frac{2q\pi h}{g} \right) \right. \\
& \left. \left. + \frac{4mq(1-\alpha)^2 \sin(m\pi\alpha)}{q^2 - m^2(1-\alpha)^2} (1 - \delta_{q,m(1-\alpha)}) \right] \right\} B_q \\
& \times \tanh [m\pi\mu\beta(1-\alpha)] \sin \left[ 2m\pi(1-\alpha) \left( \frac{0.5\alpha}{1-\alpha} + \frac{y}{g} \right) \right] \\
& = \sum_{n=0} \frac{4}{\mu\beta} \operatorname{cosech} \left( \frac{(2n+1)\pi}{2\mu\beta(1-\alpha)} \right) \sinh \left[ \frac{(2n+1)\pi}{\mu\beta} \left( \frac{1}{2} - \frac{y}{g} \right) \right] \\
& + \sum_{n=0} \frac{4}{\mu(1-\beta)} \operatorname{cosech} \left( \frac{(2n+1)\pi}{2\mu(1-\beta)} \right) \sinh \left[ \frac{(2n+1)\pi}{\mu(1-\beta)} \left( \frac{1}{2} - \frac{y}{g} \right) \right] \\
& - \sum_{m=1} 4(1-\alpha)[1 - \cos(m\pi\alpha)] \tanh [m\pi\mu\beta(1-\alpha)] \\
& \times \sin \left[ 2m\pi(1-\alpha) \left( \frac{0.5\alpha}{1-\alpha} + \frac{y}{g} \right) \right] \\
& \text{for } 0 < \frac{y}{g} < 0.5
\end{aligned} \tag{1.111}$$

where:

$$\mu = \lambda/g \text{ and } \beta = s/(s+t)$$

If  $q$  is assumed to take a maximum value of  $Q$ , the necessary number of equations can be generated from Eq. 1.111 either by Fourier analysis or leastsquares fitting, or simply by point-by-point matching, i.e., giving  $Q$  different values to  $y/g$  in the range.

Once the  $B_q$  coefficients are evaluated, the magnetic scalar potential is completely defined in both regions. The other parameters, such as the magnetic flux crossing any given area, the permeance of the air gap, and others can then be computed.

It will at once be apparent that the techniques of Schwarz-Christoffel transformation and Fourier analysis are not easily applicable to complex field topologies.

## 1.5 FINITE ELEMENT ANALYSIS OF MAGNETIC FIELDS

### 1.5.1 Motivation

The magnetic circuit or permeance method described in the previous sections is very useful for calculating approximate magnetic fields in devices of simple geometry. For more

accurate calculations, however, finite element computer programs are necessary.

The key limitation of the magnetic circuit method is that it requires assumption of the magnetic flux paths. The lengths and cross-sectional areas of all paths must be known. Usually the paths are assumed to consist of straight lines, which is erroneous to a some extent. To calculate the effects of flux fringing, saturation, and leakage flux one usually uses empirical correction factors. If a motor or other magnetic device has had essentially the same type of design for many years, then the empirical factors may be fairly well known.

Today's motor designer is often involved with new motor design concepts for which the flux paths and empirical factors are unknown. Even if the design is a well-understood older design concept, there is great need today for accurately determining the effects of geometric changes and saturation on motor efficiency and other parameters related to the magnetic field.

The finite element method can be made readily available in the form of computer software called Maxwell® [3] installed in the motor designer's office. The software requires no assumption of flux paths or related empirical factors. Finite element software accurately calculates magnetic fields and the related motor design parameters for motors of complicated geometry, with saturation and/or permanent magnets, with significant armature reaction, and with or without eddy currents.

### 1.5.2 Energy Functionals

The finite element method is based on energy conservation. The law of conservation of energy in electric motors may be derived from Maxwell's equations and can be expressed as [4]:

$$- \int_V \bar{\mathbf{E}} \cdot \bar{\mathbf{J}} dV = \int_V \bar{\mathbf{H}} \cdot \frac{\partial \bar{\mathbf{B}}}{\partial t} dV \tag{1.112}$$

where  $\bar{\mathbf{B}}$  is magnetic or flux density,  $\bar{\mathbf{H}}$  is field intensity,  $\bar{\mathbf{J}}$  is current density,  $\bar{\mathbf{E}}$  is electric field, and  $V$  is the volume enclosing the device analyzed.

The left-hand term of Eq. 1.112 is the net electrical power input  $P_E$ . It can be shown to equal voltage times current. The right-hand side can be rewritten to give [5]:

$$- \int_V \bar{\mathbf{E}} \cdot \bar{\mathbf{J}} dV = \frac{\partial}{\partial t} \int_V \left( \int_0^B \bar{\mathbf{H}} \cdot d\bar{\mathbf{B}} \right) dV \tag{1.113}$$

The term on the right-hand side is the rate of increase of the stored magnetic energy:

$$W_m = \int_V \left( \int_0^B \bar{\mathbf{H}} \cdot d\bar{\mathbf{B}} \right) dV \tag{1.114}$$

The input power  $P_E$  may be expressed in terms of magnetic vector potential  $\bar{\mathbf{A}}$  rather than  $\bar{\mathbf{E}}$  by using the definition of  $\bar{\mathbf{A}}$ :

$$\bar{\mathbf{B}} = \bar{\nabla} \times \bar{\mathbf{A}} \tag{1.115}$$

in Faraday's law:

$$\nabla \times \bar{E} = -\frac{\partial \bar{B}}{\partial t} \quad (1.116)$$

Hence:

$$\nabla \times \bar{E} = -\frac{\partial}{\partial t} (\nabla \times \bar{A}) \quad (1.117)$$

Then assuming negligible electrostatic potential, which is true if there are no power losses:

$$\bar{E} = -\frac{\partial}{\partial t} \bar{A} \quad (1.118)$$

Substituting the expression for  $\bar{E}$  in Eq. 1.118 into Eq. 1.113 gives:

$$P_E = \int_V \bar{J} \cdot \frac{\partial \bar{A}}{\partial t} dV \quad (1.119)$$

which becomes:

$$P_E = \frac{\partial}{\partial t} \int_V \left( \int_0^A \bar{J} \cdot d\bar{A} \right) dV \quad (1.120)$$

The integral is the net input electrical energy [5]:

$$W_E = \int_V \left( \int_0^A \bar{J} \cdot d\bar{A} \right) dV \quad (1.121)$$

Then Eqs. 1.138, 1.145, and 1.146 give:

$$\int_V \left( \int_0^B \bar{H} \cdot d\bar{B} \right) dV = \int_V \left( \int_0^A \bar{J} \cdot d\bar{A} \right) dV \quad (1.122)$$

that states that stored magnetic energy equals input electrical energy for lossless devices.

Variational techniques such as the finite element method obtain solutions to field problems by minimizing an energy functional  $F$  that is the difference between the stored energy and the input (applied) energy in the system volume [6]. Thus, for magnetic systems, Eqs. 1.114, 1.121, and 1.122 give

$$F = \int_V \left( \int_0^B \bar{H} \cdot d\bar{B} - \int_0^A \bar{J} \cdot d\bar{A} \right) dV \quad (1.123)$$

$F$  is minimized when:

$$\frac{\partial F}{\partial A} = 0 \quad (1.124)$$

Thus:

$$\int_V \left( \frac{\partial}{\partial A} \int_0^B \bar{H} \cdot d\bar{B} - \bar{J} \right) dV = 0 \quad (1.125)$$

The functional  $F$  is altered from Eq. 1.123 if losses due to induced currents exist. In linear induction problems  $F$  becomes [7]:

$$F = \int_V \left( \frac{B^2}{2\mu} - \bar{J} \cdot \bar{A} + j\omega \frac{1}{2} \sigma \bar{A}^2 \right) dV \quad (1.126)$$

where  $\bar{J}$  is the applied current density of angular frequency  $\omega$ ,  $\mu$  is permeability, and  $\sigma$  is conductivity.

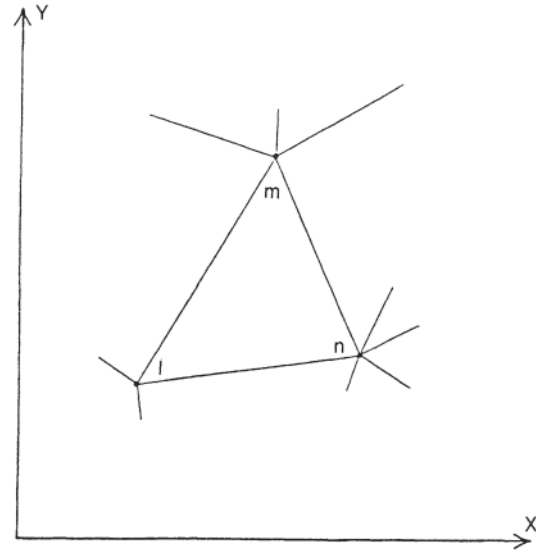


**Figure 1.23** Typical triangular finite element connected to other finite elements.

### 1.5.3 Finite Element Formulation

Minimization of the magnetic energy functional over a set of finite elements (called a model or mesh) leads to a matrix equation that can be solved for the potential  $\bar{A}$  throughout the mesh. The assembly of this matrix equation is here derived for the case of planar induction problems [8].

Figure 1.23 shows the coordinate system for planar problems, along with part of a typical finite element mesh. The entire planar mesh may represent, for example, the stator and rotor laminations and air gap of a motor. A similar two-dimensional derivation may be made for axisymmetric problems, such as for cylindrical solenoids. In either case, the device analyzed must be subdivided into triangles or quadrilaterals called finite elements, each of which has three or four vertices called grid points. Given the motor geometry, Maxwell® software automatically generates the finite element mesh for best solution accuracy.

In such two-dimensional problems,  $\bar{J}$  and  $\bar{A}$  are assumed to be directed out of or into the page. Within each triangular finite element  $A$  is assumed to vary linearly according to:

$$A = \sum_{k=l,m,n} \frac{A_k}{2\Delta} (d_k + e_k X + f_k Y) \quad (1.127)$$

where  $\Delta$  is the triangle area.

Evaluating Eq. 1.127 at the three vertices gives the solution for the  $d$ ,  $e$ ,  $f$  coefficients:

$$\begin{bmatrix} d_l & d_m & d_n \\ e_l & e_m & e_n \\ f_l & f_m & f_n \end{bmatrix} = 2\Delta \begin{bmatrix} 1 & x_l & y_l \\ 1 & x_m & y_m \\ 1 & x_n & y_n \end{bmatrix}^{-1} \quad (1.128)$$

The magnetic field in a triangle is:

$$\bar{B} = \nabla \times \bar{A} = \nabla \times A \bar{u}_z \quad (1.129)$$

$$\bar{B}(x,y) = -\frac{\partial A}{\partial y} \bar{u}_x + \frac{\partial A}{\partial x} \bar{u}_y \quad (1.130)$$

where  $\bar{u}_x$ , and  $\bar{u}_y$ , and  $\bar{u}_z$  are unit vectors. Substituting Eq. 1.127 into Eq. 1.130 gives:

$$\bar{B}(x,y) = \frac{1}{2\Delta} \sum_{k=l,m,n} [-f_k A_k \bar{u}_x + e_k A_k \bar{u}_y] \quad (1.131)$$

Thus the magnetic field is constant within a particular triangular finite element. Quadrilateral finite elements are composed of two or four triangles.

The grid point potentials  $A_k$  can be found by minimizing the functional (1.126), which becomes for planar problems:

$$F = \int_s \left( \frac{B^2}{2\mu} - JA + j\omega \frac{1}{2} \sigma A^2 \right) dS \quad (1.132)$$

where  $dS = dx dy$ . Substituting Eq. 1.132 into Eq. 1.124 and considering one triangular finite element yields:

$$\int_s \frac{\partial}{\partial A_j} \left( \frac{B^2}{2\mu} - JA + \omega \sigma A^2 \right) ds = 0, \quad j = l, m, n \quad (1.133)$$

Integration over the triangle can be shown to yield the 3x3 matrix equation:

$$[R][A] + j[M][A] = [C] \quad (1.134)$$

where:

$$[R] = \frac{v}{4\Delta} \begin{bmatrix} (e_l e_l + f_l f_l) & (e_l e_m + f_l f_m) & (e_l e_n + f_l f_n) \\ (e_m e_l + f_m f_l) & (e_m e_m + f_m f_m) & (e_m e_n + f_m f_n) \\ (e_n e_l + f_n f_l) & (e_n e_m + f_n f_m) & (e_n e_n + f_n f_n) \end{bmatrix} \quad (1.135)$$

$$[M] = \frac{\omega \sigma}{12} \begin{bmatrix} 2 & 1 & 1 \\ 1 & 2 & 1 \\ 1 & 1 & 2 \end{bmatrix} \quad (1.136)$$

$$[C] = \frac{J\Delta}{3} \begin{bmatrix} 1 \\ 1 \\ 1 \end{bmatrix} \quad (1.137)$$

Equations 1.134 through 1.137 solve for the potential  $A$  in a region containing the one triangle with nodes  $l$ ,  $m$ , and  $n$  in Fig. 1.23. For practical problems with  $N$  nodes (grid points), the above process is repeated for each finite element, obtaining matrices  $[R]$  and  $[M]$  with  $N$  rows and columns.  $[C]$  and  $[A]$  are then column vectors containing  $N$  rows of complex terms.

### 1.5.4 Boundary Conditions

An  $N \times N$  finite element matrix equation such as (1.134) can be solved for the grid point potentials  $A$  using sparse matrix techniques. Generally, all interior grid points are unconstrained, while grid points on the exterior of the mesh are constrained in a manner dependent on the boundary conditions at the exterior of the region analyzed.

In two-dimensional planar problems a flux line is a line of constant magnetic vector potential  $A$ . For most electrical machines with steel exterior surfaces, the flux is assumed confined to the steel outer boundary. By using the boundary condition,  $A=0$ , flux lines are constrained to follow the boundary.

Many electrical machines have identical poles, or even identical half-poles. The matrix equation size  $N$  can be greatly reduced if the mesh need only contain one pole or one half-pole. For example, a mesh containing one half-pole often has flux lines parallel to one radial boundary and perpendicular to the other radial boundary. Absence of any constraint on an exterior grid point can be shown to cause the flux lines to be perpendicular to the finite element mesh boundary. This perpendicularity is called the natural boundary condition.

In any electrical machine having identical poles, each pole boundary has periodic boundary conditions. For rotary planar machines, periodic boundary conditions are expressed in polar ( $r$ ,  $\theta$ ) coordinates as:

$$A(r; \theta_0 + p) = -A(r; \theta_0) \quad (1.138)$$

where  $\theta_0$  is the angle of one radial boundary and  $p$  is the pole pitch angle. This is often called a NEGA boundary condition. Figure 1.24 shows that only one pole pitch need be modeled in a machine with identical poles. This figure shows the entire eight-pole machine in (a); the fact that the motor may be divided into eight identical pieces, one of which is shown in (b); the finite element model of one piece in (c); and finally, in (d), the flux plot for the entire machine. The division shown in Fig. 1.24(b) is only one of the possible divisions. The pole pitch modeled may be a piece of any shape, as long as at all radii the radial boundaries are one pole pitch apart. Thus the rotor may be rotated by up to one pole pitch from the stator in a one-pole-pitch model representing the entire machine.

### 1.5.5 Solution Techniques

Once the matrix equation has been assembled and the  $A$  constraints have been enforced, solution for  $A$  at the unconstrained grid points may proceed. If the permeability  $\mu$  is known throughout the region, then Eq. 1.137 can be solved directly by Gauss-Jordan elimination. Grid renumbering to minimize the bandwidth of the sparse  $[R]$  matrix can be used to reduce computer storage and time. Usually the computer time is proportional to the number of unknown grid point potentials taken to a power between 2 and 3. For most electrical machine models of one pole pitch, the time ranges from a few hours on a personal computer to a few minutes on a medium-size computer.

If the permeability  $\mu$  is not constant, then the  $[R]$  matrix depends on the magnitude of  $B$  (and  $J$ ). An iterative procedure is developed by expanding Eq. 1.124 in a multidimensional Taylor series:

$$\left. \frac{\partial F}{\partial A_i} \right|_{A+\delta A} = \left. \frac{\partial F}{\partial A_i} \right|_A - \sum_j \left. \frac{\partial^2 F}{\partial A_i \partial A_j} \right|_{A+\delta A} \delta A_j + \dots \quad (1.139)$$

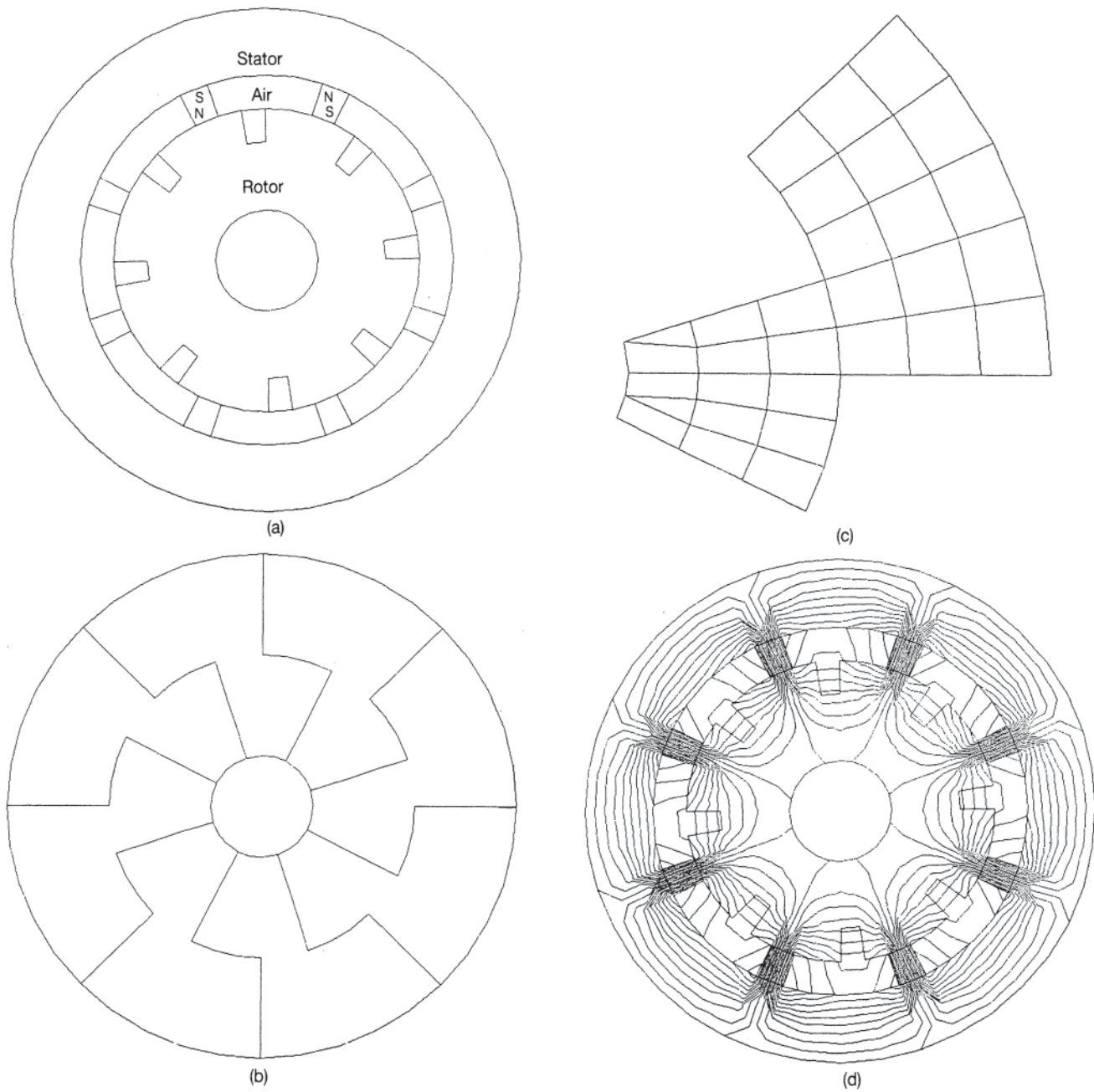


**Figure 1.24** Modeling one pole pitch of an eight-pole motor, (a) Entire motor, (b) One possible division into eight identical pieces of a puzzle, (c) Finite element model of one piece containing one pole pitch, (d) Flux plot of entire motor. An identical picture can be obtained by assembling eight copies of a flux plot of a one-pole pitch model with NEGA boundary conditions.

where  $i$  and  $j$  are integers varying from 1 to  $N$ . Substituting Eq. 1.139 in Eq. 1.124 gives the matrix equation [11]:

$$A_j = - \left[ \frac{\partial^2 F}{\partial A_i \partial A_j} \right]_{A+\partial A}^{-1} \frac{\partial F}{\partial A_i} \bigg|_{A+\partial A} \quad (1.140)$$

This equation is the basis of Newton's iterative process used to solve for  $A$  in a saturable magnetic device. The jacobian

matrix in Eq. 1.140 is first estimated from an initial solution using approximate material permeabilities. Then Eq. 1.40 is solved repeatedly until the correction  $A_j$  is negligibly small. In each solution of Eq. 1.140 both the Jacobian matrix and the residual vector in its right-hand side are reevaluated based on the latest  $A$  values, enabling rapid convergence to the correct saturable potentials  $A$  throughout the device.

The exact expressions for the Jacobian matrix and residual



vector are derived elsewhere for planar [9] and for axisymmetric [10] problems. The technique requires knowledge of reluctivity  $\nu (=1/\mu)$  and of  $\partial\nu/\partial(B^2)$  in each nonlinear material. In the program Maxwell®, these parameters are automatically computed from the  $B$ - $H$  curves supplied as input data.

### 1.5.6 Parameters from Fields

While the distribution of magnetic vector potential  $A$  obtained above has little meaning to design engineers, many useful parameters can be calculated from  $A$ . Maxwell® postprocesses  $A$  to obtain parameters of significant interest to electromagnetic device designers.

The flux density  $B$  is calculated in each finite element using the curl of  $A$  as defined in Eq. 1.115. Also, flux plots are obtained and displayed using the interactive preprocessor and postprocessor Maxwell®. Both monochromatic flux line plots and color flux density plots are created. Flux densities and flux plots tell the designer where steel should be added and where it can be removed.

From  $A$  the flux flowing between any two points is easily obtained. The definition of flux  $\phi$  is:

$$\phi = \int \bar{\mathbf{B}} \cdot d\bar{\mathbf{S}} \quad (1.141)$$

Substituting the definition of  $A$  from Eq. 1.140 gives:

$$\phi = \int \bar{\nabla} \times \bar{\mathbf{A}} \cdot d\bar{\mathbf{S}} \quad (1.142)$$

From Stokes' identity the surface integral may be replaced by a closed line integral around the surface:

$$\phi = \oint \bar{\mathbf{A}} \cdot d\bar{\mathbf{l}} \quad (1.143)$$

Thus, for two-dimensional problems the flux between any grid points 1 and 2 is simply:

$$\phi_{12} = (A_1 - A_2) d \quad (1.144)$$

where  $d$  is depth (stack) into the page.

Also calculable from the  $A$  distribution are the inductance or impedance seen by each current-carrying coil. The saturable inductance  $L$  is calculated for magnetostatic problems using [11]:

$$\frac{L}{d} = \frac{J}{3I^2} \sum_{n=1}^{N_j} \left( S_n \sum_{k=1}^3 A_k \right) \quad (1.145)$$

where  $d$  is the depth (stack height) of planar devices,  $I$  is the coil current,  $N_j$  is the number of elements containing current  $J$ , and  $S_n$  is finite element area.

The impedance calculated for problems with induced currents contains both resistive and reactive components. For example, for axisymmetric problems the impedance of a coil is [8]:

$$\bar{Z} = \frac{j\omega \bar{A}_{\text{ave}} N}{I_s} 2\pi r_0 \quad (1.146)$$

where  $r_0$  is the average radius (distance to the axis of symmetry)

of the source current,  $\bar{A}_{\text{ave}}$  is the average phasor magnetic potential over the source current region, and  $N$  is the number of conductors carrying  $I_s = J_s$  times the area of one conductor.

Other outputs by Maxwell® are the  $\bar{\mathbf{J}} \times \bar{\mathbf{B}}$  forces acting on each current-carrying finite element and the total current in each element. The current distribution in each conductor can be calculated including skin effects in single or multiple conductors [12].

The magnetic energy  $W_m$  of Eq. 1.114 is also calculated, both in every finite element as well as integrated over the volume of the entire finite element mesh. Another useful energy calculated is the magnetic coenergy:

$$W_c = \int \left( \int_0^H \bar{\mathbf{B}} \cdot d\bar{\mathbf{H}} \right) dV \quad (1.147)$$

which is very useful in calculating force [13] and torque [14, 15].

### 1.5.7 Applications in Two and Three Dimensions

Sections 4.10, 5.8, and 6.9 of this handbook describe applications of electromagnetic finite elements to a wide variety of electric motors. All types of motors can be analyzed and their design optimized with the aid of finite element software.

In addition to the two-dimensional finite elements derived in this chapter, three-dimensional, one-dimensional, zero-dimensional, and open-boundary finite elements are also useful in analyzing electric motors. Three-dimensional finite elements are needed to accurately analyze motors with short stacks and motors with three-dimensional pole and/or winding structures [16–20]. Zero-dimensional finite elements are conventional circuit elements of resistors, inductors, and capacitors [21]. By using zero-dimensional finite elements with one-dimensional finite elements representing wires and windings, arbitrary motor excitation circuits such as voltage sources can be modeled [21, 22]. Finally, open-boundary finite elements allow analysis of electromagnetic fields that extend to infinity, such as end-region fluxes in electric motors [23].

Derivation of three-dimensional, one-dimensional, zero-dimensional, and open-boundary finite element is beyond the scope of this handbook. However, applications of these element types are given in Sections 4.10, 5.7, and 6.10.

### 1.5.8 Finite Elements Compute Equivalent Circuit Parameters

There are two ways of using finite element analysis to predict the performance of electric motors. Many motor designers use equivalent electric circuits in their design, and use finite elements to obtain the values of the inductances, resistances, and/or impedances in the motor equivalent circuit. However, equivalent circuits do not predict all performance parameters, such as cogging torque and transient response, which require a second finite element technique, which is discussed in the next section.

In the first method, finite elements can obtain much more accurate values of circuit parameters than do methods based on simple equations from magnetic circuits. The values obtained by finite elements may then be used in circuit software such as SPICE or its variations to predict basic motor parameters such as torque, current, power, and efficiency. Maxwell SPICE is a version of SPICE that is part of Ansoft's Electromechanical System Simulator (EMSS) [24]. EMSS contains both finite element software and the transfer of its results to motor equivalent circuits in Maxwell SPICE. So that the finite element analyses cover the entire range of motor currents, the currents are a parameter varied in what is called *parametric finite element analysis*.

The motor types available in EMSS are alternating current (AC) reluctance motors, permanent magnet synchronous motors, direct current (DC) motors, and induction motors [24]. Detailed examples of induction motor analysis using finite element results in an equivalent circuit appears in Section 6.9 of this book and elsewhere [25]. In addition, entire drive systems can be analyzed using software called Simplorer [26], which includes all power electronics as well as the motor equivalent circuit. Both EMSS and Simplorer allow different mechanical loads on the motor to be modeled, including flywheel moments of inertia frictional and/or windage damping, and springs or opposing torques.

While equivalent circuits are often used to model motors and entire motor drive systems, equivalent circuits have inherent accuracy limitations. Most motor designs saturate their steel under some of their operating conditions, and thus inductances are not truly linear and constant. Losses also vary due to saturation, and thus resistances in equivalent circuits also vary somewhat with operating conditions. One way to improve equivalent circuit accuracy is to vary the circuit parameters with motor speed [25], as will be detailed for an induction motor in Section 6.9.

### 1.5.9 Finite Elements Directly Compute Motor Performance

The second method of using finite elements directly computes detailed motor performance. Time-stepping finite element software with zero-, one-, two-, and/or three-dimensional finite elements can directly predict essentially all motor performance parameters.

Time-stepping finite element software [24] provides more thorough and accurate prediction of motor performance than equivalent circuits. All motor performance parameters, such as torque, induced or eddy currents, and winding currents are predicted as functions of time. Thus cogging torques and harmonic currents are predicted as well as average torque and fundamental current. Such direct computation of performance eliminates the need for equivalent circuits. The time-stepping finite element software must include ways to attach drive circuits, via zero-dimensional finite elements or other means. It must also allow the rotor to move, either at a constant speed or in response to motor torque and mechanical load. Examples of applications of the time-stepping finite element software Maxwell EMPulse [26] appear later in Sections 4.10, 5.8, and 6.9.

The theory of time-stepping finite element computation of motor performance is as follows. The power source driving the motor, its electromagnetic fields, and the mechanical load are all time-dependent with optional initial conditions. Kirchoff's voltage law is used to describe the connection between the power source and the windings of the motor. Two types of winding conductors are considered: solid conductors in which eddy currents can be induced, and stranded conductors without eddy currents.

Because motion occurs in motors, the field equations for the stator and the rotor can be written in their own coordinate systems to avoid the rotational speed appearing explicitly in the formulation and to preserve the symmetry of the solution matrix. Thus the final time-dependent magnetic diffusion equation is:

$$\nabla \times \nu \nabla \times \bar{\mathbf{A}} = \bar{\mathbf{J}}_s - \sigma \frac{\partial \bar{\mathbf{A}}}{\partial t} + \sigma \nabla V + \nabla \times \bar{\mathbf{H}}_c \quad (1.148)$$

where  $\nu$ =magnetic reluctivity and  $\bar{\mathbf{A}}$ =magnetic vector potential,  $V$ =electric scalar potential in volts,  $\bar{\mathbf{H}}_c$  is permanent magnet coercive strength,  $\bar{\mathbf{J}}_s$  is source current density, and  $\sigma$  is electrical conductivity. As discussed in Section 1.5.3, in two-dimensional problems the vectors  $\bar{\mathbf{A}}$  and  $\bar{\mathbf{J}}_s$  only have one component in the  $z$  direction. Thus in the two-dimensional case, the scalar potential  $V$  has a constant value over the cross section of a conductor, and the gradient of the scalar potential is the voltage difference  $V_b$  divided by the length of the conductor in the  $z$  direction.

Conductors are normally connected to produce multiterminal windings. To represent voltage-fed windings in motors, circuit equations must be coupled with field equations. Applying Kirchoff's law gives the following equation relating terminal voltage  $U_s$  of a winding to its terminal current  $I_t$ :

$$p \left[ \frac{(N_f l)}{(S_f \alpha)} \right] f \left( \frac{dA}{dt} \right) dS + R I_t + L \frac{dI_t}{dt} + U_c = U_s \quad (1.149)$$

Where  $N_f$  is the number of conductors in the winding,  $l$  is the stack length in the  $z$  direction,  $a$  is the number of parallel branches in the winding,  $p$  is the polarity index (+1 or -1 for forward or reverse paths, respectively),  $S_f$  denotes the total area of the cross section of the winding coil group,  $R$  and  $L$  are external resistance and inductance (including those of winding endtruns) and  $U_c$  is the voltage across a capacitor (if any).

Solid conductors, such as used for rotor bars in induction motors, are large enough to require modeling of skin effects using finite elements. Since these bars may be connected at both ends using end rings, every portion of the end ring between two bars can be represented by an external  $R$  and  $L$  [25].

The equation of motion of the rotor of any motor is typically assumed to be:

$$J\alpha + \lambda\Omega = T_{em} + T_{app} \quad (1.150)$$

Where  $\alpha$ =angular acceleration,  $\Omega$ =rotational angular velocity,  $J$ =moment of inertia,  $\lambda$ =coefficient of friction,  $T_{em}$ =electromagnetic torque,  $T_{app}$ =externally applied mechanical torque.  $T_{app}$  may be either load torque (opposing sign of  $T_{em}$ ). At each time step, the electromagnetic torque is

computed using the method of virtual work involving the magnetic coenergy of Eq. 1.147. Solving the equation of motion allows computation of rotor angular acceleration versus time and thus the rotor angle versus time.

To allow the rotor to move in the finite element mesh, software such as Maxwell® [24], [26] uses the moving surface method. The idea is to share a common slip surface between the rotor mesh and the stator mesh, One side of the surface is attached to the stator and the other moves with the rotor. After any computed angular motion during the time step, the two independent meshes are coupled together by the finite element shape functions. Thus the rotor mesh is free to move to any specified angle without remeshing.

## 1.6 ENERGY STORED IN MAGNETICALLY COUPLED MULTIPLE-LOOP SYSTEMS

The energy stored in a current-carrying loop was defined earlier in Section 1.3.6. A typical electrical machine, however, consists of several current-carrying coils that are magnetically linked to each other. The energy stored in such a multiple-coil system can be obtained by considering the  $N$  loops shown in Fig. 1.25. Let  $i_m$ ,  $\phi_m$ , and  $L_{mn}$  be the current in the loop  $m$ , the flux linkage of loop  $m$ , and the mutual inductance between the loops  $m$  and  $n$ , respectively. The constant  $L_{mn}$  will be the self-inductance of loop  $m$ .

The magnetic energy in the total system is then given by:

$$W_m = \frac{1}{2} \sum_{n=1}^N i_n \phi_n \quad (1.151)$$

With linear magnetic behavior:

$$\begin{aligned} \phi_n &= \phi_{1n} + \phi_{2n} + \cdots + \phi_{Nn} \\ &= L_{1n}i_1 + L_{2n}i_2 + \cdots + L_{Nn}i_N \\ &= \sum_{m=1}^N L_{mn}i_m \end{aligned} \quad (1.152)$$

and then:

$$W_m = \frac{1}{2} \sum_{n=1}^N \sum_{m=1}^N i_n L_{mn} i_m \quad (1.153)$$

If the system constants and variables are now defined in terms of the following matrices:

$$[\mathbf{I}]' = [i_1, i_2, \dots, i_N] \quad (1.154)$$

$$[\boldsymbol{\phi}]' = [\phi_1, \phi_2, \dots, \phi_N] \quad (1.155)$$

and:

$$[\mathbf{L}] = \begin{bmatrix} L_{11} & L_{12} & \cdots & L_{1N} \\ L_{21} & L_{22} & \cdots & L_{2N} \\ \vdots & \vdots & \ddots & \vdots \\ L_{N1} & L_{N2} & \cdots & L_{NN} \end{bmatrix} \quad (1.156)$$

then the magnetic energy  $W_m$  can be written as:

$$\begin{aligned} W_m &= \frac{1}{2} [\mathbf{I}]' [\boldsymbol{\phi}] \\ &= \frac{1}{2} [\mathbf{I}]' [\mathbf{L}] [\mathbf{I}] \end{aligned} \quad (1.157)$$

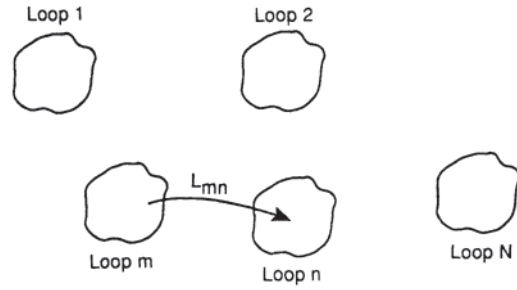


Figure 1.25 Magnetically coupled multiple-loop system.

## 1.7 FORCES AND TORQUES IN THE SYSTEM

The current-carrying loops illustrated in Fig. 1.25 will act on each other by exerting forces and torques depending on the degrees of mechanical freedom within the system. If the system has  $K$  degrees of freedom defined by displacement variables  $q_1, q_2, \dots, q_k$ , the force or the torque associated with any degree of freedom can be obtained by means of the principle of virtual work. For example:

$$F_k \text{ (or } T_k) = \frac{\partial W_m}{\partial q_k} \quad (1.158)$$

and it is considered positive if it tends to increase  $q_k$ . It must be remembered here that the partial derivative is taken with the field variables such as the current (or the flux) treated as constant.

In such a multiple-loop system, the force  $F_i$  associated with any linear motion defined by a variable  $x_i$  is then given by:

$$\begin{aligned} F_i &= \frac{\partial W_m}{\partial x_i} = \frac{1}{2} \sum_{n=1}^N \sum_{m=1}^N i_n \frac{\partial L_{mn}}{\partial x_i} i_m \\ &= \frac{1}{2} [\mathbf{I}]' \frac{\partial [\mathbf{L}]}{\partial x_i} [\mathbf{I}] \end{aligned} \quad (1.159)$$

Similarly, the torque  $T_j$  associated with any rotation defined by a variable  $\theta_j$  is given by:

$$T_j = \frac{\partial W_m}{\partial \theta_j} = \frac{1}{2} [\mathbf{I}]' \frac{\partial [\mathbf{L}]}{\partial \theta_j} [\mathbf{I}] \quad (1.160)$$

The voltages and currents in the loops can be written as:

$$\begin{aligned} v_m &= r_m i_m + \frac{d}{dt} (\phi_m) \\ &= r_m i_m + \frac{d}{dt} \left( \sum_{n=1}^N L_{nm} i_n \right) \end{aligned} \quad (1.161)$$

In matrix form:

$$[\mathbf{V}] = [\mathbf{R}][\mathbf{I}] + \frac{d}{dt} ([\mathbf{L}][\mathbf{I}]) \quad (1.162)$$

In a conventional rotating machine, there is usually only one degree of mechanical freedom—rotation. The torque  $T$  is then given by:

$$T = \frac{1}{2} [I]' \frac{\partial [L]}{\partial \theta} [I] \quad (1.163)$$

Sometimes, it is easier to solve for the voltage equations, obtain currents, and compute torque if certain transformations are used to define a new set of variables. For example:

$$[V] = [A][V]' \quad (1.164)$$

and:

$$[I] = [A][I]' \quad (1.165)$$

where  $[A]$  is the transformation matrix; it is chosen such that  $[A^{-1}] = [A]'$ .

With such a transformation, the voltage equation can then be written as:

$$\begin{aligned} [A][V]' &= [R][A][I]' + \frac{\partial [L]}{\partial t} [A][I]' + [L] \frac{\partial}{\partial t} ([A][I]') \\ &= [R][A][I]' + \frac{\partial [L]}{\partial \theta} \frac{d\theta}{dt} [A][I]' + [L] \frac{\partial [A]}{\partial \theta} \frac{d\theta}{dt} [I]' \\ &\quad + [L][A] \frac{\partial [I]'}{\partial t} \end{aligned} \quad (1.166)$$

That is:

$$\begin{aligned} [V]' &= ([A]'[R][A])[I]' + ([A]'[L][A]) \frac{d[I]'}{dt} \\ &\quad + \frac{d\theta}{dt} \left( [A]'[L] \frac{d[A]}{d\theta} + A' \frac{d[L]}{d\theta} [A] \right) [I]' \end{aligned} \quad (1.167)$$

or:

$$[V]' = [R]'[I]' + [L]' \frac{d[I]'}{dt} + \frac{d\theta}{dt} ([G]' + [T]')[I] \quad (1.168)$$

Also, the new torque equation is then:

$$\begin{aligned} T &= \frac{1}{2} ([A][I]')' \frac{d[L]}{d\theta} ([A][I]') \\ &= \frac{1}{2} [I]'' \left( [A]' \frac{d[L]}{d\theta} [A] \right) [I]' = \frac{1}{2} [I]'' [T]' [I]' \end{aligned} \quad (1.169)$$

#### Example 1. Force in a singly excited system

26 Let the coil in Fig. 1.26 have  $N$  turns and carry a current of  $I$ . If the relative permeability of the iron core of the magnetic circuit is high ( $\mu_r \gg 1$ ), the flux density  $B$  in the airgap, the flux linkage  $\psi$ , the self-inductance  $L$ , and the force  $F$  are then given by:

$$B = \mu_0 H = \mu_0 \left( \frac{NI}{x} \right) \quad (1.170)$$

$$\psi = \phi N = \frac{\mu_0 AN^2 I}{x} \quad (1.171)$$

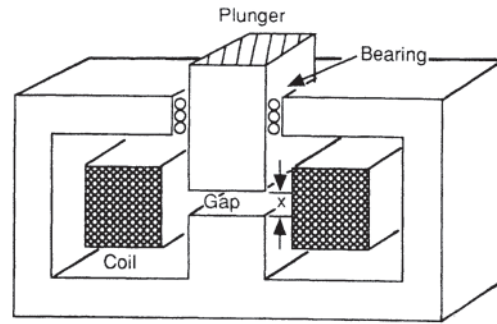


Figure 1.26 A singly excited system.

$$L = \frac{\mu_0 AN^2}{x} \quad (1.172)$$

$$W_m = \frac{1}{2} I^2 L \quad (1.173)$$

$$\begin{aligned} F &= \frac{d}{dx} \left( \frac{1}{2} I^2 L \right) = \frac{1}{2} I^2 \frac{dL}{dx} \\ &= -\frac{1}{2} I^2 \left( \frac{\mu_0 AN^2}{x^2} \right) \\ &= -\frac{1}{2\mu_0} \left( \frac{\mu_0 NI}{x} \right)^2 A \\ &= -\frac{B^2 A}{2\mu_0} \end{aligned} \quad (1.174)$$

The negative sign indicates that the force tends to decrease  $x$ , and hence is attractive.

#### Example 2. Torque in a multiply excited system

Figure 1.27 illustrates an elementary electric machine having two identical stator coils placed such that their axes are displaced by 90 degrees. A single coil is wound on a cylindrical rotor structure such that the airgap between the stator and the rotor can be assumed to be constant and independent of the rotor position. The resistance and the inductance matrices can then be defined as:

$$[R] = \begin{bmatrix} R_s & 0 & 0 \\ 0 & R_s & 0 \\ 0 & 0 & R_r \end{bmatrix} \quad (1.175)$$

$$[L] = \begin{bmatrix} L_s & 0 & L_m \cos \theta \\ 0 & L_s & L_m \sin \theta \\ L_m \cos \theta & L_m \sin \theta & L_r \end{bmatrix} \quad (1.176)$$

The torque is obtained as:

$$\begin{aligned} T &= \frac{1}{2} [I]' \frac{d[L]}{d\theta} [I] \\ &= \frac{1}{2} [i_{s1}, i_{s2}, i_r] \begin{bmatrix} 0 & 0 & -L_m \sin \theta \\ 0 & 0 & L_m \cos \theta \\ -L_m \sin \theta & L_m \cos \theta & 0 \end{bmatrix} \times \begin{bmatrix} i_{s1} \\ i_{s2} \\ i_r \end{bmatrix} \end{aligned}$$

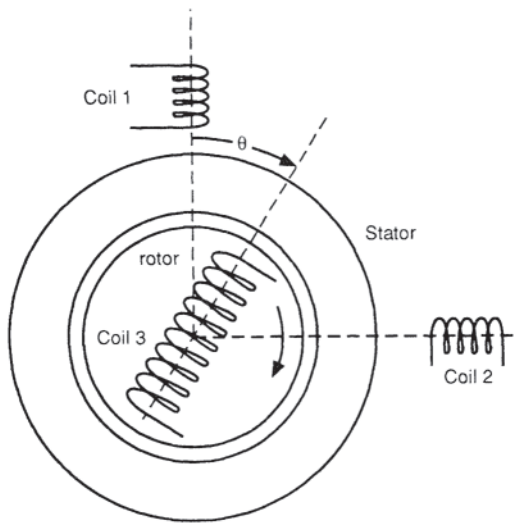


Figure 1.27 A multiply excited system.

$$=L_m i_r (-i_{s1} \sin \theta + i_{s2} \cos \theta) \quad (1.177)$$

If the two stator coils are excited by balanced two-phase currents, and the rotor is supplied by a constant direct current  $I_r$ , that is,

$$i_{s1} = I_s \cos \omega t \quad (1.178)$$

$$i_{s2} = I_s \cos \left( \omega t - \frac{\pi}{2} \right) = I_s \sin \omega t \quad (1.179)$$

$$i_r = I_r \quad (1.180)$$

then:

$$\begin{aligned} T &= L_m I_s I_r (-\cos \omega t \sin \theta + \sin \omega t \cos \theta) \\ &= L_m I_s I_r \sin(\omega t - \theta) \end{aligned} \quad (1.181)$$

If the rotor rotates at any angular speed other than  $\omega$ , the average value of the torque will be zero. If, however, it rotates at  $\omega$  such that:

$$\theta = \omega t - \delta \quad (1.182)$$

then the torque produced is constant and is given by:

$$T = L_m I_s I_r \sin \delta \quad (1.183)$$

For positive  $\delta$ , the rotor will lag behind the rotating stator field, the machine will act like a motor, and the positive sign of the torque indicates that the rotor will tend to accelerate and align itself with the stator field. A negative value of  $\delta$ , on the other hand, signifies a generator action. The negative sign of the torque then indicates that the rotor will tend to decelerate (the prime mover torque is driving it) and align itself with the stator field.

To illustrate the use of a transformation, let only the stator currents be transformed to two new variables  $i_{sd}$  and  $i_{sq}$  such that:

$$i_{sd} = i_{s1} \cos \theta + i_{s2} \sin \theta \quad (1.184)$$

$$i_{sq} = -i_{s1} \sin \theta + i_{s2} \cos \theta \quad (1.185)$$

Then:

$$[A] = \begin{bmatrix} \cos \theta & -\sin \theta & 0 \\ \sin \theta & \cos \theta & 0 \\ 0 & 0 & 1 \end{bmatrix} \quad (1.186)$$

$$[T]' = [A]^t \frac{d[L]}{d\theta} [A] = \begin{bmatrix} 0 & 0 & 0 \\ 0 & 0 & L_m \\ 0 & L_m & 0 \end{bmatrix} \quad (1.187)$$

and the torque:

$$\begin{aligned} T &= \frac{1}{2} [i_{sd} \ i_{sq} \ i_r] \begin{bmatrix} 0 & 0 & 0 \\ 0 & 0 & L_m \\ 0 & L_m & 0 \end{bmatrix} \begin{bmatrix} i_{sd} \\ i_{sq} \\ i_r \end{bmatrix} \\ &= L_m i_{sq} i_r \end{aligned} \quad (1.188)$$

If, as before:

$$i_{s1} = I_s \cos \omega t$$

$$i_{s2} = I_s \sin \omega t$$

$$i_r = I_r$$

$$\theta = \omega t + \delta$$

then:

$$T = L_m I_s I_r \sin \delta \quad (1.189)$$

It should be noted here that this is the classic direct-quadrature ( $d$ - $q$ ) transformation applied to a two-phase synchronous machine.

## REFERENCES

1. Bewley, L.V., *Two-Dimensional Fields in Electrical Engineering*, Dover Press, New York, 1964.
2. Nene, V.D., et al., "Magnetic Permeance of Identical Double Slotting of Finite Depth," Reserach Report 7201 GOUNCOS-P1, Westinghouse Research Laboratories, Pittsburgh PA, 1972.
3. Maxwell® is proprietary software available from Ansoft corporation, Four Station Square, Pittsburgh, PA 15219, USA, [www.ansoft.com](http://www.ansoft.com).
4. Stratton, J.A., *Electromagnetic Theory*, McGraw-Hill, New York, 1941, pp. 131–132.
5. Brauer, J.R., "Saturated Magnetic Energy Functional for Finite Element Analysis of Electric Machines," IEEE Power Engineering Society Meeting, January 1975.
6. Desai, C.S., and J.F. Abel, *Introduction to the Finite Element Method*, Van Nostrand Reinhold, New York, 1972, p. 58.
7. Chari, M.V.K., "Finite Element Solution of the Eddy-Current Problem in Magnetic Structures," *IEEE Transactions on Power Apparatus and Systems*, vol. PAS-93, Jan./Feb. 1974, pp. 62–72.
8. Brauer, J.R., "Finite Element Analysis of Electromagnetic Induction in Transformers," Paper A77122–5, IEEE Winter Power Meeting, Feb. 1977.
9. Brauer, J.R., L.A. Larkin, B.E. MacNeal, and J.J. Ruehl, "New Nonlinear Algorithms for Finite Element Analysis of 2D and 3D Magnetic Fields," *Journal of Applied Physics*, vol. 69, Apr. 15, 1991, pp. 5044–5046.
10. Brauer, J.R., "Improvements in Finite Element Analysis of Magnetic Devices," IEEE International Magnetics Conference, Los Angeles, CA, 1977.

11. Brauer, J.R., "Flux Patterns by the Finite Element Method," Conference Record of IEEE Applied Magnetics Workshop, IEEE No. 75CH-9064-7MAG, June 1975.
12. Brauer, J.R., "Finite Element Calculation of Eddy Currents and Skin Effects," *IEEE Transactions on Magnetics*, vol. 18, Mar. 1982.
13. Brauer, J.R., "Finite Element Analysis of Solenoids, Transformers, Generators, and Motors," Record of Cleveland Electronics Conference, IEEE No. 78CH-1300-3, May 1978.
14. Brauer, J.R., "Finite Element Calculation of Synchronous, Universal, and Induction Motor Performance," MOTORCON 82, Mar. 1982.
15. Brauer, J.R., "Finite Element Software Aids Motor Design," Small Motor Manufacturers Association Tenth Annual Meeting, Mar. 1985.
16. Brauer, John R., ed., *What Every Engineer Should Know About Finite Element Analysis*, Marcel Dekker, New York, 1993.
17. Brauer, J.R., G.A.Zimmerlee, T.A.Bush, R.J.Sandel, and R. D.Schultz, "3D Finite Element Analysis of Automotive Alternators Under Any Load," *IEEE Transactions on Magnetics*, vol. 24, Jan. 1988, pp. 500-503.
18. Brauer, J.R., S.M.Schaefer, N.J.Lambert, and B.E.MacNeal, "Mixing 2D with 3D Finite Elements in Magnetic Models," *IEEE Transactions on Magnetics*, vol. 26, Sept. 1990, pp. 2193-2195.
19. Brauer, J.R., B.E.MacNeal, and R.N.Coppolino, "A General Finite Element Vector Potential Formulation of Electromagnetics Using a Time-Integrated Electric Scalar Potential," *IEEE Transactions on Magnetics*, vol. 26, Sept. 1990, pp. 1768-1770.
20. Brauer, J.R., L.A.Larkin, and B.E.MacNeal, "Higher Order 3D Isoparametric Finite Elements for Improved Magnetic Field Calculation Accuracy," *IEEE Transactions on Magnetics*, vol. 27, Sept. 1991, pp. 4185-4189.
21. Brauer, J.R., B.E.MacNeal, L.A.Larkin, and V.D.Overbye, "New Method of Modeling Electronic Circuits Coupled with 3D Electromagnetic Finite Element Models," *IEEE Transactions on Magnetics*, vol. 27, Sept. 1991, pp. 4085-4089.
22. Brauer, John R. and Bruce E.MacNeal, "Finite Element Modeling of Multiturn Windings with Attached Electric Circuits," *IEEE Transactions on Magnetics*, vol. 28, Mar. 1993, pp. 1693-1696.
23. Brauer, J.R., S.M.Schaefer, Jin-Fa Lee, and R.Mittra, "Asymptotic Boundary Condition for Three Dimensional Magnetostatic Finite Elements," *IEEE Transactions on Magnetics*, vol. 27, Nov. 1991, pp. 5013-5015.
24. Ravenstahl M., Brauer J., Stanton S., and Zhou P., "Maxwell Design Environment for Optimal Electric Machine Design," Small Motor Manufacturing Assn. Annual Meeting, 1998.
25. Zhou P., Stanton S., and Cendes Z.J., "Dynamic Modeling of Three Phase and Single Phase Induction Motors," IEEE Int. Electric Machines & Drives Conference, 1999.
26. Maxwell, EMSS (ElectorMechanical System Simulator), Empulse, and Simplorer are proprietary products of Ansoft Corporation, Pittsburgh, PA 15219 USA, [www.ansoft.com](http://www.ansoft.com).

### SUGGESTED READING

- Churchill, R.V., *Fourier Series and Boundary Value Problems*, McGraw-Hill, New York, 1963.
- Kraus, J.D., *Electromagnetics*, McGraw-Hill, New York, 1973.
- Panofsky, W.K. H., and M. Phillips, *Classical Electricity and Magnetism*, Addison-Wesley, Reading, MA, 1962.
- Plonsey, R., and B.E. Collin, *Principles and Applications of Electromagnetic Fields*, McGraw-Hill, New York, 1961.
- Popovic, B.D., *Introductory Engineering Electromagnetics*, Addison-Wesley, Reading, MA, 1971.
- Seely, S., *Introduction to Electromagnetic Fields*, McGraw-Hill, New York, 1958.

# 2

## Types of Motors and Their Characteristics

Howard B.Hamilton (*Section 2.0*)/Howard B.Hamilton and Haran C.Karmaker (*Section 2.1*)/Howard B.Hamilton and Richard K.Barton (*Sections 2.3.1–2.3.6*)/William R.Hoffmeyer, Walter J.Martiny, and J.Herbert Johnson (*Sections 2.2–2.2.6*)/Eugene A.Klingshirn, Walter J.Martiny, and J.Herbert Johnson/(*Section 2.2.7*)/Vilas D.Nene and Gerald B.Kliman (*Section 2.2.8*)/Thomas H.Ortmeyer (*Section 2.2.9*)/Frank DeWolf and Gerald B.Kliman (*Section 2.3.7*)/Edward J.Woods (*Section 2.3.8*)/ Howard F.Hendricks, Sr., Robert N.Brigham, and Norman L.Kopp (*Section 2.3.9*)/Edward P.Priebe and Paul R.Hokanson (*Section 2.4*)/Lewis E.Unnewehr (*Section 2.5.1*)/Shailesh Kapadia and Eike Richter (*Section 2.5.2*)/Dennis L.Rimmel (*Section 2.5.3*)/Joseph C.Liu and Jacek F.Gieras (*Section 2.5.4*)/Jacek F.Gieras (*Section 2.5.5*)/Alfredo Vagati (*Section 2.5.6*)/Eike Richter (*Section 2.5.7*)/ Swarn S.Kalsi (*Section 2.5.8*)/Jerry D. Lloyd (*Section 2.5.9*)/T.J.E.Miller (*Section 2.5.10*)/Richard H. Engelmann (*Section 2.5.11*)

<b>2.0 INTRODUCTION</b>	<b>26</b>
<b>2.1 POLYPHASE SYNCHRONOUS MOTORS</b>	<b>28</b>
2.1.1 Synchronous Machine Performance Considerations	32
<b>2.2 INDUCTION MOTORS—POLYPHASE AND SINGLE-PHASE</b>	<b>35</b>
2.2.1 General Theory and Definition of Terms Used	35
2.2.2 Classification of Motors According to Size	38
2.2.3 Power Requirements, Mechanical, and Thermal Design Considerations	38
2.2.4 Standard-Efficiency Motors vs. High-Efficiency Motors	41
2.2.5 Electrical Design Options—Polyphase	41
2.2.6 Electrical Design Options—Single-Phase	42
2.2.7 Performance on Variable-Frequency Sources	43
2.2.8 Linear Induction Motors	46
2.2.9 Doubly Fed Induction Motors	54
<b>2.3 DIRECT-CURRENT MOTORS</b>	<b>58</b>
2.3.1 Introduction	58
2.3.2 General Description	58
2.3.3 Tests	62
2.3.4 Shunt Motors	64
2.3.5 Series Motors	66
2.3.6 Compound-Wound DC Motors	68
2.3.7 Permanent Magnet Motors	68
2.3.8 Brushless DC Motors	70
2.3.9 Ironless Armature DC Motors	71
<b>2.4 ELECTRIC TRACTION</b>	<b>77</b>
2.4.1 Externally Powered Vehicles	78
2.4.2 Internal Combustion Powered Vehicles	87
2.4.3 Battery Powered Vehicles	94
2.4.4 Design Considerations	98

<b>2.5 MOTORS FOR SPECIAL APPLICATIONS</b>	<b>109</b>
2.5.1 Stepper Motors	109
2.5.2 400-Hz Motors	123
2.5.3 Deep Well Turbine Pump Motors	126
2.5.4 Submersible Motors	133
2.5.5 Solid-Rotor Induction Motors	134
2.5.6 Synchronous Reluctance Motors	142
2.5.7 Aerospace Motors	153
2.5.8 Superconducting Synchronous Motor	153
2.5.9 Universal Motors	156
2.5.10 Line-Start Synchronous Reluctance and Permanent Magnet Motors	159
2.5.11 Watthour Meters	160
<b>REFERENCES</b>	<b>162</b>

## 2.0 INTRODUCTION

In general, motors are classified by type and by electrical supply requirements. There are two broad classifications of alternating current machines. One type is the polyphase synchronous motor, in which the magnetic field associated with the rotor results from a rotor (field) winding excited by direct current via slip rings or from permanent magnets on the rotor structure. The second type of alternating current machine is the single-phase or polyphase induction (or asynchronous) motor, in which the rotor magnetic field is created by electromagnetic induction effects. Direct current motors are usually classified by the field connections used, such as series, shunt, or compound field connections. In addition to these basic types of motors, there is a group of motors known as hybrid motors. These are motors that incorporate selected features of the basic motors in order to achieve special characteristics.

Some types of motors have the armature, or power winding, on the stator, or stationary frame of the motor; others (direct current) have the armature on the rotor, or rotating member of the motor. The specific configuration is dictated by mechanical and electrical considerations.

All motors, regardless of type or electrical supply, have two features in common. (1) For an average torque to be produced, the magnetic fields of the stator and rotor must be stationary with respect to each other. In alternating current machines, both fields are rotating in space; in direct current machines, both fields are stationary with respect to space and to one another. (2) For a specific rotor length, air gap diameter, and speed there is a maximum average power output rating. The limitation is determined by maximum allowable magnetic and electrical loading. Maximum magnetic loading is determined by the magnetization characteristic of the steel used. Maximum flux density in the air gap is limited to a value that does not oversaturate the armature winding teeth. Maximum electrical loading is determined by the current density in the armature winding. This in turn is limited by the effectiveness of the method used for removing joule heat loss and the permissible temperature rise, which in turn is a function

of the type of insulation utilized to insulate armature conductors from the steel slot/teeth.

The theoretical power rating is given by:

$$P = \frac{\pi^2}{60} B A l d^2 n \quad (2.1)$$

where  $B$  is air gap flux density in teslas (T).  $A$  is electrical loading in amperes per meter of circumference,  $l$  is rotor length meters (m),  $d$  is air gap diameter (m), and  $n$  is the number of revolutions per minute.

In terms of slots, current density, and so forth,  $A$  can be replaced by:

$$A = J \frac{bh}{y} \quad (2.2)$$

where  $J$  is allowable current density in amperes per square meter ( $A/m^2$ ),  $bh$  is the total cross-sectional area of the conductor in each slot in square meters ( $m^2$ ) and  $y$  is the distance between adjacent slots (m).

Typically, average airgap flux density is 1.0 T and conductor current density is  $6 \times 10^6 A/m^2$ . Actual values in a specific motor will depend upon the class of insulation used, the motor enclosure, cooling method and the magnetic steel used. Permissible temperature rise is the limiting factor in motor loading and must be considered in choosing a motor size, or rating, for a specific application. If a motor is loaded to the extent that allowable temperature rise is exceeded, the useful life of the motor insulation is decreased. A useful rule of thumb is that each  $10^\circ C$  rise over the rated temperature rise cuts the insulation life in half.

The comments in the preceding paragraphs are in general related to maximum average power or torque output. Maximum transient load is, of course, larger than the maximum average value. In the case of polyphase synchronous machines, which run at constant steady-state speed, the limiting transient torque is that at which the motor just stays in synchronism, that is, if an impact torque is applied, the rotor and stator fields (after going through an oscillatory disturbance period) return to a stationary condition with respect to each other, which is constant synchronous speed as determined by the stator frequency. In the case of induction-type motors, the motor



can absorb any transient torque up to the “breakdown” torque level, although there will be speed changes. The limitation of a direct current machine is based on the maximum current the machine can commutate. This is a function of, among other things, the presence or absence of nonpower field windings (commutating and/or compensating) that are specifically used to assist in the commutation process.

In analyzing the performance of electric motors and their loads, it is very useful to utilize the per-unit system. The perunit system is a ratioed, dimensionless system.

The use of ratios to express results as normalized dimensionless quantities is quite common. Such ratios as percent efficiency, percent regulation, percent of rated power, power factor, etc., are widely used. If a quantity such as voltage drop is expressed per unit of rated voltage, it is much more meaningful than if it is expressed in terms of its actual value. This is especially true if one is attempting to compare the performance or the parameters of one system with that of another system of different rating. In addition, as a result of standardization trends in the design of equipment, many of the performance characteristics and parameters of machines are almost constant over a wide range of ratings if they are expressed as ratios. The use of such quantities can also be applied to circuit analysis, greatly simplifying calculations in circuits involving transformers and circuits coupled magnetically, including electric machines. The advantages can be summarized as follows.

1. The use of per-unit values facilitates scaling and the programming of computers used for system studies.
2. The use of per-unit values in program solutions yields results that are generalized and broadly applicable.
3. The solution of networks containing magnetically coupled circuits is facilitated. For example, with the proper choice of unit, or base, quantities, the mutual inductance in per-unit values is the same regardless of which winding the mutual inductance is viewed from and regardless of the turns ratio of the windings.
4. Since the constants of machines, transformers, and other equipment lie within a relatively narrow range when expressed as a fraction of the equipment rating, one can make “educated guesses” as to the probable value of per-unit constants in the absence of definite design information. This is of assistance to the analyst when operating without complete device information.

Per-unit values are often converted to percentages for easy visualization. However, when doing mathematical manipulations, per-unit values should be used. By definition:

$$\frac{\text{The quantity in per-unit values}}{\text{per-unit values}} = \frac{\text{actual value of the quantity}}{\text{base value of the quantity}} \quad (2.3)$$

Actual quantity refers to its value in volts, ohms, or whatever unit is applicable. Within limits, the base values may be chosen as any convenient number. However, for machine analysis they are usually chosen based on the nameplate rating of the machine. In power systems analysis, there are many factors

that enter into the choice. In the analysis of a system, a common volt-ampere base must be used and a consistent voltage base utilized, taking the transformer turns ratios into account.

The base values must be selected so that the fundamental laws of mechanical and electrical phenomena are still valid in the per-unit system. Ohm’s law states that (in actual values):

$$\bar{V} = \bar{Z}\bar{I} \quad (2.4)$$

If *any two* values for  $V_b$ ,  $I_b$ , and  $Z_b$  (where the subscript  $b$  denotes base values) are selected, then the third value is determined by the relationship:

$$V_b = Z_b I_b \quad (2.5)$$

Dividing Eq. 2.4 by Eq. 2.5 yields:

$$\frac{\bar{V}}{V_b} = \frac{\bar{Z}}{Z_b} \frac{\bar{I}}{I_b} \quad (2.6)$$

which is, according to Eq. 2.3:

$$\bar{V}_{pu} = \bar{Z}_{pu} \bar{I}_{pu} \quad (2.7)$$

where the subscript pu denotes per-unit value.

It is common practice to select the volt-ampere base,  $VA_b$ , and the voltage base,  $V_b$ . For single-phase circuits:

$$I_b = \frac{VA_b}{V_b} \quad \text{and} \quad Z_b = \frac{V_b}{I_b} \quad (2.8)$$

from which:

$$Z_b = \frac{V_b^2}{VA_b} \quad (2.9)$$

$$Z_b = 2\pi f_b L_b = \omega_b L_b = R_b \quad (2.10)$$

where  $f_b$ ,  $\omega_b$ ,  $L_b$ , and  $R_b$  are base frequency, angular velocity, inductance, and resistance.

In three-phase circuits, base impedance is determined from the phase voltage, and base volt-amperes is the three-phase volt-amperes. Thus:

$$I_b = \frac{VA_b}{\sqrt{3} V_b} \quad (2.11)$$

and:

$$Z_b = \frac{V_b}{\sqrt{3} I_b} = \frac{V_b^2}{VA_b} = \frac{kV_b^2}{MVA_b} \quad (2.12)$$

where kV=line-line kilovolts and MVA=megavoltamperes.

Base impedance, given for a machine by the manufacturer, is based on the nameplate rating. In situations where the machine is being studied in a system using a base different from the nameplate rating of the machine, the per-unit impedance given (subscript 1) must be converted to the new conditions (subscript 2), as follows:

$$(Z_{b1}) (\bar{Z}_{pu1}) = \bar{Z}_{actual} = (Z_{b2}) (\bar{Z}_{pu2}) \quad (2.13)$$

From:

$$\bar{Z}_{pu2} = Z_{b1} (\bar{Z}_{pu1}) \frac{1}{Z_{b2}} \quad (2.14)$$

$$\bar{Z}_{pu2} = \left( \frac{kV_{b1}}{kV_{b2}} \right)^2 \left( \frac{MVA_{b2}}{MVA_{b1}} \right) \bar{Z}_{pu1}$$

It should be noted that 1.0 per-unit power corresponds to the volt-ampere rating of the machine, *not* the actual power rating. These values are the same in a direct current (dc) machine but may be different in an ac machine. As an example, for an alternating current (ac) machine rated 10,000 kVA, 0.85 pf, the rated power is 8500 kW. However, 1.0 per-unit power is taken as 10,000. Thus, on a *per-unit* basis, rated power is 0.85, not 1.0, per-unit.

Base angular velocity choice is arbitrary. However, it is usually chosen as nominal actual angular velocity. For ac machines, “nominal” is usually synchronous angular velocity, i.e.:

$$\omega_b = \frac{2\pi f}{p/2} \quad (2.15)$$

where  $p$ =number of poles of the machine.

For dc machines, it is usually calculated as:

$$\omega_b = \frac{(RPM/60)(2\pi)}{p/2} \quad (2.16)$$

where RPM is the base speed of the motor.

However, choice of base angular velocity is important if computers are being used for transient solutions. Note that for torque, speed, and power:

$$\left(\frac{\omega}{\omega_b}\right)\left(\frac{T}{T_b}\right) = \frac{P}{P'_b} \quad \text{or} \quad (\omega_{pu})(T_{pu}) = P_{pu} \quad (2.17)$$

If  $\omega_{pu}=1.0$ , that is,  $\omega_b=\omega$ , the per-unit torque and power are equal, but the mathematical solution is slowed in time by the factor  $1/\omega$ .

If  $\omega_{pu}=\omega$ , i.e.,  $\omega_b=1.0$ , the per-unit torque is equal to per-unit power divided by  $\omega$ , but the mathematical solution is in “real” time. The choice of  $\omega_b$  is made based on the problem to be solved.

Note that in using the per-unit system, for example in a power system or a single two-winding transformer, the same volt-ampere base is used throughout, or for each winding. The same requirement holds for a three-phase machine with rotor circuits. The base volt-amperes for the rotor circuits must be the same as the base volt-amperes of the three-phase or armature winding. If this is done, the per-unit value of the mutual inductance is the same when viewed from either winding and the per-unit flux linkages in each coil per unit ampere in the other coil have the same value.

In electromechanical system analysis, the moment of inertia  $J$ , in kilogram-meter squared ( $\text{kg}\cdot\text{m}^2$ ), is required. Information to determine,  $J$  is usually in terms of a defined quantity, the “inertia constant,”  $H$  seconds, or  $Wk^2\text{-lb}\cdot\text{ft}^2$ . The inertia constant turns out to be a very useful number because its value varies over a relatively small range for a wide range of machine designs of different sizes and speeds. For example, synchronous motors have an inertia constant that usually lies between 0.5 and 1.5. For induction motors,  $H$  is approximately 0.5. In the absence of specific data on the moment of inertia for a given machine, one can closely estimate the value of  $H$  based on the machine type and rating. By definition:

$$H = \frac{\text{energy stored in the rotor}}{\text{rated volt-amperes of the machine}}$$

$$= \frac{1}{2} \frac{J\omega_m^2}{\text{Rated(VA)}} \text{ seconds} \quad (2.18)$$

where  $\omega_m$  is rated mechanical angular velocity in radians per second.

If inertia information is in  $Wk^2\text{-lb}\cdot\text{ft}^2$ :

$$H = \frac{(Wk^2)(0.231)(RPM)^2}{10^6 \times \text{Rated(kVA)}} \text{ seconds} \quad (2.19)$$

$J$  can be found from Eq. 2.18 and/or Eq. 2.19; per-unit inertial torque or power can be obtained by using  $J$  with the appropriate electrical or mechanical angles and/or speed and dividing by the base torque or power as appropriate.

This chapter describes the various types of motors, their operating characteristics and supply considerations.

## 2.1 POLYPHASE SYNCHRONOUS MOTORS

Polyphase synchronous motors are usually designed for operation from a specific constant voltage (and usually constant frequency) polyphase source (that is other than a single phase source). However, there are increasing applications of synchronous motors in variable frequency/variable speed drives.

In the polyphase synchronous machine, a number of coils are distributed around the periphery of the stator and are connected in such a fashion as to form a winding of the appropriate number of phases and number of poles. The number of poles is determined by the supply frequency and desired speed. Speed, frequency, and the number of poles are related as follows:

$$f = \frac{np}{120} = p \frac{\omega_m}{4\pi} \quad (2.20)$$

where:

- $f$  = frequency (Hz)
- $p$  = number of poles
- $\omega_m$  = angular velocity (rad/sec) (mechanical)
- $n$  = angular velocity (rev/min)

The phase windings, though distributed around the periphery (for full utilization of the magnetic structure), are located so that the axes of the various phase windings are displaced in space by an angle corresponding to the “time” angle associated with the electrical supply, that is, 120 degrees in space for a three-phase source and so forth. Each phase winding is supplied with alternating current. These currents are displaced in time corresponding to 120 degrees for a three-phase system. The resulting magnetomotive force establishes a flux density in the air gap for each phase winding. The magnitude of each phase flux density pulsates with time along the axis of the particular phase winding. The coil distribution and the design of the magnetic circuit are such as to secure, as nearly as possible, a sinusoidal distribution in space of each of the phase flux density waves. The phase waves combine to form a net flux density in the air gap of,  $B(\theta, t)$ :

$$B(\theta, t) = \frac{m}{2} B_m \cos(\theta \pm \omega t) \quad (2.21)$$

where

- $B_m$  = the peak value of each phase flux density wave (T)
- $\theta$  = the electrical space angle (rad)
- $\omega$  = the electrical angular velocity of the current (rad/sec)
- $t$  = time (sec)
- $m$  = number of phases (most often  $m=3$ )

$B(\theta, t)$  is thus sinusoidally distributed in space and is revolving with angular velocity  $\omega$ . The direction in which it revolves is determined by the sign of  $\omega t$ , which is established by the phase sequence of the phase currents. If any two phases of the supply conductors are interchanged, the phase sequence is changed, the direction of rotation of  $B(\theta, t)$  is reversed and motor rotation is reversed.

The magnetic field of the rotating member (rotor) of a “conventional” synchronous motor is produced by a winding supplied with direct current via slip rings or via shaft mounted brushless exciter with rotating ac to dc converter. An alternate method is to utilize permanent magnets as a source of rotor flux density. In either configuration, the rotor field is stationary with respect to the rotor. Since average torque can be developed only when the rotor and stator fields are stationary with respect to each other, the motor operates as a synchronous motor only when the rotor is operating at synchronous speed, Eq. 2.20. At speeds other than synchronous speed, including starting conditions, no average synchronous motor torque is developed. The motor has to be started and brought nearly to synchronous speed as an induction motor. When it reaches near-synchronous speed, field excitation is applied and it is “pulled-into-step” and then runs at rated speed.

In order to perform asynchronously (as an induction machine) on startup, the rotor has an amortisseur (or damper) winding on it. This winding consists of solid conductors imbedded in the rotor in the pole face. The conductors are shorted together across each end of the rotor and thus form a squirrel-cage type winding. In some machines, the connecting, or shorting, bars extend from pole to pole and in effect form two distinct windings whose axes are centered along the axis of the rotor field winding (direct axis) and along an axis at right angle to the field winding (the quadrature axis).

Even where no deliberate pole-to-pole connection is made, the rotor iron itself forms such a circuit, allowing eddy currents to flow during transient or unbalanced conditions. During steady state, since these damper windings rotate at the same speed as the stator and rotor fields (and thus have no motion relative to magnetic fields), no induced voltage exists in them, no current flows in them, and they are completely inactive. Small currents caused by the harmonic airgap flux densities due to magnetomotive forces and slot permeances flow in damper windings at steady state. However, if a transient situation develops whereby the rotor and the stator field are rotating at different velocities, for example, the rotor is oscillating about synchronous speed, induced voltages appear, currents flow and “asynchronous” torques exist. Since the amortisseur windings tend to dampen oscillations about synchronous speed that result from electrical or mechanical

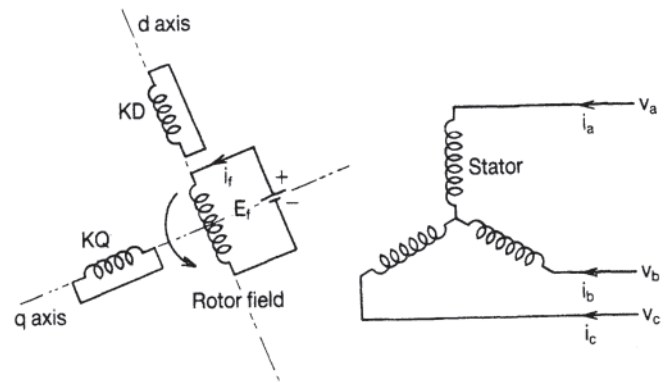


**Figure 2.1** Rotor and stator circuits of a three-phase synchronous motor, with damper circuits, KD and KQ are representative of the amortisseur windings.

perturbations, they are often referred to as damper windings. The electrical schematic of the synchronous motor, including the short-circuited damper windings, is shown in Fig. 2.1.

The actual inductances and reactances of the motor are complex to calculate and are functions of rotor position (and time). To overcome this difficulty, it is useful to resort to a mathematical transformation that resolves the stator phase magnetomotive forces into two components denoted as the direct and quadrature axis components, as defined for the rotor. This resolution results in conversion of the three stationary stator windings into two fictitious windings that are rotating synchronously with the rotor. This enables one to define fictitious reactances,  $x_d$  and  $x_q$  that are not functions of time or rotor angle. It also defines direct and quadrature (d, q) currents and voltages.

The steady-state operating characteristics of a synchronous motor are most easily visualized by means of a phasor diagram, as shown in Fig. 2.2. Resistance drops in the motor are neglected. With current in the field winding of the rotating machine, a voltage  $E_f$  will be induced. The armature current  $I_a$  will assume a magnitude and an angular position with respect to the terminal voltage  $V_t$  such as to complete the phasor diagram of Fig. 2.2.  $I_a$  will have an angle that either leads or lags the phasor  $V_t$ . That is, the armature takes a supply current having leading or lagging power factor. This is, of course, one of the advantages of choosing a synchronous motor for a specific application. It can be used as a substitute for static capacitors in correcting overall plant power factor.

Synchronous motors are of either cylindrical rotor or salient-pole rotor construction. Two-pole and four-pole motors usually have a cylindrical rotor, that is, the rotor cylinder has slots milled in the cylinder and the field winding is embedded in the slots. Some four pole motors are designed with salient poles of either solid or laminated steel. The salient-pole rotor consists of a spider with protruding poles bolted or otherwise constrained on the spider. Concentrated field coils surround the protruding pole. With salient-pole construction and little constraint on the diameter of the machine, there is a minimum restriction on the number of poles that can be utilized. Thus a synchronous motor choice may be dictated by the drive requirement, especially for applications below 900 revolutions

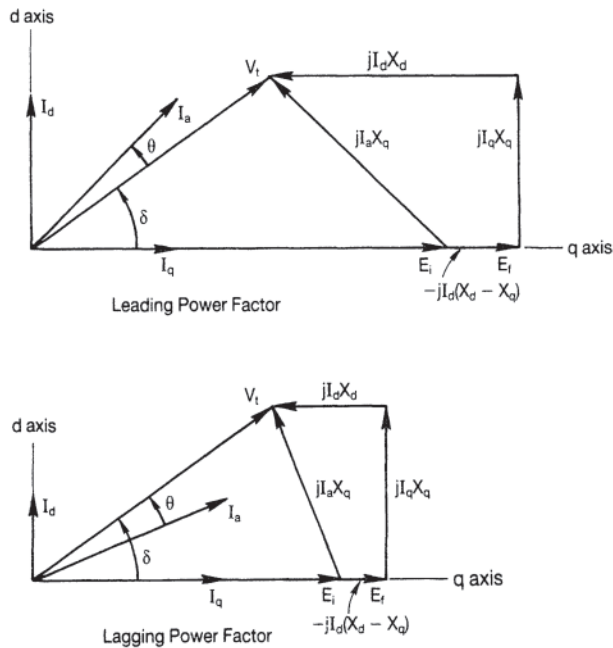


**Figure 2.2** Synchronous motor phasor diagrams for leading power factor (top) and for lagging power factor (bottom). The variables and parameters are:

$E_f$	Induced voltage in the field
$V_t$	Terminal voltage
$I_a$	Armature current
$I_d, I_q$	Direct and quadrature axis components of $I_a$
$x_d, x_q$	Direct and quadrature reactances
$\theta$	Power factor angle
$\delta$	Power angle or torque angle
$E_i$	Phasor difference between $V_t$ and $jI_a x_q$ to establish the power angle

per minute (rpm). An oft used rule of thumb is that “If the horsepower of the motor exceeds the rpm, a synchronous motor may be the economic choice,” even though the excitation source and the motor control are more sophisticated than those required for an induction motor.

The applicable standard for synchronous motors is ANSI/NEMA MG 1, Part 21 [1]. It addresses motor ratings from 20 to 100,000 horsepower (hp), speeds from 80 to 3600 rpm, and voltage ratings from 460 to 13,200 V, as well as establishing standard excitation voltages for the field windings. Among the application considerations addressed in MG 1, Part 21, are pull-in/pull-out torque; items to be included in efficiency calculations; the number of motor starts per unit of time; service conditions, that is, operation at other than rated load; variations from rated voltage and frequency; unbalanced voltages, unusual temperature or altitude conditions; and so forth. Several situations encountered in practice are not addressed. These include the necessary motor controller equipment, the torque pulsations during starting, the effect on the existing plant electrical system during abnormal situations, and motor protection provisions. All of these considerations are important and should be evaluated, as well as the economics of the

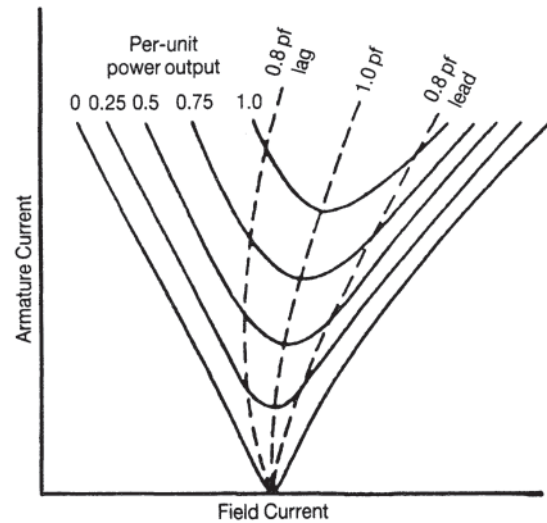


**Figure 2.3** Typical synchronous motor “V” curves.

usage of the motor vis a vis an induction motor (and gearing, if required) during the application evaluation. For detailed information on motor control and protection, refer to [Chapters 9 and 10](#).

The analysis of motor characteristics and performance under specific load conditions utilizes parameters that are obtained from the manufacturer or that may be determined by test. IEEE Std. 115 [2] details the necessary test procedures. Classic references on the parameters are in the technical literature [3, 4].

Induced voltage  $E_f$  related directly to motor speed and excitation current  $I_f$ . Armature current  $I_a$  and power factor are determined from the motor power and  $I_f$ . The relationship between  $I_a$  and  $I_f$  for various values of power is depicted in Fig. 2.3 for a typical motor with rated (constant) terminal voltage. The dotted lines indicate 0.8 lag, 1.0, 0.8 leading power factor points, and show that excitation must be changed as load conditions change in order to maintain a desired power factor.

The need for controllability and monitoring will require both field and armature current ammeters and the ability to vary excitation. A power factor meter may be desired.

From the phasor diagram, Fig. 2.2, the mathematical relations of the synchronous motor performance can be determined.

$$\begin{aligned} \text{Synchronous power, } P_s &= \frac{E_f V_t}{x_d} \sin \delta \\ &+ \frac{V_t^2}{2} \left( \frac{1}{x_q} - \frac{1}{x_d} \right) \sin^2 \delta \end{aligned} \quad (2.22)$$

$$E_i = \sqrt{(V_t + I_a x_q \sin \theta)^2 + (I_a x_q \cos \theta)^2} \quad (2.23)$$

$$\tan \delta = \frac{I_a x_q \cos \theta}{V_t + I_a x_q \sin \theta} \quad (2.24)$$

$$I_d = I_a \sin(\delta + \theta) \quad (2.25)$$

$$E_f = E_i + I_d(x_d - x_q) \quad (2.26)$$

$$\theta = \tan^{-1} \left( \frac{1}{\tan \delta} - \frac{V_t^2}{P x_q} \right) \quad (2.27)$$

$$\text{Power factor} = \cos \theta \quad (2.28)$$

$$I_d = \frac{E_f - V_t \cos \delta}{x_d} \quad (2.29)$$

$$I_q = \frac{V_t \sin \delta}{x_q} \quad (2.30)$$

$$I_a = \sqrt{I_d^2 + I_q^2} \quad (2.31)$$

Note that in Eq. 2.22 there are two distinct parts to the power expression.  $E_f V_t / x_d \sin \delta$  does not involve the “saliency” of the rotor but does depend upon the presence of an induced voltage  $E_f$ . The remaining part does depend upon saliency, that is,  $x_d \neq x_q$  but exists regardless of the induced voltage. This contribution to total power is referred to as “reluctance power.” Thus a reluctance motor can be constructed; this is a motor without field windings that depends solely on the difference in reluctance ( $x_d, x_q$ ) to develop power or torque. It will run at synchronous speed but develops considerably less torque and power than a comparably sized conventional synchronous (with field) motor. Reluctance motors commonly used are single-phase motors for electric clocks, record players, and other low-power loads requiring constant speed. However, polyphase reluctance motors in integral horsepower size have been manufactured and utilized for their simplicity and the lack of excitation requirements.

It is also possible to utilize the hysteresis characteristic of the rotor steel to achieve a cylindrical (nonsalient) motor without field excitation being required, commonly referred to as a hysteresis motor. The rotor steel is hardened magnetic steel with a wide, high-loss hysteresis loop. This steel causes the induced magnetization of the rotor (and its resulting magnetic field) to lag the stator field. Synchronous motor action results from the angular shift between the two fields. Unlike the reluctance motor, which develops torque only at synchronous speed and is thus not self-starting, the hysteresis motor develops substantially constant torque from zero speed up to synchronous speed. The actual torque developed is proportional to the hysteresis loss in the rotor steel. Thus such motors are inherently inefficient and are viable only in fractional horsepower sizes.

When a pulsating torque is present, there is a synchronizing torque, or power, due to synchronous machine effects. The parameter of interest is denoted as the synchronous power coefficient  $P_s$ :

$$P_s = \frac{\partial P}{\partial \delta} = \frac{E_f V_t}{x_d} \cos \delta + V_t^2 \left( \frac{1}{x_q} - \frac{1}{x_d} \right) \cos 2\delta \quad (2.32)$$

Any oscillation of the rotor about its equilibrium position causes the damper bars, also used for the induction start cycle of the synchronous motor, to have velocity relative to the rotating field of the motor. If the rotor angle  $\delta$  is increasing, an induction motor torque (or power) is produced. If  $\delta$  is decreasing, an induction generator torque or power results. In each case, the effect is to dampen oscillations.

Reference to an induction machine speed-torque characteristic indicates a nearly linear relationship between torque and slip,  $\sigma$  for speeds near synchronous, i.e., near zero slip. Denoting the slip  $\sigma_r$  at which rated torque  $T_r$  will be developed, the asynchronous power  $P_a$  is:

$$P_a = (\text{pf})(VA_b) \frac{\sigma}{\sigma_r} \quad (2.33)$$

Since:

$$\sigma = \frac{1}{\omega} \frac{d\delta}{dt} \quad \text{where} \quad \omega = 2\pi f \quad (2.34)$$

$$P_a = \frac{(\text{pf})(VA_b)}{2\pi f \sigma_r} \frac{d\delta}{dt} = P_d \frac{d\delta}{dt} \quad (2.35)$$

The per-unit value of  $P_d$  is:

$$P_d = \frac{(\text{pf})}{2\pi f \sigma_r} \quad (2.36)$$

$\delta$  is in electrical radians and  $P_d$  is the “damping coefficient.”

During transient conditions, nonelectrical inertia power is also present, and is given by:

$$J\omega_m \frac{d^2\delta_m}{dt^2} \quad (2.37)$$

From the definition of inertia constant  $H$ :

$$H = \frac{1}{2} \frac{J\omega_m^2}{VA_b}; \quad J\omega_m = \frac{2H}{\omega} (VA_b) \quad (2.38)$$

and inertia power can be expressed as:

$$\frac{2H}{\omega} (VA_b) \frac{d^2\delta_m}{dt^2} = P_J \frac{d^2\delta_m}{dt^2} \quad (2.39)$$

where  $P_J$  is defined as the “inertia power coefficient.” The subscript  $m$  denotes mechanical speed and angle. Since electrical and mechanical speed and angle are related by the same quantity, that is:

$$\left( \frac{p}{2} \right) \delta_m = \delta \quad \text{and} \quad \left( \frac{p}{2} \right) \omega_m = \omega = 2\pi f \quad (2.40)$$

$$\text{Inertia power} = \frac{H}{\pi f} (VA_b) \frac{d^2\delta}{dt^2} = P_J \frac{d^2\delta}{dt^2} \quad (2.41)$$

The per-unit value of  $P_J$  is:

$$P_J = \frac{H}{\pi f} \quad (2.42)$$

$H$  is the sum of the values for motor and load.

The power relationship in an electromechanical system consisting of synchronous motor, system inertia, and mechanical load is:

$$\text{Inertia power} + \text{asynchronous power} + \text{synchronous power} = \text{load power} \quad (2.43)$$

or, from Eqs. 2.22, 2.35, and 2.41:

$$P_J \frac{d^2\delta}{dt^2} + P_d \frac{d\delta}{dt} + P_s(\delta) = P_{\text{Load}} \quad (2.44)$$

### 2.1.1 Synchronous Machine Performance Considerations

Synchronous motors are commonly designed to comply with ANSI/NEMA Dtd MG 1 [1]. Important terms used in [1] are as follows

**Service Factor** At rated voltage and frequency the motors have a service factor of 1.0, that is, the rated insulation temperature rise above rated ambient will be reached at nameplate power rating. Thus there is no continuous overload capacity designed into the motor. When a service factor other than 1.0 is specified, it is preferred to have a service factor of 1.15 and temperature rise not in excess of those specified in 21.10.2 of [1] when operated at the service factor with rated voltage and frequency.

**Torques** The locked-rotor, pull-in, and pull-out torques, with rated voltage and frequency applied, shall not less than the following:

Speed (rpm)	Horsepower	Power factor	Torque <sup>a</sup> in percent of rated full-load torque		
			Locked rotor	Pull-in <sup>bc</sup>	Pull-out
500 to 1800	200 and below	1.0	100	100	150
	150 and below	0.8	100	100	175
	250 to 1000	1.0	60	60	150
	200 to 1000	0.8	60	60	175
	1250 and larger	1.0	40	60	150
450 and below	All ratings	1.0	40	30	150
		0.8	40	30	200

<sup>a</sup> Values of torque apply to salient pole machines. Values of torque for cylindrical-rotor machines are subject to individual negotiation between manufacturer and user.

<sup>b</sup> Values of normal  $WK^2$  of load are given in Eq. 2.45.

<sup>c</sup> With rated excitation current applied.

The motors shall be capable of delivering the pull-out torque for the least 1 minute.

$$\text{Normal } WK^2 \text{ of load} = \frac{(0.375) (\text{horsepower rating})^{1.15}}{(\text{speed in rpm}/1000)^2} \quad (2.45)$$

**Efficiency** The following losses are to be included in the determination of efficiency:

1.  $I^2R$  loss of armature and field
2. Core loss
3. Stray load loss
4. Friction and windage loss
5. Exciter loss (if driven from the motor shaft)

**Unbalanced Voltages** As with any motor application, any unusual service conditions, such as adverse environmental conditions, must be considered, for example, operating the motor under unbalanced supply voltage conditions. Unbalanced

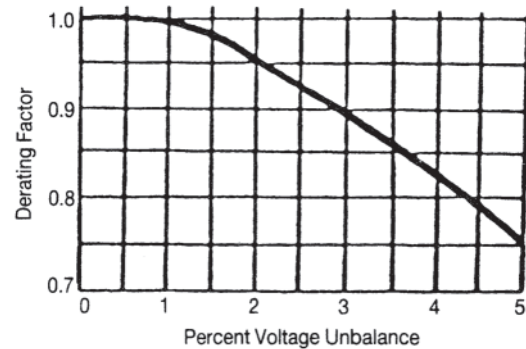


**Figure 2.4** Derating factor for voltage unbalance, where

$$\% \text{Voltage unbalance} = \frac{\text{Maximum voltage deviation from average}}{\text{average voltage}} \times 100$$

voltages result in negative sequence currents and may result in zero sequence currents. Zero sequence current results in increased  $I^2R$  loss in the stator winding. Negative sequence currents result in a torque opposite to load torque and also induce voltages, with resulting heavy currents, in the amortisseur windings. Operation of the motor with greater than 5% unbalance is not recommended. For unbalances up to that value, the rated output of the motor must be derated as shown in Fig. 2.4. Also, the locked-rotor torque, pull-in torque, and pull-out torque are decreased when the voltage is unbalanced.

In order to evaluate the effect of voltage unbalance if the specific phase voltages  $V_a$ ,  $V_b$ , and  $V_c$  are known, determine the resulting balanced positive sequence voltage,  $V_1$ , and the negative sequence voltage,  $V_2$ , by the method of symmetrical components:

$$\begin{aligned} V_1 &= \frac{1}{3} (V_a + aV_b + a^2V_c) \\ V_2 &= \frac{1}{3} (V_a + a^2V_b + aV_c) \end{aligned} \quad (2.46)$$

where:

$$\begin{aligned} a &= -0.5 + j0.866 = 1 \angle 120 \\ a^2 &= -0.5 - j0.866 = 1 \angle 240 \end{aligned}$$

The forward torque, that is, synchronous motor torque in the direction of rotation, is proportional to  $V_1^2$ . The backward torque is that torque developed asynchronously at a slip of 2.0 and is proportional to  $V_2^2$ . The net torque is the difference between the forward and backward torques.

Synchronous motors are commonly started as induction motors and thus require a more sophisticated system than induction motors. They are usually started on reduced voltage, either by virtue of impedance in series with the motor during the start sequence or by utilizing an autotransformer to reduce the voltage at the motor terminals. Generally, the constraint in motor starting is the maximum allowable current drawn from the supply and the end winding bracing system to withstand the forces due to large inrush currents.

The initial inrush current has a value determined by supply voltage/subtransient reactance ( $V_t/x_d''$ ). In the per-unit system, for  $V_t=1.0$ ,  $x_d'' = 0.2$ , for example, the current on start is 5.0 pu. If the constraint is for no more than, for example, 2.5 pu inrush current, a 1/0.7 turns ratio autotransformer will reflect the  $x_d''$  to the supply as a  $(1/0.7)^2 \times 0.2$  impedance, which is a supply impedance of  $2 \times 0.2 = 0.4$ , yielding a current of 2.5 pu. The pu voltage across the motor is 0.7. The torque developed (the square of the applied voltage) is 50% of full voltage starting. To achieve the same 2.5 pu current with impedance start would require a 0.2 pu impedance in series with the motor. This will result in 0.5 pu voltage drop across the impedance and 0.5 pu voltage at the motor terminals. The starting torque developed will be only 25% of that developed under full voltage start. The autotransformer reduced voltage starting scheme will be more expensive than the impedance method but may be required in order to meet starting torque requirements.

During the starting process, the motor field is usually shorted through a field discharge resistor in order to limit the magnitude of induced voltage across the terminals of the field winding as a result of the field winding having motion relative to the rotating magnetic field of the stator.

The start sequence, with autotransformer start, commences by closing the field discharge resistor circuit and closing the start contacts to connect the stator to reduced voltage. At a speed near synchronism, the start contacts open; the run contacts close, connecting the stator to full line voltage. Then the field discharge resistor is removed and a contactor connecting the field to the excitation source is closed. This operation is controlled by a “slip frequency” relay that detects near-synchronous speed. The motor then “pulls into step,” that is, runs synchronously.

The synchronous motor starts as an induction motor but it does not have a “smooth” torque-speed characteristic as does an induction motor. The general shape of the curve is the same except that a pulsating component is superimposed on the average value of torque at a given slip  $s$ , where slip is the difference between synchronous speed and actual speed divided by synchronous speed. The frequency of the pulsating torque is  $2f$ , where  $f$  is the supply frequency, that is, at start the pulsating torque is at twice line frequency and decreases to zero at synchronous speed. If the alternating torque frequency coincides with a resonant frequency of the load being accelerated, the magnitude of the angular mechanical oscillations may become excessive, resulting in gear or shaft failure.

There can also be problems with respect to torque pulsations during normal synchronous motor operation. Consider a synchronous motor drive on a reciprocating load compressor. The compressor is unloaded during start-up. The motor pulls into synchronism with no problem. The compressor is then loaded. Torque pulsations result due to the nature of the reciprocating load. The reciprocating load has torque harmonics. If the natural frequency of the motor approaches the frequency of torque pulsation, very large oscillations may result. The pulsations may be below the torque pull-out capability of the motor but may cause the

machine to become a generator during a portion of the oscillation. This generating portion may cause a problem if the relay protection for the motor (especially brushless excited motors) includes a power factor relay on the supply side of the motor. In effect, the power factor relay sees a very lagging power factor (indicative of loss of field) rather than a unity or leading power factor and may trip the motor off line.

In order to analyze the motor and load as an electromechanical system, the load torque,  $T_L$ , must be determined and expressed as an instantaneous torque variation with angular position. The resulting complex wave can be resolved into a Fourier series composed of an average value, a fundamental sinusoidal term, and a series of sinusoidal terms that are harmonics of the fundamental. Thus:

$$T_L = T_{ave} + \sum_{k=1}^{\infty} T_k \sin(k\omega t + \alpha_k) \quad (2.47)$$

$\alpha_k$  = the phase angle of the  $k^{\text{th}}$  harmonic

$\omega$  = the angular velocity of the fundamental term for  $n$  rpm,  $\omega = (n/60)(27\pi)$  rad/sec

If torque is in units of newton-meters (N-m), load power  $P_{Load}$  is:

$$P_{Load} = \omega T_L = P_{ave} + \sum_{k=1}^{\infty} P_k \sin(k\omega t + \alpha_k) \quad (2.48)$$

If torque is expressed in inch-pounds (in-lb), and speed  $n$  in rpm,

$$P_{Load} = 0.01183_n T_L \text{ (in-lb)} \quad (2.49)$$

$P_L$  is converted to per-unit basis by dividing by the voltampere base used (usually the motor VA<sub>b</sub>).

Using Eqs. 2.22, 2.44, 2.48, and the definition for  $\omega$  below Eq. 2.47, the equation describing the dynamic electromechanical system is:

$$\begin{aligned} P_J \frac{d^2\delta}{dt^2} + P_d \frac{d\delta}{dt} + \frac{E_f V_t}{x_d} \sin \delta + V_t^2 \left( \frac{1}{x_q} - \frac{1}{x_d} \right) \sin^2 \delta \\ = P_{ave} + \sum_{k=1}^{\infty} P_k \sin \left( \frac{2\pi n}{60} kt + \alpha_k \right) \end{aligned} \quad (2.50)$$

where  $\delta$  is the electrical angle,  $\delta(t)$ .

This is a nonlinear differential equation. A simplified analysis can be made by linearizing the equation about an “operating angle”  $\delta(0)$ . If  $\Delta\delta$  is the change in  $\delta(t)$ , then:

$$\delta(t) = \delta(0) + \Delta\delta \quad (2.51)$$

The inertia power and asynchronous power terms are unaffected since the derivatives of  $\delta(0)$ , a constant, are zero. The synchronous power term in Eq. 2.50 can be expressed as

$$\left. \frac{\partial (\text{synchronous power})}{\partial \delta} \right|_{\delta=\delta(0)} \Delta\delta = P_s \Delta\delta \quad (2.52)$$

Note that the coefficient  $P_s$  in Eq. 2.32, defined as the “synchronous power coefficient,” is treated as a constant by virtue of  $\delta$  being fixed at  $\delta(0)$ , the angle yielding average power to the load.

Since only the change in  $\delta$ , i.e.,  $\Delta\delta$ , is being evaluated, Eq. 2.50 becomes, after rearranging and applying the Laplace transformation:

$$\left(\frac{P_J}{P_s} s^2 + \frac{P_d}{P_s} s + 1\right) \Delta\delta(s) = \sum_{k=1}^{\infty} \frac{P_k}{P_s} \frac{e^{-\alpha_k s}}{k\omega(1 + s^2/(k\omega)^2)} \quad (2.53)$$

from which:

$$\Delta\delta(s) = \sum_{k=1}^{\infty} \frac{(P_k/P_s) e^{-\alpha_k s}}{\left(\frac{s^2}{\omega_n^2} + \frac{2\zeta s}{\omega_n} + 1\right)(k\omega) \left(1 + \frac{s^2}{(k\omega)^2}\right)} \quad (2.54)$$

$\omega_n$  = the system natural angular velocity =  $\sqrt{P_s/P_J}$

$\zeta$  = the damping ratio =  $P_d/(2\sqrt{P_J P_s})$

The inverse transform of Eq. 2.54 yields:

$$\begin{aligned} \Delta\delta(t) = & \sum_{k=1}^{\infty} \frac{P_k}{P_s} \left[ \frac{1}{\sqrt{(1 - (k\omega)^2/\omega_n^2) + (2\zeta k\omega/\omega_n)^2}} \right. \\ & \times \sin(k\omega t + \psi_1) + \frac{k\omega}{\omega_n \sqrt{(1 - \zeta^2)}} e^{-\omega_n \zeta t} \\ & \left. \times \sin(\omega_n \sqrt{1 - \zeta^2} t + \psi_2) \right] \quad (2.55) \end{aligned}$$

where  $\psi_1, \psi_2$  are phase angles.

Equation 2.55 reveals that the angular swing is the sum of a series of harmonic steady-state and transient oscillation. The steady-state term is at torque pulsation frequency and the transient term oscillates at system natural frequency, decaying with a time constant of  $1/\zeta\omega_n$ .

Since the magnitude of total oscillations is the item of interest, and recognizing that at times all harmonics will be in phase (worst effect) and that the transient term time constant is typically very small, the worst-case situation can be expressed as:

$$\Delta\delta(t) = \sum_{k=1}^{\infty} \frac{P_k}{P_s} A_k \sin(k\omega t) \quad (2.56)$$

where:

$$A_k = \frac{1}{\sqrt{\left(1 - \frac{(k\omega)^2}{\omega_n^2}\right)^2 + \left(\frac{2\zeta k\omega}{\omega_n}\right)^2}} \quad (2.57)$$

$A_k$  is termed the "amplification factor" and can be either greater than or less than 1.0.

As the rotor oscillates about its average angle, both synchronous power and asynchronous power also oscillate. For each harmonic  $k$ , the change in power is:

$$\Delta P_k = P_d \frac{d\Delta\delta_k}{dt} + P_s \Delta\delta_k \quad (2.58)$$

or:

$$\Delta P_k = A_k P_k \left[ \frac{P_d}{P_s} k\omega \cos(k\omega t) + \sin(k\omega t) \right] \quad (2.59)$$

In phasor form:

$$\Delta P_k = A_k P_k \left[ 1 + j\omega k \frac{P_d}{P_s} \right] \quad (2.60)$$

yielding, for the situation where all swings are in phase, the absolute magnitude

$$|AP| = \sum_{k=1}^{\infty} A_k P_k \sqrt{1 + \left(\frac{\omega k P_d}{P_s}\right)^2} \quad (2.61)$$

The significance of the ratio  $\omega/\omega_n$  is readily apparent from Eq. 2.57. As that ratio approaches 1.0, the amplification factors approach their maximum. Since:

$$\begin{aligned} \omega &= \frac{2\pi n}{60} \quad \text{and} \quad \omega_n = \sqrt{P_s/P_J} \\ \frac{\omega}{\omega_n} &= \frac{2\pi n}{60} \sqrt{P_J/P_s} \quad (2.62) \end{aligned}$$

For a fixed drive speed  $n$ , this resonance ratio,  $\omega/\omega_n$ , can be controlled by inertial additions (a flywheel) and to a limited extent by the excitation voltage.

In the linear analysis, the smaller the angular deviation, the greater the accuracy. However, for larger deviations, the more rigorous solution yields smaller values of angular deviation and power swings. Thus the results obtained from the linearized solution are conservative, the actual angular deviations being smaller. For example, calculations on a 2000-hp motor for a reciprocating compressor drive with harmonic torques of 70% (first harmonic), 122% (second harmonic), and 73% (third harmonic) of the average torque value were evaluated by both linear and nonlinear analysis. In the linear analysis,  $\delta_{(t)}$  varied from 15.3 to  $-6.32$  degrees. The solution to the nonlinear analysis showed angular variation from 1.39 to  $-1.05$  degrees, confirming the conservative nature of linear analysis.

It should be noted that  $P_s$  the synchronizing power coefficient, decreases with increasing load because as load increases  $\delta$  increases and  $P_s$  is a function of  $\cos(\delta)$ . This results in an increasing ratio of  $\omega/\omega_n$ . For the 2000-hp drive referred to above, with constant excitation to yield 0.8 pf leading at rated load, and with a specific total inertia, the system characteristics calculated are as plotted in Fig. 2.5.

The analysis of the starting performance with twice slip frequency oscillations superimposed on the average synchronous torque is much more complex and does not lend itself to a simple linearized analysis. Rather, the system must be described by a number of second order differential equations. For example, the analysis of a two-pole motor driving four axial-flow compressors via a speed-step-up bull-gear arrangement requires solution of eight simultaneous differential equations. Results of such a study [5] demonstrate that the magnitudes of the various oscillatory system torques are functions of applied starting voltage and the magnitude of the field discharge resistance.



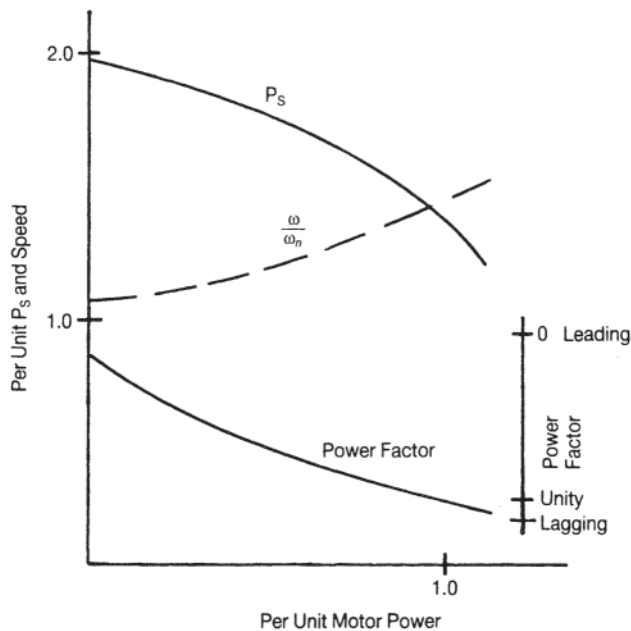


Figure 2.5 System characteristics.

MG 1, Part 21 [1], contains a compilation of torque requirements and typical  $Wk^2$  values for a large number of types of loads.

## 2.2 INDUCTION MOTORS—POLYPHASE AND SINGLE-PHASE

The most common family of motors used in homes, business, and industry is the induction motor. There is a variety to choose from, depending on power source, load requirements, mechanical interface, operating cost (efficiency), and reliability. The following is a general discussion of the theory of operation, followed by the definition of motor classification according to size, a discussion of power requirements, and mechanical and thermal alternatives. The last part discusses the electrical performance options available, including high-efficiency motors.

Standards have been developed in the United States, Canada, Europe, and Japan for mounting dimensions, ratings, and other parameters. The International Electrotechnical Commission (IEC) is in the process of developing uniform international standards. In the United States, the clearing-house for design standards is the American National Standards Institute (ANSI). The standards and usage in the United States are still in U.S. Customary units horsepower, rpm, pounds, and inches. Wherever Customary U.S. units are the fundamental units in the standards such as National Electric Manufacturers Association (NEMA) Standard MG 1–1998 [1]. A *Standard International (SI, metric)* equivalent or a conversion factor is also given.

The purpose of this chapter is to promote understanding of the variety of motors available, and to cross reference the NEMA standards wherever appropriate. Where data are presented, they are abbreviated, and the standard should be used as the precise and complete authority.

### 2.2.1 General Theory and Definition of Terms Used

The induction motor gets its name from its method of transferring power from the primary windings on the stationary part (stator) to the rotating part (rotor). The usual construction has a doughnut-shaped stack of steel laminations in the stator with insulated slots opening to the inside diameter holding the stator coils, or windings. The teeth separating the slots carry magnetic flux to the air gap that separates the stator from the rotor. The rotor is made of a stack of slotted steel laminations. The rotor stack is approximately equal to the length of the stator stack, and has an outside diameter smaller than the inside diameter of the stator laminations by twice the air gap. The rotor stack, with the slots aligned so that they are either parallel to the shaft or so that they have a uniform skew, are mounted on the shaft. The rotor conductors and the end-rings can be formed using a die cast process. In this process, a molten aluminum alloy forms the squirrel-cage configuration. Fan blades may be cast onto the end-rings at the same time, as may bosses for use in rotor balancing.

When there is relative movement between the magnetic field created by the stator windings and the conductors in the rotor, a voltage is induced in the rotor hence, the name, “induction motor.” The current produced by this induced voltage interacts with the magnetic field to produce torque.

The rotor conductors are usually made of cast aluminum. Resistance and reactance may be adjusted by changing the size and shape of the rotor slots. The rotor resistance is also changed by changing the cross section of the rotor end-rings. Other materials may be used to obtain different rotor resistances. While the most common procedure comprises a diecasting process using high-conductivity aluminum—60–62% conductivity—other methods include rotors fabricated with copper bars and end rings, rotors fabricated with aluminum bars and end rings, and also cast copper rotors. When producing aluminum die cast rotors one must take all precautions to avoid contamination with any alloying elements, especially silicon and iron. While it is true that an optimum silicon to iron ratio may produce “nice looking” end rings, it is also possible that the resultant rotor resistance may be too high. This would decrease the rotor speed, increase the rotor slip and rotor losses, and decrease the motor efficiency.

When the rotors are fabricated from either copper or aluminum, the preferred method of joining the bars and end rings is with the use of MIG or metal inert gas welding. In this process one uses argon gas and copper or aluminum welding wire. In either case, the welding wire should have the highest possible conductivity. For the copper rotors, it is also possible to use the common silver soldering technique.

The use of cast copper rotors is relatively new with special processes developed during the 1990s. Because the molten copper is at a very high temperature, it tends to absorb hydrogen and other gases if special precautions are not taken. The reader is advised to confer with his die-casting machine manufacturer for special guidance.

Other rotors have been developed using special sintered copper materials for extremely high motor efficiencies or other special performance attributes. As of this date, none are known to be in actual production.

For all rotor manufacturing processes, especially those using die-cast molten aluminum or copper, one must attempt to eliminate or significantly reduce the effects of trapped gases that would have a severe detrimental effect on the motor operation. If the process uses grease or oil to lubricate the casting molds, too much lubricant or the wrong lubricant would produce gas that would in turn create holes throughout the bars and end rings. This “Swiss cheese” effect would result in high rotor resistance, unbalanced rotors, hot spots in the end rings, and other possible defects. Likewise, the use of rotor laminations having organic surface coatings could similarly produce trapped gases. The solution to that problem is to “prebake” the laminations to burn off the coating prior to die-casting. While the surface coating intended to increase the interlaminar resistance has been essentially eliminated, the more uniformly cast rotor may more than offset any increased interlaminar losses. Also, while it is unlikely that one might totally eliminate the “Swiss cheese” effect, a more realistic goal might be to uniformly distribute the gas holes throughout the bars and end rings. This would result in more balanced rotors and fewer end ring hot spots.

Another process concern relates to the temperature of the molten aluminum or copper. If the temperature is too high, there will be excessive shrinkage during cooling and this could result in high stresses in the bars with possible bar breakage during motor operation. If the temperature is too low, the molten material could begin to solidify before the die casting is complete. Other process concerns include die-casting pressure and the number, size, shape, and placement of the orifices through which the molten material is forced into the mold. Again, the user is directed to work closely with the die-cast equipment manufacturer for guidance.

One topic that is not given adequate attention in most textbooks relates to the losses resulting from currents flowing in paths that were unintended. As stated earlier, the objective is to induce a voltage in the rotor bars so that a current is developed in the bars. Unfortunately, along with the bar current are currents flowing in the rotor surface, currents flowing axially through the laminations, and currents flowing from the bars to the steel laminations. The rotor surface currents result from poor rotor machining that produces a smeared rotor surface. The interlaminar currents result from inadequate lamination surface resistance. Finally, the bar-to-steel currents result from low bar-to-steel resistance or from molten copper or aluminum that has literally been sprayed into the rotor bar slots because of excessive die-casting pressures and/or small casting ports. Many authors tend to lump all of these resultant losses into “stray load losses” without giving proper attention to the rotor design and the rotor construction process.

The motor may have a wound rotor, with insulated wire windings similar to those on the stator. This winding is connected through slip rings to an external resistance for low-current starting and or speed control.

The stator windings are designed to create an even number of magnetic poles. A rotating magnetic field is developed by two or more current paths per pole, displaced from each other in space, and having a current that peaks at different times in the voltage cycle. A three-phase, polyphase, induction motor achieves this by having a set of stator windings for each phase, equally spaced on each pole, connected to a polyphase power source that supplies three voltages equally spaced in time.

The rotor must rotate at a speed other than that of the magnetic field in the stator in order to develop an induced voltage and torque. The field moves from one stator pole to the next in one half-cycle. Thus, in each electrical cycle the field traverses one pole pair, or 360 electrical degrees. The number of electrical cycles required for the field to complete one revolution is equal to the number of pole pairs. If the rotor were to revolve at this speed, it would be in synchronism with the field, or at synchronous speed ( $n_0$ ):

$$n_0 = 60f / (p/2) \quad (\text{rpm, Hertz, poles}) \quad (2.63)$$

While the SI unit for speed is second<sup>(-1)</sup>, common usage is revolutions per minute (rpm). The relative difference between synchronous speed and actual speed ( $n$ ) is called slip ( $S$ ) usually expressed in per-unit or percent:

$$S = \frac{n_0 - n}{n_0}; \%S = S \times 100 \quad (2.64)$$

When the load increases, the motor response is to decelerate. This increases the slip and therefore the induced voltage, the rotor current, and torque. Likewise, it accelerates to a higher speed if the load is decreased. For most induction motors, slip at rated load is less than 5%.

Speed at a given load varies somewhat even among motors that are presumed to be identical. Speed also changes by a few rpm with small changes in rotor temperature or line voltage.

For precise control of motor speed, voltage and/or frequency control is needed. For applications requiring speed control over a wide range of speeds, variable frequency power may be the best option. Motors that are designed to operate at a high value of full load slip can provide speed control by adjusting the applied voltage. Other motors can be designed to provide discrete speed ranges through the use of tapped windings, or winding arrangements that make it possible to change speed range by changing the number of poles.

Polyphase motors are classified according to size, mounting, enclosure, speed-torque, and speed-current characteristics. For a discussion of size classifications, see [Section 2.2.2](#). Enclosures are discussed in [Section 2.2.3.5](#). Mountings are discussed in [Section 2.2.3.4](#) and [Section 11.6](#).

The speed-torque characteristic can be modified by changing rotor slot shape. This changes the resistance and reactance as a function of rotor frequency. Ideally, a high resistance and reactance are desired at standstill ( $s=1$ ) to limit starting current while developing sufficient starting torque. During steady-state operation, a low resistance is desired to maximize speed and efficiency. A rotor slot shape that is deep and narrow, sometimes called deep bar, allows considerable magnetic flux to cross the slot. The induced voltage in the rotor has a frequency given by line frequency multiplied by the slip. At standstill, the rotor

current is at stator line frequency. The flux linkages, due to this high frequency current, distort the current density in the rotor to the top of the rotor bar, increasing its effective resistance. Near running speed, the slip approaches zero, with 1–4% being typical. At this low frequency, the slot flux has little effect on the current distribution, and the resistance is low. A double-cage rotor slot, features a smaller upper bar, connected to a larger lower bar by means of a narrow neck. This maximizes the flux leakage field at standstill, with a higher ratio of standstill to rated-load rotor resistance.

The smaller polyphase motors do not have double-cage or deep-bar rotor designs because the depth available is too small to be effective. Single-phase motors do not use deep slots or double cages. It will be shown later, the single-phase rotating field is imperfect. It consists of a forward and a backward field. The backward-rotating component would significantly increase losses at running speeds were the rotor to have a deep bar.

Speed-torque and speed-current characteristics of the different electrical design classifications of polyphase motors are discussed in Section 2.2.5.

A single-phase motor, as the name implies, is designed to operate from a single-phase source of voltage. There are usually two-phase windings in the stator, displaced from one another in space, wound to form poles as in the polyphase case, but both connected to the same single-phase power source. If the impedance of the two phases have different angles, the currents are “out of phase” and torque is developed to start and run the motor. This results in what may best be described as “quasi-two-phase operation.”

Once the motor starts rotating, the frequency presented to the rotor by the forward field (same direction as rotor is rotating) is  $s \times f$ , while the frequency presented by the backward field is  $(2-s) \times f$ , which is more than line frequency. The unequal impedance seen from these different frequencies result in magnetic fields of different magnitudes in the forward and backward directions, and torque can be developed even without an auxiliary winding. However, at standstill, forward and backward frequencies are equal ( $s=1$ ), so without an auxiliary stator winding there would be no net torque.

Figure 2.6 presents a speed-torque curve of a single-phase motor, showing the torque that would be developed with main winding only, and with an auxiliary winding that is switched out as the motor accelerates to normal running speed.

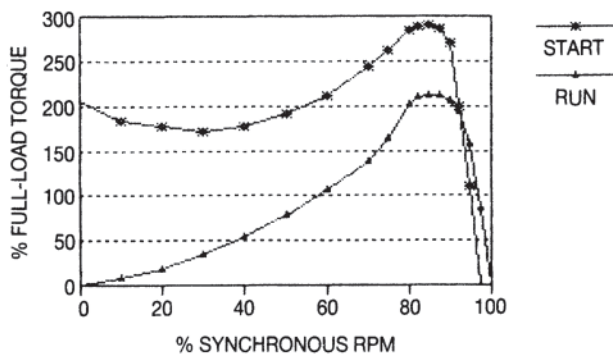


**Figure 2.6** Shape of torque-speed curve for a typical single-phase motor: START=starting condition; RUN=run winding only.

The variety of single-phase induction motor types results from the different ways for creating the impedance difference between phases. The deviation from ideal two-phase operation differs between design types, within a design type, and with load on a given motor. The pulsating, rotating magnetic field is equivalent to two non-pulsating fields of different magnitudes, rotating at synchronous speed in opposite directions. Thus, as the slip frequency for the forward-rotating field approaches zero; the slip frequency for the backward-rotating field approaches twice line frequency. The effect of the backward field is power loss and reduced torque. It is possible to design a motor to have ideal two-phase operation at one load, but at one load only. For this “balanced two-phase operation” the size of the “run” capacitor is usually very large and the cost of the capacitor usually precludes wide use of such a design. In this condition the phase angle between the main winding current and start or auxiliary winding current is 90 degrees. Also, there is pulsating torque that always exists in single-phase motors. While balanced two-phase motors are designed only infrequently, they do have their purpose. In some cases they may be used to achieve operation with no undesirable torque pulsations. Another case may be to better assess the loss distributions in the motor. At balanced operation one may easily compute the rotor and stator winding losses. If the friction and windage losses are known or computable, then the remaining losses are the iron losses.

The speed-torque-current relationships of the different types of single-phase motors and their relative performance are discussed in Section 2.2.6.

Two important terms used in comparing motors are:

$$\begin{aligned} \text{Efficiency} &= \frac{\text{Watts out}}{\text{Watts in}} \\ &= \frac{\text{Watts in} - \text{Watts Lost}}{\text{Watts in}} \end{aligned} \quad (2.65)$$

$$\text{Power Factor} = \frac{\text{Watts in}}{k \times \text{LineVolts} \times \text{LineAmps}} \quad (2.66)$$

where:

Efficiency and power factor are expressed in per unit values. To express the characteristic in percent multiply the per unit value by 100:

$$k=1.732 \text{ for three-phase}$$

$$k=1.0 \text{ for single-phase}$$

The cost of running a 10-hp motor continuously may seem high; however, with a motor efficiency of 90% only 10% of the power is dissipated in motor losses. The other 90% produces the useful work. The efficiency of a motor is increased by reducing losses. This can be done by increasing the amount and/ or quality of the steel laminations in the motor, increasing the size of the conductors in the stator windings, and reducing the rotor resistance. It may also be improved by changing the air gap distance between rotor and stator. There is an optimum air gap for each family of motors. A smaller gap length will result in high-frequency losses caused

by the effect of the slot openings in the stator and rotor on the air gap flux. Too large an air gap will increase the  $I^2R$  losses due to increased magnetizing current. These high frequency losses that occur in the stator and rotor iron comprise most of the remaining components of the so-called “stray load losses” mentioned in an earlier paragraph. One additional component not discussed is the loss induced in the end laminations of both the stator and rotor. Some authors describe this as “series iron loss” because it has the characteristics of a resistor placed in series with the main winding.

Power factor is a measure of how much of the current to the motor is producing the magnetic field compared to the current supplying losses plus output power. It is the cosine of the angle  $\phi$  between the current (amperes) and the potential (volts). The portion of the current that is equal to  $I \times \sin \phi$  is called the induction current. It is a measure of the current needed to supply the magnetic field.

This inductive component of current must be generated, but the utility usually charges only for the real power. There are additional losses produced in the power distribution system in consequence of the inductive component of the current. Some people erroneously believe that low power factor (high amperes) is also an indication of low efficiency. It often means only that the motor is running at a light load with reduced input power, and that the motor is still sized correctly for worstcase conditions. In the medium range of ratings and larger, efficiency tends to peak at a load less than the rated load. If the total electrical load for an installation results in low power factor, this can be corrected by inserting power factor-correcting capacitors somewhere in the distribution system.

Some motor design changes that reduce losses result in no change in the inductive volt-amperes or make the value larger. This has the effect of a reduction in power factor while saving energy in the motor and actually reducing total current in the system. It has been shown that it takes an improvement of about 20% in power factor to reduce motor and distribution losses as much as does a 1% gain in efficiency [6].

Power factor and efficiency are discussed further with respect to high-efficiency motors in Section 2.2.4.

## 2.2.2 Classification of Motors According to Size

A medium induction motor is defined in Ref. 1, Par. 1.4 as a motor: (a) built in a three- or four-digit frame number series in accordance with Par. 4.2.2, and (b) having a continuous rating up to and including the values in Table 1.1. A large motor is defined in Par. 1.5 as a motor built in a frame larger than that required for medium motors. Likewise, a small motor is defined in Par. 1.3 as a motor with a two-digit frame number. As a first

**Table 2.1** Maximum Ratings of Medium Induction Motors

Synchronous speed		Power rating	
(rev/see)	(rev/mm)	(hp)	(kW)
60	3600	500	373
30	1800	500	373
20	1200	350	261

Source. Adapted from [1]. Metric equivalents added by author.

approximation, small motors tend to be under 7 inches in diameter, to be single-phase, and to have a fractional horsepower ratings. Medium motors are mostly larger, polyphase, and mostly of integral horsepower rating; however, there is some overlap.

The first two digits in the NEMA frame number are an indication of the dimension D from the center of the shaft of a foot-mounted motor to the mounting plane. For medium motors, the two digits equal D times 4. Thus, frame designations of 143, 182, 184, 213, 215, and 445 have a D dimension of 3.5 in (89 mm), 4.5 in (114 mm), 4.5 in (114 mm), 5.25 in (133 mm), 5.25 in (133 mm), and 11 in (279 mm), respectively. Note that only the first two digits of the frame designation are used in this calculation [1; Par. 4.2.1].

For small motors, the two digits equal D times 16 [1; Par. 4.2.1]. Therefore, 42-, 48-, and 56-frame motors have a D dimension of 2.625 in (67 mm), 3.0 in (76 mm), and 3.5 in (89 mm). Note that the D dimension may be the same for two different frame sizes, such as 56 and 140.

## 2.2.3 Power Requirements, Mechanical, and Thermal Design Considerations

In selecting an induction motor, a series of questions must be answered with respect to input power requirements and availability, mechanical interfaces (mounting, coupling to the load), the nature and magnitude of the load, unusual temperature or environment, and protection from fire and personal injury.

The following subsections discuss the choices to be made with respect to power, load characteristics, mounting, enclosure requirements, and maximum case temperature. Discussion is limited almost entirely to general-purpose motor applications. It should be noted that there are a number of special applications with unique characteristics with sufficient volume of demand to warrant special standards, especially with respect to mounting configuration. A partial list includes motors for jet pumps, sump pumps, hermetic refrigeration and air conditioning, submersible pumps, elevators, and process pumps. These standards are presented in Ref. 1, Part 18, Definite Purpose Motors.

### 2.2.3.1 Electric Power to the Motor

Standard power generation in the United States is high-voltage, 60-Hz, three-phase. There are three-phase voltages, equal in magnitude and one third of a cycle apart in time. Small and medium motors for industrial use require the supply voltage that is transformed down, usually to a nominal value of 600, 480, 240, or 208 V. Motors have a corresponding nameplate voltage of 575, 460, 230, or 200V [1; Para. 10.30] to allow for voltage drop in the distribution system. Large induction motors are rated at 460 to 13,200 Vs, depending on horsepower [1; Para. 20.5].

Polyphase power is usually unavailable for farm, home, and office. Single-phase power is made available by connecting across two of the three-phase lines, and is available at 230 to 240 V, which may be divided further to obtain 115 to 120 V.

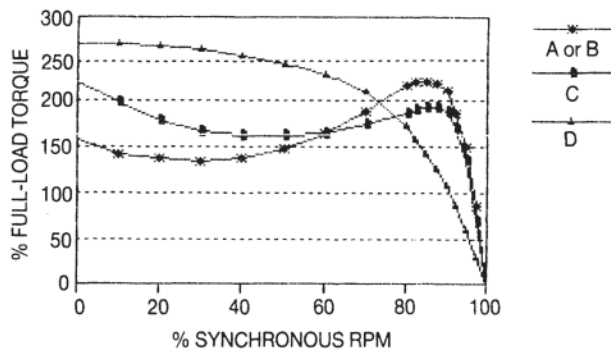


**Figure 2.7** Shape of torque-speed curves for polyphase induction motors. Curves shown are for Design Class A or B, for Class C, and for Class D.

Motors may not necessarily run satisfactorily from a power source that (1) is more than  $\pm 10\%$  from nominal voltage, (2) is  $\pm 5\%$  from rated frequency, (3) has more than 10% deviation from sinusoidal, or (4) in the case of polyphase motors, has a voltage unbalance between phases exceeding 1%. Voltage unbalance may easily occur if the various single-phase loads on the power distribution system are unevenly distributed among phases [1; Par. 12.45].

These limitations are of special concern where the power source is a standby generator or a frequency converter. Over-voltage may be most harmful to motor capacitors. Undervoltage may cause the motor to fail to start, maintain speed, or, if single-phase, to fail to switch out of the starting mode.

### 2.2.3.2 Types and Magnitudes of Loads

Figure 2.7 shows generic polyphase motor performance curves for Design A, B, C, and D motors, that are discussed further in Section 2.2.5. The percent torque values are approximate, and will vary from design to design. The figure shows the torque available to start the motor and how the torque changes with speed. Note that the torque may dip slightly at low-speed, reaching a minimum called the pull-up torque. The torque increases until it goes through a maximum. This is called the breakdown torque. The curve then becomes more and more linear, and reaches a no-load value at close to synchronous speed. (For a definition of synchronous speed, see Section 2.2.1, Eq. 2.63.) At some point in the range of half of the breakdown torque, rated torque is reached. The motor may be expected to run continuously at this speed without overheating.

Rated torque is the torque that at its corresponding rated speed delivers the rated horsepower or output kilowatts. Motors are rated in horsepower (U.S.) or kilowatts (international). Some helpful relationships are:

$$\begin{aligned} 1 \text{ horsepower (hp)} &= 550 \text{ lb-ft s} \\ &= 745.7 \text{ W} = 0.7457 \text{ kW} \end{aligned} \quad (2.67)$$

$$\begin{aligned} \text{Output power (W). } P_o &= T \times \omega \text{ (N-m-rad/sec)} \\ &= T \times N / 9.549 \text{ (N-m-rpm)} \\ &= T \times N / 84.52 \text{ (lb-in-rpm)} \\ &= T \times N / 7.043 \text{ (lb-ft-rpm)} \end{aligned}$$

$$= T \times N / 112.7 \text{ (oz-ft-rpm)}$$

$$= T \times N / 1352 \text{ (oz-in-rpm)}$$

$$1 \text{ Newton-meter} = 8.8508 \text{ lb-in}$$

As will be shown later, motors of the same horsepower rating should have close to the same breakdown torque. However, since one family may have better cooling, the motors with better cooling would run cooler at rated load, therefore, they have the ability to run continuously at a higher load. The ratio of this higher load to full load is referred to as the service factor, and this maximum continuous load is the service factor load.

Figure 2.6 shows a generic performance curve for a single-phase motor. (Traditionally, for small motors, the speed and torque are reversed on the two axes. However, in this chapter, the medium motor convention is used for all sizes.) There are typically two speed-torque curves, one for starting and one for running. The motor starts with the start or auxiliary winding energized in addition to the main winding. At some speed, the auxiliary winding or start-capacitor may be switched out, and the motor follows the running torque curve to its continuous operating point. Further description of the different types of single-phase motors is in Section 2.2.6.

To ensure that motors of the same type from different manufacturers are interchangeable, NEMA specifies that all single-phase motors of a given rating will have the same breakdown torque (within a tolerance range), and will meet a minimum starting torque limit and a maximum starting current limit [1; Part 12].

In addition, since small polyphase motors tend to have considerably higher slip at breakdown, NEMA specifies that the breakdown torque to a small general-purpose polyphase motor shall be not less than 140% of that of a single-phase motor of the same rating [1; Par. 12.37]. This tends to allow both types to operate at the same speed, so a single-phase or polyphase motor could be specified for a given application, depending on the availability of power.

The simplest load at which to size a motor is a constant load. The motor is sized to start, come up to speed and deliver the required load continuously. Other situations are more difficult. The load may be cyclic, for instance, a reciprocating pump. The rotor inertia plus load inertia must be great enough to carry through the peaks without excessive changes in speed or current. Starting torque requirements can be more severe than running torque requirements: both must be checked.

If the motor is required to start frequently, the allowable duty cycle (time on vs. time off) should be determined from Ref. 1, Par. 12.55, or in the case of high-efficiency motors, from Table 2.2 of NEMA MG 10 [7]. If the motor on-time is to be short, followed by a long off-time, it may be possible to use a smaller motor, providing that it has enough torque to start and accelerate the load. Many motors, especially in the medium and large sizes, have a 30-minute rating in addition to a continuous rating.

There are a number of ways to estimate the load. A test motor having the desired rated speed may be coupled to the load and the torque measured directly. For polyphase and the larger single-phase motors, a crude approximation may be

**Table 2.2** Nominal Speeds of Induction Motors

Poles	60-Hz				50-Hz			
	No-load		Full-load		No-load		Full-load	
	(rev/s)	(rev/min)	(rev/s)	(rev/min)	(rev/s)	(rev/min)	(rev/s)	(rev/min)
2	60.0	3600	57.5	3450	50.0	3000	47.5	2850
4	30.0	1800	28.8	1725	25.0	1500	23.8	1425
6	20.0	1200	19.0	1140	16.7	1000	15.7	940
8	15.0	900	14.2	850	12.5	750	11.7	700

obtained by measuring the current drawn by the test motor under load and dividing by the nameplate full-load amperes. If this ratio is between about 0.75 and 1.25, that number times the rated watts or horsepower of the test motor should give a good first approximation to the required watts or horsepower. If it is outside that range, it may be wise to try a different motor.

The penalty for choosing a motor larger than necessary is higher cost, greatly reduced power factor, and for most small (fractional-horsepower) motors, lower efficiency. The advantages are cooler operation (longer life) and, in the case of most integral horsepower motors higher efficiency in the load range of 0.75 to 1 times full-load.

### 2.2.3.3 Motor Speed vs. Desired Speed

The most commonly available small and medium motors have two, four, or six poles. Some eight-pole fan-motors are also standard. The possible synchronous speeds and typical fullload speeds are shown in Table 2.2. The typical full load speeds in the table are at approximately 5% slip. A high efficiency motor will have a slightly higher speed than shown in Table 2.2. This is important when matching a motor to a driven unit. Many loads, centrifugal pumps and fans, increase as the cube of the speed. Many high efficiency motors have a full load slip of 1%; therefore, the speed is 4% higher than shown in Table 2.2. The load due to the increase in speed will be 12% higher than expected. Consequently, when a high efficiency motor is applied to a load designed for the speed in the Table 2.2, the increase in load will depreciate the advantage of the improved motor efficiency. In applications such as refrigeration compressors, most systems perform best at high speed, using two-pole designs. The highest efficiency for fans occurs at lower speeds. This can make the overall system cost and efficiency best at eight poles. In other cases, the required operating speed range may not be shown in the table. In that case, it is necessary to select from the available numbers of poles, and use a belt-and-pulley system or gearing.

### 2.2.3.4 Mounting

Induction motors may be foot-mounted, face- or flange-mounted, or both (foot-mounted motor with driven device mounted to the flange). The feet on small motors may be in the form of a resilient base for vibration isolation. The most common flange mount is called a D-flange. This construction mounts the motor to the driven equipment with bolts passing through the flange into a mounting plate. The flange must therefore be of a diameter large enough to allow for access to the mounting holes from the motor side. The C-face mounts

from the opposite side. The bolts are the through the driven equipment into the motor face. The face of the motor may therefore be of a smaller diameter, but access to the opposite side of the mounting plate is necessary. A foot-mounted motor may have better heat dissipation than a flange-mounted motor.

If a motor has a C-face or D-flange, the letter C or D will appear in the model number after the frame designation. Letter designations for other special mounting configurations are listed in Ref. 1, Par. 4.22. Mounting dimensions are standardized for each frame size, and are listed in the same reference.

European mounting standards are different from NEMA. The standard ratings and dimensions used outside of North America are referenced in IEC Publication 34–10 [8].

### 2.2.3.5 Enclosures

The environment in which the motor must operate determines how the motor must be enclosed to protect the electrical parts and to protect workers from the moving parts. Since enclosures add cost and restrict cooling, one should use the most open motor consistent with the environment. Outside of North America, enclosures and cooling are defined by IEC Publication 34–5 [95], Degrees of Protection Provided by Enclosures. It uses designations IP00 through IP67, based on ability to withstand dust (first digit) and water (second digit). In North America NEMA MG 1, Part 5 address the same factors. The most recent issue of MG 1 has been harmonized with IEC 34–5. The following discussion uses NEMA MG 1 descriptive terms common before harmonizing with the IEC terms.

#### 2.2.3.5.1 Open, IP00

The simplest enclosure is open with no restriction to air flow except that needed for mechanical structure. These motors are adequate where they are inaccessible except for maintenance and away from water, dust, or chemicals that could harm internal parts of the motor. These motors usually have an internal fan. Service factor may be 1.15 to 1.35.

#### 2.2.3.5.2 Drip-Proof DP, IP02

A drip-proof motor is protected from liquid or solid particles falling at an angle of 0 to 15 degrees from the vertical. In the integral-horsepower sizes, they have a service factor of 1.15.

#### 2.2.3.5.3 Guarded, IP12

A guarded motor has all openings limited in size to prevent the passage of fingers and so forth far enough to touch electrically live or internal moving parts.

#### 2.2.3.5.4 Totally Enclosed Fan-Cooled, IP44

A totally enclosed fan-cooled (TEFC) motor is one that is enclosed to prevent the free exchange of air between the outside and inside of the motor. It has an external shaft mounted fan for cooling. This type of motor is chosen for applications where the surrounding air is dusty enough or wet enough to prevent the use of a drip-proof motor, but not dirty enough to plug up an external fan. The motor usually has an internal fan, but has poorer heat dissipation than a motor that an open motor. However, a TEFC motor rated for severe duty may have a 1.15 service factor.

#### 2.2.3.5.5 Totally Enclosed Nonventilated, IP44

A totally enclosed nonventilated motor is like a TEFC motor but does not use an external fan for cooling. It therefore has considerably poorer heat dissipation than a TEFC motor. However, TENV motors are available at the same service factors as TEFC.

#### 2.2.3.5.6 Explosion-Proof

An explosion-proof motor is not only totally enclosed but is designed to contain an internal explosion, and to prevent any flame or sparks emanating from the motor. Service factor is normally 1.0.

There are additional enclosures described in NEMA MG 1, Part 5 for large induction motors.

#### 2.2.3.6 Safety Considerations—Temperature and Noise

The selection of an enclosure must consider human safety, and the potential hazard of high temperature or even fire. The motor is designed for a maximum temperature consistent with the insulating materials, bearings, and lubrication. NEMA [1] recognizes four temperature classes: A, B, F, and H. The thermal testing of a motor to find the hottest spot under the worst-load conditions is somewhere between difficult and impossible. Therefore, the NEMA standard for medium motors specifies the limiting temperature for each insulation class based on average winding temperature, as determined by change in resistance. The test procedures and the different limits for different types of motors are beyond the scope of this discussion, but may be found in Refs. 1, 10, and 11. As a feel for the temperatures involved, according to Ref. 1, Par 12.57.1, the average winding temperature of a Class A motor may reach 140°C when the thermal protector trips, and it might reach 215°C for a class H motor. If a thermal protector is not used and the motor is misapplied, the windings can reach higher temperatures before the motor fails, and if the load is maintained, the motor may be expected to fail quickly. The methods for thermal evaluation of motor insulating systems are found in Ref. 12.

If a thermal protector is used, it may have either manual or automatic reset. A manual reset protector will not allow the motor to restart without manual intervention. Automatic reset should be used with caution, as repeated off-on cycles are likely to make the device less reliable. In addition, if the motor has been stalled, automatic reset may allow the motor to reach an excessive temperature without operation of any of the other protective devices in the circuit.

There are applications where it is not allowable to have the motor stop during the middle of a process. Rather than disable the protector, it would be better to monitor the overload device and proceed to an orderly shutdown or to immediately reduce the load if possible.

Industrial motors are normally rated for 40°C ambient temperature. Nonindustrial motors are normally rated for an ambient of 25°C. If the motor is to be applied in a different ambient, the ambient temperature will have little effect on the temperature rise. Therefore, the motor load should be adjusted down or up to allow for the difference in ambient temperatures. If the motor is to operate at an altitude above 1000 meters (3300 feet) it should be de-rated according to Ref. 1, Par. 14.4.

The motor case temperature should be somewhat below the winding temperature. If a person touches any motor that has been running under load it will feel hot and may even be well over 100°C. A motor with a lower temperature class will have a lower case temperature. In order to get the lower temperature the motor must have been made more efficient or have increased ventilation.

The windings and insulation are designed for a specific maximum temperature, however, the bearings are not selected on the basis of temperature or temperature rise. Care should therefore be taken to monitor bearing temperature if the ambient exceeds 40°C.

The sound power level of an induction motor will increase for a motor of higher speed or larger size. Overall sound power level limits for medium induction motors are listed in Ref. 1, Part 9. They are A-weighted up to 104 db. The same reference shows limits for large motors up to 120 db. Therefore, ear protection will probably be required for workers in the area.

### 2.2.4 Standard-Efficiency Motors vs. High-Efficiency Motors

An important electrical design concern is operating efficiency. Motors are designed to provide a balance between quality performance at minimum initial cost. Since 1973, greater emphasis has been placed on operating cost. In 1992 the U.S. Government enacted legislation, The Energy Policy and Conservation Act of 1992, mandating the minimum value of efficiency for induction motors rated 1–200 hp. The motors designed to comply with this act remain the best value wherever the total running time is low.

A higher efficiency design should be considered if the motor is to run much of the time. These motors generally are more costly to build and command higher prices than conventional models. One can calculate the time required to pay back the difference in price and make an economic decision based on this calculation. NEMA publications MG 10 [7] and MG 11 [13] have further discussion of this important subject.

Small motors are naturally lower in efficiency than medium motors and the trend continues to the large ratings. As is shown in Section 2.2.6, there is a large difference in efficiency among single-phase motors with respect to type and size. A standard single-phase efficiency range from 40% at 1/8 hp to 85% at 10 hp is shown in Ref. 14. Adding 20% to cost was shown to raise the range to from 60% at 1/8 hp to 86% at 10 hp.

### 2.2.5 Electrical Design Options—Polyphase

As discussed in Section 2.2.1, within the polyphase family the designer has the freedom to adjust rotor resistance and reactance. In Ref. 1, Par. 1.18, NEMA has defined four different design classes: Design A, Design B, Design C, and Design D. The most common used is Design B. Comparison speed-torque curves are shown in Fig. 2.7.

#### 2.2.5.1 Design B

These motors have lower starting current at stall than Design A motors do, and usually have higher rotor resistance. Slip at

rated output, voltage, and frequency is 5% or less. Many have slip at full load of 1–2%. They may be started at rated line voltage. Efficiency is relatively high. Starting current may be 6 to 7 times rated current. Starting torque may range from as low as 70% of rated load for large motors to 275% for the smallest medium motor. Design B motors are used in applications with relatively low starting torque requirements, such as fans, blowers, centrifugal pumps, and compressors.

#### 2.2.5.2 Design A

These motors have higher starting current than Design B motors, otherwise performance is similar. Some high-efficiency motors are Design A motors.

#### 2.2.5.3 Design C

These motors have normal starting current, but, as can be seen in Fig. 2.7, they have higher starting and accelerating torque, 190–200% of rated torque. Therefore, Design C motors can accelerate heavier loads, even though they have less breakdown torque. Slip at rated output, voltage, and frequency is slightly greater than that of Design A or B machines. The increase is in the range of 0.5–2%. Therefore, Design C motors are less efficient at rated load. They are used on reciprocating pumps, conveyers, agitators, and loads that must start under heavy load.

#### 2.2.5.4 Design D

These motors have high starting torque and high slip. Figure 2.7 shows the starting torque as 2.5 to 3.25 times rated torque. The starting current is 6 to 7 times rated for medium induction motors, and 4.5 to 6 times rated for large motors. This is the same as Design B motors. Rated load slip is between 5% and 15%. They are used on applications with high peak loads. These loads frequently use a flywheel to smooth the load on the motor. Examples for this type of load is: punch press, elevator, winch, hoist, or oil-well pumps.

#### 2.2.5.5 Wound Rotor

Wound-rotor motors usually have an external resistor bank connected to the rotor winding. By varying the amount of added resistance, the starting torque can be controlled to 1.75 to 2.75 times rated torque. Inrush current will be low, depending on the amount of starting torque required. As the motor accelerates, the added resistance can be adjusted to provide limited speed control. These motors are used where low inrush current is required, where there are frequent starts, where some speed control is desired, and where high mass must be accelerated. Wound-rotor motors are more costly to build than cast rotors for several reasons. First, the open slots in the rotor must be insulated in a manner like the stator slots. Second, instead of pouring in molten aluminum or copper, one must use preinsulated wire and hand-place or machine wind the windings into the correct rotor slots. Third, the windings must be connected internally in some acceptable manner and then the opposite ends of the wires must be connected to a set of slip rings attached to the shaft but also

insulated from the rotor shaft. Then the stator must be fitted with the appropriate brush rigging and brushes so that the external resistors can be added to the rotor windings as desired. The intent is that the added cost of the motor is offset by the motor performance that is produced.

### 2.2.6 Electrical Design Options—Single-Phase

Single-phase motors offer a set of choices, from low to high, in terms of starting torque, starting current, running current, running efficiency, and cost. A logical objective is to meet each of the other criteria at lowest cost. The discussion of single-phase motor alternatives follows in ascending order of performance and cost.

#### 2.2.6.1 Shaded-Pole Motors

Shaded-pole motors are simple in construction and are therefore relatively low-cost and reliable. The auxiliary winding is usually a simple shorted turn of conductor around one side of each stator pole, called a shading-coil. The magnetic field developed by the main winding induces a voltage in the shading-coil. This produces a current that is out of phase with the main-winding current. Thus, the necessary conditions of at least two currents displaced in space and time are met. There is no means provided to remove the shading coil from the circuit once the motor gets up to speed.

Starting current is relatively high, starting torque is relatively low, running current is relatively high, and efficiency and power factor are low. These motors are widely used to drive small fans (1/5 hp and below) because they are low in cost and reliable, and the total energy cost of operating a small fan may not be significant.

#### 2.2.6.2 Split-Phase Motors

The split-phase motor sometimes called resistance split-phase, achieves its starting torque by having a higher resistance and possibly lower reactance in the auxiliary circuit, which is usually wound 90 electrical degrees from the main winding (halfway between main poles). The higher resistance may be obtained by using smaller diameter wire than in the main winding. In some cases, the higher resistance requires using such fine wire that it would be mechanically too weak to wind, and whose current density would be so high as to cause the winding to burn out before the motor could accelerate. This problem is sometimes overcome by using a larger wire diameter, and getting the higher resistance by adding forward and backward turns so that they cancel magnetically but add resistance. An external resistance could also be used.

The “start” curve of Fig. 2.6 shows a torque-speed curve similar to that of a split-phase motor. At a speed in the region of maximum torque, the auxiliary winding is switched out, and the torque of the motor becomes that of the “run” curve, being the difference in forward and backward torque developed by the interaction of stator field and rotor currents, as discussed in Section 2.2.1. The switch may be activated by speed (centrifugal), voltage, current, or temperature (PTCR, positive temperature coefficient resistor). If the load is increased to near-



breakdown, or power is removed the start switch will close quickly, while the PTCR must cool down before resetting.

The starting torque of these motors is moderate, but the starting current is relatively high. Their size is limited by the typical electrical code limit of 12A on a branch circuit. There is also a need to keep the starting current low enough to avoid severe voltage drop during starting. This could adversely affect the operation of other nearby equipment. Efficiency and power factor are moderate, with efficiency ranging from about 40% at 1/10 hp to about 70% at 3/4 hp. Because the addition of a start switch is a potential source of failure, these motors are less reliable than shaded-pole motors but have higher starting torque and efficiency and can be applied in higher ratings than shaded-pole motors.

Split-phase motors are used in moderate starting-torque applications such as air compressors, refrigeration compressors, air conditioning fans and blowers, jigsaws, grinders, and office machines.

### 2.2.6.3 Capacitor-Start Motors

In a capacitor-start motor, the starting torque is obtained by use of a capacitor in series with the auxiliary winding while starting, then switching the auxiliary winding out as the motor reaches running speed. The capacitor causes the auxiliary winding current to lead the main current. The number of auxiliary winding turns is limited by the need to keep the capacitor voltage from exceeding its rating, which is most likely to occur at the speed at which the switch opens. The capacitor is normally designed for intermittent duty only.

These motors have the same running characteristics as a split-phase motor, since each is induction-run (runs on the main winding only). However, capacitor-start motors have up to three times the starting-torque per ampere, and therefore are designed for as much as 5 hp. Reliability is again reduced slightly by the addition of the capacitor, but the auxiliary winding has larger wire, and is less sensitive to burnout than that of a split-phase motor. Efficiency is moderate, as with the split-phase motor.

Capacitor-start motors are used in hard-to-start applications such as pumps and compressors, evaporative coolers, milking machines, saws, joiners, blowers, and conveyers.

### 2.2.6.4 Permanent-Split Capacitor Motors

In contrast to the capacitor-start motor, for which the capacitor is selected to maximize starting-torque per ampere and must be switched out for running, a permanent-split capacitor motor is designed for applications where starting torque requirements are low, but improved running performance is required. In this case, the motor is designed to have a capacitor in series with the auxiliary winding at all times. For continuous operation, the capacitor must be a more expensive oilfilled capacitor, and it must be sized for good running performance at a sacrifice in starting torque. It is possible to design a permanent-split capacitor motor to have ideal two-phase performance at a particular load. That means the turns and current in each phase are such that two equal fields are displaced by 90 electrical degrees in space and in time. In practical terms, the marginal

benefit of the much larger capacitor required does not justify its cost, and a smaller capacitor is used to come close to the ideal performance. These motors must not be used on applications where the motor can become unloaded, since the voltage on the capacitor can then exceed its allowable rating.

There are two applications where these motors are popular. Each has a different performance characteristic. Fans and blowers have low starting-torque requirements. These motors are designed to overlap the shaded-pole motor on the low end but extend to 1 hp on the upper end. They have better running performance, higher efficiency, higher power factor, and higher running torque per ampere. When fan speed control is required, high slip is desirable. Multiple speeds are obtained with a high-resistance rotor and tapped windings. Because motor cooling is less of a problem than cost-competitiveness, efficiency has traditionally not been a concern. There are now more efficient permanent-split capacitor motors available for fan applications.

For air conditioning compressors, since motor losses become part of the air conditioning load, there has always been an incentive to develop a capacitor-run motor for maximum efficiency and running torque per ampere. This has been made possible by redesigning the compressor to minimize starting torque requirements. The result is a line of very efficient permanent-split capacitor motors for hermetic compressor applications. As the demand for higher efficiency developed, only marginal improvements were needed.

### 2.2.6.5 Two-Value Capacitor Motors

A natural extension of the permanent-split capacitor motor is the two-value capacitor motor. A start-capacitor is placed in parallel with the run-capacitor. This allows the motor to be designed for optimum running efficiency without sacrificing efficiency to get starting torque. The start-capacitor is then sized to get the desired starting torque.

A practical embodiment of the two-value capacitor motor is the air conditioning compressor motor. These are designed with adequate starting torque for most conditions but not all. A start-capacitor may be added as a top-of-the-line feature or as a field modification when a compressor fails to start.

Two-value capacitor motors have been available for years in the range of 1–10 hp where, because of their high efficiency and power factor, they represented the only means of getting the desired horsepower in a single-phase motor. However, because of their higher initial cost (adding two capacitors and a switch) they must now be included in any study of energysaving alternatives. For further discussion of single-phase motor efficiency, see [Refs. 13 and 14](#).

## 2.2.7 Performance on Variable-Frequency Sources

This section introduces the basics of open loop variable speed (or frequency) operation of induction motors driven by electronic inverters. An in-depth treatment of closed loop control of inverter driven induction motors is presented in Section 15.1. An introduction to the basics of power electronics and inverters may be found in Sections 9.3 to 9.6 in the “Motor Control” chapter.

### 2.2.7.1 Torque—Speed Curves

The speed of an induction motor can be varied over a wide range by varying frequency. The no-load speed is practically equal to the synchronous speed, and this is directly proportional to frequency. With a load applied, the speed is less than synchronous speed by an amount called the slip speed ( $n_{\text{slip}}$ ). In typical polyphase induction motors,  $n_{\text{slip}}$  is between about 2 and 6 rad/sec (20 to 60 rev/mm) at rated torque.

To maintain the torque capability, and also to avoid core saturation, it is necessary to maintain normal magnetic flux as frequency is varied. This requires that voltage be varied as frequency is varied. If stator resistance is neglected, this relationship requires that applied voltage be proportional to frequency. This is referred to as constant volts per hertz (V/Hz) operation.

For variable frequency operation, a base voltage  $V_b$  and base frequency  $f_b$  are defined such that voltage  $V_b$  at frequency  $f_b$  gives normal flux. These bases are often the rated (nameplate) values. For constant V/Hz operation, the voltage is adjusted to maintain the voltage to frequency ratio of operation equal to  $V_b/f_b$  (V/Hz).

For each selected value of the variable frequency, a torque-speed curve can be plotted, resulting in a family of curves. If stator resistance were zero, and with constant V/Hz, the shape of these curves and their maximum (breakdown) torque would be independent of frequency. Only their intercepts at synchronous speed on the speed axis would be different.

In real motors, the voltage drop across the stator resistance affects the torque-speed curves. To illustrate this, the curves for a typical medium size three-phase motor rated 40 hp, 440 V, 60 Hz are plotted in Fig. 2.8. A constant value of  $V/f=440/60=7.33$  V/Hz is maintained. The stator IR drop causes a reduction in flux as current increases with load. Breakdown torque is seen to become smaller as frequency is decreased. This torque reduction becomes severe at 10 Hz and below.

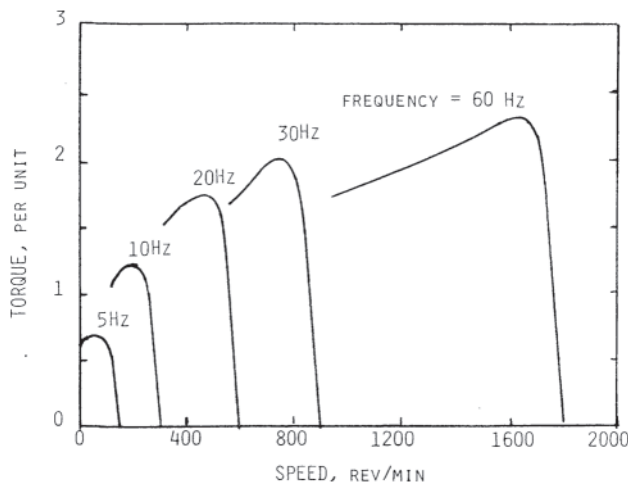


**Figure 2.8** Torque-speed curves for a typical three-phase, 40-hp, 440V, 60-Hz induction motor operated with V/Hz constant at 440/60.

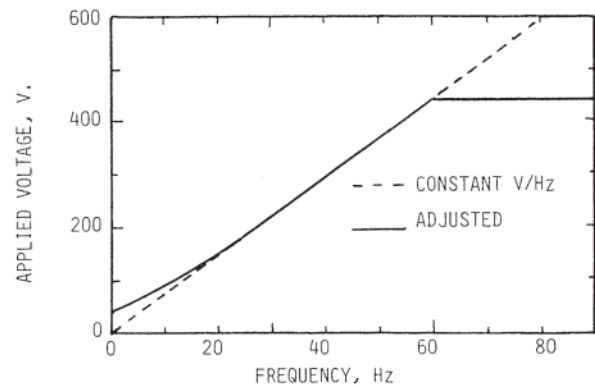


**Figure 2.9** Applied voltage vs. frequency for the 40-hp motor of Fig. 2.8.

As frequency is reduced, the applied voltage can be made increasingly larger than that indicated by constant V/Hz to overcome the torque deficiency. This voltage adjustment is shown in Fig. 2.9, where applied voltage is plotted as a function of frequency. The dashed curve is linear for constant V/Hz resulting in the torque-speed curves of Fig. 2.8. The solid line curve shows the adjusted voltage to approximate constant flux. When this voltage strategy is used, the more practical torquespeed curves of Fig. 2.10 result. If the V/Hz value is increased as described, the flux level becomes greater than normal when the motor is lightly loaded. The saturation resulting can cause an excessive magnetizing current, and a compromise value of V/Hz to give reasonable breakdown torque with a reasonable light load current is recommended. For any particular motor, data for the voltage at any frequency can be calculated by using the equivalent circuit in Fig. 4.60 of Section 4.4. In that circuit, a constant ratio of voltage  $E_1$  to frequency gives the desired constant stator flux.

In Fig. 2.10 the cross-hatched segments show the slip speed. Note that, for all frequencies up to 60 Hz,  $n_{\text{slip}}$  at a given torque is practically independent of frequency because air gap flux is maintained nearly constant.

In most variable-speed systems, the source voltage has an upper limit. It will be considered to be at voltage  $V_b$  in this discussion. Therefore, the above frequency  $f_b$  constant V/Hz can not be maintained. Figure 2.9 shows this voltage limit at 440 V (solid curve). Note that torque at any given slip speed is proportional to the square of  $V/f$ . This explains the low torque in the 90 Hz curve in Fig. 2.10. Below  $f_b$  this example system is referred to as a constant-torque drive, and above  $f_b$  it is a constant-horsepower drive.

### 2.2.7.2 Torque Pulsation

The variable-frequency sources are usually electronic inverters that produce nonsinusoidal currents in the motor. The fundamental component of current produces a smooth average torque. The harmonic components interact with the air gap flux to produce a pulsating or ripple torque having a negligible

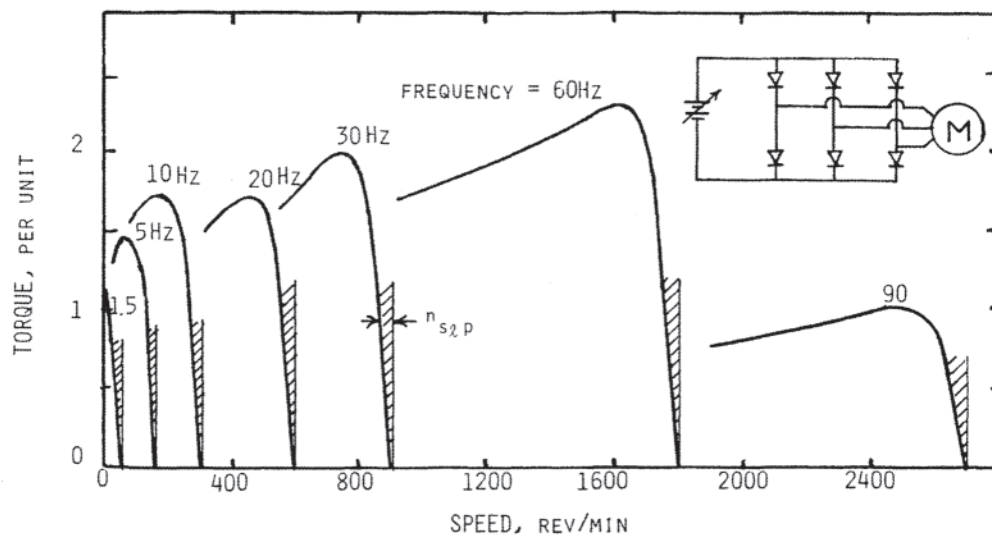


**Figure 2.10** Torque-speed curves of the 40-hp motor with voltage adjusted to maintain nearly constant flux.

average value. The result is a ripple speed superimposed on the average speed.

The waveform of pulsating torque generally has a triangular form with one dominant frequency component. Thus torque can be approximated by:

$$T = T_a + T_p \sin(2\pi f_p t) \quad (\text{N}\cdot\text{m}) \quad (2.68)$$

Where  $T_a$  is the average torque, and  $T_p$  and  $f_p$  are the amplitude and frequency of the dominant component of ripple torque. In steady-state operation,  $T_a$  is balanced by the load torque. This leaves the second term in Eq. 2.68 as an accelerating torque, and the resulting speed is:

$$\omega = \omega_a + \frac{T_p}{2\pi f_p J} \times \cos(2\pi f_p t) \quad (\text{rad/sec}) \quad (2.69)$$

where  $\omega_a$  is the average speed and  $J$  is the moment of inertia of the rotor and the driven load in  $\text{kg}\cdot\text{m}^2$ .

The second term in Eq. 2.69 is the ripple speed. This term can be kept small if  $f_p$  and  $J$  are large.

The amplitude of each pulsating torque component is dependent on the pair of time-harmonic current components associated with that torque. For most non-sinusoidal sources, even-order harmonics are small or nonexistent. Therefore, only odd-order harmonics are considered. Also, no triplen harmonic currents occur in three-phase motors.

For each value of integer  $n = 1, 2, 3, \dots, 8$ , and for harmonics of order  $k$ , the pair of harmonic currents at frequencies  $f_k = (6n \pm 1)f_1$  produce harmonic torque at frequency  $f_p = 6nf_1$ . For example, using  $n=1$ , the 5th and 7th harmonic currents produce a 6th harmonic torque, and its amplitude depends on the amplitudes of those two currents. Likewise, the 11th and 13th harmonics produce a 12th harmonic torque, and so forth.

A typical six-step inverter produces a dominant 6th harmonic torque pulsation and its amplitude is in the range of about 15–40% of rated torque [15]. For pulse-width-modulated

(PWM) waveforms, the pulsation is likely to be of somewhat larger amplitude, but at higher frequency [16].

For a given amplitude  $T_p$ , Eq. 2.69 indicates that for small  $f_p$  the ripple speed can be large. This is the case for the lower-order harmonics when  $f_1$  is very small as required for very low motor speed. The motor may rotate in an undesirable stepping fashion. This effect can be reduced by eliminating or reducing the lower-order harmonic currents. PWM schemes have been developed to accomplish this [17].

Pulsating torque can also produce large speed ripple if  $f_p$  is at or near a natural frequency mode of the mechanical system. It may be necessary to use the PWM technique to eliminate lower-order harmonics to remedy this [17].

### 2.2.7.3 Soft-Start Capability Using an Automatic Starting Device (ASD)

Induction motors that are started by applying rated voltage at rated frequency (line-start) require a current that is five times rated or more. But when a variable-frequency variable-voltage source is used the starting and accelerating torque can be rated torque with no more than rated current. This is accomplished by applying a very low frequency with a voltage value to maintain normal air gap flux. The curve in Fig. 2.10 for 1.5 Hz at about 30 V would be appropriate to provide a soft start for the motor of that example. As the motor accelerates, frequency and voltage are gradually increased to maintain a constant slip speed to give normal torque (about 40 rev/mm for the example). Using this strategy, current will remain at approximately rated value.

It should be noted that deep-bar or double-cage rotors are used to enhance starting torque using line-start. But this is not necessary for the soft-start method, and if time-harmonic currents are involved these special rotors would produce excessive  $I^2R$  losses in the steady state.

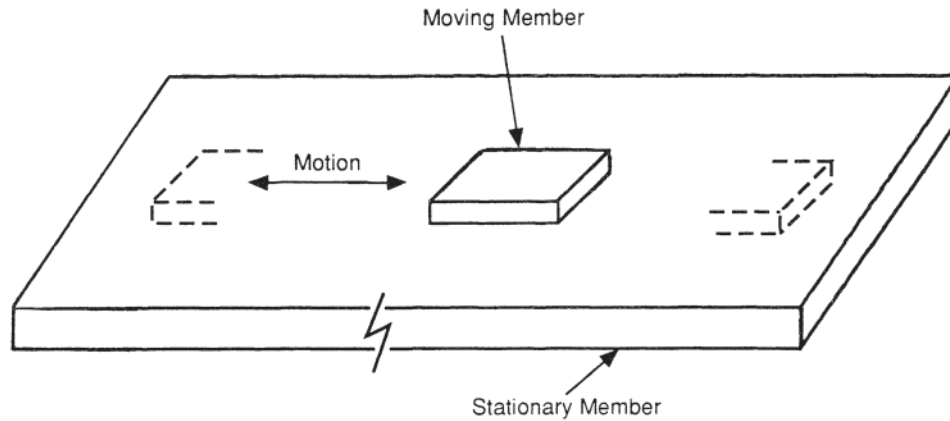


Figure 2.11 Linear machine topology.

### 2.2.8 Linear Induction Motors

In the conventional rotating motors discussed earlier the only degree of mechanical freedom is rotation: that is, the rotor revolves with respect to the stator. Linear electric motors are also possible, with the only degree of mechanical freedom being that of translation; that is, the moving member moves linearly with respect to the stationary member, as illustrated in Fig. 2.11. Obviously, in a linear motor either the moving or stationary member must extend over the entire range of motion of the moving member. The topology of linear electric machines has been known for the past several decades, and conceptually all types of motors (dc, induction, synchronous, and reluctance) are possible in a linear configuration. However, the dc motor and the synchronous motor require double excitation (field and armature), making the hardware application complex. The reluctance motor has no secondary excitation, either induced or external, and thus has a poor thrust characteristic. Hence, most attention has been focused on linear induction motors (LIMs). However permanent magnet (brushless dc) linear motors are in production and their operation is very much like the round motor. End effects are minor and speed is relatively low so end effects are not important.

Certain characteristics of LIMs can be explained with the help of Fig. 2.12(a) [18]. The linear configuration can be imagined to result from a rotary configuration that is cut radially and unrolled, as illustrated in the figure. The secondary of Fig. 2.12(b) is a linear version of a squirrel-cage rotor; that is, discrete conductors, embedded in laminated iron and shorted on both sides by end-bars. The secondary of Fig. 2.12(c), on the other hand, is a very simple configuration consisting of a sheet of conducting material, backed by iron. Normally, a nonmagnetic material such as aluminium is used to form the sheet secondary, although a magnetic material such as iron can be used. The back iron can be solid or laminated, and can be eliminated if the conducting sheet is itself made of magnetic material.

A LIM can be either a short-primary LIM or a short-secondary LIM, depending on whether the primary or the

secondary is the shorter. Furthermore, in both types of LIMs, either the primary or the secondary can be the moving member.

The linear motor shown in Fig. 2.12 has a single primary reacting with a secondary facing it, and is therefore called a single-sided linear induction motor (SLIM). Conceptually, two SLIMs can be combined effectively to obtain a double-sided linear induction motor (DLIM), as illustrated in Fig. 2.13. Two SLIMs placed back-to-back, as in Fig. 2.13(a), will

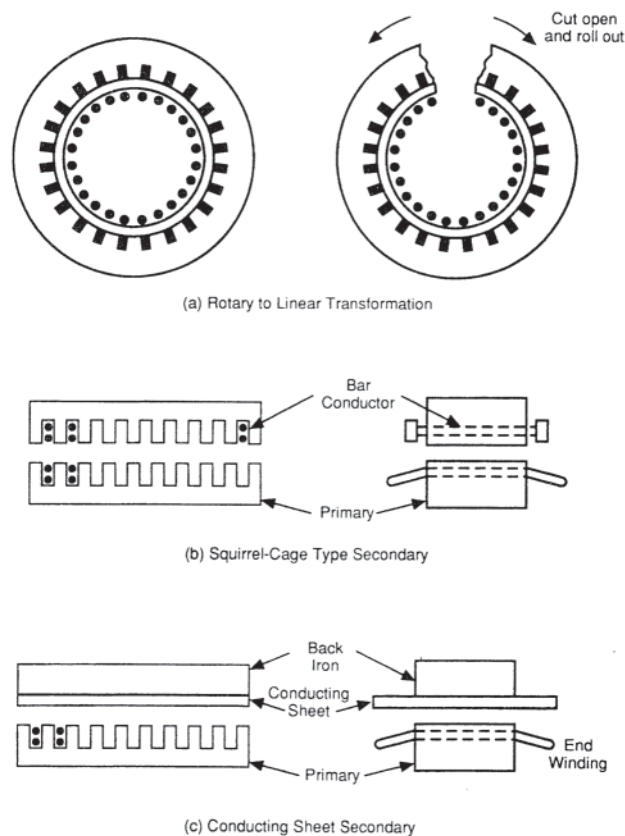
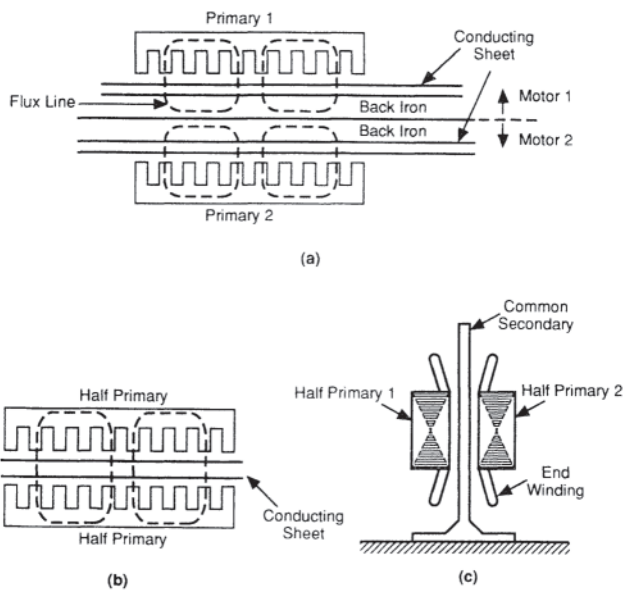


Figure 2.12 Single-sided linear induction motor (SLIM).



**Figure 2.13** Double-sided linear induction motor (DLIM).

have approximately double the force of a single unit. If the back iron were to have infinite permeability or if the primary currents were phased properly, the back iron could be eliminated without affecting the motor performance, resulting in the simpler configuration of Fig. 2.13(b). A short primary DLIM is thus possible as in Fig. 2.13(c), where two half-primaries react on two sides of a common conducting sheet secondary. The secondary can be placed either vertically or horizontally.

The problems of controlling the mechanical clearances of a linear motor are more difficult than with a rotating motor. Consequently, the linear motor must operate with a larger air gap.

The operating principles and characteristics of a linear motor are essentially similar to those of a rotating motor. The primary windings in a rotating motor close on themselves and hence the electromagnetic fields in the air gap are periodic in space, with the half-period being equal to the pole pitch. The short member of a linear motor, however, has a finite length and is open ended. Its leading and trailing edges can be clearly defined. The electromagnetic fields in the air gap of a linear motor are therefore not continuously periodic in space, but vary over the length of the motor and extend beyond the motor's length at both ends. This phenomenon is generally called the end effect in linear motors. The end effect is not symmetrical, extending more beyond the trailing edge. A linear motor and a rotary motor both have a finite width in the transverse direction, but the resulting effect, called the edge effect, is more pronounced in a linear motor because of the large air gap and the use of short secondaries. Also the efficiency and the power factor of a linear motor are generally poor compared to those of a rotating motor because of the large air gap and end effects.

### 2.2.8.1 Methods of Analyzing LIM Performance

A large number of technical articles and books have been written on the analysis of LIM performance, but even now the LIM performance cannot be said to be fully understood. The LIM topology is rather complicated and consequently very difficult to analyze theoretically. A commonly used SLIM configuration is shown in Fig. 2.14. It is a short-primary configuration. The widths of the primary, the secondary conducting sheet, and the back iron are shown as different. Furthermore, the primary is offset with respect to the center line of the secondary. When the primary windings are excited with three-phase current (or voltage), currents are induced in the conducting sheet, and three axial forces are generated by the linear motor. Due to lack of symmetry in any direction, the electromagnetic fields in the air gap can be defined only in terms of a complex three-dimensional vector potential problem. The problem has therefore been simplified by attempting to obtain one-, two-, and three-dimensional field solutions by various investigators, including, among others, Boldea, Mosebach, Nasar, Oberretl, Skalski and Yamamura [18–23].

As the name suggests, the one-dimensional analysis assumes that all quantities are functions of only one spatial variable. For example, such an analysis of a LIM would consider that the primary current  $i_1$  is a function of  $x$  and has only a  $z$ -component, that is:

$$i_{1z} = f(x) \quad 0 \leq x \leq L$$

Other quantities such as secondary current  $i_{2z}$  and flux density  $B_y$  are also functions of only the spatial variable  $x$ .

In a two-dimensional analysis, all quantities are considered to be functions of two spatial variables. The air gap flux density  $B_y$  and the  $z$ -component of the current in the secondary sheet, for example, are functions of the spatial variables  $x$  and  $y$ . In a three-dimensional analysis, all the quantities are functions of  $x$ ,  $y$ , and  $z$ .

A one-dimensional analysis is quite simple but does not adequately model all aspects of LIM characteristics, although it provides closed-form solutions as explicit functions of basic LIM parameters. It is therefore very helpful in providing insight into fundamental aspects of the end effects. The two- and three-dimensional analyses are more accurate in predicting LIM performance. The three-dimensional solutions are required to model both the end effect and the edge effect at the same time.

Some other investigators, such as Lipo and Nondahl [24], have attempted a classical circuit approach for LIM analysis, and others, such as Nene and Del Cid [25], have used a combination of electromagnetic field analysis and circuit analysis for predicting the performance of linear induction motors. The performance characteristics of a LIM supplied by constant current are discussed here on the basis of all the studies of these authors. Modern finite element analysis tools are also sometimes applied.

### 2.2.8.2 The Goodness Factor

An induction motor draws power from the primary source and transfers it to the secondary circuit across the air gap by

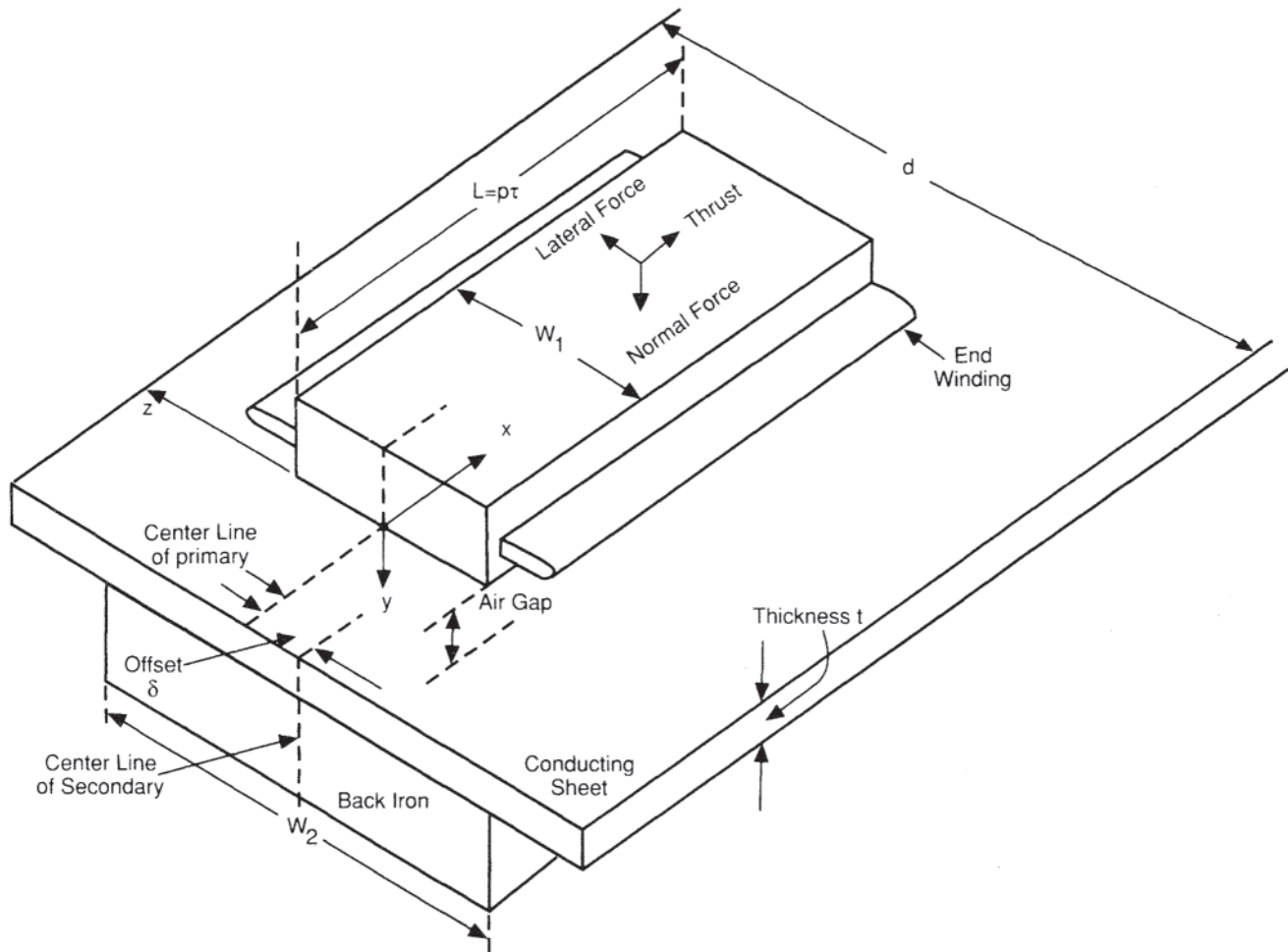


Figure 2.14 Single-sided linear induction motor (SLIM) geometry.

induction. The difference between the power transferred across the air gap and the rotor losses is available as the mechanical power to drive the load. From the point of view of energy conversion, the primary resistance and the leakage reactances of the primary and the secondary circuit are not essential. Furthermore, the energy conversion efficiency is improved as the mutual reactance  $X_m$  of the motor is increased and the secondary circuit resistance  $R_2$  is decreased. For a basic motor, therefore, one could define a goodness factor  $G = X_m/R_2$ ; the motor performance is better when the value of  $G$  is higher.

Considering a simplified LIM topology, Laithwaite [26] defines a goodness factor  $G$  for a linear motor as:

$$G = \frac{2\mu_o f \tau^2}{\pi \rho_s g} \quad (2.70)$$

$$= \mu_o \sqrt{\pi} \rho_s \times v_s \frac{\tau}{g}$$

where:

- $f$  = source frequency
- $\tau$  = pole pitch of the primary winding
- $\rho_s$  = Surface resistivity of the secondary conducting sheet

- $g$  = air gap
- $\mu_o$  = permittivity of free space
- $v_s$  = linear synchronous speed

It can be seen that a linear motor is a better energy conversion device at high synchronous speeds, and when the ratio  $\tau/g$  is large. This observation can also be explained from more fundamental considerations. For example, a linear motor, just like any other electromagnetic device, has an inherent force density limitation imposed on it by the design constraints of electric and magnetic loadings. With the resulting thrust limitation, high power (thrust times speed) for a given size of motor is possible only at high speeds. Also, if the ratio  $\tau/g$  is small, the primary leakage flux is large, and consequently the effective magnetic coupling between the primary and the secondary circuits is reduced and the LIM thus shows poor performance. The air gap is usually determined by mechanical considerations and hence, for a given linear synchronous speed, the pole pitch and therefore the ratio  $\tau/g$  are reduced as frequency is increased. High-frequency motors therefore show poor performance compared to low-frequency motors.

### 2.2.8.3 Low-Speed and High-Speed Motors

If the primary windings of a three-phase linear motor are excited by balanced sinusoidal currents, one can define an equivalent surface current sheet so that it creates an identical travelling magnetomotive force distribution. The linear current density  $j_1$  at a distance  $x$  from the front end of the LIM can be written as:

$$j_1 = J_1 \exp \left[ j \left( \omega t - \frac{\pi x}{\tau} \right) \right] = J_1 \exp \left[ \frac{j\pi}{\tau} (v_s t - x) \right] \quad (2.71)$$

where:

$$\begin{aligned} \omega &= 2\pi f = \text{angular supply frequency} \\ \tau &= \text{pole pitch of primary winding} \\ v_s &= 2f\tau = \text{linear synchronous speed} \end{aligned}$$

and:

$$J_1 = \frac{m\sqrt{2}N_{ph}K_w I_1}{p\tau} \quad (2.72)$$

where:

$$\begin{aligned} K_{w1} &= \text{winding factor of the primary winding} \\ N_{ph} &= \text{number of turns per phase of the primary winding} \\ p &= \text{number of pole-pairs of the primary winding} \\ m &= \text{number of phases (usually } m=3) \end{aligned}$$

The normal component of the air gap flux density at a distance  $x$  from the front end of the primary is a function of  $x$ . Using a simple one-dimensional LIM model, it may be written as:

$$\begin{aligned} B_n(x) &= B_0 \exp \left[ j \frac{\pi}{\tau} (v_s t - x) \right] + B_1 \exp \left( -\frac{x}{\alpha_1} \right) \\ &\times \exp \left[ j \frac{\pi}{\tau'} (v' t - x) \right] + B_2 \exp \left[ -\left( \frac{2p\tau - x}{\alpha_2} \right) \right] \\ &\times \exp \left[ j \frac{\pi}{\tau'} (v' t + x) \right] \text{ for } 0 \leq x \leq L \end{aligned} \quad (2.73)$$

where  $v_s = 2f\tau$ ,  $v' = 2f\tau'$ , and  $L$  is the length of the LIM primary.

The first term represents the normal travelling wave, which would be present even if the LIM were infinitely long. This traveling wave moves at the synchronous speed in the  $x$  direction; in fact, this is what makes  $x=0$  the front end. The second term represents an attenuating traveling wave generated at the entry end, which travels in the positive direction of  $x$ . It is caused by the discontinuity at the entry end and is called the entry-end wave. The third term represents an attenuating travelling wave generated at the exit end, which travels in the negative direction of  $x$  towards the entry end. It is caused by the discontinuity at the exit end and is called the exit-end wave. Both are called the end-effect waves.

The parameters  $\alpha_1$ ,  $\alpha_2$ ,  $v'$ , and  $\tau'$  depend on the properties of the motor, the air gap, and the resistivity of the conducting sheet. Their variation with these values has been determined by Yamamura [22]. An understanding of their influence helps to determine motor performance.

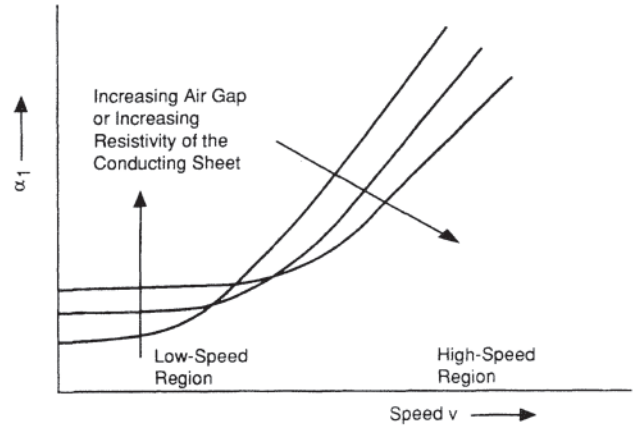


Figure 2.15 Variation of  $\alpha_1$  with speed.

The parameters  $\alpha_1$  and  $\alpha_2$  in Eq. 2.73 determine the relative strength of the end-effect waves at a particular distance from the LIM ends. The variations of these parameters with LIM velocity are quite different in the low-speed region and in the high-speed region. These relationships as a function of the relative velocity  $v$  are shown in Fig. 2.15 and Fig. 2.16 [22]

In the low-speed region,  $\alpha_1$  and  $\alpha_2$  are almost independent of the LIM velocity whereas, in the high-speed region, they both depend strongly on the LIM velocity. Furthermore, in the low-speed region, both  $\alpha_1$  and  $\alpha_2$  increase with the air gap as well as with the resistivity of the conducting sheet. In the high-speed region, however,  $\alpha_1$  decreases and  $\alpha_2$  increases with increasing air gap and resistivity of the conducting sheet. There is no clear-cut division between the low-speed and the high-speed regions. However, Yamamura has shown that the high-speed region is characterized by  $G \gg 4$ . The constant 0.25G is sometimes referred to as the Magnetic Reynold's Number (MRN). Hence the high-speed region may also be defined as the region with  $MRN \gg 1$ .

There is one more significant difference between the low-speed region and the high-speed region. The half-wavelength  $\tau'$  and the speed  $v'$  of the end-effect waves are shown as functions

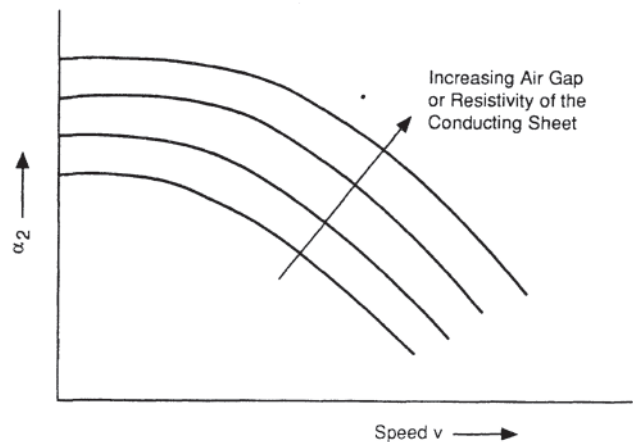


Figure 2.16 Variation of  $\alpha_2$  with speed.

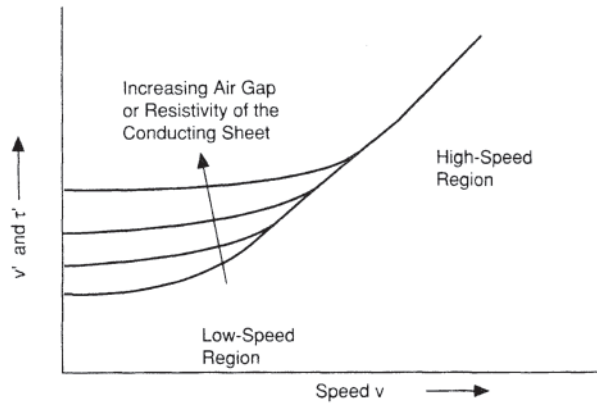


Figure 2.17 Variation of  $v'$  and  $\tau'$  with speed.

of  $v$  in Fig. 2.17. In the high-speed region, both  $\tau'$  and  $v'$  are independent of the air gap and the conductivity of the secondary sheet, and  $v'$  is approximately equal to  $v$ . In the low-speed region, however  $v'$  and  $\tau'$  are functions of these parameters, and  $v' > v$ ; that is, the end-effect waves travel faster than the secondary sheet. In fact, in this region, it is possible to have  $v' > v_s$ , and consequently, because of the end effects, the LIM can generate positive thrust at synchronous and higher speeds.

For practical high-speed LIMs,  $\alpha_1$  is much greater than  $\alpha_2$ . The numerical value of  $\alpha_1$  can be comparable to the LIM length, with the entry-end-effect wave present over the entire length of the LIM. The external LIM characteristics such as the variations of the thrust, the lift, the power factor, the efficiency, and so forth, with speed are then directly influenced by this entry-end-effect wave. The ratio  $\alpha_2/L$  however is very small for practical motors. Consequently, the exit-end-effect wave is present only near the exit end of the LIM, and has very little effect on the external LIM characteristics.

#### 2.2.8.4 Magnetic Flux Density in Front of and Behind an LIM [18–24]

The end-effect in a linear motor is clearly exhibited in the form of a nonuniform flux density distribution along the length of the motor. For a LIM supplied with a constant current, typical variation of the normal flux density with slip and position along the length is illustrated in Fig. 2.18. With constant primary current, its magnetizing component and consequently the air gap flux decrease as the load component increases with increasing slip. This is true of any induction motor, with or without the end-effect. For a given slip, the flux density builds up along the LIM length, beginning with a small flux density at the entry end. Depending on the length of penetration of the entry-end-effect wave, the flux density may not even reach the nominal level that would be found in a motor without the end effect. Since  $\alpha_1$  increases with the speed, this is more likely to happen at low slip values. Further, a significant level of flux density is found beyond the exit end of a LIM. This is known as the magnetic wake. Although this magnetic wake has little influence on the LIM thrust, it contributes significantly to the normal force between the primary and the secondary in a SLIM configuration.

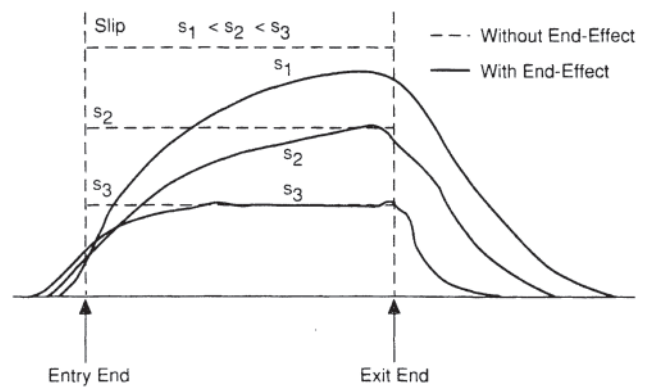


Figure 2.18 Normal flux density distribution in LIM.

#### 2.2.8.5 Thrust Characteristics of an LIM

The thrust-speed characteristics of a LIM are illustrated in Fig. 2.19. Without the end-effect, the characteristics are similar in nature to those of a conventional rotating induction motor. From a finite starting value at zero speed, the thrust increases with speed to a maximum value, and drops rapidly to zero at the synchronous speed. At speeds beyond the synchronous speed, the thrust changes sign and becomes a braking thrust. Due to the end-effect, however, the actual characteristic is different from this ideal one. For LIMs exhibiting high-speed characteristics, that is, with  $MRN \gg 1$ , the thrust is lower than the ideal value at all speeds. Such a LIM produces a braking thrust at the synchronous speed. For LIMs exhibiting low-speed characteristics, that is, with  $MRN < 1$ , the end-effect waves may travel faster than the secondary sheet even at synchronous speed and the LIM will then produce a positive thrust at synchronous speed.

The end-effect in thrust characteristics is less pronounced when the number of poles is increased. For example, variation of thrust-per-pole with speed is illustrated in Fig. 2.20 for various numbers of poles [22, 27]. As the number of poles increases, the characteristic tends to move closer to the ideal characteristic.

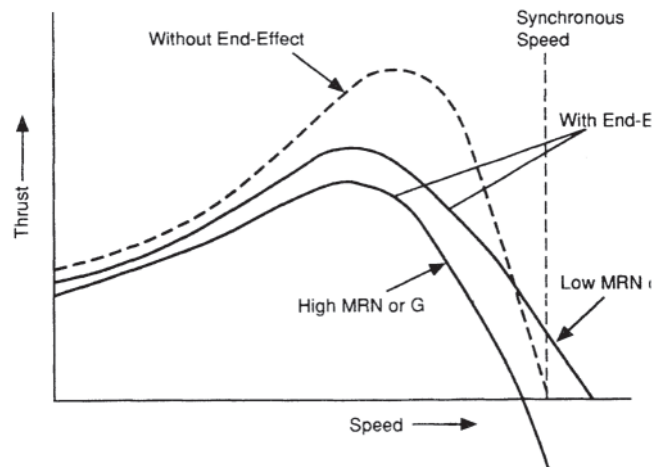


Figure 2.19 Linear induction motor (LIM) thrust characteristics.



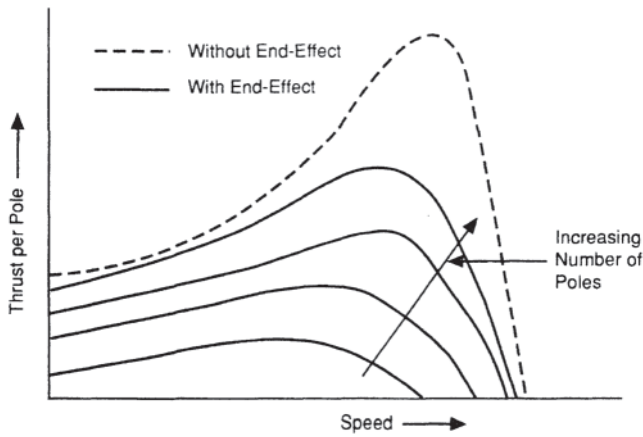


Figure 2.20 Linear induction motor (LIM) thrust per pole.

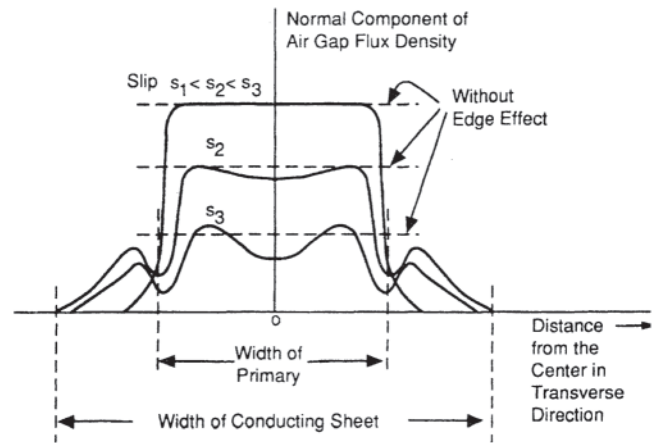


Figure 2.22 Edge-effect in a linear induction motor (LIM).

2.2.8.6 Normal Force in an LIM

In a DLIM configuration, when the secondary sheet is centrally located between the two half-primaries, the normal force between one half-primary and the secondary sheet is equal and opposite to that of the other half-primary. The resultant normal force is therefore zero. There will be a net normal force only when the secondary sheet is asymmetrically placed between the two half-primaries; this force tends to center the secondary and, for a small displacement of the secondary from the center, is directly proportional to the displacement.

In a SLIM configuration, however, there is a large net force between the primary and the secondary because of the fundamental asymmetry of the topology. The variation of the normal force with speed and frequency of primary current is illustrated in Fig. 2.21. The force is an attraction force at the synchronous speed and its magnitude is reduced as the speed is reduced; the force may even change its sign and become a repulsion force at some speed, especially for high-frequency operation. Nene and del Cid [25] have used a circuit approach to explain this behavior of the normal force of a SLIM:

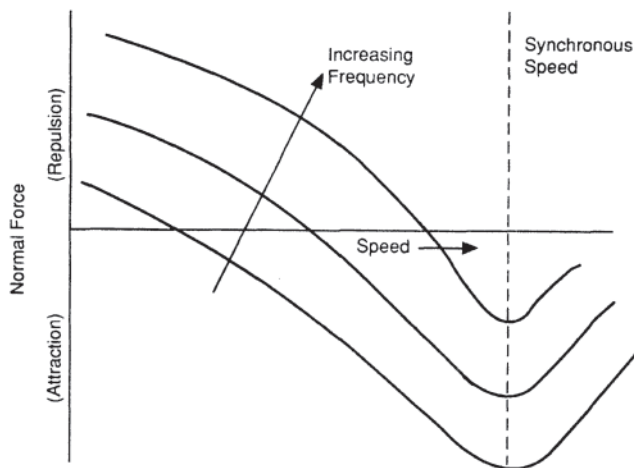


Figure 2.21 Normal force in a linear induction motor (LIM).

2.2.8.7 The Edge Effect in a Linear Motor [22, 23, 28]

The effect of having a finite width for a linear motor is generally termed the edge effect. This effect is more pronounced with lower values of the width-to-air gap ratio. The variation of the normal flux density in the transverse direction is illustrated in Fig. 2.22. The flux density distribution shows a dip at the center due to the edge-effect, and the dip is more pronounced at higher slips.

Referring back to Fig. 2.14, the LIM performance also depends on the width  $d$  of the secondary conducting sheet. Yamamura has shown, however, that the external LIM characteristics including thrust are almost independent of  $d$  if  $(d-W_1)/\tau > 0.4$ .

2.2.8.8 Solid and Laminated Back Iron

The question of whether the back iron should be laminated or solid has been debated since the inception of the SLIM configuration. For practical applications such as ground transportation, the secondary conducting sheet and the back iron will extend over great lengths, even hundreds of miles. Use of laminated back iron may, therefore, be quite expensive in terms of the costs of the material and construction. Hence it is important to know to what extent, if any, the SLIM performance is degraded if the back iron is solid instead of laminated.

With laminated back iron, the eddy currents carried by the laminations and the resulting ohmic losses and the thrust are both small enough to be ignored. However, the thrust produced by the SLIM will depend on the relative permeability of the back iron; lower permeability will result in lower thrust and poor power factor. With solid back iron, the eddy currents induced in the back iron will result in ohmic losses but will produce some thrust. The iron will also experience a saturated skin effect thus the magnetic flux will be more concentrated near the surface of the back iron closest to the primary. That portion of the back iron will tend to saturate, will have a lower value of  $\mu_r$ , and will force the flux to penetrate deeper into the back iron than if the iron were to have a linear  $B-H$  curve. The

back iron would act like a second conducting sheet, similar to a second cage in a double squirrel-cage induction motor. With constant-current excitation, an SLIM with solid back iron therefore operates at a slightly lower flux density, produces a slightly lower thrust, and has a poorer power factor compared to another SLIM with identical primary winding and conducting sheet but with laminated back iron.

### 2.2.8.9 LIM with a Solid Iron Secondary

So far we have considered a nonmagnetic conducting sheet secondary for a DLIM as well as for a SLIM with, of course, a back iron. Copper and aluminum have been used as the conducting material for the secondary sheet. However, an all-iron secondary configuration is also possible where solid iron is itself used as a conducting secondary sheet. This is a linear version of a solid-rotor induction motor. The analysis of the performance of such a LIM is inherently complex because of nonlinearity of the iron circuit.

In a DLIM with solid iron secondary, if the secondary is thick the magnetic flux caused by the two half-primaries will not cross the center line because the flux penetration is reduced as a result of skin effect. The two sides of the DLIM will then act as two independent SLIMs. With a thin secondary, the two primaries will work as a DLIM. In a DLIM the air gap between the two half-primaries is fixed, so increased saturation of secondary iron does not result in increased equivalent air gap, but results in deeper penetration of eddy currents and better utilization of secondary iron. The DLIM thrust therefore increases with iron saturation (lower values of relative permeability  $\mu_r$ ) as illustrated in Fig. 2.23 [22]. The relative permeability, however, will vary with slip. For example, if the primary current is constant, the secondary current will increase with the slip, and the effective permeability of the secondary iron will be reduced due to skin effect. The resulting thrust will therefore not fall with increasing slip in the high-slip region; it may even increase slightly with the slip as shown in Fig. 2.23.

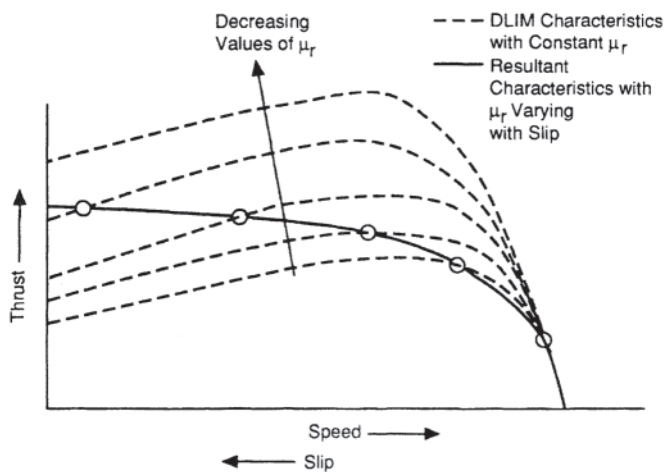


**Figure 2.23** Thrust characteristics of a double-sided linear induction motor (DLIM) with solid iron secondary.

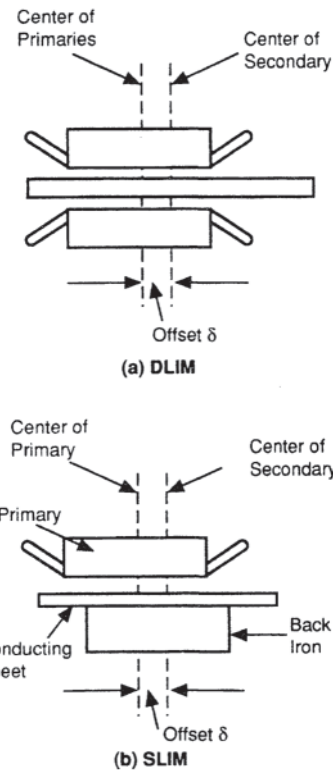


**Figure 2.24** Linear induction motors (LIMs) with transverse asymmetry.

In SLIM configuration, the secondary iron is an important segment of the LIM magnetic circuit. The effective air gap depends very much on the saturation level of the iron; higher saturation levels increase the effective gap. The SLIM performance thus deteriorates with increased saturation levels.

### 2.2.8.10 LIM Performance with Transverse Asymmetry [22, 25, 28, 29]

When LIM topology is symmetrical in the transverse direction, the net lateral force between the primary and the secondary is zero. Figure 2.24 shows DLIM and SLIM configurations with transverse asymmetry. A net lateral force then results between the primary and the secondary. In DLIM configurations, such asymmetry is usually not experienced under normal conditions; the asymmetry and the resulting lateral forces are therefore not large. This force is, however, always destabilizing in a DLIM; that is, the force tends to increase the asymmetry.

A SLIM may be designed to operate with asymmetry under normal operations because the resulting lateral force is desired for some practical applications. For example, in contactless vehicle propulsion with SLIM, the normal force and thrust can be used to lift and propel the vehicle and the lateral force resulting from transverse asymmetry can then be used to guide the vehicle along the track. The asymmetric SLIM topology has, therefore, been investigated by several authors. The thrust and the normal force of a SLIM are both reduced when the primary is offset with reference to the secondary as illustrated in Fig. 2.25. The lateral force initially increases rapidly with

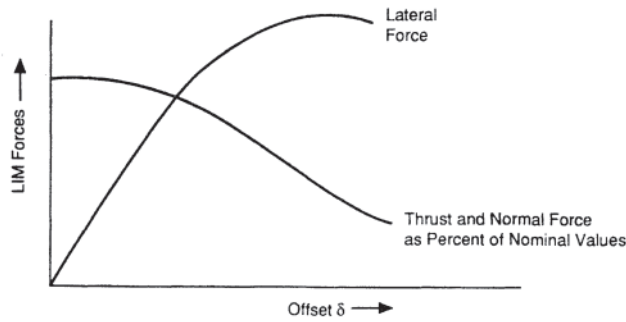
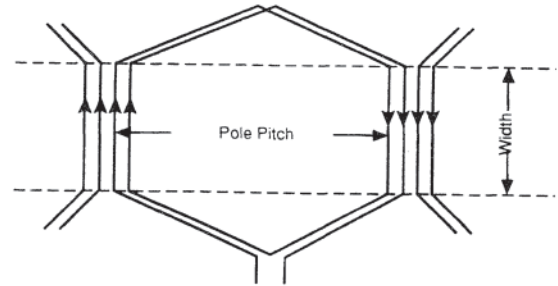


**Figure 2.25** Performance of an offset linear induction motor (LIM). (See Fig. 2.14 for offset ( $\delta$ ) measurement.)

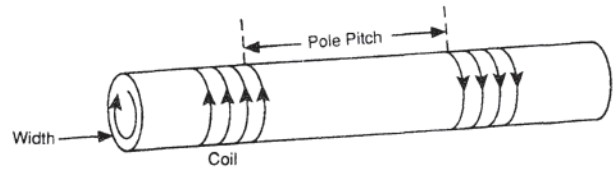
offset and reaches a maximum value; increasing the offset beyond this results in a decrease of the lateral force and also of the thrust and the normal force. The footprint of the SLIM primary on its secondary reduces with increasing offset, and beyond a certain magnitude of offset the SLIM is a very poor electromagnetic device because of very poor magnetic coupling between the primary and the secondary. All the forces will eventually drop to zero with increasing offset.

2.2.8.11 Tubular Linear Induction Motor [18, 26]

We have seen earlier that a rotary induction motor can be considered to be rolled out in arriving at a linear LIM topology. The circumference of the rotary motor is then the length of the linear motor. A typical primary winding is illustrated in Fig. 2.26(a). If the pole pitch is large compared to the LIM width, ohmic resistance and the leakage reactance of the primary winding increase because of the long end windings: the effective secondary end-turn resistance also increases. The motor will therefore be inherently inefficient. For such applications, an interesting topology can be developed by rerolling the LIM in the transverse direction; the width is rolled up in a circle as illustrated in Fig. 2.26(b). Such a motor is called tubular linear induction motor (TLIM). It will at once be clear that endwindings are now not necessary to assure continuity of primary windings. The conductors themselves can now be rolled up to form discrete coils. The motor is still linear because the degree of freedom is translational motion.



(a) LIM with a Large Pole Pitch



(b) LIM Rolled Up in Transverse Direction

**Figure 2.26** Tubular linear induction motor (TLIM).

One such TLIM is illustrated in Fig. 2.27. The magnetic flux lines close on themselves in a plane along the longitudinal or axial direction. This motor is therefore called an axialflux (or longitudinal-flux) TLIM. It can be seen that it is not necessary to have circular primary laminations; one may use a finite number of stacks of laminations around the primary circumference as shown. One could also imagine a TLIM being formed by arranging a number of LIMs in a circle, thus eliminating the need for end windings. This configuration has been used for door openers and for electromagnetic pumps.

2.2.8.12 Transverse Flux LIMs (TFLIMs) [18, 26]

The DLIMs and SLIMs considered so far have all been longitudinal-flux configurations because the main air gap flux lines were in planes parallel to the longitudinal direction. As the pole pitch of such motors is increased, the flux per pole as well as the maximum flux carried by the primary yoke (and by the back iron in SLIMs) increase proportionately. The thickness of the primary core behind the slots and the

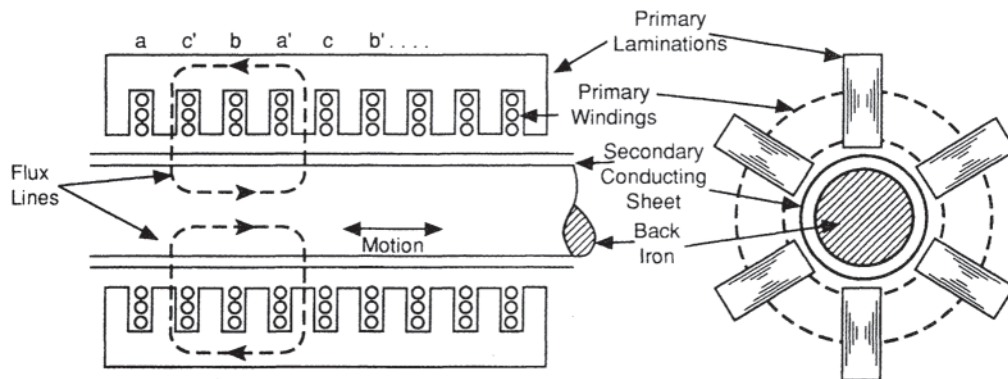


**Figure 2.27** Tubular linear induction motor (TLIM).

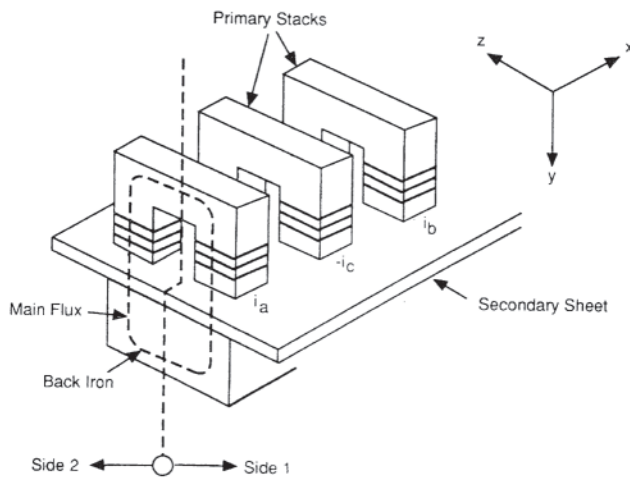


**Figure 2.28** Transverse flux linear induction motor (TFLIM).

thickness of the back iron could, therefore, increase beyond acceptable levels. The total length of the LIM is also increased because the number of poles cannot be reduced below a certain number if the end-effects are to be kept within acceptable limits. Both of these difficulties can be avoided by adopting a transverse-flux configuration for LIMs.

One such TFLIM is illustrated in Fig. 2.28. A number of primary C-core stacks are placed along the length of the motor. Primary coils are wound on each leg of the C-cores; they may be wound around more than one core so that the air gap flux is more uniform. The secondary is in the form of a conducting sheet backed by iron. The air gap flux lines are in a plane perpendicular to the direction of motion; this makes it a transverse-flux motor.

If the coils are excited with three phase currents as shown, an air gap flux distribution,  $B_r(x, t)$  will be set up under each leg of the C-core. Each side of the TFLIM can then be considered to be a SLIM. The thrust and the lateral and normal force characteristics of the TFLIM are therefore similar to those of a SLIM.

### 2.2.8.13 LIM Applications [30, 31]

Linear motors have been investigated for a variety of industrial applications. Some of the more exotic applications include liquid-metal pumps for sodium and sodium-potassium alloy in the nuclear industry and molten metal stirring in the steel industry. Other industrial applications include shuttle propulsion and threading guides for package winders for the textile industry, industrial conveyors, and actuators. However, the most extensive application of LIMs has been in the field of ground transportation. These applications include low-speed and high-speed transportation of passengers and booster-retarders for classification yards.

For linear motor applications in ground transportation, the nominal air gap is governed by operational and mechanical considerations, and not by electromagnetic considerations. The LIM air gap, therefore, may be quite large (up to 20 mm) compared to that of a rotary motor, which is typically of the order of 1 mm. With such a large gap, a LIM can never compare

favorably with a rotating motor on a one-on-one basis. LIMs are therefore used where a rotating motor, limited by operational considerations such as a necessity for contactless propulsion, a low-profile vehicle, a light truck design, and so on, cannot do an adequate job. Some attractive possibilities under these conditions include:

- Automatic door openers
- Propulsion system for tracked levitated vehicles
- LIM-rotary motor hybrid system for high-speed rail vehicles
- LIM propulsion system for urban rail vehicles
- Booster-retarder in classification yards
- Linear eddy-current brake using the running rails as the LIM secondary
- Material handling
- Machine tool positions
- Electromagnetic pumps

## 2.2.9 Doubly Fed Induction Motors

### 2.2.9.1 Introduction

Doubly fed machines are a variation of the wound-rotor induction motor, and have a symmetrical set of multiphase windings both on the stator and on the rotor. To be classified as a doubly fed machine, there must be active sources on both the stator and the rotor. In modern systems, one of these sources is electronically derived, and can be controlled to provide variable speed operation of the system, either as a motor or a generator. The other source typically has a nominally fixed frequency and voltage, which is usually a direct connection to the power grid.

Doubly fed machines offer variable speed performance. The power converter is typically connected to the rotor winding, and is rated less than the system rating, particularly in applications requiring a small speed range. Due to these characteristics, there has been a recent surge in interest in doubly fed induction motors (DFIMs) in applications including wind power generation, hydroelectric and pumped storage hydroelectric, and flywheel energy storage.

The following section provides a development of the steady-state circuit of the doubly fed machine. Following this, the voltage, current, and power relationships of the doubly fed induction motors (DFIMs) are determined. Next is a description of two alternate control strategies. The section finishes with a bibliography of related topics.

### 2.2.9.2 Steady-State Model

The DFIM consists of a symmetrical set of windings on the stator, and a symmetrical set of windings on the rotor. Consider three phase windings on both the stator and rotor (the typical case). Balanced three phase currents on the stator will set up a rotating air gap flux field which rotates at constant speed and has constant magnitude in the steady state. The following discussion considers steady-state operation of the doubly fed machine.

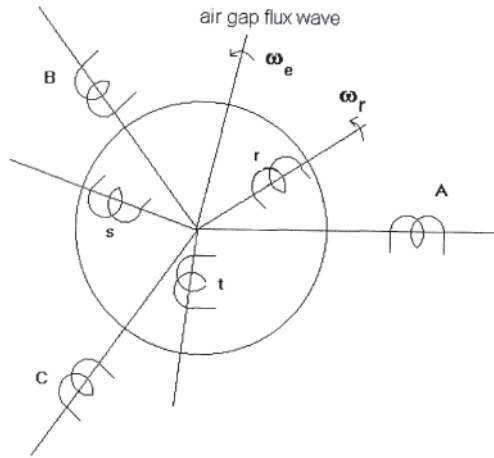


**Figure 2.29** Conceptual model of the doubly fed induction motors (DFIM) (same as for three-phase induction motor).

Figure 2.29 shows a conceptual diagram of this machine. Upper case letters refer to the stator quantities, and lower case letters refer to the rotor quantities. For the geometry shown in the figure, the stator A phase winding flux linkage due to the rotating air gap flux wave with peak magnitude  $\Phi_{ag}$  is:

$$\lambda_{A(g)} = N_s \Phi_{ag} \cos(\omega_e t) \quad (2.74)$$

$N_s$  is the number of turns of each of the stator windings.  $\omega_e$  is the speed of the air gap flux wave in electrical radians per second. The B and C phase flux linkage due to the air gap flux are both similar to  $\lambda_A$ , separated in time as the windings are separated in space.

On the rotor, the flux linking the r phase winding is :

$$\begin{aligned} \lambda_r(g) &= N_r \Phi_{ag} \cos[(\omega_e - \omega_r)t + \alpha] \\ &= N_r \Phi_{ag}(\omega_s t + \alpha) \end{aligned} \quad (2.75)$$

$\omega_r$  is the rotor speed in electrical radians per second,  $\omega_s$  is the slip frequency, and is the difference between the air gap flux speed and the rotor speed, as defined in Eq. 2.75. The slip frequency is therefore also the frequency of the induced voltages on the rotor, and should also be the frequency of any voltages and currents supplied to this winding.  $N_r$  is the number of turns of the rotor winding. Ther per unit slip  $s$  is the ratio of the slip frequency to the stator frequency,  $s = \omega_s / \omega_e$ , as in the induction motor.

Consider the stator A phase winding and the rotor r phase winding. The terminal voltage of each of these two windings is the sum of the resistive voltage drop, the leakage inductance voltage drop, and the voltage induced by the air gap flux. Therefore, with positive current defined as going into the machines, these two voltages are:

$$\begin{aligned} v_A &= R_s i_A + L_s \frac{di_A}{dt} + \frac{d\lambda_A(g)}{dt} \\ v_r &= R_r i_r + L_r \frac{di_r}{dt} + \frac{d\lambda_r(g)}{dt} \end{aligned} \quad (2.76)$$

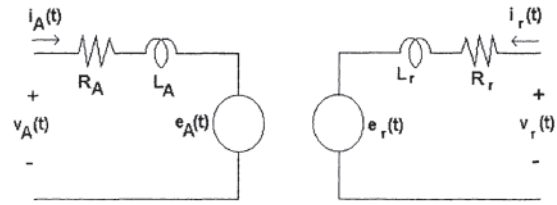


**Figure 2.30** Simplified equivalent circuit of the doubly fed induction motors (DFIM).

The equivalent circuit for these two windings is shown in Fig. 2.30. In this figure, the final terms in Eq. 2.76 have been defined as their internal voltages  $e_A$  and  $e_r$ .

Comparison of Eqs. 2.74 and 2.75 shows that the rms magnitudes of the internal stator and rotor voltages for these windings are

$$\sqrt{2}E_A = \omega_e N_s \Phi_{ag} \quad (2.77)$$

$$\sqrt{2}E_r = \omega_s N_r \Phi_{ag} \quad (2.78)$$

Therefore, these two voltage magnitudes are related by the equation:

$$E_r = \frac{\omega_s N_r}{\omega_e N_s} E_A = n \frac{\omega_s}{\omega_e} E_A = snE_A \quad (2.79)$$

where  $n$  is defined as the machine turns ratio. Equation 2.79 shows that the rotor internal voltage will vary proportionately with slip. At a slip of 0 (synchronous speed), the rotor internal voltage will be zero, and the machine would be excited by injecting direct current on the rotor windings. Positive slip represents subsynchronous speeds, while negative slips correspond to supersynchronous speeds. When the machine is operating at negative slip, the rotor electrical quantities have the reverse phase sequence as compared to those that occur at a positive slip.

The steady-state version of Eq. 2.76 is then:

$$\begin{aligned} \bar{V}_A &= R_s \bar{I}_A + j\omega_e L_s \bar{I}_A + \bar{E}_A \\ \bar{V}_r &= R_r \bar{I}_r + j\omega_s L_r \bar{I}_r + \bar{E}_r \end{aligned}$$

or

$$\begin{aligned} \frac{\bar{V}_r'}{s} &= \frac{R_r'}{s} \bar{I}_r + j\omega_e L_r' \bar{I}_r + \frac{\bar{E}_A}{s} \\ \bar{V}_r' &= \frac{V_r}{n}, \quad \bar{I}_r' = nI_r, \quad R_r' = \frac{R_r}{n^2}, \\ L_r' &= \frac{L_r}{n^2}, \quad \bar{E}_A = \frac{E_r}{n} \end{aligned} \quad (2.80)$$

The first rotor equation is a phasor equation of frequency  $\omega_s$ . The second rotor equation can be considered to have been transformed to the stator frequency for computation purposes. This is universally done in induction motor studies, but is somewhat less useful when considering the doubly fed machine. Note that the magnitude of the last term in the transformed equation is equal to the magnitude of the stator induced voltage.

### 2.2.9.3 Current Relationship

It is also necessary to know the relationship between the stator and rotor current. Neglecting the magnetizing current for the moment, the stator amp-turns must match the rotor amp-turns, as is the case in an ideal transformer. When the rotor is stationary with the A phase stator and r phase rotor windings aligned, the currents in these two phases are required to satisfy the equation:

$$N_s i_A + N_r i_r = 0 \quad (2.81)$$

where both stator and rotor currents are going into the winding. For steady-state, balanced conditions on both the stator and rotor, it can be shown through dq axis theory that the stator and rotor phasor currents are similarly related by the equation [32]:

$$N_s \bar{I}_A + N_r \bar{I}_r = 0 \quad (2.82)$$

Recall that these are per-phase currents that combine to create the rotating air gap flux. Now, if  $\bar{I}_m$  is the amount of current required to magnetize the machine from the stator windings, the current relationship becomes:

$$\bar{I}_A + n \bar{I}_r = \bar{I}_m \quad (2.83)$$

In this equation,  $\bar{I}_A$  is a phasor current of frequency  $\omega_e$ , while  $\bar{I}_r$  is a phasor of frequency  $\omega_s = \omega_e - \omega_r = s\omega_e$ . Equation 2.83 therefore appears to be untenable as it involves phasor currents which have different frequencies. Note however that  $\omega_r$  is the rotor shaft speed (in units of electrical radians per second), while the slip frequency  $\omega_s$  is the frequency of the rotor currents, which add to equal the stator frequency  $\omega_e$ . Stator currents of frequency  $\omega_e$  create a flux wave rotating at speed  $\omega_e$ . Equation 2.83, therefore, is actually a statement of the current that is required to establish the rotating flux wave.

Equations 2.79, 2.80 and 2.83 can be combined into the single-phase equivalent circuit of the machine. Figure 2.31 shows two alternate per phase equivalent circuits for this machine. Figure 2.31a contains the per phase equivalent circuit with the actual stator and rotor variables. Figure 2.31b shows the per phase equivalent circuit with rotor quantities referred to the stator. This second equivalent circuit is more commonly used in induction motor studies, particularly for squirrel cage machines where the rotor is short circuited. The first equivalent circuit can be more useful in DFIM studies as actual rotor quantities are directly computed.

Note that for a DFIM operating at constant stator voltage, frequency, and current, the rotor current will be constant while the rotor voltage will vary with the slip.

### 2.2.9.4 Power Flow

The power flow in the doubly fed machine is between the stator circuit, the rotor circuit, and the shaft. The power flowing into the stator and rotor circuit includes power lost in the winding and power which is converted. For a three phase machine, the stator power that is converted is:

$$P_{\text{stator}} = 3E_A I_A \cos \theta_A \quad (2.84)$$

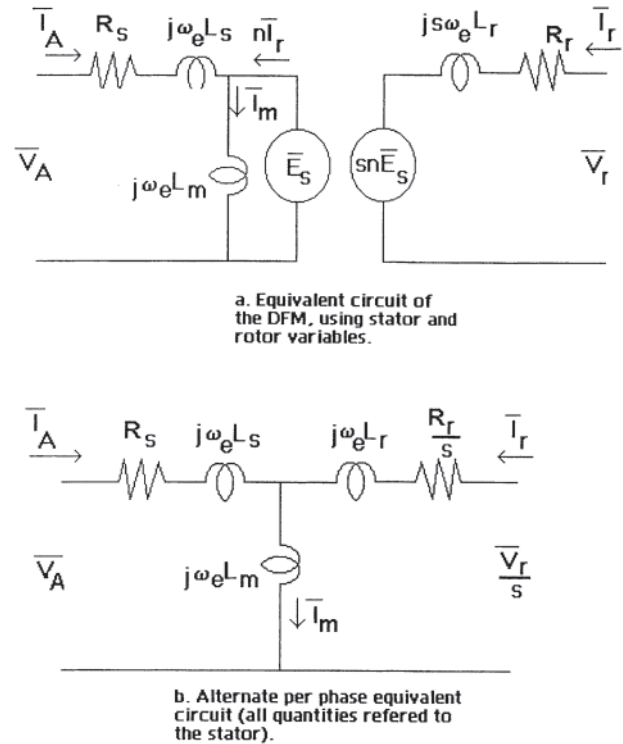


Figure 2.31 Two alternate per phase equivalent circuits.

where  $\theta_A$  is the angle between stator voltage and stator current. Similarly, the rotor power that is converted is:

$$P_{\text{rotor}} = 3E_r I_r \cos \theta_r \quad (2.85)$$

By using Eqs. 2.79, 2.80 and 2.80, the power that is converted from the rotor winding can be written as:

$$\begin{aligned} P_{\text{rotor}} &= -3snE_s \frac{I_s}{n} \cos \theta_s \\ &= -sP_{\text{stator}} \end{aligned} \quad (2.86)$$

Equation 2.86 defines the basic relationship between the stator and rotor power. The power out of the shaft must then equal the power flowing into the stator and rotor circuits:

$$P_{\text{mech}} = P_{\text{stator}} + P_{\text{rotor}} = P_{\text{stator}}(1-s) \quad (2.87)$$

#### 2.2.9.4.1 DFIM: Motoring

Equation 2.87 describes the basic relationship of a DFIM. While it neglects losses and magnetizing requirements, it usefully describes the basic conversion process. As the equation is written with the motoring convention, both the stator and shaft power will be positive when motoring. The rotor power changes sign with the slip, with power flowing out of the rotor for positive slip, and power flowing into the rotor for negative slip. These relationships are shown in Fig. 2.32, for rated stator quantities. This figure shows that both the shaft power and total electrical power vary proportionately with speed when the stator power is held constant. Note that when the stator is operating at rated voltage and current, the

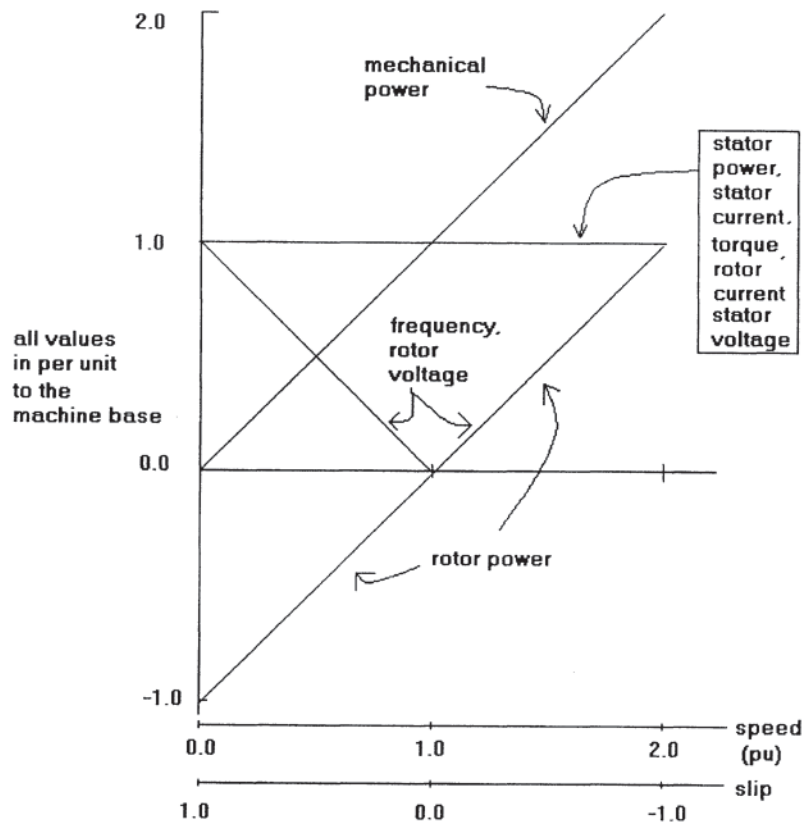


**Figure 2.32** Relationships of power, current, voltage, and frequency with doubly fed induction motor (DFIM) slip and speed. Losses and magnetizing current are neglected.

rotor current will be constant near the rated value as speed changes. The rotor voltage and power will vary proportionately with slip. Power and current values vary proportionately to changes in mechanical output power. Frequency is independent of load, as is (nominally) rotor voltage.

2.2.9.4.2 DFIM: Generating

When the doubly fed machine is used as a generator, the shaft power and stator power will both reverse, with power flowing into the machine from the shaft, and out the stator winding. From Eq. 2.86, the rotor power will flow into the rotor when slip is positive, and out of the rotor when slip is negative. The power flows for generating are also shown in Fig. 2.32, for a doubly fed generator with mechanical power going into the machine and stator and rotor electrical power flowing out of the machine. Again the shaft power into the generator and the total electrical power out of the generator will be proportional to speed when stator current (and shaft torque) are held constant.

2.2.9.5 Operating Considerations

The most common mode of operation for the doubly fed machine is with the stator directly connected to a constant frequency power system, and the rotor connected to this same

system through a static power converter, as shown in Fig. 2.33. Shaft speed and torque signals (or an estimate of torque) are fed back to the converter to control the converter frequency and voltage that are fed to the rotor. In order to take advantage of the machine’s operating range, this power converter must allow bidirectional power flow. When the operating speed range is restricted, the power rating of this converter can be substantially less than the power rating of the machine.

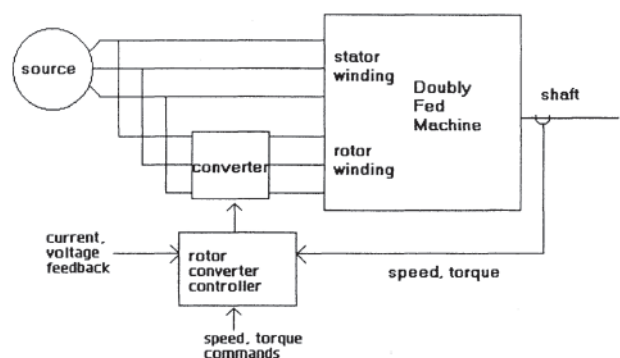


**Figure 2.33** Conceptual diagram of doubly fed induction motor (DFIM) control.

**Table 2.3** Frequency and Rotor Power Requirements for DEF Drive Speed Range

Speed range	Max motor frequency	Minimum speed (pu)	Maximum speed (pu)	Maximum shaft power (pu)	Maximum rotor power (pu)
1.25:1	0.11	0.89	1.11	1.11	0.11
1.50:1	0.20	0.80	1.20	1.20	0.20
1.75:1	0.27	0.73	1.27	1.27	0.27
2.0:1	0.33	0.67	1.33	1.33	0.33
4.0:1	0.50	0.50	1.50	1.50	0.50
—	1.00	0.00	2.00	2.00	1.00

Losses and magnetizing requirements neglected.

For example, a DFIM with a slip ranging from 0.2 to  $-0.2$  will operate from 80% of rated speed to 120% of rated speed, and will have a 1.5:1 speed range. Neglecting loss and magnetizing current, the power converter for this speed range will equal the product of the rated stator power times the maximum slip allowed in the drive. Table 2.3 shows the converter power rating for several speed ranges. While the rotor power requirement will be somewhat higher due to machine resistance and magnetizing requirements, it is clear that the power requirements of the converter feeding the rotor circuit will be a fraction of the total shaft power.

#### 2.2.9.5.1 DFIM Control

The DFIM is controlled by the magnitude and frequency of the rotor voltage. As in the synchronous machine, the rotor terminal voltage magnitude controls var flow when the stator is connected to a stiff ac system. In many operating systems, it will be preferable to control the rotor voltage magnitude to maintain unity power factor on the rotor, and in the rotor power converter. The machine is then excited with vars drawn into the stator, directly from the power system, or from a nearby var source [32].

If the rotor frequency is held constant, the shaft speed will also be constant, and the DFIM will behave similarly to a synchronous machine at that speed. In the case of generator operation, an increase in driving torque will be countered by an increase in electrical output power, and the steady-state speed will be unchanged. Alternatively, if the rotor frequency is allowed to follow the shaft speed, the machine will behave in a torque control manner, similar to a dc drive [33].

#### 2.2.9.5.2 Cascaded DFIM

The standard doubly fed machine relies on brushes to supply power to the rotor winding. While these are suitable for many applications, there are applications where brushless operation is needed. To obtain brushless operation, two doubly fed machines are operated in cascade, with rotor windings connected. The steady state performance of the cascaded doubly fed machine is similar to that of the doubly fed machine [32, 33], with the pole numbers of the two machines either adding or subtracting. The loss and magnetizing requirements of both machines must be supplied, of course.

#### 2.2.9.6 Summary

DFIMs provide variable speed operation for both motoring and generating. Aircraft applications were investigated a

number of years ago [34]. Recent applications include variable speed constant frequency generation in wind generation [35], hydro generation, and flywheel energy storage. The advantage of the doubly fed machine is that it can provide variable speed operation with a power converter which is rated at a fraction of the total drive rating.

This section has provided a brief description of the steady state performance of these machines. Dynamic analysis is readily performed using dq axis theory, with a DFIMs model similar to an induction motor model. A variety of control algorithms can be implemented on the DFIM to obtain different performance characteristics. These include synchronous operation and field oriented control, see for example, Refs. 33, and 35–38.

## 2.3 DIRECT-CURRENT MOTORS

### 2.3.1 Introduction

This section on dc motors is, in general, descriptive in nature. Mathematical derivations are kept to a minimum and are designed to develop the performance characteristics of the various types of dc motors. Transient response is treated in the section describing load characteristics.

Detailed information on the commercial aspects, such as standardized voltages, horsepower ratings, markings and nameplate data, and so forth is given in Ref. 1. IEEE Std. 113 [39] provides information on test procedures for dc machines. Some test techniques not detailed in Ref. 39 are contained in this section. (Sources of standards are listed in Appendix B.)

Many excellent textbooks yielding more detailed descriptions and theory are available. Only a few titles are listed in the References [40–45].

Chapter 6 provides detailed information on dc motor design.

### 2.3.2 General Description

Conventional dc motors consist of one or more field windings, an armature winding with commutator located on a magnetic rotor or armature, and a magnetic structure forming a stator (referred to as the yoke). Also, there are, in larger size motors, additional windings that produce flux but that are not involved directly in the electrical-to-mechanical energy conversion process. These “nonpower” windings assist in the commutation process.



Placement of dc motor windings differs from that of ac motors. The power winding, or armature winding, is on the rotor. The excitation, or field winding(s), and one nonpower winding are on the stator. The field windings are concentrated coils surrounding the steel cores that form the field poles.

The armature winding is composed of a number of coils dispersed over the surface of the rotor. Each coil spans 180 electrical degrees, that is, from a “north” pole to a “south” pole. Each coil side under a pole of one polarity has a current in one direction; the other coil side has current in the opposite direction. As the coil is rotated, the direction of current in the coil must be reversed to enable the motor to deliver continuous torque. The various coils on the armature are interconnected at the commutator to form the complete armature winding.

The net result of the current-carrying armature coils and commutator action is a magnetic field, stationary in space. If there were no magnetic flux from the field coils, the armature magnetic field would be at 90 electrical degrees with respect to the center line of the stationary field poles. In order to develop an average torque, the armature magnetic field and the magnetic field established by the stator field poles must remain stationary with respect to each other. This is accomplished if the current direction in the coil sides is reversed as the coil rotates through 180 electrical degrees, or passes from under a north pole to under a south pole. The commutator accomplishes this current reversal. In effect, it renders the armature field stationary in space.

The commutator, mounted on the rotor, consists of a number of copper segments, each insulated from the other segments by virtue of an insulated spacer, commonly mica material. One end of each segment is connected to one end of each of two different coil sides. The exact connection scheme determines whether the winding is a series (wave) or parallel (lap) armature winding.

Current is introduced into the armature winding via spring-loaded carbon brushes. The brushes wear, due to contact friction and electrical sparking. This results in “filming” of the commutator, with resulting increase of brush-commutator contact resistance and a buildup of conducting carbon dust between commutator segments. The requirement for periodic maintenance due to brush wear and necessary brush replacement is often listed as a disadvantage of dc motors. In addition, brush position must be accurately located with respect to the fixed field poles in order to secure proper commutation, or current reversal, in the armature coils. Failure to properly commutate results in electric sparking between carbon brush and copper commutator segments. Severe failure to commutate can cause “ring fire,” that is, arcing over the entire commutator periphery.

Typical dc motor components are shown in Figs. 2.34 through 2.37.

Conventional dc motors are characterized as shunt-, series-, or compound-connected. Each type has specific and different characteristics; the application determines which type is utilized.

The shunt-connected machine has field windings of relatively many turns of small wire forming the concentrated

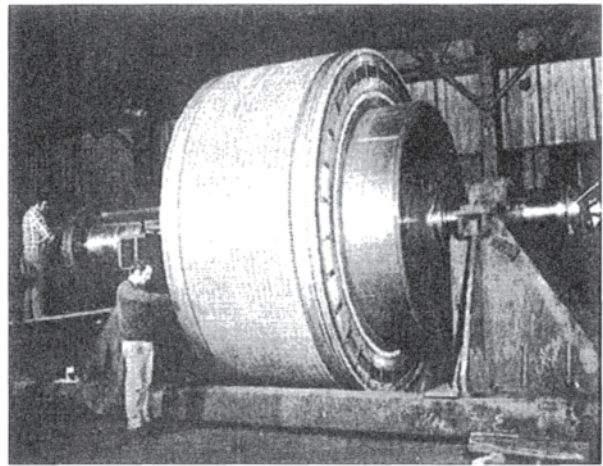


**Figure 2.34** A 7000-hp armature and commutator.

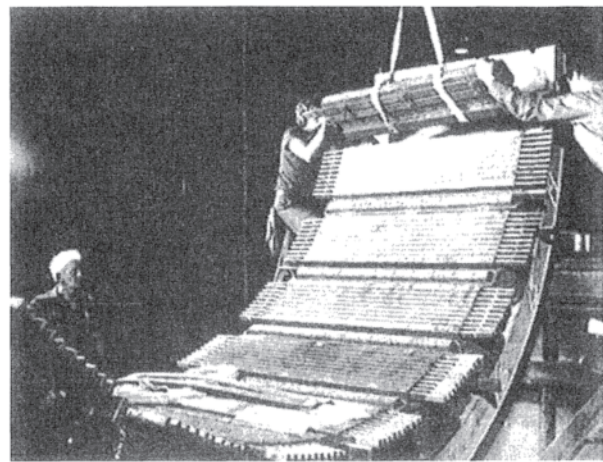


**Figure 2.35** A 7000-hp stator segment with main poles, interpoles, and pole face windings.

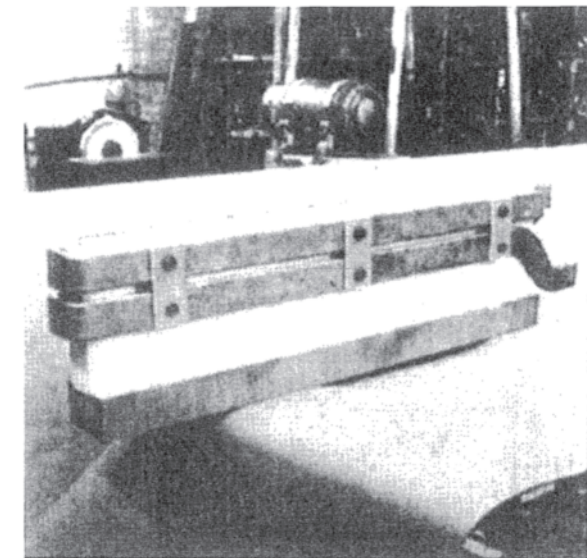


**Figure 2.36** A 7000-hp interpole with winding.

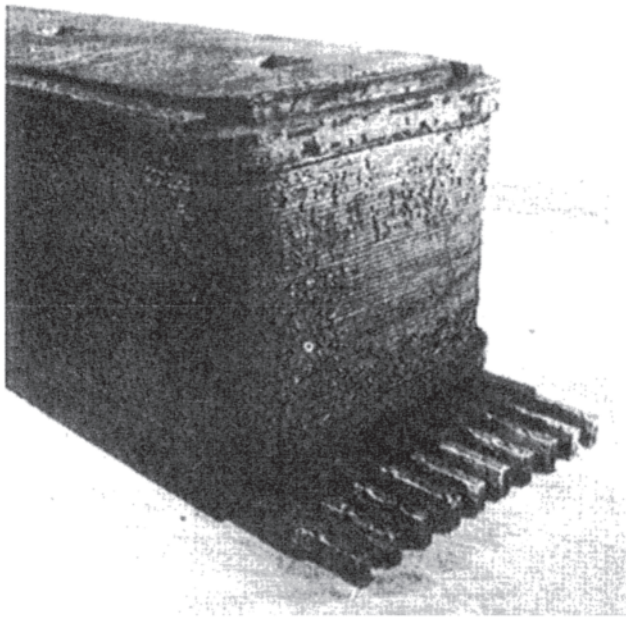


**Figure 2.37** A 7000-hp main field pole with pole face winding.

field pole winding. The field windings may be in parallel (shunt) with the armature, or may be separately connected across a constant or variable voltage supply. The flux supplied by the winding can be varied by controlling the magnitude of the current through the winding. The field flux, of course, has an important effect on the output characteristic of the motor.

The series-connected machine has relatively few turns of large wire forming the field winding, which is connected in series with the armature. Unless field bypass resistors are used, the field flux is determined by the armature current, which in turn is established by the applied voltage and the load-torque requirements.

As a generalization (theoretical but not strictly accurate), the shunt-connected motor is a “constant-speed” motor; the series-connected motor is a “constant-power” motor.

DC machine armature winding conductors are connected to the commutators in either a series (so-called wave) winding or in a parallel (so-called lap) winding configuration. Figures 2.38 and 2.39 depict developed lap and wave windings for four-pole machines. In the simplex lap winding, the armature coil leads are connected to adjacent commutator segments and the number of current paths is equal to the number of poles. In the simplex wave winding, the coil leads are connected to commutator segments two pole pitches apart and the number of current paths is always two.

As a generalization, for a given motor power rating, the voltage rating determines the choice of the lap or wave connection; that is, low-voltage, high-current machines utilize the multiple parallel paths of the lap winding, whereas a relatively high-voltage, low-current motor will likely have a wave winding with series connection of the coils.

The compound-winding connected motor has both a winding connected in shunt with the armature (the shunt winding) and a winding connected in series with the armature

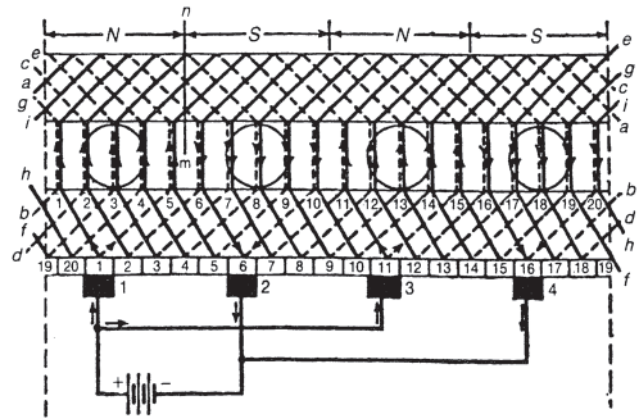


**Figure 2.38** Developed lap winding.

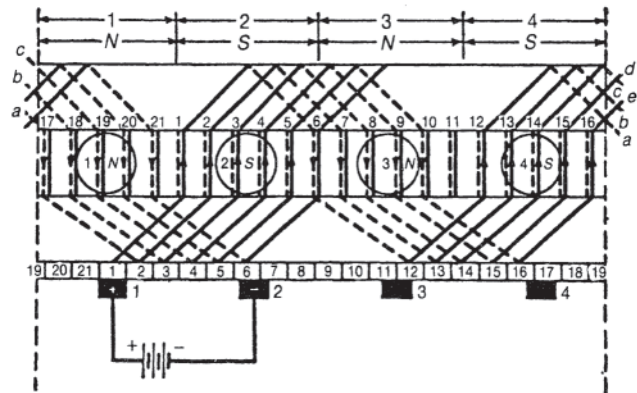


**Figure 2.39** Developed wave winding.

(the series winding) on each field pole. The windings can provide mmf in the same direction (cumulative compound) or in opposite directions (differential compound).

Regardless of the type of motor, generator action is always present by virtue of moving conductors lying in a magnetic field. The generator effect is referred to as “back” electromotive force (emf) or counterelectromotive force, cemf. The cemf opposes the impressed, or driving, voltage on the motor. The armature winding has resistance and inductance, the inductance being measured in flux linkages per ampere.

The emf,  $E$ , can be shown to be:

$$E = \frac{Zp\phi n}{60a} = \frac{Zp\phi\omega}{2\pi a} \quad (2.88)$$

where:

$E$  = cemf

$Z$  = number of active inductors (conductors)

$p$  = the number of poles

$n$  = angular speed (rev/min)

$\omega$  = angular speed (rad/sec)

$a$  = number of parallel paths through the armature

$\phi$  = flux per pole (Wb)

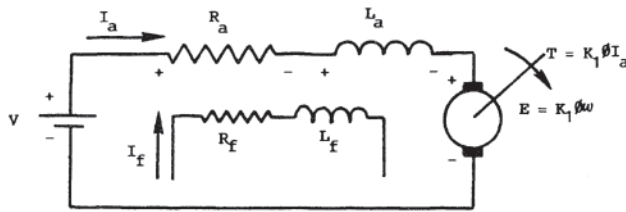


Figure 2.40 DC motor equivalent circuit.

For a simplex lap (parallel) wound machine,  $a=p$ . For a simplex wave (series) wound machine,  $a=2$ .

For purposes of formulating an equivalent circuit for a specific machine, Eq. 2.88 becomes:

$$E = K_1 \phi \omega \quad (2.89)$$

The product of induced voltage,  $E$ , and armature current,  $I_a$  is the electromagnetic power,  $P$ , in watts. Since power is also the product of torque,  $T$ , in newton-meters, and speed,  $\omega$ , in radians/second; the corresponding electromagnetic torque is:

$$T = K_1 \phi I_a \quad (2.90)$$

Actual power output is the electromagnetic power less the mechanical rotating losses (friction and windage).

The generalized equivalent circuit for dc machines can be formulated as shown in Fig. 2.40 where the symbols have the following meanings:

- $V$  = Applied voltage (V)
- $R_a$  = Armature circuit resistance (ohms)
- $L_a$  = Armature circuit inductance (H)
- $R_f$  = Field circuit resistance (ohms)
- $L_f$  = Field circuit inductance (H)
- $\phi$  = Flux per pole (Wb)
- $\omega$  = Angular velocity (rad/sec)
- $K_1$  = The machine constant (also called the torque or voltage constant)
- $T$  = Developed torque (N-m)

The connection of the field circuit(s) determines the type of dc motor, that is, shunt, series, or compound. In order to determine performance characteristics of the various types of motors, the flux is assumed to be directly proportional to the field current. In an actual motor, it is usually not; the actual relationship is the  $B$ - $H$  characteristic of the magnetic circuit (steel and air gap). Actual performance characteristics can be determined only by test.

The following procedure enables one to obtain a calculated efficiency:

1. *Joule losses,  $P_{JL}$ :*

$$I_f^2 R_f + I_a^2 R_a + V_b I_a = P_{JL}$$

$P_{JL}$  is typically 4–11% of motor rating. The voltage  $V_b$  is the contact voltage drop, that is, the voltage drop from the carbon brush to the copper commutator. It is typically 1–2 V.

2. *Rotational losses,  $P_{RL}$ :* Brush and bearing friction and the loss due to windage.  $P_{RL}$  is typically 2–13% of rating.

3. *Stray load losses,  $P_{SL}$ :* Hysteresis and eddy current losses in the iron core and the armature conductors.  $P_{SL}$  is typically 1–2% of motor rating.

Efficiency,  $\eta$ , can then be calculated as

$$\eta = \left( \frac{\text{power input} - \Sigma \text{ losses}}{\text{power input}} \right) \times 100\%$$

The transient, or short-time, overload capability of a dc motor is limited by its ability to commutate, that is, to reverse the current in the armature coils. The basic problem is that each armature coil has self- and mutual-inductance that opposes the change in current. When the ability to commutate is exceeded, sparking at the brush results, with attendant heating of the brushes and commutator.

In the commutation process, the area of contact between the fixed brush and the leaving commutator segment decreases linearly with time. Ideally, the current reversal would also change at a linear rate. The “reactance voltage” associated with the changing current and coil inductances causes the current change to lag behind the linear change of contact area. The result is that the current density increases, and when contact area goes to zero (the segment leaves the brush) the current density is extremely high. Sparking may result.

One method of aiding the commutation process is to introduce a *rotational* voltage in the coil that opposes the reactance voltage. This is accomplished by adding auxiliary poles, called commutating poles or interpoles. The latter name arises from the fact that the auxiliary poles are located in the area midway between the main field poles. These poles are connected in series with the armature circuit.

Determination of the optimal value of interpole flux by analysis is a very complex problem and has not in general been successful: that is to say, the exact number of ampere-turns and the length of the nonmagnetic interpole flux path are not readily calculable. The motor designer specifies a maximum number of turns and the insertion of several magnetic shims between interpole and yoke. By test, the correct value of interpole flux is determined. There are two measures that can be taken to adjust the interpole flux.

One method is to shunt the interpole coil with a resistor, which decreases the current through the coil and reduces the number of net ampere-turns of excitation. The disadvantage is that the current does not divide properly during transient-load impacts as it does during steady-state load situations. The preferred alternative is to design the pole with magnetic shims between the pole base and the magnetic yoke structure. The number of ampere-turns (for a given current) is constant, but the flux from the pole can be adjusted by replacing some of the magnetic shims with nonmagnetic shims, in effect increasing the reluctance of the path and decreasing the flux for a given current.

Testing to establish the interpole commutation configuration is referred to as the “black band” test. The nomenclature arises from the net result of achieving sparkless commutation. The test procedure and setup are described below.

Another type of nonpower winding is the “compensating” or “pole-face” winding. This winding compensates for

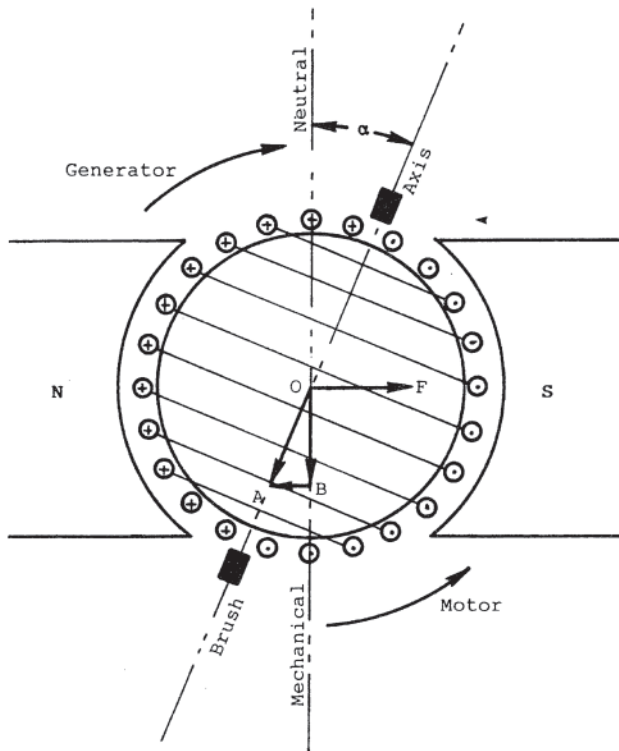


Figure 2.41 Armature reaction effects.

armature reaction and is physically on the pole face (air gap side). Armature reaction results from the magnetomotive force (mmf) established by current flow in the armature conductors. Armature reaction can be visualized by referring to Fig. 2.41. This is a simplified schematic for purposes of illustration. The vector  $OF$  represents the mmf due to the main field coils and vector  $OA$  represents the mmf due to the armature inductors. Resolving  $OA$  into components  $OB$  and  $BA$  yields a demagnetizing component and a cross-magnetizing component due to the armature mmf. The combination is armature reaction.

The armature reaction effect can be mitigated by embedding inductors in the main pole face. These inductors are connected in series with the armature with current direction opposite to the direction of the current in the adjacent armature conductors, that is, the compensating winding inductors in the south (S) pole face would have current going into the page. Thus, they neutralize the mmf due to armature current.

Commutating and compensating windings are usually found on larger machines to be used where heavy overloads or rapidly changing loads will be experienced or for shunt-connected motors that will operate over a wide speed range.

### 2.3.3 Tests

**Brush Locations** Armature reaction as described above skews the magnetic field, that is, it distorts the net flux direction. If there were no distortion, the carbon brushes would be located at the mechanical neutral position. The armature coil undergoing commutation would have no flux linkage. With

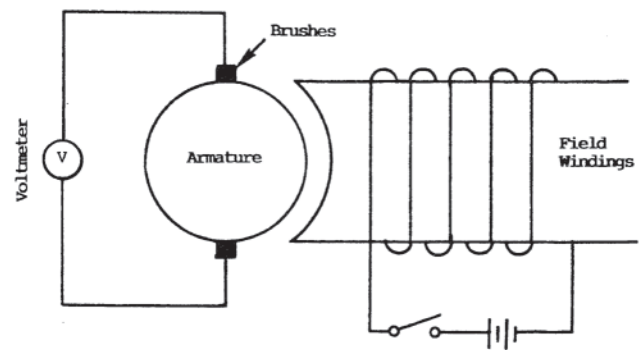


Figure 2.42 "Field flashing" test.

cross-magnetization due to armature reaction and the resulting flux directional distortion, if the brushes are on mechanical neutral, there will be flux linkage with the coil being commutated. The brushes may have to be shifted from mechanical neutral to an electrical neutral position. To accommodate the need for shifting, the brush rigging is often adjustable in position off mechanical neutral. Since the armature reaction effect is proportional to load current, frequent brush shifting may be required.

To compensate for the cross-magnetizing effect, the brushes are shifted against the direction of rotation in a motor. Hence in an application where the motor is operated under load in both directions of rotation, brush shift is not a viable solution.

To determine mechanical neutral for the brush rigging, the test known as field flashing is performed. Schematically, the test setup is as shown in Fig. 2.42. A voltmeter is placed across the brushes, with no other armature connections made. The field winding is connected to a voltage source through a switch. When the switch is closed, the time-changing flux will induce a voltage in the coil if the brushes are off mechanical neutral. A deflection of the voltmeter occurs momentarily. The brush position is moved and the test repeated until the proper location is achieved.

**Black Band Commutation Test** The simplified circuit connection for this test is shown in Fig. 2.43. This test setup

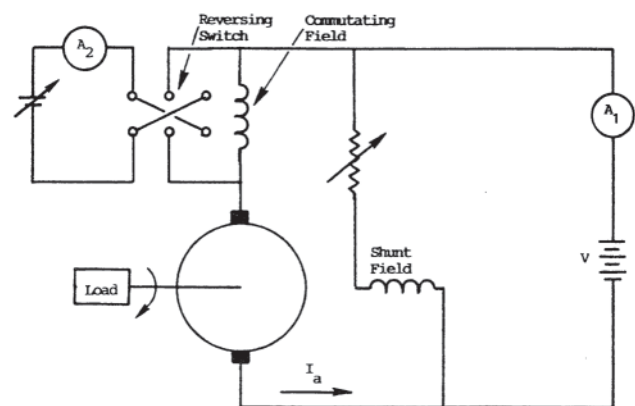


Figure 2.43 Black band commutation test.

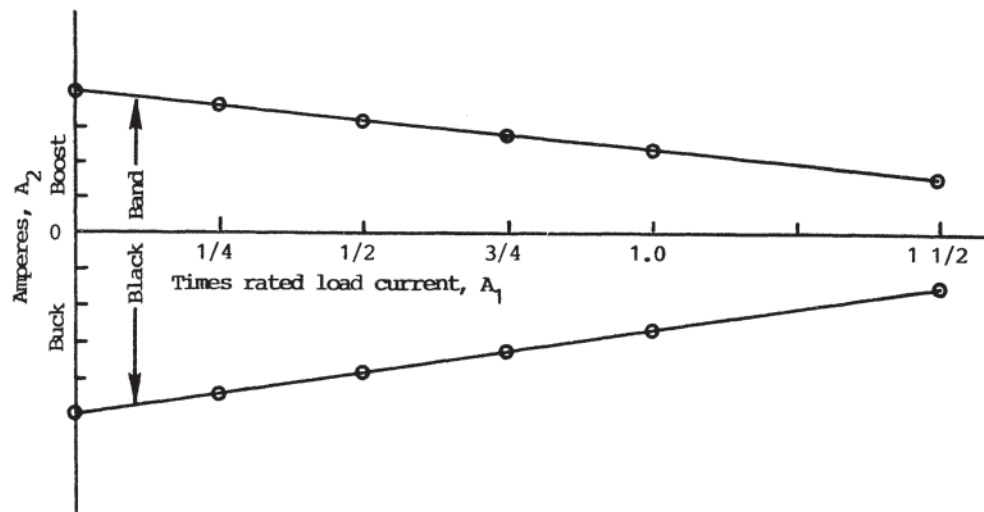


Figure 2.44 Ideal black band test results.

enables current in the interpole field winding to be boosted and to be bucked.

The boost/buck current is increased until sparking is observed at the brushes. Buck/boost data are usually taken at no load, 50% load, full load, and 150% of rated mechanical load. The data are then plotted as shown in Fig. 2.44. The ideal result, as shown, exhibits equal values of black band for buck and boost at the higher loads. Figure 2.45 depicts test results indicating that the commutating field is too strong and should be weakened by a parallel-connected shunting resistor or by increasing the magnetic reluctance of the flux path by using nonmagnetic shims or air gap increase. A brush shift with rotation will shift the band toward the boost side.

Reference to Fig. 2.44 indicates that the limits of black band commutation are decreasing with load and at some load

level the limits will go to zero, that is, the brushes will spark continuously. Figure 2.44 may well be representative of, for example, base speed of a shunt-connected motor. For speeds less than base (armature voltage control range), the band width will be increased; for speeds above base speed (weakened field current), the band width will be decreased. Also, if the motor is powered from a rectified voltage source, with resulting armature current ripple, the band width will be reduced and the zero limit (band width goes to zero) of load current will be reduced. The larger the ripple, the greater the reductions. Therefore, the black band test should be conducted with a power supply corresponding to the supply that will be used in the specific application.

Schemes for loading during tests are presented in the sections on the various types of dc motors.

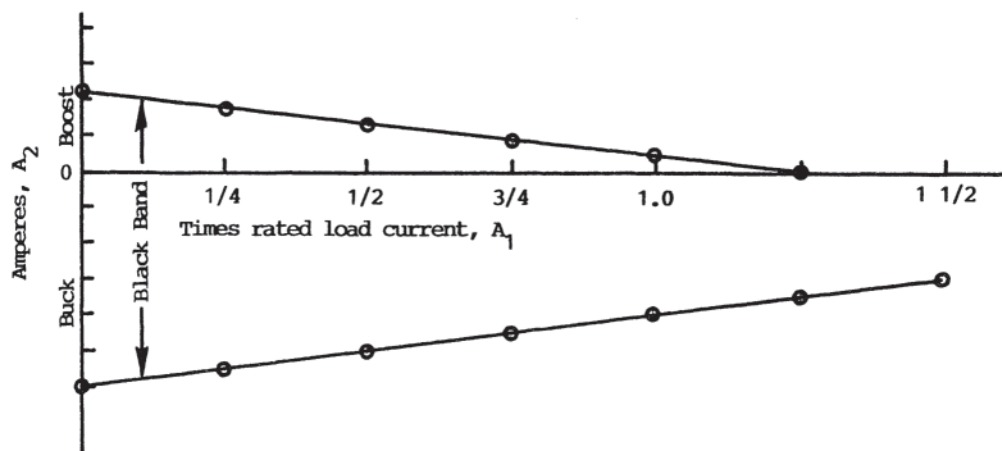


Figure 2.45 Black band test with a commutating field that is too strong.

### 2.3.4 Shunt Motors

Shunt motors were originally so designated because the excitation, or field, winding was connected in parallel, or shunt, with the source voltage. The actual field current value was controlled by varying the amount of external resistance in series with the field winding.

The shunt motor is a nearly-constant-speed motor for specific values of applied armature voltage and field current. The no-load speed can be varied over a wide speed range by control of armature voltage and field current.

From Eq. 2.89 and circuit analysis of Fig. 2.39:

$$V = R_a I_a + L_a \frac{dI_a}{dt} + K_1 \phi \omega \tag{2.91}$$

In order to visualize the operating characteristic of the shunt motor, assume it is in steady state, that is,  $dI_a/dt=0$ , and that the flux  $\phi$  is proportional to  $I_f$ , that is, no magnetic circuit saturation:

$$\phi = K_2 I_f \tag{2.92}$$

From Eq. 2.90:

$$I_a = \frac{T}{K_1 \phi} = \frac{T}{K_2 K_1 I_f} \tag{2.93}$$

Equation 2.91 can be rearranged as follows:

$$\omega = \frac{V}{K_1 K_2 I_f} - \frac{R_a T}{(K_1 K_2 I_f)^2} \tag{2.94}$$

This is a classic “straight line” equation of the form:

$$y = mx + b \tag{2.95}$$

where  $b$  is the  $y$  intercept at  $x=0$  and  $m$  is the slope. Equation 2.94, for a given value of  $V$  and  $I_f$ , is shown in Fig. 2.46.

A given motor has a rated maximum applied armature voltage and a maximum permissible field current level. If the applied armature voltage and field current are at rated values, the resulting no-load speed is characterized as base speed. If

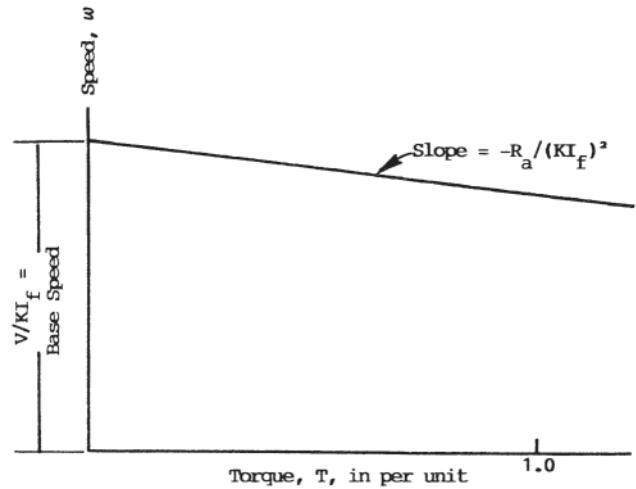


Figure 2.46 Shunt motor speed-torque characteristic.

field current is held constant at rated value and the applied armature voltage is decreased, the no-load speed will correspondingly decrease. For a specific armature voltage less than rated, the speed-torque characteristic will be a straight line parallel to and below the line shown in Fig. 2.46. If the armature voltage is at rated voltage and the field is weakened, that is,  $I_f$  is decreased, the no-load speed will increase above base speed and the slope of the  $\sim -T$  characteristic will increase.

If either  $V$  or  $I_f$  is reversed, the motor will reverse direction of rotation. As discussed in Section 2.3.3, the commutation ability of the motor decreases with field weakening. This factor determines the maximum speed at which the motor can be operated along with mechanical constraint.

Since torque is proportional to the product of armature current and field excitation, and power is proportional to the product of torque and speed, the torque and power limitations over the permissible speed range of the shunt motor are as shown in Fig. 2.47.

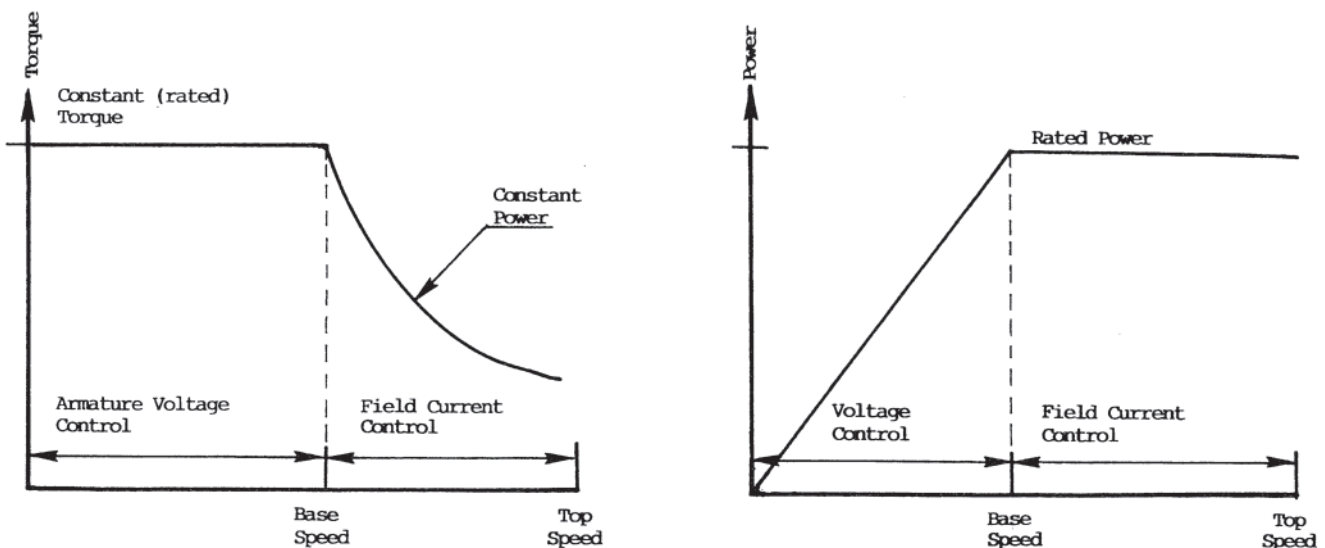


Figure 2.47 Torque-power limitations for a shunt motor.

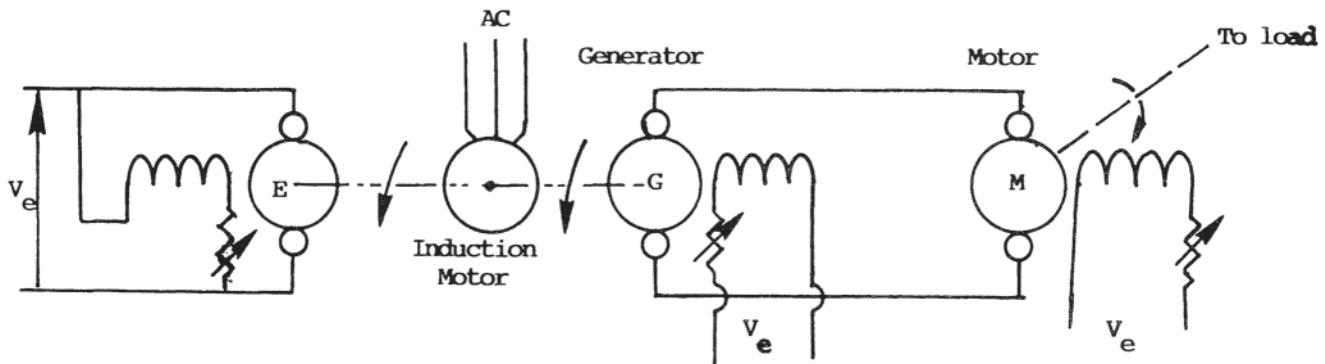


Figure 2.48 Ward-Leonard system.

Shunt motors, by virtue of their easily controlled speed-torque characteristic, find wide application in industry. Prior to the advent of controlled rectifier power sources, various schemes were utilized to obtain desired performance characteristics. For example, a commonly used variable-speed system, the Ward-Leonard system, provided adjustable armature voltage, as shown in Fig. 2.48. Although this system provided very smooth speed control over a wide range of speeds, the obvious disadvantage is that the total machine capacity required is over three times the actual power output.

Other schemes for obtaining specific speed-torque output characteristics involved adding series resistance in the armature circuit and/or shunting the armature with various values of resistance, as shown in Fig. 2.49. This scheme was used to obtain specific speed-torque characteristics, especially in the various operational modes other than conventional motoring, such as “dynamic braking” (inserting a load resistor across the armature to dissipate stored kinetic energy by causing the motor to act as a generator) and “plugging” (reversal of polarity of applied armature voltage.) Both were designed to bring the motor/load speed to zero quickly. They were also used to control an overrunning load, such as in lowering a crane or hoist load. The obvious disadvantage is the joule loss in resistors and its effect on motor drive efficiency.

Modern solid-state power electronic technology has largely replaced these control schemes. However, in small motor applications they may still be useful. In order to determine motor performance using resistor control, the resistance values can be inserted into the equivalent circuit, Fig. 2.40, and conventional analysis techniques applied. With modern-day technology, using appropriate regulators and control systems, flat speed-torque characteristics are obtainable. In effect, any

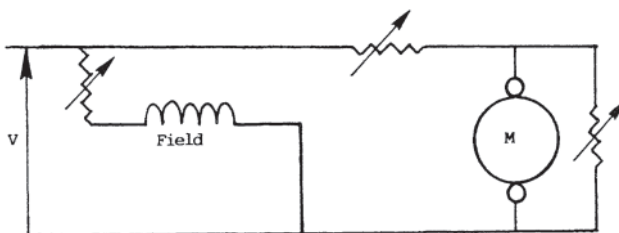


Figure 2.49 Series/shunt armature resistance connections.

desired operating point within the zero-to-maximum “rectangle” formed on the speed-torque plot can be obtained.

The foregoing has dealt with the steady-state operation of the shunt motor. To analyze the behavior under transient conditions, that is, change in armature voltage, field current, or load, differential equations involving armature and field inductance, system inertia, speed-torque characteristics of the load, and the control system response must be formulated and solved.

Motor control is discussed in detail in Chapter 9. Generally, the control must be such (for starting) as to provide maximum field current (to develop maximum starting torque consistent with inrush current limitations) and to limit the inrush current. The latter is accomplished by inserting external resistance into the armature circuit or starting on reduced armature voltage. Typically,  $R_a$  is 0.03 to 0.05 per unit. Thus rated voltage (1.0 per unit) across the armature at standstill would cause a 20 to 30 per-unit inrush current.

#### 2.3.4.1 Shunt Motor Loading for Tests

A motor-under-load test can be conducted by a friction-type prony brake, by driving a generator-type dynamometer, or by the “pump back” method. In the first two of these methods, the power output of the motor under test is dissipated as heat, either as friction for the prony brake or as joule loss in the dynamometer generator load. For larger-sized motors, the “pump back” method is preferable in that motor output is not dissipated as external friction or joule loss in generator load resistors.

The pump-back scheme requires a shunt-connected machine of rating and size similar to that of the motor under test and an external voltage source. The basic simplified connection scheme is shown in Fig. 2.50.

This test commences by applying external voltage  $V$  to the motor with the switch open. Motor  $M$  is brought up to the desired speed by adjustment of  $V$  and field excitation (controlled by  $R_{fm}$ ). The direct shaft-connected generator  $G$  is self-excited and its voltage builds up. The voltage of  $G$  is adjusted to be equal to the voltage applied to the motor by adjusting the generator excitation using  $R_{fg}$ . The voltage of  $G$  must be of the same polarity as the voltage applied to the motor; this can be checked by observation of the voltmeter connected across the switch. When that voltmeter reads zero, the generator output voltage has the correct polarity and the

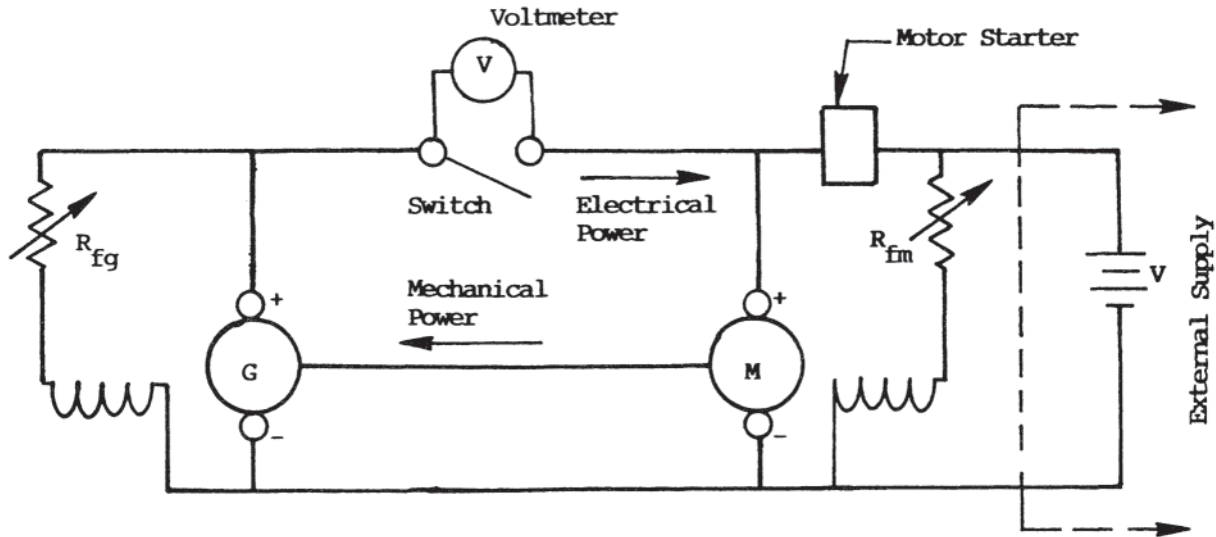


Figure 2.50 Pump-back circuit.

same voltage as the supply. When this condition is established, the switch is closed, and the generator “floats” on the line.

Motor M can now be loaded by decreasing the field excitation on M, causing its internally generated voltage (cemf) to decrease and armature current to increase (increasing its torque), and increasing its speed. Alternatively, motor M can be loaded by reducing  $R_{fg}$ , thus increasing the excitation of the generator and its output voltage. In either case, generator G sends current (and hence electrical power) toward the external supply.

That this is not a perpetual motion system is evident from the fact that there are losses involved in the conversion processes. These losses are made up by the external power supply. If M and G each have a rated power of 1.0 per unit and each is 90% efficient, the external source will supply 0.2 per unit power.

The pump-back connection can be used for commutation tests (black band), efficiency determination, actual speed-torque tests, and others. The main advantage is that it is not necessary to dissipate the total load power as joule losses in friction or in a resistance bank.

### 2.3.5 Series Motors

The series motor has the excitation, or field, winding connected in series with the armature. Thus, field current varies with load current.

To visualize the theoretical performance, refer to Eqs. 2.89 and 2.90 and the equivalent circuit shown in Fig. 2.40. Again, assuming a linear relationship between flux  $\phi$  and field current  $I_a$  and steady-state operation:

$$V = R_a I_a + K_1 K_3 I_a \omega \quad (2.96)$$

$$I_a = \sqrt{\frac{T}{K_1 K_3}} \quad (2.97)$$

from which:

$$\omega = \frac{V}{\sqrt{T} \sqrt{K}} - \frac{R_a}{K}, \quad K = K_1 K_3 \quad (2.98)$$

This is a hyperbolic relationship between speed and the square root of torque. Two important operating characteristics are easily noted.

1. At standstill, maximum torque for a given applied voltage is developed:

$$T = \frac{V^2}{R_a^2} K \quad (2.99)$$

2. If  $T$  is zero, theoretically the speed goes to infinity.

Characteristic (1) dictates the application, that is, loads that require maximum torque when starting, such as traction applications, cranes, and hoists. Torque limit is achieved either by reducing applied voltage or by inserting series resistance in the fieldarmature circuit.

Characteristic (2) dictates the requirement that a series motor should never be in a situation where it becomes unloaded. This dictates direct-drive-connected loads only (never belt-connected loads). In reality, the load never goes to zero because of the rotational loss load. However, a speed can easily be reached that develops centrifugal forces which will destroy the rotor.

The theoretical speed-torque characteristic of the series motor with no magnetic saturation is shown in Fig. 2.51. It should be noted that conventional series motors are designed to operate on the “knee” of the magnetic saturation curve and actual performance is affected by magnetic saturation.

Figure 2.52 shows actual characteristics of a 25-hp, 550-rpm, 230-V series motor with rated full-load current of 100 A. Note that because of saturation, torque is nearly linear with armature current and volts/rpm and torque/ampere (values of  $K$  in the English system of units) are not constant but rather follow the saturation curve of the magnetic circuit.



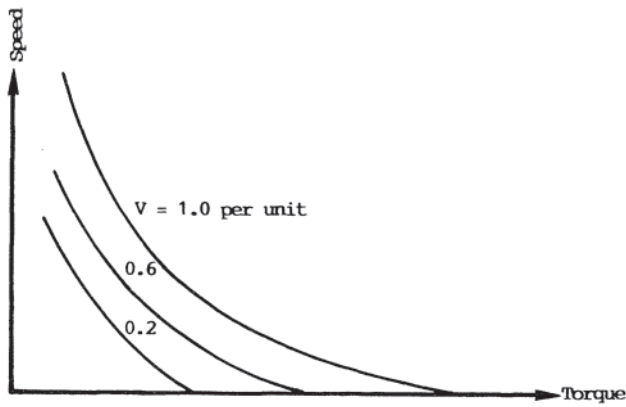


**Figure 2.51** Theoretical series motor speed-torque characteristics.

Section 3.8.2 gives sample calculations, based on test values of  $E/\omega$ , or  $K$ , as a function of field current and the procedure to calculate torque and current versus speed for various values of applied voltage.

### 2.3.5.1 Tests of Series Motors

To determine the value of  $E/\omega$ , or  $K$ , as a function of field current, the test setup shown in Fig. 2.53 can be used. The series motor is driven by the drive motor. The speed, open-circuit voltage, and field current are measured. Data taken can then be plotted and a curve-fitting technique used to establish

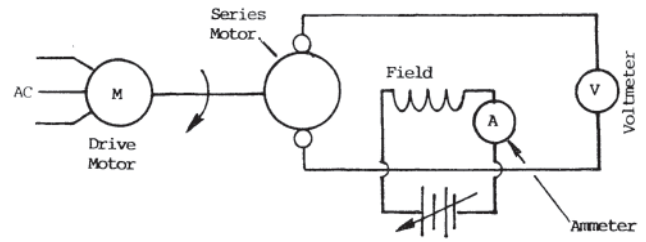


**Figure 2.53** Test to determine  $K$  as a function of field current  $I_f$ .

a mathematical relationship that can then be used in Eqs. 2.98 and 2.99.

Actual speed vs. current data can be determined by test using the test setup shown simplified in Fig. 2.54. If the value of  $K$  is known (preceding test), the speed-torque characteristic can then be calculated and plotted.

This test requires the availability of another series motor with a rating similar to the motor under test and a resistor load bank. Speed and armature current are monitored. The series fields of the two machines are connected in series, thus assuring positive generator voltage buildup and load on the motor to prevent instability and loss of motor load. Variable, adjustable resistors are utilized to adjust load and maintain precise control of the voltage applied to the motor.

### 2.3.5.2 Application of Series Motors

A series motor with laminated yoke and field poles can be operated from an alternating current supply because the field

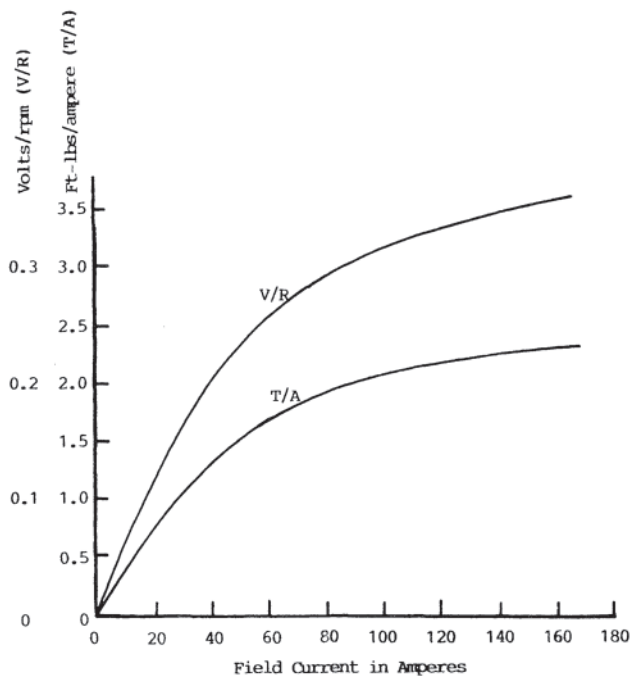
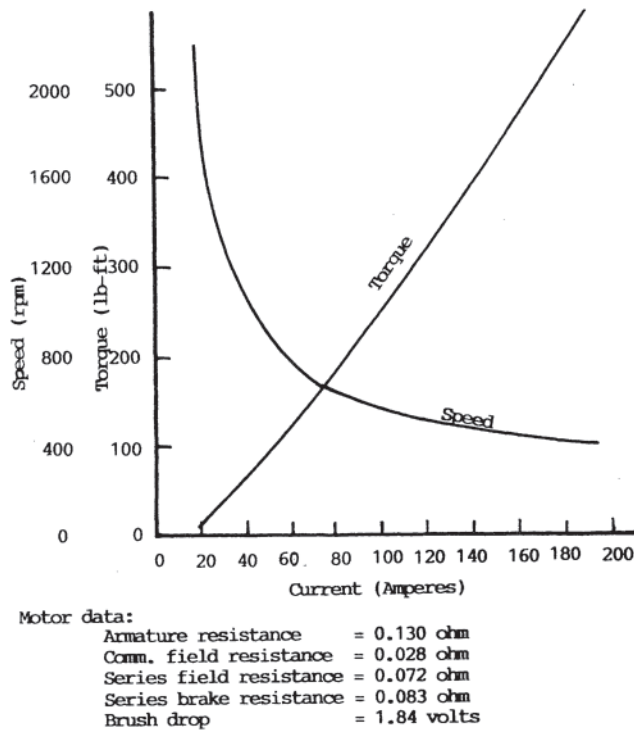


**Figure 2.52** Graphs of basic data for a 25-hp, 550-rpm, 230-V series-wound dc motor.

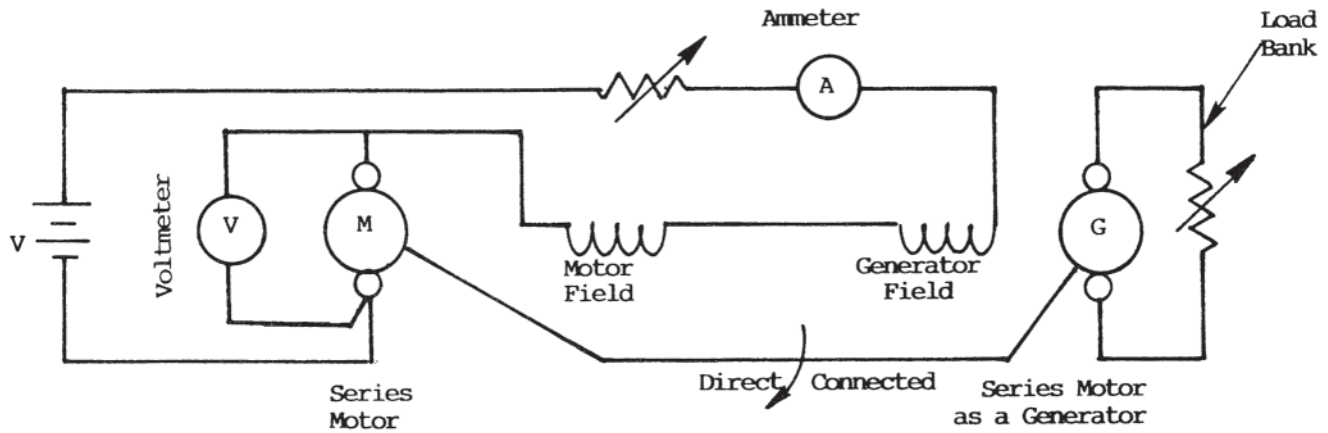


Figure 2.54 Series motor loading test.

flux and armature current are reversed simultaneously and thus torque and rotation are always in the same direction. However, the inductance of the motor will cause the motor to operate with a relatively poor power factor and poor commutation, especially at low speeds. The commutating ability decreases as supply frequency increases. Also, because of the reactance voltage drop (due to circuit inductance), the speed with ac operation is lower than it is with a dc supply for the same load torque.

The series motor speed-torque characteristic is ideal for traction applications. For relatively short run-distance systems, such as trolleys, light-rail vehicles, and subways, the series motor is usually dc supplied. However, electrified railroads, involving long distances for the power supply, use ac supply. The ac is transmitted at relatively high voltage (depending on transmission distance) and then stepped down to utilization voltage (600 V) by onboard transformers.

In order to reduce commutation problems, frequencies lower than normal usage frequencies are utilized. In the United States, 25 Hz is common; in Europe,  $16\frac{2}{3}$  Hz is used. The United States uses 25 Hz because of the availability of that frequency in the early years of electrification in this country. Today, the 25 Hz comes from motor-generator sets with an intermediate gear to obtain the frequency change. Without a gear change, the ratio of poles on the 60-Hz motor to the 25-Hz generator would be 12/5. In Europe, with 50 Hz supply for the motor and  $16\frac{2}{3}$  Hz for the generator, the pole ratio is 6/2.

Small series motors (less than 1/2 hp) are used in a variety of small appliances such as electric mowers, vacuum cleaners, blenders, sewing machines, and power tool. They are usually rated for either ac or dc supply and are referred to as “universal” motors. Unlike traction motors, universal motors usually do not have a compensating or pole-face winding.

### 2.3.6 Compound-Wound DC Motors

The compound-wound motor has two excitation windings, both on the main field poles. The majority of the flux results from the conventional shunt winding with additional excitation from a relatively small series-connected winding.

The series-connected field can be connected to add to (cumulative compounding) or subtract from (differential compounding) the flux produced by the main (shunt) winding.

The differential connection can be used in motors with a relatively small series field to reduce the speed drop with load because it weakens the total flux with an attendant increase in speed over a shunt-field only motor. However, as armature current increases, thus causing flux reduction, the developed magnetic torque decreases. The end result is that the torque characteristic of the differential compound motor is not suitable for most applications.

The cumulative compound motor combines the best of the characteristics of the shunt and series motors in that both fields contribute flux. This is especially important in applications that require a high starting torque but require the general speed-torque characteristic of the shunt motor. Because the net field flux is strengthened with load and the increased armature circuit resistance is due to the series field, the cumulative compound motor will have a greater speed drop than a straight shunt-wound motor. A typical speed-current characteristic is depicted in Fig. 2.55. Note that the rate of decrease of speed becomes less with increasing load because of saturation of the magnetic circuit. However, with modern motor control systems this is not a problem if speed sensing and appropriate control (armature voltage and/or shunt field weakening) are available.

### 2.3.7 Permanent Magnet Motors

The performance of permanent magnet-excited dc motors is similar to that of shunt-wound motors in that the motor speed is relatively independent of motor loading. The speed can be lowered by reducing the armature voltage; however, speed increase by shunt field weakening is not possible as with wound field motors. This is not a severe limitation in most modern motor applications.

The elimination of shunt field winding losses improves machine efficiency and reduces machine heating. This is particularly helpful with enclosed machines and especially when the motor is at rest or lightly loaded for lengthy periods.

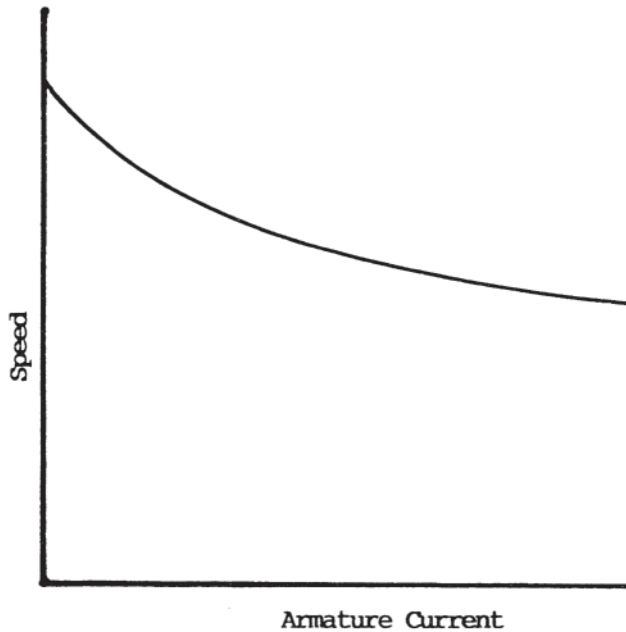


**Figure 2.55** Speed-load characteristic of a cumulative-compound dc motor.

In battery-powered applications the elimination of field excitation power losses reduces battery drain.

Several basic classes of permanent magnet materials are available, giving the opportunity to optimize motor characteristics (Table 2.4). Alnico 5–7 magnets once dominated industrial motors with ratings similar to four-pole shunt-wound motor ratings. The magnets can be designed to develop magnetic fields similar to those of shunt-wound motors using air gap lengths of similar magnitudes, although often somewhat smaller. The motors are commonly built with interpoles to aid in machine commutation. The stator and rotor diameters are similar to those of shunt-wound machines.

Permanent magnet Alnico-excited machines are usually built using laminated soft steel main pole faces adjacent to

the armature to avoid demagnetization of the magnets as a result of armature reaction flux effects when the machine is loaded. Even so, machine overloading must be limited to a degree depending on design. Alnico-excited machines are usually magnetized after the machine is assembled using a magnetizing winding located on the main poles. Such windings are small and relatively inexpensive since they are used only very briefly. Bonded Nd-Fe-B and standard Nd-Fe-B as well as better grades of ferrite and better designs have displaced Alnico in new designs.

Although permanent magnets are relatively expensive, there are offsetting savings in using these machines compared with shunt-wound motors, particularly the elimination of the heavy excitation windings, the shunt field power supply, its wiring, and its associated control equipment.

Smaller permanent magnet motors, usually less than 5 hp, are commonly built using ceramic magnets of various types, most of which are much lower in cost. These magnets are typically quite limited in magnetic flux density capability ( $B$ ), but develop a very high field intensity per unit length ( $H$ ). Hence, only a very short magnet length is needed although a large magnet cross section is required. The armature diameter and length and the main pole arc are all typically enlarged so as to increase the pole area. Further, the machine is designed to operate at a low flux level by using more armature turns than is typical of wound field machines.

The magnet frame diameter is reduced substantially because of the much shorter magnet length used and also because of the omission of the soft iron pole faces, which are not needed to avoid demagnetization when using ceramic magnets. These machines are usually built without commutating poles. The stators of the machines are magnetized using a magnetizing fixture during manufacture before machine assembly.

Other more exotic magnetic materials with energy products up to 50 MG-O<sub>e</sub> are available such that a wide variety of permanent magnet machines have been built. Some are designed with axial air gaps and are useful for special purposes. Others are especially lightweight machines for

**Table 2.4** Characteristics of Selected Permanent Magnets

Type	Residual flux density ( $B_r$ ) [T(kG)]	Coercive force ( $H_c$ ) [kA/m (Oe)]	Max. energy prod. [kJ/m <sup>3</sup> (MG-Oe)]	Recoil permeability
Alnico 5-7	1.35 (13.5)	58.9 (740)	59.6 (7.5)	17.0
Alnico 6	1.05 (10.5)	62.0 (780)	31.0 (3.9)	13.0
Alnico 9	1.06 (10.6)	119.3 (1,500)	71.5 (9.0)	7.0
Molded Ceramic 2	0.28 (2.8)	190.8 (2,400)	15.6 (1.96)	—
Ceramic 5	0.38 (3.8)	190.8 (2,400)	27.0 (3.4)	1.1
Ceramic 6	0.32 (3.2)	222.6 (2,800)	19.5 (2.45)	1.1
Ceramic 8B	0.4 (4.0)	222.6 (2,800)	32.6 (4.1)	—
Hicorex 22A (Sm-Co)	0.9 (9.0)	695.6 (8,750)	175.0 (22.0)	1.03
INCOR 26HE (Sm-Co)	1.06 (10.6)	748.0 (9,400)	207.0 (26.0)	1.03
Magnequench I (Nd-Fe-B)	0.68 (6.8)	>390 (9,900)	75 (9.8)	1.22
Magnequench II (Nd-Fe-B)	0.8 (8.0)	516.8 (6,500)	103.3 (13.0)	1.15
Magnequench III (Nd-Fe-B)	1.31 (13.1)	979 (12,300)	339 (42.0)	1.06
Neomax 27H (Nd-Fe-B)	1.1 (11.0)	811.0 (10,200)	223.4 (28.1)	1.05
Neomax 35 (Nd-Fe-B)	1.25 (12.5)	882.5 (11,100)	286.2 (36.0)	1.05

aircraft and space applications. Automotive applications are designed for extreme low cost. Variable-speed power tools constitute another field of application for fractional-horsepower permanent magnet motors.

### 2.3.8 Brushless DC Motors

This section briefly introduces the basics of brushless dc motors. Brushless dc motors are permanent magnet excited synchronous motors driven by electronic inverters triggered in accordance with rotor position. An in depth treatment of this motor is presented in Section 15.2 of Chapter 15, "Electronic Motors." An introduction to the basics of power electronics and inverters may be found in Sections 9.3 to 9.6 in Chapter 9, "Motor Control."

#### 2.3.8.1 Description

The brushless dc motor can be used for any application where torque, speed, or position control is required. The most popular brushless dc motor configuration comprises a three-phase stator winding and permanent magnets mounted on the rotor as shown in Fig. 2.56. This type of motor is driven by an electronic controller that switches the dc bus voltage between stator windings as the rotor turns. The rotor position is monitored by one or more optical or magnetic transducers that supply information to the electronic controller. Based on information supplied by the rotor position sensors, the electronic controller decides which stator phases should be energized at any instant. The controller consists of a set of power electronic devices (usually transistors, two per phase), which are controlled by low-level logic or a microprocessor. This electronic commutation of the armature voltage takes the place of the commutation that occurs in a conventional dc machine by action of the commutator and carbon brushes. Thus the name brushless dc motor. The brushless dc motor

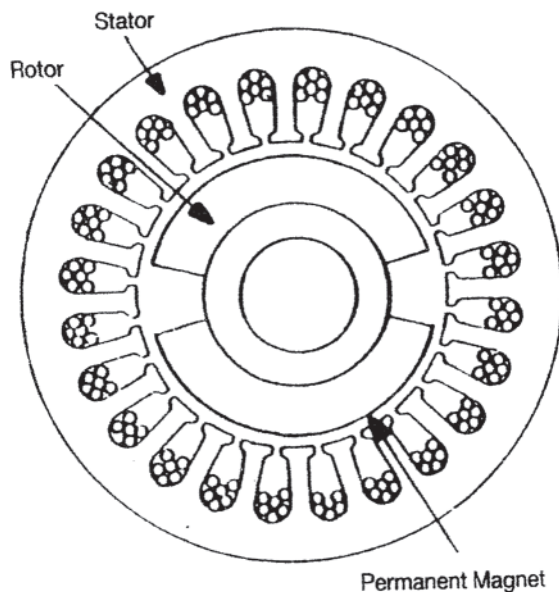


**Figure 2.56** Cross section of the structure of an electronically commutated (brushless dc) motor.

and controller eliminate rotating contacts and their associated wear and reliability problems. However, the complexity and cost of the electronics must be considered for any application.

#### 2.3.8.2 Power Supply

The power supply for a brushless dc motor is a fixed dc bus. The bus voltage can be obtained from rectified ac power or other means. It is not generally necessary to have a ripple-free dc supply, but some applications will require a smoother dc voltage to obtain the required motor control. For motor control schemes that require energy to be returned to the power system during motor braking, a more complex dc supply will be required unless other loads on the dc bus can accept the returned energy and prevent the bus voltage from exceeding required limits.

#### 2.3.8.3 Torque Control

Torque control in a brushless dc motor is usually accomplished by direct control of the armature winding current. In a brushless dc motor, the rotor permanent magnets produce a constant flux that links the armature windings. The flux density distribution along the air gap periphery is approximately a trapezoidal shape with constant flux density for about 120 electrical degrees. If the electronic current control uses 120 degree conduction that corresponds to the period of time that the stator coil sides for a given phase are located in the constant flux density region, then the dc bus current and the winding generated voltage are approximately constant. This approximation allows a simplified dc analysis of the brushless dc motor. A calculation of the air gap or rotor surface torque using a dc motor equation gives:

$$T_{\text{gap}} = K_a \times \Phi_t \times I_{\text{dc}} \text{ newton-meters} \quad (2.100)$$

where:

$$K_a = \text{armature winding constant} = \text{Poles} \times N_c / (2 \times \pi)$$

$$\text{Poles} = \text{number of motor poles}$$

$$N_c = \text{Total number of current-carrying conductors}$$

$$= 2/3 \times \text{Slots} \times \text{Coil sides per slot} \times \text{Turns per coil} / \text{Circuits}$$

The 2/3 is for the fact that only two of the three phases are conducting current at a time for 120-degree conduction. (For 180-degree conduction, one phase conducts full current for 120 degrees, and half current for the other 60 degrees, resulting in a somewhat higher torque per amp, but more complicated motor controller operation and commutation.)

$$\Phi_t = \text{total flux per pole in webers (found by integrating the flux density waveshape along the air gap periphery over one pole pitch)}$$

$$I_{\text{dc}} = \text{average dc bus current}$$

The motor-generated armature voltage or back emf can also be expressed similarly as:

$$E_a = K_a \times \Phi_t \times \text{rpm} \times 2 \times \pi / 60 \quad (2.101)$$

where:

$$\text{rpm} = \text{rotor speed in revolutions per minute}$$

This analysis shows an identical winding constant  $K_a$  being used for both torque and voltage. Some motor manufacturers provide a motor torque constant as the product of  $K_{\omega}$ ,  $\Phi_t$ , and a conversion factor for different torque units, and a voltage constant as the product of  $K_a$ ,  $\Phi_t$  and  $2\pi/60$ , which gives two numerically different values. Further analyses and derivations are given in [Chapter 15](#), where the effects of iron saturation and armature reaction are also considered.

Since output torque is nearly proportional to the product of flux and current (except for some losses), it is sufficient to use armature current as a measure of output torque. In a control system the current can be sensed and fed back to the electronics that control the power switching devices. The feedback of current is also used to limit the peak current by chopping the input voltage available at the motor terminals. When negative or braking torque is required, the motor current must be reversed, otherwise the motor would decelerate only due to losses. This requires that the controller be capable of allowing the motor to act as a generator and return power to the dc bus or a special braking circuit to dissipate energy stored in the rotating parts and load.

#### 2.3.8.4 Speed Control

Because of the nearly constant armature flux, the speed of a brushless dc motor at a steady-state condition is proportional to applied armature voltage. For applications requiring coarse speed control it is sufficient to control the voltage applied to the motor terminals by chopping the dc bus voltage. However, this form of open-loop control results in the requirement of some means of current limiting or the current will exceed the component current ratings. This is because the motor back emf is substantially less than the applied dc bus voltage. Also, the actual speed achieved will vary with load since there will be no compensation for the resistance voltage drop. A more accurate speed-control system will require a speed feedback from some form of tachometer or rotary transducer. The tachometer should also be a brushless device, to maintain the reliability of a system without rotating contacts. A controller with tachometer feedback and current control will also be able to provide braking. In some drives, the signal from the rotor position transducer used for commutation is differentiated with respect to time to obtain velocity. This method of obtaining a speed signal is not as accurate as a precision tachometer since commutation pulses come only every 60 electrical degrees.

#### 2.3.8.5 Position Control

Position control can be achieved using brushless dc motors if position feedback is used. The position transducer must be accurate enough to provide the desired position accuracy. For high-performance position controllers, velocity feedback is also added. As before, current limiting must be provided. In practice, current may be the variable that is controlled in response to position error and velocity feedback signals.

### 2.3.9 Ironless Armature DC Motors

These motors are the purest application of the basic principles of motor operation that we were all taught in our first magnetics

course. They are simple in principle, but like many applications of pure science, their construction is quite precise. Moving coil motor (MCM) is another popular name for them, which is derived from the concept that only the coils move. It is their low inertia and high pulse torque capability that combines to yield the fastest acceleration possible in the servo motor family. An added bonus is the absence of cogging and torque ripple because there is no rotating iron such as lamination teeth or magnets that cause preferred detent positions. By attaching an encoder or tachometer, this type of motor is capable of following the most demanding motion profile and position accuracy. Many motion control applications may not demand the precision and rapid acceleration offered by this technology. But when these types of motion profiles will not be compromised, the MCM must be considered.

#### 2.3.9.1 Principles of Operation

According to the earliest laws of electromagnetic motion, current moving through a conductor that is perpendicular to a magnetic field will create a force in the conductor, perpendicular to the direction of the current. Note that this law is not dependent upon the use of iron in the magnetic circuit, as found in most motors manufactured today. Iron is used because it can strengthen the field, and serve as mechanical support for the relatively weak copper conductors. The use of iron, while generally practical, brings with it certain tradeoffs. Those tradeoffs include higher inertia, higher inductance, and a tendency toward uneven torque production. Nor is there indication of how this conductor might be supported to translate the resultant force into useful torque. Those embellishments came later in history, thus the wide variety of motor types popular today. The MCM exemplifies the practical application of a motor in its simplest form: “Torque produced by a conductor carrying current in a magnetic field.” The design equations for these machines are the same as those covered in the previous section, except allowing for the absence of rotating iron.

#### 2.3.9.2 Construction

The essential MCM components that were developed after these early discoveries in the field of physics were: a respectable magnetic field, ball bearings, and a high temperature fiberglass/epoxy composite to add reinforcement and attachment of the conductors. The magnets of choice include Alnico for the highest temperature stability, samarium-cobalt for compactness and good thermal stability, and neodymium-iron-boron for compactness, ruggedness, and lower cost. Other important developments include a fast, closed loop controller, exacting manufacturing techniques, high temperature insulation systems, and an industry in need of a fast, accurate motor.

Those developments have made it possible to: wind individual conductors into coils, assemble them around a mandrel to form a cylindrical coil assembly, reinforce the coil assembly with fiberglass/epoxy and attach it to the hub/shaft, and then terminate the coils to a commutator ([Fig. 2.57](#)).

Typical construction of an MCM, exemplifying the essential developments that make it possible is shown in

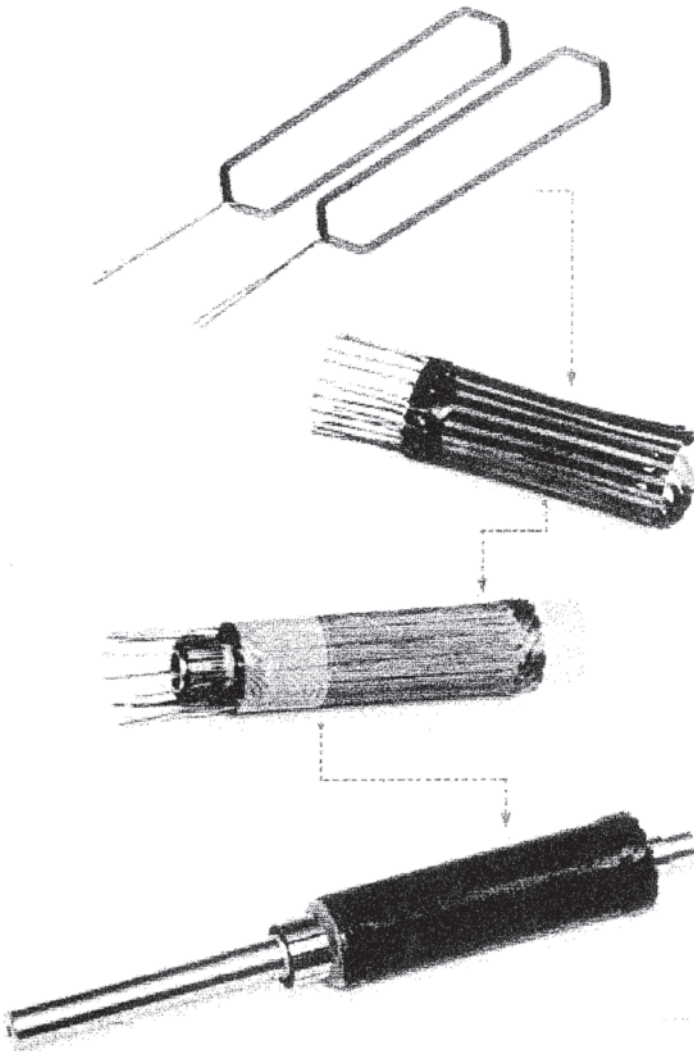


Fig. 2.58. This motor will be used in the application example in the next section.

### 2.3.9.3 Basic Equations

In this configuration, the coil structure (armature) rotates in the air gap between the inner core and the permanent magnet. To find the operating point on the magnet B-H curve, the permeance coefficient is calculated by dividing the magnet length by the air gap length, assuming that the air gap area equals the magnet area. By superimposing the load line based on the permeance coefficient on the B-H curve for Alnico 5–7 as shown in Fig. 2.59, the operating point is found to be at 12 kilogauss. However, the coercive force at this load point is only 400 Oersteds, indicating a motor design that could result in demagnetization from severely high current pulses. To counteract this tendency, a pole piece is often bonded to the face of the magnet, and then machined to the diameter of the armature plus clearance. It short-circuits the circulating current flux from the high current pulses. With this configuration, the pulse current can typically be six times the rated current before demagnetization will occur. The pole piece also serves to concentrate the lines of flux coming from the face of the magnet, resulting in a higher flux density across the

conductors. As a family, these motors are the most efficient dc machines available. Another characteristic associated with this type of motor is a low mechanical time constant, resulting from the small mass of the armature (no rotating Iron). Ironless armature motors also exhibit the lowest armature inductance, another factor that must be considered in stabilizing a servosystem using this type of motor.

Servosystems will exhibit totally different loop stability problems when an Iron armature motor is replaced by an ironless armature motor. These differences are due to the more rapid rise in armature current, providing faster torque delivery, then the lower inertia results in faster acceleration.

Since these motors use permanent-magnet fields, the flux per pole,  $\phi$  is treated as a constant. Then:

$$T_a = \frac{Zp}{2\pi a} I_a \phi_p = K_t I_a \quad (2.102)$$

and:

$$E_a = \frac{Zp}{2\pi a} \omega \phi_p = K_v \omega \quad (2.103)$$

where:

- $T_a$  = torque developed in the armature (N-m)
- $E_a$  = generated voltage (V)
- $K_t$  = torque constant (N-m/A)
- $K_v$  = voltage constant (V-sec/rad) (and  $K_t=K_v$ )
- $Z$  = total armature conductors
- $P$  = number of poles
- $a$  = number of parallel paths through the armature
- $I_a$  = armature current (A)
- $\phi_p$  = flux per pole (Wb)
- $\omega$  = shaft speed (rad/sec)

The total power loss is:

$$P_l = I_a^2 R_a + T_f \omega + D \omega^2 \quad (2.104)$$

where:

- $T_f$  = motor friction loss torque (N-m)
- $D$  = viscous damping coefficient (N-m-sec/rad)

The temperature rise is

$$\theta = R_{th} P_l \quad (2.105)$$

where:

- $\theta$  = temperature rise ( $^{\circ}\text{C}$ )
- $R_{th}$  = thermal resistance (C/W)

The armature current at the maximum allowable temperature rise may be found by combining Eqs. 2.104 and 2.105 to yield:

$$\frac{\theta_{\max}}{R_{th}} = I_m^2 R_a + T_f \omega + D \omega^2 \quad (2.106)$$

where  $I_m$  = armature current at the allowable temperature rise (A).

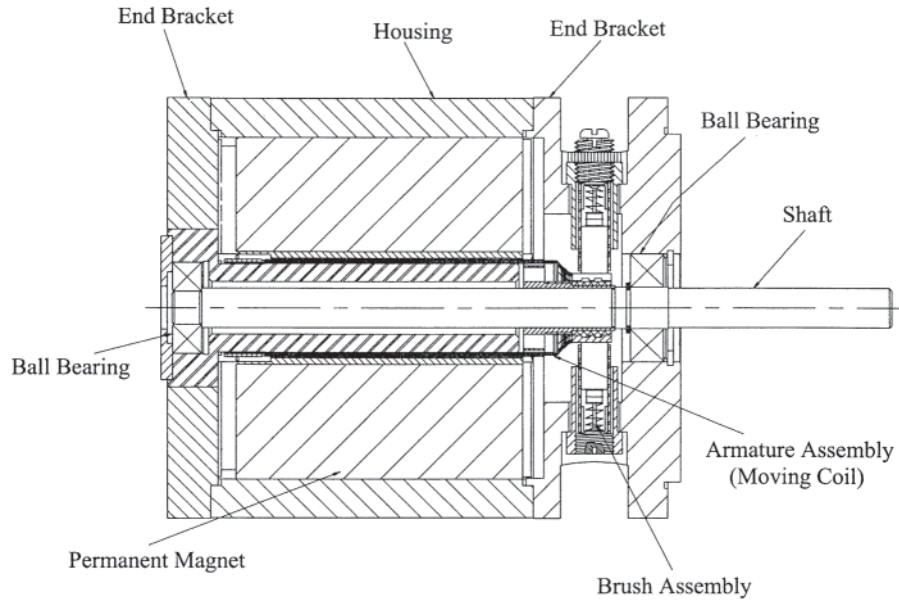


**Figure 2.58** Cross section—ironless armature motor. (Courtesy of Windings Inc., New Ulm, MN.)

Rearranging Eq. 2.106 and bringing  $R_a$  outside the resulting radical:

$$I_m = \frac{1}{\sqrt{R_a}} \sqrt{\frac{\theta_{\max}}{R_{th}} - (T_f \omega + D \omega^2)} \quad (2.107)$$

The developed torque may now be obtained by multiplying both sides of Eq. 2.107 by  $K_t$ , yielding:

$$T_a = K_t I_m = \frac{K_t}{\sqrt{R_a}} \sqrt{\frac{\theta_{\max}}{R_{th}} - (T_f \omega + D \omega^2)} \quad (2.108)$$

The shaft output torque  $T_o$  is obtained by subtracting the internal motor torque losses from the developed torque, so that:

$$T_o = T_a - T_f D \quad (2.109)$$

Combining Eqs. 2.108 and 2.109:

$$T_o = \frac{K_t}{\sqrt{R_a}} \sqrt{\frac{\theta_{\max}}{R_{th}} - (T_f \omega + D \omega^2)} - (T_f + D \omega) \quad (2.110)$$

Another constant,  $K_m$  is usually specified for servomotors. This is called the *motor constant* and is equal to the torque divided by the power loss in the armature ( $I_a^2 R_a$ ).  $K_m$  is also equal to  $K_t / \sqrt{R_a}$ .

### 2.3.9.4 Temperature Effects

Because the developed torque  $T_a$  is inversely proportional to the square root of the armature resistance  $R_a$ , the actual armature resistance at the maximum allowable armature temperature must be used to calculate the maximum continuous torque. Based on the value of  $R_a$  at 25°C, the armature resistance value can be calculated using:

$$R'_a = \frac{R_a(\theta_a + 234.5)}{259.5} \quad (2.111)$$

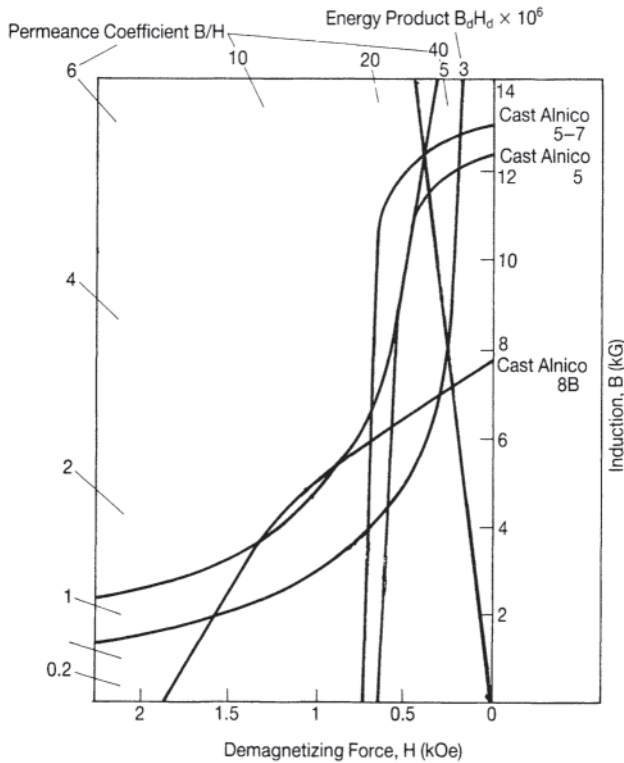


**Figure 2.59** B-H curves for various Alnico alloys.

where:

$R_a$  = armature resistance at 25°C ( $\Omega$ )

$R'_a$  = armature resistance at the maximum allowable temperature ( $\Omega$ )

$\theta_a$  = maximum allowable temperature ( $^{\circ}\text{C}$ ).

An increase in armature temperature of 130°C (to a final temperature of 155°C) results in an armature resistance equal to 1.5 times the resistance at ambient temperature, and a reduction in developed torque of 18.4%.

The developed torque is also affected by changes in magnet temperature, which may degrade the torque constant  $K_t$ , since the constant is usually specified at a temperature of 25°C. Typical  $K_t$  reduction factors are as follows:

Magnet Type	Temperature Coefficient
Ferrite	0.2%/°C
Neodymium-iron	0.11%/°C
Samarium-cobalt 1–5	0.045 %/°C
Samarium-cobalt 2–17	0.025 %/°C
Alnico	0.01%/°C

The variation in magnetic flux is dependent upon the actual temperature to which the magnet is subjected. For instance, in an iron armature structure, the magnet is located in the outer shell. In this case, the magnet is subjected to a heatgenerating source at its inner radius with the outer surface at the ambient temperature. When the magnet material is ferrite, it has been empirically demonstrated that the actual magnet temperature rise is approximately 50% of the armature temperature rise because of the poor thermal conduction characteristic of the magnet material. If neodymium-iron material is used, the magnet temperature rise is approximately -70% of the armature temperature rise. In the case of the ironless armature motor, the temperature rise of the armature is so rapid because of the small thermal mass) that there is a minimal instantaneous effect on the magnet temperature.

For an iron armature motor with ferrite magnets and an armature temperature rise of 130°C,  $K_t$  would be 13% less than at ambient temperature ( $130^{\circ}\text{C} \times 0.50 \times 0.2\%/^{\circ}\text{C}$ ). Combining this effect with the 18.4% reduction in torque due to the change in armature resistance determined above, the total developed torque with 130°C rise would be only 71% of the torque at ambient temperature. For an ironless armature design using Alnico magnet material,  $K_t$  is decreased by only 0.13% ( $130^{\circ}\text{C} \times 0.10 \times 0.01\%/^{\circ}\text{C}$ ). The developed torque is reduced to 81.5% ( $0.9987 \times 0.8162$ ) of the ambient temperature torque.

For a brushless motor with internal rotor structure, the stator housing, stator winding, and rotor magnet are closer to the same temperature. Therefore, the temperature coefficient of the magnet, for worst case analysis, can be applied directly to the winding temperature to determine the reduction in  $K_t$ . Thermal measurements of a model, of finite element analysis, are recommended to determine the temperature coefficient of a particular motor design. For example, a brushless dc motor employing samarium-cobalt magnets of the 2–17 variety would have a  $K_t$  multiplier of 96.75% for a 130°C rise. Hence the developed torque would be 79% ( $0.9657 \times 0.8162$ ) of the ambient temperature torque.

The numerical calculations above are all examples of calculation of the magnet/resistance temperature derating factor,  $k$ . That factor and the factor  $K_m$  (defined just below Eq. 2.110) may now be used to rewrite Eq. 2.110 as:

$$T_o = K_m k \sqrt{\frac{\theta_{\max}}{R_{\text{th}}} - (T_f \omega + D\omega^2) - (T_f + D\omega)} \quad (2.112)$$

This equation states that the available torque from a motor depends on the operating temperature and the thermal resistance of the motor, the thermal characteristics of the magnet material, the frictional losses, and the velocity-dependent losses of the motor. It is important to note that the velocity-dependent losses vary as the square of the velocity. This demonstrates why a motor that performs satisfactorily at rated speed may burn up if the speed is doubled.

Manufacturers of ironless armature motors specify a maximum voltage rating when characterizing the motor. The value will be low enough that, if the motor is stalled, the armature resistance will limit the current (to a value that will not demagnetize the magnet, nor will it cause the motor to self-destruct by overspeeding when operating at no load.

Another precautionary note is that, because the windings are not embedded in or surrounded by iron, the thermal time constant is relatively short. This should be accounted for when calculating the RMS current, then compare it to the rated current.

### 2.3.9.5 The Disk Motor

The disk motor is an ironless armature motor with an axial air gap. Motors using this construction have another set of performance tradeoffs. Since the torque per turn of the armature winding varies directly with the radius of the armature, doubling the radius double the developed torque. In addition, doubling the radius allows more wire turns, thus increasing the torque further. The performance tradeoff is that the inertia varies by the square of the radius, so if acceleration is important to the application, this may be the deciding factor. The other tradeoff is that the axial air gap motor will be shorter, but larger in diameter.

### 2.3.9.6 Rare Earth Magnets

MCMs are also designed using rare-earth magnets, but certain tradeoffs also occur. Because considerably less magnet length is needed, the overall diameter of the motor is reduced, but the length is the same. This results in a reduction of the surface area, which dissipates heat, thus lowers the continuous rated current. If the motor is air cooled, or of sufficient torque anyway, this may be of no consequence. Flux loss at higher temperature is greater with the rare-earth magnets than with Alnico, especially neodymium-iron-boron. And as the price of rare-earth magnets is declining faster than Alnico, a price advantage may be realized (see Fig. 2.60).

### 2.3.9.7 Application Considerations

There are several types of move profiles to be considered in the application of these servomotors. A typical move profile



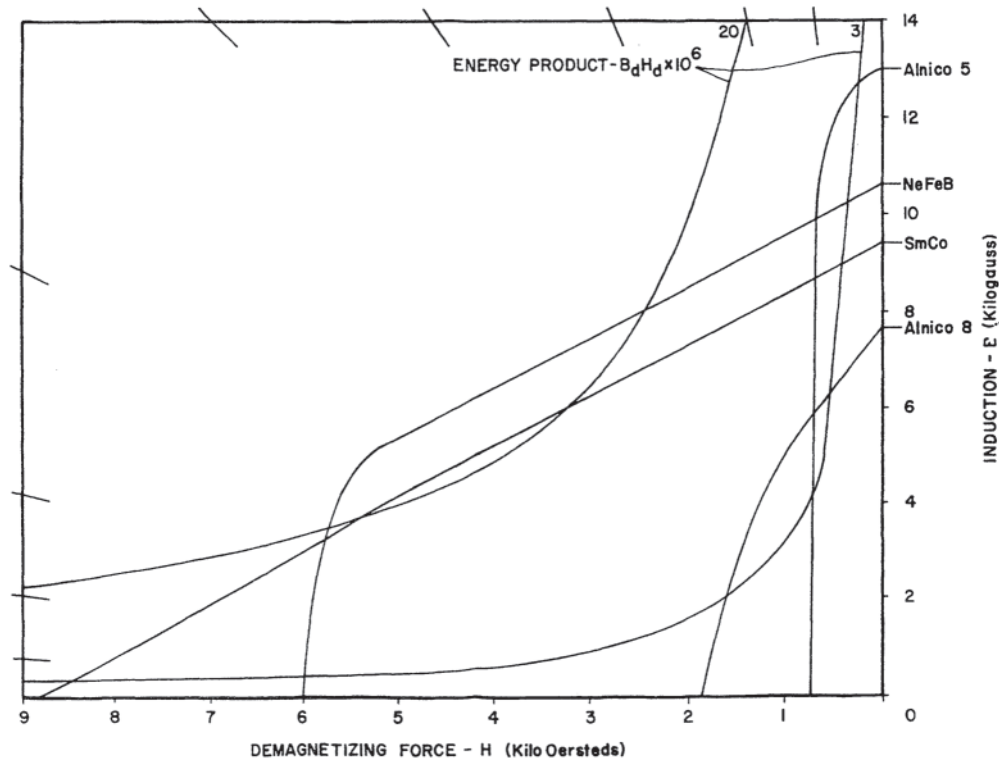


Figure 2.60  $B$ - $H$  curves for comparison of rare-earth magnets with Alnico magnets.

is usually made up of one or more of the following types of motion: precise velocity, constant acceleration/deceleration (torque), driving a load torque, or a combination to obtain accurate positioning. These profiles are obtained by putting the system in what is commonly called the velocity mode or the torque mode. A combination of both is used, with feedback, for accurate positioning in the minimum time.

MCMs are capable of following most profiles providing there is enough torque, low enough total inertia, the correct feedback, current, voltage, and the system rigidity previously mentioned. The MCM is capable of following virtually any command, but if the feedback signal is not precise, the desired motion will not be accomplished. A single, or combination of, appropriately precise feedback devices must be selected to detect velocity and/or position.

The equations will demonstrate that velocity is proportional to voltage, and torque is proportional to current. This means that the peak speed and peak torque must be known or estimated to determine the voltage and current requirements of the amplifier. It must also be noted that there are other motor constants, such as mechanical and electrical time constants, inductance, and rotational losses, which would enter into a precise simulation, but have a negligible effect when sizing a system. For the purpose of this discussion, they will not be covered.

Three related motor constants are significant when calculating for velocity or torque. The bmf constant ( $K_B$ ) governs velocity. It is the counter electromotive force generated by velocity, measured in volts/KRPM (volts/

thousand RPM). The torque constant ( $K_T$ ) governs the torque produced. It is the ability of the motor to convert current into torque, measured in oz. in./amp. A motor with a high  $K_B$  will have a proportionately high  $K_T$ . If the  $K_B$  is high, more voltage is required to reach velocity, but less current is needed to create torque. The bmf and  $K_T$  are proportional to the magnetic field, number of conductors, and their radius of rotation in the magnetic field. The terminal resistance ( $R_T$ ) is the effective or dynamic resistance of the total rotor circuit. It includes resistance of the conductors, brushes, and brush contact. The conductors' resistance is a function of their length, diameter, conductivity, and number in the circuit. It should be noted that as the armature warms up, the resistance increases by the temperature coefficient of resistance of the conductor (Cu or Al). At a maximum rated armature temperature of 155°C, the armature resistance is approximately one and one half times the terminal resistance at room ambient temperature (25°C). In this event, the power supply must have enough "headroom" to increase the voltage to maintain the desired speed. A combination of the motors' windings and the amplifier outputs are selected to optimize the system.

A popular motor that will be used in this discussion has the following performance specifications:

$$\begin{aligned}
 K_B &= \text{bmf Constant} = 6.73 \text{ V/KRPM} \\
 K_T &= \text{Torque Constant} = 9.1 \text{ oz. in. /Amp} \\
 R_T &= \text{Terminal Resistance} = 0.89 \text{ W (room ambient Temp.)} \\
 T_F &= \text{Friction Torque} = 4 \text{ oz. in.} \\
 J_R &= \text{Rotor Inertia} = 0.00047 \text{ oz. in. sec}^2
 \end{aligned}$$

$$\begin{aligned} T_R &= \text{Rated Torque}=60. \text{ oz. in.} \\ T_P &= \text{Peak Torque}=500. \text{ oz. in.} \\ I_R &= \text{Rated Current}=6.6 \text{ Amps} \end{aligned}$$

**Acceleration Rate** This motors' principle of moving only the torque-producing member (the coil assembly), is why the inertia is the lowest possible for the same diameter rotor. When combined with a magnetic circuit that will not demagnetize from high pulse currents, a motor is created with an ultra high acceleration rate capability. Using the formula:

$$\text{Acceleration}=\text{torque}/\text{inertia} \quad (2.113)$$

The resultant rate of acceleration is over 1,000,000 rad/sec<sup>2</sup>. When a reasonable load, of equal inertia is attached, the rate of acceleration is halved, but remains ultra high. The time to reach speed with these motors is commonly measured in single digit milliseconds.

The motor's armature construction is such that the fiberglass/epoxy composite results in a cylinder of extremely high torsional and lateral rigidity. This delivers a "stiff torque to the load that is needed for controlled, high acceleration rate applications. This high, stiff torque cannot be properly utilized unless the attached load and feedback components are proportionately rigid. The load should be attached as close to the motor face as possible and coupled to eliminate any windup between motor and load. Feedback devices should also be of extremely low inertia and rigidly attached. This keeps the total system's resonant frequencies high enough for the controllers closed loop to properly control the motion at the load.

**Velocity** MCMs are excellent for smooth, accurate speeds from zero, to over 5000 rpm. Because they exhibit virtually no torque ripple, they are uniquely suited for very low speeds; below 60 rpm. This low speed range is where the typical motor, with Iron as a rotating member, inherently produces undesirable torque ripple. There are relatively complicated, expensive (electronic and mechanical) ways to reduce torque ripple in a motor with rotating iron, but it is a "free" aspect of the MCM motor.

The preferred feedback device for monitoring speed is a moving coil tachometer. This device is constructed in a similar manner as the motor, adds insignificant inertia, and is integrally mounted to the motor shaft. The signal is pure to less than 1% ripple, and less than 0.2% deviation from true linearity.

The steady-state velocity is directly proportional to the dc voltage applied across the motor terminals. This applied voltage is divided between counteracting the motors generated bmf and overcoming the armature resistance to generate torque equal to the friction and load. The armature resistance is low, so generally when the speed is over 1000 RPM, and the load torque is light, most of the applied voltage is used to counter the bmf. The applicable formula for deriving voltage is:

$$E=N*K_B+T_T*R_T/K_T \quad (2.114)$$

where:

$$\begin{aligned} E &= \text{DC Voltage at the terminals (volts)} \\ N &= \text{The steady state velocity (RPM)} \\ T_T &= \text{Total system torque (oz. in.)} \end{aligned}$$

A typical high-speed application may require a minimum of 5000 rpm; have 48 V dc available and a load friction of 20 oz. in.

Using the example motor and the formula for steady-state speed:

$$\begin{aligned} E &= (5 \text{ KRPM} * 6.73 \text{ V/KRPM}) + (24. \text{ oz. in.} * 0.89 \\ &\quad \text{Ohms}) / (9.1 \text{ oz. in./Amp}) \\ E &= 35.9 \text{ volts} \end{aligned} \quad (2.115)$$

If the maximum rated armature temperature is reached, the terminal resistance would increase by 50%, and the required voltage would be 37.1 V dc. The analysis shows that the required speed is obtainable with the 48 voltage provided even at maximum motor temperature.

**Torque** The MCM's extremely low rotor inertia and high pulse torque capability (5 to 8 times rated) provide the highest acceleration rate possible for a servomotor. This same instantaneous pulse torque can be critical to overcome uneven load torques such as static or dynamic friction. The basic formula to derive motor torque for a given current is:

$$T=K_T*I \quad (2.116)$$

where:

$$\begin{aligned} T &= \text{the torque produced by the armature for a given} \\ &\quad \text{current input, (oz. in.)} \\ I &= \text{Current input (amperes)} \end{aligned}$$

If the move profile involves acceleration, the torque required for acceleration is:

$$T=J_T*\alpha \quad (2.117)$$

where:

$$\begin{aligned} T &= \text{The torque required to accelerate the load inertia} \\ &\quad \text{(oz. in.)} \\ J_T &= \text{Total inertia including the motor and the load (oz.} \\ &\quad \text{in. sec}^2\text{).} \\ \alpha &= \text{Acceleration rate (rad/sec}^2\text{)} \end{aligned}$$

Usually, when sizing a motor and amplifier, the acceleration rate and load torque are known, and the current must be derived. The formula to derive the required current is:

$$I=(J_T*\alpha+T_L+T_F)/K_T \quad (2.118)$$

where:

$$\begin{aligned} I &= \text{Current required (Amps)} \\ J_T &= \text{Total motor and load inertia (oz. in. sec}^2\text{)} \\ \alpha &= \text{Acceleration rate (rad/sec}^2\text{)} \\ T_L &= \text{Load torque (oz. in.)} \\ T_F &= \text{Friction torque including the motor (oz. in.)} \end{aligned}$$

When the current available is fixed (by motor rating or amplifier), but the resulting acceleration rate is desired, the formula can be rearranged as:

$$\alpha=(K_T*I-T_L-T_F)/J_T \quad (2.119)$$

A typical high acceleration rate application may require 250,000 rad/sec<sup>2</sup> with a load inertia equal to the rotor, load

torque of 40 oz. in., and 40 amps available. If the example motor is used in the formula for current:

$$I = \frac{((0.00047 \text{ oz. in. sec}^2 + 0.00047 \text{ oz. in. sec}^2) \times (250,000 \text{ rad/sec}^2) + 40 \text{ oz. in.} + 4 \text{ oz. in.})}{(9.1 \text{ oz. in. /Ap})}$$

$$I = 30.7 \text{ A} \quad (2.120)$$

The motor chosen is capable of a pulse current of 57A, so the desired acceleration rate is possible.

### 2.3.9.8 Summary

The MCM is often considered when the highest acceleration rates are desired. Typical applications include X-Y tables, incremental positioning, laser beam control, movie film handling, simulators, semiconductor, manufacturing, component placement, cut to length, loudspeakers, and mirror drives.

When accurate positioning and/or speed control is important, the absence of torque ripple and infinite resolution make the MCM an effective solution. Typical applications include film processing, tape drives, welding, EDM, object tracking, measurement/instrumentation, medical dispensing, medical analysis, and micromachining.

As manufactured products are becoming smaller, made at faster rates, with dynamic motions more precise, the MCM may be the best solution.

## 2.4 ELECTRIC TRACTION

Electric traction is the propulsion of vehicles with electric motors. They operate on the same basic principles as machines for other applications, but are used in environments and under conditions that are imposed on few other machines. For example, traction motor speed varies from standstill to top speed and the torque varies widely and may do so at any speed. When used for rail vehicles they can be subjected to dirt, leaves, trash, and snow along the railway. Some vehicles obtain their power from third-rail or trolley supply systems that are frequently interrupted (with consequent current surges upon regaining contact) and that certainly do not have constant voltage. Others are supplied from onboard engine-powered generators or from batteries; in these cases knowledge and proper use of the characteristics of the power sources are vital. The technology of electric traction is the understanding of the applications and how to design, manufacture, and apply electric machines that will survive and perform well under these uniquely arduous conditions.

The traction industry has a long history of specialized practice and, as a result, retains the English system of units. (The British traction industry was exempted when metrication was edicted there). Moreover, it has a vocabulary that includes terminology that may not be familiar to the unaccustomed user. One such word is adhesion, meaning the coefficient of friction required between the driving wheels and the running surface to carry the tractive effort of interest. A vehicle is said to be “motored to adhesion” when the traction motors will rate continuously all the tractive effort that maximum available adhesion will support. The available adhesion depends on the weather and many other factors; it always decreases as speed

increases. For rapid transit cars having every axle motored, about 5% adhesion is required for each 1 mph/sec of accelerating rate. A dc locomotive can typically attain 28–30% adhesion and an ac locomotive in the range of 33–35% adhesion on clean, straight rail. On rubber tired vehicles adhesion is not a factor of concern. A few more terms unique to traction:

- **Property**—A system of physical facilities and vehicles under one management.
- **Horsepower utilization**—Percent of maximum vehicle speed to which rated engine horsepower is available at the wheels (applicable only to internally powered vehicles).
- **Hotel power**—Power for amenities not involved in moving the vehicle, i.e., air conditioning, lights, heat, etc.
- **Off-highway vehicle (OHV)**—For electric transmissions these are typically large dump trucks used in open pit mining with payloads in the 150–320+ ton range.
- **Speed ratio power**—The continuous rated power output of a traction motor at its continuous rating multiplied by its maximum speed capability at rated power divided by its speed at its continuous rating (see [Section 2.4.4.8](#)). A measure of traction motor capability.
- **Consist**—A group of two or more locomotives pulling a single train.
- **Wraparound (internally powered vehicles)**—The ratio of maximum to minimum volts, amps, speed, or torque that can be maintained continuously (i.e., without overheating) at full power. The size of the machine will be proportional to its wraparound.

DC series wound machines have been the motors of choice for traction in the past because of their desirable inherent characteristics. Four pole, lap wound machines are the almost exclusive choice. Two-pole machines require too much length for endturns and the total armature current would have to be handled by one brush holder (hereafter abbreviated, BH). Due to design limitations on the thickness of the brush this could lead to a very long axial commutator length. Six-poles and higher, although not unheard of, would involve a lot of extra complication and cost (more BHs, poles, etc.). In new applications, however, three-phase inverter-driven induction motors with characteristics determined by control logic are prevalent. This trend is expected to continue, as total equipment life-cycle cost falls below that of dc drives. AC traction alternators with diode rectifiers have supplanted d' generators for all but the lowest power applications. AC auxiliary machines are supplanting dc machines as they become feasible on a case-by-case basis.

The main advantage of the ac induction motor is the elimination of the commutator and brushes and all of the associated maintenance concerns. Also, by moving the commutation function from the motor to that inverter, the case can be made that a more powerful motor can be put into the same space (see [design considerations](#)).

In addition to classification of traction motors, traction generators, and auxiliary machines as dc or ac, they may also be classified by their power source as externally powered, powered from onboard internal combustion engines, or powered

from a battery or combinations of the three (hybrid vehicles). Each of these categories is discussed in a following subsection.

Wherever economics govern, electric traction is used where it works better than the alternatives. The role of electric traction has changed and may be expected to continue to change not only with its own development but also with the development of alternatives. Its use may be driven by overriding environmental needs for clean energy, as in some locations, or just because it works better than the alternatives.

The differences in practice in various parts of the world are not only due to technical preferences, but they also reflect government policies and participation based on differing cultural, sociological, economic, and political customs and values. For example, electric traction for passenger service is utilized much more in Europe than in the United States as affected by the price of gasoline, the availability automobiles, and good road systems and government subsidies.

High-speed intercity ground transportation for passengers has been proven technically feasible in several forms. Attaining higher schedule speed on existing rail lines requires the least investment. The Northeast Corridor running between New York (and later Boston, Massachusetts) and Washington, D.C., is the most heavily traveled in the United States. A section of track was upgraded for testing, and multiple-unit externally powered trains demonstrated 150 mph capability. The equipment was put into service and schedule time has been reduced. However, the full capability has not been realized because of limited track upgrading, grade crossings for which speed must be reduced to 70 mph, and routing that snakes from track to track through other traffic with speed reductions at turnouts. The gearing has been changed to 125 mph capability. Between New York and New Haven, Connecticut, the total of all curves amounts to the equivalent of some seven complete circles. The line was electrified north of New Haven in 1999, so locomotive-hauled trains are not required anymore there. Germany's 200 km/h capability locomotive-hauled externally powered trains, British Rail's "125" (mph capability) dieselelectric services, and Canada's Montreal to Toronto trains are other examples of moderate improvement of schedule with new equipment on existing trackage. Japan's bullet trains use new high-quality trackage with 1435 mm gage to make dramatic improvement in schedule speed. (Japan's standard track gauge [width between rails] is 1067 mm [42 inches].) France's TGV trains have also made dramatic improvement in schedule speed on dedicated trackage built with another idea because no freight is to be hauled and the externally powered locomotives have plenty of power, grading of the roadbed was minimized, with considerable cost reduction. Their high-speed trains can use existing terminals. The reasons that high-speed intercity passenger ground transportation has or has not developed are economic and political.

## 2.4.1 Externally Powered Vehicles

### 2.4.1.1 Introduction

An externally powered vehicle gets its electric power from outside itself. Power is generally taken from a wayside contact system by a collector mounted on the vehicle. The

requirements of the application determine how good the collector and contact system must be. The collector and contact system characteristics greatly affect the voltage regulation, interruptions, and other transients that affect the design of motors operated from them.

External power supply gives vehicles major performance advantages. The power delivery capability of the supply is large compared to the continuous rating of the traction motors on any one vehicle or train. Excess power may be drawn within the short time ratings of the motors. Acceleration at full rate can be carried to higher speed, knowing that power demand will be below continuous rating at running speed. Schedule speed is boosted. Applications involving hill climbing can use the excess power to climb the hill faster. These performance advantages are readily apparent in a comparison of a properly equipped trolley coach with an internally powered bus.

Outdoor overhead contact wire systems usually have nominal system voltages of 600, 750, 1500, or 3000 V dc or 11–50 kV single-phase ac. The lower dc voltages favor the traction and auxiliary motor designs but require close substation spacings; they are optimum for intensive services. The higher dc voltages reduce contact system cost at the expense of making the motors bigger, heavier, and more expensive. High-voltage ac contact wire systems put the final substation transformer on the vehicle and are optimum for the extensive services of main line electrification.

Third-rail contact systems supply power through steel rails, usually alongside and somewhat higher than the running rails. Third-rail shoes, usually four per car, are mounted on insulating beams on the trucks. This system is optimum for highplatform subways, as it is out of reach of passengers in normal operation and no tunnel dimension need be increased for it. It is unsuited to services having street running or frequent grade crossings. While shoes on both sides of the car give some freedom in physical arrangement of the third rail, gaps occur at most switches and crossings. In the real world, with low and high third rail and broken shoes, motors running on these systems experience frequent power interruptions.

Collecting from one contact system with the return through the running rails has wide acceptance. The trolley coach with its dual overhead wires in the absence of steel rails also has one circuit. Although it has often been tried, collection of polyphase ac has not been reliable enough to be acceptable in high-speed service. In some low-speed (30 mph maximum) applications it has worked, for example the Personal Rapid Transit (PRT) system used to connect the campuses at West Virginia University in Morgantown, West Virginia, runs off a 575-V three-phase supply from power rails mounted at tire level, transformed down to 355-V ac on the vehicle. A compound-wound dc traction motor is motored with a combination of armature voltage (from a phase controlled rectifier) and shunt-field control.

Contact systems have wide voltage regulation compared to industrial practice. For example, for a nominal 600-V dc system, IEEE Std. 11 [46] gives 400 V minimum and 720 V maximum. These are steady-state conditions; usually, though, extremely low voltage is limited in time and extent. A vehicle would be expected to travel through a very low-voltage section in a moderate time. Sustained high voltage is most likely late

at night and close to a substation, where vehicles are likely to be parked; auxiliary motors are affected most.

In dynamic braking, traction motors are used as generators to retard vehicles. This limits wheel and brake shoe heat and wear while holding heavy loads on favorable grades or while slowing vehicles that stop frequently. Rheostatic braking is dynamic braking in which the absorbed energy is dissipated as heat in resistors. It is widely used on mass-transit, light rail vehicles, and internally powered vehicles. For the mass-transit application (short time and intermittent) air flow over the vehicle suffices to cool the resistor grids. On internal powered vehicles such as locomotives or OHVs, which can have sustained periods of retarding, the grids are typically cooled using blowers driven by dc series wound motors. This is one application where the dc motor has a unique niche, unlikely to be replaced by ac. The dc blower motor unit is self loading and designed to reach its maximum blower speed at maximum grid amps and is tapped across (put in parallel with) some portion of the grid resistor such that it will obtain the correct voltage. The beauty of this arrangement is that no control system is required since the blower motor unit operates automatically whenever power is applied to the grids—and it also uses waste power. In regenerative braking, power is returned to the line. While transit cars in principle can return energy to the line when stopping, the process has many limitations depending on the line's ability to receive power. Therefore, a full rheostatic braking system is also needed, for the foreseeable incidents when the line will be unreceptive.

Substations are generally spaced as far apart as can be tolerated. At times the system must operate with a substation out of service. Because of the separation of the conductors and the distance from the substation, contact systems have considerable inductance. Whenever a vehicle or train shuts off traction power, the line and vehicles on it see an inductive spike. On a 600-V dc system, spikes having a millisecond duration have been recorded as high as 3000 V. Traction equipment must be designed to withstand such conditions; again, the auxiliary dc motors are most affected by this high voltage. Inductive reactance is the primary line drop on high-voltage ac systems due to the great separation of the overhead catenary from the return and the long distance between substations.

In summary, it is seen that the application of motors on vehicles receiving their power from an external supply is different from any other. The supplies are more than soft; they inherently have wide regulation and severe transients.

#### 2.4.1.2 Main Line Electrification

While most railroads have been electrified in developed countries, especially so in Europe and Japan, only a few were electrified in the United States and Canada. Of those few, the lines in the Northeast Corridor are the only important ones that remain. This is directly related to the propensity of different governments and societies to subsidize this kind of service. Historically electrification with high-voltage single-phase ac had to be accompanied by methods that used ac for traction before the advent of high power electronic switches for inverters or converters.

Hence the development of the low-flux single-phase traction motor made high-voltage ac electrification possible. These were dc motors with a well laminated magnetic circuit that would run on low frequency ac. One drawback of these motors was that the alternating field current transforms ac voltage into the armature coils, upsetting commutation. The resulting heavy sparking can be tolerated in the small “universal” motors used in household appliances and tools but not in large traction motors. The recourses in motor design to minimize the transformed voltage were the use of low flux per pole and low frequency. In Europe, one-third of the commercial frequency of 50 Hz,  $16\frac{2}{3}$  Hz, became the railroad frequency at 15 kV. Two-phase 25 Hz, already in use as a commercial frequency, was chosen in the United States. Single-phase generation was avoided because of vibration. Two phase could be transmitted to transformers at a section break from which one phase powered the line at 11 kV in each direction.

The low-flux single-phase traction motor, having low flux per pole, had to have many poles and be a low-voltage highcurrent motor. Many poles meant many brush holders to carry the high current. It had to be designed as an excellent dc motor from the beginning, lap-wound with pole face compensating windings and low saturation. The motors were big, heavy, and had many brushes to maintain but proved to be reliable. The locomotives could not be motored to adhesion and thus were not good at heavy drag freight service. They were a good fit for intensive passenger service and the lighter tonnage dispatched freight trains typical of the Northeast Corridor. The European coupler design does not permit the long, heavy drag freight trains used in American practice, so the ac motor was a fit everywhere.

Developments in the 1960s and 1970s in the United States and Europe proceeded in different directions. In the United States it was recognized that a considerable advance had occurred in the state of the art in dc traction motors for diesel-electric locomotives and 600-V suburban cars. If these kinds of motors could be used for locomotives and cars for ac railroads, the advantages of large-scale production could be realized. The size, weight, cost, and maintenance savings were attractive. Rectifier equipments were developed, first with mercury arc rectifiers and then solid state. After continued development, rectifier equipments with dc traction motors became the norm in the United States.

In Europe, parallel development was limited. Small quantities of rectifier equipment were developed, sometimes to create locomotives that could pull intercity passenger (IC) trains on supplies of 1500- and 3000-V dc as well as 15-kV 16t Hz and 25-kV 50 Hz. Diesel-electric locomotive production was small and specialized. Commuter car motors remained axle hung (low performance). The traction motors were still big, heavy, special, and expensive, whether ac or dc.

By the early 1980s the inverter-driven ac induction motor drive was in experimental use in Europe. For example, in 1981 a switching locomotive was shown that had been retrofitted from single-phase traction motors to inverter-driven induction motors with a dramatic reduction in motor size, weight, and complexity. Therefore, there was a definite reason to press the

state of the art to put the inverter drive to use in Europe. In the United States, no such need existed. Rectifier equipments using standard dc diesel-electric locomotive and commuter car traction motors remained the standard until the 1990s.

#### 2.4.1.3 Commuter Lines

Externally powered commuter cars were originally operated by electrified main line railroads in suburban service. Railroad passenger size cars are, as a rule, 85-ft long. In addition to being larger than mass-transit cars, in a commuter car the availability of seats is more important than a large number of doors. Several properties offer something between commuter and mass-transit-type services.

Commuter cars have long station spacings. Their acceleration rates are usually lower than adhesion could support because top speed matters more. The power demand of greater accelerating rate cannot be justified by the slight improvement in schedule speed. Acceleration current is maintained longer than in mass transit, making thermal excursions greater.

Dynamic braking may or may not be used. With higher car speed, the amount of dirt swirled up by the train is great. That dirt at times includes salt from grade crossings in winter and wet soil that cements brushes in their holders. It was learned on the first rectifier cars that self-ventilation of the higher-voltage dc traction motors and auxiliaries was a mistake. Since then, forced ventilation with clean air taken from above the platform and preferably at roof level has been used. Moreover, it was found that the entire ventilating air system needed to be reviewed carefully to assure good winter and wet-weather performance.

#### 2.4.1.4 Mass Transit

The New York City Transit Authority operates the largest passenger railway system in the world. Their fleet is approximately 5000 cars, approximately 10% of which are ac traction. Electrically propelled multiple-unit cars, in trains to ten cars long, provide more daily passenger miles than any other system. Other systems operating in the United States and Canada include those in Boston, Massachusetts, New York (Hudson tubes and some Long Island services), Philadelphia,

Pennsylvania, Baltimore, Maryland, Washington D.C., Atlanta, Georgia, Montreal, Toronto, Cleveland, Ohio, Chicago, Illinois, and San Francisco, California. There are a number of large systems around the world, including Tokyo, Seoul, Calcutta, Moscow, Berlin, London, and Madrid. Figure 2.61 shows typical mass transit cars.

These systems are often called subways, but they also may operate outside on private right-of-way and on elevated structures. Most use third-rail power supply, an optimum fit for tunnels. Cars vary from approximately 40 to 75 feet in length, as limited by curves.

With no standard car size and varying station spacings, propulsion motor requirements vary. Acceleration at 2.5 mph/sec and braking at 3.0 mph/sec have been found tolerable for standing passengers. The historic systems all use nominal voltages near 600-V dc, but some newer systems use higher voltages. It would have been to the advantage of both users and manufacturers if a few motor designs could have covered all applications. That would have been hard enough with a common voltage, but each new voltage required a new design for dc (see [design considerations](#)). Higher voltage designs were heavier and had limited dynamic braking capability.

Figure 2.62 through 2.64 show various mass-transit traction motors.

Single-reduction parallel-drive gearing minimizes weight and gear loss, but the physical constraints on its use are severe. Clearance of approximately 2.5 inches over the rails must be provided with fully worn wheels, limiting the size of the gear. The pinion should be small to provide adequate gear ratio, although there is a minimum diameter for adequate strength. The sum of the gear and pinion pitch-line radii is the gear center spacing, which must be the spacing between axle and motor shaft centers. DC motors are designed with the frame behind a main pole at the axle, so frame section may be reduced for axle clearance to maximize motor diameter. American practice generally uses higher speed motors than the rest of the world.

Most properties use inboard journal trucks and small wheels for weight savings, severely squeezing the space available for the traction motors and their gearing. An advantage is that

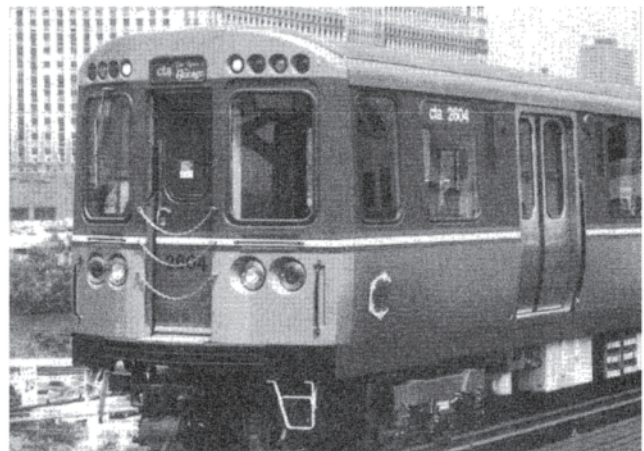
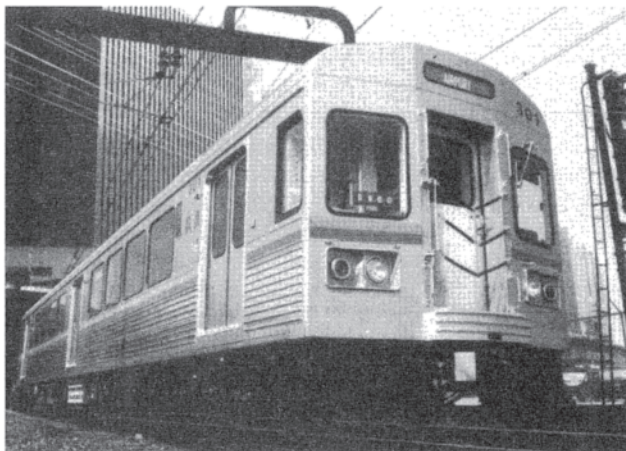
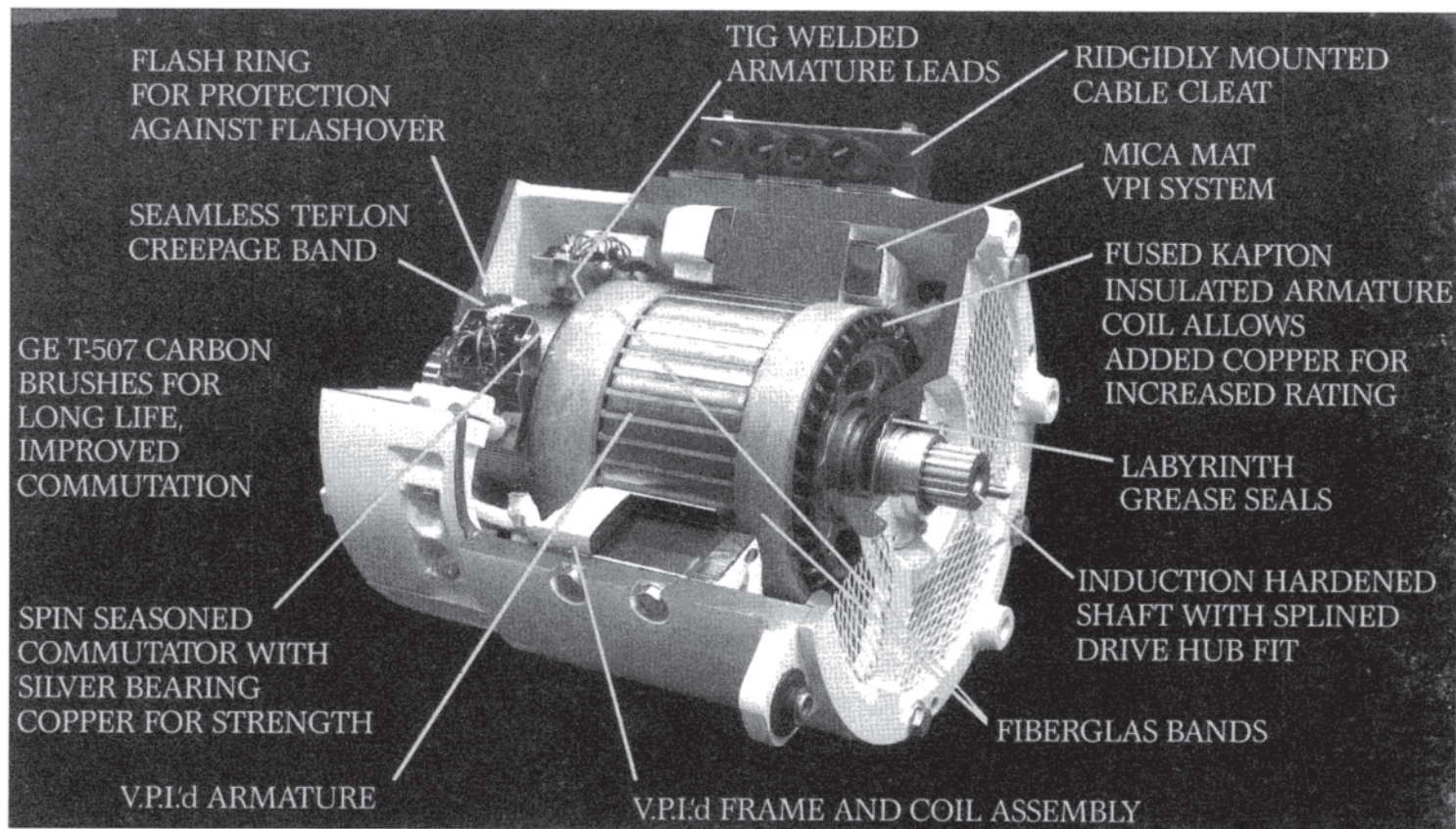
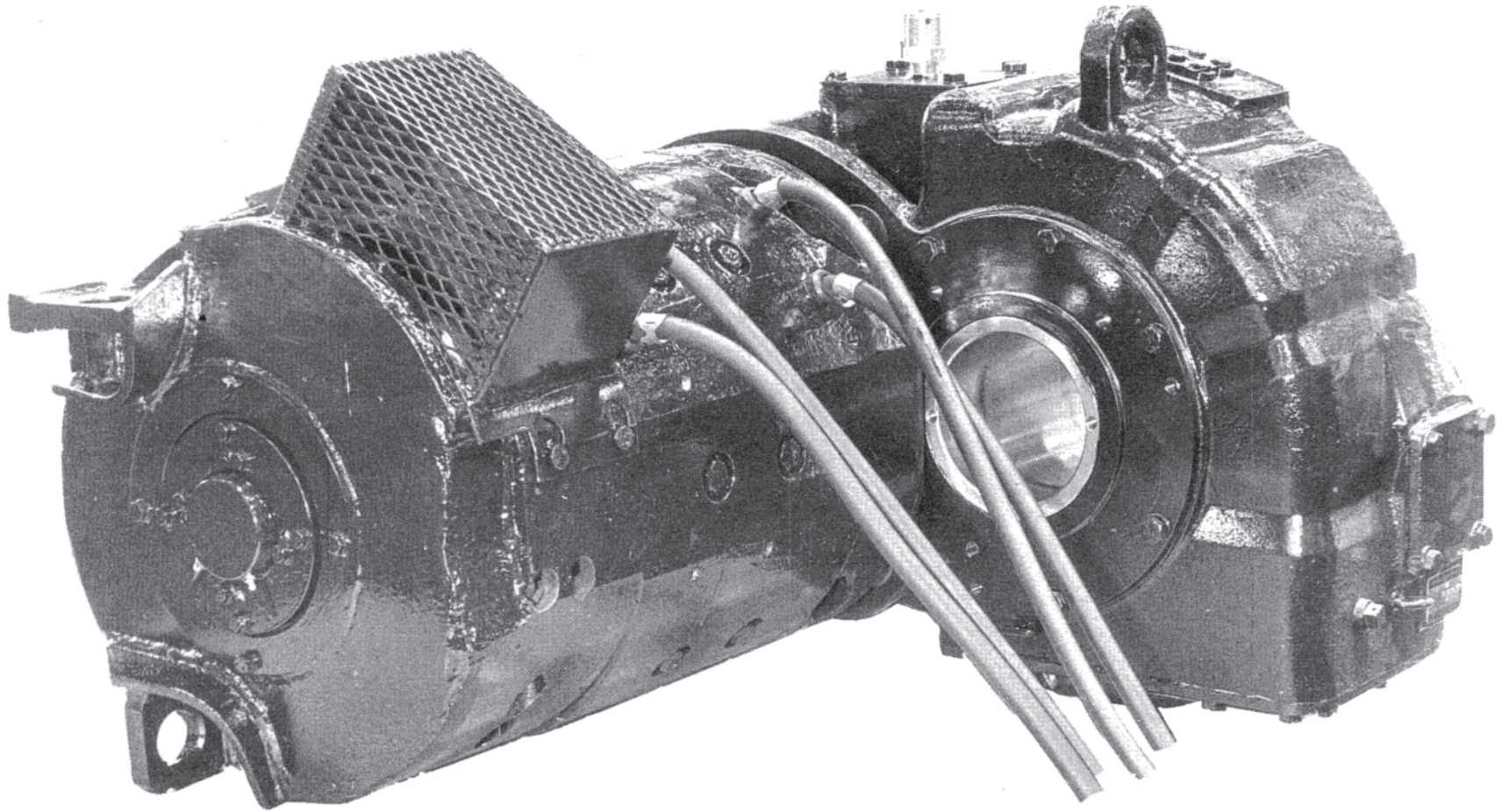


Figure 2.61 Mass-transit cars. (Courtesy of General Electric Co.)



**Figure 2.62** Cutaway view of a force ventilated dc mass-transit traction motor. (Courtesy of General Electric Co.)



**Figure 2.63** Self-ventilated dc traction motor and gear unit for lightweight mass transit car. Expanded metal box on top of motor provides increased air inlet area to decrease trash pickup. (Courtesy of General Electric Co.)



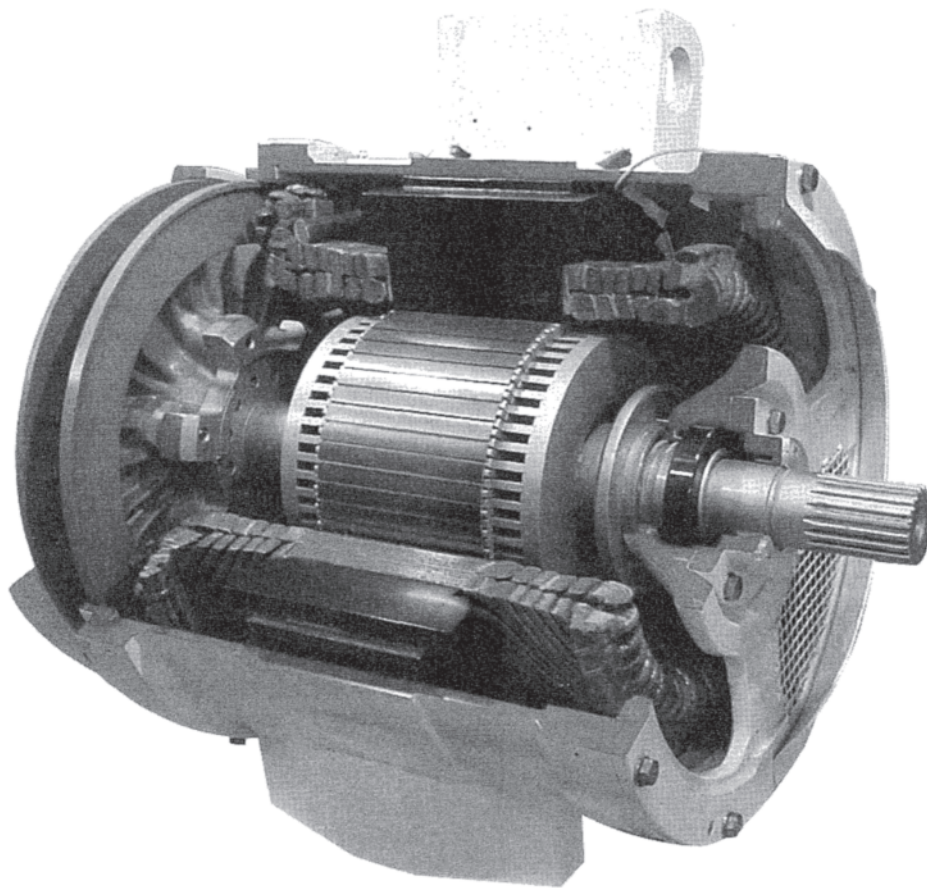


**Figure 2.64** Cutaway view of self-ventilated ac traction motor for lightweight mass transit car. Fan blades are randomly spaced and tips are recessed to reduce noise. (Courtesy of General Electric Co.)

smaller axle diameter may be used with the shorter axles. The hypoid gearing idea from the Presidents' Conference Car (PCC; see [Section 2.4.1.5](#)) development was used to position the motors at right angles to the axles. It was realized that the rubbing teeth would wear out but only much later was it realized that they consumed an added 3% of the power transmitted, more than negating the advantage of the weight saving. Alternatively, double-reduction helical gearing was used on other equipments; they consume an added 1.5% of the power transmitted. Oil-filled gear units have become universal. In American practice only the New York City Transit Authority continues to use outboard journal trucks and wheels large enough to fit their 7.235:1 ratio and 22 in motor with single-reduction helical gearing. In European practice some builders use a single-traction motor driving the two axles in one truck ("monomotor") through right-angle gear boxes. Most of the rest of the world continues to use outboard journal trucks, single-reduction gearing, and axle-hung traction motors.

Mass-transit cars generally use self-ventilated traction motors. With the swirling of the air due to train motion, the motors in effect vacuum clean the tracks. Performance requirements such as acceleration rate have been raised to the limits of passenger comfort, forcing the motor manufacturers to increase ventilation and take in more dirt. Even with the

best precautions by the manufacturers, the motors get very dirty. This is accepted by the operating properties as cheaper than using blowers with a clean air system. Maintenance instructions for dc motors call for wiping the brush holder insulators and commutator creepage band at brush inspection. Teflon\* is best for these creepage surfaces because its surface vaporizes under arc, will not track, and makes it difficult for dirt to stick. Epoxies are also used. Wiping the insulated windings is not possible at inspection, so the insulation system must be as unaffected by dirt as is possible. In New York City, it was necessary to drill the dirt out of the rotor axial air holes at motor overhaul. When a new design was required it was specified that it should not use rotor air passages. Replaceable filters can be used on the motor air inlets. To be at all effective, they must be replaced often. A few properties have chosen to add that maintenance expense to reduce the amount of dirt that gets into their motors.

AC traction is finally a reality in the United States. Being freed of design limitations on the shape of the rotor imposed on dc motors by commutation requirements, and free of the commutator itself, it allows a better arrangement of the traction equipment in the truck.

\* Teflon is a registered trademark of the Dupont Co.

For a much more thorough discussion of the design and application of traction motors for mass transportation, see “Propulsion Motor Requirements for Mass Transportation” [47].

#### 2.4.1.5 Light Rail

Light rail vehicles (LRVs) are a class of electric passenger cars used in metropolitan transit service. They are named for the light rail on which they run, as opposed to the heavy rail used by railroad commuter cars and long train subway systems. They may run as single, articulated, or multiple unit cars, but rarely over four cars in multiple. They may run on streets, reserved or unpaved lanes, or private rights-of-way at grade, in tunnel, or above grade. They collect power from overhead trolley wire systems that are nominally 600 V but occasionally reach 750 V or higher. They generally load and unload at low platforms or street level when running in the street. They are descendants of the electric street cars that used to run in every moderately large city. Major remnants never ceased operation in Boston, Massachusetts, Philadelphia, Pennsylvania, Toronto, Ontario, Pittsburgh, Pennsylvania, New Orleans, Louisiana and San Francisco, California. Many new LRV lines have been proposed and some are in operation.

The conference of the presidents of many properties operating in America sponsored the development of what came to be known as the PCC street car, beginning in the 1930s. Performance was intended to meet and exceed the internal combustion competition. The PCC had an accelerating capability (empty car) of 4 mph/sec, which could throw standing passengers to the floor if the operator was not judicious. They used sand to support the required 20% adhesion if needed. Magnetic track brakes were used to match the emergency stopping adhesion of rubber tires. There are still some of these in service as vintage vehicles, for instance in San Francisco.

The PCC trucks were inboard journal, an innovation that saved weight at the cost of truck space for the drive. The traction motors were nested at right angles to the axles, driving oillubricated hypoid single-reduction gear units. This allowed the motors to be a little higher than the axles, permitting smaller wheels and lower floors. Space in the trucks was very limited. The high-speed motors were round-frame, four-pole motors with four brush studs. They were force-ventilated with cleaned air, a first for street cars. The standard PCC had no compressed air on the car, eliminating the air compressor and other weight. Dynamic braking was the primary brake, so there was no protection in case a motor should flash over in braking. It was better that the motor be destroyed to stop the car than to protect the motor and leave the car without its primary brake. These small traction motors had to be designed to be exceptionally resistant to flashover. Even after a flashover that sustained itself until the car was almost stopped, the motor still had to have a high probability of continuing to perform normally after flashover.

In Europe, the sociological environment that made street cars obsolete in the United States did not prevail, and many operations remain and are being expanded. European streets are narrower and have tighter turns than those in America. Moreover, the cities are more compact, so shorter travel

distances are the norm. As a result, their cars are smaller than is appropriate in America.

The European articulated cars (and their American copies) have used nonpowered trucks, especially under the heavily-loaded joint of articulated cars. For equal performance, this increases the required adhesion on the powered axles. The leading axle often cannot support this performance, so performance has simply been reduced.

The European LRVs commonly use a truck and motor arrangement in which one motor with its shaft parallel to the rails drives the two axles of a truck through individual rightangle gear units. Because the two axles must run at the same revolutions per minute in spite of even microscopic wheel diameter differences, the motor shaft, couplings, and gear unit must run continuously at slip/grab adhesion. There are no known data on the extra losses involved. To brake one half a car on one commutator rather than two, the motor is bigger and has slower speed. Where performance requirements are less taxing, the single large motor can do the job.

AC traction is specified on all recent LRVs. When first applied using one inverter per truck (two motors) there was concern that driving two axles with one inverter would cause a wheel and rail wear disadvantage due to the possibility of unequal torque loading (see [design considerations](#)) but it has not proven to be a problem.

#### 2.4.1.6 Interurbans

The South Shore Line provides commuter rail service between Chicago Illinois, and South Bend, Indiana, and is operated by the Northern Indiana Commuter Transportation District. It calls itself the sole surviving true interurban line in the United States. It is not at all typical with its high floors and 1500V line (dictated by its use of the Illinois Central access to its Chicago terminal) and significant freight traffic. The concentrated commuter traffic between Chicago and Michigan City is truly a suburban railroad service. The street-running in Michigan City and private right-of-way to South Bend are more typical of an interurban line. Interurbans once tied together every major city in the eastern half of the United States from the East Coast well into Iowa.

The dc traction motors were four-pole, wave-wound for 750/1500-V operation (750 V per motor but insulated for 1500 V to ground, two motors in series per truck). The rms motor rating did not have to be high with the long spacing between stations. Many properties closed the motors during winter and opened them for ventilation the rest of the year. About half the fleet of 58 powered cars now utilize ac traction motors with plans to convert the remaining cars.

#### 2.4.1.7 Trolley and Hybrid Coaches

The trolley coach was developed to combine the advantages of the rubber-tired bus and the external power supply systems already in place for streetcars. The rubber-tired bus offers curb loading and maneuverability in traffic. The external power supply offers clean, quiet operation and the excess power needed for a short time to sustain acceleration, compared to the limited power available from an internal combustion engine.

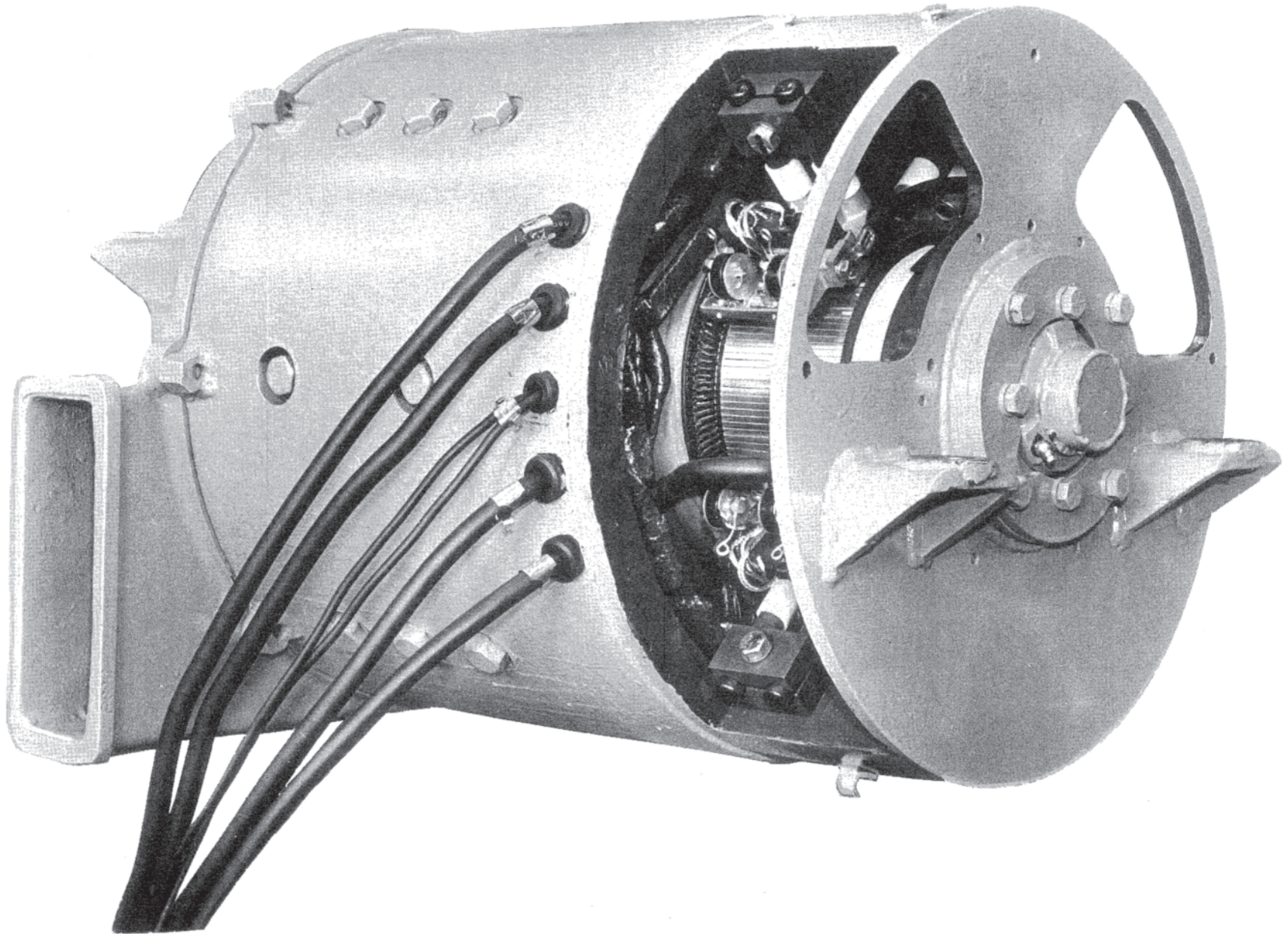


**Figure 2.65** Self-ventilated dc trolley coach motor. Fan is designed for single rotation (CW from comm. end). (Courtesy of General Electric Co.)

The trolley coach usually has only one traction motor (see Fig. 2.65) driving the rear wheels through a differential. In its fullest development, the dc motor is compound wound to give variable free running speed in city streets by pedal control of shunt field current. Regenerative braking is available as the motor becomes a differentially compounded generator. It is self-ventilated, with a fan favoring forward travel. AC traction has been introduced in San Francisco. The trolley coach can climb hills faster than a diesel coach, and it has found favor in flat services with moderately dense passenger loading as well. The reasons that many followed the street car into decline are the falling ridership that all surface systems experienced and the large investment in overhead wires and power supply that is increasingly hard to justify with ever lower use.

The trolley coach motor has a benign environment for electric traction. It is mounted in a weather protected compartment in the body of the rubber-tired vehicle, escaping much of the shock, vibration, and weather exposure other traction motors must endure. It does see the electrical environment of wide voltage range and voltage spikes, surges, steps, and interruptions. Toronto uses a common power supply for its trolley coaches, LRVs, and subway. Trolley coaches run alone and have only one traction motor, so there is no load sharing problem. There is no redundancy, either, so reliability is very important. The coaches are very quiet, so objectionable motor noise must be avoided.

The hybrid trolley coach and electric drive bus was a vehicle that was not developed to its potential. Electric equipment was developed in the late 1920s for city lines that were already served by trolley coaches and less intensively used street car lines that were candidates for conversion to trolley coaches. The theory was that, as the city expanded, new areas could be served without capital investment in extending rails or overhead wire supply. The vehicle ran as a trolley coach, with its advantages in performance, quietness, and cleanliness, on the old part of the route. Beyond the end of the trolley wires it ran as an internal combustion engine electric drive bus. The great depression brought real estate development to a stop and dried up the cash needed to buy the vehicles.

#### 2.4.1.8 Underground Mining

In mines, a “mine motor” is an electric locomotive. This terminology is mentioned because in what follows, a mine motor is a motor designed for use in a mine. A typical mining locomotive appears in Fig. 2.66.

Contact wire systems in underground mines are simply supported and located to one side to permit car loads to the tunnel roof. Trolley poles are supported on that side of the locomotives, giving room to swing a trolley pole around in the tunnel for reversal of direction. Locomotives are never turned around. The level of track maintenance is such that derailments are barely avoided. Trolley wire supports appear as hard spots in an otherwise physically soft wire. As the locomotive pitches, yaws, and rolls, the trolley pole base makes wild motions. Voltage regulation usually is high, and anything any “one” train does affects them all. Thus, interruptions and surges on the supply are to be expected.

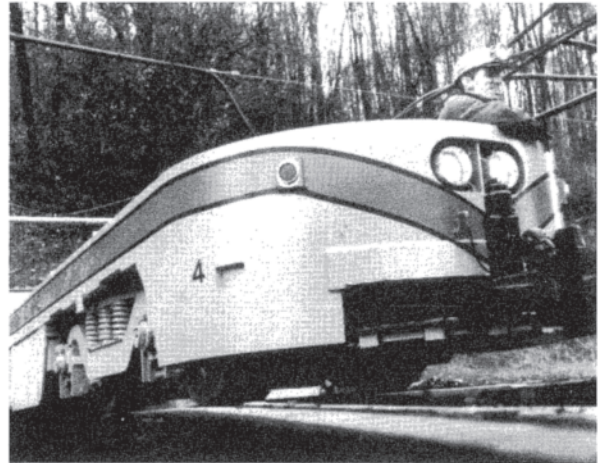


**Figure 2.66** Underground mining locomotive. (Courtesy of General Electric Co.)

There may be only one supply in a mine. Nominal system voltage is usually 250 or 500 V dc. Heavy mine haulage had favored 500 V, but 250 V is current in new mines in the United States because it is less likely to be fatal to a worker who might make accidental contact with the wire.

Most coal seams in the eastern United States are low, and tunneling is expensive, so the locomotives and haulage cars are also low. Many mines are wet, and in many the seams are folded. Side walls may go down or up. So far as is known, there have been no serious attempts to introduce ac traction or auxiliary motors on mine locomotives.

Mine haulage locomotives are sold by rated weight in U.S. tons and are motored to adhesion. Locomotives formerly weighed well over rated weight to be sure the user would not be disappointed in their hauling capabilities. Now each locomotive may be held to  $\pm 2\%$  of rated weight. Up to 20–25 tons they have two axles; 35–50 tons locomotives have two axles in each of two swivel trucks.

The constraints on the dc traction motors on mine haulage locomotives are as follows.

1. Wheel size, that with clearance under the motor and gear case, limits maximum axle-to-motor shaft spacing with single-reduction gearing and maximum motor diameter. Most wheels are 31 in diameter new. It is seen that the cross section available leads to four-pole box frame motors. The axle preparation is nested deeply into the back of an exciting pole to maximize motor diameter across flats. This constraint is similar to that imposed on the larger motors for railroad locomotives.
2. Track gauge, which governs maximum motor length. The standard track gauges for heavy mine haulage are 42, 44, and 48 inches; smaller gauges are used in precious metal mines. Outboard journals are usually used, leaving the full width between wheels for the motor and its gearing.
3. There is no pit over which to service the motors (cost of excavating underground, how to drain it). Brush access is only from the top; there cannot be bottom brush studs. The motors must be wave wound to work with only two brush studs. Commutator length is twice

what it would be if four studs were available. Being wave-wound with only two brush studs, two commutating poles may be used in lower ratings.

4. The 250-V line, dictated by Occupational Safety and Health Administration (OSHA), doubles the current compared to a 500-V line. The commutator must be longer, so the core must be shorter. Modern brush grades have permitted somewhat higher current densities.
5. Getting the needed motor rating in the space available requires forced ventilation and operation at high temperature rises. The materials and processes developed for other transportation motors are needed for mine motors.
6. The environment is dusty, dirty, and may be wet. Maintenance is minimal. The equipment is expected to last forever.

## 2.4.2 Internal Combustion Powered Vehicles

### 2.4.2.1 Introduction

Internal combustion engines drive ac or dc generators that produce power for traction motors in internal combustion powered electric traction. With mechanical, hydraulic, and other drives as alternatives, electric drive is used only where it is best.

The combination of the electric generator, traction motors and control can be thought of as an electric transmission, because it serves the same purpose, but with some important advantages, especially on very large equipment like locomotives and off-highway vehicle (OHV) dump trucks.

Diesel engines predominate, although gasoline and gas turbine engines burning residual oil have been used. The typical main line locomotive has six motored axles and a 4000–6000-hp diesel engine. The typical OHV truck has two motors with a 1800–2700 gross hp engine.

An internal combustion engine can develop its full power only at full speed. Internal combustion powered vehicles need full power over a wide range of vehicle speed, from start to full speed, unless the application calls for less. This implies low voltage and high current at low speed, and high voltage and low current at high speed for a series dc motor. On a voltampere curve, Fig. 2.67, the constant-power portion BGCD of the generator characteristic is nearly hyperbolic. Point B, beyond which the generator goes off the constant power curve and into voltage limit, is called the upper corner point. Point D, beyond which the generator goes off the constant power curve and into current limit, is called the lower corner point. Between the corner points B and D the engine has full power utilization. The upper corner point (UCP) is limited thermally by field rating and C is the continuous armature rating of the alternator or generator. The ratio of B/C (volts) or C/B (amps) is the wraparound of the machine, approximately 2.4:1 in Fig. 2.67.

On all modern locomotives, except for the very lowest powered, ac traction alternators with full-wave rectifiers have replaced the dc generator. Before the advent of the traction alternator, it was not unusual for the generator's UCP voltage

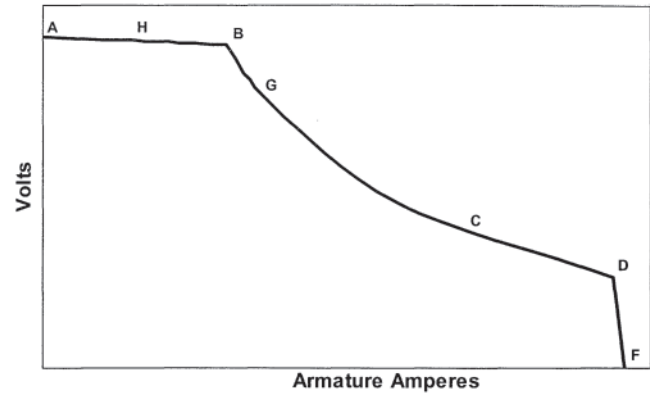


**Figure 2.67** Traction alternator/generator volt-ampere characteristic. A, no load voltage; B, upper corner point (UCP); C, continuous rating (armature); D, lower corner point; F, current limit, G, operating point immediately after field shunting at the UCP (if used); H, maximum speed operating point at <100% hp utilization.

(Fig. 2.67, Point B) to be insufficient to allow 100% horsepower utilization with 100% motor field strength. To increase utilization steps of field shunting (connecting resistance in parallel with the exciting field to reduce the current in the field) were employed (Fig. 2.68) to produce the resulting speed-tractive effort characteristic shown in Fig. 2.69. When the UCP was reached on full field the first step of field shunting would be cut in. Because the tractive effort (torque) does not change in this instant the new operating point on the reduced field characteristic is where the product of  $(E/RPM)_1 * I_1 = (E/RPM)_2 * I_2$  [constant torque implies the product of  $(E/RPM)$  and current is constant; Eq. 2.125 in Section 2.4.4.8]. Note the TE remains the same but the current has increased while the flux  $(E/RPM)$  has decreased. The motor voltage will come down by the ratio  $(E/RPM)_2 / (E/RPM)_1$  and the motor can operate to a higher speed (Fig. 2.69) on the full horsepower characteristic, until it reaches the UCP again, where

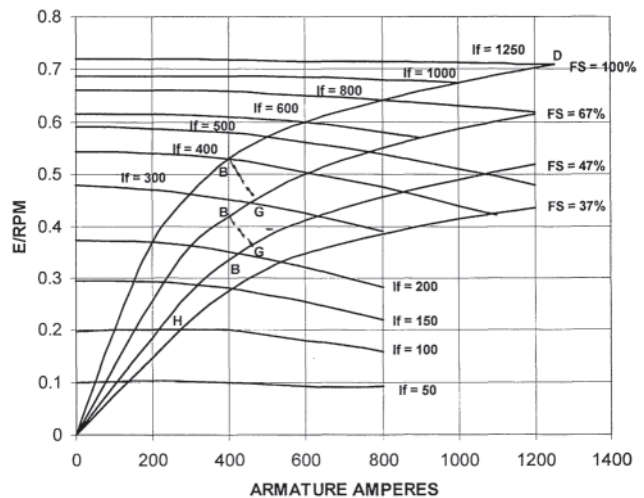


**Figure 2.68** DC traction motor load saturation characteristic with full field strength (FS) and three steps of field shunting shown. %FS is the percentage of armature current passing through the exciting field.

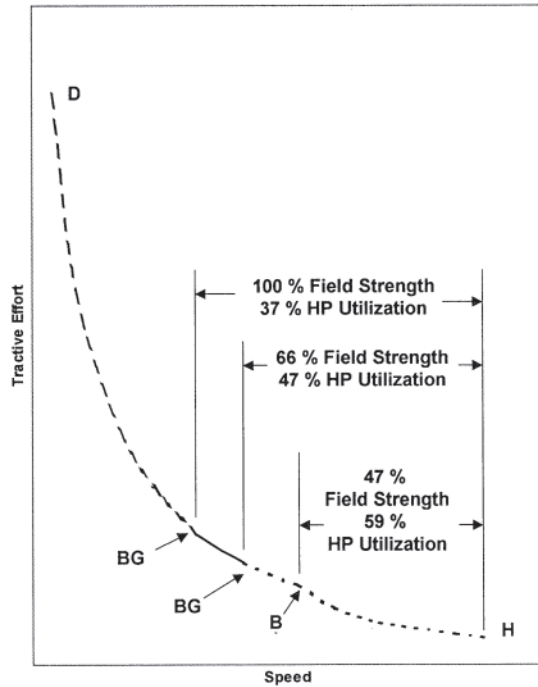


**Figure 2.69** Speed-tractive effort curve resulting from generator characteristic Figure 2.67 and motor characteristic Fig. 2.68 with two steps of field shunting.

field shunting can be repeated again down to the weakest field strength. Notice field shunting is never desirable from a commutation standpoint because it takes more current to get the same TE, and commutation difficulty is proportional to the product of RPM and current. The number of field shunting steps is determined by the maximum current step deemed acceptable at that speed. Typically the minimum field strength should not be less than a 1:1 ratio of field ampere-turns per armature reaction ampere-turns under the pole embrace to avoid high flux distortion in the armature that can result in high peak voltages between the commutator segments. Traction alternators typically can operate to much higher UCP

voltages, obtaining full horsepower utilization with 100% motor field strength (no field shunting) so it is seldom done anymore on high performance dc traction motors.

Other methods of increasing horsepower utilization is motor or alternator “transitioning,” whereby the motors can be reconnected from a series to a parallel connection say 2S3P to 6P (two motors in series, three pairs connected in parallel for low speed, high TE, to all motors in parallel for high speed, low TE). Or the alternator can be built with half of the circuits brought out to one rectifier and the other brought out to another. Then they can be put in series or parallel. The effect in either case is a doubling of the wraparound and a doubling of the horsepower utilization, but the extra contactors and complication often makes this approach unattractive. If possible, it is usually best to build the required wraparound into the equipment in the first place.

Dynamic braking with dc traction motors on internally powered vehicles can be sustained for long periods, unlike a transit car that stops relatively quickly, and is accomplished by reconnecting the motors across resistors and using them as separately excited generators (Fig. 2.70). The peak braking effort occurs with maximum field and armature amps. The characteristic on the left side of the peak is obtained by holding the field current constant so  $(E/RPM)$  is constant and voltage (and therefore current and torque) will decrease linearly with speed to the left of the peak. To the right of the peak constant armature amps can be held by field control to some higher speed where commutation and/or peak volts between commutator bars becomes limiting. In this region braking power is constant because  $(E/RPM)$  is decreasing as speed is increasing to hold constant voltage. At some speed the armature amps must be tapered down to a lower value at maximum speed. The curve shows three steps of extended range braking with lower resistances to maintain the same values of maximum braking effort to lower speeds.

Typically, the continuous rating of the armature windings of the generator/alternator, C in Fig. 2.67, exceeds the continuous rating of the traction motors, so the short-time overload capabilities are matched for starting and hill climbing. The

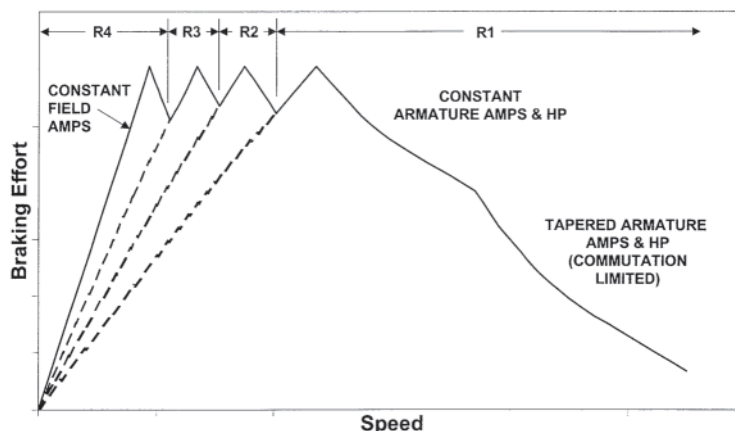


**Figure 2.70** Speed-braking effort characteristic for internally powered vehicle with three steps of extended range.

current limit, F in Fig. 2.67, should be high enough to assure that either the vehicle moves or the wheels slip with dc traction. Typically, the wraparound of an alternator used for ac traction can be lower because the LCP can be at a higher voltage.

The traction generator characteristic is seen to be quite different from usual industrial practice. The excitation source and windings must support operation at points A and B in Fig. 2.67, and the brushes or rectifiers must support the overload currents at points D and F. The power rating is not the product of the voltage at B and the current at C, although that may be used as a figure of merit in evaluating size, weight and cost.

A dc traction generator should have about 10% more current rating than the motors to have equal short-time capability. The traction motors are rated at low speed, where core loss is low. The generator at full power is at full speed, and at high current the load loss is significant. The traction motors have cool cores to sink heat into for short-time ratings, while the generator does not.

#### 2.4.2.2 Main Line Locomotives

The dominant main line locomotive in American practice is the diesel-electric freight locomotive. Design has been standardized so that while a user may choose many options, there is little that has not been predesigned. Users have become more productive, with longer through runs demanding many more miles per year of each unit. Locomotives are seldom changed on dedicated trains hauling containers or coal to utility generating plants. Users have demanded and received greatly improved availability and reliability. Fewer units are needed, creating an excess capacity situation for manufacturers. As a result, there is now only one U.S. locomotive manufacturer left. Microprocessor control and diagnostic monitoring of faults have become available and required. Most auxiliary motors are three-phase ac running off dedicated auxiliary alternators with synchronous speeds determined by the engine speed, auxiliary alternator and motor poles. One exception is the dynamic braking grid blower motor, typically series wound dc (see Section 2.4.1.1).

General-purpose freight locomotives are motored to adhesion. Wheel spin/slide systems have become more sophisticated, and trains can be dispatched at considerably higher adhesions. Motor ratings have had to be increased accordingly within the same space. Main line passenger locomotives are a small factor in American practice. Consequently, they have been designed to use available freight locomotive equipment where possible. The traction motors are the same with a gear ratio permitting higher speed. There is no need to be motored to adhesion. Trainlined “head-end power” (dedicated auxiliary alternator on the locomotive with power feed lines to the rest of the cars) is used for hotel loads.

The space available for the traction motor generally has a square cross section. Increasing its height would require larger wheels, and increasing its width would require longer truck wheelbase; neither is acceptable. Increasing motor length would require a wider track gauge, an impossibility. To get the most motor capability in the space, a four-pole box (see

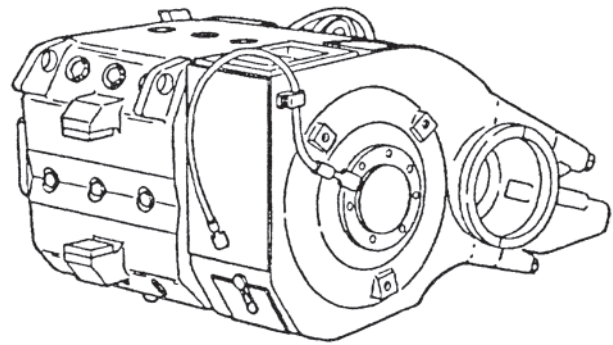


**Figure 2.71** Main line diesel-electric locomotive dc traction motor. (Drawing courtesy of General Electric Co.)

Fig. 2.71 and Section 2.4.4.8) frame dc motor is a natural choice. The exciting poles are on the top, bottom, and two sides, allowing the axle preparation to nest behind an exciting pole where full-frame cross section is not needed for flux. Commutating poles are in the corners at an effectively larger frame bore than the exciting fields. The iron is worked very hard; the flux density in the armature teeth at continuous rating is over twice that at which saturation begins to show. Starting and short-time rated tractive efforts require even higher flux densities. Copper current densities and temperatures exceed those in industrial practice. Special brush grades have been developed to withstand the high current densities and temperatures. Forced ventilation greatly exceeds that of industrial practice. Axle preparation and support bearings and nose support are integral parts of the motor.

An ac traction motor, having been relieved of the commutation function, which has been moved above deck to the inverter, might be expected to be a better fit than the dc motor. The ac motor stator is round regardless of the number of poles, therefore, it cannot utilize the corners of the box opening mentioned above, however, this space is used by the dc motor only to aid commutation that is not a need in the AC motor so that can be considered a wash. The armature winding of the dc machine is at a smaller diameter (below the air gap) than the ac machine (greater diameter than the air gap) so for the same number of poles the end turns would be longer. However, this can be regained by going to a higher number of poles (say from four to six, which will decrease the endturn axial length allowing more core length for the same length over the end windings (LOEW). Flux densities in the teeth will typically be lower in the ac motor, so a longer core length might be needed. AC stators are typically better cooled than a dc armature since the endturns have more area exposed to the cooling air. The dc armature has endturns tightly packed and banded so not much heat can get out on the same size motor. For this reason more copper might have to be in the dc design to rate. However, for this same reason the dc motor typically has more short time overload rating compared to its continuous rating.

In comparing traction motors the figure of merit to use is the concept of speed ratio power (SRP), which is the continuous rated power at the motor’s continuous rating multiplied by the ratio of maximum speed capability at that power level divided

by its speed at its continuous rating. This factors in not only the power capability but also the wraparound capability (the speed range over which that power is available) of the motor also. On this basis a study made by a major manufacturer has shown that for a 1000-hp traction motor the ac motor had 64% more SRP and 43% more SRP per pound of motor weight. This dramatic advantage is due to a good part from the higher speed capability allowed with an ac traction motor.

#### 2.4.2.3 Suburban Locomotives

Railroads in large metropolitan areas, particularly those having well located downtown passenger stations, found themselves in the suburban passenger business. Some were electrified and are covered under external power. Others were not electrified and use internally powered locomotive-hauled trains.

Double-decker cars are used on some lines to increase the number of seats per car. These lines are dead-end, rather than running through the downtown station. Push-pull trains are used to avoid having to take the locomotive from the train, turn it around if front-sensitive, and run it around to the other end for a return trip.

#### 2.4.2.4 Switching and Industrial Locomotives

As the name implies these are small, relatively low-power locomotives used to move cars about in switching yards to make up trains for main line runs or moving cars around within an industrial site. High TE capability may be needed, but not high speed. Most switching is done over humps. The locomotive pushes the cars up the hump where they are cut loose and switches are thrown to route them to desired tracks.

Yard switching and industrial locomotives seldom need full power utilization at high speed. Small, high-speed traction motors drive through double or triple-reduction gearing that is oil lubricated. Often the traction motors are self ventilated and usually dc.

#### 2.4.2.5 Off-Highway Trucks

Off-highway trucks are large electric drive trucks used mainly in open pit mining, usually copper or coal. One shovel may load a truck with overburden to be hauled to a dump while another loads ore to be hauled to the crusher or coal to its processor. Mine pits and ramps are laid out to use the short-time overload capabilities of the electric traction equipment. The maximum grade is usually 10% (10 ft of lift for every 100 ft of forward movement).

Electric drive is used where it has lower life-cycle cost than any other means. With the gradual increase in size of trucks on which mechanical drive is feasible and with the pressure for ever bigger trucks, the range where electric drive is best is gradually moving up. The first electric OHV trucks were produced in the 1960s in the 85-ton payload class and utilized two dc series-wound TMs running in parallel powered from a traction generator. By the 1970s the traction generators were replaced by traction alternators and full-wave rectifiers. Typical engine speed for OHV diesels is 1900 rpm, much

higher than locomotive (900–1050 rpm) so the traction alternator designs are specialized for the high speed service. These systems utilized equipment blowers and exciters mounted off the alternators powered from the engine drive shaft with belts and pulleys. In 1980 a major manufacturer of electric drive propulsion systems for OHV trucks introduced the STATEX (STATic EXcitation) system utilizing two separately excited dc motors with their armatures connected in series across the rectifier. Two separate single-phase tertiary windings in the alternator with phase-controlled rectifiers powered the separately excited motor and alternator fields. The belted blowers, which ran above engine speed, were replaced by a blower with a larger impeller running directly on the drive shaft at engine speed that could attain the high pressure needed to cool the equipment. This eliminated the rotating exciter, blower and all belts and pulleys. In the 1990s ac traction was introduced and is becoming predominant.

Today most of the trucks using electric drive are rated to carry 150 to 320+ U.S. tons or more of payload. Most use one traction motor for each rear wheel (see Fig. 2.72). The motorized wheel has a flange that is bolted to the axle box forming the rear axle of the truck. The axle box is a hollow tube that also serves as the air plenum providing cooling air to the motors ducted from blowers in the front of the truck. Most new trucks below 150-ton payload use mechanical drives. Consideration of the torque to be delivered makes it desirable that the final reduction gearing be in the wheel.

The dc motorized wheel concept that predominates in the industry puts the whole motor inside the wheel. Double-reduction gearing, resembling and often called planetary even though it is not, drives the rim from the inside. It includes an arrangement allowing equal sharing of motor torque among three planet gears. The ring gear drives the torque tube that drives the wheel hub mounted on very large hub bearings that seat on the outside of the motor's magnet frame, which is also the supporting structure of the wheel. Figure 2.73 shows a cutaway of a dc motorized wheel so constructed. Figures 2.74 and 2.75 show two different arrangements used for ac motorized wheels.

Off-highway truck propulsion motors, generators, and auxiliary machines are built in the same factories that make equipment for other transportation applications. The dc motors used are direct derivatives from box frame locomotive traction motors adapted to a round frame. The dc motors are arranged with the commutators outboard for brush change access and commutator inspection. This cooling arrangement is called backward blowing because it is the reverse of normal practice of blowing cool air in on the commutator end of the motor. The air that comes through the motor field coils can be up to 60°C hotter than ambient, which can make the commutator thermally limiting for the motor. Ways to alleviate this includes adding another brush path to lower the current density and increase the cooling surface and providing air deflectors that direct the air coming through the field coils down toward the commutator.

Conventional brakes cannot absorb the power needed to hold the speed of a truck going downhill and last for very long, so dynamic braking is the primary brake. The braking



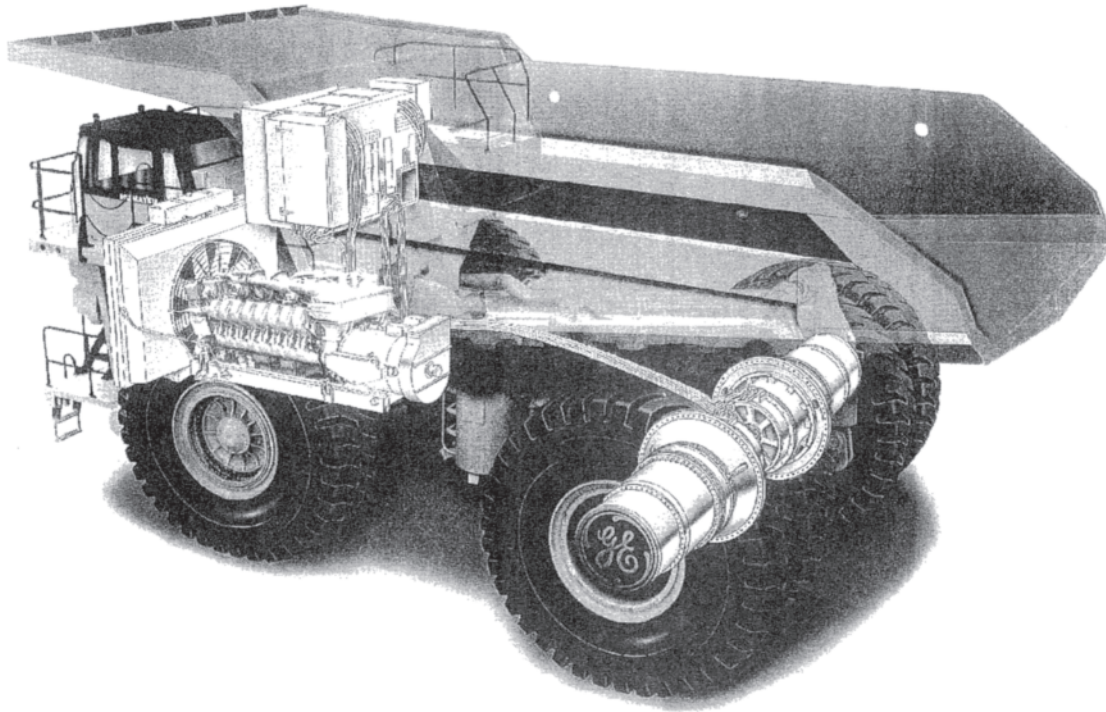


**Figure 2.72** Cutaway view of an off-highway vehicle (OHV) showing the main components of the electric propulsion system: two motorized wheels mounted to the axle box in the rear, traction alternator directly mounted to the diesel engine, control compartment on the front deck.

resistor is cooled by a dc blower motor running off braking power the same as with a locomotive. Excitation powered from tertiary windings in the alternator stator slots and “in-line” blowers (large diameter impellers in with the engine drive shaft that run at engine speed) have largely replaced belted blowers and rotating dc exciters to remove the possibility that a belt failure could cause loss of dynamic braking and consequently a runaway truck.

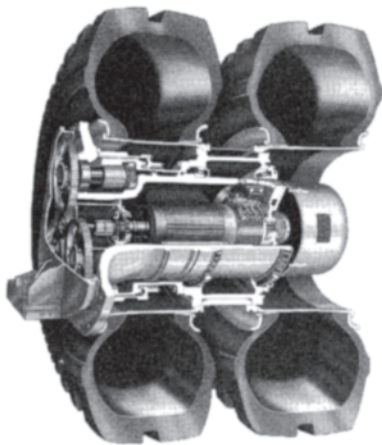


**Figure 2.73** Cutaway view of a dc motorized wheel. Commutator and brushes located outboard for accessibility. (The hubcap is at about shoulder height to a man standing on the ground.) (Drawing courtesy of General Electric Co.)

Because an uphill haul requires high tractive effort, even the full power of a large diesel engine cannot move a heavy truck very fast (6–7 mph is typical). To go uphill faster and thus make a significantly longer climb within the short-time traction motor thermal rating, some properties have found it economic to install trolley assist. If equipment blowers were installed that did not depend on engine speed (hydraulic, dc and ac motors have been used) the engine speed could be allowed to idle during trolley operation allowing a significant fuel savings also. This provided a major impetus for use of OHV trolley assist in RSA mines because they needed to import most of their petroleum and prices spiked after the 1980 oil embargo. Equipment similar to that available for trolley coaches has been further developed to permit a truck to run into the beginning of trolley power, make contact, and change over to external power for traction without slowing, using resistor stepping with the dynamic braking resistors. The separately excited motor fields had approximately four times the number of turns/pole as the series field. Operation on trolley required the exciting fields be in series with the armatures for interruption protection. To provide this the exciting fields were brought out of the motor in two circuits, one for the north poles and one for the south poles. For diesel operation all the field circuits were connected in series. For trolley operation the four circuits were connected in parallel (two circuits from each motor) and then connected in series with the armatures to provide the equivalent of 100% series field strength. More information on OHV trolley systems is available from consultants such as [www.hutnyak.com](http://www.hutnyak.com).

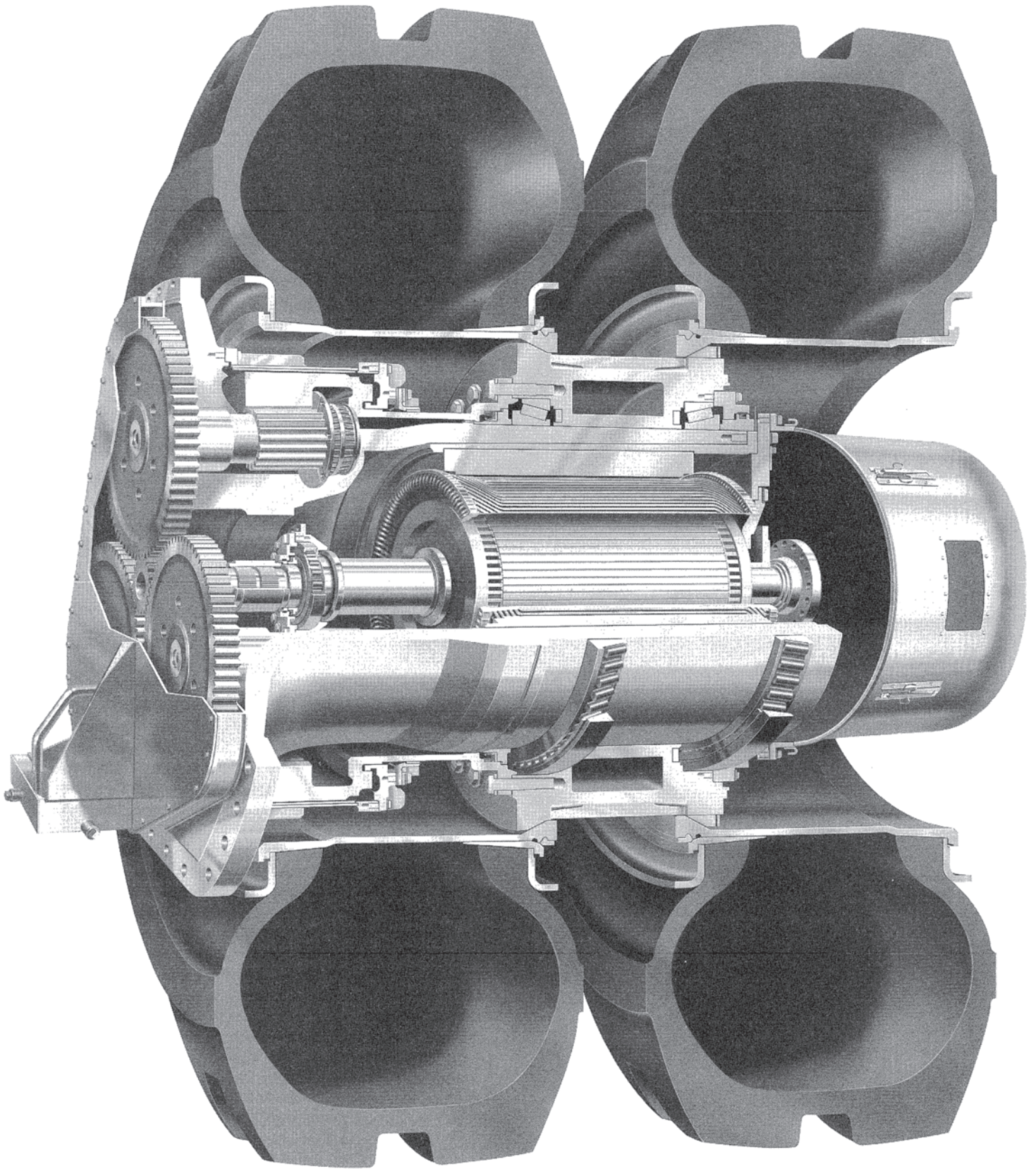


**Figure 2.74** Cutaway view of ac motorized wheel with motor inside hub bearings. (Drawing courtesy of General Electric Co.)

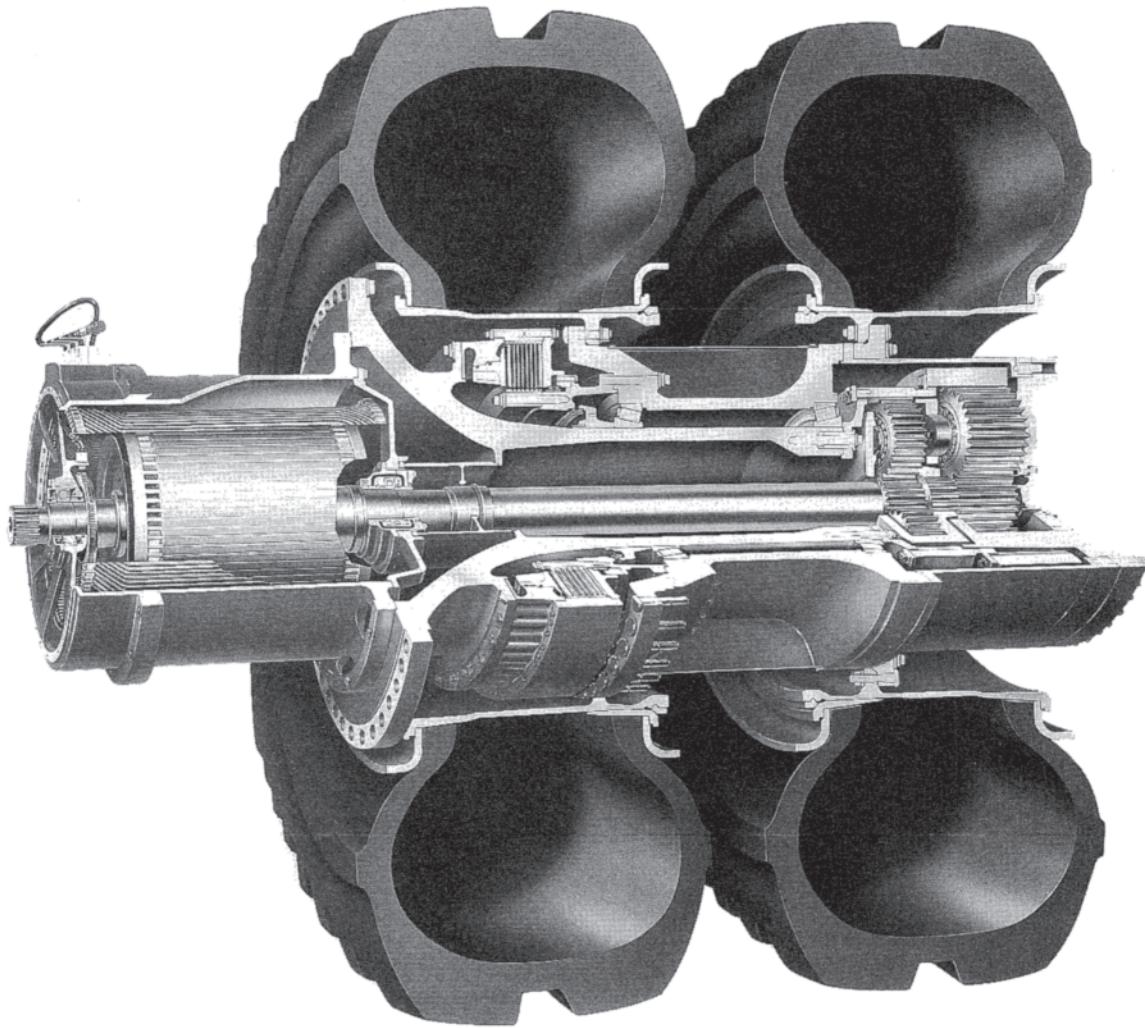


**Figure 2.75** Cutaway view of ac motorized wheel with motor cantilevered inside axle box allowing larger motor diameter and smaller hub bearings. (Drawing courtesy of General Electric Co.)

With the advent of onboard computers transient motor temperatures can be tracked with thermal models to prevent overheating of the motors. Another method that has been used with dc wheels is measuring the resistance of resistance temperature devices (RTDs) implanted in the commutating pole coils that can be used to determine the armature temperatures. Before the use of onboard computers the allowable time for thermal overloads were predicted by the use of inverse time curves. IEEE Std. 11 [14] defines a short-time overload for class H insulation to be the load that, if held constant for the defined amount of time, will result in the armature temperature going from 100°C rise to 180°C rise based on a 40°C ambient. Assuming an exponential rise, it can be derived that this results in a linear increase in current allowable plotted against inverse time (see Fig. 2.76). In this figure the short time rating for a dc motor armature is shown compared to the de-rectified amps of the traction motor alternator used with it. This figure shows a dramatic difference between the dc and ac armatures. The important point to grasp from this is that there is a substantial ratio between the

continuous rated amps for a dc armature and it's short time rating versus the corresponding ac armature. This is because the dc armature's endturns are more thermally insulated so it needs more copper mass to keep within continuous temperature rise limits than the ac winding whose endturns are well ventilated. Therefore, the dc armature will tend to have more thermal mass and a lower continuous rating than it's ac counterpart for the same short time rating.

Most OHV mines have 10% grades (10 ft of lift for every 100 ft of forward movement), which results in 10% of the truck's gross vehicle weight (GVW) required in tractive effort to move the truck up the ramp. Another 1–2% of the GVW is required for "rolling resistance" (energy lost in deforming the tire as it rotates). Therefore the total truck tractive effort required to move the truck up the grade is stated in terms of equivalent grade (EG), which if multiplied times the GVW of the truck will tell you the amount of TE required. For example, to move a 850,000-lb GVW truck up a 12% EG requires  $850,000 \times .12 = 102,000$  lbs of TE. Depending on the length of the grade and the horsepower of the truck (which determines the speed of the truck) the short

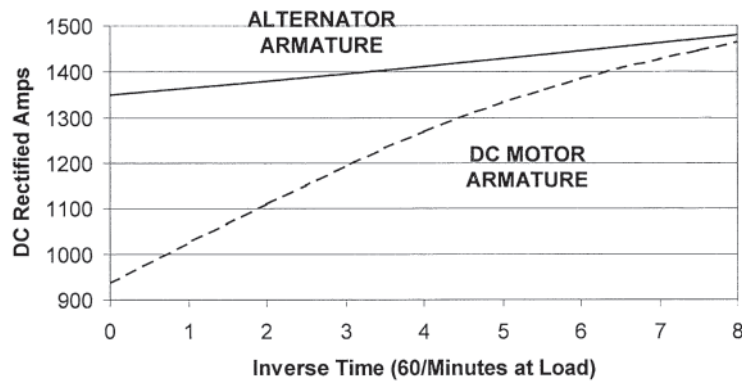


**Figure 2.76** Inverse time curve for predicting short time overload ratings.

time rating of a dc motor truck could be utilized to climb the grade without overheating the motor. For an ac motor the thermal time constant is much shorter and it is best to have the truck rated the 12% EG continuously.

The environment in which electric machines for offhighway trucks must work requires most of the same features of design and construction needed in other electric traction applications. Special attention is given to the wheel motors to be certain that no part extends beyond the tire and rim, lest it get knocked off if a truck scrapes against a wall. Hydraulic lines must often pass through the motor, so it must be designed to allow leaked fluid to drain out.

Off-highway trucks typically complete a round trip in about 20 to 45 minutes. The trip usually includes a flat run from shovel to ramp, a slow full-power climb, a flat run to the crusher or dump, a fast run back to the ramp, down the ramp with speed controlled by dynamic braking, and a flat run in the pit back to the shovel. The equipment accumulates many speed cycles in a short time. Attention must be given to design detail to avoid fatigue failure due to speed cycling.

Many mines are at high altitudes (up to 16,000 ft) in dry climates that feature wide temperature swings, including very low temperatures. Under these conditions the absolute humidity is very low, so loss of collector ring and commutator film and very short brush life would be expected. Brush manufacturers have risen to the challenge and have provided brushes having treatments that satisfy these severe conditions. Although the ambient temperature decreases with higher altitude, the density of the air also does thereby decreasing the cooling effect, and this needs to be accounted for in the machine ratings. This is usually done by basing the rating at altitude on the equivalent amount of airflow in lbs. of air per minute that would be obtained with standard air density of .075 lbs/ft<sup>3</sup>.

## 2.4.3 Battery Powered Vehicles

### 2.4.3.1 Introduction

Battery-powered vehicles share the limitations of their power source, an onboard storage battery. A battery is a group of cells in series. Each cell is inherently low voltage, so a battery of them is needed to get voltage high enough for traction

motor use. Each cell stores energy by converting electric energy to chemical energy, and produces electricity by the reverse process. The classic, economical battery types have been leadacid and nickel-alkaline. Both offer long life, but lose some of their rated capacity if discharged in less than the rated time. Nickel-cadmium cells are more expensive but have much better rapid discharge and deep cycle performance. Batteries have been greatly improved, but they still have finite energy storage capacity. The applications discussed here show economic viability with this physical limit.

Various exotic cell types have been or could be developed, but the cost or high temperature required for operation has confined each to very limited use. A fuel cell oxidizes fuel to produce electrical energy by way of a chemical link. Fuel cells can be clean-burning. Solar cells convert sunlight into electrical energy directly. Development is proceeding, but efficiently and cost are still problems at this writing. Fuel cells and solar cells are primary producers of electric energy. Their use for vehicles is usually combined with a storage battery that provides excess power during acceleration and stores excess power when the vehicle does not need all that can be produced. While much development is still required, considerable development activity is underway to develop a fuel cell as a replacement for batteries.

Generally, storage batteries are approximately 80% efficient in converting electrical to chemical energy, and the same in the other direction. Thus, in-and-out recovery of energy is about 64%, not very good. The lost energy appears as heat. This explains why charging supplies must be well filtered; trying to use a storage battery as a capacitor may destroy it.

### 2.4.3.2 Battery Trucks

Internal combustion engine powered fork lift trucks, also called jitneys, are widely used for material handling. They are acceptable outdoors, but in most factories, warehouses, and coolers, battery trucks are used because of their lack of exhaust gas. This is the main application of electric fork lifts today. Most fork lift truck use one traction motor and one hydraulic pump motor. Some trucks use two traction motors. Some also have power steering motors.

Battery maintenance and recharging stations are established, so that when a battery gets low, the operator goes there and the depleted battery is quickly replaced with a fully charged one. A pool of extra batteries is kept on charge; charging may be interrupted during periods of peak power demand to avoid added utility demand charges.

To thermally protect the motor and control, protection schemes are programmed into the control algorithm. While a motor manufacturer may develop possible mission profiles, it is widely understood that users will work the vehicles as hard as they can. Moreover, operators have been known to abuse the vehicles by such nonintended uses as snowplowing and games, like tug-of-war. The truck manufacturer wants to use the least expensive motors he can obtain that will just get by with an acceptable failure rate. The motor manufacturer tries to build a motor that will meet the truck manufacturer's speed-torque curve and rating, fit into the available space, and be as rugged as possible, all within the constraints of economics.

Battery truck traction and hydraulic pump motors have historically been open series wound motors. To reduce control complexity and gain reliability, some traction and hydraulic pump motor and control designs have been converted to use shunt-wound dc motors. The current development trend is toward use of ac motors and controls for these applications. While ac uses much more complex controls and control algorithms, it allows for brush elimination (reliability improvement) and potentially higher motor speeds that could result in smaller motor size if combined with gearbox ratio changes. AC is developed from the dc battery with an inverter in the control.

Battery truck traction motors especially, and auxiliary motors to a lesser extent, are made as simple, rugged, and

reliable as cost will allow. This dictates dc series motors without commutating poles or coils. They have armature fan ventilation unless total enclosure is required. They must be protected against grease and oil that may leak from the face-mounted gearing or pump. The insulation needs to be adequate only for the low voltage, but it must be able to withstand severe thermal overloads and all kinds of environmental conditions. For example, one common application is carrying food into and out of freezers. A typical battery truck motor is shown in Fig. 2.77.

Some users require brush wear indicators that signal when brush replacement is needed, thus eliminating regular motor inspections entirely. Brushes must have low voltage drop because of the low battery voltage, even though higher voltage drop would improve resistance commutation. As stated above, an ac system eliminates the need for brushes and the reliability issues associated with them.

Battery truck traction motors are four-pole with wavewound armatures. Many different winding combinations are needed to cover the various ratings and characteristics. Standardized iron sections are used in structured diameters and lengths of armatures, frames, and poles, with the numbers and dimensions of the armature slots chosen to maintain constant percent iron in the armature teeth. This is one of the very few places in electric traction where industrial motor product structuring methods can be used. The smallest battery truck motors may be two-pole, and may have permanent-magnet fields. Their use is for small pump and other auxiliary drives.

AC motors are typically four or six pole (traction) and four pole (pump). These motors are designed to fit in the same place and use the same gearboxes or pumps as their dc counterparts and therefore look very similar to the dc motor

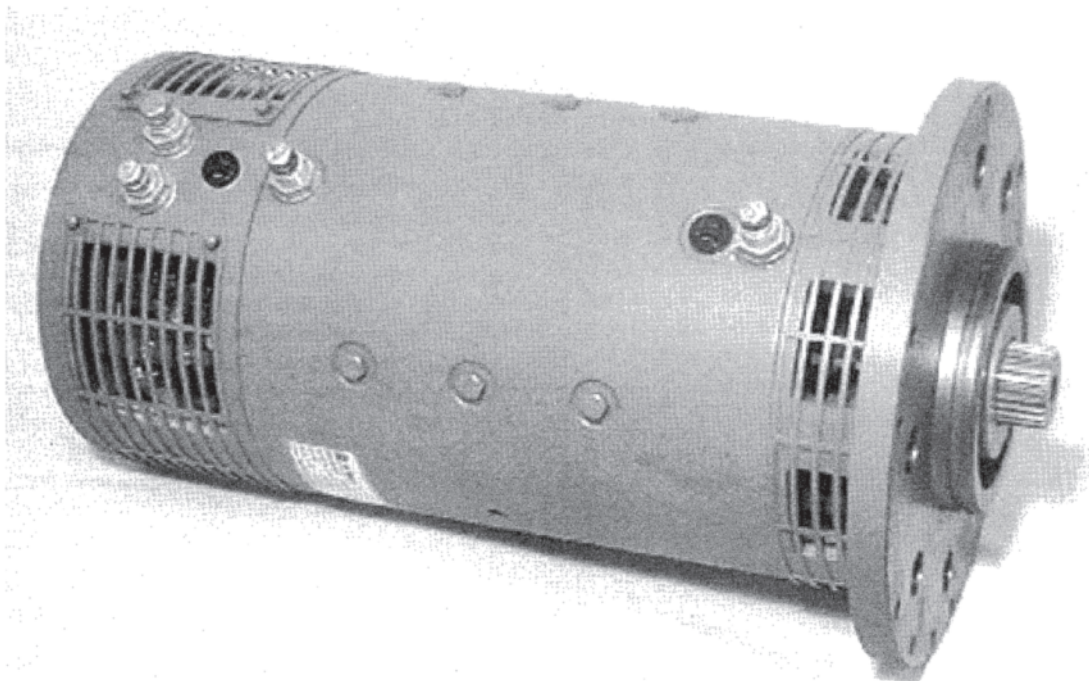


**Figure 2.77** Battery truck traction motor. (Courtesy of General Electric Co.)

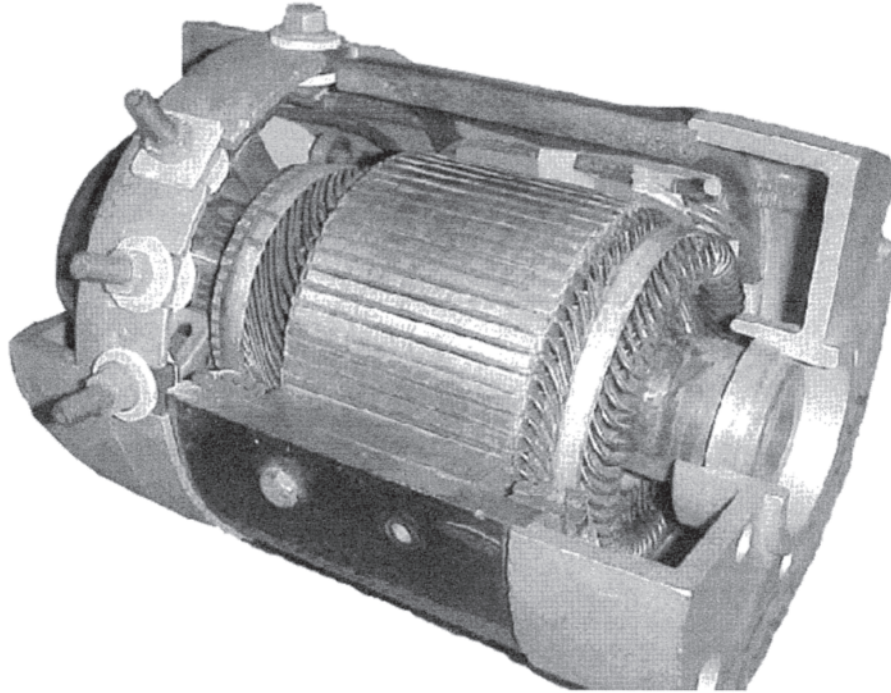


**Figure 2.78** Cutaway view of golf cart traction motor. Armature winding is machine inserted. (Courtesy of General Electric Co.)

from the outside, but are typically three phase induction motors without brushes or commutators.

#### 2.4.3.3 Golf Carts

The storage battery-powered golf car is another application of electric traction. Its mission is to run for one golf day on one charge, carrying golfers and their equipment around the course. It has often replaced the human caddy. The application is a good one for a battery vehicle; between short runs, it sits idle. Internal combustion engine driven golf cars are also used but have the disadvantages of needing a storage battery for starting, and producing noise and fumes. The application is easy enough for the battery that motor efficiency is of little concern. The traction motor (Fig. 2.78) is much like battery truck motors, and was developed and produce inexpensively by existing manufacturers of smaller battery truck motors. On a 36-V battery, motor flashover is not a problem.

#### 2.4.3.4 Underground Mining

Battery-powered mine vehicles are very specialized for the few applications where they are economical. Within the limit of energy a battery can supply for a shift, only light hauling can be done. If heavy haulage is needed, external power must be provided. One condition in which battery-powered electric traction is used in mining is in precious metal mines where the ore is rich. These tend to be deep under ground and hard to reach. The volume of ore to be hauled from the face to the hoist is too little and the path too contorted for a conveyor. Most of these vehicles, once put in place, are never taken out of the mine. Maintenance capability is limited, so equipment

must be reliable and maintenance-free.

Where haulage is needed for small volumes of ore, small battery locomotives, often called trammers, are used. One may make only one slow trip per day with a few small mine cars. Only the locomotive has brakes, and they are manual. The rail gage may be as narrow as 24 inches. Another vehicle is the personnel carrier, which carries workers to and from the face in a low vehicle.

#### 2.4.3.5 Electric Vehicles

The storage battery electric vehicle was popular as an alternative to the early hand-cranked, breakdown-prone gasoline automobile. A few survived the great depression to beat gas rationing through World War II and beyond. Speed and range limited them to short city errands. Interest has been renewed in response to smog pollution and dependence upon foreign oil. Until there is a breakthrough in battery capacity, vehicle mission capability will remain the single factor most limiting its use.

The implications for vehicle design are straightforward: minimize weight and drag. Motor considerations are less well recognized. Traction motor efficiency is crucial in getting the maximum mission capability out of available battery charge. Thus, the optimum electric vehicle will have a heavier, more efficient traction motor than the minimum possible.

In the past 20 years, the dc traction motor has been replaced by an ac induction motor small enough to be enclosed in the front or rear axle. Also, hybrid cars have been developed with both internal combustion engines and electric motors. In hybrid vehicles, the electric motor can be used as a starter for the internal combustion engine as well as a generator to

recharge the batteries and a traction motor to provide a portion of the acceleration or the vehicle can be propelled only by the electric motor in congested areas.

As an alternative to the internal combustion engine, the U.S. Government is encouraging development of the fuel cell. Fuel cells promise to be more efficient than internal combustion engines and greatly reduce pollution.

There are many electric delivery trucks in European cities. They are feasible because they are slow, are stationary for most of the time, and work in compact communities. Retirement communities provide a small market niche for personal vehicles that are based on golf carts. They are used for going to doctors, shopping, and getting to events. Local drivers' licenses may be provided to those no longer able to pass the state driver's examination.

Almost every other mission cycle given for an electric vehicle in the United States has a freeway dash in it. This is extremely hard on classic battery types. If the average current draw can be kept within the rated capacity of the battery, usually the 5-hour rate, rated capacity may be reached. The current draw required to reach freeway speed is well above rated for any existing commercial battery.

Discharging a battery causes exhaustion of the electrolyte and gassing at the interface of the metal, and dissipation of the gas takes time. The faster the discharge, the less energy may be recovered. Drawing well over rated current decreases battery efficiency and thus its usable output.

Stop-and-go inner-city traffic need not be hard on the battery. Although acceleration may exceed rated current draw, it lasts only a few seconds. During stops, electrolyte continues to mix and gas dissipates. In such short cycles, average draw may be used to calculate mission capability.

Regenerative braking can recover some energy of vehicle motion. As seen above, battery in-and-out efficiency may be approximately 64%; when gear losses and other rolling resistances are added, only about half the energy is recoverable. Perhaps the greater advantage of regeneration is the reversal of the condition at the electrolyte-metal interface. The momentary improvement of the energy recovery condition may add more mission range than the actual energy recovered.

Auxiliary loads can have major effects on the feasibility of an electric vehicle. Heating or air conditioning from the traction battery would not be feasible; a fuel-fired system would be needed. While this seems to be defeating the purpose of electric drive, such systems can be made to burn far more cleanly than the automobile engine. Lights must also be provided.

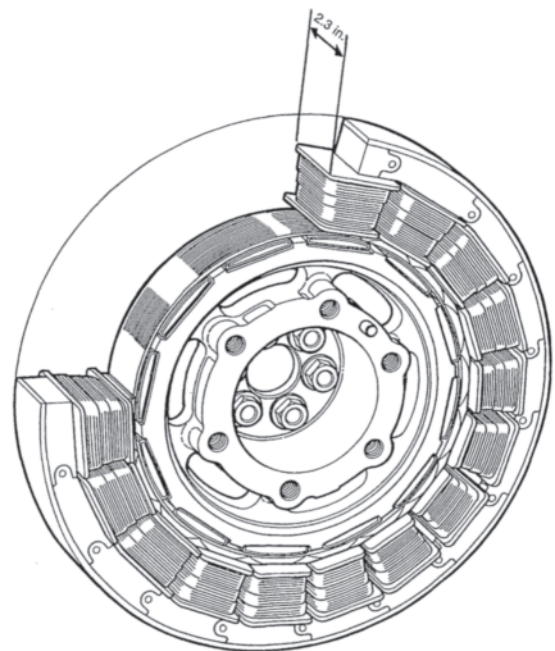
Recharging stations at best would take an order of magnitude more time than filling a gas tank. High energy demands for short times are expensive for utilities to serve. Charging slowly at night when other utility loads are low is least expensive and best for the battery. While not as desirable, recharging while the owners are working is possible, but there is little flexibility because a vehicle will not be ready for its next mission until recharging is completed. California has mandated that significant use of electric vehicles must take place as an attack on smog. Implementation should force a market large enough to attract car manufacturers.

It has become clear that it is not likely that austere electric cars will attain mass production and there will be a limited market for them. Electric vehicles cannot handle urban sprawl unaided. Special applications can be found for utility and delivery vehicles if there is sufficient demand to justify developing them. However the electric vehicle will not be an acceptable option to the general-purpose car.

#### 2.4.3.6 Hybrid Vehicles

Gasoline-electric hybrid vehicles have recently become available and appear to be a viable alternative to the pure gasolinepowered vehicle while overcoming the drawbacks of the pure electric vehicle with a significant increase in gas mileage. A hybrid vehicle combines a small, very fuel-efficient gas engine with an electric motor/generator powered by storage batteries. During acceleration, when torque and energy demand is high, the electric motor adds to the engine's output. When coasting or braking the electric motor doubles as a generator to charge the batteries. By relieving the engine of the need to handle the extreme energy overloads required for acceleration, it can be optimized to handle the average requirements resulting in much higher gas mileage and lower emissions. In one system, the brushless dc permanent magnet motor (see Fig. 2.79) provides an additional 25 lb-ft during

**Honda Insight Integrated Motor Assist System  
Electric Motor**



The electric-motor component of the integrated motor assist system consists of an ultra-thin (2.3-inch-wide), permanent-magnet electric motor with a maximum output of 10 kw, which provides power assistance to the gasoline engine. It also functions as a starter motor for the idle-stop feature, and as a generator for the IMA system and batteries.

**Figure 2.79** Electric motor used in a hybrid car. Only 2.3 inches wide, it provides a maximum output of 10 kw, assisting the gasoline engine in acceleration. (Courtesy of Honda Motor Co.)

acceleration. Also known as ECMs (electrically commutated motors) the stator poles are electronically switched between +, 0, and –dc excitation in the proper sequence to produce the desired function. A very thin (only 2.3-inch wide) design allows the motor to be sandwiched in between the engine and transmission. The motor also serves as a generator to charge the batteries (144-V nickel-metal hydride) and as a starter motor to start the engine.

The system will shut off the engine while idling if not needed. Another innovative feature is the use of the electric motor to damp engine idle vibration by application of reverse torque to the crankshaft. The reverse torque pulses are exactly in phase and opposite the 60-degree torque fluctuations of the gasoline engine. As a result the hybrid gasoline engine is remarkably smooth throughout its operation range.

The hybrid vehicle can offer the same amenities (air conditioning, power assist, etc.) and can be refueled just like a regular gasoline fueled car. This hybrid has an Environmental Protection Agency (EPA) rating of 70 mpg highway.

## 2.4.4 Design Considerations

### 2.4.4.1 Industry Standards

The industry standard covering most of the machines discussed in this section is IEEE Std. 11 [46], titled “IEEE Standard for Rotating Electric Machinery for Rail and Road Vehicles.” Off-highway trucks are covered, though not in the title. IEEE Std. 11 is a self-contained standard, including all the tests needed to prove machines. In the 2000 revision inverter-fed induction motors were added.

The International Electrotechnical Commission publication having a scope parallel to IEEE Std. 11 is IEC 349, 349–2, and 349–3 [48], “Rotating Electrical Machines for Rail and Road Vehicles.” While both of these standards claim to be “international” in practice IEEE Std. 11 tends to be used in the North America and reflect American practice and IEC 349 tends to be sited in western Europe. While agreeing in most things there are some salient differences.

Machines not covered by IEEE Std. 11 include very small auxiliary motors, battery truck motors except those used as auxiliaries on large vehicles, automotive and highway truck auxiliaries, etc. It is not yet clear whether electric automobile traction motors should be included; historically they have been derivatives of battery truck motors but quantity production could change that. IEEE Std. 113 [39], the industrial dc motor test code, and NEMA MG 1 [1] are generally used to cover battery truck motors.

### 2.4.4.2 Voltage and Insulation

Traction motor voltage affects insulation and ventilation design choices. The armature, the rotor in a dc motor and the stator in an ac motor, contains an insulated winding in slots in a grounded laminated steel stack. There are many conductors that must be insulated from each other and ground. Dielectric stress can be handled in the selection of materials. The insulation is also stressed mechanically by differential thermal

expansion, shock, and vibration. Dirt, contamination, and moisture add chemical stress. Time and temperature age the insulation thermally. The higher the motor voltage, the greater is the risk of creepage failure.

Inverter drives can produce steep voltage wavefronts that can stress winding insulation unequally (see section 8.4). The combination of motor voltage and wavefront must be kept below corona damage level if organic insulations are used. Organic insulations such as Kapton\* (polyimide) are the only high-temperature materials available that can be sealed against dirt and moisture, and is used for turn insulation. Nomex\* (polyamide) or mica-mat tape are quite commonly used for ground insulation.

Historically, the need to get the most output in limited space has forced electric traction equipment to be a leader in the use of high-temperature insulation materials. Formwound coils with rectangular shaped copper conductors are used for maximum copper in the slots. A very important development was a tape made of polyimide with a thin coating of high-temperature heat-fusible materials. It is machinetaped and induction heat-fused on bare copper wire. The heatfusible material fills any holes and seals the polyimide to produce truly waterproof wire with full insulation build at the corners for armature coils.

Insulation must have mechanical properties for electric traction that are not seen in other applications. Short-time overloads cause differential thermal expansion, with armature wire growing longer than the steel core. The insulation system must be flexible enough not to crack under this extreme stress. Thermal class is usually Class H (200°C).

Electric traction has also been a leader in the development of vacuum pressure impregnation (VPI). The core is baked to eliminate all moisture, then put in a vacuum to eliminate trapped air pockets, and then solventless varnish is impregnated into the windings under pressure and then baked until set. Properly done, VPI dramatically improves heat transfer and resistance to moisture. Two cycles are usually done on the dc and ac armatures and a single or double VPI on some dc coiled frames. The insulation needs to be tight enough that capillary attraction will hold the resin in place until it cures. The viscosity of the resin goes down as baking begins. Rolling the core slowly while baking helps keep the resin from running out. Many materials do not wet well enough to hold resin; surface treatments such as roughening help. Special mica and glass tape has been developed specifically for VPI; as a tape alone it is inferior to many others, but when filled the system is superior. When insulation failures occur, the few dielectric failures seen are due to damage in manufacture or excessive thermal aging. Most failures start with mechanical cracking and chafing in service, which lead to shorts and creepage grounds.

A quite common line voltage for North American externally powered vehicles such as mass transit, LRV and trolley buses is 600 V dc. Internally powered vehicles such as locomotives and OHVs go to 1400–1500 V dc. European practice tends to go to higher voltages, i.e., 2800 V dc link voltages on ac locomotives.

On mass transit cars the braking application calls for high torque at high speed, and holding that torque to low speed. The

\* Kapton and Nomex are registered trademarks of the Du Pont Company.



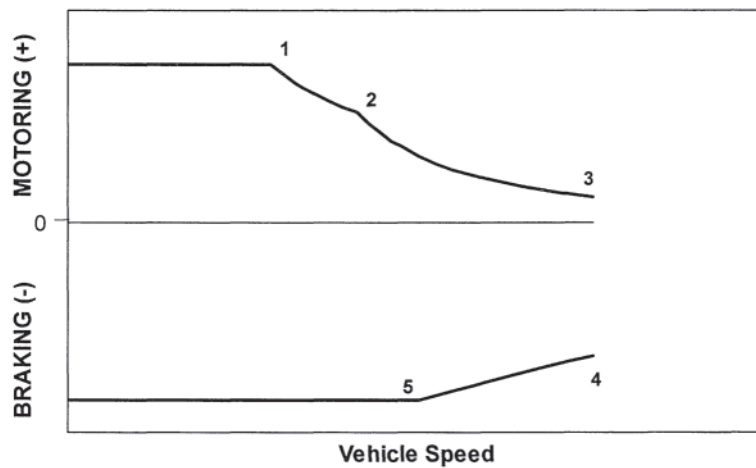


**Figure 2.80** Resulting speed-tractive effort and speed-braking effort characteristic needed to meet the performance specified in Fig. 2.82.

high-speed point is limiting; the peak power is much greater than peak motoring power. The same current and flux that produce the initial accelerating torque produce more braking torque with the reversal of losses. The peak power in braking (4 in Fig. 2.80) is the motoring full-field corner point power (1) times the ratio of braking speed to motoring corner point speed (3/1). That ratio is about 3:1 in most commuter and high-performance mass-transit applications. Commutating this power, whether electronically in the inverter for ac machines or by commutator and brushes in dc machines, is a severe design constraint.

On 600-V externally powered dc systems, the motor voltage was 600 V until high-performance dynamic braking was developed. For three times power the braking voltage would have been 1800 V or more, well beyond the capability of the commutator and insulation system. The 300/600-V traction motor developed was a 300-V motor insulated for 600 V for operation with two motors in series. The two motors on a truck are connected in series, requiring only four leads per truck. The 600-V insulation system developed to handle line transients is adequate for 1000 V and even more in braking when not connected to the line. The braking voltage can be handled on the commutators of motors that will fit in the truck, making the 300/600-V motor a natural fit.

The commutation problem is removed from the motor with ac inverter drive. AC motors used on a four-axle mass transit car are typically designed to run both motors on a truck in parallel from a single inverter.

#### 2.4.4.3 Line Characteristics, Including Transients

External traction power supplies must be expected to have voltage transients and interruptions. Transients include voltage steps and spikes, while interruptions result from loss of contact with the line. Voltage steps occur when load is shut off and when the collector passes from one line section to another. When load is shut off, an inductive spike occurs before the new steady-state voltage is reached. Spikes up to 3000 V were measured on 600-V lines before static control became

prevalent. Motors running from a line help to consume spike energy; if properly designed and applied, they run successfully. Static control is generally programmed to turn off into a spike to avoid a large current surge through the semiconductors. This can aggravate the spike situation greatly because there is little place for the inductive energy to go.

Interruptions occur at third-rail gaps and section isolators and when collectors are unable to follow the third rail or overhead wire. During an interruption on a dc motored car, motor flux begins to die, so a current surge occurs upon reclose. Crossing from one supply section to a less loaded one also causes a voltage step after the interruption. Modern control can sense loss of supply and open a line contactor in 100 ms, and static devices can be shut off even faster.

When the cemf is lower or the line voltage higher after a transient, circuit resistance is all that limits the current surge. Small dc auxiliary motors need external resistances, called buffer or running resistors, to limit surge current and avoid flashover, however they have the advantage of always operating with full field strength. Series motors have the advantage that the surge current goes through the field coil, driving up the flux and cemf to help shut off the current surge. DC traction motors running on an external power supply such as a mass transit car require field shunting to obtain maximum speed (see Section 2.4.4.8). This must be done with an inductive shunt that has an inductance similar to what the series field they are shunting have (Fig. 2.81). If the shunt was purely resistive all the current resulting from a line transient would bypass the motor fields through the shunt presenting an extremely weak field situation in the motor and probably flash it over.

On ac cars the main circuit breaker (MCB) is opened upon detection of a transient or gap and the motors are operated in a very light generating mode in coast keeping the link voltage up, until the line power returns to normal and the MCB reconnects.

The major limitation of the dc series motor is that it tends to run away and self destruct with no load. Thus, auxiliary loads that can be direct-driven by the motor shaft (such as blowers

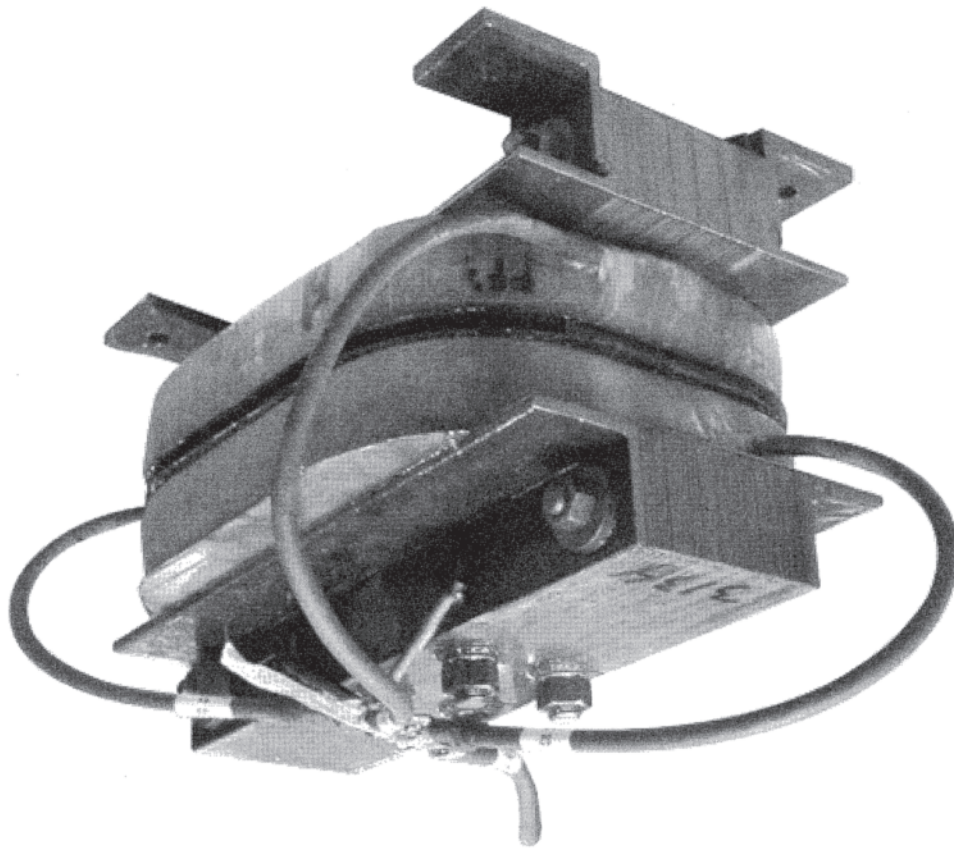


**Figure 2.81** An inductive shunt used on a dc mass-transit car.

with shaft mounted impellers) and have guaranteed minimum torque load can be and are driven by series motors. Belt drive is not used because failure of the belt would loose the load. A fan load is desirable for a series dc motor. This is one function the series dc motor still excels at: dynamic braking resistor cooling blowers (see [Section 2.4.1.1](#)). Literally all other auxiliary motors on new equipment are three-phase ac.

#### 2.4.4.4 Priority for Power

DC series motors were found to be best at surviving the electric environment on traction systems. A favorable synergism also occurs on an externally powered car. With a given torque load, the series motor draws a current almost independent of speed and runs at a speed proportional to the applied voltage. Hence, when line voltage is low, the traction motors come to the end of their maximum accelerating current demand earlier; the car accelerates somewhat more slowly but demands less average current from the line. The power being drawn from the line is down by more than the proportion by which the voltage has dropped. The end result is that the equipment inherently takes it easy on a weak line rather than dragging it down farther by trying to demand the same power. Conversely, if the voltage is high the car performance will increase.

An unregulated dc motor-driven blower varies the amount of ventilation with line voltage. The speed of a series motor and consequently the volume of air its blower delivers drops

less than the voltage because as the blower slows so its load decreases. This decrease in ventilation is permissible because the blown equipment's load has also decreased. In the case of a grid blower on a OHV truck at high altitude, the air density can be only 60% of standard air density at sea level, resulting in decreased cooling effect. However, the decreased load will cause the blower to speed up blowing more air, partially compensating for the lower cooling effect of the thinner air.

#### 2.4.4.5 Rotary Inertia

Every transportation vehicle has rotary inertia. It is the sum of the inertias of all the parts rotating with the wheels. These parts must be accelerated translationally, the same as all the other mass of the vehicle. In addition, their masses must be accelerated rotationally to change the speed of the vehicle. This makes the vehicle appear heavier than it actually is; if rotary inertia is neglected, the actual tractive effort required for acceleration will be greater than calculated.

The added tractive effort needed to accelerate a part rotationally is proportional to its  $Wk^2$ , where  $W$  is the mass or weight, and  $k$  is its radius of gyration. It is also proportional to gear ratio squared. Motor torque may be taken as proportional to  $D^2L$ , where  $D$  is rotor diameter and  $L$  is active rotor core length. A lightweight mass-transit car or light rail vehicle may have rotary inertia referred to the wheel rim that exceeds 10% of car mass. Rotary inertia is usually neglected on

locomotivehailed trains and OH Vs. The total mass of the vehicle far exceeds any rotary inertia effect.

#### 2.4.4.6 Ventilation

Almost all traction motors require ventilation to get the required rating in the space available. Traction motors are more heavily ventilated than industrial motors.

The basic types of ventilation are self, by a fan on the motor shaft, and separate, from an external blower. Figure 2.64 shows a self-ventilated ac traction motor. The main merit of self-ventilation is that it is cheap because there are no external blowers and ducting required.

A fan on a traction motor that must work equally well in both rotations must have radial blades. The maximum static efficiency to be expected is 20%. Much of the power that does not go into moving air goes into making noise; a siren and a radial fan are very similar. Making blade spacings unequal can lessen the perceived noise by dividing a single tone into multiple tones that are less objectionable to the human ear (this is called random spaced blades). Beyond that, the only way to reduce the noise generated is to reduce fan performance and ventilation by recessing the blade tips sufficiently below the air outlet struts in the frame.

Self-ventilation requires that the inlet air pressure be at a vacuum. If the inlet is at track level, as is typical, much dirt and snow will go into the motor. No active air cleaning can be used. Passive filters can be used but they must be changed often or they clog and what air does get through pulls dirt with it. Muffling noise after it has been generated has been tried but has not found much acceptance. A muffler takes up space and is prone to damage, and it also causes some reduction in air flow.

Self-ventilation gives most air at high speed, when motor losses are low, and least air at low speeds, when losses are high. Separate ventilation provides ventilation at all times, regardless of motor speed or losses. Over a duty cycle from station to station, the total losses must be removed by the air for operating temperature to stabilize. If the thermal time constant of the motor is long compared to the duty cycle the temperature excursions will be small enough to be handled by self-ventilation. This is the case for the typical mass transit duty cycle of 2–3 minutes compared to the armature thermal time constant of 15–20 minutes.

Experience has shown that self-ventilation with dirty air is economic for industrial and light switching locomotives and for many mass transportation and some light rail applications. For many mass transportation properties the simplicity of self-ventilation carries a high cost in motor maintenance, but is considered worthwhile. Self-ventilation with air ducted from a clean intake, above the platform at the minimum and preferably from roof level or the car air exhaust, has been used successfully in a few commuter applications, especially with high motor voltage.

Separate (also called forced) ventilation is provided for all applications where it can be expected that high tractive effort will be required for times equal to or exceeding the motor's thermal time constant.

There is less noise from a blower, and it's intake and outlet may be muffled by ducting. Its output is at positive pressure, so the dirtiest part of the air can be skimmed off while spilling about 10% of the output.

Main line and road switcher locomotives and OHV trucks use blowers that are engine-driven or motor-driven from supplies dependent on engine speed. Throttle position determines power demand, and ventilation is in proportion. On the locomotives air is taken from the cab side through inertial filters from which the dirtiest air is sucked away and exhausted. The cleaned air is used to ventilate the traction motors and auxiliary machines and for the engine. OHV trucks typically use unfiltered air ducted in from the highest position possible (over the control cabinet on the front deck).

#### 2.4.4.7 Auxiliaries

Auxiliary functions are often considered as nuisances by equipment designers and are not given the attention to detail that they need. As a result, auxiliaries cause a disproportionate part of vehicle problems. Auxiliaries include blowers and fans, air compressors and air conditioning. The smallest auxiliary motors are run from control voltage. This relatively benign supply allows nearly commercial motor construction. The major deviations are total enclosure to protect against the environment, extra bracing to protect against shock and vibration, and extra bearing grease for long life between overhauls.

Control voltages in American practice are 28 V on off-highway trucks, 37 V on most transit cars, and 74 V on locomotives. These systems use 24 V, 32 V, and 64 V batteries, respectively. This is suitable only for only the lowest power applications.

Large auxiliary motors used to be dc powered directly from the line on externally powered vehicles. More recently they are ac powered from three-phase static power converters which are replacing the older rotating motor-alternator sets. Large auxiliary ac machines on internally powered vehicles typically are supplied from an auxiliary alternator.

#### 2.4.4.8 DC Traction Motor

The torque and speed equations in terms of electrical input are developed as follows. First equate the power input (electrical) to the mechanical power output considering there will be losses in the conversion (we will use horsepower [hp]):

$$\frac{V \times I}{745.7} = \frac{\text{Torque} \times \text{RPM}}{5252.1 \times \text{Eff.}} \quad (2.120)$$

where:

$V$  = terminal volts across armature and series exciting field

$I$  = amperes

Torque is in lb-ft.

RPM speed in revolutions/minute

recognizing that:

$$V = E + IR + V_{bd} \quad (2.121)$$

where:

$E$  is the back emf of the armature

$R$  is total resistance of the circuit (i.e. armature, comm. Field, exciting field, etc.)

$V_{bd}$  is the contact voltage drop of the brushes (in the order of 2 volts and considered constant).

Recognizing that

$$\begin{aligned} E &= (E/RPM)*RPM \text{ 2.121 becomes:} \\ V &= (E/RPM)*RPM+IR+V_{bd} \end{aligned} \tag{2.122}$$

where the ratio  $(E/RPM)$  represents flux and is taken from the load saturation characteristic for the machine (such as Fig. 2.68), and does not represent any particular value of  $E$  or RPM.  $(E/RPM)$  is a function of exciting field amps and armature (load) amps.

$$\text{Let Eff(s)} = \frac{V - IR - V_{bd}}{V} = \text{Speed Efficiency} \tag{2.123}$$

Substituting into Eq. 2.121

$$RPM = \frac{V - IR - V_{bd}}{(E/RPM)} = \frac{V}{(E/RPM)} * \text{Eff(s)} \tag{2.124}$$

Equation 2.124 is the speed equation and implies that speed is directly proportional to voltage and inversely proportional to flux level. Eff(s) represents  $I^2R$  losses. Substituting Eq. 2.124 into Eq. 2.120 and letting Eff=Eff(s)\*Eff(t):

$$\frac{RPM*(E/RPM)*I}{745.7*Eff(s)} = \frac{\text{Torque}*RPM}{5252.1*Eff}$$

Solving for torque:

$$\text{Torque} = 7.04*(E/RPM)*I*Eff(t) \tag{2.125}$$

Equation 2.125 is called the torque equation and indicates torque is proportional to the product of flux and current. Eff(t), torque efficiency, represents the other losses other than  $I^2R$ , i.e., friction and windage, no-load core loss, and stray load loss. It can be seen that the loci of constant torque on the saturation curve (Fig. 2.68) is a hyperbola. Gear loss can be included as another torque loss and then:

$$\text{Tractive Effort (lbs. force)} = K_t * \text{Torque} \tag{2.126}$$

where  $K_t = (\text{Gear Ratio} * 24) / (\text{Wheel Diameter in inches})$  and

$$\text{mph} = \text{RPM} / (K_t * 14). \tag{2.127}$$

Inspecting the series motor saturation characteristic (Fig. 2.68) reveals why it is ideal for the traction application. When voltage is applied at standstill all of the applied voltage produces current since  $R$  is small and  $E=0$ . The high current results in a high flux  $(E/RPM)$  coincident with the high current giving the high starting torque needed for acceleration. Once running the back emf  $(E)$  will reduce the current and likewise the  $(E/RPM)$ . With a constant power generator volt-ampere curve the voltage goes up as the current decreases, therefore from 2.124,  $V$  is increasing and  $(E/RPM)$  is decreasing as  $I$  decreases, which will increase the motor speed as torque decreases. It can also be seen that since the  $(E/RPM)$  characteristic is increasing with increasing current, series motors can be run in parallel from the same voltage source and will share load. If the current increases in one motor its  $(E/RPM)$  is increased that balances the voltage between the motors. Separately excited motors in parallel have no tendency to share load.

A dc traction motor intended for rapid transit duty has to have its load saturation characteristic custom designed to meet the performance and line voltage specified as follows. While line voltage will vary considerably over and under the nominal (i.e., 400–720 V on a 600-V nominal line is allowed per IEEE Std. 11) one voltage (e.g., 575-V dc) will be specified to meet the specified performance. Specified performance will consist of an initial acceleration rate and obtaining a certain distance in a certain time with a fully loaded car (Fig. 2.82). These requirements translate directly into a speed-tractive effort characteristic as shown in Fig. 2.80. The initial acceleration rate dictates the maximum TE level at 1 in Fig. 2.80 per  $F=m*a$ . The motor is operated with full field strength initially and held at its maximum current by stepping out resistance in series with the motor as it speeds up. At point 1 all the resistance

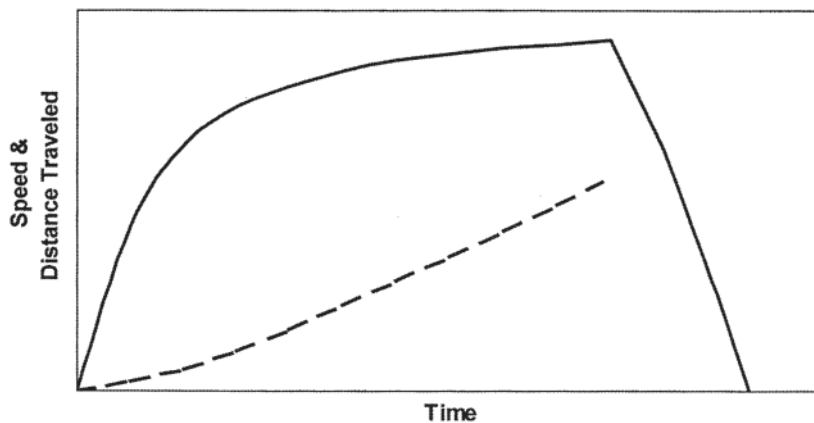


**Figure 2.82** Performance requirement for a rapid transit car. Time between stops typically 2–3 minutes. Speed, solid line; distance traveled, dashed line.

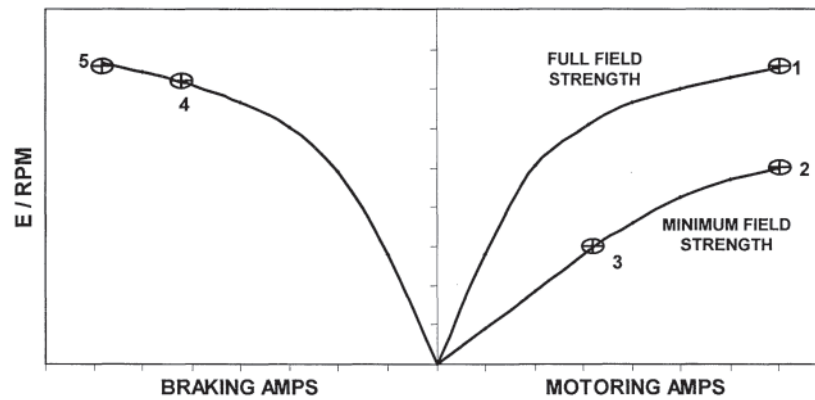


Figure 2.83 DC traction motor load saturation characteristic needed to obtain speed-tractive effort requirements in Fig. 2.82.

is out of the circuit and the motor is at line voltage. Shifting 1, 2, 3 to the right will give higher performance, shifting to the left lower, and at one point the specified distance will be covered in the specified time. Point 1 to 2 is obtained by field weakening at the maximum armature current. This is done in several steps of field shunting (diverting some current around the exciting field by connecting the appropriate resistance in parallel with it). The minimum field strength is typically one third of full field strength. Further increases in speed beyond (2) is accomplished by staying on the minimum field strength characteristic at an ever slowing acceleration rate until the TE balances the drag on the car (the balance point), or the maximum desired speed is reached, or braking is initiated. Points 1, 2, and 3 have specific motor torques and speeds and using the torque and speed equations derived above with the specified line voltage will translate into the corresponding (E/RPM), ampere points necessary on the load saturation curve (Fig. 2.83). Braking on a rapid transit car is typically always done in full field and maximum current by staging resistors to obtain maximum deceleration. Maximum speed in braking (4) is typically at three times the power level as in motoring and needs to be done at less than maximum current to stay within commutation and maximum volts between commutator

segment (peak volts/bar) limits. Braking torque can then be tapered up to maximum amps (5) at a lower speed. Typical full field characteristics for different rated voltages are shown in Fig. 2.84. Hyperbolas overlaying the saturation characteristics indicate torque levels. Compare the two 300/600 V characteristics. The one with the lower (E/RPM) characteristic will have higher performance because it will cause the curve defined by 1, 2, and 3 to shift to the right in Fig. 2.80.

For the dc traction motor used on mass-transit cars the motor rating is based on the RMS amps of the anticipated duty cycle. The exciting field is designed to rate at a lower RMS current rating than the armature circuit, since the field is shunted regularly. Minimum field strength should be no less than a 1:1 ratio of armature reaction ampere-turns times the per unit pole embrace to exciting field ampere-turns. This is to limit flux distortion which can cause unequal voltage distribution between the commutator segments. The overcompensation ratio (turns of commutator pole/turns of armature reaction per pole) should be higher than traction motors running on internal power, approximately 1.4, which provides faster response for externally powered motors which have to deal with transients. The real estate per pole pitch on the armature is divided into three zones: (1) excitation, (2)

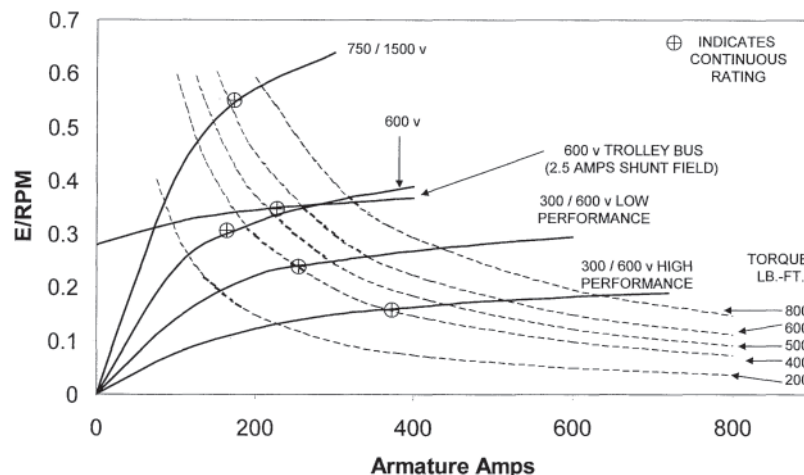
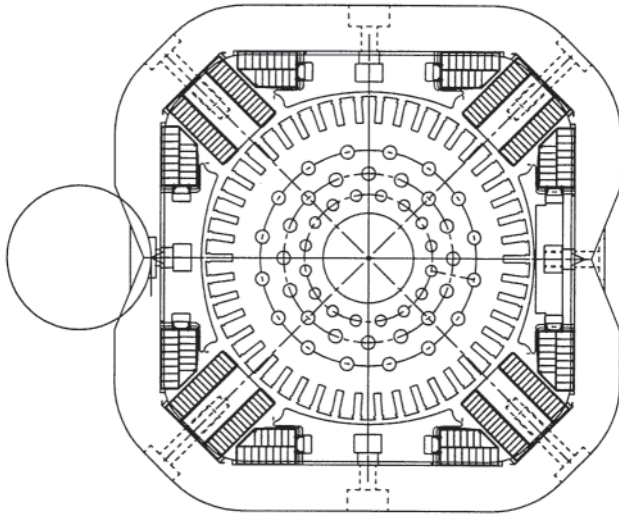


Figure 2.84 Full field saturation characteristics of dc traction motors designed for externally powered vehicles.



**Figure 2.85** Transverse section of locomotive “box” frame dc traction motor. Axle preparation is at center of exciting pole where flux is minimum. Three rows of cooling air duct holes in armature. Magnet frame carries exciting and commutating pole flux. (Courtesy of General Electric Co.)

commutating, (3) “free zone,” or what is left over. It is very desirable to have “one slot” of free zone on each side of the commutating zone for good commutation, although this is often difficult to achieve on highly rated traction motors for which the excitation zone is approximately 70%. One slot would correspond to four commutator segments with a four coil/slot armature coil.

There are strict outline limitations that must be met to fit into the allowable space. Space between the rails limits the

length. Wheel diameter and rail clearance limit the diameter. The four pole box frame maximizes the space utilization by maximizing the rail clearance and minimizing the axle prep, incursion into the frame for a given armature diameter (Figs. 2.85 and 2.86). Field coils use a molded and baked insulation system for maximum heat transfer. On very high brush current density motors a spiral groove can be cut into the commutator surface which helps maximize brush life by forcing the brush hotspots to move around.

The lap winding is used on all high performance traction motors because it commutates better than the wave winding. The wave, or “frogleg,” winding is used on lower performance high voltage auxiliary machines because it only has two circuits no matter how many poles it has. Traction motors are usually force ventilated since their highest losses ( $I^2R$ ) occur at their lowest speeds making self ventilation prohibitive (except for rapid transit duty cycles). Axial cooling ducts are used (Figs. 2.85 and 2.86) in the armature yoke to provide cooling.

It is desirable for commutation to have a shallow and wide slot since that decreases the reactance voltage in the armature coil. A higher number of slots may allow one slot of free zone on each side of the commutating zone, however more motor coils add cost. On the larger box frame traction motors a triple deck steel band is used on the pinion end to hold the endturns down on the armature head. A glass band can be used on the commutator end since the armature coil leads are tungsten inert gas (TIG) welded to the risers of the commutator segments. Smaller mass transit motors typically are glass banded on both ends. Commutating poles are provided with nonmagnetic shims between the pole and the frame and nonmagnetic bolts. This is to keep the commutation linear in

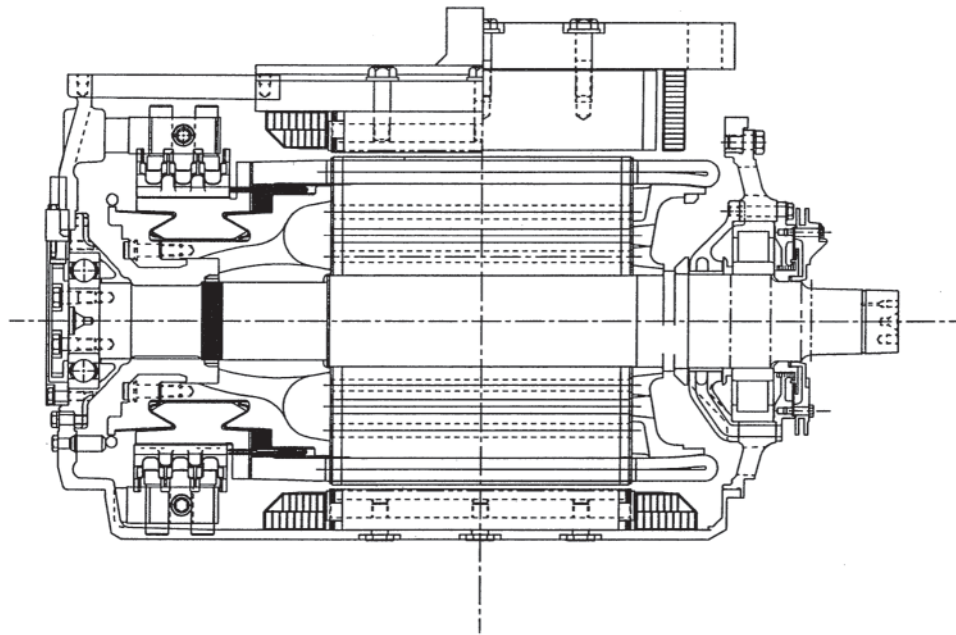


**Figure 2.86** Longitudinal section of locomotive “box” frame dc traction motor. Cooling air passes under commutator and is ducted to cooling ducts in armature core. (Courtesy of General Electric Co.)

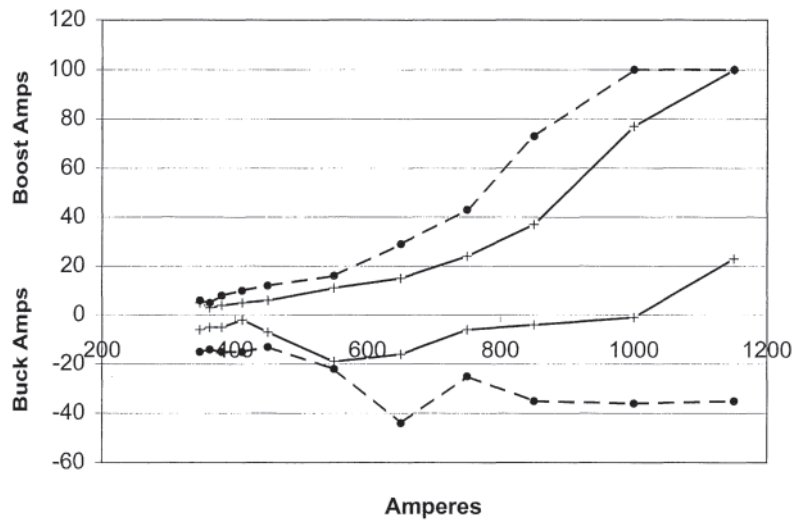


**Figure 2.87** “Black band” for dc traction motor on constant horsepower characteristic. A band is taken for each polarity and in both rotations. Dashedline, negative polarity; solidline, positive polarity.

the most important high speed region. If the bolts were magnetic they would cause overcompensation at low amps until they saturated. Most high performance traction motors have too narrow a black band at high speed to permit this.

One of the primary measures of a traction motor is its “continuous” rating defined as the maximum current capability of the motor that it can withstand continuously (i.e., until winding temperatures reach equilibrium) or, consequently the maximum tractive effort (torque) that the motor can produce continuously, with allowable temperature rise, and at a specified power level. The power level indicates the level of core losses which has a second order effect on the armature heating. This current rating will correspond to a torque level and most of the heating will be from  $I^2R$  losses. The ventilation level must also be specified in the continuous rating.

The commutator and brushes are generally the most sensitive areas to abuse and if something is wrong with the machine it usually will show symptoms at the brushes and commutator. On a new machine the proper nonmagnetic shim thickness under the comm. pole must be determined by test to get the correct amount of compensating flux. The proper amount of flux is determined by running “black band” testing on the first machines of a new design where amps are added (“boost”) or subtracted (“buck”) from the commutating field over the operating range of the motor to determine the range of sparkless commutation (the black band). If the center of the band is in the boost region the machine is said to be “undercompensated” since amps need to be added to get to the center of the band (indicating a thinner shim is needed). Likewise, if the center of the band is in the buck region the machine is “overcompensated” (indicating a thicker shim is needed). A typical black band for a locomotive traction motor after final adjustment of the shims is seen in Fig. 2.87. Note that the band is smallest at the lowest amps and widest at the highest. The band shifts toward the boost side at high amps due to the comm. pole magnetic circuit saturating. The band

is small at the low amp end because this is where the speed is the highest and the commutation is the hardest. This is where you adjust the shims on a new machine to get the band to straddle zero. If the machine runs on weak field the adjustment is done for the weakest field strength used in service (highest speed). The “zero” buck/boost line is where the machine will be running normally. Once the proper nonmagnetic shim thickness is determined it is fixed for all production machines of that design. If there is sparking at high load due to the commutating pole magnetic circuit saturating, it is not of much concern because the motor doesn’t spend that much time at high amps. However, the motor can spend considerable time at the high speed point, where the band is the smallest, so it needs to be set right at the highest speed point.

Current collection is the ability of the carbon brushes to maintain good contact with the commutator at commutator speeds of up to 12,000 ft/min. The commutator must be very round and the spring system of the brush holder must maintain adequate pressure on the brush over its entire wear range. If the spring pressure is too low the brushes will bounce causing arcing and electrical erosion. Too high and they will wear from mechanical abrasion. In transportation it is desirable to err on the side of higher spring pressure rather than too light due to the rather high vibration and shock levels on a axle hung motor. Typically, a new commutator is to have  $TIR \leq .001$  inch and less than .0001-inch difference between adjacent bars. The commutator is spin-seasoned to ensure mechanical stability at 20% over its normal maximum speed at a temperature higher than it should see in service and then tightened until stable.

It has been found that “reaction” or stabilized brush holders are most stable at very high commutator surface speeds. Reaction brush holders (Fig. 2.88A) position the brushes at a slant to the normal commutator surface as opposed to the radial position (Fig. 2.88B) common on lower performance machines. This results in part of the spring force pushing the

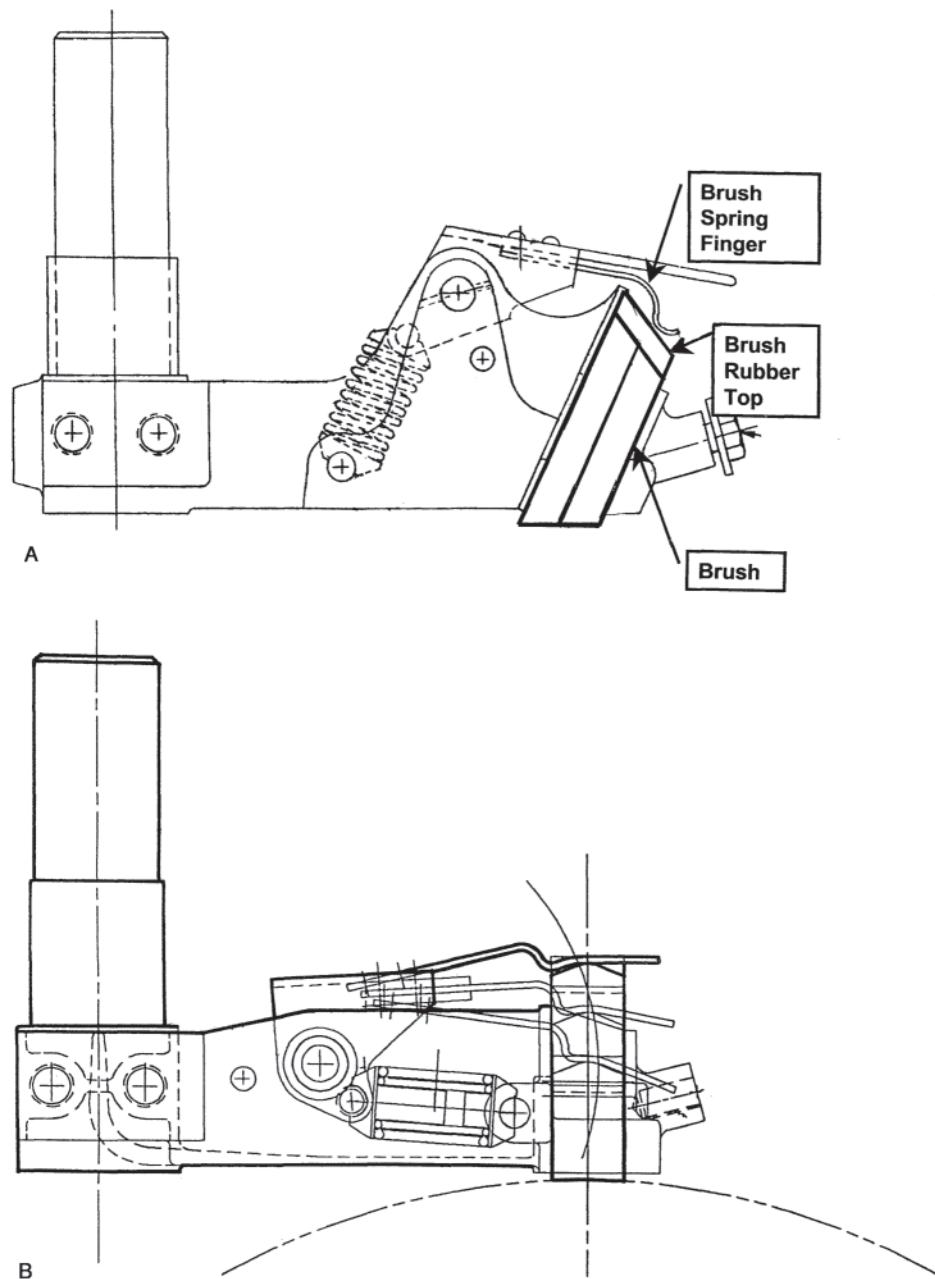


**Figure 2.88** Side view of a reaction (A) and radial (B) brush holder. Bistable spring arrangement snaps out of the way for brush replacement. (Courtesy of General Electric Co.)

brush into the long side of the carbon way so the brush is always “reacting” against and riding on this surface as opposed to the radial holder where it is possible for the brush to flop back and forth from one side of the brush box to the other (“chatter”). The force must be sufficient to keep the brush “pinned” against the long side of the brush box even if the commutator rotation is trying to push it away (“stubbing”). Care must be taken with the reaction brush holder to make sure the brush spacing is equal since the brush position can be shifted depending on the gap between the brush holder and

the commutator surface. The brush holder mounting blocks are precisely located in a fixed position so shifting the brushes is not allowed. The four brush positions are expected to be within  $4/64$  of an inch of one another.

In addition to the problem of current collection at high speed the rotor must stay together and not move appreciably under the high centrifugal forces present at high speed. The motor is mechanically designed for 20% above its maximum design speed. Armature banding to hold down the end turns is typically nonmagnetic steel banding on the pinion end and



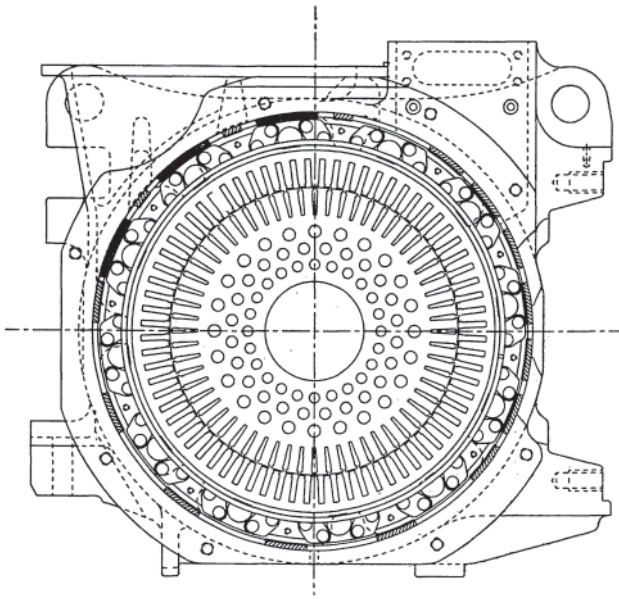


**Figure 2.89** Transverse section of an ac traction motor. Round cooling air ducts are provided in both the stator and rotor yokes. (Courtesy of General Electric Co.)

fiberglass on the commutator end. On the commutator end the coil is partially restrained by the TIG weld to the commutator riser so the weaker glass can be used. It is also an insulator so it will not conduct a flashover if one occurs. It is also, unfortunately, a good thermal insulator but this is not as important on the cool end of the motor (ventilating air is always directed at the commutator end first if possible). On the pinion end, normally the hot spot, the steel band is a better thermal conductor. In the core portion the coils are held in place with wedges.

A roller bearing is used on the drive end of the motor with the pinions where there are high side forces. A ball bearing is commonly used on the commutator end and ensures the axial location of the armature.

A good general reference on the dc traction motor is found in Ref. 49.

#### 2.4.4.9 AC Traction Motors

By the 1990s high-power electronic switching devices such as the gate turn-off silicon controlled rectifier (GTO) and later the IGBT became available at reasonable cost with good reliability for locomotive application. Prior to that they were being applied to mass transit cars. This made possible, on a large scale, the transition to ac induction traction motors, which require a variable frequency power supply to change speed and also eliminated the need for commutators and brushes. The rugged, uninsulated squirrel-cage rotor is much more suitable to the traction environment.

Typical cross sections for an ac locomotive motor are shown in Figs. 2.89 and 2.90 and a cutaway picture of a transit car motor is shown in Fig. 2.64.

AC traction motors can be applied with a single inverter per motor, which is typical for locomotive and OHVs. Or they can be applied with multiple motors per inverter such as all the motors in a truck (typical for mass transit). If more than one motor is running off one inverter some consideration needs to be made for the wheel diameter differences that will be allowed. If a low slip (low rotor resistance) design is used with a very steep torque versus slip characteristic the load sharing will be poorer than a higher slip (higher resistance) rotor for the same differences in motor speed. The motor with the larger wheels will take more load because it will run slower and have more slip. In practice, this has not proven to be a big problem.

Large motors usually have low slip rotors fabricated from copper alloy bars and endrings. The alloy increases the resistivity of the copper but greatly improves its mechanical strength. The bars are brazed into slots or grooves in the endring. Since the frequency can be varied the motor will always be operating on the right side of the maximum torque point (low slip) and never has to start “across the line” with five times or more current draw like a fixed frequency motor.

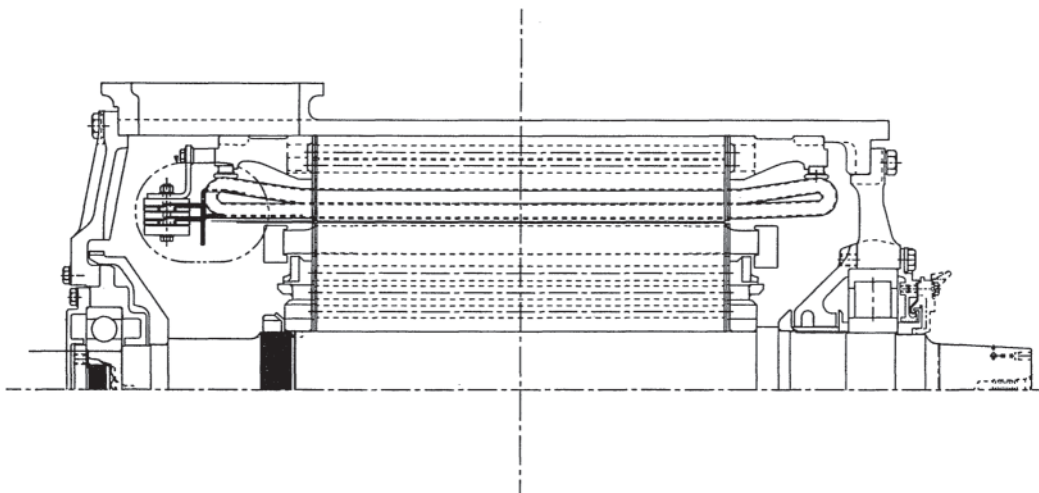


**Figure 2.90** Longitudinal section of ac traction motor. (Courtesy of General Electric Co.)

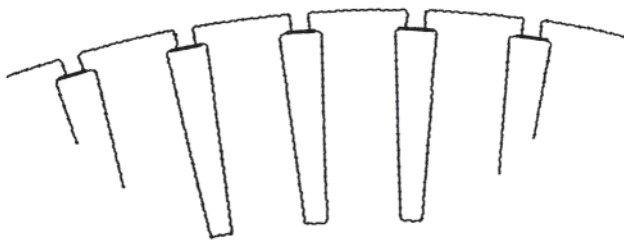


**Figure 2.91** Close up of ac traction motor transverse section of rotor bars. (Courtesy of General Electric Co.)

Therefore, no special provisions are needed to get starting torque up or starting current down, like a double cage rotor slot. Traction motors are built with trapezoidal (also called “flower pot” or “coffin”) shaped rotor slots that result in straight sided teeth (Fig. 2.91) and maximizes the bar cross sectional area for minimum resistance to harmonics.

It can be seen that the overall length of the motor is fixed by the LOEW. Since only the core portion of the motor produces torque, proportional to  $D^2L$ , the core length for a given LOEW can be increased by selecting a higher number of poles ( $P$ ). This is because for a given air gap diameter a full pitch of the coil is roughly  $D/P$  and the smaller the span between the coil sides the shorter the axial length extension of the end turns. There are other reasons why the number of poles should be minimized, such as magnetizing current proportional to  $P^2$ . Therefore, there are trade offs involved and each application must be analyzed for the best compromise. Also for the:

$$\text{RPMs (Synchronous Speed)} = \frac{120 * f}{P} \tag{2.128}$$

same maximum vehicle speed the maximum inverter frequency increases directly with the number of poles. For these and other reasons traction motors are never made two pole, small (rapid transit) motors are almost always four pole, and larger locomotive and OHV motors are typically six pole. In the case of very narrow gauge (meter) motors with limited length

but the same allowable diameter as other locomotive motors, eight poles might prove beneficial.

AC propulsion systems have an external power supply or a traction alternator’s rectified dc output feeding the dc link or bus that is filtered with capacitor banks. The inverters take their power from the dc link and create ac at the desired frequency to supply the speed call for the motors. The flux level in the motors corresponds to the V/Hz applied, or more correctly the internal or air gap V/Hz which is the voltage applied to the magnetizing inductance with the stator leakage reactance voltage drop subtracted from the terminal volts. There will be a V/Hz level that corresponds to the desired maximum flux level for each design. It is desired to operate in the full flux mode from start to well beyond the torque corner point (TCP), because this will minimize the current required, and we will want high torque to accelerate at low speed (Fig. 2.92). The inverter modulates the voltage in this region with pulse width modulation (PWM) to obtain a fairly harmonic free waveform (at least in the lower harmonic orders such as fifth, seventh, etc.). The maximum fundamental phase voltage output an inverter can produce for given dc link voltage is:

$$V_{ph} = (V_{dc} - DD) * \sqrt{2/\pi} \tag{2.129}$$

where DD=device voltage forward drop (usually about 10 V). When the inverter reaches this voltage holding constant V/Hz the voltage level is tied to the dc link voltage level at higher frequencies. This mode of inverter operation is called six-step or square wave (SW; consult Sections 9.3 to 9.6 for further details) because the line to line voltage is simply positive and negative pulses of 120-degree conduction periods. The harmonic voltages produced by the inverter in SW are very high in the nontriplen odd harmonics (i.e., 5th, 7th, 11th, 13th, ..., etc.). The amplitudes of the harmonic voltages in SW are  $V_{ph}(f)/n$  where  $n$  is the harmonic number and  $V_{ph}(f)$  is the fundamental phase voltage. The impedance to these harmonic phase voltages is the sum of the stator and rotor leakage reactances  $X_1+X_2(n)$  at their respective harmonic frequencies. Little if any harmonic current passes through the magnetizing reactance since it is very large compared to the rotor leakage

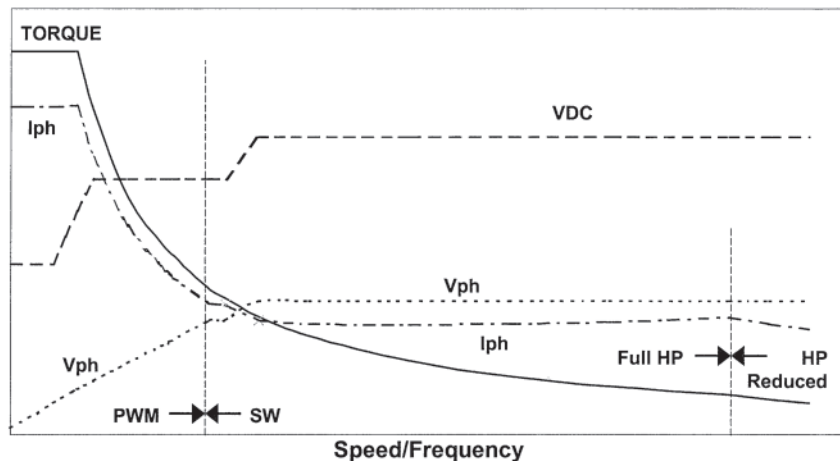


**Figure 2.92** AC traction motor characteristic.

reactance. The rotor leakage reactance is denoted  $X_2(n)$  to indicate it is a function of frequency. Due to the deep bar effect the harmonic currents are crowded into the top of the rotor bar in the rotor core. This causes the rotor leakage inductance to decrease significantly. It also increases the effective bar resistance to the harmonic currents significantly. As a result, there is a significant increase in rotor bar heating when operating in S W. It will be worst at the PWM corner point if voltage is held constant for higher frequencies because the harmonic voltage amplitudes will stay the same (if the link voltage stays the same) but the impedance increases linearly with frequency, so the harmonic currents will decrease linearly with frequency. Therefore, even though the PWM corner point is usually at a lower torque value than the continuous rating the rotor heating at this point needs to be checked to see it is not limiting.

Once on the constant voltage characteristic the motor flux (V/Hz) will decrease linearly with frequency and maximum torque (also known as pullout or breakdown torque) decreases with the square of the flux. If we are on a constant horsepower power supply (internally powered) the torque will be coming down as speed (frequency) increases. Therefore, at some speed we will have insufficient torque to continue holding constant horsepower and will have to decrease power to maintain a minimal torque margin (say 125–130%) between the breakdown torque and operating torque. For example, say you have 300% BDT at speed “X” at constant horsepower and voltage and you wish to have a minimum torque margin of 130% at the same horsepower at higher speed. You would have to start decreasing horsepower demand when the speed reaches approximately  $X \times 300 / 130$ . Also notice that since torque is the product of flux (V/Hz) and current, where torque is constant current stays about the same as long as V/Hz stays the same. If we are on the horsepower curve and the V/Hz is constant, current will come down linearly with speed increase. On constant voltage flux is decreasing as speed increases as well as torque, so the current stays relatively constant.

## 2.5 MOTORS FOR SPECIAL APPLICATIONS

### 2.5.1 Stepper Motors

#### 2.5.1.1 Introduction

Stepper motors are a class of electromechanical devices used to produce discrete or noncontinuous motion. The name “stepper motor” describes its principal functions: “motor” means that electrical input energy is converted to mechanical output energy, and “stepper” means that the energy conversion process is performed in discrete steps or increments. Stepper motors fall within a broader class of devices known as *incremental motion devices*, which includes incremental actuators and other digital control devices used in motion control. Stepper motors have been developed and are available commercially in several different physical technologies, primarily hydraulic, pneumatic, and electrical systems, and sometimes, combinations of two or more technologies. Pneumatic and hydraulic stepper motors generally have higher torque/weight ratios than electrical steppers. For very high torque positioning systems, hydraulic

and pneumatic stepper devices often provide the most cost-effective system, and are used in many robotic applications. However, where precise position, velocity, or acceleration control is required and/or when very small steps of control are necessary, electrical stepper motors have many advantages. Also, electrical stepper motors are much more compatible with digital control systems which are the norm for many control systems today. This section is concerned only with electrical stepper motors.

The input to a stepper motor is digital, that is, an electrical pulse or series of discrete pulses, in contrast to the sinusoidal ac or steady dc used to energize common household and industrial motors. If the input pulse train is continuous and applied at the proper timing intervals, a stepper motor can be operated in a constant-velocity mode just as the more common motors are. One of the most common types of stepper motors of the reluctance variety has been developed recently for continuous output speed and is known as the switched reluctance motor. The operation of stepper motors in either the stepping or continuous modes has been made economically viable by the recent rapid development and availability of low-cost power semiconductors. Thyristors (silicon-controlled rectifiers [SCRs]), power transistors, power metal oxide semiconductor field-effect transistors (MOSFETs), IGBTs, and so forth are widely used in stepper motor and switched reluctance motor control in current ratings of a few milliamperes up to hundreds of amperes. Although stepper motors can be controlled from conventional ac or dc power sources by means of mechanical switches, such as relays, contactors, or stepper switches, most modern controllers are of the semiconductor type. A stepper motor controller has two functions: supply of electrical energy to the motor so that it develops the torque required to drive the load and control the position, velocity, and or acceleration of the motor shaft. Obviously, many safety and protection features are also required, such as voltage limits and overcurrent protection.

Stepper motors are used primarily to control motion—the position, speed, or acceleration of the device connected to the motor’s output shaft, or a combination of any of these. Stepper motors can also be used to sense position and to recover energy from the output shaft motion in a regenerative mode as in continuous types of motors. Stepper motors are applied in many computer peripherals, such as printers, tape drives, disk drives, and memory access mechanisms; in machine tool control applications of many types; in robotic control; in all sorts of position control, such as antenna control, telescope positioning, gun turret control, fiber optics alignment, and optical interferometry; in automotive throttle control and other automotive applications; and in many military guidance control applications.

Stepper motors are designed and produced for both rotary and linear motion. In the latter case, the terms “motor” and “actuator” are used somewhat interchangeably. Since most applications are of the control and low-power variety, commercial stepper motors are available in relatively low torque ratings, up to about 14 N·m (2000 oz-in), except for the switched reluctance variety. Maximum electrical input

pulse rates are from 1500 to 2500 pulses per second (pps). Stepper motors are brushless and most continuous motors known as brushless dc motors can be operated in a step mode, although with relatively large step increments. Stepper motors are constructed of the same types of materials as continuous motors, generators, and transformers, which are adequately discussed in other sections of this handbook. Also, standard electromagnetic terms are used to describe most stepper motor characteristics and will not be defined except as peculiar to stepper motors. Likewise, many commercial stepper motors are designed for standard NEMA frame sizes, just as continuous machines of similar ratings.

In control applications, the stepper motor/controller system must be compared with the more conventional feedback control systems using continuous motors. Stepper motor systems are inherently open-loop systems and as such avoid the complexity, stability problems, and steady-state errors associated with feedback control. The stepper motor is a digital device, compatible with most digital power sources, and the number of input pulses determines output position and pulse frequency determines output velocity. Other merits of stepper motor systems include:

1. Freedom from drift
2. Noncumulative error
3. Low maintenance and high reliability due to their brushless design
4. For permanent-magnet and hybrid steppers, the highest developed torque per input ampere and, generally, the highest torque for a given package size of all types of motors
5. For PM and hybrid types, a holding torque at standstill
6. For all steppers, stability at zero speed
7. Capability of bidirectional operation with no switching of electrical connections

### 2.5.1.2 Basic Types and Construction

There are four basic types of stepper motors: *reluctance*, *permanent magnet (PM)*, *hybrid*, and *piezoelectric*. These designations refer to the structural differences and to the mechanism by which torque is developed in the motor. The designation “hybrid” implies that torque is developed by both reluctance and PM action. Actually, in most PM stepper motors (as well as in continuous PM motors), some reluctance torque is developed, but it may be quite small compared to the PM torque. A hybrid motor is one in which both PM and reluctance torque are significant. Within each designation, there is a great diversity of configuration and shape, in both rotary and linear designs. Only a few of the more common types will be discussed in this section.

Stepper motors are classified in motor terminology as “doubly salient”; that is, both rotor and stator are constructed with salient or projecting poles. These saliencies may consist of conventional-appearing poles, or tiny teeth, or combinations of both. The stepper motor is inherently simple due to the lack of brushes or slip rings, and consists of a salient stator magnetic member (generally laminated), insulated windings

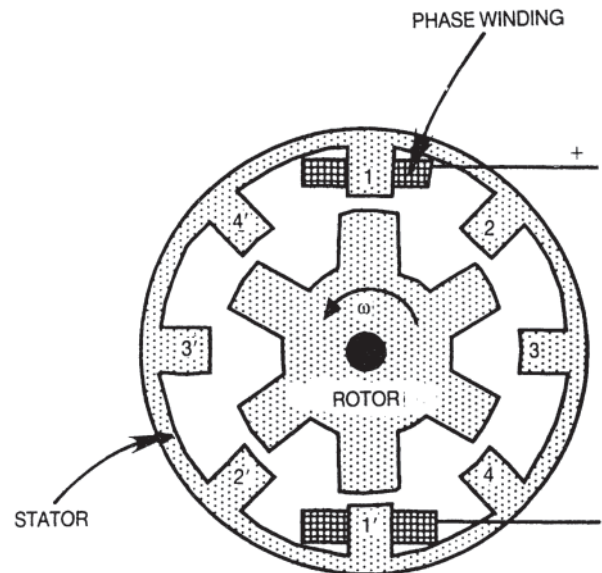


**Figure 2.93** Cross section of a reluctance stepper motor; dotted sections are composed of a soft magnetic material.

filling the slots between stator poles, a rotor consisting of soft steel (in reluctance machines) with imbedded permanent magnets in PM and hybrid machines, a stainless steel shaft, a housing containing and supporting the stator (generally constructed of aluminum or plastic), and a set of prelubricated bearings supporting the rotor. The bearings are generally the only parts requiring maintenance in stepper motors operated within the rated voltage, current, and temperature values stated on the motor nameplate.

### 2.5.1.3 Reluctance Stepper Motors

#### 2.5.1.3.1 Theory

The reluctance configuration is generally the simplest and lowest-cost type of stepper motor. The simplest reluctance motors are assembled of low-cost stamped parts using modern automated assembly techniques and are often called “tin-can” motors. The simplest form of a reluctance stepper motor is that known as the switched reluctance motor, shown in Fig. 2.93. As has been noted, this configuration is also used in higher-power, continuous-speed power applications as a replacement for induction motors [50–52]. Figure 2.93, although not the most prominent stepper configuration, will be used to illustrate some of the parameters and technical characteristics of the reluctance motor. The following symbols and abbreviations will be used.

$i$	Coil current (A)
$I$	RMS coil current (A)
$m$	Number of phase windings
$N$	Turns
$P_r$	Number of rotor poles
$P_s$	Number of stator poles
PR	Permeance (reciprocal of reluctance) (henrys)
RPM	Motor shaft speed (rev/min)

- $T_d$  Motor developed torque (N-m)  
 $\omega$  Motor shaft speed (rad/s= $2\pi$  RPM/60)

Reluctance machines are termed “singly excited” machines. That is, there is only one source of excitation of the magnetic field that sets up the conditions for producing torque or force. In Fig. 2.93, the only input to the motor is the electrical input to the windings; in the case shown, there would be four phase windings,  $m$ , each of which would be wound on two sets of diametrically opposite poles or saliencies, only the winding of phase 1 being shown in this figure. When current flows in the windings, a magnetic flux is developed in the two air gaps associated with a pair of windings. The magnitude of the flux crossing the air gap and the flux density (flux divided by the surface area of the pole) for a given applied mmf (product of current and turns in the coils) depends upon the length of the air gap and the nature of the rest of the magnetic circuit, which includes the stator and rotor poles, the stator and rotor yokes, and, to a lesser extent, the other three sets of poles and air gaps. Analysis of relatively simple magnetic circuits such as shown in Fig. 2.93 is presented in Section 1.4. The radial air gap between the stator and rotor poles is the most influential parameter in determining the flux density in most cylindrical reluctance machines; in disk or “pancake” configurations, the axial air gaps play a similar role. In Fig. 2.93, the poles of phase 1 are said to be in the *aligned* position or a *minimum reluctance* position. A magnetic circuit tends always to seek this minimum reluctance position and there is a strong force tending to maintain this position. As long as the phase 1 coils are energized, the rotor will remain in this position. In a reluctance stepper motor, this technique is used to “hold” the rotor in a certain position. The magnitude of current required for the holding phase coil depends upon the magnitude of the holding torque that must be maintained. When a rotor pole is exactly half-way between two stator poles, the poles are said to be in an *unaligned* or *maximum reluctance* position.

Theoretically, no torque is developed in the unaligned position, and it is considered a “neutral” position. In practice, it may be difficult to find an exact neutral position due to pole flux fringing effects, stator-rotor pole overlap, and dimensional inaccuracies. In Fig. 2.93, the rotor poles adjacent to phase 3 are approximately in the unaligned position. In all other relative positions of rotor and stator poles, a torque is developed when a phase is energized, always tending to move the poles into the aligned or minimum reluctance position. For example, in Fig. 2.93, if phase 1 is deenergized (current in the coils of phase 1=0) and the coils of phase 2 are energized, the rotor poles near the phase 2 stator poles will tend to move into alignment with the stator poles. This will result in a counter-clockwise “step” of motion. On the other hand, if phase 4 were energized, a clockwise step of motion would result.

Assuming that phase 2 has been energized, phase 3 will then have rotor poles in a position to produce torque resulting in another counterclockwise step of motion. Following this step, phase 4 will have rotor poles in the proper position for another counterclockwise step, and so forth. Counterclockwise motion is produced by the phase sequence 1–2–3–4; clockwise motion

by the sequence 1–4–3–2. It is important to note that the rotation (or linear) direction of reluctance stepper motors is determined by the phase switching sequence, *not by the polarity of the voltage applied to the exciting winding*. Reluctance torque is independent of the direction of the magnetic flux in the air gap.

The configuration of Fig. 2.93 is known as an 8/6 configuration, that is,  $P_s=8$  and  $P_r=6$ . Looking at the geometry of this figure, it is easily seen that the magnitude of one step is 15 mechanical degrees. In general, it can be shown that for any pole configuration:

$$\text{Step size} = 360 \times \frac{|P_s - P_r|}{P_s \times P_r} \text{ degrees} \quad (2.130)$$

Thus, a 12/10 configuration would produce steps of 6 degrees, but would require a 6-phase excitation. This type of stepper motor has a structure that becomes difficult and costly to manufacture if the number of poles is greater than 12, and thus smaller steps are not economically viable with the configuration of Fig. 2.93. There are a number of means of producing smaller steps, both through structural changes from the simple configuration of Fig. 2.93 and by altering the electrical excitation scheme by electronic techniques. Before looking at this important topic, a look at the torque developed in a reluctance stepper motor is appropriate.

It can be shown [50] that the instantaneous developed torque in a reluctance machine is:

$$T_d = \frac{(iN)^2}{2\omega} \frac{d(PR)}{dt} \text{ (N-m)} \quad (2.131)$$

In Eq. 2.131, if the two coils of the pole pair of one phase are connected in series, as is usual,  $N$  is the total number of turns per phase, that is, twice the turns per coil. Note that the speed term,  $\omega$ , will cancel out of Eq. 2.131 because the permeance change,  $d(PR)/dt$ , is also a function of speed. Equation 2.131 does not account for the effects of saturation of the magnetic circuit. Saturation is a complex phenomenon to evaluate in reluctance machines, since the regions of saturation vary as the rotor poles move into alignment with the stator poles. Equation 2.131 is adequate for low levels of saturation, such as in the pole tips. For cases where most of a rotor or stator pole or both become saturated, often called “global saturation,” the first term in parentheses in Eq. 2.131 becomes a product of  $iN$  and the saturation flux density (a constant value) in the air gap. Thus, the developed torque changes from a function of the square of the exciting coil current to a first power of the current as saturation increases in the magnetic members of the machine.

The permeance variation term in Eq. 2.131,  $d(PR)/dt$ , introduces the structural characteristics of the stepper motor. In the aligned position, the permeance (reciprocal of reluctance) is maximum and can be expressed as:

$$PR_{\max} = \frac{\mu_o A_p}{2I_g} \text{ (henrys)} \quad (2.132)$$

where:

- $\mu_o = 4\pi \times 10^{-7}$  = permeability of free space  
 $A_p =$  pole face area facing air gap ( $\text{m}^2$ )  
 $I_g =$  radial length of air gap (m)

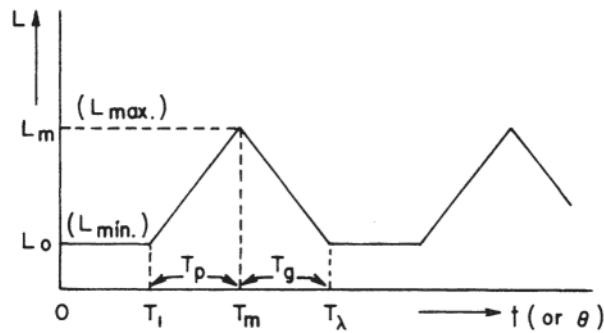


**Figure 2.94** Idealized inductance variation in a reluctance stepper motor as a function of rotor angle  $\theta$  or of time  $t$  if the rotor is turning.

The minimum permeance, which is when the poles are unaligned, is difficult to calculate analytically except by finite element methods or mapping techniques. Permeance or reluctance cannot be measured directly. However, permeance is related to inductance by the square of the turns of the exciting coil and inductance can be readily measured by many techniques. Stepper motor torque is usually expressed in terms of the inductance variation as seen at the terminals of the exciting coil. An idealized variation is illustrated in Fig. 2.94 for a motor configuration of the type shown in Fig. 2.93. Taking the average of Eq. 2.131 over a time period equal to the time for a rotor pole to move from the unaligned position to the aligned position, the average torque developed in one phase of a stepper motor is:

$$T_{d(\text{avg})} = \frac{I^2 P_s}{2\pi} (L_{\text{max}} - L_{\text{min}}) (N\text{-m}) \quad (2.133)$$

where the,  $L$  terms equal  $N^2$  times the respective permeances. This is the average torque available to move a load inertia one step as the result of the energizing of one phase winding. In practice, there may be more than one phase winding energized over some periods of time, a technique called phase overlap, which will increase the motor developed torque over that given in Eq. 2.133. But Eqs. 2.132 and 2.133 show that torque is primarily a function of the pole face area and an inverse function of the air gap between the rotor and stator poles. These two parameters largely determine the size of a stepper motor to move a given load inertia, even in physical configurations considerably different from that shown in Fig. 2.93.

The preceding analysis has been based upon a stepper motor configuration used in relatively high-torque applications. The steps available with this configuration are relatively large, as has been noted, and it is sometimes referred to as a large-angle stepper. To achieve a smaller step, many techniques and many different physical configurations are available. The most obvious technique to get a smaller step angle is to place a gearhead with the appropriate ratio on the shaft. This solution adds weight and losses and decreases the precision of the step due to gear dead band.

#### 2.5.1.3.2 Small-Angle Reluctance Stepper Motors

From Eq. 2.130 it is seen that the number of stator and rotor poles determine the step angle. To achieve small step angles, the number of poles can be increased and they are often in

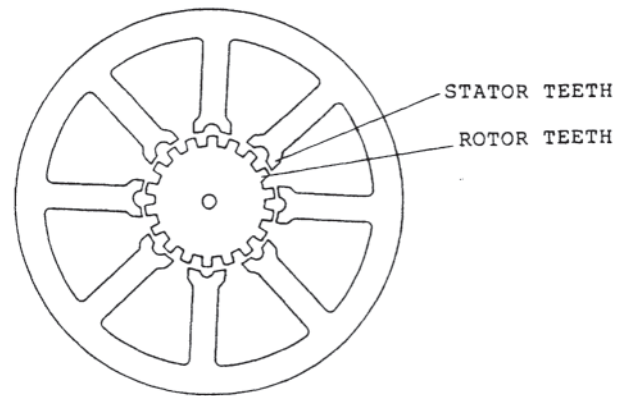


**Figure 2.95** Cross section of the magnetic circuit of a multitooth reluctance stepper motor.

appearance more like teeth than salient pole projections. Figure 2.95 illustrates a modification of the configuration of Fig. 2.93 that results in a much smaller step angle [53]. For this configuration:

$$\text{Step} = \frac{360}{mN_r} \quad (2.134)$$

The number of stator teeth is related to the number of rotor teeth by:

$$k \times \text{TH}_s = N_r \pm \frac{N_s}{m} \quad (2.135)$$

where  $\text{TH}_s$  is the number of stator teeth. For the configuration of Fig. 2.95,  $m=4$ ,  $N_r=18$ ,  $N_s=8$ , and  $\text{TH}_s=16$ , giving  $\text{Step}=5$  degrees and  $k$  (a positive integer)=1.

Investigation of a few more combinations of teeth is instructive. For example, assume a 2-degree step is desired with a 10-pole, 5-phase stator. This requires  $360/(5 \times 2)=36$  poles from Eq. 2.134; checking the number of required stator teeth using Eq. 2.135 gives the value of  $k \times \text{TH}_s=36 \pm 2$ . It is seen that there is no combination of the  $\pm$  sign and  $k$  value that results in a value of  $\text{TH}_s$  that is an integral multiple of 10 stator poles. Therefore, this combination is not realizable. If the stator is changed to 12 poles and 4 phases, then  $N_r=45$  from Eq. 2.134. Equation 2.135 then becomes  $k \times \text{TH}_s=45 \pm 3$ , and it is seen that, using the + sign, several stator tooth combinations are possible: With  $k=1$ ,  $\text{TH}_s=48$ ; with  $k=2$ ,  $\text{TH}_s=24$ ; with  $k=4$ ,  $\text{TH}_s=12$ , and all of these are multiples of 12.

The configuration of Fig. 2.95 and variations of it are among the most common and least expensive of step motors, and as pointed out earlier are often called "tin-can" motors [54]. Lamination stacks for the rotor and stator magnetic members are readily mass-produced using stamping techniques and simple lamination assembly techniques. The minimum step size is limited to about 4 degree due to stamping tolerances. As the number of rotor poles or teeth increases, such as the 45 in the example above, a larger rotor diameter is required and the difference between maximum and minimum inductance (Fig. 2.94) decreases, decreasing the developed torque per unit motor size. However, step size can be decreased through various winding and electronic techniques, as discussed below.

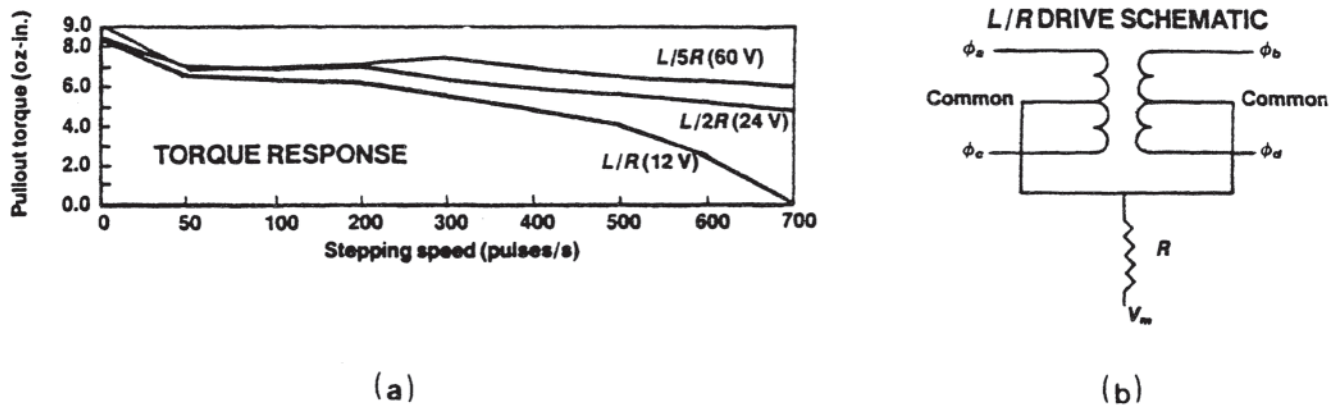


**Figure 2.96** (a) Torque response of a “tin can” stepper motor as a function of applied pulse rate, (b) Unipolar drive scheme with added resistance to decrease winding time constant.

Figure 2.96 [54] illustrates torque characteristics as a function of input pulse rate for a commercial tin-can motor; the schematic diagram for a four-phase winding is also shown in Fig. 2.96 and is discussed below.

Smaller steps can also be realized by “mechanically phasing” individual motors on the same shaft. In this approach, the individual motors are disk or pancake shaped with axial air gaps. In one mechanical phase, or individual motor, the rotor and stator have equal numbers of poles, which are constructed of radial magnetic sectors separated by nonmagnetic (usually nonconducting) radial sectors. Only one coil of solenoidal shape is required to excite a single phase. One phase of the axial gap type of reluctance stepper motor develops zero starting torque in either the aligned or unaligned position, and the torque in intermediate positions may be insufficient to overcome the load and motor inertias. However, with two or more individual motors displaced in rotary position from each other by the proper angle and affixed to a common shaft, starting torque is developed at all angular positions.

Figure 2.97 illustrates the geometry of a disk used as the rotor of one phase in this type of step motor; Fig. 2.98 illustrates a cutaway of a schematic diagram of a three-phase disk motor. Smaller versions of this configuration are manufactured with up to nine phases. Figure 2.98 shows 12 sectors per disk; in single-phase operation, each pulse in the exciting coil would result in a  $360/12=30$ -degree steps. With two additional disks on the same shaft and two additional exciting coils, steps of  $30/3=10$  degrees can be realized; with nine phases, 3.33-degree steps are realized. In low-power applications, stamped parts or powdered iron parts can be used for both rotor and stator magnetic sectors. Considering also the simplicity of the solenoidal coil, this stepper motor configuration is among the lowest in cost.

#### 2.5.1.3.3 Reluctance Motor Excitation Systems

The small-angle reluctance stepper motors described above provide steps down to the 3-degree range. Much smaller steps can be realized by various schemes of coil excitation. Thus far, a full pulse of excitation current has been assumed in one coil of systems excited as in Fig. 2.93 or in one phase of systems

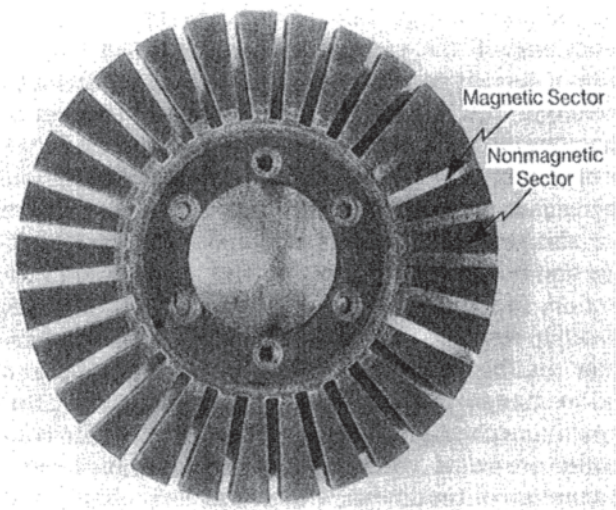


**Figure 2.97** A 29-sector disk for a radial-gap reluctance stepper motor. (Only six of the magnetic sectors have been inserted.)

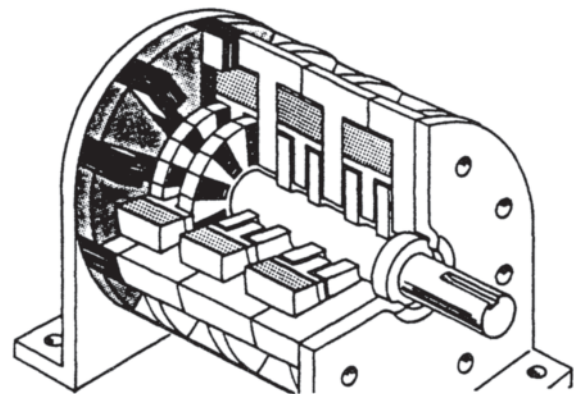


**Figure 2.98** Cutaway view of a three-phase axial gap stepper motor.

excited as in Fig. 2.98. There are two principal functions of the stepper motor controller: (1) to supply current to the motor coils that is sufficient to overcome the inertial, friction, and load torques of the system; and (2) to supply current pulses at the proper rate to achieve the shaft velocity or the time to reach a specified position that is required. There are also several ancillary functions, such as overvoltage and overcurrent protection and short-circuit protection. In more exacting applications, the controller is often required to optimize system efficiency, reduce audible noise and mechanical vibrations and aid in many other system considerations. The principal nameplate parameters of a stepper motor controller are rated voltage, maximum output current, maximum output power or power per phase, and maximum pulse rate. In applying a controller to a given motor application, it is also necessary to determine the motor torque that will be developed at maximum controller current. This requires knowledge of the motor coil characteristics and the torque constant of the motor. Most manufacturers supply speed-torque motor characteristics, examples of which are discussed below.

Almost all modern motor controllers use solid-state devices of one type or another, including power transistors, thyristors, MOSFETs, and many of the newer hybrid devices, such as IGBTs and MBTs. All semiconductors are voltage-sensitive and, in many types,  $dV/dt$ -sensitive. Therefore, the controller voltage rating is most important, and a 3:1 safety margin is generally recommended. For further safety in matching a controller to its motor and power supply, an analysis of the system voltage transients should be made due to the highly inductive nature of the motor. There is virtually no voltage overload capability in a semiconductor controller.

Figure 2.99 shows a schematic diagram of the windings in a four phase reluctance stepper motor. Note that if this diagram represents the windings of a reluctance machine of the type shown in Fig. 2.93, there will be two physical coils in each winding (on opposite poles for torque balance). This center-tapped arrangement is for *unipolar excitation*, that is, the

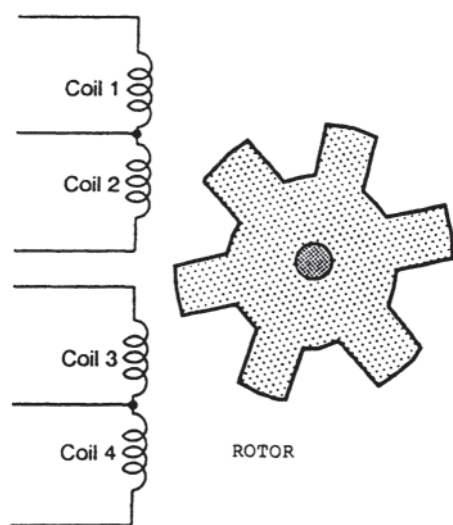


Figure 2.99 Electrical connections for a four-phase stepper motor.

current and hence its magnetic flux are unidirectional. In reluctance machines of any type, the torque developed in the machine is independent of the direction of the exciting winding current, as can be seen from Eq. 2.131. Controller configurations in which the winding current is reversed are known as *bipolar windings*. These are more common in hybrid and PM steppers, where the developed torque is reversed by current polarity. In reluctance steppers, direction of rotation can be reversed only by reversing the phase sequence, that is, the sequence in which the phase windings are excited.

Figure 2.100 shows a schematic of a simple transistor controller for two phases of a step motor. It is seen that this is a unipolar controller, since there is no means for reversing coil winding current. In Fig. 2.100 the reverse diode across the windings is present to prevent voltage buildup in the windings when the winding transistor is turned off. The energy stored in the winding at the instant of turn-off is returned to the source or used to charge another winding. Such diodes are often termed *freewheeling* diodes. The timing and sequence of the base triggers determines the speed and rotation direction of the motor.

There are many integrated circuit (IC) chips commercially available today to supply the logic and control functions for controlling stepper motors, including many of the common microcomputers, such as the Intel 8051 and Motorola 6801. These devices generally have far more capacity than required for stepper motor control alone, and there are a number of chips designed specifically for both reluctance and PM stepper motor control, such as the Sprague UCN 4204A, Siliconix Si 7250, TSC America PPMC 103, Motorola 56001, and Ericsson PBL 3774. There are also a few chips integrating both the logic and power functions, such as the Sprague UCN 5871B.

The simple controller of Fig. 2.100 is generally rather limited in control capabilities since each winding is either full on or full off. As the pulse frequency increases, the winding current rise time becomes an appreciable portion of the transistor ON time and eventually reduces the maximum and pulse RMS currents (the current required in Eq. 2.131), hence reducing the developed torque. This is illustrated in Fig. 2.96(a). A simple solution to the high-pulse-rate torque reduction is to add resistance to the excitation circuit, as shown in Fig. 2.96(b), which reduces the winding time constant, decreasing the current rise time. The effects of added winding resistance are shown in Fig. 2.96(a) for a specific tin-can stepper motor. The obvious disadvantage is the energy loss in the resistance, although this may not be an issue in small motors.

There are several more efficient means of improving high-speed response of steppers: Increasing the applied voltage is an obvious method providing this can be done while maintaining semiconductor operation within the device safe operating area (SOA). Figure 2.101 (a) illustrates the effects of increasing the applied voltage, with all other parameters remaining the same. This approach increases both the maximum steady-state current that can be reached during a pulse ( $V/R$ ) and the initial current rise rate ( $V/L$ ), and hence increases the torque level at all pulse rates. A second method is to reduce the number of turns in the exciting coils. The increase of torque at high pulse rates is primarily due to the



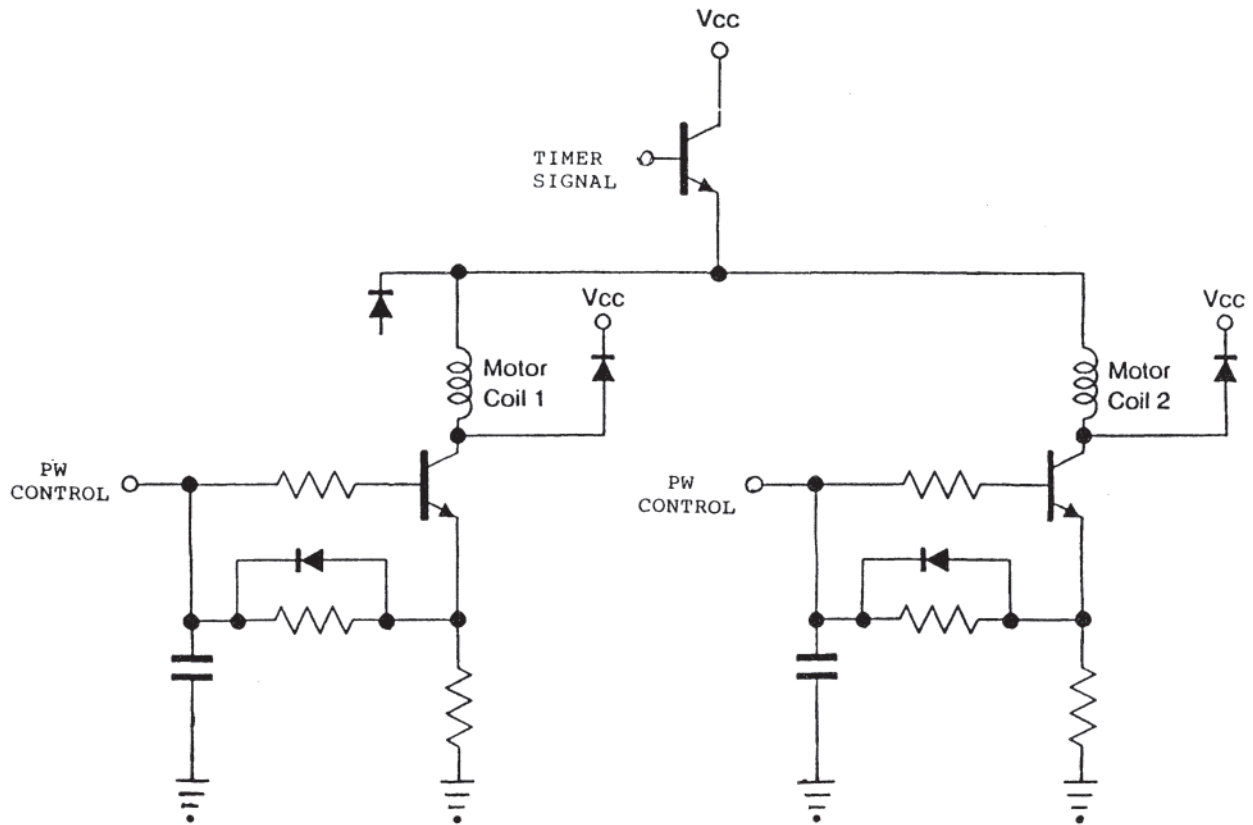


Figure 2.100 Simple pulse width (PW) controller for two phases of a stepper motor.

increase in current rise rate ( $V/L$ ). Winding resistance also decreases as the turns are reduced. Both peak and rms currents are also increased and care must be taken not to exceed heating or temperature limitations of the motor. Figure 2.101(b) illustrates the change in the speed-torque curve as exciting coil turns are reduced.

#### 2.5.1.4 Open-Loop and Closed-Loop Control

One of the principal merits of stepper motors is their ability to operate as control devices in an open-loop mode. The precision of control in open-loop is the angular step of the motor. As will be seen in subsequent sections, angular steps of hybrid steppers are commonly 1.8 degree. Finer steps can be achieved by a process known as *microstepping*, but this requires considerably more logic circuitry in the controller. The control of stepper motors in open-loop is generally simpler than the control required for competitive systems (usually closed-loop systems) such as servomotor and brushless dc motor systems. In open-loop, stepper motors are usually controlled by digital systems, in which the count of clock pulses or transistor pulses is available. The fixed relationship between count and angular or linear step gives a precise control of the motor output position and velocity. In general, there is no error between the pulse count and the position change of the motor output, provided of course that the motor develops sufficient torque to overcome system friction, inertia, and load. Using the proper conversion factors, the same may be said for the relationship between counts per second and motor velocity.

However, as in all physical systems, there are situations that may negate this relationship between pulse count and position. Discounting the obvious physical problems, such as bad bearings or some interference in the load side of the system or “glitches” in the counting system, the principal source of error is motor instability, especially at low speeds. A step motor is operated in a transient mode during each pulse, in contrast to conventional continuously excited motors that operate in a steady-state mode. Motor shaft oscillation can be caused by both electrical and mechanical time constants in the systems and cause the motor to “slip a pole” or in some other manner get out of synchronism with the input pulse rate. Demands for rapid acceleration may also cause inaccuracies between pulse count and output position or velocity. For this reason most stepper systems have a “slew rating,” which is the maximum number of steps that the system can make in a given time interval; this rating is a function of both the motor and controller parameters. There may also be problems between the pulse count and position in operations requiring frequent stop-start, reversing, or pause operations. These errors can be corrected, in general, by the logic system, but may require some sort of a position feedback signal or another counting system to count the mechanical steps.

Feedback signals other than position signals are also used in the control of stepper motors, particularly current feedback to ensure staying within current limits on semiconductors and coils and also to produce a type of current control known as “chopping.” The latter technique in stepper motor control

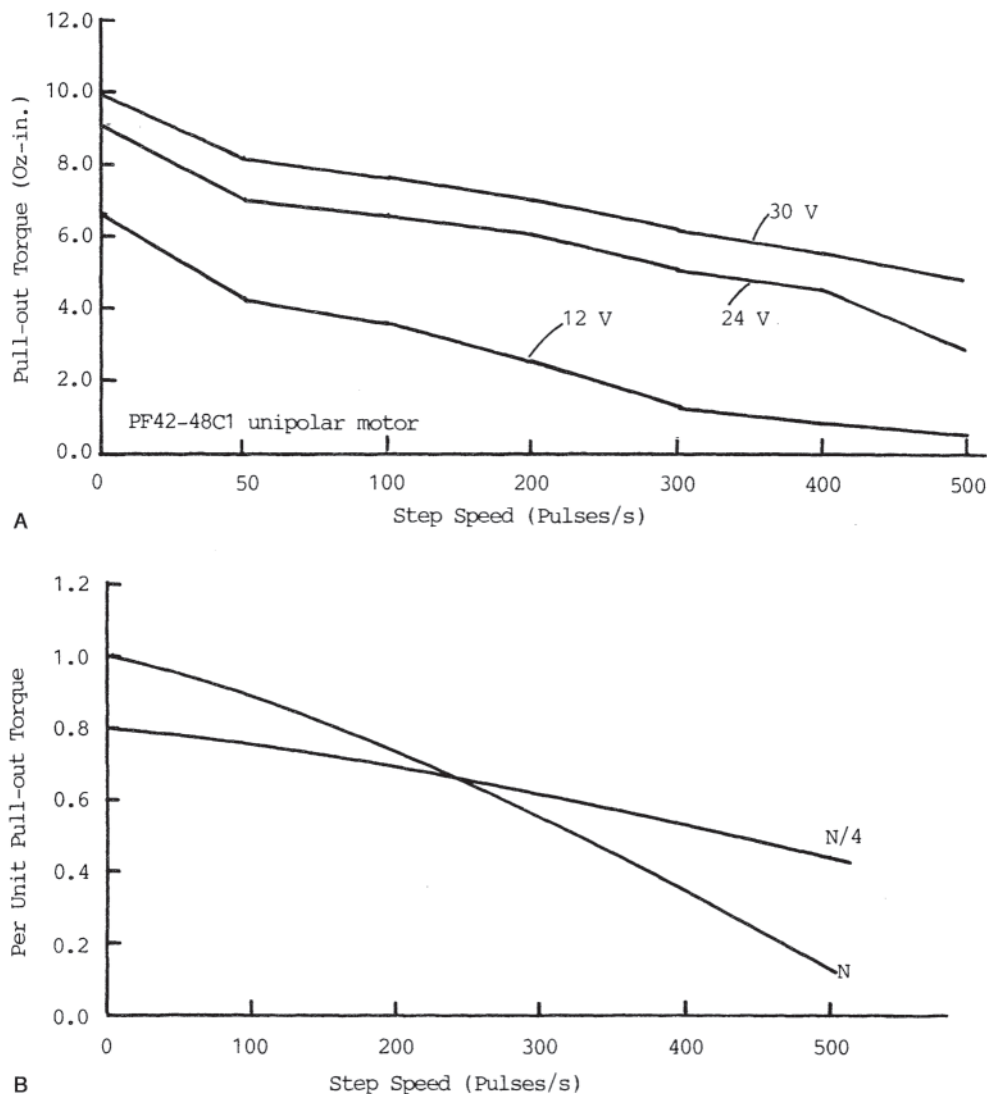


**Figure 2.101** (a) Torque-speed characteristics of a stepper motor as a function of applied voltage, (b) Improvement in high-speed torque resulting from turns reduction.

is essentially the same as that used in dc and other types of motor control. Its function is to maintain a high average or rms current to achieve high developed torque while not exceeding current ratings of the power semiconductors or the thermal ratings of the motor windings. Chopping results in typical "sawtooth" current waveforms and is discussed elsewhere in this handbook. Current feedback can be observed in some of the hybrid motor controllers discussed below.

#### 2.5.1.5 Hybrid Stepper Motors

Hybrid stepper motors contain a PM and are often called PM stepper motors. However, as noted above, the term hybrid is more appropriate since, due to the geometry of this class of motors, reluctance torque is also developed. The term hybrid has gradually become accepted as the name for this class of

motor, both for continuous and stepper motors containing permanent magnets. Hybrid motors generally develop the highest torque-to-current ratio of any type of motor. As a result, their weight and volume are often less than those of other motor types for a specific application. At the same time, the initial cost of hybrid motor is considerably more than that of reluctance machines, and the control circuitry tends to be more complex. The rotor-stator configuration of the common types of hybrid motors results in a smaller step angle than those of most reluctance steppers. The step angle of the typical hybrid step motor is 1.8 degrees, or 200 steps per revolution. Angles of 0.9 degree or less are also available, and the technique known as *microstepping* is available in the more sophisticated controllers for hybrid step motors. Microstep control can result in up to 25,000 steps per revolution.

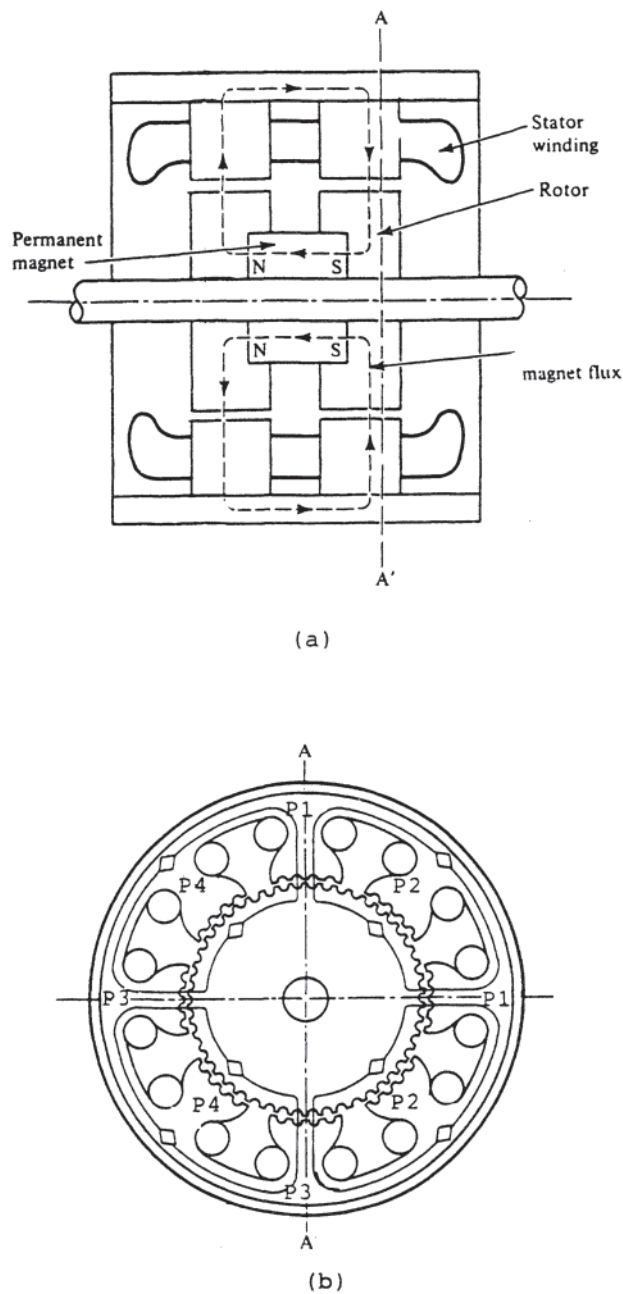


**Figure 2.102** Cross sections of a common hybrid stepper motor configuration: (a) axial cross section; (b) radial cross section.

#### 2.5.1.5.1 Hybrid Stepper Motor Configurations

Similar to reluctance stepper motors, hybrid motors are constructed in many configurations. One of the more common commercial hybrid steppers is illustrated in Fig. 2.102. This configuration has two sections of rotor laminations separated by a permanent magnet. The two rotor sections are displaced circumferentially from each other by one-half of a rotor tooth pitch. The stator has an even number of salient poles with many teeth on the air gap surfaces. The stator and its pole windings are the same throughout the axial

length, that is, not displaced circumferentially. Figure 2.102(a) shows the axial cross section and the orientation of the permanent magnet (usually cylindrical in shape). Figure 2.102(b) shows the radial cross section at one end of the rotor; the other end is displaced circumferentially by one-half of a tooth pitch. The stator coils are usually wound individually, but connected externally for either two-phase or four-phase operation with either series or parallel connection of the individual coils. It is thus seen that, in the case of the eight-pole configuration shown in Fig. 2.102(b), the stator and rotor teeth are aligned in the middle of poles P1 and P3 and fully unaligned (maximum reluctance condition) in the middle of P1' and P3'. The reverse condition is true at the opposite rotor section due to the displacement of the rotor teeth in this section. It is also seen that the primed poles of the P2 and P4 combination are aligned in Fig. 2.102(b) and the reverse would be true at the other rotor section.

The rotor of Fig. 2.102 moves in a stepping mode related to the number of rotor teeth,  $N_r$ , the number of stator teeth,  $N_s$ , and the number of poles per phase winding,  $p$ . The stator teeth are counted according to their pitch as if they were distributed around the stator periphery just as are the rotor teeth. Like the reluctance stepper described above, stepping motion in the hybrid machine also requires a relationship between teeth and poles, such that:

$$N_r = qN_s \pm \frac{p}{2} \quad (2.136)$$

where  $q$  is an integer. For the configuration shown in Fig. 2.102, the stator is wound two-phase; hence,  $p=8/2=4$ ;  $N_r=50$ ;  $N_s=48$  (if interpolar spaces are filled with teeth of the same pitch); therefore,  $q=1$  and the plus sign is used.

The electromagnetic torque developed in a hybrid stepper motor is due to both reluctance and PM torques. The latter is generally the major torque component and is a function of the interaction of the two magnetic fields in the air gap, one due to the ampere-turns of the stator current and the other due to the permanent magnet, or

$$T_{PM} \approx K(NI) \phi_p \text{ (N-m)} \quad (2.137)$$

$\phi_p$  where is the permanent magnet flux per pole and  $K$  is a constant depending upon motor geometry and winding configuration. The numerical evaluation of hybrid motor torque is complex and generally requires detailed analysis of the air gap geometry and magnetic field distribution by computer techniques such as finite elements. For more detailed analysis of hybrid motor torque, consult Refs. 55–58. The PM torque is generally larger than the reluctance torque in hybrid motors, although, of course, this depends upon many factors such as the type and size of the permanent magnets used as well as winding and geometrical considerations. One advantage of the hybrid stepper over the pure reluctance stepper is a relatively large *holding torque*, that is, the torque maintaining a specific rotor-stator position with zero exciting current in the windings. This is a requirement in many stepper motor applications and often mandates the PM type and determines the size of the motor.

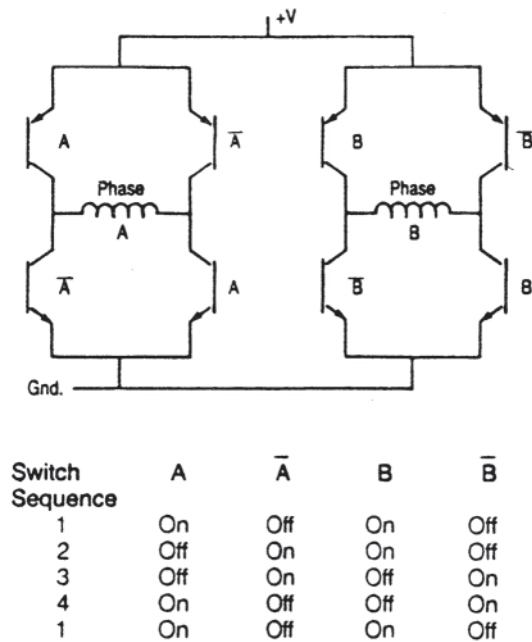


**Figure 2.103** Simplified bipolar control scheme for a hybrid stepper motor and the switching sequence for one tooth pitch rotation.

#### 2.5.1.5.2 Hybrid Control and Stepping Action

The mechanism of control in the hybrid stepper is the winding currents, just as in the reluctance machine. However, hybrid control is more complex and generally requires more logic circuitry than reluctance control. Thus, both the control electronics and the motor itself are more complex and more costly than reluctance stepper motor systems. The rewards of added complexity and cost are very fine step angle, higher torque per ampere of winding current, and holding torque.

Referring again to Fig. 2.102, stepping motion is achieved by the proper sequencing of the phase currents. As noted above, the torque analysis in hybrid machines is beyond the scope of this presentation, but it can be shown [55, 59] that four pulses of stator excitation are required to produce rotor motion of one complete tooth pitch. In the configuration of Fig. 2.102, there are 50 rotor teeth. Therefore, the number of stator current pulses to produce one revolution of rotor rotation is  $4 \times 50 = 200$ . This is equivalent to 200 steps of rotor motion per revolution, or 1.8 degree per step.

Figure 2.103 illustrates a simple schematic diagram for the control of two-phase stepper motor windings, such as those of Fig. 2.102. This diagram shows bipolar transistors as the power switches, but, as in the case of most other types of motor control, many power devices are available today, including thyristors, MOSFETs, and IGBTs. The switching sequence to result in the four-step rotor motion of one tooth pitch with a two-phase stator winding is given in the table below the schematic in Fig. 2.103. This arrangement of motor configuration and controller sequencing is the most common hybrid stepper system and is often called the 1.8-degree motor.

However, there is much more that can be done with these basic elements of motor and controls to further refine the step angle and to improve system stability. *Half-step* control doubles

the number of steps, and *micro stepping* gives an almost infinitely variable control of rotor motion. These two modes of control are illustrated in Fig. 2.104. For the purpose of clarity, a six-pole rotor and four-pole, two-phase stator are used rather than the complex pole-tooth arrangement of Fig. 2.102. In half-stepping, the phase pulse sequence shown in Fig. 2.103, by which both phases are always excited, is modified such that at every other step, only one phase is energized. This can be observed rather simply in Fig. 2.104, but is more difficult to comprehend in Fig. 2.102. However, the result is that the rotor moves only one-half of the angle it moves when excited by the sequence of Fig. 2.103, resulting in 400 steps for one revolution, or 0.9-degree per step. Microstepping is but a further extension of the concept of half-stepping in which both phases are excited at varying levels of current in a sequence such that almost smooth rotation is achieved as in a continuous motor. Figure 2.105 illustrates the “staircase” nature of microstepping motion in a hybrid step motor. The waveform of the signals applied to the excitation windings is different for these two types of control. As shown in Fig. 2.106, in half-step (and full-step) control, the excitation wave forms are relatively square, giving the discrete steps of this type of control. Microstepping requires sinusoidal excitation to achieve the more smoothly varying motion. Microstep control in commercial stepper motor systems can achieve 125 microsteps per full step, or  $125 \times 200 = 25,000$  steps per revolution. Motor speed is a function of the frequency of the sine waves shown in Fig. 2.106, and microstepping control permits motor operation at much higher speeds (the slew rate) than full stepping.

A major purpose of both half-stepping and microstepping is not only to give more precise positioning of the rotor but also to improve system stability. Figure 2.107 illustrates the typical oscillations of a full-step operation at very low speeds in many stepper motors. Such oscillations may be undesirable in many applications and can deteriorate into unstable operation under certain conditions. Obviously, causing the motor to take smaller steps will improve the transient response. Microstepping requires considerably more control logic circuitry and increases system cost.

#### 2.5.1.5.3 Permanent Magnets for Hybrid Stepper Motors

Permanent magnets for motor applications are discussed in Sections 2.3.7 and 2.3.9. Typical *B-H* curves are shown in Figs. 2.59 and 2.60 of Section 2.3.7, and Table 2.4 in Section 2.3.9 summarizes a few of the more common magnets used in stepper motors. Care must be taken in the design of hybrid stepper motors to ensure that the permanent magnet will not be demagnetized during motor operation including abnormal operations such as stall conditions. Reference 60 gives guidelines for the design of PM motor systems. PMs are also susceptible to various environmental conditions, particularly temperature, and, in some cases, continuous mechanical vibrations. These factors must be considered in the design and operation of stepper motors.

#### 2.5.1.5.4 A Linear Hybrid Motor

Many stepper motors, both reluctance and hybrid, are also built for linear motion in contrast to rotary motion. Linear stepper

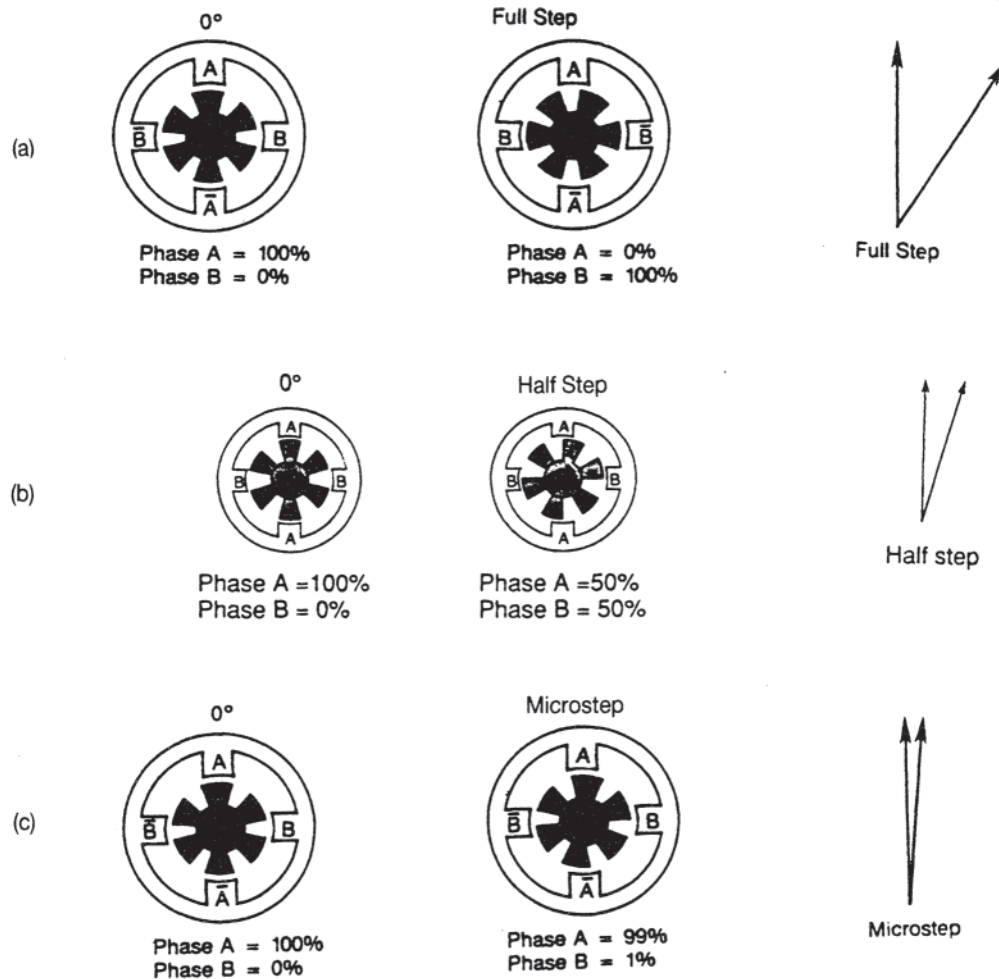


Figure 2.104 Types of step control: (a) full step; (b) half-step; (c) microstep.

motors can often reduce system size by eliminating gearing and transmission stages where relatively small linear motion is required. In such applications, a linear stepper motor may offer more precise position control and lower cost. In general, all of the principles that have been discussed for rotary motors of both reluctance and hybrid varieties can also be applied to linear motors, recognizing, of course, the different geometry.

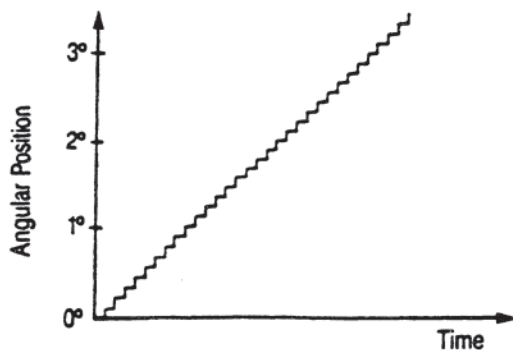


Figure 2.105 Typical smooth staircase response with microstep control.

Figure 2.108 illustrates the cross section of a prototype linear hybrid step motor capable of steps as low as 0.1 mm. Rare-earth (neodymium-iron-boron [NdFeB]) magnets were used in this prototype [61]. The principles of operation are very similar to the rotary hybrid illustrated in Fig. 2.102.

#### 2.5.1.5.5 Sensorless Control

There has been much development in recent years in the sensorless control of reluctance and PM machines of both continuous and stepper types. This term refers to controlling speed, position, and velocity by means of measured motor parameters rather than by means of a position or speed sensor which, in general reduces the cost and complexity of a position control system. Position and/or velocity can be determined by the measurement of several motor parameters, such as input inductance (see Fig. 2.94), air-gap flux, and stator current. There are many references for sensorless control, such as Refs. 62 and 86.

#### 2.5.1.6 Piezo-Stepper Motors

Piezo-stepper motors are different from other types of electric stepper motors described in this chapter in that they contain no magnetic materials. Their merits as a stepper device are very small steps (in the micro-m range), simplicity of control

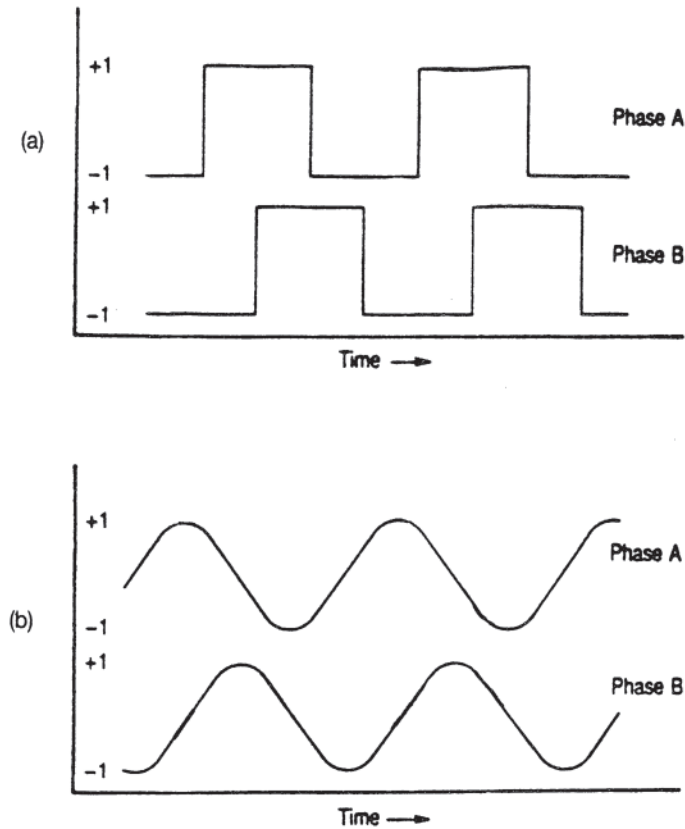


**Figure 2.106** Normalized control signals used in stepper motor control for (a) full step and (b) microstep.

in electrical systems, very fast response time as compared to electromagnetic steppers, and a relatively good torque/weight factor. Piezo-steppers are used in applications where extremely fine positioning is required, such as positioning small objects under a microscope and in fine machining operations, and many experimental and prototype stepper motors are under consideration for space, light-weight robotics, and extremely fast response-time applications [63, 87].

The principal piezo-electric materials used commercially

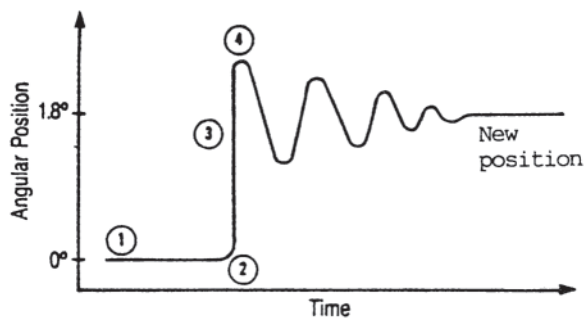


**Figure 2.107** Stepper motor transient characteristics:  
 (1) initial rotor position  
 (2) exciting coil energized for one full step of rotation  
 (3) rise time (maximum slew rate)  
 (4) initial overshoot

today include quartz, rochelle salt, and barium titanate. Quartz is insoluble in water and is used in many underwater applications. Piezo-materials are generally sensitive to high temperature (above 55°C) and humidity. Piezo-transducers have been in use for many years (the phenomena was first observed by the Curies in 1880) as ultrasonic generators, microphones, phonograph pickups, etc. In most of these older applications, the energy transformation is mechanical vibration input/electrical signal output. The reverse transformation, electrical input/mechanical output, is the principle of the piezo-stepper and other piezo-motors. Linear piezo-motors are in use for precise positioning applications. Tiny rotary piezo-motors are in use in many biomedical applications, such as fluid pumps for in-body administration of liquid medicines.

Piezo-stepper motors have a short response time (bandwidth of 10–20 kHz) and can generate large forces (1 kN or greater). Since the step of a simple piezo-stepper to an electrical input pulse is in the range of several microns, larger mechanical steps require several piezo actuators in series. Such a scheme is described in Ref. 63, a stepper developed for very precise machining applications. The limited step of a single stepper is overcome by using a stepper algorithm for a series of drive units held in a rigid frame. Spreading the drive function over a large number of units results in a high passive stiffness. Such an approach can be used in either linear or rotary motion applications.

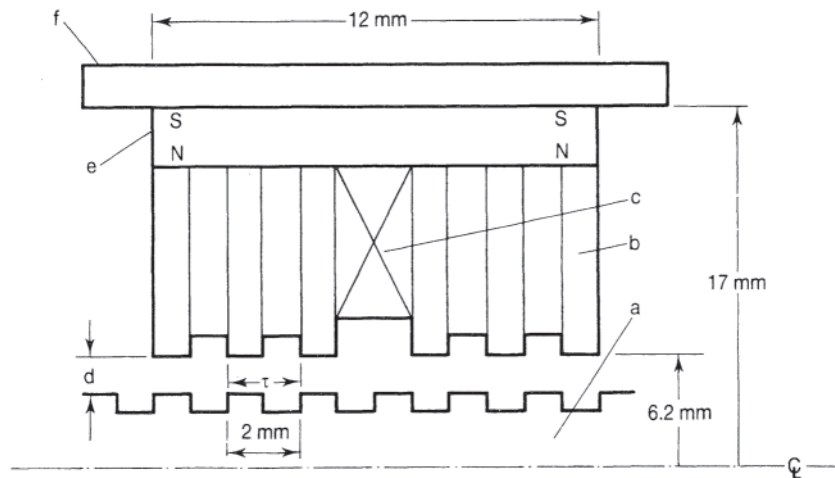


**Figure 2.108** One section of a linear hybrid stepper motor. One pulse of the exciting coil (c) will cause the forcer to move one-half of a tooth pitch, to the right; four identical sections are mounted coaxially to achieve linear movement of about 30 cm. All sections concentric with the centerline. The letters signate the parts as follows, **a**. The toothed inner core made of soft magnetic material, called a “forcer.” It is analogous to the rotor motor, **b**. The annular (stationary) outer core, made of soft magnetic material. It is analogous to the stator in a rotary motor, **c**. The electrical winding, in the form of a solenoid, **d**. Radial air gap. **e**. Annular permanent magnet, magnetized radially as shown, **f**. Housing and return magnetic path.

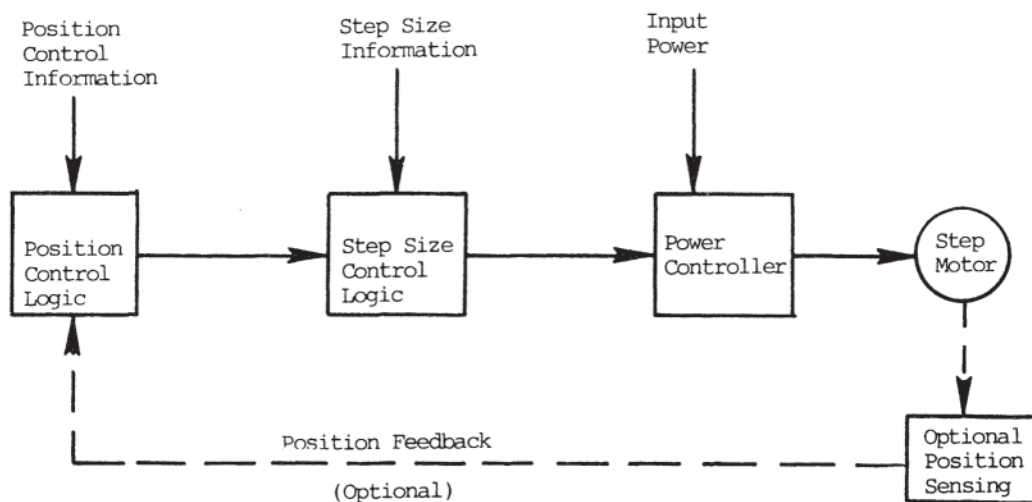
### 2.5.1.7 Stepper Motor Characteristics and Specifications

Figure 2.109 illustrates the basic elements of a position system using a step motor. Optional feedback is also shown. This simple block diagram is also generally valid for control modes other than position, although some of the nomenclature will be changed in such cases. This diagram represents the functional aspects of a stepper motor system, not hardware or software sections, which are generally overlapping in system location. Also, there may be some feedback circuits internal to the various blocks in Fig. 2.109, such as those related to system protection and safety. In many systems, the ability to change the step size (full step, half-step, and microstep) is not required.

When designing a system and designing or purchasing the components for the system, the first step is to evaluate and delineate the “load” or “output” requirements of the system. The parameters to consider are listed in [Table 2.5](#). The input considerations of [Table 2.6](#) must also be taken into account.

A number of secondary considerations should also be evaluated in the preliminary stages of design. These include:

1. Motor type-reluctance or hybrid. As has been discussed, this frequently involves trade-offs of cost vs. accuracy and precision, although there are many applications where either type of motor is suitable.



**Figure 2.109** Block diagram for the basic elements in stepper motor control.

**Table 2.5** Stepper Motor Output Parameters

- 
- Torque vs. speed characteristics
  - Maximum torque, speed, and power, including overload
  - Response time, including permissible overshoot and settling time
  - Step size
  - Slew rate, or required rate of position change at a given torque condition
  - System inertia, including that of motor rotor and shaft
  - Accuracy of shaft position (or velocity)
  - Environment-temperature, humidity, vibration
  - Size considerations, including motor mounting means and gearing, if required
  - Cost restrictions
- 

**Table 2.6** Stepper Motor Input Considerations

- 
- Available voltage source and its voltage and volt-ampere capacity
  - Input logic signals and voltages for the required control
  - Safety and protection; a principal protection circuit usually required is current limiting to maintain power semiconductor safe operating areas (SOAs)
  - Interaction with various plant or supervisory systems
  - Control philosophy
- 

2. Motor winding connection—two, three, four, and five-phase winding configurations are all common and have various attributes. The four winding motor is the most common, but the windings can be connected in a variety of ways, as shown in Fig. 2.110. The choice of connection depends upon the voltage ratings of the motor coils and the power source, the type and cost of the required power controller (often a major component of system cost), and the maximum speed and/or slew rate of the motor. Also, a selection of unipolar or bidirectional drive should be made at an early stage in the preliminary design. Two-phase (series) connection, bipolar configuration is common, partly because it reduces the number of power semiconductors required in the power controller. Figure 2.111, using MOSFETs, and Figs. 2.100 and 2.103, using power transistors, illustrate the common H-bridge type of stepper motor controller.
3. Factors affecting motor performance. Several secondary types of motor control have been discussed, such as the  $L/R$  method discussed previously and illustrated in Fig. 2.96. and torque control by varying the input voltage, as illustrated in Fig. 2.101. Also, the winding inductance can have a significant effect upon motor performance, including its transient characteristics.
4. Gearing to achieve desired output torque-speed, if required. If rotary motion is to be converted to linear

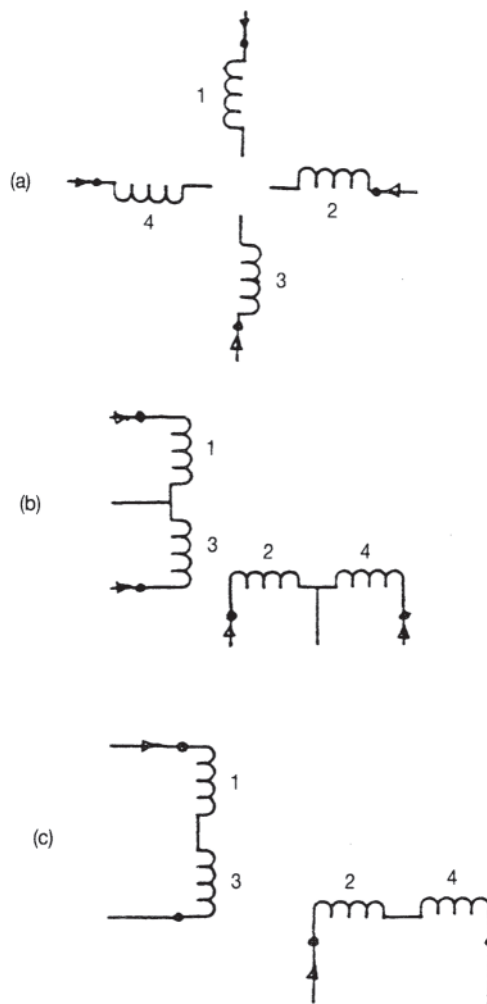


**Figure 2.110** Winding arrangements in the common 4-phase configuration: (a) 8-lead (four separate windings); (b) 6-lead (four-phase, unipolar); (c) 4-lead (two-phase, series connection).

motion, a lead screw or worm gear will be used. The motion of the motor shaft is related to linear motion by

$$\theta = \frac{360S}{L} \quad (2.138)$$

where  $\theta$ =shaft rotation degrees;  $S$ =linear movement (cm); and  $L$ =lead of screw (cm)/rev).

5. Logic family. Compatible logic will simplify power supply requirements and subsystem interaction.
6. Comparison with other types of systems. In general, many types of reliable and commercially available systems can perform the control functions of stepper motor systems, including standard dc motor feedback systems, ac servo systems, other types of continuous brushless dc drive systems, and actuators. Some evaluation of alternate systems should be made before choosing a stepper system.



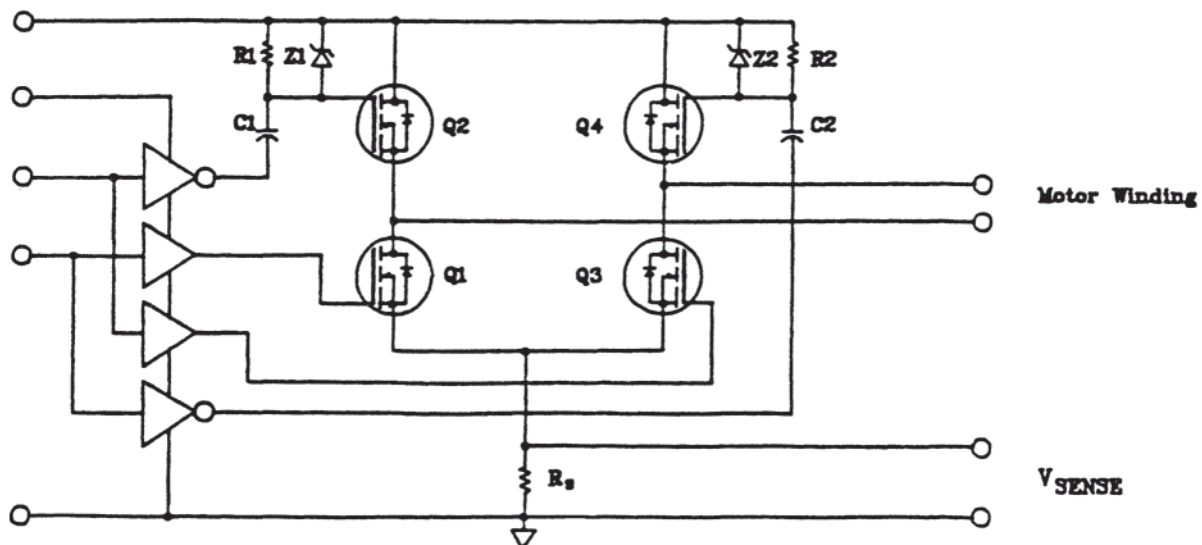


Figure 2.111 AC coupled H-bridge for one motor phase winding.

#### 2.5.1.7.1 System Specifications

Table 2.5 lists output parameters in general terms, and Table 2.6 lists input considerations, also in general terms. The system designer must take into account all of the items listed in those tables, and must then write system specifications. Table 2.7 lists the most important of these. The reader is also referred to NEMA MG 7 if the system is “intended for use in a motion/position control system that provides precise positioning, or speed control, or torque control, or in any combination” [64].

#### 2.5.1.7.2 Stepper Motor Factors of Merit

There are a number of stepper motor parameters and factors of merit that may be used in the selection of systems for commercial or industrial applications [65]:

1. Ohmic ( $I^2R$ ) losses. This is the principal loss in a stepper motor and is a major factor in the temperature rise of a

Table 2.7 Stepper Motor System Specifications

- Accuracy in  $\pm$  arc minutes
- Repeatability in  $\pm$  arc seconds
- Speed range (rpm)
- Torque vs. speed (N-m) vs. (rpm), including starting torque, if applicable
- Pull-in frequency, defined as the frequency that can be applied to an unloaded, stationary motor while maintaining synchronism [61]
- Motor type and winding connection
- Motor breakdown voltage
- Motor frame size; stepper motors are built in frame sizes used for other motors of similar VA ratings
- Controller voltage, volt-amperes, and frequency
- Short-circuit protection
- Logic supply
- Ambient temperature and humidity
- Transient characteristics, including slew rate or acceleration requirements, if applicable
- Size restrictions

motor in continuous operation. Thermal analysis of stepper motors generally proceeds along the same lines as that for continuous motors, with proper consideration of the discontinuous nature of operation [66].

2. Torque constant,  $K_t=T/I$  (N-m/A). This is identical to the parameter used in control and dc motors; it is constant only in motors with relatively high resistance and normally varies over the speed range of most stepper motors; in reluctance machines, it varies greatly with the degree of magnetic saturation.
3. Voltage constant,  $K_e=V_r/(\text{rps})(V\cdot\text{s})$ , where  $V_r$  is the rated voltage of the motor; in SI units,  $K_e=K_t$ . This constant is useful in determining the back emf,  $E$ , of a motor.
4. Maximum speed; this is approximately equal to the speed at which the back emf equals the rated voltage, or  $\text{RPM}(\text{max})=60\times V_r/K_e$ .
5. Maximum current, usually at stall or start-up at zero speed when  $I(\text{max})=V_r/R_{\text{sys}}$ , where  $R_{\text{sys}}$ =winding resistance plus added circuit resistance (as in  $L/R$  control). This is important for sizing power semiconductors.
6. Motor winding inductance. The effect of this parameter on motor performance has been noted previously. Reference 67 analyzes the effects of motor inductance variations.
7. System inertia. This is a factor in determining pull-in torque and transient response.

## 2.5.2 400-Hz Motors

### 2.5.2.1 Introduction

Four-hundred-hertz motors, also known as aerospace motors, are generally used on aircraft and other military equipment, where the power system has been chosen to minimize size and weight for the electrical equipment. The frequency of this three-phase power system has been selected at 400 Hz. This

power system provides a significantly higher power-to weight ratio than the common 50-Hz or 60-Hz power systems. Equally important as the weight is the reliability of these machines. They are designed for high performance and high mechanical integrity and to withstand the harsh environmental conditions such as salt, fog, humidity, fungus, vibration, shock, etc. These motors are designed using high-quality material, a requirement that is different from most commercial motors. The detailed characteristics are described below.

### 2.5.2.2 Applications

Originally, the majority of the applications required the motor to drive a fuel pump, fan, or compressor. More recently the applications have started to include hydraulic pumps and actuators. The fan motors are used for electronic equipment cooling systems, for air movers in cabins, or in evaporators or condensers. Most motors are three-phase, squirrel-cage induction motors operated from a 208-V (line to line) 400-Hz power supply. This relatively low voltage level has been chosen to prevent corona at the low ambient air pressure levels which the system might be exposed to when the aircraft is flying at 40,000ft altitude. More recently, especially for fuel pump and actuator drives, the motor is powered by means of a controlled electronic power converter to give the drive precise speed control capability. In this case both induction motors and PM synchronous motors can be used. The most recent developments also use switched reluctance-type motors in these adjustable speed drives.

The power and speed for the ac induction motors range from 1/4 to 25 hp and from 4000 to 24,000 rpm. However, applications for 60-hp motors or larger may also be found. The adjustable speed drives have maximum operating speeds from 8000 to 100,000 rpm and more (most recent developments) and power ratings of 100 to 200 hp will also be found in the near future. High-speed motors are found to drive fans and recently fuel pumps while lower speed motors are found in compressors and actuators. A general specification does not exist for an aerospace type motor, however very often the operational performance of the machine may be defined by several military specifications (MIL STD 7808 or similar). Every aerospace type motor is a custom design for the specific application electrically as well as mechanically.

### 2.5.2.3 Electrical Design Considerations

When designing high-frequency motors one has to realize that a machine of a given power rating tends to have a noticeably higher reactance to resistance ratio than a comparable industrial motor. That means for a similar rotor slot design the starting torque and the pull-out slip of a high-frequency motor tend to be lower than for the comparable industrial motor. Thus, special rotor slot designs and rotor conductor materials may have to be used to achieve the required starting and pull-out performance at much smaller ratings than for the industrial counterpart.

The power in aerospace-type power systems is kept as low as possible because of the weight considerations for the power generator. Therefore, it is imperative that the running current

for a given power rating of the ac motor is kept as small as possible. In other words both efficiency and power-factor need to be as high as is consistent with the requirement for a small total electrical power system. Typical requirements for efficiency and power factor ask for values in the mid-to-upper 80s, and higher for larger ratings.

#### 2.5.2.3.1 Efficiency

The primary electromagnetic losses in any electrical machine are the  $I^2R$  losses in the conductors or winding in the machine and the core losses in the iron core of the machine. The losses are generally a function of the type of material one uses in the conductors/magnetic core and the amount of the material. The second factor, the material quantity, has obvious negative impact on the motor weight, thus the losses and the weight are typically traded off against each other to provide for minimum system impact, i.e., higher motor losses result in a smaller motor but cause the generator to increase because of the increased motor input power requirement for a given motor load and vice versa.

Higher efficiency or lower losses are obtained basically in the same way as for industrial motors through the selection of the appropriate materials and design approaches. The difficulty for the high frequency motors is the weight constraint and the fact that some of the parasitic effects are much more predominant than in comparable 60-Hz motors.

**2.5.2.3.1.1 Core Losses** The core losses as for all electrical machines consist of eddy current losses and hysteresis losses. The eddy current losses are proportional to the product squared of lamination thickness, frequency, and flux density ( $\sim [d \cdot f \cdot B]^2$ ) while the hysteresis losses are proportional to the product of the frequency and flux density to the 1.6 power ( $\sim f \cdot B^{1.6}$ ). A secondary effect can be found in the impact of the lamination thickness as very thin materials are mechanically and thus also magnetically harder. This hardness also increases the hysteresis losses when selecting thinner materials because the hysteresis loop gets bigger and thus the work to remagnetize the material every cycle gets larger. In general the eddy current losses make up an ever increasing portion of the total core losses as the frequency increases. Since the need for low machine weight demands operating the core at the highest flux density level practical the only choice for the designer is to use thin lamination sheets and a lamination material with the highest specific resistivity (equivalent to lower eddy current losses).

A typical core lamination material for 400-Hz motors is fully processed M19 grade, 29 gage (0.014-inch thickness) material with inorganic C5 coating (or similar) having typically a core loss of 1.58 W/lb at 15 kg. This material has usually 3%+ silicon content higher than the commercially used M45 grade. Sometimes one uses also 6% silicon material to even further reduce the eddy current losses. The lamination material needs to be fully annealed after the punching process to achieve low core losses by removing the influence of the mechanical stress introduced through the punching process. And while the annealing process, which takes place at typically 1450°F, is expensive it is necessary to reduce the losses. The mechanical burrs introduced by the punching operation need to be minimized by using only sharp dies as

these burrs would otherwise cause lamination shorts which increase the core losses.

For extremely low weight requirements one can also use cobalt-iron lamination material as it can carry about 20% higher flux densities for the same excitation than silicon steel. However there is a large cost premium involved (factor of 60 to 80 times the \$ amount than for M19 grade) and also a core loss premium as the eddy current losses are also higher.

**2.5.2.3.1.2 Primary (Stator  $I^2R$  Losses)** The stator winding losses are proportional to the winding resistance and the square of the current. The winding resistance is expressed by the product of conductivity of the conductor material, the number of turns, the mean length of a single turn, and the number of phases divided by the total conductor cross section area of the conductor per phase. This tells the designer how to achieve low resistance and thus low losses. The only thing to choose without running into a trade situation is the conductor material. For high-efficiency and high-frequency motors, that is exclusively copper. As a side issue, one also has to consider the winding temperature as the conductivity decreases with increasing temperature. If one wants to increase the conductor cross section one runs immediately into conflict with the stator tooth flux density. Also the outer machine diameter and stator core losses and weight will increase if one assumes that the yoke flux density has been chosen at an acceptable point from the magnetization and power factor point of view. Therefore, the stator  $I^2R$  losses and the stator core losses have to be minimized in a trade study for the most significant operating point.

A second way to get more conductor area is to increase the amount of copper content in a given slot, i.e., to increase the slot fill factor. This is achieved by utilizing thin slot insulation materials with high dielectric strength. Materials like aramid paper (Nomex) or polyimide film with aramid paper (Kapton) are mostly used. A high slot fill will benefit the losses but also increase the likelihood of an electric breakdown of the insulation at the slot entrance and thus reduce the machine reliability. Another means to reduce the losses is the tightening of the end turns. Again the additional labor cost and the increased potential for insulation breakdown at the slot entrance limit the application of this approach.

**2.5.2.3.1.3 Secondary (Rotor)  $I^2R$  Losses** The process to minimize the rotor  $I^2R$  losses follows the same ideas discussed for the stator windings with the exception of the slot insulation which is mostly necessary in some form when skewed rotor slots are used. However the resistance of the rotor is significant for machine performance. In general lower resistance will also reduce the starting torque. Thus, as mentioned before, when a certain starting torque is required, one may have to utilize deep-bar effects are double-cage rotors for relatively small motor ratings to achieve the required performance. The material choices for the rotor conductors include cast aluminum, copper, and copper alloys depending upon the performance requirements. Applications such as positive displacement pumps or reciprocating compressors will generally use cast aluminum rotors or copper alloys while fan motors can utilize copper bar rotors because of the low starting torque requirements for this application.

**2.5.2.3.1.4 Windage and Friction Losses** Friction and windage losses are usually a small portion of the total losses. However, especially for high speed machines or machine where the rotors are submerged in the fluid to be pumped, the designer has to be careful to keep it that way. Most motors are either totally enclosed nonventilated, totally enclosed air over frame, or hermetically sealed. For rotors in air the air circulation inside the cavity has to be kept at the minimum required for rotor cooling purposes. That generally limits the rotor bar extension length. For rotors in a fluid, the rotor surface (and also the stator air-gap surface has to be kept very smooth with zero bar extension end-rings touching the laminations to keep the fluid churning losses within limits.

Friction losses are reduced by using high-grade bearings, which are shielded and lubricated with high temperature grease.

**2.5.2.3.1.5 Stray Load Losses** These losses include everything from losses in the rotor bars due to stator slotting, high-frequency core losses in rotor and stator core due to rotor and stator slotting, local core losses due to local saturation, eddy current losses in the frame and end-bells or other metallic parts close to the stray fields of the windings or heavily saturated parts of the magnetic circuit, as well as eddy current losses in the windings. The last effect will be more pronounced because of the high supply frequency. That means that for large motor ratings where one normally may be tempted to use bar type conductors in the stator winding one should check for current displacement in the conductors especially in the slots. Other than that the rules and practices to minimize these stray load losses are similar to those for industrial machines except that the higher supply frequency will make some of the stray load losses more pronounced.

#### 2.5.2.3.2 Power Factor

Typical values for the power factor range from 0.8 to 0.9 for higher speed motors, i.e., motors with two or four poles. As the number of poles increase the magnetization current becomes a noticeable part of the total current and tends to push the power factor to values below 0.8. Obviously this is a function of the air-gap length and some designs have reduced the gap to less than 0.01 inch to achieve reasonable power factor values. That can become very expensive from a manufacturing point of view because both rotor and stator gap surfaces need to be ground. Also this grinding process may cause additional stray load losses because the iron insulation may be smeared over forming electrical contact between the laminations. A second way out of the power factor dilemma may be capacitors if the increased weight of them is less than the increase in weight of the generator due to the low power factor.

#### 2.5.2.4 Thermal Design Considerations

One of the challenges for 400-Hz motors is the cooling or thermal design. As has been stated before the machines are totally enclosed machines that is no direct cooling of the rotor is possible. On the other hand one would like to have low weight for these machines, i.e., one would have a high-power—density machine. And typically, high-power density means also high-loss density both in the rotor and in the stator.

Thus, especially for the larger ratings one will have to perform detail thermal analysis to ensure that both stator and rotor do stay within the allowable temperature range. A typical trade-off here has to consider both weight and the required motor operational life since the insulation life is a function of the accumulated time at temperature. For air-cooled machines the air inside may have to be circulated by means of an internal fan to provide heat transfer through the end-shields.

### 2.5.2.5 Motor Construction

#### 2.5.2.5.1 Mechanical Components

**2.5.2.5.1.1 Frame and Brackets** Consistent with the goal of low-weight electrical motors the motor housing or frame as well as the brackets or end bells are made of light weight material like aluminum castings or extrusions. Aluminum alloys such as 6061 provides low weight without sacrificing mechanical strength. In addition, aluminum is a very good conductor of heat. This characteristic, combined with a finned housing, helps to transfer the heat developed inside the machine very effectively to the ambient air. As mentioned before, efficient heat transfer is vital for high power density motors.

To provide sufficient mechanical integrity aluminum castings should be tempered to T6 ensuring stability over the wide range of ambient temperatures encountered in the application for these machines. Since the aluminum is a relatively soft material one has to use helicoil inserts in threaded holes for bolted connections for increased pull-out strength and steel bearing inserts in the end bells for increased resistance to fatigue caused by the combination of vibration and continuous thermal expansion and contraction cycles.

Aluminum inherently self-protects against corrosion from water and salt by the formation of a thin film of aluminum oxide. Machined parts are generally anodized (high temperature applications) or alodined (low-temperature applications). Also during the design process one has to take into consideration that aluminum has a significantly higher thermal coefficient of expansion than steel. Thus, the stator core has to be prevented from rotating in the housing by means of either a tight interference fit or a steel pin or both. If an interference fit is used all by itself one has to make sure that the aluminum is not overstressed and does not relax over the life of the motor.

**2.5.2.5.1.2 Shaft and Bearings** The bearings, as mentioned before, are of higher grade, grease lubricated with high-temperature grease, and equipped with shields. The shafts are typically made from steel, mostly 400 series stainless, and passivated to better resist corrosion due to salt and water.

#### 2.5.2.5.2 Electrical Components

**2.5.2.5.2.1 Stator Construction** The stator core construction, because of the requirement for low weight, does not have extra material that would allow riveting or conventional welding to hold the laminations together as a core. Electron beam welding can provide a thin enough affected zone that there is little impact on the magnetic capabilities of the laminations. Most often, however, one resorts to gluing the laminations together. This is costly but also very effective in achieving a low-weight core assembly.

As mentioned before, the stator winding insulation materials have to withstand a combination of high temperatures, high dielectric stresses, and mechanical forces. This can only be obtained by using high-grade insulation materials such as NEMA class H or better. Typically these are Teflon, Kapton (polyimide), Nomex (aramid paper), silicon and glass materials. The copper wire is also coated with a double or heavy film of inorganic material which offers extremely high dielectric strength per inch of thickness. The varnishes used to hold the windings together are generally epoxies, which offer high bonding strength, high temperature capability, and high resistance to various corrosive and/or hermetic conditions. Most often epoxies use some filler material to improve its thermal conductivity.

**2.5.2.5.2.2 Rotor Construction** Rotor cores are usually made from silicon steel laminations with semi-closed or closed slots. Should the mechanical stresses for 12,000 or 24,000 rpm machines become too large (>65 KSI) then cobalt iron laminations (hyperco or vanadium permendur) can be used. This material, if properly annealed, can tolerate 50% higher stress levels at much higher costs. The rotor cages are usually made from copper bars (or copper alloy bars) inserted into the slots and brazed to copper end-laminations, which represent the end rings. Should the stress in these end laminations get too high for copper to carry high strength copper alloy end laminations have to be used. Sometimes the rotor laminations have ventilation holes stamped into them to reduce weight and provide for additional rotor cooling, provided an adequate cooling circuit has been arranged. Balancing the rotors is usually necessary to a precision grade because of the high speed requirements. The bearing arrangement and selection has been discussed before.

#### 2.5.2.5.3 Electrical Connection Hardware and Thermal Protection

The electrical connections to these motors except for very large ratings, are always made via MA-type connectors. If the current loading per pin is too high then several pins are connected in parallel. Also thermal protection is always required for these machines. Because the power ratings are quite large with respect to the physical size, there is usually not much thermal mass and thus any protection has to be fast reacting. More often than not a direct-acting thermostat is wired into the neutral of the motor connections. It acts upon the combination of motor current flowing through it as well as the winding temperature and thus, provides sufficient protection against a locked rotor condition or single phasing of the machine.

## 2.5.3 Deep Well Turbine Pump Motors

### 2.5.3.1 History

Early vertical turbine pumps were driven by standard horizontal electric motors. A quarter-turn belt with a horizontal motor engine was quite common. The pump manufacturer supplied a thrust bearing in the pump discharge head. With the advent of ball-bearing motors, it became feasible to mount the motor in a vertical position and to drive the pump by a short belt or directly. At this time, an attempt was made to place the thrust bearing in the motor, but the need for vertical

adjustment of the pump shaft and accurate alignment of the motor and pump shaft made installation and servicing difficult. Adjustment is required to lift the impellers and give a running clearance with the pump casing. The stretch of several hundred feet of shafting may require a lift of several inches at the top of the well. The impeller, at the bottom, must be positioned within a fraction of an inch. Some pumps require periodic readjustment to compensate for wear and maintain output.

The hollow-shaft motor provides a solution for these problems. With the pump headshaft extended through the hollow-shaft motor, adjustment can be made by a nut on the threaded pump headshaft, at the accessible top of the motor. Motors can be removed and replaced easily, and alignment is less critical because of the long extension of the pump shaft. It is also easy to obtain alignment by removing the drive coupling and adjusting the motor mounting to make both pump and motor shaft axis coincide, then replacing the drive coupling.

The drive coupling also provides a solution to the problem of power reversal. The pump shaft is usually composed of many lengths joined by screw thread couplings. Normal torque tightens the joints and keeps the shaft ends together. A power reversal could unscrew the joints, causing the shaft to lengthen and to buckle or break if restrained. The self-release coupling (SRC) lifts out of engagement and prevents this problem.

The first hollow-shaft motor was introduced in 1924 by U.S. Electrical Motors. Design features of vertical hollow-shaft motors have been developed to meet specific needs of the turbine pump industry.

### 2.5.3.2 Terminology

The deep-well turbine pump motor has parts unique to the design. Figure 2.112(a) illustrates most major components. Unique to the vertical hollow-shaft (VHS) motor are:

- *Drive coupling*: Supplied by the motor manufacturer, bored to the pump headshaft diameter. Connects the pump headshaft to the rotating component of the motor.
- *Pump headshafts and adjustment nut*: Supplied by the pump manufacturer. It allows adjustment of the pump line shafting and impeller clearance.
- *Locking arm*: Locks the rotating component of the motor to adjust pump line shafting and impeller clearance. It must be removed for operation.
- *Rotor locknut and washer*: Allows adjustment of the motor rotating assembly. Since large thrust bearings are separable and cannot take upthrust, the rotating assembly must be adjusted for the lower bearing to take momentary upthrust and still allow thermal expansion of the motor rotating assembly.
- *Oil lubrication parts*: Covered in more detail in Section 2.5.3.5.4. Large thrust bearings cannot be grease lubricated due to size dynamics. The most common lubrication system is the oil reservoir type illustrated in Fig. 2.112(a)
- *External thrust*: The sum of the axial forces of the weight of pump and lineshaft and the dynamic forces of the pump to lift the liquid to the surface. In the case of the deep-well turbine pump, the weight of the pump and

lineshaft is sufficient to overcome any transient dynamic up-thrust forces and the total thrust direction is always down. Therefore, thrust and horse power are independently variable within the natural laws of physics.

- *P-base*: A pump flange mounting for the Hi-Thrust vertical motor.

Figure 2.112(b) illustrates a typical deep well turbine pump installation. Static water levels depend on the particular site, however wells of 1200 feet are common. In the United States, water levels have historically been dropping requiring larger motors and higher thrust bearings.

### 2.5.3.3 Types of Vertical Motors

- *Hi-Thrust*: In addition to normal induction motor classifications, the vertical motor is also classified by thrust. NEMA does not specifically define thrust ratings for motors; each manufacturer will define thrust rating for his product offering. A typical progression is as follows:

Frame series	Four-pole 100% thrust (lb)	Optional thrust	
		175%	300%
180	1800	N/A	N/A
210	2500	N/A	N/A
250	3200	N/A	N/A
280	3200	N/A	N/A
320	5500	x	N/A
360	5600	x	N/A
400	6000	x	N/A
440	8000	x	x
500	8000	x	x

There are two additional thrust classifications, with motor construction significantly different from the Hi-thrust motor.

- *Normal Thrust*: This motor is used in general applications where there is no or very low external thrust applied to the motor bearing. It is often a footless horizontal motor with a P-flange.
- *In-line Thrust*: Sometimes called medium thrust, this is a definite-purpose motor. The pump impellers are mounted directly on the motor shaft. Since the pump impeller performance depends on close tolerance with the pump housing, the motor shaft and flange run-out tolerances must also be tighter than normal. In this construction, the thrust bearing is usually located at the bottom rather than at the top as in Hi-Thrust construction. Thus the motor rotor thermal growth will not affect the impeller clearances. Radial loads imposed by the pump on the motor are taken primarily by the lower bearing.

### 2.5.3.4 Couplings and Motor Adjustments

The standard Hi-Thrust vertical motor must be adjusted to maintain proper bearing clearance. The entire rotating pump assembly is supported by the motor thrust bearing. This large static weight ensures that the bearing will seat properly. By connecting the rotating pump assembly at the top of the motor,

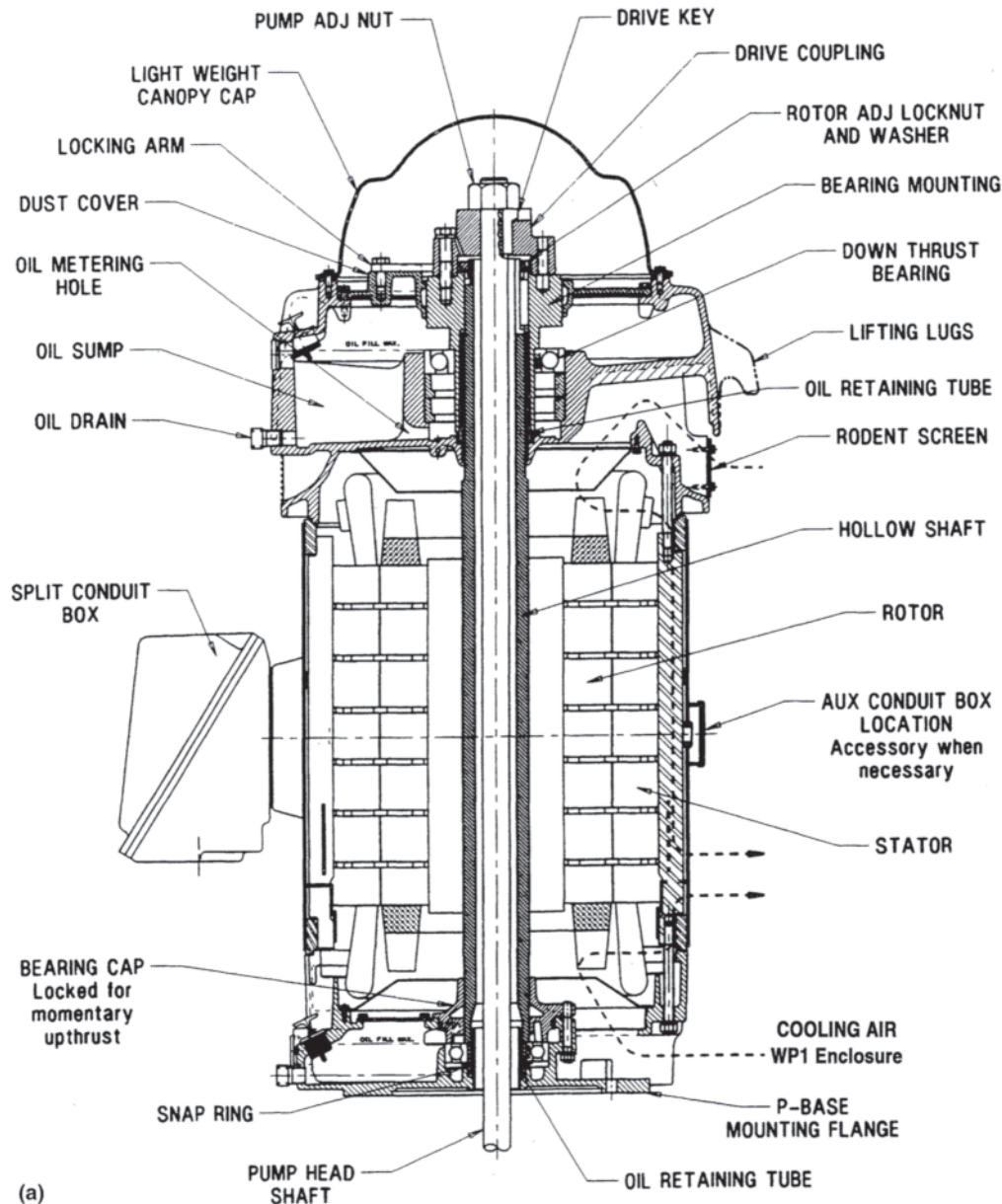


Figure 2.112(a) Nomenclature for deep well turbine pump motors.

thermal growth of the motor rotor assembly will not affect the subsequent pump impeller adjustment.

Although the exact motor adjustment procedure varies depending on motor construction, the basic procedure is to raise the rotor assembly by turning the rotor locknut with the rotor locked against rotation. This raises the rotor until the bottom bearing is locked against the bottom bearing cap. A dial indicator is used to tell when the rotor is at the correct position. The rotor is then lowered to ensure that the guide bearing is not preloaded.

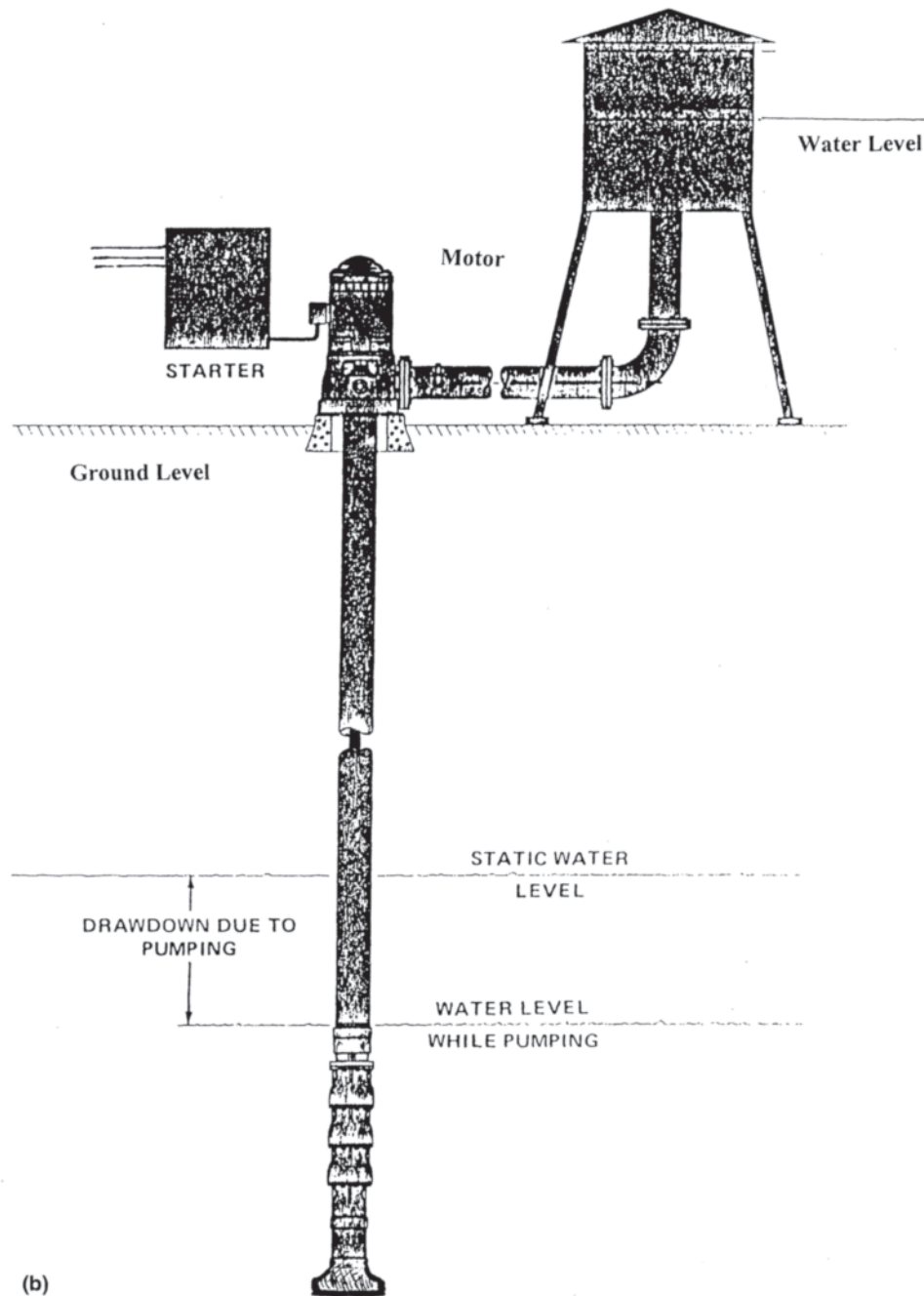
The main exception to this situation is when the thrust bearing is locked for continuous up or down loading. For vertical solid-shaft motors (VSS) with locked-thrust bearings, the rotor is simply adjusted for the proper shaft extension. Locked-thrust bearings are typical of larger two-pole (3600 rpm) motors. There is no adjustment required for VHS motors if the guide bearing is not preloaded.

After the motor rotating assembly is adjusted, the pump impeller can be positioned. With the motor rotating assembly locked, the rotating pump assembly is axially adjusted by turning the adjusting nut.

The motor hollow-shaft bore is larger than the pump headshaft to allow easy insertion during installation. The only point of contact with the motor is at the motor coupling. Occasionally it is necessary to limit pump headshaft movement by installing a steady bushing at the bottom of the motor. Figure 2.113 shows a typical example of an installed steady bushing.

#### 2.5.3.5 Thrust Bearings

The construction differences between horizontal and HiThrust vertical motors are primarily dictated by the differences in radial bearings from thrust bearings. Radial bearings are designed to handle primarily radial loads. The deep-groove



(b)

Figure 2.112(b) Typical deep well turbine pump installation.

ball bearing is a modification capable of handling moderate axial loading. A thrust bearing is designed to handle axial thrust load in only one direction and radial loading which is small compared to the axial load.

#### 2.5.3.5.1 Angular Contact

The normal Hi-Thrust bearing in vertical hollow-shaft motors is the angular contact, ball-bearing type. A typical type is shown in Fig. 2.114. This bearing has been developed specifically for pump service, having a high contact angle of up to 40 degrees. With such high contact angles the bearing

must have a considerable thrust applied in order to maintain proper operation. A motor running no load will often sound noisy because the thrust bearing is loose under this condition. The retainer in the bearing is quite important. There are four types in common use, molded plastic, pressed steel, pressed bronze, and machined bronze. Molded plastic and pressed steel are the least expensive, but still may be noisy and plastic may fail if not properly lubricated. Larger bearings at 3600 rpm usually use machined bronze cages.

Greater pumping depths require additional thrust. A convenient method of obtaining additional thrust capacity is

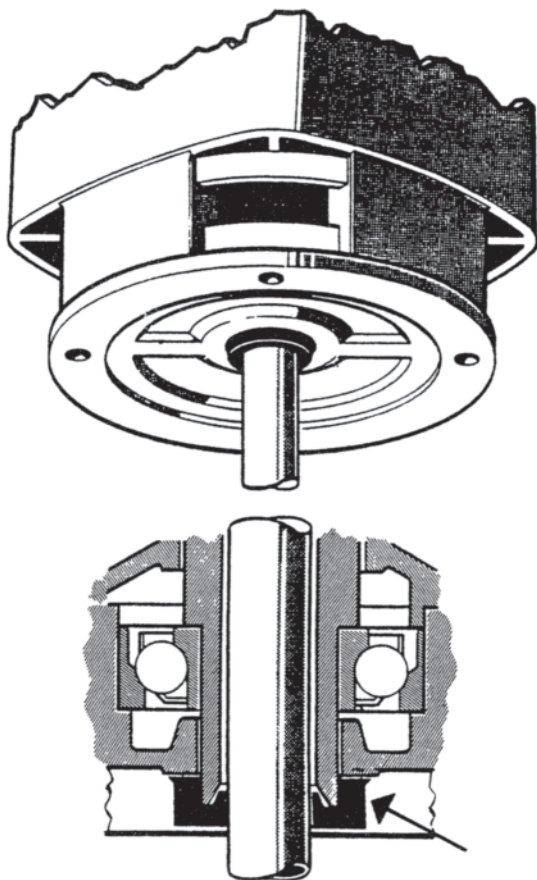


Figure 2.113 Steady bushing.

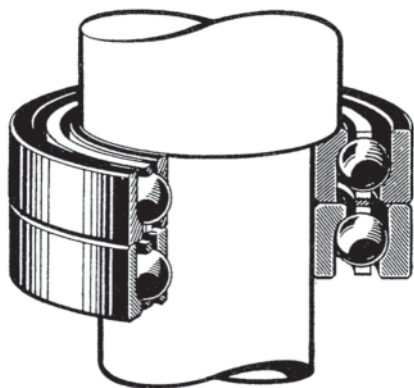


Figure 2.114 Angular contact tandem bearings.

to stack two or more bearings in tandem. Brackets can then be designed to take either one or more bearings as desired, adding flexibility and minimizing the number of brackets. Additional reasons for stacking bearings are that large-diameter balls and rollers are subject to higher dynamic stresses and become less efficient in carrying load; lubrication at high speeds is more difficult; and higher losses create additional heating that requires auxiliary cooling. By using smaller bearings in tandem, these difficulties are avoided, although lubrication

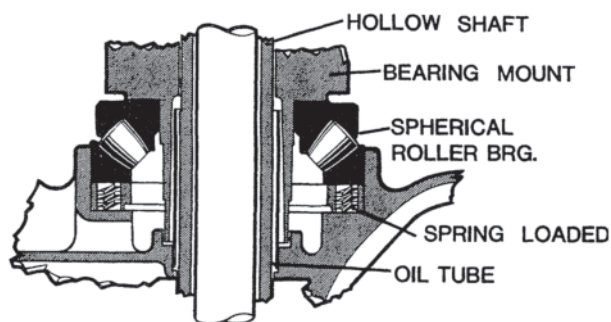


Figure 2.115 Spherical roller bearing.

of stacked bearings also requires special construction and the stack is limited in thrust capacity.

#### 2.5.3.5.2 Spherical Roller

At higher thrust ratings, when ball bearing size becomes excessively large, the spherical roller type is used. A typical construction is shown in Fig. 2.115. The rollers have a much larger contact area than do balls and are arranged to be self-aligning. Roller axis is at 45 degrees to the shaft and the bearing can carry both moderate and high thrust loads. However, the rollers must be guided and therefore develop more friction than the ball type. Water cooling is required at high speeds. Lubrication is more critical, and the bearing must also be preloaded or it may separate due to centrifugal forces if no thrust is present. A minimum downthrust, based on bearing size, is required during operation.

#### 2.5.3.5.3 Sliding Plate

For still greater thrust loads, the sliding plate bearing (Fig. 2.116) is available. Basically, this bearing consists of horizontal sliding plates separated by an oil film. The stationary plate is usually divided along the radii into a number of pie-shaped segments. In operation, a wedge shaped film of oil builds up between the rotating plate and each stationary segment.

In addition to the extraordinary high thrust capability, the bearing wear and lubrication life can be monitored by temperature measurement. The sliding plate bearing is commonly thought to have infinite bearing life. However,

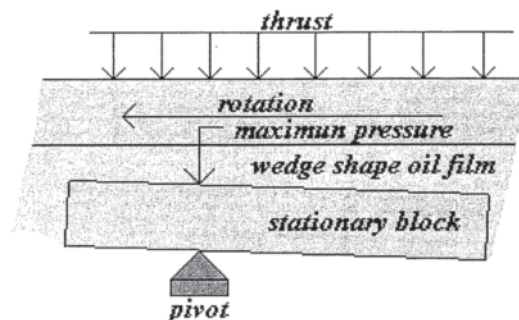


Figure 2.116 Hydrodynamic pivoted shoe thrust bearing.



infinite life requires appropriate and necessary maintenance and continuous operation. The lubrication life and the number of dry contacts starts are finite.

During starting, the plates are in direct contact without the oil film. Each start then, has dry contact between the plates causing extreme wear. Frequent starting requires a prepressurized or flood lubrication system to minimize or eliminate plate contact during starting.

Compared to antifriction bearings, the sliding plate bearing has significantly higher cost, has higher bearing losses, and requires additional or external cooling.

An optimal application for the sliding plate bearing is when thrust or shaft size exceeds the capacity of ball or roller type anti-friction bearings and the speed is low. Typically the NEMA 680 frame is the smallest housing that can accommodate this type bearing.

#### 2.5.3.5.4 Lubrication

Lubrication is determined by bearing size, loading, speed, temperature, and economics. Whereas the optimum lubrication system is full-time oil mist, it would be difficult to justify this expensive system when a simple grease-lubricated bearing will give adequate, reliable, low-maintenance, and low-replacement cost service.

The general progression for thrust bearing lubrication is:

1. Deep groove ball, grease
2. Double row ball, grease
3. Angular contact, grease
4. Angular contact, oil
5. Stacked angular contact, oil
6. Spherical roller, oil
7. Spherical roller, oil with auxiliary cooling
8. Sliding plate type, oil with auxiliary cooling

Guide bearings, which are not designed to handle continuous loading, are grease-lubricated through the NEMA 445 frame and oil-lubricated for the 500 frame series and larger. Depending on the manufacturer, the 447 and 449 frames will be either grease-or oil-lubricated.

The normal lubrication system for large thrust bearings is the metered, oil reservoir type. This allows the bearing to be completely submerged and protected during off periods, the most vulnerable time for bearings. When running, the bearing naturally pumps oil. By properly metering the returning oil, viscous losses are minimized to control lubricant heating and overall motor efficiency.

#### 2.5.3.6 Nonreverse Ratchets

When the motor is shut off, water in the column will recede to the water level, thereby causing the pump to backspin. The potential problems that may result are:

1. Damage to water-lubricated line shaft bearings.
2. Overspeed of the rotating components.
3. Silt and sand may be stirred up due to fluid flowing into the well or sump.

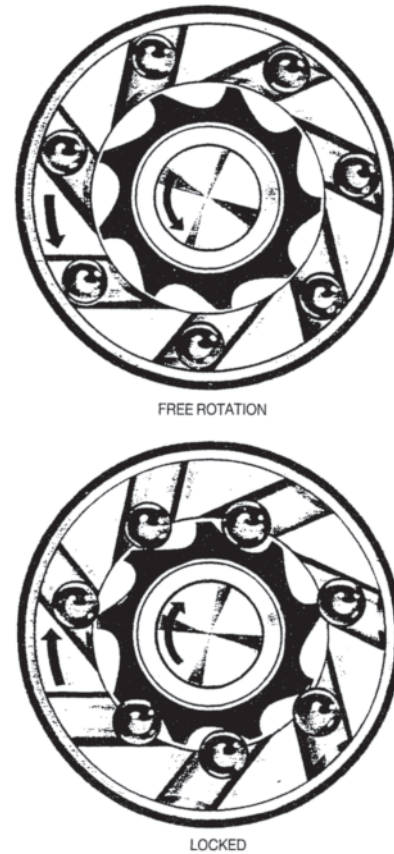


Figure 2.117 Nonreverse ratchet (NRR).

4. Resulting vacuum could cause the collapse of thin wall tubing.
5. Unscrewing of a threaded coupling in the case of a motor in an in-line service.

To avoid these problems, a nonreverse ratchet (NRR) is used.

The most common NRR is the pin type. However, this design is generally not used for deep-well operation because of the relatively large (8 to 10 degrees) rotation before it engages. A ball type with 4 degrees is generally used to limit pump shaft wrap-up. The ball type is illustrated in Fig. 2.117.

The use of ratchets with large 3600 rpm motors presents a vibration problem. Since the balls or pins never return to exactly the same place, the balls or pins then become eccentric weights at a high peripheral velocity, causing vibration.

The NRR is available with the Hi-Thrust motor construction. NRRs are not available on Normal Thrust or In-Line motors, although their inclusion is feasible.

#### 2.5.3.7 Self-Release Couplings

SRCs are the standard drive coupling on vertical motors. Typical operation is illustrated in Fig. 2.118.

If the motor reverses due to phase reversal or some other fault condition, and the line shaft pump joints start to unscrew, it will uncouple before the shaft completely unscrews.

This coupling can be bolted to take upthrust instead of self-releasing. Typical operation for either upper assembly or lower assembly locking is illustrated in Fig. 2.119.

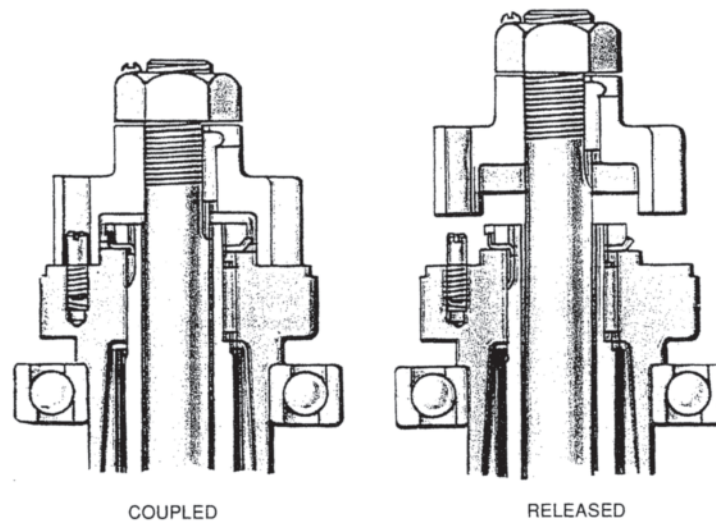


**Figure 2.118** Self-releasing coupling (SRC).

If both upthrust and nonreversing protection are required, a nonreverse ratchet must be specified.

#### 2.5.3.8 Upthrust

The direction of thrust is determined by the pump and the dynamics of the liquid flow. Even when a system is designed for thrust in one direction, transient conditions will sometimes temporarily change thrust direction. Thrust is then defined as either upthrust or downthrust.

The VHS motor was originally designed for the entire rotating pump and motor assembly to be supported by the motor thrust bearing. The high static weight precluded upthrust, which was convenient since Hi-Thrust bearings are suitable only for thrust in one direction. The standard Hi-Thrust bearing construction therefore is not suitable for sustained and/or heavy upthrust. Upthrust or even radial forces at low thrust

cause the thrust bearing to separate or move offline. The lower end guide bearing is now subjected to the full upthrust axial force. This bearing is not designed for continuous external loads. Sustained operation will eventually cause a catastrophic failure of either the thrust bearing or the guide bearing. This limitation also includes the VSS version of the VHS motor. When using the VHS or VSS Hi-Thrust motor in non-deep-well applications, it is prudent to modify the bearing construction for continuous up thrust or down-thrust.

#### 2.5.3.9 Enclosures

The VHS motor is available in standard NEMA enclosures. The open motor is most commonly supplied as Weather Protected Type I (WP-I). This enclosure includes screens to prevent contact with electrical parts. It is also most useful in preventing small animals from nesting inside the motor.

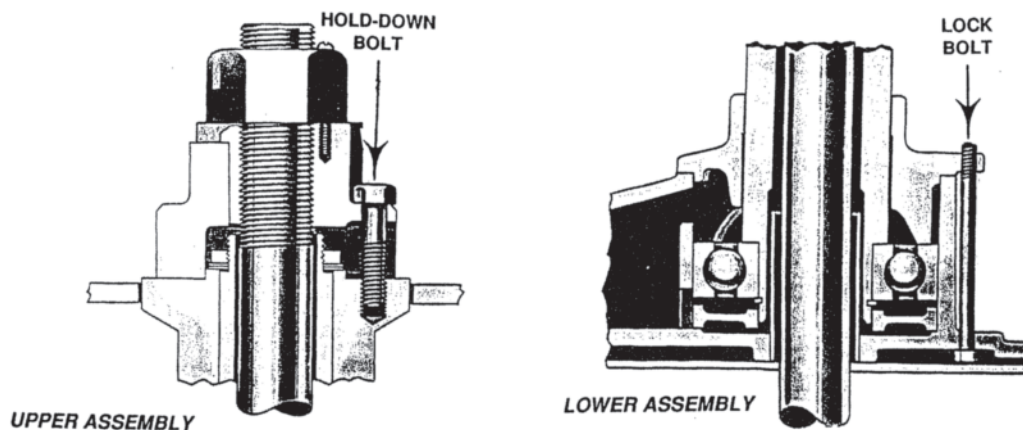


**Figure 2.119** Bolted coupling, upper or lower.

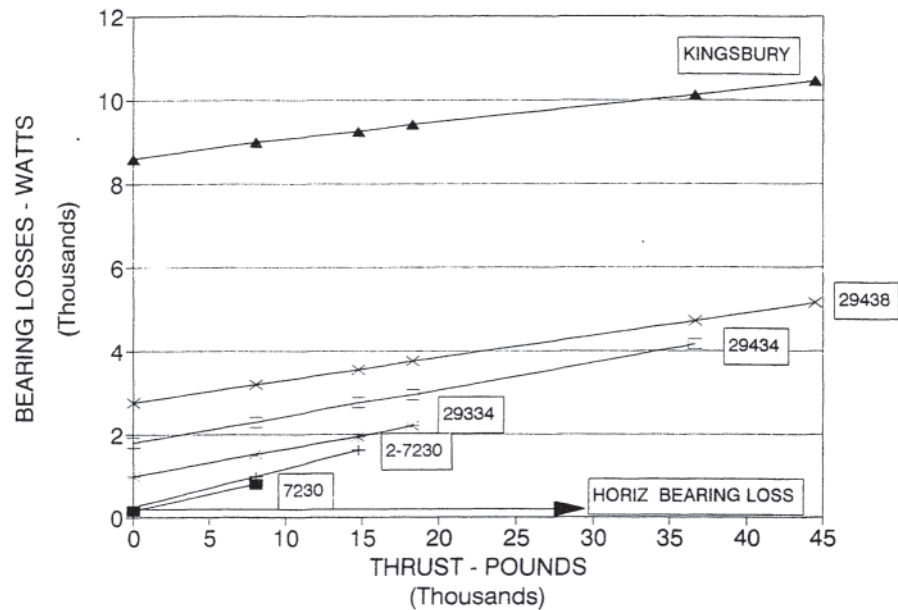


Figure 2.120 Vertical bearing losses.

### 2.5.3.10 Efficiency

The efficiency of the VHS motor will be lower than that of equivalent horizontal motors. The graph in Fig. 2.120 illustrates the increase in bearing losses for high thrust bearings. Normal thrust and inline motors use much smaller bearings and have higher efficiency.

Figure 2.120 also illustrates typical losses with thrust. Vertical mounting and thrust losses make confirming testing difficult. Vertical motors are usually converted to horizontal operation for testing on a horizontal dynamometer by replacing the thrust bearing with a horizontal type radial ball bearing. Efficiency must then be corrected to account for the difference in thrust and radial bearing losses. Since this method does not include thrust load, additional losses due to thrust have historically been included in the pump losses.

Thrust losses for ball-type thrust bearings can be estimated by the relationship of 5.6 watts per 100 rpm per 1000 pounds thrust. Losses for spherical and sliding plate-type bearings vary for several factors and must be determined individually.

## 2.5.4 Submersible Motors

### 2.5.4.1 Introduction

Submersible motors are used to drive centrifugal pumps that transfer fluid from one location to another. Submersible motors are smaller in diameter and longer than conventional motors because both space and clearance are limited in most installations. Figure 2.121 shows a typical installation of an electric submersible pump. The detailed motor description is shown in Fig. 2.122. Usually, the higher the power, the longer the motor. Two motors, upper and lower, can be bolted together mechanically and connected electrically for those applications that require additional power. In the tandem motor

arrangement, the stator windings of two motors are connected in series through plug-in type three-phase connectors. If a winding in either one of the motors is burned out, the whole system stops to prevent severe overload of the other motor.

There are some similarities between the water-well and oil-well submersible motors; however, the oil-well submersible motor is discussed in this section since the motor's operating environment is more hostile in a deep well pumping application.

### 2.5.4.2 Motor Operation

An oil-well submersible motor is a three-phase, two-pole induction motor. The three-phase power is supplied from the surface through an armored three-phase cable and a pothead. The pothead is plugged in and bolted to the motor head with O-ring seals. The typical setting depth of an oil-well submersible motor varies from 1000–3000 m (approximately from 4000–13,000 feet). The bottom hole temperature ranges from 40–180°C (100–350°F).

The internal heat generated by the motor must be transferred to the well fluid as it passes the outside diameter of the motor. The desirable rate of flow past the motor is 0.3 m/sec (1 ft/sec); the minimum is 0.15 m/sec (0.5 ft/sec). The specific heat of the well fluid is a large factor in the determination of motor internal temperature rise. The higher the oil cut, the higher the motor temperature rise. The motor temperature rise in a 100% oil well is 2 to 2.5 times the temperature rise in a water well.

The submersible motor is filled with high dielectric mineral oil for the purposes of (1) heat transfer, (2) bearing lubrication, and (3) pressure equalization. The motor oil communicates with the oil in another device called an equalizer that is bolted on the top of the motor. The equalizer mechanically seals the motor from the well fluid and equalizes the pressure

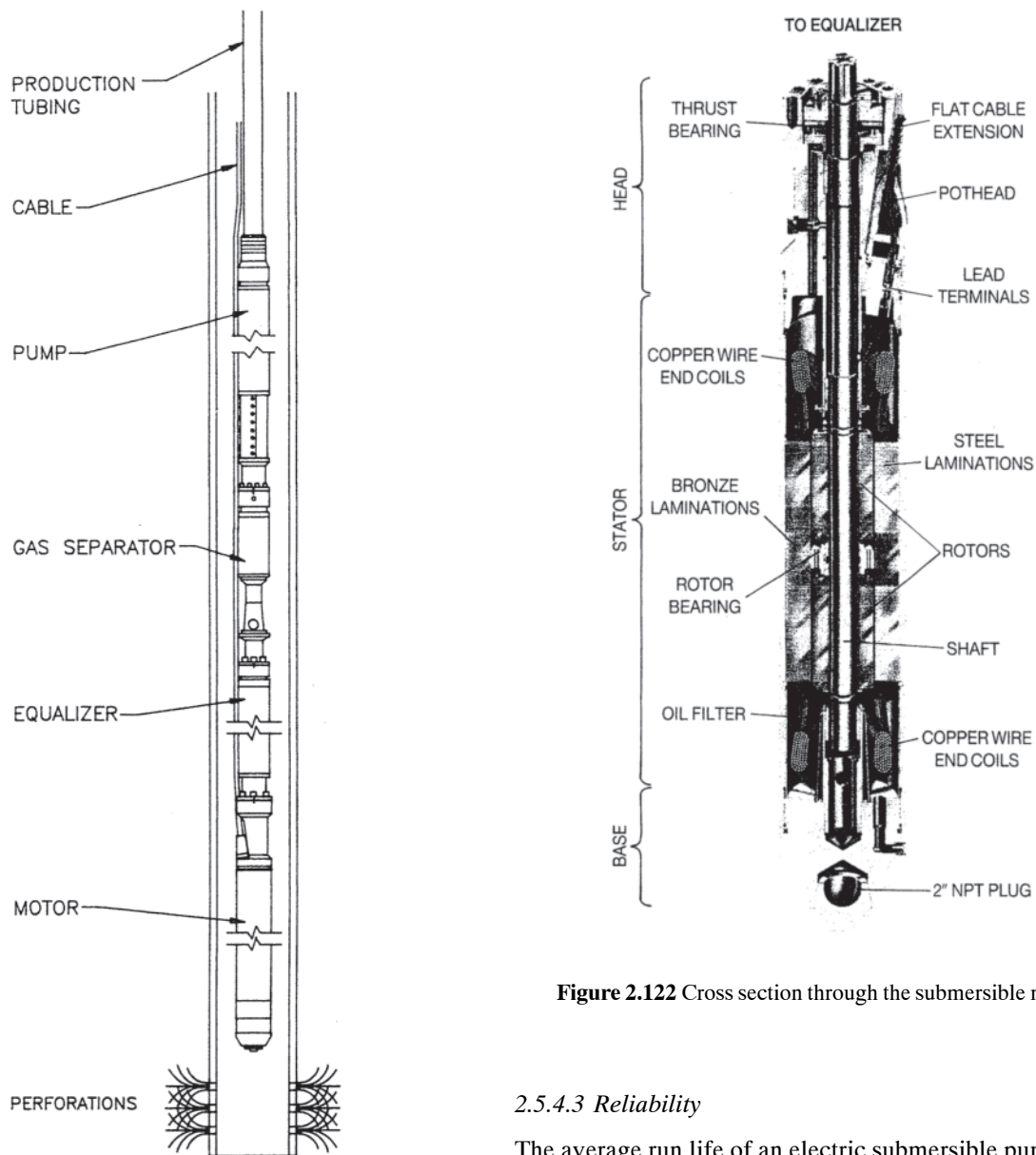


**Figure 2.121** Cross section through a well showing, from bottom to top, the submersible motor, equalizer, gas separator, pump, and production tubing. The power cable to the motor is also indicated.

between the inside and outside of the motor. It houses a thrust bearing that handles the downthrust created by the pump. As motor oil volume expands due to temperature rise, the equalizer serves as a reservoir and stores the expanded oil until its full capacity is reached. The oil then leaks out to the well bore from a check valve. When the motor is cooling down, the equalizer supplies oil to the motor. In typical operation, pressure differences between the inside and the outside of the motor are expected to be only 2 to 3 psi (13.8 to 20.7 [kpa]) kilopascal.

**Figure 2.122** Cross section through the submersible motor.

#### 2.5.4.3 Reliability

The average run life of an electric submersible pump (ESP) motor is about 2 years. The motor can be repaired mechanically or rewound if needed. The ESP is a reliable lift method. For well production larger than 300 barrels per day (1 barrel of petroleum=159 liters) it is also the most economical method for lifting the oil out of the ground. It would be advisable to add small submersible motors for residential water wells.

#### 2.5.5 Solid-Rotor Induction Motors

Solid-rotor induction motors are built with the rotor made of a single piece of ferromagnetic material. The first results of research oriented towards induction motors with solid rotors were published in the late 1920s by Schenfer [68] and Bruk [69]. Up to the early 1970s many scientists and engineers contributed to developing the theory and to perfecting the construction of solid rotors. The main motivation for such

research was to minimize the starting current and to simplify the rotor construction of an induction motor.

Further investigations have displayed other advantages of solid-rotor induction motors, namely.

- The possibility of obtaining steady-state stability and linearity of torque-speed characteristics throughout the entire speed range
- High reliability
- High mechanical integrity, rigidity, and durability
- Low level of noise and vibrations (no slots)

On the other hand, a solid-rotor induction motor has lower output power, efficiency, and power factor, and higher no-load slip than a cage induction motor of the same size. The high impedance of a solid rotor is the main reason for these disadvantages. The solid rotor impedance can be diminished in one of the following ways:

1. The solid rotor may be made of a ferromagnetic material with the ratio of magnetic permeability to electric conductivity as small as possible.
2. A layered (sandwiched) structure of the rotor may be made of appropriate ferromagnetic and nonmagnetic high-conductivity materials.
3. The effects of the high impedance may be offset by use of an optimum control system.

Solid-rotor induction motors can be used as:

- Three-phase motors for heavy-duty, fluctuating loads, reversible operation, etc.
- High-speed motors
- High-reliability motors operating under conditions of high temperature, high acceleration, active chemicals, or radioactivity as in many aviation, military equipment, deep-well pump, and nuclear applications
- Two-phase servomotors
- Gyro motors and torque transmitters incorporated into gyroscopic systems
- Auxiliary motors for starting turboalternators (the shaft of the turboalternator is utilized as a solid-steel rotor)
- Eddy current brakes and couplings

The recent development of ac variable-speed drives opens wider applications of solid-rotor induction motors [70, 71].

If the speed is high, centrifugal forces play an important role. The rotor should have sufficient mechanical strength to withstand these forces. Moreover, thyristor inverters generate higher time harmonics in the excitation voltage and current. These higher harmonics cause increased vibrations and noise. A solid rotor without slots is a good solution to minimize parasitic effects of mechanical nature.

Solid rotors are constructed in a variety of ways. The following rotors with distributed parameters are of the greatest significance.

- Homogeneous solid-steel rotor with a smooth (Fig. 2.123(a)) or slotted surface (Fig. 2.123(b))

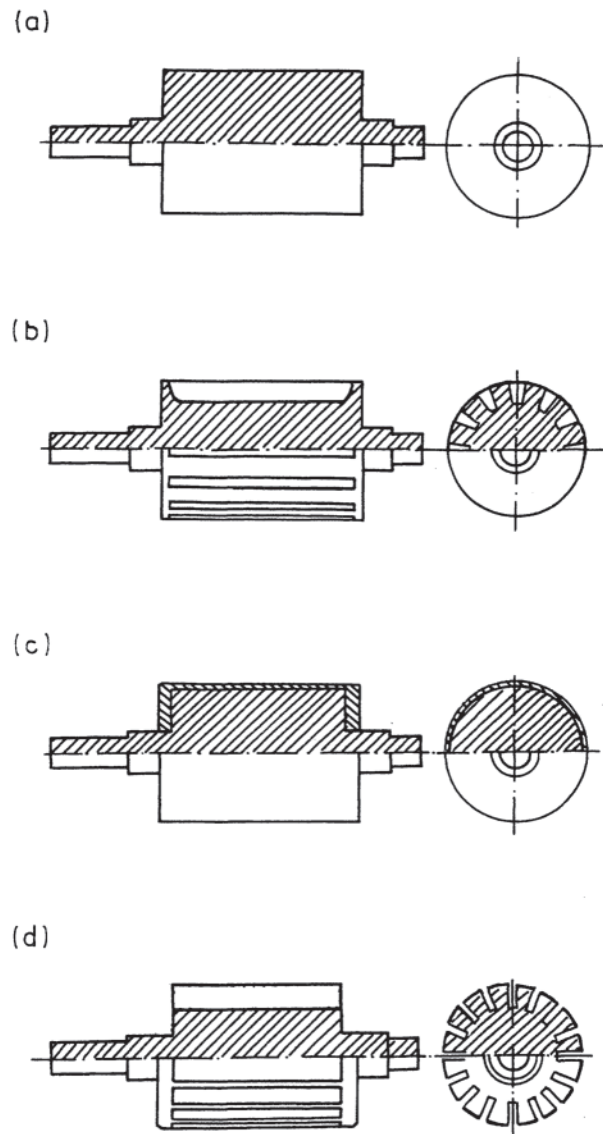


**Figure 2.123** Solid rotors: (a) homogeneous with smooth surface; (b) homogeneous with axial slots; (c) double-layer; (d) with cage winding.

- Double-layer rotor with solid or laminated back iron and nonmagnetic high-conductivity external cap (Fig. 2.123(c))
- Solid-rotor with cage winding (Fig. 2.123(d))

In this section, only the rotors of (a) and (c) in Fig. 2.123 are considered. A slotted solid rotor has recently been analyzed by Jinning and Fengli [72]. Putting the thickness of the high-conductivity layer equal to zero, the rotor of Fig. 2.123(c) becomes homogeneous. The performance for an induction motor with the rotor of Fig. 2.123(d) can be approximately calculated as that for a cage rotor with laminated stack. The analysis relates to three-phase motors.

### 2.5.5.1 Saturation and Hysteresis

In some papers, for example, that by Beckert [73], the magnetic permeability of the solid ferromagnetic rotor is assumed to be constant. In McConnel's [74], McConnel's and Sverdrup's [75], Wood's and Concordia's [76], Angst's [77], Yee's and Wilson's [78] and many other papers, an ideal rectangular magnetization curve for the solid rotor is made the basis of the analysis. Pillai [79] considered saturation assuming that the magnetization curve  $f(H)$  is expressed by the function  $B = KH^{1-2/\alpha}$ , where  $K=0.7-0.9$ ,  $\alpha \approx 2.3$ .

To take into account saturation and hysteresis in solid ferromagnetic rotors, many authors, for example, Lasocinski [80], Maergoyz and Polishchuk [81], and Voldek [82] make use of the well-known approximate Neyman's method [83]. Neyman proved that the resistance and active power losses for constant permeability should be multiplied by a constant coefficient  $a_R \approx 1.45$ . Similarly, the reactance and reactive power losses for constant permeability should be multiplied by a constant coefficient  $a_x \approx 0.85$ . Neyman's method includes approximately only the variation of permeability in the direction of wave penetration and hysteresis losses due only to the fundamental harmonic of the electromagnetic wave.

As was later shown [84], the coefficients  $a_R$  and  $a_x$  are not constant and depend on the magnetic field intensity at the surface of a ferromagnetic material.

The complex propagation constant including magnetic saturation and hysteresis in one-dimensional analysis of a ferromagnetic half-space has the form:

$$\alpha = (a_R + ja_x)k_{Fe} \quad (2.139)$$

where the coefficients are  $a_R = f_1(H)$  and  $a_x = f_2(H)$ . The attenuation coefficient for surface relative permeability  $\nu_{rs}$  is equal to :

$$k_{Fe} = (\pi f s \mu_0 \mu_{rs} \sigma_{Fe})^{1/2} \quad (2.140)$$

where  $s$  is slip for the fundamental harmonic and  $\sigma_{Fe}$  is the conductivity of the steel.

From Eq. 2.139, one can obtain the following form of the equivalent complex magnetic permeability:

$$\mu_{re} = \mu_{rs}(\mu' - j\mu'') \quad (2.141)$$

where:

$$\mu' = a_R a_x \quad (2.142)$$

$$\mu'' = 0.5(a_R^2 - a_x^2) \quad (2.143)$$

Therefore, the real part  $\mu_{rs}\mu'$  of the equivalent complex permeability and its imaginary part  $\mu_{rs}\mu''$  are functions of magnetic field intensity. The equivalent permeability from Eq. 2.141 can also be applied to a two-dimensional or three-dimensional analysis of electromagnetic fields in a ferromagnetic medium.

The values of permeabilities  $\mu_{rs}$ ,  $\mu'$ ,  $\mu''$  of carbon steels and alloy steels are given as follows.

In Fig. 2.124(a) for steel containing 0.27% C, 0.70% Mn, 0.12–0.30% Si, 0.050% P, 0.055% S and with electric conductivity  $6.2 \times 10^6$  S/m (at a temperature of 293.2°K)

In Fig. 2.124(b) for steel containing 0.32–0.40% C, 0.50–0.80% Mn, 0.17–0.37% Si, 0.25% Cr, 0.25% Ni, 0.25% Cu, 0.040% P, 0.040% S and with electric conductivity  $4.50 \times 10^6$  S/m.

In Fig. 2.124(c) for steel containing 0.52–0.60% C, 0.50–0.80% Mn, 0.17–0.37% Si, 0.25% Cr, 0.25% Ni, 0.25% Cu, 0.040% P, 0.040% S and with electric conductivity  $4.64 \times 10^6$  S/m.

In Fig. 2.124(d) for steel containing 0.62–0.70% C, 0.50–0.80% Mn, 0.17–0.37% Si, 0.25% Cr, 0.25% Ni, 0.25% Cu, 0.040% P, 0.040% S and with electric conductivity  $4.57 \times 10^6$  S/m.

### 2.5.5.2 Stator mmf and Line Current Density

The input phase voltages of an inverter-fed motor contain odd time harmonics  $n=6k+1$ , where  $k=0, 1, 2, 3, \dots$ . Triple harmonics are absent. Having only odd time harmonics present, the mmf of each phase of a three-phase machine with stator windings shifted by the space angle  $2\pi/3$  and fed with unbalanced currents can be expressed by the following set of equations:

$$\begin{aligned} F_A(x,t) &= \frac{2}{\pi} \frac{1}{p} N_1 k_{\omega 1} \cos\left(\frac{\pi}{\tau} x\right) \\ &\quad \times \sqrt{2} \sum_{n=1}^{\infty} |I_{nA}| \exp[jn(\omega t - \beta_A)] \\ F_B(x,t) &= \frac{2}{\pi} \frac{1}{p} N_1 k_{\omega 1} \cos\left(\frac{\pi}{\tau} x - 2\frac{\pi}{3}\right) \\ &\quad \times \sqrt{2} \sum_{n=1}^{\infty} |I_{nB}| \exp[jn(\omega t - \beta_B)] \\ F_C(x,t) &= \frac{2}{\pi} \frac{1}{p} N_1 k_{\omega 1} \cos\left(\frac{\pi}{\tau} x - 4\frac{\pi}{3}\right) \\ &\quad \times \sqrt{2} \sum_{n=1}^{\infty} |I_{nC}| \exp[jn(\omega t - \beta_C)] \end{aligned} \quad (2.144)$$

where  $\beta_A, \beta_B, \beta_C$  are the phase angles between currents,  $N_1$  is the number of the stator turns per phase,  $k_{\omega 1}$  is the stator winding factor for the fundamental space harmonic,  $\tau$  is the pole pitch, and  $p$  is the number of pole pairs. Subsequently,  $\beta_A$  will be set to zero, denoting:

$$I_{1n}^+ = \frac{1}{3} (I_{nA} + aI_{nB} + a^2I_{nC}) \quad (2.145a)$$

$$I_{2n}^- = \frac{1}{3} (I_{nA} + a^2I_{nB} + aI_{nC}) \quad (2.145b)$$

where  $a = \exp(j2\pi/3)$ , and  $I_{nA} = |I_{nA}| \exp(-jn\beta_A)$ ,  $I_{nB} = |I_{nB}| \exp(-jn\beta_B)$ , and  $I_{nC} = |I_{nC}| \exp(-jn\beta_C)$ , the total mmf of a three-phase machine can be expressed as:

$$\begin{aligned} F(x,t) &= F_A(x,t) + F_B(x,t) + F_C(x,t) \\ &= \frac{3\sqrt{2}}{\pi p} N_1 k_{\omega 1} \sum_{n=1}^{\infty} \{ I_{1n}^+ \exp[j(n\omega t - \pi x/\tau)] \\ &\quad + I_{2n}^- \exp[j(n\omega t + \pi x/\tau)] \} \end{aligned} \quad (2.146)$$

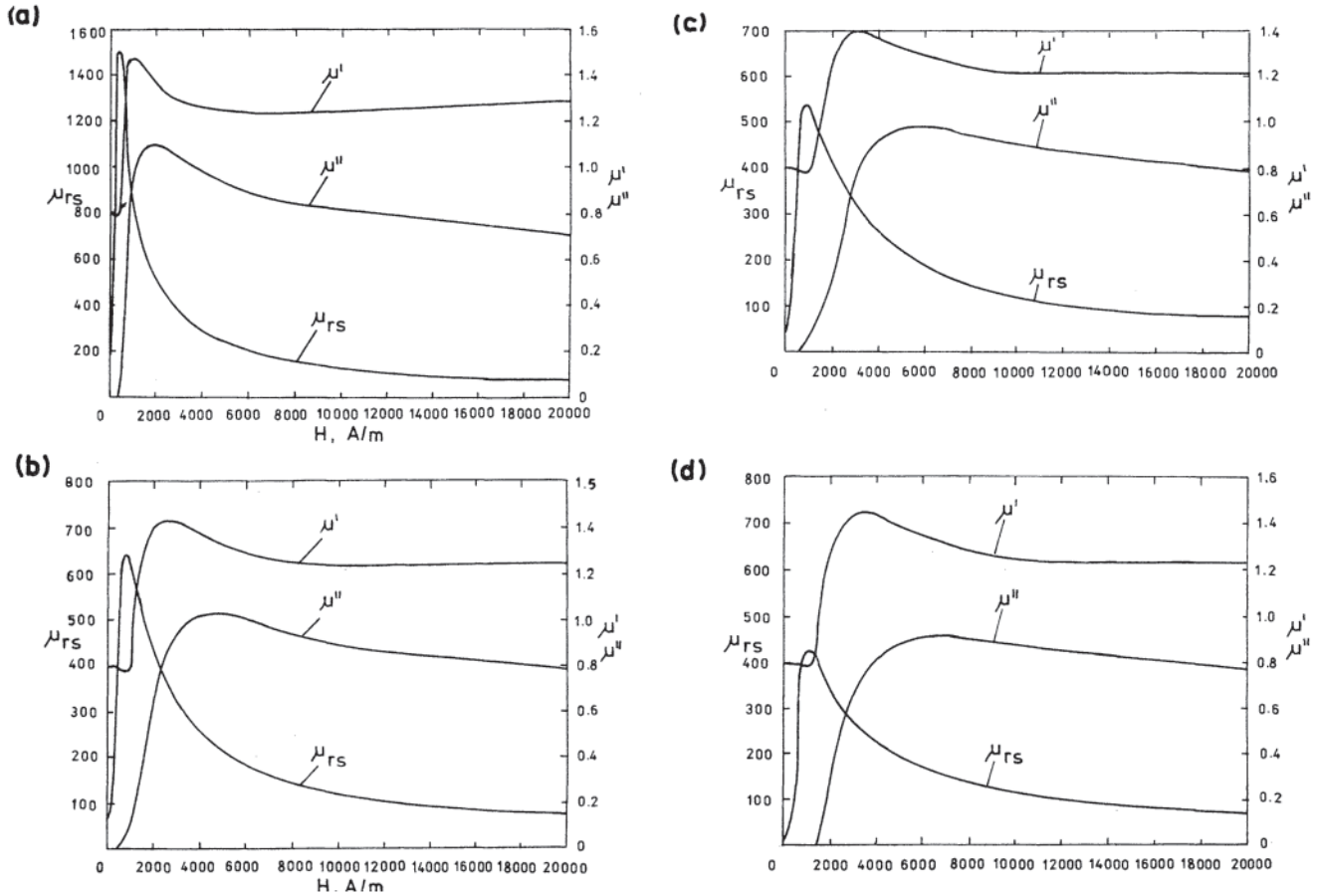


**Figure 2.124** Magnetic permeabilities  $\mu_{rs}$ ,  $\mu'$ , and  $\mu''$  of carbon and alloy steels plotted against magnetic field intensity  $H$ : (a) 0.27% C; (b) 0.32 to 0.40% C; (c) 0.52 to 0.60% C; (d) 0.62 to 0.70% C. See the complete description in the text.

Equation 2.146 describes two waves travelling in opposite directions, with the coordinate system fixed to the stator. Differentiating with respect to  $x$ , Eq. 2.146 yields the line-current density of the stator, that is:

$$a_{1n}(x, t) = A_{mn}^+ \exp [j(n\omega t - \pi x/\tau - \pi/2)] + A_{mn}^- \exp [j(n\omega t + \pi x/\tau + \pi/2)]$$

or, neglecting  $\exp(jn\omega t \pm \pi/2)$ :

$$a_{1n}(x) = A_{mn}^+ e^{-j\pi x/\tau} + A_{mn}^- e^{j\pi x/\tau} \quad (2.147)$$

where the complex amplitudes of the line-current density are

$$A_{mn}^+ = \frac{3\sqrt{2} N_1 K_{\omega 1}}{\tau p} I_{1n}^+ \quad (2.148a)$$

$$A_{mn}^- = \frac{3\sqrt{2} N_1 K_{\omega 1}}{\tau p} I_{1n}^- \quad (2.148b)$$

The summation of higher time harmonics  $n$  in Eq. 2.147 has been omitted. That is, Eqs. 2.147 and 2.148 express sinusoidal waves of the line-current density at the frequency  $nf$ .

The line-current density Eq. 2.147, together with Maxwell's equations and the boundary conditions, gives a

two-dimensional electromagnetic field distribution in the air gap and in the rotor.

From Eqs. 2.145a and 2.145b it is seen that for  $|I_{nA}| = |I_{nB}| = |I_{nC}|$  and  $\beta_A = 0, \beta_B = 120$  degrees,  $\beta_C = 240$  degrees, the first mmf harmonic in phases  $A, B$ , and  $C$  constitutes a symmetrical three-ray star with positive sequence only ( $I_{1n}^+ \neq 0, I_{1n}^- = 0$ ). The harmonics of order  $6k+1$ , where  $k=0, 1, 2, 3, \dots$ , have the same phase sequence as the first harmonic ( $I_{1n}^+ \neq 0, I_{1n}^- = 0$ ), while harmonics of order  $6k-1$ , where  $k=1, 2, 3, \dots$ , have the opposite phase sequence ( $I_{1n}^+ = 0, I_{1n}^- \neq 0$ ). The third harmonic of the mmf, and all harmonics that are a multiple of 3, that is  $6k+3$ , where  $k=0, 1, 2, 3, \dots$ , coincide in phase in the three-phase winding, that is,  $I_{1n}^+ = I_{1n}^- = 0$ . They do not exist in inverter-fed induction motors.

For  $|I_{nA}| = |I_{nB}| = |I_{nC}|$  and  $\beta_A = 0, \beta_B \neq 120$  degrees and  $\beta_C \neq 240$  degrees, the time harmonics of order  $6k+1, 6k+3$  and  $6k-1$  produce both positive-sequence and negative sequence currents.

### 2.5.5.3 Electromagnetic Fields in a Double-Layer Solid Rotor

Figure 2.125 shows a model of a double-layer rotor. The external layer, that is, the high conductivity cap, is usually

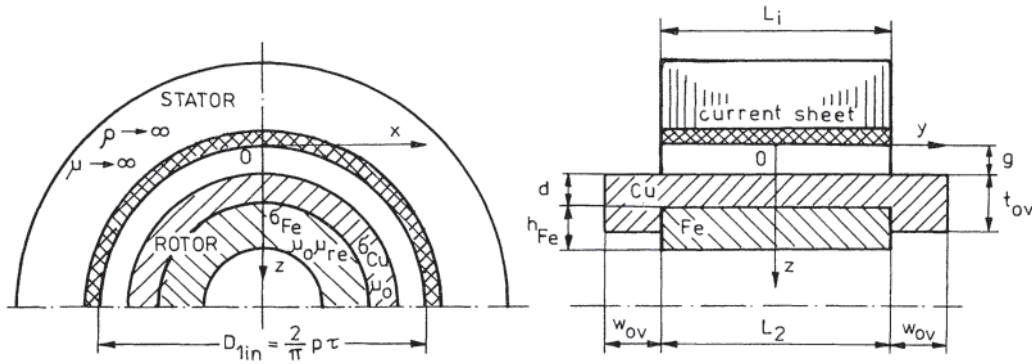


Figure 2.125 Induction motor with solid ferromagnetic rotor covered with a copper layer.

made of copper. It serves as an electric circuit. The solid back iron serves both as a magnetic and an electric circuit.

The electromagnetic field distribution in the air gap and the double-layer rotor is determined from the following assumptions.

1. The stator core is composed of thin laminations with infinite magnetic permeability and infinite resistivity.
2. The active surface of the stator with its dimensions  $L_i$  and  $2_p \tau$  ( $\tau$  being the pole pitch) is unslotted.
3. The stator windings are simulated by an infinitely thin current sheet uniformly distributed at the active surface of the core (line-current density).
4. The rotor is a smooth cylinder composed of isotropic ferromagnetic material (inside) and a high current-conducting isotropic nonmagnetic layer (outside).
5. The magnetic permeability of the ferromagnetic core is expressed by Eq. 2.141.
6. The rotor core with its length  $L_2=L_i$  (in the  $y$  direction) and the stator cylinder are coaxial.
7. The radius of curvature of the rotor is much greater than the depth of penetration of the electromagnetic wave so that the analysis can be performed in a rectangular coordinate system.
8. The equivalent magnetic permeability of the rotor core is the same for higher harmonics of magnetic field intensity as for the fundamental harmonic.
9. The rotor and stator are developed into flat bodies and the rotor core is analyzed as a half-space.
10. The space period of the electromagnetic field distribution along the pole pitch is equal to  $2\tau$ .
11. The analysis is two-dimensional so that the rotor and stator are infinitely long (in the  $y$  direction); the finite dimensions will be included later.
12. All quantities are changing sinusoidally with time.

The electromagnetic field in electrical machines is described by Maxwell's equations in which the displacement currents and convection currents can be omitted. After typical operations of vector analysis, Laplace's (for air) and Helmholtz (for a conductor) equations are obtained, as follows.

1. For  $0 \leq z \leq g$  and  $z \geq g + d + h_{Fe}$ :

$$\nabla^2 \bar{H}_n = 0 \quad (2.149a)$$

$$\nabla^2 \bar{E}_n = 0 \quad (2.149b)$$

2. For the high-conductivity nonmagnetic layer ( $g \leq z \leq g + d$ ):

$$\nabla^2 \bar{H}_{Cu n} = \alpha_{Cu n}^2 \bar{H}_{Cu n} \quad (2.150a)$$

$$\nabla^2 \bar{E}_{Cu n} = \alpha_{Cu n}^2 \bar{E}_{Cu n} \quad (2.150b)$$

3. For the ferromagnetic material ( $g + d \leq z \leq g + d + h_{Fe}$ ):

$$\nabla^2 \bar{H}_{Fe n} = \alpha_{Fe n}^2 \bar{H}_{Fe n} \quad (2.151a)$$

$$\nabla^2 \bar{E}_{Fe n} = \alpha_{Cu n}^2 \bar{E}_{Fe n} \quad (2.151b)$$

The complex propagation constants are expressed as follows:

1. In the case of forward-rotating fields ( $n=1, 7, 13, 19, \dots$ ):

$$\alpha_{Cu n}^+ = (j\omega_n^+ \mu_0 \sigma_{Cu})^{1/2} = (1+j)(\pi n f s_n^+ \mu_0 \sigma_{Cu})^{1/2} \quad (2.152a)$$

$$\begin{aligned} \alpha_{Fe n}^+ &= (j\omega_n^+ \mu_0 \mu_{re} \sigma_{Fe})^{1/2} \\ &= (a_R + ja_X) \times (\pi n f s_n^+ \mu_0 \mu_{rs} \sigma_{Fe})^{1/2} \end{aligned} \quad (2.153b)$$

2. In the case of backward-rotating fields ( $n=5, 11, 17, 23, \dots$ ):

$$\alpha_{Cu n}^- = (j\omega_n^- \mu_0 \sigma_{Cu})^{1/2} = (1+j)(\pi n f s_n^- \mu_0 \sigma_{Cu})^{1/2} \quad (2.152b)$$

$$\begin{aligned} \alpha_{Fe n}^- &= (j\omega_n^- \mu_0 \mu_{re} \sigma_{Fe})^{1/2} \\ &= (a_R + ja_X) \times (\pi n f s_n^- \mu_0 \mu_{rs} \sigma_{Fe})^{1/2} \end{aligned} \quad (2.153b)$$

where the slip for higher time harmonics is:



$$s_n^+ = 1 - \frac{1}{n} (1 - s) \quad (2.154a)$$

$$s_n^- = 1 + \frac{1}{n} (1 - s) \quad (2.154b)$$

and the angular frequency of the eddy currents and magnetic flux in the rotor is:

$$\omega_n^+ = 2\pi f n s_n^+ = \omega n s_n^+ \quad (2.155a)$$

$$\omega_n^- = 2\pi f n s_n^- = \omega n s_n^- \quad (2.155b)$$

where  $\omega=2\pi f$  is the angular frequency of the stator current for the fundamental harmonic:

The components of the electric field intensity in the  $z$  direction do not exist, that is,  $E_{Cunz}=0$  and  $E_{Fenz}=0$

Using separation of variables, general solutions for Eqs. 2.149a to 2.151b have the form:

1. For  $0 \leq z \leq g$  and  $z \geq g + d + h_{Fe}$ :

$$F_n = (C_{1n} e^{-j\beta x} + C_{2n} e^{j\beta x}) (C_{3n} e^{-\beta z} + C_{4n} e^{\beta z}) \quad (2.156)$$

2. For  $g \leq z \leq g + d$ :

$$F_{Cun} = (C_{1Cun} e^{-j\beta x} + C_{2Cun} e^{j\beta x}) \times (C_{3Cun} e^{-\kappa_{Cun} z} + C_{4Cun} e^{\kappa_{Cun} z}) \quad (2.157)$$

3. For  $g + d \leq z \leq g + d + h_{Fe}$ :

$$F_{Fen} = (C_{1Fen} e^{-j\beta x} + C_{2Fen} e^{j\beta x}) \times (C_{3Fen} e^{-\kappa_{Fen} z} + C_{4Fen} e^{\kappa_{Fen} z}) \quad (2.158)$$

where  $F_n$  represents the components of electric and magnetic field intensities in the air,  $F_{Cun}$  represents the components in the nonmagnetic layer, and  $F_{Fen}$  represents the components in the ferromagnetic material.

If  $F_n = X_n Z_n$ ,  $F_{Cun} = X_{Cun} Z_{Cun}$ , and  $F_{Fen} = X_{Fen} Z_{Fen}$ , the propagation constants  $\kappa_{Cun}$  and  $\kappa_{Fen}$  dependent on the polepitch  $\tau$  are equal to:

$$\kappa_{Cun} = (\alpha_{Cun}^2 + \beta^2)^{1/2} \quad (2.159)$$

$$\kappa_{Fen}^2 = (\alpha_{Fen}^2 + \beta^2)^{1/2} \quad (2.160)$$

where:

$$\beta = \frac{\pi}{\tau} \quad (2.161)$$

The real constant  $\beta$  is obtained from assumption (10). The complex constants  $C_{in}$ ,  $C_{iCun}$ , and  $C_{iFen}$  where  $i=1, 2, 3, 4$  in Eqs. 2.156, 2.157, and 2.158 can be found from the following boundary conditions:

$$H_{xn}(x, 0) = -a_{1n}(x) \quad (2.162)$$

$$H_{xn}(x, g) = H_{xCun}(x, g) \quad (2.163)$$

$$H_{xCun}(x, g + d) = H_{xFen}(x, g + d) \quad (2.164)$$

$$H_{xFen}(x, g + d + h_{Fe}) = H_{xn}(x, g + d + h_{Fe}) \quad (2.165)$$

$$H_{zn}(x, g) = H_{zCun}(x, g) \quad (2.166)$$

$$H_{zCun}(x, g + d) \approx \mu_{re} H_{zFen}(x, g + d) \quad (2.167)$$

$$\mu_{re} H_{zFen}(x, g + d + h_{Fe}) \approx H_{zn}(x, g + d + h_{Fe}) \quad (2.168)$$

and from the fundamental equation of electromagnetic fields,

that is,  $\text{curl } \bar{H} = \sigma \bar{E}$ ,  $\text{div } \bar{B} = 0$ , and  $\text{div } \bar{E} = 0$ , with displacement and convection current being neglected. The line-current density  $a_{1n}(x)$  is given by Eq. 2.147. The electromagnetic field decays completely for  $z \rightarrow \infty$ , hence  $C_{4n} = 0$  for  $z \geq g + d + h_{Fe}$ . After finding the complex constants  $C_{in}$ ,  $C_{iCun}$ , and  $C_{iFen}$ , the solution of the electromagnetic field equations is complete:

1. For  $0 \leq z \leq g$ :

$$H_{xn}^+ = \frac{1}{M_{4n}^+} (-A_{mn}^+) e^{-j\beta x} \left[ \frac{\kappa_{Cun}^+}{\beta} M_{3n}^+ \cosh \beta(z - g) - W_{3n}^+ \sinh \beta(z - g) \right] \quad (2.169a)$$

$$H_{xn}^- = \frac{1}{M_{4n}^-} (-A_{mn}^-) e^{j\beta x} \left[ \frac{\kappa_{Cun}^-}{\beta} M_{3n}^- \cosh \beta(z - g) - W_{3n}^- \sinh \beta(z - g) \right] \quad (2.169b)$$

$$H_{zn}^+ = \frac{1}{M_{4n}^+} j A_{mn}^+ e^{-j\beta x} \left[ W_{3n}^+ \cosh \beta(z - g) - \frac{\kappa_{Cun}^+}{\beta} M_{3n}^+ \sinh \beta(z - g) \right] \quad (2.170a)$$

$$H_{zn}^- = \frac{1}{M_{4n}^-} (-j A_{mn}^-) e^{j\beta x} \left[ W_{3n}^- \cosh \beta(z - g) - \frac{\kappa_{Cun}^-}{\beta} M_{3n}^- \sinh \beta(z - g) \right] \quad (2.170b)$$

$$E_{yn}^+ = \frac{1}{M_{4n}^+} \frac{j n \omega \mu}{\beta} A_{mn}^- e^{-j\beta x} \left[ W_{3n}^+ \cosh \beta(z - g) - \frac{\kappa_{Cun}^+}{\beta} M_{3n}^+ \sinh \beta(z - g) \right] \quad (2.171a)$$

$$E_{yn}^- = \frac{1}{M_{4n}^-} \frac{j n \omega \mu}{\beta} A_{mn} e^{-j\beta x} \left[ W_{3n}^- \cosh \beta(z - g) - \frac{\kappa_{Cun}^-}{\beta} M_{3n}^- \sinh \beta(z - g) \right] \quad (2.171b)$$

2. For  $g \leq z \leq g + d$ :

$$H_{xCun}^+ = \frac{1}{M_{n4}^+} \frac{\kappa_{Cun}^+}{\beta} (-A_{mn}^+) e^{-j\beta x} \left[ \frac{\kappa_{Fen}^+}{\kappa_{Cun}^+} M_{2n}^+ \times \cosh \kappa_{Cun}^+ (z - g - d) - \mu_{re} W_{2n}^+ \sinh \kappa_{Cun}^+ (z - g - d) \right] \quad (2.172a)$$

$$H_{xCun}^- = \frac{1}{M_{n4}^-} \frac{\kappa_{Cun}^-}{\beta} (-A_{mn}^-) e^{j\beta x} \left[ \frac{\kappa_{Fen}^-}{\kappa_{Cun}^-} M_{2n}^- \times \cosh \kappa_{Cun}^- (z - g - d) - \mu_{re} W_{2n}^- \sinh \kappa_{Cun}^- (z - g - d) \right] \quad (2.172b)$$

$$H_{zCun}^+ = \frac{1}{M_{n4}^+} jA_{mn}^+ e^{-j\beta x} \left[ \mu_{re} W_{n2}^+ \cosh \kappa_{Cun}^+ (z - g - d) - \frac{\kappa_{Fen}^+}{\kappa_{Cun}^+} M_{2n}^+ \sinh \kappa_{Cun}^+ (z - g - d) \right] \quad (2.173a)$$

$$H_{zCun}^- = \frac{1}{M_{n4}^-} (-jA_{mn}^- e^{j\beta x}) \left[ \mu_{re} W_{n2}^- \cosh \kappa_{Cun}^- (z - g - d) - \frac{\kappa_{Fen}^-}{\kappa_{Cun}^-} M_{2n}^- \sinh \kappa_{Cun}^- (z - g - d) \right] \quad (2.173b)$$

$$E_{yCun}^+ = \frac{1}{M_{n4}^+} \frac{j\omega_n^+ \mu}{\beta} A_{mn}^+ e^{-j\beta x} \left[ \mu_{re} W_{n2}^+ \cosh \kappa_{Cun}^+ (z - g - d) - \frac{\kappa_{Fen}^+}{\kappa_{Cun}^+} M_{2n}^+ \sinh \kappa_{Cun}^+ (z - g - d) \right] \quad (2.174a)$$

$$E_{yCun}^- = \frac{1}{M_{n4}^-} \frac{j\omega_n^- \mu}{\beta} A_{mn}^- e^{j\beta x} \left[ \mu_{re} W_{n2}^- \cosh \kappa_{Cun}^- (z - g - d) - \frac{\kappa_{Fen}^-}{\kappa_{Cun}^-} M_{2n}^- \sinh \kappa_{Cun}^- (z - g - d) \right] \quad (2.174b)$$

3. For  $g+d \leq z \leq g+d+h_{Fe}$ :

$$H_{xFen}^+ = \frac{1}{M_{n4}^+} \frac{\kappa_{Fen}^+}{\beta} (-A_{mn}^+) e^{-j\beta x} \left[ \frac{\beta}{\kappa_{Fen}^+} \cosh \kappa_{Fen}^+ (z - g - d - h_{Fe}) - \frac{1}{\mu_{re}} \sinh \kappa_{Fen}^+ (z - g - d - h_{Fe}) \right] \quad (2.175a)$$

$$H_{xFen}^- = \frac{1}{M_{n4}^-} \frac{\kappa_{Fen}^-}{\beta} (-A_{mn}^-) e^{j\beta x} \left[ \frac{\beta}{\kappa_{Fen}^-} \cosh \kappa_{Fen}^- (z - g - d - h_{Fe}) - \frac{1}{\mu_{re}} \sinh \kappa_{Fen}^- (z - g - d - h_{Fe}) \right] \quad (2.175b)$$

$$H_{zFen}^+ = \frac{1}{M_{n4}^+} jA_{mn}^+ e^{-j\beta x} \left[ \frac{1}{\mu_{re}} \cosh \kappa_{Fen}^+ (z - g - d - h_{Fe}) - \frac{\beta}{\kappa_{Fen}^+} \sinh \kappa_{Fen}^+ (z - g - d - h_{Fe}) \right] \quad (2.176a)$$

$$H_{zFen}^- = \frac{1}{M_{n4}^-} (-jA_{mn}^-) e^{j\beta x} \left[ \frac{1}{\mu_{re}} \cosh \kappa_{Fen}^- (z - g - d - h_{Fe}) - \frac{\beta}{\kappa_{Fen}^-} \sinh \kappa_{Fen}^- (z - g - d - h_{Fe}) \right] \quad (2.176b)$$

$$E_{yFen}^+ = \frac{1}{M_{n4}^+} \frac{j\omega_n^+ \mu \mu_{re}}{\beta} A_{mn}^+ e^{-j\beta x} \left[ \frac{1}{\mu_{re}} \cosh \kappa_{Fen}^+ (z - g - d - h_{Fe}) - \frac{\beta}{\kappa_{Fen}^+} \sinh \kappa_{Fen}^+ (z - g - d - h_{Fe}) \right] \quad (2.177a)$$

$$E_{yFen}^- = \frac{1}{M_{n4}^-} \frac{j\omega_n^- \mu \mu_{re}}{\beta} A_{mn}^- e^{j\beta x} \left[ \frac{1}{\mu_{re}} \cosh \kappa_{Fen}^- (z - g - d - h_{Fe}) - \frac{\beta}{\kappa_{Fen}^-} \sinh \kappa_{Fen}^- (z - g - d - h_{Fe}) \right] \quad (2.177b)$$

where:

$$M_{4n} = \frac{\kappa_{Cun}}{\beta} M_{3n} \cosh \beta g + W_{3n} \sinh \beta g \quad (2.178)$$

$$W_{4n} = W_{3n} \cosh \beta g + \frac{\kappa_{Cun}}{\beta} M_{3n} \sinh \beta g \quad (2.179)$$

$$M_{3n} = \frac{\kappa_{Fen}}{\kappa_{Cun}} M_{2n} \cosh \kappa_{Cun} d + \mu_{re} W_{2n} \sinh \kappa_{Cun} d \quad (2.180)$$

$$W_{3n} = \mu_{re} W_{2n} \cosh \kappa_{Cun} d + \frac{\kappa_{Fen}}{\kappa_{Cun}} M_{2n} \sinh \kappa_{Cun} d \quad (2.181)$$

$$M_{2n} = \frac{\beta}{\kappa_{Fen}} \cosh \kappa_{Fen} h_{Fe} + \frac{1}{\mu_{re}} \sinh \kappa_{Fen} h_{Fe} \quad (2.182)$$

$$W_{2n} = \frac{1}{\mu_{re}} \cosh \kappa_{Fen} h_{Fe} + \frac{\beta}{\kappa_{Fen}} \sinh \kappa_{Fen} h_{Fe} \quad (2.183)$$

The equations of electromagnetic field distribution for  $z \geq g+d+h_{Fe}$  are not important.

#### 2.5.5.4 Rotor Impedance

As is known from two-dimensional electromagnetic field analysis, the intrinsic impedance of the air half-space ( $z \geq g+d+h_{Fe}$ ) for the  $n$ th time harmonic is

$$\eta_{0n} = -\frac{j \omega_n \mu_0}{\beta} \quad (2.184)$$

Equations 2.175a, 2.175b, 2.177a, and 2.177b yield the intrinsic impedance of the ferromagnetic cylinder ( $g+d \leq z \leq g+d+h_{Fe}$ ) and the air half-space ( $z \geq g+d+h_{Fe}$ )

$$\begin{aligned} \eta_{(Fe+0)n} &= |E_{yFen}/H_{xFen}|_{z=g+d} \\ &= -\frac{j\omega_n \mu_0 \mu_{re}}{\kappa_{Fen}} \frac{(1/\mu_{re}) + (\beta/\kappa_{Fen}) \tanh \kappa_{Fen} h_{Fe}}{(\beta/\kappa_{Fen}) + (1/\mu_{re}) \tanh \kappa_{Fen} h_{Fe}} \end{aligned} \quad (2.185)$$

Inserting Eq. 2.184 into Eq. 2.185

$$\begin{aligned} \eta_{(Fe+0)n} &= \frac{j\omega_n \mu_0 \mu_{re}}{\kappa_{Fen}} \\ &\times \frac{(\omega_n/n\omega) (-\eta_{0n}) (j\omega_n \mu_0 \mu_{re}/\kappa_{Fen}) \tanh \kappa_{Fen} h_{Fe}}{(j\omega_n \mu_0 \mu_{re}/\kappa_{Fen}) (\omega_n/n\omega) (-\eta_{0n}) \tanh \kappa_{Fen} h_{Fe}} \end{aligned} \quad (2.186)$$

Denoting  $z_{0n} = j\omega_n \mu_0 \mu_{re}/\kappa_{Fen}$  and  $z_{Ln} = [(\omega_n/n\omega)]/(-\eta_{0n})$

$$\eta_{(Fe+0)n} = -z_{0n} \frac{1 + (z_{0n}/z_{Ln}) \tanh \kappa_{Fe} h_{Fe}}{(z_{0n}/z_{Ln}) + \tanh \kappa_{Fe} h_{Fe}} \quad (2.187)$$

By analogy with a transmission line,  $z_{0n}$  is the characteristic impedance of the line, and  $z_{Ln}$  is the load impedance. If  $z_{Ln} \rightarrow \infty$  is substituted, Equation 2.187 gives the input impedance of an open-circuited line or the impedance of a ferromagnetic cylinder alone, that is:

$$\begin{aligned} \eta_{(Fe+0)n} &= \eta_{Fe} = z_{0n} \frac{1}{\tanh \kappa_{Fe} h_{Fe}} \\ &= -\frac{j\omega_n \mu_0 \mu_{re}}{\kappa_{Fe}} \frac{1}{\tanh \kappa_{Fe} h_{Fe}} \end{aligned} \quad (2.188)$$

The intrinsic impedance of the copper layer for the  $n$ th time harmonic can be found in a similar way:

$$\eta_{Cu} = \frac{j\omega_n \mu_0}{\kappa_{Cu}} \frac{1}{\tanh \kappa_{Cu} d} \quad (2.189)$$

Reference 85 contains a full proof that the total impedance of the rotor is a parallel connection of  $\eta_{Cu}$  and  $z_{Fe}$ . If the length of the rotor (in the  $y$  direction) is  $L_2$ , the pole pitch is  $\tau$ , and the impedance turns ratio is  $k_{tr}$ , the impedance of the ferromagnetic cylinder and the copper layer referred to the stator winding are respectively:

$$z_{Cu}(s_n) = \frac{k_{tr} L_2}{\tau \eta_{Cu}} \quad (2.190)$$

$$z_{Fe}(s_n) = \frac{k_{tr} L_2}{\tau \eta_{Fe}} \quad (2.191)$$

For a solid rotor the number of its phases  $m_2=2p$ , the number of turns  $N_2=1/2$ , and the winding factor  $k_{w2}=1$ , so that

$$k_{tr} = \frac{m_1(N_1 k_{w1})^2}{m_2(N_2 k_{w2})^2} = \frac{6(N_1 k_{w1})^2}{p} \quad (2.192)$$

where  $p$  is the number of pole pairs.

The best estimation of the transverse edge effect is to use the equivalent conductivity  $k_{ie} \sigma_{Cu}$ , where  $k_{ie} < 1$  for the copper layer, and the impedance increase coefficient  $k_z > 1$  for the solid steel cylinder

The modified Russel and Norsworthy factor [85]:

$$k_{ie} = 1 - \frac{\tanh(\beta L_2/2)}{(\beta L_2/2)[1 + k_t(\beta L_2/2) \tanh(\beta W_{ov})]} \quad (2.193)$$

in which:

$$k_t \approx 1 + 1.3 \frac{t_{ov}-d}{d} \quad (2.194)$$

can be used to correct the copper layer conductivity, and the coefficient:

$$k_z \approx 1 + \frac{2}{\pi} \frac{\tau}{L_i} \quad (2.195)$$

can be used to correct the solid cylinder impedance on the account of the transverse edge effects:

In this way Eqs. 2.190 and 2.191 take the forms

$$Z'_{Cu}(s_n) = \frac{j\omega_n \mu_0}{\kappa_{Cu}} \frac{1}{\tanh \kappa_{Cu} d} k_{tr} \frac{L_2}{\tau} \quad (2.196)$$

$$Z'_{Fe}(s_n) = \frac{j\omega_n \mu_0 \mu_{re}}{\kappa_{Fe}} \frac{1}{\tanh \kappa_{Fe} h_{Fe}} k_{tr} k_z \frac{L_2}{\tau} \quad (2.197)$$

where  $\kappa_{Cu} = (j\omega_n \mu_0 k_{ie} \sigma_{Cu} + \beta^2)^{1/2}$  and  $\kappa_{Fe}$  is given by Eq. 2.160. The minus sign before  $\eta_{Cu}$  and  $\eta_{Fe}$  has been neglected (it has no physical meaning).

The resultant impedance of a solid rotor covered with a copper layer is [85]:

$$\begin{aligned} Z'_{2n}(s_n) &= \frac{Z'_{Cu}(s_n) Z'_{Fe}(s_n)}{Z'_{Cu}(s_n) + Z'_{Fe}(s_n)} \\ &= R'_{2n}(s_n) + jX'_{2n}(s_n) \end{aligned} \quad (2.198)$$

where  $R'_{2n}(s_n) = \text{Re}[Z'_{2n}(s_n)]$ ,  $X'_{2n}(s_n) = \text{Im}[Z'_{2n}(s_n)]$ ,  $s_n = s_n^+$  for  $n=1, 7, 13, 19, \dots$  is according to Eq. 2.154a, and  $s_n = s_n^-$  for  $n=5, 11, 17, 23, \dots$  is according to Eq. 2.154b.

### 2.5.5.5 Equivalent Circuit

Figure 2.126 shows a T-type equivalent circuit for the solid-rotor induction motor for the  $n$ th time harmonic. The rms values of the input voltage  $V_{1n}$  can be found by resolving the input voltage waveform into a Fourier series. The stator winding resistance per phase including skin effect is  $R_{1m}$ , the stator leakage reactance per phase is  $X_{1m}$ , the core loss resistance is  $R_{Fem}$  and the self-inductance (mutual) reactance is  $X_{Fe}$ . The parameters  $R_{1m}$ ,  $X_{1m}$ ,  $R_{Fem}$ , and  $X_{Fe}$  can be found as in the case of a cage induction motor subject to a sinusoidal voltage at frequency  $nf$ , as can the input current  $I_{1n}$  and the excitation current  $I_{exc}$ . The rms rotor current  $I'_{2n}$  referred to the stator is determined by the voltage  $E_{1n}$  and the impedance of the rotor circuit from Eq. 2.198, as follows:

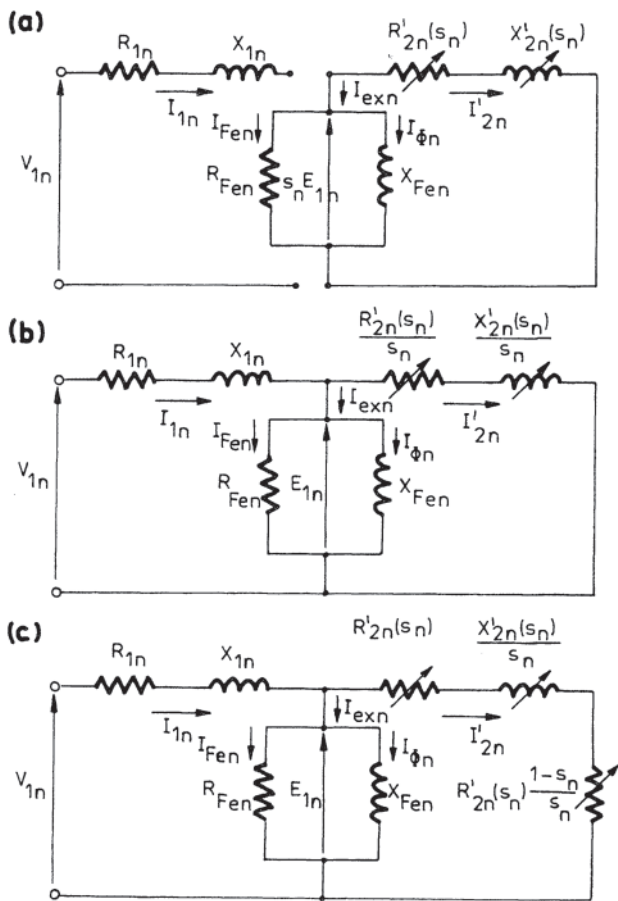
$$\begin{aligned} I'_{2n} &= \frac{s_n E_{1n}}{\sqrt{[R'_{2n}(s_n)]^2 + [X'_{2n}(s_n)]^2}} \\ &= \frac{E_{1n}}{\sqrt{[R'_{2n}(s_n)/s_n]^2 + [X'_{2n}(s_n)/s_n]^2}} \end{aligned} \quad (2.199)$$

Figure 2.126(a) shows one form of the equivalent circuit for the solid-rotor induction motor. Note that in the case of a squirrel-cage rotor only the rotor resistance is divided by slip, the rotor leakage reactance being independent of slip. For a solid-rotor induction motor, however, both the rotor resistance and the rotor leakage reactance are slip-dependent. In Fig. 2.126(b), the equivalent circuit of (a) has been rearranged into a more convenient form.

Resistance  $R_{2n}(s_n)$  from Eq. 2.198 is the rotor winding loss resistance. Just as with a cage rotor, the slip-dependent resistance may be rearranged into:

$$\frac{R'_{2n}(s_n)}{s_n} = R_{2n}(s_n) + R'_{2n}(s_n) \frac{1-s_n}{s_n} \quad (2.200)$$

The equivalent circuit may now be rearranged into that shown in Fig. 2.126(c).



**Figure 2.126** Equivalent circuit for a solid rotor induction motor and with  $n$ th time harmonic: (a) stator EMF= $s_n E_{1n}$ ; (b) stator EMF= $E_{1n}$ ; (c) stator EMF= $E_{1n}$  and mechanical load separated from the winding loss.

Multiplying Eq. 2.200  $3(I'_{2n})^2$  by results in:

$$3(I'_{2n})^2 \frac{R'_{2n}(s_n)}{s_n} = 3(I'_{2n})^2 R'_{2n}(s_n) + 3(I'_{2n})^2 R'_{2n} \frac{1-s_n}{s_n} \quad (2.201)$$

In Eq. 2.201, the left-hand side is the airgap (electromagnetic) power.

$$P_{gn} = 3(I'_{2n})^2 \frac{R'_{2n}(s_n)}{s_n} \quad (2.202)$$

On the right-hand side, the first term is the rotor winding loss:

$$P_{2wn} = 3(I'_{2n})^2 R'_{2n} s_n \quad (2.203)$$

and the second term is the developed mechanical power:

$$P_{mn} = 3(I'_{2n})^2 R'_{2n}(s_n) \frac{1-s_n}{s_n} = P_{gn}(1-s_n) \quad (2.204)$$

The torque developed by the electromagnetic energy

conversion process is given by the developed mechanical power divided by the angular velocity  $\omega_n$  of the rotor:

$$T_{dn} = \frac{P_{gn}(1-s_n)}{\omega_n} = \frac{P_{gn}}{\pm n\omega_s} \quad (2.205)$$

where  $\omega_n^+ = n\omega_s(1-s_n^+)$  for  $n=1, 7, 13, 19, \dots$ ,  $\omega_n^- = -n\omega_s(1-s_n^-)$  for  $n=5, 11, 17, 23, \dots$ , and  $\omega_s = 2\pi f/p =$  synchronous angular velocity for  $n=1$ . The synchronous velocity for  $n=1, 7, 13, 19, \dots$  is  $n\omega_s$ , and the synchronous velocity for  $n=5, 11, 17, 23, \dots$  is  $-n\omega_s$ .

### 2.5.6 Synchronous Reluctance Motors

#### 2.5.6.1 Background

The synchronous reluctance motor concept has a long history because this motor is nothing else than, in principle, a synchronous (salient) motor without rotor excitation. Reference can be made to the works of Blondel [86] and Boucherot [87], as an example. In the *Journal of AIEE*, the first paper dealing specifically with this motor appeared on 1923, by J.K.Kostko [88]. Uncontrolled (or line start) synchronous reluctance motors have been in use for some time for special applications. The primary reason for their use is to achieve synchronism of a number of shafts, such as in the fiber spinning industry, so their relatively low performance is tolerated. The usual form is similar to the controlled motors discussed here but with an induction cage integrated with the rotor for starting. The properties of such line start motors are more fully discussed in Section 2.5.10.

In spite of its long life, the evolution of the synchronous reluctance motor toward high performance and the consequent industrial application has been very slow, becoming a mature technique only in the last tenth of the 20th century. The reasons for that are twofold. On one hand, the search for a high-anisotropy rotor design started quite late, in the last 1950s [89], often with a main reference to cage-starting machines [90], for special purposes. This research led to many works [91], notably on the axially-laminated-anisotropic (ALA) rotor structure [92]. However, this structure looked unfit for industrial manufacturing.

On the other hand, widespread application of synchronous motors was not conceivable at that time without closed-loop operation, which in turn means power-electronic supply. This power supply concept was applied in the field, only in the 1980s, with the brushless dc (PM synchronous) motors. At the same time, it gave a considerable impulse to research on high-performance synchronous-reluctance motors and drives [93–95], leading to a mature design technique and finally to industrial application, first in the field of servodrives.

The actual application trend is toward general purpose applications, because of the suitability of this kind of motor to sensorless control.

#### 2.5.6.2 Fundamentals

A synchronous reluctance motor (SynR) consists of a wound-stator and a magnetically anisotropic (salient) rotor. The stator structure is analogous to that of an induction motor. In general,

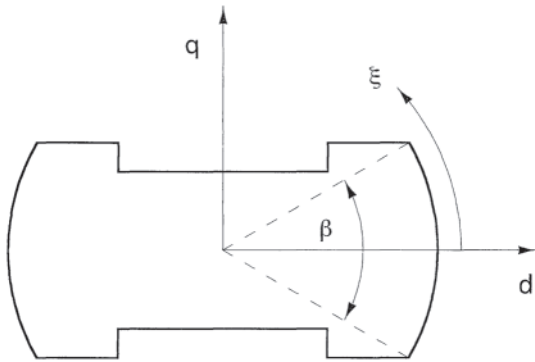


Figure 2.127 Simply salient two-pole rotor (schematic).

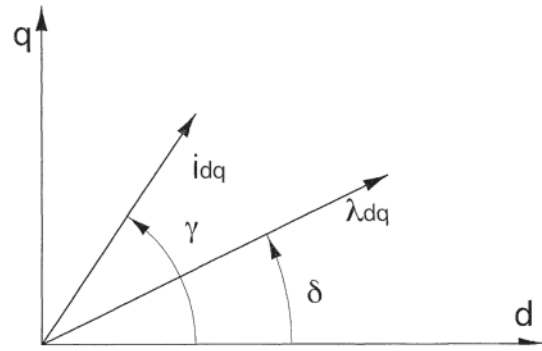


Figure 2.128 Vector diagram (motoring).

three-phase windings are used. The spatial conductor distribution is supposed to be sinusoidal, in principle. Although this is not exactly true in practice, it is a reasonable approximation because the existing third (and triple) harmonics do not contribute to torque and the higher-order harmonics are reduced by the winding design and/or skewing.

The rotor magnetic anisotropy can be obtained in different ways, as illustrated in the following. In principle, reference can be made to the simply salient, two pole structure of Fig. 2.127. A  $(d, q)$  frame synchronous to the rotor is considered. The  $d$ -axis is taken in the direction of maximum permeance. Because of the hypothesis of sinusoidal conductor distribution, a space-vector approach can be adopted, leading to Eqs. 2.206–2.208. The readers to whom space vector theory sounds unfamiliar can think of a two-phase equivalent machine, with a couple of (sinusoidal) windings synchronous with the rotor and aligned to  $d$  and  $q$  axes. The resulting (scalar) equations are obtained from Eq. 2.206 by taking  $d$  and  $q$  component of both members.

The double subscript ( $dq$ ) identifies vector quantities:  $j$  is a spatial operator ( $\pi/2$  wide rotation). Voltage, current and flux linkage have been indicated by  $v$ ,  $i$ , and  $\lambda$ , respectively;  $R$  is the phase resistance, while  $\omega$  is the rotor electrical speed (pulsation).

$$v_{dq} = Ri_{dq} + \frac{d\lambda_{dq}}{dt} + j\omega\lambda_{dq} \quad (2.206)$$

$$v_{dq} = L_{dq} \dot{i}_{dq} \quad (2.207)$$

$$T = \frac{3}{2}p(\lambda_{dq} \times i_{dq}) = \frac{3}{2}p(\lambda_{d'i_q} - \lambda_{q'i_d}) \quad (2.208)$$

While Eq. 2.206 is common to ac machines, Eq. 2.207 is specific to this machine. It states that the  $\lambda_{dq}$  flux vector is only related to the  $i_{dq}$  current vector, through an algebraic relationship: this, of course, if the effect of core loss is neglected. The relationship 2.207 describes the magnetic behavior of the machine, with reference to the  $(d, q)$  frame.  $L_{dq}$  is a (tensor) operator, which relates each current vector to the corresponding flux vector, having a different direction, in general, because of the rotor anisotropy. This is the reason for torque generation, as it is evident from Eq. 2.208, where  $p$  is the number of polepairs. In Fig. 2.128 a typical situation is shown, for motoring (positive) torque.

Coming back to Eq. 2.207, the simplest magnetic behavior is the linear one, although it is quite unrealistic in practice. In the linear case, the operator  $L_{dq}$  is constant and represented, in matrix form, by the simple diagonal matrix shown in Eq. 2.209. Of course  $L_d$  is larger than  $L_q$  as it is evident from Fig. 2.128:

$$\lambda_{dq} = \begin{vmatrix} \lambda_{d'} \\ \lambda_{q'} \end{vmatrix} = \begin{vmatrix} L_d & 0 \\ 0 & L_q \end{vmatrix} \begin{vmatrix} i_{d'} \\ i_{q'} \end{vmatrix} = L_{dq} i_{dq} \quad (2.209)$$

The linear model 2.209 represents only a rough approximation of the magnetic behavior of the machine (magnetic model). However, it is often used to gain a rough (and optimistic) idea of the machine behavior in general, because Eq. 2.209 is suited to analytical elaboration.

An example can be found in the analytical determination of the maximum obtainable anisotropy ratio from the simply salient structure of Fig. 2.127. Under the (unrealistic) hypothesis that the flux density is zero outside the pole-span  $\beta$ , Eqs. 2.210 and 2.211 are easily obtained, from integration of  $\sin \xi$  and  $\cos \xi$  functions over the pole-span  $\beta$ . They state that the inductances  $L_d$  and  $L_q$  are proportional to  $(\beta + \sin \beta)$  and  $(\beta - \sin \beta)$  functions, respectively. Since the torque is given, in this case, by Eq. 2.212, the maximum torque design implies  $\beta = \pi/2$ , which in turn implies a limit anisotropy ratio  $L_d/L_q$  equal to 4.5.

$$L_d \propto (\beta + \sin \beta) \quad (2.210)$$

$$L_q \propto (\beta - \sin \beta) \quad (2.211)$$

$$T = \frac{3}{2}p(L_d - L_q)i_{d'i_q} \quad (2.212)$$

Of course, this value is quite optimistic, because the flux density cannot be zero outside the pole span. A realistic value of the anisotropy ratio would be, in this case, not far from 3. (Note that the corresponding value for an induction motor can be much larger, up to 20.) As a consequence, the angle  $(\gamma - \delta)$  in Fig. 2.128 (torque angle) of this machine is too small, leading to a low power factor and torque density. From Eq. 2.213 it can be seen that the low torque density derives from both the low torque angle and the reduced  $L_q$  value, because of the limited pole-span. Both of these drawbacks will be overcome by the high-anisotropy design, as shown in the next section.

$$T = \frac{3}{2} p L_d \left( 1 - \frac{L_q}{L_d} \right) i_d i_q \quad (2.213)$$

As a further example of the use of the linear model Eq. 2.209, the situation of maximum torque angle can be pointed out. From Fig. 2.128, Eq. 2.214 is immediately written, which defines the general correspondence between  $\gamma$  and  $\delta$  angles:

$$\tan \delta = \frac{L_q i_q}{L_d i_d} = \frac{L_q}{L_d} \tan \gamma \quad (2.214)$$

The maximum of  $\tan (\gamma - \delta)$  is then found, after some mathematics. It defines the optimum angles  $\gamma'$  and  $\delta'$ , which are given by 2.215:

$$\tan \gamma' = \sqrt{\frac{L_d}{L_q}}; \quad \tan \delta' = \sqrt{\frac{L_q}{L_d}} \quad (2.215)$$

Equation 2.215 states that the current and flux vectors of Fig. 2.128 are, in this case, symmetric with respect to the bisecting line. If copper and iron losses are disregarded, this situation corresponds to a maximum power factor situation. This appears independent of the supply current, depending only on the anisotropy ratio. Of course this is no longer true when realistic nonlinear magnetic behavior is considered.

Finally, let us point out another notable situation, that is the maximum torque at fixed copper loss, (fixed current). Because of the linear hypothesis 2.209, it is easy to show that the maximum torque/amp situation leads to Eqs. 2.216, defining the angles  $\gamma''$  and  $\delta''$ .

$$\tan \gamma'' = 1; \quad \tan \delta'' = \frac{L_q}{L_d} \quad (2.216)$$

Equation 2.216 are realistic only for torque values much lower than rated, when the magnetic behavior can be considered as linear. In general, both maximum torque angle and maximum torque/amp situations have to be defined by proper loci, e.g., on the  $(i_d, i_q)$  plane. This will be shown in Section 2.5.7.6.

### 2.5.6.3 High Anisotropy Design

It has been shown above that a simple salient-pole structure is not suited to achieving high torque-density and good power factor. In general, a high-performance synchronous reluctance machine must exhibit both large  $L_d$  and low  $L_q$  since the torque depends on the difference  $L_d - L_q$  (Eq. 2.212), while the power factor is mainly related to the anisotropy ratio  $L_d/L_q$  (Eq. 2.215). In principle, this can be obtained by a segmental rotor, that is a rotor constituted by many iron segments, magnetically isolated from each other.

A schematic example of a three-segment rotor is shown in Fig. 2.129, for a two-pole machine. As can be seen, a  $d$ -axis mmf (proportional to  $\cos \xi$ ) magnetically polarizes the rotor, while a  $q$ -axis mmf (proportional to  $\sin \xi$ ) does not. Thus, the two lateral segments assume, at load, a magnetic potential different from that of the central segment. This fact leads to reduction of the  $q$ -flux, while the  $d$ -flux is free to flow across the whole rotor surface.

In general, the quadrature flux of a multiple-segmented rotor under sinusoidal mmf excitation can be split into a flux

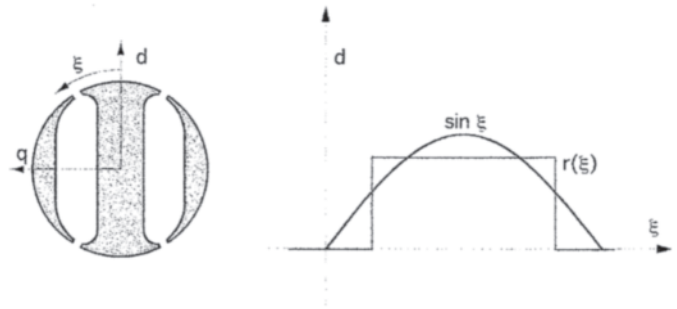


Figure 2.129 Three-segment rotor (two poles, schematic) and rotor reaction.

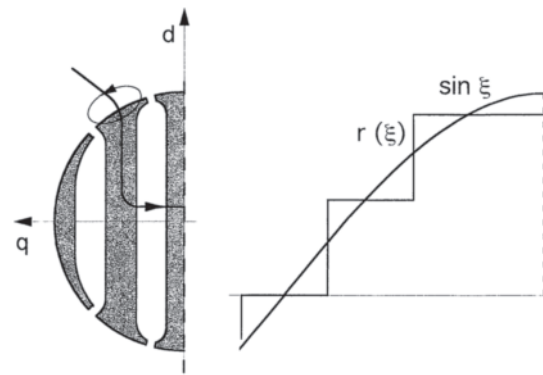


Figure 2.130 Flow-through and circulating quadrature flux components.

component which flows across the inner flux barriers (flow-through flux) and a flux that simply flows across the airgap (circulation flux). This is schematically shown in Fig. 2.130.

It is intuitive that the circulation flux rapidly vanishes as the number of rotor segment is increased, while the flow-through flux mainly depends on the total quantity of magnetic “isolation.” The latter is reasonably independent of the number of segments, while depending on the air-to-iron design tradeoff. As a consequence, a machine with a very large number of rotor segments (distributed anisotropy) could be considered as an ideal machine, from this point of view. However, the presence of stator slots and other practical considerations lead to a different conclusion.

### 2.5.6.4 ALA Design

This type of rotor construction was intensively studied in the 1960s and taken-up again cyclically: the basic idea is to lead to distributed anisotropy in a practical rotor.

A four pole schematic structure of this kind is shown in Fig. 2.131. The main part consists of axially disposed magnetic laminations, interleaved with nonmagnetic ones. The stack is held by the pole-holder, connected to a central spider structure as shown.

The pole-holder is typically nonmagnetic consequently  $d$ -flux is limited. The central spider should be magnetic, so as not

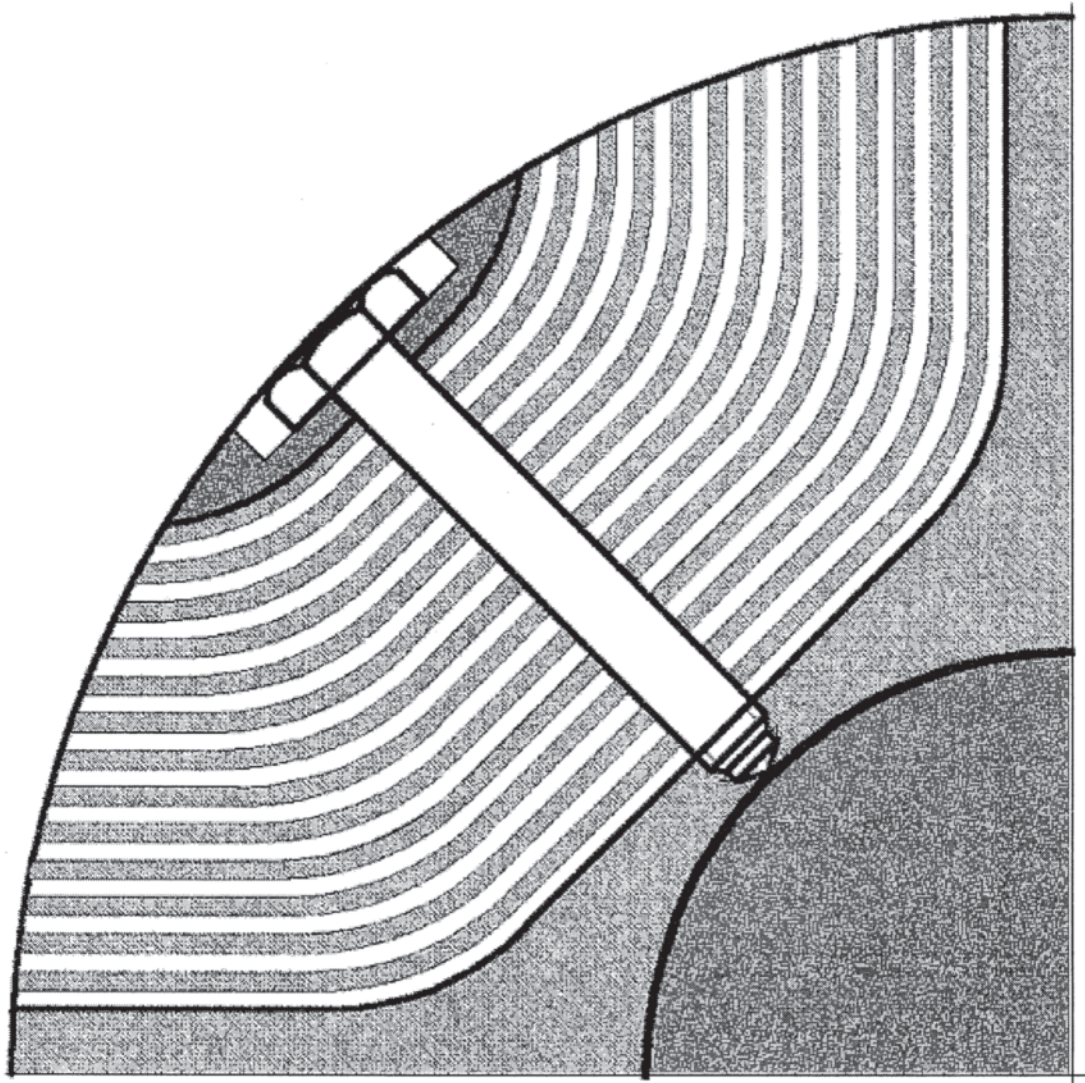


**Figure 2.131** Axially laminated (ALA) structure (four poles, schematic).

to lose a large part of the  $d$ -flux. However, in the first designs it was chosen nonmagnetic, to further reduce the  $q$ -flux component. Special attention has been devoted to the ratio between the thickness of the nonmagnetic laminae to the magnetic ones. A reasonable value is near 0.5, for anisotropy maximization. In the first designs, lower values were chosen, to pay attention to the magnetic saturation at the rotor surface: however, in this way a lower anisotropy was obtained.

The adoption of the ALA structure certainly allows high anisotropy through proper design. On the other hand, a stator-slotted structure with open slots enhances flux oscillations in the ALA rotor iron, leading to important core losses in the rotor, at no load [96] and at load as well [97], since the axially disposed laminae cannot oppose eddy currents induced by the harmonic fields. Moreover, the torque ripple due to stator slotting cannot be reduced by rotor skewing and the stator must be skewed, if a low-ripple design is wanted. Last but not the least, the ALA structure is not well suited to

industrial manufacturing, as is evident by inspection. This has prevented all serious attempts to adopt ALA motors for industrial manufacturing. To this end, a better suited structure is illustrated in the following section.

#### 2.5.6.5 Transverse-Laminated Rotor Design

An example of this rotor is shown in Fig. 2.132, for a four-pole machine. This kind of rotor is also called multiple-flux-barrier-rotor: the one in the figure shows three flux barriers per pole, as an example.

Mechanical strength is guaranteed by the thin ribs, disposed at the airgap and also in the inner rotor, for large speed values and/or large rotor diameters. The rotor laminae are obtained by traditional punching, resulting in an easy and cheap construction. The ribs are saturated, at load, by the stator mmf, thus allowing the various rotor segments to have different values of magnetic potential. Of course, an additional rotor

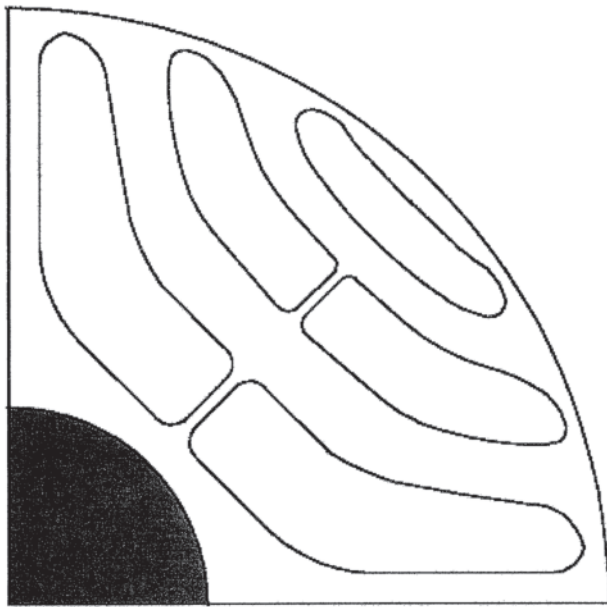


**Figure 2.132** Example of transverse-laminated rotor (four poles, schematic).



**Figure 2.133** Example of optimized rotor design.

leakage flux is added in this way (rib leakage). As a consequence, a loss of both torque and power factor has to be foreseen, in comparison to an ideal structure without any ribs.

In spite of the above discussion this type of rotor structure has many advantages, i.e., it is suited to rotor skewing, is practically free from rotor core loss and is definitely fit for mass production. Moreover, the transverse-laminated type of rotor can be optimized by proper design, in order to minimize the airgap harmonics and their effect on torque ripple. This is obtained by both the proper shaping of the various flux-barriers and the proper choice of their access points at the airgap [98, 99]. An example of optimized rotor structure is shown in Fig. 2.133, for a four-pole, two slots per pole per phase stator. The chosen rotor pitch corresponds to 16 teeth per pole, to reduce the interaction with stator slot harmonics (one flux barrier is missed, in this case).

As can be seen from the figure, the permeances of the various flux barriers can easily be tailored by design, which is practically impossible in the ALA rotor. This results in a nearsinusoidal flux-density behavior at the airgap, both at load and at no-load, with obvious advantages for torque ripple and core loss behaviors.

**2.5.6.6 Practical Performance**

Examples of practical performance are given here, mainly with reference to the transverse-laminated type of rotor. The flux-current relationships are given first in Fig. 2.134, as obtained from a 24-Nm servomotor. Both *d* and *q* components of the linked flux vector are shown, as a function of both *d*, *q* components of the current vector.

From the figure, the non linear behavior is evident. As a consequence, the linear model. Equation 2.204 cannot be representative of the realistic behavior. Let us point out that

both *d* and *q* components of flux nonlinearly depend on *d* and *q* components of current, respectively, even if the other current component is zero. While the nonlinear *d*-axis behavior is related to magnetic saturation of the main flux, the non linear *q*-axis behavior is mainly due to rotor ribs and the related flux leakage component. Moreover, from Fig. 2.134 a crosssaturation phenomenon is well evidenced: the *d*-flux is reduced when the *q*-current is growing and the same happens to the *q*-flux, when the *d*-current is increased. In conclusion, the magnetic model of this kind of machine looks quite complicated. However, in general, Eq. 2.217 can be written. The associated condition Eq. 2.218 is called the transversality condition. It must be satisfied to guarantee the existence of energy and coenergy Eq. 2.219 as state functions, that is depending only on the considered point *i*<sub>dq</sub> (or λ<sub>dq</sub>).

$$\begin{cases} \lambda_d = \lambda_d(i_d, i_q) \\ \lambda_q = \lambda_q(i_d, i_q) \end{cases} \quad \text{or} \quad \lambda_{dq} = \lambda_{dq}(i_{dq}) \quad (2.217)$$

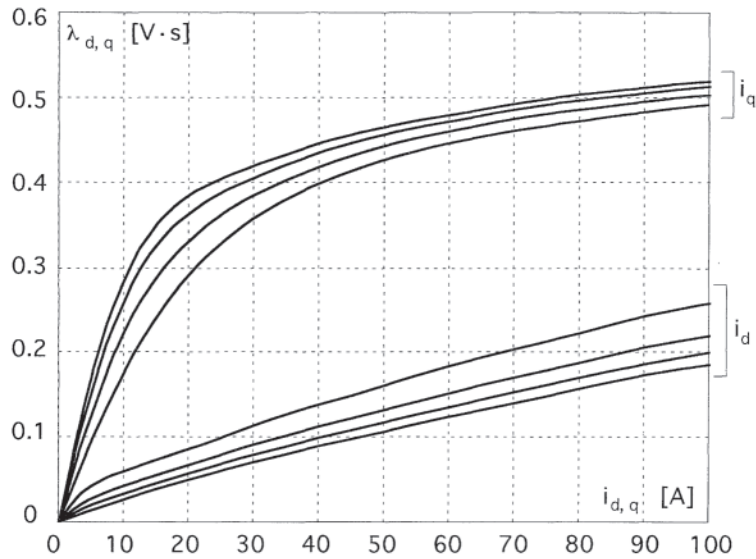
$$\frac{\partial \lambda_d}{\partial \lambda_q} = \frac{\partial \lambda_q}{\partial \lambda_d} \quad (2.218)$$

$$W' = \frac{3}{2} \int_0^{i_{dq}} \lambda_{dq}(i'_{dq}) di'_{dq} \quad (2.219)$$

To synthesize the nonlinear flux-current relationship of this machine the plot of Fig. 2.135 is also used, in alternative to that of Fig. 2.134. In Fig. 2.135 the flux modulus λ is plotted versus the current modulus *i*, for different values of the current argument γ (Fig. 2.128). Of course, the no-load curves of Fig. 2.134 that is λ<sub>d</sub>(*i*<sub>d</sub>, 0) λ<sub>q</sub>(0, *i*<sub>q</sub>) coincide with those of Fig. 2.135, for γ=0, π/2, respectively.

The λ(*i*, γ) curves describe the machine magnetic behavior in polar coordinates. This description would be completed by a set of δ(*i*, γ) curves, where δ is the flux argument. The curves in





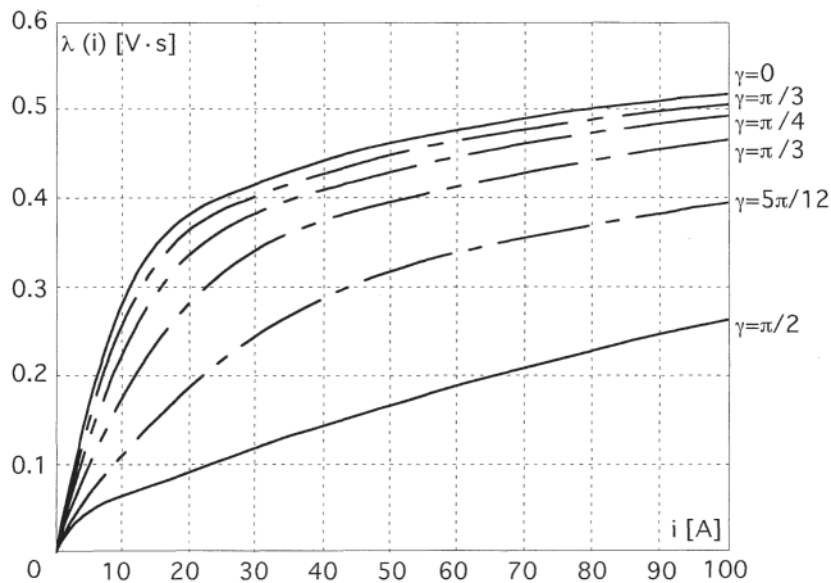
**Figure 2.134** Flux-current relationships on d, q axes (rated current 32 A peak).

Fig. 2.135 give better graphical evidence to the coenergy  $W'$ . From Eq. 2.219, if a radial integration path is chosen from zero to the working point  $i_{d,q}$  Eq. 2.220 can be written. It defines  $W'$  as a simple scalar integral, since the  $\gamma$  value is fixed.

$$W' = \frac{3}{2} \int_0^i \lambda(i') di' \quad (2.220)$$

$$T = \left. \frac{\partial W'}{\partial \vartheta} \right|_{i=\text{const}} \quad (2.221)$$

The  $\lambda(i, \gamma)$  curves of Fig. 2.135 are referred to the rotor ( $d, q$ ) frame, as the curves in Fig. 2.134 are. However, if the current vector is thought to be stationary, the same curves can describe the flux behavior when the rotor is rotated and the rotor angle  $\theta$  between rotor and stator is varied. With a proper choice of the  $\vartheta = 0$  condition (that is aligned to the set current vector) the angle  $\gamma$  of Fig. 2.135 can be simply substituted by  $\vartheta$  and the coenergy becomes a function  $W'(\vartheta)$ . Thus, the torque can be derived from Eq. 2.216, as a function of  $\vartheta$ . For the motor example reported in Figs. 2.134 and 2.135, the curves in Fig. 2.136 are obtained. They show the restoring torque when the current vector is fixed and the rotor is moved from the equilibrium point by an angle  $\vartheta$  (electrical), at different values



**Figure 2.135** Flux magnitude versus current magnitude, for various values of the current argument  $\gamma$ .

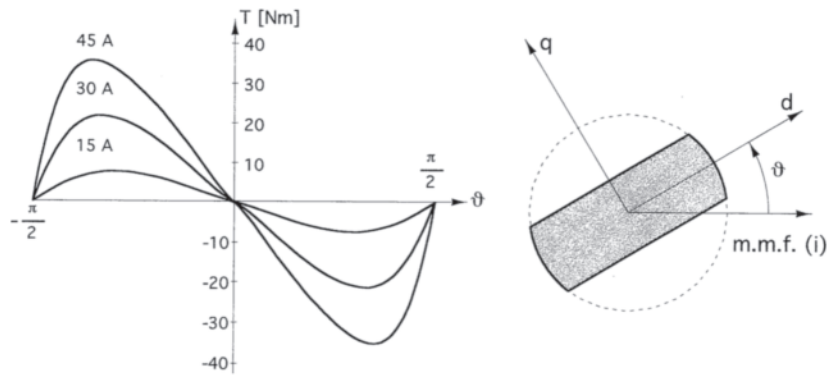


Figure 2.136 Motor torque versus rotor angle in case of stationary excitation (rated current 32 A, peak).

of the current module  $i$ . The rated current is 32 A (peak), in this case.

As can be seen, the  $T(\vartheta)$  behavior is quite far from sinusoidal, even with current values much lower than rated. This results from the inherently non linear magnetic behavior. As a consequence, the angle at which the maximum torque occurs for a given current module is quite far from and larger than  $\pi/4$ , as it would be for a linear machine, based on Eq. 2.209.

For each current magnitude the corresponding optimal angle  $\vartheta_0$  (or  $\gamma_0$ ) can be derived. Alternatively, the maximum torque-per-amp curve can be plotted, in the  $(i_d, i_q)$  plane. This is shown in Fig. 2.137, where the circle describes the rated situation. Some torque values are also shown, to illustrate the torque increasing along the optimal locus. It is apparent from the figure that the bisecting ( $\gamma = \pi/4$ ) line is left even for current values

much lower than rated. At rated, the optimal  $\gamma_0$  value is typically near 60 degrees, depending on motor size and design.

In Fig. 2.138 the torque is plotted vs. the current magnitude, when moving on the maximum Nm/A locus. In addition, the torque coefficient  $k_T$  is also shown, that is the ratio Nm/A. Its value is increasing with current, at least up to very large overcurrent values [100]. As a consequence, this kind of machine is well suited to large overload. Of course, the power factor decreases, with overload. Regarding power factor, Fig. 2.139 shows the locus of maximum power factor, on the  $(i_d, i_q)$  plane. The locus of maximum Nm/A ( $k_T$ ) is also shown (shaded), for comparison.

At a given current magnitude, a better power factor but a lower torque is obtained, on the maximum P.F. locus. For the lowest current values this locus becomes a straight-line, as defined by Eq. 2.214. For completeness, the P.F. value is plotted in Fig. 2.140 versus current magnitude, when moving on the maximum P.F. locus shown in Fig. 2.139. The given P.F. values are obtained disregarding joule and core losses: it results in slightly pessimistic values. As can be seen, the P.F. decreases with current beyond a near-to-rated current value. In Fig. 2.140

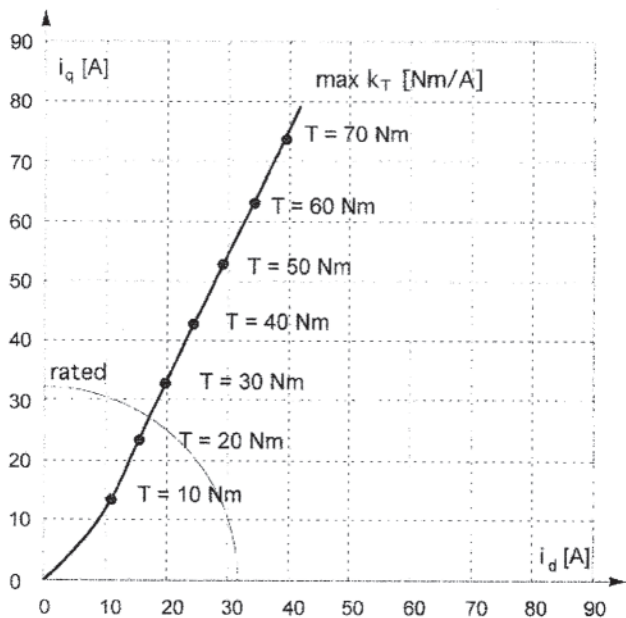


Figure 2.137 Maximum Nm/A locus, on the  $(i_d, i_q)$  plane.

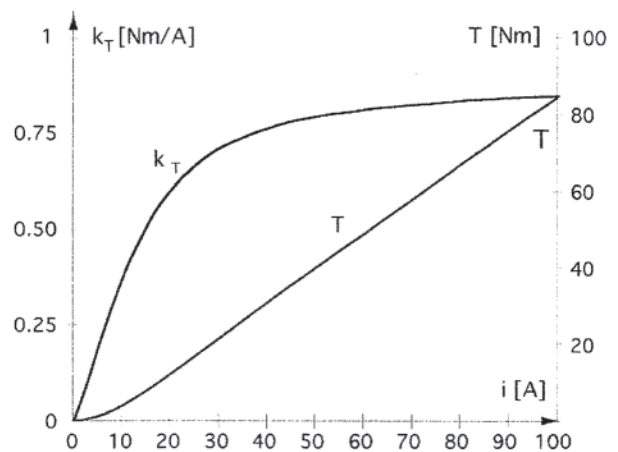


Figure 2.138 Torque and torque-over-amperes ( $k_T$ ) plots versus current magnitude (rated current 32 A).

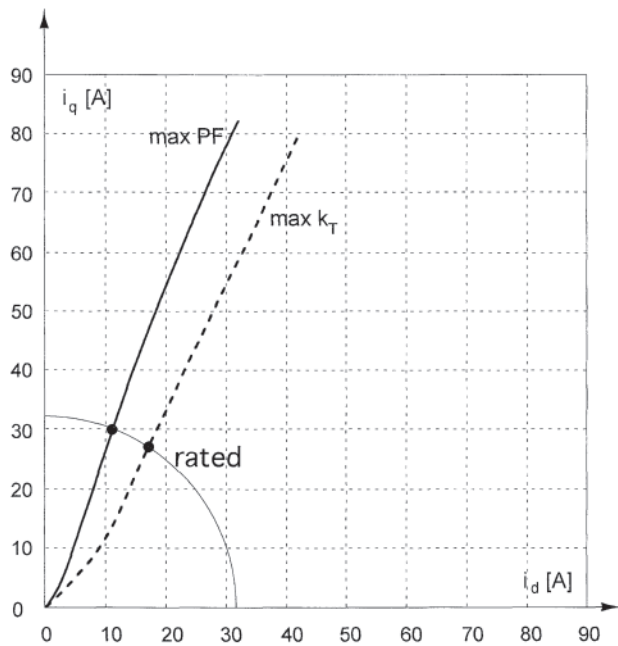


Figure 2.139 Locus of maximum power factor, on the  $(i_d, i_q)$  plane.

the  $k_T$  value is also shown, when moving on the maximum P.F. locus, to be compared with the Fig. 2.138 one. In this way, the torque drop can be evaluated, for each current value.

In conclusion, the performance of the synchronous reluctance motor is closely related to the command strategy, which in turn depends on the nonlinear magnetic behavior. Good magnetic modeling allows optimization of the motor performance, both at steady-state and in transient conditions. On the other hand, the nonlinear motor behavior cannot be described by a single valued anisotropy ratio but requires much more information.

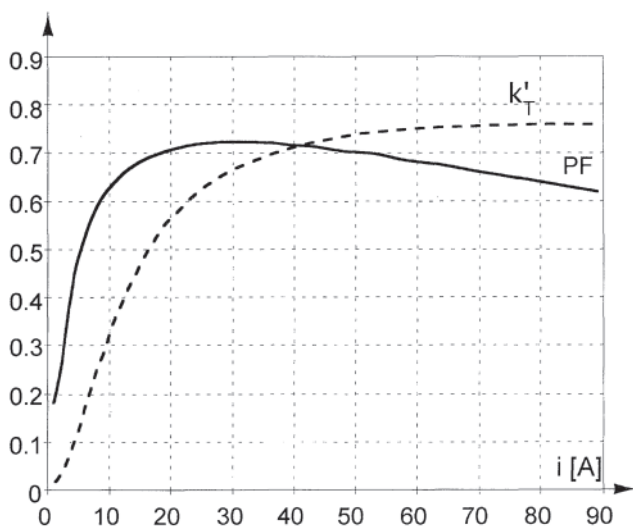


Figure 2.140 Power factor vs. current module.

### 2.5.6.7 Controlled Behavior

SynR motors are normally used under closed-loop control, supplied by a power-electronic apparatus (inverter). This represents the normal operating mode of all the motors of the synchronous type, notably PM, the so-called brushless dc motors. Then, the SynR motor may be considered as a special brushless motor, without PM excitation. The closed-loop mechanism controls the phase displacement between either the stator mmf wave or the flux wave and the rotor, thus ensuring torque performance under all working conditions.

Among the other ac machines (PM synchronous, induction), the synchronous reluctance motor exhibits the peculiarity of Eq. 2.207, that is the flux linkage depends only on the current, by an algebraic (although quite complex) relationship. In other words, disregarding the small delay due to eddy currents, the flux follows the driving current in real-time, in practice. This is different for brushless motors, that are PM excited, and for induction motors, because of the delaying action of the rotor cage. The above cited property of the synchronous reluctance motor may be seen as both an advantage and a drawback.

Real-time flux control capability allows real-time optimization of the operating point which is a welcome feature. As an example, the maximum Nm/A locus of Fig. 2.137 can be set in the control circuitry, thus optimizing the stall-torque performance at steady-state and in transient conditions as well. Alternatively, a maximum-efficiency locus can be defined in the state plane for each speed value, thus allowing optimization of the motor efficiency for all the working conditions, that is depending on both the instantaneous torque and speed values.

On the other hand, the real-time flux control capability could constitute a drawback, e.g., because of the enhanced sensitivity of the flux to various ripples and disturbances, in general. As an example, in flux-weakened conditions a ripple on the angular measurement may even lead to a loss of synchronism. On the contrary, an induction motor would be inherently protected in such a case, by the filtering action of the rotor cage.

Another consequence of the real-time flux control property is represented by the attention which must be paid to the choice of the control scheme, also depending on the desired performance. In Fig. 2.141 a standard scheme is shown, based on current-vector control. This scheme is adopted in most ac motor controls. As can be seen, at least two phase currents are measured and fed back to the current control block, which needs knowledge of the rotor position. The set (starred) current vector is obtained from the set torque and flux, depending on the preferred control strategy (max Nm/A, max efficiency, etc.). For maximum-efficiency, the rotor speed has to be known or estimated (this is represented by the dashed path).

The current control block is better shown in Fig. 2.142, where the regulator block (typically, of the proportional integrator (P.I.) type) and the motor transfer function are pointed out. The current-based scheme suffers from the non linear magnetic behavior of the machine. From Fig. 2.134, it is clear that the differential inductances depends strongly on the working point. As a consequence, the gains of the control loops of Fig. 2.142 are quite variable, particularly that of the

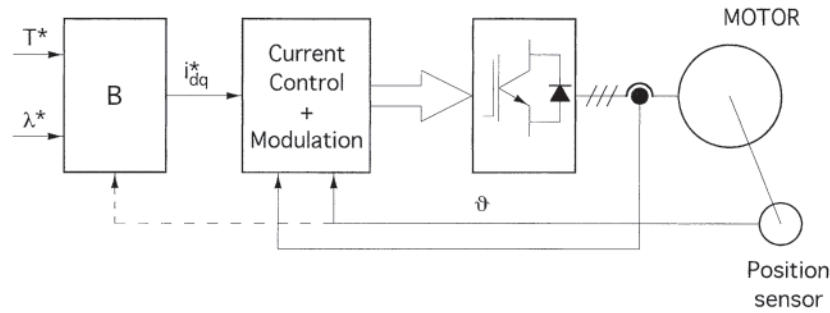


Figure 2.141 Current vector-based control scheme.

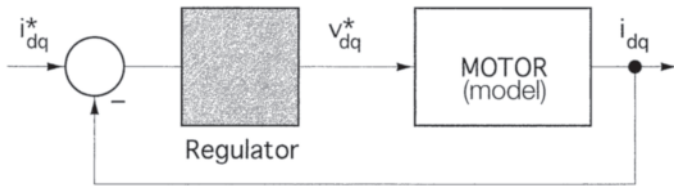


Figure 2.142 Block diagram scheme of current control.

$d$ -axis. As a consequence, a lower dynamics is generally set, to avoid improper oscillations when magnetic saturation occurs. Moreover, other problems could arise when the flux is deeply weakened, typically at high speed, because of the increased sensitivity to errors in the shaft angle measurement.

A solution to the problem of loop gain variation is to adopt a flux-based control scheme, as shown in Fig. 2.143. As can be seen, the non linear magnetic modelling (Fig. 2.134) is now included in the loop and the flux  $\tilde{\lambda}_{dq}$  is estimated from the measured currents. In this way, an approximate but effective linearization of the loop gains is obtained. Of course, this scheme does not represent a solution to the high sensitivity to angular errors, because the only measured quantities are still the motor currents. A solution is found to this problem when a flux-observer-based scheme is adopted, because a voltage measurement (or estimation) is added. Thus, at high frequency, the observed flux is mainly obtained from voltage integration. This is shown, schematically, in Fig. 2.144. Moreover, let us point out that a voltage-based flux estimation is also robust against the effect of eddy currents and of current filtering, in general.

In conclusion, the control of the SynR motor is not a trivial problem. When high performance is wanted flux observation is useful. However, this does not necessarily mean a control scheme totally based on flux components. On the contrary,

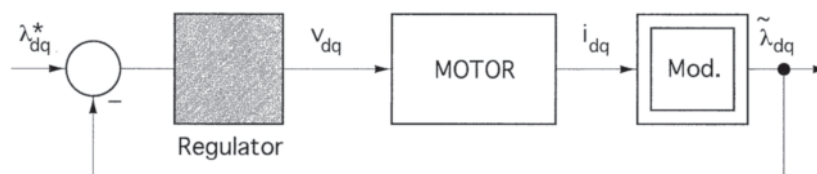


Figure 2.143 Flux-based control scheme.

mixed schemes can be profitably used, as that using  $(\lambda_d, i_q)$  as control variables [101] or those based on the stator-flux-oriented reference frame [102].

2.5.6.8 Sensorless Control

When dealing with ac drives, sensorless control means to avoid any shaft transducer, while electrical measurements are (necessarily) allowed. In this case, position sensorless control would be a more appropriate wording. In general, sensorless operation of an ac drive over the whole working area is not a trivial task. When the emf signal is sufficiently large, e.g., at high speed (frequency), the best path to sensorless operation is flux estimation from voltage integration. Reference can be made to Eq. 2.206 or to its equivalent in the stationary frame. Equation 2.206 is valid for every machine, provided that space-vector theory is applicable.

On the other hand, at low speed and at steady state, no useful information can be derived from the emf signal, since this results in a signal too small and comparable to resistive drop, noise, etc. In this case, the solution is found in some way of exciting the motor at (relatively) high frequencies and then relying on some kind of anisotropic behavior, with the goal of identifying the position of the  $(d, q)$  control frame. When the motor is inherently isotropic, as induction motors and surface-mounted permanent-magnet (brushless) motors are, second-order effects must be used. Examples are the differential inductance variations due to magnetic saturation or various effects due to stator slotting. However, the synchronous reluctance motor is inherently anisotropic, because the torque is only produced through rotor saliency. This makes the synchronous reluctance machine particularly suited to sensorless control.

The most straightforward type of motor excitation is represented by the injection of pulsating (or rotating) high

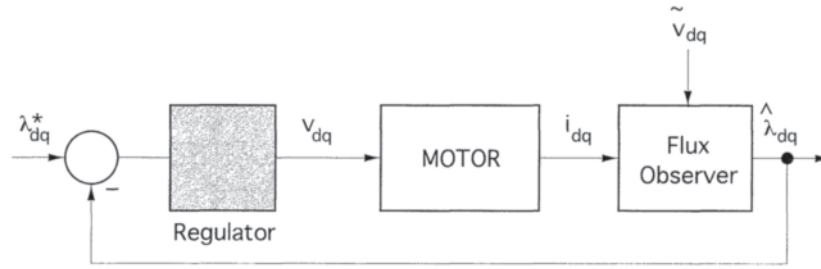


**Figure 2.144** Flux-observer-based control scheme.

frequency (~ kHz) voltage signals, superimposed on the first harmonic (alternatively, current injection or PWM modified patterns may be used). In the case of voltage excitation, the current at the corresponding frequency is sensed. This current signal depends on the rotor position and can be conveniently used, e.g., as a tracking error, to force an estimated rotor position to converge to the real one.

More details on this type of control are beyond the scope of this section but can be found in Ref. 103. However, it must be pointed out that the simple linear model Eq. 2.209 cannot be utilized in this case. Since the added high frequency signal is small, a linearized model can be derived from Eq. 2.217, leading to Eq. 2.222, in matrix form. Alternatively, Eq. 2.223 can be used, where  $\delta i'_{dq}$  represents the complex conjugate of  $\delta i_{dq}$ :

$$\delta \lambda_{dq} = \begin{bmatrix} I_d & I_{dq} \\ I_{dq} & I_q \end{bmatrix} \delta i_{dq} \quad (2.222)$$

$$I_d = \frac{\partial \lambda_d}{\partial i_d}; I_q = \frac{\partial \lambda_q}{\partial i_q}; I_{dq} = \frac{\partial \lambda_d}{\partial i_d} = \frac{\partial \lambda_q}{\partial i_d} \quad (2.223)$$

$$\delta \lambda_{dq} = \frac{I_d + I_q}{2} \delta i_{dq} + \left[ \frac{I_d - I_q}{2} + j I_{dq} \right] \delta i'_{dq}$$

Both Eqs. 2.222 and 2.223 contains the cross-coupling term  $I_{dq}$  which is due to the cross-saturation effect. From Eq. 2.223 it is pointed out that an additional backward component arises, due to  $I_{dq}$  which is in quadrature with the usual one. Because the rotor position is tracked through the backward component, disregarding  $I_{dq}$  results in a misaligned estimation of the rotor position. Moreover, attention must be paid to the operating-point dependency of  $I_b, I_p, I_{dq}$  parameters: in particular,  $I_d$  can vary by one order of magnitude, as evident from Fig. 2.134.

In conclusion, the synchronous reluctance machine is particularly well suited to sensorless control, provided that a sufficiently sophisticated magnetic model is utilized. In this case, the performance, especially at zero speed, may be greater than that obtained from other types of ac motors.

### 2.5.6.9 Permanent Magnet-Assisted Synchronous Reluctance Motors

When PMs are inserted into the rotor flux-barriers of a synchronous reluctance motor, it becomes a permanent magnetassisted synchronous reluctance (PMASR) machine.

Note that the same concept could be extended to the axially laminated structure. For the more common transverse-laminated case, an example is shown in Fig. 2.145. Observe that the magnet polarity is chosen in order to counteract the  $q$ -axis flux (e.g., at rated load) of the unassisted synchronous reluctance motor.

In principle, the PMASR motor seems nothing more than a particular case of interior permanent magnet (IPM) motor, apart from the different choice of  $d, q$  axes (the  $d$  axis is aligned to magnet flux, for IPMs). However, a substantial difference is found in the high anisotropy (low quadrature reactance) rotor structure and in the consequent low value of the PM flux, which is quite lower than the rated flux. In contrast, in the usual IPM structures (e.g., that in Fig. 2.146) the most flux

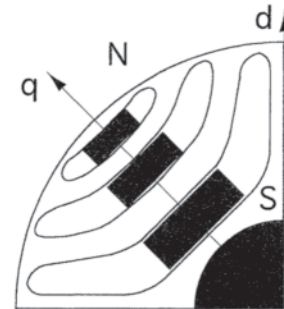


**Figure 2.145** Example of permanent magnet-assisted synchronous reluctance (PMASR) rotor (four poles).

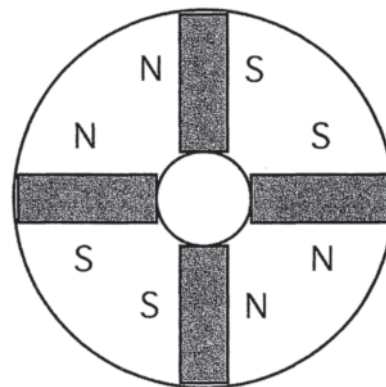


**Figure 2.146** Typical interior permanent magnet (IPM) rotor structure (four poles).

comes from the magnets and the flux produced by stator currents is seen as an unwanted reaction flux.

In practice, the above mentioned difference between PMASR and IPM machines results in a different suitability to large flux-weakening ranges. Once the inverter ratings are fixed, the maximum voltage and current values are defined, which can be supplied to the motor. The inverter kVA sizing can be then defined by Eq. 2.224, where  $V_{max}$  and  $I_{max}$  are the peak line-to-line voltage and the peak phase current, respectively. Let us observe that this  $kVA_{INV}$  value may differ from the actual reactive power, because  $V_{max}$  and  $I_{max}$  are not necessarily referred to the same working speed.

$$kVA_{INV} = \frac{\sqrt{3}}{2} V_{max} I_{max} \tag{2.224}$$

Thus, for a defined inverter ( $V_{max}$ ,  $I_{max}$ ), the maximum allowed active power (kW) from a given motor can be calculated, at each speed value. For an unassisted SynR motor (simply defined by  $L_d$ ,  $L_q$  parameters), the maximum power is met following the vector loci shown in Fig. 2.147. As the speed is increased, the voltage limit is reached and the current vector is rotated from the low speed position (point “0,” module  $I_{max}$ ). When the corresponding flux vector reaches the bisecting line (“point” 1), the situation of maximum torque with impressed voltage is met. As a consequence, at larger speed values, both current and flux modules are decreased, at fixed arguments. The corresponding active power (kW) referred to  $kVA_{INV}$  Eq. 2.224 is plotted in Fig. 2.148. Three speed zones are pointed out: constant torque ( $0 - \omega_1$ ), near constant power  $\omega_1 - \omega_2$ ), and decreasing power. Moreover, let us observe that, in the midzone, the  $kW/kVA_{INV}$  value coincides with the power factor,  $\cos \phi$ , times the motor efficiency  $\eta$ , because  $v = V_{max}$  and  $i = I_{max}$  in this zone.

$$kW = \eta \times \frac{\sqrt{3}}{2} vi \cos \phi \tag{2.225}$$

The plot of Fig. 2.148 shows that a large inverter oversizing ( $kVA_{INV}/kW$ ) is needed, if a large constant-power speed range ( $\omega_{max}/\omega_b$ ) is required (shaded rectangle). The motor suitability to flux-weakening is evidenced by a low value of the angle  $\delta_0$  (Fig. 2.147), that is by a low value of the quadrature reactance. From this point of view, the induction motor fits better, because

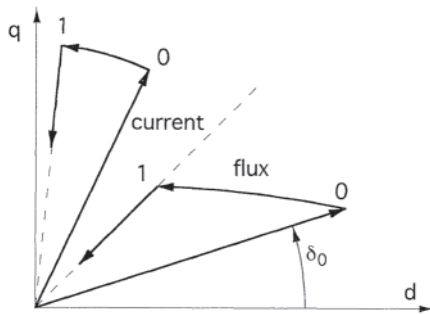


Figure 2.147 Loci of current and flux vectors for maximum motor power at a given inverter.

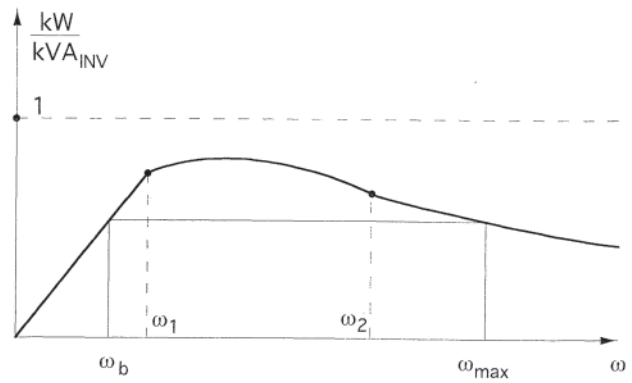


Figure 2.148 Per-unit maximum power vs. speed, for a synchronous reluctance motor.

its quadrature (short-circuit) reactance is lower than that of the corresponding synchronous reluctance motor. However, a proper amount of PM material can reverse this situation, leading to a PMASR machine.

With reference to Fig. 2.147, the flux locus can be shifted in the ( $\eta$ ) direction, by a properly added PM flux. As a result, the flux locus can cross the bisecting line at quite larger speed values or, in the limit situation, at infinite speed. Of course, this compensation is sensitive to many factors, markedly load and temperature variations. In any case, the power vs. speed diagram can be consistently improved, as qualitatively shown in Fig. 2.149. Moreover, let us observe that the added permanent magnets in the rotor also improve the Nm/Amps coefficient ( $k_T$ ). In fact, the torque is increased, since the subtractive term in Eq. 2.208 is dropped-out or strongly reduced.

As already mentioned, it is evident that the lower the quadrature reactance is, the lower the needed amount of permanent magnet is, together with the torque sensitivity to unmatched compensation. This strongly differentiates PMASR motors from most of IPM machines [104].

In the PMASR motors, a torque reversal is obtained by a  $d$ -current reversal, since the  $q$  component of current must always produce a mmf that is opposed to that of the magnets. This can constitute a minor drawback, because the needed voltage integral is larger ( $L_d \gg L_q$ ). Another drawback to be mentioned

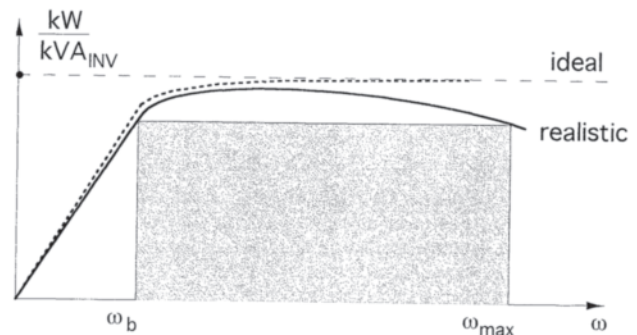


Figure 2.149 Per-unit motor power vs. speed, for a PMASR motor.

is possible overvoltage at maximum speed, in case of failure. It happens when a flux lower than that due to magnets is desired, at high speed. As a consequence, a low magnet amount is again suggested and will lead, in turn, to maximizing the rotor anisotropy.

Last, the control structure for PMASR motors is more complicated than that of uncompensated motors, because of the double nature of PMASR machines. Reference should be made to [102].

### 2.5.7 Aerospace Motors

Motors for applications in ballistic missiles, satellites, space vehicles/shuttles, etc., are the real aerospace motors. The machines are truly custom designed either for short life and absolute minimum weight (as for missiles), for applications in a vacuum, or for other extreme conditions in a space environment. The more severe requirements for these machines are usually found for man-rated applications in space shuttles, space stations, or other space vehicles. Many of these applications require the motor to function in both atmospheric and space conditions.

These motors find applications as pump drives, fans and air movers, as actuators and drives in robots as well as for gyroscopic or flywheel drives. Even though certain customers prefer induction motors for many of these applications more often than not there is a de-power system available rather than a three-phase ac system. Thus, most of these machines operate as what is commonly known as brushless de-motor. In this type of drive the ac-motor is coupled to its own dc to ac converter that also functions as the speed controller. The actual motor can be an induction motor, a permanent magnet excited motor, a switched reluctance motor, or any other kind of synchronous motor with stator side excitation.

The design approaches for these machines are generally very similar to those described in Section 2.5.2. The most significant difference is that the machine cooling has to be fully designed and analyzed especially for vacuum applications. Similarly the bearing lubrication has to be functional in those conditions. For some applications magnetic bearings have been utilized in which the emergency or auxiliary bearings have only to support the rotor for the short time it takes to stop in case of magnetic bearing failure.

The insulation materials have to be space-rated and one will have to consider whether corona discharges can take place during the operation if the machine environment is a low-to medium-level vacuum. Some applications may also be exposed to a radiation level in space and have to withstand that for the desired life of the machine. Chemical resistance of these motors may sometimes be important but in contrast to the aircraft and regular missile applications the salt water and fog resistance requirements are generally not important for space-type motors. However, very low temperature operation and a very wide operating temperature range make the mechanical design of these machines tricky because the assemblies have to accommodate the resulting thermal expansion rates of the different materials without damage to motor or system.

## 2.5.8 Superconductive Synchronous Motor

### 2.5.8.1 Introduction

The advent of high-temperature superconductivity (HTS) has created the opportunity for a quantum leap in the technology of large electric machines. HTS-based motors and generators will be smaller, lighter, more efficient, and less expensive to manufacture and operate than conventional machines. The potentially significant cost, size, weight, and efficiency benefits of superconducting machines may change the dynamics of the electrical machinery industry. This unique situation should lead to reduced manufacturing costs.

The initial use for HTS motors will likely be in transportation applications, particularly naval and commercial ship (marine) electric propulsion, where critical size and weight savings will provide a key benefit by increasing ship design flexibility. Electric drive has already penetrated the cruise ship segment of the market because of its marked advantages over competing mechanical systems. The increased power density and operating efficiency as well as other benefits of HTS-based marine propulsion systems motors will significantly further expand the attractiveness of electric propulsion systems. HTS-motors are proposed for use in pumps, fans, compressors, blowers, and belt drives deployed by utility and industrial customers, particularly those requiring continuous operation. These motors will be suitable for large process industries such as steel milling, pulp and paper processing, chemical, oil and gas refining, mining, offshore drilling, and other heavy-duty applications.

Superconducting wire in its low-temperature superconductor (LTS) form has been in widespread use now for over 30 years, and commercial applications today range from high-powered particle accelerators to sensitive resonance imaging systems utilized for medical diagnostics. General Electric and Westinghouse independently conducted large superconducting generator design studies during the 1970s; both approaches were based on LTS wire. General Electric also built and tested a 20-MVA superconducting generator in the 1970s, and a Japanese consortium built and tested a 70-MW generator during the 1990s. These machines used LTS wire made up of a niobium-titanium (NbTi) alloy. The high-current density achievable in superconducting electromagnets makes it possible to create very compact and power-dense rotating machinery. However, even at such large ratings, the complexity and cost of the refrigeration equipment, and the challenging nature of thermal isolation systems that are necessary for allowing LTS materials to operate at an ultra-low 4K, have made any conceivable commercialization of this early superconducting technology in rotating machine applications a prohibitive concept.

However, rapid advances in the development of HTS wire over the past 13 years have resulted in superconducting electromagnets that can operate at substantially higher temperatures than those made of LTS materials, and that as a consequence can utilize relatively simpler, less costly, and

---

This section is based on a paper that has been previously presented at IEEE PES Meeting, New York, January 27–31, 2002.

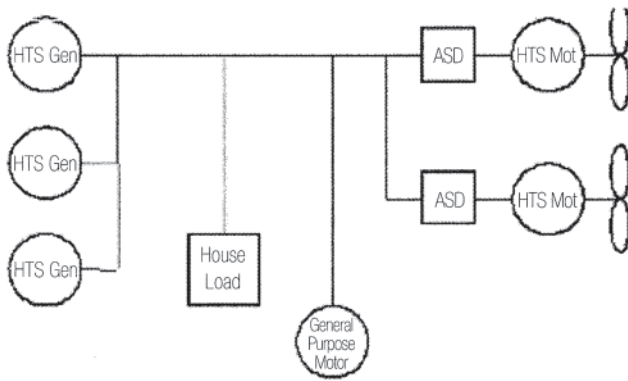


**Figure 2.150** Ship electrical system components.

more efficient refrigeration systems. These factors make HTS wire technically suitable and economically feasible for use in the development and commercialization of motor and generator applications at power ratings much lower than could be considered with LTS wire.

The discussion in this section center on applications of HTS motors to an all-electric ship. Figure 2.150 shows a single line diagram for a ship electrical system using superconducting generators, propulsion motors and general-purpose industrial motors.

#### 2.5.8.2 HTS Wire Status

Over the past 10 years, the performance of multifilamentary composite HTS wire has continually improved. At this writing one company is producing this wire at a rate of about 500 km/year and shortly will produce 10,000 km/year in a new factory. This Bi-2223 high-current density wire is available for industrial applications and prototypes. Bi-2223 high-strength reinforced wire is able to withstand close to 300 MPa tensile stress and 0.4% tensile strain at 77K. Reinforced wires provide a mechanically robust and reliable product, which are suitable for making high-performance prototype propulsion motors and generators.

#### 2.5.8.3 HTS Machine Topology

The major components of a rotating machine employing HTS winding is shown in Fig.2.151. Only the field winding uses HTS cooled with a cryocooler subsystem to approximately 35–40K. The cryocooler modules are located in a stationary frame and a gas, such as helium, is used to cool components on the rotor. The stator winding uses conventional copper windings but with a few differences. The stator winding is not housed in conventional iron core teeth because they saturate due to high magnetic field imposed by the HTS winding.

#### 2.5.8.4 HTS Generator

Compared to conventional generators, HTS generators are expected to be less expensive, lighter, more compact, efficient and reliable, and significantly superior at maintaining power system stability. They also exhibit higher efficiency under partial load conditions and could operate as a virtual condenser to deliver its rated current.

The HTS generator [105] shown in Fig. 2.152 has three major subsystems: (1) rotor, (2) rotor cooling, and (3) stator. Physically, this generator is expected to be about half the length and two-thirds the diameter of a conventional machine.

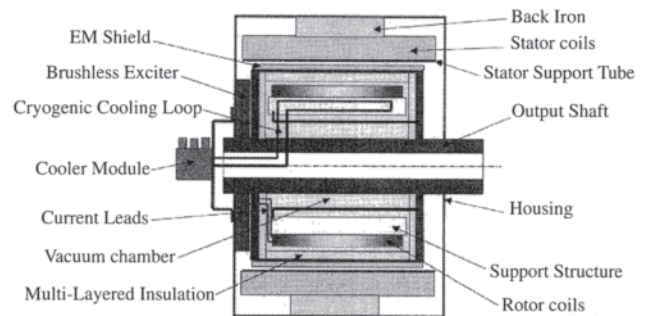


**Figure 2.151** Block diagram of an air-core high-temperature super conductivity (HTS) generator.

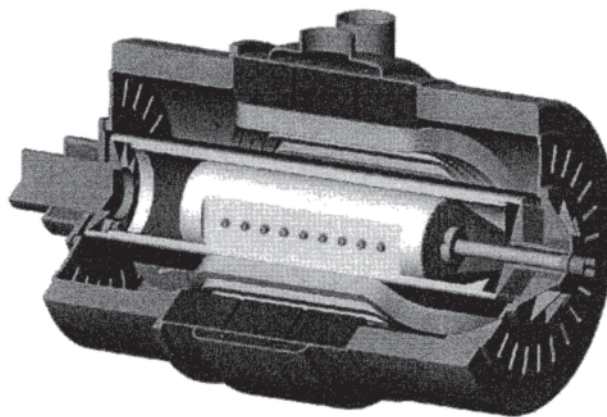


**Figure 2.152** High-temperature super conductivity (HTS) generator assembly.



This generator has a low synchronous reactance of 0.28 pu but the transient and subtransients reactances are similar to those of conventional machines. The overall efficiency of the generator is 98.6%, which is retained down to one-third of the rated load. The majority of losses (65%) are in the conventional copper armature winding. The cryogenic cooling system power consumption is merely 2% of the total losses in the machine. HTS generator produces nearly clean ac voltage in the stator winding. Both rotor and stator windings generate minimal harmonics. The field winding produces 2% of fifth harmonic voltage in stator winding; all other harmonics are negligible.

#### 2.5.8.5 HTS Drive for Ship Propulsion

Modern electric drives have many advantages over competing mechanical systems. The advantages include redundancy, reliability, better fuel economy in many circumstances, reserve power when needed, better use of internal space allowing revenue producing space elsewhere, quietness, easier maintenance and improved ship safety.

A conceptual design has been developed [106] under an Office of Naval Research (ONR) contract for a 25 MW, 120-RPM HTS motor for ship propulsion. In order to demonstrate the key technologies used in the 25-MW motor, a 5-MW motor preliminary design has been completed.

The 25-MW, 120-RPM HTS motor shown in Fig. 2.153 is 2.65 m in diameter and 2.08-m long. It weighs 60 k-kg and generates structureborne noise of 48 db at full speed. The motor uses 6.6-kV stator winding that is cooled with freshwater. The HTS rotor winding is cooled by off-the-shelf cryocoolers positioned in the stationary reference frame—a defective cooler could be replaced in less than 30 minutes without having to stop the motor. The motor has an overall efficiency of 97% at full speed and 99% at one-third full-speed; this includes power consumption by the HTS rotor cooling system, but does not include losses in the adjustable speed drive (ASD).

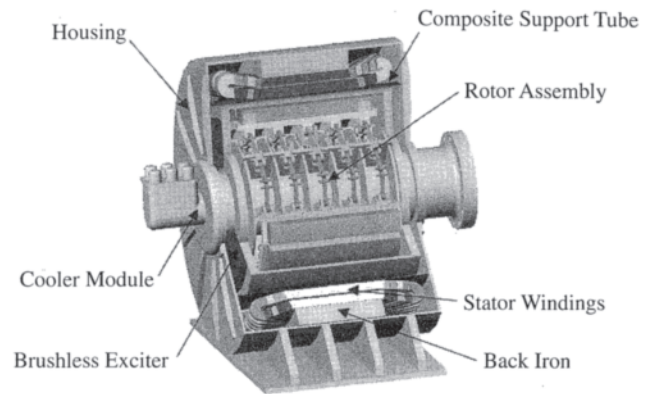


**Figure 2.153** 25-MW ship propulsion motor.

Generators and motors using HTS technologies are compact, light, and several points higher in efficiency (even at partial loads) will enable design of more economic ship for both in-hull and in-pod propulsion options.

#### 2.5.8.6 Industrial HTS Motors

A 5000-hp, 1800-rpm synchronous motor was demonstrated in July 2000. This HTS motor undergoing factory testing is shown in Fig. 2.154. The rotor assembly includes the HTS field winding operating at cryogenic temperature ( $\sim 35^\circ\text{K}$ ), its support structure, cooling loop, cryostat and electromagnetic (EM) shield. The stator assembly includes ac stator windings, back iron, stator winding support structure, bearings, and housing. This motor has met all design goals by demonstrating HTS field winding, cryocooling system, and a novel armature winding cooled with fresh water.

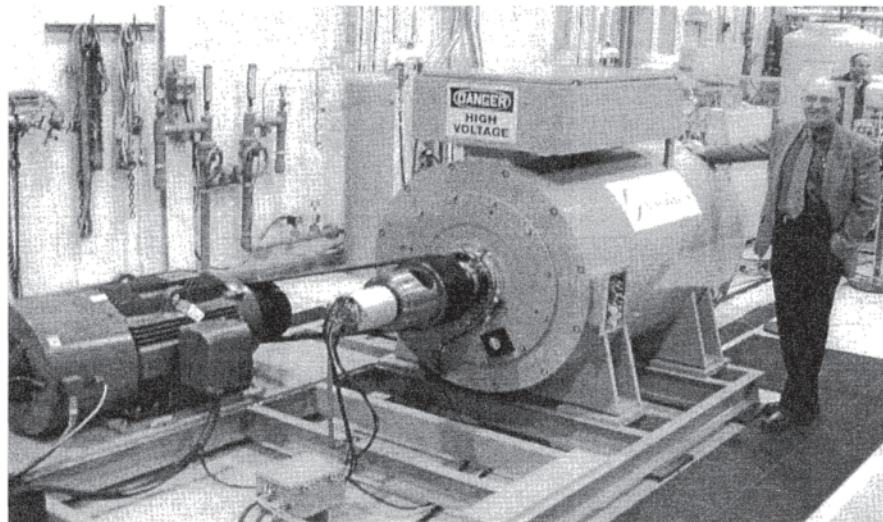


**Figure 2.154** 5000-hp high temperature superconductivity (HTS) motor under test. (Courtesy of American Superconductor Corp. (AMSC).)

### 2.5.9 Universal Motors

The universal motor, Fig. 2.155 is a commutator series motor, as discussed in Section 2.3.5, designed and connected to a single-phase ac supply. The field is produced with a wound laminated stator core, generally two salient poles, and connected in series with the armature. The armature is also wound on a laminated steel core and the windings are connected to a commutator that usually has twice as many bars as there are armature slots. The armature is connected to the field through a set of brushes mounted to the frame of the motor. The series motor has the unique characteristic that whatever voltage polarity is applied the motor terminals; the motor turns and produces torque in the same direction. The principle of operation is shown in Fig. 2.156. The field winding and the armature are connected in series, so when the voltage is reversed, the current through the field and armature are reversed simultaneously and hence, the developed torque remains in the same direction.

The name universal comes from the fact that this motor can operate on ac as well as dc current.

#### 2.5.9.1 Speed-Torque

Typical speed-torque characteristics of the universal motor are shown in Fig. 2.157, which are the same as the series dc motor. The motor produces high torque and draws high amps at low

speed and as the motor is unloaded or at light loads, the speed goes up very rapidly. Care must be taken in operating the motor without any load, as the speed could go up so high as to cause the commutator or armature windings to fly apart. The motor typically runs in the steep part of the speed-torque curve, 6000 to 8000 rpm area in the example shown in the Fig. 2.157.

The primary design difference of a universal motor, operated as an ac machine, is ac flux in the stator core that will cause eddy current and hysteresis losses in the steel so that the core must be laminated to reduce these losses. The motor also produces less torque and lower speeds on ac as opposed to dc because of the increased impedance of the windings with ac, and the fact that the applied power is varying sinusoidally. It can be shown, that there is 29.3% less torque on a machine operating on ac as opposed to dc, for a motor designed to operate at the same peak flux level and RMS value of current.

#### 2.5.9.2 Vector Diagram

The vector diagram of the series motor is shown in Fig. 2.158, [107].

1.  $V_s$  is the speed voltage of the armature, which is proportional  $\phi$  to the main flux.
2.  $V_f$  is the transformer voltage of the armature and field, which is proportional to the time derivative of the main flux.

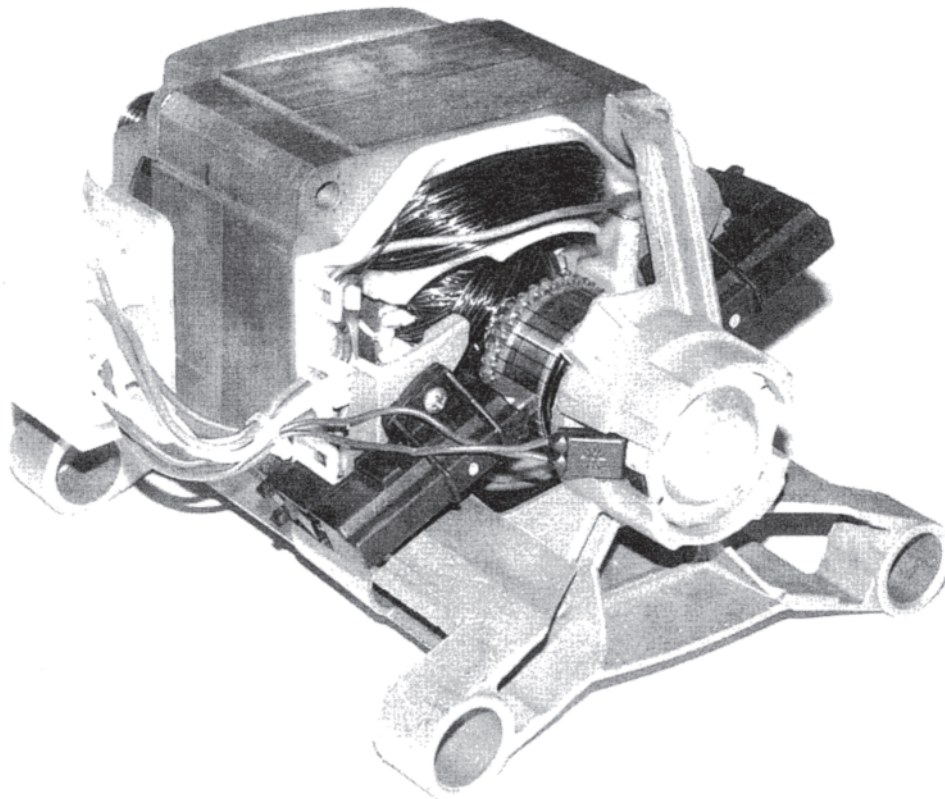


**Figure 2.155** Universal motor used in European clothes washers.

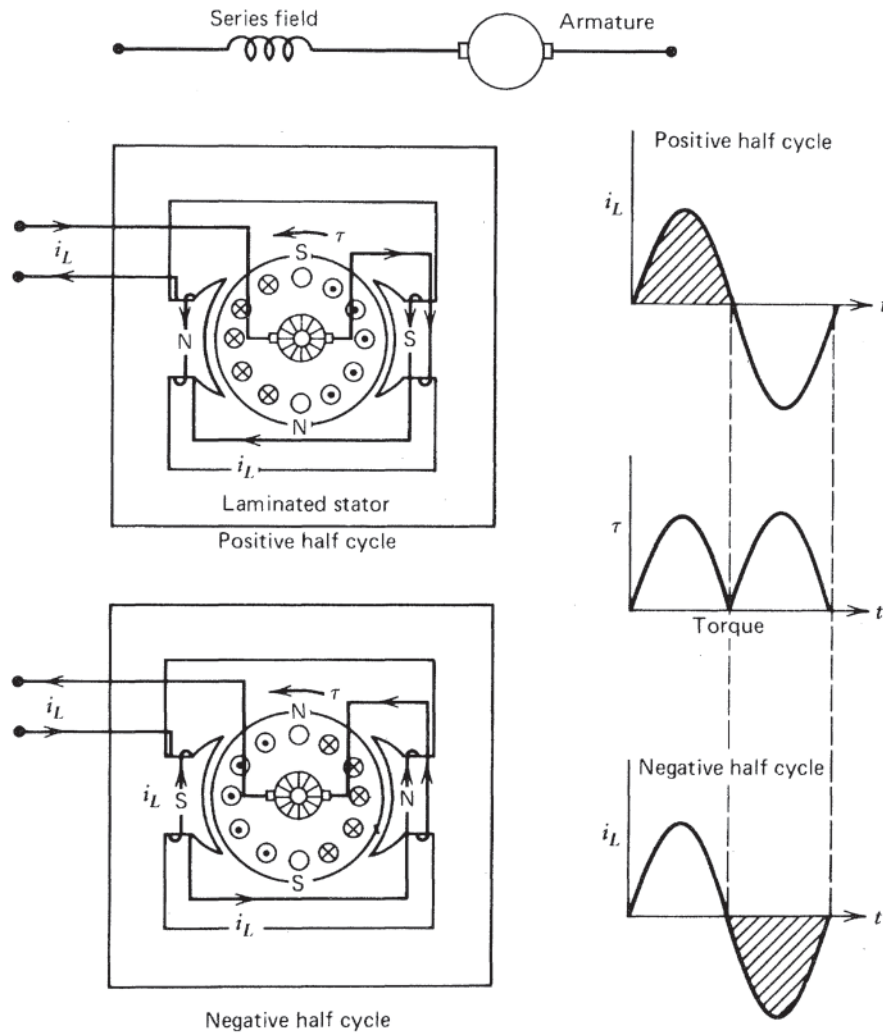


Figure 2.156 Universal motor principles.

3.  $V_t$  is the line voltage.
4.  $I$  is the current.
5.  $V_{br}$  is the brush drop.
6.  $R_a$ ,  $R_f$ ,  $X_a$  and  $X_f$  are the resistance and reactance of the armature and field.
7.  $\phi$  is the main flux.
8.  $\beta$  is the angle between main flux and current.

- $P$  = Number of poles
- $S_c$  = Number of commutator segments
- $N_a$  = Turns per coil
- $a$  = Number of parallel paths in armature
- RPM = Speed in revs per min.

Flux,  $\phi$ , is determined from the magnetization curve of the stator and armature.

There are several good references cited at the end of this section for calculating performance. Two of the better ones are by Chang and Karn [107], and Trickey [108].

### 2.5.9.3 Torque and Voltage Equations

The speed voltage or back emf is:

$$V_t = 2.36 \times 10^{-10} P \times \text{RPM} \times \phi \times \frac{S_c N_a}{a} \text{ volts} \quad (2.226)$$

torque:

$$Tq = 2.66 \times 10^{-8} P \phi I \frac{S_c N_a}{a} \cos \beta \text{ oz-ft} \quad (2.227)$$

where:

### 2.5.9.4 Brushes

Brushes are a concern because of the radio frequency interference (RFI) noise and use in hazardous locations due to sparking, and brush life, which is typically 200 to 1200 hours.

Brush life is the biggest problem encountered in the development of series motors. Brush design is based on some theory, but primarily on past experience. Brush wear is caused by:

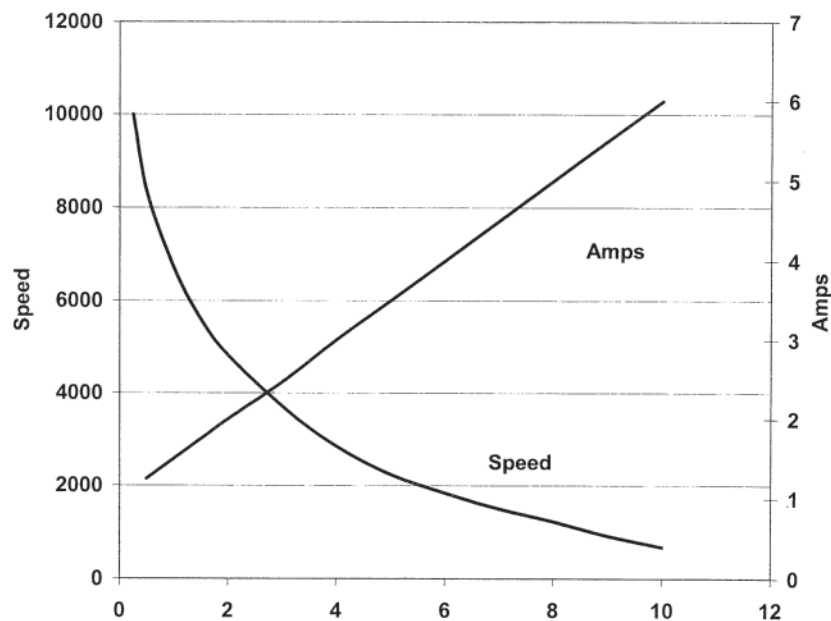


Figure 2.157 Universal motor performance.

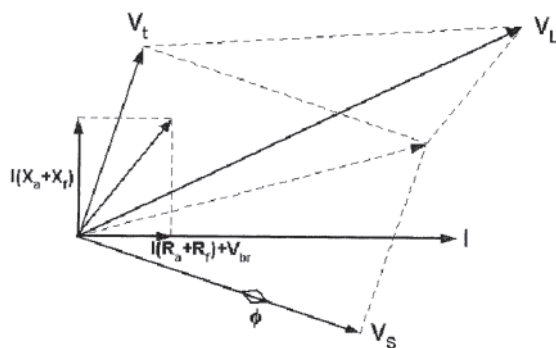


Figure 2.158 Vector diagram of ac series motor.

1. Mechanical friction and the passage of current.
2. Sparking between the brush and commutator due to jumping caused by roundness of the commutator and loose brush holders.
3. Sparking due to breaking of contact at the end of commutation.
4. Heating due to brush losses.

To obtain good brush life:

1. The commutator quality must be controlled. It must be a sturdy design and have well-machined surfaces with excellent concentricity and surface finishes.
2. Brush holder and springs must be dynamically designed to minimize brush bounce.
3. Brush materials must be selected to minimize sparking and brush loss.

4. Shifting the brushes off neutral, if the motor runs primarily in one direction.
5. Increasing the number of commutator bars.
6. Fractional pitch windings.
7. Establish a good relationship between commutation and the neutral zone between field pole tips.
8. Establish a balance of brush abrasiveness versus sparking damage to the commutator.

There are many articles and publications written on the various aspects of brush wear, some in textbooks [109, 110], but much can be obtained from the commutator, brush, and brush holder manufacturers.

The brushes wear uniformly on ac as opposed to the negative brush wearing the most in dc operation. Sparking is worse on ac because the ac commutation causes increased brush loss due to eddy current losses in the brush. Generally the use of higher resistance brush material is used to keep this loss down.

#### 2.5.9.5 Applications

The universal motor has the highest power density per dollar of any single phase machine, which makes it a very popular machine in household appliances and power tools. They are extensively used in vacuum cleaners and on horizontal axis washers in Europe. The motor is easily speed controlled with a simple triac control.

Some of the disadvantages of universal motors are the poor speed regulation due to the highly varying speed characteristic. This is typically overcome in washer applications by adding a speed sensor to the motor and controlling the speed through a triac control.

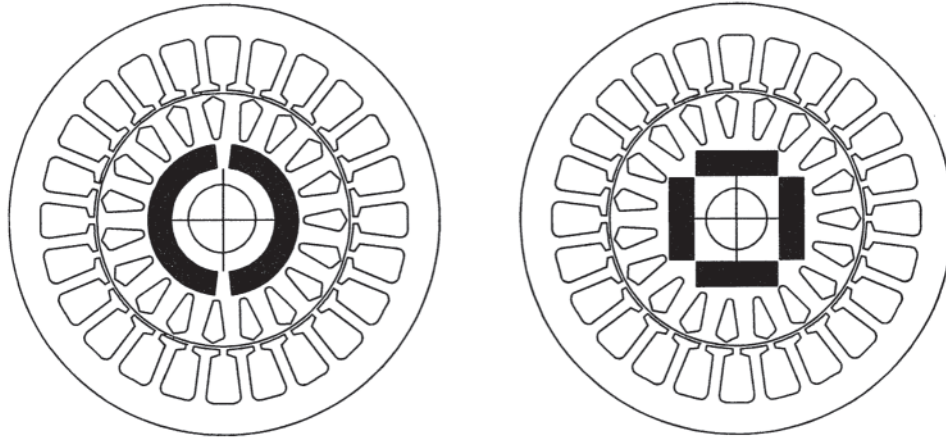


**Figure 2.159** Geometry of line-start permanent magnet (PM) motor with arc-shaped or chord-shaped interior magnets.

### 2.5.10 Line-Start Synchronous Reluctance and Permanent Magnet Motors

There is a small but important class of synchronous ac motor that can be considered as being derived from the induction motor, by incorporating magnets and/or flux-barriers in the rotor, as shown in Figs. 2.159 and 2.160. Placed in a conventional induction-motor stator with an ac rotating field, a rotor that is permanently magnetized and/or anisotropic runs at synchronous speed without slip losses, and is therefore potentially more efficient than the equivalent induction motor. In all cases the synchronous reluctance and PM rotors have a cast cage winding similar to that of the induction motor, to provide the asynchronous torque necessary for starting. Early examples are the synchronous reluctance motor of Kostko (1923) [111] and the “Permasyn” permanent-magnet motor by General Electric (1955) [112, 113]; see also Ref. 114. During the 1960s and 1970s a huge effort was made to perfect the design of the synchronous reluctance motor for applications where several motors could run from a single three-phase six-step open-loop inverter [115–118]. The applications were in textiles and glass manufacture, in process machinery that required multiple rollers to be driven in exact synchronism in order to assure the quality of the finished product. Individual motors could be switched in and started “across the line”. Analytical engineering of a high order was applied to maximise the power factor and to increase the inertial load that could be synchronized (see [119]); in both of these respects the performance was inferior to that of a good induction motor. Because the inverters were open-loop inverters without shaft position feedback, stability at low speed was an issue (in common with open-loop induction motor drives), and considerable effort was made to analyze the stability using advanced mathematical techniques [120]. Most of these machines were three-phase, but single-phase capacitor motors were also developed [121, 122].

The synchronous reluctance motors of the 1960s and 1970s achieved efficiencies and power factors comparable to those of good induction motors but still they could have been improved by using permanent magnets located in the flux-barriers and by adjusting the design to optimize the

combination of magnet alignment torque and reluctance torque, both of which contribute to the synchronous operation. Notable efforts were made with hybrid reluctance/permanent-magnet motors of this type [123–128], starting with Alnico and ceramic magnets and later taking advantage of the new rare-earth/cobalt magnets, and (since about 1985) of neodymium-iron-boron. The commercial development of these motors was limited by the cost and limited properties of the PM materials available at the time.

In the early 1980s, sudden increases in energy prices caused the motor industry to seek new ways of improving the efficiency of ac motors especially in the power range from 1 to 125 hp, which accounts for the bulk of electric energy consumption by electric motors, [129]. At first the high-energy magnet materials needed to meet the performance

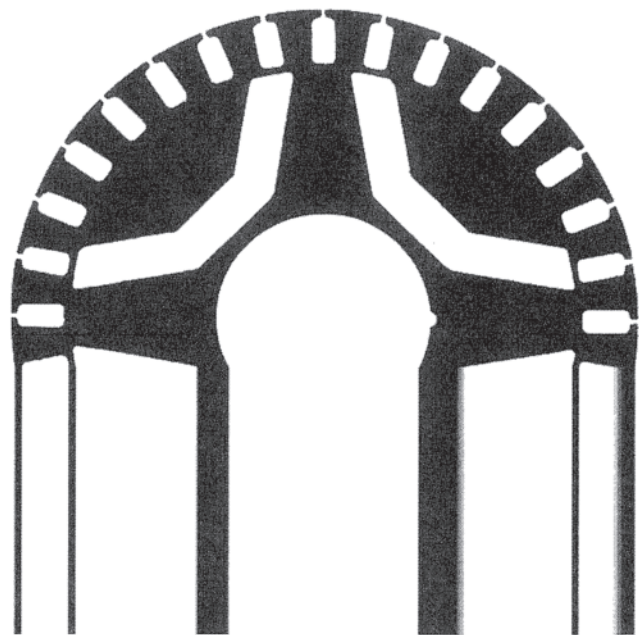


**Figure 2.160** Synchronous reluctance rotor. (Courtesy of Professor P.J.Lawrenson.)

requirements were expensive, so that the payback period required for the energy savings to pay for the additional manufacturing cost was too long to make the motors commercially viable [130]. The development of new magnet materials (especially neodymium-iron-boron) since that time has slowly lowered this barrier to the wider application of the permanent-magnet line-start motor, while competitive factors and a continuing pressure to maximize efficiency have helped to make the climate more favorable for it.

No matter how low the magnet cost, the line-start PM motor inevitably has certain limitations. For instance, it can synchronize only a load inertia that is typically less than 2–5 times the rotor inertia [131]. The higher the load torque, the less inertia it can synchronize. The synchronizing inertia limit is an electromagnetic limit, not a thermal one. Operational factors may need to be considered, such as the consequences of having a rotor that is permanently magnetized. If the rotor is overrunning or spinning for whatever reason while the stator is disconnected from the supply, the generated terminal voltage may be hazardous. If the stator is short-circuited, the short-circuit current will be sustained indefinitely since the magnet flux is persistent, unlike the trapped flux of an induction motor rotor. Overloads (both electromagnetic and thermal) may result in partial demagnetization of the magnets, downgrading the performance and even introducing serious unbalance. During starting, the permanently magnetized rotor slips poles against the rotating stator field, producing a highly oscillatory torque transient that does not disappear until the motor has synchronized. In single-phase capacitor motors, a backward-rotating field is present at all load conditions except that of perfect balance, and this introduces a pulsating torque by interaction with the permanently magnetized, salient-pole rotor.

Various means have been invented to overcome the difficulties with starting and synchronization: see, for example, [132]. Most of these involve additional windings, switches, and/or external components and so they potentially increase the cost.

### 2.5.11 Watthour Meters

The IEEE Standard Dictionary of Electrical and Electronics Terms [133] defines the motor-type watthour meter as a motor in which the speed of the rotor is proportional to the power, with a readout device that counts the revolutions of the rotor. This is the device that measures the energy supplied to a customer by an electric utility. To the layman it is known as “the electric meter.”

The configuration shown in Fig. 2.161 is not much different from the first such meter invented by Oliver B. Shallenberger and built by Westinghouse in 1895, although there have been many mechanical and material improvements that have increased the accuracy and have made it possible to use the meter under a wide range of environmental conditions.

The meter incorporates a two-winding induction motor, one winding being excited by the voltage across the line and the other by the current in the line. The potential coil is made of many turns of wire of small cross section, and is shielded

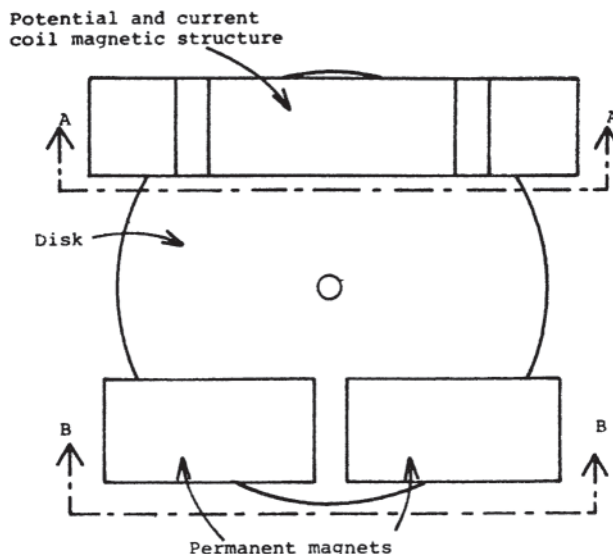


**Figure 2.161** Top view of single-phase induction watthour meter. Indicating register, gear train, and coils are not shown.

magnetically from the rotor and the current coil, as may be seen in Fig. 2.162. The current coil is made of a few turns of large cross section, and hence it has a very low impedance. By emphasizing certain parameters and deemphasizing others, the motor action is made such that the average torque on the disk is directly proportional to the average electric power passing the meter’s location in the circuit. Since the meter is an induction motor with very light load, it would tend to run up to nearly synchronous speed for any torque were it not for the viscous frictional effect of the so-called damping magnets. The net result is that the disk speed is directly proportional to

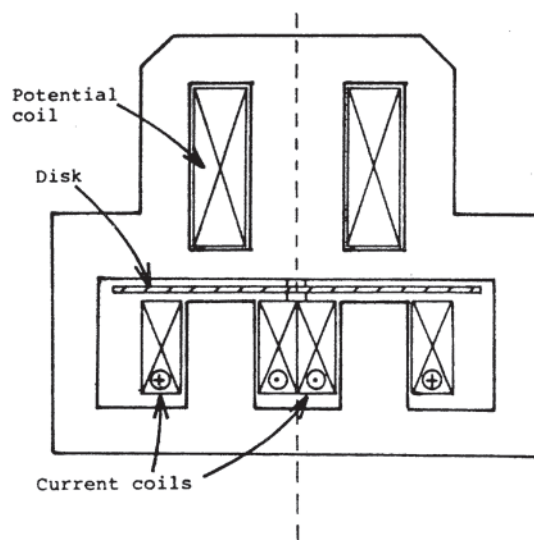


**Figure 2.162** Potential and current coil magnetic structure. Current directions shown for current coils only. (This is section A-A of Fig. 2.161.)

power. Since the disk drives a register with four or five dials, the cumulated angle of rotation as translated by the gear train and the dials is simply the integral of power over time, that is, the energy.

This unique mechanism can be seen to be a two-winding motor such as described in Chapter 1 (although with the rotor winding shorted). It is similar to a two-phase servomotor subjected to a transformation that results in the cup being flattened into a disk. The use of a disk rather than a cup makes it possible to place the winding for one phase above the disk and that for the other phase below the disk, thus making the designer's task somewhat easier in that the two windings are effectively much closer along the periphery of the disk than they could otherwise be. This results in an effective increase in the number of poles  $p$ , and there is nothing to prevent the effective number of poles from being odd or indeed fractional. The synchronous speed is given by:

$$n_s = \frac{120f}{p} \quad (2.228)$$

where:

- $n_s$  = synchronous speed of the rotor (rpm)
- $f$  = frequency (Hz)
- $p$  = the number of poles

If the power into the rotor of an induction motor is constant, a decrease in synchronous speed is accompanied by an increase in torque. In the watt-hour meter, a high torque is desirable so that friction in the gear train of the register becomes proportionately smaller in relationship to developed torque. Furthermore, a speed decrease results in a reduction in the needed gear reduction to the register, thus decreasing complexity as well as friction. Thus  $p$  should be made as large as possible.

Analysis of the motor action may begin with the general equations in Chapter 1, or with Eqs. 10.24 in Ref. 134. If the latter are used, note that the potential winding is designated by the subscript  $a$  and the winding carrying the currency the subscript  $b$ . The current  $\bar{I}_b$  is determined by the voltage  $\bar{V}_a$  and the impedance of the electrical load. Since  $\bar{I}_b$  is determined and there is little interest in the voltage across winding  $b$  other than to insure that it is negligible, the second equation in Eqs. 10.24 of Ref. 134 may be ignored and the rest rewritten as:

$$\bar{V}_a = \bar{I}_a(r_a + j\omega L_a) + \bar{I}'_{rf} \frac{jn\omega M_{ar}}{2} + \bar{I}'_{rr} \frac{jn\omega M_{ar}}{2} \quad (2.229)$$

$$\bar{I}_b \frac{n\omega M_{br}}{2} = \bar{I}_a \frac{jn\omega M_{ar}}{2} + \bar{I}'_{rr} \left( \frac{nr'_r}{2-s} + \frac{jn^2\omega L_r}{2} \right)$$

$$-\bar{I}_b \frac{n\omega M_{br}}{2} = \bar{I}_a \frac{jn\omega M_{ar}}{2} + \bar{I}'_{rf} \left( \frac{nr'_r}{s} + \frac{jn^2\omega L_r}{2} \right)$$

where:

- $\bar{I}_a$  = current in the potential winding
- $\bar{I}_b$  = current in the current winding
- $\bar{I}'_{rf}$  = current in the rotor developing forward torque
- $\bar{I}'_{rr}$  = current in the rotor developing reverse torque

- $r_a$  = resistance of the potential winding
- $L_a$  = inductance of the potential winding
- $M_{ar}$  = mutual inductance between winding  $a$  and the rotor
- $M_{br}$  = mutual inductance between winding  $b$  and the rotor
- $r'_r$  = resistance of the rotor "winding"
- $L_r$  = inductance of the rotor "winding"
- $n$  = the number of "windings" on the rotor
- $s$  = slip= ratio of the difference between synchronous speed and actual rotor speed to the synchronous speed
- $\omega$  = angular frequency of the electrical system (rad/s).

Because speed is kept low to reduce frictional effects,  $s$  is very nearly 1. The disk is made thin so that  $nr'_r$  will be much larger than  $n^2\omega L_r/2$ . To avoid large energy losses in the potential winding (winding  $a$ ) and to keep that winding current to a minimum,  $\omega L_a \gg r_a$ . (It will be seen below that this is not only desirable for the reasons given, but a necessary condition.) As noted earlier, the potential coil is well shielded from the disk. Hence  $M_{ar} \ll L_a$ , and in addition  $M_{ar} \ll M_{br}$ . The equations above then reduce to the phasor equations:

$$\bar{V}_a = j\omega L_a \bar{I}_a \quad (2.230)$$

$$\bar{I}_b \frac{\omega M_{br}}{2} = \bar{I}'_{rr} r'_r$$

$$-\bar{I}_b \frac{\omega M_{br}}{2} = \bar{I}'_{rf} r'_r$$

The torque equation for the two-winding induction motor is Eq. 10.25 in Ref. 134, which is:

$$T = \frac{nI'_{rf}}{2} [I_a M_{ar} \sin(\alpha - \beta) + I_b M_{br} \sin(\psi - \beta - 90^\circ)]$$

$$- \frac{nI'_{rr}}{2} [I_a M_{ar} \sin(\alpha - \gamma) + I_b M_{br} \sin(\psi - \gamma + 90^\circ)] \quad (2.231)$$

where:

- $\alpha$  is the angle of  $\bar{I}_a$
- $\psi$  is the angle of  $\bar{I}_b$  (the load impedance angle)
- $\beta$  is the angle of  $\bar{I}'_{rf}$
- $\gamma$  is the angle of  $\bar{I}'_{rr}$
- all with respect to  $\bar{V}_a$ . From the phasor equations above:

$$\alpha = -90^\circ, \beta = 180^\circ \pm \psi, \gamma = \psi$$

Substitution of the scalar currents  $I_a$ ,  $I'_r$ , and  $I'_r$  and of the angles into the torque equation yields

$$T = \frac{nM_{ar}M_{br}}{2} V_a I_b \cos \psi = K_T V_a I_b \cos \psi \quad (2.232)$$

and the developed torque is proportional to the power to the electrical load.

If the permanent magnets produce countertorque proportional to speed, then the disk speed will be directly proportional to the power and the cumulated disk rotation

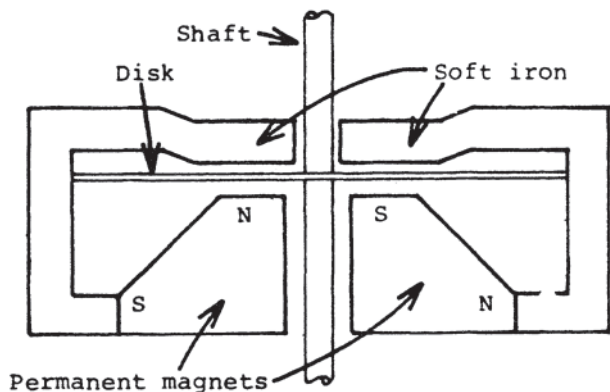


**Figure 2.163** Permanent magnet structure of the induction wattour meter. (This is section B-B of Fig. 2.161.)

exhibited by the dials will be directly proportional to the energy. To show that the permanent magnets produce the necessary counter-torque, consider the following.

The PMs in the structure of Fig. 2.163 may be thought of as windings excited by direct current. For a direct current,  $f=0$ , and hence the synchronous speed of the disk for the excitation provided by the magnets is also zero. By a derivation similar to that above, it may be shown that the torque developed in the rotor by the permanent magnets is given by:

$$T = -\frac{n\phi^2}{\sqrt{2}r_r'} \omega_m \quad (2.233)$$

where:

$\phi$  = total flux through the disk due to the permanent magnets

$\omega_m$  = angular speed of the disk in rad/s.

The total torque on the disk is then the sum of the torques of Eqs. 2.232 and 2.233, or

$$T_{\text{net}} = K_T V_a I_b \cos \psi - \frac{n\phi^2}{\sqrt{2}r_r'} \omega_m$$

and is zero for constant speed, the steady-state condition. Hence:

$$\omega_m = K_m V_a I_b \cos \psi \quad (2.234)$$

where:

$$K_m = \frac{\sqrt{2}K_{Tr}'}{n\phi^2}$$

Equation 2.233 reveals an important point. The viscous torque is proportional to the square of the flux from the permanent magnets. Hence very stable magnets must be used to maintain accuracy, a 1% reduction in magnet strength resulting in a 2% increase in the consumed energy as registered by the meter. The permanent magnet is always made stronger than necessary and then shunted to adjust the meter for accuracy at full load. It is also necessary to provide a

temperature-sensitive shunt to allow use over the wide temperature range encountered in outdoor installations.

Certain additional refinements need to be made for accuracy. One of these is a lag adjustment that compensates for the fact that the current in the potential coil does not lag the voltage by precisely 90 degrees, and hence the flux component caused by the potential coil current is not precisely 90 degrees out of phase with the voltage. By use of a shading coil or plate (called a lag plate) in the path of the flux from the potential coil, the necessary slight additional shift in the flux phase can be achieved. Moreover, by moving the lag plate to one side, a small constant torque can be produced by the potential coil only. This torque is used to overcome any coulomb friction of the gear train between the disk and the register. The adjustment of the lag plate position to accomplish this is known as the light-load adjustment.

In modern versions of the wattour meter, the magnets have been moved to the rear of the assembly, adjacent to the coils, thus allowing a decrease in depth. To reduce friction of the disk (the highest-speed element) to a minimum, the rotor may be magnetically suspended.

## REFERENCES

Note: In the following listing, abbreviations have the following meanings:

- AIEE American Institute of Electrical Engineers (predecessor to IEEE)
  - IEE Institution of Electrical Engineers(UK)
  - IEEE Institute of Electrical and Electronics Engineers
  - NEMA National Electrical Manufacturers Association
- Sources for standards are listed in [Appendix B](#).

1. NEMA MG 1–1996, rev.2 Motors and Generators.
2. IEEE Std. 115–1995—IEEE Test Procedures for Synchronous Machines.
3. Kilgore, L.A., “Calculation of Synchronous Machine Constants,” *Transactions of the AIEE*, vol. 50, 1931, p. 1201.
4. Wright, S.H., “Determination of Synchronous Machine Constants by Test,” *Transactions of the AIEE*, vol. 50, 1931, p. 1331.
5. De la Ree, J., and H.B.Hamilton, “Torque Oscillations of Synchronous Motors under Starting Conditions,” *IEEE Transactions on Industry Applications*, vol. IA-23, May/June 1987, pp. 512–519.
6. Hoffmeyer, W.R., “Motor Power-Factor vs. Efficiency—a Tradeoff,” *MOTOR-CON 1982 Proceedings*, pp. 721–734.
7. NEMA MG 10–1994 (R 1999), Energy Management Guide for Selection and Use of Polyphase Motors.
8. IEC Publication 34–10, Rotating Electrical Machines.
9. IEC Publication 34–5, Degrees of Protection Provided by Enclosures.
10. IEEE Std. 112–1984, IEEE Standard Test Procedure for Polyphase Induction Motors and Generators.
11. IEEE Std. 114–1982, IEEE Standard Test Procedure for Single-Phase Induction Motors, (withdrawn)
12. IEEE Std. 117–1974 (Reaffirmed 1991), IEEE Standard Test Procedure for Evaluation of Systems of Insulating Materials for Random-Wound AC Electric Machinery.
13. NEMA MG 11–1977 (R 1987) (R 2001), Energy Management Guide for Selection and Use of Single-Phase Motors.
14. Hoffmeyer, W.R., “Efficiency of Single-Phase Motors as a Function of Type and Rating,” *Proceedings of the IEEE Industry Applications Society*, Sept. 1979, pp. 539–541.



15. Lipo, T.A., P.C.Krause, and H.E.Jordan, "Harmonic Torque and Speed Pulsations in a Rectifier-Inverter Induction Motor Drive," *IEEE Transactions on Power Apparatus and Systems*, vol. PAS-88, 1969, p. 579.
16. Murphy, J.M.D., and M.G.Egan, "A comparison of PWM Strategies for Inverter-Fed Induction Motors," *IEEE Transactions on Industry Applications*, vol. IA-19, 1983, p. 363.
17. Patel, H.S., and R.G.Hoft, "Generalized Techniques of Harmonic Elimination and Voltage Control in Thyristor Inverters: Part I—Harmonic Elimination," *IEEE Transactions on Industry Applications*, vol. IA-9, 1973, 310.
18. Nasar, S.A., and I.Boldea, *Linear Motion Electric Machines*, Wiley, New York, 1976.
19. Oberretl, K., "Dreidimensionale Berechnung des Linearmotors mit Berücksichtigung der Endeffekte unter Wicklungsverteilung (Three-Dimensional Analysis of Linear Motors with Consideration of End Effects and of Winding Distribution)," *Archiv für Elektrotechnik*, vol. 55, 1973, pp. 181–190.
20. Oberretl, K., "Einseitiger Linearmotor mit Käfig im Sekundärteil (Single-Sided Linear Motor with a Cage Secondary)," *Archiv für Elektrotechnik*, vol. 56, 1974, pp. 305–319.
21. Mosebach, E., et al., "Finite Length Effects in Linear Induction Machines with Different Iron Contours," *IEEE Transactions on Power Apparatus and Systems*, vol. PAS-96, No. 4, 1977, pp. 1087–1093.
22. Yamamura, S., *Theory of Linear Induction Motors*, Wiley, New York, 1979.
23. Skalski, C.S., "Computer Program for 3-Dimensional Analysis of Single-Sided Linear Induction Motors," WP 10569, The Mitre Corporation, McLean, VA, 1974.
24. Lipo, T.A., and T.A.Nondahl, "Transient Analysis of a Linear Induction Machine Using the D-Q Pole-by Pole Model," *IEEE Transactions on Power Apparatus and Systems*, vol. PAS-98, No. 4, 1979, pp. 1366–1374.
25. Nene, V.D., and L.del Cid, "The Three Axial Forces of an Offset SLIM," MTR 7812, The Mitre Corporation, McLean, VA, 1979.
26. Laithwaite, E.R., *Induction Machines for Special Purposes*, Chemical Publishing Company, New York, 1966.
27. Bevan, R.J.A., "Effect of Machine Length in the Performance of Linear Induction Motors," Garrett AiResearch Manufacturing Company, Report No. 76–13171, 1976.
28. Mosebach, H., et al., "Predicted and Measured Finite Width Effects in Linear Induction Motors," *IEEE Transactions on Power Apparatus and Systems*, vol. PAS-96, No. 4, 1977, pp. 1081–86, 1977.
29. Kliman, G.B., et al., "Performance of a Single-Sided Linear Induction Motor with Solid Back Iron and with Various Misalignments," vol. II. Appendix B, Report FRA/ORD-80/53, U.S. Department of Transportation, Washington DC, 1980.
30. Katz, R.M., "Integrated Suspension and Propulsion of Guided Ground Transportation Vehicles with a SLIM," MTR 79W00013, The Mitre Corporation, McLean, VA, 1979.
31. Nene, V.D., "Use of Linear Motors for Conventional Railroad Applications," MTR 79W00369, The Mitre Corporation, McLean, VA, 1979.
32. T.H.Ortmeyer and W.U.Borger, "Brushless Generation with Cascaded Doubly Fed Machines." Proc. Of the 1983 National Aerospace and Electronics Conference, May, 1983, Dayton, Ohio. pp. 1420–1425.
33. R.Q.Li, R.Spee, A.K.Wallace, G.C.Alexander. "Synchronous Drive Performance Of Brushless Doubly-Fed Motors," *IEEE Transactions On Industry Applications*, Vol. 30(4): 963–970 Jul-Aug 1994
34. M.Riaz. "Energy-Conversion Properties of Induction Machines in Variable-Speed Constant Frequency Generating Systems." *AIEE Transactions*, Vol. 78, pt. II, 1959. pp. 25–30.
35. S.Bhowmik, R.Spee, JRH Enslin. "Performance optimization for doubly fed wind power generation systems." *IEEE Transactions On Industry Applications*, Vol. 35(4): 949–958 Jul–Aug 1999
36. T.H.Ortmeyer and W.U.Borger. "Control of Cascaded Doubly Fed Machines for Generator Applications." *IEEE Transactions on Power Apparatus and Systems*, Vol PAS-103, No.9 (Sept. 1984), pp. 2564–2571.
37. B.Hopfensperger, D.J.Atkinson, R.A.Lakin. "Stator flux oriented control of a cascaded doubly-fed induction machine," *IEE Proceedings-Electric Power Applications*, vol. 146(6):597–605 Nov. 1999.
38. B.Hopfensperger, D.J.Atkinson and R.A.Lakin. "Combined magnetising flux oriented control of the cascaded doubly-fed induction machine," *IEE Proceedings-Electric Power Applications*, Vol. 148(4): 354–362 Jul 2001.
39. IEEE Std. 113–1985, *IEEE Guide on Test Procedures for DC Machines*.(withdrawn)
40. Fitzgerald, A.E., and Charles Kingsley, Jr., *Electric Machinery*, 2d edn., McGraw-Hill, New York, 1961.
41. Liwshitz-Garik, M., and Clyde Whipple, *Direct Current Machines*, D.Van Nostrand, New York, 1956.
42. Langsdorf, Alexander S., *Principles of DC Machines*, 6th edn., McGraw-Hill, New York, 1959.
43. Sarma, M.S., *Electric Machines*, W.C.Brown Company, Boston, 1985.
44. McPherson, George, *An Introduction to Electrical Machines and Transformers*, Wiley, New York, 1981.
45. Kusko, Alexander, *Solid State DC Motor Drives*, MIT Press, Cambridge, MA, 1969.
46. IEEE Std. 11–2000, *IEEE Standard for Rotating Electrical Machinery for Rail and Road Vehicles*.
47. Priebe, E.P., "Propulsion Motor Requirements for Mass Transportation," *IEEE Transactions on Industry Applications*, vol. IA-8, No. 3, 1971, p. 310.
48. IEC Std. 349 Electric Traction—Rotating electrical machines for rail and road vehicles  
Part 1 (1999–11) Machines other than electronic converter-fed alternating current motors  
Part 2 (1993–04) Electronic converter-fed alternating current motors  
Part 3 (1995–08) Determination of the total losses of converterfed alternating current motors by summation of the component losses
49. D.A.Lightband & D.A.Bicknell. *The Direct Current Traction Motor*. 1<sup>st</sup> ed. London and Southampton, Great Britain: Camelot Press Ltd., 1970
50. Unnewehr, L.E., and W.H.Koch, "An Axial Air-Gap Reluctance Motor for Variable Speed Applications," *IEEE Transactions on Power Apparatus and Systems*, vol. PAS-93, No. 1, Jan. 1974.
51. Lawrenson, P.J., et al., "Variable Speed Switched Reluctance Motors," *IEEE Proceedings*, vol. 127, No. 4, July 1980.
52. Miller, T.J.E., "Converter Volt-Ampere Requirements of the Switched Reluctance Motor Drive," *IEEE Transactions on Industry Applications*, vol. IA-21, No. 5, Sept. 1985.
53. Nasar, S.A., *Handbook of Electric Machines*, McGraw-Hill, New York, 1987.
54. Mubeen, M., "What You Need to Know about Step Motors," *Machine Design*, Feb. 7, 1991, pp. 46–54.
55. Kuo, B.C., *Theory and Application of Step Motors*, West Publishing Company, St. Paul, MN, 1974.
56. Forghani, B., "3D Solution of a Hybrid Stepper Motor Using Finite Elements," *Proceedings of the 16th International MOTOR-CON Conference*, Oct. 1989.
57. Dawson, G.E., et al., "Switched-Reluctance Motor Torque Characteristics: Finite Element Analysis and Test Results," *IEEE Transactions on Industry Applications*, vol. IA-23, No. 3, May 1987.
58. Singh, C., and C.Folkerts, "Computer-Aided Magnetic Circuit Analysis for Performance Prediction of Step Motors," *Proceedings of the Third Annual Symposium on Incremental Motion Control Systems and Devices*, May 1974.
59. Compumotor Handbook on "Programmable Motion Control," Parker Hannifin Corp., Compumotor Division, Rohnert Park, CA, 1990.

60. Nasar, S.A., and L.E.Unnewehr, *Electromechanics and Electric Machines*, 2d edn., Wiley, New York, 1983.
61. Yoshida, K., and R.Baker, "New Manufacturing Methods Improve Permanent Magnet Stepper Motor Performance and Efficiency," *Proceedings of the 16th International MOTOR-CON Conference*, Oct. 1989, pp. 417–431.
62. Chikado, K., "A Sensorless VSR Drive for Industrial Variable-Speed Applications", *Proceedings of the American Control Conference*, June, 1998
63. Versteyhe, M. et al. "A Rigid and Accurate Piezo-Stepper Based on Smooth Learning Hybrid Force-Position Controlled Clamping" *Proceedings of the 1998 International Conference on Robotics and Automation*, May 1998
64. NEMA ICS 15–2000, Motion/Position Control Motors and Controls.
65. Taft, C.K., and S.R.Prina, "Stepping Motor Drive Chip Selection Considerations," *Proceedings of the 13th International MOTOR-CON Conference*, Oct. 1988.
66. Pellegrino, J., "Thermal Analysis for Stepping Motors," *Proceedings of the 9th International MOTOR-CON Conference*, 1986, pp. 75–88.
67. Leenhouts, A.C., "The Effect of Inductance on Step Motor Performance," *Proceedings of the 9th International MOTOR-CON Conference*, 1986, pp. 8994.
68. Schenfer, K.I., "The Rotor of an Asynchronous Motor in the Form of a Solid Iron Cylinder" (in Russian), *Elektrichestvo*, vol. 2, 1926, pp. 86–90.
69. Bruk, J.S., "The Theory of Asynchronous Motors with Solid Rotors" (in Russian), *Review of Applied and Theoretical Electrical Engineering*, vol. 2, 1928.
70. Odorico, A., M.Secco, and M.Sica, "Three-Phase Induction Motors for Adjustable Speed Drives," *Proceedings of EDS '90*, Capri, Italy, 1990, pp. A21–A24.
71. Masahiro, I., M.Hirokyuki, and E.Hideaki, "Variable Speed Motor Drive Systems with High Maximum Speeds," *Proceedings of EDS '90*, Capri, Italy 1990, pp. 295–300.
72. Jinning, L., and F.Fengli, "Calculation of Magnetic Fields and Rotor Parameters for Induction Motors with Slitted Solid Rotor," *Proceedings of Electric Energy Conference*, Adelaide, Australia, 1987, pp. 306–310.
73. Beckert, U., "Beitrag zur Theorie des Zweiphasenstellmotors mit massivem Stahllauffer (Contribution on the Theory of Two-phase Servo Motors with Solid Steel Rotor)," *Wissenschaftliche Zeitschrift der Electrotechnik*, vol. 9, 1969, p. 185.
74. McConnel, H.M., "The Polyphase Induction Machine with Solid Rotor," *IEEE Transactions on Power Apparatus and Systems*, vol. PAS-72, 1953, pp. 103–111.
75. McConnel, H.M., and E.F.Sverdrup, "The Induction Machine with Solid Rotor," *IEEE Transactions on Power Apparatus and Systems*, vol. PAS-74, 1955, pp. 343–349.
76. Wood, A.J., and C.Concordia, "An Analysis of Solid Rotor Machines: Part III, Finite Length Effects; Part IV, An Approximate Nonlinear Analysis," *IEEE Transactions on Power Apparatus and Systems*, vol. PAS-79, 1960, pp. 21–31.
77. Angst, G., "Polyphase Induction Motor with Solid Rotor; Effects of Saturation and Finite Length," *IEEE Transactions on Power Apparatus and Systems*, vol. PAS-81, 1962, pp. 902–909.
78. Yee, H., and T.Wilson, "Saturation and Finite Length Effects in Solid Rotor Induction Machines," *Proceedings of the IEE*, vol. 119, 1972, pp. 877–882.
79. Pillai, K.P.P., "Fundamental-Frequency Eddy Current Loss due to Rotating Magnetic Field: Part 1, Eddy Current Loss in Solid Rotors; Part 2, Eddy Current Loss in Hollow Rotors," *Proceedings of the IEE*, vol. 116, 1969, pp. 407–414.
80. Lasocinski, J., "Electromagnetic Field in the Airgap of a Machine with Solid Ferromagnetic Rotor Taking into Account the Finite Length (in Polish)," *Rozprawy Elektrotechniczne*, Polish Academy of Sciences, vol. 12, 1966, pp. 69–92.
81. Maergoyz, I.D., and B.I.Polishchuk, "Calculation of Magnetic Field and Equivalent Circuit Parameters of an Asynchronous Machine with Solid Ferromagnetic Rotor (in Russian)," *Elektrichestvo*, vol. 6, 1972, pp. 9–15.
82. Voldek, A.I., "Theory of Asynchronous Machine with Solid Ferromagnetic Rotor (in Russian)," *Elektrichestvo*, vol. 1, 1974, pp. 77–78.
83. Neyman, L.R., *Skin Effect in Ferromagnetic Bodies* (in Russian), GEL, Leningrad-Moscow, 1949.
84. Gieras, J.F., "Analytical Method of Calculating the Electromagnetic Field and Power Losses in Ferromagnetic Halfspace Taking into Account Saturation and Hysteresis," *Proceedings of the IEE*, vol. 124, 1977, pp. 1098–1104.
85. Gieras, J.F., "Analysis of Multilayer Rotor Induction Motor with Higher Space Harmonics Taken into Account," *IEE Proc., Part B*, vol. 138, No.2, 1991, pp. 59–67.
86. Blondel: "Synchronous motors and converters", 1913, pp. 141–145.
87. P.Boucherot: "Moteur a courant alternatif simple synchrone sans excitation continue", *L'Industrie Electrique*, Vol. 10, pp. 541–542.
88. J.K.Kostko: "Polyphase reaction synchronous motors", *Journal of AIEE*, 1923, pp. 1162–1168.
89. J.F.H.Douglas: "The theory of anisotropic field structures in synchronous machines", *Trans. American Institute Electric Engineers*, 1956, Vol. 75, PT. III, pp. 84–86.
90. V.B.Honsinger: "The inductance  $L_d$  and  $L_q$  of reluctance machines", *IEEE Transaction on Power Apparatus and Systems*, Vol. PAS-90, Jan-Feb. 1971, pp. 298–304.
91. P.J.Lawrenson and S.K.Gupta: "Developments in the performance and theory of segmental-rotor reluctance motors", *IEE Proceedings*, Vol. 114, May 1967, pp. 645–653.
92. A.J.O.Cruickshank, A.F.Anderson and R.W.Menzies: "Theory and performance of reluctance motors with axially laminated anisotropic rotors", *IEE Proceedings*, Vol. 118, No. 7, July 1971, pp. 887–893.
93. A.Fratta and A.Vagati: "A reluctance motor drive for high dynamic performances applications", *IEEE Trans. On Industry Applications*, July-Aug. 1992, Vol. 28, n. 4, pp. 873–879.
94. T.J.E.Miller, C.Cossar, A.J.Hutton and D.A.Staton: "Design of a synchronous reluctance motor drive", *IEEE Transactions on Industry Applications*, Volume: 27 Issue: 4, July-Aug. 1991, pp. 741–749.
95. L.Xu, X.Xu, T.A.Lipo and D.W.Novotny: "Control of a synchronous reluctance motor including saturation and iron loss", *IEEE Trans. on Industry Applications*, Vol. IA-27, No. 5, 1991, pp. 977–985.
96. Fratta A., Vagati A., Villata F.: "On the evolution of a.c. machines for spindle drive applications", *IEEE Trans. On Industry Applications*, Sept.-Oct. 1992, vol. 28, n. 5, pp. 1081–1086.
97. B.J.Chalmers, L.Lawrence Musaba: "Design and field-weakening performance of a synchronous reluctance motor with axially-laminated rotor", *IEEE-IAS 1997 Annual Meeting*, Vol. 1, 1997, pp. 271–278.
98. Vagati A., Pastorelli M., Franceschini G., Petrache C.: "Design of low-torque-ripple synchronous reluctance motors", *IEEE Trans. On Industry Applications*, July–Aug. 1998, vol. 34, n. 4, pp. 758–765.
99. M.J.Kamper, F.S.van der Merwe, S.Williamson: "Direct Finite Element design optimization of the cageless reluctance synchronous machine", *IEEE Transaction on Energy Conversion*, vol. 11, n. 3, Sept. 1996, pp. 547–553.
100. Vagati A., Pastorelli M., Scapino F., Franceschini G.: "Impact of cross saturation in synchronous reluctance motors of the transverse-laminated type", *IEEE Trans. On Industry Applications*, Vol. 36, n. 4, July/Aug. 2000, pp. 1039–1046.
101. Vagati A., Pastorelli M., Franceschini G., Drogoreanu V.: "Flux-observer-based high-performance control of synchronous reluctance motors by including cross saturation", *IEEE Trans.*

- On Industry Applications, May-June 1999, Vol. 35, n. 3, pp. 597–605.
102. Bilewski M., Giordano L. Fratta A., Vagati A., Villata F.: “Control of high performance interior permanent magnet synchronous drives”, IEEE Trans. On Industry Applications, Vol. 29, n. 2, March-April 1993, pp. 328–337.
  103. Vagati A., Pastorelli M., Guglielmi P., Capecchi E.: “Position Sensorless control of the transverse-laminated synchronous reluctance motor”, IEEE-Transactions on Industry Applications, November-December 2001, Vol. 37, No. 6, pp. 1768–1776.
  104. W.L.Soong, T.J.E.Miller: “Field-weakening performance of brushless synchronous AC motor drives”, IEE Proceedings—Electric Power Applications, Volume 141 6, November 1994, pp. 331–340.
  105. S.Kalsi, “A Small-size Superconducting Generator Concept”, International Electric Machines and Drives Conference, IEMDC’01, Massachusetts Institute of Technology, Cambridge, MA 02139, 17–20 June 2001.
  106. S.Kalsi, et al, “Status of the Navy HTS SuperDrive motor for ship propulsion development”, Third Naval Symposium on Electric Machines, Philadelphia, PA on December 4–7, 2000
  107. S.L.Chang, J.H.Karr. A-C Series Motors—A Design Method. AIEE Transactions, Volume 69, 1950, pp. 1257–1263.
  108. P.H.Trickey. Electric Motors and Generators Design Philosophy and Procedures. Printed by Duke University, 1974. Vols V to XIV
  109. R.H.Dijken. Optimization of Small AC Series Commutator Motors. Thesis: Stellingen, 19 Oct 1971.
  110. R.Goldschmidt. The Alternating Current Commutator Motor. London: The Electrician Printing and Publishing Co., 1909.
  111. Kostko J.K., “Polyphase reaction synchronous motors”, J. Amer. Inst. Elect. Engrs., 1923, 42, pp. 1162–1168.
  112. Merrill, F.W., “Permanent-magnet excited synchronous motors”, Trans. A.I.E.E., 1955, 74, Part II, pp. 1754–1760 (GE *Permasyn* motor)
  113. Merrill F.W., “Dynamoelectric machine magnetic core member”, U.S. Patent 2,735,952, January 4, 1954 (GE *Permasyn* motor).
  114. Cahill D.P.M. and Adkins B., “The permanent-magnet synchronous motor”, Proc. IEE, 109A, 1962, pp. 483–491
  115. Lawrenson P.J. and Gupta S.K., “Developments in the performance and theory of segmental-rotor reluctance motors”, Proc. IEE, 1967, 114(5), pp. 645–653
  116. Honsinger V.B., “Synchronous reluctance motor”, U.S. Patent 3,652,885, September 16, 1970 (*Synduction* motor)
  117. Cruickshank A.J.O., Anderson A.F. and Menzies, R.W., “Theory and performance of reluctance motors with axially laminated anisotropic rotors”, Proc. IEE, 118(7), July 1971, pp. 887–893
  118. Cruickshank A.J.O., Anderson A.F. and Menzies, R.W., “Axially laminated anisotropic rotors for reluctance motors”, Proc. IEE, 113(12), 1966, pp. 2058–2060
  119. Badr M.A., Hamouda R.M., and Alolah A.I., “Synchronization problem of high performance reluctance motors”, Proc. IEE, Electr. Power Appl., 144, (6), November 1997, pp. 455–460.
  120. Hofst R.G., “Liapunov stability analysis of reluctance motors”, IEEE Trans., PAS-87, No. 6, p. 1485.
  121. Finch, J.W. and Lawrenson, P.J., “Synchronous performance of single-phase reluctance motors”, Proc. IEE, 125, (12), 1978, pp. 1350–1356.
  122. Finch, J.W. and Lawrenson, P.J., “Asynchronous performance of single-phase reluctance motors”, Proc. IEE, 126, (12), December 1979, pp.1249–1254.
  123. Volkrodt V.W., “Polradspannung, Reaktanzen und Ortskurve des Stromes der mit Dauermagneten erregten Synchronmaschine”, Elektrotechnische Zeitschrift, July 1962, pp. 517–522.
  124. Leronze J., “Eine neue Generation von bürstenlosen Synchronmotoren”, Aktuelle Technik, 2/1978, pp. 9–12.
  125. Binns K.J., Jabbar M.A. and Barnard W.R., “Hybrid permanent-magnet synchronous motors”, Proc. IEE, 125, (3), 1978, pp. 203–208.
  126. Miyashita K. et al, “Development of a high-speed 2-pole permanent-magnet synchronous motor”, Paper F79 163–7, presented at the IEEE Power Engineering Society Winter Meeting, New York, N.Y., February 4–9, 1979.
  127. Kazdagli A., Razeq A., and Faure E., “Utilisation des aimants permanents dans les machines synchrones a vitesse variable et élevée”, R.G.E. 5/83, May 1983, pp. 337–342.
  128. Binns K.J. and Jabbar M.A., “High-field self-starting permanent-magnet synchronous motor”, Proc. IEE, 128, Pt. B, No. 3, May 1981, pp. 157–160.
  129. Miller TJE, Richter E and Neumann TW, “A permanent-magnet excited high-efficiency synchronous motor with line-start capability”, IEEE Industry Applications Society Annual Meeting (IAS), Mexico City, October 1983.
  130. Richter E., Miller TJE, Neumann T.W., and Hudson T.L., “The ferrite permanent-magnet AC motor—a technical and economical assessment”, IEEE Trans., IA-21, No. 4, May–June 1985, pp. 644–650.
  131. Miller TJE, “Synchronization of line-start permanent-magnet AC motors”, IEEE Trans., PAS-103, 1984, pp. 1822–1828.
  132. Stephens C.M., Kliman G.B. and Boyd J., “A line-start permanent magnet motor with gentle starting behavior”, Conf. Rec. IEEE IAS Annual Meeting, St. Louis, 1998 pp. 371–379.
  133. IEEE Std. 100–1996. The New IEEE Standard Dictionary of Electrical and Electronics Terms.
  134. Engelmann, Richard H., *Static and Rotating Electromagnetic Devices*, Marcel Dekker, New York, 1982.

# 3

## Motor Selection

**Robert G.Bartheld** (Section 3.1)/**Richard E.Dippery, Jr.** (Sections 3.2 and 3.3)/**Kao Chen and Richard Nailen** (Section 3.4)/**J.Herbert Johnson** (Sections 3.5 and 3.8.1)/**David M.Mullen and James H.Dymond** (Section 3.6)/**Walter J.Martiny** (Section 3.7)/**Howard B.Hamilton and Copal K.Dubey** (Section 3.8.2)

<b>3.1 STANDARDS</b>	<b>168</b>
3.1.1 Enclosures	168
3.1.2 Dimensions	175
3.1.3 Performance	176
<b>3.2 CHARACTERISTICS OF DRIVEN EQUIPMENT</b>	<b>181</b>
3.2.1 Inertia Torques	182
3.2.2 Viscous Friction Torque	182
3.2.3 Sticking Friction	182
3.2.4 Coulomb Friction	183
3.2.5 Fluid Loads	183
3.2.6 Unusual Load Situations	183
<b>3.3 INITIAL MOTOR SELECTION</b>	<b>184</b>
3.3.1 Steady-State Solutions	184
3.3.2 Dynamic Analysis	184
<b>3.4 MOTOR EFFICIENCY AND ENERGY CONSIDERATIONS</b>	<b>185</b>
3.4.1 Efficiency Considerations	185
3.4.2 Energy Considerations	188
<b>3.5 PAYBACK ANALYSIS AND LIFE-CYCLE COSTING OF MOTORS AND CONTROLS</b>	<b>188</b>
3.5.1 General-Purpose vs. Special Machines	189
<b>3.6 SAFETY CONSIDERATIONS</b>	<b>190</b>
3.6.1 Application Information	190
3.6.2 Installation	190
<b>3.7 HOW TO SPECIFY A MOTOR</b>	<b>190</b>
3.7.1 Scope	191
3.7.2 Codes and Standards	191
3.7.3 Service Conditions	191
3.7.4 Starting Requirements	191
3.7.5 Rating	192
3.7.6 Construction Features	193
3.7.7 Accessories	197
3.7.8 Balance and Vibration	198
3.7.9 Sound Levels	198
3.7.10 Paint	198
3.7.11 Nameplates	198
3.7.12 Performance Tests	199

3.7.13	Quality Assurance	199
3.7.14	Preparation for Shipment and Storage	199
3.7.15	Data and Drawings	200
3.8	<b>SPECIAL APPLICATIONS</b>	<b>200</b>
3.8.1	Hermetically Sealed Refrigeration Motors	200
3.8.2	Selection of DC Motors with Chopper Drives for Battery Powered Vehicles	209
	<b>REFERENCES</b>	<b>214</b>

### 3.1 STANDARDS

Standards provide the basis for communication between manufacturers and users. The result is a more definitive purchase specification with less opportunity for misinterpretation and the assurance that competitive products meet similar performance criteria. Good standards also provide manufacturers with the opportunity to predesign their products for maximum modular efficiency in construction and performance, resulting in shorter delivery times and lower manufacturing costs.

National Electrical Manufacturers Association (NEMA) standards for motors are predominant in North America, while the rest of the world follows International Electrotechnical Commission (IEC) publications. Harmonization of these two sets of standards is in progress wherever possible, but the ratification process is slow and some areas such as voltage and frequency will never be the same.

This section explores several of the more significant areas of motor standardization, presenting information from both the U.S. and the international perspectives. The emergence of a more uniform Europe through EC '92 has pressured the international community to eliminate trade barriers, and as a result manufacturers have reaffirmed and in some instances revised the IEC 60034 series of publications for motors. The United States, as a good international citizen, has subsequently reexamined its own standards in an effort to achieve global harmonization. Because this is a dynamic process, some of the following information reflects future standards based upon the consensus of current standards developers.

It is always good practice to check the latest revision of any standard because good standards are frequently updated.

This section has three parts:

1. *Enclosures* define the protective interface between the motor and its environment and its general configuration.
2. *Dimensions* provide the specific dimensional interface between the motor, its load, and supporting structure.
3. *Performance* covers those motor parameters affecting the application requirements and their influence on the environment.

#### 3.1.1 Enclosures

Electric machines are provided in a number of enclosures in order to satisfy the needs for a variety of environmental conditions. While the end results are generally similar, U.S.

and international standards have very different systems for defining the various configurations. In the following sections, information is presented so that each system can be used independently, and cross references are provided to relate one to the other. It is not the purpose of this part to provide an exact relationship, but rather a functionally similar relationship. For the precise differences one must refer to the individual standards listed as references.

Enclosures require three basic descriptions to completely define the machine.

*Protection*, which covers the entrance of solid objects and water, as well as personnel safety;

*Cooling*, describing the various cooling arrangements and cooling mediums; and

*Mounting*, describing how the machine will interface with its load machine and method of mounting.

Each of these is described below using both U.S. and international nomenclature as references.

##### 3.1.1.1 Protection

Electric machines are provided in a number of enclosures having various degrees of protection to meet the needs of a variety of environments. Historically, U.S. standards have relied upon generic definitions: international standards utilize a more systematic approach with a two-digit designation indicating degrees of protection. NEMA has revised MG-1 to include the IEC system.

Definitions for the IEC degrees of protection provided by enclosures [1] are:

1. Protection of persons against contact with electrically live parts and against contact with most moving parts inside the enclosure; and protection of the machine against solid foreign objects.
2. Protection of the machine from damage due to the entrance of water.

These two definitions provide the basis for the two-digit designation system in that each of the degrees of protection is covered by one of the digits. The designation used consists of the letters *IP* followed by two characteristic numerals signifying, conformity with the conditions in Fig. 3.1, respectively. Additional information may be indicated by a supplementary letter following the second characteristic numeral. The most significant such letter for the United States is *W*, which indicates suitability as weather protection of an

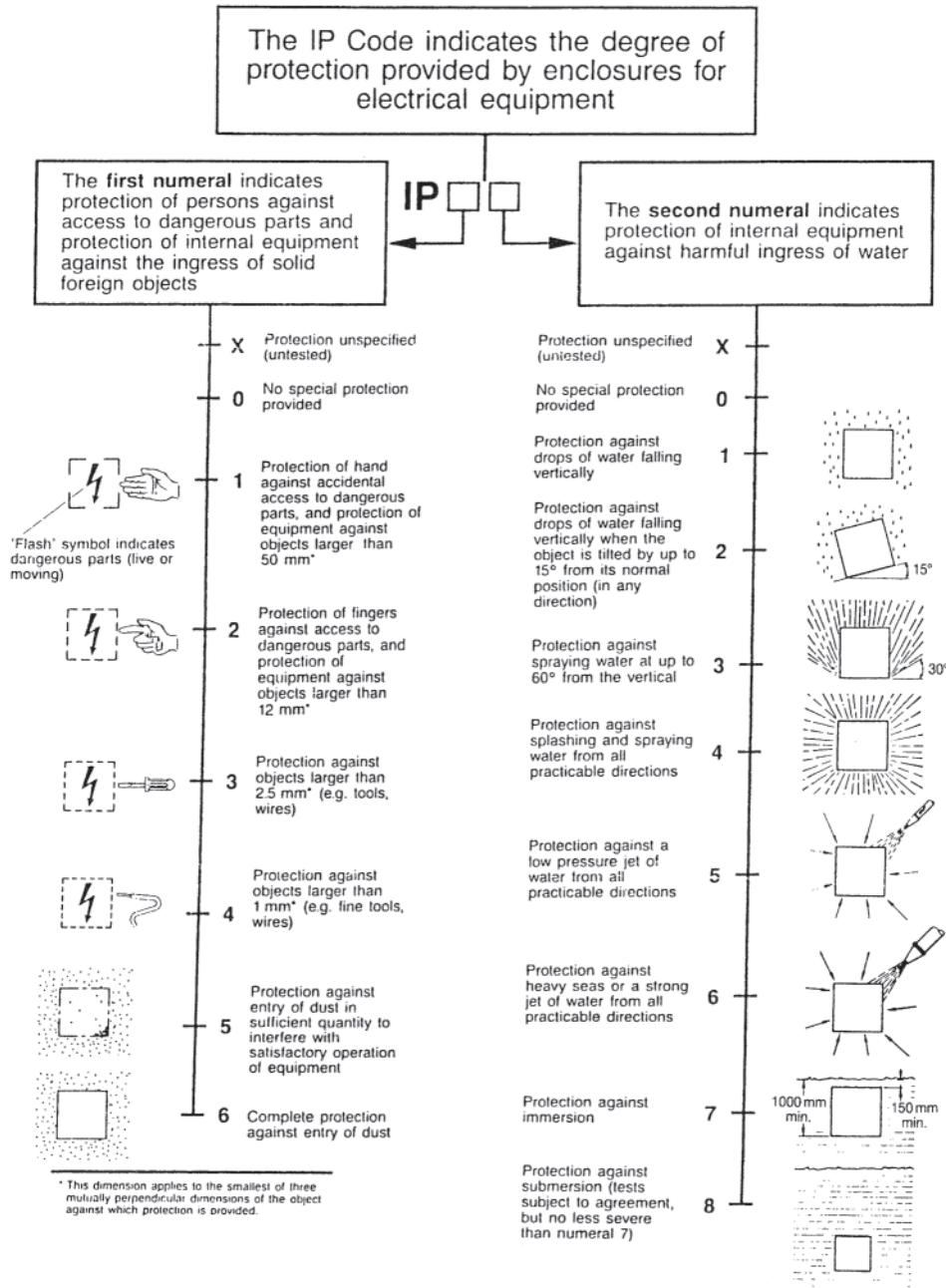


**Figure 3.1** IP Code development to indicate degree of protection provided by enclosures. (Derived from Ref. 1, courtesy Standards Australia.)

open internally air-cooled machine. For example, Table 3.1 shows for the weather-protected machine Type II (WP II) the IP designation IP24W. For each degree of protection for each of the characteristic numerals, a test must be performed to check that the machine has been designed to meet the requirements. This IEC designation does not specify types of protection for machines used in explosive atmospheres.

To provide a ready comparison, Table 3.1 lists the customary definitions and the comparable IP codes. It also lists the IC code, described in Section 3.1.1.2.

Two other generally used protection definitions are recognized in the United States [2]:

- *Explosion-proof machine.* An explosion-proof machine is a totally enclosed machine whose enclosure is designed and constructed to withstand an explosion of a specified gas or vapor that may occur within it and to prevent the ignition of the specified gas or vapor surrounding the machine by sparks, flashes or explosions of the specified gas or vapor that may occur within the machine casing.
- *Dust-ignition-proof machine.* A dust-ignition-proof machine is a totally enclosed machine whose enclosure is designed and constructed in a manner that will exclude ignitable amounts of dust or amounts that

**Table 3.1** Customary U.S. Motor Protection Definitions and the Corresponding IEC IP [1] and IC [4] Codes

Definition	IP code	IC code
<p><b>Open machine</b> An open machine is one having ventilating openings that permit passage of external cooling air over and around the windings of the machine. The term "open machine" when applied to large apparatus without qualification, designates a machine having no restriction to ventilation other than that necessitated by mechanical construction.</p>	IP00	IC01
<p><i>Drip-proof machine</i> A drip-proof machine is an open machine in which the ventilating openings are so constructed that successful operation is not interfered with when drops of liquid or solid particles strike or enter the enclosure at any angle from 0 to 15 degrees downward from the vertical.</p>	IP12	IC01
<p><i>Splash-proof machine</i> A splash-proof machine is an open machine in which the ventilating openings are so constructed that successful operation is not interfered with when drops of liquid or solid particles strike or enter the enclosure at any angle not greater than 100 degrees downward from the vertical.</p>	IP03	IC01
<p><i>Guarded machine</i> A guarded machine is an open machine in which all openings giving direct access to live metal or rotating parts (except smooth rotating surfaces) are limited in size by the structural parts or by screens, baffles, grilles, expanded metal, or other means to prevent accidental contact with hazardous parts. Openings giving direct access to such live or rotating parts shall not permit the passage of a cylindrical rod 0.75 inch in diameter.</p> <p>The openings in the machine enclosure shall be such that (1) a probe such as that illustrated in Figure A when inserted through the openings, will not touch an uninsulated live metal part or a hazardous rotating part and (2) a probe such as that illustrated in Figure B when inserted through the openings, will not touch film-coated wire. Dimensions in these figures are in inches.</p>	IP2X	IC01
<p><i>Drip-proof guarded machine</i> A Drip-proof guarded machine is a drip-proof machine whose ventilating openings are guarded.</p>	IP22	IC01
<p><i>Open externally ventilated machine</i> An open externally ventilated machine is one which is ventilated by means of a separate motor-driven blower mounted on the machine enclosure. This machine is sometimes known as a blower-ventilated or a forced-ventilated machine.</p>	—	IC06
<p><i>Open pipe-ventilated machines</i> An open pipe-ventilated machine is an open machine except that openings for the admission of the ventilating air are so arranged that inlet ducts or pipes can be connected to them. Open pipe-ventilated machines shall be self-ventilated (air circulated by means integral with the machine) IC11 or forced-ventilated (air circulated by means external to and not a part of the machine) IC17.</p>	—	IC11 or IC17

Table 3.1 Continued

Definition	IP code	IC code
<i>Weather-protected machine</i>	IP24	IC01
<i>Type I:</i> A weather-protected Type I machine is an open machine with its ventilating passages so constructed as to minimize the entrance of rain, snow and airborne particles to the electric parts and having its ventilated openings so constructed as to prevent the passage of a cylindrical rod 0.75 inch in diameter.		
<i>Type II:</i> A weather-protected Type II machine shall have, in addition to the enclosure defined for a weather-protected Type I machine, its ventilating passages at both intake and discharge so arranged that high-velocity air and airborne particles blown into the machine by storms or high winds can be discharged without entering the internal ventilating passages leading directly to the electric parts of the machine itself. The normal path of the ventilating air which enters the electric parts of the machine shall be so arranged by baffling or separate housings as to provide at least three abrupt changes in direction, none of which shall be less than 90 degrees. In addition, an area of low velocity not exceeding 600 feet per minute shall be provided in the intake air path to minimize the possibility of moisture or dirt being carried into the electric parts of the machine.	IP24W	IC01
<b>Totally-enclosed machine</b>		
A totally-enclosed machine is one so enclosed as to prevent the free exchange of air between the inside and the outside of the case but not sufficiently enclosed to be termed air-tight.		
<i>Totally-enclosed nonventilated machine</i>	IP54	IC410
A totally-enclosed nonventilated machine is a totally enclosed machine which is not equipped for cooling by means external to the enclosing parts.		
<i>Totally enclosed fan-cooled machine</i>	IP54	IC411
A totally-enclosed fan-cooled machine is a totally enclosed machine equipped for exterior cooling by means of a fan or fans integral with the machine but external to the enclosing parts.		
<i>Totally enclosed pipe-ventilated machine</i>	IP44	IC31 or IC37
A totally enclosed pipe-ventilated machine is a machine with openings so arranged that when inlet and outlet ducts or pipes are connected to them there is no free exchange of the internal air and the air outside the case. Totally enclosed pipe-ventilated machines may be self-ventilated (air circulated by means integral with the machine) IC31 or forced-ventilated (air circulated by means external to and not a part of the machine) IC37.		
<i>Totally enclosed water-cooled machine</i>	IP54	IC70W
A totally enclosed water-cooled machine is a totally enclosed machine which is cooled by circulating water, the water or water conductors coming in direct contact with the machine parts.		
<i>Totally enclosed air-to-water cooled machine</i>	IP54	IC codes as indicated in the definition
A totally enclosed air-to-water cooled machine is a totally enclosed machine which is cooled by circulating air which, in turn, is cooled by circulating water. It is provided with a water-cooled heat exchanger integral (IC7_W) or machine (IC8_W) mounted for cooling the internal air and a fan or fans, integral with the rotor shaft (IC1_W) or separate (IC5_W) for circulating the internal air.		
<i>Totally enclosed air-to-air cooled machine</i>	IP54	IC codes as indicated in the definition
A totally enclosed air-to-air cooled machine is a totally enclosed machine which is cooled by circulating the internal air through a heat exchanger which, in turn, is cooled by circulating external air. It is provided with an air-to-air heat exchanger, integral (IC5_) or machine mounted (IC6_) for cooling the internal air and a fan or fans, integral with the rotor shaft (IC1_) or separate (IC5_) for circulating the internal air and a fan or fans integral with the rotor shaft (IC1_), or separate (IC6_) but external to the enclosing part or parts for circulating the external air.		
<i>Totally enclosed air-over machine</i>	IP54	IC417
A totally enclosed air-over machine is a totally enclosed machine intended for exterior cooling by a ventilating means external to the machine.		

Source: Adapted from Ref. 2.



might affect performance or rating, and that will not permit arcs, sparks, or heat otherwise generated or liberated inside of the enclosure to cause ignition of exterior accumulations or atmospheric suspensions of a specific dust on or in the vicinity of the enclosure.

Successful operation of this type of machine requires avoidance of overheating from such causes as excessive overloads, stalling, or accumulation of excessive quantities of dust on the machine.

These definitions apply to Division 1 hazardous locations, using the classifications of Chapter 5 of the National Electric Code [3]. Exact definitions appear in the National Electric Code (NEC), which, paraphrased, suggests that motors may experience these explosive gases or dusts during normal operation, and normal operation of the motor will not produce an unsafe condition.

In addition, there are Division 2 locations in which it may be possible to use more standard enclosures. This possibility is very much application-specific and one must be cautioned that any motor suitable for one application may not be suitable if the application changes. Division 2 relies on the probability that an abnormal event involving the hazardous material will not occur at the same time as abnormal motor operation.

### 3.1.1.2 Methods of Cooling

International Standard IEC 60034-6 [4] provides for the designation of cooling arrangements and methods of moving

the coolant in rotating machines. NEMA MG -1, Part 6 is the technically equivalent U.S. standard.

Although there has been an *IC* code designation system for many years, it was redefined in 1991. This new designation system for the method of cooling is constructed as shown in Fig. 3.2, using the example of a water-cooled machine.

The most common configurations use the simplified designation and are included in Table 3.1 to provide a useful cross reference between U.S. and international practice. Additional arrangements, including the complete designation, can be constructed from Tables 3.2, 3.3, and 3.4.

### 3.1.1.3 Mounting

The interface between a motor and its supporting structure is not complicated, but there are significant differences in approach between U.S. and IEC standards.

Basically, there are two types of mounting: foot mounting and flange mounting. Some machines require both foot and flange mounting. Foot-mounted machines are designed for horizontal mounting with the feet on the floor. Because most machines have provision for water drainage, this then defines the location of any drain. Foot-mounted machines are also able to be wall- or ceiling-mounted, and when wall-mounted can have the shaft either up or down. All of these variations have different assembly considerations depending upon degree of protection, drainage, and bearing configuration. This information is communicated in different ways in the United States and by IEC, as will be seen in Refs. 2 and 6.

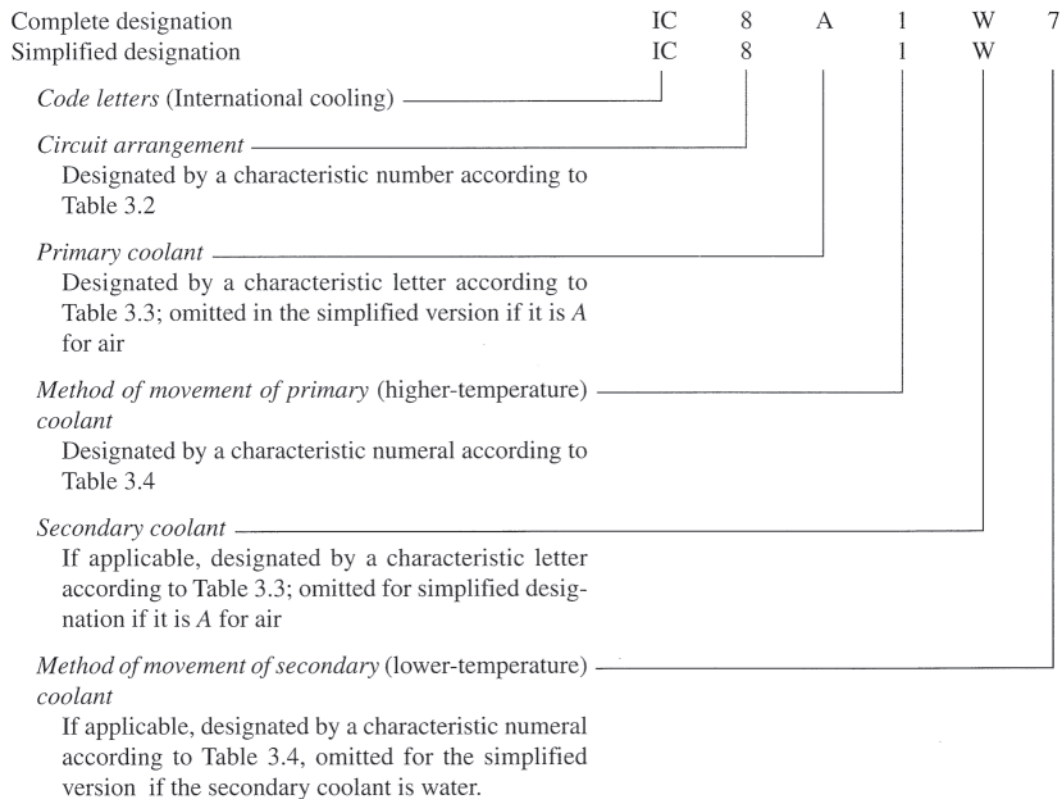


Figure 3.2 IC code designation system for cooling method.

**Table 3.2** Coolant Circuit Arrangemen

Characteristic numeral	Brief description	Definition
0	Free circulation	The coolant is freely drawn directly from the surrounding medium, cools the machine, and then freely returns directly to the surrounding medium (open circuit)
1	Inlet pipe or inlet duct circulated	The coolant is drawn from a medium remote from the machine, is guided to the machine through an inlet pipe or duct, passes through the machine and returns directly to the surrounding medium (open circuit)
2	Outlet pipe or outlet duct circulated	The coolant is drawn directly from the surrounding medium, passes through the machine and is then discharged from the machine through an outlet pipe or duct to a medium remote from the machine (open circuit)
3	Inlet and outlet pipe or duct circulated	The coolant is drawn from a medium remote from the machine, is guided to the machine through an inlet pipe or duct, passes through the machine and is then discharged from the machine through an outlet pipe or duct to a medium remote from the machine (open circuit)
4	Frame surface cooled	The primary coolant is circulated in a closed circuit in the machine and gives its heat through the external surface of the machine (in addition to the heat transfer via the stator core and other heat conducting parts) to the final coolant, which is the surrounding medium. The surface may be plain or ribbed, with or without an outer shell to improve the heat transfer.
5	Integral heat exchanger (using surrounding medium)	The primary coolant is circulated in a closed circuit and gives its heat via a heat exchanger, which is built into and forms an integral part of the machine, to the final coolant, which is the surrounding medium
6	Machine-mounted heat exchanger (using surrounding medium)	The primary coolant is circulated in a closed circuit and gives its heat via a heat exchanger, which is mounted directly on the machine, to the final coolant, which is the surrounding medium
7	Integral heat exchanger (using remote medium)	The primary coolant is circulated in a closed circuit and gives its heat via a heat exchanger, which is built into and forms an integral part of the machine, to the secondary coolant, which is the remote medium
8	Machine-mounted heat exchanger (using remote medium)	The primary coolant is circulated in a closed circuit and gives its heat via a heat exchanger, which is mounted directly on the machine, to the secondary coolant, which is the remote medium
9	Separate heat exchanger (using surrounding or remote medium)	The primary coolant is circulated in a closed circuit and gives its heat via a heat exchanger, which is separate from the machine, to the secondary coolant, which is either the surrounding or the remote medium

Source: From Ref. 4.

The IEC has two code systems: a simple code (Code I), and a complete code, (Code II). There is no correlation between them. U.S. and IEC foot-mounting configurations are compared in Fig. 3.3.

Flange-mounted machines are complicated by the variety

**Table 3.3** Characteristic Letters Used to Designate the Coolant Being Used

Characteristic letter	Coolant
A	Air
F	Freon
H	Hydrogen
N	Nitrogen
C	Carbon dioxide
W	Water
U	Oil
S	Any other coolant
Y	Coolant not yet selected

Source: From Ref. 4.

available in the United States, where there are three basic configurations:

*C-flange*: Sometimes called C-face mounting, it has a male rabbet fit and tapped holes. It is generally intended for horizontal motors supporting the load equipment, frequently a pump or brake. The two variations are shown in Fig. 3.4.

*D-flange*: Has a male rabbet fit and clearance holes external to the fit, as shown in Fig. 3.5. It is generally intended for horizontal motors attached to the load machine.

*P-flange*: Has a female rabbet fit and clearance holes external to the fit, as shown in Fig. 3.6. It is generally intended for vertical motors mounted on pumps.

The IEC, on the other hand, recognizes only one series of spigots (rabbet fits) with the possibility of either clearance or tapped holes. It is used for all applications. In all cases the mounting surface contains the mounting bolt circle.

**Table 3.4** Characteristic Numerals Used to Define the Method of Coolant Movement

Characteristic numeral	Brief description	Definition
0	Free convection	The coolant is moved by temperature differences. The fanning action of the rotor is negligible
1	Self-circulation	The coolant is moved dependent on the rotational speed of the main machine, either by the action of the rotor alone or by means of a component designed for this purpose and mounted directly on the rotor of the main machine, or by a fan or pump unit mechanically driven by the rotor or the main machine.
2,3,4		Reserved for future use
5 <sup>a</sup>	Integral independent component	The coolant is moved by an integral component, the power of which is obtained in such a way that it is independent of the rotational speed of the main machine, e.g., an internal fan or pump unit driven by its own electric motor
6 <sup>a</sup>	Machine-mounted independent component	The coolant is moved by a component mounted on the machine, the power of which is obtained in such a way that it is independent of the rotational speed of the main machine, e.g., a machine-mounted fan unit or pump unit drive by its own electric motor
7 <sup>a</sup>	Separate and independent component or coolant system pressure	The coolant is moved by a separate electrical or mechanical component not mounted on the machine and independent of it or is produced by the pressure in the coolant circulating system, e.g., supplied from a water distribution system or a gas main under pressure
8 <sup>a</sup>	Relative displacement	The movement of the coolant results from relative movement between the machine and the coolant, either by moving the machine through the coolant or by flow of the surrounding coolant (air or liquid)
9	All other components	The movement of the coolant is produced by a method other than defined above and shall be fully described

<sup>a</sup>The use of an independent component as a principal source for movement does not exclude the fanning action of the rotor or the existence of a supplementary fan mounted directly on the rotor of the main machine.

Source: From Ref. 4.

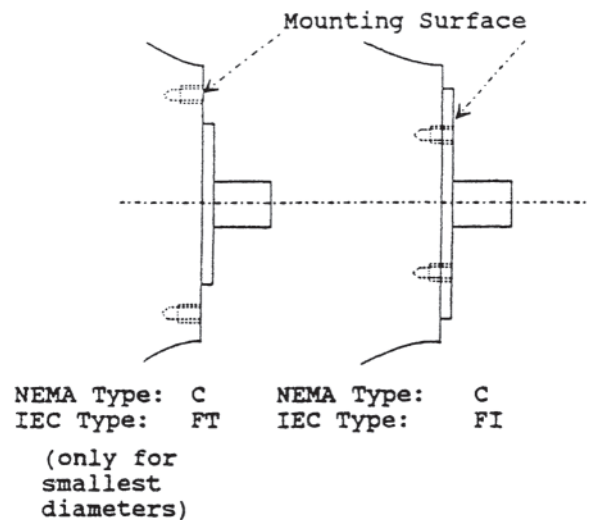
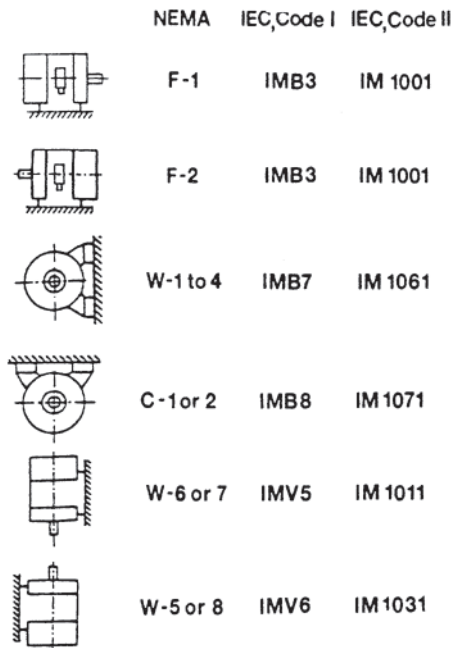


**Figure 3.3** Comparison of NEMA, IEC Code I, and IEC Code II designations for various foot-mounting configurations. (From Refs. 2 and 6.)

**Figure 3.4** Outline drawing of NEMA Type C flange mountings, with the corresponding IEC codes. (From Refs. 2 and 5.)

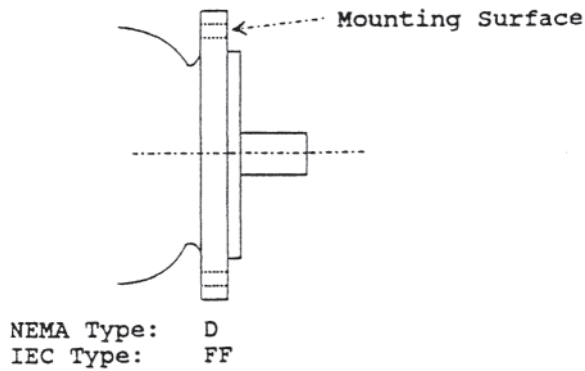


**Figure 3.5** Outline drawing of NEMA Type D and IEC Type FF flange mounting. (From Refs. 2 and 5.)

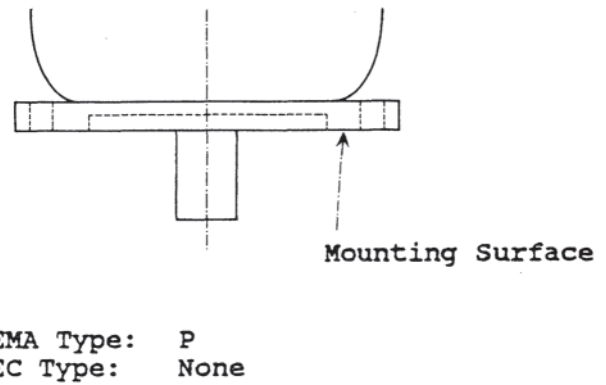


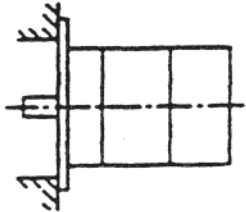
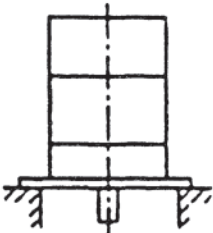
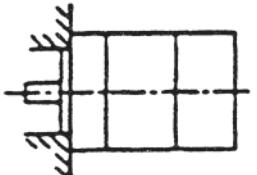
**Figure 3.6** Outline drawing of NEMA Type P flange mounting. (From Refs. 2 and 5.)

Figures 3.4, 3.5, and 3.6 show the NEMA and IEC type designations.

Flange-mounted machines do not have a standardized code in the United States, and mounting configurations must be spelled out. Figure 3.7 shows the basic comparisons among the NEMA, IEC code I, and IEC Code II designations.

**3.1.2 Dimensions**

Standardized dimensions provide the basis for physical interchangeability and, when combined as a frame size, provide all of the information necessary to mechanically mount a motor to a driven load prior to receiving the motor. A close examination of IEC [5] and NEMA [2] dimensions reveals

	<u>NEMA</u>	<u>IEC, Code I</u>	<u>IEC, Code II</u>
 <p>Flange Mounted (usually 'D' flange)</p>		IMB5	IM3001
 <p>Vertical (usually 'P' flange)</p>		IMV1	IM3011
 <p>Flange Mounted (usually 'C' flange)</p>		IMB14	IM3601

**Figure 3.7** Comparison of NEMA and IEC flange mounting descriptions and codes. (From Refs. 2 and 6.)

a great similarity. The IEC values are said to be a soft conversion of the inch values in the smaller frames up through the NEMA 500 frame. (A soft conversion from inches to metric values is one in which there is some round-off.)

Both frame size systems are based on shaft height. The IEC frame size is the shaft height in millimeters, whereas the first two digits of the three-digit NEMA frame designation give the shaft height in inches multiplied by 4. The letter following the IEC frame size defines the relative length of the frame. In the NEMA system the third digit accomplishes the length differentiation. In some NEMA frames the relative length of the motor is so great that two digits are used, for example, 5810. It should also be noted that the small NEMA motors have only a two-digit frame size, also based on shaft height. However, a multiplication factor of 16 is used rather than the previously mentioned value of 4.

Suffix letters following the NEMA frame size define shaft size and mounting arrangement. Some of these letters and their sequence for common machines are given in Table 3.5. Table 3.6 gives all of the necessary mounting dimensions for both NEMA and IEC frames with the exception of shaft extensions. Dimensions for NEMA shaft extensions are shown in Table 3.7. Additional dimensions for flange mounting can be found in reference documents IEC 60072 [5] and NEMA MG 1 [2].

Many of the dimensions that can be used to describe a machine have not been standardized. It is still, however, necessary to communicate this information. To do this a system of symbols has been established for both NEMA and IEC, a new set having recently been developed by IEC. All symbols are found in either IEC 60072 [5] or in NEMA MG 1 [2]. The most common symbols for horizontal machines are compared in Table 3.8 with the picture relating to the NEMA system.

**3.1.3 Performance**

Motor performance is required to be communicated and understood for several reasons. First, it is necessary that the motor have the ability to perform its function in driving the

**Table 3.5** NEMA Frame Size Suffix Letters

A	Industrial direct-current machine
C and CH	Type C face-mounting on drive end <sup>3</sup>
D	Type D flange-mounting or drive end <sup>4</sup>
HP and HPH	Type P flange-mounting vertical solid-shaft motors
JM and JP	Type C face-mounting close-coupled pump motor having antifriction bearings
LP and LPH	Type P flange-mounting vertical solid-shaft motors
P and PH	Type P flange-mounting vertical hollow-shaft motors
S	Standard short shaft for direct connection
T	Included as part of a frame designation for which standard dimensions have been established
U	Previously used as part of a frame designation for which standard dimensions had been established
V	Vertical mounting only
VP	Type P flange-mounting vertical solid-shaft motors
Y	Special mounting dimensions
Z	All mounting dimensions are standard except the shaft extension(s)

Suffix letters shall be added to the frame number in the following sequence:

Suffix Letters	Sequence
A	1
T, U, HP, HPH, JM, JP, LP, LPH, and VP	2
S	3
C, D, P, and PH	4
FC and FD	5
V	6
Y and Z	7

<sup>3</sup> When the face mounting is at the end opposite the drive, the prefix F shall be used.

Source: From Ref. 2.

**Table 3.6** Standardized Motor Dimensions

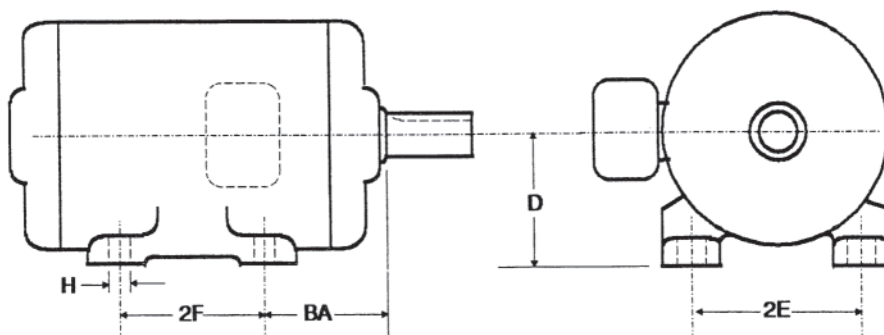


Table 3.6 Continued

Symbol:		D (H)			2E (A)			2F (B)			BA (C)			H (K)		
Frame Size:		NEMA	NEMA	IEC	NEMA	NEMA	IEC	NEMA	NEMA	IEC	NEMA	NEMA	IEC	NEMA	NEMA	IEC
NEMA	IEC	(in)	(mm)	(mm)	(in)	(mm)	(mm)	(in)	(mm)	(mm)	(in)	(mm)	(mm)	(in)	(mm)	(mm)
143	90S	3.50	88.90	90.00	5.50	139.70	140.00	4.00	101.60	100.00	2.25	57.20	56.00	0.34	8.60	10.00
145	90L	3.50	88.90	90.00	5.50	139.70	140.00	5.00	127.00	125.00	2.25	57.20	56.00	0.34	8.60	10.00
182	112S	4.50	114.30	112.00	7.50	190.50	190.00	4.50	114.30	114.00	2.75	69.90	70.00	0.41	10.40	12.00
184	112M	4.50	114.30	112.00	7.50	190.50	190.00	5.50	139.70	140.00	2.75	69.90	70.00	0.41	10.40	12.00
213	132S	5.25	133.30	132.00	8.50	215.90	216.00	5.50	139.70	140.00	3.50	88.90	89.00	0.41	10.40	12.00
215	132M	5.25	133.30	132.00	8.50	215.90	216.00	7.00	177.80	178.00	3.50	88.90	89.00	0.41	10.40	12.00
254	160M	6.25	158.80	160.00	10.00	254.00	254.00	8.25	209.60	210.00	4.25	108.00	108.00	0.53	13.50	14.50
256	160L	6.25	158.80	160.00	10.00	254.00	254.00	10.00	254.00	254.00	4.25	108.00	108.00	0.53	13.50	14.50
284	180M	7.00	177.80	180.00	11.00	279.40	279.00	9.50	241.30	241.00	4.75	120.60	121.00	0.53	13.50	14.50
286	180L	7.00	177.80	180.00	11.00	279.40	279.00	11.00	279.40	279.00	4.75	120.60	121.00	0.53	13.50	14.50
324	200M	8.00	203.20	200.00	12.50	317.50	318.00	10.50	266.70	267.00	5.25	133.40	133.00	0.66	16.80	18.50
326	200L	8.00	203.20	200.00	12.50	317.50	318.00	12.00	304.80	305.00	5.25	133.40	133.00	0.66	16.80	18.50
364	225S	9.00	228.60	225.00	14.00	355.60	356.00	11.25	285.80	286.00	5.88	149.40	149.00	0.66	16.80	18.50
365	225M	9.00	228.60	225.00	14.00	355.60	356.00	12.25	311.20	311.00	5.88	149.40	149.00	0.66	16.80	18.50
404	250S	10.00	254.00	250.00	16.00	406.40	406.00	12.25	311.20	311.00	6.62	168.10	168.00	0.81	20.60	24.00
405	250M	10.00	254.00	250.00	16.00	406.40	406.00	13.75	349.20	349.00	6.62	168.10	168.00	0.81	20.60	24.00
444	280S	11.00	279.40	280.00	18.00	457.20	457.00	14.50	368.30	368.00	7.50	190.50	190.00	0.81	20.60	24.00
445	280M	11.00	279.40	280.00	18.00	457.20	457.00	16.50	419.10	419.00	7.50	190.50	190.00	0.81	20.60	24.00
504	315S	12.50	317.50	315.00	20.00	508.00	508.00	16.00	406.40	406.00	8.50	215.90	216.00			28.00
505	315M	12.50	317.50	315.00	20.00	508.00	508.00	18.00	457.20	457.00	8.50	215.90	216.00			28.00
585	355S	14.50	368.30	355.00	23.00	584.20	610.00	20.00	508.00	500.00	10.00	254.00	254.00			28.00
586	355M	14.50	368.30	355.00	23.00	584.20	610.00	22.00	558.80	560.00	10.00	254.00	254.00			28.00
684	400S	17.00	431.80	400.00	27.00	685.80	686.00	22.00	558.80	560.00	11.50	292.10	280.00			35.00
685	400M	17.00	431.80	400.00	27.00	685.80	686.00	25.00	635.00	630.00	11.50	292.10	280.00			35.00

Source: From Refs. 2 and 5.

specified load machine in the most efficient manner, with appropriate reliability. Second, there is the need to provide the necessary coordination with devices protecting the motor and its application.

### 3.1.3.1 Torque

The speed of the driven machine establishes the speed of the motor. That, in combination with the load torque requirement, defines the rated horsepower, that is:

$$hp = (T \times N) / 5250 \quad (3.1)$$

where:

$T$  = torque in ft-lb

$N$  = speed in rpm

Because both the horsepower and speed are shown on the rating plate, the value of torque is referred to as full-load torque (FLT). Torque limits are specified as multiples (per unit) of FLT. There are three other torque values generally standardized. These are:

- *Locked-rotor torque (starting torque).* The locked-rotor torque of a motor is the minimum torque it will develop at rest for all angular positions of the rotor, with rated voltage applied at rated frequency.
- *Pull-up torque.* The pull-up torque of an alternating current motor is the minimum torque developed by the motor during the period of acceleration from rest to the speed at which breakdown torque occurs.
- *Breakdown torque.* The breakdown torque of a motor is the maximum torque it will develop with rated voltage applied at rated frequency, without an abrupt drop in speed.

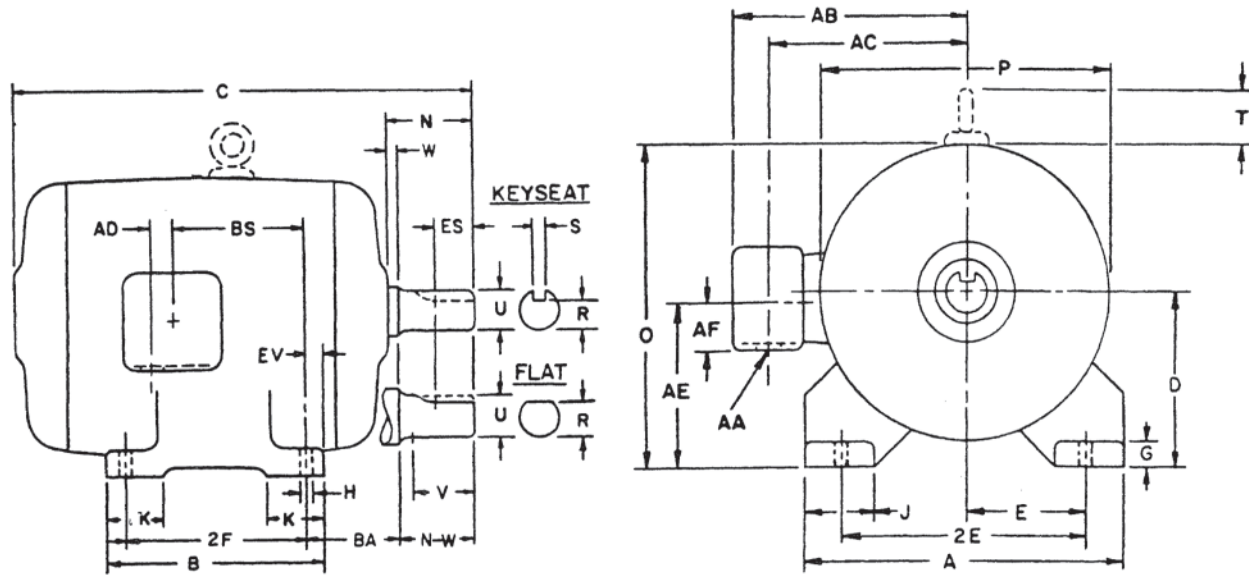
The torque limits in multiples (per unit) of FLT for normal NEMA and IEC motors are shown in Table 3.9. If the limits are different for IEC as compared to NEMA, the IEC limit is listed first. The IEC values have been normalized to

Table 3.7 NEMA Shaft Extensions

Frame size	Diameter	Length	Key stock (Sq.)
143T,145T	0.875	2.25	0.188
182T,184T	1.125	2.75	0.250
213T,215T	1.375	3.38	0.312
254T,256T	1.625	4.00	0.375
284T,286T	1.875	4.62	0.500
284TS,286TS	1.625	3.25	0.375
324T,326T	2.125	5.25	0.500
324TS,326TS	1.875	3.75	0.500
364T,365T	2.375	5.88	0.625
364TS,365TS	1.875	3.75	0.500
404T,405T	2.875	7.25	0.750
404TS,405TS	2.125	4.25	0.500
444T,445T	3.375	8.50	0.875
444TS,445TS	2.375	4.75	0.625

Source: From Ref. 2.

Table 3.8 Dimensional Designations of the NEMA System



NEMA letter	IEC letter	New IEC	Dimension indicated
A	AB	B13	Overall dimension across feet of horizontal machine (end view)
B	BB	L05	Over all dimension across feet of horizontal machine (side view)
C	L	L90	Overall length of single shaft extension machine. (For overall length of double shaft extension machine, see letter dimension FC.)
D	H	H10	Centerline of shaft to bottom of feet
2E	A	B10	Distance between centerlines of mounting holes in feet or base of machine (end view)
2F	B	L10	Distance between centerlines of mounting holes in feet or base of machine (side view)
G	HA	H13	Thickness of mounting foot at H hole or slot
H	K	D11	Diameter of holes or width of slot in feet of machine
J	AA	B14	Width of mounting foot at mounting surface
K	BA	L14	Length of mounting foot at mounting surface
N	—	—	Length of shaft from end of housing to end of shaft drive end
O	HC	G92	Top of horizontal machine to bottom of feet
P	AC	D91	Maximum width of machine (end view) including pole belts, fins, etc., but excluding terminal housing, lifting devices, feet, and outside diameter of face or flange
R	G	H02	Bottom of keyseat or flat to opposite side of shaft or bore
S	F	B01	Width of keyseat
T	—	—	Height of eye bolt above top of machine.
U	D	D01	Diameter of shaft extension. (For tapered shaft, this is diameter at a distance V from the threaded portion of the shaft.)
V	—	L02	Length of shaft available for coupling, pinion, or pulley hub, drive end. (On a straight shaft extension, this is a minimum value.)
W	—	—	For straight and tapered shaft, end of housing to shoulder. (For shaft extensions without shoulders, it is a clearance to allow for all manufacturing variations in parts and assembly.)
AA	—	—	Threaded or clearance hole for external conduit entrance (expressed in conduit size) to terminal housing
AB	AD	B80	Centerline of shaft to extreme outside part of terminal housing (end view)
AC	—	—	Centerline of shaft to centerline of hold AA in terminal housing (end view)
AD	—	—	Centerline of terminal housing mounting to centerline of hole AA (side view)
AE	—	H30	Centerline of terminal housing to bottom of feet (end view)
AF	—	R31	Centerline of terminal housing to hole AA (end view)
BA	C	L11	Centerline of mounting hole in nearest foot to the shoulder on drive end shaft. (For machines without a shaft shoulder, it is the centerline of mounting hole in nearest foot to the housing side of N-W dimension)
N-W	E	L01	Length of shaft extension from the shoulder

Source: From Refs. 2 and 5.

**Table 3.9** Torque Limits for Normal NEMA and IEC Motors<sup>a</sup>

Horsepower	Torque (per unit FLT)								
	2 Poles			4 Poles			6 Poles		
	Locked-rotor	Pull-up	Breakdown	Locked-rotor	Pull-up	Breakdown	Locked-rotor	Pull-up	Breakdown
1	NA	NA	NA	1.9/2.75	1.3/1.9	2.0/3.0	1.7	1.2	1.8/2.65
1.5	1.8/1.75	1.2	2.0/2.5	1.9/2.5	1.3/1.75	2.0/2.8	1.6/1.7	1.1/1.2	1.9/2.5
2	1.8/1.7	1.2	2.0/2.4	1.9/2.35	1.3/1.65	2.0/2.7	1.6/1.65	1.1/1.15	1.9/2.4
3	1.7/1.6	1.1	2.0/2.3	1.8/2.15	1.2/1.5	2.0/2.5	1.6/1.55	1.1	1.9/2.3
5	1.6/1.5	1.1/1.05	2.0/2.15	1.7/1.85	1.2/1.3	2.0/2.25	1.5	1.1/1.05	1.9/2.15
7.5	1.5/1.4	1.0	2.0	1.6/1.75	1.1/1.2	2.0/2.15	1.5	1.1/1.05	1.9/2.05
10	1.5/1.35	1.0	2.0	1.6/1.65	1.1/1.15	2.0	1.5	1.1/1.05	1.8/2.0
15–20	1.4/1.3	1.0	2.0	1.5	1.1/1.05	2.0	1.4/1.35	1.0	1.8/2.0
25–30	1.3	0.9/1.0	1.9/2.0	1.4/1.5	1.0/1.05	1.9/2.0	1.4/1.35	1.0	1.8/2.0
40–50	1.2	0.9/1.0	1.9/2.0	1.3/1.4	1.0	1.9/2.0	1.3/1.35	1.0	1.8/2.0
60–75	1.1/1.05	0.8/0.95	1.8/2.0	1.2/1.4	0.9/1.0	1.8/2.0	1.2/1.35	0.9/1.0	1.7/2.0
100–125	1.0	0.7/0.9	1.8/2.0	1.1	0.8/1.0	1.8/2.0	1.1/1.25	0.8/1.0	1.7/2.0
150–200	0.9/1.0	0.7/0.9	1.7/2.0	1.0	0.8/0.9	1.7/2.0	1.0/1.2	0.8/1.0	1.7/2.0
250–300	0.8/0.7	0.6/0.65	1.7/1.75	0.9/0.8	0.7	1.7/1.75	0.9/1.0	0.7/0.9	1.6/1.75
350–500	0.75/0.7	0.6/0.65	1.6/1.75	0.75/0.8	0.6/0.7	1.6/1.75	0.75/0.6	0.6	1.6/1.75
600–800	0.65/0.6	0.5/0.6	1.6/1.75	0.65/0.6	0.5/0.6	1.6/1.75	0.65/0.6	0.5/0.6	1.6/1.75

<sup>a</sup>If the IEC and NEMA torque limits are not identical, the IEC value is listed first.

Source: From Refs. 2, 7, and 8.

horsepower and some values have been adjusted for ease of comparison.

Some applications require higher torques than these normal torque values. Therefore, to recognize most applications, NEMA has defined several standard design letter classifications. The scope of design letter classifications covers polyphase squirrel-cage medium induction motors from approximately 1 to 500 hp. It is important to realize that the following tables do not apply to smaller or larger motors. The design letter definitions from [2] are as follows.

- *Design A.* A squirrel-cage motor designed to withstand full-voltage starting and developing normal torque as shown in Table 3.9, with higher locked-rotor currents than the normal values in Table 3.10 and having a slip at rated load of less than 5%.
- *Design B.* A squirrel-cage motor designed to withstand full-voltage starting and developing normal torque as shown in Table 3.9, with normal locked-rotor current not exceeding the values in Table 3.10 and having a slip at rated load of less than 5%.
- *Design C* (four-, six-, and eight-pole motors rated 3 to 200 hp). A squirrel-cage motor designed to withstand full-voltage starting and developing Design B pull-up and breakdown torques, higher locked-rotor torque than shown in Table 3.9, with locked-rotor currents (LRCs) not exceeding the normal values in Table 3.10, and having a slip at rated load of less than 5% (Table 3.11).
- *Design D* (four-, six-, and eight-pole motors rated 150 hp and smaller). A squirrel-cage motor designed to withstand full voltage starting and developing a high locked-rotor torque of not less than  $2.75 \times \text{FLT}$ , with

**Table 3.10** NEMA and IEC Normal Locked-Rotor Currents for 230-V Motors

Horsepower	Locked-rotor current (A) at 230 V	
	NEMA	IEC
0.5	20	12
0.75	25	18
1	30	24
1.5	40	37
2	50	49
3	64	73
5	92	122
7.5	127	183
10	162	225
15	232	337
20	290	449
25	365	562
30	435	674
40	580	824
50	725	1030
60	870	1236
75	1085	1545
100	1450	1873
125	1815	2341
150	2170	2809
200	2900	3745
250	3650	4688
300	4400	5618
350	5100	6554
400	5800	7490
450	6500	8427
500	7250	9363

Source: From Refs. 2 and 7.



**Table 3.11** Locked-Rotor Torque Limits for Design C Motors

Horsepower	Locked-rotor torque (per unit)		
	4 Poles	6 Poles	8 Poles
3	—	2.50	2.25
5	2.50	2.50	2.25
7.5	2.50	2.25	2.00
10	2.50	2.25	2.00
15	2.25	2.00	2.00
20–200	2.00	2.00	2.00

Source: From Ref. 2.

LRCs not exceeding the normal values in [Table 3.10](#), and having a slip at rated load of 5% or more.

IEC [7] defines only Design N and H motors. The torque limits for these designs compare in general with NEMA Designs B and C, respectively. Designs B and N limits are shown in [Table 3.9](#), while NEMA Design C locked-rotor torque limits are shown in [Table 3.11](#).

### 3.1.3.2 Current

Motor full-load current (FLC) is always listed on the motor rating plate. This is the value of current in amperes that the motor draws at rated voltage and frequency to produce rated power.

The current a motor draws during the starting cycle is generally called the LRC after the method that is used during test. All motor standards define this value as a maximum limit based on the rated power of the motor. [Table 3.10](#) compares NEMA and equivalent IEC values. LRCs for voltages other than 230 V are inversely proportional to the voltages.

Values of LRC are not provided on the motor rating plate. Instead a NEMA locked-rotor kVA code is listed on the rating plate. This code letter provides a range of values into which the actual locked-rotor current falls. [Table 3.12](#) lists these code letters.

To determine the maximum value of LRC that the motor will draw at rated voltage and frequency, apply the equation:

$$\text{LRC} = \frac{\text{Code letter maximum value} \times \text{rated horsepower}}{1.73 \times \text{rated voltage}} \quad (3.2)$$

It is important to recognize that there is no standard ratio between LRC and motor FLC. This fact should be considered when specifying motor protection, especially for energy-efficient motors, that have lower FLCs.

Whenever a motor is energized for starting, there is a transient inrush current that exceeds the actual LRC for a few cycles. Because it decays very rapidly, only the first half-cycle is of interest. The NEMA [2] standard relating to this phenomenon states that there will be a one half-cycle instantaneous peak value that may range from 1.8 to 2.8 times the LRC as a function of motor design and switching angle.

NEMA [2] has also recently developed two new standards that give additional guidance for motor protection. The first

**Table 3.12** Locked-Rotor Indicating Code Letters

Code letter	Kilovolt-amperes per horsepower with locked rotor
A	0–3.14
B	3.15–3.54
C	3.55–3.99
D	4.0–4.49
E	4.5–4.99
F	5.0–5.59
G	5.6–6.29
H	6.3–7.09
J	7.1–7.99
K	8.0–8.99
L	9.0–9.99
M	10.0–11.19
N	11.2–12.49
P	12.5–13.99
R	14.0–15.99
S	16.0–17.99
T	18.0–19.99
U	20.0–22.39
V	22.4–and up

Source: From Ref. 2.

covers occasional excess current and brings the U.S. standards into harmony with IEC standards. It reads in part:

Motors having outputs not exceeding 500 hp and rated voltages not exceeding 1 kV shall be capable of withstanding a current equal to 1.5 times the full-load rated current for not less than two minutes when the motor is initially at normal operating temperature.

Repeatedly overloading a motor for prolonged periods under this condition will result in reduced insulation life.

The second standard establishes the minimum stall time for motors. In this case, exceeding this value may cause motor failure. The standard reads in part:

Motors having outputs not exceeding 500 hp and rated voltages not exceeding 1 kV shall be capable of withstanding locked-rotor current for not less than 12 seconds when the motor is initially at normal operating temperature.

### 3.1.3.3 Temperature Rises

Allowable temperature rises are a function of insulation class. The following most common values are based on a 40°C ambient, as measured by the resistance method, and apply to all NEMA power ratings and to IEC ratings 1 to 5000 kW. For measurement by embedded thermal detectors there are some differences based upon power rating, voltage class, and class of insulation, which can be found in the respective standards. Reference may also be made to [Chapter 8](#).

Class of insulation	Temperature Rise (°C)	
	B	F
All enclosures, except NEMA TENV	80	105

### 3.1.3.4 Service Factor

The United States is unique in the world in having a standard for a dual rating system. This is called service factor and is defined [2] as follows.

When the voltage and frequency are maintained at the value specified on the nameplate, the motor may be overloaded up to the horsepower obtained by multiplying the rated horsepower by the service factor shown on the nameplate.

When the motor is operated at any service factor greater than 1.0, it may have efficiency, power factor, and speed different from those at rated load, but the locked-rotor torque and current and breakdown torque will remain unchanged.

It is important to note that service factor applies to horsepower and not to current. Depending upon the motor design, motor current may increase more rapidly than horsepower when the motor is overloaded.

Because motor performance is based upon the 1.0 service factor condition, the end result of operating a motor at a greater service factor is to operate it at higher temperatures, thus reducing insulation life. When originally conceived (during the time of Class A insulation systems), a service factor of 1.15 (15% overload) applied to a standard 1.0 service factor motor resulted in an additional temperature rise of 10°C. This is associated with decreasing the insulation thermal life to 50% of its normal design life.

With today's Class B insulation system motors, the 15% overload produces more than the additional 10°C temperature rise. It is therefore necessary to design open motors for lower than permitted temperature rise at 1.0 service factor and totally enclosed motors now utilize Class F insulation systems to achieve the 1.15 service factor.

### 3.1.3.5 Duty Types

IEC [8] has a system of defining motors for different duty types (S1-S10). The purpose is to optimize motor performance for a known duty cycle and provide a standard means for communicating this duty. The most common duty types are:

Continuous running duty	Duty type S1
Short-time duty	Duty type S2
Duty with discrete constant loads	Duty types S10

NEMA defines only continuous and short-time duty, although the procedure to establish an S10 duty type is similar to that used for standby generators and is now also being used for rating motors designed for inverter-fed operation.

### 3.1.3.6 Efficiency

NEMA now has standard efficiency limits for defining an energy-efficient motor. These limits are a function of motor enclosure, speed, and horsepower for motors rated 1–500 hp. Efficiency limits are being continually improved. For this reason the most recent edition of NEMA MG 1 [2] should always be consulted. There are no comparable efficiency standards in IEC.

Testing for efficiency is not uniform throughout the world. The United States uses a procedure that permits the determination of stator and rotor losses at actual operating temperature, while IEC standards [8] currently specify specific temperatures to be used. While this improves accuracy, the major difference occurs in the determination of stray-load losses.

During the evolution of the energy-efficient motor, the test method for determining stray-load loss was refined to such a point that the United States has the most accurate standardized method for measuring these losses in a specific machine. The current IEC method [9] assumes that stray-load has a value of 0.5% of the rated input power. This assumption does not provide the most accurate determination of efficiency. However, the new IEC 61972 is equivalent to IEC 112, Method B.

### 3.1.3.7 Tolerances

For values of performance, NEMA generally adheres to a system that uses either minimum or maximum limits. While this provides a very clear go/no-go evaluation of test results, it does not provide the user with a realistic or typical value to be expected. IEC [8] approaches this concern with a table of tolerances for guaranteed quantities used in motor performance ratings. Table 3.13 lists several of these tolerances.

When NEMA developed the efficiency tables [2], two columns were provided, one for nominal efficiency (the typical value of a large population) and another for minimum efficiency (which no motor can be less than). IEC accomplishes the same result by using a negative tolerance.

Another example is the maximum LRC. As explained above, any listed value is considered a maximum. IEC permits the issuing of an expected value with a plus 20% tolerance to recognize manufacturing and testing variances.

## 3.2 CHARACTERISTICS OF DRIVEN EQUIPMENT

Every piece of driven equipment, when viewed from the input shaft, can be characterized by a set of load torques, some of which are of interest only during the starting and run-up period, others that are of interest during normal running, and still others that are of interest in both periods. All of these torques are usually referred to the motor shaft so that a torque equation may be written with developed motor torque on one side of the equation and torques required by the equipment on the other. This will be a differential equation, and hence may be used to determine dynamic performance, or it may be used for specific conditions, such as steady state.

Various load torques are discussed in the following section. This list is not intended to be comprehensive, but should alert the reader to the variety of possibilities. For more thorough analysis than that below, the reader should consult such references as Thorpe [10], Janna [11], Shepherd [12], Shigley [13], and Streeter and Wylie [14]. The torque requirements presented by a load must be thoroughly understood before selection of a drive motor is begun.

Some of the load torques discussed are small. Examples of small loads are bearing friction under normal circumstances, the frictional effects of brushes sliding on commutators or

**Table 3.13** IEC Tolerances for Guaranteed Quantities in Motor Performance Ratings

Item	Tolerance
Efficiency, $\eta$	
By summation of losses:	
Machines up to 50 kW	-15% of $(1 - \eta)$
Machines above 50 kW	-10% of $(1 - \eta)$
By input-output test	-15% of $(1 - \eta)$
Power-factor ( $\cos \phi$ ) for induction machines	- 1/6 of $(1 - \cos \phi)$
	Minimum 0.02 Maximum 0.07
Slip of induction motors (at full load and at working temperature)	
Machines having output 1 kW (or kVA) or more	$\pm 20\%$ of the guaranteed slip
Machines having output less than 1 kW (or kVA)	$\pm 30\%$ of the guaranteed slip
Locked-rotor current of cage induction motors with short-circuited rotor and with any specified starting apparatus	+20% of the guaranteed current (no lower limit)
Locked-rotor torque of induction motors	-15% + 25% of the guaranteed torque (+ 25% may be exceeded by agreement)
Pull-up torque of induction motors	-15% of the guaranteed torque
Pull-out (breakdown) torque of induction motors	-10% of the guaranteed torque except that after allowing for this tolerance the torque shall be not less than 1.6 or 1.5 times the rated torque

Source: From Ref. 8

slip rings, and the windage due to rotation of pulleys or couplings on the motor shaft. These can generally be neglected when sizing the drive motor, but must be included if a complete energy or power balance is required.

### 3.2.1 Inertia Torques

Consider the following example. A horizontal conveyor has mass in its belt and in the material (if any) on the belt. This total mass must be accelerated at start, as must the gear train, drive pulley, and idler pulleys. Part of the motor torque equation on the load side will then be:

$$T_J = J \frac{d^2\theta}{dt^2} = J \frac{d\omega}{dt} \quad (3.3)$$

where:

$J$  =  $Wk^2$  is the sum of the polar moments of inertia of all of these parts of the conveyor reflected to the motor shaft, the inertias of the gears in the gear train reflected to the motor shaft, and the inertia of the motor itself

$d^2\theta/dt^2$  = angular acceleration in  $\text{rad/s}^2$

$\omega$  = angular speed in  $\text{rad/s}$

An equivalent rotational inertia for the belt and its load referred to the drive pulley shaft may be calculated using the drive pulley radius. The rotational inertia of the pulleys (both driven and idlers) and of the final gear in the gear train are then added to that of the belt and its load. This total inertia at the drive pulley shaft may be designated as  $J_L$ , and its value may then be reflected through the gear train. Inertias of intermediate gears in the train would each have to be reflected by the actual ratio from motor shaft to each gear.

$$J_{eqL} = J_L \left( \frac{N_m}{N_L} \right)^2 = J_L \times \left( \frac{\text{load speed}}{\text{motor speed}} \right)^2 \quad (3.4)$$

For example, if  $N_m/N_L$  is the gear ratio from the motor ( $m$ ) to the load ( $L$ ), then:

Inertias of the intermediate gears would be reflected in a similar manner and then added to  $J_{eqL}$  to obtain  $J_{eq}$  and finally motor inertia would be added to obtain  $J$  above.

### 3.2.2 Viscous Friction Torque

There are a number of frictional effects that must be considered. One of these is viscous friction, which is defined in rotational terms as a load torque that is directly proportional to speed, that is:

$$T_v = D\omega \quad (3.5)$$

Viscous friction is generally assumed to be very small, consisting of, for example, bearing friction, but even bearing friction may become quite large, as noted in the following paragraph. The power required to drive a viscous friction load is proportional to the square of the speed.

Bearing friction loss is dependent on the types of bearings (sleeve, roller, ball, and so forth), their materials, the coefficient of friction between the materials of the bearings, clearances, and the lubricant's viscosity. The operating temperature will be a factor because of its effect on lubricant viscosity; equipment that is used outdoors will experience a wide range of temperatures in every climate except in tropical and subtropical regions. If the equipment has been shut down for an appreciable length of time in subzero temperatures, the bearing torque may be so large that the motor cannot accelerate from stand-still to normal running speed. The effect of temperature on machine clearances must also be taken into account.

### 3.2.3 Sticking Friction

This is an easily observable phenomenon: if one tries to slide a box across a concrete floor, more force is required to break the box free than to keep it in motion. Sticking friction occurs

in many machines. For example, assume that a machine has sleeve bearings without an oil pump to pressurize the lower half of the bearing so as to float the shaft off the bearing surface. If the machine has been shut down, far more torque is required to start rotation than to keep the shaft turning after the oil film builds up. The same effect may be noticed in some antifriction bearings and in many kinds of machines that are started with material to be processed already in the machine. For example, mixers that contain thixotropic material will exhibit this property. From the drive motor point of view, the torque required is known as breakaway torque, and is a phenomenon that disappears once the load is in motion. The locked-rotor torque of an induction motor must be at least high enough to overcome the breakaway torque. With a direct current (dc) motor drive, breakaway torque will determine the minimum armature starting current required.

### 3.2.4 Coulomb Friction

Coulomb friction requires constant torque because the frictional effect is constant, regardless of speed. The box sliding on the concrete floor, mentioned above, tends to require a constant force to keep it in motion once breakaway has occurred, a force that is independent of speed. Another example of Coulomb friction is the frictional effect of automobile brakes; fixed pressure on the brake pedal tends to result in a constant deceleration. The power loss due to Coulomb friction is directly proportional to speed.

Brush friction usually has a Coulomb friction characteristic. The torque to overcome brush friction is dependent on brush pressure, brush grade, contact area, and the condition of the commutator or the slip rings. Typical values for brush friction power loss are given in Fink and Beaty [15] as 8 W/in<sup>2</sup> of contact area per 1000 ft/min of peripheral speed at a brush pressure of 2.5 lb/in<sup>2</sup>. Kuhlman et al. [16] give the same value for carbon and graphite brushes, but suggest 5 W rather than 8 W for metal graphite brushes. For large machines, two retardation tests, one with brushes lifted and one without brushes lifted, can be used to obtain experimental data.

Certain types of driven equipment exhibit Coulomb friction characteristics, that is:

$$T_c = K \text{ a constant} \quad (3.6)$$

For example, if the conveyor mentioned above is inclined, a certain amount of torque on the drive pulley is required to hold the conveyor belt in position at standstill because the material on the belt will tend to drive the belt in the direction to unload the belt at its lower end. Moreover, the same amount of torque is required to maintain the belt in motion at any fixed speed, assuming that material is added to the belt at one end and removed at the other.

One example of this kind of operation is a conveyor that is moving coal from a river barge to a point well above the level of the river, or an operation in which grain is moved from ground level to the top of a silo as a silo is being filled [17, 18]. Hoists and elevators are similar loads, although the required torque may be negative in those cases. Positive-displacement pumps working against a constant head are also

constant torque loads. Torque required to move a commutator or slip rings under brushes is also a constant.

Loads that exhibit a constant-torque characteristic require power that varies linearly with speed.

### 3.2.5 Fluid Loads

Any body moving through a fluid tends to drag with it the fluid immediately surrounding it, while fluid “remote” from the body is unaffected. That is, there is viscous shear between the fluid at the surface of the body and fluid layers adjacent to it. If the fluid flow is laminar, it may be shown [12] that the required torque for rotating bodies is given by:

$$T_f = C_T \rho \omega^2 d^5 \quad (3.7)$$

where:

- $C_T$  = a torque coefficient
- $\rho$  = fluid density
- $\omega$  = angular velocity
- $d$  = diameter of the body

A key point in this equation is that the torque (or force, in a translational application) is proportional to the square of the velocity. Windage in rotating electric motors, friction loss in a centrifugal pump, and the torque required by fans or blowers are similar phenomena, and in each case the square of the speed enters the torque equation. Losses may increase with accumulated operational time due to fouling of fan blades or accumulation of dirt in ventilation passages in a motor, for example. Prudent plant engineers will insist on proper maintenance, such as timely replacement of filters.

Because power equals torque times speed and the torque due to fluid friction is proportional to the square of the speed, the power required is proportional to the *cube* of the speed.

### 3.2.6 Unusual Load Situations

There are many loads that exhibit characteristics that cannot be classified as neatly as those of the preceding subsections. For example, some driven machines require torques that are cyclic in nature. Among these are reciprocating air compressors and vibrating screens. These are loads for which a cycle will correspond to a few revolutions of the motor. A different type of cyclic load is that exhibited by a reciprocating oil-well pump, for which the period of the load cycle is measured in seconds. Characterization of the torques presented by these loads will require a detailed mechanical analysis; the final result may be presented in the form of a time-dependent equation, or it may be best presented in a graphical form. Generally speaking, the load torque is predictable in the steady-state mode; it may be difficult to characterize accurately during start-up.

Another kind of load that may prove to be virtually impossible to characterize at start-up is that of a rotary kiln. Materials being processed have a certain angle of repose; with the kiln rotating, the surface of the material tends to assume that angle, with material constantly tumbling from the top of the load to the bottom as the kiln rotates. The greater the angle of repose, the larger the torque requirement.

If the kiln is stopped while loaded, it is not unusual to find on start-up that the material will initially have a new and greater angle of repose, so that torque well above the steady-state requirement is needed for an effective “breakaway” from the stationary condition.

### 3.3 INITIAL MOTOR SELECTION

Once the load has been characterized, one may write an equation of the form:

$$T_m = T_J + T_v + T_c + T_f + T_u \quad (3.8)$$

where:

- $T_m$  = torque developed by the motor
- $T_J$  = torque required to accelerate the inertia of the system
- $T_v$  = torque required by any viscous friction loads
- $T_c$  = constant torque required by the load
- $T_f$  = torque required by any fluid loading
- $T_u$  = torque required by any unusual loads

with all torques referred to the motor shaft.

In some cases, this will be a very well-defined equation except for possible temporary uncertainty as to the value of  $J$  in the term  $T_J$ . (If a specific motor has not as yet been selected, the value of  $J$  in Eq. 3.3 will not be known.) As an example, the inclined conveyor system mentioned in the preceding section may be very well characterized as to the inertias involved (except for motor inertia), down to the level of the weight per unit length of the material on the belt and the belt length. Gear losses and inertias will probably be known with reasonable precision, as well as the torques required to overcome friction in the bearings of the pulleys. Certain terms will be negligible or equal to zero, being absent by virtue of the kind of system being considered. In this case, one would not expect any fluid loading, and load torques that are unusual in character would not be anticipated. Other examples of applications that could be well-defined include machine tools, such as lathes, and take-up reels used to wind wire at the end of a wire drawing line or sheet metal at the end of a rolling mill.

However, it is possible that this will be an ill-defined equation. That is, many of the coefficients may be known only approximately, especially if a newly designed machine is being built. Experience with similar machines will very likely be the best guide in estimating some of the coefficients, but even here the application engineer may be led astray. For example, a machine being built to tumble material for drying purposes has a certain superficial resemblance to a cement kiln, but the characteristics of the material being dried may be so different from those of the material in the cement kiln that there will be no meaningful carryover of experiential knowledge from one to the other.

Whatever the situation, the engineer making the motor selection should work in a close relationship with the mechanical engineer responsible for the design and construction of the driven machine, or the renovation of an existing machine.

#### 3.3.1 Steady-State Solutions

This situation represents the easiest of the solutions to Eq. 3.8. The  $T_J$  term is zero because acceleration is zero. The other terms should be easily definable from known characteristics of the driven load. Even the  $T_u$  term should be evaluated easily. For example, in the case of the rotary kiln, in steady state the material’s angle of repose will not have a large variation, and the torque required to drive that part of the load may be calculated knowing that angle, the total weight and volume of material in the kiln, and the location of the center of gravity of the material with respect to the center of the drum.

Once the terms in the equation are known, steady-state torque required may be calculated using the synchronous speed of an induction motor or the base speed of a dc motor as the speed in the various terms on the right-hand side of Eq. 3.8. The power required will be the product of the torque and the speed. This power will be slightly larger than the actual power required in the case of an induction motor because the motor will run just below synchronous speed due to its slip, and all of the speed-dependent torque terms on the righthand side of Eq. 3.8 will be slightly smaller than the values calculated. In the case of a dc motor drive, speed may be adjusted by field control to base speed or to any other speed near base speed without serious error in the torque and power calculation.

Having established the power required from the motor, initial selection of a standard motor may be made. As an example, suppose that the required power is 85 hp. A 100-hp induction motor will easily satisfy the requirement, but there may be an initial economic benefit if a 75-hp motor with a service factor of 1.15 is chosen instead. A complete cost analysis taking into account energy costs, efficiencies of the two motors at 85 hp, and initial cost should be part of the selection process. It is desirable at this point to verify that a motor is selected having a locked-rotor torque in excess of any known breakaway torque. This may make it necessary to select a Design Class C motor rather than a Design Class B machine.

It should also be noted that selection of a drive motor, even on a tentative basis, enables the engineer to resolve the question of the moment of inertia of the motor itself, so that  $J$  in Eq. 3.3 will then be known.

#### 3.3.2 Dynamic Analysis

In some cases, the length of time required to accelerate the machine from standstill to running speed must be known. In other cases, a limitation may have been placed on the time to reach running speed. In either case, Eq. 3.8 must be solved to obtain speed as a function of time.

If an induction motor is used to drive the load, all of the terms in Eq. 3.8 are either speed-dependent or -constant, except for  $T_J$ . (The dc motor case is discussed briefly below.)  $T_J$ , from Eq. 3.3, is dependent on the rate of change of speed. If Eq. 3.8 is rearranged and  $T_J$  is replaced using Eq. 3.3.

$$T_m = T_m - T_v - T_c - T_f - T_u = J \frac{d\omega}{dt} \quad (3.8)$$

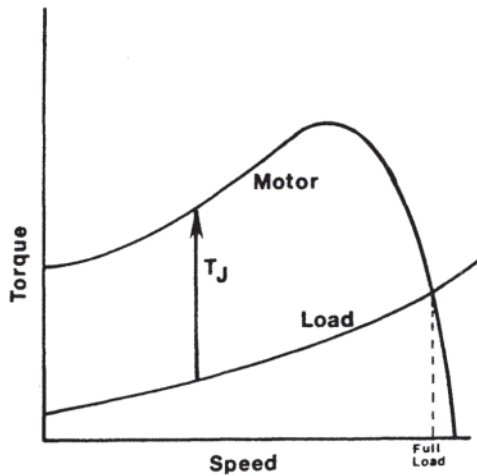


**Figure 3.8** Torque-speed curve for a typical induction motor and the speed-dependent torque required by a typical driven load.

Separating variables:

$$\int_0^t dt = \int_0^{\omega} \frac{J}{T_m - T_v - T_c - T_f - T_u} \quad (3.10)$$

If the integration is carried out from  $t=0$  and  $\omega=0$  to a final value of  $\omega$ , say 99% of full-load speed, the run-up time will be obtained. This is not feasible in closed form because of the complex form for  $T_m$  even if one uses an approximate equivalent circuit for the induction motor. Furthermore, it may not even be possible to express  $T_u$  as a function of speed, especially during the early stages of start-up. Smeaton [19, p. 1–17] shows a striking example of this condition.

Assuming that the constant load torque and the speed-dependent torques are known, their sum may be plotted versus speed as shown in Fig. 3.8. A typical torque-speed plot for an induction motor is also shown in that figure. Referring back to Eq. 3.9, it will be seen that the difference between these curves represents the middle form of that equation. That is, the difference is equal to:

$$T_J = J \frac{d\omega}{dt} \quad (3.11)$$

Rearranging and replacing the derivative by  $\Delta\omega/\Delta t$ :

$$\Delta t = J \frac{\Delta\omega}{T_J} \quad (3.12)$$

This equation may be solved numerically as follows:

1. Select a value of  $\omega$  (zero if total run-up time is desired) and calculate the sum of the load torques and the torque developed by the motor.
2. Take the difference of motor torque and the sum of the load torques to obtain  $T_J$ .
3. Select a value of  $\Delta\omega$  and use Eq. 3.12 to obtain  $\Delta t$ . (The smaller the value of  $\Delta\omega$ , the more accurate the final results.)
4. Add  $\Delta\omega$  to the value of  $\omega$  in (1) to obtain a new value of  $\omega$ . Add  $\Delta t$  to the value of  $t$  in (1) to obtain a new value of  $t$ .
5. Using the new value of  $\omega$ , repeat steps (1) through (4). As the procedure is repeated, data are accumulated for a curve of  $\omega$  versus  $t$ .

There is an additional step that would be valuable while doing these calculations. When the motor torque is calculated in (1), all of the motor variables needed to calculate losses in the motor are obtained as part of the solution for motor torque  $T_m$ . If these losses are calculated, multiplied by  $\Delta t$ , and cumulated as the solution is carried out, the total energy lost during run-up is obtained. If the motor and load are subject to a duty cycle, the energy loss during run-up is needed in order to calculate the total energy loss during one cycle.

Figure 3.8 suggests a method for approximating the run-up time. Referring back to Eq. 3.10, the denominator on the right-hand side is always the difference between the motor torque curve and the load torque curve. Obtain an average value of that difference (designated as  $T_{\text{avg}}$ ) by any convenient method. For example, the difference at a number of different but equally spaced speeds may be obtained, added together, and divided by the number of points. If the final speed is designated as  $\omega_{\text{FL}}$ , then the run-up time is given approximately by:

$$t_{\text{run-up}} = J \frac{\omega_{\text{FL}}}{T_{\text{avg}}} \quad (3.13)$$

It is obvious that the energy loss during run-up cannot be calculated if this approximation is used.

If a dc motor is used as the drive, it will probably be started using resistors in the armature circuit to limit armature current during start-up to safe values. Depending on the control used, resistors may be switched out at specific times, at specific values of back-emf of the armature, or at specific speeds. In these cases, the algorithm described above may be modified to include the switching sequence and obtain a curve of speed versus time, and losses may be tracked so that energy loss during run-up is obtained. Section 9.2 shows typical control methods.

What does one do if the run-up time is in excess of that allowable? One's first instinct may be to use a higher power motor in order to increase the available accelerating torque. While it is true that higher torque will be available, one should not forget that the inertia will also increase. A motor with a different number of poles (and a different gear train) may resolve the difficulty. It may be noted that use of Eq. 3.13 makes it easy to do a rapid comparison of run-up time using a number of different motors.

If duty cycle is important, the reader is referred to Section 12.6.

## 3.4 MOTOR EFFICIENCY AND ENERGY CONSIDERATIONS

### 3.4.1 Efficiency Considerations

#### 3.4.1.1 Definition of Motor Efficiency

The efficiency of a motor = output/input, or (input – losses)/input, where losses are chiefly a function of the electrical

environment and the design of the motor. Motor efficiency is a convenient way of relating these losses to the productive work being done by the motor.

When a motor is operating under changing loads, efficiency requires redefinition to be meaningful. If a motor is loaded to 150% of nameplate rating for 20% of the time, but is idling for 80% of the time, the rated efficiency of such a motor may have little relation to the net efficiency over the full cycle. When minimum energy cost is the objective, motor efficiency and the attendant operating costs should ideally be evaluated over a full load cycle. Unfortunately, values of motor efficiency at each of the various load conditions during the cycle will generally be difficult to obtain. An overall operating efficiency is:

$$\text{Efficiency} = \frac{0.746 \times (\text{Total output in hp-hours})}{\text{Total input in kWh}} \quad (3.14)$$

for one complete cycle. The cycle may last for only a few seconds as on a punch press; it may last for 15 minutes on a material moving system, or for a full work shift where the load is constant except for rest periods and shift changeovers. Although the equation is simple, its evaluation can be quite complex, because neither output (hp-hours) nor input (kWh) are readily measurable without complex instrumentation. More important, this efficiency number cannot be directly related to specific motor efficiencies, which always apply only at a single stated value of load.

#### 3.4.1.2 Factors Affecting Motor Efficiencies

The efficiency of all electrical equipment has a degree of sensitivity to the operating temperature, the supply voltage magnitude, phase balance, wave shape, and frequency. Motors are designed to operate successfully at terminal voltage ranging from 10% below to 10% above the nameplate value (not the power system rating or the usual power system value). However, performance—particularly efficiency—is not guaranteed to meet the nameplate or standard value under such conditions. The effects of various factors that can influence the efficiency of the motors will be more fully discussed in the following section.

1. *Phase voltage unbalance.* Any unbalance between the voltages in a three-phase system is equivalent to introducing a negative sequence voltage having a vector rotation opposite to that occurring with balanced voltages. That generates in the air gap a magnetic flux rotating against the rotation of the rotor, which requires a high input current. A small negative sequence voltage may produce currents in one or more phases of the stator and rotor conductors that considerably exceed those under balanced voltage conditions. For example, a 5% voltage unbalance can lead to a 30–50% increase in current unbalance, accompanied by a 50% increase in motor temperature rise. Table 3.14 shows the effect of voltage unbalance on a typical 200-hp motor at full load.
2. *Terminal voltage.* At full load, motor efficiency does not vary greatly with terminal voltage. However, some

**Table 3.14** Effect of Voltage Unbalance on a 200-hp Motor at Full Load

	Voltage unbalance (%)			
	0	2.0	3.5	5.0
Increase in losses (%)	0	8	25	50
Temperature rise (°C)				
Class A	60	65	75	90
Class B	80	86	100	120

motor duty cycles include significant operating time at half load or less. Under that condition, the output torque required is obviously low; so therefore is motor current and the associated  $I^2R$  losses. Iron or core loss, however, remains high because it is voltage-dependent rather than current-dependent. To reduce that loss, and therefore increase motor efficiency at the light load, some motor controls will automatically lower the motor voltage when the load drops. Tests have shown that this is a practical means of lowering energy cost when the motor must remain at light load much of the time without being shut down. The following cautions should be observed:

- If the machine is subject to a suddenly applied load, it may stall if the voltage is not adequate.
  - If the voltage is regulated to the optimum value with a thyristor or other device that creates wave distortion, the increase in losses due to the distortion may exceed the reduction in the 60-Hz losses.
3. *Harmonic distortion.* Harmonic distortions tend to increase motor losses. Although motor impedance increases at harmonic frequencies, rotor conductor resistance does also because of the so-called deep bar effect, resulting in increased rotor  $I^2R$  loss, and increased surface pulsation losses in the rotor and stator laminations adjacent to the air gap.
  4. *Voltage flicker.* Flicker is a periodic short-term voltage sag below the rated level. This can cause added motor losses for two reasons. The individual sags cause motor current to increase, which directly increases rotor and stator losses. If they occur on one phase only, the result is voltage unbalance, with the consequences described earlier. A 10% sag occurring on one phase 50% of the time will have the effect of a constant unbalance of approximately 5% with a current flow into the motor similar to starting inrush. This will likewise cause additional rotor current to flow with attendant losses.
  5. *Winding temperature.* The life of electrical insulation is a function of the operating temperature. A 10°C increase in temperature cuts the insulation life in half. Conversely, a reduction of 10°C doubles the life. Temperature also affects the resistance of the windings of all electrical equipment. Cooler equipment results in lower losses. For example, a 10°C reduction in motor temperature will reduce the dc resistance losses of the conductors by 3–4%.

### 3.4.1.3 Evaluation of Losses

1. *DC motors.* Losses for a typical dc motor are:
  - Mechanical losses—windage, brush, and bearing friction
  - Iron losses—hysteresis and eddy-current losses
  - Copper losses in field and armature coils
  - Commutator contact and resistance losses
  - Load losses

Although several methods exist to evaluate dc motor efficiency, the IEEE test standard for dc motors, No. 113, has been withdrawn. Efficiency measurement in dc machines is of little importance for these reasons:

1. In any size range, dc machines represent an extremely small portion of the total motor population.
2. The dc motor is inherently a variable speed machine, commonly operated either intermittently, at varying speed and load, or both. An efficiency evaluation at just one value of speed and load is of no use in determining overall duty cycle performance.
2. *Synchronous machines.* The losses of a synchronous machine are conventionally placed in the following six categories:
  - Core loss
  - Friction and windage
  - Field  $I^2R$  losses
  - Stator  $I^2R$  losses
  - Stray losses (or load losses)
  - Exciter or rheostat losses

Core loss and friction and windage losses are referred to as fixed losses and the others are called variable losses.

In general the total losses of large synchronous machines range from 3% to 5%, yielding a machine efficiency of 95–97%.

3. *Induction motors.* The losses of an induction motor are similarly grouped into the following:
  - $I^2R$  losses—the primary, and secondary currents and corresponding  $I^2R$  losses at any load.
  - Friction and windage losses—normally 1–2% of the rated output. This percentage value decreases with increasing motor size.
  - Core loss—typically 2–3% of rated output, the actual value dependent upon many design features.
  - Stray-load losses—typically 1–2% of the output, but values as low as 0.5% and as high as 4% are not uncommon.

### 3.4.1.4 Specifying Efficient Motors for New and/or Retrofit Projects

The passage of the 1992 Energy Policy Act (EPACT) mandated that effective October 1997 all standard three-phase low-voltage polyphase induction motors in the United States market (whether of domestic manufacture or imported) must meet stated full-load efficiencies. The ratings involved are 1 through 200 hp, open or totally enclosed, 2, 4, and 6 poles, general purpose (NEMA Designs A and B). Such machines must comply with the following requirements established ei-

ther by the EPACT legislation itself or by the U.S. Department of Energy rules created to enforce that law:

1. A nameplate efficiency marking must use one of the values tabulated in Standards MG 1 of NEMA as “nominal” for full-load operation. Associated in NEMA MG 1 with each such nominal value is a corresponding “minimum” value, which industry practice accepts as a “guaranteed” figure.
2. That nominal efficiency must be confirmed by a specific test procedure acceptable to the Department of Energy, and applied in a test facility approved by that department. The test method is to be IEEE Standard 112 Method B, involving dynamometer loading and regression analysis of stray load loss. For motors manufactured in Canada, testing per CSA Standard C390 is considered equivalent.

All such motors are defined by NEMA standards as “energy efficient.” Basic designs have been in the marketplace since the 1980s. In addition to the two-, four-, and 6-pole “general purpose” ratings defined by EPACT, motor manufacturers have tended to also include 8-pole designs and many “definite purpose” or “special purpose” ratings in the “energy efficient” category.

Keep in mind that these standardized efficiency values may be exceeded by many designs. That is up to the motor manufacturer.

In its 1993 revision of Standards MG 1, NEMA added ratings from 250 through 500-hp (depending upon speed) to its “energy efficient” design category, even though the EPACT legislation had not been changed.

Further, improvements in motor design resulted in the 2001 adoption by NEMA of a second category of higher efficiency machines formally identified as “premium efficiency.” In addition to the 1–500-hp low-voltage designs, premium ratings include medium voltage motors in the 250–500 hp range.

When any new or replacement motor is to be specified, the user should make a life cycle cost study before determining the appropriate efficiency level, with particular attention to the actual load expected. Standardized efficiency values apply only at rated or nameplate horsepower and voltage.

Contractors on new projects are primarily concerned only with first cost. Construction specifications should therefore require that the more efficient units be supplied only by acceptable bidders.

Retrofits are more complicated. Not only are electrical savings involved, but there are also considerations of removal, replacement, and repair cost; maintenance and reliability; and salvage value. Experience has proved that replacing failed units with more efficient designs is almost always cost-effective. If a less-efficient machine has not yet failed, however, such a replacement is seldom cost-effective.

Matching loads is another important consideration for retrofit projects. Although motor efficiency is relatively constant between 50% and 100% load, it is generally somewhat higher at two-third to three-quarter load than at full load. As an example: to drive an actual 7.5-hp load, a 10-hp motor operating at three-quarter load may have a slightly



higher efficiency than a 7.5-hp motor operating fully loaded. The best choice is a motor that will operate most of the time between 75% and 100% load. Maximum savings result from proper sizing as well as correct application.

### 3.4.2 Energy Considerations

#### 3.4.2.1 Energy Management Using Energy-Efficient Motors

Use of more efficient motors should always be considered whenever an electric motor is being purchased. Payback for a higher efficiency design will vary with motor loading, hours of operation, and energy cost, all of which may vary from operation to operation. Typical motor data for each alternative will provide information for such a study. One of the most useful tools for that purpose is the MotorMaster computer database, available through motor manufacturers and distributors, from the Department of Energy (for further information, the Department of Energy telephone hotline is 800-862-2086).

For example, consider an energy savings comparison for a 50-hp, 1780-rpm motor, to operate at full load 6 days per week, two 8-hour shifts per day, or about 5000 hours annually. Assume average power cost at \$0.07 per kilowatthour. "Minimum" (guaranteed) efficiency at full load for the EPACT standard energy efficient motor is 91.7%, and for a premium efficiency design is 93.6%. Motor output = 50 hp × 0.746 = 37.3 kw. Power input to the energy efficient motor = 37.3 / 0.917 = 40.68 kw. Power input to the premium motor = 37.3 / 0.936 = 39.85 kw. The annual saving in dollars = 0.83 kw × 5000 × \$0.07 = \$291.

The next step is to perform a payback analysis involving that predicted energy saving and the prices of the motors being considered. Evaluation of energy savings is discussed more fully in Section 3.5.

Prior to the 1993-1994 onset of electric utility deregulation, and to the enactment of EPACT that made higher motor efficiency mandatory, many utilities throughout the country offered substantial rebates to motor users for purchase of more efficient motors. Such financial incentives have largely disappeared since then.

#### 3.4.2.2 Application of Variable-Frequency Control

Looking beyond the motor itself, and dealing with the entire drive system from incoming power line to driven machine output, reveals opportunities for energy saving that often far exceed what can be achieved through motor design alone. Adjustable speed drives (ASD) allow variation of motor speed and load, through changes in both voltage and frequency that are well-suited to the behavior of so-called centrifugal loads—the fans and pumps that make up the largest share of motor-driven industrial machinery. When such loads operate at reduced speed, the driving power may be greatly reduced.

Not every motor application benefits from speed and load variation, however. Variable frequency inverters that supply ASD power must meet these basic requirements:

1. Ability to adjust frequency according to the desired output speed.

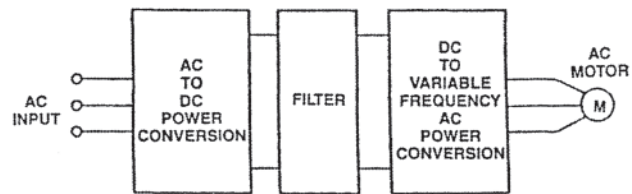


Figure 3.9 Block diagram of a variable-frequency converter.

2. Ability to adjust output voltage to maintain the proper balance between magnetic flux, current, and torque.
3. Ability to supply rated current continuously over a wide frequency range. [Note the deletion of reference to constant air-gap flux; that restriction is obsolete.]

Figure 3.9 shows the basic concept. The alternating current (ac) power input is converted to dc by a rectifier bridge. Inductive or capacitive components in the dc link maintain either a relatively constant voltage or a relatively constant current to the final stage inverter that changes the dc back to a variable frequency ac. Many different inverter configurations or topologies have been developed for various purposes. The most common today is of the so-called pulse width modulated or PWM type using a transistorized inverter. It produces a nearly sinusoidal output current by rapidly switching output voltage on and off while simultaneously varying the length of the on pulses.

Economic evaluation of the entire system must be made before committing to a given approach. Normally, so much energy can be saved through reduced-speed operation that the efficiency of the motor itself in an ASD application can be neglected. Efficiency of the electronic components of the ASD itself is likewise of little importance; a constant value of 0.95 or above may usually be assumed.

This requires detailed knowledge of the energy requirements of the load, obtained from characteristic performance curves of the gas or liquid handling equipment involved. An ASD is most cost effective when much of the operating time is spent at between 1/3 and 2/3 full speed.

When other types of loads are involved, calculations become more complex, and justifying the ASD cost more difficult. In a specific study of four induction motors driving conveyors ranging in size from 40 to 400 hp, the data were analyzed to determine if an ASD would pay for itself within three years; results indicated only a 250-hp motor was a good candidate for ASD application.

## 3.5 PAYBACK ANALYSIS AND LIFE-CYCLE COSTING OF MOTORS AND CONTROLS

This section deals with the finance aspects of motor application. Too often the engineer does an elegant job of applying a specific piece of equipment to a process or factory only to find out later that it is not cost-effective. The engineer probably did not weigh the financial benefits with the costs of the equipment. Those costs include not only the initial cost of the equipment and its installation, but also any maintenance costs that go along with it. Because this handbook deals primarily with motors, the discussion will be limited to the analysis required to determine

whether a new or different motor and its associated higher cost can be economically justified. This section is not intended to replace a comprehensive text on engineering economics. Rather, the reader is encouraged to delve into such a text. The attempt here is to introduce the reader to a number of factors to be considered when making an economic analysis of a new purchase.

A list of factors to be considered includes the following:

1. Initial cost
2. Expected life of machine
3. Application—industrial, commercial, or residential?
4. Present energy cost—consider both \$/kWh and demand costs
5. Likely inflation rate on energy costs
6. Operation hours—continuous (8760 h/year), one-shift, two-shift?
7. Expected maintenance costs
8. Motor loading profile—constant vs. variable loading
9. Interest rate on money

Although the interest rate on money was listed last, it may be the key factor in determining whether the new installation should proceed. It is one of the costs that must be considered along with the initial cost and maintenance costs. Because the discussion is limited to the justification of a single motor purchase, the engineer or owner has two choices:

1. Installing a new and better motor with the expectation of saving money because of lower energy usage.
2. Putting the money required to purchase the motor into the bank or a similar vehicle that will earn interest.

With this second choice we are assuming that the engineer has the money to spend on the new motor. Whether he has to borrow the money for the purchase or has the choice of investing the money on hand, it is still a matter of economics. The new motor must make or save money.

Some calculations to be made include the following factors.

1. Cumulative energy savings in dollars
2. Present worth of cumulative energy savings
3. Added cost of a more expensive machine vs. a standard model

If the present worth of the savings is greater than the added cost of the new motor at today's cost, then it is economically justified. The "present worth" calculation brings the savings that are accumulated over time back to today's value of money. This points out the importance of "time value of money." That is the reason for the emphasis on the alternative of investing the same amount of money in the bank. Simply, the present worth of the cumulative energy savings is equal to the cumulative savings times the present worth factor.

$$\text{PWF} = \frac{1}{(1+i)^n} \quad (3.15)$$

where:

- PWF = present worth factor  
*i* = interest rate for the period (month, year, etc.)  
*n* = number of periods used in the calculation

If the time required to accumulate enough savings to justify the installation is greater than the expected life of the machine, it is obvious the purchase should not be made. If the inflation on the energy costs is high—6% to 8% per year—the savings can accumulate faster. On the other hand, if the interest rate that can be earned on the money is high—10% to 12% per year—then the purchase may be difficult to justify.

Now we must look at the operation rate and the type of loading. Both of those factors help determine the number of kilowatt-hours that are saved. If the operation is continuous—8760 hours per year—the payback may occur fairly early. However, if the machine is used only 6 hours per day for 5 days per week and 50 weeks per year, we have 1500 hours of operation per year. This is only 17% of usage of the total hours available during the year. On top of that, if the machine is only lightly loaded during its operation, we have a still longer time to accumulate enough savings in energy usage to justify the installation.

With those factors in mind, the reader is now encouraged to make some calculations to determine whether he should purchase or invest. A fairly simple computer program, about 70 lines or less, will provide the information needed to make the decision.

### 3.5.1 General-Purpose vs. Special Machines

In the selection of motors or generators one may have the choice of applying a standard catalog item or going to the manufacturer with a request for a machine to match a set of definite requirements. The choice could also be between a machine with "normal" performance and one with high efficiency. The high-efficiency machine may be one with a longer stack core made with thin laminations and/or better steel chemistry, resulting in low hysteresis and eddy-current losses. The "better" machine could cost the customer 25–100% more than the standard machine. This is an ideal time to apply lifecycle costing. It is important for the user to determine his own set of ground rules. The user may find that the motor advertisements neglected to consider the "cost of money."

Another choice becoming more prevalent is the selection of variable-speed motors. In previous years the only candidate for variable-speed applications was the dc machine, which generally commanded a significant premium over single-speed induction machines. More recently we have seen three major types of variable-speed machines offered to the public. The likely applications include fans, pumps, compressors, and so forth, where the loading conditions may not be constant. These three machine types include inverter-fed induction motors, electronically commutated permanent-magnet motors, and switched-reluctance motors. All three types use electronic power supplies. Depending on the complexity of the electronic supply, that portion may cost significantly more than the motor itself. The important point is that these machines can be programmed to follow the particular load characteristic of variable speed, torque, or power. Furthermore, they can be programmed to set the conditions to achieve minimum power input to the electronic

supply. Again, one needs to apply the life-costing concepts to such an application to determine whether the special machine with its unique characteristics can be economically justified or whether the standard machine will suffice.

### 3.6 SAFETY CONSIDERATIONS

Most motor manufacturers specifically include safety criteria in the design and construction of electric motors. Such provisions alone do not ensure the practical safeguarding of persons and property in use of motors. In addition to construction and design features, it is equally essential that motors be applied and installed with safety as a consideration.

#### 3.6.1 Application Information

The following guidelines should be reviewed as part of the application process.

1. The performance characteristics of the motor selected for a particular application must be properly matched to the requirements of the driven load.
  2. Usual and typical unusual service conditions are defined in NEMA MG 1 [2].\* In order to ensure a safe application, any unusual service conditions must be reported to the motor supplier.
  3. The motor supplier must be advised if the motor is to be used in a hazardous environment. Include details on zone, groups, division and temperature limits.
  4. The motor supplier must be advised if anticipated variations in the power supply voltage and frequency will exceed the standard allowable variations as defined in NEMA MG 1.
  5. The motor supplier must be advised if the starting requirements will exceed the standard as defined in NEMA MG 1.
  6. The motor must be provided with the proper enclosure for the application. For a safe application, enclosure selection involves not only the operating environment but the degree to which the motor will be exposed to personnel as well.
  7. The motor supplier must be advised of any anticipated conditions under which the motor will be required to operate either above or below the normal speed range.
  8. The sudden and unanticipated reenergization of a motor using automatic reset protective devices can produce a potentially hazardous condition in some applications. Worst case scenarios involving personnel and equipment should be carefully constructed before applying such devices.
2. The connection of the motor to the power supply should be made by a qualified person in accordance with instructions provided by the motor manufacturer.
  3. Motors having brushes or collector rings emit sparks during normal operation. In the event of a winding failure, flame and/or molten metal may be expelled from open-type motors. Consequently, flammable or combustible materials should not be permitted in the proximity of these types of motors.
  4. Rotating parts such as couplings, pulleys, and unused shaft extensions should be provided with guards. This is particularly true when the parts have surface irregularities such as keys, keyways, or set-screws.
  5. The lifting and movement of larger motors can be a particularly hazardous operation. Reasonable care and knowledge of proper lifting techniques are required to assure the safety of personnel and to prevent damage to the equipment. Lifting instructions provided by the motor manufacturer should be followed carefully. For odd-shaped equipment, know the center of gravity before lifting.
  6. In some applications, exposed motor surfaces may reach temperatures that could cause discomfort or injury in the event of physical contact. The need for protection against accidental contact is a consideration in such cases.
  7. The motor manufacturer will provide hold-down bolt holes in the motor base designed to accept bolts of sufficient size to hold the motor securely in place. The largest diameter bolt that will fit the nominal hole should be used to mount the motor. The length of a steel bolt should be such that the minimal thread engagement is equal to the bolt diameter after allowing for washers under the head of the bolt and shims under the feet. If a material other than steel is used the minimum thread engagement should be adjusted in conformity to the strength of the material.
  8. Motors connected to drives require extra care for grounding otherwise damaging shaft currents may exist.

#### 3.7 HOW TO SPECIFY A MOTOR

A motor specification is used to document and communicate the requirements of the motor user to the motor supplier. The specification should be clear and concise. Short sentences limited to one point should be used. Good transition and flow are essential. A well-written specification can do much to help prevent misunderstandings, delays in manufacturing, and unnecessary additional costs.

Most electric motors manufactured in the United States for domestic usage are designed and manufactured in accordance with NEMA MG 1, Motors and Generators. The prospective author of a motor specification should have this standard available for reference and be generally familiar with its contents. Frequent references will be made to sections of NEMA MG 1. Because of the frequency with which this reference is cited in Sections 3.7, a reference number does not identify later references to MG1.

The terms “medium” and “large” motors, as defined in

#### 3.6.2 Installation

1. Although there are some exceptions, in most cases, the metal exterior parts of a motor should be grounded to limit the potential to ground in the event of a contact between a live electrical part and the enclosure.

\* Because of the frequency with which this reference is cited in Sections 3.6 and 3.7, later references to MG 1 are not identified by a reference number.

NEMA MG 1 will be used frequently. Most motor specifications are written to cover medium and large, polyphase, ac, squirrel-cage, induction motors. The contents of this section are therefore oriented toward that general group of motors. Much of the information contained in this section applies to other groups of motors as well.

### 3.7.1 Scope

The specification should begin with a statement defining the scope or coverage of the document. In the case of a general specification intended for use with a group of motors, the horsepower range, voltage range, and type of motors to which the specification will apply should be stated.

*Example:* This specification shall govern the design, material, construction, tests, and inspection of all polyphase, squirrel-cage induction motors rated 600 V and below, 100 hp and below for use on a constant frequency sine wave source.

### 3.7.2 Codes and Standards

The specification should contain a statement defining the industry codes and standards that, along with the specification, will apply.

*Example:* Unless otherwise specified, the equipment shall be designed, constructed, and tested in accordance with the applicable provisions of the following standards:

NEMA MG 1 Motors and Generators NEMA MG 2 Safety Standards for Construction and Guide for Selection, Installation and Use of Electric Motors and Generators [21]

IEEE Std. 112. Test procedure for Polyphase Induction Motors and Generators [20]

ANSI S12.43 Engineering Method for the determination of Sound Power Levels of Noise Sources [22]

### 3.7.3 Service Conditions

The specification should contain a statement defining the service conditions under which the equipment will be required to operate. Motor design and construction is based on the following normal service conditions:

- An ambient temperature in the range of 0°—40°C;
- Altitude not exceeding 3300 feet;
- A location in which ventilation of the motor is not restricted;
- Seismic requirements not exceeding those described in NEMA MG 1–20.32.4;
- Variations in the supply voltage not exceeding  $\pm 10\%$ ;
- Variation in the supply frequency not exceeding  $\pm 5\%$ ;
- A combined variation from rated values of  $\pm 10\%$  in frequency and voltage, provided the variation in frequency does not exceed  $+5\%$ ; and
- While running at rated load, a phase voltage unbalance not exceeding 1%.

Unusual service conditions such as those described in NEMA MG 1–20.29.3. must be included in the specification. At minimum, this section should state whether the motor is to be located indoors or outdoors, the minimum and maximum ambient temperature, and altitude. Any unusual environmental conditions should be mentioned.

*Example:* Motors shall be designed for continuous outdoor operation without protective shelter. They shall be suitable for operation in an atmosphere made corrosive by traces of chemicals and environmental conditions such as high humidity storms, salt-laden air, insects, plant life, rodents, blowing sand, fungus, etc.

Elevation:	Sea level
Maximum ambient temperature:	40°C
Minimum ambient temperature:	–10°C
Maximum humidity:	100%

#### 3.7.3.1 Adjustable Voltage Adjustable Frequency Applications

When 60-Hz NEMA Design A or B motors are purchased for use on an adjustable voltage adjustable frequency power source to obtain speed adjustment the conditions of the source shall conform to NEMA MG 1–30.

Definite purpose inverter fed polyphase motors shall conform to NEMA MG 1–31.

*Example:* The motor will be supplied from a PWM inverter using IGBT switching with a 2-kHz chopping frequency. The motor must be capable of continuous duty over a 10:1 speed range at constant torque.

### 3.7.4 Starting Requirements

The specification should contain a statement defining the starting requirements.

Unless otherwise stated, the supply voltage and frequency during the starting period are assumed to remain within the limits for normal service conditions. If the supply system characteristics are such that the voltage drop may exceed 10% of the rated voltage during starting, it must be so stated in the specification. Similarly, if a reduced-voltage motor starter is to be used, the type of starter and starting voltage must be stated.

The torque developed by an ac, polyphase, squirrel-cage induction motor during starting is approximately proportional to the square of the applied voltage. Therefore, it is essential that the supply voltage conditions during starting are correctly identified in order to assure that the motor will produce enough torque to start and accelerate the driven load to running speed.

Any specific starting current restrictions must be stated. The maximum permissible rated voltage starting currents for medium motors having standard NEMA design designations are stated in NEMA MG 1–12. The maximum permissible starting currents of large motors covered by NEMA MG 1–20 are not similarly restricted.

Large motors having normal torque characteristics are usually designed to have starting currents in the range of 5 to

7 times rated full load current. It should be noted that excessively severe starting current restrictions will result in a reduction of motor efficiency during normal running and of torque-producing capability during the starting period.

In order to start and accelerate, a motor must produce a torque that exceeds the torque required by the driven load at all speeds during acceleration to running speed. In addition, the design of the motor must be such that the heat generated within the motor during starting will not exceed acceptable limits. The amount of heat generated during starting and acceleration depends upon the inertia of the driven load and the length of time required to accelerate. Unless otherwise specified, motors will be designed with a starting capability in accordance with NEMA MG 1–12.45.2, MG 1–20.11, and MG 1–20.12, as applicable.

Any requirements involving load inertia values or starting frequencies that exceed the NEMA standard values must be stated. If the inertia of the load, the required load torque during acceleration, the applied voltage, and the method of starting are those for which the motor is designed, it will normally be capable of two starts in succession, coasting to rest between starts, with the motor initially at rest, or one start with the motor initially at a temperature not exceeding the rated operating temperature. This permissible starting cycle can be repeated without potential damage to the motor only after it has had an opportunity to cool to ambient or normal operating temperature. If specified, a special “Starting Duty Nameplate” can be provided showing permissible starting frequency. The information shown on the plate will be based on the starting duty for which the motor was originally designed and will not necessarily apply for other applications.

Any acceleration time requirements must be specified. If the inertia and speed vs. torque characteristics of the driven load are known, a motor can be designed, within limits, to develop the amount of torque required during acceleration to meet a desired time parameter.

*Example:* Motors shall be designed for across-the-line starting. Starting duty shall be in accordance with NEMA MG 1–12.45.2 for medium ratings and NEMA MG 1–20.11 and MG 1–20.12 for large motors. Motors shall be able to overcome the starting load inertia and accelerate to rated speed at 80% rated voltage. Starting current at rated voltage shall not exceed 650% of rated full-load current.

### 3.7.5 Rating

Information relating to the specific rating or ratings required must, of course, be specified. In the case of a general type of specification intended for repeated use, this information is usually given on separate data sheets.

1. *Horsepower.* The horsepower rating is normally determined by the horsepower requirements of the driven load. The standard horsepower ratings are listed in NEMA MG 1–10.32 and NEMA MG 1–20.3
2. *Speed.* The required speed in revolutions per minute is determined by that of the driven load.

3. *Voltage and frequency.* The rated voltage and frequency of the motor must be specified. Standard voltage and frequency ratings are listed in NEMA MG 1–10.30 and MG 1–10.31, MG 1–20.5, and MG 1–20.6, as applicable. Standard voltage ratings are lower than associated standard system voltage levels in anticipation of system voltage drops.
4. *Duty (time rating).* Most integral-horsepower and large motors are designed and manufactured for continuous operation. In some applications, the motor may be required to operate only intermittently. Standard time ratings for integral-horsepower motors are listed in NEMA MG 1–10.36. It is normal practice to state in the specification whether continuous or intermittent operation at rated horsepower is required.
5. *NEMA design designation.* NEMA design designations are applicable only to those ratings specifically listed in NEMA MG 1–12. The design designation establishes torque and starting current characteristics in accordance with the values listed in NEMA MG 1–12. NEMA design designations do not apply to motors covered by NEMA MG 1–20.
6. *Service factor.* The service factor is a multiplier that, when applied to the rated horsepower, indicates a permissible loading that may be applied to the motor under the conditions outlined in NEMA MG 1–14.37. The standard service factors for general purpose, open type, ac, motors are listed in NEMA MG 1–12.52. Motors not specifically listed will have a service factor of 1.0 in accordance with NEMA MG 1–12.52.2, unless specified otherwise.
7. *Direction of rotation.* Most ac, polyphase, induction motors are bidirectional. A substantial number of ratings are, however, designed mechanically for unidirectional operation. If a motor is to be capable of operation in both directions, this must be specified. Otherwise, the required direction of rotation must be specified.
8. *Performance characteristics.* Minimum efficiency and power factor values, if desired, must be specified. Most motor manufacturers are able to provide motors having higher than normal efficiency values. Improvements in efficiency values usually involve special features that increase the cost of a motor. These improvements are incremental in nature as they are incorporated into the design. In most cases, some incremental increase in efficiency values can be economically justified by a decrease in operating costs. Normal efficiency values tend to increase with the horsepower rating. Efficiency values attainable for large motors may not be available for medium motor ratings.

AC induction motors inherently have a lagging power factor. Motor manufacturers may be able to provide motors having higher than normal power factor values; however, such designs tend to increase the cost of the motor and reduce efficiency values. In most cases, the use of power factor correction capacitors is a desirable alternative.

Minimum values of locked-rotor (starting), pull-up, and

breakdown torque are stated in MG 1–12 for motors having NEMA design designations. Similarly, minimum torque values are stated in MG 1–20.10 for large motors. If other than standard torque values are required, they must be included in the specification.

*Example:* Motors shall be rated for continuous operation at the horsepower and speed stated on the data sheet. Motors 300 hp and below shall be rated 460 V, 60 Hz, three-phase. Motors above 300 hp shall be rated 4000 V, 60 Hz, three-phase. Motors shall be provided with the service factor stated on the data sheet.

Normal torque motors, 300 hp and below, shall have NEMA Design B characteristics. Normal torque motors above 300 hp shall have the following minimum torque values at rated voltage and frequency:

	Percent of Rated Full-Load Torque
Locked-rotor	60
Pull-up	60
Breakdown	175

Motors shall have minimum efficiency and power factor values as stated on the data sheet. Direction of rotation shall be as stated on the data sheet.

### 3.7.6 Construction Features

Certain construction features such as the type of enclosure and accessory items are optional and must be specified. Avoid the inclusion of special construction features that are not normally considered to be optional.

#### 3.7.6.1 Frame Size

Most low-voltage, integral-horsepower ratings are assigned specific frame sizes in accordance with NEMA standards. The basic dimensions of standard NEMA frames are shown in NEMA MG 1–4.

In the case of large motors covered by NEMA MG 1–20 and high-voltage, 440 frame motors, NEMA has made no frame assignments. In these cases, the frame size of a specific rating is a matter of the design criteria of the motor manufacturer. A rating may be offered in a frame size that is not a NEMA standard frame. In the case of replacement motors, it may be necessary to specify mounting dimensions and shaft locations.

*Example:* Frame size shall be the manufacturer's standard for the rating involved.

#### 3.7.6.2 Enclosure

The two basic enclosure types, open and totally enclosed, are available for most ratings. The variations of these two basic enclosure types are described in NEMA MG 1–1.25 and MG 1–1.26. The availability of most of these variations in enclosure types is limited to particular ranges of frame size. Opentype enclosures may not be provided with restrictive devices over the ventilation openings unless classified as fully guarded. If required, screens, grilles, or baffles should be

specified. Most large totally enclosed motors are provided with tubular air-to-air heat exchangers. If a specific tube material is required, it must be specified. Many specifications include a statement defining acceptable enclosure materials. Enclosure materials are normally cast iron, fabricated steel, or a combination of both.

Holes are normally provided in the bottom of motor enclosures for drainage. The drain holes of totally enclosed motors are normally threaded and furnished with plugs that must be removed to drain the enclosure. Breather drain devices that permit the drainage of condensate or water from the motor can be provided if specified.

Any particular welding requirements that apply to the fabrication of the motor enclosure or parts must be specified.

*Example:* The motor enclosure shall be totally enclosed, fan-cooled (IP44) for NEMA 440 frames and smaller. The motor enclosure shall be NEMA Weather Protected, Type II, (IP2HW) for frame sizes larger than NEMA 440. Major enclosure parts of all motors shall be made of cast iron or fabricated steel.

Louvers or screens shall be provided for the ventilation openings of all open-type motors.

TEFC motors shall have drilled and tapped drain holes located so as to permit drainage from the motor. Drain holes are to be provided with automatic breatherdrain devices.

Stainless-steel cooling tubes shall be provided for motors equipped with air-to-air heat exchangers.

The manufacturer's standard welding procedures shall be acceptable in the construction of steel fabrications.

#### 3.7.6.3 Stator

Stators of low-voltage motors, 600 V and below, are normally provided with random-wound coils of round copper wire coated with insulating enamel. Stators of higher-voltage motors are provided with form-wound coils of rectangular copper conductor covered with either a Dacron glass-covered tape or coated with insulating enamel. Individual form-wound coils are covered with layers of insulating and armor tape before insertion into the stator core. The specific type of winding to be furnished should not be specified unless form-wound coils are specifically required for larger low-voltage ratings in lieu of the random-wound coils normally provided. The various types of insulation systems used in electric motors are classified according to thermal endurance limits. The classification of the various insulation systems is outlined in NEMA MG 1–1.66. The thermal limits of each system are shown in NEMA MG 1–12.42, and MG 1–12.43, and MG 1–20.40, as applicable. Currently, Class F insulation systems are normally used in the manufacturing of electric motors. Class H systems are available, but must be specified.

Integral-horsepower and large motors are frequently provided with Class F insulation but are designed to have temperature rises near the limits established for Class B insulation when operating at rated horsepower, thus extending the life of the Class F system. The additional thermal capability

of the Class F system can be used to accommodate the higher temperatures associated with service factors above 1.0, higher than standard altitudes or ambient temperatures, or operation from a variable-frequency power source. Any stator temperature limits other than standard limits associated with the particular insulation system used must be specified.

After the windings are inserted into the core and the connections made, the stator assembly receives further treatment. Random-wound stators normally receive multiple dips in an insulating varnish with a baking period after each dip. Formwound stators normally receive multiple vacuum pressure impregnation treatments with a baking period after each treatment. If a specific type or number of treatments is required, it must be specified. It should be noted that the vacuum pressure impregnation process is appropriate only for formwound stators and should not be specified for motors having random-wound coils. Although standard form-wound, vacuum impregnated, stator windings are moisture-resistant, a sealed insulation system may be specified. Sealed insulation systems are limited to stators having form-wound coils in accordance with NEMA MG 1–1.27.2.

In applications involving open-type motors and cooling air having a high concentration of abrasive particles, a special abrasive-resistant coating may be specified. This coating, normally silicone rubber, is placed over the winding end turns. In applications involving operations in warm, humid, tropical environments. Special antifungus and tropical winding treatments are available but must be specified.

Standard large motors are designed to withstand bus transfer or reclosing surges in accordance with NEMA MG 1–20.34. If the motor is to be subjected to any unusual stresses resulting from anticipated bus transfer or switching surges, this must be stated in the specification. In such applications the motor manufacturer may elect to design the winding with additional bracing or insulation.

In the case of polyphase, alternating current motors, phase connections are normally made within the motor in an arrangement specified by the designer. If a special connection arrangement is required or if the leads are to be brought out for both ends of each phase winding, this must be specified.

*Example:* Motors rated 460 V and furnished in frame sizes larger than 449 shall be provided with form-wound coils. All motors shall be provided with a Class F, or better, insulation system. The maximum winding temperature rise at rated horsepower shall be limited to the maximum values for Class B insulation as stated in NEMA MG 1.

Stator windings having form-wound coils shall be provided with an insulation system utilizing epoxy vacuum pressure impregnation with a combination of materials and processes that will provide a fully sealed winding as defined in NEMA MG 1–1.27.2. Form-wound stator windings shall be capable of passing a conformance test performed in accordance with NEMA MG 1–20.18.

If specified on the data sheet, open-type motors shall be provided with a silicone rubber abrasion-resistant coating on the winding end turns. Windings shall be braced for an occasional energized transfer from one power source to

another within a transfer time not to exceed five cycles.

### 3.7.6.4 Rotor

Squirrel-cage rotors are manufactured in one of three basic cage design configurations, that is: die-cast aluminum, fabricated aluminum, or fabricated copper or copper alloy. Manufacturers are limited to maximum die-cast rotor dimensions depending upon the capability of their die-casting equipment. Larger rotors must be fabricated. In some cases, fabricated rotors can be provided instead of die-cast rotors. Fabricated copper rotors are frequently used in applications involving severe starting requirements, above normal torque, or higher than normal efficiency values. If a specific cage construction or material is required, it must be specified. The bars of fabricated copper rotors are brazed to the shorting rings. In some environments, the use of phosphorus-free brazing materials may be preferred. If so, it must be specified.

Any specific directional or material requirements for rotor-mounted fans must be specified. Squirrel-cage rotors are designed for overspeed capability in accordance with NEMA MG 1–12.48 or MG 1–20.44. If an overspeed capability in excess of the NEMA standard is required, it must be specified.

*Example:* All induction motors shall have squirrel-cage rotors. Rotors shall be adequately sized to avoid overheating during acceleration of the motor and driven equipment. Rotors may be aluminum die-cast construction; copper or copper alloy cage materials, or fabricated aluminum. Phosphorus-free brazing material shall be used in the fabrication of copper bar rotors. Ventilating fans shall be suitable for rotation in either direction and shall be made of steel, bronze, or cast aluminum.

### 3.7.6.5 Bearings and Lubrication

Both antifriction and sliding-type bearings are used in the construction of electric motors. Integral-horsepower ratings are normally available only with antifriction bearings. In general, large motor ratings are available with either antifriction or sliding-type bearings. Design parameters limit the use of antifriction bearings to a maximum size and speed, beyond which sliding-type bearings must be used. Antifriction bearings must be used for belt-drive applications involving radial bearing loads and, unless special provisions are made, for applications involving axial thrust loads. Normally, sleeve-type sliding bearings have no axial thrust capability and the motor must be connected to the driven load through a limited end-float coupling. For vertical motors, special sliding-type thrust bearings are available for the more extreme thrust loads. The type of bearings required should be stated in the specification.

When choosing between antifriction and sleeve bearings there are some notable considerations. Antifriction bearings are standardized and widely used, consequently, replacement bearings are relatively easily obtained. Sleeve bearings are usually obtainable only from the motor manufacturer's authorized service shops. Antifriction bearings are more easily maintained and do not require frequent inspection, as do sleeve bearings. Within limits, motors having antifriction bearings

may be mounted in positions other than horizontal. Sleeve bearing motors must be mounted in a horizontal position. If properly maintained, sleeve bearings are subject to little wear and will remain in service indefinitely. Antifriction bearings will eventually wear to the point that replacement is required.

Antifriction bearings are selected by the motor manufacturer to provide a reasonable  $L_{10}$  life. Belt driven applications require special consideration because  $L_{10}$  life is affected by the amount of belt pull.

NEMA MG 1–14.42 lists the parameters within which standard integral-horsepower motors having antifriction bearings may be used in belt-drive applications. For applications beyond the limits shown in NEMA MG 1–14.42, detailed information regarding the belt-drive arrangement must be given to the motor manufacturer. In most cases, special bearing arrangements can be provided to meet the application requirements. Typically, antifriction bearings are selected to provide a 15-year  $L_{10}$  life in direct-drive applications and a 3-year  $L_{10}$  life in belt-drive applications. If a particular  $L_{10}$  life is required for antifriction bearings, it must be specified. Antifriction bearings are usually grease-lubricated, although in some applications, antifriction bearings may be lubricated with an oil mist or bath. Sliding-type bearings are oil-lubricated.

Sleeve bearings used in large motors are normally self-lubricating with an oil ring and reservoir arrangement. External pressurized lubrication systems may be required for higher speeds or very large motors and for certain types of sliding bearings. If the application involves a pressurized lubrication system and it is not required by the bearing design, this must be specified. Normally, the pressure lubrication system is provided by others and the motor manufacturer will furnish the motor with the necessary provisions for operation with the pressurized system.

The external thrust requirements for vertical pump motors must be specified in order to assure adequate bearing thrust capability. Bearing temperatures are limited by design criteria to those maximum levels considered to be acceptable. If bearing temperatures are to be limited to a particular level, it must be specified.

Shaft currents are limited by design criteria to those maximum levels considered to be acceptable. If necessary, at least one bearing will be insulated. If bearing insulation is specifically required, it must be specified.

Motor manufacturers will normally provide integral-horsepower and large motors having antifriction bearings with provisions for relubrication. Threaded fill and drain openings with plugs are usually furnished. Any particular devices other than plugs must be specified.

Motors having sliding-type, oil-lubricated bearings are provided with oil fill and drain openings. A gauge or sight-glass is normally furnished to provide a visual indication of the oil level in the reservoir. If particular devices such as oil ring sight-glasses, external oil level gauges, or constant-level oilers are required, they must be specified.

Sleeve bearing motors are designed to have a small amount of free axial rotor movement between the bearings. This is called end-float. When the motor is energized, the rotor moves axially to a point approximately halfway between the extremes

of end-float, to a point called magnetic center. In order to prevent damage to the bearings resulting from external thrust loads, limited end-float couplings are used. Standard rotor and coupling end-float values are stated in NEMA MG 1–14.39 and MG 1–20.30. Any particular end-float requirements must be specified.

#### *Example*

1. Horizontal motors rated 1000 hp and below shall be furnished with grease-lubricated, antifriction bearings. Horizontal motors rated above 1000 hp shall be furnished with sleeve bearings.
2. Antifriction bearings shall be manufactured to AFBMA standards and selected for electric motor service. Antifriction bearings for horizontal applications shall have an  $L_{10}$  life of 15 years in direct-coupled service and 3 years in belt-drive applications.
3. The bearing housings of motors having antifriction bearings shall have threaded and plugged lubrication fill and drain holes.
4. Sleeve bearings shall be split-type, self-lubricating, and be provided with one-piece oil rings. The bearing housings shall be split to permit replacement of the bearings without removing the bottom section of the housing.
5. Sleeve-bearing motors shall have oil reservoirs of adequate capacity with fill and drain openings. Oil level gauges and oil ring inspection sight-glasses shall be provided.
6. Insulation shall be provided, as required, to prevent damage to the bearings as the result of circulating shaft current.
7. Motors requiring pressure lubrication shall be furnished with provisions only for flood lubrication. The lubricating oil pumping system, including all auxiliary motor driven pumps, piping, and controls will be supplied by others.
8. Horizontal sleeve-bearing motors shall be provided with openings in the bearing housings for measurement of the air gap.

#### *3.7.6.6 Terminal Boxes*

Main terminal or conduit boxes are normally designed for wire-to-wire connections. Minimum dimensions and usable volumes are listed in NEMA MG 1–4.19. The dimensions of the main conduit box depend upon the size of motor lead and supply cable, voltage, and any special termination requirements such as stress cones. If protective equipment such as lightning arresters, surge capacitors or current transformers are required, they are normally mounted in an oversized main terminal box.

Terminal boxes are normally made of cast iron or pressed steel. Larger boxes are fabricated from steel plate. Most motor manufacturers have designed a series of standard boxes and will select a box that best suits the particular application. An attempt to include a particular type of construction or specific dimensions in the specification is not recommended. Terminal



box dimensions are normally specified as minimum dimensions. Specific conduit size openings may be specified.

The location of the main terminal box is defined by an assembly symbol. The various assembly symbols are shown in NEMA MG 1-4.02 and MG 1-4.3. Any arrangement other than the standard F-1 assembly must be specified. It is appropriate only to specify the side of the motor on which the main and auxiliary terminal boxes are to be mounted. The exact location of the terminal boxes along the side is often dictated by the basic design of the motor.

Terminal boxes are normally mounted in such a way as to accommodate the entrance of incoming leads from the bottom. If the incoming leads are to enter the box from any other direction, this must be specified. Most smaller terminal boxes are bolted to the enclosure and may be fully rotated in 90-degree increments providing there are no obstructions. Oversize terminal boxes containing protective equipment are not normally rotatable. In the case of larger terminal boxes, the bottom of the box may extend below the horizontal plane of the motor base. If this is not acceptable, it should be so stated in the specification.

Terminal boxes are not usually provided with drains or breathers. If required, they must be specified. Accessory leads of low-voltage motors are normally brought to the main terminal box. In the case of motors having higher voltages, accessory leads are brought to one or more auxiliary boxes.

Medium and large motors are normally provided with a means of grounding within the main terminal box. If a specific grounding arrangement is required, it must be specified.

*Example:* Motors rated 600 V and below shall be provided with a diagonally split, cast iron, main terminal box. The main terminal box shall be designed for full rotation in 90-degree increments to receive conduit from any of four directions.

Motors rated above 600 V shall be provided with a main terminal box for the power leads and separate auxiliary terminal boxes for the accessory leads. Leads insulated for different voltage classes shall not occupy or terminate in the same box. Terminal boxes shall be cast iron or fabricated steel and be either diagonally split or provided with a bolted front cover plate. All terminal boxes shall have threaded hubs for connection to rigid conduit.

A nonconducting lead positioner and gasket shall be furnished between the enclosure and the main terminal box.

The main box shall contain a bolt-type-grounding lug suitable for stranded copper cable size 1/0 through 4/0 AWG.

### 3.7.6.7 Leads and Terminals

Medium and large motors are normally provided with flexible leads that extend from the winding into the main terminal box. The motor leads are usually furnished with compression-type terminals suitable for wire-to-wire connection to the incoming power supply leads. If a particular lead length or type of terminal is required, it must be stated in the specification.

Motor leads are identified in accordance with NEMA MG

1-2. The specific method of lead identification is a matter of the manufacturer's standard practice.

Leads for accessory devices are usually brought to terminal boards in the auxiliary boxes. If a particular auxiliary box or accessory lead termination arrangement is required, it must be specified.

*Example:* Motor leads shall be fully insulated, fitted with compression terminals, and provided with permanent identification within the terminal box. All motors shall have their leads tagged and the nameplates stamped to indicate the direction of rotation when a specific phase sequence is applied.

### 3.7.6.8 Mounting

Most medium and large motors are mounted horizontally on a floor or base. Standard symbols for the various mounting arrangements are shown in NEMA MG 1-4.3. Mounting arrangements other than F-1 and F-2 are restricted depending upon the size and type of motor.

The basic mounting dimensions of motors manufactured in standard NEMA frames are listed in NEMA MG 1-4.4; however, it is recommended that dimensional information be based on outline drawings or specific information provided by the motor manufacturer. Motors used in belt-drive applications may be mounted on adjustable subbases or rails. These devices can be provided by the motor manufacturer, if specified. Large horizontal motors are frequently mounted on soleplates that are imbedded in the foundation or base on which the motor is mounted. If soleplates are required, they must be specified.

In applications involving replacement motors, adapter bases can be provided to compensate for differences in shaft height and location of foot mounting holes. If required, specific details of the existing mounting arrangement must be made available to the motor manufacturer.

Dowel pins are frequently used in the mounting of large motors. If specified, the motor manufacturer can provide the motor with dowel pin pilot holes drilled in the motor base. Dowel pins and mounting bolts are not normally furnished by the motor manufacturer. If required, they must be specified.

Shims are used to assist in the proper leveling and alignment of a motor. The motor manufacturer can furnish shims, if specified. If a particular material or thickness is desired, it must be specified. Jacking screws may also be used for leveling and alignment. If specified, jacking screws for vertical alignment can be provided in the motor base. Jacking screws for horizontal alignment are also available if specified, but the motor must be mounted on a subbase or soleplate.

*Example:* Unless otherwise stated on the data sheet, all motors shall be mounted horizontally with the main conduit box in the F-1 position.

Large horizontal motors shall be provided with dowel pin pilot holes.

Large motors shall be provided with stainless-steel laminated shims for each foot having a total thickness of 3/8 inch per foot.

Large horizontal motors shall be provided with two-piece soleplates.

Large horizontal motors shall be provided with vertical and horizontal jacking screws.

### 3.7.7 Accessories

Most accessory devices are optional and must be specified. Motor accessories are usually protective in nature and are intended in some way to prevent damage to the motor. Because the cost of a motor is increased with the addition of most accessory devices, their use is influenced by the invested cost of the basic motor, the critical nature of the application, and the ease of replacement should a failure occur.

#### 3.7.7.1 Winding Temperature Measurement

Winding temperature sensing devices are used in motors of all sizes. On-off switching devices such as thermostats and thermistors are frequently used to deenergize a motor when the winding temperature reaches a predetermined level. These devices are normally mounted on the surface of the winding end turns.

Resistance temperature detectors (RTDs) and thermocouples are available for use with larger motors. These devices are normally embedded between coils in the middle of the stator slots. When used with the appropriate external instrumentation, these devices are able to measure specific temperature values. When specified, the motor manufacturer will provide thermal sensors embedded in the stator during the winding operation with the leads brought to a terminal box. Normally, others supply all instrumentation and monitoring equipment. Various types of RTDs and thermocouples are available. The particular type required must be specified. Embedded-winding temperature detectors are discussed in NEMA MG 1–20.63.

#### 3.7.7.2 Bearing Temperature Measurement

Thermal sensing devices are available for use with sliding-type bearings to provide advance warning of impending bearing malfunction. Thermal devices are not recommended for use with antifriction bearings. Normally, antifriction bearings do not experience an elevation in temperature until near the time of failure, consequently, thermal devices will not provide an early warning function as in the case of sliding-type bearings.

Bearing RTD and thermocouple arrangements are available for monitoring bearing temperature. As in the case of winding detectors, the motor manufacturer will normally provide only the sensing devices. Others furnish instrumentation and monitoring equipment. If required, the particular type of RTD or thermocouple must be specified.

Dial-type thermometers are available for bearing temperature monitoring. These devices can be provided with alarm contacts or relays, if specified. Bearing temperature relays only can be provided, if specified. All types of bearing temperature-sensing devices must be specified, if required.

#### 3.7.7.3 Space Heaters

Although one of the most commonly used accessory items for medium and large motors, space heaters are not normally

considered to be a standard feature and must be specified. In most cases, space heaters are supplied by a single-phase power source and the voltage and frequency must be specified. Standard space heater arrangements may result in heater sheath temperatures of up to approximately 400°C. In some applications, it may be necessary to limit sheath temperatures to lower values. If lower than standard space heater sheath temperatures are required, this must be specified.

#### 3.7.7.4 Filters

Filters are often used with WP 2 construction. If required, filters and differential pressure devices must be specified.

#### 3.7.7.5 Surge Protection

Higher-voltage motors are frequently exposed to excessive voltage surges caused by switching, line faults, or lightning. These surges assume the familiar traveling-wave form. If specified, the motor manufacturer can provide surge protection.

Lightning arresters are used to protect the ground wall insulation of the motor winding by reducing the magnitude of the surge waveform. Surge capacitors are used to protect the turn-to-turn insulation by reducing the slope of the wavefront. Full surge protection, therefore, involves the use of both arresters and capacitors. These are usually mounted in an oversize main conduit box.

Large motors are frequently provided with current transformers arranged for ground fault protection or line metering. Current transformers are usually mounted in the main conduit box. Ring- or window-type transformers are normally furnished with one or more motor leads passing through the center of each transformer. The leads of the current transformers are usually brought to a terminal board in a separate auxiliary terminal box. If current transformers are required, their purpose and their current ratio must be specified.

#### 3.7.7.6 Vibration Detection Devices

Any type of vibration detection equipment must be specified. Normally, the motor manufacturer will provide only the pickup transducers or sensors mounted in or on the motor. Others provide monitoring and alarm equipment.

#### Example

1. *Winding temperature detectors.* Medium motors, rated 600 V and below, shall be furnished with thermostats, one per phase, mounted on the winding end turns.

Medium motors rated above 600 V and all large motors shall be furnished with six 10–11 three-wire, RTDs, two per phase, evenly spaced around the stator and embedded between the coils in the stator slots.

2. *Bearing temperature detectors.* Horizontal sleeve bearing motors shall be furnished with one 10-V, three-wire RTD per bearing. Bearing RTDs shall have a stainless-steel sheath and be spring-loaded with the leads brought to a connection head.
3. *Space heaters.* All medium motors rated above 25 hp and all large motors shall be furnished with space heaters.

Space heaters rated 1200 W and below shall be suitable for operation from a 120-V, single-phase, 60-Hz power source. Heaters rated above 1200 W shall be suitable for operation from a 208-V, three phase, 60-Hz power source. Space heaters shall be sized as required to maintain the internal temperature above the dew point when the motor is idle.

4. *Filters and differential pressure switches.* WP 2 enclosures shall be provide with washable filters. Differential pressure switches shall be provided to indicate a reduction in airflow.
5. *Surge protection.* Motors rated 2000 hp and above shall be provide with a surge capacitor and lightning arresters mounted in the main conduit box.
6. *Current transformers.* Motors rated 2000 hp and above shall be provided with three 50:5 ratio current transformers in the main conduit box arranged for self-balancing differential protection.
7. *Vibration detection.* Motors rated 200 hp and above having antifriction bearings shall be provided with one vibration detection switch at each bearing. Detection switches are to be located so as to sense the horizontal radial vibration level.

### 3.7.8 Balance and Vibration

Standard medium and large motors are designed and the rotors are balanced to achieve vibration levels within the maximum permissible levels stated in NEMA MG 1–7.8. The maximum vibration levels listed are based on vibration measurements made in accordance with NEMA MG 1–7. In both cases, the vibration levels are measured radially and axially with the motor running at no load. Motors having dynamic balance characteristics within the NEMA standard limits are satisfactory for most applications.

In some applications, it may be desirable to limit the maximum permissible vibration to levels that are lower than those listed in NEMA MG 1. Generally speaking, vibration levels that are within 50% of the NEMA MG 1 standard levels are achievable with special high-precision designs and manufacturing techniques. Any dynamic balance requirements other than those contained in NEMA MG 1 must be specified.

Careful consideration should be given to the inclusion in the specification of any method or condition of vibration measurement other than that stated in NEMA MG 1. Vibration levels measured on the shaft are usually higher than and do not necessarily correlate to bearing housing readings. Vibration measurements taken under loaded conditions will be influenced by the mounting arrangement and alignment achieved in connecting to the test load. In addition, vibration of the loading device may well be transmitted to the motor under loaded conditions.

*Example:* Motors shall have the rotors dynamically balanced so as to achieve vibration characteristics within the limits stated in NEMA MG 1 when measured in accordance with NEMA MG 1.

### 3.7.9 Sound Levels

The airborne sound level of standard medium and large, polyphase, squirrel-cage induction motors will be within the limits stated in NEMA MG 1–9.6. The limits shown are stated in terms of sound power. Sound power is a measure of the absolute sound produced by a particular source but does not reflect the conditions to which the human ear is exposed. Sound level requirements are normally expressed in terms of sound power because pressure must be stated at a specific reference distance, usually 3 feet, 5 feet, or 1 meter. Normally, maximum permissible sound levels are stated in terms of adjusted decibel (dB(A)). The sound levels of medium and large motors are measured in accordance with ANSI S12.34 and NEMA MG 1–9 at no load. Motors having sound levels lower than the manufacturers standard may be available but must be specified.

*Example:* Motors shall be provided having a maximum overall airborne sound power level of 90 as measured in accordance with ANSI s12.34 [22].

### 3.7.10 Paint

Normally, motor manufacturers will furnish motors having their standard paint system applied over a suitably prepared surface. In most cases, these standard systems have evolved from years of field experience by the manufacturer and are adequate for most applications. Special colors normally present little difficulty for the manufacturer; however, special paint systems may not be available. Environmental restrictions may prevent the use of certain types of paint within the confining area of the manufacturing facility. In some cases, the motor manufacturer may not be able to provide the surface preparation required for a particular paint system. Careful thought should always be given to the acceptability of the manufacturer's standard paint system whenever a special paint system is considered.

*Example:* All motors will be cleaned, primed, and finish painted in accordance with the motor manufacturer's standard specification. The total dry film thickness of primary and finish coat shall be a minimum of 3 mils.

### 3.7.11 Nameplates

The nameplates of medium and large motors must provide at least the information indicated in NEMA MG 1–10.40 and MG 1–20.25. Motor manufacturers will provide additional information, either on the main nameplates or on separate plates, if specified. If a particular nameplate material is required, it must be specified.

*Example:* Each motor shall have a main stainless steel nameplate providing information in accordance with NEMA MG 1-10.40 or NEMA MG 1–20.25, as applicable. In addition, LRC, total motor weight, and winding temperature rise at service factor load shall be shown on the main nameplate.

A separate stainless-steel plate stating the starting limitations shall be provided.

A separate stainless-steel plate stating lubrication instructions shall be provided.

### 3.7.12 Performance Tests

Medium and large polyphase induction motors normally receive, as a minimum, a routine test in compliance with NEMA MG 1–12.56 and MG 1–20.16, as applicable. Tests are performed in accordance with IEEE Std. 112 [20]. The routine test includes a no-load running test and provides the motor manufacturer with information to confirm that the motor is as designed and is suitable for service. If a certified test report is required, it must be specified.

The following special tests are available and can normally be performed, if specified.

1. A complete test will provide performance information and efficiency values in accordance with NEMA MG 1–12.59, and MG 1–20.21, as applicable. The various methods of performing a complete test are outlined in IEEE Std. 112, Test Procedure for Polyphase Induction Motors and Generators [20]. In general, the use of Method A in the standard is restricted to small motors. Availability of test equipment may limit the use of Method B to medium motors and specific ranges of large motor ratings. Methods E or F are normally used for large motors.

If a loading device is available, Method E will probably be used. If a loading device is not available, Method F is the likely choice. Both Methods E and F utilize the segregation of losses; however, power input under load is measured in Method E, whereas Method F is a no-load test and performance information is calculated from the equivalent circuit.

2. If specified, sound level tests will be performed in accordance with ANSI S12.34 [22] and NEMA MG 1–9, as applicable.
3. For stators having a form-wound coil sealed insulation system, a special conformance test in accordance with NEMA MG 1–20.18 and IEEE SW. 429. Evaluation of Sealed Insulation Systems for A-C Electric Machinery Employing Form Wound Coils [23] may be specified.
4. If specified, a bearing temperature stabilization test will be performed. In this test, the motor is run under idle conditions until the bearing temperatures stabilize. If a complete test has been specified and a heat run is included, bearing temperatures will normally be monitored during the heat run.
5. Vibration levels are measured during the routine test in accordance with NEMA MG 1–7. Normally, unfiltered measurements only are made. Any special test requirements such as measurement of both unfiltered and filtered vibration levels, vibration levels during coast down, and so forth, must be specified.

Additional and special testing can be time consuming and is normally expensive. Care should be exercised in the selection of special tests to assure that they are appropriate and are not redundant.

If specified, a representative or the purchaser may witness tests. However, this can result in shipment delays and adds to the cost of the motor. If contemplated, it is recommended that

serious consideration be given to the necessity of including this requirement in the specification. Unless a qualified observer is available to witness the test, the practice is of questionable value.

*Example:* Each integral-horsepower motor shall receive a routine test in accordance with NEMA MG 1–12.56 and IEEE Std. 112 [20]. The motor manufacturer shall provide four copies of a certified test report for each motor tested.

Each large motor shall receive a routine test in accordance with NEMA MG 1–20.16 and IEEE Std. 112. The motor manufacturer shall provide four copies of a certified test report for each motor tested.

Motors rated 2500 hp and above shall receive a complete test, including heat run, performed in accordance with Method E. One motor only of each rating shall receive a complete test. The remaining identical motors shall receive a routine test. The motor manufacturer shall provide four copies of a certified test report for each motor tested.

### 3.7.13 Quality Assurance

Typically a motor manufacturer will have a standard quality assurance program in place with specific documented procedures. Normally, the standard program will not include such features as 100% inspection of parts, tractability of materials, certificates of conformance, and so forth. Any specific quality assurance requirements must be specified. It should be emphasized that any special quality assurance requirements must be made known to the motor manufacturer at the time of order placement. After an order is placed, it may be difficult if not impossible to implement many special quality assurance features.

*Example:* All motors shall be manufactured utilizing the manufacturer's standard quality assurance program.

### 3.7.14 Preparation for Shipment and Storage

Medium and large motors manufactured for domestic use within the continental United States are normally prepared for under cover, land transportation to the specified shipping destination. This type of shipping preparation is usually limited to placing the motor on a wooden pallet or skid that is bolted to the motor base. Exposed unpainted or unprotected metal surfaces are covered with a removable protective coating. The rotors of motors having sleeve bearings are blocked to prevent axial movement during shipment.

Motors provided with standard packaging are suitable for storage under cover in clean, dry, well-ventilated location free from vibration and rapid or wide variations of temperature. If storage suitability is required for periods in excess of 6 months, it must be specified. Any special shipping or storage requirements must be specified.

*Example:* All motors shall be prepared for shipment utilizing the manufacturer's standard domestic packaging procedure.

### 3.7.15 Data and Drawings

Motor manufacturers will normally provide a minimum of data and drawings. If specific information is required, it must be specified.

*Example:* The manufacturer shall provide four copies of the following information for installation, maintenance, and record purposes:

1. Certified outline drawings of the motor and all auxiliary equipment.
2. Certified wiring diagrams of the motor and all auxiliary equipment.
3. Installation, maintenance and operating instructions, including drawings, illustrations, and complete parts list.
4. Bearing reference data consisting of part numbers and quantities recommended for stock including oil rings, oil guards, oilers, and so forth.
5. Performance data.

## 3.8 SPECIAL APPLICATIONS

Although many motors are labeled “general purpose,” a high percentage of motors are in fact designed with a special purpose in mind. If the application requirements are well defined, both the motor manufacturer and the customer will benefit. Some of the major requirements to be defined include torque loading, duty cycle, chemical and thermal environment, and number of start-up cycles. With points such as these defined, the design engineer can begin to determine the amount of steel, the conductors, and the insulation system that will result in a life expectancy that is agreeable to both the initial customer and the end user. For example, the amount of steel will be dictated by the voltage range to which the motor will be subjected. A motor designed for a 200/240 V range will require more steel than a motor applied to a stiff line held at exactly 230 V. The reason, of course, is that at 200 V the motor must have enough torque (or flux) to operate properly at the heaviest load. However, since the flux level at 240 V is 20% greater than that at 200 V, a longer stack is required to keep the magnetizing current and core loss at acceptable levels with respect to winding temperature and operating efficiency.

A similar argument can be made for the selection of the amount of cross section of the stator and rotor conductors. If the motor is lightly loaded a high percentage of the time, the motor can be designed at a higher level of rated load current density than one operating at a heavy load almost continuously. The heat developed by the winding losses can be transferred to both the stator and rotor steel and also to the cooling medium surrounding the motor.

Another major factor in motor designs is the type of insulation system. This includes such items as slot liners and wedges, phase insulators, magnet wire enamel, and the amount and type varnish used to securely bond the stator conductors to each other. Motors rated at 2300 or 4000 V will have a much higher electrical stress from turn to turn, phase to phase, and winding to ground than will motors operating at ordinary residential and commercial voltages of 115 and 230 V.

Consequently, the higher the operating voltage, the thicker the ground and magnet wire insulation.

In many cases, the chemistry of the insulation system is as important as the thickness. Motors intended for duty in a steel mill or petroleum refinery may be subjected to acid fumes likely to attack both the metallic and nonmetallic parts of the motor. Without proper protection, a shortened motor life could ensue. Similar cases could be made for motors used in gasoline pumps, submersible water pumps, and deep-well pumps used in the petroleum fields.

The cooling system and the means for lubricating the motor bearings must be well designed. Motors in hazardous applications will most likely be totally enclosed and fan-cooled by the air within the motor enclosures. Motors intended for submersible pumps will rely on transfer of the motor heat through the stator core to the outside enclosure, which is in contact with the water or fluid being pumped. Depending on the application, the bearings might be grease-filled ball bearings or sleeve bearings lubricated by an oil-filled wicking material.

### 3.8.1 Hermetically Sealed Refrigeration Motors

#### 3.8.1.1 Insulation Selection

*[Editors' note:* Motors to be applied to a refrigeration compressor operate in an unusual environment, in which the motor operates in a refrigerant atmosphere. With the mandated phasing-out of the chlorofluorocarbons (CFCs) as refrigerants, refrigeration motors will continue to operate in an unusual environment, but an environment that will not initially be as well understood as the refrigerant environment of today. Nevertheless, one may expect interactions between newer refrigerants and the materials of the drive motor that are somewhat similar to those encountered with refrigerant. The following discussion illustrates some of the possible effects to be evaluated.]

The motors to be applied to a refrigeration compressor have special considerations. First, the refrigerant, such as R-12, R-22, or R-134a, turns out to be an excellent solvent. If any of the insulating components is slightly soluble, the refrigerant will partially dissolve them and cause the material to migrate throughout the system. In some cases, the dissolved material could coat any of the moving parts such as the pistons, valves, or the inside of the tiny capillary tube that is often used in place of an expansion valve. If the tube becomes clogged or if the parts become excessively coated with this migrating material, the refrigeration system could malfunction or have seriously degraded performance. Consequently, the motor designer must select refrigerant compatible organic materials for the insulation system.

Of particular importance in the material selection are the ground insulation (slot liners and wedges), phase insulation, wire enamel, and any varnish that may be used to tightly bond together the magnet wires and laminations. The vendors supplying the magnet wire and ground insulation are generally in a good position to supply the proper materials to meet the refrigeration-compatible requirements. The varnishing process must be controlled by the motor

manufacturer. In essence, the manufacturer must be sure that any baking process fully converts the monomer into a fully polymerized material to prevent the refrigerant from “leaching out” the monomer and causing it to be dispersed in the refrigerant and oil.

The compressor motor is nearly always subjected to both refrigerant and oil during its operation. In a high percentage of compressors the motor is on the low-pressure side of the system. In this situation, the refrigerant is less active than when the motor is on the high-pressure side of the system. In the “low side,” the motor is subjected to low-pressure, warm gas returning from the evaporator to the compressor. In high-side compressors the motor “sees” hot, high-pressure gas before it goes to the condenser to be condensed to a liquid. Any improperly selected insulation or undercured varnish will be readily attacked by the refrigerant. Such systems often use polyester insulating films that have been processed in boiling benzene or refrigerant to extract any unpolymerized monomer that would otherwise be dissolved in the refrigeration system to the detriment of the compressor.

During the development of wire enamels to withstand attack by refrigerants, it was found that some enamels allowed the refrigerant to migrate into the enamel. If the pressure in the compressor was reduced, the enamels would balloon out. Pressure reduction is not uncommon in motors and compressors subjected to the rigors of air conditioning and heat-pump operation. Today’s enamels for refrigeration applications have been highly refined to satisfy almost any situation. Various wire manufacturers have formulations involving polyester imides, polyimides, polyamides, or combinations involving undercoats, overcoats, etc.

The primary purpose of the varnishing process is to make a tight bond between the individual wires, both in the slots and in the end turns. A “rule of thumb” has been adopted by many motor manufacturers to varnish only motors of about 1 hp or greater. The major deciding factor is the magnitude of forces on the conductors themselves. Just as the rotation of the rotor is caused by the magnetic force acting on a current-carrying conductor, the current-carrying conductors in the stator are also subjected to the magnetic field both in the slots and in the end turn region. Motors carrying hundreds of amperes within the conductors are likewise subjected to hundreds of pounds of force. Since the conductors are carrying ac, the forces are pulsating. Without sufficient bonding enamel and lacing cord to bond together the wires or wire bundles, the strong pulsating forces will literally tear the stator winding apart.

High-speed movies have demonstrated how the rapid movement of the conductors both against themselves and against the stator core can quickly erode the wire enamel until shorted turns or shorts to ground cause catastrophic failure. Great care is taken to monitor the integrity of the wire enamel, the winding process itself, and other manufacturing processes to ensure long life of the motor. A further complicating factor is the softening of the varnish and wire enamel because of the motor temperature and the presence of gas or liquid refrigerant flowing over the winding. While the motor designer appreciates the cooling nature of the refrigerant

gas flowing over the motor, the designer is also cognizant of the detrimental nature of its solvent action.

### *3.8.1.2 Steel Selection and Processing; Core Construction*

The steel used by most motor manufacturers has gradually been changed from a high-silicon steel to a steel with little or no silicon. Early developments in the 1960s showed that the addition of small amounts of phosphorus and manganese together with thinner gauge material resulted in a level of core loss quite comparable to the thicker-gauge steel using 2–3% silicon. Later refinements included the use of a “critical strain” plus a close control on the carbon level in the incoming steel and the furnace atmosphere to reduce the carbon level to about 0.003–0.005%. The purpose of critical strain is to induce grain growth during annealing, thus assuring an acceptable permeability level. The low carbon level ensures the designer of an acceptable level of hysteresis loss, and the addition of the alloying element, keeps the steel resistivity level high enough so that eddy current losses are at an acceptable level.

Steel manufacturers have further improved today’s steels through the application of “oxygen-blowing” to remove carbon and also through the use of argon and nitrogen bubbling from the bottom of the molten steel to further remove impurities that would otherwise raise the core loss and reduce the permeability. It is not uncommon to obtain steel with core loss levels of 2.5–2.75 W/lb (5.51–6.06 W/kg) at 1.5 Tesla. Also, the relative permeability at 1.5 Tesla is in the range of 2000–2500.

Through the judicious selection of chemistry and gauge, the motor designer can find an acceptable steel for the application. The designer must also keep in mind the operating frequency of the motor. The core loss and permeability levels mentioned previously are at 60 Hz. Also, one should be aware that the stator and rotor tooth frequencies are many times higher than the fundamental yoke flux frequency. It is generally accepted that the high-frequency losses in the stator and rotor teeth account for about 25% of the total iron losses. Another factor precluding the need for extremely high permeability is the fact that most motors have about 85% of their ampere-turns of mmf in the air gap with the remaining ampere-turns in the steel. Therefore, a slight improvement in steel permeability is seldom significant.

Since the purpose of using laminated steel is the reduction of the eddy current component of the iron losses, the manufacturer must use care that the manufacture of the complete stator core retains most of those characteristics. Ideally, one would desire that the stator core has the electrical characteristics of laminations that are perfectly insulated from each other but also retains the mechanical characteristics of a solid block of steel. Even though that goal is not completely met, the stator core in today’s hermetic motor is a highly efficient “conductor” of magnetic flux. Most manufacturers process the punched laminations through one or more annealing operations that together produce the desired magnetic characteristics within the steel and also produce a surface finish that insulates the laminations from one another. This insulation, while not perfect, is sufficient to keep the

eddy-current losses to an “economically acceptable” level. Assuming the motor manufacturer is not using “fully-processed” or preannealed steel, it must be conditioned prior to stator core assembly such that the core losses and permeability are acceptable.

Depending on the exact chemistry and mechanical condition of the as-punched steel, the laminations are processed in an atmosphere-controlled furnace at a temperature of 730°C (1350°F) or higher. The atmosphere is often a mixture of partially burned natural gas and air. This mixture is rich in hydrogen, having a “reducing” characteristic capable of lowering the carbon content to acceptable levels while minimizing oxidation of the steel. Without this carbon removal, the steel would have high losses and low permeability. Care is taken to prevent excessive annealing temperatures, which would cause internal oxidation and render the steel useless.

The next most important factor is the growth of large grains, which affect both the core loss and the permeability. Not only are the temperature and the time at that temperature important factors in the annealing process, but also the time rate at which the laminations are heated and cooled. Many manufacturers use minimum times of 30–45 minutes at the “cold spot” temperatures. Cold spot refers to those laminations or cores that are subjected to the lowest temperature within the oven. Obviously, this treatment applies to entire stator cores or groups of loose laminations being processed.

So far, the preceding discussion has addressed only the magnetic characteristics *within* the lamination itself. The next step is the formation of a high-resistance coating on the surface of the lamination. This is done in a separate furnace at a lower temperature and in an oxidizing atmosphere, or in another zone within the main annealing furnace. The goal is to build a thin layer of blue magnetic oxide,  $\text{Fe}_3\text{O}_4$ , on the surface of the lamination. This oxide, like the blue coating on a gun, can be a rust deterrent and also an electrical insulation between individual laminations. The combination of the “full” or magnetic anneal together with the blue anneal process results in a stator core that exhibits most of the desired characteristics: high permeability, low loss, and high interlaminar resistance to reduce the flow of cross-current or interlaminar current.

While the discussion has been directed toward the annealing of separate laminations, it also applies to the annealing of complete stator cores. High mechanical strength can be achieved by use of numerous welds on the outer periphery of the stator core. If this construction is used, it is generally advisable to weld unannealed laminations and then process the welded cores through the annealing furnaces. This procedure is not without its own problems, however. Since the magnetic anneal is achieved only when the cores become “yellow hot” in the furnace, the combination of both temperature and furnace atmosphere is highly conducive to lamination sticking, which must be alleviated prior to winding. If it is not, the core will exhibit high core loss and the resultant motor will have degraded performance and possible attendant shorter life. The solution is the addition of a procedure that hammers, vibrates, or by various other methods causes the laminations to become “unstuck.”

A procedure that has been used by a number of foreign and

domestic manufacturers is the use of “cleared” cores. In this process, strips of metal, called cleats, are inserted into slots in the outer periphery of the core. While the laminations are compressed, the cleats are pressed into the slots and the ends of the cleats are bent over to form holding tabs. The use of cleats now permits the motor manufacturer to use preannealed laminations. This essentially eliminates interlaminar sticking and the increased core loss that it causes.

### 3.8.1.3 Stator Mounting

While most of the early refrigeration compressors used round motors, more recent compressor manufacture has seen the adoption of motors bolted down to the compressor. Heretofore, the round motors were pressed or shrunk into compressor shells. That procedure was expensive both for the motor manufacturer and the compressor manufacturer. Most U.S. compressor manufacturers now use “bolt-down” motors for air conditioning and heat pump compressor applications up to 10–12 hp.

Since a uniform air gap between rotor and stator can be achieved only by having coincidence between the axes of the rotor and stator bores; the motor manufacturer must now ensure that the stator mounting surface is perpendicular to the axis of the stator bore. This has been achieved by manufacturing processes generally unique to each manufacturer. Some of the important factors include close control of punching burrs, use of lamination bonding agents, proper control of the location of the bonding material and its cure, together with close control of the clamping procedure. The net result has been stator cores with high mechanical strength and low magnetic core losses. The resultant motor/compressor combination has been a high-performance, high-quality product at an acceptable cost level reflected accordingly in consumer prices. The compressor manufacturers have done a remarkable job in continued performance improvements while holding prices that are affordable to the public.

### 3.8.1.4 Rotor Construction

A discussion of the rotor is now in order. Because of the backward-rotating field in the single-phase motor, double cages and deep bars are never used. Although some special applications can affordably use copper cage rotors, few if any hermetic compressors use rotors with fabricated copper cages. Today’s high-volume production necessitates the use of cast aluminum squirrel-cage rotors. Depending on some of the performance requirements, most of the hermetic rotors use aluminum of 99% purity or higher. This corresponds to a conductivity relative to copper of about 62% or higher. Since aluminum of this purity level poses special casting problems, the manufacturer must closely monitor such process variables as aluminum temperature, casting pressure, casting time, and number and size of the ports or gates through which the molten aluminum is allowed to enter the casting cavity.

If the temperature of the aluminum is too high, excessive shrinkage will occur in both the bars and end rings. This means less actual conductor than intended. Too much die lubricant could cause gases to form bubbles in the aluminum and form a “Swiss cheese” effect, particularly in the end rings. This in

turn can cause hot spots in the end ring or undesirable mechanical unbalance. The number and size of the rotor bar slots, together with the length of the stack of the iron, are all important factors that the rotor casting engineer must include in the design of the rotor casting tooling and the overall casting process.

Practically all single-phase rotors are skewed to reduce the effect of harmonic currents flowing in the rotor. In most split-phase and capacitor-start motors a skew of one stator slot is used. In permanent-split capacitor (PSC) motors a skew of about 30% more, or 1.3 stator slot pitch is used. The objective is the reduction of the “dip” torque (i.e., pull-up torque) that occurs at low speed. If the load is greater than the dip torque, the motor will not accelerate any further. The primary source of the undesirable harmonic currents is the forward and backward components of the stator slot-order harmonics. For example, if a 24-slot, 2-pole lamination is under consideration, there will be the mathematical equivalent of the  $S1\ 1-1$  and  $S1\ 1+1$  harmonics, each with its own speed-torque characteristics. Also, each has a forward and backward component. The resultant speed-torque curve will include the torques generated by each of those harmonic values. In this case the main culprits contributing to the torque dip are the backward 23rd and forward 25th harmonics. Because the insulation between the rotor bars and steel core is imperfect, a one-slot mechanical skew is generally less than a one-slot skew from an electrical standpoint. Hence, a PSC motor is generally designed with a slot skew greater than one.

One might now wonder what improvement might be realized if the bar-to-steel insulation resistance were made infinite. First of all, it would *not* eliminate the pesky low-speed torque dip. It would merely reduce it by the amount that the bar-to-steel cross-currents contribute to the harmonic currents. Further, high electrical resistance is generally accompanied by high thermal resistance. Consequently, an infinite resistance between the rotor cage and the steel rotor core would prevent the rotor losses from being transferred to the steel and thus to the air or other cooling medium. A typical level of bar-to-steel resistivity in cast aluminum squirrel-cage rotors used in hermetic compressor applications is in the vicinity of  $0.02\text{--}0.04\ \Omega\text{-in}^2$  ( $0.13\text{--}0.26\ \Omega\text{-cm}^2$ ). The unusual form of the unit of resistivity is the result of the inability to separate the true surface resistivity,  $\rho$ , and the length of the path. The resistivity levels stated are for typical rotors that have been steam-blued or gas-blued.

What is the optimum iron-to-aluminum resistivity? There is no single value that applies to all applications and all designs. Based on work by Adnan Odok, the author has determined that about 1.5 to 2 orders of magnitude increase would be necessary to significantly reduce the deleterious harmonic effects in both the low-speed region (about 0.0833 times synchronous speed) and the breakdown region (about 0.833 times synchronous speed).

Fortunately, most polyphase motors using non skewed rotors do not need a high level of bar-to-steel resistivity. Of more concern in those motors are the surface losses and the interlaminar currents that contribute to the so-called “stray-load losses.” In the case of the surface losses, the machining

technique used plays an important role in minimizing the rotor surface smear. The lamination surface resistivity and the presence of burrs are both important factors in causing interlaminar currents and their attendant losses that subtract from the rotor output.

So far, the discussion concerning the rotor has been focused on its electrical characteristics. An important role played by the hermetic rotor is that of helping to balance the crankshaft in the compressor. Because practically all compressors require an oscillating member whose volume increases and decreases during a revolution of the shaft, there is usually a mechanical unbalance that if not corrected or compensated will cause vibration and noise. In reciprocating compressors much or all of the counterbalancing can be accomplished on the crankshaft itself. In other compressors it may be easier and less costly, or even the only solution, to attach counterweights to the rotor. This is usually done by casting lugs as part of the end ring itself. The weights are then firmly attached to the cast lugs. Depending on the nature of the unbalanced moment, these balance weights may be attached to one or both ends of the rotor. Motors that ordinarily have a large starting torque, such as polyphase or capacitor-start motors, often use ordinary steel balance weights. However, PSC motors, because of the low level of starting torque, often have balance weights made of copper, brass, or nonmagnetic stainless steel. The presence of a magnetic material passing through the strong end turn leakage flux field causes rather large starting torque pulsations that could impede the starting of the compressor under conditions of low voltage, high head pressure in the system, or both. Often the compressor unbalance can be satisfied by casting an unbalance in the rotor end ring itself. Since the cast unbalance is pure aluminum, there is a limit as to the amount of unbalance that can be achieved.

### 3.8.1.5 Stator Conductors and Connectors

In an earlier discussion about the stator, no mention was made of the winding except that care must be taken to secure the wires and wire bundles together mechanically to minimize bending, abrasion, and any movement that might damage the insulation and thereby shorten the life of the motor. The two major types of conductor used in hermetic motors are copper and aluminum. The relative world prices of the base metals have much to do with the actual use of those metals in motor magnet wire. Until reliable methods of aluminum wire termination were developed, all motor magnet wire was made of copper. It is a material that can be reliably terminated by mechanical crimping, torch brazing, and soft soldering. In motors, the primary method of wire termination had been torch brazing. This is the method of fusing the wires together by melting the copper under a gas flame. Often the brazed joint was further mechanically enhanced by the use of a silver-bearing brazing material, but the electrical joint itself was formed by the copper wires melting together.

At a time when the world prices of copper were rising and the supply of aluminum made the price of aluminum attractive, considerable work was done by several motor manufacturers together with magnet wire and terminal manufacturers to



develop a means of mechanically connecting aluminum to aluminum and aluminum to copper. The problems encountered included “creep” of the aluminum because of thermal expansion, the tenacious aluminum oxide that forms almost instantly upon exposure to air, and the glassy copper-to-aluminum interface that forms during hot welding of the metals. Perhaps the most widely used solution from these efforts has been the mechanical crimp connector.

Several terminal manufacturers now offer crimp connectors that utilize holes, serrations, or similar means to literally bite through the aluminum oxide while the terminal is being squeezed. Since the newly crimped joint is essentially air free, no further oxidation can take place and therefore a good electrical joint is maintained. Where several aluminum wires are joined to copper magnet wires or to stranded copper cable, it is generally advisable to prestrip the magnet wires prior to crimping. In other cases, depending on the toughness of the wire enamel, it has been shown that a highly reliable wire termination can be effected without stripping the enamel from the wire. Each motor manufacturer will usually develop techniques based on the particular terminals selected, the size and type of wire and type of wire enamel, and tooling that can be shown to produce wire terminations with a long life expectancy.

Several other application factors are advantageous if aluminum wire is used in a hermetic motor. First, many motors of approximately of 1 hp and larger are varnish-treated. This coating will further impede any oxidation of the aluminum wire inside the crimped joint. Second, the environment within the compressor is free of air and water, consisting entirely of refrigerant and oil. This further keeps the connection in a pure metal-to-metal contact. If the design is made with reasonable current densities in the wire, the “creep” problem resulting from numerous large temperature cycles is essentially nonexistent.

With the concern for improved compressor performance brought on largely by the energy crisis of the 1970s, the emphasis in motor design and manufacture has returned to copper for windings. Where aluminum magnet wire is still used, motor size can still be a constraining factor because the aluminum-wound motor will generally be 10–20% larger than its equivalent copper-wound motor.

One characteristic of aluminum wire that has been successfully exploited is its ability to be deformed and yet maintain good integrity of the wire enamel. During initial use of aluminum wire in hermetic motors, much concern was expressed over any slight impressions that may have been

made in the wire during the manufacturing processes. Later investigations showed that the wire could withstand relatively deep indents before any “life-threatening” conditions would arise that could affect the reliability of the motor. Further, it was found that the aluminum wire could be compacted both in the slot and in the end turns. The compaction tended to improve heat transfer and reduce wire movement during periods of high current and consequent high forces. It also allowed the motor design engineer to keep the equivalent aluminum design within 10–15% of the shorter or smaller-diameter copper design.

It was found that typical copper designs had a “press factor” or compaction factor of about 70%. That meant that when the first winding was inserted into the bottom of the stator slot and mechanically pressed to keep it in that position, the space taken up by the conductors was between 68% and 72%. The remaining 28–32% was taken up by air between the conductors. When aluminum was used, it was found that the first winding could be compacted to about 78–82% without serious degradation of the wire or its enamel. A compaction factor of that level meant that 18–22% of the volume occupied by the conductors was used by air. Furthermore, when aluminum wire was pressed down into the slots, it tended to stay there and not to spring back. That left the remaining slot space to be taken up by the top layer of wire and slot separating insulation and the wedge, which would often be mechanically inserted into the slot simultaneously.

### 3.8.1.6 Stator Coil Windings

Except for motors of about 60 hp or larger, practically all motors for today’s hermetic applications are wound with concentric-coil windings. The underlying reason is that concentric-coil windings are more adaptable to machine winding and placement. The advantage is primarily economic. A machine-wound motor is less costly and can be produced in higher volumes than a hand-placed motor. While the concentric windings can result in unbalanced slot and end turn reactances, this is of concern only in high-power motors. These are always polyphase motors. The unbalance in single-phase motors is of little concern. In fact, the unbalance is used to advantage in resistance split-phase motors where the start winding, placed on top of the main winding, has a lower reactance than the main winding. An additional advantage of the concentric windings is the ability to adjust the distribution of the turns in the individual coils to increase certain harmonics and reduce

**Table 3.15** Typical Single-Phase Winding Distribution<sup>a</sup>

P	S <sub>1</sub>	S <sub>1</sub> /P	Main winding		Start winding	
			Teeth enclosed	Turns	Teeth enclosed	Turns
2	20	10	3, 5, 7, 9	18–29–36–40	5, 7, 9	31–39–44
2	24	12	3, 5, 7, 9, 11	13–20–27–31–33	5, 7, 9, 11	21–28–33–35
4	32	8	2, 5, 7,	28–42–50	5, 7	50–59
4	36	9	4, 6, 8	30–41–46	5, 7, 9	31–38–41

<sup>a</sup>P=poles; S<sub>1</sub>=slots. The windings illustrated are arranged to give approximately 100 effective turns per pole.

others. While a high harmonic content is generally discouraged from the standpoint of harmonic cusps and their effect on performance, a judicious level has been shown to be beneficial in the starting of PSC motors. Table 3.15 illustrates typical winding distributions that may be used with several of the widely used stator slot combinations for single-phase applications.

The equation to give a sinusoidally distributed winding is:

$$N_x = \frac{N_{le} \sin \theta_x}{\sum (\sin^2 \theta_x + \dots + \sin^2 \theta_n)} \quad (3.16)$$

where:

- $N_x$  = turns in slot  $x$
- $N_{le}$  = effective turns=100
- $\theta_x$  = angle subtended by coil  $x$
- $\theta_n$  = angle subtended by the  $n$ th coil

While the windings given in Table 3.15 do not specifically indicate the slot placement, one generally assumes that the main and start windings are in “quadrature,” or displaced 90 electrical degrees. Perhaps the largest percentage of single-phase motors are wound with this arrangement. In most 115-V PSC air conditioning compressor motors, one finds that a “shifted” start winding provides a significant performance improvement. The “shift” means that the start winding is angularly displaced by one or more slots in the direction opposite to the motor rotation. The result of this winding placement is a higher capacitor voltage, higher start winding current, and lower line current. This phenomenon was discovered in the 1930s but it seemed impractical at that time because the slot space factors were too high. (In that period the slot space factors were about 35%. Today it is common to use space factor values in the range of 55–60%.) Most computerized motor design programs allow the motor design engineer to iterate or search for the turns ratio or “a-ratio” that will result in the lowest rated-load line current for the given capacitor size and main and start wire sizes. Other routines may allow the engineer to iterate the a-ratio for maximum efficiency at the load point. Such programs remove much of the tedium from the design work and let the engineer apply his ingenuity to more complex problems.

If one is using concentric-wound coils for polyphase motors, it is most desirable to have a sinusoidal magnetomotive force wave (mmf). Two commonly used stator slot combinations are 24 slots and 36 slots. For a 24-slot, 2-pole winding, it can be shown that a winding ratio of 1–2–3 with the coils encompassing 7, 9, and 11 teeth results in a fairly good sinusoidal distribution. To check this one must look at the effect of all three windings. This can be done by looking at the instant when the current is at a peak in one phase and equal to one half the peak value, but of the opposite sign in the other two phases. The resultant mmf wave will be found to be acceptable. For example, one might use 20 turns around 7 teeth for the inner coil, 40 turns around 9 teeth for the middle coil, and 60 turns around 11 teeth for the outer coil. One would soon discover that the slot with 20 turns

would also contain 40 turns from another phase. Hence, the slot fullness remains constant except for the addition of a slot separator.

For a 24-slot, 4-pole motor, one would use the ratio of 1–2 with the turns around 3 teeth and 5 teeth, respectively. For a 36-slot, 4-pole stator, one would use the same 1–2 ratio of turns with the coils encompassing 6 teeth and 8 teeth, respectively. As stated previously, the concentric windings lend themselves to machine placement, which is much faster and more economical than hand-placed windings. This assumes, of course, that the manufacturer is already well equipped with machine winding.

There is a penalty that accompanies the concentric coils as they are normally used. In most cases one places all of “phase A” coils in the stator first. Next are placed all of “phase B” coils. Finally, “phase C” coils are placed in the stator. It soon becomes obvious that “phase A” has the highest reactance because it is in the bottom of the slots. Likewise, “phase C” has the lowest reactance. The resultant reactance differences cause unbalanced currents and different heating rates in the windings. Compounding the reactance differences are any unbalanced voltages that may exist in the system. Usually the unbalanced voltages are the greater concern. Fortunately, most hermetic motor applications have sufficient cooling because of the refrigerant and oil that is passing over the stator. However, if more balanced reactances are desired, one may choose to “lap” the pole-phases around the stator. To do this, phase A-north is placed first, then phase B-north, and so forth, until all of the pole phases are placed. Another scheme patented by one company is the “modified concentric-lap” method. This starts out like the first method, except that phase A-south is skipped and is placed last. When the poles are connected in series (and this is required), each phase has an equal number of phase conductors in the top and also the bottom of the slots. Likewise, the end-turn reactance is more balanced than the ordinary concentric placement.

### 3.8.1.7 Torque and Horsepower

Although the previous sections have addressed the magnet wire types, winding distributions, and insulation systems, the subject of torque requirements has not been discussed. It should be noted at the outset that the type of refrigerant, number of cylinders, motor speed, and operating temperatures of the evaporator and condenser are the key factors in determining the motor loading requirements. To a large extent, motor horsepower rating for refrigeration applications is somewhat nebulous. There is an obvious correlation between motor size and horsepower, but it is significantly different from general purpose or NEMA sizes. For the purposes of this discussion only residential heat pump and air conditioning applications will be addressed. The reader can then use this information as a starting point for other applications.

For the most part, residential air conditioning compressor motors are two-pole units. The change from four-pole to two-pole motors started in the late 1950s and was essentially completed during the 1960s. The reason for change was

largely economic. Assuming that the same shaft horsepower and therefore thermal energy conversion is required from a motor of a given outside diameter, it was found that the stator stack length of a two-pole motor was about 40% shorter than for the equivalent four-pole motor. Equation 3.17 has been used by many motor designers:

$$L_{2p} = \frac{L_{4p}}{(p_4/p_2)^{0.646}} = \frac{L_{4p}}{1.565} = 0.64 L_{4p} \quad (3.17)$$

where:

$$\begin{aligned} L_{2p} &= \text{stack length of the two-pole motor} \\ L_{4p} &= \text{stack length of the four-pole motor} \\ p_4 &= 4 \\ p_2 &= 2 \end{aligned}$$

For a given British thermal unit (BTU) requirement, the change from four-pole to two-pole resulted in both the compressor and motor being smaller and the resultant air conditioners being both smaller and lighter. This type of change has been reflected in maintaining the “value” per dollar in air conditioning units.

The following relationships may be used as starting points in determining the torque requirements for a new two-pole application:

$$\begin{aligned} \text{MRT} &= 6.0 \text{ oz-ft per 1000 BTU} \\ \text{FLT} &= 3.0 \text{ oz-ft per 1000 BTU} \\ \text{HPL} &= 0.55\text{FLT} = 1.65 \text{ oz-ft per 1000 BTU} \end{aligned} \quad (3.18)$$

where:

$$\begin{aligned} \text{MRT} &= \text{maximum running torque} = \text{torque at } 0.833 \\ &\quad \text{Synchronous speed or 3000 rpm for a 60 Hz motor.} \\ \text{FLT} &= \text{full-load torque or rated-load torque} \\ \text{HPL} &= \text{heat pump load torque} \end{aligned}$$

The relationships have been found to be quite acceptable for two-pole compressor motors in R-22 applications for BTU requirements ranging from 10,000 BTU to 100,000 BTU.

As mentioned previously, a horsepower rating is usually given to each compressor motor, but it bears only a faint resemblance to horsepower ratings for general purpose motors. For air conditioning motors, one usually rates the motors about 1 hp per 12,000 BTU or 1 hp per ton of air conditioning, since the two are equivalent. However, in the low-BTU sizes, one might find that compressors ranging from 8000 BTU to 14,000 BTU also have motors rated at 1 hp. As a result, the horsepower rating becomes a “name” to put on the motor. Of more importance to both the motor design engineer and the compressor engineer are the maximum running torque (MRT), the locked-rotor torque (LRT), and the locked-rotor amperes (LRA). The MRT determines whether the compressor will continue to operate with heavy load and reduced voltage. The LRT determines whether the compressor will start, and the LRA will dictate the size of the contactor required. One point that is not obvious is the selection of the MRT speed of 0.833 times synchronous speed. The reason is that it is close to the actual breakdown speed in a single-phase motor. In a polyphase motor the breakdown speed is much lower—usually about 0.67 times synchronous speed or about 2400 rpm for a 60-Hz, 2-pole motor. However, the design engineer still looks at the MRT point in a polyphase motor.

### 3.8.1.8 Capacitor Voltage

Next in importance in the single-phase PSC motor is the capacitor voltage,  $V_c$ . This is determined both by the applied motor voltage and the turns ratio, or  $a$ -ratio. The  $a$ -ratio is defined as follows:

$$a\text{-ratio} = \frac{N_{1es}}{N_{1e}} \quad (3.19)$$

where:

$$\begin{aligned} N_{1es} &= \text{effective turns of the start winding} \\ N_{1e} &= \text{effective turns of the main winding} \end{aligned}$$

If a 440-V capacitor is applied to the motor, the highest voltage that can be continuously applied to the capacitor is 484 V, or 110% of its rating. This condition must apply to the lightest load (where the capacitor voltage is highest) and the highest line voltage, which is assumed to be 110% of the rated line voltage. The most commonly used “run” capacitors used in PSC applications for air conditioners are 330-V, 370-V, and 440-V capacitors. For typical air conditioner motors, one might find the following  $a$  ratios used:

Capacitor voltage	$a$ -ratio
330	1.2
370	1.35
440	1.6

The actual  $a$ -ratio used will vary slightly from design to design.

### 3.8.1.9 Wire Sizes

Of no less importance is the selection of wire sizes in the motor, since that is the determining factor in both the steady-state heating of the windings and also the temperature rate of rise (ROR) at standstill or locked-rotor conditions. One method of determining the relative sizes of the main-to-start wire sizes in a single-phase motor is the determination of the  $q$ -ratio of the motor. It can be shown that this dimensionless ratio is proportional to the weight ratio of the main and start windings. The  $q$ -ratio is determined as follows:

$$q\text{-ratio} = \frac{R_{1s}}{a^2 R_1} \quad (3.20)$$

where:

$$\begin{aligned} R_{1s} &= \text{resistance of start winding} \\ R_1 &= \text{resistance of the main winding} \\ a &= \text{turns ratio} \end{aligned}$$

For most PSC single-phase motors the  $q$ -ratio ranges between 1.5 and 3.5. For motors with a relatively small “run” capacitor the  $q$ -ratio may be in the 3.0–3.5 range. If the capacitor is very high in microfarad rating, the  $q$ -ratio will be in the range of 1.5–2.0. The use of dimensionless ratios like  $a$  and  $q$  makes it easy to design a range of motors in the same frame size.

The reader might now wonder how much capacitance is enough? Let us define the term,  $C_{bal}$ :

$$C_{bal} = \text{capacitance in microfarads required to give zero backward field losses or zero backward current} \quad (3.21)$$

“Balanced” operation is obtained when the design can be shown to have no backward field losses. The condition does not physically occur, of course, since it is a mathematical representation of the pulsating currents that occur in a single-phase motor. It can be shown that balanced operation occurs under the following condition:

$$\begin{aligned}\alpha_m + \beta_s &= 90.0 \text{ degrees} \\ I_m &= aI_s \\ R_{1s} + R_c &= a^2R_1\end{aligned}\quad (3.22)$$

where:

- $R_1$  = main winding resistance
- $R_{1s}$  = start winding resistance
- $R_c$  = internal resistance of capacitor
- $I_m$  = main winding current
- $I_s$  = start winding current
- $\alpha_m$  = phase angle of main winding current
- $\beta_s$  = phase angle of start winding current

From experience, this author has found that balanced capacitor operation can be obtained with the following approximate motor design conditions:

$$\begin{aligned}a &= 0.8 \\ q &= 0.8 \\ C_{\text{bal}} &= 0.8 \text{ times MRT in oz-ft. This is the capacitance in microfarads for a 230-V motor. A 115-V motor would require four times that capacitance}\end{aligned}$$

With a nested-loop iterative routine added to a computer program, one can determine the exact values of  $a$ ,  $q$ , and  $C_{\text{bal}}$  to give balanced operation at a specified load point and at the same time give the required MRT that the compressor requires. Although balanced operation is seldom required it is a useful condition to know, since the single-phase motor in balanced operation produces the highest efficiency possible. One can then back off to a lower value of capacitor, namely 60% of the balanced amount, and adjust  $a$  and  $q$  for optimum performance with that capacitance. This results in a more economical design.

### 3.8.1.10 Protection

Now that the windings and capacitor have been selected to produce the designed MRT, LRT, and the optimum performance at the FLT, a question remains whether the motor can be protected from severe thermal excursions. Three basic types of thermal protection are available to the motor designer: linebreak thermostats, pilot-duty thermostats, and solid-state thermistors.

Line-break thermostats do just what the name says. They are thermostats placed in the end turns of the motor winding to sense the temperature of the winding. Some are configured to be attached to the end turns and are also internally fitted with a calibrated resistive heater that senses the current in one of the windings. Some thermostats have two heaters to sense both windings. When the thermostat reaches the temperature to which it was calibrated, it will open the motor circuit and shut down the motor. Both the sensed winding temperature and the internal heater temperature can cause the thermostat contacts to open.

The pilot-duty thermostat merely detects winding temperature. It is used where a line-break thermostat cannot handle the motor current. This kind of thermostat is primarily used on large polyphase motors, where it is imbedded in the end turns of the winding. The pilot-duty thermostat then causes a larger contactor to remove the motor from the power line.

Solid-state thermistors are used on large polyphase motors where three or more protection devices are required. Often they are arranged with three on one end and three on the other end of the motor. Because they are quite small—about the size of a large grain of rice—they can be imbedded in the end turns. When used with part-winding start motors, the engineer must be sure the thermistor is placed in the winding that will be energized during starting. Otherwise, it will provide protection only during the running operation.

The thermistor itself is a semiconducting device made generally of barium titanate that is “doped” to give the desired characteristics of resistance versus temperature. When subjected to an elevated temperature, the thermistor will change resistance drastically, usually by about four to five orders. Connected to an electronic circuit that controls a contactor, it prevents thermal damage in very large polyphase motors.

The selection of the thermal protector for hermetic applications depends on several factors: cost of the protection system relative to the cost of the motor and compressor, cost of replacing the compressor and motor if failure should occur, space available inside the compressor for the protector, and speed of response. In large polyphase motors the locked-rotor current and corresponding current density in the stator winding are quite high. As a result, the only protector that might sense the winding temperature fast enough could be the thermistor. Also, the thermistor and its electronic module are probably a small percentage of the entire motor and compressor cost.

Polyphase motors in the 5 hp to 15 hp rating might well be good candidates for line-break protectors that are connected to the wye of the motor. Since that type usually senses stator winding temperature in addition to the current at the wye connection—both the motor manufacturer and the compressor manufacturer must make accommodations for a relatively large-sized protector to be tied or otherwise fastened to the end turns of the motor. Single-phase motors in the 1 hp to 5 hp range have adopted the line-break units with good success for many years. One of the key factors in successful application of thermal protectors to hermetic motors is good communication among the protector supplier, motor design engineer, and the compressor design engineer. For more detailed information on thermal protectors, see [Chapter 10](#).

### 3.8.1.11 Starting of Single-Phase Motors

A final area of concern in hermetic applications is that involving the starting of single-phase motors. Since exposed contacts such as those used in centrifugal starting mechanisms cannot be used inside a compressor filled with oil and refrigerant vapor, another means has had to be devised. Two such means are now available: current- or voltage-actuated relays, and positive temperature coefficient resistors (PTCRs). Both types are applied

externally to the compressor and do not require extra leads from the motor. This is important because the motor leads must be brought through the compressor case with special sealed connectors. For motor sizes up to 15 hp, this is usually done with three-pronged connectors that are sealed in glass or ceramic to a steel body, which is then welded to the compressor housing. Any extra connections obviously require more seals, which add to the cost of the unit.

With these restrictions placed on the motor design engineer, it soon became apparent that a relay that could sense the main winding current or one that could sense the start winding voltage would be an excellent candidate for a hermetic application. Current relays have been used successfully for decades in refrigerator and freezer applications, as well as in small window air conditioner units. Current relays are primarily used in resistance split-phase motors up to about one-half hp and capacitor-start motors up to about 1 hp. The maximum rating is largely governed by the amount of main winding current since that determines the size and number of turns in the relay coil. If the relay coil wire gets too large and there are only a few turns, a change of one turn in the relay coil might be unacceptable with respect to the effect on the starting performance of the motor.

Three factors relative to protection using relays are of primary concern to the motor engineer: (1) relay pick-up current, (2) relay drop-out current, and (3) motor drop-out torque. The pick-up current is the level of current that causes the relay plunger to rise and close the contacts that connect the start winding to the circuit. As the motor speed rises, the main winding current falls off to a level where the weight of gravity causes the plunger to fall and thereby open the start winding contacts. Since the relay engineer is governed by the same laws of magnetism and gravity that apply to the motor engineer, there is a limit to the number of tricks the relay engineer can use in designing the relay. As a result, one will see that the margin between the “maximum pick-up current” and the “minimum drop-out current” is generally about 18–20%. Some relay manufacturers have up to 90 standard relays available with pick-up settings ranging from 2.3 A to 24.4 A. The corresponding drop-out settings range from 1.9 A to 20.4 A.

With that information in mind, the motor engineer concentrates on drop-out torque and current density in the start winding. Drop-out torque is that torque delivered by the motor at the time the relay opens the contacts to remove the start winding from the circuit. The torque at that instant, either with the start winding connected or with it removed, must be greater than the compressor load torque, even when the motor voltage is only 85% of the rated line voltage. A usually acceptable torque level is 85% of MRT at rated voltage.

When a refrigerator is just being started with the entire cabinet at room temperature, a large amount of liquid refrigerant will be evaporated in the evaporator to start the cooling process. This in turn will mean that the compressor will be required to compress a large amount of the gas. With a high mass flow rate, the corresponding load on the compressor motor will be high. If the motor stops momentarily and is started again, the torque in the starting condition at the time of relay drop-out must be sufficient to cause the motor to continue running on the main

winding. If the relay picks up again, it may continue to cycle between the start and run conditions until something catastrophic occurs: The relay contacts may weld, the start winding may burn out, or both. If the thermal overload is sized properly, the motor will be protected.

To avoid this dilemma, the motor engineer resorts to two design factors under his control: the  $a$ -ratio and the  $q$ -ratio. The shape of the curve of the main winding current versus speed—referred to as the current-relay curve—is affected by those two design variables. Typical values of the  $a$ -ratio for resistance split-phase designs are 0.7 to 0.9. The values of the  $q$ -ratio for good relay performance are about one order of magnitude higher—typically 8.0 to 10.0. Referring back to the definition of the  $q$ -ratio, one can see that a high start winding resistance is required to obtain a high  $q$ . If that is achieved by using extremely small wire, one might find that the current density and resultant temperature rate of rise of the start winding is totally unprotectable by any existing overload devices. A common solution to this problem is the use of “backlash” start windings. This is done by winding extra turns in the forward direction and then an equal number of backward turns. This preserves the original forward start winding net turns but adds noninductive turns that therefore add resistance to the start winding. The motor “thinks” it has a smaller start wire than it really has. This backlash winding is generally used with copper windings.

One alternative to the use of backlash windings is the substitution of an alloy material having higher resistance so as to eliminate the extra forward and backward turns. However, the resistivity of the wire is only one of the factors of concern. The other two are the specific heat and the weight density. Fortunately, one can find a combination of all three that can be used to provide a high-resistance start winding with a low  $a$ -ratio such as required for resistance split-phase motors. One such alloy is an aluminum alloy described in Patent No. 3,774,062. It is an alloy that allows one to replace a long, thin copper wire with a short, alloy wire of larger diameter having the same temperature rate of rise and resistance. The result is a motor with acceptable relay performance and rate of rise at standstill, and no backlash turns.

For motors of about 1 hp and higher, one must resort to voltage relays that sense the changing voltage across the start winding. Whereas the current relay has normally-open contacts that close when the motor is energized, the voltage relay has normally closed contacts that open only when the start winding voltage reaches a predetermined level. Since motors in these ratings are generally capacitor-run motors, the  $a$ -ratio is usually 1.1 or higher. As in the case of the current relays, the engineer must be concerned with the drop-out torque when the relay contacts are opened. Motors with high  $a$ -ratios and high capacitance start capacitors could result in voltage relay curves that are nearly straight. A desirable voltage relay curve is one that has a significant change in start winding voltage as the motor accelerates from standstill to its operating load speed. Also, there must be a significant difference between the speed-voltage characteristic in the start condition when the start capacitor is in the circuit and the corresponding speed-voltage characteristic in the run

condition when the start capacitor is no longer in the circuit. If not, the relay could cycle back and forth between the run and start modes, causing the relay contacts to weld, the capacitor to explode, the protective device to open the motor circuit, or the start winding to burn out.

The engineer again uses a general rule that the drop-out torque must be equal to or greater than 85% of the MRT. The three design variables that are used to achieve the desired starting and drop-out torque are the  $a$ -ratio, start wire size, and start capacitor size in microfarads. Since the start capacitors are always electrolytic units, the voltage across the capacitor during the entire starting period must not exceed the levels established by the capacitor manufacturer. One further constraint on the motor design is the amount of current that is interrupted by the start relay contacts. That, of course, is the current that flows through the start capacitor. Knowing the capacitance and the voltage across the capacitor, one can readily compute the current. If that point is overlooked, one might have a relay with welded contacts and, again, a possible failed capacitor.

While current relays are either custom-designed for the particular motor or selected from a large number of semicustom relays, there is a limited variety of voltage relays from which to select. If there is a question about a particular application, usually a slight change in the motor start winding will result in a satisfactory motor-relay-compressor application. An oscilloscopic trace of many start-up cycles is usually made to verify successful relay operation with no relay “bounce” that could indicate marginal operation in the drop-out region.

The PTCR mentioned earlier is a more recent addition to the engineer’s repertory of start-assist devices. These are from the same family as the PTCRs used to sense the winding temperature. The difference is in the application and size. Since PTCRs are affected by both temperature and voltage (or current), one may use a properly-sized PTCR in series with the start winding of a resistance split-phase motor. After a certain amount of current has passed through the PTCR, the heating effect of the current will cause the resistance to increase by several orders of magnitude and reduce the start winding current to a very low level—usually on the order of milliamperes, but not zero. Because it stays in the circuit, it does add some loss to the motor circuit, which reduces the motor efficiency somewhat. It has the advantage of having no moving components and therefore is not affected by mounting position. It is however, affected, by any heat-sinking or heat sources. Also, one must be aware that its ability to start immediately after the motor is turned off for some other reason may be different than expected. As long as one recognizes these temperature-voltage effects, a successful application can be made. They have been in use for at least a decade.

Still another application of the PTCR is to assist the PSC motor to handle hard-start loads. Probably 75% or more of the residential heat-pump and air conditioning applications are made with PSC motors. There are situations in which the PSC motor needs a start assist. Depending on the choice of the compressor manufacturer in conjunction with the motor designer, one might find a PTCR placed in parallel with the oilfilled run capacitor. Usually these PTCRs are made with a limited range of resistance values. Typical sizes include 12.5,

25,50, and sometimes 100 $\Omega$ . One can easily show with a computer model of the motor that placing a low resistance value in parallel with the run capacitor will result in an equivalent series resistor and capacitor that will increase the starting torque of the motor by 20–30%. However, it also changes the entire speed-torque characteristic. Since one is mainly interested in getting the motor to accelerate to at least a few hundred rpm, a device that quickly returns the motor to its original PSC mode of operation might be quite acceptable. The PTCR is just such a device.

As in the case of the split-phase application, the PTCR will heat rapidly and increase its resistance by four or five orders of magnitude. Depending on the level of heat-sinking, the final level of steady-state losses of this device may be on the order of 10–20 W. These also show up as a reduction in system efficiency. The simplicity, ease of field application, cost, and other factors have made them an attractive start-assist device in heat-pump and air conditioning applications.

### 3.8.2 Selection of DC Motors with Chopper Drives for Battery Powered Vehicles

Chopper drives are used to power dc motors when the available power supply is constant-voltage dc and the application requires a variable voltage in order to obtain the desired speed-torque characteristic. By definition, a chopper drive consists of a power electronic device, such as a self-commutated switching device (IGBT, MOSFET), which acts as a controllable switch to convert the constant voltage to a desired average level, as shown in Fig. 3.10. In this figure,  $T_o$  is ON time;  $T$  is the period and  $1/T$  is the chopper frequency,  $f$ . The device is operated at the highest frequency the device is capable of. Tests have shown that motor efficiency increases with increasing frequency because of reduced harmonic content of the current at higher frequencies [24]. Figure 3.11 depicts source current and motor current in a chopper circuit (neglecting circuit resistance).

The current excursion,  $\Delta i$ , is given by

$$\Delta i = \frac{E}{Lf} \left( 1 - \frac{T_o}{T} \right) \frac{T_o}{T} \text{ amperes} \quad (3.23)$$

where  $L$  is circuit inductance (henry);  $f$  is frequency (hertz);  $E$  is source voltage (volt), and  $T_o/T$  is the “duty cycle.” The greater  $\Delta i$ , the higher the harmonic content of the current. This in turn introduces additional Joule loss with increased

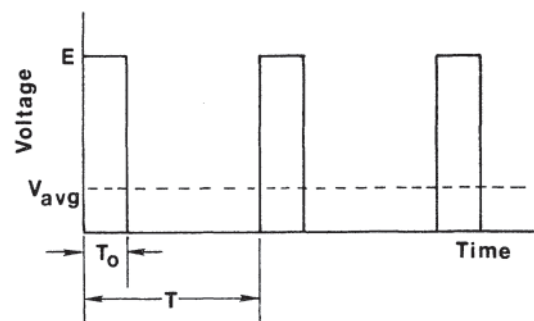


**Figure 3.10** Output voltage of the controller for a chopper drive ( $V_{avg} = E(T_o/T)$ ).

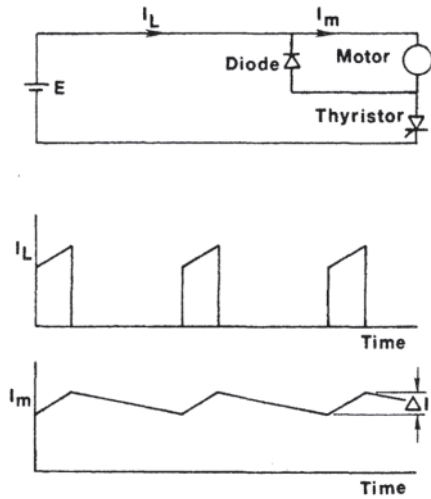


**Figure 3.11** Basic chopper circuit; source current ( $I_L$ ) and motor current ( $I_m$ ) as a function of time.

heating and reduced efficiency, reduced motor commutation capability, and derating. Increasing the chopper frequency and the circuit inductance will reduce  $\Delta_i$  and increase the efficiency and reduce the derating of the motor. A further consideration is that power electronic devices capable of gate (or input signal) turn-on have a maximum  $di/dt$  rating. At turn-on,

$$\frac{di}{dt} = \frac{E - V_{avg}}{L} = \frac{E}{L} \left(1 - \frac{T_o}{T}\right) \quad (3.24)$$

Thus, from the standpoint of operating efficiency and matching the electronic drive to the motor, circuit inductance is an important factor.

At a specific chopper frequency, the motor inductance typically decreases by 20% from no-load to full-load current. In addition, for a specific load current, inductance has been noted to decrease by 20% in going from a chopper frequency of 20 Hz to 600 Hz [25]. Motor inductance can be controlled in the design of the motor [26]. The important parameters that affect the inductance are as follows:

For the armature:

$$L = \frac{K_1 Z^2 l (h_1 + h_2)}{3 Q a^2 b} \quad (3.25)$$

$$\text{For the poles: } L = \frac{K_2 h n^2 l p}{g a^2} \quad (3.26)$$

where:

$K_1, K_2$  are constants

$Z$  = armature inductors

$l$  = stack length

$Q$  = number of slots

$a$  = number of parallel paths in armature

$b$  = slot width

$h_1$  = depth of copper in slot

$h_2$  = depth from top of tooth to top of conductor in slot

$h$  = pole height

$n$  = number of pole turns

$p$  = number of poles in series

$g$  = air gap length

These equations are greatly simplified and are presented only to indicate how inductance varies with motor design. It is not possible to assign values to the constants  $K_1$  and  $K_2$  because actual inductance is a function of the presence of compensating windings, commutating windings, the end turn connection method, brush shift, and so forth.

An approach to estimating the machine inductance,  $L$ , is based on the per-unit value of inductance,  $C_x$ , as follows:

$$L_{base} = \frac{E}{I \omega_{base}} \quad (3.27)$$

$$\omega_{base} = \frac{N}{60} \left(\frac{p}{2}\right) 2\pi = \frac{Np}{19.1} \quad (3.28)$$

where  $E$  and  $I$  are rated voltage and current:

$N$  = speed in rev/min

$p$  = number of poles

$\omega_{base}$  = rated angular (base) speed (rad/s)

$$L = L_{base} C_x \quad (3.29)$$

Typical values of  $C_x$  are as follows:

Shunt-wound [27] (compensating windings)	$0.06 < C_x < 0.4$
(noncompensated)	$C_x \approx 0.35$
Series-wound [24], [25] (non-compensated)	$C_x \approx 0.35$

It should be noted that use of compensating windings (pole-face windings) decreases the motor circuit inductance, permitting a faster rate of rise of current. This in turn is a limiting factor in the selection of the chopper switching device. A determination must be made of the  $di/dt$  limitations of the chopper controller and the minimum  $V_{avg}$  to be used in order to specify a minimum circuit inductance that can be tolerated. As will be seen later in the motor size selection example, the magnitude of current that can be commutated influences the size of the motor required for a specific application. That is, the use of compensating windings is highly desirable from the standpoint of permitting use of a smaller motor but, because the inductance is smaller due to the compensating winding, the rate of rise of current increases, complicating the device selection.

In addition to changes in inductance with frequency and load, the apparent resistance of the motor circuit and the torque/voltage constant also change with frequency in a chopper drive [24]. Because of these changes, the conventional equivalent circuit of the dc motor may not yield the performance that will actually be observed by test. If motor performance is to be obtained by test, special precautions in instrumentation must be observed. Conventional instruments will yield substantial errors. Noninductive current shunts and wide-bandwidth electronic wattmeters are essential [24].

When selecting a motor size for a specific load, it should be recognized that the chopper-controlled motor will be operating at reduced efficiency, typically 70% of the efficiency realized from a ripple-free voltage source at rated load. DC motors with chopper drive are utilized extensively in electric vehicles, such as automobiles, golf carts, and forklift

trucks. The selection of a motor size for an electric vehicle will be used as an example of the analysis process to be followed.

A number of factors enter into the determination of the motor and control scheme for the drive train in electric vehicles. Basic decisions to be made (not necessarily in this order) are:

1. Type of motor, that is, series or shunt.
2. If shunt wound,
  - a. Shall constant field excitation or controlled variable excitation be used?
  - b. Will armature voltage be controlled by chopper or switched in finite, discrete steps?
  - c. What transmission gear ratio will be necessary?
  - d. Is regeneration to be utilized?
3. Tire size.
4. System voltage.
5. Vehicle performance, based on frontal area and weight, to include the following:
  - a. Maximum acceleration
  - b. Maximum speed on a specified maximum grade for a minimum time period
  - c. Cruise speed
  - d. Top speed
  - e. Regeneration, if utilized

Since the performance specifications require varying speed/torque and speed/power combinations and result in an intermittent load on the motor, a standardized duty cycle must be used in order to establish a rating, based on thermal and commutation considerations, for the motor. The speed requirements will fix the drive-train gear ratio and the motor speed-torque relationships.

Assume that the speed follows the duty cycle shown in Fig. 3.12. During the cruise period (constant 30 mph speed period), the car will be required to climb a grade for 5 seconds. It is to be capable of a top speed of 55 mph, and is to be designed for urban driving, 5-mile trips, six trips during a 12-hour day.

The motor must be capable of supplying sufficient power to accommodate the following load conditions:

1. Aerodynamic drag
2. Rolling resistance
3. Change of grade
4. Acceleration requirements

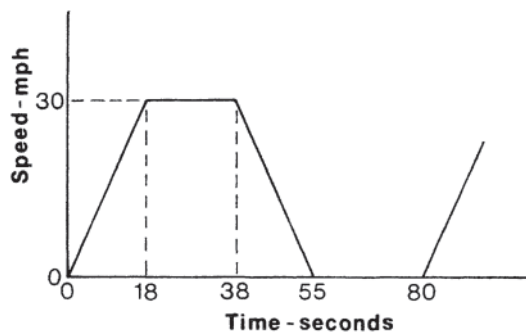


**Figure 3.12** Electric vehicle speed duty cycle. Acceleration, 0–18 s; cruise, 18–38 s (including 5 s climbing a 10% grade); coast and brake, 38–55 s; idle, 55–80 s.

5. Losses in the mechanical gearing and bearing friction in the mechanical drive train

### 3.8.2.1 Equations for Various Load Conditions

The power in hp to overcome aerodynamic drag is calculated from:

$$P_d = \frac{6.762}{10^6} (C_d A)(\text{mph})^3 \quad (\text{hp}) \quad (3.30)$$

where:

$A$  = frontal area in  $\text{ft}^2$

$C_d$  = drag coefficient

mph = speed in miles per hour

A typical electric vehicle will have a frontal area of  $20 \text{ ft}^2$  and a value for  $C_d$  of 0.3.

The power used when changing grade can be calculated from:

$$P = \frac{2.7}{10^5} (W)(\text{mph})(\%) \quad (\text{hp}) \quad (3.31)$$

where:

$W$  = vehicle weight in pounds

$\%$  = percent grade (increase in elevation in feet per 100 ft of travel)

The same equation is used to calculate the power required to overcome the rolling resistance due to tire friction by substituting  $100\mu$  for  $\%$ ,  $\mu$  being the coefficient of friction between the tires and the road. Typically,  $\mu$  lies between 0.012 and 0.017, with conventional-bias tires at the upper value and steel-belted radial tires at the low end.

The power requirements for acceleration are based on accelerations rates expressed in  $\text{ft}/\text{s}^2$ . The equation is:

$$P_a = \frac{8.28}{10^5} (W)(a)(\text{mph}) \quad (\text{hp}) \quad (3.32)$$

where  $a$  = the acceleration rate in  $\text{ft}/\text{s}^2$ .

If the electric vehicle has a weight of 3000 lb with  $C_d A = 6.0$  and  $\mu = 0.012$ , a drive-train efficiency assumed to be 95%, and the vehicle encounters a 10% grade during the cruise period, the power requirements during the speed duty cycle may be calculated for each part of the cycle and for the top speed condition:

Accelerating	0–30 mph in 18 s	25.58 hp
Cruising	30 mph	6.51 hp
Grade climbing	10% at 30 mph	31.77 hp
Top speed	55 mph	27.67 hp

**Figure 3.13** is a plot of the motor power required during the driving cycle. As can be seen, grade climbing is the most demanding of the various operations; the motor selected must be capable of delivering 31.77 hp on a short-time overload basis.

### 3.8.2.2 Continuous Power Rating and Motor Selection

To determine the continuous power rating of the motor, the root mean square (rms) power (heating effect) must be deter-



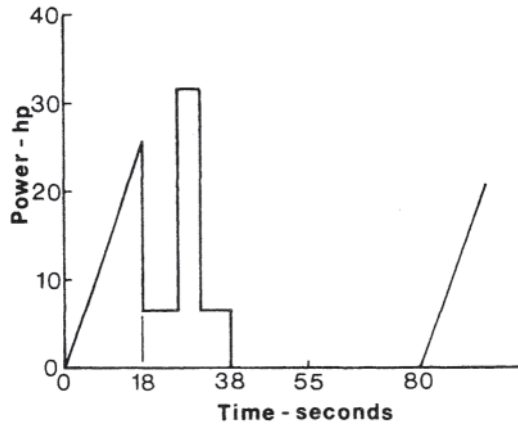


**Figure 3.13** Electric vehicle power duty cycle for the speed duty cycle of Fig. 3.12.

mined. The worst-case scenario is repeated duty cycles. The rms power is:

$$P_{rms} = \sqrt{\frac{\sum(p)^2 \times \text{time}}{\text{running time} + \text{standstill time}/k}} \quad (3.33)$$

where the constant  $k$  accounts for the poorer ventilation at standstill and is commonly taken as 4 for an open motor. Thus:

$$P_{rms} = \sqrt{\frac{\int_0^{18} \left(\frac{25.58}{18}\right)^2 t^2 dt + 6.51^2 \times 15 + 31.77^2 \times 5}{38 + 17 + 25/4}}$$

$$= 12.5 \text{ hp}$$

Note that the ratio of peak power to rms power is:

$$\frac{31.77}{12.5} = 2.54$$

Thus the motor size will probably be determined not on the basis of continuous load but on its ability to handle peak load, that is, its commutation ability.

Assuming that a series motor is to be used, data available from the manufacturer may be presented as a plot of the open-circuit saturation curve, that is, voltage versus series field current at a specific rotor speed. For a series motor:

$$E = K(I_f)\omega \quad \text{and} \quad T = K(I_f)I_a \quad (3.34)$$

where  $E$  is open circuit voltage.  $T$  is torque in Newton-meters,  $\omega$  is speed in rad/s and  $I_f$  and  $I_a$  are field and armature currents in amperes. If  $E$ ,  $\omega$ ,  $T$ , and  $I$  are per unit,  $K(I_f)$  is also a per-unit value. Figure 3.14 is a typical saturation curve reduced to perunit values.

Applying a curve-fit routine to the data yields:

$$K(I_f)_{pu} = \left(\frac{T}{I_a}\right)_{pu} = \left(\frac{E}{\omega}\right)_{pu} = 0.95 I_f^{0.454} \quad (3.35)$$

Assuming that  $I_a = I_f$  (a series motor), the equations describing the motor can then be formulated as:

$$T_{pu} = 0.95 I^{1.454} \quad (3.36)$$

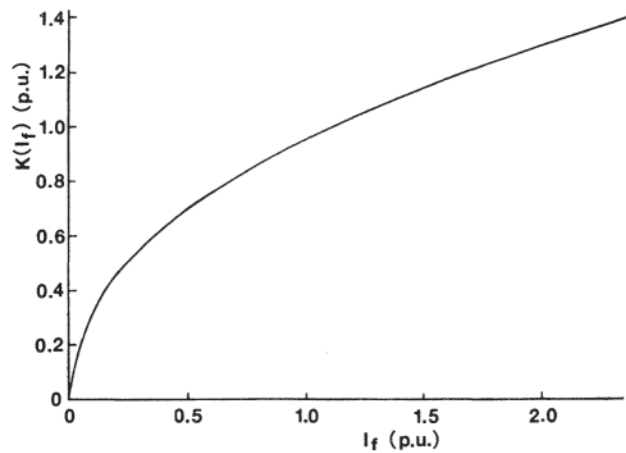


**Figure 3.14** Typical motor saturation curve.  $K(I_f) = (E/\omega) = T/I_a = 0.95 I_f^{0.454}$  pu.

$$\omega_{pu} = \frac{V - IR}{0.95 I^{0.454}} \quad (3.37)$$

$$P_{pu} = (T_{pu})(\omega_{pu}) \quad (3.38)$$

where:

- $V$  = per-unit applied voltage = source voltage  $\times (T_o/T)$ , and
- $R$  = per-unit armature and field resistance

Based on an assumed value of  $R = 0.045$  per unit, values of  $I$  from 0.2 to 3.0 per unit, and values of  $V = .0, 0.8, 0.6$ , and so forth per unit, values of  $T$ ,  $\omega$ , and  $P$  were calculated, resulting in the curves of Figs. 3.15 and 3.16. In Fig. 3.15, the per-unit current loci are also indicated.

The electric vehicle power requirements can be used with these typical motor characteristics to demonstrate how a motor rating can be determined and to illustrate the influence that a motor's ability to commutate overloads has on the motor size required. In order to relate motor size to vehicle power and speed requirements, it is necessary to specify tire diameter,  $D$ , step-down gear ratio,  $G/I$ , and drive efficiency of the motor and gearing. For vehicle velocity  $v$  in ft/s and tire diameter in ft, the motor speed  $\omega_m$  in rad/s will be:

$$\omega_m = \frac{2Gv}{D} \quad (3.39)$$

or, in terms of speed in mph and rev/min,  $N$ :

$$N = 27.89 \frac{G}{D} \text{ (mph)} \quad (3.40)$$

If the vehicle uses a 5.21/1 gear differential and 2-ft. diameter tires, motor speed at 55 mph will be

$$N = (27.89) \frac{(5.21)}{2} (55) = 4000 \text{ rpm} \quad (3.41)$$

Now a "cut and try" process begins. Assume the motor chosen has a rated speed of 5000 rpm. Vehicle speed of 55 mph represents 0.8 per-unit (pu) speed. Net power at top speed was calculated earlier at 27.67 hp. From Fig. 3.15, at 0.8 pu speed and  $V = 1.0$ , per-unit power is 1.45 and  $I = 1.5$  pu.

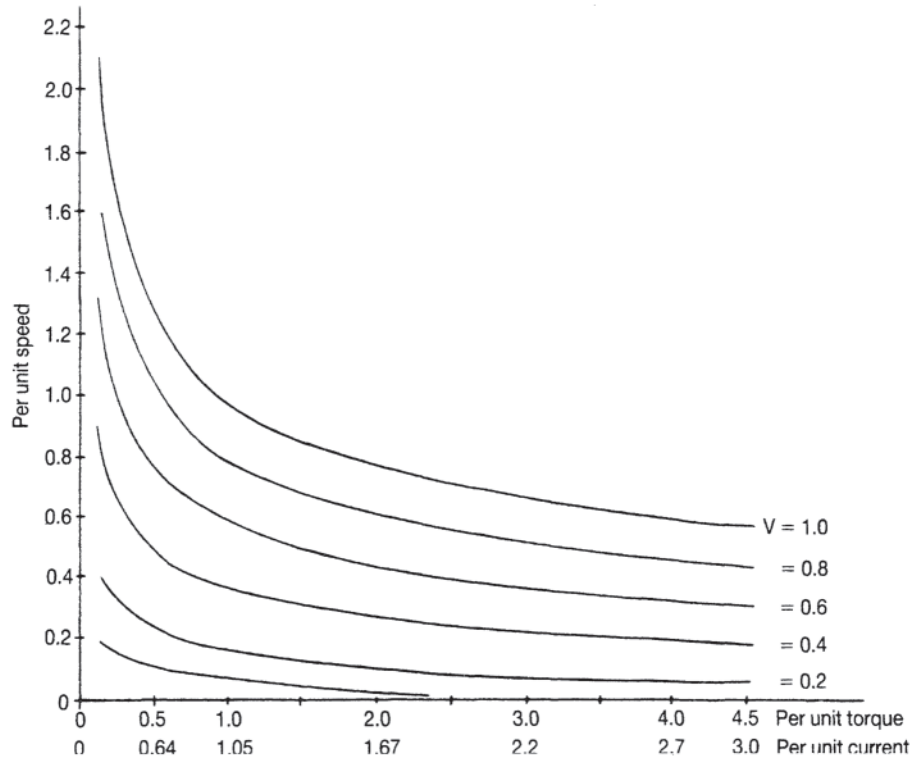


Figure 3.15 Per-unit speed vs. per-unit torque (with auxiliary per unit current scale) for a typical series motor.

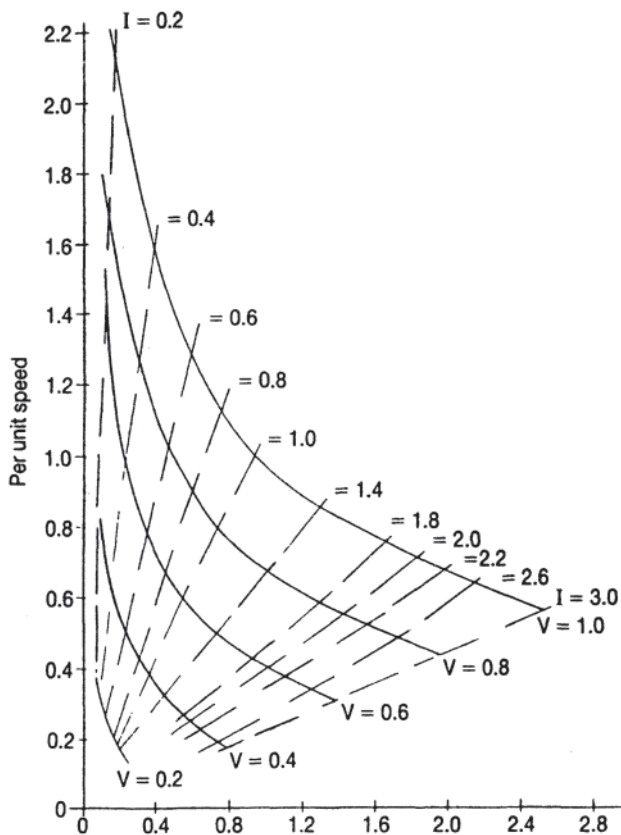


Figure 3.16 Per-unit speed vs. per-unit power for a typical series motor.

Motor size is then  $27.67/1.45=20$  hp.

The per-unit speed, power, current, and voltage are calculated for the driving conditions for a 20-hp, 5000-rpm motor as follows.

20-hp, 5000-rpm Motor				
Condition	Speed	Power	Voltage	Current
Top speed	0.8	1.45	1.0	1.5
Cruise	0.44	0.33	0.42	0.8
Accelerating	0.44	1.28	0.7	2.1
Grade climbing	0.44	1.59	0.75	2.6

If this series of calculations is repeated for a motor of 4000 rpm rated speed (1.0 pu), full voltage (1.0 pu), and perunit power=0.95, then motor size is calculated as approximately 30 hp.

30-hp, 4000-rpm Motor				
Condition	Speed	Power	Voltage	Current
Top speed	1.0	0.95	1.0	1.0
Cruise	0.55	0.22	0.4	0.5
Accelerating	0.55	0.85	0.68	1.4
Grade climbing	0.55	1.06	0.73	1.6

These two evaluations illustrate the method used to relate the variables of interest. The designer is often constrained in his choice of motor by the maximum current. A 20-hp, 4000-rpm motor is smaller, weighs less and should be more economical, not only in first cost but in decreased losses while running. However, note that, in order to use the smaller motor, that motor must be capable of commutating 260% of rated

current while grade climbing; the larger motor requires maximum commutating current ability of only 160% of rated current. From the rms power loading (thermal capability) 12.5 hp was required. Calculations similar to those above indicate that if a 15 hp, 5880 rpm motor were used, the current during grade climbing would be 3.2 pu. As can be seen from these calculations, the limiting factor in motor selection is its commutating ability. This is especially important in chopper-drive applications because the “black band” of commutation decreases with harmonics in the motor supply current.

## REFERENCES

Note: In the following listing, abbreviations have the following meanings:

AIEE	American Institute of Electrical Engineers (predecessor to IEEE)
ANSI	American National Standards Institute
IEC	International Electrotechnical Commission
IEEE	Institute of Electrical and Electronics Engineers
NEMA	National Electrical Manufacturers Association
NFPA	National Fire Protection Association

Sources for standards are listed in [Appendix B](#).

- IEC Standard 60034–5: Rotating Electrical Machines (Part 5: Classification of degrees of protection provided by enclosures for rotating electrical machines (IP Code)).
- NEMA MG 1–1998, Motors and Generators.
- ANSI/NFPA 70, National Electric Code, 1999.
- IEC Standard 60034–6: Rotating Electrical Machines (Part 6: Methods of cooling (IC Code)).
- IEC Standard 60072: Dimensions and Output Series for Rotating Electrical Machines.
- IEC Standard 60034–7: Rotating Electrical Machines (Part 7: Symbols for types of construction and mounting arrangements of rotating electrical machinery).
- IEC Standard 60034–12: Rotating Electrical Machines (Part 12: Starting performance of single-speed three-phase cage induction motors for voltages up to and including 660 V).
- IEC Standard 60034–1: Rotating Electrical Machines (Part 1: Rating and performance).
- IEC Standard 60034–2: Rotating Electrical Machines (Part 2: Methods for determining losses and efficiency of rotating electrical machinery from tests).
- Thorpe, J.F., *Mechanical System Components*, Allyn & Bacon, Boston, 1989.
- Janna, W.S., *Introduction to Fluid Mechanics*, 2d edn, PWS Publishers, Boston, 1987.
- Shepherd, D.G., *Principles of Turbomachinery*, Macmillan, New York, 1956.
- Shigley, J.E., *Mechanical Engineering Design*, 3d edn, McGrawHill, New York, 1977.
- Streeter, V.L., and E.B.Wylie, *Fluid Mechanics*, 8th edn, McGraw-Hill, New York, 1985.
- Fink, D.G., and H.W.Beaty, *Standard Handbook for Electrical Engineers*, 11th edn, McGraw-Hill, New York, 1979.
- Kuhlmann, John H., and N.F.Tsang, *Design of Electrical Apparatus*, 3d edn, Wiley, New York, 1950.
- Hetzl, Frederic V., and Russell K.Albright, *Belt Conveyors and Belt Elevators*, 3d edn, Wiley, New York, 1941.
- Colijn, R., *Mechanical Conveyors for Bulk Solids*, Elsevier, Amsterdam, New York, 1985.
- Smeaton, Robert W., Editor, *Motor Application and Maintenance Handbook*, 2d edn, McGraw-Hill, New York, 1987.
- IEEE Std. 112–1996—IEEE Standard Test Procedure for Polyphase Induction Motors and Generators.
- NEMA MG 2–1989, Safety Standard for Construction and Guide for Selection, Installation, and Use of Electric Motors and Generators.
- ANSI Std. S-12.34–1988 (R1993) Engineering Methods for the Determination of Sound Power Levels of Noise Sources for Essentially Free-Field Conditions over a Reflecting Plane.
- IEEE Std. 429—Evaluation of Sealed Insulation Systems for AC Electric Machinery Employing Form-Wound Coils.
- Hamilton, H.B., “Losses in Chopper Controlled DC Series Motors,” DOE/NAS A/3163–1, NASA CR-167845, 1982.
- Hamilton, H.B., and E.Strangas, “Series Motor Parameter Variations as a Function of Frequency and Saturation,” *IEEE Transactions on Power Apparatus and Systems*, vol. PAS-99, July/Aug., 1980, pp. 1567–1574.
- Snively, H.D., and P.S.Robinson, “Measurement and Calculation of DC Machine Armature Inductances,” *Transactions of the AIEE*, vol. 69, 1950, pp. 1228–1237.
- AIEE Technical Paper 52–71, “Rate of Rise of Short Circuit Current of DC Motors and Generators,” AIEE Subcommittee on DC Machines, 1952.

# 4

## Induction Motor Analysis and Design

**Hamid A.Toliyat, Peregrin L.Timár, and Sheo P.Verma** (Sections 4.0 and 4.1)/**Colin E.Tindall** (Sections 4.2 and 4.3)/**Eugene A.Klingshirn** (Section 4.4)/**Vilas D.Nene** (Sections 4.5, 4.6.1, 4.7.1, 4.7.2, and 4.8)/**Gerald B.Kliman** (Section 4.6.1)/**Jacek F.Gieras** (Section 4.6.2)/**Sheo P.Verma** (Sections 4.7.1 and 4.7.2)/**Nils E.Nilsson** (Section 4.7.3)/**T.J.E.Miller** (Section 4.9)/**John R.Brauer** (Section 4.10)

<b>4.0 INTRODUCTION</b>	<b>216</b>
<b>4.1 INDUCTION MOTOR FIELD ANALYSIS</b>	<b>219</b>
4.1.1 Generation of the Rotating Field	219
4.1.2 Winding of the Stator	223
4.1.3 Spatial Harmonics in the Field Curve	237
4.1.4 Reactances of the Induction Motor	241
4.1.5 Radial Force Waves	245
4.1.6 Homopolar Flux and Unbalanced Magnetic Pull in the Two-Pole Induction Motor	247
4.1.7 Tangential Forces Caused by Harmonics	249
4.1.8 Components of Air Gap Flux Caused by Inverter Supplies	251
4.1.9 Switching Transients	252
<b>4.2 ROTOR CONSTRUCTION</b>	<b>256</b>
4.2.1 Introduction	256
4.2.2 Squirrel-Cage Design	257
4.2.3 Wound-Rotor Design	257
<b>4.3 INDUCTION MOTOR EQUIVALENT CIRCUITS</b>	<b>258</b>
4.3.1 Introduction	258
4.3.2 Steady-State Equivalent Circuit	258
4.3.3 Transient or Dynamic Equivalent Circuit	260
<b>4.4 EQUIVALENT CIRCUITS FOR VARIABLE FREQUENCY</b>	<b>261</b>
4.4.1 Introduction	261
4.4.2 Rotor Deep-Bar Effect	262
4.4.3 Solution of Equivalent Circuits	263
<b>4.5 IMPORTANT DESIGN EQUATIONS</b>	<b>263</b>
4.5.1 Output Equation and Main Dimensions	263
4.5.2 Design of Stator Winding	264
4.5.3 Fractional Slot Winding	265
4.5.4 Squirrel-Cage Rotor Design	265
<b>4.6 SPECIAL INDUCTION MOTOR DESIGNS</b>	<b>271</b>
4.6.1 Linear Induction Motor Design	271
4.6.2 Solid-Rotor Induction Motor Design	273
<b>4.7 MECHANICAL DESIGN</b>	<b>277</b>
4.7.1 Crawling and Cogging	277
4.7.2 Vibration and Noise	278
4.7.3 Lamination Fatigue Mechanisms	279

<b>4.8 THERMAL DESIGN</b>	<b>282</b>
4.8.1 Methods of Cooling	283
4.8.2 Design of the Ventilation Circuit	284
<b>4.9 COMPUTER-AIDED DESIGN OF ELECTRIC MACHINES</b>	<b>284</b>
4.9.1 Why We Need Computers in the Design of Electric Machines	284
4.9.2 The Nature of the Design Process	285
4.9.3 Steps Needed to Design an Electric Machine	286
4.9.4 Examples of Specialized Computer Analysis	290
4.9.5 Automation of the Design Process	292
<b>4.10 FINITE ELEMENT ANALYSIS OF INDUCTION MOTORS</b>	<b>293</b>
4.10.1 Motivation for Induction Motor Finite Element Analysis	293
4.10.2 Three-Phase Induction Motor Finite Element Analysis	293
4.10.3 Single-Phase Induction Motor Finite Element Analysis	296
<b>REFERENCES</b>	<b>297</b>

## 4.0 INTRODUCTION

Electric machines in general provide energy transformation. Although machines using electrostatic forces can be built, the magnetic field is the medium of choice because energy densities  $10^4$  times that of the electrostatic field are possible.

Multiphase induction machines, especially those with squirrel-cage rotors, are the simplest and least expensive electrical machines devised. Their development had to await the advent of alternating current systems, which in turn had to wait on the development of the transformer. With alternating current systems available, serious work began on motors designed to take advantage of the characteristics of such systems.

The fundamental principle on which induction motors are based is the rotating magnetic field concept. The original work was done by Galileo Ferraris in Italy and Nikola Tesla in the United States, both of whom announced the results of their work in 1888. Both based their designs on two-phase systems, but Tesla recognized that more than two phases could be used. Although Ferraris made his first announcement 2 months before Tesla, the weight of the evidence presented in later court cases was on Tesla's side, and his patents, both in the United States and abroad, were upheld in subsequent litigation.

Westinghouse proceeded at once to acquire Tesla's patents, and had induction motors in commercial service in 1890, settling on 60 Hz as the frequency of choice in 1892. Although Westinghouse favored a two-phase system, General Electric began installation of three-phase systems in 1893. Both two-phase and three-phase systems existed for some years, but the economic advantage of the three-phase system led to its eventual adoption as a nearly universal standard for generation, transmission, and distribution.

When analyzing the electric machine as a system, the description of the system and the input data are given, and the output variables of the system are determined [1]. In the case of synthesis, the input and output variables are given and a system is designed to provide the correct relationships between them. Since the analysis of the real system is complicated, models and simulation procedures are used in both analysis and synthesis, with experimental procedures being used for verification.

The simulation procedure includes choosing the proper modeling process, creating a reasonably simple model, exercising it, improving the model, and introducing into practice the information obtained from the model.

The classic model of the induction motor was developed from recognition of the electrical parameters of the various components that make up the machine. This model came to be known as the equivalent circuit. In the case of multiphase machines, the equivalent circuit represents only one phase under the assumption that all phases are identical. Such a circuit is shown in Fig. 4.55 (p. 259).

The equivalent circuit is a two-loop network with resistance  $R_1$  and reactance  $X_1$  of the stator winding in the first loop, the resistance  $R_2$  and reactance  $X_2$  of the rotor conductors in the second loop, and a branch common to both loops contains a reactance  $X_m$ . This reactance accounts for the working magnetic flux. A resistance  $R_i$  in parallel with the reactance  $X_m$  accounts for the hysteresis and eddy current losses. The mechanical output power per phase is equal to the  $I^2R$  loss in the resistance  $R_2(1-s)/s$ , where  $s$  is the ratio of the difference between the speed of the rotating field and the speed of the rotor to the speed of the rotating field.

A phasor diagram of the currents and voltages can be drawn from the analysis of the equivalent circuit. With the applied voltage and the parameter values assumed or known from measurements, the magnitude and phase angle of all currents and voltages can be calculated. In other words, these lumped parameters and circuit loops form a representation from which predictions of the physical operation of the machine can be made by repeated analysis.

The equivalent circuit and the phasor diagram developed from it were and still are satisfactory models for the quick, qualitative analysis of the machine's operating characteristics. Kirchhoff's laws applied to the relatively simple circuit make it possible to write mathematically complete equations for those physical quantities that are of importance to the engineer. In many cases even today, this modeling procedure—the classic description—is often used.

The preceding assumes that three-phase machines have absolutely symmetrical stators and rotors; that is, that the number of turns in the phase windings are equal, that the placement of

the conductors is identical from phase to phase, that the windings for each phase are at 120 electrical degrees with respect to each other, and that the excitation voltages are precisely equal in magnitude and their phase differences are precisely 120 degrees [2]. Given these conditions, it is necessary to look at only one phase. With a symmetrical three-phase supply, the current and voltage relationships of the phases are identical. That is, the three-phase symmetric machine with symmetric operating conditions does not have a dominant phase. This makes it possible to use only the equivalent circuit of one phase instead of examining the entire machine, and variables such as torque and power for the entire machine can be obtained by multiplying those for one phase by 3.

As induction motors are used in a wide range of applications, analysis of the machine during transient conditions has become important. Designers have tried to add additional lumped parameters to the simple equivalent circuit, thus making it suitable for the new demands. This effort was effective for a while, but later such enormous and complicated equivalent circuits were required, sometimes with several hundred additional parameters, that they were practically unusable. More accurate analysis also led to the realization that the machine as well as the supply circuit could no longer be considered symmetrical, thus further complicating the problem. In practice, it often happens that asymmetric operating conditions arise. Moreover, symmetric conditions are sometimes artificially changed to asymmetric conditions to bring about special operating conditions. In these cases, the operation of the machine cannot be analyzed from one phase only, and the total effect of all three phases has to be examined [3]. However, there is a way of analyzing asymmetric systems by considering the overall effect of several symmetric systems.

This method is called the *symmetrical components method*. In this method, the current and voltage relationships of the asymmetric machine or system can be considered as the combined effect of several machines operating with symmetric conditions, and only one phase need be analyzed for each. In practice, because asymmetrical operating conditions frequently appear, it is important to examine the effects on induction machines. Some of the asymmetrical operating conditions in which this method would be used are:

- *Supply circuit asymmetry.* The asymmetry may be steady or transient. Steady circuit asymmetry may appear when asymmetric loads are connected to the network (e.g., single-phase welding transformers, single-phase motors, melting furnaces, and so forth) or on the occurrence of conditions such as blown fuses, circuit breakers and switches with defective contacts, prolonged ground faults, and so forth. Transient asymmetry is created with every asymmetrical breakdown in the network (e.g., intermittent ground or line-to-line faults).
- *Internal asymmetry.* This condition may arise as the result of an open circuit or a short circuit in one phase winding, but will also arise as a consequence of certain winding arrangements, as will be seen later.

A three-phase system is said to be asymmetric if the voltage and current phasors are of different magnitudes and have different angles between them. The starting point in the symmetrical components method is that the three-phase system, having three asymmetric phasors, can always be resolved into three symmetrical systems. Conversely, one asymmetric three-phase system can always be derived from three symmetric three-phase systems.

In the case of symmetrically built multiphase machines with a spatially sinusoidal winding distribution, another method (known as the Park-vector method) may be used to relate the multiphase variables and to simplify the equations. The spatially sinusoidal distribution makes it possible to sum the three magnetomotive forces (mmfs) into a single resultant space vector and do all the necessary operations with that vector. A great advantage of the method is that it demonstrates the physical conditions directly.

In examining the circuits of electric machines, the voltage equations of the circuits are used and solved as simultaneous equations. In electromechanical energy transducers, the voltage equations must be supplemented by the mechanical equation describing the equilibrium of the torques or forces. The simplicity of the calculations depends on the number of equations; thus the model to be used for general analysis should contain the required cases with the minimum number of windings.

For the sake of completeness, the model includes salient poles. (The cylindrical machine is subsumed in this model as well if the parameters in the *d* [direct] and *q* [quadrature] directions are equal.) The model has two windings perpendicular to each other in the stator as well as in the rotor. The axis of the winding of the salient pole is, according to practice, the direct (*d*) axis. Hence the *d* axis lies along the line of maximum flux density, and falls in the same place as the magnetic symmetry axis.

A general model that contained all the special characteristics of the machines would be almost too complicated to solve. For simplicity's sake several assumptions are often made, which may require the neglect of certain factors. The degree of neglect depends on the complexity of the model and the depth of analysis. The basic assumptions are summarized below.

1. The construction of the machines is magnetically symmetrical. Magnetic symmetry is a natural consequence of the construction of the cylindrical machine. In the salient-pole machine, symmetrical mechanical placement of the salient poles is required.
2. The magnetic circuit of the machine has salient poles on either the rotor or the stator, but not on both. The effect of the slots in the cylindrical section on the magnetic field is neglected and the cylindrical section is considered to have a uniform surface from a magnetic point of view. The effect of the salient poles is taken into consideration in designing the magnetic circuit.
3. The magnetic permeability of iron is considered to be infinitely large. The magnetic relationships are then linear; thus the inductances are independent of the current and the magnitudes of the mutual inductances are equal in both senses.

4. In cylindrical machines, both the mmf and the flux density have sinusoidal distributions along the periphery. In machines with salient poles, the windings on the salient-pole side have an mmf distribution of optional form, but the flux density has sinusoidal distribution. The distributions of the mmf and flux density on the cylindrical side are both sinusoidal, but the amplitude of the flux density distribution depends on the relative position of the salient pole and the pole on the cylindrical side.

5. Based on the flux density distribution in the air gap, periodically repetitive magnetic poles having opposite polarities will be formed along the periphery of the air gap; the circumferential spacing of these poles, the pole pitch, is constant.

6. The windings on the cylindrical side are designed identically and are placed so that their axes have the same mechanical angle between them. (The mechanical angle between the axes of the windings is the quotient of 360 degrees and the number of windings.) On the salient-pole side the designer has the option of a number of different windings only in the d and q directions, but in the case of several pairs of poles the pairs of poles are designed identically.

7. The hysteresis and eddy current losses due to change in flux and all of the effects of the electric fields present in the machine are neglected.

These assumptions are not valid for all machines, and due to this lack of validity some phenomena may occur in the machine that cannot be examined with this kind of model. *Regardless of the assumptions, the basic characteristics of the machine cannot change.* The effects of these assumptions are usually examined separately.

Variables that describe the state of the dynamic system in the past, present, and future are called *state variables*. If these systems are described with simultaneous first-order differential equations (e.g., the differential equations of the independent energy storage), then these equations are called the *equations of state*.

To ease calculations, it is best to express the differential equations in matrix form and to use matrix analysis methods. For better understanding, it may be advisable to consider the variables of state to be components of an n-dimensional vector, and thus the concept of vector fields can be applied. The state method is thus frequently called the state field method or the vector field of state method. One of the reasons the state method has been developed is that the transformation methods are not applicable to variable-coefficient, nonlinear differential equations. For this reason and because computers lend themselves well to state variable simulation, formulation of the necessary equations in the state variable form has become widespread.

The name of this method originates from “the state of the system,” because with knowledge of the present state, the future state can be deduced when the input signals of the system, that is the forcing functions, are known. The “present state” is frequently not a stationary one as a result of previous inputs or load disturbances. The energy stored in various parts of the system is a consequence of this past history; that is why it is advisable to choose as state variables the currents in

inductances, the voltages across capacitors, the angular speeds of rotating bodies, and so forth. The state of a dynamic system is then the collection of those numbers that define the forcing functions and the equations describing the system, thus pointing to the future state and the output of the system.

By the expression “the state of a system” is meant that smallest set of number that must be given at time  $t=t_0$  to be able to deduce unequivocally, using the given input signals, the reaction of the system at any given time  $t \geq t_0$ . The state of the system at any time  $t$  is defined unequivocally by the state at time  $t_0$  and the forcing functions used for  $t \geq t_0$ . This state is independent of the state or the forcing functions before the time  $t_0$ .

The state method describes the first-order differential equation system in the form used in analog or digital modeling and usually solves it directly in real time. Laplace transform methods may be used to gain insight and also for verification. The generalized theory of machines is a development of the state method. While the usual matrix analysis of electric machines is done with the help of matrix algebra, the state method is based on the analysis of the matrix itself. Thus, the required variables are found at the same time, not one after the other, and tiresome inversions and Laplace transformations can be avoided. Moreover, the state method is applicable to changing coefficients and nonlinear differential equations of the first order, although in these cases the solutions are usually only numerical. Actually, this is not really a disadvantage.

In today’s technical literature, the complete model is being sought due to the more frequent use of analog and digital computers. A supplementary “equationless” method and concept is developing where, instead of the equations, the effect of the variables is obtained through running the program several times, and the solution is either plotted or listed. In many cases the engineer has only to state the problem and model it, while the search for a solution is the machine’s job, usually with available software. This does not deny the importance of the complete form from a theoretical as well as a practical point of view.

The generalized theory of machines is accepted all over the world [4]. The basis of the generalized theory is a coordinate transformation, just as the vector method was also a coordinate transformation. At the same time, it is becoming evident that direct simulation with the phase quantities is sometimes more advisable. Similarly, the “direct” nonlinear and time-variant state methods will also place heavy demands on Laplace and Fourier transformation methods. In all probability, the computer will overshadow transformation methods in both cases. It is also easy to imagine that the engineers of the future will think in time functions again instead of the complex numbers used in alternating current analysis.

When electric machines are examined within the more general sphere of concepts of an energy system or control system (e.g., generalized machine theory, the system, simulation, and mathematical studies connected with them, matrix algebra, matrix analysis, state systems, and state fields examined in the wider perspective of the theory of sets), only the concept of the physical image changes; the physical facts being mirrored are the same as before. The machines rotate for

the same reasons and in the same manner as before. Only the concept and the accompanying method of analysis is changed.

The method of analysis is changed on the one hand because different groups of phenomena have been emphasized, such as transients, stability, and so forth; on the other hand, the possibilities in calculation have improved to a great degree in general and also in specific areas. Another reason is that the machines are seldom used as stand-alone units; they have become parts of control systems, e.g., a current or voltage inverter, controls, and a machine are parts of a complex unit.

The aim of this chapter is to describe analysis and synthesis; that is why it is especially important to choose optimal models and mathematical aids. At the beginning of this chapter, emphasis was put on analysis to establish the physical image. The most appropriate methods were described in broad terms in the case of the cited physical phenomena, including equivalent circuits, symmetrical components, and the Park-vector method, although other models may be used as well. Each method makes it possible to construct a relationship in a complete form for the whole system, including the input and output variables of the system elements. They demand only simple computer techniques and can be used with hand-calculator computations as well.

In later sections of this chapter, where the viewpoints of the design engineer dominate, computer methods and numerical analysis are emphasized. Use of these computer techniques in analyzing research of scientific depth (for

instance, the complexity of the problem) and in achieving design objectives (economy, optimization, and so forth) is almost unavoidable. The following material deals mainly with three-phase symmetric machines with special emphasis on physical phenomena and relationships, and indicates how special uses and asymmetric machines are derived from the three-phase machine [5]. Where necessary, the effect of the saturation of iron is also taken into account. Steps needed to design an electric machine are described.

## 4.1 INDUCTION MOTOR FIELD ANALYSIS

### 4.1.1 Generation of the Rotating Field

Suppose a direct-current excited coil is situated in the iron ring as seen in Fig. 4.1 (a). The construction of the iron ring is as follows: The interior cylindrical surface with diameter  $D$  is the so-called bore of the ring. There are slots in the bore in the axial direction and a distributed coil is placed in them along the circumference. This is actually a solenoid coil with vertical axis. In order to ensure low reluctance of the flux path, there is a cylindrical-shaped iron body in the bore placed in such a way that an air gap separates it from the exterior cylindrical ring.

Beginning from the starting point  $x=0$  as seen in Fig. 4.1 (a), the stepped mmf curve  $f_{ml}(x)$  is spread out along the direct current-carrying coil as a function of the  $x$  coordinate of the bore, as shown in Fig. 4.1(b). Two poles are created due to the direct

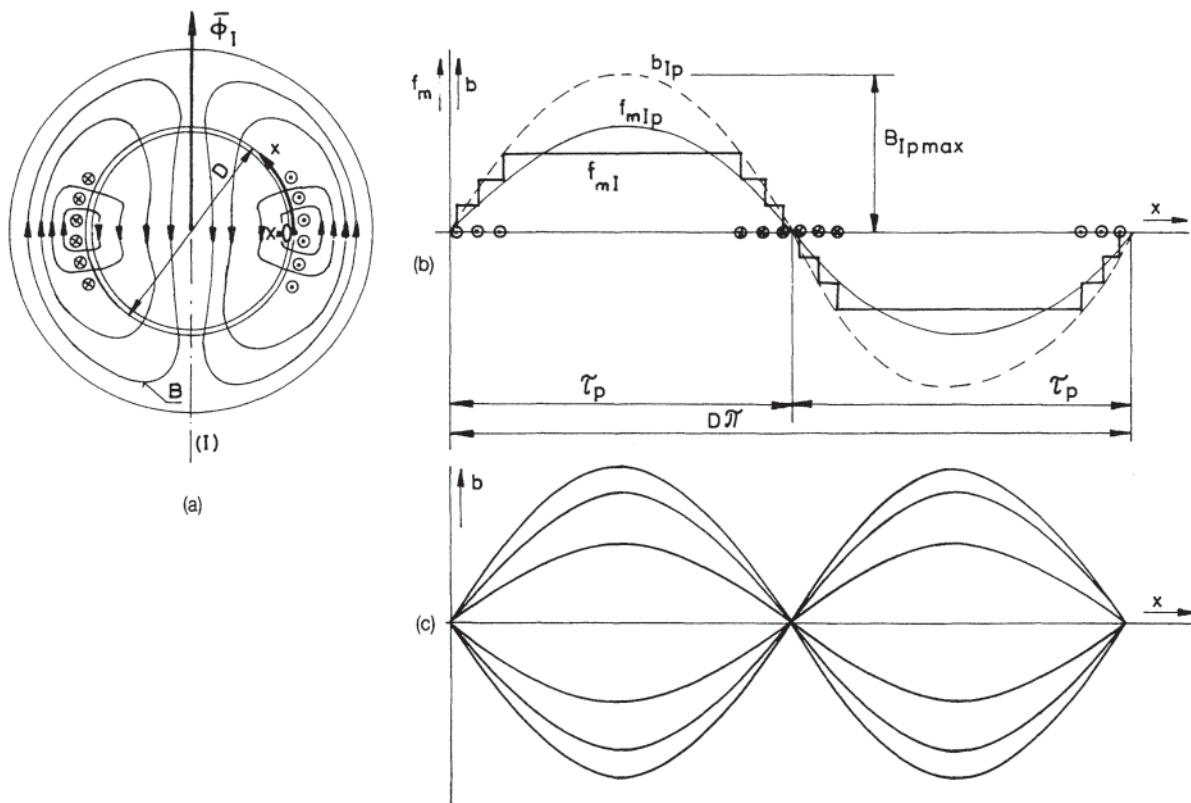


**Figure 4.1** One phase, two-pole winding, (a) Winding position, (b) Magnetomotive force (mmf) and flux density distribution along the periphery induced by direct current, (c) The distribution of fundamental-component of flux density excited by alternating current.



current flowing in the coil. That part of the circumference belonging to one pole is the pole pitch  $\tau_p = (D\pi)/2p$ , where  $p$  is the number of pairs of poles. The  $f_{ml}(x)$  mmf curve is periodic along the circumference, and thus can be expanded in a Fourier series.

The Fourier series of a general function  $f(x)$  that is periodic in space is:

$$f(x) = F_0 + \sum_{\mu=1} F_{a\mu} \sin \mu x + \sum_{\mu=1} F_{b\mu} \cos \mu x$$

Since the mmf of the coil under the two poles is equal, as seen in Fig. 4.1 (a), the term  $F_0$  is equal to zero. By choosing a suitable starting point for the coordinate system, the cosine terms (the coefficients of  $F_{b\mu}$ ) will also be zero. Thus, the mmf curve of the coil (I) has a Fourier series as follows:

$$f_{ml}(x) = \sum_{\mu=1} F_{ml\mu} \sin \left( \mu \frac{x}{\tau_p} \pi \right) \quad (4.1)$$

To understand the generation of rotating fields, the stepped mmf curve can be replaced by the first term of the Fourier series ( $\mu=1$ ). That is, the distribution of mmf along the circumference can be considered sinusoidal. (A later section will deal with the terms for which  $\mu>1$ , that is, the harmonics.) The mmf equation for  $p$  pole pairs is approximately:

$$f_{ml}(x) \cong f_{mlp} = F_{ml} \sin \left( \frac{x}{\tau_p} \pi \right) \quad (4.1a)$$

and may be plotted as shown in Fig. 4.1(b). The flux density distribution is radially sinusoidal, exactly like the mmf distribution in the air gap, because of the constant permeance (or reluctance) of the flux path. The curve  $b_{lp}(x)$ , shown dashed in Fig. 4.1(b), is given by:

$$b_{lp}(x) = B_{lp\max} \sin \left( \frac{x}{\tau_p} \pi \right) \quad (4.1b)$$

If the current in the coil is alternating current having frequency  $f_i$ , then all the values of the  $b_{lp}$  sinusoidal curve in space will change according to a sinusoidal curve in time (see Fig. 4.1(c)), with the angular frequency  $\omega_1$  of the alternating current. The flux density distribution of one coil is:

$$b_{lp}(x,t) = B_{lp\max} \sin \left( \frac{x}{\tau_p} \pi \right) \sin \omega_1 t \quad (4.1c)$$

Equation 4.1c is the equation of the alternating field, which can be characterized graphically with the  $\phi_l$  flux vector. The direction of the flux vector coincides with the axis of the solenoid coil, and its magnitude changes sinusoidally with time.

Assume now that there are two additional coils placed in the iron core. The original coil seen in Fig. 4.1 (a) may be designated as the (I)–(I') coil, shown diagrammatically in Fig. 4.2. It occupies one-third of the total circumference. The axes of the three coils (I), (II), (III) are displaced 120 degrees from each other, and the coils are called phase coils. The alternating current in coil (II) lags 120 degrees and the current in coil (III) lags 240 degrees behind the current in coil (I). Similar to the previous train of thought, the equation of flux density distribution due to coil (II) is:

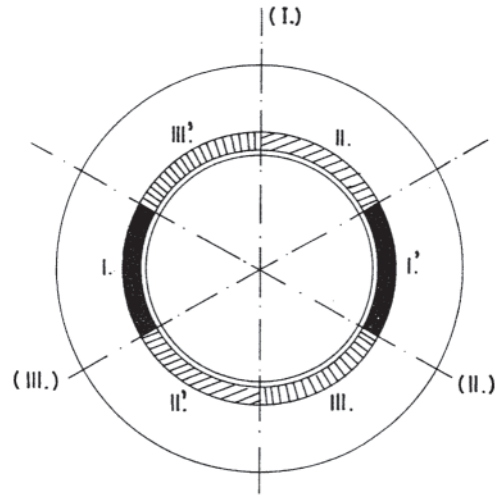


**Figure 4.2** Positioning of a three-phase two-pole winding along the periphery.

$$b_{IIp}(x,t) = B_{IIp\max} \sin \left( \frac{x}{\tau_p} \pi - \frac{2\pi}{3} \right) \sin \left( \omega_1 t - \frac{2\pi}{3} \right) \quad (4.2)$$

and the equation of flux density distribution due to coil (III) is:

$$b_{IIIp}(x,t) = B_{IIIp\max} \sin \left( \frac{x}{\tau_p} \pi - \frac{4\pi}{3} \right) \sin \left( \omega_1 t - \frac{4\pi}{3} \right) \quad (4.3)$$

To determine the resultant of the fields produced by the three phase coils, use is made of the identity:

$$\sin \alpha \sin \beta = \frac{1}{2} [\cos (\alpha - \beta) - \cos (\alpha + \beta)]$$

The flux density equations of the separate coils then become:

$$b_{Ip}(x,t) = \frac{1}{2} B_{Ip\max} \cos \left( \frac{x}{\tau_p} \pi - \omega_1 t \right) - \frac{1}{2} B_{Ip\max} \cos \left( \frac{x}{\tau_p} \pi + \omega_1 t \right) \quad (4.4)$$

$$b_{IIp}(x,t) = \frac{1}{2} B_{IIp\max} \cos \left( \frac{x}{\tau_p} \pi - \omega_1 t \right) - \frac{1}{2} B_{IIp\max} \cos \left( \frac{x}{\tau_p} \pi + \omega_1 t - \frac{4\pi}{3} \right) \quad (4.5)$$

$$b_{IIIp}(x,t) = \frac{1}{2} B_{IIIp\max} \cos \left( \frac{x}{\tau_p} \pi - \omega_1 t \right) - \frac{1}{2} B_{IIIp\max} \cos \left( \frac{x}{\tau_p} \pi + \omega_1 t - \frac{8\pi}{3} \right) \quad (4.6)$$

The resultant of the field distribution produced by the three phase coils is the sum of Eqs. 4.4, 4.5, and 4.6.

If the three coils have the same numbers of turns and the amplitudes of the three phase currents are equal, the resultant field distribution is of the form:

$$b_p(x,t) = \frac{3}{2} B_{p \max} \cos \left( \frac{x}{\tau_p} \pi - \omega_1 t \right) \quad (4.7)$$

because the second terms of the right-hand sides of Eqs. 4.4 to 4.6 add to zero. Equation 4.7 is such that it describes a sinusoidal flux density distribution along the circumference of the bore that advances with constant velocity  $v = \omega_1 D/2p$  along the circumference of the bore. That is, it rotates.

The mechanical angular velocity is given by  $\Omega_0 = \omega_1/p$ . This is called the synchronous angular velocity. If, for instance, all the coil sides seen in Fig. 4.2 situated along the circumference are crowded together so that each occupies 1/12 of the circumference, then in total they will occupy only one-half the circumference, still producing two poles. Now the winding may be repeated in the unoccupied half, creating two more poles. The iron core has a four-pole winding, and the synchronous angular velocity is only half that of the two-pole winding. At a given frequency, the synchronous angular velocity depends only on the number of poles.

Summarizing, it can be said that the rotating magnetic field is a magnetic wave with sinusoidal distribution, advancing along the periphery of the machine in the air gap, with constant velocity. Half of the wavelength of the wave is equal to the pole pitch  $\tau_p$  of the machine. The relationship between the mechanical angular velocity  $\Omega_0$  of the magnetic field and the number of pairs of poles  $p$  of the winding is given by:

$$\omega_1 = 2\pi f_1 = p\Omega_0 \quad (4.8)$$

A rotating field of constant magnitude and constant angular velocity will be developed if the spatial shift of each phase coil is equal to  $1/p$  times the phase shift of the current in each coil, and the current amplitudes are all equal. Thus it is possible to create a circular rotating field not only with a three-phase system, but with any  $m$ -phase numbered winding system as well. In the case of a coil system with  $m$  phases, the angular displacement of the axes of the coils is equal to  $(2\pi)/(mp)$  and the phase difference between the currents in time is equal to  $2\pi/m$ .

In this case, the expression for the magnetic field is:

$$b_p(x,t) = \frac{m}{2} B_{p \max} \cos \left( \frac{x}{\tau_p} \pi - \omega_1 t \right) \quad (4.9)$$

If the sequence of the coils is changed along the periphery of the bore, the equation of the field is:

$$b_p(x,t) = \frac{3}{2} B_{p \max} \cos \left( \frac{x}{\tau_p} \pi + \omega_1 t \right) \quad (4.10)$$

which differs from the previous field given in Eq. 4.7 only in that it rotates in the opposite direction, with a synchronous angular velocity:

$$\Omega_0 = -\omega_1/p.$$

Referring back to Eq. 4.4, which describes the field generated by the alternating current in the phase winding, it can be shown

that the alternating field can be replaced by two fields of half the amplitude, rotating in opposite directions. Conversely, the resultant of two equal magnetic fields rotating in opposite directions produces a stationary wave in space with double amplitude, varying in time. If just one of the symmetry conditions that result in a circular rotating field is not met, then the magnitude of the distribution of the rotating field will change in a periodic manner when rotating around the periphery of the bore. This kind of rotating field is called an elliptical field.

The following conditions may cause asymmetry:

1. The phase coils not being symmetrically placed in space.
2. The number of turns of the coils not being equal.
3. The coil currents not having the correct phase shifts.
4. The amplitudes of the phase currents not being the same.

#### 4.1.1.1 The Vector Description of the Field of Induction Machines

The flux density wave in space can be described vectorially independently of whether it is stationary or rotating. Equation 4.1b describes a distributed field that is sinusoidal in space and constant in time. The following vectorial form corresponds exactly to the harmonic form of Eq. 4.1b:

$$\bar{B}_{lp \text{ const}} = B_{lp \max} \exp \left( j \frac{x}{\tau_p} \pi \right) \quad (4.1b\bullet)$$

The projection of the vector on the imaginary axis gives the harmonic form

$$b_{lp} = \text{Im}[\bar{B}_{lp \text{ const}}]$$

The complex coordinate system used has its center at the center of the cross section of the iron core. At this moment the sinusoidal flux density wave, constant in time (see Fig. 4.3), is characterized by a vector of constant position and magnitude. Projecting the vector on the separate radii, the flux density wave may be constructed at given points of the periphery. The vector is also shown in Fig. 4.4(a). An alternating field is created if the magnitude of the vector,

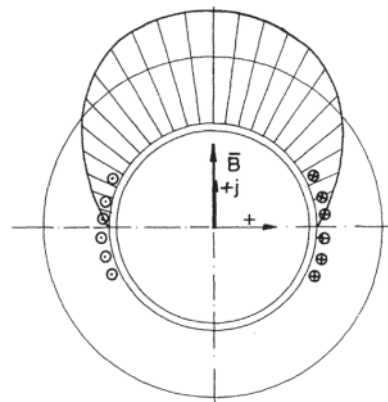


**Figure 4.3** The vector of a field stationary in space and constant in time.

which symbolizes the distribution in space, varies sinusoidally in time (see Fig. 4.4(b)) so that:

$$b_{fp} = \bar{B}_{fp \text{ const}} \cos \omega t \quad (4.1b'')$$

If the rotating field is to be described vectorially, then the vector in Fig. 4.4(a) has to be multiplied by the unit vector  $\exp(j\Omega_0 t)$ , resulting in the vector of Fig. 4.4(c), rotating at constant velocity, and yielding an equation analogous to Eq. 4.1c:

$$\bar{B}_p = B_{p \text{ max}} \exp\left(j \frac{x}{\tau_p} \pi\right) \exp(j\Omega_0 t) \quad (4.1c')$$

This expression describes such a field that is of the same magnitude, has a sinusoidal shape, and advances along the periphery of the bore with constant velocity. The projections of the vector give the peripheral distribution of the field for a given value of  $t$  for all directions, and also give the variation of flux density with time at a fixed point on the bore.

The alternating field in Fig. 4.4(b) can be resolved into two fields rotating oppositely, each having half the size. In vectorial form, this situation is represented by the equation:

$$\begin{aligned} \bar{B}_{fp \text{ const}} \cos \omega t &= \frac{1}{2} \bar{B}_{fp \text{ const}} \exp(j\Omega_0 t) \\ &+ \frac{1}{2} \bar{B}_{fp \text{ const}} \exp(-j\Omega_0 t) \end{aligned} \quad (4.4a)$$

and can be seen in Fig. 4.5(a).

It has previously been shown that if there is an asymmetry in either the winding or the alternating current excitation, than an elliptical field will evolve instead of a circular rotating field. This can be described vectorially as the sum of two vectors of different magnitudes, rotating with equal angular velocity but in opposite directions.

$$\begin{aligned} &\bar{B}_+ \exp(j\Omega_0 t) + \bar{B}_- \exp(-j\Omega_0 t) \\ &= \bar{B}_+ (\cos \Omega_0 t + j \sin \Omega_0 t) + \bar{B}_- (\cos \Omega_0 t - j \sin \Omega_0 t) \\ &= (\bar{B}_+ + \bar{B}_-) \cos \Omega_0 t + j(\bar{B}_+ - \bar{B}_-) \sin \Omega_0 t \end{aligned} \quad (4.11)$$

According to Eq. 4.11, the end of the resultant vector moves along an ellipse whose long axis is in the direction of the bisector of the original  $\bar{B}_+$  and  $\bar{B}_-$  vectors and with a magnitude  $B_+ + B_-$ , with its short axis perpendicular to the long axis and with a magnitude of  $B_+ - B_-$ . A field such as this is called an elliptical field, and the ellipse will look like the one in Fig. 4.5(b). The equation for the elliptical field (Eq. 4.11) can be written in another way after rearranging, resulting in

$$(\bar{B}_+ - \bar{B}_-) \cos \Omega_0 t + 2\bar{B}_- \cos \Omega_0 t + j(\bar{B}_+ - \bar{B}_-) \sin \Omega_0 t$$

Then, by combining the first and third terms, the expression becomes:

$$(\bar{B}_+ - \bar{B}_-) \exp(j\Omega_0 t) + 2\bar{B}_- \cos \Omega_0 t \quad (4.12)$$

thus demonstrating that an elliptical field is the sum of a symmetrical circular rotating field and an alternating field.

#### 4.1.1.2 The Park-Vector Description of the Magnetic Field of Induction Motors

In theoretical work on alternating current electric machines, Park-vector modeling can be a helpful aid. When plotting the mmf curve of Fig. 4.1 and the field curve of Fig. 4.3, the spatial sinusoidal distribution of the curves can be seen. This spatial distribution can be represented by  $\bar{F}_m$  and  $\bar{B}$  space vectors with magnitudes proportional to their maxima, placed at the positive maximum point. The space vector of the current is assumed in the direction of the mmf space vector. The magnitude of the vectors differ from each other only by the effective number of turns.

For any given time  $t$ , the current of each phase winding may be assigned a current phase vector of magnitude and sign determined by the magnitude and sign of the current at that specific instant, the vector being fixed in the direction of the axis of the winding. The axis of each phase coil can be assigned mathematically by use of the unit vectors  $\bar{1}$ ,  $\bar{a}$  and  $\bar{a}^2$ , which have phase shifts of 0, 120, and 240 degrees, respectively, in space. (See Fig. 4.6(a).) Properly summing up in a vectorial manner the  $i_a$ ,  $i_b$ , and  $i_c$  space vectors of the currents of the three phase coils at the given time, one obtains the space vector of the three-phase winding.

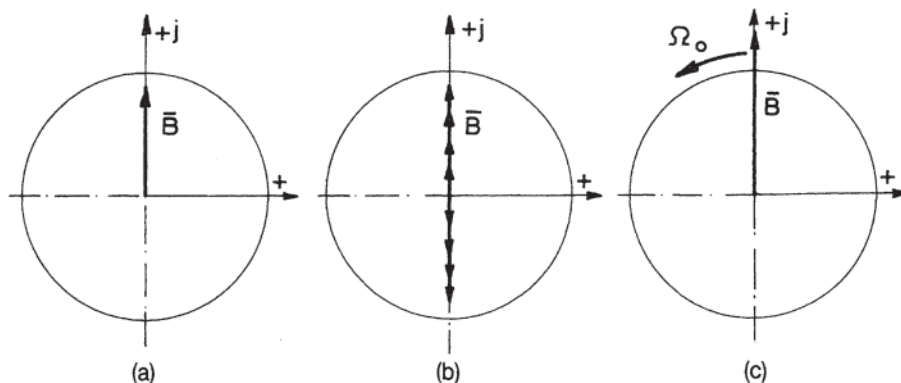


**Figure 4.4** Vector description of the fields, (a) Constant in time, stationary in space, (b) Sinusoidal in time, stationary in space, (c) Rotating field.

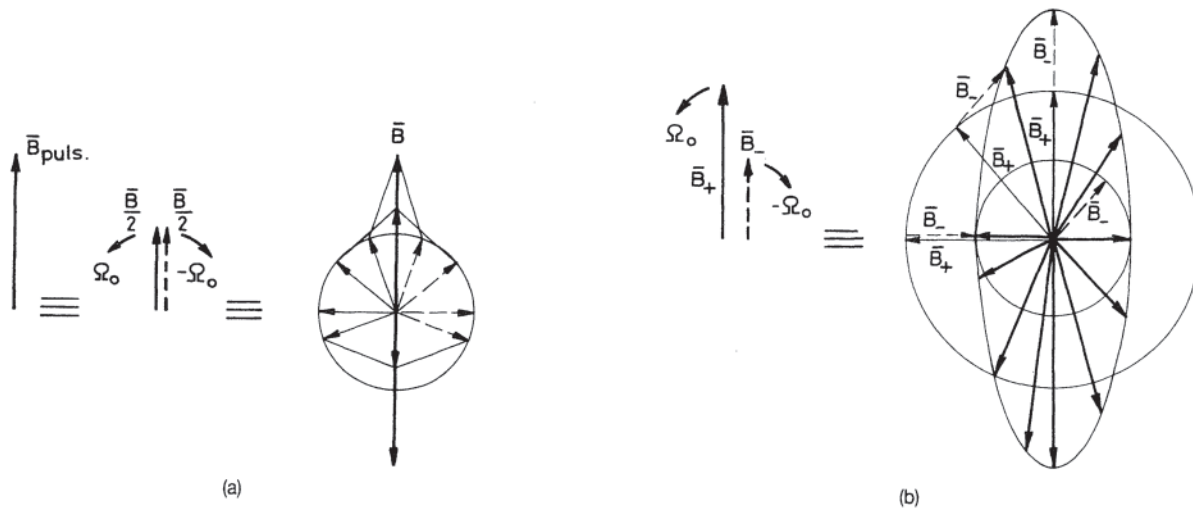


**Figure 4.5** Disjoining and summing up of fields, (a) An oscillating field produced by two rotating fields of equal magnitude and rotating at equal angular speeds in opposite directions, (b) An elliptic field resulting from two rotating fields of different magnitude, rotating in opposite directions.

The resultant three-phase current vector is:

$$\bar{i}_a + \bar{a}i_b + \bar{a}^2i_c$$

and the resultant three-phase mmf vector is:

$$\bar{i}f_{ma} + \bar{a}f_{mb} + \bar{a}^2f_{mc}$$

with the three-phase flux density vector:

$$\bar{i}b_a + \bar{a}b_b + \bar{a}^2b_c$$

Figure 4.6(b) shows the graphic summation of the current vectors in the case of a three-phase symmetrical supply. As a definition, the Park-vector is 2/3 of the current:

$$\bar{i} = \frac{2}{3}(\bar{i}_a + \bar{a}i_b + \bar{a}^2i_c) \tag{4.13.}$$

The Park-vector can be used even when the currents change arbitrarily with time. The condition for summing up the phase vectors was that they should be sinusoidally distributed along the periphery. In a symmetrical steady state, the Park-vector has constant magnitude and thus its end point plots a circle (see Fig. 4.6(c)), its angular velocity being constant.

The Park-vector can also be plotted when the supply current system is asymmetric. The end point of the Park-vector does not plot a circle in this case, but an ellipse. In addition to the steady-state case (the circular plot) and the asymmetric case (the ellipse), still other variations in the plot of the end point are possible, such as periodic functions (the sum of the fundamental and the harmonics), transient conditions (see Fig. 4.6(d)), or other changes with time.

The Park-vector is the general model of the rotating field, or excitation. Within this model, the magnitude and even the velocity of the Park-vector can change. In fact, it can have jumps as well, as in the case of controlled semiconductor switches.

The projection of the Park-vector on the phase axes shows the momentary phase magnitudes with correct signs. In machines without an external neutral point, such that  $(i_a+i_b+i_c=0)$ , using the complex form of the unit vectors results in

$$\begin{aligned} \bar{a} &= -0.5 + j\sqrt{3}/2 & \text{and} & & \bar{a}^2 &= -0.5 - j\sqrt{3}/2 \\ \text{Re}[\bar{i}] &= i_a & & & \text{Re}[\bar{a}^2\bar{i}] &= i_b & & \text{Re}[\bar{a}\bar{i}] &= i_c \end{aligned}$$

In the case of an external neutral point, the zero-sequence currents must be considered in separate equations [6].

### 4.1.2 Winding of the Stator

#### 4.1.2.1 Fundamentals of Winding Design

The excitation needed to create the rotating field is produced by a multiphase alternating-current-carrying winding that is periodically distributed along the periphery of the bore. The *m*-phase winding (in practice, *m* usually equals 3) consists of identically designed phase coils that are displaced by equal angles along the periphery. The phase coils are placed into slots in the inner surface of the cylindrical stator iron. That is why this kind of winding is called a distributed winding. As shown in Fig. 4.7, the distributed winding can be transformed from the solenoid coil (or concentrated winding) in two ways. In Fig. 4.7, the solenoid coil is made of three elementary coils.

A distributed, concentric winding is shown in Fig. 4.7(a). In this case the symmetry axes of the distributed elementary coils coincide, but the widths of the separate elementary coils are different. In Fig. 4.7(b), the widths of all elementary coils are identical in the distributed winding and the symmetry axis of the winding is a spatial average of the symmetry axes of the elementary coils. This type of winding is called a consequent-pole winding.

The coils of induction machines are placed in slots so that the air gap is smaller than if the coils were on the surface of the

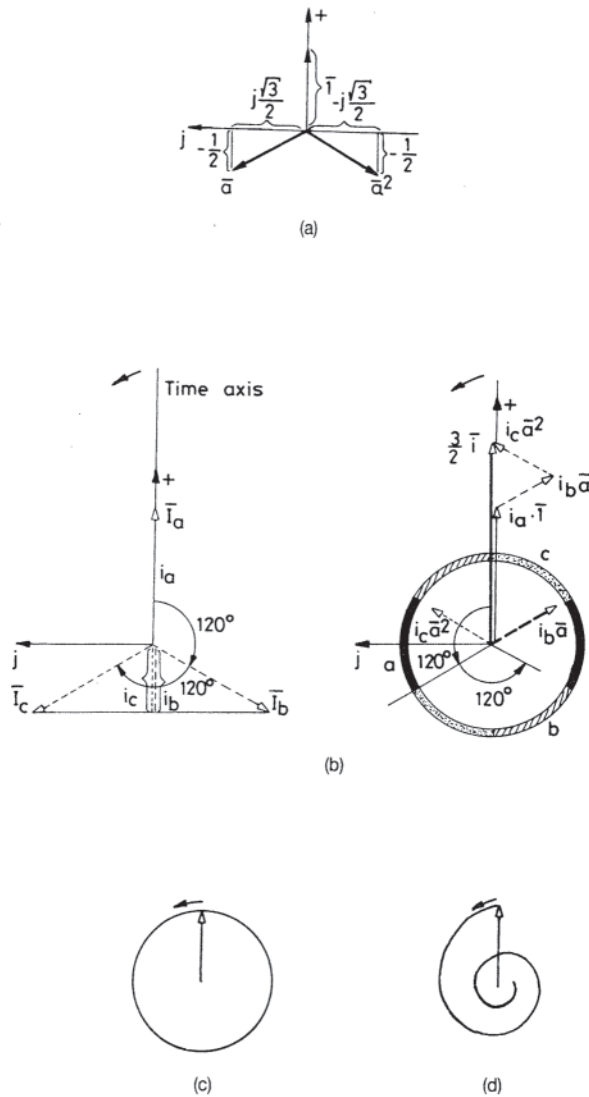


**Figure 4.6** Definition of the space vector, (a) Complex representation of the three-phase unit vector, (b) Plot of the Park-vector for three-phase current, (c) Trace of the end point of the Park-vector in steady-state operation, (d) Trace of the end point of the Park-vector in transient operation.

iron and also so that the coils are more easily fixed in position. The portions of the elementary coils that lie in the slots are called the coil sides, and those portions connecting the coil sides outside the iron core are called coil heads or end turns. Each elementary coil is made of two coil sides and two coil heads. If the elementary coil has many turns it is made of a small circular cross section conductor, but if it has only a few turns it is made of a rectangular cross section conductor.

The width of the elementary coils is stated in terms of a number of slots, and is the same as the number of teeth surrounded by the coil sides of the elementary coils. The steps (pitch) of the concentric winding's elementary coils are different, while the steps (pitch) of the consequent pole winding are the same.

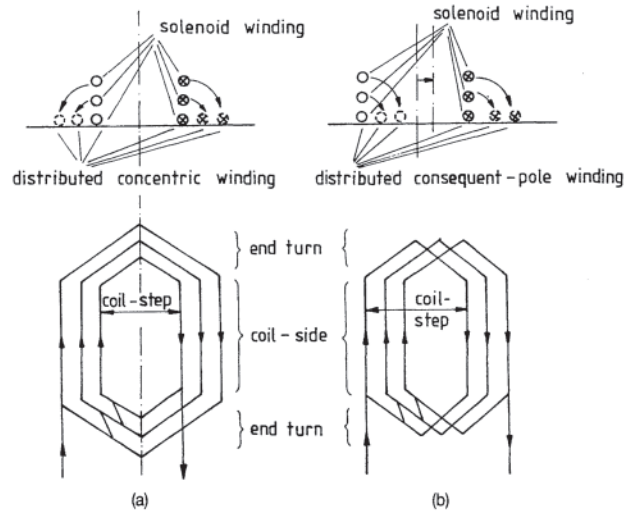


**Figure 4.7** Derivation of a distributed winding from a solenoid winding, (a) Concentric winding, (b) Consequent-pole winding.

If the number of conductors in one slot is equal to the number of turns of the elementary coil, then the winding is called single-layered (see Fig. 4.8(a)). In many cases, there are two coil sides in one slot, and the coil sides belong to different elementary coils (see Fig. 4.8(b)). In this case, half of the number of conductors belong to one coil side, and the winding is called two-layered.

In the windings of multipole machines, the series connection of the elementary coils belonging to one phase winding can be made in two ways. If one coil side under each pole is connected in series and the winding is continued to the coil sides in the adjacent slots until all coil sides for the phase winding have been used, as in Fig. 4.9, the resulting winding is called a wave winding. It is difficult to break this mode of winding into parallel branches, but it has the advantage that the end turn connections are short.

If the winding arrangement is such that first all coil sides are connected that lie under one pair of poles and only then is the connection made for the next pair of poles, it is called a looped or lap winding. Its advantage is that it can be divided into equal parts that may be connected in parallel. Its drawback is that the connections between the coils are long. An example can be seen in Fig. 4.10.

Up to this point, several types of alternating-current-carrying windings have been described. Almost any

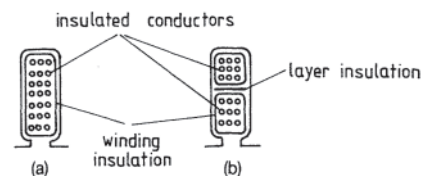


**Figure 4.8** Position of (a) a single-layer and (b) a double-layer winding in a slot.

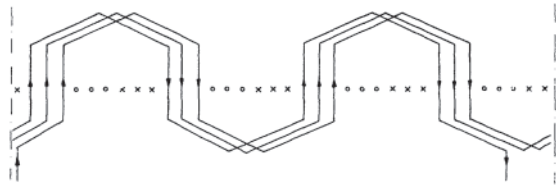


**Figure 4.9** Consequent-pole wave winding ( $S_1=36$ ,  $2p=4$ ,  $m=3$ ,  $q_1=3$ ).

combination of these can be constructed. As can be seen in Figs. 4.7, 4.9, and 4.10, the coil sides are placed beside each other in several slots under one pole when constructing a distributed winding. In general, if the number of slots of the stator is  $S_1$  and a rotating field with  $2p$  poles is to be created with  $m$  phases, then the number of slots lying beside each other for each phase is:

$$q_1 = \frac{S_1}{2pm} \quad (4.14)$$

The number of slots per pole per phase,  $q_1$ , may be an integer, as may be supposed from the figures above (for instance, 3 in Fig. 4.10). An integral number of slots is relatively easy and simple to manufacture.

If the geometric dimensions of the stator bore are so small that it is impossible to provide enough stator slots, or if another winding having a different number of poles has to be designed for a given stator core, then windings having a fractional number of slots have to be manufactured. (Under successive poles the number of slots belonging to a given phase is different; hence  $q_1$  is an average and is not a whole number.) In designing induction machines, noninteger values of  $q_1$  should be avoided if possible, otherwise the resulting flux density curve will be rich in space harmonics, thus increasing the harmonic leakage reactance and tending to increase noise and vibration.

Good windings have the following characteristics.

1. The winding will be symmetrical in every phase. (This will occur only if the phase voltages, which are induced by the rotating field in the phase windings, are large enough, and if the electric angle between the phase voltages is exactly 360 degrees/m.)
2. The phase voltage induced in the distributed phase windings with a given flux density should be as large as possible; that is, the winding factor should be high. (This will later be discussed in detail.)
3. The stepped mmf curve created by the winding should contain as few harmonics as possible.

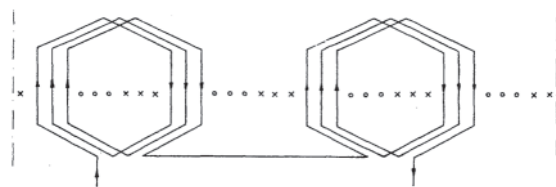


**Figure 4.10** Consequent-pole lap (loop) winding ( $S_1=36$ ,  $2p=4$ ,  $m=3$ ,  $q_1=3$ ).

4. The technology of manufacturing the coils and placing them into the slots should be as simple as possible.

In the illustrations up to this point, the two sides of the coil have always been 180 degrees apart electrically. This is possible in the consequent-pole winding only when the slot steps of all the elementary coils, or the coil span  $S$ , is exactly equal to the pole pitch. That is,  $S=\tau_p$  where  $\tau_p$  is the number of slots in the stator belonging to the pole, being  $\tau_p=S_1/2p$ . In concentric coils,  $\tau_p$  is an average. If, for instance,  $q_1=2$  and the coil span of one of the elementary coils is  $S_k$  and the coil span of the other elementary coil is  $S_l$ , then  $\tau_p=(S_k+ S_l)/2$ .

This kind of winding is called a full-pitch winding. One of the effective means of decreasing the side effects of the spatial harmonics in the flux density wave is so-called step-shortening (or short pitch) for two-layered coils. In this case the two sides of the coil are at an angle to each other that is smaller than 180 electrical degrees.

In motor operation, one of the largest flux harmonics is the seventh, and its effects are among the most deleterious. If the coil pitch is shortened by one-sixth of a pole pitch, the flux density curves of Fig. 4.11 result. The positive and negative areas of the seventh harmonic flux wave are equal, resulting in a net seventh harmonic flux of zero. Thus this harmonic does not induce voltage in the coil. At the same time, the hatched area of Fig. 4.11 will also be lost from the fundamental flux, and the effectiveness of the coil will decrease. This is an unavoidable cost of reducing the effect of the harmonics.

#### 4.1.2.2 Frequently Used Windings for Induction Machines

The stator windings of multiphase alternating current machines are essentially identical. Much of the following therefore applies to synchronous machines as well as to induction machines.

When designing a winding, it is advisable to first lay out the slots along the stator's bore, as shown in Fig. 4.12. In this figure, there are 24 slots along the periphery. For 3 phases and 4 poles,  $q_1=2$ . The conductors laying in two slots next to each other belong to the same phase and pole; thus the conductors in those slots create one effective "coil side." Initially, only the winding of one phase is drawn with only one conductor in each slot; that is, a bar winding is created such as those in Figs. 4.9 and 4.10. Current directions may be assigned from the knowledge that the direction of the induced voltage changes under successive poles. In practice, every coil layout shows the winding from the air gap side.

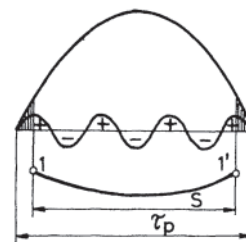


**Figure 4.11** Elementary winding (1-1') with short pitch.

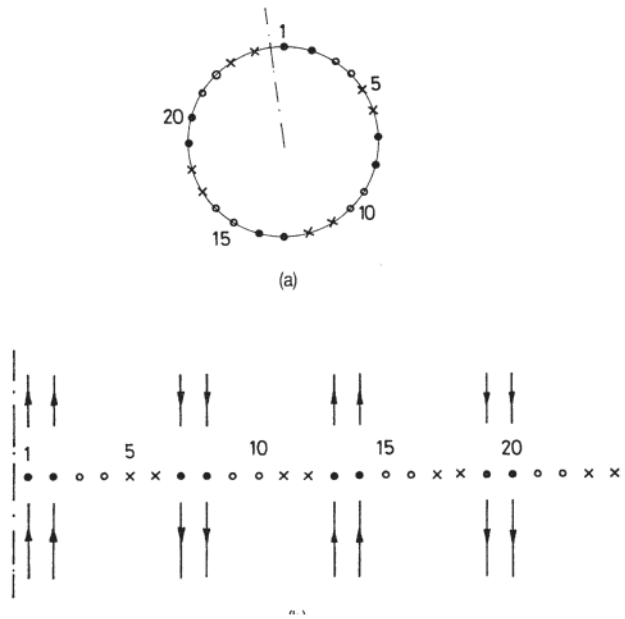


**Figure 4.12** Conductors belonging to one phase of a three-phase, four-pole winding for 24 slots in the stator.

The next problem is that of connecting the coil sides in series. The connections have to be made by taking into consideration the directions of the voltages or currents. The coil sides are connected in series so that the instantaneous voltages are additive. The end turns, which do not take part in the induction, are needed for continuity. The end turns increase the resistance of the winding and thus the copper loss, but do not increase the voltage output or the power of the machine. That is why the coil ends are designed to be as short as possible.

The  $m$ -phase winding has  $m$  independent phase windings that are constructed identically. If the windings of the first phase have been placed properly, the rest of the phases will occupy the remaining slots without any problem. The phase winding ends are  $360/m$  electrical degrees from each other: that is, for 3 phases they are 120 electrical degrees apart. In the case of machines with  $p$  pole pairs, the phase ends repeat  $p$  times around the periphery of the machine, and any of these is suitable for starting a phase. The starting points of the individual phases will be close to each other if  $k=1$  in the equation  $\gamma=360k/m$  electrical degrees, where  $\gamma$  is the angle between starting points and  $1 \leq k \leq p$ . This is advantageous for stators in that the terminals are all available in the same area.

Care should be taken not to commit the serious mistake of connecting the source to the windings at 60-degree intervals. For instance, if the B phase in Fig. 4.13 is not connected to the marked B position, but 60 degree from the A phase, at the Z position, the motor will not start.

In the following, a few of the more frequently used windings are described. Many of the winding layouts shown are prepared for the same number of slots and poles in the stator as the previous example. These values are not used because this number of slots is preferred, but to demonstrate to the reader that various layouts can accomplish the same results. The

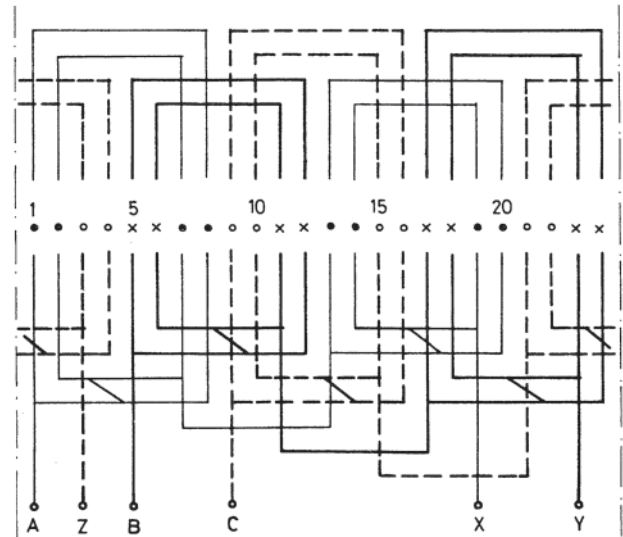


**Figure 4.13** Single-layer, concentric, two-plane winding ( $S_1=24$ ,  $2p=4$ ,  $m=3$ ,  $q_1=2$ ).

confusion resulting from simultaneously illustrating a different winding layout possibility and also changing the number of slots has been avoided.

Integer-slotted ( $q_1$  is an integer) single-layer windings will be discussed first. One of the most frequent variations of single-layer windings is the concentric winding with  $p$  windings per phase and  $q_1$  slots per pole per phase (see Fig. 4.13). In this case the end-turns are placed in two planes outside the stator core (see Fig. 4.18(a)). The concentric winding can be built with end-turns in three planes. (See Figs. 4.14 and 4.18(b).) In this case, the dimensions of the coils belonging to one phase are equal while in the previous

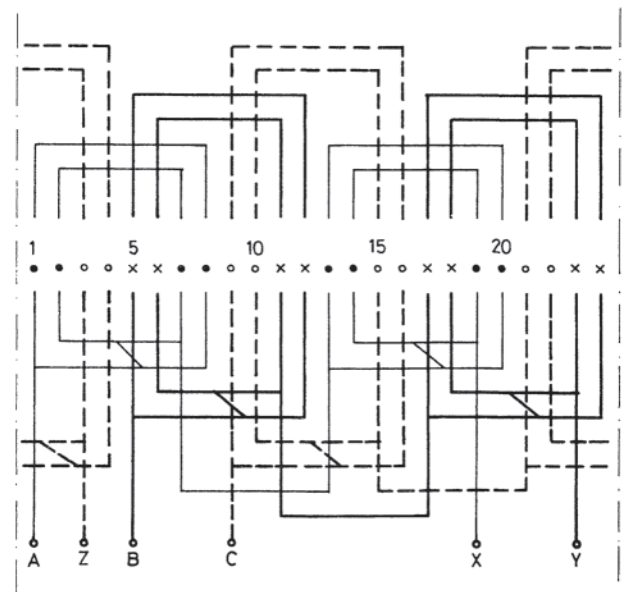


**Figure 4.14** Single-layer, concentric, three-plane winding ( $S_1=24$ ,  $2p=4$ ,  $m=3$ ,  $q_1=2$ ).

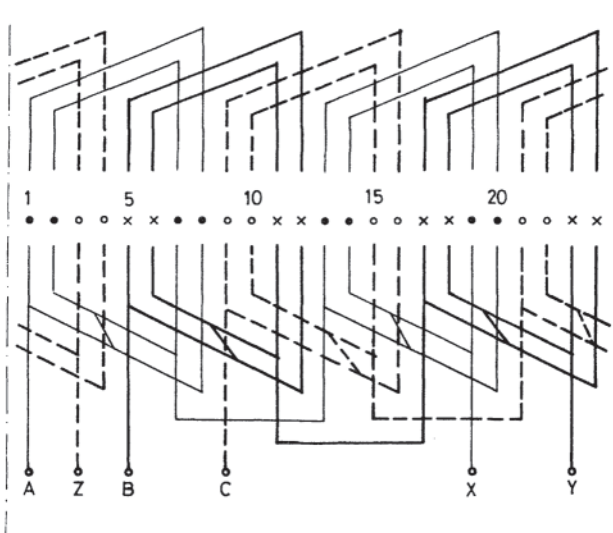


**Figure 4.15** Single-layer, concentric winding with winding groups of similar forms ( $S_1=24$ ,  $2p=4$ ,  $m=3$ ,  $q_1=2$ ).

case coils of two different sizes belong to each phase; thus the resistance of the phase windings is not the same. In the previous case, if  $p$  were an odd number, symmetry would be lost and a distorted coil would have to be inserted, with coil sides not of the same length. If this is not to be permitted, identically shaped concentric coils are made from distorted coils only (see Fig. 4.15). If the winding shown in Fig. 4.14 is to be produced with  $q_1$  being an odd number, then  $q_1$  under one pole is to be divided in such a way that they form concentric coil groups with  $(q_1+1)/2$  and  $(q_1-1)/2$  coil sides.

Figure 4.16 shows a consequent-pole winding. Consequent-pole windings can also be created with all distorted coils (see

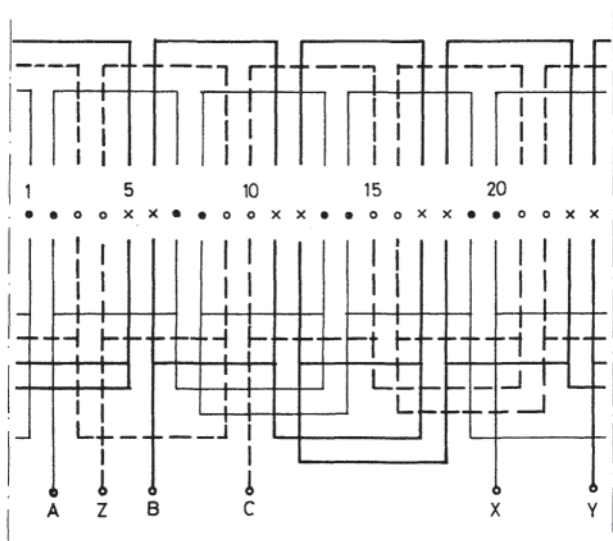


**Figure 4.16** Single-layer consequent-pole winding ( $S_1=24$ ,  $2p=4$ ,  $m=3$ ,  $q_1=2$ ).

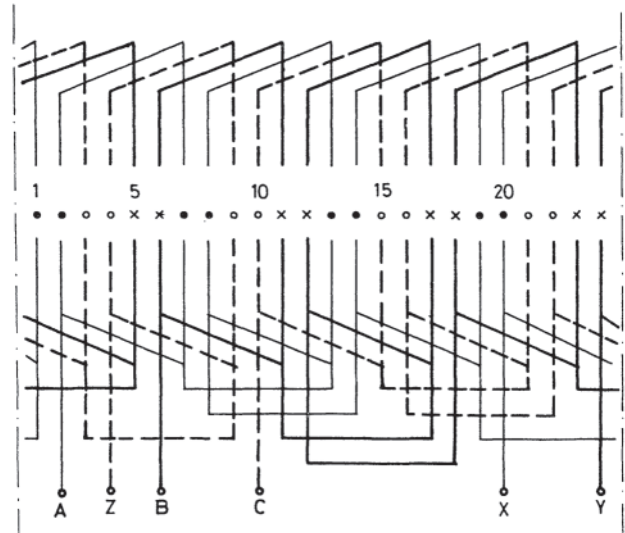


**Figure 4.17** Single-layer consequent-pole winding, with groups of windings of similar form ( $S_1=24$ ,  $2p=4$ ,  $m=3$ ,  $q_1=2$ ).

Fig. 4.17). Due to the shape of the end-turns, this is called a crown winding. Since it is easy to manufacture, it is quite widespread for fractional-horsepower induction machines. In the case of end-turns in two planes, there may be a cooling problem due to the lack of room. In the case of larger machines, the end-turns may have to be placed not in two planes but in four planes as shown in Fig. 4.18(e).

In very large machines having a segmented stator core, coil groups may also be designed in such a way (Fig. 4.19) that there will be empty spaces between them on the periphery. (The dash-dot lines indicate the boundaries between segments.) Only three connections have to be made or unmade when assembling or disassembling. Due to the difference in the shape of the end-turns, a difference arises in the end turn leakage reactance in the separate phases and thus in the phase currents and voltages.

In double-layer windings, two coil sides lie in every slot. One side of each coil is in the upper part of one slot, while the other side is in the lower part of another slot. The coils may be wound with short pitch. Concentric double-layer windings (see Fig. 4.21) are rarely used because their manufacture and assembly into the stator is difficult, although they are sometimes used in small machines. Most often double-layer windings are used in consequent-pole designs, and the coils are easily produced by coil-formers. The wide acceptance of the double-layer winding is due to the advantage of having uniform coils, the merits of short pitch, the excellent cooling possibilities, and the ease of bracing the end turns.

In Fig. 4.20, it will be seen that, if the two layers are slid with respect to each other, the symmetry lines of the coil sides belonging to one phase will remain at 180 degrees distances from each other, but the coil span decreases by one or two slots, as shown in Fig. 4.20(b) and 4.20(c) respectively. The disadvantage is the coil sides placed into one slot may belong to different phases; for this reason the insulation of the coil sides must be increased, and the ratio of copper cross section



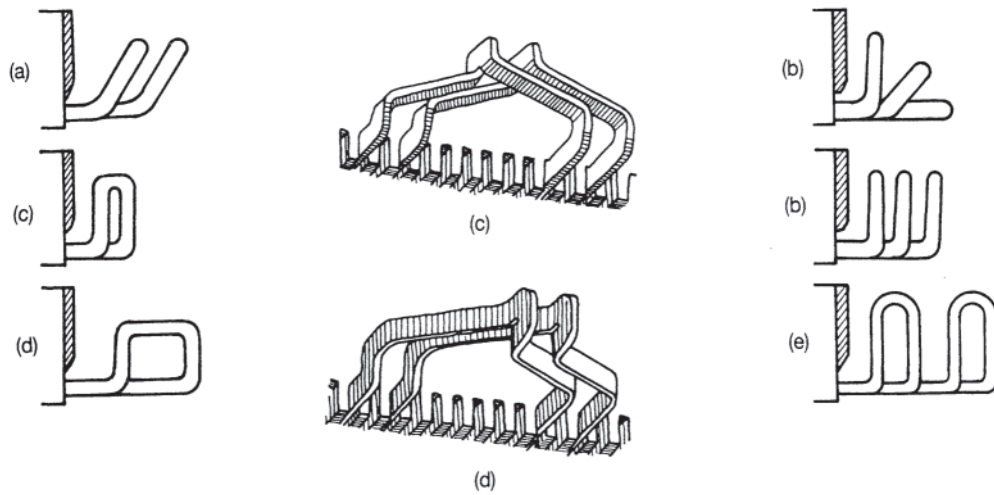


**Figure 4.18** End-turns of single-layer windings, (a) Two-planed.  $q_1$ =number of sides of windings in one group (for concentric coils), (b) End-turns uniformly distributed in three planes, (c) End-turns for consequent-pole windings with the coil heads situated in a plane, with an isometric view, (d) End-turns for consequent-pole windings with the coil heads along a cylindrical surface, with an isometric view, (e) Four-plane end-turns.

to slot area is reduced. The short pitch configuration of Fig. 4.20(b) may be implemented either in a concentric winding as shown in Fig. 4.21 or in a lap winding as in Fig. 4.22. In the case of single-layer windings, the short pitch arrangement is helped by using mixed phase windings, as may be seen in Fig. 4.23.

The end-turns of double-layer windings can be seen in Fig.

4.24. In Fig. 4.24(a) a two-planed and in Fig. 4.24(b) a four-planed end-turn arrangement can be seen. The latter is used when the two-planed end-turns are too close to each other, which occurs when the radial dimension of the endturns has to be decreased. The condition for the four-planed variation is that  $q_1$  be an even number.

Purely single-phase windings are rare. In the case of single-phase windings, theoretically all the conductors can be connected in parallel along the periphery of the stator, but this is not economical because the voltages induced in the conductors in the first and last slots are almost of opposite polarity. For this reason, only two-thirds of the periphery is used; in the other one-third of the periphery the slots are left empty as is shown in Figs. 4.25 and 4.26.

Single-phase split-phase windings are used in the stator of fractional-horsepower induction motors connected to residential supply circuits. The most common design in this category is basically a two-phase motor with the current of the starting winding shifted from that in the main winding. Such a winding is shown in Fig. 4.27. A symmetrical three-phase winding can be used by connecting two of its phase windings in series as the main winding and using the third phase as the starting winding.

#### 4.1.2.3 The Winding Factor

If the winding is full pitch and there is one slot per pole per phase ( $q_1=1$ ), then at a given moment, a voltage of identical magnitude and direction is induced in all of the turns belonging to one phase coil. That is, when calculating the induced phase voltage, the voltage induced in one conductor has to be multiplied by the number of turns  $N_1$ . The equation for the induced phase voltage is:

$$U_i = 4.44f_1N_1\phi_p \tag{4.15}$$

where:

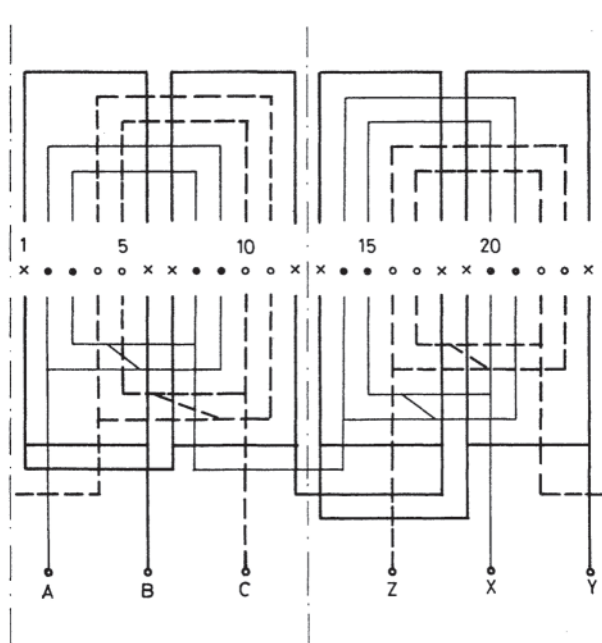


**Figure 4.19** Single-layer winding for a machine with a stator that may be split into two parts, with three-plane end-turns ( $S_1=24, 2p=4, m=3, q_1=2$ ).

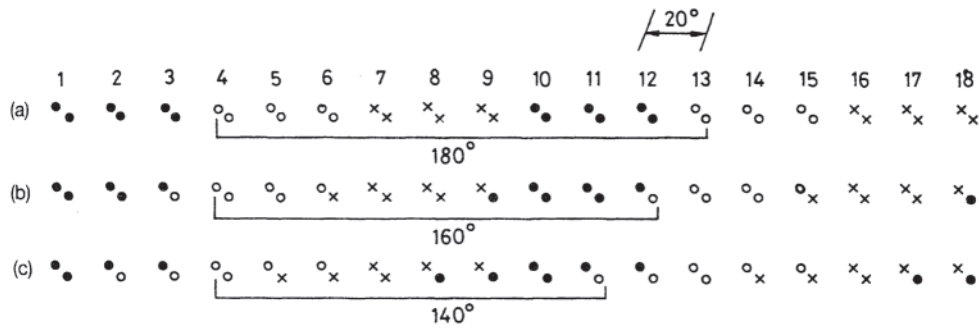


**Figure 4.20** Double-layer winding with different pitches ( $S_1=18, 2p=2, m=3, q_1=3$ ). (a) With full pitch,  $S/\tau_p=9/9$ . (b) With pitch shortened by one slot,  $S/\tau_p=8/9$ . (c) With pitch shortened by two slots,  $S/\tau_p=7/9$ .

- $U_i$  = the rms value of the induced phase voltage
- $f_i$  = the frequency of the supply circuit
- $N_1$  = the number of turns belong to one phase
- $\phi_p$  = the flux originating from one pole

The phase angle between the voltages induced in two neighboring slots is:

$$\alpha = p \frac{2\pi}{S_1} \tag{4.16}$$

It is more usual for  $q$  to be greater than 1. The voltage induced in one coil of a phase winding will have the same magnitude as that of an adjacent coil but a different phase angle because of the spatially sinusoidal flux density distribution in the air gap. Thus, the series connection of the coils does not give, the algebraic sum of the induced voltages, but a value somewhat less. The calculated value of the induced voltage from Eq. 4.15 has to be multiplied by the winding distribution factor  $K_d$  which is smaller than 1.

Figure 4.28 shows a case in which  $q_1=3$  and the induced voltage phasors in the elementary coils are  $\bar{U}_{i1}, \bar{U}_{i2}$  and  $\bar{U}_{i3}$ . The relationship between the resultant voltage  $\bar{U}_i$  and the three coil voltages is known as the distribution factor  $K_d$ , where:

$$K_d = \frac{U_i}{U_{i1} + U_{i2} + U_{i3}} = \frac{U_i}{q_1 U_{i1}} \tag{4.17}$$

Using the geometrical relationships seen in Fig. 4.28, the distribution factor becomes:

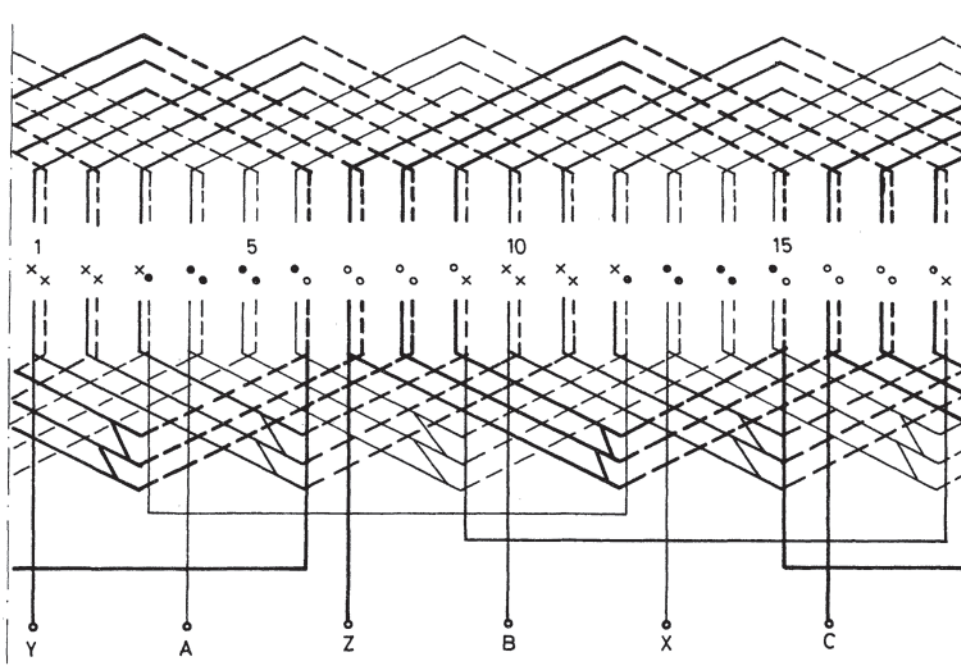


**Figure 4.21** Double-layer, concentric winding with short pitch ( $S_1=18, 2p=2, m=3, q_1=3, S/\tau_p=8/9$ ).

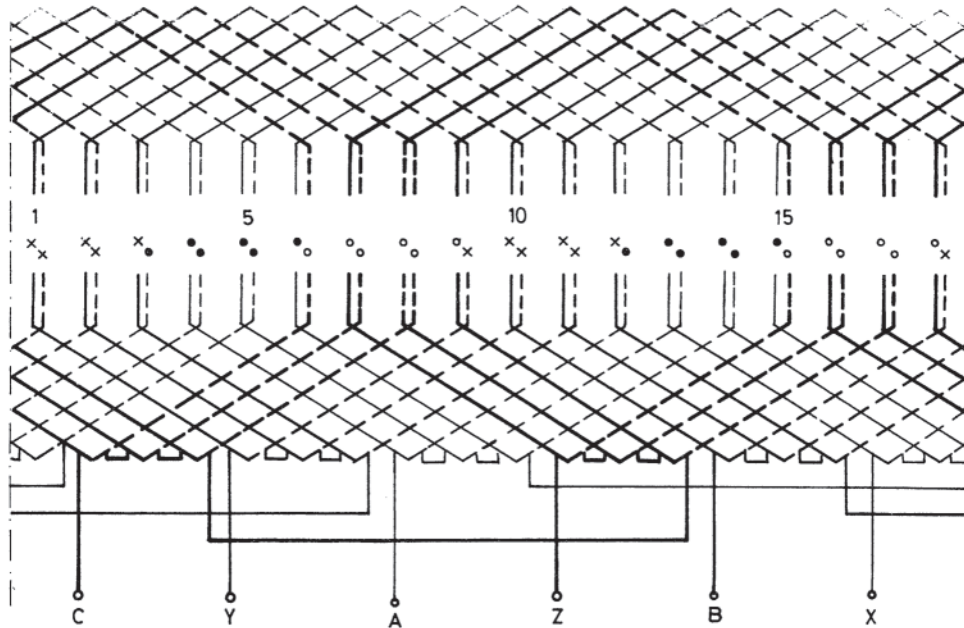


**Figure 4.22** Double-layer, consequent-pole winding with short pitch ( $S_1=18, 2p=2, m=3, q_1=3, S/\tau_p=8/9$ ).

$$K_d = \frac{\sin(q_1 \alpha/2)}{q_1 \sin(\alpha/2)} = \frac{\sin(\pi/2m)}{q_1 \sin(\pi/2mq_1)} \quad (4.18)$$

If the winding is not full pitch, that is, the winding pitch  $S/\tau_p \neq 1$ , one coil will never surround the entire pole flux. Hence, for further calculations of the induced voltage an even smaller factor is used, the so-called pitch factor  $K_p$ .

The idea of the pitch factor is demonstrated in Fig. 4.29,

with  $q_1=1$ . The short pitch coil is shorter by  $\gamma$  electrical degrees than the angle  $\pi$  belonging to the pole pitch  $\tau_p$ . Thus, between the voltages induced on the two sides of the elementary coil, a lag of  $\gamma$  appears, corresponding to Fig. 4.29(b). The ratio of the resultant  $\bar{U}_i$  phase voltage and the induced voltages of the elementary coils is the pitch factor  $K_p$  given by:

$$K_p = \frac{U_i}{2U_{i1}} = \cos\left(\frac{\gamma}{2}\right) \quad (4.19)$$

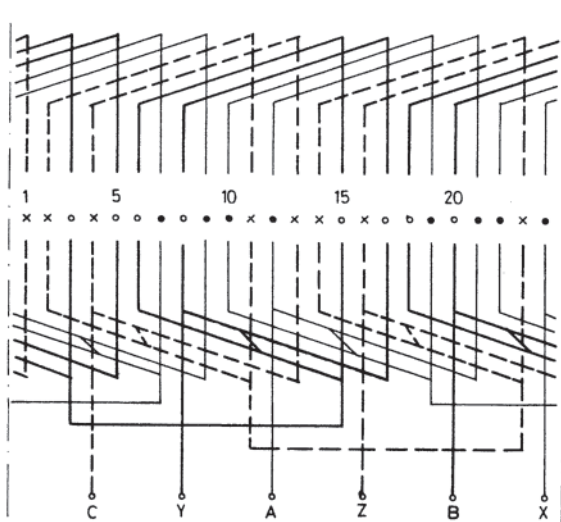


**Figure 4.23** Single-layer, consequent-pole windings, with similar shapes, and short pitch (mixed-phase windings) ( $S_1=24, 2p=2, m=3, q_1=4, S/\tau_p=9/12$ ).

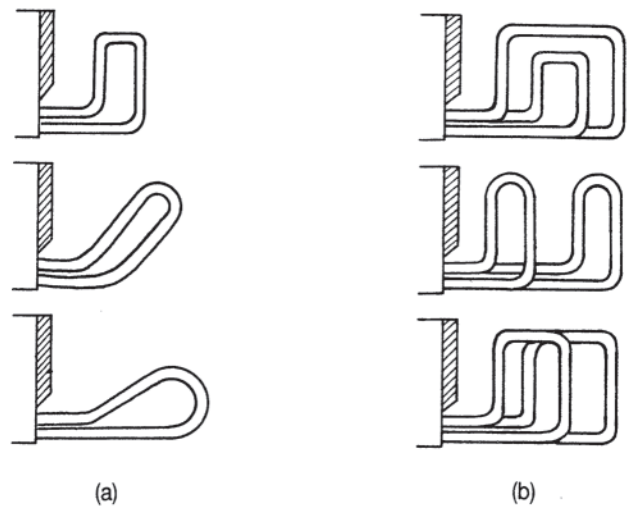


**Figure 4.24** End-turns of double-layer windings, (a) In two planes, (b) In four planes.

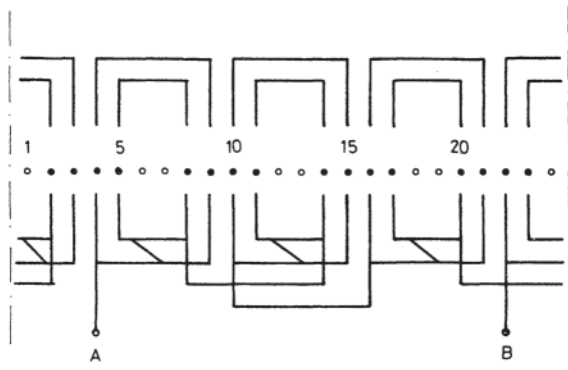


**Figure 4.25** Single-phase, single-layer concentric winding (the empty circles denote the empty slots) ( $S_1=24, 2p=4, q_1=4$ ).

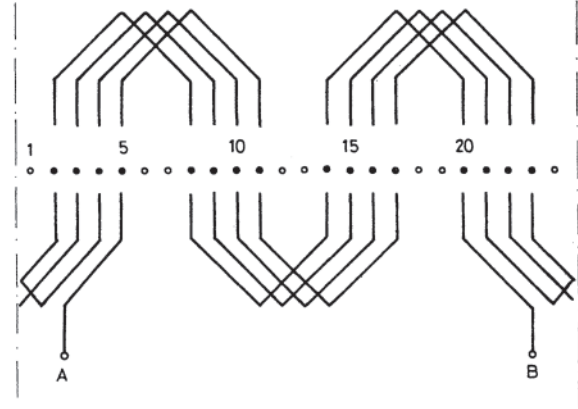


**Figure 4.26** Single-phase, single-layer bar-winding running in one direction (the empty circles denote the empty slots) ( $S_1=24, 2p=4, q_1=4$ ).

With winding pitch  $S/\tau_p$ , Eq. 4.19 can be expressed in the form:

$$K_p = \sin\left(\frac{\pi S}{2\tau_p}\right) \quad (4.20)$$

The equation of the induced phase voltage then becomes:

$$U_i = 4.44 K_d K_p f_1 N_1 \Phi_p \quad (4.21)$$

in which the product  $K_d K_p$  may be replaced by the winding factor  $K_w$ .

As a result of the use of short pitch, the voltage falls slightly, which is a disadvantage. The advantageous effect on the space harmonics is discussed below.

#### 4.1.2.4 Parallel Branches

In fractional-horsepower motors, the flux and hence the induced voltage in the winding is small due to the small geometric dimensions. In the smallest machines, the three-phase winding is connected in a star or wye; thus only  $1/\sqrt{3}$  of the line voltage is across one phase winding, the coils belonging to the same phase

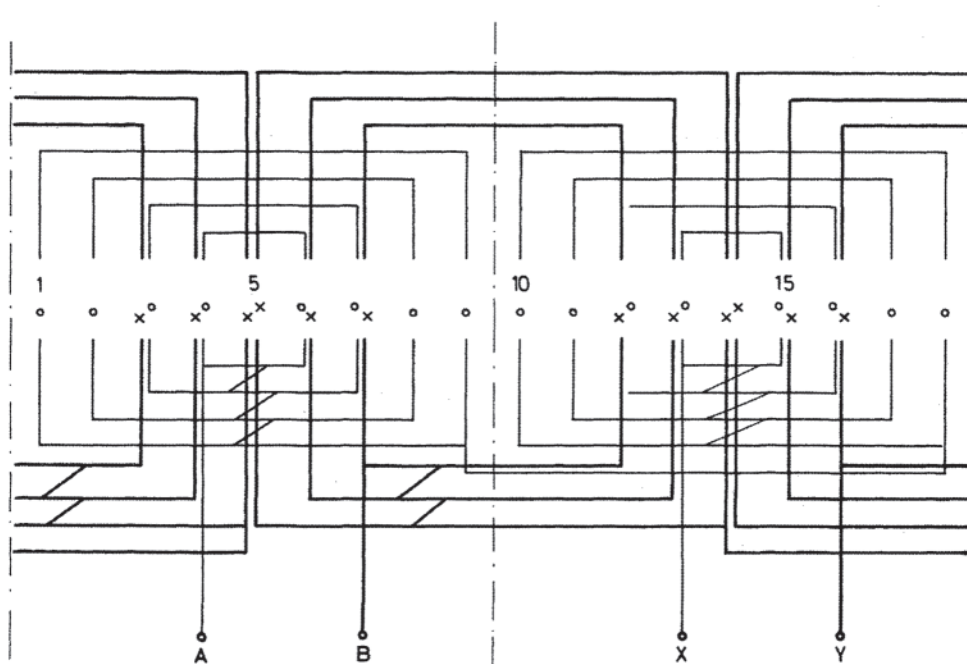


**Figure 4.27** Single-phase winding with split phase ( $S_1=18, 2p=2$ ). The main phase is between A and X, and the split phase is between B and Y.

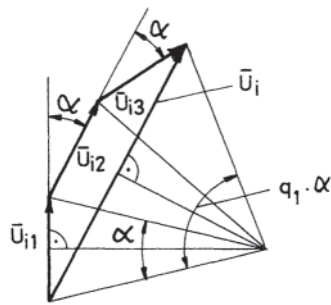


**Figure 4.28** Diagram for calculation of the distribution factor from the induced voltages.

being connected in series under the poles. The line current is equal to the phase current. The line voltage is fixed, thus an increase in power is possible only by increasing the current. An increase in the diameter of the elementary conductor is limited by the slot dimensions. An increase in the power output of the motor is possible only if two or more parallel-connected conductors are used in the winding; in the case of multipole machines the coils under the poles are connected in parallel.

It is advisable to connect the coil groups or conductors in parallel only if it is certain that voltages of equal magnitude will be induced in all parallel coils in all cases. For this reason, care must be taken to ensure that the magnetic relationship between the parallel conductors and the slots of the stator are absolutely identical and the position of the conductors within the stator slots should be kept identical by systematic transpositions and placement at the same radial positions. This is the only way to avoid the presence of circulating currents in the parallel branches. In motors with more than two poles, the parallel branches can be arranged in several ways, but it is advisable to adhere to the following practical advice.

In the case of single-layer windings, three cases are considered.

1. With consequent-pole (crown) windings, the elementary number of coils is  $q_1 p$ , where  $q_1$  is the number of slots per pole per phase and  $p$  is the number of pairs of poles. The number of parallel branches  $a$  is chosen so that  $q_1 p/a$  is an integer.
2. End-turns lying in two planes can be realized only with symmetric parallel branches if the ratio  $p/2a$  is an integer. It should be noted that a winding with an odd number  $p$  can be realized only with distorted coils, which are difficult to manufacture.
3. In the case of windings with end-turns in three planes, there are  $q_1/2$  elementary coils in one coil group and the number of coil groups is  $2p$  per phase. With a parallel connection, a number of elementary coils have to be placed in the parallel branches, and the resultant coil length has to be identical for total symmetry. If the ratios  $2p/a$  and  $q_1 p/a$  are both integers, the winding is totally symmetrical.

In the case of double-layer windings, the number of elementary coils is equal to the number of slots. There are fewer obstacles to creating parallel branches in this case.

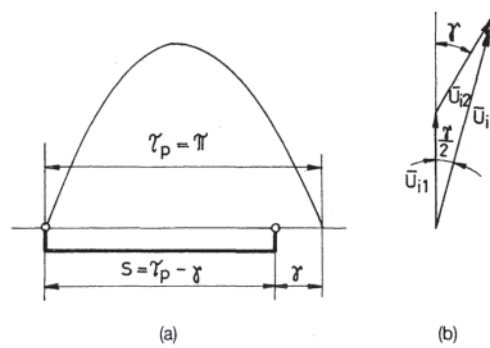


**Figure 4.29** Diagram for calculation of the pitch factor from the induced voltage.

If the elementary coils are not identical in the two layers in the slots (that is, the coils do not have the same number of conductors), then the rules for creating parallel branches are the same as in the case of single-layer crown windings. However, in this case the winding pitch, which is otherwise optional with double-layer windings, cannot be chosen freely.

Let the number of turns of one elementary coil be designated by  $a$  and of the other be designated by  $b$ . In practice, the coils can be arranged in the following ways:

(a)	Top layer	$a b a b a b a b a b \dots$
	Bottom layer	$b a b a b a b a b a \dots$
	Slot number	12.4.6.8.10...
(b)	Top layer	$a a b b a a b b a a b b \dots$
	Bottom layer	$b b a a b b a a b b a a \dots$
	Slot number	1.3.5.7.9.11...
(c)	Top layer	$a a a a b b b b a a a a b b b b \dots$
	Bottom layer	$b b b b a a a a b b b b a a a a \dots$
	Slot number	1...5...9...13...

The total number of slots must be divisible by 2 in case (a), by 4 in case (b), and by 8 in case (c).

The arrangement of (a) can be used by every three-phase winding that has an integer value for  $q$  because the number of slots in the stator is always divisible by 2. Case (b) can be used only in machines with an odd number of pole pairs ( $2p=2, 6, 10, \dots$ ) if  $q$  is an even number.

The case (c) variation can be used with machines with an odd number of pairs of poles ( $2p=2, 6, 10, \dots$ ) only if  $q$  is divisible by 4. With machines with an even number of pairs of poles ( $2p=4, 8, 12, \dots$ ), if  $q$  is an even number the only possibilities are machines with a number of pole pairs that can be divided by 4 ( $2p=8, 16, \dots$ ). In this case, it can be used with every integer value of  $q$ .

In case (a), only an odd number of slot steps may be used; that is, from the slot marked 1, one may only step into an even-numbered slot. In cases (b) and (c), only an even number of slot steps may be taken; that is, from the slot marked 1, one may step only into odd-numbered slots. Thus there will be slot steps that cannot be realized with an odd number of conductors per slot. The following slot steps can never be used:

1:9, 1:17, 1:25, 1:33, and so forth

In case (c), the following slot steps may be used only with certain  $p$  and  $q$  values:

1:5, 1:13, 1:21, 1:29, and so forth

All other slot steps may be used without restriction in cases (a) and (b) subject to the earlier restrictions that odd numbers are used in case (a) and even numbers in case (b).

One further technological restriction must be taken into account. If the dimensions of the heights of the two coils differ significantly, difficulties can appear in bracing the endturns. For this reason, double-layer windings with an odd number of conductors per slot should have at least five conductors.

#### 4.1.2.5 Questions of Production Technology

The usual shape of the slot in fractional-horsepower induction motors is similar to a liquid drop, as shown in Fig. 4.30(a). The drop shape is used because the teeth should have uniform width to maintain constant flux density in the teeth. To avoid damaging the insulation in the slots, large radii are used at the slot openings. Circular cross-section conductors are usually twisted into place. The coils are made separately with a coilformer or automated machine.

The loosely formed coils are twisted into the half-closed slot through the opening of the slot (see Fig. 4.30(b)). The opening of the slot has to be wide enough that the conductor can be placed in the slot between the protruding slot insulation, or a separate protecting lining can be placed in the slot opening. This is necessary to avoid damage to the insulation of the conductor by the edges of the iron

laminations. The dimensions of the slot opening should be  $(d+2v+0.5)$  mm, where  $d$  is the diameter of the insulated conductor and  $v$  is the thickness of the slot insulation. The twisting operation is used with both circular cross section and smaller rectangular crosssection conductors.

In the case of conductors with rectangular cross section as in Fig. 4.30(c), the slot has parallel sides and the cross section of the teeth decreases toward the air gap; that is, the tips of the teeth tend to saturate. If flat-copper conductors are twisted into the slot and if their final position is to be as shown in Fig. 4.30(c) (lying on their larger face), the depth of the slot must be large enough that the last conductor that is slid into place in a standing position through the slot opening may be laid down flat (Fig. 4.30(b)).

Application possibilities are limited in the case of twisted-in windings because coils with a diameter above 1.5 mm are stiff, and the number of parallel branches should not be too high because of circulating currents. In practice, flat copper is generally used above 50 kW, and above 100 kW only flat copper is used for the winding of low-voltage machines. Machines with voltages higher than 1 kV are called high-voltage machines. Machines with power greater than 200 kW are almost always built as high-voltage machines.

For high-voltage windings, thick insulation and large air gaps are needed, and long leakage paths result. High-voltage windings today are almost always manufactured with open slot entrances, and are built by placing the windings through the slot opening, an entire coil side being placed in the slot at the same time.

If there are only one, two, or four large conductors in the slot, a bar winding is built. The bar windings are placed into half-open slots and the bars are usually connected to form coils on the machine. A maximum of two bars can be placed into the slot on top of each other or beside each other. The endturn on one side can be made before placement, and on the other side the turn is bent when the coil is in place in the machine or, in the case of larger copper cross sections, the end connectors can be soldered or welded onto the ends of the bars projecting out of the slot.

Mechanical forces are exerted on current-carrying conductors in a magnetic field. It is this effect that causes motor action. That portion of the winding in the slot is held in place by the slot wedge. However, forces are also developed on the end-turns, and these forces may cause deformation of the coil unless the end turns are braced.

In small machines, which generally have twisted windings, the end-turns are secured to each other by lacing. In addition, the windings are impregnated, thus stiffening the endturns. Impregnation also tends to eliminate movement of conductors in the slots. In larger machines, the greater lengths of the endturns and the higher currents create forces so large that positive steps must be taken to brace the endturns. The worst case is that of a large two-pole induction motor, and especially so during start-up or reversal.

The force between two parallel current-carrying conductors with currents  $I_1$  and  $I_2$ , respectively, is easily calculated. The calculation of the forces on the end-turns of induction motors is much more complicated. Not only will the forces be affected by the current in adjacent coils of different phases will also

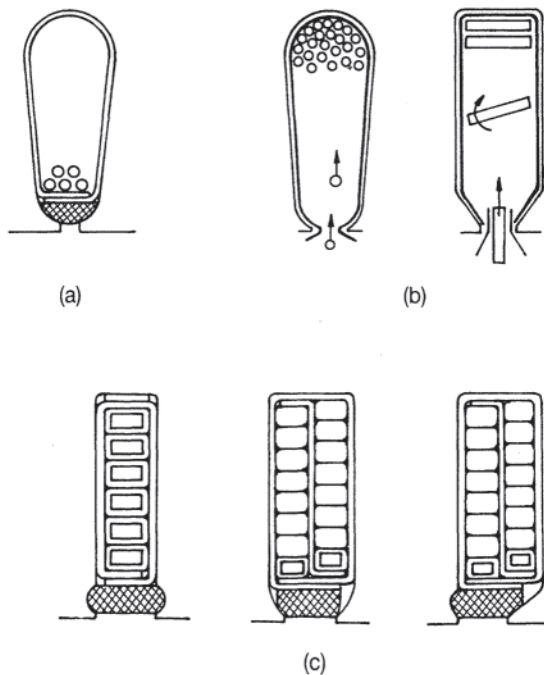


**Figure 4.30** (a) Slot cross section of the twisted-in stator winding, (b) Twist-in of circular and rectangular cross section conductors, (c) Laid-in winding in open, half-closed, and asymmetrical half-closed slots.

contribute. Calculations may be carried out using numerical methods programmed on a digital computer.

For approximate calculations, Eq. 4.22 is used. The force acting on the conductor of the end turn is:

$$F = \mu_0 \frac{l}{2a\pi} I_{\max}^2 \sum_{i=1}^{n-1} \frac{1}{i} \quad (4.22)$$

where:

$l$  = the average length of the conductor in the end turn

$a$  = the distance between the neighboring, parallel conductors or bundle of conductors

$n$  = the number of conductors parallel to each other

$I_{\max}$  = the peak value of the current in the conductor

If there are  $n$  conductors in the bundle of conductors making up the endturn of the elementary coils, then  $I_{\max}$  has to be substituted for the current value in Eq. 4.22.

#### 4.1.2.6 Special Stator Windings

The speed of an induction motor depends on the number of poles of the winding and the supply frequency. If the windings of an induction machine can be reconnected from  $p_1$  pole pairs to  $p_2$  pole pairs, the motor will rotate at a different speed. In fact, the speed may be changed during operation.

Changing the number of poles is done in one of two ways. In the first case, smaller winding sections are formed from the phase windings by tapping. Suitable switching of these winding sections will cause the currents in the sections to change their directions. The most frequent case for this solution is the Dahlander connection, for which  $p_1/p_2=2$ . Another pole-pair change realized with one winding is the pole-amplitude-modulated (PAM) winding. In this case, the ratio of the number of pairs of poles usually differs from 2. Both of these methods are discussed below.

Another possibility for changing the number of poles is to use two independent windings. Since only half of the cross section of the slot can be occupied by one winding, the efficiency of these machines is inferior to normal machines. If more than two pole-pair values are needed, a combination of the two possibilities may be used. Machines with more than four values of pole pairs are not manufactured. The rotors of multiple-speed induction motors are usually squirrel-cage rotors because the current distribution in a squirrel-cage rotor can accommodate any number of poles within reason.

#### 4.1.2.7 Dahlander Windings

The basis of the two-speed motor can be demonstrated most simply with the Dahlander connection, which changes the number of poles by the ratio of 2:1. The phase windings of the four-pole stator as shown in Fig. 4.31(c) may be divided into two half-windings as shown in Fig. 4.31(a) for a two-pole motor.

The winding scheme of one phase with  $q=1$  is indicated in Fig. 4.31(b) and 4.31(d), the direction of the currents also being shown. In two-pole operation, two parallel star (or wye) circuits are formed (a double wye) and in four-pole operation a delta circuit is used. In Fig. 4.32, the simplified winding arrangement of a single-layer Dahlander winding for a stator

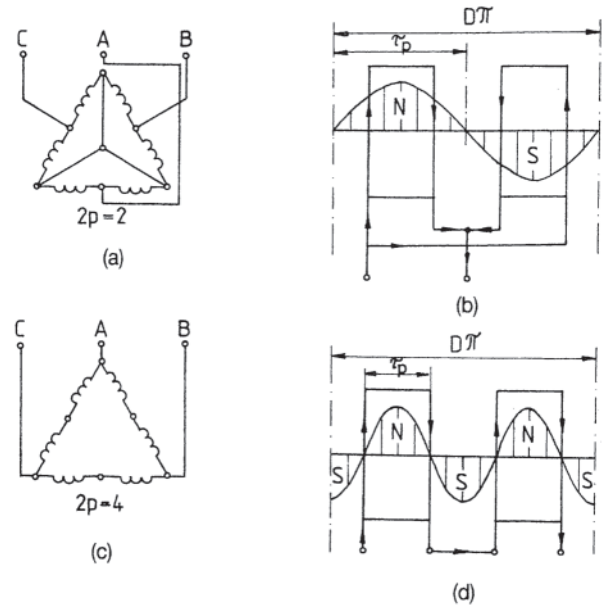


**Figure 4.31** Dahlander winding for changing the number of poles, (a) Connection of the winding for two-pole operation, (b) Field distribution in two-pole operation, (c) Connection of the winding for four-pole operation, (d) Field distribution in four-pole operation.

having 24 slots is shown, as is the distribution of the mmf along the periphery.

It follows from the doubling of the number of poles that the width of a phase belt in electrical degrees is 60 for two-pole operation and 120 for four-pole operation; that is, the winding is full pitch in the four-pole connection and a chorded winding (short pitch) in the two-pole connection. The result is that the winding factors in the two different connections will be different. The pitch factor in the four-pole circuit is larger, while the distribution factor is larger in the two-pole circuit. Calculated exactly, the winding factor for four poles is 0.83, while for two poles it is 0.68.

The utilization of the winding is poorer for both speeds than for the normal 60-degree full pitch, one pole-pair, three-phase winding, where the resultant winding factor is 0.96. The winding is particularly poorly utilized if the machine has fewer poles (and hence higher speeds).

Examining Fig. 4.32, it can be seen that the distance between two neighboring phases in the two-pole connection of Fig. 4.32(b) becomes 120 degrees when shifting the winding to four-pole operation. This same geometrical distance will equal  $2 \times 120 = 240 = -120$  electrical degrees; that is, the sequence of the phases has been changed. For this reason, the pole changing control has to include two phase switches to keep the same direction of rotation for the motor. The winding of Fig. 4.32(a) is connected to reflect both switch operations.

As can be seen in the mmf curve of Fig. 4.32(b), the mmf distribution is far from sinusoidal. The amplitudes of the space harmonics are large. The deleterious effects of these harmonics are discussed in detail below.

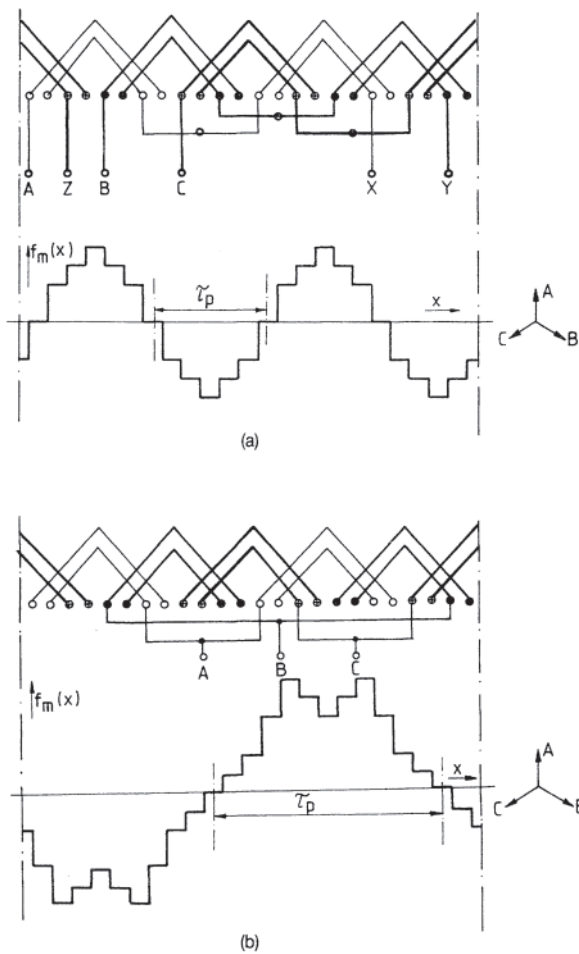


**Figure 4.32** Simplified circuit diagram of a single-layer Dahlander winding ( $S_1=24$ ) and the distribution of the mmf along the periphery, (a)  $p=2$  and  $q_1=2$ . (b)  $p=1$  and  $q_1=4$ .

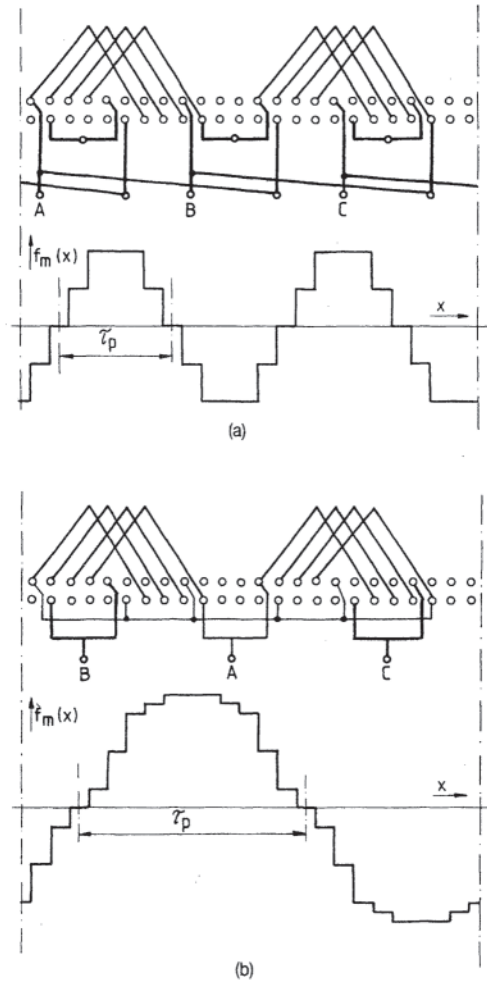


**Figure 4.33** Simplified circuit diagram of one phase of the double-layer Dahlander winding ( $S_1=24$ ) and the mmf distribution of the three-phase winding along the periphery at a given instant. (a)  $p=1$  and  $q_1=4$ . (b)  $p=2$  and  $q_1=2$ .

To improve the unfavorable mmf curves and to eliminate the large space harmonic content (which is actually a general characteristic of pole-changing windings), the Dahlander winding may be designed in two layers. Figure 4.33 shows this kind of winding. For simplicity the connection of the windings is shown only for one phase, but the connection between the different phase coils is shown in detail. The mmf curve shows smaller space harmonics.

Starting from the point where the phase windings are divided into two half-windings, changing of the number of poles from  $p_1$  to  $p_2=0.5p_1$  can be done in several ways. The different winding schemes influence the output and the torque of the motor differently. The most frequent Dahlander connections are shown in Fig. 4.34. The A variation is designed for approximately constant power (for instance, rolling mills); the B variation is mainly for constant torque (for instance, machine tools); and variation C is mainly designed for power output that increases more rapidly than speed (for instance, pumps and blowers).

The poor utilization of the Dahlander windings shown previously can be corrected by dividing the phase windings into four equal parts, as shown in Fig. 4.35. In this case, the windings for both numbers of poles have a 60-degree belt width. The utilization has increased, but the number of terminals has also increased from 6 to 12. It should be emphasized that this circuit also is capable of only a 2:1 ratio of the number of poles.

One of the advantageous forms is a winding designed with a smaller number of poles and winding pitch  $S/\tau_p=2/3$ , because with the larger number of poles this becomes  $S^*/\tau_p=4/3$ , that is, a step-lengthening of 4/3. The resultant winding factor for both speeds is 0.83. At lower speeds the utilization of the winding is equal to that of the traditional Dahlander, but at higher speeds the utilization is 25% better. In large machines, the Krebbs-type double-layer winding may be used. This actually consists of two double-layer windings pushed together; it has small space harmonic content.

Summarizing, it may be said that in designing good



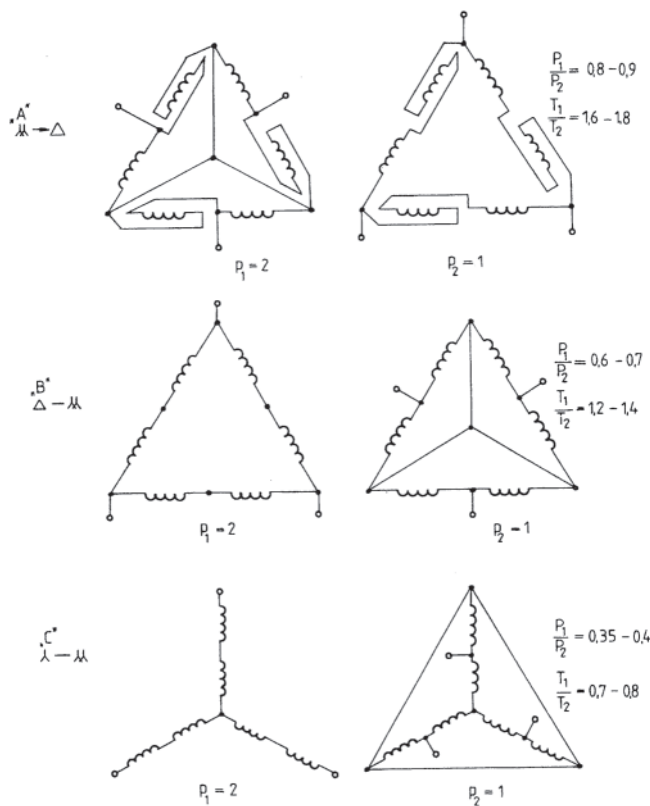


**Figure 4.34** Dahlander connection strategies with  $p_1=2p_2$ . The motor develops rated power  $P_1$  and torque  $T_1$  with  $p_1$  pole pairs, and rated power  $P_2$  and torque  $T_2$  with  $p_2$  pole pairs. The connections used are: Star (or wye) connected:  $\lambda$ . Parallel star (double wye) connected:  $\lambda\lambda$ . Delta connected:  $\Delta$ .

speed-changing windings the phase windings have to be divided and the two sets of pole pairs have to be connected in such a way that

1. As few terminals as possible should be created.
2. The winding factor should be favorable for both numbers of pole pairs.
3. The mmf curve should have small harmonic content.

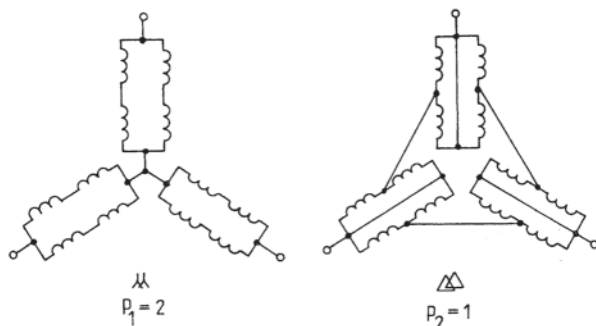


**Figure 4.35** Modified Dahlander connection.

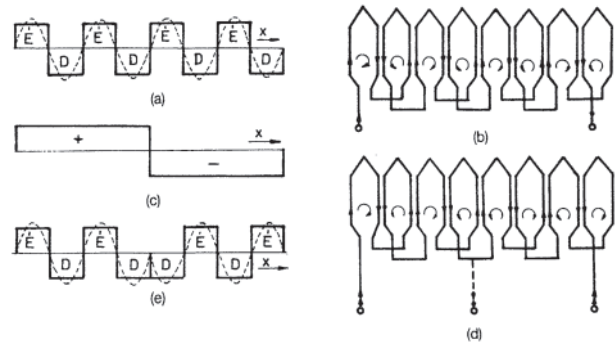


**Figure 4.36** PAM principle, (a) Basic field, (b) One phase of the winding and the direction of currents in the winding for the basic field, (c) The modulating sign-function, (d) Modulated winding and the direction of currents for one phase, (e) Modulated field.

#### 4.1.2.8 Pole Amplitude Modulation

PAM may be explained using Fig. 4.36. The name of the method is taken from the field of telecommunications, where high-frequency oscillations are modulated by low-frequency oscillations. In the case of windings, the term spatial modulation is also used.

In Fig. 4.36(a), the eight-pole basic field shown was created by the excited coils of Fig. 4.36(b). Figure 4.36(c) shows the modulating sign-function, which can be obtained as shown in Fig. 4.36(d). It can be seen that the winding is that of Fig. 4.36(b) modified by tapping the winding in the middle. Thus the direction of the current in the half-winding on the right is reversed. The resultant field distribution is shown in Fig. 4.36(e).

The expression for the spatial fundamental of the basic field with amplitude  $A$  is:

$$b_1(x, t) = A \sin px \tag{4.23}$$

where  $p$  is the number of polepairs and  $A$  is a sinusoidal function of time. The general expression of the modulating field is

$$b_2(x, t) = B \sin kx \tag{4.24}$$

where  $k$  is the number of modulating cycles and  $B$  is a sinusoidal function of time having the same frequency as  $A$ . (In this case,  $p=4$  and  $k=1$ .) The resultant field distribution, using familiar trigonometric identities, is:

$$b_{res}(x, t) = \frac{AB}{2} [\cos (p - k)x - \cos (p + k)x] \tag{4.25}$$

In this case, fields having 6 and 10 poles are created, a result that has no practical application. One of the fields must be eliminated, and this is relatively easy to do. The series of figures and Eqs. 4.23 and 4.25 are for one phase. By choosing the displacement in time and the starting point of the modulated waves in the three phases properly, either the 6-pole or the 10-pole fields may be made to coincide in space. Thus the resultant is equal to zero at each moment because of the 120-degree displacement. The other field remains and is used. It can be shown that the Dahlander connection corresponds to a special kind of pole amplitude modulation.

Pole-modulating windings have six terminals. For one pole number, their utilization is nearly equal to that of the unmodulated machine, but for the second pole number the utilization is only about 75%.

#### 4.1.2.9 Change of Number of Poles with Two Independent Windings

Instead of a pole-changing winding, windings with differing number of pole pairs can be used independently of each other on the stator. These have to be designed in such a way that they do not influence each other. The small pole-pair winding is placed near the opening of the slot because the end-turns of the winding are longer than for the low-speed winding. Thus, the end-turn leakage reactance is larger, but this can be balanced to some extent with smaller slot leakage. In large machines bracing of the end-turns of the two windings is a serious design problem. In high-voltage machines, the insulation will occupy so much space that the use of two independent windings is not feasible.

#### 4.1.3 Spatial Harmonics in the Field Curve

A major objective in the design of an induction motor is to create a sinusoidally distributed magnetic field with  $2p$  poles in the air gap of the motor. With conventional construction, a magnetic field is developed in the air gap by windings made of current-carrying conductors lying in slots, as described at the beginning of this chapter and shown in detail in the preceding section.

Slotting results in a number of phenomena, which must be considered. The current-carrying conductors for each phase winding develop a stepped mmf curve along the periphery of the stator bore, rather than a sinusoidal curve. Since the stepped mmf curve is periodic, it can be expanded into a Fourier series. Besides the fundamental wave for  $p$  pairs of poles, harmonic mmfs also develop with ordinal numbers  $\mu p$ , where  $\mu$  is the spatial ordinal number of the stator. Due to the symmetry of three-phase windings,  $\mu$  will be only an odd number and will be equal to or greater than 3. The amplitudes of the harmonics decrease in inverse proportion to the ordinal number. The mmf wave for the machine as a whole is the resultant of the mmf waves created by each of the phase windings.

Another consequence of slotting, especially with open slots, is that uniformity of the air gap along the periphery is not possible. The air gap, which constitutes the greatest part of the magnetic circuit's reluctance, fluctuates periodically due to the relative displacement of the stator and rotor teeth. The tooth-to-tooth position gives the maximum magnetic permeance, while the slot-to-slot position gives the minimum. This fluctuation in permeance is greater in induction motors than in any other rotating machine because the induction motor is the machine most likely to have teeth on both rotor and stator. Moreover, it takes all its magnetizing current from the supply circuit, and in order to reduce this current the air gap is made as small as possible. Magnetic permeance harmonics are also caused by eccentricity of the rotor and local iron saturation in the magnetic circuit, principally in the teeth.

The mmf waves may be multiplied by the average value of

the spatial permeance, thus producing the stator winding's flux density fundamental and harmonics. The number of pairs of poles of the mmf waves will equal the number of pairs of poles  $p$  of the machine. But, in addition, all of the mmf waves interact with all of the permeance waves to create new flux density waves that have numbers of pairs of poles and frequencies that are either the sum or the difference of the ordinal numbers of the mmf and permeance waves. This infinite series of flux density waves of the stator affects the winding of the rotor through the air gap and induces harmonic voltages of the same ordinal number.

The induced voltages create circulating currents in the closed rotor circuits dependent on the impedance of the rotor windings. This impedance is a function of the frequency, number of turns or, in the case of squirrel-cage machines, the number of slots, the permeability of the iron, the shape of the slots, and so forth. All of these currents develop mmf waves of their own with a theoretically infinite number of harmonics with separate and new ordinals  $\lambda$  due to the slotting of the rotor. As a result of the interaction of the mmf waves of the rotor and the permeance waves of the air gap, still other flux density waves are created. Those flux density waves produced by the rotor that have an ordinal number equal to the ordinal numbers of the flux density wave of the stator (that is,  $\lambda = \mu$ ) modify the corresponding flux density harmonics of the stator (armature reaction). The unmodified flux density waves of the stator are called the residual flux density waves.

The residual rotor fields induce voltages in the stator windings with frequencies differing from the frequency of the supply. The stator winding at these frequencies is practically short-circuited through the supply circuit, and the resulting currents are largely dependent only on the stator impedances. In the case of parallel branch stator windings, the residual field of the stator has to be considered because it can cause several additional effects. The damping effect of the rotor, which is the essence of armature reaction, can be neglected in the case of slip-ring machines, and is large only in the case of squirrel-cage rotors with fields of low ordinal numbers.

The magnitudes of the induced voltages in the windings created by the spatial harmonic flux density waves may be calculated using equations similar to Eq. 4.21, which was derived for fundamental voltages. In place of the fundamental flux, the magnitude of the harmonic flux has to be used, and the fact that the voltage harmonics induced by the spatial harmonic flux density waves have a different winding factor than the fundamental must be taken into account. In calculating the winding coefficients of the harmonics, it should be noted that the  $\mu$ th harmonic has an electric angle  $\mu p$  times the geometric angle.

Thus, there is a phase shift of magnitude  $\mu\alpha$  between the voltages induced in the separate slots, and Fig. 4.28 must be modified accordingly when calculating the distribution coefficient. The distribution coefficient relating to the  $\mu$ th space harmonic is:

$$K_{d\mu} = \frac{\sin(\mu\pi/2m)}{q_1 \sin(\mu\pi/2q_1m)} \quad (4.26)$$

In the case of short pitch, the harmonic pitch factor is:

$$K_{p\mu} = \sin\left(\mu \frac{\pi}{2}\right) \sin\left(\mu \frac{\pi}{2} \frac{S}{\tau_p}\right) \quad (4.27)$$

Since  $\sin(\mu\pi/2) = \pm 1$  if  $\mu$  is an odd integer, as it generally is in practice, this coefficient only yields the sign of  $K_{p\mu}$ . Analyzing Eq. 4.27, it can be noted that the pitch factor is zero if the value of  $\mu S/2\tau_p$  is a whole number; that is, however large the spatial field flux of the  $\mu$ th harmonic is, it will not induce any voltage. Thus, in choosing the winding pitch, one space harmonic can be eliminated or at least can be decreased to a very small value.

To eliminate the effect of just one spatial field harmonic, there is another possibility. If the slot center line of the rotor (or of the stator) is not a straight line parallel to the axis of the machine, but is a spiral line along the cylinder (for instance, the surface of the rotor), then the slot is said to be skewed. Slot skewing is used only for small or medium size machines for technical production reasons, and is usually done on rotors.

The conductor lying in a skewed slot may be visualized as an infinite number of elementary conductors connected in series but shifted parallel to each other, each one remaining parallel to the machine's axis. Due to the shift, the voltages induced in the separate elementary conductors are not in phase. Thus, in calculating the induced voltage, the winding factors so far discussed are multiplied by another pitch factor, which can be approximated by the chord/arc ratio, due to the constant skewing.

Considering the meaning of the pitch factor as given in Eq. 4.19 and expanding to the  $\mu$ th harmonic, the skewing factor  $K_{sk}$  can be calculated from:

$$K_{sk\mu} = \frac{\sin(\mu pb/D)}{\mu pb/D} \quad (4.28)$$

where  $b$  is the circumferential displacement of one end of the slot from its unskewed position as shown in Fig. 4.37 and  $D$  is the diameter of the rotor.

If the amount by which the slot is skewed is such that the argument of the sine function in the numerator of Eq. 4.28 is  $\pi$  or any integral multiple of it for a given value of  $\mu$ , then the value of the slot skewing coefficient is theoretically zero and in practice vanishingly small. Thus, for a selected space harmonic, the effect is zero. That harmonic does not take part

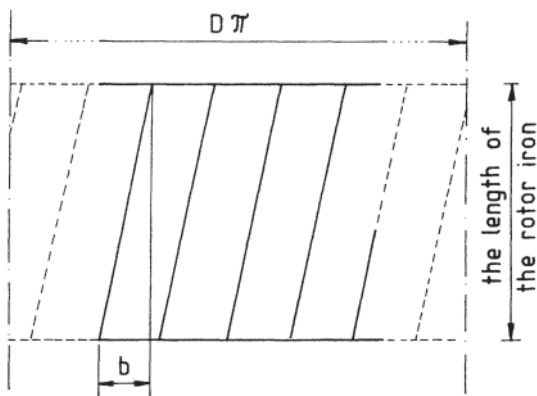


**Figure 4.37** Cylindrical surface of the rotor with skewed slots spread out in a plane.

in inducing voltages or in developing noise and vibrations [7]. Due to slot skewing, the short-circuit current and torque of the motor decrease.

It must be noted that if the conductors in the rotor are not properly insulated from the laminated iron, then circulating currents will flow in the iron perpendicular to the slots and additional local losses will be developed. The losses due to the cross currents are especially high in the case of an inverter supply because of the inherent harmonic richness of the output. There is further discussion of this phenomenon below.

Combining all of the concepts above, the mmf function in the air gap of the induction machine may be expressed as:

$$\bar{F}_m(x,t) = \bar{F}_{mp}(x,t) + \bar{F}_{m\mu}(x,t) + \bar{F}_{m\lambda}(x,t) + \bar{F}_{m\lambda\mu}(x,t) \quad (4.29)$$

The complex expression of the fundamental of the mmf is:

$$\begin{aligned} \bar{F}_{mp}(x,t) &= \frac{\sqrt{2} m N_1 K}{p\pi} I_0 \exp[j(px - \omega_1 t - \phi_0)] \\ &= F_{mp} \exp[j(px - \omega_1 t - \phi_0)] \end{aligned} \quad (4.30)$$

where:

- $m$  = the number of phases
- $N_1$  = the number of turns in the stator winding of one phase
- $K$  = the resultant winding factor for the fundamental
- $I_0$  = the no-load current
- $p$  = the number of pole pairs
- $x$  = the coordinate along the periphery of the bore in radians
- $\phi_0$  = the phase angle of the no-load current
- $\omega_1$  = the angular frequency of the supply
- $t$  = time

Under load, the value of  $F_{mp}$  has to be multiplied by a factor of value smaller than 1, thus taking the armature reaction into consideration as well.

The complex Fourier series for the spatial mmf harmonics of the stator is:

$$\begin{aligned} \bar{F}_{m\mu}(x,t) &= \sum_{\mu} I_1 \frac{\sqrt{2} m N_1 K_{\mu}}{p\pi\mu} \frac{\sum F_m}{F_m \text{ air gap}} \\ &\times \exp[j(\mu px - \omega_{\mu} t - \psi_{\mu})] \\ &= \sum F_{m\mu} \exp[j(\mu px - \omega_{\mu} t - \psi_{\mu})] \end{aligned} \quad (4.31)$$

where:

- $\mu = 2mg+1$  = the ordinal of the spatial harmonic of the stator
- $I_1$  = the stator phase current
- $\omega_{\mu} = \omega_1$
- $\psi_{\mu} = \psi_1$  = the phase angle of the stator phase current
- $K_{\mu}$  = the resultant winding factor of the  $\mu$ th harmonic
- $g = \pm 1, \pm 2, \dots$

When substituting values of  $g$  with different signs into the ordinal equation for  $\mu$ , ordinal numbers of different signs are obtained. The positive sign means a harmonic mmf rotating in the same direction as the fundamental, and the negative

sign means that it rotates in the direction opposite to the fundamental. Noting that  $\mu$  half-waves correspond to the  $\mu$  value of the space harmonic for one half-wave of the fundamental, it will be seen that the number of pairs of harmonic poles is  $\mu p$ .

The change in frequency from one spatial harmonic to the next is always  $f_1$ : thus the synchronous angular frequency of the flux density for the  $\mu$ th spatial harmonic is  $\Omega_\mu = \omega_1 / (\mu p)$ , which is the  $1/\mu$  part of the angular frequency of the fundamental.

The rotor mmf for squirrel-cage rotors with rotor current  $I_2$  at frequency  $s f_1$  is given in complex Fourier series form by:

$$\begin{aligned} \bar{F}_{m\lambda}(x,t) &= \sum_{\lambda} -(-1)^g \frac{\sqrt{2} m N_1 K K_{\lambda} I_1 \cos \phi_1}{p \pi \lambda} \\ &\quad \times \exp [j(\lambda p x - \omega_{\lambda} t - \psi_{\lambda})] \\ &= \sum_{\lambda} F_{m\lambda} \exp [j(\lambda p x - \omega_{\lambda} t - \psi_{\lambda})] \end{aligned} \quad (4.32)$$

where:

$\lambda = (gS_2/p)+1$  = the ordinal of the spatial harmonic of the rotor

$K_{\lambda}$  = the winding factor for the  $\lambda$ th harmonic

$$\omega_{\lambda} = \omega_1 \left( \frac{gS_2}{p} (1-s) + 1 \right)$$

$$\psi_{\lambda} = \phi_1 + \arctan \frac{I_0 S_m / I_{sc}}{S}$$

$s_m$  = the slip for maximum torque

$s$  = the actual slip

$I_{sc}$  = the short-circuit current

$S_2$  = the number of slots on the rotor

For wound rotors, calculation of the harmonic mmfs is done in a manner similar to that of the stator using suitable modifications of Eq. 4.31.

The complex Fourier series for the space harmonic mmf waves created by the time harmonics of the currents in the rotor conductors is:

$$\bar{F}_{m\lambda\mu}(x,t) = \sum_{\lambda\mu} F_{m\lambda\mu} \exp [j(\lambda_{\mu} p x - \omega_{\lambda\mu} t - \psi_{\lambda\mu})] \quad (4.33)$$

where:

$$\lambda_{\mu} = \frac{gS_2}{p} + \mu$$

$$\omega_{\lambda\mu} = \omega_1 \left( \frac{gS_2}{p} (1-s) + 1 \right)$$

$$\psi_{\lambda\mu} = \phi_1 + \arctan \frac{I_0 S_m / I_{sc}}{S}$$

These residual mmf waves and their effects are taken into account only in an extremely detailed analysis of induction motors.

For the magnetic permeance  $G_m$  only the harmonics of slotting, eccentricity, and saturation are taken into account:

$$\begin{aligned} \bar{G}_m(x,t) &= \bar{G}_{m0} + \bar{G}_{m\mu}(x) + \bar{G}_{m\lambda}(x,t) \\ &\quad + \bar{G}_{me}(x,t) + \bar{G}_{ms}(x,t) \end{aligned} \quad (4.34)$$

The average permeance of the air gap  $G_{m0}$  can be calculated for increased air gaps using the Carter factors, referring to the stator and rotor separately:

$$G_{m0} = \frac{\mu_0}{\delta_g k_{c1} k_{c2}} \quad (4.35)$$

where  $\delta_g$  is the length of the air gap (measured from rotor outside diameter to the stator bore).

In the case of rotors without slots, the complex Fourier series for harmonics of the magnetic permeance due to the slots of the stator is:

$$\begin{aligned} \bar{G}_{m\mu}(x) &= G_{m0} k_{c1} \sum_{g=1}^{\infty} -(-1)^g \frac{\sin g\pi}{g\pi} 2 \frac{k_{c1} - 1}{k_{c1}} \\ &\quad \times \exp (jgS_1 x) \end{aligned} \quad (4.36)$$

In the case of stators without slots, the complex Fourier series for the space harmonics of the magnetic permeance due to the slots of the rotor is:

$$\begin{aligned} \bar{G}_{m\lambda}(x,t) &= G_{m0} k_{c2} \sum_{g=1}^{\infty} -(-1)^g \frac{\sin g\pi}{g\pi} 2 \frac{k_{c2} - 1}{k_{c2}} \\ &\quad \times \exp [jgS_2(x - \omega t)] \end{aligned} \quad (4.37)$$

The first term of the complex Fourier series of the magnetic permeance wave due to eccentricity is:

$$\bar{G}_{me}(x,t) = \frac{\mu_0 \varepsilon}{\delta_g^2 k_{c1} k_{c2}} \exp [j(x - \omega_e t - \phi_e)] \quad (4.38)$$

where  $\varepsilon$  = eccentricity, and:

$$\omega_e = \begin{cases} 0 & \text{in the case of static eccentricity} \\ \omega_1(1-s)/p & \text{in the case of dynamic eccentricity} \end{cases}$$

The first term of the complex Fourier series of the magnetic permeance wave due to saturation is:

$$\begin{aligned} \bar{G}_{ms}(x,t) &= -G_{m0} \frac{\delta_s}{\delta_g k_{c1} k_{c2}} \left( \frac{F_{m \text{ air gap}}}{\sum F_m} \right)^2 \\ &\quad \times \exp [j(2px - 2\omega_1 t - 2\phi_0)] \end{aligned} \quad (4.39)$$

where  $\delta_s$  = a virtual air gap increase in millimeters that has the same effect on the air gap flux as the saturation has.

The radial air gap flux density is given in the following series:

$$\bar{B}(x,t) = (\bar{F}_m(x,t) \bar{G}_m(x,t)) \quad (4.40)$$

For practical calculations, the following should be taken into consideration.

1. The product of the constant term of the magnetic permeance and of the fundamental of the mmf gives the fundamental of the air gap flux density. That is, using Eqs. 4.30 and 4.35 in complex form yields:

$$\bar{B}_p(x,t) = G_{m0} F_{mp}(x,t) = B_p \exp [j(px - \omega_1 t - \phi_0)]$$

The instantaneous value of the fundamental of the flux density wave is the real part of the complex wave, so that:

$$b_p(x, t) = B_p \cos(px - \omega_1 t - \phi_0) \quad (4.41)$$

where the amplitude  $B_p = G_{m0} F_{mp}$ .

In the following, the origin and the harmonic form of the space harmonics of the flux density are given.

2. The product:

$$G_{m0} [\bar{F}_{m\mu}(x, t) + \bar{F}_{m\lambda}(x, t)]$$

gives the flux density harmonics or, in other words, the winding harmonics of the air gap flux density. The Fourier series of the winding harmonics of the stator is:

$$\bar{B}_\mu(x, t) = G_{m0} \bar{F}_{m\mu}(x, t)$$

The form of the instantaneous value of the general term of the winding harmonics of the stator is:

$$b_{\mu w}(x, t) = B_{\mu w} \cos(\mu_w px - \omega_{\mu w} t - \psi_{\mu w}) \quad (4.42)$$

where the index  $w$  refers to the winding harmonic, and the amplitude is:

$$B_{\mu w} = G_{m0} F_{m\mu}$$

3. The Fourier series of the harmonics of the rotor is:

$$\bar{B}_\lambda(x, t) = G_{m0} \bar{F}_{m\lambda}(x, t)$$

The instantaneous value of the harmonic with ordinal number  $\lambda_w$  in the case of a squirrel-cage rotor is

$$b_{\lambda w}(x, t) = B_{\lambda w} \cos(\lambda_w px - \omega_{\lambda w} t - \psi_{\lambda w}) \quad (4.43)$$

where  $B_{\lambda w} = G_{m0} F_{m\lambda}$ .

4. The following product gives the permeance waves of the air gap flux density:

$$\bar{F}_{mp}(x, t) \times [\bar{G}_{m\mu}(x) + \bar{G}_{m\lambda}(x, t) + \bar{G}_{me}(x, t) + \bar{G}_{ms}(x, t)]$$

The Fourier series of the stator slot harmonics is:

$$\bar{B}_{\mu s1}(x, t) = \bar{F}_{mp}(x, t) \bar{G}_{m\mu}(x)$$

Performing the multiplication with complex values, the complex series for  $\bar{B}_{\mu s1}(x, t)$  will be found to be:

$$\bar{B}_{\mu s1}(x, t) = \frac{1}{2} [\bar{F}_{mp}(x, t) \bar{G}_{m\mu}(x) + \bar{F}_{mp}(x, t) \bar{G}_{m\mu}^*(x)]$$

Thus, the instantaneous value of the general term of the slot harmonics of the stator is:

$$b_{\mu s1}(x, t) = b_{\mu s1} \cos(\mu_{s1} px - \omega_1 t - \phi_0) \quad (4.44)$$

where the harmonic ordinal is:

$$\mu_{s1} = \frac{gS_1}{p} + 1$$

and its amplitude is:

$$B_{\mu s1} = (-1)^g B_p (k_{c1} - 1) K_{\mu s1}$$

where:

$$K_{\mu s1} = \frac{\sin [g(k_{c1} - 1)\pi/k_{c1}]}{[g(k_{c1} - 1)\pi/k_{c1}]}$$

5. The Fourier series of the slot harmonics of the rotor is given by:

$$\bar{B}_{\lambda s1}(x, t) = \bar{F}_{mp}(x, t) \bar{G}_{m\lambda}(x, t)$$

which may also be written as:

$$\bar{B}_{\lambda s1} = \frac{1}{2} [\bar{F}_{mp}(x, t) \bar{G}_{m\lambda}(x, t) + \bar{F}_{mp}(x, t) \bar{G}_{m\lambda}^*(x, t)]$$

The instantaneous value of the general term is:

$$b_{\lambda s1}(x, t) = B_{\lambda s1} \cos(\lambda_{s1} px - \omega_{\lambda s1} t - \psi_{\lambda s1}) \quad (4.45)$$

where  $\lambda_{s1}$  and  $\omega_{\lambda s1}$  are equivalent to  $\lambda$  and  $\omega_\lambda$  of Eq. 4.32, and the phase angle is:

$$\psi_{\lambda s1} = \phi_0$$

The amplitude is:

$$B_{\lambda s1} = (-1)^g B_p (k_{c1} - 1) K_{\lambda s1}$$

where:

$$K_{\lambda s1} = \frac{\sin [g(k_{c2} - 1)\pi/k_{c2}]}{[g(k_{c2} - 1)\pi/k_{c2}]}$$

The angular frequencies of the winding and slot harmonics are equal. The set of ordinals of the winding harmonics contains the slot harmonics as well. The slot and winding harmonics appear together only when  $g2pm/S_1$  is a whole number. The two field components have different phase angles. Hence the summation has to be done vectorially separately for the stator and for the rotor. The angular frequency of the resultant harmonic remains unchanged.

6. The flux density harmonic of the eccentricity is:

$$\bar{B}_{\mu e}(x, t) = \bar{F}_{mp}(x, t) \bar{G}_{me}(x, t)$$

$$\bar{B}_{\mu e}(x, t) = \frac{1}{2} [\bar{F}_{mp}(x, t) \bar{G}_{me}(x, t) + \bar{F}_{mp}(x, t) \bar{G}_{me}^*(x, t)]$$

Its instantaneous value is:

$$b_{\mu e}(x, t) = B_{\mu e} \cos(\mu_e px - \omega_{\mu e} t - \phi_{\mu e}) \quad (4.46)$$

where:

$$B_{\mu e} = B_p e / (2\delta_g)$$

$$\mu_e = 1 \pm 1/p$$

$$\omega_{\mu e} = \omega_1 \pm \omega_e$$

$$\phi_{\mu e} = \phi_1 \pm \phi_e$$

7. The flux density harmonic due to saturation is:

$$\bar{B}_{\mu s}(x, t) = \bar{F}_{mp}(x, t) \bar{G}_{ms}(x, t)$$

which may also be written as:

$$\bar{B}_{\mu s}(x, t) = \frac{1}{2} [\bar{F}_{mp}(x, t) \bar{G}_{ms}(x, t) + \bar{F}_{mp}(x, t) \bar{G}_{ms}^*(x, t)]$$

The instantaneous value of the term with  $3p$  as the ordinal from among the flux density harmonics due to saturation is:

$$b_{\mu s}(x, t) = B_{\mu s} \cos(3px - 3\omega_1 t - 3\phi_0) \quad (4.47)$$

Its amplitude is:

$$B_{\mu s} = \frac{F_{mt}}{3(F_{mp} + F_{my})} B_p$$

where:

$F_{mt}$  = the mmf belonging to the tooth

$F_{my}$  = the mmf belonging to the yoke

To analyze the residual fields originating from saturation and eccentricity of the rotor, the rotor and the waves of the residual flux density have to be recalled. It was stated that the random origin flux density harmonics of the air gap induce harmonic currents in the rotor that react upon the fields developing them, and cause the undamped residual field of the rotor. This causes random origin mmf in the rotor, with air gap flux density harmonics of the form of Eq. 4.33:

$$\bar{B}_\mu(x,t) = B_\mu \exp [j(\mu p x - \omega_\mu t - \psi_\mu)]$$

The instantaneous value of the residual rotor field that develops as a result of this mmf and the eccentricity of the rotor is

$$b_{\lambda_e}(x, t) = B_{\lambda_e} \cos(\lambda_e p x - \omega_{\lambda_e} t - \psi_{\lambda_e}) \quad (4.48)$$

which has an ordinal of:

$$\lambda_e = \frac{gS_2}{p} + \mu_e = \frac{gS_2}{p} + 1 \pm \frac{1}{p}$$

an angular frequency of:

$$\omega_{\lambda_e} = \omega_{\mu_e} + \frac{gS_2}{p} (1 - s)\omega_1$$

and a phase angle of:

$$\psi_{\lambda_e} = \psi_{\mu_e} + \arctan \frac{I_0 S_m / I_{sc}}{s}$$

The instantaneous value of the residual field due to saturation is:

$$b_{\lambda_s}(x, t) = B_{\lambda_s} \cos(\lambda_s p x - \omega_{\lambda_s} t - \psi_{\lambda_s}) \quad (4.49)$$

where:

$$\lambda_s = \frac{gS_2}{p} + 3$$

$$\omega_{\lambda_s} = \omega_1 \left( 3 + \frac{gS_2}{p} (1 - s) \right)$$

$$\psi_{\lambda_s} = 3\phi_m + \arctan \frac{I_0 S_m / I_{sc}}{s}$$

#### 4.1.3.1 Summary

The air gap flux density is the sum of the fundamental flux density and the stator and rotor harmonic flux densities, and has the form:

$$b(x,t) = b_p(x,t) + \sum_\mu b_\mu(x,t) + \sum_\lambda b_\lambda(x,t) \quad (4.50)$$

The harmonic spatial fields rotate alternately in the same direction as the fundamental field and in the opposite direction if the stator winding is three-phase and symmetric. Their ordinals are odd numbers not divisible by 3 for symmetry reasons, and their amplitudes are inversely proportional to the ordinal. In the flux density wave of a two-phase winding, harmonics with ordinals divisible by 3 also appear.

#### 4.1.4 Reactances of the Induction Motor

The induction motor can be considered as two winding systems in inductive relationship with each other with current in each of them. The resulting fluxes may be divided into two parts.

1. Those fluxes that take part in energy transfer, are linked with both windings, and are related to the fundamental field wave are called useful or magnetizing fluxes
2. Those fluxes that do not satisfy the definition given in (1) in one or more respects are called leakage fluxes

These fluxes are modeled for circuit analysis by the reactances of the equivalent circuits, using  $X_m$  for the magnetizing flux and  $X_l$  for leakage flux. It is desirable to have  $X_m$  as large and  $X_l$  as small as possible to obtain good motor performance ( $\phi_l$ ).

##### 4.1.4.1 Magnetizing Reactance

A good approximation to the magnetizing reactance  $X_m$  in a typical induction machine is the ratio of the terminal voltage to the exciting current. The magnetizing reactance of one phase can be calculated using the following equation, which is based on the winding data, the geometrical configuration of the machine, and the supply frequency:

$$X_m = 2\mu_0 m f_1 (N_1 K_\omega)^2 \frac{D_1 l_i}{p^2 \delta_i} K_{sk} \quad (4.51)$$

where:

$$\mu_0 = 4\pi \times 10^{-7} \text{hm}^{-1}$$

$m$  = the number of phases in the stator

$f_1$  = the frequency of the supply circuit (s<sup>-1</sup>)

$N_1 K_\omega$  = the number of turns per stator phase, corrected by the winding factor

$D_1$  = the diameter of the bore of the stator (m)

$l_i$  = the actual length of the iron (the geometric length shortened by a factor to account for lamination insulation).

$p$  = the number of pairs of poles

$K_{sk}$  = the skewing factor

$$\delta_i = \delta_g k_{c1} k_{c2} \frac{\sum F_m}{F_{m \text{ air gap}}}$$

$\delta_i$  being the effective air gap length ( $m$ ).

When calculating  $\delta_i$ , factors to be taken into account include the geometric air gap dimension  $\delta_g$ , the Carter coefficients  $k_{c1}$  and  $k_{c2}$ , and the saturation of the magnetic circuit as indicated by the ratio of  $\sum F_m / F_{m \text{ air gap}}$  where  $\sum F_m$  is the total mmf required by the magnetic circuit.

As the magnetic path becomes more saturated,  $\sum F_m$  increases, thus increasing  $\delta_i$ . Since the magnetizing reactance  $X_m$  is inversely proportional to  $\delta_i$ , increasing saturation reduces  $X_m$ . Figure 4.38 shows a typical curve of  $X_m$  vs. the magnetizing current  $I_m$ . The magnetizing reactance will generally lie in the 0- $M$  range of the curve.

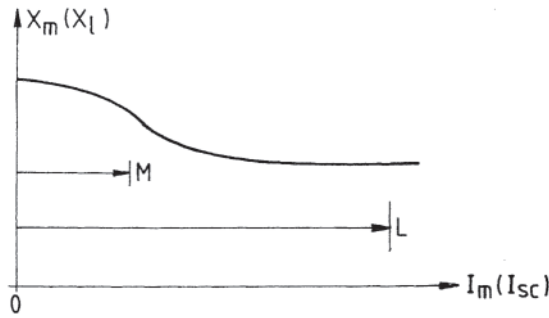


**Figure 4.38** Variation of the magnetizing reactance and leakage reactance as a function of saturation.

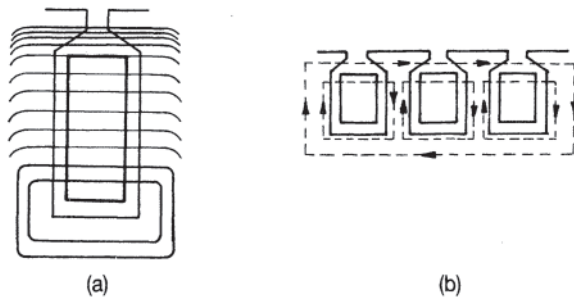
4.1.4.2 Leakage Reactances

Except for fractional-horsepower motors, where the winding resistance is particularly important, the value of the leakage reactance is of major importance from the point of view of overloading and torque.

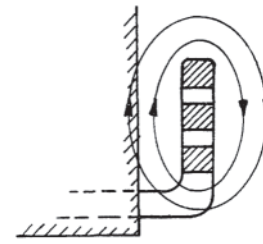
The leakage flux is composed of two parts, one of which links either the stator winding or the rotor winding; this part of the flux surrounds the slots and end turns. The other part of the flux links both windings, and is caused by the harmonic mmfs.

Figure 4.39(a) shows flux lines that link the conductors in one slot, and are thus part of the slot leakage flux. Figure 4.39(b) shows how the leakage of the individual slots combines to become the resultant leakage of a phase band, in this case for  $q_1=3$ . Slot leakage can be defined and calculated separately for the stator and the rotor. In the case of induction machines, because of the complicated interactions between the stator and rotor end-turns, the end-turn leakage is taken into consideration by a common leakage reactance. (A part of the end-turn leakage related to the stator end-turn may be seen in Fig. 4.40.)

In earlier sections, the spatial flux density harmonics were discussed. The fluxes of the spatial harmonics are linked with both windings. With their rotating speeds  $\omega_1/(\mu_p)$  and their number of pairs of poles  $\mu_p$ , they induce voltages of line frequency in the stator winding. Since the magnitude of the terminal voltage is fixed by the supply, the induced voltage or magnetic flux related to the fundamental field wave is decreased. The method of calculation of this kind of leakage flux and of the harmonic leakage reactance that is modeled by this effect was unclear for a long time.



**Figure 4.39** Flux lines illustrating slot leakage, (a) For one slot, (b) In the case of  $q_1=3$ .



**Figure 4.40** Flux lines typical of end-turn leakage.

From experience, there must be some other kind of leakage besides the slot leakage and end-turn leakage to ensure that the calculated and measured values are in agreement with each other. In technical literature, the so-called zig-zag and belt leakage reactances were calculated using an empirical or semiempirical formula for both the stator and the rotor. Slot skewing also creates a leakage effect, since it decreases the short-circuit current and the magnetizing flux.

Hence, the total leakage reactance can be divided into the following parts.

For the stator:

$$X_{l_s} = X_{sl_s} + 0.5X_e + X_{hs} + X_{sk_s} \tag{4.52}$$

where:

- $X_{sl_s}$  = the slot leakage reactance of the stator
- $X_e$  = the end turn leakage reactance
- $X_{hs}$  = the harmonic leakage reactance of the stator
- $X_{sk_s}$  = the slot skewing leakage reactance of the stator

For the rotor as reflected to the stator:

$$X'_{l_r} = X'_{sl_r} + 0.5X_e + X'_{hr} + X'_{sk_r} \tag{4.53}$$

where:

- $X'_{sl_r}$  = the slot leakage reactance of the rotor
- $X'_{hr}$  = the harmonic leakage reactance of the rotor
- $X'_{sk_r}$  = the slot skewing leakage reactance of the rotor

In the short-circuit condition, the large currents cause saturation in certain cross sections of the magnetic path. Hence the leakage reactance decreases in a manner similar to that shown in Fig. 4.38. Although the current producing the magnetizing flux varies only within the 0– $M$  range, the current producing the leakage fluxes varies over the 0– $L$  range (up to the short-circuit current of the motor), and therefore changes occur in the leakage reactance:

$$X_l = X_{l_s} + X'_{l_r}$$

When calculating the slot leakage reactance, the number of conductors lying in the slot, the current in the conductors, and the equivalent magnetic permeance of the slot have to be taken into consideration. Given the magnetic circuit with its geometric dimensions and by using the magnetic circuit equivalent of Ohm's law, the resultant slot flux is as follows.

In the stator:

$$X_{sl_s} = 8\pi f_1 \frac{mN_1^2}{S_1} l_t \lambda_{sl_s} \tag{4.54}$$

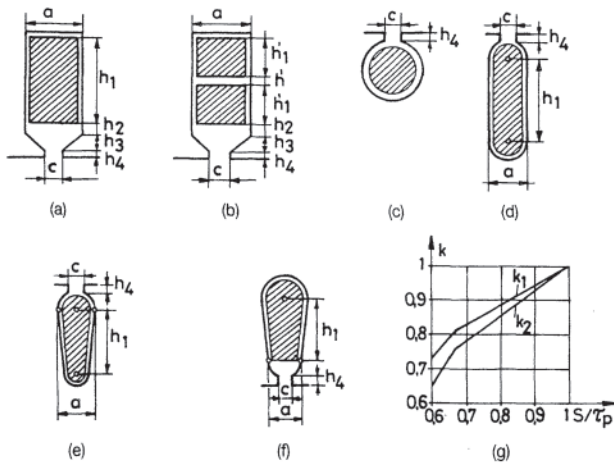


**Figure 4.41** (a–f) Different shapes of slots and their dimensions for calculating slot leakage, (g) Pitch factor.

where:

- $N_1$  = the number of turns per phase winding of the stator
- $S_1$  = the number of slots in the stator
- $\lambda_{s1s}$  = the magnetic permeance of the stator per unit length of iron

In a wound rotor with reactance referred to the stator.

$$X'_{slr} = 8\pi f_1 \frac{mN_1^2}{S_2} \left( \frac{K_s}{K_r} \right)^2 l_i \lambda_{s1r} \quad (4.55)$$

where:

- $S_2$  = the number of slots in the rotor
- $K_s$  = the winding factor of the stator winding
- $K_r$  = the winding factor of the rotor winding
- $\lambda_{s1r}$  = the magnetic permeance of the rotor per unit length of iron

For squirrel-cage rotor, leakage reactance referred to the stator may be calculated from Eq. 4.55 if  $K_r=1$  is used.

In the following the specific permeance expressions are shown for generally used slot shapes in induction motors. For the half-closed partially parallel walled slots of Fig. 4.41 (a), which has a single-layer winding,

$$\lambda_{s1} = \mu_0 \left( \frac{h_1}{3a} + \frac{h_2}{a} + \frac{2h_3}{a+c} + \frac{h_4}{c} \right) \quad (4.56)$$

The indices may be supplemented with an  $s$  or an  $r$  index, depending on whether it is a stator or a rotor slot.

If the winding is double-layer and is full pitch, if the slot is half closed, and if the slot is partially parallel walled as in Fig. 4.41 (b), then:

$$\lambda_{s1} = \mu_0 \left( \frac{2h'_1}{3a} + h_2 + \frac{0.25h'}{a} + \frac{2h_3}{a+c} + \frac{h_4}{c} \right) \quad (4.57a)$$

Short pitch coils can decrease the slot leakage because there will be slots in which the two coil sides belong to different phases. For this reason, their leakage magnetic field does not sum up algebraically but vectorially; thus it will be smaller than if both coil sides belonged to the same phase. For a

double-layer short pitch winding, the factors  $k_1$  and  $k_2$  should be put into Eq. 4.57, the values of  $k_1$  and  $k_2$  being obtained from Fig. 4.41(g). Then:

$$\lambda_{s1} = \mu_0 \left[ k_1 \frac{2h'_1}{3a} + k_2 \left( \frac{h_2}{a} + \frac{2h_3}{a+c} + \frac{h_4}{c} \right) + \frac{h'}{4a} \right] \quad (4.57b)$$

If the slot is parallel walled from top to bottom ( $a=c$ ), then:

$$\lambda_{s1} = \frac{\mu_0}{a} \left( k_1 \frac{2h_1}{3} + k_2 h_2 + \frac{h'}{4} \right) \quad (4.57c)$$

If the slot has a circular cross section (as in the case of squirrel-cage rotors) and the conductor fills the slot cross section completely, as in Fig. 4.41(c), then:

$$\lambda_{s1} = \mu_0 \left( 0.623 + \frac{h_4}{c} \right) \quad (4.58a)$$

For the slot of Fig. 4.41(d),

$$\lambda_{s1} = \mu_0 \left( 0.623 + \frac{h_1}{3a} + \frac{h_4}{c} \right) \quad (4.58b)$$

In many cases trapezoidal slots are used so that the teeth have constant width for better magnetic utilization. If the winding is double-layer and is full pitch, then in the case of the slot shapes of Figs. 4.41(e) and 4.41(f). Equation 4.58b may be used. In the case of a double-layer short pitch winding with a half-closed slot shape with semicircular cross section, Eq. 4.58b has to be supplemented with the  $k_1$  and  $k_2$  factors shown in Fig. 4.41(g). The specific permeance of the slot shape is:

$$\lambda_{s1} = \mu_0 \left[ k_1 \frac{h_1}{3a} + k_2 \left( \frac{h_4}{c} + 0.623 \right) \right] \quad (4.58c)$$

The end-turn leakage reactance in induction motors is extremely complicated for theoretical calculations, so the specific permeance of the end-turns has been established on the basis of model experiments as the combined leakage reactance of the end-turns of the stator and rotor. To calculate the specific magnetic permeance of the end-turns  $\lambda_e$  the type of construction of the winding must be taken into account. The leakage reactance can be calculated using:

$$X_e = 4\pi f_1 \frac{N_1^2}{p} \left( \frac{l_{av}}{2} - l_i \right) \lambda_e \quad (4.59)$$

where  $l_{av}$  is the average length of the turns of the winding.

The value of the specific magnetic permeance of the endturn ( $\lambda_e$ ) may be taken from Table 4.1 on the basis of measurements. The uncertainty of the end-turn leakage reactances calculated from the average values of  $\lambda_e$  from Table 4.1 can be as much as 10–20%.

Having calculated the harmonic leakage reactance, one must take into consideration the fact that the voltages induced by the flux harmonics behave in the same way as the voltages induced by the slot or end-turn fluxes. Since the voltage induced by the (useful) fundamental flux changes due to the effect of the harmonic fluxes, it is advisable to correlate the harmonic leakage reactance with the magnetic reactance. The



**Table 4.1** The Specific Magnetic Permeance of End-Turns

	Winding system <sup>a</sup>							
	Stator		2s		3s		cro	
	2s	3s	2s	3s	2s	3s	cro	cro
	Rotor		2s		3s		cage	
	2s	3s	cro	cro	cage	cage	cro	cage
$\lambda_e \times 10^6$ ( $H m^{-1}$ )	0.54	0.41	0.45	0.40	0.43	0.40	0.40	0.41

<sup>a</sup> Winding systems: 2s, two-planed; 3s, three-planed; cro, crown; cage, squirrel cage.

harmonic leakage factor  $\sigma_{is}$  of the winding of the stator can be defined as the ratio of the resultant of the induced harmonic voltages and the induced fundamental voltage: where:

$$\sigma_{1s} = \frac{\sum U_{i\mu}}{U_{i1}} = \frac{\sum (K_{\mu}/\mu)^2}{K_{\omega}^2} \tag{4.60}$$

- $U_{i\mu}$  = the voltage induced in the stator winding by the  $\mu$ th spatial flux harmonic
- $U_{i1}$  = the voltage induced in the stator winding by the fundamental flux
- $K_{\omega}$  = the fundamental's winding factor
- $K_{\mu}$  = the spatial harmonic winding factor for the  $\mu$ th term

If the rotor is also wound, Eq. 4.60 may be used for calculating the harmonic leakage factor  $\sigma_{ir}$  of the rotor also using the winding factors for the rotor.

Values of the harmonic leakage factors  $\sigma_l$  are found in Fig. 4.42 for the values of  $q$  usually used in practice for short pitch and full-pitch three-phase and two-phase windings in Figs. 4.42(a) and 4.42(b), respectively. Figure 4.42(a) shows that in the case of  $q=2$ , the winding pitch  $S/\tau_p=5/6=0.833$  gives the smallest harmonic leakage factor. This agrees with the fact that for such a winding pitch the two largest harmonics, the fifth and the seventh, will be very small or will even disappear. In the case of two-phase motors, the minimum usually appears in the little used range of  $S/\tau_p < 0.65$  because of the third harmonic. Reference 8 gives more information.

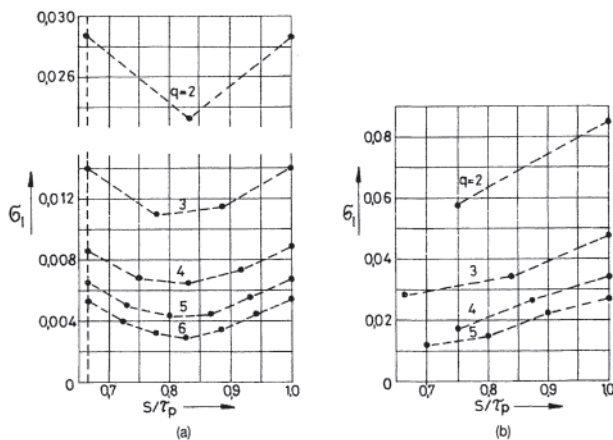


**Figure 4.42** Harmonic leakage factor of a squirrel-cage rotor (From Ref. 8. Reproduced by permission of Springer Verlag.)

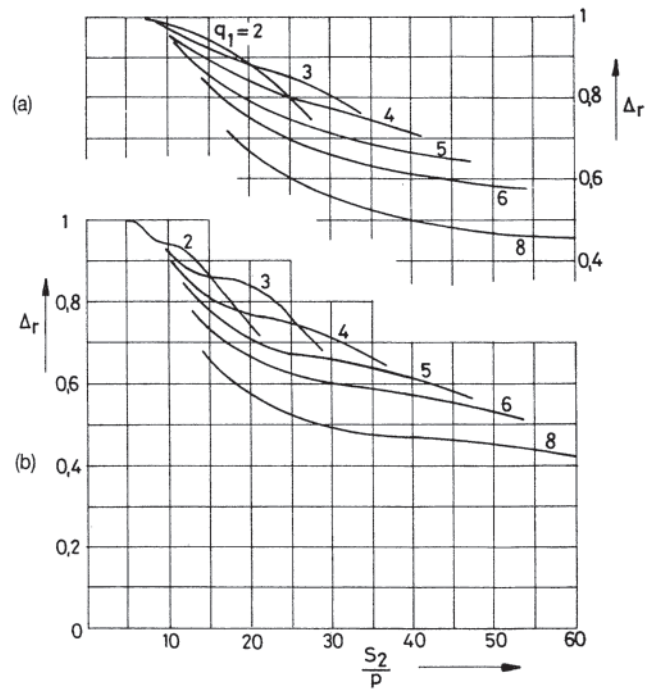


**Figure 4.43** The damping factor  $\Delta_r$  of squirrel-cage rotors for various values of  $q_1$ . (a) For skewed rotor slots (where  $b$  in Fig. 4.37 equals  $D\pi/S_2$ ). (b) Unskewed rotor slots. (From Ref. 8. Reproduced by permission of Springer Verlag.)

In the case of wound rotor induction motors, the harmonic leakage reactances are both easily calculated from:

$$X_{\sigma_{ls}} = X_m \sigma_{ls} \quad \text{and} \quad X'_{\sigma_{lr}} = X_m \sigma_{lr} \tag{4.61}$$

The stator harmonics do not induce any voltage in the rotor winding because the number of pairs of poles of the space harmonics of the stator does not equal that of the number of poles of the wound rotor.

If the rotor is of the squirrel-cage type, it adapts to every number of pole pairs and thus damps the spatial flux harmonics of the stator. The harmonic leakage factor  $\sigma_{ls}$  has to be multiplied by a damping factor  $\Delta_r$ . This damping factor can be calculated from:

$$\Delta_r = 1 - \sum_{\mu \neq 1} \frac{\sin(\mu p b/D)}{(\mu p b/D)} \frac{\sin(\mu p \pi/S_2)}{(\mu p \pi/S_2)} \tag{4.62}$$

The damping factor  $\Delta_r$  is shown in Fig. 4.43(a) for skewed rotor slots and in Fig. 4.43(b) for unskewed slots. When calculating  $\sigma_{lr}$ , the harmonic leakage factor of squirrelcage rotors, Eq. 4.60 has to be used as a basis, taking into consideration that, for squirrel-cage rotors,  $K_r=K_{\lambda}=1$  and, as seen in Eq. 4.32,  $\lambda=(gS_2/p)+1$ . The harmonic leakage factor of the squirrel cage rotor can be written as:

$$\sigma_{lr} = \sum_{\lambda \neq 1} \frac{1}{\lambda^2} = \sum_g \frac{1}{(gS_2/p + 1)^2} \tag{4.63a}$$

In the denominator, 1 may be neglected compared to  $gS_2/p$  and, considering all the values of  $g=\pm 1, \pm 2, \dots$ ,

$$\sigma_{lr} = 2 \left( \frac{p}{S_2} \right)^2 \sum_g \frac{1}{g^2} = 3.29 p^2 / S_2^2 \quad (4.63b)$$

On increasing the number of slots in the rotor, the harmonic leakage decreases, as would be expected.

The harmonic leakage factor can also be calculated with the help of the accumulated energies in the air gap. Knowing values of  $B$  and  $H$  in the air gap and the geometric dimensions  $l_i$  and  $\delta_i$ , then (assuming that the relative permeability  $\mu_{Fe}$  of iron is infinite) the total energy in the air gap is:

$$\begin{aligned} W_a &= \frac{1}{2} \int BH \, dV = \frac{1}{2} \int_0^{D\pi} B(x) H(x) l_i \delta_i \, dx \\ &= \frac{\mu_0 l_i}{2 \delta_i} \int_0^{D\pi} f_m^2(x) \, dx \end{aligned} \quad (4.64)$$

where:

- $B$  = flux density
- $H$  = magnetic field strength
- $f_m(x)$  = the mmf distribution along the periphery of the bore
- $l_i$  = the length of the stator or rotor core
- $\delta_i$  = the effective air gap length (see Eq. 4.51)

Similarly, the magnetic energy of the fundamental flux is:

$$W_p = \frac{\mu_0 l_i}{2 \delta_i} \int_0^{D\pi} f_{mp}^2(x) \, dx \quad (4.65)$$

where  $f_{mp}(x)$  = the fundamental wave of the mmf along the periphery of the bore.

The magnetic energy of the harmonic waves is the difference of Eqs. 4.64 and 4.65:

$$W_h = W_a - W_p = \frac{\mu_0 l_i}{2 \delta_i} \int_0^{D\pi} [f_m^2(x) - f_{mp}^2(x)] \, dx \quad (4.66)$$

The harmonic leakage factor may then be defined by:

$$\sigma_l = \frac{W_h}{W_p} = \frac{\int_0^{D\pi} [f_m^2(x) - f_{mp}^2(x)] \, dx}{\int_0^{D\pi} f_{mp}^2(x) \, dx} \quad (4.67)$$

In the case of windings with integral numbers of slots (i.e.,  $q$  is a whole number), it is enough to integrate for only one half of the pole pitch because of the periodicity of the mmf curves. Figure 4.44 shows the mmf curve (labeled 1) and the fundamental mmf wave (labeled 2) for one half pole pitch in the case of  $q=2$  at the instant when the current is equal to zero in the II phase. Curve 3 gives the square of the stepped curve and curve 4 gives the square of the fundamental wave. For this case,  $\sigma_l=0.0284$ .

When using Eq. 4.51 to calculate the reactance  $X_m$  of the magnetizing branch in the equivalent circuit of a machine having skewed slots, it may be noted that the value of the magnetizing reactance is decreased by the factor  $K_{sk}$ . Under no-load conditions, when there is practically no current in the rotor, there is no difference between the skewed and the straight slotted machine, whether it is supplied from the stator side or the rotor side.

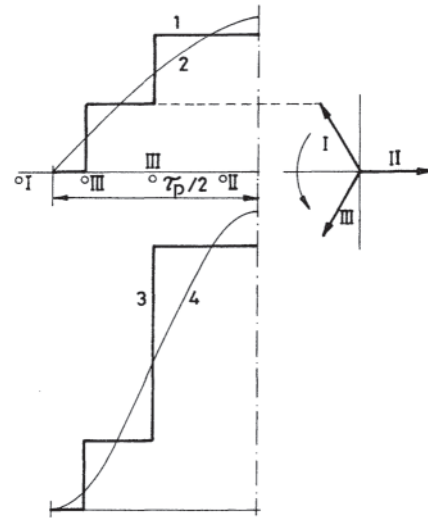


**Figure 4.44** Determination of the harmonic leakage factor using an energy approach ( $q_1=2$ ).

It is for this reason that both the rotor leakage reactance and that of the stator in the equivalent circuit have to be expanded with a new leakage reactance term in the case of skewed machines. This additional reactance is the skew leakage reactance. Following an earlier line of thought, the skew leakage reactance of the stator, which is also the skew leakage reactance of the rotor referred to the stator, is:

$$X_{sk_s} = \frac{X_m(1 - K_{sk})}{K_{sk}} = X'_{skr} \quad (4.68)$$

Now that all of the expressions are available for calculating the reactances of the induction motor, it is worthwhile to look at typical values of the reactances and trends in those values as machine power increases. The machine's parameters can be put into per-unit or percent by comparing the machine parameters to the nominal or base impedance ( $Z_n=U_n/I_n$ ), which is defined as the ratio of the rated phase voltage and the rated phase current of the machine.

The percent values of typical reactances of induction machines are shown in Fig. 4.45, where the rated power of the machine is on the horizontal axis. The leakage reactances of the stator and of the rotor as referred to the stator are of the same order of magnitude.

### 4.1.5 Radial Force Waves

In the air gap of an induction motor, there are radial flux density waves as seen from Eq. 4.50. As a result, Maxwellian tensile stresses are developed that act on both the stator bore and the cylindrical surface of the rotor. The tensile stress expressed in tensile force per unit surface area is proportional to the square of the flux density. Equation 4.69 gives a general expression for the tensile stress  $p(x, t)$ :

$$p(x, t) = \frac{b^2(x, t)}{2\mu_0} = \frac{1}{2\mu_0} \left[ b_p^2 + \sum_{\mu} b_{\mu}^2 + \sum_{\lambda} b_{\lambda}^2 \right]$$

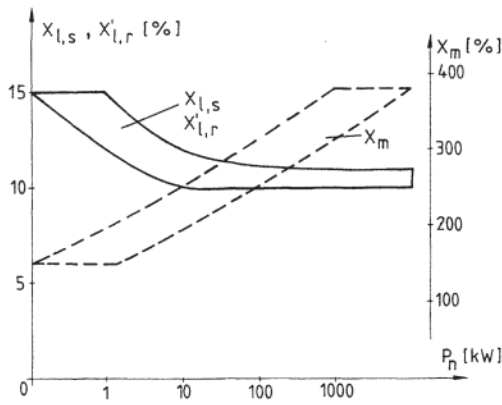


**Figure 4.45** Typical ranges of reactances (in percent) as a function of the rated power of machines.

$$\begin{aligned}
 &+ 2 \left( \sum_{\mu} b_p b_{\mu} + \sum_{\lambda} b_p b_{\lambda} + \sum_{\substack{\mu \\ (\mu' \neq \mu'')}} b_{\mu'} b_{\mu''} \right. \\
 &\left. + \sum_{\substack{\lambda \\ (\lambda' \neq \lambda'')}} b_{\lambda'} b_{\lambda''} + \sum_{\lambda \mu} b_{\mu} b_{\lambda} \right) \quad (4.69)
 \end{aligned}$$

Maxwell's tensile forces thus consist of three groups of an infinite number of radial force waves. The squares of the flux density waves create force waves of zero frequency and of double line frequency, that is,  $2p$ . The double line frequency and the  $2p$  mode number force waves have to be taken into consideration when investigating vibrations. The unbalanced magnetic pull, which has an angular frequency of  $\omega_e$  is created by the product of the first harmonic originating from eccentricity  $b_{\mu e}$  and the fundamental  $b_p$  of the stator. In some cases the unbalanced magnetic pull is so great that it is worth examining in more detail, and this is done below.

Those stator and rotor flux density waves that are multiplied by themselves have mode numbers that are large and amplitudes that are vanishingly small and thus do not significantly affect the operation of the motor.

The mixed products of the space harmonics of the stator and the rotor play an important role in creating vibrations and noise [9]. A typical term of the tensile stress wave resulting from these mixed products is:

$$p_r(x, t) = P_r \cos(rx - \omega_r t - \psi_r) \quad (4.70)$$

where:

$r = p(\mu_i \pm \lambda_j)$  is the mode number of the tensile stress wave, a mode number with negative sign signifying that the harmonic tensile stress wave rotates in the direction opposite to that of the fundamental flux wave

$\omega_r = \omega_{\mu_i} \pm \omega_{\lambda_j}$  = the angular frequency of the tensile stress wave

$\psi_r = \psi_{\mu_i} \pm \psi_{\lambda_j}$  = the phase angle of the tensile stress wave

$P_r = \frac{B_{\mu_i} B_{\lambda_j}}{2\mu_0}$  is the amplitude of the tensile stress wave

The product of the tensile stress and the cylindrical surface area of the bore gives the radial tensile force.

Examining the expressions for frequency in Eq. 4.70, it will be seen that the following frequencies appear.

1. The frequencies resulting from mixed products of the winding harmonics of the stator and of the rotor are:

$$f_r = f_1 \left[ \frac{gS_2}{p} (1-s) + (0 \text{ or } 2) \right]$$

2. Those due to mixed products of the space harmonics created by the eccentricity of the rotor and the space harmonics due to the windings of the stator are:

$$f_r = f_1 \left[ \frac{gS_2}{p} (1-s) + (0 \text{ or } 2) \pm \left( 0 \text{ or } \frac{1-s}{p} \right) \right] \quad (4.71b)$$

3. Those due to a mixed product of the harmonic due to saturation in the rotor and space harmonics of the stator are:

$$f_r = f_1 \left[ \frac{gS_2}{p} (1-s) + (2 \text{ or } 4) \right] \quad (4.71c)$$

The 2 or 0 and the 4 or 2 found in the brackets depend on whether the argument of the harmonic terms developed from a product of the harmonic flux density components is a sum or a difference of the argument of the component. In Eq. 4.71b, zero or  $(1-s)/p$  is used depending on whether static or dynamic eccentricity is present.

Equations 4.71a, 4.71b, and 4.71c show that the frequency of the magnetic force depends on the speed and that it changes linearly with it. At standstill ( $s=1$ ), the frequency is zero,  $2f_1$ , or  $4f_1$ , and these increase linearly during starting.

It can be shown by calculation and in some cases can be noticed in practice also that even those air gap force waves that have large mode numbers (equal to the slot number or even higher) cause lower frequency yoke forces and deformation waves due to the teeth. The radial force wave, acting directly on the head of a tooth, is passed through the tooth from the air gap to the yoke.

The surface of the stator bore is not smooth, but changes from slot to tooth. Force waves appear even in those parts interrupted by slots. The total force acting on the teeth is equal to the integral of the force per-unit surface area within a tooth pitch. This force propagates along the tooth to the yoke, and the mechanical stress changes along the periphery of the yoke depending on the cross section at the root of a tooth.

If the frequency of the force wave is small compared to the number of teeth, above a certain number of teeth the amplitude of the force wave will show only insignificant changes. If the mode number of the air gap force wave falls close to the number of teeth, then a significant bending torque will appear in the yoke due to the large variation in the stress distribution in the tooth head. It is shown in Ref. 10 that, for those force waves that have mode numbers  $r > S_1/2$ , the force wave does not pass on to the yoke unchanged and, a most important point, that the harmonic number of the yoke wave decreases. This phenomenon is called subharmonic wave generation.

The time function of the specific radial force wave acting on the yoke of the stator is:

$$p_y(x, t) = P_y \cos(r_y x - \omega_1 t - \psi_r) \quad (4.72)$$

where:

$$\begin{aligned} r_y &= gS_1 - r = \text{the mode number of the subharmonic wave} \\ P_y &= K_i K_j P_r = \text{the amplitude of the subharmonic wave} \\ K_i &= \frac{(\sin r\pi/S_1)}{(r\pi/S_1)} \\ K_j &= \frac{(\sin r_y b_t/D)}{(r_y b_t/D)} \end{aligned}$$

In these expressions,  $b_t$  is the width of the tooth neck, and  $D$  is the diameter of the bore.

If  $g=0$ , then  $r_y=|r|$ . If the value of  $r/S_1$  is close to zero (that is, if the mode number of the force wave is small compared to the number of teeth), then the values of  $K_i$  and  $K_j$  are nearly 1, and the general calculation method is correct. Errors are due to  $K_i$  and  $K_j$ , which are indirectly dependent on  $r/S_1$ .

#### 4.1.6 Homopolar Flux and Unbalanced Magnetic Pull in the Two-Pole Induction Motor

In the two-pole induction motor, homopolar fluxes are developed due to manufacturing asymmetries and material inhomogeneities. It is characteristic of the homopolar flux that it is unidirectional along the whole air gap; that is, it passes into the stator, then the yoke, housing, end frames, bearings, and finally the magnetic circuit closes through the shaft and the rotor iron.

The most frequent reason for homopolar flux is eccentricity of the rotor. Only the fundamental mmf wave and the permeance waves originating from the first static and dynamic eccentricity flux density waves are considered in the following. The spatial fundamental mmf of a three-phase two-pole induction motor can be expressed as:

$$f_{mp}(x, t) = F_{mp} \cos(x - \omega_1 t - \phi_m) \quad (4.73)$$

The magnetic permeance can be written in the following form if there is static as well as dynamic eccentricity ( $\epsilon_s$  and  $\epsilon_d$ ) in the machine with normalized values below 0.2 to 0.3:

$$\begin{aligned} G_m(x, t) &= G_{m0} + G_{mes} \cos(x - \phi_{es}) \\ &+ G_{med} \cos[x - (1 - s)\omega_1 t - \phi_{ed}] \end{aligned} \quad (4.74)$$

where:

$$\begin{aligned} G_{mes} &= G_{m0}\epsilon_s & \text{and} & & G_{med} &= G_{m0}\epsilon_d \\ \epsilon_s &= \frac{e_s}{\delta} & \text{and} & & \epsilon_d &= \frac{e_d}{\delta} \end{aligned}$$

The product of Eqs. 4.73 and 4.74 gives the air gap flux density. The air gap flux density consists of five terms:

$$\begin{aligned} b(x, t) &= B_p \cos(x - \omega_1 t - \phi_m) + B_{esh} \cos[\omega_1 t - (\phi_m - \phi_{es})] \\ &+ B_{es} \cos[2x - \omega_1 t - (\phi_m - \phi_{es})] \\ &+ B_{edh} \cos[s\omega_1 t - (\phi_m - \phi_{ed})] \\ &+ B_{ed} \cos[2x - (2 - s)\omega_1 t - (\phi_m - \phi_{ed})] \end{aligned} \quad (4.75)$$

The index  $h$  refers to the homopolar term. It can be seen that the second and fourth terms are independent of  $x$  and therefore have a constant value along the periphery at a given instant. The flux passes through the air gap either from the rotor to the stator or in the opposite direction; that is, these terms represent the homopolar flux. The homopolar flux originating from static eccentricity has line frequency, while that originating from dynamic eccentricity has slip frequency. The amplitude of the radial flux density wave due to static eccentricity is:

$$B_{es} = 0.5B_p\epsilon_s$$

while the amplitude of the radial flux density wave due to dynamic eccentricity is:

$$B_{ed} = 0.5B_p\epsilon_d$$

When calculating the amplitude of the homopolar flux densities, it must be noted that the magnetic reluctance of the machine parts in the flux path cannot be neglected in comparison to the magnetic reluctance of the air gap. That is why the technical literature [11] uses a factor  $Q'$ :

$$Q' = \left[ 1 + \frac{D\pi l}{2\delta_g} \sum_n \frac{l_n}{\mu_r A_n} \right] \quad (4.76)$$

where:

$$\begin{aligned} \delta_g &= \text{the actual length of the air gap.} \\ l &= \text{the length of the rotor reduced by the interlaminar insulation} \\ D &= \text{the diameter of the rotor} \\ l_n &= \text{the length of the } n\text{th section of the homopolar flux path} \\ A_n &= \text{the cross section area of the } n\text{th section of the homopolar flux path} \\ \mu_n &= \text{the relative permeability of the } n\text{th section of the homopolar flux path} \end{aligned}$$

Then:

$$B_{esh} = 0.5B_p\epsilon_s Q' \quad \text{and} \quad B_{edh} = 0.5B_p\epsilon_d Q'$$

The existence of the homopolar flux has many adverse consequences. It does not contribute to the production of electromagnetic torque, but does increase the losses due to local saturation and due to hysteresis and eddy currents in the shaft, end frames, and housing. Moreover, since the homopolar flux is alternating, alternating voltage will be induced in the shaft, end frames, and housing. If this voltage has a magnitude of even a few volts, current will flow in this loop, which of course includes the bearings. The resulting spark discharges through the lubricant will cause deterioration and early failure of the bearings. Since homopolar flux is unavoidable, large machines (above approximately 200 hp) include insulation between the bearing and the end frame, thus effectively providing an open circuit in the shaft current loop.

In addition, the homopolar flux adds to the leakage

magnetic field that already exists due to the heteropolar flux. This may have an adverse effect on any electronic instruments used in the vicinity of the motor.

Using Eq. 4.75 when calculating Maxwell's radial tensile stress and multiplying the radial tensile stress by the cylindrical surface of the bore, several forces with ordinal  $r=1$  can be found. These tensile forces are very dangerous in the case of heavy-duty rotors with long bearing spans. Forces with one maximum and one minimum point along the periphery result in unbalanced magnetic pull. References to this force will be found in the technical literature.

It should be noted that not only the two-pole induction motor may have a force with ordinal  $r=1$ , but this force can also develop in motors with larger pole numbers, being created as a result of slot harmonics, saturation harmonics, or magnetic asymmetry.

From the product of the  $B_{es}$  heteropolar, the  $B_{esh}$  homopolar, and the  $B_p$  spatial fundamental flux density waves in two-pole induction motors with static eccentricity, the unbalanced magnetic pull may be written as:

$$f_{es}(x,t) = \frac{D\pi l}{8\mu_0} B_p^2 \epsilon_s [(1+Q') \cos x + Q' \cos (x-2\omega_1 t)] \quad (4.77a)$$

which is directly proportional to the static eccentricity.

The results of analyses published in Ref. 12 show that the amplitude of this unbalanced magnetic pull should be multiplied by a factor  $Q$ , which has been established experimentally and depends on the number of poles of the motor. The value of  $Q$  in the case of a two-pole machine is 0.25, in the case of a four-pole machine it is 0.712, for a six-pole machine it is 0.86, and for an eight-pole machine it is 0.896.

The unbalanced magnetic pull in Eq. 4.77 has one component that is independent of time and another one that rotates with angular velocity  $2\omega_1$ . Consider how these two forces affect the two directions of space perpendicular to each other. The projection of the unbalanced magnetic pull pointing in the direction of the minimum air gap is:

$$f(x=0,t) = \frac{D\pi l}{8\mu_0} B_p^2 \epsilon_s Q \times \sqrt{1 + 2Q' + 2Q'^2 + 2Q'(1+Q') \cos 2\omega_1 t} \quad (4.77b)$$

In other words, the magnitude of the unbalanced magnetic pull pointing in the direction of the minimum air gap oscillates at twice the line frequency.

A harmonic force

$$f(x=\pi/2,t) = \frac{D\pi l}{8\mu_0} B_p^2 \epsilon_s Q Q' \sin 2\omega_1 t \quad (4.77c)$$

acts perpendicular to it in space.

The ratio of the maximum to minimum value of the oscillating magnetic pull pointing in the direction of the minimum air gap is  $(1+2Q')$ . If the reluctance of that part of the homopolar flux path that falls outside of the air gap can be neglected, then  $Q'=1$ . Thus the ratio of the largest to smallest unbalanced magnetic pull possible is 3.

The other extreme case,  $Q'=0$ , occurs if in some way the reluctance is increased (thus nearly eliminating the homopolar

flux). For instance, a nonmagnetic end frame or nonmagnetic rings surrounding the bearings will cause sizable reluctance increases. If  $Q'$  approaches zero, the pulsations in magnetic pull nearly disappear.

If there is dynamic eccentricity in the induction motor, then two unbalanced magnetic pulls are created from the mixed product of the  $B_p$  spatial fundamental flux density wave, the  $B_{ed}$  heteropolar flux density wave, and the  $B_{edh}$  homopolar eccentricity flux density wave. One pull rotates with angular velocity  $(1-s)\omega_1$  and the other with angular velocity  $(1+s)\omega_1$ . The resultant of the two force waves of equal ordinals acts on the induction motor.

The magnitude of the unbalanced magnetic pull due to dynamic eccentricity is:

$$F_{ed}(t) = \frac{D\pi l}{8\mu_0} B_p^2 \epsilon_d Q \times \sqrt{1 + 2Q' + 2Q'^2 + 2Q'(1+Q') \cos 2s\omega_1 t} \quad (4.78a)$$

Its amplitude pulsates with a frequency twice that of the slip frequency and rotates at rotor speed.

The instantaneous value is given by:

$$f_{ed}(x,t) = F_{ed}(t) \cos [x - (1-s)\omega_1 t] \quad (4.78b)$$

The ratio of the largest to smallest value of the unbalanced magnetic pull due to dynamic eccentricity is  $(1+2Q')$ , just as with the static eccentricity force. The earlier remarks about pull ratios and means of reduction or elimination apply in the same way.

It must be noted that the expressions above do not give the magnitude of the unbalanced magnetic pull in the machine with high precision. On the one hand, it is usually overestimated because the flux reduction effect of saturation is not taken into consideration, nor how the flux density distribution under the tooth arch is affected by the slotting. On the other hand, the force is underestimated because the unbalanced magnetic pull components originating from the interaction of the slot and winding harmonics with larger ordinals are also not considered.

The evaluation of the factor  $Q'$ , the fact that the factor  $Q$  is empirical, and the approximate values of the most important input values (that is, the extent of the static and dynamic eccentricities) all contribute to increased inaccuracy of the calculations. Only the static eccentricity can be measured in the machine as built, and that generally only by disassembly of the motor, but the value of the dynamic eccentricity can usually be measured only indirectly. If the extent of specific eccentricity exceeds 0.2 to 0.3, use of only the first term of the permeance wave is definitely inadequate, and the harmonics must be taken into consideration as well.

The deleterious effects of homopolar flux and the resulting unbalanced magnetic pull can be summarized as follows.

1. Homopolar flux is created in two-pole machines by eccentricity. This flux is a shaft flux and can lead to shaft stresses.
2. The amplitude of certain mmf waves oscillates with frequency  $2sf_l$  due to the homopolar flux, which causes

low-frequency modulation of the motor's noise near the nominal speed of the motor. (This is most frequently noticeable at no load.)

3. In a parallel branch stator winding, the fields due to eccentricity induce voltages that create circulating currents.
4. The unbalanced magnetic pull originating from eccentricity tries to bend the shaft so that the extent of eccentricity and unbalanced magnetic pull continues to grow. This self-excitation effect, especially in the case of flexible shafts, can cause the rotor to rub the stator bore surface and do serious damage.
5. Since an increase in eccentricity leads to an increase in the deflecting force on the shaft, the phenomenon can be represented by a spring with a negative characteristic; the mechanical spring constant of the shaft decreases, thus decreasing the critical angular frequency of the shaft in the bending mode.

The critical angular frequency due to the mechanical properties of the rotor and to the unbalanced magnetic pull is:

$$\Omega_{\text{crit}} = \sqrt{\frac{C_{\text{mech}} + C_{\text{magn}}}{m_2}} \quad (4.79)$$

where:

$C_{\text{mech}}$  = the mechanical spring constant of the shaft in the bending mode, with the units  $\text{N}\cdot\text{cm}^{-1}$ . (This constant is the ratio of the weight of the rotor to the sag caused by the weight.)

$C_{\text{magn}}$  = the magnetic spring constant, in  $\text{N}\cdot\text{cm}^{-1}$ . The constant is the negative of the ratio of the eccentricity  $\varepsilon\delta$  to the constant term in the unbalanced magnetic pull.

$m_2$  = rotor mass in kg.

The change (measured in percent) in the critical angular frequency because of eccentricity is:

$$100(1 - \sqrt{1 + C_{\text{magn}}/C_{\text{mech}}})$$

Not only does the amplitude of the unbalanced magnetic pull pulsate as a result of the force waves whose existence follows from the flux density components of Eq. 4.75, but another force is present when both static and dynamic eccentricity exist at the same time. This force appears from the mixed products of  $B_{\text{esth}}B_{\text{ed}}$  and  $B_{\text{es}}B_{\text{edh}}$ . It is a four-pole force wave with angular velocity  $(1-s)\omega$ , and an amplitude which pulsates with a frequency which is twice slip frequency. The equation for this force wave is:

$$f_{\text{esd}}(x,t) = \frac{D\pi l}{8\pi_0} B_p^2 \varepsilon_s \varepsilon_d Q Q' \sqrt{5 + 4 \cos(2s\omega t)} \times \cos[2x - (1-s)\omega t] \quad (4.80)$$

If the homopolar flux is eliminated, this force wave will of course disappear.

#### 4.1.7 Tangential Forces Caused by Harmonics

According to the Biot-Savart law, tangential forces are created due to the interaction of the flux density waves of the air gap

and currents along the periphery of the rotor. The tangential force wave acting on a unit surface area of the bore can be expressed as:

$$p_{\text{tg}}(x,t) = \sum_{\mu} \sum_{\lambda} b_{\mu}(x,t) a_{\lambda}(x,t) \quad (4.81)$$

where:

$b_{\mu}(x,t) = B_{\mu} \cos(\mu px - \omega_{\mu} t - \psi_{\mu})$ , and is one component of the spatial flux density harmonics of the stator  
 $a_{\lambda}(x,t) =$  one component of the rotor current

The relationship between the spatial flux density waves of the rotor and the current of the rotor is:

$$a_{\lambda}(x,t) = \frac{2\delta \partial b_{\lambda}(x,t)}{\mu_0 \partial x} \quad (4.82)$$

where:

$b_{\lambda}(x,t) = B_{\lambda} \cos(\lambda px - \omega_{\lambda} t - \psi_{\lambda})$ , and is one component of the spatial flux density harmonics of the rotor

$\delta$  = the length of the air gap

Substituting the values of  $b_{\mu}$  and  $a_{\lambda}$ , Eq. 4.81 becomes:

$$p_{\text{tg}}(x,t) = - \sum_{\mu} \sum_{\lambda} \frac{2p\lambda B_{\mu} B_{\lambda}}{\mu_0 D} \sin(\lambda px - \omega_{\lambda} t - \psi_{\lambda}) \times \cos(\mu px - \omega_{\mu} t - \psi_{\mu}) \quad (4.81')$$

Using well-known trigonometric identities, this becomes:

$$p_{\text{tg}}(x,t) = - \sum_{\mu} \sum_{\lambda} \frac{p\lambda B_{\mu} B_{\lambda}}{\mu_0 D} \sin(r_{\text{tg}} x - \omega_{\text{tg}} t - \psi_{\text{tg}}) \quad (4.81'')$$

where:

$$r_{\text{tg}} = p(\lambda_j \pm \mu_i)$$

$$\omega_{\text{tg}} = \omega_{\lambda_j} \pm \psi_{\mu_i}$$

$$\psi_{\text{tg}} = \psi_{\lambda_j} \pm \psi_{\mu_i}$$

Comparing Eqs. 4.70 and 4.81'', it can be seen that the mode numbers, angular frequencies, and phase angles of the radial and tangential force waves are equal; that is, the tangential vibration spectrum due to force waves is the same as that for radial vibrations. On comparing the amplitudes of the two force waves, it will be seen that the amplitude of the tangential force wave is  $2p\lambda\delta/D$  times that of the radial. For usual dimensions, this ratio is much smaller than 1. Thus the tangential vibrations are usually much smaller than the radial vibrations.

##### 4.1.7.1 Parasitic Torques

By multiplying the expression for the tangential force wave acting on a unit surface area of the bore (Eq. 4.81) by the differential element of surface area  $lR dx$ , a differential force is obtained. Then, multiplying by the radius  $R=D/2$ , the differential torque is obtained. That is:

$$dT = \left( - \sum_{\mu} \sum_{\lambda} b_{\mu}(x,t) a_{\lambda}(x,t) dx \right) lR^2 \tag{4.83}$$

On substituting the expressions for  $b_{\mu}$  and  $a_{\lambda}$ , the torque is given by the integral equation:

$$T = - \sum_{\mu} \sum_{\lambda} \frac{pDl\lambda\delta B_{\mu}B_{\lambda}}{4\mu_0} \int_0^{2\pi} \sin(r_{ig}x - \omega_{rig}t - \psi_{rig}) dx \tag{4.84}$$

where  $l$  is the length of the rotor.

The torque will be zero for every nonzero value of  $r_{ig}$ . If the absolute value of the ordinals of the space harmonics for the stator and the rotor are equal [ $|\lambda|=|\mu|$ ], then  $r_{ig}=0$ , and the integral of Eq. 4.84 is nonzero. The torque developed is referred to as a parasitic torque. There are two types of parasitic torques.

The angular velocity of a spatial harmonic of the stator in a stationary coordinate system is constant and depends on the line frequency, the number of pole pairs, and the ordinal of the harmonic. The velocity is:

$$\Omega_{\mu} = \frac{\omega_1}{\mu p}$$

In addition the angular velocity of a spatial harmonic of the rotor depends on the speed of the rotor in the stationary coordinate system, yielding:

$$\Omega_{\lambda} = \frac{\omega_1[(\lambda - 1)(1 - s) + 1]}{\lambda p}$$

If the two angular velocities are equal at a given speed, the rotor will develop a torque with magnitude  $pD\pi l\lambda\delta B_{\mu}B_{\lambda}/(2\mu_0)$ . The rotor will “crawl” at this speed if the torque magnitude exceeds that normally developed by the rotor at the “synchronous crawling” speed. At other speeds, the pulsating torque acts in the induction motor with angular frequency  $(\omega_{\lambda}+\omega_{\mu})$  and the amplitude of the torque pulsation is the same as that for synchronous parasitic torque.

If  $p=2$  and  $S_1=24$ , the definition of  $\mu$  below Eq. 4.31 yields 13 as one value of  $\mu$ . If  $S_2$ , the number of slots in the rotor, is 28, the expression  $\lambda=(gS_2/p)+1$  with  $g=-1$  yields  $-13$ . That is, one condition for creating torque, that of equality of the number of pairs of poles on stator and rotor, is thereby satisfied.

The equation:

$$\frac{\omega_1}{\mu p} = \frac{\omega_1}{\lambda p} [(\lambda - 1)(1 - s) + 1]$$

that describes the equality of the angular velocities of the harmonics, is satisfied if  $s=6/7$ . That is, at 1/7 of the synchronous speed of the fundamental ( $n=n_0/7$ ), synchronous crawling will develop, as seen in Fig. 4.46. Certain kinds of loads will prevent the rotor from exceeding this speed when accelerating. An example is the load presented by an inclined conveyor belt with materials on the belt. This kind of load requires a torque nearly independent of speed.

If the spatial harmonics of the stator and rotor, besides having the same number of pairs of poles ( $\mu=\lambda$ ), rotate with the same angular velocity independent of the actual speed ( $\Omega_{\mu}=\Omega_{\lambda}$ ), then asynchronous parasitic torque results and asynchronous crawling develops, with a torque magnitude of:

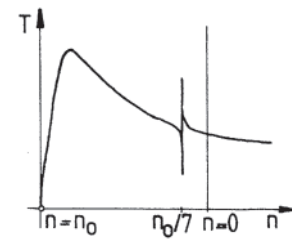


**Figure 4.46** Effect of a synchronous-type parasitic torque on the normal speed-torque curve of a machine.

$$\frac{pD\pi l\lambda\delta B_{\mu}B_{\lambda}}{2\mu_0} \cos(\psi_{\lambda} \pm \psi_{\mu})$$

The physical explanation for this phenomenon is as follows: the  $\mu$ th spatial harmonic of the stator flux density acts as if there were a winding of  $\mu p$  pairs of poles on the stator, which is supplied at frequency  $f_1$ . The angular velocity of the resulting rotating field is  $\Omega_{\mu}=\omega_1/(\mu p)$ . The squirrel-cage rotor has no definite number of poles and tries to reach angular velocity  $\Omega_{\mu}$ .

The ordinal of the currents induced by the  $\mu$ th harmonic of the stator is  $\lambda=(gS_2/p)+\mu$ . If  $g=0$  (that is, the spatial fundamental of these currents), the ordinal of the rotor harmonic is  $\lambda=\mu$ . From previous equations, the angular frequency of the rotor harmonic is:

$$\omega_{\lambda} = \omega_1 \left( \frac{gS_2}{2} (1 - s) + 1 \right) = \omega_1 \quad (\text{at } g = 0)$$

The rotating angular velocity of the harmonic of the rotor is  $\Omega_{\lambda}=\omega_1/(\lambda p)$ ; that is, the condition  $\Omega_{\mu}=\Omega_{\lambda}$  is fulfilled.

The shape of the asynchronous parasitic torque-speed curve is similar to that of the torque-speed curve due to the fundamental flux wave. The synchronous speed is different, and the magnitude of the torque is decreased by the factor  $1/\mu^2$ . In Fig. 4.47 the torque-speed curve of the first two spatial harmonics of the stator (those for  $\mu=-5$  and for  $\mu=7$ ) are shown. There are “saddles” on the resultant torque-speed curves that are again able to prevent the motor from reaching normal running speed with certain kinds of loads.

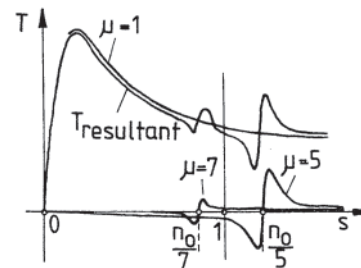


**Figure 4.47** Effect on the speed-torque curve of the asynchronous parasitic torques due to the sixth and seventh stator spatial flux density harmonics.

Asynchronous crawling caused by the seventh harmonic is, for instance, capable of preventing the motor from accelerating beyond one-seventh of the fundamental synchronous speed, the slip being

$$s_{\mu} = \frac{n_0 \pm n_0/\mu}{n_0} = 1 \pm \frac{1}{\mu} = 1 - \frac{1}{7} = 0.86$$

Asynchronous crawling is most likely to occur in the case of unskewed squirrel-cage motors. It is well known that by using short pitch windings in the stator or by proper skewing of the rotor slots, the largest spatial harmonics of the stator will decrease to nearly zero. Asynchronous crawling does not ordinarily disturb the running up of induction motors with wound rotors and slip rings, because adequate accelerating torque is usually ensured as a result of shifting the maximum torque point to lower speeds by use of external resistors in the rotor circuit.

#### 4.1.8 Components of Air Gap Flux Caused by Inverter Supplies

Rapid development of electronics has made it possible to solve more and more controlled drive problems with semiconductor controls. Induction motor drives with inverters for changing frequency are especially important, uniting the advantage of control technology with the simple, robust, and service-free construction of induction motors. But the application of inverters brings with it the complication that the voltage output of the inverter, while periodic in time, is not a simple sinusoid.

The supply voltage can be expanded into a time-dependent Fourier series. Thus it can be modeled by the superposition of the fundamental and its harmonics as a three-phase voltage supply connected to the motor. The voltages at different frequencies act simultaneously on the motor and cause several unfavorable side effects. For instance, the motor's losses, vibration, and noise will increase, and unfavorably large torque oscillations will appear.

The time-dependent Fourier series of the voltage supplied to the stator winding is:

$$u(t) = \sum_v U_v \cos v \omega_1 t \quad (4.85)$$

For symmetry reasons, the ordinal of the harmonics is  $v = 6k+1$  (where  $k=\pm 1, \pm 2, \dots$ ). However, if back-to-back semiconductor pairs are in series with each of the phase windings, one being a thyristor and the other a diode, then harmonics of ordinal  $v=3k+1$  are also created.

In steady state, the amplitude of the  $v$ th current harmonic is determined by the impedance  $Z_v$ . for angular frequency  $v \omega_1$ :  $I_v = U_v / Z_v$ . Keeping in mind that the harmonic voltages create symmetric three-phase voltage systems, to determine the harmonic impedance  $Z_v$  of the motor the same equivalent circuit is used as for the fundamental except that the slip  $s$  for the  $v$ th harmonic (at frequency  $v f_1$ ) is:

$$s_v = \frac{v\Omega_0 - \Omega}{v\Omega_0} = 1 - \frac{1}{v} \frac{\Omega}{\Omega_0}$$

The second term of this expression tends toward zero very quickly due to the  $1/v$  factor. Thus, apart from the first two

harmonics, it can be said with good approximation that  $s_v \cong 1$ . The harmonic currents flow in the stator winding of  $p$  pairs of poles. Every harmonic develops its own space fundamental and harmonics, just as the fundamental with frequency  $f_1$  does.

The amplitude of the time harmonics is smaller than that of the fundamental. Taking into consideration the fact that the amplitude of the force wave depends on the square of the voltage, the space harmonics resulting from the time harmonics have to be considered only if the amplitudes of the time harmonics are greater than 70% of the fundamental. If the amplitude of the time harmonics is greater than 30% and less than 70% of the fundamental, then the space harmonics due to the time harmonics can be neglected as secondary components. But If the amplitude of the time harmonics is greater than 30% of the fundamental, even the space fundamental wave of the time harmonic may be neglected.

The Fourier-series of the spatial fundamental of the flux density waves created by the time fundamental and harmonics of the supply is:

$$b_{pv}(x,t) = \sum B_{pv} \cos(px - v\omega_1 t - \psi_v) \quad (4.86)$$

The phase angle  $\psi_v$  is, with good approximation,  $\pi/2$ .

The Fourier series of the instantaneous values of the spatial harmonics of the flux density created by the time fundamental and harmonics of the supply is:

$$b_{\mu}(x,t) = \sum_{\mu} B_{\mu} \cos(\mu px - v\omega_1 t - \psi_{\mu}) \quad (4.87)$$

Just as with the stator, space fundamental and harmonic flux density waves are created on the rotor as well, which together with the slotting harmonics have a Fourier series as follows:

$$b_{\lambda}(x,t) = \sum_{\lambda} B_{\lambda} \cos(\lambda px - \omega_{\lambda} t - \psi_{\lambda}) \quad (4.88)$$

where:

$$\lambda = \left( \frac{gS_2}{p} \right) + 1 \text{ is the ordinal}$$

$$\omega_{\lambda} = \omega_1 \left( \frac{gS_2}{p} (1 - s) + v \right) \text{ is the angular frequency}$$

These waves are created by the voltages induced in the rotor winding by the stator's temporal fundamental and harmonic flux density waves.

The rotor's space flux density harmonics due to eccentricity are

$$b_{\lambda e}(x,t) = \sum_{\lambda e} B_{\lambda e} \cos(\lambda_e px - \omega_{\lambda e} t - \psi_{\lambda e}) \quad (4.89)$$

where:

$$\lambda_e = \frac{gS_2}{p} + 1 \pm \frac{1}{p}$$

$$\omega_{\lambda e} = \omega_1 \left( \frac{gS_2}{p} (1 - s) + v \pm \frac{1 - s}{p} \right)$$

Based on the equality of the ordinals, the flux density waves detailed above can be grouped in the following way:



$$b(x,t) = \sum_{\nu} b_{p\nu} + \sum_{\mu} b_{\mu} + \sum_{\lambda} b_{\lambda} + \sum_{\lambda e} b_{\lambda e} \quad (4.90)$$

Maxwell’s tensile stress expression uses the square of the flux density. Thus, as with Eq. 4.69, the force waves can be calculated. After listing the squares of all the possible terms and all of the mixed products, the set of exciting force waves from Eq. 4.90 may be compared with the set of exciting force waves developed due to a sinusoidal supply, leading to the following conclusions.

1. New mode numbers cannot be found; that is, the set of exciting force wave mode numbers does not expand.
2. The number of exciting force waves and the number of their frequencies will be greater if an inverter is used to supply the motor, although the set of mode numbers of the exciting forces remains unchanged.

Because the supply is rich with time harmonics, parasitic torques will develop in induction motors supplied by inverters. These torques are usually much larger than the pulsating torques created by space harmonics. The space fundamental of all the time harmonics has an ordinal  $p$ : in other words, the condition for creating torque—an equal number of pairs of poles—is satisfied.

Since the ordinal of the time harmonics is given by  $\nu = 6k+1$ , the frequency of the pulsation in torque is  $6kf_1$ . The largest of the torques is that due to the interaction of the lowest harmonic and the fundamental (that is,  $k=1$ ). This torque can be as much as 20% of the nominal torque of the machine.

A large number of inverters have an intermediate direct current link between the rectifier on the supply side and the inverter, as shown in Fig. 4.48. The rectified voltage is not smooth, and hence harmonic currents flow in the direct current link also. New torque oscillations arise from these harmonics in the induction motor, thus further disturbing the ideal torquespeed curve of the motor. The amplitudes and frequencies of the oscillations of torque developed by a simple inverter supply (no pulse-width modulation) are listed in Table 4.2.

The torque oscillations usually affect the performance of the motor most at no load or at light loads because the useful torque is very small under those conditions. Hence the oscillating torques are relatively quite large. Under load, the amplitudes of the oscillating torques do not change. Because the useful torque

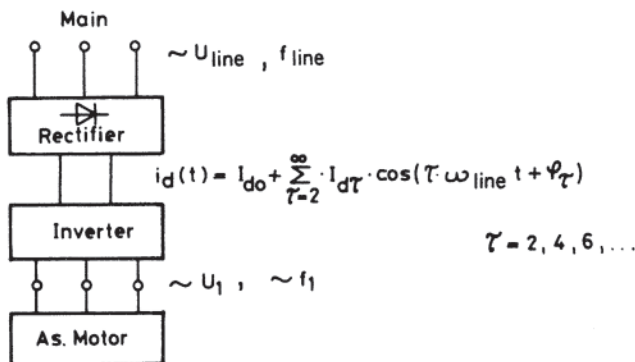


Figure 4.48 Harmonic currents due to the intermediate direct-current circuit.

Table 4.2 Torque Oscillations with an Inverter Supply

Peak value	Frequency
$1.83 p L_m I_{d0} \hat{I}_{d\tau} \frac{1}{s\omega_1 T_{r0} + (1/s\omega_1 T_{r0})}$	$\tau f_{line}$
$\frac{\hat{U}_1^2}{\omega_1^2} \frac{1}{L_r} \left( \frac{1}{(6k-1)^2} - \frac{1}{(6k+1)^2} \right)$	$6kf_1$
$\frac{\hat{U}_1^2}{\omega_1^2} \frac{1}{L_r} \left( \frac{1}{(6k-1)^2} - \frac{1}{(6k+1)^2} \right) \frac{\hat{I}_{d\tau}}{2I_{d0}}$	$6kf_1 \pm \tau f_{line}$

- $p$  = number of pole pairs of the motor
- $L_m$  = magnetizing inductance of the motor,  $L_m = X_m/\omega_1$
- $L_r$  = leakage inductance of the motor  $L_r = (X_{ls} + X_{lr})/\omega_1$
- $I_{d\tau}$  = direct current flowing in the intermediate direct-current circuit
- $\hat{I}_{d\tau}$  = peak value of the  $\tau$ th harmonic current in the intermediate direct current circuit
- $s$  = slip
- $\omega_1$  = angular frequency of the fundamental voltage of the motor
- $\hat{U}_1$  = peak value of the fundamental voltage of the motor
- $T_{r0} = L_m + \frac{L'_{lr}}{R'_r}$
- $R'_r$  = the rotor circuit resistance of the motor referred to the stator
- $\tau$  = the ordinal of the harmonic current caused by the rectifier in the intermediate direct current circuit ( $\tau = 2, 4, 6, \dots$ )
- $k = \pm 1, \pm 2, \pm 3, \dots$

increases with load, the relative effect of the torque oscillations decreases.

The torque oscillations due to time harmonics can be decreased and certain components can be eliminated by use of optimized pulse-width modulation in the inverter. Thus, the creation of the most trouble some time harmonics can be prevented. In addition, the harmonics resulting from the rectification process may be filtered out in the direct-current link.

### 4.1.9 Switching Transients

Various transient conditions develop in an induction motor when starting the motor from rest. In order to separate the conditions in the motor from those which may occur in the supply, an infinite bus is assumed. Several different phenomena will be found, briefly summarized as follows.

1. The stator current will have the following components:
  - a. A direct current component that decays quickly, but which increases the peak value of the alternating current in the first few cycles.
  - b. A large short-circuit alternating current (inrush current) that decreases continuously during rotor run-up. Its decrease as a function of time is usually slower by at least one order of magnitude than the direct current of (a).
  - c. The phase angle between the phase current and the phase voltage changes continuously during run-up.
2. The following components will appear in the electromagnetic torque:

- a. Transient torques of short duration with alternating and direct components due to the unidirectional flux created when connecting the motor to the supply.
  - b. The electromagnetic torque of the motor changes during running-up, following the torque-speed curve.
  - c. Asynchronous and synchronous parasitic torques appear, caused by the spatial harmonic flux density waves.
3. New components appear in the radial harmonic forces of the induction motor due to the direct current created at switching on.
  4. During running-up, there will be local maximum points in vibration and noise because the frequencies of the mmfs, which change dynamically during acceleration, will temporarily coincide with resonant frequencies of the mechanical system of the machine. These phenomena are discussed in more detail in Section 4.7.2.

The eight transient phenomena listed above may be separated into three groups. The phenomena of the first group are those that are present throughout the running-up period. This group consists of the phenomena described in (1.b), (1.c), and (2.b). The parameters associated with these phenomena are in constant change. The time duration of these changes depends on the size of the machine and the loading during run-up. Hence their duration will extend from as little as a few hundred milliseconds to as much as several seconds. Because of the relatively long duration of these transients, they may be referred to as quasi-stationary phenomena.

The phenomena of the second group are those of (1.a), (2.a), and (3). These appear immediately after connecting to the line. Their time duration is very short, shorter than 100 ms. These phenomena are the actual switching-on transients.

The phenomena of the third group, (2.c) and (4), are those that appear for only a short time during acceleration, after which they disappear. These are called the transients of running-up.

#### 4.7.9.1 Currents

The Park-vector form of the voltage equations for the stator and the rotor in a stationary coordinate system is:

$$\bar{u}_s = \bar{i}_s R_s + \frac{d\bar{\Lambda}_s}{dt} = \bar{U}_s e^{j\omega_1 t} \quad (4.91a)$$

$$\bar{u}_r = \bar{i}_r R_r' + \frac{d\bar{\Lambda}_r}{dt} = 0 \quad (4.91b)$$

where:

- $\bar{u}_s, \bar{u}_r$  = the Park-vectors of the stator and rotor voltages
- $\bar{i}_s, \bar{i}_r$  = the Park-vectors of the stator and rotor currents
- $R_s$  and  $R_r'$  = the ohmic resistances of the stator and rotor winding
- $\bar{\Lambda}_s$  and  $\bar{\Lambda}_r$  = the flux linkages of the stator and rotor

The flux linkages may be expressed using self- and mutual inductances and the currents as:

$$\bar{\Lambda}_s = (L_m + L_{ls}) \bar{i}_s + L_m \bar{i}_r \quad (4.92a)$$

$$\bar{\Lambda}_r = (L_m \bar{i}_s + (L_m + L_{lr}') \bar{i}_r \quad (4.92b)$$

where:

- $L_m$  = the magnetizing inductance
- $L_{ls}$  and  $L_{lr}'$  = the leakage inductances of the stator and of the rotor (referred to the stator)

Substituting Eqs. 4.92a and 4.92b into Eqs. 4.91a and 4.91b, differential equations for the currents follow:

$$\bar{i}_s R_s + \frac{d}{dt} (L_m \bar{i}_s + L_{ls} \bar{i}_s + L_m \bar{i}_r) = \bar{U}_s e^{j\omega_1 t} \quad (4.91a\bullet)$$

$$\bar{i}_s R_r' + \frac{d}{dt} (L_m \bar{i}_s + L_m \bar{i}_r + L_{lr}' \bar{i}_r) = 0 \quad (4.91b\bullet)$$

Solving these inhomogeneous differential equations, the short-circuit currents of the stator  $\bar{i}_s$  and of the rotor  $\bar{i}_r$  are obtained, as shown in Fig. 4.49. The circle diagram for the conventional equivalent circuit is also shown in that figure.

During the transient investigation, it may be presumed that because the time constant of the electromagnetic transients is much smaller than that of the mechanical transients, the electromagnetic transients disappear while the rotor is still at standstill. The so-called free direct currents (which decay exponentially) arise from the solution of Eqs. 4.91a and 4.91b, starting at  $t=0$ , the time of connection to the supply. The complete solution of the differential equations is:

$$\bar{i}_s = \bar{I}_s e^{j\omega_1 t} + \bar{A}_0 e^{-t/T_a} + \bar{B}_0 e^{-t/T_b} \quad (4.93a)$$

$$\bar{i}_r = \bar{I}_r e^{j\omega_1 t} + \bar{A}_0 e^{-t/T_a} - \bar{B}_0 e^{-t/T_b} \quad (4.93b)$$

In these equations:

$$\bar{A}_0 = -\frac{\bar{I}_s + \bar{I}_r}{2} \quad \text{and} \quad \bar{B}_0 = \frac{\bar{I}_r - \bar{I}_s}{2}$$

are the free direct currents, and:

$$T_a = L_m \left( \frac{1}{R_s} + \frac{1}{R_r'} \right) \quad \text{and} \quad T_b = \frac{L_{ls} + L_{lr}'}{R_s + R_r'}$$

are the time constants.

The free direct currents  $\bar{A}_0$  and  $\bar{B}_0$  are shown in Fig. 4.49. With typical machine parameters,  $|\bar{A}_0| \ll |\bar{B}_0|$ , and as a first approximation one may set  $\bar{A}_0=0$  and  $\bar{B}_0 = \bar{I}_s$ . Examination of the equations for the time constants shows that  $T_a \gg T_b$ . That is, even though the free current  $\bar{B}_0$  is much larger than  $\bar{A}_0$ , it disappears much more rapidly.

If the Park-vector of the supply voltage has an angle  $\alpha$  with respect to the positive real axis at the moment of switching on, then the expression for the Park-vector of the current in the stator is the following:

$$\begin{aligned} \bar{i}_s = & \bar{I}_s \exp [j(\omega_1 t + \alpha - \phi_{sc})] \\ & - \bar{I}_s \exp [j(\alpha - \phi_{sc})] \exp (-t/T_b) \end{aligned} \quad (4.94a)$$

where  $\phi_{sc}$  = the phase angle between the stator short circuit current and the supply voltage.

Rewriting Eq. 4.94 into harmonic form, the time function of the phase current after a switching-on is:

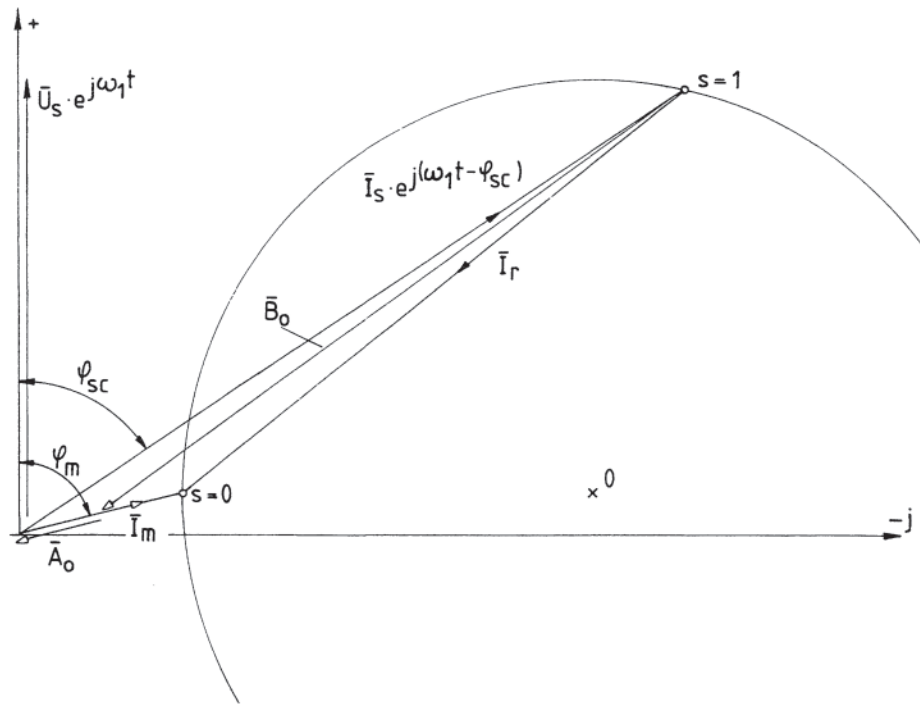


**Figure 4.49** The free direct-current components  $\bar{A}_0$  and  $\bar{B}_0$  of Eqs. 4.93a and 4.93b.

$$i_{sa}(t) = \hat{I} \cos(\omega_1 t + \alpha - \phi_{sc}) - \hat{I}_s \cos(\alpha - \phi_{sc}) e^{-t/T_b} \tag{4.94b}$$

These currents appear in Fig. 4.50, where the time constant  $T_b$  is typical of fractional-horsepower induction motors and the notation  $\hat{I}$  indicates the peak current.

4.1.9.2 Torques

The electromagnetic torque may be calculated from the vectorial product of the flux linkage and the current Park-vectors, yielding:

$$T = \frac{3}{2} \bar{\Lambda}_s \times \bar{i}_s = \frac{3}{2} (L_m + L_{is}) \bar{i}_s \times \bar{i}_s + \frac{3}{2} L_m \bar{i}_r \times \bar{i}_s \tag{4.95}$$

The first term of the torque expression is zero because the product  $\bar{i}_s \times \bar{i}_s$  is also zero. The following four components of torque may be calculated by substituting the stator and rotor currents of Eqs. 4.93a and 4.93b into Eq. 4.95 for the

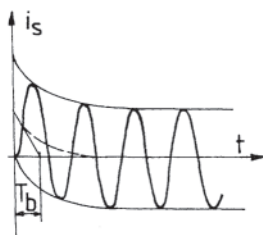


**Figure 4.50** Current in one phase in a fractional-horsepower induction motor after switching-on with the rotor at standstill.

electromagnetic torque. The torque components below are shown in Fig. 4.51.

The product of the alternating current components gives the starting torque:

$$T_1 = T_{st} = \frac{3}{2} L_m (\bar{i}_r e^{j\omega_1 t}) \times (\bar{i}_s e^{j\omega_1 t}) = \frac{3}{2} L_m \bar{i}_r \times \bar{i}_s \tag{4.96}$$

The product of the free direct current is:

$$T_2 = \frac{3}{2} L_m (\bar{A}_0 e^{-t/T_a} - \bar{B}_0 e^{-t/T_b}) \times (\bar{A}_0 e^{-t/T_a} + \bar{B}_0 e^{-t/T_b}) \tag{4.97a}$$

Substituting the expressions for the free direct currents into Eq. 4.97 and putting the starting torque into the expression for  $T_2$  as well,  $T_2$  becomes:

$$T_2 = T_{st} \exp[-t(T_a^{-1} + T_b^{-1})] \tag{4.97b}$$

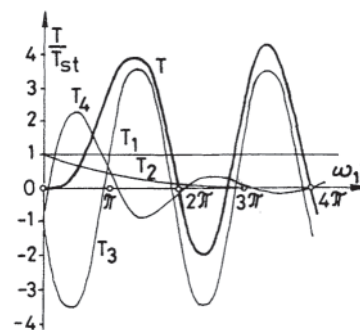


**Figure 4.51** Torque components in a motor after switching-on with the rotor at standstill.

The torque corresponding to this expression decays without oscillations, as shown in Fig. 4.51. Considering the relative magnitudes of  $T_a$  and  $T_b$ , a good approximation to  $T_2$  is:

$$T_2 = T_{st} e^{-t/T_b} \quad (4.97c)$$

From the product of the alternating currents and the free direct current  $\bar{A}_0$ , torque component  $T_3$  is found to be:

$$T_3 = \frac{3}{2} L_m \bar{A}_0 \times (\bar{I}_s - \bar{I}_r) e^{j\omega_1 t} e^{-t/T_a} \quad (4.98a)$$

Substituting for the currents and rearranging:

$$T_3 = -\frac{T_{st}}{\cos\phi_{sc}} \cos(\omega_1 t - \phi_{sc}) e^{-t/T_a} \quad (4.98b)$$

This component of torque alternates with line frequency  $f_1$  and decays with the rather large time constant  $T_a$ . In medium-horsepower induction motors,  $T_a$  is on the order of 100 to 150 ms. The magnitude of  $T_3$  is also large, as much as twice that of the starting torque. Hence, this oscillating torque component has a sizable effect on the running-up of the motor.

The fourth torque component is obtained by multiplying the free direct  $\bar{B}_0$  current and the alternating currents:

$$T_4 = \frac{3}{2} L_m [(\bar{I}_s + \bar{I}_r) e^{j\omega_1 t}] \times [\bar{B}_0 e^{-t/T_b}] \quad (4.99a)$$

Expanding the equation for  $T_4$  and neglecting small terms, it can be shown that a good approximation is:

$$T_4 = -\frac{T_{st}}{\cos\phi_{sc}} \cos(\omega_1 t - \phi_{sc}) e^{-t/T_b} \quad (4.99b)$$

Although the magnitude of the  $T_4$  component is as large as that of  $T_3$ ,  $T_4$  does not cause problems in practice because it decays rapidly as a result of the small time constant  $T_b$ .

Figure 4.51 shows the four torque components and their sum, the torque  $T$ . Note that  $T$  is zero at the moment of connecting the motor to the supply ( $t=0$ ). Torque components  $T_2$  and  $T_4$  decay rapidly, while components  $T_1$  and  $T_3$  decay slowly. If the rotor of the motor remains blocked after  $t=0$ , the time function of the torque is:

$$T(t) = T_{st} \left( 1 - \frac{\cos(\omega_1 t - \phi_{sc})}{\cos\phi_{sc}} e^{-t/T_a} \right) \quad (4.100)$$

It is the mean value of the electromagnetic torque that, in practice, causes the motor to accelerate. During running-up, the magnitudes of the stator and rotor currents decrease, and the phase angle between them changes. Thus, in Eq. 4.100, the electromagnetic torque for the slip at any point in time must be used instead of  $T_{st}$ . As a consequence, the torque oscillations decay faster than they would with a blocked rotor.

#### 4.1.9.3 Effects of Harmonics

In the foregoing, it has been assumed that the stator current, the rotor current, and the free direct currents in the machine exist in the form of their space fundamentals. When examining the transients of the harmonic force and torque waves, the space harmonics must be taken into consideration. The resultant mmf of the induction motor should be written as follows:

$$\bar{F}_m(x,t) = \bar{F}_{mp}(x,t) + \bar{F}_{m\mu}(x,t) + \bar{F}_{m\lambda}(x,t) + \bar{F}_{mdc}(x,t) \quad (4.101)$$

where:

- $\bar{F}_{mp}$  is the fundamental mmf due to the currents  $\bar{I}_s$  and  $\bar{I}_r$ ,
- $\bar{F}_{m\mu}$  is the Fourier series of the space harmonics of the mmf of the stator (shown in more detail in Eq. 4.29)
- $\bar{F}_{m\lambda}$  is the Fourier series of the space harmonics of the mmf of the rotor (see Eq. 4.34)
- $\bar{F}_{mdc}$  is the Fourier series of the fundamental and harmonics of the mmf due to the free direct currents.

The Fourier series of the direct current mmf components in detail is:

$$\begin{aligned} \bar{F}_{mdc}(x,t) = & \sum_{\mu} F_{ma\mu} e^{-t/T_a} \cos(\mu p x - \phi_m) \\ & + \sum_{\mu} F_{mb\mu} e^{-t/T_b} \cos(\mu p x - \phi_t) \\ & + \sum_{\lambda} F_{ma\lambda} e^{-t/T_a} \cos(\lambda p x - \phi_m) \\ & - \sum_{\lambda} F_{mb\lambda} e^{-t/T_b} \cos(\lambda p x - \phi_t) \end{aligned} \quad (4.102a)$$

where:

- $\bar{F}_{ma\mu}$  and  $\bar{F}_{mb\mu}$  are the mmfs of the space harmonics in the stator due to the free direct currents  $A_0$  and  $\bar{B}_0$ , and
- $\bar{F}_{ma\lambda}$  and  $\bar{F}_{mb\lambda}$  are the mmfs of the space harmonics in the rotor due to the same currents

Because the mmfs  $\bar{F}_{ma\mu}$  and  $\bar{F}_{ma\lambda}$  are unidirectional and the two distributions are very similar, summing them up with minor approximations yields a result equal to twice  $\bar{F}_{ma\mu}$ . The terms  $\bar{F}_{mb\mu}$  and  $\bar{F}_{mb\lambda}$  cancel each other in the resultant mmf (see Eq. 4.93.) Thus, with good approximation:

$$\bar{F}_{mdc}(x,t) = \sum_{\mu} F_{ma\mu} e^{-t/T_a} \cos(\mu p x - \phi_m) \quad (4.102b)$$

If the eccentricity and saturation harmonics are neglected, the permeance of the magnetic circuit can be written in the form:

$$\bar{G}_m(x,t) = G_{m0} + \bar{G}_{m\mu}(x) + \bar{G}_{m\lambda}(x,t) \quad (4.34\bullet)$$

The product of the mmf and the magnetic permeance gives the air gap flux density, as in Eq. 4.40. Those flux density waves that do not originate from the free direct currents have already been discussed. The goal of the present investigation is to see the effect of the free direct currents; thus only the flux density waves originating from the decaying direct currents  $\bar{A}_0$  and  $\bar{B}_0$  will be detailed:

$$\bar{B}_{dc}(x,t) = \bar{F}_{mdc}(x,t) [G_{m0} + \bar{G}_{m\mu}(x)] \quad (4.103a)$$

Substituting the expressions for mmf and for magnetic permeance and by reducing the winding and slotting waves:

$$\bar{B}_{dc\mu}(x,t) = \sum_{\mu} B_{dc\mu} e^{-t/T_a} \cos(\mu p x - \phi_m) \quad (4.103b)$$

The resultant air gap flux density can be written as the sum of several flux density groups:

$$\bar{B}(x,t) = \bar{B}_p(x,t) + \sum_{\mu} \bar{B}_{\mu}(x,t) + \sum_{\lambda} \bar{B}_{\lambda}(x,t) + \sum_{\mu} \bar{B}_{dc\mu}(x,t) \quad (4.104)$$

Developing the radial Maxwell's forces in the same manner as in Eq. 4.69 and concentrating attention on the effects of the free direct currents, it will be seen that the supply when switched to the motor at standstill will generate force waves of frequency  $f_1$  as well as the usual radial forces. The amplitudes of these waves will decay with time constant  $T_a$ .

The quasi-stationary currents and torques mentioned in the discussion of the switching-on phenomena will be discussed again in a later chapter, while the parasitic torques mentioned among the accelerating transients are already known. Vibrations due to the running-up transients are discussed in Section 4.7.2.

#### 4.1.9.4 Useful Strategies

The current peak of the switching-on transient and the torque oscillation at line frequency are unfavorable side effects from many points of view. If the phase windings of the three-phase motor are not connected to the supply at precisely the same instant but with a properly chosen time asymmetry, one direct current component can be eliminated. To eliminate the different free direct currents, different switching strategies must be used. If the transient current peak is deemed to be the more unfavorable side effect, then the free direct current  $\bar{B}_0$  has to be eliminated; if the object is to get rid of the oscillating torque at line frequency, then the free direct current  $\bar{A}_0$  has to be eliminated.

In the case of a star-connected stator winding without a neutral return, one possible connection strategy is the following. To eliminate the free direct current  $\bar{B}_0$ , phases  $a$  and  $b$  of the motor are connected simultaneously to the line when the line voltage  $U_{ab}$  is at the angle  $\alpha_1 = \phi_{sc}$  past a zero crossing. ( $\phi_{sc}$  is the phase angle of the short-circuit current of the motor.) Only after this connection is made should phase  $c$  be connected to the supply, and with phase lag  $\alpha_2=90$  degrees. The rationale for this strategy is that transient currents in inductive circuits can be eliminated if the circuit is connected to the supply at a time when the steady-state current is at a natural zerocrossing. Thus the transient current peak disappears from the phase current of the motor.

The free direct current  $\bar{A}_0$  can be eliminated by connecting phases  $a$  and  $b$  simultaneously to the supply when the line voltage  $U_{ab}$  is at an angle  $\alpha_1 = \phi_m$  past a zero crossing. ( $\phi_m$  is the phase angle of the magnetizing current.) The  $c$  phase is then connected to the supply with a phase lag of  $\alpha_2=90$  degrees after the first connection. Because the magnetizing current has a phase angle  $\phi_m = 90$  degrees, the connection strategy can be characterized by  $\alpha_1=90$  degrees with a further phase lag of 90 degrees for  $\alpha_2$ . With this connection strategy, the oscillating torque at line frequency disappears, and the motor will run up more smoothly.

It should be noted that if the asymmetrical connection strategy is not carried out correctly, the value of the transient oscillating torque may be even larger than in the case of simultaneous connection of all three phases to the line, reaching as much as  $k$  times that value, where  $k$  is:

$$k = \sqrt{\cos^2 \alpha_1 + \sin^2 (\alpha_1 + \alpha_2)}$$

In the case of simultaneous connections,  $\alpha_1$  has a random value, but  $\alpha_2$  is zero. Hence  $k=1$ . If the oscillating torque is to be eliminated,  $\alpha_1=\alpha_2=90$  degrees and  $k=0$ . The worst case is that for which  $\alpha_1$  is zero and  $\alpha_2=90$  degrees, yielding  $k = \sqrt{2}$ .

## 4.2 ROTOR CONSTRUCTION

### 4.2.1 Introduction

An overwhelming proportion of induction motors are provided with rotors of squirrel-cage construction. Cage rotors are mechanically robust and relatively inexpensive compared with the phase-wound equivalents. This cost advantage is particularly the case for small machines, where the large price differential is due as much to economies of scale in manufacture as it is to the inherently more complex and costly construction of a wound rotor.

For small ratings (up to 250 kW) the rotor cage will invariably be cast aluminum alloy. In addition to low manufacturing costs, this allows the possibility of specially shaped bars for increased torque and reduced current at starting and low speed, although machines with rotor bars of this type are not common. The use of aluminum rotor conductors results in machines that are slightly larger than would be the case if copper bars were employed; this is due to the higher resistivity of aluminum, the lower current densities thus allowed, and the consequent larger cross-sectional areas required for the rotor bars. Since most stock motors are totally enclosed (i.e., TEFC), the stator current densities and specific electric loadings are also low, which leads to a further increase in core volume relative to drip-proof machines. However, at these ratings, manufacturing costs and operational versatility are more significant than marginal increases in mass, volume, and material cost.

Above approximately 250 kW (depending on voltage), batch production (or manufacture of a single machine) is more usual, and for ratings in excess of 400 kW copper bars are invariably used. There is still scope for modification of the torque/slip characteristics, even though very complex bar shapes cannot now be cast in punched slots, since large and deep bars can be shaped by machining or rolling, and then inserted into slots of appropriate profile. In large sizes a simple deep bar is often adequate; alternatives are sash ("or tee") and taper bars, which enhance the "deep-bar" effect.

Wound-rotor machines are usually manufactured with ratings in excess of 75 kW, although some smaller machines are produced for special applications. For ratings in excess of 150 kW they would normally be single machines or produced in small batches. In large and particularly in low-speed machines, the price differential between wound and cage rotor construction is not significant, the cost of slip rings and brush gear being a relatively minor item, and the benefits that accrue from the use of external resistance for starting are often considered to be well worth any extra cost.

Speed control using slip-power recovery is also possible where access, via slip rings, to a wound rotor is available. Depending upon the speed range, the power semiconductor

equipment can be much less expensive than its equivalent used on the stator.

#### 4.2.2 Squirrel-Cage Design

As on the stator, the magnetic path is provided by laminated silicon steel. For maximum utilization of material, the rotor and stator laminations are usually cut from the same sheet of steel and are often separated only after slot and vent-duct punching is complete. Large-diameter and slow-speed machines are an exception to this rule, segmented laminations being used either on the stator alone or on both stator and rotor.

Neither the use of high-quality material nor lamination is strictly necessary on the rotor for basic operational purposes, particularly at rated speed, but it is much simpler to punch slots in steel laminate than to machine rotors from a solid cylinder. The use of silicon steel does reduce iron losses by a small degree, although not those losses due to slip frequency fluxes in the rotor core but rather, at normal speeds, those associated with the fluxes due to higher-frequency slot harmonics, which are mainly restricted to the air gap surface of the rotor teeth.

The rotor slots are virtually filled with either copper or aluminum rather than by a combination of conductors, air and insulation; thus the rotor slots have a smaller combined cross-sectional area than those on the stator. This reduction in cross-sectional area is also due, in part, to the higher current densities that are allowed on the rotor as a result of superior heat conduction from rotor conductor to rotor core, although the difference is not so marked with aluminum rotors.

The number of rotor slots can be greater or less than on the stator, the number being chosen according to well-established rules [13]. In practice, aluminum rotors tend to have numbers of rotor slots less than on the stators for reasons associated with the die-casting process, whereas the copper rotors of larger machines tend to have numbers of slots in excess of those on the stators, the superior performance that results assuming greater importance at higher ratings. It is also normal practice to skew the rotor slots, typically by one stator slot pitch, the purpose being to attenuate the effects of stator slot harmonics, which produce both parasitic torques and noise. However, with skewed slots, the rotor is a virtual open circuit to induced voltages at the stator slot harmonic frequencies; the corresponding harmonic fluxes become a source of additional rotor iron (or “stray”) loss. Such is the nature of engineering compromise.

The cross-sectional area of the rotor conductors depends on the machine rating, the number of slots and the conductor material. It is, of course, closely associated with the rotor-specific electric loading, which is itself dependent on the methods used for cooling both the rotor and the stator. The procedure for determination of rotor bar cross-sectional area is to balance the ampere-turns of rotor and stator and then design the bar according to the number of slots, the allowable current density, and any special requirements regarding low-speed characteristics.

Given the rotor bar cross-sectional area, the slot shape is then chosen both to produce the desired performance characteristics and, as far as possible, to satisfy manufacturing requirements. These latter include the longevity of punch

presses and punch and die sets and, with aluminum bars, the efficiency of the die-casting process. Both rotor resistance and leakage reactance are important parameters and the latter is especially influenced by slot shape. With small machines, slot shape is itself heavily influenced by manufacturing considerations. Where high starting torque and reduced starting current are deemed essential, double cage and trislot designs are available. These designs are produced in small numbers, and only for special applications. For larger machines, in which copper rotor bars are employed, improved starting performance can be provided by the use of specially shaped bars and slots. Common shapes are sash (or tee), taper, and deep bars.

Insulation between copper, bars, and the steel core is sometimes used to prevent electrical contact and consequent circulating currents between bars via the rotor laminations. Such currents are deemed to reduce performance and increase stray losses. This latter consideration is typical of contemporary trends in machine design and construction that have, probably by coincidence, accompanied globalization. Until relatively recently there were many manufacturing organizations producing broadly similar machines but each with its distinctive design quirks. These often resulted in spectacular improvements in performance under specific conditions (e.g., very high starting and low-speed torque) but almost inevitably led to increased manufacturing cost and, usually, to reduced efficiency or power factor at rated speed. Now there are many fewer manufacturers each producing far more machines but with much less variety. Design rationalization and economies of scale in manufacture are the prime concern and any further emphasis is now upon efficiency, almost all recent design innovation being concentrated upon reduction of losses.

The temperature rise of a cage rotor is not in itself as immediate a problem as for a stator winding. However, because the heat generated in the rotor may have to be removed either by way of the stator or by common cooling fins, as in TEFC machines, it clearly has an important influence on the overall thermal design. In addition, excessive rotor temperatures may damage bearings or, in the extreme, die-cast aluminum rotor bars. With small totally enclosed machines, few special arrangements are made to cool the rotor core or cage, although a small fan, often cast with the end rings and being little more than cooling fin projections from the rotor end rings may be provided for internal air circulation. In the case of the less common small drip-proof designs, an internally mounted fan will draw cooling air through the machine from the local environment and the rotor may well be provided with a number of axial vents.

As machines increase in size and rating, these cooling arrangements become more significant and more sophisticated, with both axial and radial vents being required in the design of most large machines. The design of the fans and the cooling air passages within the machine will also receive much more attention during the design stage.

#### 4.2.3 Wound-Rotor Design

Wound rotors always use laminated material, slotted and assembled in a fashion similar to that employed with cage

rotors. The slots will, however, be of larger cross-sectional area, because they must accommodate a number of insulated conductors. The number of slots, although different from that used on the stator, will be chosen according to the same basic rules to accommodate a balanced, polyphase, integral, or fractional-slot winding.

The rotor winding (if three-phase) can be connected in either star or delta and is terminated at slip rings mounted on and insulated from the shaft. The presence of the slip rings either within or external to the enclosure of the machine makes for a larger motor. The increase in size is in addition to the inherently larger core dimensions resulting from somewhat lower specific electric loadings allowed in wound rotor design. A wound rotor is clearly of less robust construction than a cage design and its manufacture is more labor-intensive. With the further inclusion of slip rings and brush gear, wound-rotor machines are, except in large sizes, much more expensive than the cage-rotor equivalents. However, for certain applications, the benefits that accrue from either slip power recovery or improved starting performance provided by external rotor resistance, inserted by way of the brushes and slip rings, are sufficiently persuasive to generate a small but steady demand for wound-rotor machines.

### 4.3 INDUCTION MOTOR EQUIVALENT CIRCUITS

#### 4.3.1 Introduction

The purpose and great value of machine equivalent circuits is to represent an electromagnetic device comprising a complicated arrangement of interlinked electric and magnetic paths by a simple electric circuit. The lumped parameters of this circuit represent either the apparent resistances or the inductances associated with the various current or flux paths within the machine.

The steady-state equivalent circuit for one phase of a polyphase induction motor is sufficiently simple to allow easy calculation of not only phase currents and power factor but also torque, power, losses, and efficiency, and to a surprising degree of precision if the parameters are calculated or measured with suitable accuracy. Indeed, the ease of calculation is such that performance predictions can be made with little more than mental arithmetic and common sense.

Derivation of the transient, or dynamic, equivalent circuit either requires a more rigorous and simultaneously more abstract approach than the steady-state version or relies on a combination of empiricism and intuition. For present purposes the latter methodology will be adopted, but suitable reference will be made to expositions of the alternative approach.

Finite element methods are commonly used in the calculation of the equivalent circuit reactances [14, 15] and, with the addition of time-stepping, can provide quite accurate prediction of transient performance [16]. The advantage of this latter technique is that saturation can be accounted for, although the consequent nonlinearity often leads to lengthy computation time.

#### 4.3.2 Steady-State Equivalent Circuit

At standstill the induction motor is merely a short-circuited transformer with relatively poor linkage between primary and secondary windings because of the air gap. There is electrical power transfer between stator and rotor, all of which is dissipated as rotor copper and iron losses. However, the rotating magnetic fields in the air gap produce torque and, if this is sufficient to overcome the load on the shaft, then rotation results. Under these circumstances the power transfer accomplished by interaction between the air gap fields is rather more complex because electrical power crossing the air gap from the stator is dissipated both as mechanical output and rotor electrical losses. There is, in other words, conversion of electrical energy into both heat and mechanical energy. It will be seen that these various phenomena and interactions can be identified, represented, and quantified from the simple, six-element equivalent circuit, which will now be developed.

The stator of a balanced polyphase induction machine can be treated in a fashion similar to that used for the primary of a transformer, with inductive voltages representing the fluxes by which they are assumed to be induced (Fig. 4.52). The corresponding phasor equation is:

$$\bar{V}_1 = \bar{E}_1 + \bar{I}_1 (R_1 + jX_1) \quad (4.105)$$

where:

$\bar{E}_1 = j\bar{I}_m X_m$  the voltage or “back” emf induced in one stator phase by the mutual air-gap flux.

$\bar{V}_1 =$  the applied stator phase voltage

$\bar{I}_1 =$  the total stator phase current

$\bar{I}_m =$  the magnetizing current

$R_1, X_1,$  and  $X_m$  the stator resistance, leakage reactance and magnetizing reactance per phase.

Now the mutual airgap flux also induces voltages in the balanced rotor windings, the magnitude of which depends upon the flux linking the rotor, the number of rotor turns and the relative velocity of the resultant field and the rotor windings.

If  $\bar{E}_2$  is the voltage induced in a rotor phase at standstill, where  $\bar{E}_2 = \bar{E}_1/n$ ,  $n$  being the effective turns ratio, then with rotation,  $\bar{E}_2 = s\bar{E}_1/n$ , where the slip is:

$$s = \frac{f_2}{f_1} = \frac{N_1 - N}{N_1}$$

where:

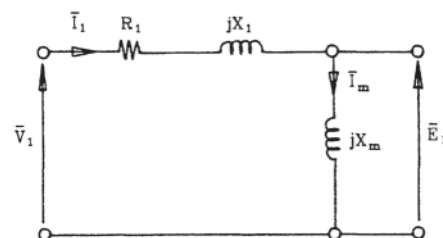


Figure 4.52 Stator equivalent circuit.

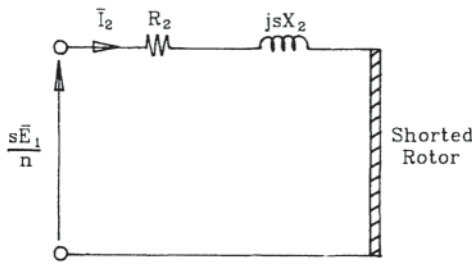


Figure 4.53 Rotor equivalent circuit.

$f_1$  and  $f_2$  = the stator and rotor frequencies, respectively  
 $N$  and  $N_1$  = the rotor speed and the speed of the stator field in the air gap (i.e., the synchronous speed), respectively

The value of  $E_2$  is dependent on slip because electromotive force (emf) is proportional to rate of change of flux linkage and hence is directly proportional to the relative speed between the stator air gap field and the rotor winding.

The rotor equivalent circuit is thus as depicted in Fig. 4.53 and the phasor equation is:

$$\frac{s\bar{E}_1}{n} = \bar{I}_2 (R_2 + jsX_2) \tag{4.106}$$

where:

- $\bar{I}_2$  = the rotor phase current
- $R_2$  = the rotor resistance per phase
- $X_2$  = the rotor leakage reactance per phase measured at stator frequency. At any other frequency  $X_2$  will be modified by  $s$ .

Now, with an ampere-turn balance between stator and rotor, there can be assumed a current  $I'_2$  that is the equivalent of  $I_2$  referred to the stator so that:

$$\bar{I}_2 = \frac{\bar{I}'_2}{n} \quad \text{or} \quad \bar{I}_2 = n\bar{I}'_2$$

and Eq. 4.106 becomes:

$$\frac{s\bar{E}_1}{n} = n\bar{I}'_2 (R_2 + jsX_2)$$

or:

$$s\bar{E}_1 = n^2\bar{I}'_2 (R_2 + jsX_2) = \bar{I}'_2 (n^2 R_2 + jsn^2 X_2)$$

The rotor current and voltages in this equation are at rotor frequency, but a transformation to the common base of stator frequency is achieved by operating on both sides of the equation by  $1/s$ ; thus:

$$\bar{E}_1 = \bar{I}'_2 \left( n^2 \frac{R_2}{s} + jn^2 X_2 \right) \tag{4.107}$$

where the rotor resistance, as observed from the stator, *appears* to vary with speed (or rotor frequency).

If, in both Eqs. 4.105 and 4.107, the substitution  $\bar{E}_1 = j\bar{I}_m X_m$ , is made, there follows:

$$\bar{V}_1 = \bar{I}_1 (R_1 + jX_1) + j\bar{I}_m X_m \tag{4.108}$$

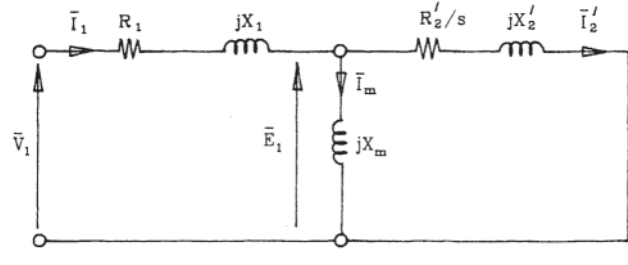


Figure 4.54 Composite equivalent circuit.

$$0 = \bar{I}'_2 \left( \frac{R'_2}{s} + jX'_2 \right) - j\bar{I}_m X_m \tag{4.109}$$

where  $R'_2 = n^2 R_2$  and  $X'_2 = n^2 X_2$  are, respectively, the rotor resistance and leakage reactance per phase measured from, or “referred” to, the stator.

Equations 4.108 and 4.109 have voltages and currents of the same (i.e., line) frequency and can be said to be the Kirchhoff voltage equations for the composite equivalent circuit of Fig. 4.54, where:

$$\bar{I}_1 = \bar{I}'_2 + \bar{I}_m$$

Now stator iron losses, for which hysteresis and induced eddy currents are responsible, are primarily associated with mutual flux and can thus be accounted for by a resistance  $R_l$  in parallel with the magnetizing reactance  $X_m$ . Rotor iron losses are significant only at high values of slip and are normally neglected. The simple, six-element equivalent circuit is then as illustrated in Fig. 4.55. The stator iron loss per phase is given by:

$$W_{Fe} = I_l^2 R_l \quad \text{and} \quad \bar{I}_0 = \bar{I}_l + \bar{I}_m$$

is the phase current drawn by the machine at synchronous speed. If  $\bar{I}_0$  is measured with the machine running light, the input power and thus the value of  $R_l$  is taken to include friction and windage loss.

Values for current, torque, power, and power factor can be deduced quite easily from the equivalent circuit of Fig. 4.55, but even simpler expressions are available if, following common practice, the magnetizing branch is removed to a new location across the input terminals. This is justified by the assumption of constant mutual air gap flux, and results in the circuit of Fig. 4.56. The electrical power supplied at the

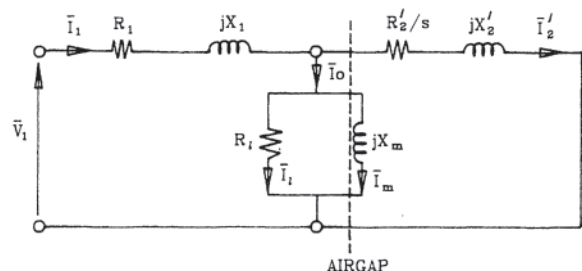


Figure 4.55 Equivalent circuit with iron losses.



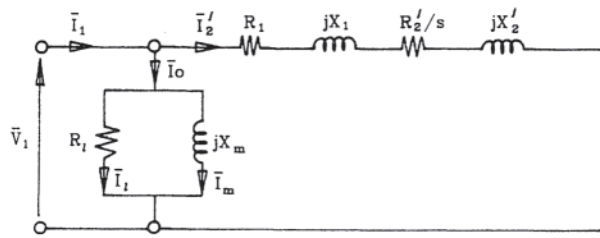


Figure 4.56 Modified equivalent circuit.

stator terminals is either dissipated as losses or is converted to mechanical output power at the rotor shaft. The air gap torque  $T_1$  is a result of interaction between the stator and rotor air gap fields, both of which rotate at synchronous speed, so that the power transmitted by field interaction across the air gap is:

$$P_1 = \frac{\omega_1 T_1}{p}$$

where:

$\omega_1$ =the field angular velocity in electrical rad/s  
 $p$ =the number of pole pairs

Similarly, the mechanical output power is:

$$P = \frac{\omega T}{p}$$

where:

$\omega$ =the rotor angular velocity in electrical rad/s  
 $T$ =output torque

In the steady state there is no acceleration of the rotor, so  $T_1 = T$ ,  $P_1 \neq P$ , but since there are electrical losses in the rotor. At normal speeds these are predominantly copper losses, so:

$$\frac{\omega_1 T}{p} = \frac{\omega T}{p} + 3I_2'^2 R_2'$$

or:

$$T = \frac{3p}{\omega_1 - \omega} I_2'^2 R_2' \text{ N-m}$$

and since slip,  $S$ , is:

$$s = \frac{f_2}{f_1} = \frac{(\omega_1 - \omega)}{\omega_1}$$

then  $(\omega_1 - \omega) = s\omega_1$ , whence:

$$T = \frac{3p}{\omega_1} I_2'^2 \frac{R_2'}{s} \text{ N-m}$$

for the case of a three-phase machine.

Inspection of Fig. 4.55 indicates that the  $3I_2'^2 R_2'/s$  term represents the power that crosses the air gap, called air gap power, so that:

$$T = \frac{P}{\omega_1} \times (\text{airgap power})$$

and the mechanical output power,  $P$ , is:

$$P = \frac{\omega T}{p} = 3 \frac{\omega}{\omega_1} I_2'^2 \frac{R_2'}{s}$$

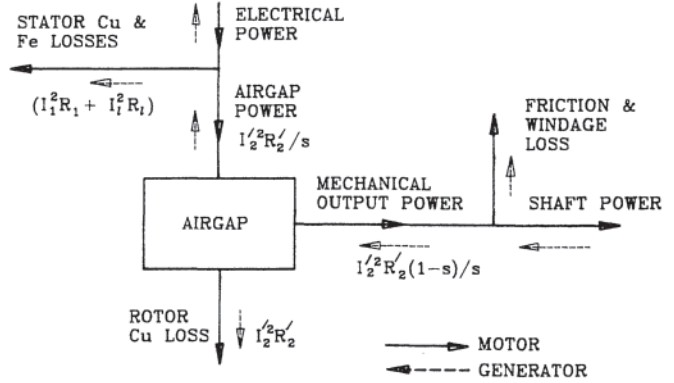


Figure 4.57 Power flow diagram for one phase of a balanced polyphase induction motor.

And because:

$$s = 1 - \frac{\omega}{\omega_1} \quad \text{or} \quad \frac{\omega}{\omega_1} = 1 - s$$

then:

$$P = 3I_2'^2 R_2' \frac{1-s}{s}$$

That is, air gap power=mechanical power+rotor Cu losses

$$3I_2'^2 \frac{R_2'}{s} = 3I_2'^2 R_2' \frac{1-s}{s} + 3I_2'^2 R_2'$$

and the power flow diagram of Fig. 4.57 can be drawn. The modifications required to represent induction generator operation with  $s < 0$  (or  $s$  negative) are indicated as appropriate.

Expressions for stator and rotor currents can be derived from either of the equivalent circuits of Figs. 4.55 or 4.56. With knowledge of the supply voltage and the machine parameters, values can then be calculated for phase and line current, power factor, and torque. Prediction of the electrical losses is likewise a straightforward matter so that, with a suitable estimate of friction and windage loss, both shaft output and efficiency can also be calculated.

### 4.3.3 Transient or Dynamic Equivalent Circuit

The complexity, method of derivation, and ultimate adequacy of the transient equivalent circuit depend to a large extent upon the uses to which it is likely to be put. There are two particular operational conditions for which such a circuit is uniquely applicable. In the first case the results primarily concern the machine designer or applications engineer; the second case is of greater interest to the power systems analyst. These circumstances are:

1. *Three-phase short circuit at the machine terminals.* The machine may be operating as either a motor or an induction generator, but in either event it is the stator current which will flow into the fault from the machine that is of concern here. At the instant of the short circuit there will be rotor current that

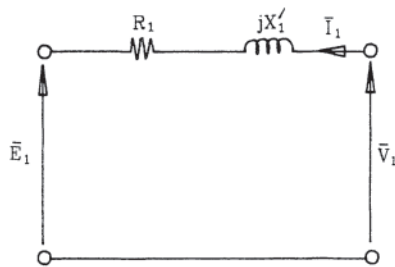


Figure 4.58 Transient equivalent circuit.

will decay, reaching zero when the initial stored energy is dissipated. The decaying current in the rotor generates voltages in the stator windings and the machine is transiently analogous to a short-circuited alternator. This is reflected by the equivalent circuit of Fig. 4.58, where  $R_1$  is the stator resistance per phase and the transient reactance per phase is

$$X'_1 = X_1 + X_m - \frac{X_m^2}{X'_2 + X_m}$$

$$\approx X_1 + X'_2$$

the various parameters being as defined in Section 4.3.2.  $V_{w1}$  is the prefault terminal voltage and  $E_{w1}$  is known as the initial voltage behind the transient reactance of the machine.

The procedure for calculation of fault current [17, 18] is then to calculate  $E_{w1}$  from the prefault stator phase current, short circuit the stator terminals, and determine the initial current fed into the fault. The short-circuit time constant also follows approximately from the quotient:

$$\tau = \frac{X'_1}{2\pi f R_2}$$

where  $R'_2$  is the referred rotor resistance.

The initial short-circuit current may be of the order of three or four times the rated value, but, with a short time constant, the fault current usually decays to zero within less than ten cycles of the supply frequency. It is thus considered acceptable to neglect any change in speed during the transient.

Machines for which such transient analysis is considered appropriate are usually large devices, that is, in the megawatt range, and may well be provided with deep rotor bars. This somewhat complicates the estimate of transient reactance but it is possible to produce a transient equivalent circuit based on the treatment of double-cage motors to which deepbar rotor machines may be considered analogous.

2. *Power system fault conditions.* The behavior and influence of induction motor loads following a power system fault can be assessed by the use of the transient equivalent circuit of Fig. 4.58.

In fact, power system engineers use various models to represent induction motor loads in transient stability studies, the complexity of the models depending upon the degree of refinement required and the degree of influence (or significance) assigned to this dynamic component of the load. A simple impedance representation may sometimes be adopted or as an alternative, the steady-state equivalent circuit of Fig. 4.55 or 4.56 may be deemed adequate, either with or without consideration of the load inertia and mechanical transients. The use of the transient equivalent circuit, with suitable account being taken of mechanical transients, is then a further option with time-stepping, finite element techniques for a complete transient solution being available if necessary.

## 4.4 EQUIVALENT CIRCUITS FOR VARIABLE FREQUENCY

### 4.4.1 Introduction

Most variable-frequency sources are inverters that supply nonsinusoidal voltage and current to the induction motor. For a voltage source inverter (VSI), the Fourier series method can be used to represent the voltage by a fundamental and harmonics. The fundamental alone determines average torque, but the fundamental as well as the harmonics produce loss in the motor. Reference 19 gives complete details on the method.

Even-order harmonics and triplen harmonics are seldom present with three-phase motors. The harmonic order numbers are then  $6n \pm 1$  where  $n=1, 2, 3, \dots, \infty$ . Based on the Fourier method, the currents for the fundamental and each significant

Table 4.3 Nomenclature Used in Section 4.4

Symbol	Quantity	Units
$E_1$	Fundamental voltage induced by stator flux	V/phase
$f_1, f_k$	Frequency of stator fundamental and $k$ th harmonic, respectively	Hz
$f_r$	Frequency of rotor current	Hz
$k$	Harmonic order number ( $k = 1$ for fundamental)	None
$L_1, L_m$	Stator leakage and magnetizing inductances	H/phase
$L_{2k}$	Rotor leakage inductance for $k$ th harmonic, referred to stator	H/phase
$n$	Sequence of integers 1, 2, 3, ..., $\infty$	None
$n_{slp}$	Slip speed	rad/s or rev/min
$s_1, s_k$	Fractional slip for fundamental and for $k$ th harmonic, respectively	None
$p$	Number of poles	None
$V_1, V_k$	Applied voltage for fundamental and for $k$ th harmonic, respectively	V/phase

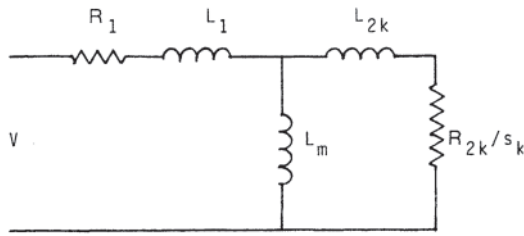


Figure 4.59 Alternate form of the equivalent circuit.

harmonic are found separately using the appropriate equivalent circuit.

Figure 4.59 is the conventional, per-phase equivalent circuit of a polyphase motor. In it, the value of  $s_k$  is frequency dependent. Also, the values of  $R_{2k}$  and  $L_{2k}$  for squirrel-cage rotors are dependent on the frequency of rotor current because of deep-bar effect. This phenomenon is similar to skin effect in conductors, which causes current to crowd to the outer surface. In the bars of a rotor, the current crowds to the section of the bar nearest the air gap. As a result,  $L_{2k}$  becomes smaller and  $R_{2k}$  becomes greater as frequency  $f_r$  increases [1].

The circuit of Fig. 4.60 is convenient for the fundamental frequency. The impedance of each element is explicitly given in terms of the fundamental frequency  $f_1$ . The slip speed  $n_{slip}$  is used rather than fractional slip  $s_1$  because  $n_{slip}$  is more nearly constant than  $s_1$  when frequency is varied. When the motor runs at normal, low, slip speed, the rotor frequency in Fig. 4.60 is very low and therefore the direct current (dc) resistance  $R_{dc}$  is used for  $R_{2k}$ .

But for harmonic currents, deep-bar effect causes  $R_{2k}$  to exceed  $R_{dc}$ . Also, for the  $k$ th harmonic of stator current, fractional slip is given by:

$$s_k = \frac{k \pm 1}{k} \tag{4.110}$$

The plus sign is used for  $k=6n-1$ , and the minus sign for  $k=6n+1$  to account for backward- or forward-rotating fields. Eq. 4.110 may be approximated by  $s_k \approx 1$  for  $k \geq 5$ .

Figure 4.61 for the  $k$ th harmonic comes from Fig. 4.59, but with  $s_k=1$ , and with the shunt branch neglected because its impedance is very large compared to rotor impedance. At harmonic frequencies, the reactances in Fig. 4.61 are much larger than the resistances and the resistances can be neglected when currents are computed. Figure 4.62 uses this approximation.

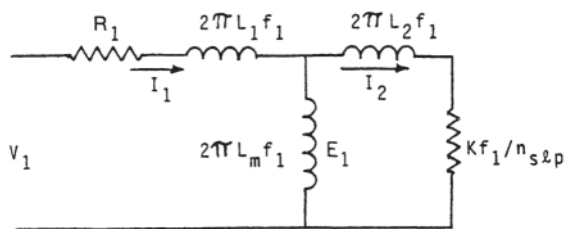


Figure 4.60 Equivalent circuit at the fundamental frequency.  $K=(4\pi/p)R_{dc}$  for  $n_{slip}$  in rad/s;  $K=(120/p)R_{dc}$  for  $n_{slip}$  in rpm.

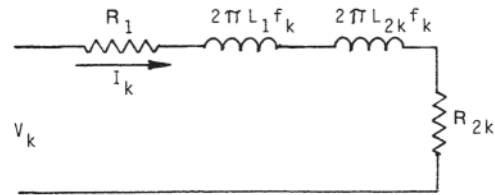


Figure 4.61 Equivalent circuit for the  $k$ th harmonic.

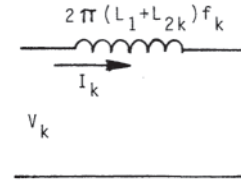


Figure 4.62 Approximate equivalent circuit at harmonic frequencies.

Table 4.4 Rotor Frequency  $f_r$  for Each Stator Harmonic  $k(k=1$  for fundamental)

$k$ :	1	5 and 7	11 and 13	...	$6n \pm 1$
$f_r$ :	$s_1 f_1$	$6f_1$	$12f_1$	...	$6n f_1$

#### 4.4.2 Rotor Deep-Bar Effect

The effective rotor resistance  $R_{2k}$  depends on rotor frequency  $f_r$ . For the various values of  $k$ , Table 4.4 gives the relationship between  $k$  and  $f_r$  when the motor is running. This is for a three-phase induction motor neglecting the even-order and triplen harmonics. This table indicates that, for  $k \geq 5$ ,  $f_r \approx k f_1$ .

For frequency above approximately 50 Hz, effective rotor resistance may be estimated within approximately 25% by:

$$R_{2k} \approx R_{dc}(C_r d \sqrt{f_r}) \text{ ohms} \tag{4.111}$$

where  $d$  is the radial depth of a rotor bar, in centimeters, and  $C_r$  is a constant whose value depends on bar shape and conductivity, and on how much of  $r_{dc}$  is for the end ring, where deep-bar effect does not occur. See Table 4.5 for approximate values of  $C_r$ . Equation 4.111 shows that, for higher frequency harmonics,  $R_{2k}$  can be several times  $R_{dc}$ .

The rotor inductance  $L_{2k}$  becomes somewhat smaller as frequency increases because of deep-bar effect. Reference 1 gives details. If accurate results are not required,  $L_{2k}$  may be considered independent of frequency.

Table 4.5 Values of  $C_r$  for Various Rotor Bars

Bar shape:	Rectangle	Trapezoid	Rectangle	Double cage
Material:	Aluminum	Aluminum	Copper	Aluminum
$C_r^a$	0.05	0.035	0.07	>0.1

<sup>a</sup> Value assumes end ring resistance is  $\frac{1}{2} R_{dc}$ .

### 4.4.3 Solution of Equivalent Circuits

To determine torque and speed behavior, only the fundamental circuit, Fig. 4.60, is needed. Assuming a voltage source inverter, and with values of  $f_1$  and  $V_1$  specified, currents  $I_1$  and  $I_2$  can be found at any selected value of  $n_{slp}$ . From  $I_2$ , the power across the gap and then torque can be found using standard equations for sine-wave operation. Also, power losses due to the fundamental can be found in the usual way.

Section 2.2.7 points out the need for constant flux. The voltage  $E_1$  in Fig. 4.60 is that induced by stator flux, and keeping  $E_1/f_1$  constant gives constant flux. Figure 4.60 can be solved with the required  $E_1$ , and then inclusion of the phasor  $I_1 R_1$  drop gives  $V_1$  for constant flux as frequency is varied. In this way, a curve similar to Fig. 2.9 can be determined for any motor.

For each of the harmonic voltages produced by the source, Fig. 4.62 is used to find current. The Fourier series of source voltage gives each  $V_k$  then:

$$I_k = \frac{V_k}{2\pi k f_1 (L_1 + L_{2k})} \text{ amperes} \quad (4.112)$$

If a current source inverter (CSI) is used, the fundamental and harmonic currents are determined directly from the Fourier series of the source current, and there is no need to solve the equivalent circuit to find these currents.

The harmonic currents are used to compute the loss in stator and rotor windings as:

$$P_{\text{har}} = 3 \sum_{k=5}^{\infty} I_k^2 (R_1 + R_{2k}) \text{ watts} \quad (4.113)$$

Because  $R_{2k}$  is increased with deep-bar effect, the rotor harmonic loss may become large, resulting in increased temperature rise of the rotor. The temperature-corrected values of  $R_1$  and  $R_{2k}$  should be used.

The  $I^2 R$  losses due to harmonics are easily evaluated. The harmonic currents also cause other losses that are not easy to calculate. These include eddy current loss in the steel laminations at each end of the stator and rotor core [19] and loss in the rotor bars due to skew [20]. These additional losses are significant, being approximately half the value for harmonic  $I^2 R$  in Eq. 4.113.

The total harmonic losses are nearly independent of load. The harmonic losses may be evaluated by subtracting no-load loss with sinusoidal excitation from no-load loss when the machine is inverter-driven. Total harmonic loss for typical sixstep and PWM waveforms with a VSI is between 15% and 25% of motor loss at rated load on a sine wave.

## 4.5 IMPORTANT DESIGN EQUATIONS

### 4.5.1 Output Equation and Main Dimensions

Consider a full-pitch, one-turn coil in a magnetic field that is sinusoidally distributed in space and is sinusoidally varying in time. The flux linkage of this coil is then given by:

$$\phi = \phi_p \sin 2\pi f t \quad (4.114)$$

and the voltage induced in the coil is:

$$e = \frac{d\phi}{dt} = 2\pi f \phi_p \cos 2\pi f t \quad (4.115)$$

The rms value is then

$$E = \frac{2\pi}{\sqrt{2}} f \phi_p = 4.44 f \phi_p \quad (4.116)$$

The rms voltage induced in the entire phase winding with the number of turns equal to  $N_{ph}$  and a winding factor of  $k_w$  is then:

$$\begin{aligned} E_{ph} &= 4.44 f k_w N_{ph} \phi_p \\ &= 4.44 \left( \frac{pn}{120} \right) k_w N_{ph} \left( B_{gav} \frac{\pi D}{p} L \right) \end{aligned} \quad (4.117)$$

where:

$D$  = diameter of the stator bore (m)

$p$  = number of poles

$n$  = speed (rpm)

$L$  = active length of the core (m)

$B_{gav}$  = average air gap flux density (Wb/m<sup>2</sup>), also called the specific magnetic loading

Now if  $q$  (ampere-conductors per meter) is the specific electric loading, then:

$$q = \frac{2(3 N_{ph})}{\pi D} I_{ph} \quad (4.118)$$

The machine kVA can now be written as:

$$\begin{aligned} \text{kVA} &= 3 I_{ph} E_{ph} \times 10^{-3} \\ &= 3 \left( \frac{\pi D q}{6 N_{ph}} \right) \frac{4.44 p n}{120} k_w N_{ph} B_{gav} \frac{\pi D L}{p} \times 10^{-3} \\ &= \frac{4.44 \pi^2}{240} k_w q B_{gav} D^2 L n \times 10^{-3} \end{aligned} \quad (4.119)$$

If  $\eta$  is the efficiency and  $\cos \theta$  is the power factor of the machine, then:

$$\frac{\text{kW}}{\eta \cos \theta} = \frac{4.44 \pi^2 \times 10^{-3}}{240} k_w q B_{gav} D^2 L n$$

i.e.:

$$\begin{aligned} D^2 L n &= \frac{240 \times 10^3}{4.44 \pi^2} \frac{\text{kW}}{\eta \cos \theta k_w q B_{gav}} \\ &= \left( \frac{5.48 \times 10^3}{\eta \cos \theta k_w q B_{gav}} \right) \text{kW} \end{aligned} \quad (4.120)$$

The above equation relates machine dimensions to its power rating, and is generally known as the *output equation*. The following basic aspects of machine design are apparent from this equation:

1. For a given output, high-speed machines are smaller in size than low-speed machines.
2. Machine size can generally be reduced by using higher values of specific electric and magnetic loadings. However, higher loadings result in increased temperature rises and magnetic saturation, thus creating an effective lower limit on size.

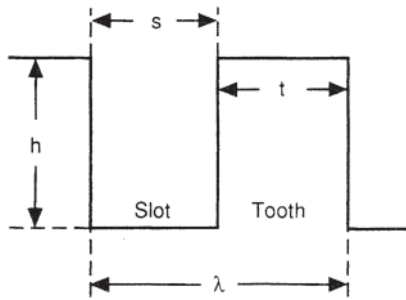


Figure 4.63 Slot geometry.

#### 4.5.1.1 Specific Electric Loading $q$

The permissible value of the electric loading is limited essentially by the ability of the cooling system to carry the heat away from the conductors. Referring to Fig. 4.63, if the slot is entirely filled with the conductor, the slot current is:

$$I_s = Jsh \quad (4.121)$$

where  $J$  is the current density in  $A/m^2$  in the conductor. The specific electric loading is:

$$q = \frac{I_s}{\lambda} = Jh \left( \frac{s}{\lambda} \right) \quad (4.122)$$

Furthermore, the heat generated within the slot is equal to the ohmic loss  $W_s$  in the slot:

$$W_s = I_s^2 \rho \frac{L}{sh} = J^2 \rho (shL) \quad (4.123)$$

where  $\rho$  is the resistivity of the conductor.

The volume density of the ohmic loss in  $W/m^3$  is:

$$\frac{W_s}{shL} = \rho J^2 \quad (4.124)$$

The maximum permissible  $J$  is, therefore, limited by the effectiveness of the cooling system. This in turn depends on several factors such as the machine speed, type of cooling (air, oil, water, and so forth), open or closed slots, thermal conductivity of slot insulation, slot height, air gap, and similar factors. The maximum value of  $q$  is thus limited by permissible  $J$ .

The nominal value of  $q$  is 15–35 ampere-conductors per millimeter for air-cooled induction motors, with lower values used for lower power rating [13]. For water-cooled machines with water flowing through hollow conductors, however, the specific electric loading could be as high as 150 ampere-conductors/per millimeter [21].

#### 4.5.1.2 Specific Magnetic Loading $B_{gav}$

The permissible value of  $B_{gav}$  is essentially limited by the maximum value of flux density in the teeth. With sinusoidal flux density distribution:

$$B_{rmax} = \frac{\pi}{2} B_{gav} \frac{\lambda L}{tL_{eff}} \quad (4.125)$$

where  $L_{eff}$ , the effective magnetic length of the machine, is smaller than  $L$  because of the presence of cooling vents.

$B_{gav}$  is usually 0.35–0.60  $Wb/m^2$  for 60-Hz machines so that the maximum tooth flux density can be limited to a high of 1.6  $Wb/m^2$  [13].

#### 4.5.1.3 Aspect Ratio $L/\tau$

The ratio of length ( $L$ ) to pole pitch ( $\tau$ ) is called the aspect ratio. This ratio is also chosen on the basis of several factors such as peripheral velocity ( $v=2f\tau$ ), the end winding leakage flux, and other economic considerations such as cost of assembling the machine. Generally, high-speed machines are longer so that the peripheral velocity can be limited to acceptable levels. The ratio  $L/\tau$  is usually between 1.00 and 4.00, with the lower range applicable to lower speeds.

The main dimensions  $D$  and  $L$  can thus be determined for a given power rating of the machine. As an illustrative example, consider the design of a 7.5-kW, 60-Hz, 220-V, 1800-rpmsquirrel-cage induction motor:

$$p = 120 \frac{f}{n} = \frac{120(60)}{1800} = 4$$

$$V_{ph} = \frac{ZZV}{\sqrt{3}} = 127 \text{ V}$$

Assuming, as a first step:

$$\eta = \cos \theta = 0.85$$

$$k_w = 0.95$$

$$q = 20,000 \text{ ampere-conductors/m}$$

$$B_v = 0.4 \text{ Wb/m}^2$$

$$D^2 L n = \frac{5.48 \times 10^4 (7.5)}{(0.85)(0.85)(0.95)(2.0 \times 10^4)(0.4)} = 7.485$$

$$D^2 L = \frac{7.485}{1800} = 4.158 \times 10^{-3} \text{ m}^3$$

Using  $L/\tau=1$ , i.e.,  $L=\pi D/4$ ;

$$D^3 = 5.295 \times 10^{-3}$$

$$D = 0.174 \text{ m}$$

and  $L = 0.137 \text{ m}$

#### 4.5.2 Design of Stator Winding

The stator winding is designed as follows:

1. The flux per pole  $\phi_p = B_{gav}(\pi DL/p)$ .
2. Conductors in series per phase =  $V_{ph} / (2.22fk_w\phi_p) =$  integer. The winding factor  $k_w =$  distribution factor  $\times$  pitch factor. For infinitely distributed full pitch coils,  $k_w = 3/\pi$ . As a first step, therefore, assume  $k_w = 3/\pi$ .
3. The number of stator slots ( $N_1$ ) is obtained in one of several ways. First, one could select one of the standard frame sizes established by the American Standards Association. Alternatively, for a machine with small number of poles, one could select an integer number of slots per pole per phase (2, 3, 4, etc.), calculate  $N_1 = 3p$  (slots/pole/phase), and check the slot pitch

( $\lambda = \pi D / N_1$ ).  $N_1$  is then selected such that the slot pitch is not too small. For a machine with large number of poles, slots/pole/phase is not an integer, and the winding is called a fractional-slot winding; this is discussed in the next section. For such a machine,  $N_1$  is chosen such that it is a multiple of 3, and conductors/slot given by:

$$\text{Conductors/slot} = \frac{q\pi D}{N_1 I_1} \text{ is an even number,}$$

$$\text{where } I_1 = \frac{kw}{\eta \cos \theta} \frac{1}{3V_{ph}}$$

4. Recalculate  $\phi_p$  and  $B_{gav}$ .
5. Calculate  $B_{60^\circ} = \frac{\sqrt{3}}{2} \frac{\pi}{2} B_{gav}$ .
6. Calculate slot pitch  $= \pi D / N_1$ .
7. Obtain slot and tooth dimensions by having the ratio of tooth depth/tooth width less than or equal to 7 to avoid noise [22].
8. Lay out a double-layer winding by assuming a certain coil span, usually a short pitch coil spanning less than a pole pitch. With a short pitch coil, the length of the end turns is reduced with only a small reduction in the useful flux. Also, specific winding harmonics can be eliminated by using an appropriate coil pitch. For low power ratings, a single-layer stator winding can be designed; such a winding, however, cannot be short pitched.

Continuing the illustrative example:

$$\phi_p = \frac{0.4\pi(0.174)(0.137)}{4} = 7.5 \times 10^{-3} \text{ Wb}$$

$$\text{Conductors/phase} = 12(36/3) = 144$$

Using integer slot winding, slots/pole/phase of 1 or 2 will give a rather large slot pitch for such a small diameter of the stator. So using 3 slots/pole/phase, we get  $N_1 = 36$ . Conductors/slot would then be  $144(36/3) = 11$ . Selecting an even number 12, we recalculate:

$$\text{Conductors/phase} = 12(36/3) = 144$$

$$N_{ph} = 72$$

$$\phi_p = \frac{127}{2.22(60)(3/\pi)(144)}$$

$$= 6.93 \times 10^{-3} \text{ Wb}$$

$$B_{gav} = \frac{6.93 \times 10^{-3}}{\pi(0.174)(0.137)/4} = 0.37 \text{ Wb/m}^2$$

$$\text{Stator copper loss} = 3I_1^2 R_1$$

Using  $s/t = 1$ , we get

$$s = t = \frac{\lambda}{2} = 0.0076 \text{ m (7.6 mm)}$$

### 4.5.3 Fractional Slot Winding [23, 24]

With a low-speed machine having a large number of poles, it is not practical to have an integer number of slots per pole per phase. These windings are called fractional slot windings; they drastically reduce the tooth-ripple voltages, although their distribution factor is inherently small. The design of such a winding can best be explained with the help of a sample calculation, such as, for example, a winding design for a machine with  $N_1 = 108$ ,  $p = 16$  and phases = 3.

1. Obtain slots per phase,  $N_1/p = 108/16 = 6.75$ .
2. Find the greatest common factor (GCF) of  $N_1/p$  and  $p$ ; this gives the number of repeatable sections of the total stator winding. The unit section covers  $N_1/\text{GCF}$  slots and  $p/\text{GCF}$  number of poles; both these numbers are integers. In the example,  $\text{GCF}(6.75, 16) = 1.6$ . Hence the unit winding covers  $108/1.6 = 67.5$  slots and the unit section is  $16/1.6 = 10$  poles.
3. Obtain slots per phase for the unit winding,  $N_{su}/p = (N_1/\text{GCF})/p$ . In the example,  $N_{su}/p = 67.5/16 = 4.21875$ . This means that 9 slots must be distributed over 4 poles to each of the three phases A, B, and C.
4. In the absence of any other considerations, such as winding harmonics, the slots should be distributed as evenly as possible. In the example, distribute the 9 slots as 3, 2, 2, 2 over the poles. Write down these numbers in sequence for three sets  
3 2 2 2 3 2 2 2 3 2 2 2

These will add to the number of slots for the unit winding. Then assign these numbers of slots in phase order such as A C B A C B and so forth as shown:

Phase A C B A C B A C B A C B  
3 2 2 2 3 2 2 2 3 2 2 2

Slots 1 4 6 8 10 13 15 17 19 22 24 26  
2 5 7 9 11 14 16 18 20 23 25 27  
3 12 21

This pattern is then repeated four times to cover 108 slots.

5. Lay out a double-layer winding by assuming a certain coil span (short pitch).

### 4.5.4 Squirrel-Cage Rotor Design [1, 13, 22–26]

Several designers have presented certain empirical rules for choosing the number of rotor slots in relation to the number of stator slots. These are based on considerations such as vibration, noise, starting and harmonic torques, harmonic losses, and others. These factors are considered elsewhere in the handbook. Without going into a complete analysis of all the undesirable slot combinations, all the empirical rules are presented here without explanation.

If  $N_1$  and  $N_2$  are the numbers of stator and rotor slots, respectively, the number of rotor slots should be selected such that:

1.  $N_1 \cdot N_2 \neq \pm 1, \pm 2, \pm(p \pm 1), \pm(p \pm 2), \pm p, \cdot 2p, \cdot 5p, \pm 3p$  or any multiple of  $\pm 3p$  for 3-phase motors,  $\pm p, \pm 2p$  or any multiple of  $\pm 2p$  for 2-phase motors.

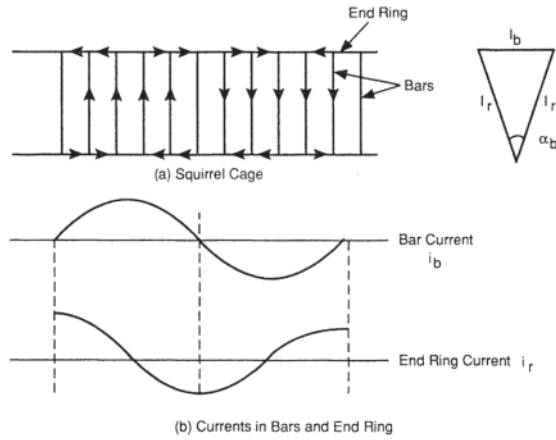


Figure 4.64 Squirrel-cage currents.

2.  $N_2 > 0.80N_1$
3.  $N_2 \approx 0.9N_1$
4.  $N_2 \neq \text{odd number}$
5.  $N_2 \leq 1.25N_1 + p$  for nonreversible drives  $\leq 1.25N_1$  for reversible drives

It is obviously not possible to abide by all of the above rules, especially with a small number of poles. Many designers have, therefore, developed allowable slot combinations based on their own experience.

A part of a squirrel-cage rotor of an induction motor is illustrated in Fig. 4.64. It behaves like a polyphase system with the number of phases  $m_2 = N_2$ , where  $N_2$  is the number of rotor bars or slots and the number of conductors in series per phase equals unity. The bar currents and the end-ring current are related as shown in Fig. 4.64(b). The angle:

$$\alpha_b = \pi p / N_2 \quad (4.126)$$

$$I_b = 2I_r \sin(\pi p / 2N_2) \quad (4.127)$$

i.e.,

$$I_r = \frac{I_b}{2 \sin(\pi p / 2N_2)} \quad (4.128)$$

The bar current can be obtained as follows:

The power in the rotor circuit

$$\begin{aligned} &= m_2 V_b I_b \\ &= N_2 [4.44 f (1/2) \phi_p] I_b \\ &= N_2 \frac{V_1}{2k_w N_{ph}} I_b \\ &= \text{output watts} / \text{rotor efficiency} = \frac{(\text{kW})}{\eta_R} \\ I_b &= 2k_w N_{ph} (\text{kW}) \times 10^3 / \eta_R N_2 V_1 \end{aligned} \quad (4.129)$$

As a start, the rotor efficiency  $\eta_R$  may be assumed to be 0.9–1.0. The bars and the end-ring cross section can now be determined by assuming a certain current density.

Generally, round-bar rotors use closed slots, whereas deep-bar rotors use open slots.

For selecting the number of rotor slots, we calculate the following guidelines.

1.  $N_1 - N_2 \neq \pm 1, \pm 2, \pm 3, \pm 5, \pm 6, \pm 4, -8, -20, \pm 12 \dots$
2.  $N_2 > 36 \sqrt{1.25}$ , i.e.,  $N_2 > 29$
3.  $N_2 \approx 0.9(36) \approx 32$
4.  $N_2 \neq \text{odd number}$

As stated earlier, it is not possible to satisfy all these constraints, especially with a small number of poles. In this example, we select  $N_2 = 31$ . The bar current and the end-ring current are then computed as:

$$I_b = \frac{2(3/\pi)(72)(7.5) \times 10^3}{0.9(31)(127)} = 291 \text{ A}$$

$$I_r = \frac{291}{2 \sin [4\pi/2(31)]} = 723 \text{ A}$$

Using a current density of  $4 \times 10^6 \text{ A/m}^2$ ;

$$\text{Bar cross-section} = \frac{291}{4 \times 10^6} = 7.25 \times 10^{-5} \text{ m}^2 (72.5 \text{ mm}^2)$$

$$\text{Rotor slot pitch} = \frac{\pi(0.174)}{31} = 0.01763 \text{ m} (17.63 \text{ mm})$$

A rotor bar of  $5 \text{ mm} \times 15 \text{ mm}$  may be selected. With a 2 mm tooth lip, the slot height will be 17 mm. The tooth width at the bottom of the tooth will be approximately 9 mm. The flux density at the bottom of the tooth is now checked as follows:

$$\text{Diameter at the bottom of the teeth} = 0.174 - 2(0.017) = 0.14 \text{ m}$$

$$\text{Slot pitch at the bottom} = \frac{\pi(0.14)}{31} = 0.014 \text{ m} (14 \text{ mm})$$

$$B_{\text{gav}} \text{ at the bottom} = \frac{6.93 \times 10^{-3}}{\pi(0.14)(0.137)/4} = 0.46 \text{ Wb/m}^2$$

$$B_{\text{max}} = \frac{\pi}{2} (0.46) \frac{14}{9} = 1.12 \text{ Wb/m}^2$$

This flux density at the bottom of the tooth is quite acceptable.

#### 4.5.4.1 Magnetizing Reactance

The main flux of an induction machine is that portion of the air gap flux that links totally with both the stator conductors and the rotor conductors. The reactance associated with this flux is called the magnetizing reactance  $X_m$  of the machine. The reactive component of the primary current that is responsible for producing the main flux is called the magnetizing component  $I_m$ . It is desirable to have  $X_m$  as large as possible so that  $I_m$  is small and the machine exhibits better power factor.

At any given instant of time, the air gap flux density is sinusoidally distributed in space. It is, therefore, customary to base the magnetic circuit computations on the value of the flux density  $B_6$  defined earlier as

$$B_{60^\circ} = \frac{\sqrt{3}}{2} \frac{\pi}{2} B_{\text{gav}} \quad (4.130)$$

Because each flux line crosses the air gap twice, the mmf relating to this flux density is:

$$\begin{aligned} AT_{60}^g \text{ per pole pair} &= \frac{B_{60}^g}{\mu_0} 2g_e \\ &= \frac{\sqrt{3}}{2} \frac{\pi}{2} \frac{2}{1} (B_{gav} g_e) \frac{10^7}{4\pi} \\ &= 0.2165 \times 10^7 B_{gav} g_e \end{aligned} \quad (4.131)$$

where the effective airgap  $g_e$  is given by:

$$g_e = g k_e \quad (4.132)$$

and  $k_e$  is a constant, greater than 1, that accounts for slotting in the stator and the rotor structure. In the absence of any detailed two- or three-dimensional field analysis, one can use the classic Carter's coefficient computed for the stator and the rotor geometries as [27]:

$$\begin{aligned} k_e &= \frac{5 + 2(\lambda_1/g) (s_1/\lambda_1)}{5 + 2(\lambda_1/g) (s_1/\lambda_1) (t_1/\lambda_1)} \\ &\times \frac{5 + 2(\lambda_2/g) (s_2/\lambda_2)}{5 + 2(\lambda_2/g) (s_2/\lambda_2) (t_2/\lambda_2)} \end{aligned} \quad (4.133)$$

where  $g$  is length of air gap,  $\lambda$ , is slot pitch,  $s$  is slot width,  $t$  is tooth width, and subscripts 1 and 2 refer to the stator and the rotor, respectively.

If a three-phase winding is excited by a set of balanced three-phase currents, the amplitude of the fundamental component of the air gap mmf distribution due to the winding is given by:

$$AT_{lm}^w = \frac{3}{2} \frac{4}{\pi} \left( \frac{N_{ph} k_w}{p} \right) \sqrt{2} I_m \text{ ampere-turns/pole} \quad (4.134)$$

and:

$$AT_{60}^w = \frac{6\sqrt{2}}{\pi} \left( \frac{N_{ph} k_w}{p} \right) I_m \sin 60 \text{ ampere-turns/pole} \quad (4.135)$$

If the permeability of the iron is assumed infinite,  $AT_{60}^g$  and  $AT_{60}^w$  may be equated, leading to:

$$\begin{aligned} AT_{60}^g &= 2 \frac{6\sqrt{2}}{\pi} \frac{\sqrt{3}}{2} \left( \frac{N_{ph} k_w}{p} \right) I_m \\ &= 4.678 (k_w N_{ph}/p) I_m \end{aligned} \quad (4.136)$$

That is:

$$\begin{aligned} I_m &= \frac{AT_{60}^g \text{ per pole pair}}{4.678 \text{ (effective turns per pole per phase)}} \\ &= \frac{0.2165 \times 10^7 B_{gav} g_e}{4.678 N_{ph}/p} \\ &= 4.63 \times 10^5 \frac{B_{gav} g_e}{(N_{ph}/p)} \end{aligned} \quad (4.137)$$

The magnetizing inductance  $L_m$  is then obtained as

$$L_m = \frac{1}{2\pi f} \frac{V_{ph}}{I_m}$$

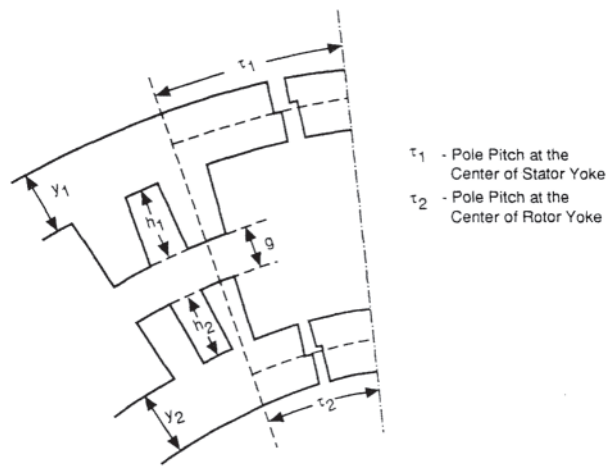


Figure 4.65 Ferromagnetic part of the magnetic circuit.

and can be shown to be:

$$L_m = 4.8 \times 10^{-5} \frac{DL}{g_e} \left( \frac{k_w N_{ph}}{p} \right)^2 \text{ Henrys} \quad (4.138)$$

It should be noted that only the mmf across the air gap was considered above and that the magnetizing current will actually be somewhat higher (20–40%) than this to account for the mmf requirements of the ferromagnetic portion of the magnetic circuit illustrated in Fig. 4.65. This increase can be estimated for the machine geometry for a flux density level such as  $B_{gav}$  or  $B_{60}^g$ .

#### 4.5.4.2 The Air Gap

The air gap in an induction machine is made as small as possible, and is mainly governed by mechanical considerations such as the unbalanced magnetic forces on the rotor and the stiffness of the shaft. The unbalanced magnetic pull on the rotor can be approximated by considering the geometry of Fig. 4.66.

Assuming that the flux density is inversely proportional to the air gap, the vertical components  $P_1$  and  $P_2$  are given by:

$$P_1 = \frac{B_{rms}^2}{2\mu_0} \left( \frac{1}{1 + \epsilon \sin \theta} \right)^2 \left( \frac{D_r}{2} d\theta L \right) \sin \theta \quad (4.139)$$

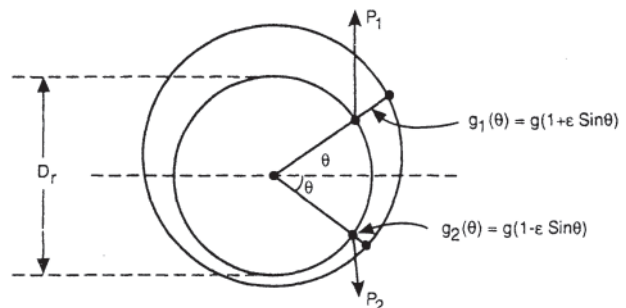


Figure 4.66 Rotor eccentricity.



$$P_2 = \frac{B_{rms}^2}{2\mu_0} \left( \frac{1}{1 - \varepsilon \sin \theta} \right)^2 \left( \frac{D_r}{2} d\theta L \right) \sin \theta \quad (4.140)$$

The differential force  $dp$  directed downward is then:

$$dP = P_2 - P_1 \cong \frac{B_{rms}^2}{2\mu_0} (4\varepsilon \sin^2 \theta) \frac{D_r L}{2} d\theta \quad (4.141)$$

It should be noted here that since the magnetic force is proportional to  $B^2$ , the rms value of the flux density is used in this equation.

The total unbalanced magnetic pull on the rotor is then:

$$\begin{aligned} P &= \frac{\varepsilon D_r L B_{rms}^2}{\mu_0} \int_0^x \sin^2 \theta d\theta \\ &= \frac{\varepsilon \pi D_r L B_{rms}^2}{2\mu_0} \\ &= \frac{\varepsilon (\pi D_r L)}{2\mu_0} \left( \frac{\pi}{2\sqrt{2}} B_{gav} \right)^2 \\ &= 1.54 \times 10^7 \varepsilon B_{gav}^2 D_r L \text{ newtons} \end{aligned} \quad (4.142)$$

The weight of the rotor can be added to this unbalanced magnetic force and the deflection of the rotor shaft can then be estimated. The nominal air gap of the machine must be sufficiently large to avoid contact between the stator and the rotor. If the air gap is made very small, the tooth harmonics and the tooth core losses will increase. Still and Siskind [13] give the following empirical formula for the air gap:

$$g \text{ (air gap in miles)} = 15 + D \text{ (diameter in inches)} \quad (4.143)$$

In addition to the main flux that links both the stator and the rotor conductors, there are several components of the total flux in an electric machine that link, totally or partially, only the stator or the rotor windings. Different reactances can be defined to account for the voltages induced in the stator and the rotor windings because of these flux components; these are the leakage reactances of the machine. In the absence of magnetic saturation, it is possible to consider these individual components independently.

#### 4.5.4.3 Stator Slot Leakage Reactance [1, 13, 23]

A winding placed in a slot is illustrated in Fig. 4.67. The slot leakage flux lines cross the slot width at various slot heights and, assuming unsaturated iron, they all close on themselves behind the slots in the yoke. Each flux line is caused by the amount of current in the slot under the flux line. The line integral of  $\vec{H} \times d\vec{l}$  around the flux path PQRS for example, is equal to the current in the slot under the level PQ shown by the shaded area. If the slot insulation is thin, the conductor width is nearly equal to the slot width and the flux lines in the slot can be assumed to be straight lines as shown. Consider the differential flux  $d\phi$  crossing the slot between the height  $x$  and  $(x+dx)$  in the conductor. If the current in the conductor is  $I$ :

$$d\phi = (dx L) \mu_0 H_x$$

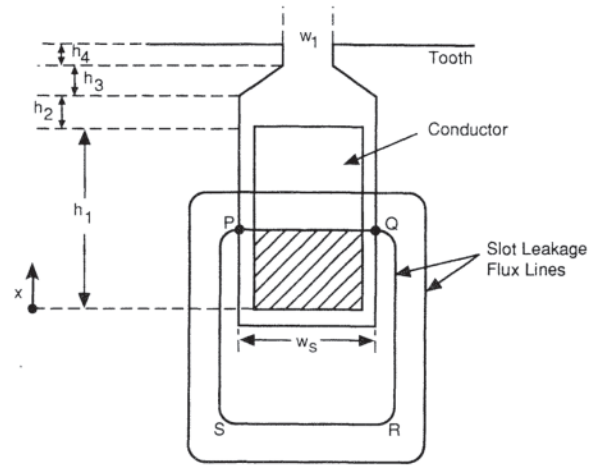


Figure 4.67 Slot leakage flux.

$$\begin{aligned} &= (dx L) \mu_0 \frac{I(x/h_1)}{w_s} \\ &= \frac{\mu_0 L I}{h_1 w_s} x dx \end{aligned} \quad (4.144)$$

This differential flux does not link the entire conductor, but only the fraction  $x/h_1$ . The elemental flux linkage  $d\psi$  is then given by

$$d\psi = \frac{\mu_0 L I}{h_1 w_s} \frac{x}{h_1} x dx \quad (4.145)$$

and the flux linkage of the total conductor caused by the flux between the height 0 to  $h_1$  is then given by:

$$\begin{aligned} \psi_1 &= \frac{\mu_0 L I}{h_1^2 w_s} \int_0^{h_1} x^2 dx \\ &= \mu_0 L I \left( \frac{h_1}{3 w_s} \right) \end{aligned} \quad (4.146)$$

Considering the total slot geometry, the total flux linkage is given by:

$$\begin{aligned} \psi &= \mu_0 L I \left( \frac{h_4}{w_1} + \frac{2h_3}{w_1 + w_s} + \frac{h_2}{w_s} + \frac{h_1}{3w_s} \right) \\ &= \mu_0 L I P_s \end{aligned} \quad (4.147)$$

The constant  $P_s$  is dimensionless and depends only on the conductor-slot topology; this constant is called the *slot permeance ratio*. This ratio can be defined for specific slot geometries. For example, for a round slot of Fig. 4.68:

$$P_s = 0.66 + \frac{h_1}{w_0} \quad (4.148)$$

If the slot has  $N_s$  conductors, each carrying a current of  $I_{ph}$ , the flux linkage per slot will be:

$$\begin{aligned} \Psi_{\text{per slot}} &= N_s (\mu_0 L N_s I_{ph}) P_s \\ &= \mu_0 L I_{ph} N_s^2 P_s \end{aligned} \quad (4.149)$$

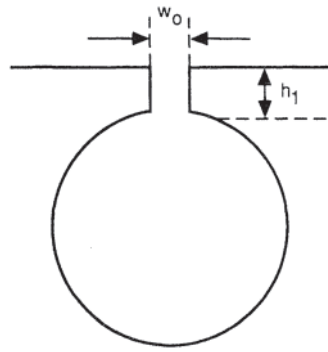


Figure 4.68 A round slot.

Furthermore, if the total number of stator slots is  $N_1$ , the slots per phase will be  $N_1/q$ , and the flux linkages of the phase winding will be:

$$\Psi_{ph} = \left(\frac{N_1}{q}\right) \mu_0 L I_{ph} \left(\frac{2q N_{ph}}{N_1}\right)^2 P_s \quad (4.150)$$

and the leakage inductance  $L_{ph}$  per phase will be:

$$L_{ph} = \frac{\Psi_{ph}}{I_{ph}} = \mu_0 L \left(\frac{N_1}{q}\right) \left(\frac{2q N_{ph}}{N_1}\right)^2 P_s \quad (4.151)$$

The leakage reactance associated with the slot leakage flux is then given by:

$$\begin{aligned} X_{sph} &= 2\pi f L_{ph} \\ &= 32\pi^2 \times 10^{-7} \frac{qf L N_{ph}^2}{N_1} P_s \\ &= 3.16 \times 10^{-5} \left(\frac{qf L N_{ph}^2}{N_1}\right) P_s \end{aligned} \quad (4.152)$$

It must be remembered that  $L$  is the length of the machine, representing the length of the stator conductors embedded in the iron. This calculation of the slot leakage reactance can be modified appropriately to take into account the influence of factors such as slot skewing, the coil pitch, magnetic saturation, and others. Various authors have presented different formulas to account for these factors.

#### 4.5.4.4 Rotor Slot Leakage Reactance

The rotor slot leakage is calculated using the same technique. The reactance value must, however, then be referred to the stator circuit by the transformation ratio, yielding:

$$X'_2 = X_2 \frac{k_{w1} N_{ph1}^2}{k_{w2} N_{ph2}^2} \quad (4.153)$$

#### 4.5.4.5 Zigzag Leakage

The leakage flux that zigzags across the air gap by hopping between stator teeth and rotor teeth as shown in Fig. 4.69 is called the *zigzag leakage* of the machine. The zigzag flux shown in the figure represents a component of stator leakage flux because it links only with the stator winding. The rotor also has a similar zigzag leakage flux.

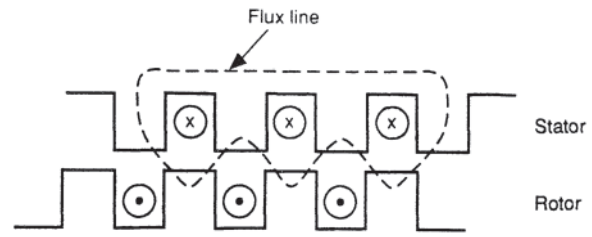


Figure 4.69 Zigzag leakage of the stator winding.

Several authors have given various formulas for estimating this reactance. For example, Alger [1] gives the following expressions.

Stator zigzag reactance:

$$X_{z1} = \frac{\pi^2 X_m P^2}{12 N_1^2} \left[ 1 - \frac{a(1+a)(1-k)}{2k} \right] \text{ ohms/phase} \quad (4.154)$$

Rotor zigzag reactance:

$$X'_{z2} = \frac{\pi^2 x_m P^2}{12} \left[ \frac{1}{N_2^2} - \frac{a(1+a)(1-k)}{2k N_1^2} \right] \text{ ohms/phase} \quad (4.155)$$

where  $a=t/\lambda$  and  $k=g/g_c=1/k_e < 1$ . If the slots are closed,  $g$  is almost equal to  $g_o$  and then:

$$X_z = X_{z1} + X'_{z2} = \frac{\pi^2 x_m P^2}{12} \left( \frac{1}{N_1^2} + \frac{1}{N_2^2} \right) \text{ ohms/phase} \quad (4.156)$$

If the slots of either the stator or the rotor are skewed, the following component is added to this value [1]:

$$X_{skew} = \frac{\pi^2 \sigma^2 X_m P^2}{12 N_1^2} \quad (4.157)$$

where  $\sigma$  is the angle of the skew in radians.

The zigzag leakage is essentially due to air gap harmonics that would be produced if the winding had only one slot per pole per phase; each slot would then carry the same rms current, equally displaced in space and time.

#### 4.5.4.6 Belt Leakage

When the machine winding has phase belts that are several slots wide, that is, when the winding has a large number of slots per pole per phase, an additional component of leakage flux can be defined. This leakage flux results from the nonsinusoidal mmf distribution of the winding, and is called the *belt leakage*. The belt leakage of the winding is therefore a function of the winding factors for the individual harmonics, and may be calculated as:

$$X_b = X_m \left[ \sum_n \frac{1}{n^2} \left( \frac{k_{pn}}{k_{p1}} \right) \left( \frac{k_{dn}}{k_{d1}} \right) \right] \quad (4.158)$$

where  $k_{pn}$  and  $k_{dn}$  are the pitch and the distribution factors for the  $n$ th harmonic. For full-pitch three-phase windings with 60-degree or 120-degree phase belts,  $X_b \approx 0.00214 X_m$ .

The sum of the zigzag reactance and the belt leakage reactance is commonly referred to as the *differential reactance*.

#### 4.5.4.7 Peripheral Leakage

This component of the air gap flux closes on itself in the air gap without crossing over to the rotor at all. Nominally, this leakage may be ignored because the ratio  $g/\tau$  is very small. A peripheral leakage can, however, be defined as:

$$X_p = X_m \left[ \sum_n \frac{1}{2} \frac{p^2 g^2}{D^2} \left( \frac{k_{pn}}{k_{p1}} \right)^2 \left( \frac{k_{dn}}{k_{d1}} \right)^2 \right] \quad (4.159)$$

For three-phase windings, the ratio  $X_p/X_m$  is usually between  $9.9(g/\tau)^2$  and  $10.9(g/\tau)^2$  depending on the winding pitch.

#### 4.5.4.8 End- Winding Leakage

The leakage flux components considered so far are all contained within the air gap between the stator and the rotor. In addition, the current in the end turns of the stator and the rotor cause a flux distribution in the end winding region; this flux mainly links the end turns. The varying topology of the end turns and the adjacent ferromagnetic parts make exact determination of this flux component very difficult. It can, however, be roughly estimated as [1]:

$$X_{1e} = X'_{2e} = \frac{4.2 \times 10^{-5} f N_{ph}^2 D}{p^2} \text{ (winding pitch)} \\ - 0.3) \text{ ohm/phase} \quad (4.160)$$

where the winding pitch is expressed in per unit.

#### 4.5.4.9 Deep-Bar Rotor [1,27]

Referring back to Fig. 4.67, it can be seen that the flux linkages of the lower section of the squirrel-cage bar are greater than those of the upper section of the bar. The reactive impedance of any section of the bar is therefore a function of its location in the slot; the lower section has a higher impedance. Consequently, the rotor current is not uniformly distributed over the cross section of the bar. The current tends to crowd up toward the top of the bar and the effective ac resistance of the bar is higher than its dc resistance. The ratio  $R_{ac}/R_{dc}$  is a function of the frequency of the rotor currents and the bar height.  $R_{ac}$  increases with motor slip and bar height. A deep-bar rotor thus behaves like a high-resistance rotor during starting when the slip is very large; it behaves like a low-resistance rotor in the normal low-slip operating region.

The classic depth of penetration of the electromagnetic field in the rotor bar is:

$$\delta = \frac{\sqrt{2}}{\mu_0 \gamma \omega} \quad (4.161)$$

where  $\gamma$  is the conductivity of the bar and  $\omega$  is the frequency of rotor currents in rad/sec. The quantity  $\delta$  is often called the *skin depth*. The ratio  $R_{ac}/R_{dc}$  is given by:

$$\frac{R_{ac}}{R_{dc}} = \zeta \frac{\sinh(2\zeta) + \sin(2\zeta)}{\cosh(2\zeta) - \cos(2\zeta)} \quad (4.162)$$

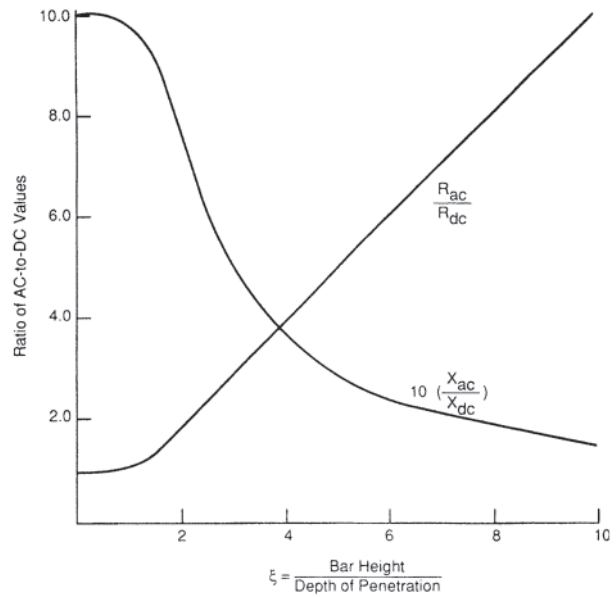


Figure 4.70 Skin effect in deep-bar rotors.

where  $\zeta = \text{bar height}/\delta$ . This ratio is plotted in Fig. 4.70. It can be seen that for  $\zeta > 2$ , the ratio  $R_{ac}/R_{dc} \cong \zeta$ .

As a result of this skin effect, the rotor slot leakage reactance  $X'_{2ac}$  is now different from that given by earlier slot leakage formulas,  $X'_{2dc}$ , by the equation:

$$\frac{X'_{2ac}}{X'_{2dc}} = \frac{3}{2\zeta} \frac{\sinh(2\zeta) - \sin(2\zeta)}{\cosh(2\zeta) + \cos(2\zeta)} \quad (4.163)$$

which is approximately equal to  $3/2\zeta$  for  $\zeta > 2$ .

For 60-Hz motors with copper bars, the depth of penetration would be nearly 10 mm at the start and over 50 mm in the low-slip region.

#### 4.5.4.10 Check on Performance

By following the design procedure outlined above, it is possible to obtain a preliminary design of an induction motor for a given power rating. At this stage, the performance characteristics of the machine designed above should be checked.

#### 4.5.4.11 Estimation of Machine Losses

Once the machine size, the stator windings, and squirrel-cage rotor are designed, and the equivalent circuit parameters are determined, it is necessary to estimate machine losses so that the machine's performance can be determined.

The copper losses are calculated as:

$$\text{Stator copper loss} = 3I_1^2 R_1 \quad (4.164)$$

$$\text{Rotor copper loss} = 3I_1^2 R_2' \text{ for wound rotor} \\ \text{or} = \text{Copper losses in all} \\ \text{bars} + \text{copper losses} \\ \text{in both end rings} \quad (4.165)$$

The core loss in the machine generally has two components, the eddy current loss and the hysteresis loss in the stator core.

Under normal operating conditions, the rotor core loss can be ignored due to low rotor frequency. The stator core loss is estimated by computing core weight separately for teeth and for the rest of the core. Core loss is then obtained by referring to the loss curves for the core material. The loss in the teeth is estimated on the basis of the flux density at a depth equal to one 1/3 third tooth depth measured from its smallest width.

Several authors have given different formulas for estimating the friction and windage losses of a machine. For an induction machine, these losses may be estimated as [22]:

$$F \& W \text{ losses} = 8 \times 10^{-18} (D^2 L) (Dn^2) \text{ kW} \quad (4.166)$$

In addition to the core loss, copper loss, and the friction and windage losses, there are other losses in the machine caused largely by harmonic currents and flux components. These are generally referred to as *stray load losses*, and may be 0.5–3.0% of the machine output.

4.5.4.12 Starting Torque, Maximum Torque, and Efficiency

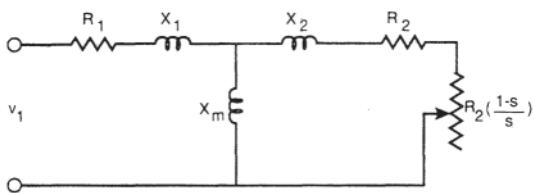
The machine equivalent circuit is shown in Fig. 4.71 (a), and its Thévenin equivalent circuit is shown in Fig. 4.71 (b). The constants in the Thévenin equivalent circuit are:

$$R_{1t} + jX_{1t} = \frac{jX_m(r_1 + jX_1)}{R_1 + j(X_1 + X_m)} \quad (4.167)$$

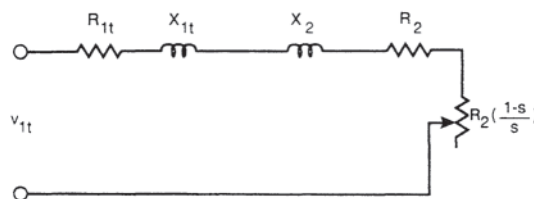
$$V_{1t} = V_1 \frac{jX_m}{R_1 + j(X_1 + X_m)} \quad (4.168)$$

The starting and pull-out torques are then:

$$T_{st} = \frac{3}{\omega_s} \frac{V_{1t}^2 R_2}{(R_{1t} + R_2)^2 + (X_{1t} + X_2)^2} \text{ N-m} \quad (4.169)$$



(a) Equivalent Circuit of an Induction Motor



(b) Thévenin Equivalent

Figure 4.71 Induction motor equivalent circuit, with its Thévenin equivalent.

$$T_{max} = \frac{3}{2\omega_s} \frac{V_{1t}^2}{R_{1t}^2 + \sqrt{R_{1t}^2 + (X_{1t} + X_2)^2}} \text{ N-m} \quad (4.170)$$

and the slip at maximum torque  $s_T \text{ max}$  is given by:

$$s_{Tmax} = \frac{R_2}{\sqrt{R_{1t}^2 + (X_{1t} + X_2)^2}} \quad (4.171)$$

$$\text{Mechanical output} = \frac{3V_{1t}^2 R_2 [(1-s)/s]}{(R_{1t} + R_2/s)^2 + (X_{1t} + X_2)^2} \text{ watts} \quad (4.172)$$

$$\begin{aligned} \text{All losses} = & \text{stator copper loss} + \text{rotor copper loss} \\ & + \text{stator core loss} + F \& W \text{ loss} \\ & + \text{stray load loss} \end{aligned} \quad (4.173)$$

$$\text{Power input} = \text{mechanical output} + \text{all losses} \quad (4.174)$$

$$\text{Efficiency } \eta = \text{output/input} \quad (4.175)$$

The power factor of the machine is given by

$$\text{Power factor} = \cos \theta = \frac{\text{power input}}{3V_{ph} I_1} \quad (4.176)$$

If the performance of the machine is not acceptable, the design parameters of the machine can be changed appropriately. This is essentially a trial-and-error method and is essentially accomplished by using a digital computer.

4.6 SPECIAL INDUCTION MOTOR DESIGNS

4.6.1 Linear Induction Motor Design

The performance characteristics of linear induction motors (LIMs) have been discussed earlier in Section 2.2.8. A general basis of LIM design is now presented. In conventional industrial drives with rotating motors, the frequency of the supply is ordinarily 50 or 60 Hz. In variable-speed drives such as traction systems, however, the nominal speed of the load is specified: the operating frequency of the motor is the designer's choice. The primary application of LIMs is in variable-speed drives, especially in the field of ground transportation and services. For such applications, the thrust-speed characteristic is usually specified as the basic requirement. For a given characteristic, several modes of motor operation can be identified as illustrated in Fig. 4.72. Not of all these modes may be present for every motor application. Because of the end effect, it is not possible to predetermine the region that will constrain the LIM design; the motor may be either

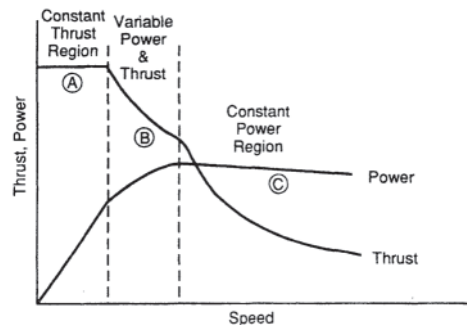


Figure 4.72 Typical traction application characteristics.

thrust-limited or power-limited. As a first step, however, one can determine the nominal rating of the machine from the thrust-speed requirements. Furthermore, the air gap is also specified on the basis of mechanical considerations such as minimum clearances.

The LIM design essentially involves the following.

1. Choice of frequency, pole pitch, and operating slip; only two of these can be independently chosen for a given operating speed.
2. Choice of voltage per phase.
3. Selection of reaction rail parameters.  
For DLIM: rail thickness and overhang.  
For a SLIM: rail thickness, overhang, and back iron.
4. Primary design consisting of number of poles, winding layout, slot and tooth geometry, and yoke width.

Many conflicting factors must be taken into account in designing a LIM to the system specifications and constraints. Magnetic loading, for example, is determined by the geometry, magnetizing current, iron losses, and most importantly, by the maximum flux density allowed in different parts of the magnetic circuit. The electric loading, on the other hand, depends, among other things, on slot geometry, wire insulation, and cooling method, the numerous parameters that must be handled simultaneously as well as the various trade-offs required make the design of the motor a challenging task. Some design criteria have been proposed to achieve good design of a motor. High power factor, high efficiency, and light weight are some of the important criteria of design evaluation.

In practice, it is not easy to implement a design procedure that would incorporate all these elements and one or more design criteria. Alternately, a combination of motor analysis and synthesis can be followed. Basically this method consists of a two-step iteration: (1) The performance characteristics of the motor are computed for a set of initial design parameters, and (2) the necessary design parameters are then adjusted to obtain the desired motor characteristics. This procedure thus requires that some LIM model is available to the designer for computing the thrust-speed characteristics of a LIM for given parameters.

#### 4.6.1.1 Choice of Frequency and Pole Pitch

The choice of the frequency and the pole pitch depends on factors that are partially external to the linear motor. For given electric and magnetic loadings, there is a fundamental limit to the force density of a LIM. A certain area of the footprint of the primary on the secondary is therefore necessary for a given thrust requirement. The minimum footprint required would be that of a LIM that exhibits no end effect. For a given operating speed, as the frequency is increased, the pole pitch will be lower, the number of poles will be higher, and the end effect will be reduced. This will result in a higher thrust-to-weight ratio and in a lower cost. The frequency can, however, be increased within limits; if the pole pitch to air gap ratio is too small, the effective coupling between the primary and the secondary will be reduced to an unacceptable level. With increasing frequency, the reactive volt-amperes will also increase proportionally and the cost of the static power

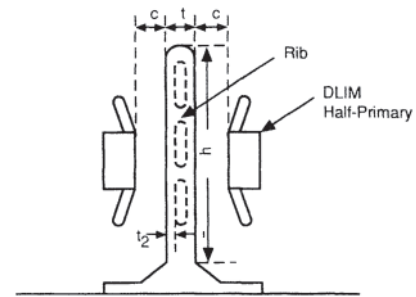


Figure 4.73 DLIM secondary.

conditioning unit (PCU), such as an inverter, will increase. The frequency must therefore be chosen such that the combined cost of the LIM and the PCU is minimum. For LIMs designed for high-speed ground transportation applications (350 km/hr and more), the optimum frequency may be within a wide range of 80–200 Hz. The high-speed LIMs are normally high-slip motors. The pole pitch can therefore be obtained initially by assuming an operating slip of 0.10 per-unit (pu).

#### 4.6.1.2 DLIM Secondary

The secondary of a DLIM is essentially a thick conducting sheet placed between two half primaries as shown in Fig. 4.73. The clearance  $c$  between the primary and the secondary and the thickness  $t$  are determined by the LIM suspension characteristics and the required stiffness of the secondary. If, however, the secondary sheet needs to be made thinner to obtain the required thrust characteristics, this may be accomplished by taking the conducting material out of the center of the rail, leaving a sufficient number of ribs for mechanical strength. It should be noted here that the total clearance between the two half-primaries is sometimes referred to as the magnetic gap and should be kept as low as possible. The height  $h$  of the rail is determined so that sufficient overhang is available beyond the LIM core even with the maximum vertical displacement of the primary.

#### 4.6.1.3 SLIM Secondary

The design of the SLIM secondary (Fig. 4.74) involves determining the thickness and the width of both the conducting sheet and the back iron. The width of the conducting sheet can be initially chosen such that the overhang is approximately 40% of the pole pitch; the thickness  $t$  must be chosen using simulation modeling to obtain required thrust. The thickness  $y_2$  of the back iron should be as low as possible to reduce cost, with the constraint that

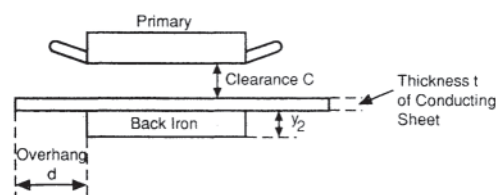


Figure 4.74 SLIM secondary.

the saturation level in the back iron is held at an acceptable level. Solid back iron should be used as far as possible to reduce the cost of the secondary.

#### 4.6.1.4 LIM Primary Design

The LIM primary is designed using procedures presented earlier for rotating motors with some exceptions. The slot leakage, end winding leakage, and other leakage components can be estimated using the earlier formulas. The LIM windings, however, are not closed on themselves, and some slots at both ends carry only one layer of the winding; the total number of slots is greater than the product of the slots per pole and the number of poles. The design of additional windings to compensate for the end effect is beyond the scope of this book, and the reader is referred to earlier work by Yamamura and others. Furthermore, the determination of the yoke depth in linear motors is different from that in the rotary motors. In rotary machines with circular symmetry, the yoke depth can be based on one-half of the flux per pole. In linear machines, the flux density varies along the length of the machine, and due to lack of circular symmetry the yoke may carry more than half the maximum flux per pole at some locations. It is not possible to give a unique value for the ratio between the yoke flux and the air gap flux. The designer essentially has to decide how much saturation to accept and over what portion of the yoke length; a factor between 0.5 and 1.0 may be then chosen by examining the predicted air gap flux density variation along the length of the linear motor.

### 4.6.2 Solid-Rotor Induction Motor Design

The theory of solid-rotor induction motors appears in Section 2.5.5. This section is concerned with factors to consider in the design of such motors.

#### 4.6.2.1 General Requirements

The development of gate turn-off (GTO) inverters capable of accommodating high currents and high voltages and operating at high frequencies leads to consideration of the design of variable high-speed (3000 to 12000 rpm) induction motor drives, for example, for compressors, pumps, fans, blowers, and so forth. High-speed operation creates significant centrifugal forces. The rotor must have sufficient mechanical strength to withstand these forces. From a mechanical point of view, the rotor should be designed on the basis of a stress analysis using, for example, the finite element method. If a laminated core cannot withstand the stresses, the use of a solid layer or with a cage winding located in closed slots should be considered.

The measures taken to overcome vibration and noise problems include torque ripple reduction, minimization of unbalance, use of a high-rigidity rotor, selection of a favorable combination of the number of stator and rotor slots, elimination of rotor slots, and so forth. If the vibrations or noise are not significant, a solid rotor with a cage winding is preferred since it allows better drive performance than that of a solid rotor with distributed parameters. For high-speed drives with reduced levels of noise, a solid rotor without slots is best.

Table 4.6 presents the specification data for two variable high-speed drives using induction motors, one with solid rotor core and one with laminated core [28]. Both rotors are equipped with a cage winding.

#### 4.6.2.2 Main Dimensions

The main dimensions, i.e. the stator inner diameter  $D_{lin}$  and the effective length of stator core  $L_i$  can be chosen using the output coefficient  $C = S_g / (\pi^2 D_{lin}^2 L_i n_s)$ , the same as for other induction machines. The apparent power crossing the air gap is  $S_g = 3E_1 I_1$ ;  $E_1$  and  $I_1$  are for the fundamental harmonic ( $n = 1$ ), and  $n_s$  is the synchronous speed of the fundamental harmonic of the rotating magnetic field. Because the impedance of a solid rotor is higher than that of a cage rotor, and very often the rotor is covered with a copper layer resulting in a larger effective air gap, the apparent power  $S_g$  is lower than that of a motor with a rotor cage winding. Therefore, the output coefficient  $C$  for a solid-rotor induction motor should be approximately 70–90% of that for a cage-rotor induction motor as shown in Fig. 4.75. For example, if  $C = 12,000$  VAs/m<sup>3</sup> for a 10-kW, two-pole cage induction motor,  $C \sim 8400$ – $10,800$  VAs/m<sup>3</sup> for a similar solid-rotor induction motor. For given values of  $S_g$  and number of pole pairs, the product  $D_{lin}^2 L_i n_s$  for solid-rotor induction motors is higher than that for cage-rotor induction motors. The volume of a solid rotor is higher than that of a cage rotor.

#### 4.6.2.3 Air Gap (Mechanical Clearance)

Factors to be considered when selecting the air gap include magnetizing current, power factor, stray (surface) losses, unbalanced magnetic pull, rigidity of the shaft, and cooling from the gap surface.

From a mechanical and manufacturing point of view, the air gap can be the same as that for a cage-rotor induction motor, e.g.,  $g \approx (0.2 + 2\sqrt{D_{lin} L_i}) \times 10^{-3}$ , where  $D_{lin}$  and  $L_i$  are in meters.

#### 4.6.2.4 Rotors with Conductive Layers

The outer surface of a solid ferromagnetic rotor should be covered with a thin layer of a good conductor, usually copper or sometimes silver (micromotors). The thicker the high-conductivity layer, the lower the rotor impedance (both resistance and inductance), and the higher the developed torque. On the other hand, the high conductivity nonmagnetic layer thickness  $d$  affects the magnetizing current and power factor in the same way as the air gap  $g$ . For induction motors up to 100W, the recommended thickness of the copper layer is  $d = 0.15$ – $0.20$  mm, and for three-phase induction motors from 0.1 to 10 kW,  $d = 0.2$ – $0.5$  mm. For larger motors a detailed analysis of magnetizing current, power factor, and sometimes surface losses is required. The high-conductivity layer can reduce the transient unbalanced magnetic force because radial repulsive forces are produced by eddy currents.

The high-conductivity layer at the ends of a solid ferromagnetic core is generally thicker than that over this core, forming the end rings (Fig. 2.115). The thickness  $t_{ov}$  of an end ring can be of the same thickness as that of a cage winding.

**Table 4.6** Specifications of Two High-Speed AC Drives with Cage-Rotor Induction Motors: MELDRIVE 4000 with Solid-Core Rotor and MELDRIVE 2000 with Laminated-Core Rotor

Unit	MELDRIVE 4000	MELDRIVE 2000
<i>Input transformer</i>		
Type	3-phase rectifier transformer	—
Output	6000 kVA	—
Frequency	60 Hz	—
Voltage	3.3 kV/1100 V × 2	—
<i>Inverter</i>		
Type	24-phase voltage source GTO inverter	Voltage source transistor inverter
Output	4800 kVA	400 kVA
Frequency	2–191.5 Hz	2–200 Hz
Voltage	936 × 8	400 V
Modulation	PAM/PWM	Multipulse PAM/PWM
Control	VF control	VF control
Cooling	Forced	Forced
<i>Output transformer</i>		
Type	24-phase multiplex transformer	—
Output	4800 kVA	—
Frequency	191.5 Hz	—
Voltage	936 × 8/6.6 kV	—
<i>Motor</i>		
Type	3-phase cage induction motor	3-phase cage induction motor
Output	3300 kW	250 kW
Number of poles	2	2
Frequency	191.5 Hz	200 Hz
Voltage	6.6 kV	400 V
Speed	11,430 rpm	12,000 rpm
Cooling	Totally enclosed internal cooled. Separately powered ventilation	Drip-proof; separately powered ventilation
Rotor core	Solid	Laminated

#### 4.6.2.5 Solid Ferromagnetic Core of a Rotor

Solid ferromagnetic cores are made of carbon steels (Fig. 2.115) or alloy steels.

Consider the impedance of a solid ferromagnetic core for  $n=1$  given by Eq. 2.166. If  $h_{Fe} > 1.5\delta_{Fe}$ , it can be assumed that  $|\kappa_{Fe}h_{Fe}| > 1$  and  $\tanh \kappa_{Fe}h_{Fe} \approx 1$ , where:

$$\delta_{Fe} = \frac{1}{k_{Fe}} = \frac{1}{(\pi f s \mu_0 \mu_{rs} \sigma_{Fe})^{1/2}} \quad (4.177)$$

is the equivalent depth of penetration of the electromagnetic wave for  $n=1$ . Moreover, if  $\beta \ll a_{Fe}$  in Eq. 2.129,  $\kappa_{Fe} \approx a_{Fe}$ . The

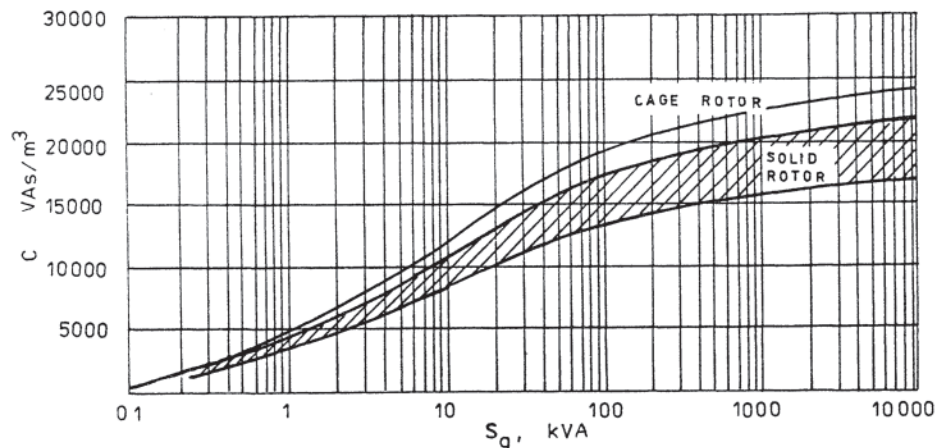


**Figure 4.75** Output coefficient  $C$  plotted against apparent air gap power  $S_g$  for two-pole solid-rotor induction motors.

impedance given by Eq. 2.166 then takes the following simpler form:

$$\begin{aligned} Z'_{Fe}(s) &\approx \sqrt{\frac{j s \omega \mu_0 \mu_{re}}{\sigma_{Fe}}} k_{tr} k_z \frac{L_2}{\tau} \\ &= (a_R + j a_x) \sqrt{\frac{s \pi f \mu_0 \mu_{rs}}{\sigma_{Fe}}} k_{tr} k_z \frac{L_2}{\tau} \end{aligned} \quad (4.178)$$

The solid core is characterized by  $\mu_{rs}$  and  $\sigma_{Fe}$ . The best material should have good magnetic properties and also the parameter  $\sqrt{\mu_{rs}/\sigma_{Fe}}$  should be small. The steel with electric conductivity  $\sigma_{Fe}=4.57 \times 10^6$  S/m containing 0.62–0.72% carbon has the lowest parameter  $\sqrt{\mu_{rs}/\sigma_{Fe}}$  of all the steels presented in Figure 2.114.

To reduce the moment of inertia, it is recommended that the core be a hollow ferromagnetic cylinder. Its thickness  $h_{Fe}$  should be approximately  $3\delta_{Fe}$  as calculated from Eq. 4.177 for  $n=1$  and  $s=1$ . If the thickness is too small, a decrease in both torque and power factor will result.

Assuming  $n=1$ , the ratio:

$$\begin{aligned} \frac{I_2}{I_\phi} &= \frac{j X_{Fe}}{Z_2'(s)/s} \\ &= \frac{\tau^2 \kappa_{Fe} [\tanh(\kappa_{Fe} h_{Fe}) + (\mu_{re} \kappa_{Al}/\kappa_{Fe}) k_z \tanh(\kappa_{Cu} d)]}{\pi^2 k_c k_{sat} \mu_{re} k_z} \end{aligned} \quad (4.179)$$

expresses the so called “goodness factor” [29] in which  $k_c$  is Carter’s coefficient,  $k_{sat}$  is the saturation factor of the magnetic circuit, and  $k_z$  is the rotor impedance increase factor given by Eq. 2.164. Equation 4.179 provides the basis by which the most appropriate solid steel cylinder thickness may be selected for a given stator design. For large  $h_{Fe}$ , the “goodness factor” approaches an asymptotic limit. For a given application, the optimum  $h_{Fe}$  is determined by balancing the degradation in motor performance against the gain from the reduction in moment of inertia.

The length  $L_2$  of the ferromagnetic cylinder can be estimated as:

$$L_i \leq L_2 \leq L_i + 0.1\tau \quad (4.180)$$

#### 4.6.2.6 Magnetic Permeability and the Electric Circuit

The rotor impedance of Eqs. 2.166 and 2.167 is a function of magnetic permeability  $\mu_{rs}$  of the solid ferromagnetic core at its surface; see also Eq. 2.110. From a practical point of view, the relative permeability  $\mu_{rs}$  at the surface ( $z=g+d$ ) is estimated at the origin of the coordinate system, that is, at  $x=0, y=0$ . The permeability  $\mu_{rs}$  is a function of the magnetic field intensity at the solid ferromagnetic core surface, that is:

$$H_{Fes} = [H_{xFe}^2(x=0, z=g+d) + H_{zFe}^2(x=0, z=g+d)] \quad (4.181)$$

where  $H_{xFe}$  is given by Eq. 2.144a and  $H_{zFe}$  is according to Eq. 2.145a for  $n=1$ . For a given steel  $\mu_{rs}$  and  $\mu'$  and  $\mu''$  may be found from the curves of Fig. 2.114. The rotor impedance calculated using Eq. 4.178 is obviously nonlinear.

The relationship between  $V_1$  (or  $I_1$ ) and  $H_{Fes}$ ,  $\mu_{rs}$  and slip  $s$

for the fundamental can be found using an iterative procedure. For a given frequency, current, and slip, computation is started for the no-load slip. Initially,  $H_{Fes}$  is taken to be equal to the line current density of the stator:

$$A_m = \frac{3\sqrt{2} N_1 k_{w1}}{\tau p} I_1 \quad (4.182)$$

where  $I_1$  is the rms value of the fundamental ( $n=1$ ) of the stator current. (See also Eqs. 2.117(a) and 2.117(b).) This represents the highest value of  $H_{Fes}$  and, after computation of the electromagnetic field components and impedances of the equivalent circuit, it is iteratively brought to its correct value for any finite slip. The most appropriate value of relaxation factor for  $H_{Fes}$  was found to be 1.0.

#### 4.6.2.7 Magnetic Circuit

The analysis of the magnetic circuit of an inverter-fed motor should be done only for the first time harmonic. It is assumed that the magnetic circuit is saturated by the first harmonic  $n=1$  of the input voltage. In this way the equivalent circuit (Fig. 2.116) can be used for each harmonic separately in an agreement with the superposition theorem. From Ampeère’s circuital law the mmf per pole pair is equal to:

$$F = 2U_g + 2U_d + 2U_{lr} + U_{ly} + U_2 = \frac{3\sqrt{2} N_1 k_{w1}}{\pi p} I_\phi \quad (4.183)$$

where  $I$  is the rms magnetizing current (first harmonic). The mmf wave is expressed by Eq. 2.115. The magnetic potential differences across the stator teeth,  $U_{1b}$  and yoke,  $U_{1y}$ , are calculated in the same way as for any other ac machine. The magnetic potential differences across the airgap,  $U_g$ , copper layer,  $U_\delta$  and solid rotor,  $U_2$ , should be calculated on the basis of the equations of electromagnetic field distribution (Section 2.5.5).

The magnetic potential difference across the air gap (mechanical clearance) is:

$$U_g = \left| \int_0^{k_{cg}} H_z(x=0, z) dz \right| \quad (4.184)$$

where  $k_c$  is the Carter’s coefficient for the stator and  $H_z(x=0, z)$  is according to Eq. 2.139a for  $n=1$ . After integrating:

$$U_g = \left| \frac{1}{M_4} \frac{j A_m}{\beta} \left( W_3 \sinh(\beta k_{cg}) - \frac{\kappa_{Cu}}{\beta} M_3 [1 - \cosh(\beta k_{cg})] \right) \right| \quad (4.185)$$

where  $A_m$  is according to Eq. 2.117a,  $\kappa_{Cu}$  is according to Eq. 2.128,  $M_4$  is according to Eq. 2.147,  $M_3$  according to Eq. 2.149,  $W_3$  according to Eq. 2.150, all quantities for  $n=1$ , and  $\beta$  is according to Eq. 2.130.

Similarly, using Eq. 2.142a, the magnetic potential difference across the copper layer can be found, i.e.:

$$\begin{aligned} U_g &= \left| \int_g^{g+d} H_{zCu}(x=0, z) dz \right| \\ &= \left| \frac{1}{M_4} \frac{j A_m}{\kappa_{Cu}} \left( \mu_{re} W_2 \sinh(\kappa_{Cu} d) \right) \right| \end{aligned}$$



$$-\frac{\kappa_{Fe}}{\kappa_{Cu}} M_2 [1 - \cosh(\kappa_{Cu} d)] \Bigg) \quad (4.186)$$

where  $M_2$  is according to Eq. 2.151,  $W_2$  is according to Eq. 2.152,  $\kappa_{Fe}$  is according to Eq. 2.129, all quantities for  $n=1$ , and  $\mu_{re}$  is according to Eq. 2.110.

One of the most difficult tasks is to calculate the magnetic potential differences in ferromagnetic portions of the magnetic circuit made of solid steel. To find the magnetic potential difference across the solid ferromagnetic core, the mean tangential flux should be calculated first, i.e.:

$$\begin{aligned} \phi_{xFe} &= L_2 \mu_0 \mu_{rs} \int_{g+d}^{g+d+h_{Fe}} H_{xFe}(x, z) dz \\ &= \frac{L_2}{M_4 \beta} \mu_0 \mu_{rs} (-A_m) e^{-\beta x} \left( \frac{\beta}{\kappa_{Fe}} \sinh(\kappa_{Fe} h_{Fe}) \right. \\ &\quad \left. - \frac{1}{\mu_{re}} [1 - \cosh(\kappa_{Fe} h_{Fe})] \right) \end{aligned} \quad (4.187)$$

where  $H_{xFe}$  is according to Eq. 2.144a for  $n=1$ .

The average value of magnetic field strength in the secondary of thickness  $h_{Fe}$  is equal to:

$$\begin{aligned} H_{xFeav}(x) &= \frac{\phi_{xFe}(x)}{L_2 h_{Fe} \mu_0 \mu_{rav}} \\ &= \frac{1}{h_{Fe}} \frac{\mu_{rs}}{\mu_{rav}} \frac{(-A_m)}{M_4 \beta} e^{-\beta x} \left( \frac{\beta}{\kappa_{Fe}} \sinh(\kappa_{Fe} h_{Fe}) \right. \\ &\quad \left. - \frac{1}{\mu_{re}} [1 - \cosh(\kappa_{Fe} h_{Fe})] \right) \end{aligned} \quad (4.188)$$

where  $\mu_{rav}$  is the average relative magnetic permeability at  $z=g+d+d_{av}$ .

If the depth of penetration [28]  $\delta_{Fe} < 0.5h_{Fe}$  then  $d_{av} = \delta_{Fe}$  (Fig. 4.76(a)). If  $\delta_{Fe} \geq 0.5h_{Fe}$  then  $d_{av} = 0.5h_{Fe}$  (Fig. 4.76(b)).

The magnetic field strength

$$\begin{aligned} H_{Fe} &= [H_{xFe}^2(x=0, z=g+d+d_{av}) \\ &\quad + H_{zFe}^2(x=0, z=g+d+d_{av})]^{1/2} \end{aligned} \quad (4.189)$$

obtained from Eq. 2.144 and 2.145 corresponds to  $\mu_{rav}$ .

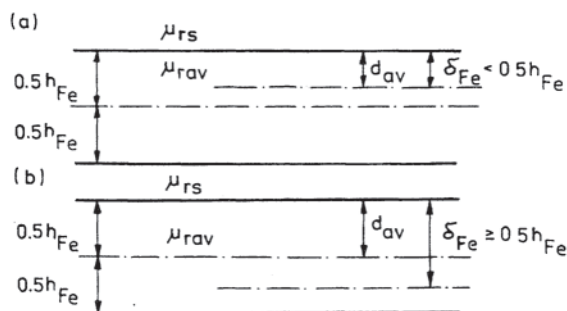


**Figure 4.76** Estimation of an average relative magnetic permeability of a solid ferromagnetic core, (a)  $\delta_{Fe} < 0.5h_{Fe}$ , (b)  $\delta_{Fe} \geq 0.5h_{Fe}$ .

The magnetic potential drop in the back iron is

$$U_2 = \left| \int_{-0.5\tau}^{0.5\tau} H_{xFeav}(x) dx \right| = \frac{2}{\pi} \tau |H_{xFeav}(x=0)| \quad (4.190)$$

The permeabilities  $\mu_{rs}$  and  $\mu_{rav}$  in Eq. 4.188 are to be determined using a magnetization curve  $\mu_r = f(H)$  for  $H = H_{Fe}$  ( $x=0, z=0$ ), and  $H_{Fe}$ , according to Eq. 4.189, respectively.

The saturation factor of the magnetic circuit due to main (linkage) flux is defined similarly as for rotary induction motors, i.e.:

$$k_{sat} = \frac{F}{2(U_g + U_d)} \quad (4.191)$$

The magnetizing current  $I$  can be found using Eq. 4.183.

#### 4.6.2.8 Losses

The stator winding loss  $P_{1w}$  is calculated in the same way as for other alternating current (ac) machines, i.e., as a sum of loss harmonics each produced by a current harmonic  $I_{1n}$  with its own skin effect coefficient; see, for example, Ref. 30. The different winding types must be considered: preformed coils from flat copper bars for larger power ratings and random windings from conductors with circular cross section for smaller power ratings.

The total rotor losses both in copper layer and solid ferromagnetic core can be calculated on the basis of the Poynting vector. The normal component of the Poynting vector for the  $n$  the time harmonic,

$$S_{zn} = -0.5 [E_{yCun} H_{xCun}^*]_{z=g} \quad (\text{VA/m}^2) \quad (4.192)$$

expresses the losses (active and reactive) per-unit area of the cylindrical rotor external surface  $2\pi\tau L_2$ , i.e., the active losses:

$$P_{2w} = 2\pi\tau L_2 \sum_{n=1}^{\infty} \text{Re}[S_{zn}] \quad (4.193)$$

The transverse edge effect in the solid steel core and losses in the end rings are not included.  $E_{yCun}$  is according to Eq. 2.143a or 2.143b and  $H_{xCun}^*$  is the conjugate of Eq. 2.141a or 2.141b.

The rotor resistance  $R'_{2n}$  ( $S_n$ ) multiplied by  $3(I'_{2n})^2$  gives the rotor losses, i.e.:

$$P_{2w} = 3 \sum_{n=1}^{\infty} (I'_{2n})^2 \text{Re}[Z'_{2n}(S_n)] = 3 \sum_{n=1}^{\infty} (I'_{2n})^2 R'_{2n}(S_n) \quad (4.194)$$

where  $I'_{2n}$  is the rotor current referred to the stator winding. Equation 4.194 includes the skin effect and transverse edge effects in both the copper layer and the solid core.

The losses in the stator laminated core  $P_{1Fe}$  can be calculated using the same relationships as for any ac motor.

Because the slots are only in the primary stack and the rotor has a smooth surface, the mechanism of the additional high-frequency losses is simpler than that for a cage induction motor. The stray high-frequency losses in a solid rotor are surface losses due to the stator slots and teeth. The method described by Heller and Hamata [31] can be adapted to the

calculation of surface losses due to the fundamental time harmonic in a solid rotor. However, good accuracy is not guaranteed. Therefore, it is better to evaluate the stray losses for  $n=1$  on the basis of mandatory standards and then to include stray losses on account of the higher time harmonics. According to National Electrical Manufacturers Association (NEMA) the stray-load losses  $P_{\text{str}|n=1}$  for a sinusoidal supply are equal to 1.2% of the rated output power for induction motors smaller than 2500 hp (1840kW) and 0.9% of the rated output power for larger motors. Heller and Hamata [31] insist that these values are too small. Hentschel and Shehata [32] propose the following empirical formula for stray-load losses with higher time harmonics being included.

$$P_{\text{str}} = P_{\text{str}|n=1} \sum_{n=1}^{\infty} \left( \frac{I_{ln}}{I_l} \right)^2 n^x \quad (4.195)$$

where  $x=1.0-1.5$ , and  $I_1$  is the stator current for  $n=1$ . It is recommended for a solid rotor to assume  $x=1.4-1.5$ .

The rotational losses (friction, windage and ventilation losses) are the same as in the case of a smooth cage rotor. There are many empirical formulas for calculation of rotational losses, e.g.,  $P_{\text{rot}} = 40(D_{\text{lin}} + 0.15)^4 \sqrt{L_i(n/100)^{2.5}}$  (watts), where  $D_{\text{lin}}$  and  $L_i$  are in meters, while speed  $n$  is in rpm.

## 4.7 MECHANICAL DESIGN

### 4.7.1 Crawling and Cogging [1, 13, 31, 33, 34]

Consider an induction motor with a uniform air gap having a distributed winding on the stator as well as on the rotor. Considering a general expression for space harmonics, one can write the air gap flux density due to stator excitation as

$$B_1(\theta, t) = \sum B_{tm} \cos(m\theta \mp \omega t) \quad (4.196)$$

It should be realized that the integer  $m$  can take any value as

$$m = \alpha N_1 \pm \beta p \quad (4.197)$$

where  $\alpha, \beta$  are integers,  $N_1$  is the number of stator slots, and  $p$  is the number of pole pairs.

For any arbitrary order of harmonic  $m$ , the synchronous speed is  $\pm\omega/m$ , and if the rotor rotates at a speed of  $\omega_r$ , the air gap flux density due to rotor currents, referred to the rotor coordinates, can be written as:

$$B_{2m}(\theta', t) = \sum_n B_{2mn} \cos[n\theta' \mp (\pm\omega - m\omega_r)t - \phi_m] \quad (4.198)$$

where  $\theta'$  is the air gap position referred to the rotor, and  $\phi_m$  is an arbitrary angle. It must be noted here that  $n$  can take values of:

$$n = \gamma N_2 \pm \delta p \quad (4.199)$$

where  $N_2$  is the number of rotor slots and  $\delta$  is an integer. Considering all harmonic orders of the rotor, and referring to the stator coordinates ( $\theta' = \theta - \omega_r t$ ).

$$B_2(\theta, t) = \sum_m \sum_n B_{2mn} \cos[n(\theta - \omega_r t) \mp (\pm\omega - m\omega_r)t - \phi_m] \quad (4.200)$$

From the principle of virtual work, one can obtain the electromagnetic torque as:

$$T = \frac{\partial W_m}{\partial \lambda} \quad (4.201)$$

where  $W_m$  is the energy stored in the magnetic field in the air gap, and  $\lambda$  is the position of the rotor.  $W_m$  is given by:

$$W_m = \frac{1}{2\mu_0} \int_0^{2\pi} [B_1(\theta, t) + B_2(\theta, t)]^2 d\theta \quad (4.202)$$

and because  $B_1(\theta, t)$  does not depend on the rotor position:

$$T = \frac{dW_m}{d\lambda} = \frac{1}{2\mu_0} \int_0^{2\pi} 2[B_1(\theta, t) + B_2(\theta, t)] \frac{dB_2(\theta, t)}{d\lambda} d\theta \quad (4.203)$$

It will quickly be apparent that the second term does not give any torque because:

$$\int_0^{2\pi} \sin \alpha \cos \alpha d\alpha = 0 \quad (4.204)$$

Furthermore, the first term will produce a torque if and only if  $m=n$ . Therefore, a torque is produced if for any given stator harmonic of order  $m$ , a rotor harmonic of order  $n=m$  can be found. Both the stator and the rotor harmonics will then have equal numbers of poles.

Considering one such harmonic pair, the torque  $T$  can be written as:

$$T_k = \frac{1}{\mu_0} \int_0^{2\pi} \left[ B_{1k} \cos(k\theta \mp \omega t) \times \sum_m B_{2km} \sin\{k(\theta - \omega_r t) \mp (\pm\omega - m\omega_r)t - \phi_m\} \right] d\theta \quad (4.205)$$

The total torque  $T$  can now be obtained as:

$$\begin{aligned} T &= \sum_k T_k \\ &= \sum_k \sum_m T_{km} \sin[k\omega_r t \pm (\pm\omega - m\omega_r)t + \phi_m \mp \omega t] \\ &= \sum_k \sum_m T_{km} \sin[\{k\omega_r \pm (\pm\omega - m\omega_r) \mp \omega\}t + \phi_m] \end{aligned} \quad (4.206)$$

It is obvious that a finite average torque can result only if:

$$k\omega_r \pm (\pm\omega - m\omega_r) \mp \omega = 0 \quad (4.207)$$

Generally it is possible to satisfy this equation in two ways:

1.  $k=m$  for all values of  $\omega_r$ .
2.  $k \neq m$ , and

$$\omega_r = \frac{\pm 2\omega}{k \mp m} \quad (4.208)$$

*Case 1:  $k=m$*  This type of operation results when both the stator field and the rotor field exhibit a component having an identical space harmonic. A torque is developed that shows a typical induction motor characteristic, with a synchronous speed of  $\omega/m$  as shown in Fig. 4.77. This torque when added to the

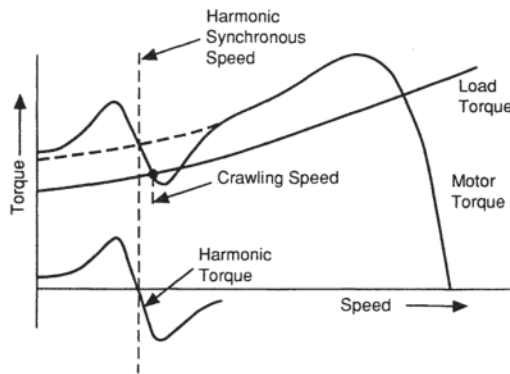


Figure 4.77 Asynchronous crawling of induction motors.

fundamental torque produces the resulting torque-speed curve as shown. If the load torque characteristic intersects the resulting motor torque characteristic as shown, the motor will crawl at a speed near the harmonic synchronous speed. This phenomenon is called *asynchronous crawling* of an induction motor.

From earlier definitions of  $k$  and  $m$ , one can satisfy  $k=m$  when:

$$\alpha N_1 \pm \beta p = \gamma N_2 \pm \delta p \quad (4.209)$$

where  $\alpha$ ,  $\beta$ ,  $\gamma$ , and  $\delta$  are all integers. That is,

$$\alpha N_1 - \gamma N_2 = (\pm \delta \mp \beta)p \quad (4.210)$$

Since  $N_1$  and  $N_2$  are both usually quite large compared to  $p$ , the practical solution to the above equation essentially means:

$$N_1 - N_2 = \pm \text{integer multiple of } p \quad (4.211)$$

**Case 2:  $k \neq m$**  This kind of operation results when a particular harmonic field is generated both by the stator and by the rotor, but with different harmonic orders. These two harmonic fields can then lock in synchronism with each other only at a particular rotor speed. For example, the magnetic field of the harmonic order  $m$  generated by the stator will rotate in space at a speed of  $\pm (\omega/m)$ .

Let us now assume that this harmonic field of the rotor is due to a stator harmonic of order  $k$  (not equal to  $m$ ). If the rotor is rotating at  $\omega_r$ , the rotor slip for this stator harmonic is given by:

$$\text{Slip} = \frac{\pm \omega/k - \omega_r}{\pm \omega/k} = \frac{\pm \omega - k\omega_r}{\pm \omega} \quad (4.212)$$

The rotor field will then rotate in space at a speed given by:

$$\omega_r \pm \frac{\pm \omega - k\omega_r}{\pm \omega} \frac{\pm \omega}{m} = \omega_r \pm \frac{\pm \omega - k\omega_r}{m} \quad (4.213)$$

The stator field and the rotor field can lock in synchronism when:

$$\pm \frac{\omega}{m} = \omega_r \pm \frac{\pm \omega - k\omega_r}{m} \quad (4.214)$$

This operation is very similar to a synchronous motor operation where a small change in load results in angular displacement of the rotor field with respect to the stator field. This phenomenon is therefore called *synchronous crawling* of induction motors. The torque speed curve is as illustrated in Fig. 4.78.

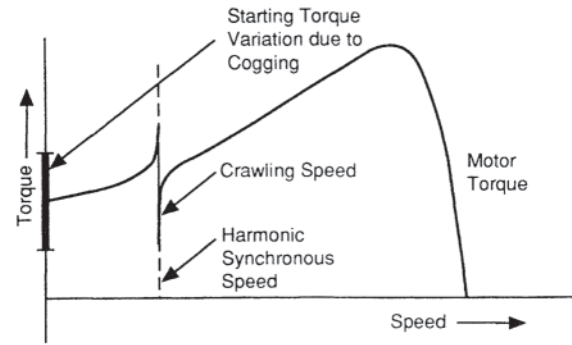


Figure 4.78 Synchronous crawling and cogging.

As an example, consider a machine with  $N_1=36$ ,  $N_2=28$  and  $p=2$ . For the working stator field at  $k=2$ , the rotor will generate harmonic fields of the order  $m=26$ . The stator will, however, also generate its own harmonic field of the order  $N_1-4p=26$ . These two fields will produce synchronous crawling at a speed of  $\omega_r=2\omega/(2+26)=\omega/14$ . Additional pairs of  $k$  and  $m$  that will produce a synchronous crawling at  $\omega/14$  may also be identified as  $m \pm k=28$ .

It may be seen that if the harmonic fields of the stator and the rotor are such that they both rotate in the same direction when the rotor is at standstill, the above equation is satisfied at rotor speed  $\omega_r$  equal to zero. A steady torque will therefore be generated at zero speed due to these harmonic fields. The magnitude of this torque depends on the position of the rotor slots with reference to the stator slots, because the equivalent permeance of the air gap and hence the stored energy in the magnetic field are both functions of the rotor position. This phenomenon is called *cogging* in induction motors.

The effects of crawling and cogging in induction motors resulting from space harmonics are usually reduced by avoiding certain combinations of stator and rotor slots, by skewing of rotor bars, and by appropriate chording of stator windings.

#### 4.7.2 Vibration and Noise

We have seen earlier that the magnetic flux in the air gap varies in time and space. The magnetic forces resulting from this flux are also functions of time and space. These forces acting on the stator and rotor cores produce unwanted vibration and noise, especially if the frequencies of the force variation are equal to or near the natural frequencies of the machine. The vibrations may lead to fatigue failures of components, and with large machines, the machine vibrations may cause vibrations in the surrounding equipment. Vibration is also a principal cause of noise, although additional sources of machine noise such as the bearings and certain siren effects can be identified.

In the most general form, the radial vibrations of the stator and the rotor may be expressed as:

$$A(\theta, x, t) = \sum_m A_m \cos(m\theta - \Omega_m t) \left[ B_0 + \sum_n B_n \sin\left(\frac{n\pi x}{L}\right) \right]$$

where  $A$  is the amplitude of vibration at a location defined by the angle  $\theta$  along the periphery and the distance  $x$  from one

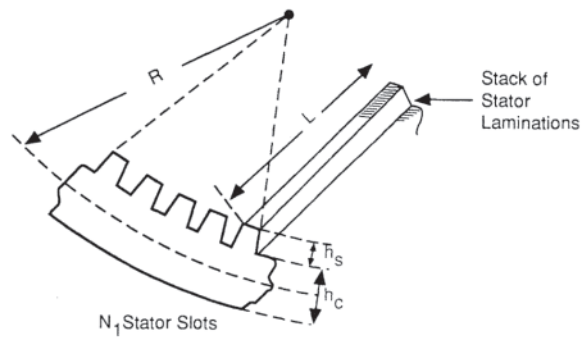


Figure 4.79 Stator geometry.

end of the machine. Except for very long machines, all the longitudinal nodes  $n > 0$  can usually be ignored, that is, the radial vibration can be considered to be independent of the longitudinal variable  $x$ .

The radial vibration for mode  $m=0$  is a pulsating vibration. It is analogous to a ball with a variable internal pressure that is higher than the ambient pressure. The vibration for mode  $m=1$  is caused by a circularly rotating unbalanced resultant force on the rotor. This force could be the unbalanced magnetic pull caused by rotor eccentricity, or two harmonic fields with their number of pole pairs differing by unity, or by permeance variations resulting from certain stator and rotor slot combinations. If the frequency of force excitation for this mode ( $m=1$ ) is anywhere near the resonant frequency of the machine, it will result in heavy machine vibration.

Yang [35] gives the following formulas for the natural frequencies ( $\Omega$ ) for machine stators having dimensions of Fig. 4.79.

$$\Omega_0 = \frac{1}{2\pi R} \sqrt{\frac{E}{\rho \Delta}}$$

where  $R$  is the radius of the stator yoke halfway behind the slots,  $E$  is the modulus of elasticity,  $\rho$  is the density of the stator core, and  $\Delta$  is the ratio of total weight of the stator to the weight of the stator yoke.

$$\Omega_1 = \Omega_0 \sqrt{\frac{2}{1 + i^2(\Delta'/\Delta)}}$$

$$\Omega_{m \geq 2} = \Omega_0 \frac{im(m^2 - 1) \phi_m}{\sqrt{m^2 + 1}}$$

where:

$$i = \frac{1}{2\sqrt{3}} \frac{h_c}{R}$$

$$\Delta' = 1 + \frac{N_s \theta_z}{2\pi R} \left( \frac{12}{L h_c^3} \right)$$

$$\theta_z = A_i^* h_s^3 \left[ \frac{1}{3} + \frac{h_c}{2h_s} + \left( \frac{h_c}{2h_s} \right)^2 \right]$$

$A_i^*$  = mean tooth area × (weight of teeth and winding/weight of teeth)

$$\phi_m = \left[ 1 + \frac{i^2(m^2 - 1)\{m^2[4 + \Delta'/\Delta] + 3\}}{m^2 + 1} \right]^{-1/2}$$

As an example, consider a 10-hp, 4-pole motor with following design parameters [13]:

Bore diameter	7 inches
Slot height	1.34 inches
Yoke depth	1.41 inches
Stator slots	36
Slot width	0.302 inches
Weight of yoke	58.7 lb
Weight of teeth	24.4 lb
Weight of copper	10.4 lb

Then one may compute the following constants:

Mean tooth area	= 2.235 inches
$R$	= 5.545 inches
$i$	= 0.0735
$\Delta$	= 1.6
$\Delta'$	= 8.4

The above Yang formulas yield the following frequencies:

$\Omega_0$	= 4670 Hz
$\Omega_1$	= 6500 Hz
$\Omega_2$	= 860 Hz
$\Omega_3$	= 2240 Hz
$\Omega_4$	= 3830 Hz
$\Omega_5$	= 5460 Hz

If the force excitation frequencies are anywhere near the above natural frequencies, the stator vibration amplitudes will be quite large. From the noise point of view, modes  $m=0-5$  will be significant for small motors: higher-order modes may also be important for larger motors because these frequencies are inversely proportional to the physical size of the machine.

The space harmonics in the air gap field having large numbers of poles induce high-frequency voltages in the windings and result in high-frequency torque and force components. These frequencies should be kept away from the natural frequencies of the machine structure.

Noise in electrical machines can be substantially reduced by reducing the excitation forces and the vibration amplitudes, and by using a larger  $L/D$  ratio. The excitation forces can generally be reduced by using a large air gap, by appropriate slot combinations, by skewing either stator or rotor slots, and by using a number of parallel paths in the windings so that effects of rotor eccentricity are reduced. The amplitudes of vibrations can generally be reduced by mismatching the natural and exciting frequencies, by increasing stiffness in the structure, and by providing adequate damping. The aerodynamic noise can be controlled by advanced fan designs, by the use of sound-absorbing materials near duct openings, and by using silencers at the entrance and exit of cooling air.

#### 4.7.3 Lamination Fatigue Mechanisms

In order to reduce eddy current heating losses and their resultant temperature rises in the core of a large squirrel-cage induction

motor, the rotor core, rather than being a solid body, is usually made up from a stack of thin laminated sheets. These laminations are coated with an electrical insulating material to prevent interlaminar eddy currents. For smaller motors, both the stator and rotor laminations can be punched from the same sheet of core steel. For larger motors, it is not practical to punch the stator core laminations from one piece of core steel and so 60-degree segments are often fabricated. Only for very large motors is it also necessary to make segmented laminations for the rotor core. A typical lamination is 24 standard gauge or 0.0635 cm (0.025 inches) thick for a large motor rotor.

When performing the mechanical design of the motor, the engineer needs to consider a number of wear and vibration modes. The stator core has to have adequate frame support so that there will be no structural failure over the lifetime of the motor. The base plate and housing should be designed to avoid resonance during start-up. The motor end-turns must be adequately braced to minimize flexing in the overhang region. The rotor spider, that connects the core to the rotor shaft, must have sufficient stress relief at each end to prevent low-cycle fatigue in itself as well as the rotor shaft, especially where the spider is welded to the shaft. The rotor core should not be over-looked in this analysis.

To maintain the rigidity of the rotor core in the axial direction, the lamination stack is compressed during stacking. The finished core is kept tight in the axial direction by through-bolts or a set of pressure plate and finger assemblies. It is also necessary to design the rotor slots to keep the circumferential movement of the rotor core lamination teeth to a minimum. This is not a problem with a cast cage rotor because the conductor fills the slot. For a fabricated rotor, conductor bars are driven into the slots and they cannot be exactly the same size as the slot because of stagger in the laminations. In other words, the laminations have some amount of misalignment as a result of the punching and stacking process. This stagger is on the order of a few mils (1 mil=0.00254 cm). In the future, it is anticipated that laser or hydraulic cutting methods will result in more perfectly aligned lamination slots. Nevertheless, punching is presently the most economic method of making slotted laminations.

Different manufacturers have different tolerances for the empty space between the bar and the sidewall slots. For the slot section shown in Fig. 4.80, these tolerances have been known to vary between 4 mils and 16 mils.

Before assembling a rotor with bar to slot clearances at the larger end of the tolerance range, the manufacturer needs to verify that the natural frequency of the rotor lamination teeth in the circumferential direction is not at the critical frequency ( $f_r$ ) that can be excited by slot harmonics of the stator:

$$f_r = nS_s \quad (4.215)$$

where:

$$\begin{aligned} f_r &= \text{critical or resonant frequency} \\ n &= \text{speed in revolutions per second} \\ S_s &= \text{number of stator slots} \end{aligned}$$

For example, in a six-pole squirrel-cage induction motor with 108 stator slots, 133 rotor slots and an operating speed at

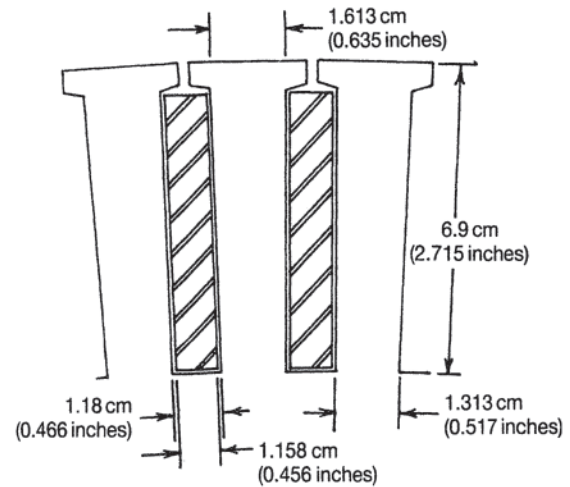


**Figure 4.80** Typical rotor slot section for a large squirrel-cage induction motor.

load of 1190 revolutions per minute, the frequency,  $f_r$ , equals 128,520 cycles per minute or 2142 cycles per second.

Figures 4.81 and 4.82 illustrate what happens when there is free circumferential vibration of rotor lamination teeth at resonance.

The weakest point is normally expected to exist at the base of the lamination tooth. The tooth is narrowest at this location

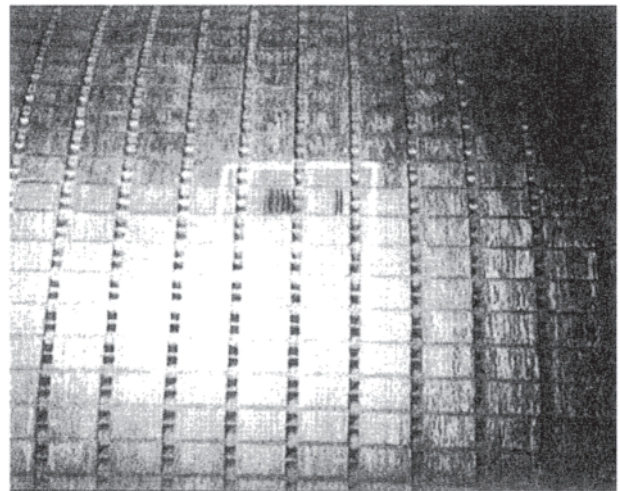


**Figure 4.81** Missing rotor lamination teeth. (Courtesy of Ohio Edison Company.)

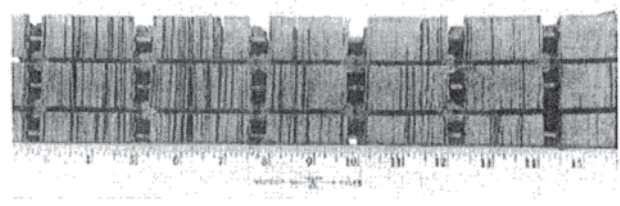


**Figure 4.82** More serious missing rotor lamination teeth condition. (Courtesy of Ohio Edison Company.)

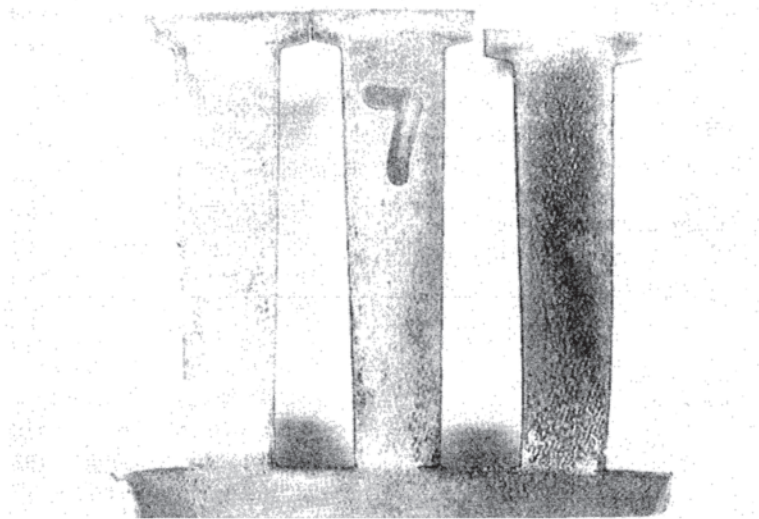


**Figure 4.83** Rotor lamination tooth cracking at the base of the slot. (Courtesy of Ohio Edison Company.)

and, in the case of square-bottomed slots, normally contains stress risers at the corners of the slot, which exacerbates the likelihood of crack initiation. Crack inception at the bottom corner of the slot is clearly shown in Fig. 4.83. Scanning electron microscopy of the fracture surfaces illustrates striations formed by cyclic stress resulting in fatigue crack propagation (Fig. 4.84).

There are countermeasures that can be taken if the number of slots cannot be readily changed

1. The stress riser can be eliminated by using slots with rounded bottoms as shown in Fig. 4.85.
2. Nailen [37] suggests that closing the rotor slot

eliminates the free body movement at the surface of the rotor.

3. Where a closed slot is not practical, the rotor bar can be swaged. The swaging process involves driving a wedge into the top of the conductor bar expanding it to fill the slot. This countermeasure will not be successful if the swaging is incomplete or substandard.

Fortunately, the design of rotor laminations with a circumferential critical frequency at the full-load operating speed of the induction motor occurs infrequently. Nevertheless, a wide range of failure scenarios is possible when this situation exists.

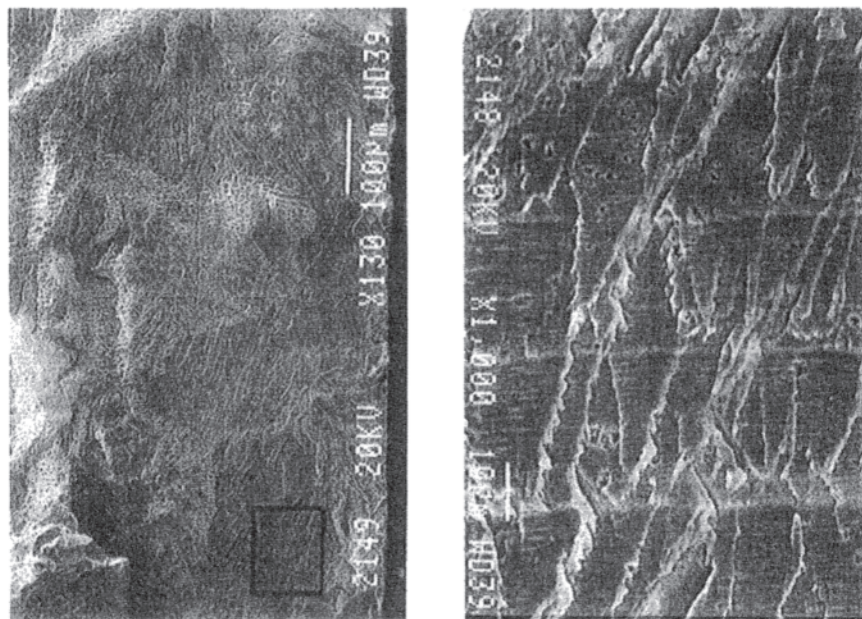


**Figure 4.84** Scanning electron micrographs showing the rotor lamination crack surface. (Courtesy of Ohio Edison Company.)

## Induction Motor Analysis and Design

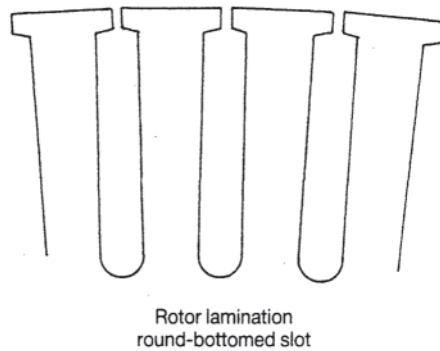
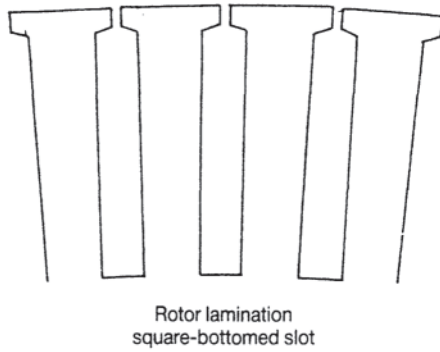


**Figure 4.85** Comparison of rotor lamination changes to eliminate stress risers at the bottom corners.

1. There is a benign failure mode in which the clamping force of the rotor pressure plates keeps the teeth from flying out of the rotor reacting to centrifugal force. In this mode, the broken tooth moves outward slowly until it contacts the stator core. It curls over as it continues to move into the air gap until a small ball breaks off. This process continues until several small balls have been formed and the broken tooth has completely worked its way out of the rotor. These steel balls become distributed in the stator core ventilating spacers and in the bottom of the motor. In an open motor, they will be redistributed and some will be ejected from the cooling air exhaust during start up of the motor. Obviously, there is a limit to the number of broken teeth that can develop before something more serious will occur.

2. At the other extreme, broken teeth can act as a cutting tool during migration into the air gap. If they enter the air gap in large enough pieces, they can behave like any other foreign object, damaging the stator core, slot wedges, and conductors. The loss of a sufficient number of teeth from adjacent iron packs or the iron packs along the same pair of rotor slots can cause severe mechanical unbalance and related bearing

problems. If the pack moves into the air gap as a single mass, the motor might jam, resulting in a locked-rotor failure.

#### 4.8 THERMAL DESIGN

There are several components of losses in electrical machines. These include, among others, ohmic losses in the primary and secondary circuits, commonly referred to as the copper losses; eddy current and hysteresis losses in the ferromagnetic material, commonly referred to as the core losses; stray-load losses in the frame structure parts and strands and the mechanical losses such as bearing friction and windage losses. When a machine operates continuously at any given load, a steady-state temperature distribution is established in the machine such that the heat generated within the machine is equal to the heat transferred from the machine to the surrounding medium. The temperature rise within the machine has to be limited for two reasons: mechanical stress and the deterioration of the insulating materials.

Temperature rise is accompanied by expansion when the material is not constrained. If  $\alpha_T$  is the coefficient of linear expansion at any temperature  $T$ , one may write:

$$\alpha_T = \frac{\Delta l/l}{\Delta T}$$

i.e.:

$$\text{Strain } \epsilon = \frac{\Delta l}{l} = \alpha_T \Delta T$$

If the material is constrained from expanding freely, any temperature rise is then accompanied by a mechanical stress  $\sigma$  given by:

$$\sigma = \epsilon E$$

where  $E$  is the modulus of elasticity. The temperature rise must therefore be limited such that the mechanical stresses are within permissible values. In a deep-bar rotor, for example, the classic skin effect results in an uneven distribution of current in the bars especially during standing and acceleration. The current, and consequently the heat, tend to concentrate near the top of the bars. The resulting uneven bending of the bars causes additional stresses at the point where the bars and the end rings meet. These stresses must be considered in determining allowable temperature rise in the rotor.

The life of insulating materials is also significantly reduced if they are operated at temperatures higher than the recommended operating limit. As a general rule, the life of insulation is almost halved for every  $10^\circ\text{C}$  rise in the operating temperature. Possible high temperatures at different hot spots within a machine are therefore an important factor in determining the operating limits for the load on a machine.

It will be apparent that the permissible temperature rise and hence the permissible maximum load depend very much on the ambient temperature: the higher the ambient temperature, the lower is the permissible maximum load on the machine on the temperature rise allowed.

### 4.8.1 Methods of Cooling

Heat is transferred from one location to another by conduction, convection, and radiation. Conduction is the principal method of heat transfer through metallic materials; it is the first stage in dissipating copper and core losses of any machine. Convection occurs at any interface between a solid and a fluid. The fluid that acts as a cooling medium absorbs the heat at one location and carries it away with its own movement. The movement of the fluid may be caused either by temperature gradients themselves or by fans or blowers; the flow may be either laminar or turbulent depending upon the characteristics and the speed of the fluid. Radiation is the process in which heat is transferred by means of electromagnetic waves. This mode of cooling is important when heat must be dissipated across a vacuum, such as in space.

Modern electrical machines exhibit large heat losses per unit area of the surfaces across which the heat may be removed. These machines, therefore, have to be artificially cooled to avoid excessive temperatures. In most cases, this is achieved by convection using flow of air: this is also called the ventilation of electrical machines. High-speed turbo/generators and synchronous condensers are generally hydrogen-cooled. Some special-application machines are also cooled by forcing water through hollow current-carrying conductors.

Ventilation of an electrical machine is achieved either by air ducts in the rotor, built-in fans, or by a separately driven external fan. The fan might be centrifugal or axial. A centrifugal fan forces air from the center to flow outward, irrespective of the direction of rotation. A propeller-type axial fan can move air axially in either direction depending on the direction of rotation.

There are four basic schemes of machine ventilation:

1. *Natural ventilation:* The air flow is produced without the help of any fan, caused only by rotation and temperature gradients.
2. *Self-ventilation:* The air flow is caused by air ducts or built-in fans that are an integral part of the machine.
3. *Frame ventilation:* The external surface of the frame of a totally enclosed machine is cooled by means of a built-in fan. A separate fan may be used to circulate air inside the enclosed machine.
4. *Separate ventilation:* The flow of cooling air is caused by an external fan, separately driven.

If separate ventilation is used, the fan may be placed either at the point of air discharge (suction ventilation) or at the inlet (forced ventilation). In terms of cooling effects, there is no practical difference between the two. However, if filters are to be used to clean the air flowing through the machine, placement of the fan at the inlet (forced ventilation) is advantageous. The air pressure throughout the machine will be greater than that outside, and the inevitable leakage of air will be from inside (cleaned air) to the outside. Air leakage with suction ventilation brings unfiltered air into the machine and is not recommended for pressuring machine in hazardous locations.

In the ventilation schemes illustrated in Fig. 4.86, the heat is directly transferred to the cooling air, which is being continuously replaced. This is called *open-circuit ventilation*.

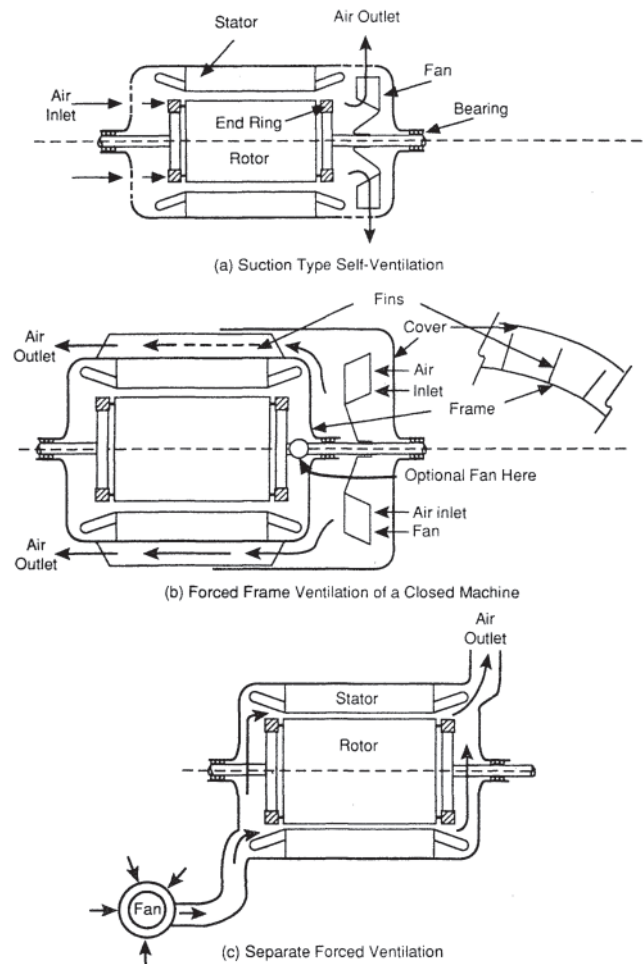


**Figure 4.86** Open-circuit machine ventilation.

In *closed-circuit ventilation*, the heat is transferred to the cooling fluid via an intermediate fluid medium; the intermediate fluid circulates in a closed circuit as illustrated in Fig. 4.87. Hydrogen gas is sometimes used as the intermediate fluid; it is lighter than air and is a better conductor of heat.

In medium- and large-size machines, the surface area in contact with the cooling air is usually increased by providing radial and axial ducts in the stator and the rotor as required.

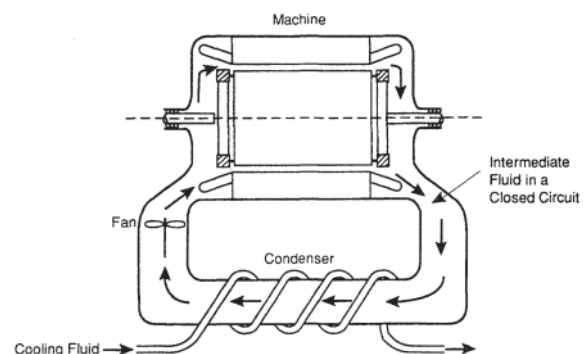


**Figure 4.87** Closed-circuit ventilation.



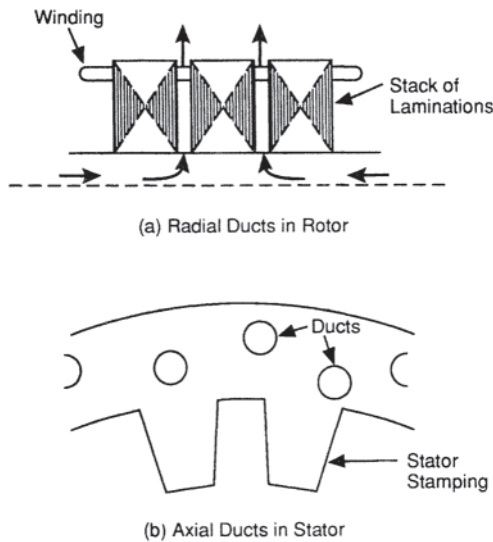


Figure 4.88 Radial and axial ducts.

This is illustrated in Fig. 4.88. The radial ducts allow air to be sucked in from both ends of the machine and provide similar cooling for both end windings. It is, however, not very effective with lower values of peripheral speed. The axial ducts of Fig. 4.88(b) are highly effective except when the machine length is very large.

The volume of air flow can be estimated by knowing the density and the specific heat of air and by knowing the temperature rise permitted for the machine.

#### 4.8.2 Design of the Ventilation Circuit [38]

The ventilation circuit of an electric machine essentially consists of a system of axial and radial ducts joined together in series and parallel. Each element of this circuit offers a certain hydrodynamic resistance to the flow of a cooling fluid such as air. This resistance depends on the dimensions of the circuit element and the density of the cooling fluid. The hydrodynamic pressure  $H$ , the resistance  $Z$ , and the rate of air flow  $V$  (volume per second) are related by

$$H = ZV^2$$

Hence, if two elements are in series as shown in Fig. 4.89, the resultant resistance  $Z_s$  is given by:

$$Z_s = Z_1 + Z_2$$

If, however, the two elements are in parallel:

$$V_a = \sqrt{\frac{H}{Z_a}}$$

$$V_b = \sqrt{\frac{H}{Z_b}}$$

$$V = V_a + V_b = \sqrt{H} \left( \frac{1}{\sqrt{Z_a}} + \frac{1}{\sqrt{Z_b}} \right)$$

and the resultant resistance  $Z_p$  is given by:

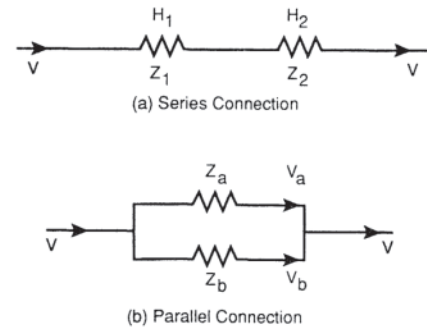


Figure 4.89 Connections of ventilation circuit elements.

$$\frac{1}{\sqrt{Z_p}} = \frac{1}{\sqrt{Z_a}} + \frac{1}{\sqrt{Z_b}}$$

i.e.:

$$Z_p = \frac{Z_a Z_b}{(\sqrt{Z_a} + \sqrt{Z_b})^2}$$

Once the total hydrodynamic resistance of the ventilation circuit and the volume of the air flow is known, it is possible to select a proper built-in centrifugal fan. It should be noted here that if the machine is used for variable-speed duty it may not be possible to use self-ventilation, depending on the duty cycle involved. For short duty cycles and/or for wide speed variations, separate ventilation may be necessary.

## 4.9 COMPUTER-AIDED DESIGN OF ELECTRIC MACHINES

### 4.9.1 Why We Need Computers in the Design of Electric Machines

Techniques for *designing*, *analyzing*, and *driving* electric motors have developed rapidly with computers and power electronics. Today we rely on numerical methods to understand the electromagnetic, thermal, and mechanical behaviour of machines. *Design* is distinct from *analysis*. It requires imagination and judgement that go beyond the realm of mere computation.

Most of the key tasks in electric machine design are software-based:

1. Basic electrical and magnetic design
2. Thermal management
3. Control and system performance analysis
4. Mechanical computer-aided design (CAD)
5. Mechanical analysis (dynamics, stress, noise)
6. Optimization
7. Database management of designs, manufacturing details, inventory, etc.

The most fundamental tasks are (1) and (2), because they determine all the basic dimensions of the motor, the materials used to construct it, and the performance. This section focuses on these tasks.

In the simplest cases, task (3) is a matter of ensuring that the motor will start when it is switched on, or stop when it is switched off. Much more complex simulations may be required when the motor design is being coordinated with the design of a complete

system, such as an automotive electric power steering gear. Task (4) is a necessary part of design for manufacture and is frequently integrated with Task (5). Task (6) is for the refinement of the design, but optimization software depends on having a fast and reliable computer engine or model for tasks (1) and (2). Task (7) is not really motor design *per se*, but it is often important for motor design software (task 1) to interface closely with a company's database or catalog of designs, and/or with its inventories of standard components such as punchings, ending dies, etc. Because of this, software for task A may be required to calculate cost functions based on material weights and other parameters related to performance and manufacturing factors.

Electric machines are usually designed by specialist engineers skilled in electrical and mechanical engineering. More and more, these specialists need knowledge of power electronics and system simulation. In larger companies, there may be separate specialists for all the tasks 1–7, but this is a luxury beyond the reach of smaller companies. These factors make it increasingly important to have good communication between the various software tools, especially because there is no single software package that performs all the tasks.

The easiest task in electric machine design is to make a small modification to an existing design. A simple example is to reconnect the windings of a 230-V motor to make it operate at 115 Vs. It is easy to predict the resulting changes in the motor's parameters, such as the winding resistance and the current, the efficiency and the temperature rise. But even for such simple modifications it is convenient to perform the calculations on a computer model, because of the organized way which the data can be managed.

At the other end of the scale, imagine the difficulty of designing a completely new motor for a new application, such as a special kind of actuator on a spacecraft. Often, not even the type of motor is known at the outset. Even after the envelope dimensions and the details of the power supply have been determined, hundreds of parameters must be optimized. The design must be analyzed in detail to assess the reliability, to optimize the interaction between the motor and its load, and to provide for fault conditions. It is unthinkable to fulfil these requirements without computer models.

### 4.9.2 The Nature of the Design Process

A “design” is defined as a set of “design parameters.” The design parameters include all the dimensions of the laminations, windings, magnets, etc., together with the numbers of turns in the winding, the layout of the windings, and many details of the supply. For motors that run from electronic drives, the design may include details of control parameters such as commutation angles and set-point values of controlled voltages or currents.

The design process is concerned with determining the design from a set of specified performance requirements. It also includes performance calculations to ensure that the design meets the performance requirements. Because there is no general procedure for synthesizing a design to meet a set of performance requirements, most designers rely on an iterative or recursive process in which the parameters are adjusted recursively until

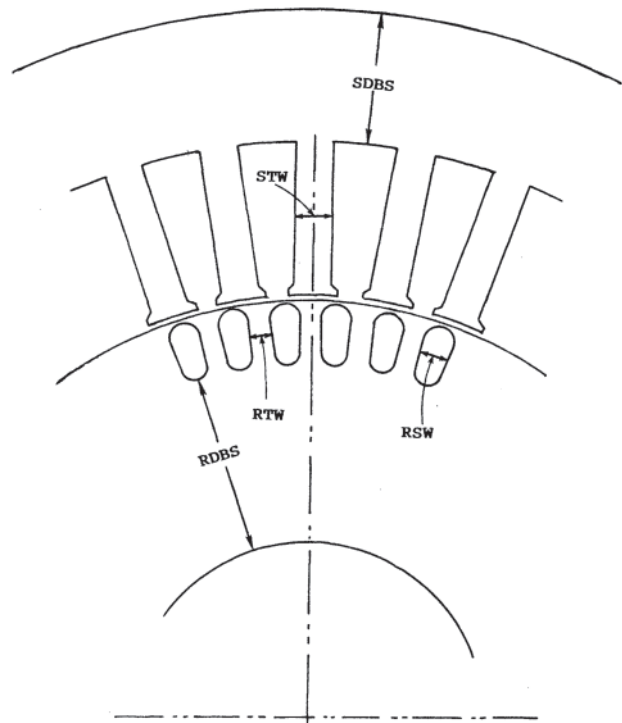


**Figure 4.90** Design process using manual repetition of performance calculations.

the performance calculations indicate that the design will meet the performance requirements. The final result is a design sheet summarizing all the design parameters and many aspects of performance, including graphical data.

In Fig. 4.90 this recursion is described as manual repetition. Even when a computer program is available to perform the performance calculations, the design engineer make all the decisions about parameter adjustments. In other words, all the intelligence and creativity is contributed by the design engineer, while the computer does nothing more than model the current version of the design. Although the words manual repetition may suggest a crude and approximate approach, the performance calculations may be complex and sophisticated, while the design decisions can be delicate and may involve difficult compromises and matters of judgment. The partition of responsibility between the computer software and the design engineer is generally very effective in this model.

**Figure 4.91** shows the same basic design process with three enhancements:

1. The incorporation of finite-element analysis in the performance calculations;
2. The automation of some or all of the manual repetition; and
3. The storage and management of the design in a database.

Finite-element analysis is generally specialized to one technology (such as electromagnetic field analysis), and is still relatively slow in spite of the advances made in computer processing speed. For these reasons it is not a trivial matter to integrate finite-element analysis into the design process. In the

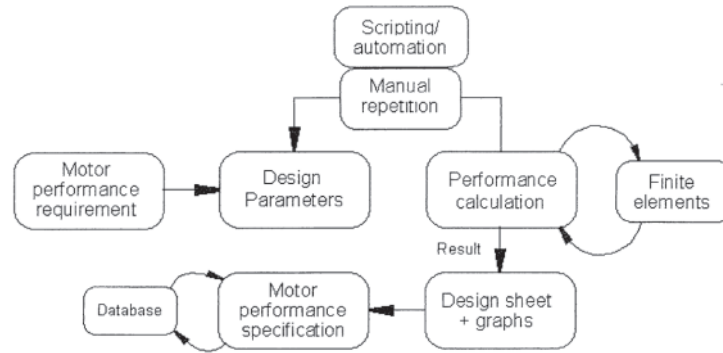


**Figure 4.91** Design process enhanced with finite-element computations, database facilities, and automation.

examples given below, the finite-element process is automated as far as the generation of data that can be readily fed back into the performance calculations, so that for standard calculations the design engineer need not concern himself with the details of meshing or controlling the solution or the post processing.

Automation of the manual repetition is possible only if a sensible algorithm is provided. Consider, for example, the automatic determination of the number of turns required in a winding by a search process. The search must follow the basic relationship between voltage and flux, expressed mathematically in the correct form for the particular type of motor. But it must also work within the practical constraints of discrete wire sizes, maximum slot-fill factor, etc. Once the process is automated, the designer's role becomes one of supervision and evaluation, rather than of execution. Therefore the automatic algorithm must be written carefully and efficiently to avoid hidden errors and produce reliable, practical results.

Design automation becomes extremely complex if the computer is entrusted with the control of more than one or

two design parameters, because of the interactions between parameters and their constraints. The constraints and objectives are usually highly particular to one company or one product, and therefore it is important that software capable of this type of automation or optimization be easily programmable by the user. By the same token there is no serious market for software that purports to synthesize or optimize the design automatically without detailed programming by the user. Not only the results, but often also the constraints and process of achieving particular results are proprietary. Accordingly there are few publications describing these processes, even though there are some published examples of the use of formal tools such as genetic algorithms, Monte Carlo methods, and others.

#### 4.9.3 Steps Needed to Design an Electric Machine

In CAD of electric machines, an important part of the design process is the definition of input data for the performance calculation. This can be divided into distinct sections:

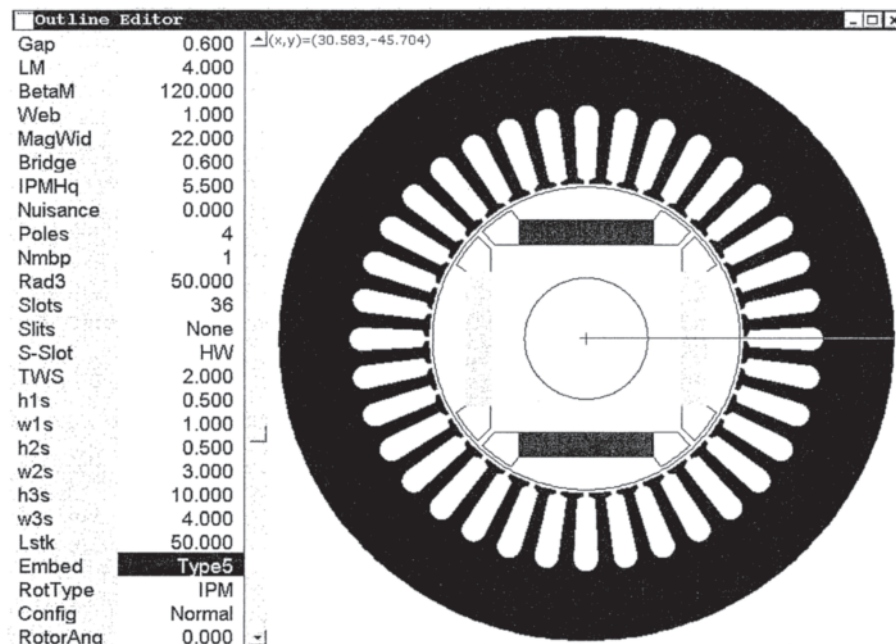


**Figure 4.92** Parameterized graphical data entry for the motor cross section: the “outline editor.”

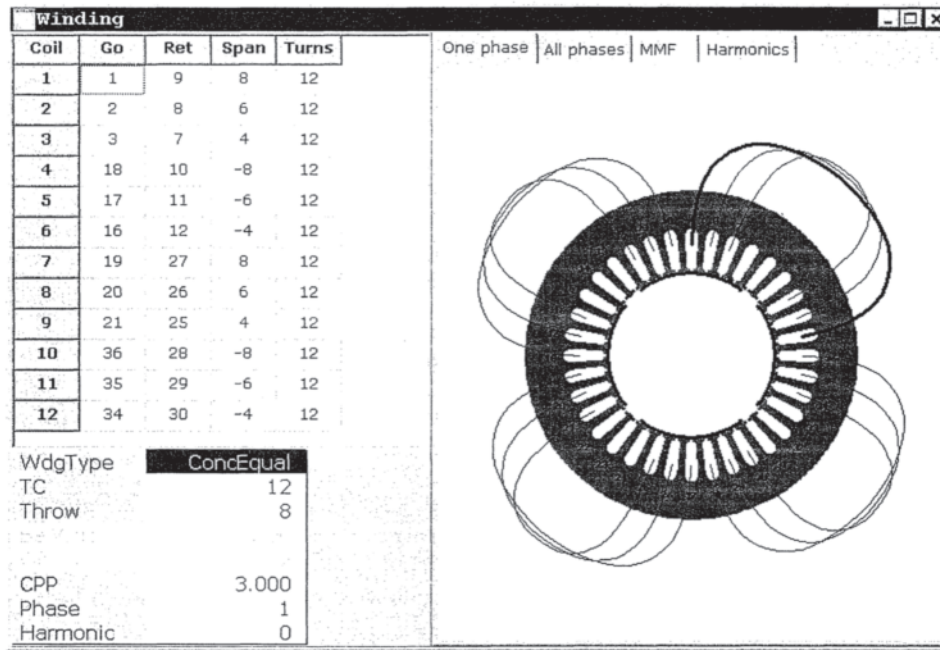


Figure 4.93 “Winding editor” for the construction of standard or custom windings.

1. *Drawing the cross-section:* The best starting point is a cross section of the machine such as in Fig. 4.92, which is “parameterized” so that dimensional changes can be viewed instantly, giving the engineer a powerful tool for developing a visual image of the relationship between the performance and the shape and size of the motor and its elements. Later this same cross section

will be overlaid with flux-lines and color maps of flux-density and other functions.

2. *Defining the winding layout:* Related to Fig. 4.92 is the *winding editor*, Fig. 4.93, in which the cross section is overlaid by a diagram of the winding layout. Again the parameterization permits instant visualization of changes in the pitch and layout of the coils. The slot-

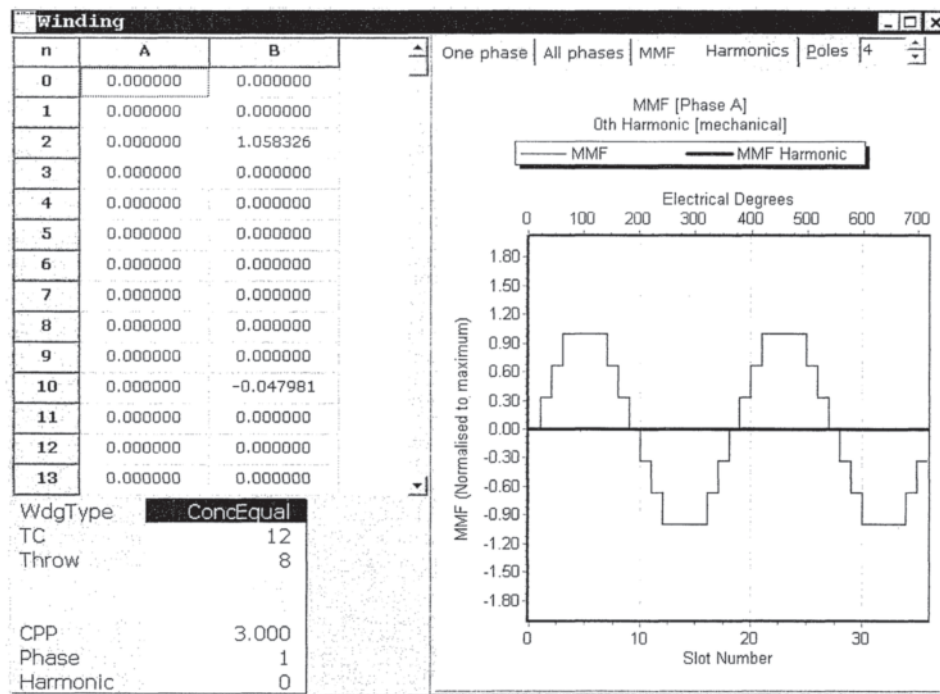


Figure 4.94 Magnetomotive force (mmf) distribution around the airgap, displayed by the winding editor.

Template Editor							
<b>Dimensions</b>							
Config	Normal	RotType	IPM	Poles	4	Slots	36
Lstk	50.000	Embed	Type5	LM	4.000	S-Slot	HW
Rad3	50.000	Rad1	25.000	BetaM	150.000	SD	14.000
Stf	0.970					SO	2.000
MOH	0.000	Bridge	0.600	SOAng	20.000	TWS	2.000
RotorAng	0.000	RadSH	10.000	TGD	1.000	Gap	0.700
<b>Windings</b>							
WdgType	ConcEqual	Throw	8	CPP	3.000	TC	12
NSH	1	PPATHS	1	Ext	0.000	Liner	0.400
WireSpec	BareDia	Wire	2.000	XET	1.000	InsThick	0.000
Skew	1.000						
<b>Control</b>							
RPM	3000.000	Vs	300.000	Drive	Sine	Connex	3-Ph Wye
ISP	15.000	fChop	0.000	Sw_Ctl	dq_VV_CR	gamma	0.000
				Tol_ISLA	Auto	Tol	8.000
EMFCalc	BLV	ChopType	Soft	RTorq	On	Dwell	0.000
<b>Thermal</b>							
TempCalc	DegCW	Templt	IterX	Wdg2Mag	0.800	Ambient	20.000
T_Mag	25.000	T_Wdg	25.000	T_Brg	25.000	T_Gap	25.000
DegCW	0.000					ThTol	1.000

Figure 4.95 “Temple editor” for input data.

fill factor can be displayed for every slot, to confirm that all slots have equal numbers of conductors. In Fig. 4.94 is shown the mmf distribution of the winding in Fig. 4.93, with ideal current values in the individual phases according to the type of drive (sinewave or squarewave current waveforms). A harmonic analysis of this mmf distribution can also be displayed graphically, along with the winding factors.

3. *Definition of numerical and other parameters:* As simple as Figs. 4.92 and 4.94 appear, a complete design may have as many as 500 input parameters, many of which cannot be represented graphically. In the *SPEED* software this data is made accessible in two types of *template editor*, one of which contains *all* the parameters organized by type (dimensions, winding, controls, materials, etc.); see Fig. 4.95. The other one is a *custom editor* that contains only a subset of parameters chosen by the user, Fig. 4.96. Several custom editors can be open at the same time, and they can be made to overlay a window of graphical results, so that the effect of parameter changes can be seen instantly without switching back and forth between windows. The custom editor is useful when frequent changes are made to a small number of parameters. It is also useful in training because it hides the complexity of the entire parameter set in the main template editor.
4. *Graphical and numerical representation of results:* A motor design calculation involves hundreds of computations of varying levels of complexity, producing a mass of data covering basic performance (torque, power, efficiency, current, power factor, etc.); electric circuit parameters (currents in individual windings and power semiconductor devices), magnetic fluxdensities at different points in the cross section, temperature rise at different points in the cross-section, and a detailed breakdown of losses (core losses, stray load losses, frictional losses and copper losses). The representation of this data is both graphical and numerical. Figure 4.97 is an example of graphical output data—a set of waveforms of current, emf and torque in a brushless permanent-magnet motor of the type shown in Fig. 4.92. The output data presents the same problem of organizing large quantities of information as the input data, and the same approach is used to represent it: a comprehensive *design sheet* containing every calculated parameter as well as all the input parameters, organized into sections; and a set of *custom design sheets* containing subsets of output parameters, similar to Fig. 4.96.
5. *Ranging:* One of the most useful performance calculations is a complete graphical representation of the torque/speed characteristic including the variation of current, efficiency, power-factor, etc., as the load and/or speed varies. This involves the repetition of the performance calculation over a range of load and/or speeds—a process known as *ranging*. A common example is the calculation of torque, current, efficiency, etc., over a range of speeds.
6. *Thermal analysis:* Thermal analysis is essential in the design of electric machines. Because the insulation life is sensitive to the winding temperature, it is desirable to estimate the maximum winding temperature (“hotspot” temperature) as accurately as possible. The temperatures of the windings, the iron, and any magnets have a significant effect on the

The screenshot shows a window titled "TED - TJEM" with a close button (X) in the top right corner. The window contains a list of parameters, each with a text input field or a dropdown menu. The parameters and their values are as follows:

Parameter	Value
ISP	15.000
gamma	0.000
Tol	8.000
Drive	Sine
ISLA	24.000
HBA	8.000
RPM	3000.000
BetaM	150.000
Sw_Ctl	dq_VV_CR
SO	2.000
dqD	true
fChop	0.000
Vs	300.000
FixfChop	Yes
HBtype	Constant
Tol_ISLA	Auto
XL	1.000

Figure 4.96 “Custom editor” for simplifying the data entry.

efficiency. The temperature of the frame is important for environmental reasons, and the temperatures of the shaft and bearings and other structural components are important in determining stress levels and thermal expansion. For these reasons the calculation of the temperature distribution within the machine requires a thermal equivalent-circuit model of the type shown in Fig. 4.98.

In Fig. 4.98 the thermal equivalent-circuit contains heat sources, thermal resistances, and thermal capacitances. The circuit is solved transiently by integrating its differential equations, which basically represent thermal diffusion (conduction), convection, and radiation from and within the various components of the machine. The transient solution is usually necessary because it is often the case that electric machines are used intermittently, or with a variable duty-cycle. In other cases the greatest rate of heat generation may occur under transient conditions, for example, during the starting of induction motors the rotor cage heats up at a rapid rate that cannot be sustained for more than a few seconds. Figure 4.99

shows a typical set of transient temperatures at several nodes in such a model after start-up.

The individual elements of the thermal equivalent circuit must be calculated one by one, including the loss components (which generally themselves vary with temperature). This requires the exercise of a considerable range of engineering theory, particularly in calculating the losses and several of the thermal resistances that depend on convection. Because of the indefinite nature of some of the elements (such as the thermal interface resistance between components that are only in partial contact), calibration of the thermal equivalent circuit model is usually necessary, using test data typically from machines wired up with thermocouples. Sophisticated numerical analysis such as the finite-element method and various methods in computational fluid dynamics can help to resolve the values of certain thermal resistances, but no one method is available to calculate all of them.

Because of the need to compute the loss components at the correct temperature, the thermal calculation must be integrated into the design program, and its solution must be

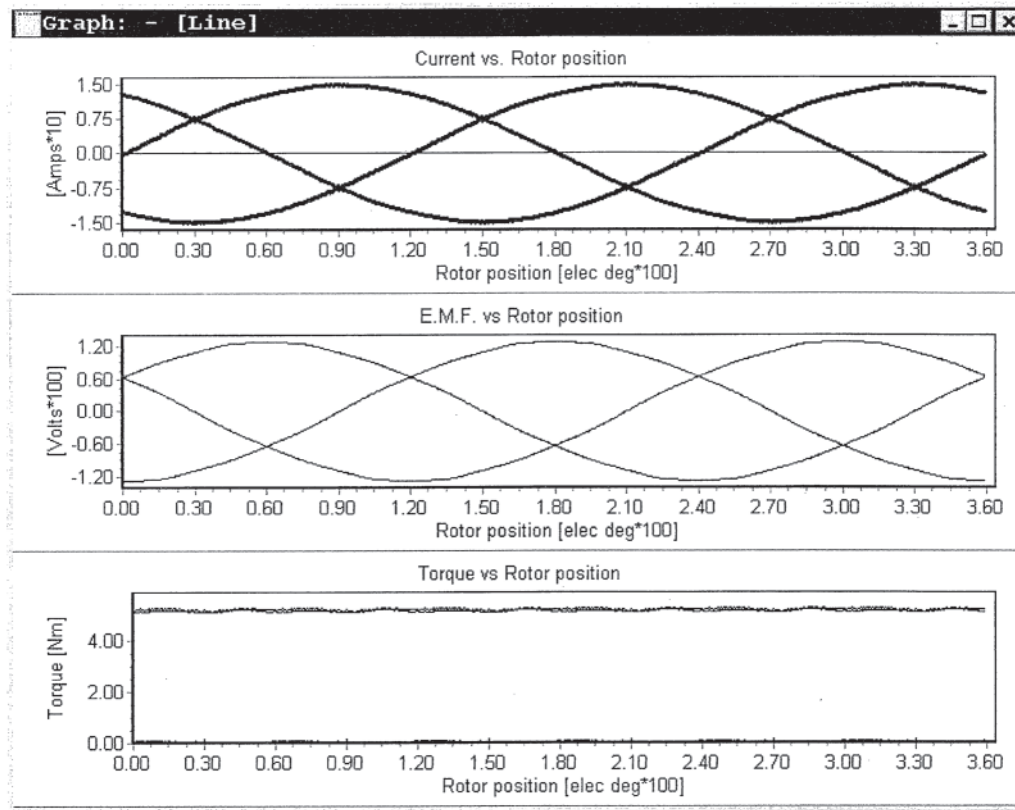


Figure 4.97 Graphs of current, electromotive force (emf), and torque waveforms produced by the design program.

iterated along with all the other iterative calculations of the magnetic field, controller currents, etc.

#### 4.9.4 Examples of Specialized Computer Analysis

Many aspects of electric machine design require specialized analysis tools. One of the commonest examples is the use of finite-element analysis for a more precise estimate of the magnetic field distribution inside a machine. Figure 4.100 shows an example of the calculation of the magnetic field in a permanent-magnet motor in which the stator current is producing a strong demagnetizing effect on the magnet. The estimation of local demagnetization effects is hardly possible by classical analytical methods in such a complicated nonlinear structure.

Figure 4.101 shows the distribution of airgap flux-density in a permanent-magnet motor of the type shown in Fig. 4.92. The ordinate is azimuthal position. The deeply notched graph is the finite-element computation of the actual airgap flux-density, while the smooth graph following more or less the averaged finite-element curve is produced by an analytical magnetic lumped-circuit circuit analysis that uses empirical functions for the shape of the airgap flux-density wave. The analytical method does not model the slotting in detail, but uses Carter's coefficient. Although the finite-element graph is very interesting, it cannot be used directly to calculate the generated emf because the notches caused by the slot-

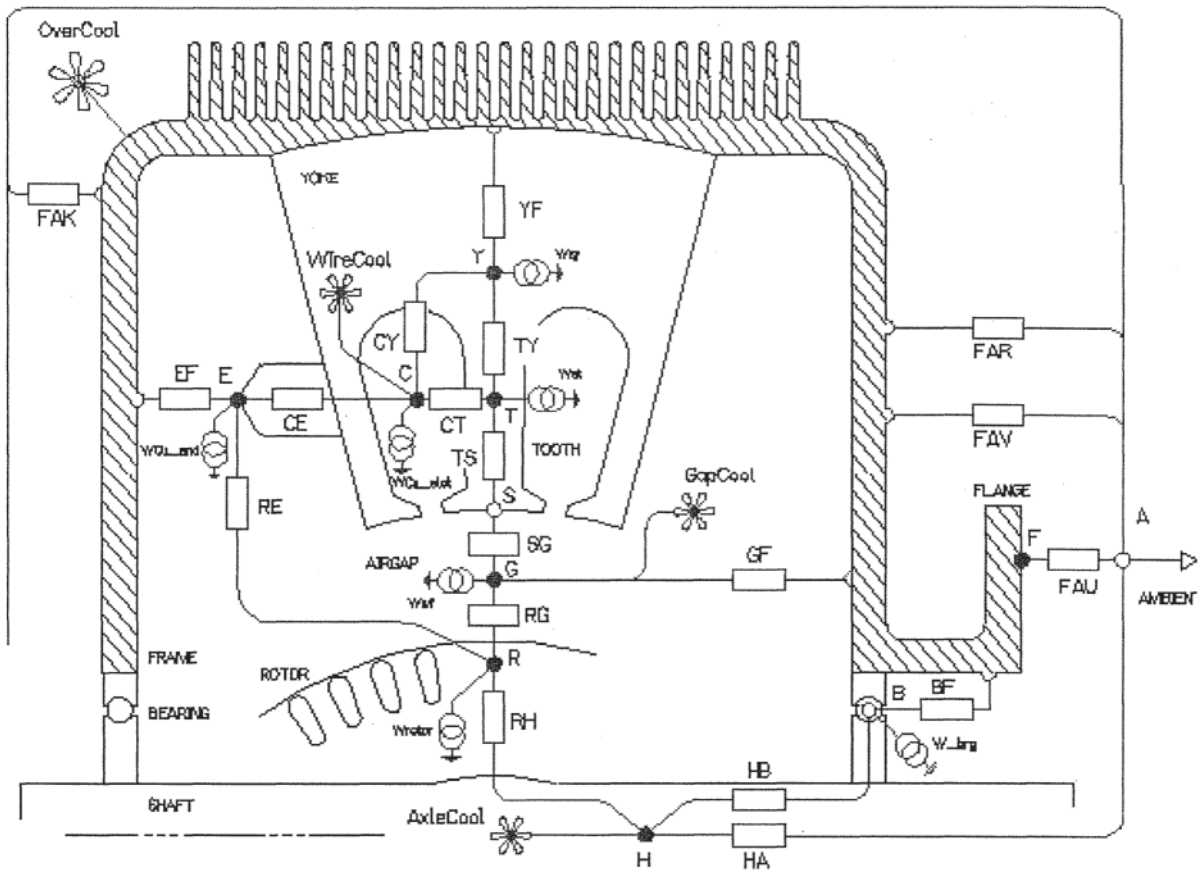
openings do not move relative to the stator conductors. The smooth analytical graph is better for this purpose, but even so its value may be modulated as the rotor rotates, so producing a modulation in the emf waveform that is not apparent from a single plot such as Fig. 4.101. A more rigorous technique is to compute the flux-linkage of a test coil wound around a single tooth as the rotor rotates. From this flux-linkage the flux-linkage of any winding distribution can be computed, and from its derivative with respect to rotor position the EMF.

Figure 4.101 also shows the fundamental space-harmonic component of the airgap flux-density distribution, in which the finite-element method and the analytical method agree closely.

General design software such as the *SPEED* software described in earlier sections is well adapted for the following tasks:

- Preliminary design (including routine simple finite-element analysis)
- Calibration of product designs
- Providing a unified, complete machine model covering many technical disciplines
- Providing instantaneous calculations
- Training
- What-if analysis

Because of its convenience and range, it is useful in providing a set of standard templates for communication between manufacturer and user.



**Figure 4.98** A 10-node thermal equivalent-circuit model representing transient and steady-state heat transfer within the motor and between the motor and the environment.

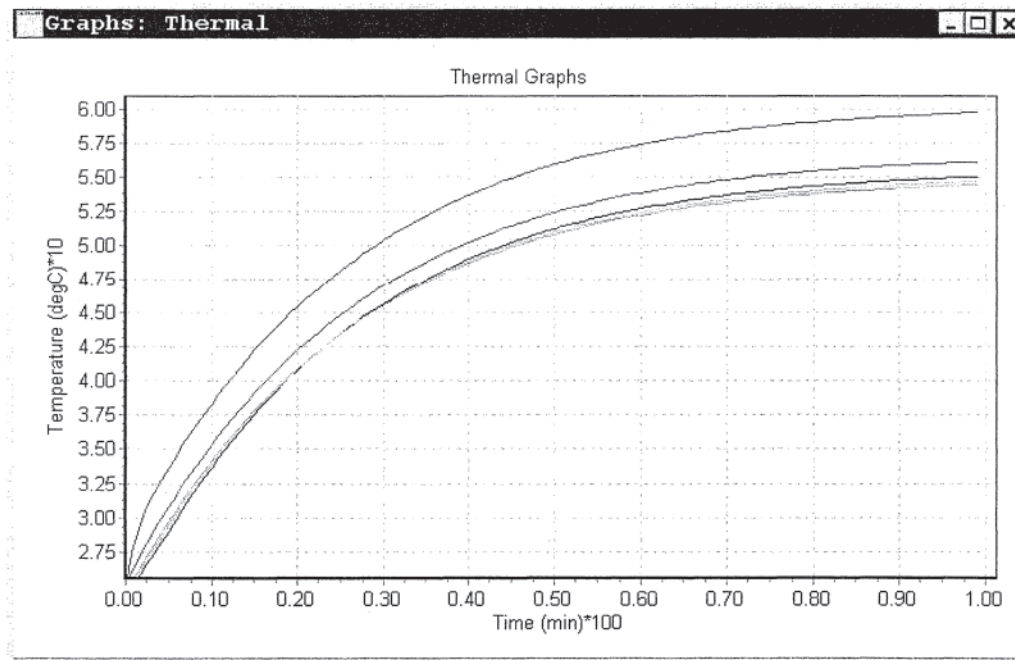


**Figure 4.99** Temperature-vs.-time graphs computed by the 10-node thermal equivalent circuit model.



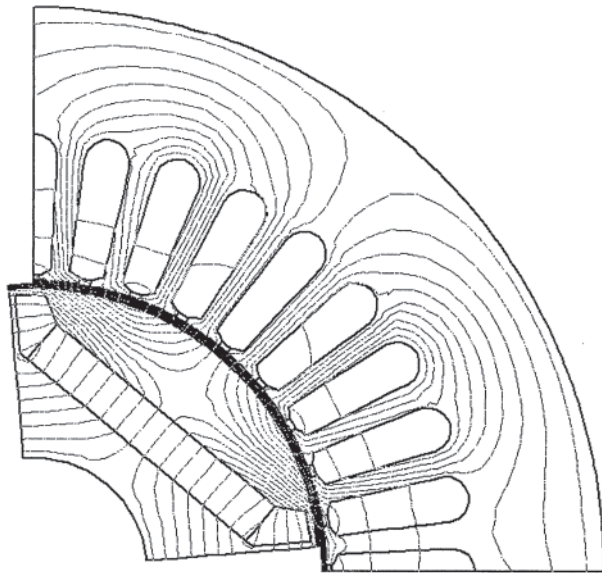


**Figure 4.100** Finite-element computation of the magnetic field in a permanent-magnet brushless motor with a strongly demagnetizing current in the negative direct axis.

On the other hand, the finite-element method is well adapted for the following tasks:

- Checking design calculations and improving the precision of analytical calculations
- Analysis of difficult problems (eddy currents, complex geometry, etc.)

Finite-element tools are generally restricted to a single discipline, for example, electromagnetic analysis, and they are relatively slow to produce results (especially when three-dimensional formulations are used); but of course they can

analyze very complex problems and can be expected to provide more precise results than analytical methods.

#### 4.9.5 Automation of the Design Process

It is natural to ask whether computer methods can be used to automate the design process, given the speed at which data can be processed. The subject of “optimization” has been studied for at least 50 years and yet there is no single best way to invest a computer program with autonomy in the design process. The problem of devising an “optimum” design is that of determining optimal values for at least a hundred parameters, most of which interact with one another in somewhat complex ways, and almost all of which are constrained. The constraints are usually proprietary and may be particular to a single factory or even to a single tool used in the manufacture of a lamination, so that it is virtually impossible to write a general approach that will work in all circumstances. The fact is that most designs today are still optimized by hand, and the process still relies heavily on the wisdom, experience, judgement, invention and intuition of the design engineer.

Early work on design optimization used mathematical concepts such as hill-climbing, penaltyfunction methods, and so on, which tied the methods to parameters that could be expressed by suitable functions. In particular they required the definition of “optimum” in terms of an objective function whose value was to be maximized or minimized by varying the dimensions and parameters of the design (subject to constraints in most cases). The nonlinearity and the incidence of discontinuities in the constraints made it difficult to retain mathematical rigor of the type that would prove that the optimum really was the optimum.

A further difficulty characteristic of electric machine design is that the optimum value of a typical objective function (such as efficiency per unit cost) tends to be a rather flattened function of most of the important variables. Conse

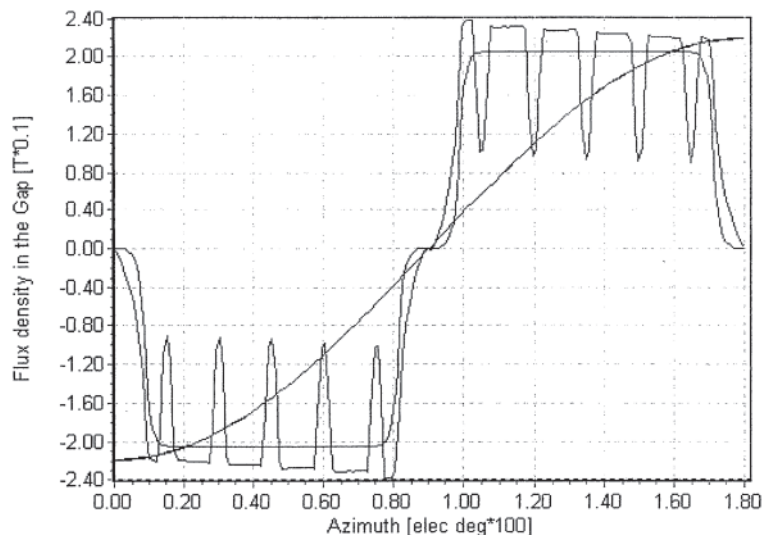


**Figure 4.101** Airgap flux-density distribution in a permanent-magnet brushless motor, computed by finite-element and analytical methods, together with the fundamental space-harmonic component. The deep notches are caused by slotting.

quently the optimum design may not be very distinct, and it may take a great deal of computation to find it.

To circumvent these problems, more sophisticated methods for optimization were developed since the 1980s, such as genetic algorithms and others. Basically these methods attempt to evolve an optimal design rapidly by establishing a hierarchy of “better or worse” from one generation of designs to the next.

An improvement in the prospects for design optimization has been generated by the development of scripting capabilities within the software environment. This is illustrated schematically in Fig. 4.91. If there is available a reliable parameterized machine model, it can be used as the calculating engine in an optimization process written by the design engineer in any common programming language or mathematical analysis software, including spreadsheet software. The importance of this is that the design engineer can specialize the optimization algorithms to his/her own local requirements while still retaining the power and accuracy of an advanced design program. The scripted optimization process can be as simple or as complex as is necessary, and of course it can draw on the theory of genetic algorithms, penaltyfunction methods, hill-climbing algorithms, etc., with good effect.

## 4.10 FINITE ELEMENT ANALYSIS OF INDUCTION MOTORS

### 4.10.1 Motivation for Induction Motor Finite Element Analysis

The equivalent-circuit method discussed above has been used for many years to calculate induction motor performance. The saturable reactances in the equivalent circuits are customarily estimated by using the magnetic circuit or permeance method.

As discussed in Section 1.5.1, the magnetic circuit method requires assumption of flux paths, including flux path length and area. In induction motors the circuit method usually estimates reactances by assuming that the magnetic flux follows straight lines through stator and rotor teeth, slots, and yokes or cores. This assumption restricts the stator yoke to be perfectly circular and the stator slots to be uniform, and does not allow for stator bolt holes or rotor vent holes. To account for saturation and for flux fringing, various empirical factors have been developed.

Today for competitive reasons many induction motors have noncircular stator yokes, nonuniform stator slots, and bolt or vent holes. Such geometric complexities, along with new lamination materials and winding distributions, are usually beyond the capabilities of equivalent-circuit computer programs used by induction motor designers.

The finite element analysis method of Section 1.5 can be used to analyze induction motors [39–41]. A three-phase induction motor will be analyzed first, both to obtain equivalent circuit parameters and also to directly compute total motor performance. Then a single-phase induction motor will be analyzed directly using finite elements.

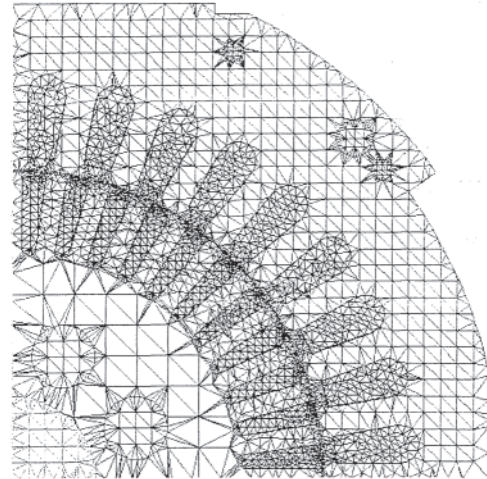


**Figure 4.102** Finite element model of one pole of four-pole three-phase induction motor.

### 4.10.2 Three-Phase Induction Motor Finite Element Analysis

#### 4.10.2.1 Equivalent Circuit Obtained Using Finite Elements

As mentioned in Section 1.5.8, finite elements can obtain much more accurate values of circuit parameters than do methods based on simple equations from magnetic circuits. Here the Maxwell finite element solver is used to obtain a Maxwell SPICE equivalent circuit of a three-phase motor. The complete software is called EMSS (Electromechanical System Simulator) [42].

For three-phase induction motors, the equivalent circuit model includes impedance variations due to both saturation and induced rotor currents. Assuming an applied terminal voltage, the stator currents of the equivalent circuit are input to the finite element model. The induced voltage in each phase winding and the total power loss in the rotor bars are outputs of the finite element analysis and are then input into the equivalent circuit to update its load-dependent parameters. Because of the high degree of nonlinearity of the steel magnetization ( $B-H$ ) curves, an iterative procedure coupling the field computation with the equivalent circuit is needed to determine the true operating point associated with the specified terminal voltage. Thus EMSS performs the following sequence of steps to cover the entire range of slip frequency (motor speed) [43]:

1. The design engineer enters the terminal voltage, frequency, three-dimensional end-turn and/or skew leakage inductance and resistance, and an initial estimate of the stator winding current  $I$ . These values can be obtained from a standard equivalent circuit model such as the commercial program RMxpert [44].
2. Starting from locked rotor (slip=1), the software

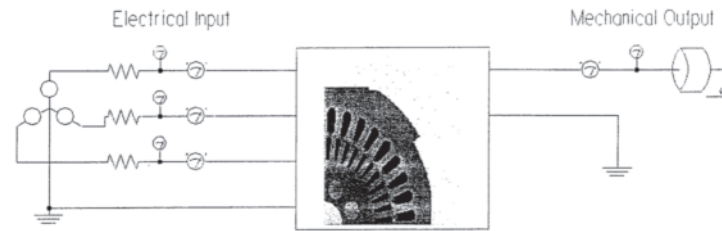


**Figure 4.103** Equivalent circuit model of three-phase induction motor of preceding figure, displayed by ElectroMechanical System Simulator (EMSS).

- computes the induced voltage from the nonlinear finite element solution.
3. Using Kirchoff's law, the software computes the estimated terminal voltage. Then it modifies  $I$  until the terminal voltage equals the specified value.
4. The nonlinear permeability is now "frozen" to its  $B-H$  values in all finite elements and a linear field solution is computed at zero slip (top or idle speed).
5. From the above linear solution, the magnetizing reactance is computed.
6. All other equivalent circuit parameters are also obtained at this slip frequency.
7. The software then uses the above computed parameters to provide an initial estimate of stator current  $I$  at the next slip frequency, and then steps 2–7 are repeated for slips frequency varying from zero to line frequency.
8. The equivalent circuit is used to compute motor performance curves over the entire speed (slip) range. The curves, all plotted versus speed, include torque, input power, efficiency, and power factor.

Note that the finite element solutions obtain accurate equivalent circuit parameters and thereby obtain accurate performance curves. It is recognized that core loss and friction and windage also have an affect on performance prediction, and thus these

quantities can be input as functions of motor speed. Typically the above procedure implemented in the software EMSS provides predictions within approximately 10% of measured results.

The equivalent circuit generated above is also available as a d-q (direct and quadrature) circuit for use by other software and for systems models. For example, software called Simplorer [44] is widely used for power electronic circuits for motor drives, etc., and can be used to model entire induction motor drives. The drive systems can be modeled and coupled to the motor equivalent circuit. Thus the design engineer can easily change the drive system model and quickly determine and optimize the performance of the entire drive and motor system.

As an example, a three-phase induction motor to be analyzed has 36 stator slots, 44 rotor bars, and 4 poles. It is shown in Fig. 4.91 after its finite element mesh for one pole pitch has been generated automatically by Maxwell [44]. Its finite element model is represented in Fig. 4.103 as an EMSS [44] "schematic capture" motor equivalent circuit. Note that in Fig. 4.103 the input electric energization is added to the left of the motor schematic with whatever SPICE circuit elements are desired. In this case the motor is simply energized by balanced wye-connected three-phase ac voltages. To the right of the motor schematic is a mechanical model containing whatever mechanical elements are desired; in this case simply rotor inertia is included.

Computed performance curves are shown in Fig. 4.104. They agree reasonably well with measurements.

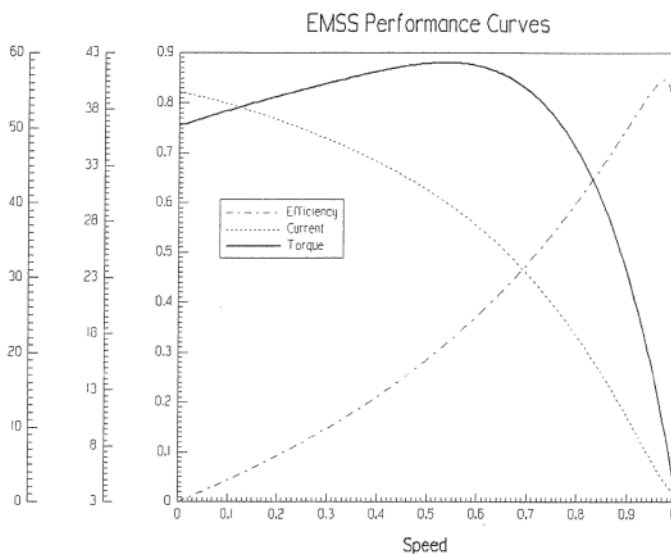


**Figure 4.104** Performance curves of three-phase induction motor computed by ElectroMechanical System Simulator (EMSS).

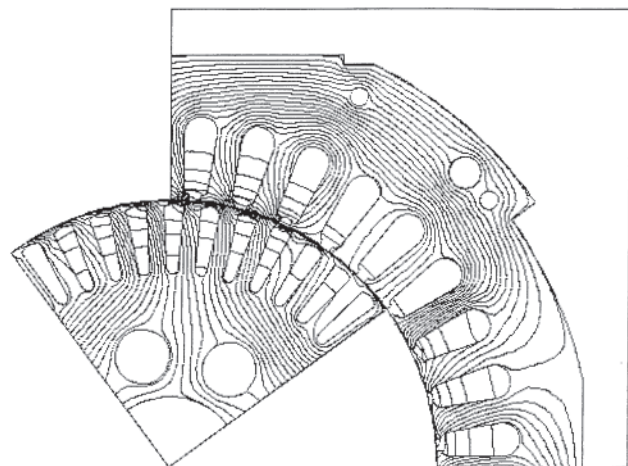


**Figure 4.105** Computed flux line plot of three-phase induction motor. (From Ref 44, copyright 1999 IEEE.)

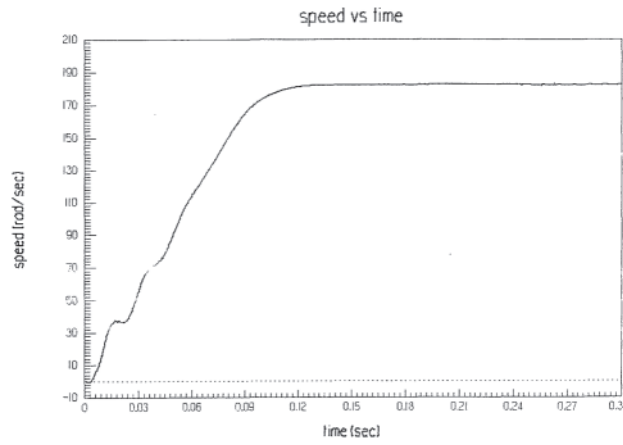


**Figure 4.106** Computed speed vs. time of three-phase induction motor. (From Ref. 44, copyright 1999 IEEE.)

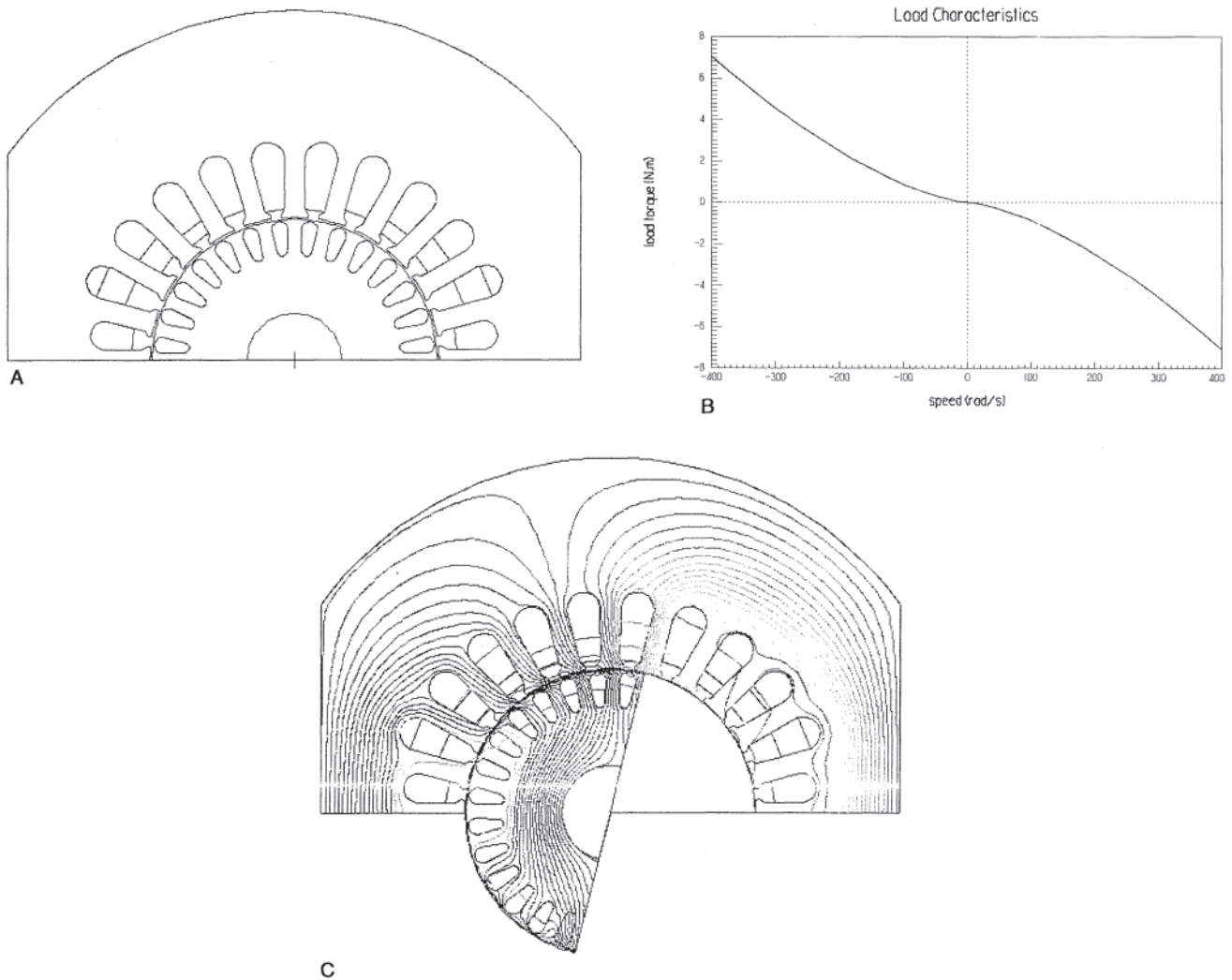


**Figure 4.107** One-half (one pole) of two-pole capacitor-run single-phase induction motor, (a) Geometry, including smaller stator slots containing portions of the auxiliary winding, (b) Load torque vs. speed computed magnetic flux plot at (c) typical instant when rotor has rotated approximately 80 degrees.

#### 4.10.2.2 Direct Performance Computation Using Time-Stepping Finite Element Analysis

As mentioned in Section 1.5.9, time-stepping finite element computations can obtain the most accurate and complete predictions of motor performance, including instantaneous speeds, torques, and currents. Here the same three-phase induction motor as in the preceding section, with 36 stator slots, 44 rotor bars, and 4 poles, is analyzed using time-stepping software EMpulse [44]. A special parameterized input program called RMxpert [44] is used to quickly input the motor geometry and excitation. Its wye-connected stator is assumed energized by 460 V 60 Hz. The moment of inertia of the rotor is assumed to be  $0.021 \text{ kg}\cdot\text{m}^2$  and its frictional damping is assumed to be  $1.5 \text{ MN}\cdot\text{m}\cdot\text{s}$ .

Figure 4.94 shows the finite element model for a particular rotor position at a typical instant. Note that only one pole pitch of the four pole motor need be modeled for any rotor position. Figure 4.105 shows the computed speed versus time after acceleration from standstill at time zero.

If the speed is specified as constant, performance can be

computed at any desired speed. Not only can average torque and current be computed, but torque ripple and current ripple (if any) can also be obtained. For comparison with measurements, average torque and current are often computed. For example, at speeds of 0, 1230, and 1747 rpm computed and measured average torques are respectively 47.1 and 49 N-m, 56.3 and 57.9 N-m, and 12.03 and 12.2 N-m. At the same speeds, computed and measured 60-Hz rms currents are respectively 37.3 and 39 amps, 23.1 and 24 amps, and 4.28 and 4.5 amps.

#### 4.10.3 Single-Phase Induction Motor Finite Element Analysis

The single-phase induction motor to be analyzed by time-stepping finite element analysis is shown in Fig. 4.107a. It is a 3 hp, 2-pole, capacitor-start motor. Note that the stator (half shown in Fig. 4.107a) has 20 large slots and 4 small slots; the small slots can be small because they contain no main winding turns, only auxiliary winding turns.

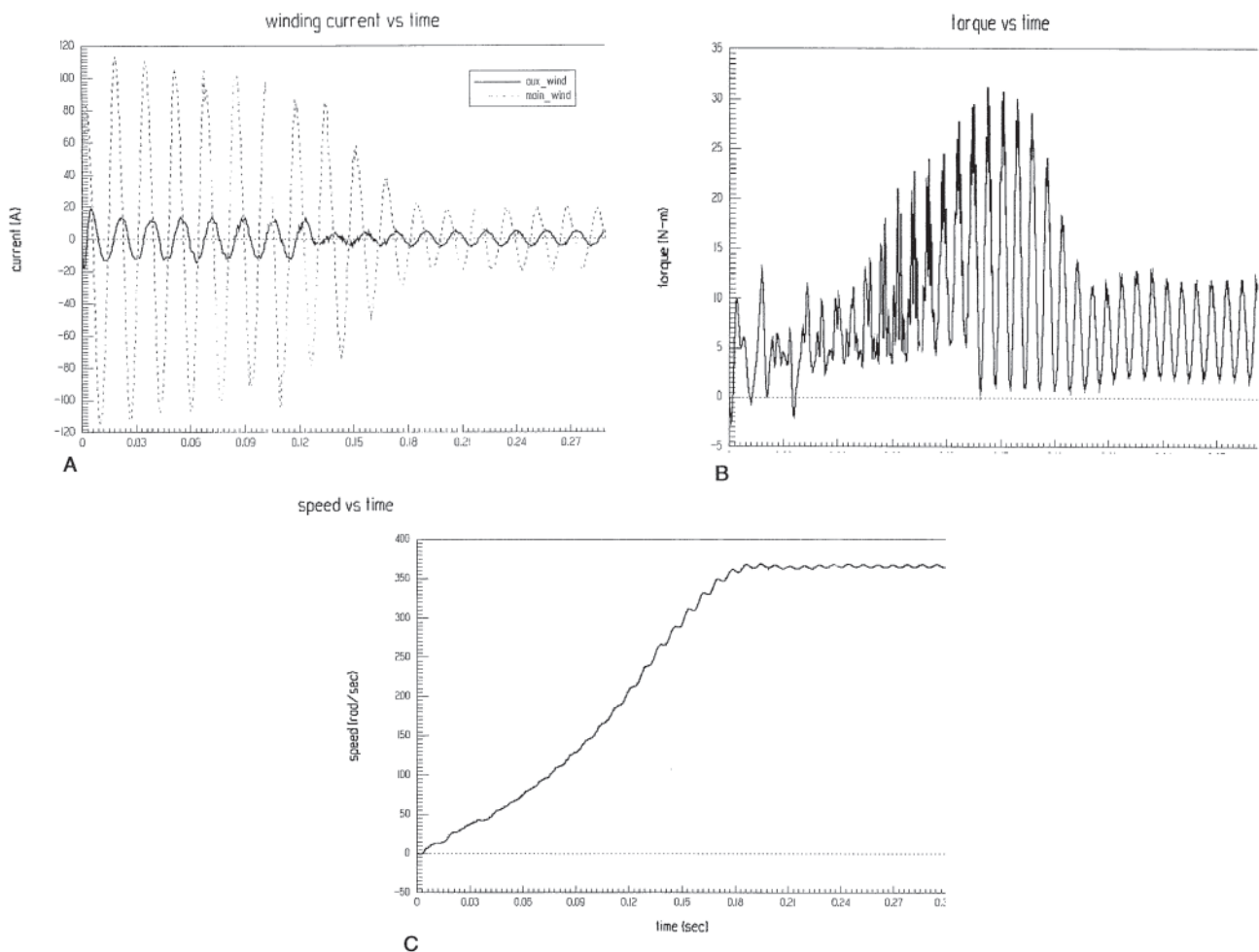


**Figure 4.108** Computed performance parameters vs. time (in seconds) for single-phase induction motor of Fig. 4.96. (a) Currents in main and auxiliary windings, (b) Torque, (c) Speed. (From Ref. 44, copyright 1999 IEEE.)

One of the two capacitors is used only for starting and is removed from the circuit by a centrifugal switch at 70% of synchronous speed. The total capacitance as a function of speed is input into the time-stepping finite element software EMPulse [44]. The rotor moment of inertia is 3.5 millikg-m<sup>2</sup> and the friction damping coefficient is 1.4 MN-m-s. The load torque varies with speed as graphed in Fig. 4.96b. A typical computed flux plot is shown in Fig. 4.107c.

The computed performance versus time, computed directly by EMPulse [44], is shown in Fig. 4.108. The current waveforms in the main and auxiliary windings are seen in Fig. 4.108a to be maximum at start-up (zero speed) and then to decay to steady-state sinusoids. Note that Fig. 4.108b shows that the torque is pulsating, as expected for a single-phase motor. The speed vs. time is shown in Fig. 4.108c.

For given steady-state speeds, the average torques and currents were computed. At zero speed (locked rotor), the main and auxiliary currents were computed to be 80.2 and 9.2 amps, compared to 78.6 and 9.0 amps measured. At rated speed of 1745 rpm, the main and auxiliary currents were computed to be 13.3 and 3.4 amps, compared to 12.8 and 3.3 amps measured. The computed torques agreed with measured torques within 3%.

## REFERENCES

Note: In the following listing, abbreviations have the following meanings:

AIEE American Institute of Electrical Engineers (predecessor to IEEE)

ICEM International Conference on Electrical Machines

IEE Institution of Electrical Engineers

IEEE Institute of Electrical and Electronics Engineers

- Alger, P.L., *The Nature of Induction Machines*, 2nd edn., Gordon and Breach, New York, 1970.
- Fitzgerald, A.E., and C.Kingsley, Jr., *Electric Machinery*, 2d edn., McGraw-Hill, New York, 1961.
- Kron, G., *Equivalent Circuits of Electric Machinery*, Dover Press, New York, 1967.
- Retter, G., *Az Egyseges Villamosgep Elmelet (Unified Theory of Electrical Machines)*, Müszaki Könyvkiado, Budapest, 1976.
- Veinott, C.G., *Fractional Horsepower Electric Motors*, 2d edn., McGraw-Hill, New York, 1948.
- Kovacs, K.P., and I.Racz, *Transiente Vorgänge in Wechselstrommaschinen, I—II, (Transient Phenomena in Alternating Current Machinery, I•II)*, Verlag der Ungarischen Akademie des Wissenschaften, Budapest, 1958.
- Timár, P.L., "Noise Problems of the Asynchronous Machine Fed by an Inverter," ICEM'76 Conference Paper, Vienna, 1976.
- Schuisky, W., *Induktionsmaschinen (Induction Machines)*, Springer Verlag, Vienna, 1957.
- Timár, P.L., *Noise and Vibration of Electric Machines*, Publisher of the Hungarian Academy of Sciences, Budapest, 1989.
- Weh, H., "Zur Elektromagnetischen Schwingungsanregung bei Asynchronmaschinen (On Electromagnetic Excitation of Vibrations in Asynchronous Machines)," *Electrotechnische Zeitschrift, Part A* vol. 85, no. 7, 1965, pp. 193–197.
- Kovacs, K.P., "Two-Pole Induction Motor Vibrations Caused by Homopolar Alternating Fluxes," *IEEE Transactions on Power Apparatus and Systems*, vol. 96, no. 4, 1977, pp. 1105–1108.
- Wright, M.T., D.S.M.Gould, and J.J. Middlemiss, "The Influence of Unbalanced Magnetic Pull on the Critical Speed of Flexible Shaft Induction Machines," *Proceedings of the International Conference on Electric Machine Design and Application*, London, 1982.
- Still, A., and C.S.Siskind, *Elements of Electrical Machine Design*, McGraw-Hill, New York, 1954.
- Stephen Williamson and Danielle R.Gersh, "Finite element calculation of double-cage rotor equivalent circuit parameters," *IEEE Trans. Energy Conversion*, vol 11, March 1996, pp 41–48.
- N.A.Demerdash and P.Baldassari, "A combined finite elementstate space modeling environment for induction motors in the abc frame of reference: the no-load condition," *IEEE Trans. Engery Conversion*, vol 7, No 4, December 1992, pp 698–709.
- John Brauer, Hamid Sadeghi and Robert Oesterlei, "Polyphase Induction Motor Performance Computed Directly by Finite Elements," *IEEE Trans. Vol. 14, No 3, September 1999*, pp 583–588.
- Sarma, M.S., *Electric Machines—Steady-State Theory and Dynamic Performance*, West, St. Paul, MN, 1985.
- Adkins, B., and R.G.Harley, *The General Theory of Alternating Current Machines*, Chapman and Hall, 1975.
- Klingshirn, E., and H.E.Jordan, "Polyphase Induction Motor Performance and Losses on Nonsinusoidal Voltage Sources," *IEEE Transactions on Power Apparatus and Systems*, vol. PAS-87, Mar. 1968, p. 624.
- Chalmers, B.J., and B.R.Sarkar, "Induction Motor Losses Due to Nonsinusoidal Supply Waveforms," *Proceedings of IEE*, vol. 115, no. 12, Dec. 1968.
- Nene, V.D., "Use of Linear Motors for Conventional Railroad Applications," MTR 79W00369, The Mitre Corporation, McLean, Virginia, U.S.A., 1979.
- Mukherji, K.C., "General Basis of Induction Machine Design," Lecture Notes, Indian Institute of Technology, Bombay, 1962.
- Say, M.G., *Alternating Current Machines*, Halsted Press, 1984.
- Singh, B., *Electric Machine Design*, (Vikas India) Advent, New York, 1981.
- de Jong, H.C.J., *AC Motor Design with Conventional and Converter Supplies*, Clarendon Press, Oxford, 1976.
- Liwschitz, M., *Die Elektrischen Maschinen (Electric Machines)*, Verlag und Druck von B.G. Teubner, Leipzig and Berlin, 1934.
- Levi, E., *Polyphase Motors: A Direct Approach to Their Design*, Wiley, New York, 1984.
- Masahiro, I., M.Hiroyuki, and E.Hideaki, "Variable Speed Motor Drive Systems with High Maximum Speeds," *Proceedings of EDS'90*, Capri, Italy, 1990, pp. 295–300.
- Laithwaite, E.R., *Induction Machines for Special Purposes*, George Newnes Ltd., London, 1970.
- Andresen, E.C., and K.Bieniek, "On Torques and Losses of Voltage- and Current-Source Inverter Drives," *IEEE Transactions on Industry Applications*, vol. IA-20, 1984, pp. 321–327.
- Heller, B., and V.Hamata, *Harmonic Field Effects in Induction Machines*, Elsevier Scientific, Amsterdam, 1977.
- Hentschel, F., and M.A.Shehata, "Comparative Study of the Losses in Inverter-Fed Standard Squirrel-Cage Induction Motors," *Proceedings of ICEM'86*, München, Germany, 1986, pp. 320–323.
- Graham, Q., "Dead Points in Squirrel Cage Motors," *Transactions of the AIEE*, vol. 59, 1940, pp. 637–642.
- Hansen, K.L., "Torque Components due to Space Harmonics in Induction Motors," *Journal of the AIEE*, 1922, pp. 929–932.
- Yang, S.S., *Low-Noise Electrical Motors*, Clarendon Press, Oxford, 1981.
- Morill, W.J., "Harmonic Theory of Noise in Induction Motors," *Transactions of the AIEE*, vol. 59, 1940, p. 474.
- Nailen, R.L., "Rotor Tooth Vibration," *Electrical Apparatus*, vol. 40, no. 10, Sept. 1987, pp. 26–29.

38. Yermolin, N.P., *Construction of Electrical Machines*, Academic Books Private Ltd., New Delhi, 1968.
39. Brauer, J.R., "Finite Element Analysis of Single-Phase and Polyphase Induction Motors," *Conference Record of the IEEE Industry Application Society Annual Meeting*, Oct. 1981.
40. Mark Ravenstahl, John Brauer, Scott Stanton, and Ping Zhou, "Maxwell design environment for optimal electric machine design," Small Motor Manufacturing Assn. Annual Meeting, 1998.
41. Ping Zhou, Scott Stanton, and Zoltan J. Cendes, "Dynamic modeling of three phase and single phase induction motors," IEEE Int. Electric Machines & Drives Conference, 1999.
42. Electromechanical System Simulator is a proprietary product of Ansoft Corporation, Pittsburgh, PA 15219 USA, [www.ansoft.com](http://www.ansoft.com).
43. Ping Zhou, J. Gilmore Z. Badics, and Z. Cendes, "Finite element analysis of induction motors based on computing detailed equivalent circuit parameters," *IEEE Trans. Magnetics*, Sept. 1998, pp. 3499–3502.
44. Maxwell, RMxprt, EMpulse, EMSS, and Simplorer are proprietary products of Ansoft Corporation, Pittsburgh, PA 15219 USA, [www.ansoft.com](http://www.ansoft.com).

# 5

## Synchronous Motor Analysis and Design

Edward J.Woods and Haran C.Karmaker (Sections 5.0–5.5)/Jacek F.Gieras (Section 5.6)/Vilas D.Nene and Haran Karmaker (Section 5.7)/John R.Brauer (Section 5.8)

<b>5.0 INTRODUCTION</b>	<b>300</b>
<b>5.1 FLUX AND FLUX DISTRIBUTION</b>	<b>300</b>
<b>5.2 ARMATURE WINDINGS</b>	<b>300</b>
5.2.1 Armature Inductance	301
5.2.2 Slot Leakage	301
5.2.3 Harmonics in the Flux Distribution	302
5.2.4 Effects of Inverters	302
<b>5.3 FIELD WINDINGS</b>	<b>302</b>
5.3.1 Leakage Flux	302
5.3.2 Field Winding Ampere-Turns	302
<b>5.4 DAMPER WINDINGS</b>	<b>303</b>
5.4.1 Leakage Flux	303
<b>5.5 EQUIVALENT CIRCUITS</b>	<b>303</b>
5.5.1 Steady-State Operation	303
5.5.2 V-Curves	304
5.5.3 Equivalent Circuits During Transients	304
5.5.4 Starting Equivalent Circuits	305
<b>5.6 LINEAR SYNCHRONOUS MOTORS</b>	<b>305</b>
5.6.1 Definitions, Geometries, and Principle of Operation	305
5.6.2 Topologies	306
5.6.3 Performance Calculation	313
5.6.4 Applications	317
<b>5.7 DESIGN EQUATIONS FOR A SYNCHRONOUS MACHINE</b>	<b>318</b>
5.7.1 Magnetic and Electric Loading	318
5.7.2 Main Dimensions and Stator Windings	318
5.7.3 Cylindrical Rotor Design	319
5.7.4 Salient-Pole Rotors	320
5.7.5 Field Winding Design	320
5.7.6 Full-Load Field Ampere-Turns	320
5.7.7 Machine Oscillations and the Damper Winding	321
<b>5.8 FINITE ELEMENT ANALYSIS OF SYNCHRONOUS MOTORS</b>	<b>321</b>
5.8.1 Advantages of Finite Element Analysis of Synchronous Motors	321
5.8.2 Motors with Permanent Magnet Rotors	321
5.8.3 Variable-Reluctance Stepper Motors	323
5.8.4 Axial Flux Machines	323
<b>REFERENCES</b>	<b>325</b>



## 5.0 INTRODUCTION

Performance of synchronous motors has been discussed in Sections 2.1 and 2.1.1. Additional information on their characteristics and design are discussed in this chapter.

### 5.1 FLUX AND FLUX DISTRIBUTION

The fundamental rms phase voltage induced in the armature winding of a synchronous motor is given by:

$$E_{ph} = 4.44f\phi_p N_{eff} \quad (5.1)$$

where:

- $f$  = applied frequency (Hz)
- $\phi_p$  = fundamental flux per pole (Wb)
- $N_{eff}$  = number of effective series armature turns per phase =  $N_{rph} K_p K_d$
- $N_{rph}$  = actual series turns per phase
- $K_p$  = winding pitch factor ( $\leq 1.0$ )
- $K_d$  = winding distribution factor ( $\leq 1.0$ )

In a synchronous motor the air gap flux is produced by a rotor field winding supplied with direct current. The air gap flux density distribution is determined by the shape of the rotor iron surface (or pole face as it is called for salient-pole synchronous motors), the air gap dimensions, the armature winding configuration and current relative to the field winding, and the stator slot and surface configuration. Round-rotor machines have a uniform air gap while salient-pole motors will generally have an air gap shaped to control the flux density as a function of distance along the pole face. A correction factor must be applied to the actual total flux per pole to obtain the fundamental flux used in Eq. 5.1. This applies to either round-rotor or salient-pole motors because the field and armature mmf's are not sinusoidally distributed in either machine. The correction factor can be obtained from flux plots produced by graphical approximation or finite element analysis (see Refs. 1 and 2).

Figure 5.1 shows the rotor/stator configuration for a salient-pole machine, and Fig. 5.2 shows the configuration for a round-rotor machine. (In both figures, the circular configuration has been transformed into a flat one.)

The flux density distribution produced by a field winding can be flat-topped or peaked depending on the rotor surface shape, as shown in Fig. 5.3. The flat-topped wave will usually

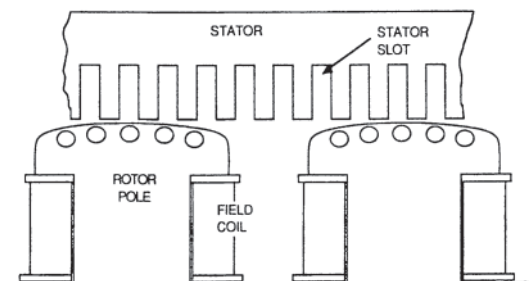


Figure 5.1 Salient-pole rotor/stator configuration.

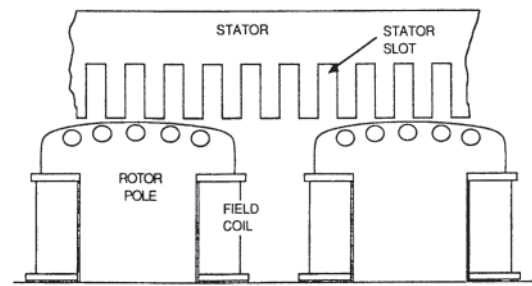


Figure 5.2 Round-rotor rotor/stator configuration.

have more total flux per pole for a given fundamental flux than will the peaked waveshape. This will require more core and pole body iron cross section to carry the flux. The peaked waveshape, however, will have a higher center air gap and stator tooth flux density, requiring wider teeth and more air gap field ampere-turns. The effect of armature slotting can be seen in Fig. 5.4. The slots produce a waveshape of flux density having slot harmonics that remain stationary with respect to the armature winding. A change in total reluctance, however, will induce some voltage harmonics in the armature winding as the rotor moves past the stator teeth. This is especially true of motors with open slots that have few slots per pole and an integral number of slots per pole.

### 5.2 ARMATURE WINDINGS

Armature (stator) windings for three-phase synchronous motors are wound such that there are an integral number of slots per phase (i.e., the number of slots is an integral multiple of 3). The number of slots per pole per phase is not necessarily an integer. However, the fractional part of the slots/pole/phase when expressed as an integer plus a fraction reduced to its lowest level, will have a denominator that is not an integral multiple of 3. For example, a four-pole motor with 42 slots will have a number of slots/pole/phase equal to  $3\frac{1}{2}$ . This is an acceptable number because the denominator of the fraction is 2, which is not divisible by 3. A 12-pole motor with 114 slots yields  $3\frac{3}{6}$  slots/pole/phase. This is unacceptable because the denominator of the fraction is divisible by 3. The reason for such a rule is that the winding can be distributed around the stator periphery in such a way that the coil groupings will have the same pattern in each phase. This ensures that the same voltage will be generated in each phase winding.

In addition, if the motor has more than one circuit per phase, then the number of poles must be an integral multiple of the denominator of the fractional part of the slots/pole/phase times the number of circuits so that each circuit will have the same number of coils in the same locations, thus producing equal voltages. An example of the application of this rule is a 3-phase 10-pole motor with 66 slots and 2 circuits. The number of slots per pole per phase is  $2\frac{1}{5}$ . This is an acceptable number, because the denominator of the fractional part of the result (5) multiplied by the number of circuits (2) is 10, the number of poles. However, if the number of slots is increased to 69, the number of slots per pole per phase is  $2\frac{3}{10}$ ,



**Figure 5.3** Flux density distributions, (a) Peaked wave compared to a sine wave, (b) Flat-topped wave compared to a sine wave.

for which the denominator (10) times the number of circuits equals 20, and there is no way to lay out the coils so that the three phases and two circuits are identical except for circumferential shifts along the bore of the stator.

The rules above for armature windings are always applied to large motors with form-wound coils, because all coils must be identical, except in a very few special cases where some efficiency can be sacrificed due to circulating currents between circuits or phases. For smaller machines with random-wound coils the rules are more often broken because manufacturers must work with existing stator laminations that may not have the desired number of slots. A random winding allows more flexibility to change the number of turns in each coil to compensate for unbalanced winding patterns.

The use of fractional slots/pole/phase and fractional pitch windings results in a voltage or current that is more nearly sinusoidal and can have some benefit in reducing torque pulsations in motors used on certain application.

Larger motors having voltages greater than approximately 1000 V per phase will usually have form-wound coils with strand insulation as well as turn insulation. Smaller motors with voltages below several hundred volts per phase will usually have random-wound coils with wire enamel used for strand insulation as well as turn insulation. Motors between these can have either winding depending on the particular application. Figure 5.5 shows the two types of windings and their slot configurations. Note that the form-wound coil requires an open slot while a semiclosed slot is used for random windings.

### 5.2.1 Armature Inductance

Armature inductance can be calculated by considering the various flux linkages that are present in a synchronous machine.

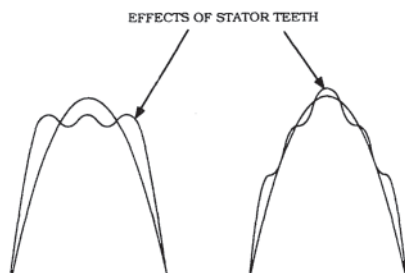


**Figure 5.4** Effects of stator teeth on the flux distribution.

The leakage inductance is associated with that flux that does not cross the air gap but links only armature conductors. The magnetizing inductance is associated with that flux that crosses the air gap and links the field winding. The magnetizing inductance in a salient-pole motor is dependent on the rotor angular position relative to the armature current peak, because a flux generated by a current-carrying coil in the stator will be greater when the salient-pole centerline is aligned with the coil centerline. The two inductances associated with the two rotor positions are  $L_{ad}$  for the direct axis and  $L_{aq}$  for the quadrature axis.

### 5.2.2 Slot Leakage

The primary contribution to armature leakage inductance is the slot leakage shown in Fig. 5.6. This leakage flux crosses the slot from side to side, from tooth tip to tooth tip in the air gap, and as a zig-zag flux that exits the stator tooth face and crosses the air gap, entering the rotor face and then back to an adjacent stator tooth.

These three components are combined in formulas to provide a calculation of leakage inductance  $L_1$ . The cross-slot leakage flux is further divided into several components depending on whether the flux crosses through copper or through an insulating material. For a thorough treatment of armature leakage inductance calculations see Ref. 3 for closed form analytical formulas and Ref. 2 for finite element analysis.

The armature leakage flux, when added to the air gap flux, determines the flux density level in the stator teeth as well as the stator core. The flux density in core and teeth contributes to the ampere-turns of the field winding required to pass flux through the air gap for a given field and armature excitation level.

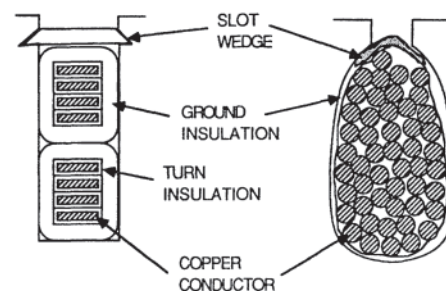


**Figure 5.5** Cross sections through typical slots with form-wound coils (left) and random-wound coils (right).

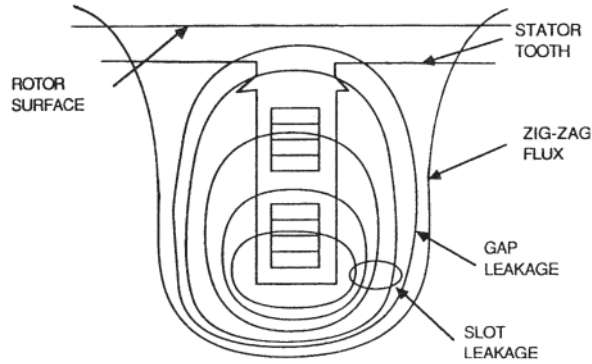


Figure 5.6 Armature slot leakage.

### 5.2.3 Harmonics in the Flux Distribution

Harmonics that exist in the air gap flux density distribution will have some effect on the generated phase voltage, the torque pulsations, and the excitation requirements of the field winding. In salient pole machines, an effort is made to produce a somewhat sinusoidal flux density distribution by using a nonuniform air gap along the periphery of the pole face. Generally the radial air gap dimension is larger near the pole tips than at the pole centerline. In a round-rotor machine, the flux density distribution will depend on the location along the periphery of the rotor slots used to hold the field winding in place. Nonuniform spacing of these slots along the periphery can produce a more sinusoidal flux density distribution. The effects of these harmonics in terms of generated voltage is somewhat reduced by design of the armature winding, as pointed out in Section 5.1.

### 5.2.4 Effects of Inverters

Nonsinusoidal voltages and currents are frequently applied to motors, depending on the type of electronic converter used to power the motor. For a voltage source inverter where the voltage is applied to the motor windings from a dc bus that is switched between phases, voltage harmonics other than the fundamental exist in the applied waveshape. These voltage harmonics cause additional core loss and, depending on the motor reactances, current harmonics that cause additional copper and stray loss.

A current source inverter, which forces current into the motor windings from a more or less constant-current source, will have large-amplitude current harmonics and associated copper and stray-load loss.

An electronic motor drive that synthesizes a sinusoidal wave by pulse width modulation or other high-frequency switching will have small current harmonics due to the filtering action of the motor reactances. One consequence of an electronic controller is the voltage spikes caused by the very short turn-off times of the electronic devices. Switching times in the microsecond range will cause voltage spikes several times the rated motor voltage and can possibly damage the motor insulation.

## 5.3 FIELD WINDINGS

The pole construction of a salient-pole synchronous motor requires that the field winding be capable of placement around the pole body (see Fig. 5.1). For small motors, the field winding can usually be random-wound, and placed in rotor slots or inserted in the space between rotor poles. This can be accomplished after the assembly of the complete stack of rotor laminations, which include poles. For larger motors, however, the poles are assembled separately, the windings are placed on them, and each pole assembly is either bolted or wedged onto the rotor center.

Because of the need to supply dc current to the field winding, slip rings are used on the rotor shaft, and current is passed through brushes riding on the slip rings. Another way to provide excitation is by a rotating rectifier exciter. This is a generator on the same shaft as the motor, having a three-phase winding excited across an air gap to produce a three-phase voltage. This voltage is rectified and applied directly to the motor field winding. The individual field coils must have interpolar electrical connections to complete the rotor field circuit.

### 5.3.1 Leakage Flux

The leakage flux from pole to pole of a synchronous motor is an important factor that determines how the motor behaves under transient conditions as well as the saturation level of the pole body. Figure 5.7 shows the field leakage flux paths in the interpolar space.

Knowledge of the field leakage flux is required to calculate the field leakage inductance, which in turn is required for the transient reactance calculation of the motor. Direct calculation of the flux can be accomplished by assuming that the flux path area and length are known, or a finite element field calculation can be used for greater accuracy. Once the field leakage flux is known, it can be added to the air gap flux to obtain an estimate of the pole body flux and calculate the required pole body ampere-turns.

### 5.3.2 Field Winding Ampere-Turns

The total field winding ampere-turns required to operate a motor at a given voltage, power factor, and output power are determined by the combined contributions from stator core, stator tooth, air gap, pole face, pole body, pole base, and rotor

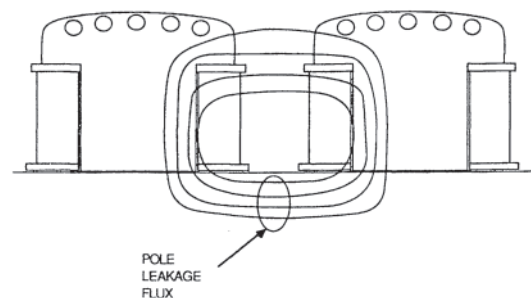


Figure 5.7 Pole body leakage flux paths.

center. These sections of the motor all add reluctance to the magnetic circuit and all but the air gap are nonlinear magnetic circuit elements. In order to accurately determine the correct amount of field ampere-turns to apply for a given condition, an iterative process must be used. This iteration requires a value of total flux and an estimate of field leakage flux. The field ampere-turns are then calculated for the load condition specified. Based on the field ampere-turns and the pole body flux density, a new field leakage is calculated and the iteration continues until a solution is reached.

Likewise, an iteration is required to determine the air gap and stator tooth ampere-turns accurately, because tooth saturation at the pole face centerline will cause the air gap flux to spread out toward the pole tips, thus reducing the gap and tooth center flux densities.

## 5.4 DAMPER WINDINGS

Damper windings on synchronous motors are buried in slots in the pole face iron. The windings consist of cast aluminum bars or bars of copper, bronze or other alloys inserted axially into pole face slots and connected at the ends to form a complete winding quite similar to the squirrel-cage of an induction motor. The end connections are either complete rings of conducting rectangular cross section material or a high-conductivity pole body end lamination to which the pole face bars are brazed. The winding is required to produce an induction motor torque, when the motor is started from standstill and three-phase alternating voltage is applied to the armature terminals. By selecting the rotor bar material, the torque from such a winding can be tailored to start the motor reasonably well even with an inertia load. The pole face winding is used only for starting and not for continuous operation and is designed to dissipate the heat energy in the rotor bars during starting without exceeding the temperature limits.

### 5.4.1 Leakage Flux

The starting winding of a synchronous motor has a component of leakage flux across the rotor bar slot as shown in Fig. 5.8. This flux determines the rotor bar circuit leakage inductances  $L_{kd}$  and  $L_{kp}$  which contribute to the subtransient reactances of the motor and when combined with the other motor inductances and resistances will determine the motor starting performance.

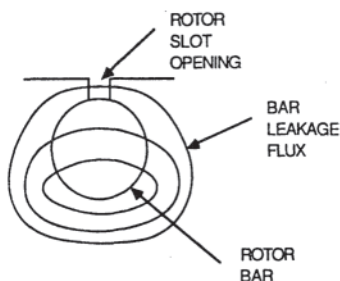


Figure 5.8 Rotor bar leakage flux.

## 5.5 EQUIVALENT CIRCUITS

The equivalent circuit of a synchronous motor depends on the mode of operation. During synchronous operation, the motor can be represented by the direct and quadrature axis armature reactances and the leakage reactance and armature resistance. During transients the field leakage reactance and resistance must also be considered. During starting or rapidly changing synchronous conditions, the leakage reactance and resistance of any pole face windings must be included.

### 5.5.1 Steady-State Operation

When the motor is running at synchronous speed under steady-state, balanced conditions, the motor per-phase equivalent circuit may be approximated by that shown in Fig. 5.9. This circuit assumes no saliency, no saturation, and zero armature resistance, and that the motor reactance is equal to the direct axis air gap reactance plus the armature leakage reactance ( $X_d = X_{ad} + X_l$ ). The equivalent circuit is simply a reactance in series with a voltage source. This circuit represents a per-phase equivalent looking into the stator terminals and the circuit parameters are line to neutral values. The voltage source is the voltage generated in the armature winding by the rotating field poles. A phasor diagram can be used to describe the motor operation for this circuit. The phasor diagram describes the relationship between the armature voltages and currents, the field requirements, and the rotor angular position relative to stator windings. Figure 5.10 shows a phasor diagram for a synchronous motor running at steady-state conditions.

This phasor diagram can be used for either a round-rotor motor or a simplified salient-pole motor neglecting saliency and using direct axis quantities only. The diagram shows the armature terminal voltage  $V_t$ , the armature current  $I_a$ , the power factor angle  $\theta$ , the reactance drop  $jI_a X_d$ , the load angle  $\delta$ , and the required armature generated voltage  $E_d$ . The field excitation requirements can be obtained by calculating the field ampere-turns required to supply the flux to generate voltage  $E_d$ . This diagram also neglects saturation effects.

Some insight into motor performance can be obtained from this simplified diagram. The power delivered from the source is given by  $V_t I_a \cos(\theta)$ . The power delivered to the load is given by  $E_d I_a \cos(\delta - \theta)$ . As  $E_d$  is increased, the current into the motor decreases, thus reducing the phasor  $jI_a X_d$ . This brings  $E_d$  more in phase with  $V_t$ , reducing  $\delta$ , and swinging  $jI_a X_d$  counterclockwise to remain perpendicular to  $I_a$ . This in turn

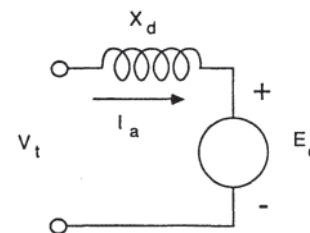
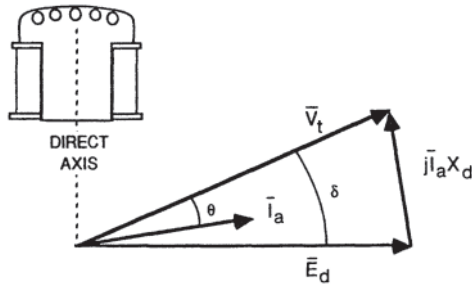


Figure 5.9 Motor per-phase equivalent circuit for synchronous operation.



**Figure 5.10** Synchronous motor phasor diagram for a round-rotor motor operating at lagging power factor. (Note: A salient-pole is shown in the figure to establish the position of the direct axis.)

reduces the power factor angle  $\theta$ . If  $E_d$  is increased further by increasing the field current, then the power factor angle will become zero and eventually leading. This condition is called overexcitation and the motor can be used to correct for lagging power factor loads on the electrical system. A more complete phasor diagram, including saliency and saturation, is shown in Fig. 5.11.

For either of these equivalent circuits, the load angle  $\delta$  is useful to estimate motor performance neglecting losses. For the simplified diagram, the output power is given by:

$$P_{out} = 3E_d V_t \frac{\sin(\delta)}{X_d} \tag{5.2}$$

while for the more complete diagram, the output power is:

$$P_{out} = 3E_d V_t \sin(\delta) / X_d + 3 V_t^2 \left( \frac{1}{X_q} - \frac{1}{X_d} \right) \sin(2\delta) / 2 \tag{5.3}$$

The second equation includes the saliency effect and uses the direct and quadrature axis reactances. A further refinement of the synchronous motor phasor diagram accounts for armature resistance and separates stator saturation from rotor saturation. To achieve this, the stator leakage reactance  $X_l$  is separated from  $X_{ad}$  and  $X_{aq}$  and the voltage “behind the stator leakage,”  $E_l$ , is calculated. This is the voltage necessary to

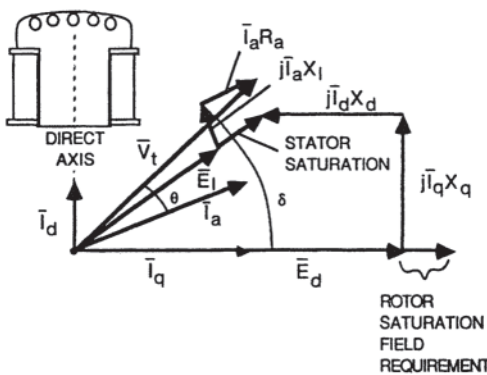


**Figure 5.11** Phasor diagram for a motor with lagging power factor, including the effects of saliency and saturation.

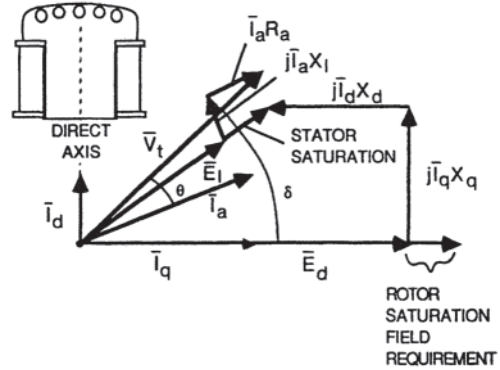


**Figure 5.12** Complete phasor diagram.

support the terminal voltage in addition to the stator resistance and reactance drop. The stator flux density and saturation level are determined from the voltage  $E_l$  instead of  $V_t$  and then the rest of the phasor diagram is constructed. Rotor excitation and saturation are then determined. The phasor diagram is shown in Fig. 5.12.

**5.5.2 V-Curves**

A useful way to view motor field requirements for various load conditions is through the use of V-curves. These curves are a result of calculating motor excitation requirements at rated voltage for loads from zero up to as high as desired and at power factors from zero power factor lagging to zero power factor leading. Figure 5.13 shows a set of V-curves. Some points of operation on these curves will result in the motor current increasing when field current is reduced. Continued reduction of field current beyond a certain point results in the motor becoming self-exciting and uncontrollable.

**5.5.3 Equivalent Circuits During Transients**

During transients, the motor can be represented by the circuit shown in Fig. 5.14. This circuit includes the reactance and resistance of the field winding referred to the stator winding.

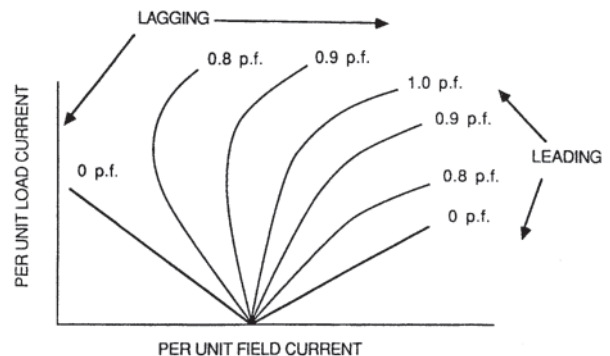


**Figure 5.13** V-curves for a synchronous motor.

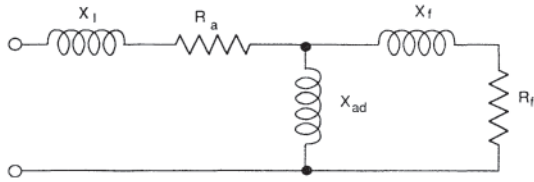


Figure 5.14 Transient equivalent circuit.

The transient reactance is given by the parallel combination of  $X_f$  and  $X_{ad}$  in series with  $X_l$ .

$$X'_d = X_l + \frac{X_f X_{ad}}{X_f + X_{ad}} \quad (5.4)$$

### 5.5.4 Starting Equivalent Circuits

During starting, the motor equivalent circuit is the same as for an induction motor except that the direct and quadrature axis effects are both considered and averaged to obtain motor performance. Figure 5.15(a) and 5.15(b) shows the two equivalent circuits.  $R'_f$  in the direct axis circuit is the sum of the field resistance in series with any added resistance known as discharge resistor used during starting. This total resistance is referred to the stator winding. The subtransient circuit of a synchronous motor is the same as the direct axis circuit during starting except that the field winding is considered to be shorted through the field supply and no extra resistance is added to the field resistance. The subtransient reactances are given by the starting winding leakage reactance in parallel with the field and air gap reactances, this combination being in series with the stator leakage reactance as follows:

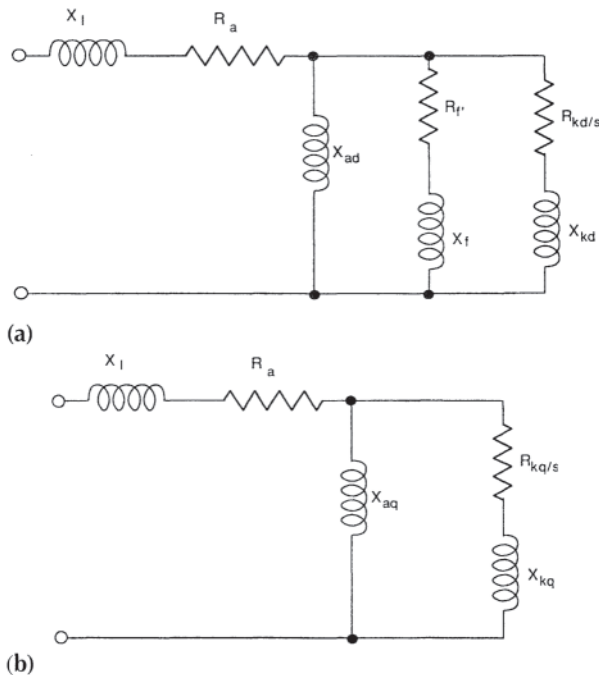


Figure 5.15 (a) Direct axis starting equivalent circuit, (b) Quadrature axis starting equivalent circuit.

$$X''_d = X_l + X_{kd} \frac{X_a X_{f'} (X_{ad} + X_f)}{X_{kd} + X_{ad} X_{f'} (X_{ad} + X_f)} \quad (5.5)$$

and for the quadrature axis subtransient reactance:

$$X''_q = X_l + \frac{X_{aq} X_{kq}}{X_{aq} + X_{kq}} \quad (5.6)$$

## 5.6 LINEAR SYNCHRONOUS MOTORS

### 5.6.1 Definitions, Geometries, and Principle of Operation

Linear electric motors can drive a linear motion load without intermediate gears, screws or crank shafts. A *linear synchronous motor* (LSM) is a linear motor in which the mechanical motion is in synchronism with the magnetic field, i.e., the mechanical speed is the same as the speed of the travelling magnetic field. The thrust (propulsion force) can be generated as an action of

- Traveling magnetic field produced by an alternating current (ac) polyphase winding and an array of magnetic poles N, S, ..., N, S or a variable reluctance ferromagnetic rail;
- Magnetic field produced by electronically switched direct current (dc) windings and an array of magnetic poles N, S, ..., N, S or variable reluctance ferromagnetic rail (linear stepping or switched reluctance motors).

The part producing the traveling magnetic field is called the *armature* or *forcer*. The part that provides the dc magnetic flux or variable reluctance is called the *field excitation system* (if the excitation system exists) or *salient-pole rail*, *reaction rail* or *variable reluctance platen*. The terms *primary* and *secondary* should rather be avoided, because they are only justified for linear induction motors [4] or transformers. The operation of a LSM does not depend on which part is movable and which is stationary.

Traditionally, ac polyphase synchronous motors are machines with dc electromagnetic excitation, the propulsion force of which has two components: (1) produced by the traveling magnetic field and dc magnetic flux (synchronous component) and (2) produced by the traveling magnetic field and variable reluctance in the *d* and *q* axis (reluctance component). Replacement of dc electromagnets by permanent magnets (PMs) in LSMs is common, except for LSMs for magnetically levitated vehicles. PM brushless LSMs can be divided into two groups:

1. PM LSMs in which the input current waveforms are sinusoidal and produce a traveling magnetic field;
2. PM dc linear brushless motors (LBMs) in which the input rectangular or trapezoidal current waveforms are precisely synchronized with the speed and position of the moving part using a position feedback.

Construction of magnetic and electric circuits of LSMs belonging to both groups is the same. In dc PM brushless motors the information about the position of the moving part is usually provided by an absolute position sensor. This control scheme corresponds to an *electronic commutation*,

functionally equivalent to the mechanical commutation in dc commutator motors. Therefore, motors with square (trapezoidal) current waveforms are called *dc brushless motors*. The operation of LBMs can be regarded as a special case of the operation of LSMs.

Instead of dc or PM excitation, the difference between the *d*- and *q*-axis reluctances and the traveling magnetic field can generate the reluctance component of the thrust. Such a motor is called the ac *reluctance* LSM. Different reluctances in the *d* and *q* axis can be created by making salient ferromagnetic poles, using ferromagnetic and nonferromagnetic materials or using anisotropic ferromagnetic materials.

In the case of LSMs operating on the principle of the traveling magnetic field, the speed  $v$  of the moving part:

$$v = v_s = 2f\tau = \frac{\omega}{\pi}\tau \quad (5.7)$$

is equal to the *synchronous speed*  $v_s$  of the traveling magnetic field and depends only on the input frequency  $f$  (angular input frequency  $\omega=2\pi f$ ) and pole pitch  $\tau$ . It does not depend on the number of poles  $2p$ .

The polyphase (usually three-phase) armature winding can be distributed in slots, distributed uniformly on the slotless surface of the armature core, made in the form of concentrated-parameter coils or made as a coreless (air-cored) winding layer. The peak value of the armature line current density or *specific electric loading* is defined as the number of conductors in all phases  $2m_1N_1$  times the peak armature current  $\sqrt{2}I_a$  divided by the armature stack length  $2p\tau$ , i.e.:

$$A_m = \frac{m_1 \sqrt{2}N_1 I_a}{p\tau} \quad (5.8)$$

where  $m_1$  is the number of phases,  $N_1$  is the number of series turns per phase,  $I_a$  is the phase *rms* armature current, and  $p$  is the number of pole pairs. PMs are the most popular excitation systems for short traveling distances (less than 10 m), e.g., factory transportation or automation systems. A long rare-earth PM rail is expensive.

For PMs with linear demagnetization curve, i.e., neodymium-iron-boron (NdFeB) magnets, the coercive field strength  $H_c$  at room temperature can simply be calculated on the basis of the remanent magnetic flux density  $B_r$  and relative recoil magnetic permeability  $\mu_{rrec}$  as:

$$H_c = \frac{B_r}{\mu_0 \mu_{rrec}} \quad (5.9)$$

The magnetic flux density produced in the air gap  $g$  by a PM with linear demagnetization curve and its height  $h_M$  placed in a magnetic circuit with infinitely large magnetic permeability and air gap  $g$  is, approximately:

$$B_g \approx \frac{B_r}{1 + \mu_{rrec}g/h_M} \quad (5.10)$$

Equation 5.10 has been derived assuming  $H_c h_M \approx H_M h_M + H_g g$ , neglecting magnetic voltage drops (MVDs) in mild steel portion of the magnetic circuit, putting  $H_c$  according to Equation 5.9,  $H_M = B_g / (\mu_0 \mu_{rrec})$  and  $H_g = B_g / \mu_0$ . The relative recoil magnetic permeability  $\mu_{rrec}$  for NdFeB PMs is from 1 to 1.15.

Electromagnetic excitation is used in high-speed passenger transportation systems operating on the principle of magnetic levitation (maglev). The German system, *Transrapid*, uses vehicle-mounted steel core excitation electromagnets and stationary track-mounted armature core with windings located in slots. Japanese MLX001 test train sets use on-board superconducting air-cored electromagnets and a stationary three-phase air-cored armature winding distributed along the guideway (Yamanashi Maglev Test Line).

A *linear stepping motor* has a concentrated armature winding wound on salient poles and PM excitation rail or variable reluctance platen. The thrust is generated as an action of the armature magnetic flux and PM flux (active platen) or the armature magnetic flux and salient ferromagnetic poles (variable reluctance platen). Stepping motors have no position feedback.

The topology of a linear switched reluctance motor (LSRM) is similar to that of a stepping motor with variable reluctance platen. In addition, the LSRM is equipped with position sensors. The *turn-on* and *turn-off* time instant of the input current is synchronized with the position of the moving part. In the case of a linear stepping motor or LSRM, the speed  $v$  of the moving part is:

$$v = v_s = f_{s\omega}\tau \quad (5.11)$$

where  $f_{s\omega}$  is the fundamental switching frequency in one armature phase winding and  $\tau$  is the pole pitch of the reaction rail. For a rotary stepping motor or switched reluctance motor  $f_{s\omega} = 2p_r n$  where  $2p_r$  is the number of rotor poles and  $n$  is rotational speed in rev/s.

## 5.6.2 Topologies

LSMs can be classified according to their geometry and construction, i.e.,

- Flat (planar) or tubular (cylindrical);
- Single-sided or double-sided;
- Slotted or slotless;
- Iron-cored or air-cored;
- Transverse flux or longitudinal flux.

The above topologies are possible for nearly all types of excitation systems. LSMs operating on the principle of the traveling magnetic field can have the following excitation systems:

- PMs in the reaction rail;
- PMs in the armature (passive reaction rail);
- Electromagnetic excitation system (with winding);
- Superconducting excitation system;
- Passive reaction rail with saliency and neither PMs nor windings (reluctance motors).

LSMs with electronically switched dc armature windings are designed either as linear stepping motors or LSRMs.

### 5.6.2.1 Permanent Magnet Motors with Active Reaction Rail

Figure 5.16(a) shows a single-sided flat LSM with the armature winding located in slots and surface PMs. Figure 5.16(b) shows

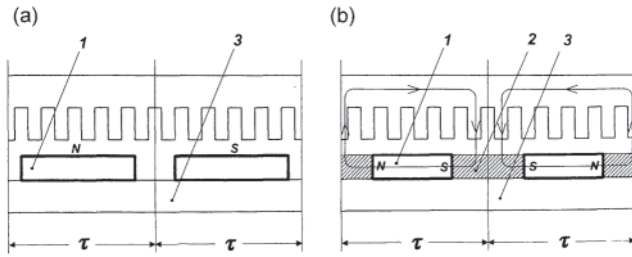


**Figure 5.16** Single-sided flat permanent magnet (PM) linear synchronous motors (LSMs) with slotted armature core and: (a) surface PMs, (b) buried PMs. 1, PM; 2, mild steel pole; 3, yoke.

a similar motor with buried-type PMs. In surface arrangement of PMs the yoke (back iron) of the reaction rail is ferromagnetic and PMs are magnetized in the normal direction (perpendicular to the active surface). Buried PMs are magnetized in the direction of the traveling magnetic field and the yoke is nonferromagnetic, e.g., made of aluminum. Otherwise, the bottom leakage flux would be greater than the linkage flux, as shown in Fig. 5.17. The same effect occurs in buried-type PM rotors of rotary machines in which the shaft must also be nonferromagnetic [5].

The so called *Halbach array* of PMs also does not require any ferromagnetic yoke and excites stronger magnetic flux density and closer to the sinusoids than a conventional PM array [6, 7]. The key concept of the Halbach array is that the magnetization vector should rotate as a function of distance along the array (Fig. 5.18).

It is recommended to furnish a PM LSM with a *damper*. A rotary synchronous motor has a cage damper winding embedded in pole shoe slots. When the speed is different than the synchronous speed, electric currents are induced in damper circuits. The action of the armature magnetic field and damper currents allows for asynchronous starting, damps the oscillations and helps to return to synchronous operation when the speed decreases or increases. Also, a damper circuit reduces

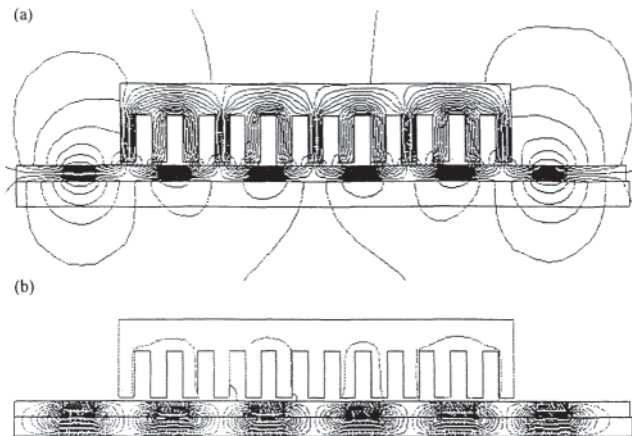


**Figure 5.17** Magnetic flux distribution in the longitudinal sections of buried-type PM LSMs: (a) non-ferromagnetic yoke, (b) ferromagnetic yoke (back iron).

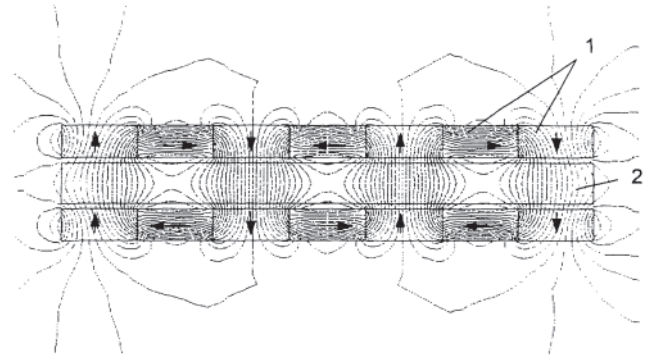


**Figure 5.18** Double sided LSM with Halbach array of PMs. 1, PMs, 2, coreless armature winding.

the backward traveling magnetic field. It would be rather difficult to furnish PMs with a cage winding so that the damper of PM LSMs has the form of an aluminum cover (Fig. 5.19(a)) or solid steel pole shoes (Fig. 5.19(b)). In addition, steel pole shoes or aluminium cover (shield) can protect brittle PMs against mechanical damage.

The *detent force*, i.e., attractive force between PMs and armature slotted core, force ripple and some higher space harmonics can be reduced with the aid of skewed assembly of PMs. Skewed PMs can be arranged in one row (Fig. 5.20(a)), two rows (Fig. 5.20(b)) or even more rows.

Specification data of flat, single-sided PM LBMs manufactured by *Kollmorgen* are shown in Table 5.1 [8]. The temperature 25°C or 130°C for the thrust, current, resistance, emf constant, and thrust constant is the temperature of the armature winding.

The emf constant  $k_E$  in Table 5.1 for sinusoidal operation is defined by equation expressing the emf (induced voltage) as a function of the excitation flux  $\Phi_f$  and linear synchronous speed  $v_s$ , i.e.:

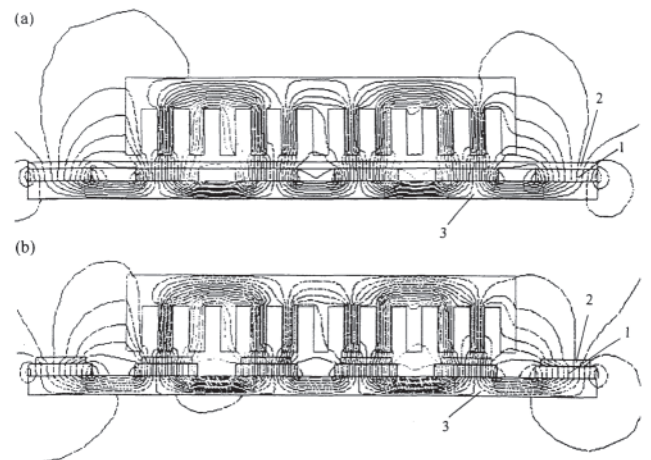


**Figure 5.19** Dampers of surface-type permanent magnets (PM) linear synchronous motors (LSMs): (a) aluminum cover (shield), (b) solid steel pole shoes. 1, PM; 2, damper; 3, yoke.



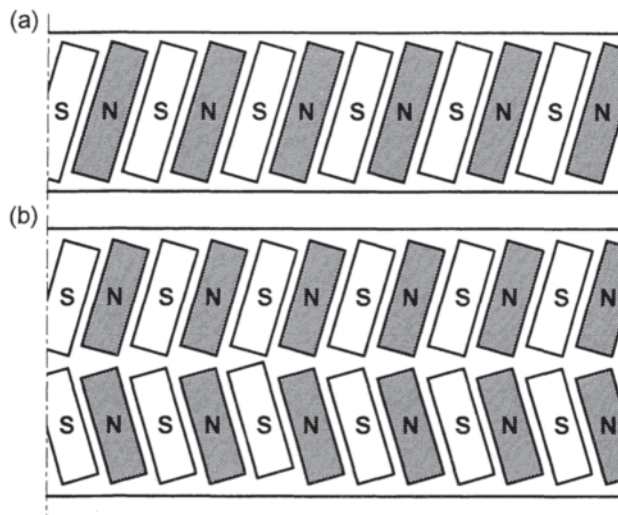


**Figure 5.20** Skewed permanent magnets (PMs) in flat linear synchronous motors (LSMs): (a) one row, (b) two rows.

$$E_f = c_E \Phi_f v_s = k_E v_s \quad (5.12)$$

where  $k_E = c_E \Phi_f$ . Thus, the emf constant  $k_E$  multiplied by the synchronous speed  $v_s$  gives the emf  $E_f$ .

The thrust constant  $k_F$  in Table 5.1 is defined by simplified equation for the electromagnetic thrust [9], i.e.:

$$F_{ax} = k_F I_a \cos \psi \quad (5.13)$$

for a sinusoidally excited LSM with equal reluctances in the  $d$  and  $q$  axis and for the angle between the armature current  $I_a$  and the  $q$  axis  $\psi = 0^\circ$  ( $\cos \psi = 1$ ). Thus, the thrust constant  $k_F$  times the armature current  $I_a$  gives the thrust. Derivations of Eqs. 5.12 and 5.13 are given in [9]. The same equations, i.e.,  $E_f = k_E v$  and  $F_{ax} = k_F I_a$ , can be used for a LBM with square wave current waveforms.

Double-sided, flat PM LSMs consist of two external armature systems and one internal excitation system (Fig.

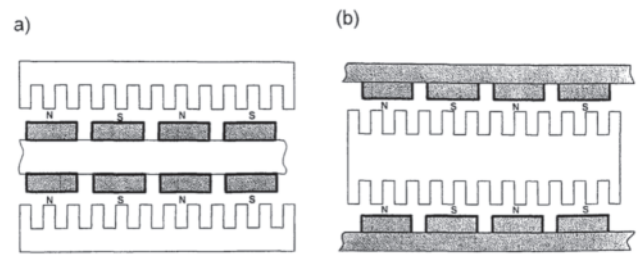


**Figure 5.21** Double-sided flat PM LSMs with: (a) two external armature systems, (b) one internal armature system.

5.21 (a)) or one internal armature system and two external excitation systems (Fig. 5.21(b)). In the second case a linear Gramme's armature winding can be used.

In *slotless motors* the primary winding is uniformly distributed on a smooth armature core or does not have any armature core. Slotless PM LSMs are detent force-free motors, provide lower thrust ripple, and can achieve higher efficiency in the higher speed range than slotted LSMs. On the other hand, larger nonferromagnetic air gap requires more PM material and the thrust density (thrust per mass or volume) is lower than that of slotted motors. The input current is higher as synchronous reactances in the  $d$  and  $q$  axis can decrease to a low undesired value due to absence of teeth. Figure 5.22(a) shows a single-sided flat slotless motor with armature winding (moving coil motor).

Table 5.2 contains performance specifications of doublesided PM LBMs with inner three-phase air-cored armature winding manufactured by *Trilogy Systems Corporation*, Webster, TX [10]. *Trilogy* also manufactures motors with parallel wound coils as well as miniature motors and high-force motors (up to 9000 N continuous thrust).

By rolling a flat LSM around the axis parallel to the direction of the traveling magnetic field, i.e., parallel to the direction of thrust, a tubular (cylindrical) LSM can be obtained

**Table 5.1** Flat Three-Phase, Single-Sided PM LBMs with Natural Cooling Systems Manufactured by *Kollmorgen*, Radford, VA

Parameter	IC11-030	IC11-050	IC11-100	IC11-200
Continuous thrust at 130°C, N	150	275	600	1260
Continuous current at 130°C, A	4.0	4.4	4.8	5.0
Peak thrust, N	300	500	1000	2000
Peak current, A	7.9	7.9	7.9	7.9
Continuous power losses at 130°C, W	64	106	210	418
emf constant, at 25°C, $k_E$ , Vs/m	30.9	51.4	102.8	205.7
Thrust constant (three phases) at 25°C, $k_F$ , N/A	37.8	62.9	125.9	251.9
Resistance, line-to-line, at 25°C, $\Omega$	1.9	2.6	4.4	8.0
Inductance, line-to-line, mH	17.3	27.8	54.1	106.6
Electrical time constant, ms	8.9	10.5	12.3	13.4
Thermal resistance winding-to-external structure, °C/W	1.64	0.99	0.50	0.25
Maximum winding temperature, °C			130	
Armature assembly mass, kg	2.0	3.2	6.2	12.2
PM assembly mass, kg/m	5.5	7.6	12.8	26.9
Normal attractive force, N	1440	2430	4900	9850

PM, permanent magnet; LBMs, linear brushless motors.

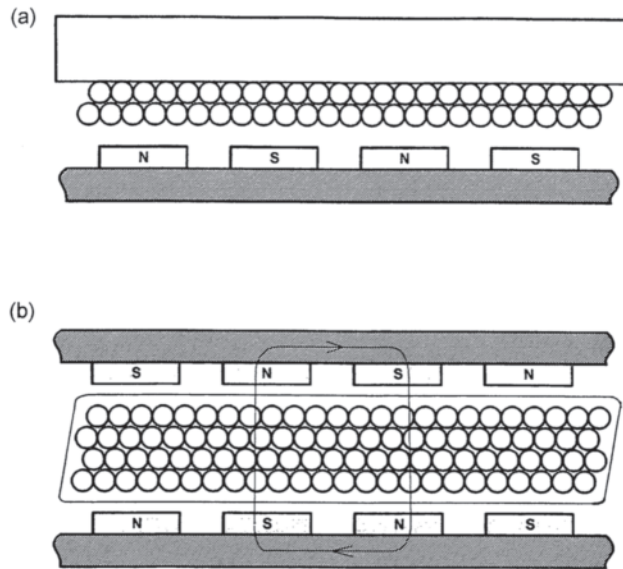


**Figure 5.22** Flat slotless PM LSMs: (a) single sided with armature core, (b) double sided with inner air-cored armature winding.

(Fig. 5.23). A tubular PM LSM can also be designed as a double-sided motor or slotless motor.

Tubular single-sided LSMs LinMoT<sup>®</sup> with movable internal PM excitation system (slider) and stationary external armature\* are manufactured by *Sulzer Electronics AG*, Zürich, Switzerland (Table 5.3). All active motor parts, bearings, position sensors and electronics have been integrated into a rigid metal cylinder [11].

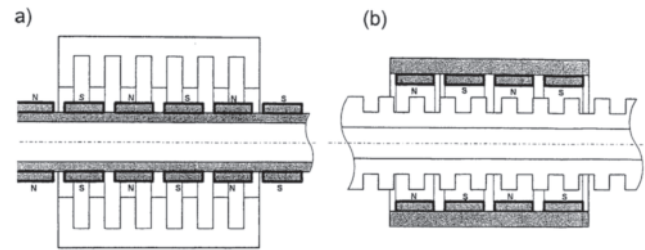


**Figure 5.23** Single-sided slotted tubular permanent magnet (PM) linear synchronous motors (LSMs): (a) with external armature system, (b) with external excitation system.

All the abovementioned PM LSMs are motors with *longitudinal magnetic flux*, the lines of which lie in the plane parallel to the direction of the traveling magnetic field. LSMs can also be designed as *transverse magnetic flux* motors, in which the lines of magnetic flux are perpendicular to the direction of the thrust [12]. Figure 5.24 shows a single-sided transverse flux LSM in which PMs are arranged in two rows. A pair of parallel PMs creates a two-pole flux excitation system. A double-sided configuration of transverse flux motor is possible; however, it is complicated and expensive.

#### 5.6.2.2 PM Motors with Passive Reaction Rail

The drawback of PM LSMs is the large amount of PM material that must be used to design the excitation system. Normally, high-energy density rare earth PMs are the best option. If a small PM LSM uses, for example, 10 kg of NdFeB per 1 m of the reaction rail, and 1 kg of good quality NdFeB costs US

**Table 5.2** Flat Double-Sided PM LBMs with Inner Three-Phase Air-Cored Series-Coil Armature Winding Manufactured by *Trilogy Systems Corporation*, Webster, TX

Parameter	310-2	310-4	310-6
Continuous thrust, N	111.2	209.1	314.9
Continuous power for sinusoidal operation, W	87	152	230
Peak thrust, N	356	712	1068
Peak power, W	900	1800	2700
Peak/continuous current, A	10.0/2.8	10.0/2.6	10.0/2.6
Thrust constant $k_F$ for sinusoidal operation, N/A	40.0	80.0	120.0
Thrust constant $k_F$ for trapezoidal operation with Hall sensors, N/A	35.1	72.5	109.5
Resistance per phase, $\Omega$	8.6	17.2	25.8
Inductance $\pm 0.5$ mH	6.0	12.0	18.0
Heat dissipation constant for natural cooling, W/°C	1.10	2.01	3.01
Heat dissipation constant for forced air cooling, W/°C	1.30	2.40	3.55
Heat dissipation constant for liquid cooling, W/°C	1.54	2.85	4.21
Number of poles	2	4	6
Coil length, mm	142.2	264.2	386.1
Coil mass, kg	0.55	1.03	1.53
Mass of PM excitation systems, kg/m	12.67 or 8.38		

PM, permanent magnets; LBMs, linear brushless motors.

\*LinMot<sup>®</sup> is a registered trademark of *Sulzer Electronics AG*, Zürich, Switzerland.

**Table 5.3** Data of tubular LSMs LinMot<sup>®</sup> Manufactured by *Sulzer Electronics AG*, Zürich, Switzerland

Parameter	P01	P01	P01	P01
	23 × 80	23 × 160	37 × 120	37 × 240
Number of phases	2			
Permanent magnets	NdFeB			
Maximum stroke, m	0.210	0.340	1.400	1.460
Maximum force, N	33	60	122	204
Maximum acceleration, m/s <sup>2</sup>	280	350	247	268
Maximum speed, m/s	2.4	4.2	4.0	3.1
Stator (armature) length, m	0.177	0.257	0.227	0.347
Stator outer diameter, mm	23	23	37	37
Stator mass, kg	0.265	0.450	0.740	1.385
Slider diameter, mm	12	12	20	20
Maximum temperature of the armature winding, °C	90			

\$100, the cost of the reaction rail without assembly amounts to US \$1000 per 1 m. This price cannot be acceptable, e.g., in passenger transportation systems.

A cost-effective solution is to apply the PM excitation system to the short armature that magnetizes the long reaction rail and creates magnetic poles in it. Such a linear motor is called the *homopolar* LSM.

The homopolar LSM as described in [13, 14] is a doubled-sided ac linear motor that consists of two polyphase armature systems connected mechanically and magnetically by a ferromagnetic U-type yoke (Fig. 5.25). Each armature consists of a typical slotted linear motor stack with polyphase armature winding and PMs located between the stack and U-type yoke. Because the armature and excitation systems are combined together, the armature stack is oversized as compared to a conventional steel-cored LSM. The PMs can also be replaced by electromagnets [14, 15]. The variable reluctance reaction rail is passive. The saliency is created by using ferromagnetic (solid or laminated) cubes separated by a nonferromagnetic material. The reaction rail poles are magnetized by the armature PMs through the air gap. The traveling magnetic field of the polyphase armature winding and salient poles of the reaction rail produce the thrust. Such a homopolar LSM has been proposed for the propulsion of maglev trains of *Swissmetro* [14].

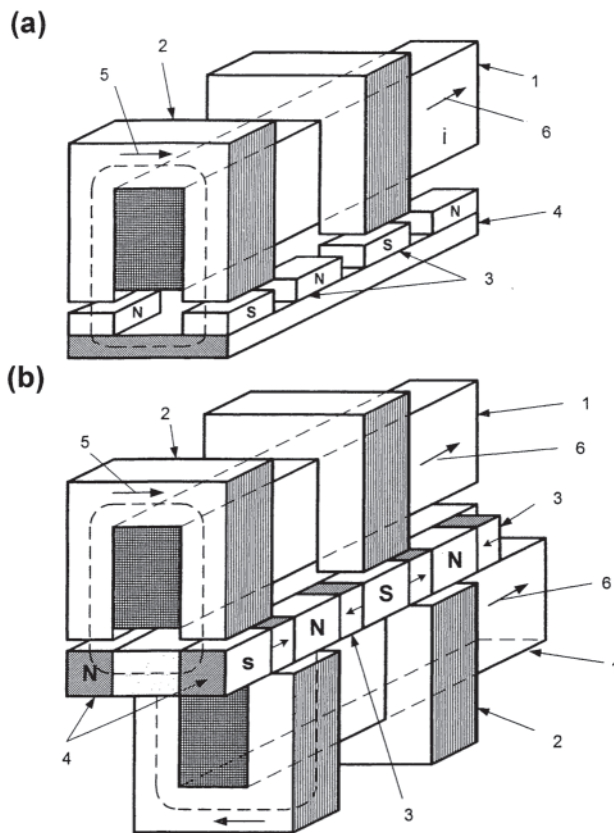


**Figure 5.24** Transverse flux permanent magnet (PM) linear synchronous motors (LSMs): (a) single-sided, (b) double-sided. 1, armature winding; 2, armature laminated core; 3, PM; 4, mild steel; 5, magnetic flux; 6, current.

### 5.6.2.3 Motors with Electromagnetic Excitation

The electromagnetic excitation system of a LSM is similar to the salient pole rotor of a rotary synchronous motor. **Figure 5.26** shows a flat single-sided LSM with salient ferromagnetic poles and *dc field excitation winding*. The poles and pole shoes can be made of solid steel, laminated steel or sintered powder. If the electromagnetic excitation system is integrated with the moving part, the dc current can be delivered with the

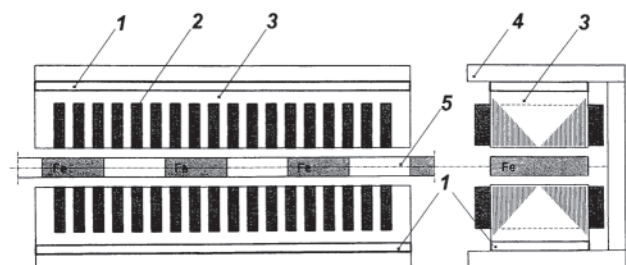


**Figure 5.25** Double-sided homopolar permanent magnet (PM) linear synchronous motor (LSM) with passive reaction rail. 1, PM; 2, armature winding; 3, armature stack; 4, yoke; 5, reaction rail.

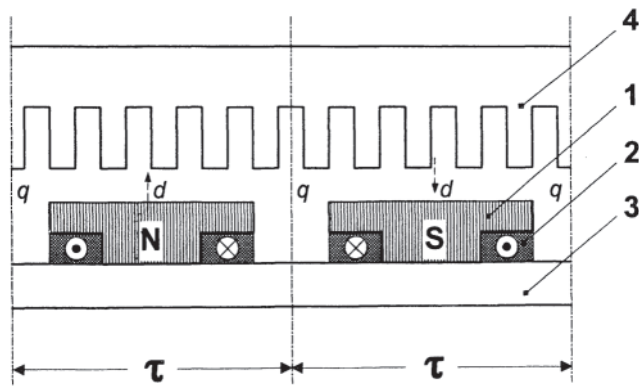


**Figure 5.26** Electromagnetic excitation system of a flat single-sided iron-cored linear synchronous motor (LSM). 1, salient pole; 2, direct current (dc) excitation winding; 3, ferromagnetic rail (yoke); 4, armature system.

aid of brushes and contact bars, inductive power transfer (IPT) systems [16], linear transformers or linear brushless exciters.

#### 5.6.2.4 Motors with Superconducting Excitation System

In large-power LSMs, the electromagnets with ferromagnetic core that produce the excitation flux can be replaced by coreless *superconducting electromagnets*. Because the magnetic flux density produced by the superconducting electromagnet is greater than the saturation magnetic flux density of the best laminated alloys ( $B_{sat} \approx 2.4$  T for cobalt alloy), there is no need to use the armature ferromagnetic core. An LSM with super-conducting excitation system is a totally air-cored machine (Fig. 5.27).

#### 5.6.2.5 Synchronous Reluctance Motors

The simplest construction of a *reluctance LSM* is shown in Fig. 5.26 with dc excitation winding being removed. However, the thrust of such a motor would be low as the ratio of *d*-axis permeance to *q*-axis permeance is low. Better performance can be obtained when using *flux barriers* [17] or steel laminations [18]. To make flux barriers, any nonferromagnetic material can be used. To obtain high permeance (low reluctance) in the *d* axis and low permeance in the *q* axis, steel

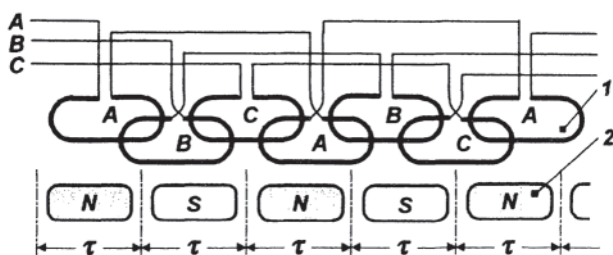


**Figure 5.27** Three-phase air-cored linear synchronous motor (LSM) with superconducting excitation system. 1, armature coils; 2, superconducting excitation coils.

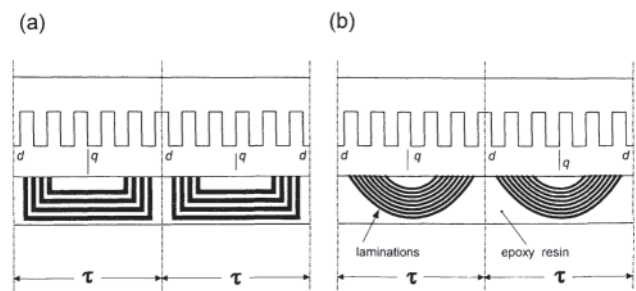


**Figure 5.28** Reluctance linear synchronous motors (LSMs) with: (a) flux barriers, (b) steel laminations.

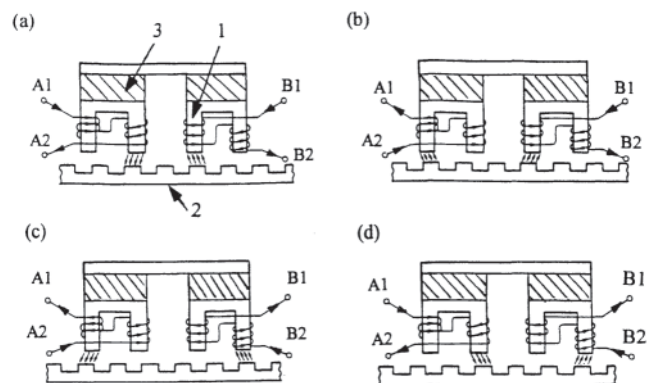
laminations should be oriented in such a way as to create high permeance for the *d*-axis magnetic flux.

Figure 5.28(a) shows a variable reluctance platen with flux barriers and Fig. 5.28(b) shows how to arrange steel laminations to obtain different reluctances in the *d* and *q* axis. The platen can be composed of segments the length of which is equal to the pole pitch  $\tau$ . Each segment consists of semicircular *lamellas* cut out from electrotechnical sheet. A filling, e.g., epoxy resin, is used to make the segment rigid and robust. By putting the segments together, a platen of any desired length can be obtained [19].

#### 5.6.2.6 Stepping Motors

So far, only stepping linear motors of hybrid construction (PM, winding and variable reluctance air gap) have found practical applications.

The *hybrid linear stepping motor (HLSM)*, as shown in Fig. 5.29, consists of two parts: the *forcer* (also called the *slider*) and the variable reluctance platen [20]. Both of them are evenly toothed and made of high permeability steel. The forcer is the moving part with two rare earth magnets and two concentrated parameter windings. The tooth pitch of the forcer matches the tooth pitch on the platen. However, the tooth pitches on the forcer poles are spaced one-fourth or one-half pitch from one pole to the next. This arrangement allows for



**Figure 5.29** Principle of operation of a hybrid linear stepping motor (HLSM): (a) initial position, (b) 1/4 tooth pitch displacement of the forcer, (c) 2/4 tooth pitch displacement, (d) 3/4 tooth pitch displacement. 1, forcer; 2, platen; 3, PM.

**Table 5.4** Data of HLSMs Manufactured by *Tokyo Aircraft Instrument Co., Ltd.*, Tokyo, Japan

Parameter	LP02-20A	LP04-20A	LP04-30A	LP60-20A
Driver	Bipolar chopper			
Voltage, V	24 dc			
Resolution, mm	0.2	0.4	0.4	0.423
Holding force, N	20	20	29.5	20
Step-to-step accuracy, mm	± 0.03			
Cumulative accuracy, mm	± 0.02			
Maximum start-stop speed, mm/s	60	120	120	127
Maximum speed, mm/s	400	600	500	600
Maximum load mass, kg	3.0	3.0	5.0	3.0
Effective stroke, mm	330	300	360	310
Mass, kg	1.4	1.2	2.8	1.4

HLSMs, hybrid linear stepping motors; dc, direct current.

the PM flux to be controlled at any levels between minimum and maximum level by the winding so that the forcer and the platen lines up at a maximum permeance, position. The HLSM is fed with two phase currents (90 degree, out of phase), similarly as a rotary stepping motor. The forcer moves one-fourth tooth pitch per each full step.

There is a very small air gap between the two parts which is maintained by strong air flow produced by an air compressor [21, 20]. The average air pressure is about 300 to 400 kPa and depends on how many phases are excited.

Table 5.4 shows specification data of HLSMs manufactured by *Tokyo Aircraft Instrument Co., Ltd.*, Tokyo, Japan [22]. The *holding force* is the amount of external force required to break the forcer away from its rest position at rated current applied to the motor. The *step-to-step accuracy* is a measure of the maximum deviation from the true position in the length of each step. This value is different for full step and microstepping drives. The *maximum start-stop speed* is the maximum speed that can be used when starting or stopping the motor without ramping that does not cause the motor to fall out of synchronism or lose steps. The *maximum speed* is the maximum linear speed that can be achieved without the motor stalling or falling out of synchronism. The *maximum load mass* is the maximum allowable mass applied to the forcer against the scale that does not result in mechanical damage. The *full-step resolution* is the position increment obtained when the currents are switched from one winding to the next winding. This is the typical resolution obtained with full step drives and it is strictly a function of the motor construction. The *microstepping resolution* is the position increment obtained when the full step resolution is divided electronically by proportioning the currents in the two windings. This resolution is typically 10 to 250 times smaller than the full-step resolution [22].

HLSMs are regarded as an excellent solution to positioning systems that require a high accuracy and rapid acceleration. With a microprocessor-controlled *microstepping mode* [23], smooth operation with standard resolution of a few hundred steps per millimeter can be obtained. The advantages such as high efficiency, high throughput, mechanical simplicity, high reliability, precise open-loop operation, low inertia of the system, etc., have made these kind of motors more and more

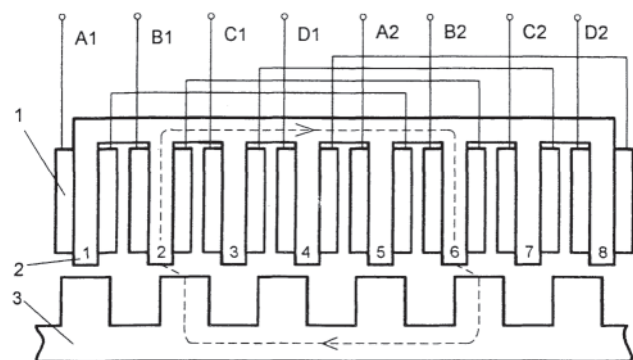
attractive in such applications as factory automation, high speed positioning, computer peripherals, facsimile machines, numerically controlled machine tools, automated medical equipment, automated laboratory equipment and welding robots. This motor is especially suitable for machine tools, printers, plotters and computer controlled material handling in which a high positioning accuracy and repeatability are the key problems.

When two or four forcers mounted at 90 degree and a special grooved platen (waffle plate) are used, the *x-y* motion in a single plane is obtained (Fig. 5.30). Specification data of the *x-y* HLSMs manufactured by *Normag Northern Magnetics, Inc.*, Santa Clarita, CA, U.S.A. are given in Table 5.5 [24].

#### 5.6.2.7 Switched Reluctance Motors

An LSRM has a doubly salient magnetic circuit with a polyphase winding with concentrated parameters on the armature as shown in Fig. 5.31. Both linear speed and position can be controlled with high accuracy. Low speed is not subject to design constraints, i.e., minimum speed limited by minimum feasible pole pitch as in linear ac motors [25]. An LSRM can also be designed as a linear transverse flux motor [25].

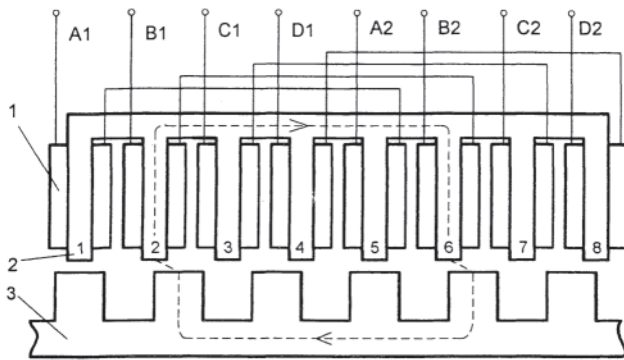
The inductance of a LSRM (Fig. 5.31) can be approximated by the following equation:



**Figure 5.30** Hybrid linear stepping motor (HLSM) with a four-unit forcer to obtain the *x-y* motion: 1, forcers for the *x* direction; 2, forcers for the *y* direction; 3, platen; 4, air pressure.

**Table 5.5** Data of *x-y* HLSMs Manufactured by *Normag Northern Magnetics, Inc.*, Santa Clarita, CA

Parameter	4XY0602-2-0	4XY2002-2-0	4XY2004-2-0	4XY2504-2-0
Number of forcer units per axis	1	1	2	2
Number of phases	2	2	2(4)	2(4)
Static thrust, N	13.3	40.0	98.0	133.0
Thrust at 1 m/s, N	11.1	31.1	71.2	98.0
Normal attractive force, N	160.0	400.0	1440.0	1800.0
Resistance per phase, $\Omega$	2.9	3.3	1.6	1.9
Inductance per phase, mH	1.5	4.0	2.0	2.3
Input phase current, A	2.0	2.0	4.0	4.0
Airgap, mm		0.02		
Maximum temperature, $^{\circ}\text{C}$		110		
Mass, kg	3.2	0.72	2.0	1.5
Repeatability, mm		0.00254		
Resolution, mm		0.00254		
Bearing type		air		

**Figure 5.31** Construction of a linear switched reluctance motor (LSRM). 1, armature winding; 2, armature stack; 3, platen.

$$L(x) = \frac{1}{2}(L_{\max} + L_{\min}) - \frac{1}{2}(L_{\max} - L_{\min}) \cos \frac{\pi}{\tau} x$$

$$= L_0 - \frac{1}{2}(k_L - 1)L_{\min} \cos \frac{\pi}{\tau} x \quad (5.14)$$

where:

$$L_0 = \frac{1}{2}(L_{\max} + L_{\min}) \quad (5.15)$$

$$k_L = \frac{L_{\max}}{L_{\min}} \quad (5.16)$$

$L_{\max}$  is the maximum inductance (armature and platen poles are aligned) and  $L_{\min}$  is the minimum inductance (complete misalignment of armature and platen poles). If the magnetic saturation is negligible, the electromagnetic thrust (in the  $x$  direction) is:

$$F_{dx} = \frac{dW}{dx} = \frac{1}{2} I_a^2 \frac{dL(x)}{dx} = F_{\max} \sin \frac{\pi}{\tau} x \quad (5.17)$$

where:

$$F_{\max} = \frac{1}{4} \frac{\pi}{\tau} (k_L - 1) L_{\min} I_a^2 \quad (5.18)$$

The electromagnetic thrust of an LSRM is directly proportional to the armature current squared  $I_a^2$  and the

parameter  $k_L \tau 1$  and it is inversely proportional to the pole pitch  $\tau$ . The ratio of the maximum to minimum inductance  $k_L$  should be as high as possible. Equations 5.16 and 5.17 do not take into account the current waveform shape (current turn-on and turnoff time instants).

For example, an LSRM with  $L_{\max}=0.015$  H,  $L_{\min}=0.002$  H, pole pitch  $\tau=0.038$  m and rms current  $I_a=15$  A develops the maximum force  $F_{\max}=0.25(\pi/0.038)(7.5-1) \times 0.002 \times 15^2=60.5$  N, where  $k_L=0.015/0.002=7.5$ .

## 5.6.3 Performance Calculation

### 5.6.3.1 Synchronous Reactance

For a salient-pole synchronous machine, the  $d$ - and  $q$ -axis synchronous reactances are:

$$X_{sd}=X_1+X_{ad} \text{ and } X_{sq}=X_1+X_{aq} \quad (5.19)$$

where  $X_1=2\pi f L_1$  is the armature winding leakage reactance,  $L_1$  is the armature winding leakage inductance,  $X_{ad}$  is the  $d$ -axis armature reaction reactance also called the  $d$ -axis mutual reactance, and  $X_{aq}$  is the  $q$ -axis armature reaction reactance also called the  $q$ -axis mutual reactance. The *direct* or  $d$ -axis is the center axis of the magnetic pole while the *quadrature* or  $q$ -axis is the axis parallel (90 degree electrical) to the  $d$  axis. The reactance  $X_{ad}$  is sensitive to the saturation of the magnetic circuit while the influence of the magnetic saturation on the reactance  $X_{aq}$  depends on the excitation system design. In Salient-pole synchronous machines with electromagnetic excitation  $X_{aq}$  is practically independent of the magnetic saturation. Usually, in PM synchronous machines  $X_{sq}>X_{sd}$ .

The  $d$ -axis armature reaction reactance:

$$X_{ad} = 4m_1 \mu_0 f \frac{(N_1 k_{\omega 1})^2}{\pi p} \frac{\tau L_i}{g'} k_{fd} \quad (5.20)$$

where  $\mu_0$  is the magnetic permeability of free space,  $N_1$  is the number of turns per phase,  $k_{\omega 1}$  is the armature winding factor for the fundamental space harmonic,  $L_i$  is the effective length of the stator core,  $g' \approx k_C k_{sat} g + h_M / \mu_{rec}$  is the equivalent air gap in the  $d$  axis,  $k_C$  is the Carter's coefficient for the air gap [26,

27],  $k_{sat} > 1$  is the saturation factor of the magnetic circuit, and  $k_{fd}$  is the form factor of the armature reaction in the  $d$  axis. The saturation factor  $k_{sat}$  depends on the magnetic saturation of armature teeth, i.e., the sum of the air gap MVD and the teeth MVD divided by the air gap MVD. Similarly, for the  $q$  axis:

$$X_{aq} = 4m_1\mu_0f \frac{(N_1k_{\omega 1})^2}{\pi p} \frac{\tau L_i}{k_C k_{saq} g_q} k_{fq} \quad (5.21)$$

where  $g_q$  is the air gap in the  $q$  axis,  $k_{saq}$  is the saturation factor in the  $q$  axis, and  $k_{fq}$  is the form factor of the armature reaction in the  $q$  axis. For salient pole excitation systems the saturation factor  $k_{saq} \approx 1$ , because the  $q$ -axis armature reaction fluxes, closing through the large air spaces between the poles, depend only slightly on the saturation. For surface configuration of PMs the form factors of the armature reaction  $k_{fd} \approx k_{fq} = 1$ . For other configurations of PMs the coefficients  $k_{fd}$  and  $k_{fq}$  are given in [25, 27].

The leakage reactance  $X_1$  consists of the slot, endconnection, differential, and tooth-top leakage reactances [26]. Only the slot and differential leakage reactances depend on the magnetic saturation due to leakage fields.

### 5.6.3.2 Voltage-Induced (emf)

The no-load rms voltage-induced (emf) in one phase of the armature winding by the dc or PM excitation flux  $\Phi_f$  is:

$$E_f = \pi\sqrt{2}fN_1k_{\omega 1}\Phi_f \quad (5.22)$$

where  $f$  is the input frequency,  $N_1$  is the number of the armature turns per phase,  $k_{\omega 1}$  is the armature winding factor, and the fundamental harmonic  $\Phi_{f1}$  of the excitation magnetic flux density  $\Phi_f$  without armature reaction is:

$$\Phi_{f1} = L_i \int_0^\tau B_{mg1} \sin\left(\frac{\pi}{\tau}x\right) dx = \frac{2}{\pi} \tau L_i B_{mg1} \quad (5.23)$$

Similarly, the voltage  $E_{ad}$  induced by the  $d$ -axis armature reaction flux  $\Phi_{ad}$  and the voltage  $E_{aq}$  induced by the  $q$ -axis flux  $\Phi_{aq}$  are, respectively:

$$E_{ad} = \pi\sqrt{2}fN_1k_{\omega 1}\Phi_{ad} \quad (5.24)$$

$$E_{aq} = \pi\sqrt{2}fN_1k_{\omega 1}\Phi_{aq} \quad (5.25)$$

The emfs  $E_f$ ,  $E_{ad}$ ,  $E_{aq}$  and magnetic fluxes  $\Phi_f$ ,  $\Phi_{ad}$  and  $\Phi_{aq}$  are used in construction of phasor diagrams and equivalent circuits.

### 5.6.3.3 Armature Currents and Input Power

On the basis of the phasor diagram of a salient pole synchronous motor [28] the currents in the  $d$  and  $q$  axis are [41]:

$$I_{ad} = \frac{V_1(X_{sq} \cos \delta - R_1 \sin \delta) - E_f X_{sq}}{X_{sd} X_{sq} + R_1^2} \quad (5.26)$$

$$I_{aq} = \frac{V_1(R_1 \cos \delta + X_{sd} \sin \delta) - E_f R_1}{X_{sd} X_{sq} + R_1^2} \quad (5.27)$$

where  $R_1$  is the winding resistance per phase and  $\delta$  is the load angle between the input voltage  $V_1$  and emf  $E_f$ . The rms armature current as a function of  $V_1$ ,  $E_f$ ,  $X_{sd}$ ,  $X_{sq}$ ,  $\delta$ , and  $R_1$  is:

$$I_a = \sqrt{I_{ad}^2 + I_{aq}^2} = \frac{V_1}{X_{sd} X_{sq} + R_1^2} \times \sqrt{[(X_{sq} \cos \delta - R_1 \sin \delta) - E_f X_{sq}]^2 + \sqrt{[(R_1 \cos \delta + X_{sd} \sin \delta) - E_f R_1]^2}} \quad (5.28)$$

The phasor diagram can also be used to find the input power [30]:

$$P_{in} = m_1 V_1 I_a \cos \phi = m_1 V_1 (I_{aq} \cos \delta - I_{ad} \sin \delta) \quad (5.29)$$

### 5.6.3.4 Electromagnetic Power and Thrust

Neglecting the core losses, the electromagnetic power is the motor input power minus the armature winding loss, i.e.,

$\Delta P_{1\omega} = m_1 I_a^2 R_1 = m_1 (I_{ad}^2 + I_{aq}^2) R_1$ . Thus:

$$P_{elm} = P_{in} - \Delta P_{1\omega} = m_1 [I_{aq} E_f + I_{ad} I_{aq} (X_{sd} - X_{sq})] = \frac{m_1 [V_1 (R_1 \cos \delta + X_{sd} \sin \delta) - E_f R_1]}{(X_{sd} X_{sq} + R_1^2)^2} \times [V_1 (X_{sq} \cos \delta - R_1 \sin \delta) (X_{sd} - X_{sq}) + E_f (X_{sd} X_{sq} + R_1^2) - E_f X_{sq} (X_{sd} - X_{sq})] \quad (5.30)$$

Putting  $R_1=0$ , Eq. 5.30 takes the following simple form:

$$P_{elm} = m_1 \left[ \frac{V_1 E_f}{X_{sd}} \sin \delta + \frac{V_1^2}{2} \left( \frac{1}{X_{sq}} - \frac{1}{X_{sd}} \right) \sin 2\delta \right] \quad (5.31)$$

Small PM LSMs have rather high armature winding resistance  $R_1$  that is comparable with  $X_{sd}$  and  $X_{sq}$ . That is why Eq. 5.30 instead of 5.31 is recommended for calculating the performance of small, low-speed motors.

The electromagnetic thrust developed by a LSM is:

$$F_{dx} = \frac{P_{elm}}{v_s} \quad \text{N} \quad (5.32)$$

Neglecting the armature winding resistance ( $R_1=0$ ):

$$F_{dx} = \frac{m_1}{v_s} \left[ \frac{V_1 E_f}{X_{sd}} \sin \delta + \frac{V_1^2}{2} \left( \frac{1}{X_{sq}} - \frac{1}{X_{sd}} \right) \sin 2\delta \right] \quad (5.33)$$

In a salient pole-synchronous motor the electromagnetic thrust has two components, i.e.:

$$F_{dx} = F_{dxsyn} + F_{dxrel} \quad (5.34)$$

where the first term:

$$F_{dxsyn} = \frac{m_1}{v_s} \frac{V_1 E_f}{X_{sd}} \sin \delta \quad (5.35)$$

is a function of both the input voltage  $V_1$  and the excitation emf  $E_f$ . The second term:

$$F_{dxrel} = \frac{m_1 V_1^2}{2v_s} \left( \frac{1}{X_{sq}} - \frac{1}{X_{sd}} \right) \sin 2\delta \quad (5.36)$$

depends only on the voltage  $V_1$  and also exists in an unexcited machine ( $E_f=0$ ) provided that  $X_{sd} \neq X_{sq}$ . The thrust  $F_{dxsyn}$  is called

the *synchronous thrust* and the thrust  $F_{d_{\text{rel}}}$  is called the *reluctance thrust*. The proportion between  $X_{sd}$  and  $X_{sq}$  strongly affects the shape of the curve  $F_{dx}=f(\delta)$ . For surface configurations of PMs  $X_{sd}\approx X_{sq}$  (if the magnetic saturation is neglected) and:

$$F_{dx} \approx F_{d_{\text{syn}}} = \frac{m_1}{v_s} \frac{V_1 E_f}{X_{sd}} \sin \delta \quad (5.37)$$

Reluctance LSMs do not have any excitation system so that the emf  $E_f=0$ . The thrust is expressed by Eq. 5.36 and is proportional the the input voltage squared  $V_1^2$ , the difference  $X_{sd}-X_{sq}$  between the  $d$ - and  $q$ -axis synchronous reactances and  $\sin 2\delta$  where  $\delta$  is the load angle (between the terminal voltage  $V_1$  and  $q$  axis).

The thrust of a PM LSM can be calculated directly on the basis of the electromagnetic field distribution [29, 30]. For two dimensional electromagnetic field distribution the electromagnetic thrust developed by a PM LSM is [31].

$$F_{dx} = \frac{4}{\pi} p \tau L_i B_r A_m \sin \left( \frac{\alpha_i \pi}{2} \right) \times \frac{\tanh(\beta h_M)}{\mu_{r\text{rel}} \sinh(\beta k_C g) + \tanh(\beta h_M) \cosh(\beta k_C g)} \quad (5.38)$$

where  $\alpha_i = b_p/\tau$ ,  $\beta = \pi/\tau$ ,  $\tau$  is the pole pitch,  $g$  is the air gap in the  $d$ -axis,  $k_C$  is Carter's coefficient,  $b_p$  is the width of pole shoe (or width of magnet  $\omega_M$ ) and  $h_M$  is the magnet height.

#### 5.6.3.4.1 Numerical Example

A falt, short-armature, single-sided, three-phase ( $m_1=3$ ) LSM has a long reaction rail with surface configuration of PMs. Sintered NdFeB PMs with the remanent magnetic flux density  $B_r=1.1$  T and coercive force  $H_c=800$  kA/m have been used. The armature magnetic circuit has been made of cold-rolled steel laminations with stacking factor  $k_f=0.95$ . The following design data are available: armature phase windings are Y-connected, number of pole pairs  $p=4$ , pole pitch  $\tau = 56$  airgap in  $d$  axis (mechanical clearance)  $g=2.5$  mm, airgap in  $q$  axis  $g_q=6.5$  mm, effective width of the armature core  $L_i=84$  mm, width of the core (back iron) of the reaction rail  $\omega=84$  mm, height of the yoke of the armature core  $h_{1y}=20$  mm, number of armature turns per phase  $N_1=560$ , number of parallel wires  $a_\omega=2$ , number of armature slots  $z_1=24$ , slot opening  $b_{s1}=0.0103$  mm, slot depth  $h_{s1}=0.032$  mm, diameter of armature wire  $d_{\text{wir}}=1.02$  mm, height of the PM  $h_M=4.0$  mm, width of the PM  $\omega_M=42.0$  mm, length of the PM (in the direction of armature conductors)  $l_M=84$  mm, width of the pole shoe  $b_p=\omega_M=42.0$  mm, armature winding resistance  $R_1=2.5643$   $\Omega$ , armature winding leakage inductance  $L_{l1}=0.0331$  H, saturation factor of the magnetic circuit  $k_{\text{sat}}\approx 1.1$ . The coil pitch of the armature winding is equal to the pole pitch  $\tau$  (full pitch winding).

The LSM is fed from a VVVF inverter. The input voltage  $V_{1L-L}=200$  V (line-to-line) and input frequency  $f=20$  Hz. The LSM has been designed for continuous duty cycle to operate with the load angle  $\delta \approx 22^\circ$ , which corresponds to the maximum efficiency. Find the steady-state performance.

The phase voltage  $V_1 = V_{1L-L}/\sqrt{3} = 200/\sqrt{3} = 115.47$  V, the pole shoe-to-pole pitch ratio  $\alpha_i = b_p/\tau = 42/56 = 0.75$ , slot pitch  $t_1=2p\tau/z_1=2\times 4\times 0.042/24=0.01867$  m, the relative recoil permeability  $\mu_{r\text{rec}}=B_r/(\mu_0 H_c)=1.1/(0.4\pi \times 10^{-6}\times 800,000)=1.094$ , Carter's coefficient  $k_C=1.336$  [27] and winding factor for the coil pitch equal to pole pitch is  $k_{\omega 1}=1$  [30]. The equivalent air gap in the  $d$  axis:

$$g' = k_C k_{\text{sat}} g + \frac{h_M}{\mu_{r\text{rec}}} = 1.336 \times 1.1 \times 0.0025 + 0.004 \times 1.094 = 0.00733 \text{ mm}$$

The armature reaction reactances in the  $d$  and  $q$  axis according to Eqs. 5.20 and 5.21 are:

$$X_{ad} = 4 \times 3 \times 0.4\pi \times 10^{-6} \times 20 \times (560 \times 1.0)^2 \pi \times 4 \times 0.056 \times 0.084 \times 0.00733 \times 1.0 = 4.829 \Omega$$

$$X_{aq} \approx X_{ad} = 4.829 \Omega$$

where for surface PMs  $k_{fd}=k_{fg}=1.0$ . The armature winding leakage reactance  $X_{l1}=2\pi f L_{l1}=2\pi \times 20 \times 0.0331=4.159$   $\Omega$ . Synchronous reactances in the  $d$  and  $q$  axis according to Eq. 5.19 are equal, i.e.,  $X_{sd}=X_{sq}=4.829+4.159=8.989$   $\Omega$ . The air gap magnetic flux density according to Eq. 5.10 is:

$$B_g = \frac{1.1}{1 + 1.094 \times 0.0025} = 0.653 \text{ T}$$

Because in most cases Eq. 5.10 gives higher value of  $B_g$  than obtained from measurements, in further considerations  $B_{mg1}\approx B_g$ . The excitation magnetic flux and the emf per phase are calculated on the basis of Eqs. 5.24 and 5.22, i.e.:

$$\Phi_f \approx \frac{2}{\pi} \times 0.056 \times 0.084 \times 0.653 = 0.00196 \text{ Wb}$$

$$E_f = \pi \sqrt{2} \times 20 \times 560 \times 1.0 \times 0.00196 = 97.345 \text{ V}$$

Armature *rms* currents according to Eqs. 5.26–5.28 are:

$$I_{ad} = \frac{115.47(8.989 \cos 22^\circ - 2.5643 \sin 22^\circ) - 97.345 \times 8.989}{8.989 \times 8.989 + 2.5643^2} = -0.27 \text{ A}$$

$$I_{aq} = \frac{115.47(2.5643 \cos 22^\circ + 8.989 \sin 22^\circ) - 97.345 \times 2.5643}{8.989 \times 8.989 + 2.5643^2} = 4.735 \text{ A}$$

$$I_a = \sqrt{(-0.27)^2 + 4.735^2} = 4.743 \text{ A}$$

The current density in the armature winding is:

$$j_a = \frac{I_a}{a_\omega s_a} = \frac{4.743}{2 \times 0.817 \times 10^{-6}} = 2.902 \times 10^6 \text{ A/m}^2$$

where  $s_a = \pi d_{\text{wir}}^2/4 = \pi 0.00102^2/4 = 0.817 \times 10^{-6}$   $\text{m}^2$ . The peak value of the armature line current density according to Eq. 5.8:

$$A_m = \frac{3\sqrt{2} 560 \times 4.743}{4 \times 0.056} = 50,305.5 \text{ A/m}$$

The input active power according to Eq. 5.29



$$P_{in} = 3 \times 115.47 [4.735 \cos 22^\circ - (-0.27) \sin 22^\circ] \\ = 1555.9 \text{ W}$$

The mass of armature teeth  $m_r = 7760_{z_1}(t_1 - b_{s1}) h_{s1} k_i L_i = 7760 \times 24 (0.01867 - 0.0103) 0.032 \times 0.95 \times 0.084 \times 3.979 \text{ kg}$ , the mass of the armature yoke  $m_y = 7760 (2p\tau + t_1) h_{1y} k_i L_i = 7760 (2 \times 4 \times 0.056 + 0.01867) 0.02 \times 0.95 \times 0.084 = 5.78 \text{ kg}$ , the magnetic flux density in the armature tooth  $B_r \approx B_g \times t_1 / [(t_1 - b_{s1}) k_i] = 6.53 \times 0.01867 / [(0.01867 - 0.0103) \times 0.95] = 1.534 \text{ T}$ , and the magnetic flux density in the armature yoke  $B_y \approx (\Phi_f - 0.1\Phi_f) / (2h_{1y} k_i L_i) = (0.00196 - 0.1 \times 0.00196) / (2 \times 0.02 \times 0.95 \times 0.084) \times 0.552 \text{ T}$ . The armature leakage flux has been estimated as  $0.1\phi_f$ . The armature core losses according to [28, 29] are:

$$\Delta P_{Fe} = \Delta p_{1/50} \left( \frac{f}{50} \right)^{4/3} (k_{adt} B_r^2 m_r + k_{ady} B_y^2 m_y) \\ = 2.4 \left( \frac{20}{50} \right)^{4/3} (1.9 \times 1.534^2 \times 3.979 + 3.5 \\ + 0.552^2 \times 5.78) = 16.8 \text{ W}$$

where  $\Delta p_{1/50} = 2.4 \text{ W/kg}$  is the specific core loss at 1 T and 50 Hz,  $k_{adt} \approx 1.9$ , and  $k_{ady} \approx 3.5$ . The armature winding losses are:

$$\Delta P_a = m_1 R_1 I_a^2 = 3 \times 2.5643 \times 4.743^2 = 173 \text{ W}$$

the electromagnetic power is:

$$P_{elm} = P_{in} - \Delta P_a - \Delta P_{Fe} = 1555.9 - 173.0 - 16.9 = 1365.9 \text{ W}$$

Neglecting the stray losses and mechanical losses the efficiency is:

$$\eta \approx \frac{P_{elm}}{P_{in}} = \frac{1365.9}{1555.9} = 0.878$$

The power factor  $\cos \phi$  is:

$$\cos \phi = \frac{P_{in}}{m_1 V_1 I_a} = \frac{1555.9}{3 \times 115.474 \times 4.743} = 0.947$$

The electromagnetic thrust developed by the LSM according to Eq. 5.32 is:

$$F_{dx} = \frac{1365.9}{2.24} = 609.8 \text{ N}$$

where the linear synchronous speed  $v_s = 2 \times 20 \times 0.056 = 2.4 \text{ m/s}$  is calculated on the basis of Eq. 5.7.

### 5.6.3.5 Normal Force

The Force  $F_i$  associated with any linear motion defined by a variable  $s_i$  of a device utilizing a magnetic field is given by:

$$F_i = \frac{\partial W}{\partial s_i} \quad (5.39)$$

where  $W$  is the field energy in joules,  $F_i$  denotes the  $F_x$ ,  $F_y$ , or  $F_z$  force component and  $s_i$  denotes the  $x$ ,  $y$  or  $z$  coordinate. Eq. 5.39 can be used to find the attractive force between two poles separated by an air gap  $z=g$ . Let us consider a linear electromagnetic actuator, electromagnet, or relay mechanism. The following assumptions are usually made: (a) leakage flux paths are neglected, (b) nonlinearities are neglected, and (c)

all the field energy is stored in the air gap ( $\mu_0 \mu_r \gg \mu_0$ ) where the magnetic permeability of free space  $\mu_0 = 0.4\pi \times 10^{-6} \text{ H/m}$  and  $\mu_r$  is the relative permeability. The volume of the air gap is  $Az$  and the stored field energy is  $W = 0.5 (B_g^2 / \mu_0) Az$ . With the displacement  $dz$  of one pole the new air gap is  $z+dz$ , new stored energy is  $W + dW = 0.5 (B_g^2 / \mu_0) A (z + dz)$ , change in stored energy is  $0.5 (B_g^2 / \mu_0) Adz$ , work done  $F_z dz$  and the force:

$$F_z = \frac{dW}{dz} = \frac{1}{2} \frac{B_g^2}{\mu_0} A = \frac{1}{2} \frac{\mu_0 (NI_f)^2}{g^2} A \quad (5.40)$$

where  $B_g = \mu_0 H = \mu_0 (Ni/z) z = g$ ,  $I_f$  is the excitation current (for electromagnetic excitation and  $A$  is the cross section of the air gap (surface of a single pole shoe). Equation 5.40 is used to find the normal (attractive) force between the armature core and reaction rail of linear motors. For a LSM the surface  $A \approx (p\tau - 0.5z_1 t_1) k_i L_i$  where  $p$  is the number of pole pairs,  $z_1$  is the number of slots,  $t_1$  is the slot (tooth) pitch,  $k_i$  is the stacking factor, and  $L_i$  is the effective length of the armature core.

For the LSM considered in Section 5.6.3.4 the normal attractive force according to Eq. 5.40 is:

$$F_z = \frac{0.653^2}{2 \times 0.4\pi \times 10^{-6}} \times 0.008013 = 1507.4 \text{ N}$$

where  $A = (4 \times 0.056 - 24 \times 0.0103) \times 0.95 \times 0.084 = 0.008013 \text{ m}^2$ . The normal attractive force is  $F_z / F_{dx} = 1507.4 / 609.8 \approx 2.5$  times greater than the electromagnetic thrust.

### 5.6.3.6 Main Dimensions

The pole pitch  $\tau$  and the effective length of the stator core  $L_i$  (in the direction of the traveling wave) are the main dimensions of the LSM that are estimated on the basis of the thrust, speed, magnetic loading, and electric loading.

On the basis of Eqs. 5.7, 5.8, 5.22, and 5.23, the apparent electromagnetic power is:

$$S_{elm} = m_1 E_f I_a = v_s p \tau L_i k_{\omega 1} B_{mg} A_m \quad (5.41)$$

Because the efficiency  $\eta = P_{out} / P_{in} = P_{out} / (m_1 V_1 I_a \eta \cos \phi)$  and the ratio of the phase emf-to-the phase voltage  $\epsilon = E_f / V_1$ , the output power in connection with Eq. 5.41 is

$$P_{out} = \frac{1}{\epsilon} v_s p \tau L_i k_{\omega 1} B_{mg} A_m \eta \cos \phi \quad (5.42)$$

Because the load thrust  $F_x = P_{out} / v_s$ , the output coefficient:

$$\sigma_p = \frac{F_x \epsilon}{2p\tau L_i} = 0.5 k_{\omega 1} B_{mg} A_m \eta \cos \phi \quad (5.43)$$

links the main dimensions  $\tau$  and  $L_i$  with the magnetic  $B_{mg}$  (peak value of the air gap magnetic flux density) and electric  $A_m$  (peak value of the line current density) loadings. For example, if  $F_x = 650 \text{ N}$ ,  $p = 4$ ,  $k_{\omega 1} \approx 1.0$ ,  $\epsilon = 0.84$ ,  $B_{mg} = 0.65 \text{ T}$ ,  $A_m = 54,000 \text{ A/m}$ ,  $\eta = 0.85$ , and  $\cos \phi = 0.9$ :

$$\sigma_p = 0.5 \times 1.0 \times 0.65 \times 54,000 \times 0.85 \times 0.9 \\ = 13,425.75 \text{ N/m}^2$$

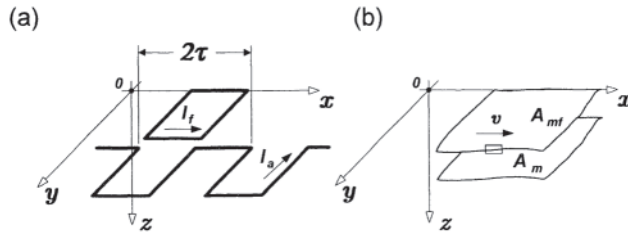


**Figure 5.32** Model of an air-cored linear synchronous motor (LSM) with superconducting excitation system for the electromagnetic field analysis: (a) winding layout, (b) armature and field excitation current sheets.

The area of the active surface of the armature core according to Eq. 5.43:

$$2p\tau L_i = \frac{F_x \epsilon}{\sigma_p} = \frac{650 \times 0.84}{13,425.75} = 40,668.1 \times 10^{-6} \text{ m}^2$$

Assuming  $L_i=0.09$  m, the pole pitch is:

$$\tau = \frac{40,668.1}{2 \times 4 \times 0.09} \approx 0.0565 \text{ m}$$

### 5.6.3.7 Careless LSM with Superconducting Electromagnets

The model of a *careless LSM with superconducting electromagnets* is shown in Fig. 5.32 [31–34]. The armature winding can be represented by the following space-time distribution of the line current density (current sheet) expressed as a complex number:

$$a(x, t) = A_m e^{j(\omega t - \beta x)} \quad (5.44)$$

and the excitation winding can be described by the following space time distribution of the complex line current density:

$$a_f(x, t) = A_{mf} e^{j(\omega t - \beta x - \epsilon_f)} \quad (5.45)$$

where the peak values of line current densities are:

- for the armature winding—see Eq. 5.8

$$A_m = \frac{m_1 \sqrt{2} N_1 k_{\omega 1} I_a}{p\tau} = \frac{2m_1 \sqrt{2} N_{1p} k_{\omega 1} I_a}{\tau} \quad (5.46)$$

- for the field excitation winding (dc current excitation)

$$A_{mf} = \frac{2N_f k_{\omega f} I_f}{p\tau} = \frac{4N_{fp} k_{\omega f} I_f}{\tau} \quad (5.47)$$

The number of series armature turns per phase is  $N_1=2pN_{1p}$  where  $N_{1p}$  is the number of armature series turns per phase per pole and the number of field series turns  $N_f=2pN_{fp}$  where  $N_{fp}$  is the number of field turns per pole.

The so-called force angle  $\epsilon_f = 90^\circ \mp \psi$  is the angle between phasors of the excitation flux  $\Phi_f$  in the  $d$  axis and the armature current  $I_a$ .

The two-dimensional distribution of the magnetic vector potential of the field excitation winding is described by the Laplace's equation [31–34]. The electromagnetic forces in the  $x$  and  $z$  direction per unit area can be found on the basis of Lorentz equations, i.e.:

$$\begin{aligned} f_{dx} &= \frac{1}{2} \text{Re}[a(x, t) \mathbf{B}_{fz}^*] \\ &= -\frac{1}{4} \mu_0 A_m A_{mf} e^{-\beta z} \sin \epsilon_f \quad \text{N/m}^2 \end{aligned} \quad (5.48)$$

$$\begin{aligned} f_{dz} &= -\frac{1}{2} \text{Re}[a(x, t) \mathbf{B}_{fx}^*] \\ &= -\frac{1}{4} \mu_0 A_m A_{mf} e^{-\beta z} \cos \epsilon_f \quad \text{N/m}^2 \end{aligned} \quad (5.49)$$

Multiplying Eqs. 5.48 and 5.49 by the area  $2pr$  of the superconducting electromagnet

- the electromagnetic thrust

$$F_{dx} = -F_{\max} \sin \epsilon_f \quad (5.50)$$

- the normal repulsive force

$$F_{dz} = -F_{\max} \cos \epsilon_f \quad (5.51)$$

where the peak force:

$$F_{\max} = 4\sqrt{2} \mu_0 m_1 p N_{1p} k_{\omega 1} N_{fp} k_{\omega f} \frac{L_i}{\tau} I_a I_f e^{-\beta z} \quad (5.52)$$

Let us consider a single-sided air-cored LSM with superconducting excitation winding with the following design data:  $m_1=3$ ,  $p=2$ ,  $N_{fp} k_{\omega f} I_f=700 \times 10^3$  A,  $k_{\omega 1}=1.0$ ,  $I_a=1000$  A,  $g=0.1$  m,  $\tau = 1.35$  m, and  $L_i=1.07$  m. The maximum force for  $N_{1p}=2$  is:

$$\begin{aligned} F_{\max} &= 4 \times 0.4\pi \times 10^{-6} \times 3 \times 2 \times \sqrt{2} \\ &\quad \times 2 \times 1.0 \times 700 \times 10^3 \times 1000.0 \\ &\quad \times \frac{1.07}{1.35} e^{-0.1\pi/1.35} = 37,501.4 \text{ N} \approx 37.5 \text{ kN} \end{aligned}$$

for  $N_{1p}=5$ ,  $F_{\max}=93.75$  kN;  $N_{1p}=10$ ,  $F_{\max}=187.5$  kN; for  $N_{1p}=15$ ,  $F_{\max}=281.25$  kN, and for  $N_{1p}=20$ ,  $F_{\max}=375.0$  kN. The  $-$  sign has been neglected.

The forces  $F_{dx} = F_{\max} \sin \epsilon$  and  $F_{dz} = F_{\max} \cos \epsilon$  as functions of the force angle  $\epsilon$  are plotted in Fig. 5.33.

### 5.6.4 Applications

There are two main areas of applications of LSMs: industrial automation systems and transportation systems.

Industrial automation systems include:

- Positioning stages [10, 20, 24, 35, 36]
- Machining centers [37–40]
- Friction welding [43]
- Welding robots [44]
- Thermal cutting
- Two-dimensional orientation of plastic films [45]
- Electrocoating [9]
- Laser scribing systems [48, 49]
- Material handling, e.g., monorail material handling, semiconductor wafer transport [16], capsule filling machines [20]
- Testing, e.g., surface roughness measurement [9], generation of vibration [47]
- Diamond processing laser systems [46].

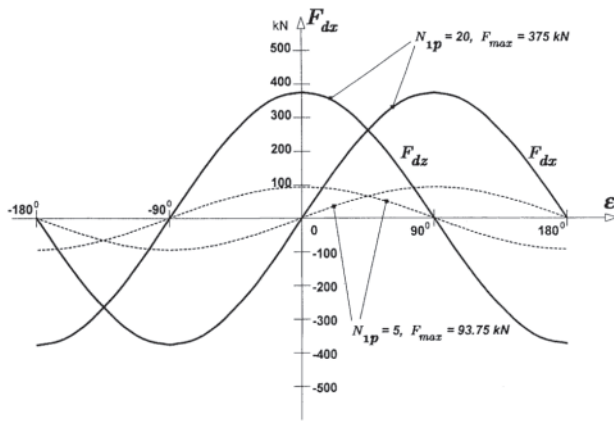


**Figure 5.33** Electromagnetic thrust  $F_{dt}$  and normal force  $F_{dz}$  as functions of the force angle  $\epsilon$  for typical parameters of an aircored LSM.

In factory transportation systems LSMs can simplify the transfer of bulk and loose materials, small containers, pallets, bottled liquids, parts, hand tools, documents, etc. It is possible to design both on-floor and overhead transportation systems. Linear motor transportation lines can be arranged on one level or on two or more levels.

In the future, LSMs are predicted for high speed maglev trains [14, 45–50] and ropeless elevators [51–53].

## 5.7 DESIGN EQUATIONS FOR A SYNCHRONOUS MACHINE [1, 56–62]

A synchronous machine, being a doubly excited device, can be designed to operate at any power factor, lagging or leading. Furthermore, the voltage regulation of a generator or the pullout torque for a motor depends on the synchronous reactance of the machine. With modern solid-state devices, used in variable speed motors, the commutation reactances of the machine and hence the subtransient reactances of the machines are also of critical importance. A synchronous machine is therefore designed for a given power rating, power factor, the synchronous reactances  $X_{sd}$ ,  $X_{xq}$ , and the subtransient reactances  $X''_{sd}$ ,  $X''_{xq}$ .

In the absence of any special considerations, for a machine to operate at a power factor of 0.8,  $X_{sd}$  may be taken as 1.0 per-unit (pu). For such a generator, the voltage rise on throwing off rated load would be approximately 30%; for a motor, the pull-out torque would be approximately 250% of the rated torque [57]. This should meet normal machine requirements. For very close voltage regulation or very large pull-out torque at normal excitation, a lower value of  $X_{sd}$  possibly down to 0.5 pu, may be necessary.

In a generator with a higher power factor, the reactance  $X_{sd}$  can be increased to 1.25 pu without excessively worsening voltage regulation; in a motor with a higher power factor, the reactance  $X_{sd}$  must be reduced to 0.8 pu or so to maintain a sufficient pull-out torque [57]. For machines without overload requirements,  $X_{sd}$  can usually be increased by 25%; for very large machines, which usually have lower load fluctuations, it may be increased by 50%. However, for machines operating

under zero power factor, weak-field conditions,  $X_{sd}$  may have to be much lower, down to 0.5 pu for machine stability.

Lower synchronous reactance implies a larger field excitation relative to the stator ampere-turns, and results in a larger machine for a given output.

### 5.7.1 Magnetic and Electric Loading

The electric loading  $q$  depends upon several variables such as power rating, speed, frequency, and voltage rating. The nominal value of  $q$  is 15–35 ampere-conductors per millimeter for air-cooled machines, with the lower values used for the lower power ratings. For machines with a smaller number of poles, a small diameter, or a large pole pitch, a smaller value of  $q$  should be used. Similarly, in high-voltage machines requiring larger slot insulation,  $q$  must be smaller. For machines with a larger number of poles, low voltage, and low frequency,  $q$  may be increased by up to 20%. For water-cooled machines, a value of  $q$  as high as 150 ampere-conductors per millimeter may be used.

The average flux density  $B_{gav}$  is limited primarily by saturation and core loss. For 60 Hz machines, it is usually 0.35–0.8 T.

### 5.7.2 Main Dimensions and Stator Windings

The main dimensions of a synchronous machine and its stator windings are designed by following the approach presented in Section 4.5 for induction machines, except for certain modifications that are required for a salient-pole machine.

When the field winding of a salient-pole machine is excited, the resulting air-gap flux density distribution is usually not sinusoidal because of magnetic saturation, the spatial configuration of the pole face and permeance variations due to stator and rotor slotting and concentration of conductors in slots. The effects of the spatial configuration may be taken into account in the following way.

The arc subtended by the pole compared to the pole pitch varies from one machine to another, and the air gap at the pole edges is generally greater than that at the center of the pole. Hence the ratio  $A_1$  of the amplitude of the fundamental of the flux density wave to the maximum flux density under the pole is a function of the machine geometry. To obtain  $A_1$ , enter the curves of Fig. 5.34 [1] with the ratio of the minimum air gap to the pole pitch. Factor  $A$  is taken from Fig. 5.34(a) for the pole arc to pole pitch ratio and factor  $B$  from Fig. 5.34(b) for the ratio of the maximum gap to the minimum gap.  $A_1$  is then given by the product of  $A$  and  $B$ .

For example, if the ratio of the minimum gap to the pole pitch is 0.03 and the ratio of pole arc to pole pitch is 0.65,  $A = 1.14$ . If the air gap at the pole edges is 2.00 times that at the center of the pole,  $B = 0.83$ . The amplitude of the fundamental is then given by  $A_1 = 1.14 \times 0.83 = 0.95$  times the maximum flux density.

The factor  $A_1$  is used to compute the maximum flux density in the stator teeth as (see Eq. 4.125):

$$B_{\max} = \frac{\pi}{2} B_{gav} \frac{L/L_i}{A_1(t/\lambda)} \quad (5.53)$$

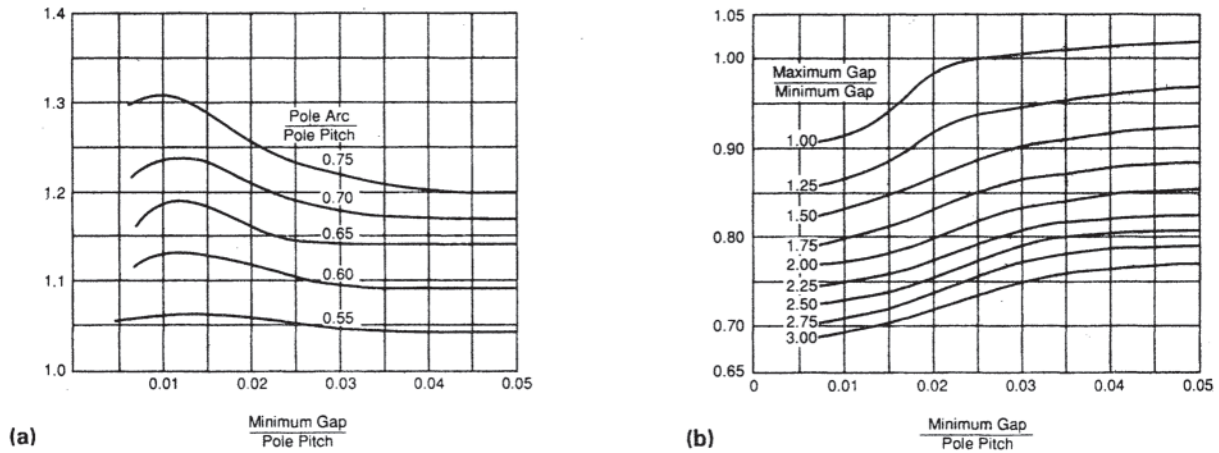


**Figure 5.34** (a) Form factor  $A$  for air gap flux with field excitation. (Copyright by the American Institute of Electrical Engineers, 1927.) (b) Form factor  $B$  for air gap flux with field excitation. (Copyright by the American Institute of Electrical Engineers, 1927.)

In the absence of specific field plots,  $AI$  may be taken to be 1.05.

### 5.7.3 Cylindrical Rotor Design

The air gap is first determined on the basis of the required synchronous reactance  $X_s$ , which is the sum of the armature reaction reactance  $X_a$  and the stator leakage reactance  $X_l$ . With a cylindrical rotor, the armature reaction reactance  $X_a$  can be calculated by using the magnetizing inductance equation presented earlier for an induction machine; the leakage reactance  $X_l$  can also be obtained by using pertinent leakage reactance formulas given earlier.

The cylindrical rotor carries two separate circuits: the field winding, and the damper cage. The damper cage is a squirrel cage as in an induction motor, and is designed to provide the required starting torque for a motor, or the desired damping for an alternator. In the case of solid-state motor drives, the

squirrel cage is also designed so that the commutation reactance of the power circuit is acceptable. The damper cage of a motor can thus be designed by using the procedure described earlier.

The field winding is placed in rotor slots under the damper cage as illustrated in Fig. 5.35. The field ampere-turns must be sufficient to induce a voltage  $E_f$  in the stator winding as obtained from the phasor diagrams of Fig. 5.36.

The field ampere-turns  $AT_f$  per pole are then given by:

$$AT_f = \frac{B_{\max}}{\mu_0} g_e \frac{E_f}{V} = \frac{\pi}{2} \frac{B_{gav}}{\mu_0} g_e \frac{E_f}{V} \tag{5.54}$$

These ampere-turns are then provided by designing a distributed field winding in the slots under the damper cage.

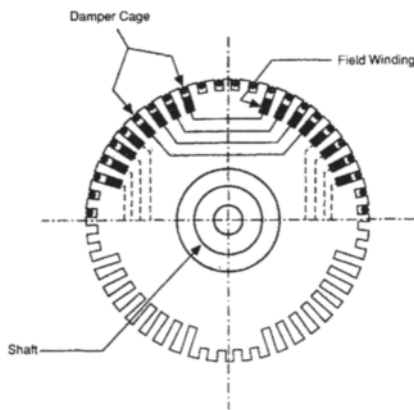


**Figure 5.35** Cylindrical rotor with damper cage.

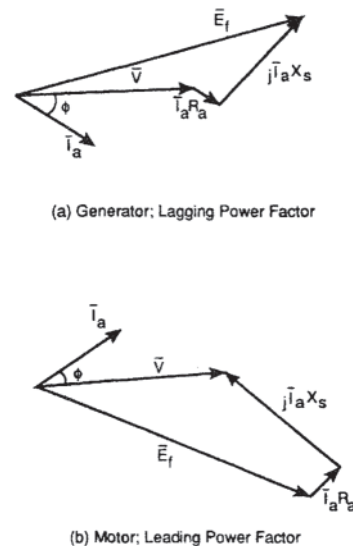


**Figure 5.36** Phasor diagrams (cylindrical rotor).

### 5.7.4 Salient-Pole Rotors

There are certain features of a salient-pole rotor that must be understood before a design procedure can be presented. The pole-arc/pole-pitch ratio  $\alpha$  is usually approximately 0.65 for a machine with a small number of poles and runs as high as 0.75 for a machine with a large number of poles. Furthermore, as shown in Fig. 5.37 the pole face is shaped such that a nearly sinusoidal flux density distribution is obtained in the air gap when the field winding is excited. The air gap  $g_2$  under the pole tip is usually 50–125% greater than the gap  $g_1$  at the pole center. The thickness of pole tips is chosen for mechanical strength, allowing for damper slots if necessary. The pole body width is chosen such that the flux density  $B_p$  at the root of the pole is limited to 1.4–1.8 T. A leakage factor of 1.25 is usually considered in calculating  $B_p$  [56], as

$$B_p = 1.25 B_{gav} \text{ (pole pitch/pole body width)} \quad (5.55)$$

### 5.7.5 Field Winding Design

In a salient-pole machine, the armature reaction, i.e., the air gap flux generated by stator currents, depends on the position of the rotor with reference to the axes of the phase windings. It is therefore customary to define two separate armature reaction reactances for a salient-pole machine. The *direct-axis armature reaction reactance*  $X_{ad}$  is defined as that reactance associated with the armature reaction when it is centered on the direct axis, i.e., on the center of the rotor pole. The *quadrature-axis armature reaction reactance*  $X_{aq}$  is defined as that reactance associated with the armature reaction when it is centered on the quadrature axis, i.e., on the interpolar axis. If  $X_a$  is defined as the armature reaction reactance with a constant air gap, the ratios:

$$A_d = \frac{X_{ad}}{X_a} \quad \text{and} \quad A_q = \frac{X_{aq}}{X_a}$$

are functions of rotor geometry. Considering a uniform air gap under the pole face, and an infinite air gap in the interpolar region, the ratios  $A_d$  and  $A_q$  can be obtained as functions of  $\alpha$  by using simple Fourier analysis as:

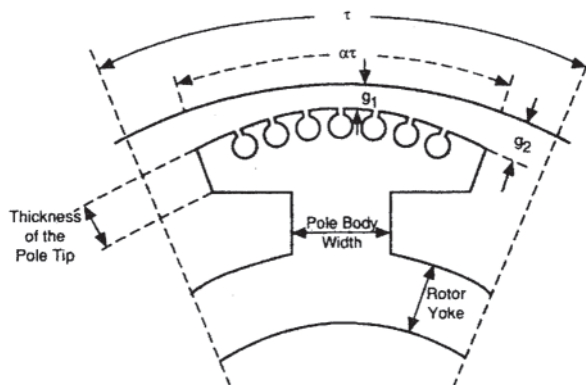


Figure 5.37 Salient pole geometry

$$A_d = \frac{\alpha\pi + \sin(\alpha\pi)}{4 \sin(\alpha\pi/2)} \quad (5.56)$$

$$A_q = \frac{\alpha\pi - \sin(\alpha\pi) + \frac{1}{2} \cos(\alpha\pi/2)}{4 \sin(\alpha\pi/2)} \quad (5.57)$$

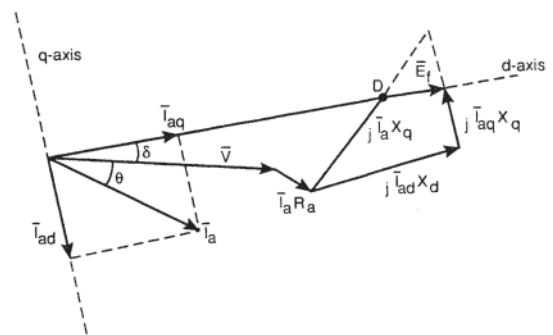
For  $\alpha$  between 0.65 and 0.75,  $A_d$  lies between 0.86 and 0.83, and  $A_q$  between 0.41 and 0.50.

### 5.7.6 Full-Load Field Ampere-Turns

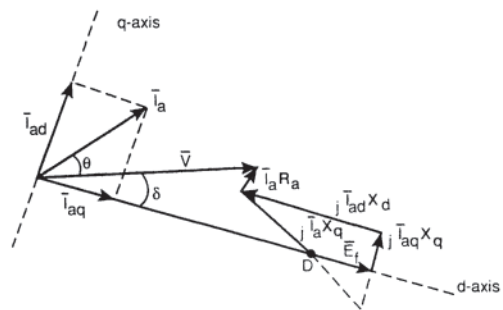
As in the cylindrical rotor, the phasor diagram for machine operation is first constructed as illustrated in Fig. 5.38. Here it must be noted that the location of the direct axis is established by adding vectorially  $V, I_a R_a$ , and  $jX_q I_a$  as shown as a first step in constructing the conventional phasor diagram. Once the voltage  $E_f$  is known, the required ampere-turns  $AT_f$  are computed by using the equation given in Section 5.7.3:

$$AT_f = \frac{\pi}{2} \frac{B_{gav}}{\mu_0} g_e \frac{E_f}{V} \quad (5.58)$$

The field winding is designed such that the required total field voltage, with all the field windings connected in series, is 80–100 V in small machines and 160–200 V in large machines. Furthermore, the current density in the field winding is usually limited to 2.5 A/mm<sup>2</sup> because of thermal considerations.



(a) Generator; Lagging Power Factor



(b) Motor; Leading Power Factor

Figure 5.38 Phasor diagrams (salient-pole machine).

### 5.7.7 Machine Oscillations and the Damper Winding

Consider a cylindrical-rotor synchronous motor operating at a load angle  $\delta$  ( $E_f$  lagging  $V$  by  $\delta$ ) so that the power output  $P$  is given by:

$$P = \frac{E_f V}{X_a} \sin \delta \quad (5.59)$$

Now, if the load on the motor is suddenly removed, the angle  $\delta$  must become zero; that is, the pole structure must move forward by an angle  $\delta$ . This cannot happen instantaneously because of the rotor and load inertia. The motor torque, which previously counterbalanced the load torque, accelerates the rotor so that the rotor is running above synchronous speed. Although the torque becomes smaller and  $\delta$  becomes smaller and becomes zero when  $\delta$  equals zero, the machine is running above synchronous speed and the kinetic energy stored in the inertia will force the rotor to move ahead of the stator field. The phasor  $E_f$  will now lead the phasor  $V$ , and the machine will act as a generator. Since there is no prime mover, this generator action cannot be sustained, the machine will decelerate, and the angle  $\delta$  will again tend to become zero. The angle  $\delta$  thus will oscillate around a mean value of zero. In fact, any sudden change of load on a synchronous machine results in such oscillations.

If damper windings are present, the machine produces a positive torque due to induction machine action at speeds under the synchronous speed, tending to accelerate the machine. At speeds above the synchronous speed, the damper windings cause a braking torque to be produced. Any oscillations in speed of the synchronous machine are therefore damped out. The phenomenon of synchronous machine damping can be analyzed by defining individual damping circuits, some centered on the direct (polar) axis and some centered on the quadrature (interpolar) axis. Design of these circuits is clearly beyond the scope of this book, and any interested reader should refer to the classical work on this subject [58–61].

## 5.8 FINITE ELEMENT ANALYSIS OF SYNCHRONOUS MOTORS

### 5.8.1 Advantages of Finite Element Analysis of Synchronous Motors

The finite element analysis (FEA) method can be of great help in the analysis and design of synchronous motors, including so-called brushless dc motors, stepper motors, and axial flux machines. The theory behind the finite element method is described in Section 1.5.

Many synchronous machines use PMs in their rotors. PM rotors are advantageous over wound-coil rotors in that they do not need brushes and they do not consume  $I^2R$  power. PM materials have improved greatly over the last few years; in chronological order the material types available include Alnico, ferrite, samarium-cobalt, and neodymium-iron.

The finite element method can accurately analyze

permanent magnets of any shape and material. There is no need to calculate reluctance factors, load lines, or leakage factors if finite element software is used. Also there is no need to assume that the permanent magnet is operating at any one “point” or  $B$  value. Instead the magnet’s demagnetization  $B$ - $H$  curve is input to the finite element software, and the software computes  $B$  and how it varies throughout the permanent magnet and throughout the entire motor. Even two-dimensional permanent magnet motors often have considerable three-dimensional end region leakage fluxes, which makes three-dimensional finite element analysis very helpful. Finite elements can also be used to aid the design of magnetizing fixtures [15] needed to manufacture permanent-magnet motors, as described in Section 6.9.3.

### 5.8.2 Motors with Permanent Magnet Rotors

There are two ways to use finite elements to analyze synchronous motors with PM rotors. As explained previously in Sections 1.5.8 and 1.5.9, one can either use magnetostatic finite element analysis to compute parameters of equivalent circuits, or one can use time-stepping finite element software to directly compute time-varying motor performance.

Figure 5.39 shows the geometry of the four-pole 550-W synchronous motor to be analyzed, with a rotor made of permanent magnets on the outside of a steel core. Similar motors have been analyzed elsewhere [63] and are sometimes called brushless dc motors. The brushless dc description applies here because electronic switching on the stator converts a dc supply voltage (here 220 V) to two-phase waveforms of variable frequency. Figure 5.40 shows the circuit containing eight transistors that is used to convert the dc supply into a cross-type two-phase circuit. Note that each transistor has a

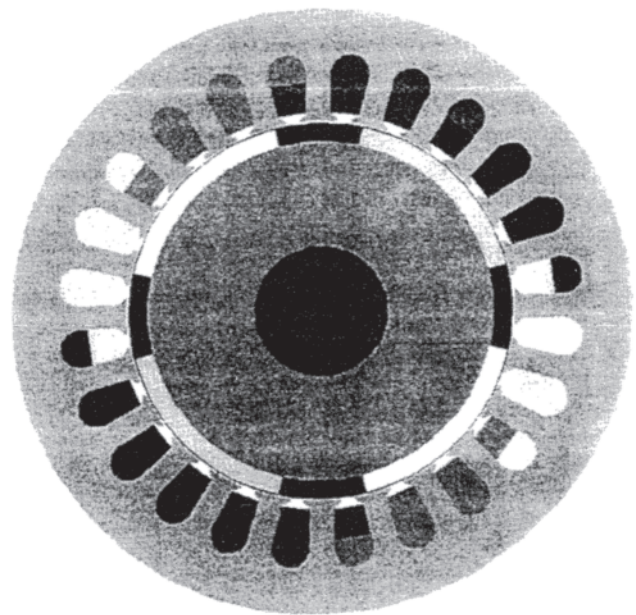


**Figure 5.39** Geometry of brushless two-phase synchronous motor to be analyzed.

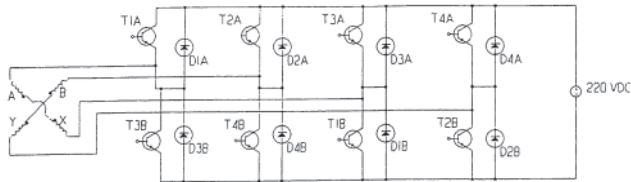


**Figure 5.40** Circuit that uses 220 VDC to drive synchronous motor shown in Fig. 5.39.

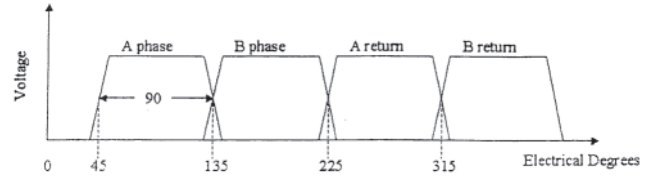


**Figure 5.41** Voltages applied to two-phase stator windings of synchronous motor shown in Fig. 5.39.

flyback diode for discharge during transistor turn-off. Figure 5.41 shows the waveforms of the transistor-switched voltages applied to the two phases.

The method used here to analyze the above synchronous (or brushless dc) motor is time-stepping finite element analysis. As explained in Section 1.5.9, time-stepping FEA involves dynamic rather than static finite element analysis. The finite element software Maxwell [64] was used to generate the finite element model of 180 degrees, or two-pole pitches, of the

geometry of Fig. 5.39. The motor model was then turned on at zero speed and allowed to accelerate against a steady load torque of 3.6 N-m. The assumed moment of inertia is 1.45 g/m<sup>2</sup>. The assumed damping, based upon windage and friction loss estimates, is 452E-6 N-m-sec/rad.

The results versus time computed by EMPulse [63, 64] are shown in Fig. 5.42. Figure 5.42(a) shows the back emfs in the two stator phases, and Fig. 5.42(b) shows their currents. Figure 5.42(c) shows the speed vs. time and Fig. 5.42(d) shows the

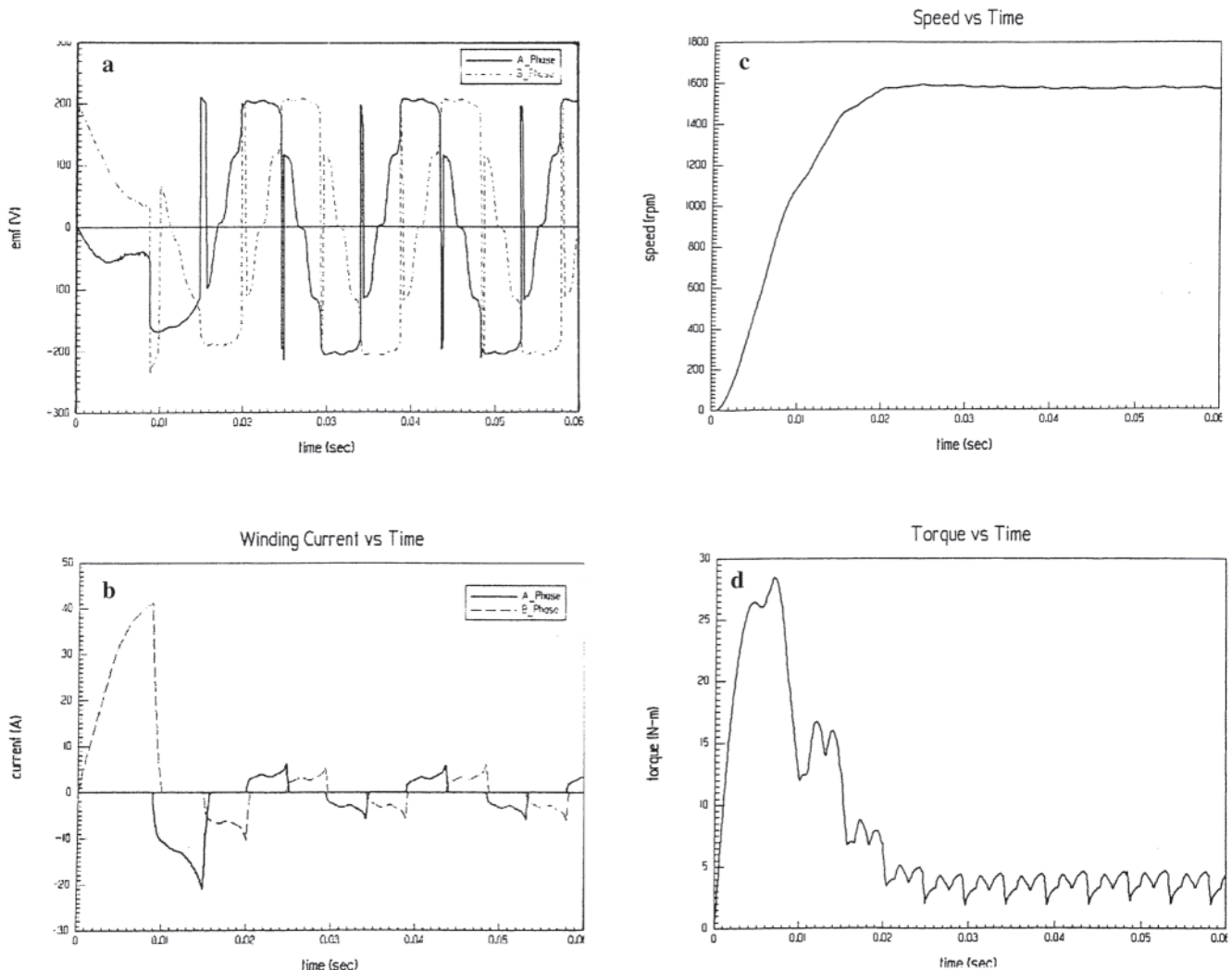


**Figure 5.42** Computed performance vs. time for synchronous motors shown in Fig. 5.39. (a) EMF. (b) Winding currents, (c) Speed, (d) Torque.

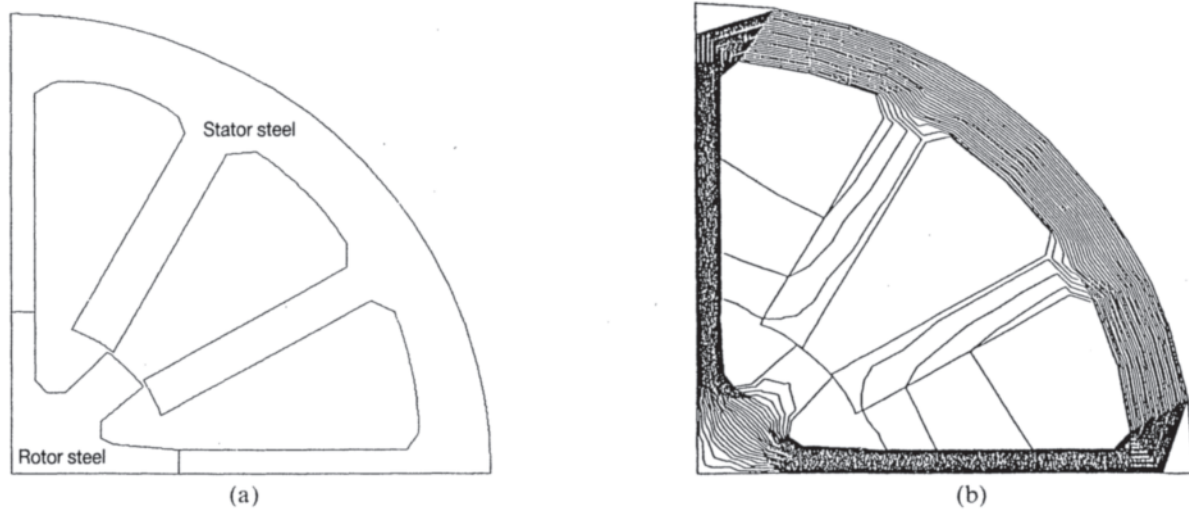


**Figure 5.43** Variable reluctance stepper motor, (a) Configuration of one quarter, (b) Calculated flux plot.

computed torque. Note that the average steady-state torque is indeed the expected 3.6 N-m, but the initial transient torque greatly exceeds that value so that the motor may be accelerated up to its load speed of 1600 rpm.

### 5.8.3 Variable-Reluctance Stepper Motors

A stepper motor (also called a step motor or a stepping motor) is a synchronous machine that is excited by current pulses of variable frequency. It can be “stepped” pulse by pulse to any desired incremental position [65–68].

One very common type of stepper motor is the variable reluctance (VR) stepper. Figure 5.43(a) shows a typical VR motor, which has essentially planar two-dimensional magnetic fields. The unexcited rotor tends to rotate to positions dependent on which stator coils are excited.

Figure 5.43(b) shows the computed saturable magnetic flux pattern. The torque calculated by the change in conenergy is within a few percent of measured torque. For accurate torque calculation it is found that air gap finite elements need to have radial edges at the end of each stator or rotor tooth.

### 5.8.4 Axial Flux Machines

Several kinds of synchronous machines and stepper motors have highly three-dimensional flux paths. The flux flows not only in the plane normal to the shaft axis but also in the axial direction. There are two ways to analyze such devices with finite elements.

One way is to perform one or more planar and/or axisymmetric two-dimensional analyses of the device. Certain approximations are involved, but often results can be obtained fairly quickly and accurately. An example is a novel axial flux stepper motor finite element analysis with three two-dimensional models [67].

Another type of axial flux motor is the hybrid stepper motor. Figure 5.44 shows its rotor, which has an axially magnetized permanent magnet sandwiched between two stacks of steel laminations. The rotor laminations have teeth that are offset by one half tooth pitch from one stack to the other.

The stator of the hybrid stepper motor is also laminated and is seen in the flux plot of Fig. 5.45. The flux plot is a two-dimensional planar plot in the plane of the stator and rotor laminations, but also has added flux paths to account for axial flux as well as laminar flux. A color flux density plot has been published [67].

The second way of analyzing three-dimensional problems is to use three-dimensional finite elements. This technique avoids the approximations involved in developing and/or combining two-dimensional models. However, three-dimensional modeling is much more difficult than two-dimensional modeling.

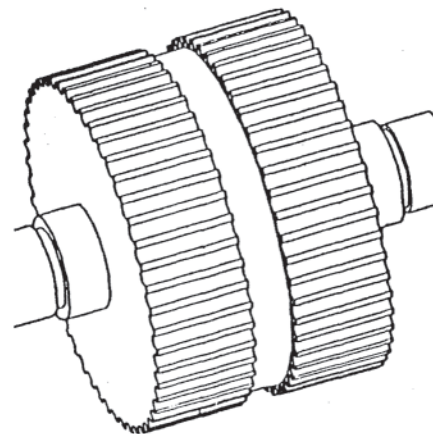


**Figure 5.44** Rotor of hybrid stepper motor.



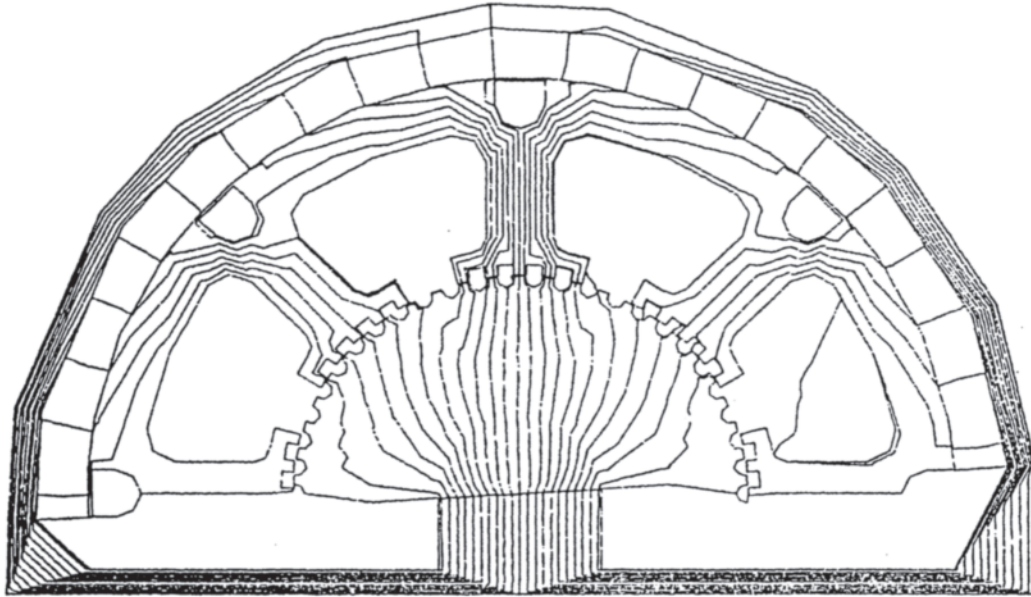


**Figure 5.45** Flux plot of one half of hybrid stepper motor, showing rotor and stator laminations and added flux paths.

One type of axial flux machine is called the Lundell type and is shown in Fig. 5.46. While commonly used as alternator in automobiles [69], the Lundell machine can also be used as a synchronous motor. Figure 5.47 shows portions of a three-dimensional finite element model developed for one pole pitch of a Lundell machine. Approximately 1800 finite elements are used in the model, consisting of hexahedrons

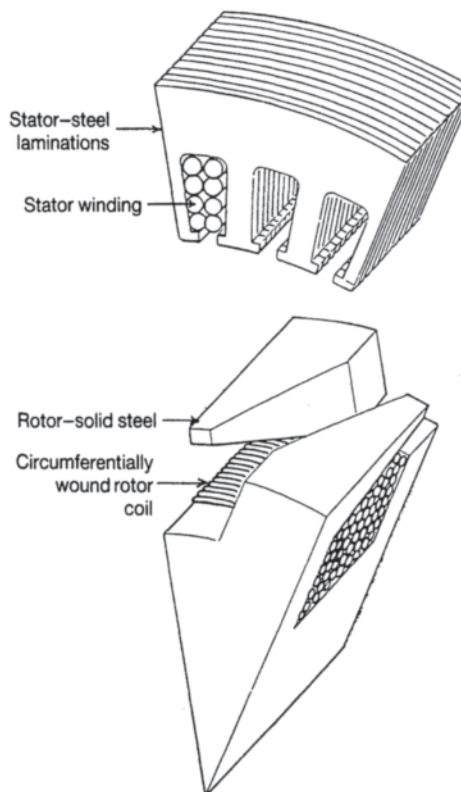


**Figure 5.46** Lundell axial-flux machine, showing one pole pitch.

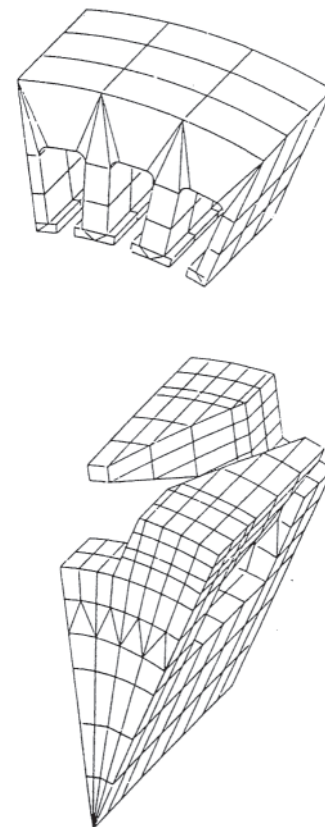


**Figure 5.47** Three dimensional finite element model of a portion of a Lundell machine, showing steel elements only.

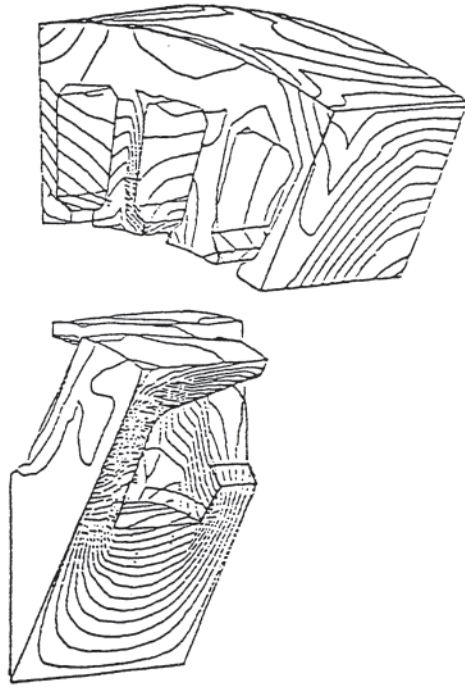


**Figure 5.48** Flux line plot for three dimensional Lundell machine.

(six-sided bricks), pentahedron (five-sided wedges) and tetrahedrons (four-sided pyramids).

The three-dimensional model of Fig. 5.47 was input to MSC/EMAS, a three-dimensional electromagnetic program [21], which calculated the  $A$  and  $B$  distributions throughout the machine. In three-dimensional problems both  $A$  and  $B$  are three-component vectors. Plotting the magnitude of gives the flux line plot of Fig. 5.36. Color displays of  $B$  may also be obtained. Calculated fluxes, inductances, and voltages for various stator currents have been shown to agree quite well with measurements. MSC/EMAS has been used extensively to optimize the design of various sizes of Lundell machines [69, 21].

## REFERENCES

Note: In the following listing, abbreviations have the following meanings:

AIEE American Institute of Electrical Engineers (predecessor to IEEE)  
 IEEE Institute of Electrical and Electronics Engineers

1. Wieseman, R. W., "Graphical Determination of Magnetic Fields," *Transactions of the AIEE*, vol. 46, 1927, pp. 141–154.
2. Salon S.J., # Finite Element Analysis of Electrical Machines, Kluwer, 1995
3. Alger, P.L., *The Nature of Induction Machines*, 2d edn., Gordon and Breach Science Publishers, New York, 1970.
4. Nasar, S.A., and I. Boldea, *Linear Motion Electric Machines*, Wiley, New York, 1976.
5. Nondahl, T.A., and E. Richter, "Comparisons between Designs for Single-Sided Linear Electric Motors: Homopolar Synchronous and Induction," Report FRA/ORD-80/54, U.S. Department of Transportation, Washington D.C., 1980.
6. Halbach, K., *Design of Permanent Multipole Magnets with*

*Oriented Rare Earth Cobalt Material*, Nuclear Instruments and Methods, vol. 169, 1980, pp. 1–10.

7. Halbach, K.: *Application of Permanent Magnets in Accelerators and Electron Storage Rings*, J. Appl. Physics, vol. 77, 1985, pp. 3605–3608.
8. *Kollmorgen Linear Motors Aim to Cut Cost of Semiconductors and Electronics Manufacture*, Kollmorgen, Radford, VA, U.S.A., 1997.
9. Gieras, J.F. and Piech, Z.J.: *Linear Synchronous Motors—Transportation and Automation Systems*, CRC Press, Boca Raton, FL, U.S.A., 1999.
10. *PM Linear Motors*, Trilogy Systems Corp., Webster, TX, U.S.A., 1999, [www.trilogysystems.com](http://www.trilogysystems.com)
11. *LinMot Design Manual*, Sulzer Electronics, Ltd, Zürich, Switzerland, 1999.
12. Evers, W., Elschenbroich, H., and Henneberger, G.: *A Transverse Flux Linear Synchronous Motor with a Passive Secondary Part*, 16th Int. Conf. on Magnetically Levitated Systems and Linear Drives MAGLEV'2000, Rio de Janeiro, Brazil, 2000, pp. 393–397.
13. Evers, W., Henneberger, G., Wunderlich, H. and Selig, A., *A Linear Homopolar Motor for a Transportation System*, 2nd Int. Symp. on Linear Drives for Ind. Appl. LDIA'98, Tokyo, Japan, 1998, pp. 46–49.
14. Rosenmayr, M., Casat, Glavitsch, A. and Stemmler, H., *Swissmetro—Power Supply for a High-Power-Propulsion System with Short Stator Linear Motors*, 15th Int. Conf. on Magnetically Levitated Systems and Linear Drives Maglev'98, Mount Fuji, Yamanashi, Japan, 1998, pp. 280–286.
15. Seok-Myeong, J. and Sang-Sub, J., *Design and Analysis of the Linear Homopolar Synchronous Motor for Integrated Magnetic Propulsion and Suspension*, Int. Symp. on Linear Drives for Ind. Appl. LDIA'98, Tokyo, Japan, 1998, pp. 74–77.
16. *The Contactless Power Supply System of the Future*, Wampfler AG, Weil am RheinMaerkt, Germany, 1998.
17. Sanada, M., Morimoto, S. and Takeda, Y., *Reluctance Equalization Design of Multi Flux Barrier Construction for Linear Synchronous Reluctance Motors*, 2nd Int. Symp. on Linear Drives for Ind. Appl. LDIA'98, Tokyo, Japan, 1998, pp. 259–262.
18. Locci, N. and Marongiu, I., *Modelling and Testing a New Linear Reluctance Motor*, Int. Conf. on Electr. Machines ICEM'92, vol. 2, Manchester, U.K., pp. 706–710.
19. Hamler, A., Trlep, M. and Hribernik, B., *Optimal Secondary Segment Shapes of Linear Reluctance Motors Using Stochastic Searching*, IEEE Trans, on Magn., vol. 34 (1998), No. 5, pp. 3519–3521.
20. Beakley, B., *Linear Motors for Precision Positioning*, Motion Control, October 1991. *Compumotor Digiplan: Positioning Control Systems and Drives*, Parker Hannifin Corporation, Rohnert Park, CA, U.S.A., 1996.
21. Kajioka, M., Torii, S. and Ebihara, D., *A Comparison of Linear Motor Performance Supported by Air bearings*, 2nd Int. Symposium on Linear Drives for Industry Applications, LDIA'98, Tokyo, Japan, 1998, pp. 252–255.
22. *Linear Step Motor* (information brochure), Tokyo Aircraft Instrument Co., Ltd., Tokyo, 1998.
23. Gieras, J.F., *Linear Induction Drives*, Clarendon Press, Oxford, U.K., 1994.
24. *Northern Magnetics Linear Motors Technology*, Normag (Baldor Electric Company), Santa Clarita, CA, U.S.A., 1998.
25. Krishnan, R., Byeong-Seok Lee, and Vallance, P.: *Integral Linear Switched Reluctance Machine Based Guidance, Levitation, and Propulsion System*, 16th Int. Conf. on Magnetically Levitated Systems and Linear Drives MAGLEV'2000, Rio de Janeiro, Brazil, 2000, pp. 281–286.
26. Adamiak, K., Barlow, D., Choudhury, C.P., Cusack, P.M., Dawson, G.E., Eastham, A.R., Grady, B., Ho, E., Yuan Hongpin, Pattison, L. and Welch, J., *The Switched Reluctance Motor as a*

- Low-Speed Linear Drive*, Int. Conf. on Maglev and Linear Drives, Las Vegas, U.S.A., 1987, pp. 39–43.
27. Heller, B. and Hamata, V., *Harmonic Field Effects in Induction Motors*, Academia, Prague, 1977.
  28. Honsinger, V.B.: *Performance of Polyphase Permanent Magnet Machines*. IEEE Trans, on PAS Vol. 99, 1980, No. 4, pp. 1510–1516.
  29. Kostenko, M. and Piotrovsky, L., *Electrical Machines, Vol. 2: Alternating Current Machines*, Mir Publishers, Moscow, 1974.
  30. Gieras, J.F. and Wing, M., *Permanent Magnet Motors Technology: Design and Applications*, Marcel Dekker, Inc., New York, U.S.A., 1996.
  31. Mosebach, H., *Direct Two-Dimensional Analytical Thrust Calculation of Permanent Magnet Excited Linear Synchronous Machines*, 2nd Int. Symp. on Linear Drives for Ind. Applications LDIA'98, Tokyo, Japan, 1998, pp. 396–399.
  32. Mosebach, H. and Canders, W.R., *Average Thrust of Permanent Magnet Excited by Linear Synchronous Motors for Different Stator Current Waveforms*, Int. Conf. on Electr. Machines ICEM'98, Istanbul, Turkey, 1998, vol. 2, pp. 851–865.
  33. Atherton, D.L. et al, *Design, Analysis and Test Results for a Superconducting Linear Synchronous Motor*, Proc. IEEE, vol. 124, No. 4, 1977, pp. 363–372.
  34. Gieras, J.F. and Miszewski, M., *Performance Characteristics of the Air-Core Linear Synchronous Motor* (in Polish), Rozprawy Elektrot. PAN, Warszawa, Poland, vol. 29, 1983, No. 4, pp. 1101–1124.
  35. Lingaya, S. and Parsch, C.P., *Characteristics of the Force Components on an Air-Core Linear Synchronous Motor with Super-conducting Excitation Magnets*, Electric Machines and Electromechanics, Hemisphere Publishing Corp., No. 4, 1979, pp. 113–123.
  36. Skalski, C.A., *The Air-Core Linear Synchronous Motor: An Assessment of Current Development*, MITRE Technical Report, VA, U.S.A., 1975.
  37. Afonin, A., Szymczak, P. and Bobako, S., *Linear Drives with Controlled Current Layer*, 1st Int. Symp. on Linear Drives for Industry Applications LDIA'95, Nagasaki, Japan, 1995, pp. 275–278.
  38. Ayoma, H., Araki, H., Yoshida, T., Mukai, R. and Takedoni, S., *Linear Motor System for High Speed and High Accuracy Position Seek* 1st Int. Symp. on Linear Drives for Industry Applications LDIA'95, Nagasaki, Japan, 1995, pp. 461–464.
  39. *Anorad Linear Motors* (information brochure), Anorad, Hauppauge, NY, U.S.A. 1998, [www.anorad.com](http://www.anorad.com)
  40. Kakino, Y., *Tools for High Speed and High Acceleration Feed Drive System of NC Machine Tools*, 2nd Int. Symposium on Linear Drives for Industry Applications, LDIA'98, Tokyo, Japan, 1998, pp. 15–21.
  41. Karita, M., Nakagawa, H. and Maeda, M., *High Thrust Density Linear Motor and its Applications*, 1st Int. Symp. on Linear Drives for Industry Applications LDIA'95, Nagasaki, Japan, 1995, pp. 183–186.
  42. Muraguchi, Y., Karita, M., Nakagawa, H., Shinya, T. and Maeda, M., *Method of Measuring Dynamic Characteristics for Linear Servo Motor and Comparison of their Performance*, 2nd Int. Symp. on Linear Drives for Ind. Appl. LDIA'98, Tokyo, Japan, 1998, pp. 204–207.
  43. Howe, D. and Zhu, Z.Q., *Status of Linear Permanent Magnet and Reluctance Motor Drives in Europe*, 2nd Int. Symp. on Linear Drives for Ind. Appl. LDIA'98, Tokyo, Japan, 1998, pp. 1–8.
  44. Yamada, H., *Handbook of Linear Motor Applications* (in Japanese), Kogyo Chosaki Publ. Co. Ltd, 1986.
  45. Breil, J., Oedl, G. and Sieber, B., *Synchronous Linear Drives for many Secondaries with Open Loop Control*, 2nd Int. Symp. on Linear Drives for Ind. Appl. LDIA'98, Tokyo, Japan, 1998, pp. 142–146.
  46. Eidelberg, B., *Linear Motors Drive Advances in Industrial Laser Applications*, Industrial Laser Review, 1995, No. 1, pp. 15–18.
  47. Atzpodien, H.C., *Magnetic Levitation System on Route from Berlin to Hamburg—Planning, Financing, State of Project*, 14th Int. Conf. on Magnetically Levitated Systems Maglev'95, Bremen, Germany, 1995, pp. 25–29.
  48. Nakashima, H. and Isoura, K., *Superconducting Maglev Development in Japan*, 15th Int. Conf. on Magnetically Levitated Systems and Linear Drives Maglev'98, Mt. Fuji, Yamanashi, Japan, 1998, pp. 25–28.
  49. Wiescholek, U., *High-Speed Magnetic Levitation System Transrapid*, 14th Int. Conf. on Magnetically Levitated Systems Maglev'95, Bremen, Germany, 1995, pp. 17–23.
  50. *Yamanashi Maglev Test Line—Guide of Electric Facilities*, Central Japan Railway Company, Tokyo, 1992.
  51. Yoshida, K., Muta, H. and Teshima, N., *Underwater Linear Motor Car*, Int. Journal of Appl. Electromagnetics in Materials, vol. 2, Elsevier, 1991, pp. 275–280.
  52. Yoshida, K., Liming, S., Takami, H. and Sonoda, A., *Repulsive Mode Levitation and Propulsion Experiments of an Underwater Travelling LSM Vehicle ME02*, 2nd Int. Symp. on Linear Drives for Industry Applications LDIA'98, Tokyo, 1998, pp. 347–349.
  53. Cruise, R.J. and Landy, C.F., *Linear Synchronous Motor Propelled Hoist for Mining Applications*, The 31st IEEE Ind. Appl. Conf., San Diego, CA, 1996.
  54. Ishii, T., *Elevators for Skyscrapers*, IEEE Spectrum, No. 9, 1994, pp. 42–46.
  55. *Linear-Motor-Driven Vertical Transportation System*, Elevator World, September, 1996, pp. 66–72, [www.elevator-world.com](http://www.elevator-world.com)
  56. Mukherji, K. C., “General Basis of Synchronous Machine Design,” Lecture Notes, Indian Institute of Technology, Bombay, 1962.
  57. Still, A., and C.S. Siskind, *Elements of Electrical Machine Design*, McGraw-Hill, New York, 1954.
  58. Park, R.H., and B.L. Robertson, “The Reactances of Synchronous Machines,” *Transactions of the AIEE*, vol. 47, 1928, pp. 514–536.
  59. Kilgore, L.A., “Effects of Saturation on Machine Reactances,” *Transactions of the AIEE*, vol. 54, 1935, pp. 545–550.
  60. Rankin, A.W., “Per Unit Impedances of Synchronous Machines, Part I,” *Transactions of the AIEE*, vol. 64, 1945, pp. 569–572.
  61. Rankin, A.W., “Per Unit Impedances of Synchronous Machines, Part II,” *Transactions of the AIEE*, vol. 64, 1945, pp. 839–842.
  62. Alger, P.L., “The Calculation of the Armature Reactance of Synchronous Machines,” *Transactions of the AIEE*, vol. 47, 1928, pp. 493–513.
  63. Maxwell, RMXprt, EMpulse, EMSS, EMAS, and Simplorer are proprietary products of Ansoft Corporation, Pittsburgh, PA 15219 USA, [www.ansoft.com](http://www.ansoft.com).
  64. Mark Ravenstahl, John Brauer, Scott Stanton, and Ping Zhou, “Maxwell design environment for optimal electric machine design,” Small Motor Manufacturing Assn. Annual Meeting, 1998.
  65. Horber, R.W., “Higher Torque from Hybrid Stepper Motors,” *Machine Design*, Apr. 25, 1985.
  66. Brauer, J.R., “Finite Element Analysis of DC Motors and Step Motors,” *Proceedings of Incremental Motion Control Symposium*, IMCS Society, Champaign, IL, pp. 213–222, May 1982.
  67. Kenecny, Karl F., “Analysis of Variable Reluctance Motor Parameters Through Magnetic Field Simulation,” *MOTORCON 1981 Proceedings*, Intertec Communications Inc., Oxnard, CA.
  68. Zeisler, F.L., and J.R. Brauer, “Automotive Alternator Electromagnetic Calculations Using Three Dimensional Finite Elements,” *IEEE Transactions on Magnetics*, vol. 21, no.6, pp. 2453–2456, Nov. 1985.
  69. Brauer, J.R., G.A. Zimmerlee, T.A. Bush, and R.D. Schultz, “3D Finite Element Analysis of Automotive Alternators Under Any Load,” *IEEE Transactions on Magnetics*, vol. 24, Jan. 1988, pp. 500–503.

# 6

## Direct-Current Motor Analysis and Design

Edward J.Woods (Sections 6.0–6.5 and 6.8)/Chauncey Jackson Newell (Section 6.6)/Gopal K.Dubey (Section 6.7)/John R.Brauer (Section 6.9)

<b>6.0 INTRODUCTION</b>	<b>328</b>
<b>6.1 ARMATURE WINDINGS</b>	<b>328</b>
6.1.1 Wave Windings	328
6.1.2 Equalizers	328
6.1.3 Lap Windings	329
6.1.4 Machines with Reduced Numbers of Slots	330
<b>6.2 COMMUTATORS</b>	<b>331</b>
6.2.1 Commutator Construction	331
6.2.2 Brushes and Holders	331
<b>6.3 FIELD POLES AND WINDINGS</b>	<b>332</b>
6.3.1 Pole Laminations	332
6.3.2 Main Field Windings	332
6.3.3 Commutating Poles and Windings	332
6.3.4 Pole Face Windings	333
<b>6.4 EQUIVALENT CIRCUIT</b>	<b>334</b>
6.4.1 Steady-State Analysis	334
6.4.2 Transient Analysis	334
<b>6.5 DESIGN EQUATIONS</b>	<b>334</b>
6.5.1 Magnetic Circuit	335
6.5.2 Saturation	335
6.5.3 Detailed Magnetic Circuit Calculations	335
<b>6.6 DC MOTORS IN CONTROL SYSTEMS</b>	<b>338</b>
6.6.1 Basic Motor Equations	338
6.6.2 Basic Mechanical Equation	339
6.6.3 Block Diagrams	340
6.6.4 Typical Motor Characteristics and Stability Considerations	341
6.6.5 Field Control	341
<b>6.7 DC MOTORS SUPPLIED BY RECTIFIER OR CHOPPER SOURCES</b>	<b>343</b>
6.7.1 List of Symbols	343
6.7.2 Analysis	343
6.7.3 Rectifier Sources	344
6.7.4 Chopper Sources	347
<b>6.8 PERMANENT MAGNET DC MOTORS</b>	<b>349</b>
6.8.1 Magnetic Materials	349
6.8.2 Design Features	351
6.8.3 Servo and Control Motors	354

## 6.9 FINITE ELEMENT ANALYSIS OF DC MOTORS

6.9.1	Advantages of FEA of DC Motors	354
6.9.2	Permanent Magnet Brush DC Motors	355
6.9.3	Magnetization of Permanent Magnets	355
6.9.4	Wound-Field Brush DC Motors	356
6.9.5	Universal Motors	356

## REFERENCES

364

## 6.0 INTRODUCTION

Direct current (dc) motors are used where a source of dc voltage is available and variable-speed motor operation is required. Motor speed can be varied by controlling applied armature voltage, applied field voltage, or both. The armature voltage can be varied by using a controlled rectifier source or a chopper control. Field voltage is varied by the same means. Either voltage can also be supplied by a dc generator whose output can be controlled. Series dc motors have the field windings in series with the armature; shunt motors have the field windings in parallel with the armature, or the field windings may be supplied by a separate source.

## 6.1 ARMATURE WINDINGS

DC motor armature or rotor windings are designed to produce a voltage between adjacent brushes on the commutator. Usually, every other brush around the commutator periphery is connected together to form one armature terminal while the alternate brushes are connected together to form the other terminal, one terminal being positive and the other negative. The voltage  $E_a$  generated by a dc motor armature winding is given by:

$$E_a = \frac{Z \times \phi_p \times \text{RPM} \times \text{POLES}}{60 \times \text{PATHS}} \quad (6.1)$$

where:

$Z$  = the total number of armature conductors  
= SLOTS  $\times$  CSPS  $\times$  TURNS PER COIL

CSPS = coil sides per slot

$\phi_p$  = total flux per pole (webers)

POLES = number of stator or field poles

PATHS = number of parallel armature winding paths

RPM = motor speed in revolutions per minute

The number of armature winding parallel paths is determined by the type of winding employed and the pattern of connections to the commutator bars. There are two basic types of dc motor windings, as shown in Fig. 6.1, the wave winding and the lap winding. The coil pitch shown in the figure is close to one pole pitch. For example, a motor with 4 poles and 25 slots would have a pole pitch (expressed in slots/pole) of 25/4, or 6.25. A coil pitch or span of 6 is close to the pole pitch. This would result in a coil throw of 1 to 7 (that is, coil sides would be located in slots 1 and 7). A motor with 4 poles and 27 slots would have a pole pitch of 6.75, and a coil pitch of 7 could be used. The coil throw would be from slot 1 to slot 8.

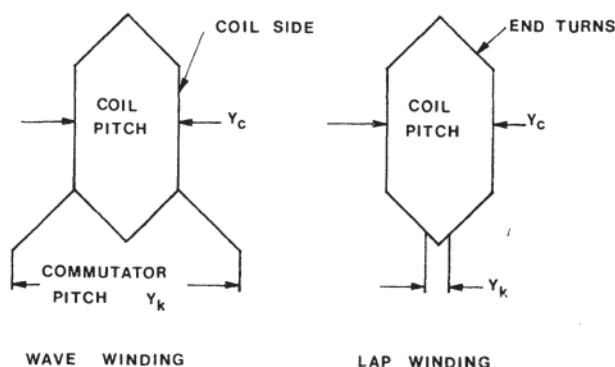


Figure 6.1 Two basic armature winding types.

### 6.1.1 Wave Windings

The commutator pitch depends on whether the winding is wave or lap wound. For a wave winding, Fig. 6.2(a) shows the commutator connection configuration. In this figure, a simplex wave winding is shown. This winding has two circuits or parallel paths regardless of the number of poles. The coil commutator pitch (in bars) is given by:

$$Y_k = \frac{2(\text{NSEG} \pm 1)}{\text{POLES}} \quad (6.2)$$

where NSEG = number of commutator bars (and NSEG/SLOTS must be an integer). For a motor with 4 poles and 25 slots and 25 commutator bars or segments,  $Y_k = 12$  or 13.

A duplex wave winding is shown in Fig. 6.2(b). This winding has four circuits or parallel paths in the motor winding. For a duplex wave winding, the coil commutator pitch is given by:

$$Y_k = \frac{2(\text{NSEG} \pm 2)}{\text{POLES}} \quad (6.3)$$

where NSEG/SLOTS is an integer. For example, for a 4-pole motor with 50 commutator bars,  $Y_k = 24$  or 26.

### 6.1.2 Equalizers

When windings with more than two parallel paths and more than two poles are used, each armature circuit can generate slightly different voltages between brushes of opposite polarity due to different flux levels of the poles. These windings

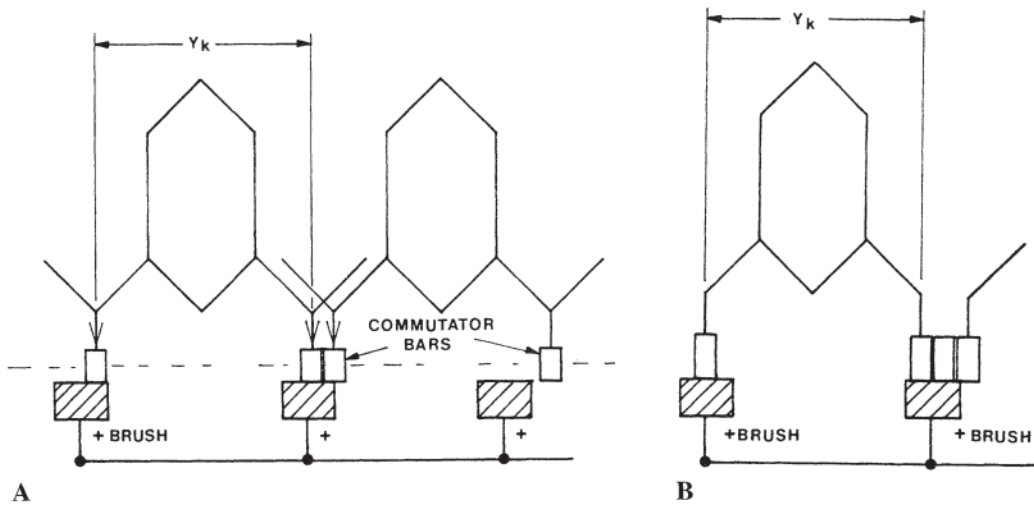


**Figure 6.2** (a) Commutator connection for a four-pole simplex wave winding, (b) Commutator connections for a four-pole duplex wave winding.

often require equalizers connecting commutator bars that are 360 electrical degrees apart. The equalizers are extra copper conductors fastened to the commutator bars, and are sized to carry the circulating current that would otherwise flow through the brushes and impede commutation.

### 6.1.3 Lap Windings

The simplest form of dc motor armature winding has the number of paths equal to the number of poles. This type of winding is called a simplex lap winding and is shown diagrammatically in Fig. 6.3 for a two-pole motor. It can be seen from this figure that the voltage  $E_a$  is generated in the coils between brushes. There are two paths for the current to flow between brushes. In this case, coils are connected between

adjacent commutator bars and the number of coils equals the number of commutator bars. The coil sides are located approximately one pole pitch apart, and are placed in armature slots. The actual coil shape is shown in Fig. 6.4.

A more complex winding is a duplex lap winding, for which the number of parallel paths is equal to  $2 \times \text{POLES}$  and the coil leads attach to commutator bars that are spaced two bar pitches apart. As before, the number of commutator bars is equal to the number of coils, but the arrangement is as shown in Fig. 6.5 for a two-pole motor. Here there are two complete armature circuits with four parallel paths leading from each brush. The actual coil shape is shown in Fig. 6.6. If the winding shown in Fig. 6.5 is made with an odd number of slots, then the winding of Fig. 6.7 results.

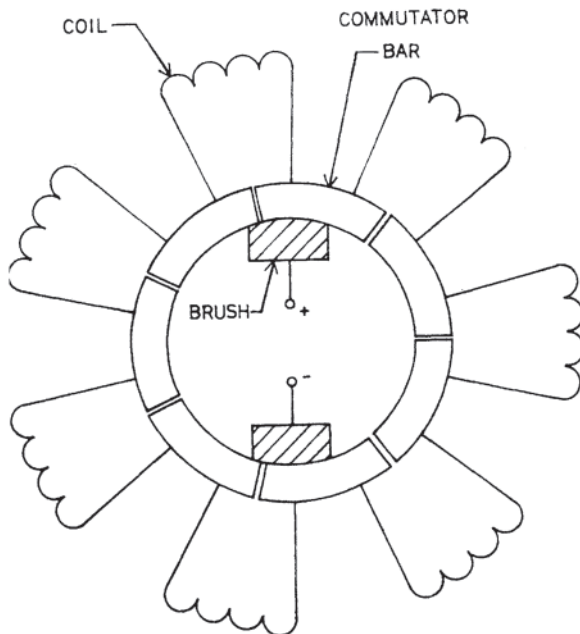


**Figure 6.3** Two-pole simplex lap winding.

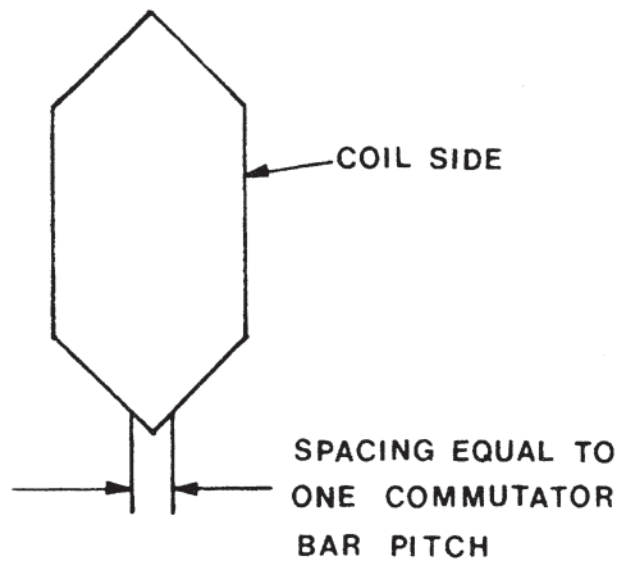


**Figure 6.4** Actual coil shape for a simplex lap winding.

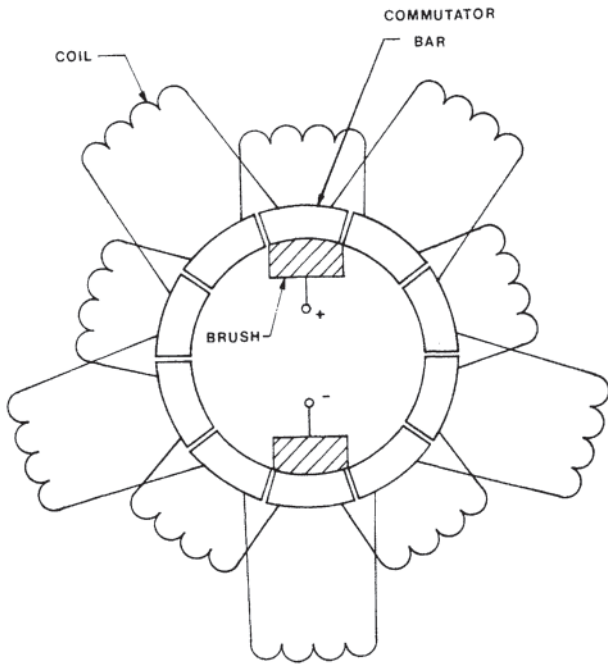


Figure 6.5 Two-pole duplex lap winding.

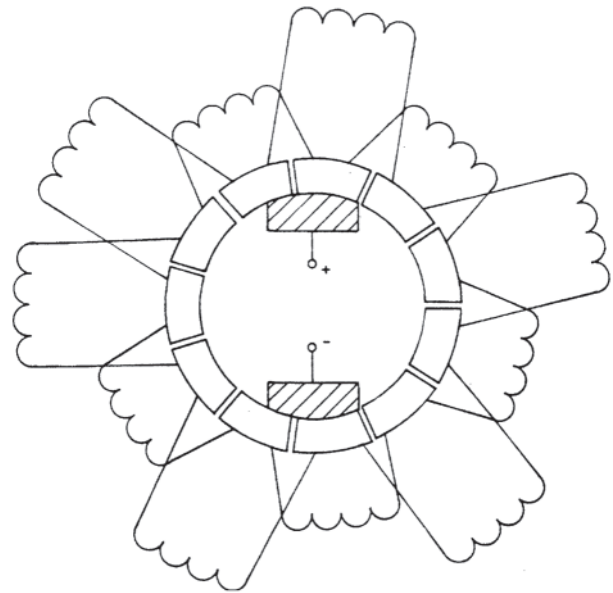


Figure 6.7 Duplex lap winding with an odd number of slots.

Armature windings can be either retrogressive or progressive as shown in Fig. 6.8, depending on whether the coil leads are crossed or uncrossed to make the connection to the commutator.

### 6.1.4 Machines with Reduced Numbers of Slots

In some machines, the number of slots is reduced so that there are several coil sides (and commutator bars) per slot. In that case, the coil sides are wound and insulated together to form a coil with multiple leads for connection to the commutator as shown in Fig. 6.9. For the case shown, the total number of coil sides per slot is equal to six for a conventional two-layer winding.

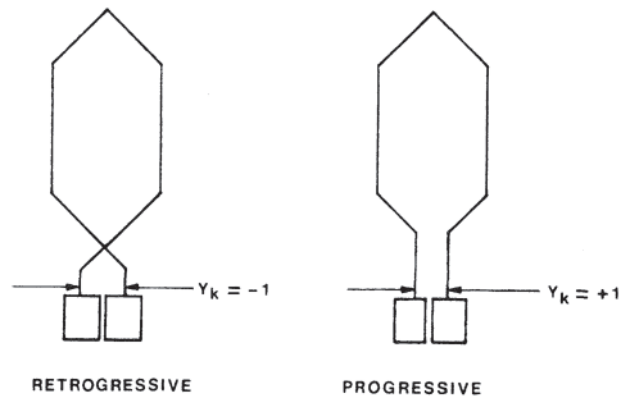


Figure 6.8 Lap winding progression.

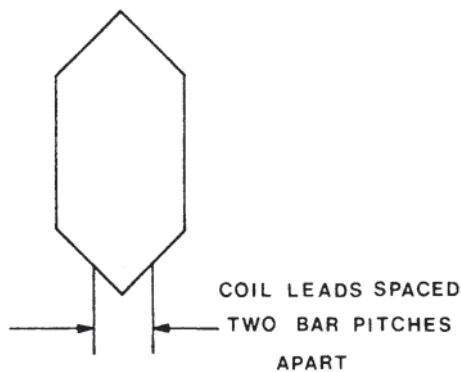


Figure 6.6 Actual coil shape for a duplex lap winding.

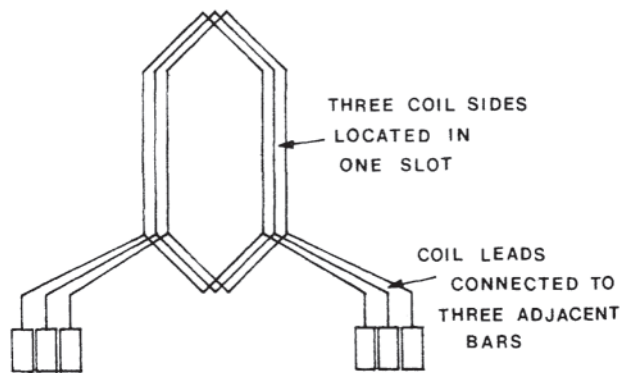


Figure 6.9 Multiple lead commutator connection.

## 6.2 COMMUTATORS

### 6.2.1 Commutator Construction

Most commutators are made from copper bars with some form of insulation between bars and a means of mechanical clamping to prevent centrifugal forces from moving the commutator bars radially. The clamping method must be designed so as to ensure that the bars are held firmly in position under loading from radial forces, axial forces during and after assembly, and thermally induced forces. The difficulty is compounded by the fact that any metallic clamping device must be insulated from the commutator to prevent reporting between adjacent bars. Figure 6.10 shows one form of commutator construction for larger motors, that is, motors above a few horsepower.

Smaller motors have used molded commutators, where some kind of insulating and molding compound is impregnated between commutator bars and between commutator and shaft to prevent the bars from moving. Molded commutators are generally limited to lower temperatures than mechanically clamped commutators with mica insulation. Excessive temperature or stress cycling of a commutator will eventually cause bars to loosen and move outward, causing poor commutation and rapid brush wear.

For further information on commutators, see [Section 14.3](#).

### 6.2.2 Brushes and Holders

DC machine brushes are used to collect current from the commutator surface and to provide a resistive path to aid in dissipating the inductive energy of a coil undergoing commutation, during which coil current changes from one direction to the other. Brushes are held against the cylindrical surface of the commutator by springs in the brush holders.

The brushes must remain in contact with the commutator surface so that current flow from the surface is not interrupted. If brushes are allowed to bounce on the commutator surface due to commutator eccentricity, uneven commutator bars, weak springs, or vibration, then poor commutation and rapid brush wear will result.

Brushes are composed of some amount of carbon held together with a high-temperature binder. Metal such as copper is added to make the brushes more conductive at the cost of more rapid wear. For short-time motor operation such as with

starter motors, the metal content is increased so that high current density and low voltage drop can be achieved.

For long life and continuous duty operation, brushes have an increased carbon content. Higher-resistance brushes can sometimes be substituted to solve a brush sparking problem in a dc motor by adding more resistance to the commutating circuit and causing the current to be reversed before the brush edge leaves a bar. The penalties are greater brush drop and more loss.

The brush-to-commutator interface is where all the action takes place during commutation and current collection. This interface is composed of a film on the commutator surface which conducts by allowing current to punch tiny holes through the film. These holes move about on the film and distribute the heating over the entire interface and thus the commutator surface as the commutator moves relative to the stationary brushes. The film is maintained by action of sparking, oxidation, motion, and the presence of carbon, oxygen, and water vapor. Lack of a film will cause rapid brush and commutator wear and may cause excessive sparking. Too thick a film will also cause sparking and variable commutation performance as parts of the film are removed in chunks.

Brush holders must be designed to allow stable contact between the brush and commutator while applying the right amount of pressure on the brush. Stable contact is achieved when the brush does not rock back and forth or “chatter” in the holder. Brush holders must also allow the brush to slide radially in the holder without sticking. Brush holder natural frequencies that could be excited by motor operation must also be avoided.

It is important that brush holder springs be designed to allow movement of the brushes in the holder and to keep a nearly constant pressure of the brush on the commutator throughout the life of the brush. As shown in [Fig. 6.11](#), there are several types of springs used to apply a force to the back of a commutator brush.

Brushes can be aligned to the commutator surface in several different ways. The brushes in [Fig. 6.11](#) are angled and the spring contact face is angled to keep the brush against the lefthand side of the brush holder. This method works well for either direction of rotation provided the coefficient of friction between brush and commutator is not excessive. Radial brush holders, where the brush is perpendicular to the commutator, are also used for bidirectional rotation, although small

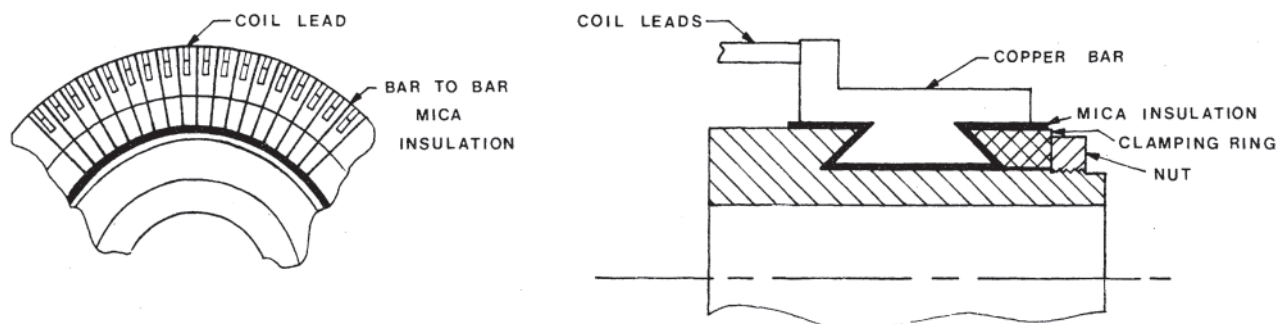


**Figure 6.10** Clamped commutator construction.



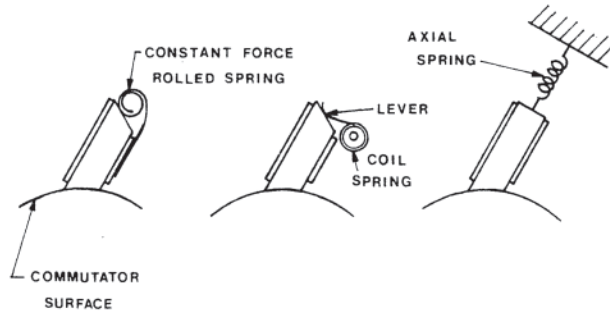


Figure 6.11 Brush spring types.

clearances between the brush and holder are necessary to prevent brush chatter.

A more complete discussion of brushes appears in Sections 11.5, 13.3, and 14.4.

### 6.3 FIELD POLES AND WINDINGS

The stator or frame of a dc motor carries the field poles and windings. In most dc machines, the main poles are laminated and bolted to the inside of the stator frame. The frame may be either solid or laminated.

#### 6.3.1 Pole Laminations

The main poles of dc motors carry magnetic flux from the air gap to the frame, and the main field windings are wrapped around the main pole body. Figure 6.12 shows the configuration of a main pole bolted to the motor frame. The main pole laminations are riveted together and the pole body is assembled together with the field coil for bolting to the stator frame.

Voltage is induced in the armature winding coil sides during the time that they are moving opposite the main pole face. When they reach the edge of the pole face, commutation can begin to take place by action of the brushes on the commutator. If the main pole face is made too wide, then the main pole tip leakage flux will cause poor commutation. A pole face that is too narrow will require a larger air gap flux density and a correspondingly larger field current. Similarly, the pole body must be wide enough to support the pole body main flux plus pole body leakage flux without saturating, but allow enough room between poles for the field windings. The pole body height is made large enough for the main field winding space.

The main pole body is usually laminated to aid in reducing pole face loss due to armature slot ripple flux. In larger

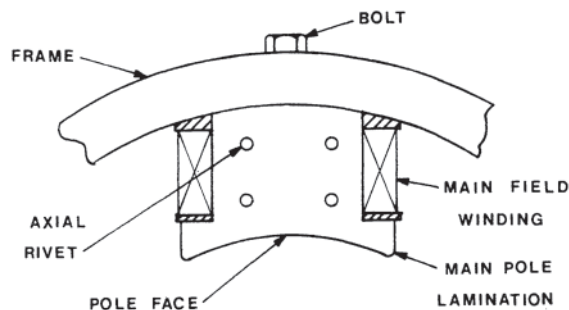


Figure 6.12 Main pole configuration.

machines, the pole laminations are bolted or riveted together axially, while in smaller machines, the laminations are welded together along their sides.

#### 6.3.2 Main Field Windings

The main field winding is required to drive flux through the frame, pole body, air gap, armature teeth, and armature core. The copper field winding must produce enough ampere-turns to provide for saturation effects in the iron paths as well as the air gap mmf drop. In addition, the field must account for increased ampere-turns due to additional saturation from the effects of armature reaction.

##### 6.3.2.1 Shunt or Separately Excited

The shunt machine has a field voltage comparable to the motor armature voltage and comprises many turns of small wire. The wire is individually coated with insulation and wound around a form or directly on the pole body with appropriate thicknesses of insulation to keep the winding from contacting the pole body or frame. The field is supplied by a separate power supply, or in parallel or “shunt” with the armature supply with appropriate resistor or chopper control.

##### 6.3.2.2 Series Field Windings

A series field winding comprises a few turns of large copper cross section designed to carry armature current with a voltage drop that is a small fraction of the armature voltage.

The series field produces main pole flux proportional to armature current when the motor is not saturated, and more or less constant flux for a saturated magnetic circuit.

In many motors, a few series turns are added on top of a shunt field winding to compensate for the effects of armature reaction.

#### 6.3.3 Commutating Poles and Windings

In most direct current machines of integral horse power and larger, commutating poles (or interpoles) are used to aid commutation. The pole is a thin, straight-sided pole with a winding of few turns and large cross section to carry armature current. The purpose of the interpole is to cancel the effect of increasing flux in the interpolar space as armature current increases.

The interpole induces a voltage in coils undergoing commutation in such a direction as to aid the commutation process and reverse current flow in the coil. Figure 6.13 shows an interpole configuration for a dc traction motor. Nonmagnetic shims are sometimes added to the base of the interpole to prevent main pole leakage flux from saturating the interpole and affecting commutating ability at high main field strengths. Magnetic shims can be used to adjust the distance from rotor surface to commutating pole tip and thereby affect commutating performance.

##### 6.3.3.1 Commutation

Some calculations and rules for commutation performance are presented in this section. If the commutator insulation

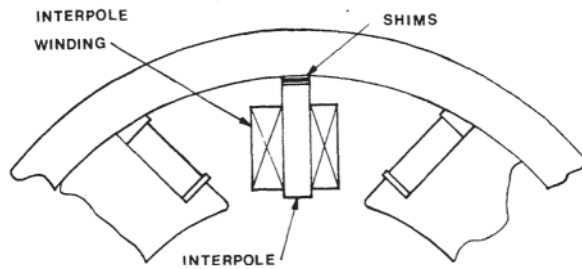


**Figure 6.13** Commutation pole (interpole) configuration.

between segments is approximately 1.0 mm thick, then the average bar-to-bar voltage should be limited to approximately 18V. This defines the minimum number of commutator segments for a given motor design as shown here:

$$V_{\text{bav}} = V_t \text{ POLES}/N_{\text{seg}} \text{ less than or equal to } 18 \text{ V} \quad (6.4)$$

where:

$$N_{\text{seg}} = \text{total number of commutator segments}$$

$$V_t = \text{motor terminal voltage}$$

The commutation zone is defined as the distance, in slot pitches, that a coil will travel while undergoing commutation, and is given by:

$$C_z = (\text{SLOTS}/N_{\text{seg}})(B + F_\lambda + (N_{\text{seg}}/\text{SLOTS}) - (\text{CIRC}/\text{POLES})) \quad (6.5)$$

where:

$$B = \text{BW } N_{\text{seg}}/(\pi D_{\text{comm}})$$

= brush overlap is commutator segments

BW = brush width along the peripheral direction of the commutator surface in meters

$D_{\text{comm}}$  = commutator diameter in meters

$F_\lambda$  = absolute value of  $|(N_{\text{seg}}/\text{POLES}) - Y_c N_{\text{seg}}/\text{SLOTS}|$   
= the short pitch of coil in commutator segments

$Y_c$  = coil pitch in slots

A term known as slots per neutral is defined as:

$$\text{SLPN} = ((\pi D_a/\text{POLES}) - \text{PA}) \text{SLOTS}/(\pi D_a) \text{ in slot pitches} \quad (6.6)$$

where:

PA is the pole arc peripheral length in meters

$D_a$  is the armature (rotor) diameter in meters

POLES = the total number of stator main poles

In general, SLPN should be greater than the commutating zone,  $C_z$ , so the coil has a chance to finish reversing current direction in the interpolar space before coming under the influence of the next main pole. A term called the single clearance is used as a measure of the margin between SLPN and  $C_z$ . It is given by:

$$\text{SC} = (\text{SLPN} - C_z) (\pi D_a) / (2 \text{SLOTS}) \quad (6.7)$$

Reference 2 recommends the minimum SC for traction motors to be slightly greater than a tooth-face width at the air gap, with further consideration given to increased commutation difficulty because of higher than normal air gap flux densities, higher than normal rotor speeds, larger air gap producing increased fringing flux at pole tips, and increased bar to bar voltage.

### 6.3.3.2 Commutating Pole Considerations

The commutating pole is designed to induce a voltage in the coil undergoing commutation that opposes the voltage induced by the armature reaction magnet motive force (mmf) at the interpole center. In an uncompensated machine the interpole mmf is designed to be approximately 1.15 to 1.2 times the armature reaction mmf. The interpole tip width is generally approximately 0.5 to 0.8 times the commutating zone  $C_z$ , while the axial length is approximately 0.75 times the axial length of the armature. In a fully compensated machine with interpole and pole face winding, the total compensation should add to approximately 1.15 to 1.2 times the armature reaction mmf.

### 6.3.4 Pole Face Windings

Because the armature windings produce a flux that is in quadrature with (or 90 electrical degrees from) the main pole flux, a severe distortion of the air gap flux can occur in larger, more highly loaded machines. In many designs, it is not sufficient to add series turns and commutating poles. In these cases, some of the turns that would otherwise be placed on the commutating pole are placed in slots in the main pole face. Armature current passed through these pole face windings (also known as compensating windings) mirrors the armature current with reverse direction, and compensates for armature reaction effects on the main pole flux. Figure 6.14 shows a compensating winding slot configuration. The windings in each pole face slot are insulated from the pole laminations and from each other. In order to complete the circuit, each conductor of the pole face winding is connected to an equivalent conductor on the nearest adjacent main pole.

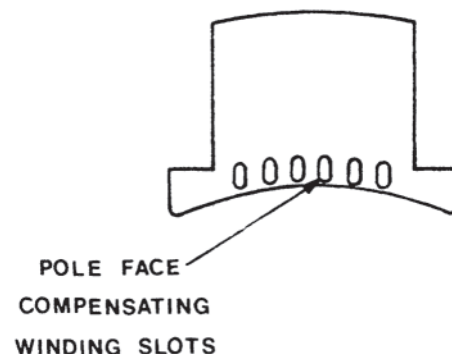


**Figure 6.14** Compensating winding slot configuration.

This construction is very expensive, but is justifiable for large, heavily loaded machines because of the elimination of the demagnetizing effects of armature reaction on the main field and because of the improved commutation.

## 6.4 EQUIVALENT CIRCUIT

The equivalent circuit of a dc motor is shown in Fig. 6.15.

### 6.4.1 Steady-State Analysis

For steady-state calculations, the equation describing this circuit is:

$$V_t = E_a + I_a R_a + V_{br} \quad (6.8)$$

where:

$V_t$  = applied terminal voltage (V)

$E_a$  = generated armature voltage (V) as given by Eq. (6.1)

$I_a$  = armature current in amperes

$R_a$  = armature circuit resistance in ohms, including resistance of any series field, interpole windings, and pole face windings

$V_{br}$  = brush drop voltage (in the range of 1 to 2 V for two brushes in series)

The shunt field shown in Fig. 6.15 is controlled by a variable resistor in series with the field. Other means of control of the shunt field current are by use of a solid-state field control, or by means of a completely separate power supply. (For a series motor, the shunt field is eliminated and control is achieved by varying the applied voltage,  $V_t$ .)

Because  $E_a$  is very nearly equal to  $V_t$  (except for a few volts drop for brushes and series resistance), a small change in the voltage applied to either the armature or the main field will produce a large change in armature current. For an increase in armature current, the motor torque is increased and the motor speeds up until Eq. 6.8 is again satisfied and the armature current is that needed to supply the load torque. The motor will slow down for a decrease in armature current.

The motor developed power is given by the product of  $E_a$  and  $I_a$ ; motor shaft power is given by:

$$P_{\text{shaft}} = E_a I_a - \text{LOSSES} \quad (6.9)$$

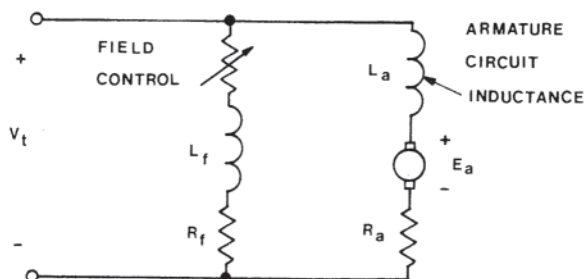


Figure 6.15 Direct current (dc) motor equivalent circuit.

where LOSSES includes friction, windage, iron, and strayload losses.

Dividing both sides of Eq. 6.9 by the rotational speed in radians per second will give the torque in newton-meters:

$$T_{\text{out}} = \frac{P_{\text{shaft}}}{2\pi \times \text{RPM}/60} \quad (6.10)$$

Substitution of  $E_a$  from Eq. 6.1 and  $P_{\text{shaft}}$  from Eq. 6.9 yields:

$$T_{\text{out}} = \frac{Z \times \phi_p \times I_a \times \text{POLES}}{2\pi \times \text{PATHS}} - T_{\text{loss}} \quad (6.11)$$

where  $T_{\text{loss}}$  is the drag torque associated with the losses in Eq. 6.9.

### 6.4.2 Transient Analysis

For transient or time-varying conditions, the motor inductances must be considered, and Eq. 6.8 becomes

$$V_t = E_a + I_a R_a + V_{br} + L_a \frac{dI_a}{dt} \quad (6.12)$$

where  $L_a$  is the armature circuit inductance.

If the armature voltage is chopper controlled, external inductance may be added to reduce current ripple. For a series motor with solid iron parts such as interpoles and frame, the armature inductance will vary with frequency of the applied armature voltage changes due to eddy currents in the solid iron. These eddy currents cause additional iron losses and, for large machines, reduction in these losses may require lamination of the motor frame and interpoles. (The main poles would probably be laminated in any case.) For a shunt or separately excited motor, the voltage equation for the field circuit will include a field inductance term, which has to include the effects of motor frame eddy currents for time-varying field voltages.

## 6.5 DESIGN EQUATIONS

The torque that may be developed by a motor is proportional to the size (or active volume) of the motor:

$$T = k D_a^2 L_a B_{av} J \quad (6.13)$$

where

$k$  = a constant depending on the units used and the type of machine

$D_a$  = armature diameter

$L_a$  = armature length

$B_{av}$  = average air gap flux density

$J$  = armature current loading in ampere-conductors per unit of armature periphery, having a range that depends on duty and size of motor and the heat transfer from the armature surface

The first step in the iterative design process is to select a motor size based on a  $D_a^2 L_a$  known and torque from an existing design with a known performance. The motor performance

and design parameters are then calculated. Subsequent iterations are used to drive the design toward a preselected optimum.

### 6.5.1 Magnetic Circuit

The motor magnetic circuit is comprised of the frame, main pole body, main pole tip, air gap, rotor (armature) teeth, and rotor core. The field winding must supply enough mmf (ampere-turns) to drive the flux through all of this series path. For low values of flux, only the air gap ampere-turns need be considered, but as motor flux increases, additional ampere-turns are required by the iron parts because of saturation. Additional ampere-turns may also be required by a main pole that does not fit snugly against the frame. The main field current required is given by the equation

$$I_f = \frac{AT_{\text{tot}}}{N_{\text{ft}}} \quad (6.14)$$

where:

- $N_{\text{ft}}$  = number of main field turns per pole
- $AT_{\text{tot}}$  = total magnetic circuit ampere turns/pole  
=  $AT_{\text{gap}} + AT_{\text{iron}} + (0.1 AT_{\text{ar}})$ , in which
- $AT_{\text{gap}}$  = ampere-turns required by the air gap  
=  $(B_g \times \text{GAP} \times C_{\text{slot}}) / (4\pi \times 10^{-7})$ , the variables being
- $B_g$  = air gap flux density (tesla)
- $\text{GAP}$  = length of the air gap
- $C_{\text{slot}}$  = Carter or slot coefficient
- $AT_{\text{iron}}$  = total iron ampere-turns from curves for the steel
- $AT_{\text{ar}}$  = total armature reaction ampere-turns per pole  
=  $(I_a \times Z) / (2 \times \text{POLES} \times \text{PATHS})$

If the machine is fully compensated (having interpole and pole face windings),  $AT_{\text{ar}}$  is set to zero.

### 6.5.2 Saturation

The ampere-turns required by the air gap and by armature reaction in Eq. 6.14 are linear quantities and can be plotted as shown in Fig. 6.16(a). When steel parts of the magnetic circuit are included, saturation becomes evident at higher levels of flux, the excitation curve deviating from the straight line relationship of Fig. 6.16(a) and becoming that shown in Fig. 6.16(b).

In the design and sizing of the iron paths of a dc motor, it is very important to include enough field current capability to allow for some error in the ampere-turns required by the iron. Since the material is very nonlinear, a small error in flux density can lead to large errors in required ampere-turns. This is especially true at high levels of flux density, around 2 T and greater.

### 6.5.3 Detailed Magnetic Circuit Calculations

The magnetic circuit ampere-turn requirements referred to in Eq. 6.14 are determined by considering the magnetic flux

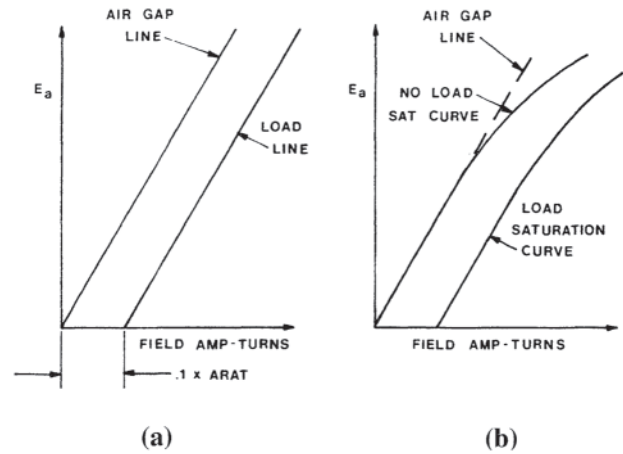


**Figure 6.16** Magnetization curves at fixed speed, with and without armature reaction effects: (a) without saturation; (b) with saturation.

passing through each portion of the magnetic circuit. This section presents a method of calculation for each portion in turn. The coefficients for determining the effects of flux fringing such as the pole face coefficient can be obtained from the published work of Wieseman [2] at the end of this chapter. More detailed values of these coefficients as well as the effects of saturation and armature reaction can be obtained from finite-element magnetic-field calculations such as those presented in Section 6.9.

The dimension variables used in the equations of the following sections are referenced in Fig. 6.17. The equations shown in the following sections are approximations used to allow quick calculation of the magnetic circuit performance.

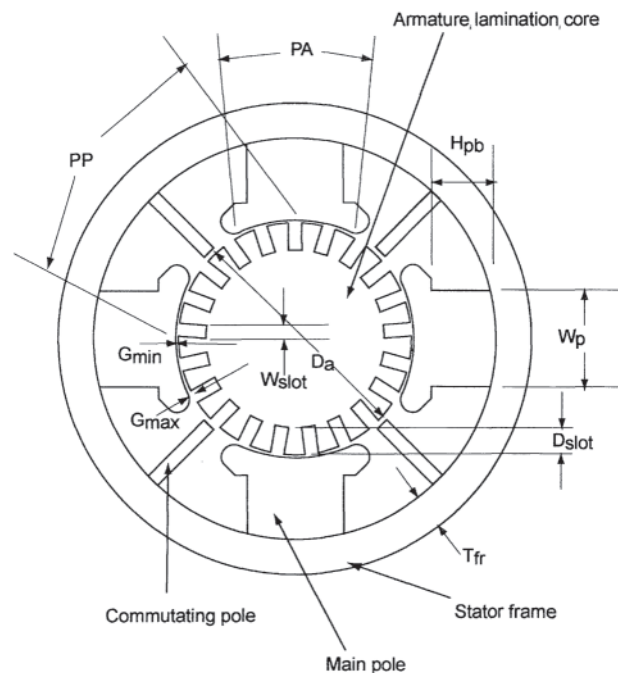


**Figure 6.17** Cross section of four-pole direct current (dc) motor with main and commutating poles showing dimensional quantities used in equations.

### 6.5.3.1 Air Gap

The air gap flux is the total flux per pole that crosses the air gap and is the value of magnetic flux used to calculate the generated voltage of Eq. 6.1 and the generated torque of Eq. 6.11. This flux is designated  $\Phi_p$  with a value in webers.

To calculate ampere-turns of the air gap, the following value of flux is used:

$$\begin{aligned}\Phi_\lambda &= \Phi_p K_\lambda & (6.15) \\ &= \text{total air gap flux per pole entering the pole face} \\ & \quad \text{only in webers}\end{aligned}$$

where:

$K_\lambda$  is the air gap flux coefficient (ratio of pole face flux to total flux per pole)

The equivalent air gap area for flux density calculations is given by the product of the average of rotor and stator lengths and the pole arc peripheral length:

$$A_{\text{gap}} = PA(L_p + L_a)/2 \text{ in square meters} \quad (6.16)$$

where:

PA is the pole arc peripheral length in meters

$L_p$  is the pole axial length in meters

$L_a$  is the armature (rotor) axial length in meters

The appropriate radial air gap length to use with the value of  $\Phi_\lambda$  flux is the average gap,  $G_{\text{av}}$  as given by:

$$G_{\text{av}} = (2G_{\text{min}} + G_{\text{max}})/3 \quad (6.17)$$

(this is actually a weighted average for this method)

where:

$G_{\text{min}}$  is the minimum air gap (usually at the center of the pole face arc) in meters

$G_{\text{max}}$  is the maximum air gap in meters

The air gap flux density is then:

$$B_g = \Phi_\lambda / A_{\text{gap}} \quad (6.18)$$

And the air gap ampere-turns are given by:

$$AT_{\text{gap}} = G_{\text{av}} C_{\text{slot}} B_g / \mu_0 \quad (6.19)$$

where:

$\mu_0 = 4\pi \cdot 10^{-7}$  = permeability of air in webers per amp-m

$C_{\text{slot}}$  is the well-known slot or Carter coefficient for armature slot flux fringing. An alternative method uses a constant  $K_m$  instead of  $K_\lambda$ , and gives a slightly different result. In this method,  $B_{\text{gm}}$  replaces  $B_g$ , and  $G_{\text{min}}$  replaces  $G_{\text{av}}$  in Eq. 6.19.  $B_{\text{gm}}$  is obtained by:

$$B_{\text{gm}} = K_m B_a \quad (6.20)$$

where:

$K_m$  is obtained from flux plots

$B_{\text{av}}$  is the average flux density over a pole pitch given by

$$B_{\text{av}} = \Phi_p / A_{\text{gtot}} \quad (6.21)$$

$$A_{\text{gtot}} = PP(L_p + L_a)/2 \quad (6.22)$$

$$PP = \pi D_a / \text{POLES}$$

$D_a$  is the armature (rotor) diameter

POLES = the total number of stator main poles

An additional factor  $K_{\text{ag}} (>1)$  is sometimes used in Eq. 6.20 to account for the fact that as the armature teeth saturate, the air gap flux distribution along the air gap changes, with more flux crossing the larger air gap closer to the pole tips. This factor is obtained from flux plotting or finite element field calculations, and can increase the air gap ampere-turns by as much as a third for tooth densities greater than two teslas with a  $G_{\text{max}}$  to  $G_{\text{min}}$  ratio of four. For uniform air gaps  $K_{\text{ag}}$  is unity. A value of 1.07 can be used for a first approximation with armature tooth density equal to 2.0 teslas, and maximum to minimum gap ratio around 1.5.

### 6.5.3.2 Armature Teeth

The air gap flux  $\Phi_\lambda$  opposite the pole face is used to calculate the armature tooth flux density as follows:

$$B_{\text{teeth}} = \Phi_\lambda / A_{\text{teeth}} \quad (6.23)$$

where:

$$\begin{aligned}A_{\text{teeth}} &= \text{tooth area opposite pole face} \\ &= \text{TOP } L_a (S_{\text{pav}} - W_{\text{slot}}) FS_a & (6.24)\end{aligned}$$

TOP = PA/SLPT

SLPT =  $\pi D_a / \text{SLOTS}$  = slot pitch at armature surface

$$\begin{aligned}S_{\text{pav}} &= \pi(D_a - 4D_{\text{slot}}/3) / \text{SLOTS} \\ &= \text{weighted average slot pitch}\end{aligned}$$

$D_{\text{slot}}$  is the total depth of an armature slot

$W_{\text{slot}}$  is the armature slot width (use average width if slot width is not uniform)

$FS_a$  is the armature stacking factor (typically 0.95 to 0.98)

After the flux density of the armature teeth is found, the  $H_{\text{teeth}}$  for the armature material is found from a  $B-H$  curve such as shown in Fig. 6.18 for the value of  $B_{\text{teeth}}$  calculated. The ampere-turns for the teeth are:

$$AT_{\text{teeth}} = D_{\text{slot}} H_{\text{teeth}} \quad (6.25)$$

Figure 6.18 shows a plot of typical values of  $H$  vs.  $B$  for two steel types used in motor manufacture, compared to ingot iron. From above the value of 2.0 T, the curves of  $H$  vs.  $B$  start to approach the slope of the magnetic susceptibility of air,  $1/\mu_0$ . This  $B-H$  information is available from steel suppliers for the particular material being used. Iron or low carbon steel might be used for the motor frame and the pole laminations because the magnetic flux is essentially dc and does not vary rapidly. The armature steel would likely be a motor grade containing more silicon for larger motors to improve motor efficiency, because the armature flux is varying proportionally

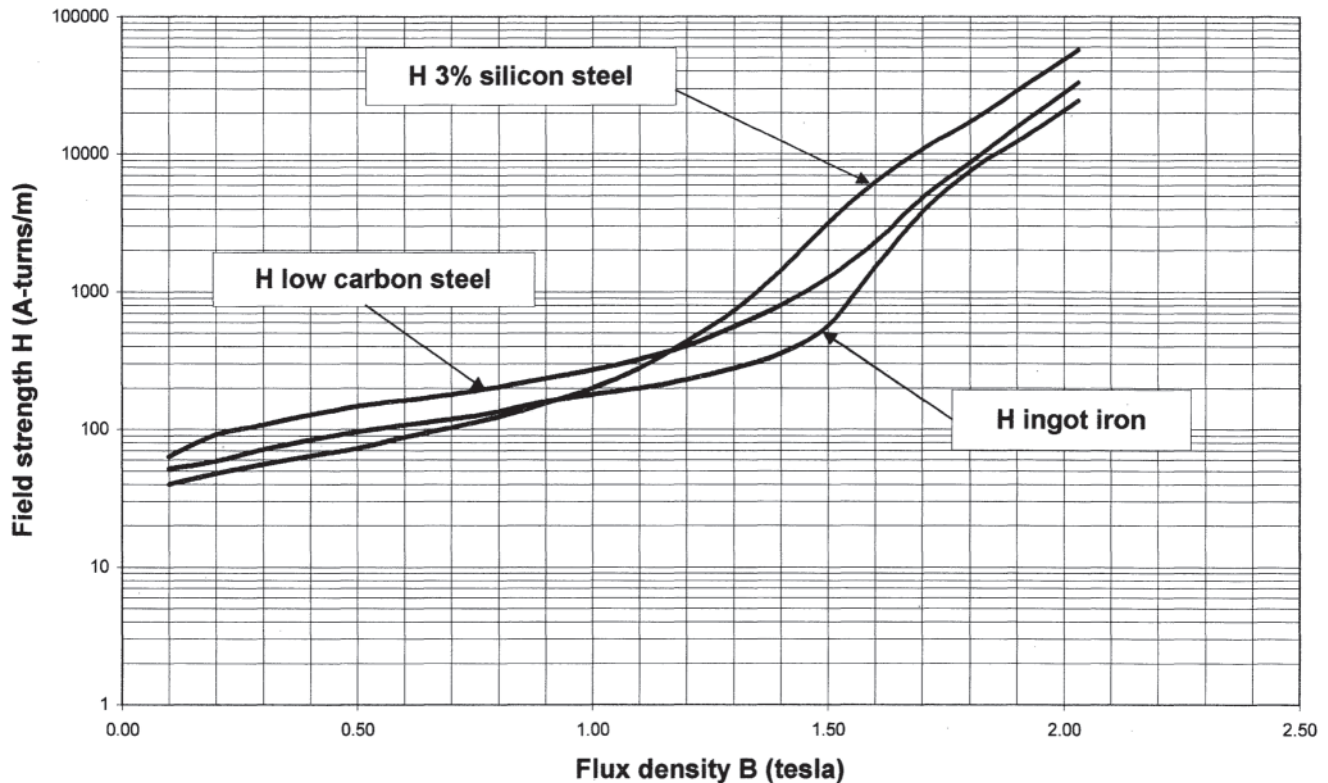


Figure 6.18 Typical  $B$ - $H$  curves for two direct current (dc) motor materials compared to ingot iron.

with the motor speed, and the higher resistance of the steel resulting from the addition of silicon helps to reduce iron losses caused by eddy currents in the individual laminations. For chopper controlled motors, where the field is chopper controlled, or rectifier supplied with a high ripple content, the poles and even the frame might be laminated with higher quality steel.

### 6.5.3.3 Armature Core

The total flux per pole  $\Phi_p$  is used to calculate the armature core flux density (the flux splits two ways, so a factor of two is used in the flux density equation) as follows:

$$B_{\text{core}} = \Phi_p / (2 A_{\text{core}}) \quad (6.26)$$

where:

$$A_{\text{core}} = L_a ((D_a - 2D_{\text{slot}}) / 2) FS_a \quad (6.27)$$

= the core area below armature teeth perpendicular to the peripheral direction (assuming a solid magnetic rotor path to the center of the shaft or rotor structure)

After the flux density of the armature core is found, the  $H_{\text{core}}$  for the armature material is found from a  $B$ - $H$  curve for the value of  $B_{\text{core}}$  calculated. The ampere-turns for the core are:

$$AT_{\text{core}} = L_{\text{core}} H_{\text{core}} \quad (6.28)$$

where:

$$L_{\text{core}} = \pi(RC_{\text{avg}}) / (2 \text{ POLES})$$

= one half the pole pitch length at the core geometric average radius

$$RC_{\text{avg}} = ((D_a/2 - D_{\text{slot}})^2 / 2)^{0.5}$$

= core geometric average radius in meters

### 6.5.3.4 Stator Pole

The total flux per pole  $\Phi_p$  is used to calculate the pole body flux density as follows:

$$B_{\text{pole}} = \Phi_p K_{1p} / A_{\text{pole}} \quad (6.29)$$

where:

$$K_{1p} = L_p W_p \text{ FS}_p$$

= pole leakage factor determined by flux plots (1.05 to 1.15)

Pole body leakage flux is that flux that links some of the field turns, and also enters the frame, but does not cross the air gap:

$$A_{\text{pole}} = L_p W_p \text{ FS}_p = \text{pole body area in square meters} \quad (6.30)$$

where:

$W_p$  is the main pole body width

$\text{FS}_p$  is the pole stacking factor (typically 0.95 to 0.98)

After the flux density of the pole is found, the  $H_{\text{pole}}$  for the armature material is found from a  $B$ - $H$  curve for the value of  $B_{\text{pole}}$  calculated. The ampere-turns for the pole are:

$$AT_{\text{pole}} = H_{\text{pb}} H_{\text{pole}} \quad (6.31)$$

where:

$H_{\text{pb}}$  = the pole body height from frame to bottom of pole tip

For a pole with a compensating winding, the flux is constricted as it passes between the bars of the pole face, and instead of pole body height, the total pole height from frame to air gap should be used in Eq. 6.36.

### 6.5.3.5 Stator Frame

The total flux per pole  $\Phi_p$  is used to calculate the frame flux density (the flux splits two ways, so a factor of two is used in the flux density equation) as follows:

$$B_{\text{frame}} = \Phi_p K_{\text{ifr}} / (2 A_{\text{frame}}) \quad (6.32)$$

where:

$K_{\text{ifr}}$  = frame leakage factor determined by flux plots (1.07 to 1.20)

Frame leakage flux is some of the same flux that was described above as pole leakage flux, caused by the pole winding mmf but not crossing the air gap:

$$A_{\text{frame}} = L_{\text{fa}} T_{\text{fr}} = \text{the peripheral core area below the pole base} \quad (6.33)$$

$L_{\text{fa}}$  = axial frame length in meters

$T_{\text{fr}}$  = frame radial thickness in meters

After the flux density of the frame is found, the  $H_{\text{frame}}$  for the frame material is found from a  $B$ - $H$  curve for the value of  $B_{\text{frame}}$  calculated. The ampere-turns for the frame are:

$$AT_{\text{frame}} = L_{\text{frame}} H_{\text{frame}} \quad (6.34)$$

where:

$L_{\text{frame}} = \pi(RF_{\text{avg}})/(2 \text{ POLES}) - W_p/4 = \text{one half the pole pitch length at the frame geometric average radius minus one fourth of the pole body width, all in meters}$

$RF_{\text{avg}} = (((OD_{\text{frame}}^2 - ID_{\text{frame}}^2)/2)^{0.5})/2 = \text{core geometric average radius in meters}$

$OD_{\text{frame}}$  is the frame outside diameter in meters

$ID_{\text{frame}}$  is the frame inside diameter in meters

The magnetic circuit values of ampere-turns are summed along with the fraction of the armature reaction ampere-turns as shown in Eq. 6.14 to obtain the total field mmf required per pole. This value is divide by the number of field turns per pole to obtain the field current. As stated earlier, for a fully compensated dc motor with a pole-face winding, the armature reaction effect is considered to be zero for the main pole mmf.

## 6.6 DC MOTORS IN CONTROL SYSTEMS [1]

### 6.6.1 Basic Motor Equations

A dc machine used in a position or motion control system is frequently referred to as a servomotor. Motors specifically intended to be used in a closed-loop system are covered in NEMA MG 7-1993 Motion/Position Control Motors and Controls [1]. There are, however, many closed-loop systems whose load characteristics require the use of dc motors that fall outside the scope of that standard. For any of these machines, the variables of interest on the electrical side are voltage and current; on the mechanical side, the variables to be considered are torque and speed. Two basic equations relate these four variables, and form the foundation of control system analysis. These are the equation for developed torque:

$$T = Zp/2\pi a i_a \phi_p = K_t i_a \phi_p \quad (6.35)$$

which is the first term on the right in Eq. 6.11, and the equation for internally generated voltage:

$$E_a = \frac{Zp}{60a} n \phi_p \quad (6.36a)$$

where:

$Z$  = the total number of armature conductors

$p$  = the number of poles (POLES in Section 6.1)

$a$  = the number of parallel paths through the armature (PATHS in Section 6.1)

$i_a$  = armature current ( $I_a$  in Section 6.4.1)

$\phi_p$  = the flux per pole (webers)

$n$  = speed (rpm) (RPM in Section 6.1)

$K_t = Zp/2\pi a = \text{torque constant}$

Since  $n=60\omega/(2\pi)$ , where  $\omega$ =angular speed in radians/s, then:

$$E_a = \frac{Zp}{2\pi a} \omega \phi_p = K_v \omega \phi_p \quad (6.36b)$$

The factor  $Zp/(2\pi a)$  appearing in both Eq. 6.35 and Eq. 6.36b is frequently referred to as the torque constant  $K_t$  in Eq. 6.35 and the voltage constant  $K_v$  in Eq. 6.36b. Since  $K_v=K_t$ , a new constant  $K'$  may be defined by

$$K' = K_v = K_t = \frac{Zp}{2\pi a} \quad (6.37)$$

If the machine is to be used with fixed-field strength in a control system, the flux per pole  $\phi_p$  is commonly merged with  $K'$  to yield another constant:

$$K = \frac{Zp}{2\pi a} \phi_p \quad (6.38)$$

where  $K$  is generally referred to as the machine constant. Equations 6.35 and 6.36 may then be expressed as:

$$T = K i_a \quad (\text{N}\cdot\text{m}) \quad (6.39)$$

and:

$$E_a = K \omega \quad (\text{V}) \quad (6.40)$$

The machine constant  $K$  from Eq. 6.39 has dimensions of N-m/A. In the SI system of units, these dimensions are identical to V-s/rad, the units needed in Eq. 6.40. If the machine constant is given by the manufacturer in other units, it should be converted to either of these dimensional forms before being used in control system analysis in order to avoid having to bring dimensional conversions into those equations, with complications that can easily lead to errors.

In addition to Eqs. 6.39 and 6.40, at least one Ohm's law type of equation is needed. Figure 6.19 shows the equivalent circuit for the motor. If the field strength is fixed, the field loop is ignored,  $i_f$  having been set to produce the value of  $\phi_p$  in Eq. 6.38. For the armature loop:

$$v_a = R_a i_a + L_a \frac{di_a}{dt} + E_a \quad (6.41)$$

where:

- $R_a$  = armature circuit resistance (ohms)
- $L_a$  = armature circuit inductance (henrys)

Equations 6.39, 6.40, and 6.41 are the relationships on the electrical side of the motor and at the energy conversion interface that are needed for control system analysis if the machine is used in an armature voltage control mode, such as a positioning system or a system that controls speed from zero speed to base speed in either direction. If the motor is used in a speed control system above base speed, which is achieved by field weakening, there are additional complications in control system implementation and analysis. These are discussed briefly in Section 6.6.5 below.

### 6.6.2 Basic Mechanical Equation

The load driven by the motor may be characterized in various ways, but in every case some of the parameters needed for the differential equation relating the mechanical variables ( $T$  and  $\omega$ ) are partially dependent on the mechanical characteristics of the motor. For example, the armature has a polar moment of inertia, which is part of the total inertia  $J$  in Fig. 6.19. In many cases, the value of  $J$  is dominated by the armature inertia, and

the armature inertia can rarely be neglected. Its value is one of the parameters the manufacturer should supply.

There are internal frictional effects in the motor from the bearings, brush-commutator friction, windage, and eddy current and hysteresis losses. The torques due to these various effects are difficult to place into neat categories. Some of them are Coulomb friction effects, that is, frictions that result in a torque that is independent of speed. Others are viscous friction effects, resulting in a torque that is directly proportional to speed. Still others, such as fans on the armature shaft, produce torques proportional to the square of the speed. Fortunately, most of these effects due to the motor are small compared to the torques required by the load, which is generally far easier to characterize.

Load characteristics are of the same general type as those mentioned in the preceding paragraph. The load itself may be direct-coupled to the motor shaft, or it may be coupled through a speed-changing device, such as a set of gears. If it is direct-coupled,  $J$  in Fig. 6.19 is simply the sum of the motor and load inertias,  $D$  is the sum of the motor and load viscous friction factors, and  $T_L$  is the constant torque required by the load.

If the load is not direct-coupled, the effects of the speed change must be taken into account. If a gear set is interposed between the motor and the load with a gear ratio  $N=N_1/N_2$ , where  $N_1$  is the number of teeth on the gear on the motor shaft and  $N_2$  the number of teeth on the load shaft, the load effects may be reflected back to the motor shaft using  $N^2 J_L$  to reflect the load inertia  $J_L$  and using  $N D_L$  to reflect the viscous friction effects of the load. If the load presents a constant torque  $T_L$ , that torque is reflected back to the motor shaft using  $N T_L$ . Once the load effects are reflected back to the motor shaft and added to those of the motor itself, the analysis proceeds using Fig. 6.19.

The torque equation for Fig. 6.19 is:

$$T = J \frac{d\omega}{dt} + D\omega + T_L \quad (6.42)$$

Equations 6.39 through 6.42 may now be combined and rearranged to yield a single equation relating source voltage  $v_a$  and shaft angular speed  $\omega$ , resulting in

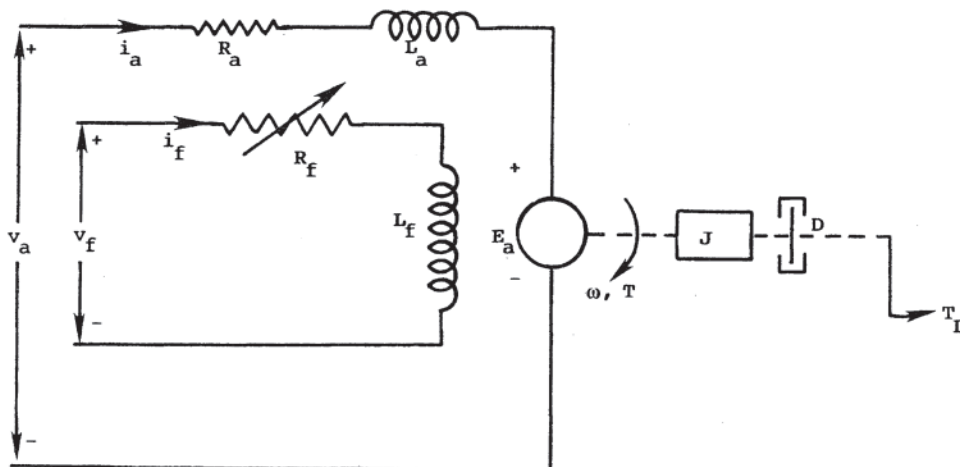


Figure 6.19 Equivalent circuit of a dc motor with mechanical loading.



$$v_a = \frac{JL_a}{K} \frac{d^2\omega}{dt^2} + \frac{(R_a J + L_a D)}{K} \frac{d\omega}{dt} + \frac{(R_a D + K^2)}{K} \omega + \frac{R_a T_L}{K} + \frac{L_a}{K} \frac{dT_L}{dt} \quad (6.43)$$

Various simplifications of Eq. 6.43 may be made to investigate special conditions. For example, if the motor is not loaded ( $T_L=0$ ) and the viscous friction factor  $D$  is small, Eq. 6.43 reduces to:

$$v_a = \frac{JL_a}{K} \frac{d^2\omega}{dt^2} + \frac{R_a J}{K} \frac{d\omega}{dt} + K\omega \quad (6.44)$$

which may be rewritten as:

$$v_a = K \left( \tau_a \tau_m \frac{d^2\omega}{dt^2} + \tau_m \frac{d\omega}{dt} + \omega \right) \quad (6.45)$$

where:

$$\tau_a = \frac{L_a}{R_a} \quad \text{and} \quad \tau_m = \frac{J R_a}{K^2}$$

Taking the Laplace transform of Eq. 6.45 and defining:

$$\omega_n = 1/\sqrt{\tau_a \tau_m} = \text{the undamped natural angular frequency (rad/s)}$$

$$\zeta = \frac{1}{2} \sqrt{\tau_m/\tau_a} = \text{the damping factor}$$

$$\Omega(s) = \frac{V_a(s)/K}{(s^2/\omega_n^2) + (2\zeta/\omega_n)s + 1} \quad (6.46)$$

For this equation, the response to a step function of voltage (normalized by division by  $K$ ) as a function of  $\omega_n t$  appears in Fig. 6.20. Note the overshoot and “ringing” that occurs for small values of  $\zeta$ , effects that virtually disappear for values of  $\zeta$  greater than 0.7.

Examination of  $\tau_a$ ,  $\tau_m$ , and  $\zeta$  shows that the damping factor becomes larger as  $L_a$  is decreased. Moreover,  $\omega_n$  also increases, and the time to reach steady state decreases.

### 6.6.3 Block Diagrams

Neither Eq. 6.43 nor Eq. 6.44 can be represented by a block diagram having a single input and a single output unless  $T_L$  is set to zero. Although this is reasonable in some cases, there are many control systems for which the load torque acts as a second input. For example, a roll-turning lathe with a speed control system will have the set speed as one input. The second input, the load torque  $T_L$ , is controlled by the lathe operator by setting the depth of cut and the speed of the slide or cross slide. If the roll being turned is an “as-cast” roll, the depth of cut when first beginning to remove material will vary widely for a single circumferential pass, possibly being zero at some points on the circumference. In this latter case, the load torque may come on suddenly, almost in a step-function mode, or may come on more gradually, in the form of a ramp. It is obvious that this is a two-input system, and the block diagram must provide for analysis using either speed or torque as the input.

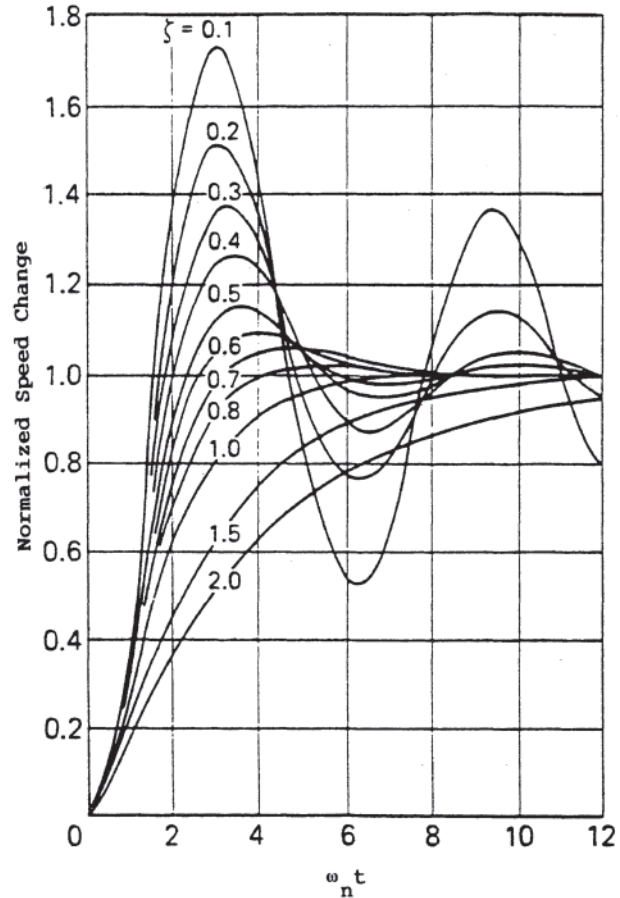


**Figure 6.20** Normalized speed change for a direct current (dc) motor versus  $\omega_n t$  following a step function of armature voltage.

The block diagram of Fig. 6.21 is based on Eqs. 6.39 through 6.42 and represents the motor in the fixed-field mode. In this diagram and in those that follow,  $s$  is the Laplace operator; it may be replaced by  $p$  (the differential operator) if one is more familiar with that notation. The transfer functions, summing points, and time constants ( $\tau_s$ ) arise directly from Eqs. 6.39 through 6.42, and the intermediate variables, armature current  $i_a$  and developed torque  $T$ , may be obtained as time functions if desired. Output speed is generally the variable of interest. When the block diagram of the remainder of the system is added to that of Fig. 6.21, the complete system may be analyzed using speed as the input or using load torque as the input.

Block diagram reduction or rearrangement is frequently done so that stability of the system and compensation tactics can be more easily investigated. For example, the block diagram of Fig. 6.22 may be shown to be identical to that of Fig. 6.21. It should be noted that, in this process, the intermediate variables of Fig. 6.21 disappear. For example, there are no points in this diagram where one may identify the internally generated voltage  $E_a$ , the armature current  $i_a$ , or the developed torque  $T$ .

The transfer function  $G(s)$  relating input voltage  $v_a$  to output speed  $\omega$ , with the viscous friction factor  $D$  set equal to zero, is the same as Eq. 6.46 if both sides of Eq. 6.46 are

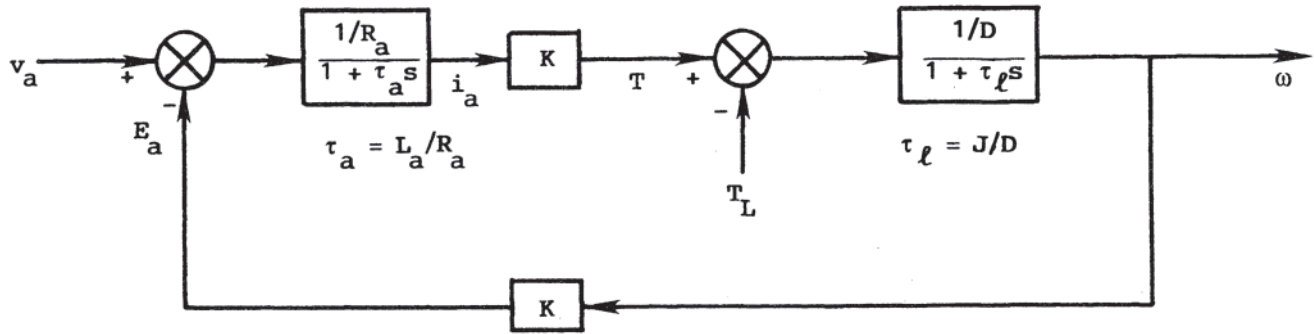


Figure 6.21 Block diagram for a direct current (dc) motor.

divided by  $V_a(s)$ . This form lends itself to investigations of frequency response,  $s$  being replaced by  $j\omega_d$ , where  $\omega_d$  is the angular frequency of the driving function. Figure 6.23 shows the magnitude of the transfer function in dB and the angle of the transfer function in degrees, both being shown versus the normalized frequency  $\omega_d/\omega_n$ .

### 6.6.4 Typical Motor Characteristics and Stability Considerations

The electrical time constant  $\tau_e$ , the mechanical time constant  $\tau_m$ , and the undamped natural angular frequency  $\omega_n$  are important characteristics of dc motors used as servomotors. Another parameter of importance is the torque-to-inertia ratio,  $T/J$ . The larger this ratio, the higher the acceleration of the motor and the more rapid the response of the system. The polar moment of inertia of a motor is proportional to the armature diameter  $D$  to the fourth power, whereas the torque is proportional only to  $D^2$ . Hence the  $T/J$  ratio is proportional to  $1/D^2$ . The smaller the motor, the larger  $T/J$ . Table 6.1 shows typical values of the various parameters for four motors in integral horsepower sizes, and for a miniature dc motor (5 cm outside diameter) having an output capability of about 200 W.

As will be noted from the table, the electrical and mechanical time constants are of the same order of magnitude for these machines. Hence the damping factor  $\zeta$  for the motor

without load varies from approximately 0.8 to about 0.35. The undamped natural frequency  $\omega_n$ , however, covers a range of almost 30 to 1, and the  $T/J$  ratio spans a range of 130 to 1. Because the damping ratio for most of these machines is below 0.7, they may be said to be “unstable” in the sense that the transient response of Fig. 6.20 exhibits overshoot and damped oscillations, and the frequency response of Fig. 6.23 exhibits peaks in the response for the smaller damping ratios.

There is another sense in which a motor may be said to be unstable. Motors are generally expected to have a drooping speed-torque characteristic. Some machines, however, will exhibit a rising speed-torque curve for high load torques. This characteristic may be the consequence of armature reaction, which has the effect of weakening the field. If the load speedtorque curve does not rise faster than the motor curve, there will be an excess of torque available, which will accelerate the motor and load, leading to runaway. In spite of such a dangerous characteristic, a good speed control system will adjust armature voltage to avoid the runaway condition.

### 6.6.5 Field Control

If a motor is to be operated above base speed, field weakening is required. Some of the equations used to analyze the speed control system appear earlier in this section. The armature voltage is kept constant, so that  $v_a$  is replaced by  $V_a$ . The equations are:

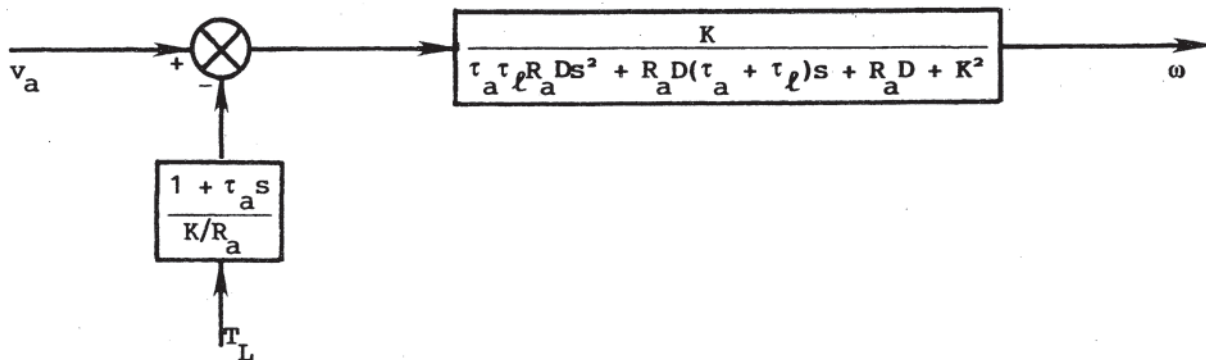


Figure 6.22 Modified block diagram for a direct current (dc) motor.

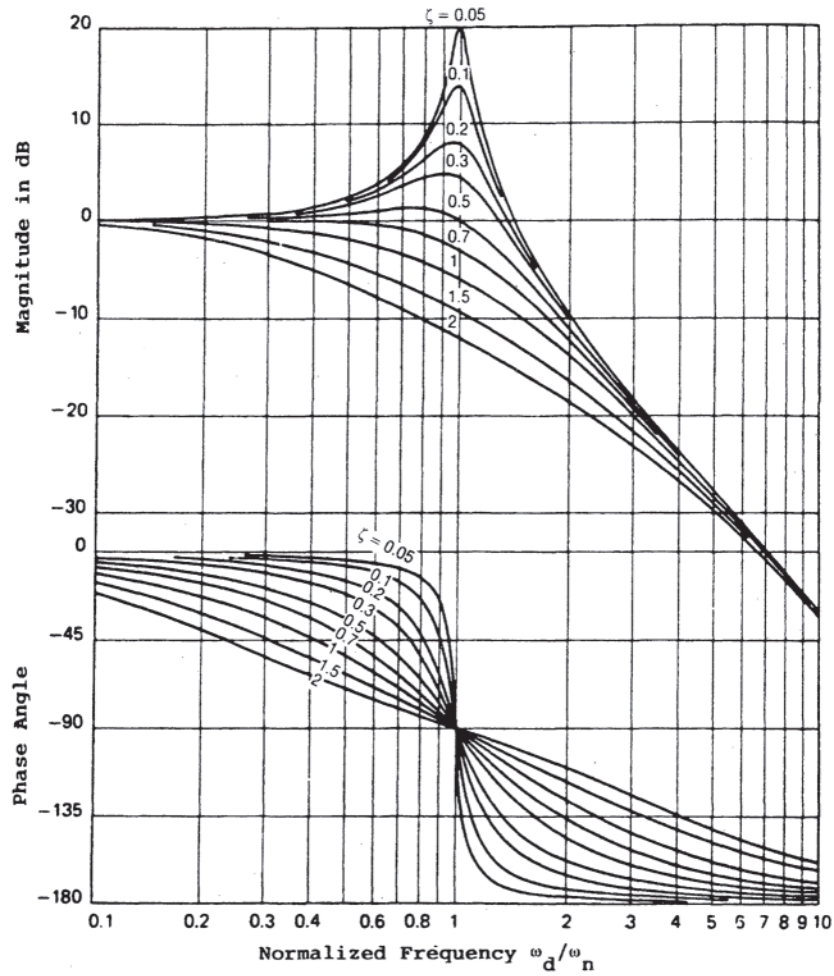


Figure 6.23 Frequency response of a direct current (dc) motor.

$$T = K_t i_a \phi_p \tag{6.35}$$

$$E_a = K_v \omega \phi_p \tag{6.36}$$

$$V_a = R_a i_a + L_a \frac{di_a}{dt} + E_a \tag{6.41}$$

$$T = J \frac{d\omega}{dt} + D\omega + T_L \tag{6.42}$$

The second term in this equation appears in the form of a derivative of  $L_f i_f$  (flux linkage) with respect to time because saturation of the field causes  $L_f$  to be a function of field current.

The other equation relates  $\phi_p$  to  $i_f$ . This is generally a nonlinear relationship, and may be expressed as:

$$\phi_p' = f(i_f) \tag{6.48a}$$

Two additional equations are needed. One of these is:

$$v_f = R_f i_f + \frac{d(L_f i_f)}{dt} \tag{6.47}$$

Even if Eq. 6.48 is linear and  $L_f$  is independent of  $i_f$ , there is an inherent nonlinearity in Eq. 6.35 because the right-hand side is a *product* of two of the variables,  $i_a$  and  $\phi_p$ . Hence analysis of the system must depend on the techniques used in

Table 6.1 Dynamic Motor Characteristics

	Electrical time constant $\tau_a$ (ms)	Mechanical time constant $\tau_m$ (ms)	Undamped natural frequency $\omega_n$ (rad/s)	Torque/inertia (rad/sec <sup>2</sup> )
Standard dc motors	15	22	55	500
Compensated motors	10	22	67	1,000
Super servo (low-speed PM)	7.4	6	150	1,150
Hyper-servo	1.7	2	540	10,000
Miniature dc (5 cm diameter)	0.88	0.46	1,570	66,300

nonlinear analysis. Rather than attempt to predict performance using analytical techniques, it is better to use one of the simulation programs available for digital computers, using look-up tables as necessary. With this approach, various forms of compensation may be examined rapidly.

The speed control system for the roll lathe mentioned in Section 6.6.3 is designed to operate with fixed field and variable armature voltage below base speed, and with variable field current above base speed. In the armature control mode the speed is controlled from nearly zero speed to base speed; in the field control mode the speed range is from base speed to about  $2\frac{1}{2}$  times base speed. For most of the speed range, therefore, the speed control is operating in a nonlinear fashion.

### 6.7 DC MOTORS SUPPLIED BY RECTIFIER OR CHOPPER SOURCES

The speed of a dc separately excited motor can be controlled from zero to base speed by varying the terminal voltage while the field current is maintained at the rated value. Because the maximum torque capability of the motor remains constant, the motor operates in the constant torque mode. The speed control above base speed is realized by varying field current with armature voltage maintained constant at the rated value. Because, the maximum power capability of the motor is constant in field current control, the motor operates in constant power mode. When operating with weak field and at high speed, the motor's ability to commutate current without sparking reduces. Therefore, approximately twice the rated speed motor operation is restricted below the rated current, and therefore, the machine operates at reduced power. The maximum speed attainable from the field control is twice the rated speed in a normally designed machine and is specially designed machines it can be six times rated speed. Variable dc voltages for armature voltage and field current controls are obtained using rectifier when the source is alternating current (ac) and using chopper when the source is dc. The speed of a dc series motor can be controlled from zero to base speed by armature voltage control. The field control is not used as the available methods allow change of flux in steps. Change of flux in steps produces severe current transients in armature, which has adverse effect on armature rectifier or chopper [3]. Because of this limitation and also because of the problems associated with regenerative braking, series motor is not used; even in traction where it was widely used in the past. Instead separately excited or compound motor is used. In low-power servos, permanent magnet dc motor is used and separately excited motor is used in higher power applications.

#### 6.7.1 List of Symbols

- $E$  = Armature back emf, V
- $K$  = Motor constant
- $i_a$  = Instantaneous value of armature current, A
- $I_a$  = DC component (or average value) of armature current, A
- $L_a$  = Armature inductance, H

- $R_a$  = Armature resistance,  $\Omega$
- $t_{on}$  = On period, S
- $T$  = Period of a cycle, S
- $T_m$  = Developed motor torque, N-m
- $v_a$  = Instantaneous motor terminal voltage, V
- $v_s$  = Instantaneous source voltage, V
- $V_a$  = Average value (or dc component) of motor terminal voltage, V
- $V_d$  = DC source voltage, V
- $V_m$  = Peak of source voltage, V
- $\alpha$  = Rectifier firing angle, Degrees
- $\tau_a = L_a/R_a$  = armature circuit time constant, S
- $\omega$  = AC source frequency, rad/S
- $\omega_m$  = Motor speed, rad/S
- $\delta$  = Duty cycle of chopper

#### 6.7.2 Analysis

The output voltage of a rectifier or chopper is not perfect dc, but consists of harmonics in addition to dc component. Consequently the motor armature current consists of a dc component and harmonics. Because the flux in dc separately excited motor is constant, only the dc component produces steady torque. Harmonic components produce alternating torque components; the average value of these is zero. The motor torque can, therefore, be calculated from the dc component. Because of their high frequency, the alternating torque components are filtered out by motor inertia. Therefore, the fluctuations in motor speed and back emf are negligible. From the dc equivalent circuit of a separately excited motor shown in Fig. 6.24 when flux  $\phi$  is constant:

$$E = K_e \phi \omega_m = K \omega_m \quad (6.48b)$$

$$V_a = E + I_a R_a \quad (6.49)$$

$$T_m = K_e \phi I_a = K I_a \quad (6.50)$$

and

$$\omega_m = \frac{V_a}{K} - \frac{R_a}{K^2} T_m \quad (6.51)$$

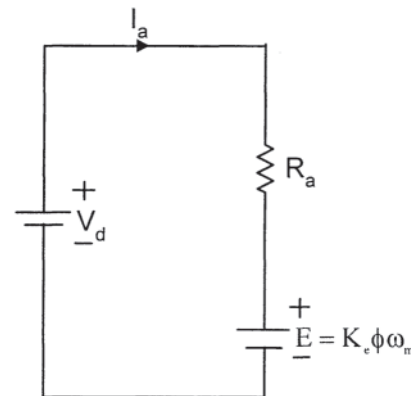


Figure 6.24 Equivalent circuit of a direct current (dc) motor.

6.7.3 Rectifier Sources [3]

DC motors supplied by rectifiers are used in applications requiring adjustable speed in wide range, good speed regulation, and frequent starting, braking and reversing. Some important applications are servos for positioning and tracking, rolling mills, paper and textile mills, traction, mine winders, machine tools, hoists and cranes, excavators, and printing presses. The ratings range from fractional horsepower permanent magnet dc motors for servos to few thousand horsepower motors for rolling mills and mine winders. Because of the problems associated with commutator and brushes, such as frequent maintenance, their applications have reduced, but they are still widely used in variable speed applications because of lower cost, reliability, simple control, and high part load efficiency.

Commonly used rectifier circuits are shown in Fig. 6.25. Because the thyristors are capable of conducting current only in one direction, all these rectifier circuits are capable of providing current in one direction. Rectifiers of Fig. 6.25(a) and (c) provide control of dc output voltage in either direction and therefore, allow motor operation in quadrants I and IV as shown. They are known as fully controlled rectifiers. In quadrant I power flows from ac source to motor. In quadrant IV the power flows from the motor to the ac source and the rectifier operates as an inverter and motor operates in regenerative braking. Two fully controlled rectifiers connected in antiparallel can provide motor operation in all four quadrants. Rectifier cost is reduced when half of the thyristors in fully controlled rectifiers are replaced by diodes, giving halfcontrolled rectifiers of Fig. 6.25(b) and (d), which provide operation in quadrant I only. The rectifier circuits are also identified by the number of pulses in their output dc voltage in a cycle of ac source voltage. The one-phase rectifiers of Fig. 6.25(a) and (b) are called two-pulse rectifiers, and three-phase rectifiers of Fig. 6.25(c) and (d) are known as six-pulse and three-pulse rectifiers, respectively. The output voltage of the rectifiers is controlled by controlling the angle at which thyristors are turned on in a cycle of input ac voltage. This angle  $\alpha$ , known as firing angle, is measured from the reference angle at which thyristor would turn on if it were a diode. Two-pulse rectifiers have two modes of operation: discontinuous conduction mode and continuous conduction mode. The motor terminal voltage and armature current waveforms for these two modes for the rectifier circuit of Fig. 6.25(a) are shown in Fig. 6.26. When the source voltage is:

$$v_s = V_m \sin \omega t \tag{6.52}$$

In continuous conduction dc component in motor terminal voltage is given by:

$$V_a = \frac{1}{\pi} \int_{\alpha}^{\pi+\alpha} V_m \sin \omega t d(\omega t) = \frac{2V_m}{\pi} \cos \alpha \tag{6.53}$$

and in discontinuous conduction it is given by:

$$V_a = \frac{1}{\pi} \left[ \int_{\alpha}^{\beta} V_m \sin \omega t d(\omega t) + \int_{\beta}^{\pi+\alpha} E d(\omega t) \right] \tag{6.54}$$

$$= \frac{V_m (\cos \alpha - \cos \beta) + (\pi + \alpha - \beta) E}{\pi}$$

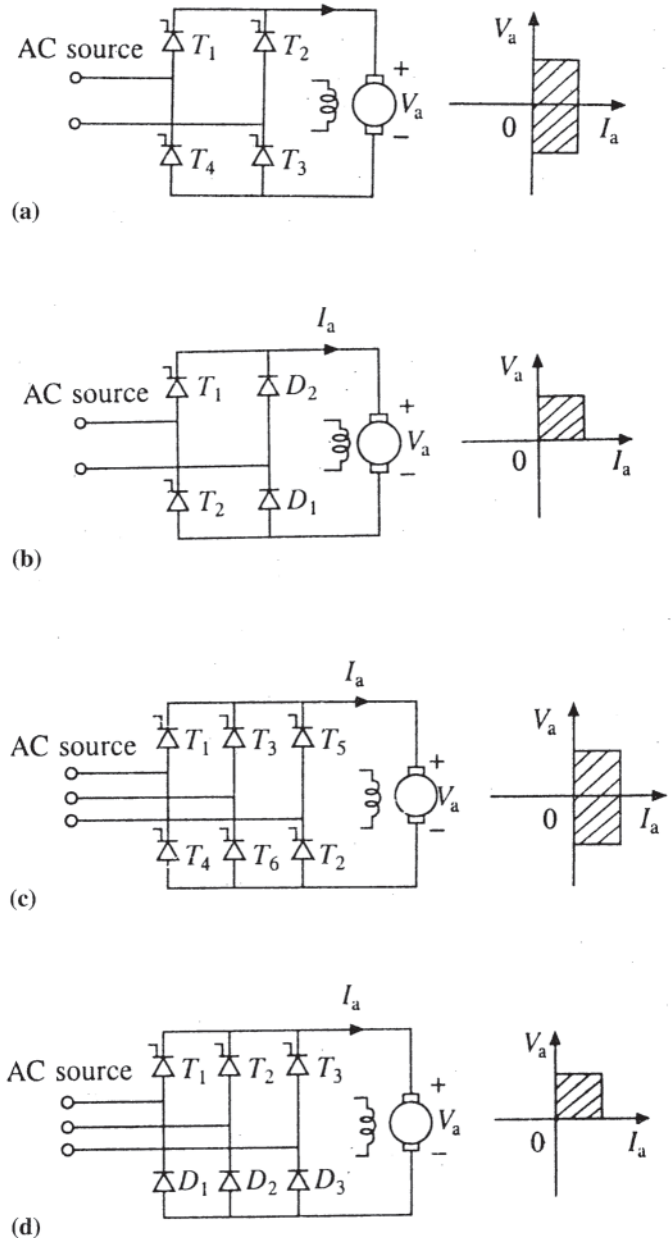


Figure 6.25 Single-phase and three-phase controlled rectifier circuits: (a) single-phase fully-controlled rectifier, (b) single-phase half-controlled rectifier, (c) three-phase fully-controlled rectifier, and (d) three-phase half-controlled rectifier.

where  $\beta$  is the angle at which current falls to zero.

$\beta$  is obtained from the following equation:

$$\frac{V_m}{Z} \sin(\beta - \phi) - \frac{E}{R_a} + \left[ \frac{E}{R_a} - \frac{V_m}{Z} \sin(\alpha - \phi) \right] e^{-(\beta - \alpha) \cot \phi} = 0 \tag{6.55}$$

where  $Z = \left[ R_a^2 + (\omega L_a)^2 \right]^{1/2}$  (6.56)

and

$$\phi = \tan^{-1} (\omega L_a / R_a) \tag{6.57}$$

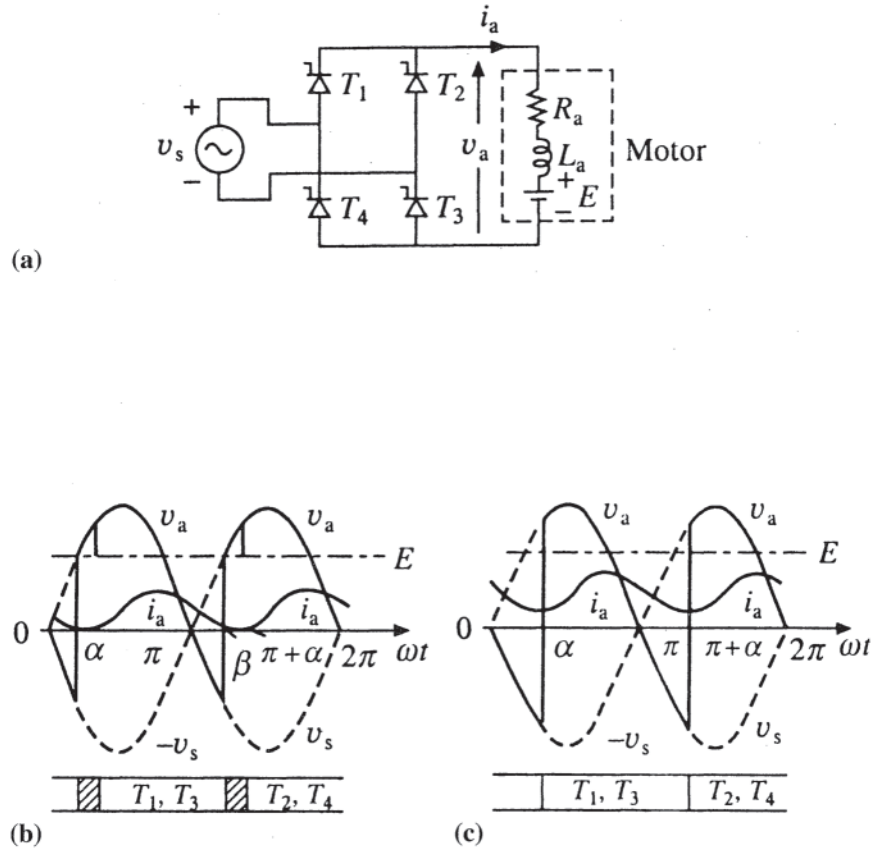


**Figure 6.26** Single-phase fully-controlled rectifier fed dc separately excited motor: (a) rectifier motor circuit, (b) waveforms in discontinuous conduction, and (c) waveform in continuous conduction.

The nature of speed-torque curves is shown in Fig. 6.27. The motor mostly operates in discontinuous conduction mode where speed regulation is poor. In continuous conduction mode the curves are similar to those obtained when the motor is fed from a perfect dc source (source with zero harmonic content).

For the rectifier of Fig. 6.25(b) the dc component of motor terminal voltage is given by:

$$V_a = \frac{V_m}{\pi} (1 + \cos \alpha) \tag{6.58}$$

when conduction is continuous, and by:

$$V_a = \frac{1}{\pi} \left[ \int_{\alpha}^{\pi} V_m \sin \omega t d(\omega t) + \int_{\beta}^{\pi+\alpha} E d(\omega t) \right] = \frac{V_m (1 + \cos \alpha) + (\pi + \alpha - \beta)E}{\pi} \tag{6.59}$$

when conduction is discontinuous,  $\beta$  is obtained from the following equation:

$$e^{\beta \cot \phi} = \frac{R_a V_m}{Z E} \left[ \sin \phi e^{\pi \cot \phi} - \sin (\alpha - \phi) e^{\alpha \cot \phi} \right] + e^{\alpha \cot \phi} \tag{6.60}$$

where  $\phi$  and  $Z$  are given by Eqs. 6.56 and 6.57.

The nature of speed torque curves is shown in Fig. 6.28. The motor operates in quadrant I only and predominantly in discontinuous conduction, where speed regulation is poor.

When supplied by three-phase rectifiers of Fig. 6.25(c) and (d), the motor operates mostly in continuous conduction.

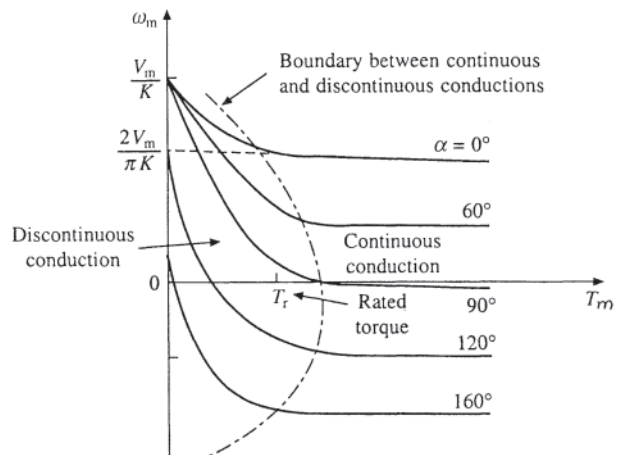


**Figure 6.27** Speed-torque curves of single-phase fully controlled rectifier fed separately excited motor.

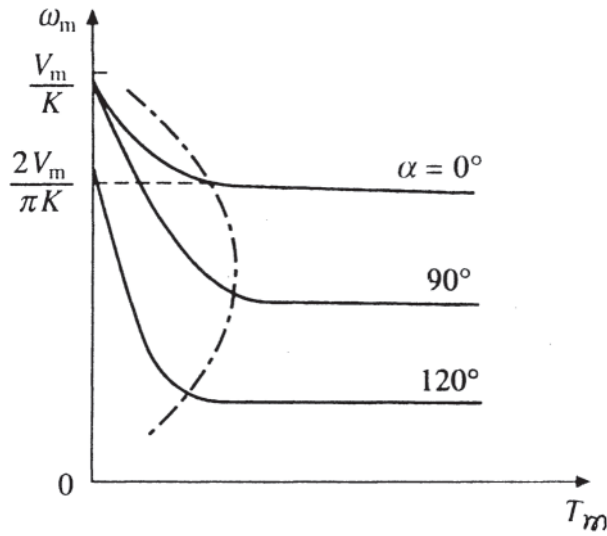


**Figure 6.28** Speed-torque curves of single-phase half-controlled rectifier fed separately excited motor.

Therefore speed-torque curves are similar to those obtained when fed from a perfect dc source. The nature of waveforms of motor terminal voltage and armature current of separately excited motor fed from the six-pulse rectifier of Fig. 6.25(c) is shown in Fig. 6.29. The dc component of the terminal voltage is given by:

$$V_a = \frac{3\sqrt{3}}{\pi} V_m \cos \alpha \tag{6.61}$$

where  $V_m$  is the peak value of phase voltage of ac source.

The nature of speed-torque curves is shown in Fig. 6.30. The discontinuous conduction has been ignored as it occurs in a narrow region for low torques. The speed-torque characteristics are similar to those obtained when fed from a perfect dc source. The motor operates in quadrants I and IV. The three-pulse rectifier of Fig. 6.25(d) operates in quadrant I only and has speed torque characteristics similar to those of Fig. 6.30 but confined to quadrant I only. The average motor terminal voltage is given by:

$$V_a = \frac{3\sqrt{3}V_m}{2\pi} (1 + \cos \alpha) \tag{6.62}$$

The one-phase rectifiers are generally used for motors of low power ratings (10 kW or less). For higher ratings three-phase rectifiers are used. Exception is made in traction where one-phase rectifiers are used in high power ratings.

The performance of a rectifier-fed dc motor is significantly different from a dc motor fed from a perfect dc source (source with no harmonics in the output voltage). Two major differences are the presence of discontinuous conduction and the ripple in armature current [3, 4]. Discontinuous conduction has three adverse effects on motor performance: (i) Poor speed regulation as shown in Fig. 6.27. When used in closed-loop variable speed applications it become difficult to achieve

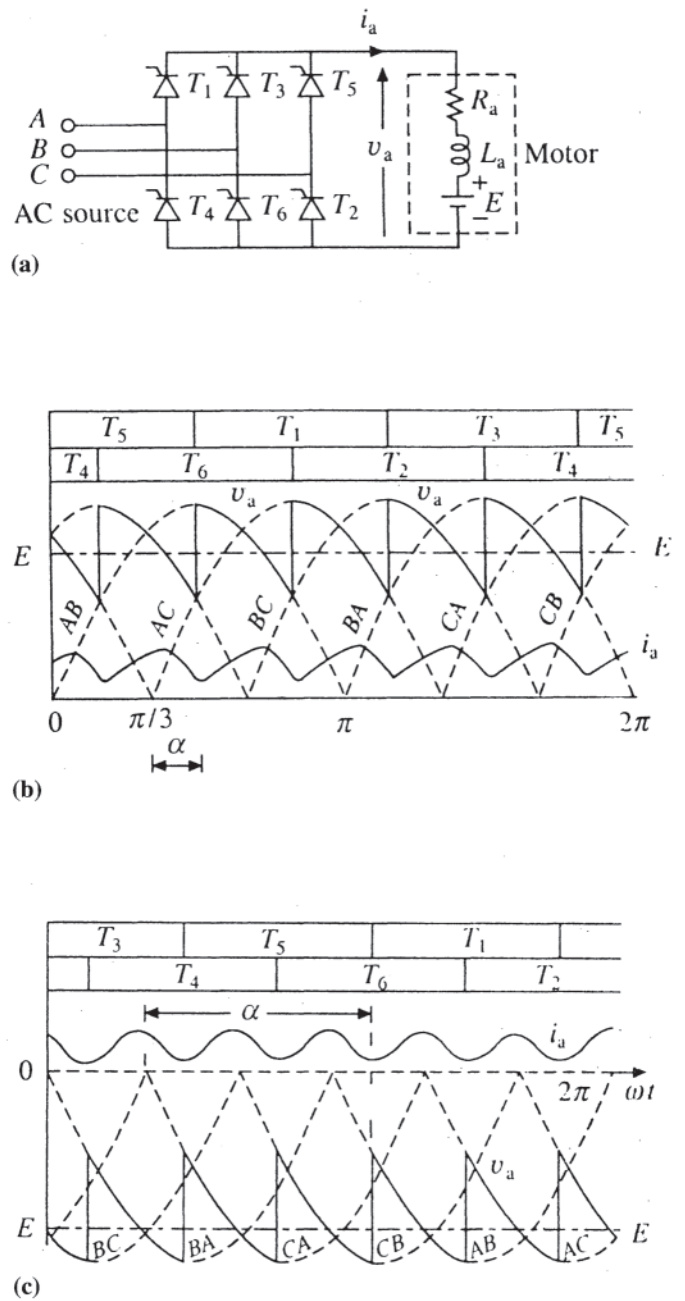


**Figure 6.29** Three-phase fully-controlled rectifier fed separately excited motor: (a) rectifier motor circuit, (b) waveforms for motoring operation with  $\alpha=30^\circ$ , and (c) waveforms for regenerative braking operation with  $\alpha$  nearly  $140^\circ$ .

good steady state accuracy (ii) Discontinuous conduction increases the peak value of current for a given average value. The sparking between commutator and brushes occurs even when the average current is small compared to rated motor current. The ripple is armature current  $\Delta I_a$  is defined as:

$$\Delta I_a = \frac{i_{amax} - i_{amin}}{2} \tag{6.63}$$

where  $i_{amax}$  and  $i_{amin}$  are maximum and minimum instantaneous

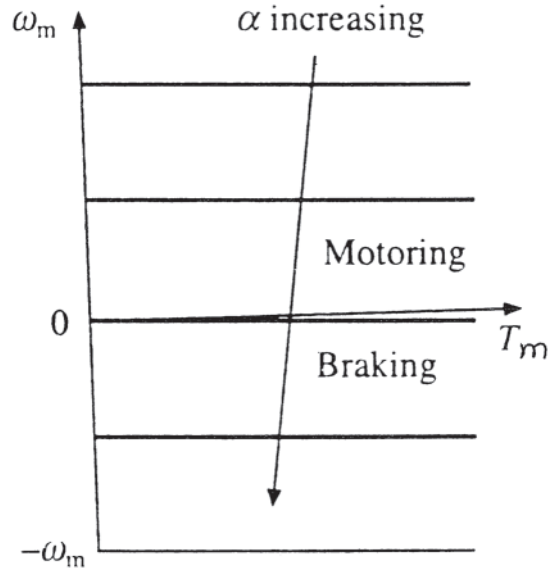


**Figure 6.30** Speed-torque curves of separately excited motor fed from three-phase fully-controlled rectifier, neglecting discontinuous conduction.

values of armature current. When conduction is continuous, an approximate value of ripple can be calculated by the following equation:

$$\Delta i_a = \sqrt{2} \frac{V_{nd}}{pX} \quad (6.64)$$

where  $V_{nd}$  = the rms value of dominating harmonic component in the rectifier output voltage,  $p$  = rectifier pulse number and  $X$  = reactance of motor armature inductance at ac source frequency. The denominator in Eq. 6.64 is the armature circuit reactance at dominant harmonic frequency.

Because of ripple, the mis and peak values of armature current have higher values than its average value. While the torque is contributed by the average value, the armature copper loss depends on rms value and the ability of the motor to commutate current without sparking between brushes and commutator depends on the peak value of current. When fed from a perfect dc source, the average, rms and peak values are same. Because of increase in rms value of armature current and because of increase in armature circuit resistance caused by skin effect because of presence of harmonics the copper loss is substantially increased. The core loss is also increased because of the harmonics in the input voltage. Because of higher peak value and because of pulsating interpole flux, the armature current that the motor can commutate without sparking at the brushes has lower average value than the rated motor current. Often a motor with a laminated yoke is used to improve the motor commutation capability. Even then the current that the motor can carry without sparking has a lower value than the rated current. The increase in losses and reduction in the value of the current the motor can carry without sparking, substantially derates the motor. The increase in rectifier pulse number reduces the ripple (Eq. 6.64), because with increase in pulse number  $V_{nd}$  reduces but  $pX$  increases. The large rating motors are often fed by 12-pulse rectifiers

that are obtained by connecting two 6-pulse rectifiers in parallel on dc side and feeding them from Y-Y and Y- $\Delta$  connected transformers connected to common ac supply.

The ripple in armature current can be reduced and boundary between continuous and discontinuous conduction can be shifted to the left (Figs. 6.27 and 6.28) by increasing the armature circuit inductance by connecting an external inductance in series with the armature. This is rarely done because of increase in cost, weight, and volume, and as a result of adverse effect on the dynamic response due to increase in electrical time constant of the motor.

Other problems associated with rectifier supplies is that their ac source current has harmonics and they operate at low power factor at low output voltages. This has adverse effect on power quality. When the rating is large, provision is made to counter these adverse effects either by using different rectifier circuits or by installing harmonic filters and VAR compensators.

In spite of the abovementioned limitations dc motor fed from rectifier source has wide acceptance because of the advantages of (i) high efficiency, (ii) fast dynamic response, and (iii) flexible control.

#### 6.7.4 Chopper Sources [3]

The dc motors supplied from choppers have applications in servos, battery-powered vehicles such as forklift trucks, trolleys, cars and buses, and traction consisting of electric buses, underground transit, and suburban and mainline trains. Choppers have several advantages such as high efficiency, control flexibility, lightweight, small size, quick response, and regenerative braking down to low speed.

A dc separately excited motor supplied from a step-down chopper also known as buck converter, is shown in Fig. 6.31 (a). The motor is shown by its equivalent circuit. The switch  $S$  is a self-commutated semiconductor switch. A semiconductor switch is called self-commutated if it can be turned on and turned off by its control signal  $I_c$ . The switch is operated periodically with a period  $T$  and remains on for a duration  $t_{on}$ . The motor terminal voltage and armature current waveforms are shown in Fig. 6.31 (b). When the switch is closed, motor terminal voltage is  $V_d$  and armature current rises from  $i_{a1}$  to  $i_{a2}$ . When the switch opened, armature current freewheels through diode  $D_F$  and terminal voltage becomes zero. During the off period the current drops from  $i_{a2}$  to  $i_{a1}$ . The dc component in the output voltage of the chopper is:

$$\begin{aligned} V_a &= \frac{1}{T} \int_0^{t_{on}} V_d dt \\ &= \frac{t_{on}}{T} V_d = \delta V_d \end{aligned} \quad (6.65)$$

$\delta$  is known as duty ratio or duty cycle of chopper. Equation 6.65 shows that the motor terminal voltage can be varied from 0 to source voltage  $V_d$  by varying  $\delta$  from 0 to 1. The average armature current is given by the following equation:

$$I_a = \frac{\delta V_d - E}{R_a} \quad (6.66)$$



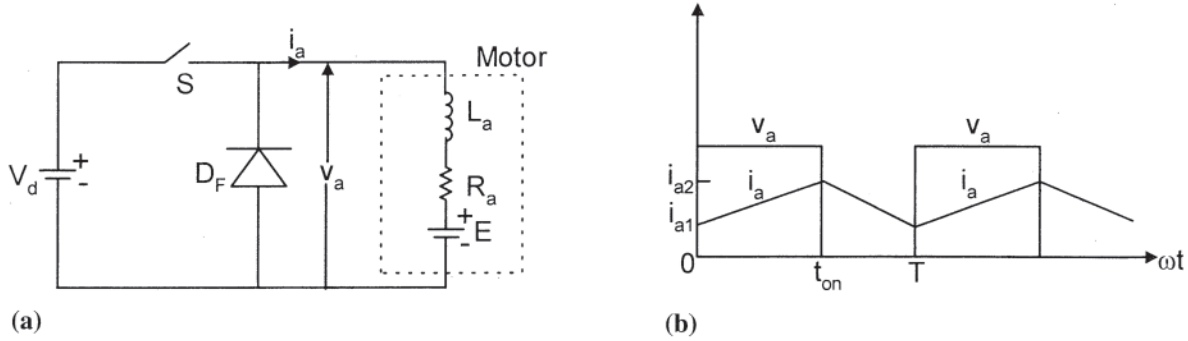


Figure 6.31 Step-down chopper control of separately excited motor: (a) chopper motor circuit and (b) waveforms.

Noting that the maximum value of armature current occurs at the end of an on period and the minimum value occurs at the end of the cycle, the following expression is obtained for the current ripple:

$$\Delta i_a = \frac{V_d}{2R_a} \left[ \frac{1 + e^{T/\tau_a} - e^{\delta T/\tau_a} - e^{-(1-\delta)T/\tau_a}}{e^{T/\tau_a} - 1} \right] \quad (6.67)$$

The maximum value of ripple occurs at  $\delta=0.5$  and is given by:

$$\Delta i_{am} = \frac{V_d}{2R_a} \left[ \frac{e^{0.5T/\tau_a} - 1}{e^{0.5T/\tau_a} + 1} \right] \quad (6.68)$$

For low-power and low-voltage applications MOSFET switch is used, for medium voltage and medium power applications insulated gate bipolar transistor (IGBT) is used, and for high-voltage and high-power applications gate turn-off (GTO) is used. MOSFET and IGBT operate at sufficiently large frequency to restrict the discontinuous conduction to such a narrow region that it can be neglected. Although high-power GTO operates at low frequency (200 to 500 Hz), but because of large armature inductance of high-power dc motors, discontinuous conduction is restricted to a narrow region, and therefore, can be ignored. The problem associated with discontinuous conduction, i.e., poor speed regulation, is not present in chopper-fed dc motor. This is an important

advantage for servo applications. Because of high frequency of the dominant harmonics in the output voltage of choppers using MOSFET and IGBT, the ripple in armature current is low. Because the high-power dc motor has high armature inductance, armature current ripple is also low with GTO chopper. Because of low ripple in armature current with chopper control, compared to rectifier control, the derating of motor is significantly lower.

The most important advantage of chopper control is the regenerative braking down to very low speed. With regenerative braking, energy saving from 15–30% has been reported in traction applications. In battery driven vehicles, the energy saving increases the distance the vehicle can travel before battery gets discharged. In regenerative braking the motor works as a generator. At speeds below the rated speed, the induced electromotive force (emf) will have a value lower than the source voltage, which is fixed. For regenerative braking energy must be supplied from the induced emf to the dc source at a higher voltage. This is achieved by connecting a step-up chopper between the motor and the source as shown in Fig. 6.32(a). The self-commutated switch  $S$  is operated periodically with a period  $T$ . It remains on for a period  $(1-\delta)T$  and remains off for a period  $\delta T$ , where  $\delta$  is the duty cycle of the switch and given by:

$$\delta = \frac{\text{Period for which motor is connected to source}}{T} \quad (6.69)$$

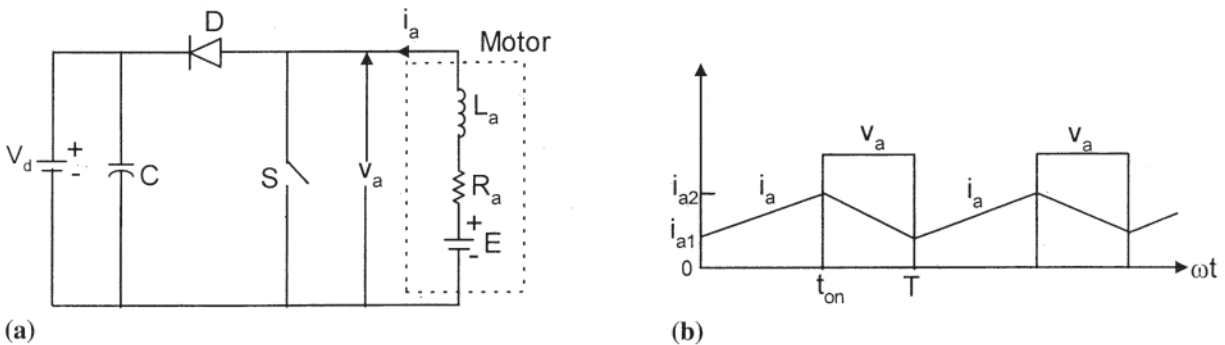


Figure 6.32 Regenerative braking of separately excited motor with step-up chopper control: (a) chopper motor circuit and (b) waveforms.

When the switch is closed, the energy supplied by the motor working as generator is stored in the inductance  $L_a$  and armature current increases. When the switch is opened, the inductance transfers the current to the path consisting of armature, diode  $D$  and the source. During the off period, energy supplied by the back emf and energy stored in the inductance is supplied to the source and armature current decreases. The waveforms are shown in Fig. 6.32(b). The average motor terminal voltage:

$$V_a = \frac{1}{T} \int_{t_{\text{on}}}^T V_d dt = \delta V_d \quad (6.70)$$

and

$$I_a = \frac{E - \delta V_d}{R_a} \quad (6.71a)$$

Since  $I_a$  has reversed, motor torque is negative and power flows from the motor to the source giving regenerative braking.

The chopper used for motoring is a step-down chopper (also commonly known as buck converter) and the chopper used for regenerative braking is a step-up chopper (also commonly known as boost converter). These two choppers are combined in the two-quadrant chopper of Fig. 6.33(a). In this chopper switch  $S_1$  and diode  $D_1$  constitute the step-down chopper and switch  $S_2$  and diode  $D_2$  form step-up chopper. They can be operated separately. They can also be operated simultaneously by applying control signal to  $S_1$  from 0 to  $\delta T$  and to  $S_2$  from  $\delta T$  to  $T$ . The motor terminal voltage waveform will then be as shown in Fig. 6.33(b). Now:

$$I_a = \frac{\delta V_d - E}{R_a} \quad (6.71b)$$

Motoring operation is obtained when  $\delta V_d > E$  and regenerative braking operation is obtained when  $\delta V_d < E$ . The  $\delta$  can be set to obtain motoring or braking operation. The speed-torque curves are shown in Fig. 6.34. A four-quadrant chopper for servo-motor control is obtained by connecting 2 two-quadrant choppers in antiparallel.

The value of  $T_d$  can be made smaller by increasing inductance  $L_a$  or by increasing chopper frequency. For the two-quadrant type of chopper, current is continuous at any value of torque [2].

## 6.8 PERMANENT MAGNET DC MOTORS

### 6.8.1 Magnetic Materials

Although magnetic materials are generally assumed to contain iron, it was already known in the nineteenth century that alloys containing copper, silver, gold, and zinc made superior permanent magnets. With the advent early in this century of the Alnico magnets (alloys containing aluminum, copper, iron, nickel, and cobalt), it became possible to replace the electromagnetic field of the dc motor with a permanent-magnet field. Although permanent-magnet motors do not have the advantage of field strength control for speed adjustment, they have a simpler design than the wound-field motor, and they are lighter and more efficient, having no copper losses in the field winding.

Compared with ferrous magnetic materials, the Alnicos have high flux densities (thus producing high output torques) and high coercive force (thus resisting demagnetization from the effects of armature reaction). The first Alnico magnets were isotropic; that is, they had the same properties in every direction. Later developments produced anisotropic characteristics, providing superior magnetic properties along one axis. Motor performance could therefore be enhanced by using this type of magnet configured so that the flux path coincides with the preferred axis. Anisotropic characteristics are also available in the higher-performance materials discussed below.

With the development of ceramic magnets (barium ferrite and strontium ferrite), lower cost motors could be produced, although output torque was sacrificed due to their lower flux densities. However, the ceramic magnets have much higher coercive forces than the Alnicos, and are thus better able to resist demagnetization due to armature reaction. This in turn allows high intermittent loads to be applied without permanent degradation of motor performance.

As a design type, ceramic magnet motors constitute one of the highest-volume motors produced in the world today. Their range of sophistication runs from functional toys to actuators in space environments. Their simple design and lowcost magnet material combine to make them very cost effective. Because ceramic magnets have the same permeability as air, the motors can be disassembled without the magnets being demagnetized. These magnets provide a flux level substantially higher than that of electromagnetic fields in motor structures of comparable physical size.

Within the past 20 years, other magnetic materials have been developed for high-performance motors. Rare-earth magnets, which are usually samarium-cobalt alloys, are still among the highest-performing magnet materials. The most recent developments are the neodymium-iron-boron alloys. Magnetic performance of these alloys is about 30% better than that of samarium-cobalt magnets. See Table 2.4, page 69.

In addition to the magnetic performance of these materials, temperature limits and corrosion effects must be considered. The effect of temperature is discussed in Section 2.3.9. Corrosion resistance of neodymium alloys is poor, but magnet producers have developed protective coatings to overcome this deficiency.

Magnet materials are characterized by three parameters:

Residual induction,  $B_r$  (gauss)

Coercive force,  $H_c$  (oersteds)

Maximum energy product,  $(BH)_{\text{max}}$  (megagauss-oersteds)

$B_r$  is the intercept of the plot of induction versus magnetizing force with the  $B$  axis on the descending (demagnetization) branch of the hysteresis loop.  $H_c$  is the intercept of that branch with the  $H$  axis. The plot of the product of  $B$  and  $H$  along the demagnetization branch is known as the energy product curve; the maximum value of this product is  $(BH)_{\text{max}}$ . (Reference 5 gives examples.) The units used for the magnetic quantities are those used by many engineers who work with permanent magnets.

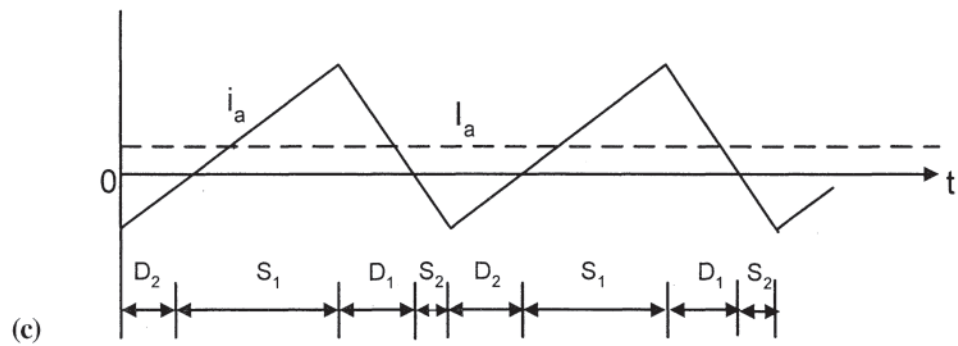
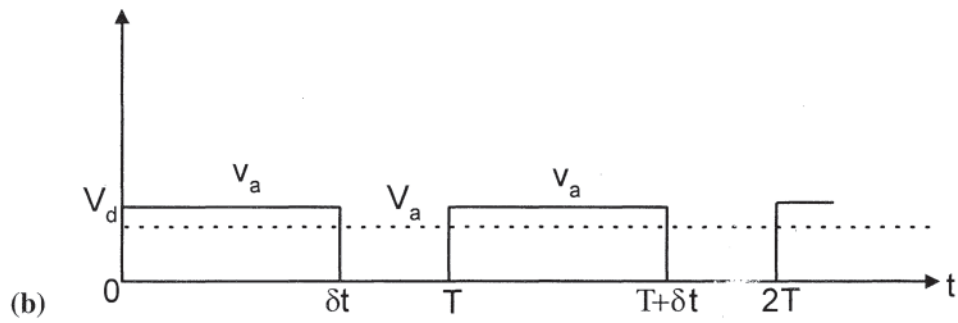
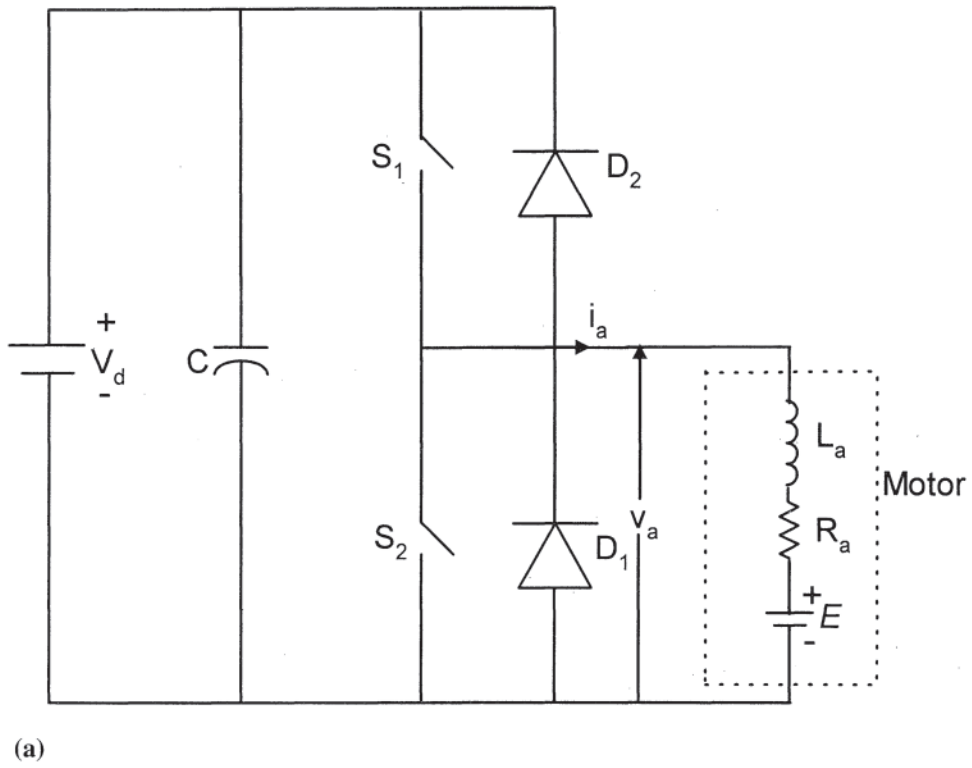


**Figure 6.33** Two-quadrant chopper fed separately excited motor: (a) two-quadrant chopper and motor, (b) armature terminal voltage, and (c) armature current.

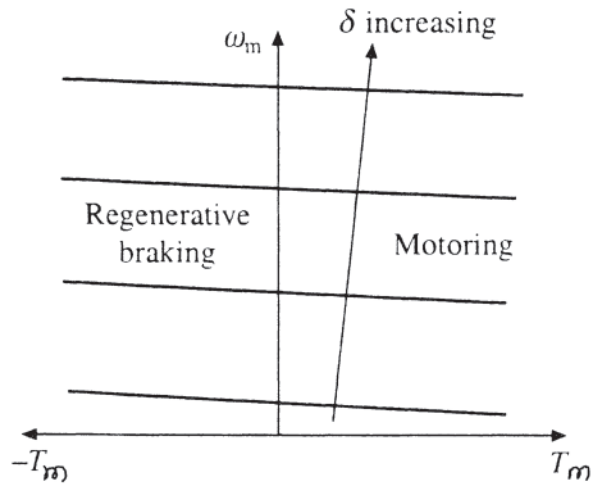


**Figure 6.34** Speed torque curves of motoring and regenerative braking operations of two-quadrant chopper fed separately excited motor.

### 6.8.2 Design Features

Because of the space required for the field structure of a wound-field motor, the outside diameter of the motor is usually approximately twice that of the armature. If ceramic or rare-earth magnets are used in a permanent magnet motor, the high coercive force allows the magnet to be relatively thin. Hence the outside diameter of the motor can be considerably smaller than that of a comparable wound-field motor, and there will be an accompanying weight reduction.

When anisotropic magnets are used, the preferred axis is oriented radially to coincide with the radial flux path. The return flux path is provided by a magnetic steel shell which forms the motor housing. The magnet segments are usually secured to the inside diameter of the housing with an adhesive.

#### 6.8.2.1 Magnetic Circuit Considerations

Because the magnetic flux is supplied by a permanent magnet, the magnetic circuit analysis is similar to that presented in Section 15.3 for brushless dc motors. Of course, the motor is inside-out and the equations must be modified where necessary. This section presents the basic elements of magnetic circuit analysis and torque and voltage equations. The magnetic properties are characterized by a  $B-H$  curve showing the basic demagnetization properties of the material independent of the magnetic circuit in which it will be used. This  $B-H$  curve is a second-quadrant plot of magnet flux density ( $B$ ) vs. mmf per unit length ( $H$ ). Figure 6.35 shows a  $B-H$  plot for several magnet material types. The curves show only gross characteristics for each magnet family, and not for a specific member of the family. The units used on the two axes are teslas (webers per square meter) for flux density and kiloampere-turns per meter for flux density and kiloampere-turns per meter for magneto-motive force per unit length.

##### 6.8.2.1.1 Magnet Flux-mmf Curves

While a magnet material  $B-H$  curve is a second-quadrant plot of the intrinsic magnet material properties of flux density and

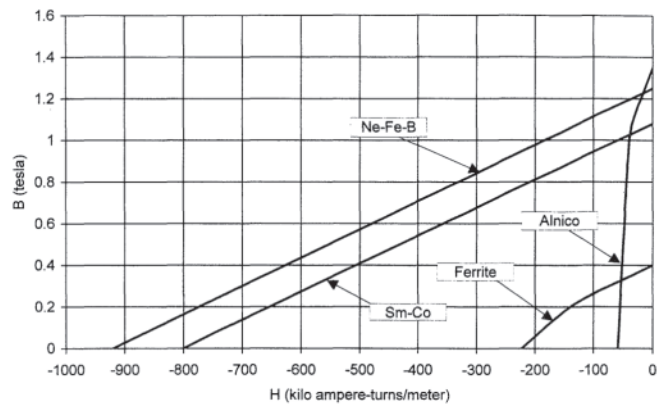


**Figure 6.35** Typical  $B-H$  Curves for four magnet material types.

ampere-turns per unit length, the actual magnet capability for a given configuration is represented by a second-quadrant plot of the magnet flux vs. magnet ampere-turns. The magnet flux is obtained by multiplying flux density  $B$  by magnet area, and the magnet ampere-turns obtained by multiplying magnetizing force  $H$  by the magnet length.

Magnet flux and mmf are given by:

$$\Phi_m = B A_m = \text{magnet total flux per pole in webers} \quad (6.72)$$

$$\mathcal{F}_m = H t_m = \text{magnet total mmf in ampere-turns} \quad (6.73)$$

where:

- $B$  = magnet flux density in tesla
- $A_m$  = magnet area per pole in square meters
- $H$  = magnet strength in ampere-turns per meter
- $t_m$  = magnet radial thickness in meters

The complete magnetic circuit comprises magnet, air gap, magnetic steel, and stator winding mmf. The effect on the magnet operation is shown in Fig. 6.36 with a samariumcobalt magnet an approximate thickness of 0.01 m and approximately 0.1 m<sup>2</sup> area. The vertical axis shows the magnetic flux and the horizontal axis shows the ampere-turns available to force the magnetic flux through the magnetic circuit. A load line drawn

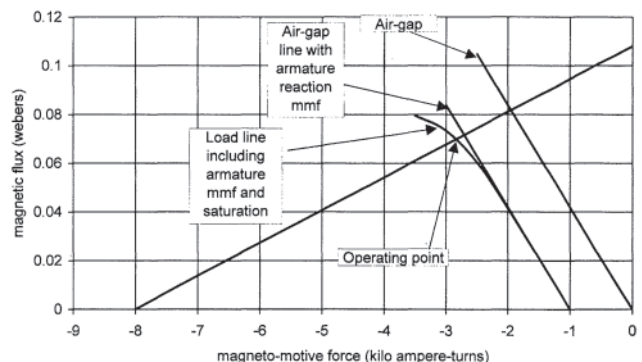


**Figure 6.36** Load lines superimposed on magnet characteristics for permanent magnet direct current (dc) motor.

from the origin represents the magnetic circuit without any iron saturation or demagnetizing ampere-turns due to stator winding mmf. The intersection of the load line with the magnet curve defines the no-load operating point of a given magnet in terms of magnet total flux and ampere-turns. This load line is also the air-gap line, because it represents the mmf consumed by the air gap for the given flux density (and is of course linear.)

The air-gap or load line mmf is:

$$\mathcal{F}_g = L_{ge} B_{gm} / \mu_0 = \text{air gap mmf in ampere-turns} \quad (6.74)$$

where:

$B_{gm}$  = maximum air gap flux density in tesla

$L_{ge}$  = air gap effective radial length in meters

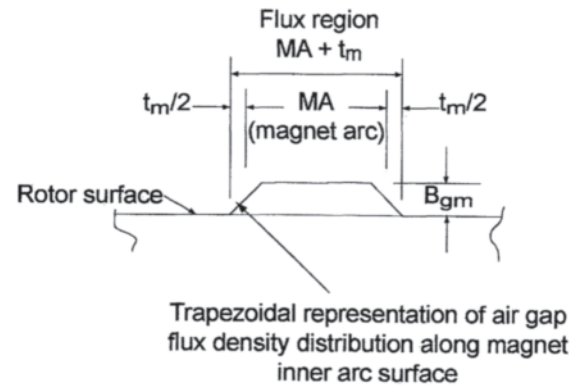
$\mu_0 = 4 \pi 10^{-7}$  = permeability of air in webers per amp-m

An additional load line parallel to the first load line represents the addition of demagnetizing armature reaction ampere turns. A curve diverging away from the straight line represents magnetic saturation of the iron circuit (mostly in the stator lamination core and teeth) as shown in Fig. 6.36. The resultant operating point is shown as the intersection of the load line and the magnet characteristic.

#### 6.8.2.1.2 Magnet Shape and Flux Density Distribution

The air gap flux is the flux that crosses the air gap and interacts with the armature winding to produce a generated voltage or back-emf in the armature winding. The magnet leakage flux is that which does not cross the air gap, but travels peripherally to the adjacent magnets, and also back to the frame. The portion of the magnet adjacent to the interpolar space will produce leakage flux, and actually be on a different demagnetization curve than the total average magnet curve shown in Fig. 6.36. To determine the exact shape of the air gap flux density distribution, a detailed flux plot performed by hand or preferably from a finite-element magnetic field analysis computer program, should be used. A computer analysis that uses the finite-element method (FEM) can include the effects of saturation and armature reaction demagnetization on the magnet operating point for each load condition and rotor position relative to the current-carrying armature windings.

A simplified method to determine the no-load radial air gap magnetic flux, for an initial design effort, is to assume that the radial air gap flux density distribution is trapezoidal along the periphery, with the total radial air gap flux being the area under the trapezoid as shown in Fig. 6.37. Because there is tangential space between adjacent magnets along the frame to allow for a region in the air gap for proper coil commutation, an assumption can be made that the radial magnetic flux density distribution has a zero value for some distance along the armature periphery. A further assumption is that the radial air gap flux density goes to zero in approximately one half a magnet thickness away from the magnet tip. The magnet total flux is the sum of the radial gap flux and the leakage flux. The trapezoid of flux density starts



Four-pole dc motor frame and magnets

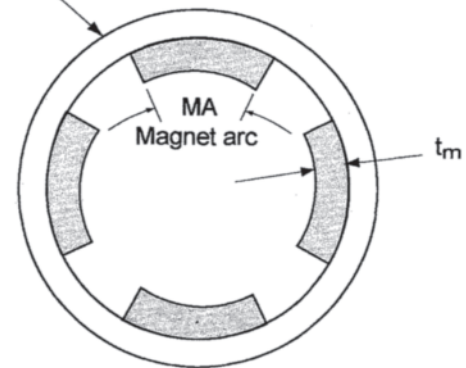


**Figure 6.37** Trapezoidal air-gap flux density distribution for permanent magnet direct current (dc) motor analysis.

with a zero value at one half magnet thickness away from the pole tip and rises to a maximum at one half the magnet thickness from the corner of the magnet. The maximum value of air gap flux density is constant along the trapezoid and equal to the value obtained from solving Eq. 6.74 for  $B_{gm}$ .

$$B_{gm} = \mu_0 \mathcal{F}_g / L_{ge} \quad (6.75)$$

where:

$L_{ge}$  equals the effective radial air gap taking into consideration the armature slotting

The solution of this will require iteration to determine the intersection of the air gap line with the actual magnet demagnetization curve. This iteration can be performed by graphically plotting a point on the magnet demagnetization curve and drawing a line from the origin. Remember that the leakage flux must be added to the air gap flux before plotting total magnet flux versus magnet mmf at the magnet average area (magnet axial length multiplied by tangential length at the magnet radial midpoint.)

After performing the integration of the trapezoidal flux density distribution over one pole pitch from Fig. 6.37, the air gap flux per pole is, approximately:

$$\Phi_g = B_{gm}(MA-t_m)(L_m+L_a)/2 + 2B_{gm}(t_m/2)(L_m+L_a)/2$$

that can be simplified to:

$$\Phi_g = B_{gm}MA(L_m+L_a)/2 \text{ webers} \quad (6.76)$$

where:

- $L_m$  = magnet axial length in meters
- $L_a$  = armature axial length in meters
- MA = magnet face arc length in meters
- $t_m$  = radial magnet thickness in meters

The magnet leakage flux is approximately the difference between the magnet flux at the magnet radial midpoint and the magnet flux at the magnet surface arc. Assuming that the magnet flux density at the radial midpoint is the same as the magnet face maximum, the total magnet flux is given by:

$$\Phi_m = L_m B_{gm} ((D_m + t_m)/D_m) MA \text{ in webers} \quad (6.77)$$

where:

- $D_m$  = the magnet face inside diameter

The leakage flux is then:

$$\Phi_l = \Phi_m - \Phi_g \text{ leakage flux per pole in webers} \quad (6.78)$$

The air gap load line crosses the magnet demagnetization characteristic where the mmfs are equal:

$$\mathcal{F}_g = \mathcal{F}_m \quad (6.79)$$

To solve for the point where the two mmfs are equal, the following procedure can be used:

1. Assume a value for  $B_{gm}$ .
2. Calculate  $\Phi_g$ ,  $\Phi_l$ , and  $\Phi_m$  from above Eqs. 6.76, 6.77, 6.78.
3. Calculate  $\mathcal{F}_g$  from Eq. 6.76.
4. Locate  $\Phi_m$  on the magnet curve.
5. If the corresponding value of  $\mathcal{F}_m$  is not equal to  $\mathcal{F}_g$  select a new value of  $B_{gm}$  and repeat steps 2 through 4 or go to step 6.
6. For a graphical solution, plot the point  $\mathcal{F}_g$ ,  $\Phi_m$  on the magnet mmf-flux plot and draw a straight line through the point from the origin.

Other approximations can be made to obtain a magnetic circuit solution for the permanent magnet dc motor. It is best to perform a detailed FEM analysis to obtain at least a verification of a particular approximating calculation such as the one presented above. Values of mmf for armature reaction and saturation effects can be calculated using procedures for conventional wound field dc machines presented in Section 6.5.3. The results are shown on Fig. 6.36 as a second curve due to the addition of armature reaction intersecting the magnet characteristic, and finally a third curve which includes saturation and defines the final operating point.

### 6.8.2.1.3 Voltage and Torque Calculations

The equations for generated armature voltage and torque for a permanent magnet dc motor are the same as for a

conventional dc motor in Eqs. 6.1 and 6.11 in Sections 6.1 and 6.4, respectively. The value of flux in these equations is replaced by  $\Phi_g$  from the analysis of the previous section. The equivalent circuit for a permanent magnet dc motor is the same as Fig. 6.15 except that there is no field winding branch.

### 6.8.2.2 Commutation Considerations

A permanent magnet dc motor has brushes for coil commutation, the same as a conventional wound-field dc motor. The analysis of Section 6.3.3.1 applies to permanent magnet dc motors except as noted in the following material.

As in conventional wound field dc motors, the bar-to-bar voltage should be limited to approximately 18V. This defines the minimum number of commutator segments for a given motor design as shown here:

$$V_{bav} = V_t \text{ POLES}/N_{seg} \text{ less than or equal to } 18 \text{ V.} \quad (6.80)$$

where:

- $N_{seg}$  = total number of commutator segments
- $V_t$  = motor terminal voltage

The commutation zone is defined as the distance, in slot pitches, that a coil will travel while undergoing commutation, and is given by:

$$C_z = (\text{SLOTS}/N_{seg})(B + F_\lambda + (N_{seg}/\text{SLOTS}) - (\text{CIRC}/\text{POLES})) \quad (6.81)$$

where:

- $B$  =  $BW N_{seg}/(\pi D_{comm})$  = brush overlap in commutator segments
- BW = brush width along the peripheral direction of the commutator surface in meters
- $D_{comm}$  = commutator diameter in meters
- $F_\lambda$  = absolute value of  $|(N_{seg}/\text{POLES}) - Y_c N_{seg}/\text{SLOTS}|$
- = the short pitch of coil in commutator segments
- $Y_c$  = coil pitch in slots

A term known as slots per neutral is defined as:

$$\text{SLPN} = ((\pi D_a/\text{POLES}) - \text{MA}) \text{SLOTS}/(\pi D_a) \text{ in slot pitches} \quad (6.82)$$

where:

- MA is the magnet arc peripheral length at the air gap in meters
- $D_a$  is the armature (rotor) diameter in meters
- POLES = the total number of stator magnet poles

In general, SLPN should be greater than the commutating zone,  $C_z$ , so the coil has a chance to finish reversing current direction in the interpolar space before coming under the influence of the next magnet pole. A term called the single clearance is used as a measure of the margin between SLPN and  $C_z$ . It is given by:

$$\text{SC} = (\text{SLPN} - C_z)(\pi D_a)/(2 \text{SLOTS}) \quad (6.83)$$

Reference 8 recommends the minimum SC for traction motors to be slightly greater than a tooth face width at the air gap, with further consideration given to increased commutation difficulty due to higher than normal air gap flux densities, higher than normal rotor speeds, larger air gap producing increased fringing flux at pole tips, and increased bar to bar voltage. In general, permanent magnet dc motors are not used for traction or other high-power applications due to the lack of control of the field strength. Also, in a permanent magnet dc motor, interpole and pole face windings are not present to aid in commutation, so the motor is designed to have much more commutation margin.

### 6.8.3 Servo and Control Motors

The performance characteristics of the permanent magnet motor make it ideal for use in servomechanisms and control systems. Because of the constant field flux and the lack of demagnetization of the field by armature reaction, the speed-torque characteristic of the permanent magnet motor tends to be linear. This allows the motor to be characterized by a linear transfer function, facilitating analysis of the system under dynamic conditions. See Section 6.6 and Ref. 6 for details of motor equations and transfer functions, and Ref. 1 for definitions of important terms.

#### 6.8.3.1 Peak Torque vs. Maximum Continuous Torque

*Peak torque* is the value of torque that the motor can deliver to the load on a repetitive basis without overheating the motor or demagnetizing the field magnets. It is usually less than the *stall torque rating*, since operating the motor at stall even for short periods of time will almost always result in damage to the motor. To test for stall torque, constant voltage is applied to the motor and torque is gradually increased to the point where speed is reduced to zero. Motors are seldom tested to this point because internal heating causes the point to move during the test.

Consider a typical motor whose terminal resistance is 1  $\Omega$ , having a thermal resistance of 8°C/W and operating at 24 V. The instantaneous input current at stall would be 576 W [(24)<sup>2</sup>/1.0]. The ultimate temperature rise of the winding would be 4608°C [576×8]. In approximately 51 seconds, the armature would reach a temperature of 155°C, and the armature resistance would have increased 50%. This change in resistance would result in a 33.3% decrease in armature current and a reduction in stall torque by the same percentage. A more thorough analysis would include the effect of the negative temperature coefficient of the magnet material, which would cause a further reduction in stall torque. Some authors have recommended that peak torque be limited to 4 to 5 times the maximum continuous torque, with a maximum duty cycle of 10%. (For this condition, it is assumed that the ON period of the peak current does not exceed 0.5 second.)

The motor in the example given above has a rated stall torque of 1.45 N-m and a rated maximum continuous torque of 0.17 N-m. Using the assumption above, the peak torque would be 0.68 to 0.85 N-m. Using the 0.68 N-m figure (four times maximum continuous torque), we find that the rms current is within the thermal limits of the motor at a 10% duty cycle:

Torque constant,  $K_t=0.061$  N-m/A

Armature current,  $I_a=0.68/0.061=11.14$  A

RMS current= $(11.14)^2 \times 0.1=3.52$  A

Armature resistance,  $R_a$  at 115°C=1.5  $\Omega$

Temperature rise at 3.52 A= $(3.52)^2 \times 1.5 \times 8=149^\circ\text{C}$ .

Based on these calculations, a peak torque of four times the maximum continuous torque would be acceptable, but at five times the motor would over-heat.

Although the motor is within thermal limits with this current, the resultant torque may be less than expected because of the negative temperature coefficient of the magnet material. See Section 2.3.9.2 for a calculation of this effect.

#### 6.8.3.2 Thermal Resistance

*Thermal resistance* is another parameter that is defined in Ref. 1. It is defined as “the opposition to the flow of heat in the materials of which the motor is constructed, expressed in degrees Celsius per watt. All measurements shall be taken under specified conditions.”

Testing for thermal resistance is done either at continuous stall or slow-speed load. Each of these test modes will result in a different value. At continuous stall, heat will build up in the armature in certain areas of the windings, resulting in hot spots. At slow speed under load, hot air is circulated around the magnets, which are poor thermal conductors if they are ceramic. This effect is less pronounced in electronically commutated (“brushless”) motors because the windings in those machines are generally located in the stator. On the other hand, it poses a more serious problem in ironless armature motors because the armature has only a high thermal resistance path to the ultimate heat sink.

Another factor that contributes to test errors is the method of mounting the motor for the test. Since each motor manufacturer employs its own (unique) test method, users must understand the conditions under which the tests were performed. For stall tests, a motor can be suspended by wires. For lowspeed tests on load, a very rigid mount may add to the thermal mass and improve heat transfer paths. This is important when comparing motors made by different manufacturers.

## 6.9 FINITE ELEMENT ANALYSIS OF DC MOTORS

### 6.9.1 Advantages of FEA of DC Motors

Finite element analysis (FEA), described theoretically in Section 1.5, can be very useful in the analysis and design of dc motors. In addition to finite element analysis of brushless dc motors described in Section 5.8.2, several other kinds of dc motors are analyzed here.

One advantage of FEA over other methods of analyzing dc motors is the inherent ability of the FEM to calculate accurately the armature reaction effects. High armature currents have significant effects on flux distribution and torque. Also, armature reaction in permanent magnet machines may permanently demagnetize the magnets. The finite element method can predict the current at which demagnetization occurs.

Another inherent advantage of FEA is its ability to calculate

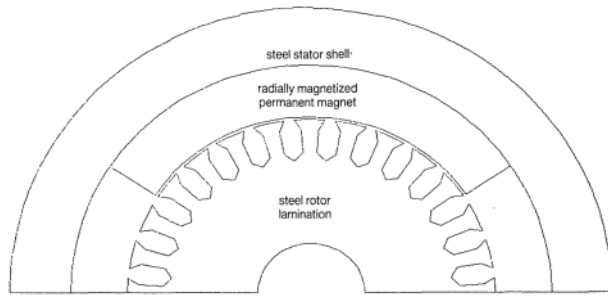


**Figure 6.38** One pole of a two-pole permanent-magnet brush-type direct current (dc) motor.

torque variation with position, called cogging torque. This advantage and others are mentioned in Section 5.8.2.

The following subsections describe FEA of three types of motors. The first subsection discusses FEA of the permanent magnet dc motor, and the next subsection describes how FEA aids the design of permanent magnet magnetizers. The final subsections describe FEA of wound-field motors, both dc and universal.

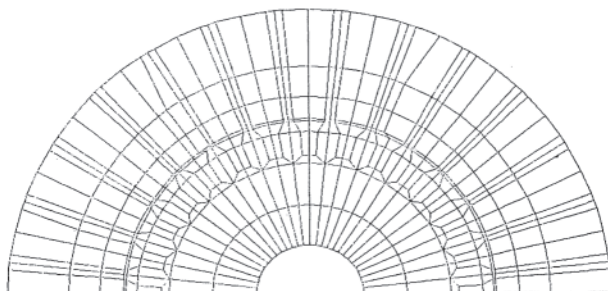
### 6.9.2 Permanent Magnet Brush DC Motors

Figure 6.38 shows a typical permanent magnet dc motor with brushes. The brushes (not shown) are required to feed dc current to the coils in the rotor.

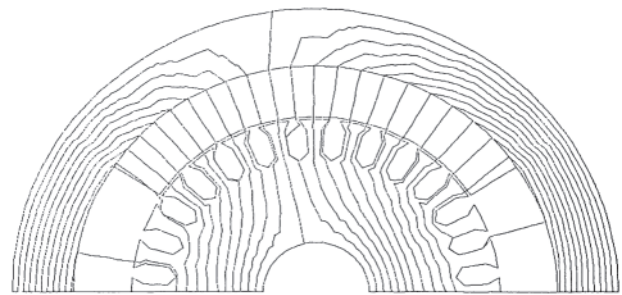
Figure 6.39 shows the finite element model developed for the motor. Periodic boundary conditions (see Section 1.5.4) are applied along the radial boundaries one pole pitch apart.

Figure 6.40 is a flux plot for a given current in the motor calculated by the program EMAS [9]. Armature reaction is seen because the flux density in the left half of the permanent magnet is greater (indicated by the closer spacing of the flux lines) than in the right half. The torque can be calculated for any rotor position by rotating the rotor slightly and dividing the change in coenergy by the change in angle, as described in Sections 1.5.6 and 4.10.3.2. Both average torque and cogging torque can be obtained as functions of rotor current. FEA has been used to investigate alternative designs of this type of dc motor and has helped achieve a 10-fold reduction in cogging torque of a particular motor [10].

Also of great interest is the speed-torque curve of the motor. The speed corresponding to the above average torque and current can be calculated using the familiar relation for dc machines:



**Figure 6.39** Finite element model for Fig. 6.38.



**Figure 6.40** Flux plot calculated for Fig. 6.38.

$$T\omega = E_b I \quad (6.84)$$

where  $T$  is torque (averaged over 360 degrees of rotation),  $\omega$  is rotational speed in radians per second,  $E_b$  is back-emf in volts, and  $I$  is the armature (rotor) current in amps. Now from Kirchhoff's voltage law:

$$E_s = E_b + IR \quad (6.85)$$

where  $E_s$  is the dc source voltage and  $R$  is the armature resistance. Substituting Eq. 6.85 in Eq. 6.84 gives:

$$\omega = (E_s - IR) / (I/T) \quad (6.86)$$

Hence Eq. 6.86 can be used with the finite element results for torque per ampere to obtain the speed—torque curve of the dc motor. The only inaccuracy in the above derivation is due to the fact that Eq. 6.84 neglects the effects of core loss and stray losses, which may be significant at extremely high motor speeds.

### 6.9.3 Magnetization of Permanent Magnets

The manufacturer of today's permanent magnet motors, including certain dc and synchronous motors, must usually magnetize the permanent magnets. Most permanent-magnet suppliers no longer magnetize their magnets. The permanent magnets of today are too powerful to be shipped after magnetization and before insertion in the motors; the shipper would complain that the magnet packages were attracted to steel surfaces.

The magnetization of permanent magnets is not necessarily an easy task. Because today's magnets are more powerful than ever, the magnetization ampere-turns required are larger than ever. Such large ampere-turns can be obtained only by supplying a large current to a magnetization winding that has many turns. To avoid burning up the winding, the large current must exist for only a few milliseconds, and thus it is usually supplied by discharge of a large capacitor. To obtain a high magnetic flux density  $B$  in the permanent magnet material, the magnetization winding is placed on a steel magnetizing fixture. The fixture can be specially made or can be the motor itself, with the magnetization winding consisting of one or more of the motor windings. The advantage of using the motor itself as a fixture is that the permanent magnets need not be moved after magnetization, which can be a dangerous process because of the possibility of pinching of fingers due to the powerful attractive forces of these powerful magnets.



FEA of the magnetization process can be very helpful in designing a magnetizer. Hand calculations are often practically useless, because today's magnets require such large values of  $B$  that the steel fixture is often saturated. Also, the current supplied by the capacitive-discharge system is influenced by the geometry and materials of the magnetizing fixture and winding. Finally, today's magnet materials, especially Alnico, samarium-cobalt, and neodymium-iron, have high conductivities. The high magnet and fixture conductivities can allow high eddy currents that oppose the pulsed current of the discharging capacitor and reduce the peak  $B$  in the permanent magnet.

The type of finite element analysis required to analyze a magnetizer is therefore nonlinear transient analysis, for such analysis includes the effects of saturation and eddy currents. In addition, however, the finite element model must include the capacitive discharge electric circuit. Zero-dimensional finite elements are required to model the circuit and its interaction with the two-dimensional or three-dimensional finite element model of the magnetizing fixture. In addition, one-dimensional finite elements are required to represent the multiterm winding on the fixture. Finite element software is available commercially that can analyze fixtures for magnetizing permanent magnets in motors and other apparatus [11].

#### 6.9.4 Wound-Field Brush DC Motors

There are two ways to use finite elements to analyze dc motors with brushes and wound fields without permanent magnets. As explained previously in Sections 1.5.8 and 1.5.9, one can either use magnetostatic FEA to compute parameters of equivalent circuits, or one can use time-stepping finite element software to directly compute time-varying motor performance.

Parametric magnetostatic finite element analysis has been used in conjunction with classical motor equations to analyze wound-field DC motors. Equation 6.85 is used along with Eq. 6.86 in which  $R$  must include both armature and field resistance for series DC motors. A series dc motor has been analyzed in this manner using Maxwell parametric finite element software [12].

Figure 6.41 shows the geometry of the series dc motor analyzed [12]. Figure 6.42 shows one of its typical computed flux plots. A total of 108 magnetostatic analyses were made over a range of winding current and rotor position. Figure 6.43 shows the computed speed-torque curves for several different values of applied dc voltage. Note that the computed curves agree closely with the measured curves.

The other way to analyze dc motors is to use timestepping FEA [13]. As explained in Section 1.5.9, time-stepping FEA involves dynamic rather than static FEA. The dynamic approach for the same dc motor of Fig. 6.41 can involve specifying speed vs time as shown in Fig. 6.44(a). The resulting torque and current vs. time are shown in Fig. 6.44(b) and 6.44(c), and show torque and current ripples due to commutation and cogging. Using the time-average torques and currents, the steady-state performance curves of Fig. 6.45

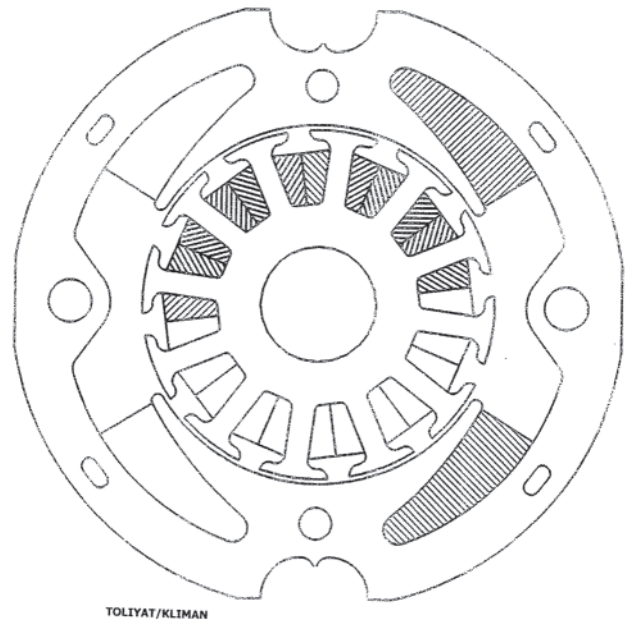


**Figure 6.41** Geometry of series motor to be analyzed, first as a direct current (dc) motor and later as a universal motor.

are plotted. Note the extremely good agreement with measured curves of both current and torque versus speed.

#### 6.9.5 Universal Motors

As mentioned in Section 6.9.1, the geometry of universal motors can be identical to that of wound-field dc motors, such as the one shown in Fig. 6.41. The field and armature windings must be connected in series in order for the motor to produce useful torque when energized by ac, in which case it is called a universal motor.

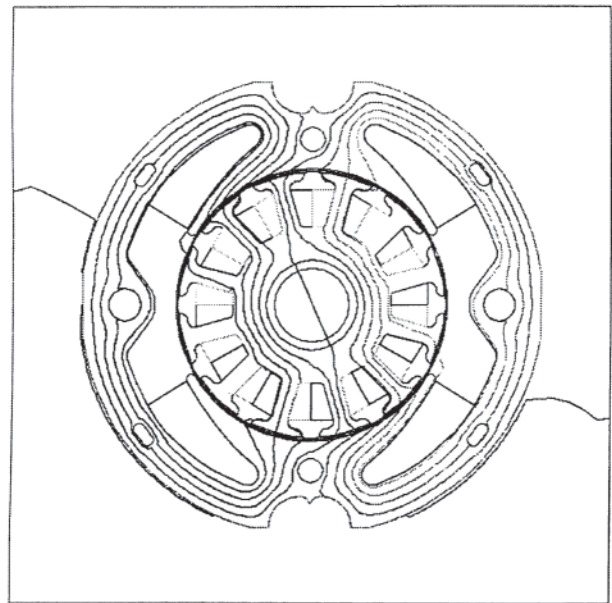


**Figure 6.42** Typical computed magnetic flux line plot in series motor of Fig. 6.41.

## Comparison of Calculated and Measured Results

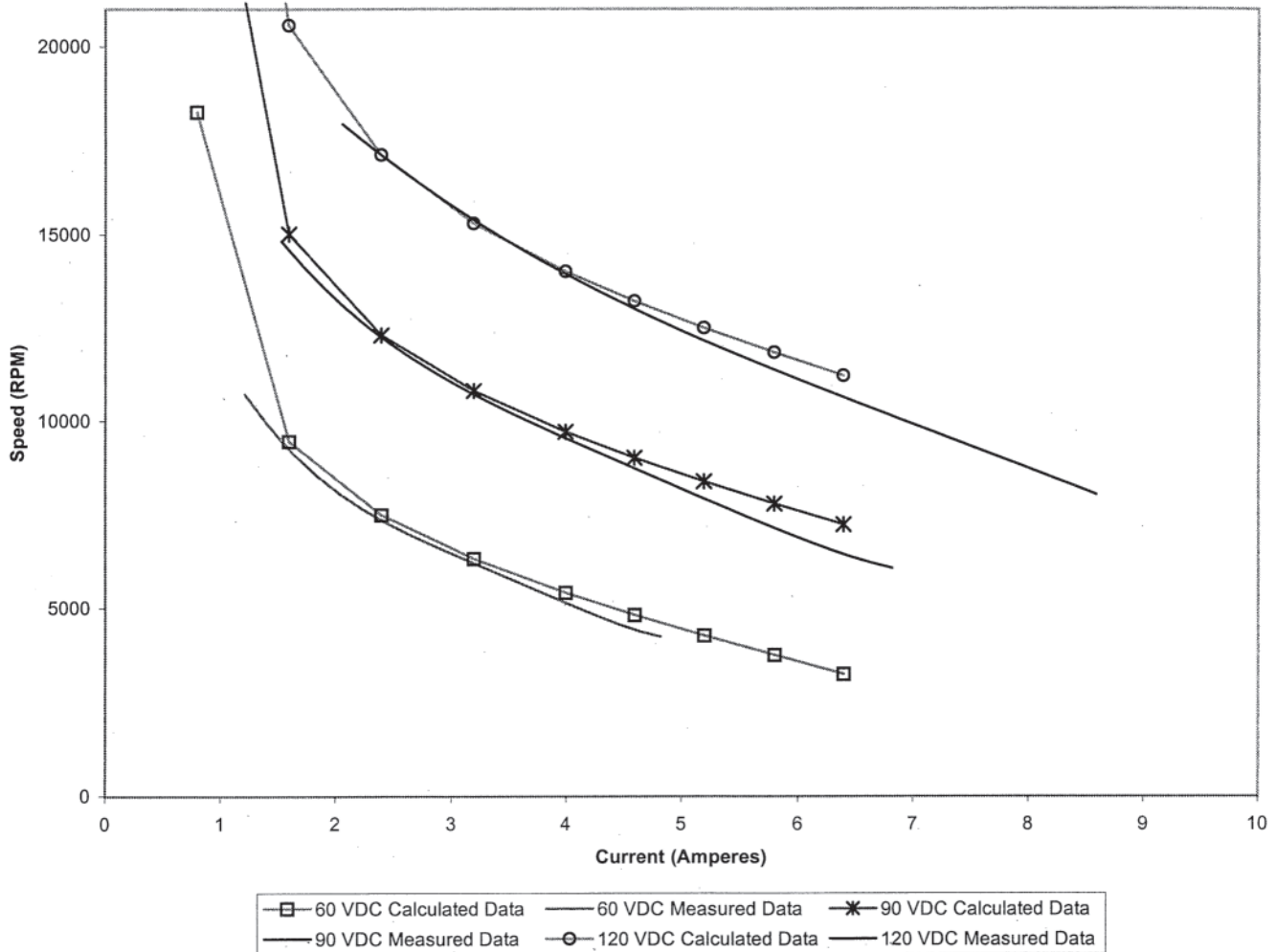


**Figure 6.43** Computed speed-torque curves using magnetostatic analysis with equivalent circuit equations compared with measured speed-torque curves for various direct current (dc) voltages applied to motor of Fig. 6.41. (From Ref. 10, copyright 1999 IEEE.)

Finite element flux plots for universal motors are of the type shown previously in Fig. 6.42. However, the current and torque now vary with time over the period  $D$  of the applied ac frequency. The time-average torque  $T_{av}$  is calculated from the instantaneous torque  $T(i)$  using:

$$T_{av} = \frac{1}{D} \int_0^D T(i) dt \quad (6.87)$$

As described in the preceding section of dc motor analysis using finite elements, there are again two ways to use finite elements to predict the performance of universal motors. They are using magnetostatic analysis to compute parameters of equivalent circuits, or using time-stepping finite element software to directly compute time-varying motor performance. Both methods are applied in this section to the series motor of Fig. 6.41 here energized with 120-V, 60-Hz ac as a universal motor.

The same parametric magnetostatic runs used previously for the dc case can be used with the proper equivalent circuit

equations to predict the performance as a universal motor. The dynamic equivalent circuit and its equations are all given elsewhere [14]. Results computed by Maxwell [15, 16] are shown in Figs. 6.46 and 6.47. Note that the performance curves of Fig. 6.46 agree well with measurements in terms of current, torque, and input power versus speed. For best estimation of input power at high speeds, the core loss should be computed with the aid of finite element techniques for high frequency eddy current loss [17]. Note also that the current waveforms of Fig. 6.47 are quite nonsinusoidal, both computed and measured.

The same universal motor (of Fig. 6.41) has also been analyzed directly using time-stepping finite element software EMPulse [13, 15, 16]. Figure 6.48 shows the computed current and torque waveforms at no load (including a short start-up transient). Figure 6.49 shows the computed performance curves of current and torque versus speed. Their comparison with measurements is excellent, even better than the curves in Fig. 6.46(a) and 6.46(b).

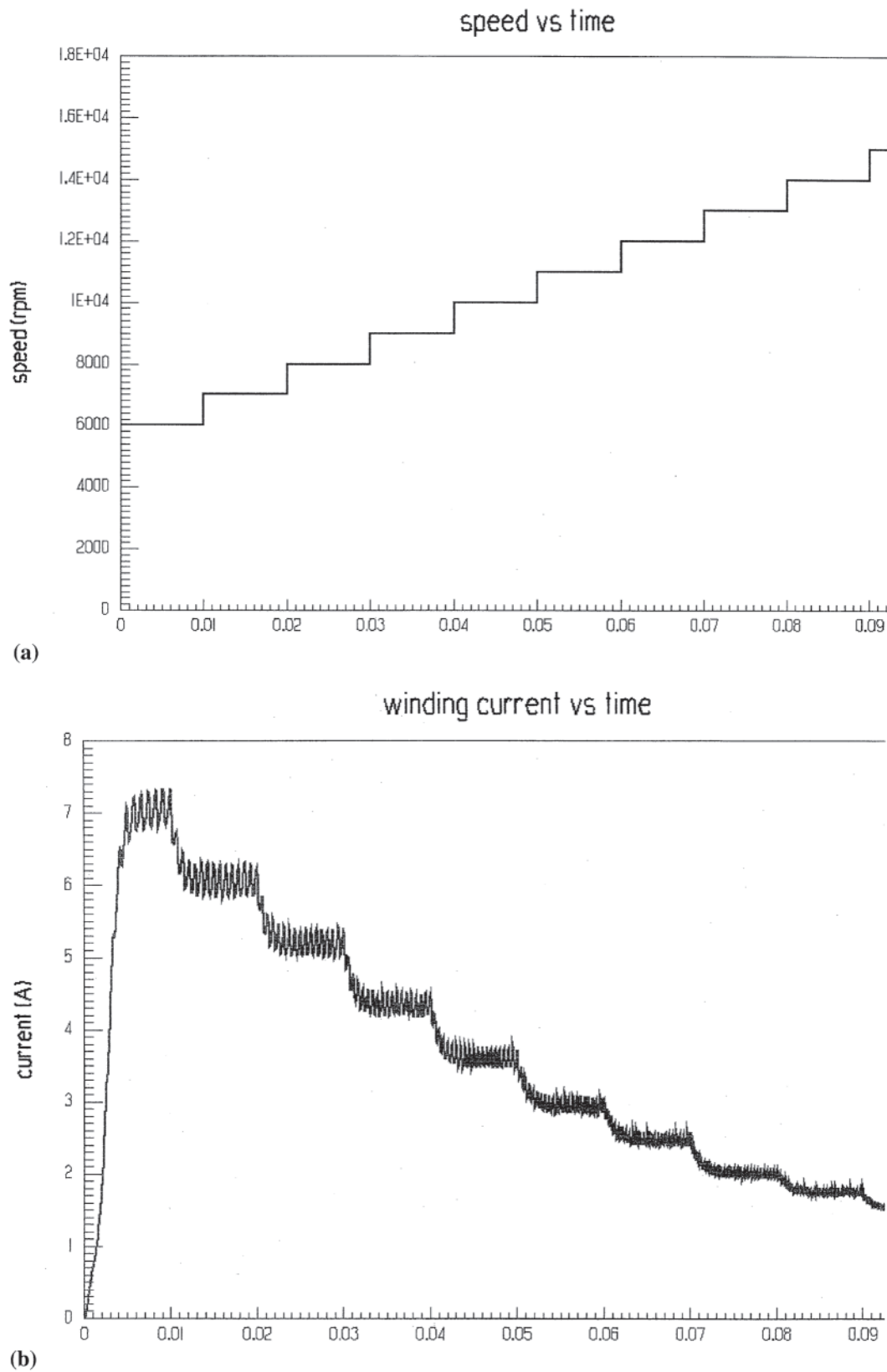


**Figure 6.44** Computed performance versus time for motor of Fig. 6.41 with 90-V direct current (dc) applied using time-stepping finite element analysis (FEA). (a) Specified speed vs. time, (b) computed current vs. time. (Copyright 1999 IEEE.)

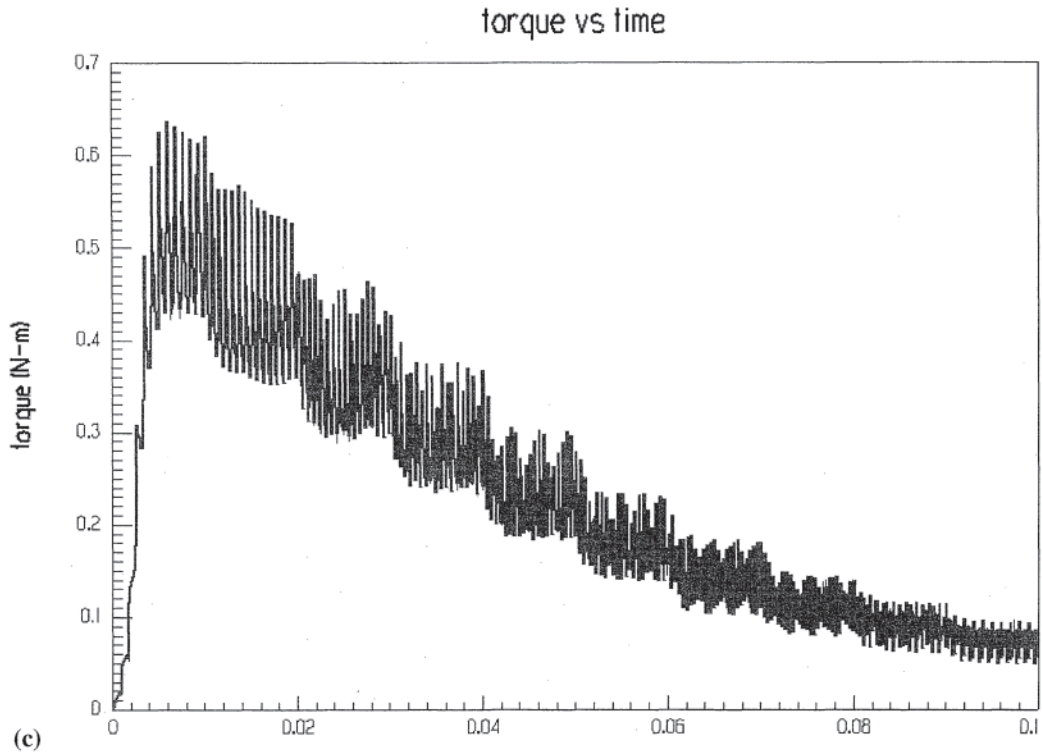
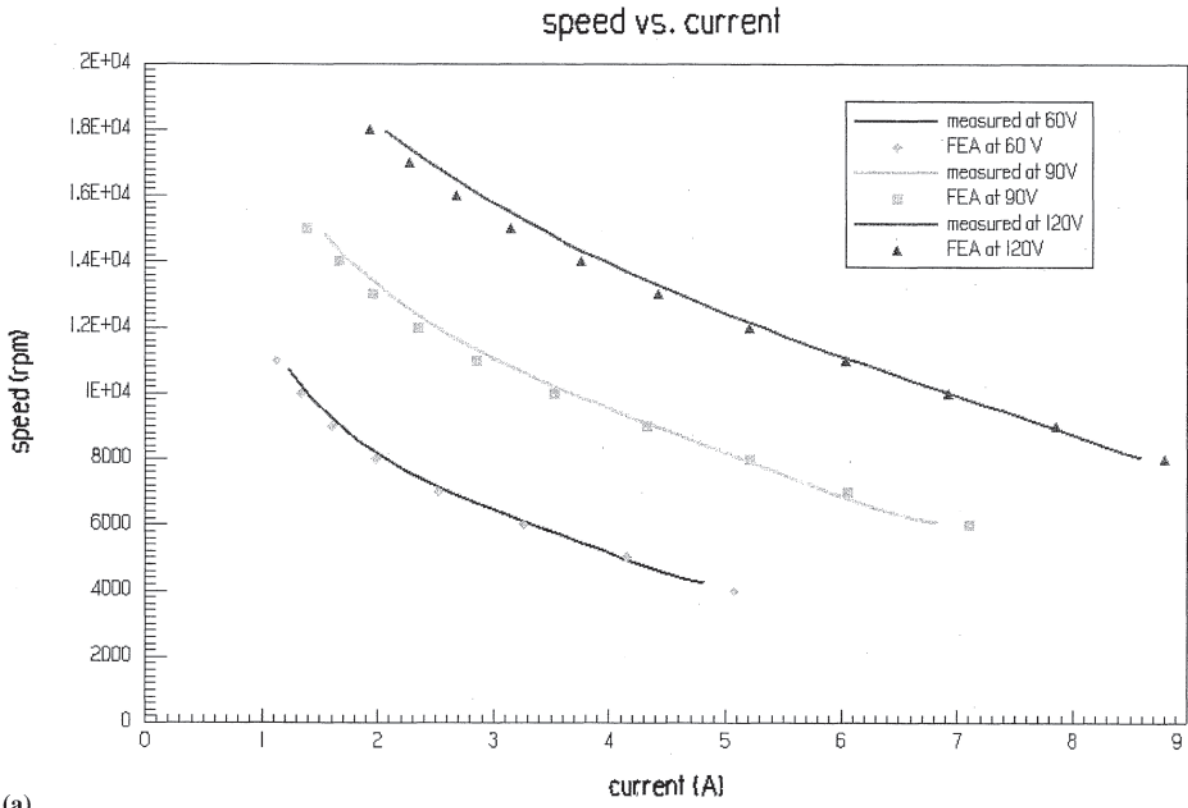
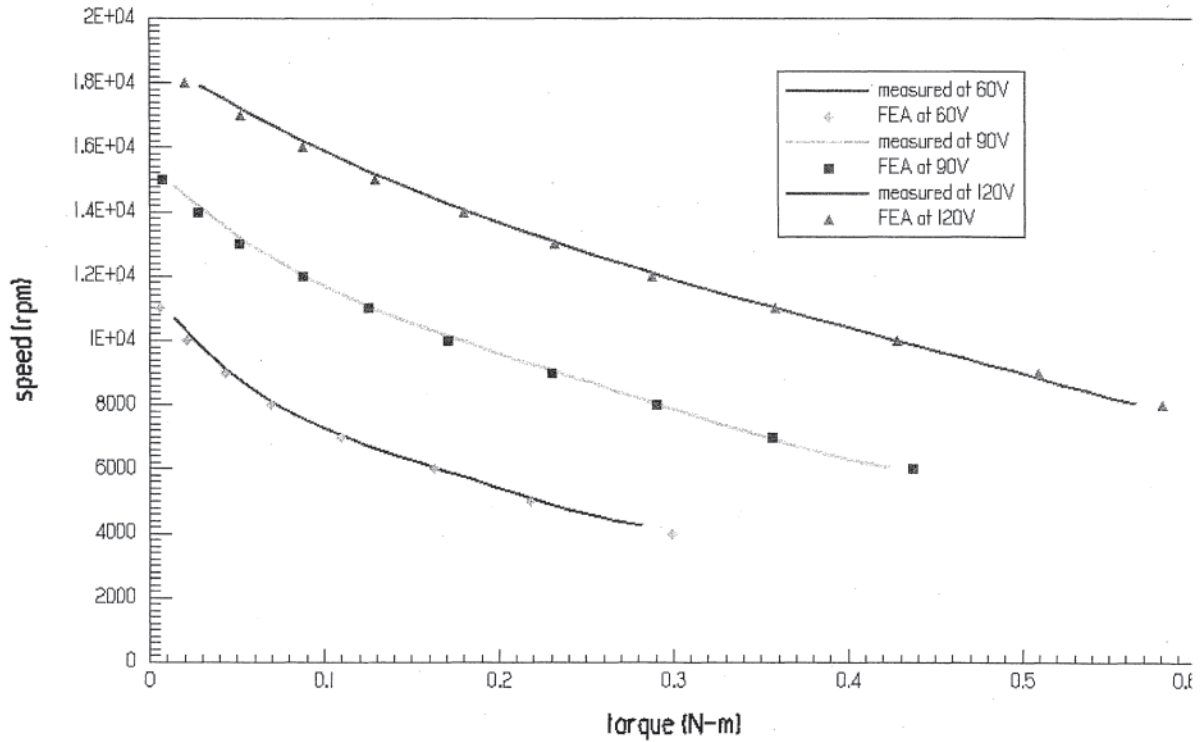


Figure 6.44 (cont'd.) (c) Computed torque vs. time. (From Ref. 11, copyright 1999 IEEE.)



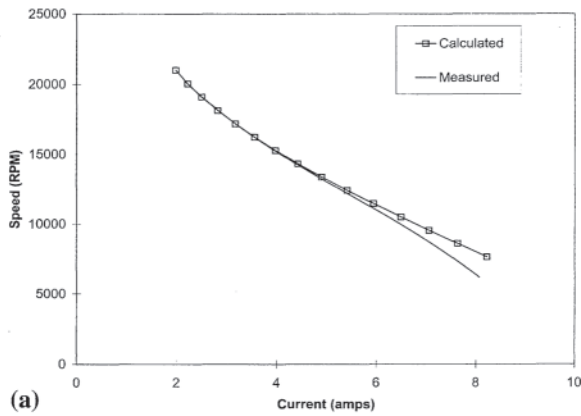
(a)

Figure 6.45 Performance curves computed for direct current (dc) motor of Fig. 6.41 using time-stepping finite element analysis, (a) Current vs. speed. (Copyright 1999 IEEE.)

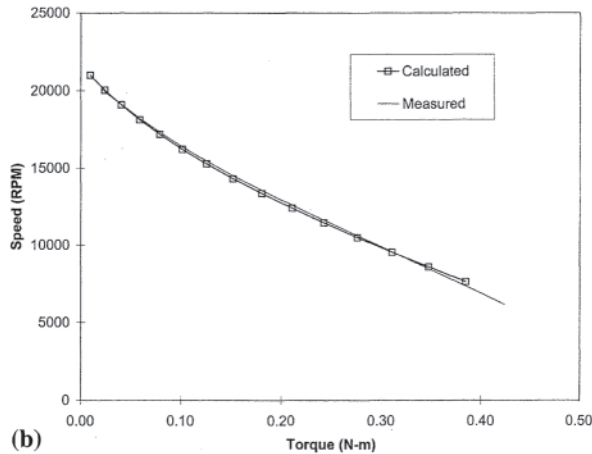


(b)

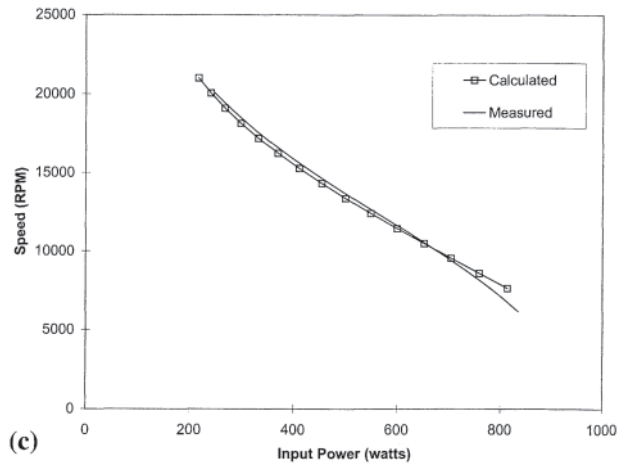
Figure 6.45 (cont'd.) (b) Torque vs. speed. (From Ref. 11, copyright 1999 IEEE.)



(a)

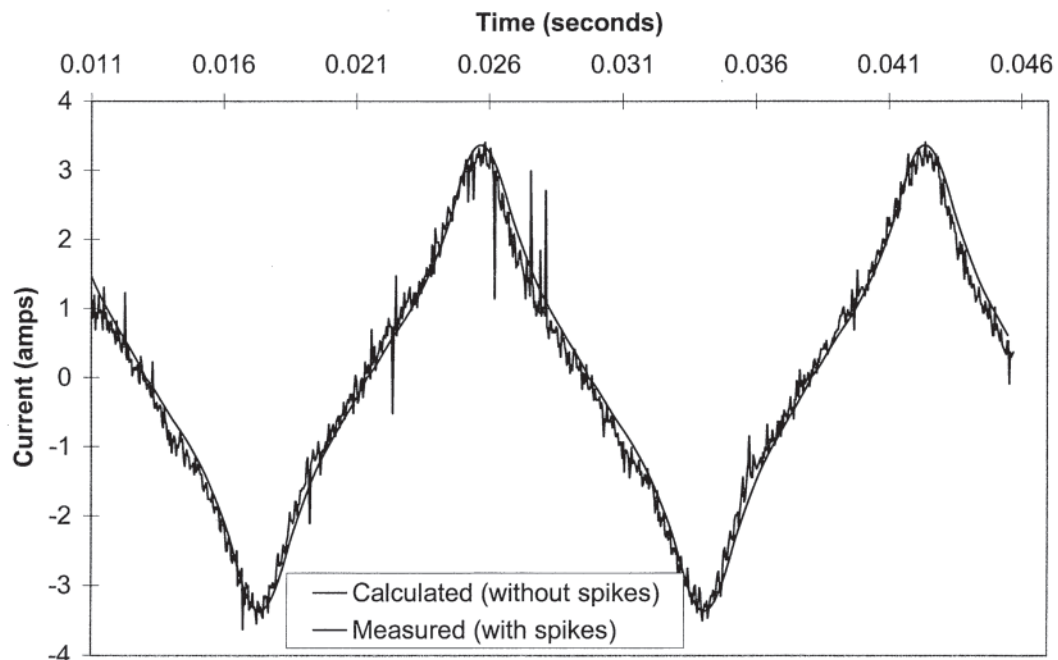


(b)

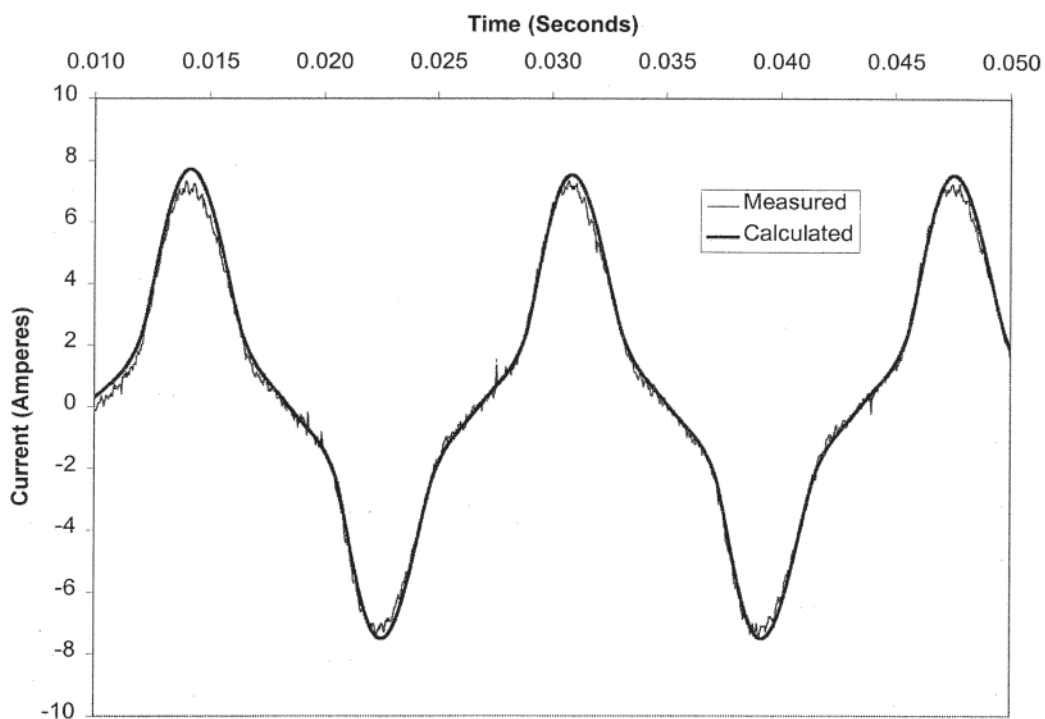


(c)

Figure 6.46 Performance curves for universal motor of Fig. 6.41 energized with 120-V 60-Hz alternating current (ac) computed using magnetostatic finite element analyses with equivalent circuit and equations of Ref. 12. (Copyright 1999 IEEE.) (a) Current, (b) torque, (c) input power, all vs. speed and compared with measurements.



(a)



(b)

**Figure 6.47** Current vs. time for universal motor of Fig. 6.41 energized with 120-V 60-Hz alternating current (ac) computed using magnetostatic finite element analyses with equivalent circuit and equations of Ref. 12, compared with measurements. (Copyright 1999 IEEE.) (a) At 21,500 rpm (no-load), (b) at 14,363 rpm (normal load).

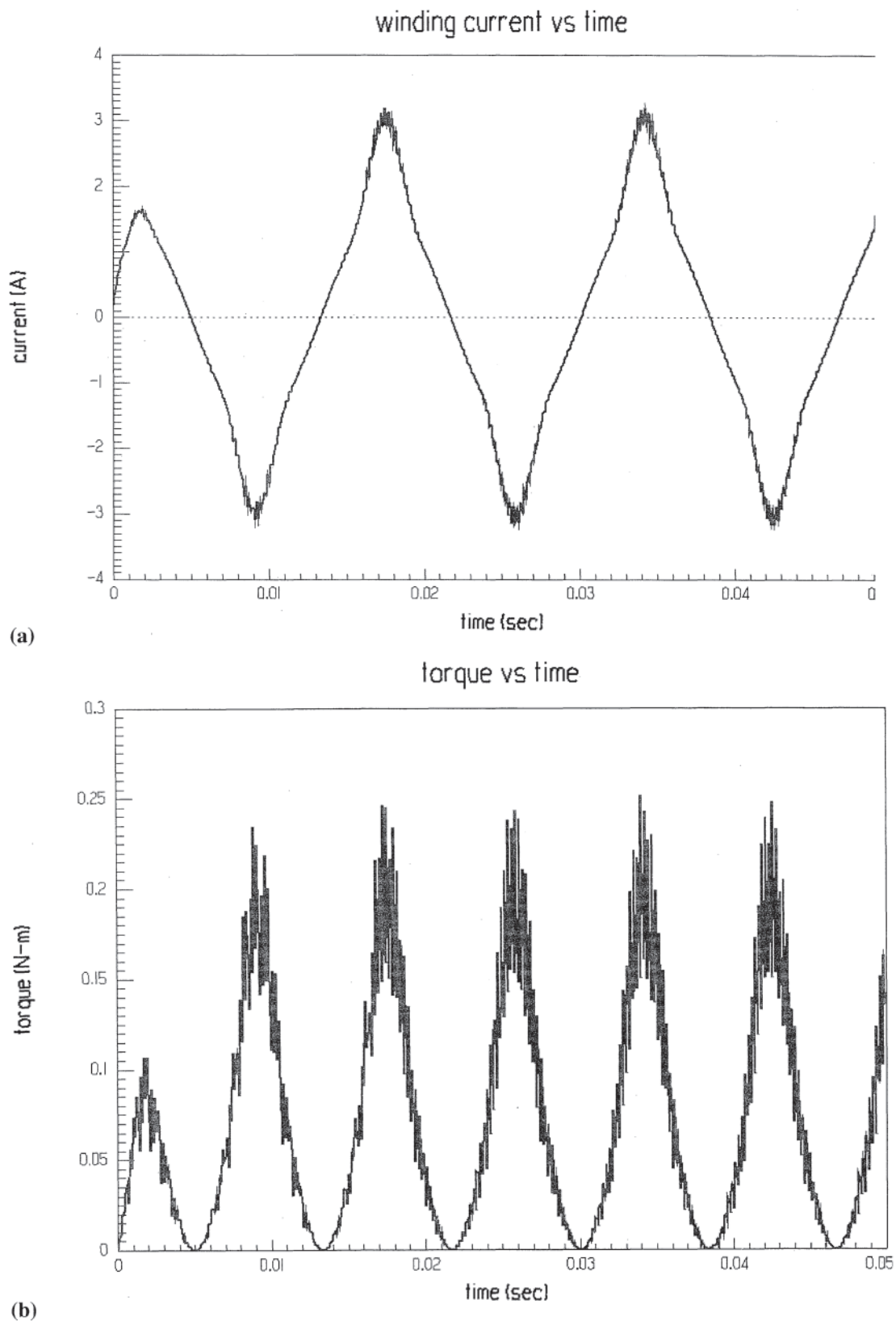


**Figure 6.48** Time-dependent performance of universal motor of Fig. 6.41 at no-load energized with 120-V 60-Hz alternating current (ac) computed using time-stepping finite element analysis: (a) current, (b) torque.

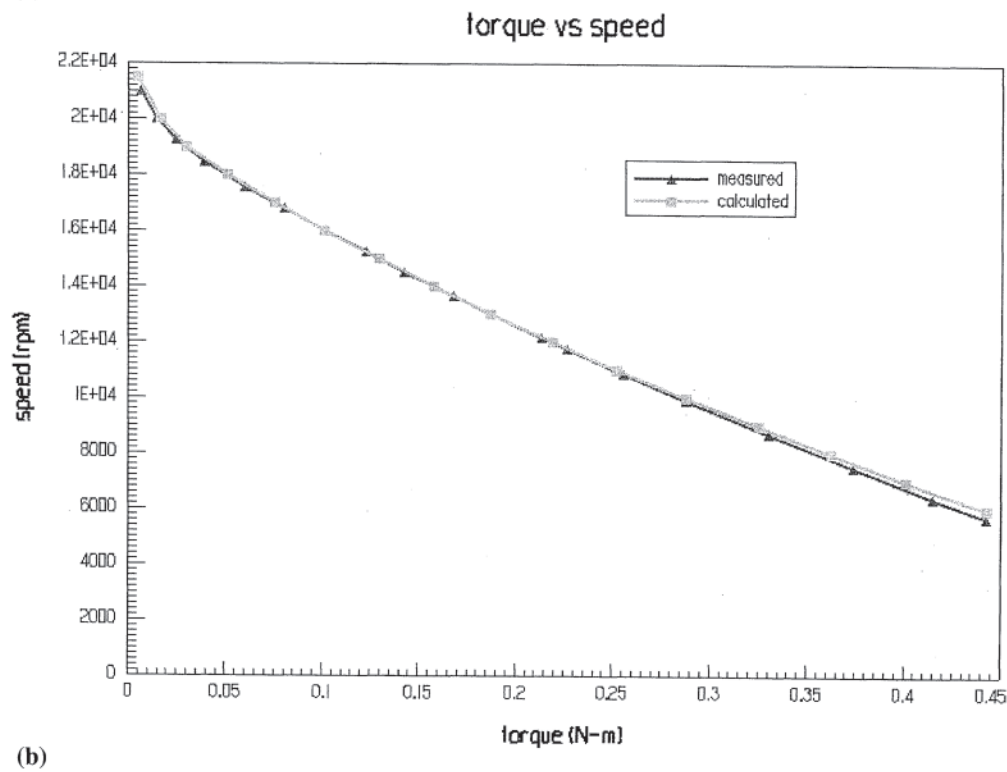
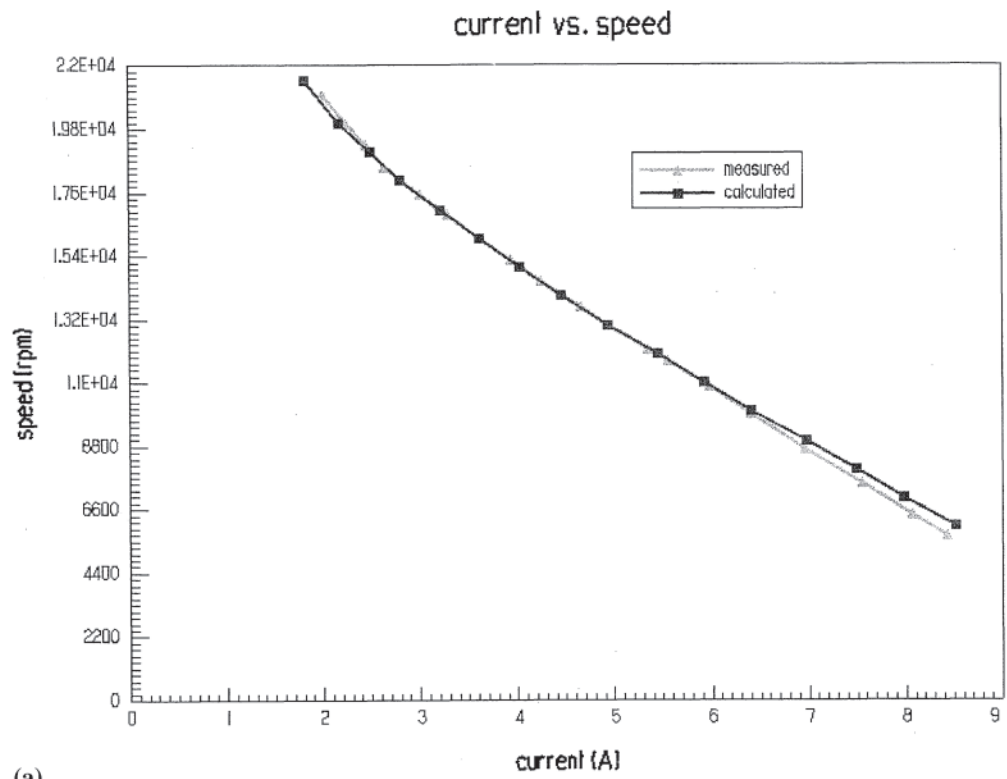


**Figure 6.49** Performance curves for universal motor of Fig. 6.41 energized with 120-V 60-Hz alternating current (ac) computed using time-stepping finite element software (From Ref. 11, copyright 1999 IEEE.) (a) Current, (b) torque.



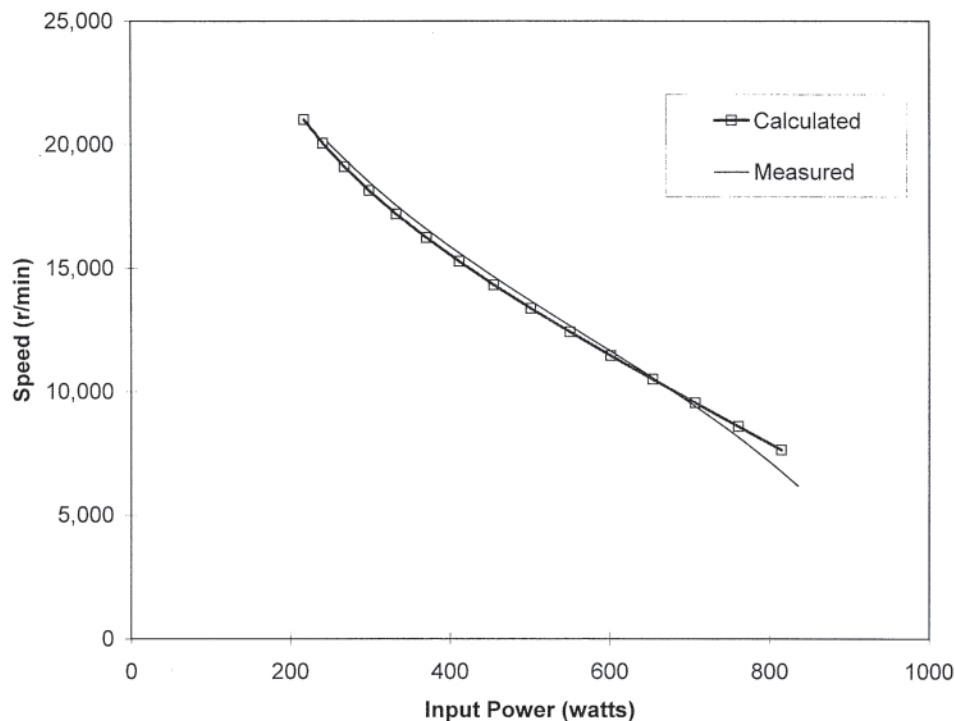


Figure 6.45 (cont'd.) (c) Input power, all vs. speed and compared with measurements.

## REFERENCES

- Selected references on dc servomotors
  - NEMA MG 7–1993, Motion/Position Control Motors and Controls. (See Appendix B for source of this standard.)
  - Fitzgerald, A.E., Charles Kingsley, Jr., and Stephen D. Umans, *Electric Machinery*, McGraw-Hill, New York, 1990, 5th ed.
  - Kuo, Benjamin C., *Automatic Control Systems*, Prentice-Hall, Englewood Cliffs, NJ, 1987, 5th ed.
  - Direct Current Machine Design Course Notes*, Direct Current Motor and Generator Department, Engineering Section, General Electric Company, Erie, PA, 1958.
  - Regulating Systems Course Notes*, Speed Variator Products Department, Engineering Section, General Electric Company, Erie, PA, 1956.
  - Roters, H.C., *Electromagnetic Devices*, Wiley, New York, 1946.
- Wieseman, R.W., “Graphical Determination of Magnetic Fields,” *Transactions of the AIEE*, vol. 46, 1927, pp. 141–154.
- G.K.Dubey, “Fundamentals of Electrical Drives”, Narosa, New Delhi, Second Edition 2001.
- G.K.Dubey, “Power Semiconductor Controlled Drives”, Prentice-Hall, Englewood Cliffs, 1989.
- Parker, Rollin J., and Robert J.Studders, *Permanent Magnets and Their Applications*, Wiley, New York-London, 1962.
- DC Motors, Speed Controls, Servo Systems*, 5th edn., Electro-Craft Corporation, August 1980.
- Saner, Floyd E., *Servo Motor Application Notes*, Pittman Division of Penn Engineering & Manufacturing Corporation, 1983, 1987, 1990.
- Franklin, P.W., “Design Theory of the Chopper Controlled D.C. Motor,” Seminar course notes, University of Missouri, Columbia, MO, 1976.
- EMAS is a proprietary product of Ansoft Corporation, Pittsburgh, PA 15219, USA, [www.ansoft.com](http://www.ansoft.com).
- Brauer, J.R., “Finite Element Software Aids Motor Design,” presented at Small Motor Manufacturing Association Tenth Annual Meeting, March 1985.
- Vander Heiden, R.H., A.A.Arkadan, and J.R.Brauer, “Nonlinear Transient Finite Element Modeling of a Capacitive Discharge Magnetizing Fixture,” *IEEE Transactions on Magnetics*, vol. 28, Mar. 1993, pp. 2051–2054.
- R.N.Ebben, J.R.Brauer, G.C.Lizalek, and Z.J.Cendes, “Performance curves of a series DC motor predicted using parametric finite element analysis,” *IEEE Trans. Magnetics*, v 35, May 1999, pp. 1294–1297.
- Ping Zhou, John R.Brauer, Scott Stanton, Zoltan J.Cendes, and Roderick N.Ebben, “Dynamic modeling of universal motors,” *Proc. IEEE Int. Electric Machines & Drives Conf.*, 1999.
- R.N.Ebben, J.R.Brauer, Z.J.Cendes, and N.A.Demerdash, “Prediction of performance characteristics of a universal motor using parametric finite element analysis,” *Proc. IEEE Int. Electric Machines & Drives Conf.*, 1999.
- Mark Ravenstahl, John Brauer, Scott Stanton, and Ping Zhou, “Maxwell design environment for optimal electric machine design,” Small Motor Manufacturing Assn. Annual Meeting, 1998.
- Maxwell, RMxpert, EMPulse, EMSS, and Simplorer are proprietary products of Ansoft Corporation, Pittsburgh, PA 15219 USA, [www.ansoft.com](http://www.ansoft.com).
- J.R.Brauer, Z.J.Cendes, B.C.Beihoff, and K.P.Phillips, “Laminated steel eddy current losses versus frequency computed with finite elements,” *IEEE Trans. Industry Applications*, v 36, July/Aug 2000, pp. 1132–1137.

# 7

## Testing for Performance

**Robert Oesterle** and **Walter J.Martiny** (Section 7.1)/**J.Herbert Johnson** (Sections 7.2, 7.5, 7.6, and 7.7)/**Mulukutla S. Sarma** (Section 7.3)/**Frank DeWolf** and **Richard K.Barton** (Section 7.4)

<b>7.0 INTRODUCTION</b>	<b>366</b>
<b>7.1 POLYPHASE INDUCTION MOTOR TESTING</b>	<b>366</b>
7.1.1 Electrical Test Standards	366
7.1.2 Types of Tests	366
7.1.3 Sample Calculations	369
7.1.4 Variation in Testing	369
7.1.5 Miscellaneous Tests	371
<b>7.2 SINGLE-PHASE INDUCTION MOTORS</b>	<b>371</b>
7.2.1 Electrical Test Standards	371
7.2.2 Types of Tests	371
7.2.3 Choices of Tests	371
7.2.4 Variations Due to Uncontrolled Factors	372
7.2.5 Curve Fitting of Performance Data	373
7.2.6 Miscellaneous Tests	373
<b>7.3 SYNCHRONOUS MOTOR TESTS</b>	<b>374</b>
7.3.1 Electrical Test Standards	374
7.3.2 Types of Tests	374
7.3.3 Choices of Tests	388
7.3.4 Variations Due to Uncontrolled Factors	388
7.3.5 Curve Fitting of Performance Data	388
7.3.6 Miscellaneous Tests	390
<b>7.4 DC MOTOR TESTS</b>	<b>391</b>
7.4.1 Electrical Test Standards	391
7.4.2 Preparation for Tests	391
7.4.3 Performance Tests	392
7.4.4 Special Tests	393
<b>7.5 HERMETICALLY SEALED REFRIGERATION MOTORS</b>	<b>394</b>
7.5.1 Electrical Test Standards	394
7.5.2 Types of Tests	394
7.5.3 Choices of Tests	394
7.5.4 Variations Due to Uncontrolled Factors	396
7.5.5 Curve Fitting of Performance Data	397
7.5.6 Miscellaneous Tests	397
<b>7.6 SPECIALTY TESTING</b>	<b>397</b>
7.6.1 Induction Motor Stators	397
7.6.2 Induction Motor Rotors	398
7.6.3 Permanent Magnet Motors	400

<b>7.7 SELECTION AND APPLICATION OF TEST EQUIPMENT</b>	<b>400</b>
7.7.1 Reasons for Testing	400
7.7.2 Functional Specifications of Test Equipment	400
7.7.3 Recommended Steps in Purchasing Test Equipment	401
7.7.4 Types of Tests	401
7.7.5 Types of Data Recording Devices	401
7.7.6 Mechanical and Electrical Loading Devices	402
7.7.7 Instrumentation	403
<b>REFERENCES</b>	<b>404</b>

## 7.0 INTRODUCTION

Electric motors convert electrical energy into mechanical energy. How efficiently they perform this task depends on how well their characteristics fit into the systems requiring their services. While advances in theory and computer analysis in the past 25 years have helped to better define characteristics, a complete performance study requires a testing program. Testing is still the final judge of motor performance.

This chapter covers basic testing procedures and discussion of standards on a variety of electric machines. Not everything on testing can, of course, be written in one chapter. The objective of this chapter is to introduce the reader to the subject of testing and to cite references that are useful for more in-depth study.

## 7.1 POLYPHASE INDUCTION MOTOR TESTING

### 7.1.1 Electrical Test Standards

#### 7.1.1.1 Background

Test standards for polyphase induction motors have been formulated by various agencies to establish consistent and reliable procedures for determining motor performance. These standards are kept up-to-date through periodic review by agency committees. It is important for the user to have the latest version of the standard before applying it to any testing program.

#### 7.1.1.2 General Descriptions

The major standards that cover polyphase induction motor testing are as follows.

*AN SI/IEEE 112 IEEE Standard Test Procedure for Polyphase Induction Motors and Generators* [1]. This is the U.S. standard for testing polyphase motors. It includes a variety of methods for determining the steady state performance characteristics of a wide range of machine types and sizes.

*International Electrotechnical Commission (IEC) Publication 34-2, Part 2, Methods for Determining Losses and Efficiency of Rotating Electrical Machinery from Test* [2]. This standard is followed by many European countries. Like the ANSI/IEEE 112 it includes different test procedures for a wide range of machines. Studies [3] have indicated, however, it is less rigorous than 112 as regards temperature

specification and loss determination when testing for motor efficiency.

*JEC-37 Induction Machine, Standard of Japanese Electrotechnical Committee* [4]. This is the Japanese standard for motor testing. Like the IEC, it is also considered [3] less rigorous than 112 in its handling of motor loss and temperature rise specification when determining efficiency.

*Canadian Standards Association C390 Energy Efficiency Test Methods for Three-Phase Induction Motors* [5]. This standard deals primarily with the determination of polyphase motor efficiency using a dynamometer type loading system. It is limited in scope, as it covers only one method for testing and evaluating motor efficiency performance.

*ANSI/NEMA Standards Publication No. MG 1, Motors and Generators* [6]. NEMA is a trade organization that has established standards to assist users in the proper selection and application of motors and generators. Many different test procedures are recommended in this group of standards. For induction machine testing, MG 1-12.58.1 recommends following ANSI/IEEE 112.

#### 7.1.1.3 Sources of Standards

It is recommended that any serious attempt to set up a testing program should begin with a review of the latest copies of the standards. The agencies from which the major standards can be obtained are as follows:

- Institute of Electrical and Electronics Engineers
- International Electrotechnical Commission
- Japanese Electrotechnical Committee
- Canadian Standards Association
- National Electrical Manufacturers Association

Addresses and some telephone numbers are found in Appendix B.

### 7.1.2 Types of Tests

#### 7.1.2.1 General Descriptions

The general-purpose polyphase induction motor has typical performance characteristics as shown in Fig. 7.1 and Fig. 7.2. Figure 7.1 illustrates the important low-slip (high-speed) characteristics and Fig. 7.2 shows the major features of the first-quadrant speed-torque curve. Table 7.1 defines the various

**Table 7.1** Motor Torques

Torque	Description
Full-load	The torque necessary to produce rated horsepower at full-load speed
Locked-rotor	The minimum torque that will develop at rest for all angular positions of the rotor
Pull-up	The minimum torque developed by the motor during the period of acceleration from rest to the speed at which breakdown occurs
Breakdown	The maximum torque that will develop with rated voltage applied at rated frequency without an abrupt drop in speed

torques of that figure. These characteristics are typical of the steady-state performance of the machine. This generally means that measurements are made with sinusoidal power applied to the motor and recorded after the electrical and mechanical transients have disappeared. In standards such as IEEE 112, specific ranges are defined for acceptable steady-state voltage, waveform, and frequency variations.

The test procedures can be grouped according to what characteristics are being sought. The low-slip characteristics as illustrated in Fig. 7.1 require methods that deal with accurate procedures for determining efficiency and power factor. The selection of the methods to determine the speed-torque characteristics as given in Fig. 7.2 are generally dependent upon the motor size and available testing facilities.

**7.1.2.2 Low-Slip Testing**

For low-slip testing the test methods can be grouped into direct measurement methods and segregated loss methods. In the direct measurement methods both the input and output power to the motor are measured directly. In the segregated loss approach one or both are not measured directly.

Different expressions are used to determine motor efficiency as a function of the test method used. For direct measurement methods the expression is:

$$\text{Efficiency} = \frac{\text{output}}{\text{input}} \times 100 \tag{7.1}$$

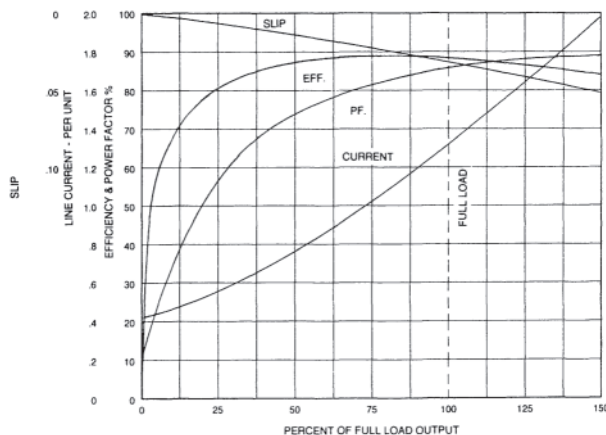


**Figure 7.1** Low-slip (high-speed) characteristics.

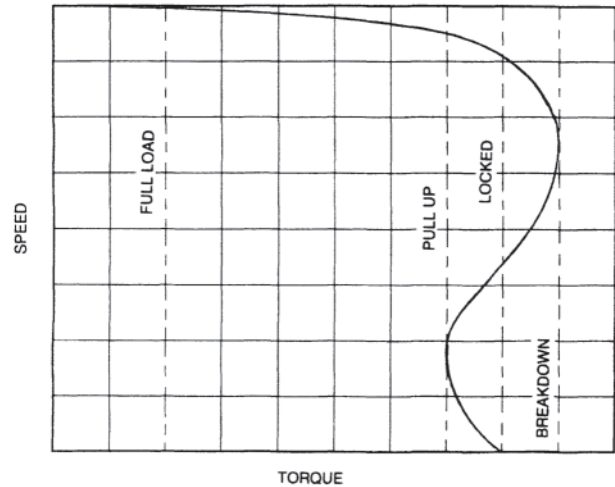


**Figure 7.2** First-quadrant speed-torque characteristics.

For the segregated loss method it is:

$$\text{Efficiency} = \frac{\text{input} - \text{losses}}{\text{input}} \times 100 \tag{7.2}$$

or

$$\text{Efficiency} = \frac{\text{output}}{\text{output} + \text{losses}} \times 100 \tag{7.3}$$

**7.1.2.2.1 Auxiliary Tests**

The basic losses requiring determination in the segregated loss methods are defined in Table 7.2. Special (auxiliary) tests are needed to determine the (a), (b), and (e) losses of the table.

*No-load test* Core loss and friction and windage loss are determined by this test. The machine is operated at rated voltage and frequency without connected load. It should be run until the temperature stabilizes to obtain accurate values of friction and windage.

*Stray-load tests* There are both indirect and direct methods available for determining stray loss. The loss is determined in the indirect method by subtracting the known losses (a) to (d) as given in Table 7.2 from a direct measured total loss.

**Table 7.2** Induction Motor Losses

Type of loss	Description
(a) Friction and windage	Mechanical loss due to bearing, friction, and windage
(b) Core	Loss in iron at no load due to fundamental magnetic field
(c) Stator $I^2R$	$I^2R$ loss in stator winding due to resistance of the windings
(d) Rotor $I^2R$	$I^2R$ loss in rotor windings due to resistance of the windings
(e) Stray load	Stray loss in iron and eddy-current losses in conductors

The reverse rotation test [7, 8] is used for the direct measurement of stray losses. This test requires two operations, during which reduced voltages are applied to the test motor to establish currents near the actual load currents. The line frequency stray-load losses are measured with the rotor removed. The high-frequency stray-load losses are measured with the rotor in place and driven in the reverse direction.

Standard stray-loss values have also been established as guidelines when the above tests cannot be conducted. These usually are expressed as a percentage of the rated output or input of the motor. Percentage values proposed by IEEE 112 are 1.8% of the output for motors between 1 and 125 horsepower (hp) and 1.5% for motors between 126 and 500 hp. The IEC standard, on the other hand, assumes the stray losses to be 0.5% of rated input for all motor sizes.

#### 7.1.2.2.2 Test Methods

Specific procedures have been classified using the terminology “methods” by different standards. The methods are basically the same among the IEEE 112, IEC, and JEC standards. The following discussion of the methods uses the IEEE 112 identification scheme.

There are five basic methods. A, B, and C are considered direct measurement methods, and E and F are considered indirect or segregated loss methods. A brief description of each follows:

**Method A: Brake** In this method a mechanical brake is generally used to load the motor. The output power is dissipated in the mechanical brake. The brake’s limited ability to dissipate power limits this method primarily to smaller sizes of induction motors, generally of fractional horsepower.

**Method B: Dynamometer** In this method the energy from the motor is transferred to a rotating machine (dynamometer), which acts as a generator to dissipate the power into a load bank. The dynamometer is mounted on bearings and reaction torque is measured by a load scale, a strain gage, or torque table. This is a very flexible and accurate test method for motors in the range from 1 to 500 hp.

To enhance the accuracy of this method for efficiency determination, a loss segregation adjustment to the test data is recommended. This includes adjusting the stray losses, determined indirectly, by subtracting the sum of the conventional losses from the direct measured total test loss at each load point. A trend line is established by linear regression analysis for the stray losses by plotting them against the load torque squared. The adjusted stray value is recorded from the trend line for each load point and added to the conventional losses to produce an overall adjusted loss. The adjusted total loss is then combined with the measured input to produce a corrected output.

Method B has been adopted by NEMA as the preferred method for determining motor efficiency.

**Method C: Duplicate machines** This method uses two identical motors mechanically coupled together and electrically connected to two sources of power, the frequency of one being adjustable. Readings are taken on both machines, and computations are made to calculate efficiency. This is also known as a pump-back test because power is returned to the line during the course of the test. Special equipment needs usually limit this method to testing the efficiency of large motors.

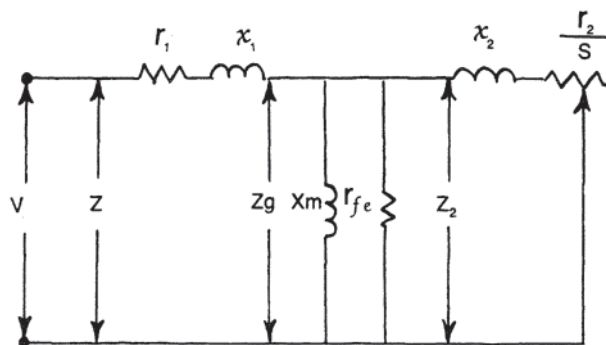


Figure 7.3 Per-phase polyphase induction motor equivalent circuit.

**Method E: Input measurements** In this method the motor output power is determined by subtracting the losses from measured motor input power at different load points. For each load point, the measured  $I^2R$  losses are adjusted for temperature and added to the no-load friction, windage, and core losses. The stray losses, which may be determined directly, indirectly, or by use of an agreed standardized value, are included in this total.

**Method F: Equivalent circuit calculations** When load tests cannot be made, operating characteristics are calculated from no-load and impedance data by means of an equivalent circuit. The basic type of circuit is shown in Fig. 7.3. Because of the nonlinear nature of these circuit parameters, they must be determined with great care to insure accurate results. Procedures for determining these parameters are outlined in the standards.

#### 7.1.2.3 Speed-Torque Testing

The speed-torque characteristic is the relationship covering the range from zero to synchronous speed as illustrated in Fig. 7.2. Several different methods are available for obtaining this data. IEEE 112 has grouped these methods as follows:

**Method 1: Measured output** In this method a calibrated direct current (dc) generator is used to load the test motor. At different speed settings the output of the generator is carefully measured and combined with previous known losses of the generator to determine the torque of the test motor.

**Method 2: Acceleration** In the acceleration method the motor is started with no load and the value of acceleration is determined at various speeds. The torque at each speed is determined from the mass of the rotating parts and the acceleration at each speed.

**Method 3: Input** In this method the torque is determined by subtracting the losses in the machine from the input power at each load point. The motor does not have to be unloaded for this test. Because the motor losses cannot be determined directly at each load point, the procedure is considered approximate.

**Method 4: Direct measurement** A dynamometer is used to directly load the motor in this method. This means of loading is relatively easy and accurate and offers the ability to simulate different load cycles that the motor might experience in special applications. At each speed setting, simultaneous readings of

**Table 7.3** Temperature Correction

Class of insulation	Temperature (°C)
A	75
B	95
F	115
H	130

Source: IEEE Std. 122–1996.

voltage, current, speed, and torque can be taken. It should be considered the preferred method of testing.

The basic relationships needed to transform the test data of these different methods into torque values can be found in the IEEE 112 Standard [1].

#### 7.1.2.4 Temperature

The losses in the motor are the reason its temperature rises above ambient temperature. It is important to know these temperatures to produce accurate final performance results. The use of thermometers, embedded detectors, and local temperature detectors is described in the different standards.

Since it is not possible to obtain a stabilized heat run on every motor, it is necessary in many cases to correct the resistances of the motor for expected operating temperatures to establish its performance characteristics. When direct measurement data are not available, it is permissible to correct the winding resistances by using temperatures such as those given in Table 7.3 for different insulation classes.

Since the rotor resistance in an induction motor cannot conveniently be measured directly, it is acceptable practice to assume that the rotor is at the same temperature as the stator winding. Indications are that the rotors of open motors tend to be somewhat cooler than the stator windings, and in enclosed motors somewhat hotter.

### 7.1.3 Sample Calculations

#### 7.1.3.1 Low-Slip Performance

A sample calculation is given in this section using IEEE Method B with segregation of losses to correct for stray-load loss. This is the NEMA-recommended procedure for accurate determination of induction motor efficiency.

#### 7.1.3.2 Test Data

The machine analyzed in this sample calculation is a 15-kW (20-hp) four-pole polyphase induction motor. The test results were obtained using a dynamometer such as that shown in Fig. 7.4 as a loading device. The summary test data and corrections are given in Table 7.4.

The core loss and friction and windage loss were determined by no-load tests. These are illustrated in Fig. 7.5. In this figure, the no-load losses measured at voltages between 350 and 500 V form a smooth curve. The sum of the core loss and the friction and windage loss at rated voltage, 460 V, is 0.345 kW.

To separate the friction and windage loss from the total no load loss, the curve must be extrapolated back to zero voltage,

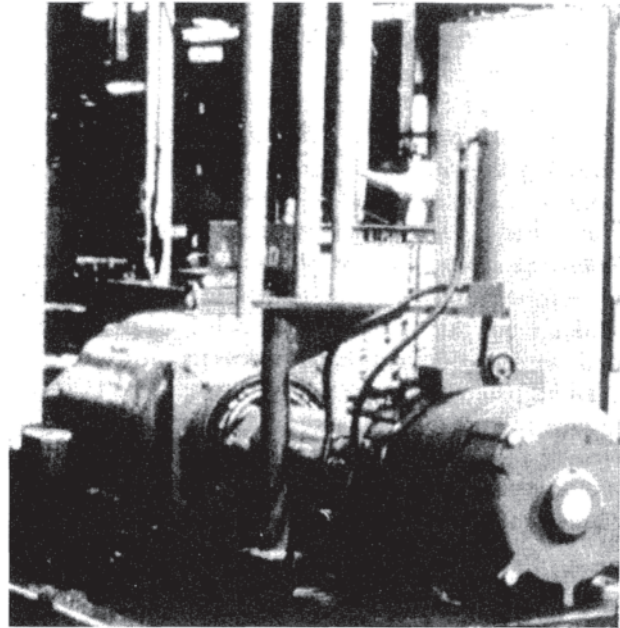


**Figure 7.4** Dynamometer. (Courtesy of Magnetek, Inc., St. Louis, MO.)

at which point the core loss disappears. This is most accurately done by plotting the loss versus the square of the voltage as indicated in the figure. The justification for this procedure is that the core loss is proportional to the square of the voltage, but the friction and windage loss depends only on the motor speed.

#### 7.1.3.3 Efficiency

The efficiency is determined at each point using Eq. 7.2. The output power is the input power minus the total adjusted losses.

The stray-load losses are calculated indirectly. All known conventional losses ( $I^2R$ , friction and windage, core loss) are subtracted from the total apparent loss. The remaining loss is plotted against the torque squared and a straight line leastsquares regression technique is used to fit the data. The corrected stray load is obtained by drawing a line parallel to the regression line through the zero axis. The stray-load losses for each torque load are recorded from this line. The slope for this line is given in Table 7.4.

In this procedure the full-load temperature is used to correct all load point resistances. This tends to make the lightload efficiency values lower and the high-load values higher than under steady-state temperature conditions.

Since the actual winding temperatures of this motor were determined during full-load testing, it was not necessary to use Table 7.3.

### 7.1.4 Variation in Testing

#### 7.1.4.1 Preferred Method Differences

Studies [9, 10] have shown that there are differences in efficiency results due to the preferred efficiency methods used.

**Table 7.4** Calculation of Motor Efficiency<sup>a</sup>

Description	Load					
	1	2	3	4	5	6
Ambient temperature (°C)	25	25	25	25	25	25
Stator winding temperature (°C)	49	51	52	53	56	60
Speed (rpm)	1789	1779	1769	1757	1744	1729
Line current (A)	10.3	14.4	19.2	24.2	30.6	36.9
Power input (kW)	4.535	8.519	12.567	16.855	21.095	25.615
Core loss (kW)	0.295	0.295	0.295	0.295	0.295	0.295
Stator I <sup>2</sup> R loss (kW)	0.106	0.207	0.374	0.593	0.959	1.413
Rotor I <sup>2</sup> R loss (kW)	0.025	0.094	0.205	0.381	0.617	0.943
Friction and windage loss (kW)	0.050	0.050	0.050	0.050	0.050	0.050
Total conventional loss (kW)	0.476	0.646	0.924	1.319	1.921	2.701
Torque (N-m)	20.2	40.4	60.6	80.8	100.9	121
Dynamometer correction (N-m)	0.54	0.54	0.54	0.54	0.54	0.54
Torque correction (N-m)	20.74	40.94	61.14	81.34	101.44	121.54
Power output (kW)	3.894	7.632	11.331	14.972	18.553	22.051
Apparent loss (kW)	0.641	0.887	1.236	1.883	2.542	3.564
Stray-load loss (kW)	0.165	0.241	0.312	0.564	0.621	0.863
Slope 0.048. Regression factor 0.987						
Stator I <sup>2</sup> R loss at 82°C	0.118	0.230	0.413	0.653	1.044	1.519
Corrected speed (rpm)	1788	1777	1766	1753	1739	1724
Rotor I <sup>2</sup> R loss at 82°C	0.027	0.102	0.224	0.415	0.670	1.004
Corrected stray-load loss (kW)	0.021	0.080	0.179	0.316	0.493	0.708
Corrected total loss (kW)	0.517	0.757	1.161	1.729	2.552	3.577
Corrected output (kW)	4.023	7.760	11.404	15.121	18.541	22.031
Efficiency (%)	88.7	91.1	90.7	89.7	87.9	86.0
Power factor (%)	55.4	74.5	82.0	87.4	86.5	87.1

<sup>a</sup> Rating: 15 kW. Phase: 3, Speed: 1800 rpm. Line voltage: 460 V  
Stator resistance: 0.610 ohms at 25°C. Temperature correction: 82°C

These studies generally show the IEEE 112 Method B as yielding lower efficiencies than the IEC 34-2 and the JEC 37 methods. Table 7.5 compares the efficiencies of three different machines calculated by the above preferred methods.

The major reason for the differences is the way in which stray-load losses are handled. The IEEE 112 method stray-load losses are included in the direct input and output measurements. In the IEC method the losses are estimated as 0.5% of the input, and in the JEC method they are set equal to zero. The comparison shows the importance the method can have in establishing the final efficiency value.

**7.1.4.2 Test Variations**

The results from any motor test procedure will vary as a function of the measurement system accuracy. A study [9] conducted by NEMA developed data to aid in quantifying

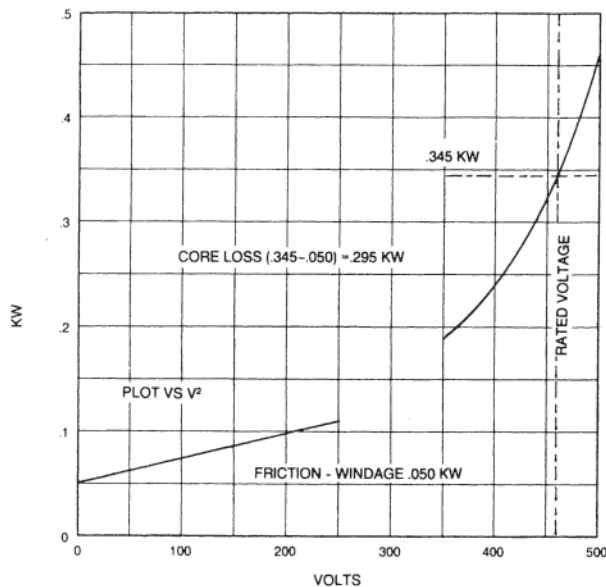


**Figure 7.5** Core loss and friction and windage loss of a 15-kW motor.

**Table 7.5** Efficiency Differences Due to Preferred Methods

hp	JEC 37 Circle diagram	IEC 34-2 Loss summation	IEEE 112 Method B
5	88.8	88.3	86.2
10	89.7	89.2	86.9
20	91.9	91.4	90.4

**Table 7.6** Efficiency Variations Due to Testing Techniques Using IEEE 112 Method B

Motor Power (hp)	Average	$\pm 2$ S.D. <sup>4</sup>
5	87.1	0.7
25	89.5	0.8
100	91.9	0.9

<sup>4</sup>S.D.=standard deviation.

this variation. In this study, three motors (5 hp, 25 hp, and 100 hp) were tested by a number of different motor manufacturers. After a preliminary round of testing, each manufacturer tested the motors in accordance with IEEE Method B. The results are given in Table 7.6.

These results illustrate the variation that can occur in testing. For example, the variation was less than 1% with the stray smoothing technique. This shows that careful maintenance of testing equipment and following defined procedures can keep the variations under good control.

### 7.1.5 Miscellaneous Tests

There are test procedures outlined for determining other performance characteristics of the induction motor. Included among these characteristics are insulation resistance, high potential capability, shaft current and bearing insulation, noise and vibration. Each of these is covered in various standards listed earlier in this section. It is important to know that not only electrical but also mechanical and insulation characteristics must be tested to ensure proper motor performance in many different application areas.

## 7.2 SINGLE-PHASE INDUCTION MOTORS

### 7.2.1 Electrical Test Standards

The recommended test procedure for single-phase induction motors is outlined in IEEE Standard 114-\* (this standard is on the process of being reapproved at this time) "IEEE standard Test Procedure for Single-Phase Induction Motors" [11]. This standard was prepared by the Single-phase and Fractional Horsepower Subcommittee, of the IEEE Rotating Machinery Committee, which is now called the Electric Machine Committee of the IEEE Industry and Applications Society. The reader is encouraged to take advantage of that standard since it gives further references to other standards involving temperature measurement, resistance measurement, etc.

### 7.2.2 Types of Tests

Before a detailed discussion of testing is given, a review of the motor types would be in order. IEEE Standard 114 covers a number of single-phase motors that are becoming increasingly less popular and will not be covered in this section. Also, those single-phase motors used in hermetic compressor applications for air conditioning and refrigeration are dealt with in Section 7.5.

### 7.2.2.1 Most Popular Single-Phase Induction Motors

The single-phase induction motors to be covered in this section include the following types:

- PSC (permanent-split capacitor)
- CSCR (capacitor-start, capacitor-run)
- CS (capacitor-start)
- Split-phase
- Shaded-pole

All of the above mentioned single-phase induction motors are found in pumps, fans, blowers, bench-grinders, table saws, and a host of other residential, commercial, and light industrial applications. For this reason, most of the attention will be given to these motor types.

### 7.2.2.2 Motor Tests

The motor tests are best understood if the particular motor function to be studied is considered. For this purpose, the motor functions will be divided into starting and running performance tests.

#### Starting performance

- LRA, locked-rotor amperes
- LRT, locked-rotor torque
- LST, low-speed torque, also known as pull-up torque
- SWT, switching torque
- Locked-rotor temperature rate of rise

#### Running performance

- BDT, breakdown torque
- speed
- Efficiency
- Power factor
- Temperature rise above ambient

It is common for most manufacturers to perform the motor tests in an ambient of 25°C to 30°C. The starting tests especially are taken with the motor at room temperature. Most running performance curves and associated tabulated data are also based on room-temperature conditions for the motor. However, it is common for rated-load tests to be made after the motor temperature has stabilized. The necessary readings are then taken to obtain the performance characteristics listed above, as well as the motor and ambient temperatures. If the motor has a service factor rating such as 1.15, the motor tests may be performed at the overload condition. This also provides assurance that the motor temperature rise and associated performance will meet the nameplate rating and the customer's requirements.

### 7.2.3 Choices of Tests

The test choices are delineated in Table 7.7. The reader is referred to Section 7.7, Selection and Application of Test Equipment, and also IEEE Standard 114 [11] for comments and specific recommendations. The following are some suggestions for the single-phase tests.

- LRA: This is usually taken with the rotor locked to prevent rotation. Sufficient time must be given to allow the



**Table 7.7** Test Choices for Various Types of Motors

Motor type		Test choice	PSC	CSCR	CS	Split-phase	Shaded-pole
Starting performance							
Measured	LRA	×	×	×	×	×	×
	LRT	×	×	×	×	×	×
	LST	×	×	×	×	×	×
	SWT	—	×	×	×	—	—
Running performance							
Measured	BDT	×	×	×	×	×	×
	TORQ	×	×	×	×	×	×
	SPEED	×	×	×	×	×	×
	WATTS	×	×	×	×	×	×
	AMP	×	×	×	×	×	×
	T-RISE	×	×	×	×	×	×
Calculated	PF	×	×	×	×	×	×
	EFF	×	×	×	×	×	×

meter or current transducer to settle out and give a stable reading. It is common for some instruments to have a response time of 0.3 to 0.5 second. Another important factor is line voltage and the associated voltage regulator in the test system. For these reasons, a locked-rotor current reading is usually taken at 3 or 4 seconds.

- **LRT:** Single-phase motors with a starting torque of 50% of breakdown (BDT) or more can be sufficiently tested with the rotor locked or traversing through zero speed as with an inertia tester. Low-torque motors such as PSC motors and some split-phase motors are best measured with the “revolving torque” method, where the motor is allowed to revolve at a speed of about 6 to 8 rpm. During that time the torque is measured with the aid of an inline torque transducer or load cell in conjunction with a trunnion mount. As long as the speed is close to zero, the envelope enclosing the high- and lowtorque readings gives the best measurement of the starting capability of the motor. The torque variations are the result of the varying air gap permeance due to presence of stator and rotor teeth. The selection of the slot combinations can have a pronounced effect on the number of these variations and the size of the torque envelope.
- **LST:** The low-speed torque dip, or pull-up torque as it is often called, is best measured with a dynamic tester. It is nearly futile to measure this in a point-by-point test. An inertia tester, programmed dynamometer, or an eddy current or particle brake are good choices to use for this measurement of torque as the motor is traversing the speed range where this torque dip is likely to occur.
- **SWT:** The torque delivered by the motor at the time the switching occurs is usually measured dynamically. If action of a solenoid or a mechanical switch occurs, the use of an oscillograph or oscilloscope may be desirable

to record the speed and torque during actual motor acceleration. Care must be taken, however, to ensure that the speed and torque transducers are responding correctly in the transient condition. It may be sufficient to make these measurements during a normal 6- to 8-second dynamic test. If the pick-up and drop-out of the switches are different, as they usually are, it may be preferable to make the test both for motor acceleration and deceleration. The torque measurements of interest are the torque readings in both the start and run connections.

- **BDT:** Breakdown torque is another motor attribute that is best measured with a dynamic tester because the speed at breakdown is a function of the specific design itself. During the test, one must be sure that data are not taken too quickly so that the change in the torque signal can be observed within the reading or writing capability of the instrument used for the recording.
- **TORQ, SPEED, WATTS, AMP:** All of these load-point readings comprise data that can be taken during a steady-state test or dynamically “on-the-fly.” If the readings are taken during a steady-state test, it is quite likely that the instruments can be simultaneously locked so that the data can be recorded after the load has been reduced or removed entirely. Of course, if the load is a heat-run test, then the readings are best taken while the motor is loaded.
- **T-RISE:** The temperature rise above ambient is always taken after the motor has been loaded for a period of time so that the operating temperature has stabilized. Depending on the application requirements, this may be taken as the winding temperature or it may be the temperature of the motor case or frame. In the first case, resistance measurements both cold and hot may be required. For a continuous test the Seely method [12] is preferred since it allows the test operator to continuously monitor the winding resistance while it is energized. One of the points often overlooked is that resistance measurements are useless without an accurate temperature measurement of the winding when it is cold. The temperature rise above ambient is not to be confused with “temperature-rate-of-rise” listed earlier as a possible starting performance test. That test is commonly taken with hermetic motors but used only occasionally with “standard” motors because of the difficulty in gaining visual access to the windings during the locked test.

#### 7.2.4 Variations Due to Uncontrolled Factors

As indicated in other sections, the major factors that cause errors or differences to occur include temperature and voltage variations, variation of frequency (although this is now less common), and the non-sinusoidal characteristic of the applied voltage wave. The use of many high-power electronic devices without proper filtering can cause difficulties in motor performance testing. High-current welders that put intermittent loading on the incoming bus can cause voltage changes with undesirable effects, especially when a 6- to 8-second dynamic

test is under way. If analog meters are used, care must be taken to avoid parallax errors.

When using computerized data acquisition systems one must exercise care that all readings intended to be acquired simultaneously are in fact so acquired. Phasing of all signals is vitally important. Usually shielded cables are required and single grounding points are mandatory to avoid ground currents.

### 7.2.5 Curve Fitting of Performance Data

It is worth repeating that if performance curves are plotted from individual test points, one should use at least seven test points that are spaced fairly evenly in the region of plotting. Since most curves start from no-load, the test points should be evenly spaced from no-load to about 1.5 to 2.0 times full load. Most personal computers now have curve-fitting programs that allow one to fit the data to a fourth-degree polynomial. Rather than attempting to fit efficiency and power factor curves to a polynomial, one should fit watts input, watts output, and line current to load torque. Then, from the fitted equations, one can compute and plot efficiency and power factor, obtaining smooth curves. As a test on the “goodness” of the test data, the program should check the error from the data point to the fitted curve and also determine  $R^2$ , or the correlation coefficient squared. If the data point is in error by more than 0.25% and if the  $R^2$  is less than 0.9999, one should look for data that are suspect or repeat the test.

The same rigorous scrutiny should apply even if the data are taken in a continuous acquisition process. It is not uncommon for small aberrations in test data to occur if line transients happen while the test sequence is under way.

An example of curve fitting is given in tables Table 7.8 and Table 7.9. Table 7.8 is a list of data taken from an actual test on a PSC single-phase induction motor. The speed, load torque, and watts input were taken from their respective reading meters. The watts output is computed directly from the speed and torque using the equation:

$$\text{Watts out} = \frac{\text{torque (oz-ft)} \times \text{speed (rpm)}}{112.7} \quad (7.4)$$

**Table 7.8** Data from Test on a PSC Single-Phase Induction Motor

Load torque (oz-ft)	Speed (rpm)	Watts input	Watts output	Efficiency (%)
0	3594	199	0	0
5	3576	341	159	46.6
10	3558	486	316	65.0
12.5	3548	562	394	70.1
15	3538	628	471	75.0
20	3517	790	624	79.0
28.5	3477	1076	880	81.8
30	3470	1124	924	82.2
34	3449	1264	1040	82.3
40	3415	1482	1212	81.8
50	3343	1916	1483	77.4
60	3235	2472	1722	69.7
65	3146	2732	1814	66.4

**Table 7.9** Corrected Data Using Least-Mean Squares CurveFitting Routine

Load torque (oz-ft)	Fitted watts input <sup>a</sup>	Fitted watts output <sup>b</sup>	Efficiency (%)
0	198.1	0	0
5	342.1	160.2	46.8
10	487.0	316.8	65.0
12.5	560.4	394.1	70.3
15	634.9	470.9	74.2
20	788.0	623.2	79.1
28.5	1066.0	878.6	82.4
30	1117.9	923.1	82.6
34	1261.8	1040.8	82.5
40	1493.5	1213.4	81.2
50	1931.4	1484.2	76.8
60	2448.4	1718.9	70.2
65	2741.7	1815.6	66.2

<sup>a</sup> Fitted watts in= $198.1+28.83T-0.0227T^2+0.002787T^3$

<sup>b</sup> Fitted watts out= $0+32.48T^2+0.1011T^3-0.00002826T^4$

Where  $T$ =torque in oz-ft.

The efficiency values are simply the watts output divided by the watts input. While these numbers look fairly respectable, there are undoubtedly some ordinary test errors in the readings of speed, torque, and watts.

Table 7.9 comprises data fitted to a polynomial to “smooth” the readings and minimize the error using what is called the least-squares error technique. As shown in the equations following Table 7.9, the watts input were fitted to a third-degree polynomial as a function of torque. The curve-fitting program showed that the third-degree equation had the least residual error based on the data entered into the program. Likewise, the watts out resulted in a fourth-degree equation with the least residual error. The efficiency values were simply computed using the fitted watts out and watts input values. The value of such a routine is that the curves can simply be plotted with a PC and a plotter to get both smooth and statistically correct curves. The same routine can be used to compute and plot power factor, if desired.

### 7.2.6 Miscellaneous Tests

The temperature-rate-of-rise test was mentioned briefly earlier. (See Section 7.5.3.2 for a description of the calculation that can be made to estimate the temperature-rate-of-rise.) This test, which is common with hermetic motor parts, is taken with the rotor locked. Visual access to the stator winding and rotor end rings is required since a thermal-acting paint or wax is applied to the parts to be measured. When the parts have reached the transformation temperature of the applied material, the paint or wax will melt and change appearance. Another method that is highly preferred uses an infrared sensing “gun” that is aimed at the part to be measured. When used with a black paint having an emissivity of 1.00, the system can be calibrated for that emissivity and the temperature continuously recorded and plotted.

The friction and windage test is important if a complete separation of losses is desired. Historically this has been taken at no-load with decreasing voltage until the line current begins to rise. Then the resultant input power is plotted on cartesian coordinate graph paper against an abscissa of voltage. This works in theory, but in actual practice it has many problems. The author has found that using semi-logarithmic paper is a great improvement. Power is plotted on the log scale and the voltage on the linear scale. A straight line with four or five points gives a fairly accurate determination of friction and windage.

## 7.3 SYNCHRONOUS MOTOR TESTS\*

### 7.3.1 Electrical Test Standards

Adequate safety precautions should be taken for all tests because of the possibly dangerous currents, voltages, and forces that may be encountered. No attempt is made here to list all possible applicable standards or to review the manifold general safety precautions that are well established in industry.

The references at the end of this chapter include a large number that are applicable to synchronous motors. Of these, Refs. 13 and 14 are probably the most relevant, but anyone with the responsibility for testing synchronous motors should consult Refs. 6, 12, and 15 through 44 in order to understand the full scope of synchronous motor testing.

### 7.3.2 Types of Tests

It is not intended that this section cover all possible tests, or tests of a research nature, but only those more general methods that may be used to obtain performance data. For further details, one is referred to ANSI/IEEE Standard 115–1983 [13]. The following kinds of tests are discussed below: torque tests; temperature tests; load excitation; saturation curves, segregated losses, and efficiency; sudden short-circuit tests and machine parameters; standstill frequency response tests and machine parameters; miscellaneous tests.

#### 7.3.2.1 Torque Tests

While the pull-out torque is a synchronous quantity, the asynchronous quantities are locked-rotor torque, pull-up torque, breakdown torque, pull-in torque, and locked-rotor current.

##### 7.3.2.1.1 Locked-Rotor Current and Torque

When saturation effects can be neglected, the locked-rotor current varies directly with the voltage and the power with the square of the voltage. Otherwise, the test should be taken at enough values to plot a curve of current versus voltage that may be extrapolated to give the current at the specified voltage. Typical test data are shown in Fig. 7.6.

\* Portions of this section have been reprinted from IEEE Std. 115–1983, *IEEE Test Procedures for Synchronous Machines*, copyright © 1983 [13] and IEEE Std. 115A-1987, *IEEE Standard Procedures for Obtaining Synchronous Machine Parameters by Standstill Frequency Response Testing*, copyright © 1987 [14] by the Institute of Electrical and Electronics, Inc., with the permission of the IEEE.

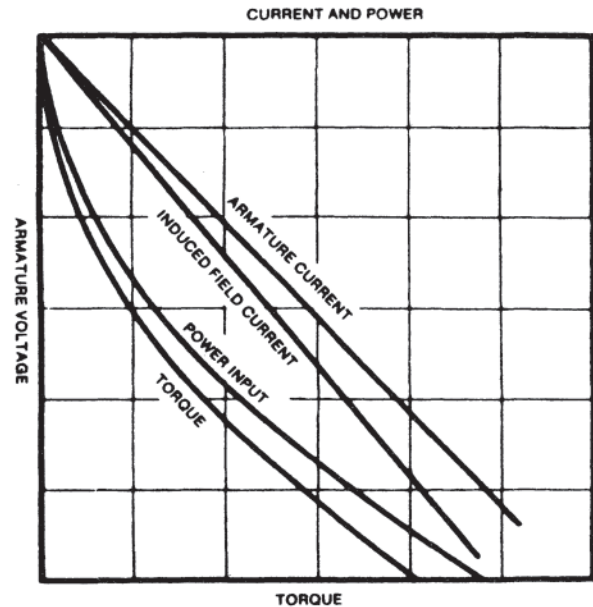


Figure 7.6 Torque characteristics with locked rotor.

*Method 1: Torque by scale and beam* The air gap torque in this case equals the mechanical output torque and hence may be calculated as follows:

$$T_g = \frac{T_l}{T_n} \text{ (per-unit)} \quad (7.5)$$

where

$T_g$  = the air-gap torque at test conditions, per-unit on the output base

$T_l$  = the mechanical output torque of motor at test condition, given by  $F l$ , where  $F$  is the net force (newtons in the SI system or pounds in the English system) and  $l$  is the lever arm (meters in the SI system or feet in the English system)

$T_n$  = the base mechanical output torque of the motor, given by

$$T_n = \left( \frac{k P_{MN}}{n_s} \right) \quad (7.6)$$

where  $n_s$  is the synchronous speed in rpm,  $P_{MN}$  is the rated output of the motor being tested (kW in the SI system or hp in the English system), and  $k$  is 9549 in the SI system or 5252 in the English system.

*Method 2: Torque by electric input* The per-unit air gap torque is computed as power input to the rotor in kilowatts divided by rated power output converted to kilowatts. The input to the rotor is calculated by subtracting the short-circuit loss at the test current from the test power input.

The locked-rotor torque, which is defined as the value for the rotor position giving the minimum torque with rated voltage applied, may be adjusted to a value corresponding to specified voltage as follows:

$$T_{L,R} = T_g \left( \frac{I_s}{I_t} \right)^2 \text{ per-unit} \quad (7.7)$$

where:

- $T_{L,R}$  = the locked-rotor torque corresponding to the specified voltage, per-unit on the output base
- $T_g$  = the air gap torque at test conditions (per-unit)
- $I_s$  = the locked-rotor current at the specified voltage, usually rated, and
- $I_t$  = the value of locked-rotor current from the same test as used to determine  $T_g$ .

### 7.3.2.1.2 Speed-Torque Tests

In order to determine sufficient data to plot a speed-torque curve for a motor, any one of the following four methods may be used. The selection of the method will depend upon the size and the speed-torque characteristics of the machine and the testing facilities. From the results of the following tests, adjusted to the specified voltage, plots of per-unit torque, per-unit armature current, and induced field current in amperes should be obtained as a function of speed.

*Method 1: Measured output* A direct-current generator with predetermined losses is coupled or belted to the motor being tested. The total power output of the motor is the sum of the output and the losses of the dc generator. The air gap torque,  $T_g$ , at each speed is calculated as follows:

$$T_g = \frac{k(P_{GO} + P_{GL})n_s}{P_{MN}(n)} + T_{FW} \text{ (per unit on the output base)} \quad (7.8)$$

where:

- $P_{GO}$  = the output of the dc generator (kW)
- $P_{GL}$  = the losses of the dc generator (including friction and windage) (kW)
- $T_{FW} = k(P_{FW})n_s | P_{MN}^n$  represents motor friction and windage torque in per unit on the output base
- $P_{FW}$  = the motor friction and windage loss (kW) at the test point speed
- $n_s$  = the synchronous speed of the motor (rpm)
- $n$  = the test speed of the motor (rpm)
- $P_{MN}$  = is the rated output of the motor being tested (kW in the SI system or hp in the English system)
- $k$  = is 1.0 in the SI system or 1.341 in the English system.

*Method 2: Acceleration* In this method the motor is started as an induction motor with no load and the value of acceleration is determined at various speeds. The torque at each speed is calculated from the acceleration and the moment of inertia of the rotating parts. Accurate measurements of speed and acceleration are essential requirements of this method. Speed-time curves should be plotted very carefully to a large scale. The air gap torque,  $T_g$ , at each speed is computed from the acceleration as follows:

$$T_g = \left( \frac{(k \times 10^{-6}) J n_s (dn/dt)}{P_{MN}} \right) + T_{FW} \text{ (per unit on the output base)} \quad (7.9)$$

where:

- $n_s$  = the synchronous speed (rpm)
- $dn/dt$  = the acceleration at each speed in (rpm/s)
- $T_{FW}$  = the torque due to friction and windage at each speed in per unit on the output base
- $J$  = the moment of inertia of rotating parts (kg-m<sup>2</sup> in the SI system of lb-ft<sup>2</sup> in the English system)
- $P_{MN}$  = the rated output of motor being tested (kilowatts in the SI system, or horsepower in the English system)
- $k$  = 10.97 in the SI system or 0.6197 in the English system

*Method 3: Input* The torque in this method is computed by subtracting the losses in the machine from the input power. This method is particularly useful when the machine cannot be unloaded to determine torque by acceleration. The air gap torque,  $T_g$ , at each speed is computed from the input power as follows;

$$T_g = k \left( \frac{P_{si} - P_{sc} - P_c}{P_{MN}} \right) \text{ (per unit on the output base)} \quad (7.10)$$

where:

- $P_{si}$  = the input power to the stator (kW)
- $P_{sc}$  = the short-circuit loss at the test current (kW)
- $P_c$  = the open-circuit core loss at the test voltage (kW)
- $P_{MN}$  = the rated output of the motor being tested (kW in the SI system or hp in the English system)
- $k$  = 1.0 in the SI system or 1.341 in the English system

*Method 4: Direct measurement* The torque may also be measured by loading the machine at various speeds with a dynamometer or prony brake. The use of a prony brake is limited to tests on very small machines because of its limited capacity to dissipate heat. The air gap torque,  $T_g$ , at each speed is calculated from the torque readings,  $T_t$ , as follows:

$$T_g = \frac{T_t}{T_n} + T_{FW} \text{ (per unit on the output base)} \quad (7.11)$$

where:

- $T_t$  = the mechanical output torque of the motor at the test condition
- $T_n$  = the base mechanical output torque of the motor
- $T_{FW}$  = the torque due to motor friction and windage at each speed (per-unit on the output base)

### 7.3.2.1.3 Pull-Out Torque

Two methods are described below.

*Method 1: Direct measurement* This method is not usually practical for large machines. In this method the motor is running at synchronous speed and the load is increased while the voltage, frequency, and field current are kept at normal rated-load values. At various points up to the maximum stable load, the armature input power and current are read. The losses of the motor at this maximum load are determined and subtracted from the input to obtain the maximum output power.

The maximum output power divided by rated output in consistent units is the per-unit pull-out torque.

*Method 2: Calculation from machine constants* For machines for which it is not practical to use Method 1, an approximate value of the pull-out torque,  $T_{PO}$ , at specified voltage and field current (normally rated-load values) may be calculated by the following equation:

$$T_{PO} = \frac{KI_{FL}E_S}{I_{FSI}\eta \cos \theta} \quad (\text{per unit}) \quad (7.12)$$

where:

$T_{PO}$  = the pull-out torque (per-unit of the base mechanical output torque)

$E_S$  = the specified terminal voltage (per-unit)

$I_{FL}$  = the specified field current (amperes or per-unit)

$I_{FSI}$  = the field current corresponding to base armature current on the short-circuit saturation curve in the same units as  $I_{FL}$

$\cos \theta$  = the rated power factor

$\eta$  = the efficiency at rated load (per unit)

$K$  = a factor to allow for reluctance torque and for positive-sequence  $PR$  losses. This is usually in the range of 1.00 to 1.25; it can be calculated from the maximum value of the following equation as a function of  $\delta$ :

$$K = \sin \delta + \frac{I_{FSI}E_S(x_d - x_q)}{2I_{FL}x_dx_q} \sin 2\delta \quad (7.13)$$

in which:

$x_d$  = is the direct-axis synchronous reactance (per-unit)

$x_q$  = the quadrature-axis synchronous reactance (perunit)

$\delta$  = the load angle between terminal voltage and the voltage that would be generated by the field current acting alone.

### 7.3.2.2 Temperature Tests

Temperature tests are made to determine the temperature rise of certain parts of the machine above the ambient temperature, when running under a specified loading condition. The following four methods of loading are most commonly used for temperature testing.

*Method 1: Conventional loading* The preferred method of making a temperature test is to hold the specified conditions of armature current, power, voltage, and frequency (with a constant field current) until the machine reaches constant temperature, taking readings every half hour or less.

*Method 2: Synchronous feedback* Considerable energy savings result from this method of loading if another synchronous machine similar to the one being tested is available. This method also enables full-load testing of machines rated far in excess of the available supply capability. The two machines are coupled together and connected electrically so that one serves as a motor and the other as a generator. The output of the generator is fed electrically to supply the motor. The losses of the two machines may be supplied by a third machine (a motor), deriving its power from the local electrical utility.

*Method 3: Zero power factor* The machine is operated at no load as a synchronous capacitor, maintaining appropriate conditions of armature current, voltage, and frequency until the machine reaches constant temperature.

*Method 4: Open-circuit and short-circuit loading* This method consists of three separate heat-run tests with the motor being driven as a generator:

1. Specified voltage with the armature terminals open-circuited
2. Specified armature current with the terminals short-circuited
3. Zero excitation

The armature temperature rise is then computed as the sum of the temperature rises for the open-circuit and short-circuit tests, corrected for the duplication of heating due to windage, for which the data can be obtained from the zero-excitation no-load test.

#### 7.3.2.2.1 Duration of Tests

Continuous loading tests should be continued until machine temperatures have become constant within  $\pm 2\%$  of the rise value for three consecutive half-hourly readings. For loads corresponding to the short-time rating of the machine, the test should be started from conditions as specified, and continued for the time specified. For intermittent loads, the load cycle specified should be applied and continued until the temperature rise at the end of the load causing greatest heating varies by less than  $2^\circ\text{C}$  for three consecutive cycles.

#### 7.3.2.2.2 Methods of Measuring Temperature

There are four ways to determine temperatures or changes of temperature of various motor parts, namely by (1) thermometers (including alcohol and mercury thermometers and temperature-sensitive resistive devices), (2) thermocouples, (3) infrared detectors, and (4) winding resistance changes. Each of these schemes has characteristics that make it most suitable for a specific task and deficiencies that make it unsuitable for others.

Thermometers are most likely to be selected for temperature measurements on the machine's outer surface. Thermocouples and some temperature-sensitive resistive devices are used when the temperature at a specific stationary location inside or outside the motor is of interest. Infrared detectors are capable of reading temperatures of moving parts and of locating hot spots by thermography techniques. The increase of winding resistance with temperature is used when the average winding temperature is of interest. Thermocouples and temperature sensitive-resistive devices cannot determine the average winding temperature, and the increase in winding resistance is not directly related to the existence and location of hot spots, if any.

#### 7.3.2.3 Load Excitation

When field current exceeds that corresponding to unity power factor at the test voltage and power, the machine is considered to be overexcited. Conversely, when the field current is less than that corresponding to unity power factor, the machine is underexcited. The load field current of a synchronous machine may be determined by any of the following methods.

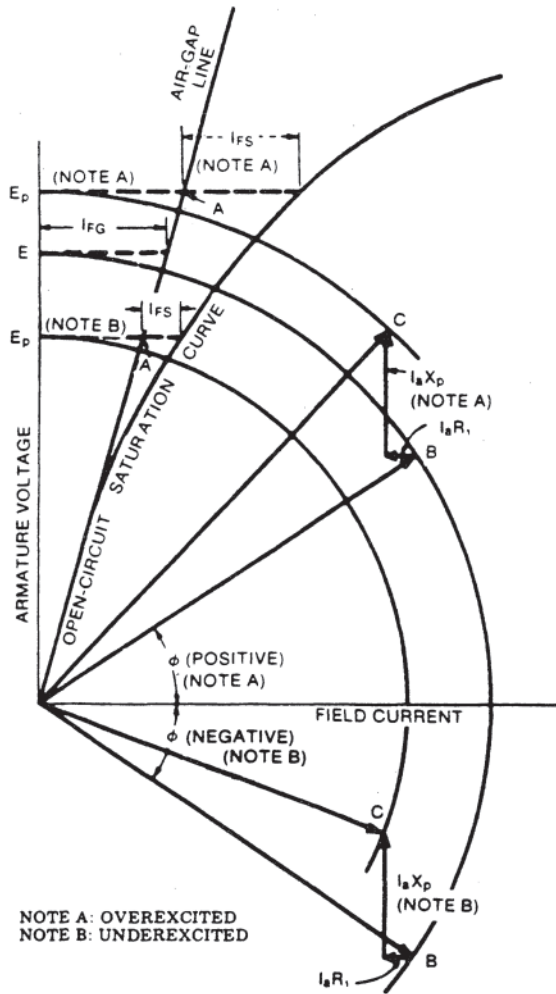


**Figure 7.7** Diagram for the voltage back of the Potier reactance for a synchronous motor.

*Method 1: Loading at specified conditions* The field current for a specified armature current, power factor, and voltage may be obtained directly by loading the machine at the specified conditions and measuring the field current required. Particularly on large machines, this method is not generally applicable to factory tests. The synchronous feedback method of loading can be used in factory testing when two similar machines are available.

*Method 2: Potier reactance method* The field current for specified conditions can be determined approximately by this method in situations where machines cannot be loaded to specified conditions. Using a load value of Potier reactance,  $X_p$ , the excitation under the specified load can be calculated. If the machine cannot be loaded, a test value of zeropower-factor Potier reactance may be used.

Calculation of load excitation from test data using Potier reactance is illustrated in Fig. 7.7 for the case of a synchronous motor.

The voltage  $E_p$  back of the Potier reactance may be calculated from the following equation:

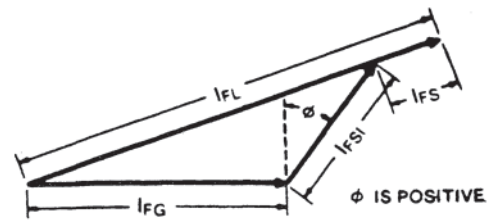


**Figure 7.8** Determination of load field current: over-excited operation.

$$E_p = \sqrt{(E \cos \phi - I_a R_i)^2 + (E \sin \phi + I_a X_p)^2} \text{ (per unit)} \quad (7.14)$$

where

- $x_p$  = the Potier reactance (per unit)
- $E$  = the specified armature terminal voltage (per unit)
- $I_a$  = the specified armature current (per unit)
- $R_i$  = the positive-sequence resistance (per unit)
- $\phi$  = the power-factor angle (positive for overexcited operation and negative for underexcited operation)

The load field current for a specified armature current, power factor and voltage may be obtained as shown in Figs. 7.8 and 7.9. The value of  $I_{FL}$  the load field current, can be determined from the following equation:

$$I_{FL} = I_{FS} + \sqrt{(I_{FG} + I_{FSI} \sin \phi)^2 + (I_{FSI} \cos \phi)^2} \quad (7.15)$$

where:

- $I_{FS}$  = the difference between the field current on the open-circuit saturation curve and the field current on the air gap line, both for the voltage  $E_p$
- $I_{FG}$  = the field current for the air gap line at the specified armature terminal voltage
- $I_{FSI}$  = the field current corresponding to the specified armature current on the short-circuit saturation curve
- $\phi$  = the power-factor angle (positive for overexcited operation and negative for underexcited operation)

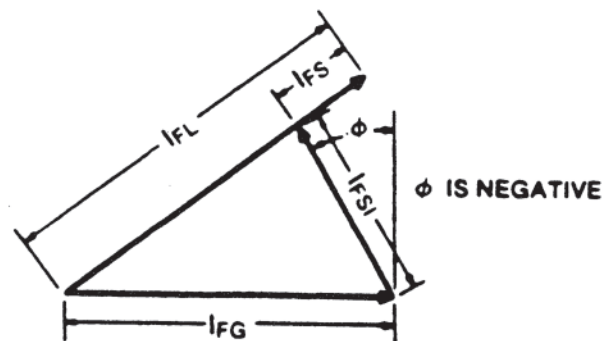


**Figure 7.9** Determination of load field current: under-excited operation.

All values of field current should be in amperes or in per unit on any suitable base.

The load Potier reactance is best obtained from the load test at approximately the specified load conditions with the machine operating overexcited or at unity power factor. Readings should be taken simultaneously of armature voltage, current, active and reactive power, and field current. Along with the test data on the open- and short-circuit saturation curves,  $I_{FS}$  may be calculated as:

$$I_{FS} = I_{FL} - \sqrt{(I_{FG} + I_{FSI} \sin \phi)^2 + (I_{FSI} \cos \phi)^2} \quad (7.16)$$

The voltage,  $E_p$  for the test load can be obtained graphically from the open-circuit saturation curve and the air gap line and the calculated value of  $I_{FS} \cdot x_p$  the Potier reactance at test load, may be calculated as :

$$x_p = \frac{\sqrt{E_p^2 - (E \cos \phi - I_a R_1)^2} - E \sin \phi}{I_a} \quad (\text{per unit}) \quad (7.17)$$

The equivalent Potier reactance from the no-load test may be calculated as

$$x_{p0} = \left( \frac{I_e x_p}{I_a} \right)$$

in per-unit, where  $I_e$  is the equivalent zero-power-factor armature current during the test in per unit,  $I_a$  is the specified armature current in per unit, and:

$$k = \frac{I_e}{I_a} = \frac{\sqrt{(I_{FG} + I_{FSI} \sin \phi)^2 + (I_{FSI} \cos \phi)^2} - I_{FG}}{I_{FSI}} \quad (7.18)$$

in per-unit. Two key features of this method are that the classical  $x_p$  is empirically adjusted down by a factor  $k$ , and the zero-power-factor data are taken near rated field current instead of at rated armature current. In addition to the open- and short-circuit saturation curves from tests, this method requires operating the machine at zero power factor overexcited at rated voltage with the armature current adjusted to an equivalent value,  $I_e$ . The intersection of the no-load  $V$ -curve with the value of armature current  $I_e$  defines  $I_{FL}$  and locates the point  $d'$  shown in Fig. 7.10.

Following the construction illustrated in Fig. 7.10, the equivalent Potier reactance is calculated as  $(I_e x_p / I_a)$  in per unit. This equivalent Potier reactance is used to determine the internal  $E'_p$  voltage corresponding to the specified current and power factor from the following equation:

$$E'_p = \sqrt{E \cos \phi - I_a R_1)^2 - [E \sin \phi + (I_e x_p)]^2} \quad (\text{per unit}) \quad (7.19)$$

The value of  $I_{FS}$  is then determined from the open-circuit saturation curve for the voltage  $E'_p$ . The value of  $I_{FL}$ , the load field current, is then determined from

$$I_{FL} = I_{FS} + \sqrt{(I_{FG} + I_{FSI} \sin \phi)^2 + (I_{FSI} \cos \phi)^2} \quad (7.20)$$

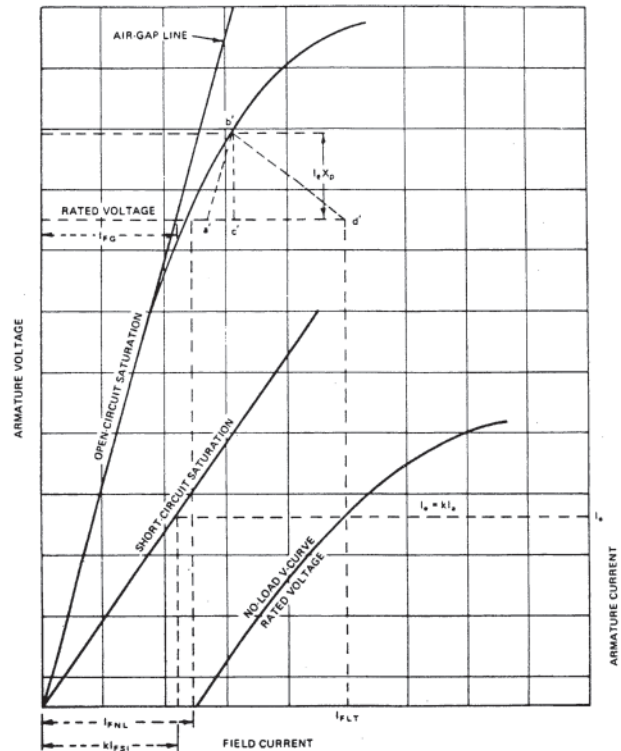


Figure 7.10 Determination of equivalent Potier reactance voltage drop.

for the specific value of  $I_{FSI}$  and power-factor angle. Thus, this method provides an empirical adjustment to the classic Potier reactance method for classes of machine where it is felt that the classic Potier reactance method has historically overstated rated-load field current.

The Potier reactance is determined from the open-circuit saturation curve and from the zero-power-factor overexcited saturation curve. Typical curves are shown in Fig. 7.11. The Potier reactance is obtained by dividing the voltage  $b_e$  in that figure by the per-unit value of current.

### 7.3.2.4 Saturation Curves, Segregated Losses, and Efficiency

The efficiency is the ratio of output power to input power under specified conditions. On small machines, these can be measured directly. On larger equipment where the mechanical power cannot be measured accurately, a conventional efficiency, based on segregated losses, is used. The losses to be considered are:

1. Armature  $I^2R$  loss (corrected to a specified temperature)
2. Field  $I^2R$  loss (corrected to a specified temperature)
3. Friction and windage loss
4. Core loss (on an open circuit)
5. Stray-load loss (on a short circuit)

There are four methods available to measure the losses of a synchronous machine, separate-drive method, electric-input method, retardation method, cooler method. If one of the first

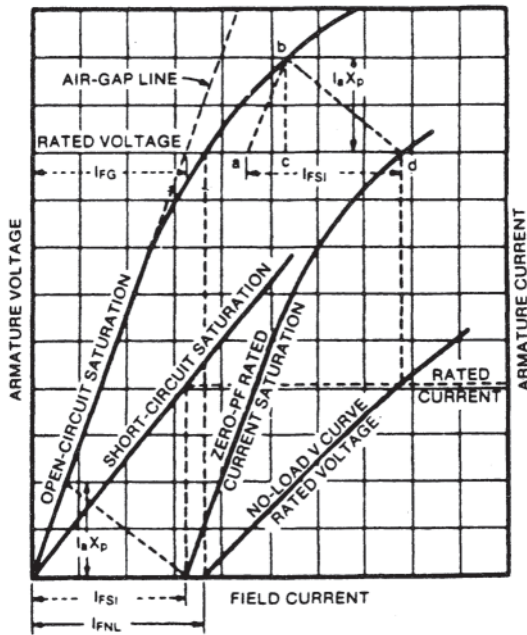


Figure 7.11 Determination of Potier reactance voltage.

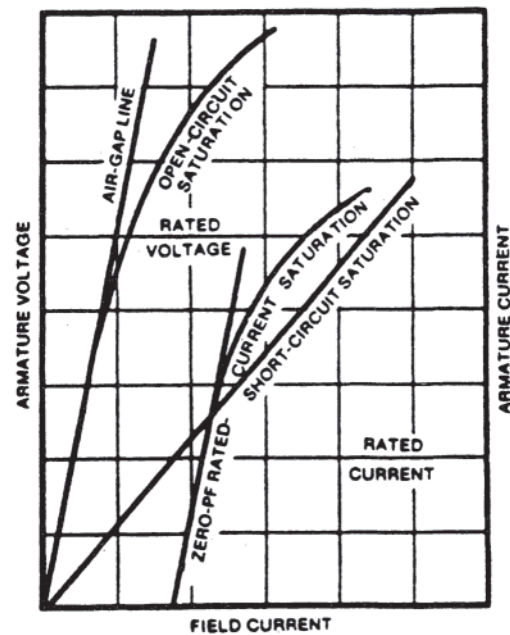


Figure 7.12 Saturation curves.

three methods is used, data for the open-circuit and short-circuit saturation curves are needed for determination of losses. For the first three methods, the machine is to be operated for two series of runs to simulate load conditions, one with the armature terminals open-circuited and the other with them shortcircuited. For the cooler method, the machine may be operated either with load or with simulated load conditions as for the first three methods.

With armature terminals open-circuited, the total loss includes friction and windage of all mechanically connected apparatus and the open-circuit core loss corresponding to the armature voltage and frequency. With armature terminals short-circuited, the total loss includes friction and windage of all mechanically connected apparatus and the armature copper loss as well as stray-load loss corresponding to the armature current and frequency.

*Method 1: Separate-drive method for saturation curves and losses* The machine under test is usually driven by a motor, directly or through a belt or a gear. The driving motor should be capable of operating the driven machine at its rated speed. The input to the driving motor minus the losses of the driving motor (and belt or gear, if any) equals the input to the tested machine.

The open-circuit saturation curve is obtained by driving the machine being tested at rated speed, open-circuited, and recording its armature terminal voltage and field current. Readings for this curve should always be taken with increasing excitation. The results may be plotted as in Fig. 7.12.

The air gap line is obtained from the open-circuit saturation curve by extending the straight-line lower portion. Core loss as well as friction and windage loss can be determined from additional readings taken at the time the open-circuit saturation curve is made. At each value of terminal voltage, the power input to the driving motor is measured. By subtracting

the losses of the driving motor from the power input to the driving motor, the power input to the machine being tested is obtained. The friction and windage loss is the power input to the machine being tested with zero excitation. The core loss at each value of armature voltage is determined by subtracting the friction and windage loss from the total power input to the machine being tested. The core loss may be plotted as in Fig. 7.13.

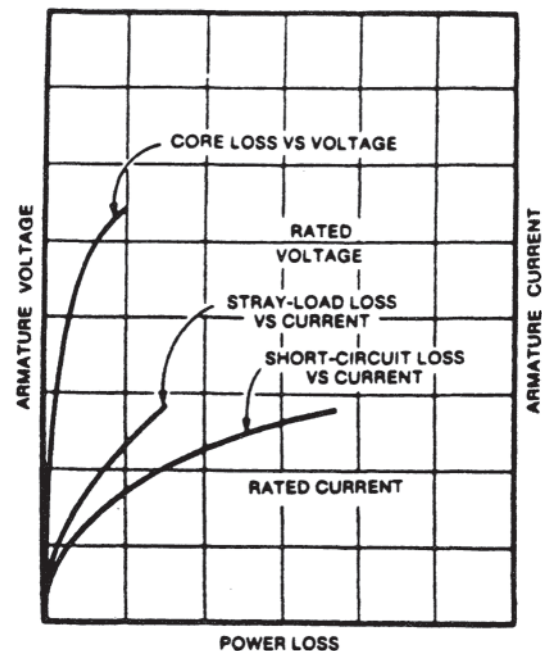


Figure 7.13 Loss curves.



The short-circuit saturation curve is obtained by driving the machine being tested at rated speed, short-circuited, and recording its armature and field currents. Current readings should be taken with decreasing excitation, starting with the value that will produce an armature current equal to the maximum allowed. The results may be plotted as in Fig. 7.12.

The stray-load loss can be determined from additional readings taken at the time the short-circuit saturation curve is made. At each value of armature current, the power input to the driving motor is measured. The driving motor loss should be subtracted from the measured power input to obtain the loss of the machine being tested. The friction and windage loss is subtracted from the loss of the machine to obtain the short-circuit loss, which includes the stray-load loss is obtained by subtracting the armature  $I^2R$  loss calculated for the measured current values and with the dc resistance corrected to the average temperature of the winding during the test.

The zero-power—factor saturation curve may be obtained by overexciting the machine being tested while it is connected to a load consisting of idle-running, underexcited, synchronous machines. By proper adjustment of the excitation of the machine being tested and that of its load, the terminal voltage may be varied while the armature current of the machine being tested is held constant at the specified value. The zero-power-factor saturation curve, for the machine being tested, is the plot of terminal voltage against field current as shown in Fig. 7.12. This characteristic is used to obtain the Potier reactance. For this purpose, the point at rated current and voltage is often sufficient.

**Method 2: Electric-input method for losses and saturation curves** The machine is run as an unloaded synchronous motor from a power supply of adjustable voltage and steady frequency equal to the rated frequency of the machine being tested. Power input is measured by wattmeters or watt-hour meters under various conditions of voltage and current to obtain the losses. In testing for the open-circuit losses, the machine under test is operated at approximately unity power factor by adjusting for minimum armature current. The measurement of the power input is a very important item in the application of this test method.

If the neutral of the test machine is brought out and is connected to the system during the test, the three-wattmeter connection as in Fig. 7.14 should be used. If the neutral of the test machine is brought out but not connected to the system during the test, either the 3-wattmeter connection (Fig. 7.14)

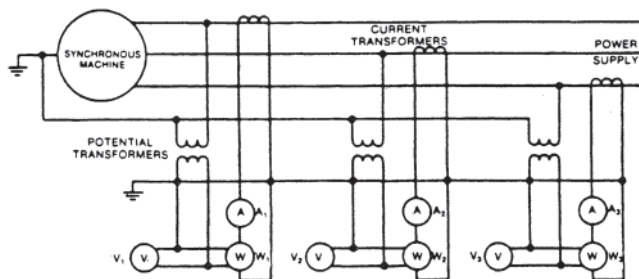


**Figure 7.14** Connection diagram: three-wattmeter method of measuring power.

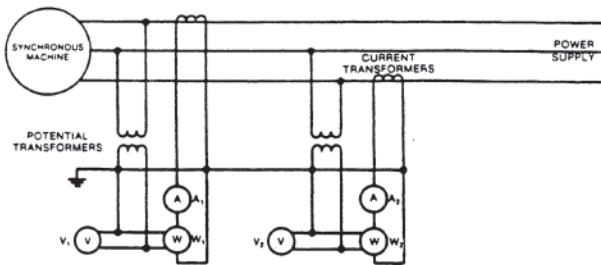


**Figure 7.15** Connection diagram: two-wattmeter method of measuring power.

or the 2-wattmeter connection for measuring three-phase power (Fig. 7.15) may be used.

The electric-input method can be used to determine the open-circuit loss, open-circuit saturation curve, and short-circuit saturation curve with sufficient accuracy using normal instruments and procedures. However, to obtain satisfactory measurement of stray-load loss, special procedures and instruments are necessary. Since the power factor in the measurement for stray-load losses is low and measurements also include two relatively large losses (friction and windage plus  $I^2R$  losses), it is necessary to make corrections for ratio and phase-angle errors of the instrument transformers and for the scale corrections for the wattmeters or error of the watt-hour meters.

The test machine is run as a synchronous motor at approximately unity power factor and at a number of voltages. Readings should be taken of power input (or energy and time), armature voltage, and field current. Open-circuit core loss at each point is equal to the power input less the friction and windage loss and the armature  $I^2R$  loss. The results may be plotted as in Fig. 7.12. Loss data from a typical test are shown in Fig. 7.16.

If the data could be taken to zero voltage, the intercept at the bottom would be the friction and windage loss. In order to find this intercept, a curve, as shown in Fig. 7.17, is plotted with the voltage squared as ordinate and power input as abscissa. For low values of saturation, the core loss varies approximately as the square of the voltage. Therefore, the lower part of the curve of voltage-squared versus power loss is a straight line and can easily be extended to give the intercept on the horizontal axis.

The open-circuit saturation curve can be plotted from the readings of armature voltage and field current taken from the open-circuit loss test. Figure 7.18 shows data from a typical test using the electric-input method. The curve of total loss is composed of friction and windage, core, and short-circuit losses. This may be extrapolated to zero current by first plotting separately the total loss against the square of the armature current and extrapolating this separate curve to zero current as indicated earlier. The total loss at zero current is the sum of core loss plus friction and windage loss. By subtracting this sum from the total loss at any armature current, the short-circuit loss for that armature current is obtained. The short-circuit loss is the sum of  $I^2R$  and stray-load loss. The stray-load loss is then determined by subtracting the armature  $I^2R$  loss calculated for the temperature of the winding during the test.

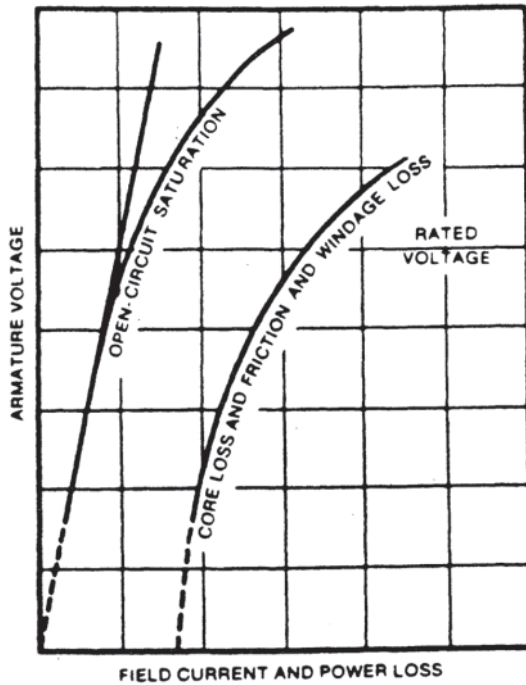


Figure 7.16 Open-circuit saturation and core loss curves by the electric-input method.

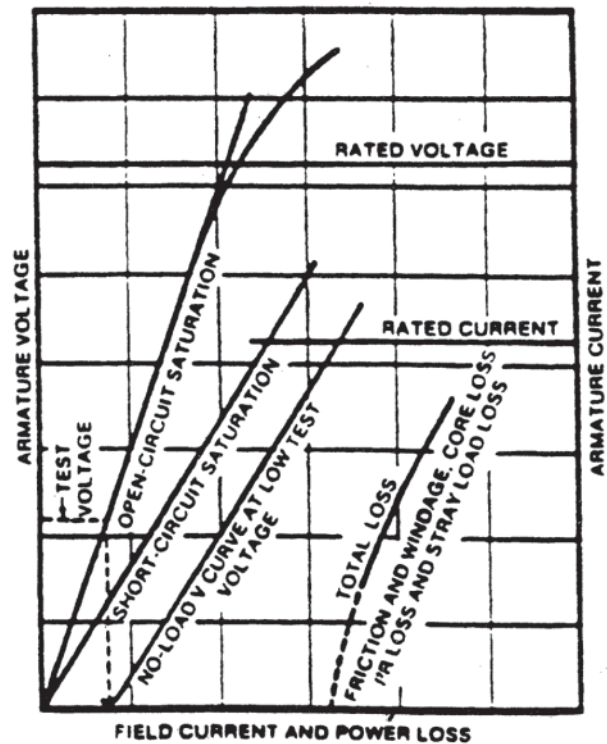


Figure 7.18 Curves from the electric-input method.

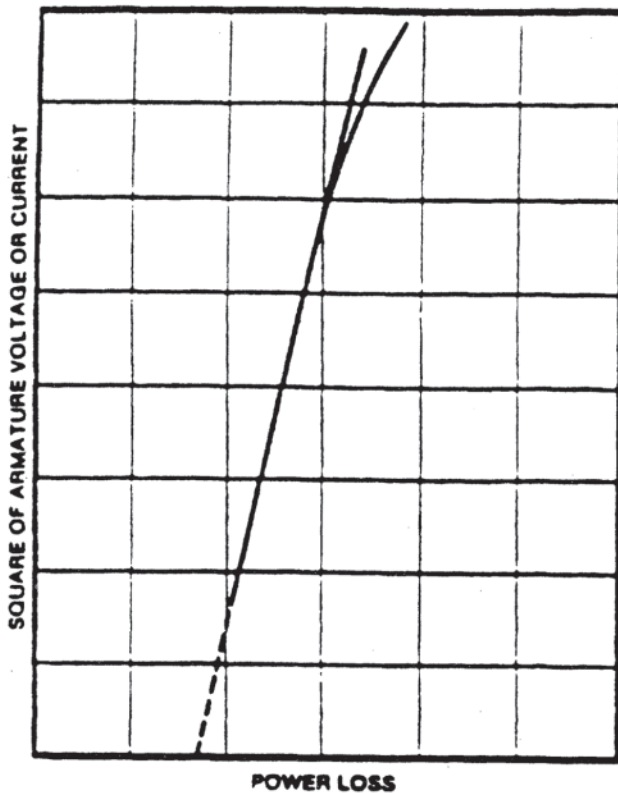


Figure 7.17 Construction curves for extrapolating loss curves from the electric-input method.

The curve resulting from the plotting of armature current versus field current is the overexcited part of a zero-powerfactor V-curve. This curve, extended to zero armature current, should give the same field current as the no-load saturation curve at the voltage at which the test was made. A straight line passing through the origin, parallel to this part of the V-curve, is approximately the same as the short-circuit saturation curve.

*Method 3: Retardation method for losses and saturation curves* This method is useful in factory tests where use of a separate driving motor is not practical or convenient. It is based on the relationship between the rate of deceleration of a rotating mass, its mass and radius of gyration, and the power loss tending to decelerate it. The loss can be determined by:

$$\text{Loss in kilowatts} = k \times 10^{-6} J n \frac{dn}{dt} \tag{7.21}$$

where:

- $n$  = the rotational speed (rpm)
- $dn/dt$  = the rate of deceleration as determined from the slope of speed-time curve at  $n$  (rpm/s)
- $J$  = the moment of inertia of rotating parts ( $\text{kg}\cdot\text{m}^2$ ) in the SI system or  $\text{lb}\cdot\text{ft}^2$  in the English system, and
- $k$  = 10.97 in the SI system or 0.4621 in the English system.

When a motor is permitted to decelerate without any excitation and with its terminals open-circuited, the power tending to decelerate it is the friction and windage loss. The

total open-circuit loss is obtained by providing constant excitation during a retardation test with the armature terminals open-circuited. This test should be made at several values of excitation in order to make a plot of open-circuit core loss versus voltage at rated speed. By subtracting the friction and windage loss from the total open-circuit loss for each test, the open-circuit core loss is obtained.

The short-circuit loss plus friction and windage loss is obtained by providing constant excitation during a retardation test with the armature terminals short-circuited. This test should be made at several values of excitation in order to make a plot of short-circuit loss and stray-load loss versus armature current at rated speed. By subtracting the friction and windage loss, the short-circuit loss for each test is obtained. By subtracting the  $I^2R$  loss calculated at the temperature of the winding from the short-circuit loss for each test, the stray-load loss is obtained.

Figure 7.19 shows typical retardation curves.

**Method 4: Cooler method for losses** This method can be used on machines with water coolers in which the ventilating medium circulates in a closed system. It is based on the fact that the loss is equal to the heat added to the water plus the heat lost by radiation and convection. The equation for the loss absorbed by the water is:

$$\text{Loss} = 0.264(t_h - t_c) Q \text{ (kW)} \quad (7.22)$$

where:

$t_h$  = the temperature of the water leaving the cooler ( $^{\circ}\text{C}$ )

$t_c$  = is the temperature of the water entering the cooler ( $^{\circ}\text{C}$ ) and

$Q$  = is the rate of water flow (gallons per minute)

Because the difference between  $t_h$  and  $t_c$  is usually small, it is very important that all temperature measurements be accurate within  $0.1^{\circ}\text{C}$ . The rate of flow of water can be measured by a calibrated flowmeter. The heat lost by radiation and convection may be estimated by:

$$\text{Loss} = 0.008(t_r - t_a) \text{ (W/in}^2\text{)} \quad (7.23)$$

where

$t_r$  = the average temperature of the entire radiating surface ( $^{\circ}\text{C}$ )

$t_a$  = the ambient temperature ( $^{\circ}\text{C}$ )

The conventional efficiency is related to the sum of the segregated losses as follows:

$$\text{percentage efficiency} = 100 - \frac{\text{losses} \times 100}{\text{input}} \quad (7.24)$$

The efficiency from the input-output method is determined by:

$$\text{Percentage efficiency} = \frac{\text{output}}{\text{input}} \times 100 \quad (7.25)$$

The preferred method of measuring output of a motor is to use a dynamometer. Power input is obtained from:

$$\text{Power} = \frac{nT}{k} \text{ (kW)} \quad (7.26)$$

where:

$n$  = the rotational speed in revolutions per minute

$T$  = the torque N-m or lb-ft.

$k$  = 9549 if  $T$  is in N-m, or 7043 if  $T$  is in lb-ft

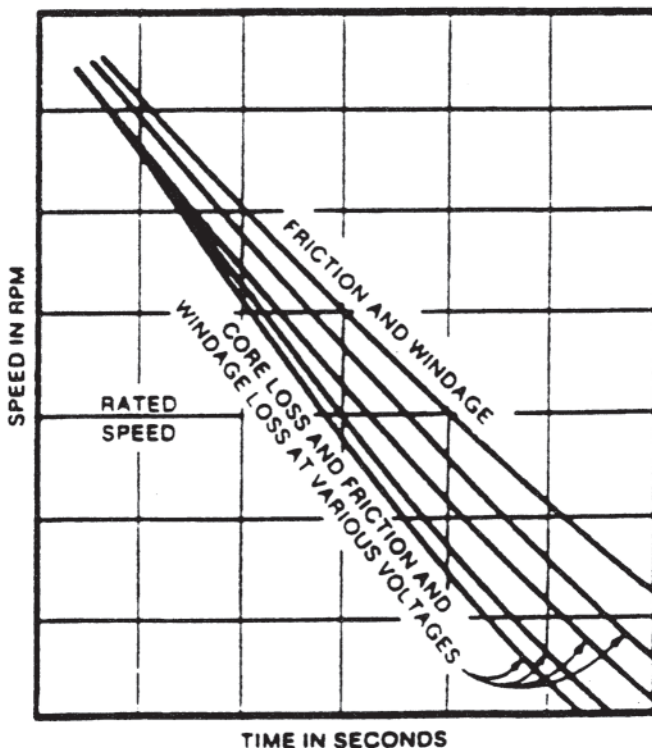
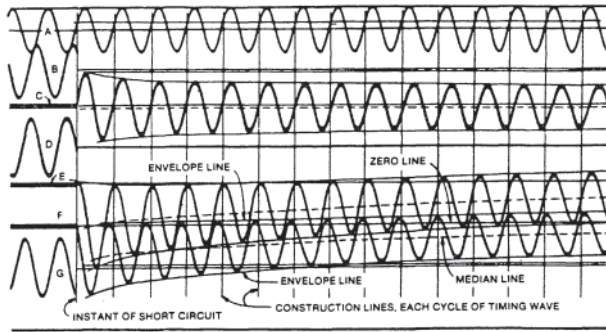


Figure 7.19 Typical retardation curves.

### 7.3 2.5 Sudden Short-Circuit Tests and Machine Parameters

Sudden short-circuit tests are conducted to show that the mechanical design of the machine is adequate to withstand the stress due to short circuits and related abnormal operating conditions, and also to determine certain characteristics, such as reactances and time constants. When test results are to be determined from the varying values of current and voltage during the early stages of a short circuit before steady state has been reached, the currents and voltages should be determined from oscillograms. Extreme care in calibration of the oscillograph and in scaling values from the oscillograms is required to obtain the desired accuracy. The derivation of transient and subtransient reactances and time constants from sudden shortcircuit test data is based on the assumption that the generator field voltage is maintained constant during the transient. Typical data of a three-phase short-circuit suddenly applied to the machine operating open-circuited at rated speed is shown in Fig. 7.20.

For a motor, base three-phase power is taken as the apparent power input to the machine when operating at rated voltage and power factor and delivering rated load.



**Figure 7.20** Oscillogram of three-phase sudden short-circuit. Trace A, timing wave. Traces B, D, and G, armature voltages. Traces C, E, and F, armature currents.

### 7.3.2.5.1 Direct-Axis Synchronous Reactance, $x_d$

For machines of normal design, the magnitude of the direct-axis synchronous reactance is so nearly equal to that of the direct-axis synchronous impedance,  $z_d$ , that the two may be taken to have the same numerical value in per unit  $z_d$  in per unit is equal to the ratio of the field current,  $I_{FSI}$ , at base armature current (from the short-circuit test) to the field current,  $I_{FG}$ , at base voltage on the air gap line (from the open-circuit test):

$$z_d = \frac{I_{FSI}}{I_{FG}} = x_d \text{ (per unit)} \quad (7.27)$$

### 7.3.2.5.2 Quadrature-Axis Synchronous Reactance, $x_q$

**Method 1: Slip test** The slip test is conducted by driving the rotor at a speed very slightly different from synchronous with the field open-circuited and the armature energized by a three-phase, rated frequency, positive-sequence power source at a voltage below the point on the open-circuit saturation curve where the curve deviates from the air gap line. Figure 7.21 illustrates the method even though the slip shown to illustrate the relationships is higher than that which should be used in practice.

Approximate values of  $x_q$  and  $x_{ds}$  designated by  $x_{qs}$  and  $x_{ds}$  are found as:

$$x_{qs} = \frac{E_{\min}}{I_{\max}} \text{ (per-unit)} \quad (7.28)$$

$$x_{ds} = \frac{E_{\max}}{I_{\min}} \text{ (per-unit)} \quad (7.29)$$

More accurately, if  $x_d$  has already been determined by short-circuit and open-circuit test data, the following relationships can be applied:

$$x_q = x_d \left( \frac{x_{qs}}{x_{ds}} \right) \text{ (per unit)} \quad (7.30)$$

$$x_q = x_d \left( \frac{E_{\min}}{I_{\max}} \right) \left( \frac{I_{\min}}{I_{\max}} \right) \text{ (per unit)} \quad (7.31)$$

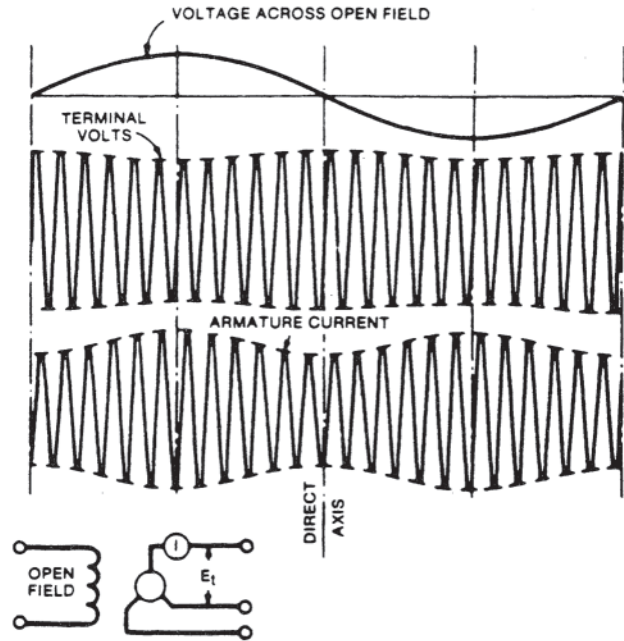


**Figure 7.21** Slip method of obtaining quadrature-axis synchronous reactance.

If the slip is not extremely low, currents induced in the damper winding will produce an appreciable error.

**Method 2: Maximum lagging current** The machine to be tested is run as a synchronous motor with no driven load, with applied test voltage not greater than 75% of normal, and with approximately normal no-load excitation. The field excitation is then reduced to zero, reversed in polarity, and then gradually increased with the opposite polarity, causing an increase in armature current. By increasing the negative excitation in small increments until instability occurs, the per-unit line current  $I_t$  corresponding to the maximum stable negative excitation is determined.  $x_q$  is then obtained as:

$$x_q = \frac{E}{I_t} \text{ (per unit)} \quad (7.32)$$

where  $E$  is the per-unit armature voltage.

### 7.3.2.5.3 Direct-Axis Transient Reactance, $x'_d$

Following a three-phase short-circuit from no load, neglecting armature-circuit resistances and assuming constant exciter voltage, the alternating current rms components of armature current in per unit are assumed to be given by:

$$I = \frac{E}{x_d} + \left( \frac{E}{x'_d} - \frac{E}{x_d} \right) e^{-0t\tau'_d} + \left( \frac{E}{x''_d} - \frac{E}{x'_d} \right) e^{-0t\tau''_d} \quad (7.33)$$

where:

- $E$  = ac rms voltage before short-circuit (per unit)
- $t$  = the time (S) measured from the instant of short-circuit
- $x''_d$  = the subtransient reactance (per unit)
- $\tau'_d$  = the transient time constant (S)
- $\tau''_d$  = the subtransient time constant (S)

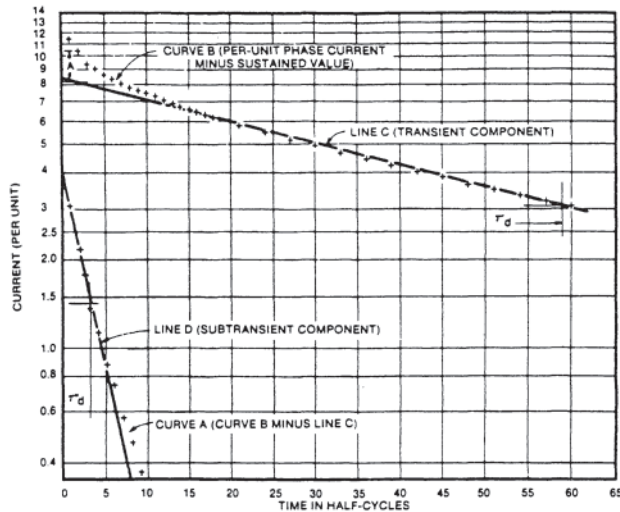


**Figure 7.22** Analysis of alternating-current components of short-circuit current (a typical phase).

The current is taken to be composed of a constant term and two decaying exponential terms, where the third term of the equation decays very much faster than the second. Subtracting the first constant term and plotting the remainder on semilogarithmic paper as a function of time, the curve appears as a straight line after the rapidly decaying term decreases to zero. The subtransient current is the rapidly decaying part of the current, while the straight line is the transient current. Because of several factors such as saturation and eddy-current effect, the actual short-circuit may not follow the above form of variation precisely. The range of time to be used in making the semilog plot is usually the first half second following the short-circuit. Typical results are shown in Fig. 7.22:

$x'_d$  is then given by

$$x'_d = \frac{E}{I'} \text{ (per unit)} \tag{7.34}$$

where:

- $E$  = the per-unit open-circuit armature voltage at normal frequency immediately before short-circuit
- $I'$  = the per-unit transient component of current at the moment of short-circuit, plus the steady-state component

Table 7.10 gives an example of determination of transient and subtransient reactances.

### 7.3.2.5.4 Direct-Axis Subtransient Reactance, $x''_d$

The direct-axis subtransient reactance is given by

$$x''_d = \frac{E}{I''} \text{ (per unit)} \tag{7.35}$$

where:

- $E$  = the per-unit open-circuit voltage at normal frequency immediately before short-circuit
- $I''$  = the per-unit initial ac component of short-circuit current

The three-phase suddenly applied short-circuit test used for determination of  $x'_d$  can also be used to determine  $x''_d$ . A typical procedure is shown in Fig. 7.22 and typical calculations are shown in Table 7.10.

### 7.3.2.5.5 Quadrature-Axis Subtransient Reactance, $x'_q$

For the applied-voltage test used, the rotor is stationary and the field winding is short-circuited through a suitable alternating current (ac) ammeter or current transformer supplying an ammeter. Single-phase voltage of rated frequency is applied to any two stator terminals, the third being isolated. The connections are shown in Fig. 7.23.

The armature voltage and current as well as the field current are recorded. A quantity  $A$  is calculated as:

$$A = \frac{E}{I} \text{ (per unit)} \tag{7.36}$$

**Table 7.10** Example of Determination of Transient and Subtransient Reactances

	Phase 1	Phase 2	Phase 3	Average
(1) Initial voltage	—	—	—	0.994
(2) Steady-state current	1.4	1.4	1.4	
(3) Initial transient component	9.4	10.2	9.3	
(4) $I' = (2) + (3)$	10.8	11.6	10.7	11.0
(5) Transient reactance $x'_d = (1)/(4)$	—	—	—	0.0904
(6) Initial subtransient component	3.6	5.8	3.8	
(7) $I'' = (4) + (6)$	14.4	17.4	14.5	15.4
(8) Subtransient reactance $x''_d = (1)/(7)$	—	—	—	0.0645
(9) Initial direct-current component	11.0	25.0	13.6	
Identified as	c	a	b	
Weighted average	$I''_{(1)}$	$I''_{(2)}$	$I''_{(3)}$	
(10) $I''$	17.7	17.7	17.4	17.6
(11) $x''_d = (1)/(10)$	—	—	—	0.0565

All values in per unit.

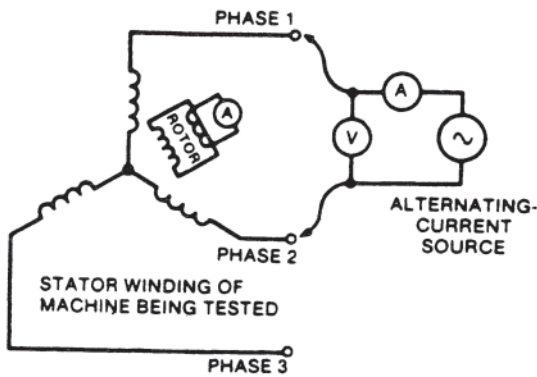


**Figure 7.23** Diagram for determination of direct-axis sub-transient reactance.

where:

$E$  = the applied line-to-line voltage, in per-unit of base line-to-neutral voltage

$I$  = is the line current, in per unit of base line current

As quickly as possible the test voltage is removed and the same voltage is applied to another pair of terminals in the same way. A quantity  $B$  is determined similarly from these readings. Then the test voltage is applied to the third pair of terminals, from which a quantity  $C$  is calculated similarly. It is important that the rotor position remain the same throughout this test. A quantity  $K$  is then calculated as:

$$K = \frac{A + B + C}{3} \quad (7.37)$$

and the amplitude of the sinusoidal component of variation is given by

$$M = \sqrt{(B - K)^2 + \frac{(C - A)^2}{3}} \quad (7.38)$$

The rated-current value of  $x''_q$  is then usually given by

$$x''_q = \frac{K + M}{2} \quad (\text{per unit}) \quad (7.39)$$

corresponding to the largest stationary-rotor reactance.

#### 7.5.2.5.6 Negative Sequence Reactance, $x_2$

The machine to be tested is operated at rated speed with its field winding short-circuited. Symmetrical sinusoidal three-phase currents of negative phase sequence are applied from a suitable source. If the rated-current value of negative-sequence reactance is to be determined, the current should be adjusted until it is approximately equal to rated current of the machine. This test produces abnormal heating in the rotor of the machine being tested and should be concluded as quickly as possible. The line-to-line terminal voltages, the line currents, and the electric power input are measured and expressed in perunit.

The test negative-sequence impedance in per-unit is given by:

$$z_{2t} = \frac{E}{I} \quad (7.40)$$

The test negative-sequence resistance in per unit is given by:

$$R_{2t} = \frac{P}{I^2} \quad (7.41)$$

and the test negative-sequence reactance in per-unit is given by:

$$x_{2t} = \sqrt{z_{2t}^2 - R_{2t}^2} \quad (7.42)$$

where:

$E$  = the average of rms values of the fundamental component of the three line-to-line voltages (per unit)

$I$  = the average of rms values of the fundamental components of the three line currents (per-unit)

$P$  = the electric power input (per-unit)

#### 7.3.2.5.7 Zero-Sequence Reactance, $x_0$

With the neutral terminals of the windings connected together as for normal operation, the three line terminals are also connected together so that the three phases are in parallel. A single-phase alternating voltage is applied between the line terminals and the neutral. It is preferable that the machine be driven at normal speed, with the field short-circuited and with normal cooling. The zero-sequence impedance is obtained by:

$$z_0 = \frac{3E}{I} \quad (\text{per unit}) \quad (7.43)$$

where:

$E$  = the test voltage, expressed in per-unit of base line-to-neutral voltage

$I$  = is the total test current, expressed in per-unit of base line current

In most cases the zero-sequence reactance may be taken as equal to the zero-sequence impedance.

#### 7.3.2.5.8 Positive-Sequence Resistance, $R_1$

This resistance is determined by:

$$R_1 = \frac{1}{z_N} \left( R_a + \frac{W_{LO} \times 10^3}{3I_N^2} \right) \quad (\text{per unit}) \quad (7.44)$$

where:

$R_a$  = the armature resistance per phase corrected to a specified temperature (ohms)

$W_{LO}$  = the stray-load loss at base line current (kW)

$I_N$  = the base line current (A) and

$Z_N$  = the base armature impedance (ohms)

The temperature,  $t_s$ , for which  $R_1$  is determined should be stated.

#### 7.3.2.5.9 Negative-Sequence Resistance, $R_2$

As applied sinusoidal negative-sequence current test is made as in determining the negative-sequence reactance  $x_2$ ,  $R_2$  is obtained from  $P/I^2$  in per-unit.

#### 7.3.2.5.10 Zero-Sequence Resistance, $R_0$

Making a parallel-circuit test as for determining  $x_0$ , the power input  $P$  is measured by a single-phase wattmeter.  $R_0$  is obtained by:

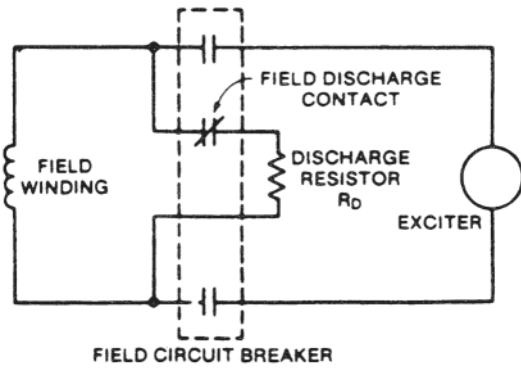


**Figure 7.24** Field winding circuit for direct-axis transient open-circuit time constant.

$$R_0 = \frac{3P}{I^2} \quad (\text{per unit}) \quad (7.45)$$

where:

$P$  = the test power input expressed in per-unit of base single-phase power

$I$  = the total test current, expressed in per-unit of base line current  $\tau'_{d0}$

#### 7.3.2.5.11 Direct-Axis Transient Open-Circuit Time Constant, $\tau'_{d0}$

The machine is operated at rated speed and specified voltage with the armature open-circuited. The field is excited from an exciter through a field circuit breaker using the connections shown in Fig. 7.24.

The field current and voltage should first be measured simultaneously by instruments to obtain the field temperature by resistance at the time of the test. Immediately thereafter, the field circuit breaker is deenergized to short-circuit the field winding, and the armature voltage of one phase, field current, and field voltage are recorded by oscillograph.

The rms residual armature voltage is determined with the field winding open and with the machine operated at rated speed. This residual voltage is subtracted from the rms values of armature voltage obtained from the oscillogram at selected points of time. The resulting varying component of voltage is plotted against time on semilog paper with the armature voltage on the logarithmic scale, as shown in Fig. 7.25.

Normally, the curve is approximately a straight line if a few initial points of rapid decay are neglected. Extrapolation of the curve, neglecting the first few cycles, back to the moment of closing of the field-discharge contact gives the effective initial voltage. The time in seconds for the armature voltage to decay to  $(\Lambda_e)$  or 0.368 times the effective initial voltage is the open-circuit transient time constant,  $\tau'_{d0}$ . It can be corrected to a specified temperature,  $t_s$ , using the following equation:

$$\tau'_{d0} = \tau'_{d0r} \left( \frac{k + t_r}{k + t_s} \right) \quad (\text{seconds}) \quad (7.46)$$

where:

$\tau'_{d0r}$  = the direct-axis transient open-circuit time constant from test

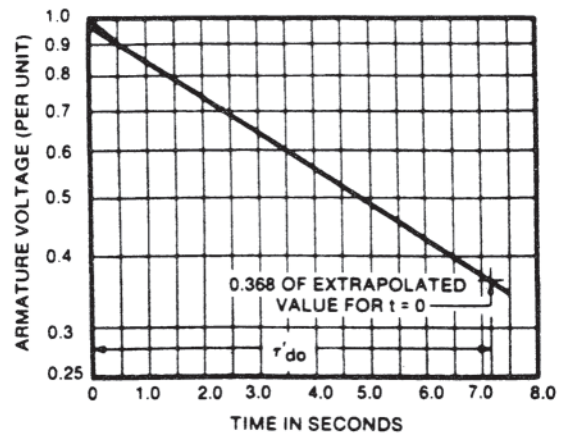


**Figure 7.25** Determination of direct-axis transient open-circuit time constant.

$t_t$  = the field winding temperature during test ( $^{\circ}\text{C}$ )

$t_s$  = the specified temperature ( $^{\circ}\text{C}$ )

$k$  = 234.5 for pure copper or 225 for aluminum, based on a volume conductivity of 62% of pure copper.

#### 7.3.2.5.12 Direct-Axis Transient Short-Circuit Time Constant, $\tau'_{d0}$

This is obtained from the sudden short-circuit test data used to determine  $x'_d$ . It is the time, in seconds, required for the transient alternating component of the short-circuit current (see line C in Fig. 7.22) to decrease to 0.368 times its initial value, as shown in that figure. It may be corrected to a specified temperature in the same way as for  $\tau'_{d0}$ .

#### 7.3.2.5.13 Direct-Axis Subtransient Open-Circuit Time Constant, $\tau''_{d0}$

In a voltage-recovery test, an oscillographic record is made of the line-to-line armature voltages following the sudden opening of a steady-state three-phase short-circuit of the armature when the machine is running at rated speed with a selected value of excitation. The values of armature current in each phase are measured prior to opening the circuit. The differential voltage  $E_{\Delta}$  is obtained at frequent intervals by subtracting the average of the three rms voltages from the average of the three rms steady-state voltages. A semilog plot of the differential voltage is made versus time with the differential voltage on the logarithmic axis (see curve B in Fig. 7.26).

The transient component of differential voltage is the slowly varying portion of the plot and should be extrapolated back to the instant at which the circuit was opened, neglecting the first few cycles of rapid change (see line C of Fig. 7.26). The subtransient voltage (see curve A) is obtained by subtracting the transient component of differential voltage (line C) from the differential voltage (curve B). A semilog plot of the subtransient voltage is made vs. time with the voltage on the logarithmic axis. A straight line D is fitted to this plot, giving preference to the earliest points.  $\tau''_{d0}$  is the time in seconds on the straight line corresponding to 0.368 of the ordinate of the line at the instant of opening the circuit, as shown in the figure.

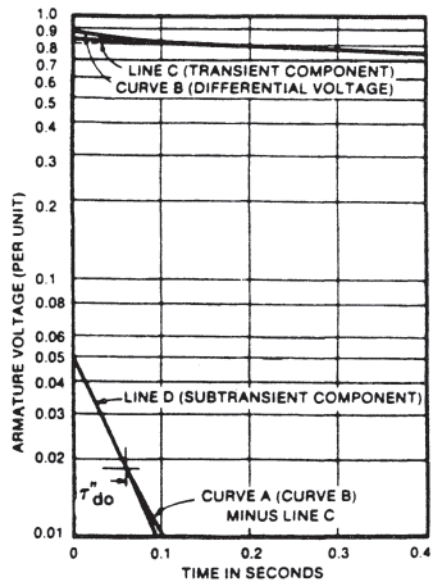


**Figure 7.26** Voltage recovery test for direct-axis subtransient open-circuit constant.

#### 7.3.2.5.14 Direct-Axis Subtransient Short-Circuit Time Constant, $\tau_d''$

This is obtained from the sudden short-circuit test data used to determine  $x_d''$ . It is the time, in seconds, required for the subtransient alternating component of the short-circuit current (see line D in Fig. 7.22) to decrease to 0.368 times its initial value, as shown in that figure.

#### 7.3.2.5.15 Short-Circuit Armature Time Constant, $\tau_a$

From the sudden short-circuit test data, values of the dc components for the three-phase currents are obtained and plotted on a semilog paper as shown in Fig. 7.27.

A resolved value of the dc component,  $I_{dc}$  in per-unit, is calculated for each value of time as follows:

$$I_{dc} = \sqrt{\frac{4}{27}(a^2 + b^2 - ab)} + \sqrt{\frac{4}{27}(a^2 + c^2 - ac)} + \sqrt{\frac{4}{27}(b^2 + c^2 - bc)} \quad (\text{per unit}) \quad (7.47)$$

where:

- $a$  = the largest value of dc component of the three-phase currents at the selected time
- $b$  = the second largest value of dc component (per unit)
- $c$  = the smallest value of dc component (per unit)

The values of resolved current are plotted as a function of time on semilog paper with current on the logarithmic axis. By extrapolating the curve back to the moment of the short circuit, the effective initial current is obtained.  $\tau_a$  is then determined as the time, in seconds, required for the resolved current to reach 0.368 of its initial value. It can be corrected to a specified temperature in the same way as for  $\tau_{d0}'$ .

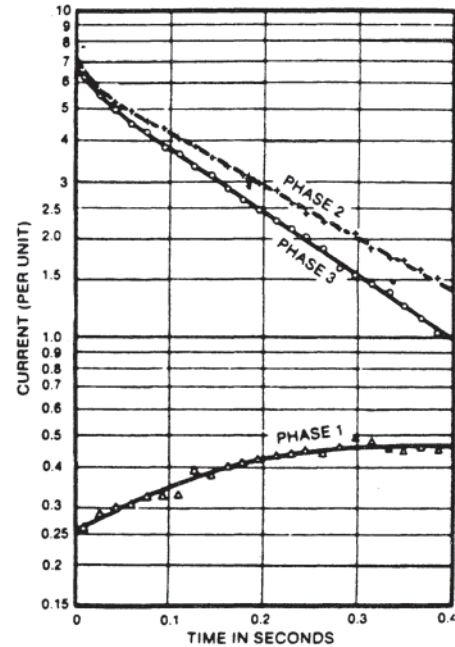


**Figure 7.27** Direct-current components of phase currents.

#### 7.3.2.5.16 Load Angle, $\delta$

The load angle can be approximately calculated using:

$$\delta = \tan^{-1} \frac{I x_q \cos \phi}{E + I x_q \cos \phi} \quad (\text{electrical radians}) \quad (7.48)$$

where:

- $I$  = the per-unit armature current
- $E$  = the per-unit armature terminal voltage
- $\phi$  = is the power-factor angle
- $x_q$  = the per-unit quadrature-axis synchronous reactance.

#### 7.3.2.5.17 Short-Circuit Ratio, SCR

This is given by:

$$\text{SCR} = \frac{I_{FNL}}{I_{FSI}} \quad (7.49)$$

where:

- $I_{FNL}$  = the field current for rated voltage, rated frequency and no load, as obtained from the open-circuit saturation curve and
- $I_{FSI}$  = the field current for rated armature current on a sustained three-phase short circuit at rated frequency, in the same units as  $I_{FNL}$ , as obtained from the short-circuit saturation curve

#### 7.3.2.6 Standstill Frequency Response Tests and Machine Parameters

It has been customary to assume a two-rotor-circuit direct-axis model to describe the synchronous machine mathematically in stability and other related analyses. Figure 7.28 shows the corresponding equivalent circuit. The assumed quadrature-axis



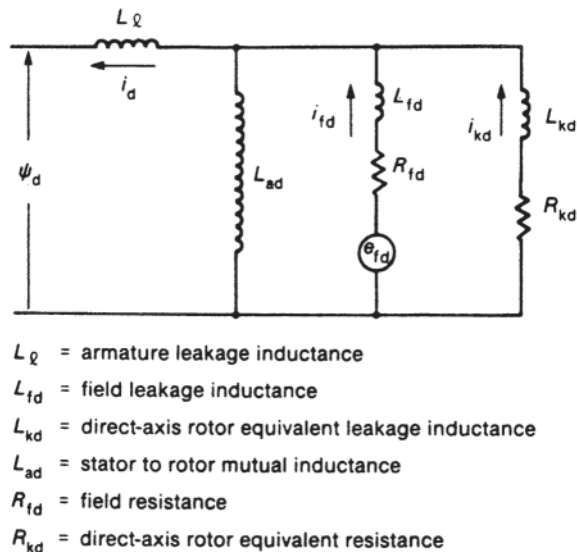


Figure 7.28 Conventional d-axis equivalent circuit.

equivalent circuit is similar in structure, except that the field winding is replaced by a second (equivalent) iron circuit.

Accurate identification of the field circuit is a desirable feature for present-day stability analyses where excitation controls play an important role. This is not possible with the tests described in Section 7.3.2.5. An additional difficulty lies in defining adequate tests for quadrature-axis quantities. Present-day stability studies require quadrature-axis as well as direct-axis values for an accurate and adequate synchronous machine stability simulation.

A new approach has demonstrated that stability parameters for synchronous machines can be obtained by performing frequency response tests with the machine at standstill. Frequency response data describe the response of machine fluxes to stator current and field voltage changes in both the direct and quadrature-axes of a synchronous machine. However, this method requires measurement accuracy and adds to the complexity of data-reduction techniques. Instrumentation capable of resolving magnitudes and phase angles of fundamental components of ac signals at low frequencies (possibly down to 0.001 Hz) is needed. In addition, the procedure for translating the test data into synchronous machine stability study constants requires a computerized, curve-fitting technique. This entire approach was developed in order to improve turbogenerator models for power-system stability studies or for other applications such as excitation control analyses.

The presentation of this method in detail is not pursued here except to give a reference to IEEE Standard 115A-1987 [14], in which an illustrative example is also included in an appendix.

### 7.3.3 Choices of Tests

This entire section on synchronous motors contains information about the more generally applicable and accepted tests to determine the performance characteristics. Three-phase

synchronous motors of larger than fractional horsepower are considered. The schedule of factory and field tests that may be required on new equipment is normally specified by applicable standards or by contract specifications. To minimize the risk of damage to the machine, it is recommended that all tests be performed either under the manufacturer's supervision or in accordance with the manufacturer's recommendations. Alternative methods of making many of the tests that are suitable for different sizes and types of machines and different conditions may have to be considered. In the absence of prior agreement or contract specification, the manufacturer's choice of method for factory or field tests on new equipment will govern.

Specified conditions for tests will generally be considered as rated conditions unless otherwise agreed upon. Since the development of improved practices and new equipment (such as electronic and automatic devices) will result in new and improved methods of carrying out the intent of a standard, such new or modified methods may be used as substitutes provided their results are reliable and consistent.

It is important that instruments of proper type and range be used. The tests usually require considerable care to obtain the desired accuracy. Information relating to the proper use of instrument transformers and instruments for obtaining the measurements is contained in IEEE Standard 120-1989 [38]. Calibrated high-accuracy instrumentation and accessory equipment should be used. Suitable automatic data acquisition systems or high-speed recorders may be used.

All tests should be performed by knowledgeable and experienced personnel.

### 7.3.4 Variations Due to Uncontrolled Factors

Many of the tests described in Section 7.3 may subject the machine to thermal or mechanical stresses, or both, beyond normal operating limits. Variations due to uncontrolled factors in testing methods and their effect on test results should be carefully analysed and documented.

### 7.3.5 Curve Fitting of Performance Data

Nonlinearity of the  $B$  (magnetic flux density) versus  $H$  (magnetic field intensity) relationship of magnetic materials (shown in Fig. 7.29) stands out as a principal impediment to the accurate analysis of electromechanical systems. Some analytical relationships between  $B$  and  $H$  may be convenient for digital computations. Typical expressions (out of the many proposed) are:

$$B = \frac{aH}{1 + bH}$$

$$B = \frac{a_0 + a_1 H + a_2 H^2 + \dots}{1 + b_1 H + b_2 H^2 + \dots}$$

$$H = [k_1 \exp(k_2 B^2) + k_3]B \quad (7.50)$$

where  $a$ ,  $b$ ,  $a_0$ ,  $a_1$ ,  $a_2$ , ...,  $b_1$ ,  $b_2$ , ...,  $k_1$ ,  $k_2$ , and  $k_3$  are constants to be determined from the experimental points on a measured

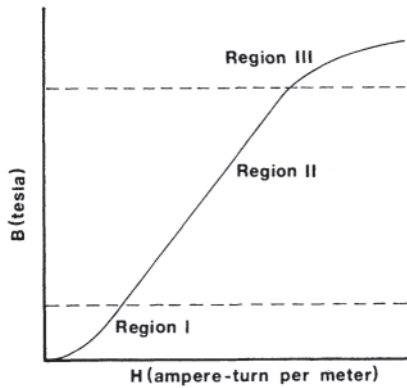


**Figure 7.29** Typical magnetization characteristic showing three regions of domain behavior.

$B-H$  curve for a given material in a given region of interest. Alternatively, by choosing a sufficiently large number of points on the  $B-H$  curve and storing the data in the computer, either linear interpolation or some other curve-fitting technique can be used for obtaining the intermediate values of the magnetic characteristic. In region II of Fig. 7.29, the  $B-H$  curve for many materials is relatively straight, so that linear theory can be applied if a magnetic device is operated only in this region.

A short-circuit current oscillogram is utilized to evaluate some of the reactances and time constants of a synchronous machine. Consider a three-phase, initially unloaded, synchronous generator operating at synchronous speed with constant excitation. Let a three-phase short-circuit be suddenly applied at the armature terminals. Typical oscillograms are shown in Fig. 7.30.

The field current is assumed to have sustained dc, damped dc with time constant  $\tau_d'$ , damped dc with time  $\tau_d''$ , constant and

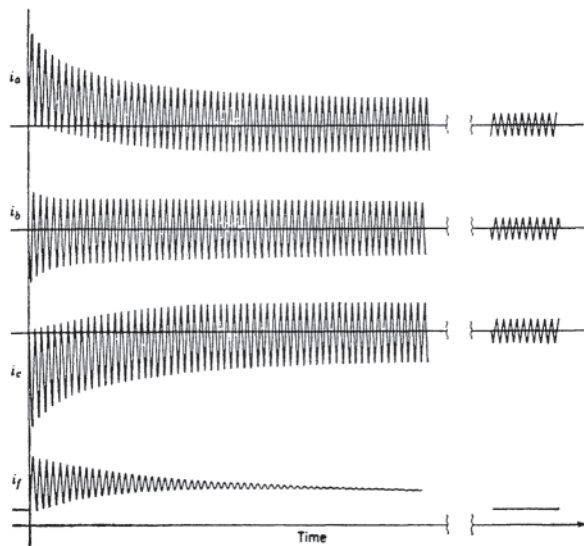


**Figure 7.30** Short-circuit three-phase armature current and field current waves. (Adapted with permission from E.W.Kimbark, *Power System Stability: Synchronous Machines*, Vol. 3, Dover Publications, New York, 1968.)

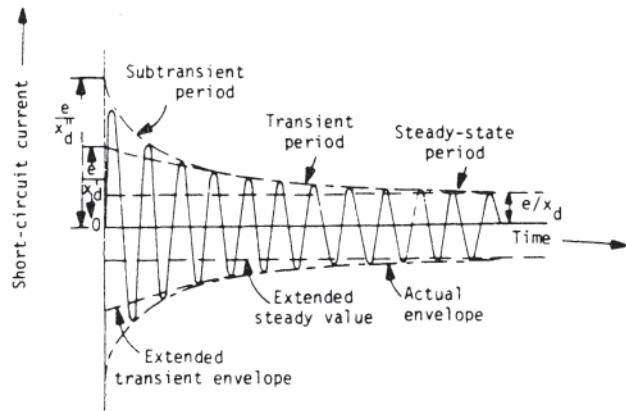


**Figure 7.31** Alternating component of a symmetrical short-circuit armature current of a synchronous machine. (Reproduced with permission from M.S.Sarma, *Synchronous Machines*, Gordon & Beach, 1979.)

damped fundamental ac component with time constant  $\tau_a$ . Detailed discussion is given in Ref. 45.

The armature phase windings are assumed to have sustained fundamental ac, damped fundamental ac with time constant  $\tau_d'$ , damped fundamental ac with time constant  $\tau_d''$ , damped dc components with time constant  $\tau_a$ , which depend on the instant the fault occurs, and damped second-harmonic ac with time constant  $\tau_a$ . Thus, each current wave in general consists of two kinds of components: (a) ac components, and (b) dc components, the former of which are equal in all the three phases and the latter of which are dependent upon the particular point on the cycle at which the short-circuit occurs. Figure 7.31 shows an enlarged view of the ac component of a symmetrical short-circuit armature current of a synchronous machine.

The time constants can be evaluated from logarithmic plots of the transient and subtransient components, as shown Figs. 7.32, 7.33, and 7.34.

Semilog plots of the dc components of the armature currents and the ac component of the field current can be used for obtaining the time constant  $\tau_a$ .

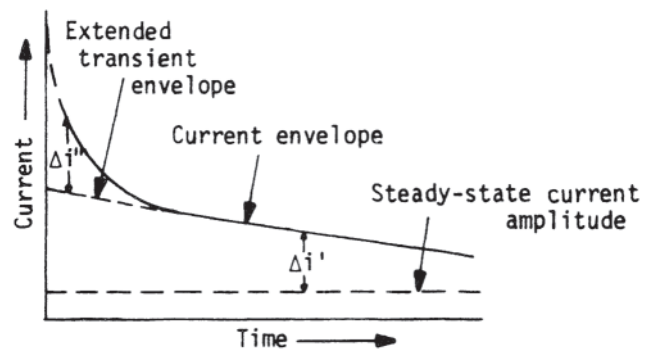


**Figure 7.32** Envelope of the symmetrical short-circuit current. (Reproduced with permission from M.S.Sarma, *Synchronous Machines*, Gordon & Beach, 1979.)

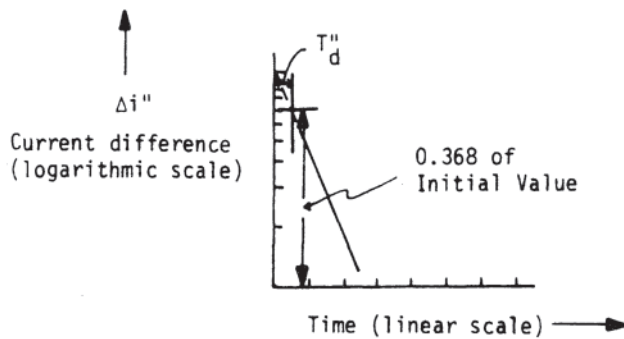


**Figure 7.33** Semilog plot of  $\Delta i''$  as a function of time. (Reproduced with permission from M.S.Sarma, *Synchronous Machines*, Gordon & Beach, 1979.)

Several factors, such as saturation and eddy current effects, may cause the actual short-circuit current not to follow precisely the variation described above. The assumed exponential functions only approximate the true current behavior.

Curve fitting and approximation of functions are discussed in textbooks on applied numerical analysis. Topics such as least-squares, approximations, fitting nonlinear curves by least squares, Chebyshev polynomials, approximation of functions with truncated power series, approximation with rational functions, approximation of functions with trigonometric series, and fast Fourier transforms (FFTs), as well as relevant computer programs, are presented in Ref. 46. The topic of splines is discussed in Chapter 9 of Ref. 47 and “Polynomial Regression with Plotting” is presented in Chapter 8 of Ref. 48.

Standstill frequency response (SSFR) testing requires data reduction techniques and a procedure for translating the test data into synchronous machine stability study constants through a computerized curve-fitting technique applicable to nonlinear functions (also known as nonlinear regression analysis). Programs that could be suitable for curve fitting the results from SSFR tests are described in Refs. 49 and 50.

### 7.3.6 Miscellaneous Tests

#### 7.3.6.1 Insulation Resistance

The recommended methods for testing insulation resistance are given in ANSI/IEEE 43–1974 (Reaffirmed 1991) [18].

#### 7.3.6.2 High-Potential (Dielectric) Tests

This test is usually, but not necessarily, applied after all other tests have been completed. The recommendations are given in ANSI C50.10–1977 [15] and ANSI/NEMA MG 1–1989 [6]. For high-voltage testing procedures, one is also referred to ANSI/IEEE Standard 4–1978 [16] and IEEE Standard 62–1978 [34].

#### 7.3.6.3 Resistance Measurements

The procedures are given in IEEE Standard 118–1978 for determining dc resistance measurements of armature and field

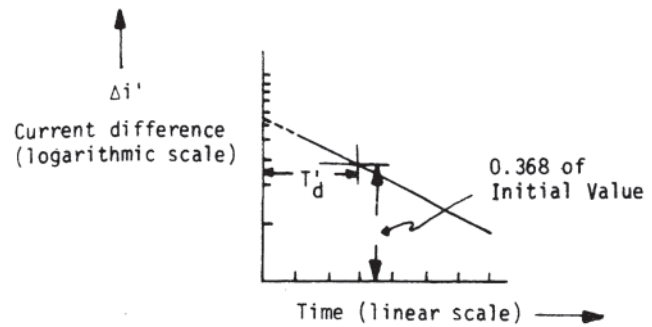


**Figure 7.34** Semilog plot of  $\delta_i'$  as a function of time. (Reproduced with permission from M.S.Sarma, *Synchronous Machines*, Gordon & Beach, 1979.)

windings [37]. Correction to a specified temperature can be done using the following equation:

$$R_s = R_t \left( \frac{t_s + k}{t_t + k} \right) \text{ ohms} \quad (7.51)$$

where :

- $R_s$  = the winding resistance, corrected to a specified temperature,  $t_s$
- $t_s$  = the specified temperature ( $^{\circ}\text{C}$ )
- $R_t$  = the test value of winding resistance
- $t_t$  = the temperature of the winding when its resistance was measured ( $^{\circ}\text{C}$ )
- $k$  = the characteristic constant for the winding material

#### 7.3.6.4 Tests for Short-Circuited Field Turns

Tests may be performed to detect field coils that have shortcircuited turns, an incorrect number of turns, or incorrect conductor size. At standstill, not all short-circuited field turns are apparent by test; a test at speed may also be required.

#### 7.3.6.5 Polarity Test for Field Poles

The polarity of the field poles may be checked by means of a small permanent magnet mounted so that it may turn and reverse its direction freely.

#### 7.3.6.6 Shaft Current and Bearing Insulation

Irregularities in the magnetic circuit may cause a small amount of flux to link the shaft, with the result that an electromotive force (emf) is generated between the shaft ends. The emf may cause a current to flow through the shaft, bearings, bearing supports, and machine framework, and back to the other end of the shaft unless the circuit is interrupted by insulation. While the machine is running at rated speed and excited at rated armature voltage (open circuit), the presence of shaft voltage may be determined by measuring the voltage from end to end of the shaft with a high-impedance voltmeter.

#### 7.3.6.7 Phase Sequence

The phase-sequence test is made to check the agreement of the machine with the specified terminal markings and phase

rotation, or with the requirements of ANSI/NEMA MG 1–1989 [6]. The results are used when connecting the line leads to the armature terminals to obtain correct direction of rotation for motors.

### 7.3.6.8 Line-Charging Capacity

The line-charging capacity of a synchronous machine is its reactive power in kVA when operating synchronously at zeropower—factor rated voltage, and with the field current reduced to zero. The machine is operated as a synchronous motor at no load, preferably uncoupled, and at rated voltage and frequency, with excitation reduced to zero. Because machine losses are supplied from the driving units, the line-charging capacity is approximately the reactive power input in kVA. Note that a limit for reduction of field current of cylindrical rotor machines at rated voltage may be set by the manufacturer to avoid local heating in the armature.

## 7.4 DC MOTOR TESTS

### 7.4.1 Electrical Test Standards

The recommended reference test standard for dc machines is IEEE Std 113–1985 IEEE Guide: Test Procedures for Direct Current Machines [51]. This standard was prepared by the D.C. and Permanent Magnet Subcommittee of the Rotating Machinery Committee. It contains information relating to most of the test guides contained herein although it does not deal with commutation testing. It contains references to other related IEEE Standards such as those covering generalized techniques for resistance measurement, temperature measurement, airborne sound measurement, and measurement of radio noise emission.

### 7.4.2 Preparation for Tests

#### 7.4.2.1 Winding Resistances

Cold winding resistance measurements should be made before power is applied to any of the windings to check correctness of manufacture compared with published data and to serve as a basis for calculating winding temperature rise by resistance in subsequent heating tests. The ambient temperature should be measured and recorded so that the measured values can be corrected to the nominal cold temperature, usually 25°C.

The shunt field winding resistance may be calculated from initial measurements of voltage and current at the winding terminals. The resistances of the series field and commutating field windings may be measured using a Kelvin double-bridge or other appropriately accurate instrumentation. The commutating field winding resistance can usually be measured between the brush stud connected to the winding and the A2 terminal. Measurement of armature resistance should be made from marked commutator segments one brush span apart, with the brushes raised. During heating tests, cold and hot armature resistance measurements are often made using marked segments less than a pole span apart so that measurements can be made quickly after termination of the heat run without raising the brushes.

A comparison of the cold and hot resistance measurements of any winding allows calculation of the average hot winding temperature using the relation:

$$R_1 = R_2 \frac{(k + t_1)}{(k + t_2)} \quad (7.52)$$

where:

- $R_1$  = resistance of the winding (ohms) measured at a cold temperature standard  $t_1$ , such as 25°C
- $R_2$  = resistance of the winding (ohms) measured at temperature  $t_2$
- $t_1$  = cold temperature standard, °C, such as 25°C
- $t_2$  = hot temperature (°C) (including effects of ambient temperature changes during the run)
- $k$  = temperature constant (234.5 for copper; 225 for EC grade aluminum, based on a volume conductivity of 62%)

#### 7.4.2.2 Brush Preparation

The brushes should be inspected carefully to see that they are free to move in the holders and that the brush springs contact the brushes uniformly and properly. With the motor running in the specified direction of rotation, if one exists, the brushes should be seated using seater stone and blown clean with an air hose. After a run-in period at no load of a several minutes, the motor should be stopped and the brushes removed and inspected carefully as to the completeness of the brush fit. The fit should be essentially 100%, especially in the thickness direction of the brush face. If not, the run-in period should be extended using seater stone at the locations needing further attention.

If the motor is to be run in both directions of rotation, the brushes should be seated in one direction as discussed above and then the motor should be run at no load in the opposite direction for approximately 30 minutes. The brushes should then be examined. A careful inspection for a double fit of the brushes should be made, indicating brush tilt in the boxes. If such a fit is found, the brush rigging should be reexamined and if the cause of the trouble cannot be corrected, at least it should be noted conspicuously on the test report. A brush fit depending on direction of rotation will affect speed neutral tests, speed regulation tests and commutation tests.

#### 7.4.2.3 Neutral Setting

Motor designs differ as to whether the brush rigging is fixed in position or whether it is intended that the brush position be adjustable. For this subsection it is assumed that the brushes are adjustable. The most useful method of locating the brush rigging consists of position adjustments such as to render equal full-load speeds in both directions of rotation. This is termed *full-load speed neutral*. The brush rigging should be examined and the brushes properly fitted as discussed in Section 7.4.2.2 before neutral setting is begun. The motor should then be run in one direction of rotation, measuring the full-load speed with the armature voltage, armature current, and shunt field current

held constant. Then the motor should be reversed by changing the polarity of the armature voltage maintaining the series field, if one is used, in the original polarity. As the brush position is changed, the speed will increase in one direction of machine rotation and decrease in the other. The brush position in which the full-load speed is essentially the same in either direction of rotation should be determined and the brush position marked. If the motor is rated for operation with the shunt field weakened, the brush position should be set at weak field.

Several factors affecting motor speed cause apparent neutral inconsistencies and must be guarded against. These include: (1) main field magnetic hysteresis, (2) hysteresis in the magnetic fields relating to the armature circuit, and (3) variations in effective brush position caused by brush fit variations. These can be minimized by conducting tests without any shunt field current variation during speed reversals and by minimizing armature current surges during speed and load changes.

#### 7.4.2.4 Commutation Adjustments (refer also to Section 7.4.3.2)

Any changes made to improve commutation performance should be undertaken as a preliminary adjustment because these changes will affect other machine performance characteristics. The most common method of measurement as to the quality of commutation performance is the black-band test, the name of which becomes obvious as the test is described. This test consists of observing the limits of black (sparkless) commutation as the commutating strength is artificially boosted above or bucked below the design level. When the test results are plotted against the armature current the horizontally shaped zone or band within which machine commutation is black is termed the *black band*.

The test is usually taken at no load and at loads such as 50%, 75%, 100%, 125%, and 150% of rated load current in both directions of rotation with full field excitation and with field excitation adjusted for maximum rated operating speed. By analyzing these test results it may be determined that the commutating field should be strengthened or weakened for better commutation performance. This can be done by changing the number of turns on the commutating field or, more commonly, by increasing or decreasing the effective commutating field air gap by changing shims behind the commutating poles.

If adjustments are not to be made, further tests as described in Section 7.4.3.2 may not be required.

### 7.4.3 Performance Tests

#### 7.4.3.1 Rated Speed and Speed Regulation Tests

These tests are to be conducted with the motor hot, as resulting from continuous operation at rating. The shunt field current should be maintained at the hot value during subsequent regulation tests. Full load should be gradually applied and removed several times until readings are consistent. Then full-load and no-load speeds should be recorded and speed regulation calculated:

$$\begin{aligned} \text{Percent speed regulation} &= 100 \\ &\times \left[ \frac{(\text{speed at no load} - \text{speed at rated load})}{\text{speed at rated load}} \right] \end{aligned} \quad (7.53)$$

For reversible motors the test should be repeated in the opposite direction of rotation. For more complete information the test can be conducted by applying and removing load in 25% steps from no-load to overloads such as 150%. Variation of the full-load speed may be observed depending on whether the load is being increased or decreased. This is mainly the result of magnetic hysteresis in the commutating field of the motor.

#### 7.4.3.2 Commutation Tests (refer also to Section 7.4.2.4)

The brushes should be seated and inspected carefully after which the motor should be run at rated load for about an hour before black-band tests are begun. Buck-boost tests should then be taken at no-load and at loads such as 50%, 75%, 100%, 125%, and 150% of rated load in both directions of rotation with full-field excitation and with field excitation that will result in maximum rated operating speed. Overheating can be avoided by running the motor at no-load between test points. It will be found that when the bucking or boosting current is raised and lowered, sparking does not begin and end at the same current. The test should be conducted in a consistent manner such as always noting when the sparking is terminated, not when it is initiated.

There are other measures of detecting sparking which will not be dealt with here. These include sparking meters which detect high frequency line disturbances resulting from sparking. Such meters are particularly useful with enclosed machines if sparking is impossible to detect visually.

It should be recognized that although the black-band test is an effective tool in motor evaluation, satisfactory commutating performance can best be measured by suitable brush life and commutator wear in service.

#### 7.4.3.3 Heating Tests

Motor temperatures should be measured at the machine surfaces using thermometers and thermocouples and calculated from winding resistance measurements using the relation given at the end of Section 7.4.2.1. Temperatures derived from resistance measurements, when properly taken, accurately indicate the average temperature of the windings. They are usually significantly higher than surface temperatures.

Thermocouples are usually used to measure the temperature of stationary parts: the magnet frame, bearings, field windings, and brush holders. They should be mounted on the surfaces and covered with thermal insulation so as to measure the machine surface temperatures, not the surrounding air. The temperature of the entering and leaving ventilating air should also be measured. When a heat run is terminated and the armature is no longer rotating, thermometers and other contact devices should be applied quickly to measure the temperature of the armature core, the armature winding, and the commutator.

Before the run is begun, careful measurements of the cold resistances of the armature and of the field windings should be made using the techniques discussed in Section 7.4.2.1. The shunt field temperature rise should be calculated and all of the surface temperature measurements should be monitored

periodically as the test progresses. When these measurements indicate that steady state has been reached, preparations for shutdown should be made. After the armature power has been removed and the motor has stopped, the shunt field excitation should be discontinued and timed temperature measurements should begin. As quickly as possible thermometers should be applied to measure the armature and commutator temperatures and double-bridge connections to the marked bars on the commutator should be made. Measurements of the winding resistances should be made at brief intervals at the machine cools so that cooling curves can be drawn and extrapolated to the time of shutdown to yield the hot average temperature rise of the windings measured by resistance.

Heat runs are usually taken at the motor name-plate rating but they may be taken all other agreed conditions such as at reduced speeds when achieved by armature voltage control.

#### 7.4.4 Special Tests

##### 7.4.4.1 Saturation Tests

The no-load saturation curve provides the nonlinear relationship between field excitation and resulting magnetic flux as indicated by the generated armature voltage when the armature rotates. The motor should be driven at any convenient speed and measurements taken of the shunt field current, armature voltage, and speed of rotation. Inconsistencies resulting from magnetic hysteresis can be minimized by increasing the field excitation smoothly from zero to 150% rated excitation and reducing it to zero before recording measurements. Then measurements should be taken of the armature voltage and speed as the shunt field is increased from zero to 150% of rated excitation without reversing the direction of change. Similar measurements should be taken as the field current is decreased to zero.

Two other methods of test are suggested for providing more complete data: (1) Measurements made in a fashion similar to that indicated above, the field being cycled first in the positive direction and then in the reverse direction so as to provide a four-quadrant hysteresis loop; (2) a single ascending magnetization curve starting from an unmagnetized state. The unmagnetized state can be achieved by repeatedly reversing the field current while gradually reducing the magnitude to zero, thereby reducing the residual flux to zero.

##### 7.4.4.2 Loss Measurement Tests

Mechanical and magnetic losses of a motor can be determined by measuring the power required to drive the machine when electrically disconnected using a small calibrated dc drive motor or a dynamometer. To calibrate a dc drive motor, run it uncoupled and measure the input armature power as it is run over its speed range by armature voltage control. Then raise the brushes of the motor to be tested, couple it to the drive motor and measure the increased input power caused by friction and windage of the motor being tested. Next, lower the brushes of the test motor and, after driving it at rated speed until the input power is constant, measure the added brush

friction over the speed range. Finally, raise the brushes and, with the motor at rated speed, measure the input power as the field is applied in steps. The increased power is caused by core losses in the test motor.

A simpler but less complete means of determining the mechanical and magnetic losses of a motor is to run the machine at no load, uncoupled, at rated shunt field current and rated speed and measure the input armature circuit power. This power is the sum of the windage and friction of the motor, including brush friction, the rotational core loss, and the  $I^2R$  losses of the armature circuit windings and the brush contact losses, both at very light load. By subtracting the calculated values of the latter two loss components, the sum of the mechanical and magnetic losses can be determined.

With motors having multiple brushes, it is possible to measure brush friction by raising all but two of the brushes and measuring the resulting decrease in losses. With this information, total brush friction can be determined. Loss test at various speeds and field currents can be used to separate loss components.

##### 7.4.4.3 Dynamometer Tests

Using a dynamometer the power output of a motor at rated load can be determined and the accuracy of the current rating can be established. By comparing the output with the electrical input power, the motor efficiency can be determined and the total losses of the machine can be measured.

These losses consist of the no-load losses of the motor: the shunt field excitation power, windage and friction including brush friction and the magnetic core loss, plus the load losses. The load losses consist of the  $I^2R$  losses of all of the windings of the armature circuit, including the brushes and the stray-load loss. The stray-load losses occur for many reasons, for example, losses resulting from distortion of the magnetic flux in the main pole faces at load. The dynamometer test, when accurately conducted, allows determination of the sum of the motor losses. These can be compared with the sum of the losses at no load and the  $I^2R$  losses in the windings to determine the  $I^2R$  losses in the brushes and also the stray-load losses.

The dynamometer can also be used as a test tool in the measurement of some of the individual motor losses as indicated in 7.4.4.2.

##### 7.4.4.4 Rectifier Tests

###### 7.4.4.4.1 Test Power Supplies and Instrumentation

Tests should be conducted with the rectifier circuitry that will be used with the motor in service, including the specified supply voltage and frequency, the number of phases, and freewheeling rectifiers and smoothing reactances, if used.

Instrumentation should include measurements of both the ac and dc components of the motor current and the input power to the motor. An oscilloscope allows observation of the proper phase balance of the current waveform.

###### 7.4.4.4.2 Extra Losses

Rectifier operation causes extra losses in the motor. These losses are equal to the difference between the motor input

power and the product of the average values of the armature voltage and current:

$$\text{Extra losses} = \text{Watts input} - (v_{dc} J_{dc}) \quad (7.54)$$

The true power input is measured by wattmeters; the dc volts and amperes each have the same significance as with normal operation on direct current. The torque developed is essentially proportional to the average current since the field flux is nearly constant, even though some field current variation may be observed. The extra losses consist of added  $IR$  losses and iron losses caused by the current pulsations.

Measurement of the rms value of the ac component of the current should be made using appropriate instrumentation. The rms value of the current can be measured directly or calculated:

$$I_{\text{rms}} = \sqrt{I_{\text{dc}}^2 + I_{\text{ac}}^2} \quad (7.55)$$

#### 7.4.4.4.3 Motor Testing

Heating tests should be taken as discussed earlier for dc operation, except that ac instrumentation should be included to allow evaluation of extra losses during the tests. These losses may increase motor temperatures considerably and require derating, particularly if continuous operation is required at reduced speeds by armature voltage control.

Measurement of the extra losses is a common and useful test. This can be done by running the motor at rated voltage, or preferably, with a much lower voltage adjustment, first at no load and then increasing the armature current in gradual steps while measuring the input armature ac and dc voltages and currents, and the power. At light loads the current is usually intermittent. As the dc current is increased, the ac component current is also increased and the losses are increased accordingly. When the current becomes continuous, the added losses reach their maximum value. Further increase of current is unnecessary as far as measurement of extra losses is concerned. A much greater range of ac current can usually be attained by conducting this test at the lower voltage setting.

## 7.5 HERMETICALLY SEALED REFRIGERATION MOTORS

### 7.5.1 Electrical Test Standards

The most recent test guide directly applying to motors used in refrigeration compressors is the "IEEE Guide: Procedures for Testing Single-Phase and Polyphase Induction Motors for Use in Hermetic Compressors." This guide, IEEE Standard 839-1986 [52], is the culmination of several years of effort by the Hermetic Working Group assigned to the task by the Single-Phase and Fractional Horsepower Subcommittee of the Rotating Machinery Committee. The request for such a test guide originated from the Motors Committee of ASHRAE, the American Society of Heating, Refrigeration, and Air Conditioning Engineers, Inc. The lack of standard test procedures among the compressor manufacturers had been the source of differences in motor performance for identical applications. The availability of this guide is a step toward better motor/compressor applications.

### 7.5.2 Types of Tests

The tests on hermetic motors may be divided into three main categories: (1) running performance, (2) starting performance, and (3) relay tests. It should be noted at the outset that a hermetic motor comprises only two parts, a stator and a rotor. In the industry it is known as a "hermetic motor" because the compressor housing in which the compressor and motor are mounted is hermetically sealed from the atmosphere either with a welded seam or a bolted flange assembly. Because of the difficulty in monitoring the complete thermal performance of the motor inside the compressor or in simulating the compressor-loaded motor, the tests have been standardized at a temperature of 25°C. Furthermore, since it is impractical to maintain the motor temperature at 25°C during the test, the IEEE Test Guide recommends that the test be initiated with the motor (stator and rotor) at 25°C (77°F). If the test is of sufficiently short duration, the slight increase in motor temperature will have only minor or correctable effects on motor performance. The purpose of these tests is to determine whether the motor will provide acceptable performance when it is placed in the compressor environment.

With proper dynamometer fixturing, the hermetic motor parts (stator and rotor) can be coupled to the test bench in a matter of minutes and given a fairly complete set of tests in 30 minutes or less. This assumes that sufficient cooling means are available to cool the motor parts between each test segment. A preferred method is to force dry, chilled air through the motor air gap and vents after completion of each test segment. To avoid cooling the motor below 25°C, one might sense the temperature of the exiting air and warm the cooling air gradually to a temperature of 25°C. With electronic devices such as thermistors and proportional controllers, this can be done very simply.

In addition to determining performance acceptability, a second purpose for the motor tests is obtaining diagnostic information. Occasionally one has the problem of determining whether the stator or rotor is not functioning properly. This could be the result of mechanical damage, overheating, or a manufacturing process that may have gone out of control. Locating the source of the problem can be vitally important to either the user or the manufacturer.

### 7.5.3 Choices of Tests

A number of choices are now available to obtain sufficient information about the motor relating to the operation in the compressor application. The following descriptions apply to the types of tests generally used.

#### 7.5.3.1 Running Performance

In the running mode one is concerned mainly with motor operation from a speed of about 70% of synchronous speed up to no-load speed. The highest torque developed or breakdown torque is not of major importance. A term MRT, for maximum running torque, is of greater value to the hermetic compressor engineer. MRT is defined as the torque at 83.3% of synchronous speed; this speed is usually above the speed

at which breakdown torque (BDT) occurs in single-phase motors. In polyphase motors BDT often occurs at approximately 65% of synchronous speed. In this test, the motor is loaded to run at a speed just above the MRT speed, but at a reduced voltage. During this operation the motor must continue running without overheating. Hence, a primary test point in the running mode is the measurement of MRT.

The remaining points of concern are in the speed range of about 90–98.5% of synchronous speed. For a two-pole, 60-Hz motor this corresponds approximately to 3200 to 3550 rpm. While a refrigerator or freezer motor may operate at the lower speed during “cabinet pull-down,” it probably will not operate at the higher speed mentioned. A motor used in an air conditioning/heat pump application could traverse the entire speed range. During heat pump operation with very cold outdoor temperatures, the load on the motor is fairly light because the refrigerant cannot absorb much heat from the outdoor air. This will cause the motor to run at a light load and high speed. On a hot day calling for maximum air conditioning, the load is heavy and the speed may approach a level of 3200 rpm. For these reasons one is concerned with motor efficiency and winding temperatures, which are related to the  $I^2R$  losses in the windings. Because the compressor engineer usually thinks of torque loading on the motor, the major performance attributes are plotted against torque. A complete test on a permanent-split capacitor (PSC) motor will usually include the following attributes measured and plotted against torque:

- Speed
- Efficiency
- Power factor
- Power input
- Capacitor voltage
- Capacitor voltage
- Capacitor voltage
- Main winding current
- Start winding current

These curves together with a tabulation of numerical data at the critical load points will usually provide both the motor engineer and the compressor engineer with sufficient information to determine whether a particular motor will run properly or what redesign changes will result in satisfactory operation.

Test on a polyphase motor will not include the start winding measurements, but may include individual phase voltage and current measurements to determine whether the current balance is reasonable. If current unbalance does exist, the major cause is usually voltage unbalance among the three lines. Also, tests on a split-phase motor will only include the line readings since the start winding is not in the circuit during the running operation.

### 7.5.3.2 Starting Performance

In the starting mode the two major points of concern are standstill torque and the accelerating torque. Standstill or locked rotor torque (LRT) is better measured when the rotor is revolving at a speed of 6 to 8 rpm. Because the torque has normal pulsations due to the presence of rotor and stator slots, one looks at the graphical envelope that encloses the starting torque trace (see Ref. 52, p. 17). The reported torque is taken at 3 seconds. The predominant preference seems to be the average value of torque at 3 seconds as representative of the starting capability of the motor. In polyphase motors and capacitor-start motors the LRT is often measured when the motor is accelerating from a negative

speed through the zero speed point. This is not always either the minimum or the average value but is reasonably representative of the torque at zero speed.

The accelerating torque or low-speed torque (LST) is defined as the torque at 8.33% of synchronous speed. For a 60Hz, two-pole motor this is 300 rpm. This torque is of little value in polyphase motors because of their high starting capability, but is of major importance in split-phase and PSC motors where the starting torque is in the range of 10% to 15% of the breakdown torque. Significant torque dips in the low-speed range could prevent the motor from accelerating to the normal full-load point. The LST point is best measured dynamically when the motor is accelerating from standstill to a speed of about 500 rpm. The speed-torque trace is then done graphically on an X-Y recorder or stored and displayed on an oscilloscope or computer monitor using known computer software techniques. If a severe dip or cusp in the LST region is detected, a close examination of the rotor is in order. The torque dip itself is caused by the stator “slot-order” harmonic currents flowing in the rotor but is greatly accentuated if the rotor cage is sticking to the rotor laminations. This suggests that a process in the rotor manufacture is out of control.

A speed-torque trace from standstill to no-load is included in the starting mode tests. Because the starting and running modes of a PSC motor are identical there is only one speed-torque trace. If it is a split-phase or capacitor-start motor, the presence of winding harmonics will be detected. The complete starting speed-torque trace is useful when applying voltage or current relays for assurance that the motor will provide adequate torque at the time the relay switches from the start to the run mode. As in PSC motors, the polyphase start and run modes are the same. The entire speed-torque trace is useful in determining both the breakdown torque and the speed at which it occurs.

Two additional measurements taken during starting are the locked-rotor current (LRA) and the temperature rate of rise. The LRA may be taken simultaneously with the LRT trace but most prefer to measure the stator current with the rotor actually locked. The current value reported may be at either 3 or 4 seconds, depending on the preference of the compressor manufacturer. Simultaneously during this test one measures the temperature rate of rise of both the stator winding and one or both of the rotor end rings. The compressor engineer must be assured that any thermal protector used with the motor will disconnect it from the line before the stator insulation is degraded or damaged or before any oil on the surface of the rotor is carbonized. The oil is present because the motor is constantly flooded with oil and refrigerant during its normal operation.

The temperature rate of rise test may be done with temperature-activated waxes painted on the windings or rotor, but a preferred method is the use of infrared sensing detectors aimed at the surfaces to be measured. One approach uses a black paint that is sprayed on the rotor end ring and the stator end winding. Only a small spot about 0.5 in or 1.25 cm in diameter needs to be painted since the infrared sensing lens can focus on a small area. The infrared sensing device can be coupled to timers, plotters, or computers to display time-temperature plots.

In addition to testing the temperature rate of rise (ROR),



one may wish to compute it, especially for the stator conductors. In doing so, one assumes an adiabatic condition where all of the heat is stored and none is transferred. This is a reasonable assumption in many cases where the time involved is approximately 15 seconds, or less. The calculation uses the current density squared, together with the resistivity ( $\rho$ ), specific heat ( $C_p$ ), and density ( $d$ ) for the conductor of concern. The formula for this calculation is given below:

$$\text{ROR} = (\text{current density})^2 \times (\rho) / C_p \times d$$

At 20°C the following characteristics apply to copper:

$$\begin{aligned} \rho &= 0.6788 \times 10^{-6} \text{ ohm-in} \\ C_p &= 176.5 \text{ watt-sec/}^\circ\text{C per pound} \\ d &= 0.321 \text{ pounds per in}^3 \\ \text{current density} &= \text{amp/in}^2 \end{aligned}$$

Using those material characteristics in the definition of ROR, one arrives at the following formula for temperature rate of rise for copper:

$$\text{ROR} = 0.01198 \times 10^{-6} \times (\text{current density})^2$$

If one is using EC (electrical conductor)-grade aluminum, the coefficient in the formula is 0.0282. For cast aluminum with a conductivity of 56%, one may use a coefficient of 0.0311.

### 7.5.3.3 Relay Tests

The name suggests that relays are tested, but that is not the case. The motor must be tested to see whether its characteristics are such that a current- or voltage-actuated relay can be connected to the single-phase motor to be sure that the motor will start properly and then switch to the run mode. Current and voltage relays are used with hermetic motors because the motor is in an oil and refrigerant environment that is not acceptable for arcing contacts. The relays are connected externally to the compressor and sense main winding current in the case of the current relay and start-winding voltage in the case of the voltage relay.

For the current relay tests the motor is allowed to accelerate from standstill to no-load, during which time a plot of main winding current versus speed is made on an X-Y plotter. The plot may also be made by utilizing a computer with software so as to store and display the curves on a computer monitor and also make a "hard copy" with a printer. The test bench must be fitted with the proper loading so that this acceleration time is between 3 and 8 seconds. If the test is taken too rapidly, the current transducer or the X-Y recorder may not be able to follow the changing current signal. If the test is too slow, the motor may get too hot and give erroneous readings. In the actual application, the motor accelerates to its load in about five cycles, but only a transient recording device could follow the signal properly. Furthermore, the relay manufacturers and compressor engineers have become accustomed to use the quasi-steady-state data taken in the 3- to 8-second tests.

The relay test described is taken at three different voltages applied to the motor: 85%, 100%, and 110% of rated line voltage. This would correspond to 98, 115, and 126 V for a 115-V rated motor. These curves are taken with the start winding both connected and disconnected from the circuit, corresponding to the start and run modes of the motor.

For voltage-actuated relays the same kind of accelerating test is taken, except that curves of capacitor voltage versus speed and start winding voltage versus speed are plotted on the X-Y plotter. As in the case of the current relay, curves are taken both in start and run modes. In the case of a capacitor-start motor, the capacitor is in the circuit in the start mode and is disconnected from the circuit during the run mode. This difference is generally sufficient to cause a displacement in the voltage curves between the two modes so that the relay will pick up at standstill and will drop out at a predetermined speed and will not pick up again. If that were to happen, the relay would continue to cycle and chatter. Ultimately, the relay contacts would likely weld and the start winding would burn out or the electrolytic start capacitor would vent or explode. Analysis of the motor characteristics together with the data supplied by the manufacturer of the relay itself should permit the application engineer to properly apply a relay to a given motor design.

The same kind of voltage curves would be plotted for a capacitor-start, capacitor-run motor. In that case, the run mode would consist of only the run capacitor connected in the start winding circuit. The start mode would consist of the run and start capacitors in the circuit. In both cases, of course, the main winding is connected in parallel with the start winding and capacitor. In actual operation, the relay disconnects the electrolytic start capacitor when the desired speed is reached. When very large start capacitors are used, the current in the capacitor circuit may be measured and plotted to be sure that the relay has contacts that are adequate to make and break the current level. The worst case is at overvoltage and high speed.

### 7.5.4 Variations Due to Uncontrolled Factors

Variations in the reported test data can be a source of real frustration to the engineer designing the motor as well as the compressor designer trying to apply it to his compressor. A number of factors can contribute to these variations, some mechanical, some electrical, and some thermal. The following guidelines are suggested as a means of reducing the test variance.

All tests are to be taken at the rated voltage and frequency unless other conditions are specified. Because many motors are rated at both 50 and 60 Hz, it is common to test at both frequencies and their respective voltage ratings. For example, a motor may be rated at 460 V, 60 Hz and also 400 V, 50 Hz. Because wave shape, voltage balance, and frequency variations could have a definite effect on the resultant performance, the Test Guide offers specific recommendations in this area. The applied voltage shall approximate a sinusoidal waveform. The waveform deviation factor, which is a measure of the shape, should not exceed 5%. The frequency should be held at the required level within 0.1%. Finally, the voltage balance of the phases or lines connected to polyphase motors should be of such an order that the negative-sequence voltage should not be greater than 0.1% of the positive-sequence voltage. While these restrictions may seem somewhat tight, controls on those variables are necessary to obtain both accurate and repeatable test measurements.

All of the electrical quantities to be measured are to be rms (root mean square), unless the IEEE Guide [52] indicates

differently. Instruments that sense the average signal but display the rms value should be avoided. Different types of instruments may be selected. One type is the self-contained meters with analog dials for steady-state readings. Another type is electronic (usually with digital outputs) that are connected to transducers feeding X-Y plotters for continuous curves displayed while the motor is dynamically tested.

Measurement of the electrical quantities is by no means the only source of test errors. The measurement of torque can often be a source of errors. Measurement of the angular acceleration of an inertia disk is commonly used but has no real source of calibration such as with a hanging weight. The method can be highly reliable but requires attention to the electronic means used to measure the acceleration. This is usually done with an analog differentiating circuit, which is inherently unstable if not properly designed. Care must also be given to the inertia disks to insure that the disks and any other rotating elements have not changed due to wear.

Trunnion-mounted dynamometers provide an excellent means of deadweight calibration, but undulating bearing friction due to worn-out grease or brinelled bearings can cause variations in the torque readings. The same holds true if the motor itself is trunnion-mounted instead of the load. In both cases the leads either to the dynamometer or to the motor must be extremely flexible and positioned so as not to add to or subtract weight from the load. If either a trunnion-mounted test motor or dynamometer load is used in conjunction with a dynamic test system, one must predetermine whether a critical speed exists within the test speed range. Unless the load cell used to measure the torsional load has an extremely high  $K$  factor or spring constant, the large mass or inertia, which is free to rotate within its constraints, could result in a very low resonant frequency.

The same resonance problem exists when one is using a rotating in-line torque meter. Here the rotating masses include the test rotor, couplings, and so forth. While the masses are smaller, the spring constants also may be smaller. It is likely that the system actually comprises several springs and several rotating masses, all of which contribute to a plurality of resonant speeds. Gear boxes used to achieve high speeds may have backlash that could contribute to a pulsating torque reading. Selection of these mechanical elements in motor testing is extremely important.

Improper cooling of the test motor is often a source of errors. Because the motor designer has no control of the final operating environment of the hermetic motor, the IEEE Guide [52] recommends that the motor test be started with the motor initially at 25°C. In most cases, the test segment can be fairly short in duration so that the heat generated during the test will not significantly raise the motor temperature. If the end temperature is measured, the measured performance data can be corrected fairly easily with access to a computerized motor design program. It is important that both the stator and rotor are cooled to the same initial temperature.

### 7.5.5 Curve Fitting of Performance Data

Performance data taken in a series of point-by-point tests or collected by a computerized test system are all subject to test

errors. Regardless of the care taken during the test, one will usually find small aberrations in the plotted curves when using the “raw” data. When using point-by-point data the Guide recommends at least seven points relatively evenly spaced for a curve-fitting routine. One will generally find that trying to curve-fit data directly to efficiency and power factor curves is doomed to failure. A better method consists of curve-fitting the input power data versus torque and similarly fitting the output power to the same abscissa. With the resulting equations one can compute the final efficiency values. Assuming a small computer and plotter are available, the program can then compute and plot in small increments to get a continuous efficiency curve. The power factor curve can be obtained similarly. Curve-fitting routines such as this inherently eliminate some of the test errors since they use the least-squares technique in the program.

One should always keep in mind that the purpose of the final curve plots is a fairly accurate *picture* of the data. Specific numbers should come from the equations used to plot the curves and not from the curves themselves.

### 7.5.6 Miscellaneous Tests

One change in motor applications introduced in the 1970s relates to the use of positive temperature coefficient resistors (PTCRs). In some cases they are used in series with the start winding of a split-phase motor and have taken the place a current relay. In other cases they are placed in parallel with the run capacitor of a PSC motor to provide a boost in starting torque. In that case they have replaced the start capacitor and its associated voltage relay. Because the PTCR device is current-, voltage-, and temperature-sensitive, it is difficult to get a realistic test with the PTCR device itself. Usually one substitutes an ordinary resistor in the place of the PTCR device and the desired starting test is then taken with existing equipment.

## 7.6 SPECIALTY TESTING

In this section details of several tests not covered in other sections are presented. They may be useful in diagnosing problems in specific parts of the motors.

### 7.6.1 Induction Motor Stators

Because the stator is made of only two parts, the winding and the core, one can concentrate on specific tests relating to those parts. The function of the winding is to create a magnetic field that will ultimately cause rotation of the rotor. The function of the core is to carry the magnetic flux and direct it across the air gap to the rotor. A faulty winding will likely create a magnetic field that may be too weak or too strong. Shorted turns or unbalanced turns may cause overheating of the winding during operation. Likewise, a faulty stator core may require excessive excitation current or have excessive iron losses. These increased losses may be the result of poor-quality steel, improper annealing, or possibly sticking laminations. Any of the three conditions could show up as high hysteresis losses and/or high eddy current losses.

### 7.6.1.1 Winding Resistance

This is perhaps the most elementary measurement in electricity, but a factor often overlooked is the measurement of winding temperature when the resistance is measured. With both values available, one can compute the winding resistance at the desired temperature.

Usually the motor manufacturer reports all winding resistances at 25°C. For any other temperature one can easily compute the correct resistance using Eq. 7.56:

$$R_2 = \frac{R_1(t_2 + k)}{t_1 + k} \quad (7.56)$$

where:

- $R_2$  = the resistance at a temperature,  $t_2$
- $R_1$  = is the measured resistance at temperature,  $t_1$
- $k$  = 234.5 for copper and 225.0 for electrical-grade aluminium conductor

### 7.6.1.2 Hipot and Surge Tests

A measurement of the quality of the ground insulation is a high-potential or hi-pot test. The voltage is impressed from the winding to the stator core. The voltage often used is twice rated voltage plus 1000 V. Specific cases may require different voltage levels. High-potential tests are discussed in general in NEMA MG 1, Part 3 [6], which contains additional references to other NEMA and IEEE standards.

A second test of winding integrity is the surge test. The surge test requires specially designed equipment usually found only in large motor service shops or in motor manufacturing facilities. In this test, a high voltage, e.g., 4000–6000 V, is rapidly sequenced between the ends of the winding. It is then usually compared with a master stator that has the correct winding. The surge pattern may also be compared to a “correct” master pattern which has been measured and stored in a computer. An incorrect winding will show up as a distinct pattern change when the waves are displayed on a special oscilloscope. An amplified description appears in MG 1–12.05 [6] and in Section 8.2.2.

### 7.6.1.3 Core Loss and Exciting Current

A final measure of the “goodness” of the stator is the magnetic quality of the stator core. A perfect core would require no energy to drive the magnetic flux through the steel, nor would there be any losses in the steel. The current required to achieve a certain flux density in the steel will indicate whether the steel is acceptable. If the input power is also measured, one can determine the level of steel losses. The motor winding is not used for these measurements. Instead, a number of turns are looped through the stator bore. The more turns the better, but 10 turns of heavy insulated wire are probably sufficient. Then a similar number of turns of small-gauge insulated wire is looped through the bore. If possible, this second coil should be wound tightly against the stator core. The second coil, or pick-up coil, is connected to an *average-sensing* voltmeter and also to the voltage coil of a wattmeter. The first coil is connected through an ammeter and also the current coil of the wattmeter. Depending on the current required, one may have to use a

current transformer in conjunction with the ammeter and wattmeter. By knowing the yoke dimensions of the stator core plus the number of turns in the pick-up coil, one may compute the voltage required to achieve a flux density of 15,000 G or 96,774 lines per square inch. This flux density is often used by steel manufacturers as a reference point when comparing steels. A good electrical steel may test only 1.5 to 2.0 W/lb at that flux density level. Small motor manufacturers may use steel measuring 3 to 4 W/lb when properly processed. Together with the power measured as described, one should also measure or estimate the weight of the yoke of the stator core. Because the magnetic flux is not in the teeth in this test, the weight of the teeth is not used. Using both the power and pound values, one can compute the watts per pound. If it appears to be excessively high, the steel was improperly processed or the laminations may be stuck together, or both conditions may exist. The user must now decide whether the stator core should be discarded or replaced, or whether an attempt should be made to repair the present one through reannealing. The user must keep in mind that if the steel has given an improper anneal through incorrect temperatures, atmosphere, or annealing time, a second anneal will not necessarily produce the desired steel characteristics. Keep in mind that if one were baking a loaf of bread and the incorrect time or temperature had been applied, a second baking effort will most likely produce a poor loaf of bread. The same concept applies to annealing steel.

## 7.6.2 Induction Motor Rotors

Like the stator, the rotor is also made of two parts, the core and the winding. In wound-rotor motors the rotor has a separate winding much like the stator. In this section the concentration is on cast squirrel-cage rotors because the rotor processing can have a profound effect on the final motor performance. It is also assumed that the cage is cast aluminum. Because the rotor bars are joined at the ends to end rings, the winding has an effective turn of one with respect to the stator winding. Whereas in the stator the winding is insulated with enameled wire, the cast aluminum cage winding depends on aluminum oxide and iron oxide to insulate the bars and end rings from the steel core. Also, the aluminum casting process can have imperfections, usually in the form of gas pockets or voids. The poor insulation and holes in the cage winding can produce undesirable performance and are the reason for process-control testing during manufacture.

### 7.6.2.1 Rotor Impedance Testing

Because one cannot directly connect a resistance bridge to the rotor to measure its resistance, one must resort to transformer theory to measure the impedance in the rotor. In essence, the induction motor is a rotary transformer. The stator winding is the primary winding and the rotor cage is the secondary winding. With this knowledge one can indirectly measure the resistance and reactance of the rotor. Instead of using a standard stator for this measurement, one uses a special impedance head or stator that has two windings, an exciting winding placed in the bottom of the stator slots, and a pick-up or sensing winding placed in the top of the slots. Both windings are sinusoidally distributed with respect to the

number of turns and both are placed in the same slots. The number of coils in these windings depends on the number of stator slots. A 20-slot stator could have a 4-coil winding and a 36-slot stator could have a 6-coil winding.

The impedance head stator is essentially a single-phase stator with both the exciting and pick-up windings wound on the same axis. Voltage is applied to the exciting winding such that a low level of current flows in that winding. The ends of the pick-up winding are connected to the voltage coil of a wattmeter. The current flowing through the exciting winding is directed through an ammeter and the current coil of the wattmeter. Through either some experimentation or computation one can determine the level of current required to obtain an up-scale wattmeter reading and at the same time keep the flux density in the stator iron to about 15000 lines per square inch or 2.3 kG. The purpose of the test is to induce a current in the rotor and at the same time keep the iron losses at a very low level. It should be noted that the connection is essentially the same as an Epstein test or the stator core loss test referred to in Section 7.6.1.3.

Upon further inspection one will see that the wattmeter reading essentially comprises the  $I^2R$  losses in the rotor winding. It also includes iron losses in both the stator and rotor, but by keeping the flux density at a low level those losses can be held to 5% or less of the total power measured by the wattmeter. This means that the wattmeter reading may be correlated directly to the resistance of the rotor. If the aluminum has a high level of impurities, particularly iron, the rotor resistance and its corresponding power measurement will be high. The power measurement is really a relative reading since the resistance measured in this manner is a function of the square of the turns of the primary or exciting winding.

One can go a step further with this rotor impedance tester and connect a varmeter to it instead of a wattmeter. Since a varmeter measures  $I^2X$ , the reading can detect changes in rotor reactance. The factors that are of concern include rotor skew angle, rotor bridge thickness, rotor slot geometry, and so forth. It should be noted that the rotor impedance test measuring either resistance or reactance is performed with the rotor revolving slowly at 5 to 10 rpm.

#### 7.6.2.2 Open Bar Testing

The rotor impedance head can be reconnected in another manner to detect open bars. Whereas the impedance test is performed with both the exciting and pick-up windings connected in a standard north-south polarity, the open bar test is performed with the pick-up windings connected in like polarity, for example north-north. For this test the pick-up winding is connected to a high-impedance voltmeter, preferably one that is peak reading. As the rotor slowly revolves, the voltage will show moderate fluctuations. If an open bar exists in the rotor cage, the voltmeter will show a substantial increase in voltage.

#### 7.6.2.3 Surface Losses

An additional test that can be performed with the impedance tester is a measure of rotor surface losses resulting from smearing of the rotor outside diameter during the turning or grinding operation. In this test the rotor is driven at the

synchronous speed of the stator. If the impedance head is wound as a 2-pole stator and energized with 60-Hz power, then the rotor should be driven at 3600 rpm. The pick-up winding is connected in the standard north-south manner and connected to the wattmeter. Again, the reading is relative, but the reading can be calibrated to good and bad rotors.

#### 7.6.2.4 Iron-to-Aluminum Resistance

One of the rotor characteristics that contributes to parasitic losses and dips in the speed-torque curve is poor insulation between the aluminum bars and the steel laminations. In an ideal situation the bars would be perfectly insulated electrically from the steel but would have perfect thermal conduction to the steel. In the real situation the bar-to-lamination insulation is not perfect and there is thermal resistance between the two. Most induction motor rotors applied to hermetic refrigeration compressors have a fairly good bar insulation, comprising both the normal aluminum oxide on the bars plus a blue magnetic oxide produced in the final rotor process. Often it is necessary to measure the level of insulation formed by this process. This measurement is done in a somewhat round-about way. A suggested procedure is as follows.

First, remove the end rings on each end of the rotor by turning the rotor in a lathe. Then peel off one lamination on each end. This will expose the bars for better access by probes. Using a constant current source of 10 to 20 A, direct the current into one end of one bar and out the other end of an adjacent bar. Simultaneously, measure the voltage across the other ends of the same two bars. The voltage will generally be in the millivolt level.

Digital meters are preferred for both the current and voltage readings. The resistance obtained by dividing the voltage by the current is the resistance created by the thin film of aluminum oxide and magnetic iron oxide. Now recall that:

$$R = \frac{\rho L}{A} \quad (7.57)$$

where:

$\rho$  = the resistivity of the thin film

$L$  = the thickness of the film

$A$  = the area of current path=twice the circumference of one bar times the length of the bar being measured

Since the length of the oxide film cannot be measured, the quantity  $\rho L$  best defines the quality of the insulation. If the units of measurements are in inches,  $\rho L$  has the units of ohm-in<sup>2</sup>. Many doctoral dissertations and papers have been written on the importance of the iron-to-aluminum resistance on induction motor performance. Past experience has shown that good hermetic motor rotors have a resistivity of about 0.02 to 0.04 ohm-in<sup>2</sup>. If one could achieve levels between 0.2 and 2.0 ohm-in<sup>2</sup>, the parasitic losses and accompanying torque dips could be significantly reduced.

#### 7.6.2.5 Bar Density

Normal aluminum in the ingot or rod form usually has a specific gravity of 2.702 at 20°C. Because of gas pockets and voids formed during the casting process, the density is somewhat less than this. To check this, one takes rotor bars that have been

chemically removed from the rotor by nitric acid and makes a specific gravity measurement by weighing the bar in air and in water. Because some gas pockets in any casting process are unavoidable, a bar density of 2.64 to 2.66 g/cm<sup>3</sup> is usually acceptable. The end rings have a lower density and a density of 2.58 to 2.62 g/cm<sup>3</sup> may be found to be acceptable.

#### 7.6.2.6 Percent Fill

Even though the rotor bars may have a high specific gravity, they may be too small in area due to shrinkage. This is the result of the aluminum being too hot during the casting process. One can check this by measuring the volume of the bar. If the metric measurements of weight from the specific gravity test are used, the bar volume is:

$$\text{Bar volume (cm}^3\text{)} = \frac{\text{weight in air (g)} - \text{weight in water (g)}}{\text{density (g/cm}^3\text{)}} \quad (7.58)$$

Neglecting any reduction in volume due to the stair-step of the skewed laminations, the volume of the bar can be readily computed from the bar dimensions. To keep the units consistent, one must use metric dimensions. The percentage fill is then:

$$\text{Percent fill} = \frac{\text{bar volume (cm}^3\text{)}}{\text{slot volume (cm}^3\text{)}} \times 100 \quad (7.59)$$

For rotors having normal shrinkage one might expect a percent fill of 95–97%.

### 7.6.3 Permanent Magnet Motors

The continued advances in power electronics have brought a corresponding increase in numbers of permanent magnet motors with the emphasis on brushless dc motors in which the commutator of the motor is replaced by power transistors. The speed-torque characteristic is much like that of a series ac motor. Two basic machine characteristics are of importance: the voltage constant and the torque constant. Both are related. In fact, if one is using the metric system of newton-meters per ampere and volts per radian per second, the torque constant and voltage constant are equivalent. In other cases one expresses the voltage constant as volts per 1000 rpm and the torque constant as oz-ft or even oz-in per ampere. They are related by equivalent conversion factors.

#### 7.6.3.1 Voltage Constant

Assume that the magnets are fastened to the rotor and that the stator winding is a 3-phase, wye-connected winding. The simplest method of measuring the voltage constant is to drive the rotor at 1000 rpm and display the line-to-line voltage on a digital oscilloscope so that an accurate measurement of zero to peak voltage can be obtained. By convention, the voltage constant is the peak voltage at a speed of 1000 rpm. Note that the voltage wave displayed in this test is essentially of sinusoidal nature. The torque constant can now be derived from the voltage constant:

$$K_T = 0.1127 K_e \quad (7.60)$$

where  $K_T$  has units of oz-ft/A and  $K_e$  has units of volts/1000 rpm.

#### 7.6.3.2 Torque Constant

Instead of driving the rotor at high speed, this test is done by slowly revolving the rotor at 5 to 10 rpm. A low level of dc current is forced through two of the three phases of the wye-connected winding. The level of current selected must be compatible with the particular design so that the magnets are not demagnetized. If the motor will be operating at a current level of 10 to 15 A, it is not unreasonable to use 10 A through the winding as the rotor rotates. The torque is measured using a torque table or with an in-line torque transducer. With the torque signal displayed on one axis of an X–Y plotter and time from the built-in time base on the other axis, the display will be sinusoidal. The torque constant is:

$$K_T = \frac{\text{peak torque}}{0.866 \times \text{current}} \quad (7.61)$$

The value 0.866 is the sine of 60 degrees. This is used because in a three-phase connection the current in one phase is zero when the other two phase currents are at 60 degrees. For this test, the current passes through only two phase windings. The voltage constant can now be derived from the torque constant:

$$K_e = \frac{K_T}{0.1127} \quad (7.62)$$

where  $K_T$  has units of oz-ft/A and  $K_e$  has units of volts/1000 rpm.

Because of saturation effects, the two methods may differ by 6–8% in the values obtained.

## 7.7 SELECTION AND APPLICATION OF TEST EQUIPMENT

### 7.7.1 Reasons for Testing

Before one attempts to assemble, purchase, or lease motor test equipment, the real reasons for testing should first be decided so that test equipment may be specified that meets the requirements and that may be economically justified for the business. It must be kept in mind that selection of inadequate test equipment may lead to erroneous decisions based on incorrect data, leading to a serious negative impact on the business. The following list describes a few reasons for motor tests

- Verification of design calculations
- Monitoring of factory quality
- Diagnostic testing to determine reasons for performance defects
- Heat runs for temperature measurement

### 7.7.2 Functional Specifications of Test Equipment

If test equipment is to be purchased from an outside vendor, it is imperative that the vendor be given a detailed description of the functions the equipment is expected to perform. Attempts to avoid the time-consuming process of writing detailed specifications by reliance on the vendor will almost inevitably result in equipment that does not meet the needs.

### 7.7.3 Recommended Steps in Purchasing Test Equipment

The following guidelines are recommended to gain assurance that the test equipment will provide the test functions needed.

- Prepare a detailed set of functional specifications.
- Send out a request for quotation (RFQ) to one or more reliable equipment vendors.
- If extensive design work is required, insist on the preparation of design specifications.
- The vendor is to build the equipment to the agreed design specifications.
- Insist that the vendor demonstrate that the equipment meets specifications. If the equipment does not perform to agreed specifications, the vendor has not fulfilled his contract.
- Provide progress payments based upon established milestones.
- Before the equipment is delivered to the purchaser's facility, the purchaser should insist on test verification at the vendor's facility.
- After the equipment is delivered, give the equipment extensive tests for an appropriate length of time before the final payment is made.

Precautions such as those outlined above will go a long way in obtaining the correct equipment with the proper use of funds.

### 7.7.4 Types of Tests

Before a description of test equipment is attempted, it would be wise to understand some of the major test procedures. Performance testing can be classified as steady-state or dynamic testing.

#### 7.7.4.1 Steady-State Testing

Steady-state tests include all of those tests where the load condition is held long enough for the instruments to display a constant reading. The period may be only 3 seconds or it could be as long as 1 hour. The entire test procedure, loading equipment, and instrumentation can be rather simple for this type of test. Since the signals being measured are essentially constant, one does not need to worry about proper signal phasing or delay lines since all of the instruments can be read sequentially and the data recorded. A first step in automating this recording would be the use of locking meters so that the data can be "frozen" on the instruments and then recorded after the power to the motor is turned off. This type of test is justified when the motors to be tested come in great varieties and there is little continuity from one test to another.

#### 7.7.4.2 Dynamic Testing

In dynamic testing the motor is allowed to traverse part or all of its speed-torque range in a relatively short time, usually 3 to 8 seconds, depending on its electrical and thermal time constants. The dynamic test is really a quasi—steady-state test in that the motor provides the same information as in a steady-state test but

in only a fraction of the amount of time and effort. However, ordinary analog or digital instruments will not suffice since the signals are changing so rapidly that it would not be possible to record the data manually. Dynamic testing requires automatic or continuous data recording. If simultaneous recordings of several signals are to be made, it is imperative that any signal conditioners, filters, amplifiers, etc. have the same time constants so that the data are truly recorded or stored simultaneously.

Simultaneous measurement of motor signals requires that attention be given to the time constants of the transducers and all of the associated circuitry between the transducer and the final device recording the data. This is particularly important if the signal frequency is changing during the test.

Dynamic testing is particularly advantageous when similar motors and similar tests are confronted on a daily basis. High-quality test equipment yields the benefits of increased worker productivity.

### 7.7.5 Types of Data Recording Devices

Depending on the complexity of the motor to be tested and the quantity of motors to be tested, one may select a simple meter system or go to a more complex computerized setup.

#### 7.7.5.1 Instruments for Steady-State Testing

Analog instruments are perhaps the oldest of the instruments in use. There will be situations when average-reading meters are desired, but for most motor testing one should use true rms meters for voltage and current. The measurement of power is by definition the average of the instantaneous volt-ampere products, so rms does not have any meaning in power measurements. In any event, one should select meters that have an accuracy of at least 0.25% of full scale. Analog meters do have an advantage over digital meters if the signal is varying or cycling, even though it is supposed to be steady state. By watching the needle swing, one can get an indication of the high and low readings. However, the frequency response and damping of the movement will affect the excursions. The method of recording is obvious: pencil and paper.

In general, digital instruments are replacing most analog meters and they have the advantage of providing consistent readings regardless of the person reading the meter. With analog meters, one has to be concerned with parallax, the situation when one does not look squarely at the meter. This is not a problem with digital meters. In addition, most digital meters have a higher accuracy than analog meters.

Instrumentation systems to read voltage, current, and power are likely to be composed of individual digital meters that read ac and dc voltage and current with high precision. For measurements outside of the instrument's ranges, separate transducers are required.

If instrument transformers are required, they should be selected carefully by examining the ratio and phase-angle errors. This is particularly important when using both current and voltage transformers to measure power. Seemingly small ratio and phase-angle errors can produce significant errors in power measurements.

### 7.7.5.2 Continuous Curve Plotting

Dynamic motor testing by its very nature requires a continuous capturing of the data. Instead of using analog or digital instruments for steady-state tests, one can connect the transducers to an  $X$ — $Y$  recorder and get a continuous plot of the data. Most analog  $X$ — $Y$  plotters are designed to accept 0 to 50 mV. This system allows one to get complete plots of quantities such as voltage, current, and power plotted against speed or torque. Care should be exercised that the data are not received faster than the writing rate of the plotter selected. This is particularly important when plotting curves that have dips or humps that change rapidly. This could happen when approaching the breakdown torque region of the motor. The use of  $X$ — $Y$  plotters has greatly speeded up motor testing since it allows the tester to traverse a large section of the motor performance curve in about 5 seconds. Taken manually this could take 15 to 20 minutes or more. Furthermore, the continuous plot allows one to examine harmonic torque dips in a manner not possible with steady-state metering techniques.

### 7.7.5.3 Computerized Data Acquisition

An alternative to the continuous curve plot made during the test is the use of analog-to-digital (A/D) converters connected to the transducers and bus-connected to a dedicated computer for simultaneous acquisition of ten or more signals. Most desktop personal computers are now capable of such data acquisition. After the test is complete, the computer is given the task of smoothing the data, which are then output to a plotter, printer, or both. In addition, the computer can calculate the efficiency and power factor directly from the online acquired points or from the statistically-smoothed data. The latter method is generally preferred since slight errors appearing in both the numerator and denominator in those calculations can result in exaggerated errors in the efficiency and power factor curves.

More recent test systems have essentially eliminated the analog and digital meters and have concentrated on the greatly improved capabilities of today's high-speed computer systems. Again, that speed is available in desk-top PCs. Using sampling techniques one may obtain simultaneous readings of both voltage and current values. If these instantaneous readings are taken at small intervals, one may use numerical techniques to compute power, average voltage and current (if desired), and the rms values of current and voltage.

If the sampled waves are essentially sinusoidal, trapezoidal, or of similar shape without discontinuities, one may realize a relatively high accuracy with as few as 60 to 100 samples per cycle. To achieve that level of accuracy one must use Simpson's rule and the trapezoidal rule to reduce the error of integration from point to point and as the signal crosses zero. With such numerical analysis techniques one can easily sense three voltage signals, three current signals, and also speed and torque, and transfer all of the instantaneous data into a direct memory access (DMA) of a computer for later computation while the motor is being cooled and readied for the next test sequence. With today's 32-bit microprocessors using high clock speeds one can perform sophisticated tests in less time than with the older test systems, which required further laborious hand calculations.

## 7.7.6 Mechanical and Electrical Loading Devices

A number of devices are available for use in loading the motor. These range from simple disks or inertia wheels to four-quadrant regenerative dynamometers.

### 7.7.6.1 Inertial Loading Wheels

One form of dynamic test uses disks or wheels whose moment of inertia is precisely known. If the motor accelerates those wheels and the acceleration is measured during the test, the delivered torque can be readily computed "on the fly" with a simple analog computer using the principle:

$$T = I\alpha \quad (7.63)$$

where:

$T$ =delivered motor torque  
 $I$ =moment of inertia  
 $\alpha$ =acceleration

If the moment of inertia is in units of oz-ft-s<sup>2</sup>, and the acceleration is in units of radians/s<sup>2</sup>, then the units of torque will be in oz-ft. Torque can be computed in other units with appropriate units for the moment of inertia.

It must be understood that the moment of inertia includes *all* of the mass that is being accelerated. That includes not only the inertial disks, but also the motor rotor itself, the shaft, and any couplings or similar devices that are caused to rotate by the system. The moments of inertia must be measured by comparing their time periods to that of known, calibrated inertial disks. With good digital timing devices these inertial values can be obtained to five or six significant figures rather easily.

The acceleration of the system is determined by measuring the angular speed of rotation and then taking the first derivative of that speed. The best tachometers using commutators will not suffice because their output is clouded with extraneous high-frequency noise. Because a differentiating circuit inherently accentuates high-frequency components, the noise will create havoc; that is, a clean signal cannot be obtained. A good light-beam encoder coupled to a frequency-to-voltage converter is the best choice.

Because the inertial test bench can only be used when the test motor is accelerating, the speed-torque curves and other variables measured are always taken from low speed to high speed. When properly used and maintained, the inertial test method will result in high test productivity and accuracy.

### 7.7.6.2 Regenerative Dynamometer

Perhaps the most versatile of all loading devices is the dynamometer, which operates as a motor or generator in either direction. This gives it the name of four-quadrant dynamometer. While most dynamometers presently use dc machines, the advent of the regenerative ac drive (inverter) used in conjunction with an induction machine makes it a strong candidate for motor test systems. The fact that the induction motor rotor is inherently rugged makes it an ideal unit for high-speed testing because a gearbox can be eliminated.

The dynamometer can be used for both steady-state and

dynamic testing. With proper feedback control circuitry, it can be used to hold the test motor at constant speed or constant torque. When testing very large motors it is almost imperative to use its regenerative capability, since that mode of testing requires that only the system losses be supplied by the power bus.

### 7.7.6.3 String-and-Pulley Tester

This tester is also known in the literature as a prony brake. This system is low cost and versatile but it requires a special technique on the part of the operator. A disadvantage is that the motor must bring itself up to speed and be connected all during the test. This, of course, means that the motor will increase in temperature during the test. In the case of the dynamometer machine, the dynamometer can keep the test motor running even when power to the test motor is turned off. Very few brakes of this type are now used.

### 7.7.6.4 Eddy Current and Particle Brakes

Both of these loading schemes use the principle of induced losses in a solid drum or disk, or in iron particles. The torque load is proportional to the losses induced by a magnetic field surrounding the drum or particles. Because the field is created by current flowing in a field winding, it is readily controllable either manually or automatically with the appropriate feedback. As with the string-and-pulley tester, this is strictly a onequadrant device. The test motor must bring itself up to speed, during which time heating in the test motor will occur. A modification that can be made is the addition of a separate drive motor that could accelerate the test motor and eddy-current drum up to speed before power was applied to the test motor. This same concept is often used with the inertial loading system.

### 7.7.6.5 Motor Test Precautions

Each of the motor test systems previously described has its own sets of advantages and disadvantages. Some are in first cost, others in test simplicity, and others in increased equipment cost but greater versatility. There are some major concerns that must not be overlooked. If trunnion bearings are used with either the dynamometer or test motor, attention must be given to the method of lubrication to be sure that the bearings are free to move with negligible friction. Sticky bearings could cause increased variance or uncertainty in the torque readings. In any dynamic test bench one must consider resonant frequencies based on the known geometry and physical characteristics. In a rotating system one can compute the resonant frequency by the relationship:

$$f = \frac{1}{2\pi} \sqrt{\frac{K}{I}} \quad (7.64)$$

where:

- $K$  = the torsional spring constant
- $I$  = the moment of inertia of the rotating mass

Since the test system is likely to comprise several torsional “springs” or shafts and several masses, there will be several

resonant frequencies or speeds. During the time the system is accelerating through those resonant speeds, it is likely that the torque readings will be in error. If at all possible, the system should be designed so that the top operating speed is below the lowest resonant speed. If not, the data gathered in the area of resonance should be discarded or considered suspect. This problem of resonance occurs both in trunnion-mounted systems using a load cell for torque and in systems using an inline torque meter. Caution is advised in any system.

## 7.7.7 Instrumentation

A number of performance variables will be measured. Each has its own unique types of instrumentation best suited for it.

### 7.7.7.1 Electrical Input Measurements

The units to be measured are voltage, current, and power. The preferred instruments for current and voltage are rms reading instruments. Average-sensing instruments should be avoided. Although many average-sensing meters are calibrated to read rms on a sine wave, the reading will be in error if a distorted wave is to be measured. An example would be the capacitor voltage in a single-phase motor operating at over voltage.

Preference should be given to digital meters because high accuracy can be obtained with relatively modest cost. The use of digital meters completely eliminates the problem of parallax. If several digital meters are to be used to give a complete set of readings, it is probable that the system will require several transducers for measuring voltage, current, and power. These could be standard devices that provide a small dc voltage output proportional to the ac input signal. They are generally quite satisfactory for steady-state tests but care must be exercised if they are applied to dynamic tests. Many have a time constant in the range of 0.5 seconds, which is too long for a dynamic test. An additional problem is that the time constants may be different, thus giving the false impression that the signals were measured simultaneously. The use of isolation amplifiers and filters must similarly be applied with care and scrutiny. Watch for phase and common-mode errors. A high common-mode rejection ratio (CMMR) is advised.

The advent of the personal computer and its associated instrumentation interfaces, such as the A/D amplifiers, has been a boon to the motor test engineer. A number of computer device manufacturers are making interface units that will allow one to connect the present transducers to the PC and simultaneously record 10 or more signals and store them in memory for later printout or plotting. If the test sequence is in the period of 8 to 12 seconds, there is a good possibility that multiplexing or sequential sampling will present negligible error. This may be easier and more cost effective than true simultaneous sample-and-hold devices applied to the system, although this method is no doubt the preferred one. If the voltage, current, and power are computed from a set of instantaneous sample measurements, it is imperative that simultaneous sample-and-hold devices be used. If not, there is likely to be a significant skew error.



### 7.7.7.2 Mechanical Output Measurements

Because the power output of the motor is proportional to the product of torque and speed, it is necessary to have accurate measurements of both quantities. The old standard of torque measurement had been the torque arm and a spring scale. There are many applications where that system is cost justified, but most of the newer systems use either a load cell or an in-line torque transducer. Both of these can be output to digital meters, X–Y recorders, or computers. If the in-line torque transducer is used, one should give preference to the rotary transformer type that does not use slip rings. Shaft alignment of the entire system is vitally important even though flexible couplings are used. Also important is the stability of the test bed. It, too, can resonate in the same manner as the rotating elements, so the bed should be made with high stiffness but with low mass. The principal goal is to achieve a test bed that does not resonate at any of the speeds encountered during the test sequence.

Speed can be measured with a hand-held tachometer, but it is not likely that that measurement will be satisfactory if high accuracy is desired. Another option is the stroboscopic method of measuring slip speed. This is highly accurate, especially at speeds close to synchronous speed, but that measurement is not likely to be capable of interfacing with a computer. Still another approach is a dc tachometer, like the hand tachometer mentioned but more adapted to direct connection to either the dynamometer or the load motor. The output voltage is proportional to speed and can be calibrated accordingly.

Some of the better speed-measuring devices are the steel gear with a plain magnetic pick-up or the preferred “zeroveLOCITY” pick-up to sense low speeds and direction of rotation. These gears usually have either 60 or 120 teeth for easy conversion to rpm. Perhaps the best speed measurement is that taken with an optical encoder having a number of lines scribed radially on a glass or plastic disk. Dual disks can be mounted to determine direction of rotation. A 7-bit encoder will have 128 lines while a 12-bit encoder will have 4096 lines. Lowspeed measurements may require the high-bit encoder while high speed measurements will necessitate the use of the lowbit encoder. Careful consideration is obviously required. Often the encoder is output to a frequency-to-dc voltage converter to give a voltage proportional to speed. That voltage can be input to the PC via the A/D converter.

## REFERENCES

Note: In the following listing, abbreviations have the following meanings:

ANSI	American National Standards Institute
CSA	Canadian Standards Association
EPRI	Electric Power Research Institute
IEC	International Electrotechnical Commission
IEEE	Institute of Electrical and Electronics Engineers
JEC	Japanese Electrotechnical Committee
NEMA	National Electrical Manufacturers Association

Sources for standards are listed in Appendix B.

1. IEEE 112–1996, IEEE Standard Test Procedure for Polyphase Induction Motors and Generators (ANSI recognized).
2. IEC Publication 34–2, Part 2, Methods for Determining Losses and Efficiency of Rotating Electrical Machinery from Test.
3. Cummings, P.G., W.D.Bowers, and W.J.Martiny, “Induction Motor Efficiency Test Methods,” *IEEE Industry Applications Society Conference Record*, 1979.
4. JEC-37 Induction Machine, Standard of Japanese Electrotechnical Committee.
5. CSA C390.1 Energy Efficiency Test Methods for Three Phase Induction Motors.
6. ANSI/NEMA Standards Publication No. MG1–1998, Motors and Generators.
7. Morgan, T.H., W.E.Brown, and A.J.Schumar, “Reverse-Rotation Test for Determination of Stray Load Loss in Induction Machines,” *Transactions of the American Institute of Electrical Engineers*, vol. 58, Jul. 1939, pp. 319–324.
8. Working Group on Stray Load Loss of the AIEE Rotating Machinery Committee, “Stray Load Loss Measurement in Induction Machines,” *Transactions of the American Institute of Electrical Engineers*, vol. 78, part III, 1959, pp. 67–71.
9. Oesterlei, R.E., “Measurement of Induction Motor Performance Using Standard Methods,” *Proceedings of the 7th National Conference on Power Transmission*, Cleveland, OH, 1980.
10. Jordan, H.E., and A.Gattozzi, “Efficiency Testing of Induction Machines,” *IEEE Industry Applications Society Conference Record*, 1979.
11. IEEE 114–2001, IEEE Standard Test Procedure for Single-Phase Induction Motors (ANSI recognized).
12. IEEE 119–1974, IEEE Recommended Practice for General Principles of Temperature Measurement as Applied to Electrical Apparatus.
13. IEEE 115–1983 (Reaffirmed 1991), IEEE Test Procedures for Synchronous Machines (ANSI recognized).
14. IEEE 115A-1987, IEEE Standard Procedures for Obtaining Synchronous Machine Parameters by Standstill Frequency Response Testing.
15. ANSI C50.10–1977. American National Standard General Requirements for Synchronous Machines.
16. IEEE 4–1978, IEEE Standard Techniques for High Voltage Testing (ANSI recognized).
17. IEEE 11–1980 (Reaffirmed 1992), IEEE Standard for Rotating Electric Machinery for Rail and Road Vehicles (ANSI recognized).
18. IEEE 43–1974 (Reaffirmed 2000), IEEE Recommended Practice for Testing Insulation Resistance of Rotating Machinery (ANSI recognized).
19. IEEE 56–1977 (Reaffirmed 1991), IEEE Guide for Insulation Maintenance of Large AC Rotating Machinery (10,000 k V A and Larger) (ANSI recognized).
20. IEEE 86-, \*IEEE Recommended Practice: Definitions of Basic Per-Unit Quantities for AC Rotating Machines (ANSI recognized).
21. IEEE 95–1977 (Reaffirmed 1991), IEEE Recommended Practice for Insulation Testing of Large AC Rotating Machinery with High Direct Voltage (ANSI recognized).
22. IEEE 100–1996, IEEE Standard Dictionary of Electrical and Electronics Terms—Fourth Edition (ANSI recognized).
23. IEEE 117–1974 (Reaffirmed 1991), IEEE Standard Test Procedure for Evaluation of Systems of Insulating Materials for Random-Wound AC Electric Machinery (ANSI recognized).
24. IEEE 275–1992 (reaffirmed 1990), IEEE Recommended Practice for Thermal Evaluation of Insulation Systems for AC Electric Machinery Employing Form-Wound Pre-Insulated Stator Coils, Machines Rated 6900 V and Below.
25. IEEE 286-\*, IEEE Recommended Practice for Measurement of Power-Factor Tip Up of Rotating Machinery Stator Coil Insulation.
26. IEEE 290-\*, IEEE Recommended Test Procedure for Electric Couplings.

27. IEEE 421.1–1986, IEEE Standard Definitions for Excitation Systems for Synchronous Machines (ANSI recognized).
28. IEEE 421.2–1990, IEEE Guide for Identification, Testing, and Evaluation of the Dynamic Performance of Excitation Control Systems (ANSI recognized).
29. IEEE 421.4–1990, IEEE Guide for the Preparation of Excitation System Specifications (ANSI recognized).
30. IEEE 432–1992 (Reaffirmed 1998), IEEE Guide for Insulation Maintenance for Rotating Electrical Machinery (5 hp to more than 10 000 hp) (ANSI recognized).
31. IEEE 433–1974 (Reaffirmed 1991), IEEE Recommended Practice for Insulation Testing of Large AC Rotating Machinery with High Voltage at Very Low Frequency (ANSI recognized).
32. IEEE 434–1973 (Reaffirmed 1991), IEEE Guide for Functional Evaluation of Insulation Systems for Large High-Voltage Machines (ANSI recognized).
33. IEEE 1–1992, IEEE Standard General Principles for Temperature Limits in the Rating of Electric Equipment and for the Evaluation of Electrical Insulation (ANSI recognized).
34. IEEE 62–1995, IEEE Guide for Field Testing Power Apparatus Insulation.
35. ANSI std S–12.34–1988 RI 1993, Engineering Methods for the Determination of Sound Power Levels of Noise Sources for Essentially Free-Field Condition over a Rotating Plane.
36. IEEE 95–1977 (Reaffirmed 1991), IEEE Recommended Practice for Insulation Testing of Large Rotating Machinery with High Direct Voltage (ANSI recognized).
37. IEEE 118–RI 1992, IEEE Standard Test Code for Resistance Measurements.
38. IEEE 120–RI 1997, IEEE Master Test Guide for Electrical Measurements in Power Circuits.
39. IEEE 522–1992, (Reaffirmed 1998), IEEE Guide for Testing Turn-to-Turn Insulation on Form-Wound Stator Coils for AC Rotating Electric Machines.
40. IEEE 792–, \*IEEE Trial-Use Recommended Practice for the Evaluation of the Impulse Voltage Capability of Insulation Systems for AC Electric Machinery Employing Form-Wound Stator Coils.
41. EPRI Report EL 1424, vol. 1, “Determination of Synchronous Machine Stability Study Constants” (Westing-house Electric Corp.), EPRI Project 997, Sep. 1980.
42. EPRI Report EL 1424, vol. 2, “Determination of Synchronous Machine Stability Study Constants” (Ontario Hydro), EPRI Project 997, Dec. 1980.
43. IEEE Joint Working Group on Determination of Synchronous Machine Stability Constants, “Supplementary Definitions and Associated Test Methods for Obtaining Parameters for Synchronous Machine Stability Study Simulations,” *IEEE Transactions on Power Apparatus and Systems*, vol. PAS-99, no. 4, July/Aug. 1980, pp. 1625–1633.
44. Rankin, A.W., “Per Unit Impedance of Synchronous Machines, Parts I and II,” *Transactions of the American Institute of Electrical Engineers*, vol. 64, 1945, pp. 569–572 and pp. 839–842.
45. Sarma, M.S., *Electric Machines*, chap. 10, West, St. Paul, MN, 1985.
46. Gerald, C.F., and P.O. Wheatley, *Applied Numerical Analysis*, 3d edn., chap. 10, Addison-Wesley, Reading, MA, 1984.
47. Schaum’s Outline Series, *Theory and Problems of Numerical Analysis*, 2d edn., McGraw-Hill, New York, 1988.
48. Carnahan, B., H.A. Luther, and J.O. Wilkes, *Applied Numerical Methods*, Wiley, New York, 1969.
49. Biomedical Computer Programs, P Series, Sections 14.1 and 14.2 University of California Press, Berkeley, CA, 1979.
50. Hooke, R., and T. Jeeves, “Direct Search Solution of Numerical and Statistical Problems,” *Journal of the Association of Computers*, vol. 8, no. 2, Apr. 1961.
51. IEEE 113–1985, IEEE Guide on Test Procedures for DC Machines (ANSI recognized).
52. IEEE 839–1986,\* IEEE Guide on Procedures for Testing Single-Phase and Polyphase Induction Motors for Use in Hermetic Compressors.

---

\* Withdrawn

# 8

## Motor Insulation Systems

Gregory C.Stone (Sections 8.1, 8.3, and 8.4)/L.Edward Braswell III (Section 8.2)

<b>8.1 INTRODUCTION</b>	<b>407</b>
8.1.1 Insulation and Ratings	408
8.1.2 Influence of Insulation on Motor Efficiency	408
8.1.3 Influence of Insulation on Motor Life	408
8.1.4 Random- and Form-Wound Motors	409
<b>8.2 RANDOM-WOUND MOTORS</b>	<b>410</b>
8.2.1 Insulation System of Random-Wound Motors	410
8.2.2 Insulation Testing of Random-Wound Motors	412
8.2.3 Causes of Insulation Failure	415
<b>8.3 FORM-WOUND MOTORS</b>	<b>416</b>
8.3.1 Insulation Systems	416
8.3.2 Factors Affecting Insulation System Design	419
8.3.3 Insulation Testing	422
<b>8.4 EFFECT OF INVERTER DRIVES ON STATOR INSULATION</b>	<b>427</b>
8.4.1 Surge Voltage Environment	427
8.4.2 Distribution of Voltage Surges within Stator Windings	428
8.4.3 Mechanisms of Insulation Deterioration	429
<b>REFERENCES</b>	<b>429</b>
<b>GENERAL REFERENCES</b>	<b>430</b>

### 8.1 INTRODUCTION

Most of this handbook has concentrated on the electromagnetic and mechanical aspects of motor design and operation. However, some very important aspects of a motor's rating, such as voltage and temperature, strongly influence the electrical insulation that is an inherent component of motor windings. In particular, various conductors in a motor winding are at different voltages. If these conductors come into contact, then currents will flow in unexpected paths, usually with substantially less impedance, resulting in large circulating currents that prevent or impair motor operation. The electrical insulation in the motor prevents these circulating currents. The insulation system design must be adequate to perform this function for the motor's expected life.

Electrical insulation can be used in three locations in a modern motor:

The stator winding

The rotor winding

To separate the steel laminations in stator and rotor cores

For both the stator and rotor windings, the purpose of the insulation is to prevent short circuits to the steel, or shorts between the various turns in the winding. If such shorts occur, the magnetic fields are not the desired ones, and large circulating currents can flow that melt the conductors. For the lamination insulation, the purpose is to prevent axial eddy current flow in the steel, which produces  $I^2R$  losses in the core, resulting in reduced motor efficiency.

Whether and how much insulation is used in each of these motor components depends on the type of motor. For example, squirrel-cage induction motors normally contain stator winding and core lamination insulation, but no insulation on the rotor cage winding. Other ac motors, such as the wound rotor induction motors and synchronous motors, contain insulation in all three components. Similarly, direct current (dc) motors also require stator and rotor insulation, as well as core lamination insulation.

### 8.1.1 Insulation and Ratings

The voltage rating of a three-phase induction motor almost always refers to the normal phase-to-phase rms voltage impressed across the stator winding leads. For single-phase induction motors and dc motors, the rating is the normal stator line-to-ground voltage. In induction motors, there is no voltage directly applied to the rotor winding, and the induced rotor voltage is usually only a few volts. For synchronous ac motors and dc motors, a voltage is applied to the rotor winding, but it is usually less than the stator winding voltage, and typically a maximum of a few hundred volts.

The electrical insulation used in motor windings must be substantial enough to prevent short circuits over the expected life of the motor. The insulation must withstand voltages ranging from only a few volts (core lamination insulation and interstrand insulation) to more than 20,000 V across the main stator ground wall insulation in very large motors. The insulation thickness depends on the voltage across the insulation and the electrical strength of the insulation material used. Some materials have a higher breakdown (electrical) strength than others, and thus thinner insulation can be used.

In the smaller motors that operate up to approximately 600 V, the electrical insulation provides more of a physical barrier between conductors, and the thickness is more a function of the amount of insulation needed to ensure that the winding survives the physical process of winding manufacture. For motors rated 2300 V and above, the stator winding insulation must be thick enough to withstand the electrical stresses that can occur at high voltages. In such large motors, the thickness of the insulation and the need to maintain adequate distances between parts of the winding at different voltages have an overriding impact on the design of the stator, requiring that form-wound coils with long end-turns be used. Thus the physical size of the motor is very dependent on the winding's voltage rating. Similarly, the core steel laminations have thin layers of insulation to reduce eddy current losses. To accomplish the task of concentrating the magnetic fields in the motor, a larger overall core is required, because a considerable amount of the core is composed of insulation that is not magnetically active.

Most of the electrical insulation used in motor windings is made from organic materials such as varnish, polyester, and epoxy. Such materials have a maximum operating temperature, above which the insulation loses its mechanical and electrical strength. Each material has a characteristic temperature, above which it should not operate. Standard test procedures have been developed to rate the capability of the insulation to resist deterioration at high temperature. These standards group the various types of insulation into a restricted number of maximum operating temperatures such as 105°C (or class A), 130°C (class B), 155°C (class F) and 180°C (class H). Insulation materials rated for 155°C can, on average, be expected to operate 20,000 hours without failure at the maximum insulation temperature of 155°C. The thermal rating of winding insulation systems is discussed in considerably more detail later.

The motor must be designed to ensure that insulation does not operate above the maximum temperature capability of the insulation, otherwise electrical shorts will occur, and motor failure results. Heat in a motor is primarily created by  $I^2R$  losses in the copper conductors, eddy current and hysteresis losses in the core, plus windage losses. The maximum operating temperature of a winding depends on a complicated interaction of the winding current, the thermal resistance of the insulation, the rate of cooling air flow, the ambient temperature, and whether the motor had been subjected to recent starts and/or overloads. Thus the motor designer has a complex set of trade-offs to make, i.e., set the maximum winding currents, develop an adequate cooling system, and select the least expensive insulation material that can survive the expected maximum operating temperature.

### 8.1.2 Influence of Insulation on Motor Efficiency

The amount and type of insulation has a direct effect on the voltage and temperature rating of the motor. The insulation also has an influence on the motor's efficiency. The electrical insulation plays a passive role in motor operation, unlike the role of the magnetic cores or the copper (or aluminum) windings. In general, the motor's efficiency in converting electrical power to mechanical power is increased if the thickness of the insulation is decreased.

In the stator winding, coupling between the current in the winding conductors and the magnetic field would be greatest if the insulation thickness around the copper conductors was reduced to near zero. (It cannot be zero because the parts of the winding at higher voltage would short to the grounded steel core, diverting the current from its intended path, and destroying the carefully-shaped magnetic field.) With near-zero thickness, all the magnetic flux created by the current in the stator conductors would be directed by the core to link with the rotor. With thicker insulation, some of the magnetic flux immediately surrounding the conductors does not couple into the steel core, and thus a greater current in the stator winding is required to achieve the same flux linkage with the rotor. Thus, increasing the insulation thickness results in greater leakage flux, the use of more steel, and ultimately lower efficiency.

Increasing the insulation thickness also has a second-order effect on efficiency. With thicker insulation, the thermal impedance between the conductors and the steel core (heatsink) is increased. Thus, all other things being equal, the winding conductors operate at a higher temperature, increasing the conductor resistance, resulting in greater  $I^2R$  loss and thus lower efficiency.

### 8.1.3 Influence of Insulation on Motor Life

A motor is said to have failed when it becomes excessively noisy, the motor or bearings vibrate excessively, the motor can no longer drive its load, or a short circuit occurs in the stator winding that causes a surge in supply current and a tripping of the circuit breaker. In an extensive survey of large squirrelcage induction motor users, 37% of motor failures were due to stator insulation breakdown that resulted in a

short circuit [1]. Another 10% of the failures were due to rotor winding failures that manifested themselves as high vibration and noise or inability to drive the load, as a result of cracked rotor bars. Thus, winding problems are a major determinant of motor life.

Other studies have shown that the root cause of winding failure is gradual deterioration of the insulation due to thermal, electrical, mechanical, and environmental stresses [2]. The aging of the insulation reduces the electrical and mechanical strength of the insulation. At some point, a voltage surge or mechanical shock from a motor start will fracture or break down the insulation, resulting in a short circuit and motor failure. Motor winding failure can sometimes occur without prior aging, but this is very rare if the motor has been properly specified and operated.

Because winding aging is a major factor in determining motor life, designers expend considerable effort to design an insulation system that will operate without failure for its intended life. Thus, designers must determine what insulation deterioration modes occur in service. They must then determine the ability of a particular insulation to resist the deterioration modes, and estimate the design (materials and thickness) needed to achieve the expected life. This usually requires extensive laboratory evaluation of the insulation systems, and the use of accelerated aging tests.

For example, manufacturers have devoted considerable effort to ensuring that insulating materials will operate properly at the design operating temperature. The thermal aging process in insulation is a complex one, but it is essentially a continuation of those processes used in production of the insulation to bring it to a usable condition. The inevitable result is the eventual loss of desirable characteristics such as tensile strength, electrical strength, and so forth. The degradation mechanism is usually a complex combination of effects due to scission of molecular chains, oxidation, changes in oxidation, loss of plasticizer, formulation of dense cross-linked skin, and so forth.

In 1948, T.W.Dakin [3] realized the connection between the thermal aging phenomenon and the Arrhenius law of chemical reaction rates. The equation that expresses aging of plastics is:

$$k = Ae^{-E/RT}$$

where:

$k$  = the specific reaction rate

$A$  = the frequency of molecular encounters

$E$  = the activation energy (constant for a given reaction)

$R$  = the universal gas constant

$T$  = the absolute temperature

Taking the natural logarithm of this equation results in:

$$\ln k = - \left( \frac{E}{R} \right) \left( \frac{1}{T} \right) + \ln A$$

which is the equation of a straight line.

One of the important results of Dakin's work is that the expected life of new formulations of insulation can be obtained within a short time by accelerated aging of insulation

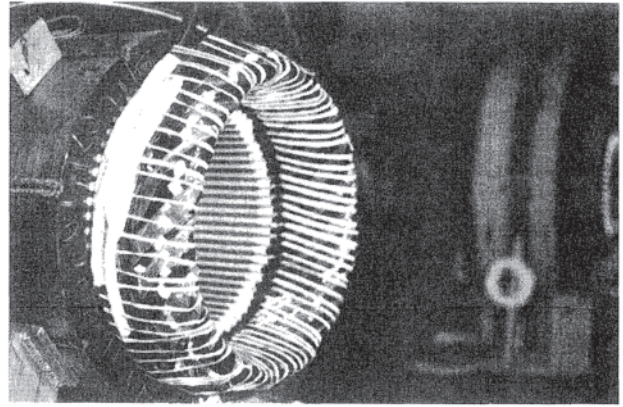


**Figure 8.1** A random-wound stator. (Courtesy of Westinghouse Motor Company, Canada, Ltd.)

using four (or more) elevated temperatures. Using the criterion that the end of life occurs when the test variables (usually dielectric strength and flexural strength) degrade to one-half the preaged values, the data points of time vs. temperature are plotted on log-log paper. If the aging test has been run correctly, the results will be a straight line that can be extrapolated to estimate the expected life of the insulation at a target temperature, or the temperature at which the insulation can be expected to perform reliably for a given time. The Arrhenius relationship is the basis of test methods (e.g., those of Ref. 4) used to classify the capabilities of various insulation materials to operate at high temperatures.

The effect of thermal aging, as well as mechanical, electrical, and environmental aging, is discussed in more detail later.

#### 8.1.4 Random- and Form-Wound Motors

With regard to the design of motor insulation systems, there are two broad classes of motors: form-wound stators and random-wound stators. Random-wound stators are usually used for motors less than 2300 V. In a random-wound stator, insulated copper (magnet wire) is wound around the steel and/or into slots in the steel core (Fig. 8.1). A copper turn that is at high voltage (i.e., connected to the terminal) may be adjacent to a turn that is near ground potential. Sufficient insulation thickness is used on the magnet wire that the insulation can withstand the full operating voltage (and normal transient voltages) without breakdown.

A typical form-wound stator is shown in Fig. 8.2. Such windings are used if the rated voltage is 2300 V or above. In form-wound motors, the coils are preshaped into diamonds, and then inserted into slots in the motor. The principal distinction from form-wound windings is that there is separate turn insulation and ground insulation. (For random-wound stators, the turn insulation is the same as the ground insulation.) Another distinction is that the position of adjacent turns is carefully controlled to prevent turns with significantly different voltage from being close to one another. This ensures that in even very large motors, turns that are adjacent to one another have only a few tens of volts across the turn insulation. This reduces the necessary thickness of the turn insulation.

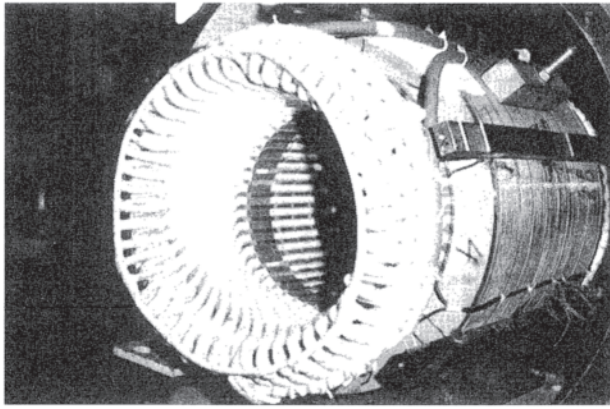


**Figure 8.2** A form-wound stator in a large machine. (Courtesy of Westinghouse Motor Company, Canada, Ltd.)

Due to the completely different design and deterioration aspects of random-wound and form-wound stators, these two types of machines will be dealt with separately. In addition, the impact of inverters on stator winding insulation design is also discussed in Section 8.4.

## 8.2 RANDOM-WOUND MOTORS

The more efficient and less expensive random-wound motors can be found in a variety of applications in commercial and industrial facilities throughout the world. In normal applications, random-wound motors are usually rated up to 600 horsepower (hp) and operate at 115, 200, 230, 460 and 575 V. Random windings are generally used on machines that have partially closed slots in their magnetic cores. The motors are called random-wound because the layers of round conductor in each coil are applied with no particular effort being made in the placement of the magnet wire; the conductors lie in whatever random position they happen to be laid as they are inserted into the slot. This random placement of coil loops could result in current circulating through the entire coil before reaching an adjacent conductor. Under this condition the maximum electrical stress could be applied on the turn-to-turn insulation at that point.

In random-wound motors, the loose individual conductors are inserted directly by hand or machine into the insulated core slots. In many cases the magnet wire is wound on a form to shape the coils, which are then inserted into semiclosed slots and braced in place with top sticks, or wedges, that are inserted afterwards.

### 8.2.1 Insulation System of Random-Wound Motors

The insulation system of a random-wound motor consist of several insulation materials that provide specific functions. The cross section of a typical random-wound motor slot is shown in Fig. 8.3.

**Ground insulation** The major part of the insulation system of a motor is the ground insulation, usually identified as the slot cell. It is inserted in each core slot before the insulated conductors are placed in the slot and must extend beyond the core to insure mechanical separation between the conductors

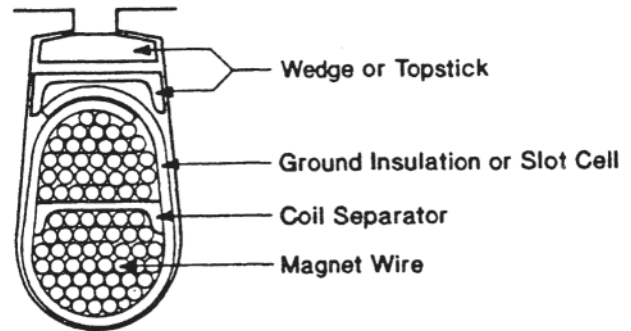


**Figure 8.3** Cross section of a typical random-wound motor slot.

and the core. During motor assembly the slot cell is subjected to physical abuse. During motor operation the slot cell generally must withstand higher voltages than the turn-to-turn insulation. The slot cell provides important electrical and mechanical protection to the winding and requires the highest degree of attention in design and manufacture to assure maximum service reliability of the motor. The slot cell must have a high dielectric strength, which is a measure of its ability to withstand the passage of current, expressed as a breakdown value in volts per mil or kilovolts per millimeter. Typical slot cell materials are mica, Nomex, and Dacron-Mylar-Dacron (DMD).

**Strand or Conductor Insulation** The wire used in the winding of motor coils is known as magnet wire. The purpose of magnet wire, as distinguished from other insulated conductors that are used for the transmission of electrical energy, is to form a useful magnetic field within a motor. Copper magnet wire is normally used; however, under certain economic and supply conditions, aluminum magnet wire has also been used. The strand insulation is a coating applied to the magnet wire to form a thin, flexible insulation film. Strand insulation for low-voltage random wound motors is usually of the resinous coating type because of its good dielectric strength and ability to withstand the bending and stretching that occurs during coil forming operations and high-speed winding. The thinness of the coating itself (0.002 to 0.005 inch) is a contributing factor to flexibility.

Many types of round and shaped magnet wires are available in thermal ratings from 105°C to 220°C. The selection of the proper magnet wire is made by considering the required properties. Thermal stability, resistance to heat shock, and thermal overload characteristics determine the temperature level at which the wire must operate. Mechanical properties of abrasion resistance and windability are determined in order to provide successful application. The chemical properties define processing capabilities with treating varnishes or general compatibility with other insulation materials. Electrical and chemical properties also limit the environment in which the wire can operate. Unusual environments may require special resistance to moisture, oil, refrigerants, chemicals or encapsulation compounds.

Magnet wire standards are issued and available from the National Electrical Manufacturers Association (NEMA) and

are affirmed as national standards by the American National Standards Institute (ANSI). The magnet wire standards publication is NEMA MW 1000 [5] and applies to round, rectangular and square, plated or unplated, copper or aluminum magnet wire. It includes definitions, type designation, dimensions, constructions, performance, and methods of testing magnet wire generally used in the winding of coils for electrical equipment.

A federal specification titled 'Federal Specification Wire, Magnet, Electrical J-W-1177' was developed by the Naval Ship Engineering Center. Products that meet the J-W-1177 specification can be listed on a qualified products list and their use is allowed in government-related electrical equipment.

Typical film-coated magnet wire types are (1) oleoresinous enamel, polyvinyl formal, solderable acrylic, and polyurethane for 105°C thermal class; (2) epoxy, polyurethane nylon, and polyurethane nylon butyral for 130°C thermal class; (3) polyester, polyester nylon, and polyester with amideimide overcoat with a high-temperature bondable topcoat for 155°C thermal class; (4) modified polyester with amide-imide overcoat and modified aramid overcoat for 180°C thermal class; (5) polyamide-imide and polyester with amide-imide overcoat for 200°C thermal class; and (6) aromatic polyimide for 220°C thermal class.

*Coil separators and phase insulation* Often two or more coils lie adjacent to or on top of one another. Because the voltage gradient between coils is usually much higher than turn-to-turn voltages within a coil, it is desirable to place an added piece of insulation between the coils. Coil separators are placed on top of coil sides as they are laid in the iron core slots.

Phase insulation prevents the ends of coils in different groups from touching each other. Coil separators and phase insulation provide a high-voltage barrier between coils, with good formability and mechanical strength to resist the softening and shrinking action of varnishes and heat. Materials used for these applications are made from such basic insulation materials as paper, pressboard, fibre, mica, laminated cloths, and laminated papers. There are also laminated combinations of materials such as rag paper and polyester film (RMR), polyester mat and polyester film (DMD), and glass mat and polyester film (CMC).

*Wedges* Wedges, or top sticks, are placed over the winding in each slot to close the slot and keep the wires compact and guard against vibration. Typical wedges are made of paper, canvas, and fiber glass impregnated with a thermosetting resin such as phenolic, melamine, silicone, and epoxy, high-temperature resin reinforced with glass fibers, and high-temperature synthetic paper.

*Tapes and tie cords* Tape is the most easily applied form of electrical insulation. It is used for physical support and for dielectric barrier purposes. Most tapes are easily applied to odd shapes and are therefore used extensively. Tapes are relatively narrow, woven or cut, strips of fabric, paper, or film material. They may be plain or impregnated with oleoresinous or polyester varnish as well as epoxy or polyester resin. Tapes are made in both treated and untreated forms from materials such as cloth, glass, and synthetic resin monofilaments. Tapes are also made of rubber, synthetic films, and mica. Pressure-

sensitive adhesive tapes are also used for insulating end-turns and to retain components as winding aids. Pressure-sensitive tapes differ from other tapes in that there is an adhesive coating on the backing material that is activated by the application of pressure.

Tie cords are an essential element of a random-wound motor. They perform important mechanical functions in tying and lashing coils to each other and in supporting members as well as binding other insulating parts to prevent looseness, motion, and wear as the result of certain stresses applied to the motor windings by the service it sees. Braided polyester lacing tape is the most popular tying cord presently being used by the motor industry. Cords are also constructed of woven cotton and glass polyester.

*Varnishes and resins* Resinous materials found in varnishes and insulating compounds provide important characteristics to electrical insulation. These materials can be considered as imparting life and reliability to many of the basic solid insulation materials, which by themselves have serious limitations. Organic resins are not only important as insulators, but as protection to other insulating materials. The proper processing of fibrous materials with resinous products will raise their dielectric level from spacing insulation to true dielectric barrier insulation.

Windings are treated with varnish to improve their resistance to moisture; to increase the electric strength of the insulation by replacing air with solid dielectric; to bond turns together and to other parts of the structure so as to prevent damage by abrasion and vibration; to improve heat dissipation and to prevent the entry of dirt, metal particles, and other contaminants that may be detrimental to the insulation system. Varnishes and resins should also provide good resistance to moisture, good adhesion, strength and flexibility, high dielectric strength, and a smooth, impervious surface with good chemical resistance. Additional important qualities are penetration and wetting properties.

All varnishes absorb water and are permeable to water vapor to some extent and afford only partial protection. Measurements of the dielectric strength of varnish-treated paper before and after exposure to wet conditions give a good indication of the varnish's vulnerability to moisture. Dielectric strength measurements are more easily interpreted and are of greater significance than data on the water absorbed by a specimen, or on the readiness with which it is wetted by water.

Varnishes and resins are often no more than 1–2 mils thick and seldom more than 15–20 mils. They do not contribute physical strength to the total insulation system because they are not present in sufficient amounts. Therefore, their structural properties (tensile, compressive and flexural) are of no direct design consequence. These properties are important only because they are reflected indirectly in terms of bend strengths, peel resistance, scrape resistance, heat shock, and environmental factors.

A varnish cannot be effective unless it is present as a continuous film; therefore, the ease with which it wets the surface to be treated is important. This is best assessed by a test using the actual materials involved. Varnish build, or the amount of varnish picked up per treatment, is a function of the percentage

solid content and viscosity. Electrical rotating machinery can be coated or impregnated with a variety of insulating varnishes and resins. The chemical industry over the years has developed a number of more suitable insulating materials that have been a major contribution to the evolution of today's modern electrical motors and generators. The industry has progressed from the use of organic oils, to asphalt compounds, to synthetic solvent varnishes, and finally to organic solventless polymers. Solvent-containing varnishes have been used for many years; however, most solvent varnishes for random-wound motors contain from 25%–50% solids. Solventless polymers have made it possible to achieve excellent void-free impregnation using vacuum pressure technology. While vacuum pressure impregnation (VPI) is not new, early attempts using materials available at that time did not come close to achieving the results that are possible today.

With the use of vacuum to remove air and gas entrapped in the winding, and the use of pressure to assist the varnish in more thorough and rapid wetting and fill, it is possible to obtain 100% void-free fill. However, 50%–75% of the volume (solvent) would be driven off during cure. Varnishes containing solvents cannot provide the desirable slot fill when used as an impregnant.

A solventless resin impregnant, properly processed by the use of vacuum and pressure, can produce the desired fill and protection. Solventless resins contain 100% solids, thereby eliminating the loss of volume during the curing process. In addition, a thixotropic material is used to retain a sufficient coating on the coils. Thixotropy is the property of a coating that, after it is no longer agitated, it sets to a semi-gelled state. At this point, the material will stay on the motor windings and the amount drained in the curing open is minimal.

Some common varnishes and resins used in the insulation of random-wound motors are acrylic, epoxy, phenolic, polyamide, polyimide, polyester, and silicone.

## 8.2.2 Insulation Testing of Random-Wound Motors

Modern electric motor insulation systems are very reliable. If a motor is operated within its ambient design temperature and not overloaded electrically or abused chemically or mechanically, its insulation system could be expected to have a life expectancy of as much as 100,000 operating hours. However, these ideal conditions are never met in practice, and motors and their insulation systems are exposed to many factors that accelerate the deterioration process. High temperature, vibration, environment, mechanical effects from thermal expansion and contraction, electromagnetic forces, motor start-up forces in the end turns, and voltage stresses at operation levels and due to power surges and transients contribute to irreversible changes and loss of insulation integrity and reliability.

Insulation testing evaluates the integrity of the insulating medium. This usually consists of applying a high potential (voltage) to the motor under test and determining the leakage current that flows under test conditions. Excessive leakage current may indicate a deteriorated condition or impending failure of the insulation. Insulation testing can be performed

by applying either a dc voltage or an alternating current (ac) voltage. The testing of random-wound motor insulation with these voltages can be categorized as nondestructive testing and destructive testing, respectively. The destructive test may cause windings under test to fail or render them unsuitable for further service. Nondestructive tests are performed at low voltage stress or in a controlled manner so that the motor under test is rarely damaged. The ac high-potential test is primarily a go or no-go test. The voltage is raised to a specified level and if the equipment fails or shows excessive leakage current, the equipment under test is unusable. If the equipment does not fail, it has passed the test. This test can only indicate whether the winding is good or bad. It cannot indicate with what safety margin the test was passed. The dc high-potential test can indicate more than a go or no-go condition. It can indicate that equipment is functioning properly at the present time but may fail in the future. Direct-current testing is conducted to obtain information for comparative analysis on a periodic basis. With direct-current testing, the leakage current is measured during the progress of the test and compared to leakage current values of previous tests.

### 8.2.2.1 Insulation Resistance Testing

In an electric machine, insulation resistance is the resistance of the parallel combination of all the insulation that can be found between the conductors of the random winding and ground, or the frame of the motor. The instrument used to measure insulation resistance is known as a megohmmeter or Megger™ and the readings are known as “megger™” readings. For many years megohmmeters were all of the hand crank variety, and many are still in use today. The most popular testers currently being used, however, are battery-operated models. In operation, the instrument imposes a dc voltage from winding terminals to ground and interprets leakage current to ground in terms of megohms of insulation resistance. Testers are commonly available in output voltage ranges from 100 through 5000 V.

The quality of insulation is evaluated based upon the level of insulation resistance. The measured insulation resistance is a variable, dependent upon temperature, humidity, and other environmental factors. Therefore, all readings must be corrected to a standard temperature for the class of equipment under test. The insulation resistance values by themselves do not indicate the weakness of the insulation nor its total dielectric strength. However, they can indicate contamination of the insulation and predict trouble ahead within the insulation system if a downward trend continues over time in the insulation resistance values.

Long-term trends in insulation resistance can be plotted accurately only if all readings are taken at the same temperature or if they are all corrected to a common reference temperature, normally 40°C. Alternately, the measurements may all be made under similar conditions, for example, immediately after shutting down a motor that always carries the same load and for which the ambient temperature is essentially constant.

The resistance of most insulating materials is contravariant with temperature, and can often be represented by a



function of the same form as the Arrhenius equation, which was mentioned earlier in the discussion of insulation life. The relationship is a complex one from a theoretical point of view, but from a practical point of view and for the temperature range in which insulation is normally used, insulation resistance is halved for every 10°C rise in temperature. That is, insulation that has a resistance of 10 mΩ at 20°C will have a resistance of 2.5 megohms at 40°C. To avoid cumbersome calculations, a resistance  $R$  measured at a temperature that is not some multiple of 10°C from the reference temperature being used (e.g., 40°C) may be corrected to the reference temperature by use of the chart in IEEE Std. 43–1974 [6].

Moisture and humidity affect insulation in two important ways. First, moisture can be absorbed into solid insulation pores, reducing its insulation resistance. Surface moisture can turn an insulating system into a conducting path. Second, water distributed throughout the volume of an insulation produces interfacial polarization. This will cause increased capacitance and power factor as well as reduced insulation resistivity.

The degree by which moisture absorbed into insulation will affect these factors depends on the relative humidity of surrounding air and the frequency at which insulation measurements are made. The rate at which porous insulation absorbs water and retains moisture depends on material porosity. At 100% relative humidity and commercial frequencies, insulation capacitance may double, power factor may approach 100% and insulation resistance may decrease by several orders of magnitude. When measuring insulation resistance the amount of relative humidity should be noted and taken into consideration in determining the overall condition of the insulation system.

The measured value of insulation resistance will increase with the time that the voltage is applied, changing rapidly at first and later less rapidly, with the readings gradually approaching a stable value. Values at 30 Seconds may be as low as 10% of the final value. The insulation resistance of clean, dry insulation may continue to increase for hours with continuous voltage application. However, an approximately steady value will generally be reached in 10–5 minutes. In wet or dirty insulation, the steady value of insulation resistance is usually reached quickly. The change in apparent insulation resistance is a dielectric absorption phenomenon. It is dependent upon the character and condition of the insulation material rather than equipment size or voltage rating.

There are four useful methods of measuring insulation resistance of random wound motors: (1) short-time readings, (2) time-resistance measurements, (3) step-voltage measurements, (4) polarization index test.

1. Short time testing simply measures the insulation resistance values for a short duration of time, such as 30 or 60 seconds. The reading only allows a rough check of the insulation condition. However, comparison of this value with previous values is of importance. A continued downward trend is indicative of ongoing insulation deterioration.
2. The time-resistance method of measuring insulation

resistance is independent of temperature and equipment size. It can provide conclusive results as to the condition of insulation. The ratio of time-resistance readings can be used to indicate the condition of the insulation system. The ratio of the resistance read at 60 seconds to that read at 30 seconds is called the dielectric absorption ratio (DAR). A DAR ratio below 1.25 is cause for investigation and possible repair of the motor.

3. The step-voltage method is performed by applying voltage in steps to the insulation under test through a multivoltage test set. As voltage is increased, the weak insulation will show lower resistance that was not obvious at lower voltage levels. Moisture, dirt, and other contaminants can be detected at lower voltage levels, whereas aging and physical damage in clean, dry insulation systems can only be revealed at higher voltages. The step-voltage test can be very valuable when conducted on a regular periodic basis.
4. The polarization index (PI) test method of measuring insulation resistance is the ratio of the reading at 10 minutes to the reading at 1 minute. The PI provides information on the moisture and deterioration of the winding insulation. The PI values can vary from above 2 to a low of less than 1. An acceptable value should be at least 2 or higher, values between 2 and 1 indicate marginal condition, and values below 1 indicate poor condition. There are no hard and fast rules or criteria for a “good” polarization index. It is important to maintain records from past tests that can be used as a standard of comparison.

DC voltages for insulation resistance testing of random-wound motors depend on the motor’s normal operating voltage. Motor voltages up to 200 V ac are tested at 100 to 200 V dc; motors operating at 440 to 600 V are tested at 500 and 1000 V dc.

The values of measured resistance may range from kilohms to 1000 megohms and even higher; however, typical motor insulation resistance is in the range of tens or hundreds of megohms. An accepted formula for minimum insulation resistance as defined by IEEE Std 43–1974 is:

$$R_{\min} = kV + 1$$

where:

$$R_{\min} = \text{recommended minimum insulation resistance in megohms at } 40^{\circ}\text{C of the entire machine winding}$$

$$kV = \text{the rated machine terminal potential (rms kV)}$$

For example, a motor operating at 440 V ac would have a minimum insulation resistance of  $0.440 + 1$  or 1.44 mΩ.

Typically, results of dc tests are relative and therefore evaluation is based on trends over time. For this reason, it is best to keep records of the test and a plot of the insulation resistance versus time for each motor. It is also important for the person making the evaluation to be aware of any possible test problems or conditions that might cause sudden changes in the insulation resistance. In many cases, low values are caused by the effects of humidity and drying out the windings is all that is required as a remedy.

### 8.2.2.2 Direct-Current High-Potential Testing

The discussion of insulation resistance testing to this point has been focused on using dc test voltage levels at or below the full working voltage of the motor. These methods are very useful in determining the condition of the insulation; however, the use of dc high potential testing can provide information about the dielectric strength of the motor's insulation system. The dielectric strength of an insulation material is defined as the maximum potential gradient that the material can withstand without rupture. A dc high-potential, or hi-pot, test is a deliberate application of a higher than normal potential across the motor's insulation. If the insulation withstands the higher potential for a certain period of time, and does not pass exceptionally high leakage current, it is assumed that it will be able to function properly at its normal operating voltage. A dc hipot can reveal defects in insulation integrity as well as conductor spacings that are too close. These deficiencies result in high leakage current to ground or arcing as a result of the potential difference and ionization of the air. Evidence of arcing and excessive leakage current are usually monitored during a dc hi-pot test.

A dc hi-pot tester should be able to vary voltage smoothly from zero up to the maximum required, usually 5000 V. The tester should have a microammeter with sufficient range to provide readings from less than one microampere to a least 2500  $\mu$ A. It should also contain a protective current relay that can be set to trip at any given percentage of the microammeter range. This is to prevent insulation failure when the leakage current rises sharply.

The selection of the test voltage is important and is based on the ac peak value, so that it is related to the maximum stress the insulation carries in normal ac operation. An often used rule of thumb is two times the normal operating voltage plus 1000 V. If the normal operating voltage is ac then the result must be multiplied by a factor to obtain a level for an equivalent dc test. Based solely on the peak voltage of a sine wave, the factor would be the square root of 2, or 1.414. However, multipliers may range from 1.1 to 2 depending on the age of the equipment.

The test potential is not applied all at once. The voltage is usually divided into eight or more increments and raised one increment at a time, allowing the current to stabilize after each increase. While the test is being conducted, a graph of the leakage current at each applied voltage is plotted on cross-section paper. If there is no insulation problem, the plot is an ascending straight line. The actual magnitude of leakage current and the corresponding slope of the plotted line are not the fundamental concern. The important consideration is that the plot should be, in fact, a straight line. Should the plot take an abrupt upswing, the test should be discontinued. An abrupt rise in leakage current indicates a defective winding that is likely to fail if the test is continued. Actual insulation breakdown is indicated by a sharp rise in the current and is often accompanied by arcing at the location of the breakdown. However, if the last step to the full voltage is taken without breakdown and without exceeding the leakage current specification, the motor has passed the test.

In general, dc testing of motor insulation is widely accepted as providing a very good means for testing phaseto-ground

insulation in motors. It does, however, check insulation *condition* as opposed to insulation *integrity*. One severe drawback of the dc resistance test is its inability to detect turn-to-turn or phase-to-phase faults.

### 8.2.2.3 Alternating-Current High-Potential Testing

An ac hi-pot test is conducted by applying an ac voltage potential (usually 60 Hz) that is higher than the rated operating voltage between the insulated windings and ground. This stresses the insulation and indicates a defect in the insulation system or whether a margin of safety above the operating voltage is available. Testing with ac results in a charging current that is extremely large. The winding of a large random-wound motor can have so much capacitance to ground that the test voltage source may have to supply 100 kVA.

To conduct the test, the ac voltage from the instrument is increased to some specified point to see whether the insulation can stand that particular voltage. As stated previously, it is a go, no-go type of test and causes deterioration of the insulation. An ac hi-pot test should never be conducted on a winding that has a low or minimum megger reading. If the insulation is dirty, the hi-pot test voltage will creep and flash to ground. Also, if the insulation is wet, the test voltage will rupture the insulation.

Motor manufacturers commonly use ac hi-pot testing as an acceptance test on new windings. The test is usually conducted with an applied voltage of  $2E+1000$  V where  $E$  is the rated line-to-line operating voltage of the machine. However, after the motor has been in service, the test voltage is usually 1/2 to 2/3 of the acceptance test level or between 100% and 150% of the rated line-to-line voltage of the motor. When conducting the test, the voltage is usually increased to the maximum test voltage as rapidly as possible without overshooting the maximum value and maintained for one minute. The voltage is then reduced at a rate that will bring it to 1/4 the value or less in not more than 15 seconds. Any defect in the insulation system will result in high leakage current to ground and a tripping of the hipot tester's overcurrent protection device, usually a circuit breaker.

### 8.2.2.4 Surge Comparison Testing

Surge comparison testing is used to evaluate the integrity of random-wound coils and windings. The test provides information about insulation conditions over and above that which can be obtained by insulation resistance or hi-pot testing. Many winding failures begin as turn-to-turn, coil-to-coil, or phase-to-phase insulation defects that eventually propagate into ground faults. Megohmmeter and high-potential tests can detect existing and immediately incipient faults to ground, but they cannot detect conditions such as turn-to-turn shorts. Surge testers are so sensitive that even a single-turn short circuit can be detected.

The surge comparison tester is an electronic device designed specifically to apply a surge voltage stress between turns of a coil, between phases, and from the windings to ground, and to detect short-circuited turns in windings under test. As the name implies, it is the application of two identical high-voltage, high-frequency pulses to two separate but equal parts of a

winding. For example, with a three-phase random wound motor, each winding phase is tested or compared against the others (phases A/B, B/C, and C/A). If the windings of the two phases under test are identical and have no deficiencies, the two reflected waveforms will be identical, overlap each other, and appear on the instrument's oscilloscope as a single trace.

The surge comparison tester uses the principle of impedance balance to test windings. Almost all electrical windings are made up of several identical coils or phases. The surge tester compares the impedance of these windings to detect faults. The instrument applies a very brief surge to two matched windings by capacitor discharge. The resulting voltage decay pattern of each of the two windings is then displayed on the oscilloscope. If the windings have no faults and are balanced in impedance, the two patterns will be identical. One wave pattern will be superimposed over the other so that a single wave pattern will appear on the screen. If one of the windings has an insulation fault or winding defect, its pattern will not be the same as the trace from the good winding, so a double line will be shown. Figure 8.4 provides examples of faults and the waveforms they produce on the oscilloscope.

The surge comparison tester applies current as a series of pulses that stress the entire winding system. The voltage of these pulses rises very quickly. As this pulse travels along the winding, it produces a voltage distribution across the coil. For example, when the pulse has penetrated to turn number 10, it may be at 2000 V, while other turns (numbers 20, 30, 40, etc.) have not been pulsed and are at a lower voltage. If this voltage difference is greater than the dielectric strength of the turn insulation, one or more turns may be shorted out of the circuit. If this shorted circuit is compared to a good winding, their patterns will not match. In addition, the shorted winding will almost always give an unstable, or flickering, pattern. This is caused by the arcing of the short. Generally, shorted or missing turns will cause fairly small differences in waveform amplitude. Misconnections causing gross alteration of magnetic field patterns within the winding, such as coil reversal, or interphase shorts, tend to cause large irregularities in waveform shape.

Test voltages for random-wound motors are determined by the operating voltage of the winding. The test voltage is calculated from the high-potential test voltage calculation of two times operating voltage plus 1000 V. A multiplier of 1.4, based on the rms to peak conversion, is used to obtain the actual surge comparison test voltage. Therefore, a winding rated at 220 V would have a test level of 2016 V.

The surge comparison test, unlike the insulation resistance test and dc hi-pot test, does not provide numbers to plot or trend. The test does provide a "picture" that allows the detection of potential insulation faults and failures in random-wound motors. Faults that pertain to the integrity of the windings themselves, such as turn-to-turn, coil-to-coil and phase-to-phase shorts, as well as opens and grounds, can be very easily detected by surge comparison testing.

### 8.2.3 Causes of Insulation Failure

Insulation and its proper design, application, and maintenance have a very important part in the successful operation of any

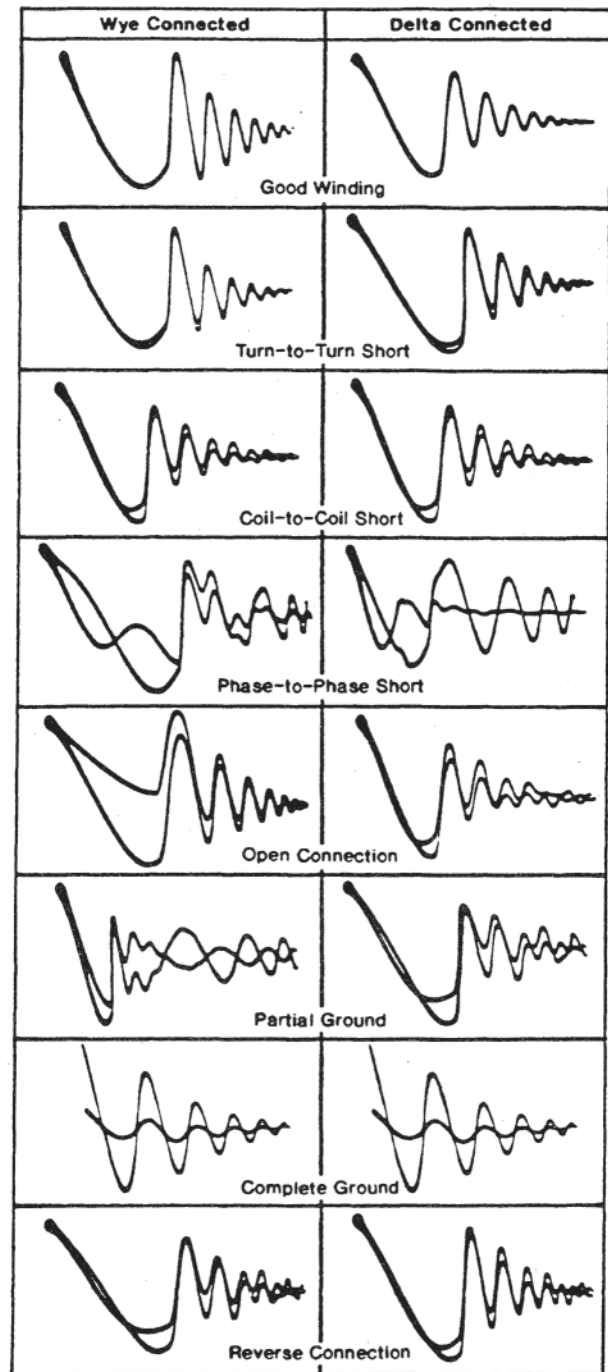


**Figure 8.4** Waveshapes for winding faults in three-phase alternating current (ac) windings.

electrical machine. The failure of electrical insulation of motors is frequently associated with serious thermal aging except where there is physical damage from some external source or serious contamination of the insulation with foreign matter. Thermal aging is generally evidenced by loss of resistance to moisture and subsequent looseness of the winding and loss of adhesion of the insulation components. The following are major causes of in-service motor insulation failure

- Unusual surge voltages that may be caused by lightning, switching surges, or system malfunction.
- Mechanical damage due to some foreign matter being introduced into the machine, or some failure of the mechanical supports or ties as a result of short circuits.
- An accumulation of dirt, oil, and other chemical contaminants due to improper operating conditions or faulty maintenance.
- Damage caused by improper handling or coils and insulation during winding.
- Corona deterioration at points of high voltage stress.
- Faulty design with insufficient safety margin or unsuitable stress.
- Moisture absorption, which reduces insulation resistance and dielectric strength levels.
- Thermal aging caused by excessive operating temperatures that result in the insulation system being vulnerable to many other causes of failure.

Also, there are failures that occur simply from the normal deterioration to which motor insulation is subjected in service. Under low stress levels, this may be preceded by a long period of progressive erosion, pitting, and chemical degradation, with the insulation life decreasing as stresses increase.

A properly designed and tested winding will have a reasonable life expectancy if it is manufactured with the specified insulating materials and operated within its thermal rating.

It is not the intent of this section to cover every aspect of random-wound motor insulation systems or testing of these systems. For more information, the reader is directed to the general (unnumbered) references at the end of the chapter.

## 8.3 FORM-WOUND MOTORS

### 8.3.1 Insulation Systems

#### 8.3.1.1 Physical Construction

Most large motors rated 2300 V or above have stator windings composed of form-wound multiturn coils (Fig. 8.2). The coils are preformed outside of the stator and have a diamond shape (Fig. 8.5). Each coil is then inserted into the slots in a stator core. There may be from 40 to over 100 slots in the stator, depending on the motor design and speed. The coil has two “legs” and end winding or endturn portions (Fig. 8.5). In manufacturing the stator, the coil is placed in two slots, with a leg in each slot.

The cross section of a typical stator slot is shown in Fig. 8.6. In almost all modern form-wound motors there are two coil legs from different coils in each slot. The coil leg closer to the rotor is the top coil leg (or just coil), whereas the coil leg farther from the rotor is the bottom coil. Normally one leg of a coil is in the bottom position of one slot and the other coil leg is in the top position of another slot.

In a typical stator slot, the coil is held rigidly in place by depth packing or separators, side packing and wedges (Fig. 8.6). The purpose of these components is to hold the coils within the slot and prevent movement under the magnetically induced forces that are inherent in all motors. The connections

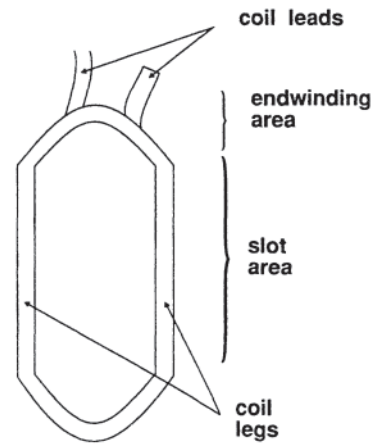


**Figure 8.5** A form-wound, multiturn, diamond-shaped motor stator winding coil.

between coils are made outside the stator slot, in the end winding area (Fig. 8.5). The end windings can be very long in high-speed motors. The portions of the coils in the end winding area must be well supported against the magnetic forces; thus various types of end winding blocking and bracing are required.

Each coil has at least two and perhaps three different insulating components (Figure 8.6). The main, thick insulation is the groundwall insulation, which must be capable of operating at the rated voltage of the motor, i.e., 2300 V, 4100 V, and so forth. The turn insulation separates the various copper turns from one another. The voltage across the turn insulation may be from a few volts to approximately 100 V ac. Motor coils may typically have from 2 to 12 turns in the coil. Finally, the strand insulation insulates the copper strands from one another. One turn is typically made of 2 to 6 or more copper strands. If the strand insulation were not present and each turn were instead a single copper wire, significant eddy currents would flow within the copper, reducing motor efficiency. There is usually less than a volt across the strand insulation. In some coil designs, the strand and the turn insulation may be combined. Figure 8.7 shows the cross section of a 3 turn, 3 strands per turn motor coil.

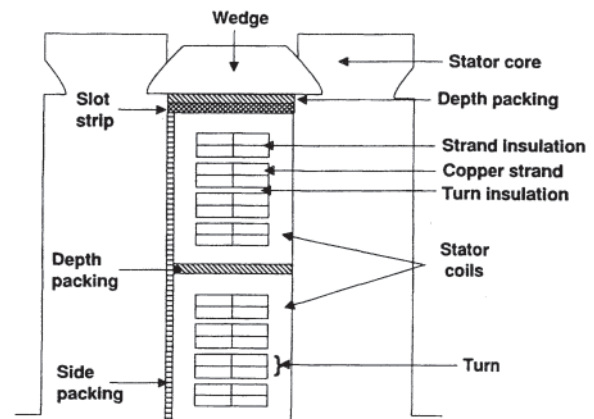


**Figure 8.6** Cross section of a stator slot showing two legs of form-wound coils, as well as slot packing materials.

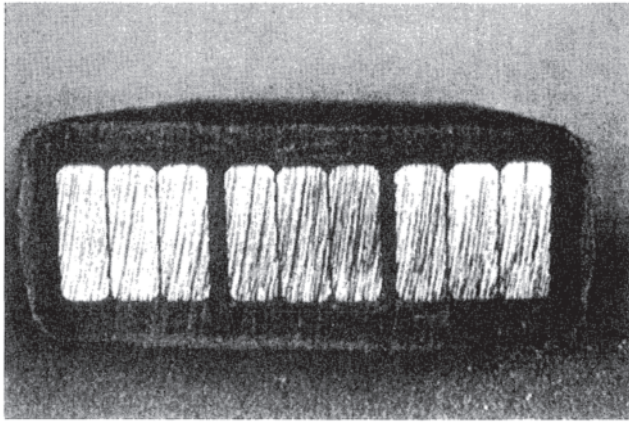


**Figure 8.7** Cross section of a three-turn stator coil, with three strands per turn.

Coils are made using sophisticated machines to bend and shape the copper, as well as to apply the insulation layers. The copper strands are normally insulated by the magnet wire manufacturer. The coil shop cuts the magnet wire into the required length and assembles the specified number of strands in each turn into a rectangular cross section. The turn insulation, if separate from the strand insulation, is then taped over the strands. A machine then loops the copper strand bundle around a mandrel to create the desired number of turns. Another machine then forces (pulls) the loop into the desired diamond shape (Fig. 8.5), a process can obviously cause distress to the strand and turn insulation. Finally, the groundwall insulation is taped over the entire coil.

### 8.3.1.2 Strand and Turn Insulation

The strand insulation is form-wound stator coils must withstand an environment similar to the insulation used in random-wound stators. The primary stresses are temperature from  $I^2R$  losses in the copper and mechanical abuse, especially during coil manufacture. The voltage across the strand insulation is usually negligible, even under voltage surge conditions. Thus an insulated copper strand is usually rectangular magnet wire. The insulated copper strand is made in the same way and often uses the same materials as described above for random-wound stators (see Section 8.2.1). In motors built before the 1940s, the insulation was typically a varnish film. Since the 1950s there has been a variety of synthetic materials developed that operate at higher temperature before losing mechanical or electrical strength, are more abrasion-resistant, and are more flexible. The last characteristic is needed to withstand the rigors of coil forming.

In modern motors rated 4100 V and below, the strand insulation is usually a film made from synthetic materials such as polyimide (Kapton) or polyamide-imide. These materials can operate at temperatures up to 220°C before softening or losing mechanical strength. At the 4100 V level and above it is not uncommon for the film to be overcoated with a material composed of fused glass fiber and polyester fiber (Daglas), which has a temperature rating of 155°C or more. The Daglas coating gives enhanced partial discharge resistance (see Section 8.3.2.3). For similar reasons, especially when the turn and the strand insulation are the same, the film-

covered copper wire may also be covered in mica-paper tape. Mica-paper tape consists of small bits of mica that are bonded to either a fiber-glass tape or a Dacron™ tape. (Dacron is a trade mark of Dupont.)

In stators where the turn insulation and the strand insulation are distinct, the turn insulation is usually a mica-paper tape that is wrapped over all the insulated copper strands in the turn (Fig. 8.6). Depending on the voltage rating of the motor, one to three layers of tape may be applied, either half-lapped or butt-lapped. The mica paper tape is usually impregnated with epoxy or polyester after the groundwall insulation is applied (see below.)

In recent years there has been a tendency to enhance the strand insulation and not use dedicated turn insulation. The advantage is that one step in the coil manufacturing process (applying the turn insulation) is not required, resulting in a less expensive motor. Inevitably, however, the reliability of the winding is decreased to some degree. Where there is no dedicated turn insulation, the strand insulation is built up with either Daglas or mica-paper tape to withstand the required electrical stress.

### 8.3.1.3 Groundwall Insulation

There are two basic types of groundwall insulation used in motor stator windings. The older type is referred to as thermoplastic, because, as the temperature increases, the insulation becomes softer and tends to deform or flow. The thermoplastic insulation system is characterized by asphaltic-mica insulation, and was popular before the 1960s. The more modern insulation system is composed of thermosetting insulation, which does not tend to soften or deform as the temperature increases. Typical thermosetting insulation systems are micapaper impregnated with polyester or epoxy. The thermoset and thermoplastic systems are discussed separately.

In common with both insulation systems is the use of mica. Mica is an inorganic crystalline material that is completely nonconducting and has a very high electrical breakdown strength. In addition, mica can be used to very high operating temperatures without degradation. Furthermore, mica is extremely resistant to deterioration by partial discharges (see Section 8.3.2.3). Unfortunately, mica has relatively poor mechanical properties in that it is easy to split it apart, and it cannot be shaped. For this reason, mica cannot be used alone, and is instead used in combination with various backing materials to support it during application, and bonded together by thermoplastic or thermosetting materials.

*Thermoplastic insulation* Asphaltic compound bonded mica tape systems were used fairly extensively and with good success in motors until the early 1960s. When this type of insulation was first introduced in the 1930s, large flakes of mica were bonded to a backing material (usually a special paper), which was hand taped over the copper bundle. The mica flakes were then impregnated with a special asphalt using a vacuum pressure impregnation (VPI) process. In this process the coils were typically placed in a tank and a vacuum was pulled to remove air trapped between the layers of tape. The tank was then filled with a hot asphalt, which seeped between

the taped layers, bonding the layers together. Pressure was then applied to the coil leg sides to obtain a good rectangular coil shape while the coil was cooled. There are many variations of this basic process.

In the 1950s the following improvements were introduced. (1) The replacement of the paper backing material with glass fiber or Dacron™ tapes. This improved the mechanical strength of the supported mica tape and allowed it to be more tightly applied. It also reduced the susceptibility of the insulation to thermal, electrical and mechanical aging. (2) Improvements in the properties of the asphaltic bonding materials that allowed them to reach higher temperatures before they started to flow.

In general, asphaltic-mica insulation systems have a thermal rating of 110°C (Class B). When not overheated or subjected to excessive mechanical stress, such insulation systems can be very long-lived. There are still many motors built in the 1950s and using asphaltic-mica insulation that are operating part 2000.

*Thermosetting insulation* The use of asphalt as a binder for the mica implied that the groundwall could not operate at very high temperatures. Advances in polymer research in the 1940s and 1950s led to new and improved bonding materials that would remain stable at higher operating temperatures. Polyester and epoxy were found to be suitable for stator winding applications. These bonding agents gave coil groundwall insulation the desired thermal and mechanical stability.

By the mid 1950s, these synthetic resins were widely used by machine manufacturers. At first polyesters were much more popular than epoxies because solventless forms of polyester had been developed that could directly replace the asphaltic bonding compounds being used in a VPI process. The new polyesters did not expand appreciably in comparison to thermoplastic systems, retained good mechanical strength when heated, and had very low viscosities in the uncured state. In fact, they flowed so easily through the winding insulation that difficulties were experienced in retaining them until they were polymerized by heating.

The first major manufacturer to introduce a thermosetting synthetic resin bonded groundwall insulation system was Westinghouse with their Thermalastic system, initially developed for turbine generators [7]. This was a continuous tape system consisting of large mica flakes sandwiched between two layers of paper backing material and vacuum-pressure impregnated with a thermosetting polyester resin and cured prior to placement in the core.

The first use of epoxy as the bonding material was by General Electric [8]. The development of this system produced two important components of groundwall insulation that are still being used today.

- Mica-paper that consists of very small platelets of mica held together by electrostatic forces to form a continuous, self-supporting sheet. The main reason for changing to this form of mica from the large-flake material previously used was its uniformity and thus much more predictable properties.
- A thermosetting synthetic epoxy resin bonding material which remained stable at high temperatures.

From these materials a groundwall insulation was developed consisting mainly of half-lapped layers of mica-paper tape with a few layers of mica flake tape material interspersed between them. Another important feature of this system was that the epoxy bonding resin was impregnated into the tapes prior to their application. After applying the tapes to the coil, the resin was then cured by placing the coils in an autoclave and applying heat and pressure. This tape is now commonly known as a resin-rich material.

The use of epoxy to bond layers of mica-paper tape together is now pervasive in modern motors. However, there are now three significantly different processes to accomplish the same epoxy-mica groundwall.

#### (a) Resin-Rich Process

As for the first epoxy-mica system described above, the modern resin-rich process involves applying mica-paper tapes that have been impregnated with “B-stage” epoxy that will rapidly polymerize (solidify) above a critical temperature. These tapes are then applied to the copper bundle. These are two main methods to consolidate the impregnated tapes in this system. The first method is to confine the coil side in metal molds while applying heat and pressure. The second method uses an autoclave where, after application of the preimpregnated tape to the conductor coil, it is usually vacuum and pressure treated in the autoclave while enclosed in hydraulic molds or shaping aids. The following tasks are accomplished during this procedure.

- Under applied heat, the resin in the tape begins to flow.
- Under the combined effects of vacuum and pressure, uniform impregnation of the resin throughout the groundwall is further improved. Trapped air and volatiles are drawn off at the same time as the insulation is compacted to minimize voids.
- The coil side is molded to the required dimensions and shape. The molding of the slot section and the overhang may be accomplished separately.
- Further heating in the autoclave cures the thermosetting resin to a hard and homogeneous condition.

On removal from the autoclave or molds, the coil is ready to be placed into the stator core.

#### (b) Coil VPI Process

The insulation tape is applied to the shaped copper bundle in a “dry” or “green” state in which only a minimal amount of resin is present for the purpose of holding the mica paper and backer together during handling and taping. The taped coils are placed in a vacuum/pressure tank. The dry insulation is first evacuated in order to remove air and obtain a high degree of fill with the impregnant that is introduced later under pressure. The coils are then removed from the tank and heat cured to final dimension and the required shape by pressing.

#### (c) Global VPI

In the above two processes, complete, hard coils are made, which are then placed into the stator core. Because epoxy-mica insulation produces a rigid, hard coil, the winding process is often difficult. It is not uncommon to crack the insulation on

some of the coils during the winding process in an effort to force the coils into the slots. In the global VPI process (also known as post-VPI or simply VPI stator process), the coils are taped with mica-paper tapes and directly placed into the stator. The winding process is relatively easy since the coils are still somewhat flexible because the epoxy has not yet been introduced.

Once the coils are in the slots and the connections between the coils are made, the entire stator core is placed in a tank. The tank is first evacuated and then is filled with epoxy, which proceeds to impregnate the tapes. The stator is then removed from the first tank and placed in a second tank where the epoxy is cured at high temperature and high gas pressure. The latter shrinks any air voids that may remain.

The result is a stator where the coils are intimately bonded to the core. The global VPI process tends to be a less expensive process than the first two above because it is easier to wind the stator, there are fewer damaged coils during processing, and all the coils are impregnated at one time. The size of the motor stator that can be impregnated is limited by the VPI tank size. Most major manufacturers can make motors up to about 15,000 hp with this process.

Today, polyester is still used as the impregnant in either the coil VPI process or the global VPI process by some organizations that rewind motors. In general, less sophisticated process controls are required with polyester, and the basic resin is cheaper than for epoxy. Although epoxy has superior mechanical and electrical properties to polyester, especially in the presence of moisture [9], polyester-mica windings are quite satisfactory for many motor applications.

#### 8.3.1.4 Wedging, Blocking, and Bracing

Stator windings must be held rigidly to the stator core to prevent their movement under the 120-Hz continuous magnetically induced force or the force created by large inrush currents during motor starting (see Section 8.3.2.2). Within the stator slot, wedges and sidepacking are used to keep the coils from moving (Fig. 8.6). These components are now made from epoxy-glass laminates, typically NEMA G 10 grade. Such materials can withstand large compression forces, and are rated for 155°C operation or better. The function of the wedging is less critical in the case of global VPI stators where the epoxy or polyester directly bonds the coils to the core.

Because the end winding area is not in contact with the grounded stator core, special provisions are necessary to ensure that the end windings do not move. Several means of mechanically securing the end windings are usually used.

- End-winding extensions that slope away from the rotor at an angle up to 60 degrees to the longitudinal axis of the stator bore, allowing adequate radial bracing to be applied by fitting supports that extend from the stator core end support structure.
- The insertion of rows of blocking between coils and end winding connections to control distortion resulting from circumferential and axial electromagnetic forces.
- An insulated steel ring for radial bracing.
- Ropes or ties to lash the coils to the insulated steel ring.

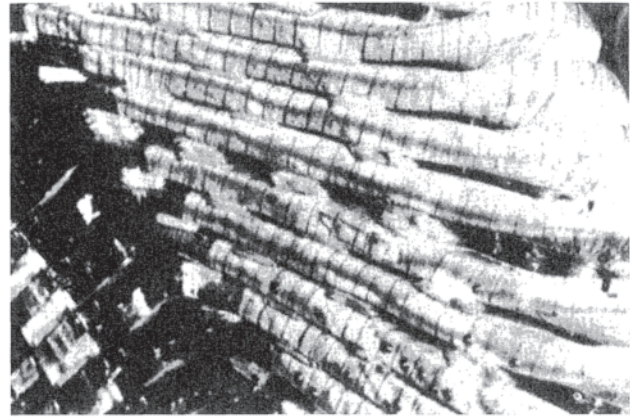


**Figure 8.8** End winding area of a large motor, showing bracing system made with conformable packing materials.

Glass-fiber ropes or tapes are used for lashing, whereas Dacron or conformable resin-impregnated synthetic felts are used for blocking (Fig. 8.8). In global VPI motors, the felts and ropes are applied dry, and they are impregnated during the VPI process.

#### 8.3.1.5 Partial Discharge Control

In motors rated approximately 6000 V or more, an additional component is required to ensure proper motor performance at such high voltages. As explained in Section 8.3.2.3, at high enough operating voltages, any air gaps between the copper conductors and the grounded steel core may cause partial discharges to occur. Partial discharges (sometimes also called corona) are small electrical sparks that result when the breakdown strength of the air is exceeded. If such partial discharges occur, the energy in the sparking rapidly degrades materials such as epoxy or polyester (although mica is much more resistant). If allowed to continue, the discharges will destroy the groundwall insulation. Since it is likely that some air gaps will occur between the outside of the coil and the core, a semiconducting coating is often applied to the outside of coils rated 6000 V or more. This carbon-loaded coating is grounded against the core, and ensures that all the applied voltage is across the epoxy-mica, and not across any air gaps. Thus there is no sparking.

### 8.3.2 Factors Affecting Insulation System Design

The electrical insulation in the motor stator winding is one of the most challenging applications for an insulation. The insulation must simultaneously withstand continuous and transient electrical, thermal, mechanical, and environmental stresses. These stresses gradually degrade the insulation, and will most likely be the cause of scrapping or rewinding a motor. The insulation system designer must determine which stresses will predominate in any particular motor application, and develop a system that will not seriously deteriorate within the design life of the motor.

Before designing a motor insulation system, the designer must translate the operating environment into insulation system stresses, and be cognizant of the various ways the stator winding will age in the presence of these stresses. The

following presents an overview of the stresses, and how these stresses age the stator coil insulation.

### 8.3.2.1 Thermal Duty

During operation, the main source of heat in a motor is  $I^2R$  losses in the copper conductors, i.e., by the stator current creating losses in the non-zero resistance of the copper winding. There is also some heat created by eddy-current losses in the copper conductors, as well as stator core losses caused by eddy currents and hysteresis losses in the magnetic steel. In addition, there is heating from dielectric losses in the groundwall insulation. The latter losses are normally minor, although older thermoplastic insulation systems are more lossy. All these heat sources raise the temperature of the copper and steel, and thus of the insulation. Because the primary source of heat is  $I^2R$  loss in the copper conductors, and the heat sink is the air-cooled stator core, the highest temperature in the winding is adjacent to the copper conductors, i.e., at the strand and turn insulation. In a typical application, the temperature at the strand insulation is approximately 10°C higher than the temperature at the surface of the groundwall insulation.

The operating temperature in a stator winding is sometimes higher than normal for one or more of the following reasons.

- High cooling medium temperatures; that is, the air that circulates in the air gap, over the end windings and through ducts in the stator core is at too high a temperature because of plugged filters, blockages, or inadequate cooling water in the heat exchangers.
- Overloading of the motor, which increases the current in the stator winding, and thus the losses in the copper. The copper temperature will increase with the square of the overload current.
- Starting frequency well above design values. When starting a motor there are inrush currents that may be ten times the normal operating current, since during starting, the stator winding does not have a significant back-emf. The extra  $I^2R$  heating created during starting will take several minutes to dissipate. If the motor is started again before this heat has dissipated and the temperature returned to normal, the additional heat created from the second start will further increase the winding temperature. With several starts in a short time period, the winding temperature can quickly attain dangerous levels.
- Negative-sequence currents in stator windings due to system voltage unbalance between the three phases. Even if the magnitude of the negative-sequence voltages is low, they may cause significant negative sequence currents to flow in a winding because the negative-sequence impedance of the motor may be only 20% of its positive-sequence impedance. These negative-sequence currents cause additional heating in certain phases of the motor, e.g., a 3.5% voltage unbalance can produce as much as a 25% increase in the temperature rise of at least part of the winding. The most severe form of voltage unbalance is single-phasing, which can induce currents close to 200% of rated in the phase windings that remain connected to the power supply.

The effect of high temperature on the insulation depends on the nature of the materials used, the design of the motor, and where the highest temperatures are occurring. The following are some effects of high temperatures, and how failure might result.

The first step in the thermal breakdown process due to general, continuous overheating is often failure of the interstrand and strand-to-ground wall bonds, because the temperature is usually highest there. Failure of the bond occurs because the bonding strength of both thermoplastic and thermoset materials decreases as the temperature increases, especially for the thermoplastic materials. Once debonding occurs, individual copper strands become loose and thermal and magnetic forces produce relative motion that causes abrasion of the strand insulation and distortion of the conductors. This leads to a further acceleration of the aging process due to reduced heat transfer between the conductors and groundwall. Ultimately turn-to-turn failures occur from turn insulation abrasion or mechanical failure. Failures due to high temperatures at the strand insulation are much less likely to occur in present-day insulation systems since the conductor stack is usually consolidated with a thermosetting resin that can withstand much higher temperatures than older materials.

Even if modern thermoset materials are used, continuous operation at high temperatures will result in the epoxy or polyester becoming brittle and shrinking to some degree. The shrinkage, together with the embrittlement, can lead to easier abrasion of the groundwall under the magnetically induced forces. Also, embrittled insulation is more likely to crack under the very high mechanical force caused by motor starting.

Similarly, operation at high temperature can cause the end winding blocking and bracing to gradually shrink and become embrittled. Looseness can lead to relative movement between the coils and the blocking, leading to abrasion or cracking of the insulation during motor starting.

For motors that are started frequently, thermal cycling can lead to failure. When a motor is first turned on, the highest temperature is in the copper, and copper expands more than the insulation. The result is that the copper expands along the slot more than the groundwall insulation. This difference in expansion creates a shear stress between the copper and the groundwall insulation. The longer the slot length of the core, the greater is the shear stress. The higher the operating temperature, the lower the ability of the bonding materials to resist this shear stress. Thus, under certain circumstances, the bond between the copper and the groundwall is lost, creating gaps or delamination in the insulation, leading to even higher temperatures, and failure as described above. In global VPI stators, the shear stresses are even higher since the coil cannot slip in the slot. A motor that is started frequently sees many thermal cycles, which slowly fatigue the bond between the insulation and the copper.

Thermal cycling due to frequent starting can also fatigue the bonds between the coils and the blocking and bracing in the end winding. On motor starting, the coil in the end winding tends to expand, which exerts a mechanical force at the blocking and bracing points. The more thermal cycles there are, the more likely it is for some components to become loose, which under



normal magnetic forces can lead to abrasion. Such problems are more likely in high-speed motors, where the end windings are longer and there is more thermal expansion.

### 8.3.2.2 Mechanical Duty

Mechanical forces are generated in motor stator windings as a result of thermal expansion, as described above, or as a result of currents flowing in magnetic fields. Every time a rotor pole passes over a stator slot there is a magnetic force on the stator coils that tends to move the coils. The force produced by this electromagnetic phenomenon is proportional to the square of the current flowing through the conductors and occurs at a rate of 120 Hz for a 60-Hz machine. These forces are highest in coils near the air gap. Furthermore, the current in each of the coils in a slot creates an additional force between the two coils. The thermoset “hard” insulation systems are more likely to degrade under the influence of these cyclic forces since they are less flexible and it is more difficult to ensure that coils are tightly wedged in the slots; that is, the older thermoplastic systems were much more flexible and tended to swell and flow to fill the slot and restrict coil movement.

If a coil is allowed to move in the slot under the influence of these cyclic electromagnetic forces, the conductor and groundwall insulation will be stressed by flexing and compression. The insulation may also be abraded by relative movement between copper strands or between the outside of the groundwall and the slot or slot packing. This will lead to the following failure mechanisms.

- Cracking of the groundwall insulation leading to a ground fault.
- Abrasion of strand or conductor insulation causing strand-to-strand or turn-to-turn faults.
- Abrasion of the groundwall insulation resulting in loss of the semiconducting coating (if present) and consequently partial discharges can occur that slowly bore a hole in the groundwall. Modern global VPI stators are much less likely to suffer from this problem, since the coils are bonded to the core.

The same 120 Hz magnetic forces can lead to relative movement between coils and/or bracing points in the end winding. If the end winding becomes loose, these mechanical forces will lead to abrasion of the insulation and eventual failure.

Another mechanical aging mechanism can occur as a result of motor starting. Extremely high radial, axial, and circumferential end winding forces are induced by the inrush current each time a motor is started. Adequate winding bracing systems have to be designed to prevent excessive coil movement and loosening under the influence of these forces. Both the magnitude and frequency of the forces have to be considered when assessing the amount of bracing required; for example, a motor that is started once per hour would require substantially more end-winding bracing than one that is started two or three times per year.

The failure mechanisms associated with high transient end winding forces in combination with inadequate bracing are the same as those for machines with high continuous end-winding forces.

In the early days of the hard insulation systems, bonded with thermosetting epoxy or polyester resins, there were many problems due to inadequate end winding bracing. Most of these resulted from insufficient appreciation of the differences between hard and soft insulation systems; the older systems with thermoplastic insulation tended to conform to radial bracing rings, and intercoil blocking to prevent relative movement and could tolerate a certain amount of flexing. When manufacturers realized that conformable packing materials such as felts and ropes impregnated with compatible thermosetting resins were required to ensure that coil movement was restricted, these problems started to diminish. Present-day designs are based on a good understanding of the end winding forces involved under the worst operating conditions, and the use of conformable packing materials has substantially reduced problems due to excessive end winding vibrations.

### 8.3.2.3 Electrical Duty

A motor failure is usually a consequence of the groundwall insulation puncture, so that the insulation can no longer prevent short circuits between various parts of the winding at different potentials. Normally the insulation is weakened by thermal or mechanical forces. However it is possible for electrical stress alone to cause winding failure.

In motors rated 4000 V and below, the continuous 60 Hz stress causes little aging, except when there has been severe thermal or mechanical aging first, leading to a severely debonded (or delaminated) groundwall. In such a case, there are usually air pockets within the insulation. Due to the capacitive voltage division effect, some voltage will be placed across these air pockets. If the voltage is high enough, the electric stress (approximately the voltage divided by the thickness of the air pocket) will be higher than the breakdown strength of air, and a spark will occur in the air pocket. (Note that the breakdown strength of air is only about 1% of the breakdown strength of epoxy-mica.) The spark is stopped by the solid groundwall insulation, but repeated sparking will gradually erode a hole in the insulation. This process, called partial discharging or delamination discharging, can be the means by which thermal and mechanical aging leads to failure. For motors rated greater than about 6000 V, this discharging mechanism can directly lead to failure if the air pockets were created during manufacturing. Such voids are most likely to occur in global VPI stators, where very careful process control is needed to ensure that the insulation is fully impregnated by epoxy or polyester.

For motors rated 6000 V or more, another partial discharge-related mechanism can occur. Most motors with this voltage rating have a semiconducting coating over the outside of the groundwall insulation in the slot area. This semiconducting coating keeps the electric field entirely within the epoxy-mica insulation, and thus partial discharges will not occur in any air gap between the coating and the stator core. In a nonglobal VPI stator, if the coil becomes loose in the slot as a result of overheating, thermal cycling or inadequate wedging and sidepacking, the semiconducting coating can abrade, permitting partial discharges to occur. This process is called

slot discharge, and is more common on motors rated 11 kV or more. If the stator winding is made by global VPIing, sometimes the electrical connection of the semiconducting coating to the stator slot is not continuous. The capacitive charging current of the coil may then flow through a few points where the semiconducting coating touches the core, creating high-current densities, burning of the coating, and possibly completely isolating the coating from ground. If allowed to persist, slot discharges and groundwall puncture can occur.

Electrical tracking i.e., the formation of permanent conductive (carbonized) paths over the insulation surface in the end winding region, is caused by ac electrical stress in combination with pollution. The surface of a stator coil, in the endwinding region, is normally highly resistive. However, slightly conductive areas can occur in normal operation due to pollution, such as coal dust, in combination with moisture and/or oil films. These conductive regions will pick up a capacitive charge from the high-voltage conductors. Leakage currents will flow between conductive patches at different voltages on adjacent coils or from such patches to the core, with scintillations and/or sparking at surface discontinuities. These currents or sparks degrade the insulation surface, and create conducting, carbonized paths to ground or between phases. Areas adjacent to phase-end bars are particularly susceptible as well as interphase support packing. Failures resulting from this type of aging are ground or phase-to-phase faults. Winding designs that maximize the spacing between components of different voltages, as well as clean, dry windings are least susceptible to this type of aging.

A very important failure mechanism that can occur in motors is failure of the turn insulation by voltage surges. The voltage between turns under normal supply conditions is relatively low, i.e., usually less than 100 V rms. If a fast-rise-time voltage surge strikes the stator winding (for example, from switching on a motor), then a voltage of several kilovolts can appear across the turn insulation in the line end coil for a short time. This voltage can puncture the turn insulation, causing a shorted turn and thus high circulating currents, which eventually burn the groundwall insulation [10]. In principle, this failure mechanism is not due to aging, but is rather due to random external switching events. The turn insulation strength can be poor or can degrade due to other factors such as the following.

- The use of magnet wire insulation with a low electrical and partial discharge strength, rather than mica paper.
- The presence of turn insulation that has been weakened by manufacturing processes, such as coil forming, which can stress and weaken wire coverings at the points where the conductors are bent to give the required coil shape.
- Thermal, electrical, or mechanical aging that reduces the electrical strength of the turn insulation. Such failures are relatively common in old windings with thermoplastic insulation systems, which allow the turns freedom to rub against one another, abrading the turn insulation.
- Inadequate filling with or retention of binding resins or compounds during manufacture.

Turn insulation failure is associated with extreme insulation burning and conductor melting at the fault location.

#### 8.3.2.4 Environment

The environment in which a motor operates can have a major influence on the life of the stator winding. As mentioned in Section 8.3.2.3, if the end windings become polluted with moisture, dust, oil, or the like, a conducting film will occur that can lead to electrical tracking and puncture. Another obvious environmental factor is ambient temperature for motors that are not cooled by means of water heat exchangers. As the ambient increases, so will the winding temperature. If the resulting temperature is too high for the insulation, deterioration can occur as discussed in Section 8.3.2.1.

Open type machines operating in dusty environments can experience groundwall insulation aging due to erosion from the impingement of abrasive materials on the coil surfaces. This may eventually lead to ground, phase-to-phase, or interturn faults resulting from the exposure of conductors and electrical tracking between points with high potential differences between them. Winding failures from abrasion can best be prevented by applying special protective coatings such as elastic rubbery materials to the windings, or by the use of filtered open-types or totally sealed-type motor enclosures.

Insulation deterioration can result from operation in special environments. Motors operating within the containment buildings of nuclear power stations may be subjected to high doses of radiation. Such radiation can affect many types of organic insulation, with many of the same symptoms as thermal aging. Similarly, some motors in certain industries operate in an environment that contains acids, alkalis, or oils, which chemically attack the binder in the groundwall, reducing the mechanical and electrical strength of the insulation. In all these cases, motor manufacturers can use special materials that are resistant to such aging. Alternatively the designer can protect the insulation from exposure to such environments by the use of suitable motor enclosures.

#### 8.3.3 Insulation Testing

Maintenance personnel have at their disposal a variety of tests that may be used as tools to track the condition of the stator winding insulation in the motor and, perhaps more significantly, the rate at which aging is taking place [2]. This information is essential for the allocation of sometimes scarce resources for the most efficient and cost-effective programs to schedule maintenance, make repairs, and otherwise contribute to trouble-free operation. Experience has shown that the more sensitive the test, the sooner a developing deterioration process can be detected, and the less costly will be the repair.

Unfortunately, there is not single test that can determine the condition of a motor stator winding. In fact, even the results from a variety of tests cannot always determine the condition of the insulation with complete assurance. Thus it is always prudent to confirm the winding condition by means of a careful visual inspection of the motor. An inspection is best done by an experienced individual who is alert to the visible symptoms of deterioration.

The following summarizes many of the tests that are generally available to help maintenance personnel determine the stator winding condition. Since there are a large number of possible tests, many of which give duplicate information, maintenance personnel should consider carefully which tests are most useful and cost-effective. Some guidelines on this aspect are presented later. However, it is note-worthy that computer programs are now available to help maintenance personnel select and interpret tests [11].

### 8.3.3.1 AC and DC Hipot

AC or dc high potential (hipot) withstand tests may be applied to a motor stator winding to gain some assurance that the groundwall may safely be stressed to normal operating voltage. Hipot tests are not diagnostic tests, since the outcome is simply pass or fail. Some users do a hipot test whenever maintenance has been done on the winding to ensure the winding has not been damaged. The consequences of a hipot failure should always be considered, and appropriate spare parts and time should be available before proceeding with such testing.

The principle behind a hipot test is that weakened insulation will puncture if it is subjected to a high enough voltage. The test voltage is selected such that good insulation will survive the test, whereas damaged insulation will break down during the test. In principle, insulation that fails a hipot test could be expected to fail in a relatively short period of time if placed in service. The electric stress distribution within the insulation during a dc test is different from that in normal ac operation, since the dc electric field is determined by resistances rather than capacitances. Thus some users prefer to do ac hipot tests, since ac stress is experienced during normal operation.

To perform a hipot test, the winding must be isolated and a high voltage connected between the winding and ground, as shown in Fig. 8.9. Note that most motors are Y-connected, with the neutral point inaccessible. Thus usually the high voltage supply need only be connected to one phase. The stator frame should be grounded and accessory devices such as current and potential transformers shorted or disconnected. Any temperature sensors should also be grounded. For acceptance of a new winding, NEMA Standard MG 1 suggests using two times the rated line-to-line voltage (rms) plus 1 kV for ac hipots and 1.7 times the rms ac test voltage for dc hipot tests. Subsequent tests for purposes of periodic maintenance or following major winding repairs are scaled down in proportion to the corresponding ac maintenance test levels. A

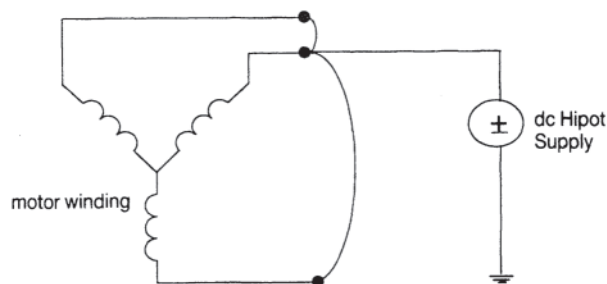


**Figure 8.9** Electrical circuit arrangement for a dc hipot and/or insulation resistance test.

typical routine ac maintenance test is suggested to be 1.25 to 1.5 times the rated ac line-to-line voltage. As described in IEEE 95 a dc voltage of  $(2 \times V_{L-L})$  kV dc is popular with power utility users [12].

It must be kept in mind that a hipot test is little more than a proof test indicating that no serious cracks have yet appeared in the groundwall, and that the test voltage level can be withstood at the time of test. Test levels are, in general, based on long experience of confirmation (with minimal risk of damage) that the insulation system has a good probability of withstanding normal operating stresses at least until the next scheduled maintenance test. Although many consider the ac hi-pot test to be more realistic in testing the insulation, the dc test is much more popular because the dc high voltage source is smaller, less expensive, and easier to use than the ac hipot supply.

### 8.3.3.2 Insulation Resistance and Polarization Index Tests

The insulation resistance (IR) and polarization index (PI) tests are useful indicators of contamination and moisture on the stator end windings or when there are cracks or fissures in the groundwall insulation. These tests are easily done and are the most common tests performed on any motor winding.

The insulation resistance is the ratio of the dc voltage applied between the winding copper and ground to the resultant current. When a dc voltage is applied, three current components flow: a charging component into the capacitance of the winding; a polarization or absorption current involving various molecular mechanisms in the insulation; and a “leakage” component over the surface between exposed conductors and ground, which is highly dependent on the state of dryness of the winding.

The first two current components decay with time. The third component of current is determined primarily by the presence of moisture or a ground fault and is relatively constant with time. Moisture may be absorbed within the insulation and/or condensed on the end winding or connection surfaces, which are often dirty. If this leakage current is larger than the first two components, then the total charging current (that is, the insulation resistance) will not change significantly with time. Thus, to help determine how dry and clean the winding is, the insulation resistance is often measured after 1 minute and after 10-minute, and the ratio of the 10-minute reading over the 1-minute reading is called the polarization index.

Several suppliers offer insulation resistance meters that can provide test voltages of 500 to 10,000 V dc. For motors rated 2.3 kV and below, 1000 V is normally used for the test voltage, whereas 5000 V is used for higher-voltage windings. To test the stator winding, the phase leads must be isolated and the test instrument connected between one or more phase leads and the stator frame. When doing an insulation resistance test, the test leads should be clean and dry.

When an actual fault or insulation puncture has occurred, the insulation resistance will be close to zero, and this is easily recognized as being unacceptable. However, it is difficult to set a practical pass/fail criterion for the insulation resistance test when the insulation is not punctured. An IEEE Standard

[6] recommends that the resistance should exceed 100 megohm.

The insulation resistance is highly dependent on the temperature and humidity of the winding. Unless the winding is always measured under exactly the same humidity and temperature conditions, it is virtually meaningless to track the resistance over time. As described in Ref. 6, the insulation resistance values can be corrected for the winding temperature (as determined from imbedded temperature indicators). If corrected measurements over the years on the same winding reveal gradually decreasing resistance, then the insulation may be deteriorating. However, it is much more probable that the resistance will swing wildly from measurement to measurement due to humidity conditions, making interpretation impossible. Similarly, in comparisons between two windings, a higher resistance in one does not imply that this winding is in better condition [13].

For very moist and dirty windings, the relatively constant surface leakage component of the current will predominate over the time-varying components, so that the total current will rapidly reach a near steady value. Thus the PI is a direct measure of how dry and clean the insulation is [6]. Since the PI is a ratio of resistances, it is not affected by temperature, and thus better for trending over time. The index is high ( $>2$ ) for a clean, dry winding, but approaches unity for a wet and dirty winding. If the IR is above about 5000 M $\Omega$ , the PI becomes an erratic indicator of winding condition, especially for modern epoxy-mica windings. Thus if very high IRs are measured, the PI can be disregarded.

### 8.3.3.3 Dissipation Factor and Tip-Up Tests

An important ac test that is sensitive to the internal condition of the groundwall insulation is the dissipation factor test. The dissipation factor test can be performed on any form wound stator winding of any size or rating. The test requires an outage for at least half a day. By itself, a single dissipation factor measurement on a complete winding is of limited use. However, measurements on coils or coil groups over the years may provide useful trend information. The dissipation factor test is most useful when done at both low and high voltage [14]. Usually the dissipation factor will increase from low to high voltage, i.e., tip-up. The greater the increase, the greater the delamination within the insulation (see Section 8.3.2.1).

Dissipation factor is a property of electrical insulation. It is a measure of the electrical losses in the insulation. A low dissipation factor is generally desirable, but a high dielectric loss does not necessarily imply that the insulation is inferior. The dissipation factor is normally measured with a capacitance bridge, and is expressed as a percentage. For example the dissipation factor for good epoxy-mica insulation is typically approximately 0.5%, whereas for good asphaltic insulation it is approximately 3%.

In a perfect insulation, the dissipation factor will not increase as the applied voltage increases. However, in the groundwall insulation of stator windings, air-filled voids can be present within the insulation or between the insulation and the stator core. When a high enough voltage is applied to

the winding, these voids may experience partial discharges (see Section 8.3.2.3). Because discharges give off heat and light, they consume energy, which increases the electrical losses in the winding. This in turn results in a higher dissipation factor as the voltage is increased. The greater the tip-up, the greater the partial discharge activity, and the worse the condition of the winding.

The dissipation factor can be measured on a bridge or similar instrument that effectively measures the ratio of the inphase 60-Hz current in the sample to the capacitive (or quadrature) current. The resulting ratio is with respect to the total current in the sample, and thus represents the average loss over the entire sample. That is, the dissipation factor does not respond directly to the worst area of the insulation. Thus a high in-phase current for one bad coil in a winding can be swamped by the high number of good coils that individually have a low in-phase current component. The dissipation factor test is therefore not sensitive to a few deteriorated coils in a winding, unless the winding is partly disassembled for testing.

In windings rated above 6.6 kV, the coils normally have an electric-stress-grading coating at the exit of the coil from the slot. This coating is commonly made from a nonlinear resistive material. As the voltage on the bar or coil increases, the power loss in this coating changes even faster. This is normal and desirable. Unfortunately, the apparent tip-up caused by this stress relief coating can dominate the tip-up of the insulation itself. Thus the tip-up test can be misleading in high-voltage windings. In normal quality control tests in the factory, special measures are taken to eliminate errors introduced by the grading coating.

Guidance on doing a tip-up test is given in Ref. 14. The dissipation factor is normally measured at 100% and 25% of rated line-to-ground voltage. The tip-up is the difference between the two readings. To increase the sensitivity of the tip-up test, it is desirable to isolate the winding into the three phases, which requires the disconnection of the neutral busbar. Unfortunately, in an installed motor winding, there is no practical way to overcome the influence of the stress-grading coating on the tip-up.

It is not practical to infer insulation condition on the basis of a single measurement of dissipation factor or tip-up. This is due to the effect of the stress-grading coatings and the fact that tip-up can have a wide range of values among different insulation systems. It is better to do these tests routinely, i.e., every one or two years, since failure can occur in this time frame. If a steady increase in tip-up is seen on the same winding, then it is desirable to visually inspect the winding.

As a general guide, the tip-up on an epoxy-mica insulation should be below 1%. The tip-up for a winding using mica splittings and bonded with polyester, asphalt, or varnish can exhibit much higher tip-ups and not be in trouble. However, steady increases in tip-up from test to test could be a sign of insulation deterioration.

As a measure of a winding's partial discharge activity, the tip-up test is inferior to a partial discharge test (see Section 8.3.3.4). The tip-up test is most successful with the older asphaltic and shellac-mica-folium windings, where delamination predominates and occurs throughout the winding.

### 8.3.3.4 Partial Discharge Test

In a conventional partial discharge (pd) test, the winding is energized to normal line-to-ground ac voltage with an external supply, and a commercial pd detector is used to measure the pd activity in the winding. Usually about a 1-day outage is necessary to do the test.

Partial discharges are electric sparks that occur in gas voids within the insulation when the voltage is high enough. The spark is a fast current pulse that travels through the stator winding. The larger the pd pulse, the higher is the current pulse (and the accompanying voltage pulse) that reaches the terminals of the winding.

The conventional test requires isolation of the winding from ground, and a 60-Hz power supply capable of energizing the three phases to rated line-to-ground voltage. To energize a large motor stator winding to normal voltage often requires a 10 kVA test set. The pd test equipment comprises a power separation filter (essentially a high-voltage pd-free capacitor, and a high-pass filter to block the power frequency and its harmonics), an amplifier, and an oscilloscope display (Fig. 8.10). PD pulses may be observed directly on the oscilloscope display, and the most meaningful result is the magnitude of the highest pd pulse on the display. Although the pulse magnitudes are measured in millivolts on the oscilloscope screen, some calibrate the pulse magnitudes in terms of picocoulombs (pC). The relationship between the charge transfer at the pd site, and the apparent charge detected at the machine terminals may be difficult to establish in a real machine because of the complexity of the route to the machine terminal. The detected pulse may, however, be considered as a direct gauge of the size of the discharge spark.

The usual test procedure is to gradually raise the ac voltage applied to the motor until pd pulses are observed on the oscilloscope screen. The voltage at which pd starts is noted, and is called the discharge inception voltage, or DIV. When the test voltage reaches normal line-to-ground operating voltage, the highest pd pulse magnitude is then read from the screen. A pulse height analysis may also be recorded. As the ac voltage is decreased, the discharge extinction voltage (DEV) is determined. This is the voltage at which the pd pulses disappear. The DIV is usually higher than the DEV.

The actual pd measurements take about 30 minutes. However, test setup and disassembly can take up to a day per machine, depending on the experience of the plant staff.

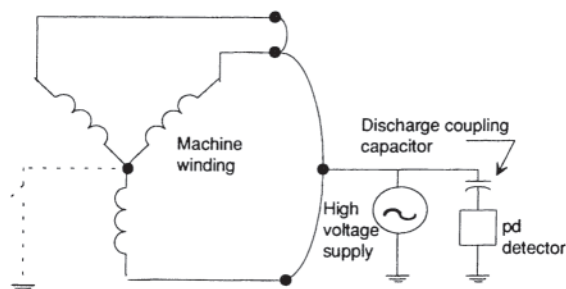


**Figure 8.10** Electrical circuit arrangement for a stator winding partial discharge (pd) test.

There is no agreement on acceptable levels of pd magnitude, DIV, or DEV for stator windings. The inductive nature of a stator winding makes the calibration procedure [15] for converting millivolts on the oscilloscope screen into picocoulombs uncertain. Thus the pulses measured at the detector may not be a true measure of the actual pd activity: and they cannot readily be calibrated from machine to machine, or even amongst different types of commercial detectors.

The most powerful method for the interpretation of pd test results is to perform the test at regular intervals and watch for a trend. For example, every 3–5 years is suggested for motors. As insulation damage progresses, pd magnitudes will increase and the DIV and DEV will decrease. Observation of any continuous increase in pd activity from test to test is an indication that aging is occurring and visual inspection of the winding condition is necessary. Likewise, comparison of data on identical machines can focus awareness on a developing problem in a particular machine. Due to the calibration problems noted above, any comparisons should be done with exactly the same test equipment and test procedure.

Since the pd test described above requires a lengthy testing outage, and is therefore difficult to perform frequently, a pd test that can be performed by nonspecialized maintenance personnel while the motor is operating normally has been developed [16]. The TGA test requires the prior installation of special sensors in the stator winding. The TGA test is most cost effective on large motors rated 6000 V or more, and where winding failures have expensive consequences. Continuous on-line PD monitors have also been found effective for motors rated 4 kV and above [17].

### 8.3.3.5 Turn Insulation Surge Test

None of the above procedures is sensitive to the condition of the interturn insulation in multiturn coils. Surge tests function as a hipot test to check the integrity of the interturn insulation, as well as to test the capability of the groundwall insulation to withstand steep-fronted transients likely to be encountered in normal service. Guidelines for the magnitudes and the front time of the surges for the test have been given in IEEE 52 [18]. The surge tests are normally used to test new windings in the factory or to detect whether a fault exists in a machine before repair. The surge test applies a voltage to the turn insulation for a very short time, causing weak insulation to fail. Thus the surge test is a hipot test for the turn insulation, rather than a diagnostic test.

Older commercial surge testers compare impedances of two matching sections (usually coils in parallel, or separate phases) of the winding. An instrument applies voltage surges of about  $0.2 \mu\text{s}$  rise time and adjustable magnitude to the two winding sections  $L_1$  and  $L_2$  simultaneously (Fig. 8.11) and the shapes of the surges are superposed on an oscilloscope (Fig. 8.4). The fast rise time of the surge ensures that a high voltage is developed across the turns in the winding, if both parts of the winding are free from faults, their impedances will be the same and the two waveforms will be indistinguishable. Any discrepancy in the two waveforms may indicate a shorted turn in one of the them. The magnitude and the nature of the discrepancy between the two waveforms can be used by an

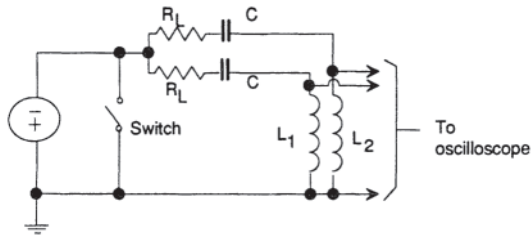


**Figure 8.11 Schematic of a surge comparison test.**  $L_1$  and  $L_2$  represent two phases of the motor stator winding.

experienced operator to identify the nature of the fault [19]. Usually the manufacturers of the surge testing equipment provide information on relating the observed discrepancy in the superposed waveforms to the nature of the fault.

Turn insulation surge testers are most often used by winding manufacturers to ensure that the turn by turn insulation in new coils or complete phases is intact. Testing the insulation in an older machine is more difficult since the individual coils cannot easily be separated from one another. At best, only complete phases can be tested without dismantling the winding. The high-voltage output of the surge tester is connected to two of the phases. The third phase is grounded to the surge tester. The voltage is applied and increased to the specified limit, such as in IEEE 522. Note that the surge test voltage should not exceed the ground wall dc hi-pot voltage (see Section 8.3.3.1). If there is no difference between the surge waveforms up to the test voltage limit, the turn insulation has not broken down, and is presumed sound.

The validity of conclusions drawn from a comparison of the shapes of surges applied to two winding sections depends on the matching of their impedance in the absence of insulation faults. If the two winding sections being tested have slightly different impedances, due either to variations in insulation thickness, dimensions of coils and circuit parallels, and so forth, or to their positions in the winding (e.g., a parallel circuit winding with different lengths of the ring bus), the two surge shapes may not overlap completely, and thus suggest a fault, even for an otherwise perfect insulation system. Also, it may be practically difficult to detect a turn fault in a coil tested in a circuit parallel with more than, say, 10 coils, because a shorted turn will cause only a very minor change in the total winding impedance. The more coils in series, the more subjective is the judgment that a defective coil is present. Thus a great deal of experience is required to interpret results from this test on complete phases. Since minor differences in inductance between phases can lead to unmatched waveforms, modern surge testers digitally compare waveforms on the same phase at low and high voltages.

As with the ac and dc hi-pot tests for the stator ground-wall insulation, the surge test is a go/no-go proof test. It does not indicate the relative condition of the turn insulation in different coils other than whether shorts exist.

### 8.3.3.6 Process to Determine Stator Winding Condition

To assess insulation condition, a wide variety of information should be considered. The general procedure for motors is as follows:

- Collect background information.
- Perform electrical tests that do not require dismantling of the motor.
- Remove the rotor and perform a visual inspection.

This process is described more fully in Ref. 20, and recently a personal-computer-based expert system is available to guide maintenance personnel through this process [11].

An important first step is to collect background information that can help determine which aging processes may occur, and thus the signs to look for. The following describes some of the types of information that should be known prior to undertaking an assessment of a particular machine.

#### (a) Operating Practice and Environment

Aging and failure of motor insulation depends on the stresses imposed on it. Some of these stresses are a direct result of the operating practice and environment in which the machine operates. The same insulation would last longer in a continuously operated motor compared to a motor that sees a lot of starts, due to the effect of thermal cycling (see Section 8.3.2.1). Another important factor is the environment in which the machine operates. System and lightning conditions causing surges at the machine terminals, high ambient temperature, vibration and shock loading transmitted back from the driven equipment, coal dust in the air, high humidity, salt in the air in maritime locations, oil mist, bearing oil problems, and corrosive fumes are some of the environmental factors that affect the condition of the insulation (see Section 8.3.2.4).

The effect of these factors will be small where the machine design incorporates special features to withstand these conditions. However, the effect can be significant when the special features malfunction or where they are nonexistent. These environmental factors should therefore be considered in the assessment of machine insulation because they can provide useful clues to the condition of the insulation and the type of aging process that might be underway.

#### (b) Past Experience

Experience by the owner of a motor, and also others with the same equipment, is an important basis for understanding findings and planning strategy. Records of past failures, inspections, and repairs can be invaluable indicators of the likely problem areas, the types of damage that can be expected, and the relative usefulness of tests and techniques that could be used in the assessment.

Where repair shops are used frequently, some of these records might be located at these shops. Sometimes, records from factory testing of equipment when new can provide an important clue. Past experience of others on similar equipment can also prove to be quite valuable. The exchange of information at regular industry seminars can be very useful. Feedback on experience with particular equipment at such meetings frequently motivates design improvements by manufacturers.

#### (c) Insulation Systems

As described in Section 8.3.1, there are a variety of materials used in motor stator winding insulation systems. Each material and system has certain abilities to resist the applied stresses. The insulation life consumed during operation depends on

the severity of the stresses and the type of insulation system used. It may be minimal if the insulation system is well matched with operating duty. However, a mismatch could result in serious deterioration. For instance, in a motor exposed to steep surges, the turn insulation would require careful checking if it contained dielectrics other than mica. The type of insulation used is, therefore, an important factor in the assessment of its condition. Similarly, if a motor is frequently overloaded, more thermal deterioration is likely to occur if the insulation is thermoplastic than if it is epoxy-mica.

#### *Diagnostic Tests*

As described above, there are several nondestructive tests available for checking the condition of machine insulation, the probable extent of aging, and the rate at which aging is taking place. The results from these tests can have a major impact on the smooth running of the plant in terms of proper scheduling of maintenance and repair work. Moreover, the test results are also important to the efficient operation of the plant by helping in the economic evaluation of alternative action plans, such as when to shut down and whether disassembly, other tests, rehabilitation, or repair is warranted.

The results from diagnostic tests are not always clear-cut and are often subject to interpretation due to the complexity of rotating machines and changes in the test environment beyond the control of maintenance personnel.

#### *Visual Inspection*

Visual inspection becomes necessary to confirm any problem found by diagnostic testing and to evaluate the extent of the damage. At times, it may also be required to locate deterioration that cannot be identified by diagnostic testing.

In any of the above situations, the assessment enters a critical stage when visual inspection is being considered because of its impact on the extent of the disassembly required, the components to be examined, the method of inspection, the down-time of the machine and, finally, any corrective action required. In essence, visual inspection by skilled people can provide an essential opportunity, along with tests, for obtaining the best possible assessment of the condition of insulation and its remaining life.

Techniques for visually examining different components of the machine insulation are outlined in Refs. 2 and 11. Past experience with insulation system inspections will greatly enhance both the quality and quantity of the information. Unfortunately, it is beyond the scope of this book to describe visual inspection procedures.

### **8.4 EFFECT OF INVERTER DRIVES ON STATOR INSULATION**

Rapid advances in power electronic components in the 1990s have led to new stresses that may adversely affect the life of motor insulation in both random- and form-wound stators. The four main impacts of modern invertors on stator windings include:

- Increased operating temperature due to reduced cooling airflow when operating at reduced speeds. In most motors, the cooling air is forced to flow through the motor

by means of a fan attached to the rotor. If the rotor is spinning more slowly, the effectiveness of the cooling is reduced. The increased operating temperature at reduced speeds may accelerate the thermal deterioration of the insulation (see Sections 8.1.3 and 8.3.2.1).

- Invertors tend to result in more harmonic currents flowing in the stator winding, which increases the copper and dielectric losses. In addition, the higher frequency harmonics in the current tend to induce greater stator core lamination circulating currents. The result is that the stator winding operates at a high temperature when inverter driven, than occurs with sinusoidal 50/60 Hz operation at the same speed.
- For form-wound motors with semiconductive coatings and stress grading coatings (see Section 8.3.1.5), higher capacitive currents flow in these coatings due to the high frequency voltages associated with drives. This also raises the temperature of the winding, and can accelerate the thermal deterioration of these coatings and the adjacent insulation.
- Inverter-fed drives (IFDs) of the pulse-width-modulated (PWM) type that use insulated gate bipolar junction transistors (IGBTs) can create tens of thousands of fast-rise-time voltage surges per second. There is anecdotal evidence that the huge number of voltage surges from IFDs can lead to gradual deterioration and eventual failure of the turn, ground or phase insulation by partial discharges, both in low voltage (less than 1000 V) and medium voltage (2.3–4.16 kV) motors [21–24].

The first three impacts increase the rate of thermal deterioration, as described in earlier sections. In any particular application, whether these thermal effects due to the IFDs are significant, can be determined by monitoring the stator winding temperature. The fourth impact is somewhat related to failure caused to switching surges, as discussed in Section 8.3.2.3, but deserves a more in depth explanation.

#### **8.4.1 Surge Voltage Environment**

A PWM type of IFD generates fast-rise-time rectangular pulses of fixed amplitude voltage that have varying width and frequency. The voltage of the pulses at the output of the inverter are not more than the dc bus voltage. This level depends on the rectified ac voltage or braking voltage level or power factor correction regulation voltage.

Modern inverter output voltage rise times may be in the 50–400 ns range due to IGBT switching characteristics. The rise-time at the motor terminals depends on the grounding system, the dielectric of the power cable to the motor, as well as if filters are present which slow the rise-time of the pulse.

The invertors can generate repetitive voltage overshoot. Figure 8.12 shows the power frequency voltage applied to the motor terminals in a conventional motor. Figure 8.13 shows a plot of the voltage surges measured at the terminals of a motor fed from an inverter drive. Figure 8.14 shows an expanded view of a single surge as measured at the motor terminals.

Depending on the rise-time of the voltage pulse at the inverter output, and on the cable length and motor impedance,

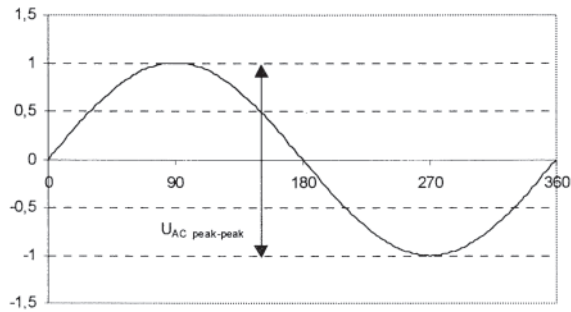


**Figure 8.12** Power frequency sine wave-ac-voltage

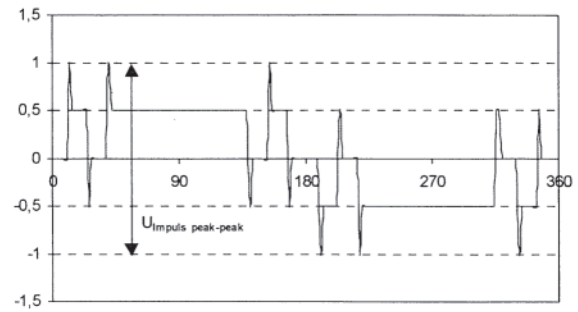


**Figure 8.13** Surge voltage (including spikes due to voltage reflection).

the pulses generate voltage overshoots at the motor terminals. This over voltage is created by reflected waves at the interface between cable and motor terminals due to impedance mismatch. This phenomenon is fully explained by the transmission line and traveling wave theory. Oscilloscope traces of voltage surges from a typical inverter drive are given in Figs. 8.13 and 8.14. Even higher voltage stress can be produced by drive double transition and by an IFD algorithm that does not allow a minimum time between successive pulses:

- Double transition occurs for example when one phase switches from minus to plus DC bus voltage at the same instant that another phase switches from plus to minus.
- There is no minimum pulse time control in the drive, and if the time between two pulses is matched with the time constant of the cable between the drive and the motor.

Typically and IFD will produce a wide range of surges with different risetimes and magnitudes (Fig. 8.15).

#### 8.4.2 Distribution of Voltage Surges within Stator Windings

The dielectric stress across the ground and phase insulation is determined by the magnitude of the voltage applied to the motor terminals. However, both the peak voltage and the peak rise time of the surge at the motor terminals determine the dielectric stress across the turn insulation and between coils. Short rise times surges result in the voltage being unevenly distributed throughout the coils with high levels of stress present within the first several turns of the individual winding phase. Figure 8.16 shows the distribution of the voltage across a coil as a function of risetime. Fast rise time surges at

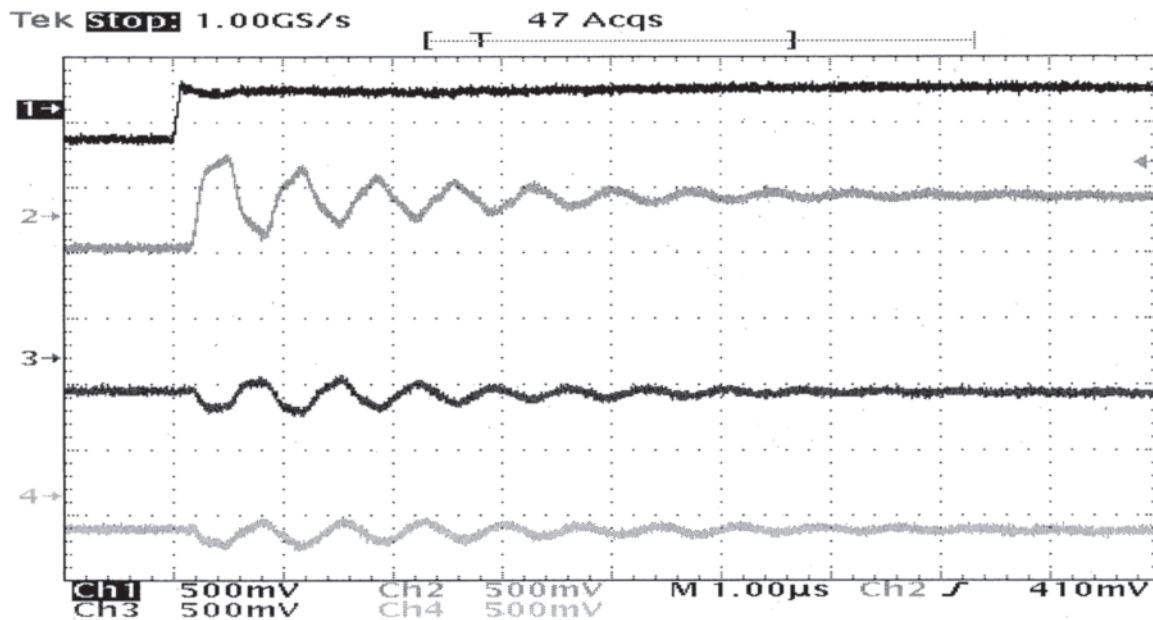


**Figure 8.14** Typical high-resolution oscilloscope image of a fast risetime surge as measured at the motor terminals (trace 2) of a 460-V rated motor. The top trace shows the pulse as measured at the drive. The vertical scale is 500 V per division.



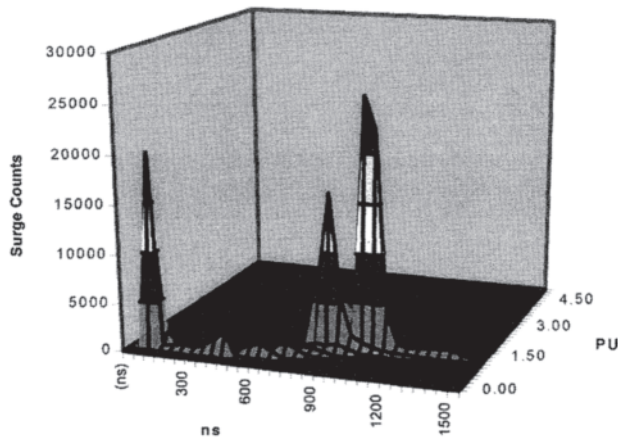


**Figure 8.15** Surge monitor output from a pulse-width modulated (PWM), insulated gate bipolar junction transistor (IGBT), inverter-fed drive (IFD) into a 40-hp, 600-V motor through 300 m of power cable [24]. Note that short-rise-time surges tend to be associated with low magnitude surges. 1 pu is rated line-ground voltage.

motor terminals also generate high turn to turn voltages in the first coils of each winding phase.

### 8.4.3 Mechanisms of Insulation Deterioration

If a specific motor does experience fast-rise-time surges with a significant magnitude, this will create a high-voltage stress in the following locations:

- Between a conductor and ground
- Between conductors in different phases
- Between the first and last turns in the first coil, which in a random wound coil may be in contact with one another
- Between conductors in different phases in three phase stators

In a random-wound stator, the stator winding's conductor insulation has a small diameter, and there is often some air surrounding the wire. With sufficient electric stress between turns, or to ground or to another phase, the air between the wires or to ground may experience electrical breakdown (i.e., a spark) in the air, called a partial discharges (see [Section 8.3.2.3](#)). The electrons and ions created by the discharge in air bombard the wire, ground or phase insulation. In random

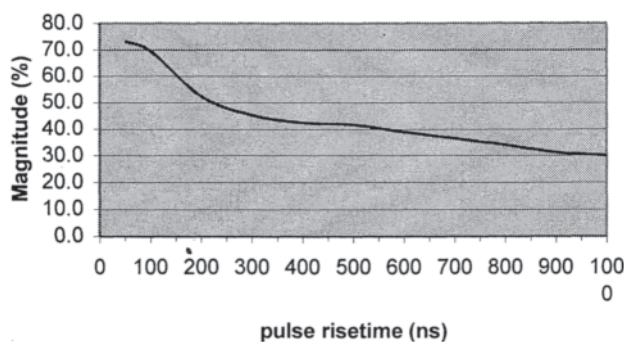


**Figure 8.16** Typical distribution of the voltage across the first coil in a random wound stator, as a function of the rise-time of the surge.

wound stators, conventional wire insulation in a thin organic film. This film is eventually eroded by the PD, leading to insulation failure and a shorted coil. Pitting of the wire insulation and white powders are typical observable indications that PD has occurred in service.

In form-wound stators, turn insulation deterioration can occur due to PD between the turns. In addition, the PD may attack the ground insulation. If the coils have a semiconductive coating, then the high frequency capacitive currents in the shield caused by drive can overheat the coating and deteriorate it, as discussed above.

To prevent these processes, the motor designer can design the stator to prevent the occurrence of PD. Alternatively, the stator designer can allow for the presence of PD by incorporating materials that are resistant to deterioration by PD.

### REFERENCES

Note: In the following listing, abbreviations have the following meanings:

AIEE	American Institute of Electrical Engineers (predecessor to IEEE)
ANSI	American National Standards Institute
ASTM	American Society for Testing Materials
IEEE	Institute of Electrical and Electronics Engineers
NEMA	National Electrical Manufacturers Association

Sources for standards are listed in [Appendix B](#).

1. Mighdoll, P. et al, "Improved Motors for Utility Applications—Industry Assessment Study," Electric Power Research Institute Report EL-2678, Oct. 1982.
2. Culbert, I., H.Dhirani, and G.C.Stone, "Handbook to Assess the Insulation Condition of Large Rotating Machines," Electric Power Research Institute Report EL-5036, vol. 16, June 1989.
3. Dakin, T.W. (1948). "Electrical Insulation Deterioration Treated as a Chemical Rate Phenomenon." *Transactions of the AIEE*, vol. 67(1), pp. 113–122.
4. IEEE Std. 1–1986, General Principles for Temperature Limits in the Rating of Electric Equipment and for the Evaluation of Electrical Insulation (ANSI recognized).
5. NEMA Std. MW 1000–1987. Magnet Wire.
6. IEEE Std. 43–2000, Recommended Practice for Testing Insulation Resistance of Rotating Machinery.
7. Laffoan, C.M., C.F.Hill, G.L.O.Moses, and L.J.Berberich, "A New High Voltage Insulation for Turbine Generator Stator Windings," *Transactions of the AIEE*, vol. 70, 1951, pp. 721–730.
8. Flynn, E.J., C.E.Kilbourne, and C.D.Richardson, "An Advanced Concept for Turbine-Generator Stator Winding Insulation," *Transactions of the AIEE*, vol. 77, June 1958, pp. 358–371.
9. Fort, E.M. and J.C.Botts, "Development of Thermalastic Epoxy for Large High Voltage Generators," IEEE International Symposium on Electrical Insulation, June 1982, p. 56.
10. Gupta, B.K., et al, "Turn Insulation Capability of Large AC Motors, Parts 1, 2, and 3," *IEEE Transactions on Energy Conversion—Dec.* 1987, p. 658.
11. Lloyd, B.A., G.C.Stone, and J.Stein, "Development of an Expert System to Diagnose Motor Insulation Condition," *Proc. IEEE Industry Applications Society Annual Meeting*, vol. 1. Sept. 1991, p. 87.
12. IEEE Std. 95–2001, Recommended Practice for Insulation Testing of Large AC Rotating Machinery with High Direct Voltage.

13. Stone, G.C. and M.Kurtz, "Interpretation of Megohm Tests on Electrical Apparatus and Circuits," *IEEE Electrical Insulation Magazine*, vol. 2, no. 1, Jan. 1986, pp. 14–17.
14. IEEE Std. 286–2001, Recommended Practice for Measurement of Power-Factor Tip-Up of Stator Coil Insulation.
15. IEEE 1434–2000, "Guide to the Measurement of Partial Discharges in Rotating Machinery.
16. Sedding, H.G., et al, "A New Sensor for Detecting Partial Discharges in Operating Turbine Generators," *IEEE Transactions on Energy Conversion*, Dec. 1991, p. 700.
17. G.C. Stone, S.Tetranlt, H.G.Sedding, "Monitoring Partial Discharges on 4.1 k V Motors," IEEE Petroleum and Chemical Industry Conference, Banff Canada, Sept 1997, pp. 159–165.
18. IEEE Std. 522–1992, IEEE Guide for Testing Turn-to-Turn Insulation on Form Wound Stator Coils for AC Rotating Electric Machines (in revision).
19. Schump, D.E. and G.L.Shook, "Winding Fault Diagnosis by surge Comparison," *Proc. 14th IEEE Electrical/Electronics Insulation Conference*, Oct. 1979.
20. Culbert, I., H.G.Sedding, and G.C.Stone, "A Method to Estimate the Insulation Condition of High Voltage Stator Windings," *Proc. IEEE Electrical Insulation Conference*, Oct. 1989, p. 236.
21. A.L.Lynn, W.A.Gottung, D.R.Johnston, *Corona Resistant Turn Insulation in AC Rotating Machines*, Proc. IEEE Electrical Insulation Conference, Chicago, October 1985, p. 308.
22. W.Yin, et al, *Improved Magnet Wire for Inverter-Fed Motors*, Proc. IEEE Electrical Insulation Conference, Chicago, September 1997, p. 379.
23. E.Persson, *Transient Effects in Applications of PWM Inverters to Induction Motors*, IEEE Trans IAS, September 1992, p. 1095.
24. G.C.Stone, S.Campbell, S.Tetreault, "Inverter-Fed Drives: Which Motors are at Risk", IEEE Industry Applications Magazine, Sept 2000.

## GENERAL REFERENCES

- Annual Book of ASTM Standards. Electrical Insulation and Electronics, Section 10, vols. 10.01, 10.02, and 10.03, American Society for Testing and Materials, Philadelphia PA.
- Barlow, A., "The Chemistry of Polyethylene Insulation," *IEEE Electrical Insulation Magazine*, Jan./Feb. 1991.
- Battisit, A.J. and C.Lin, "New Developments in Solventless Polyester Varnishes," *IEEE Electrical Insulation Magazine*, Sept./Oct. 1991.
- Beaty, H.W., *Electrical Engineering Materials Reference Guide*. McGraw-Hill, New York, 1990.
- Bergstrom, R. and G.W.Smith, *An Introduction to the Testing of Insulation Systems in Electrical Apparatus*, Baker Instrument Company, Fort Collins, CO.
- Bucek, G.E., "Converting to Water-Soluble Organic Varnishes Makes Environmental, Economic, and Processing Sense" *IEEE Electrical Insulation Magazine*, July/Aug. 1988.
- Crawford, D.E., "A Mechanism of Motor Failure," *Proc. 12th Electrical Insulation Conference*, Boston, 1975
- "Electrical Insulation and High Voltage, Selected References by the DEIS Education Committee," *IEEE Electrical Insulation Magazine*, Jan. 1987.
- Gill, A.S., *Electrical Equipment Testing and Maintenance*, Reston Publishing, Reston V A. 1982.
- Harrington, A.W., "VPI System Considerations when Impregnating Multilayers of Insulation," *IEEE Electrical Insulation Magazine*, Mar. 1986.
- IEEE Std. 56–1977 (Reaffirmed 1991), Guide for Insulation Maintenance of Large AC Rotating Machinery (10 000-k V A and Larger).
- IEEE Std. 95–1977 (Reaffirmed 1991), Recommended Practice for Insulation Testing of Large AC Rotating Machinery with High Direct Voltage.
- IEEE Std. 112–1991, Standard Test Procedure for Polyphase Induction Motors and Generators.
- IEEE Std. 117–1974 (Reaffirmed 1991), Test Procedure for Evaluation of Systems of Insulating Materials for Random-Wound AC Electric Machinery.
- IEEE Std. 275–1981, Recommended Practice for Thermal Evaluation of Insulation Systems for AC Electric Machinery Employing FormWound Pre-Insulated Stator Coils, Machines Rated 6900-V and Below.
- IEEE Std. 304–1977 (Reaffirmed 1982), Standard Test Procedure for Evaluation and Classification of Insulation Systems for DC Machines.
- IEEE Std. 432–1974 (Reaffirmed 1982), Guide for Insulation Maintenance for Rotating Electric Machinery (5-hp to less than 10000-hp).
- IEEE Std. 433–1974 (Reaffirmed 1991), Recommended Practice for Insulation Testing of Large AC Rotating Machinery with High Voltage at Very Low Frequency.
- IEEE Std. 434–1973 (Reaffirmed 1991), Guide for Functional Evaluation of Insulation Systems for Large High-Voltage Machines.
- Jenkins, J.E. Jr. and W.L.Hall, "Stressing Insulation in Motor Repair Testing," *IEEE Electrical Insulation Magazine*, Sept./Oct. 1990.
- Miller, H.N., *DC Hypot Testing of Cables, Transformers, and Rotating Machinery*, Manual P-16086. Associated Research, Inc., Skokie IL.
- Nailen, R.L., "For Electrical Insulation, What is the Best Test?," *Electrical Apparatus Magazine*, Sept. 1985.
- NEMA Std. RE 2–1987. Electrical Insulating Varnish.
- NEMA Std. MG 1–1987. Motors and Generators.
- Rejda, L.T. and K.Neville. *Industrial Motor Users' Handbook of Insulation for Rewinds*, Elsevier, New York, 1977.
- Reynolds, A.O., *The Lowdown on High-Voltage DC Testing*, Biddle Instruments, Blue Bell PA. 1988.
- Schaible, M., "Electrical Insulating Papers—An Overview," *IEEE Electrical Insulation Magazine*, Jan. 1987.
- Schump, D.E., "Reliability Testing of Electric Motors," *IEEE Transactions on Industry Applications*, vol. 25, no. 3, May/June 1989.
- Smeaton, R.W., *Motor Application and Maintenance Handbook*, McGraw-Hill, New York, 1987.
- Steffens, H.G., "Structure and Bonding in Matter: A Primer for the Users of Electrical Insulation," *IEEE Electrical Insulation Magazine*, May 1987.
- A Stüch in Time ...A Manual on Electrical Insulation Testing for the Practical Man*, Biddle Instruments, Blue Bell PA. 1984.
- Stone, G.C. and J. Kuffel, "Digital Recording Techniques for Electrical Insulation Measurements," *IEEE Electrical Insulation Magazine*, May/June 1989.
- Thurman, C.E., "Trickle Impregnation of Small Motors," *IEEE Electrical Insulation Magazine*, May/June 1989.
- Van Vooren, E.J., "Electrical Insulation systems-How the Pieces Fit Together," *IEEE Electrical Insulation Magazine*, Sept. 1985.
- Westinghouse Electrical Maintenance Hints*, Westinghouse Electric Corporation Printing Division, Trafford PA 1976.
- Winkeler, M., "A Comparison of Solvent Versus Solventless Electrical Insulating Varnishes via Systems Testing," *IEEE Electrical Insulation Magazine*, Sept. 1986.

# 9

## Motor Control

**Hamid A.Toliyat** (Section 9.0)/**Nils E.Nilsson** (Sections 9.1.1–9.1.7)/**Edgar F.Merrill** (Section 9.1.8)/**Richard H. Engelmann and Hamid A.Toliyat** (Sections 9.1.9–9.2)/**Richard H.Engelmann and Robert L.Steigerwald** (Sections 9.3–9.6)/**Marc Bodson and John N.Chiasson** (Section 9.7)

<b>9.0 INTRODUCTION</b>	<b>432</b>
<b>9.1 INDUCTION MOTORS</b>	<b>432</b>
9.1.1 Electrical Voltage Surges	432
9.1.2 Voltage Drop During Start-Up	437
9.1.3 Starting Torque Characteristics	447
9.1.4 Reduced Starting Duty Schemes	451
9.1.5 Accelerating Torque and Multispeed Applications	456
9.1.6 Starting Duty Thermal Limitations	461
9.1.7 Miscellaneous Induction Motor Starting Topics	464
9.1.8 Bus Transfer and Reclosing of Induction Machines	467
9.1.9 Induction Motor Speed Control	473
9.1.10 Induction Motor Braking	474
<b>9.2 DIRECT-CURRENT MOTORS</b>	<b>475</b>
9.2.1 DC Motor Starting	475
9.2.2 DC Motor Speed Control	477
9.2.3 Braking of Direct-Current Motors	480
<b>9.3 GENERAL CONSIDERATIONS CONCERNING SOLID-STATE CONVERTERS AND CONTROLLERS</b>	<b>482</b>
9.3.1 Converters	482
9.3.2 Controllers	483
<b>9.4 POWER ELECTRONIC DEVICES</b>	<b>483</b>
9.4.1 Diodes	484
9.4.2 Thyristors	484
9.4.3 Gate Turn-Off Thyristors	485
9.4.4 Bipolar Transistors	486
9.4.5 Metal Oxide Semiconductor Field-Effect Transistors	487
9.4.6 Insulated-Gate Bipolar Transistors	488
9.4.7 Integrated Gate-Commutated Thyristor	488
<b>9.5 CONVERTER CIRCUITS</b>	<b>488</b>
9.5.1 Rectifier Circuits	489
9.5.2 Cycloconverters	492
9.5.3 Chopper Circuits	493
9.5.4 Six-Step Inverters	493
9.5.5 Pulse-Width Modulation Inverters	495
9.5.6 Multilevel Converters	498
<b>9.6 CONTROLLERS</b>	<b>498</b>
<b>9.7 OPEN- AND CLOSED-LOOP CONTROL OF A PERMANENT MAGNET STEPPER MOTOR</b>	<b>500</b>
9.7.1 Open-Loop Operation of the Stepper Motor	501
9.7.2 Closed-Loop Control of a Stepper Motor	503
9.7.3 Experimental Results	509
<b>REFERENCES</b>	<b>511</b>

## 9.0 INTRODUCTION

During the past 30 years, there have been major advances in the kinds of motors that can be built and that are in common use, but the advances in motor control have been even more striking. Some of the advances in motor controls have been driven by the developments in motors, but other advances in the control area have resulted in controllers that are as useful with motors built 50 years ago as they are with motors coming off the line today.

Solid-state motor controls were only beginning to come over the horizon 30 years ago; they have now displaced the traditional controls (relays, contactors, circuit breakers, and magnetic amplifiers) of the 1950s and 1960s in many new installations, as well as in installations that are being retrofitted. For small machines, controllers are off-the-shelf items; for large machines, the controller itself may be identical to that of a small machine, only the power-handling devices being different. Customization to a particular machine or installation can be done within normally accepted lead times. Yet the traditional magnetic controls still exist in many installations and will continue to be used for many years to come.

The editors were thus faced with a dilemma as to which topics should be covered in a chapter on motor control. The fact that the solid-state motor control field is still advancing rather rapidly served only to make the dilemma more difficult to resolve. In the end, the decision was made to cover both the more traditional methods (those using magnetic devices and auxiliary machines) and the modern methods (those using solid-state devices), but with one exception: not to go to great depth in either area. The references in the following material to the relevant literature and to standards should enable the reader to build, as necessary, on the base presented in this chapter. The exception, covered in more depth, is that of control of large induction motors, including such topics as bus transfer and reclosing. We know that this area will change, but not at so rapid a rate that extensive coverage will soon be out-dated.

Traditional controls are covered in Sections 9.1 and 9.2, with control of induction motors (including ac supply system considerations) in Section 9.1 and control of direct current (dc) motors in Section 9.2. Sections 9.3 through 9.6 include discussion of the external characteristics of several types of solid-state power devices, a sampling of configurations of converter circuits, and the capabilities of present-day controllers including multilevel converters. Finally, Section 9.7, after a review of the operation of stepper motors, presents a control strategy for closed-loop operation that yields superior performance, as evidenced by experimental results. Due to their importance we have included [Chapter 15](#) in this revised edition on electronic motors. More advanced materials on vector control of induction motors are presented in this chapter. More in-depth control of dc motors is presented in [Chapter 6](#).

## 9.1 INDUCTION MOTORS

One of the classic electrical engineering problems is the across-the-line starting of an alternating current (ac) three-phase in-

duction motor. This problem has many aspects. The motor stator must be capable of withstanding steep-fronted electrical voltage surges of submicrosecond rise times. The electrical supply system needs to be evaluated in conjunction with the motor characteristics to guarantee adequate starting capability. The coordination of protective devices such as relays must be evaluated against subtransient and accelerating induction motor starting currents. Mechanically, the motor must develop sufficient torque to reach operating speed rapidly enough to avoid overheating. Overheating can also be caused by closely spaced repetitive starts.

### 9.1.1 Electrical Voltage Surges

Boehne and colleagues (1930) [1] reported the first study on steep-fronted electrical voltage surges, hereafter simply called surges, produced by lightning striking overhead lines to which rotating electrical machines were connected. It was not long before it was discovered that circuit-breaker switching could cause steep-fronted surges in motors. This discovery was published by Calvert and Fielder in 1936 [2].

Most electrical devices are designed so that there is adequate, but not excessive, electrical insulation surrounding conductors and other live parts. Accordingly, they contain graded insulation systems, which means that they contain thicker electrical insulation or shielding at locations where the voltage stress is higher (greater voltage gradients). Three-phase induction motor stator windings (and generator stator windings) are an exception to this rule. All the windings have the same amount of turn-to-turn and phase-to-ground insulation whether comprising the lead coil or a grounded coil in a wyeconnected winding. In low-horsepower and low-voltage motors, stator coils are random-wound, also called “mush” wound. The coil consists of many turns of round copper wire coated or covered with one or more layers of insulating material. Larger motor stators employ form-wound coils. Figure 9.1 illustrates the typical diamond-shaped form-wound coil.

The formed coil consists of strands protected by a coating or covering of electrical insulating material to provide turn-to-turn electrical isolation (minor insulation). The entire coil then has layers of phase-to-ground insulating material (major insulation), which can be applied generally in one of three ways: (1) tape wrapped in half-lapped fashion, (2) tape wrapped in butt-lapped fashion, (3) sheet wrapped along the slot portion

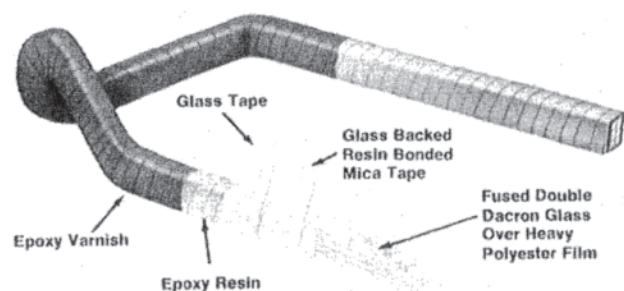


**Figure 9.1** Large induction motor form-wound stator coil. (Courtesy of Magnetek/Louis Allis.)

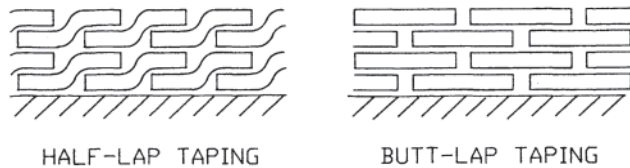


**Figure 9.2** Comparison of half-lapped and butt-lapped coil taping.

of the coil. Figure 9.2 shows diagrammatically the half-lapped and the butt-lapped configurations.

#### 9.1.1.1 Electrical Voltage Surge Standards

Using a special measurement apparatus and an electrical voltage surge generator capable of  $0.12 \mu\text{s}$  rise times, it was shown in the classic Russian paper by Petrov and Abramov [3] that the voltage distribution across the turns within formed stator coils during energization is nonuniform, especially when the surges have fast rise times. In the context of this section, the peak voltage is the absolute value of the voltage peak (not root mean square [rms]) or highest scalar voltage during energization, and the rise time is the amount of time from energization to the voltage peak. When the voltage distribution is nonuniform, there is often an initial peak voltage that occurs in tens or hundreds of nanoseconds and a second somewhat higher peak voltage that occurs in microseconds.

The early standards evolved from some basic ideas about electrical voltage surges. The per-unit base voltage comprising the basis of this theory is the peak phase-to-ground motor terminal voltage:

$$V_{\text{base}} = \sqrt{\frac{2}{3}} V_{\text{LL}} \quad (9.1)$$

In cases where the voltage surge relaxes to form a long wavefront, it distributes uniformly across the turns in the motor coils such that the phase-to-ground insulation, or groundwall insulation, becomes the limiting factor in the design. The ac high-potential (hi-pot) test level has been defined as:

$$V_{\text{hipot}} = 2E + 1000 \quad (9.2)$$

where  $E$  is the rated motor rms line-to-line terminal potential in volts (NEMA MG 1-1999 [4], Par. 20.17.2, and following). Note that the equivalent dc hipot test level is higher by a factor of 1.7.

The American Institute of Electrical Engineers (AIEE) published a Committee Report [5] in 1960 that established a surge envelope of:

$$V_s \text{ (per unit)} \leq 1.25 \times \sqrt{2} \frac{V_{\text{hipot}}}{V_{\text{base}}} \quad (9.3)$$

between  $0.2 \mu\text{s}$  and  $10 \mu\text{s}$  for rotating machines. The concept of surge envelope in this instance means a continuous range of absolute values between zero voltage and a defined maximum peak voltage between two specified time values.

Maintaining an effective insulation coordination margin was the rationale for selection of this envelope. This level should permit adequate protective margin when using 100%

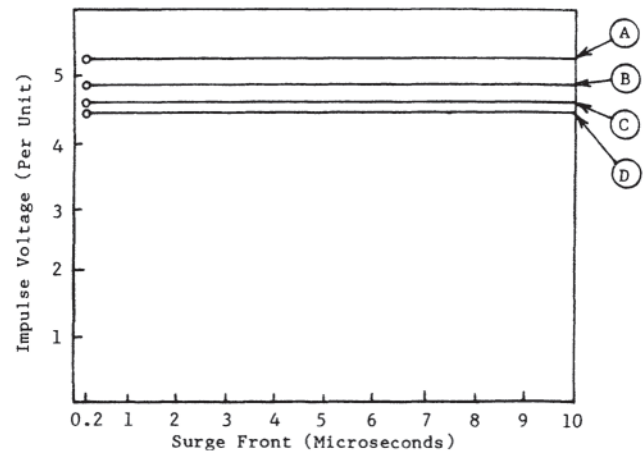


**Figure 9.3** 1960 AIEE rotating machine impulse voltage withstand envelope. Terminal voltages: A, 2.3 kV; B, 4.0 kV; C, 6.6 kV; D, 13.2 kV.

rated lightning (or electrical voltage surge) arresters. The need for 100% arresters arises when applying lightning arresters on delta systems or high-impedance grounded circuits. Figure 9.3 illustrates this surge envelope. In actuality, it consists of a family of curves due to the constant in the righthand expression of Eq. 9.2.

By 1981, a Working Group (WG) in the IEEE Power Engineering Society Electric Machinery Committee (formerly the Rotating Machinery Committee) reporting to the Insulation Subcommittee (ISC) determined that voltage surges with rise times of less than  $5 \mu\text{s}$  do not distribute uniformly across the turns of an induction motor stator winding. Therefore, the turn-to-turn voltage insulation, or minor insulation, becomes the limiting factor in the voltage insulation design. Accordingly, this WG determined that the machine voltage surge envelope, or impulse voltage withstand envelope, should be lowered in the short-time region as shown in Fig. 9.4. At zero time, the motor stator winding should be

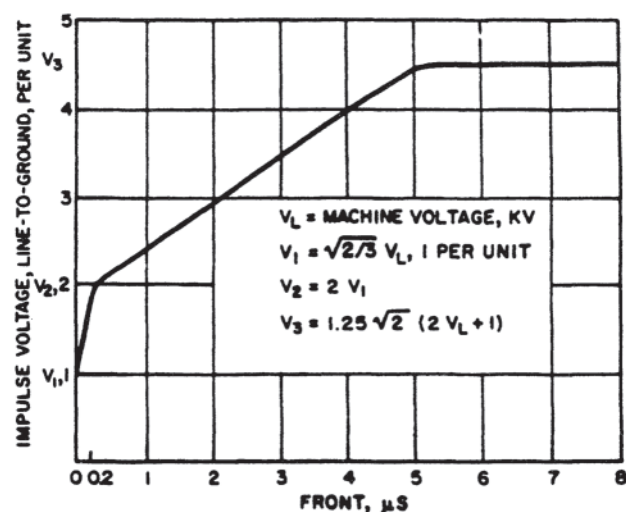


**Figure 9.4** 1981 IEEE rotating machine impulse voltage withstand envelope. (Copyright by IEEE, 1981.)

able to withstand 1 per-unit voltage such that  $V_s(t)$  at time  $t=0$  is given by:

$$V_s(0)=V_{\text{base}} \quad (9.4)$$

Another way of looking at this is that the motor should be able to withstand a step-function voltage wave with a magnitude of unity.

With a wavefront of  $0.2 \mu\text{s}$ , the motor stator winding should be able to withstand a voltage surge with a magnitude of 2 per unit. This value accommodated the dispersive or attenuating effect of lossy cables on voltage surges with a magnitude greater than 1 per unit as well as reflected voltages from the motor. These points, along with  $V_s(5 \mu\text{s})$ , as calculated in Eq. 9.3, were connected by straight lines on a linear scale to demarcate the upper limits of the new machine impulse voltage withstand envelope as shown in Fig. 9.4.  $V_s(5 \mu\text{s})$  equals  $V_3$  in Fig. 9.4. It should be pointed out that Fig. 9.4 is in error beyond  $5 \mu\text{s}$  because the surge envelope is again a family of curves as was the case in Fig. 9.3. This is because  $V_3$  has different values depending on the induction motor terminal voltage rating.

Although much theoretical work transpired during the ensuing years, not much information was forthcoming on the actual electrical voltage surges arriving at the terminals of motors in either industrial electrical systems or electric utility systems. Actual motor winding failure data were of limited value for the following reasons:

- Turn-to-turn winding failures are difficult to identify. During in-service energization, turn-to-turn failures will evolve into additional turn shorting until the winding fails to ground. As a result, many failures reported as ground faults actually started out as turn-to-turn failures.
- Turn-to-turn failures never show up during maintenance hi-pot testing because all the turns are at the same potential.
- Surge comparator testing during maintenance will show a turn-to-turn failure in the lead coil: however, a turn-to-turn short circuit whose location is several coils into the winding does not have much impact on the surge waveform and may be masked during a surge comparator test.

In 1982, the Electric Power Research Institute (EPRI) initiated a study, project RP2307, "Turn Insulation Capability of Large AC Motors," to monitor electrical voltage surges at motor terminals during operation and to determine the surge capability of typical existing electrical insulation systems. Additionally, motor electrical insulation systems were tested to failure to determine actual electrical strength of insulation systems in common usage.

Surges On 33 motors at 11 North American electric utilities were monitored over a period of 3 years using high-speed recording equipment [6]. Air magnetic metal-clad switchgear was utilized to switch 26 of the motors and vacuum devices were used to switch seven of the motors. Numerous surges were recorded during energization of each motor, which permitted an average and a worst-case electrical voltage surge to be defined. No surges were identified during deenergization.

During the tests to failure, it was discovered that all the turn-to-turn insulation systems tested had greater surge withstand capability than that defined by the impulse voltage withstand envelope illustrated in Fig. 9.4. These were not the results expected given the reduction in capability of the 1981 IEEE Rotating Machine Impulse Voltage Withstand Envelope compared with the 1960 AIEE Rotating Machine Impulse Voltage Withstand Envelope. The conclusions reached by analyzing the destructive test data were as follows [7].

- Most motors have a turn-to-turn impulse strength of 5 per unit or more.
- Manufacturers of modern motor insulation systems have the capability and expertise to produce motors with turn-to-turn impulse strength of 10 per unit or more.

A figure of merit, called the slew rate, can be defined as the electrical surge magnitude divided by the rise time:

$$\text{Slew rate (SR)} = \frac{V_{s,\text{max}}}{\text{rise time}} \text{ (pu}/\mu\text{s)} \quad (9.5)$$

The worst case monitored in the EPRI study was a wound-rotor induction motor used in a reversing duty application. The motor was applied to raise and lower a coal barge calmshell unloader. It therefore experienced many switching operations in close succession. A peak magnitude electrical voltage surge of 4.6 per unit was recorded with a peak rise time of  $0.2 \mu\text{s}$ . The slew rate was  $22 \text{ pu}/\mu\text{s}$ . Thirty of the monitoring situations are plotted in Fig. 9.5 [8].

It is clear from Fig. 9.5 that the 1981 IEEE Impulse Voltage Withstand Envelope does not adequately define the environment in which motors operate. Fortunately, the destructive tests performed as part of the EPRI study verified that typical motor electrical insulation systems are capable of operating in actual surge environments without a failure being likely to occur during a worst-case surge. The IEEE Insulation Subcommittee Working Group, which revised IEEE Std. 522 (1977), "IEEE Guide for Testing Turn-to-Turn Insulation on FormWound Stator Coils for Alternating Current Rotating Electric Machines" [9], adopted a new impulse-withstand envelope similar to the one shown in Fig. 9.6 in the 1992 revision of IEEE Std. 522 (reaffirmed 1998) to address this issue. ANSI Std. C50.41-2000 "American National Standard for Polyphase Induction Motors for Power Generating Stations," also adopts this impulse-withstand envelope [10].

### 9.1.1.2 Methodology for Reducing Stator Winding Surge Failures

When coils are made, they can be cured in several ways. The two most common techniques are as follows: (a) After the coils are formed, they can be put through one or more vacuum, pressure resin impregnation (VPI) cycles. This process may include slot section pressing, (b) The soft coils may be installed in the stator slots. Then the entire stator-coil assembly may be cycled through a VPI process. This technique permits easier slot insertion as the coils are not as rigid as would otherwise be the case.

It was discovered during the EPRI study that forming the coil into the diamond shape and inserting the coil into the

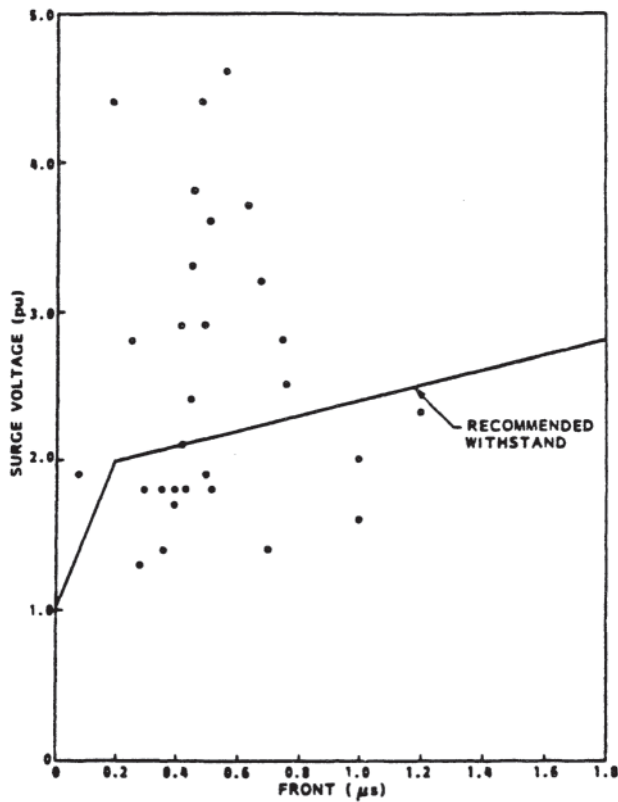


**Figure 9.5** Worst-case start-up voltage surges recorded during the Electric Power Research Institute (EPRI) motor voltage surge study. (Copyright by IEEE, 1987.)

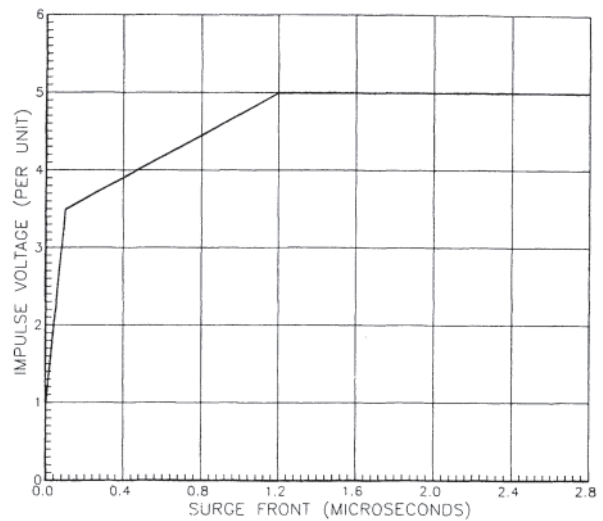
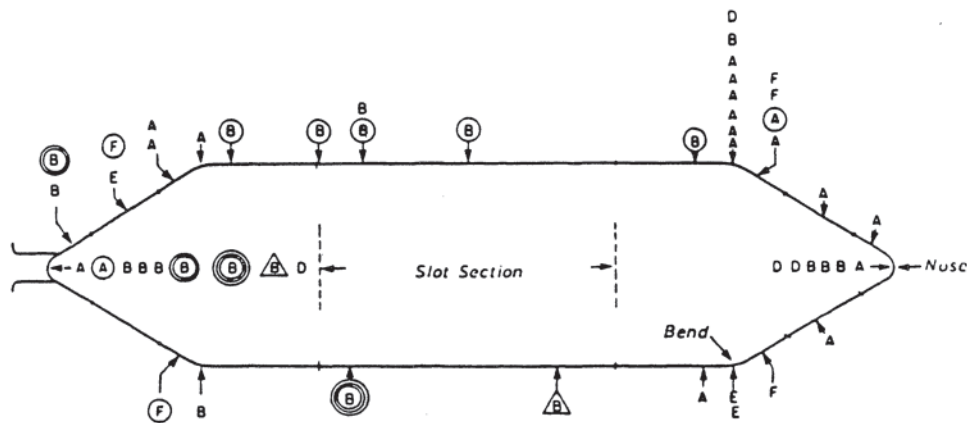


**Figure 9.6** Proposed rotating machine impulse voltage withstand envelope.

stator slot distresses the coil. Gupta et al. [11] located almost all of the destructive test failures at bends or knuckles of the coils or in the end turn overhang region. These dramatic data are reproduced in Fig. 9.7. It is postulated that the process of forming the coil into the diamond shape can disturb either the minor insulation or the major insulation or both.

Nilsson [12] has reported cases where the VPI process has not been completely successful for wrapper insulation systems where the slot length exceeds 0.9 meters. Bunching-up and



Insulation classification	Single-turn	Multiturn
A	13	3
B	8	4
C	0	4
D	3	0
E	1	3

**Figure 9.7** Electrical voltage surge breakdown locations in a typical diamond coil. (Reprinted by permission of the Electric Power Research Institute.)

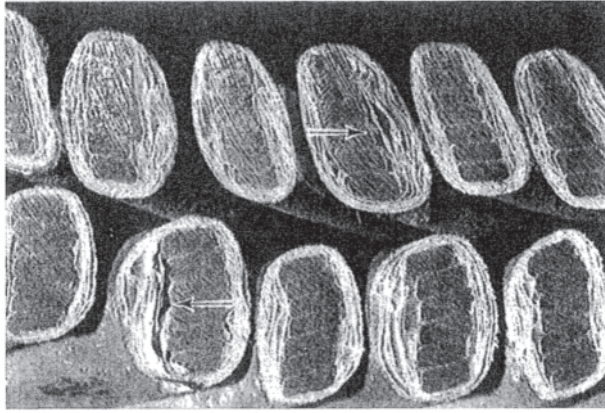


**Figure 9.8** Cross section of coils with inadequate resin filling. (Courtesy of Ohio Edison Company.)

separation of insulation in uncured regions during on—off cycling of the motor is the postulated failure mechanism. While it is difficult to remove the slot section of the coil from the slot after the VPI process has been completed, removal of the motor end-turns from a motor with a failed winding can provide some evidence of problems that are more severe in the slot section of the coil. It is recommended that the owner inspect failed motors in order to determine the cause of failure rather than simply sending the motor out to be rewound. Information can be obtained this way that can be used to improve the owner's new motor specification. Such an inspection was performed on the motor windings illustrated in Fig. 9.8, which shows a typical example of a defective resin impregnation process. Note that the voids are located in the first few turns of the electrical ground insulation and in the turn-to-turn electrical insulation.

Coils that have these latent defects are termed weak coils. Since it takes only one coil failure to necessitate a major motor repair or complete rewind of the motor, a significant reduction in motor stator winding failure rates can be realized simply by weeding out the weak coils. The following three steps are suggested as a methodology for addressing this issue:

1. In order to compensate for damage during the coilforming process, a redundant insulation system can be utilized. An example of this would be the use of a taped electrical insulation over a film or coating for the turn-to-turn insulation system.
2. One hundred percent coil surge testing rather than random sampling would locate and identify almost all of the weak coils. This can be implemented as one feature of an improved quality control program. Also, more sophisticated methods such as power factor tipup testing can supplement other testing programs and can be used to identify voids in solid insulation systems (see [Chapter 7](#), Testing for Performance).
3. In order to check the success of the VPI process, a complete extra coil with a dummy slot section can be put through the VPI process with the motor stator. The test coil can then be dissected to verify the VPI process.

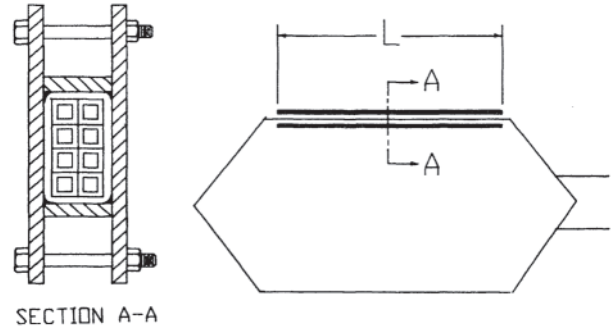


**Figure 9.9** Test coil prepared for the vacuum pressure impregnation (VPI) process with a simulated slot.

Resins that are too thick or too thin can be identified. Figure 9.9 shows the arrangement of the dummy slot.

### 9.1.1.3 Application of Surge Capacitors

On occasion, surge capacitors have been used in the industry to reduce the rate-of-rise of surges impinging on the motor coils. Typical values of capacitance are shown in Table 9.1.

As an example, consider a 9000-horsepower (hp) 13,200-V motor connected to the supply bus by two, 200-foot long, triplexed 350 MCM cables with a dielectric constant of 3.5. A typical voltage surge calculation will be performed in this section to illustrate the effectiveness of surge capacitors in decreasing the rate-of-rise of a severe voltage surge such that it does not exceed the 1981 IEEE Rotating Machine Impulse Voltage Withstand Envelope.

The CIGRE Working Group [13] suggests that a motor surge impedance can typically be computed as follows:

$$Z_m = (200)V^{0.32}P^{-0.64} \text{ (ohms)} \quad (9.6)$$

where  $V$  is the voltage in kilovolts and  $P$  is the power rating in thousands of horsepower. For the example motor,  $Z_m$  equals 112 ohms. The cable capacitance,  $C_{cab}$ , can be shown to equal  $0.0486 \mu\text{F}$  per phase, and the cable inductance,  $L_{cab}$ , can be shown to equal  $7.2 \mu\text{H}$  per phase. Then:

$$Z_{cab} = \left( \frac{L_{cab}}{C_{cab}} \right)^{1/2} \quad (9.7)$$

For the capacitive and inductive parameters specified,  $Z_{cab}$  equals 12.24 ohms. Finally, assume that the surge capacitor was tested at  $0.276 \mu\text{F}$ .

At the motor terminals,  $V_2$  is the reflected surge and  $V_3$  is the refracted surge. Hence,  $V_3$  is the surge that impinges on the motor windings. As a worst case, the incoming surge,  $V_1$ , will be modeled by a rated voltage step function. The incoming

**Table 9.1** Typical Values of Motor Surge Capacitor Ratings

Motor voltage (V)	Surge capacitor rating ( $\mu\text{F}$ )
4,000	0.50
13,200	0.25



surge will be 1 per unit. The rate-of-rise of the step function surge approaches infinity and so the motor surge impedance is large relative to the surge capacitor impedance. Accordingly, the motor surge impedance is not used in the calculation. The relationship for determining the refraction coefficient can be found in Greenwood [14], which is restated as follows:

$$k_{\text{refr}} = 2 \frac{Z_{\text{cap}}}{Z_{\text{cab}} + Z_{\text{cap}}} \quad (9.8)$$

Using Laplace transforms one can then write the following:

$$\mathcal{P}\{V_1\} = \frac{1}{s} \quad (9.9)$$

Where  $s$  is the Laplace transform variable:

$$\mathcal{P}\{k_{\text{refr}}\} = \frac{2/[0.276(10^{-6})s]}{12.24 + 1/[0.276(10^{-6})s]} \quad (9.10)$$

Simplifying,

$$\mathcal{P}\{k_{\text{refr}}\} = \frac{2/[3.378(10^{-6})]}{s + 1/[3.378(10^{-6})]} \quad (9.11)$$

$$V_3(s) = k_{\text{refr}}(s)V_1(s) = \left( \frac{2/[3.378(10^{-6})]}{s + 1/[3.378(10^{-6})]} \right) \left( \frac{1}{s} \right) \quad (9.12)$$

Transforming to the time domain:

$$V_3(t) = 2 - 2e^{-t/3.378[10^{-6}]} \quad (9.13)$$

Figure 9.10 shows the refracted surge at the motor terminals. Note that an initial peak is included that accounts for a small amount of surge capacitor lead length. This lead length must be minimized for the surge capacitors to be effective. One way of visualizing the effects of surge capacitor lead length is to recognize that the delay time associated with the lead length permits the initial portion of the surge to enter the motor

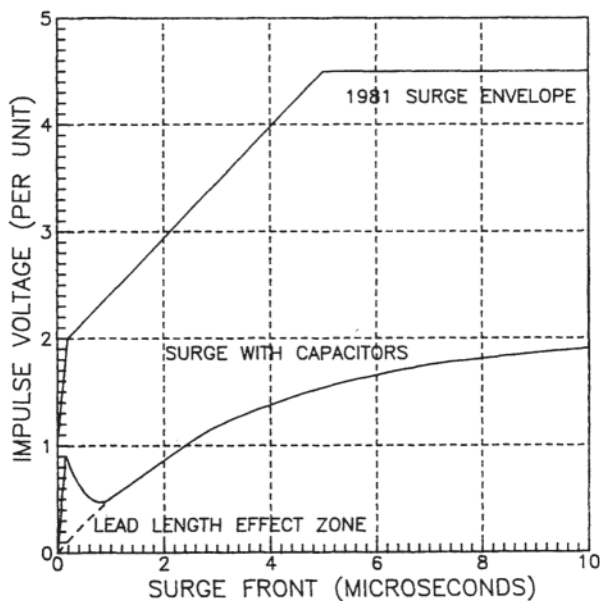


**Figure 9.10** Worst-case surge where a 0.25- $\mu\text{F}$  surge capacitor is connected to the motor terminals.

before the onset of the clamping action of the surge capacitor. For the example given, it is clear that the step function surge will be “sloped” effectively to a level within the 1992 IEEE Std. 522 surge-withstand envelope. This will be true for any reasonable set of values of cable capacitance and inductance. A surge characteristic of this nature will distribute uniformly across the motor winding.

On the other hand, there are reasons that militate against the use of motor surge capacitors. There is a cost factor in applying surge capacitors; users only consider surge capacitors for large motors in cases where the cost of the surge capacitors is less than 1–2% of the cost of the motor. Surge capacitors can also complicate maintenance procedures. Because some capacitors contain drain resistors, they must be disconnected before an accurate “megger” or insulation resistance reading can be achieved when testing a motor circuit. Many surge protective capacitors presently in service contain polychlorinated biphenol (PCB) fluids. The United States Code of Federal Regulations (1999) [15] poses PCB handling requirements: “Any PCB large high or low voltage capacitor which contains 500 ppm or greater PCBs...shall be disposed of...in an incinerator that complies with §761.70.”

Gupta et al. [16] note that “conventional wisdom suggests that if a device has a design weakness, it is more-effective in the long run to cure the problem than to address it with a second device which has a host of additional failure modes.” Jackson [17] has surveyed the rate of failure for surge capacitors and has determined that “if surge protective capacitors had been applied in most installations, they could have prevented fewer outages than they contributed.”

### 9.1.2 Voltage Drop During Start-Up

After the initial electrical voltage surge has become evenly distributed across the induction motor stator windings, the reference frame of interest changes from microseconds to cycles. This is illustrated in the time line shown in Fig. 9.11. The event regions will vary slightly from motor to motor; however, the relative event regions are characteristically the same for all squirrel-cage induction motors started across-the-line (rated voltage energization).

The highest electrical current during start-up occurs during the first few cycles after energization. It is important to know what the rms magnitudes of these currents are in order to set instantaneous fault protection relays high enough to avoid a false tripping.

At zero speed (locked-rotor condition), the induction motor is a constant-impedance device when viewed conceptually from a two-port connection to the electrical system equivalent circuit. This contrasts greatly with steady-state operation, wherein the induction motor appears to the electrical system as essentially a constant-power device within the bounds of the standard voltage range for induction motors.

Since the induction motor’s rated locked-rotor current (LRA) is approximately six times as much or more than the rated load or nameplate current (FLA), the voltage drop across the system’s equivalent circuit impedance during across-the-line starting will cause a momentary drop in voltage at the

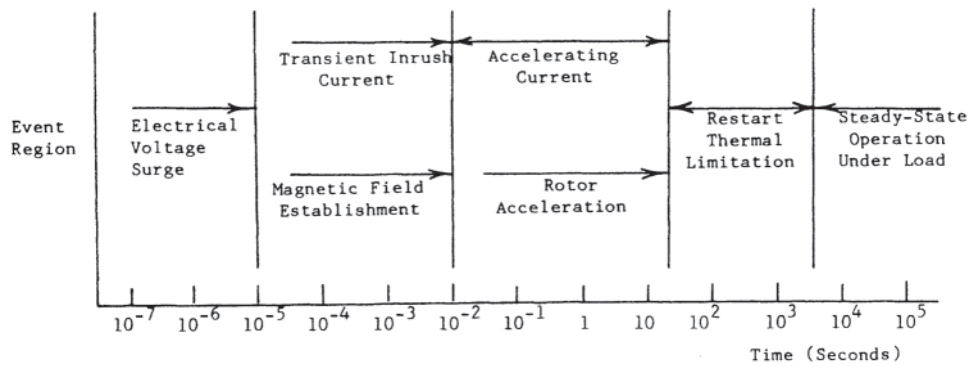


**Figure 9.11** Induction motor starting time line.

terminals of a large induction motor. This voltage reduction is less severe at locations in the electrical system that are located away from the motor terminals. Nevertheless, for high-power machines, a disturbance, known as *flicker*, is created by repetitive induction motor starting.

If the LRA is sufficiently large and the system’s equivalent impedance is high, the induction motor terminal voltage will sag to a level that will adversely impact the ability to start the induction motor and will affect other electrical equipment connected to the electrical power supply bus. Other induction motors that are under load will draw higher stator currents in an effort to maintain their shaft horsepower outputs. These higher currents will result in even greater voltage drops and thus lower bus and terminal voltages. If the voltage drop is severe, these motors can pull out and stall. Additionally, contactors and undervoltage relays can drop out.

**9.1.2.1 Transient Inrush Current**

In this section, the maximum current that can occur during the start-up of an induction motor will be considered with the intention of determining instantaneous fault protection relay settings that are secure from false tripping. This worst-case current, which will be designated as the transient inrush current, occurs during the first cycle or two after energizing the induction motor. The term cycle is used as a time period in this context with a value of 16.67 ms on a 60-Hz system. By convention, the initial ac component of the transient inrush current is called the locked-rotor current. The rotor is not “locked” in the sense that it is prevented from moving. The

locked rotor current derives its name from the testing procedure by Bartheld [18] to determine starting current and starting torque. This ac current tends to be about six times the full-load current for large induction motors, and exceeds seven times the full-load current in some cases.

$$\bar{I}_{LRA} = \frac{\bar{V}_t}{\bar{Z}_{LR}} \tag{9.14}$$

where  $\bar{Z}_{LR}$  is defined in Section 9.1.2.3 as the locked-rotor impedance.

As is evident in Fig. 9.12, this initial ac current decays by only a small amount until the motor begins to approach full-load speed.

Figure 9.12 also reveals a dc offset current component in the transient inrush current. The theorem of constant flux linkages applies to each induction motor stator phase separately and so one phase will usually exhibit a higher dc offset current than the other two phases. To see why this is so, assume that the closing times for all three phases of the circuit breaker are identical (pole closure times differing by 1 ms or less) and that a pole closure results only rarely in an initial voltage of zero on any terminal of the motor. If no initial terminal voltage is zero, then the initial voltages on the three terminals will all differ, and the resulting dc offset current in one phase will be higher than in the other two.

This dc offset current has a time constant of a few cycles or less. Even so, this dc offset current can add substantially to the maximum rms current.

$$I_{DC,max} = \sqrt{2} |\bar{I}_{LRA}| \tag{9.15}$$

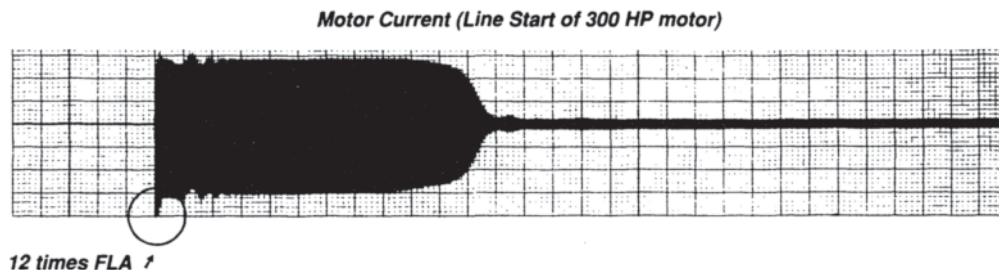


**Figure 9.12** Chart recorder trace of an across-the-line start. (Courtesy of Magnetek/Louis Allis.)

Therefore:

$$\begin{aligned} I_{\text{INRUSH.max}} &= (\bar{I}_{\text{LRA}}^2 + I_{\text{DC.max}}^2)^{1/2} \\ &= \sqrt{3} |\bar{I}_{\text{LRA}}| = \sqrt{3} I_{\text{LRA}} \end{aligned} \quad (9.16)$$

There are other factors to be considered that can cause higher levels of transient inrush current. In Eq. 9.14,  $V_t$  is normally assumed to be 100% voltage. It can be substantially less when starting a large induction motor across-the-line on a heavily loaded auxiliary electrical supply network. On the other hand, it can be as high as 110% voltage when starting a small induction motor on a lightly loaded electrical auxiliary network. Therefore:

$$I_{\text{INRUSH.max}} (V_t = 110\%) = (1.1)\sqrt{3} I_{\text{LRA}} = 1.91 I_{\text{LRA}} \quad (9.17)$$

The “Guide for Induction Motor Protection,” ANSI Std. C37.92 (1972) [19] uses a similar analysis for determining locked rotor protection settings.

$$I_{\text{RELAY}} = 1.5 K_{\text{err}} K_{\text{sf}} I_{\text{LRA}} \approx 2.065 I_{\text{LRA}} \quad (9.18)$$

where:

$$\begin{aligned} K_{\text{err}} &= 1.10, \text{ including the relay trip device tolerance of } 10\% \\ K_{\text{sf}} &= 1.25, \text{ including a safety factor of } 25\%. \end{aligned}$$

The safety factor appears to compensate for the low level of 1.5 used as the dc offset current multiplier as well as to provide for other contingencies not specifically identified in the equation.

One might ask what limits the setting that can be applied to the instantaneous fault protection relays. Clearly, this setting should not be any higher than necessary because of the possibility of resistive faults that will not be cleared if the fault current magnitude is less than the instantaneous fault protection relay pick-up setting. It is this consideration that accounts for the following portion of Section 430–52(a) of the National Electric Code (1993) [20]:

Where the setting specified in Table 430–152 is not sufficient for the starting current of the motor, the setting of an instantaneous trip circuit breaker shall be permitted to be increased but shall in no case exceed 1300% of the motor full load current.

Section 7.2.10.4.2 of ANSI/IEEE Std. C37.96–2000, IEEE Guide for AC Motor Protection [21], also makes reference to the 1300 percent of the motor full load current restriction.

This can be a real constraint given the levels calculated in Eqs. 9.17 and 9.18. If the locked-rotor current is six times the full load current, the maximum short circuit current pick-up level to  $I_{\text{LRA}}$  ratio is 2.165, but if the locked rotor current is seven times the full load current, the maximum ratio is only 1.857. This ratio is less than the value of 2.065 computed in Eq. 9.18, which means that the relay setter will have to settle for a lower safety factor.

The induction motor application engineer should also be aware of the fact that higher transient inrush currents have

been measured during testing than are predicted using the analysis presented above. Buckley [22] describes this phenomenon. In essence, this means that higher transient inrush currents are being measured than were calculated by the motor designers. These higher transient inrush currents can be attributed, in some cases, to eddy currents that tend to decrease the leakage inductance at high rotor slip frequencies and saturation that tends to reduce stator and rotor leakage reactances (and thus increase stator and rotor currents). It is also possible that there are subtransient current characteristics in rotors with double squirrel-cages. It is difficult to quantify these additional phenomena; however, the multiplier of 2.065 in Eq. 9.18 when applied to the calculated  $I_{\text{LRA}}$  may be too low when these additional phenomena are present.

### 9.1.2.2 The Impedance of Induction Motors Started in Parallel

There are network connections in which two or more induction motors may be started from the same circuit breaker or motor starting contactor. A typical example of this is a coal-fired power plant pulverizer mill motor and its associated primary air fan motor. The subtransient impedance for this circuit can be computed in the traditional manner for parallel impedances:

$$\bar{Z}_{\text{LR.TOTAL}} = \frac{1}{1/\bar{Z}_{\text{LR.MOTOR1}} + 1/\bar{Z}_{\text{LR.MOTOR2}}} \quad (9.19)$$

Nevertheless, once the rotors begin to spin, the accelerating currents interact in a more complicated manner that is also a function of the mechanical moment of inertia and the torque characteristics of both the induction motors and the driven loads. See Section 9.1.8 on ac motor bus transfer for a more comprehensive explanation of this interaction.

### 9.1.2.3 Locked-Rotor Current and Accelerating Current

The induction motor equivalent circuit will now be used in a more traditional manner to describe the accelerating phase of induction motor starting. When the induction motor is energized at rest, the slip of the rotor is unity ( $s=1$ ) and the variable lumped circuit resistance,  $(1-s)R_2/s$ , is zero. The rotor circuit impedance thus consists of the resistive and reactive elements  $R_2$  and  $X_2$ . As in the case of transformer equivalent circuits, these are not values measured at the secondary (the rotor itself) but rather the parameters reflected into the primary circuit, taking into account the apparent turns ratio between the primary and the secondary.

Thus, the locked-rotor current is limited by the air gap impedance, reflected to the primary, in series with the stator impedance as shown in Fig. 9.13.

$$\bar{I}_{\text{LRA}} = \frac{\bar{V}_t}{\bar{Z}_{\text{LR}}} = \frac{\bar{V}_t}{\bar{Z}_1 + \bar{Z}_m \parallel \bar{Z}_2} \quad (9.20)$$

Fitzgerald et al. [23, p. 344] have summarized an empirical distribution of leakage reactances between the stator and rotor for the four National Electrical Manufacturers' Association (NEMA) Induction Motor Design Classes as shown in

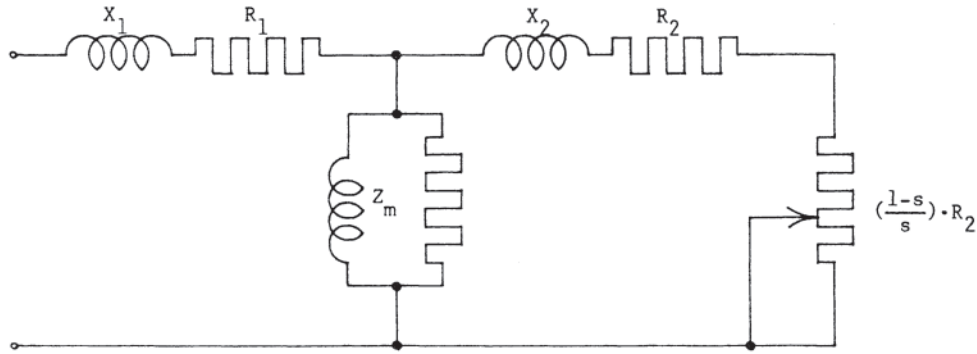


Figure 9.13 Induction motor equivalent circuit.

Table 9.2. This summary is based on materials addressed in IEEE Std. 112–1984, “IEEE Standard Test Procedure for Polyphase Induction Motors and Generators” [24]. This information is retained in the 1991 revision and the 1996 revision of IEEE Std. 112.

$\bar{Z}_m$  is large compared to  $\bar{Z}_2$  and so:

$$\bar{I}_{LRA} = \frac{\bar{V}_r}{\bar{Z}_1 + \bar{Z}_2} \tag{9.21}$$

As the rotor begins to spin, the value of the variable resistance,  $(1-s)R_2/s$ , increases. This resistance accounts for the electrical energy that is converted to rotating mechanical energy to drive the load (plus rotational losses). The accelerating current can be calculated using Eq. 9.20, but note that  $\bar{Z}_2$  now includes the variable parameter.

$$\bar{I}_{acc} = \frac{\bar{V}_r}{\bar{Z}_1 + \bar{Z}_m \parallel \bar{Z}_2} \tag{9.22}$$

where:

$$\bar{Z}_2 = R_2 + \frac{(1-s)R_2}{s} + jX_2 = \frac{R_2}{s} + jX_2 \tag{9.23}$$

9.1.2.4 Locked-Rotor kVA

The starting characteristics of an induction motor are critical to the application engineer. These characteristics are necessary

to determine the impact on the rest of the electrical auxiliary system due to starting the motor and to design an adequate protective relaying scheme for both the motor and the system.

The NEMA Motors and Generators Standard (1998) [4], Par. 10.37, requires that “the nameplate of an alternating current motor...shall be marked with the caption ‘code’ followed by a letter...to show locked rotor kVA per horsepower.” Table 9.3 summarizes the “code” ranges. Note that there is no “I” or “O” letter designation in the table.

To illustrate the use of the code, assume that a computation of the locked-rotor current and impedance of a 500-hp, 2300-V motor with a code of “G” is desired.

$$kVA_{LR} = HP \times code \tag{9.24}$$

$$kVA_{LR} = 500 \times 6.3 = 3150 \text{ kVA} \tag{9.25}$$

$$I_{LRA} = 3150 / (2.3 \times \sqrt{3}) = 790.7 \text{ A} \tag{9.26}$$

$$Z_{LR} = (2.3 \times 1000) / (790.7 \times \sqrt{3}) = 1.679 \text{ ohms} \tag{9.27}$$

Locked-rotor current is predominantly reactive and hence it has a low power factor. There are no standards addressing power factor ranges and analogous to the locked rotor kVA code. Starting power factors can range between 0.25 and 0.50 according to one source (Westinghouse Electrical Transmission & Distribution Reference Book, 1964) [25] while another source specifies a range between 0.10 and 0.40 [26, p. 259].

Table 9.2 Distribution of Induction Motor Leakage Reactances

Stator leakage reactance $X_1$	Rotor leakage reactance $X_2$	NEMA motor design class	Design class characteristics
0.5	0.5	A	Normal torque, normal starting current
0.4	0.6	B	Normal torque, low starting current
0.3	0.7	C	High torque, low starting current
0.5	0.5	D	High starting torque, high running slip

Table 9.3 Locked-Rotor kVA

Code letter	kVA/horsepower	Code letter	kVA/horsepower
A	0.00 to < 3.15	L	9.0 to < 10.0
B	3.15 to < 3.55	M	10.0 to < 11.2
C	3.55 to < 4.00	N	11.2 to < 12.5
D	4.00 to < 4.50	P	12.5 to < 14.0
E	4.50 to < 5.00	R	14.0 to < 16.0
F	5.00 to < 5.60	S	16.0 to < 18.0
G	5.60 to < 6.30	T	18.0 to < 20.0
H	6.30 to < 7.10	U	20.0 to < 22.4
J	7.10 to < 8.00	V	22.4 and up
K	8.00 to < 9.00		

For this analysis, the locked-rotor power factor is presumed to be 0.30. Therefore:

$$\bar{Z}_{LR} = (0.30 + j0.954) \times 1.679 = 0.5 + j1.6 \text{ ohms} \quad (9.28)$$

Network analysis is also usually performed on a per-unit basis. In actuality, the current is in per unit and the voltage and impedance are in percent. Note that the base voltage is that of the auxiliary network rather than the terminal voltage of the induction motor. For reasons that will be explained later, a 2300-V induction motor will normally be supplied from a 2400-V bus. The normal power base for performing transmission system network analyses is 100 MVA. Since a typical plant auxiliary network operates at much lower power levels, a smaller power base, say 100 kVA, will be used in this section. The base impedance for a 100-kVA, 2400-V electrical network is 57.6 ohms. Therefore:

$$\begin{aligned} \bar{Z}_{LR} (100\text{-kVA base}) &= (100/57.6) (0.5 + j1.6) \\ &= 0.864 + j2.778 \text{ percent} \end{aligned} \quad (9.29)$$

#### 9.7.2.5 Flicker

The IEEE Dictionary [27] defines flicker as the “impression of fluctuating brightness...occurring when the frequency of the observed variation lies between a few hertz and the fusion frequencies of the images.” Incandescent lightbulb illumination is very susceptible to fluctuating voltage. A 1% change in voltage can cause as much as a 3.8% change in brightness. This characteristic makes a voltage change or fluctuation visible to electric lighting customers.

In the past, the consequences of flicker did not typically include misoperation of equipment, although flicker could be an annoyance to customers. Recently, flicker has been shown to have the potential of causing complications in the operation of electronic equipment, including computers, process control equipment, and biomedical apparatus. This is particularly true of devices that are not adequately designed for operation on typical electrical networks.

Electric utilities have to be responsive to complaints resulting from annoying flicker as well as those resulting from problems with the operation of connected electrical equipment. The policing of flicker creates a dilemma for electric utilities that are charged with its control. Flicker is often created by one class of customers (industrial) and affects another class of customers (residential) because there exists a point of common coupling in the power grid that connects these customers. In order to analyze a flicker situation, the following steps are suggested:

1. The level of flicker that causes irritation must be known.
2. The magnitude of the voltage fluctuation and the rate (frequency) of fluctuation should be measured and recorded.
3. When flicker exceeds the borderline of irritation, corrective measures should be implemented.

Flicker studies indicate that, on the average, between 3 and 8 fluctuations per second at 0.5% change in voltage magnitude can be irritating. A typical flicker envelope used in the electric utility industry is shown in Fig. 9.14. A more extensive treatment of the variation of electric utility flicker standards can be found in Seebald [28].

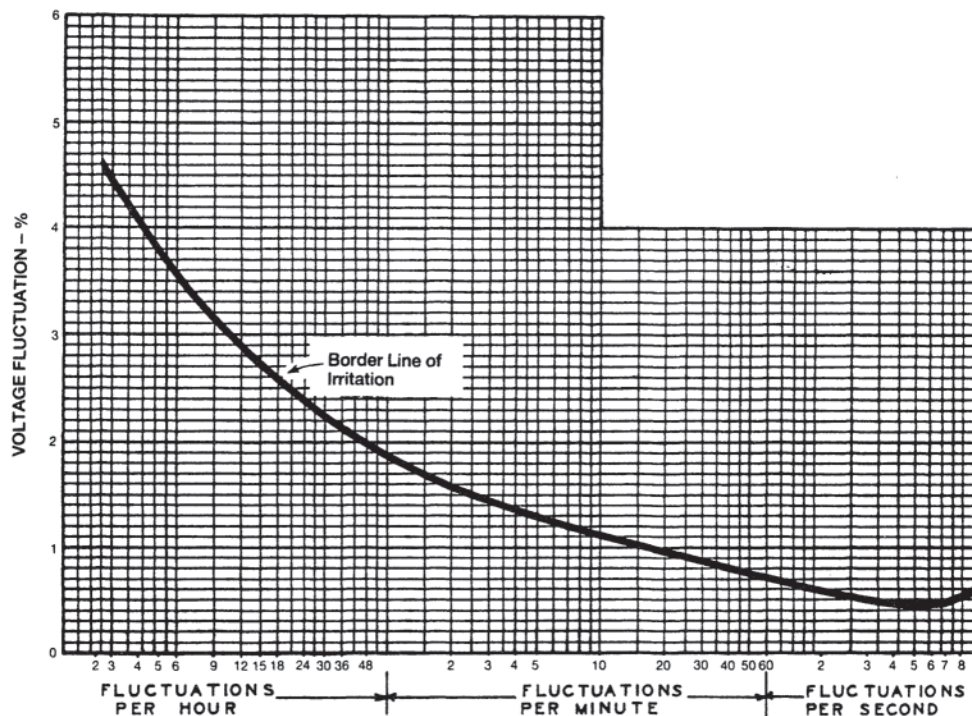
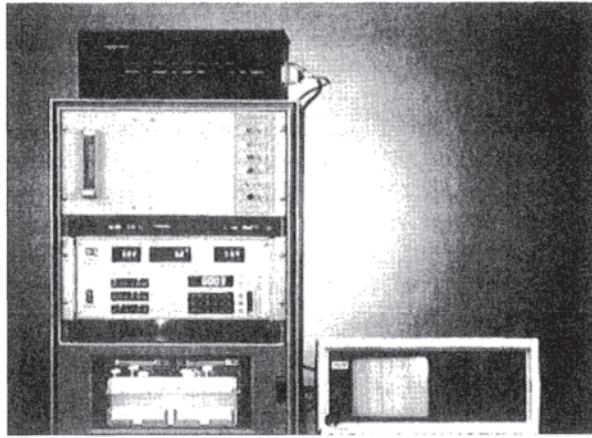


Figure 9.14 Typical maximum permissible voltage fluctuation envelope. (Courtesy of Ohio Edison Company.)



**Figure 9.15** Portable flicker monitoring equipment. (Courtesy of Ohio Edison Company.)

Flicker can be caused by many things. The Westinghouse Transmission and Distribution Reference Book [25] (1984) asserts on page 723 that “probably most of the flicker problems are caused by the starting of motors.” The switching of electrical capacitors and intermittent loads, especially electric arc furnaces, can also cause flicker.

Briggs [29] describes the use of the flicker monitoring equipment shown in Fig. 9.15 for digitally sampling and storing data. These data can then be analyzed on a PC class computer. Fig. 9.16 is a graphical display of an analysis illustrating the flicker recorded for a 9-hour period during which the flicker exceeded the irritation level 29% of the time. In this situation, the application of a static VAR compensator increased the fluctuation rate and reduced the fluctuation magnitude at the most sensitive flicker frequency such that it exceeded the irritation envelope only 4% of the time. The improvement is shown in Fig. 9.17.

There are a number of countermeasures that can be used to reduce flicker. When induction motor starting is the culprit, the most practical countermeasure is to reduce the magnitude of the induction motor starting current in addition to reducing, if possible, the frequency of induction motor starts. This topic is addressed in Section 9.1.4.

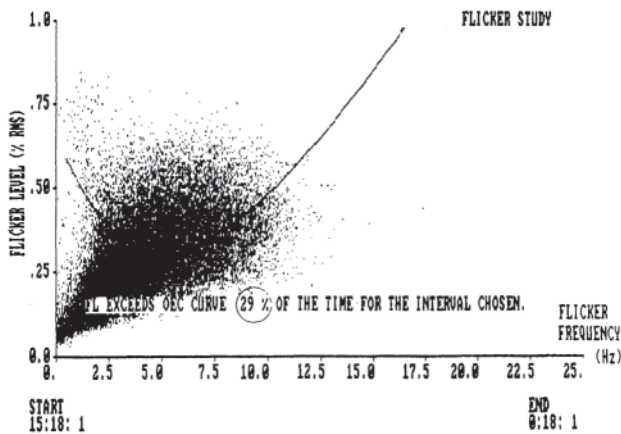


**Figure 9.16** Flicker exceeding the irritation envelope 29% of the time. (Courtesy of Ohio Edison Company.)

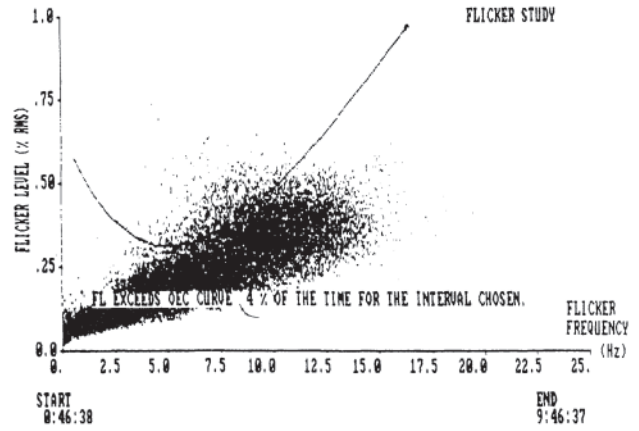


**Figure 9.17** After corrective measures, flicker exceeds the irritation envelope only 4% of the time. (Courtesy of Ohio Edison Company.)

### 9.1.2.6 Starting Voltage Standards

In addition to problems that can arise affecting the electrical network to which an induction motor is connected, low voltage at the terminals of the induction motor can cause a problem for the motor as well. Since the starting torque is approximately proportional to the square of motor terminal voltage, the induction motor may not be able to accelerate a load with a high torque characteristic. If not, the rotor (and sometimes even the stator windings) will overheat to the point of damage unless the proper relay protection is applied.

Because the induction motor will see voltage drop, even during normal operation at rated speed, due to the voltage drop across transformers and feeder cables, the induction motor terminal voltage rating will be 3% to 10% less than the bus voltage rating. This is known as “building voltage regulation” into the induction motor terminal voltage rating. Table 9.4 illustrates this voltage regulation.

There are standards that specify the starting voltage capability requirements. There is a substantial variation in these standards. Additionally, the owner can specify lower starting voltage capability than specified in these standards. Nevertheless, if starting voltage capability is not specified, the manufacturer will defer to whatever standard is common in the industry. Truly, the rule of *caveat emptor* (buyer beware) applies to motor starting voltage capability.

ANSI Standard C50.41 (2000) [10] specifies the following with regard to induction motor starting:

**Table 9.4** Electric System and Induction Motor Nominal Voltage Ratings

System voltage (V)	Motor nameplate voltage (V)	Other motor nameplate voltage (V)
480	460	440
2400	2300	2200
4160–4300	4000	—
6900–7200	6600	—
12,000	11500	—
13,800	13200	—

- 13.2 Starting. Motors having performance characteristics in accordance with this standard shall, at rated frequency, start and accelerate to running speed a load that meets the torque characteristics and inertia requirements specified in...this standard, provided, that the voltage at the motor terminals during starting is not less than 85% of the rated voltage.
- 13.3 Momentary Operation. Motors shall be capable of operating at rated load for a minimum of 60 seconds when 75% of rated voltage and voted frequency is applied at the motor terminals.

NEMA Standard MG 1 (1998) [4.120.14] has a different induction motor voltage requirement:

- 20.14.1 Running. Induction machines shall operate successfully under running conditions at rated load with a variation in voltage...:
1. Plus or minus 100% of rated voltage, with rated frequency.
- 20.14.2 Starting Induction machines shall start and accelerate to running speed a load which has a torque characteristic not exceeding that listed in 20.10 and an inertia value not exceeding that listed in 20.11 with the voltage and frequency variations specified in paragraph 20.14.1.

There is more. Motors supplied with driven equipment as a package system may be manufactured outside the United States. Induction motors manufactured in Europe, for example, may be designed in accordance with IEC Publication 34-1 (1969) [30]. It specifies the following:

13. Voltage Variations During Operation. Motors complying with these requirements shall be capable of providing their rated output when they are supplied (in the case of ac machines at their rated frequency) by a voltage that may vary between 95% and 105% of their rated voltage.

New IEC requirements are covered in a new IEC standard with a revised numbering system. IEC International Standard 60034-1, Rotating Electric Machines (1999) [31] states:

- 6.3. Voltage and frequency variations during operation ...A machine shall be capable of performing its primary function...continuously within zone A [motors-95 to 105 percent voltage]. A machine shall be capable of performing its primary function within zone B but may exhibit...deiratures from its performance at rated voltage ...Extended operation [in] zone B [motors-90-110% voltage] is not recommended.

There are a number of reasons why it might be beneficial to have an induction motor that can successfully start at termi-

nal voltages of 85% or less. A few typical examples are as follows.

- An industrial user may have an induction motor that is large relative to the capacity of the supply system. In the absence of any reduced starting duty schemes, a weak electrical supply network may not be able to sustain voltages above 85% or less during the period of induction motor acceleration.
- While electric utility plant auxiliary systems may be stiff systems (low equivalent circuit impedance to an infinite bus) during normal plant operation, they may not be stiff systems in the case where the plant design criteria calls for “black start” capability. Black start is the ability to start the electrical auxiliaries of a unit at a plant with no units online either from the cranking transformer (start-up transformer) or onsite black start or peaking generating units. The black start situation presumes a weak auxiliary network and/or sagging transmission voltage.

#### 9.1.2.7 Network Studies

Calculations of voltage drops during motor starting were originally done by hand. As networks increased in size and complexity, it became necessary to automate this process. First, the network must be described in a one-line diagram similar to the one shown in Fig. 9.18. Although a simple network, it does demonstrate all the elements necessary for a network study of any size. For the purposes of this section, protective devices are omitted.

From the one-line diagram, an impedance diagram is developed. Fig. 9.19 illustrates the impedance of the electrical equipment in the one-line diagram. Note that the impedances are in percentages on a 100-kVA base. The following simplifying assumptions will be made.

1. Since motor starting is deemed to be a balanced three-phase event, the network will be an impedance type network rather than a positive phase sequence network of the kind used in an unbalanced fault symmetrical component short circuit study. Thus, it will not be necessary to track the 30-degree phase shifts through wye-delta transformers.
2. Actual percentage impedances must be adjusted for the transformer turns ratios used to obtain regulation for full-load operation. It will be assumed that all transformer taps and secondary ratings are at nominal values such that the transformers will have a unity turns ratio. If adjustments need to be made for nonunity turns ratios, they are normally made on the high-voltage side of the transformer to minimize the number of circuit elements that need to be recalculated.

The network that will be modeled contains a 13.8-kV to 2400-V, 150-kVA transformer with five high-voltage side, 2.5% voltage taps, two above nominal and two below nominal. For this example, the transformer is set on the middle or nominal tap. Note that these are *not* TCUL (tap changing under load)

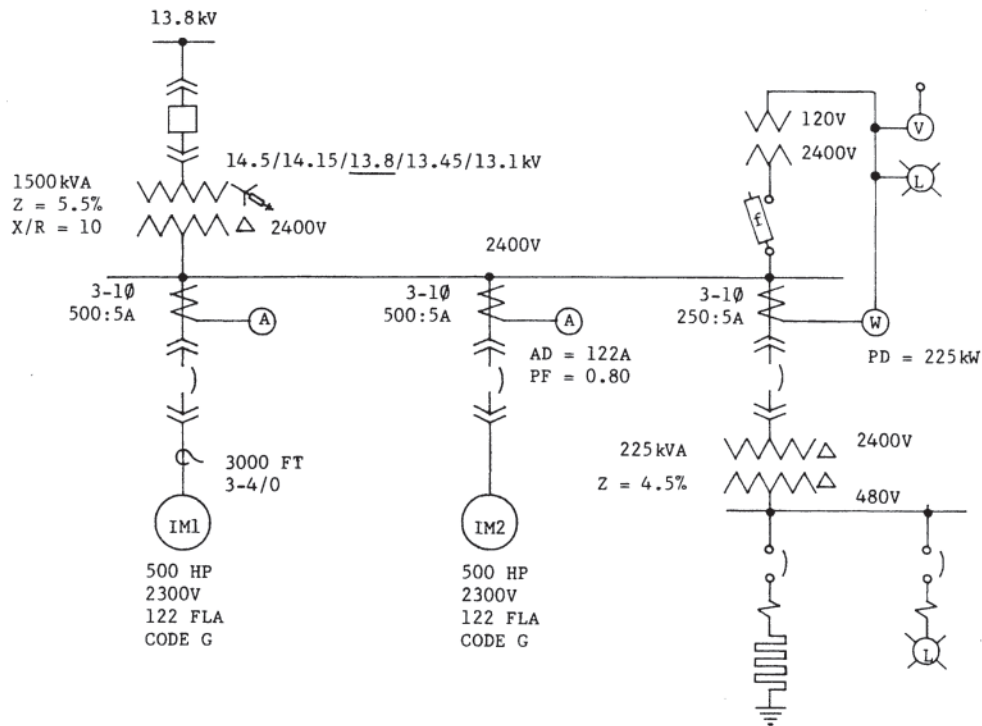


Figure 9.18 Typical network one-line diagram.

taps and so the turns ratio will remain constant during the start-up analysis. The transformer impedance, which can be located on the transformer nameplate, is 5.5%. In cases where the resistive and reactive components are not known, the transformer X/R ratio can be assumed to be approximately 10.

If the manufacturer's transformer test report is available, the resistive component of the impedance can be determined from the load loss watts test data. For this transformer, the tested load loss (LLW) at the nominal tap is 8209 W. Since the transformer rated current is 361 A:

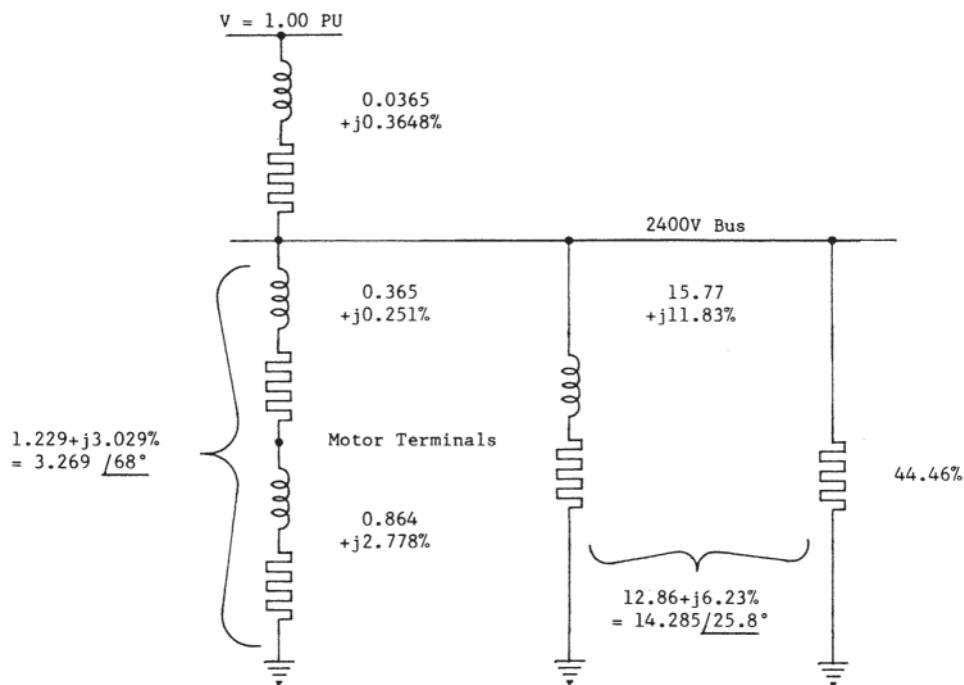


Figure 9.19 First-pass impedance diagram.



$$3^2 R_{TR} = LLW \quad (9.30)$$

$$R_{TR} = \frac{8209}{(3 \times 361 \times 361)} = 0.021 \text{ ohms} \quad (9.31)$$

The transformer base impedance is:

$$Z_{TR(\text{base})} = \frac{V^2}{P} = \frac{2400^2}{1,500,000} = 3.84 \text{ ohms} \quad (9.32)$$

Then:

$$R_{TR}(\%) = \frac{0.021 \times 100}{3.84} = 0.547\% \quad (9.33)$$

Using the Pythagorean theorem,  $X_{TR}$  can be computed as:

$$X_{TR}(\%) = (5.5^2 - 0.547^2)^{1/2} = 5.473\% \quad (9.34)$$

Then:

$$\bar{Z}_{TR}(\%) = 0.547 + j5.473\% \quad (9.35)$$

The transformer lumped element impedance to be used in the voltage drop study can be computed simply by making a power base transformation.

$$\begin{aligned} \bar{Z}_{TR} &= (100/1500) \times (0.547 + j5.473) \\ &= 0.0365 + j0.3648\% \end{aligned} \quad (9.36)$$

The 480-V bus feeds a resistive process and the plant lighting. A 2400-V to 480-V, 225-kVA transformer is the power source for this bus. It is known from the wattmeter on the operator's control panel that the peak demand for this load is 225 kW. For this analysis, the load power factor will be assumed to be unity and the 225-kVA transformer reactance will be assumed to be negligible. (In an actual study, this assumption would not be made; however, the additional level of detail introduced by using this small transformer reactance is not needed for the principles being discussed in this section.)

One 500-hp motor is operating at rated load. The ammeter on the operator's control panel indicates a peak current of 122 A. Performance testing has proven that the induction motor operates at 0.80 power factor. In this example, the load currents will be added before conversion to an impedance. Therefore,

$$\bar{I}_{IM2} = 122 \text{ A } \angle 0.80 \text{ P F} = 97.6 - j73.2 \text{ A} \quad (9.37)$$

$$\bar{I}_{RES} = 225 \text{ kW} / (2.4 \sqrt{3}) = 54.1 \text{ A} \quad (9.38)$$

$$\begin{aligned} \bar{I}_{LOAD} &= \bar{I}_{IM2} + \bar{I}_{RES} = 151.7 - j73.2 \text{ A} \\ &= 168.4 \text{ A } \angle 0.90 \text{ P F} \end{aligned} \quad (9.39)$$

$$\begin{aligned} \bar{Z}_{LOAD} &= 2400 / [(168.4 \angle 0.90 \text{ P F}) \sqrt{3}] \\ &= 8.23 \text{ ohms } \angle 0.90 \text{ P F} \end{aligned} \quad (9.40)$$

$$\begin{aligned} \bar{Z}_{LOAD}(\%) &= (8.23 \angle 0.90 \text{ P F}) \times 100/57.6 \\ &= 14.285 \angle 0.90 \text{ P F}\% \end{aligned} \quad (9.41)$$

Normally, the highest horsepower induction motor with the

longest feeder cable is the subject of the starting voltage study. Accordingly, its feeder cable impedance becomes significant and cannot be neglected as was done for the running loads of this particular model. The cable does not have a nameplate like other electrical equipment does. Impedances per hundred feet can be obtained from the manufacturer of the cable. Often the manufacturer will not be known to the person performing the study, as in this case, and so an impedance for 3000 feet of 4/0 single-phase cable can be determined from a reference book such as Beeman [26, p. 99]. Note that this impedance will be put on a 100-kVA base (57.6 base ohms) as discussed previously.

$$\begin{aligned} \bar{Z}_{CAB} &= (0.007 + j0.00482) \times 30 \\ &= 0.21 + j0.14465 \text{ ohms} \end{aligned} \quad (9.42)$$

$$\begin{aligned} \bar{Z}_{CAB}(\%) &= (0.21 + j0.1446) \times 100/57.6 \\ &= 0.3646 + j0.251\% \end{aligned} \quad (9.43)$$

The induction motor locked-rotor impedance is known from Eq. 9.23 to be 0.864 + j2.778% impedance. This impedance, added to the cable impedance, will be designated as the starting impedance,  $\bar{Z}_{ST}$ .

$$\bar{Z}_{ST} = \bar{Z}_{CAB} + \bar{Z}_{LR} = 1.229 + j3.029\% \quad (9.44)$$

The impedance connected to the 2400-V bus is the starting impedance paralleled with the load impedance.

$$\bar{Z}_{BUS} = \bar{Z}_{ST} \parallel \bar{Z}_{LOAD} = \frac{\bar{Z}_{ST} \bar{Z}_{LOAD}}{\bar{Z}_{ST} + \bar{Z}_{LOAD}}$$

Substituting:

$$\bar{Z}_{BUS} = (3.27 \angle 68^\circ) \cdot (14.28 \angle 25.8^\circ) / (1.23 + j3.03 + 12.86 + j6.23)\% \quad (9.46)$$

$$\begin{aligned} \bar{Z}_{BUS} &= (46.7 \angle 93.8^\circ) / (14.09 + 9.26) \\ &= (46.7 \angle 93.8^\circ) / (16.86 \angle 33.3^\circ)\% \end{aligned} \quad (9.47)$$

$$\bar{Z}_{BUS} = 2.77 \angle 60.5^\circ = 1.364 + j2.411\% \quad (9.48)$$

The total impedance in the circuit can now be determined:

$$\begin{aligned} \bar{Z}_{TOT} &= \bar{Z}_{TR} + \bar{Z}_{BUS} = 0.0365 + j0.3648 \\ &\quad + 1.364 + j2.411\% \end{aligned} \quad (9.49)$$

$$\bar{Z}_{TOT} = 1.4 + j2.776 = 3.109 \angle 63.2^\circ\% \quad (9.50)$$

Next, the total per-unit (pu) current in the circuit can be determined:

$$\bar{I}_{TOT} = 100/3.109 \angle 63.2^\circ = 32.16 \text{ pu } \angle -63.2^\circ \quad (9.51)$$

Since the base current of a 2.4-kV system at 100 kVA is 24 A, the current in the transformer is:

$$I_{TOT} = |32.16 \angle -63.2^\circ| \times 24 = 772 \text{ A} \quad (9.52)$$

Now the voltage drops at various locations in the circuit can be determined:

$$\begin{aligned} \bar{V}_{BUS} &= 100 - \bar{I}_{TOT} \cdot \bar{Z}_{TR} \\ &= 100 - [(32.16 \angle -63.2^\circ) \cdot (0.3666 \angle 84.3)]\% \end{aligned} \tag{9.53}$$

$$\begin{aligned} \bar{V}_{BUS} &= 100 - 11.79 \angle 21.1^\circ \\ &= 100 - 11.0 - j4.24 = 89.0 - j4.24\% \end{aligned} \tag{9.54}$$

$$\bar{V}_{BUS} (V) = |89.10 \angle -2.73^\circ| \times 2400/100 = 2138 V \tag{9.55}$$

$$\begin{aligned} \bar{V}_{IM1} &= \bar{V}_{BUS} - \bar{Z}_{CAB} \cdot \bar{I}_{ST} \\ &= \bar{V}_{BUS} - \bar{Z}_{CAB} \cdot [\bar{I}_{TOT} \cdot \bar{Z}_{LOAD} / (\bar{Z}_{LOAD} + \bar{Z}_{ST})]\% \end{aligned} \tag{9.56}$$

Calculating the induction motor starting current,  $\bar{I}_{ST}$ , first:

$$\bar{I}_{ST} = \bar{I}_{TOT} \cdot \bar{Z}_{LOAD} / (\bar{Z}_{LOAD} + \bar{Z}_{ST}) \text{ pu} \tag{9.57}$$

$$\begin{aligned} \bar{I}_{ST} &= (32.16 \angle -63.2^\circ) \cdot (14.28 \angle 25.8^\circ) / (12.86 \\ &\quad + j6.23 + 1.23 + j3.03) \text{ pu} \end{aligned} \tag{9.58}$$

$$\begin{aligned} \bar{I}_{ST} &= 459.4 \angle -37.4^\circ / (14.09 + j9.26) \\ &= 459.4 \angle -37.4^\circ / 16.86 \angle 33.3^\circ \text{ pu} \end{aligned} \tag{9.59}$$

$$\bar{I}_{ST} = 27.25 \angle -70.7^\circ \text{ pu} \tag{9.60}$$

$$I_{ST} (A) = |27.25 \angle -70.7^\circ| \times 24 = 654 A \tag{9.61}$$

Then:

$$\begin{aligned} \bar{V}_{IM1} &= \bar{V}_{BUS} - \bar{Z}_{CAB} \cdot \bar{I}_{ST} \\ &= 89.0 - j4.24 \\ &\quad - (0.44 \angle 34.5^\circ) \cdot (27.25 \angle -70.7^\circ)\% \end{aligned} \tag{9.62}$$

$$\begin{aligned} \bar{V}_{IM1} &= 89.0 - j4.24 - 12.072 \angle -36.2^\circ \\ &= 89.0 - j4.24 - 9.74 + j7.13\% \end{aligned} \tag{9.63}$$

$$\bar{V}_{IM1} = 79.26 + j2.89 = 79.3 \angle 2.09^\circ \tag{9.64}$$

$$V_{IM1} = |79.31 \angle 2.09^\circ| \cdot 2400/100 = 1903 V \tag{9.65}$$

Since the motor is rated at 2300 V, the starting voltage must be recalculated on the motor base.

$$\begin{aligned} V_{IM1} (\text{motor base voltage}) &= (1903/2300) \times 100 \\ &= 82.7\% \end{aligned} \tag{9.66}$$

The computation made indicates that the starting of the 500-hp induction motor, IM1, causes a voltage drop of 11% at the 2400-V bus and 20.7% at the induction motor terminals. It is known that the model is correct for induction motor IM1 and for the lighting loads because they are constant-impedance devices. But the motor running load is a constant power device with the model impedance calculated at 100% bus voltage. Since the bus voltage fell to 89% as a result of the first-pass study, another iteration must be made using a revised impedance for running motor IM2 as shown in Fig. 9.20.

It will be assumed for this calculation that the change in power factor (PF) of the running motor, IM2, is negligible. Then:

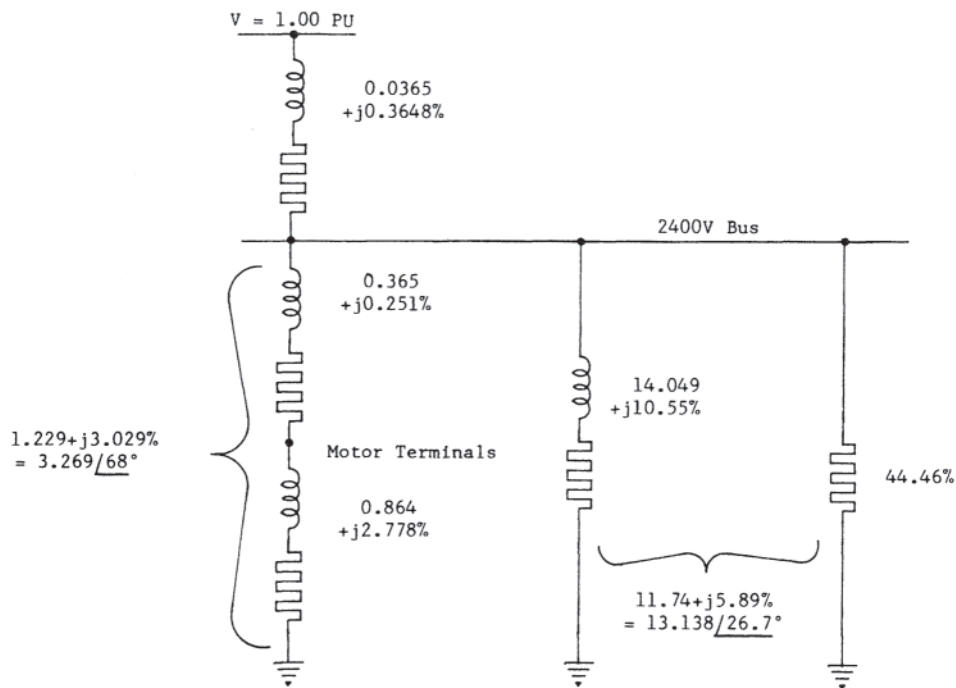


Figure 9.20 First-iteration impedance diagram.

$$\begin{aligned}\bar{I}_{IM2} &= 122 \text{ A} \angle 0.80\text{PF}/0.891 \\ &= 136.92 \text{ A} \angle 0.80\text{PF} = 109.54 - j82.15 \text{ A} \quad (9.67)\end{aligned}$$

Since the resistive load is a constant-impedance characteristic, the resistive load current decreases with voltage.

$$I_{\text{RES}2} = 0.891 \times 54.1 = 48.23 \text{ A} \quad (9.68)$$

Then:

$$\begin{aligned}\bar{I}_{\text{LOAD}2} &= \bar{I}_{IM2} + \bar{I}_{\text{RES}2} \\ &= 157.77 - j82.15 \text{ A} = 177.87 \text{ A} \angle 0.887\text{PF} \quad (9.69)\end{aligned}$$

$$\begin{aligned}\bar{Z}_{\text{LOAD}2} &= 2400 / [(177.87 \angle 0.887\text{PF}) \times \sqrt{3}] \\ &= 7.79 \Omega \angle 0.887\text{PF} \quad (9.70)\end{aligned}$$

$$\begin{aligned}\bar{Z}_{\text{LOAD}2}(\%) &= (7.79 \angle 0.887\text{PF}) \times 100 / 57.6 \\ &= 13.525 \angle 0.887\text{PF}\% \quad (9.71)\end{aligned}$$

$$\bar{Z}_{\text{BUS}2} = \bar{Z}_{\text{ST}} \parallel \bar{Z}_{\text{LOAD}2} = \bar{Z}_{\text{ST}} \cdot \bar{Z}_{\text{LOAD}2} / (\bar{Z}_{\text{ST}} + \bar{Z}_{\text{LOAD}2}) \quad (9.72)$$

$$\begin{aligned}\bar{Z}_{\text{BUS}2} &= (3.27 \angle 68^\circ) \cdot (13.525 \angle 27.5^\circ) \\ &\div (1.23 + j3.03 + 12.0 + j6.25)\% \quad (9.73)\end{aligned}$$

$$\begin{aligned}\bar{Z}_{\text{BUS}2} &= (44.21 \angle 95.5^\circ) / (13.23 + j9.28) \\ &= (44.21 \angle 95.5^\circ) / (16.16 \angle 35^\circ)\% \quad (9.74)\end{aligned}$$

$$\bar{Z}_{\text{BUS}2} = 2.736 \angle 60.5^\circ = 1.347 + j2.381\% \quad (9.75)$$

$$\begin{aligned}\bar{Z}_{\text{TOT}2} &= \bar{Z}_{\text{TR}} + \bar{Z}_{\text{BUS}2} = 0.0365 + j0.3648 \\ &\quad + 1.347 + j2.381\% \quad (9.76)\end{aligned}$$

$$\bar{Z}_{\text{TOT}2} = 1.3835 + j2.7458\% = 3.075 \angle 63.3^\circ \quad (9.77)$$

$$\bar{I}_{\text{TOT}2} = 100 / 3.075 \angle 63.3^\circ = 32.52 \text{ pu} \angle -63.3^\circ \quad (9.78)$$

$$I_{\text{TOT}2}(\text{A}) = |32.52 \angle -63.3^\circ| \times 24 = 780.5 \text{ A} \quad (9.79)$$

$$\begin{aligned}\bar{V}_{\text{BUS}2} &= 100 - \bar{I}_{\text{TOT}2} \cdot \bar{Z}_{\text{TR}} \\ &= 100 - [(32.52 \angle -63.3^\circ) \cdot (0.3666 \angle 84.3^\circ)]\% \quad (9.80)\end{aligned}$$

$$\begin{aligned}\bar{V}_{\text{BUS}2} &= 100 - 11.922 \angle 21^\circ \\ &= 100 - 11.13 - j4.27 = 88.87 - j4.27\% \quad (9.81)\end{aligned}$$

$$V_{\text{BUS}2}(\text{V}) = |88.97 \angle 2.75^\circ| \times 2400 / 100 = 2135 \text{ V} \quad (9.82)$$

This iteration is within 0.13% of the first-pass calculation and so the answer is assumed to be close enough to the final value that another iteration will not be required. The results are listed in Table 9.5.

As noted at the outset of this section, starting voltage studies made by hand are laborious, even for this very simple model. Fortunately, these studies can now be done utilizing computer programs designed for circuit calculations. All the circuit

**Table 9.5** Summary of Starting Voltages

Location	Percent voltage (%)	Actual (V)
13.8-kV bus	100	13,800
2400-V bus	89	2,135
Motor terminals	79.2	1,900
Motor terminals (at the motor base voltage)	82.6	1,900

elements, including all the cable and bus bar impedances can be incorporated into the model for more precise results. It goes without saying that the results of a computer generated study are only as good as the information that is used as input data for the computer program. It is necessary for the engineer or technician running the computer program to be as meticulous as possible in preparing and checking the data.

The following pitfalls should be guarded against.

- Beware of voltage base changes due to transformer turns ratios. There voltage base changes are necessary when off-nominal transformer voltage taps are used. There will be actual problems (circulating currents) as well as computational problems in grid networks with transformers with different turns ratios.
- Make sure that the induction motor percentage starting voltage is computed on its terminal voltage rating, which is usually not the same as the system base voltage.
- Be alert for variable impedance loads. Some computer network analysis programs lack the sophistication needed to handle impedance circuit elements that vary with voltage. In such cases, several iterations may be required before an accurate solution is obtained.

The values shown in Table 9.5 are not unreasonable when a large induction motor is started across the-line. This was not a worst-case analysis. Often, the real question is whether or not a specific motor will start when there are degraded voltage conditions on the high-voltage power supply network. In cases where these voltage drops are deemed excessive because of their impact on the electrical system or where the motor has not been specified for such a low starting voltage, some form of reduced starting duty method is recommended.

### 9.1.3 Starting Torque Characteristics

The theory of induction motors was developed in Chapter 4. This section will paraphrase some of the earlier material in order to provide a foundation for understanding the rotor acceleration phase of the induction motor starting phenomenon. This section applies specifically to three-phase induction motors.

#### 9.1.3.1 Torque Development

As the induction motor stator starting current decays from the current that was established during the subtransient interval, a secondary current develops in the rotor cage by transformer

action. A magnetomotive force (mmf) wave begins to travel either clockwise or counterclockwise in the air gap, depending on the stator phase rotation.

If the rotor is not blocked, the forces created by the interaction of the fundamental air gap flux with the fundamental rotor bar current will cause the rotor to begin to rotate in the direction of the mmf wave. By the laws of action and reaction, the stator would begin to rotate in the opposite direction but for the fact that it is bolted down to prevent such movement. The torque imparted to the rotor [32, p. 182] is:

$$T(\text{lb-ft}) = \frac{7.04}{n_s} m \frac{I_2^2 R_2}{s} \quad (9.83)$$

where:

- $I_2$ =the rotor current reflected to the primary (A)
- $m=3$ , the number of phases
- $n_s$ =the synchronous speed in rpm
- $R_2$ =the rotor resistance reflected to the primary (ohms)
- $s$ =per-unit slip

If it is desired to compute the torque in newton-meters (N-m), the coefficient used is 9.5393 instead of 7.04. The torque in Newton-meters can be calculated directly as follows:

$$T(\text{N-m}) = \frac{1}{\omega_s} m \frac{I_2^2 R_2}{s} \quad (9.84)$$

where

- $\omega_s$ =the synchronous angular velocity (rad/s).

The IEEE Dictionary (1996) defines specific torque values at various points on the speed-torque curve for induction motors [27].

1. Breakdown torque is “the maximum shaft-output torque that an induction motor... develops when the primary winding is connected for running operation, at normal operating temperature, with rated voltage applied at rated frequency. Note: A motor with a continually increasing torque as the speed decreases to standstill, is not considered to have a breakdown torque.”

2. Locked-rotor torque is “the minimum torque that a motor will provide with locked rotor, at any angular position of the rotor, at a winding temperature of 25° Celsius plus or ±5°C, with rated voltage applied at rated frequency.”

3. Pull-up torque is “the minimum torque developed by the motor during the period of acceleration from rest to the speed at which breakdown torque occurs with rated voltage applied at rated frequency.”

The speed-torque curve is one of the most interesting characteristics in all of engineering science. For a standard induction motor design, the torque increases to a maximum, called the breakdown torque (or stall torque), at about 80% of synchronous speed, or 0.20 per-unit slip. Reference 23 gives a closed-form solution for the slip at this operating point as:

$$s_{\text{MAX-T}} = \frac{R_2}{[R_{e1}^2 + (X_{e1} + X_2)^2]^{1/2}} \quad (9.85)$$

where:

- $R_2$  = the rotor resistance reflected to the primary
- $R_{e1}$  = the Thevenin equivalent resistance of the stator impedance and magnetizing impedance seen by the rotor reflected to the primary
- $s_{\text{MAX-T}}$  = slip at maximum torque
- $X_2$  = the rotor reactance reflected to the primary
- $X_{e1}$  = the Thevenin equivalent reactance of the stator impedance and magnetizing impedance seen by the rotor reflected to the primary

Knowing this, the maximum torque ( $T_{\text{max}}$ ) can be computed from Eq. 9.83 or Eq. 9.84.

### 9.1.3.2 Rotor Deep-Bar Effect

In actuality, the torque calculation made in Section 9.1.3.1 is more complicated because  $R_2$  is not constant.  $R_2$  varies at different rotor speeds due to “skin effect”, which means that at high slip (low rotor speed), the current is crowded to the top of the rotor conductor bar. The current at the bottom of the bar is also more lagging because of the additional reactance at the bottom of the rotor bar. Since rotor bars tend to be tall and narrow, this phenomenon has acquired the appellation of deep-bar effect.

Alger [33, pp. 265–271] has developed a closed-form solution deep-bar effect model. He first defines  $R_0$  as the “maximum permissible bar resistance in primary terms at low slip to obtain desired full-load speed.” This is essentially  $R_{dc}$ . Then the increase in starting resistance,  $\Delta R_2$ , is as follows:

$$\Delta R_2 = (\alpha d - 1) R_0 \quad (9.86)$$

where:

$d$ =depth of the bar (cm)

$$\alpha = 2\pi \sqrt{\frac{rf}{10^9 \rho}}$$

$r$ =ratio of bar width to slot width

$f$ =frequency (cycles/s)

$\rho$ =resistivity of the bar (ohm-cm)

Often the deep-bar effect can be modeled with sufficient accuracy using a linear approximation of  $R_2$  as a function of rotor slip (Nilsson et al. [34]) as shown in Fig. 9.21. The equation for this model is simply:

$$R_2 = R_{2dc} = k_{\text{DEEP BAR}} R_{2dc} S \quad (9.87)$$

where:

$k_{\text{DEEP BAR}}$  = deep-bar model constant

$R_{2dc}$  = the rotor dc resistance reflected to the primary

$s$  = slip

The deep-bar effect can be accentuated by using very tall and very narrow rotor bars. Additional accentuation can be achieved by using a double-cage rotor.

Alger’s purpose in deriving this complex solution for  $R_2$  was to demonstrate the trade-off between high  $R_2$  when the rotor is blocked and high rotor bar inductance at running

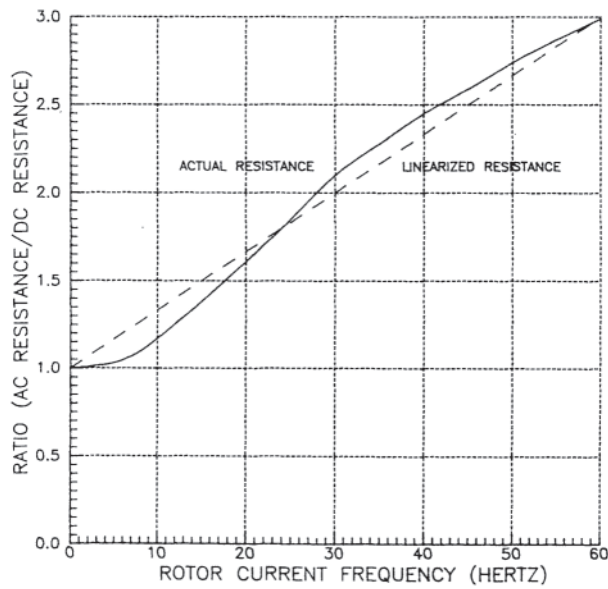


**Figure 9.21** Linear approximation of the deep-bar effect.

speed. He also wanted to demonstrate the impact of the deep-bar effect at higher frequencies. The value of  $R_2$  when starting the rotor from reverse rotation will be higher than when the rotor is at rest. Thus, the induction motor will develop higher torque when plugged (energized during reverse rotation) than when started at rest.

**9.1.3.3 Effects of Rotor Bar Shape on Starting Torque**

It is clear that the shape of the speed—torque curve of the induction motor can be modified by varying the circuit parameters of the induction motor equivalent circuit. This can be accomplished by modifying the shape and the material of the rotor bar. Figure 9.22 shows a common rotor bar configuration, using a rectangular copper bar, and its resultant speed-torque curve. Figure 9.23 shows some modification to the bar and its impact on the speed-torque curve.

A further modification and a switch to a more resistive rotor bar material is illustrated in Fig. 9.24. As expected, the higher resistance of  $R_2$  increases the developed torque at all speeds. The trade-off is that the efficiency at full load decreases

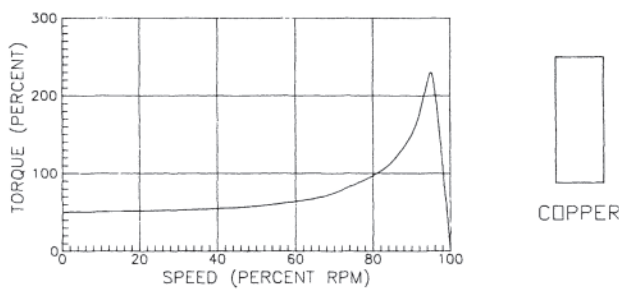


**Figure 9.22** Rectangular bar speed-torque curve. (Courtesy of Magnetek/Louis Allis.)

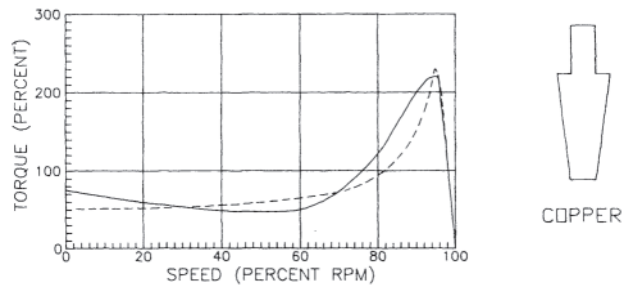


**Figure 9.23** Effects of reducing the conductor area at the top of the slot. (Courtesy of Magnetek/Louis Allis.)

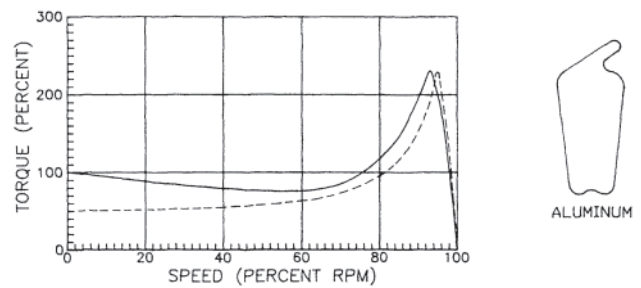


**Figure 9.24** Application of a higher-resistance rotor bar material. (Courtesy of Magnetek/Louis Allis.)

and the full-load slip increases. Figure 9.25 illustrates increases in pull-up torque using a notched rotor bar made from a high-resistance material. Additional increases in torque are achieved by using a tall bar to take advantage of the deepbar effect as illustrated in Fig. 9.26.

Utilizing these principles, any of the four NEMA design class speed-torque curves can be achieved. Figure 9.27 illustrates their respective speed-torque curves.

The NEMA design class characteristics are listed in Table 9.2. These characteristics are repeated in Table 9.6 for the purpose of including a description of the characteristics of Class E and Class F induction motors [35]. These additional characteristics involve low starting torques. Accordingly, they use low-resistance rotor bar materials and generally work best

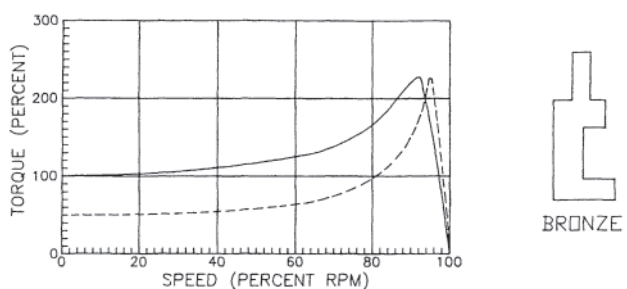


**Figure 9.25** Speed-torque curve characteristic using a notched bronze bar. (Courtesy of Magnetek/Louis Allis.)

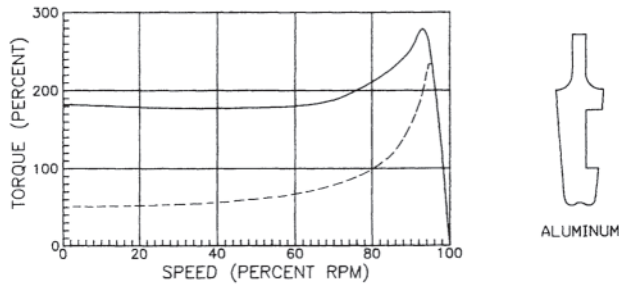


**Figure 9.26** Speed-torque characteristic using a tall rotor bar. (Courtesy of Magnetek/Louis Allis.)

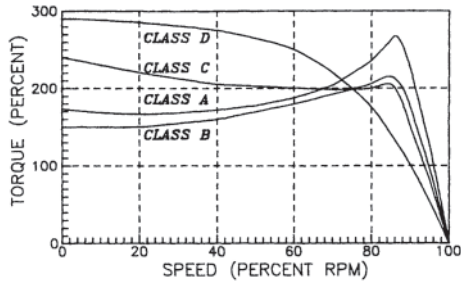


**Figure 9.27** NEMA design class speed-torque curves.

with driven loads with cubic speed-torque curves (torque being a function of speed to the third power).

**9.1.3.4 Countermeasures for Cracked Rotor Bar Problems**

When the rotor accelerates, forces act in different directions at varying locations in the squirrel-cage. As the rotor begins to spin, the rotor bars are pulled towards the air gap, and they deflect in a bow shape, the maximum deflection being near the middle of the rotor. At the squirrel cage shorting ring, a twisting force is imparted at the bar-to-shortring joint, which amplifies the unrestrained deflection of the bars with the least slot support. This phenomenon is particularly wearing on round and trapezoidal bars in fabricated squirrel-cage rotors. Following repetitive starts, a bar can crack as shown in Fig. 9.28.

The reason trapezoidal bars and bars with round shapes are more susceptible to broken bar damage is that the laminations forming the slot boundary tend to provide linear restraint (line contact) rather than surface restraint. The factors described

**Table 9.6** Characteristics of Induction Motor Design Classes

Design class	Induction motor characteristics
A	Normal starting torque, normal starting current
B	Normal starting torque, low starting current
C	High starting torque, low starting current
D	High starting torque, high running slip
E	Low starting torque, normal starting current
F	Low starting torque, low starting current

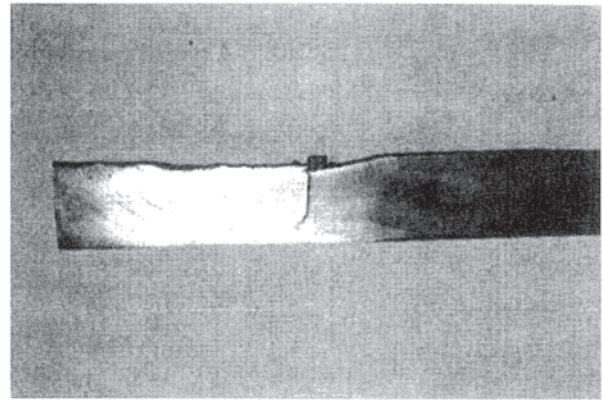


**Figure 9.28** Cracked rotor bar. (Courtesy of Ohio Edison Company.)

in Section 4.7.3 covering rotor lamination fatigue mechanisms, such as excessive clearances to accommodate lamination stagger, can also exacerbate this problem.

Fabricated squirrel-cage rotor designs that have shown tendencies to produce bar cracking after a limited number of start-ups should be reevaluated. There are countermeasures that can be used to remedy this undesirable characteristic. Some of these countermeasures are as follow.

1. A redesigned bar similar to the one shown in Fig. 9.23 or Fig. 9.25 ensures better surface contact and support. Consequently, the force is more uniformly distributed along the bar. The disadvantage in making this change is that new rotor laminations must be punched.
2. On 3600-rpm induction motors and other high-speed machines, centering rings can be used under the shorting rings to minimize the deformation of the shorting ring. This also has the beneficial affect of minimizing bar bending during motor acceleration.
3. A retaining ring with an interference fit over the shorting ring can also minimize shorting ring deformation and bar movement. Some designs use fiberglass banding for this purpose. It is also used occasionally for sound reduction. Fiberglass banding must be applied carefully. If it is not carefully applied, the bandings may shred and the stator end-turns will usually be damaged, resulting in a multiphase short circuit necessitating a rewind.
4. Stronger bar material can reduce failure due to cracking, but many of these materials do not have a resistivity that is in the range of the design specification. When the bar material is changed, the impact on motor parameters such as torque and efficiency must be reviewed.

**9.1.3.5 Part-Winding Starting**

Unusual starting torques are obtained when only part of the winding in each phase is energized. This can be accomplished when an induction motor has two or more phase groups in parallel, when the leads for these phase groups are brought out of the induction motor, and when the induction motor does not have any intraphase group connections, known as equalizers. There is a practical reason for using part-winding

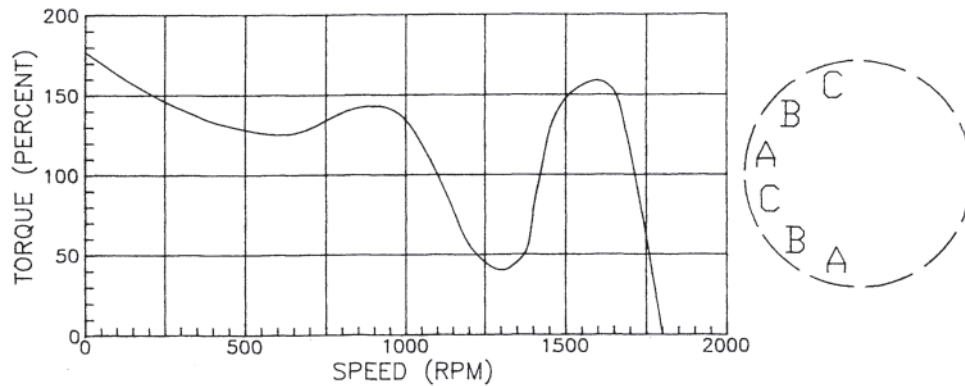


**Figure 9.29** Starting torque with a short-throw part-winding connection.

starting methods. The inrush current is reduced during starting, which tends to minimize the impact of the start-up on the electrical network.

An induction motor can have more than one phase group in parallel for various reasons related to the design of the motor. For the purposes of this example, a four-pole induction motor containing 12 phase groups will be used. An obvious way of attempting the part-winding start is to energize the phase groups on one side of the induction motor. This technique allows the use of the same coil throw in the stator slots as used in the standard motor. (The letter symbols in Fig. 9.29 represent the top coils in the energized phase groups.) The mmf wave in the air gap will no longer be symmetrical. It will contain even harmonics, as well as odd harmonics, which will result in peaks and valleys in the speed-torque curve. A predominant cusp will appear, as shown in Fig. 9.29, at approximately two thirds synchronous speed, that is, somewhere in the vicinity of 1200 rpm for this motor. Depending on the torque requirements of the driven load, the induction motor may not accelerate past this speed. Hence, it may be necessary to connect the other part of the winding before the induction motor can be accelerated above 1200 rpm. Since the cusp speed is relatively high, and higher than for most other part-winding connections, this part-winding

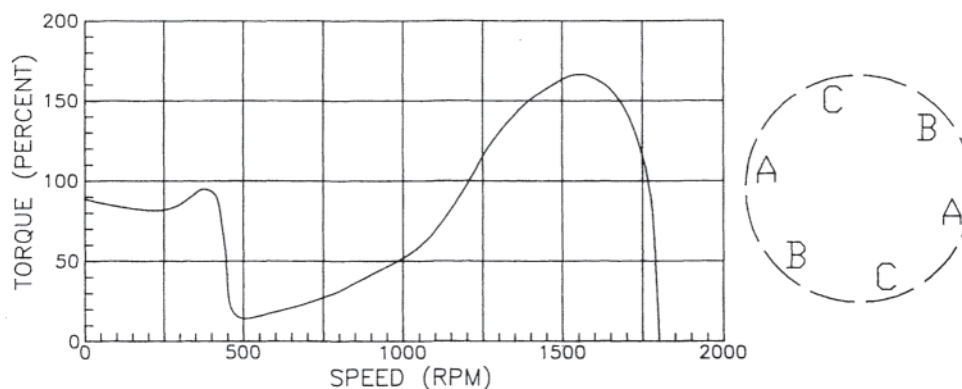
connection can be used as a viable reduced starting duty circuit connection. However, the motor specification should clearly alert the manufacturer that a part winding starting application is contemplated as not all induction motor designs are suitable for this application.

Figure 9.30 shows a connection with alternate phase groups energized. The winding scheme will require some physical modification to facilitate the winding arrangement shown. The major disadvantage of this part-winding connection is that it has a cusp at one quarter speed (450 rpm in this case).

Figure 9.31 illustrates another modified part-winding connection. While it displays an improved starting torque characteristic (900 rpm cusp) when compared to the connection in Fig. 9.30, it is not practical because of the loud noise emitted from the motor when at the cusp speed of 900 rpm.

#### 9.1.4 Reduced Starting Duty Schemes

Some general guidelines are noted for across-the-line induction motor starting circuits that also apply to reduced starting duty schemes. The starting control circuit will consist of a control (isolating) transformer, often 480-V (motor nominal



**Figure 9.30** Starting torque with a long-throw part-winding connection.

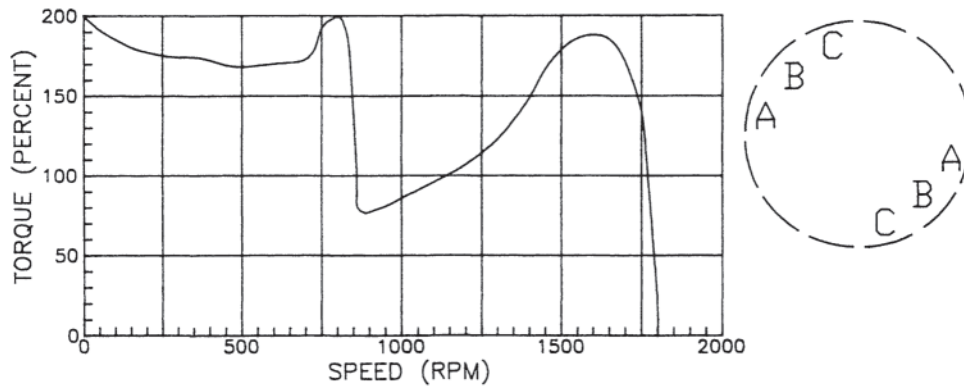


Figure 9.31 Starting torque with a modified long-throw connection.

voltage) to 120-V rated. The overload relays are permissives. They have “b” contacts in the control scheme, which are closed when the overload device is in the deenergized state. If an overload device operates, it opens its control contact to prevent further energization of the motor circuit. Stop pushbuttons are normally connected in series while “push-to-start” devices are wired in parallel as shown in Fig. 9.32. These pushbuttons can be located at remote parts of the plant. For example, it is common to have a stop pushbutton at the motor (e.g., 3 stop in Fig. 9.32) for safety reasons. Since it usually takes much less energy to hold the M coil closed than to close it initially, care must be taken in designing the control circuit to make sure that there is not so much capacitance in the

remote stop pushbutton lead circuit that the M coil remains energized when this stop pushbutton is depressed.

Not all electrical networks are stiff enough to start a large induction motor across-the-line. Likewise, not all induction motors nor all their driven loads are designed to be started across-the-line. In these situations, some form of reduced starting duty scheme is recommended.

9.1.4.1 Resistance Starting

A simple method of reducing the starting current of low-voltage motors (up to about 200 hp) is to switch phase resistors in series with the motor as shown in Fig. 9.33.

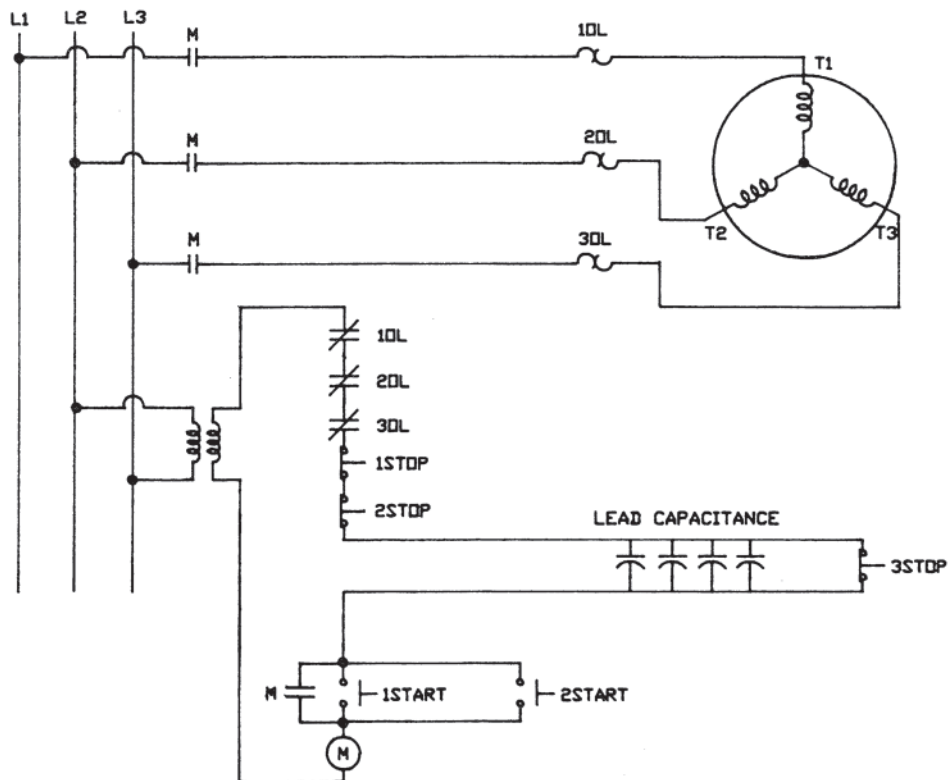


Figure 9.32 Starting circuit fundamentals.



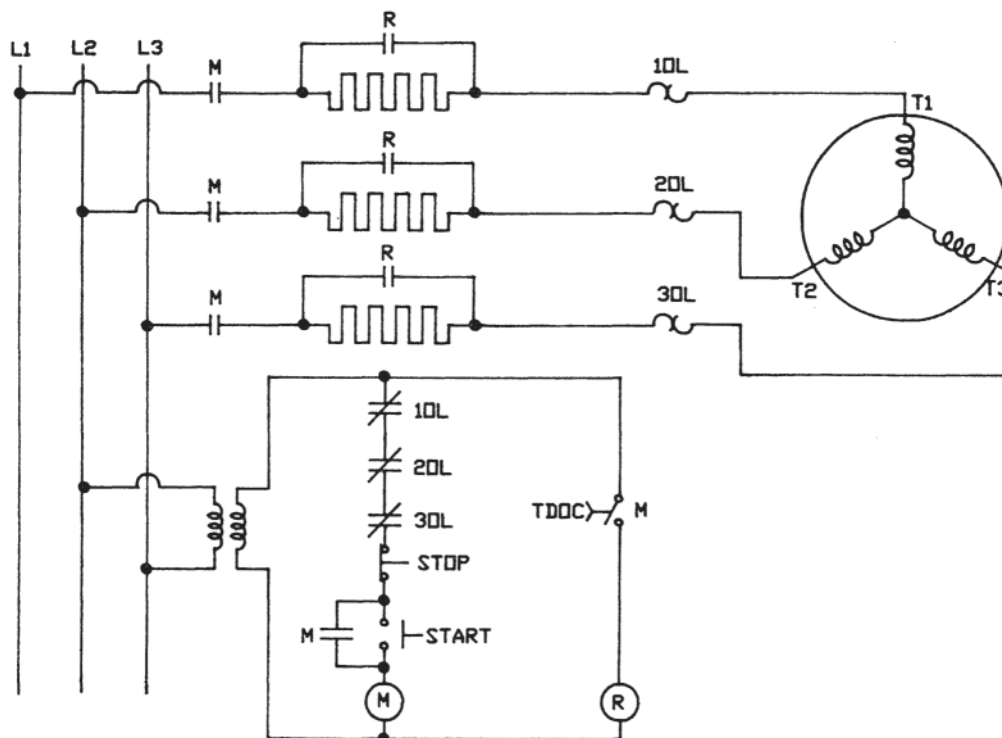


Figure 9.33 Resistance starting schematic diagram.

The M contactor closes when the start pushbutton is depressed provided the overload devices, 1OL, 2OL, and 3OL, are not in the tripped position. The M coil seals itself in and after a time delay, the R coil closes, shorting out the starting resistors. This function can also be accomplished by some sensor that would detect that the motor has accelerated. A more sophisticated scheme would include a second step in order to provide smoother starting. When the R coil closes, full voltage is applied to the terminals of the motor. The M and R contacts need to be rated for inductive current duty at the motor terminal voltage rating. In addition to reducing the starting current, this starting method has the following advantages:

1. Lower cost than other reduced starting voltage schemes.
2. For a given initial starting torque, the accelerating time is faster than other reduced starting voltage schemes, such as autotransformer starting. This is because the motor starting current decreases as the motor accelerates. Therefore, the  $IR$  drops across the starting resistors decrease and the voltage at the motor terminals rises. As a result, the developed torque increases and the motor accelerates faster.
3. The voltage transient upon shorting out the starting resistors is minimal.

#### 9.1.4.2 Reactance Starting

For higher voltage applications, a reactance starting method can be used. It is similar to resistance starting; however, the

reactors are sometimes installed in the neutral leads of the motor to minimize the amount of electrical insulation required for the reactors. In order to connect this circuit, all six induction motor leads must be brought out. Where only three motor leads are available, the reactors will have to be installed on the line side of the induction motor. In this case, the reactors will have to be fully insulated for line voltage.

Fewer reactance ohms are needed for the reactance starting method than ohms of resistance for the resistance starting method for a given reduction in voltage at the terminals of the motor. This is because the  $X\bar{I}$  voltage drop phasor tends to align with the line voltage phasor and motor voltage phasor during the low-power-factor starting current condition as shown in Fig. 9.34.

#### 9.1.4.3 Autotransformer Starting

An autotransformer has a common winding, designed for high voltage and low current, connected in series with a low-voltage and high-current winding [36]. The starting voltage will be limited to the voltage rating of the common winding. On a per-unit basis, this value,  $k_{TR}$ , will equal the number of turns in the common winding divided by the sum of the turns in the common and series windings. Viewing the induction motor again as a constant-impedance device, the locked-rotor current in the induction motor will be reduced to  $k_{TR}$  times the locked-rotor current that would have existed without the autotransformer. Since the current on the supply bus side of the autotransformer is reduced by transformer action to  $k_{TR}$  times

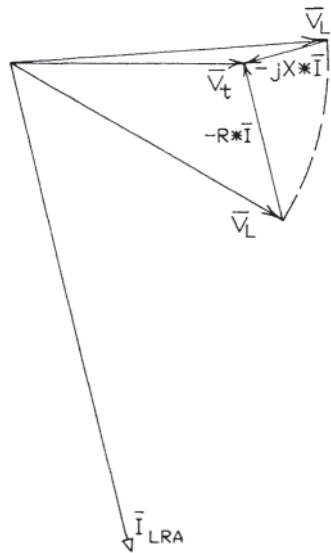


**Figure 9.34** Phaser diagram for reactance starting and resistance starting.

the current on the motor side of the autotransformer, the locked rotor current is effectively reduced by  $k_{TR}$ . Accordingly, the voltage ratio of the autotransformer can be selected to limit the current seen by the electrical network to a specified level using Eq. 9.77. That is:

$$k_{TR} = \left( \frac{I_{LINE}}{I_{LRA}} \right)^{1/2} \tag{9.88}$$

Millermaster [37] describes a circuit for autotransformer starting as shown schematically in Fig. 9.35. The following should be noted. Figure 9.35 shows only two single-phase transformers. While three transformers are normally used to provide balanced currents, this starting method will work with two transformers. However, with just two single-phase transformers, unbalanced voltages will occur at the motor terminals; thus appreciable levels of negative-sequence current will be developed, which will increase the heating in the induction motor during the acceleration phase. It is not a good idea to omit the third single-phase autotransformer in a severe starting duty application such as a high-inertia load. Starting autotransformers normally come equipped, unless specified otherwise, with three taps: a 0.81 ratio tap, a 0.65 ratio tap, and a 0.50 ratio tap. Only the connected tap is shown in Figure 9.35.

The start pushbutton is depressed, which will energize the AUX relay if the overload devices are not in the tripped position. The AUX relay seals itself in and energizes coil S through a time-delay-drop-out (TDDO) AUX contact. Coil S contacts connect the autotransformer neutrals together in the induction motor power circuit and energize the M coil in the control circuit. The M coil seals itself in and energizes the auto transformer in the power circuit.

Once the motor is up to speed, a dead-time transfer or “open transition” can be made in order to connect the induction motor to the main power supply. However, in the circuit shown, the TDDO operates first to open the autotransformer neutral connection. Then, only the series winding of the autotransformer remains in the induction motor starting circuit, making it analogous to the reactance starting circuit. This is called the closed transition method. The switching is completed when the time-delay-on-closing (TDOC) contact

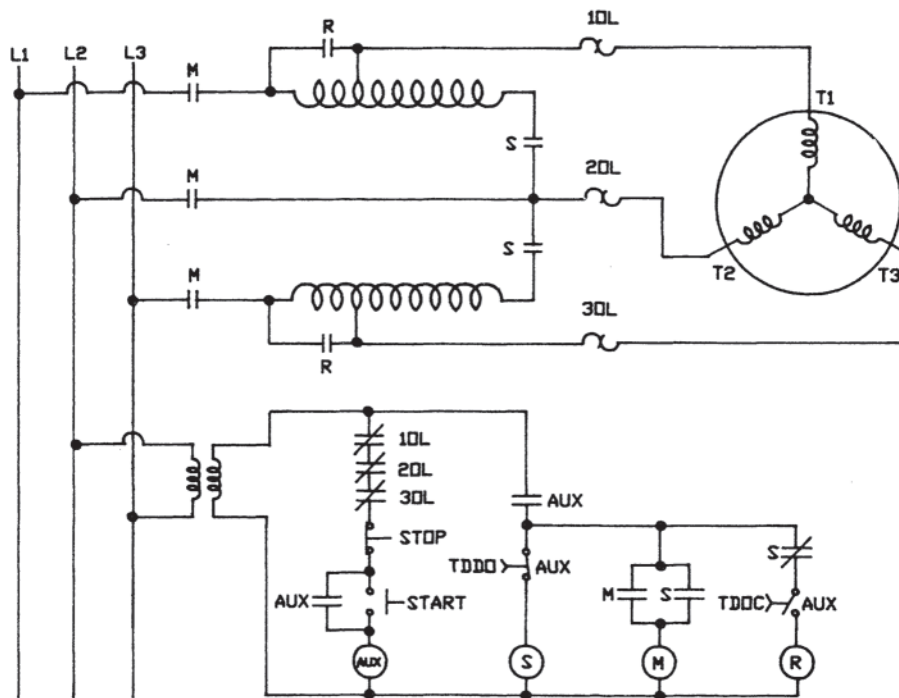


**Figure 9.35** Autotransformer starting schematic.

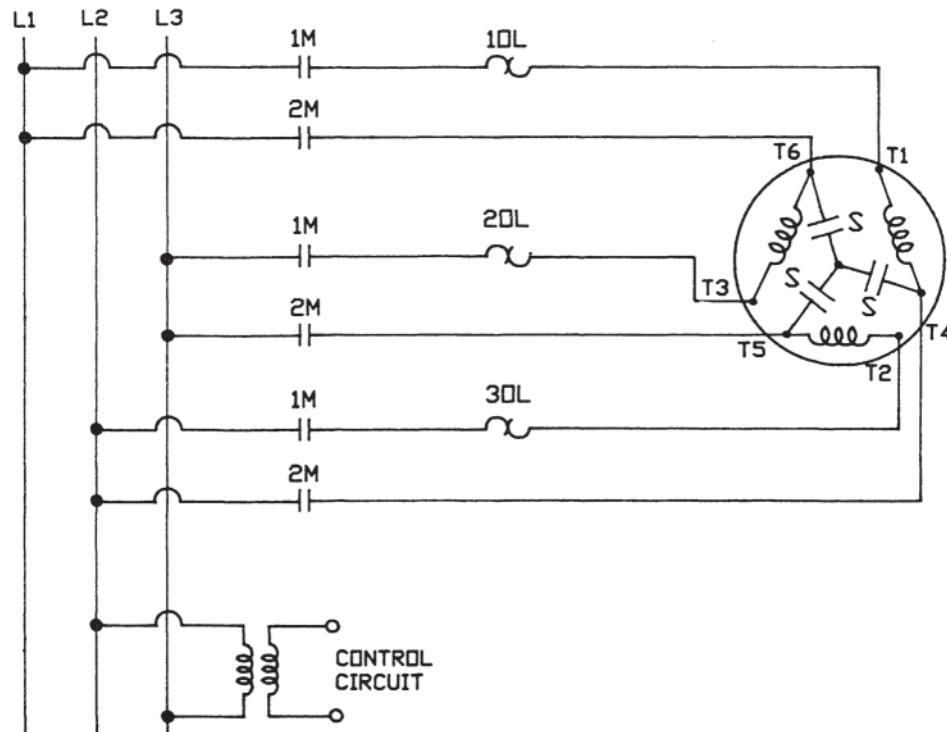


Figure 9.36 Wye-delta starting circuit.

energizes the R coil, shorting out the series winding of the autotransformer. The S coil b contact (normally closed when the S coil is deenergized) prevents operation of the R coil until the autotransformer neutral is opened.

#### 9.1.4.4 Wye-Delta Starting

A motor that is delta connected during normal operation can be reconnected wye for starting if all six leads are brought out. Figure 9.36 illustrates how this is done. The S contacts are closed first to make up the wye at terminals T4, T5, and T6 of the induction motor. Note that only two S contacts are required if one of the induction motor terminals is connected directly between the other two S contacts. If the two-contact method is used, the neutral point will have to be fully insulated as it will “float” at line voltage during normal operation.

The IM contacts are closed next, which energizes the induction motor across-the-line connected wye.

After the motor is up to speed, the S contacts are opened and the 2M contacts are closed in sequence. Closing the 2M contacts connects T1 to T6, T2 to T4, and T3 to T5, thus making up the delta. Note that it is imperative to open the S contacts before closing the 2M contacts, known as an “open transition” connection, or else a three-phase fault will be thrown on the electrical network.

The wye connection imposes  $1/\sqrt{3}$  or 57.7% of the line-to-line voltage across each phase. Accordingly, the motor winding current is 57.7% of what the winding current would have been in a delta-connected induction motor. Since the winding current in delta-connected windings is 57.7% of the line current, the starting current seen by the electrical system

is only one third of the delta-connected starting current. It then follows that the starting torque is only one third of the starting torque in the delta connected motor.

The disadvantage of this starting method is that the starting torque is sometimes too low to overcome the load torque of a direct-coupled load. Figure 9.37 compares the speed-torque characteristics of the reduced starting duty schemes described

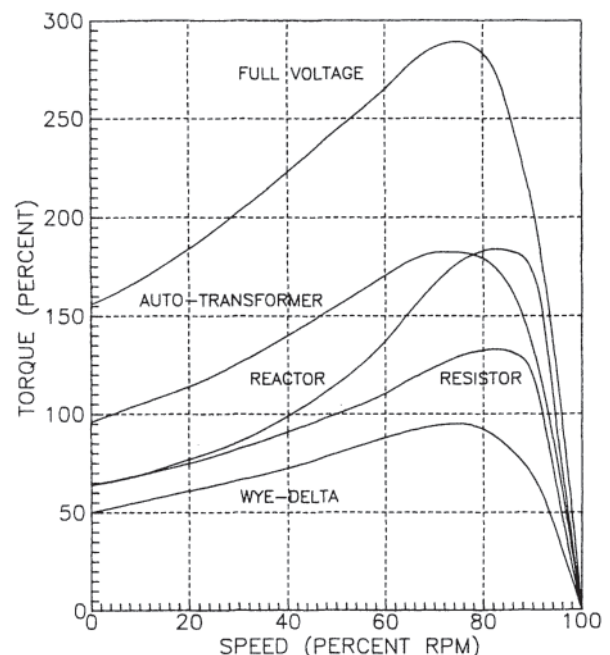


Figure 9.37 Speed-torque curves for various starting methods.

**Table 9.7** Starting Efficiency Comparison

Starting method	Torque	Locked-rotor current	Starting efficiency
Across-the-line (S)	$T_S$	$I_{LRA}$	$T_S/I_{LRA}$
Series resistor (SR)	$k_{SR}^2 T_S$	$k_{KS} I_{LRA}$	$k_{SR} T_S/I_{LRA}$
Series reactor inductance (SI)	$k_{SI}^2 T_S$	$k_{SI} I_{LRA}$	$k_{SI} T_S/I_{LRA}$
Autotransformer (TR)	$k_{TR}^2 T_S$	$k_{TR} I_{LRA}$	$T_S/I_{LRA}$
Wye-delta	$0.33 T_S$	$0.33 I_{LRA}$	$T_S/I_{LRA}$
Series-parallel	$0.25 T_S$	$0.25 I_{LRA}$	$T_S/I_{LRA}$

in this section up to this point. The line current was reduced by 36% for the autotransformer method, the starting resistor method, and the starting reactor method in order to put them on a comparative basis.

#### 9.1.4.5 Series-Parallel Starting

Another method of reduced-voltage starting for a motor with more than one parallel phase group (but an even number of phase groups) is series-parallel starting. Since the voltage across each phase group is one-half of what it will be in the parallel connection, the starting torque will be 25% of the starting torque during normal across-the-line starting with parallel-connected phase groups.

The disadvantages of this starting technique are the same as those for wye-delta starting: the starting torque is too low to accelerate a direct-coupled load.

#### 9.1.4.6 Starting Efficiency

It is instructive to compare various methods of reduced-voltage starting with across-the-line starting. A figure of merit system for this comparison known as torque efficiency or starting efficiency (SE) can be used:

$$SE = \frac{\text{Torque}}{I_{LRA}} \quad (9.89)$$

Table 9.7 summarizes the SE values of some of the reduced-voltage starting techniques with across-the-line starting. Table 9.7 illustrates that autotransformer starting, wye-delta starting, and series-parallel starting all provide as much starting torque per locked-rotor ampere as across-the-line starting. This is not strictly true in all cases as there is some loss in the autotransformer. However, the autotransformer losses are not appreciable. Series resistor starting and series reactor starting produce less starting torque per locked rotor ampere than the other methods tabulated.

### 9.1.5 Accelerating Torque and Multispeed Applications

The shaft torque developed by the induction motor was described in previous sections. Additional information is needed to determine the accelerating characteristics of the driven load-induction motor rotor system. Once the induction motor achieves an operating speed at which its shaft torque decreases to the point where it equals the load torque, the induction

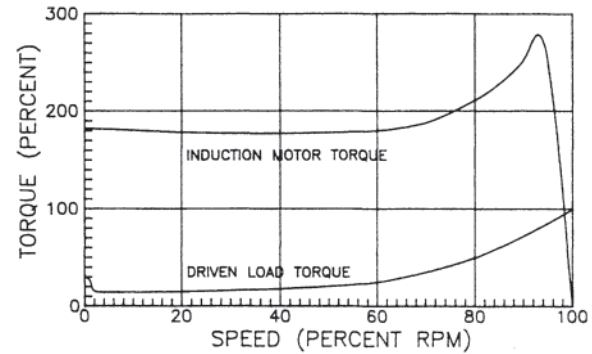


**Figure 9.38** Induction motor speed-torque curve with a load speed-torque curve.

motor stops accelerating. This operating point may be acceptable for continuous load operation. On the other hand, there may be cases where operation may be required at higher speeds for peaking conditions. There are also other reasons why operation may be required at a different speed. There are various induction motor winding configurations that permit two-speed operation. One two-speed application where the desired operating speeds are two rotor poles apart is the pole amplitude modulated motor.

#### 9.1.5.1 Motor Torque Less Load Torque

Figure 9.26 illustrated a typical NEMA Class B induction motor speed-torque curve. Note that the driven equipment such as a fan or pump will resist rotation; that is, it will coast to a stop when the prime mover (in this case an induction motor) is deenergized. It will require a specific shaft torque at any given speed to continue spinning at that speed. Figure 9.38 illustrates a typical fan speed-torque curve imposed on the induction motor speed-torque curve introduced in Fig. 9.26.

It should be clear from Fig. 9.38 that at speeds below normal operating speed, the induction motor shaft torque exceeds the load torque and so the induction motor-driven load system will accelerate.

#### 9.1.5.2 Inertia

One more parameter must be known to determine how fast the induction motor will accelerate. That parameter is the moment of inertia of the induction motor rotor-driven load about the shaft axis. Halliday and Resnick [38] provide a method for calculating the moment of inertia,  $J$ , for a continuous mass as follows:

$$J = \int_{\text{rotor system}} r^2 dm \quad (9.90)$$

where:

$dm$ =an infinitesimal element of mass

$r$ =the distance of that element from the axis

For motor problems, the moment of inertia is commonly designated as  $Wk^2$  in the units of pound-feet squared. Fortunately, the problem is simplified by the fact that the motor supplier and the driven equipment supplier provide the  $Wk^2$  as part of the design data for their equipment.

**Table 9.8** Load  $Wk^2$  Limits for Motors up to 500 hp ( $Wk^2$ , exclusive of motor  $Wk^2$ , in lb-ft<sup>2</sup>)

HP	Synchronous speed (rpm)						
	3600	1800	1200	900	720	600	514
1	—	5.8	15	31	53	82	118
1 1/2	1.8	8.6	23	45	77	120	174
2	2.4	11	30	60	102	158	228
3	3.5	17	44	87	149	231	335
5	5.7	27	71	142	242	375	544
7 1/2	8.3	39	104	208	356	551	798
10	11	51	137	273	467	723	1048
15	16	75	200	400	685	1061	1538
20	21	99	262	525	898	1393	2018
25	26	122	324	647	1108	1719	2491
30	31	144	384	769	1316	2042	2959
40	40	189	503	1007	1725	2677	3881
50	49	232	620	1241	2127	3302	4788
60	58	275	735	1473	2524	3819	5680
75	71	338	904	1814	3111	4831	7010
100	92	441	1181	2372	4070	6320	9180
125	113	542	1452	2919	5010	7790	11310
150	133	640	1719	3456	5940	9230	—
200	172	831	2238	4508	7750	—	—
250	210	1017	2744	5540	—	—	—
300	246	1197	3239	—	—	—	—
350	281	1373	3723	—	—	—	—
400	315	1546	—	—	—	—	—
450	349	1714	—	—	—	—	—
500	381	1880	—	—	—	—	—

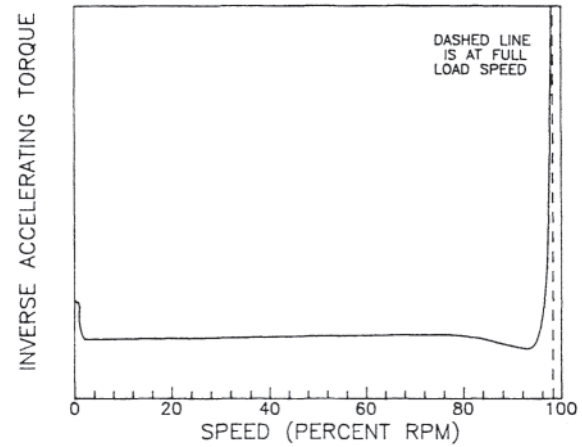
Nevertheless, there is a limitation on the  $Wk^2$  of the load that a typical induction motor can accelerate without the need for redesign of the induction motor for high-inertia accelerating duty. The application engineer must verify that this limitation is not exceeded when putting together a package system (induction motor and driven load). Table 9.8 (NEMA MG1–1998) Table 12-b [4] summarizes load  $Wk^2$  limits for motors up to 500 hp.

Typically, induction motor manufacturers will provide similar tables for ratings above 500 hp. Also, NEMA MG1–1998 Table 20–1 provides additional load  $Wk^2$  limits for induction motor ratings above 500 hp and for lower-speed induction motors of 100 hp and up.

For acceleration studies then:

$$Wk^2 = Wk_{\text{motor}}^2 + Wk_{\text{load}}^2 \quad (9.91)$$

Often the load  $Wk^2$  will be known and the induction motor rotor  $Wk^2$  will not be known. Since the load  $Wk^2$  is usually larger, a multiplying factor applied to the load  $Wk^2$  can some times be used to get an approximate  $Wk^2$  for the total shaft system. Care must be taken in this instance as the induction motor may have a flywheel. This will change the  $Wk_{\text{motor}}^2/Wk_{\text{load}}^2$  ratio. An example of this is a reactor coolant pump motor application in a nuclear power plant where a flywheel is needed to permit the motor-pump system to maintain coolant flow during certain loss-of-power events. There are other aspects of this ratio that can impact balancing and vibration problems that are discussed in Sections 11.2 and 11.3.

**Figure 9.39** Inverse accelerating torque as a function of speed.

### 9.1.5.3 Accelerating Torque

Having determined the total shaft system  $Wk^2$ , the induction motor-driven load accelerating time can be calculated. Referring to Fig. 9.38, it is clear that the accelerating torque at any speed can be computed as follows:

$$T_{\text{acc}} = T_{\text{motor}} - T_{\text{load}} \quad (9.92)$$

Since  $T_{\text{acc}}$  varies at each different speed, the accelerating time,  $t_{\text{acc}}$ , is computed as follows assuming that the induction motor is being started from zero speed:

$$t_{\text{acc}} = \int_0^{\text{rpm}_{\text{FLA}}} \left( \frac{Wk^2}{308} \right) \left( \frac{d[\text{RPM}]}{T_{\text{acc}}} \right) \quad (9.93)$$

where  $T_{\text{acc}}$  is expressed in pound-feet.

This is not an easy equation to solve since  $T_{\text{acc}}$  is not a simple function of speed. Nevertheless, an accurate answer can be obtained by performing a graphical integration using a plot of  $1/T_{\text{acc}}$  as a function of speed. A typical plot is shown in Fig. 9.39. One of the advantages of using this technique is that the time to accelerate to any partial speed can be determined. This also permits the development of a graph of speed as a function of time.

There is another factor that complicates the accelerating time computation. The accelerating torque is a function of motor terminal voltage. As an example, assume that a motor has a 100% torque at zero speed and the load torque at that speed is 44%. Now assume that the voltage at the terminals of the motor is 85%. Thus the motor torque will be reduced to 72% and the accelerating torque is only half as much as that at rated voltage.

There is another method that can be used to compute acceleration time. The time  $t_{\text{acc}}$  can be solved for by breaking the speed-torque curves of the induction motor rotor and the load into intervals wherein the average accelerating torque over the interval can easily be determined. Utilizing the speed-torque curves in Fig. 9.38, the technique for establishing these speed-torque intervals is illustrated in Fig. 9.40.

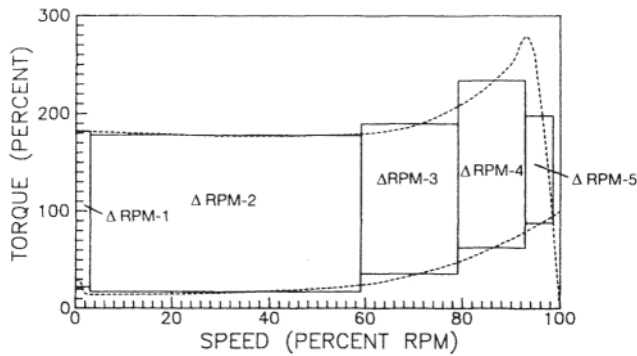


**Figure 9.40** RPM intervals with equivalent accelerating torque.

Having done this:

$$t_{\text{acc}} = \sum_{i=1}^{i=n} \left( \frac{Wk^2}{308} \right) \left( \frac{\Delta \text{RPM}_i}{T_{\text{acc,ave}}} \right) \quad (9.94)$$

#### 9.1.5.4 Two-Speed Induction Motors

Some induction motor operating situations do not require the induction motor to operate at full load except during peak or unusual conditions. Accordingly, a multispeed motor application may be suitable. The first type of multispeed motor that will be considered is the two-speed squirrel-cage induction motor in which the speed is changed by changing the number of poles in the stator winding. Increasing the number of poles decreases the speed at which the flux wave moves around the air gap between the rotor and stator and therefore the angular speed of the rotor is decreased. For a number of years after the development of the induction motor, speed changing with one winding was performed with a consequent-pole connection, which always produces an approximate 2:1 speed ratio. This connection can be designed to have one of the following characteristics: constant horsepower, constant torque, variable torque.

Figure 9.41 illustrates how the consequent-pole connection works. For operation at high speed, the windings are connected so that the current produces four poles. The currents in adjacent coil sides of the two windings are in phase. When the phase is reversed in one of the windings, the number of phase reversals doubles, forcing a pole between adjacent coil sides of the two

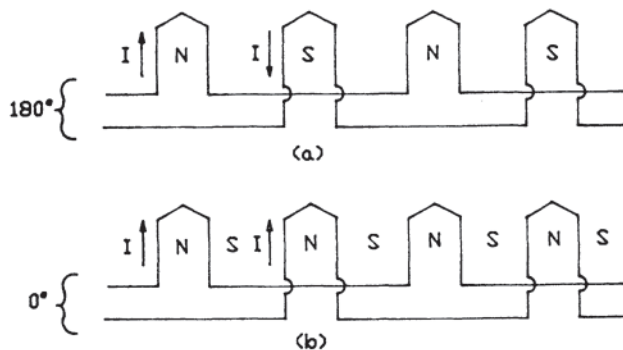


**Figure 9.41** Winding configuration for a consequent-pole connection.

separate windings. Thus, the rotor will spin at low speed, approximately one-half of the original speed. It is the forced pole, in this case the S pole, that is the consequent pole, and so this winding connection is called a consequent-pole connection.

#### 9.1.5.4.1 Constant-Torque Consequent-Pole Windings

While the winding configuration shown in Fig. 9.41 is common to all consequent-pole motors, the terminal connections are different for the constant-horsepower, constant-torque, and variable-torque characteristics. The constant-torque consequent-pole induction motor, as the name implies, is designed to develop the same torque no matter what steady-state speed is. Typical applications are compressors, positive-displacement loads such as hoists and elevators, and friction loads such as conveyors, grinders, and stokers.

Power is a function of both torque and speed. The constant-torque consequent-pole induction motor will be rated for twice the horsepower at the higher speed. The high-speed connection will also have a much greater locked-rotor current.

A circuit that will start a constant-torque consequent-pole motor can be found in Millermaster [37, p. 374]. The circuit works as illustrated in Fig. 9.42. This circuit is known as a compelling starter because the motor will not accelerate to high speed from rest, even if the fast pushbutton is depressed. The motor must be started at slow speed first.

When the slow pushbutton is depressed, the S coil will pick up if the overload permissives are reset and the high-speed circuit (1F) is deenergized. An “a” contact from the S coil picks up the FR coil, which seals itself in and seals in the S coil. The motor is energized at terminals T1, T2, and T3. Motor terminals T4, T5, and T6 are open outside the motor. Although it is not intuitively obvious from the motor circuit in Fig. 9.42, the currents in both windings of each phase have zero phase shift, thus creating the consequent-poles necessary for low-speed operation.

To switch to high speed, the fast pushbutton is depressed. The S coil drops out, which permits the 1F coil to pick up. This connects T1, T2, and T3 together in the motor circuit after T1, T2, and T3 have been separated from the feeder circuit. An “a” contact from the 1F coil energizes the 2F coil which, in turn, connects T4, T5, and T6 to the feeder circuit. Now the currents in both windings of each circuit are 180 degrees out of phase and the motor operates at high speed.

#### 9.1.5.4.2 Constant-Horsepower Consequent-Pole Windings

Constant-horsepower loads have decreasing torque requirements at higher speeds. Typical applications are machine tools such as lathes, boring mills, winches, and mixers. Not only is the motor horsepower constant, but locked-rotor current tends to be about the same for each speed connection.

The T1, T2, and T3 motor terminals are connected to the feeder circuit at low speed as was the case for the constant torque induction motor. However, the T4, T5, and T6 motor terminals are shorted together at low speed rather than open-circuited. At high speed, motor terminals T4, T5, and T6 are

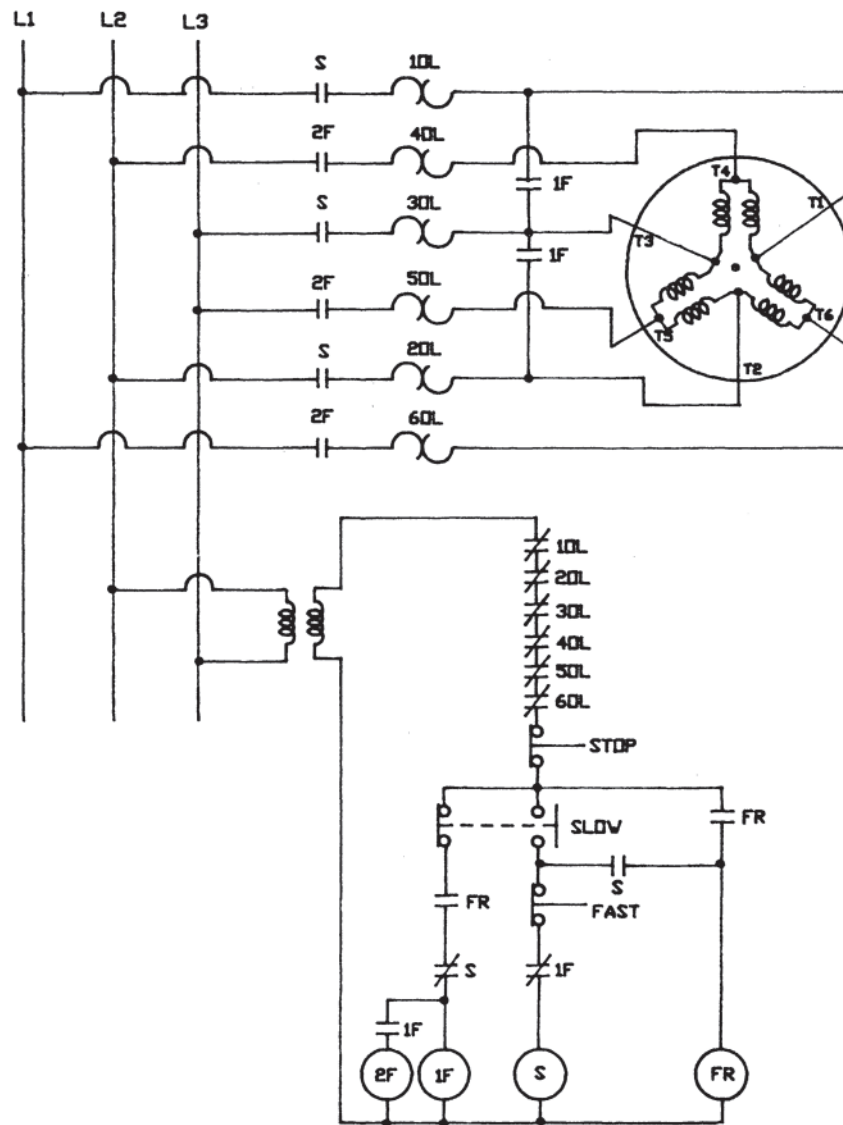


**Figure 9.42** Constant-torque consequent-pole starter.

connected to the feeder circuit and motor terminals T1, T2, and T3 are open-circuited.

**9.1.5.4.3 Variable-Torque Consequent-Pole Windings**

Variable-torque loads have higher torque requirements at higher speeds. Accordingly, they have horsepower ratings that are the third power or more as a function of speed. Variable-torque consequent-pole induction motors have locked-rotor currents that are substantially greater at higher speeds. Typical applications include fans, blowers, and centrifugal pumps.

The starting circuit external to the motor is identical to the constant-torque connections described above. The terminal connections inside the motor are quite different, as illustrated in Fig. 9.43. At low speed the windings in each phase are connected in series, while at high speed they are effectively in parallel. This is an obvious switching connection to make since the low-speed current and power are much lower than at high speed.

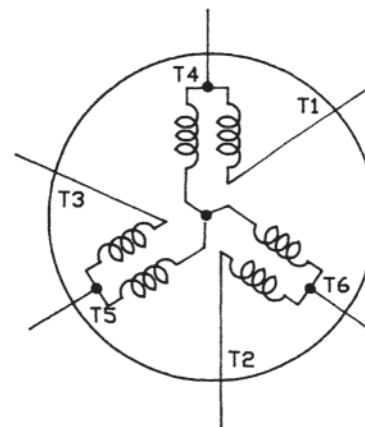


**Figure 9.43** Variable-torque consequent-pole motor internal terminal connections.

**Table 9.9** Variable-Torque, Two-Winding, Consequent-Pole Induction Motor

Speed (rpm)	Winding used	Winding connection used
600	1	Consequent-pole
900	2	Consequent-pole
1200	1	Conventional-pole
1800	2	Conventional-pole

#### 9.1.5.5 Pole-Amplitude-Modulated Motors

The last section concluded with a description of the variable-torque requirement of fan loads. In actuality, a consequent-pole winding connection does not provide an ideal set of speeds for most fan drive applications. For small variable-torque loads, this difficulty can usually be overcome by using an induction motor with two separate consequent-pole windings to achieve a rating such as 60/900/1200/1800 rpm. A typical application is described in Table 9.9.

For very large loads, such as a utility power plant induced-draft fan application, two-winding consequent-pole induction motors are not practical due to the cost of the multiple winding induction motor and the complexity of the switching apparatus. The induced-draft fan drive system is sized for test block (TB) requirements but it normally operates at maximum continuous rated (MCR) conditions. Various drive options are available to the application engineer, including the following.

1. Utilize a single-speed induction motor and damper down the fan output to achieve the desired operating conditions.
2. Apply an induction motor configuration that will accommodate two-speed operation.
3. Employ a variable-speed drive system. (Variable speed drive systems can be applied over a wide speed range for situations where variable operating conditions are required, such as unit load-cycling or boiler sliding pressure operation.)

A two-speed induction motor application can overcome some of the drawbacks inherent in dampering the single-speed motor load.

1. Operation at full speed and dampering down is less efficient than operating at a lower speed.
2. If the fan blade erosion rate is a fourth-order function of speed, then operating at MCR (about 80% speed) reduces the fan blade erosion rate to 40% of that experienced under TB conditions.
3. Starting duty is reduced both when accelerating to MCR speed and later when switching to TB speed.

At one time, two-speed induced-draft fan operation was accomplished by installing one induction motor at each end of the fan shaft; one for high speed and one for low speed. The low-speed induction motor would be started first, driving both the fan rotor and the unenergized high-speed induction motor rotor. To achieve high speed, the low-speed induction motor would be deenergized and then the high speed induction motor

would be energized. This is an open transition technique. It is a method that works well but has the cost disadvantage of dual electrical components (i.e., two motors).

Two-speed operation can be achieved using one induction motor. One way to do this is to use an induction motor with two separate stator windings, one for MCR speed and one for TB speed. An induction motor with two separate stator windings would be up to 80% larger than a similarly rated single-speed induction motor and it could have lower efficiency. (A large stator with three or more separate windings is costprohibitive.) Two-speed operation with a speed ratio of 2:1 can be achieved with a single stator winding induction motor using a consequent-pole winding connection as described previously. Unfortunately, a 2:1 speed ratio is not a useful one for a fan application, where the MCR speed is on the order of 80% of the TB speed. There is another two-speed induction motor alternative.

A pole-amplitude-modulated (PAM) induction motor can provide the desired speed ratio utilizing a single stator winding. Consider an eight-pole induction motor. Using modulation terminology, the carrier frequency would be 900 rpm. One alternating frequency can be superimposed upon another, producing the sum and the difference of those frequencies. The carrier frequency can be modulated to frequencies characteristic of induction motors with two more poles or two fewer poles than the carrier frequency has. For this situation, the induction motor can be made to perform either as a 10-pole, 720-rpm induction motor or a 9-pole, 1200-rpm induction motor. The PAM effect is obtained by changing the phase angle of the stator current 180 degrees in part of the stator winding in all three phases as described in Say [39]. In this case, 10-pole operation is desired. The PAM motor efficiency at 720 rpm (10 poles) and at 900 rpm (8 poles) is within a few tenths of a percent of that of a single-speed induction motor at either speed. However, at low speeds some performance is sacrificed. The power factor for the 720 rpm connection is lower than for a similar single-speed induction motor.

A set of speed-torque curves for a typical 720/900 rpm PAM induction motor and the load is illustrated in Fig. 9.44. The PAM induction motor windings can be designed for optimum performance at each speed. The induction motor shown in Fig. 9.44 has a rating of 4000/7000 hp. The accelerating current of the 720 rpm connection is less than that for the 900 rpm connection. The 720 rpm configured motor can come up to speed in 20 seconds, which is less than the 22.5-second accelerating time of the 900-rpm connection accelerating from standstill. This lower accelerating current and accelerating time results in lower starting duty. Running at low speed for a while before switching to high speed permits the rotor to cool down to continuous running temperature. When the PAM induction motor is switched to high speed, the acceleration time is much less than 22.5 seconds. Thus, the two-speed start-up reduces heating in both the rotor and the stator.

An "open transition" is required during the speed change to permit the flux to decay in the part of the winding in which the current angle reversal takes place. This can be accomplished with a 2-second time delay without an



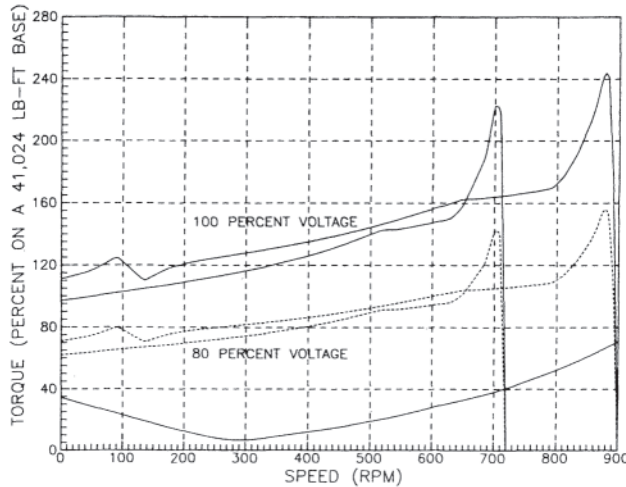


**Figure 9.44** Typical pole-amplitude-modulated (PAM) induction motor speed-torque curves. (Data courtesy of the Westinghouse Motor Company for a 720/900-rpm PAM motor rated at 4000/7000 hp.)

appreciable loss of rotor speed. The switching control can be accomplished with a simple device such as a programmable controller or it can be implemented as part of a more sophisticated plant computerized control scheme. At one time when a PAM motor was procured from the Westinghouse Motor Company, Westinghouse could supply a step logic sequencer that could be used to control the PAM induction motor speed change switching. The design of the speed change control needs to be done carefully as any lack of coordination with other control elements and devices, such as dampers or vanes, can cause boiler transients or other more severe problems.

### 9.1.6 Starting Duty Thermal Limitations

Many people who are not familiar with power electrical equipment tend to believe that this equipment is designed for a specific power rating based on abstract principles of electromagnetism. In actuality, what defines the power rating of an electrical device is its ability to expel waste heat caused by electrical and mechanical losses and its ability to operate without damage at an elevated temperature due to limitations on the rate at which it can dispose of this waste heat.

#### 9.1.6.1 Energy Storage and Dissipation

When the induction motor is energized, locked current develops in the rotor cage as the rotor begins to spin (assuming the rotor is being started from a dead stop). Since the rotor is initially at rest, it has no kinetic energy. The initial energy in the rotor is due to the  $I^2R$  heating loss in the rotor bars. As the motor accelerates, its kinetic energy increases and the heating loss in the rotor decreases. Once the induction motor is up to speed, half the total energy of accelerating the induction motor has gone into kinetic energy and the other half has gone into heating the induction motor. This is often illustrated by the model shown in Fig. 9.45.

If a motor design is limited to the energy characteristic shown in Fig. 9.45, it will fail thermally when accelerating

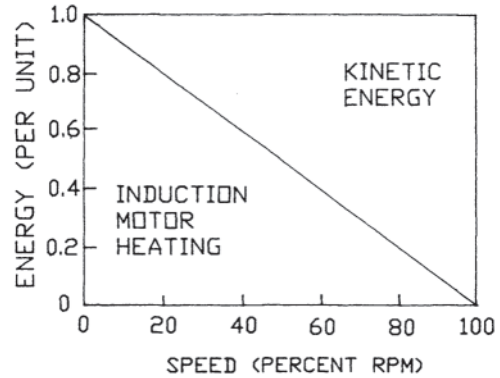


**Figure 9.45** Energy inventory as a function of rotor speed.

the driven load in a short period of time. The reason for this is that the model depicted in Fig. 9.45 does not include load torque and load inertia. Rearranging this model and adding the load characteristic, the energy inventory looks a lot more like that displayed in Fig. 9.46 [40]. The motor designer must take this physical property into consideration when designing the induction motor.

#### 9.1.6.2 Impact of Starting Current on the Rotor Bars

When the rotor bars are tall and thin, the locked-rotor current is concentrated in a small portion of the rotor bar closest to the air gap. (See Section 9.1.3.2 on Deep-Bar Effects.) Thus, a substantial part of the rotor bar heating is taking place in that small portion of the rotor bar at the top of the rotor slot. Furthermore, tall bars in a large induction motor cannot conduct the heat away to the bottom of the bar fast enough to equalize the heating in the bar before the starting cycle is completed. This is an additional factor tending to bow the rotor bars out as described in Section 9.1.3.4 on Countermeasures for Cracked Rotor Bar Problems. The motor designer needs to minimize the propensity of rotor bars to fail because of localized heating and high mechanical stress.

It is difficult to identify countermeasures for this particular phenomenon. Nevertheless, one technique for reducing the bowing stress on the rotor bars and at the bar-to-shortening-ring connection is to employ a double-cage design.

#### 9.1.6.3 Starting Requirements Specified by Industry Standards

NEMA Standard MG 1–1998, [4, Par. 10.36] describes the requirements for short-time rated induction motors.

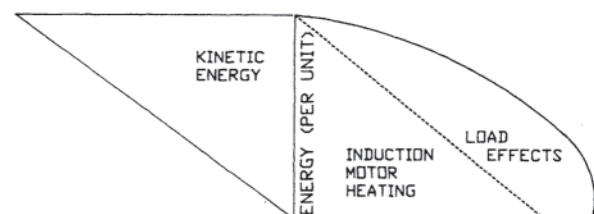


**Figure 9.46** Energy inventory including load effects.

10.36 The time ratings for single-phase and polyphase induction motors shall be 5, 15, 30, and 60 minutes and continuous.

All short-time ratings are based upon a corresponding short-time load test which shall commence only when the winding and other parts of the machine are within 5°C of the ambient temperature at the time of the starting of the test.

Most utility induction motor applications call for continuous-rated electric machines. The limitations for the number of repetitive starts for continuous-rated induction machines can be found in ANSI Standard C50.41 (2000) [10].

11.1 Starting Capabilities. Motors shall be designed for across-the-line starting, and shall be capable of making either of the starts described in 11.1.1 and 11.1.2, provided that the load inertia ( $Wk^2$ ), the load torque during acceleration, the expected voltage and frequency, and the method of starting are those for which the motor was designed.

11.1.1 Two starts in succession, coasting to rest between starts with the motor initially at ambient temperature.

11.1.2 One start with the motor initially at a temperature not exceeding its rated-load operating temperature.

11.2 Number of Starts. It should be recognized that the number of starts should be kept to a minimum since the life of the motor is affected by the number of starts. If the normal starting duty exceeds three starts per day, the starting duty shall be specified.

11.3 Starting Information Nameplate

11.3.1 A starting information nameplate, setting forth the starting capabilities specified in 12.1.1 and 12.1.2, shall be mounted on the motor.

12.3.2 If specified, the starting information nameplate shall also include the minimum time at standstill and the minimum time running prior to an additional start.

9.1.6.4 Thermal Limitations

Previous sections in this chapter have described the variation of torque as a function of speed during the induction motor accelerating phase. To fully understand the thermal limitations on a three-phase induction motor during start-up, the accelerating current needs to be analyzed. Figure 9.47 shows the phase current in the stator as a function of speed. This curve is overlaid on the speed-torque curve illustrated in Fig. 9.38. When the information available in this figure is used to compute the accelerating time for the induction motor using Eq. 9.94 (see Section 9.1.5.3), a current versus time characteristic can be developed. The result is usually plotted on semi-log paper as shown in Fig. 9.48.

The major component of induction motor heating during the accelerating phase is the  $I^2R$  loss in both the stator and the rotor. It is not uncommon to have a locked-rotor current 6 to 7 times the normal running current. Accordingly, the  $I^2R$  heating in the stator will be as much as 50 times that which occurs at

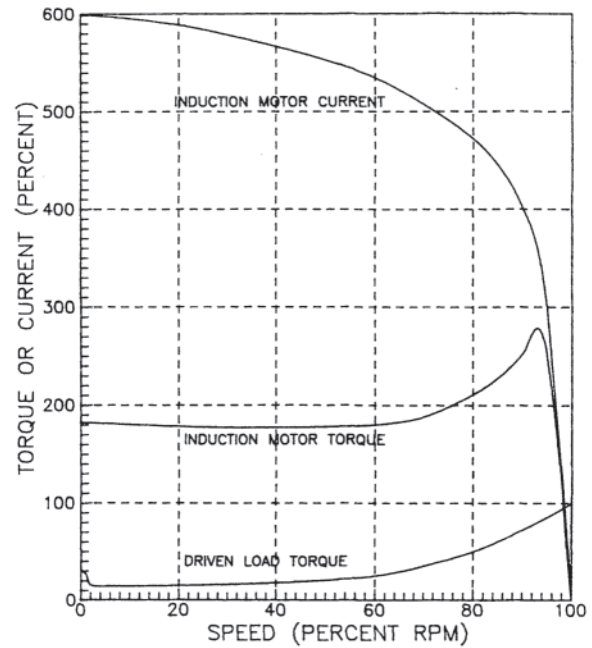


Figure 9.47 Accelerating current as a function of speed.

full-load operation. The induction motor will be able to withstand this elevated thermal loading for only a short period of time. Figure 9.49 illustrates the locus of points forming the locked-rotor thermal capability characteristic and the locus of points forming the running thermal capability characteristic, both characteristics being at the induction motor's normal operating temperature. The situation can arise wherein a motor running at normal temperature is shut down momentarily and then restarted without having cooled to ambient temperature. This is a more restrictive condition than starting the induction motor from ambient temperature.

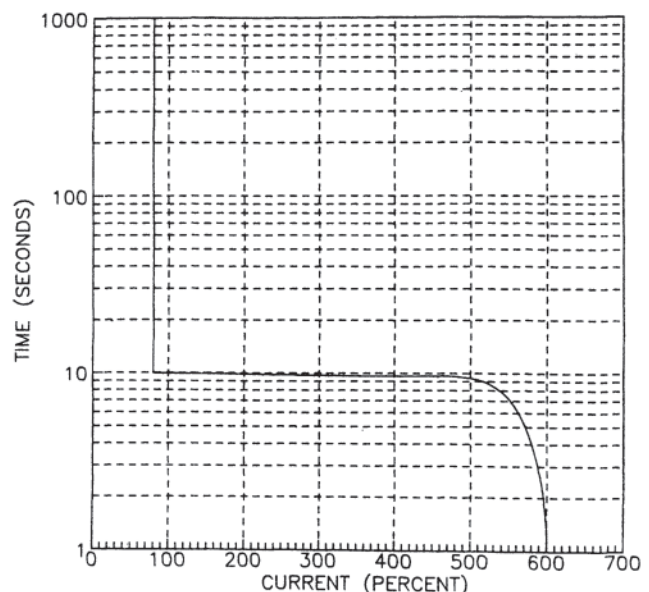
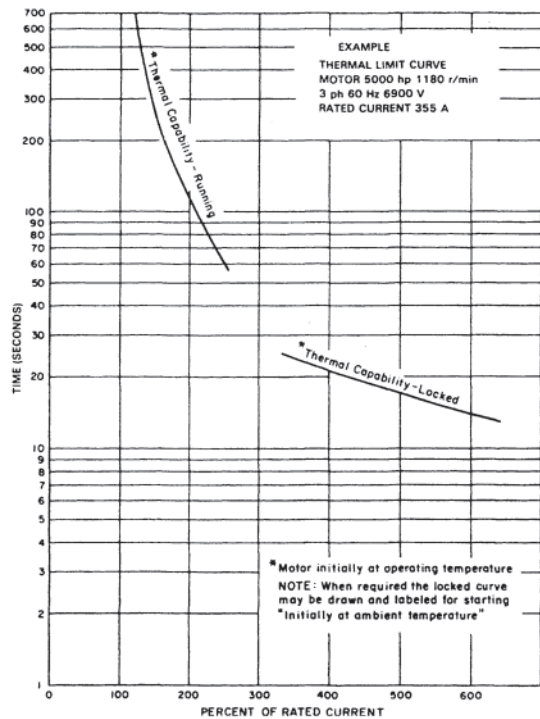


Figure 9.48 Induction motor time-current curve.



**Figure 9.49** Induction motor thermal limit characteristics. (Reproduced from Ref. 41, with the permission of the IEEE.)

The running and locked rotor thermal limit characteristics are not continuous. There are a number of reasons for this including the following.

1. Once the rotor begins to spin, the cooling fan, that is connected to or is part of the rotor shorting ring, begins to circulate air through the air gap. This increases the rate at which heat can be removed from the induction motor.
2. The two characteristics may represent different limits. For example, the running thermal limit characteristic may represent a stator conductor limit, whereas the locked-rotor thermal limit may represent a rotor temperature limitation.
3. As the rotor accelerates, the rotor bars are subjected to slip frequency current. This current has a lower frequency than locked-rotor current and so the current in the rotor tends to spread more uniformly across the rotor bars (deep-bar effect). The larger the useful cross-sectional bar area, the lower the  $I^2R$  heating.

Since the voltage at the terminals of the machine will be depressed during the accelerating phase due to the voltage drop in the feeder circuit because of the high-magnitude accelerating current, the accelerating time will increase. It is not uncommon to show multiple induction motor time-current curves as in Fig. 9.50 with their respective locked rotor and accelerating current thermal limit curves to account for variability in the motor starting voltage. See Figure 6(b), ANSI/IEEE Std. C37.96–2000 *IEEE Guide for AC Motor Protection* [21].

Induction motor relay protection will be addressed in a

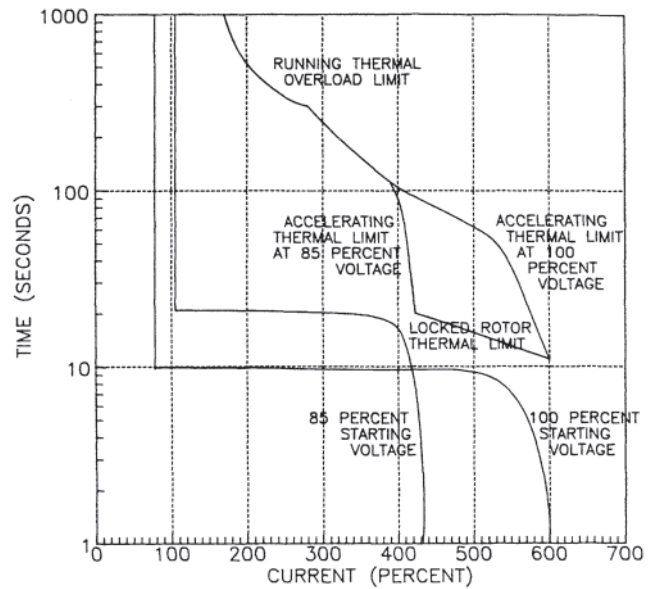


**Figure 9.50** Time-current and thermal limit curves for two starting voltages.

subsequent section. Nevertheless, there is a potential locked-rotor protection problem that needs to be addressed while discussing the locked-rotor thermal limit curve. It would appear after reviewing Fig. 9.50 that it would be very easy to fit an inverse over/current relay characteristic just under the locked-rotor thermal limit curve without risk of a false relay trip. This may not be the case. The text *Applied Protective Relaying* [42, p. 7–5] uses a linear—linear plot of the induction motor time-current curve to demonstrate the equal-area criterion to verify adequate thermal margin. Figure 9.51 illustrates this

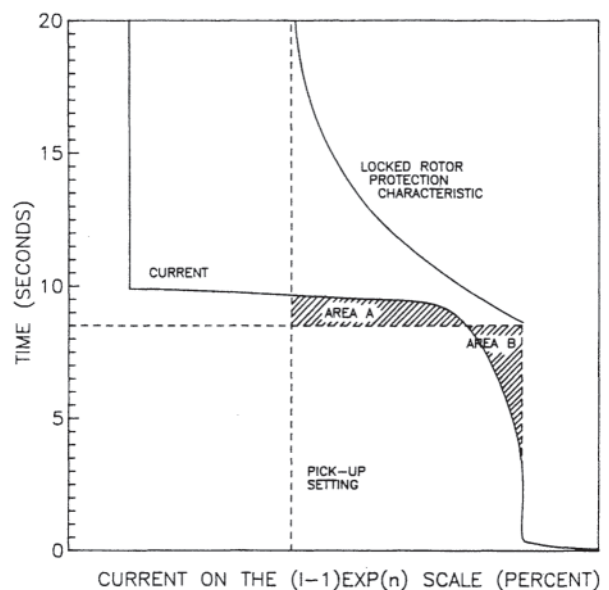


**Figure 9.51** Equal-area criteria.

concept. For this example, it will be presumed that the inverse overcurrent relay curve is virtually congruent with the locked-rotor thermal limit curve. This assumption will permit the longest time to trip at any current without damage to the induction motor. While it is true that the accelerating current at all times is less than the overcurrent locus of trip points, it can be seen that the overcurrent relay disk begins rotating during the locked rotor interval because the accelerating current is above the overcurrent relay pickup point. In fact, the overcurrent relay disk will continue moving its trip contacts until the accelerating current of the induction motor (at the current transformer secondary) is less than the overcurrent relay pickup level. If the accelerating current falls below the pickup level before the area of region A in Fig. 9.51 becomes as large as area B, the relay trip contacts will not make up and the overcurrent relay will begin to reset (assuming no overtravel). If area A is greater than area B, the overcurrent relay will trip.

There are two observations that should be made when area A is approximately equal to area B.

1. If area A is approximately equal to or greater than area B, then overcurrent relay protection is not the best locked-rotor protection scheme for the induction motor application.
2. The motor manufacturer should be questioned as to the validity of the locked-rotor thermal limit data being provided for the induction motor. Remembering that an overcurrent relay inverse current curve is a relative measure of the losses being thermally generated in the motor, one of two scenarios is likely:
  - a. The locked rotor thermal limit data are in error.
  - b. The induction motor has very little thermal margin and may not be an adequate design for the application contemplated.

### 9.1.7 Miscellaneous Induction Motor Starting Topics

The materials covered in this chapter so far have all pertained to three-phase squirrel-cage induction motors. There are additional topics that will be addressed briefly in this section for the sake of complete coverage of induction motor starting.

#### 9.1.7.1 Single-Phase Induction Motor Starting

Small motors in the fractional horsepower range are normally single-phase devices for two reasons. First, there is rarely a three-phase circuit available for the voltages used in small-motor applications. These motors are used primarily in the residential and commercial sector rather than the industrial sector. Secondly, a single-phase motor can often be built at a lower cost than a three-phase motor in small-horsepower sizes.

In a single-phase induction motor with one winding, the magnetic field created by the stator currents is a pulsating field rather than the rotating field that exists in a three-phase motor. Accordingly, such a single-phase induction motor on starting does not develop torque. In order to start a single-phase induction motor, two fluxes that are out of phase are required. This can be accomplished by using an auxiliary winding with

a different impedance than the main winding. This causes a phase shift in the auxiliary winding current (and flux), which creates a rotating field. The auxiliary winding may be permanently connected or it may be switched open when the single-phase induction motor approaches operating speed. The phase shift in flux can be achieved in different ways:

1. Winding techniques
  - a. The auxiliary winding can have a higher resistance to reactance ratio than the main winding.
  - b. The auxiliary circuit can have a capacitor in series with the auxiliary winding.
  - c. As in (b), the auxiliary circuit can have a series capacitor but this capacitor is disconnected as the motor reaches normal operating speed, leaving only the main winding connected.
  - d. In order to optimize starting and running characteristics, two capacitors connected in parallel can be used in series with the auxiliary winding. As the rotor approaches operating speed, one of the capacitors is open-circuited, leaving the other capacitor in series with the auxiliary winding in the running circuit. The auxiliary winding will then operate in parallel with the main winding during steady-state operation.
2. Flux control. A flux shifting technique can be employed wherein the stator poles are split. A low-resistance copper coil is fitted around the pole piece, which is split off from the main pole. This coil is called a shading coil. To keep the flux linkage constant, the shading coil will develop a current that opposes flux build-up when the current increases in the main coil. When the main coil current decreases, the shading coil current will reverse polarity in an effort to maintain the flux in the shaded pole piece. This creates a rotating magnetic field in the air gap.

The circuit and phasor diagrams for the single switched capacitor case are shown in Fig. 9.52.

#### 9.1.7.2 The Impact of a Double-Cage Rotor on Induction Motor Starting

In Section 9.1.3.3, the shape of the rotor bar was discussed as it affects starting torque. The logical extension of the deep-rotor-bar effect is a double cage, that is, a second cage inside the first cage. The motor laminations need to be punched with openings for an upper and a lower bars. The bars can then be

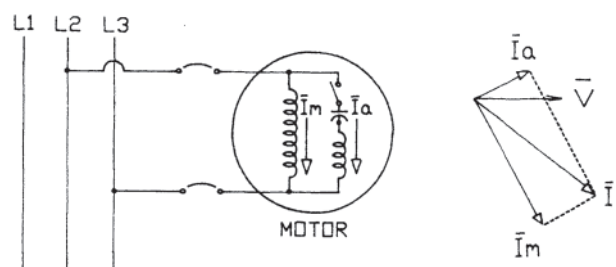
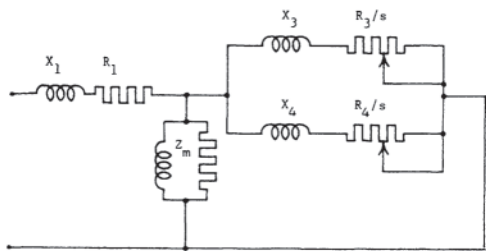


Figure 9.52 Single-phase switched capacitor-start induction motor.



**Figure 9.53** Equivalent circuit for a double-cage induction motor with separate rotor end rings.

connected to one large shorting ring at each end of the rotor, or two separate rings, one for each cage.

A class D, high locked-rotor torque can be developed by employing a high-resistance material for the outer cage. Since the rotor frequency is relatively high during acceleration, the low-inductance outer cage will carry the current. At steady-state slip frequency, the rotor reactances are substantially reduced, allowing the cage with the lowest resistance to carry most of the rotor current. A low-resistance inner cage is used to reduce rotor slip and to minimize rotor  $I^2R$  losses. Figures 9.53 and 9.54 show lumped-parameter circuits that are used by Engelmann [43] to model double-cage induction motor starting.

Figure 9.53 is a modification of Fig. 9.12 in which the single-cage rotor parameters indicated by the subscript 2 are replaced. Parameters with the subscript 3 represent the outer cage and the parameters with the subscript 4 represent the inner cage. In order for the outer cage to carry the locked rotor current:

$$X_4 > X_3 \tag{9.95}$$

In order for the inner cage to carry low-slip, steady-state current:

$$R_3 > R_4 \tag{9.96}$$

Figure 9.54 illustrates the lumped-parameter circuit for a double-cage rotor with a single end ring at each end of the cage. The parameters with the subscript 5 represent the end ring characteristics. As suggested in Section 9.1.6.2, the proclivity for rotor bar bowing because of thermal expansion is increased when the current is constrained to reside in the top portion of the rotor bar during locked-rotor conditions. This phenomenon is amplified in a double-cage rotor with a single

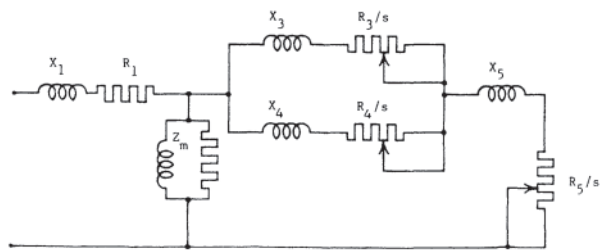


**Figure 9.54** Equivalent circuit for a double-cage induction motor with a single rotor end ring.

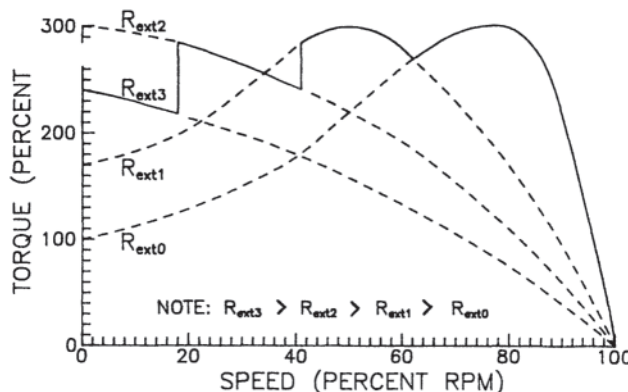


**Figure 9.55** Wound-rotor motor speed-torque characteristic.

end ring at each end of the rotor. Accordingly, double-cage rotors with separate end rings for each cage, that permit the cages to thermally expand and contract independently, are preferable.

### 9.1.7.3 Wound-Rotor Induction Motor Starting

The preceding section described how a double-cage rotor achieves a high rotor resistance characteristic in order to develop high locked-rotor torques and a low steady-state resistance for low slip and high efficiency. A further extrapolation of these desired characteristics can be achieved by introducing an external switchable resistance to the rotor circuit. This resistance can be sized to produce the maximum torque, or breakdown torque, at locked-rotor speed (unity slip). As the motor accelerates, the resistance is shorted out. The motor's natural speed-torque characteristic controls the rest of the accelerating time period. Additional resistance steps in the rotor circuit can be used to tailor the motor accelerating torque. An example of a switched multiple external-resistance motor speed-torque characteristic is illustrated in Fig. 9.55.

A special type of motor, known as a wound-rotor motor, is needed to accommodate the external switchable resistors. The rotor has insulated windings, similar to the stator, rather than the uninsulated rotor bars found in a squirrel-cage induction motor. The rotor windings are brought out to slip rings on the rotor shaft. The external resistance is connected to carbon brushes that contact the slip rings to make up the rotor circuit. The wound rotor may have a different number of phases than the stator has. However, a three-phase wound-rotor motor will usually have three phases on the rotor and, accordingly, three slip rings in the rotor circuit to permit connection to a three-phase resistor bank.

As one might expect, the resistor bank can become hot during motor acceleration due to the high momentary currents and their resultant  $I^2R$  losses. These losses are not significant, because the accelerating time is short compared to the overall operating time of the wound-rotor induction motor. Nevertheless, a wound-rotor motor can also be used at about full load to adjust operating speed. This application requires a resistor with a continuous rating rather than the short time rating of a starting resistor bank. When the motor is used as a

variable-speed device, the losses in the resistor bank are no longer negligible. Since improved controllability is also desirable in a variable-speed regime, various techniques have been developed to eliminate the stepped resistor bank and recover the associated losses. Several manufacturers employed unique names for these techniques; however, the names used below are generally known in the industry for the devices described.

#### 9.1.7.3.1 Kraemer Drive

This drive was originally configured with the wound-rotor slip rings connected to the slip rings of a rotary converter. This device converts ac power to dc power, which can be reclaimed rather than given off as heat loss. A variation of this drive uses a synchronous motor coupled to a dc generator instead of a rotary converter. The essential element of a Kraemer drive is the dc link between the wound-rotor motor and the energy recovery system.

#### 9.1.7.3.2 Kramer stat Drive

In the 1960s, it was discovered that a solid-state (electronic) thyristor inverter could be substituted for the dc generator and synchronous motor in a Kraemer drive. The recovered power can be fed into a lower voltage ac auxiliary system. If a step-up transformer is utilized, the recovered power can be fed back into the motor feeder circuit. This transformer provides the secondary benefit of attenuating some of the ac harmonics and preventing the flow of any residual dc unbalance current in the stator feeder circuit. Accordingly, this transformer is known as an isolating transformer. A typical Kramerstat drive system is illustrated in Fig. 9.56.

#### 9.1.7.4 Electromechanical Induction Motor Starting Methods

Because the motor accelerating interval places heavy-duty requirements on the squirrel-cage motor, a number of devices have been used over the years to reduce this duty. Some of these devices can be used for variable-speed operation as part of the drive system.

One technique that has been used in multiple boiler plants with common steam headers is the application of small steam turbines that can develop enough torque to get the drive system up to part speed. This technique is particularly helpful for high-inertia loads. The turbine is mechanically coupled to the induction motor-load shaft system.

Another apparatus is the eddy current clutch, a device that is coupled between the induction motor and the load. This apparatus consists of concentric drums separated by a small air gap. The induction motor is started first unloaded. When it is up to speed, an external excitation coil induces eddy currents in the drums. The magnetic fields created by the eddy currents interact to develop torque to accelerate the load. For large drives, a coolant system is required to dissipate the heat generated by the eddy current coupling.

An analogous device is the hydraulic coupling. The actual coupling between the concentric drums is created by a fluid film. The fluid also provides the coupling cooling. The power required to operate the coolant pump is equivalent to the power in the excitation coil of the eddy-current clutch. Reason [44] reports that at one time, 20% of boiler induced-draft fans were driven through hydraulic couplings. See Fig. 9.57 for a typical hydraulic coupling installation. This device can also be used to achieve variable-speed operation. Because the hydraulic coupling is relatively inefficient, new drive systems

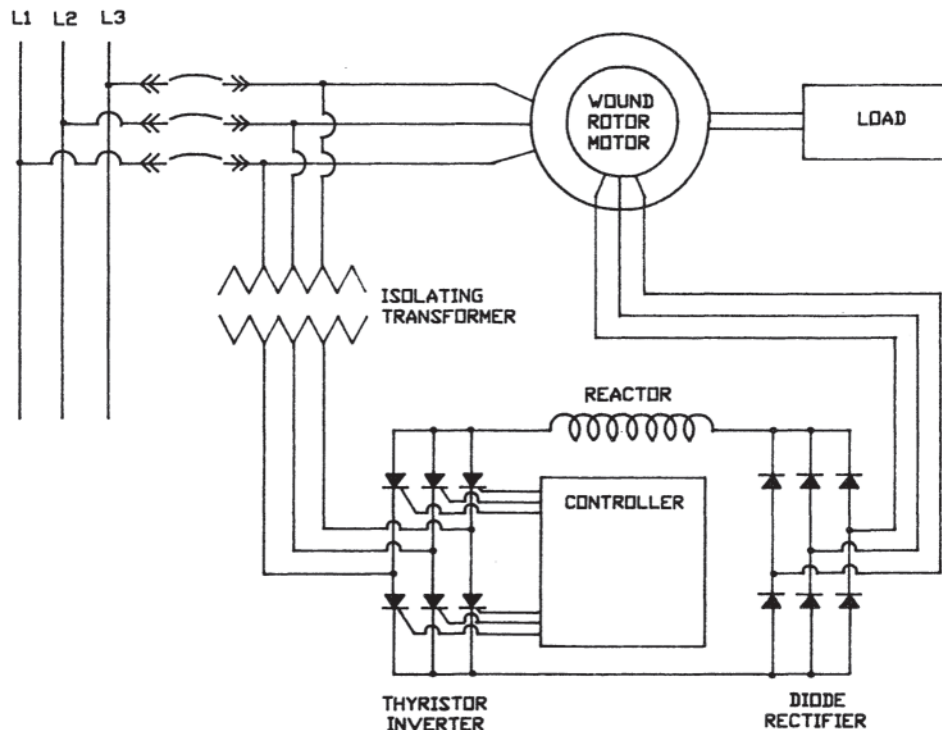
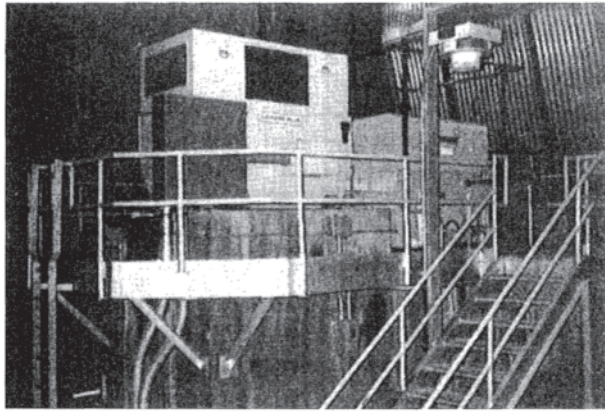


Figure 9.56 Wound-rotor motor slip energy recovery control system.



**Figure 9.57** Hydraulic coupling between a motor and an induced draft fan. (Courtesy of Ohio Edison Company.)

are utilizing electronic adjustable-speed drive (ASD) systems, that have high efficiencies. ASDs are addressed in Section 9.5.

[A number of individuals reviewed the foregoing material and provided helpful comments. These were greatly appreciated by the author. Of this group, special acknowledgement is due to Dr. S.D.Umans of MIT and to Professor Emeritus R. S.Grumbach of the University of Akron, who went to considerable effort to provide constructive criticism and to suggest improvements in the presentation.]

## 9.1.8 Bus Transfer and Reclosing of Induction Machines

### 9.1.8.1 Bus Transfer and Reclosing Considerations

Modern steam power stations, fossil-fueled or nuclear-fueled, must start “cold plants” from power sources in the grid they ultimately supply. This power is needed to supply auxiliary equipment: fans, pumps, coal pulverizers, and so forth. Once the generator is brought online, these auxiliaries are transferred to an auxiliary bus fed from the generator’s own terminals.

Large industrial complexes are supplied power by radial feeders from the utilities or from a utility grid. Some systems include cogenerative generators feeding power into the grid to which they are connected. These systems require relaying coordination and, frequently, reclosing of breakers tripped under fault conditions to maintain or restore service continuity.

Each of the above situations involves separating either single-systems or subsystems from the principal power supply. The dynamics, both electrical and mechanical, result in transient current, power, and mechanical forces when the circuits are again joined. These affect the ability to maintain system stability and individual machine integrity.

If both the separated circuit and the supply system contain large synchronous machines, the problem becomes one of synchronous system stability and is beyond the scope of this section. This section, then, deals with the transfer or reclosing of loads containing induction machines as the major dynamic loads.

### 9.1.8.2 Historical Background

The problems of bus transfer and reclosing have been addressed by machine designers and system application engineers for many years. The effects of the transient forces on machine windings and mechanical parts were known, if not well understood. Some user specifications in the late 1950s, particularly by European contractors, began to call for the bracing of stator windings to withstand the effects of reclosing or transferring with the motor residual voltage, maintained at rated voltage, 180 electrical degrees out of phase with the oncoming bus. Because of the nonlinear effects of saturation, it was impossible to predict the resulting electrical and mechanical forces with the mathematical tools available at the time. Rather than to merely “take exception” to these requirements, the major U.S. motor manufacturers elected to establish conditions under which they would agree to out-of-phase switching and to state these limits in their proposals. The result of these studies stated that the vectorial voltage difference between the oncoming bus voltage and the residual voltage for the machine or bus being switched should not exceed 1.33 perunit voltage on the machine base. One manufacturer published this information in 1961 and other U.S. motor manufacturers implicitly agreed to this value. In 1977, ANSI C50.41–1977 [10] included the 1.33 criterion for bus transfer is that Standard.

There has been some discussion of the applicability of this Standard (ANSI C50.41) to the industry as a whole. A major point of contention has been that ANSI C50.41 is a “power plant” document but is cited by industrial users and contractors. It is necessary to keep C50.41 in perspective: It was intended as a guide to address the mechanical effects of outof-phase switching on machine stator windings. It does not address, nor was it intended to address, the mechanical stresses resulting from switching at motor and drive speeds near torsional system critical speeds. These matters still require additional system analysis. Nevertheless, C50.41 provides the user with a published criterion to support relaying and control decisions even though additional investigation may be essential for specific applications.

### 9.1.8.3 Technical Analysis of Bus Transfer and Reclosing

The following symbols are used in the remainder of Section 9.1.8.

Symbol	Description
$e$	Instantaneous voltage
$f$	System frequency (hertz)
$i$	Instantaneous current
$t$	Time (seconds)
$t_{d0}'$	Open-circuit time constant
$t'$	Short-circuit time constant
$t_c'$	Open-circuit time constant with capacitors
$\sim$	Cycles
$E$	RMS voltage, per unit, per phase
$E_M$	Voltage at motor terminals ( $E_T \times \text{RPM}$ )
$E_R$	Resultant voltage between $E_s$ and $E_M$
$E_S$	System voltage at motor starter
$E_T$	Motor terminal voltage at synchronous speed

<i>I</i>	RMS current
kVA	Kilovolt-amperes
kVAC	Kilovolt-amperes (capacitive)
kVAR	Kilovolt-amperes (reactive)
kW	Kilowatts
<i>L</i>	Circuit inductance (Henrys)
<i>N</i>	Rotor speed (rpm)
RPM	Rotor speed, per unit of synchronous speed

EQUIVALENT CIRCUIT CONSTANTS

<i>r</i> <sub>1</sub>	Primary (stator) resistance
<i>r</i> <sub>2</sub>	Secondary (rotor) resistance
<i>X</i> <sub>1</sub>	Primary leakage reactance
<i>X</i> <sub>2</sub>	Secondary leakage reactance
<i>X</i> <sub><i>m</i></sub>	Magnetizing (mutual) reactance
<i>s</i>	Slip

Note: All constants are in per unit on the motor output base

A practical interpretation of Faraday’s laws of magnetic induction is: If a magnetic field in a core of magnetic material is enclosed within a coil of current-carrying conductors such that all of the field is enclosed by the coil, the flux-linkage (product of current and magnetic flux) is constant. The voltage (*e*) across the coil is given by the equation:

$$e = L \frac{di}{dt} \tag{9.97}$$

where:

- e*=instantaneous voltage across the coil
- L*=inductance of the coil and core circuit
- di/dt*=rate of change of current in the coil

From this it is seen that if the current flowing in the circuit is suddenly interrupted, the voltage across the coil will increase very rapidly. (This effect is well known to those having worked on automotive ignition systems having distributors and induction coils!)

It is also seen from this equation that, if the flux (proportional to *e*) tries to change under some external influence, the current will change to maintain the constant flux-linkages. In short, the flux will be “trapped” within the circuit by an increase in the current resisting the change in flux. The only way the flux can change with time is for the energy in the magnetic circuit to be dissipated as *I*<sup>2</sup>*R* loss in the winding resistance.

Consider a single induction motor connected to a power system by a radial feeder through a circuit breaker. With the motor operating normally, the mmf (field) produced by the motor rotor is in-phase but opposite to the rotating magnetic field in the air gap. This is true even though the rotor is moving at less than the speed of the air gap flux [32]. Opening the supply breaker instantly removes the source of the air gap flux. The field attempts to collapse to zero. However, currents flow in the rotor bars (winding) to prevent the flux changing. The rotor then is decelerating with the trapped field and is moving back in angle relative to the voltage of the system from which it was disconnected. The rotor is generating a voltage at the motor terminals that is decreasing exponentially

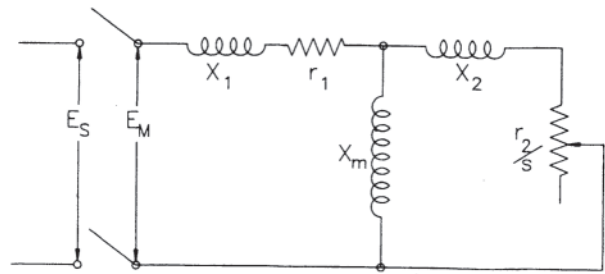


Figure 9.58 Induction motor equivalent circuit, circuit open.

with time as well as moving, angularly, farther from the system. The decreasing voltage is the result of the field energy being dissipated as *I*<sup>2</sup>*R* losses in the rotor bars. This rate of decay is a function of the inductance of the circuit enclosing the flux and the resistance and is the reciprocal of the “open-circuit time constant,” *t*<sub>d0</sub>. The motor residual voltage is given by:

$$E_T = E_S \exp [-(r_2/L) t] = E_S \exp [-2\pi f r_2 / X] t \tag{9.98}$$

where:

- E*<sub>*T*</sub>=motor terminal voltage
- E*<sub>*S*</sub>=rms voltage at motor terminals at time of switching
- L*=inductance of rotor and air gap
- r*<sub>2</sub>=rotor winding resistance
- X*=reactance of rotor and air gap = *X*<sub>*m*</sub>+*X*<sub>2</sub>
- X*<sub>*m*</sub>=magnetizing reactance
- X*<sub>2</sub>=rotor reactance
- f*=system frequency (Hertz)
- t*<sub>d0</sub>=*L*/*r*<sub>2</sub>=*X*/*2πf**r*<sub>2</sub>

All circuit constants per unit on motor output base. (Refer to equivalent circuit, Fig. 9.58.)

At the time the exponent (*2πf**r*<sub>2</sub>/*X*) is equal to 1.0, *E*<sub>*T*</sub> will be 36.8% of *E*<sub>*S*</sub>. This is defined as occurring at “one open-circuit time constant.”

Should the breaker connecting the motor to the system be reclosed, the voltage at the motor terminals is then the vectorial difference between the residual voltage of the motor and the system voltage. The currents that flow into the motor, and the

$$E_R = \sqrt{E_S^2 + E_M^2 - 2E_S E_M \cos \delta} \quad X_M = X_1 + \frac{X_m X_2}{X_m + X_2}$$

$$I_M = \frac{E_R}{X_M} \quad \delta = \text{angle between } E_S \text{ and } E_M \tag{9.99}$$

torques at the air gap, are the result of this resultant voltage, *E*<sub>*R*</sub>, divided by the total motor reactance, *X*<sub>*M*</sub>:

The most severe condition will result from a high-inertia load, such as an induced-draft fan motor with a long open-circuit time constant, closing 180 degrees behind the system. A low-inertia drive, having a short time constant, will approximate a normal across-the-line start. In between are an infinite combination of circumstances that may be “safe” or “unsafe” for reclosing.



Transferring a bus with many connected motors is a much more complicated condition to analyze, but is still the same situation. The high-inertia drives tend to hold up the residual bus voltage while the heavy loads with short time constants tend to extract both mechanical and magnetic energy from the system to reduce the residual bus voltage. The analysis of such a system requires a degree of sophistication beyond the scope of this section. Nevertheless, the methods employed here are fully applicable to this more complex analysis.

#### 9.1.8.4 The 1.33 Mystique and Other Switching Criteria

In Section 9.1.8.2 it was noted that reclosing criteria were developed by the U.S. motor manufacturers in the late 1950s. These were in response to user and contractor specifications attempting to require reclosing or transfer with the motor 180 electrical degrees out of phase with the oncoming bus.

The first published data of which this author is aware appeared in 1961 in a “District Engineering Letter” by Merrill [44] written to state one company’s policy on bus transfer and reclosing. This document was distributed to the company’s application engineers in the field. From there it was disseminated to various users, consultants, and contractors for their guidance. Other manufacturers either tacitly agreed to these conditions or adopted similar conditions of their own. Three conditions for switching were established:

1. *Fast Transfer:* The transfer must be completed in less than 8.0 cycles of dead time. Dead time is defined as the period between the clearing of the opening breaker and the restoration of voltage by the oncoming breaker.
2. *Differential Voltage Transfer:* This is permitted if the voltage difference (vectorial) between the motor residual voltage and the oncoming bus does not exceed 1.33 per unit.
3. *Delayed Reclosing:* If the conditions in (1) or (2) above cannot be met, the oncoming breaker should be locked out for a time equal to or greater than one open-circuit motor time constant.

The rationale for these conditions is somewhat empirical but still based on sound motor theory. It is necessary to establish a maximum voltage at the motor terminals that permits the designer to predict the inrush current and consequently the winding forces and air gap torques with confidence. The effects of saturation in the motor are nonlinear and become unpredictable at high levels of core saturation. It is also necessary that the user have some relationship relating this voltage condition to the timing of the control scheme.

The 6- to 8-cycle dead-time condition for fast transfer relates to the timing of circuit breaker operation. If the same signal is used to trip the active breaker and initiate closing of the oncoming breaker, the actual dead time should be between 2.0 and 6.0 cycles. This time is sufficiently short to conclude that neither the residual motor voltage, nor the angle between the buses, can change sufficiently to exceed the recommended switching criteria. Any breaker or relay malfunction can, however, create a difficult to-predict situation. The

responsibility for the consequences properly rest with the party making the application.

Some electrical utilities investigated sequential switching. This involved the transfer of a loaded bus having several motors of differing characteristics on it. A back contact on the opening breaker picked up the closing coil for the oncoming breaker. In nearly every case they found that the dead time was between 15 and 20 cycles and the resulting voltages were unsafe for transfer.

A rule-of-thumb used by some machine designers is that for a 10% increase in voltage (flux density), the saturation ampere-turns doubled. Thus, if at 1.0 (rated) voltage a motor saturation curve has 1500 ampere-turns per pole (AT) in the air gap and 300 AT in the iron (a total of 1800 AT), then at 1.1 voltage the air gap has 1650 AT and the iron 600 AT, or a total of 2250 AT. Two 10% voltage increments higher (1.33), the air gap requires 1995 AT and the iron requires 2400 AT, a total of 4395 AT, or 144% increase in magnetizing current alone. In addition the locked-rotor current, excluding the magnetizing branch, will increase 33%. This appears to be the upper level of saturation at which the performance of motor magnetic circuits remains predictable.

The open-circuit time constant, by definition, is the time in which the field decays to 36.8% of its initial value. If relay and switching times are considered, the residual terminal voltage should be less than 0.33 per unit. Thus, a one open-circuit time constant lock-out will meet the 1.33 per unit criterion regardless of angle.

#### 9.1.8.5 Methods of Calculation

The general method of analysis is very similar to the calculation of stability analysis for a single synchronous machine swinging against an infinite bus. The induction motor, with the flux trapped in its rotor, acts as a generator while the oncoming bus (presumably part of the same primary system as the bus being cleared) can be considered an infinite system. A step-by-step iteration process is described in the Westinghouse Transmission and Distribution Reference Book [25], [Chapter 13](#). This step-by-step approach should be used whenever long transfer times are involved or where special voltage conditions exist (such as power factor correction capacitors being switched with the motor).

For short transfer times (15 to 20 cycles), step-by-step integration may not be necessary. If it can be assumed that there is no voltage decay during the transfer and that the retarding torque is constant for the transfer period, a very simple calculation can be used. If this calculation gives marginal results, a more precise analysis should be made.

Both methods use per-unit notation and an inertia or kinetic energy constant,  $H$ . The per-unit base is output power in kilowatts ( $0.746 \times \text{rated horsepower}$ ). The voltage base is rated motor terminal voltage (line-to-line). Motor equivalent circuit data are not necessary if the calculation is to determine the resultant voltage at the motor terminals.

If, however, it is desired to determine the motor current and air gap torques at transfer, the resultant per-phase voltage must

be applied to the motor equivalent circuit, Fig. 9.58. The circuit constants in Fig. 9.58 are in per-unit per phase, on an output base. The output base is used here because load (real) current, kilowatts, shaft torque, and output kVA are all 1.0 on this base.

### SIMPLIFIED METHOD

1. Calculate the kinetic energy for the drive:

$$A_2 = (2.31)(Wk^2)(\text{RPM})^2(10^{-7})$$

where

$A_2$ =kinetic energy in kilowatt-sec.

$Wk^2$ =total  $Wk^2$ , in lb-ft<sup>2</sup>, of rotating elements (motor, gear, load, etc.)

RPM=full-load speed in rpm

2. Calculate the  $H$  Constant:

$$H = A_2 / \text{kW}$$

where

kW=rated kilowatt output of motor (0.746×hp).

3. Calculate the angular rate of deceleration:

$$\alpha = \frac{(180)(f)(\Delta P)}{(H)(\text{kW})}$$

where

$\delta$ =angular deceleration in degrees/sec<sup>2</sup>

$f$ =line frequency in hertz

$\Delta P$ =retarding power in per unit

kW=rated kW=1.0 in per-unit (output base)

$$\alpha = \frac{(180)(60)}{H} = \frac{10,800}{H} \text{ degrees/sec}^2$$

for 60-Hz motors and constant, full-load retarding torque.

4. Calculate the angular change:

$$\delta = \frac{1}{2} \alpha t^2$$

where

$\delta$ =angular change in degrees

$\alpha$ =angular deceleration

$t$ =dead time of transfer in seconds

5. Calculate resultant voltage between buses or motor and bus:

$$E_R = \sqrt{E_S^2 + E_M^2 - 2E_S E_M \cos \delta}$$

where

$E_R$ =resultant vectorial voltage in per-unit volts/hertz

$E_S$ =system equivalent volts/hertz (usually 1.0)

$E_M$ =motor residual volts/hertz=motor terminal voltage in per-unit of motor rated voltage multiplied by motor speed in per-unit of synchronous speed

Note:  $E_M=1.0$  if no voltage decay is assumed for fast transfer.

Example 1 A 6000-hp, 900-rpm motor is driving an in-

duced draft fan having a  $Wk^2$  of 207,750 lb-ft<sup>2</sup>. The motor  $Wk^2$  is 19,500 lb-ft<sup>2</sup> and has an open-circuit time constant of 1.0 sec. The customer desires a transfer dead-time of 12 cycles. Is this acceptable?

Assume no voltage decay and constant retarding torque.:

$$1. A_2 = (2.31)(207,750 + 19,500)(900)^2(10^{-7}) = 42,520 \text{ kW-s}$$

$$2. H = \frac{42,520}{(0.746)(6000)} = 9.5$$

$$3. \alpha = \frac{10,800}{9.5} = 1137 \text{ degrees/sec}^2$$

$$4. \delta = (0.5)(1137)(12/60)^2 = 22.74 \text{ degrees}$$

$$E_R = \sqrt{(1.0)^2 + (1.0)^2 - 2(1.0)(1.0) \cos 22.74^\circ}$$

$$5. = \sqrt{2 - 2 \cos 22.74^\circ} = 0.394 \text{ per unit}$$

0.394 < 1.33, so acceptable for 12 cycle transfer.

Example 2 A 5000-hp, 1800-rpm, 1.15 service factor motor drives a pipeline pump having a  $Wk^2$  of 825 lb-ft<sup>2</sup>. The motor  $Wk^2$  is 4650 lb-ft<sup>2</sup>. The open-circuit time constant is 2.9 sec. Customer is considering transfer schemes having dead-times of 3, 6, 8, and 10 cycles. Which, if any, can be used?

Assume no voltage decay and full service factor load on motor at time of transfer:

$$1. A_2 = (2.31)(4650 + 825)(1800)^2(10^{-7}) = 4098 \text{ kW-s}$$

$$2. H = \frac{4098}{(0.746)(5000)} = 1.099 = (1.1)$$

$$3. \alpha = \frac{10,800(\Delta P)}{H} = \frac{(10,800)(1.15)}{1.1} = 11,291 \text{ degrees/sec}^2$$

- a. For 3 cycles:

$$\delta = (0.5)(11,291)(3/60)^2 = 14.1 \text{ degrees}$$

$$E_R = \sqrt{(1.0)^2 + (1.0)^2 - 2 \cos 14.1^\circ}$$

$$= \sqrt{2 - 2 \cos 14.1^\circ} = 0.245 \text{ O.K.}$$

- b. For 6 cycles:

$$\delta = (0.5)(11,291)(6/60)^2 = 56.46 \text{ degrees}$$

$$E_R = \sqrt{2 - 2 \cos 56.46^\circ} = 0.946 \text{ O.K.}$$

- c. For 8 cycles:

$$\delta = (0.5)(11,291)(8/60)^2 = 100.36 \text{ degrees}$$

$$E = \sqrt{2 - 2 \cos 100.36^\circ} = 1.48 \text{ NO}$$

- d. For 10 cycles:

$$\delta = (0.5)(11, 291)(10/60)^2 = \underline{156.8 \text{ degrees}}$$

$$E_R = \sqrt{2 - 2 \cos 156.8^\circ} = \underline{1.71 \text{ NO}}$$

It is safe to transfer in either 3 or 6 cycles but not 8 or 10. The 8-cycle case could be examined more closely using step-by-step analysis to include the voltage decay. However, the time constant is so long that it is doubtful that it could reduce  $E_R$  to 1.33.

**Step-by-Step Analysis**

The step-by-step analysis accounts for the rate of decay of the field in the motor, the change of rotor speed and the effects of speed on the decelerating torque from the load. Example 3 and Table 9.10 demonstrate this method.

*Example 3* Motor rating 11,000 hp, 12,470 volts, 3-phase, 60 Hz, 438 A, 1792 rpm, efficiency 0.96 p-u.  $T_d' = 3.23$  sec; load  $Wk^2 = 54,500$  lb-ft<sup>2</sup>; motor  $Wk^2 = 11,530$  lb-ft<sup>2</sup>.

1. Calculate kinetic energy:

$$A_2 = (2.31)(66,030)(1792)^2(10^{-7}) = 48,981 \text{ kW-s}$$

2. Calculate  $H$  constant:

$$H = \frac{48,981}{(0.746)(11,000)} = 5.97 \text{ Use (6.0)}$$

Refer to Table 9.10. The analysis consists of calculating the angular change ( $\delta$ ) and residual volts-per-hertz ( $EM$ ) over small intervals of time. The angular velocity ( $\omega$ ) is assumed constant over the period but the acceleration ( $\alpha$ ) is assumed constant from the middle of one period to the middle of the

next. This is done by calculating the angular velocity for one-half of the first time interval. After that, the full interval is used in each calculation.

Note that two lines are used for zero time, 0- and 0+. 0- is the initializing condition and represents the situation the instant prior to the breaker opening. 0+ represents the dynamic forces acting upon the system as a result of the breaker opening.

Each of the columns will be discussed in turn together with the calculations required. Note that the columns that represent *end results* (columns 7, 10, 11, 12, 13, 14) are the conditions that exist at the *beginning* of the next interval. *Be cautious* of this when plotting curves from the table.

Col. 1: Time—1(a) in cycles, 1(b) in seconds.

Col. 2:  $\delta$ —Initial angle at time in Col. 1.

Col. 3:  $\Delta P$ —Per-unit power acting to decelerate (or accelerate) the load. Motor losses are included.

$$\Delta P = \frac{1}{\text{Eff.}} \left( \frac{\text{RPM}}{\text{RPM}_0} \right) \text{ for centrifugal loads}$$

$$\Delta P = \frac{1}{(0.96)} \left( \frac{1.0}{1.0} \right)^2 = \underline{1.04} \text{ at } t = 0+$$

Col. 4:  $\alpha$ —Angular acceleration

$$\alpha = \frac{(180)(f)(\Delta P)}{H} = \frac{(180)(60)(1.04)}{6} = \underline{1872 \text{ degrees/sec}^2}$$

**Table 9.10** Step-by-Step Analysis of Speed and Voltage During Bus Transfer

(a)	(1)	(2)	(3)	(4)	(5)	(6)	(7)	(8)	(9)	(10)	(11)	(12)	(13)	(14)
	(b) Time	$\delta$	$\Delta P$	$\alpha$	$\Delta t$	$\Delta \omega$	$\omega$	$\Delta' t$	$\Delta \delta$	$\delta_2$	RPM	$E_{TT}$	$E_M$	$E_R$
~	SEC													
0-	0-	0					0			0	1.00	1.00	1.00	0
0+	0+	0	1.04	1872	0.041	76.8	76.8	0.083	6.4	6.4	0.996	0.975	0.971	0.114
5	0.083	6.4	1.03	1854	0.084	155.7	232.5	0.084	19.5	25.9	0.989	0.950	0.940	0.439
10	0.167	25.9	1.02	1831	0.083	152.0	384.5	0.083	31.9	57.8	0.982	0.926	0.900	0.926
15	0.250	57.8	1.00	1800	0.083	149.4	533.9	0.083	44.3	102.0	0.975	0.902	0.879	1.462
20	0.333	102.0	0.99	1782	0.084	149.7	683.6	0.084	57.4	159.4	0.968	0.879	0.851	1.820
25	0.417	159.4	0.98	1764	0.083	146.4	830.0	0.083	68.9	228.3	0.961	0.857	0.824	1.666
30	0.500	228.3	0.96	1728	0.083	143.4	973.4	0.083	80.8	309.1	0.955	0.835	0.797	0.794
35	0.583	309.1	0.95	1710	0.084	143.6	1117	0.083	92.7	41.8	0.948	0.813	0.771	0.667
40	0.667	41.8	0.94	1692	0.083	140.4	1257	0.083	104.3	146.1	0.942	0.793	0.747	1.672
45	0.750	146.1	0.92	1656	0.083	137.4	1394	0.083	115.7	261.8	0.935	0.773	0.723	1.315
50	0.833	261.8	0.91	1638	0.084	137.6	1532	0.084	128.7	30.5	0.929	0.753	0.700	0.533
55	0.917	30.5	0.90	1620	0.083	134.5	1666	0.083	138.3	168.8	0.923	0.733	0.677	1.670
60	1.000	168.8	0.89	1602	0.083	133.0	1799	0.083	149.3	318.1	0.917	0.715	0.656	0.666
65	1.083	318.1	0.88	1584	0.084	133.0	1932	0.084	162.3	120.4	0.910	0.697	0.634	1.429
70	1.167	120.4	0.87	1566	0.083	130.0	2062	0.083	171.1	291.5	0.904	0.679	0.614	0.963
75	1.250	291.5	0.85	1530	0.083	127.0	2189	0.083	181.7	113.2	0.899	0.661	0.594	1.349
80	1.333	113.2	0.84	1512	0.084	127.0	2316	0.084	194.5	307.7	0.893	0.645	0.576	0.792
85	1.417	307.7	0.83	1494	0.083	124.0	2440	0.083	202.5	150.2	0.887	0.628	0.557	1.509
90	1.500	150.2												

Col. 5:  $\Delta t$ —Time interval for calculating velocity change. Use 1/2 of first period, full time for succeeding periods.

$$\Delta t = 0.041 \text{ for } t = 0+ \text{ to } t = 0.083$$

$$\Delta t = 0.084 \text{ for } t = 0.083 \text{ to } t = 0.167$$

Col. 6:  $\Delta\omega$ —Change in angular velocity ( $\omega$ ) by  $\Delta P$  for time  $\Delta t$ .

$$\Delta\omega = (\alpha)(\Delta t) = 1872(0.041)$$

$$= 76.8 \text{ degrees/sec}$$

Col. 7:  $\omega$ —Angular velocity change from base speed at end of time interval, degrees/s.

$$\omega = \Delta\omega(\text{col.6}) + \omega[\text{col.7}(n - 1)]$$

$$\omega = 76.8 + 0 = 76.8 \text{ degrees/s}$$

Col. 8:  $\Delta t'$ —Angle-time increment at  $\omega^\circ/\text{sec}$ .

$$\Delta t' = 0.083 \text{ sec}$$

Col. 9:  $\Delta\delta$ —Change in angle during total time interval.

$$\Delta\delta = (76.8)(0.083) = 6.4$$

Col. 10:  $\delta_2$ —Final angle at end of period (enter in Col. 2, next line).

$$\delta_2 = (0 + 6.4^\circ) = 6.4 \text{ at } t = 0.083$$

Col. 11: RPM—Per-unit speed at end of interval.

$$\omega_0 = (180)(\text{Poles})(\text{rev/s}) = (180)(4)(30)$$

$$= 21,600 \text{ degrees/sec}$$

$$\text{RPM} = \left(1.0 - \frac{\omega}{\omega_0}\right) = \left(1.0 - \frac{76.8}{21,600}\right)$$

$$= 0.996 \text{ at } t = 0.083$$

Col. 12:  $E_{TT}$ —Per-unit terminal voltage from decay of flux only during period.

$$E_{TT} = (1.0) \exp(-t/t'_{d0})$$

$$E_{TT} = (1.0) \exp(-0.083/3.23)$$

$$= 0.975 \text{ at } t = 0.083$$

Col. 13:  $E_M$ —Per-unit motor volts-per-hertz (Note: volts-per-hertz here is intended to account for the reduction in terminal voltage,  $E_M$ , caused by the decreasing velocity of the rotor and not any change in frequency. Therefore,  $E_M$  is the product of  $E_{TT}$  and RPM.)

$$E_M = E_{TT}(\text{RPM}) = (0.975)(0.996) = 0.971$$

$$\text{at } t = 0.083$$

Col. 14:  $E_R$ —Resultant, per-unit vectorial voltage difference between system and motor.

$$E_R = \sqrt{E_S^2 + E_M^2 - 2E_S E_M \cos \delta}$$

$$E_R = \sqrt{(1.0)^2 + (0.971)^2 - 2(1.0)(0.971)(\cos 6.37)}$$

$$E_R = 0.114 \text{ at } t = 0.083. \text{ Plot these values.}$$

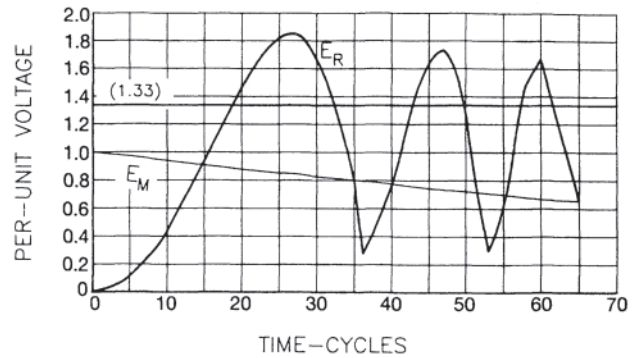


Figure 9.59 Per-unit voltage vs. time curves, open-circuit transfer.

The values for the line  $t=5$  cycles, 0.083 sec are calculated below for reference.

Col. 1:  $t=5$  cycles  $t=0.083$  s

Col. 2:  $\delta=6.4$  degrees (from col. 10)

Col. 3:  $\Delta P=(1.04)(0.996)^2=1.03$

Col. 4:  $\alpha=(1.03)(1800)=1854$  degrees/s<sup>2</sup>

Col. 5:  $\Delta t=(0.167-0.083)=0.084$  s

Col. 6:  $\Delta\omega=(0.084)(1854)=155.7$  degrees/s

The per-unit voltage vs. time curves are plotted in Fig. 9.59.

### 9.1.8.6 Reclosing on a Faulted Bus

There are common situations when a machine connected to a faulted bus is tripped from the system and reclosed after the fault is cleared. While the reclosing criteria are still valid, the time constants are considerably different.

In the equivalent circuit, Fig. 9.58, assume the circuit constants (per-unit, per phase) to be:

$$x_1 = 0.10 \quad r_1 = 0.01$$

$$x_2 = 0.10 \quad r_2 = 0.02$$

$$x_m = 4.00$$

Under open-circuit conditions the circuit reactance is  $X_m+X_2$  and the circuit resistance is  $r_2$ . The open-circuit time constant is then;

$$t'_{d0} = \left(\frac{X_m + X_2}{2\pi f r_2}\right) = 0.544 \text{ s} \quad (32.6 \sim)$$

Now consider the equivalent circuit in Fig. 9.60, having the stator terminals short-circuited. Now the circuit reactance (seen from the fault) is:

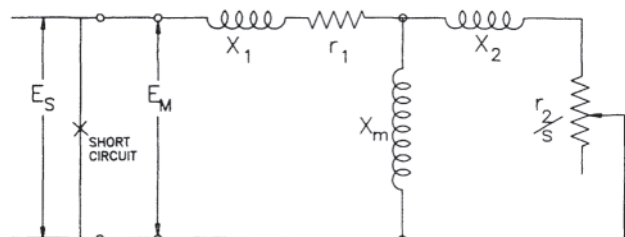


Figure 9.60 Equivalent circuit with short-circuit at motor terminals.

$$X_M = X_1 + \left( \frac{X_m X_2}{X_m + X_2} \right) = 0.198$$

The short-circuit time constant (in terms of the open-circuit time constant) is given by:

$$t' = t'_{d0} \left( \frac{X_M}{X_m + X_2} \right) = 0.026 \text{ s} \quad (1.6 \sim)$$

Thus, the flux decays at a rate nearly 21 times faster than for the open-circuit condition.

For the example shown, the initial fault current from the motor (for a bolted three-phase fault at the motor terminals) is 8.4 per-unit (output base). It is apparent that the switching time is not a consideration here. However, the initial fault current must be included when determining the momentary rating of the motor starter or breaker.

### 9.1.8.7 Machines with Switched Capacitors

Good engineering practice suggests that the maximum capacitive kVA switched with the motor should not exceed the magnetizing, or no-load reactive kVA, ( $\text{kVAC} \leq \text{kVAR}$ ). Were there no resistance, at no-load the motor circuit would be a true “tank-circuit”; a fixed voltage source at the terminals would result in the magnetic and electrical energy oscillating between the capacitor and the motor winding inductances with no current (or power) input from the voltage source. The presence of resistance in the motor stator winding provides damping to remove energy from the system and damp the oscillation. Consider the equivalent circuit in Fig. 9.61. The effect of the capacitors at the machine terminals is to maintain the voltage at the air gap, and at no-load only the stator resistance is effective in damping the residual terminal voltage. Under load, the rotor resistance also contributes to the damping. The open-circuit time constant with capacitors,  $t'_c$ , in terms of the open-circuit time constant,  $t'_{d0}$ , may be considered as:

$$t'_c = t'_{d0} \left( \frac{X_m + X_2}{X_1 + X_2} \right) \left( \frac{r_1}{r_1 + r_2} \right) = 5.58 \text{ s} \quad (335 \sim) \text{The}$$

open-circuit time constant, with capacitors, has now increased by a factor of 10, from 0.54 sec to 5.6 sec. For practical open-circuit switching situations, then, it may be assumed that the terminal voltage magnitude will not change. The motor becomes an infinite system as far as residual voltage is concerned. One “open-circuit time constant” lock-out is no longer a practical condition. A step-by-step analysis is required for all except high “H constant” situations.

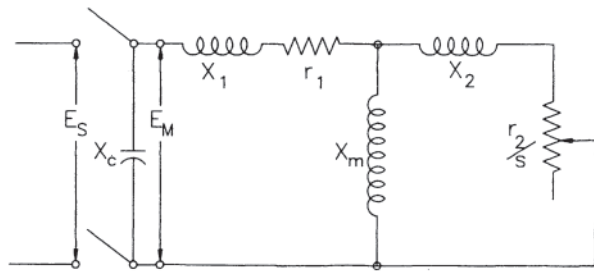


**Figure 9.61** Equivalent circuit with switched capacitors on the motor feeder.

### 9.1.8.8 Induction Generators

The induction generator is an induction motor operating at negative slip (i.e., above synchronous speed). While the same switching criteria are applicable from the standpoint of transient torques and currents, reclosing an induction generator is usually a dangerous procedure. When the electrical load is removed from the machine, the prime-mover torque accelerates the drive. Most induction generators are high-speed (1800–3600 rpm) and have low inertia ( $H$ ) constants. They also have low-resistance rotor windings, resulting in long open-circuit time constants. Should the machine be disconnected under full load, it could accelerate above its designed overspeed in less than one time constant. If the generator is equipped with power factor correction capacitors the overspeed will also generate an over-voltage condition in the windings. Good engineering practice suggests that, as soon as the generator loses its load, the power to the prime mover should be removed. Generators driven by hydraulic turbines may require flywheels or special rotors to avoid reaching dangerous overspeeds before the shaft power can be removed.

### 9.1.9 Induction Motor Speed Control

The speed-torque curve of an induction motor is determined by the machine parameters, the applied voltage and the frequency of the supply. The curve may be altered by change of voltage or frequency or by changing the rotor impedance.

Change of rotor impedance is, of course, not possible in squirrel-cage machines. Moreover, in the normal running range of a squirrel-cage motor, change of voltage has little effect on speed because the running speed is only a few percent below synchronous speed. Reduction in voltage can have a major effect on slip at full load, but a large change in slip translates into only a small change in speed. For example, doubling the slip from 3–6% results in a reduction in speed from 97% of synchronous to 94% of synchronous speed—hardly what one would call speed control.

Due to the shape of the torque-speed curve, only change of frequency can offer real speed control of a squirrel-cage machine. Until the advent of solid-state frequency changers, a change of frequency required the use of additional machines. For example, a dc motor-alternator combination could be used to supply power to a squirrel-cage motor, the frequency of the alternator output being controlled by the speed of the dc motor, and the output voltage of the alternator being controlled by the excitation of the alternator field. The control of the dc motor-alternator set would have to take into account the desirability of maintaining a nearly constant ratio of alternator output voltage to frequency. Furthermore, the shape of the torque-speed curve is frequency dependent. Starting torque may increase as the frequency is reduced, but will reach a maximum and fall for further frequency reductions. Breakdown torque will also fall as the frequency is reduced. These factors must be taken into account when considering starting scenarios. Like the Ward-Leonard system, this is a three-machine system, but it lacks the advantages of the Ward Leonard system.

The speed of a wound-rotor induction motor may be

adjusted by variation of voltage, frequency, or rotor impedance. Control of speed by adjustment of voltage or frequency suffers from the same limitations as for the squirrel-cage machine, although the slip under full load when rated voltage is applied to the motor is generally one or two percent higher for the wound rotor machine than for the squirrel cage machine. Hence, real speed control cannot be achieved by voltage control, and control by adjustment of the frequency (and voltage simultaneously) of the stator supply requires the addition of more rotating machines.

Control of speed by change of rotor resistance (or impedance) is feasible because of the access to the rotor circuit by way of the slip rings. Introduction of external resistance into the rotor circuit moves the breakdown torque point toward lower speeds without changing the magnitude of that torque, as will be seen in Fig. 9.62. This figure shows torque-speed curves for a 2-hp, 4-pole motor, with various external resistances ranging from zero (for  $r_{r1}$ ) to  $3 \times r_{r1}$  (for  $r_{r4}$ ). The value of  $r_{r4}$  was selected so that the peak of the torque-speed curve occurs at zero speed (unity slip).

It will be noted that no-load speed is essentially unaffected by the external resistance. Furthermore, if the load torque is always equal to the rated torque, the speed range possible with external resistances is limited to those indicated in the figure, which is only a little more than 200-rpm; that is, from 1730-rpm down to 1520-rpm. To achieve a wider speed range requires that the external resistance be increased further, moving the peak of the torque-speed curve into the negative speed range. Speed regulation is high, and becomes increasingly so as the external resistance is increased.

There are two additional factors to consider. The first of these is that this method of speed control is very inefficient, large amounts of power being dissipated in the external resistors. The second factor follows from the first. Because of the high power dissipation, power-type resistors (such as stainless-steel grid resistors) must be used; change in external resistance can therefore be made only in steps (and probably by use of contactors), and hence speed changes will occur in steps also. Speed control of induction motors by this method

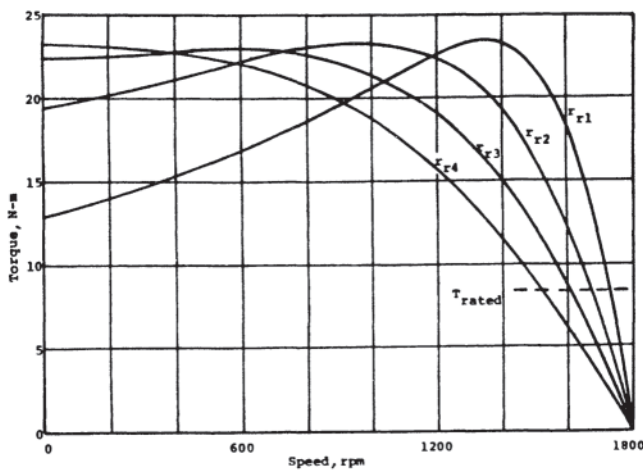


**Figure 9.62** Torque-speed curves for a wound-rotor motor with external resistors.

may be fairly characterized as being inefficient, imprecise, and incapable of control over the entire range of loads that may be encountered.

Several ingenious schemes have been devised that avoid the inefficiency just described and that lend themselves to more accurate speed control. These operate in the rotor circuit, replacing external resistors by combinations of additional machines. Among these schemes are the Kraemer and the Scherbius systems. Both require either two or three additional machines. For a constant-power drive, the Kraemer system requires a dc motor (with a dc supply) and a rotary converter; for a constant-torque system, an induction motor is also required. This system and a solid-state adaptation thereof were described earlier in Sections 9.1.7.3.1 and 9.7.1.3.2. The Scherbius system requires an induction motor and a specially built machine (the Scherbius machine) in one embodiment, and an additional machine to act as a frequency converter in another version. The interested reader will find more detailed descriptions in Ref. 45.

The speed control methods described briefly above were intended to enable one to make adjustments in speed over a given speed range. None was completely satisfactory, nor were other methods such as the doubly fed wound-rotor motor and the unbalanced voltage or unbalanced impedance control schemes that were implemented. The resulting controls either were inefficient, or, if efficient, required a large investment in additional machines.

### 9.1.10 Induction Motor Braking

In some applications, it is necessary to bring the motor to a stop as rapidly as possible. Mechanical brakes may be used, but there are also several methods of braking the motor using electrical means.

One of these methods is to disconnect the motor from the line and to pass direct current through the windings. A separate dc source may be used if available, but the dc may also be supplied by use of rectifiers connected to the ac line. Since the dc current will be limited only by the stator resistance, a fixed resistance is generally included in the circuit so that the dc current is limited to about four times the ac rms current at full load. Since large currents drive the magnetic circuit into saturation, any current greater than that needed to produce saturation will provide only a negligible increase in braking torque while causing substantial increase in the  $I^2R$  losses.

In this mode of operation, the flux field is stationary with respect to the stator; it is revolving with respect to the rotor, and at nearly synchronous speed at the beginning of the braking period. Hence, when braking begins, the frequency of the rotor voltages and currents will be nearly equal to the line frequency; at the end of the braking period, when the rotor is nearly stopped, the frequency of the rotor currents will be very small, becoming zero at stand still.

The resulting torque-speed curve in the dc braking mode will therefore be essentially that of the motor between starting and no load when excited from the line, except that the slip axis is reversed. That is, when braking begins the rotor conditions are

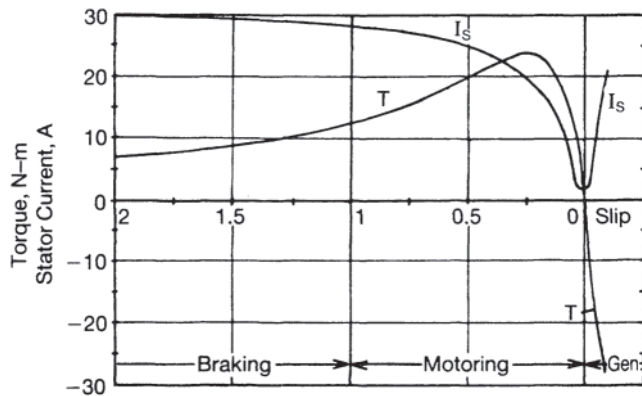


**Figure 9.63** Torque-speed curve for a 2-hp, 230-V, 3-phase induction motor for slip between—0.10 and 2.0

similar to those that exist in the rotor during a normal start (slip=1 in Fig. 9.63), whereas at the end of the braking period the rotor conditions are similar to those in the normal running range of the motor (slip nearly zero in Fig. 9.63). Braking torque therefore has an initial value comparable to starting torque, increases in magnitude as speed falls, and peaks at a speed approximately equal to the difference between synchronous speed and the speed at which break down torque occurs when the motor is operating in the induction motor mode.

A second common method of braking electrically is known as the plugging method. Figure 9.63 shows the torque-speed curve for a 2-hp, 230-V, squirrel-cage induction motor over the range of slip from 2 (synchronous speed in the reverse direction) to approximately  $-0.10$  (above synchronous speed in the forward direction). When a motor is plugged, the phase sequence of the supply is reversed, and the slip immediately becomes nearly 2. The torque is in such a direction as to drive the rotor in the direction opposite to that in which it has been running, thus being a braking torque.

As will be note from the  $I_s$  curve of the figure, line current will be only slightly larger than the locked-rotor value even at the time of initiation of plugging. The windings are therefore not subjected to currents much in excess of those that exist in the motor during a normal start. Providing the duty cycle is not too short, the motor will not be adversely affected by the increased heating.

The braking torque for this motor in the plugging mode will initially be approximately 7 N-m (newton-meters), rising as the speed falls to about 12 N-m at standstill. If dc braking were used with that current that produces the (reversed) torque-speed curve of Fig. 9.63, braking torques would always be above 12 N-m except when very near standstill. Plugging is thus less effective than dc braking, and the braking period will then be longer with plugging.

A plugged motor will decelerate to zero speed and, if the motor is not disconnected from the line, will then accelerate in the reverse direction. If reverse operation is to be avoided, the motor must be disconnected from the line when standstill is reached. This is frequently done by incorporating a zero-speed switch into the control circuitry.

Small induction motors are plugged without special precautions being taken with the control circuitry. The situation

is different with large machines. The plugging operation sequence requires that the machine be disconnected from the line and then reconnected with the opposite phase sequence. The flux in the motor that existed at the time of disconnection (trapped flux) decays with time, but some of that flux (and hence induced voltages in the stator windings) still exists at the time of reconnection to the line with the opposite phase. The situation is analogous to that discussed in Section 9.1.8, Bus Transfer and Reclosing of Induction Machines. As pointed out in Reference 46, torque pulsations with maxima as much as six times the steady-state torque value can occur during the first few cycles after reconnection occurs.

## 9.2 DIRECT-CURRENT MOTORS

### 9.2.1 DC Motor Starting

Starting of dc motors, except very small ones, is considerably different from starting an induction motor. Induction motors, by virtue of their impedance at standstill, draw currents that at start are typically five to ten times full-load current if the motor is started directly across the line. By contrast, a direct-current motor started directly across the line can easily draw 30 times full-load current (assuming that the supply is from an infinite bus), a value that will doubtless be greater than the commutating ability of the machine.

The reason for the high current draw is that the motor, at standstill, generates no counter electromotive force (emf), current is therefore limited only by brush drop (negligible), armature resistance, and, if present, resistance of the series field. It is evident that the starting current must be limited in some manner, both to protect the machine and to protect the supply. This has been done historically by introduction of one or more external resistors into the armature circuit in series with the armature.

#### 9.2.1.1 Counter-emf Starters

A simple starting circuit for a shunt motor is that of Fig. 9.64. This is known as a counter-emf starter. In this circuit, an external resistor  $R$  is placed in series with the armature in order to

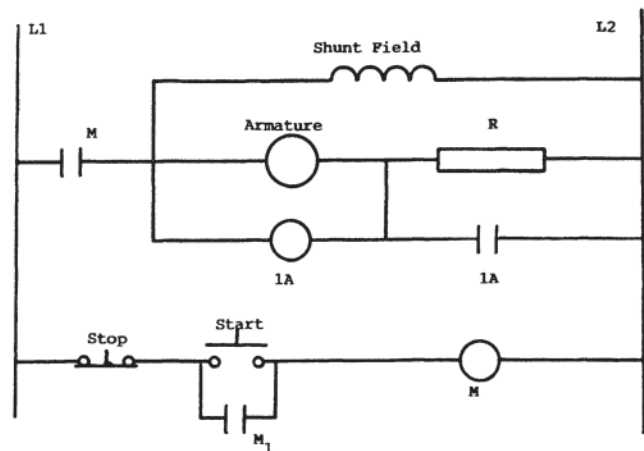


**Figure 9.64** Counter electromotive force (emf) starter for a shunt motor.

limit the armature current. Resistor  $R$  is sized so that armature current at standstill is greater than full-load current, thus insuring that starting torque will exceed full-load torque and a constant-torque load can be accelerated.

When the start button is pressed, contactor  $M$  picks up, latching itself in by means of auxiliary contacts  $M_1$ , and connecting the motor circuit to the line by main contacts  $M$ . Contactor  $1A$  is the accelerating contactor. At start, the only voltage across the coil of  $1A$  is that due to brush drop and armature  $IR$  drop. As the motor accelerates, the armature develops counter-emf, and the increasing voltage across coil  $1A$  will eventually reach the point at which  $1A$  picks up, its contacts shorting out resistor  $R$  and placing the armature directly across the line.

It may not be possible to use only a single accelerating resistor as shown in this figure. The armature current just before the point at which  $1A$  picks up may be too small to sustain acceleration, or the armature current just after  $R$  has been shorted may be higher than desired. Two or more series resistors may be required in the armature circuit, being shorted out at different points in the starting sequence by contacts  $2A$  on a second contactor  $2A$ , by contacts  $3A$  on a third contactor  $3A$ , and so forth. The coils of the additional contactors are placed in parallel with the coil of  $1A$ , but they each operate at different voltages.

Accelerating contactor  $1A$  must be designed to pick up on partial voltage, and any additional contactors  $2A$ ,  $3A$ , ... must be designed to pick up on different partial voltages. Standard contactors may be used instead, each one obtaining its excitation from the dc line by contacts on control relays (CR1 for contactor  $1A$ , CR2 for contactor  $2A$ , and so forth). The control relays are placed across the armature, each with a series resistor to adjust its pickup point.

### 9.2.1.2 Current Limit Acceleration

An alternate starting method is shown in Fig. 9.65. The motor shown here is a series motor, although with slight modification the circuit will serve for a shunt motor as well, just as the preceding circuit may be adapted to a series motor. There are numerous variations on both of these circuits, as well as those below.

The key to the operation of this circuit is that the armature current is to be sensed and used to control the acceleration sequence. The devices used to sense the current are the relays  $1AR$  and  $2AR$ . These are fast-acting relays with coils designed to carry the currents that appear in the armature circuit on starting, dropping out at a set value as the current falls. As the sequence of relay/contactor action is followed, it will become obvious that timing of contact opening and closing of the relays and contactors in this circuit is critical.

When the start button is depressed, contactor  $M$  picks up, closing main contacts  $M$  and holding contacts  $M_1$ . Contacts  $M_2$  are purposely arranged so that they do not close until after contacts  $M$  are closed and  $1AR$  has picked up. With  $1AR$  energized, the normally closed contacts  $1AR$  in series with contactor  $1A$  are open, and neither  $1A$  nor  $2A$  is energized. The motor starts with the full value of the tapped resistor  $R$  limiting the motor current to a predetermined value.

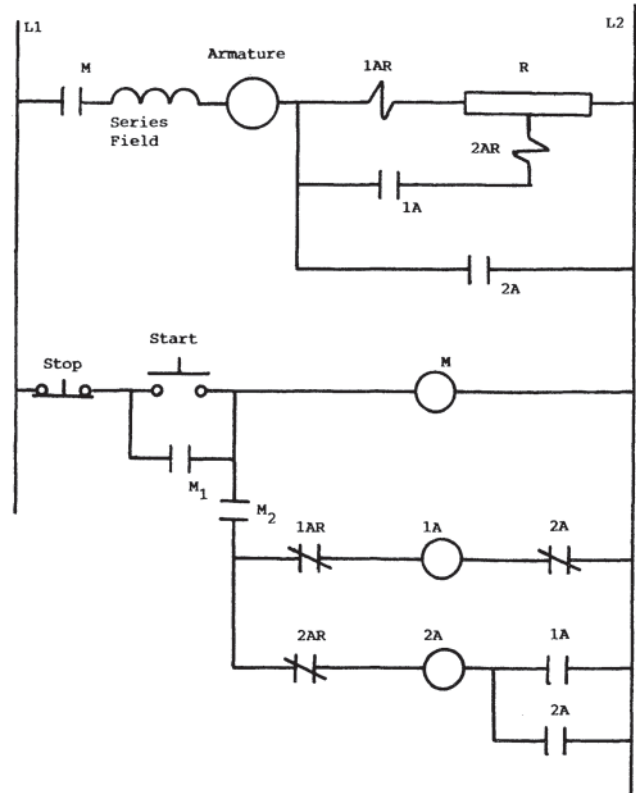


Figure 9.65 Current limit starter for a series motor.

As the motor accelerates and develops counter-emf, armature current falls. When it reaches the value at which  $1AR$  drops out, contactor  $1A$  picks up, shorting out part of tapped resistor  $R$  through contacts  $1A$  and the coil of relay  $2AR$ , thus allowing armature current to rise to a value nominally equal to the current at the beginning of the starting sequence. The normally closed contacts on  $2AR$  open quickly so that contactor  $2A$  is prevented from being energized when the  $1A$  contacts in series with the coil of  $2A$  close.

Armature current falls again as speed (and counter-emf) increase, eventually falling to the point at which  $2AR$  drops out. Contactor  $2A$  is then energized through normally closed contacts  $2AR$  and the normally open contacts of energized contactor  $1A$ . Contacts  $2A$  in the armature circuit now short out the entire accelerating resistor  $R$ . Contactor  $2A$ , being energized, drops  $1A$  out but maintains itself through its own auxiliary contacts.

### 9.2.1.3 Definite Time Acceleration Starting

A variety of circuits have been devised to cause the starter to run through its starting sequence in a fixed period of time. The starter shown diagrammatically in Fig. 9.66, which relies on a mechanical timer, is probably the simplest of these conceptually. Other circuits have been devised that rely on the time constant of the magnetic circuit of a relay or on the time constant of an  $RC$  circuit associated with a relay coil.

The operation of the circuit in Fig. 9.66 relies on the time delay relay  $TR$ . This may be a solenoid-type device, or may



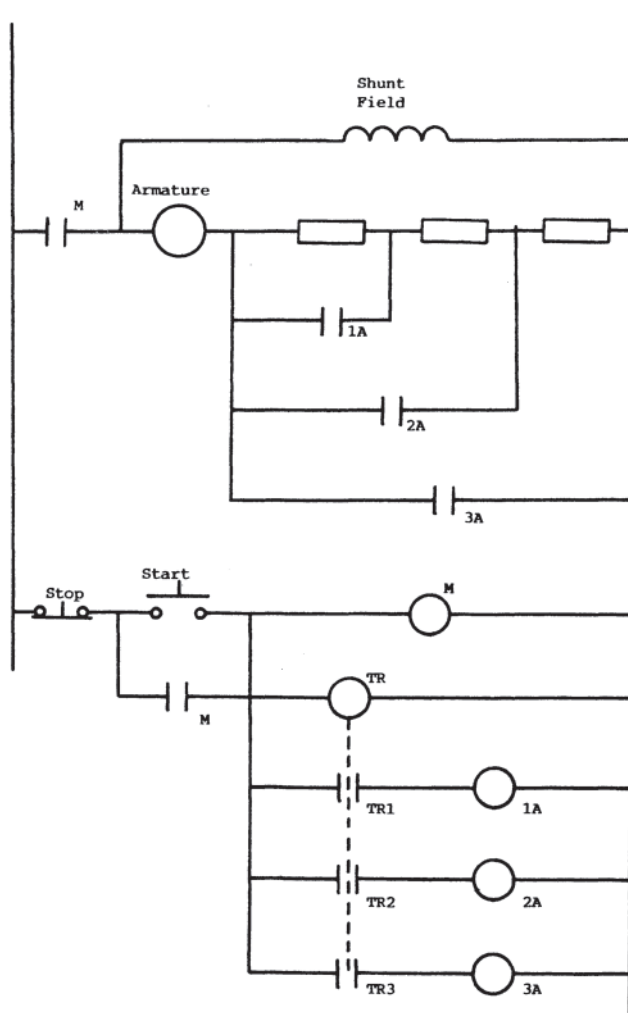


Figure 9.66 Definite time acceleration starter.

be a small motor. In either case, it closes contacts TR1, TR2, and TR3 in sequence, thus causing sequential energization of the coils of contactors 1A, 2A, and 3A, and the sequential shorting out of the resistors in the armature circuit. The time delays must be adjustable, and the relay TR must reset on deenergization of the circuit.

### 9.2.2 DC Motor Speed Control

The counter-emf generated by a dc motor is directly proportional to the flux in the machine and to the speed of the machine. That is:

$$E_a \propto \phi n \tag{9.100}$$

where:

- $E_a$  = the voltage generated internally in the armature
- $\phi$  = the flux in the machine, which is largely dependent on the mmf produced by the field(s) (and hence the field currents)
- $n$  = the speed of the machine.

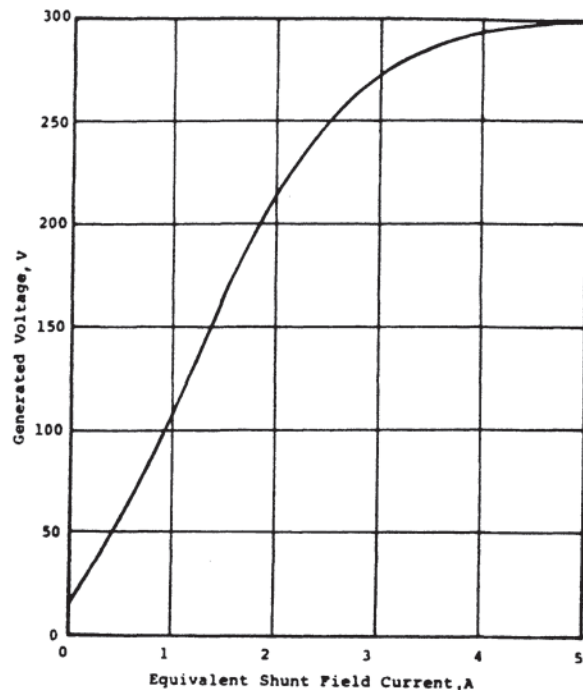


Figure 9.67 Magnetization curve of a 74-hp direct current (dc) machine at 1800 rpm.

Figure 9.67 shows a typical curve of  $E_a$  vs. field current  $I_f$  from data taken at 1800 rpm, where:

$$I_f = I_{sf} \pm N_s I_a / N_f$$

$I_{sf}$  = shunt field current,  
 $I_{sa}$  = series field current,  
 $N_s$  = number of turns on the series field, and  
 $N_f$  = number of turns on the shunt field.

The sign of the second term in the equation for  $I_f$  above depends on whether the motor is cumulatively compounded (+) or differentially compounded (-).

The curve of Fig. 9.67 is generally referred to as the magnetization curve (or “mag” curve) of the machine. It is sometimes referred to as the saturation curve; the fact that the magnetic path of the machine goes into saturation is clearly evident from the flattening of the curve above 250 V. It may also be noted that the curve does not pass through the origin, but that there will be generated voltage even with no field current. This voltage is due to the residual flux in the magnetic circuit, flux that is present because of the hysteresis loop of one or more parts of the magnetic circuit. The speed at which data were obtained for the curve must be specified; if the machine is running at a different speed,  $E_a$  may be obtained for the new speed by use of the proportionality above.

This curve also makes evident the highly nonlinear nature of the relationship between  $E_a$  and  $I_f$ . Recognition of this non-linearity must be taken into account when considering various methods of speed control. This is especially so in analysis of closed-loop systems using field control of speed. (See Section 6.6.)

If the armature of the motor is connected directly across the line,  $E_a$  is less than the line voltage  $V$  by the amount of the brush drop (about 2 V) plus the  $IR$  drop in the armature resistance and in the series field resistance (if present). This difference is small, even under full-load conditions, unless the motor is very small or the line voltage quite low. As a first approximation, line voltage  $V$  may be taken as being equal to the internally generated voltage  $E_a$ , especially under no-load conditions. Therefore the speed of the motor is almost directly proportional to line voltage after completion of the starting period.

It is therefore apparent that the speed of a dc motor may be adjusted by adjusting the voltage supplied to the armature, and that the armature voltage and the speed are directly proportional to each other. The proportionality above also shows that the speed may be adjusted by changing the flux (field current) in the machine, and that flux and speed are inversely proportional to each other. Every method of speed control of dc machines uses armature voltage control or field current control (that is, control of the flux), or both.

A shunt-connected dc motor is designed for a specified voltage and is intended to deliver a specified output power at a specified speed. That speed is known as the base speed. Base speed will be achieved if the shunt field current is about 85–90% of the ratio of line voltage to field resistance and with rated (specified) line voltage at the armature terminals.

#### 9.2.2.1 Speed Control by Field Current Adjustment

It was noted above that base speed is achieved with field current smaller than the current obtainable with the field rheostat set to zero. Increasing the field current will increase the flux in the machine and hence reduce the speed. However, most machines are designed so that the steel in the magnetic circuit is at or near saturation under rated conditions. An increase in field current will therefore not produce an increase in flux in the same proportion as at lower flux levels. For example, Fig. 9.67 is for a 250-V, 1800-rpm machine. If the machine is connected to a 250-V line and the field current is set to 2.5 A, then the machine will run at 1800 rpm at no load because the internally generated voltage  $E_a$  is equal to the line voltage at that speed and that field current.

If the field current were doubled (to 5.0 A), the armature would generate 300 V at 1800 rpm; as a motor it must run at a lower speed so that the generated voltage (the counter-emf) remains at 250 V. This requires a reduction in speed from 1800 rpm to  $1800 \times (250/300) = 1500$  rpm. That is, doubling field current has resulted in speed reduction of only one sixth of base speed. When trying to bring the speed below base speed, speed control by adjustment of field current is generally ineffective.

On the other hand, suppose that the field current were reduced by one-half, to 1.25 A. The generated voltage from Fig. 9.67 would be about 140 V at 1800 rpm, and motor speed would have to increase to  $1800 \times (250/140) = 3200$  rpm in order to generate the 250 V required to equal the line voltage. The motor speed has not quite doubled in response to halving of the field current, but the inverse speed-field current relationship discussed above is approached much more closely when the field is weakened than when it is strengthened.

In general, if speed is to be adjusted and controlled by adjustment of the field current, the adjustment is such as to weaken the field and the resulting speed is above base speed. For most machines, 150–200% of base speed is possible. Higher speeds (up to 400% or 500% of base speed) are possible with some specially built motors. Maximum speed may be limited by mechanical considerations (centrifugal forces on the armature) or by electrical considerations (commutation limits). If a motor is to be operated above base speed, the suitability of the motor for the service contemplated needs to be investigated very thoroughly and carefully. Consult the motor manufacturer.

Since output power is proportional to torque times speed, one might conclude that the rated output power of the motor is increased as the field is weakened (the speed increased). This conclusion is not correct. Another limitation comes into play, that being the ability of the motor to commutate the armature current. This limit falls as speed rises, the net result being that the motor has a constant-power limit at speeds above base speed: the motor is said to be in a constant-power region.

Field current control has been implemented using a wide variety of devices and circuits, ranging from the “operator setting a rheostat” level to closed-loop controls using binary-coded disks on the output shaft and digital input of the desired speed. Detailed discussion of the large number of schemes possible is beyond the scope of this handbook.

#### 9.2.2.2 Speed Control by Armature Voltage Control

The relationship between generated armature voltage (counter-emf) and motor speed is a linear relationship. Because motors are generally connected to sources that are at voltages reasonably close to the rated voltage of the motor, the only change of armature voltage that is practical is reduction of voltage. As discussed earlier, armature voltage and speed are directly related to each other. Hence reduction in armature voltage causes a corresponding reduction in speed. That is, armature voltage control results in control of motor speed below base speed.

In this region the motor is spoken of as being in a constant-torque mode; armature current is limited by brush loss, armature  $I^2R$  loss, and commutation limits, and field flux is nearly constant. Since torque is proportional to the product of armature current and field flux, a limitation on armature current imposes a similar limit on the torque that may be produced.

Typical speed-torque curves are shown in Fig. 9.68 for the machine having the magnetization curve of Fig. 9.67. Two curves are shown, one for the machine as a shunt motor, and the other as a cumulatively compounded motor. (Differentially compounded motors are rarely used, there being a tendency for the machine to run away.) The speed of the motor falls as load comes on due to the increased  $IR$  drop in the armature circuit (thus decreasing  $E_a$ ), although this is offset to some extent by the field weakening effect of armature reaction. The shunt motor shown has a no-load speed around 1660 rpm, and a full load speed around 1550 rpm, or speed regulation of  $(1660 - 1550)/1550 = 0.071$ .

Implementation of armature voltage control is not as simple as implementation of field current control. Armature currents

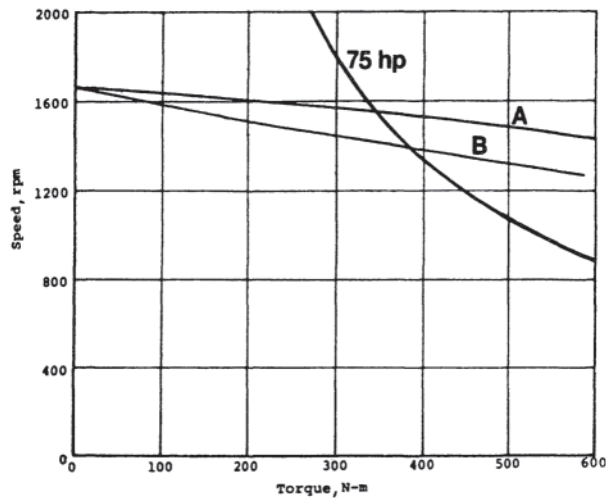


**Figure 9.68** External characteristics of a typical 75-hp direct current (dc) motor. A, shunt connection; B, cumulatively compounded connection.

at full load are typically 20 to 100 times as large as field currents with full field excitation. Hence external resistors in series with the armature must dissipate far more power than those used in series with a field circuit. Not only does efficiency suffer, but the motor speed-torque curve from no load to full load will no longer be like those of Fig. 9.68, that is, having a slow droop from no load to full load, but will be much steeper curves.

To see why this is so, consider the motor whose characteristics are shown in these two figures some what more closely, with the assumption that armature reaction effects are negligible. As a shunt motor, no-load speed is about 1660 rpm with a 250 V supply. No-load armature current  $I_a$  is 8.4 A, and armature resistance  $R_a=0.10$  ohm. Brush drop and armature resistance drop at no load may be taken to be 2 V [brush drop]+(8.4 A×0.10 ohm)=2.8 V, so that  $E_a=250-2.8=247.2$  V. The point of operation on the magnetization curve of Fig. 9.67 is therefore at  $E_a=247.2\times(1800/1660)=268$  V. (Field current is about 2.8 A.) At full load, speed is about 1550 rpm, and actual  $E_a=268\times(1550/1800)=231$  V. Full-load armature current may then be calculated from  $75\text{ hp}\times(746\text{ W/hp})/231\text{ V}=242$  A.

If speed is to be reduced to 1000 rpm at rated torque,  $E_a$  will be  $268\text{ V}\times(1000/1800)=149$  V. Since armature current  $I_a$  will be the same as at full load (242 A), resistance must be inserted into the armature circuit equal to  $(231\text{ V} - 149\text{ V})/242\text{ A}=0.339$  ohm.  $I^2R$  loss in this resistor will be about 20 kW.) No-load speed may be calculated using the original no-load armature current and the new total resistance in the armature circuit, 0.339 ohm externally plus the internal resistance of 0.10 ohm. Brush drop plus  $IR$  drop will be 5.7 V,  $E_a$  will be  $250\text{ V}-5.7\text{ V}=244.3$  V. No-load speed will then be  $1800\times(244.3/268)=1640$  rpm, only 20 rpm below the no-load speed with no additional armature resistance. Speed regulation will be  $(1640-1000)/1000=0.64$ , about nine times that for the shunt motor with no additional armature circuit resistance.

The first conclusion that may be drawn from this discussion

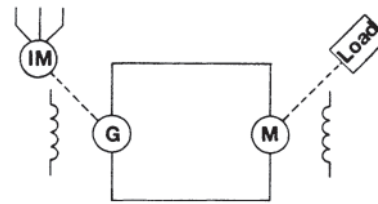


**Figure 9.69** Ward-Leonard system with induction motor drive. IM, induction motor; G, dc generator; M, dc motor.

is that speed control by use of armature resistance is not feasible if the torque that the load demands varies. Speed regulation will be larger than for a simple shunt motor, and increases in magnitude as the speed under load is reduced. The second conclusion is that the added  $I^2R$  losses are a sizable fraction of the output power under load and, if extremely low speeds at rated torque are to be achieved, the losses in the external armature circuit resistances will very likely be larger than the output power. A discussion of this type of control appears in Chapter 12, Ref. 46.

The shortcomings in the external armature resistance scheme have led to other and much more satisfactory methods of adjusting the speed of shunt motors below base speed. Two of these methods are briefly described below. Both require two additional machines, and both control the armature voltage without introduction of external resistors into the armature circuit.

The older of the two methods is the Ward-Leonard system, illustrated diagrammatically in Fig. 9.69. In this figure, the drive motor for the dc generator is usually an induction motor (because of its low cost), although any prime mover may be used. Probably the most popular alternative is a synchronous motor, used with the objective of improving line power factor.

The generator field is supplied from an adjustable dc source. This may be a constant-voltage bus with a rheostat in series with the generator field, a full-wave rectifier fed by an adjustable transformer, a magnetic amplifier, or an electronic controller using transistors or thyristors. Whatever the method selected, the control circuit needs to control only a very small power compared to the output power being controlled in the armature loop.

Another method for controlling the armature voltage is to use an amplidyne generator in place of the conventional dc generator shown in Fig. 9.69. A description of this machine will be found in Ref. 23. The amplidyne had the advantage that the control power is reduced by another order of magnitude from that required in the Ward-Leonard system, but that advantage was offset by the increased cost for the amplidyne itself. With the high-power electronic devices available today, the major advantage enjoyed by the amplidyne has been lost.

In both the Ward-Leonard system and the amplidyne system, the field of the motor may be excited from a fixed dc source, or it may be excited by a controller similar to that used by the generator/amplidyne. The generator field control allows motor speeds to be set at or below base speed. Control of the motor field then gives speed control above base speed, with a cutover from generator field control to motor field control

somewhere in the vicinity of base speed. Speed ranges of 70:1 to 100:1 are possible.

Speed control systems of the kinds just described are being replaced by single machine drives with solid-state controls of the type described below, and Ward-Leonard and amplidyne systems would very likely not be considered for any new installations. However, many of these systems are still in service, although the controllers are being upgraded to today's capabilities. In some cases, the motor-generator sets of either system are being replaced with modern controls; in other cases the three-machine system is being retained because it provides some isolation of the ac supply from the load being driven by reason of the ability of an induction motor-generator set to supply additional energy to the load on a temporary basis, drawing on the stored kinetic energy. This enables the ac supply to "ride through" transient conditions caused by a sudden increase in load torque. As an example, such changes occur frequently on roll lathes on which "as cast" rolls are being turned. The cutting tool may be clear of the work at one instant, and taking a full cut a fraction of a second later.

### 9.2.3 Braking of Direct-Current Motors

Every rotating machine and connected load contains stored kinetic energy. In addition, electrically driven vehicles will have varying amounts of potential energy if the route traversed has changes in elevation. The objective of every method of braking is to take stored energy and to convert it into another form. This is most frequently done by converting the energy into thermal energy. Mechanical brakes, for example, perform this function. The energy converted during dynamic braking from the kinetic or potential form into thermal energy is rarely, if ever, utilized.

The only way to brake a dc motor electrically is to shift its operation from motor action to generator action. As noted in the preceding subsection on speed control, the armature of a dc motor in its normal running range already has an internally generated voltage, the counter-emf, which is the principal factor in limiting armature current. A small increase in field excitation will cause the internally generated voltage  $E_a$  to exceed the line voltage. Armature current will then reverse direction, as will the power flow. In a stationary installation, energy will be abstracted from the rotating parts of the motor and load, resulting in a reduction of speed. In an electric vehicle, potential energy changes that occur simultaneously must be taken into account to determine what speed change will occur.

#### 9.2.3.1 Dynamic Braking

In dynamic braking, the energy being abstracted from the system is transformed into thermal energy. The circuit diagram of Fig. 9.70 is for a cumulatively compounded motor that is to be dynamically braked. (Portions of the circuit used for starting are not shown.) In this circuit, contactor DB controls the dynamic braking action. When the motor is started, DB picks up and its normally closed contacts open the armature-braking resistor loop, and a pair of normally open contacts pick up M. Main contactor M is held in by the normally

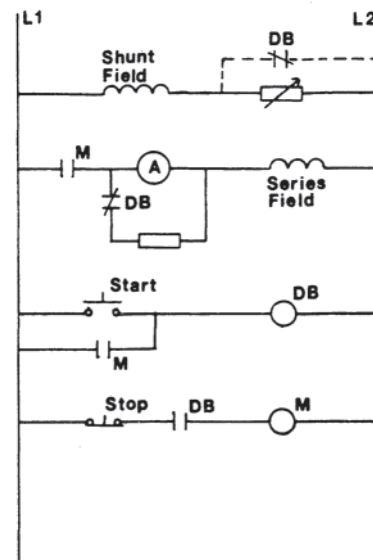


**Figure 9.70** Circuit for dynamic braking of a cumulatively compounded direct current (dc) motor.

open contacts on DB, and DB is held in by normally open contacts on M.

The braking sequence is initiated by pressing the "stop" button. This drops out contactor M, which in turn drops out contactor DB. The armature and series field are disconnected from the line, and the armature is connected to the braking resistor. Since the machine is running and flux is provided by the shunt field (which is maintained across the line), the machine shifts to the generator mode, and armature current now leaves the positive terminal of the armature and returns by way of the braking resistor. Reversal of the direction of armature current causes a reversal of the direction of armature torque, and the machine slows down.

Note that the dynamic braking resistor is connected directly across the armature, inside the series field. If the series field were included in the braking loop, the reversed armature current through the series field would reduce the total mmf of the armature circuit, thus weakening the braking action.

The resistance of the dynamic braking resistor is selected so as to keep the maximum (that is, initial) current during braking within the commutation limits of the machine. The power rating of the resistor must be sufficiently large that the resistor is capable of absorbing the energy transferred to it during the braking period. To a first approximation, that energy is the total kinetic energy stored at the beginning of braking, adjusted in the case of electric vehicles for any change in potential energy. Unless the motor is braked only infrequently, the duty cycle will also have to be considered when selecting the resistor.

Braking action changes during the braking period. At the beginning, maximum braking torque is developed because the armature current is high. As the motor slows, generated voltage, becomes smaller, being directly proportional to the speed, and the armature loop current falls in the same proportion. As the motor approaches zero speed, braking torque is approaching zero asymptotically. It is sometimes necessary to initiate mechanical braking action toward the end of the

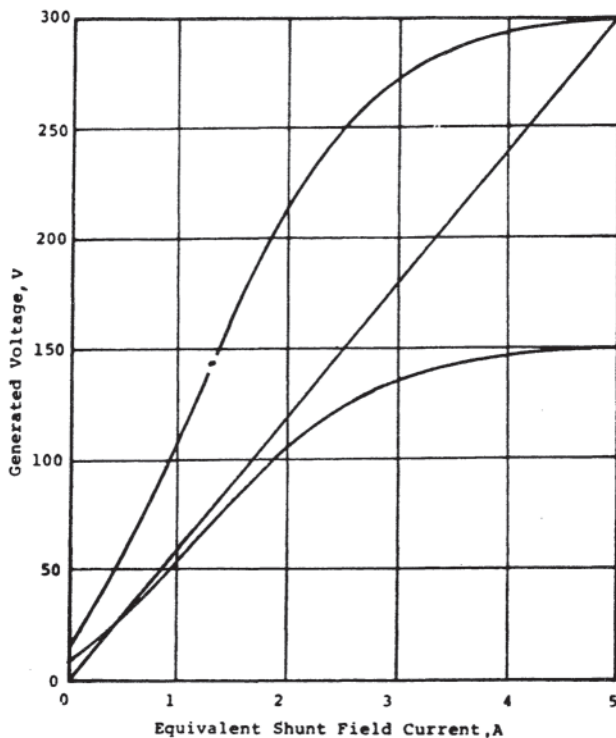


**Figure 9.71** Magnetization curves at 1800 rpm and at 900 rpm, with 60-ohm field resistance line.

braking period, and a mechanical brake is required if the motor and load are to be held stationary after stopping.

The shunt field is usually not at its full strength when the motor is running, especially if field weakening is used to adjust the speed. The auxiliary normally closed contacts on DB, which are shown dashed across the field rheostat, may be added to insure full field for braking purposes.

If dynamic braking is required in the event of loss of voltage on the dc bus, a different connection must be used. Instead of the shunt field being connected to the bus, it must be connected across the armature so that its excitation is maintained. The motor will then operate as a self-excited generator. As speed falls, braking torque will be smaller at every speed than for the fixed-field case because field excitation will fall with speed.

Figure 9.71 gives a graphical example of this effect. The upper magnetization curve is that of Fig. 9.67, the machine being at 1800 rpm. Drawn on these axes is a field resistance line for a 60-ohm field circuit, so that the intersection of the magnetization curve and the field resistance line occurs at 300 V.

The lower magnetization curve is that of the same machine at 900 rpm. The intersection of that magnetization curve with the field resistance line occurs at about 25 V. Assuming that the motor was running at 1800 rpm and field resistance was 60 ohms at the initiation of braking, it can be seen that the armature current when the machine has reached 900 rpm is only one twelfth of its initial value. By contrast, if the field were on fixed excitation at 5 A, the generated voltage at 900 rpm would be 150 V, and the armature current would have only been halved.

It is obvious that self-excited dynamic braking is not nearly as effective as dynamic braking with fixed field current.

### 9.2.3.2 Regenerative Braking

Dynamic braking transforms kinetic energy (and sometimes potential energy) into thermal energy. Regenerative braking, on the other hand, transfers energy from the rotating system back into the supply. The motor “regenerates” power back into the line. This is especially useful in those regimes in which the load is driving the motor and a relatively constant speed is desired. Examples of loads for which regenerative braking is useful and desirable include hoists that are lowering loads, elevators under some loadings, and electric traction vehicles on down grades. There are two principal advantages: Reduction in energy costs, and elimination of the capital expense of braking resistors. The second advantage may be reduced in importance or even eliminated if dynamic braking is required during the braking sequence. For example, electric trains descending long grades at speeds below that at which regenerative braking is effective may still be dynamically braked, but all of the energy must be dissipated in the resistor banks.

The shift from motoring to generating requires only that the field be strengthened so that internally generated voltage is above line voltage. Control of the braking process is by control of the field current.

If substantial reductions in speed are to be achieved by regenerative braking or if the speed is to be held considerably below normal running speed, the motor must be designed so that it operates on a weak field at normal running speeds, that is, with the magnetic circuit flux well below the saturation level. If this is done, the field can be strengthened so much that line voltage may be generated at speeds well below the speeds usually achieved when running. Further discussion of this point appears in Section 2.4.1.1.

Regenerative braking becomes less effective as the speed is reduced, and there is a lower limit to the speed at which it has any effect at all. That lower limit is determined largely by the speed at which the motor with saturated field has an internally generated voltage that equals the line voltage. If further speed reduction is needed, resort must be had to dynamic or mechanical braking.

If the electrical system in which the motor(s) to be regeneratively braked is closed—that is, if energy from the system cannot be returned to the main supply—regenerative braking may not be fully effective or may result in unexpected motor operation. An example of a closed system is an electric railway using dc for the locomotives that is fed by conventional rectifiers from an ac supply. If there are several locomotives in the system and some of them are operating at light loads or are perhaps standing in a station, regenerative braking of other locomotives can produce more power than can be absorbed by those locomotives drawing power. This effectively disconnects the system from the ac supply by raising the voltage above the peak of the ac supply voltage to the rectifiers. This increased voltage can then cause unanticipated modes of operation by all locomotives, both those drawing power

and those returning power to the system. Those that are regenerating will lose some of their braking torque, and those in normal motoring will be subject to unwanted acceleration.

### 9.3 GENERAL CONSIDERATIONS CONCERNING SOLID-STATE CONVERTERS AND CONTROLLERS

The combination of a motor, converter, and controller is frequently referred to in present-day terminology as a “drive.” One definition of a converter in the *IEEE Standard Dictionary* [27] is “a device that changes electrical energy from one form to another.” There are also a number of definitions of “controller” in Ref. 27, one being “a device that regulates the state of a system by comparing a signal from a sensor located in the system with a predetermined value and adjusting its output to achieve the predetermined value.” This definition is so broad that an entire drive may be subsumed under the term “controller.”

For purposes of this discussion, the term “converter” will be restricted to mean power semiconductor devices with their necessary firing or driver circuits. The term “controller” will be used to refer to that part of the drive that accepts input signals, whether from a local control panel, from the drive output, from internal feedback paths, or from remote stations, and which processes those signals so that the controller output sends the necessary signals to the converter. Output signals may also be sent to other units.

#### 9.3.1 Converters

The definition of a converter covers conversion from ac to dc, from dc to ac, from dc to dc, or from ac at one voltage and frequency to ac at another voltage and frequency. A converter that converts ac to dc is referred to as a rectifier. If it converts dc to ac it is referred to as an inverter. One embodiment of a dc to dc converter is known as a chopper, an application being discussed in Section 3.8.2.

Equipment that converts from ac at one frequency to ac at another frequency is known as a frequency changer. In the process of changing the frequency, the voltage may or may not be changed. Frequency changers may consist of a rectifier followed by an inverter, or they may utilize circuitry that converts energy at one frequency directly to energy at another frequency without an intermediate conversion into dc. (Some engineers prefer to use the term “converter” for the ac-dc-ac conversion process and to reserve the term “frequency changer” for conversion without the intermediate dc link. The term “cycloconverter” is also used for circuits that convert directly from ac to ac without a dc link.)

Many converters are one-quadrant circuits. That is, they provide energy to the motor so as to drive the motor in the forward direction; they operate only in quadrant I of Fig. 9.72. Other converters have the capability of operation in quadrants I and II. Consider, for example, a separately excited shunt motor on a hoist. When raising a load, energy is being supplied to the motor from the line through the converter; operation is in quadrant I. If a load is being lowered, the motor is running in the reverse direction and must be braked. This is operation

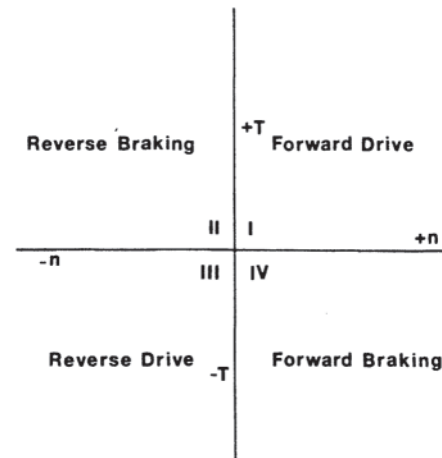


**Figure 9.72** The four possible quadrants of motor operation:  $n$ =speed;  $T$ =torque.

in quadrant II, and energy may be returned to the line using the same converter. Other (and more complex) converters and controllers have capability in all four quadrants shown in Fig. 9.72. That is, they supply power to the motor and connected load or accept power from the combination (regenerative braking) in the “normal” forward direction, and they can also operate in the reverse direction in either a motoring mode or in a braking mode.

Whether ac power is supplied to an ac motor by an ac-dc-ac conversion or by a direct ac-ac conversion, the output voltage waveshapes are not sinusoids. They exhibit a variety of waveforms, all of which contain harmonics of different orders and magnitudes. Because the loads contain active elements (such as internal generators) and in addition none of them contains passive elements that are strictly resistive in nature, the output currents may exhibit a markedly different appearance from the output voltages. The harmonics in the output of the converter are frequently supplied by the input circuit, resulting in harmonics in the supply that may or may not have an effect on other parts of the system. Similar comments may be made with respect to rectifiers that supply power to dc motors. The output voltage is not a pure dc, and the output current will frequently contain strong harmonics that must be supplied from the ac supply circuit.

For a thorough discussion of harmonics in electric power systems and recommended practices and requirements, the reader is referred to IEEE Std. 519–1992—IEEE Recommended Practices and Requirements for Harmonic Control in Electrical Power Systems [48]. As pointed out in that standard, harmonics are produced in electrical power systems, both in the current and the voltage waveforms, by nonlinear loads. Such nonlinear loads include static power converters, arc discharge devices (electric arc furnaces), saturated magnetic devices, and some rotating machines. Of these, static power converters now constitute the largest nonlinear loads, and their share will certainly continue to increase.

The presence of harmonics in the ac power system can cause interference with communication circuits and may produce other deleterious effects. For example, if capacitors are used for power factor improvement, the harmonics may excite unanticipated

resonances, resulting in elevated levels of harmonic voltages and currents. Moreover, the static converters on the system may be affected by harmonics, either self-generated or generated by other equipment on the system. There is the possibility that harmonics on the supply side of a converter may cause misfiring or failure to commute. Functional failure or component destruction are distinct possibilities.

For all of these reasons, IEEE 519 establishes goals concerning waveform distortion. These goals are established only for steady-state operation; the limits set forth may be exceeded under transient conditions. A partial list of other relevant IEEE standards and excerpts from their stated scopes is as follows. Anyone concerned with the selection and application of converters should consult the appropriate standards.

1. ANSI/IEEE Std. 444–1973—IEEE Standard Practices and Requirements for Thyristor Converters for Motor Drives: Part I—Converters for DC Motor Armature Supplies [49]. This standard applies to all types of line-commutated semiconductor power converters, using monocrystalline semiconductor thyristors or diodes, when used in industrial motor drive applications requiring adjustable direct voltage for dc motor armature of field, or adjustable voltage and frequency in the case of ac motor drives (cycloconverter).

2. IEEE Std. 597–1983—IEEE Standard Practices and Requirements for General Purpose Thyristor DC Drives [50]. This standard applies to line-commutated semiconductor power converters for general purpose industrial direct-current motor drives powered from three-phase or single-phase ac supplies.

3. IEEE Std. 428–1981—IEEE Standard Definitions and Requirements for Thyristor AC Power Controllers [51]. These recommendations apply to thyristor ac power controllers that are low-voltage, power electronic, industrial-class equipment for the control or switching of ac power. Switching, multicycle control and phase control are included. Cycloconverters are excluded. Examples of application include, but are not limited to, industrial oven controls, static motor starters, static relays, and so on.

4. ANSI/IEEE Std. 995–1987—IEEE Recommended Practice for Efficiency Determination of Alternating-Current Adjustable-Speed Drives: Part I—Load Commutated Inverter Synchronous Motor Drives [52]. This recommended practice proposes a method for determining the efficiency of large, adjustable-speed ac motor drive systems consisting of a load-commutated inverter and a synchronous machine, in which a dc-linked converter is connected between the line and the load.

### 9.3.2 Controllers

The controller may be a relatively simple circuit, such as an analog phase shift circuit in which the phase shift is controlled by a hand-set potentiometer so as to control the firing angle of a thyristor in a rectifier. On the other hand, the controller may be largely digital in nature, processing outputs of tachometer generators, current and voltage sensors, and torque sensors so as to control speed, torque, or both, to keep currents within allowable limits, to control acceleration and deceleration, or to provide other functions needed in the drive.

It may also contain compensation networks to stabilize closed-loop systems.

Beginning in the late 1960s, “black boxes” became available in which these functions could be performed. These devices, known as programmable logic controllers (PLCs), or simply as programmable controllers, provide the user with the capability of selecting the desired functions without having to design any of the circuits. Nowadays, microprocessors, introduced in 1971 are used in the control of more complex power electronic systems. Depending on the system requirements, a wide range of processors can be used. These include general purpose microprocessors, microcontrollers, and any one of several advanced processors (DSPs, Rise processors, etc.).

See [Section 9.6](#) for more detailed discussion of controllers.

## 9.4 POWER ELECTRONIC DEVICES

There are seven types of solid-state power electronic devices used in motor control circuits: (1) diodes, (2) thyristors (silicon-controlled rectifiers [SCRs]), (3) gate turn-off thyristors (GTOs), (4) bipolar transistors, (5) metallic oxide semiconductor field-effect transistors (MOSFETs), (6) insulated gate bipolar transistors (IGBTs), and (7) Integrated Gate-Commutated Thyristor (IGCTs).

The diodes, as their name indicates, are two-terminal devices; one terminal is connected to the anode and the other to the cathode. The remaining devices have at least three terminals. One of these is connected to the anode and one to the cathode. Control of the anode-cathode conduction characteristic is achieved by use of appropriate signals on the remaining electrode(s).

The order in which these seven devices are listed corresponds roughly to the chronological order in which they became important in the motor control field. The semiconductor diode was originally looked on as a replacement for selenium and copper oxide rectifiers. It very quickly supplanted those devices by virtue of its lower forward voltage drop and its near-ideal reverse characteristics, having far lower leakage current and being able to withstand higher inverse voltage. As higher-current devices were developed, the semiconductor diode also replaced the mercury arc rectifier.

The thyristor appeared quite early in the development of semiconductor devices. This device, also known as the SCR, was an early replacement for the thyratron and later, as the capabilities of the device were improved, as a replacement for the controlled mercury arc rectifier, the ignitron. However, the thyristor has the same limitation as the thyratron and the ignitron in that once conduction has been initiated by the control electrode it can be terminated only by reducing the anode-cathode voltage to a very low level or by reversing it. That is, the control electrode has turn-on capability, but no turn-off capability. In the five remaining devices, the control electrodes have both turn-on and turn-off capability.

The following discussion is general in nature, and is intended only to set forth the most important points about each of these devices. Although device construction may be shown in diagrammatic form, attention is directed to the

external characteristics. If more detailed information is needed, the reader should consult other sources. Mazda [53] includes information on semiconductor fabrication and the characteristics of diodes, bipolar transistors, thyristors, GTOs, and other power semiconductor devices. Hoft [54] discusses diodes, power transistors, and thyristors. Finney [55] confines discussion of devices to the thyristors only. Reference [60] discusses the characteristics of most of the devices discussed above from an application point of view. Extensive coverage of diodes, thyristors, bipolar transistors, and MOSFETs appears in Fisher [56]. Pearman [57] discusses thyristors, and includes manufacturer's data sheets for typical devices. Murphy and Turnbull [58] has one chapter on devices. All of these references also contain discussion of various circuits in which these devices are used. Reference 58 has very complete discussions of circuits, and is particularly useful because of the large number of references cited.

### 9.4.1 Diodes

Semiconductor crystals without impurities are referred to as intrinsic semiconductors. Intrinsic material has very few charge carriers and therefore exhibits a high resistance. The semiconductor used in power devices is silicon (valence 4). Useful semiconductor devices contain impurities that have been introduced deliberately into the intrinsic material. If the impurity has a valence of 5, the resulting material is known as N-type material. Not all of the outer shell electrons of the impurity atoms are needed to form the valence bonds of the crystal; the excess electrons are available to carry current. If the impurity has a valence of 3, the resulting material is referred to as P-type material. Some of the valence bonds are not filled. These "holes" have the characteristics of positive charges which are free to move through the P-type material as current carriers. In a semiconductor device, some regions are P-type and others are N-type. The regions in which a transition is made from one type to the other are known as PN junctions. There are one or more junctions in power semiconductor devices.

As shown in Fig. 9.73(a), a semiconductor diode has one PN junction and two external terminals. The conventional graphic symbol is shown in Fig. 9.73(b). If the anode-to-cathode voltage is positive, current flows through the diode in the arrow direction of the symbol. The diode is said to be forward biased. A typical current versus voltage ( $I$ – $V$ ) characteristic in the forward-biased region is shown in the first quadrant of Fig. 9.73(c). (The voltage scale and the current scale for the first quadrant of that figure are considerably different from the scales for the third quadrant.) The maximum allowable forward current (the rated current) can be as high as 2000 A. Voltage drop in the forward direction is typically 1–2 V.

If reverse voltage is applied, a small reverse current will flow. This current, known as the leakage or saturation current, is typically only a few microamperes or less, and is nearly constant for reverse voltages larger than a very few volts. As the voltage in the reverse direction is increased, a voltage is eventually reached at which a phenomenon known as avalanche breakdown occurs. In the avalanche breakdown region, the reverse voltage drop across the diode is essentially

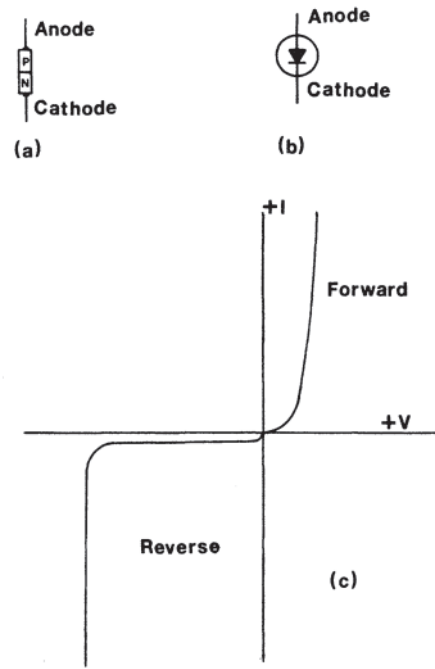


**Figure 9.73** (a) Diagrammatic representation of a diode; (b) graphic symbol; (c) current-voltage characteristic.

independent of the current. Unless the avalanche breakdown voltage is small (as is the case for the so-called Zener diodes), operation in the avalanche breakdown region results in dissipation of large amounts of power and rapid device destruction. The reverse voltage rating of the diode is set somewhat smaller than the avalanche breakdown value, and ranges in commercial devices from levels around 50 V to as much as 5000 V. The reverse voltage rating is also known as the peak inverse voltage (PIV).

The characteristics just described and shown in Fig. 9.73(c) do not include dynamic effects. Diodes used in rectifier circuits will be subjected to a rapid reversal of voltage when the supply voltage goes negative. In an ideal diode, there would be instantaneous switching from a conducting state to a blocking state when voltage reversal occurs. Practical diodes, however, when in the conduction mode, have charges moving through the junction region to supply the external current. Upon voltage reversal, the charge in the junction (referred to as  $Q_{rr}$ ) must be swept out before blocking is actually established. The resulting current is known as the reverse recovery current,  $i_{rr}$ ; it persists for a time  $t_{rr}$ . This effect is of most importance in rectifier circuits for use at high frequencies, where  $t_{rr}$  begins to become a sizable portion of the period of the voltage wave. If this effect is important, diodes known as fast-recovery diodes are used. These diodes have a small value of  $Q_{rr}$  and short  $t_{rr}$ .

### 9.4.2 Thyristors

A thyristor is a four-layer device, having three junctions between P and N regions. A diagrammatic representation of the structure is shown in Fig. 9.74(a), and the corresponding graphic symbol is shown in Fig. 9.74(b). For purposes of the following discussion, the junctions are labelled J1, J2, and J3



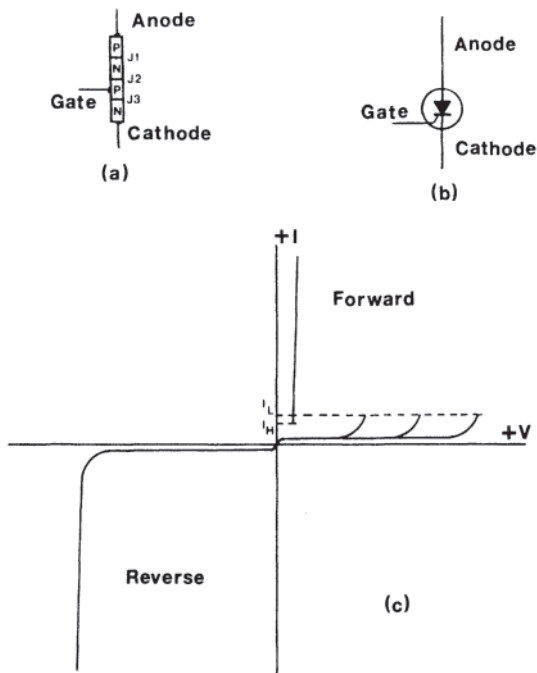


**Figure 9.74** (a) Diagrammatic representation of a thyristor; (b) graphic symbol; (c) current-voltage characteristic.

from anode to cathode. The gate (control electrode) is connected to the layer between junctions J2 and J3.

As long as no signal is applied to the gate, the thyristor exhibits similar characteristics for either polarity of voltage applied from anode to cathode, as is shown in Fig. 9.74(c). In the forward direction (positive voltage on the anode with respect to the cathode), the characteristic is that exhibited by J2, which is reverse-biased. It is the right-hand branch of the curve in the “Forward” quadrant, originating at the origin and ending when avalanche breakdown begins to occur and thyristor current reaches a (low) value indicated as  $I_L$ . The other two branches, having the same general shape, will result if pulses of gate current are injected at voltages lower than the forward avalanche breakdown voltage. The forward voltage rating of the thyristor is somewhat lower than the forward avalanche breakdown voltage. In the reverse direction, both junctions J1 and J3 are reverse-biased, but the characteristic is essentially that of J1 only because J3 normally has only a small reverse breakdown voltage (avalanche voltage).

If the anode-cathode voltage is positive, the thyristor may be put into a conducting state by injecting a positive current pulse into the gate. For complete turn-on to occur, the thyristor current must reach a value known as the latching current,  $I_L$ . Once full turn-on has occurred, the current may fall to a slightly smaller value, the holding current  $I_H$ . These currents are a very small fraction of the rated current.

With the thyristor in conduction, the gate current is no longer necessary. In fact, the gate has lost control over the action of the thyristor. To turn the thyristor off, anode current must be reduced below  $I_H$ . This will occur when the anode-cathode voltage reverses polarity, as in a rectifier circuit. It is also possible to divert the anode current temporarily into

another path to force thyristor current below  $I_H$ . If current falls below  $I_H$  as a result of reversal of voltage, the process is known as self- or line-commutation. If current is diverted to another path so as to cause turn-off, the process is known as forced commutation.

If the anode-cathode voltage is reversed (from positive to negative), reverse current occurs during the turn-off interval in junctions J1 and J3, just as in the diode. In addition, there are carriers near J2 that must be removed by a process known as recombination. This is a somewhat slower process. The total time for complete turn-off is on the order of 100 to 200  $\mu\text{s}$  in thyristors commonly used in phase-controlled rectifiers. The turn-off time limits the frequency of the supply for phase-controlled rectifiers using these thyristors to a value under 1 kHz.

The turn-off time may be reduced to 15–30  $\mu\text{s}$  by proper design of the thyristor (the “fast” thyristor), but with an attendant increase in the voltage drop during conduction. For a given mechanical configuration and a specified upper limit on device temperature, the total allowable internal heat losses in the thyristor are determined by the rate at which that heat can be transferred. With increased voltage drop, it is then necessary to reduce the rated current. Fast thyristors are desirable in chopper circuits, in which forced commutation is required, in order to minimize the size of the components in the commutation circuit.

A rapid increase in anode to cathode voltage when the thyristor is in the blocking state can cause significant charge to flow through the capacitance of junction J2. If this charge is high enough it can act as a gate current and trigger the device into conduction. Thyristors therefore have a maximum  $dv/dt$  rating. To limit the  $dv/dt$  applied, practical applications use a resistor-capacitor (RC) “snubber” circuit connected directly across the device.

Thyristors having breakdown voltages up to 4000 V and higher are available. Rated currents may run as high as 3000 A. Thyristors may carry nonrepetitive surge currents up to 10 times their rated value.

### 9.4.3 Gate Turn-Off Thyristors

GTOs have the same turn-on capability as conventional thyristors. In addition, it is possible to turn them off by use of a negative gate current. The symbol for the GTO shown in Fig. 9.75 is intended to show graphically that negative gate current can turn off the device. GTOs have voltage and current ratings comparable to those of conventional thyristors.

In a conventional thyristor, initial turn-on is localized in the vicinity of the gate terminal. The turned-on area spreads rapidly (approximately 100 m/s), and within a matter of microseconds the entire turn-on has occurred. Since negative gate current can turn off only that part of the device in the vicinity of the gate terminal and there is little or no spreading of the turn-off area, thyristor turn-off cannot occur with negative gate currents. However, if the structure is altered so that the cathode and gate are interdigitated, negative gate current may be visualized as turning off many very small areas, with the cumulative effect of turning off the entire

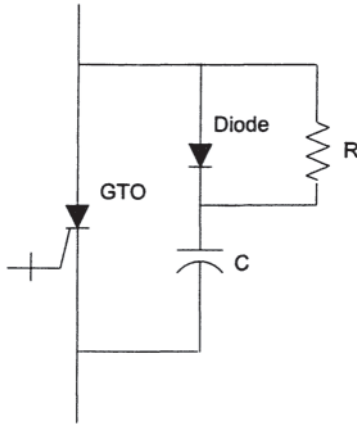


**Figure 9.75** Gate turn-off thyristor (GTO) with snubber circuit.

device. The negative gate current required is quite large, the gate turn-off gain being in the range of 3 to 5. After turn-off, it is usual practice to reverse bias the gate at about 15 V in order to prevent retriggering.

Power loss in the GTO may be calculated using the product of anode—cathode voltage drop, anode current, and the duty cycle, and adding to that value the gate power required for turn-on and turn-off. This power must be successfully dissipated through the GTO case and its heat sink to the ambient. Because turn-on and turn-off power rises linearly with the switching frequency, the switching frequency is limited to approximately 2 kHz.

An additional point that must be taken into account with GTOs is that forward voltage is reapplied immediately after turn-off, unlike the situation with the conventional thyristor. That is, the GTO is subjected to a rapid rise of voltage (high  $dv/dt$ ) in the circuits in which it is used. The capacitance of the reverse-biased junction (J2) will have a current directly proportional to  $dv/dt$ , and this current, if sufficiently large, will retrigger the GTO. To prevent retriggering from occurring, the resistor-capacitor-diode (RCD) snubber circuit of Fig. 9.75 is often used to limit the rate of rise of voltage after turn-off.

#### 9.4.4 Bipolar Transistors

Bipolar transistors are three-layer devices, either NPN or PNP. Transistors used as power devices are almost invariably NPN because they have better characteristics than the PNP devices for this type of service. The discussion which follows is based entirely on the NPN configuration.

The structure is shown diagrammatically in Fig. 9.76(a) and the symbol used in circuit drawings is shown in Fig. 9.76(b). The collector-to-emitter voltage  $V_{CE}$  is positive; most of that voltage appears across junction J1, which is reverse-biased. Base current  $I_B$  controls the collector current  $I_C$ . Because the base-emitter junction (J2) is forward biased, the voltage from base to emitter is very low. The ratio of  $I_C$  to  $I_B$  is known as the common emitter forward current transfer ratio,  $h_{FE}$ , and  $h_{FE} \gg 1$ . Currents  $I_C$  and  $I_B$  are constant (direct) currents. Since the collector voltage is high (a few volts to many hundreds of volts in power transistors) while the base voltage

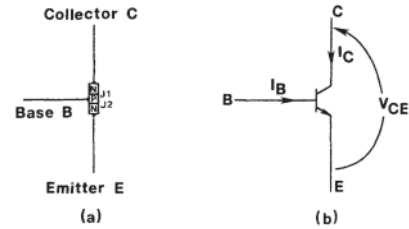


**Figure 9.76** (a) Diagrammatic representation of a bipolar transistor; (b) graphic symbol.

is very low (a volt or so), and because the collector and base currents have this same magnitude relationship, it is easily seen that a small amount of power in the base circuit controls large amounts of power in the collector circuit. That is, there is considerable power gain.

Transistor characteristics are usually shown as curves of collector current  $I_C$  versus collector to emitter voltage  $V_{CE}$  for various values of  $I_B$ . A typical set of curves appears in Fig. 9.77. There are three modes of operation that are referred to in the following.

One of these modes is the cut-off mode;  $I_B$  is zero. In this mode,  $I_C$  is very small for all  $V_{CE}$  until a high voltage is reached, the  $I_C$  curve then beginning to turn up. Rated collector voltage is set at a lower value. A second mode is the saturation mode, in which  $I_C$  varies almost linearly with  $V_{CE}$  independently of the current  $I_B$  (provided only that  $I_B$  is large). Collector-emitter voltage  $V_{CE}$  is small, being only 2 to 3 V at high collector currents. This mode is identified by the legend saturation line in Fig. 9.77. The third mode is the active mode, which comprises the entire area between the  $I_B=0$  curve and the saturation line.

Power dissipated in a transistor is very nearly equal to the product of  $V_{CE}$  and  $I_C$ . (There is an additional component equal to  $V_{BE} I_B$ , but this is very small compared to  $V_{CE} I_C$ .)

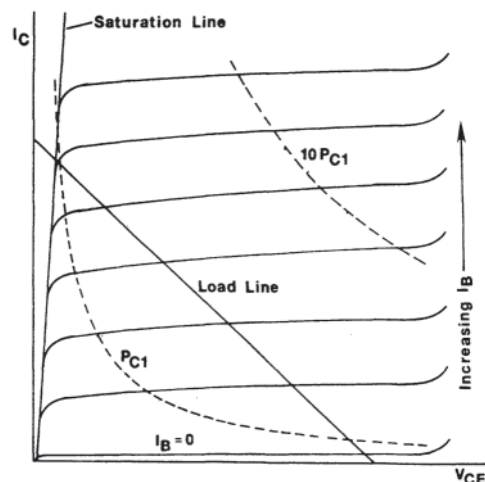


**Figure 9.77** Typical characteristic curves of a bipolar transistor.

Curves of constant power are hyperbolic in form; two constant-power curves are shown. Because of the large power dissipation in the transistor in the active region, converters using power transistors are designed so that the transistor is either in the cut-off mode ( $I_B=0$ , and  $I_C$  quite small) or in saturation ( $V_{CE}$  quite small). That is, the transistor is not used in the active mode region of the characteristics. It is used as a switch, being either open (switch off;  $I_B=0$ ) or closed (switch on;  $V_{CE}=V_{CEsat}$ ). Power dissipation under either of these conditions is small.

Even though the active region is to be avoided, the transistor must traverse the region from cutoff (switch off) to saturation (switch on) when performing its function as a switch. The path followed depends on the impedance of the load. For a resistive load, that path is the straight line shown as a load line on the  $I_C$ — $V_{CE}$  axes. The time to make the transition is finite; hence, additional power is dissipated in the transistor during the transition from off to on or vice versa. The energy dissipated during these transitions must be taken into account when calculating the total energy dissipated in the transistor during operation of the circuit in which the transistor is used. Rapid turn-on and turn-off will minimize this additional loss.

Power transistors have rated voltages about one third those of thyristors and current capabilities that are proportionately even smaller. They also have a much smaller overcurrent ratio, that ratio being only about 2 as compared to 10 for thyristors. However, they can be used at higher switching speeds, up to 25 kHz. As the characteristics of Fig. 9.77 show, to maintain the transistor in the On condition, base current must continue to flow. Turn-off, however, can be achieved merely by reducing the base current to zero, a much simpler process than achieving turn-off with thyristors. However, to achieve fast switching speeds the base current needs to be reversed to pull charge out of the base region.

#### 9.4.5 Metal Oxide Semiconductor Field-Effect Transistors

Field-effect transistors (FETs) are three-terminal devices. The terminology used for the electrodes differs from that used for other semiconductor devices, and is a reflection of the way in which the FET is constructed and the way in which it operates. Principal current flow is in a narrow channel between “source” and “drain”; this current is referred to as the drain current,  $I_D$ . Control of the drain current is achieved by use of an electric field created within the channel by application of voltage to the gate. The MOSFET, unlike devices considered above, is not current-controlled. It is a voltage-controlled device, the gate in the diagrammatic representation of Fig. 9.78(a) being isolated from the remainder of the structure by a layer of silicon dioxide. The graphic symbol is shown in Fig. 9.78(b).

In the structure shown in this figure, the channel for drain current is from one N+ region to the other through the P-material of the substrate. The gate, the silicon dioxide layer, and the substrate form a capacitor. In the absence of gate voltage, the channel from drain to source is closed. Application of a positive voltage on the gate opens the channel so that conventional current may flow from drain to source. As the

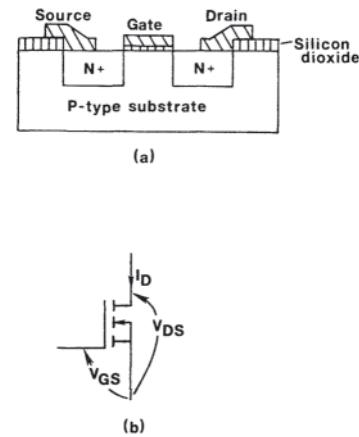


Figure 9.78 (a) Structure of a MOSFET; (b) graphic symbol.

gate voltage is increased, the channel is widened and drain current increases.

Figure 9.79 shows typical characteristics of drain current,  $I_D$ , vs. drain to source voltage,  $V_{DS}$ , with gate to source voltage  $V_{GS}$  as the control variable. Characteristics are shown only for positive  $V_{DS}$ . Although not shown in Fig. 9.78, there is a parasitic diode present between source and drain, with the diode’s anode connected to the MOSFET source and the diode’s cathode to the MOSFET drain. Hence  $V_{DS}$  cannot become more than a volt or two negative.

As with the bipolar transistor, there is a cutoff region ( $V_{GS}=0$ ), a full-on region (labeled “constant resistance”), and an active region between these extremes. For the same reasons as in the case of the bipolar transistor, the MOSFET is used as a switch, being in the off condition for  $V_{GS}=0$ , and in the on state along the constant resistance line. (The resistance between drain and source in the on condition is given the symbol  $R_{DS(on)}$ .)

MOSFET voltage ratings are somewhat below those of the bipolar transistor, running up to about 1000 V. Rated currents of 20 A–46 A are typical values. Devices may be paralleled to increase the current rating of a circuit,  $R_{DS(on)}$  has a positive temperature coefficient. Hence a MOSFET that has a tendency to carry more than an equal share of the current will also develop more internal heating, thus diverting current to other MOSFETs because of its rise in  $R_{DS(on)}$ .

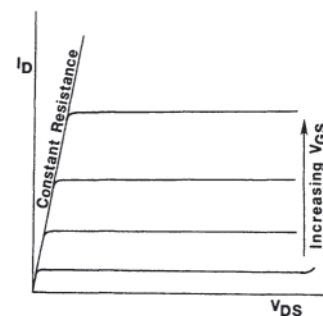
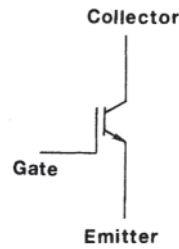


Figure 9.79 Typical characteristics of a MOSFET



**Figure 9.80** Circuit symbol of an insulated-gate bipolar transistor (IGBT).

The MOSFET has switching characteristics that are superior to those of all of the other power semiconductors. Typical switching times are on the order of 100 ns, considerably shorter than with other power semiconductors. Switching frequencies of 100 kHz to 200 kHz are typical while frequencies as high as 500 kHz are possible with lower rated devices.

#### 9.4.6 Insulated-Gate Bipolar Transistors

The IGBT is a voltage-controlled device with input characteristics that are generally like those of an FET and output characteristics similar to those of a bipolar transistor. Figure 9.80 shows the circuit symbol and the designations of the terminals.

The IGBT may be thought of as a PNP transistor whose base current is controlled by a FET. As with previously considered devices, it is operated as a switch. The potential from collector to emitter is typically approximately 2 to 3 V in the on state. As with the bipolar transistor and the power MOSFET, the gate signal must be maintained during the on period.

The gate presents a capacitive load to the gate drive circuit. Turn-on will take place in approximately 100 ns. Turn-off of the MOSFET portion of the structure is very rapid. As would be expected, turn-off of the bipolar part of the structure is much slower. Typical turn-off times are on the order of 400–600 ns. These transition times are not as short as those of a MOSFET, but are better than those of bipolar transistors. Switching losses are about one third those of a comparable bipolar transistor.

As might be expected, with shorter transition times and smaller switching losses than the bipolar transistor, the maximum switching frequency of the IGBT is increased, with an upper limit around 20 kHz. Voltage ratings and current ratings of the IGBT are much larger than those of the bipolar transistor and have essentially displaced the bipolar transistor in newer designs.

#### 9.4.7 Integrated Gate-Commutated Thyristor

The IGCT evolved from the GTO thyristor by realizing that if the entire anode current was extracted from the gate, the cathode current would be reduced to zero and the device would turn off as a PNP transistor. This can be seen by referring to Fig. 9.81 (a). If a gate current equal to the anode current is extracted from the gate terminal, the cathode is essentially open (the gate cathode junction is reversed biased), and the PNP transistor portion of the device is left to turn off the anode current and block voltage. There is now no  $dv/dt$  effect

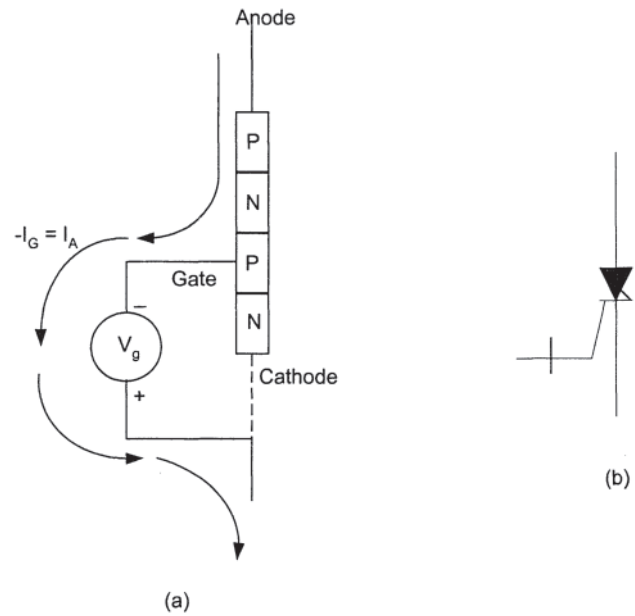


**Figure 9.81** (a) IGCT at turn off; (b) symbol illustrating integral feedback diode.

and the device can be operated without a snubber circuit. The IGCT has been optimized for this type of operation [59]. Due to the large reverse gate current, the IGCT switches faster than the GTO. Since most applications require an inverse parallel diode, IGCT devices have been implemented with an integral inverse diode fabricated on the same silicon. This leads to the often used symbol of Fig. 9.81(b) where the little reverse triangle represents the inverse parallel diode.

A disadvantage of this device is that the gate circuit must be able to extract the entire load current at a relatively low gate voltage (e.g., 20 V). This leads to a relatively elaborate, very low inductance gate circuit that must be physically located very close to the device. Most manufacturers supply this gating circuit and its integral low-inductance interconnect circuit board already interfaced with the device. Very high-power IGCT devices are available. Voltages up to 4500 V and currents up to 4000 A are available and larger devices can be expected in the future. They are used in very high power drives up to 25 MVA as well as utility applications where the gate circuit complexity can be justified in order to obtain the high power device capability.

## 9.5 CONVERTER CIRCUITS

Development of the power semiconductor devices described briefly in the preceding section was accompanied by development of a variety of converter circuits to transform electrical energy from one form to another. Without even attempting to determine the number of converter circuits that are possible, it becomes obvious rather quickly when considering one's choices that only a small selection can be discussed. Among those choices are the electrical energy at the converter input, which can be either ac or dc; for either form of the

electrical input energy, the converter output can also be of either form. Voltage levels can be changed, and, if the input is ac, the output can also be ac at a different frequency or voltage, or both. With an ac output, the waveform can be chosen in such a way as to modify the harmonic content so that harmonics that would have a deleterious effect on motor performance can be minimized or eliminated. Circuits can be designed to minimize the effect of harmonics on the supply circuit. One or more of several different power devices can be selected for use. In addition, the circuit can be designed for the single-quadrant, two-quadrant, or four-quadrant operation discussed in Section 9.3.

The converters discussed in the remainder of this section were selected to illustrate the range of possibilities. Some (for example, the PWM converters) have far wider application than others (such as the cycloconverter). Where controlled semiconductor devices are shown, they are shown as IGBTs. In many of these circuits other devices have been and are being used but the IGBT is considered the workhorse of the motor control industry at P. The reader will find additional information in the references (53–62) already cited. Additional references appear in the remainder of this section.

### 9.5.1 Rectifier Circuits

Rectifier circuits change ac energy into dc energy. In an ideal rectifier circuit, the dc output voltage and current are perfectly ripple-free and the ac input voltage and current are pure sinusoids. In practice, this ideal situation is never achieved. How close one comes to the ideal depends on a number of choices, such as three-phase input versus single-phase and whether to use a half-wave rectifier circuit or a full-wave circuit. Other choices, such as whether to use transformers or not, may be dictated by the ac voltage level of the supply in the plant and by the dc voltage required for the application. (It should be noted, however, that transformers are always encountered in an ac supply as one goes from load back toward the source.) Is the dc output to be fixed, or must it be adjustable? If it is to be adjustable, are discrete steps in the output voltage acceptable or must continuous adjustment be possible? (Discrete steps might be satisfied by taps on a transformer winding and semi-conductor diodes, whereas continuous adjustment would require the use of thyristors and an adjustable-delay firing circuit.)

The rectifier circuit will probably be full-wave rather than half-wave. There are advantages to this choice on both the input side and the output side. On the output side, filtering is much easier in those cases in which filtering is needed, and dc motors have better performance on full-wave rectification than on half-wave. On the input side, there is no direct current component in the supply current, as there would be with a half-wave rectifier. A direct current in one winding of a transformer offsets the magnetic operating point of the transformer from the origin. If the offset is large, the transformer will draw excessively large magnetizing currents. Transformer overheating and burn-out have been known to occur.

If a low-ripple output with minimum filtering is desired, a

three-phase source is far superior to a single-phase source. For example, a single-phase full-wave rectifier has a form factor on an unfiltered output of 1.11, where the form factor,  $f$ , is defined as the ratio of the effective value of the output current to the average value. Since the harmonic content (ripple) in percent is given by  $100(f^2 - 1)^{1/2}$ , the single-phase rectifier has 48% ripple. By contrast, the three-phase full-wave rectifier has a form factor of 1.001 and a ripple factor of 4.2%. The superiority of the three-phase circuit over the single-phase circuit evidenced by these numbers is offset by the observation that the single-phase full-wave rectifier has no harmonics in the supply current for a resistive load, whereas the three-phase rectifier does.

Given the large number of rectifier circuits that are used, it is clearly not feasible to include more than a limited number within the scope of this handbook. Those discussed below are the single-phase full-wave bridge rectifier using diodes or thyristors and a single-phase four-quadrant converter using thyristors. Single-phase circuits have been selected so that the principles may be illustrated in as simple a configuration as possible. Other circuits, including circuits with a three-phase supply, will be found in references previously cited.

#### 9.5.1.1 Full-Wave Rectifiers

In the full-wave rectifier circuit of Fig. 9.82, the supply voltage  $v_s$  may be directly from the ac line, or it may be the voltage at the secondary of a transformer. (In the following, voltage supplies are assumed to be from an infinite bus.) The bridge consists of the four diodes D1 through D4. With this configuration, diodes D1 and D4 are forward-biased during the positive half-cycle of the supply voltage; D2 and D3 are reverse-biased. On the negative half-cycle, the role of the diodes is reversed, but, in either case, current flow  $i_l$  in the load is from left to right. During conduction, the voltage drop across the diodes may be assumed to be zero unless the supply voltage is quite small. In the reverse-biased mode, diode current may be assumed to be zero unless the load has an extremely high impedance. That is, the diodes are assumed to be ideal. Three possible loads are shown at (a), (b), and (c) of Fig. 9.82.

If the resistive load of Fig. 9.82(a) is used, diodes D1 and D4 will conduct during the first half-cycle shown for  $v_s$  in Fig. 9.83, and  $v_l$  will be the same as  $v_s$ . In the second half-cycle, diodes D2 and D3 conduct, and  $v_l$  will be  $v_s$  inverted. Since the load is resistive, the load current  $i_l$  will be proportional to  $v_l$ , as shown. The load voltage and current have average values (direct voltage and direct current) equal to 0.637 times the respective maximum values. (The average value of the load current is indicated by the dashed line.) In addition to their average values, the load variables will contain a strong second harmonic as well as other higher frequency harmonics. The source, on the other hand, sees a resistive load, and there are no harmonics in the source current.

If it is necessary to reduce the harmonic content of the load voltage and current, either of the filter circuits shown at (b) and (c) in Fig. 9.82 may be used. In (b), an inductor is placed in series with the load so as to present a high impedance to the harmonic currents and (ideally) zero resistance to the

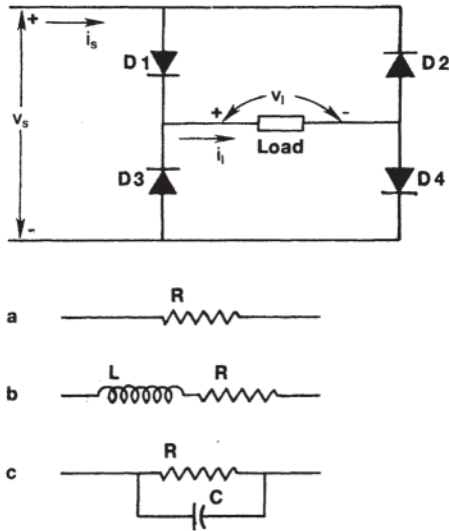


Figure 9.82 Full-wave diode bridge circuit.

direct-current component. Figure 9.84 shows waveshapes for the resulting voltages and currents. The voltage across the load resistor will be directly proportional to  $i_L$ , the difference between that voltage and the voltage  $v_L$  appears across the inductor. Harmonic content of the load variables has been substantially reduced. However, harmonics now appear in the source current.

Figure 9.82(c) shows a parallel combination of load resistance and filter capacitor. The waveshapes of voltage and current that result are shown in Fig. 9.85. The capacitor will be charged to the maximum of the source voltage on the first half-cycle after the circuit is energized. The load voltage  $v_L$

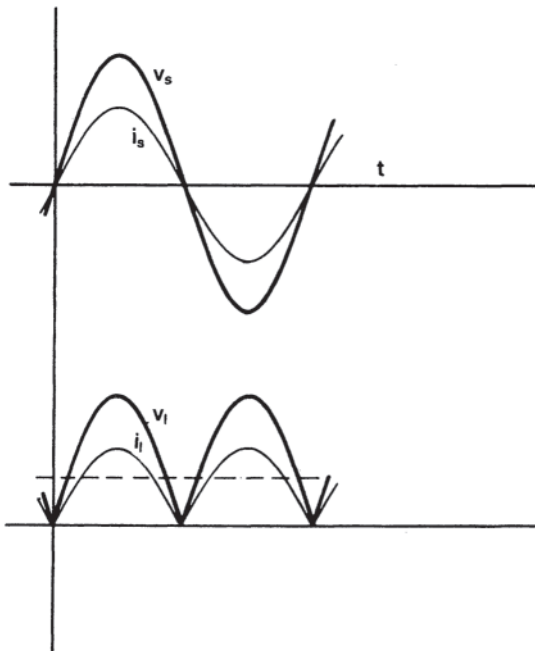


Figure 9.83 Supply and load voltages and currents for a full-wave bridge with resistive load.

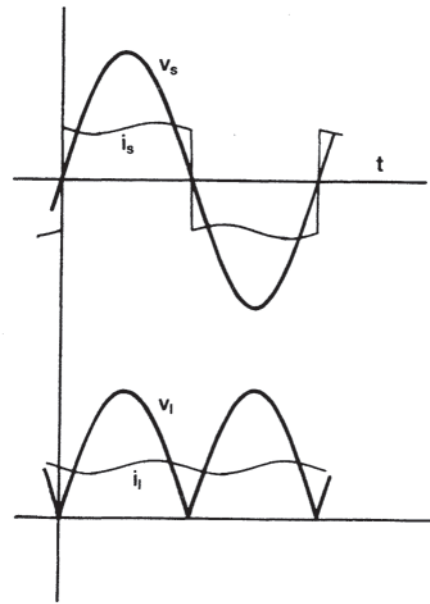


Figure 9.84 Supply and load voltages and currents for a full-wave bridge with inductive filter.

then decays in an exponential manner. Because the supply voltage falls faster than the load voltage, the diodes become back-biased just after the peak of the supply voltage has been reached (the cut-out point), and conduction does not occur again until the voltage wave of the next half-cycle exceeds the decaying load voltage. At that point, the forward-biased diodes come into conduction (the cut-in point) and remain in conduction until the next cut-out point is reached.

The load voltage is relatively smooth, and is higher than in either of the two previous cases. Current in the load resistance is not shown, but will be proportional to load voltage. Harmonic content of the load voltage and current is greatly reduced from the unfiltered case. The current in the diodes, shown separately in Fig. 9.85, has the form of a narrow pulse, beginning at the cut-in point and ending at the cut-out point. During the pulse of diode current, sufficient charge must be stored in the capacitor to supply the load during the remainder of the half-cycle. These pulses of current are supplied by the source, as shown, creating harmonics in the supply current.

Harmonic content in the load can be reduced by increasing the capacitance, thus reducing the rate of decay of  $v_L$  and delaying the cut-in point. (The cut-out point, even for small values of  $C$ , is not much beyond the peak of the voltage wave.) The width of the diode current pulse being reduced, the amplitude of the pulses must increase so as to meet the requirement for stored charge, and the harmonic content of the source current is increased.

Figure 9.85 has been drawn for an  $\omega RC$  product of 20. For this value with a 60-Hz supply, the cut-in angle is 61 degrees from the zero-crossing of the voltage wave, and the cutout angle is 93 degrees. The maximum current through the load resistance is, of course,  $V_m/R$ , and the diode current has a peak value 10.5 times as large. The fact that the peak diode current

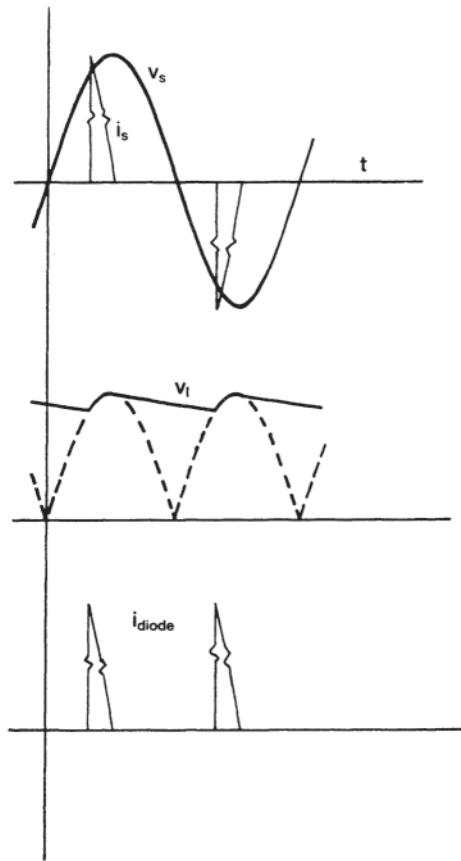


**Figure 9.85** Supply voltage, current and load voltage, and diode currents for a full-wave bridge with capacitive filter.

is much larger than the average value must be kept in mind when selecting diodes; the selection may be dictated by the surge current required of the diode rather than the average value.

Finally, Fig. 9.86 shows the control possible with an unfiltered resistive load if the diodes are replaced by thyristors. If firing of the thyristors is delayed for some time after the zero crossing point of the supply voltage, the average load voltage and load current are reduced. Magnitudes of the harmonics in the output are increased with respect to the average value, and harmonics now appear in the source current. Moreover, the fundamental of the source current is delayed, and the source sees a lagging power factor load even though the load itself is resistive.

Either of the filter circuits of Fig. 9.82 may be used with the thyristor bridge. Satisfactory filtering will probably require the use of larger values of  $L$  or  $C$  than with the diode bridge. With the capacitor filter, the time-constant of the  $RC$  combination will limit the rate at which output voltage can be reduced, and there is little or no control of the output voltage for firing angles much less than 90 degrees because the thyristor will be back-biased. Since a back-biased thyristor will not fire, a single firing pulse must be delayed until after the cut-in point has been reached. A train of pulses with close spacing initiated at the desired firing angle will ensure that the thyristor is fired after the cut-in point has been reached.

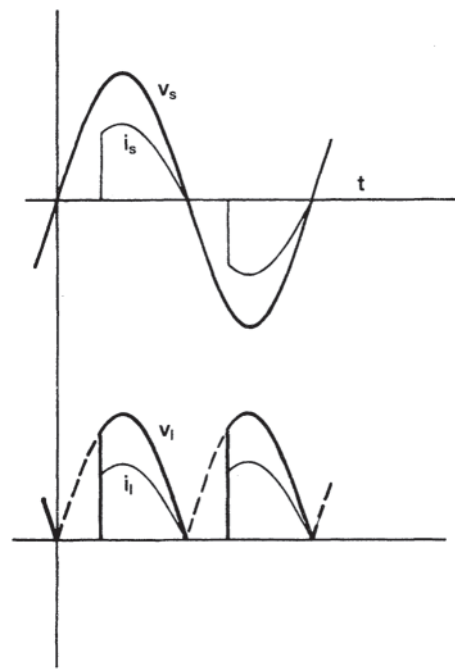
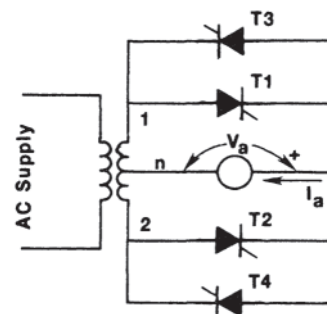


**Figure 9.86** Supply and load voltages and currents for a full-wave thyristor bridge with resistive load and 60-degree firing angle.

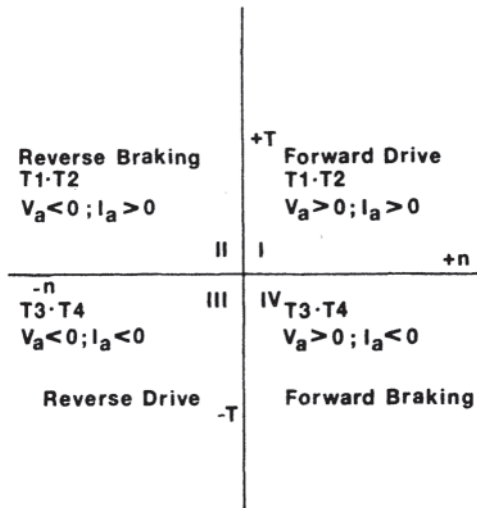
### 9.5.1.2 Single-Phase Four-Quadrant Converter

Figure 9.87 shows a dc motor control circuit using a centertapped transformer and thyristors to rectify power from the ac supply to provide dc to a motor armature, or to invert dc power from the armature so that it can be fed into the ac supply. The field circuit of the machine is not shown; it would probably be excited from the ac supply using a full-wave diode rectifier, with provision being made for some adjustment of the field current so that a desired full-load speed could be set. Moreover, the controller must insure that field current is established before power is applied to the armature.

Thyristors T1 and T2 are used for one direction of operation (arbitrarily designated as “forward”), and T3 and T4 are used for the reverse direction. For forward running, T1 and T2 are fired during alternate half-cycles of the transformer secondary voltage. Conduction through these thyristors results in



**Figure 9.87** Single-phase four-quadrant motor control.



**Figure 9.88** Four quadrants of motor control of Fig. 9.72 with identification of thyristors used in each quadrant by the circuit of Fig. 9.88, with voltage polarities and current directions.

positive voltage at the right end of the armature and current flow into that terminal. Most operation is then in quadrant I of Fig. 9.88. If T3 and T4 were used instead of T1 and T2, the armature voltage and current would have the opposite polarity and direction; since field current direction remains the same, the armature would run in the reverse direction. Motor operation would then be in quadrant III of Fig. 9.88.

Suppose that the motor is running in the forward direction and is to be brought to a standstill (and possibly reversed). Removal of firing signals from T1 and T2 will result in zero armature current, but continued rotation of the armature will insure that  $V_a$  remains positive. Armature current flow can be reversed using T3 and T4 to transfer energy from the armature back into the source. This is the (regenerative) braking mode shown in quadrant IV of Fig. 9.88. If firing signals are not removed when stand-still is reached, the armature voltage will reverse and the motor will accelerate in the opposite direction, moving into quadrant III. In an exactly analogous manner, operation can be shifted from quadrant III (reverse drive) into quadrant II (reverse braking). If a three-phase supply is used, more precise control of the dc motor will be achieved and the harmonic content of the energy returned to the source will be reduced. See Refs. 57 and 58 for further discussion.

Controllers are discussed in Section 9.6. However, it may be noted at this point that sensing of the armature current and the use of ramp circuits is almost always necessary in the controller in order to prevent thyristor currents from exceeding device limits.

### 9.5.2 Cycloconverters

Very low (a few cycles per second) and adjustable frequency alternating-current sources are needed for certain applications. For example, drive motors used in icebreakers are required on occasion to run at low speeds, they must be reversible, and they must be capable of developing several thousand horse-

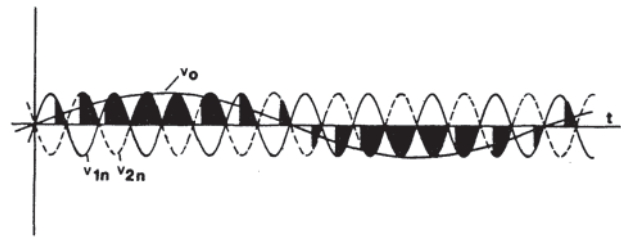


**Figure 9.89** Waveshapes in a single-phase cycloconverter.

power. Conventional approaches to generating ac power under these conditions would require the use of alternators having large numbers of poles driven by engines capable of developing high torque over a large speed range, possibly as large as 20 to 1. Reversibility would require the use of contactors. The resulting installation would be massive in scale, expensive, and inefficient. An efficient and far less expensive system is an engine-driven alternator running at constant or nearly constant speed, generating power at normal frequencies (50 to 60 Hz), together with means for transforming the output to the low frequencies desired. The transforming means used is the cycloconverter.

Cycloconverters have been in use since at least the 1930s. One of the early installations was for conversion of standard three-phase 50-Hz power to single phase at 16 2/3 Hz for the German State Railway system, the devices used being controlled mercury arc rectifiers. A modern application of direct ac-to-ac conversion is in the aircraft industry. Electrical energy is generated by engine-driven alternators at variable frequency and voltage; it is then converted to fixed-frequency, constant-voltage power.

The principle involved can be understood by referring to Figs. 9.87 and 9.89. In Fig. 9.87 the motor armature is replaced by a resistive load. The voltage  $V_a$  is the voltage across the load and current  $I_a$  is the current through it. In Fig. 9.89, the voltage between points 1 and  $n$  of Fig. 9.87 is shown as the solid sinusoid labeled  $v_{1n}$ ; the voltage between 2 and  $n$  is shown by the dashed sinusoid labeled  $v_{2n}$ .

If thyristors T1 and T2 of Fig. 9.87 are fired alternately during the first four cycles (eight half-cycles) of the supply voltage and if the firing angle is advanced during the first four half-cycles and then delayed in the next four, conduction through the load will occur as shown by the blacked-out portion of each half cycle. During the next eight half-cycles of the supply voltage, thyristors T4 and T3 would be fired on alternate half-cycles, following the same firing angle advance and delay pattern as in the first eight half-cycles. The result is a low-frequency voltage wave across the load, indicated by  $V_0$ , with a fundamental as shown in Fig. 9.89. (The fundamental is not to the same scale as the incoming wave.)

In the case shown, the output frequency is one eighth of the input frequency, and the amplitude of the fundamental of the output is set by the full-wave rectification that occurs at the 4th and 5th half-cycles and again at the 12th and 13th, assuming that the firing angles on the other half-cycles have been properly chosen. A number of observations may now be made.



1. The frequency of the output is adjustable by changing the number of half-cycles during which T1 and T2 (T4 and T3) provide the positive (negative) half-cycle of the output. Firing angles would, of course, have to be adjusted if a greater or lesser number of half-cycles of the source voltage were used for one cycle of the output voltage in order to ensure that each conduction pulse contributed properly to the output wave.

2. The amplitude of the output voltage is adjustable from a maximum (the condition shown) to lower values. If, for example, T1 and T2 were fired at the 90-degree point on half-cycles four and five and the firing delay on the remaining half-cycles of the first eight half-cycles in Fig. 9.89 were increased, an output wave having half as large an amplitude as that shown would result.

3. The phase of the output wave can be changed by changing the half-cycles for which certain thyristors are used. For example, if the firing delay scheme of Fig. 9.89 were used except that T3 and T4 were used in the first four half-cycles, T1 and T2 for the next eight, and so forth, the output voltage would be delayed by 90 degrees from that shown. Such control would have significance, of course, only if there were a second low-frequency voltage wave of the same frequency to which the phase could be compared. With both low-frequency waves present, a two-phase low-frequency supply has been created.

4. If a three-phase source were used in a bridge configuration, the output voltage would be a much closer approximation to a true sine wave. (Harmonic content would be reduced substantially.) The number of thyristors would increase to 12 to provide a single-phase output. If a three-phase output were wanted, the number of thyristors would increase to 36. Reference 57 shows circuits of this type.

5. If load voltage and current are not in phase, as would be the case with an inductive load, the cycloconverter operation must include the capability of regeneration for those portions of the output cycle during which energy is being returned to the source from the load. This increases the complexity of the controller. This condition is illustrated on page 219 of Ref. 54 or page 201 of Ref. 53.

Finally, it must be pointed out that the cycloconverter is only one of the broader class of direct ac-to-ac converters. The most complete discussion of the various possibilities is probably that of Ref. 61.

### 9.5.3 Chopper Circuits

Conversion of direct voltage from one level to another (dc-dc conversion) may be achieved using a number of different circuits. The name “chopper” arises from the fact that the output voltage is obtained by “chopping” the constant input voltage into a train of pulses. The output voltage may be at a lower level (often called a “buck” regulator), at a higher level (often called a “boost” regulator), or at either a lower or a higher level (often called a “buck-boost” regulator). (Reference 60 shows examples of all three types of circuits.) Thyristors used in earlier circuits have largely been supplanted by MOSFETs and IGBTs as the switch of choice. The chopper circuits may be configured for one, two, three, or four quadrant operation.

Figure 9.90 shows a two quadrant chopper in which the output voltage,  $v_o(t)$  is less than the input voltage,  $V_{dc}$ . In this figure, it is assumed that the load is the armature of a dc motor. Motor flux may be provided by permanent magnets or by a separate circuit to a wound field; flux is assumed to be constant. For one quadrant operation, only the transistor Q2 and the diode D1 are needed. The transistor Q2 is switched on and off at the chopper switching frequency producing the waveforms of Fig. 9.90(b) and 9.90(c) or 9.90(d). When Q2 is on, the dc input voltage,  $V_{dc}$ , is applied to the motor armature inductance (and any external inductance in series with the armature) and the motor counter emf,  $V_{cemf}$ . As shown in Fig. 9.90(b) and 9.90(c), the motor current rises during Q2s on time,  $t_1$ , at a rate determined by the voltage across the motor inductance ( $V_{dc} - V_{cemf}$ ) divided by the value of armature inductance. When Q2 switches off, load current is maintained by the armature inductance and diode D1 comes into conduction. This brings the voltage  $v_o(t)$  to ground potential as seen in Fig. 9.90(b) of the figure. During the OFF time of transistor Q2 ( $t_2$ ), the load current decreases at a rate determined by the counter-emf,  $V_{cemf}$ , divided by the armature inductance as seen in Fig. 9.90(c) of the figure. The average output voltage of the chopper is simply given by the duty ratio of switch Q2 ( $t_1/T$ ) times the dc input voltage,  $V_{dc}$ . Note that in the steady state, this average output voltage is equal to the motor counter emf-voltage,  $V_{cemf}$  (neglecting any IR voltage drops in the load).

If operation in the fourth quadrant (forward braking), transistor Q1 and diode D2 are needed. In this case the load current is negative and is controlled by the duty cycle of transistor, Q1. During time  $t_2$ , Q1 is ON, current builds up in the negative direction at a rate determined by the counter-emf,  $V_{cemf}$ , divided by the armature inductance as seen in Fig. 9.90(d) of the figure. When Q1 turns OFF, diode D2 comes into conduction as the armature inductance maintains current. Note that when D2 conducts, energy is being returned to the dc source and thus the braking is regenerative. Also note that in this case the chopper is “boosting” the counter-emf voltage,  $V_{cemf}$ , up to the source voltage,  $V_{dc}$ . Again, the average output voltage of the chopper is controlled by the duty cycle of the transistor, Q1, and in the steady state is equal to the counter-emf voltage,  $V_{cemf}$ . This average voltage is given by the source voltage,  $V_{dc}$ , multiplied by the appropriate duty ratio ( $t_1/T = 1/(1-t_2/T)$ ).

Chopper circuits are widely used for dc motor control in servo and traction applications or as dc machine field exciters. They are also widely used to establish a regulated dc bus from which other converters operate. For example, a chopper is often used to establish a dc bus from which a dc-ac inverter operates (often a simple six-step inverter as discussed in the next section). References 54–60 contain numerous other chopper circuits. Several transistor chopper circuits are shown in Ref. 60.

### 9.5.4 Six-Step Inverters

Induction motors are generally the motor of choice because of their low initial cost, reliability, low maintenance, and the near-universal availability of alternating-current power. Their

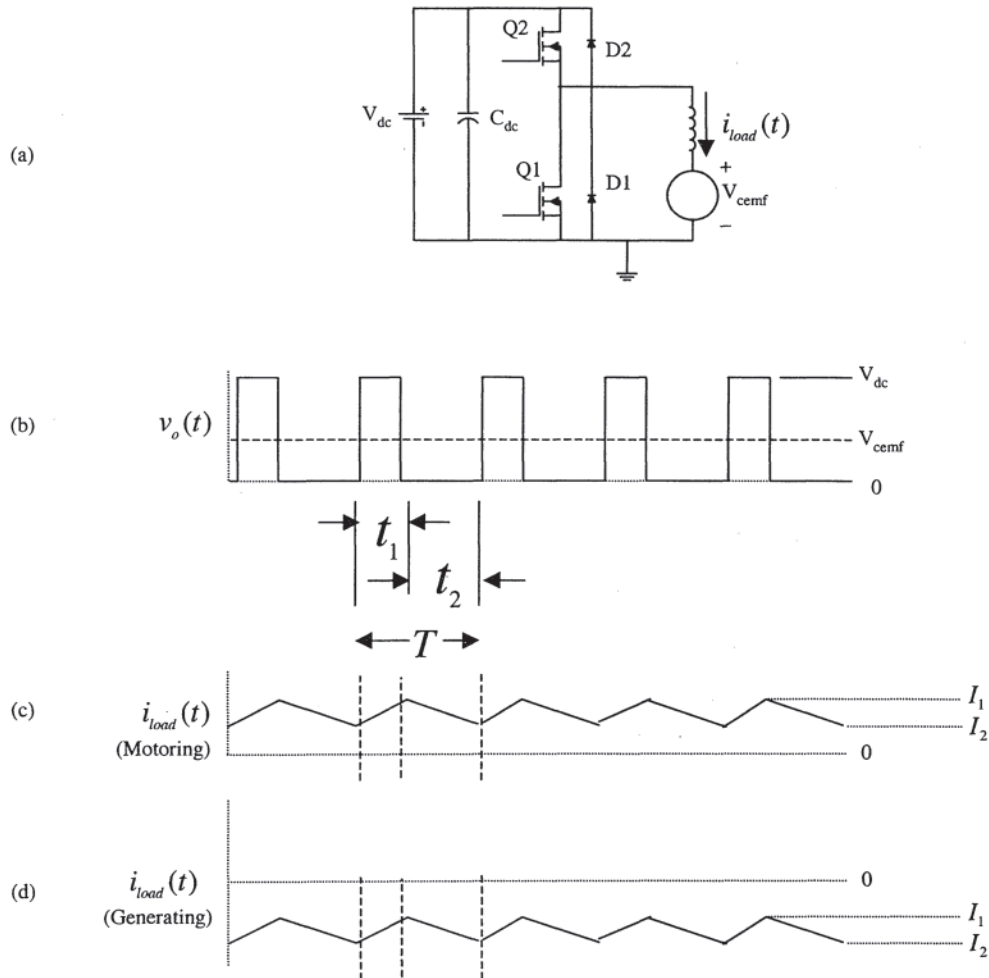


**Figure 9.90** (a) Two quadrant chopper circuit; (b) output voltage waveform; (c) load current during motoring operation; (d) load current during generating (braking) operation.

principal short-coming has been the inability to adjust their speed in a satisfactory and economical fashion. In their operating range, especially with a squirrel-cage rotor, they run at a speed that is determined largely by the number of poles and the frequency of the supply. As soon as power semiconductors became available with current and voltage ratings comparable to the currents and voltages encountered in motor circuits, engineers began to devise rectifier/inverter circuits to provide a variable-frequency supply so that induction motor speed could be adjusted. The converter of Fig. 9.91 is one such circuit.

This circuit is composed of three parts. The first part is a controlled rectifier. To maintain a constant magnitude of flux in the motor, the voltage supplied to the inverter must vary in a nearly direct proportion to the output frequency of the inverter, as is discussed in Section 2.2.7. An alternative to the controlled rectifier is to use an uncontrolled rectifier followed by a chopper circuit (as described in the previous section) to control the dc bus. This has the advantage of presenting a higher power factor to the ac source. The second part of the

circuit, the filter, insures that the dc voltage applied to the inverter is reasonably smooth. The third part of the circuit is the inverter.

The inverter shown is known as a six-step inverter. It uses six IGBTs, labeled Q1 through Q6, and six diodes in inverse parallel with the IGBTs. The function of the diodes is to take

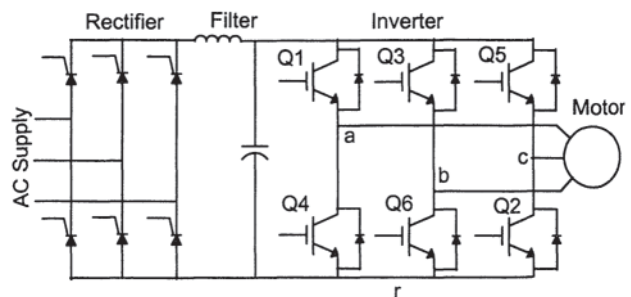


**Figure 9.91** Six-step inverter circuit.

care of any regeneration necessary because of the inductive nature of an induction motor load. The IGBTs are gated in the sequence 1 through 6, each IGBT being allowed to conduct for just under 180 degrees of the output wave. The reason that conduction is limited to less than 180 degrees is that, just after Q1 is turned off, Q4 is turned on. If Q1 has not regained a complete blocking state before Q4 begins to turn on, they may both go into conduction, placing a short circuit across the filter capacitor and potentially damaging the IGBTs.

The voltages that result between terminals a, b, and c of the motor are shown in Fig. 9.92. Each voltage wave goes from  $+V_{dc}$  to  $-V_{dc}$  during the course of one cycle, where  $V_{dc}$  is the voltage across the filter capacitor.

If the motor is connected in delta, these are the phase voltages of the fundamental of this wave has an amplitude of  $(2\sqrt{3}/\pi) \times V_{dc}$ . The harmonics that are present are all odd and have amplitudes equal to the fundamental amplitude divided by the harmonic number. None of the triplen harmonics is present. Figure 9.93 shows the voltages from a, b, and c to the common point, o, of a wye-connected motor. The amplitude of this wave is  $(2/3) \times V_{dc}$  and the amplitude of the fundamental of the wave is  $(3/\pi) \times V_{dc}$ . The same harmonics are present with the same relative magnitudes, but the phase of some of them has shifted by 180 degrees.

Only the fundamental of the voltage wave and the resulting fundamental of the current produce useful torque. The harmonics in the voltage will cause harmonic currents in the motor, and those currents cause increased  $I^2R$  losses and greater temperature rise without contributing to the useful torque. If the motor is running at low speed at or even below rated torque and if it is cooled by a shaft fan, temperature rises in excess of rated should certainly be expected.

In addition to the heating effect of the harmonic currents, the 5th and 7th harmonics that are present create a 6th-harmonic pulsation in the torque and speed. (The 11th and 13th produce a 12th-harmonic torque, but this is considerably smaller than the 6th and the dynamics of the system make significant 12th-harmonic speed variations unlikely.) In spite

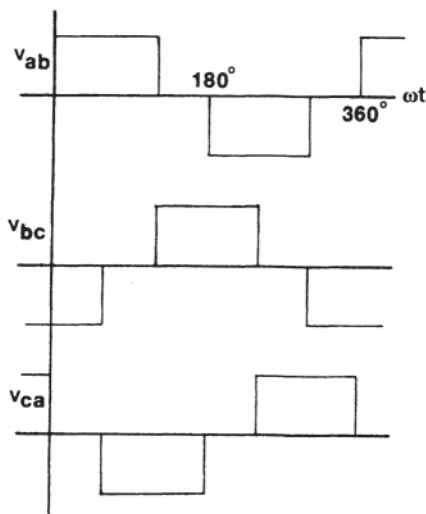


**Figure 9.92** Line-to-line voltages for the motor of Fig. 9.91.

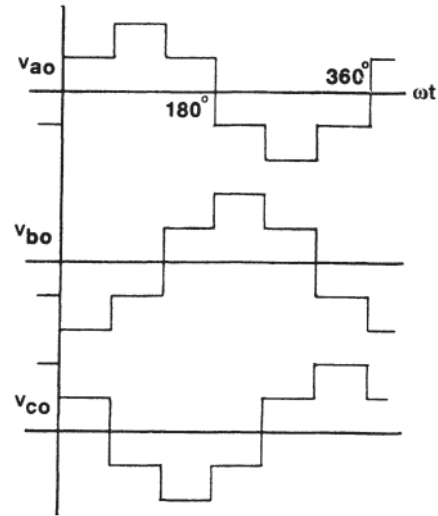


**Figure 9.93** Phase voltages for a wye-connected motor in Fig. 9.91.

of the fact that the 5th and 7th harmonics are relatively small, it has been shown [61] that the sixth-harmonic torque and speed pulsations can become quite troublesome at low inverter output frequencies.

To avoid these problems, alternate inverter schemes have been devised, two of which are described in the next section.

### 9.5.5 Pulse-Width Modulation Inverters

As was pointed out in the preceding section, regardless of the speed, the motor of a six-step inverter motor combination carries harmonic currents that produce added heat without contributing useful torque. Moreover, there is a sixth-harmonic torque that can cause unwanted speed fluctuations at low speeds. Added to these disadvantages is the fact that as speed is reduced, the output voltage of the controlled rectifier must be reduced so that the motor flux remains constant. At low speeds, the thyristors in the rectifier bridge must be fired very late in the cycle, with the result that the input current to the filter may consist of spaced pulses of current. These pulses are difficult to filter, and yet  $V_{dc}$ , the voltage at the output of the filter, must be smooth enough for proper operation of the inverter.

If both the output voltage and the frequency could be controlled in the inverter, the rectifier thyristors could be replaced by diodes, eliminating the control circuitry for the rectifier thyristor gates and simultaneously easing the requirements on the filter. Moreover, if the most troublesome harmonics (the fifth and the seventh) could be reduced or even suppressed completely, there would be no sixth-harmonic torque and corresponding speed fluctuation at low speeds. Various inverters have been devised that produce several pulses of variable width in each cycle of the voltages (referred to below as “pole” voltages) between  $a$  and  $r$ ,  $b$  and  $r$ , and  $c$  and  $r$  of Fig. 9.91, rather than a single pulse that extends over almost a half-cycle.

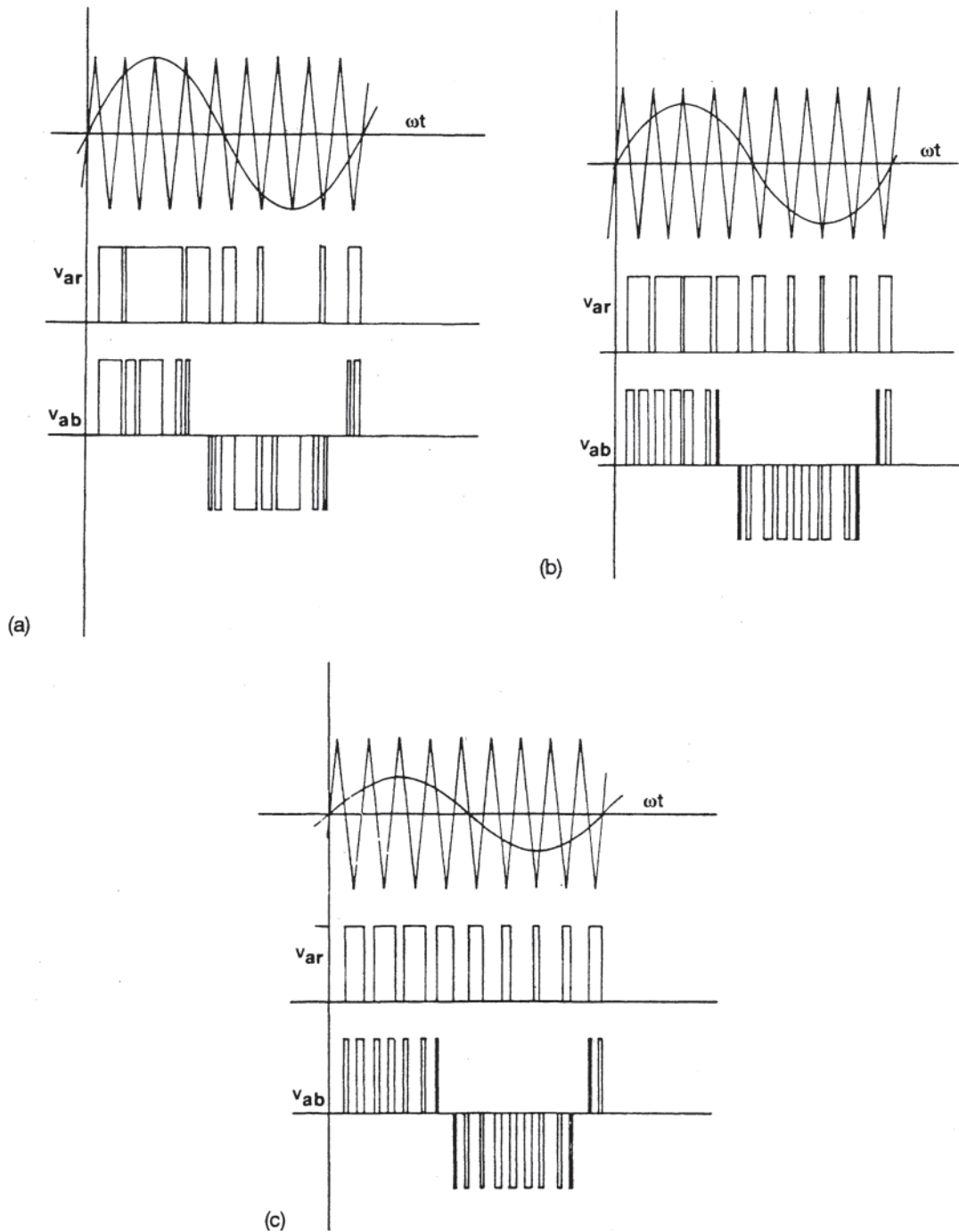


**Figure 9.94** Pulse generation method for a PWM inverter, (a)  $M=1.0$ ; (b)  $M=0.8$ ; (c)  $M=0.5$ .

By proper control of the width and spacing of these pulses, the fundamental frequency of the output and its amplitude may be controlled, and the unwanted harmonics suppressed. Such inverters are known as pulse width modulation (PWM) inverters. Because of the more frequent switching of the power devices in PWM inverters, most of these inverters make use of power transistors rather than thyristors because of the ease of control of transistors.

Figure 9.94 shows one way in which pulse location and width can be selected and controlled in a PWM inverter. In the upper portion of each part of this figure, a triangular wave is shown with a superimposed reference sine wave having an amplitude  $M$  times the amplitude of the triangular wave,  $M$  being 1.0, 0.8, and 0.5 in (a), (b), and (c) respectively. The triangular wave must be selected so that second and third reference waves, displaced in angle by  $\pm 120$  degrees from the

**Table 9.11** Pole Voltage Harmonic Content

	<i>M</i>		
	1.0	0.8	0.5
Average	0.500	0.500	0.500
$b_1$	0.500	0.326	0.250
$b_3$	0	0	0
$b_5$	0.015	0.114	0.001
$b_7$	0.159	0.110	0.047
$b_9$	0.300	0.409	0.542
$b_{11}$	0.160	0.110	0.047
$b_{13}$	0.026	0.010	0.001
$b_{15}$	0.106	0.070	0.022

reference wave shown, will exhibit exactly the same relationship with the triangular wave as the reference wave shown in the figure. That is, when a reference sine crosses zero going positive, it must coincide with a zero crossing of the triangular wave at a point at which it is also going positive. The triangular wave shown meets these requirements.

The reference sine wave and the triangular wave may be used to control the pole voltage  $v_{ar}$  in Fig. 9.91 using the following rule: Whenever the reference voltage is higher than the voltage of the triangular wave, Q1 is turned on and Q4 is off; when the reference voltage falls below that of the triangular wave, Q1 is off and Q4 is on. A train of positive pulses having varying widths and a height of  $V_{dc}$  is then generated as shown by plots of  $v_{ar}$  in Fig. 9.94. With reference sinusoids displaced by  $\pm 120$  degrees from that shown, identical trains of pulses will appear as  $v_{br}$  and  $v_{cr}$  having  $\pm 120$  degrees displacement from  $v_{ar}$ . Using the equation  $v_{ab} = v_{ar} - v_{br}$  gives the trains of positive and negative pulses shown as  $v_{ab}$  in Fig. 9.94.

Table 9.11 shows the harmonic content of the pole voltage for the three values of  $M$  is used in Fig. 9.94, all values being in per unit with  $V_{dc}$  as base. Regardless of the value of  $M$ , the average value of pole voltage is 0.500 V. Because of the subtraction of instantaneous pole voltages to obtain the line-to-line voltages, the average value disappears from the line-to-line voltage harmonic tabulation of Table 9.12, as do all of the triplen harmonics. (The fact that the third harmonic of the pole voltages is zero is interesting, but irrelevant.) The ninth harmonic is large for  $M=1.0$ , and grows in magnitude as  $M$  is reduced, reaching a maximum when  $M=0$ .

The other harmonics have magnitudes that vary in both absolute and relative (with respect to the fundamental) magnitude as  $M$  is varied. Of these, the fifth and thirteenth are small and become negligible as  $M$  is decreased, as will be seen in Table 9.12 in which both the per-unit values of the line-to-line harmonics are given and their magnitudes as a percentage of the fundamental. The 7th and 11th harmonics are considerably larger, both of them remaining above the relative magnitudes they would have in a square wave (14.3% and 9.1% of the fundamental, respectively) for the range of  $M$  in the table.

Because the amplitude of the fundamental becomes smaller as  $M$  is reduced, the frequency of the pole and line-to-line

**Table 9.12** Line-to-Line Voltage Harmonic Content

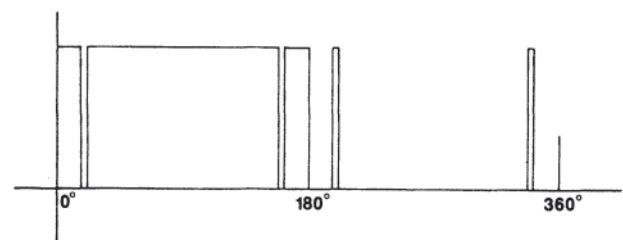
	<i>M</i>		
	1.0	0.8	0.5
$b_1$	0.866	0.565	0.433
$b_5$	0.026 (3.0%)	0.006 (1.1%)	0.001 (0.3%)
$b_7$	0.275 (31.8%)	0.191 (33.8%)	0.081 (18.7%)
$b_{11}$	0.277 (32.0%)	0.191 (33.8%)	0.081 (18.7%)
$b_{13}$	0.045 (5.2%)	0.018 (3.1%)	0.002 (0.5%)

voltages may also be reduced so that the voltage/frequency ratio is kept constant. If the synchronous speed is  $N_s$  for  $M=1.0$ , it can then be set at  $0.65N_s$  for  $M=0.8$  and at  $0.50N_s$  for  $M=0.5$ .

Two of the objectives of PWM control are achieved with this inverter: The voltage is adjusted in the inverter rather than in the rectifier, and the frequency may be changed to achieve the nearly constant volts/hertz criterion. The third objective, to eliminate or at least reduce the unwanted harmonics, has not been completely achieved.

With increasing use of microprocessors in the controllers, it has become feasible to generate wave shapes of the pole voltages (and hence of the line-to-line voltages) in which certain harmonics can be suppressed completely. Since the fifth and the seventh harmonics are the source of low-speed pulsations in torque and speed, these are the ones whose elimination is desired. The pole voltage shown in Fig. 9.95 contains neither of these harmonics if the notches in the first half-cycle are placed between 16.2471 degrees and 22.0684 degrees from the 0- and 180-degree points, and the pulses in the second half-cycle appear between those angles, measured forward from 180 degree and backward from 360 degrees. The harmonic content of this wave is shown in Table 9.13; the amplitudes are based on an amplitude of unity for the wave shown in Fig. 9.95. Because the triplen harmonics disappear when the line-to-line voltage is considered, the first harmonic above the fundamental that will appear at the motor terminals will be the eleventh. Although the degree of precision given above for the angles is much greater than can be achieved in practice, approximations to these angles will still result in substantial reductions in the fifth and seventh harmonics.

The PWM inverter schemes shown are only two examples of a wide variety of possible inversion methods, and neither has been given more than a passing review. The interested engineer will find much to explore further, even in these two methods. For example, in the method shown in Fig. 9.93, there will be a different harmonic content if the triangular

**Figure 9.95** Wave with no fifth or seventh harmonic.

**Table 9.13** Harmonic Content of a Wave with Suppressed Fifth and Seventh Harmonics

	Absolute value	Percentage of fundamental.
$b_1$	0.594	100.0
$b_3$	0.104	17.4
$b_5$	0.000	0.0
$b_7$	0.000	0.0
$b_9$	0.054	9.1
$b_{11}$	0.121	20.3
$b_{13}$	0.161	27.1
$b_{15}$	0.154	26.0

wave is at a different frequency with respect to the reference than that shown, and  $M$  need not necessarily be restricted to 1.0 as an upper limit. References 55 and 58 show other possibilities. Given the large number of possible methods and the desirability of suppression of certain harmonics, the reader should consult the current literature. Reference 64 gives an excellent treatment of pulse width modulation.

**9.5.6 Multilevel Converters**

For higher voltage designs, multilevel converters are applied. Multilevel converters are usually classified as of the “flying capacitor” type, “diode clamped” type, or “cascaded inverter” type [85]. Multilevel voltage source converters typically synthesize a staircase voltage wave from several levels of dc capacitor voltage. As an example of a diode-clamped type, Fig. 9.96 shows a three-level neutral-point-clamped (NPC) type of inverter [86]. Each phase is capable of outputting three voltage levels ( $+V_{dc}/2, -V_{dc}/2$ , and zero) to the load that allows for sophisticated PWM schemes. This can be seen in Fig. 10 by considering the inverter “leg” consisting of Q1 through Q4 and diodes D1 through D6. With Q1 and Q2 on (or, in the case of a reactive load, diodes D1 and D2 conducting), the voltage

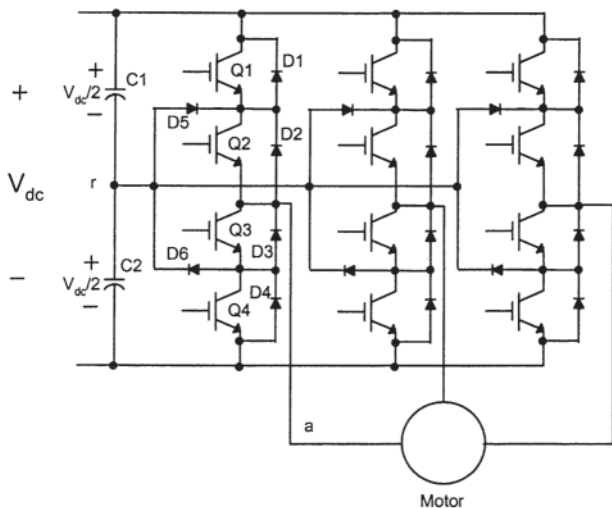


**Figure 9.96** Neutral-point-clamped multilevel inverter circuit.

at point a is  $+V_{dc}/2$  relative to the reference voltage,  $r$ ; at the center point of the seriesed dc bus capacitors, C1 and C2. With Q1 off and Q2 conducting, point a is clamped to zero (point  $r$ ) by Q2 through either diode D5 or D2 depending on which way the load phase current is flowing. Likewise, the voltage at point a can be negative with respect to point  $r$  by turning off Q1 and Q2 and turning on Q4 and Q5 (or diodes D3 and D4 by reactive current flow). A major advantage of the converter for high-voltage applications is that the dc maximum voltage applied to the switching devices is one half the rail-to-rail dc bus voltage. This is because of the clamping of the diodes connected to the dc bus midpoints (which in turn are established by the split capacitors across the high-voltage dc bus). It is noted that the voltage at the midpoint of these bus-splitting capacitors is not guaranteed to stay at one half of the rail-to-rail dc voltage. Many schemes have been proposed for maintaining this midpoint. Active control of the midpoint by proper control of the device switching intervals while still maintaining acceptable output voltage waveforms has proven to be an attractive solution. Reference 67 describes a 10 MVA, 3300-V converter using 4.5 kV IGCT devices operating from a nominal 5.4 kV dc bus. This converter, developed for heavy duty rolling mill applications, uses voltage clamps, space vector modulation, and active control of the capacitor midpoint.

**9.6 CONTROLLERS**

In Section 9.3, a distinction was made between the terms converter and controller. As defined there, converter refers to power-handling elements and controller refers to “those elements that accept input signals, process the information, and use the processed information to control the power handling components.” The elementary block diagram of Fig. 9.97 follows this usage, and the controller is further subdivided into logic circuitry and firing circuits. In this figure, there may be a single input signal, such as a voltage corresponding to a desired speed; there may be two signals, one corresponding to a desired voltage level at the output and another for a desired frequency or speed; there may be an input signal that sets a current that is not to be exceeded at the output of the converter. The feedback signals can be voltage or current at the output of the converter, output frequency, motor speed, motor current, or other signals that contain needed information.

If the power electronic devices are thyristors, the term “firing circuits” is appropriate. In some converters (for example, chopper circuits and PWM inverters), it is necessary to turn the power devices off. If forced turn-off (forced commutation)

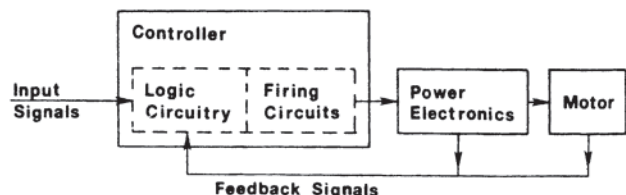


**Figure 9.97** Generic controller/converter block diagram.

is necessary, GTOs may be used, and the turn-off circuitry will take a different form from that used with thyristors. If a converter is implemented using power transistors, the firing circuits block will be replaced by one containing driver circuits designed to switch the transistors from the off state into the saturation mode (the on condition) and to hold them in that condition until the end of the desired pulse.

There are many variations of firing circuits, turn-off circuits, or driver circuits. Their nature is frequently determined by the kind of circuit to be controlled (rectifier, cycloconverter, PWM inverter, and so forth). References 53–60 may be consulted for specific circuits, such as circuits used for forced commutation, as well as for more general concepts, many of which are illustrated in block diagram form. References 68 and 69 give excellent discussions on interfacing to and driving modern gate commutated devices such as power MOSFETs, and IGBTs. Control of these circuits was originally achieved using an analog implementation. The availability of a wide variety of solid-state integrated circuits, such as programmable read-only memories (PROMs), digital logic circuitry, and microprocessors (which can be used for real-time waveform generation and control) has virtually supplanted the analog circuitry.

Control circuit diagrams were shown earlier in this chapter. Each one can be subdivided into blocks similar to those in Fig. 9.97, although engineers accustomed to designing such circuits generally do not think of them in that fashion. Part of each of those circuits is designed to carry out specific logic functions and part is designed to control power.

The power handling functions are carried out using contactors capable of carrying the motor currents. These circuits require large volumes in control cabinets, they are slow in operation, are time-consuming for design and installation, and are not easily or quickly modified if necessary.

Logic functions were often implemented using logic elements such as transistor-transistor logic (TTL), emittercoupled logic (ECL), or complementary metal oxide semiconductor (CMOS) logic. These logic functions are now implemented directly in most drives using microprocessors, microcontrollers or DSPs.

The power-handling functions of the contactors may continue to be carried out in the same way, or their contacts may be replaced by thyristors GTOs, IGBTs or is other solid-state switches. For example, each of the  $M$  contacts of Fig. 9.32 may be replaced by a thyristor with a diode connected in reverse parallel. Turning each thyristor on for a full half-cycle provides a direct replacement for the contacts on the contactors, or they may be fired initially for only part of the cycle, giving the capability of a soft start. Because of the voltage alternation of ac supplies, self-commutation occurs. Use of thyristors in control circuits for dc motors is less attractive because turn-off capability must be incorporated. IGBTs or MOSFETs can be used for these cases.

The development of microprocessors over the last 30 years has allowed most of the control functions for power electronic systems to be performed digitally under software control. This has allowed great simplification of control hardware and also

allowed sophisticated motor control algorithms to be implemented (such as field oriented control of ac motors and space vector modulation of inverters and converters). Microprocessors have evolved from early 4-bit architectures to today's 64-bit complex architectures running at hundred of megahertz. Depending on the application, many types of processors are available. These include general purpose microprocessors (used mostly in computing and data processor applications), microcontrollers, and advanced processors such as digital signal processors (DSPs) and RISC processors. Many of these advanced processors contain specialized functions needed to implement a power electronics system such as dedicated PWM functions and on-chip analog-to-digital (A-to-D) converters. DSPs were developed specifically for realtime computations for signal processing applications. Conventional control algorithms used in power electronic systems (such as PID control, feed forward control, and PWM) and advanced algorithms (such as adaptive control, observers, and Kalman filtering) utilize the same fundamental operations as the signal processing applications. Thus, the controls needed for power electronics benefit from the DSP's capabilities. The DSP's high computational power can be used to increase sampling rate and implement complex control algorithms. Real-time control of power electronic systems demands that several tasks be performed essentially simultaneously. Real-time operating systems are available for popular microprocessors to allow the processor to be used in a multitasking environment. To generate real-time code for microprocessor based power electronic systems, several higher-level programming languages are available including C and C++. An excellent overview of microprocessor control for power electronics can be found in Ref. 70.

Figure 9.98 show in block diagram form a power electronic system and its control. An ac or a dc power source supplies a power circuit such as an inverter, dc-dc converter (chopper), rectifier, or cycloconverter. The power circuit processes the power under control of the microprocessorbased control circuit to supply the load with either ac or dc power at the desired quality (voltage level, current level, frequency, harmonic content, ripple, etc.). The input voltage and/or current is often sensed and input to the control circuit to increase performance and stability. Note that these quantities must be attenuated to logic voltage levels and converter to digital form (with an A-to-D converter) for input to the digital control. As mentioned above many modern processors have on-chip A-to-D converters to minimize the external hardware needed. The converter output and load variables are also sensed and fed back to the control circuitry to complete the feedback loops. These output variables for a motor drive are usually motor voltage, current, speed, torque and/or position. Because of the processing power of modern processors and the advanced control algorithms that have been developed over the last several decades, many of these variables can be estimated by measuring only a few of the output variables. This is advantageous because any measurement requires a sensor, attenuator, and an A-to-D converter (which however, may be on-chip as discussed above). The microprocessor then performs its programmed

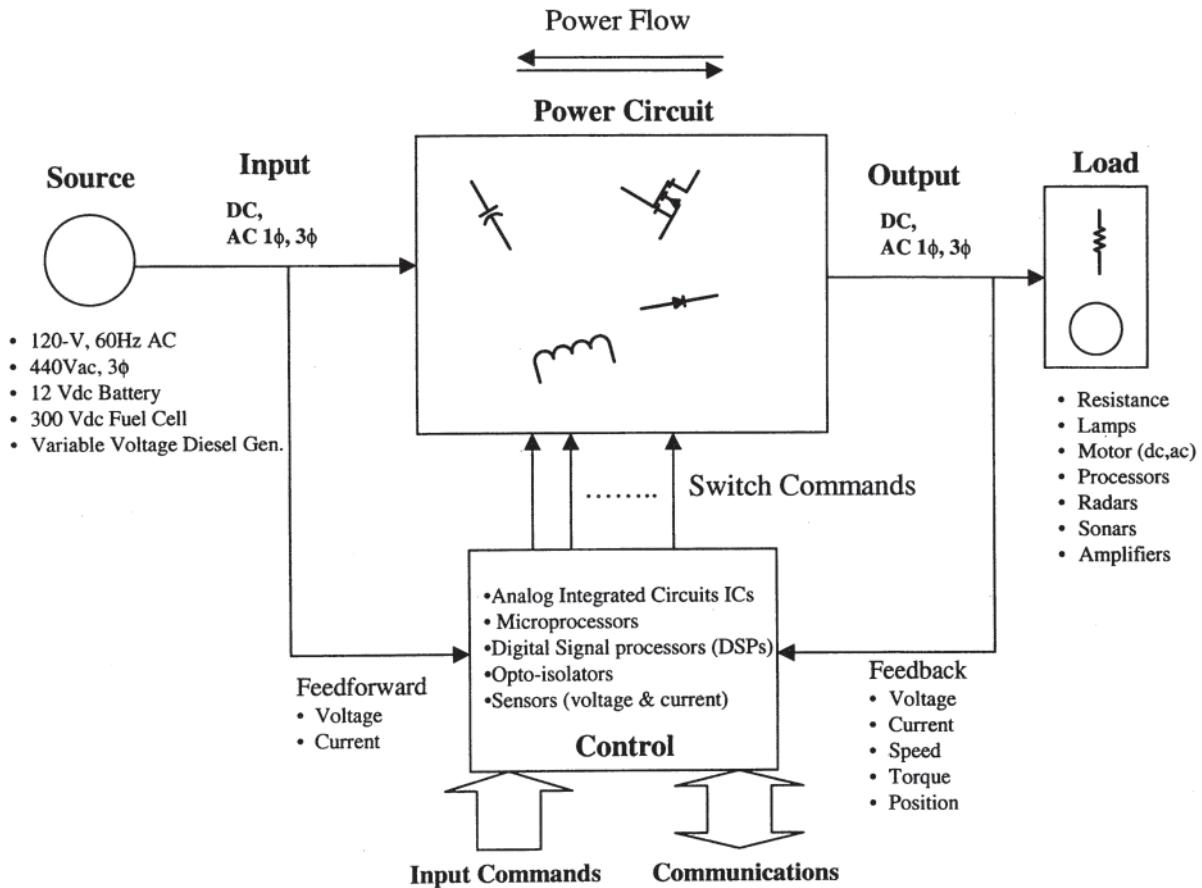


**Figure 9.98** Generic power electronic system showing power and control interfaces.

function to stabilize the system and control the load as commanded by the input commands. The input commands may come from another computer or may be programmed directly in the main controlling processor. The processor may also communicate with a central computer or display devices to indicate the status of the system (volts, amps, watts, VARs, temperatures, etc.) for both the input and the output of the converter.

Finally, the interface to the power circuit is through the firing circuits (gate drivers). In older systems, the gate drive signals may be generated from discrete analog circuitry, which performs some of the high-speed protection and modulation functions (thus relieving these critical functions from the microprocessors). In more modern systems the processor itself performs most of these functions and outputs the gate firing digital switch commands directly. It remains to provide an interface between the low-level gate command and the gate-firing power pulses required for the particular power switches being used. These gate-drivers are solid-state analog circuits with voltage isolation between control and power circuit (often being supplied by small isolation pulse transformers). In many cases the drive signals from the processor are provided to the gate-driver circuits using opto-couplers. The gate drivers in turn receive their power source from a separate isolated power supply. Special gate drive interface circuits employing high-

voltage integrated circuit (HVIC) technology are also available. These special integrated circuits are able to provide the voltage level shifting and voltage standoff capability required between the control and power circuits. They provide low voltage circuit functions (the gate driver functions) on separate parts of the chip, which in turn can be operated up to 1200 V apart. Signaling between the two parts of the chip is via an on-chip lateral high-voltage transistor operated as a current source. Power for nongrounded gate circuits is obtained using a bootstrapping technique. The advantage of these circuits is that no magnetic devices are needed and the gate driver can be implemented in a small space. The disadvantage is that there is no galvanic isolation between the power circuit and the control electronics, which may expose the control electronics to damage in the event of a gate driver failure. Details of these types of gate driver circuits can be found in Ref. 71.

## 9.7 OPEN- AND CLOSED-LOOP CONTROL OF A PERMANENT MAGNET STEPPER MOTOR

Permanent magnet (PM) stepper motors are synchronous electric machines with permanent magnet rotors, but are quite different in structure from standard permanent magnet synchronous machines. A typical PM stepper motor consists of a



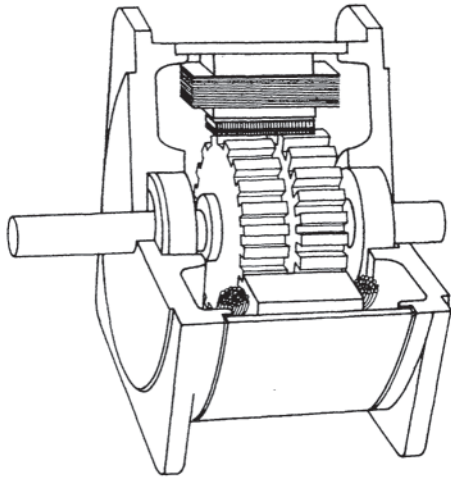


**Figure 9.99** Cutaway view of a stepper motor.

stator equipped with four phases (windings/coils) and a permanent magnet rotor with no windings. The rotor has two sets of teeth on it (with typically 50 teeth on each (that are out of alignment with each other by a tooth width). Figure 9.99 shows a cutaway view of a PM stepper motor. The rotor is magnetized so that the teeth on the left-hand side of Fig. 9.99 are all south poles while the teeth on the right-hand side are all north poles.

**Figure 9.98** (adapted from Figure 9-1 of [72]) shows the left-hand and right-hand side views of the PM stepper motor of Fig. 9.99 (simplified to five teeth on the rotor). The rotor has a cylindrical permanent magnet core assembled with a set of rotor teeth made of soft iron and pressed onto each end of the core. The permanent magnet magnetizes the rotor teeth making one set of teeth (left-hand side in Fig. 9.100) a south pole and the other set a north pole. The motor is typically operated as a two-phase machine, that is, phases A–A' are connected in series to make up one phase and phases B–B' are connected in series to make up the second phase. This will be the assumed connection in all that follows.

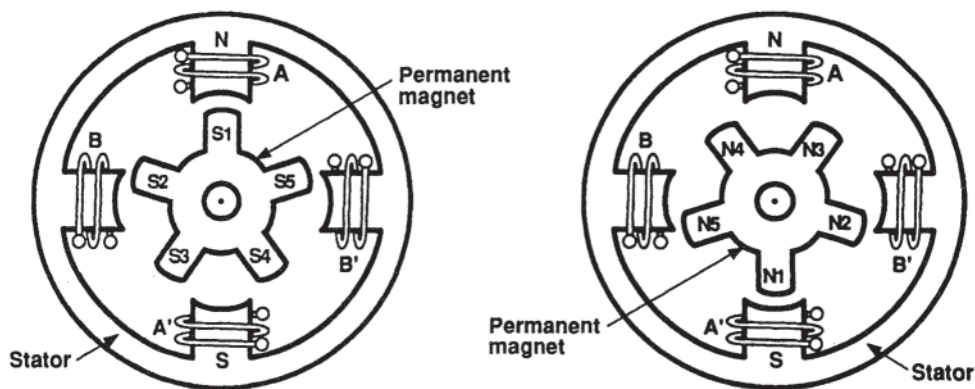


**Figure 9.100** Side views of the permanent magnet (PM) stepper motor.

### 9.7.1 Open-Loop Operation of the Stepper Motor [70–73]

The sign convention for the currents is as follows: When positive current is passed through phase A–A', side A of the stator is magnetized as a north pole while side A' is magnetized as a south pole. Conversely, when negative current is passed through phase A–A', side A of the stator is a south pole and side B is a north pole. A similar convention holds for phase B–B'. In Fig. 9.101 (a), a constant positive current  $i_0$  is shown that magnetizes stator side A as a north pole and stator side B as a south pole. In Figs. 9.101 (a)–(e) inclusive, the series connections between phases A and A' and B and B' are not shown but are assumed to be in effect.

The manner in which the PM stepper motor is operated in open-loop mode is illustrated by the diagrams in Fig. 9.101 (adapted from Figure 9-2 of [72]). We follow the presentation given in Deltoro [72]. Figure 9.101(a) illustrates the starting point with phase (winding/coil) A–A' energized for a N–S orientation and phase B–B' deenergized. The left-hand side of Fig. 9.101 (a) shows the south end of the PM motor while the right-hand side of Fig. 9.101(a) shows the north end. Neglecting electrical transients, the current  $i_0$  and voltage  $v_0$  are related by  $v_0 = Ri_0$  where  $R$  is the resistance of phase A–A' (equals the resistance of phase B–B').

Figure 9.101(b) illustrates the fact that when coil A–A' is deenergized, and coil B–B' is energized for a N–S orientation, the rotor rotates counterclockwise one step.

Note that Fig. 9.101(e) is identical to Fig. 9.101(a) except for numbering of the rotor teeth. In other words, after four steps, the rotor has rotated by an angle equal to the (angular) distance between two successive rotor teeth. Thus, the step size is given by  $360/(4N_r)$  degrees where  $N_r$  is the number of rotor teeth. Finer resolution can be achieved by increasing the number of rotor teeth. For example, with  $N_r = 50$ , this expression evaluates to 1.8 degrees for the step size.

In order to achieve finer resolutions, techniques such as half-stepping can be used. For example, in Fig. 9.101(a), one could leave  $v_a = v_0$  and set  $v_b = v_0$  so that the motor rotates to the new equilibrium point  $\theta = 9$  degrees, that is, a half-step. **Table 9.14** gives the voltage sequence needed to step the motor from  $\theta = 0$  to  $\theta = 72$  degrees in steps of 9 degrees.

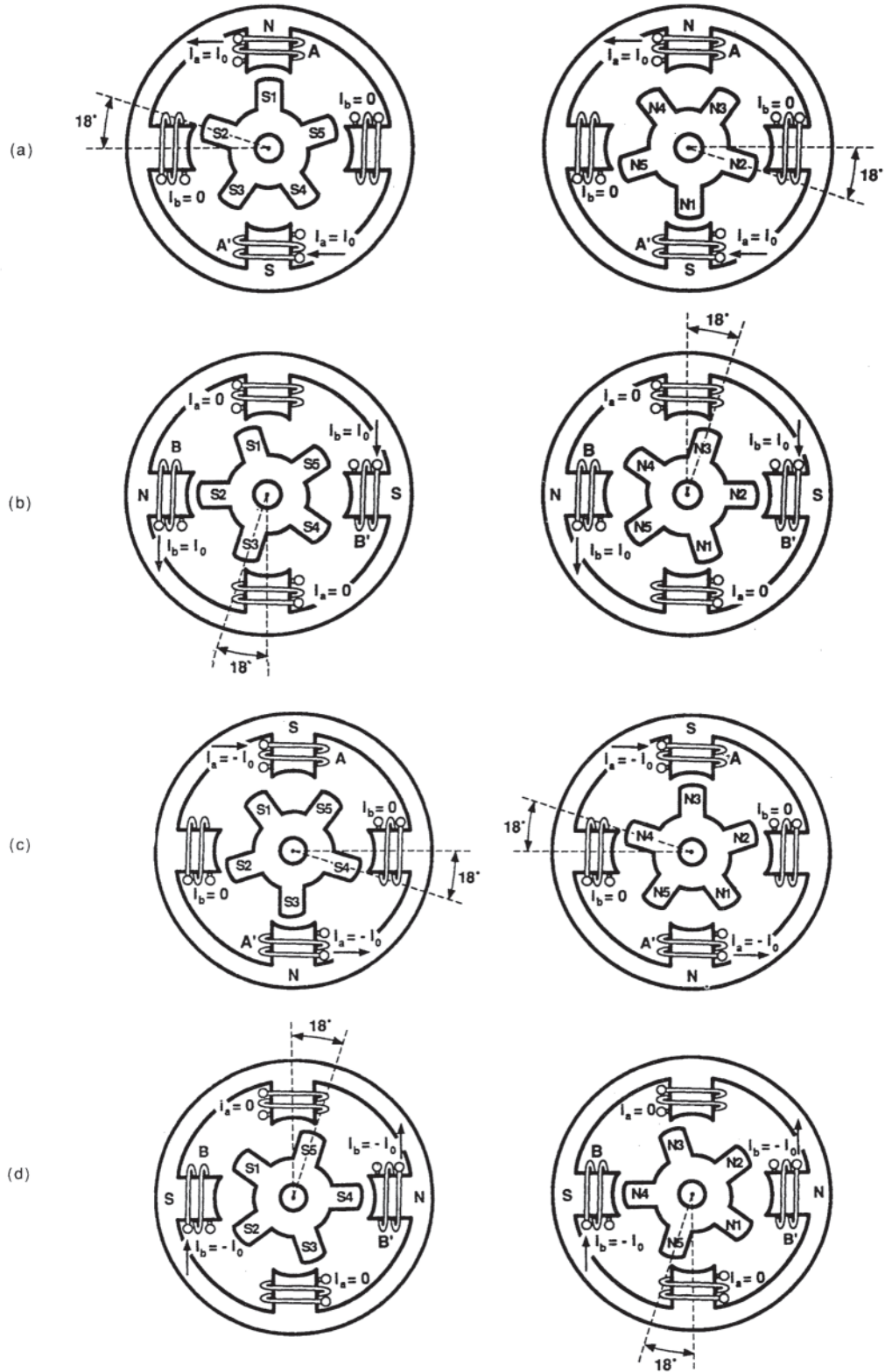


**Figure 9.101** PM motor rotation, (a) Starting point ( $\theta=0$ );  $v_a=v_0, v_b=0, i_a=i_0, i_b=0$ . (b) One-step rotation of the motor ( $\theta=18$  degrees);  $v_a=0, v_b=v_0, i_a=0, i_b=i_0$  (c) Second step ( $\theta=36$  degrees);  $v_a=-v_0, v_b=0, i_a=-i_0, i_b=0$ . (d) Third step ( $\theta=54$  degree);  $v_a=0, v_b=0-v_0, i_a=0, i_b=-i_0$ .

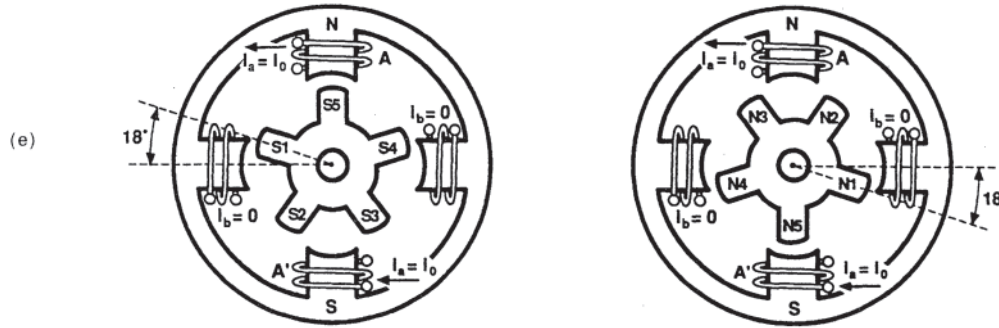


**Figure 9.101** PM motor rotation (*Continued*) (e) Fourth step ( $\theta=72$  degree);  $v_a=v_0, v_b=0, i_a=i_0, i_b=0$ .

In general, if fractional combinations of the voltages  $v_a = \alpha v_0, v_b = \beta v_0$  with  $|\alpha|, |\beta| \leq 1$  can be produced, arbitrary equilibrium positions will be achievable. Explanations of microstepping techniques are given in Deltoro [72] and Kuo [75].

A typical step response of a PM stepper motor with  $N_r=50$  is shown in Fig. 9.102; it is seen that the position settles out to 1.8 degrees. Such a response occurs, for example, when the motor is initially in the position shown in Fig. 9.101 (a) and then  $v_a$  is set to zero and  $v_b$  is set to  $v_0$ . The oscillatory nature of the response can be traced to the fact that, for constant phase currents, the equations describing the rotor motion are approximately those of a pendulum (this can be seen from the mathematical model that is developed later). Attenuation of the oscillations occurs only through the natural energy dissipation present in the system, namely friction and ohmic losses. Note that the transients do not settle out for approximately 50 ms. To run the motor open-loop at constant speed requires sequentially stepping the rotor at a constant rate as shown in Fig. 9.101 and Table 9.14. If such steps are initiated before the transients have settled sufficiently, it is possible for the motor to lose synchronism, with the result that the position is off by a step or more, a situation from which it cannot recover [73]. Consequently, the open-loop operation is traded off with a relatively long settling time and thus low-speed performance. To obtain fast and precise positioning, closed-loop operation is required.

**Table 9.14** Voltage Sequencing for Half-Stepping

$v_a$	$v_b$	$\theta$ (deg)
$v_0$	0	0
$v_0$	$v_0$	9
0	$v_0$	18
$-v_0$	$v_0$	27
$-v_0$	0	36
$-v_0$	$-v_0$	45
0	$-v_0$	54
$v_0$	$-v_0$	63
$v_0$	0	72

### 9.7.2 Closed-Loop Control of a Stepper Motor

Although stepper motors were originally designed for open-loop operation, they are now often used in closed-loop servo systems. One major advantage of the stepper motor over standard PM synchronous motors is its large stiffness. That is, due to the fact that a typical stepper motor has 50 teeth (50 pole-pairs), a small deflection of its shaft from the desired position results in a large restoring torque compared to standard PM synchronous motors. This will be elaborated upon below after the expression for the torque of a stepper motor has been derived.

#### 9.7.2.1 Mathematical Model of a Permanent Magnet Stepper Motor [73–75]

With  $\lambda_a$  the flux in phase A–A' due to the permanent magnet rotor,  $L$  the stator inductance, and  $R$  the stator resistance, the equation describing the electrical dynamics of phase A–A' is:

$$v_a = L \frac{di_a}{dt} - Ri_a - \frac{d\lambda_a}{dt} = 0$$

A similar equation holds for phase B–B'.

The surface of the rotor teeth and the surface of the stator are shaped so that the fluxes due to the permanent magnet in the rotor linking phases A–A' and B–B' are, respectively [74],

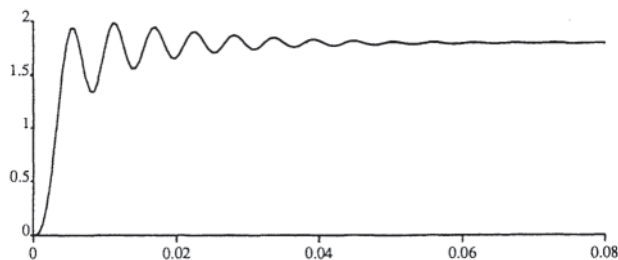


**Figure 9.102** Step response of a permanent-magnet stepper motor. (Position in degrees versus time in seconds.)

$$\lambda_a = \lambda_M \cos(N_r \theta) \quad \lambda_b = \lambda_M \sin(N_r \theta)$$

where  $\lambda_M$  is the maximum possible flux linking either phase and  $\theta=0$  corresponds to the position of the rotor in Fig. 9.101 (a). The voltages induced in windings A-A' and B-B' due to this flux are, respectively:

$$e_a = -\frac{d\lambda_a}{dt} = K_m \omega \sin(N_r \theta)$$

$$e_b = -\frac{d\lambda_b}{dt} = -K_m \omega \cos(N_r \theta)$$

where  $K_m \triangleq N_r \lambda_M$  and  $\omega = d\theta/dt$  is the angular velocity (in rad/sec). The power absorbed (negative power) by the windings from the voltage source is given by:

$$i_a e_a + i_b e_b = i_a K_m v \sin(N_r \theta) - i_b K_m v \cos(N_r \theta)$$

By conservation of energy, this power is equal to the negative of the mechanical output power  $\tau_m \omega$ , that is,  $\tau_m \omega = -i_a e_a - i_b e_b$ . Canceling  $\omega$  results in:

$$\tau_m = -K_m i_a \sin(N_r \theta) + K_m i_b \cos(N_r \theta)$$

*Remark:* The above expression for torque indicates the large stiffness of the stepper motor. Specifically, assume that the motor is in the equilibrium position shown in Fig. 9.101 (a), that is,  $\theta=0$ ,  $i_a=i_0$  and  $i_b=0$ , so that the torque is  $\tau_m = -K_m i_a \sin(N_r \theta)$ . The slope of the torque curve  $\tau(\theta)$  at  $\theta=0$  is  $-K_m i_a N_r$ , which is large if  $N_r$  is large. In other words, a slight disturbance in the position  $\theta$  from<sup>2</sup> results in a correspondingly large change in the argument  $N_r \theta$  of  $\sin(\cdot)$  and hence a large restoring torque.

Using the above relationships, the dynamic equations for the PM stepper motor are [74, 76]:

$$\frac{di_b}{dt} = \frac{v_b - Ri_b + K_m \omega \cos(N_r \theta)}{L}$$

$$\frac{d\omega}{dt} = \frac{-K_m i_a \sin(N_r \theta) + K_m i_b \cos(N_r \theta) - f\omega}{J} \quad (9.101)$$

$$\frac{d\theta}{dt} = \omega$$

where  $i_a$ ,  $i_b$  and  $v_a$ ,  $v_b$  are the currents and voltages in phases A-A' and B-B', respectively.  $L$  and  $R$  are, respectively, the self-inductance and resistance of each phase winding,  $K_m$  is the motor torque constant,  $N_r$  is the number of rotor teeth,  $J$  is the rotor inertia,  $f$  is the coefficient of viscous friction,  $\omega$  is the rotor speed, and  $\theta$  is the motor position. Other forms of friction (for example, Coulomb friction) and load torques  $\tau_L$  may be easily added to the model of Eq. 9.101. This model neglects the slight magnetic coupling between phases and the small change in  $L$  as a function of position  $\theta$  due to the rotor teeth [78, 79]. (These have negligible effect on the control problem of the PM stepper motor.)

*Remark:* In *variable-reluctance* stepper motors, the inductance  $L$  is a function of the position  $\theta$  and is not negligible.

It is in fact the mechanism for torque production in such motors (they do not have permanent magnet rotors). An introduction to variable-reluctance motors is given by Kuo in [75]. An approach to the closed-loop control of variable-reluctance motors is given by Taylor in [77].

### 9.7.2.2 Direct-Quadrature Transformation

In order to control the PM stepper motor, it is useful to consider the direct-quadrature (DQ) transformation of electric machine theory [76, 77, 82, 83]. The DQ transformation is defined by:

$$\begin{bmatrix} i_d \\ i_q \end{bmatrix} \triangleq \begin{bmatrix} \cos(N_r \theta) & \sin(N_r \theta) \\ -\sin(N_r \theta) & \cos(N_r \theta) \end{bmatrix} \begin{bmatrix} i_a \\ i_b \end{bmatrix} \quad (9.102)$$

New inputs are also defined using the DQ transformation:

$$\begin{bmatrix} v_d \\ v_q \end{bmatrix} \triangleq \begin{bmatrix} \cos(N_r \theta) & \sin(N_r \theta) \\ -\sin(N_r \theta) & \cos(N_r \theta) \end{bmatrix} \begin{bmatrix} v_a \\ v_b \end{bmatrix} \quad (9.103)$$

In terms of these new inputs and state variables, the system Eq. 9.101 becomes:

$$\frac{di_d}{dt} = \frac{v_d - Ri_d - N_r \omega Li_q}{L}$$

$$\frac{di_q}{dt} = \frac{v_q - Ri_q - N_r \omega Li_d K_m \omega}{L} \quad (9.104)$$

$$\frac{d\omega}{dt} = \frac{K_m i_q - f\omega}{J}$$

$$\frac{d\theta}{dt} = \omega$$

The inverse of the DQ transformation (Eq. 9.103), denoted as I DQ, is given by:

$$\begin{bmatrix} v_a \\ v_b \end{bmatrix} \triangleq \begin{bmatrix} \cos(N_r \theta) & -\sin(N_r \theta) \\ \sin(N_r \theta) & \cos(N_r \theta) \end{bmatrix} \begin{bmatrix} v_d \\ v_q \end{bmatrix} \quad (9.105)$$

The significance of the DQ transformation (see the third of equations of Eq. 9.104) is that the torque is linearly related to the quadrature current  $i_q$  (similar to a brush dc motor). The control problem is then reduced to using  $i_q$  to obtain the desired motion.

### 9.7.2.3 Closed-Loop Control Using Current Command

The simplest approach to closed-loop control is to use inner PI (proportional plus integral) current feedback loops to operate the system under current-command. This configuration is shown in Fig. 9.103. Choosing  $i_d=0$  and, assuming the  $i_d = i_{d^*} = 0$ , Eq. 9.104

$$\frac{di_q}{dt} = \frac{v_q - Ri_q - K_m \omega}{L}$$

$$\frac{d\omega}{dt} = \frac{K_m i_q - f\omega}{J}$$

$$\frac{d\theta}{dt} = \omega$$

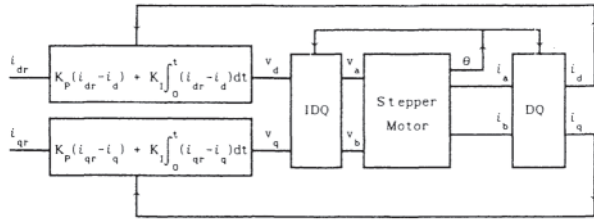


**Figure 9.103** Block diagram for closed-loop current-command control.

Note that these equations are *identical in form* to those for a brush dc motor. Assuming that the current feedback loop for  $i_q$  is also effective, the position/speed feedback controller can be designed using the reduced-order system:

$$\frac{d\omega}{dt} = \frac{K_m i_{qr} - f\omega}{J}$$

$$\frac{d\theta}{dt} = \omega$$

Again, these equations are comparable to those of a current-command brush dc motor, so that similar control strategies can be used. For example, with  $\theta_r, \omega_r = d\theta_r/dt, \alpha_r = d\omega_r/dt$  as the position, speed and acceleration references, respectively, one may choose the PID (proportional plus integral plus derivative) control law:

$$i_{qr} = \frac{J}{K_m} \left( K_I \int_0^t (\theta_r - \theta) dt + K_p(\theta_r - \theta) + K_D(\omega_r - \omega) + \alpha_r + \frac{f}{J} \omega \right)$$

to achieve position/speed tracking.

### 9.7.2.4 Field Weakening—Choice of $i_{dr}$

At low speeds, the current reference  $i_{dr}$  can be set to zero as in the previous section. However, for high speeds, it is necessary to control  $i_d$  as a function of  $\omega$  to avoid saturation of the input voltages. This is understood by considering the back-emf term  $-K_m\omega$  in Eq. 9.104. With a typical  $K_m$  taken to be 0.2 (V/rad)/sec, the back-emf voltages at speeds of 500 rpm, 1000 rpm, 1500 rpm, and 2000 rpm are 10.5 V, 21 V, 31.5 V, and 42 V, respectively. The PI current-command loop forces  $v_q$  to cancel the back-emf term (along with the other terms  $-Ri_q$  and  $-N_r\omega Li_d$ ) in order to achieve current tracking. If the voltage source is 40 V, it will not be possible to do this, that is, the phase voltages will saturate.

If  $i_d$  were forced to be negative (referred to as *field weakening* [80]), then the term  $-N_r\omega Li_d$  would help to cancel out the back-emf term  $-K_m\omega$  in the second part of Eq. 9.104. This would then allow  $v_q$  to be used to build up  $i_q$  and hence the torque. Careful consideration must be given to choosing the input  $v_d$  to control  $i_d$  in order to maximize the available torque.

#### Optimal Choice for $i_d(t)$ [78]

The limits on the voltage are given as  $|v_a|, |v_b| \leq V_M$ . The problem then is how to choose  $v_{\omega}, v_b$  to maximize the torque

with out violating the voltage constraints. As stated, this a difficult nonlinear control problem for which no analytic solution exists. However, an approximate solution can be found by assuming that the speed is constant (or varies slowly). In that case, the DQ variables are all constant and the phase voltages  $v_a$  and  $v_b$  are sinusoids of the form  $v_a = V \cos(N_r\omega + \phi)$  and  $v_b = V \sin(N_r\omega + \phi)$ . The equality  $v_d^2 + v_q^2 = v_a^2 + v_b^2$  holds and the constraint is  $v_d^2 + v_q^2 = V^2 \leq V_M^2$ . The problem is then to find the inputs  $v_d, v_q$  that maximize the torque  $K_m i_q$  subject to  $v_d^2 + v_q^2 \leq V_M^2$ . With the assumption of constant speed,  $i_b, i_{\phi}, v_d$  and  $v_q$  are constant. Thus, setting  $d\omega/dt=0, di_d/dt=0,$  and  $di_q/dt=0$  in Eqs. 9.104 and then solving for  $i_d$  and  $i_q$  results in:

$$i_q = \frac{Rv_q - N_r\omega Lv_d - K_m R\omega}{R^2 + (N_r\omega L)^2} \tag{9.106a}$$

$$i_d = \frac{N_r\omega Lv_q + Rv_d - K_m N_r L\omega^2}{R^2 + (N_r\omega L)^2} \tag{9.106b}$$

The optimization problem is to maximize  $i_q$  subject to  $v_d^2 + v_q^2 = V_M^2$ , that is, maximize  $Rv_q - N_r\omega Lv_d$  with the constraint  $v_d^2 + v_q^2 = V_M^2$ . Use of the Lagrange multiplier technique gives:

$$\frac{v_d}{v_q} = \frac{-N_r L\omega}{R} \tag{9.107}$$

This formula gives the well-known *optimal lead-angle* [73–75]. Note from Eq. 9.107 that, at low speeds, where  $\omega \approx 0$ , the optimal  $v_d \approx 0$  and the control effort is primarily  $v_q$ . In contrast, at high speeds, where  $\omega$  is large, the optimal  $v_q$  is small and  $v_d$  is  $< 0$  and large in magnitude. This corresponds to a lead-angle of 90 degrees on the voltages to compensate for the 90-degree phase-lag due to the inductive effects. Use of Eq. 9.107 and  $v_d^2 + v_q^2 = V_M^2$  in Eq. 9.106 results in the optimal currents being given by:

$$i_{qopt} \triangleq \frac{(R^2 + (N_r\omega L)^2)^{1/2} V_M - K_m R\omega}{R^2 + (N_r\omega L)^2} \tag{9.108}$$

$$i_{dopt} \triangleq - \frac{K_m N_r L\omega^2}{R^2 + (N_r\omega L)^2} \tag{9.109}$$

If current-command is used, Eq. 9.109 can be used instead of Eq. 9.107 to define the reference for the direct current  $i_d$  as:

$$i_{dr} \triangleq \frac{-K_m N_r L\omega^2}{R^2 + (N_r\omega L)^2} \tag{9.110}$$

Note that  $i_{dr}$  is negative for all speeds, which in turn helps to counteract the back-emf (optimal field-weakening). At low speeds  $\omega \equiv 0$  and  $i_q \equiv V_M/R, i_d \equiv 0$ . At high speeds, the direct current tends to  $i_d \equiv K_m/(N_r L)$ . The transition between  $i_d=0$  and  $i_d=-K_m/(N_r L)$  occurs around the critical speed  $\omega_c \triangleq (R/N_r L)$ . For stepper motors where  $N_r$  is large, this speed can be quite low. The reference current, Eq. 9.110, is then used in the current-command feed-back system as shown in Fig. 9.103 to maximize the range of speeds over which torque can be produced.

### 9.7.2.5 Speed Estimation

#### 9.7.2.5.1 Estimation of Speed by Differentiation of Position

In a typical servo (positioning) control system, a sensor such as an optical encoder is used for the position measurement, but a speed measurement is usually not available. With a 2000-line optical encoder, a straightforward way to compute the speed is as:

$$\hat{\omega}(kT) \triangleq \frac{2\pi}{2000} \frac{N(kT) - N(kT - T)}{T} \quad (9.111)$$

where  $T$  is the time between samples and  $N(kT)$  is the optical encoder count at time  $kT$ . However, this method of estimating the speed by differentiation of the position measurements can be very inaccurate at low speeds. At any time  $kT$ ,  $N(kT)$  can be in error by up to one encoder count. Specifically,  $N(kT)$  can be too *small* by up to one encoder count ( $N(kT)$  is never too large because of the way the encoder works). Thus, with  $\theta(kT)$  the true position of the motor in radians, we may write:

$$\theta(kT) = \frac{2\pi}{2000} N(kT) + \frac{2\pi}{2000} e(kT)$$

where  $e(kT)$  represents the *positive fractional* count that the encoder cannot sense, that is,  $0 \leq e(kT) < 1$  for all  $k$ . Then, the speed may be written as:

$$\begin{aligned} \omega(kT) &= \frac{\theta(kT) - \theta(kT - T)}{T} \\ &= \frac{2\pi}{2000} \frac{N(kT) - N(kT - T)}{T} \\ &\quad + (2\pi/2000) \frac{e(kT) - e(kT - T)}{T} \end{aligned}$$

where, as  $0 \leq e(kT) < 1$  and  $0 \leq e((k-1)T) < 1$ , it follows that  $|e(kT) - e(kT - T)| < 1$ .

It is now straightforward to compute a bound on the error in estimating the speed. As the speed estimate is given by Eq. 9.111 and the difference  $e(kT) - e(kT - T)$  is bounded by  $\pm 1$ , we have

$$|\text{Error in } \omega(kT)| \leq \frac{2\pi}{2000} \frac{|e(kT) - e(kT - T)|}{T} = \frac{2\pi/2000}{T}$$

As the sampling rate increases ( $T$  gets smaller), the error gets larger. On the other hand, as the sampling rate decreases, the approximation

$$\omega(kT) \approx \frac{\theta(kT) - \theta(kT - T)}{T}$$

becomes less and less valid. One way to decrease the error would be to use an encoder with higher resolution. Such encoders are typically more expensive and cannot operate at higher speeds (as the speed increases, the frequency of the pulses becomes too high for the pulse detection circuitry).

#### 9.7.5.2.2 Speed Estimation Using an Observer [81]

An estimate of the speed can be found by using a *speed observer*. To do this, one measures  $i_\omega$ ,  $i_b$  and  $\theta$  to calculate  $i_q$  and then implements:

$$\frac{d\hat{\theta}}{dt} = \hat{\omega} - l_1 (\hat{\theta} - \theta) \quad (9.112)$$

$$\frac{d\hat{\omega}}{dt} = \frac{K_m i_q - f\hat{\omega}}{J} - l_2 (\hat{\theta} - \theta)$$

in *real-time*, with the solution  $\hat{\omega}$  being the estimate of  $\omega$ . To understand why this works, let  $\epsilon_1 = \hat{\theta} - \theta$ ,  $\epsilon_2 = \hat{\omega} - \omega$  be the estimation error whose dynamics are found by subtracting Eq. 9.112 from

$$\begin{aligned} \frac{d\theta}{dt} &= \omega \\ \frac{d\omega}{dt} &= \frac{K_m i_q - f\omega}{J} \end{aligned} \quad (9.113)$$

resulting in:

$$\begin{aligned} \frac{d\epsilon_1}{dt} &= \epsilon_2 + l_1 \epsilon_1 \\ \frac{d\epsilon_2}{dt} &= -\frac{f}{J} \epsilon_2 + l_2 \epsilon_1 \end{aligned} \quad (9.114)$$

The characteristic equation of this error system is then

$$s^2 + \left( l_1 + \frac{f}{J} \right) s + l_2 + \frac{f}{J} l_1 = 0$$

Choosing the observer gains as  $l_1 = p_1 + p_2 - f/J$ ,  $l_2 = p_2 p_2 - (f/J) l_1$ , the roots of this characteristic equation are  $-p_1, -p_2$ . Consequently, by choice of  $p_1, p_2$ , the error in speed  $\epsilon_2(t) = \hat{\omega}(t) - \omega(t)$  can theoretically be made to converge to zero with any desired time constants, resulting in  $\hat{\omega}(t)$  being a good estimate of  $\omega$ . In practice, the gains are chosen so that a satisfactory trade-off is reached between speed of convergence and sensitivity to noise.

#### 9.7.2.6 A State-Space Trajectory Tracking Controller [78, 82]

A distinctive feature of PM stepper motors is the large number of pole-pairs on the rotor. With  $N_r = 50$  as a typical number for the pole-pairs, the machine goes through 50 electrical cycles for each single mechanical revolution. Equation 9.104 shows that there are strong cross-couplings, even after transforming to the DQ axes. Specifically, the term  $N_r \omega L i_q$  appears in the equation for  $i_d$  and  $-N_r \omega L i_d$  in the equation for  $i_q$ . Because  $N_r$  is large, these terms become dominant at high speeds. While high-gain feedback can be used to cancel these cross-couplings, a more effective solution consists in using the knowledge of the current dynamics to create a multivariable voltage control law. Such a method is now described.

Reconsider the DQ system (Eq. 9.104). The idea here is to use feedback to eliminate the nonlinear terms. That is, let:

$$\begin{aligned} v_d &= -N_r \omega L i_q + L u_d \\ v_q &= N_r \omega L i_d + K_m \omega L u_q \end{aligned} \quad (9.115)$$

to obtain the system:

$$\frac{di_d}{dt} = -\frac{R}{L} i_d + u_d$$

$$\frac{di_q}{dt} = -\frac{R}{L}i_q + u_q \quad (9.116)$$

$$\frac{d\omega}{dt} = \frac{K_m}{J}i_q - \frac{f}{J}\omega$$

$$\frac{d\theta}{dt} = \omega$$

The original system (Eq. 9.104) has now been decoupled into two linear subsystems of first and third order, respectively. However, this *particular* feedback cancellation (Eq. 9.115) requires  $v_q$  to cancel both  $-N_r\omega L i_d$  and  $-K_m\omega$ , which was shown above to lead quickly to saturation of the phase voltages as the motor speed increases. This difficulty is circumvented by consideration of a full state trajectory tracking controller that incorporates the reference current (9.110) developed for  $i_d$ . Specifically, let  $\theta_r, \omega_r = d\theta_r/dt, \alpha_r = d\omega_r/dt$ , and  $j_r = d\alpha_r/dt$  be, respectively, the references for the position, speed, acceleration, and jerk. Choosing  $i_{qr} \triangleq (J\alpha_r + f\omega_r)/K_m$  results in  $[i_{dr}, i_{qr}, \omega_r, \theta_r]^T$  as the state reference trajectory where  $i_{dr}$  is given by Eq. 9.110. Let  $[v_{dr}, v_{qr}]^T$  denote the corresponding reference input, which must be chosen such that:

$$\frac{di_{dr}}{dt} = \frac{v_{dr} - Ri_{dr} + N_r\omega_r Li_{qr}}{L}$$

$$\frac{di_{qr}}{dt} = \frac{v_{qr} - Ri_{qr} - N_r\omega_r Li_{dr} - K_m\omega_r}{L} \quad (9.117)$$

$$\frac{d\omega_r}{dt} = \frac{K_m i_{qr} - f\omega_r}{J}$$

$$\frac{d\theta_r}{dt} = \omega_r$$

is satisfied. That is, differentiating the expression for  $i_{dr}$  gives

$$\frac{di_{dr}}{dt} = -\frac{2K_m N_r L R^2 \omega_r \alpha_r}{R^2 + (N_r \omega_r L)^2}$$

which is then substituted into the first of Eq. 9.117 to solve for  $v_{dr}$ . Similarly, one substitutes  $di_{qr}/dt = (J\alpha_r + f\omega_r)/K_m$  into the second of Eq. 9.117 and solves for  $v_{qr}$ . The control designer must choose the desired trajectory in such a way that the corresponding reference inputs  $v_{dr}, v_{qr}$  do not exceed the voltage limits.

To design a state feedback controller to track this trajectory, define the error state variables as  $\varepsilon_1 = i_d - i_{dr}, \varepsilon_2 = i_q - i_{qr}, \varepsilon_3 = \omega - \omega_r$ , and  $\varepsilon_4 = \theta - \theta_r$ . Subtracting Eq. 9.117 from Eq. 9.114 gives:

$$\frac{d\varepsilon_1}{dt} = -\frac{R}{L}\varepsilon_1 + \frac{v_d - v_{dr}}{L} + N_r\omega i_q - N_r\omega_r i_{qr}$$

$$\frac{d\varepsilon_2}{dt} = -\frac{R}{L}\varepsilon_2 - \frac{K_m}{L}\varepsilon_3 + \frac{v_q - v_{qr}}{L} - N_r\omega i_d - N_r\omega_r i_{dr}$$

$$\frac{d\varepsilon_3}{dt} = \frac{K_m}{J}\varepsilon_2 - \frac{f}{J}\varepsilon_3 \quad (9.118)$$

$$\frac{d\varepsilon_4}{dt} = \varepsilon_3$$

Letting:

$$\begin{aligned} v_d &= v_{dr} + (-N_r\omega i_q + N_r\omega_r i_{qr} + u_d)L \\ v_q &= v_{qr} + (-N_r\omega_r i_{dr} + N_r\omega i_d + u_q)L \end{aligned} \quad (9.119)$$

results in the *linear error system*:

$$\frac{d\varepsilon_1}{dt} = -\frac{R}{L}\varepsilon_1 + u_d$$

$$\frac{d\varepsilon_2}{dt} = -\frac{R}{L}\varepsilon_2 - \frac{K_m}{L}\varepsilon_3 + u_q \quad (9.120)$$

$$\frac{d\varepsilon_3}{dt} = \frac{K_m}{J}\varepsilon_2 - \frac{f}{J}\varepsilon_3$$

$$\frac{d\varepsilon_4}{dt} = \varepsilon_3$$

In order to eliminate any steady-state error due to constant disturbances, let  $\varepsilon_5 = \int_0^t (\theta - \theta_r) dt$  be used to provide integral feedback. Then with  $\varepsilon = [i_d - i_{dr}, i_q - i_{qr}, \omega - \omega_r, \theta - \theta_r, \int_0^t (\theta - \theta_r) dt]^T$ , it follows that:

$$[\dot{\varepsilon}] = \begin{bmatrix} -R/L & 0 & 0 & 0 & 0 \\ 0 & -R/L & -K_m/L & 0 & 0 \\ 0 & K_m/J & -f/J & 0 & 0 \\ 0 & 0 & 1 & 0 & 0 \\ 0 & 0 & 0 & 1 & 0 \end{bmatrix} [\varepsilon] + \begin{bmatrix} 1 & 0 \\ 0 & 1 \\ 0 & 0 \\ 0 & 0 \\ 0 & 0 \end{bmatrix} \begin{bmatrix} u_d \\ u_q \end{bmatrix} \quad (9.121)$$

Through the use of a nonlinear state transformation, input transformation and nonlinear feedback, a *linear time-invariant error system* has been obtained. Further, Eq. 9.121 is decoupled into two subsystems of orders 1 and 4, respectively. With the obvious definitions for  $A$  and  $b$ , Eq. 9.121 may be written compactly as:

$$[\dot{\varepsilon}] = [A][\varepsilon] + [b][u]$$

where  $[u] = [u_b, u_q]^T$ . The inputs  $u_b, u_q$  are then chosen to force  $[\varepsilon(t)] \rightarrow 0$  as  $t \rightarrow \infty$ . Specifically, letting  $[u] = -[K]\varepsilon$  where

$$[K] \triangleq \begin{bmatrix} k_{11} & 0 & 0 & 0 & 0 \\ 0 & k_{22} & k_{23} & k_{24} & k_{25} \end{bmatrix}$$

Equation 9.121 becomes:

$$[\dot{\varepsilon}] = ([A] - [b][k])[\varepsilon]$$

As the pair  $\{[A], [b]\}$  is controllable, the feedback gain  $[K]$  may be chosen to assign the eigenvalues of  $[A] - [b][k]$ . Software Packages such as MATLAB [83] facilitate such a procedure

**Figure 9.104** is a block diagram of the state-space (non-linear) feedback controller. In Fig. 9.104, the currents  $i_b, i_q$  are computed in real-time using the direct-quadrature (DQ) transformation:

$$\begin{aligned} i_d &= i_a \cos(N_r\theta) + i_b \sin(N_r\theta) \\ i_q &= -i_a \sin(N_r\theta) + i_b \cos(N_r\theta) \end{aligned} \quad (9.102)$$

The speed estimate  $\hat{\omega}$  is the real-time solution to:

$$\frac{d\hat{\theta}}{dt} = \hat{\omega} - l_1(\hat{\theta} - \theta) \quad (9.112)$$

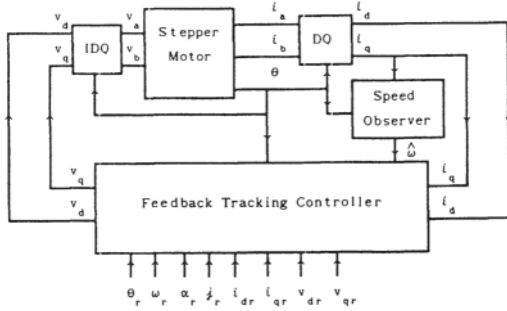


Figure 9.104 System block diagram for the state-space controller.

$$d\hat{\omega}/dt = \frac{(K_m i_q - f \hat{\omega})}{J} - l_2(\hat{\omega} - \omega)$$

The complete feedback law is given by:

$$\begin{aligned} v_d &= v_{dr} - N_r \hat{\omega} L i_q + N_r \omega_r L i_{qr} - L k_{11}(i_d - i_{dr}) \\ v_q &= v_{qr} - N_r \omega_r L i_{dr} + N_r \hat{\omega} L i_d \\ &\quad - L \left( k_{22}(i_q - i_{qr}) + k_{23}(\hat{\omega} - \omega_r) + k_{24}(\theta - \theta_r) \right. \\ &\quad \left. + k_{25} \int_0^t (\theta - \theta_r) dt \right) \end{aligned}$$

The phase voltages  $v_a$ ,  $v_b$  are computed using the inverse direct-quadrature (IDQ) transformation:

$$\begin{aligned} v_a &= v_d \cos(N_r \theta) - v_q \sin(N_r \theta) \\ v_b &= v_d \sin(N_r \theta) + v_q \cos(N_r \theta) \end{aligned} \quad (9.105)$$

For further details, see [78].

#### 9.7.2.7 Identification of the Motor Parameters [84]

The values of the motor parameters  $R$ ,  $L$ ,  $K_m$ ,  $f$ , and  $J$  must be determined to implement the state feedback controller. As the model of the stepper motor is linear in the parameters, a *least-squares* procedure may be used. To do so, the DQ model Eq. 9.104 is rewritten as:

$$\begin{bmatrix} i_d & (di_d/dt) - N_r \omega i_d & 0 & 0 & 0 \\ i_q & (di_q/dt) + N_r \omega i_q & \omega & 0 & 0 \\ 0 & 0 & -i_q & d\omega/dt & \omega \end{bmatrix} \begin{bmatrix} R \\ L \\ K_m \\ J \\ f \end{bmatrix} = \begin{bmatrix} v_d \\ v_q \\ 0 \end{bmatrix} \quad (9.122)$$

The idea here is that  $v_d$ ,  $v_q$  are commanded to the motor for a short period of time using the inverse DQ transformation:

$$\begin{aligned} v_a &= v_d \cos(N_r \theta) - v_q \sin(N_r \theta) \\ v_b &= v_d \sin(N_r \theta) + v_q \cos(N_r \theta) \end{aligned}$$

and the measured position to obtain the phase voltages  $v_a$ ,  $v_b$  commanded to the amplifier. Over this same period of time, the currents  $i_a$ ,  $i_b$  are measured to compute  $i_d$ ,  $i_q$  using the DQ transformation with the measured value of  $\theta$ . The derivatives  $di_d/dt$ ,  $di_q/dt$ ,  $\omega = d\theta/dt$ ,  $d\omega/dt$  are then computed offline using a digital filter. With the use of these data in Eq. 9.122, the

parameter values  $R$ ,  $L$ ,  $K_m$ ,  $f$ , and  $J$  are found that “best” satisfy Eq. 9.122. Rather than work with the  $5 \times 3$  system of Eq. 9.122, the calculation can be further separated into two stages: Stage 1 is the identification of the electrical parameters  $R$ ,  $L$ , and  $K_m$ . Specifically, with  $t = nT$ , the  $n$ th sample:

$$\begin{aligned} [W_1(nT)] &\triangleq \begin{bmatrix} i_d(nT) \frac{di_d}{dt}(nT) - N_r \omega(nT) i_d(nT) & 0 \\ i_q(nT) \frac{di_q}{dt}(nT) + N_r \omega(nT) i_q(nT) & \omega(nT) \end{bmatrix} \\ [y(nT)] &\triangleq \begin{bmatrix} v_d(nT) \\ v_q(nT) \end{bmatrix}, \quad [K_E] = \begin{bmatrix} R \\ L \\ K_m \end{bmatrix} \end{aligned}$$

and using Eq. 9.122, it follows that:

$$[W_1(nT)][K_E] = [y(nT)] \quad (9.123)$$

Multiplying this equation by  $[W_1(nT)]^T$ , the transpose of  $[W_1(nT)]$ , and summing over  $N$  time samples results in

$$\left( \sum_{n=1}^N [W_1(nT)]^T [W_1(nT)] \right) [K_E] = \sum_{n=1}^N [W_1(nT)]^T [y(nT)]$$

If  $[R_{W_1}] \triangleq \sum_{n=1}^N [W_1(nT)]^T [W_1(nT)] \in \mathbb{R}^{3 \times 3}$  is invertible, then:

$$[K_E] = [R_{W_1}^{-1}] [R_{W_y}] \quad (9.124)$$

where  $[R_{W_y}] \triangleq \sum_{n=1}^N [W_1(nT)]^T [y(nT)] \in \mathbb{R}^3$ . It turns out that the value for  $[K_E]$  given by Eq. 9.124 minimizes the squared error defined by

$$\begin{aligned} \varepsilon_1^2 &\triangleq \sum_{n=1}^N \left[ [W_1(nT)][K_E] - [y(nT)] \right]^T \\ &\quad \times \left[ [W_1(nT)][K_E] - [y(nT)] \right] \end{aligned}$$

thus making  $[K_E]$  the *least-squares estimate*.

Using the identified value of  $K_m$ , step 2 is the identification of the mechanical parameters  $J$  and  $f$  using:

$$\left[ \frac{d\omega}{dt}(nT) \quad \omega(nT) \right] \begin{bmatrix} J \\ f \end{bmatrix} = K_m i_q(nT)$$

Similarly, with:

$$[W_2(nT)] \triangleq \left[ \frac{d\omega}{dt}(nT) \quad \omega(nT) \right], \quad z(nT) = K_m i_q(nT),$$

$$[K_M] = \begin{bmatrix} J \\ f \end{bmatrix}$$

so that:

$$[W_2(nT)][K_M] = z(nT)$$

it follows that:

$$[K_M] = [R_{W_2}^{-1}] [R_{W_z}] \quad (9.125)$$

assuming that  $[R_{W_2}] \triangleq \sum_{n=1}^N [W_2(nT)]^T [W_2(nT)] \in \mathbb{R}^{2 \times 2}$  is invertible and defining:



$$[R_{w2}] \triangleq \sum_{n=1}^N [W_2(nT)]^T z(nT) \in \mathbb{R}^2.$$

Further,  $[K_M]$  minimizes the squared error

$$\varepsilon_2^2 \triangleq \sum_{n=1}^N [W_2(nT)[K_M] - z(nT)]^2.$$

The invertibility of  $[R_{w1}]$  and  $[R_{w2}]$  is usually not a problem as long as the speed is not kept constant over the length of the experiment. For more information on identification theory, the reader is referred to Refs. 83–85. For more information on the implementation consideration for stepper motors, see Ref. 82.

### 9.7.3 Experimental Results [78]

Experimental results of the implementation are given to illustrate the performance of the controller. The state-space controller of Section 9.7.2.6 is considered. The stepper motor is attached to a linear positioning table through a ball screw, which moves the table 4 millimeters per revolution of the motor. The position measurement is obtained from a 2000-line optical encoder on the motor, which gives a resolution of 360 degrees/2000=0.18 degrees. The voltage limit for  $v_a$  and  $v_b$  is 40 V.

The parameters were identified using the above leastsquares technique on collected data [82, 86]. The motor used to do the experimental work was found to have the following parameter values:  $N_r=50$ ,  $R=0.55$  ohms,  $L=1.5$  mH,  $J=4.5 \times 10^{-5}$  kg-m<sup>2</sup>,  $K_m=0.19$  (N-m)/amp,  $f=8.0 \times 10^{-5}$  (N-m/rad)/sec. The values for/ and/include the contributions of the linear positioning table.

#### 9.7.3.1 1.8-Millimeter Move of a Positioning Table

The first experiment consists in having the motor move the table 1.8 mm, which corresponds to having the motor rotate 2.83 radians or 162 degrees. Figure 9.105 is a plot of the actual and reference position responses. The last part of the position response is shown in more detail in Fig. 9.109. The reference speed and estimated speed (by the observer) are shown in Fig. 9.106. Note the close tracking of both the position and speed responses.

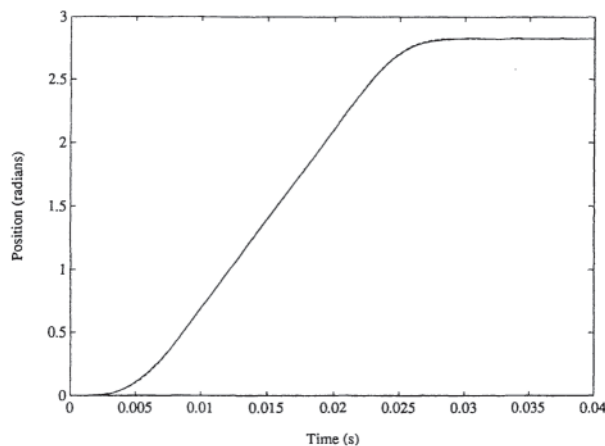


Figure 9.105 Measured and reference position for the 1.8-mm move.

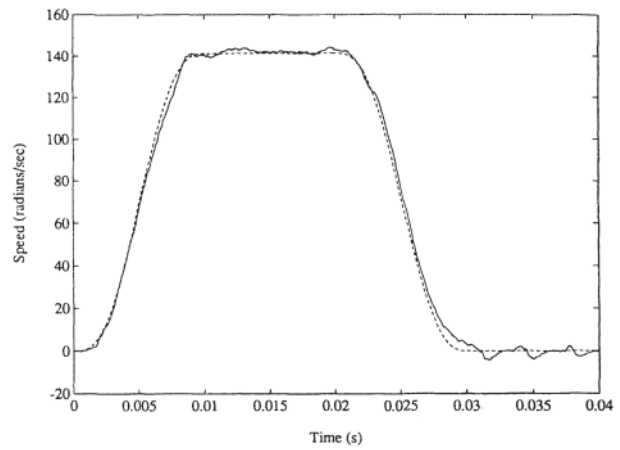


Figure 9.106 Estimated and reference speed for the 1.8-mm move.

Figures 9.107 and 9.108 show, respectively, the tracking of the direct and quadrature currents to their reference. The fluctuation in the currents about their references is due to the limited resolution of the encoder. That is, the direct and

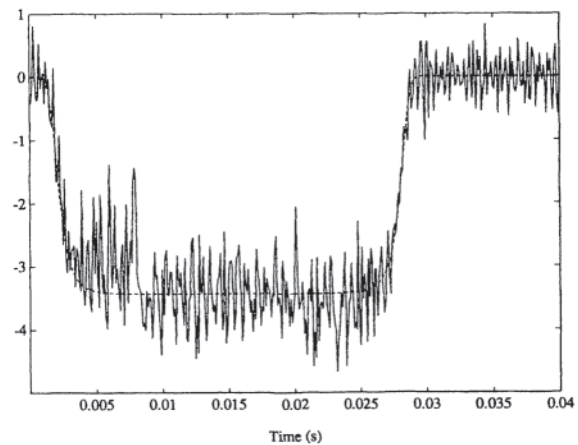


Figure 9.107 Actual and reference direct current for the 1.8-mm move.

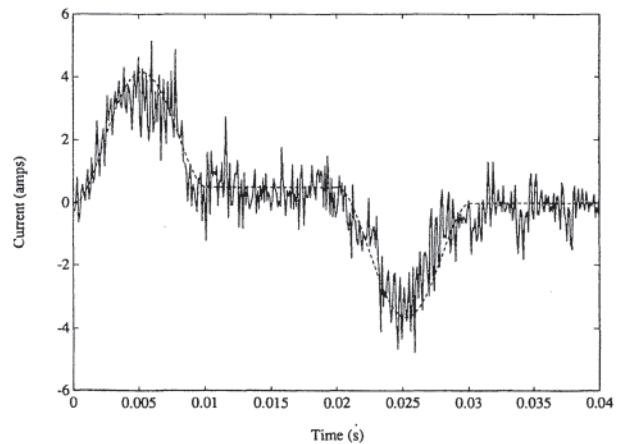
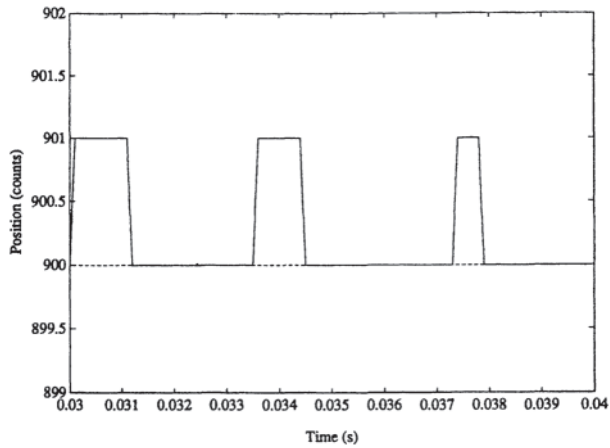


Figure 9.108 Actual and reference quadrature current for the 1.8-mm move.



**Figure 9.109** Measured position in counts after 30-ms. Final reference position is 900 counts= $(900/2000)\pi$  radians.

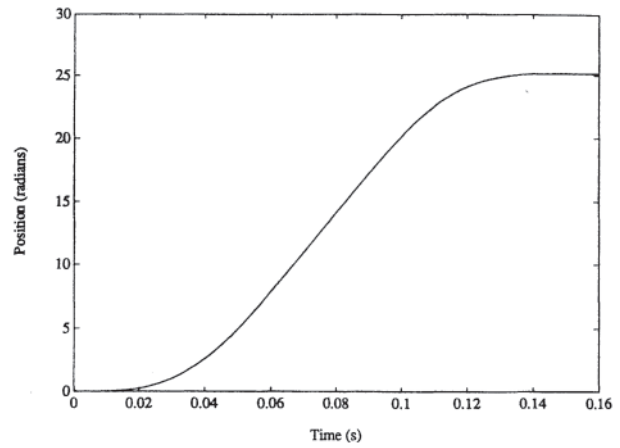
quadrature currents are found using the DQ transformation Eq. 9.102, in which the position measurement  $\theta$  is only known to within 0.18 degree. It was found that the high-frequency oscillations in the currents were due to this quantization noise in the position measurement [78]. The oscillatory behavior of the estimated speed  $\hat{\omega}$  is a direct result of integrating the fluctuating quadrature current  $i_q$  in the observer of Eq. 9.112. That is, the motor comes into position and stays there within one encoder count. This is demonstrated in Fig. 9.109 (note that the units are *counts* not radians), in which the position is within one count of the final position after 30 ms. Consequently, the estimate of speed  $\hat{\omega}$  is responding to the noisy oscillations in  $i_q$  and does *not* indicate that the controller is not maintaining the correct final position. The oscillations in  $i_d$  in Fig. 9.107 are also due to limited resolution of the encoder.

In the implementation of the 1.8-mm run, the gains of the feedback controller were set at  $k_{11}=1.06\times 10^4$ ,  $k_{22}=3.4\times 10^2$ ,  $k_{23}=3.4\times 10^2$ ,  $k_{24}=3.8\times 10^6$  and  $k_{25}=1.07\times 10^8$ , which placed the (closed-loop) poles of the error system at  $s=-11047, -28.3, -54.86\pm j190.7$  for the fourth-order system. The observer gains were chosen as  $l_1=5272$ ,  $l_2=7.0\times 10^6$  resulting in the closed-loop poles of the observer error system (9.114) being at  $-2646, -2646$  rad/sec.

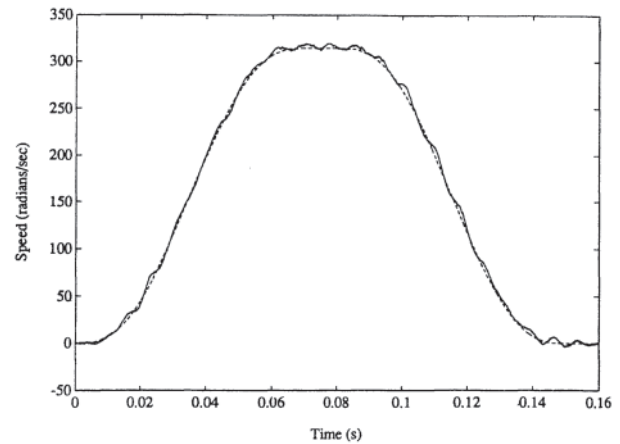
### 9.7.3.2 3000 RPM Move

Figure 9.110 shows the measured and reference positions for a move that was designed to bring the motor up to 3000 rpm. The reference and estimated speed are shown in Fig. 9.111, where the oscillatory behavior is due to the oscillation in  $i_q$ . The direct and quadrature currents are shown in Figs. 9.112 and 9.113 respectively, with the fluctuations being a result of the limited resolution of the position measurement. Note also that the reference input  $v_{dd}$  shown in Fig. 9.114 reaches below  $-30$  V, leaving less than 10 V for the feedback controller.

In the implementation of this run, the gains of the feedback controller were changed to  $k_{11}=2.58\times 10^4$ ,  $k_{22}=2.45\times 10^2$ ,  $k_{23}=6.0\times 10^2$ ,  $k_{24}=2.9\times 10^6$  and  $k_{25}=1.0\times 10^8$ , which placed the (closed-loop) poles of the error system at  $s=-24727, -3.4, -101\pm j893$  for the fourth-order system.



**Figure 9.110** Measured and reference position for the 3000-rpm run.



**Figure 9.111** Estimated and reference speed for the 3000-rpm run.

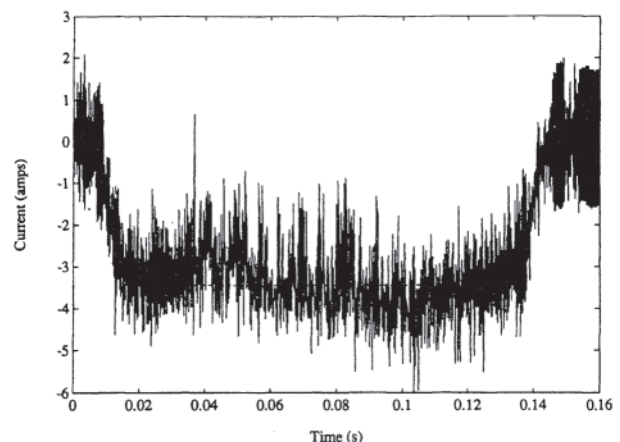


**Figure 9.112** Actual and reference direct current for the 3000-rpm run.

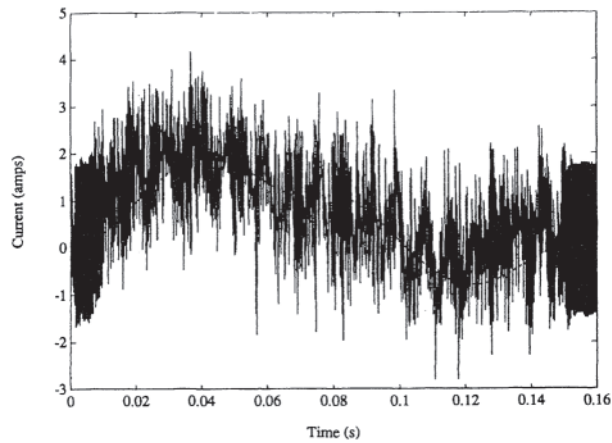


**Figure 9.113** Actual and reference quadrature current for the 3000-rpm run.

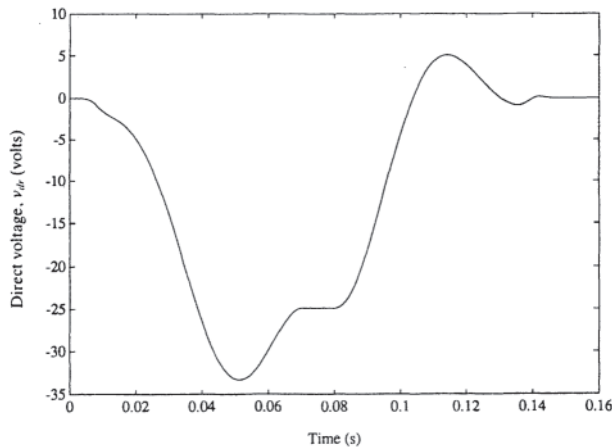


**Figure 9.114** Reference direct voltage  $v_{dr}$  for the 3000-rpm run.

## Acknowledgments

The authors would like to take this opportunity to thank Sharon Katz for drawing Figs. 9.99, 9.100, and 9.101.

## REFERENCES

Note: In the following listing, abbreviations have the following meanings:

AIEE	American Institute of Electrical Engineers (predecessor to IEEE)
ANSI	American National Standards Institute
CIGRE	Conference Internationale des Grands Reseaux Electriques
EPRI	Electric Power Research Institute
IEC	International Electrotechnical Commission
IEEE	Institute of Electrical and Electronics Engineers
NEMA	National Electrical Manufacturers Association
NFPA	National Fire Protection Association

Sources for standards are listed in [Appendix B](#).

- Boehne, E.W., "Voltage Oscillations in Armature Windings under Lightning Impulses—Part I," *Transactions of the AIEE*, vol. 49, 1930, p. 1587.
- Calvert, J.D., and F.D.Fielder, "Switching Surges in Rotating Machines," *Transactions of the AIEE*, vol. 55, 1936, p. 376.
- Petrov, G.N., and A.I.Abramov, "Overvoltage Stresses in Turn Insulation of Electric Machine Windings during Electromagnetic Transients," *Electrichestov*, vol. 7, Mar. 1954, p. 24.
- NEMA Standard MG 1–1998, "Motors and Generators."
- AIEE Committee Report, "Impulse Testing of Rotating AC Machines," AIEE Transactions on Power Apparatus and Systems, no. 48, June 1960, pp. 182–188.
- Gupta, B.K., B.A.Lloyd, G.C.Stone, S.R.Campbell, D.K.Sharma, and N.E.Nilsson, "Turn Insulating Capability of Large AC Motors, Part I—Surge Monitoring," *IEEE Transactions on Energy Conversion*, vol. EC-2, no. 4, Dec. 1987, pp. 658–665.
- Gupta, B.K., B.A.Lloyd, G.C.Stone, D.K.Sharma, and J.P.Fitzgerald, "Turn Insulation Capability of Large AC Motors, Part 2—Impulse Strength," *IEEE Transactions on Energy Conversion*, vol. EC-2, no. 4, Dec. 1987, pp. 666–673.
- Gupta, B.K., B.A. Lloyd, G.C.Stone, D.K.Sharma, N.E.Nilsson, and J.P.Fitzgerald, "Turn Insulation Capability of Large AC Motors, Part 3—Insulation Coordination," *IEEE Transactions on Energy Conversion*, vol. EC-2, no. 4, Dec. 1987, pp. 674–679.
- IEEE Std. 522–1992 (Reaffirmed 1998). IEEE Guide for Testing Turn-to-Turn Insulation on Form-Wound Stator Coils for Alternating Current Rotating Electric Machines.
- ANSI Std. C50.41–2000, American National Standard for Polyphase Induction Motors for Power Generating Stations.
- Gupta, B.K., G.C.Stone, B.A.Lloyd, E.P.Dick, A.Narang, P. R.Pillai, and A.Greenwood, *Turn Insulation Capability of Large AC Motors*, EPRI Project RP 2307–1, Final Report, EPRI EL-5862, vols. 1 and 2, 1988.
- Nilsson, N.E., "Opportunities for Improving Motor Reliability," *International Conference on Electrical Machines*, Massachusetts Institute of Technology, Cambridge MA, August 13–15, 1990, pp. 963–970.
- CIGRE Working Group 13.02, "Interruption of Small Inductive Currents: Chapter 3, Part A," *Electra*, no. 75, 1981, p. 5.
- Greenwood, A., *Electrical Transients in Power Systems*, Wiley-Interscience, New York, 1971, p. 205.
- United States 40 CFR, Ch. 1, Subpart D, §761.60(b)(iii), p. 414, 1999.
- Gupta, B.K., N.E. Nilsson, and D.K. Sharma, "Protection of Motors Against High Voltage Switching Surges," presented at the IEEE Power Engineering Society 1990 International Conference in India, October 30, 1990.
- Jackson, D.W., "Survey of Failures of Surge Protective Capacitors and Arresters on AC Rotating Machines," Report by Working Group 3.4.9 of the Surge Protective Devices Committee, *IEEE Transactions on Power Delivery*, PWRD, vol. 4, no. 3, July 1989, pp. 1725–1730.
- Bartheld, R.G., "Motor Starting Coordination," IEEE Paper No. PCIC-86–21, 1986, pp. 63–67.
- ANSI/IEEE Std. C37.92 (1972), Guide for Induction Motor Protection.
- NFPA 70, National Electric Code.
- ANSI/IEEE Std. 37.96–2000, IEEE Guide for AC Motor Protection.
- Buckley, G.W., "Calculation of the Locked Rotor Currents and Torque in Induction Machines," *Electric Machines and Electromechanics*, vol. 4, nos. 2–3, Sept.–Oct. 1979, pp. 217–232.
- Fitzgerald, A.E., Charles Kingsley, Jr., and Stephen D. Umans, *Electric Machinery* 5th edn., McGraw-Hill, New York, 1990.
- IEEE Std. 112–1946, IEEE Standard Test Procedure for Polyphase Induction Motors and Generators.

25. *Electrical Transmission and Distribution Reference Book*, 4th edn., 5th printing, Westinghouse Electric Corporation, 1984.
26. Beeman, D., *Industrial Power Systems Handbook* 1st ed., McGraw-Hill, New York, 1955.
27. IEEE Std. 100–1996, *The New IEEE Standard Dictionary of Electrical and Electronics Terms*.
28. Seebald, R.C., J.F.Buch, and D.J.Ward, “Flicker Limitations of Electric Utilities,” *IEEE Transactions on Power Apparatus and Systems*, vol. PAS-104, no. 9, Sept. 1985, pp. 2627–2631.
29. Briggs, S.B., “Voltage Flicker Measurement Program,” *Proceedings: Power Quality for End-Use Applications Conference—1990*, EPRI CU-7125, Project 2935–1.
30. IEC Standard 34–1, Rotating Electric Machines.
31. IEC Standard 60034–1, Edition 10.2, 1999–98. Rotating Electric Machines.
32. Liwshitz-Garik, M., and Clyde C.Whipple, *Electric Machinery, Vol. II, A-C Machines*, 6th printing, Van Nostrand, New York, 1946.
33. Alger, Philip, *Induction Machines, Their Behavior and Uses*, 2d edn., Gordon and Breach Science Publishers, New York, 1965.
34. Nilsson, N.E., and R.S.Grumbach, “Modelling of a Large Induction Motor Started from a Medium Power Synchronous Generator,” Midwest Power Symposium, October 23 and 24, 1975, sponsored by the University of Akron in Cooperation with the IEEE Power Engineering Education Committee, Akron OH.
35. Anderson, E.P., and R.Miller, *Electric Motors*, 3d edn., 2nd printing, Theodore Audel & Company, a Division of Howard W. Sams & Company, Inc., Indianapolis IN, 1978, pp. 74–76.
36. Blume, L.F., A.Boyajian, G. amilli, T.C.Lennox, S.Minneci, and V.M.Montsinger, *Transformer Engineering*, 2d edn., Wiley, New York, 1951, pp. 250–274.
37. Millermaster, R.A., *Harwood’s Control of Electric Motors*, 4th edn., Wiley-Interscience, New York, 1970, pp. 253–256.
38. Halliday, D., and R.Resnick, *Physics, Parts I and II*, Wiley, New York, 1960, p. 270.
39. Say, M.G., *Alternating Current Machines*, Halsted Press, New York, 1976, p. 316.
40. Nailen, R.L., *Managing Motors*, Barks Publications, Chicago, 1991, pp. 3–8 and 3–9.”
41. IEEE Std. 620–1987; IEEE Guide for Construction and Interpretation of Thermal Limit Curves for Squirrel Cage Motors Over 500 HP.
42. *Applied Protective Relaying*, Westinghouse Electric Corporation, Relay Instrument Division, Newark NJ, 1976.
43. Engelmann, Richard H., *Static and Rotating Electromagnetic Devices*, Marcel Dekker, New York, 1982, p. 316.
44. Reason, John, “AC Motor Control,” *Power Magazine*, vol. 125, no. 2, Feb. 1981, pp. S1-S23.
45. Merrill, E.F., “The Effect of Short Duration Interruption of Power Connected to Large Induction Motors,” Westinghouse District Engineering Letter 61–5, East Pittsburgh PA, 1961.
46. Heumann, Gerhart W., *Magnetic Control of Industrial Motors*, 2d edn., Wiley, New York, 1954.
47. Jones, Richard W., *Electric Control Systems*, Wiley, New York, 1953.
48. IEEE Std. 519–1992, IEEE Recommended Practices and Requirements for Harmonic Control in Electrical Power Systems.
49. ANSI/IEEE Std. 444–1973, IEEE Standard Practices and Requirements for Thyristor Converters for Motor Drives: Part I—Converters for DC Motor Armature Supplies.
50. IEEE Std. 597–1983, IEEE Standard Practices and Requirements for General Purpose Thyristor DC Drives.
51. IEEE Std. 428–1981, IEEE Standard Definitions and Requirements for Thyristor AC Power Controllers.
52. ANSI/IEEE Std. 995–1987, IEEE Recommended Practice for Efficiency Determination of Alternating-Current Adjustable-Speed Drives: Part I—Load Commutated Inverter Synchronous Motor Drives.
53. Mazda, F.F., *Power Electronics Handbook: Components, Circuits, and Applications*, Butterworths, London, 1990.
54. Hoft, Richard G., *Semiconductor Power Electronics*, Van Nostrand Reinhold, New York, 1986.
55. Finney, David, *The Power Thyristor and Its Applications*, McGraw-Hill, London, 1980.
56. Fisher, Marvin J., *Power Electronics*, PWS-Kent Publishing Co., Boston, 1991.
57. Pearman, Richard A., *Power Electronics: Solid State Motor Control*, Reston Publishing Company, Reston VA, 1980.
58. Murphy, J.M.D., and F.G.Turnbull, *Power Electronic Control of AC Motors*, Pergamon Press, Oxford and New York, 1988.
59. Steiger, P., O.Apeldoorn, E.Carrol, A.Nagel, “IGCT Technology Baseline and Future opportunities,” in Transmission and Distribution Conference and Exposition, 2001 IEEE/PES, Oct. 28–Nov. 2, 20001, pp. 1182–187.
60. Krein, P., *Elements of Power Electronics*, Oxford, 1998, pp. 125–135.
61. Gyugyi, L., and B.R.Pelly, *Static Power Frequency Changers*, Wiley, New York, 1976.
62. Slonim, Michael A., *Theory of Static Converter Systems*, Elsevier, Amsterdam, 1984.
63. Lipo, Thomas A., Paul C.Krause, and Howard E.Jordan, “Harmonic Torque and Speed Pulsations in a Rectifier-Inverter Induction Motor Drive,” *IEEE Transactions on Power Apparatus and Systems*, vol. PAS-88, no. 5, May 1969, pp. 579–587.
64. Mohan, N., Undeland, T., Robbins, W., *Power Electronics, Converters, Applications, and Design*, Second Edition, John Wiley & sons, Inc, 1995.
65. J.S.Lai and F.Z.Peng, “Multilevel Converters-A new breed of Power converters,” *IEEE Trans, on Ind. Applic.*, vol. 32, No. 3, May/June 1996, pp. 509–517.
66. A.Nabae, I.Takahashi, and H.Akagi, “A New neutral-point-clamped PWM inverter,” *IEEE Trans. Ind. Applicat.*, vol. IA-17, No. 5, pp. 518–523, Sep./Oct. 1981
67. J.P.Lyons, V.Vlatkovic, P.M.Espelage, F.H.Boettner, E. Larsen, “Innovation IGCT Main Drives,” IAS Annual Meeting Conf. Record, 1999, pp. 2655–2661.
68. *Power Electronics, Devices, Drives and Applications*, John Wiley & Sons, B.W.Williams, 1987.
69. *Elements of Power Electronics*, Oxford University Press, Philip T. Krein, 1998.
70. *Power Electronics and Variable Frequency Drives, Technology and Applications*, Edited by Bimal K.Bose, IEEE Press, 1997, Chapter 10 by H. Le-Huy.
71. S. Clemente and Ajit Dubhashi, “HV Floating MOS-Gate Driver IC,” International Rectifier Application Note AN-978B.
72. Deltoro, Vincent, *Electric Machines and Power Systems*, Prentice-Hall, Englewood Cliffs NJ, 1985.
73. Acarnley, P.P., *Stepping Motors: A Guide to Modern Theory and Practice*, P.Peregrinus, Ltd., Stevenage, UK, 1982.
74. Kenjo, T., *Stepping Motors and Their Microprocessor Controls*, Clarendon Press, Oxford, 1984.
75. Kuo, B.C., *Incremental Motion Control Volume II, Step Motors and Control Systems*, SRL Publishing, Champaign, IL, 1979.
76. Kuo, B.C., *Automatic Control Systems*, 5th edn., Prentice-Hall, Englewood Cliffs NJ, 1987.
77. Taylor, D.G., “An Experimental Study on Composite Control of Switched Reluctance Motors,” *IEEE Control Systems Magazine*, vol. 11, no. 1, pp. 31–36, Feb. 1991.
78. Bodson, M., J.Chiasson, R.Novotnak, and R.Rekowski, “High Performance Nonlinear Feedback Control of a Permanent Magnet Stepping Motor,” *IEEE Transactions on Control Systems Technology*, vol. 1, no. 1, pp. 4–14, Mar 1993.
79. Aiello, M., R.Rekowski, M.Bodson, J.Chiasson, and D. Schuerer, “Experimental Results of using an Exact Linearization

- Controller on a PM Stepper Motor,” in *Microprocessors in Robotic and Manufacturing Systems*, Spyros G.Tzafestas, Editor. Kluwer Academic Publishers, 1991, pp. 353–368.
80. Leonhard, W., *Control of Electrical Drives*, Springer-Verlag, Berlin and New York, 1985.
  81. Kailath, T., *Linear Systems*, Prentice-Hall, Englewood Cliffs NJ, 1980.
  82. Zribi, M., and J.Chiasson, “Position Control of a PM Stepper Motor by Exact Linearization,” *IEEE Transactions on Automatic Control*, vol. 36, no. 5, May 1991, pp. 620–625.
  83. MATLAB User’s Guide, The MATHWORKS Inc., Natick, MA.
  84. Blaich, A.J., M.Bodson, and J.Chiasson, “High-Speed Parameter Estimation of Stepper Motors,” *IEEE Transactions on Control Systems Technology*, vol. 1, no. 4, Dec. 1993, pp. 270–279.
  85. Ljung, L., *System Identification: Theory for the User*, PrenticeHall, Englewood Cliffs NJ, 1987.
  86. Ljung, L., and P.Stoica, *System Identification*, Prentice-Hall, Englewood Cliffs NJ, 1989.
  87. Sastry, S., and M.Bodson, *Adaptive Control: Stability, Convergence, and Robustness*, Prentice-Hall, Englewood Cliffs NJ, 1989.
  88. Schuerer, David P., *Parameter Identification of a Permanent Magnet Stepper Motor*, M.S. Thesis, University of Pittsburgh, 1990.

# 10

## Motor Protection

Neil Nichols (Sections 10.1–10.6)/Jeffrey Massereeuw (Section 10.2.5.1)/David M.Mullen and James H.Dymond (Section 10.7)/Vincent I.Saporita (Section 10.8)/Lloyd W.Buchanan, George E.Herzog, and Edwin Fisher (Sections 10.9–10.11)

<b>PART A OVERVIEW</b>	<b>516</b>
<b>10.1 INTRODUCTION</b>	<b>516</b>
<b>10.2 PROTECTION AGAINST OVERLOADS</b>	<b>516</b>
10.2.1 Fuses	517
10.2.2 Thermal Overload Relays	517
10.2.3 Switchgear-Type Thermal Relays	517
10.2.4 Imbedded Temperature Detectors	517
10.2.5 Microprocessor Motor Protection Relays	518
10.2.6 Damper Bar Protection	520
10.2.7 Special Current Detection	520
10.2.8 Pull-Out Protection	520
<b>10.3 UNBALANCED VOLTAGE PROTECTION</b>	<b>520</b>
10.3.1 Phase Loss Relays	521
10.3.2 Negative-Sequence Voltage Relays	521
10.3.3 Current Unbalance Relays	521
10.3.4 Microprocessor Devices	521
<b>10.4 PROTECTION FOR INTERNAL ELECTRICAL FAILURES</b>	<b>521</b>
10.4.1 Stator Insulation Failure Protection	521
10.4.2 Microprocessor Protection for Internal Faults	522
<b>10.5 SELECTION OF SWITCHING DEVICES</b>	<b>522</b>
10.5.1 Contactors	522
10.5.2 Electrically Operated Circuit Breakers	522
<b>10.6 MECHANICAL PROTECTION</b>	<b>523</b>
10.6.1 Vibration Detectors	523
10.6.2 Bearing Temperature Monitors	523
10.6.3 Microprocessor Protection	524
<b>10.7 ACCESSORIES</b>	<b>524</b>
10.7.1 Filters	524
10.7.2 Ventilation Opening Guards	524
10.7.3 Space Heaters	524
<b>PART B FUSES AND PROTECTION COORDINATION</b>	<b>524</b>
<b>10.8 INTRODUCTION</b>	<b>524</b>
10.8.1 Single-Element Fuses	525
10.8.2 Protection Coordination with Single-Element Fuses	525
10.8.3 Dual-Element Fuses	527
10.8.4 Protection Coordination with Dual-Element Fuses	528
10.8.5 Single-Phasing Protection	529

<b>PART C BIMETALLIC THERMAL PROTECTORS</b>	<b>532</b>
<b>10.9 INTRODUCTION</b>	<b>532</b>
10.9.1 Definitions	532
10.9.2 Typical Devices	533
10.9.3 Considerations in Device Selection	535
10.9.4 Selection of Bimetallic Thermal Protectors for Shaded-Pole, Permanent-Split Capacitor, and Other Slow Heat Rise Single-Phase Motors	536
10.9.5 Selection of Bimetallic Thermal Protectors for Single-Voltage Split-Phase, Capacitor-Start, Capacitor-Start/Capacitor-Run, and Other Single-Phase Motors	537
10.9.6 Selection of Bimetallic Thermal Protectors for Dual-Voltage Split-Phase, Capacitor-Start, Capacitor-Start/Capacitor-Run Single-Phase Motors	540
10.9.7 Selection of Bimetallic Thermal Protectors for Three-Phase Motors	541
<b>10.10 TESTING AGENCY REQUIREMENTS FOR MOTOR THERMAL PROTECTORS</b>	<b>542</b>
10.10.1 General	542
10.10.2 Protection Types	542
10.10.3 Test Voltages and Frequencies	542
10.10.4 Protector Calibration Ranges	543
10.10.5 Temperature Measurements	543
10.10.6 Ambient Temperature	543
10.10.7 Multispeed Motors	543
10.10.8 Motor Mountings	543
<b>10.11 PERFORMANCE REQUIREMENTS AND TESTS</b>	<b>543</b>
10.11.1 Running Heating Tests	543
10.11.2 Running Overload Tests	543
10.11.3 Locked-Rotor Tests	544
10.11.4 Locked-Rotor Endurance Test	544
10.11.5 Dielectric Tests	544
10.11.6 Limited Short-Circuit Tests	544
<b>REFERENCES</b>	<b>545</b>

## PART A OVERVIEW

### 10.1 INTRODUCTION

Protection of motors falls into two categories. The first is protection against conditions external to the motor that could be damaging to the motor. The second is protection against further damage to the motor or the power system from a failure within the motor. In this second category the motor is obviously not completely protected; it requires the presence of internal damage to invoke this protection.

Most of the undesired external influences cause excessive temperatures in the motor. These influences include overloading during running or starting, excessively frequent starting, improper or unbalanced voltages, and inadequate cooling due to high ambient temperatures or restricted ventilation. Excessive temperature reduces the useful life of the insulation, the amount of reduction being dependent upon both the temperature and the time it persists. The amount of life lost is not clearly defined, nor is the expected life. There is an industry rule of thumb that has persisted throughout much of the past century that says that there will be a 50% loss of insulation life for each 10°C increase in operating temperature, even though new insulation characteristics have been developed during the existence of this rule. Motors with a service factor of 1.15 are allowed by NEMA Standards [1] to

have a temperature 10°C higher at the 115% loading than is allowed at full load on a motor without a service factor.

Protective devices perform two functions, detection of an undesirable condition, such as an overload or short circuit, and disconnection of the circuit. Fuses and low voltage circuit breakers perform both functions in one unit. Contactors and medium voltage circuit breakers require external relays.

### 10.2 PROTECTION AGAINST OVERLOADS

An overload is defined as a mechanical duty imposed on the motor that could result in destructive overheating of the motor, affecting primarily the insulation. A number of devices and methods are used to detect overloads, with various levels of cost and sophistication. Most depend on measuring motor current and attempting to predict the resulting thermal behavior. These devices seldom consider ambient temperatures, ventilation problems, or voltage levels, the ambient-compensated devices being designed to ignore ambient temperature.

Voltage has a significant effect on motor heating because it affects core losses. Contrary to popular belief, rated current will produce rated temperature rise only when rated voltage is applied; if the voltage is higher, the allowable current is lower. Motor efficiencies do not vary significantly over a voltage

range of 10% or so; thus the losses and the temperature rise will remain nearly the same for a given power output even though the current will vary inversely with the voltage.

Starting a motor creates a temporary overload condition, because the initial stator current is approximately 600% of the rated current. The rotor fares even worse, because at zero speed almost 100% of the energy going into the motor is heating the rotor. The heating of the rotor decreases as a function of the slip frequency of the rotor, but remains above normal until the rotor reaches full load speed with a slip of less than 1%. If the starting period is extended past the design starting period by a high inertia load, motor life may be lost and classified area restrictions may be violated. The permissible loading and inertia of the driven equipment for standard motors is listed in Section 20.42 of NEMA MG 1 [1]. NEMA permits a temperature rise greater than the rated temperature rise during starting because of the short duration and presumed infrequency of starts. NEMA also restricts successive starts as necessary to avoid a cumulative temperature rise. Although NEMA does not further restrict the number of starts, frequent starting of larger motors, particularly synchronous motors [2], has been observed to reduce the motor's life. Small IHP motors are less critical.

Overcurrent protection during starting is traditionally based upon rated locked-rotor time with locked rotor current. Thus the motor is protected even if it fails to turn. An exception to this is noted in Section 10.2.2. Generally motors are able start their loads within the rated locked-rotor time. When they cannot, it may be necessary to consult the motor manufacturer for a separate rated time of acceleration during which rotor heating is less than during locked-rotor. The protection would then be switched from locked-rotor protection to the more generous acceleration protection as soon as the motor rotation is detected. Motor rotation can be detected by a zero speed switch, or in some cases by measuring motor impedance [3].

In the following subsections, various types of devices used to detect overloads and to protect the motor are discussed.

### 10.2.1 Fuses

Fuses are one-time protective devices. They are designed so that a fusible element melts as a result of excessive current, thus opening the circuit and removing voltage from the motor. A wide variety of fuses is available. The fusing current-versus-time characteristic of a fuse must be known in order to determine whether it will actually protect a motor from damage and in order to determine that it will not “blow” under conditions that are safe for the motor, the so-called “nuisance” events.

A fuller discussion of fuses and their application appears below in Part B, Section 10.8.

### 10.2.2 Thermal Overload Relays

These economical devices are the most widely used protective devices. They are characterized by relatively poor accuracy, with 200–300% allowable time variation at lower overloads, little thermal lag compared to the motor, and a delayed

response at locked-rotor current levels. This delayed response can cause the relay to operate after the starting current has subsided [3]. Partly for this reason, the common practice in the United States has been to apply the Class 20 relay, which allows six times full-load current for 20 seconds even though this may exceed the allowable locked-rotor time for the motor [3]. IEC Standard overload relays are normally Class 10.

This relay is suitable for the large number of motor applications where the driven load will not normally impose a running or starting load in excess of the motor capability, and where the probability of abnormal loads, the cost of the motor, and the cost of downtime are all relatively low. It is not suitable for protection when there are frequent moderate overloads of short duration, which can result in cumulative heating of the motor. It cannot differentiate between occasional or continuous operation at the service factor level, even though continuous operation at this level would be expected to reduce motor life. It will not provide adequate voltage unbalance protection [3, 4], nor in most cases will it provide protection against high ambient temperatures.

### 10.2.3 Switchgear-Type Thermal Relays

These relays are an improvement over the standard thermal overload relay in terms of accuracy, dependability, and to some extent, thermal delay. However, their cost compared to the modern microprocessor makes them less attractive for new applications.

### 10.2.4 Imbedded Temperature Detectors

Imbedded temperature detectors include bimetal snap switches (see [Section 10.9](#)) or their solid-state equivalent, thermocouples, and resistance temperature detectors (RTDs). All of these have the advantage of measuring actual winding or bearing temperatures, thus being cognizant of high ambient temperatures of cooling difficulties and temperatures resulting from nonstandard voltages. Restriction of the cooling ducts in the motor core is a common problem. The RTD is the predominant choice except in small motors.

An RTD is normally placed in a slot between the top and bottom coil sides at two locations in each phase. It is recognized as the measuring method by NEMA [1] for determining temperatures in large motors. In the past, it was the practice on large medium-voltage machines to ground all RTDs to the machine frame for safety reasons, since the detector is only a fraction of an inch from the medium-voltage conductor in the coil. To avoid noise pickup due to voltage unbalance to ground of the leads and to have a more rugged detector, the 10-ohm copper element was the general choice, even though it required a third wire for lead compensation. More recently, process-type measuring devices have been used that do not allow grounding of the RTD at the motor or, in some cases, not at all. Solid-state devices introduced by the motor controller or switchgear relay industries have, in some cases, been unsuitable for RTDs grounded at the machine frame. As a precaution, any unused detector should have one lead grounded at the machine, but



the other lead should not be grounded in order to prevent induced circulating currents in the detector.

### 10.2.5 Microprocessor Motor Protection Relays

More microprocessor motor protection relays (MPRs) have become available in recent years and their use has increased significantly on larger motors where the higher cost can be justified. They are a multifunction device offering a fairly complete menu of protective functions. Though their principle function remains detection of overloads, they can also detect the effects of unwanted voltage and frequency excursions, unbalance supply voltage as discussed in Section 10.3, internal faults as discussed in Section 10.4, and mechanical functions as discussed in Section 10.6. They now offer sophisticated record keeping and the ability to transmit this data to remote locations. They may also be able to control the motor contactor or breaker, and to receive control signals from remote locations.

The overload current function offers greatly improved accuracy as compared to thermal overload relays or fuses, and improved selectable and adjustable characteristics which can represent the heating effects of currents much better than thermal overload relays, fuses, or overcurrent relays designed for fault protection. These characteristics are adjustable in small increments. They may have the capability to utilize a userdefined curve that may be used to address the difference between locked-rotor and accelerating ratings. They can have selectable reset rates to replicate the cooling rate of the motor after overloads or starting for both running and stopped conditions. They may use this replication of cooling rates to develop a mathematical quantity known as thermal capacity, which can be used to change the response to a successive overload or to delay a start if it would cause the thermal capacity to be exceeded, i.e., the motor temperature would exceed the maximum allowable value before the start was completed.

Although the accuracy and repeatability of the devices are excellent, their temperature predictions may not be. Motor characteristics set into the MPR may have to be based more on soft assumptions than on hard data. Ambient temperature is not in the equation. Effects of applied voltage are not normally in the equation. Although changing the applied voltage may change the motor current for a given horsepower load it may not change the temperature accordingly due to an opposing change in iron losses. Thus the heating effect for a given value of current has been changed. The manufacturers of the MPRs recommend the use of resistance temperature detectors (RTD) for better accuracy, and provide capability for accepting the RTD outputs. And after the investment in the MPR the investment for RTDs in the motor and in ambient air is relatively modest.

Utility generating plants have long eschewed close protection of critical motors by overload relays. They do not want critical motors to trip unnecessarily, even if temporarily overloaded in emergencies, and previous protective devices have been found wanting. They have depended upon human judgment and intervention to intelligently protect the motors. In recent years changes in conditions and practices has caused an increase in motor failures. Introduction of MPRs for more

realistic protection is being accepted in the industry, without significant complaints of unwarranted trip-outs. Protection of these motors without reducing reliability is simplified by the practice of specifying a motor full-load temperature rise less than the maximum allowed for the insulation class. This practice has long been followed by those desiring long and dependable motor life, and has been encoded into the new IEEE 841 motor standard.

The data collecting and disbursement function of the MPR is significant to motor protection. The MPR can protect the motor from loss of life due to starting and overloads based upon conventional criteria that is expected to limit the loss of life to an acceptable value. These criteria are based upon an assumed (in)frequency of these events. If the frequency of overloads, and particularly of starting, is greatly increased, the motor life will be severely diminished. It is beyond the capacity of the existing microprocessors to control the long time frequencies of these events by a protective algorithm. But the events will appear in the data, suggesting that the use of the motor should be modified to prevent rapid deterioration. Such operating abuse of the motor may not otherwise be detected by management.

Temperature monitoring records can allow scheduling of maintenance before reduction of cooling results in prolonged high temperature.

#### 10.2.5.1 Microprocessor Motor Protection Examples

Microprocessor-based motor protection relays have become standard for medium voltage motors (Fig. 1) and recently, they have become cost-effective for low voltage applications (Fig. 2). These multifunction devices can protect the motor, the driven load, the power system, and personnel. The motor protection typically includes thermal protection during starting, overload, and unbalance conditions as derived from the measured motor current. With stator and bearing RTDs connected to the relay, detection of absolute machine temperature for protection due to loss of motor ventilation or bearing lubrication is also possible. The driven load is protected with “mechanical jam” overcurrent and “loss of load” undercurrent elements. Short circuit and ground fault elements protect the power system and personnel.

Motor thermal limits are dictated by the design of both the stator and the rotor. Motors have three modes of operation: locked-rotor or stall (when the rotor is not turning), acceleration (when the rotor is coming up to speed), and running (when the rotor turns at near synchronous speed). Heating occurs in the motor during each of these conditions in very distinct ways. Typically, during motor starting, locked-rotor, and acceleration conditions, the motor is rotor-limited. That is to say that the rotor will approach its thermal limit before the stator. Under locked rotor conditions, voltage is induced in the rotor at line frequency, 50 or 60 Hz. This voltage causes a current to flow in the rotor, also at line frequency, and the heat generated ( $I^2R$ ) is a function of the effective rotor resistance. At 50 or 60 Hz, the reactance of the rotor cage causes the current to flow at the outer edges of the rotor bars. The effective resistance of the rotor is therefore at a maximum during a locked rotor condition as is rotor heating. When the motor is running at rated speed,



**Figure 10.1** Medium-voltage motor protection relay. (Courtesy of GE/Multilin.)

the voltage induced in the rotor is at a low frequency and therefore, the effective resistance of the rotor is reduced quite dramatically. During running overloads, the motor thermal limit is typically dictated by stator parameters. Some special motors might be all stator or all rotor limited. During acceleration, the dynamic nature of the motor slip dictates that rotor impedance is also dynamic, and a third overload thermal limit characteristic is necessary.

For most motors, the distinct characteristics of the motor thermal limits are formed into one smooth homogeneous curve. Sometimes only a safe stall time is provided. This is acceptable if the motor has been designed conservatively and can easily perform its required duty without infringing on the thermal limit. In this case, the protection can be conservative and process integrity is not compromised. If a motor has been designed very close to its thermal limits when operated as required, then the distinct characteristics of the thermal limits become important. For a high inertia load, it is quite possible and acceptable that the acceleration time exceeds the safe stall time (bearing in mind that a locked-rotor condition is quite different than an acceleration condition). In this instance, each distinct portion of the thermal limit curve must be known and protection must be coordinated against that curve. The relay that is protecting the motor must be able to distinguish between a locked-rotor condition, an accelerating condition, and a running condition.

An intelligent microprocessor-based motor protection relay may have a very comprehensive motor thermal replica. One manufacturer's product has a thermal model that uses not only current inputs, but also temperature as measured from stator RTDs and motor terminal voltage. The basic model uses the traditional thermal limit curves or a user programmable "custom-curve." The model may be biased to account for the additional heating caused by an unbalanced supply (described in Section 10.3), as shown in Fig. 3. With RTDs, stator temperature is used to correct the model to account for conditions not reflected in the motor current drawn. For high



**Figure 10.2** Low-voltage motor protection relay. (Courtesy of GE/Multilin.)

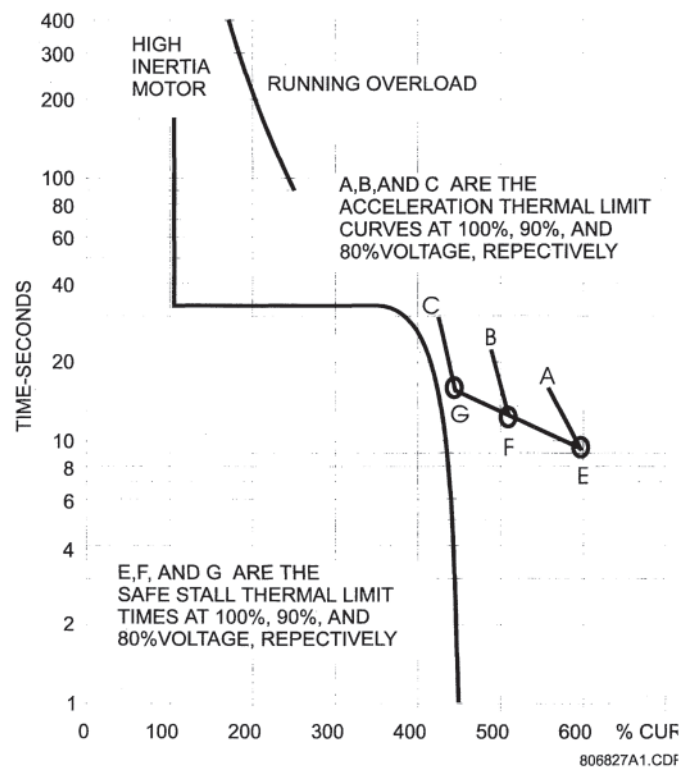


**Figure 10.3** Typical time-current thermal limit curves. (ANSI/IEEE C37.96.)

inertia loads, voltage is monitored constantly during motor starting and the acceleration thermal limit curve is adjusted accordingly to account for the change in motor speed as an impedance relay would.

More than a simple overload device, the digital relay may provide metering, event recording, and control functions. With communications capability, it may also serve as an integral component of an automated system.

### 10.2.6 Damper Bar Protection

This is a special protection for brush-type synchronous motors during starting. The alternating current output of the wound field is monitored during starting. This measurement is used to determine the heating during starting in both the wound field and the starting cage (damper or amortisseur winding).

### 10.2.7 Special Current Detection

This protective category covers devices that detect sudden current changes, such as a sudden current increase that may signify a jam, or a sudden decrease, which may signify loss of fluid flow in a pump. This type of relaying is intended to protect the equipment being driven by the motor. Sudden overcurrent or undercurrent detection is normally available in microprocessor motor protection relays. The MPR will normally block tripping by sudden overcurrent during starting, and possibly during reacceleration after a severe voltage depression.

### 10.2.8 Pull-Out Protection

Synchronous motors may lose synchronism due to application of loads exceeding their torque capability, or by reduction in torque output due to voltage reduction or loss of excitation. Most synchronous motors have pull-in (synchronizing) torques less than full load, particularly with the field applied. Thus a loaded motor will usually not be able to resynchronize, and the motor will be damaged if the motor continues to run.

On brush-type machines, pull-out can be detected by an induced ac component in the field current. The relay sensitivity or delay needs to be set so as to ignore currents induced by sudden load applications or line voltage dips. On brushless machines, the motor field current cannot be measured, so it is necessary to measure the effect of loss of field or pull-out as seen by the stator. The devices that are commonly used are directional impedance or directional reactive current relays, which detect an apparent low impedance and the consequent reactive current (VAR) flow into the motor. The VAR relay may be a power factor relay whose operating point varies as a function of the motor kilowatts (constant VAR/kW). The response to loss of field is predictable, but there is a problem in differentiating between stable transient swings and actual out-of-step operation, not unlike the detection of pull-out by measuring field current. There has been a suggestion that the number of successive swings be used as a measure of pullout [5].

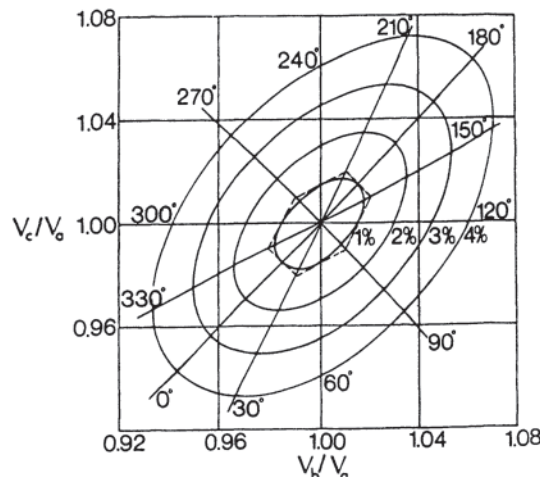


**Figure 10.4** Constant-magnitude loci of the ratio of the negative sequence voltage ( $V_2$ ) to the positive sequence voltage ( $V_1$ ) displayed on axes of  $V_c/V_a$  versus  $V_b/V_a$ , where  $V_2/V_1$  is expressed in percent. For comparison purposes, the NEMA 1% unbalance locus is shown dashed.

## 10.3 UNBALANCED VOLTAGE PROTECTION

By NEMA Standard MG 1 [1], a motor is to be capable of operating at full load with a voltage unbalance of 1% without derating, but should be derated for greater unbalance, with a derating to 75% at a maximum allowable unbalance of 5%. The voltage unbalance is calculated as:

$$\% \text{Unbalance} = \frac{\text{maximum deviation from average voltage}}{\text{average voltage}} \times 100$$

Cummings et al. [4] show that the percentage unbalance in this equation is a close approximation to the ratio of negativesequene to positive-sequence voltage, that is, negativesequene voltage expressed per unit. This is also evident from Fig 10.4.

When there are unbalanced phase currents, a given point on the rotor is subject to a change in flux as it travels from one stator phase to another, resulting in circulating currents in the rotor, which produce heat. The unbalance of the stator currents for a given voltage unbalance is a function of the negativesequene reactance of the individual motor, and this unbalance will be typically 6 to 10 times the voltage unbalance at full load [4].

Since the amount of current unbalance does not change with load, as the load decreases the percentage current unbalance will become larger, although the total heating in the motor becomes less because of the lower load current. Thus the rotor heating due to unbalance is a function of the voltage unbalance (or, more precisely, of the negative sequence voltage), but the total heating of the motor is a function of the voltage unbalance and the load, as is expressed in the NEMA derating factor described in the first paragraph.

Severe voltage unbalances can be caused by complete loss of one phase, such as that caused by fuse operation either at the motor voltage level or on the primary of the supply transformer. Such incidents have resulted in substantial damage

to motors, demonstrating the lack of ability of the basic thermal overload relay to provide protection for this condition. Smaller voltage unbalances can be caused by unbalanced single-phase loads on utility distribution lines. These loads often vary in a manner that precludes redistribution of these loads between phases to obtain a satisfactory balance throughout the day.

### 10.3.1 Phase Loss Relays

A number of relatively unsophisticated relays are available that will detect loss of phase and in some cases severe undervoltage. These relays will not protect for those slight unbalances discussed above, and some have undesirable time delay responses.

### 10.3.2 Negative-Sequence Voltage Relays

Since the NEMA unbalance formula above coincides so closely with the negative- to positive-sequence voltage ratio, a negative-sequence voltage relay, if sensitive enough, can protect all the motors on a bus with a single relay. However, it may overprotect, since it cannot determine individual motor loading. Motors at 75% load or less can accommodate 5% voltage unbalance. There is a relay available that can be set to operate as low as 2% negative-sequence voltage. It may be desirable to set the relay to alarm at that point so that heavily loaded motors can be disconnected, but to trip only at 5%. With harmonic pollution created by nonlinear loads, the relay response to harmonics should be examined, since some negative-sequence relays have undesirable responses to harmonics.

### 10.3.3 Current Unbalance Relays

Some current unbalance relays are responsive to the amount of unbalance or to the magnitude of negative-sequence current. Other relays may respond to percentage unbalance. Since the current unbalance for a given voltage unbalance will vary as a function of the motor design, these motor data will be required to set the relay properly. At light loads, the percentage unbalance will become greater for a given voltage unbalance [4], yet will be less damaging to the motor. In general, these relays lack the capability to match their inverse timing characteristic to the rate of heating for the unbalance levels being considered; timing is unrealistically short. This may not be a significant handicap if unbalance is rarely encountered.

### 10.3.4 Microprocessor Devices

Multiprocessor-based devices may offer simple current unbalance protection or more sophisticated responses. The simplest response may be a settable pickup point and a settable definite or inverse time delay. The sophisticated response uses an algorithm to calculate the combined heating effect of the unbalanced and balanced currents. This algorithm may be used to trip the motor directly though accuracy can be improved if used in conjunction with RTD data. In other relays the algorithm may be used to bias the tripping by the RTDs,

so that it does not function unless RTD data is present. It is usually necessary to calibrate the algorithm by an often soft assumption of the motor characteristics that will relate temperature rise to the measured data. Although this assumption introduces some inaccuracy this methodology is a vast improvement over arbitrarily tripping with a short time delay based upon exceeding 1% voltage unbalance or an arbitrary current unbalance regardless of motor load.

The simple unbalance protection remains available as a backup and also may detect shorted turns.

## 10.4 PROTECTION FOR INTERNAL ELECTRICAL FAILURES

As mentioned earlier, protection for internal failures does not prevent damage, but is intended to prevent the spread of damage, either in the motor or in the power system. Accurate and timely detection and shutdown are essential to these objectives.

### 10.4.1 Stator Insulation Failure Protection

Stator insulation failure can occur between coils of different phases, between phase and ground, or between turns in a single coil. Phase-to-phase or phase-to-ground faults occurring close to the line terminals of the motor will result in large, and thus easily detected, fault currents. Since the coil voltage is highest at the line end of the winding, this is the most probable fault location. In contrast, turn-to-turn failures are characterized by unspecified but comparatively low currents that may produce a very slow response in the overcurrent devices. The fault may escalate to a phase or ground fault before it is detected. In older or larger machines, there was some advantage to early detection of this type of fault because the coil could be replaced or patched. Many of the modern insulating materials do not lend themselves to such repair work.

For most low-voltage motors, the fault protection of choice is a molded-case circuit breaker, known as a motor circuit protector (MCP). Since the motor is otherwise protected thermally, this device has an instantaneous response only and features a very fast operating time. These devices are now made with interrupting capacities up to 100,000 A at 480 V. Fuses may also be used, but, being single-pole devices, they have the disadvantage that they can cause single-phasing of the motor as a result of a ground fault in the wiring to the motor. Fuses should be selected with characteristics appropriate for the motor, and care should be taken upon replacement to use the same type of fuse. (See [Section 10.8](#).)

Medium-voltage motors more commonly use fuses for short-circuit protection since there is a large cost difference between fuses and circuit breakers at this voltage. Circuit breakers for this voltage range do not offer the current-limiting action provided by fuses or the low-voltage molded-case circuit breakers. Because these fuses may operate rather slowly at the short-circuit current levels usually encountered, and to minimize any damage to the motor laminations, protective relays are also used in many cases.

A differential protection relay compares the current at one end of a motor winding with the current at the other end of the same winding. If the currents are not equal, it is assumed that some current has been diverted by an insulation failure, and the motor is tripped. While the difference in current should be a positive indication of an internal motor fault, some error may be introduced by current transformers, particularly with high or asymmetrical currents. A better response to transient inrush at a considerable cost saving can be achieved by passing the leads from the two ends of each winding through a single current transformer, thus comparing the currents magnetically. This method does not include the motor branch circuit in the differential protection, so that a conductor fault must be cleared by the fuses or breaker. These devices are normally adequate to detect and clear the lead faults, which are usually higher than can be interrupted by the contactor.

A ground relay is commonly used on medium-voltage motors, partly because of the cost and importance of the motor. In addition, ground faults that are closer to the neutral end of the winding will have lower fault currents, low enough that they may not operate the fuses promptly, but which can be interrupted by the contactor. Often a resistance grounded system is used to supply medium-voltage motors in order to minimize damage in case of ground faults in the winding. Thus the available ground fault current may be less than the normal motor current and not recognized by the phase overcurrent devices. The most common ground relay uses a single current transformer (the zero sequence system) with all three motor leads passing through it. The sum of the three currents is not zero if a ground fault is present, and the current transformer will operate a relay. Since the current transformer and relay do not have to accommodate load current, the trip point can be made extremely sensitive. If subject to extremely high currents due to a stiff supply system or charging of power factor capacitors, small inaccuracies such as those that may be caused by the leads not being centered in the current transformer may cause false tripping in the first cycle with relays having no time delay. Charging currents in surge-suppression capacitors caused by sudden unbalance of the voltage to ground will be recognized as a ground current. A few cycles delay of the sensing relay is recommended.

Short circuits between turns of a single coil will not be detected by either the differential or ground relay, but can be detected by a negative-sequence or phase current balance relay. It would be advantageous to trip promptly at the minimum level of a turn-to-turn fault, but it is likely that this will cause nuisance trips from unbalanced currents caused by unbalanced voltages. During an unbalanced fault on the power system that severely depresses the voltage on one phase, the momentary current unbalance may well exceed that of a turn-to-turn fault without being hazardous to the motor. Thus close protection for turn-to-turn faults may not be beneficial.

#### 10.4.2 Microprocessor Protection for Internal Faults

High-speed ground fault detection is normally available. Ground fault detection can be set with lower pickup and time delay if a core balance current transformer is used. High speed

may be somewhat of a misnomer with some MPRs since the response time for some microprocessor instantaneous relays may be as high as 50 ms. An additional time delay of 50 ms with a core balance (zero sequence) current transformer, or more if using a residual detection scheme or if surge capacitors are present, is often necessary to avoid false tripping.

There is a high-speed phase overcurrent (50 ms) included. Again the response time may be up to 50 ms, but additional time delay may be needed. Pickup setting should allow for transient asymmetry during motor starting unless fundamental only current detection is available. This feature will normally respond to motor feeder faults, though the fault will normally be cleared by the separate short circuit protection device.

Differential protection may be available. Experience to date with microprocessor machine differential relays indicates that the more sensitive settings and small or no time delay can produce false tripping. Core balance differential current transformers in each phase will normally allow better settings, but do not detect motor feeder faults. Fundamental only current sensing can also produce better performance with either differential scheme.

### 10.5 SELECTION OF SWITCHING DEVICES

Except for very small motors, switching of the motor to start or stop and to disconnect the motor in case of trouble is done by an electrically operated contactor or breaker.

#### 10.5.1 Contactors

Contactors are used for the majority of motors. The contactor is designed to endure many more operations than a circuit breaker and often at a lower initial cost. It automatically disconnects the motor upon loss of power. The contacts, which suffer erosion when closing and opening, can be changed more easily and at less cost than breaker contacts.

Contactors are required to interrupt locked-rotor currents, but not large short-circuit currents. Medium-voltage contactors are designed to have a delayed dropout to allow fuses to clear a large fault current first. Low-voltage contactors depend upon fast operating MCPs or current limiting fuses clearing larger fault currents.

#### 10.5.2 Electrically Operated Circuit Breakers

For large motors (from about 200 hp and up), there is a perception that the larger and less frequently used low-voltage contactors are less reliable than smaller contactors. In addition, there can be a significant first-cost saving in using electrically operated air circuit breakers for very large low-voltage motors. At medium voltage the circuit breaker does not enjoy a cost advantage, and contactors are not generally available above 700 A or 7200 V.

The importance of the motor and its operating mode can affect the choice of contactor or circuit breaker. If a motor is to be started and stopped frequently, a contactor should be used if available, even at a higher first cost. A circuit breaker may not provide satisfactory service. If continuous motor

output is essential and it would be costly if the motor were shut down inadvertently, a latched circuit breaker should be considered, since it will not fall open as the result of a voltage dip. This is of prime importance in a generating plant, where the plant's status must be preserved even though there may be disturbances on the power system.

A contactor may drop open during a voltage dip, and, if the motor is to be kept running, the contactor would have to be reclosed at the end of the dip. However, this may subject the motor to damaging currents or torques if the internal voltage in the motor has not decayed, since it can be expected to be out of phase with the supply voltage. NEMA limits the phasor sum of the internal and external voltages during reclosing to 133% of rated voltage [1]. In very large motors, it may take several seconds for the internal voltage to decay to 33% of rated voltage. However, if the motor is kept connected to the system, the internal voltage will remain in phase with the system voltage unless the system voltage becomes zero. In this case the motor voltage will have decayed before the fault can be cleared and the system voltage can be restored.

The motor will remain on line during a controlled source transfer, such as is practiced in generating plants. However, motors should not be subjected to an uncontrolled rapid reclosing of an upstream breaker. If experience has shown that a motor can be started and stopped frequently, it probably can also be started again after a voltage dip. Thus, the contactor would be preferable in such a case.

For further considerations on bus transfer and reclosing, see [Section 9.1.8](#).

## 10.6 MECHANICAL PROTECTION

A majority of motor failures are mechanical in nature, primarily in the bearings [2]. Large-amplitude vibration, inadequate lubrication, and deterioration are the greatest contributors, often resulting in mechanical failure. The failure may be initiated by factors external to the motor, including vibration of the driven equipment, misalignment, excessive thrust, coupling deterioration, loose hold-down bolts, or failure of an external lubrication supply.

No coupling is completely flexible. With gear-type couplings, misalignment produces a force as a function of the degree of misalignment and shaft torque loads. With a bending-member—type coupling, the amount of force is a function of the misalignment. These forces are imposed on the motor shaft and bearings, increasing the temperature and wear of antifriction bearings and the temperature of sleeve bearings. At some point, dependent upon oil viscosity, excessive load on a sleeve bearing will break down the oil film and damage the babbitted surface, leading to rapid and catastrophic failure. If the coupling is not completely symmetrical, the forces will be imposed cyclically, resulting in vibration. This further loads the bearings. When a sleeve bearing temperature rises, the oil viscosity falls. This lower viscosity provides less damping of the vibration, thus allowing increased amplitude of motion. The process may become cumulative to the point of destruction. Loose bolts may contribute to both misalignment and vibration.

Internal contributors to mechanical motor failure can include breakage of rotor parts such as fan blades, wear or damage to a bearing that allows the shaft to rub, or wear of antifriction bearings, all of which can cause increased vibration or heating. Loosening of fasteners may allow relative movement between rotor and stator, which, barring electrical failure, will be manifested by vibration, heat, or noise. Failure can also be caused by loss of lubrication, which usually results in a temperature rise preceding the failure. With a sleeve bearing, the time between lubrication loss and bearing failure can be very short.

Antifriction bearings fail primarily from wear. Wear increases as a function of loading or lack of lubrication. Failure can be relatively gradual, and often can be detected by frequent monitoring of audible noise or changes in high-frequency vibration. If properly maintained, sleeve bearings are essentially nonwearing because there is no metal-to-metal contact while running. Lack of maintenance or excessive loading in either the radial or axial direction can cause breakdown of the oil film, with consequent metal-to-metal contact. This contact is often preceded by increased bearing temperature, which raises the oil temperature, decreasing the film strength. When metal-to-metal contact does occur, the failure is usually rapid and catastrophic. The failure changes the bearing dimension by removal of bearing material, frequently allowing the shaft or rotor to rub on the frame or core. Shaft bending, excessive vibration with possible failure of motor brackets or feet, damage to core laminations by smearing or to windings by frictional overheating, damage to the rotor bars, and the disgorging of parts from the rotor are all possible consequences.

### 10.6.1 Vibration Detectors

There are rudimentary devices that can be mounted on the motor frame or bracket with a seismic response that will operate an electrical contact. More sophisticated devices can produce an output calibrated in displacement, velocity, or acceleration. The relationship between these three quantities is constant only if the motor speed is constant. Some machine designs or mountings have resulted in insignificant stator vibration during periods of excessive shaft and rotor vibration. By use of proximity probes, the movement of the shaft with respect to the bearing can be measured. This measurement is more relevant to the effect on the bearing. Where machines are attended, it is often beneficial to use an alarm point somewhat lower than the trip point so that corrective action or orderly shutdown may be instituted.

### 10.6.2 Bearing Temperature Monitors

These monitors may be capillary tube devices that operate an indicating gauge and/or provide a contact closure. Thermocouples or RTDs provide electrical signals that can be monitored in various ways. Measurement is normally made on the shell of sleeve bearings and on the outer race of antifriction bearings, although the oil temperature may be measured. Oil temperatures tend to be less responsive during

transient conditions than the bearing element temperatures. With antifriction bearings, the best results are obtained by spring loading the probe against the outer race of the bearing. With sleeve bearings, the best results are obtained by being in contact with the interior of the bearing shell as close as possible to the babbitt at the bottom of the bearing. Once again, it is recommended that an alarm point as well as a trip point be used if the installation is attended, so that corrective action or orderly shutdown can be attempted.

### 10.6.3 Microprocessor Protection

MPRs are capable of monitoring bearing RTDs as well as winding RTDs. They will often be capable of accepting a contact input to initiate a trip and/or alarm and provide a record of the initiating cause. Thus a vibration monitor or filter pressure drop contact output can be processed by the MPR, providing a record that the vibration monitor or pressure device may not be capable of providing. There may be shutdown signals from mechanical malfunctions in the driven equipment which historically have not been identified, resulting in considerable delay in corrective action. With multiple input contact capability in the MPR these trip functions can also be processed and may even produce a sequence-of-events report.

## 10.7 ACCESSORIES

### 10.7.1 Filters

The various types of open motors are designed for the passage of external cooling air over and around the winding. Outside air is drawn or forced into the enclosure, circulated, and discharged. Ambient air may contain electrically conducting dust particles or other contaminants, which, when deposited on the surface of the winding, can be potentially degrading. Over a period of time, airborne dirt will accumulate in the interior ventilation passages. Air filters are frequently used to minimize the inflow of dust and dirt into the motor enclosure. Permanent, dry, washable-type filters are available using one of several types of metallic media. Filters having zinc electroplated steel, copper, Monel, aluminum, or stainless steel filter media are available. Disposable fiberglass filters are also available. Choose filter media which does not corrode in the environment and deposit on the winding.

In the normal course of operation, dust and dirt will eventually accumulate in the filter media and restrict the amount of air flowing into the motor. Restricted air flow will cause inadequate motor cooling and result in an increase of motor temperature to a prohibitive level. To prevent overheating and provide a warning of clogged filters, either stator thermal protective devices or differential pressure monitoring equipment are recommended.

### 10.7.2 Ventilation Opening Guards

Unless further qualified, motors having open or drip-proof enclosures have no restrictions to ventilation other than that necessitated by the mechanical construction. The term

“guarded” is used to indicate that openings giving direct access to live metal or rotating parts (except smooth rotating surfaces) must be limited in size by the structural parts or by the use of screens, louvers, baffles, and so forth. Openings giving direct access to such live or rotating parts shall not permit the passage of a cylindrical 3/4-inch diameter rod. Although a standard feature for guarded and weather-protected enclosures, screens or louvers are considered accessory items for open and drip-proof enclosures.

### 10.7.3 Space Heaters

Space heaters are used to maintain the temperature of the air inside the motor enclosure at a level 5°C to 10°C higher than that of the exterior ambient temperature during nonoperating periods. By maintaining the internal temperature above the dew point, condensation of moisture within the enclosure is prevented. Space heaters are recommended for installation in damp locations or location where there are large variation in the ambient during the night and day, and should be activated only when the motor is not operating.

Depending on mechanical or space limitations, several types of heaters are commonly used. Flexible heaters consisting of a heating element enclosed in a silicone rubber jacket are frequently used with smaller motors where space within the enclosure is limited. These heaters are mounted on the winding end-turns. Exercise caution when working in the terminal boxes of deenergized machines if the end-winding type space heaters are energized. The leads may be energized if there is a failure in the end-winding insulation and the heater insulation. Tubular immersion-type and strip-type heaters are used when space and mechanical considerations permit.

## PART B FUSES AND PROTECTION COORDINATION

### 10.8 INTRODUCTION

Fuses, thermal magnetic circuit breakers, and “instantaneous only” MCPs are the three major types of overcurrent protective devices used to provide motor branch-circuit, shortcircuit, and ground-fault protection. In addition, dual-element time-delay fuses, when properly sized, can provide overload (motor running) protection for motors where a motor starter is not utilized and can also provide backup overload protection where an overload relay/contactors (motor starter) is used.

Current-vs.-time curves in electric motors may be shown in a variety of ways. One way that is especially useful when considering motor protection is that shown in Fig. 10.5, where current appears on the horizontal axis and time on the vertical axis. Two curves are shown in this figure. One is a motor starting curve, which clearly illustrates the high current at the beginning of the starting period and the way it tapers off to steady-state current after the starting period is over. Any branch-circuit, short-circuit, or ground-fault protective device and any overload protective device must be able to “ride through” the inrush of motor starting current without operating.

The second curve is a motor damage curve, one that is typical of single- and three-phase motors. Provided the motor

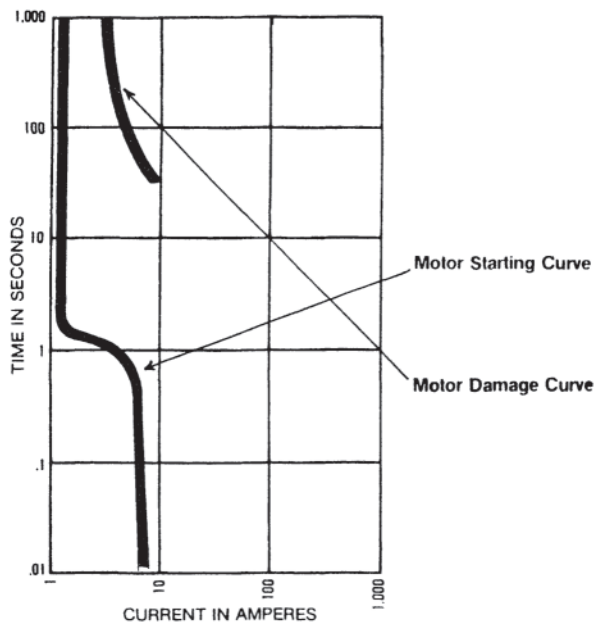


**Figure 10.5** Motor starting curve and motor damage curve for the motor of the example (three-phase, 1/3 hp, 208 V). Full-load current is 1.4 A.

operates in the area below and to the left of the curve, no damage results. If the motor operates in the area above and to the right of the curve, some damage will result. The motor is not necessarily destroyed if the damage curve is crossed, but its life has been shortened. At some point, when the combination of current and time extend beyond the motor damage curve, the motor will need to be rewound or will have to be scrapped. The practical objective of overload protection is to prevent motor damage. In terms of the figures and discussion that follow, that means that a protective device must operate before the motor damage curve is reached. The damage curve shown is that for a three-phase, 1/3-horsepower, 208-V motor, with a full-load current of 1.4 A.

### 10.8.1 Single-Element Fuses

Figure 10.6 shows a curve for a 2-A fast-acting fuse, sized at approximately 140% of the motor full-load current rating. It is seen that the motor starting curve crosses over the fuse curve, indicating that the fuse will open due to the inrush current of the motor. If the fast-acting fuse is sized at 5 A, which is large enough to allow the motor to start (Fig. 10.7), the fuse cannot possibly prevent an overload from reaching the motor damage curve, as can be seen in Fig. 10.8. In this case the fast-acting fuse provides branch-circuit, short-circuit, and ground-fault protection, but not overload or running protection.

It should be noted that the National Electrical Code (NEC) [6] allows up to a 6-A fuse to be used. That is, Table 430.52 of the NEC specifies a maximum fast-acting fuse rating of 300% of the full-load current (1.4 A), or 4.2 A, and an exception to Section 430.52 allows the next larger standard size fuse to be used. Standard size fuses are 1, 3, 6, 10, 15 A and so forth.

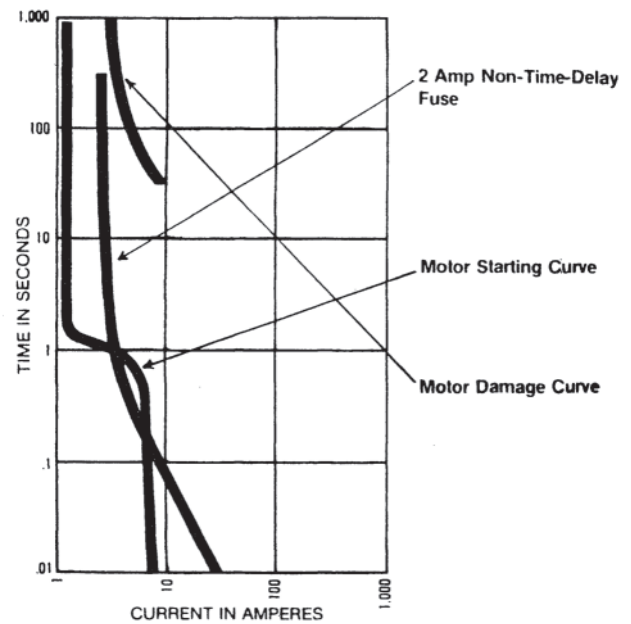


**Figure 10.6** Curves for the motor of the example with the addition of the curve for a 2-A non-time-delay fuse.

### 10.8.2 Protection Coordination with Single-Element Fuses

An overload relay must be added as shown in Fig. 10.9 to provide the necessary overload protection. The overload relay is a Class 10, which means that it will open within 10 seconds at

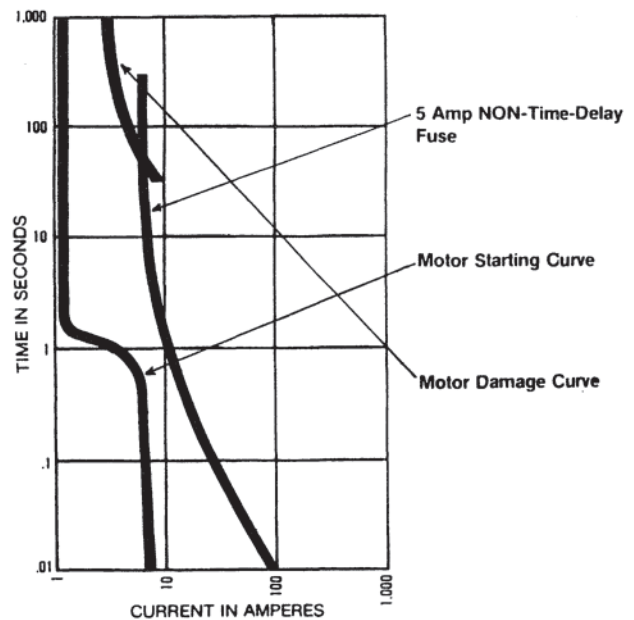


**Figure 10.7** Curves for the motor of the example with the curve for a 5-A non-time-delay fuse.



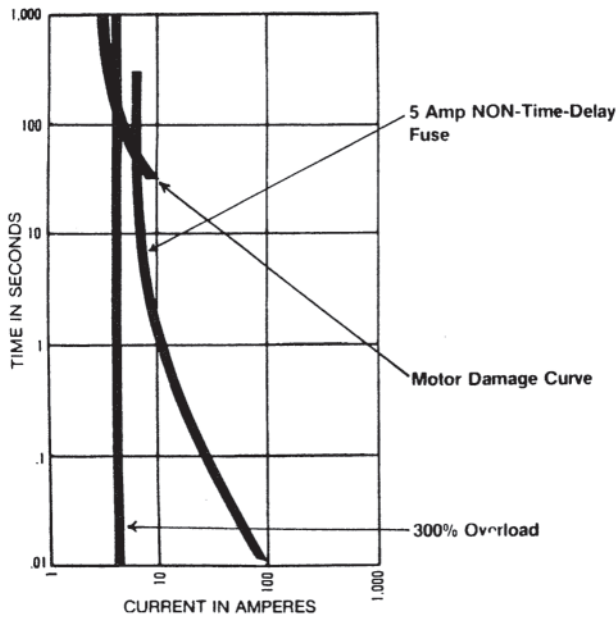


**Figure 10.8** Curves for the motor of the example with 300% overload and a 5-A fuse.

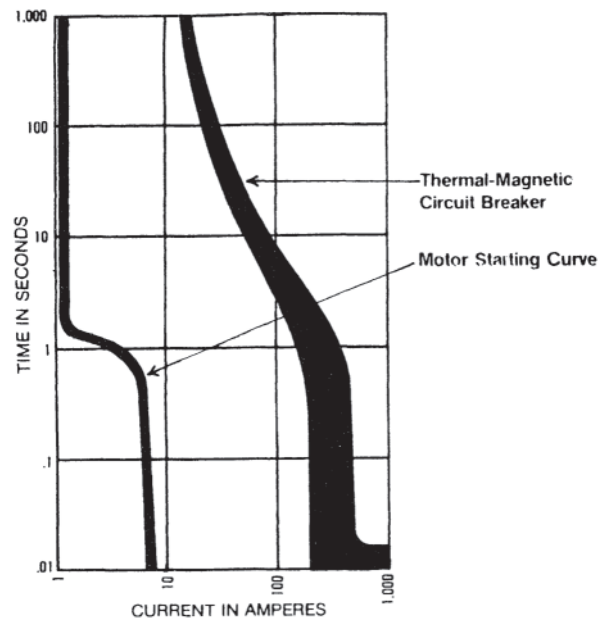


**Figure 10.10** Starting curve for the example motor with the curve for a thermal-magnetic circuit breaker.

600% of its current rating. Should the overload relay fail to take the motor offline because of purposeful interference with its function or as the result of poor maintenance, the motor will be damaged.

Figure 10.10 includes the time-current curve for a 15-A thermal magnetic circuit breaker (the smallest standard size). Since it is oversized, it can easily handle the motor inrush. But as Fig. 10.11 shows, the thermal magnetic circuit breaker cannot prevent the motor damage curve from being reached. Thermal magnetic circuit breakers are typically sized at 250% of the

motor full-load current, too large to provide overload protection. If an overload relay is added, it provides the overload protection while the thermal magnetic circuit breaker provides the branch-circuit, short-circuit, and ground-fault protection. If the overload relay failed, for whatever reason, Fig. 10.11 shows that the motor damage curve would be reached.

The time-current curve for a 3-A instantaneous trip circuit breaker or MCP, set at the lowest setting (8 A), is depicted

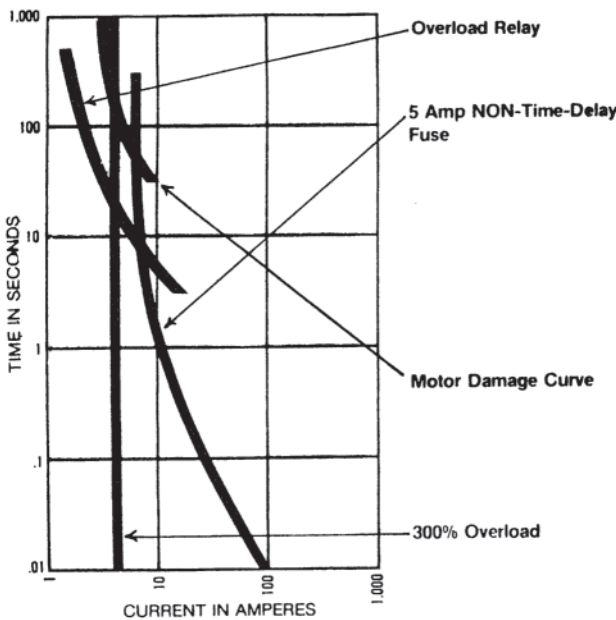


**Figure 10.9** Figure 10.4 with the addition of the curve for an overload relay.

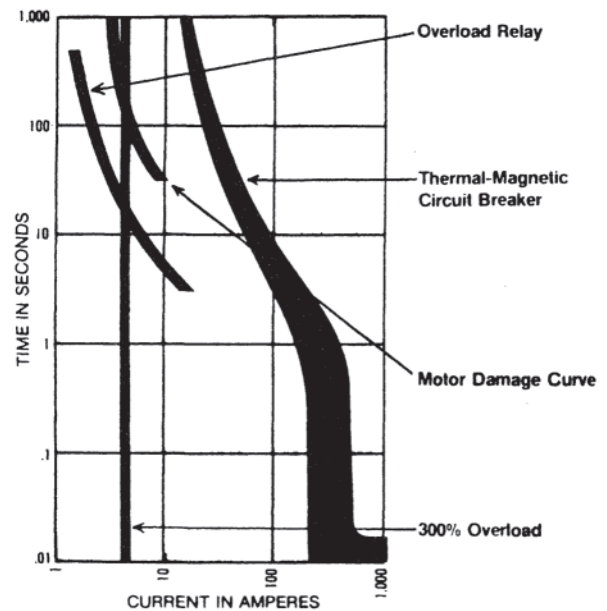


**Figure 10.11** Example motor at 300% overload with the motor damage curve, overload relay curve, and circuit breaker curve.

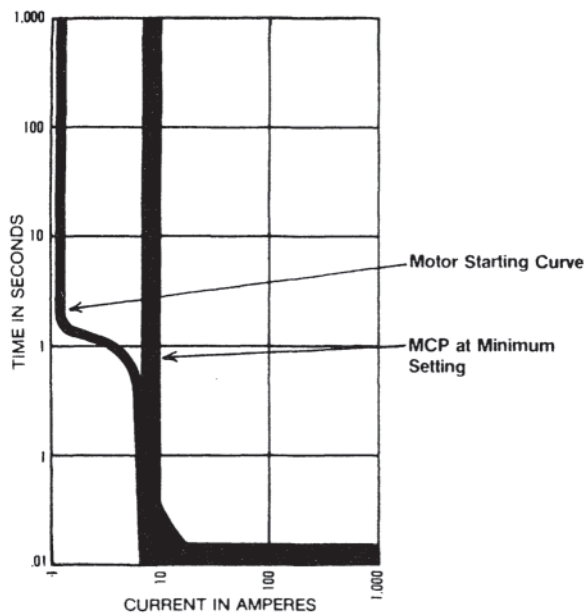


**Figure 10.12** Motor starting curve for the example motor with the curve for an MCP at minimum setting.

in Fig. 10.12, in which the motor starting current curve is again shown. The coincidence of these curves for very short times shows that the MCP might (or might not) open because of the inrush current. Turning the setting to 13 A allows the motor to start, as may be seen in Fig. 10.13, but allows the motor damage curve to be reached. Again, an overload relay is required

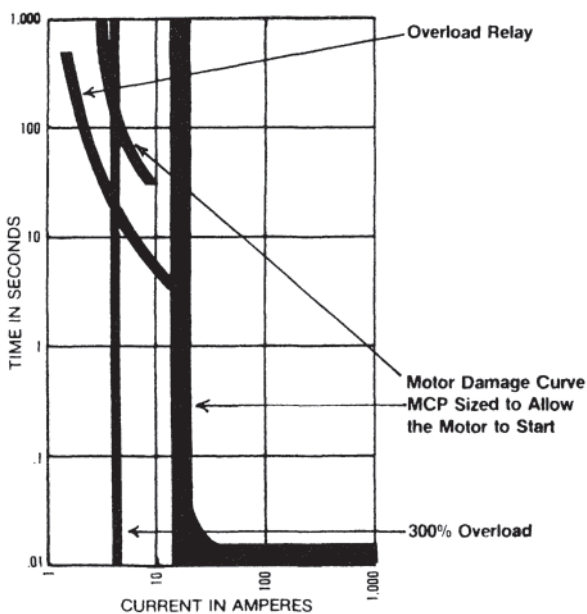
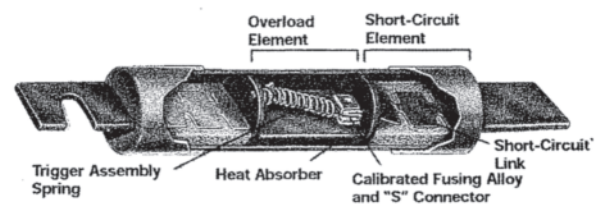


**Figure 10.13** Example motor at 300% overload with an MCP sized to allow the motor to start reliably, and showing the necessity for an overload relay to prevent the damage curve from being reached.

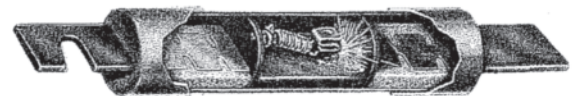
to provide overload protection while the MCP provides branch circuit, short circuit, and ground fault protection. As before, if the overload relay and contactor fail to take the motor offline, the damage curve will be reached.

### 10.8.3 Dual-Element Fuses

Fast-acting (non-time-delay) fuses that are sized to provide overload protection are unable to survive the inrush currents of a motor. These fuses, if adequately sized for inrush current, will not provide overload protection. Another type of fuse, called a dual-element fuse or time-delay fuse, includes in one envelope mechanisms to provide both functions. (See Fig. 10.14.)



The true dual-element fuse has distinct and separate overload and short-circuit elements.



Under sustained overload conditions, the trigger spring fractures the calibrated fusing alloy and releases the "connector".



The "open" dual-element fuse after opening under an overload condition.



Like the single element fuse, a short-circuit current causes the restricted portions of the short-circuit elements to melt. Arcing to burn back the resulting gaps occurs until the arcs are suppressed by the arc quenching material and the increased arc resistance.



The "open" dual-element fuse after opening under a short-circuit condition.

**Figure 10.14** Dual-element fuses showing various opening mechanisms.

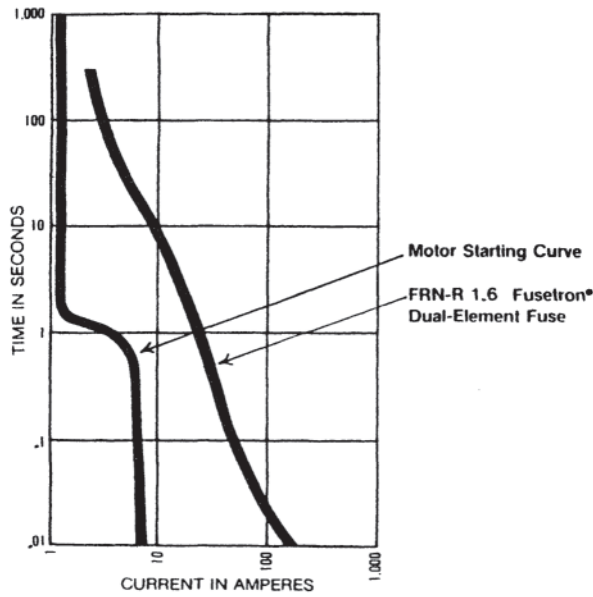


**Figure 10.15** Example motor starting curve and the curve for a FRN-R 1.6 Fusetron® (Bussman Div. of Cooper Industries, St. Louis, MO) dual-element fuse.

As an example, Fig. 10.15 shows the time-current curve for a 1.6-A dual-element, time-delay fuse (sized just below 125% of motor full-load current), and also shows the motor starting curve. (The NEC in Section 430-32(c) sets upper limits for fuse sizes for the motor under consideration.) It is obvious that the fuse will withstand the motor inrush. Figure 10.16 shows that this fuse will also prevent the motor damage curve from being reached.

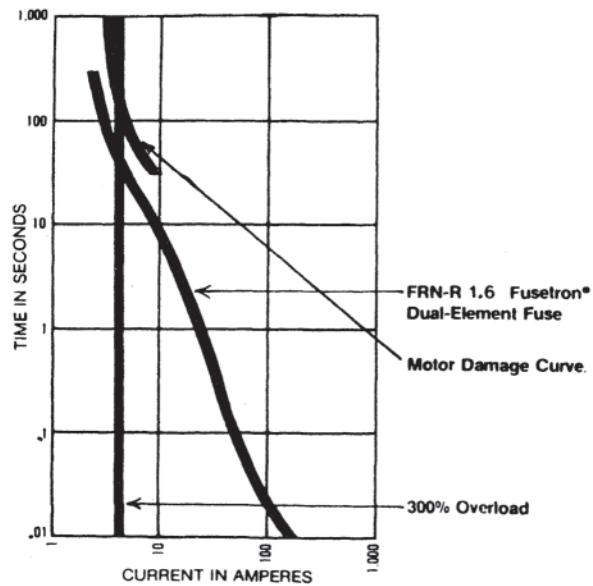


**Figure 10.16** Example motor at 300% overload, illustrating the protection of the motor by the FRN-R 1.6 Fusetron® (Bussman Div. of Cooper Industries, St. Louis, MO) dual-element fuse.

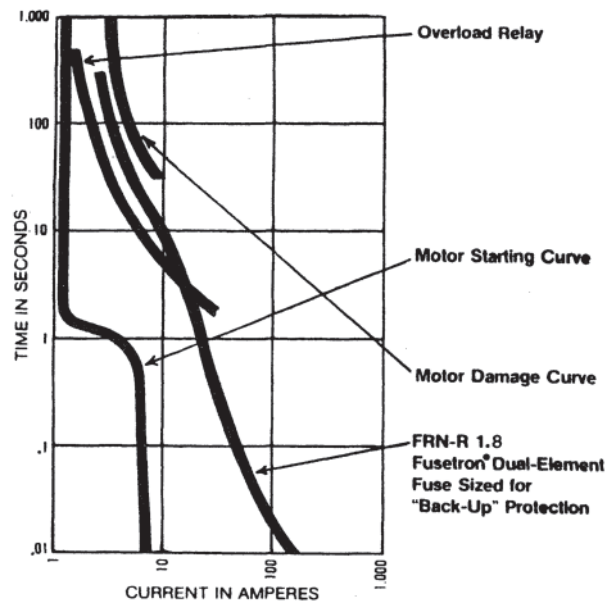


**Figure 10.17** Starting curve for the example motor, together with curves illustrating use of a Fusetron® (Bussman Div. of Cooper Industries, St. Louis, MO) dual-element fuse to back up an overload relay.

In this case, the dual-element, time-delay fuse provides both motor running and branch circuit, short circuit, and ground fault protection, and this is permitted under NEC rules. That is, motors may be protected with properly sized fuses and a properly sized horsepower-rated safety switch instead of a motor starter. The advantage of “fuse-only” protection is that it is very inexpensive. The disadvantage of fuse-only protection is that fuses need to be replaced when the motor is overloaded.

**10.8.4 Protection Coordination with Dual-Element Fuses**

If the options of start/stop buttons, remote control, and the like are desired, a motor starter must be used. When properly sized overload relays are installed, the dual-element, time-delay fuses can be sized one step larger than the overload relays. In Fig. 10.17, the curve for a 1.8-A dual-element, time-delay fuse is shown with the properly sized overload relay. Note that neither opens due to current inrush. If an overload exists, the overload relays will take the motor offline before the fuses open or before the motor damage curve is reached, as is shown in Fig. 10.18. Thus, the overload relays are selectively coordinated with the dual-element, time-delay fuses. However, if the overload relays fail to take the motor offline, the fuses are still sized closely enough to prevent the motor damage curve from being reached. When dual-element, time-delay fuses are sized one step larger than the properly sized overload relays, the fuses are said to be providing backup running overload protection in addition to the functions of branch-circuit, short-circuit, and ground-fault protection.

Overloads can be the result of various problems, including overworking, bearing failure, locked rotor, and single

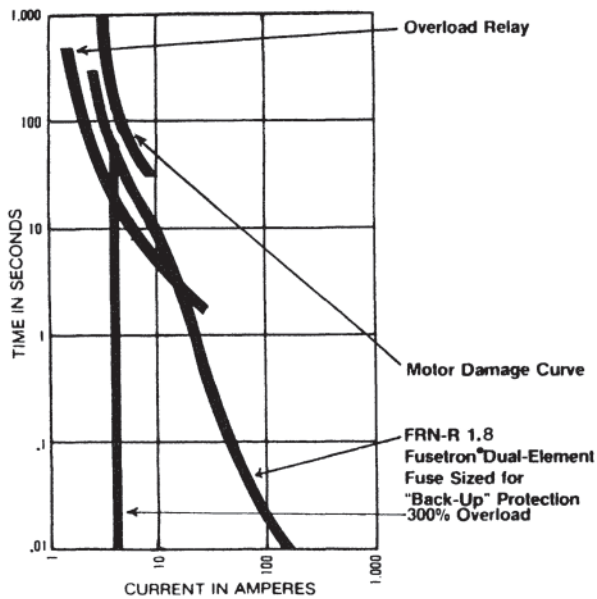


**Figure 10.18** Example motor overload curve, illustrating backup protection at 300% overload.

phasing. Fig. 10.6 through 10.18 depict various situations with “overworking” types of overloads. Figure 10.19 depicts a properly sized dual-element, time-delay fuse protecting the motor from a locked-rotor condition (600% of full-load current). Figure 10.20 shows an overload relay protecting against a locked-rotor condition; the properly sized dual-element, time-delay fuses provide protection even if the overload relay fails.

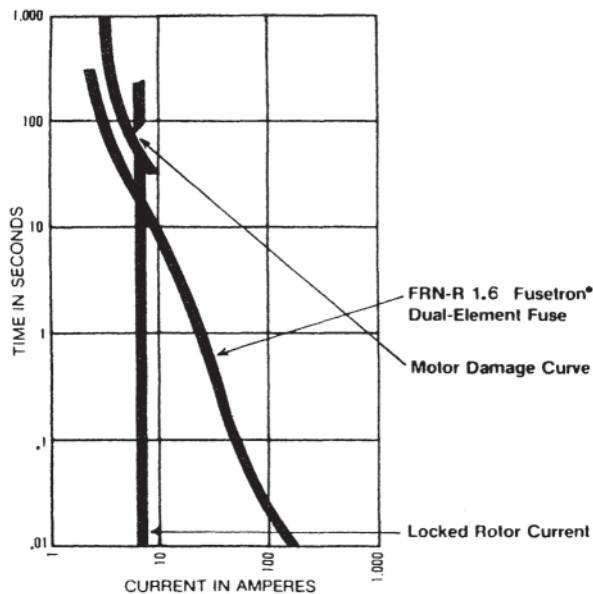


**Figure 10.19** Protection of the example motor under locked rotor conditions by a Fusetron® (Bussman Div. of Cooper Industries, St. Louis, MO) dual-element fuse.

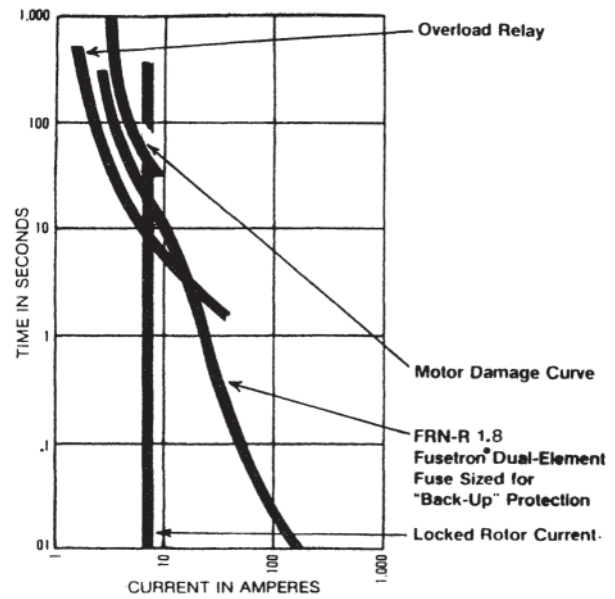


**Figure 10.20** Protection of the example motor under locked rotor conditions by an FRN-R 1.8 Fusetron® (Bussman Div. of Cooper Industries, St. Louis, MO) dual-element fuse to back up an overload relay.

### 10.8.5 Single-Phasing Protection

The motor damage curve may be crossed because of mechanical overloading, but it may also be crossed due to single phasing of the supply. There are two basic types of single-phasing conditions. The first and most destructive type is primary single phasing, that is, the opening of one phase of a three-phase system on the primary side of a delta—wye or a wye-delta transformer or transformer bank. Typical causes of primary single phasing are listed in Table 10.1. The second type of single phasing is secondary single phasing, where the open phase occurs on the secondary of the transformer, between it and the motor. Typical causes of secondary single phasing are shown in Table 10.2.

**Table 10.1** Single Phasing on Transformer Primary—Typical Causes

1. Primary wire broken by:
  - a. Storm, wind
  - b. Ice, sleet, hail
  - c. Lightning
  - d. Vehicle or plane striking pole
  - e. Falling tree limbs
  - f. Construction mishaps
2. Primary wire burned out from short-circuit created by birds or animals
3. Defective contacts on primary breaker—failure to make up on all three poles
4. Failure of three-shot automatic reclosers to make up on all three poles
5. Open pole on three-phase automatic voltage tap changer
6. Open winding in one phase of transformer
7. Primary fuse open

**Table 10.2** Single Phasing on Secondary—Typical Causes

1. Damaged motor starter contact—one pole open
2. Burned-open overload relay (heater)
3. Damaged switch or circuit breaker on the main, feeder, or branch circuit
4. Open fuse or open pole in breaker on main, feeder, or branch circuit
5. Open cable or bus on secondary of transformer terminals
6. Open cable caused by overheated lug on secondary side-connection to service head
7. Open connection in wiring such as in motor junction box (caused by vibration) or any pull box
8. Open winding in motor
9. Open winding in one phase of transformer winding

During a primary single-phasing event, motor current increases to 115% of normal in two of the motor phases while the current in the third phase rises to 230%, as shown in Fig. 10.21. The curves of Fig. 10.22 show that a dual-element, time-delay fuse, sized for motor running overload protection, will prevent this single-phasing overload condition from reaching the motor damage curve. (When the first fuse opens, the motor sees a secondary single-phasing condition described below.)

Figure 10.23 depicts the situation with an overload relay and a dual-element, time-delay fuse sized for back-up protection; the motor damage curve will not be reached.

In a secondary single-phasing situation as shown in Fig. 10.24, the current in one leg is, of course, zero, but the currents in the other two legs increase to 173% of normal. In Fig 10.25, it can be seen that the dual-element, time-delay fuse

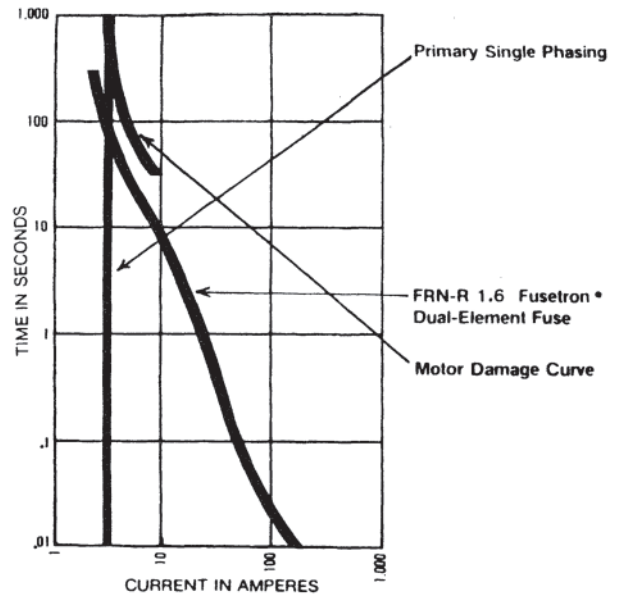


**Figure 10.22** Motor protection with transformer primary singlephasing using a Fusetron® (Bussman Div. of Cooper Industries, St. Louis, MO) dual-element fuse.

sized for motor running overload protection will act to prevent the motor damage curve from being reached. In Fig. 10.26, the overload relay takes the motor offline before the backup fuse opens or before the motor damage curve is reached, and the motor will still be taken offline even if the overload relay does not operate.

It should be noted that for close protection against single

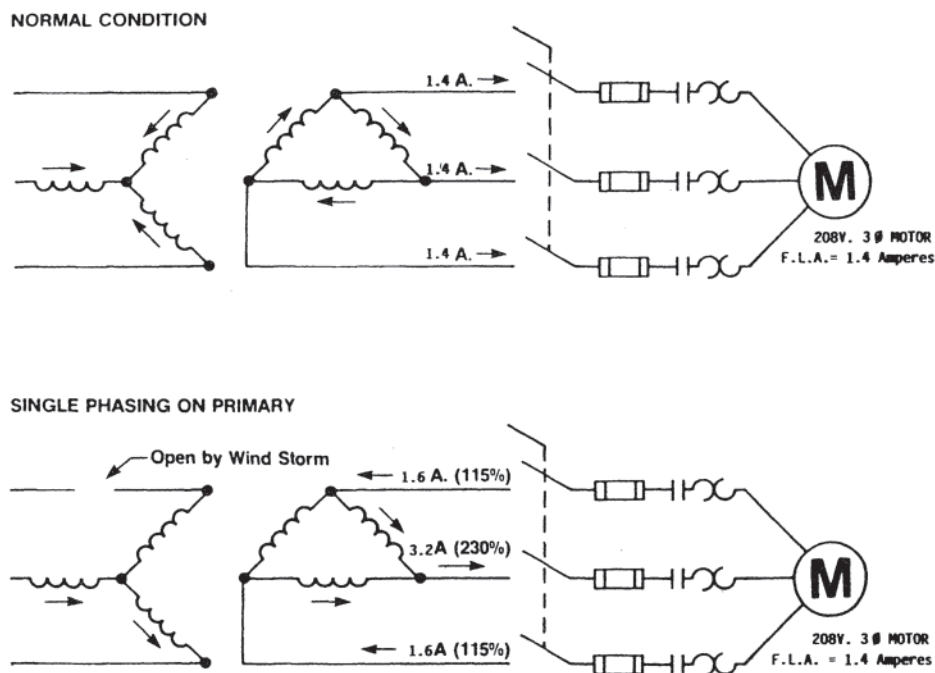


**Figure 10.21** Currents in the example motor with transformer primary single-phasing.

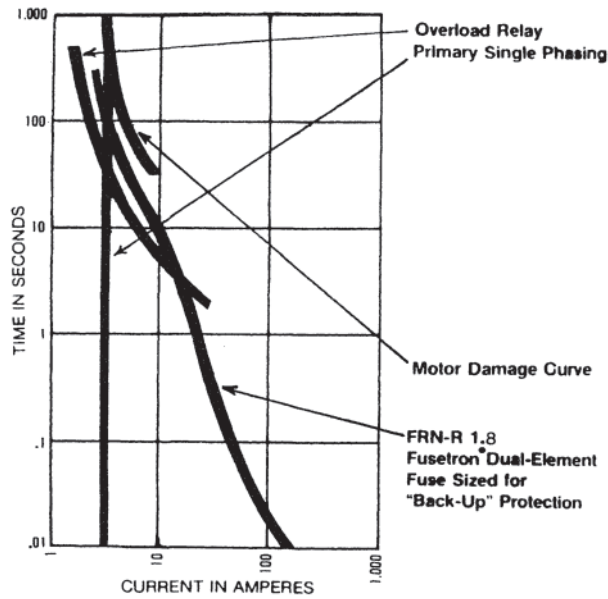


**Figure 10.23** Motor protection with transformer primary single-phasing using a Fusetron® (Bussman Div. of Cooper Industries, St. Louis, MO) dual-element fuse as backup for an overload relay.

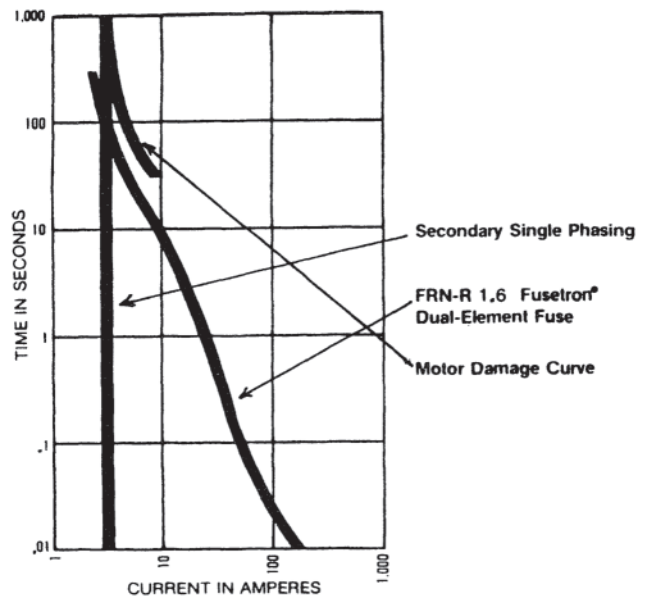


**Figure 10.25** Motor protection with secondary single-phasing using a Fusetron® (Bussman Div. of Cooper Industries, St. Louis, MO) dual-element fuse.

phasing damage, as described above, the overload relays and fuses must be sized to the motor's actual full-load running current, not to the nameplate current (assuming that full-load running current is less than nameplate current). This is especially important when three-phase motors are single-phased while they are lightly loaded. Circulating currents

can still damage the motor if the overloads/fuses are sized to the nameplate and the lightly loaded motor is single-phased. The actual running current of the motor should be measured with an ammeter and the overload relays and fuses should be sized in accordance with the actual measured current. While no overcurrent device can prevent single phasings from occurring, properly sized overload relays and dual-element, time-delay fuses-can protect motors from the damaging effects caused by single-phasing conditions.

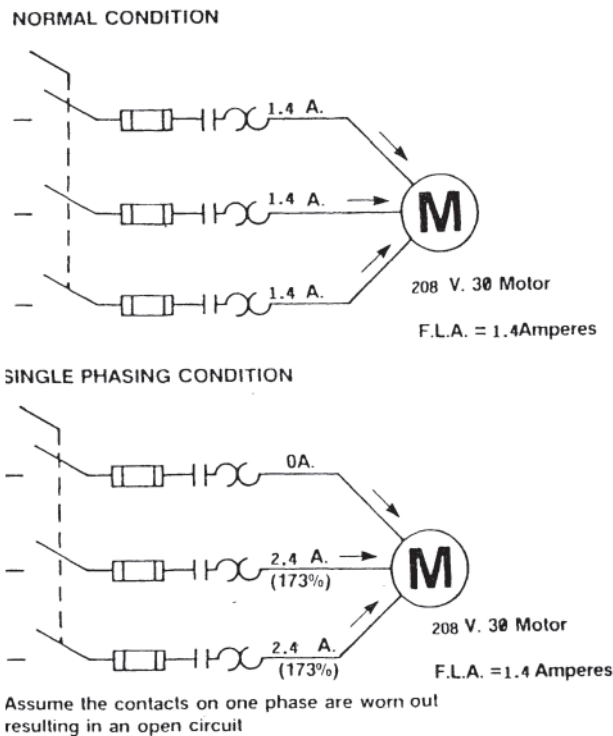


**Figure 10.24** Currents in the example motor with transformer secondary single-phasing.

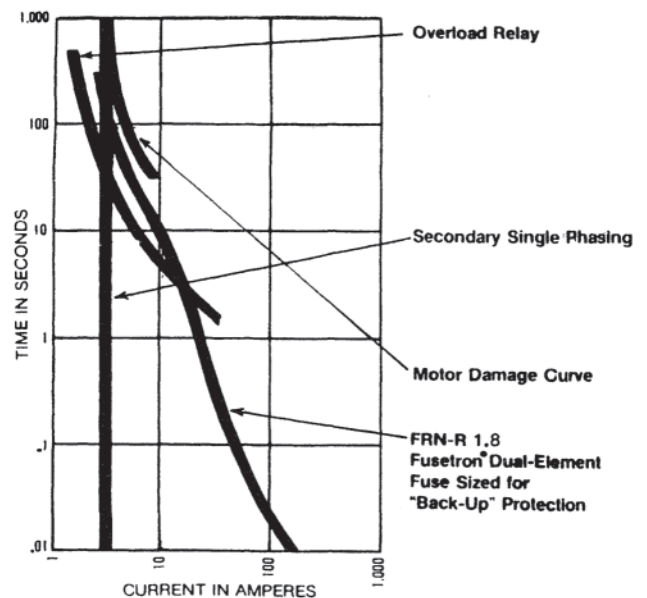


**Figure 10.26** Motor protection with secondary single-phasing using a Fusetron® (Bussman Div. of Cooper Industries, St. Louis, MO) dual-element fuse to backup an overload relay.

**WARNING:** On motors of 50 hp and greater or for motors critical to continuous processes, one of the electronic “black boxes” can be added to provide a third level of protection. For expensive motors or key processes, these devices can easily be justified economically. They can sense overvoltage, undervoltage, phase reversal, and single phasing, to name just a few functions.

## PART C BIMETALLIC THERMAL PROTECTORS

### 10.9 INTRODUCTION

Article 430 of the NEC [6] requires motors connected to branch circuits and rated 600 V or less to be thermally protected. This requirement does not apply where thermal protection might introduce additional or increased hazards, as in fire pump motors. Requirements for inherent thermal protection are covered in Under-writers Laboratories Standard UL 2111–2001 [7] and Canadian Standards Association Standard C22.2 No. 77–1988 [8].

This section applies to induction motors. It describes available motor thermal protectors that can be reset and reused, reviews the theory of protection using bimetallic devices, outlines testing procedures required to determine compliance with applicable standards, and describes methods for determining the most suitable device. Testing agency requirements for motor thermal protectors are discussed in Section 10.10. Thermal protectors installed outside the motor housings are not covered.

Bimetallic thermal protectors are normally used on fractional and small integral-horsepower (up to 5 hp), alternating current motors, and are characterized as “inherent overheating protection.” The primary objective of this protection is to prevent fires and hazardous conditions from occurring. A secondary objective is to protect motors from damage when operating under abnormal conditions.

#### 10.9.1 Definitions

- *Automatic reset protector:* After the protector trips, the contacts of an automatic reset protector will reclose when the motor windings have cooled to a safe temperature.
- *Bimetallic strip or disk:* A bimetallic strip or disk consists of two metals with different coefficients of expansion that are rigidly bonded together. The combination bends in a predictable manner when its temperature is changed.
- *Calibration temperature:* The calibration temperature is the temperature of the bimetal disk at which it is calibrated to open the contacts.
- *Circular mils per ampere (CM/A):* CM/A is the square of a round conductor’s diameter, in mils (1 mil = 0.001 inch), divided by the current in the conductor in amperes. This ratio is frequently referred to as the copper loading. Its reciprocal is referred to as the current density.
- *Cycling up:* Starting with a motor at the ambient temperature and with its rotor locked, the winding temperature will be  $T_1$  at the first trip point and the winding will cool to temperature  $T_2$  before the thermal protector resets automatically (or can be reset if it is a manual reset device). The winding temperature will then rise to  $T_3$  at the second trip point and cool to temperature  $T_4$  before resetting. The cycle repeats for each trip point. The second opening temperature,  $T_3$  will be greater than  $T_1$ , and  $T_5$  will be greater than  $T_3$ . This increase follows for subsequent cycles until a maximum temperature is reached. It may require 20 or more cycles to reach maximum temperature. This phenomenon is known as cycling up.
- *Delta T ( $\Delta T$ ):*  $\Delta T$  is the increase in the temperature of the bimetallic strip or disk caused by current through the internal resistance of the protector. Current through the resistance of the bimetal disk and through the heater elements of a protector results in  $I^2R$  resistance heating which increases the internal temperature of the protector.
- *Effective protector ambient (EPA):* EPA of the bimetallic device installed in a motor is the internal temperature that would occur in the thermal protector with the motor running and with no current passing through the protector.
- *Locked-rotor protection:* When a motor is energized and its shaft is prevented from turning, a thermal protector providing locked-rotor protection will trip before the motor windings exceed specified limiting temperatures.
- *Manual reset protector:* When a manual reset protector trips, its electrical contacts are locked in the open position until they are reset manually.
- *Nuisance trip:* A nuisance trip is the undesirable tripping of the thermal protector when a motor is running at expected overload conditions.
- *Off-winding protector:* An off-winding protector is a thermal protector mounted away from the winding, but within the motor housing. It may be mounted on or in the end shield or housing.
- *On-winding protector:* An on-winding protector is a thermal protector mounted or fastened to the motor windings. Integral wire insulation and varnish are the only materials separating the protector from the conductor wire of the windings.
- *Running overload protection:* A thermal protector providing running overload protection will trip before motor windings exceed a specified limiting temperature when the motor is operating under overload or abnormal load conditions.
- *Safety factor load (SAF):* SAF is a load greater than normal or expected overload conditions selected as the minimum load at which the thermal protector will trip to provide a safety factor and to prevent nuisance trips.
- *Thermal cutoff protector:* A thermal cutoff protector uses an alloy or other material that melts at a specific temperature and permanently opens the electrical circuit of a motor. A thermal cutoff protector is a single-event device and cannot be reset.

- $T_{max}$ : When the motor is running, the maximum permitted winding temperature as measured by a thermocouple is identified as  $T_{max}$ . Maximum temperatures for each insulation class may be found in Section 10.11.2.
- *Trip time*: Trip time is the elapsed time after a motor is energized that it takes for the protector to trip under locked-rotor conditions. Trip time is usually measured in seconds.
- $T_{trip}$ : The temperature of the bimetallic disk that will cause it to trip and open the contacts is identified as  $T_{trip}$ . It is equal to the calibration temperature.
- *Ultimate trip current*: Ultimate trip current is the motor current at the greatest load a motor can carry without tripping its thermal protector.

### 10.9.2 Typical Devices

Thermal protectors with bimetallic disks were introduced in fractional-horsepower motors by Westinghouse Electric Corporation in 1930. Motors with thermal protectors were listed by Underwriters Laboratories (UL) in 1938 and the first standard for motor thermal protection was issued by UL in 1939. Veinott and Schaefer [9] described a method for selecting bimetal thermal protectors for motors in 1949.

A bimetallic thermal protector for motors, in its simplest form, consists of a bimetal strip with an electrical contact attached to its free end, a matching fixed contact and terminal assembly, and a case that provides mechanical stability for the parts. The case also prevents the entry of damaging or disabling materials. Examples of simple thermal protectors are shown in Fig. 10.27. A cutaway view of a simple protector is shown in Fig. 10.28. Opening and closing of the contacts at predetermined temperatures are controlled by the bimetal material and its mechanical configuration. Contacts in these devices open gradually as the bimetal reaches the calibration temperature. This type of gradual contact opening is often

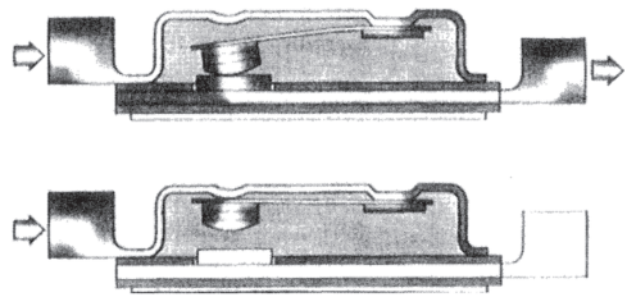


**Figure 10.28** Cutaway view of a simple thermal protector without heater. (Courtesy of Texas Instruments, Inc.)

referred to as a “creeper” and is satisfactory for most low-current applications. When a metal outer case is used in a protector, the opening temperature calibration is often accomplished by bending the case. Protectors are widely available with fixed opening temperatures with tolerance ranges of  $\pm 8^{\circ}\text{C}$  and  $\pm 5^{\circ}\text{C}$ .

In Fig. 10.28, the upper diagram shows the current path through the protector. Current enters through the case crimp terminal and flows through the case member, bimetal disk, and the mating contacts. The current completes its path by exiting through the plate member and the integral plate crimp terminal. Special shaping of the bimetal disk makes it possible to have a “snap” action such that the contacts remain closed until the opening temperature is reached. The disk then snaps like an oil can and opens the contacts quickly, as shown in the lower diagram. This quick opening action increases contact life in high-current applications. When the reset temperature is reached, the bimetal disk snaps the contacts closed.

A major disadvantage of the simple bimetal device is that it cannot protect against rapidly rising temperatures since there is a time delay between actual motor winding temperatures and the internal temperature of the thermal protector.

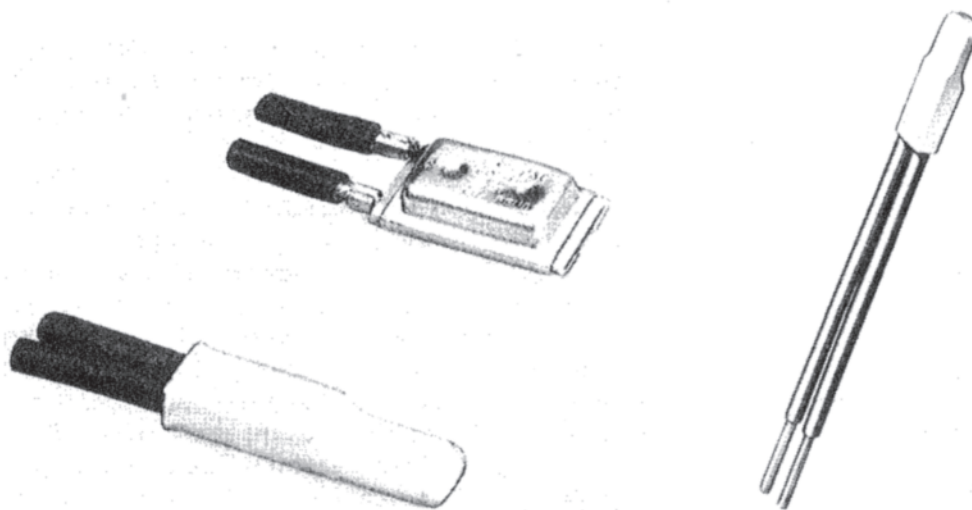


**Figure 10.27** Simple motor thermal protectors without heaters. (Courtesy of Texas Instruments, Inc.)



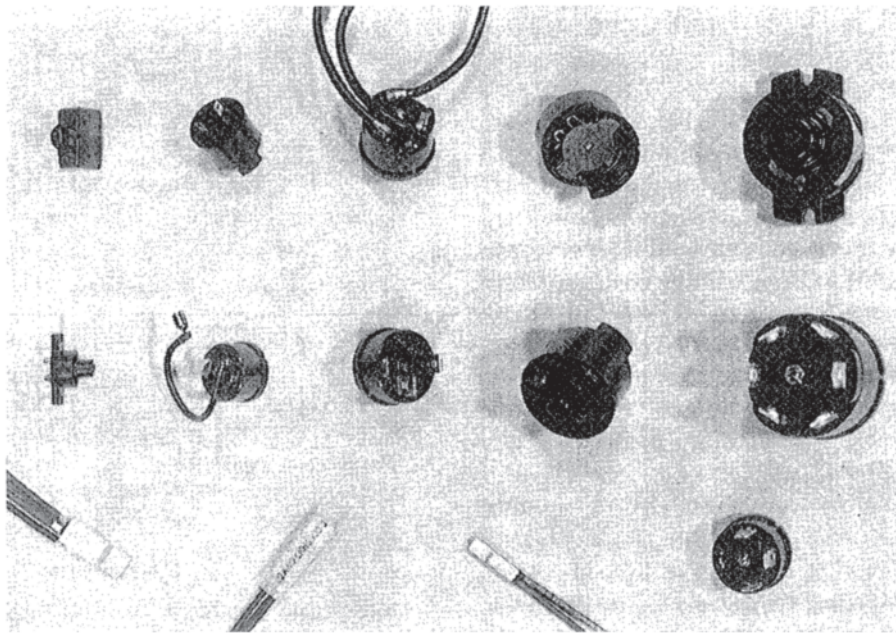


**Figure 10.29** On-winding and off-winding, single- and three-phase, automatic and manual reset protectors. (Courtesy of Texas Instruments, Inc.)

However, simple bimetal protectors are used successfully in shaded-pole, permanent-split capacitor, and other motors where rapidly rising temperatures are not encountered.

To protect split-phase and capacitor-start, single-phase motors, and three-phase motors from the rapidly rising temperatures of locked-rotor conditions, resistance heater elements are added to thermal protectors. With part or all of the motor line current passing through the heater elements, the temperature rise of the internal parts of the protector is proportional to the current squared and, under locked-rotor conditions, quickly reaches the preset bimetal opening temperature. Thermal protectors are manufactured with one, two, or three heater elements depending on the application and the type of motor. Protectors for three-phase motors have

three heater elements, one for each phase. Typical thermal protectors with heaters are shown in Fig. 10.29. A cutaway view of a protector with a heater is shown in Fig. 10.30.

Bimetallic disk and strip thermal protectors for motors are available in a variety of sizes and shapes and can be roughly divided into two categories, on-winding and offwinding mountings. Protector costs range from a few cents to several dollars. Three-phase motor protectors are expensive and represent a significant percentage of the motor cost.

On-winding protectors were introduced in the mid-1950s; these protectors are installed in intimate contact with the motor windings. On-winding protectors are usually applied to motors rated 1 hp or less and are laced on or strapped in place after the motor windings are placed in the stators. Clamps or clips can

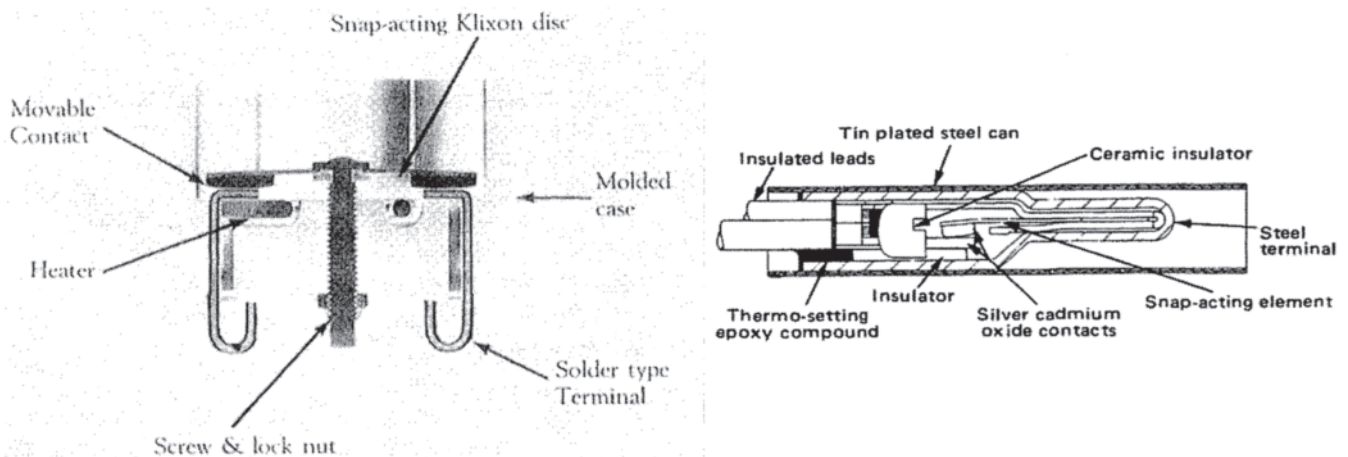


**Figure 10.30** Cutaway of automatic reset protectors. (Courtesy of Texas Instruments, Inc.)

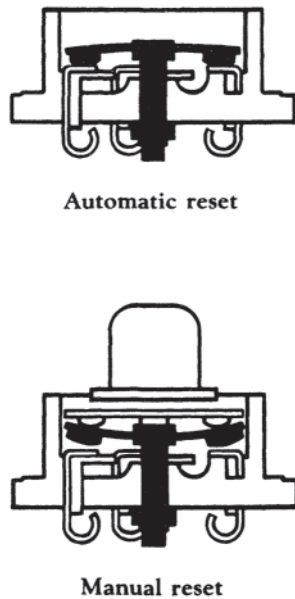


**Figure 10.31** Cutaways of automatic and manual reset protectors. (Courtesy of Texas Instruments, Inc.)

also be used to hold protectors tightly against the windings. If the protectors have metal cases, sleeves are used to insulate the cases from the wire of the motor windings and from other live and dead metal parts in the motors. Onwinding protectors, for the most part, are two-lead, single voltage devices, with or without heater elements. However, there is at least one three-lead, on-winding protector available that is usable in dual-voltage motors. Thermal protectors normally used in off-winding, dual voltage applications may be strapped to the motor windings. On-winding protectors reset automatically when the temperature of the bimetal falls below predetermined values. On-winding protectors are shown in Figs. 10.27 and 10.29.

Off-winding thermal protectors intended for mounting away from the windings in motor end shields or in other locations within the motor housing have cases made from insulating materials, such as phenolic, and are available in automatic reset or manual reset configurations. A manual reset protector has a lock-out feature that prevents the contacts from reclosing after tripping until the bimetal reaches the reset temperature and the reset button is pushed. Manual reset protectors are required where sudden, unexpected restarting of motors might be hazardous. Table saws, meat slicers, food grinders, and oilfired furnaces are typical applications where manual reset thermal protectors are required. Off-winding protectors are installed using mounting ears molded into the cases or with spring clips and clamps. Typical off-winding devices are shown in Figs. 10.29 to 10.31.

### 10.9.3 Considerations in Device Selection

To prevent fires and to protect motors from damage or burnout, motor windings must be prevented from reaching damagingly high temperatures. The actual values of these temperatures

depend on the insulation materials used. Most motors are manufactured with Class A, B, F, or H insulation systems as defined by UL or ANSI standards. Limiting temperatures have been selected so that motors subjected to such temperatures for an extended period of time will continue to be safe to operate once the abnormal conditions are corrected. Abnormal conditions to be protected against include locked rotor, running overload, no load (fan and blower motors), and single phasing of polyphase motors.

When a motor is energized, the temperature of the bimetal of an on-winding protector with no current through it will be less than the motor winding temperature even though the protector is in intimate contact with the windings, because heat-insulating materials (metal protector cases, sleeves, and air) separate the bimetal of the protector from the windings. The temperature at the bimetal with no current through it or through the heater elements is known as the effective protector ambient (EPA). The EPA temperature rise above the ambient temperature external to the motor is proportional to the winding temperature rise. The temperature rise of the onwinding protector will be a fraction, less than but approaching unity, of the winding temperature rise. Temperature differences between motor windings and the bimetal of an off-winding protector are much greater than those of an onwinding device.

Under normal operation and during overload conditions, motor current generates heat inside a thermal protector that is proportional to the  $I^2R$  heating in the bimetal and the heater element(s). The temperature rise inside a thermal protector caused by this heating is known as the  $\Delta T$  temperature. The internal temperature of the protector is equal to the EPA plus  $\Delta T$ . A protector will trip when the internal temperature of the device (EPA+ $\Delta T$ ) reaches the bimetal opening temperature,  $T_{\text{trip}}$ . Motor winding temperatures at the protector trip point will be higher than the EPA.

When its internal temperature equals the preset trip temperature, a thermal protector will trip. If motor windings are to be limited to a certain maximum temperature,  $T_{\text{max}}$ , under running and overload conditions, the preset trip temperature of the protector,  $T_{\text{trip}}$  must be:

$$T_{\text{trip}} \leq \text{EPA at } T_{\text{max}} + \Delta T \text{ at } T_{\text{max}}$$

$\Delta T$  is determined from the motor current at the loading required for the winding temperature to reach  $T_{\text{max}}$ .

Protectors must not trip under normal or expected operating conditions. A trip under these conditions is defined as a nuisance trip. Thermal protectors are usually selected to trip at load points 10–25% greater than normal or expected operating conditions so that variations in motor manufacture, protector calibration, and unusual short-time operating events do not cause nuisance tripping. These load points are designated SAF (SAFety factor loads). Therefore:

$$T_{\text{trip}} \geq \text{EPA(SAF)} + \Delta T(\text{SAF})$$

where EPA(SAF) and  $\Delta T$  are temperatures at the SAF load point.  $T_{\text{trip}}$  can be higher than  $T_{\text{max}}$  if the winding temperature at the ultimate trip point is close to  $T_{\text{max}}$  since  $\Delta T$  is often

**Table 10.3** Operating Conditions at Maximum Winding Temperature and at SAF Load Point

	Max.	SAF
Voltage (V)	120	120
Load	*	SAF
Winding temperature (°C)	130	90
Motor current (A)	8	6
Ambient temperature (°C)	25	25
EPA (on-winding protector) (°C)	125	87
$\Delta T$ (on-winding protector) (°C)	11	6
EPA (off-winding protector) (°C)	80	58
$\Delta T$ (off-winding protector) (°C)	27	16

\* Load at which winding reaches a 130°C temperature limit.

greater than  $T_{\max}$ -EPA. The winding temperature, of course, must not exceed  $T_{\max}$ .

For example, a motor operates with a maximum winding temperature of 90°C in a 25°C ambient at a load that is 15% above service factor loading. The winding temperature is not to exceed 135°C. In this case, a maximum temperature of 130°C is used for device selection to allow for differences in thermal protector calibration and for motor manufacturing differences. Operating conditions are shown in Table 10.3. For the on-winding protector of the table:

$$T_{\text{trip}} \leq (125^\circ\text{C} + 11^\circ\text{C}), \text{ or } 136^\circ\text{C} \text{ (column \#1)}$$

$$T_{\text{trip}} \geq (87^\circ\text{C} + 6^\circ\text{C}), \text{ or } 93^\circ\text{C} \text{ (column \#2)}$$

For the off-winding protector of Table 10.3:

$$T_{\text{trip}} \leq (80^\circ\text{C} + 27^\circ\text{C}), \text{ or } 107^\circ\text{C} \text{ (column \#1)}$$

$$T_{\text{trip}} \geq (58^\circ\text{C} + 16^\circ\text{C}), \text{ or } 74^\circ\text{C} \text{ (column \#2)}$$

Note in Table 10.3 that  $\Delta T$  for both the on-winding and the off-winding protectors at maximum load (8A, 130°C) is greater than  $\Delta T$  at SAF load (6 A, 90°C). In this case, onwinding protectors calibrated between 93°C and 136°C can be used and off-winding protectors calibrated to trip between 74°C and 107°C can also be used. Such devices will trip when the motor is severely overloaded while permitting loading up to the SAF point without tripping. Winding temperatures will not exceed 130°C. Methods used to select specific thermal protectors are covered in the following subsections.

Split-phase, capacitor-start, capacitor-start/capacitor-run, and other types of single-phase motors have auxiliary windings that are energized for short periods of time while the motors start and accelerate to operating speeds. To reduce winding material cost and to enhance motor performance, auxiliary windings operate with current densities much higher than main or run windings. Temperature rise in auxiliary windings is rapid and, if no heat is lost from the windings, the time to reach a given temperature is proportional to the square of the inverse of the current density. The inverse of the current density is expressed in CM/A. The actual time to reach a specific temperature is longer than the (CM/A)<sup>2</sup> ratio indicates because of heat loss from the winding. For a given limiting temperature, a graph of time to reach that temperature versus CM/A can be generated. The resulting plot will be accurate

enough to use with a variety of motor types and configurations. If the current of an auxiliary winding under locked-rotor conditions is known and the auxiliary winding wire size is known, the time to reach a limiting temperature can be found on the time versus CM/A graph for that temperature. Thermal protectors that trip in less than the limiting time can then be selected.

Thermal protector selection methods for locked-rotor protection are covered in the following subsections. Testing agency requirements for motor thermal protectors are discussed in Section 10.10.

#### 10.9.4 Selection of Bimetallic Thermal Protectors for Shaded-Pole, Permanent-Split Capacitor, and Other Slow Heat Rise Single-Phase Motors

The temperature rise of shaded-pole and permanent-split capacitor motors under locked-rotor conditions is relatively slow when compared to other single-phase motors. This slow rate of temperature rise makes it possible to use temperature-sensitive thermal protectors without internal heater elements. Protector trip temperatures are selected to allow the windings to approach the limiting ultimate trip or no-load temperature, whichever is applicable.

For example, a thermal protector for a 0.25-hp, 115-V, 60-Hz, air-over, shaded-pole motor used to drive a directconnected fan is mounted on-winding. Rated motor current is 7 A and the insulation is Class A. Running temperature at 120 V with the fan attached to the shaft is 90°C in a 40°C ambient. The limiting no-load trip temperature is 140°C (see Section 10.11.2). Locked-rotor limits are shown in Table 10.4. Since 7 A through the bimetal of the protector will generate some internal  $I^2R$  heating, protectors with zero-current trip temperatures of 125°C to 145°C should be tested for suitability. The 125°C minimum temperature selection is used to avoid the possibility of nuisance tripping when the ambient temperature is higher than 40°C, when the line voltage is above 120 V, or when the ambient temperature and line voltage are both high. Another reason for selecting higher calibration temperatures is that the protectors will be usable on a wide range of motor ratings.

To determine whether a candidate protector is suitable for a slow heat rise application, locked-rotor performance should be checked first. Locked-rotor trip time should be long enough to allow the fan or blower to accelerate to its full-load speed under low-voltage conditions but short enough so that the winding will stay below limiting temperature at high line voltages. All speed connections should be tested.

No-load, no-fan, or ultimate trip temperature must be checked to make sure the margin between it and the full-load winding temperature is great enough to avoid nuisance tripping. All speed connections must be checked. Protectors are connected in series with the common leads in these motors as shown in Figs. 10.32 and 10.33.

The application of an off-winding protector in slow heat rise motors should be approached in the same manner as for fast heat rise applications in the next subsection.

**Table 10.4** Maximum Permitted Locked-Rotor Temperatures

	Insulation Class			
	A	B	F	H
Automatic reset thermal protectors				
Peak temperature, 1st hour (°C)	200	225	250	275
Peak temperature after 1st hour (°C)	175	200	225	250
Average temperature after 1st hour (°C)	150	175	200	225
Thermal cutoff protectors				
Peak temperature (opens during 1st hour) (°C)	200	225	250	275
Peak temperature (opens after 1st hour) (°C)	150	175	200	225
Manually reset protectors				
Peak temperature during 10 cycles (°C)	200	225	250	275

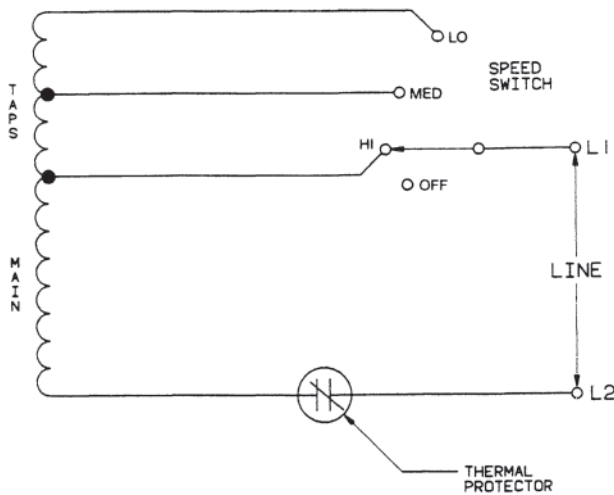


**Figure 10.32** Shaded-pole motor connection diagram. (Courtesy of A.O.Smith Corp.)

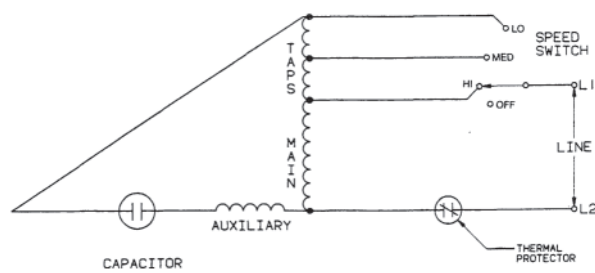


**Figure 10.33** Permanent-split capacitor motor connection diagram. (Courtesy of A.O.Smith Corp.)

**10.9.5 Selection of Bimetallic Thermal Protectors for Single-Voltage Split-Phase, Capacitor-Start, Capacitor-Start/ Capacitor-Run, and Other Single-Phase Motors**

Thermal protectors are connected in series with the common lead in single-phase motors as shown in Figs. 10.32, 10.33, and 10.34. Motor line current flows through the bimetal and

contacts and through the heater elements when used as in Fig. 10.34.

Under locked-rotor conditions in split-phase, capacitorstart, and capacitor-start/capacitor-run motors, the current densities in auxiliary windings are much higher than those in the main windings. As a result, the temperature rises of auxiliary windings are very rapid. Simple bimetallic thermal protectors cannot follow rapidly changing temperatures quickly enough to trip reliably before temperature limits are exceeded. To increase the internal temperature of thermal protectors rapidly and in proportion to winding temperatures, internal heater elements are added to the protectors. Motor current flowing through the heater elements produces internal *I*<sup>2</sup>*R* heating that rapidly increases the internal temperatures of the protectors to the calibrated trip points.

To apply thermal protectors to such motors properly, the following basic information is needed:

- A. Motor rating
- B. Test voltages and temperature limits from UL and CSA standards
- C. Motor performance and construction data, including:
  1. Motor winding wire sizes and materials
  2. Locked-rotor currents with the motor at 25°C and at a selected elevated temperature of 140°C, 165°C, 190°C, or 215°C
  3. Full-load and service factor motor performance under normal conditions
  4. For directly connected fan and blower motors, noload, no-fan performance at a stabilized

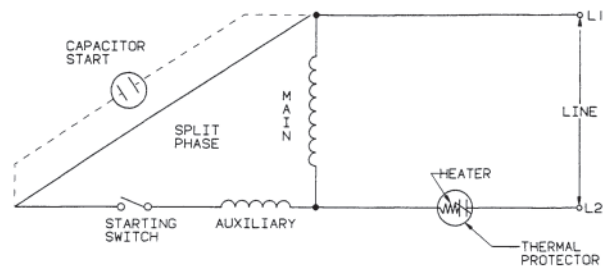


**Figure 10.34** Single-voltage, split-phase, and capacitor-start diagram. (Courtesy of A.O.Smith Corp.)

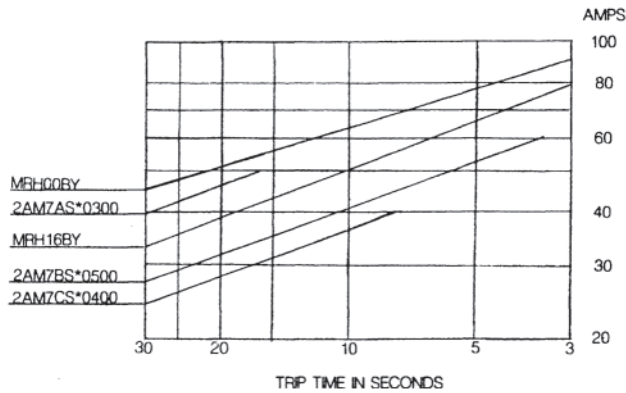


**Figure 10.35** Average first-cycle trip time vs. current for thermal protectors. (Courtesy of Texas Instruments, Inc.)

temperature or at the maximum permissible temperature, whichever is lower

5. Performance with motor windings at the maximum permissible ultimate trip temperature and at the required test voltage
- D. The temperature of the thermal protector (see EPA in Sections 10.9.1 and 10.9.3) in relation to the motor winding temperature when the protector is mounted in the motor.
- E. Current versus trip time data for the type of thermal protectors that will be used. See Fig. 10.35 for an example.
- F.  $\Delta T$  for the protectors in (E). See Fig. 10.36 for an example.
- G. Maximum permissible locked-rotor trip time vs. CM/A. CM/A is the reciprocal of the current density.

Items (A) through (D) will be available from engineering test records and design calculations. Items (E) and (F) are available from the thermal protector manufacturer. Item (G) requires some testing, but once generated for one motor type and frame

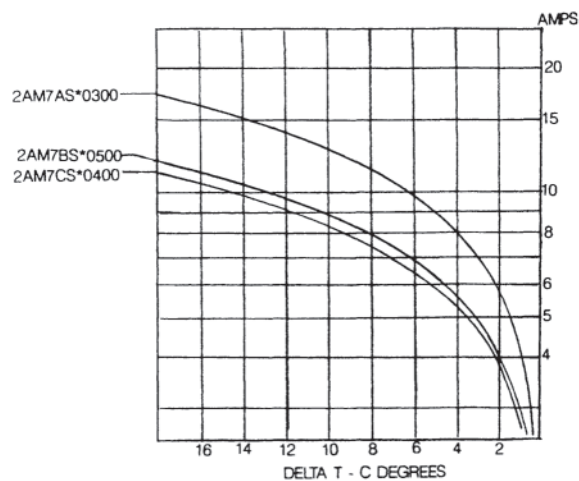


**Figure 10.36**  $\Delta T$  versus protector current for on-winding thermal protectors. (Courtesy of Texas Instruments, Inc.)

size, the data can be applied to other types and frame sizes with acceptable accuracy.

The temperature selected in (C.2) should be sufficiently below the limiting locked-rotor temperature of Section 10.11.3 to allow for the cycling up of the peak and average temperatures at the second and subsequent trips. Recommended first-cycle trip temperatures are as follows: 140°C for Class A insulation, 165°C for Class B insulation, 190°C for Class F insulation, and 215°C for Class H.

Data to establish the relationship of CM/A and time required to reach selected temperatures for each winding material can be generated from tests of one or two motors having reasonably high winding slot fill. The shaft is locked and the current is manually controlled at a constant value by adjusting the applied voltage. The time required for the motor winding to rise from a 25°C ambient to a selected temperature is recorded. CM/A can be calculated using the locked-rotor current and the known wire sizes of the winding tested. Second and subsequent points for other CM/A values can be obtained by cooling the motors to the ambient temperature and repeating the procedure with different applied voltages. If the ambient is not 25°C, test temperatures should be adjusted to produce the same temperature rise. For example, when testing in a 20°C ambient, a Class A temperature of 135°C should be used (20°C+[140°C–25°C]=135°C). Minimum and maximum CM/A values should be tested along with several points in between. Separate tests should be made on copper and aluminum windings. Insulation Class B curves can be estimated from Class A data by multiplying the maximum trip times by 1.15 to allow for the 15+% increase in the allowable temperature rise. Insulation Class F and H curves can be obtained using the same approach, but some points should be tested to check the accuracy. Careful records of thermal protector applications should be kept so that the limiting temperatures shown above can be adjusted to reflect the actual amount of cycling-up that occurs with each motor type. This adjustment will make it easier to accurately predict thermal protector performance in given applications.

#### 10.9.5.1 Procedure and Example

To select a protector for locked-rotor and running-overload protection of an insulation Class B, single-voltage, 115-V, 60Hz motor, the procedure is as follows.

- A. Determine the UL and CSA test voltage (120 V in this case).
- B. Calculate or test to obtain motor performance at the test voltage and frequency (120 V, 60 Hz) with windings at 25°C or some other selected temperature. (Using the same temperature each time facilitates the comparison of tests.) When testing, do not connect the thermal protector in the circuit for (B) and (C), but determine the EPA temperature at the metal thermal protector case of an on-winding device or at the bimetal of an off-winding device.
- C. Calculate or test for performance at the UL voltage by increasing the load until the total winding temperature reaches 155°C for Class B insulation (or 130°C for Class A). This is the performance at 10°C less than the

**Table 10.5** Example of On-Winding Thermal Protectors

Candidate thermal protector	2AM7BS*0500	2AM7AS*0300
Line voltage (V)	120	120
Line current (A)	10.0	10.5
Winding temperature at ultimate trip (°C)	128	134
EPA (°C)	122	129
Calibrated protector trip temperature (°C)	135	135
$\Delta T$ at line current (°C)	13	6
Protector calibration – $\Delta T$ (°C)	122 (135–13)	129 (135–6)
Average auxiliary winding CM/A	32 (copper)	32 (copper)
Average locked rotor line amps (A)	45	45
Maximum permissible trip time (s)	15.4	15.4
Locked rotor trip time (s)	6.9	23.5

- maximum allowable Class B ultimate trip temperature. Variations in motor construction, thermal protector calibration, and testing make it prudent to reduce the maximum allowable temperature by 10 degrees. Measure the temperature at the protector as in (B).
- D. Calculate or determine by test at the UL voltage the locked-rotor line current, main winding current, and auxiliary winding current at 25°C and 165°C (25°C and 140°C for Class A). Average the cold and hot values of the auxiliary winding current and determine the average CM/A using the bare diameter of the auxiliary winding wire, taking the number of strands used into consideration. Do the same for the main winding. Determine the maximum allowable trip time from the Time vs. CM/A data for each winding. Select the lower trip time value.
- E. Plot rpm, watts loss (watts input—watts output), and line current vs. torque using data from Section 10.11.2. Draw constant-torque lines at the full load or service factor load and at the 155°C load point from (C). Tripping must occur in the region between the two lines but, as explained in Section 10.9.3, a SAF load at least 10% greater than the service factor load is desirable as a minimum load point. The watts loss at the 155°C load point can be used as a limit for other Class B motors with similar construction and ventilation systems. In the absence of test data, 80% of the Class B watts loss can be used for Class A motors.
- F. The maximum locked-rotor trip time (D) and the ultimate trip range (E) have now been established. The minimum locked-rotor trip time can be any value below the maximum as long as there is enough time for the motor to accelerate its load to the operating speed. Trip times below 4 seconds should be avoided and require careful testing to make sure nuisance tripping will not occur.
- G. Using current versus trip time and  $\Delta T$  data supplied by the protector manufacturer, as well as the maximum allowable trip time from (D), protectors can now be selected. For example, a motor is to have an on-winding protector and conditions are as listed in Table 10.4. Protector 2AM7BS\*0500 of Fig. 10.35 will trip in 6.9 seconds with an average current of 45 A. It will be a satisfactory locked-rotor application since the trip time is greater than 4 seconds and less than the maximum allowable trip time of 15.4 seconds. The 2AM7AS\*0300 protector will trip in 23.5 seconds. It is not satisfactory because it exceeds the 15.4-second maximum trip time limit.
- H. The running performance for all devices that meet the locked-rotor requirements is determined using the  $\Delta T$  curves (Fig. 10.36) and the line current in the ultimate trip range established in (E). A  $\Delta T$  under running overload conditions is established for all thermal protectors being considered.
- For example, a motor is to have an on-winding protector and conditions are as listed in Table 10.5. When the EPA plus  $\Delta T$  equals the protector calibration trip temperature, the protector will trip. A 2AM7BS\*0500 protector calibrated to trip at 135°C will trip when the winding temperature reaches 128°C. The current at that point is 10.0 A,  $\Delta T$  is 13°C from Fig. 10.35 and the EPA is 122°C. The EPA temperature rise, determined by test, is 95% of the winding temperature rise. Another 135°C calibrated protector, 2AM7AS\*0300, has a  $\Delta T$  of 6°C at 10.5 A and will trip when the winding temperature is 134°C. However, it has an unsatisfactory locked trip time as determined in (G).
- Checking the performance of all possible thermal protectors is a difficult task without a computer. However, application experience will quickly point to ways to narrow the choices to manageable levels.
- I. An off-winding protector may also be considered for the same motor. Off-winding protectors are checked in the same manner. Conditions are as shown in Table 10.6. Off-winding protector MRH16BY will trip in 12.5 seconds with a current of 45 A (Fig. 10.35).  $\Delta T$  for this device is shown in Fig. 10.37, and the protector will trip when the winding temperature reaches 128°C. This will be satisfactory application.
- J. When selecting protectors, it is important that the current limits of the heater elements and contacts of the protectors are not exceeded. Both the 2AM7BS\*0500 and the MRH16BY protectors have heaters that will not burn out and are therefore satisfactory. The choice

**Table 10.6** Example of an Off-Winding Protector

Thermal protector	MRH16BY
Line voltage (V)	120
Line current (A)	10.0
Winding temperature at ultimate trip (°C)	128
EPA (°C)	93
Protector calibrated trip temperature (°C)	120
$\Delta T$ at 10.0 A (°C)	27
Protector calibration $-\Delta T$ (°C)	93(120-27)
Average start winding CM/A	32(copper)
Average locked rotor line amp (A)	45
Maximum permissible trip time (s)	15.4
Locked rotor trip time (s)	12.5

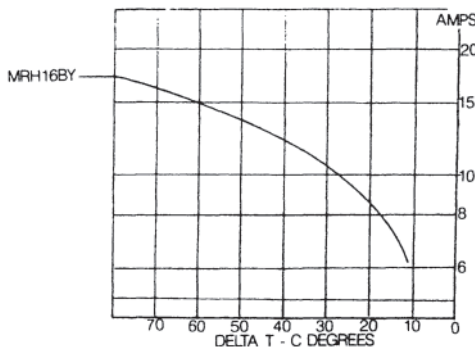


**Figure 10.37**  $\Delta T$  versus protector current for an off-winding thermal protector. (Courtesy of Texas Instruments, Inc.)

of a 2AM7CS \*0400 would also appear to be a good one since it would trip in an overloaded motor when the winding reached 127°C and the locked rotor trip time would be 5.7 seconds. However, the measured locked rotor current of the motor in Table 10.5 is 45 A and a 2AM7CS\*0400 protector has a heater current limit of 40 A. If this protector were used in the example, the heater would burn open during the 72-hour locked-rotor test or during the 15day locked-rotor endurance test described in Sections 10.11.3 and 10.11.4. Limiting heater and contact currents are shown on the thermal protector information sheets issued by the protector manufacturer.

**10.9.6 Selection of Bimetallic Thermal Protectors for Dual-Voltage Split-Phase, Capacitor-Start, Capacitor-Start/ Capacitor-Run Single-Phase Motors**

Dual-voltage motors, such as 115/230 V, are connected as in Figs. 10.38 through 10.41. Dual-voltage motors usually have two sections in the main or running winding. The sections are connected in parallel on low voltage and in series on high voltage. In others motors, poles are connected in parallel on low voltages and in series on high. The volts per turn are the same with the low and high voltage connections. In both cases, running performance is similar on either voltage connection except that the current on high voltage is half the low-voltage

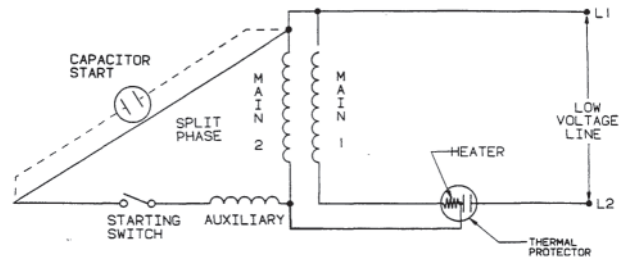


**Figure 10.38** Dual-voltage, split-phase, and capacitor-start standard low-voltage connection. (Courtesy of A.O.Smith Corp.)

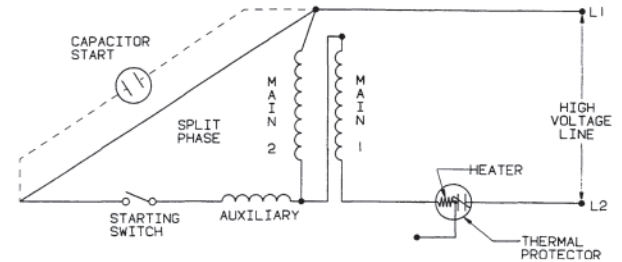


**Figure 10.39** Dual-voltage, split-phase, and capacitor-start standard high-voltage connection. (Courtesy of A.O.Smith Corp.)

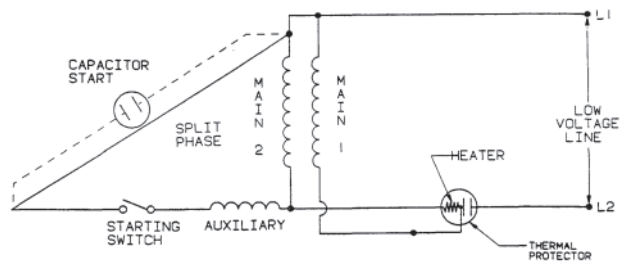


**Figure 10.40** Dual-voltage, split-phase, and capacitor-start special low-voltage connection. (Courtesy of A.O.Smith Corp.)

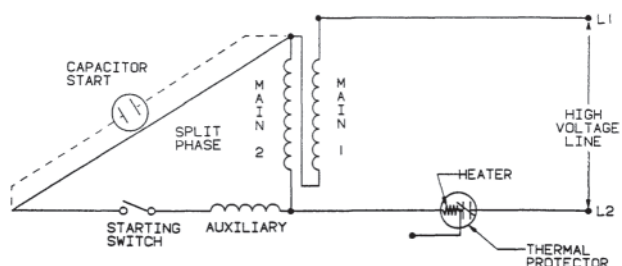


**Figure 10.41** Dual-voltage, split-phase, and capacitor-start special high-voltage connection. (Courtesy of A.O.Smith Corp.)

value. A single, low-voltage auxiliary winding is most often used, and it is connected across the line on low-voltage connection and across one section of the main winding on the high-voltage connection across. This is commonly referred to as a swing connection.

Locked-rotor torque on high voltage is less than that on low because the voltage across the main section and auxiliary winding in parallel is less than one-half the line voltage, and hence the auxiliary current is lower on the high-voltage connection. To protect such motors with a single thermal protector, a connection point is made between the bimetal and the heater element of the protector and the motor is connected so that half of the main winding current flows through the heater on the low-voltage connection. Line current flows through the heater on the high-voltage connection. See Figs. 10.38 and 10.40 for details of the connections.

In capacitor-start motors, the locked-rotor currents through the heater of the thermal protector are very nearly equal on either voltage connection. This simplifies the protector selection process. In dual-voltage split-phase motors, the currents through the heater of a thermal protector on high voltage are much greater than on low voltage under locked-rotor conditions, and this can cause great difficulty in selecting protectors. Figures 10.40 and 10.41 show a special connection that is sometimes used to increase the low-voltage heater currents in dual-voltage split-phase motor protectors. This connection is used sparingly since it requires added connection points on motor terminal boards and the connection procedure to change voltage is more complicated.

#### 10.9.6.1 Procedure

The selection of dual-voltage thermal protectors is accomplished in a manner similar to the single voltage process.

- A. The high-voltage connection is used for the initial selections.
- B. Two CM/A values are calculated for the main winding at locked rotor; the first uses high-voltage line current and the second uses half of the low-voltage main winding current. CM/A for the auxiliary winding is calculated using auxiliary current on the low-voltage connection.
- C. Maximum locked-rotor trip times are determined for the three CM/A values in (B) using CM/A vs. maximum allowable trip time data described in the single-voltage selection process. (See [D] in Section 10.9.5.1.)
- D. Determine a trip time for each protector using high-voltage locked-rotor current. Eliminate all protectors with trip times greater than the lowest of the three values in (C) and eliminate all protectors with trip times of less than 4 seconds. (See [F] in Section 10.9.5.1.)
- E. Eliminate all selections remaining in (D) that fall outside the trip time limits when the current is equal to one-half the low-voltage main winding locked-rotor current.
- F. For all selections remaining in (E), eliminate those where the heater current limits of the protectors are exceeded by currents used in (D) and (E).
- G. Line current flows through the bimetal on either voltage connection and the low-voltage line current is twice that at high voltage. If the resistance of the bimetal is high, the  $I^2R$  heating in the bimetal may be enough on the low-voltage connection to cause the protector to

trip in a very short time. To check for this possibility, examine the zero or no-heater performance curve of the protector. (See MRH00BY in Fig. 10.35, the “00” indicates no heater.) If a MRH 16BY protector were selected for a dual voltage motor with 45 A locked-rotor current on high voltage, the high-voltage trip time would be 12.5 seconds. The low-voltage line current of this motor would be 90 A. Figure 10.35 shows that a MRH00BY protector will trip in 3 seconds with 90 A through the bimetal disk. If the total locked rotor line current at low voltage produces a trip time of less than 4 seconds with no heater in the protector, the locked-rotor trip time with a heater will be unsatisfactory. Therefore, all selections from (F) with “00” trip times of less than 4 seconds are eliminated.

- H. Compare the  $\Delta T$  performance of the selections remaining in (G) with the high-voltage, running-overload performance of the motor. Determine  $\Delta T$ , EPA, winding temperature, and the motor current at the trip point for each protector. Eliminate selections where winning temperatures exceed  $T_{\max}$ .
- I. Determine motor loading for the currents at the trip points for the protectors remaining in (H) and eliminate those falling below the safety factor load (SAF).
- J. Compare the  $\Delta T$  performance of the selections remaining in (I) with the running-overload performance of the motor on the low-voltage connection. Determine  $\Delta T$ , EPA, winding temperature, and the motor current at the trip points with one-half of the line current through the heater of the protector. Again, eliminate selections that fall outside the established limits. Selections that remain will perform satisfactorily on both high and low voltages.
- K. The selection procedure for dual-voltage motors that use the special connections of Figs. 10.40 and 10.41 are similar to steps (A) through (J) except that the currents through the heaters at locked rotor are different from those used in (D), (E), and (F). These currents, determined by test or calculation, are used to modify the selection procedure.

#### 10.9.7 Selection of Bimetallic Thermal Protectors for Three-Phase Motors

A three-phase thermal protector has a single bimetal disk, three heater elements, and three sets of contacts. Three of the contacts are welded to the bimetal disk and the mating contacts are connected individually to the ends of the three heaters. A wye connection must be used in the motor. The bimetallic disk serves as the star point of the wye-connected motor. For dual-voltage applications, terminals are located between each protector heater element and its contacts so that one-half of the phase current flows through the heaters on low voltage. Heater currents are equal on high and low voltage, but the bimetallic disk current on low voltage is twice that on the high-voltage connection. A dual-voltage, three-phase protector has six terminals, compared to three for a single-voltage device.



Thermal protectors for three-phase motors are selected in a manner similar to the single-phase motor process. CM/A is calculated for the windings under locked-rotor conditions and a maximum permissible trip time is determined from CM/A versus trip time data established for three-phase motors. If three-phase data are not available, single-phase data will serve. Locked-rotor trip times of candidate thermal protectors are determined using the high-voltage connection in dualvoltage motors. The low-voltage connection must also be checked to make certain its trip time is not less than 4 seconds. Ultimate trip points,  $\Delta T$ , winding temperatures, phase current, line current, motor loading, and heater current limits are determined from motor performance data and the protector manufacturer's data.

It has been found that protectors with locked-rotor trip times of 10 seconds or less have the best chance of being acceptable if primary single-phasing thermal protection is required. Primary single-phasing tests are conducted with the motor connected to the secondary side of a three-phase transformer. The motor shaft is locked, a standard test voltage is applied to the motor terminals, and one phase lead on the primary of the transformer is disconnected. The motor thermal protector must prevent the winding from exceeding the temperature shown in Table 10.4. Three-phase motors will not start with one open primary phase. Primary single-phasing tests should be repeated, opening each phase in the primary. If limiting temperatures are exceeded, select a protector with a lower locked-rotor trip time and repeat the tests.

## 10.10 TESTING AGENCY REQUIREMENTS FOR MOTOR THERMAL PROTECTORS

### 10.10.1 General

UL Standard No. UL 2000–2001, Thermal Protectors for Motors [7], outlines requirements for inherent overheating protection for motors. This standard is limited to direct current motors and alternating current, single-, and polyphase motors rated 15 hp or less, 600 V or less, and having frame diameters of 11 inches or less. Motor insulation Classes A and B are specifically covered and provisions are made for other classes. Automatic reset, manual reset, and thermal cutoff type protectors are included. Thermal cutoff protectors must also comply with the requirements of UL 1020, Thermal Cutoffs for Use in Electrical Appliances and Components [10] and/or Canadian Standards Association CSA 22.2 No. 209, Thermal Cut-Offs [11].

Canadian Standards Association Standard C22.2, No. 77–1988, Motors with Inherent Overheating Protection [8] is essentially the same as UL 2000–2001 except that it includes limiting temperatures for insulation Classes F and H. Common UL and CSA values for insulation Classes A and B are used in this section along with CSA values for Classes F and H.

UL 2000–2001 covers motor thermal protectors, that is, inherent overheating protective devices that are responsive to motor current and temperature in order to protect the motor against overheating due to overload or failure to start. It does

not cover protective devices responsive to current alone, manually operated devices for opening motor circuits, protectors combined with motor controllers, or protectors that control relay coils in motor starters. Protectors in motors in hazardous locations, such as gasoline pump motors, and motor protectors in hermetically sealed compressor units are covered in UL and CSA standards developed for those specific applications, and are excluded from UL 2000–2001 and CSA C22.2 No. 77. These standards may also be modified by other standards for specific products and applications.

The remainder of this section and Section 10.11 contain the authors' interpretation of UL and CSA requirements currently in effect. Anyone embarking on a test program should consult the latest revisions of the standards.

### 10.10.2 Protection Types

Single- and polyphase motors may be listed at UL and CSA under several thermal protection types as follows:

- Locked-rotor only (Thermally Protected L. or T.P.L.)
- Locked-rotor and running-overload protection (Thermally Protected or T.P.)
- Locked-rotor and running no-load protection (Thermally Protected or T.P.)
- Time-rated and intermittent duty protection (Thermally Protected)

These types apply to both automatic and manual reset protectors.

### 10.10.3 Test Voltages and Frequencies

Standard test voltages have been established for certain motor voltage ratings as listed in Table 10.7. Motors with voltage ratings not included in the table will be tested at 100–105% of the rated voltage unless the intended source of supply dictates a higher test voltage. Motors with two or more voltage ratings requiring reconnection for operation at two or more voltages will be tested using each voltage connection. For example, motors rated 110/220 V will be tested at 120 V on the lowvoltage connection and at 240 V on the high-voltage connection. Motors rated 115/208–230 V will be tested at 120 and 240 V since the 208-V connection is the same as that used for 230 volts.

Test frequencies will be as specified in the motor rating.

**Table 10.7** Standard Test Voltages

Motor nameplate voltage rating (V)	Standard nominal test voltage (V)
110, 115, or 120	120
200 or 208	208
220, 230, or 240	240
265 or 277	277
440, 460, or 480	480
550, 575, or 600	600

### 10.10.4 Protector Calibration Ranges

If the thermal protector opening temperature calibration exceeds  $\pm 5^{\circ}\text{C}$  or if the closing temperature calibration exceeds  $\pm 15^{\circ}\text{C}$ , certain tests will be conducted at both extremes of the calibration ranges to determine Suitability. One protector calibrated to open at the maximum temperature will be subjected to all tests and one protector calibrated to the lowest opening temperature will be subjected to an 18-day locked-rotor endurance test. (See Sections 10.11.3 and 10.11.4.)

### 10.10.5 Temperature Measurements

UL temperature measurements are made by use of thermocouples attached to the surfaces of all windings and parts. Nothing other than the integrally applied insulation on the conductor surface and the motor insulating varnish is to be placed between the thermocouples and the conductors of the motor windings. CSA temperature measurements are made by thermocouple or by the rise-of-resistance method.

### 10.10.6 Ambient Temperature

Tests may be conducted at any ambient temperature between  $10^{\circ}\text{C}$  and  $40^{\circ}\text{C}$ .

### 10.10.7 Multispeed Motors

Motors having more than one speed connection may be tested on all speeds to check compliance.

### 10.10.8 Motor Mountings

Nonintegral parts of motors, such as blades, couplings, and brackets, will be removed during running-heating and locked-rotor tests. Resilient bases, rigid bases or feet, and gear units are not removed but are mounted on wood or other poor thermally conductive material during the tests. A motor intended for an application with a special mounting condition, such as an oil-fired furnace motor, may be mounted in a manner representing the field conditions.

## 10.11 PERFORMANCE REQUIREMENTS AND TESTS

This section lists requirements to be met and tests to be conducted.

### 10.11.1 Running Heating Tests

Motors rated for continuous duty must carry nameplate fullload current and service factor current (if a service factor is included in the motor rating) without tripping the thermal protector. Time-rated motors (for example, 1/2 hour) must carry nameplate current for the time rating without tripping.

Full-load and service factor-load temperature limits can

**Table 10.8** Maximum Ultimate Trip Current in Amperes for Motors Rated Above 1 hp

Power rating (hp)	110–120 V 1 $\phi$ /3 $\phi$	220–240 V 1 $\phi$ /3 $\phi$	440–480 V 1 $\phi$ /3 $\phi$	550–600 V 1 $\phi$ /3 $\phi$
1.0	25.0/12.2	13.6/6.1	6.8/3.1	5.4/2.4
1.5	31.2/16.2	15.6/8.8	8.5/4.4	6.8/3.6
2.0	33.6/21.2	18.7/11.6	10.2/5.8	8.2/4.6
3.0	47.6/30.0	26.5/16.3	14.5/8.2	11.6/6.6
5.0	78.4/42.6	39.2/23.7	21.8/12.9	17.5/10.4

be found in standards published for specific motor applications and are not included in CSA C22.2 No. 77, or in UL 2000–2001.

### 10.11.2 Running Overload Tests

For running overload or ultimate trip tests, the ultimate trip current is the motor current at the greatest load a motor can carry without tripping its thermal protector. The stable winding temperature at this load point is the ultimate trip temperature. Thermal protectors in motors with running overload protection must trip under overload conditions before the windings exceed  $T_{\text{max}}$ .  $T_{\text{max}}$  is  $140^{\circ}\text{C}$  for Class A insulation,  $165^{\circ}\text{C}$  for Class B insulation,  $190^{\circ}\text{C}$  for Class F insulation, and  $215^{\circ}\text{C}$  for Class H insulation. Tests are conducted by loading a motor at full-load or service factor-load current with the appropriate test voltage applied and allowing the winding temperatures to stabilize. The load is then increased in steps of 0.1 or 0.2 A. Temperatures are stabilized at each step and the procedure is followed until the thermal protector trips. Ultimate trip current and temperature are those at the test condition immediately preceding the trip point.

Maximum ultimate trip currents for motors rated more than 1 hp are listed in Table 10.8. These limiting currents do not apply to polyphase motors operating under single-phasing conditions.

In air-over, direct-connected fan applications, motors must operate in the air stream in order to meet temperature limits for normal operation. For these motors, the thermal protectors must trip before the windings exceed the temperatures in column 1 of Table 10.9. Tests are conducted at no-load with the fan removed and the shaft running free. If the thermal protector does not trip under these conditions, the winding temperatures cannot exceed the temperatures in column 2 of Table 10.9.

**Table 10.9** Winding Temperature Limits for Direct-Connected Fan Applications

Column 1 Protector trip ( $^{\circ}\text{C}$ )	Insulation class	Column 2 No load, no trip, max. temp. ( $^{\circ}\text{C}$ )
140	A	150
165	B	175
190	F	200
215	H	225

Winding temperatures of intermittent-duty and time-rated motors cannot exceed 140°C for Class A insulation, 165°C for Class B insulation, 190°C for Class F insulation, and 215°C for Class H insulation. To check compliance, a motor at room ambient temperature is loaded to nameplate current at the applicable test voltage. If the protector trips, the elapsed time must exceed the time rating of the motor. If the protector does not trip, the motor load is increased in 0.1- or 0.2-A steps and the temperatures are stabilized. This procedure continues until protector trip occurs.

If the protector trips when an intermittent-duty motor is loaded at rated current and at the required test voltage, the motor is allowed to cool. When the thermal protector resets, the motor is operated at the test voltage with no load applied. If the protector trips under no-load conditions, the trip time and temperatures are recorded and the motor is again allowed to cool. When the protector resets, the line voltage is reduced and the motor is operated at no load until the protector trips. The voltage is reduced until a condition is reached where the protector does not trip. Data from these tests are used to establish a maximum duty cycle for the intermittent-duty motor.

### 10.11.3 Locked-Rotor Tests

Automatic reset protector tests under locked-rotor conditions begin with a motor at room ambient (10°C to 40°C). The motor shaft is locked so that it cannot turn and the test voltage, measured at the motor terminals, is applied. Since this test is conducted for 72 hours, recording instruments are used to measure elapsed time, motor terminal voltage, motor line current, winding temperatures (all windings), thermal protector trip times or thermal cutoff points, thermal protector reset time, and ambient temperature. During the 72-hour test, permanent damage to the motor or the introduction of a fire hazard is unacceptable. Permanent damage includes deterioration of the insulation systems such as charring, brittleness, melting or destruction of insulating barriers, grounding of windings, flashover to the frame, severe or prolonged smoking or flaming, and electrical failure of components such as capacitors and relays. Insulation that flakes or comes off when windings are rubbed with a thumb is unacceptable, but discoloration of the winding insulation is permitted. Locked-rotor temperature limits during these tests are listed in [Table 10.4](#).

Average temperature is calculated by adding all peak temperatures and all minimum temperatures recorded during the 2nd and the 72nd hours and dividing by the number of included points. A motor that employs a capacitor mounted separately from the motor will be locked-rotor tested with the capacitor in the circuit or with the capacitor terminals shortcircuited, whichever is the more severe.

Testing specifications for locked-rotor thermal cut off protectors require that three thermal cutoff protectors be tested on each voltage and on each speed connection. Locked-rotor temperature limits for thermal cutoff protectors are shown in [Table 10.4](#).

Locked-rotor tests for a motor with a manual reset protector begin with the motor at ambient temperature. The manual

reset protector is tripped and reset 10 times with the rotor locked. The protector is reset as quickly as possible after each trip. The reset button is operated manually during this test and is not clamped or otherwise prevented from tripping and resetting normally. Locked-rotor winding temperature limits for manually reset protectors for each insulation class are also shown in [Table 10.4](#). Manual reset thermal protectors shall not reset automatically at temperatures higher than -5°C.

### 10.11.4 Locked-Rotor Endurance Test

In addition to the 72-hour locked-rotor test described in the preceding subsection, motors with automatic reset thermal protectors must complete a 15-day locked-rotor endurance test. At the end of 15 days, no permanent damage to the motor, including deterioration of the insulation as described in the 72-hour test, is permitted. An automatic reset protector may permanently open the circuit during this test provided it was specifically designed to do so and testing of three samples shows that the protectors operate consistently. For the endurance test at UL, the motor enclosure is connected to the power supply ground through a 30-A non-time-delay cartridge fuse. Opening of the fuse constitutes a test failure. CSA specifications are similar except that a 3.0-A fuse is used.

For a motor rated more than 1.0 hp, the thermal protector must complete 2000 cycles in the combined 72-hour locked-rotor test and the 15-day endurance test. If 2000 cycles are not completed in that time interval, additional testing is required until 2000 cycles are completed. Additional testing can be accomplished by continuing the 15-day endurance test or by testing the protector separately. No permanent damage to the motor or to the protector as described in the preceding section is permitted as a result of this test.

### 10.11.5 Dielectric Tests

UL requires that motors rated 0.5 hp or less and 250 V or less withstand a dielectric test of 1000 V to ground for 1 minute without breakdown. All other motors are subjected to a voltage of 1000 V plus twice rated motor voltage. The voltage is increased rapidly and uniformly from zero to the test voltage and then held for 1 minute. CSA requires 1000 V plus twice rated voltage on all motors. See [Chapter 8](#) for more detailed information.

### 10.11.6 Limited Short-Circuit Tests

Limited short-circuit tests are conducted to ensure that no fire hazard will occur if there is a short circuit through the motor/thermal protector combinations. The amount of shortcircuit current varies with the horsepower and voltage ratings of the motor being tested because the capacity of the power source normally varies with the size of the load connected to it.

Limited short-circuit tests may be conducted with protectors mounted inside the motor or with protectors alone in the circuit. Protectors are connected to a nonrenewable, nontime-delay cartridge fuse rated at a minimum of 20 A for 150 V or less and 15 A for 151 to 600 V. The fuse must be rated for at least 4 times the motor nameplate current. The outer enclosure

**Table 10.10** Limited Short-Circuit Current Tests

Motor power rating (hp)	Motor voltage rating (V)	Limited short-circuit current (A)
0.5 or less	250 or less	200
>0.5 to 1	250 or less	1000
>1.0 or less	>250	1000
>1.0 to 3	250 or less	2000
>1.0	>250	5000
>3.0 to 7.5	250 or less	3500
>7.5	250 or less	5000

of the protector or the motor is wrapped in cotton gauze. Short-circuit currents are passed through the protector as listed in Table 10.10. The protector may cycle during the test and the test is continued until the fuse blows or the protector permanently opens the circuit. No ignition of the cotton gauze is permitted during the limited short-circuit test.

## REFERENCES

Note: In the following listing, abbreviations have the following meanings:

ANSI American National Standards Institute  
 CSA Canadian Standards Association

IEEE Institute of Electrical and Electronics Engineers  
 NEMA National Electrical Manufacturers Association  
 NFPA National Fire Protection Association  
 UL Underwriters Laboratories, Inc.

Sources for standards are listed in [Appendix B](#).

1. ANSI/NEMA Standards Publication No. MGI-1998, Motors and Generators.
2. IEEE Power Systems Engineering Committee, "Report of Large Motor Reliability Survey of Industrial and Commercial Installations. Parts I and II," *IEEE Transactions on Industry Applications*, Vol. 1A-21, No.4, July/August 1985, pp. 853–872.
3. Brighton, P., and P.Renade, "Why Overload Relays Don't Always Protect Motors," *Siemens-Allis Bulletin CP 3821*, 1981.
4. Cummings. P.G., J.R.Dunke-Jacobs, and R.H.Kerr, "Protection of Induction Motors Against Unbalanced Voltage Operation," *IEEE Transactions on Industry Applications*, May/June 1985.
5. Elmore, W.A., "Some New Thoughts on Large Motor Protection," *Silent Sentinels RPL 76-2*, Westinghouse Electric Corporation, 1976.
6. NFPA 70, 2002 National Electrical Code.
7. ANSI/UL 2000–2001, Thermal Protectors for Motors.
8. CSA C22.2 No. 77–1998, Motors with Inherent Overheating Protection.
9. Veinott, C.G., and L.C.Schaefer, "Fundamental Theory of Inherent Overheating Protection under Running Overload Conditions," *Transactions of the American Institute of Electrical Engineers*, Vol. 68, 1949, p. 266.
10. UL 1020, Thermal Cutoffs for Use in Electrical Appliances and Components.
11. CSA 22.2 No. 209—Thermal Cut-Offs.

# 11

## Mechanical Considerations

**Peregrin L.Timár and Sheo P.Verma** (Sections 11.1, 11.1.1, 11.1.5, 11.2, and 11.2.1)/**Robert G.Bartheld** (Sections 11.1.2–11.1.4, 11.2.2–11.2.5, and 11.3)/**Paul L.Cochran** (Section 11.4.1)/**Walter E.Littmann** (Section 11.4.2)/**National Electrical Carbon\*** (Section 11.5)/**Chauncey Jackson Newell** (Section 11.6)

<b>11.1 NOISE</b>	<b>548</b>
11.1.1 Noises of Electromagnetic Origin	551
11.1.2 Influence of Motor Configuration and Design	554
11.1.3 Regulation of Noise: Typical Levels	555
11.1.4 Reduction of Noise Levels: Special Treatment	560
11.1.5 Experimental Investigation of Noise	561
<b>11.2 VIBRATION</b>	<b>566</b>
11.2.1 Vibration Measurement and Evaluation	568
11.2.2 Housing and Shaft Vibration	571
11.2.3 Mounting	572
11.2.4 Variable-Speed Motors	572
11.2.5 Standards	573
<b>11.3 BALANCING THE ROTOR</b>	<b>575</b>
11.3.1 Rigid Rotors	575
11.3.2 Flexible Rotors	575
11.3.3 Unbalance Quality	576
<b>11.4 BEARINGS</b>	<b>576</b>
11.4.1 Sleeve Bearings	576
11.4.2 Antifriction Bearings	591
<b>11.5 BRUSHES</b>	<b>596</b>
11.5.1 Introduction	596
11.5.2 Grade Characteristic Definitions	597
11.5.3 Specialty Brushes	601
11.5.4 Summary	602
<b>11.6 MOTOR HANDLING, MOUNTING, AND MECHANICAL CONNECTION</b>	<b>602</b>
11.6.1 Motor Handling	602
11.6.2 Motor Mounting Dimensions	603
11.6.3 Shaft Connections—Belts	610
11.6.4 Shaft Connections—Chain and Sprocket Drives and Flat Belt Drives	613
11.6.5 Shaft Connections—Couplings	613
11.6.6 Shaft Connections—Splines	614
11.6.7 Initial Operation	614
<b>REFERENCES</b>	<b>614</b>

---

\* The National Electrical Carbon Group includes Kenneth A.Bruni, Richard D.Hall, George G.Kalinovich, and Roland Roberge.

### 11.1 NOISE

Noise is an audible sound or a mixture of sound that has an unpleasant effect on human beings, disturbs their ability to think, and does not convey any useful information. This definition clearly implies that noise is a subjective concept, associated with human beings.

In general, the unpleasantness and disturbing effect of sound is related to its uncertainty and the overall random nature of the environment. For example, an electric motor may be called “silent” if the noise produced by the milling machine or blower driven by the motor is louder than the motor’s own noise by at least 10 dB. On the other hand, almost any electric motor would be characterized as noisy in a watchmaker’s shop. The operation of an elevator may be unnoticed during the day when environmental noise is high, but one’s rest is disturbed by it during the night when environmental noise is low. An added complication is that the hearing response curve differs from one person to another, and the curve for any one person changes with age [1].

Standards of noise measurement are used in an attempt to provide a certain degree of objectivity when assessing the subjective concept of noisiness. Noise-measuring systems model the average human hearing (e.g., by using the A-weighting network), and the standards set noise limits for various kinds of electric machines. These limits, however, are not derived from physical laws but rather reflect the typical technical level at a given time. This clearly implies that the mere fact that an electric machine complies with standards as far as its noise characteristics are concerned does not necessarily mean that it is considered to be silent under all circumstances or at all times. The acoustic phenomenon produced by the electric machine is an undesirable concomitant of the energy-transforming function of the

machine, and is considered as noise, regardless of its magnitude, nature, or spectrum.

Noise is an undesirable environmental phenomenon, and has a doubly adverse effect on everyone subjected to it. If sufficiently intense, it will damage the organs of hearing; even at more moderate levels it may induce a vegetative nervous system reaction. Because noise reduces human performance, it gives rise indirectly to economic losses.

By the end of the 1960s, engineers had achieved substantial progress in decreasing steady-state noise levels due to electromagnetic exciting forces [2–4]. Attention was then turned to noise of aerodynamic origin, that is, to ventilation noise. The problem of aerodynamic noise had been exacerbated by increased exploitation of active materials in motors, which in turn resulted in increased losses and consequently created an increased demand on the ventilation system [5].

Solid-state drive systems, which first appeared in the 1970s, have created new problems as a result of the time harmonics of voltage present at the motor terminals, which in many cases considerably enhanced the noise level generated by the machine. Currently, engineers encounter new challenges, such as short-time noise phenomena occurring during transient operation of electric machines and the measurement techniques required to quantify these phenomena [6]. Specifications on noise levels of electric machines are becoming increasingly stringent and wider in scope because of the importance of noise reduction for reasons of health, economy, and productivity.

The objects, elements, and human beings involved in the noise generation process, from the subjective point of view, constitute a well-defined, clear-cut system, as shown in Fig. 11.1. This system consists of three major sections. On the left side is the noise source, a device that generates vibrational energy. On the right side, the noise is perceived by a human

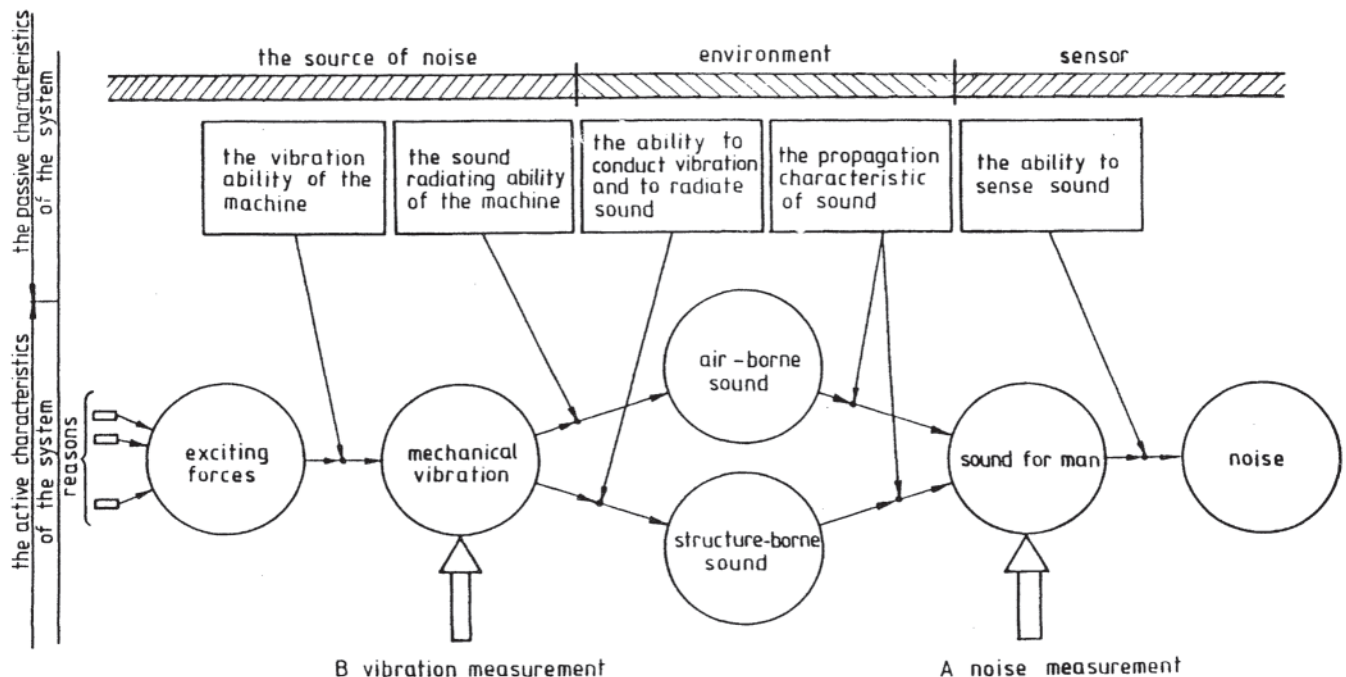


Figure 11.1 Flow chart showing the generation of noise by an electric machine.

being or sensed by a measuring instrument. Between source and sensor, there is the so-called ambient, the medium that connects them.

The characteristics of this system may be divided into two main groups. Parameters that are independent of time are called passive parameters. These parameters of the system determine the response of the system to outside interference. They are determined by the geometry, materials, and other conditions of the system or its components. The active parameters include physical phenomena that vary with time and influence the passive parameters.

In Fig. 11.1, a circle is used to designate each of the active system parameters and a rectangle for each passive parameter. Arrows indicate the causal relations and the process flow. At the starting point of the system, there are causes that give rise through complex interactions to exciting forces. Because the exciting forces are periodic in nature, the use of Fourier series allows the forces to be expressed as the sum of numerous sinusoidal waves. Any exciting force can be characterized by its amplitude, mode number (vibration mode), frequency, and angular position. These exciting forces give rise to the vibratory motion characteristic of a driven mechanical system.

The vibrating capability of the electric machine can be thought of as a transfer function of the system, since the exciting force applied at the input produces vibration at the output. The vibrating capability of the machine is a function of the mode number and the frequency. At least one natural frequency of the machine corresponds to each vibration mode. Of course, the most adverse (and possibly dangerous) situation is the one where the frequency of the periodic exciting force is identical with or close to one of the resonance frequencies of the machine.

Part of the vibrational energy within the audible range is transformed directly into airborne sound energy. The "efficiency" of this transformation depends on the radiating ability of the machine, which is in turn dependent on the mode number and the frequency [5]. The radiation coefficient appears as a term in the equation describing the sound-radiating capability of the machine.

The acoustic properties of the surroundings determine how much of this power is transmitted to the observer and how it is transmitted. The end point of the process is perception of noise by the human ear. The human response is determined by the ear, with its own transfer characteristic, which is dependent on frequency, sound intensity, and exposure time. The human response is also affected by one's mental state.

A second, and probably major part of the vibrational energy in the audible range is transmitted to the surroundings by the mechanical connection between the machine and its environment through the base plate or mounting flange, the shaft, or even through a vibration damper. This energy is known as structure-borne sound. The transmission process spreads the vibrational energy through the structure. Lighter elements, especially those with large surface area, act as secondary radiators, the end product again being airborne noise that adds to the airborne noise emitted directly by the machine. The two components together make up the actual noise.

Measurement of noise in the proximity of a machine (as at

A in Fig. 11.1) always results in a measurement of the combined noise. Care must be taken in the evaluation of the resulting data. The airborne sound power of the electric machine depends quite unambiguously on the parameters and working condition of the machine. The airborne sound power measurement gives reproducible results and thus can be taken as a well-defined parameter of the machine. However, the sound resulting from the structure-borne energy depends greatly on the elements that conduct the structure-borne sound and on the nature of assembly and installation. Hence, when a noise measurement of an electric machine is given, it refers only to the airborne sound power, every effort having been made to reduce the structure-borne sound to negligible levels. However, when measuring the operational noise of a machine in a specific situation, the resultant noise level is wanted, independent of the place of origin or the path of propagation. It is this level that is of significance when considering the effect on a worker.

If the vibrational effect on the mechanical environment of the electric machine is the main reason for examination, then vibration has to be measured at B in Fig. 11.1. In engineering and vibration safety measurements, the low-frequency part of the vibration energy of the machine is measured (in the 10–1000 Hz range), and this is called the vibration measurement of the machine. Noise and vibration measurements of electric machines complement each other, the same group of phenomena being examined for the same machine, but from different points of view and with different methods. By measuring both the noise and the vibrations, information is obtained on the vibro-acoustic condition of the electric machine.

Before examining the machine in detail from a noise point of view, it is advisable to summarize the basic concepts in acoustics, especially since these concepts are usually not part of the everyday practice of the electric power engineer.

The sound power radiated by electric machines covers a very large range, from that radiated by the quiet motor of a cassette player ( $\sim 10^{-9}$  W) to that from a high-power, high-speed machine ( $\sim 10^3$  W). Moreover, the human ear can sense sound pressures from 20  $\mu$ Pa to 20 Pa (the threshold of feeling). These are wide dynamic ranges. If the fact that the human ear responds in a logarithmic or near-logarithmic manner to changes in sound pressure is taken into account, it is seen that a logarithmic measure will yield more meaningful data. The use of a logarithmic measure requires that a reference value be established against which the measured variable may be normalized so that the argument of the logarithm is dimensionless.

The measurements of sound level used are:

$$L_W = 10 \log_{10} \left( \frac{P}{P_0} \right) \quad \text{the sound power level in dB}$$

where:

$P$  = the radiated sound power

$P_0 = 10^{-12}$  W, the reference level

or alternately:

$$L_p = 20 \log_{10} \left( \frac{p}{p_0} \right) \quad \text{the sound pressure level in dB}$$

where:

$p$ =the effective value of the sound pressure at a given point  
 $p_0=20 \mu\text{Pa}$ , the reference level

Using these measures, it is found that the human ear cannot sense changes below 1 dB.

If the electric machine is enveloped by a closed surface of any optional shape, the radiated sound power may be calculated from:

$$P = \oint_s \bar{I} d\bar{S} \tag{11.1}$$

where:

- $P$ =sound power
- $\bar{I} = p\bar{v}$ =the sound intensity vector
- $S$ =the closed surface enveloping the machine
- $d\bar{S}$ =the surface element vector
- $p$ =the sound pressure and
- $\bar{v}$ =the velocity vector of the particle propagation of sound

At a sufficient distance from the machine radiating the sound, the equation:

$$v = \frac{P}{\rho c}$$

relates the pressure of the sound wave and the velocity of the particle,  $\rho$  being the density of the air, and  $c$  being the velocity of the propagation of sound in air. Hence the sound intensity may be considered to be a scalar quantity given by:

$$I = \frac{p^2}{\rho c}$$

If the machine radiates sound uniformly in all directions, Eq. 11.1 may be simplified:

$$P = \frac{p^2}{\rho c} S \tag{11.1'}$$

Equation 11.1' may be written for the reference values as well. If this is done, the following relationship may be developed relating sound power and sound pressure levels:

$$L_W = L_p + 10 \log_{10} \left( \frac{S}{S_0} \right) + 10 \log_{10} \left( \frac{\rho c}{\rho_0 c_0} \right) \tag{11.2}$$

where:

- $S_0=1 \text{ m}^2$
- $c_0=344 \text{ m/sec}$

For noise measurements made at room temperature,  $\rho c=\rho_0 c_0$  is a very close approximation, and the last term of Eq. 11.2 disappears.

When making acoustical calculations using sound levels, the physical meaning should always be considered. Summing, subtracting, and calculating averages are not just simple arithmetic operations. If there are  $n$  different sound pressure levels,  $L_{p1}, L_{p2}, L_{p3}, \dots, L_{pwn}$  the resultant sound pressure level is given by:

$$L_{pres} = 10 \log_{10} \sum_{i=1}^n 10^{0.1L_{pi}} \tag{11.3}$$

The average of the  $n$  sound pressure levels is:

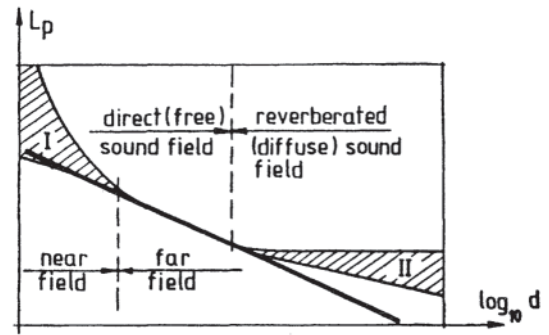


**Figure 11.2** Variation of the sound pressure level as a function of the distance ( $d$ ) from the sound source.

$$\bar{L}_p = 10 \log_{10} \left( \frac{1}{n} \sum_{i=1}^n 10^{0.1L_{pi}} \right) \tag{11.4}$$

The difference between two levels of sound pressure is

$$L_{pdif} = 10 \log_{10} (10^{0.1L_{p1}} - 10^{0.1L_{p2}}) \tag{11.5}$$

Assuming the ideal spherically symmetric sound radiator, the sound pressure level at distance  $d$  from the sound source can be given if the conditions surrounding the source are ideal, that is, if there is no sound source other than the machine being measured and there is no sound reflecting surface nearby. That is:

$$L_p(d) = L_W - 20 \log_{10} \left( \frac{d}{d_0} \right) - 8 \tag{11.6}$$

where  $d_0=1 \text{ m}$ .

In this ideal case, the sound pressure level changes as a function of distance  $d$  as shown by the heavy line in Fig. 11.2. For twice the distance, there is a decrease of 6 dB. However, the acoustic field surrounding the sound source is in reality not ideal. The first uncertainty is shown by the area denoted in the figure by I. If the measuring microphone is too near the sound source, the velocity vectors of the particles and the sound pressure wave are not in phase, and in the case of electric machines with complicated shapes, the direction of propagation near the sound source may differ from the radial direction at a given point in the sound field. These phenomena result in what is called the near-field effect or near-field error. The usual result is that the measuring microphone senses greater pressure than would be expected on the basis of the radiated sound power and the distance from the machine. That section of the sound field where the near-field error appears is called the acoustic near field, and it is not advisable to measure noise in that region. That section of the sound field where the near-field error does not appear is called the acoustic far field, and is the region in which noise measurements should be made.

Measurement of noise is usually made in a closed sound field (for example, a workshop) where the wall surfaces surrounding the sound source reflect the sound waves with some damping, and the wall surfaces are some distance from the source and the measuring apparatus. If these reflected sound waves raise the level of sound pressure significantly, the resulting field is called a reflected or diffuse acoustic field; if



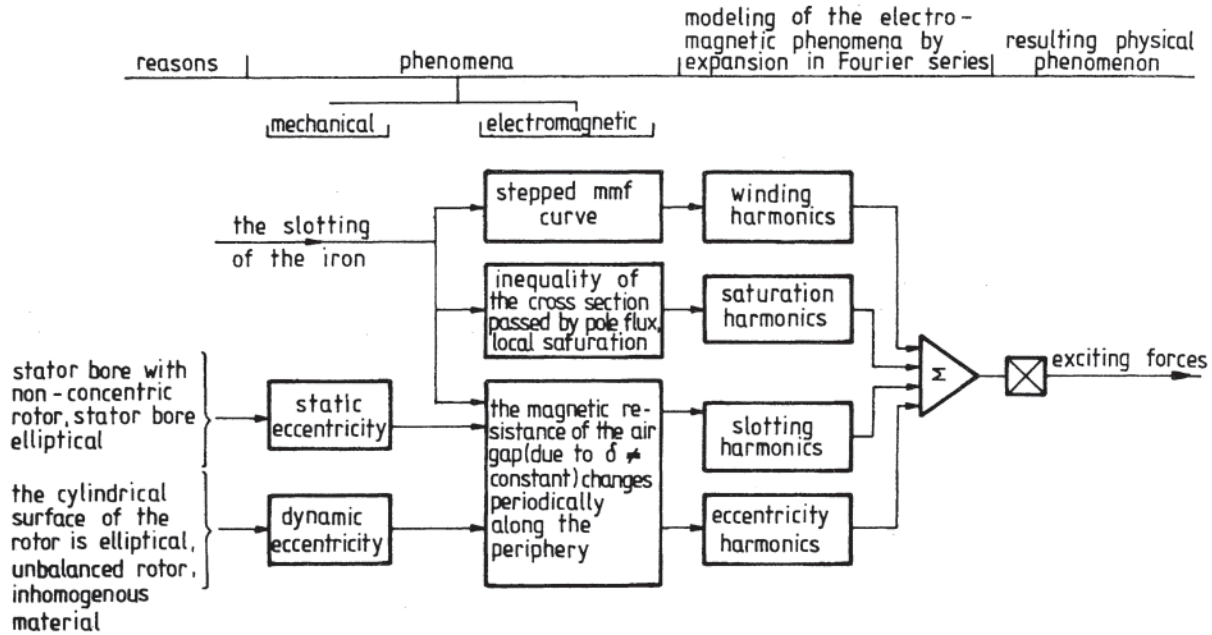


Figure 11.3 Generation of exciting forces from electromagnetic origins.

the sound waves directly radiated from the source are the dominant elements, the field is referred to as a direct or free sound field. Because of the reflected sound waves, the level of sound pressure in the area denoted II in Fig. 11.2 rises to a level given by:

$$L_p = L_w + 10 \log_{10} \left( \frac{S_0}{S} + \frac{4}{A} \right) \quad (11.7)$$

where:

- $A = \bar{\alpha}S_v$ =the absorption number of the room ( $m^2$ )
- $\bar{\alpha}$ =the medium absorption factor of the enveloping surfaces of the room in which the measurements are being made
- $S_v$ =the area of the enveloping surfaces of the room ( $m^2$ )

The absorption number  $A$  may be calculated to a close approximation from the volume  $V$  and the reverberation time  $T$  of the room, where  $T$  is the time for the sound pressure level to fall by 60 dB after switching off a test sound source (not the machine under consideration).  $A=0.164V/T$ , where  $V$  is in cubic millimeters and  $T$  is in seconds.

Equation 11.7 may be rewritten as:

$$L_p = L_w - 10 \log_{10} \left( \frac{S}{S_0} \right) + 10 \log_{10} \left( 1 + \frac{4S_0}{A/S} \right) \quad (11.7')$$

If the machine does not create a spherical field, a direction factor  $D$  may be included in the last term of Eq. 11.7' as follows:

$$10 \log_{10} \left( D + \frac{4/S_0}{A/S} \right) \quad (11.7'')$$

According to international agreement, the sound power level is referred to as the acoustic characteristic of the noise source in electric machines. It is determined by measuring the level

of sound pressure taking into consideration the acoustic conditions (for example, the reflected sound field) and the geometric dimensions of the measured surface as well as of the machine.

### 11.1.1 Noises of Electromagnetic Origin

In Section 4.1, radial force waves acting on the rotating electric machine were determined. These forces were found to be waves of different mode numbers and different distribution in the air gap around the periphery. The waves propagate with different angular velocities around the rotor, some in the same sense as the rotor rotation and some in the opposite sense, and they act on both rotor and stator. The development of the exciting forces in induction motors is summarized in Fig. 11.3.

With the exception of the bending force wave of mode number  $r=1$ , all exciting forces result in a significant deformation of the stator. For  $r=1$ , the rotor seems to be more flexible. Bending forces of mode number  $r=1$  present the greatest problem in high-power rotating machines with a flexible rotor and large bearing span. (A rotor is called "flexible" if its first critical speed\* is below or just above the rotational speed of the rotor.) The calculation of critical speeds for such machines is feasible using the section matrix method run on digital computers.

\* Any frequency at which a structure (mechanical structure or an electrical circuit) will oscillate if excited by an impulse function will be designated as a natural frequency. When the structure has internal damping, the frequency is the damped natural frequency, usually referred to in practice as the resonance frequency. When the structure has no internal damping, the frequency is the undamped natural frequency, usually referred to as an eigenfrequency. In the case of rotating bodies, such as a shaft, 60 times the resonance frequency gives the first critical speed (in revolutions per minute).

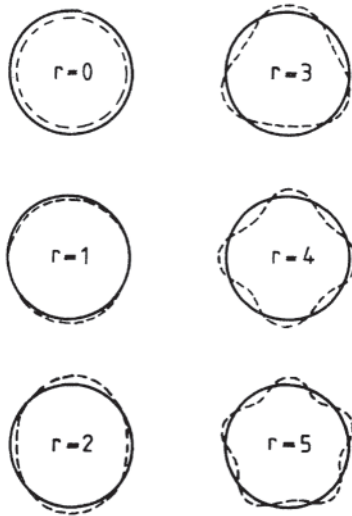


**Figure 11.4** Vibration patterns with various mode numbers.

Any force wave of frequency  $f_r$  and mode number  $r$  gives rise to a set of vibrations of order  $j$  and frequency  $f_r$  in the rotating electrical machine. The instantaneous values of the deformational waves are shown in Fig. 11.4 for different vibrational mode numbers. The magnitudes of the vibration components depend on the geometric dimensions of the machine, on the magnitude of the exciting force, on the difference between the frequency  $f_r$  of the exciting force and the resonance frequencies  $f_{resj}$  and on the damping conditions inside the machine.

If the frequency  $f_r$  of the exciting force is close to or equal to any of the resonance frequencies  $f_{resj}$  of the machine, then resonance occurs, which results in potentially dangerous deformations and vibration and a substantial increase in noise. The rms value of the vibrational velocity produced by a force wave with amplitude  $P_r$ , frequency  $f_r$ , and mode number  $r$  is given by:

$$v_{fr} = \sqrt{2} \pi f_r \sum_j H_j P_r \quad (11.8)$$

where:

$H_j$  = the system function of the electrical machine as a vibrating mechanical system.

The crucial step in the calculation of the system function is the determination of the correct value of the resonance frequency.

Resonance may occur in steady-state operation (at constant speed) or may occur in transient operation. The equation for the frequency of the electromagnetic exciting forces in the induction motor, for instance, shows that the value of  $f_r$  changes linearly with the speed.

Therefore, resonance may occur during the acceleration period even in cases where the resonance frequency of the machine in steady-state operation is much lower than the frequency of the exciting force. In other words, the smoothly running machine might “roar up” during the acceleration period. This transient resonance may show up under other types of transient operating conditions, such as reversing, or in the generator braking mode of multispeed motors.

Based on theoretical considerations and practical experience, the force waves classified as dangerous in terms of vibration or noise can be selected on the basis of their mode number and frequency. Low- and medium-power induction machines prove to be extremely rigid against force waves with mode number greater than six; therefore one can neglect these force waves in analysis. From experience, the following frequency ranges must be considered for induction machines:

For noise:  $200\text{Hz} < f_r < 6000\text{ Hz}$

For vibration:  $10\text{Hz} < f_r < 2000\text{ Hz}$

For a rough estimate of the resonance frequencies of ac rotating machines, assuming an ideal symmetrical stator, consult the formulas in Ref. 4.

The system function  $H_j$  introduced in Eq. 11.8, which represents the relationship between the force acting on the system and the resulting vibration deformation, is divided into two components. These are commonly found in the literature. One of them,  $H_{js}$ , contains the geometrical dimensions of the machine, the quality of the material, and the deformation mode number  $j$ . This component provides the deformation for the case when the mode number  $r$  of the exciting force equals the ordinal; of deformations and the frequency  $f_r$  is zero, that is, the deforming force does not vary in time.

The second component,  $H_{jn}$ , depends on the separation between  $f_r$  and the resonance frequency  $f_{resj}$  that is characteristic of the vibration mode,  $r=j$ , and on the internal damping conditions. The  $H_{jn}$  component is sometimes referred to as the magnification factor. The two components of the system function  $H_j$  are shown in Table 11.1, together with the formula for the resonance frequency corresponding to the individual vibration modes.

It is worth noting that the propensity for vibration of the machine increases with increasing size; the resonance frequencies become lower so that the resonance frequencies corresponding to higher mode numbers appear within the audible range.

The main source of damping is the friction between the contacting surfaces of the winding and the laminated core. The theoretical determination of the damping factor is extremely complex; it is therefore usually obtained experimentally. For induction motors, the damping factor is generally in the range of 0.01 to 0.03.

The sound power radiated by the electric machine into the environment by vibration of magnitude  $v_{fr}$  at frequency  $f_r$  can be calculated as follows:

$$P_{fr} = \rho c \sigma v_{fr}^2 S_{rad} \quad (11.9)$$

where

$\sigma$  = the radiation coefficient

$v_{fr}$  = the effective value of the mechanical vibration velocity measured on the surface of the machine (see Eq. 11.8)

$S_{rad}$  = the area of the machine surface contributing to sound radiation.

Because electric machines have complex shapes, determining

**Table 11.1** The Characteristic Function of the System of Small- and Medium-Horsepower Alternating Current Machines

Ordinal	$H_{js}$ The static factor of the characteristic function of the system	$H_{jn}$ The magnifying factor	$f_{resj}$ The mechanical natural frequency
$r = 0$	$\frac{R_s R_{yav}}{E \cdot h_y}$	$\frac{1}{\left\{ \left[ 1 - \left( \frac{f_0}{f_{res0}} \right)^2 \right]^2 + \left( 2D_{s0} \frac{f_0}{f_{res0}} \right)^2 \right\}^{1/2}}$	$f_{res0} = \frac{83750}{R_{yav} \sqrt{\Delta}}$
$r = 1$	$\frac{4R_r l l_r^3}{3d^4 E}$	$\frac{1}{\left\{ \left[ 1 - \left( \frac{f_1}{f_{res1}} \right)^2 \right]^2 + \left( 2D_{r1} \frac{f_0}{f_{res1}} \right)^2 \right\}^{1/2}}$	$f_{res1} = \left( \frac{3}{16\pi} \frac{Ed^4}{M_r l_r^3} \right)^{1/2}$
$r = 2$	$\frac{12R_s R_{yav}^3}{E(j^2 - 1)^2 h_y^3}$	$\frac{1}{\left\{ \left[ 1 - \left( \frac{f_r}{f_{resj}} \right)^2 \right]^2 + \left( 2D_{sj} \frac{f_r}{f_{resj}} \right)^2 \right\}^{1/2}}$	$f_{resj} = f_{res0} \left[ \frac{B}{2A} \left( 1 \pm \left( 1 - \frac{4AC}{B^2} \right)^{1/2} \right) \right]^{1/2}$

$R_s$  = the radius of the stator bore  
 $R_{yav}$  = the average radius of the stator yoke  
 $h_y$  = the height of the stator yoke  
 $E$  = the modulus of elasticity in iron  
 $R_r$  = the external radius of the rotor lamination  
 $l$  = the length of the rotor lamination  
 $l_r$  = bearing span  
 $d$  = diameter of shaft  
 $D_s$  = the internal damping of the stator  
 $D_r$  = the internal damping of the rotor  
 $G_t$  = the weight of the stator teeth  
 $G_w$  = the weight of the stator windings  
 $G_y$  = the weight of the stator yoke  
 $j$  = ordinal  
 $l_r$  = the tooth-length of the stator  
 $b_t$  = the average width of the stator tooth

$S_1$  = the number of slots in the stator.

$$\Delta = 1 + \frac{G_t + G_w}{G_y}$$

$$A = 1 + \frac{h_y^2}{12R_{yav}^2} \left[ j^2 \left( 3 + \frac{\Delta_m}{\Delta} \right) - 3 \right]$$

$$B = \frac{h_y^2}{12R_{yav}^2} (j^2 - 1) \left[ j^2 \left( 4 + \frac{\Delta_m}{\Delta} \right) + 3 \right] + (j^2 + 1)$$

$$C = \frac{h_y^2}{12R_{yav}^2} j^2 (j^2 - 1)^2$$

$$\Delta_m = 1 + \frac{S_1}{2\pi} \frac{l_r h_t}{R_{yav} h_y^3} (4l_r^2 + 6l_r h_y + 3h_y^2)$$

$$M_r = 2\pi 10^3 [(4R_r^2 - d^2) + l_r d^2]$$

the value of  $S_{rad}$  in the case of some electric machines is quite difficult. From experience, the role of ribs in emitting sound is not significant; thus  $S_{rad}$  may be calculated from the cylindrical or rectangular surface enveloping the machine.

The sound radiation coefficient may be determined for simplified models. In Ref. 7, the machine is considered to be an infinitely long cylinder. This model gives a satisfactory result only for the central section of long machines with a large  $l/D$  ratio, where  $l$  is the length of the assembled machine and  $D$  is the diameter of the cylinder enveloping the machine. With this model, the end effect due to the finite length of the cylinder can be neglected. Reference 8 assumed a spherical model to be suitable. If the surface of the machine is made of large planes, such as the rectangular shape frequently used today, it is sufficient to assume that the machine is a plane radiator.

The most characteristic dimension of the machine is the diameter  $D$  of the cylinder enveloping the machine. The force waves causing the vibration, which deform the machine, brings about a deformation going around the external diameter  $D$  of the cylinder. This dimension is used as the diameter of the cylinder for the cylindrical radiation model; if a spherical

radiation model is used, diameter  $D$  is the diameter of the radiating sphere.

The radiation coefficient is usually described by a complicated formula. For example, in the case of the ideal spherical radiator with ordinal  $r$ , the formula is:

$$\sigma_r = \text{Re} \left\{ \frac{jkd}{2} \frac{\sum_{i=1}^{r-1} \frac{(r+i)!}{(r-i)!} \frac{r!}{i!} (jkD)^{r-i}}{\sum_{i=1}^{i-1} \frac{(r+i)!}{(r-i)!} \frac{r!}{i!} (jkD)^{r-i} (1 + 0.5jkD + i)} \right\} \tag{11.10}$$

where:

$$j = \sqrt{-1}$$

$k = 2\pi f_r / c =$  the wavenumber

$D =$  the diameter of the cylinder enveloping the machine

$r =$  the mode number of vibration

$f_r =$  the frequency of vibration

$i =$  an integer

If  $r = 0$ , then:

$$\sigma_0 = \frac{k^2 D^2}{4 + k^2 D^2} \quad (11.10a)$$

Equation 11.10 illustrates the fact that the radiation coefficient  $\sigma$  depends on the dimensions of the machine, the mode number, and the frequency. However, the calculation of the radiation coefficient using the formula is not easy, and resort is usually made to the curves of Fig. 11.5.

Some limiting cases can be derived easily. If the frequency  $f_r$  is low and the size of the machine  $D$  is very small, the machine acts as a point source of sound, and  $\sigma = k^2 D^2 / 4$ . If the frequency is high and the size of the machine is large, the machine will act as a plane radiator, with  $\sigma = 1$ . Independently of the type of sound-radiating model, it can be shown that machines of small dimensions are poor radiators of sound, while machines of large dimensions are good radiators. If many independent components of vibration take part in creating the noise from the electric machine, the resultant sound power of the machine is given by the sum of the sound powers of the components, using Eq. 11.3.

Noise of electromagnetic origin is influenced by the magnitude and type of load, and in fact in different ways depending on the components of the noise. Theoretical analysis based on experimental data [9] showed that the electromagnetically driven noise component of a loaded induction motor can be larger by 36 dB or, in some cases, smaller by 24 dB, than it was in no-load operation. Predictions of increase or decrease in noise or the magnitude of such changes due to load cannot usually be made. Examination of the changes have to be carried out for every component of noise separately and the components of the noise have to be summed; only then will the nature of the change be known.

When the first inverter and stator voltage control drives appeared in industry, they caused many problems in terms of

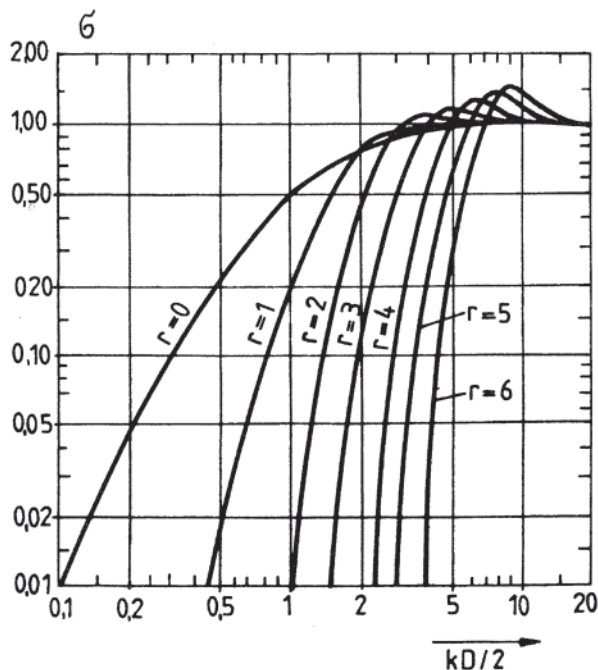


Figure 11.5 Curves of the radiation factor of a spherical radiator.

noise and vibration, as well as in terms of additional losses and torque oscillations. At low speed, the noise and vibration of mechanical and aerodynamic origin decreased sharply, while that of electromagnetic origin increased due to the large amplitudes of low-order time harmonics fed to the motor terminals which, in many cases, fell into the range of the fundamental of the voltage. The set of electromagnetic exciting forces has expanded, and the possibility of coincidence in the frequencies of resonance and exciting force has also increased.

These shortcomings in the low speed range can be overcome as a result of developments in power electronics. To eliminate the lowest-order time harmonics ( $|v|=5, 7, 11, 13, \dots$ ), the three phases are modulated in symmetrical cycles. Optimal switching times are predetermined by calculation in order to eliminate the unwanted low-order harmonics, and these times are stored in memory. The programs in memory must be selected to match the frequency of the time fundamental so that the number of commutations is constant. This optimized inverter control can eliminate the low-order harmonics in the low-speed range, although it is not the best solution as far as additional losses are concerned. Now the harmonics produced by the modulation replace the previous low-order harmonics, being responsible for a substantial part of the voltage amplitude with quite high orders, that is,  $\approx 35$  or even higher.

The frequencies of these higher voltage harmonics produce currents of only relatively small amplitudes in the winding of the stator. Thus at low speeds, the previously high sound pressure level can be decreased. The fact that when changing the speed the need to change the supply voltage frequency causes the frequencies of the exciting forces to change over a wide range (within which stable operation may be achieved) makes the noise rates of the inverter drives unfavorable. The probability of stationary resonance can rarely be avoided, although a proper choice of the number of slots, type of winding, and slot skewing can make marked improvements.

### 11.1.2 Influence of Motor Configuration and Design [10–14]

Motors have two basic configurations, that is, open drip-proof (ODP) or totally enclosed fan cooled (TEFC). In larger power machines the open motor is modified to create a weatherprotected design (WPII) that provides additional protection for outdoor service. Examination of Tables 11.2 and 11.3 provides an understanding of the noise generated by each configuration.

The first configuration is the ODP, in which the magnetic noise and windage noise combine unattenuated. This configuration is the most difficult to correct after the motor is built, so low-noise features must be designed into the original motor, with most attention addressing the magnetic design. TEFC motors produce more noise than ODP for a given power and speed. Because the magnetic components are effectively enclosed, they have minimal influence on the noise level; windage noise is the main noise contributor for this configuration. Again, there is little opportunity for noise level correction once a TEFC motor has been built. The WPII motor is designed for low-velocity ventilation and has several

**Table 11.2** Sound Power Levels for Squirrel-Cage Induction Motors (NEMA Sizes)

Frame designation	Synchronous speed (rpm)	Overall sound power level, $L_{WA}$ (dB; reference $10^{-12}$ W)	
		Drip-proof	Totally-enclosed fan-cooled
143T, 145T	3600	76	85
182T, 184T	3600	80	88
213T, 215T	3600	82	91
254T, 256T	3600	84	94
284T, 286T	3600	86	94
324T, 326T	3600	89	100
364T, 365T	3600	94	101
404T, 405T	3600	98	102
444T, 445T	3600	101	104
143T, 145T	1800	70	70
182T, 184T	1800	72	74
213T, 215T	1800	76	79
254T, 256T	1800	80	84
284T, 286T	1800	80	88
324T, 326T	1800	84	89
364T, 365T	1800	86	95
404T, 405T	1800	89	98
444T, 445T	1800	93	100
143T, 145T	1200	65	64
182T, 184T	1200	67	67
213T, 215T	1200	72	71
254T, 256T	1200	76	75
284T, 286T	1200	81	80
324T, 326T	1200	83	83
364T, 365T	1200	86	86
404T, 405T	1200	88	90
444T, 445T	1200	91	94
143T, 145T	900	67	67
182T, 184T	900	69	69
213T, 215T	900	70	72
254T, 256T	900	73	76
284T, 286T	900	76	80
324T, 326T	900	79	83
364T, 365T	900	81	86
404T, 405T	900	84	89
444T, 445T	900	87	93

90-degree bends in the air flow. Both of these features tend to mask the generated noise and yield lowest total noise levels. This design also lends itself to being more easily modified to lower the noise level after the motor has been built and tested.

An examination of Tables 11.2 to 11.5 also reveals that as the rated power and speed increase, so does the noise level. Remember that these values are expressed on a logarithmic scale and an increase of 3 dB represents a doubling of the sound level. It should also be noted that for 3000–3600 rpm motors there is not a uniform increase in noise. This is because small motors have bidirectional fans and larger motors have unidirectional fans, which provide more air at less power and are also quieter.

Before discussing specific motor design parameters,

**Table 11.3** Sound Power Levels for Large Squirrel-Cage Induction Motors

Rated horsepower	rpm	Overall sound power level, $L_{WA}$ (dB; reference $10^{-12}$ W)		
		Open drip-proof	Totally enclosed fan-cooled	Weather-protected type II
200–250	3600	101	107	—
300–450	3600	107	110	102
500–800	3600	110	113	105
900–1500	3600	111	116	106
1750–2500	3600	112	118	107
3000–5000	3600	114	120	109
200	1800	—	103	—
250–400	1800	103	105	99
450–700	1800	106	108	102
800–1250	1800	108	111	104
1500–2250	1800	109	113	105
2500–4000	1800	110	115	106
150	1200	96	98	—
200–350	1200	99	100	97
400–700	1200	102	103	99
800–1250	1200	105	106	101
500–2500	1200	107	109	103
3000–3500	1200	109	111	105
125	900–600	93	96	92
150–250	900–600	95	97	92
300–400	900–600	98	100	96
450–700	900–600	99	102	98
800–1250	900–600	101	105	100
1500–2250	900–600	103	107	102

something should be said about noise level. Until the late 1980s there was no convenient procedure for performing noise evaluation under loaded conditions. This is now changing due to the introduction of sound intensity measurement equipment and standards.

Earlier studies suggest that loaded motors produce a 2–3 dB increase over the levels of unloaded motors. This statement, however, requires several qualifications. For example, the motor must be designed and constructed as a low-noise motor and it must be correctly and adequately mounted. Ignoring these qualifications has been shown to yield an increase in levels in the range of 6–10 dB. It must also be noted that an increase in applied voltage from rated voltage generates an abnormally high noise level.

### 11.1.3 Regulation of Noise: Typical Levels

The primary reason for noise regulation is to protect against hearing loss; sound levels are therefore expressed in terms of values experienced at the operator's ear. The regulations are also expressed as a function of exposure time, for example, 85 dB for 8 hours.

Regulations pertain to the worker and cannot be transformed directly to motor specifications. For example, the regulations can be met by reducing the exposure time from 8 hours to 4 or

**Table 11.4** Maximum Permissible Sound Power Levels,  $L_{WA}$ ,<sup>a</sup> for IEC Rotating Electric Machines IEC 60034–9

Rated speed $n_N$ (rev/min)	$n_N \leq 960$		$960 < n_N \leq 1320$			$1320 < n_N \leq 1900$			$1900 < n_N \leq 2360$			$2360 < n_N \leq 3150$			$3150 < n_N \leq 3750$			
	IC01	IC411	IC31	IC01	IC411	IC31	IC01	IC411	IC31	IC01	IC411	IC31	IC01	IC411	IC31	IC01	IC411	IC31
Methods of cooling (simplified code) <sup>b</sup>	IC11	IC511	IC71W	IC11	IC511	IC71W	IC11	IC511	IC71W	IC11	IC511	IC71W	IC11	IC511	IC71W	IC11	IC511	IC71W
	IC21	IC811	IC81W	IC21	IC811	IC81W	IC21	IC811	IC81W	IC21	IC811	IC81W	IC21	IC811	IC81W	IC21	IC811	IC81W
	IC8A1W7		IC8A1W7			IC8A1W7			IC8A1W7			IC8A1W7			IC8A1W7			
	c	d	d	c	d	d	c	d	d	c	d	d	c	d	d	c	d	d
Rated output $P_N$ (kW or kVA)	Maximum permissible sound power level $L_{WA}$ (dB)																	
$1 \leq P_N \leq 1.1$	73	73		76	76		77	78		79	81		81	84		82	88	
$1.1 < P_N \leq 2.2$	74	74		78	78		81	82		83	85		85	88		86	91	
$2.2 < P_N \leq 5.5$	77	78		81	82		85	86		86	90		89	93		93	95	
$5.5 < P_N \leq 11$	81	82		85	85		88	90		90	93		93	97		97	98	
$11 < P_N \leq 22$	84	86		88	88		91	94		93	97		96	100		97	100	
$22 < P_N \leq 37$	87	90		91	91		94	98		96	100		99	102		101	102	
$37 < P_N \leq 55$	90	93		94	94		97	100		98	102		101	104		103	104	
$55 < P_N \leq 110$	93	96		97	98		100	103		101	104		103	106		105	106	
$110 < P_N \leq 220$	97	99		100	102		103	106		103	107		105	109		107	110	
$220 < P_N \leq 550$	99	102	98	103	105	100	106	108	102	106	109	102	107	111	102	110	113	105
$550 < P_N \leq 1100$	101	105	100	106	108	103	108	111	104	108	111	104	109	112	104	111	116	106
$1100 < P_N \leq 2200$	103	107	102	108	110	105	109	113	105	109	113	105	110	113	105	112	118	107
$2200 < P_N \leq 5500$	105	109	104	110	112	108	110	115	106	111	115	107	112	115	107	114	120	109

<sup>a</sup>dB, referred to  $10^{-12}$  W.

<sup>b</sup>See IEC 60034–6

<sup>c</sup>ODP configuration.

<sup>d</sup>TEFC configuration.

even 2 hours. A sound-absorbing barrier could be placed between the worker and the noise source, or, in some extreme cases, hearing protection for the worker could be required.

Because motors are a prime source of noise in any worker’s environment, many specifications are written to control motor noise emission to 85 dBA sound pressure at 3 feet. As a result, there is significant difficulty in relating a motor test to the noise level at the worker’s ear, which is a function of the distance between motor and worker and is also a function of the environment.

For purposes of testing for sound pressure, these variables have been standardized to the extent that the measurement distance from the motor surface is 3 feet (1 meter), the motor is tested alone and unloaded, and the environment is specified as being free-field over a reflecting plane. There is obviously great disparity between these situations and normal working conditions.

To overcome these ambiguities, motor noise levels are reported in terms of sound power. Sound power eliminates the variables of distance and environment. Recent standardization of intensity measurement now also permits the testing of motors under load in most environments, although load measurements could and can still be made by isolating the machine that loads the motor to achieve an acceptable ambient for testing the motor noise.

Typical sound power levels for motors conforming to U.S. (NEMA) standards are given in Tables 11.2 and 11.3. These levels are for polyphase induction motors.

The IEC standards presently published are for all rotating electrical machines (see Table 11.4). This broad treatment

has allowed polyphase asynchronous motors to have noise levels higher than generally permitted by specification. Table 11.5 is now included in IEC 60034–9 and provides lower noise levels for this class of asynchronous motors. Although the standards are presented in different formats, slight revisions have brought the U.S. standards into harmony with the IEC standards.

Air-borne induction motor noise can be categorized according to its source, and there is no general rule to establish the relative importance of each source. Individual design

**Table 11.5** Maximum Permissible A-Weighted Sound Power Levels in Decibels for IEC Squirrel-Cage Induction Motors of TEFC Configuration

Number of poles	8	6	4	2 (50 Hz)	2 (60 Hz)
Rated output (kW)	Maximum permissible sound power level, $L_{WA}$ in dB				
$1.1 < P_N \leq 2.2$	71	71	71	81	85
$2.2 < P_N \leq 5.5$	76	76	76	86	88
$5.5 < P_N \leq 11$	80	80	81	91	91
$11 < P_N \leq 22$	84	84	88	94	94
$22 < P_N \leq 37$	87	87	91	96	100
$37 < P_N \leq 55$	89 <sup>a</sup>	90 <sup>a</sup>	94 <sup>a</sup>	98	101
$55 < P_N \leq 110$	92 <sup>a</sup>	94 <sup>a</sup>	97 <sup>a</sup>	100	104
$110 < P_N \leq 220$	96 <sup>a</sup>	98 <sup>a</sup>	101 <sup>a</sup>	103	107
$220 < P_N \leq 400$	98 <sup>a</sup>	101 <sup>a</sup>	105 <sup>a</sup>	107	110

<sup>a</sup> Increase by 1 dB for 60 Hz.

characteristics set the pattern that makes one or the other a major noise source. The three categories are as follows.

1. *Magnetic noise* that is objectionable usually has loud single-frequency components in the high-frequency range.
2. *Windage noise* is largely broadband in character, but single-frequency components associated with resonant volumes within the frame of the motor, the flow of the ventilating air through or over the motor, the number of fan blades, or a siren effect caused by the rotor bars periodically interrupting the flow of air may also appear.
3. *Mechanical noises* are often associated with the bearing assembly and can be appreciable if, for example, the bearing parts are deformed in some manner, or if excessive clearances permit axial travel of the shaft. Unbalance or magnetic forces can excite natural frequencies of the motor structure that radiate noise to the surrounding air.

11.1.3.1 Magnetic Noise

Magnetic noise of induction motors has two predominant sources: (1) radial force waves created by the air gap flux density and (2) the magnetostrictive expansion of the core steel. Whereas the force waves are imposed on the air—iron surface of the air gap, the magnetostrictive expansion is an internally generated variation in dimension. Both of these sources of magnetic noise produce noise that is twice the line frequency (the induction motor hum).

The first source of the magnetic noise is the periodic forces that exist primarily in the air gap between stator and rotor. These forces, which are proportional to the square of the flux density, produce radial components that appear as harmonics of the line frequency and at frequencies related to the slip and line frequency. *Flux densities should be kept low to minimize these twice-line-frequency noises.* In some commercial motors it is the practice to employ unbalanced fractional slot windings to obtain maximum utilization of standard laminations. Such unbalanced windings are not admissible in motors that are to be quiet, since unbalanced line currents and hence twice-line-frequency vibrations will result.

The forces in the air gap can be effectively reduced by altering either the electromagnetic or the mechanical characteristics of the rotor-stator assembly. It is not always practical to make these changes, since they also affect the

torque characteristics, core losses, and other electrical characteristics.

Induction motors have other magnetic noise sources in addition to the induction motor hum. These are from the basic slot harmonic force field, which occurs at the following frequencies:

$$f_r = Rn \quad f_i = Rn + 2f \quad f_o = Rn - 2f$$

where

- $R$  = number of rotor slots
- $n$  = rotor speed (rev/sec)
- $f$  = line frequency (Hz)

In well-designed motors, the appropriate skewing of either the rotor or the stator slots will decrease the magnitude of these slot harmonics. For more detailed discussion of forces causing magnetic noise and of the frequencies, see [Sections 11.1.1 and 14.1.5](#).

11.1.3.2 Rotor and Stator Slotting

The selection of the rotor and stator slot combination is the most important single parameter in the electrical design of a quiet motor. In general the slot combination should be chosen so that the number of exciting-force pole pairs is as high as possible, since the motor frame will usually be stiffer in these modes. Factors other than noise, such as elimination of hunting, crawling and cogging, eliminate many possible combinations. Table 11.6 lists the best slot combinations resulting from the computation of rotor and stator harmonics whose interaction produces the greatest number of force pole pairs.

Squirrel-cage induction motors have either closed or semiclosed rotor slots and semiclosed or open stator slots. The partial or complete steel bridge over the slots reduces the abrupt permeance variation as sensed by the opposing member. A decrease in permeance variation will result in lower magnitudes of slot harmonics. A closed rotor slot causes less permeance variation than a semiclosed slot unless there is a relatively small bridge thickness that becomes saturated. As the steel bridge saturates, the permeance variation approaches that of a completely open slot. In such situations the closed slot may not appreciably reduce magnetic noise. Since the use of closed slots never causes an increase in noise, it is recommended that rotors with closed slot configuration be used.

For similar reasons, stators should utilize semiclosed rather than open-slot configurations. The width of the slot opening

**Table 11.6** Preferable Rotor-Stator Slot Combinations for Three-Phase Motors

Stator slots	Number of rotor slots									
	2-pole		4-pole		6-pole		8-pole			
24	32	34	32	34	32	36				
36	26	28	44	26	28	44	46	48	48	52
48	38	40	56	38	40	56	58	60	64	68
54	46	62		46	62		42	66		
60	52	68	78	44	46	52	76	44	48	72
72							60			
									56	58

**Table 11.7** Skew-Test Sound Levels

Band	0 slot	1 slot	1.3 slot	1.75 slot
125	35	29	30	28
250	39	34	33	38
315	49	42	40	43
800	52	42	42	48
1250	49	41	42	45
4000	44.5	31.5	33	36
5000	40	34.5	36.5	34.5
Overall	59	53	52	55

The skew is referenced to the component having the fewer slots.

should be kept at a minimum. The ability to wind the motor will determine the minimum opening that may be used.

An increase in the air gap radial length will also decrease the magnitude of the permeance variations.

Slip noise is a low-frequency beating of higher frequency components. Because of its intermittence, this noise may be objectionable even though its level is relatively low. Being a function of slip, it is more noticeable under load, with the frequency varying directly with the slip. The noise is often associated with a defect in the uniformity of the squirrel-cage rotor, in which case a new rotor is required.

#### 11.1.3.3 Skew of Rotor Bars

The practice of skewing either the rotor or the stator slots with respect to the axis of rotation to reduce noise and provide for smooth acceleration has become so prevalent that the vast majority of induction motors are skewed. There is general agreement that skewing reduces magnetic noise, but there is no clear agreement on the optimum amount of skew. The noise produced by varying amounts of skew cannot be calculated accurately. One test made is shown in Table 11.7. It is suggested that the rotor be skewed at least one rotor or stator slot, whichever has fewer slots. Skewing less than one slot is not effective in appreciably reducing the unit's sound level. Larger skews may be used, but these generally sacrifice motor performance.

#### 11.1.3.4 Windage Noise

Windage noise is most common in high-speed rotating machines. It is caused by the presence of obstructions in the vicinity of the rotating part that moves air and creates turbulence. The acoustic power generated varies approximately as the fifth power of the air flow rate, and the fundamental frequency is a function of the rotational speed. Windage noise differs from the majority of motor noise in that it is created in the airstream rather than in the motor components. In most cases it is broadband noise with essentially no significant pure-tone components. In large motors that use radial ventilating ducts and in some motors with large cooling fans, discrete frequencies manifest themselves as a series of peaks superimposed on the broadband noise.

Air flowing around or against surfaces produces turbulence, a potential source of sound. The turbulence energy content determines the magnitude of the radiated sound. For

this reason wire cloth is preferable to expanded metal for screening purposes.

While the housing, fan, and other components are designed to minimize noise due to turbulence, the constrictions, bends, and obstructions are usually not aerodynamically designed and may still produce severe turbulence. Minimizing this noise calls for the elimination of sharp edges and burrs on all parts in contact with the airstream. It requires aerodynamically designed fans and an airstream path designed with the following criteria.

1. Use a short, streamlined flow path in which the motion of air is orderly and predictable.
2. Keep the flow-path cross section as large as possible throughout as much of its length as possible.
3. Minimize abrupt discontinuities and changes in flow direction.
4. Eliminate unnecessary obstructions in the flow path.
5. Keep boundary surfaces smooth.
6. Provide gradual changes in flow-path cross section.

Reducing fan-tip speed (the product of rotational speed and fan diameter) produces low maximum air velocity with respect to the rotating fan blades and thus minimizes the energy content of turbulence in the wake of the blades.

#### 11.1.3.5 Fan-Blade Noise

Fan-blade noise is the result of an air impulse every time a blade passes a protruding stationary member, or a standingwave resonance point. The blade frequency is:

$$f_b = Nn \text{ Hz}$$

where:

$N$  = number of blades on the fan

$n$  = rotational speed (rev/sec)

Totally enclosed motors with external fans produce discrete fan-blade frequencies superimposed on a broadband noise level. The fan-blade-frequency noise level may be reduced by increasing the clearance between fans and stationary parts or by using a nonsymmetrical group of blades in relation to the stationary protrusions. A directional fan that decreases the effective air impulse leaving the blades will also decrease noise levels.

Large open motors may exhibit standing-wave resonances that can be reduced at the source by changing the number of fan blades, or in the motor frame by changing the critical dimension.

#### 11.1.3.6 Siren Effect

Open motors with radial air ducts through the rotor and stator may produce pure-tone components of airborne noise that are highly irritating. The frequency is usually above 1000 Hz and is called the siren effect. The noise itself is produced by the sudden interruption of the flow of air from the radial ducts in the rotor. The frequencies associated with this type of noise are:

$$f_s = Rn \text{ Hz} \quad f_{s2} = 2Rn \text{ Hz}$$



where:

$R$  = number of slots in the rotor

$n$  = rotational speed of the motor (rev/sec)

The offsetting of rotor ducts with respect to stator ducts can be beneficial in reducing noise levels. The elimination of stator or rotor ducts by design considerations is the best approach for low-noise—level motors.

### 11.1.3.7 Bearing Noise

Bearings used in induction motors are a source of noise and vibration because of the sliding or rolling contact of bearing components. Sleeve or ball bearings are the types usually used, with the former having a sliding contact between components, while the latter has a combination of rolling and sliding contact.

#### *Sleeve Bearings*

Induction motors may be equipped with sleeve bearings when low noise levels are required and when the bearing noise is predominant. Sleeve bearings do not cause objectionable motor noise unless they are unstable. If there is large clearance, the oil film in the bearing may lift the shaft, unloading the oil film, thereby reducing the pressure. Consequently the shaft drops, hitting the bearing material, causing noise. This instability may be rectified by decreasing clearances in the bearing, by changing the location of the oil grooves, or sometimes by changing the viscosity of the oil.

Bearing oil film is based on the eccentric pump action inherent in a sleeve bearing. Just as a common pump must turn to produce a pressure, the shaft must turn to pressurize the oil. The pressurized oil is capable of transmitting sufficient force to lift the shaft from the mating sleeve. The lubricant film may be considered as a series of laminar layers. The innermost layer of the oil will whirl around with the shaft; the outermost layer will be stationary on the sleeve surface. The viscosity of the oil will determine the ease of relative motion of layers between these two. Note that without relative motion, there is no pressure and thus no support from the lubricant. At standstill, the oil is pressed from between the two bearing members, and during starting there will be metal-to-metal contact that will create noise. Oil with insufficient viscosity will permit intermittent metal-to-metal contact during shaft rotation. In addition to wear, the contact generates an impact noise. For very quiet operation, bearings made from plastics, graphite, or similar materials may be used. These bearings are limited to small motor applications where the surface velocity is low.

Axial bumping may be another impact-noise source. The bumping occurs when the shaft shoulder oscillates axially, with one boundary being the bearing face. Motors whose sleeve bearings are designed to take axial-thrust loads should have the shaft shoulder in continuous contact with the bearing. When thrust capabilities are not present, the rotor shaft should “float” between bearing faces without contact. Close control of design clearance and coupling type generally overcomes this problem.

#### *Antifriction Bearings*

Excessive noise in antifriction ball bearings may be caused by nonuniform balls, poor surface finish, ball-retainer rattle,

and eccentricity, which result in impact noise or resonance excitation of the bearing housings, air baffles, and other parts that are efficient noise radiators.

Precision-grade bearings are usually quieter than the more common industrial grade because of closer tolerance and better surface-finish control during manufacture. Bearings made as “electric-motor quality” possess the necessary features for most induction-motor applications.

The most common sources of noise in antifriction ball bearings of induction motors are listed below, along with their possible causes.

1. *Noise due to bearing configuration*
  - Mounted-bearing radial clearance too tight or too loose
  - Retainer too tight and rubbing or too loose and rattling
  - Poor race finish
  - Excessive eccentricity and runout
  - Shield or retainer resonance
  - Shield interference with retainer or race
  - Improper retainer material for application
2. *Noise due to lubricant*
  - Grease tacky (remedy: use softer grease)
  - Ball skidding in race (remedy: add lubricant, preload bearing)
  - Excessive oil present (remedy: clean bearings)
  - Residue present on races because of long storage
3. *Noise due to machining*
  - Housing or shaft fit too tight or too loose
  - Out-of-round housing
  - Poor shaft or housing finish (shaft finish should be 16 to 32  $\mu$  inch)
  - Bent shaft
  - Misalignment (shoulder against which bearing rests is not perpendicular to axis)
  - Interference from adjacent parts
4. *Noise due to abuse or neglect*
  - Brinnelled races and damaged balls
  - Dirt and dust inclusions
  - Corrosion
  - Damage to shield
  - Ball skidding and fatigue damage

Increasing the bearing size and the rotating speed of the induction motor has an increasing effect on the bearing noise level generated.

The noise due to some of these sources is distinct enough to be easily identified. For example, brinelling can be recognized by a low-pitched noise; the presence of dirt in the bearings causes a shrill noise; and skidding at low temperatures with insufficient lubrication results in destruction of the surface, causing a high-frequency noise. An intermittent crackle is often due to grease. A noise in the frequency range of 100–300 Hz may be caused by the passage of the balls or rollers and is characteristic of antifriction bearings. This noise is generally of low level and not disturbing unless it excites motor parts to vibrate at their natural frequencies.

The discrete frequencies of ball-bearing noise are produced by irregularities of the ball-bearing components and may be

**Table 11.8** Possible Noise Sources and Remedies in Electric Motors

Noise source	Cause	Component causing noise	Noise-control remedy
Mechanical	Impact	Sleeve bearings	Correct end play of shaft, decrease clearance between shaft and sleeve, modify oil grooves
		Ball bearing	Reduce radial play by preloading, reduce shaft or housing tolerances; natural frequency of end shield should not equal characteristic ball-bearing frequency
	Friction	Loose laminations	Improve clamping of laminations
		Sleeve bearings	Increase clearance, increase oil viscosity, scrape sleeve surface
Windage	Unbalance	Ball bearings	Increase preload pressure, change type of grease
		Rotor	Mechanical balance required
	Instability	Bearings	Change oil grooves in bearings, change oil viscosity
		Modulation	Siren effect
Turbulence	Fan blades	Fan	Change number of fan blades, remove stationary obstacles from airstream, or use aerodynamic directional fan
Magnetic	Radial	Air gap	Correct eccentricity of rotor or stator by machining and adjustment
	Variable force field radial in direction	Slotting of rotor and stator punchings	Skew stator or rotor slots, use closed rotor and semiclosed stator slots
		Dissymmetry harmonics due to higher harmonics in stator current	Reduce dissymmetry by improved magnetic-circuit design; avoid resonance of rotor frame, particularly at lower modes, which are more effective sound radiators

determined if the bearing geometry and shaft speed are known. The following symbols are defined:

$d$	Diameter of rolling element (inches)
$E$	Pitch diameter (inches)
$N$	Number of rolling elements
$n$	Speed of rotating member (rev/s)
$B$	contact angle (degrees)

The fundamental rotational frequency  $n$  is apparent with the slightest unbalance or race eccentricity. Any irregularity of rolling element or the cage causes noise with a train frequency of

$$f_i = \frac{n}{2} \left( 1 - \frac{d}{E} \cos B \right) \text{ Hz} \quad (11.11)$$

The speed of the train of rolling elements  $f_i$  is roughly one-half the rotational speed of the inner race  $n$ . The spin frequency of a rolling element is:

$$f_s = \frac{E}{2d} n \left[ 1 - \left( \frac{d}{E} \right)^2 \cos^2 B \right] \text{ Hz} \quad (11.12)$$

A rough spot or indentation of an element causes a frequency component:

$$f_e = 2f_s \text{ Hz}$$

because the spot contacts the inner and outer races alternately.

Another frequency occurs if there is an irregularity (high spot or indentation) on the inner raceway:

$$f_i = N(n - f) \text{ Hz}$$

The frequency due to an irregularity on the stationary raceway is:

$$f_0 = Nf_i \text{ Hz}$$

In case of many spots, the harmonics of  $f_i$  or  $f_0$  will be more pronounced.

#### 11.1.4 Reduction of Noise Levels: Special Treatment

Some of the noise sources in electric motors and possible noise controls are shown in Table 11.8. The noise sources are normally identified by a frequency analysis. No general rule can be given for induction motors as to the relative importance of these three types of noise. Individual design characteristics set the pattern that makes one or the other a major noise source. During the initial design stage of a motor, the designer should keep the possibilities for excessive sound generation to the minimum. Once a motor is designed and manufactured, it is much more costly to effect a suitable noise reduction.

##### 11.1.4.1 Preloading Bearings

One of the best-known methods in the suppression and damping of bearing noise is the use of a thrust washer to preload the bearings axially. Wavy-spring washers are one of the more common types of thrust washer. This washer acts as a spring to exert a force, usually on the outer race of the ball bearing. The reactive force is supplied by the shaft pressing against the inner race of the bearing. This force couples across the bearings, takes up the internal clearances, and causes each ball to follow the same path on each bearing raceway.

Preloading bearings decreases noise caused by the balls rattling within the raceway and cage, decreases the generation of high-frequency vibration, and improves balance by the removal of bearing looseness. But preloading also causes the

balls to follow the surfaces of the raceways closely. Good surface finish of the raceways and of the balls will permit the bearing to run smoothly and thus more quietly. Too much bearing preload produces low-frequency noise and possibly bearing overheating.

#### 11.1.4.2 Bearing Friction Noise

Friction noise arises from a lack of sufficient lubrication between two sliding surfaces and is caused by a high-impact type of vibration resulting from rapid intermittent contacting of the surfaces. Sleeve bearings exhibit this phenomenon when there is insufficient oil film, whereas ball bearings commonly experience sliding contact due to a lack of preload. The noise at the point of contact occurs at a high frequency, like that of hissing air, and when the impact vibration is transmitted to a resonant point in the adjacent structure, the audible sound is best described as a screech. The frequency at which the noise occurs cannot be described by an equation, but it is related to the surface finish of the areas in contact. Both surface finish and normal loading values affect the noise level. An additional effect of the high vibration rate is the breakdown of the lubricant at the surfaces.

#### 11.1.4.3 Vibrating Surfaces

Any structural part of a motor may act as a source of airborne noise if it is excited with sufficient energy. For example, rotational unbalance itself may not emit airborne noise of any magnitude, but it may act as an energy source for vibrations that are then transmitted through the support structure to be converted to airborne sound waves at some resonant point. Thus the vibrating member or housing sets the air into motion, making it appear as if it were the noise source.

Air baffles, drip covers, and similar parts may perform their particular function but tend to resonate. Under such conditions two remedies can be effected:

1. Deadening or damping material can be applied to change vibratory motion into heat energy by making use of the internal friction of the material.
2. The stiffness characteristics of the structure can be changed so that resonance will occur at another frequency.

Usually, rigid parts produce less vibration and noise than parts that are more flexible. Consideration should also be given to the use of cast and molded plastic parts to decrease vibration-originated noise.

#### 11.1.4.4 Sound Absorption

The emission of airborne noise generated within the motor can be reduced by using sound-absorbing materials. Sound-absorbing materials are porous materials that absorb the energy from the sound waves passing into their pores and convert it to heat energy. The absorption capability of this type of material increases with its density, tightness, or pore structure, and thickness. For best results, the barrier should completely enclose the source, or at least intercept the direct path between the source and the receiver.

A further advantage is gained by introduction of 90 or 180 degree bends into the ducts, in particular for the control of low frequencies (up to 400 Hz), where the absorption coefficients of commercially available sound-absorptive materials are low.

### 11.1.5 Experimental Investigation of Noise

Around a sound source in a closed space, two different types of sound fields may be established, depending on which energy component is the dominant one in determining the magnitude of energy density. In the zone close to the sound source the direct energy is predominant, while farther away the reflected energy predominates. The zone where the sound pressure level is determined only by the parameters of the sound source is called the direct field, while the one where the reflected sound waves dominate is called the diffuse field. There are two basic methods of determining the power level depending on whether the measurement is done in the direct field or in the diffuse field. In practice, one always tries to select the measuring points so that the energy component to be measured is predominant over the other component at the points selected.

There is no measuring instrument that is suitable for the direct measurement of sound power; therefore the determination of sound power is reduced to the measurement of sound pressure level. The basic difference between sound pressure measurements conducted in the direct field and in the diffuse field is that in the direct field the intensity is determined, whereas in the diffuse field the energy density is determined from the sound pressure.

In the direct field, one can generally assume that the relationship between the pressure and the particle velocity of the sound wave may be expressed as  $v = p/(\rho c)$ ,  $\rho$  being the density of the air and  $c$  being the speed of sound propagation in air, as in Section 11.1. Hence the intensity  $I = p^2/(\rho c)$ . This simple formula is based on the assumption that the intensity vector and the normal of the measuring surface are pointing in the same direction, and that the pressure wave and the particle velocity wave are in phase.

One of the promising trends in sound measurement is the direct measurement of intensity [15]. For this purpose, two microphones are used to sense the sound pressure level. From their output signals the gradient of pressure is also determined. In principle, the intensity can be determined without error from the pressure and the pressure gradient.

Direct measurement of intensity is feasible using digital analyzers that utilize the fast Fourier transformation or by means of a computer through an analog-to-digital converter (ADC). The accuracy of the procedure that uses two pressure microphones is strongly dependent on the distance between the microphones.

For diffuse-field measurements, the sound source should be located so as to allow the establishment of a sound field that can be considered to be diffuse at the place of measurement, being some distance from both the sound source and the walls of the room. The energy density of this diffuse sound field may be determined by measuring the sound pressure at various points in the space. The sound power is

calculated from the energy density. Because no transducer is available that can measure particle velocity correctly, pressure microphones are also used for these measurements.

The actual measured energy density is not the total energy density, but only the density of potential energy. When the power level is determined, one implicitly assumes that the total energy density is twice the density of potential energy. This means that the density of potential energy is equal to the density of kinetic energy at any point in the space. In reality, however, this is true only for the averages taken for the whole of the diffuse field. From the sound pressure level averaged for the entire diffuse field, the sound power level is found as:

$$L_W = \bar{L}_p + 10 \log_{10} \left( \frac{V}{V_0} \right) - 10 \log_{10} \left( \frac{T}{T_0} \right) - 14 \quad (11.13)$$

where:

$\bar{L}_p$  = the sound pressure level averaged for the whole of the diffuse field

$V$  = volume of the room, and  $V_0 = 1 \text{ m}^3$

$T$  = reverberation time, and  $T_0 = 1 \text{ s}$

As may be seen, the accuracy of a diffuse-field measurement depends partially on the accuracy of the average sound pressure calculated from the sound pressure levels for the whole of the diffuse field, that is, on how the mean value of the discrete samples approximates the expected value of the entire set of data, and partially on the accuracy of the measured reverberation time. It must also be pointed out that reverberation time can be different for different frequencies; therefore, when the average  $T$  is used, as it generally is in practice, error in the measurement of a noise with a dominant pure tone component may be significant.

The comparison theorem is frequently used in the case of both direct-field and diffuse-field measurements. In this method, the sound power level of a so-called reference sound source with known sound power level is measured under the same conditions as for the tested noise source. Comparing the known sound power level with the levels measured during the comparative test, one can identify the deviations due to local acoustic conditions and use them to correct the results obtained for the noise source by measurement.

The accuracy of the direct field measurements depends on the acoustic conditions in the test room. For accurate measurements, a completely free sound space is required. In many cases this means an anechoic chamber, that is, an acoustic laboratory with nonreflecting walls. Such an installation is expensive, but the lack of reverberation means that the direct sound field is easily measured. The practical use of these measurements is mostly technical or informative, as in the case of direct-field measurements. The machine to be tested should be placed on a sound-reflecting plane so as to use the principle of acoustic reflection.

When measuring the sound pressure level, capacitor microphones are usually used as transducers. The capacitor microphone has good dynamic response over a wide frequency range; its transfer characteristics are good; and it is stable with time. Environmental disturbing effects, such as humidity

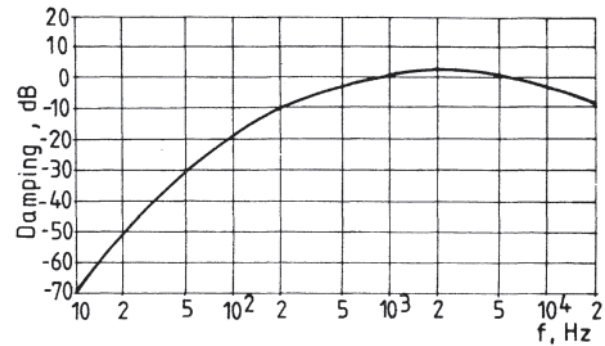


Figure 11.6 The damping factor of the A-weighting filter.

of the air and magnetic fields, affect it very little; it is easy to calibrate; and it has small dimensions.

The electrical signal proportional to the sound pressure at the capacitor microphone is amplified and passes through a weighting filter. The weighting filter is actually a bandpass filter with defined frequency-response characteristics. It is used so that the measuring system will produce a result that conforms to the subjective noise-sensing ability of the human ear. The most frequently used weighting filter is the A-weighting filter, which simulates the average sound sensing ability of the human ear in the 60–90 dB range of sound pressure levels. The damping curve of this filter is shown in Fig. 11.6. The cutoff frequencies of the A-weighting filter are around 700 Hz at the low end of the frequency spectrum and around 10,000 Hz at the high end.

It is often important to know what components of the frequency spectrum make up the vibration or noise of the tested machine. In such a case a spectrum analysis is carried out. The objective of this analysis is to determine the frequency and amplitude of each component in the spectrum. Both analog and digital instruments are available to do the frequency analysis, and both have similar displays. In one implementation, an electrical signal which is proportional to a desired characteristic of the vibration or noise, such as amplitude, velocity, or acceleration, passes through a filter system having a number of bandpass filters in parallel. Each bandpass filter is characterized by an upper and a lower cutoff frequency ( $f_u$  and  $f_b$  respectively), which define the edges of the pass band. In the pass band the signal is practically unaltered. At the band edges, the response is 3 dB down. In the signal rejection portions of the spectrum (the so-called stop band), the slope of the response is in the order of 45 to 50 dB per octave. The center frequency  $f_c$  is defined as the geometric mean of the upper and lower cutoff frequencies, that is  $f_c = \sqrt{f_b f_u}$ .

In industrial practice, constant percentage or constant relative bandwidth analysis is used most often. That is, the filters are all constructed so that  $f_u/f_b$  is a constant, where the index  $i$  specifies one of the set of filters. Constant percentage analysis may be implemented in one of two ways. The first of these uses a set of filters with standardized center frequencies  $f_{c,i}$  and bandwidths such that  $f_{u,i} = f_{u,i-1}$ . There are therefore as many filters in the spectrum analyzer as there are bands to be covered in the measurement. A second way to implement constant percentage bandwidth analysis is to use a single filter whose center frequency  $f_c$  can be tuned continuously.

For simple applications, the ratio of the upper cutoff frequency to the lower cutoff frequency is 2 for every band so that  $f_{u,i}/f_{l,i} = f_{c,i}/f_{c,i-1} = 2$ . Using the fact that the center frequency is the geometric mean of the cutoff frequencies, the respective upper and lower cutoff frequencies may be obtained by multiplying and dividing the center frequency by  $\sqrt{2}$ . Analysis using filters having these characteristics is referred to as octave-band analysis. A more detailed picture of the spectrum is obtained from third-octave-band analysis, for which  $f_{u,i}/f_{l,i} = f_{c,i}/f_{c,i-1} = \sqrt[3]{2}$ . For third-octave-band analysis, the cutoff frequencies are obtained from the center frequency using the factor  $\sqrt[3]{2}$ .

The band center frequencies are specified by international standards. The constant percentage fixed-center-frequency filters normally satisfy the analysis requirements for factory measurements. Although the bandwidth of the individual filters increases with increasing frequency, the discrete frequencies of the components present in the noise produced by electric machines are also farther and farther apart as the frequency increases. An absolute bandwidth that increases with increasing center frequency facilitates economic execution of the measurements, since the analyzer runs quickly through the high-frequency range with its few components.

The frequency spectrum obtained by fixed-center-frequency constant bandwidth analysis looks like a histogram in that one cannot separate the individual components, if any, within a given band because a measurement made through a given bandpass filter yields the rms value of the vibration or noise components within the frequency range of the particular filter.

Constant percentage filters with a continuously variable center frequency provide a more accurate picture of the dominant vibration and noise components both as to their frequencies and as to their magnitudes. The largest value of  $f_u/f_l$  generally used is 1.26 (the third-octave band filter case); this is spoken of as having a resolution of 26%. The smallest ratio of cutoff frequencies is 1.01 (1% resolution) in the case of precision filters. This resolution is sufficient for even the most delicate operating requirements.

The frequency spectrum obtained from a constant percentage filter with continuously variable center frequency is a continuous curve with local maxima and minima, the maxima giving the frequencies of the individual noise components as well as the amplitudes. A spectrum showing a flat peak and having moderate slopes on the rising and falling edges indicates that the bandwidth is too wide; more than one component has merged into a single local maximum.

Too much reduction in bandwidth is to be avoided, although the narrower the bandwidth the more accurate the results. The time involved in locating the components increases and, in addition, the long time constant associated with narrow-bandwidth filters poses an additional problem.

With a great deal of idealization, small- and medium-horsepower electric machines that actually create a spherical acoustical field may be assumed to be point sources. The sound field of this kind of field is described in the technical literature [1, 9]. The ideal acoustic condition is the free sound field, where only the sound waves originating from the sound source exist;

there is no reflecting surface (thus no reflected sound field), nor is there sound from any other source. That is, the background noise level is zero. In this case, the sound pressure level in a spherical sound field at a distance  $d$  from a sound source radiating sound power level  $L_w$  can be calculated from:

$$L_p = L_w + 10 \log_{10} \frac{S_0}{4d^2\pi} \quad (11.14)$$

For a free sound field above a reflecting plane:

$$L_p = L_w + 10 \log_{10} \frac{S_0}{2d^2\pi} \quad (11.15)$$

where:

$$S_0 = 1 \text{ m}^2$$

$d$  = the distance of the measuring point from the point source

From Eq. 11.14 it can be seen that in the ideal case it is sufficient to carry out one distance and one sound pressure level measurement to be able to calculate  $L_w$  unambiguously.

In reality, electric machines are not ideal point-like spherical radiators and measurements cannot be done in an ideal acoustic environment. The points used for measuring noise are on a measuring surface whose shape depends on the type of machine and the standards used. The surface can be a hemisphere, a parallelepiped, or a conformal surface resting on a rigid floor. The position and density of the points used are determined by the geometric dimensions of the machine and by the difference between the sound pressure levels of neighboring measuring points. (A conformal surface is defined as one that is everywhere a fixed distance from the machine.)

The measuring surface most often used is a rectangular parallelepiped placed at a distance  $d=1$  m from the reference surface, which is the smallest parallelepiped containing the electric machine. These parallelepipeds are shown in Fig. 11.7, and the measuring points are also identified in that figure.

From a practical point of view, the number of measuring points must be finite. Assume that the measuring points belong to approximately equal-size surface units. Assume further that the orientation of the machine is such that the values of the sound pressure levels at the measuring points are characteristic for the intensity values, having a normal distribution as the elements of a group. Assuming also that the expected value of the normal distribution equals the average value, the standardized evaluation calculates the sound power from the weighted average  $\bar{L}_p$  of the measured sound pressure levels:

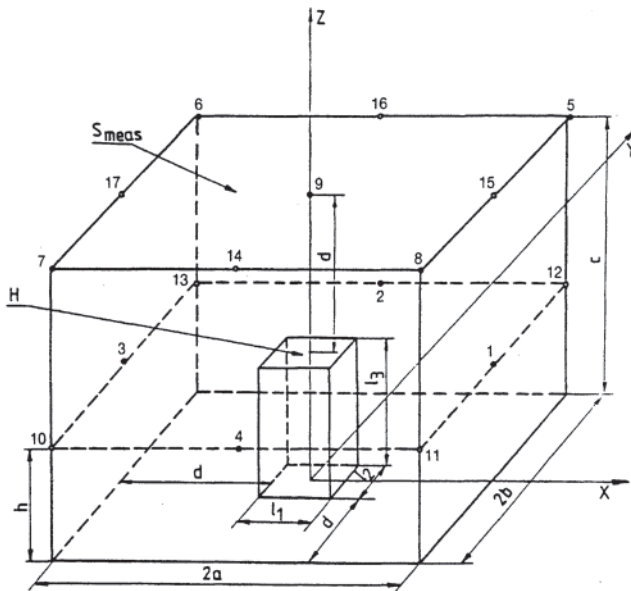
$$L_w = \bar{L}_p - 10 \log_{10} \frac{S_0}{S} \quad (11.16)$$

where  $\bar{L}_p$  = the average sound pressure level calculated using Eq. 11.4,

and  $S$  = the area of the measuring surface previously defined, in  $\text{m}^2$ .

Experience has shown that using the average value  $\bar{L}_p$  to calculate the sound power  $L_w$  using Eq. 11.16 gives smaller values than the actual sound power level values. The procedure as described to this point assigns too small a weight to large values of  $L_p$ .

Suppose, for example, that the 9 key measuring points of



The coordinates of the key measuring points

Serial Number	X	Y	Z
1	a	0	h
2	0	b	h
3	-a	0	h
4	0	-b	h
5	-a	b	c
6	-a	b	c
7	a	-b	c
8	a	-b	c
9	0	0	c

Smeas Measuring surface  
 H The parallelepiped surface containing the machine  
 1-9 The key measuring points  
 10-17 Additional measuring points  
 l<sub>1</sub>, l<sub>2</sub>, l<sub>3</sub> The linear dimensions of the parallelepiped  
 d The measuring distance

Figure 11.7 The rectangular parallelepiped measuring surface and the measuring points.

Fig. 11.7 are to be used. To add weight to the large values of  $L_p$  it is advisable to add a tenth measuring point. The extra point should be adjacent to that point having the largest of the 9 measured values. If, for instance, the fifth measuring point is the point at which  $L_p$  (max) occurs, then 20 to 30 cm from it, at the same height, another measurement is made. All 10 data points are used in subsequent calculations. By following this procedure, the largest value will be weighted more heavily when calculations are made, and the calculated sound power level will more closely approach the actual value.

The real electric machine is usually a directed sound source. A sound source is said to be directed if the range of measured sound pressure levels at the same distance  $d$  is greater than 5 dB. Directedness is denoted by the directivity index at the given point of the measuring surface, which is the difference between the measured sound pressure level at the given point from that which would be measurable in the case of a spherical sound source radiating uniformly in every direction and having the same sound power as that of the investigated machine. In the practice of noise measurement of electric machines, measurements are made above the sound-reflecting plane. In this case the directivity index  $G$  is calculated from:

$$G = L_{pi} - \bar{L}_p + 3 \tag{11.17}$$

and the directivity factor  $D$  by:

$$D = 10^{0.1G} \tag{11.18}$$

The directivity of an electric machine is one of the factors that cause sound pressure levels at the measuring points to fail to represent their measuring surface element accurately.

In practice, the reading of sound pressure level  $L'_p$  when measuring the noise of the machine is the resultant of the background noise  $L_{pb}$  and the sound pressure level  $L_p$  radiated by the machine. By subtracting the background noise  $L_{pb}$  measured with the machine switched off from the sound pressure level  $L'_p$ ,  $L_p$  may be calculated:

$$L_p = 10 \log_{10}(10^{0.1L'_p} - 10^{0.1L_{pb}}) \tag{11.19}$$

If  $L'_p - L_{pb} \geq 10$  dB, the maximum error will be 0.4 dB if one simply uses  $L'_p = L_p$ .

To simplify calculations, Eq. 11.19 can be rearranged. If the measurable difference  $L'_p - L_{pb}$  is defined as  $\Delta$ , then a correction factor  $K_1$  for background noise can be calculated so that:

$$L_p = L'_p - K_1 \tag{11.20}$$

$$\text{where } K_1 = 10 \log_{10} \left( \frac{10^{0.1\Delta}}{10^{0.1\Delta} - 1} \right)$$

The correction  $K_1$  for background noise is shown as a function of  $\Delta$  in Fig. 11.8.

In Section 11.1 it was pointed out that in addition to the direct sound waves radiated from the operating electric machine, reflected sound waves exist as well that raise the level of sound pressure. The sound pressure level increase should be considered with the environmental correction  $K_2$  to account for the influence of reflected sound.  $K_2$  is the last term in Eq. 11.7', and is given by:

$$K_2 = 10 \log_{10} \left( 1 + \frac{4/S_0}{A/S} \right) \tag{11.21}$$

For easier use,  $K_2$  is shown in Fig. 11.9 as a function of the ratio  $A/S$ .

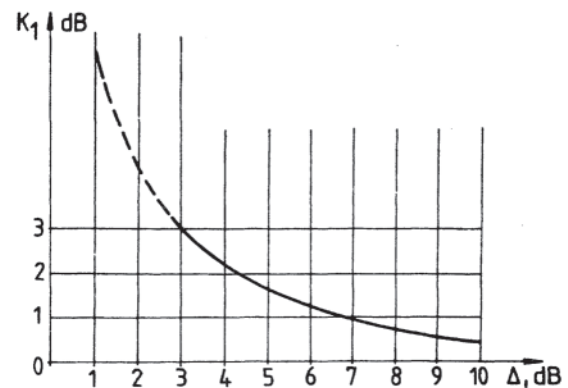
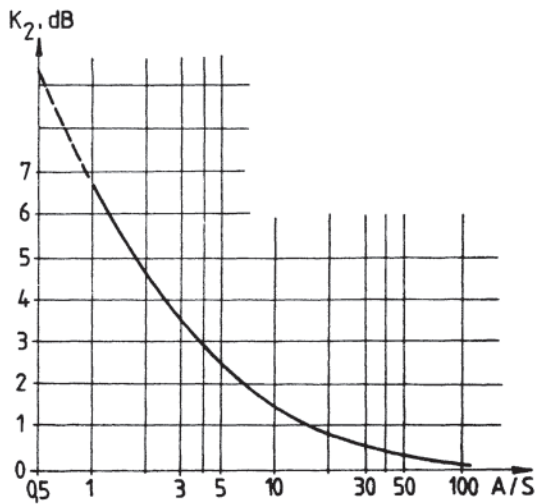


Figure 11.8 The correction factor  $K_1$  for background sound pressure levels.



**Figure 11.9** The environmental correction factor  $K_2$  to account for the influence of reflected sound.

Noise measurement of an electric machine is usually made in a direct sound field. These measurements are made to accuracies suitable for engineering or survey purposes. Since the goal of measuring noise is to determine the level of airborne sound power, the direct sound field measurement is made with the machine installed in such a way that it does not pass structure-borne sound to its environment so that the environment does not become an additional sound source. The machine to be tested is placed on a rigid floor that acts as a sound-reflecting plane, and as close as possible to the reflecting plane. There should not be a sound-reflecting wall or other object close to the machine. Using the usual 1-m measuring distance, it is advisable not to have any object within 3 m of the machine.

The sound power level radiated by the electrical machine should be determined under rated operating conditions, that is, rated supply voltage, frequency, speed, and load. In many cases these conditions are hard to achieve. If the tested electric machine is a generator, then the driving motor is indispensable; if the machine is a motor, then some device must provide the necessary load. Additional machines are themselves noise sources, and from the point of view of the machine on test they manifest themselves as background noise. Due to their proximity, however, these background noises are very hard to separate.

Most of the electric rotating machines tested are electric motors, which can easily be run under no-load conditions. An aspect that deserves some consideration is that the load dependency of electric rotating machine noise is ambiguous, as pointed out in Section 11.1. The effort to simplify the noise measurement procedure as much as possible, and also the consideration that noise measurement of electric motors aims at the qualification of the motor as a product, led the framers of the standards to accept the measurement of noise in no-load operation [9].

The dimensions of the electric machine determine the shape of the reference surface. Small-size electric rotating machines can usually be considered to be pointlike sound sources. The

most suitable measuring surface in this case is the hemisphere. For medium and large electric machines, the conformal or the parallelepiped surface is used. The conformal surface is a better fit to the shape of the machine to be measured and the constant measuring distance  $d$  can easily be used. The parallelepiped makes execution of the measurement procedure simpler and faster.

At least eight to nine measuring points should be used on the measuring surface, the so-called key measuring points. If the electric machine is not a directed noise source, the range of the sound pressure level values measured at the different key measuring points will not be larger than 8 dB. If it is, the number of measuring points has to be increased. In calculations for the measuring surface area  $S$ , the standards and the shape of the measuring surfaces must be taken into consideration.

When carrying out the noise measurement, the first step is to determine the effect of the acoustic environment. The environmental correction  $K_2$  to account for the influence of reflected sound has to be determined. The measuring points have to be introduced on the measuring surface, the background noise level has to be measured, so that later the correction for background pressure level  $K_1$  can be determined. The measurement of noise for the machine has to be carried out at the measuring points, determining the sound pressure level  $L'_{pi}$  for every point. Correcting these with  $K_1$  (see Fig. 11.8), the sound pressure  $\bar{L}_p$  (Eq. 11.4) may be computed by the averaging calculation. Correcting this average sound pressure level with  $K_2$  and adding the correction for the measuring surface, the sound power level radiated by the electric machine can be calculated:

$$L_W = \bar{L}_p - K_2 + 10 \log_{10} \left( \frac{S}{S_0} \right) \quad (11.22)$$

The algorithm above is carried out with an A-weighting filter, yielding a sound power level designated as  $L_{WA}$ . If needed, the measurement is also carried out with octave-band and third-octave band filters as well. Band analysis of the sound power level requires a great deal of time but gives useful information.

The basis for qualifying electric machines is the sound power level measured with the A-weighting filter and calculated to yield  $L_{WA}$ . The standards give tables of permissible values of  $L_{WA}$  for normal sound quality based on the speed and for nominal power of the electric machine. For example, see Table 11.4.

A frequently encountered situation in industry is that of making noise measurements on a source that cannot be moved. These machines cannot be transported to an acoustic laboratory for measurements and the classic method of substitution, that is, the use of a reference sound source, cannot be used either due to the difference in sizes and the inability to move the test source. In such situations, *in situ* noise measurement must be done, but under such circumstances the acoustic conditions specified in the standards cannot be satisfied. The answer is found in substantial expansion of the list of noise-measuring possibilities by carefully applying the concept of reference sound sources.

The measuring surface should be located around the noise

source. The recommended measuring distance is  $d=1$  m. Over the measuring surface,  $n$  measuring points should be selected. At these points the background noise levels  $L_{piB}$  are measured with the machine switched off. The average background noise level  $\bar{L}_{pb}$  is then calculated. After the machine has been switched on, the sound pressure level  $L'_{piF}$  is measured at each measuring point.

The values of  $L'_{piF}$  must be corrected in terms of the background noise by an amount that depends on the difference between the average background noise and the individual values of  $L'_{piF}$  to obtain values of  $L_{piF}$ . Now the reference sound source is to be used, again with the motor switched off. The reference source emits a reference sound power level  $L_w(\text{ref})$  (calibrated in an acoustic laboratory) for  $m$  operating positions. These operating positions are located along the sides of the motor (side-by-side procedure) or on top of the motor (superpositional procedure). For each reference source position the sound pressure level at each measuring point is obtained, yielding the levels  $L'_{pij}(\text{ref})$  (where  $i$  is the subscript indicating the measuring point and  $j$  is the subscript indicating the operating position of the reference sound source). Each value of  $L'_{pij}$  is to be corrected for background noise, thus determining the values of  $L'_{pij}(\text{ref})$ .

The sound pressure levels measured for the different positions of the reference sound source are averaged at each measuring point.

$$L_{pi}(\text{ref}) = 10 \log_{10} \left( \frac{1}{m} \sum_{j=1}^m 10^{0.1L_{pij}(\text{ref})} \right) \quad (11.23)$$

Knowing the geometric configuration of the measuring points (that is, their distances from the operating positions of the reference sound source), one calculates the values of  $L_{pij}(\text{ref-comp})$  from  $L_w(\text{ref})$  for each measuring point, and these values are averaged for each measuring point:

$$L_{pi}(\text{ref-comp}) = 10 \log_{10} \left( \frac{1}{m} \sum_{j=1}^m 10^{0.1L_{pij}(\text{ref-comp})} \right) \quad (11.24)$$

Now the correction terms that take into account the acoustic conditions must be determined for each measuring point:

$$K_{2i} = L_{pi}(\text{ref}) - L_{pi}(\text{ref-comp}) \quad (11.25)$$

The average of these correction terms is  $K_2$ .

Next the sound pressure levels have to be averaged over the measuring surface and corrected for the acoustic environment using Eq. 11.4, which is:

$$\bar{L}_p = 10 \log_{10} \left( \frac{1}{n} \sum_{i=1}^n 10^{0.1L_{pi}} \right) \quad (11.4)$$

Finally, corrected for the measuring surface, the sound power level emitted by the motor is found to be:

$$L_w = \bar{L}_p - K_2 + 10 \log_{10} \left( \frac{S}{S_0} \right) \quad (11.26)$$

where  $S_0=1$  m<sup>2</sup>.

If the spectral characteristics of the motor noise and the reference sound source noise are similar, the algorithm is directly applicable to the sound pressure levels measured using an A-weighted filter to determine the A-weighted sound power

level. However, if the spectral characteristics are different, the procedure discussed should be applied to the octave-band sound pressure levels, and the A-weighted sound pressure level can be calculated from the octave-band sound pressure levels only at the end, taking into account the A-weighting curve.

## 11.2 VIBRATION

Mechanical vibration of electric machines cannot be separated from noise produced by the machine, as shown above. The various sources of vibration and noise act in different ways. For example, noise produced by electromagnetic effects is characteristically produced by a process that begins with vibration, and part of the vibrational energy is radiated as sound energy. Among mechanical causes of noise, an out-of-balance rotor is a major source; the low-frequency noise (at rotational frequency) is felt by an individual only after much damping. Another mechanical source of noise is the bearings. The mechanism by which bearings generate noise is similar to the mechanism for production of electromagnetic noise; that is, significant cyclical deformation appears in the body of the machine, and these cyclical deformations generate the noise. There are also mechanical noise sources such as sliding contacts (brushes on slip rings and/or on commutators) that do not create vibration in the body of the machine but radiate noise directly. Aerodynamic noises also do not create measurable mechanical vibrations in the body of the machine.

In everyday practice, vibration is defined as the mechanical motion measurable on the surface of the machine. Vibration means deformation. Vibration of the machine decreases the lifespan of the machine. Some of the vibrational energy of the electric machine is transferred to the environment, for example, to machine tools driven by a motor, and these units will vibrate in turn. Machine tool vibration may make it difficult or even impossible for satisfactory work to be produced. Vibration reaches those who are using the machine or are in the vicinity of the machine, and may be harmful to their health.

Vibrational velocity due to electromagnetic driving functions in an electric machine can be determined from Eq. 11.8. The physical effects represented by this equation are valid in stable operation or transient operation, and with line supply or with inverter supply. The expression is valid for any component of vibration. The electromagnetic noise phenomena discussed in Section 11.1.1 are valid for the vibration of machines supplied by inverters. With simple inverters and especially at low speeds, the time harmonics in the supply cause a significant increase in vibration. These effects are eliminated by modulation of the optimized impulse width of the inverter.

In Section 4.1, switching-on phenomena of induction motors were discussed and the switching-on and accelerating transient vibrations were mentioned. A transient radial vibration of frequency  $f_1$  develops in the stationary induction motor when switching-on due to  $A_0$ , the free direct current. This transient vibration decays with time constant  $\tau_a$ . Elimination of the transient vibration is achieved in a manner similar to the elimination of the transient torque oscillations due to the free direct current  $A_0$  [16]. The solution is the



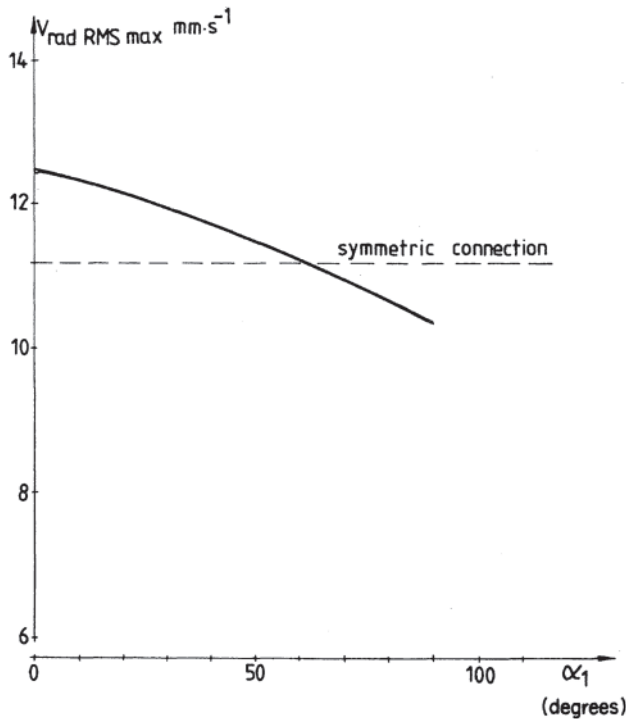


**Figure 11.10** Variation of the maximum value of the transient radial vibration velocity as a function of retarding angle  $\alpha_1$  with  $\alpha_2=90$  degrees. For the symmetric connection,  $\alpha_1$  is optional.

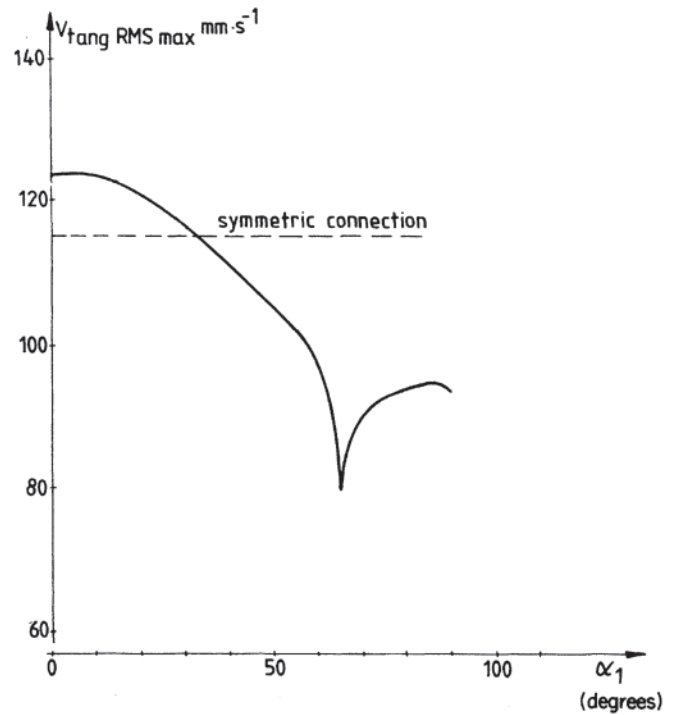


**Figure 11.11** Variation of the maximum value of the transient tangential vibration velocity as a function of retarding angle  $\alpha_1$  with  $\alpha_2=90$  degrees. For the symmetric connection,  $\alpha_1$  is optional.

asymmetrically retarded switching-on strategy, with lags from a zero-crossing point of voltage of  $\alpha_1 = \phi_m = 90$  degrees and  $\alpha_2=90$  degrees, as shown in Ref. 6, with the results displayed in Fig. 11.10. This figure shows the change of the effective values of the transient radial vibration velocities as a function of  $\alpha_1$  with  $\alpha_2=90$  degrees. Since there are other vibration sources present that are independent of the switching-on method, the vibration velocity does not decrease to zero even at the optimum of  $\alpha_1=\alpha_2=90$  degrees, but substantial improvement is effected over symmetrical switching.

When examining the switching-on transients, it was shown earlier that there are transient oscillating torques of network frequency that decay with a time constant  $\tau_w$ , the same time constant as for the radial vibrations, and others that decay with a time constant  $\tau_b$ . Though the oscillating torques with a time constant  $\tau_b$  decay rapidly, they can still affect the torque peak at the beginning of the switching-on.

Oscillating torques create tangential vibrations and can be detected on the surface of the machine. Since both free direct currents take part in creating the tangential vibration (see Eqs. 4.98 and 4.99) and the two free direct currents cannot be eliminated simultaneously, the transient tangential vibration velocity will have two minima, corresponding to the two switching strategies. The correctness of the theory has been proved experimentally [6], and a plot of rms tangential velocity is shown in Fig. 11.11. The first vibration minimum was at a phase lag of  $\alpha_1 = \phi_{sc}$  with  $\alpha_2=90$  degrees, and the second (local) minimum was at a phase lag of  $\alpha_2=90$  degrees, again

with  $\alpha_2=90$  degrees. The transient vibrations of running-up mentioned in Section 4 should be noted separately in the case of induction motor, the most common electric machine.

It can be seen in Eq. 4.70 for electromagnetic exciting force that the exciting forces depend on the speed. Assuming constant acceleration of the rotor during running-up, the expression for the electromagnetic exciting force can be written as  $P \sin(\frac{1}{2} \epsilon t^2 + \phi_0)$ , where  $\epsilon$  is the acceleration of the rotor and  $P$  is the amplitude of the force as a function of the current during acceleration. The vibrating electric machine can be modeled as a vibrating mass  $m$ , with a damping factor  $k$  and a spring constant  $c$ . The following inhomogeneous linear differential equation can describe the model:

$$m\ddot{y} + k\dot{y} + \frac{1}{c}y = P \sin\left(\frac{1}{2} \epsilon t^2 + \phi_0\right) \quad (11.27)$$

$y$  = the displacement due to the vibration

$\dot{y}$  = the velocity

$\ddot{y}$  = the acceleration

The homogeneous part of Eq. 11.27 may be solved by well-known methods. The roots of the characteristic equation are  $\lambda_1$  and  $\lambda_2$ . One solution is obtained by varying the constants in the inhomogeneous equation. The solution in the case of  $\lambda_1 \neq \lambda_2$  is:

$$y_{inhom.part} = \frac{P}{m(\lambda_2 - \lambda_1)} \left[ e^{\lambda_2 \tau} \int_0^t e^{-\lambda_2 \tau} \sin\left(\frac{1}{2} \epsilon \tau^2 + \phi_0\right) d\tau - e^{\lambda_1 \tau} \int_0^t e^{-\lambda_1 \tau} \sin\left(\frac{1}{2} \epsilon \tau^2 + \phi_0\right) d\tau \right] \quad (11.28)$$

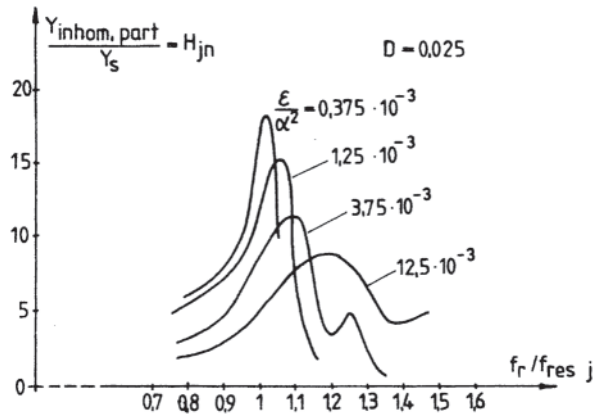


**Figure 11.12** The enveloping curves of the excited part of vibration in the case of  $D=0.025$ .

Evaluation of these integrals is quite difficult. For the usual induction motor internal damping  $D=0.025$  to  $0.030$ , the resonance curves are shown in Fig. 11.12 as a function of  $\epsilon/\alpha^2$ , where  $\alpha=2\pi f_{resj}$ . Each resonance curve is actually the upper enveloping curve of the excited oscillation spectrum. If the frequency of the exciting force changes rapidly, as in the case of transient resonance during running up, the vibration will not grow infinitely large, not even the case of zero damping, because of the short time during which the oscillating system takes energy from the excitation, the frequency of the excitation equaling the resonance frequency for only a short time.

There are two consequences of the change of excitation with angular frequency. The first of these is that the peak of the resonance curve is displaced in frequency and lags in time. That is, as the induction motor accelerates, the frequency of the exciting force increases and instead of the resonance appearing at the static resonant frequency  $f_{resj}$  it appears at a higher frequency  $f'_{resj}$ . The greater the acceleration  $\epsilon$  the greater the difference between  $f'_{resj}$ . In Fig. 11.12, choosing  $\epsilon/\alpha^2$  as a parameter, four curves are shown. If the acceleration  $\epsilon$  is sufficiently large,  $f'_{resj}$  may differ from  $f_{resj}$  by as much as 20%.

If the frequency of the exciting force is reduced, as happens in motor braking during reversing,  $f_{resj}$  shifts to a lower frequency. That  $f'_{resj} < f_{resj}$ . The extent of the shift is similar to that during acceleration, although for the usual values of acceleration of induction motors during reversing the resonant frequency shift will be in the range of 5–10%.

The shift of the peak of the resonance curve from  $f_{resj}$  to  $f'_{resj}$  is approximated from the following equation:

$$f'_{resj} \cong f_{resj} \left[ 1 \pm \frac{15.5}{5t_{res} \cdot \sqrt{\epsilon} + Dt_{res}^2 \epsilon} \right] \quad (11.29)$$

where:

$\epsilon = d\omega_r/dt$  = the rate of change in the frequency (which may be considered to be constant)

$t_{res}$  = the elapsed time from starting-up until resonancy is reached

$D$  = internal damping factor

The second consequence of the change of excitation with angular frequency is a decrease of the maximum magnifying factor. As can be seen in Fig. 11.12, with an increase in the velocity of frequency change, the amplitude of the vibration decreases. (For this figure,  $Y_s$  is the static deformation due to a constant force, and  $H_{jn}$  is the factor by which  $Y_s$  is magnified as a function of frequency.) With the usual accelerations of induction motors, the decrease in the resonance peak may be as much as 50%. This will not occur when heavy loads are started, but will occur with no-load or light-load running-up. Thus low critical speeds can be passed without danger.

The magnifying factor at the peak of the resonance curve is:

$$H_{jn}(\max) \cong \frac{1}{2D \sqrt{1-D^2}} [1 - \exp(-2.53 Dt_{res} \sqrt{\epsilon})] \quad (11.30)$$

### 11.2.1 Vibration Measurement and Evaluation

In the last 20 years or so, both general practice and international standards have used the effective value of the resultant vibration velocity in the frequency range between 10 Hz and 1000 Hz to describe the vibration condition of a machine. This practice has developed for the following reasons.

- Of the three vibration characteristics, namely, acceleration, velocity, and displacement, the vibration velocity is related linearly to the subjective sensation of vibration intensity, independently of frequency.
- It is the vibration velocity with which the kinetic energy of the vibrating body is in closest relationship. A given energy content corresponds to a given vibration velocity, while the acceleration signal enhances the importance of high-frequency components and the displacement signal enhances the low-frequency ones.
- The vibration velocity that corresponds to a given vibrational energy is independent of the frequency. This means that if a limit is specified for the vibrational energy, there is an inherent limit to the vibration velocity due to the unique relationship between the vibrational energy and the velocity.
- The vibration components most common in electric machines can be studied on the basis of frequency analysis of vibration velocity since this choice provides the best opportunity to take advantage of the dynamics of sensitivity that characterize the measuring system over the widest frequency range.

Mechanical vibration measurements of electric machines are made using contact sensors. The piezoelectric acceleration transducer is used most often and the signal proportional to the vibration velocity is obtained by integrating the output signal proportional to the vibration acceleration. The value of vibration velocity to be measured is a multifold rms value. The rms value of the individual harmonic vibration components is defined by Eq. 11.31:

$$v_{ie} = \left( \frac{1}{T} \int_0^T v_i^2(t) dt \right)^{1/2z} \quad (11.31)$$

where:

$v_{ie}$  = the effective value of the  $i$ th harmonic vibration component

$v_i(t)$  = the instantaneous value of the  $i$ th harmonic vibration component

$t$  = time

$T$  = the duration of the integration period

The duration  $T$  of the integration period is determined by the frequency of the signal to be measured. When measuring low-frequency signals, a larger  $T$  is needed than that used in high-frequency signal measurements. The most commonly used values of  $T$  are two standardized values, the “slow” (1 sec) and the “fast” (0.125 sec).

Having determined the effective value  $v_{ie}$  for each of the harmonics in the range 10 Hz to 1000 Hz, the resultant effective value is determined from:

$$v_e = \left( \sum_{i=1}^n v_{ie}^2 \right)^{1/2} \quad (11.32)$$

where:

$v_e$  = the resultant effective (rms) vibration velocity

$i$  = the serial number of the harmonic vibration components in the 10 Hz to 1000 Hz range

$n$  = the number of such components

and

$$f_u = 1000 \text{ Hz.}$$

To describe vibrations of long duration and different magnitudes, an equivalent value has been defined, one that is actually the rms value for a long period of time. The equivalent value of the vibration velocity is

$$v_{eq} = \left( \frac{1}{T_m} \int_0^{T_m} v^2(t) dt \right)^{1/2} \quad (11.33)$$

where  $T_m$  = the total measuring time.

Product standards emphasize isolation of the machine mechanically from its environment and try to ensure the reproductibility of measurements by specifying the measuring conditions. They also specify limiting values. As such, they must be understood by both the purchaser and the manufacturer of a product. Important standards are listed as Refs. 17–19. It is obvious that the conditions will be met with different degrees of success for various machine sizes, and the methods used in an attempt to meet all conditions are dependent on machine size. In the case of small- and medium-sized machines, flexible mounting is the method of choice, the machine being isolated from its surroundings by means of soft springs. For large machines, a completely rigid mounting is better. Rigid mounting should be used, of course, for small machines as well if the vibration of a motor and associated mechanical components is to be measured.

In the case of flexible mountings, the degree of softness of the springs must be checked. The spring-mounted machine (or the machine placed on a flexible base plate) forms a vibrating system that should have a natural frequency lower than one-fourth of the number of revolutions of the rotating machine per second. This requirement will be met if the static deformation of the elastic element is within the range given by:

$$0.5l \geq \delta \geq 4.2/n^2 \quad (11.34)$$

where:

$l$  = the unloaded length of the elastic element

$\delta$  = the change in length of the elastic element due to the weight of the machine

$n$  = machine speed in revolutions per second (rev/s)

The relevant product standards (for example, Ref. 18) strictly specify the operating conditions during vibration measurements. For induction motors, vibration measurement is normally done under no-load condition with rated supply voltage.

The number and the location of measuring points are dependent on the type and design of the machine, but in general the points with high dynamic requirements should be selected, those where vibration is transmitted to the surroundings. In the case of rotating electric machines, important measuring points are the bearing planes and the points where the machine is coupled to its surroundings. Vibration is measured in three mutually orthogonal directions,  $x$ ,  $y$ , and  $z$ , as shown in Fig. 11.13, the  $z$ -axis always corresponding to the axis of rotation.

Product qualification of an electric motor with respect to vibration is typically based on a single value of vibration velocity, spoken of as vibration severity. That value is the greatest of the velocities measured at appropriate points on the motor. Three grades of product qualifications are set forth in standards based on international agreement (see Ref. 8). The three grades are N (normal), R (reduced), and S (special).

The allowable velocities for the three grades are related to each other in such a way that those for grade R are 60% (4 dB) larger than those for grade S, and the same relationship applies to the velocities for grades N and R. Table 11.9 shows the allowable velocities for the three grades for ranges of motor speeds and shaft heights. Products of factories with average manufacturing capabilities and technology should be capable of meeting the qualifications specified for grade N.

A frequently encountered situation, especially in the case of large machines, is one where the bearing housing and the bearing bracket are rigidly mounted separately from the machine body. Consequently a mechanical vibration

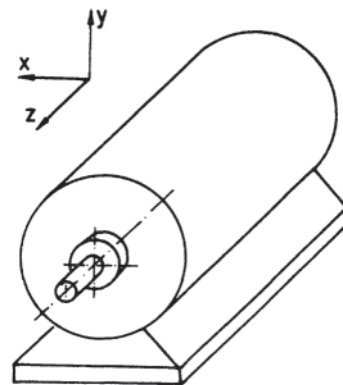


**Figure 11.13** Orthogonal coordinate conventions for vibration measurements on rotating machines with bases.

**Table 11.9** Allowable Vibration Velocities for Various Electric Motors

Vibration quality grade	Rated speed (rpm)	Maximum vibration velocity $v$ (mm/s) for machines with shaft height $h$ (mm)		
		$80 \leq h \leq 132$	$132 < h \leq 225$	$225 < h \leq 400$
N (normal)	600–3600	1.8	2.8	4.5
	3600–6000	2.8	4.5	7.1
R (reduced)	600–1800	0.71	1.12	1.8
	1800–3600	1.12	1.8	2.8
	3600–6000	1.8	2.8	—
S (special)	600–1800	0.45	0.71	1.12
	1800–3600	0.71	1.12	1.8
	3600–6000	1.12	—	—

measurement on the surface of the bearing housing does not provide in-depth information on the vibration of the shaft and rotor. In such a case, direct measurement of the vibration of the rotating part by means of a noncontact transducer is important in analytical, diagnostic, and safety testing.

Noncontact transducers measure displacement; hence the characteristic quantity in vibration of rotating shafts is always the vibrational displacement. If the noncontact transducer is mounted on a stationary and rigid bracket (clamping device) fastened to the bearing bracket or to the bearing housing itself, the transducer output will give the displacement of the shaft relative to the transducer. Hence comparison of shaft vibrational displacement between two machines is most meaningful if the same clamping device is used. Since the mounting point of the transducer may itself vibrate, the measurements made do not give the absolute displacement of the shaft.

To obtain an absolute measurement, the displacement of the mounting point of the noncontact transducer may be measured with respect to the reference inertial system by means of a contact transducer, such as a piezoelectric acceleration sensor. By integrating the signal from the piezoelectric acceleration sensor twice, absolute displacement of the noncontact transducer is obtained. The absolute displacement of the contact transducer and the relative displacement from the noncontact transducer may now be summed (taking care to use the correct sign) to yield the absolute displacement of the rotating shaft.

Although measurement of shaft vibrations is generally done over the frequency range 10 Hz to 1000 Hz, it must be remembered that many ultrahigh-power machines, such as hydrogenerators, operate at lowspeed, and the frequency range when making vibration measurements must be extended downward to include the rotational frequency of the shaft.

It is advisable to measure the vibration of rotating shafts in two mutually perpendicular directions, that is, vertically and horizontally. The measuring arrangement shown in Fig. 11.14 allows the measurement of both the absolute and the relative shaft displacement. When only the noncontact transducers, designated E1, are clamped in the clamping device B, then the relative displacement is measured. However, if the absolute vibration sensors, designated E2, are also put into position and the measuring and processing instrument M calculates

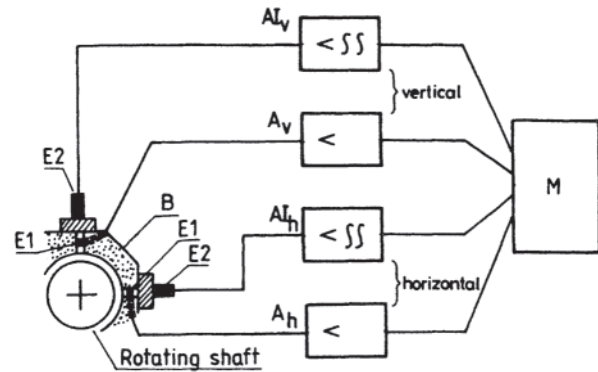


**Figure 11.14** Arrangement for the simultaneous measurement of absolute and relative displacements of a rotating shaft.

the sum (with appropriate sign) of the two kinds of vibration signals, then the absolute vibrational displacement of the rotating shaft is obtained. That is, using the output signals from amplifier-integrator  $AI_v(h)$  and amplifier  $A_v(h)$ , one can obtain the vertical (horizontal) displacement as a function of time.

Figure 11.15 shows the trajectory of the center of the rotating shaft in the plane perpendicular to the shaft. If it is assumed that the cross section of the shaft is circular, then Fig. 11.15 also shows the trajectory of a surface element while the shaft turns under the sensor. If the instantaneous coordinates of the shaft center  $K$  are  $x(t)$  and  $y(t)$  in the horizontal and vertical directions, respectively, then the integrated mean position of the shaft center with respect to time, that is, the coordinates of the origin  $O$ , are given by:

$$\bar{x} = \frac{1}{t_2 - t_1} \int_{t_1}^{t_2} x(t) dt \tag{11.35}$$

and

$$\bar{y} = \frac{1}{t_2 - t_1} \int_{t_1}^{t_2} y(t) dt \tag{11.36}$$

The displacement with respect to the origin  $O$  is indicated by the rectangular coordinates  $S_{h1}$  and  $S_{v1}$ , while the distance is given by  $S_1$ , where:

$$S_1^2 = S_{h1}^2 + S_{v1}^2$$

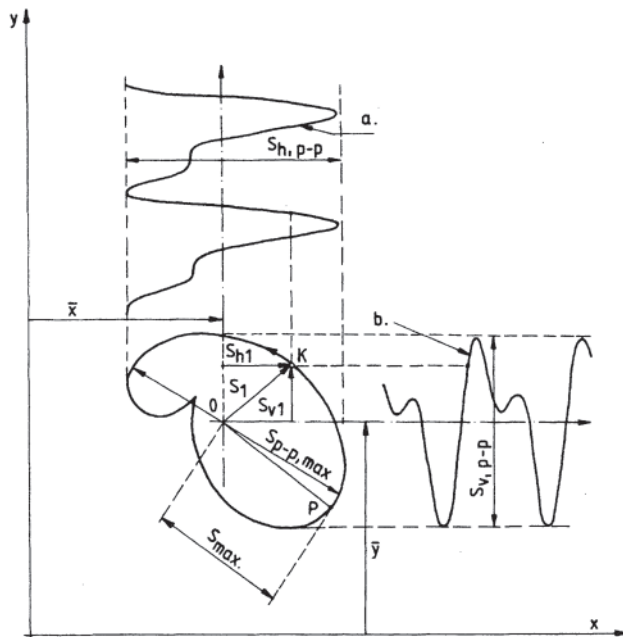


**Figure 11.15** Trajectory of the center of a rotating shaft, (a) Displacement vs. time in the horizontal direction, (b) Displacement vs. time in the vertical direction.

Figure 11.15 also shows the measurable time functions of vibrational displacement that correspond to the given shaft center trajectory, both in the vertical and the horizontal directions. The peak-to-peak values  $S_{h,p-p}$  and  $S_{v,p-p}$  can be read from the time functions of vibrational displacement.

The largest peak-to-peak value,  $S_{p-p(max)}$ , should be considered as characteristic of the shaft vibration, being the longest chord that can be drawn inside the trajectory of the shaft center. The correct value of  $S_{p-p(max)}$  can be determined by measurement only if the rigid clamping device that holds the vibration sensor can be adjusted concentrically about the shaft center. In such a case, the clamping device should be moved slowly until one of the sensors gives maximum signal, that is, the signal decreases if the adjustment is turned any farther. However, the position of the clamping device is fixed in most designs. In this latter and more typical case, the value of  $S_{p-p(max)}$  may be computed from the peak-to-peak values measured in the vertical and horizontal directions, using the following expression as a good approximation:

$$\frac{1}{2} \left[ (S_{v,p-p} \text{ or } S_{h,p-p}) + \sqrt{(S_{v,p-p})^2 + (S_{h,p-p})^2} \right] \quad (11.37)$$

In the first term inside the brackets, the larger of the values of  $S_{v,p-p}$  and  $S_{h,p-p}$  should be used. The value of the largest unidirectional shaft center displacement may be defined  $S_{max}$ . By definition:

$$S_{max} = [S_1(t)]_{max} \quad (11.38)$$

In most cases, only  $S_{v,p-p}$  or  $S_{h,p-p}$  is known, so the value of  $S_{max}$  may be approximated as:

$$S_{max} = 0.5S_{p-p(max)} \quad (11.39)$$

This equation gives the correct value only if the time function of the vibrational displacement of the shaft is a single sinusoidal wave.

In addition, Ref. 20 sets forth certain instructions regarding the evaluation of the shaft vibration measurement results. If each of the absolute displacements measured by the sensor clamping device (that is, the output signals of amplifier-integrator  $AI_h$  and  $AI_v$  in Fig. 11.14) is respectively smaller than 20% of the output signal of the corresponding amplifier  $A_h$ , or  $A_v$  (which measure the relative shaft displacements), then the qualification in terms of vibration may be carried out on the basis of the relative shaft displacement only. In any other case, the absolute displacement must be used for this purpose.

### 11.2.2 Housing and Shaft Vibration

The selection of vibration criteria is largely dependent upon the mechanical configuration of the machine. As shown in the previous section, either housing or shaft measurements may be made. Housing measurements are the more meaningful as they provide a better evaluation of the total machine. There is no direct relationship between housing and shaft measurements.

It is also necessary to understand that vibration criteria for a new motor will differ from the criteria for a motor connected to its driven equipment. Evaluation of new machines establishes viability of rotor balance and whether there are any resonances of machine parts coincident with the operating speed. This is generally the only vibration performance over which the motor manufacturer has control. Evaluation of installed machines is beyond the scope of this handbook.

“New,” as used in the previous paragraph, is intended to describe a machine that has not been operated for any period of time. It is generally considered that such machines produce vibrations that are without many of the harmonics that appear with wear and use. Nor should “new” be construed to apply to a rebuilt machine, even though a rebuilt machine may have the same warranty, because it is not certain that a rebuilt machine necessarily reverts completely to the condition of a new machine.

#### 11.2.2.1 Housing Measurements

For most motors, housing measurements made on the stationary frame are adequate to evaluate the machine with regard to reliable operation. Machines having antifriction bearings are best evaluated by the housing measurement method. Since the rotor shaft is closely contained by the bearings, any rotor-induced vibration is readily transmitted to the housing. Housing measurements also permit evaluation of vibration velocity, which provides a better interpretation of the health of the machine.

#### 11.2.2.2 Shaft Measurements

Shaft vibration is only significant on machines having sleeve bearings. Sleeve bearings provide an oil film to damp vibration transmission between the rotor and the enclosure.

Shaft measurements are also the preferred procedure to be used when rotors are operating above their first critical speed.

These flexible rotor shafts have a node between the bearing supports and are generally furnished with sleeve bearings, all of which suggests shaft measurements as the procedure of choice.

Although shaft vibration measurements are common for compressors, they are less common for motors. It should be recognized that motors are not constructed in the same way as are pumps and compressors. The vast majority of motors are configured to direct the flow of cooling air, provide protection from entry of moisture, and prevent access to dangerous parts by foreign objects (including protection of personnel). In this respect motors are structurally different from pumps and compressors where the enclosure must also contain the high pressures of working fluids. The result is that motors have a higher ratio of rotating to stationary mass. This in turn causes the enclosure to respond more effectively to rotor vibration, making frame measurements acceptable locations for most installations. Motor speeds are also relatively modest when compared with compressor speeds.

As a practical matter, therefore, shaft vibrations are only useful for high-speed, high-power motors that have sleeve bearings.

### 11.2.3 Mounting

Having made the decision as to the vibration measurement procedure, one must then understand that evaluation criteria are different for the acceptance of a new machine as compared to one that is in service. NEMA and IEC standards suggest that for new machines measurements be made with elastic mounting and with the machine unloaded. Measurements made in this manner have the advantage of evaluating the vibration quality of the basic machine, thereby eliminating motor vibration as a basic source of vibration after installation.

#### 11.2.3.1 Elastic Mounting

New machines should be evaluated on elastic mounts whenever possible. This truly reflects the condition of the machine and the vibration levels are not compromised by the type of mounting or foundation. Elastic mounting criteria are satisfied if the minimum deflection of the supporting elastic mounting is in accordance with Fig. 11.16.

#### 11.2.3.2 Rigid Mounting

Large motors may require rigid mounting. Acceptable rigid mounting of the new motor requires two separate evaluations:

1. The plane of the feet must be flat and they must be mounted on a flat surface. Unless this condition is met the motor frame may be stressed, causing abnormal resonances in the motor. This condition can be checked by selectively loosening the mounting bolts to see if there is a change in the overall vibration level.
2. The mass of the foundation must be great enough that the natural frequency of the test installation is not coincident with the predominant motor frequencies. This criterion will be met if measurements on the motor feet

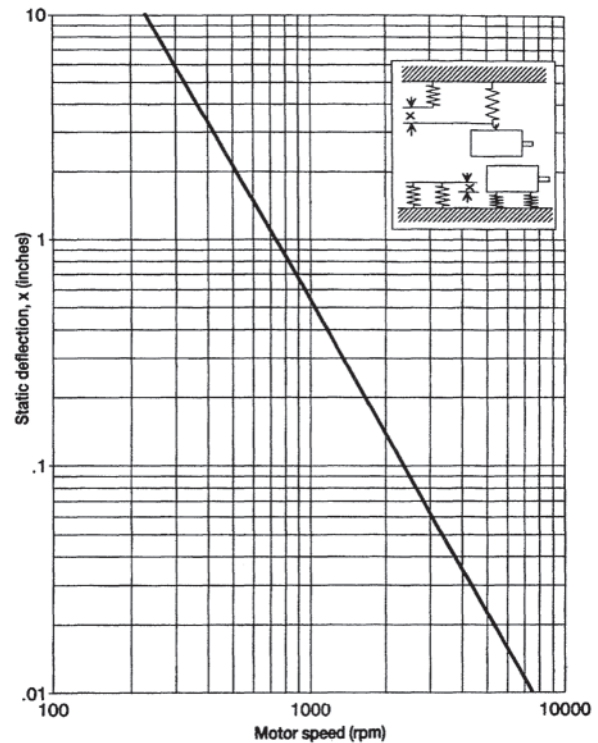


Figure 11.16 Minimum static deflection for motor vibration testing.

are less than 25% of housing measurements on the closest bearing, both measurements being taken in the same direction.

Satisfactory machine vibration is closely associated with the actual mounting of the motor. It is often desirable to make vibration measurements under actual installed conditions before connection to the driven equipment. These vibration levels may then be compared to the levels of the factory-tested motor. Vibration levels of installed motors should be comparable if the factory test used rigid mounting, but should be less if the factory test used elastic mounting. This latter situation results from the increased stationary mass. Unacceptable levels at this time are more easily identified and corrected.

#### 11.2.3.3 Shaft Key Convention

Vibration measurements are made with a half-key occupying the shaft keyseat. This is now the international standard and displaces the previous convention of using a full key in many areas of the world. A half-key has always been used by the motor industry in the United States.

### 11.2.4 Variable-Speed Motors

For machines intended to be operated at more than a single speed, vibration should be evaluated at all speeds of interest. Multispeed motors have well-defined speed ratings, but adjustable-speed motors have only a speed range. Since most of these motors have rigid rotors, rotor vibration (from unbal

ance) will increase as a function of the square of the motor speed. Therefore, maximum rotor-induced vibration usually occurs at maximum operating speed. On the other hand, resonance can occur whenever a resonance frequency is excited. This phenomenon is observed as a noticeable increase and then decay of the vibration level as a resonance frequency is passed during variable-speed operation. When this occurs the offending resonant part should be modified. Improving the rotor balance may provide only a temporary solution.

#### 11.2.4.1 Measurement Locations

Vibration measurement locations are dependent upon the type of machine enclosure and the application.

#### 11.2.4.2 Housing Measurements

Housing vibration measurements are made on bearing supports because vibration in the vicinity of bearings reflects the dynamic forces and the overall vibration of the motor.

Housing measurements are made in three mutually perpendicular directions as close to each bearing as possible. Directions are usually designated as vertical, horizontal, and axial. The maximum reading in any of these six locations establishes the vibration level of the motor. Typical measurement locations are shown in Fig. 11.17.

Operational evaluation measurements can then be reduced to a single radial measurement with an occasional monitoring of the axial position. Each location characterizes different sources of vibration and can be used as a diagnostic test to determine maintenance actions to be taken.

#### 11.2.4.3 Shaft Displacement Measurements

Shaft vibration measurements are made with two noncontact proximity probes, 90 degrees apart, which should be located inside the bearing, measuring the shaft's bearing journal displacement.

Figure 11.18 shows a typical mounting arrangement. Shaft displacement vibration measurements reflect imperfections in the bearing journal surface and may also indicate electrical

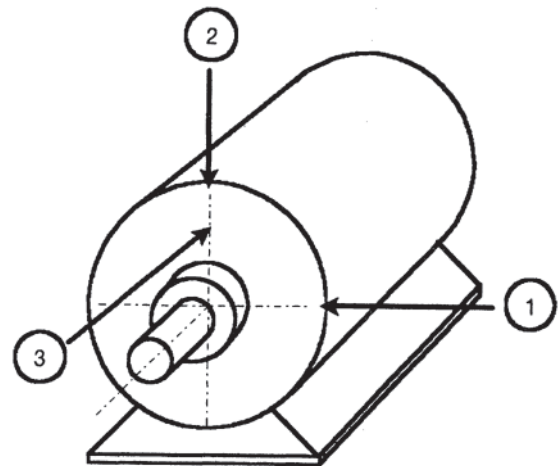


**Figure 11.17** Measurement locations for housing vibration evaluation.

abnormalities due to nonhomogeneous structure of the shaft material. It is generally necessary to have a special machining of the shaft bearing journal to achieve a minimum acceptable runout. These abnormalities can be isolated either with instrumentation or by isolating the abnormalities during a slow-speed rotational test.

#### 11.2.5 Standards [20–22]

The representation of vibration limits has recently gone through an evolution.

##### 11.2.5.1 Housing Measurements

United States standards have historically been based upon vibration displacement, which provides only a qualitative evaluation of the machine unbalance.

Based upon work originating in the international community, the trend during the last 20 years has been toward expressing machine vibration limits in vibration velocity. While the United States has moved toward vibration velocity, there still exists a difference in that the United States generally

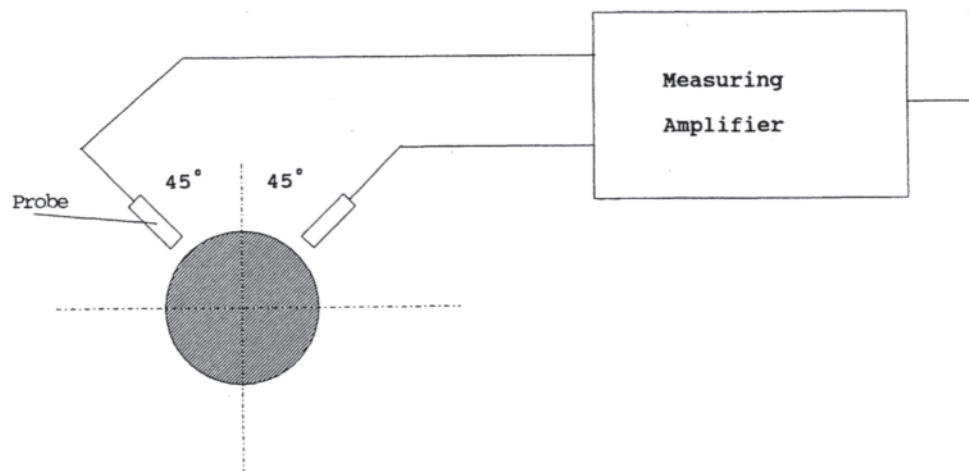


**Figure 11.18** Preferred installation of transducers for measurement of shaft displacement.

**Table 11.10** Limits of Maximum Vibration Magnitude in Displacement, Velocity, and Acceleration (rms) for Shaft Height H (mm)

Shaft Height, mm		$56 \leq H \leq 132$			$132 < H \leq 280$			$> 280$		
Vibration grade	Mounting	Displac. [ $\mu\text{m}$ ]	Vel. [mm/s]	Acc. [ $\text{m/s}^2$ ]	Displac. [ $\mu\text{m}$ ]	Vel. [mm/s]	Acc. [ $\text{m/s}^2$ ]	Displac. [ $\mu\text{m}$ ]	Vel. [mm/s]	Acc. [ $\text{m/s}^2$ ]
A	Free Suspension	25	1.6	2.5	35	2.2	3.5	45	2.8	4.4
	Rigid mounting	21	1.3	2.0	29	1.8	2.8	37	2.3	3.6
B	Free Suspension	11	0.7	1.1	18	1.1	1.7	29	1.8	2.8
	Rigid mounting	—	—	—	14	0.9	1.4	24	1.5	2.4

specifies peak velocity vibration values, whereas rms velocity vibration values are preferred elsewhere in the world. It is therefore important to note the reference system when comparing vibration limits. While it can be assumed that the ratio of the limits is the square root of 2, there can be significant variations from this ratio depending upon the harmonics present. Justification for either representation is left to others.

Table 11.10 gives the IEC limits for housing measurements. U.S. vibration standards have progressed from single values as a function of machine size or power rating to families of curves consisting of constant displacement, constant velocity and constant acceleration zones. Such a curve for U.S. standards is shown by Fig. 11.19. Simply stated, the constant displacement zone addresses unbalance for slow machines and subharmonics of rotation speed, the constant velocity zone covers most of the vibration concerns and the constant acceleration zone evaluates the integrity of the bearing system

and its lubrication quality. IEC has introduced a similar set of values, using a table, format (see Table 11.10).

The upper curve (level=0.15) represents a standard machine with the lesser levels available for those applications requiring lower vibration limits. These limits are for uncoupled, elastically mounted motors. Motors that are rigidly mounted shall have the limits of Fig. 11.19 reduced by multiplying them by 0.8.

It should be noted that some large 3600-rpm motors may exhibit a twice-line-frequency vibration, excited from the electromagnetic field within the air gap. These motors require additional evaluation with the motor rigidly mounted.

*11.2.5.2 Relative Shaft Displacement*

Relative shaft displacement limits are presently equivalent in both U.S. and international standards.

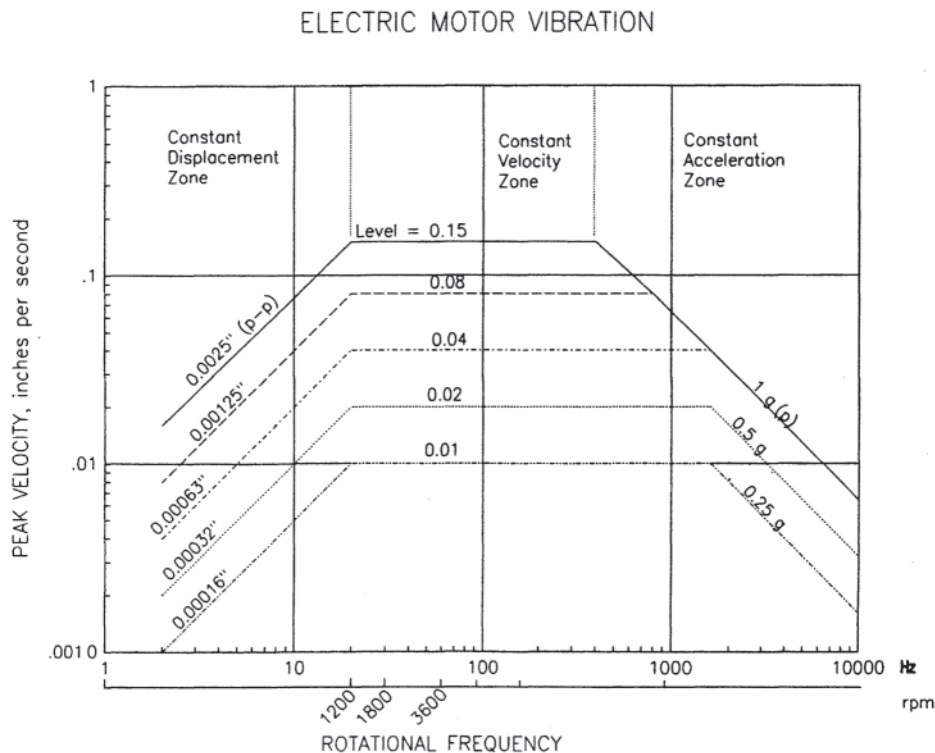


**Figure 11.19** Vibration velocity limits for elastically mounted motors.



**Table 11.11** Limits for Unfiltered Relative Shaft Displacement ( $S_{pk-pk}$ )

Motor	Number of poles	Maximum relative shaft displacement
Standard	2	0.0028 in (70 $\mu\text{m}$ )
	4	0.0035 in (90 $\mu\text{m}$ )
Special	2	0.0020 in (50 $\mu\text{m}$ )
	4	0.0028 in (70 $\mu\text{m}$ )
	>4	0.0030 in (76 $\mu\text{m}$ )

All of the above limits include electrical and mechanical runout. This total combined runout shall not exceed 25% of the maximum allowed vibration displacement in the table.

Motors having special provision for measuring shaft displacement should not exceed the limits specified in Table 11.11 when rigidly mounted.

The runout limits may be determined by rotating the shaft of an assembled motor at a slow speed of 100–400 rpm while measuring the peak-to-peak amplitude.

### 11.3 BALANCING THE ROTOR [23]

Minimum machine vibration is not possible without an adequate rotor balance. An unbalanced rotor provides the forcing frequency and energy that causes other components to vibrate in resonance. In addition to the fundamental unbalance amplitude, these resonant parts also contribute to the overall vibration levels and may cause the specification level for the motor to be exceeded even though the rotor balance is within acceptable limits.

There is no direct correlation between the residual unbalance of rotors and final machine vibration. A manufacturer can establish an empirical relationship based upon the ultimate vibration of the finally assembled machine as a function of the magnitude of the rotor unbalance. This relationship can change for each motor configuration. As a result, it is best for the user to specify a final machine vibration level and rely upon the motor manufacturer to provide a rotor balance that will achieve the specified level.

Rotor unbalance is characterized by a once-per-revolution unbalance force vector whose angular orientation (phase) remains constant with rotor rotation.

Rotor balancing is the process of adding (or removing) weight to balance planes that are as close as possible to the location of the unbalance. In motors there are usually two correction planes provided by the motor designer and they are located at each end of the rotor. These planes are used by the motor manufacturer for the initial balancing process and in some designs may also be used for final or field balancing of the complete machine. Motors with rigid rotors, which use two correction planes, are said to be dynamically balanced.

For the motor user it is not necessary to know the specific rotor dynamics of the motor. It is, however, important that the motor manufacturer know whether the rotor assembly is rigid or flexible.

#### 11.3.1 Rigid Rotors [24]

ISO defines a rigid rotor as follows.

A rotor is considered rigid when it can be corrected in any two (arbitrarily selected) planes and, after that correction, its unbalance does not significantly exceed the balancing tolerances (relative to the shaft axis) at any speed up to the maximum service speed when running under conditions which approximate closely to those of the final supporting system.

Practically this means that a rigid rotor does not have a rotor critical (resonance) speed within its operating speed range. Such rotors have a single flexural (bending) mode that is characterized by the residual unbalance inducing additional bending of the rotor assembly as the operating speed increases (see Fig. 11.20(a)). With a rigid rotor the unbalance amplitude increases as the square of the speed.

A rigid rotor can be balanced at a speed less than operating speed and generally provide acceptable performance. This slow-speed balance is best accomplished in a dynamic balancing machine. Instructions provided by each balance machine manufacturer provide adequate balancing procedures.

While the vast majority of motors have rigid rotors, there is a growing trend that 3600 rpm motors in the higher power range may have flexible rotors.

#### 11.3.2 Flexible Rotors [25]

ISO defines a flexible rotor as follows.

A rotor not satisfying the rigid rotor definition due to elastic deflection.

A flexible rotor will exhibit a significant increase in vibration in a narrow range (its critical speed) as it accelerates to operating speed. These rotors can be characterized as being rigid rotors with a single flexural mode at the lower speeds while at higher speeds they develop a second flexural mode (see Fig. 11.20(b)). The transition between the first and second flexural mode operation occurs when the mass center (location of the residual unbalance) shifts from being a radial force increasingly displaced from the axis of rotation to a position coincident with the axis of rotation. This area of transition is considered the critical speed (resonance) of the rotor and should occur at least 15% below the operating speed of the motor.

The residual unbalance now appears as being in two locations, that is, between the mass center and each bearing. The unbalance phase angle as seen at one end of the motor has also shifted about 180 degrees from the other end. This phase shift is one way of identifying a flexible rotor.

Flexible rotors are most effectively balanced when using three balance planes. Ideally one of these planes passes through the mass center and this is the plane where unbalance is corrected when operating in the first flexural (rigid rotor) mode.

By using a center correction plane for the initial balance correction in a balancing machine, it is then possible to do the final balancing at operating speed. Final balancing may be accomplished in a high-speed balancing machine with

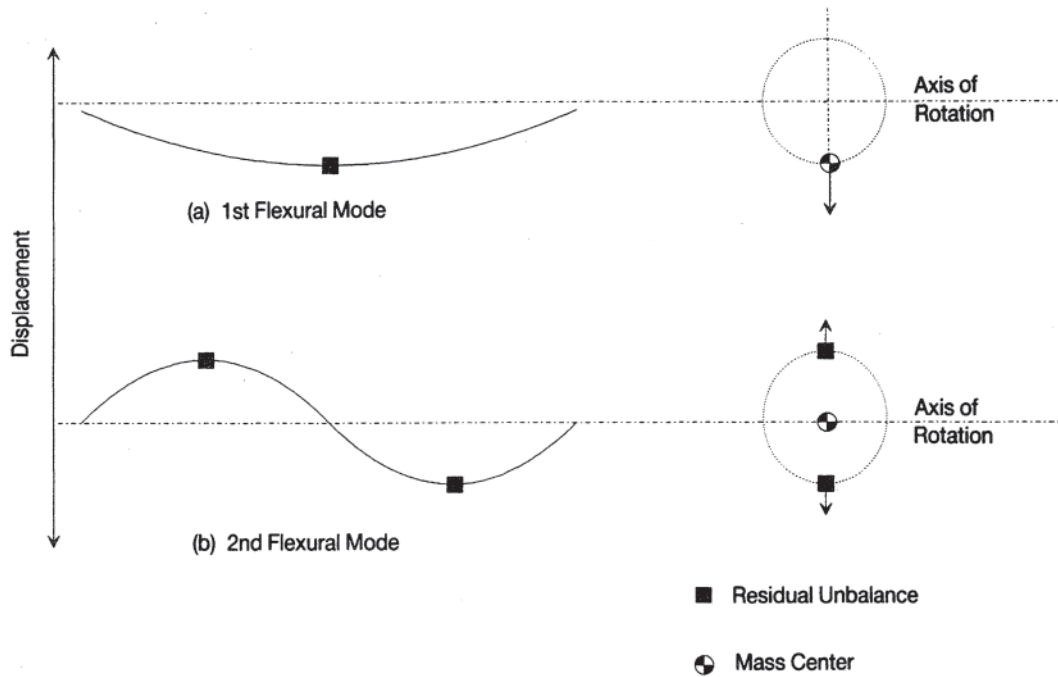


Figure 11.20 Rotor assembly flexural modes.

proper bearing supports or after the motor has been assembled and is operational. In the latter case the motor design must be such that access is provided to the balance correction planes.

Balancing of flexible rotors must be performed by a knowledgeable operator. ISO 5406 [25] is a good reference for flexible rotor balancing for those wishing detailed information.

### 11.3.3 Unbalance Quality

It must always be recognized that the first time a rotor reaches its operating speed and final temperature there may be a change in the unbalance amplitudes due to movement or stress equalization of some components. In some cases this is a one-time adjustment that can be corrected by rebalancing. Motors with die-cast rotors fall into this category.

In other cases unbalance quality is reflective of components that move as a result of centrifugal force. Some fabricated rotors are an example of this type of configuration. These cases can be corrected either by balancing at operating speed in a balance machine or by balancing the assembled motor.

There is a third case, generally associated with loose components, for example, parts manufactured out-of-tolerance or poorly designed so that they can become loose at operating speed. These can only be corrected by changing the offending part(s) and rebalancing. Of the three types, only the last exhibits unpredictable vibration levels as a function of speed.

## 11.4 BEARINGS

### 11.4.1 Sleeve Bearings

#### 11.4.1.1 Introduction

Functionally, an electric drive motor is a system for transforming electrical power into mechanical power and for converting it into usable torque, delivered to a rotating shaft. This power conversion is possible because of the electromagnetic linkage between the stator and rotor and such a conversion results from the interaction of the various components of that linkage, that is, the stator winding, rotor winding, stator core, and rotor core. However, the bearing assembly provides the only mechanical linkage between the rotor and stator and is, therefore, vital to the delivery of torque at the shaft extension. The magnitude of the forces acting upon, and the complexity of, the bearing assembly increase rapidly with the size of the motor. Accordingly, it is important that the basic design requirements of the bearing be defined, that the design be in accordance with fundamental principles, and that the specific application requirements expected to be encountered in service be considered in the overall design for (1) special bearings for special requirements and (2) a standard line of bearings for general application to a product line.

Some basic design requirements for the bearing assembly include: (1) capability to withstand the various forces acting between the stator and rotor; (2) capability for continuous operation; (3) in some cases capability for high peripheral speed; (4) capability to coordinate with the configuration of

other adjacent motor parts, such as to allow no oil leakage from the bearing housing; (5) ease of replacement, if necessary; (6) capability of being manufactured within small dimensional tolerances; and (7) conformity to limitations in available space of adjacent parts. To appreciate and to put into perspective the significance of the diverse design requirements of high peripheral speed and continuous duty on one hand and high reliability on the other hand, a point on a 5-inch journal that rotates in a 3600 rpm drive motor for 30 years would describe a distance equal to 25 trips to the moon and back.

#### 11.4.1.2 Scope of Application

Rolling-type bearings are normally used in the NEMA frame sizes of electric drive motors, although sleeve-type journal bearings may also be used in certain cases in such frames. However, because of the increase in journal size, peripheral speed, and loading encountered as the rating of the motor increases, a point is eventually reached for which sliding-type journal bearings are applied as standard. This results from such considerations as lubrication, centrifugal force of the rolling elements, bearing life at higher peripheral speeds and loads, cost of rolling-type bearings, and the need for increased damping provided by sliding-type bearings to counteract the tendency for vibration to increase with motor size.

There is no specific demarcation line between the use of rolling-element (so called antifriction) bearings and the use of sliding-element bearings. In this transitional region, where either type of bearing may be satisfactorily used for normal applications, several of the motor manufacturers will supply the type the customer desires and specifies in the purchase order. One demarcation line, which is somewhat typical of normal practice, is shown in Fig. 11.21, with either type of bearing being available for one or more ratings on either side of the demarcation line.

Figure 11.21 represents normal practice for drive motors, the shafts of which are oriented in a horizontal position. Such horizontal machines represent a large percentage of all motors sold. Although they represent a much smaller percentage of applications, sliding-type bearings are also used for vertical motors, the shafts of which are oriented in a vertical position. Vertical motors are typically used to drive centrifugal pumps

of various kinds, where the motors are mounted above the pumps they drive. For this type of application, a thrust bearing carries the axial load due to the weight of the motor rotor and pump impeller, as well as the hydraulic thrust of the pump. Also, two sleeve-type guide bearings, located near the two ends of the shaft, are used to hold the shaft in vertical alignment. In the usual design of a vertical motor, the thrust bearing and the upper guide bearing are incorporated into one upper bearing assembly and are contained within one bearing housing. The mechanical configuration of sliding-type horizontal sleeve bearings and vertical thrust bearings will be discussed subsequently.

#### 11.4.1.3 Forces Acting on the Bearing

The bearing system provides the only mechanical linkage that exists between the rotor and stator. In order for a sliding-type bearing to operate effectively, it must maintain a continuous oil film between the journal and bearing during operation and must withstand all forces that act between the rotor and stator. For a typical medium to large drive motor, the rotor weight is approximately equal to one-third of the total weight. For units weighing from 4000 kg (8800 pounds) to 20,000 kg (44,000 pounds), the rotor weight would vary from 1300 kg (2870 pounds) to 6700 kg (14,700 pounds). Another significant force acting on the bearings is unbalanced magnetic pull, a force that is a function of the amount of displacement of the rotor outer diameter relative to the stator bore. The rotor is never exactly centered in the stator bore of a large motor, nor is it desirable for it to be so, from a stability standpoint. Accordingly, there is always unbalanced magnetic pull present in large machines due to a nonuniform air gap. Although the magnitude of the unbalanced magnetic pull can, within reasonable limits, be controlled by the design of the stator winding and by the amount of air gap offset permitted, it varies from a fraction of the rotor weight to an amount equal to it.

There are occasional applications that impose additional forces on the bearings. These include overhung exciters for synchronous motors, flywheels, axial thrust from the driven equipment, nonuniform motion of the entire unit, such as is encountered in shipboard service and in shovel sets, and lateral belt pull, for belted drive motors. Concerning belted applications, both the magnitude and direction of belt pull can be significant and not all motors are designed to be suitable for such applications. When ordering a new drive motor for a belted application, it is important to so state on the purchase order and to give the magnitude and direction of the force. Also, when reapplying an existing drive motor from a direct-coupled application to a belted application, it is important to verify that the motor is suitable for the new application. This can be accomplished by identifying the model number and serial number of the unit to the manufacturer and requesting information on its suitability for the belted application.

In providing mechanical linkage between the rotor and stator, bearings are also subject to dynamic forces. Even though considerable care is taken to machine the rotor parts within close tolerance and to balance the complete rotor, some amount of unbalance will inevitably exist. This unbalance is manifested

HP POLES	400	450	500	600	700	800 UP
2						
4	ANTIFRICTION					
6				SLEEVE		
8						
10 UP						

**Figure 11.21** Typical demarcation between sleeve bearing and antifriction bearing ratings for normal horizontal motor applications.

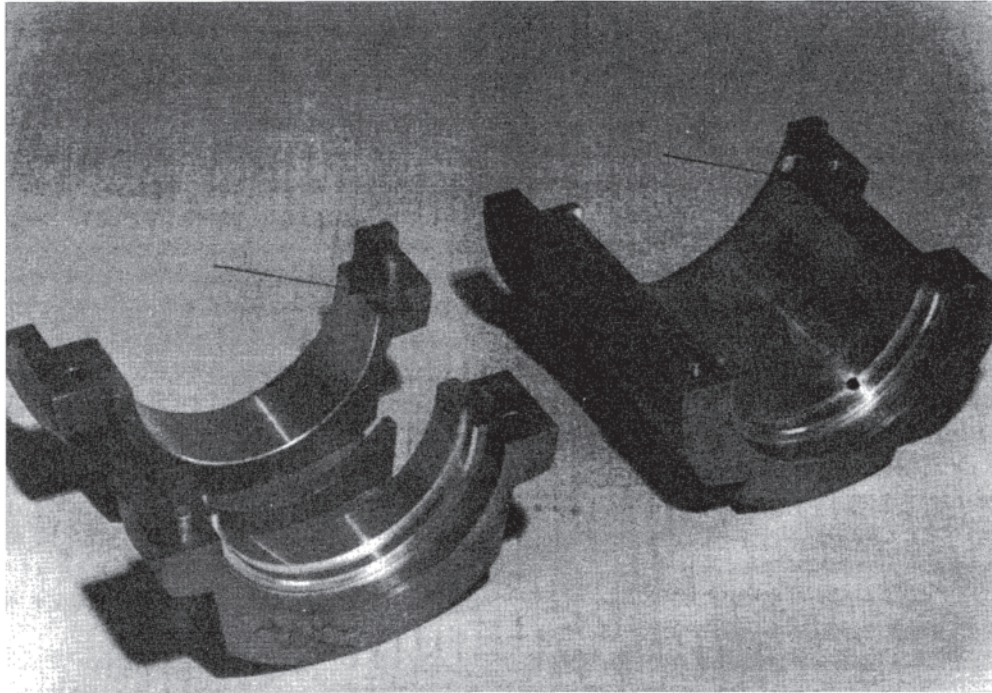


**Figure 11.22** Cylindrical-type, horizontal, split-sleeve bearing, showing lateral oil grooves on each side. Left: top bearing half. Right: bottom bearing half. (Courtesy of the General Electric Company.)

as a dynamic exciting force that is transferred across the oil film from the rotating journal to the stationary bearing at a frequency equal to operating rpm. The magnetomotive force produced by the stator winding also causes dynamic forces, the most significant of which is that corresponding to twice the line frequency. The effect of such dynamic exciting forces is to produce some amount of vibration. The overall design of the machine is coordinated so as to limit vibration to insignificant amplitudes from an overall application standpoint, say 0.025 mm (0.001 inch). However small this may appear, it is of the order of magnitude of the minimum oil film thickness within the bearing. The oil film must be maintained continually, which means that it must withstand such dynamic forces, as well as the previously mentioned steady-state forces.

#### 11.4.1.4 Configuration of Sleeve Bearings

Sleeve bearings have existed for most, or all, of recorded history. A cart wheel, the hollow hub of which rotates about an axle, is typical of a simple sleeve bearing that has existed from the dawn of history. With the advent of the industrial revolution, sleeve bearings have become increasingly important. Accordingly, during that period, and in particular during the past 75 years, great improvements have been made in sleeve-bearing design and in the development and use of proper lubricants.

Based on the type of bore that forms the bearing surface, horizontal sleeve bearings used on drive motors may be classified as cylindrical, elliptical, and pivoted-shoe. The cylindrical type is probably the most commonly encountered sleeve bearing and, as the name would suggest, has a cylindrically machined inside diameter to form the bearing surface. This mates with the shaft journal. This type of bearing

may be split horizontally, so that the complete bearing is formed by a top half and a bottom half, or it may be continuous. The splitsleeve bearing has the advantage that it is easier to remove for inspection or replacement in the field without disturbing the coupling alignment. This feature makes it desirable for larger machines.

The bearing shell is made from steel stock, cast iron, or cast steel, and the outside diameter is machined to seat in the lower half of the end shield, end bell, or pedestal. For a cylindrical bearing the inside diameter (ID) of the bearing shell is machined to a true circle, or is cast to very close tolerances, but this ID is somewhat larger than the eventual ID of the finished bearing. Molten babbitt is then applied to the ID of the bearing shell, usually by a centrifugal casting process, after which the desired inside diameter of the bearing is achieved by machining the babbitt to the correct diametrical dimension. Lateral oil grooves are then machined into each side of the bearing at the horizontal centerline, as indicated by the arrows in Fig. 11.22. Although other systems of oil grooving have been used for drive motors, side grooves provide the maximum uninterrupted bearing area on the bottom bearing half and are generally favored for most motor applications.

Lightly loaded sleeve bearings are somewhat susceptible to a fluid phenomenon called “oil whip,”\* which can cause significant vibration. In such situations, so-called elliptical bearings are frequently used, in which the ID is slightly greater in the horizontal plane than in the vertical plane. This is achieved by placing shims in the split between the two bearing

\* Oil whip (or oil film whirl) is the name ascribed to a condition of instability that is characterized by movement of the journal shaft in a closed path at a frequency that is generally equal to or less than one-half the rotational speed. The force and resulting motion are self-excited.

halves prior to final machining of the bearing inside diameter. When the shims are subsequently removed after machining, the inside of the bearing has an ellipsoid contour, with a maximum clearance with the journal in the horizontal plane. This allows a greater quantity of oil to flow through the bearing, which tends to reduce oil whip.

A type of sleeve bearing that has proven to be very stable, in particular at light loading and higher speeds, is the pivotedshoe, or tilting-pad type. It consists of three or four segments around the bearing, the inside surfaces of which form an interrupted circle of babbitt, to mate with the journal. The center of the outside surface of each segment is pivoted to a fixed circumferential shell or similar structure that allows each of the segments to tilt and to form an oil wedge at the leading edge. This type of construction has the overall effect of forcing the journal toward the geometric center of the bearing and of reducing oil whip. This design of bearing has the disadvantage of greater cost and fewer options in methods of oil delivery to the bearing, but it is a viable option at speeds and bearing loads at which oil whip can occur.

#### *11.4.1.5 Configuration of Thrust Bearings*

Sleeve bearings on horizontal drive motors are not normally designed to accept any significant amount of axial thrust. Such motors normally operate with their rotors on “magnetic center” and with the axial end play of their journals essentially equal at each end of the bearings. It is usual practice to have the two ends of the bearing babbitted in the vertical plane. This provides a flat surface with which corresponding faces at each end of the journal can mate and thereby carry a small amount of axial thrust on a temporary basis. However, if a horizontal motor with sleeve bearings must carry significant axial thrust on a continuous basis, an auxiliary thrust bearing will be required, designed somewhat along the line of that discussed below for vertical motors.

Vertical motors are primarily applied as drives for centrifugal pumps. Accordingly, the bearing system must carry the axial thrust in the vertical direction due to the motor’s rotor weight and pump’s impeller weight, as well as hydraulic thrust from pump action. In smaller sizes of vertical motors, antifriction thrust and guide bearings are used, such as angular-contact ball bearings, spherical-seat roller bearings, and so forth. However, in the larger sizes of vertical motors, sliding-element thrust bearings are used to a significant extent. There are two types of sliding-element thrust bearings that are widely used for such application, i.e., the pivoted-shoe type and the spring-supported, segmented-plate type of bearing.

The pivoted-shoe, or Kingsbury, type of thrust bearing is a highly reliable type that has been widely used. The bearing surface consists of several individual segments around a circle. Each segment is free to pivot about a radial line, which allows the individual segment to tilt in the plane perpendicular to the shaft and thus to form an oil wedge and to adjust the oil film to the load and oil hydrodynamics that exist at any point in time. Thrust is delivered to the bearing by means of a collar, attached to the shaft, which acts as the runner. For smaller applications, for which the bearing losses can be dissipated by

conduction and convection from the bearing housing, the bearing is sufficiently submerged in oil so as to allow the pumping action of the bearing to force oil between segments in a radial direction, where it can form an oil wedge on the leading edge of each segment or shoe. For intermediate applications, the above scheme can also be used, but with an oil-to-water cooling coil located inside the bearing housing. For larger applications, oil is supplied to the center of the bearing housing, near the “standpipe” that surrounds the shaft. The oil then passes through the bearing, as discussed above, and leaves the bearing housing near its outer diameter. The hot oil then passes through an oil-to-water heat exchanger, through an oil pump (usually) and back to the center of the bearing.

For very high values of thrust at moderate to low speeds, say 600 rpm or less, the spring-supported, segmented-plate type of thrust bearing is useful. Although it is used for some large vertical drive motors with high thrust requirements, it is also used on hydroelectric generators, which can have thrusts of 1,000,000 kg (2,200,000 pounds). This type of thrust bearing consists of some number of individual segments around the circle, similar to the pivoted-shoe thrust bearing just described. It differs in that, instead of being pivoted, the individual bearing segments are positioned over an array of coil springs. Thus, when the thrust collar, or runner, is positioned over the segments, the weight of the rotor will preload the springs. When the rotor starts to rotate, the leading edges of the segments will deflect sufficiently to permit the formation of an oil wedge and the capability to carry load. In order to ensure adequate distribution of oil, the bearing segments and the mating collar, or runner, are frequently grooved. Oil flow is achieved in the same manner as described for the pivoted-shoe thrust bearing. Because of the amount of loss associated with the thrust encountered with such bearings, the bearing losses are usually removed by an external oil-to-water heat exchanger. It is not unusual to use hydraulic oil lift at start-up for segmented-plate bearings. It is provided by exerting hydraulic oil pressure through small openings in the bearing segments.

Other designs of sliding-type thrust bearings have occasionally been used on vertical drive motors, such as solid annular plates with several radial grooves to permit radial oil flow. The bearing segments are formed by the annular spaces between radial oil grooves. This design of bearing can be either a flat-land or a tapered-land type. As the name suggests, the bearing surfaces of the individual lands, or segments, of the flat-land type are in a fixed, horizontal position. Usually, however, there is a chamfer in the leading edge, which assists in forming the oil wedge. As might be expected, this bearing is limited to light loads. For the tapered-land type, a taper is machined on the leading 75–80% of the land of each segment, which significantly increases the permissible unit loading over that of the flat-land type. However, the most reliable thrust bearings for heavy values of thrust are the pivoted-shoe type and the spring-supported, segmented-plate type, which were discussed earlier. These bearings are available from only a few suppliers and should be applied to machines at loads and speeds and with lubrication systems in accordance with the application data provided by such suppliers.

### 11.4.1.6 History of Sliding-Bearing Technology

Prior to the middle to late part of the nineteenth century, bearing design and application was a highly inexact art and improvements resulted from trial and error. Consequently, many earlier practices were not optimal and were even unsound. However, toward the end of the last century and the beginning of this century, scientists and engineers started to address the concept of sliding bearings on a more fundamental basis, and since then insight into the theory and application of such bearings has greatly improved. Today it is possible to design and apply sleeve bearings for a given motor application in accordance with sound physical principles. These improvements resulted over the years from the work of scientists and engineers such as Sommerfeld, Lord Rayleigh, Reynolds, Petroff, Shaw, Wilcock, Cameron, Rosenblatt, Wood, Booser, Baudry, and others.

The hydrodynamic concept of operation of a sliding bearing is incorporated into Reynolds' equation, and such operation results from shear and flow considerations of a somewhat idealized lubricating fluid. Even though the lubricating fluid (such as oil) is somewhat idealized in its physical properties, the resulting equation has been found to give sufficiently valid results for a wide range of operating conditions. Reynolds' equation, in three dimensions, is:

$$\frac{\partial}{\partial x} \left( h^3 \frac{\partial p}{\partial x} \right) + \frac{\partial}{\partial z} \left( h^3 \frac{\partial p}{\partial z} \right) = 6\mu v \frac{\partial h}{\partial x} \quad (11.40)$$

where  $x$  represents distance in a tangential direction,  $z$  represents distance in an axial direction,  $h$  represents oil-film thickness,  $p$  represents pressure,  $v$  represents velocity, and  $\mu$  represents absolute viscosity, all in a consistent set of units. This is a formidable equation for which a general mathematical solution is not available, to the best of the author's knowledge. However, numerical solutions have been made, as well as mathematical solutions for certain limiting cases, such as for very long and for very short bearings. Fortunately, as a result of this, it is now possible to design sliding-type bearings based on working equations derived from fundamental principles.

### 11.4.1.7 Physical Units

A sliding-type bearing, such as a sleeve bearing, operates primarily due to the property of viscosity of the lubricating oil in the oil film. Thus, the units chosen for viscosity are central in determining the units used in the analysis of sliding bearings. Viscosity is the resistance of a fluid to motion and is associated with the internal friction of that fluid. The coefficient of absolute viscosity,  $\mu$ , is defined as the force required to move a plane surface of unit area at unit speed, parallel to a second plane, located a unit distance from the first plane. Then, absolute viscosity is equal to:

$$\mu = \frac{Fh}{VA} \quad (11.41)$$

where  $F$  is the force that is required to move the first surface, having area  $A$ , at a velocity of  $V$ , and positioned a distance  $h$  from the second parallel area. Thus, the dimensions of absolute viscosity  $\mu$  in terms of more fundamental units are:

$$\mu = \frac{(\text{force})(\text{time})}{(\text{length})^2} \quad (11.42)$$

In the centimeter-gram-second (cgs) system of units, the unit of absolute viscosity is the poise, or:

$$1 \frac{\text{dyne} \cdot \text{second}}{\text{cm}^2} = 1 \text{ poise} \quad (11.43)$$

However, the poise is about two orders of magnitude greater than desirable for practical calculations. Thus the centipoise (cP) has become the favored unit. Then, in centipoise units:

$$\frac{1}{100} \text{ poise} = \frac{1}{100} \frac{\text{dyne} \cdot \text{second}}{\text{cm}^2} = 1 \text{ centipoise} \quad (11.44)$$

The meter-kilogram-second (mks) system of units is becoming increasingly important in electrical and mechanical engineering within the United States. The unit of absolute viscosity, in the mks system, is:

$$1 \frac{\text{newton} \cdot \text{second}}{\text{meter}^2} = 10 \text{ poise} = 1000 \text{ centipoise} \quad (11.45)$$

However, because of the size of the mks unit of absolute viscosity relative to the more favored unit of centipoise, it is not used to any extent in calculations. Also, for the same reason, the cgs unit of length, the centimeter (or even the millimeter), is usually favored over the meter—the mks unit of length—in bearing calculations.

Within the British system of units, the unit of absolute viscosity is the reyn, named after Reynolds. The reyn has units of:

$$1 \frac{\text{pound-seconds}}{\text{foot}^2} = 1 \text{ reyn} \quad (11.46)$$

One reyn is such a large unit that the microreyn, which is 1/1,000,000 of a reyn, is occasionally used. The quantitative comparison of the reyn to the poise and centipoise is

$$1 \text{ reyn} = 68,950 \text{ poise} = 6,895,000 \text{ centipoise} \quad (11.47)$$

Other physical quantities used in sliding-bearing technology are energy, power, rate of oil flow, and temperature. The "pure" units for these physical quantities, as well as those mentioned earlier, for each of the three systems of units, are:

Quantity	System of units		
	mks	cgs	British
Force	newton	dyne	pound
Distance	meter	cm	foot
Time	second	second	second
Energy	joule	erg	foot-pound
Power	watt	ergs/s	horsepower
Flow rate	liters/s	cm <sup>3</sup> /s	gal/s
Viscosity	10 poise	poise	reyn
Temperature	°C	°C	°F

However when considering motor bearings, common practice in engineering offices and in the technical literature is to use a set of units that deviates somewhat from those shown above. For the metric system, the kilogram is occasionally used for

force, the centimeter (or millimeter) is frequently used for distance and the centipoise is used for viscosity. For the British system, the inch is frequently used for distance, the joule is used for energy, the watt is used for power, the centipoise (as well as the reyn) is used for viscosity and degree Celsius is used for temperature. In the following discussion, the units that are used will be identified when necessary.

#### 11.4.1.8 Fundamentals of Operation

Sleeve bearings represent a large percentage of the sliding type, oil-lubricated bearings that are used on medium and large drive motors. Accordingly, this configuration will be used to explain the fundamentals of operation of sliding-type bearings. As would be expected, the same fundamentals apply in general to the configurations of sliding-type thrust bearings used on large vertical machines, such as the pivoted-shoe type and the tapered-land type, as well as the spring-supported, segmented-plate type of thrustbearing configuration.

A sliding-type journal bearing operates by virtue of the geometry of the bearing and the properties of the lubricating oil. Lubricating oil in sufficient quantity must be delivered to the axial side grooves shown in Fig. 11.22. This may be accomplished by oil rings, oil disks, or by an auxiliary oil pump, depending upon the application. In general, oil rings similar to those shown in Fig. 11.23 are used for most motor applications for which journal diameter  $D$  multiplied by speed in rpm does not exceed 25,000 cm-rpm or 10,000 inch-rpm.

Oil disks are usually used for reversing duty applications, such as for steel mill reversing drives. A typical oil disk is shown in Fig. 11.24. Auxiliary pumps are used to provide oil to the side grooves for applications requiring high peripheral speed, such as large, 3600 rpm, boiler feed pump drives, where the product (journal diameter) $\times$ (rpm) exceeds 25,000 cm-rpm. An auxiliary oil pump is shown in Fig. 11.25.

However it is delivered, oil in sufficient quantity must be available in the axial side grooves. As the surface of the rotating journal passes the region of the side groove, some portion of the contained oil tends to adhere. It is then forced into a wedge by the decreasing clearance between the journal and the bearing (see Fig. 11.26). Since oil is essentially an incompressible fluid, its pressure must increase as the oil film is formed from the wedging action. The clearance between the journal and bearing in the load-carrying area will adjust itself such that the pressure corresponds to the load. The product of the average oil film pressure and the bearing area subjected to this pressure is equal to the load on the bearing, that is,  $W = p_{av}A$ . In more general terms, the surface integral of the pressure is equal to and in equilibrium with the load, that is,  $W = \int p dA$ .

That the oil film can sustain a pressure and not collapse from a sudden, equalizing flow is due to the fact that oil can exhibit a momentary resistance to shear, that is, it has the property of viscosity. The property of viscosity has mixed blessings, however. It is also the cause of power loss in the oil film.

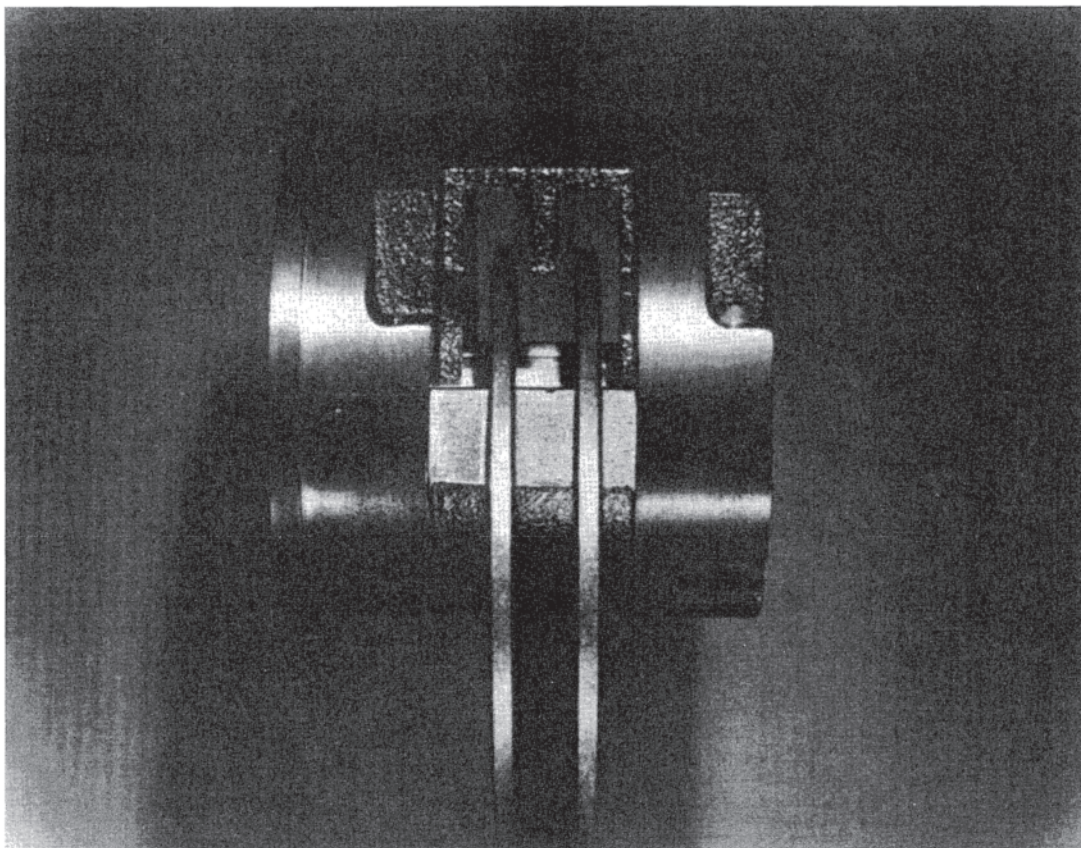


**Figure 11.23** Assembled split-sleeve bearing, showing oil rings. (Courtesy of the General Electric Company.)

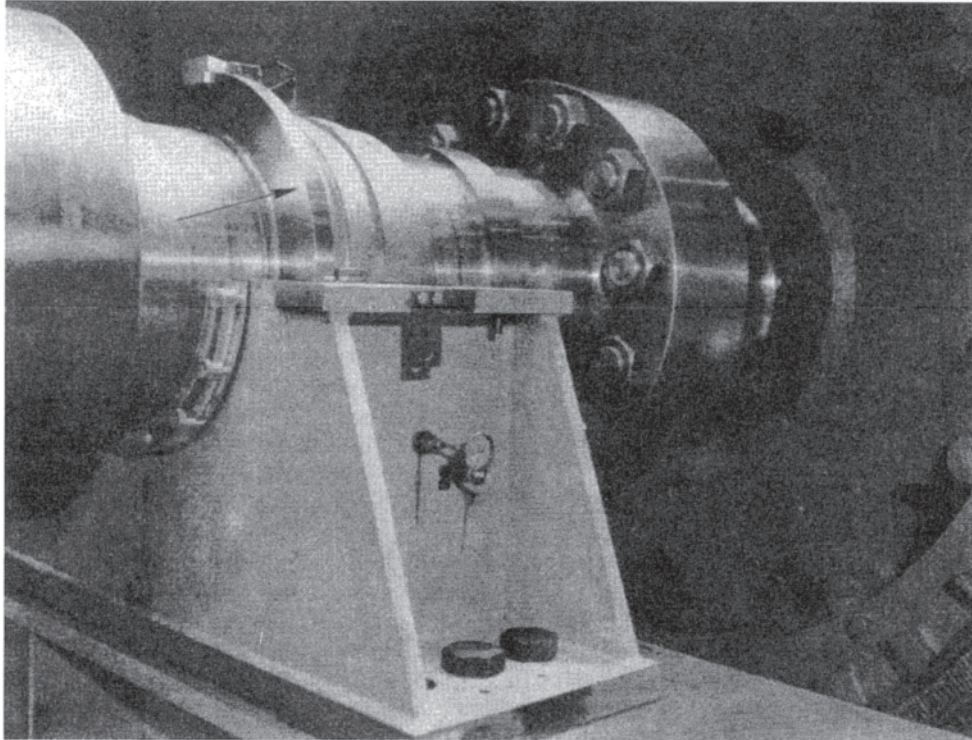


**Figure 11.24** Disk-oiled, split-sleeve bearing, used on a reversing mill motor, with upper bearing half removed, showing oil disk (arrow). (Courtesy of the General Electric Company.)

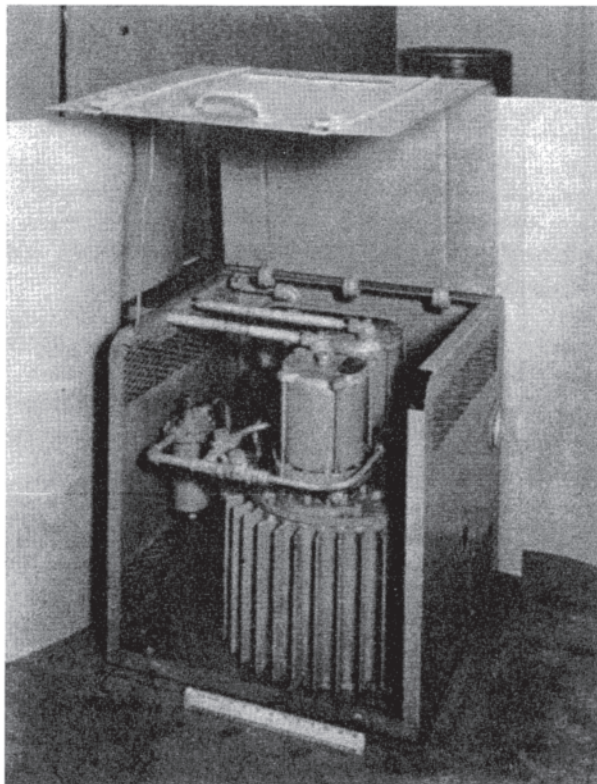


**Figure 11.25** Lubricating oil system used for external provision of oil to bearings. (Courtesy of the General Electric Company.)

Since oil exhibits a resistance to shear, shearing action within the oil film as the journal rotates requires the expenditure of energy. The rate at which this energy is dissipated is the power loss and for a lightly loaded bearing can be calculated from the definition of viscosity given in Eq. 11.41, or:

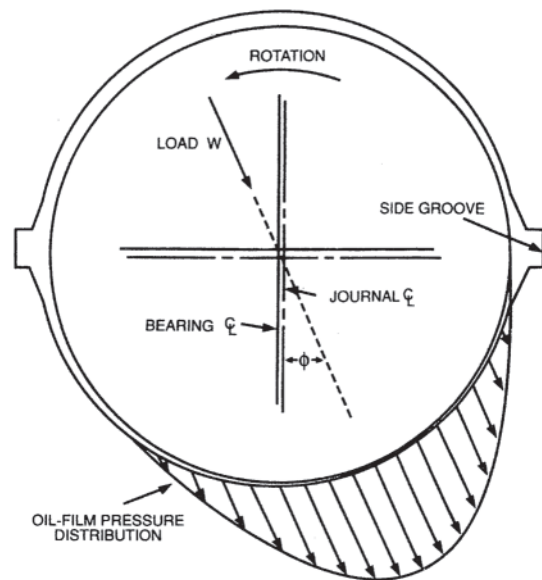


**Figure 11.26** Cross-sectional view of bearing and journal, showing typical load direction and pressure distribution.



$$\mu = \frac{Fh}{VA} \tag{11.48}$$

In the following derivation, the mks system of units given in the previous tabulation will be used because of its simplicity. Solving Eq. 11.48 for  $F$ , the force produced by the shearing action within the oil gives:

$$F = \frac{\mu VA}{h} \tag{11.49}$$

where  $F$  is in newtons,  $V$  is in meters/second,  $A$  is in square meters ( $m^2$ ) and  $h$  is in meters. Expressing Eq. 11.49 in terms of the journal diameter  $D$ , bearing length  $L$ , diametrical clearance  $C$ , and shaft speed  $N$  in rpm:

$$F = \mu \frac{\pi DN}{60} \frac{\pi DL}{C/2} \text{ newtons} \tag{11.50}$$

As stated earlier, the bearing is assumed to be lightly loaded, such that the journal tends to be centered in the bearing by the action of the oil. A correction for nonuniform clearance, as the bearing is loaded, will be considered subsequently. Simplifying Eq. 11.50:

$$F = \frac{\mu \pi^2 D^2 LN}{30C} \text{ newtons} \tag{11.51}$$

The corresponding torque is:

$$T = \frac{FD}{2} = \frac{\mu \pi^2 D^3 LN}{60C} \text{ newton-meters} \tag{11.52}$$

and the corresponding power loss is:

$$H^1 = \frac{2\pi N}{60} T = \frac{2\pi N}{60} \frac{\mu \pi^2 D^3 LN}{60C} \text{ watts} \tag{11.53}$$

Simplifying:

$$H^1 = \frac{0.0172 \mu D^3 LN^2}{C} \text{ watts} \tag{11.54}$$

Also, it is convenient to express Eq. 11.54 in the practical units of inches for  $D$ ,  $L$ , and  $C$ , and of reyns for  $\mu$ , which are widely used within the United States. Then:

$$H^1 = \frac{(0.0172)(6895)}{(39.37)^3} \frac{\mu D^3 LN^2}{C} \text{ watts} \tag{11.55}$$

which reduces to:

$$H^1 = \frac{1943 \mu D^3 LN^2}{10^6 C} \text{ watts} \tag{11.56}$$

The equation above for  $H^1$  is called Petroff's equation because Petroff first called attention to it about a century ago.

Equations 11.54 and 11.56 were derived on the basis of assuming a lightly loaded bearing. Although these equations give reasonable results as formulated above for a fully loaded bearing, more accurate results can be obtained by making an adjustment for the effect of load on the oil film. Wilcock and Rosenblatt [26] presented a paper before the American Society of Mechanical Engineering in 1951 in which the dimensionless parameter  $j$  was defined as:

$$j = \frac{H}{H^1} \tag{11.57}$$

where  $H$  is the actual bearing loss at a given load  $W$  and  $H^1$  is the loss, as calculated by Petroff's equation, as shown in Eq. 11.54 and Eq. 11.56. Solving Eq. 11.57 for the actual loss  $H$ :

$$H = jH^1 \text{ watts} \tag{11.58}$$

The dimensionless parameter  $j$  results from the hydrodynamic state of the oil film at the actual bearing load  $W$ . This parameter is a function of another dimensionless parameter, called the Sommerfeld number  $S$ , which is equal to:

$$S = \left(\frac{D}{C}\right)^2 \frac{\mu}{p} \frac{N}{60} \tag{11.59}$$

where the terms  $D$ ,  $C$ , and  $N$  are as defined earlier, and where  $p$  is the pressure on the bearing due to the bearing load. For the mks system of units,  $p$  is equal to:

$$p = \frac{W}{DL} \text{ pascals} \tag{11.60}$$

when  $W$  is the total force on the bearing in newtons, and  $D$  and  $L$  are bearing dimensions in meters. For the British system of units:

$$p = \frac{W}{DL} \text{ pounds/inch}^2 \tag{11.61}$$

where  $W$  is the total force on the bearing in pounds, and  $D$  and  $L$  are bearing dimensions in inches. If the mks system of units is used,  $\mu$  in Eq. 11.59 is in units of  $10 \times$ poise or  $1000 \times$ centipoise, and if the British engineering system of units is used,  $\mu$  is in units of reyns. A curve of the dimensionless number  $j$  vs. the Sommerfeld number  $S$  is given in Fig. 11.27.

The power loss  $H$  in a sliding bearing can become large, equaling several kilowatts in a large motor bearing. This loss is manifested as heat, which if not removed at about the same rate at which it is being produced by the shearing action within

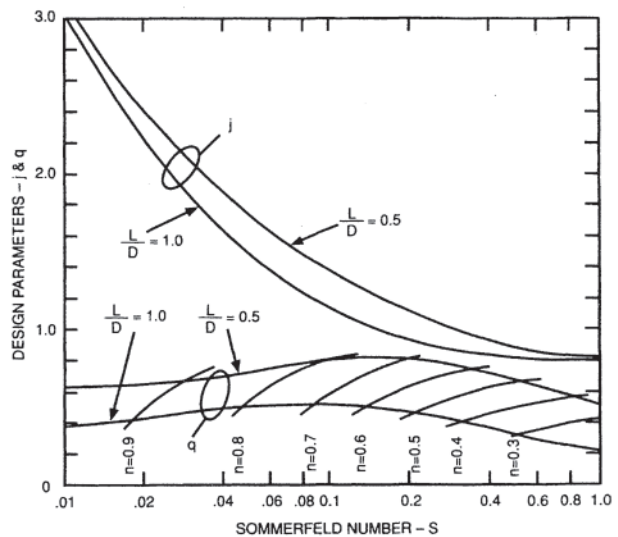


**Figure 11.27** Dimensionless hydrodynamic parameters  $j$ ,  $q$ , and  $n$  vs. the Sommerfeld number  $S$ .

the oil, will cause the bearing to reach an unsafe temperature. Fortunately, another property of lubricating oil, specific heat  $c_p$ , provides the means for removing that heat. The side groove shown in Fig. 11.22 acts as a local reservoir to collect the lubricating oil that has been deposited by action of the oil rings, oil disk, or external oil pump. The oil then tends to adhere to the rotating journal and is pulled into the continually forming oil wedge in the direction of rotation. From the oil-wedge region, the oil is then drawn into the heavily loaded portion of the oil film because of the viscous property of the oil. From there the oil flows out of the two ends of the bearing, as end leakage.

As the oil flows through the bearing, the heat energy produced by viscous shearing causes the oil temperature to rise. The temperature will rise by an amount proportional to the heat energy being produced by the shearing action in the oil, inversely proportional to the quantity of oil flow, and inversely proportional to the specific heat of the oil. Thus the temperature rise is given by:

$$\theta = \frac{H}{c_p Q} \text{ } ^\circ\text{C} \quad (11.62)$$

In the mks system,  $H$  is the rate at which losses are produced in watts, or joules/sec,  $Q$  is the rate of oil flow in liters/sec and  $c_p$  is the specific heat of oil in joules/(liter C). Thus it is apparent that, to keep the increase in temperature of the oil and of the bearing within reasonable limits, a sufficient quantity  $Q$  of oil must flow through the bearing. Because the specific heat of oil, although varying slightly with type of oil, is essentially fixed, the value of  $\theta$  is almost wholly dependent on  $Q$ . This being the case, Eq. 11.62 can be formulated in terms of more convenient units, to give:

$$\theta = \frac{0.044H}{Q} \text{ } ^\circ\text{C} \quad (11.63)$$

where  $H$  is in watts and  $Q$  is in liters/min of oil flow. The equivalent equation, in practical units, typically used in bearing calculations for electric motors, is:

$$\theta = \frac{0.010H}{Q} \text{ } ^\circ\text{C} \quad (11.64)$$

where  $H$  is in watts and  $Q$  is in gallons/min of oil flow. In calculating the temperature rise by Eq. 11.63 and Eq. 11.64, it is tacitly assumed that all of the heat is removed by convection by the oil and that none is removed by radiation or by conduction through the metal of the bearing and bearing seat. For motor sizes in which sleeve bearings are normally used, the assumption is essentially correct and any error is on the conservative side.

From the two equations above it is apparent that it is necessary to be able to reasonably predict oil flow  $Q$  for a given design or a given line of bearings in order to use such bearings in actual machines. In 1949, Cameron and Wood [25] presented an important paper to the Institute of Mechanical Engineers in the United Kingdom. This paper, together with the previously mentioned paper by Wilcock and Rosenblatt [26], presented to the American Society of Mechanical Engineers in 1951, provided a methodology for the calculation of oil flow through sleeve bearings.

Total oil flow through the bearing is divided into two categories; flow at zero speed  $Q_0$ , due to any external source of oil pressure, and flow due to hydrodynamic action  $Q_R$ , associated with rotation of the journal. The total oil flow is then equal to:

$$Q = Q_0 + Q_R \quad (11.65)$$

Rotational oil flow is a function of the pumping action of the rotating journal and of the hydrodynamic effect of the oil film. The bearing parameters that affect oil flow due to rotation are  $N$ ,  $D$ ,  $L$ , and  $C$ . The hydrodynamic effect of the oil film is represented by the dimensionless parameter  $q$ , which is a function of the Sommerfeld number. This parameter is defined as:

$$q = \frac{Q_R}{913NDLC} \quad (11.66)$$

Solving for  $Q_R$ :

$$Q_R = 913NDLCq \text{ liters/min} \quad (11.67)$$

when using mks units of meters for  $D$ ,  $L$ , and  $C$ . Also:

$$Q_R = \frac{NDLCq}{294} \text{ gallons/min.} \quad (11.68)$$

when using practical units of inches for  $D$ ,  $L$ , and  $C$ . A curve of the dimensionless number  $q$  vs. the Sommerfeld number is shown in Fig. 11.27.

Oil flow at zero speed,  $Q_0$ , is, of course, zero for ringoiled or for disk-oiled bearings, since there is no source of external pressure and no oil is deposited in the side grooves until rotation has started. Thus,  $Q_0$  occurs only when an external source of pressurized oil is used, but for such externally fed bearings, it is a significant part of the total oil flow,  $Q$ ,  $Q_0$  is determined (1) by measuring the rate of oil flow through the bearing with the external oil pressure established and with the journal not rotating, or (2) by calculation. Of the two methods, measuring the rate of oil flow will consistently give the more accurate results. However, reasonable results can be obtained by calculation.

As would be expected, a variety of methods have been proposed for calculating  $Q_0$ , and the more involved methods are not necessarily more accurate than less complicated methods, across a wide span of bearing sizes. Oil flow through the bearing at zero speed is tantamount to flow through the clearance space in the bearing, between the bearing ID and the journal outside diameter (OD). Using the concept of oil flow through a long thin slot and assuming a typical distribution pattern of the oil flow over the bearing surface, the rate of flow  $Q_0$  is proportional to the inlet oil pressure  $p_0$ , to the third power of the bearing clearance (that is,  $C^3$ ) and inversely proportional to the absolute viscosity  $\mu$ . Thus, for the mks system of units:

$$Q_0 = 22.5 \times 10^3 \frac{p_0 C^3}{\mu} \text{ liters/min} \quad (11.69)$$

where  $p_0$  is in pascals,  $C$  is in meters, and  $\mu$  is as defined in Eq. 11.45. For the practical system of units:

$$Q_0 = 0.084 \frac{p_0 C^3}{\mu} \text{ gallons/min} \quad (11.70)$$

where  $p_0$  is in pounds/inch<sup>2</sup>,  $C$  is in inches, and  $\mu$  is in reyns.

As stated in Eq. 11.65, total oil flow for a sleeve bearing is equal to the sum of  $Q_R$  and  $Q_0$ . Substituting Eqs. 11.67 and 11.69 into Eq. 11.65 for the mks system of units:

$$Q = 913NDLC_q + 22.5 \times 10^3 \frac{p_0 C^3}{\mu} \text{ liters/min} \quad (11.71)$$

Similarly, substituting Eqs. 11.68 and 11.70 into Eq. 11.65 for the practical system of units:

$$Q = \frac{NDLC_q}{294} + 0.084 \frac{p_0 C^3}{\mu} \text{ gallons/min} \quad (11.72)$$

As mentioned earlier, the oil delivered to the bearing is used to remove the heat produced by the bearing and to provide a continuous reservoir of oil in the side grooves for forming the oil wedge. Oil from the oil wedge, under the influence of hydrodynamic action, then distributes itself into the pressure pattern shown in Fig. 11.26 to carry the bearing load. Within the oil film, the point of maximum pressure corresponds to the point of minimum oil-film thickness  $h$ . The minimum thickness  $h_m$  is equal to:

$$h_m = (1 - n) \frac{C}{2} \quad (11.73)$$

where  $n$  is a dimensionless parameter that depends upon the hydrodynamic state of the oil. The value of  $n$  may be obtained, as a function of the Sommerfeld number, from Fig. 11.27. In this equation  $h_m$  will have the same dimensional unit as that used for  $C$ .

It will be noticed in Fig. 11.26 that the direction of the bearing-load vector  $W$  is displaced counterclockwise from the vertical centerline due to the hydrodynamic action of the oil. The angle between the vertical centerline and the load line is called the attitude angle  $\phi$ . This angle is given in a curve of  $\phi$  vs. Sommerfeld number in Fig. 11.28.

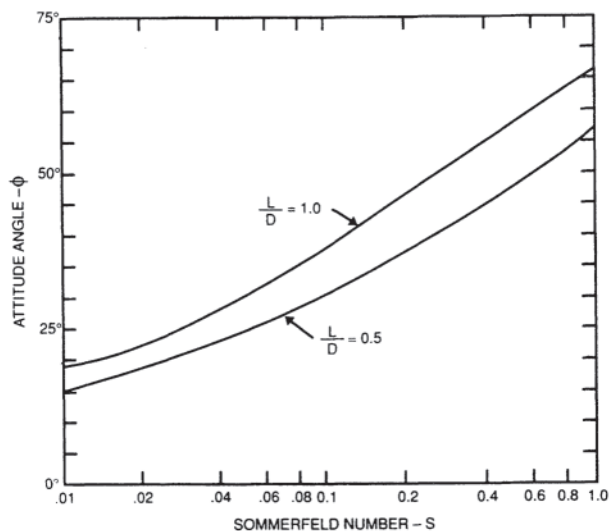


Figure 11.28 Attitude angle  $\phi$  vs. the Sommerfeld number  $S$ .

#### 11.4.1.9 Application of Sleeve Bearings

Application requirements, including the rating and the characteristics of the driven equipment, constitute the starting point for applying bearings to large motor drives. The horsepower and speed determine the torque to be delivered through the journal. The relationship between torque  $T$ , in newton-meters, and power HP, at a rotational speed of  $N$  rpm, is:

$$T = \frac{(60)(746)HP}{2\pi N} = 7124 \frac{HP}{N} \text{ newton-meters (N-m)} \quad (11.74)$$

In British engineering units:

$$T = 5252 \frac{HP}{N} \text{ pound-feet} \quad (11.75)$$

It should be noted that, to be consistent, horsepower HP as used in both Eqs. 11.74 and 11.75 is based on the horsepower unit as defined in the United States, which is equal to 746 watts. In the SI system of units (mks), the horsepower unit is equal to 735.5 watts. Thus, in those countries for which the SI system of units is normally used, Eq. 11.74 should be  $T = 7024 \times HP/N$  (N-m).

Torque is delivered to the load through the shaft, including the journal, which must pass through the bearing. The journal must have sufficient diameter  $D$  to limit the torsional stress  $\tau$  to a safe value, such as to prevent fatigue failure. Torsional stress in the journal is equal to:

$$\tau = \frac{16T}{\pi D^3} \quad (11.76)$$

for a consistent set of units. Substituting Eq. 11.74 into Eq. 11.76 for the mks system of units:

$$\tau = 36,300 \frac{HP}{D^3 N} \text{ N/m}^2 \quad (11.77)$$

Similarly, substituting Eq. 11.75 into Eq. 11.76, for the practical system of units:

$$\tau = 321,000 \frac{HP}{D^3 N} \text{ pounds/inch}^2 \quad (11.78)$$

Depending upon the steel used in the shaft, rated-load torsional stress is limited to about  $27.6 \times 10^6$  N/m<sup>2</sup> or 27,600 kPa, or the equivalent in practical units of 4000 pounds/inch<sup>2</sup>. As a practical matter, the diameter of the shaft extension is frequently made about 3 mm, or about 1/8 inch, less in diameter than the journal. Then, in the improbable event of a torsional failure of the shaft, the failure would occur at the coupling, instead of inside the bearing.

Having established the diameter  $D$  of the journal and hence of the bearing, and using accepted values of oil pressure  $p$ , the length  $L$  of the bearing can also be established. The projected load on the bearing due to the weight of the rotor is equal to half of the rotor weight divided by  $LD$ . See Eqs. 11.60 and 11.61. To this load should be added a load due to normal magnetic pull exerted on the rotor. Also, as will be discussed subsequently, any belt pull should also be added to bearing loading. The total unit pressure on the bearing should be limited to about 2000 kPa or to about 300 pounds/inch<sup>2</sup>. Because bearing loss increases as the third power of  $D$ , there is a tendency to increase  $L$ , in order to reduce the bearing load

pressure  $p$ . However, the ratio  $L/D$  should not exceed about 1.0 because of considerations of shaft misalignment and effective use of the bearing area. Usually, the selection of  $D$ , such as to limit the torsional stress in the journal, will also provide sufficient  $DL$  to prevent excessive loading pressure on the bearing. There are certain cases, however, for which the physical size of the motor is greater than normal for the hp and speed rating, such as for high maximum torque or for a stator voltage that is greater than normal for the horsepower rating. For such cases, the bearing pressure may set the bearing size.

Most large drive motors are direct-coupled. However, an occasional medium-sized unit, through several hundred horsepower in rating, may be belted. For such cases, the forces associated with belt pull must be considered in selecting the bearing. For a sheave to drive a belt, there must be a difference in belt tension between the “tension” and the “slack” sides of the belt. The ratio of tension is:

$$F_1/F_2 = e^{f\alpha} \quad (11.79)$$

where  $e$  is the base of natural logarithms,  $f$  is the coefficient of friction between the belt and driving sheave,  $\alpha$  is the angle of embrace of the belt with the sheave in radians, and  $F_1$  and  $F_2$  are in newtons or in pounds. The delivered torque is equal to:

$$T = (F_1 - F_2)r \text{ N-m; pound-feet} \quad (11.80)$$

where  $r$  is the effective radius of the driving sheave in meters or in feet. The belt pull on the shaft extension is equal to the total lateral force  $F_d$  on the shaft extension, or:

$$F_d = F_1 + F_2 \text{ N, pounds} \quad (11.81)$$

The force of belt pull must be added to the other forces acting on the bearing, in both direction and magnitude. The bearing must have adequate  $DL$  to keep the pressure within good working limits. Also, since the direction of belt pull is frequently lateral to the drive motor, the vectorial resultant of all forces acting across the bearing must be determined in order to make certain that there is adequate bearing surface in the desired location, uninterrupted by the lateral oil grooves, to accommodate the load.

Belt pull will occur perpendicular to the shaft in a vertical plane outboard from the vertical plane passing through the centerline of the drive-end bearing. Let  $l_1$  be the distance from the centerline of the drive-end bearing to the centerline of the opposite-drive-end bearing and let  $l_2$  be the distance from the centerline of the drive-end bearing to the centerline of the drive sheave. Also, let  $F_d$  be the total belt pull on the sheave and let  $F_b$  be the resulting force exerted on the drive-end bearing. Taking moments about the opposite-drive-end bearing:

$$(l_1 + l_2)F_d = l_1 F_b \text{ N-m, pound-feet} \quad (11.82)$$

and solving for the force  $F_b$ , which the belt pull exerts on the bearing:

$$F_b = \frac{l_1 + l_2}{l_1} F_d \text{ N, pounds} \quad (11.83)$$

This force must be added vectorially to the force that the rotor also exerts on the bearing to obtain the total force and force direction acting on the bearing.

#### 11.4.1.10 Environmental Considerations

There are environmental conditions that must be considered in the design of the bearing and the associated bearing housing. Some of these conditions are common to all units and some are peculiar to certain applications.

There is, in general, a pressure differential across the bearing housing due to normal operation of the motor ventilating system. The inboard side of the housing is adjacent to the vortex of the rotor fan, whereas the outboard side is usually exposed to atmospheric pressure. To prevent axial oil leakage along the shaft, it is necessary to use a system of shaft seals or venting to atmosphere of an annular chamber mating with the shaft and located between the bearing and the inboard side of the bearing housing. In extreme cases, such as for large 3600-rpm drive motors, for which the pressure differential across the bearing housing is great, it may be necessary to charge this annular chamber with a pressure above atmospheric to prevent axial oil leakage. Such air pressure is usually obtained from the pressure discharge of the fan.

Drive motors are occasionally applied in high-temperature locations. If hydrocarbon lubricating oil is to be used for such applications, as would normally be the case, it may be necessary to use an auxiliary oil pump and an external cooler. Conversely, the application may be in a low-temperature location, such as for weather-protected motors for the northern tier of states. Such low-temperature locations may require that the lubricating oil be heated prior to start-up by electric heaters located in the oil reservoir.

#### 11.4.1.11 Shaft Currents

In ac drive motors, voltage across the bearing, in some minute degree, is frequently present. Because of small magnetic dissymmetries in the stator core, some of which are unavoidable, low-order voltages may be induced in the shaft. Such voltages are usually of so low a value that they may be ignored in smaller motors. In larger motors, and in certain cases for smaller motors, however, the shaft voltage may be sufficient to cause current to flow in the circuit consisting of the shaft, bearings, and frame. If such a current does flow, it causes progressive damage to the bearing babbitt and failure will eventually result. To prevent this, it is necessary to provide an insulated barrier in the circuit, usually between the OD of the bearing and the bearing seat. Such a bearing is called an insulated bearing.

During the first half of this century, bearing failures from shaft current were observed and, over a period of time, correlated with various magnetic core dissymmetries as well as machine size. These observations were discussed in trade meetings, trade journals, and so forth until about 1950, at which time general criteria were reasonably well established as given below. To prevent shaft currents from flowing in large motors and even in medium-sized motors in some cases, bearings should be insulated for the following cases:

- Two-pole motors of approximately 1000 hp or more.
- All ac motors of approximately 2500 hp or more, for any number of poles.
- When 2 times the number of stator slots, divided by the number of poles, equals an odd integer.

- When 4 times the number of punching segments, divided by the number of poles, equals an odd integer.
- When, in general, 2 times the number of stator punching segments, divided by the number of poles equals  $A/B$ , where  $A$  is an odd integer and  $A/B$  has been reduced to its lowest terms.

Although earlier practice was to insulate only one bearing to interrupt current flow, more recent practice has been to insulate both bearings. This allows both bearings to be identical, thereby requiring only one bearing to be carried in stock and allowing a reduction in overall production cost to the manufacturer and a reduction in maintenance cost to the user.

#### 11.4.1.12 Bearing Materials

When a sliding-type bearing is operating within the hydrodynamic domain, a metallic journal rotates within the bearing, with a sustained oil film separating the two members. For drive motors in general usage, this oil-film separation is continually maintained except for the first revolution or so at startup and the last revolution or so at shutdown, so that the journal is separated from the bearing by an oil film. Nevertheless, the physical properties of the bearing material are important to the successful operation of the bearing system. The more important of these physical properties are discussed below.

The journal is made of steel of medium hardness and it is therefore desirable that the bearing material be somewhat softer than the journal. It is possible to “harden” the journal portion of the shaft so that the bearing material can be correspondingly harder than otherwise. Although this has been done in some cases, it is more costly and may present other problems. Thus, the bearing material is normally selected to be considerably softer than the steel journal with which it mates. The hardness and the modulus of elasticity should be as low as possible, while still being capable of carrying the total bearing load without extruding or flowing. This allows the bearing to conform to misalignment and to dimensional variations; this property is called conformability. Also, if foreign particles somehow get into the bearing, a softer bearing material will allow such particles to become embedded into the bearing and thus to prevent the journal from scoring or the bearing from “plowing.” This property of a bearing material is called embeddability.

Compatibility is another significant property that is desired in a bearing material. Even for a properly machined journal and bearing, operating within acceptable hydrodynamic limits, metal-to-metal contact is occasionally possible. The minimum oil-film thickness can be as small as 0.025 mm, or 0.001 inch, and still be entirely operational. However, certain momentary load perturbations and motor vibration can result in microscopic high points of the bearing contacting the journal, causing momentary melting of localized bearing metal so that the two surfaces tend to weld together at such high points. The amount of resulting tearing and other damage is a function of the lubricating oil and of the chemical and physical properties of the bearing and journal material. There are good reasons for using medium steel for the shaft journal, such as fatigue strength, availability, cost, and so forth, associated

with steel. Thus, the bearing material should be selected so as to be compatible with the steel journal, as discussed above.

Another property of a bearing material that should be considered is that of corrosion resistance. Compounds of oxygen and organic acids can form in lubricating oil, particularly at higher temperatures. This can result in corrosion of the metal and in the formation of insoluble organic compounds, both of which are undesirable. Bearing materials containing cadmium, lead, and copper are more susceptible to oxidation than materials primarily containing tin. Corrosion resistance and formation of insoluble sludge within the lubricating oil can be reduced or prevented by use of an oil with proper oxidation inhibitors, by more frequent change of oil, by limiting oil temperature, and by selection of tin-based bearing material.

An important property of bearing material is compressive strength. A suitable material should have a low to moderate compressive strength. If the compressive strength is too low, the babbitt will tend to flow or extrude under load. On the other hand, too high a compressive strength may result in some flaking, crumbling, or spalling under heavy cyclical loading. Tin-based and lead-based babbitts, which have proven to be very successful bearing materials for most motor applications, have ultimate strengths of 10,000 to 11,000 pounds per square inch (psi).

The last property of a bearing material to be considered is fatigue strength. If the bearing load alternates in magnitude, fatigue of the bearing material can result. However, fatigue is not as great a consideration for bearings used on electric motors as for crankshaft bearings used on reciprocating engines. Problems from fatigue will be manifested by cracks, scallops, and so forth, on the bearing surface. However, as stated above, bearing fatigue is not normally a problem with correctly applied electric motors.

The bearing materials that most nearly meet the above set of desirable bearing properties for application on electric drive motors are tin-based and lead-based babbitt, known as white metal. In 1839, Isaac Babbitt was awarded an American patent for a bearing material with a composition of about 89% tin, about 9% antimony, and about 2% copper. This proved to be an unusually useful bearing material and approximately the same composition of material is still in common use. Lead, which is also a good bearing material, has been substituted for much of the tin in some applications to give a lower overall cost. These two materials are referred to as “white metal” and as babbitt in the industrial art.

Babbitts are classified as tin-based and as lead-based babbitts. Tin-based babbitt consists of a pure tin matrix, with compounds of copper and tin and of antimony and tin interspersed throughout the matrix. Lead-based babbitt consists of a pure lead matrix, with compounds of tin and antimony interspersed throughout the lead matrix. A small amount of copper may also be present. The lead content is approximately 84%.

Babbitt metal has very desirable frictional characteristics and bearing-metal characteristics. It has low surface hardness, in the range 10 to 15 Brinell at 100°C, and the hardness

decreases rapidly at high temperatures. The modulus of elasticity of lead-based babbitt is approximately  $2 \times 10^6$  pounds/inch<sup>2</sup> and of tin-based babbitt is approximately  $6 \times 10^6$  pounds/inch<sup>2</sup>. This permits good conformability of the bearing to the journal and the journals do not usually need to be hardened beyond the degree inherently present in the shaft steel.

Babbitt metals have a low compressive strength and low fatigue strength in bulk amounts, with these strengths decreasing with temperature. However, the fatigue strength and compressive strength increase significantly as the thickness of the material is decreased, with a dramatic increase at thicknesses of about 0.35 mm (about 0.014 inch). In order to support and to back such a thickness, the babbitt is bonded to a bearing shell, made of steel or cast iron. The steel shell must be machined to a reasonably close tolerance of inside diameter and the cast-iron shell, when used, must also be machined to a reasonably close tolerance of inside diameter (or cast to a correspondingly close tolerance). The molten babbitt is deposited onto the machined bearing surface by centrifugal casting. In order to obtain a metallurgical bond between the steel or cast iron shell and the cast babbitt lining, the machined inside surface of the liner must be deoxidized and cleaned of oil by treatment with an appropriate cleaning agent, washing with water, and drying. In order to obtain a suitable bond, the molten babbitt must be cast into the shell immediately before any significant oxidation or other fouling can occur following cleaning. The bearing, with the cast-in babbitt contained within the shell, is then machined to the correct inside diameter. Whereas the final babbitt layer is as thin as a few mils for such applications as connecting-rod bearings for reciprocating engines, a babbitt thickness of about 2.5 mm, or about 0.10 inch or even greater, will give sufficient compressive and fatigue strength for electric motors.

Babbitt, or white metal, has become the bearing material of choice for medium and large drive motors. However, it is of interest to list other metallic bearing materials that have been and continue to be used in various other applications. Some of the more significant of these materials are brass (copper and zinc), bronze (copper and tin), copper-lead, bronze-lead, silver-lead-indium, hardened lead, tin-bronze, and aluminum. In addition, nonmetallic materials have been and continue to be used, such as carbon graphite, wood (oil-impregnated maple and oak), and some plastics (Teflon, cotton phenolics, and so forth).

#### 11.4.1.13 Lubricating Oil

The oil used for lubricating sleeve bearings and sliding-type thrust bearings for electric motors is, with few exceptions, a mineral-based oil, that is, a petroleum oil. Although some organic and some synthetic oils might be used in unusual applications, this occurs so infrequently as not to warrant any discussion (except to follow the manufacturer's instruction book in such a case). Thus, only petroleum oil will be considered in the following. All petroleum oils used for lubrication contain paraffin, naphthene, and aromatic-type hydrocarbon molecules. In the process of refining, a considerable portion of the paraffin wax and of the aromatic-type compounds are

removed, thus reducing the pour point and reducing the tendency to form sludge at higher temperatures.

It was seen in Section 11.4.1.8 that hydrodynamic bearing theory was dependent on the properties of lubricating oil and that the working equations used for calculating bearing performance involved the physical properties of the oil, prime among which was absolute viscosity  $\mu$ . As discussed in Section 11.4.1.7, absolute viscosity is measured in terms of poise and reyn for the metric and the British unit systems, respectively. Thus, absolute viscosity, in units of poise and reyn, is important for engineering calculations. It has been found, however, that kinematic viscosity  $\gamma$ , in units of stokes and centistokes, is proportional to the flow time. Thus, for describing or specifying grades of oil, kinematic viscosity is an important property and the unit of kinematic viscosity is the stoke. One stoke is equal to the absolute viscosity in poise divided by the oil density  $\rho$ , in grams/centimeter<sup>3</sup>, or:

$$\gamma = \frac{\mu}{\rho} \quad \text{stokes} \quad (11.84)$$

The centistoke unit is equal to 1/100 of a stoke, or:

$$\text{centistoke} = \frac{\text{stoke}}{100} \quad (11.85)$$

If it is desired to convert kinematic viscosity of oil in stokes or centistokes to absolute viscosity in units of reyns, it should first be converted to metric units of poise. Then the absolute viscosity in poise can be easily converted to reyn by use of Eq. 11.47.

An additional unit for kinematic viscosity that has come into widespread usage for electric motors, generators, and turbines is the Saybolt Universal Second or the SUS. It is the time in seconds required to drain a container of a specific size by free flow of the oil through a capillary opening of a specific size. The flow time in seconds from this Saybolt viscometer is the kinematic viscosity of the oil in units of SUS. It should be noted, however, that the flow time associated with the SUS unit is not exactly proportional to the kinematic viscosity as defined by the stoke, particularly for the more viscous oils.

The viscosity of lubricating oil varies significantly with temperature. Light turbine oil, which is typically used for electric-motor bearings, has a kinematic viscosity of about 150 SUS at 100°F and of about 44 SUS at 210°F. Also, medium turbine oil, which is recommended by some motor manufacturers, has a kinematic viscosity of about 300 SUS at 100°F and about 55 SUS at 210°F. Since it is common commercial practice to specify and to purchase lubricating oil with the viscosity specified in kinematic units of SUS, it is necessary to convert the value of the kinematic viscosity of the oil to centistokes, and then to the corresponding value of absolute viscosity, in centipoise, at the temperature desired. As shown in Eq. 11.84 absolute viscosity  $\mu$  is equal to kinematic viscosity  $\gamma$  multiplied by the oil density  $\rho$ . Since oil density  $\rho$  varies with temperature, the density of the oil at the particular temperature being considered must first be calculated. The density of light turbine oil is 0.872 g/cm<sup>3</sup> at 60°F and it varies with temperature approximately as:

$$\rho = 0.872 \left( \frac{1}{1 + 0.000426(T - 60)} \right) \text{ g/cm}^3 \quad (11.86)$$

where  $T$  is the oil temperature in degrees Fahrenheit ( $^{\circ}\text{F}$ ).

To prepare a curve of absolute viscosity in units of poise or centipoise vs. temperature in degrees Celsius for use in performing engineering calculations, the following steps should be taken.

1. Select a value of kinematic viscosity, in centistokes, for a given temperature  $T$ , usually given in degrees F, from the oil supplier's data sheet.
2. Calculate the oil density at the same temperature  $T$ . If it is light turbine oil with a kinematic viscosity of about 32 centistokes at  $100^{\circ}\text{F}$ , such as is typically used for electric-motor bearings, Eq. 11.86 may be used to calculate the density.
3. Multiply the kinematic viscosity  $\gamma$  by the density  $\rho$ , both determined at temperature  $T$ , to obtain the absolute viscosity  $\mu$ , in centipoise, at the same temperature  $T$ .
4. Repeat for several different temperatures to cover the temperature range desired. Then plot  $\mu$  vs.  $T$ , so that absolute viscosity  $\mu$  is available, throughout the temperature range, for engineering calculations.
5. If it is desired to use temperature in Celsius for  $T$  in performing engineering calculations, the oil temperatures  $T$  can be transformed from degrees F to degrees C and then plotted vs.  $\mu$ .

Figure 11.29 shows such a curve for a typical light turbine oil, for which  $\mu$ , in centipoise, is given as a function of oil temperature  $T$ , in degrees C.

#### 11.4.1.14 Numerical Example

Sleeve bearings, 5.5 inches in diameter and 3.5 inches in length, are being considered for use in a 2000-hp, 4-pole, 60-Hz motor, with a synchronous speed of 1800 rpm. The bearing assembly is provided with oil rings and has also been drilled and tapped to accept piping from an external pressurized-oil source, if forced lubrication is required. However, it is known that the oil ring will deliver not less than 0.60 gallons/min of light turbine oil to each bearing, with the journal rotating at 1800 rpm. Thus, the bearings can (1) be lubricated by use of an external source of oil pressure with the oil rings serving as a backup source in case the external source of oil fails, or (2) they can be lubricated by use only of the oil rings if the resulting operating temperature is permissible. It is known that the ambient temperature of the oil reservoir and of the oil within that reservoir into which the lower part of the oil rings are submerged is  $40^{\circ}\text{C}$  when normal ventilating air is passing over the bearing housing. Thus,  $40^{\circ}\text{C}$  is the ambient temperature of the oil. It is desired to limit the total temperature of the bearing and oil to  $70^{\circ}\text{C}$  because of viscosity considerations. Then the temperature rise of the oil should not exceed  $70-40=30^{\circ}\text{C}$ . The engineering problem is to determine, subject to these constraints, whether the bearings require forced lubrication or whether oil rings will provide adequate lubrication. The light turbine oil being used has an absolute viscosity of 12 cP at  $60^{\circ}\text{C}$  oil temperature. Also, the diametrical clearance  $C$  between the bearing and journal is 0.007 inch.

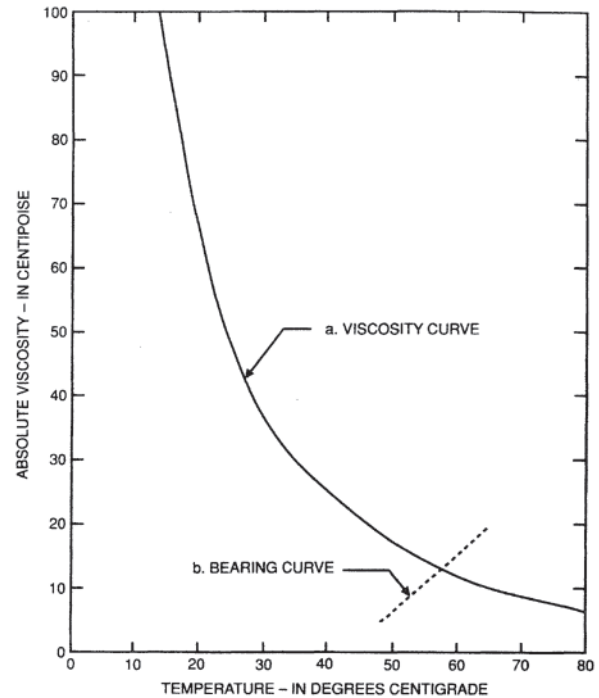


**Figure 11.29** Curve of absolute viscosity vs. temperature for a light turbine oil. (a) Viscosity curve of the oil. (b) Characteristic curve of a specific bearing design.

As is apparent from curve a, Fig. 11.29, absolute viscosity varies significantly with temperature. Thus, it is necessary to assume a temperature and to calculate the corresponding viscosity at that temperature. Then, using that value of viscosity, calculate the bearing loss  $H$  and the oil flow  $Q$ , from which the temperature rise  $\theta$  can be calculated. The bearing temperature rise  $\theta$  is then added to the ambient temperature to give a bearing temperature (and the oil temperature). In all probability, the bearing temperature just calculated and the viscosity used as a starting point will not plot as a point on the viscosity curve. However, this temperature and viscosity give one point on a second curve, referred to as the “bearing curve” (curve b of Fig. 11.29). The process is repeated until sufficient points are determined to provide a “bearing curve” that intersects the “viscosity curve.” The point of intersection is the actual operating point of the bearing.

Selecting the first trial temperature as  $60^{\circ}\text{C}$ , the corresponding absolute viscosity is  $\mu=12$  cP. However, when using the British system of units, viscosity is in units of reyns. From Eq. 11.47,  $1 \text{ reyn}=6.895 \times 10^6 \text{ cP}$ . Then:

$$\mu = \frac{12}{6.895 \times 10^6} = 1.74 \times 10^{-6} \text{ reyns} \quad (11.87)$$

From Eq. 11.56, Petroff's equation is given as:

$$H^1 = \frac{1943 \mu D^3 L N^2}{10^6 C} \text{ watts} \quad (11.88)$$

Substituting the value of  $\mu$  from Eq. 11.87 and the values of  $D$ ,  $N$ , and  $C$ , given above into Eq. 11.88:

$$H^1 = \frac{(1943)(1.74)(5.5)^3(3.5)(1800)^2}{10^{12}(0.007)} = 911 \text{ watts} \quad (11.89)$$

which is the Petroff loss for one bearing. The actual bearing loss, considering the hydrodynamic state of the oil, is given by

Eq. 11.58 as:

$$H = jH^1 \text{ watts} \quad (11.90)$$

where the dimensionless number  $j$  is a function of the Sommerfeld number  $S$ . From Eq. 11.59, the Sommerfeld number is equal to:

$$S = \left(\frac{D}{C}\right)^2 \frac{\mu}{p} \frac{N}{60} \quad (11.91)$$

where  $p$  is the total pressure exerted on one bearing. For the machine being considered, the rotor weight is 4000 pounds and the force of magnetic pull is 2000 pounds, giving a total load  $W$  of 6000 pounds on two bearings, or approximately 3000 pounds/bearing. The total pressure on the bearing is defined as:

$$p = \frac{W}{DL} \text{ pounds/inch}^2 \quad (11.92)$$

or

$$p = \frac{3000}{(5.5)(3.5)} = 156 \text{ pounds/inch}^2 \quad (11.93)$$

Substituting the value of  $p$  from Eq. 11.93 and the values of  $D$ ,  $C$ ,  $\mu$ , and  $N$  given earlier into Eq. 11.91, the Sommerfeld number is equal to:

$$S = \left(\frac{5.5}{0.007}\right)^2 \left(\frac{1.74}{10^6}\right) \left(\frac{1}{156}\right) \left(\frac{1800}{60}\right) = 0.207 \quad (11.94)$$

From Fig. 11.27 the value of the dimensionless loss parameter  $j$ , corresponding to the above value of  $S$ , is:

$$j = 1.02 \quad (11.95)$$

Then, substituting Eq. 11.89 and Eq. 11.95 into Eq. 11.90:

$$H = (1.02)(911) = 929 \text{ watts} \quad (11.96)$$

It is necessary to calculate the oil flow through the bearing in order to determine the corresponding temperature rise of the oil and bearing. Since it is desired to determine if the oil rings alone will provide sufficient oil to limit the temperature rise to 30°C or less without the use of external pressurized oil, the oil flow at zero speed  $Q_0$  will not be calculated. Thus the only oil flow to consider is  $Q_R$  which is due to hydrodynamic action of the bearing associated with rotation. From Eq. 11.68,  $Q_R$  is equal to:

$$Q_R = \frac{NDLCq}{294} \text{ gallons/minute} \quad (11.97)$$

when using British units. From Fig. 11.27 the value of the dimensionless flow parameter  $q$ , corresponding to the value of the Sommerfeld number given in Eq. 11.94, is:

$$q = 0.67 \quad (11.98)$$

Substituting the value of  $q$  given in Eq. 11.98 and the values of the other variables as given above, into Eq. 11.97:

$$Q_R = \frac{(1800)(5.5)(3.5)(0.007)(0.67)}{294} = 0.553 \text{ gallons/minute} \quad (11.99)$$

From Eq. 11.64, the temperature rise of the oil is equal to:

$$\theta = \frac{0.010H}{Q} \text{ } ^\circ\text{C} \quad (11.100)$$

Since no external source of pressurized oil is being used, the total oil flow through the bearing  $Q = Q_R$ . Substituting the value of  $H$  from Eq. 11.96 and the value of  $Q = Q_R$  from Eq. 11.99 into Eq. 11.100:

$$\theta = \frac{(0.010)(929)}{0.553} = 16.8^\circ\text{C} \quad (11.101)$$

Thus, for an assumed viscosity of 12 cP, the resulting oil and bearing temperature rise is equal to 16.8°C or the total temperature is equal to 40+16.8=56.8°C, and these values of viscosity and total temperature establish one point on the "bearing curve."

If the above process is repeated for assumed viscosities of  $\mu=8$  cP  $\mu=16$  cP the resulting coordinates are:

Total oil temperature=52.2°C at a viscosity of 8 cP.

Total oil temperature=61.4°C at a viscosity of 16 cP.

These two sets of values provide two more points on the bearing curve. If all three points as determined are plotted on the coordinates in Fig. 11.29 and a smooth curve is drawn, the result is the bearing curve for this application, as shown in the figure. The intersection of the bearing curve and the viscosity curve is the operating point when the machine is operated without an external pressurized-oil supply. It can be seen that the total temperature is about 58°C and that, at this operating temperature, the light turbine oil has an absolute viscosity of about 13 cP.

Having determined the operating point of the bearing, the final operating characteristics may be determined. The viscosity of the oil at the operating temperature, from Eq. 11.47, is equal to:

$$\mu = \frac{13}{6.895 \times 10^6} = 1.89 \times 10^{-6} \text{ reyns} \quad (11.102)$$

and the Petroff loss, from Eq. 11.56, is equal to:

$$H^1 = \frac{(1943)(1.89)(5.5)^3(3.5)(1800)^2}{10^{12}(0.007)} = 990 \text{ watts} \quad (11.103)$$

Also, from Eq. 11.59, the Sommerfeld number is equal to:

$$S = \left(\frac{5.5}{0.007}\right)^2 \left(\frac{1.89}{10^6}\right) \left(\frac{1}{156}\right) \left(\frac{1800}{60}\right) = 0.225 \quad (11.104)$$

From Fig. 11.27, the corresponding value of the dimensionless loss parameter  $j$  is equal to:

$$j = 1.01 \quad (11.105)$$

Then, from Eq. 11.58, the bearing loss is:

$$H = (1.01)(990) = 1000 \text{ watts} \quad (11.106)$$

for each bearing. For the value of the Sommerfeld number at the operating point, given in Eq. 11.104, Fig. 11.27 shows the dimensionless parameter  $q$  to be:



$$q=0.68 \quad (11.107)$$

From Eq. 11.68, the actual oil flow through the bearing due to hydrodynamic action is equal to:

$$Q_R = \frac{(1800)(5.5)(3.5)(0.007)(0.68)}{294} \quad (11.108)$$

$$= 0.561 \text{ gallons/minute}$$

Since the oil ring of each bearing can deliver at least this amount of oil to the side grooves, there will be sufficient oil available for the hydrodynamic action of the bearing without use of an external source of oil.

Using the value of the Sommerfeld number calculated in Eq. 11.104, the value of the dimensionless number  $n$ , from Fig. 11.27 is:

$$n=0.605 \quad (11.109)$$

This number is called the eccentricity number and, as shown in Eq. 11.73, has the following relationship to the minimum oil-film thickness:

$$h_m = (1 - n) \frac{C}{2} \quad (11.110)$$

Substituting the value of  $n$  given in Eq. 11.109 and the design value of  $C=0.007$  into Eq. 11.110:

$$h_m = (1 - 0.605) \left( \frac{0.007}{2} \right) = 0.0014 \text{ inch} \quad (11.111)$$

which is acceptable

It is of interest to calculate the temperature rise at the operating point and to compare it with the curve in Fig. 11.29. From Eq. 11.64, it is equal to:

$$\theta = \frac{(0.010)(1000)}{0.561} = 17.8^\circ\text{C} \quad (11.112)$$

When the bearing temperature rise is added to the ambient temperature, the total temperature is equal to  $40+17.8=57.8^\circ\text{C}$ . This agrees with the operating temperature on the curve of Fig. 11.29, as would be expected.

Figure 11.26 shows the attitude angle  $\phi$  which is the angle between the line of action of the force on the bearing and the vertical centerline of the bearing. This angle is a function of the hydrodynamic state of the oil and hence a function of the Sommerfeld number  $S$ . Figure 11.28 gives  $\phi$  the parameter  $S$ . For the value of  $S$  given in Eq. 11.104, at the operating point the attitude angle  $\phi$  is equal to 43 degrees.

## 11.4.2 Antifriction Bearings

### 11.4.2.1 Design Consideration

#### 11.4.2.1.1 Rolling Contact Bearings vs. Sleeve Bearings

The primary decision with regard to bearings in electric motors is whether to use a sliding-contact or a rolling-contact bearing. Because the starting friction in rolling-contact bearings is due to the rolling motion within the bearing, such

bearings are sometimes called antifriction bearings, although all bearings are designed to provide relative motion with low friction. The most common sliding bearings are hydrodynamic, in which bearing loads are carried by a pressurized liquid lubricant film that is generated by relative motion between the inner and outer portions of the bearing. Section 11.4.1 contains detailed information on sliding bearings, including Kingsbury tilting-pad bearings. Other sliding bearings are self-lubricated bushings, made of dry lubricant polymers or porous, oil-impregnated metal bushings.

Neale [28] has discussed the ranges of application conditions that favor the selection of rolling-contact bearings in preference to sliding bearings. Table 11.12 provides a summary of design considerations and bearing characteristics.

Halling [29] has compared the load capacity of hydrodynamic, dry rubbing and rolling-contact bearings over a wide range of load and speed, as shown in Fig. 11.30. For the shaft sizes in most electric motors, the load capacity of rolling-contact bearings within a given space is higher than for the other types until the speed provides enough film thickness in the hydrodynamic bearings to be competitive with or preferred over rolling-contact bearings.

#### 11.4.2.1.2 Selection of Rolling Element Bearing Type

Because the principal loads in many electric motors are radial as a result of the weight of the rotor, unbalanced magnetic

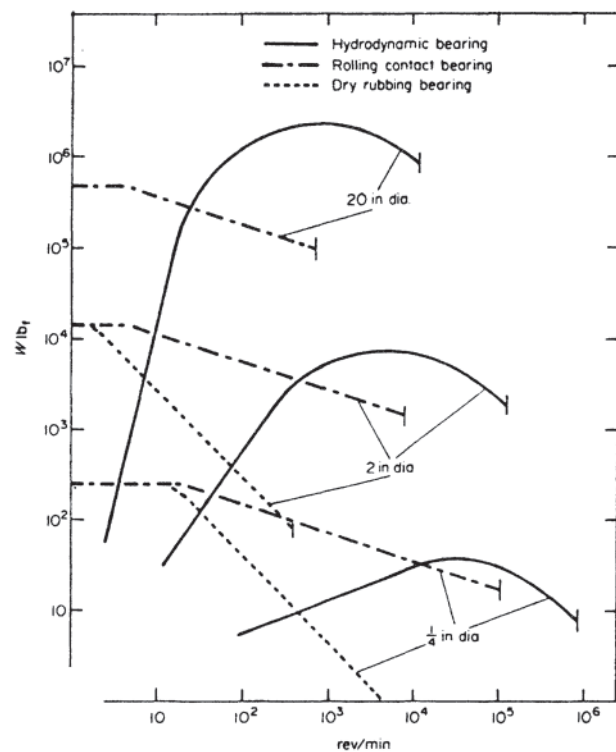


**Figure 11.30** Schematic comparison of load capacity vs. rotational speed for three bearing types indicating relative load capacities,  $W$  (pounds force) vs. bearing speed (rpm). (According to J.Halling, *Principles of Tribology*, The MacMillan Press, Ltd. [29]; by permission of The MacMillan Press, Ltd.)

**Table 11.12** Considerations in Selection of Bearings for Electric Motors

Design consideration	Rolling contact bearings	Hydrodynamic bearings	Dry sliding bearings
Load capacity in given space	Higher at low rpm Lower at high rpm Combined radial and thrust load capability	Lower at low rpm Higher at high rpm	Limited by PV of bushing material. (PV = product of unit pressure $\times$ relative sliding velocity)
Life vs. load	Fatigue life prediction, Weibull life distribution for individual bearings	Infinite life with adequate lubrication	Life limited by wear rate under application conditions
Starting torque, running torque vs. rpm	Low	Higher than rolling bearings	Higher than rolling bearings
Structural stiffness	High, maximum stiffness with preload	Lower	Lowest
Standardization, availability	ANSI, ISO and AFBMA <sup>a</sup> standards assure interchangeability; available from many vendors	Wide variety of materials and configurations, mostly proprietary to individual vendors	Wide variety of materials, mostly proprietary
Environmental effects, i.e., temperature, lubricant contamination with water, chemicals or solid contaminants	Must be protected from water and corrosive environments by effective seals. Can be used at low and high temperatures.	Can be designed for operation with water lubrication; depends on sealing from corrosive and abrasive particle environments	Can tolerate water and some corrosive environments; susceptible to solid particle contamination
Failure characteristics	Progressive, warning from damage before failure	Overheating after loss of effective lubrication	Progressive wear
Initial and lifetime cost	Depends on lubrication system	Depends on lubrication system	Lowest
Maintenance, condition monitoring, inspection, replacement	Depends on lubrication system. Noise and vibration provide warning of impending failure. Unit configuration allows easy replacement.	Depends on lubrication system. Temperature rise and noise at failure; shaft damage may influence ease and cost of replacement	Progressive increase in clearance with wear

<sup>a</sup>ANSI=American National Standards Institute; ISO=International Standards Institute; AFBMA=Anti-Friction Bearing Manufacturers Association.

forces, and departures from perfect dynamic balance, the dominant choice among the various rolling-contact bearings is deep-groove (Conrad type) ball bearings. Axial location is maintained with the deep groove configuration at the fixed end of the rotor. Provision for thermal expansion of the rotor shaft between bearing supports is usually provided by having one bearing fixed and the other end floating (free); the housing fit allows axial movement of the bearing at the free end of the rotor shaft.

Additional radial loads from belts, chains, or other power output devices on the motor shaft are a major consideration in bearing selection. For higher radial loads, double-row ball bearings or cylindrical roller bearings may be used. If angular misalignment or shaft deflection is expected, self-aligning ball bearings or spherical roller bearings could be considered. Cylindrical roller bearings are also available with self-aligning seats for special situations. [Table 11.13](#) compares the characteristics of the rolling-contact bearings most widely used in electric motors. If axial loads are present, angular contact ball bearings may be used. Thrust bearings for vertical rotors, as in some pumps, are discussed in Section 2.5.3.5.

#### 11.4.2.2 Internal Clearance and Preload

The internal clearance of rolling bearings is controlled by the as-manufactured dimensions of the bearing components and by the fitting practice used in mounting the bearing. It is

important that the designer or user consider the shaft and housing materials in the determination of internal radial clearance. Light metals have lower elastic properties and a steel insert is often used between the light-metal housing or shaft and the bearing. Since interference fits of the inner ring on the shaft and of the outer ring in the housing decrease the internal radial clearance, they must be considered before specifying the appropriate radial internal clearance designation, indicated by the suffixes C1, C2, C3, or C4 after the bearing part number, when ordering cylindrical and spherical roller bearings. Bearing number without any suffix will indicate a “normal” clearance bearing. During operation, the flow of heat generated within the bearing causes the temperature of the inner ring to be greater than that of the outer ring, which decreases the running clearance. If the net internal clearance during operation becomes negative, the radial load within the bearing is increased and the bearing temperature is higher than when adequate clearance is maintained. If a balance of heat generation and bearing cooling is not maintained, the bearing will over-heat and be destroyed.

Some bearings require preloading to achieve optimum performance. Preloading can be used to increase stiffness, reduce running noise, optimize shaft guidance, compensate for run-in wear, and improve bearing life. The internal clearance and preloading of rolling bearings also influences the center and axial location of shaft rotation. A controlled

**Table 11.13** Types and Characteristics of Rolling Bearings

Bearing type	Load capacity	Speed	Noise, torque, heat generation	Tolerance for misalignment	Fixed or free end use	Rigidity
Deep-groove ball	Radial and axial, both directions	High	Low	Angular OK	Fixed or free	
Angular contact ball	Radial and axial, one direction; double row, both axial directions	High		Low	Double row may be used on fixed or free end	Duplex angular contact type has good rigidity
Self-aligning ball	Radial	High		Excellent	May be used on fixed or free end	
Cylindrical roller	Good radial load capacity, light axial load (with bearings having integral flanges only), excellent radial capacity with double row	High	Low	Limited	Free end	Good
Needle (large ratio of roller length to diameter)	Good radial capacity, no axial capacity	High	Poor tolerance for angular misalignment	Poor	Free end	Good
Tapered roller (two row)	Excellent for combined radial and axial loads	High	Higher heat generation than ball or cylindrical roller types	Limited	Fixed end for single row; fixed or free end for double row	Good for single row, excellent for double row or if pre-loaded
Spherical roller	Good radial capacity; axial capacity in both directions	Moderate		Excellent tolerance for angular misalignment; capable of self-alignment	Fixed or free end	
Thrust bearings: single or double direction ball; angular contact ball; cylindrical, spherical or tapered roller types	Predominant axial load capacity; used with vertical axis motors	Low				

preload that is consistent with adequate lubrication and cooling is often used to provide the desired control of rigidity and vibration in a given rotating assembly. Axial preload is used in deepgroove ball bearings in conjunction with optimum radial clearance to control ball motion and minimize bearing noise under light loads. A preload spring or shims are used at the floating bearing end of the motor shaft to provide the desired axial preload. [Figure 11.31](#) illustrates the use of a preload spring in conjunction with steel inserts and light metal housings in an electric motor. A detailed discussion of bearing preload for all of the rolling bearing types can be found in bearing manufacturers' catalogs and other engineering application literature [30, 31].

Recommendations for shaft and housing fits are provided in product catalogs by bearing manufacturers, together with

information on dimensional tolerances for each bearing type and quality level. It is important that tolerances on shafts and housings be considered in conjunction with bearing tolerances to assure control of the internal clearance under expected operating conditions. Shoulder and shaft fillet dimensions should also be chosen in accordance with manufacturers' recommendations to avoid harmful deflections within rolling bearings during operation.

#### 11.4.2.3 Lubrication System Design

The performance of all rolling bearings is critically dependent on an adequate supply of an appropriate lubricant for the prevailing operating conditions. A discussion of lubricant functions and the selection of an appropriate lubricant material is given in Section 14.1.2. In the design of the bearingsystems in

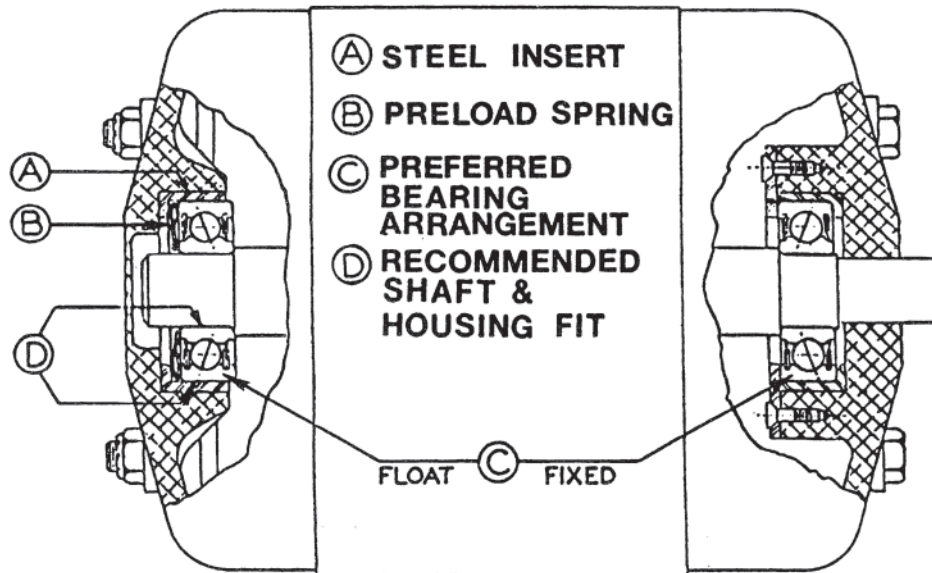


**Figure 11.31** Typical application of ball bearings to an electric motor, showing the preload spring at the floating end of the rotor shaft. (Courtesy of Fafnir Division of the Torrington Company.)

electric motors, the decision is made first between oil and grease lubrication. If oil splash lubrication is used, a sight-glass or other means to assure control of the proper oil level must be provided. If circulating oil is used, the location of inlet(s) and outlet(s) must be designed to assure maximum cooling and control of the oil level for the expected operating conditions. An oil pump of adequate capacity is critical and an oil filter must be provided in the scavenge line between the bearings and the oil pump. If the environment allows ingress or condensation of water in the lubrication system, a means for water separation should be provided in the circulating oil system. The bearing enclosure and seals must prevent contamination of the bearing and lubricant by liquid or solid particle contamination. A breather is also needed to avoid pressure buildup in the bearing enclosure that could cause lubricant leakage or seal damage.

If grease lubrication is used and a means for relubrication is provided, directions must be provided to the motor user to avoid overfilling. The bearing enclosure must have an escape path for excess grease in the event of overfilling. Otherwise, heat generated from churning of the grease will cause rapid overheating and catastrophic bearing failure. A wide variety of bearing shields or seals is available for bearings that are supplied with grease prelubrication. Detailed designs for appropriate grease lubrication systems, including the grease and seal materials as well as the configuration of the enclosures, can be found in bearing catalogs and manufacturers' lubrication literature. Comprehensive discussions of electric motor lubrication can be found in Refs. 32 and 33.

#### 11.4.2.4 Load Ratings and Expected Life

##### 11.4.2.4.1 Catalog Load Ratings

Manufacturers provide catalogs containing engineering information needed for the selection and application of rolling

bearings. Such catalogs contain rated load capacities, speed limits, dimensional data needed for control of shaft and housing fits, and recommendations for lubrication for the range of products offered. The expected bearing life is calculated from the basic dynamic load rating of a given bearing and the expected operating conditions. Because of improvements in bearing materials and in the understanding of how elastohydrodynamic lubrication affects rolling bearing life, it is important to use current product and application engineering data from bearing suppliers in selecting rolling bearings and calculating expected bearing life. The load ratings and method for calculating bearing life published in bearing catalogs are an area of competitive activity among bearing suppliers, so it is worth the effort to compare bearing life based on the ratings and calculation methods of two or more reputable bearing suppliers.

The static load capacity and basic dynamic load capacity for a given bearing can be calculated from bearing dimensions according to ANSI/ISO/AFBMA Standards [34, 35]. However, the dimensions needed for such calculations are not typically provided in the catalogs. Furthermore, most manufacturers incorporate proprietary details in the design and manufacture of their bearings that influence the bearing life. Therefore, it is best to use the manufacturer's most recent published load ratings and methods for calculation of expected life. The basic static and dynamic load ratings in such catalogs are based on the contact fatigue properties of AISI 52100 (AMS 6440)\* steel or carburized alloy steels of vacuum degassed, bearing quality. For applications at high temperatures or when higher

\* Steel type designations are from AISI, American Iron and Steel Institute, and AMS, Aerospace Material Standards of the Society of Automotive Engineers.

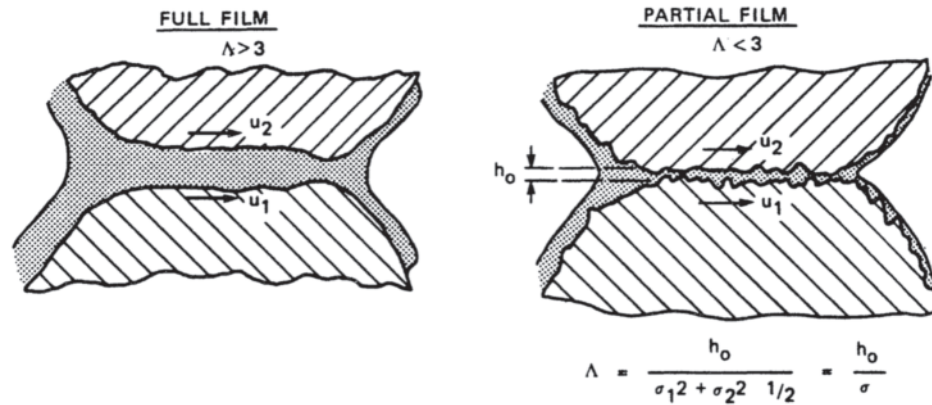


**Figure 11.32** Schematic cross section of EHL film in a roller/raceway contact. (From Ref. 36, by permission of CRC Press, Inc., Boca Raton, FL.)

load capacity or reliability is required, the bearings can be made from special materials. Premium bearing materials are discussed later in this section (see also Section 13.2.3 for a discussion of premium performance bearings).

The factors that have the greatest influence on bearing life are the bearing material, the magnitude and direction of bearing loads, the bearing speed, the ambient temperature, and the lubrication conditions. As a first approximation, the bearing life may be calculated from the following formula:

$$L_{10} = \left( \frac{16667}{N} \right) a_1 a_2 a_3 \left( \frac{C}{P_e} \right)^p \quad (11.113)$$

where

$C$  = basic radial load rating

$P_e$  = equivalent radial load

$N$  = bearing speed (rpm)

$L_{10}$  = estimated bearing life in hours, with 90% survival probability (see Section 13.2.3 for a discussion of individual bearing life and bearing system reliability) for given application conditions

$p$  = exponent relating load and life:  $p=3$  for ball bearings;  $p=10/3$  for roller bearings

$a_1$  = life factor for reliability, that is, survival probability other than 90%

$a_2$  = life factor for special bearing material and bearing processing

$a_3$  = life factor for application conditions

The  $a_1$  factor may be used to adjust the expected life for higher reliability, that is, lower or higher probability of failure than  $L_{10}$ . The  $a_2$  factor accounts for nonstandard bearing material, the life improvement due to premium bearing materials, for example, VIM-VAR M50 double-vacuum-melted steel\*; adjustment for material hardness at the operating temperature; and other processing effects, such as forged raceways. The  $a_3$  factor includes all effects of the operating environment, the most important being the bearing lubrication. Misalignment and housing deflections, preload, vibration, and the hoop stress from press fitting may also be considered.

\*VIM-VAR, vacuum-induction-melted plus vacuum-arc-remelted steel.

#### 11.4.2.4.2 Elastohydrodynamic Lubrication

The pressurized oil film between the rolling elements and the raceways exerts a powerful influence on the life of rolling bearings. Figure 11.32 illustrates the elastohydrodynamic lubricant (EHL) film at the center of a ball or roller/raceway contact [36].

When the oil enters the region of high contact stress due to the elastic deflection of the contact surfaces, the viscosity of the oil is greatly increased, which limits the flow of lubricant out of the high-pressure region. The thickness of the EHL film can be computed from the inlet viscosity, the pressure/viscosity and thermal properties of the oil, the contact geometry, and the bearing speed. If the EHL film thickness is greater than the composite surface roughness of the contact surfaces, metallic contact is prevented and surface-origin fatigue failure is prevented or delayed. In many applications, full separation of the contact surfaces is not possible, and surface-origin fatigue damage will occur. Since the EHL film thickness depends on the bearing speed, some surface damage can occur during start-up and at low speed. Additionally, if the size of solid debris contaminants in the oil exceeds the EHL film thickness, denting of the contact surfaces will occur and surface-origin contact fatigue is more likely.

Bearing suppliers provide tables and charts to calculate the  $a_3$  factor. The inlet oil temperature in the EHL calculation will usually be the same as the contact surface temperature, which is 5–20°F (3–11°C) above the bearing housing temperature. Extensive research and bearing life tests have provided the basis for calculation of the  $a_3$  factor. Some bearing suppliers have used a combined  $a_{23}$  factor for material, processing, and lubrication effects. Because of improved internal quality of commercial bearing steels in recent years, classical inclusion-origin contact fatigue failures are infrequent and bearing life is primarily limited by surface flaws, debris damage, and corrosion.

The combination of factors indicated by Eq. 11.113 must be used with caution because they simply indicate the factors to be considered in modifying the rating life to account for reliability other than 90% survival, for premium bearing materials, and for those operating conditions that influence

bearing life, for example, lubricant viscosity at the bearing temperature and EHL film thickness compared with contact surface textures. One cannot use a premium bearing material to overcome an application conditions factor less than 1 for a low lubricant film thickness. One can, however, use special high-temperature bearing materials, or even ceramics, if operating temperatures will exceed the limit for standard bearing products. If the oil inlet temperature or the bearing temperature is over 375°F (190°C) the standard material will progressively lose hardness and premature failure will occur by fatigue or plastic flow. The values of life adjustment factors are different for some bearing types and may be different for some bearing manufacturers. Since the basic dynamic load capacity in a given manufacturer's catalog includes the fatigue properties of their basic bearing material, the internal geometry, and the surface texture of their standard product, it is important to use the life adjustment factors that are consistent with the given bearing manufacturer's calculation method.

#### 11.4.2.4.3 Bearing Materials

Nearly all ball, cylindrical, and spherical roller bearings are made from AISI 52100 (AMS 6440) or modifications with different chromium content. For bearings of larger cross section, alloy modifications of 52100 for higher hardenability may be used. For high-temperature bearings, VIM-VAR M-50 (AMS 6491) permits operation or exposure to temperatures to 900°F (482°C) with no permanent size change or loss of hardness. VIM-VAR M-50NIL (AMS 6278) is a carburizing variation of VIM-VAR M-50 and provides all of the properties of M-50 plus high fracture toughness in a softer core. The higher fracture toughness of carburized inner rings allows operation at higher speeds while avoiding section fracture due to high centrifugal forces and interference fits. CEVM 52100 (AMS 6444)\* can be used to obtain longer fatigue life at temperatures up to 375°F (191°C), but only with regard to the inclusion origin mode of contact fatigue damage, that is, the EHL film thickness, surface texture, and lubricant filtration must be adequate to avoid surface-origin modes of failure (see Section 13.2.1).

AISI 440C stainless steel (AMS 5880) or special coatings may be used in special bearings requiring corrosion resistance. Ceramics such as silicon nitride can be used in corrosive environments and at temperatures up to 1800°F (982°C). Metal-ceramic hybrid bearings have also been developed for ultrahigh-speed applications to reduce the radial loads from centrifugal force on the orbiting balls or rollers.

## 11.5 BRUSHES [37]

### 11.5.1 Introduction

The term carbon brush was developed around 1889. Before 1889 bundles of copper wires (brushes) were used to collect current from rotating armatures of motors and generators. Thanks to a suggestion made by Mr. Charles J. Van Depoele, carbon replaced copper wires as the device to collect current from rotating machinery. Over the past 100 years, carbon brush

development has created four main brush grade families. These families are classified according to manufacturing processes, the types of carbons and graphites, or other ingredients used. The four main families are carbon graphites, electrographites, graphites, and metal-graphites.

#### 11.5.1.1 Carbon Graphite Brushes

Carbon graphite brushes made their entrance early in the brush industry. They are high-strength materials with a pronounced cleaning action. Carbon graphite brushes are generally limited to lower current densities (45 A/inch<sup>2</sup>) and are used on older, lower-speed machines that reach maximum commutator surface speeds of approximately 4000 feet/min. The high friction generated with this type of material also makes it unattractive for present use on commutators.

#### 11.5.1.2 Electrographitic Brushes

Electrographitic brushes are baked at temperatures in excess of 2400°C, which changes the material physically to a more graphitic structure. Apparent density, strength, hardness, and resistivity can be closely controlled through raw material composition and processing to achieve superior commutating ability while providing long life.

The high processing temperature volatilizes impurities, which makes electrographitic brushes generally free from abrasive ash. Therefore, commutators must have undercut mica since very little mechanical wear results.

Electrographitic materials are generally fairly porous, thus permitting treatment with various organic resins. The treatments increase strength and lubricating ability, which generally increases brush life significantly at high operating temperatures and at lower humidities. The curves shown in Fig. 11.33 and Fig. 11.34 illustrate typical improvements through the addition of treatments to the electrographitic base material.

Treatment can also permit electrographitic materials to operate satisfactorily in a variety of contaminated atmospheric environments.

Friction characteristics with electrographitic materials can be controlled through raw material combinations before graphitization and also by treating the finished product with organic resins. Brush face temperature is a primary influence in determining the coefficient of friction, as shown by the typical curve of Fig. 11.35.

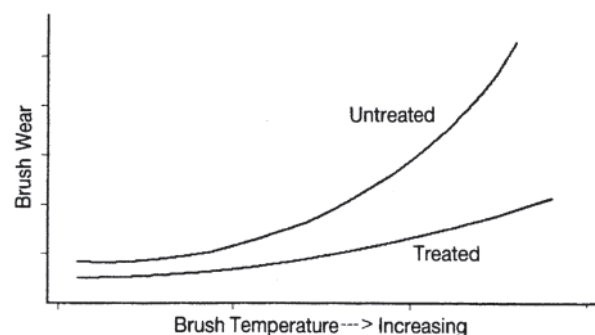


**Figure 11.33** Brush wear vs. brush temperature for treated and untreated brushes.

\* CEVM, consumable-electrode vacuum-remelted steel.

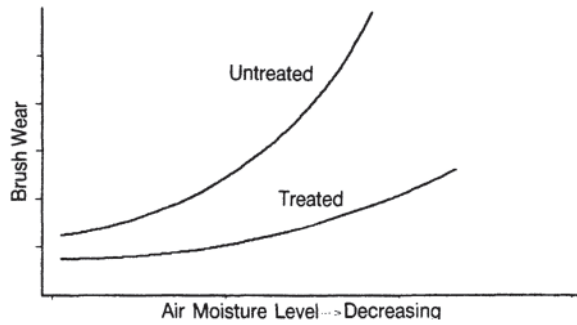


**Figure 11.34** Brush wear vs. air moisture level.

### 11.5.1.3 Graphite Brushes

Graphite brushes are composed of natural or artificial graphite bonded with resin or pitch to form a soft brush material. Natural graphite usually contains ash that gives the brushes an abrasive or cleaning action. Artificial graphite generally does not contain ash, nor does it have the flaky structure of natural graphite.

Graphite brushes are characterized by their controlled filming and excellent riding qualities on both commutators and slip rings at brush current densities used with electrographitic brushes; however, higher surface speeds are often permitted with some types of graphite materials.

The fast filming properties of graphite brushes are beneficial in protecting the commutator or slip ring during operation in contaminated atmospheres such as those existing in papermills. Their low porosity is also valuable in reducing commutator threading, which is often encountered in contaminated environments (see [Section 13.3.4](#)).

### 11.5.1.4 Metal-Graphite Brushes

Metal-graphite brushes are generally made from natural graphite and finely divided metal powders. Copper is the most common metallic constituent, but silver, tin, and other metals are sometimes used.

Metal graphites are ideal for a variety of applications because of their low resistivity. Metal graphites are used on commutators of plating generators where low voltage and

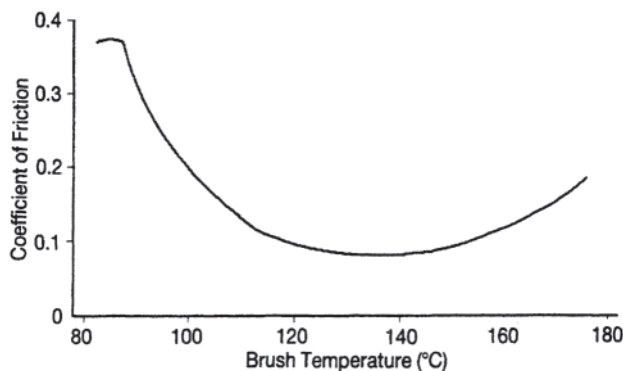


**Figure 11.35** Coefficient of brush friction vs. brush temperature.

**Table 11.14** Applications Table for Metal-Graphite Brushes

Metal content (%)	Application
50 or less	Low-voltage (24–72 V) motors for forklift and battery trucks Battery charging and welding generators in the 24–72 V range
65–85	Brass slip rings at brush current densities less than 100 A/in <sup>2</sup> Plating generators in the 6–24 V range Brass slip rings at brush current densities less than 125 A/in <sup>2</sup>
75 and above	DC machines at less than 6 V Brass slip rings at brush current densities less than 150 A/in <sup>2</sup> Grounding brushes

high brush current densities are encountered. They operate on slip rings of wound-rotor induction motors where high brush current densities are common. Metal graphites are used for grounding brushes because of their low contact drop.

Table 11.14 describes some general applications where metal-graphite brushes are used.

### 11.5.2 Grade Characteristic Definitions

Various static tests are performed on carbon materials to ensure the material is properly manufactured. These carbon materials also are dynamically tested to quantify the desired operating properties. Detailed values for various brushes are shown in [Table 11.15](#). The following is an explanation of these tests.

#### 11.5.2.1 Specific Resistance

Unless otherwise specified, specific resistance (or resistivity) in ohm-inches is equal to the resistance that a specific volume of the brush material offers to the passage of current. Specific resistance is measured in the length direction of the slab, since resistance in the direction of width or thickness may be considerably different. Specific resistance is calculated from measurements on a test specimen as follows.

$$R = \frac{EWT}{IL} \quad (11.114)$$

where:

$R$  = the specific resistance (ohm-inch)

$E$  = voltage drop over length  $L$  (V)

$I$  = current passed through the specimen (A)

$W$  = width of specimen (in)

$T$  = thickness of specimen (in)

$L$  = that portion of the length, over which the drop  $E$  is measured (in)

#### 11.5.2.2 Scleroscope Hardness

The scleroscope hardness is determined by dropping a special diamond-tipped weight on a specimen and measuring the height of the rebound. This hardness measurement is, to some

**Table 11.15** Characteristics, Descriptions, and Typical Applications for Various Types and Grades of Brushes

Brush grade	Specific resistance [Ohm-in meter]	Density (g/cm <sup>3</sup> )	Scleroscope hardness	Transverse strength [psi (MPa)]	Abrasive-ness	Contact drop	Friction	Surface speed [ft/min (m/s)]	Normal current density [A/in <sup>2</sup> (A/cm <sup>2</sup> )]	Description and application
<b>Electrographitic</b>										
561	0.0030 (76)	1.54	53	1700 (11.7)	L	VH	L	8000 (40)	80 (12.5)	A brush for use where excellent commutating is of primary importance
571	0.0027 (69)	1.57	61	2400 (16.5)	L	VH	L	7000 (35)	80 (12.5)	An excellent commutation grade with higher strength than grade 561
591	0.0020 (51)	1.66	70	4000 (30.3)	L	VH	L	6000 (30)	80 (12.5)	A very strong grade for use under severe mechanical conditions and where long life is particularly important
T563	0.0030 (76)	1.58	58	2400 (16.5)	L	VH	L	8000 (40)	80 (12.5)	A treated grade of excellent commutating and riding ability. Has been used in many industrial applications
T573	0.0027 (69)	1.62	65	3100 (21.4)	L	VH	L	7000 (35)	80 (12.5)	A grade similar to, but stronger than, grade T563
T593	0.0020 (51)	1.73	80	5000 (34.5)	L	VH	L	6000 (30)	80 (12.5)	Recommended for diesel electric locomotive traction motor service
T566	0.0030 (76)	1.62	60	2500 (17.2)	L	VH	L	8000 (40)	70 (11)	Recommended for contaminated atmospheres seen in paper mills and where load requirements are high
T416	0.0030 (76)	1.62	60	2700 (18.6)	L	VH	L	8000 (40)	70 (11)	A treated grade with excellent commutating and riding properties. Applied on high-voltage machines used in steel mills, paper mills, dc excavators, etc.
T659	0.0030 (76)	1.63	65	4000 (27.6)	L	VH	L	8000 (40)	80 (12.5)	A good commutating grade treated to improve friction—successful where friction chatter has been a problem
T758	0.0027 (69)	1.68	70	4700 (32.4)	L	VH	L	8000 (40)	80 (12.5)	Similar to T659 but with higher strength and longer life. Successful on high-speed transit car motors
F799	0.0035 (89)	1.70	38	2800 (19.3)	L	VH	L	7000 (35)	70 (11)	Recommended for application where friction chatter is encountered
T606	0.0035 (89)	1.73	50	3600 (24.8)	L	VH	L	7000 (35)	70 (11)	Treated brush grade that is very effective in reducing threading in contaminated atmospheres and in minimizing friction
T777	0.0015 (38)	1.63	55	3300 (22.8)	L	VH	L	7000 (35)	80 (12.5)	Elevator grade treated to provide good leveling qualities
T900	0.0020 (51)	1.68	72	4500 (31.0)	L	VH	L	8000 (40)	80 (12.5)	Excellent low-humidity and high-brush-temperature grade used extensively in traction motor service
D	0.0005 (13)	1.65	41	4200 (29.0)	L	VH	L	5000 (25)	80 (12.5)	A dense strong grade used extensively on steel and cast-iron rings of synchronous machines and brass
G	0.0013 (33)	1.65	52	3300 (22.8)	L	VH	L	6000 (30)	70 (11)	Good for medium-duty commutating service
T869	0.0013 (33)	1.71	60	4000 (27.6)	L	VH	L	6000 (30)	70 (11)	Treated material used on brass collector rings and medium-duty commutating service
T300	0.0008 (20)	1.72	57	4000 (27.6)	L	VH	L	7000 (35)	80 (12.5)	A treated grade for high temperature and low humidity. Used on 24–80 V dc generators
<b>Graphite</b>										
H	0.0010 (25)	1.36	18	1300 (9.0)	M	VH	M	12000 (60)	55 (7.8)	A low-density graphite material for high-speed service. Used on steel slip rings of turbine-generators and on ac generators of motor-generator sets
K816	0.00036 (9)	1.83	25	2900 (20)	L	M	L	8000 (40)	65 (10)	Special contaminated atmosphere brush for light loads and low-voltage machines



**Table 11.15** Characteristics, Descriptions, and Typical Applications for Various Types and Grades of Brushes (*Continued*)

Brush grade	Specific resistance [Ohm-in (micro-ohm meter)]	Density (g/cm <sup>3</sup> )	Scleroscope hardness	Transverse strength [psi (MPa)]	Abrasive-ness	Contact drop	Friction	Surface speed [ft/min (m/s)]	Normal current density [A/in <sup>2</sup> (A/cm <sup>2</sup> )]	Description and application
R310	0.0022 (56)	1.75	40	3600 (24.8)	L	VH	L	5000 (25)	45 (7.0)	A graphite grade of exceptional riding and commutating ability. Has been successful on 3600 rpm turbo exciters up to about 60 kW size and on motors and generators in papermill and steel mill service
R312	0.0020 (51)	1.73	40	2400 (16.5)	L	VH	L	6000 (30)	55 (8.5)	Similar to R310 but with load capacity
R318	0.00055 (14)	1.75	35	3200 (22.1)	L-1	H	L	10000 (50)	65 (10)	Very successful on steel slip rings of alternators and synchronous motors
R320	0.0013 (51)	1.35	18	1000 (33)	L	H	L	12000 (60)	65 (10)	A low-density graphite material formulated to reduce selectivity. This grade has a very low coefficient of friction for high-speed service on steel rings of turbine generators, alternators and synchronous motors
R420	0.013 (330)	1.60	65	2700 (18.6)	L	VH	L	6000 (30)	40 (6.2)	Brush used on small amplidyne for high commutating ability
R782	0.044 (1118)	1.60	25	4000 (27.6)	L	VH	L	6000 (30)	35 (5.4)	A very high-resistance grade useful on small, hard-to-commutate machines such as small amplidyne and noncommutating pole motors used with SCR packages
T341	0.0020 (51)	1.79	45	4500 (27.6)	L	VH	L	6000 (30)	55 (8.5)	Similar to R312 but treated for higher strength, lower friction and good filming characteristics. Useful to minimize threading
T990	0.0025 (64)	1.83	42	3700 (32.4)	L	VH	L	8000 (40)	80 (12.5)	Battery truck grade with superior commutating ability
T999	0.00036 (9)	1.88	30	3400 (19.3)	L	M	L	8000 (40)	65 (10)	Used very successfully on brass rings. Can be used at lower humidities and in contaminated atmospheres
<b>Metal graphite</b>										
L	0.000015 (0.4)	6.2	11	20000 (9.0)	M	L	M	3500 (18)	150 (23.3)	A very high-metal contact brush having a low contact resistance and high current-carrying capacity. Used on slip rings of rotary converters and for grounding brushes
L4	0.000014 (0.6)	4.57	15	3100 (21.4)	L	L	M	5000 (25)	125 (19.4)	A very smooth-grained brush of high metal content and low contact resistance designed for collector rings where high capacity is required. Used on low-voltage motors, particularly switch and signal equipment; used on plating generators up to 15 V, also on brass slip rings of induction motors
M407	0.000008 (0.2)	5.10	14	2400 (16.5)	L	L	L	4500 (23)	150 (23.3)	A silver-grade brush having very low contact drop and low friction. Used where low contact drop and temperature are of primary importance. Also used on controllers and control equipment where low, stable contact drop is required
M540	0.000015 (0.4)	5.40	10	8300 (16.5)	L	L	M	5000 (25)	140 (21.7)	A brush of approximately 85% metal that is used on low-voltage dc machines and grounding brushes
M753	0.0003 (8)	3.25	15	2600 (22.1)	L	L	M	6000 (30)	100 (15.5)	Similar to M785 with additive to improve low-humidity life
M783	0.00035 (9)	2.50	25	2900 (20.0)	L	M	M	6000 (30)	80 (12.5)	A metal graphite of low metal content recommended for collector rings and low-voltage dc machines

*(Continued)*

Table 11.15 (Continued)

Brush grade	Specific resistance [Ohm-in (micro-ohm meter)]	Density (g/cm <sup>3</sup> )	Scleroscope hardness	Transverse strength [psi (MPa)]	Abrasive-ness	Contact drop	Friction	Surface speed [ft/min (m/s)]	Normal current density [A/in <sup>2</sup> (A/cm <sup>2</sup> )]	Description and application
M785	0.00027 (7)	3.20	17	3000 (20.7)	L	L	M	6000 (30)	100 (15.5)	A brush of approximately 50% metal. Used on low-voltage dc motors and generators in the 24–72 V range and on brass slip rings of induction motors.
ME31	0.00008 (2)	2.48	80	13000 (89.6)	M	L	L	6000 (30)	100 (15.5)	Metal-impregnated grade designed to provide long and trouble-free life as wear shoes for pantograph applications
<b>Carbon graphite</b>										
B2	0.0012 (30)	1.65	65	6400 (44.1)	M	H	H	4000 (20)	45 (7.0)	Hard, strong carbon graphite brush with no abrasive but some polishing action because of its texture and hardness. Used on noncommutating pole railway motors with undercut mica. Also used on vehicles, crane, elevator and mill motors when the service is such as to require a moderate polishing action

extent, an indication of the resilience of the carbon material. Hardness measurements obtained in this manner are not interpreted as absolute units, but as relative values for comparative purposes. Hardness alone should not be used as the sole basis for determining the quality of a brush. Several points of variation in hardness alone may have no pronounced effect on brush performance.

The hardness of a brush is not a direct indication of its abrasiveness. Some very hard brushes have low abrasiveness, whereas others of almost identical hardness are highly abrasive. It is the combination of hardness, grain structure, and ash content that determines abrasiveness.

#### 11.5.2.3 Apparent Density

For a brush material, the apparent density is equivalent to its weight in grams divided by its volume in cubic centimeters. Density must be considered jointly with other brush characteristics in estimating brush quality.

#### 11.5.2.4 Abrasiveness

Corrosive or oily atmospheres frequently cause an excessive buildup of film on the commutator/slip rings. The ability of the brush to prevent this excessive buildup is called the abrasiveness or “polishing action.” Abrasive brushes are usually required on flush-mica commutators. The abrasiveness of a brush may be influenced by its hardness, grain structure, and ash content. Brushes are classified according to abrasiveness as follows: “Low” indicates very little abrasiveness (commonly referred to as nonabrasive by the trade). “Medium” indicates some polishing action. “High” indicates pronounced polishing action, which is usually obtained by using a material with high ash content or by the addition of a polishing agent. In the resin-bonded series, the abrasion has been calibrated L4 to L, the brush with the higher number having the greater polishing ability.

#### 11.5.2.5 Contact Drop

Contact voltage drop between the brushes and rotating surface is influenced by many variables that cause the values to fluctuate. Brush current density, temperature, pressure, speed, and contamination all influence the magnitude of contact drop.

Values of contact drop for brushes listed in Table 11.15 are approximate values only and represent the total voltage drop (positive plus negative) obtained on a copper ring at 50 A/in<sup>2</sup> (7.8 A/cm<sup>2</sup>) while rotating at 2500 feet/min. Contact drop classifications are as in Table 11.16.

#### 11.5.2.6 Current-Carrying Capacity

The actual current-carrying capacity of a brush is widely influenced by operating conditions such as type of ventilation, continuous or intermittent duty, speed, and other factors. The data sheet ratings are conservative, some allowance having been made for overloads. Brushes have been run at densities considerably above those listed in the table. Metal graphites, for example, have been operated at 180 A/in<sup>2</sup> on certain high-current generators. Electrographitic brushes have been used at 150 A/in<sup>2</sup> on similar equipment with reasonably good results.

The current-carrying capacity of a brush depends on the operating temperature. On well-ventilated machines having small brushes, with large surface area in proportion to their volume, and where brushes cover only a small percentage of

Table 11.16 Voltage Drops for Various Contact Drop Designations

Contact drop designation	Contact drop (V)
VH = very high	1.7 and above
H = high	1.2 to 1.7
M = medium	0.6 to 1.2
L = low	Below 0.6

the commutator or ring surface, conventional current densities can usually be doubled without seriously jeopardizing the performance. On the other hand, increasing the current density without making provisions for maintaining a low brush temperature may reduce the brush life many times. The brush current density of a given machine can be calculated as follows.

$$D = \frac{1}{(N/2)TW} \quad (\text{for commutator machines}) \quad (11.115)$$

$$D = \frac{1}{NTW} \quad \text{for slip rings}$$

where:

$D$  = the brush current density (A/in<sup>2</sup>)

$I$  = total current (A)

$N$  = total number of brushes on a commutator, or the number of brushes on an individual ring

$W$  = width of the brush (in)

$T$  = thickness of the brush (in)

#### 11.5.2.7 Maximum Speed

The highest peripheral speed in feet per minute recommended for the collector or commutator on which the brush is to ride is referred to as the maximum speed. The allowable speed depends not only upon the characteristics of the brush material but also upon the spring pressure, current density, type of brush holder, brush angle, condition of ring or commutator, and atmospheric conditions. Consequently, the maximum speed, conventionally listed as a brush characteristic, is only an approximation.

#### 11.5.2.8 Friction Coefficients

Brush friction is influenced by many variables including brush temperature, brush pressure, current, atmospheric conditions, mechanical conditions, ring or commutator materials, surface films, speed, and other factors. Even under favorable conditions, the commutator surface is continually undergoing changes caused by oxidation, abrasion, and moisture.

Certain brush holder configurations may increase friction chatter noise and accelerate the associated brush wear. This is especially true under conditions of light loads and lower brush temperatures when the coefficient of friction is relatively high (refer to Fig. 11.35). Specific brush grades are used to lessen the severity of friction chatter under these conditions.

Friction between the brush and rotating surface can be a major source of heat generation that causes serious temperature-related problems. Commutators can distort, slip rings can move, and brush wear can become excessive when the coefficient of friction becomes too high.

Brush friction designations and coefficient ranges are tabulated in Table 11.17.

#### 11.5.2.9 Transverse Strength

The standard specimen is supported near the ends on two knife edges. A third knife edge presses on the top of the specimen midway between the two supporting edges. The force is

**Table 11.17** Coefficients of Friction for Various Friction Designations

Friction designation	Friction coefficient
High	0.40 and above
Medium	0.22 to 0.40
Low	Below 0.22

increased on the top knife edge until the specimen breaks. The transverse strength is computed by using the beam formula:

$$S_t = \frac{3PL}{2WT^2} \quad (11.116)$$

where:

$S_t$  = transverse strength (psi)

$P$  = the total force applied at the upper knife edge (pounds)

$L$  = distance between supports (in)

$W$  = width of specimen (in)

$T$  = thickness of specimen (in)

#### 11.5.3 Specialty Brushes

In addition to the four brush families there are two brush types that are for unique applications. They are laminated brushes and surface rounding brushes. Both of these brushes are patented by National Electrical Carbon.

Laminated brushes are used when a premium brush is required. The laminated series was developed to aid the designer and the ultimate user in obtaining more effective performance from commutator-type machines.

The laminated brush is a composite assembly of two or more grades of electrographitic carbon that are of varying resistivities. These brushes will improve commutation, reduce commutator temperatures, and reduce commutator cutting. Reduction of the resistivity of the various parts will reduce the commutating ability slightly, but will increase the brush life. Several combinations of materials have been produced for special commutation conditions.

The surface rounding brush (SRB) is a preventive maintenance tool designed to give the best possible performance in rotating equipment. The SRB fits in the brush holder of the motor or generator and smooths the commutator or collector ring to a specific roundness as the machine operates. The SRB does not limit the apparatus output since it is made of a material compatible with the other brushes. The SRB has also been used as a trouble-shooting tool that removes undesirable films that can cause commutation distress.

An additional specialty brush is the fluted brush. Many larger machines shipped are equipped with a fluted brush face to reduce the running time necessary to get a good brush fit and commutator polish. When replacement brushes are installed a few at a time, the fluted brush does not have to be fitted. Using a fluted brush for replacement will decrease the possibility of tearing of the commutator film surface when brushes are replaced and not sanded to fit the commutator contour.

On critical threading conditions, it is recommended that

fluted brushes be used, as the brush allows for quick brush fit and a more even film. It is not necessary to remove the brush after the flutes are worn away; they may be used until they reach the normal minimum wear length.

Rubber hardtops are installed on brushes instead of steel clips to soften the impact from a rough commutator, giving longer brush wear and reduced brush breakage. However, rubber hardtops are not a “cure-all” solution. If the spring force applied to the rubber hardtop is not properly positioned, differential brush wafer wear can result. Proper technical assistance should be consulted when applying rubber hardtops.

#### 11.5.4 Summary

Carbon brushes have been manufactured for the past hundred years. During this time many different types of base materials have been developed to be used on multiple applications. Treatments impregnated into the base carbon have improved the performance of the brush in various applications. Carbon brushes carry current to and from rotating surfaces. In dc machines, carbon brushes also aid in the commutation process. Improvements in manufacturing processes and new organic materials for treatments have allowed the carbon brush to maintain its leadership as the method for transferring electrical energy to mechanical energy.

### 11.6 MOTOR HANDLING, MOUNTING, AND MECHANICAL CONNECTION

#### 11.6.1 Motor Handling

Manufacturers of electrical equipment provide instruction books that are usually shipped with the equipment. These instructions are periodically revised and updated to cover the latest information on safely handling and installing the equipment. Many have carefully worded “Caution” and “Warning” notices throughout in order to minimize accidents and possible liabilities. The following excerpts from General Electric Company instruction books [38, 39] are typical examples.

##### *Handling*

Individual motors and generators can be lifted by using hooks or slings in the lifting lugs on the frame. Do not lift the machine by the shaft extensions.

**Warning:** Before attempting to lift any machine, check the outline drawing for the lifting points and their limitations. Unless otherwise specified on the outline drawing, lifting devices are intended to support only the part to which they are attached. They are not to be used to lift the machine plus additional equipment such as pumps or other driven equipment.

Failure to observe these precautions may result in damage to the equipment, injury to personnel, or both.

##### *Installation*

**Warning:** Installation should be in accordance with the National Electrical Code and consistent with all local codes. Coupling, belt, and chain guards should be installed as needed to protect against accidental contact with moving parts.

**Warning:** Disconnect power before touching any internal part. High voltage may be present even when the machine is not rotating. Failure to observe these precautions may result in injury to personnel.

Totally enclosed and waterproof motors must have all covers securely in place with gaskets intact in order to exclude dirt, oil, and water.

##### *Location*

Motors and generators should be installed so that they will be readily accessible for routine inspection and maintenance. They are suitable for use in ambient temperatures from 0°C (32°F) to 40°C (104°F). An adequate supply of clean, dry, room air is required for self-ventilated and blown motors. Where motors must operate in dirty, wet, or contaminated environments, protection in the form of filters or totally enclosed construction must be used to insure long life with normal maintenance.

Do not obstruct ventilating openings.

When filters are supplied, service them regularly. Dirty filters shut off ventilating air.

Beware of recirculation. Install motors so that hot exhaust air will not re-enter the motor.

##### *Mounting*

Motors and generators should be mounted on rigid and solid foundations. Level the base (or the machine). Hold down bolts should be inspected regularly and kept tight. The feet of the machine may be doweled to the foundation or base when alignment procedures are completed. Sliding bases, when used, should be securely anchored to the foundation.

Further examples of manufacturer’s instructions for the proper and safe handling and installation of large motors appear in Tippins Machinery Company’s Instructions No. TMI-702 and 703 [40]. Excerpts from important sections follow.

##### *Supervision of Erection*

The process of installing a rotating electrical machine will vary widely with the construction and the available handling facilities. A small end-shield bearing motor may require little more than leveling the machine on the foundation, properly aligning it with the load, and connecting the machine terminals to the control. A motor-generator set consisting of many machines may require, in addition, assembly of the larger machines, mounting them on a common base and foundation and carefully aligning them with respect to each other. The erection of large machines is highly complex and should be supervised by an experienced erection engineer.

##### *Construction of Foundation*

The chief requirement of a machine foundation is that it must have sufficient rigidity and mass to support the machine and minimize vibration. Actual design and construction of the foundation are governed largely by local conditions. Therefore, the responsibility for providing ample foundations rests with the purchaser of the machine.

The foundation should not interfere with the ventilation or accessibility of the machine. If a pit is located under the unit, it should be large enough to provide access to machine terminals and to the bottom of the machine for cleaning, inspection, and repairs. The pit should be provided with a drain or other means of preventing the accumulation of water or oil.

#### Handling Heavy Machines

The handling of heavy machines should be supervised by experienced personnel. Primary considerations are the safety of those working near the machine and the avoidance of damage to the machine itself.

Overhead cranes, derricks, or mobile boom rigs are the best means of lifting heavy machinery. Where they are not available, it is necessary to move the machine by such means as jacks, pinch bars, and rollers. To avoid strains on any part of the machine, the weight must be evenly distributed over as many points as possible. Skids used in shipping are usually sufficient for normal handling in field erection, but should be carefully checked before being depended on for handling in this manner.

#### Slings

Either rope or wire cable may be used as slings. It may be necessary to use chains or chain hoists in some cases, but great caution should be exercised in their use for rigging. However, if the use of chains cannot be avoided, they should be rigidly inspected for fatigue, overstrains and deformed hooks, rings, and links. [Slings should be placed so that the center of gravity is nearly midway between the slings, and the slings should be as far apart as possible.]

#### Eyebolts

As a matter of safety, eyebolts should never be used for lifting heavy machinery. When manufacturer's equipment is fitted with eyebolts, a liberal safety factor is allowed, provided the eyebolt is sound and the pull is directly along the axis of the thread. For example, when the load is applied at an angle of 45 degrees with respect to this axis, the safe load will be only 5% or 6% of the allowable load on a straight pull. Small machines are more readily handled by means of eyebolts, but precautions should be taken that the bolt is screwed in tight and careful examination made for flaws. Tap the eyebolt with a hammer to test for tightness or fractures.

These examples stress some of the important concerns of manufacturers for the safety of personnel handling electrical equipment. In addition to the manufacturer's instructions, the reader is directed also to the industry standard, NEMA MG 2-1989 [4], Safety Standard for Construction and Guide for Selection, Installation, and Use of Electric Motors.

#### 11.6.2 Motor Mounting Dimensions

Mounting dimensions for motors made in the United States are standardized by the National Electrical Manufacturers Association (NEMA) in Standard MG 1-1993 [13]. The dimensional units used are inches. Domestic manufacturers will conform to this standard whether they belong to NEMA or not so that their frames will fit with the same mounting dimensions as all others.

#### Foot-Mounted Dimensions

Figure 11.36 defines the letters used to describe the various dimensions for foot-mounted direct current machines, as

**Table 11.18** Dimensions for Foot-Mounted Industrial Direct-Current Machines<sup>a,b,c</sup>

Frame designation	A max	B max	D <sup>d</sup>	E <sup>e</sup>	2F <sup>e</sup>	BA hole	H <sup>c</sup>	AL	AM	AO	AR	AU	AX	AY max bases	BT
182AT	9.00	6.50	4.50	3.75	4.50	2.75	0.41	12.75	9.50	4.50	4.25	0.50	1.50	0.50	3.00
183AT	9.00	7.00	4.50	3.75	5.00	2.75	0.41	12.75	10.00	4.50	4.50	0.50	1.50	0.50	3.00
184AT	9.00	7.50	4.50	3.75	5.50	2.75	0.41	12.75	10.50	4.50	4.75	0.50	1.50	0.50	3.00
185AT	9.00	8.25	4.50	3.75	6.25	2.75	0.41	12.75	11.25	4.50	5.12	0.50	1.50	0.50	3.00
186AT	9.00	9.00	4.50	3.75	7.00	2.75	0.41	12.75	12.00	4.50	5.50	0.50	1.50	0.50	3.00
187AT	9.00	10.00	4.50	3.75	8.00	2.75	0.41	12.75	13.00	4.50	6.00	0.50	1.50	0.50	3.00
188AT	9.00	11.00	4.50	3.75	9.00	2.75	0.41	12.75	14.00	4.50	6.50	0.50	1.50	0.50	3.00
189AT	9.00	12.00	4.50	3.75	10.00	2.75	0.41	12.75	15.00	4.50	7.00	0.50	1.50	0.50	3.00
1810AT	9.00	13.00	4.50	3.75	11.00	2.75	0.41	12.75	16.00	4.50	7.50	0.50	1.50	0.50	3.00
213AT	10.50	7.50	5.25	4.25	5.50	3.50	0.41	15.00	11.00	5.25	4.75	0.50	1.75	0.50	3.50
214AT	10.50	8.25	5.25	4.25	6.25	3.50	0.41	15.00	11.75	5.25	5.12	0.50	1.75	0.50	3.50
215AT	10.50	9.00	5.25	4.25	7.00	3.50	0.41	15.00	12.50	5.25	5.50	0.50	1.75	0.50	3.50
216AT	10.50	10.00	5.25	4.25	8.00	3.50	0.41	15.00	13.50	5.25	6.00	0.50	1.75	0.50	3.50
217AT	10.50	11.00	5.25	4.25	9.00	3.50	0.41	15.00	14.50	5.25	6.50	0.50	1.75	0.50	3.50
218AT	10.50	12.00	5.25	4.25	10.00	3.50	0.41	15.00	15.50	5.25	7.00	0.50	1.75	0.50	3.50
219AT	10.50	13.00	5.25	4.25	11.00	3.50	0.41	15.00	16.50	5.25	7.50	0.50	1.75	0.50	3.50
2110AT	10.50	14.50	5.25	4.25	12.50	3.50	0.41	15.00	18.00	5.25	8.25	0.50	1.75	0.50	3.50
253AT	12.50	9.50	6.25	5.00	7.00	4.25	0.53	17.75	13.88	6.25	6.00	0.62	2.00	0.62	4.00
254AT	12.50	10.75	6.25	5.00	8.25	4.25	0.53	17.75	15.12	6.25	6.62	0.62	2.00	0.62	4.00
255AT	12.50	11.50	6.25	5.00	9.00	4.25	0.53	17.75	15.88	6.25	7.00	0.62	2.00	0.62	4.00
256AT	12.50	12.50	6.25	5.00	10.00	4.25	0.53	17.75	16.88	6.25	7.50	0.62	2.00	0.62	4.00

(Continued)



**Table 11.18** Dimensions for Foot-Mounted Industrial Direct-Current Machines<sup>a,b,c</sup>

Frame designation	A max	B max	D <sup>d</sup>	E <sup>e</sup>	2F <sup>c</sup>	BA hole	H <sup>c</sup>	AL	AM	AO	AR	AU	AX	AY max bases	BT			
	Drive end—for belt drive					Drive end—for direct-connected drive <sup>f</sup>					End opposite drive—straight							
	Keyseat					Keyseat					Keyseat							
Frame designation <sup>g</sup>	U	N-W	V min	R	ES min	S	U	N-W	V min	R	ES min	S	FU	FN-FW min	FV min	FR	FES min	FS
182AT–1810AT	1.1250	2.25	2.00	0.986	1.41	0.250	—	—	—	—	—	—	0.8750	1.75	1.50	0.771	0.91	0.188
213AT–2110AT	1.3750	2.75	2.50	1.201	1.78	0.312	—	—	—	—	—	—	1.1250	2.25	2.00	0.986	1.41	0.250
253AT–259AT	1.625	3.25	3.00	1.416	2.28	0.375	—	—	—	—	—	—	1.3750	2.75	2.50	1.201	1.78	0.312
283AT–289AT	1.875	3.75	3.50	1.591	2.53	0.500	—	—	—	—	—	—	1.625	3.25	3.00	1.416	2.28	0.375
323AT–329AT	2.125	4.25	4.00	1.845	3.03	0.500	—	—	—	—	—	—	1.875	3.75	3.50	1.591	2.53	0.500
363AT–369AT	2.375	4.75	4.50	2.021	3.53	0.625	—	—	—	—	—	—	2.125	4.25	4.00	1.845	3.03	0.500
403AT–409AT	2.625	5.25	5.00	2.275	4.03	0.625	—	—	—	—	—	—	2.375	4.75	4.50	2.021	3.53	0.625
443AT–449AT	2.875	5.75	5.50	2.450	4.53	0.750	—	—	—	—	—	—	2.625	5.25	5.00	2.275	4.03	0.625
502AT–509AT	3.250	6.50	6.25	2.831	5.28	0.750	—	—	—	—	—	—	2.875	5.75	5.50	2.450	4.53	0.750
583A–588A	3.250	9.75	9.50	2.831	8.28	0.750	—	—	—	—	—	—	2.875	5.75	5.50	2.450	4.28	0.750
683A–688A	3.625	10.88	10.62	3.134	9.53	0.875	—	—	—	—	—	—	3.250	6.50	6.25	2.831	5.03	0.750

<sup>a</sup>All dimensions in inches.

<sup>b</sup> For the meaning of the letter dimension, see MG 1<sup>4</sup>.01.

<sup>c</sup> It is recommended that all machines with keyseats cut in the shaft extension for pulley, coupling, pinion, and so forth be furnished with a key unless otherwise specified by the purchaser.

<sup>d</sup> Frames 182AT to 329AT, inclusive. The tolerance on the D dimension shall be +0.00 inch, “0.03 inch. Frames 363AT to 688A, inclusive: The tolerance on the D dimension shall be +0.00 inch, “0.06 inch.

<sup>e</sup> The tolerance for the 2E and 2F dimensions shall be ±0.03 inch and for the H dimension shall be +0.05 inch, -0.00 inch.

<sup>f</sup> When frames 583A through 688A have a shaft extension for direct-connected drive, the frame number shall have a suffix letter “S” (that is, 583AS).

<sup>g</sup> Source: Reproduced by permission of the National Electrical Manufacturers Association from NEMA Std. MG 1–1993; 1993 © NEMA.

viewed from the side. Figure 11.37 shows the end view. Table 11.18 lists the standard dimensions in inches that have been established for some of these letters. Note that not all of the letter dimensions have been standardized, only those that affect foot and shaft location. Length C in Fig. 11.36 and height O in Fig. 11.37 are not standardized. Table 11.18 gives dimensions for frame designations from 182AT to 688A.

There is some significance to the frame number. The first two digits divided by two closely approximate the outside diameter, although the dimension O is not standardized. A 182AT frame, for instance, is approximately 9 inches in diameter. In addition, the first two digits divided by 4 yield exactly the shaft height, or dimension D. The third digit of the frame number is related to the distance between the feet in the side view (Fig. 11.36), or the dimension 2F. The larger the number, the greater the spacing between feet and the longer the machine.

The second part of Table 11.18 lists the shaft dimensions assigned to the various frame sizes. There is now only one standard shaft diameter and length for each frame size. Previously, there were two standard shafts, one slightly smaller in diameter and shorter in length which was designed for direct connection to the load shaft through a coupling, and the other larger and longer, and intended to be used for belted connections. The adoption of one shaft size per frame has simplified interchangeability.

Figures 11.36 and 11.37 and Table 11.18 are examples of the information in NEMA MG 1–1993 [13]. There are, in

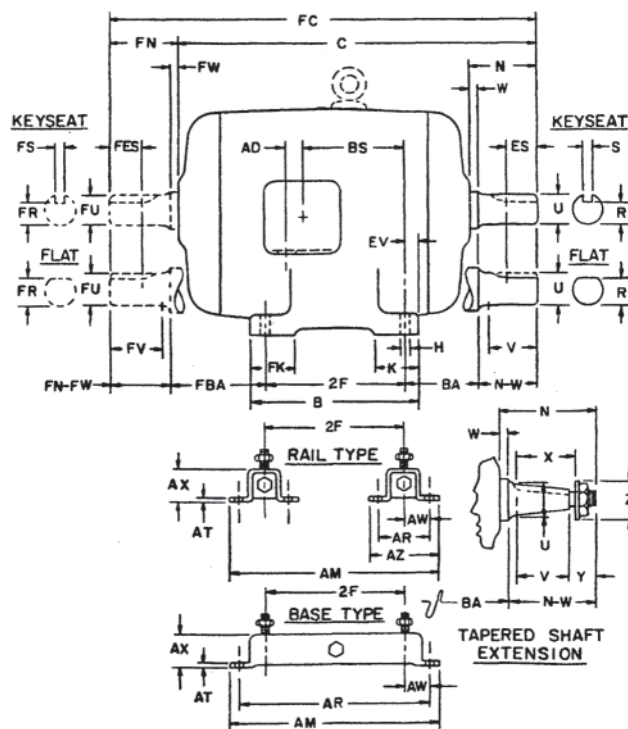


**Figure 11.36** Lettering of dimension sheets for foot-mounted machines, side view. (Reproduced by permission of the National Electrical Manufacturers Association from NEMA Std. MG 1–1993; 1993 © NEMA.)

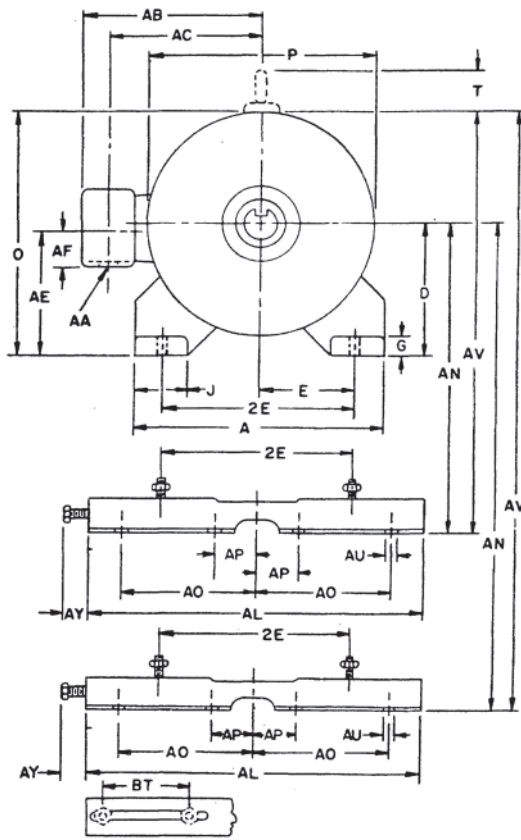


**Figure 11.37** Lettering of dimension sheets for foot-mounted machines, end view. (Reproduced by permission of the National Electrical Manufacturers Association from NEMA Std. MG 1-1993; 1993 ©NEMA.)

addition, many more tables covering smaller sizes and other types of motors. Tables for ac motors assign a horsepower rating for each frame size and speed, so that rating as well as dimensions are the same for all manufacturers. Standards for dc motors, by contrast, do not assign a rating to a frame size. There can be as much as a 50% difference in horsepower rating for the same frame size between dc motors manufactured by different companies.

*Flange-Mounted Dimensions*

In many applications, it is convenient to close-couple the motor to the load. Standard flange mountings have been established for Type C face-mountings and type D flangemountings. Figure 11.38 shows the lettering for dimensions for the type C mounting, and Table 11.19 lists the values. The type C face has a male rabbet diameter and, except for the very small sizes, the tapped mounting bolt holes are inside, that is, at a smaller diameter than, the mounting rabbet. This type of flange is used when it is more convenient for the bolts to be entered from the load side and threaded into the motor bracket.

Figure 11.39 and Table 11.20 show the lettering and standard dimensions for the type D flange. This likewise has a male rabbet, but the mounting clearance holes are beyond (at a larger diameter than) the rabbet diameter. This type of flange is used when it is more convenient for the bolts to be entered from the motor side and threaded into the load structure.

For both of these flanges, it is possible to furnish motors with or without feet. The figures show the foot in dotted lines to emphasize this choice. In addition to these outline and dimension prints, Figs. 11.40 and 11.41 show photographs of a type C face and a type D flange motor, respectively. These show more clearly the relation between the mounting flange and the mounting bolt holes for these two popular standard mounting methods.

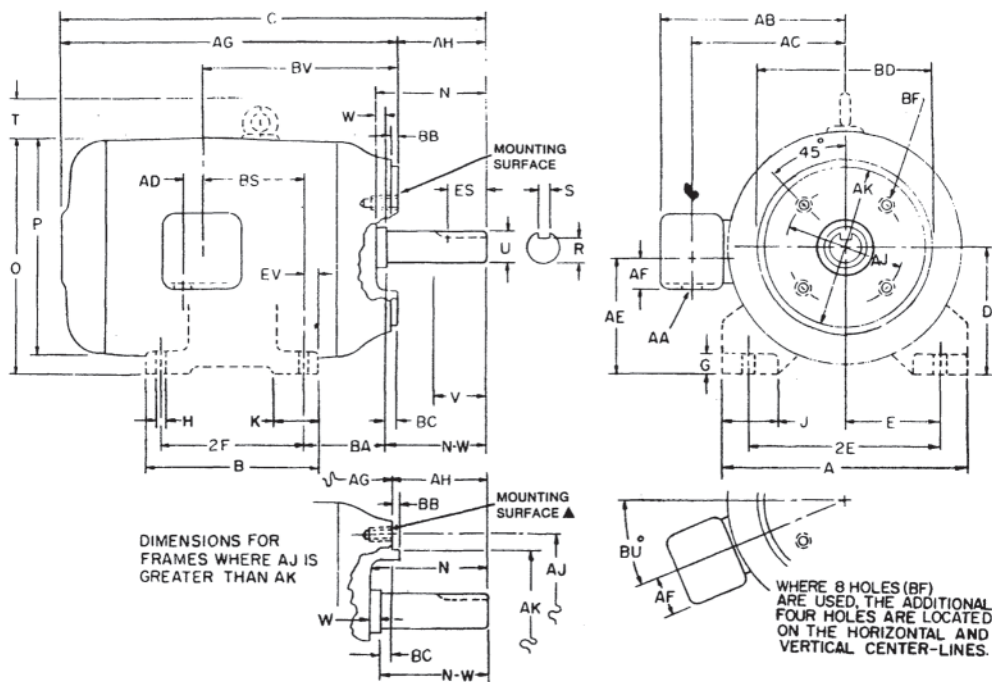


**Figure 11.38** Lettering of dimension sheets for type C face-mounting foot or footless machines. (Reproduced by permission of the National Electrical Manufacturers Association from NEMA Std. MG 1-1993; 1993 © NEMA.)



**Table 11.19** Dimensions for Type C Face Mounting Small and Industrial Direct-Current Motors<sup>a</sup>

Small motors <sup>b-c</sup>													
Frame designations	AJ	AK	BA	BB	BC	DF hole			U	AH	Keyseat		
						BD nom	Number	Tap size			R	ES min	S
42C	3.750	3.000	2.062	0.16 <sup>g</sup>	-0.19	5.00	4	1/4-20	0.3750	1.312 <sup>h</sup>	0.328	—	Flat
48C	3.750	3.000	2.50	0.16 <sup>g</sup>	-0.19	5.625	4	1/4-20	0.500	1.69 <sup>h</sup>	0.453	—	Flat
56C	3.875	4.500	2.75	0.16 <sup>g</sup>	-0.19	6.50	4	3/8-16	0.6250	2.06 <sup>h</sup>	0.517	1.41	0.188

Industrial motors <sup>b,d-f</sup>														
Frame designations	AJ	AK	BA	BB	BC	BD max	Number	Tap size	Bolt penetration allowance	U	AH	Keyseat		
												R	ES min	S
182ATC-1810ATC	7.250	8.500	2.75	0.25	0.12	9.00	4	1/2-13	0.75	1.1250	2.12	0.986	1.41	0.250
213ATC-2110ATC	7.250	8.500	3.50	0.25	0.25	9.00	4	1/2-13	0.75	1.3750	2.50	1.201	1.78	0.312
253ATC-259ATC	7.250	8.500	4.25	0.25	0.25	10.00	4	1/2-13	0.75	1.625	3.00	1.416	2.28	0.375
283ATC-289ATC	9.000	10.500	4.75	0.25	0.25	11.25	4	1/2-13	0.75	1.875	3.50	1.591	2.53	0.500
323ATC-329ATC	11.000	12.500	5.25	0.25	0.25	14.00	4	5/8-11	0.94	2.125	4.00	1.845	3.03	0.500
363ATC-369ATC	11.000	12.500	5.88	0.25	0.25	14.00	8	5/8-11	0.94	2.375	4.50	2.021	3.53	0.625

<sup>a</sup> All dimensions in inches.

<sup>b</sup> For the meaning of the letter dimensions, see MG 1-4.01.

<sup>c</sup> See MG 1-11.60 for dimensions D, E, and 2F when the motor is provided with feet.

<sup>d</sup> For tolerances on shaft extension diameters and key seats, see MG 1-4.05.

<sup>e</sup> For tolerances on, AK dimensions face runout, and permissible eccentricity of mounting rabbet, see MG 10-4.08.

<sup>f</sup> See MG 1-11.61 for dimensions A, B, D, E, 2F, H, and BA when the motor is provided with feet.

<sup>g</sup> These BB dimensions have a tolerance of +0.00, "0.06 in.

<sup>h</sup> If the shaft extension length of the motor is not suitable for the application, it is recommended that deviations from the length be in 0.25-in increments.

Source: Reproduced by permission of the National Electrical Manufacturers Association from NEMA Std. MG 1-1993; 1993 © NEMA

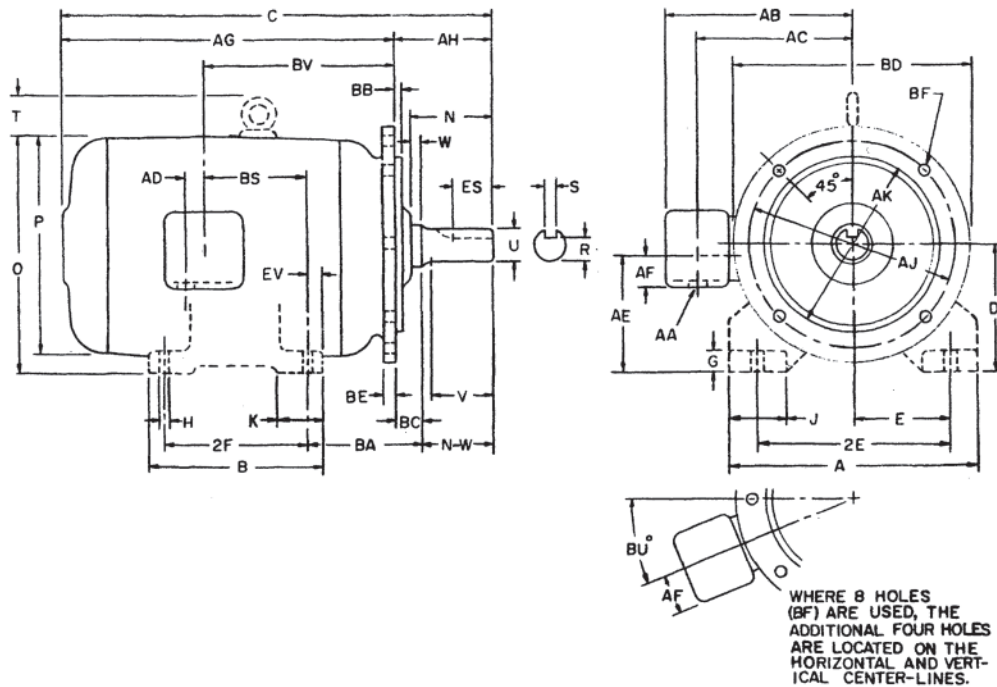


**Figure 11.39** Lettering of dimension sheets for type D flange-mounted foot or footless machines. (Reproduced by permission of the National Electrical Manufacturers Association from NEMA Std. MG 1-1993; 1993 © NEMA.)

**Table 11.20** Dimensions for Type D Flange-Mounting Industrial Direct-Current Motors <sup>a-c</sup>

Frame designations	AJ	AK	BB <sup>f</sup>	BC	BD max	BE nom	BF clearance hole		Keyseat					
							Size	Number	Recommended bolt length	U	AH	R	S	
182ATD-1810ATD	10.00	9.000	0.25	0	11.00	0.50	0.53	4	1.25	1.1250	2.25	0.986	0.250	
213ATD-2110ATD	12.50	11.000	0.25	0	14.00	0.75	0.81	4	2.00	1.3750	2.75	1.201	0.312	
253ATD-259ATD	16.00	14.000	0.25	0	18.00	0.75	0.81	4	2.00	1.625	3.25	1.416	0.375	
283ATD-289ATD	16.00	14.000	0.25	0	18.00	0.75	0.81	4	2.00	1.875	3.75	1.591	0.500	
323ATD-329ATD	16.00	14.000	0.25	0	18.00	0.75	0.81	4	2.00	2.125	4.25	1.845	0.500	
363ATD-369ATD	20.00	18.000	0.25	0	22.00	1.00	0.81	8	2.25	2.375	4.75	2.021	0.625	
403ATD-409ATD	22.00	18.000	0.25	0	24.00	1.00	0.81	8	2.25	2.625	5.25	2.275	0.625	
443ATD-449ATD	22.00	18.000	0.25	0	24.00	1.00	0.81	8	2.25	2.875	5.75	2.450	0.750	
502ATD-509ATD	30.00	28.000	0.25	0.38	32.00	1.00	0.81	8	2.50	3.250	6.88	2.831	0.750	
583AD-588AD	30.00	28.000	0.25	0.38	32.00	1.00	0.81	8	2.50	3.250	10.12	2.831	0.750	
583ASD-588ASD	30.00	28.000	0.25	0.38	32.00	1.00	0.81	8	2.50	2.875	6.12	2.845	0.750	
683AD-688AD	35.25	33.250	0.25	0.38	37.25	1.00	0.81	8	2.50	3.625	11.25	3.134	0.875	
683ASD-688ASD	35.25	33.250	0.25	0.38	37.25	1.00	0.81	8	2.50	3.250	6.88	2.831	0.750	

<sup>a</sup> All dimensions in inches.

<sup>b</sup> For the meaning of the letter dimensions, see MG 1-4.01.

<sup>c</sup> See MG 1-11.61 for dimensions A, B, D, E, 2F, H, and BA.

<sup>d</sup> For tolerances on shaft extension diameters and keyseats, see MG 1-4.05.

<sup>e</sup> For tolerances on AK dimensions, face runout, and permissible eccentricity of mounting rabbet, see MG 1-4.08.

<sup>f</sup> These BB dimensions have a tolerance of +0.00, “0.06 in.

Source: Reproduced by permission of the National Electrical Manufacturers Association from NEMA Std. MG 1-1993; 1993 © NEMA.

In addition to C and D flanges, there is a P base mounting defined in the standard. This is used primarily for vertical pump motors. It has a female motor mounting rabbet and threaded holes at a diameter greater than the rabbet diameter.

#### Belly Bands

For some small motors used in forklift trucks, it is common practice to support the motor with a metal strap around the frame, anchored to a solid surface above the motor. Even though the motors have mounting flanges on the drive end,

the vibration and shock to which these motors are subjected requires additional support.

#### Sliding Bases and Sole Plates

Sliding bases are shown in Fig. 11.36 and are used when the motor is to be belted to the load and a means of belt tightening is necessary. Standard sliding bases should not be used for wall mounting. Special, heavy-duty bases are required for such mounting. Sole plates are flat steel plates grouted into cement to form a firm, flat, and smooth mounting surface for

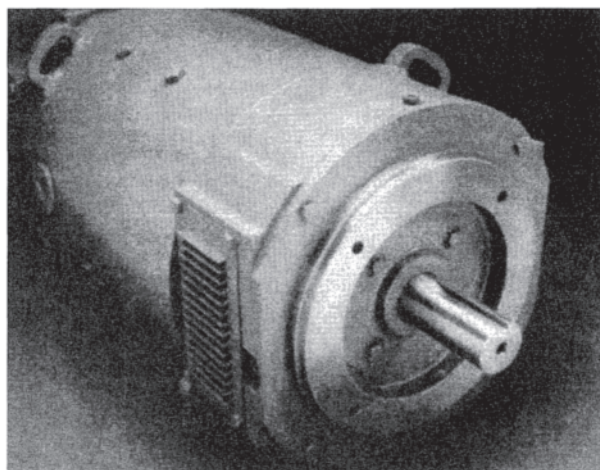


**Figure 11.40** Direct-current motor with a NEMA “C” face-mounting flange. (Courtesy of the Drive Motor and Generator Operation, General Electric Company, Erie, PA.)

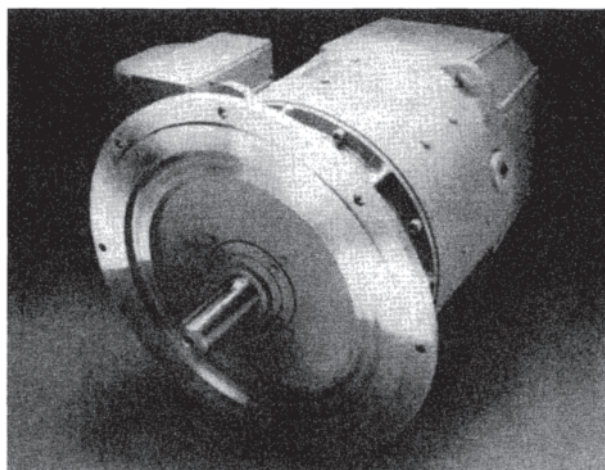


**Figure 11.41** Direct-current motor with a NEMA “D” mounting flange. (Courtesy of the Drive Motor and Generator Operation, General Electric Company, Erie, PA.)

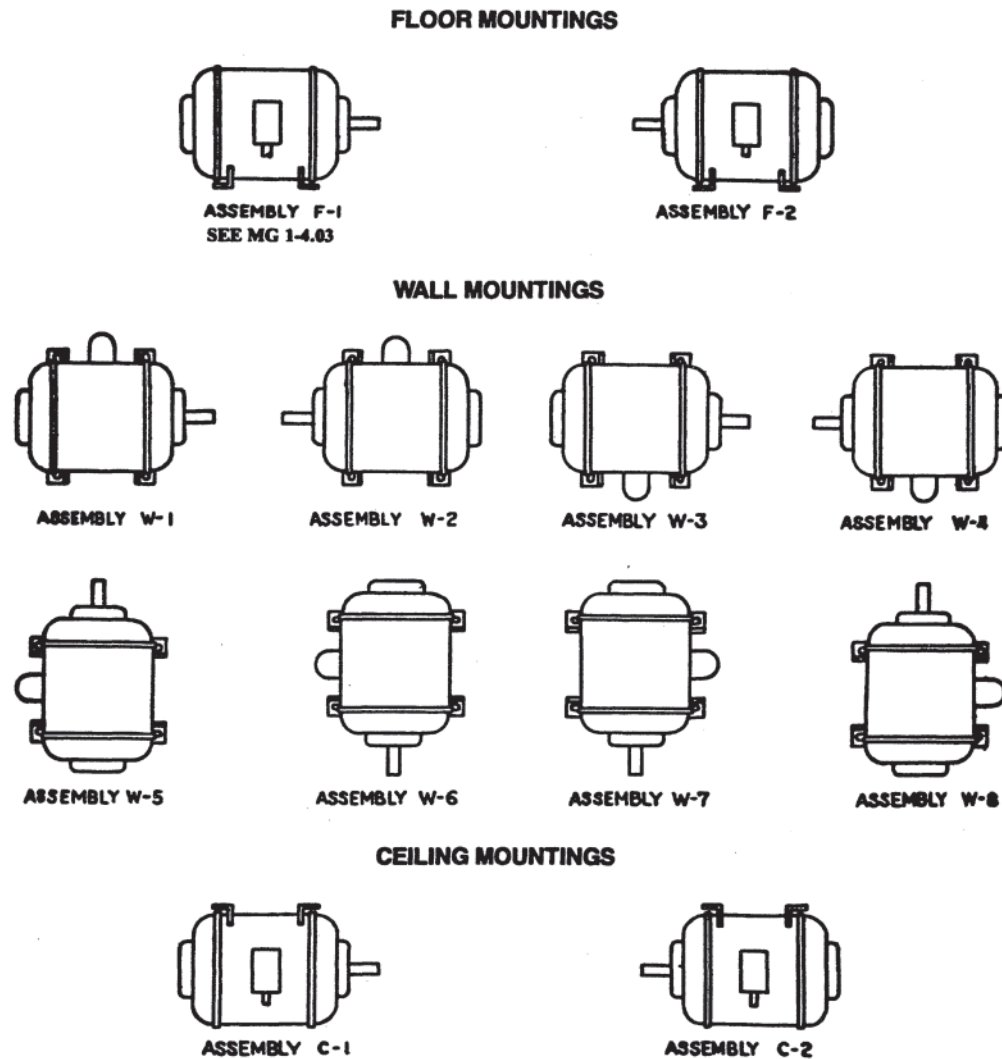


**Figure 11.42** Symbols for machine-mounting assemblies. (Reproduced by permission of the National Electrical Manufacturers Association from NEMA Std. MG 1–1993; 1993 © NEMA.)

large motors. They can be supplied with the motor or furnished separately by the user.

#### *Mounting Assembly Symbols*

Figure 11.42 shows the standard designations for wall, floor, and ceiling mounting. It is especially useful because it shows the location of the feet and the location of the conduit box in relation to the feet and shaft. Simply specifying that the motor is to conform to outline W-2, for instance, clearly depicts the feet, shaft, and connection box in relation to each other. Not all of these mounting arrangements are safe with any given motor. Vertical mountings especially (W-5 through W-8) should be approved by the manufacturer to be sure that bearings and brackets are suitable.

#### *European Standards*

The NEMA Standard for Motors, MG 1–1993 [13] does not apply anywhere except in the United States. All European and Asian manufacturers use the metric measurement system and

have a much more widely accepted motor standard, IEC Publication No. 72 [42]. [The International Electrotechnical Commission (IEC) is a worldwide organization founded in 1906 to facilitate the unification of electrotechnical standards. More than 40 countries participate in the work of the IEC.]

Table 11.21 is a comparison from Ref. 43 of the NEMA and IEC dimensions. It will be noted that there is reasonably close dimensional correspondence between NEMA frame sizes and IEC frame sizes for NEMA frames from 180 through 500. Table 11.22 (from the same reference) compares the shaft diameters and lengths. The differences, although small, require an adaptation to be interchangeable. Most U.S. manufacturers can, by the use of special machining, shimming, and the use of the larger IEC bolt hole, adapt NEMA standard motors to meet IEC standards. Unlike NEMA standards, the IEC standards do not assign a horsepower or kilowatt rating to a frame size for either ac or dc motors.

**Table 11.21** Comparison of IEC Metric vs. NEMA Mounting Dimensions<sup>a</sup>

Frame size		D		2E		2F		BA		H	
IEC	NEMA	IEC	NEMA	IEC	NEMA	IEC	NEMA	IEC	NEMA	IEC	NEMA
90S	143	90	88.9	140	139.7	100	101.6	56	57.2	10	8.6
90L	145	90	88.9	140	139.7	125	127	56	57.2	10	8.6
112S	182	112	114.3	190	190.5	114	114.3	70	69.9	12	10.4
112M	184	112	114.3	190	190.5	140	139.7	70	69.9	12	10.4
132S	213	132	133.4	216	215.9	140	139.7	89	88.9	12	10.4
132M	215	132	133.4	216	215.9	178	177.8	89	88.9	12	10.4
160M	254	160	158.8	254	254	210	209.6	108	108	15	13.5
160L	256	160	158.8	254	254	254	254	108	108	15	13.5
180M	284	180	177.8	279	279.4	241	241.3	121	120.6	15	13.5
180L	286	180	177.8	279	279.4	279	279.4	121	120.6	15	13.5
200M	324	200	203.2	318	317.5	267	266.7	133	133.4	19	16.8
200L	326	200	203.2	318	317.5	305	304.8	133	133.4	19	16.8
225S	364	225	228.6	356	355.6	286	285.8	149	149.4	19	16.8
225M	365	225	228.6	356	355.6	311	311.2	149	149.4	19	16.8
250S	404	250	254	406	406.4	311	311.2	168	168.1	24	20.6
250M	405	250	254	406	406.4	349	349.2	168	168.1	24	20.6
280S	444	280	279.4	457	457.2	368	368.3	190	190.5	24	20.6
280M	445	280	279.4	457	457.2	419	419.1	190	190.5	24	20.6
315S	504	315	317.5	508	508	406	406.4	216	215.9	28	—
315M	505	315	317.5	508	508	457	457.2	216	215.9	28	—
355S	585	355	368.3	610	584.2	500	508	254	254	28	—
355M	586	355	368.3	610	584.2	560	558.8	254	254	28	—
400S	684	400	431.8	686	685.8	560	558.8	280	292.1	35	—
400M	685	400	431.8	686	685.8	630	635	280	292.1	35	—

<sup>a</sup>All dimensions in mm.

Letter dimensions as in [Figs. 11.36](#) and [11.37](#).

### *Bolt Torques and Doweling*

Many larger motors (500 mm diameter and above) are furnished with dowel holes in the feet, usually on two diagonally opposite feet, so that the motor can be returned to exactly the same position if it becomes necessary to remove it for repair or maintenance. These holes are drilled and reamed together with corresponding holes in the foundation once the motor has been correctly aligned, and the dowel pins are then inserted.

It is important that the proper foot bolt size and type be used to secure the motor to the foundation. The correct bolt torque for the type bolt being used should be applied with a torque wrench and checked after 24 hours of operation, after 3 months, and every 6 months thereafter. [Table 11.23](#) gives the recommended torque for various thread sizes.

### *Enclosures and Cooling Options*

When motors are being lifted, handled, installed, and mounted, it is helpful to know what type of enclosure is employed and what cooling method is used. The more protection the motor has, the better it is able to tolerate dirty and wet conditions. [Table 11.24](#) gives NEMA codes for various types of enclosures and ventilation systems. IEC standards have both an enclosure code and a cooling code. The table also lists the IEC code nearest to the NEMA enclosure code.

### **11.6.3 Shaft Connections—Belts**

The most economical way to connect a motor to a load shaft when a speed change is required is by belts and sheaves. (The

more expensive alternative is a gearbox and two couplings.) Belts with a trapezoidal cross section, called V-belts, are most popular because they can transmit the most power per belt, up to 40 kW per belt. The application is limited by the maximum sheave rim speed permitted by belt manufacturers. This limit is about 6500 feet/min (3300 cm/sec), and results in a maximum power that can be transmitted by belts to about 520 kW at 1800 rpm for ac machines, where no constant-horsepower speed range is involved. In addition, at the upper end of belting capability, special motor shaft material and size, as well as special oversized bearings, will almost always be required because of the resulting high radial load on the shaft. This adds to the cost of this method of shaft connection.

The radial load on the shaft is an important consideration whenever a belt or chain-and-sprocket connection is used. The resultant shaft radial force is equal to the product of a multiplier, called the tension factor, and the ratio of torque to sheave radius.

To demonstrate the horsepower limitation with an example, assume that a machine tool spindle drive requires a top motor speed of 3000 rpm and is to be belted with a 2:1 ratio to 1500 rpm. The maximum sheave diameter to limit the belt speed to 6500 feet/min (3300 cm/sec) would be 8.3 inches, or 21 cm. With special bearings, a motor of NEMA 500 frame size could safely sustain a shaft radial load of 3500 pounds (15568 N). V-belts must be tightened to transmit torque without slipping. The tension factor for V-belts is approximately 1.8. The maximum torque that can be transmitted can now be calculated from:

**Table 11.22** Comparison of IEC Metric and Inch Shaft Extension Dimensions

Metric series				Inch series	
Nominal values		Conversion values			
Diameter (mm)	Length (mm)	Diameter (in)	Length (in)	Diameter (in)	Length <sup>a</sup> (in)
19	40	0.7480	1.57	0.7500	2.25
22	50	0.8661	1.97	0.8750	2.25
24	50	0.9449	1.97	(1.000) <sup>b</sup>	—
28	60	1.1024	2.36	1.125	2.75
32	80	1.2598	3.15	1.375	3.38
38	80	1.4961	3.15	(1.500) <sup>b</sup>	—
42	110	1.6535	4.33	1.625	4.00
48	110	1.8898	4.33	1.875	4.62
55	110	2.1654	4.33	2.125	5.25
60	140	2.3622	5.51	2.375	5.88
65	140	2.5591	5.51	(2.500) <sup>b</sup>	—
70	140	2.7559	5.51	(2.750) <sup>b</sup>	—
75	140	2.9528	5.51	2.875	7.25
80	170	3.1496	6.69	(3.125) <sup>b</sup>	—
85	170	3.3465	6.69	3.375	8.50
90	170	3.5433	6.69	(3.500) <sup>b</sup>	—
95	170	3.7402	6.69	(3.750) <sup>b</sup>	—
100	210	3.9370	8.27	(3.875) <sup>b</sup>	—
110	210	4.3307	8.27	(4.375) <sup>b</sup>	—

<sup>a</sup> IEC publication 72 lists only one shaft length per frame. The indicated inch series values are current NEMA values for long shaft which are in process of approval by the IEC to replace obsolete values currently listed.

<sup>b</sup> These are diameters listed in NEMA but not assigned to a frame and not listed in Publication 72.

$$T = (\text{maximum radial load}) \times (\text{sheave radius}) / (\text{tension factor})$$

$$= (15568 \text{ N} \times 0.21 \text{ m}) / (2 \times 1.8) = 908 \text{ N}\cdot\text{m}, \text{ or } 670 \text{ lb}\cdot\text{ft}$$

(11.117)

If the motor accelerates at 150% torque, then rated torque is limited to 605 N m, or 446 lb-ft. If the dc motor had a constant-horsepower speed range of 3:1, then the base speed would be one-third of 3000 rpm, or 1000 rpm. The maximum power  $P$  that can be transmitted by belts in this example is:

$$P = (\text{torque} \times \text{speed in rpm}) / 5252 \text{ hp}$$

$$= 446 \text{ lb}\cdot\text{ft} \times 1000 \text{ rpm} / 5252$$

$$= 85 \text{ hp}, \text{ or } 63 \text{ kW}$$

(11.118)

Belting of higher-power dc motors with wide speed ranges is very difficult for the reasons made apparent by this example. High speed requires small sheaves to limit belt speed, and small sheaves result in high radial loads. Moreover, the tension factor varies with the angle of belt engagement on the sheave, which in turn varies with the speed ratio. A 7:1 speed ratio is a common maximum and results in the shortest arc angle on the smaller sheave, but the tension factor even for this worst case may be only 2.0 instead of the 1.8 used above.

Minimum sheave diameters have been established by NEMA for ac motors and are shown in Table 11.25, taken from Reference 44. This table is for NEMA 500 frame sizes with 6000 feet/min as the maximum belt speed.

Radial loads from belts cause high bearing loads. The bearing load is about 1.8 times the belt pull and varies depending on where the center of the belt pull is located with respect to the bearings. The closer the center of belt pull is to the shaft-end bearing, the smaller the bearing loads. The shaft stress from the bending moment will also be reduced. Bearing life varies inversely with the cube of bearing load, so if a sheave can be moved 5 cm closer to the bearing the bearing load will be reduced by about 10% but the resulting bearing life will be increased by 33%. It is for this reason that manufacturers recommend putting the sheave as close to the bearing as possible. In addition, improved V-belts are now available that reduce the number of belts and therefore the width of the sheave, keeping the center of pull closer to the bearing. In any case, the sheave should not be so wide that the center is beyond

**Table 11.23** Bolt Tightening Torque Values—Metallic Parts

Thread sizes (UNC-2A)	Hex head (CIC5), medium-carbon steel (hold down, electrical connections main pole, frame eye bolts, etc.)		Socket head (hex) CIA7, high-strength alloy steel (coupling bolts)		Hex head CIE1, silicon bronze (Commutator pole bolts)		Hex head B7Y7, nonmagnetic steel (commutator pole bolts)	
	(lb-ft)	(N-m)	(lb-ft)	(N-m)	(lb-ft)	(N-m)	(lb-ft)	(N-m)
1/4–20	7–9	10–12	8–10	11–14			5–6	7–8
5/16–18	13–17	18–23	16–20	22–27			9–11	12–15
3/8–16	24–30	33–40	28–35	38–47			16–20	22–27
1/2–13	60–75	80–100	72–90	98–120	32–40	43–54	36–45	49–61
5/8–11	120–150	160–200	140–180	190–240	70–86	95–120	72–90	98–120
3/4–10	210–260	280–350	255–320	350–430	90–115	120–160	100–125	140–170
7/8–9	320–400	430–540	400–500	540–680	145–178	197–241	155–195	210–260
1–8	460–580	620–790	615–770	830–1040			210–260	290–350
1–1/8–7	640–800	870–1080	865–1080	1170–1460				
1–1/4–7	900–1200	1220–1520	1220–1520	1660–2060				
1–1/2–6	1540–1940	2090–2630	2130–2160	2890–3610				

Source: Reproduced by permission of General Electric Company from Publication GEH-4963, "Drive Motor and Generator Operation," June 1981.

**Table 11.24** Alternate NEMA Enclosures

Enclosure type	Designation	Description	IEC Reference Code		
			Protection	Cooling	
Drip-proof (DP)	DPFG	Drip-proof fully guarded, self-ventilated	IP-22	IC-01	
	DPFG-SV	Drip-proof fully guarded, separately ventilated	IP-22	IC-17	
	DPFG-BV	Drip-proof fully guarded, blower-ventilated	IP-22	IC-06	
	ESV	Enclosed separately ventilated, air ducted in and out	IP-54	IC-37	
	SPFG	Splash-proof fully guarded, self-ventilated	IP-23	IC-01	
	SPFG-SV	Splash-proof fully guarded, separately ventilated	IP-23	IC-17	
	SPFG-BV	Splash-proof fully guarded, blower-ventilated	IP-23	IC-06	
	Totally enclosed (TE)	TENV	Totally enclosed nonventilated	IP-54	IC-410
TEFC		Totally enclosed fan-cooled	IP-54	IC-411	
TEAO		Totally enclosed air-over-frame	IP-54	IC-416	
TEUC		Totally enclosed unit-cooled (air-to-air)	IP-54	IC-666	
TEWAC		Totally enclosed unit-cooled (air-to-water)	IP-54	IC-86W	
TENV-WP		Totally enclosed nonventilated, water-proof	IP-54	IC-410	
TEFC-WP		Totally enclosed fan-cooled, water-proof	IP-55	IC-411	
TEAO-WP		Totally enclosed air-over-frame, water-proof	IP-55	IC-416	
TENV-DP		Totally enclosed nonventilated, dust-proof	IP-55	IC-410	
TEFC-DP		Totally enclosed fan-cooled, dust-proof	IP-54	IC-411	
TEAO-DP		Totally enclosed air-over-frame, dust-proof	IP-54	IC-416	
Explosion-proof (XP)		TENV-XP	Totally enclosed nonventilated, explosion-proof	n.d. <sup>a</sup>	n.d.
		TEFC-XP	Totally enclosed fan-cooled, explosion proof	n.d.	n.d.
		TEAO-XP	Totally enclosed air-over-frame, explosion-proof	n.d.	n.d.

<sup>a</sup> n.d.=not defined

Source: Reproduced by permission of General Electric Company from Publication GEA-11948, "Drive Motor and Generator Operation," September 1990.

**Table 11.25** 3, 5, 8 V-Belt Drive

509 Frame							5011 Frame							
Horsepower at rpm			Voltage				Min. sheave diameter (in)	Horsepower at rpm			Voltage			
1800	1200	900	230/460	2300	4000	1800		1200	900	230/460	2300	4000	Min. sheave diameter (in)	
—	—	150			*	11	—	—	300			*	25	
—	—	200	*	*	*	16	—	—	350	*	*	*	30	
—	—	250	*	*	*	22	—	—	400	2	2	2	32	
—	—	300	*	*	*	28	—	—	450	1, 2	1, 2		22	
—	250	—	*	*	*	16	—	350	—			*	23	
—	300	—	*	*	*	19.5	—	400	—			*	25	
—	350	—	*	*		24	—	450	—	1, 2	1, 2		18	
—	400	—	*	*		27	—	500	—	1, 2	1, 2	1, 2	20	
300	—	—			*	14	—	600	—	1, 2	1, 2		22	
350	—	—			*	16	600	—	—			1, 2	16	
400	—	—	1, 2	1, 2	1, 2	15	700	—	—		1, 2	1, 2	17.5	
450	—	—	1, 2	1, 2	1, 2	17	800	—	—		*	*	N/A	
500	—	—	1, 2		1, 2	14								
600	—	—	1, 2	1, 2		17								

<sup>a</sup> Bearing, shaft material, and end shield are indicated in the table by:

\*=Standard bearing and shaft construction.

1=Drive end shield must be 320 roller bearing.

2=Shaft material B5F4C4 stress proof material required.

<sup>b</sup> Maximum sheave width 12.75 inches.

<sup>c</sup> 6000 fpm is the maximum sheave speed suggested by the sheave manufacturers for cast iron sheave. Therefore, the maximum suggested sheave diameters are 32 inches for 900 rpm, 27 inches for 1200 rpm and 17.5 inches for 1800 rpm.

Source: Reproduced by permission of General Electric Company, Fort Wayne, IN, from Publication GEH-4092A, December 1989.

**Table 11.26** Tension Factors for Various Types of Drives

Drive	Tension factor
Chain and sprocket	1.0
Timing belt	1.2
V-belt, 1:1 ratio	1.5
V-belt, 2:1 ratio	1.8
Flat belt	2.0

the end of the shaft. Making the shaft longer to fully engage the bore of the sheave does not alleviate the problem of excessive bearing load.

It is important to remember that bearing life for V-belt applications is independent of the motor load. Once the belts have been tightened just enough to prevent slipping when the maximum torque is being delivered by the motor, the radial load on the shaft and bearing is established and remains constant regardless of the motor load.

Belt tensioning methods are crude and are usually established by the belt's sound, look, and feel while operating. There are measurement methods in Section 14.67.2 of Ref. 13 for checking belt tension. These involve measuring the force required to produce a certain amount of belt deflection, but good performance and normal bearing life depend principally on the knowledge and carefulness of the installer.

#### 11.6.4 Shaft Connections—Chain and Sprocket Drives and Flat Belt Drives [45]

Chain and sprocket drives have essentially a slack side, which results in radial load being simply the torque divided by the sprocket radius, or a tension factor of 1.0. For timing belts, the tension factor is 1.2. Other belts have increased tension factors, as shown in Table 11.26.

For timing belts and chain drives, the radial load varies somewhat with motor load and hence the load duty cycle as well as the average speed should be considered in estimating bearing life.

#### 11.6.5 Shaft Connections—Couplings

When no speed change is required between motor and load shaft and the shafts can be in-line, couplings are used to connect the motor to the load. If either the motor or load lacks a shaft-supporting bearing, then a rigid, flanged face coupling must be used. Alignment must be very accurate to reduce vibrations. Since in most applications both shafts have bearings, a more common coupling type is the flexible coupling, so named because it can tolerate a certain amount of both offset and angular misalignment without excessive wear or maintenance.

There are several types of flexible couplings, depending on the driving medium. Elastomer (usually rubber), steel grid, gear teeth, and thin steel disks. The amount of misalignment that can be tolerated by these couplings is largest for the rubber coupling and less for the others, with the grid type least flexible. Rubber-type couplings, such as the Dodge Paraflex or Lovejoy, will allow a maximum parallel misalignment of 0.125 in (3 mm) and a maximum angular misalignment of 4 degrees. Table 11.27, taken from Ref. 46 gives a comparison of the several characteristics of flexible couplings. Gear-type and grid-type couplings require lubrication and seals, while rubber and disk types do not.

Torsionally soft couplings with elastomer mediums are best suited for applications where the load is subjected to high impact and vibration. These couplings tend to isolate the load shocks from the driving motor. Stiff couplings, using steel disks as the medium, are ideal for coupling tachometers to motors in high-performance drives for which the speed signal must closely follow the actual motor shaft speed. Gear-type couplings have proven to be the most satisfactory for motor-generator sets, where several electric machines are coupled together and must operate with rapidly changing torques while maintaining low vibration levels.

If couplings are not aligned more accurately than the limits allowed by coupling manufacturers as shown by the values in Table 11.27, the performance of both ac and dc machines is quite often unacceptable, and they require more frequent maintenance. Electric motor manufacturers specify an alignment tolerance of not more than 0.002 inch (0.05 mm) for both parallel and angular misalignment. This alignment

**Table 11.27** Characteristics of Flexible Couplings (10 hp/100 rpm size)

Characteristic	Coupling Medium			
	Elastomer	Grid	Gear	Steel disk
Lubrication required	No	Yes	Yes	No
Parallel misalignment allowed	0.0125 in (3.2 mm)	0.011 in (0.25 mm)	0.015 in (0.38 mm)	0.07 in (1.8 mm)
Angular misalignment allowed	4 degrees	0.011 in (0.25 mm)	0.015 in (0.38 mm)	2 degrees
End float	High	High	High	Low
Backlash	High	Medium	Low	Zero
Torsional stiffness	Low	Medium	High	High
Isolation from vibration	Best	Medium	Low	None
Use in M-G sets	Worst	Medium	Best	Medium
Maximum speed (rpm)	2500	5500	5500	5500

Source: Data from Dodge Engineering Catalog, vol. 1.1, Dodge/Reliance Electric Industrial Co., Greenville, SC.

**Table 11.28** Vibration Tolerance Values and NEMA Limits (Peak-to-Peak Vibration Displacement in mils and mm)

Operating speed (rpm)	Vibration quality				NEMA allowance
	Good	Normal	Fair	Poor	
1150	0.8 mil (0.02 mm)	1.8 mil (0.05 mm)	4 mils (0.1 mm)	9 mils (0.23 mm)	2 mils (0.05 mm)
1750	0.5 mil (0.01 mm)	1.0 mil (0.03 mm)	3 mils (0.08 mm)	6 mils (0.15 mm)	1.5 mil (0.04 mm)
3500	0.18 mil (0.005 mm)	0.44 mil (0.01 mm)	1.4 mils (0.04 mm)	4 mils (0.1 mm)	1 mil (0.03 mm)

Source: Data from “Kinematic Application Manual,” Direct Current Motor and Generator Department, General Electric Company, Erie, PA, 1979.

precision is especially important in motor—generator sets where several machines are connected together with flexible couplings.

### 11.6.6 Shaft Connections—Splines

Splined shafts are shafts with teeth cut parallel to the shaft centerline by use of special hob-cutting tools. The teeth may be on the outside or on the inside of the shaft extension. They are designed to mate with matching teeth on the driven machine. The teeth are crowned to allow for misalignment. Splined shafts are commonly used in electric lift truck motors because of the ease of assembly and disassembly. When many motors of the same design are being made, the tooling cost can be easily justified. Splines do not allow alignment adjustment and therefore can result in more motor vibration than flexible couplings. In addition, splines wear and have to be replaced. Sometimes the shaft extension with the splined teeth is designed to be removable and replaceable.

### 11.6.7 Initial Operation

The most common indication of a problem during initial operation of electric motors is unusual noise or vibration. The most likely cause of vibration is misalignment due to improper installation, loose foot bolts, or uneven shimming under the feet. In addition, vibration is a function of the dynamics of the system, which includes the base, foundation, piping, and all associated parts and structures. Motors overhung from flanges must have a sufficiently stiff mounting surface that the resulting system’s critical (reed) frequency is above the maximum operating speed.

Table 11.28 is taken from the General Electric “Application Manual” [47] and shows the amount of vibration that would be considered as good, normal, fair, or poor by “feel” at several different speeds. It is interesting to note that the amount of vibration allowed to be present as a result of residual unbalance of the rotating member, as listed under the “NEMA allowance” column, is higher than the “normal” values, thus confirming that mounting, coupling, and alignment must be done carefully to assure that vibration levels after installation are at least no higher than levels of the uncoupled motor.

## REFERENCES

Note: In the following listing, abbreviations have the following meanings:

AFBMA Anti-Friction Bearing Manufacturers Association  
 ANSI American National Standards Institute  
 IEC International Electrotechnical Commission  
 IEEE Institute of Electrical and Electronics Engineers  
 ISO International Organization for Standardization  
 NEMA National Electrical Manufacturers Association  
 Sources for standards are listed in [Appendix B](#).

- Beranek, L.L., *Noise and Vibration Control*, McGraw-Hill, New York, 1971.
- Alger, P.L., and E.Erdélyi, “Calculation of the Magnetic Noise of Polyphase Induction Motors,” *Acoustical Society of America Journal* vol. 28, Nov. 1956, pp. 1063–1067.
- Erdélyi, E., “Predetermination of Sound Pressure Levels of Magnetic Noise of Polyphase Induction Motors,” *Transactions of the AIEE*, vol. 74, pp. 1268–1280.
- Frohne, H., “Über die Primären Bestimmungsgrößen der Lautstärke bei Asynchronmaschinen [On the Primary Noise Intensity Data of Asynchronous Machines],” Dr. Ing. Thesis, Technical University of Hanover, 1959.
- Yang, S.J., *Low-Noise Electrical Motors*, Clarendon Press, Oxford, 1981.
- Timár, P.L., “Noise and Vibration of Asynchronous Motors, Theory and Experimental Investigation, Doctoral Thesis, Hungarian Academy of Sciences, Budapest, 1985.
- Alger, P.L., *The Nature of Induction Machines*, Gordon and Breach, New York, 1965.
- Jordan, H., *Der Geräuscharme Elektromotor [The Low-Noise Electric Motor]*, Girardet, Essen, 1950.
- Timár, P.L., *Noise and Vibration of Electrical Machines*, Technical Publisher, Budapest, 1986.
- ANSI S12.34–1988, Engineering Methods for the Determination of Sound Power Levels of Noise Sources for Essentially Free-Field Conditions over a Reflecting Plane.
- ANSI S12.36–1990, Survey Methods for the Determination of Sound Power Levels of Noise Sources.
- IEEE Std. 85–1973, Test Procedure for Airborne Noise Measurements on Rotating Electric Machinery.
- NEMA MG 1–1993, Motors and Generators.
- IEC Publication 60034–9 (1990), Rotating Electrical Machines Part 9, “Noise Limits.”
- Yang, S.J., and A.J.Ellison, *Machinery Noise Measurement*, Clarendon Press, Oxford, 1985.



16. Geszti, P., A.Pongó, E.Solymoss, and P.L.Timár, "Method and Apparatus for Switching Three-Phase Loads with an Ohmic-Inductive Character," Hungarian patent 22511/1708/82/7.
17. ISO 2372–1983, Mechanical Vibration of Machines with Operating Speeds from 10 to 200 rev/s. [Basis for specifying evaluation standards.]
18. ISO 2373, Mechanical Vibration of Certain Rotating Electrical Machines with Shaft Heights between 80 and 400 mm. (Measurement and evaluation of vibration severity.)
19. ISO 3945–1985, Mechanical Vibration of Large Rotating Machines with Speed Range from 10 to 200 rev/s. [Measurement and evaluation of vibration severity *in situ*.]
20. ISO 7919/1–1989, Mechanical Vibration of Nonreciprocating Machines. [Measurements on rotating shafts and evaluation of results.]
21. IEC 60034–14–1994, Mechanical Vibration of Certain Machines with Shaft Heights 56 mm and Higher: Measurement, Evaluation, and Limits of Vibration.
22. NEMA Standards Publication No. MG 1–1993, Part 7, Motors and Generators: Mechanical Vibration—Measurement, Evaluation, and Limits.
23. ISO 1925–1990—Mechanical Vibration, Balancing, Vocabulary.
24. ISO 1940–1986, Mechanical Vibration, Balancing Quality Requirements of Rigid Rotors.
25. ISO 5406–1980, The Mechanical Balancing of Flexible Rotors.
26. Wilcock, D.F., and M.Rosenblatt, "Oil Flow, Key Factor in Sleeve-Bearing Performance," *ASME Transactions*, vol. 74–5 1952, pp. 849–865.
27. Cameron, A., and W.L.Wood, "The Full Journal Bearing," *ME Proceedings*, vol. 161, 1949, pp. 59–64.
28. Neale, M.J. "Selection of Bearings," *Proceedings of the Institute of Mechanical Engineers*, vol. 182(3A), 1970, pp. 547–556.
29. Halling, J., *Principles of Tribology*. The MacMillan Press Ltd., London, 1978, pp. 360–368.
30. SKF General Catalog, Catalog 400 U.S. Reg. 47.50000. 1991–01 SKF Group, King of Prussia, PA, pp. 114–121.
31. Duplex Bearings and Preload, The Torrington Company Service Catalog, Form No. 100–292–75M First Edition, Fourth Printing, The Torrington Company, Torrington, CT, pp. E59–60.
32. Booser, E.R., "Electric Motors," Chapter 35, *Standard Handbook of Lubrication Engineering*, McGraw-Hill, New York, 1968.
33. Beebe, Theodore J., "Industrial Electric Motors," *CRC Handbook of Lubrication (Theory and Practice of Tribology)*: Volume I, *Application and Maintenance*, E. Richard, Booser, editor, CRC Press Inc., Boca Raton, FL, 1984, pp. 181.
34. ANSI/AFBMA Std. 9–1978, American National Standard/AFBMA Standard Load Ratings and Fatigue Life for Ball Bearings.
35. ANSI/AFBMA Std. 11–1978, American National Standard/AFBMA Standard Load Ratings and Fatigue Life for Roller Bearings.
36. Cheng, Herbert S., "Elastohydrodynamic Lubrication," *CRC Handbook of Lubrication (Theory and Practice of Tribology)*: Volume-II, *Theory and Design*, E.Richard Booser, editor, CRC Press Inc., Boca Raton, FL, 1984, p. 140.
37. Carbon Products Operation Inc., *How to Select Carbon Brushes for Motors and Generators One Horsepower and Above*, February 1991, pp. 1–10.
38. "Direct-Current Motors and Generators," Publication GEH-4963, General Electric Company, 1981.
39. "Direct-Current Motors and Generators," Publication GEH-39671, General Electric Company, 1984.
40. Moore, R.E., *Electrical Rotating Machines—Mechanical Features of Installation and Handling Instructions*, Tippins Machinery Company, Inc., for Integrated Industrial Systems Company, Yalesville, CT, 1980.
41. NEMA Std. MG 2–1989, Safety Standard for Construction and Guide for Selection, Installation, and Use of Electric Motors.
42. IEC Publication No. 60072 (1991), Dimensions and Output Ratings for Rotating Electrical Machines—Frame Numbers 56 to 400 and Flange Numbers F55 to F1080.
43. Cummings, P.G., "Comparison of IEC and NEMA/IEEE Motor Standards—Part II," *IEEE Transactions on Industry Applications*, no. PCI-82–12, vol. IA-20, Jan./Feb. 1984.
44. "GE-Motors—500 Diameter Line Horizontal Induction Motors," Publication No. GEH-4092A, General Electric Company, Fort Wayne, IN, 1989.
45. "GE Drive Motors—Kinematic Direct Current Motors, 1–4500 HP, Buyers' Guide," Publication No. GEP-387G, General Electric Company, Erie, PA, 1989.
46. Dodge Engineering Catalog vol. 1.1, Dodge/Reliance Electric Industrial Company, Greenville, SC, 1989.
47. "Kinematic Application Manual," Direct Current Motor and Generator Department, General Electric Company, Erie, PA, 1979.

# 12

## Environmental Considerations

Robert M.McCoy and Edward L.Owen

<b>12.1</b>	<b>INTRODUCTION</b>	<b>618</b>
<b>12.2</b>	<b>HEAT TRANSFER</b>	<b>619</b>
	12.2.1 Modes of Heat Transfer	620
	12.2.2 Ventilation	623
<b>12.3</b>	<b>COOLING OF BASIC MOTOR TYPES</b>	<b>626</b>
	12.3.1 Induction Motors	626
	12.3.2 Synchronous Motors	627
	12.3.3 DC Motors	627
	12.3.4 Special Cooling	627
<b>12.4</b>	<b>ENCLOSURES</b>	<b>628</b>
	12.4.1 IEC Enclosures	628
	12.4.2 NEMA Enclosures	628
<b>12.5</b>	<b>THERMAL CIRCUITS</b>	<b>629</b>
	12.5.1 Steady-State Circuits	630
	12.5.2 Time-Varying Circuits	632
	12.5.3 Simplified Circuits	633
<b>12.6</b>	<b>DUTY CYCLES</b>	<b>636</b>
	12.6.1 RMS Loading Analysis	636
	12.6.2 Time-Constant Analysis	638
<b>12.7</b>	<b>AMBIENT AND ENVIRONMENTAL EFFECTS</b>	<b>639</b>
	12.7.1 Ambient Temperature	640
	12.7.2 Altitude	640
	12.7.3 Moisture	641
	12.7.4 Solid Contaminants	641
	12.7.5 Chemicals	642
	12.7.6 Hazardous Locations	642
	12.7.7 Seismic Activity	643
	12.7.8 Nuclear Plant Safety	643
<b>12.8</b>	<b>POWER SYSTEM QUALITY</b>	<b>644</b>
	12.8.1 Parameters of Power System Quality	644
	12.8.2 Adjustable Speed Drives	650
	<b>REFERENCES</b>	<b>653</b>

## 12.1 INTRODUCTION

Electric motors are ubiquitous in the modern world. Motors are found at home, in commercial establishments, and in industry. Most household motors are fractional-horsepower motors. As motors are applied commercially and in industry, the physical size and the ratings increase significantly. Pumped-storage hydroelectric sites, for instance, may have hundreds of thousands of horsepower in a single synchronous motor-generator unit. Equivalent powers are found in multiunit wound-rotor induction motors, such as those driving the compressors installed at NASA's wind tunnel facilities. Also included are the effects of power system quality on the motor and the influence of the motor on power system quality.

The philosophy of design, application, and use changes as the size and economic value of the units change. Fractional and small integral-horsepower motors are manufactured on automated assembly lines. First-cost economics are emphasized. Removal and replacement of these units is less expensive and faster than is removal, repair, and reinstallation. Generally, all environmental considerations are handled in terms of a few standardized enclosures and enclosure materials, unless the quantity of production is sufficient to justify a definite-purpose motor, such as the hermetically sealed units used for refrigerator application.

Larger motors, on the other hand, may be of sufficient size and cost to justify tailored design and manufacture for individual machines. More enclosures and materials are chosen to meet application requirements for these larger motors. Removal, repair, and reinstallation is far more economical than removal and replacement. This chapter has been written primarily on the basis of the larger motors defined by the National Electrical Manufacturers Association (NEMA) [1] as Large Apparatus. For induction motors NEMA defines Large Apparatus as horsepower (hp) from 600 hp to 100,000 hp, but the bulk of these ratings are generally in the range from 600 hp to 10,000 hp.

There are three basic motor types in popular use. These are alternating current (ac) squirrel-cage induction motors, ac synchronous motors, and direct current (dc) motors. The most popular type of motor in use is the squirrel-cage induction motor. It has the greatest usage and variety of applications due to its simple and economical construction. In the case of the larger higher speed units, the synchronous motor, as compared to the induction motor, offers the advantage of a fixed speed and of supplying reactive kilovars to the power system. It offers a significant advantage in power factor and machine size in very low-speed motors. The dc motor offers the advantage of inherent speed-changing capability for duty cycle applications. Generally the vehicle used for purposes of example in this chapter is the large squirrel-cage induction motor. The principles covered in this chapter apply to all sizes and types of motors. These electric motors are used as the prime movers for a vast array of machinery in many industries and geographic locations. Each industry and application has its own set of special environmental conditions. Whether the motor is installed indoors or outdoors will affect these conditions.

In considering the effects of the environment on electric motors, it is necessary to evaluate motor construction including enclosure, motor materials, the cooling medium and method, the temperature of the machine surroundings, the atmospheric conditions, and the contaminants that may be present at the installation site.

While motor materials can be and often are chosen to provide resistance to the many atmospheric, chemical, and mechanical conditions found at the operating sites, the large variety of enclosures provide the first degree of defense. These enclosures are the major selection factor in dealing with the environment and provide mechanical protection in varying amounts for the basic motor operating components.

The basic operating components of a motor are the stator, rotor, and bearings. These components are those that make the machine an electric motor rather than some other piece of machinery. The mechanical structure supports these components as an entity. It is this mechanical structure that is modified to provide the various motor enclosures.

For induction and synchronous motors, the stator component generally consists of a stack of electrical-grade magnetic punching sheets. Each sheet is insulated to maintain electrical separation since the varying magnetic flux carried in the steel during operation induces an electric potential between the laminations. These sheets are slotted to receive an electrical winding. This electrical winding consists of coils fabricated from an insulated conductor, usually copper. The coil itself is insulated from the punching slot walls either by a slot tube or by the application of insulating wraps and/or tapes. The inserted coils are frequently mechanically reinforced or braced to withstand the forces on the coil ends. These forces occur during operation, particularly during motor starting when the stator winding is subjected to large forces due to current much higher than rated current. The coil bracing may include intercoil spacers and ties, and a steel bracing ring or rings of insulated steel or composite material. Generally this entire structure will be impregnated with an insulating resin.

The squirrel-cage induction rotor is also generally manufactured with electrically separated laminations punched with slots for a squirrel-cage winding. The squirrel cage winding is typically a set of copper-base or aluminum-base bars either brazed or welded to a shorting ring at each end of the rotor. For NEMA size polyphase integral-horsepower induction motors that range in size to 500 hp, the squirrel-cage winding is most frequently cast aluminum. The squirrel-cage punching assembly is mounted on a shaft. [Figure 12.1](#) is illustrative of the construction defined for squirrel-cage induction motors.

In the case of a synchronous motor, a set of field poles may be mounted directly on a shaft or onto a stack of laminations that are mounted on a shaft. The field poles are typically stacks of laminations with insulated field coils wrapped around them. For field coil excitation, either a set of collector rings or the rotor of a brushless exciter completes the rotor assembly. The collector rings mate with a set of stationary brushes and the rotor of the brushless exciter mates with its stationary stator. [Figure 12.2](#) is illustrative of the construction defined for synchronous motors.

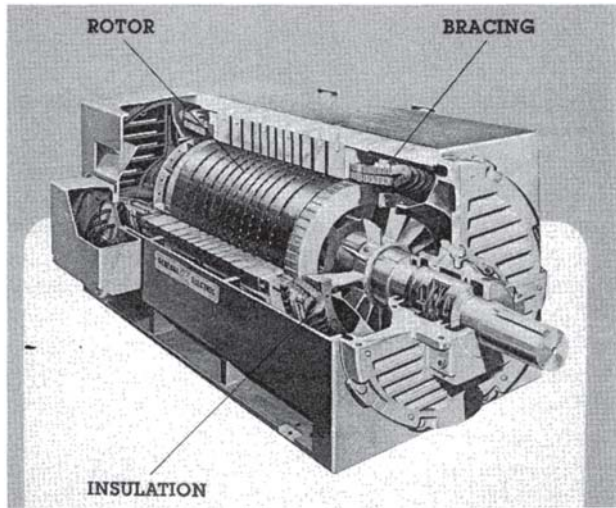


**Figure 12.1** Squirrel-cage induction motor with drip-proof enclosure and cutaway of enclosure. (Courtesy of General Electric.)

DC machine construction typically inverts synchronous machine construction. The wound-field poles are stationary. The armature winding rotates and is connected to a commutator.

Other types of machines have different specific constructions, but these types of motors also have stators and rotors, insulated or uninsulated magnetic parts, insulated machine windings, and bearings.

Bearings may be grease-lubricated or oil-lubricated antifriction bearings, or oil-lubricated sleeve-type bearings. The insulating and lubrication materials have operating temperature requirements that are the most limiting in terms of the allowable temperatures for electric motors. Over the years, it has become common practice to limit lubricant temperatures so that infrequent changes of lubricant are required. Thermal standards have been established for various classes of insulations [1–6] by NEMA and IEEE. Insulating materials and lubricants are subject to degradation with temperature. Over a significant range of temperature these changes have been found to vary inversely as a power of temperature. Insulation life has been found as a rule of thumb to decrease in life by one-half for every 8°–10°C increase in

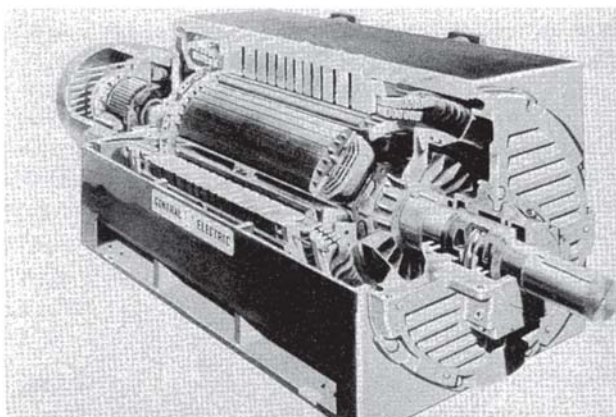


**Figure 12.2** Synchronous motor with drip-proof enclosure and cutaway of enclosure. (Courtesy of General Electric.)

temperature. This relationship is sometimes referred to as the Arrhenius rule. The IEEE and NEMA insulation temperature standards have been established on this basis to insure a long operational life for the motor.

During the operation of an electric motor, energy is lost due to hysteresis and eddy currents in the magnetic materials and resistance losses in the electrical conductors. These energy losses must be removed in such a way that the temperature limitations established for the motor materials are maintained. In addition to the insulating materials and the lubricants, the performance of the brushes used for commutators and slip rings is also dependent on temperature.

It should be noted that due to the temperature coefficient of resistance, machine winding losses increase with temperature. Thus there is an efficiency advantage to lowering operating temperatures.

Heat transfer, therefore, is an important science in the design, application, installation, and maintenance of electric motors. Heat transfer is a vital ingredient when considering the compatibility of the motor to the environment.

This chapter deals with environmental considerations in the design and operation of motors. This includes the subjects of heat transfer, motor ventilation, motor enclosures and their relationship to the ambient temperature, moisture conditions, pollutants, and other conditions found at the operating sites of the motors.

## 12.2 HEAT TRANSFER

Heat transfer deals with the flow of thermal energy from a heat source to a heat sink. In the case of an electric motor this heat transfer is normally from the windings and magnetic steel where the thermal energy is generated to the air surrounding the motor. The heat flow may also occur from the air cooling the motor to an air-to-air heat exchanger or an air-to-water heat exchanger. Special machines may be designed for direct water cooling, hydrogen cooling, cooling by air conditioning compounds, or by other special means. The basic principles of heat transfer apply for all of these cases. Very often heat transfer in electric motors is modeled on the basis of dc electrical circuits. In these models, the various modes of heat transfer are represented as resistance elements. The thermal capacities of the materials are represented as electrical capacitors. Thermal energy is input as a current source. Figure 12.3 is an electrical circuit representation of a simple thermal circuit with constant heat input into an insulated metal conductor, such as a stator coil. The figure shows an electrical circuit with a single electrical resistance,  $R$ , in parallel with a single electrical capacitance,  $C$ . A

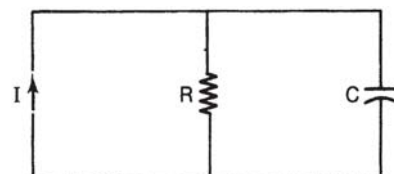


**Figure 12.3** Representation of heat flow using an  $RC$  electric circuit.

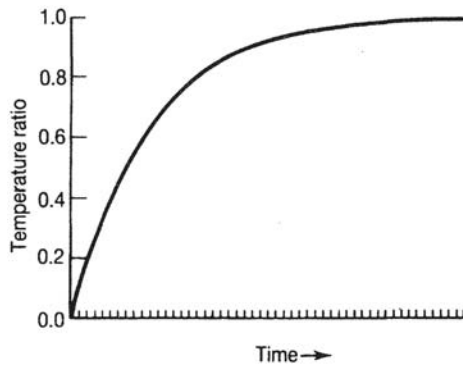


**Figure 12.4** Ratio of temperature rise to steady-state temperature rise vs. time (Eq. 12.2).

constant direct current,  $I$ , flows in the circuit. The resulting voltage,  $V$ , for such a circuit is:

$$V = IR(1 - e^{-t/\tau}) \quad (12.1)$$

where:

- $t$  = time
- $\tau$  = time constant  $RC$
- $V$  = voltage
- $I$  = current
- $R$  = electrical resistance
- $C$  = electrical capacitance

The corresponding thermal relationship is

$$\frac{\Delta\theta}{\Delta\theta_0} = (1 - e^{-t/\tau}) \quad (12.2)$$

where:

- $\Delta\theta$  = temperature rise
- $\Delta\theta_0 = q R_\theta$  = steady-state temperature rise
- $q$  = heat flow rate
- $R_\theta$  = thermal resistance
- $C_\theta$  = thermal capacitance
- $\tau$  = time constant =  $R_\theta C_\theta$

Figure 12.4 shows the time-temperature relationship for  $\Delta\theta/\Delta\theta_0$  vs. time. This particular circuit demonstrates the time versus temperature effects of including both the thermal resistance and the capacitance. Frequently, only the steady-state conditions are represented by the thermal equivalent circuits. The steady-state representations include only thermal resistance and heat flow rate inputs.

### 12.2.1 Modes of Heat Transfer

Three modes of heat transfer are generally recognized in the literature [7,8]: conduction, radiation, and convection.

There are two types of convection, natural convection and forced convection. Additionally, the processes of evaporation and condensation may be used to utilize the latent heat of

vaporization. The application of the processes of evaporation and condensation for electric motors is generally limited to hermetically sealed motors. These motors are used to drive refrigerant compressors for heat pumps, air conditioners, and refrigeration units.

#### 12.2.1.1 Conduction

In the conductive mode, heat flows directly through the material without movement of the material except for the incident thermal expansion and contraction. For unidirectional heat flow through a solid:

$$q = \left( \frac{kA}{l} \right) \Delta\theta = \frac{\Delta\theta}{R_\theta} \quad (12.3)$$

where:

- $q$  = heat flow rate
- $k$  = thermal conductivity
- $A$  = area of flow path
- $l$  = length of flow path
- $\Delta\theta$  = temperature difference between the start and end of the heat flow path.
- $R_\theta = \frac{l}{kA}$  = thermal resistance

This mode is directly comparable mathematically to Ohm's law, which governs the flow of an electrical current through a material of electrical resistance from a location of higher voltage potential to a point of lower voltage potential.

$$I = \left( \frac{\gamma A}{l} \right) V = \frac{V}{R} \quad (12.4)$$

where:

- $I$  = current
- $\gamma$  = conductivity
- $A$  = area
- $l$  = length
- $V$  = potential difference
- $R = \frac{l}{\gamma A}$

Thus if heat is conducted through several solid materials in series such as copper, electrical insulation, and magnetic steel, the resistances may be added directly:

$$R_{\text{series}} = R_{\text{Cu}} + R_{\text{ins}} + R_{\text{steel}} \quad (12.5)$$

In like manner, if parallel paths are available:

$$\frac{1}{R_{\text{parallel}}} = \frac{1}{R_1} + \frac{1}{R_2} + \dots \quad (12.6)$$

Interestingly the thermal conductivities of metals are generally proportional to the electrical conductivity of the metal, and with some exceptions, including aluminum and brass, the value of thermal conductivity decreases as temperature increases [8]. For aluminum and brass the value of thermal conductivity increases with temperature. Over the range of interest for electric motors, these variations are not

**Table 12.1** Thermal Conductivities of Materials Used in Electric Motors

Material	Conductivity <sup>a</sup>		Relative conductivity <sup>b</sup>	Relative resistivity <sup>b</sup>
	[W/(°C-m)]	[W/(°C-in)]		
Copper	383.85	9.75	1.00	1.00
Aluminum	203.94	5.18	0.53	1.88
Carbon steel	44.88	1.14	0.12	8.55
Motor-grade steel	22.83	0.58	0.06	16.81
Varnished cambric	1.99	0.050	0.005	192.9
Mica	0.433	0.011	0.001	886.5

<sup>a</sup> References 7, 8, and 14.

<sup>b</sup> Relative to copper.

large but are significant. They may be accounted for by using a value corresponding to an average temperature, or conservatively by using a value of conductivity corresponding to the largest value in the operating temperature range.

Also, in the case of composite materials, it is necessary to account for the effects of contact resistance between the different materials. Often the same type of test used to measure material conductivity, such as temperature measurements of materials sandwiched between plates, may also be used to include the contact resistance. This may be accomplished by proper selection of the test material specimens and the testing setup.

As implied in the discussion, conductivity is the mode by which heat transfers from the motor winding conductors through the winding insulation and through the magnetic steel to the motor enclosure. A brief review of the relative conductivities of various materials used in motors is of interest.

Table 12.1 provides the thermal conductivities of some of the materials commonly used in the construction of electric motors. The table clearly demonstrates that electrically conducting materials also conduct heat well and that electrically insulating materials serve equally well as thermally insulating materials. Improved electrical insulations should not only allow better utilization of space for active materials such as copper and motor-grade steel, but also need to provide good heat transfer capabilities. Improved thermal conductivity allows a designer the option to increase efficiency, or performance, or to reduce machine size, or to accomplish a combination of these factors.

### 12.2.1.2 Radiation

Heat is transferred by radiation from the surface of a body at higher temperature to the surface of a body at lower temperature.

The quantity of radiated energy is a function of the absolute temperature of the radiating and absorbing bodies as well as the surface characteristics of these bodies. Surfaces that absorb all incident energy (no reflection) are called black bodies. The Stefan-Boltzmann law defines the amount of energy radiated from a black body to black surroundings as [7–10]:

$$q = \sigma A_1 \left[ \left( \frac{\theta_1}{100} \right)^4 - \left( \frac{\theta_2}{100} \right)^4 \right] \times 10^8 \quad (12.7)$$

where:

$q$  = heat flow rate

$\sigma$  = Stefan-Boltzmann constant

$A_1$  = area of surface 1

$\theta_1$  = absolute temperature of surface 1

$\theta_2$  = absolute temperature of surface 2

“The ratio of the emissive power of an actual surface to that of a black body is called the emissivity  $\epsilon$  of the surface” and Kirchhoff’s law states “at thermal equilibrium, the emissivity and absorptivity of a body are the same” [8].

Thus, for a body with emissivity  $\epsilon_1$ , the amount of energy radiated to black surroundings is:

$$q = \sigma \epsilon_1 A_1 \left[ \left( \frac{\theta_1}{100} \right)^4 - \left( \frac{\theta_2}{100} \right)^4 \right] \times 10^8 \quad (12.8)$$

If the product of the emissivity and the area of the surface surrounding surface 1 (surface 2) is very much larger than the product of the emissivity and the area of surface 1, then the surrounding surface appears black to surface 1 and Eq. 12.8 may be used to determine radiant heat flow from surface 1 to the surroundings. Frequently, when heat is transferred by radiation some degree of convection is also present, so that the additional heat flow due to convection must also be evaluated to determine the total heat flow.

The radiation mode of heat transfer is not usually of great significance in the steady-state cooling of operating electric motors. The absolute surface temperature of motors is not particularly high either in absolute terms or in relation to the motor surroundings. Thus, the heat flow rate due to radiation is not generally sufficient to maintain the required operating temperature. An exception is the totally enclosed nonventilated (TENV) motor. For the TENV motor, this mode together with natural convection cools the machine. Also, motors applied out of doors in hot areas may absorb significant solar radiation. Thus, solar radiation should be considered when applying motors to these or similar operating sites.

### 12.2.1.3 Convection

In this mode, heat is transferred from the surface of a solid to a fluid, such as air, by movement or circulation of the fluid. This circulation also causes mixing and heat transfer within the fluid.

Natural convection occurs in heating of a fluid, such as air, by the surface of a solid object. As the fluid heats, it rises and

is replaced by cooler fluid from the general environment. Thus, a fluid circulation is established by the surface heat transfer from the warmer solid to the cooler fluid. If the temperatures are reversed, the direction of fluid flow will reverse. Most people are familiar with this mode of heat transfer in homes constructed with wall-type tube-and-fin, hot-water-to-air heat exchangers. Heat flow with this mode is generally described by an equation of the form:

$$q = h A (\theta_1 - \theta_2) \quad (12.9)$$

where:

- $q$  = heat flow rate
- $h$  = surface heat transfer coefficient
- $A$  = effective surface area
- $\theta_1$  = surface temperature of the solid
- $\theta_2$  = temperature of the fluid

The value for  $h$  is related in a complex manner to the geometrical configuration, including the surface characteristics of the solid, and to various parameters of the fluid such as viscosity ( $\mu$ ), thermal conductivity ( $\kappa$ ), velocity ( $v$ ), density ( $\rho$ ), and specific heat ( $c$ ). Heat transfer experts have determined these relationships by the use of dimensional analysis [7,9,10] and experimental data on physical models. The various parameters have been combined into dimensionless ratios by the use of dimensional analysis and by a theoretical understanding of the general effect that each parameter has upon the phenomenon of surface heat transfer. A few of the combined dimensionless ratios together with their associated area of application are shown in Table 12.2. Using these and other such numbers, experimental data is plotted, typically on log-log paper. Frequently the data clusters so that linear or curvilinear correlations result. Thus, for known values of geometry and fluid parameters it is possible to determine a useful value of  $h$ .

Natural convection in conjunction with radiation is the method by which TENV motors are cooled. This is also the way by which virtually all self-ventilated motors cool after shutdown.

**Table 12.2** Selected Dimensionless Numbers Applied in Heat Transfer

Name	Parameters <sup>a</sup>	Application
Reynolds	$DV\rho/\mu$	Laminar and turbulent flow
Nusselt	$hD/k$	Free and forced convection
Prandtl	$c\mu/k$	Fluid characteristic
Grashof	$D^3\rho^2g\beta\Delta\theta/\mu^2$	Free convection

<sup>a</sup> $D$  = critical dimension

$v$  = velocity

$\rho$  = density

$\mu$  = viscosity

$h$  = surface heat transfer coefficient

$k$  = thermal conductivity

$c$  = specific heat

$g$  = acceleration of gravity

$\beta$  = coefficient of expansion

$\Delta\theta$  = temperature difference

Forced convection is similar to natural convection, but in this mode the fluid is blown or pumped across the heated surface. This greatly enhances the heat transfer. The forced warm air heating system is a familiar household example of this type of heating system. In addition, many room-type electrical heaters act in this mode. Room air is blown across the electrically heated elements and then either circulated within the room or blown directly onto a surface. The heat flow rate is described by the same type of equation as for natural convection. The value of  $h$  is determined by the same method of dimensionless ratios and experimentation in a manner similar to that for natural convection. In the case of forced convection, the velocity of the fluid is a key consideration. The value of  $h$  has been found to be a power function of the mass flow of the fluid. The range of the exponent has been reported to be between 0.78 and 0.82 for air flowing inside pipes [8]. This relationship generally applies for turbulent flow. In the laminar flow regime, the value of  $h$  is also influenced by natural convection so that this power function relationship no longer holds. Forced convection is far more effective in cooling surfaces than is natural convection and it is the preferred mode for cooling the surfaces of electric motors during operation.

It is instructive to consider the relative surface heat transfer capabilities per unit of surface area for radiation, natural convection, and forced convection. McAdams [8] provides the following formulas for the convection coefficient for free convection on plates:

$$h_c = 0.38(\Delta\theta)^{0.25} = \text{horizontal up} \quad (12.10)$$

$$h_c = 0.2(\Delta\theta)^{0.25} = \text{horizontal down} \quad (12.11)$$

$$h_c = 0.27(\Delta\theta)^{0.25} = \text{vertical} \quad (12.12)$$

where:

$$h = \text{BTU}/(\text{h}\cdot\text{ft}^2\cdot^\circ\text{F})$$

$$\Delta\theta = ^\circ\text{F}$$

This suggests an average corresponding to the vertical condition. To determine the convection coefficient ( $h$ ) for values that might be representative for a motor, use Eq. 12.12. Consider a surface temperature 60°C above an ambient temperature of 40°C.

Then:

$$h_c = 0.87 \text{ BTU}/(\text{h}\cdot\text{ft}^2\cdot^\circ\text{F}) = 4.94 \text{ W}/(\text{m}^2\cdot^\circ\text{C})$$

To determine the heat transfer coefficient due to radiation for a surface with an emissivity  $\epsilon$  of 0.9 with a temperature of 60°C above the ambient temperature, use Eq. 12.13. [7,8]:

$$h_r = \frac{\sigma\epsilon[(\theta_1/100)^4 - (\theta_2/100)^4]}{\theta_1 - \theta_2} \times 10^8 \quad (12.13)$$

Table 12.3 shows heat transfer coefficients for radiation at surface temperatures of 100°C, 90°C, and 80°C with an ambient of 40°C.

Thus, for the case considered, the radiation effect exceeds the free convection effect. The combined coefficient is in the order of:

$$h = 2.37 \text{ BTU}/(\text{h}\cdot\text{ft}^2\cdot^\circ\text{F}) = 13.46 \text{ W}/(\text{m}^2\cdot^\circ\text{C})$$

**Table 12.3** Surface Heat Transfer Coefficient Representation for Radiation with Differing Surface Temperatures and a 40°C Ambient

Surface temperature (°C)	Ambient temperature (°C)	Surface heat transfer coefficient, $h_r$	
		[W/(m <sup>2</sup> -°C)]	[BTU/(h-ft <sup>2</sup> -°F)]
100	40	8.52	1.5
90	40	8.01	1.41
80	40	7.67	1.35
$\varepsilon = 0.9$			
$\sigma = 5.71 \times 10^{-8}$		W(m <sup>2</sup> -k <sup>4</sup> )	
$\sigma = 0.173 \times 10^{-8}$		BTU/(h-ft <sup>2</sup> -°R <sup>4</sup> )	

$\varepsilon$  is the surface emissivity.

$\sigma$  is the Stefan-Boltzmann constant.

Compare these values of convection coefficient to those for the case of air flowing over smooth plates. For convenience, Eq. 12.14 from King [7] will be used to evaluate  $h$ . While the data available from McAdams [8] and General Electric [11] are more particularized in terms of the specific geometry of plates and ducts, that data is also more complexly presented in multiple curve plots. Equation 12.14 highlights the important variables as determined by dimensional analysis. The results from the use of this equation can be conveniently used for the comparison of convection coefficient,  $h$ , by forced convection with those obtained for radiation and free convection. Use of Eq. 12.14 is not recommended below about 4.6 m/s (15ft/s) because of free convection effects below this velocity.

$$h = \frac{0.56[v]^{0.75}}{L^{0.25}} \quad \text{BTU/(h-ft}^2\text{-°F)} \quad (12.14)$$

where:

$v$  = velocity in ft/s

$L$  = length of the surface in feet

Consider three different four-pole motors. Each runs at a speed of 1800 rpm. Each motor has a different rotor diameter ( $D$ ). The air surface velocity for each motor is one-quarter of the peripheral speed and has a critical  $L$  dimension of 10% of the rotor diameter. Typically air velocities in the air passages of self-ventilated motors are limited to one-quarter of the peripheral speed in order to avoid excessive pressure head drop. This value will be selected for comparative purposes, recognizing that the air velocities such as those impinging on

the stator coils may be significantly higher. Ten percent of the rotor diameter has been selected as the  $L$  dimension for comparison.

Table 12.4 provides the value of the heat transfer coefficient for the three different 1800 rpm motors described. The heat transfer coefficient increases as the machine size and rotor peripheral velocity increases. This surface heat transfer coefficient for even the smallest motor is in the order of 4.5 times the combined coefficient calculated for natural convection and radiation and is over 10 times the coefficient for free convection alone. Since the effectiveness of forced convection is highly dependent upon cooling fluid velocity, the next item considered will be motor ventilation. Before considering ventilation, however, it should be noted that it is sometimes useful to represent the radiation and convection modes of heat transfer as equivalent resistances for use in thermal circuits. This is done by using the methods that have been described. For the convective mode the equivalent resistance is equal to the inverse of the product of  $h$  and  $A$ . For the radiation mode a similar procedure is followed except that the value of  $h_r$  is used. In the cases of natural convection and radiation, an iterative thermal calculation procedure is required to obtain appropriate values of resistance.

### 12.2.2 Ventilation

Certain parameters are used as yardsticks for the relative performance of different motors. The parameter  $D^2L$  is frequently used in this regard.  $D^2L$  is a simple measure of machine volume or size. If  $D_0$  is the outer diameter of the

**Table 12.4** Surface Heat Transfer Coefficient for Three Different 1800-rpm Motors of Differing Rotor Diameter, Air Velocity, and Length of Cooling Surface

$h$		$D$		$V$		$V/4$	
[W/m <sup>2</sup> -°C]	[BTU/(h-ft <sup>2</sup> -°F)]	(m)	(ft)	(m/s)	(ft/s)	(m/s)	(ft/s)
60	10.6	0.305	1	28.7	94	7.2	23.6
85	15.0	0.610	2	57.3	188	14.3	47.0
104	18.4	0.914	3	86.0	282	21.5	70.7

$h$  = the surface heat transfer coefficient

$D$  = the rotor diameter

$V$  = the rotor peripheral velocity

$V/4$  = 1/4 of the rotor peripheral velocity



punchings and  $L$  the total punching stack length, then  $D_0^2L$  is the volume of the machine space as determined by the punchings with the constant  $\pi/4$  dropped. Most frequently this term is used in a ratio with machine horsepower or kilowatts (kW), that is,  $hp/D_0^2L$ . This parameter is a measure of the output obtained from a given volume of electromagnetic material. If the volume is divided by the surface area of punching stack length ( $\pi D_0L$ ), the ratio obtained is  $D_0/4$ . It is clear then that as the machine punching diameter increases, the volume to surface area ratio increases in proportion. Thus, as machine size and horsepower increase, less and less relative outside punching surface area is available for machine cooling.

In the case of a machine with TENV enclosure, cooling depends upon natural convection. Thus, as machine rating and size increase, cooling the machine becomes more and more difficult. While efficiency generally increases with machine size and the losses per unit of volume diminish, the reduction in losses is not sufficient to offset the relative loss in peripheral cooling surface. Thus TENV machines become increasingly unavailable in higher power ratings and the time ratings decrease as power increases.

This cooling capability may be significantly increased if the natural convection is replaced by forced convection, such as is done for the totally enclosed fan-cooled machine enclosure.

Further improvement in cooling capability may be attained by use of an ambient breathing or open-type enclosure. In this case the machine end turns and rotor may be more easily cooled. Modification of the punching stack to allow for radial ventilating ducts permits a very significant advance in cooling capability. This modification allows for cooling machines in the largest sizes. These items are discussed below.

Thus, the major modes of heat transfer for electric machines are forced convection and conduction. It is important to understand the principles of fans and ventilation, upon which the effectiveness of forced convection depends.

### 12.2.2.1 Fans

The radial fan is the principal fan used in the ventilation of squirrel-cage induction motors. Generally the radial fan will provide a greater increase in pressure than a single-stage axial fan of the same diameter, and it can be designed with sufficient flow to meet most electric machine requirements. In addition the radial flow fan can be very simple in terms of fabrication requirements. It fits well into the overall machine design.

Axial flow fans increase in importance as machine speed increases. Their use has generally been limited to larger machines at speeds of 3600 rpm or higher as these fans fulfill the unique ventilation requirements of these machines. Axial type fans are also frequently used as inducers to assist the fan action of synchronous field poles.

For illustrative purposes a simple model of a radial flow fan will be considered (see Fig. 12.5). First, however, Bernoulli's theorem, which defines pressure relationships, will be developed [9]. Figure 12.6 illustrates a pipe of differing flow areas and elevations. The energy relationship for an incompressible fluid without friction flowing through the pipe

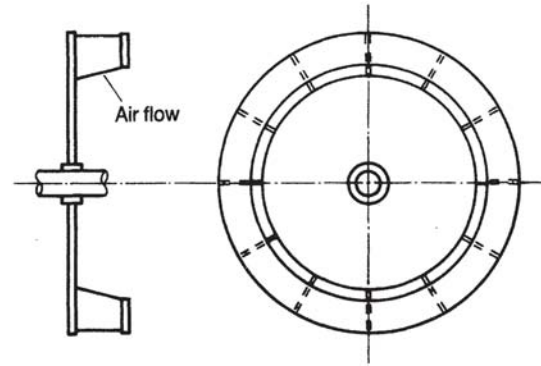


Figure 12.5 Radial flow fan with 12 blades mounted on a shaft.

at positions 1 and 2 is expressed in Eq. 12.15. For the radial fan and the air flow under consideration, the pressure differentials are small compared to atmospheric pressure, so that the cooling air may be treated as incompressible. For any period of time  $t$ , the mass of fluid passing each point will be constant for this steady-state analysis. Then the energy involved is [9]:

$$mgh_1 + \frac{1}{2}mv_1^2 + p_1V = mgh_2 + \frac{1}{2}mv_2^2 + p_2V \quad (12.15)$$

where:

- $m$  = mass of the fluid
- $v$  = velocity
- $V$  = volume
- $p$  = pressure
- $h$  = altitude

Substitute  $m/\rho$  for  $V$ , where  $\rho$ =mass density. Divide by  $mg$  and rearrange to obtain:

$$(h_1 - h_2) + \frac{v_1^2 - v_2^2}{2g} + \frac{p_1 - p_2}{\rho g} = 0 \quad (12.16)$$

Note that if  $(p_1 - p_2)/(\rho g)$  is interpreted as the height of a fluid column, then  $\Delta p = (p_1 - p_2)/(\rho g)$  is me pressure difference expressed in fluid height. The energy equation has now been converted to a pressure equation expressed in the dimension of elevation or "head." This is Bernoulli's theorem. The first term represents head due to elevation difference; the second term represents head due to velocity; and the final term

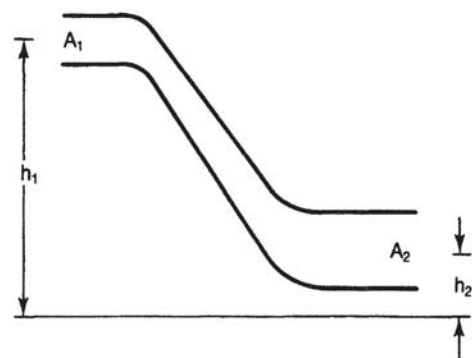


Figure 12.6 Pipe of differing flow areas and differing elevations.

represents head due to pressure. For the case of motor ventilation with air, the elevation term is negligible and the equation may be reduced to:

$$\frac{v_1^2 - v_2^2}{2g} + \Delta p = 0 \quad (12.17)$$

As a matter of interest, for air at a density of 0.075 lb/ft<sup>3</sup> (approximately room temperature at sea level) and a velocity of 4000 ft/min,  $v^2/2g$  is equal to one inch of water in velocity head.

For fans used on motors, the peripheral velocity pressure is generally not recovered, and the fan characteristics are normally expressed in developed static pressure  $p_s$  and volume flow  $Q$ . The power output ( $W_s$ ) developed may be expressed as:

$$W_s = p_s Q \quad (12.18)$$

The static efficiency,  $\eta_s$ , is defined as:

$$\eta_s = \frac{p_s Q}{\text{power input}} \quad (12.19)$$

It may be shown by dimensional analysis that fans of similar geometric proportions may be represented by a pressure coefficient  $\psi$  and a flow coefficient  $\phi$  [10,11] where:

$$\psi = \frac{p_s}{\rho v_t^2 / 2} \quad (12.20)$$

$$\phi = \frac{Q}{A v_t} \quad (12.21)$$

where:

- $p_s$  = static fan pressure (not head)
- $\rho$  = air mass density
- $v_t$  = peripheral speed of the fan tip
- $A$  = discharge area of the fan
- $Q$  = volume flow

Figure 12.7 shows the relationship of the pressure coefficient  $\psi$  and the flow coefficient  $\phi$  for a specific fan with a geometry similar to the fan of Fig. 12.5. The upper curve starting at a  $\psi$  value of 0.46 and a  $\phi$  value of zero represents the fan pressure/flow characteristics. This fan has 12 blades that are equally spaced around the periphery of the fan. This particular fan may operate in either direction of rotation with the same characteristics. The pressure coefficient and volume coefficient for this fan have a linear relationship. As the radial fan blade is slanted or curved, the relationship between pressure and flow tends to include more curvature. Pressure may drop less with light flow and more steeply with high flows. These changes may also improve fan efficiency.

The relationships of Eqs. 12.20 and 12.21 indicate that pressure is a function of peripheral speed squared and fluid density, and that volume flow is a function of peripheral speed and the fan discharge area. Fan discharge area is dependent upon fan blade width and fan blade outer diameter. Fan diameter is generally limited either to motor rotor diameter or to stator punching outer diameter. Even for machines with external fans, site requirements or industry dimensional

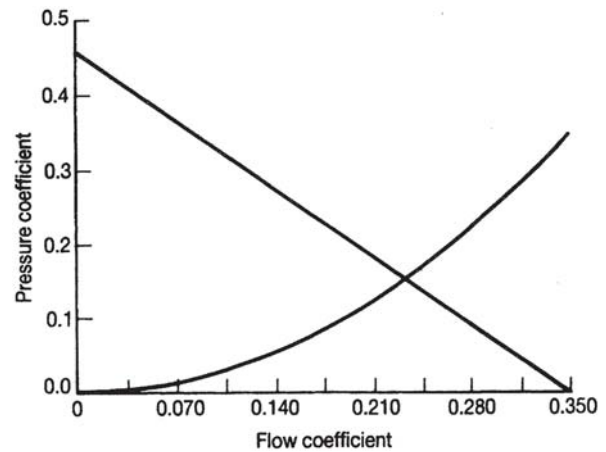


**Figure 12.7** Radial flow fan operational curves. Upper curve provides the pressure-flow characteristic for a radial fan. Lower curve provides a typical parabolic air flow resistance characteristic for a motor.

standards will restrict the available diameter essentially as stated. Radial ventilating ducts when used and when located in the rotor of a motor perform as radial fans.

The pressure drops throughout the machine may also be determined. The energy to force the air through the motor is provided by the fan or fans. In the case of motors with rotor air ducts, each air duct acts as a fan. As the air passes through the machine, the flow passages will change shape. The passages may enlarge or they may contract. The air will change direction, as well, during its traverse through the machine. Loss coefficients or coefficients of discharge have been determined for these various condition [11]. These losses are described in the form of Eq. 12.22, which is similar in form to the velocity head terms in Bernoulli's equation:

$$\Delta p = C_D \frac{v^2}{2g} \quad (12.22)$$

$C_D$  thus expresses the pressure change in terms of velocity head. The determination of the values of  $C_D$  is complex. It is a function of the specific geometry of the flow path and the medium. It is generally determined by test. For instance, for a contraction the value of  $C_D$  is a function of the flow characteristics of the fluid or gas (Reynolds number) as well as the areas associated with both the smaller and larger passages. The  $L/D$  ratio associated with each passage is also very significant. The value of  $C_D$  may vary from about 1.45 to about 2.80 depending upon the particular conditions. In the case of an expansion,  $C_D$  will be negative as a pressure recovery will occur as the fluid velocity decreases. As pointed out, the values of these coefficients are available in handbooks [10,11] and engineering periodicals such as those of ASME and ASHRAE. The various velocities may be determined on the basis of total machine volume flow.

Thus, the pressure drop for the machine may also be expressed as a product of a constant and the square of the volume flow. The flow resistance curve may be plotted on a fan curve such as shown in Fig. 12.7. The lower parabolic curve starting at the zero values of  $\psi$  and  $\phi$  represents the motor flow resistance. The intersection of the fan curve and

the flow resistance curve determines the pressure and the volume at the operating point. With the operating point known, the velocity of the fluid flow at various points throughout the machine can be determined. From these velocities, the surface heat transfer coefficients may be determined. From the surface heat transfer coefficient data, the thermal conductivity data and the machine losses, the temperature rise of the machine can be calculated. If necessary, the design may be modified and the procedure reiterated until a satisfactory result is obtained.

In addition to the determination of the heat transfer coefficients, ventilation design is also important in several other respects. In order for the cooling medium to transport the heat from the motor, the mass flow must be sufficient so that the heating of the coolant does not significantly contribute to the temperature rise of the machine. A kilowatt of loss transported by an air flow of 100 ft<sup>3</sup> per minute will increase the air temperature 18°C. Thus on the average for this flow, the cooling air temperature rise will contribute 9°C to the total temperature rise of the motor. The air flow must therefore provide sufficient mass flow to remove the heat without excessive air temperature increases, as well as sufficient velocity to provide effective values of heat transfer coefficients.

The total volume of air is also important to the user. Sufficient space must be allowed from the air intakes to prevent excessive entrance pressure drops. For motors operating indoors, sufficient air exchange with the outside must be allowed so that the indoor air does not exceed the allowable ambient air temperature requirement.

## 12.3 COOLING OF BASIC MOTOR TYPES

### 12.3.1 Induction Motors

Figure 12.1 shows a cutaway of a polyphase induction motor with open drip-proof construction. The louvered end shields provide the drip-proof protection at the air inlet. The machine frame provides the protection for the air outlet. The motor construction includes a stator wound with formed coils. Radial air ducts are formed by the use of interpunching packet spacers. The spacers are not shown in the figure. The rotor also has axial packages of punchings and the rotor ducts align with the stator ducts. The rotor has an aluminum winding with the end ring adjacent to the end punching packet. The radial fan is mounted directly on the rotor shaft. A stationary air shield is mounted near the air inlet and is formed to provide a close axial clearance with the fan blades.

Air enters the machine through the louvered shields at each end. At the fan inlet a portion of the air is directed by the fan through the stator end-turns and then axially past the outer diameter of the core in the space between the core and the frame at the four frame corners and thence to the outside through openings on the sides of the frame. Another portion of the air is pulled through axial openings in the rotors by the fan action of the rotor bars, which act as fan blades where they cross the rotor ducts. The axial openings are formed either by the use of a shaft-mounted spider with arms on which the rotor punchings are mounted or by openings in the punchings

themselves when the punchings are shaft-mounted. This air is blown by the rotor through the mating stator ducts and thence out of the side of the machine. Frequently, the air directed over the end turns is controlled by the use of metering openings in the frame plates and by judicious placement of these plates. This technique allows for control over the relative quantities of air flowing over the stator coil end-turns compared to the air flowing through the air ducts.

Smaller motors have a smaller stack length-to-diameter ratio and are built without core ventilating ducts. For these machines none of the cooling air is directed through the machine core. All of the cooling air passes through or over the machine end turns and bathes the outer diameter of the machine core. These motors usually have cast aluminum rotors with fan blades cast as a part of the rotor winding end rings. These fan blades provide a high degree of fin cooling effect for the squirrel-cage rotor winding.

A totally enclosed fan-cooled motor of double-shell construction is shown in Fig. 12.8. This particular frame has an inner shell and outer shell spaced from the inner shell by ribs and pins. The pins are included to enhance heat transfer. The stator core may be press fit or interference fit with the stator frame. An external radial fan located on the opposite end of this motor blows air through the passages between the double shell. Internally, rotor fans provide a limited circulation of air at each end. This circulation transports heat from the rotor end ring and the stator winding end turns to the end shields of the motor. The major heat flow, however, is by conduction from the rotor windings radially, across the air gap from the rotor to the stator punchings, as well as from the stator windings through the stator punchings. From the stator punchings the heat flows to the surfaces of the cooling shell. The shell is cooled by the flow of the ambient air. This type of construction is most typical for the intermediate-power ratings. Smaller units typically omit the pins and outer shell.

For larger motors, a variation of the cooling system described for open-type motors with axially spaced air ducts is frequently used. Instead of utilizing ambient air, the internal air is

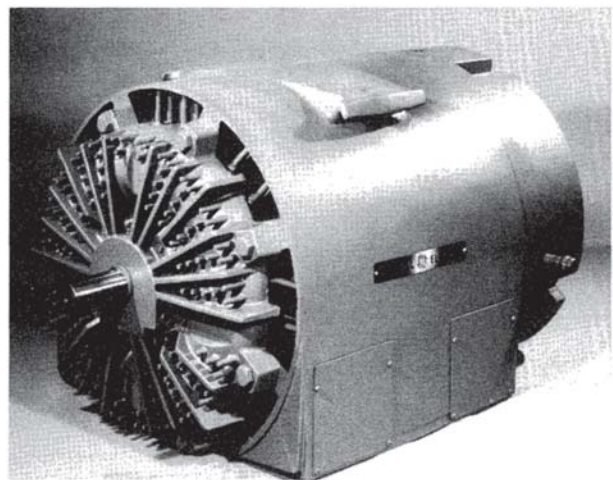


**Figure 12.8** Totally enclosed fan-cooled (TEFC) motor with double-shell frame construction and pin-type cooling fins. (Courtesy of General Electric.)

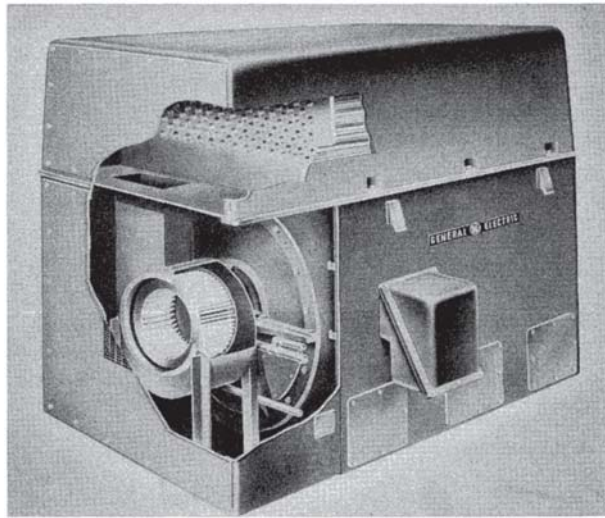


**Figure 12.9** Totally enclosed air-to-air cooled (TEAAC) motor cutaway showing external fan and air-to-air heat exchanger. (Courtesy of General Electric.)

recirculated through a heat exchanger, often placed in a “top hat” mounted on top of the frame. The internal air is discharged from the frame center up through the heat exchanger. The cooled air returns from the top hat to the frame from above at each end. Figure 12.9 shows a motor of such construction. This totally enclosed air-air cooled (TEAAC) type of motor utilizes an air-to-air heat exchanger. A sirocco type of radial external fan, for the machine shown, has been used to circulate the external ambient cooling air through the heat exchanger.

The other enclosures defined by NEMA [1] are generally variations of those already described. For instance, the weather-protected type II enclosure is arranged so that winds may blow through the intake and exhaust sections and the entering air takes a path with at least three 90-degree bends. The internal cooling is the same as that described for the open drip-proof machines. Similarly, air-to-water heat exchangers may replace air-to-air heat exchangers.

### 12.3.2 Synchronous Motors

Synchronous motors can use cooling systems similar to those described for induction motors. The synchronous motor shown in Fig. 12.2 has an open drip-proof enclosure similar to that of the induction motor. The air flow is very similar. Air enters at both ends through the end shields and is exhausted through the openings on the side of the frame. The shaft-mounted rotor fan provides air to the stator winding end turns and provides an inducing action to bring the air up to speed prior to entry into the openings between the synchronous field poles. The field poles themselves provide fan action to drive the air through the stator core air ducts and thence through the openings on the side of the motor frame.

The particular machine shown is a relatively high-speed machine (1200 rpm) with a center interpolar winding support bracket and a relatively long stack length. Some synchronous motors, usually smaller units or shorter lower-speed units that

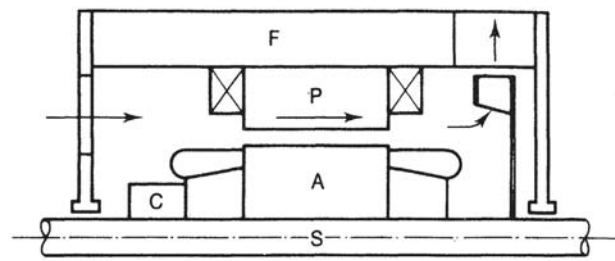


**Figure 12.10** Schematic diagram of a dc motor with end-to-end ventilation.

do not require an interpolar winding bracket, are designed for single end ventilation. These machines might have a larger centrifugal fan at one end to pull the air completely through the machine. The unit might or might not have radial stator air ducts depending on its length. It would probably be arranged to pull air over the core outer diameter as well as through the interpolar space from the air entry end by the oversize radial fan. Air would be discharged out of the sides of the frame at the location of the fan.

### 12.3.3 DC Motors

As pointed out in Section 12.1, dc motors are inverted synchronous motors, or vice versa, depending upon the viewpoint taken. Figure 12.10 shows a ventilating schematic for a dc motor. The wound poles, P, are mounted on a frame, F. These parts are stationary. The wound armature, A, and commutator, C, are mounted on shaft, S, and rotate. The end-to-end ventilation scheme shown is similar to the one described for synchronous motors. DC motors are frequently supplied with separate ventilation because of their use for applications requiring speed changes and speed reversals. The end-to-end ventilation scheme is quite suitable for external separately driven blowers since only a single air inlet and a single air outlet location are involved. The schematic of Fig. 12.10 shows air blowing through only the stator interpolar area. On larger units, air may also be blown through axial holes located in the armature punchings similar to those described for induction motor rotors.

### 12.3.4 Special Cooling

Some motors are cooled by special means. Inert gas-filled construction has been used for large motors installed at hazardous locations. Special sealing techniques are used to minimize the internal gas leakage to the ambient. These units are otherwise similar to totally enclosed motors with air-to-water heat exchangers. Smaller units are sometimes used with water-cooled jackets. These are similar to the double-shell TEFC motors previously described except that the fan parts are removed and the shells are sealed at each end so that water may be circulated to cool the machine. Hermetically sealed units for refrigeration service are commonplace. These units use the refrigerant as the cooling medium. Except for these hermetically sealed motors, large motors with special cooling

are not at this time in popular use. Experimental work proceeds on using advanced technology to improve motor thermal performance. It is feasible to build motors with direct water-cooled windings similar to turbine generators, or even with cryogenic cooling. Units of the latter type are not yet in common service but may have important future applications for shipboard or land transportation propulsion service.

## 12.4 ENCLOSURES

Enclosures are a major line of defense in protecting motors from the degrading effects of the environment. The use of enclosures inherently impacts the type and effectiveness of the cooling techniques used. Two of the major groups that have established motor standards, the IEC and NEMA have defined standards for enclosures. In the United States, the NEMA classifications are the recognized standard. However, in the climate of the international market place, it is important to recognize the IEC standards.

### 12.4.1 IEC Enclosures [12]

IEC Publication 34–5, “Degrees of Protection by Enclosure for Rotating Machines,” defines enclosure by numeric coding. The first numeral defines protection from foreign solid objects and protection for personnel safety. The second numeral defines the protection against water. For instance, an IP 45 enclosure protects the machine interior from objects exceeding 1 mm in diameter (0.039 inches) and from water projected by a nozzle in any direction. While not directly comparable to NEMA, a NEMA waterproof motor would generally comply with this definition.

A second IEC Publication, 34–6, “Methods of Cooling Rotating Machinery,” defines the cooling of a motor with a capital letter and two numerals. The capital letter defines the cooling medium. The first numeral defines the technique for cooling the motor, such as open, surface cooled, or heat exchanger. The second numeral defines the technique of circulating the coolant, such as by natural convection, self-circulated, or separately driven fan. For further information on IEC enclosures, refer to the IEC publications (see [Appendix B](#)) and Cummings [12].

### 12.4.2 NEMA Enclosures [1]

The IEC categorizes machines by type of enclosure and method of cooling. NEMA, on the other hand, categorizes machines as either open machines (MG 1–1.25) or totally enclosed machines (MG 1–1.26) [1]. An open machine permits ambient air to circulate within the motor, over and around the windings. Machines defined as open are

Drip-proof machine	(DP)
Splash-proof machine	(SP)
Semiguarded machine	
Guarded machine	
Drip-proof guarded machine	(DPG)
Open externally-ventilated machine	(OEV)
Open pipe-ventilated machine	(OPV)

Weather-protected machine: type I	(WPI)
Weather-protected machine: type II	(WPII)

Totally enclosed machines have barriers to stop the ambient air from circulating within the machine, but are not airtight. Machines defined as totally enclosed are

Totally-enclosed nonventilated	(TENV)
Totally-enclosed fan-cooled	(TEFC)
Explosion-proof machines	
Dust-ignition—proof machines	
Waterproof machines	
Totally-enclosed pipe-ventilated	(TEPV)
Totally-enclosed water-cooled machine	(TEWC)
Totally-enclosed water-air-cooled machine	(TEWAC)
Totally-enclosed air-air-cooled machine	(TEAAC)
Totally-enclosed fan-cooled guarded machine	(TEFCG)
Totally-enclosed air-over-machine	(TEAO)

The complete definitions for these motor types are available by reference to the appropriate standards documents [1]. As noted, the enclosures are used both to protect the motor and to protect personnel from possible safety hazards. Generally, open motors are easier to cool and hence smaller and lower in first cost than are enclosed motors. The protection of the interior usually involves directing the air flow to a lesser or greater degree prior to impingement on the electrical parts. For instance, adding screens to the air inlet and to the air outlet openings of a drip-proof motor converts the enclosure to drip-proof guarded construction. These screens provide protection for personnel and also prevent rodents and solids from entering the motor. The solid portion of the screening obstructs the air and reduces the air flow. The motor winding will increase in temperature for the same loading when the screens are added. Interestingly, the drip-proof enclosure does not necessarily result in a higher temperature rise for the motor as compared to a wide open enclosure. For instance, a motor as open as that in Fig. 12.11 does not provide direction to the

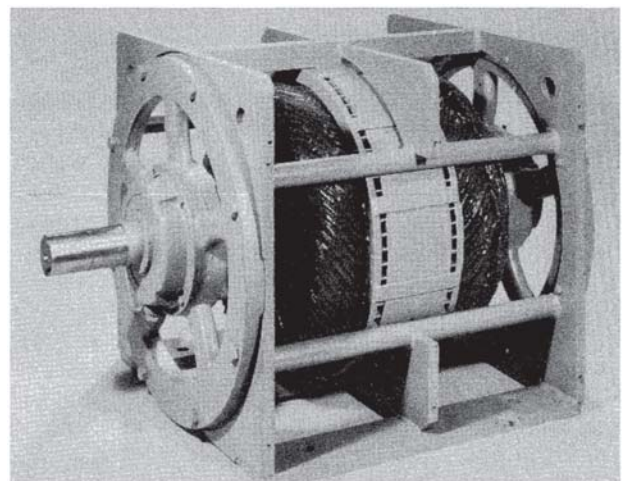


**Figure 12.11** Open induction motor with encapsulated stator windings. (Courtesy of General Electric.)

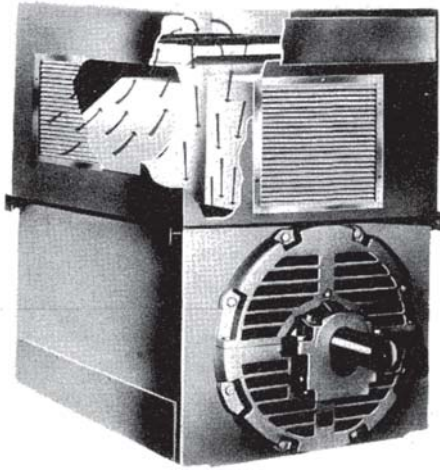


**Figure 12.12** Weather-protected type II enclosure with cutaway of the top hat showing inlet air path. (Courtesy of General Electric.)

air flow. A motor with more enclosure may better direct the air over the end windings and the back of the punchings. Use of baffles and enclosing sheet metal can accomplish this.

Figure 12.12 shows a weather-protected type II enclosure where the weather protection features are provided by the use of a “top hat.” This particular figure is a cutaway that shows the air inlet provisions. The air enters through louvers on both sides of the motor top hat. The air turns 90 degrees upwards through a screen or filter. The air is free to blow through from one side of the motor to the other in high winds. After going through the screen the air turns 90 degrees axially toward each end of the motor and then 90 degrees downwards to enter openings in the frame. The inlet air thus has three 90-degree bends and the presence of a screen or filter to protect the internals of the motor from the environment. This enclosure generally provides the greatest degree of environmental protection of all of the open-type motor enclosures, as well as the most restrictive ventilation scheme. While not specifically a part of the NEMA definition, motors to be applied outdoors frequently have bearing seals to effectively protect the bearings and bearing oil reservoirs from the entry of rainwater.

Enclosed motors will also usually have seals to protect the bearings and lubricants from the surroundings, although this requirement is not a part of the definition. It is important, therefore, that the user specify requirements when ordering a motor needing special protection. A variety of enclosed motors has been defined for special purposes. The variety is also needed because of the change in preferred machine design as machines increase in size. Both the TENV and TEFC machine enclosures are limited in size application as covered in Section 12.2.2. The explosion-proof and dust-ignition-proof enclosures are variations of the TEFC enclosure that are used where environments may be hazardous. The explosionproof enclosure will contain both an internal explosion and any incidental sparking or flashing so that the surrounding hazardous atmosphere cannot be ignited by an internal fault. The dust-ignition-proof enclosure prevents the entry of dust mixtures that might be ignited by internal faults, nor should the motor cause the ignition of external dust mixtures. The

TEFCG and the TEAO are other variations of the TENV and TEFC enclosures. The TEAAC, the TEWAC, and the TEPV machine enclosures provide protection for machines where the TENV and TEFC type enclosures are not economic or where these enclosures may not be feasible. The TEPV machines also find application in hazardous locations, and so has the TEAWC when it has inert gas-filled construction.

These two enclosures allow the application of larger machines in certain hazardous locations. For the TEPV motor, the application to a hazardous area is dependent upon the internal air pressure provided by air from a nonhazardous area. This nonhazardous air prevents the entrance of any hazardous vapor into the motor. This application requires a thorough purging of the internals of the enclosure prior to start-up as well as a protected maintenance of pressure during operation.

Similarly, the inert gas-filled motor requires the presence of the inert gas (typically nitrogen) prior to start-up and during all operating periods. This enclosure, to be practical, requires minimal loss of inert gas from within the enclosure to the outside. Seal-welded frames and special oil-filled bearing seals with gas separating oil tanks have been used for this purpose.

## 12.5 THERMAL CIRCUITS

Lumped-parameter circuits have been used extensively to represent the complex distributed thermal parameters of electric motors. Section 12.2 covered basic modes of heat transfer and presented a method of representing these modes as resistance elements in a direct-current type of electrical circuit. Mc Adams [8] and General Electric [11] provide information on how to evaluate the thermal resistance for complex geometrical configurations. In the conductive mode, this is done by proper selection of lengths and areas. For the radiant and free convection modes of heat transfer, particular care must be used in the calculation of resistances. These heat transfer coefficients are highly dependent upon both the temperature of the part and the temperature of the surroundings. For the forced convection mode, the air velocity is a major determinant of the heat transfer coefficient. Thus, for self-ventilated motors the forced convection heat transfer coefficient is a function of rotor speed and diameter. By using lumped parameter circuits it is possible to represent the heat transfer networks of machine components and complete machines.

Representative thermal circuits are presented in this section to illustrate their application to specific motor constructions as well as to illustrate their application to different operating conditions. Table 12.5 provides a listing of the various circuits presented. This table delineates the figure number for the thermal circuitry, the motor components represented, the general construction of the motor, and the applicable operating mode. Each figure is explained in the text. While the text is centered upon explaining these figures for the open type of construction, the circuits may be applied in most cases to enclosed construction as well by modifications or additions to the circuitry. The terminology “single element” has been used when singular thermal inputs, resistances, and capacitances have been used to thermally represent particular motor parts.

**Table 12.5** Listing of Figures Showing Thermal Circuits

Figure no.	Component	Construction	Mode	Comment
12.14	AC motor stator	Open—no air ducts	Steady state	Single element
12.15	AC motor stator	Open—no air ducts	Steady state	Dual element
12.16	AC motor stator	Open—no air ducts	Time varying	Single element
12.17	AC motor stator	Open—no air ducts	Time varying stall	Fig. 12.16 simplified to calculate stator core and core copper temperature
12.19	AC motor stator	Open—no air ducts	Steady state	Fig. 12.14 simplified
12.20	AC motor stator	Open—multiple air ducts	Steady state	Single element

These motor parts are the stator winding end-turns, the stator winding in the core slots, the core teeth, the core yoke, and so forth.

### 12.5.1 Steady-State Circuits

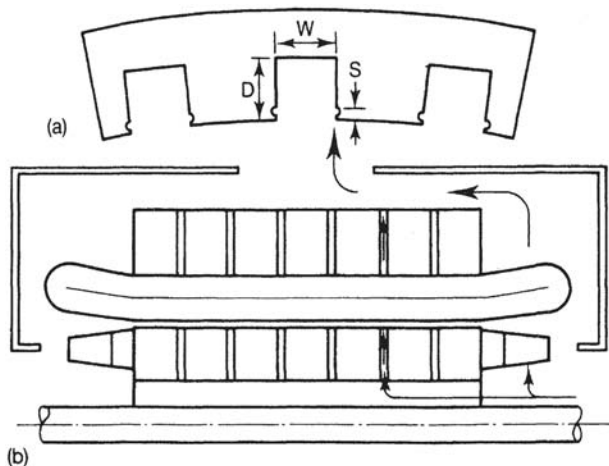
Figure 12.13 presents a sketch of an induction motor. View (a) shows the stator punching configuration. View (b) shows the motor in axial cross section. This view includes the motor rotor, the motor stator, and the motor air flow within the enclosure. The stator punching configuration of (a) shows the yoke, stator slot, and stator tooth, with  $D$  being the depth of the slot and  $W$  being the width of the slot.  $S$  is the setback from the stator bore to the edge of the wedgegroove. Table 12.6 provides technical information for this motor. This motor is representative of a motor that was tested thermally for a large number of operating modes. The motor and tests have been described by Martiny et al. [13]. The data are readily available to use for analysis, and for this reason this motor was chosen to illustrate several points in this section. Although the motor has six air ducts, it will initially be assumed that the machine has no air ducts. Thus, the only air flow is that which passes the end-turn regions and thence around the back of the core. For thermal evaluation, it is advantageous to take advantage of the machine symmetries. The motor stator is symmetrical from a heat transfer perspective from the machine

center to the tip of the stator winding end turns. Each half of the machine from the machine center mirrors the other half. No heat flows across the machine centerline.

The heat input is generally symmetrical in the stator slot and in the stator tooth. The heat flow in this portion of the machine is conductive. A static thermal field plot would demonstrate that heat would not conduct peripherally across either the tooth centerline or the slot centerline. Thus, symmetry from a heat transfer viewpoint occurs from the centerline of a slot to the centerline of a tooth. Figure 12.14 represents a steady-state thermal circuit for the stator of Fig. 12.13 with the air ducts eliminated. The circuit lumps the end winding and the stack into representative parameters. The effect of the cooling air temperature rise is lumped and represented by the adjustable battery. The symmetries are utilized in the development of the thermal circuits and the calculations of the circuit parameters. Figure 12.14 shows a heat flow rate input,  $I_1$ , to the stator winding conductor end turns due to the end turn  $I^2R$  losses. This heat may flow in two

**Table 12.6** Parameters for an Eight-Pole, 350-hp, 900-rpm, 3-Phase 440-V, 60-Hz Squirrel-Cage Induction Motor

Parameter	Parameter value
Stator winding	4 circuit 75% pitch
Coil	7 turns of $0.090 \times 0.250$ copper wire
Insulation	Class A
Stator resistance	0.0265 ohms/phase delta—25°C
Core loss	4.85 kW
Windage and friction	1.12 kW
Full-load current	407 A—line
Starting current	2400 A—line
Rotor speed	883 rpm
Stator OD	28 in
Stator ID	21.5 in
Rotor OD	21.43 in
Rotor ID	15.75 in
Stack length	15 in
Air ducts	6 each 0.5-in wide
Stator slots	96
Rotor slots	116
Stator slot width, $W$	0.31 in
Stator slot depth, $D$	1.61 in
Stator wedge setback, $S$	0.11 in

**Figure 12.13** Induction motor sketch, (a) Stator core slot and tooth configuration, (b) Axial cross section.

Data from Ref. 13 by permission. © 1961 AIEE (now IEEE).

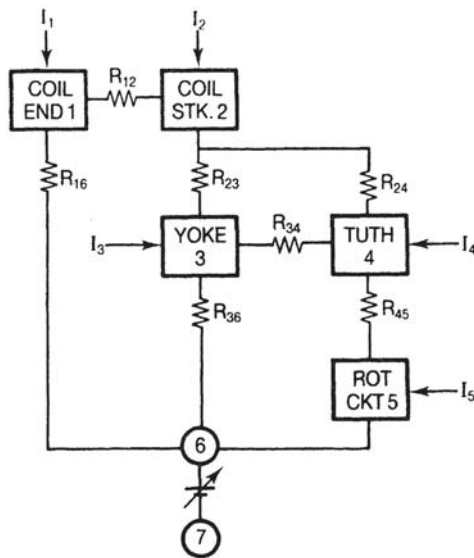


**Figure 12.14** Single-element steady-state stator thermal circuit for an open motor without air ducts.

directions. In one path the heat travels through the winding insulation resistance, through the convective resistance between the insulation surface and the end turn cooling air, and then via the cooling air to the ambient represented by the circled number 7.  $R_{16}$  represents these resistances. The end turn conductors are also shown as connected by the axial thermal conductivity of the winding conductors to the winding conductors located within the stator core slots.  $R_{12}$  represents the resistance in the path. The heat may flow in either direction in this leg depending upon the particular parameters of the circuit.

Generally, at rated steady-load conditions, for the drip-proof enclosures, heat flows from the stator core copper to the stator end-turn copper. The remainder of this descriptive text will be on the basis of the expected direction of heat flow for the drip-proof enclosure. It must be recognized, however, that heat may actually flow in either direction depending upon the parameters of the circuit and the specific heat input conditions. For instance, if the enclosure were TEFC, then the heat might flow from the end turn copper towards the stator core. Heat will also flow from the stator winding conductors in the core slots through the stator winding insulation,  $R_{23}$  and  $R_{24}$ , to the stator core iron. The flow is peripheral to the stator core teeth represented by TUTH 4 and radially out to the stator core yoke represented by YOKE 3. Core loss heat inputs are included in the stator core yoke and the stator core tooth heat flow rate inputs,  $I_3$  and  $I_4$ . Load loss heat inputs are included in the stator core tooth and stator copper inputs. Heat may flow through the stator core iron between the tooth and the yoke,  $R_{34}$ , as well as from the yoke radially to the outer surface of the stator core,  $R_{36}$ . Heat may also flow axially through the core iron to the end surfaces of the core. The heat then flows to the cooling air and to the ambient. Figure 12.14 does not include this path. In practice the axial flow of heat through the core iron is sometimes neglected because the laminated core has

a significantly higher thermal resistance axially as compared to radially. This higher axial thermal resistance in the core iron is due to the laminated construction. In addition, the core end surfaces may not be as effectively cooled by the cooling air as the core outer surfaces. Heat may also flow axially from the rotor tooth as well as radially between the rotor surface and the tooth through the machine air gap,  $R_{45}$ . The transfer of heat between the rotor and the stator across the air gap is also sometimes neglected, especially in the case of motors with air ducts. The transfer of heat across the air gap may be handled in a number of different ways.

1. A complete heat network may be established for the rotor and interconnected to the stator across the air gap. Figure 12.14 shows a representation of this circuit. If only stator heating is of interest and the machine stack length is long so that the axial flow of heat is small, then the analysis may proceed using a representative center section of the machine. The appropriate rotor loss  $I_5$  can then be applied directly into the stator tooth. This approach has been used for Fig. 12.15. For Figs. 12.16, 12.17, and 12.18, the rotor heat flow rate inputs are not separately shown but must be included as a part of the detailed rotor circuit.
2. If the heat transferred is small, it may be neglected. This, however, needs to be established by calculation, test, a combination of the two, or by similarity to a motor for which this has already been established.
3. The cooling system can be designed so that the rotor and stator circuits are nearly independent thermally, as is the case for certain motors such as some of those with air ducts. The air ducts tend to decouple the cooling circuits by carrying the cooling air to the components rather than requiring heat to flow between them. Thus the assumption of little interaction can be established as valid by design.

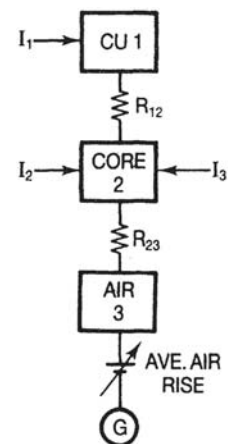


**Figure 12.15** Steady-state stator thermal circuit for Fig. 12.14 utilizing only simplified stator core elements.



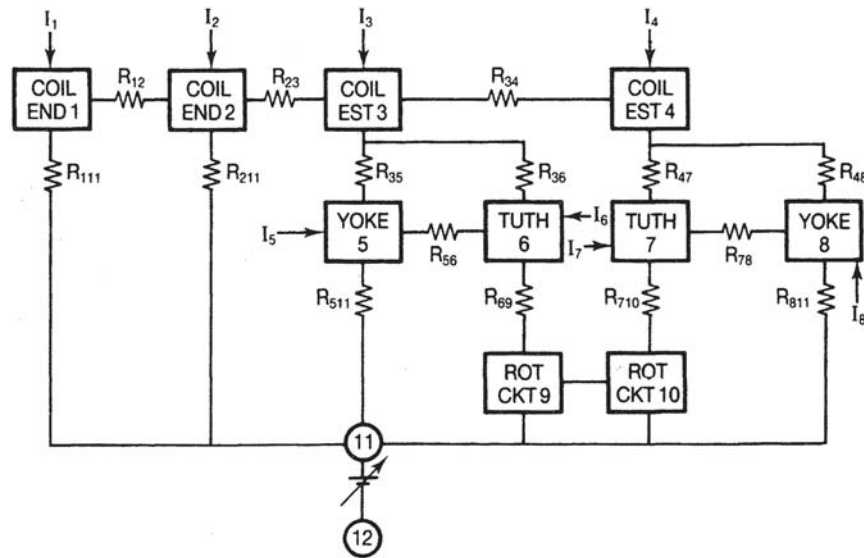


**Figure 12.16** Dual-element steady-state stator thermal circuit for an open motor without air ducts.

Returning to the heat flow description for Fig. 12.14, the heat flows from the stator tooth and yoke to the outer surface of the stator core and thence to the cooling air.  $R_{36}$  represents the thermal resistance for this path. The effects of the cooling air are represented by the variable battery. For the circuit of Fig. 12.14, the average air temperature rise for the condition being considered may be used for the temperature rise of the battery element. The circled number 6 represents a convenient nodal point to represent contact with the cooling air.

Figure 12.16 shows a circuit where the elements of Fig. 12.14 are doubled. Generally, as circuit elements and heat input nodal points are increased, accuracy of representation is increased. The comments for the circuit of Fig. 12.14 generally apply to Fig. 12.16 as well. Since greater accuracy

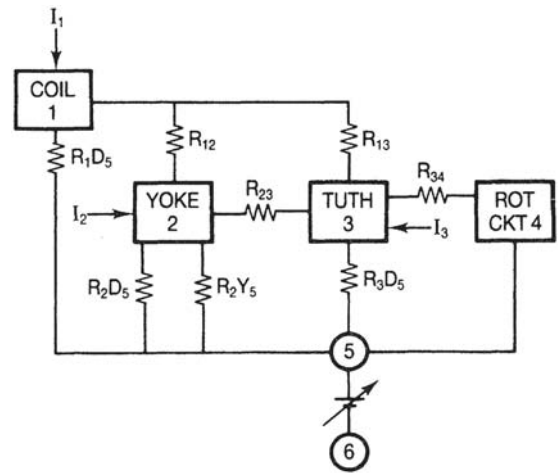


**Figure 12.18** Steady-state thermal circuit of a central stator packet for a motor with multiple radial air ducts.

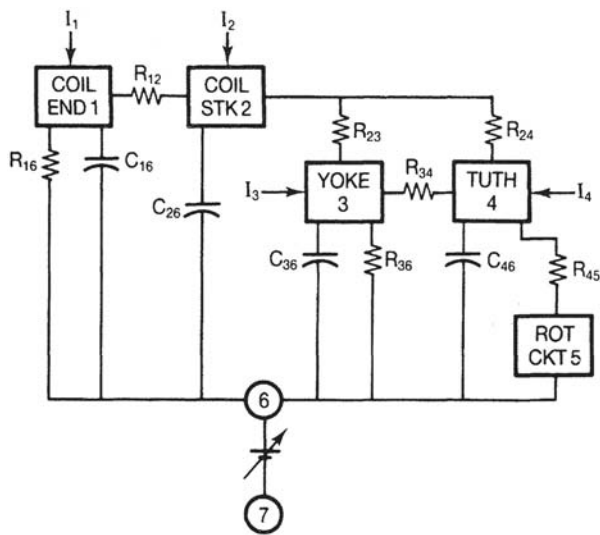


**Figure 12.17** Single-element time-varying stator thermal circuit for an open motor without air ducts.

is normally the goal for multielement circuits, the use of axial connections between the stator core elements is more likely. For simplicity, none are shown in Fig. 12.16. A connection is shown for the two rotor circuit elements in the figure. This connection is representative. The connection is to show that if the rotor circuit were also broken into two elements, that connection would be needed between the elements in a manner similar to the case for stator elements.

### 12.5.2 Time-Varying Circuits

Figure 12.6 is a circuit that adds capacitance to represent the major masses. The masses and the capacitances of the stator winding insulation and any stator lamination insulation have been neglected. Similarly, the heat flow to the frame mass has

been neglected, as was also the case for Fig. 12.14. The rotor circuit would also contain suitable capacitive elements. This circuit may be used to evaluate the time history of the thermal relationships of a motor. It can be used to evaluate situations where the temperature may be transient, such as for motor stall or acceleration. It can also be used for situations that vary with time due to changes in motor loading, such as motors with duty cycle loading. These loading conditions may include the following

1. The motor accelerates in a normal manner to full speed.
2. The motor is operated at full speed at various loads and for differing time periods.
3. The motor is operated at different specific speeds, loads, and time periods.
4. The motor is at standstill without load.
5. The motor is subjected to cycles of multiple starts to full speed as might occur in dynamic balance operations.

The simplest thermal circuits to evaluate are those used to evaluate conditions for fixed continuous loads and speeds. The circuits used for time history evaluations involve more complex calculations. The algorithms used for these evaluations require significant additional time to develop, as do the capacitive parameters needed in the thermal circuits. Thus the steady-state conditions that form the basis for rating are the most frequently evaluated. A number of approximate methods have been developed for the time history evaluations. Some of these approximations will be considered in this section. Some of these methods that are used for duty cycle calculations are considered in Section 12.6.

Rosenberry [14] and Griffith et al. [15] consider induction motor rotor thermal response for several loading conditions and are useful references. Rosenberry [14] defines a representative thermal circuit and makes use of an electronic differential analyzer to reach a solution for the temperature response of an induction motor rotor winding when the rotor is stalled. McCoy et al. [15] utilize the finite element analysis technique. This is an advanced mathematical technique that allows the representation of motor thermal characteristics by a multielement approach that can closely replicate the actual distributed system. This analysis is also of an induction motor rotor winding. The computer program developed in Ref. 15 has capabilities for thermal analysis together with the capability of evaluating the mechanical fatigue life of the rotor winding for a defined duty cycle of motor loading. The analysis has the capability to evaluate the loading situations listed above. In Section 12.1, it was noted that the motor stator winding insulation temperature is limited by standards in order to insure a long insulation life. In the case of a squirrel-cage rotor, the squirrel-cage winding is not normally insulated. Nevertheless, temperature still plays a key role in squirrel-cage winding life. The temperature must be limited first to insure that no melting of the winding or gross distortion occurs. In addition, the material of the winding may be subject to fatigue by a combination of both centrifugal and thermal strains. The thermal strain is generally the more significant

and the rotor winding temperatures must be obtained to determine the mechanical fatigue life of the winding.

### 12.5.3 Simplified Circuits

In this section the circuits evaluated for illustrative purposes are simpler than for Rosenberry [14] or McCoy et al. [15]. As an example of the use of simplified thermal circuits, consider the motor of Fig. 12.13 and Table 12.6. The stator slot is shown in some detail. Table 12.6 provides sufficient information on the dimensions and losses to allow thermal evaluation if some assumptions are made in the evaluation of the heat transfer parameters and inputs. The information used for the evaluation is essentially all supplied in this chapter. The stator winding endturns will be thermally evaluated for the stalled-rotor condition.

For this condition, the motor losses are significantly larger than at rated load and speed. The time to reach maximum allowable temperature is relatively short compared to the machine thermal time constant.

In addition, if the end turns are long, the thermal resistance from the very ends (the points on the end-turns farthest from the stator core) to the stator core may be sufficiently large that the heating at the end is not materially influenced by the winding losses in the core or by the core losses. Additionally, the resistance to the air at standstill involves free convection and radiation. At least initially, this resistance is very large. The calculation of the temperature rise in the copper can be approximated by thermal storage in the stator winding end turn copper and may be described by the following set of generally equivalent forms of the same equation.

$$\Delta\theta = \frac{It}{C_\theta} \quad \text{or} \quad \Delta\theta = \frac{It}{C_p W} \quad (12.23)$$

where:

- $\Delta\theta$  = temperature rise
- $I$  = heat flow rate into the stator winding conductor (stator  $I^2R$  loss)
- $C_\theta$  = thermal capacitance of the winding
- $C_p$  = thermal capacitance per unit of winding conductor weight
- $t$  = time
- $W$  = weight of the winding conductor

For a copper conductor, the rate of temperature rise is [13]:

$$^\circ\text{C/s} = 0.014(\text{current density}/1000)^2 \quad (12.24)$$

For the machine in question, the rate of rise from Eq. 12.24 is about 3°C/sec for the rated voltage standstill or stalled condition. The stalled condition is considered an abnormal condition [13]. The allowable stalled temperature for the stator and rotor windings of large machines is provided by the motor manufacturer in the form of an allowable stalled time. Insulation life has been found to follow the Arrhenius or 10°C life rule (Section 12.1) over a wide temperature range. There are, however, upper temperature limits to this rule. Above these limits, severe damage may occur rather quickly in forms such as embrittlement, melting, or even burning. The stalled time is

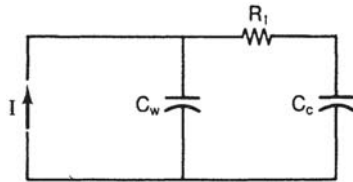


**Figure 12.19** Time-varying stator thermal circuit simplified to represent the stator winding in the stator core under motor stall conditions.

generally selected so that the insulation will not be subject to such sudden loss of life. For fractional-and integral-horsepower motors, NEMA MG 1–12.53 [1] defines allowable winding temperatures for motors with overtemperature protection. However, for this example, the limiting allowable temperature has been selected as 156°C, which corresponds to the average allowable temperature reported by a group of manufacturers [13]. Then, from an ambient temperature of 40°C, with an allowable temperature rise of 116°C, the allowable stall time would be 39 seconds. With the machine hot (that is, shutdown from a fully loaded condition), the stator winding copper might, for a class A machine, be at 105°C when the unit was stalled. The stall time would then be 17 seconds for this 51°C rise. If a second starting attempt is made after a hot stall, then sufficient time should be allowed for the machine copper to return to a lower temperature. This temperature should be low enough to allow a full acceleration or another stall without the winding exceeding 156°C.

Suppose, however, that the stator stack is relatively long and without air ducts. Then the evaluation of the temperature for the copper at the center of the stack may be made with a different approximation. Then, Fig. 12.17 may be simplified to Fig. 12.19. Again the machine is at standstill and surface heat transfer resistance is very large, especially at the moment that the motor is stalled. Only the copper losses are considered. The core losses are negligible compared to the copper losses. This is because the effective flux is at a level corresponding to about one-half of rated voltage, whereas the copper losses at rated-voltage stall are about 35 times larger than rated copper losses, and over 50 times larger than the core loss. The

winding heat loss rate,  $I$ , is initiated within the stator copper and is shown at this point. As the copper temperature rises, as represented by the voltage of  $C_w$ , heat flows from the copper,  $C_w$ , through the stator winding insulation resistance,  $R_i$ , to the iron in the stator core,  $C_c$ . The capacitance of the stator winding insulation is relatively small and has been neglected.

The total heat flow  $I$  divides as  $i_1$  and  $i_2$  between the two capacitance elements:

$$i_1 = I \left[ \left( \frac{C_w}{C_w + C_c} \right) + \left( \frac{C_c}{C_w + C_c} \right) e^{-t/\tau} \right] \quad (12.25)$$

$$i_2 = I \left( \frac{C_c}{C_w + C_c} \right) (1 - e^{-t/\tau}) \quad (12.26)$$

where:

$i_1$  = the heat flow rate into the copper

$i_2$  = the heat flow rate into the iron

$I$  = the total heat flow rate

$C_w$  = the capacitance of the stator winding

$C_c$  = the capacitance of the stator core

$t$  = time

$\tau$  = a time constant  $\frac{C_w C_c R_i}{(C_w + C_c)}$

$R_i$  = the insulation resistance

The temperature rises for the winding and the core are:

$$\Delta\theta_w = \frac{It}{C_w + C_c} + \frac{I\tau^2}{C_w\tau_w} (1 - e^{-t/\tau}) \quad (12.27)$$

$$\Delta\theta_c = \frac{It}{C_w + C_c} - \frac{I\tau}{C_w + C_c} (1 - e^{-t/\tau}) \quad (12.28)$$

where the terminology is the same as for Eqs. 12.25 and 12.26 and where:

$\Delta\theta_w$  = the winding temperature rise

$\Delta\theta_c$  = the core temperature rise

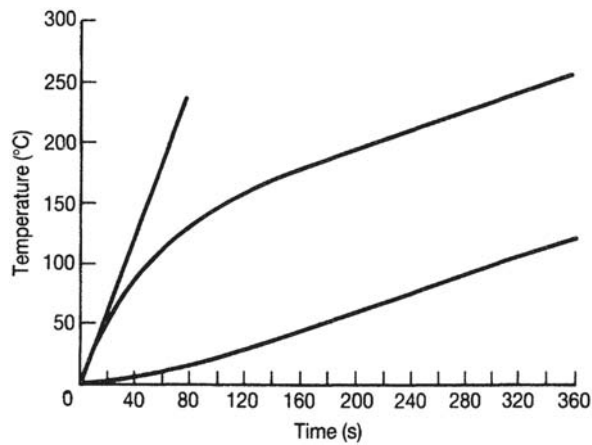
$\tau_w$  = a time constant  $C_w R_i$

Table 12.7 provides appropriate values for the required

**Table 12.7** Parameters Used in Eqs. 12.27 and 12.28 Based on the Sample Motor of Table 12.6 and the Thermal Circuit of Fig. 12.17

Item	Quantity
Heat flow rate, $I$	28 W
Capacitance of winding, $C_w$	9.17 Ws/°C
Capacitance of core, $C_c$	64.9 Ws/°C
Resistance of insulation, $R_i$	5.6 °C/W
Time constant, $\tau$	45 sec
Time constant, $\tau_w$	51 sec
Thermal capacitance of core steel	460 Ws/(kg °C) [209 Ws/(lb °C)] <sup>a</sup>
Thermal capacitance of winding copper	388 Ws/(kg °C) [176 Ws/(lb °C)] <sup>a</sup>
Density of core steel	7640 kg/m <sup>3</sup> [0.276 lb/in <sup>3</sup> ] <sup>a</sup>
Density of winding copper	9020 kg/m <sup>3</sup> [0.326 lb/in <sup>3</sup> ] <sup>a</sup>
Thus	
	$\Delta\theta_w = 0.378t + 120(1 - e^{-t/45})$
	$\Delta\theta_c = 0.378t - 17(1 - e^{-t/45})$

Parameters of core steel and winding copper may be found in Ref. 14 and elsewhere.



**Figure 12.20** Temperature rise-time relationships for a motor under stalled conditions. Upper curve:  $\Delta\theta_w$ , vs. time with no heat transfer to the core. Middle curve:  $\Delta\theta_w$ , vs. time with heat transfer to the core. Bottom curve:  $\Delta\theta_c$ , vs. time with heat transfer to the core.

parameters for the sample machine. Figure 12.20 shows the temperature rise of the copper,  $\Delta\theta_w$ , and the temperature rise of the iron,  $\Delta\theta_c$ , for the sample machine as described by Eqs. 12.27 and 12.28. At the first instant, all of the heat flows into the stator copper. As time progresses, the heat flow rate into the iron increases. With total heat storage persisting, as is the case with this model, then as the time ( $t$ ) becomes very large as compared to the time constant ( $\tau$ ), the heat flow divides between the copper and the iron in proportion to their respective thermal capacitances. As a result, the temperatures for both elements will eventually rise at the same rate.

Equation 12.28 may also be interpreted in another way. If a thermal detector were taped to the sides of a coil in the end winding of the sample machine with the long ends, then the equation describing the temperature rise of the detector would be of the same form as Eq. 12.28. The specific values would be different as compared to the iron core. However, the detector would experience a lag in temperature due to the resistance of the winding insulation and the thermal capacitance of the detector just as the core iron experienced such a lag. This illustrates the problem of detecting rapid changes in copper temperature by the use of thermal detectors on the outside of the insulation.

By utilizing Eqs. 12.23 and 12.27, it is possible to compare the temperature rise with all heat stored in the copper alone as compared to heat storage in the copper plus the stator iron. Figure 12.18 provides this comparison also.

For the heat stored in the winding copper alone, the temperature rise was 51°C in the 17-second hot stalled time. For the case of the copper winding in the slot, the comparable temperature rise is 44°C in 17 seconds. For the case of the cold stall time of 39 seconds, with all the heat stored in the copper, the temperature rise was 116°C. For the case of the winding in the slot, the comparable temperature rise in 39 seconds is 84°C and for 116°C rise the comparable time is 65 seconds. This clearly demonstrates that for the stalled condition the stator winding end-turns are generally at a greater thermal risk than the winding in the slot.

For the running condition, for an open machine, the stator winding in the core is normally the controlling thermal condition. Refer again to Fig. 12.14. This figure may be simplified to Fig. 12.15 with the following assumptions.

1. The winding stack is sufficiently long that the center is not affected by the winding ends.
2. The center portion of the stator core may be represented by a single element.
3. The winding stack is sufficiently long that the rotor losses at the center of the core are transmitted across the air gap to the stator bore and thence are transmitted through the stator core to the cooling air.

For Fig. 12.15,  $I_1$  includes the stator copper losses and the winding portion of the load losses.  $I_2$  includes the core losses and the portion of the load losses assignable to the stator teeth.  $I_3$  represents the rotor losses transferred across the air gap.  $I_3$  includes the rotor copper losses and the rotor portion of the load losses.  $R_{12}$  represents the resistance between the stator winding and the stator core.  $R_{23}$  represents the resistance between the stator core and the cooling air. Values for the sample machine have been estimated as

$$I_1 = 0.875 \text{ W}$$

$$I_2 = 2.36 \text{ W}$$

$$I_3 = 2.39 \text{ W}$$

$$R_{12} = 5.6^\circ\text{C/W}$$

$$R_{23} = 13^\circ\text{C/W}$$

$$\text{Air rise}_{\text{ave}} = 9^\circ\text{C}$$

For these parameters, a steady-state temperature rise of 87°C is calculated. This exceeds the allowable temperature rise of 50°C for the machine of Ref. 13. This confirms the need for the air ducts used in the design of that machine.

Finally, the thermal circuit for a machine with a significant number of air ducts will be presented. If the motor is constructed with a large number of air ducts, then the center packet or packets will be relatively unaffected by the remainder of the packets or the machine end-turns. Then the machine may be represented by modeling a single half-packet and half-duct. Figure 12.18 represents such a model.  $I_1$ ,  $I_2$ , and  $I_3$  represent the thermal inputs.  $I_1$  represents the stator winding resistance losses plus the load losses that occur in the stator winding.  $I_2$  represents the stator iron losses occurring in the stator core.  $I_3$  represents the iron losses and load losses occurring in the stator tooth. The rotor circuit includes all of the rotor losses.  $R_1D_5$  is the resistance through the insulation including the resistance to the cooling air in the duct.  $R_{12}$  represents the resistance through the insulation to the yoke.  $R_{13}$  similarly represents the resistance to the tooth.  $R_2D_5$  represents the resistance axially through the yoke to the cooling air in the duct.  $R_3D_5$  is a similar resistance for the tooth.  $R_2Y_5$  represents the resistance through the yoke to the air at the yoke periphery.  $R_{23}$  is the resistance between the yoke and the tooth radially.  $R_{34}$  is the resistance between the tooth and the rotor across the air gap.

If the number of ducts were limited, it would be necessary to expand this circuit to fully represent one-half of the motor including the end windings.

Here again the rotor circuit may be treated in different ways.

1. A complete heat network may be established for the rotor and interconnected to the stator across the air gap.
2. If the heat transferred is small it may be neglected.
3. It may be represented as a fixed-temperature battery connected to the stator bore surface across the resistance of the air gap. To do this some method must be used to separately assess the rotor surface temperature.

For the duct circuit, the major portion of the heat flow is usually to the air in the duct, especially for the stator winding conductor. To enhance heat flow axially in the stator iron, the ducts must be spaced so that the axial thermal resistance of the stator iron is kept relatively low. The design of the cooling system represents an accommodation of machine temperature, axial length, and cost.

This section has introduced both steady-state and time-varying thermal circuits. A series of simplified circuits have been developed and utilized. Particular steady-state and stalled-motor situations were used to illustrate the power of the circuits as engineering models. These same examples provide some understanding of motor thermal performance for the particular situations illustrated. The next section, 12.6, will consider models and methods for analyzing the thermal response of electric motors to changing load conditions of a repetitive nature. These conditions are frequently referred to as duty cycle calculations.

## 12.6 DUTY CYCLES

The models and methods of Section 12.5 may be used to calculate the temperature rise of motors subject to the different acceleration, speed, loading, and deceleration requirements of a specific duty cycle. When this is done, the appropriate model including thermal capacitance and thermal resistance is used for each successive requirement of the duty cycle. In order to obtain the maximum temperature reached during a repeating duty cycle, a sufficient repetition of thermal calculations is required so that the thermal history during each successive cycle repeats closely enough that the thermal condition may be considered as in quasi-steady state.

However, other mathematical models are available for thermal analysis of motors subjected to duty cycles. These models were initially developed for dc motors. Historically, dc machines were the machines of choice for duty cycle application because of the relative simplicity of speed control for these machines. One of the methods developed is sometimes referred to as an rms loading analysis because it evaluates the armature loading based upon the rms value of the different magnitudes of the armature dc current as the load changes. The other method covered here involves utilizing a thermal time constant as defined in Section 12.1 as a part of the calculation.

### 12.6.1 RMS Loading Analysis

The dc motors used for duty cycle applications are frequently separately excited, externally ventilated, shunt-wound motors. Because of the external ventilation, the cooling capability of the motor is essentially unaffected by speed. If the iron losses

do not exceed rated iron losses, then the motor will not exceed rated temperature rise if the duty cycle rms current does not exceed rated current. A more complete discussion follows.

A set of relatively simple equations may be used to understand the performance of this motor.

$$E = K_1 \phi n \quad (12.29)$$

where:

$E$  = the back electromotive force (emf)

$K_1$  = a constant

$\phi$  = the magnetic flux

$n$  = the motor speed

$$T = K_2 \phi I \quad (12.30)$$

where:

$T$  = the torque

$K_2$  = a constant

$\phi$  = the magnetic flux

$I$  = the armature current

$$HP = K_3 T n = K_2 K_3 \phi I n = \frac{K_2 K_3}{K_1} E I = \frac{K_2 K_3}{K_1} W \quad (12.31)$$

where:

$HP$  = power in horsepower

$K_3$  = is a constant

$W$  = power in watts

If the armature resistance drop is neglected, then the back-emf and the applied voltage are equal. Clearly then for constant flux, the basic speed of the motor is directly proportional to the applied voltage. On the other hand, if the voltage is held constant, then the motor speed is inversely proportional to the value of the motor flux. With armature voltage speed control, constant-torque output may be obtained at rated armature current. Similarly, if armature voltage (the product of  $\phi n$ ) is maintained constant, then constant power may be obtained at constant armature current as the speed is increased by weakening the machine magnetic flux.

For a separately ventilated motor, the cooling remains essentially constant. Thus, a dc motor rated for a specific horsepower at a base speed has two adjustable-speed operational modes. From standstill to base speed is a constant-torque mode, and above base speed to the top rated speed is a constant-horsepower mode. This conclusion is based on the further assumption that the dc power supply characteristics do not degrade as the applied motor voltage is reduced. If a rectifier power supply characteristic degrades, then the dc machine is subject to additional harmonic losses. General industrial motors are capable of frequently applied momentary loads of 125% of rated or more depending upon the speed compared to base speed. These overloads may be a part of a regular duty cycle, but the temperature rise of the machine should not be exceeded during the overload time period [1]. Special motors, such as metal rolling mill motors, reversing hot mill motors, and other specials, may be capable of driving even a higher momentary percentage value of rated power.

On the simplest basis, for the dc motor described, it is only necessary to calculate the rms value of armature current over

the duty cycle. Then, compare this rms current to rated current to determine if the motor will perform within rated temperature rise.

$$I = \sqrt{\frac{\sum_{j=1}^{j=f} i_j^2 t_j}{T}} \quad (12.32)$$

where:

- $I$  = the rms current
- $i_j$  = the value of current for each specific load
- $t_j$  = the time at each specific load
- $T$  = the total time over the period of the duty cycle

In addition, if the rms current is close to rated current, and the period of time for an overload is significant, an investigation is necessary to determine if the rated motor temperature is exceeded during this portion of the duty cycle.

Additional insight may be obtained by considering the heat-producing losses individually and by determining the contribution of each loss to motor heating. The losses that need to be considered are:

- Field winding ( $I_f^2 r_f$ ) losses
- Armature winding ( $I_a^2 r_a$ ) losses
- Core losses
- Stray-load losses
- Brush contact losses
- Brush friction, bearing friction, and windage losses

The field winding  $I_f^2 L_f$  losses are a function of the flux density level of the machine. The field current required to produce a particular flux density level is generally linear at low flux density levels and increases at a greater rate as the magnetic structure saturates. Thus, during field weakening, the field  $I_f^2 r_f$  losses will decrease somewhat faster than the square of the flux level, or inversely with the square of speed, especially for the initial increases in speed above base speed. The losses will also increase as field winding temperature increases due to the increase in field winding resistance. Frequently, for simplicity in thermal calculations, the resistance is assumed to be at a value corresponding to rated temperature rise.

The armature  $I_a^2 r_a$  losses are directly proportional to the armature current squared or to the torque squared in the constant-torque range and to the horsepower squared in the constant-horsepower range.

The core losses are a function of the flux density and the fundamental electrical frequency. This frequency is proportional to armature speed. The core losses are due to these electrical frequency eddy current losses and hysteresis losses, as well as certain higher-frequency losses. The eddy current losses are proportional to flux density squared and to the speed (frequency) squared. The hysteresis losses are proportional to about the 1.6 power of flux density and directly with speed (frequency). For the constant-torque range, the flux is held constant. In the constant-horsepower range the flux density is reduced inversely to the speed. The core losses are mainly located in the armature magnetic circuit, although some high-frequency core losses are located in the magnetic iron of the pole faces.

The stray-load losses are also mainly located in the armature and are proportional to the armature current squared.

The brush contact losses are electrical and are located at the brush-commutator interface. They are proportional to armature current. The brush friction and bearing friction losses are generally proportional to speed. The windage losses are a function of the fan pressure, the air volume, and the fan efficiency. The major result of the friction, windage, and brush contact losses is chiefly in the heating of the air so far as armature and field winding heating are concerned.

In the initial discussion on duty cycle heating, the approach used essentially evaluated armature current as compared to rated load current. A somewhat more sophisticated heating approximation may be made by evaluating total losses for each loading defined for the duty cycle. In this case the temperature rise is calculated as:

$$\theta = \left( \frac{\sum_{j=1}^{j=f} L_j t_j}{L_R T} \right) \theta_R \quad (12.33)$$

where:

- $\theta$  = temperature rise
- $L_i$  = losses at a specific load
- $t_j$  = time at a specific load
- $T$  = time period of the duty cycle
- $L_R$  = losses at rated load
- $\theta_R$  = rated load temperature rise

This calculation for open-type machines is made separately for the armature and for the field. The losses must be known and are assigned based on the variation and distribution of losses as previously described. Frequently, the friction and windage losses are ignored for this calculation, although, where known, they may be treated as an air temperature rise as discussed in Section 12.5. If the actual temperature rise at rated load is not known, then the allowable rated load temperature rise may be used in Eq. 12.33.

These general methods may also be used for modern adjustable-speed ac motor drives. The loss distribution and variation with speed is generally the same for adjustable-speed ac drives utilizing synchronous motors, recognizing that for synchronous machines the armature is stationary and the field rotates. For drives with induction motors only the constant-torque mode is directly comparable. In this mode the flux level is maintained constant by holding the voltage-to-frequency ratio constant. Also, for either the synchronous or the induction motor, the effect of power factor on the stator current must be considered. For an adjustable-speed ac drive with an induction motor, a form of field weakening can be used for speeds above rated speed by means of line voltage reduction. This reduces the flux density and offsets the increase in core loss due to the higher line frequency needed for higher-speed operation. Voltage reduction, however, reduces the value of motor maximum torque in proportion to the per-unit value squared of the ratio of volts per hertz.

The discussion to this point has assumed an external ventilation system that provides constant pressure and

nearconstant air flow. If the motor is self-ventilated, the calculations become far more complex. The fan air pressure developed is a function of the square of the fan peripheral speed and the volume of flow is directly proportional to fan peripheral speed. The flow resistance curve for the motor is the product of a motor air pressure loss characteristic constant and the square of the volume flow. The intersection of this flow resistance curve with the fan pressure-flow characteristic determines the operating point and air flow for each motor speed (see Section 12.2.2.1). For each change of speed, the heat transfer characteristics must be determined by calculations or test. Thus the method of Section 12.5 or other methods must be used at least to define the motor thermal capabilities at each speed point.

### 12.6.2 Time-Constant Analysis

In the discussion of thermal circuits (Section 12.1), the concept of thermal time constants was introduced. For normal thermal events, thermal circuits involve thermal inputs at different locations as well as several independent *RC* networks. Each thermal input makes a contribution to the temperature rise at each node or junction of the circuit. Similarly, each separate *RC* circuit contributes a time constant for each of the inputs. Thus the temperature rise at a particular point in the circuit is dependent upon each of the thermal heat flow rates. Similarly, the temperature rise at each point is a function of more than one time constant. Thus the temperature rise versus time at any individual point in the circuit might better be thought of as an expression of the following form:

$$\Delta\theta = \Delta\theta_0 - \Delta\theta_1 e^{-t/\tau_1} - \Delta\theta_2 e^{-t/\tau_2} \dots - \Delta\theta_x e^{-t/\tau_x} \quad (12.34)$$

where:

- $\Delta\theta$  = temperature rise
- $\Delta\theta_1$  = temperature rise due to thermal input 1
- $\Delta\theta_x$  = temperature rise due to thermal input  $x$
- $\Delta\theta_0$  = steady-state temperature rise
- $t$  = time
- $\tau_x$  = time constant at 1, 2, ...,  $x$
- $\Delta\theta = 0$  at  $t=0$

and:

$$\sum_{j=1}^{j=x} \Delta\theta_j = \Delta\theta_0$$

Nevertheless, it has been found from experience with a large variety of machines that a thermal time history expression showing a single time constant can be sufficiently accurate to be useful in forecasting the thermal behavior of a motor, as in Eq. 12.2.

$$\Delta\theta = \Delta\theta_0(1 - e^{-t/\tau}) \quad (12.2)$$

This expression is also useful in the understanding of shorttime ratings. For instance, MG 1–10.35 [1] lists standard time ratings of “5, 15, 30, and 60 minutes and continuous.” It is apparent from this expression and from Fig. 12.4 that, as the time rating is decreased for the same temperature rise, the losses and therefore the horsepower of any particular motor may be increased at least from a thermal standpoint.

Accepting that Eq. 12.2 provides an appropriate engineering thermal model for a particular motor operating at rated power and rated speed, specific values used for the model will change for each load and speed condition. As covered in Section 12.5, the most appropriate thermal model to choose is dependent upon the thermal design of the machine. In some instances, the component temperature rise is primarily dependent upon the loss attributable to the component. In other cases, the total loss may be more significant. For this latter case, the steady-state temperature rise  $\Delta\theta_0$  for a particular load condition may be assumed to be proportional to the total loss of the motor for the particular load as compared to the total loss at rated load. This total loss case was discussed in Section 12.6.1 for the rms loading analysis. This assumption has been found to be relatively conservative at loads below rating, but somewhat optimistic for significant overloads. Generally, with overloads of short duration compared to the lighter loadings, this representation has been found to be a very useful tool in estimating duty cycle thermal conditions.

Another caveat to observe is that both the steady-state temperature rise,  $\Delta\theta_0$ , and the time constant  $\tau$  will change with motor speed since the thermal resistance is affected by speed, except for separately ventilated motors. The cooling of some nonventilated motors also is not greatly affected by speed.

An example of this method will be reviewed to illustrate the essential points. The motor chosen for illustrative purposes is an open drip-proof squirrel-cage induction motor. The stator core has no air ducts, and the motor has cooling fans at each end that circulate air over the stator winding end turns and the outer periphery of the stator core. Thus, rotor conductor losses are dissipated through the ends and through the stator core, the same as for the stator copper losses. The thermal circuit of Fig. 12.19 described in Section 12.5.3 applies to the steady-state calculations.

The significant motor data are as follows: The motor has a rated load efficiency of 90.9% and a rated load power factor of 90. The power factor at one-half rated load is 65 and the power factor at 125% load is 90. The losses and steady state temperature rises at these loads are shown in Table 12.8.

**Table 12.8** Losses and Steady-State Temperatures at Different Motor Loads Experienced During Duty Cycle Loading<sup>a</sup>

Load	Loss <sup>a</sup>			
	125%	100%	50%	No load standstill
<b>Constant losses</b>				
Windage and friction	2.00	2.00	2.00	—
Core loss	2.00	2.00	2.00	—
<b>Variable losses</b>				
Stator copper losses	3.21	2.00	1.03	—
Rotor copper losses	3.13	2.00	0.50	—
Stray-load losses	3.13	2.00	0.50	—
<b>Total losses</b>	<b>13.47</b>	<b>10.00</b>	<b>6.03</b>	<b>—</b>
Temperature rise (°C)	114	80	41	—
<b>Total temperature (°C)</b>	<b>154</b>	<b>120</b>	<b>81</b>	<b>40</b>

<sup>a</sup>Losses are in percent of rated output. Ambient is 40 °C.

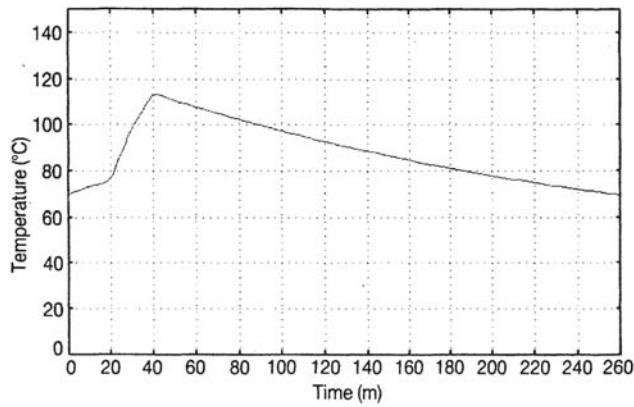


**Figure 12.21** Motor stator winding temperature under duty cycle loading calculated by time-constant analysis.

The rated motor temperature rise is 80°C and motor tests have confirmed this value with an air rise of 14°C. Thus the windage losses contribute about 7°C to the total temperature rise of the motor. The temperature rise for loadings other than rated were estimated as proportional to the total losses excluding windage and friction losses. The windage and friction contribution to the temperature rise was estimated as one-half of the air rise due to the total losses at each load.

The duty cycle to be evaluated involves three loading conditions that continuously repeat: (1) 50% load for 20 minutes, (2) 125% load for 20 minutes, and (3) standstill condition for 220 minutes.

The acceleration and deceleration times are very small compared to the loaded times, as are the comparable energies involved, and need not be considered. The full-speed time constant is 30 minutes and the standstill time constant is 240 minutes.

Figure 12.21 shows the temperature variation for the duty cycle loading described. Each portion of the temperature curve is described by the following basic equations:

$$\theta = \theta_p + (\theta_b - \theta_p)(1 - e^{-(t-t_x)/\tau}) \quad (12.35)$$

where:

$\theta$  = motor temperature

$\theta_p$  = motor temperature at the end of the preceding condition and at the start of the condition being evaluated

$\theta_b$  = motor temperature for continuous operation at the condition being evaluated

$t$  = time at the condition being evaluated in minutes

$t_x$  = total time elapsed during the prior duty cycle loading conditions in minutes

$\tau$  = motor thermal time constant in minutes

For:

Condition 1:	$t_x = 0$	$0 \leq t \leq 20$	$\tau = 30$
Condition 2:	$t_x = 20$	$20 \leq t \leq 40$	$\tau = 30$
Condition 3:	$t_x = 40$	$40 < t < 260$	$\tau = 240$

For the standstill condition Eq. 12.35 reduces to:

$$\theta = \theta_a + (\theta_p - \theta_a)e^{-(t-t_x)/\tau} \quad (12.36)$$

where  $\theta$ ,  $\theta_p$ ,  $t$ , and  $\tau$  are defined in the same way as for Eq. 12.35 and  $\theta_a$  = ambient temperature.

For the condition described, the initial motor temperature is 70°C. During operation at 50% load the temperature of the winding climbs 5°C to 75°C. After operation at 125% load, the temperature has climbed an additional 39°C to 114°C. The motor is shutdown for 220 minutes and  $\theta$  falls 44°C to 70°C. For this duty cycle, the peak temperature rise is 74°C over the 40°C ambient as compared to the allowable 80°C. If the loading time at either load was increased or the standstill time decreased, then the motor would cycle higher in temperature and eventually reach in equilibrium at a higher temperature, assuming that the resistances remained relatively stable. The peak temperature would rise until  $\theta$  was sufficiently large enough that during the final loading period  $\theta$  would return to a temperature above 70°C. If the peak temperature exceeded the allowable temperature of 120°C, then the motor thermal life would be shortened at an accelerated rate for the time period during which the motor winding temperature exceeded the allowable temperature.

Sometimes, when the differential between the peak temperature and the allowable temperature, as well as the time period involved, are small, the loss in insulation thermal life may be acceptable. This acceptability is enhanced if major time periods involve time at lower operating temperatures that are equivalent in life-extending capabilities. This type of decision must be made with due care to be sure that the motor is not harmed because of some other factor. For instance, the thermal design may need a detailed review to insure that the higher loading has not resulted in a peak temperature significantly higher than the measurable temperature. In addition, if this high temperature should result from excessive mechanical loading, then component mechanical failures may well occur.

This section completes the description of motor heat transfer and thermal modeling and analysis. The next section, Section 12.7, covers the ambient and environmental effects that influence motor design and type as well as enclosure selection.

## 12.7 AMBIENT AND ENVIRONMENTAL EFFECTS

There are a number of factors in the motor environment that affect motor design, selection, and performance. These items include ambient temperature, altitude, moisture, solids, chemicals, hazardous locations, seismic activity, and nuclear plant safety.

Motors may be subject to contaminants whether located indoors or outdoors. Indoor locations will preclude environmental factors due to weather conditions such as wind, rain, snow, and air-borne sand and leaves. Indoor locations, however, are not free from the presence of moisture or other airborne contaminants as evidenced by the logging, lumber, pulp and paper, chemical, and other industries. There are two basic lines of defense against these environmental factors. One involves selection of the materials and processes used to manufacture the motor. The other involves the selection of the enclosure.



The basic enclosures involve different degrees of protection from the environment. A major design difference occurs between open motors intentionally utilizing ambient air for internal cooling and the enclosed motors where barriers exist to obstruct the interchange of internal air with ambient air. Even enclosed motors will, due to the laws governing gases, develop some interchange of internal and external gases. For the special case of inert gas-filled units, the interior of the motor is maintained at a pressure above the outside atmospheric pressure and no inward interchange occurs. The standard enclosed motor has fits and tolerances that do allow some interchange of gases. These leakages are exacerbated by the normal changes in pressure within the motor that occur between standstill and run. These pressure changes are caused by the increase in internal gas pressure relative to the outside due to the fan action, and due to the reduction in internal pressure relative to the outside pressure as flow occurs within the internal cooling passages. Thus even in the case of enclosure protection it is also desirable to select materials that will help prevent excess maintenance or failure.

### 12.7.1 Ambient Temperature

NEMA standards [1] define standard ambient temperature as not exceeding 40°C. Thus, motors designed to these standards are suitable for operation in ambients up to this temperature. There are, however, areas of the United States and the world, such as the desert areas of the southwestern part of the United States, where the temperature may exceed 40°C. There are also situations in industry where temperature may exceed 40°C within the building enclosure, and where for environmental or other reasons it is not desirable to interchange the air within the building freely with the air outside of the buildings. In these cases, it is often possible to obtain motors suitable for higher than normal ambient temperature.

The main concerns for suitability are the performance of the insulation system, the bearing lubricants, and brushes if they are present. The insulation system may be made suitable in a number of ways. The first and simplest solution, where the departure from standard ambient may be small, is to operate the motor outside of the standard and accept a reduced insulation thermal life. The next simplest way may be to use a motor of a higher output rating and thus allow for the higher ambient temperature by a reduction in motor temperature rise through use of the motor at partial rating. In both of these cases it is wise to first determine that other factors such as lubrication difficulties do not preclude these solutions.

Another method to deal with ambient is to order the motor suitable for the higher ambient by use of a higher insulation thermal classification. This often may involve only the substitution of a different stator winding in the motor. For instance, a motor winding with class F insulation may be used with a lower temperature rise corresponding to class B insulation.

The lubrication considerations may prove more difficult. For lower speed and smaller motors there may be sufficient margin in the lubricant to allow use of the motor in the higher ambient. For grease-lubricated antifriction bearings, lubricants suitable for higher temperatures may be substituted for the

standard lubricants. For sleeve-type bearings, the oils suitable for higher temperature are often incompatible with motor electrical insulations. Thus any leakage or misting can represent hazards to long insulation life. Standard lubricating oils, however, can frequently be retained by the use of auxiliary oil-to-water or oil-to-air heat exchangers. These heat exchangers may require the use of complete pump-driven lubrication systems separate from the motor.

In some cases, brushes may also have sufficient thermal margin for higher than normal ambient. It may also be possible to gain some benefit by a change in the number or grade of the brushes. Commutators, collector rings, and brushes are frequently located adjacent to the rotor winding connections and between those connections and the bearings at the outboard bearing end of the motor. In order to easily assemble these parts at this location, their diameter must be greater than the outboard bearing diameter. If the location of the collector rings is changed from inboard of the bearing to outboard of the bearing, it is possible to reduce the ring diameter, and hence the peripheral speed and brush loss. This is a significant modification that involves the drilling of shaft holes to route the electrical cable through the holes past the bearing surfaces to the rotor winding connections. Such modifications may or may not be available from motor manufacturers depending upon overall economics.

If the ambient is sufficiently high, it may also be necessary for the manufacturer to review the design to be sure that differential thermal expansion between dissimilar materials will not cause a problem.

The other ambient temperature concern involves temperatures below freezing, such as may occur for Arctic pipeline application. A major concern in this regard is material embrittlement due to low temperature, and also thermal differential contraction for materials of different expansion and contraction characteristics. Steels and other metals must be selected to insure sufficient ductility, particularly in selection of material for the motor shaft. The compatibility of the cold insulation and expanding copper under stall and acceleration loading must also be reviewed so that mechanical failure of the insulation by cracking will not occur.

Lubricants must frequently be preheated prior to starting the machinery to insure proper lubrication of the bearings.

Other factors must also be considered. For instance, the driven equipment may have a greater starting load at the low ambient as compared to a 40°C ambient. Fluids such as oils have both a greater density and a higher viscosity at the lower temperature. The starting loads for oil pumps may be greatly affected by low temperature. In addition, the motor protective devices in the standardized types of motor controllers may not be satisfactory in low ambients, and may need to be modified to properly protect the motor from stall or overload.

### 12.7.2 Altitude

As altitude increases, the barometric pressure of the atmosphere decreases. This phenomenon is generally explained as the result of the gravitational pull of the earth on the atmosphere, and is similar to the effect of the earth's gravitational pull on the waters of the oceans.

The atmosphere is, however, composed of gases that generally comply with the law for ideal gases:

$$PV=MR\theta \quad (12.37)$$

where:

- $P$  = absolute pressure
- $V$  = volume
- $M$  = mass
- $R$  = constant
- $\theta$  = absolute temperature

Thus, at constant temperature when the absolute pressure decreases, the volume increases. This means the gas density decreases. Thus the capability of the cooling gas to carry away heat is reduced because mass flow decreases. Since the heat transfer coefficient is dependent upon the mass flow of the gas, this coefficient will also decrease. Because of these effects, standard machines must be derated at altitude. NEMA standards [1] provide this derating factor.

For every increase in altitude of 330 feet, above an altitude of 3300 feet at an ambient temperature of 40°C, the allowable temperature rise of a standard motor decreases 1°C when the motor is designed for test at an altitude not exceeding 3300 feet.

In addition to the need to derate at altitude, elevation may also affect the reliability of the insulation system. As motor voltage increases, the voltage stress loading on the insulation is also normally increased. If voltage stresses increase sufficiently, electrical discharges will be initiated in whatever voids may be present. These discharges normally occur between the surface of the insulation and the surface of the stator core at the ends of the core. They also occur between the surface of the stator coil and the surface of the slot. Discharges will also occur in whatever voids may be present internally within the insulation structure.

Historically, many insulation systems have been manufactured that contain mainly organic materials at voltage levels up to 2300 V. Generally systems at 4000 V and above utilize tapes and fabrics where the material content is primarily inorganic and voids are minimized. The inorganic materials are corona resistant, whereas the organic materials are subject to corona degradation. The use of an organic insulation structure may extend to voltages as high as 3300 V or more at sea level.

As elevation increases and air density decreases, the corona start voltage stress decreases. Thus, it is important to specify altitude requirements for all machines that are 2300 V and higher, but especially for voltages between 2300 and 4000 V to ensure that the insulation selected is suitable for the service.

### 12.7.3 Moisture

Relative humidity is a measure of the moisture content of the air. For conditions of rain, snow, fog, and steam, the relative humidity is generally at 100% at the location where the precipitation is formed. Even when the relative humidity may initially be below 100%, it is possible to have condensation of the liquid “on a solid surface if the surface is cooler than the surrounding gas. Such condensation is frequently encountered in the form of dew. The reduced temperature at

which the condensation occurs is called the dew point. The relative humidity of the air may be determined from the dew point temperature and the air temperature. For instance, air at 20°C and 94% relative humidity has a dew point temperature of 19°C. In general, when a nonoperating motor at standstill has a significant reduction in temperature compared to ambient air of high relative humidity, condensation will occur both internally and externally. This temperature reduction most frequently occurs on outdoor installations due to night-time radiation. This condensation in many geographic locations may contain conducting contaminants such as salt (in seashore areas), acidic elements from smog, or other chemical elements at various industrial sites. If the condensation is frequent and, for whatever reason, the motor insulation absorbs this moisture when at standstill, then the motor may fail on start-up. As possible causes of absorption, the insulation may have material that can absorb moisture, or the insulation may have minute crevices, cracks, or interlamination separations due to thermal aging, mechanical stresses, or other reasons.

Actions can be taken to prevent moisture absorption. First, the motor can be supplied with space heaters. These heaters should be wired so that power is applied whenever the motor is shut down. This should prevent condensation. In addition, a motor with sealed insulation may be available. Such a machine is defined as an alternating-current squirrel-cage machine with formed coils where the windings and connections are sealed against contaminants, and which is capable of passing the submerged or spray tests defined in NEMA MG1–20.48 [1]. See NEMA [1] for the complete definition and for the test details. Similarly, NEMA [1] defines an encapsulated machine as an alternating-current squirrel-cage machine having random windings filled with an insulating resin that also forms a protective coating. Both of these types of windings are frequently used for moisture conditions.

In addition to condensation, machines may be subject to other forms of moisture such as spray from hoses. To protect the motor in these cases, sealed insulation should also prove very beneficial. In addition, however, there are many enclosures available to protect the entire structure and not just the insulation systems. These enclosures were described earlier and range from drip-proof to totally enclosed varieties of machines such as the water-proof motor.

In addition to the problem of excessive moisture, lack of moisture may also cause problems for motors. Some materials, particularly organic materials, are subject to embrittlement and resultant fracture in locations of low relative humidity. Brushes, in particular, may be subject to dusting and high wear rates when the atmosphere is extremely dry. Very large enclosed machines are sometimes humidified to obtain satisfactory brush life performance.

### 12.7.4 Solid Contaminants

Frequently, airborne solids will be part of the content of the cooling air. Those that may be active chemically will be considered in the section following. The concern for the remainder of these particles is for those that may clog the cooling passages and for those that may abrade the insulation

system. Leaves, wood chips, and similar materials can readily block cooling passages. This is especially true for the relatively narrow air duct used for electric motors. This duct is about 3/8 of an inch in width, more or less. In addition to the obstruction of the coil, the ducts normally include separating spacers at the location of each tooth. These spacers also obstruct the air passages. Dust such as some desert sands and some mineral ore particles have proven very abrasive to insulations.

Frequently these problems may be resolved by indoor motor locations or by special enclosures such as TEFC or TEPV. The TEFC enclosure may preclude the entry of the solid contaminants within the enclosure. The TEPV enclosure utilizes cooling air piped in from a location not subject to the presence of the contaminants. In some circumstances, where machines are relatively large, the TEFC enclosures may be impractical or very expensive. In these circumstances, there is still the possibility of using the weather-protected type II enclosure. For the abrasive dusts, elastomeric treatments may be applied to the stator coil end-turns and the slot sections at the air ducts. These have proven effective in resisting abrasion for many of the abrasive particles at site locations.

The 600 ft/min contaminant dropout feature as well as the blow-through feature of the weather-protected type II enclosure have proven effective for many of the airborne particles encountered. Air filters may be added to this enclosure, but if the dust is fine and copious, the filters will require a significant amount of cleaning maintenance.

Other solids of concern include people, rodents, and tools. Screens are frequently used to protect personnel from possible injury and to exclude tools and rodents from entering the machinery.

### 12.7.5 Chemicals

Motors are made from a variety of materials. The structural materials generally used are fabricated steel, cast iron, and aluminum alloys in the form of castings and/or extrusions. Aluminum, alloyed with silicon and/or magnesium and of low copper content, may be heat treated to obtain moderately high strength and good resistance to corrosion [16]. Shafting stock is frequently made from magnetic steel bars or forgings as the shaft is frequently a part of the magnetic structure. The laminated magnetic structures are of electrical-grade silicon steel or magnetic low-carbon steel. High-purity copper and aluminum are generally used as the conductive material for the coils and connections of the windings. Motor insulating materials may utilize glass fabric, Dacron fabric or sheet, Nomex, and other good dielectric, materials of relatively high strength, as well as mica and mica mat for dielectric, thermal, and coronaresistant characteristics. The insulation materials may be filled and bonded with an electrical-grade polyester or epoxy resin. Most of these materials are subject to some degree of degradation in the presence of certain chemicals found in the multitude of modern manufacturing, industrial, and process plants.

With the general concern for the environment and the safety of the work place, protection from chemicals and pollutants for both motors and humans has been improving. Nevertheless, there are still applications where protection and/or resistance

of equipment to chemicals is necessary. Acids may be particularly active with all structural materials.

Aluminum alloys may prove sensitive to caustic atmospheres and steels and aluminum may be troublesome in seacoast regions due to the wet salt-laden atmosphere. Motor storage over sustained periods of shutdown in these atmospheres requires special attention such as periodic shaft turning. This is done to renew a protective lubricant coating on the shaft and bearings. An adequate quantity of heat from space heaters should also be provided to prevent condensation within the motor enclosure [17].

In addition to the selection of resistive materials and enclosures, for the most difficult cases special protective coatings in the form of paints and resins are sometimes available to increase the resistance of the enclosure materials, the machine's internal materials, or both.

### 12.7.6 Hazardous Locations

The National Electric Code (NEC) [18], Articles 500 through 504, cover the requirement for electrical equipment and wiring for all voltages in locations where fire or explosion hazards may exist. Locations are classified depending on the properties of the flammable vapors, liquids, or gases, or combustible dusts or fibers that may be present and the likelihood that a flammable or combustible concentration or quantity is present.

Class I hazards generally require explosion-proof motors and are concerned with hazardous gases, liquids, or vapors. Class II hazards generally require dust-ignition-proof motors, and are concerned with metal dusts such as magnesium dusts, coal dusts, and grain dusts.

Group letters A, B, C, and D have been assigned by the NEC to define the degree of explosive pressure, safe clearances, and minimum ignition temperatures for the various class I gases. Similarly, group letters E, F, and G define the required exclusion clearances and minimum ignition temperatures for the various class II dusts and fibers.

In addition, division numbers have been assigned to the hazardous locations. Division 1 locations generally have continuous, frequent, and likely hazardous materials, whereas division 2 locations are not normally subject to hazardous materials. Division 2 locations, however, may well be subject to the presence of hazardous materials because of failure of equipment or of a preventative mechanism.

Determination of the classification of a hazard is usually the responsibility of the user and the code-enforcing authority with jurisdiction over the operating site. Approval for a specific motor application is generally obtained by the user through the code-enforcing authority.

Explosion-proof machines and dust-ignition-proof machines are specifically designed for hazardous locations. "An explosion-proof machine is a totally enclosed machine whose enclosure is designed and constructed to withstand an explosion of a specified gas or vapor which may occur within it and to prevent the ignition of the specified gas or vapor surrounding the machine by sparks, flashes, or explosions of the specified gas or vapor which may occur within the machine casing" [1].

A motor manufacturer will generally qualify such a class I machine by submitting the appropriate design calculations and details to a testing laboratory, such as the Underwriters Laboratory (UL). The machine will be qualified by the UL after undergoing the pertinent tests, design review, and test review. Motors must be specifically qualified for the gas group for which the machine is to be applied.

The dust-ignition-proof machine is a totally enclosed machine whose enclosure is designed to fulfill NEC requirements for class II hazards. As for class I hazards, the manufacturer should obtain approval and a UL listing for the specific group of hazards for which the motor will be applied.

UL listed motors are not available for all motor ratings, primarily because of size effects. In these cases and for economic reasons, class I and class II division 1 locations may be serviced by other special motor enclosures and designs. These motors, however, depend upon exclusion of the hazard from the motor enclosure. To accomplish this, operational procedures and failsafe protective measures are essential for successful operation.

Motor types applied for this service are the inert gas-filled TEWAC motor and the totally enclosed pipe-ventilated motor with a forced air ventilation system. The inert gas-filled motor must never be operated without an internal inert gas pressure higher than the surrounding hazardous ambient. Similarly, the TEPV motor must be prepurged of hazardous gas prior to start-up, and the clean air coolant must remain clean and above ambient pressure during machine operation.

For all of the machines, great care must be exercised in selecting accessories. Space heater surface temperatures may not exceed allowable temperatures and all accessories subject to possible sparking must meet the same requirements as the motor. Enclosures have been developed for some of these accessories such as bearing temperature relays, temperature switches, and pressure switches.

For class I division 2 applications, squirrel-cage induction motors may prove satisfactory with open-type enclosures, so long as fans are nonsparking and all sources of ignition have been excluded or properly protected by enclosure.

### 12.7.7 Seismic Activity

Nuclear safety requirements have highlighted the importance of specific motors having the capability of operation through and beyond a seismic event. Actually it is important that safety-related motors be capable of operating during seismic activity. For instance, it is desirable that any motors driving water pumps essential for firefighting should meet such a requirement. Such requirements are finding their way into state and local building codes especially in the western portion of the United States.

Seismic requirements may be stated in different ways depending upon the sophistication of the specification. Seismic waves may be described by a frequency range and by a magnitude for each portion of the frequency range. The resultant frequencies and magnitudes are a function of both the shock force of the earthquake and the response of the earth, soil, and rock structure. Since the earth mass is large with respect to man-made structures, the magnitude is usually expressed as an

acceleration per unit of gravity accelerations. The range of frequencies corresponding to the spectrum of seismic time period is normally from 0 to 30 cycles per second with the larger amplitudes concentrated at the lower end of the frequency scale. In considering the frequency effects of an earthquake, it is necessary to evaluate the amplification that may occur due to building construction and electrical equipment construction. Expected amplification factors for various constructions may be available on the basis of preevaluation.

Where the combination of amplitude and amplification is relatively small (i.e., less than 1g), a single value of amplitude may be specified for the seismic requirement. More generally, however, a spectrum of amplitude and frequency may be specified first for the seismic event in three planes and then translated to include the building amplification with consideration given to the mass of the motor. Finally, the motor manufacturer must consider possible resonance in the motor components and the total motor assembly together with the capability of the motor to withstand the accelerations specified. Considerations for the motor include frame structural resonances, end shield flexibility response, and rotor beam response to the seismic activity defined as an amplitude-frequency input.

### 12.7.8 Nuclear Plant Safety

Because of the requirement for safe shutdown of nuclear plants, special standards have been set to cover the basic requirements for qualifying class 1E electrical equipment. These requirements include normal operation, abnormal operation, and design basis event as well as in-service test requirements. The class 1E electrical system provides electric power to the reactor trip system, engineered safety features, and auxiliary supporting features. The class 1E system includes the electric motors necessary for implementing these requirements.

IEEE Standard 323 [19] has been the recognized standard for qualifying class 1E equipment. IEEE Standard 334 [20], covering continuous duty class 1E motors, was issued in mid-1994. The first step of the qualification procedure is the preparation of the requirements for the motor including:

- The life objective
- Operating time
- Ambient pressure and temperature
- Relative humidity
- Radiation conditions
- Seismic operating basis earthquake
- Operating cycles
- Design basis accident
- Aging consideration

To qualify the equipment, a qualification program is developed based upon the requirements for the equipment. This program must demonstrate by test or by calculation that the equipment can perform the specified safety function at the end of its required design life. This involves the evaluation of those components of the motor subject to aging. These materials are usually the insulations, the lubricants and other nonmetallic materials such as structural plastic components, gaskets, and other seals. The aging mechanisms are usually temperature and nuclear

radiation. If the materials are not satisfactory for the complete time period, then periodic replacement of the material is allowed. The actual qualification testing and/or analysis must be done on equipment preaged by a recognized aging mechanism such as accelerated thermal aging accomplished by shorter times at higher temperature than specified.

## 12.8 POWER SYSTEM QUALITY

Power quality was an early concern with respect to the operation of power systems. This concern traced back at least to 1893 when a problem with motor heating was diagnosed as due to a resonance in the power system. This resonance was driven by a generator space harmonic and the response involved the transmission line and the motor [21]. At that time frequencies were significantly higher than the current standards for power lines. This particular problem was solved by the introduction of a then new method of suppressing space harmonics in ac rotating machinery output waveforms. The method is now well known as the short pitching of stator windings. By judicious choice of slots and pitch, particular space harmonics may be reduced or eliminated. Subsequently, it was realized that ac machines such as transformers, generators, and motors were producing third harmonics that might introduce other problems in power systems. These problems were resolved by the appropriate selection of transformer connections, the use of transformer tertiary windings, and the appropriate selection of winding pitch for motors and generators.

The introduction of nonlinear devices, such as power transistors and rectifiers that are used in adjustable speed drives has provided a revived interest in electric power quality especially with the presence of sensitive electronic equipment on the line. As noted, electric motors are a part of the power system quality story, and since the introduction of the ac motor, power system quality has influenced the motor and the motor has influenced the power system quality. The flicker of incandescent light bulbs was another harbinger of this relationship. When an ac electric motor drives a reciprocating compressor, the periodic pulsating torque of the compressor produces pulsations in the current of the drive motor. This pulsating current flowing through the supply side impedance creates a low-frequency modulation of the power system voltage. If the motor represents a relatively large load on the feeder bus and the modulation is sufficiently large in magnitude, then light flicker will occur in incandescent lights connected to the bus. Owen [22] provides an historical perspective on this subject plus additional insight. Pulsating currents and the associated power pulsations caused by one motor may also react with other motors on the same bus, or react with other equipment such as electronic timing devices on the bus causing unwanted equipment operation interruptions.

These pulsation conditions may be corrected by the judicious choice of a flywheel for the drive. Because a synchronous motor has a torsional magnetic restoring force or spring constant,  $P_r$ , and a damping constant,  $P_d$ , special calculations are needed to select the flywheel.  $P_r$  is a measure of the torsional magnetic restoring force when the poles of a synchronous machine are periodically oscillated from their

normal steady-state position when rotating at synchronous speed.  $P_d$ , the torsional damping torque factor, is due to the response of the amortisseur winding to these same oscillations. Halberg [23] provides guidance on the flywheel selection calculations for a synchronous motor, and Concordia [24] demonstrates that torsional perturbations in an induction motor will also trigger a restoring torque and a damping torque. Thus, since both induction and synchronous motors may cause light flicker when pulsations are significant, the methods of Halberg [23] can be modified to calculate the necessary flywheel required for an induction motor [25].

The American Society of Refrigeration Engineers selected 66% total current variation as a normal limit, where current variation is defined as the maximum amplitude minus the minimum amplitude of current divided by the current at rated amplitude expressed as a percentage [23]. This value was adopted, as a part of ANSI standard C50. Additional information is available in Ref. 1 [NEMA MG-1]. Reduced limits of current variation may be desirable for special situations.

Pulsating currents affect other parameters. A current modulating in amplitude above and below rated currents, results in an increase of the rms current as compared to a sinusoidal rms current. Since power factor is defined as the ratio of the value of the power to the product of the value of the voltage and the current, the resulting increase in the product of voltage and current reduces the power factor. Additionally, the increase in current raises copper losses. This increase in loss decreases efficiency and increases the machine temperature rise. Motors should, however, operate successfully for pulsations complying with the standards.

### 12.8.1 Parameters of Power System Quality

Parameters of power system quality, which affect ac motors, include:

- Voltage
- Frequency
- Voltage balance
- Voltage surges
- Voltage sags
- Harmonics

Electric motors are rated on the basis of a sinusoidal waveform of specific voltage magnitude at a specific value of horsepower, speed, and frequency. Any departure of the power system from this rated condition represents a reduction in power system quality for the motor, and represents a change in the motor environment. Fundamental sinusoidal waveforms are considered as the normal operating condition. Performance testing of motors is done with power supplies that closely approximate the ideal waveform. It is recognized that actual operating conditions frequently depart from the ideal so that limits have been addressed in the technical literature for many of the conditions of departure. In many cases operational guidelines and operating standards have been established.

#### 12.8.1.1 Voltage, Frequency, and Voltage Balance

The effects of voltage and frequency variation and voltage unbalance are of significant importance for motors. NEMA

Standard MG-1 addresses these issues in detail for integral horsepower three phase induction motors for NEMA frame sizes 143 through 445 at ratings ranging from 1 to 250 hp. The details of the standards applicable to general purpose motors are quoted directly as they provide a succinct description of the effects and provide general guidance on the subject. [26].

NEMA 12.44 specifies allowable variations from rated voltage and frequency.

Motors shall operate successfully under running conditions at rated load with a variation in the voltage or frequency up to the following:

- a. Plus or minus 10 percent of rated voltage with rated frequency.
- b. Plus or minus 5 percent of frequency, with rated voltage.
- c. A combined variation in voltage and frequency of 10 percent [sum of absolute values] of the rated values provided the frequency variation does not exceed plus or minus 5 percent of rated frequency.

Table 12.9 prepared by the Electrical Apparatus Service Association illustrates the effects of these variations on a typical motor [26].

NEMA 14.35 provides a description of the effect of unbalanced voltages on motor operation:

The effects of motor unbalanced voltages on polyphase induction motors is equivalent to the introduction of a “negative-sequence voltage” having a rotation opposite to that occurring with balanced voltages. This negativesequence voltage produces in the air gap a flux rotating against the rotation of the rotor, tending to produce high currents. A small negative-sequence voltage may produce in the windings currents considerably in excess of those present under balanced voltage conditions. The voltage unbalance in percent may be defined as follows:

With voltages of 460, 467, and 450, the average is 459, the maximum deviation from average is 9, and the percent unbalance is

$$V_u = 100 * 9 / 459 = 1.96\%$$

The locked-rotor torque and breakdown torque are decreased when the voltage is unbalanced. If the voltage unbalance is severe, the required accelerating torques might not be adequate for the application. The full-load speed is reduced slightly when the motor operates at unbalanced voltages. The locked-rotor current will be unbalanced to the same degree that the voltages are unbalanced, but the locked rotor KVA will increase only slightly. The motor efficiency may also be significantly reduced. The currents at normal operating speed with unbalanced voltages will be greatly unbalanced in the order of approximately 6 to 10 times the voltage unbalance. The performance of the machine will be affected as shown in Fig. 14.1 [Fig. 12.22 of this chapter] and the change in loss distribution will result in higher rotor temperatures. The motor noise and vibration may also increase.

It should be further noted that NEMA 12.45 states that for successful operation it is recommended that voltage unbalance should not exceed 1%.

The standards referenced in 12.8.1.1 were established based on the study of lower ratings of horsepower designs of induction motors. While these rules also are applicable to many of the higher horsepower ratings, some of these higher horsepower machines may have designs of differing capabilities. Reference should be made to the specific NEMA standards for these machines.

#### 12.8.1.2 Voltage Surges

Voltage surges on power systems occur due to incidents such as lightning strikes, circuit breaker actions such as for motor starting and shutdown, and to ground faults such as may occur in arcing faults on ungrounded systems. An historical and users perspective on voltage surges is presented in Section 9.1.1. The events that cause voltage surges have been found to result in traveling waves on transmission lines. The major voltage surges of concern for motors are those that occur during

**Table 12.9** General Effect of Voltage and Frequency Variations on Induction Motor Characteristics

Characteristics	Voltage		Frequency	
	110%	90%	105%	95%
Starting torque	Up 21%	Down 19%	Down 10%	Up 11%
Maximum torque	Up 21%	Down 19%	Down 10%	Up 11%
Percent slip	Down 15–20%	Up 20–30%	Up 10–15%	Down 5–10%
Efficiency	Down	Down	Up	Down
Full load	+ or –2%	0–3%	Slightly	Slightly
3/4 load	0 to down slightly	Little change	Up slightly	Little change
1/2 load	Down 0–5%	Up 3–10%	Up slightly	Down slightly
Power Factor				
Full load	Down 5–15%	Up 1–7%	Up slightly	Down slightly
3/4 load	Down 5–15%	Up 2–7%	Up slightly	Down slightly
1/2 load	Down 10–20%	Up 3–10%	Up slightly	Down slightly
Full load current	Down slightly to up 5%	Up 5–10%	Down slightly	Up slightly
Starting current	Up 10%	Down 10%	Down 5%	Up 5%
Maximum overload capacity	Up 21%	Down 19%	Down slightly	Up slightly
Magnetic noise	Up slightly	Down slightly	Down slightly	Up slightly

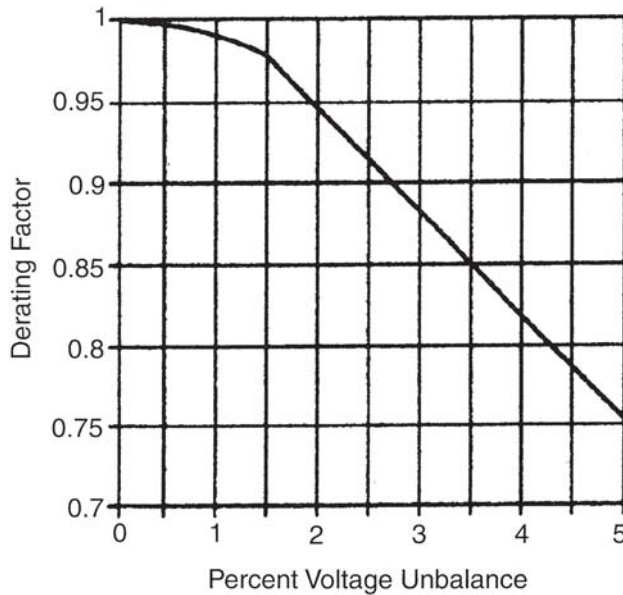


**Figure 12.22** Derating factor due to voltage unbalance [NEMA MG1, Fig. 14-1].

motor starting mainly because of the relative frequency of starting as compared to the frequency of the other events.

Methods have long been established to analyze traveling waves on transmission lines. These analyses have shown that traveling waves are affected by the value of the transmission line surge impedance,  $Z_o$ , where  $Z_o=L/C$  and  $L$  is the value of the line inductance per unit length and  $C$  is the value of the line shunt capacitance per unit length. If the termination impedance matches the line surge impedance, then no reflections occur. This is not the normal case. If the termination is open circuit, then the voltage wave will reflect back on the line essentially doubling the voltage on the line. [This assumes a rectangular front on a constant value of surge voltage.] The current wave will reverse direction and polarity essentially canceling the incoming wave. For a short circuit the situation changes, and the voltage wave must have no amplitude at the fault and the current will flow into the fault. Actual conditions may approach one of these limiting conditions, depending upon the termination impedance. The transmission line analogy has been found useful in the analysis of a motor connected to a bus by switchgear and cable. For a motor and for the frequencies represented in the surges of interest, the inductance of the motor is high and may approach the values of an open circuit. For some conditions multiple voltage reflections can result in peak values above twice the peak to ground value of the surge voltage. These severe conditions are generally a function of cable length. It is desirable to keep the cable length short [27, 28].

The peak value of the surge voltage front and the slope of the front are important. The peak value is a measure of the value of voltage, which may be imposed across the motor ground insulation and turn insulation, and the slope determines the distribution of the voltage across the motor turns. The steeper the voltage front, the higher the percentage of the peak value of voltage imposed across the initial coil. Rhudy et al. [29] presented a paper providing valuable insight

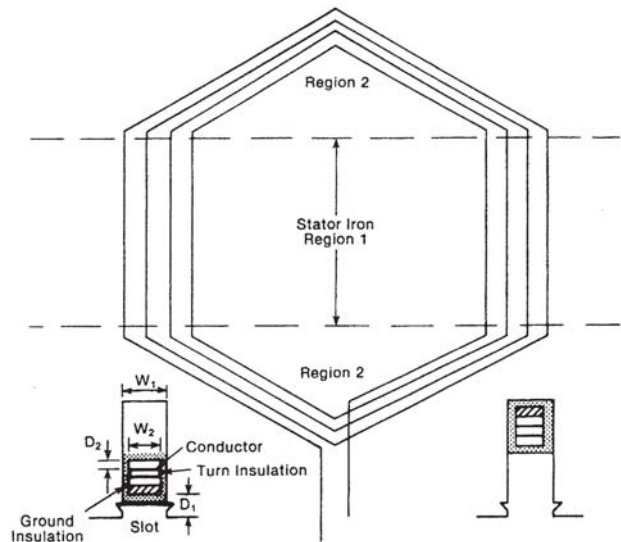


**Figure 12.23** Schematic of a formed coil with a cross section of the coil as inserted in slots.

into the impulse voltage distribution in form wound stator voltage coils. The analysis used a lumped parameter equivalent circuit representation of the machine stator winding and a Fourier series representation of the voltage impulse wave. Figure 12.23 shows a schematic of a formed coil, as well as a cross section showing the coil in slots. The cross section shows the coil conductor, turns insulation and ground insulation. Figure 12.24 shows the equivalent circuit. This equivalent circuit can be used to evaluate the voltage distribution across the coils and turns of the motor for wave fronts of different rise times and different magnitudes. It may also be used for other evaluations such as to demonstrate the advantage of the thinnest adequate turn insulation in helping to distribute the surge voltage more uniformly across the winding turns. This thinner turn insulation also allows for the design of a smaller and more economical motor with a lower stator copper loss and a possible higher efficiency.

Historically, the recommendation for motors on high and medium voltage systems has been to protect them from voltage surges by the use of voltage arrestors and surge capacitors.

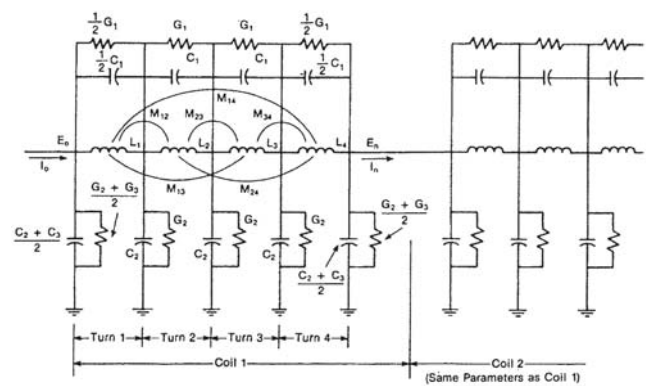


**Figure 12.24** Equivalent circuit representing a machine stator winding to be analyzed for an imposed voltage impulse.

While some motors were not so protected, large important motors usually were. The higher the voltage the greater has been the degree of protection. The arrestors limit the surge voltage peak and the capacitor reduces the rise time of the voltage surge. For effective use, the capacitor should be connected and located as close to the motor terminals as possible. Otherwise the surge front may reach the motor prior to the surge front reaching the capacitor. Forecasting a standard requirement for an allowable motor impulse voltage standard is complex. There is a philosophical question as to whether to use motors with an historical impulse voltage capability for the turn insulation and to use surge voltage protection as required, or whether to use motors with a higher standard of impulse voltage capability for the turn insulation and no surge protection. An IEEE working group report [28] was published in 1981 tracing the history of surge voltage capability for motor windings. Prior to the working group report, the ground insulation impulse voltage capability was expected to be limiting. The ground voltage capability was and is expected to be at least 1.25 times the crest value of the voltage of the high potential test. The expectation was that with the use of surge voltage protection, the turn insulation would not be in jeopardy and that the ground-wall capability would be limiting. With the use of surge capacitors, steep fronted waves are expected to be no less than 10  $\mu\text{sec}$  in rise time. With this value of rise time, the surge voltage will distribute relatively uniformly between the coils. Thus the ground-wall insulation is limiting rather than the turn insulation. The report does, however, include a proposed new representation of the capability of ac rotating machine insulation to withstand impulse voltage as limited by the turn insulation. The proposed envelope of capability is shown in Fig. 12.25. Subsequently the IEEE guide for testing turn-to-turn insulation on form-wound stator coils [30] was revised and reissued. This report suggests acceptance test values for form-coils, both as individual coils and for coils in completely wound stators. Two acceptance criteria are defined. The acceptance values for the first criteria are shown in Fig. 12.26. These values are higher than recommended by the working group, and require a higher level of turn insulation capability.

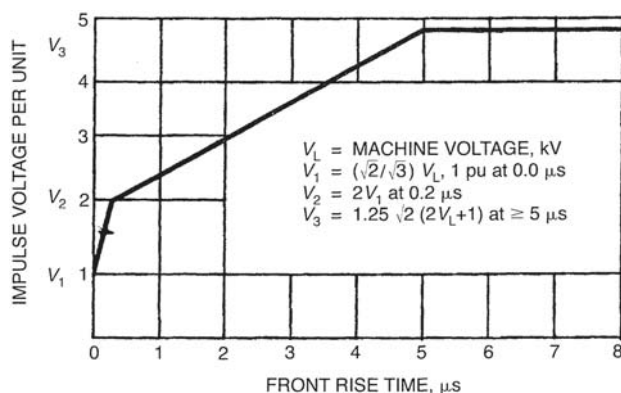


**Figure 12.25** Impulse voltage withstand envelope [Ref. 28 proposal and Ref. 30 alternative standard].

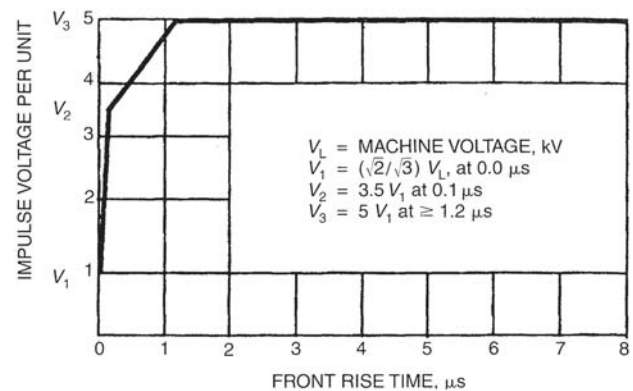


**Figure 12.26** Impulse voltage withstand standard [Ref. 30 standard].

This implies increased size and cost of motors as compared to the motors evaluated by the working group. A second acceptance standard is provided which corresponds to the values proposed by the working group as shown in Fig. 12.25. This second standard is recommended in the guide for machines that are not expected to encounter surges with rapid rise times. Thus each power system may be reviewed to determine which motor impulse voltage capability is the best overall technical, reliable and economic choice for the power system bus of concern.

### 12.8.1.3 Voltage Sags

Voltage sags are distinguished from voltage regulation. Voltage sag may be described as a short duration [cycles to seconds] reduction in voltage magnitude. Here again motors may be a source, a recipient and a participant in the total phenomenon and it is these voltage sags where the motor is involved that are considered in this text.

When a motor, which represents a significant portion of the load on a line, is started, the motor starting current will cause voltage sag. Depending upon the inertia of the load, the torque of the load during starting, and the motor starting torque, the sag may last from cycles to minutes.

Conversely, if there is a system fault, such as a ground fault, an induction motor as well as a synchronous motor will generate additional current to feed the fault. The amount of this contribution will depend on the motor loading, the total inertia of the drive, the breaking torque of the driven equipment and the power delivered to the fault by the motor. The induction motor provides generator action because when short-circuited at the terminals, the current flowing in the squirrel cage winding of the rotor continues to flow for a time period determined by the time constant of the rotor winding. This current acts to maintain the air gap magnetic field. This action generates a stator voltage, which in turn causes the additional current flow to the fault.

Perhaps of most interest, in so far as the motor is concerned, are the consequences of acceleration of the motor on a bus where the electrical power has been momentarily interrupted and then suddenly reapplied. This sudden reapplication is



done to minimize the time of power loss. This particular condition has long been of concern to electric utilities and is also a concern for other applications where adjustable speed drives and other critical electronic equipment may be affected. The concern for electronic equipment is generally for the effects of electrical disruption on the equipment and the processes controlled by the equipment, whereas the concern for the motor utility installation includes the concern for the reliability of the motor and the driven equipment. Adjustable speed drive control strategies during the time between power interruption and power reapplication are also of interest. Studies of the control strategies were sponsored and reports published by EPRI [30]. ANSI C50.51 paragraph 15 [31] addresses the reclosure situation for utility applications and reads as follows:

#### Bus Transfer or Reclosing

A motor is inherently capable of developing transient torque [and current] considerably in excess of rated torque when exposed to out of phase bus transfer or momentary voltage interruption and reclosing on the same bus. The magnitude of this transient torque can range from approximately 2 to 20 times rated torque and is a function of the machine operating conditions, switching times, system inertia, etc.

To limit the possibility of damaging the motor or driven equipment, or both, it is recommended that the power supply be designed so that the resultant vectorial volts per hertz between the motor residual volts per hertz and the incoming source volts per hertz at the instant of transfer or reclosing is completed does not exceed 1.33 per unit Volts per Hertz on the motor rated voltage and frequency bases.

NEMA also adopted this standard as a part of standard MG 1. NEMA later withdrew the criteria because of concern for the mechanical response of the motor and the driven equipment. NEMA, in essence, added the recommendation for a mechanical analysis. Two significant studies sponsored by EPRI have been performed on this subject. The first study [31] investigated two representative power station auxiliary motor power buses. Each bus had a complement of typical motors. Calculations covered various transfer conditions of interest. The resulting motor currents and air gap torques were also calculated and guidelines were developed for the application of the bus transfer criteria to multi-machine situations. Based on this study the second study [32] used the same buses and machines, but was expanded to include the mechanical response of the equipment. As a result of the work completed, additional work was recommended in order to generalize the conclusions. Still, it may be concluded from the two studies and from the historical performance of motors subject to bus transfers, that for most cases, polyphase induction motors, for many applications, will operate successfully with fast bus transfers. A preliminary evaluation study of the particular application should be able to determine the required detailed analysis, if any, and the criteria to insure reliable mechanical operation.

#### 12.8.1.4 Harmonics

The use of solid-state converter equipment on supply power lines introduces harmonic currents to the power system. The values of the harmonic currents are a function of the converter power rating and are further influenced by the converter design. In the case of a constant current, ac to ac, converter with a dc link, if the current smoothing inductance is properly sized, and the current on the dc side is constant, then a relatively constant current flows on both the ac and dc sides of the converter. Figure 12.27 [33] illustrates a representative six-pulse, ac-to-ac, controlled current converter with a dc link. Thus for this case, each cycle of current on both ac sides is essentially in the form of a quasi square wave. A Fourier series may be used to represent this waveform. The representation consists of a fundamental sinusoidal wave together with a series of harmonic waves. To increase power or to influence the value of the amplitude of the harmonics, then two such circuits may be connected to provide a 12-pulse converter as shown in Fig. 12.28 [31]. Additional bridges may be arranged to provide still larger numbers of pulses and this further influences the magnitude of the harmonic currents. Generally there is a reduction in some of the harmonics as additional bridges are added. Refer to Table 12.10 [34, 35]. The harmonics of the current wave follow a pattern of rotation for each order of harmonic: the fundamental is forward rotation. The second harmonic is backward rotation. The third harmonic is in phase or zero rotation. The pattern continues to repeat. For a symmetrical wave, there are no even harmonics needed to represent the wave. For a three-phase system there are no triplen harmonics needed to represent the wave. Typical values of the amplitudes of the harmonics for the waves for various bridge arrangements and the harmonic rotations are summarized in Table 12.10. Also shown is the value of the harmonic order induced in the induction motor cage winding by the stator harmonics at running speed, when slip speed is neglected.

The converter generates constant harmonic currents. These harmonic currents flow back through the power system through the power system impedance. The power system surge impedance is generally representative of the harmonic impedances when adjusted to the frequency of the harmonic. For this case, each harmonic voltage on the bus is the product of the harmonic current times the system harmonic surge impedance. Thus in addition to the normal supply voltage, the other equipment on the bus is also exposed to these harmonic voltages. The actual harmonic currents and voltages will depend upon the design of the converter and the design of the power system. A harmonic voltage factor [HVF] has been adopted as a measure of the total harmonic voltage on the bus.

$$\text{HVF} = \sqrt{\sum_{n=5, n \text{ odd and not divisible by } 3}^{\infty} \frac{V_n^2}{n}}$$

The major concern for motors operating on a power system with harmonic content is the increased losses, which affect motor heating and motor efficiency. Cummings [34] has analyzed the response of over 20 typical induction motors rated

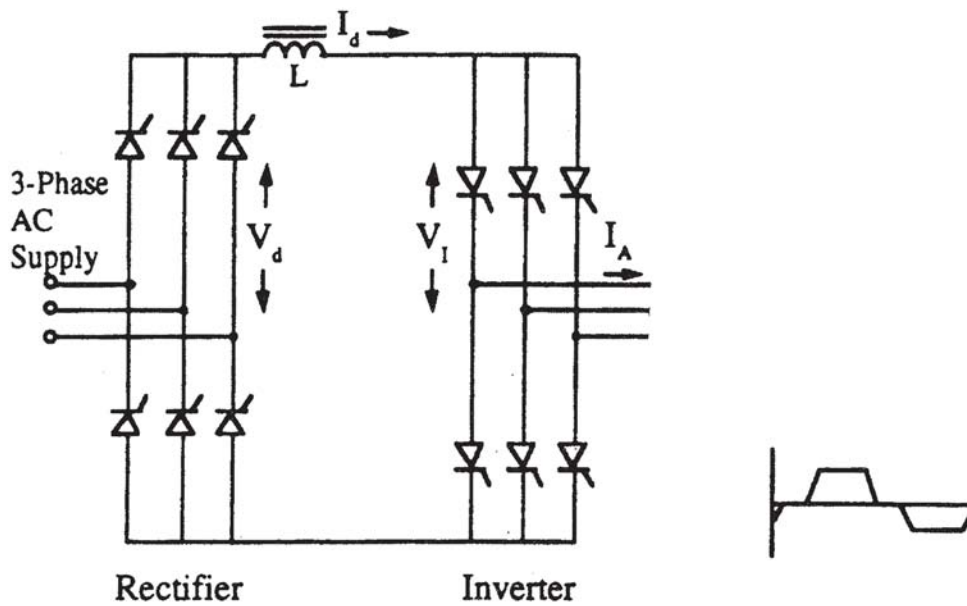


Figure 12.27 Representative six-pulse, ac-to-ac, constant-current converter with a dc link.

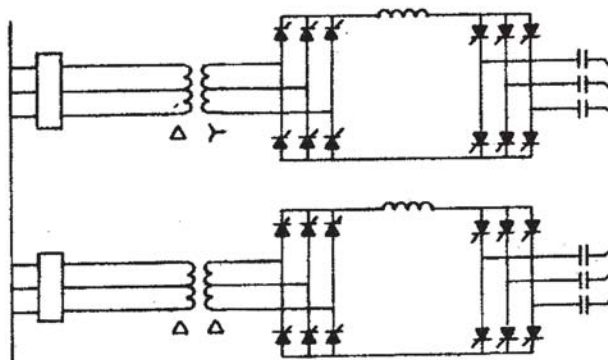


Figure 12.28 Representative 12-pulse, ac-to-ac, constant-current converter with a dc link.

from 15 to 5000 hp to 4 different sets of harmonic content that are representative of what might be expected in practice. Based on the analysis it is suggested that a limit for HVF of 0.045 may be appropriate as a general guideline for 1.0-service factor polyphase motors of normal design. NEMA has chosen a conservative limit for HVF of 0.03 and has provided a derating curve for the presence of larger values of HVF in NEMA 30.10.2 [35].

It should be noted that harmonics might also cause shaft torque oscillations and additional motor noise. This fact provides an additional incentive to avoid high harmonic voltage factors. The torques and additional noise will be covered in greater detail in the section on adjustable speed drives.

Table 12.10 Harmonic Orders of Current Showing: Direction of Rotation, Order of Motor Rotor Harmonic, and Typical Per Unit Value of Harmonic Current in Power Bus

Harmonic order	1	5	7	11	13	17	19
Rotation	+	-	+	-	+	-	+
Induction rotor harmonic <sup>a</sup>	0	6	6	12	12	18	18
Converter pulse order	Per Unit Harmonic Current						
6	1	0.175	0.11	0.045	0.029	0.015	0.010
12	1	0.026	0.016	0.045	0.029	0.002	0.009
18	1	0.026	0.016	0.007	0.004	0.015	0.010
24	1	0.026	0.016	0.007	0.004	0.002	0.001

<sup>a</sup>Rotor harmonic at synchronous speed

## 12.8.2 Adjustable Speed Drives

Technical advances in solid-state devices and the need for energy conservation have been the driving forces behind the increasing use of ac adjustable speed drives for polyphase induction motors. Prior practice was to use induction motors fed by a constant voltage and constant frequency bus. When reduced flow was needed from driven equipment such as pumps and fans, flow restrictors were used. In the case of pumps, adjustable valves might be used. For fans, adjustable dampers might be used for flow control. When such a flow restrictor is introduced it creates a pressure drop. In the case of a pump operating at constant speed and constant pressure, the insertion of an additional pressure drop reduces the flow. Significant energy losses occur because of the pressure across and flow through the valve. Flow recirculating schemes have also been used to regulate flow, but these are also inefficient. Adjustable speed drives control the flow by changing the drive motor speed. When the speed is reduced, the pressure in the hydraulic system is reduced, and the total output of the motor is less as well. Most or all of the energy reduction in the mechanical system may be saved, particularly as the flow is reduced. The adjustable speed drive converter has relatively high efficiency since the voltage across the switching devices is small and the controller losses are not great. For the motor the reduction in voltage and frequency to obtain the lower speed reduces the fundamental flux core losses. The reduced fundamental current corresponding to the smaller load at the reduced speed may reduce the current losses to a greater extent than the harmonic current due to the inverter increases the losses. Thus a significant overall reduction in losses occurs in the motor that provides an offset to the converter losses. In the adoption of adjustable speed drives, questions of efficiency determination for the combined effects of motor and drive were a major concern. An industry standard was created to provide assistance with this issue [36].

Adjustable speed ac motor drives have a constant torque range and a constant power range. These operating characteristics are discussed in Section 12.6.1. These characteristics provide the drives with the capability of being used for a large number of applications. It is noted in the referenced section that for successful operation, careful consideration must be given to cooling at reduced speeds. The torque requirements for pump and fan drives reduce basically as the square of the speed ratio for differing speed points as the speed is reduced. These applications therefore present an easier cooling situation than some other applications, such as constant torque applications. In any event adequate cooling must be supplied for all applications or the application must be restricted to the speed range where the cooling is adequate.

Other items of significant interest relate to the quality of the power provided by the converter, which are dependent on the inverter design and the control strategy of the ac adjustable speed drive. The items are:

- Harmonics
- Torsional vibrations
- Voltage surges
- Shaft voltage
- Noise

Various systems have been developed for use as ac motor adjustable speed drives. Refer to Sections 9.3 through 9.6. Particular systems are sometimes chosen based on the horsepower rating and the type of motor selected. For large three-phase synchronous motors both cycloconverter drives and load commutated inverter (LCI) drives have been designed, manufactured and installed. Cycloconverter equipment fabricates a new three-phase adjustable voltage and adjustable frequency supply by directly selecting portions of the wave form from an existing constant voltage and constant frequency three phase system to fabricate the new three phase supply. Cycloconverters and large slow speed synchronous motor designs have been coordinated as ac adjustable speed drives for the large ball mills that are used in the mining and cement industries. These drives may be soft started. These drives may also be run at a speed selected to provide optimum performance in the pulverization process needed at a particular site or for a particular product.

LCI designs and large, high-speed synchronous motor designs have been coordinated for both pump and fan drives. The rated motor speeds for these designs do not have to match the standard 60-Hz speeds. Rather these motors may be designed for speeds that are optimum for the particular pump or fan output, and thus enhance pump or fan operation and efficiency. Furthermore, motor drives for pumps and fans do not need to maintain the constant volts/hertz that is required to maintain a fixed maximum torque capability. The ratio of volts to hertz may be reduced as the speed and torque requirements are reduced. Thus the proportion of iron and copper losses may be adjusted to minimize the overall drive and motor losses as the speed is reduced.

Such tailored designs may also be available with specialpurpose induction motors designed for specific applications where the volume and value justify the design and coordination effort. Other adjustable speed drives can be tailored to take advantage of other motor types such as permanent magnet motors, reluctance motors and Blondel-type motors. It is probable that these tailored designs will gain a growing share of the market because of the overall cost and performance advantage of special purpose components coordinated as power supply, motor and driven equipment, in one overall performance package.

This still leaves a very large area of application where it is necessary to coordinate polyphase induction motors with adjustable frequency inverter drives.

### 12.8.2.1 LCI Drives

The adjustable speed drive, with a LCI supplying power to a large synchronous motor was an early development and has been popular in the higher horse power ratings. Because of the lack of availability of fast acting transistors in ratings with sufficient power, this drive continues to maintain its dominance for larger motors. Hundreds of units are in operation. These successful units have been designed with drive components that are coordinated.

#### 12.8.2.1.1 Harmonic Considerations

Section 12.8.1.4 considered the effects of a constant current being fed to the power line from a dc converter. In the case of an

inverter, the constant current supply, in the form of a quasisquare wave of current, is supplied to a synchronous motor. The current is described as a quasi-square wave because in practice it takes a finite amount of time for the current to rise to the value of relatively constant amplitude and to decrease to zero amplitude. Since the harmonic portion of the current will flow in to the motor and will follow the path of least impedance, the synchronous machine is designed with a special amortisseur winding. With the machine started in an essentially synchronous mode from the adjustable frequency supply, the amortisseur winding does not need to be designed to provide the torque to accelerate to full speed. Thus this winding may be designed for low impedance and a low loss rather than for torque. Nevertheless, the motor must be designed to accommodate the additional stator and amortisseur winding copper losses due to the flow of harmonic currents.

#### 12.8.2.1.2 Torsional Vibration

The square wave of current also gives rise to torsional excitations. Table 12.10 of Section 12.8.1.4 of this chapter lists the production of sixth harmonic rotor currents due to the fifth and seventh harmonic currents flowing in the stator winding. These are the major harmonics for a six-pulse constant current inverter or converter. This sixth harmonic rotor cage winding current interacting with the stator flux causes a sixth harmonic oscillating torque to act on the rotor. A similar situation occurs for the eleventh and thirteenth stator harmonic currents. These stator currents cause a twelfth harmonic current to flow in the rotor cage winding and cause a corresponding oscillating torque to act on the rotor. Torsional excitations will occur at the sixth harmonic frequency and its multiples. If the converter is designed for higher multiples of pulse rate, a pattern of reduction of certain harmonic orders occurs as can be seen in Table 12.10.

Because torsional excitations are present, there is a high probability that an excitation frequency will occur that corresponds to a mechanical torsional resonant frequency of the motor-driven equipment shaft system [37]. This correspondence is likely for a full-range adjustable speed drive. In this case the drive frequency can range from say 4–60 Hz. Torsional exciting frequencies ranging from 24 to 360 cycles will be present over the speed range due to the sixth harmonic exciting frequency. For some applications, shaft resonances are likely to be present in this frequency range. When this correspondence occurs, the shaft may be subject to fatigue due to the amplified shaft strain. A torsional analysis is desirable to identify any possible coincidence of resonance with an exciting frequency. If an analysis identifies such a correspondence, then corrective action is recommended. As pointed out previously, it is possible that changing the pulses of the inverter may reduce the degree of excitation and/or the use of a resilient coupling may resolve the problem or provide some alleviation of the problem. Generally the use of a resilient mechanical coupling is desirable.

#### 12.8.2.1.3 Voltage Surges

Just as circuit breakers give rise to voltage surges when motors are started or disconnected, the opening and closing of the switching components of the inverters used for adjustable speed

drives also create voltage surges. These surge voltages propagate in the same manner as described in Section 12.8.1.2. These may occur with each action of a switching component of the inverter. This increases the number of surges by orders of magnitude compared to the number experienced by motors supplied directly from the power system. In the event that these surges result in partial discharge of the insulation between turns or from the ground insulation to ground, there is the possibility of failure of the insulation from electrical aging [38, 39]. The LCI drives, using silicon-controlled rectifiers, have switching speeds limited by their inherent characteristics. With the addition of snubbers, the surge rise times are further reduced. These rise times may be in the order of 2–5  $\mu$ sec and the impulse voltage magnitude may be quite high. For motors used with these LCI drives, both the turn and the ground insulation should be reviewed. The expected surge conditions of the specific drive should be compared to the capability of the insulation provided on the motor to insure compatibility.

#### 12.8.2.1.4 Shaft Voltage

Shaft voltage is produced in an ac squirrel-cage motor due to several types of actions [40]. The underlying principles of these actions may also be used to analyze the response of synchronous machines. These actions include the production of asymmetrical flux due to certain numbers of lamination joints when used with machines of particular pole pairs. These joints are caused by the use of segmental punchings for the stator core. This is perhaps the oldest recognized cause of shaft voltage [41]. Other causes of shaft voltage cited in the references, which are also influenced by discontinuities and pole pairs are: air gap eccentricity, saturation of the stator teeth due to air gap flux, stator and rotor tooth harmonics and spider shafting configuration.

These shaft voltages become detrimental when the magnitude is sufficient to cause shaft currents. Machines supplied with ball bearings are more sensitive to shaft voltage than are machines with sleeve bearings. A full hydrodynamic oil film in a sleeve bearing provides a higher resistance to the flow of current than the thin film in a ball bearing. When sufficient current due to shaft voltage is present, bearing failure will eventually occur. The normal correction for the condition is to provide a machine with an insulated bearing on the opposite drive end of the machine. In the case of double end drive extensions, an insulated coupling is also used on the drive end. NEMA [42] recommends the use of bearing insulation when the shaft voltage exceeds 300mV peak.

In addition to the shaft currents caused by asymmetry and poles, capacitance effects produce other shaft currents. These are of most concern in the presence of higher frequency voltage and will be considered for the pulse width modulated inverter (PWMI). While the six-pulse LCI may have increased shaft voltage due to harmonics compared to a machine supplied from a conventional power supply, the larger machines used for this application are normally supplied with insulated bearings. Thus, the machines are already protected from shaft voltage.

It should be noted that when sleeve bearings are used on adjustable speed drives and the motor bearings are supplied with oil by the use of oil rings, the low-speed operating points

are limited. Oil rings may not supply sufficient oil at reduced speeds. The use of a separate oil supply system will extend the speed range of the motor and the drive.

#### 12.8.2.1.5 Noise

Motor noise is produced in two basic ways. In the first way the electromagnetic forces in the active motor parts cause vibrations in the motor components. The resulting noise is transmitted through the motor structure and mounting through the air to the human ear. The second method involves the flow of the cooling medium, which is usually air. The rotation of the rotor itself can cause turbulence in the air. The turbulence causes noise. The fan and air ducts that force air through the machine will also produce noise.

All of the motor components including the active electromagnetic components are assembled from mechanical pieces. Each of these components has natural modes of vibration and associated frequencies of vibration. As a forcing frequency approaches the natural frequency of a part, the vibration of a part increases. When the forcing frequency and the natural frequency correspond, the amplitude of vibration is limited by the damping in the system. This condition is sometimes referred to as resonance [43]. Thus the parts of the motor such as the stator yoke, the stator frame, the air deflectors, the conduit boxes and the covers are subject to electromagnetic forces that may correspond to resonance or near resonance.

Similarly, the passages of the cooling system may also be excited to produce significant noise. For instance the air ducts may be excited to produce a pipe organ effect by the passing frequency between the rotor and the stator. Refer to [Section 11.1](#) for a detailed review of motor noise.

As indicated in the section on torsional vibration, the use of an adjustable speed converter provides a rich selection of driving frequencies as the drive changes speed virtually insuring a match to the natural frequency of some part. Fortunately the mechanical response that produces noise is not usually of a damaging nature to the part, but the amplitude of the noise may be objectionable to the human ear. Several actions may be undertaken to at least partly mitigate the noise:

1. Recognize from the start that additional noise may be present. Locate the motor in a relatively isolated area, and/or in such a way that a sound absorbing barrier or enclosure can be installed if necessary.
2. Analyze the major internal components of the motor such as the motor yoke and the air ducts for natural modes to preidentify possible problem speeds. These speeds may be avoidable for continuous operation. If the speed is not avoidable, it may be possible to slightly shift the response frequency by a design change to an avoidable speed.
3. Investigate the inverter design to determine if inverter design modifications may reduce the noise and /or be a more economical solution.
4. Determine if either a more rigid or a more flexible mount would reduce the noise.

#### 12.8.2.2 Pulse Width Modulated Drives

The solid-state power devices used for adjustable frequency inverter drives have progressed from thyristors to transistors to gate turn off transistors to insulated gate bipolar transistors (IGBT). At each step the speed and the power capacity have also increased. The fast acting IGBT is now the transistor of choice for the pulse width modulated inverter (PWMI). The features of the PWM drive with the IGBT have made the six-pulse square wave voltage and current source inverters outmoded in so far as squirrel cage induction motors are concerned. Section 9.5.5 describes the operation of the PWM I.

In the case of adjustable speed drives of the applied voltage type such as the PWM drive, the waveform is impressed directly on the motor terminals. The output voltage and frequency wave of a PWMI is constructed as the sum of a series of voltage square wave type pulses that may have differing elapsed times for the half wave whereas the output wave of a six-pulse inverter may be a single pulse per half wave. The faster acting IGBT allows an inverter design of increased numbers of pulses in the output for each wave. These multiple pulses provide great opportunity to shape the inverter current wave. Section 9.5.5 describes the operation of the inverter in greater detail.

The pulse rate may be of the order of 1–10 kHz. With this repetition rate the output wave may be designed to virtually eliminate the lower harmonics from the current wave. The major current harmonic is at a high frequency that is a function of the pulse rate.

##### 12.8.2.2.1 Harmonics, Torsional Vibration, and Noise

As a result of eliminating certain lower order harmonic currents, the power system environment of the motor is changed as compared to the LCI drive. The higher order harmonic currents still cause extra heating that must be accounted for in the motor design.

For this design, certain lower order harmonics have been eliminated. These are the harmonics most likely to correspond with the most responsive modes and frequencies of the shaft. The probability of fatigue due to a resonant condition at the higher harmonic frequency is far less probable than at a lower frequency. Nevertheless, it is still conservative to review the harmonics produced by the converter so that any frequency of concern may be reviewed. The forcing frequencies that produce noise are changed. The higher frequencies produce noises in a frequency range where the human ear is more sensitive. Thus noise still is of concern and should be analyzed.

NEMA standard MG 1–1998 part 31 [42] sets performance standards for definite-purpose inverter-fed polyphase motors. The standard is silent on the additional motor heating from harmonic currents. This leaves the coordination of this matter to the system coordinator and the manufacturers. It is prudent to have a review of the drive for possible torsional vibrations and noise production.

##### 12.8.2.2.2 Surge Voltage

The faster firing and shut-off rate of the IGBT causes higher voltage spikes and steeper wave fronts as compared to the silicon-

controlled rectifier (SCR) devices used for the LCI drive of Section 12.8.2.1. In addition since the pulse rate is significantly higher than for the LCI, the motor winding insulation is subject to many more repetitive voltage impulses. This increases the exposure of the insulation to possible voltage fatigue [38, 39].

Historically 600-V insulation systems have not been designed with the corona-resistant materials that are frequently used to resist electrical fatigue on the higher voltage systems. The materials used for both the ground and turn insulation have been from the “organic” class of materials. These materials are subject to electrical aging above the corona start voltage as demonstrated by Les Mans [39]. NEMA [42] has defined the level of surge voltage capability for definite purpose inverter fed polyphase motors. For motors with rated voltage equal to or less than 600 V, the peak voltage should not exceed 3.1 times the rated voltage. The surge voltage rise time should not be less than 0.1 microseconds. With this fast rise time for the wavefront, a high percentage of the surge voltage will be imposed on the initial coil of the phase winding and will be divided among the turns of that coil. If the turn voltage exceeds the value at which partial discharge occurs, the turn insulation will be subject to electrical aging.

The wire used for turns on random-wound machines is usually round film-coated wire. This film is relatively thin and has a high dielectric strength. Film-coated wire is also used for the wires of the turns of the coils of the lower voltage form-coil motors. A corona-resistant wire was developed for medium voltage machines designed with form-coils [44]. This type insulating coating is now available on round wires and is available for inverter application. Les Mans [36] reviews this subject in some detail.

It should also be noted that NEMA MG 1 part 30 [35] defines the surge voltage capability for general purpose motors when the power source is an inverter. The surge voltage capability is considerably lower than for definite purpose motors designed for inverter operation. The peak of the applied voltage should not exceed 1000 V and the surge rise time should be at least 2  $\mu$ sec.

It is clear that the motor insulation system and the inverter surge voltage output must be closely coordinated at any voltage to ensure satisfactory motor insulation life and a reliable drive system.

### 12.8.2.2.3 Shaft Voltage

In addition to the bearing currents caused by shaft voltage that were covered in Section 12.8.2.1.4, a motor with a PWMI power supply is subject to additional types of bearing currents. Both circulating and noncirculating bearing currents may occur from the use of a PWMI power supply [45]. Both types of currents in a PWMI have been attributed to the common mode voltages and the common mode currents of the inverter [46]. At the higher frequencies of the common mode, parasitic capacitance between the parts of the drive components allows currents to flow. These capacitors have too high an impedance at normal line frequency to allow significant current flow.

The circulating currents flow from end to end in the shaft, through one bearing to the stator, through the stator, and back

to the rotor through the other bearing. The shaft currents due to dyssymmetry are circulating currents. The noncirculating current, rather than circulating around the motor parts as the circulating current does, flows from the inverter to the motor stator and rotor and through both bearings to ground and back to the inverter [46].

Shaft currents of the circulating type may be eliminated by the use of one insulated bearing. Shaft currents of the noncirculating type require two insulated bearings and insulated couplings, or a shaft grounding brush. If there is a concern for voltage buildup on the rotor, the shaft grounding brush should be used. Note that special care is required for the selection of the shaft grounding brush system [47]. The voltage drop through the system must not exceed the breakdown voltage across the bearing and the lubrication film.

NEMA has published an application guide for ac adjustable speed drives [45]. It contains a section on shaft voltages and sections on many of the other topics included in this chapter concerning motors used for adjustable speed drives.

## REFERENCES

Note: In the following listing, abbreviations have the following meanings:

ANSI American National Standards Institute  
IEC International Electrotechnical Commission  
IEEE Institute of Electrical and Electronics Engineers  
NEMA National Electrical Manufacturers Association  
NFPA National Fire Protection Association  
Sources for standards are listed in [Appendix B](#).

1. ANSI/NEMA Standards Publication No. MG 1–1993, Motors and Generators.
2. IEEE 1–1986, IEEE Standard General Principles for Temperature Limits in the Rating of Electric Equipment and for the Evaluation of Electrical Insulation (ANSI recognized).
3. IEEE 117–1974 (Reaffirmed 1991), IEEE Standard Test Procedure for Evaluation of Systems of Insulating Materials for Random-Wound AC Electric Machinery (ANSI recognized).
4. IEEE 275–1981, IEEE Recommended Practice for Thermal Evaluation of Insulation Systems for AC Electric Machinery Employing Form-Wound Pre-Insulated Stator Coils, Machines Rated 6900 Volts and Below.
5. IEEE 304–1977 (Reaffirmed 1991), IEEE Standard Test Procedure for Evaluation and Classification of Insulation Systems for DC Machines (ANSI recognized).
6. IEEE 429, Standard Test Procedure for the Evaluation of Sealed Insulation Systems for AC Electrical Machinery Employing Form-Wound Stator Coils.
7. King, W.J., “The Basic Laws and Data of Heat Transmission,” *Mechanical Engineering*, Mar.—Aug. 1932.
8. Mc Adams, William H., *Heat Transmission*, McGraw-Hill, New York, 1942, 2nd edition.
9. Hausmann, Eric, and Edgar P. Slack, *Physics*, Van Nostrand, New York, 1939, 2nd edition.
10. Eshbach, Ovid W., *Handbook of Engineering Fundamentals*, Wiley, New York, 1936.
11. *Heat Transfer Data Book*, General Electric Company Corporate Research and Development, Schenectady, New York.
12. Cummings, Paul G., “Comparison of IEC and NEMA/IEEE Motor Standards, Parts I and II,” *IEEE Transactions on Industry Applications*, Part I, vol. IA-18, no. 5, Sept./Oct. 1982; Part II, vol. IA-20, Jan./Feb. 1984.
13. Martiny, W.J., R.M. McCoy, and H.B. Margolis, “Thermal Relationships in an Induction Motor under Normal and Abnormal

- Operation," *Transactions of the American Institute of Electrical Engineers*, vol. PAS-80, Apr. 1961, p. 66–77.
14. Rosenberry, G.M., Jr., "The Transient Stalled Temperature of Cast Aluminum Squirrel Cage Rotors for Induction Motors," *Transactions of the American Institute of Electrical Engineers*, vol. PAS-74, Oct. 1955.
  15. Griffith, J.W., R.M.McCoy, and D.K.Sharma, "Induction Motor Squirrel Cage Rotor Winding Thermal Analysis," *IEEE Transactions on Energy Conversion*, vol. EC-1, no. 3., Sept. 1986.
  16. Johnson, T.C., and W.R.Morton, "Design Considerations for the Use of Aluminum Alloys for Integral Horsepower Motors," *IEEE Transactions on Industry Applications*, vol. IA-13, no. 6, Nov./Dec. 1977.
  17. Pai, V.S., "Preservation of Large Motors and Generators from Weather on Offshore Platforms," *IEEE Transactions on Industry Applications*, vol. IA-26, no. 5, Sept./Oct. 1990.
  18. NFPA 70, National Electrical Code, 1993.
  19. IEEE 323–1983, IEEE Standard for Qualifying Class 1E Equipment for Nuclear Power Generating Stations (ANSI recognized).
  20. IEEE 334–1994, IEEE Standard for Qualifying Continuous Duty Class 1E Motors for Nuclear Power Generating Stations.
  21. Owen, E.L., "A History of Harmonics in Power Systems," *IEEE Industry Application Magazine*, January/February 1996.
  22. Owen, E.L., "Power Disturbance and Quality: Light Flicker Voltage Requirements," *IEEE Industry Application Magazine*, January/February 1996.
  23. Halberg, M. N., "Calculating the Size of Flywheel Required for a Synchronous Motor Driving a Reciprocating Compressor," ASME Fall Meeting September 1956 Paper Number. 56-F-18.
  24. Concordia, Charles, "Induction Motor Damping and Synchronizing Torques," *AIEE [IEEE] Transactions*, Volume 71, 1952.
  25. Mc Coy, R.M., "Power and Current Pulsations of an Induction Motor Driving a Pulsating Torque Load," *GE TIS DF62 MMG* 34, November 1962.
  26. Bonnett, A. H, and G. C. Soukup, "NEMA Motor—Generator Standards for Three Phase Induction Motors," *IEEE Industry Application Magazine*, May/June, 1999.
  27. Berth, Matthias, Lucas King, and Evert Limbeck, "Switching Overvoltages in Motor Circuits," *IEEE Transactions on Industry Applications*, Vol. 37, No.6, Nov./Dec.2001, p1562–1589.
  28. IEEE Working Group progress Report," Impulse Strength of ac Rotating Machines, *IEEE Transactions on Power Apparatus and Systems*, Vol. PAS-100, No.8 August 1981.
  29. Rhudy, R.G., E.L. Owen and D.K.Sharma, "Voltage Distribution Among the Coils and Turns of a Form Wound ac Rotating Machine Exposed to Impulse Voltage," *IEEE Power Engineering Review*, June 1986 p.50–60.
  30. IEEE Std 522–1992, IEEE Guide for Testing Turn-to Turn Insulation on Form-Wound Stator Coils for ac Rotating Electric Machines.
  31. Appiarius, J.C., E.L.Owen, R.M.Mc Coy, and A. Murdoch, "Improved Motors for Utility Applications-Bus Transfer Studies" EPRI EL-4286, Volume 2, Project 1763–2, October 1986.
  32. Appiarius, J.C., G.E.Boukarim, E. L. Owen et al, "Bus Transfer Criteria for Plant Electrical Auxiliary Systems", EPRI-TR-03185, Project 2626–01, October 1993.
  33. EPRI Applications of Motors and Drives Course, Section 19, Power Quality Basics, 1992.
  34. Cummings, P. G, "Estimating Effect of System Harmonics on Losses and Temperature Rise of Squirrel-Cage Motors" *IEEE Transactions on Industry Applications*, Vol. IA-22, No. 6, p1 121–1126, November/December 1986.
  35. MG-1998 Part 30, Application considerations for Constant Speed Motors Used on a Sinusoidal Bus with Harmonic Content and General Purpose Motors used with Adjustable Voltage or Adjustable Frequency Controls or Both.
  36. ANSI/IEEE Std. 995–1987, IEEE Recommended Practice for Efficiency Determination of Alternating-Current Adjustable-Speed Drives.
  37. Sheppard, David J, "Torsional Vibration Resulting from Adjustable-Frequency ac Drives," *IEEE Transactions on Industry Applications*, Vol. 24, No.5, September/October 1988.
  38. Owen, E.L, "History-Motor Insulation Life-Aging Factors and Arrhenius" *IEEE Industry Application Magazine*, July/August 1997.
  39. Mans, Les, "Motor Insulation System Quality for IGBT Drives" *IEEE Industry Applications Magazine*, January/February 1997.
  40. Ong, R, et al, "Shaft Current in ac Induction Machine-An online monitoring System and Prediction Results," *IEEE Transactions on Industry Applications*, Vol.37, No. 4, July/August 2001.
  41. Alger, P.L and H.M.Samson, "Shaft Currents in Electric Machines," *AIEE [IEEE] Transactions*, Vol.43, p235–244, February 1924.
  42. MG1–1998 Part 31, Definite-Purpose Inverter-Fed Polyphase Motors.
  43. Yacamini, R, and S.C.Chang, "Noise and Vibration from Induction Machines Fed from Harmonic Sources," *IEEE Transactions on Energy Conversion*, Vol. 10, No.2, June 1995.
  44. Lynn, A. L, W.H.Gottung, D.Johnston and J.T.LaForte, "Corona Resistant Turn Insulation in ac Rotating Machines," 17<sup>th</sup> EEIC conference, CH2133–7/85 IEEE, p308–310
  45. NEMA Standards Publication, Application Guide for ac Adjustable Speed Drives Systems, 2001.
  46. Chen, Shaotang and Thomas A.Lipo, "Circulating Type Motor Bearing Current in Inverter Drives," *IEEE Industry Application Magazine*, January/February 1998.
  47. Boyanton, Hugh E., "Bearing Fluting," *IEEE Industry Application Magazine*, September/October 2002.

# 13

## Reliability

Charles R.Heising (Section 13.1)/Walter E.Littmann (Section 13.2)/Carbon Products Operation Group\* (Section 13.3)/  
R.Gene Smiley and Stewart V.Bowers (Section 13.4)/Russell J.Kerkman (Sections 13.5 and 13.6)

<b>13.1</b>	<b>RELIABILITY OF LARGE MOTORS</b>	<b>656</b>
13.1.1	Introduction	656
13.1.2	IEEE 1983–1985 Survey	656
13.1.3	Failure Rate and Downtime Data	656
13.1.4	Data on Failed Components	657
13.1.5	Causes of Failure	658
13.1.6	Comparison: 1973–1974 and 1983–1985 IEEE Surveys	659
13.1.7	Comparison: AIEE 1962 and 1983–1985 IEEE Surveys	659
13.1.8	Comparison: 1983 EPRI and 1983–1985 IEEE Surveys	660
<b>13.2</b>	<b>RELIABILITY OF ANTIFRICTION BEARINGS</b>	<b>660</b>
13.2.1	Failure Modes of Rolling Bearings	660
13.2.2	Damage Progression to Failure	662
13.2.3	Statistical Variation of Bearing Life	663
<b>13.3</b>	<b>GUIDELINES FOR SUCCESSFUL COMMUTATOR AND BRUSH OPERATION</b>	<b>663</b>
13.3.1	Summary	663
13.3.2	Introduction	663
13.3.3	Acceptable Commutator Conditions	663
13.3.4	Destructive Commutator Conditions	664
13.3.5	Conclusion	669
13.3.6	Reference Note	669
<b>13.4</b>	<b>MONITORING FOR SIGNS OF WEAROUT</b>	<b>669</b>
13.4.1	Introduction	669
13.4.2	On-Line Tests	669
13.4.3	Off-Line Tests	670
13.4.4	Continuous (On-Line) or Periodic (Off-Line)?	672
<b>13.5</b>	<b>RELIABILITY IMPACT OF ADJUSTABLE SPEED DRIVES (ASDs) ON BEARINGS</b>	<b>672</b>
13.5.1	Introduction	672
13.5.2	Bearing Currents Induced by Supply Voltage	673
13.5.3	An Equivalent Circuit for Bearing Displacement and EDM Currents	677
13.5.4	Methods to Mitigate Bearing Currents and Their Cost	688
<b>13.6</b>	<b>RELIABILITY IMPACT OF ADJUSTABLE SPEED DRIVES (ASDs) ON INSULATION</b>	<b>690</b>
	<b>REFERENCES</b>	<b>690</b>

---

\*The Carbon Products Operation Group includes Kenneth A.Bruni, Richard D.Hall, George G.Kalinovich, and Roland Roberge.



## 13.1 RELIABILITY OF LARGE MOTORS

### 13.1.1 Introduction

The most significant information on the reliability of large motors is found in a 1983–1985 IEEE survey of the reliability of motors larger than 200 horsepower (hp) in industrial and commercial installations [1–3]. These references include data collected on 360 failures from 75 industrial plants on motors no older than 15 years. Failure rates are given for induction, synchronous, wound-rotor, and direct-current motors, and several pertinent factors that affect the failure rate are identified. Data are also given on downtime per failure, failed component, causes of failure, and under what circumstances the failure was discovered. These results are compared with three other motor reliability surveys:

1. The 1973–1974 IEEE survey of motors larger than 50 hp in industrial plants [4].
2. The 1962 AIEE survey of motors 250 hp and larger in industrial plants [5].
3. The 1983–1985 survey sponsored by the Electric Power Research Institute (EPRI) of motors 100 hp and larger in electric utility power plants [6, 7].

### 13.1.2 IEEE 1983–1985 Survey

A Working Group of the IEEE Industry Applications Society began by enumerating the reasons for conducting the 1983–85 IEEE motor reliability survey. These reasons had an impact on the questionnaire that was used; both the reasons and the questionnaire are given in Ref. 1. A decision was made to focus on motors that were of a critical nature and thus only motors larger than 200 hp were selected to be included in the survey. In addition, data were desired on motors similar to those presently being manufactured and used; thus another decision was made to limit the survey to include only motors that were 15 years old or less. Data were submitted by 33

companies on 1141 motors with a population of 5085 unit-years. Some respondents to the survey did not submit data for every category listed in the questionnaire. Where the response was insufficient to identify the motor and/or the period reported, the response was not used.

The IEEE followed a policy of not publishing a failure rate when the sample size was considered too small. If there were fewer than eight failures, an asterisk (\*) was used to indicate a small sample size.

### 13.1.3 Failure Rate and Downtime Data

Failure rate results are shown in Table 13.1 for induction, synchronous, wound-rotor, direct-current, and “all” motors. Calendar time was used when calculating the unit-years of service rather than running time; this was done in order to simplify the data that were collected. Motors with intermittent duty operation had a failure rate that was about half that of those with continuous duty and it is not known how different this would have been if running time had been used rather than calendar time. Data were also collected on the number of starts per day in order to see if this would have any significant effect on the failure rate; motors with fewer than one start per day had approximately the same failure rate as motors with between 1 and 10 starts per day.

Induction motors and synchronous motors had approximately the same failure rate, 0.07–0.08 failures per unit-year. Induction motors, 0–1000 V and 1001–5000 V, had approximately the same failure rates. The sample size on motors above 5000 V was too small to draw any conclusions. Wound-rotor motors 0–1000 V had a failure rate that was about the same as that of squirrel-cage induction motors 0–1000 V. The sample size on direct current motors was too small to draw any meaningful conclusions.

The downtime per failure data are shown in Table 13.2 for all types of motors grouped together as one group. The

**Table 13.1** Overall Summary—Large Motors Above 200 hp

Number of plants in sample size	Sample size (unit-years)	Number of failures reported	Equipment subclass	Failure rate (failures per unit-year)	Average hours downtime per failure	Median hours downtime per failure
75	5085.0	360	All	0.0708	69.3	16.0
			Induction			
33	1080.3	89	0–1000 V	0.0824	42.5	15.0
52	2844.4	203	1001–5000 V	0.0714	75.1	12.0
5	78.1	2*	5001–15,000V	*	*	*
1	13.5	—	Not specified	—	—	—
			Synchronous			
19	459.3	35	1001–5000 V	0.0762	78.9	16.0
2	29.5	3*	5001–15,000 V	*	*	*
			Wound rotor			
5	137.0	10	0–1000 V	0.0730	*	*
9	251.1	8	1001–5000 V	0.0319	*	*
2	39.0	4*	5001–15,000 V	*	*	*
			Direct current			
5	122.7	6*	0–1000 V	*	*	*
1	30.0	—	1001–5000 V	—	—	—

\* Small sample size.

Source: From the IEEE Survey of Industrial and Commercial Installations, 1983–1985 [1–3]. Permission of the American Society for Quality Control; © 1985.

**Table 13.2** Downtime per Failure vs. “Repair or Replace” and “Urgency for Repair,” All Types of Motors Above 200 hp

	Number of failures	Average hours downtime/failure	Median hours downtime/failure
Repair—normal working hours <sup>a</sup>	87	97.7	24.0
Repair—round the clock	45	81.4	72.0
Replace with spare <sup>b</sup>	111	18.2	8.0
Low priority	4*	370.0*	400.0*
Not specified	6*	288.0*	240.0*
Total	251	69.3	16.0

\* Small sample size.

<sup>a</sup> 6570 hours for one failure omitted.

<sup>b</sup> 960 hours for one failure omitted.

Source: From the IEEE Survey of Industrial and Commercial Installations 1983–1985 [1–3]. Permission of the American Society for Quality Control; © 1985.

**Table 13.3** Numbers of Failures for Various Failed Components—Large Motors Above 200 hp

Failed <sup>a</sup> component	Induction motors	Synchronous motors	Wound-rotor motors	DC motors	Total all types
Bearings	152	2	10	2	166
Windings	75	16	6	—	97
Rotor	8	1	4	—	13
Shaft or CLPG	19	—	—	—	19
Brushes or S.R.	—	6	8	2	16
External dev.	10	7	1	—	18
Not specified	40	9	—	2	51
Total	304	41	29	6	380

<sup>a</sup> Some respondents reported more than one failed component per motor failure.

Source: From the IEEE Survey of Industrial and Commercial Installations 1983–1985 [1–3]. Permission of the American Society for Quality Control; © 1985.

comparison of the downtime per failure data for “repair” versus “replace with spare” is of importance when deciding whether a spare motor should be purchased when designing a new plant. Both average downtime per failure data and median downtime per failure data are given so that the effect of a few very long outages on the average downtime can be indicated by a large difference between the average and median values. Table 13.2 also shows the effect on the “repair” time that the “urgency for repair” has had. There were 45 cases of motor failures where the “repair” was carried out on a “round the clock all out effort basis.” There were four cases of motor failures where “low priority” urgency resulted in a very long downtime; it is important to exclude these cases when making decisions on the design of industrial or commercial power systems. In general, the “average downtime per failure” is about five times larger for “repair” than for “replace with spare.”

### 13.1.4 Data on Failed Components

The data on failed components are shown in Table 13.3 for induction, synchronous, wound-rotor, direct current, and “all” motors. It can be seen that the two largest categories reported are bearings and windings, with 166 and 97 failures, respectively, out of a total of 380 failures. Bearings and windings represent 44% and 26%, respectively, of the total failures.

Table 13.4 shows data on failed component versus the “time discovered.” It can be seen that 60.5% of the failures found

during “maintenance or test” are bearings. Many industrial plants consider that it is important to find as many failures as possible during “maintenance or test” rather than “normal operation.” Bearings and windings represent 36.6% and 33.1%, respectively, of the failures discovered during “normal operation.”

**Table 13.4** Failed Component in Percent of Total Failures vs. Time Discovered—All Types of Motors Above 200 hp

Failed component	Time discovered		
	Normal operation	Maintenance or test	Other
Bearing	36.6%	60.5%	50.0%
Winding	33.1%	8.3%	28.6%
Rotor	5.1%	1.8%	0.0%
Shaft or coupling	5.8%	8.3%	14.3%
Brushes or slip rings	3.1%	7.3%	0.0%
External device	5.0%	3.7%	0.0%
Not specified	11.3%	10.1%	7.1%
Total percent	100.0%	100.0%	100.0%
Total no. of failures	257	109	14

Source: From the IEEE Survey of Industrial and Commercial Installations 1983–1985 [1–3]. Permission of the American Society for Quality Control; © 1985.

### 13.1.5 Causes of Failure

The causes of failure are shown in Table 13.5 for induction, synchronous, and “all” motors. This includes the failure initiator, the failure contributor, and the failure underlying cause. “Mechanical breakage” is the largest failure initiator for induction motors, and “electrical fault or malfunction” and “other insulation breakdown” are large failure initiators for synchronous motors. “Normal deterioration from age” is the largest failure contributor for both induction and synchronous motors, but “high vibration” and “poor lubrication” are also large failure contributors for induction motors.

“Inadequate maintenance” and “defective component” are the largest underlying causes of induction motor failures. “Defective component” is the largest underlying cause of synchronous motor failures.

Table 13.5 also shows a correlation between bearing and winding failures and the causes of failure: 50.3% of bearing failures were initiated by “mechanical breakage”; 31.3% and 21.8%, respectively, had “poor lubrication” and “high vibration” as failure contributors; and 27.6% blamed “inadequate maintenance” as the underlying cause. “Other insulation breakdown” was given as the initiator of 36.7% of the winding failures; 18.5% and 18.5%, respectively, had

**Table 13.5** Causes of Failure vs. Bearing and Winding Failures and vs. Motor Type—Motors Above 200 hp

Causes of failure	All motor types— failed component				
	Bearings %	Windings %	All types of motors %	Induction motors %	Synchronous motors %
<i>Failure initiator</i>					
Transient overvoltage	0.0	4.1	1.5	1.4	0.0
Overheating	12.4	21.4	13.2	14.7	0.0
Other insulation breakdown	1.9	36.7	12.3	11.9	21.1
Mechanical breakage	50.3	10.2	33.1	37.4	5.2
Electrical fault or malfunction	3.7	11.2	7.6	5.8	23.7
Stalled motor	0.0	2.1	0.9	0.7	2.6
Other	31.7	14.3	31.4	28.1	47.4
Total %	100.0	100.0	100.0	100.0	100.0
Total no. of failures	161	98	341	278	38
<i>Failure contributor</i>					
Persistent overloading	1.4	6.5	4.2	4.9	2.7
High ambient temperature	0.7	7.6	3.0	3.4	0.0
Abnormal moisture	2.7	18.5	5.8	6.7	2.7
Abnormal voltage	0.0	5.4	1.5	1.5	2.7
Abnormal frequency	0.0	1.1	0.6	0.7	0.0
High vibration	21.8	8.7	15.5	17.6	5.4
Aggressive chemicals	5.4	6.5	4.2	4.5	2.7
Poor lubrication	31.3	5.4	15.2	16.9	8.1
Poor ventilation or cooling	0.0	7.6	3.9	2.2	2.7
Normal deterioration with age	20.4	18.5	26.4	24.0	51.4
Other	16.3	14.1	19.7	17.6	21.6
Total %	100.0	100.0	100.0	100.0	100.0
Total no. of failures	147	92	330	267	37
<i>Failure underlying cause</i>					
Defective component	17.8	10.9	20.1	20.3	22.2
Poor installation/testing	14.5	10.9	12.9	15.9	0.0
Inadequate maintenance	27.5	19.6	21.4	22.8	11.1
Improper operation	2.0	6.5	3.6	3.3	2.8
Improper handling/shipping	0.7	0.0	0.6	0.8	0.0
Inadequate physical protection	7.9	7.6	6.1	6.5	2.8
Inadequate electrical protection	2.6	15.2	5.8	5.3	11.1
Personnel error	7.2	5.4	6.8	5.7	5.6
Outside agency—not personnel	2.0	3.3	3.9	2.8	13.9
Motor-driven equipment mismatch	5.9	4.3	4.9	4.9	0.0
Other	11.8	16.3	13.9	11.8	30.6
Total %	100.0	100.0	100.0	100.0	100.0
Total no. of failures	152	92	309	246	36

Source: From the IEEE Survey of Industrial and Commercial Installations 1983–85 [1–3]. Permission of the American Society for Quality Control; © 1985.

“normal deterioration from age” and “abnormal moisture” as failure contributors; and the “failure underlying cause” had 19.6% “inadequate maintenance” and 15.2% “inadequate electrical protection.” It is of interest to note that “inadequate maintenance” is the largest underlying cause of both bearing failures and winding failures.

A special study of the 71 failures attributed to “inadequate maintenance” is shown in Table 13.6; it can be seen that 59.1% are bearings, that 52.1% are initiated by “mechanical breakage,” and 43.7% had “poor lubrication” as a failure contributor.

### 13.1.6 Comparison: 1973–1974 and 1983–1985 IEEE Surveys

Table 13.7 shows the results from the 1973–1974 IEEE motor reliability survey [4] of industrial plants; this survey covered motors 50 hp and larger and had no limit on the age. These results can be compared to Table 13.1 for the 1983–1985 IEEE survey of motors above 200 hp and not older than 15 years. The 1983–1985 failure rates for induction motors and synchronous motors are about double those from the 1973/1974 survey for motors 601–15,000 V.

### 13.1.7 Comparison: AIEE 1962 and 1983–1985 IEEE Surveys

Table 13.8 shows the results from the 1962 AIEE motor reliability survey [5] of industrial plants; this survey covered motors 250 hp and larger and had no limit on the age. The failure rates for both induction and synchronous motors from the 1962 AIEE survey are within a factor of 1.3 of those shown in Table 13.1 for the 1983–1985 IEEE survey of motors above 200 hp and not older than 15 years. These two surveys conducted 21 years apart show remarkably similar results.

**Table 13.6** Failures (Expressed as Percentages) Caused by “Inadequate Maintenance” vs. Failed Component, Failure Initiator, and Failure Contributor—All Types of Motors Above 200 hp

<i>Failed component</i>	<i>%</i>
Bearing	59.1
Winding	25.4
Rotor	1.4
Shaft or coupling	0.0
Brushes or slip rings	8.5
External device	1.4
Other	4.2
Total % (No. of failures = 71)	100.0
<i>Failure initiator</i>	<i>%</i>
Transient overvoltage	0.0
Overheating	4.2
Other insulation breakdown	14.1
Mechanical breakage	52.1
Electrical fault or malfunction	2.8
Stalled motor	0.0
Other	26.8
Total % (No. of failures = 71)	100.0
<i>Failure contributor</i>	<i>%</i>
Persistent overloading	0.0
High ambient temperature	4.2
Abnormal moisture	7.0
Abnormal voltage	0.0
Abnormal frequency	0.0
High vibration	4.2
Aggressive chemicals	9.9
Poor lubrication	43.7
Poor ventilation/cooling	1.4
Normal deterioration with age	18.3
Other	11.3
Total % (No. of failures = 71)	100.0

Source: From the IEEE Survey of Industrial and Commercial Installations 1983–1985 [1–3]. Permission of the American Society for Quality Control; © 1985.

**Table 13.7** 1973–1974 IEEE Overall Summary—Motors 50 hp and Larger [4]

Number of plants in sample size	Sample size (unit–years)	Number of failures reported	Equipment subclass	Failure rate (failures per unit–year)	Average hours downtime per failure	Median hours downtime per failure
—	42,463	561	All Induction	0.0132	111.6	—
17	19,610	213	0–600 V	0.0109	114.0	18.3
17	4,229	172	601–15,000 V Synchronous	0.0404	76.0	91.5
2	13,790	10	0–600 V	0.0007	35.3	35.3
11	4,276	136	601–15,000 V	0.0318	175.0	153.0
6	558	31	Direct current	0.0556	37.5	16.2

**Table 13.8** 1962 AIEE Overall Summary—Motors 250 hp and Larger, U.S.A. and Canada [5]

Number of plants represented	Sample size (unit–years)	Failures reported	Equipment subclass	Failure Rate (failures per unit–year)	Average hours downtime per failure	Median hours downtime per failure
46	1,420	140	Induction	0.0986	78.0	70.0
53	600	39	Synchronous	0.0650	149.0	68.0

**Table 13.9** Size and Scope Comparison of the IEEE 1983–1985 Motor Survey [1–3] with the EPRI Sponsored Motor Survey in Electric Utility Power Plants [6]

Parameter	IEEE working group	EPRI phase I
Horsepower	>200	100 and up
Number of companies/utilities	33	56
Number of plants or units	75	132
Number of motors	1,141	4,797
Total population (unit–years)	5,085	24,914 <sup>a</sup>
Total failures	360	872 <sup>a</sup>
Failure rate (all motors)	0.0708	0.035 <sup>a</sup>

<sup>a</sup>To first failure.

### 13.1.8 Comparison: 1983 EPRI and 1983–1985 IEEE Surveys

Tables 13.9, 13.10, and 13.11 show a comparison between a 1983 EPRI-sponsored study [6] for motors 100 hp and larger that were installed during or after 1969 and the 1983–1985 IEEE survey of motors above 200 hp and not older than 15 years. The failure rate of 0.035 failures per unit-year in the EPRI sponsored study in the electric utility industry is about half the IEEE failure rate of 0.0708 failures per unit-year. Similar results were obtained in these two studies on the failed component, with bearings and windings and rotor related percentages that were each about the same. Table 13.11 shows some differences between the these two studies on the causes of failures. The IEEE survey found inadequate maintenance, poor installation/testing, and misapplication to be a much larger percentage of the causes, while the EPRI study attributed a larger percentage to the manufacturer; in addition, the EPRI study had a much larger percentage attributed to “other or not specified.”

Additional results from the EPRI-sponsored study are given in a second paper [7]. Table 13.12 shows how the application

**Table 13.10** Comparison of Percentage Failure by Component Between the IEEE 1983–1985 Motor Survey [1–3] and the EPRI Sponsored Survey [6]

IEEE working group		EPRI phase I	
Bearings	44%	Bearing related	41%
Windings	26%	Stator related	37%
Rotor/shaft/coupling	8%	Rotor related	10%

can have an effect on the failure rate in the electric utility industry. The applications with the highest failure rates and the lowest failure rates are shown. Additional data in Ref. 7 showed that much of the failure rate for “cooling tower fan” applications was attributed to “misapplication.”

## 13.2 RELIABILITY OF ANTIFRICTION BEARINGS

### 13.2.1 Failure Modes of Rolling Bearings

The various types of damage that can cause failure of rolling bearings are listed in Table 13.13. Photographic illustrations of these damage modes can be found in several references [8–11] and in literature that is available from bearing manufacturers. The presence of electrical currents passing through the bearing can be recognized by the distinctive appearance of the resulting damage, as shown in Fig. 13.1. The characteristic fluted appearance of damage from prolonged passage of electric current through a bearing is the result of a multiplicity of tiny electrical arcs between the rolling contact surfaces causing local melting of the surfaces. Liquid metal detachment and changes in microstructure and hardness lead to rapid and progressive degradation of surface geometry, resulting in premature failure. Larger electrical currents cause discrete electrical pits on rolling contact surfaces.

One of the most frequent causes of rolling bearing failures

**Table 13.11** Comparison of Failure Cause Between the IEEE 1983–1985 Motor Survey [1–3] and the EPRI Sponsored Motor Survey [6]

Failure cause	EPRI phase I		Failure cause	IEEE working group	
	Number	%		Number	%
Manufacturer Design	401	32.8	Defective component	62	17.2
Workmanship	124	10.2	Improper operation/personnel error	32	8.9
Misoperation			Improper operation Personnel error		
Misapplication	83	6.8	Misapplication	52	14.5
—	613	50.2	Motor-driven equipment mismatch	66	18.3
—			Inadequate electrical protection		
—			Inadequate physical protection		
—	613	50.2	Inadequate maintenance	40	11.1
—			Poor installation/testing	12	3.3
—			Outside agency other than personnel	2	0.6
Other or not specified	613	50.2	Improper handling/shipping	94	26.1
Total	1221	100.0	Other or not specified	360	100.0
			Total		

**Table 13.12** Failure Rate vs. Application in the Electric Utility Industry—EPRI-Sponsored Survey for Motors 100 hp and Up [7]

	Number of failures	Exposure time (years)	Estimated failure rate (%/year)	95% confidence limit (%/year)
<i>Applications with high failure rate</i>				<i>Lower limit</i>
Boiler feed pump	59	695	8.5	6.8
Induced-draft fan	88	1318	6.7	5.6
Boiler circulating pump	50	966	5.2	4.0
Heater drain pump	41	806	5.1	3.9
Primary air fan	44	980	4.5	3.4
Cooling tower fan	150	3345	4.5	4.0
Air compressor (large)	36	811	4.4	3.3
Ash slurry pump	52	1300	4.0	3.1
<i>Applications with low failure rate</i>				<i>Upper limit</i>
Misc. fan (nuclear)	0	109	0	2.8
Boiler feed booster pump	1	568	0.2	0.8
Low-pressure injection pump	1	163	0.6	2.9
Not specified	41	3056	1.3	1.7
High-pressure injection pump	4	294	1.4	3.1
Condensate booster pump	11	606	1.8	3.0
Oil pump	29	1480	2.0	2.7
Misc. pump (special)	71	3568	2.0	2.4
Vacuum pump	18	865	2.1	3.1
Pulverizer	70	3213	2.2	2.7

**Table 13.13** Classification of Damage in Rolling Bearings

Damage classification	Description
<b>Wear</b>	
Adhesive wear	Local rupture of the lubricant film allows microscopic welding of contact surfaces and transfer or detachment of wear particles
“Normal” mild, smooth wear	Adhesive wear is confined to local high spots in the surface roughness and effective lubrication is maintained
Scuffing, scoring, smearing, galling, seizure	Adhesive wear is more extensive, causing irreversible damage to the contact surfaces; unless effective lubrication is reestablished, progressive damage and heat generation cause lubrication failure
Abrasive wear	Hard, solid particles in the lubricant scratch the contact surfaces, removing tiny chips of bearing material
Corrosion wear	Corrosion products from reaction of the bearing material with chemicals in the lubricant wear away
Fretting damage	Vibratory motion in press-fit contact surfaces causes adhesive wear; oxidation of the wear debris promotes subsequent abrasive wear
<b>Plastic flow</b>	
Debris denting	Metallic or other solid debris in the lubricant enters the rolling contacts, causing denting of the surfaces
Brinelling	Static overload causes mutual indentation of the raceways and balls or rollers
Burn-up (lubrication failure)	Loss of effective lubrication causes progressive adhesive wear and smearing of sliding and/or rolling contact surfaces; heat generation and loss of thermal equilibrium leads to catastrophic overheating and destruction of the bearing
<b>Electrical damage</b>	
Fluting	Electric current passing through the bearing causes arcing, local melting, and progressive damage to rolling contact surfaces
Arcing, electrical pitting	
<b>Fatigue</b>	
Contact fatigue—See Table 13.14 for competitive modes of contact fatigue in rolling bearings	Cyclic contact stresses at local stress risers cause initiation and propagation of contact fatigue cracks at and/or just below the contact surfaces
Fracture	Cyclic tensile or bending stresses cause fatigue cracks to grow through the inner or outer ring section

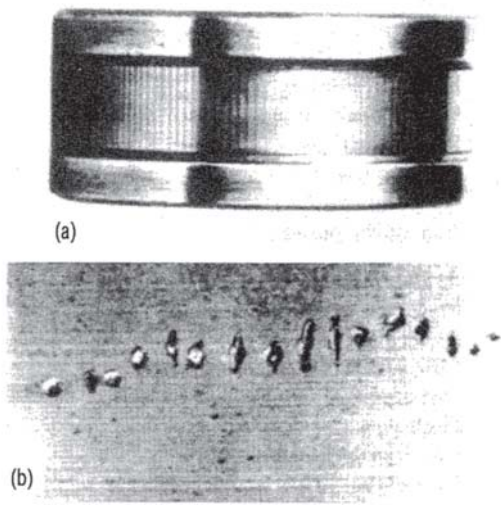


**Figure 13.1** (a) Electrical fluting damage from prolonged passage of electric current, (b) Discrete arcing damage from electrical current. (Courtesy of SKF USA, Inc.)

is overheating (burn-up) because of inadequate lubrication. When the appropriate rolling bearings are properly installed in a given electric motor with the correct running clearance and operated with an adequate supply of clean, cool lubricant, the life of the bearings is ultimately limited by one or more modes of contact fatigue damage described in Table 13.14. Because of the number of balls or rollers in a bearing, the number of contact stress cycles causing fatigue damage of the rolling elements or raceways is a multiple of the number of shaft revolutions, and typical bearing life may be the result of many millions of contact stress cycles. Because contact fatigue life is exponentially related to load and contact stress, the origin of contact fatigue failures is associated with local stress concentrations. These may be inclusions or other discontinuities within the bearing material or on the contact surfaces. Surface roughness heights that are locally or generally greater than the elasto-hydrodynamic lubrication (EHL) film

thickness, debris dents, or other flaws in the contact surfaces are surface stress concentrators that cause surface-origin modes of contact fatigue. Denting of the surfaces due to solid particles (metallic or nonmetallic) in the lubricant that pass through the rolling contacts is another type of surface stress concentration at which contact fatigue originates.

The information in Table 13.14 will be helpful in recognizing contact fatigue modes of damage in electric motor bearings.

### 13.2.2 Damage Progression to Failure

With the exception of lubrication failure, which can occur very rapidly after lubricant supply and thermal equilibrium are lost, most bearing failures are preceded by damage to the contact surfaces and a degradation of performance. The damage is manifested as changes in bearing noise, vibration and/or temperature, as well as the appearance of metal particles in the lubricant. Condition monitoring (see Section 13.4) can be used to detect such damage so that appropriate action can be taken before bearing failure.

The definition of bearing failure depends on the application and required bearing functions. Some damage can sometimes be tolerated before unacceptable changes in bearing noise, vibration, and metal particles in the lubricant. Damage to adjacent components from contact fatigue and wear debris should be considered as well as the changing condition of the bearing itself. The interval of propagation life after initial contact fatigue damage can be significant for some bearing types, especially if lubricant viscosity and chemical activity are favorable [12].

Carburized bearings with line contact, for example, cylindrical or tapered roller bearings, typically exhibit longer propagation life than through-hardened bearings, such as ball bearings and spherical roller bearings. Bearings that operate with widely varying loads and speeds are less likely to have useful propagation life than bearings that run under relatively constant load and speed.

**Table 13.14** Classification of Contact Fatigue Damage/Failure Modes

Damage/failure mode	Distinguishing characteristics	Morphology/appearance
Subsurface inclusion origin	Origin is subsurface at nonmetallic inclusion(s)	Early stages, intact spall; later, semielliptical spall
Geometric stress concentration	Multiple origins at a geometric discontinuity, e.g., at the end of a misaligned line contact or an area of superficial pitting	Multiple adjacent pits along the edge of the contact area, e.g., at the end of line contact or at the boundary of superficial pitting (peeling)
Point Surface Origin	Discrete surface origin, cracking at a shallow angle to the surface, propagating in the direction of rolling motion	Early stage, surface micro-pits; later arrowhead spall, pointing opposite the direction of rolling motion
Superficial pitting (peeling, frosting)	General superficial microspalling; depth of spalling less than 0.001 inch (25 $\mu$ m)	Early stage, multiple micropitting, polished appearance of unpitted surface; later, areas of very shallow spalling (peeling)
Subcase fatigue (case crushing)	Deep subsurface cracks at the junction of case and core	Early development of deep intact spalls, multiple cracks visible at the surface
Section fracture	Fracture through the section, perpendicular to the contact surface	Brittle, flat fracture; beach marks or circumferential jogs may be visible

**Table 13.15** Life Adjustment for Higher Reliability

Reliability (survival probability of individual bearings)	$L_n$	Life adjustment factor, $a_1$
90%	$L_{10}$	1.00
95%	$L_5$	0.62
96%	$L_4$	0.53
97%	$L_3$	0.44
98%	$L_2$	0.33
99%	$L_1$	0.21

### 13.2.3 Statistical Variation of Bearing Life

Bearing life tests conducted with constant load, speed, and controlled lubrication have demonstrated that the life of individual bearings can vary by a factor of 20 to as much as 50 between the first and last failure in a large population of a given bearing, even when the test sample is drawn from a single lot of material and manufacture. For this reason, the catalog load ratings of rolling bearings correspond to the  $L_{10}$  life (sometimes called  $B_{10}$  life), that is, 10% failure or 90% survival probability. Table 13.15 lists the values of the factor ( $a_1$  of Eq. (11.113)) that is used to adjust the calculated life for higher reliability. When the application requires the maximum load capacity and/or reliability, a premium performance bearing can be considered. Such bearings, made from ultraclean bearing steels with customized internal geometry and surface texture, can provide almost infinite life under favorable lubrication conditions. Specialized bearing application analysis can be provided by bearing suppliers to address the need for premium performance in rolling bearings.

Since most machines contain more than one bearing, the reliability of the system will be less than that of the individual bearings. Methods for calculation of system reliability can be found in most manufacturer's catalogs and engineering service guides.

## 13.3 GUIDELINES FOR SUCCESSFUL COMMUTATOR AND BRUSH OPERATION

### 13.3.1 Summary

The production of mechanical or electrical energy using motors and generators is a common practice throughout industry. Successful operation of many of these machines depends on the satisfactory performance of carbon brushes riding on commutators. Unfortunately, there appears to be a considerable amount of confusion and controversy surrounding the criteria used to judge satisfactory brush and commutator performance. Examples of acceptable commutator conditions that may appear unattractive at first glance are provided. The primary impetus then focuses on a discussion of various destructive commutator conditions with related causes. Pictorial views of commutators are included to help relate word descriptions to actual operating conditions.

### 13.3.2 Introduction

A carbon brush riding on a commutator conducts current from a stationary member to a rotating collector. The primary function of the brush is to form the necessary interface at the brush—commutator junction so that current may be conducted successfully. Therefore, the brush must properly lubricate the sliding contact by establishing the commutator film necessary to ensure a smooth ride and uninterrupted current flow. In addition, a brush must aid in the dc machine commutation process to keep circulating currents and associated sparking and heating to a minimum.

A collector system that is functioning properly results in satisfactory performance characterized by the following interrelated criteria:

1. Nondestructive sparking
2. Satisfactory brush life
3. Acceptable commutator life

These three qualities are used to establish guidelines for judging satisfactory brush and commutator performance.

Nondestructive sparking is classified as “black commutation” or fine pinpoint sparking that does not cause brush and commutator deterioration. Destructive sparking will electrically erode both the brush and commutator surfaces, which can eventually lead to equipment failure if not corrected.

Satisfactory brush life is a comparative index usually established by comparing past and present performance on a particular machine or by comparing similar machines. Unsatisfactory brush life may not be caused by the brush itself, for there are many factors that can have a negative influence on brush life. High brush temperatures, low humidity, excessive sparking, destructive vibration, and abrasives are the most common factors that contribute to a reduction in brush life. It must be noted that the brush is a replaceable item that will eventually wear out, but it is important that brush life be reasonably predictable to avoid unexpected and expensive shutdowns.

Acceptable commutator life is another comparative index established through experience with a particular machine or by a comparison with similar machines. Commutator bar burning, grooving, and general deterioration must be nonexistent or controlled within satisfactory levels before acceptable commutator life is attained. Some commutator wear is expected and most designs enable resurfacing when necessary with grinding stones or other appropriate tools.

### 13.3.3 Acceptable Commutator Conditions

Most people are familiar with the textbook description of what a normal and healthy commutator should look like. This leads to classifying every commutator that is not “chocolate brown in color with a medium polish” as unfit for service. This is simply not an accurate assumption, for there are many commutators in service throughout industry that do not comply with the textbook definition but have been successfully performing their duties for many years. The three previously mentioned qualities, nondestructive sparking,



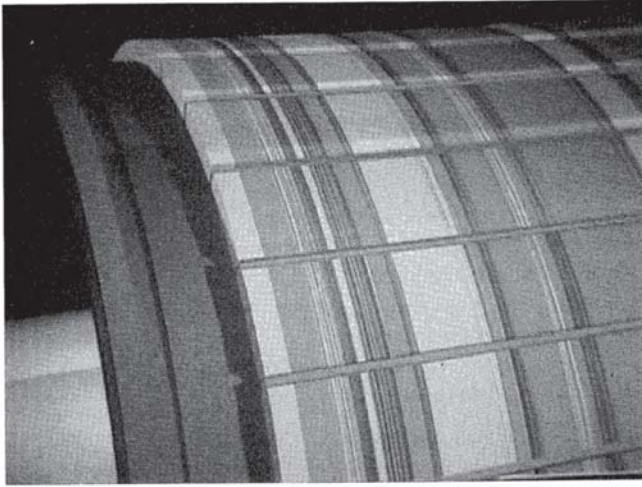


**Figure 13.2** Streaking. Not harmful if there are just streaks in the film and the commutator is not damaged. (Courtesy of National Electrical Carbon.)

satisfactory brush life, and acceptable commutator life, should be the primary criteria in determining satisfactory performance. Successful operation can and does occur on commutator films that are not pleasing to the eye. For example, the brush face is constantly changing during commutator rotation, which may produce uniform circumferential streaks in the film as shown in Fig. 13.2. Streaking is not harmful to the operation if this is a surface condition in the film only and the commutator is not being damaged.

Film color is an appearance factor that is often discussed at great length. Dark or light film colors can be caused by the type of brush being used or by atmospheric contamination. Some brush materials produce dark films, while others provide satisfactory performance with a much lighter color. Both are acceptable if the equipment is functioning properly and commutator and brush distress is not detected. Contamination can cause the film to be very nonuniform in color, such as that shown in Fig. 13.3. Oil contamination can cause this mottled

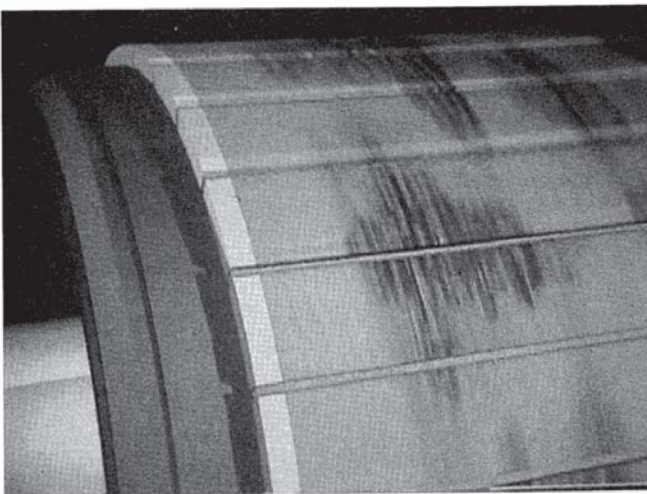


**Figure 13.3** Mottled. Satisfactory operation can result with a film color that is not uniform. (Courtesy of National Electrical Carbon.)

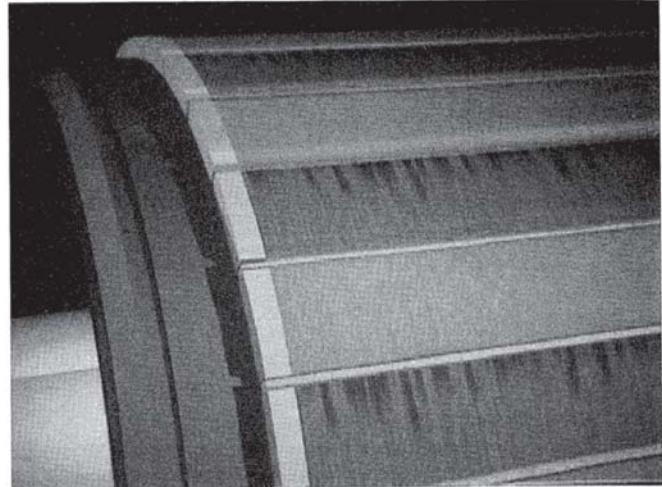


**Figure 13.4** Nondestructive slot bar pattern. Darker film color pattern related to the number of conductors per slot. (Courtesy of National Electrical Carbon.)

appearance, in which random dark and light colored areas are observed on the commutator surface.

The number of conductors in the armature slot can influence commutator bar coloration, resulting in a keyboard appearance or pattern. This is commonly referred to as a slot bar pattern and is characterized by every second, third, or fourth bar being of a darker color than the others. Figure 13.4 illustrates a two-bar pattern where every second bar is darker in color. This pattern occurs in regular intervals around the commutator circumference. Slot bar patterns are related to the electrical design of the machine and are not considered harmful if the commutator has not been damaged. This is readily determined by erasing the film on darker colored bars with a pencil eraser and looking for burned or etched areas on the trailing edges.

### 13.3.4 Destructive Commutator Conditions

Destructive commutator conditions must be avoided if possible to extend equipment life and to prevent unnecessary shutdowns. Unfortunately, this is not always possible, for both brushes and commutators experience distress on occasion, leading to an increase in operational expense. Therefore, it is important to recognize commutator distress symptoms and to take corrective action as soon as possible. Listed in Table 13.16 are the most common destructive commutator conditions observed in a variety of industries. They are not

**Table 13.16** Destructive Commutator Conditions

- 
- Slot bar burning
  - Pitch bar burning
  - Threading
  - Copper drag
  - Grooving
  - Selectivity, stripping, and grooving
  - Nonconductive filming
-

necessary listed in order of importance to any particular industry, for they represent common complaints registered in the operation of direct current motors and generators worldwide. Each condition is defined and examined below for its respective causes.

### 13.3.4.1 Slot Bar Burning

Both the nondestructive slot bar pattern described earlier and destructive slot bar burning are influenced by the number of conductors in the armature slot. Also, both are characterized by second, third, or fourth bar discoloration in regular intervals around the commutator circumference. However, slot bar burning is more than just an integral part of the film. Sparking levels have become high enough to remove metal from the trailing edges of the commutator bars, which will appear burned or etched when the film is removed. These electrically eroded areas usually enlarge with continued operation and become readily detectable without film removal if the destructive process is allowed to continue. This situation is analogous to a pothole in a road progressively increasing in size with the continuing passage of traffic. The commutator illustrated in Fig. 13.5 has experienced slot bar burning on two of every three bars in a repeated pattern around the commutator surface.

Slot bar burning is influenced by factors that reduce the commutating ability of a dc motor or generator. These factors are numerous, but the most common ones can be grouped in the following three categories:

1. Use of a carbon brush material or brush design with insufficient commutating ability.
2. Improper electrical adjustment of the machine.
3. Exceeding the machine load or transient load design limits.

An electromotive force (emf) of self- and mutual induction is induced in an armature coil undergoing commutation when current reversal occurs. This induced emf, commonly called the reactance voltage, acts to oppose current reversal and can be expressed in its simplest form by:

$$E_R = (L + M) \frac{di}{dt}$$

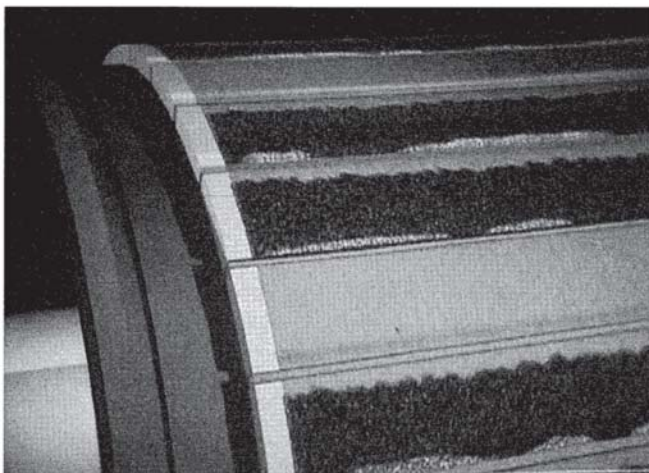


**Figure 13.5** Slot bar burning. Etching on the trailing edges in a regular pattern. (Courtesy of National Electrical Carbon.)

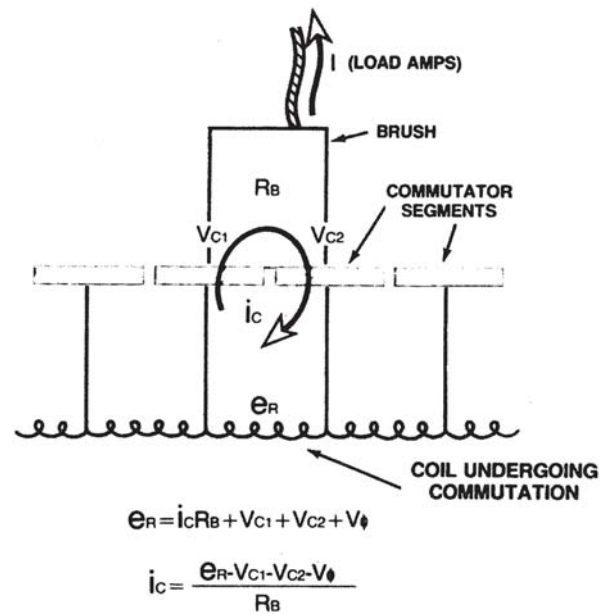


**Figure 13.6** High-resistivity brush materials reduce circulating currents. (Courtesy of Carbon Products Operation.)

where  $E_R$  is the reactance voltage,  $L$  is the self-inductance,  $M$  is the mutual inductance, and  $di/dt$  is the rate of change of current with time in the short-circuited coil. High reactance voltage values increase brush circulating currents, temperatures, and sparking, which can lead to slot bar burning and flashovers.

It is very important to have the correct brush material and brush design at higher reactance voltages ( $E_R$ ) to maintain lower levels of brush circulating currents and associated sparking. The simplified drawing shown in Fig. 13.6 illustrates the importance of brush material resistivity in reducing circulating currents. Higher resistivities reduce circulating currents ( $i_c$ ) by increasing brush cross resistance ( $R_B$ ) and increasing contact drop voltage ( $V_{C1}$  and  $V_{C2}$ ) since contact drop usually increases as brush resistivity increases. These are reasons why higher resistivity brushes are used on the more difficult-to-commutate motors and generators, which have elevated sparking levels that cannot be neutralized by the generated commutating pole flux voltage ( $V_\phi$ ) alone.

The drawing shown in Fig. 13.7 is similar to that in Fig. 13.6 except that a three-wafer brush design is shown instead of a single thick wafer. The additional increase in cross resistance between the wafers ( $R_W$ ) also helps to reduce circulating currents. In addition, a multiwafer brush generally has a better opportunity to follow irregular commutator contours, accounting for a further decrease in sparking and associated bar burning.

Correct circumferential brush positions and commutating pole air gaps are essential to the proper electrical adjustment of dc machines. Improper adjustments of either can lead to higher reactance voltages in the coil undergoing commutation. Some machines have narrow commutating zones that make proper electrical adjustment paramount to successful operation.

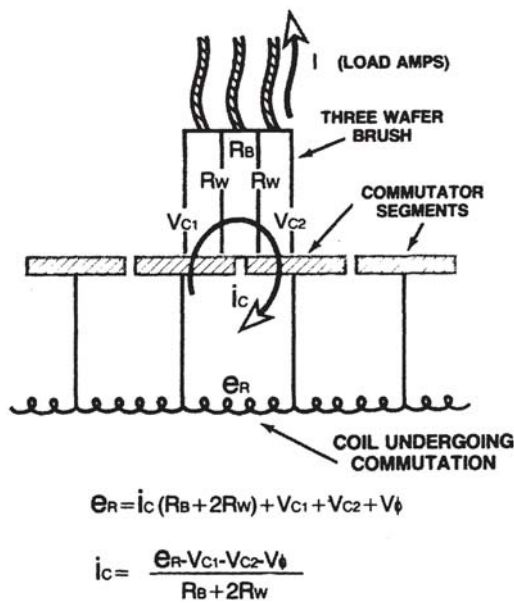


**Figure 13.7** Multiple wafer brushes aid in improving commutation. (Courtesy of Carbon Products Operation.)

Exceeding the machine load design limits can create higher than normal reactance voltages because commutating pole magnetic saturation and insufficient neutralizing flux can result. The commutating pole flux can also lag the armature reactive flux under severe transient loads, leading to severe sparking at the brushes and to slot bar burning and flashovers.

#### 13.3.4.2 Pitch Bar Burning

Pitch bar burning starts under the cathode brush when certain mechanical or electrical disturbances are in phase with armature rotation. Excessive arcing, metal transfer, and associated burning occur every time the same commutator bars pass under the cathode brushes. Usually, the burned bars will be spaced initially in a uniform pattern around the commutator, with angular separations between burned bars equal to  $2 \times 360$  degrees/ $p$ , where  $p$  is the number of poles. That is, a four-pole machine will have burned bars 180 degrees apart, a six-pole machine 120 degrees apart, and so forth. The commutator will develop burned areas related to the total number of poles if operation continues. Each burned area may contain one or more bars, such as shown in Fig. 13.8, which cause the brush to bounce and eventually break if the commutator is not resurfaced.

At times, it is difficult to determine the cause of pitch bar burning since there are a number of possible electrical and mechanical contributing factors. Open-circuit and high-resistance connections in the armature circuit are leading electrical contributors. This applies to the equalizer circuit in addition to the riser/armature conductor connection. Another electrical contributor in the presence of vibration is an unbalanced main field magnetic circuit caused by shorted turns or unequal pole gaps. Sources of vibration such as armature unbalance, worn bearings, misalignment, and rough or eccentric commutators are leading mechanical conditions

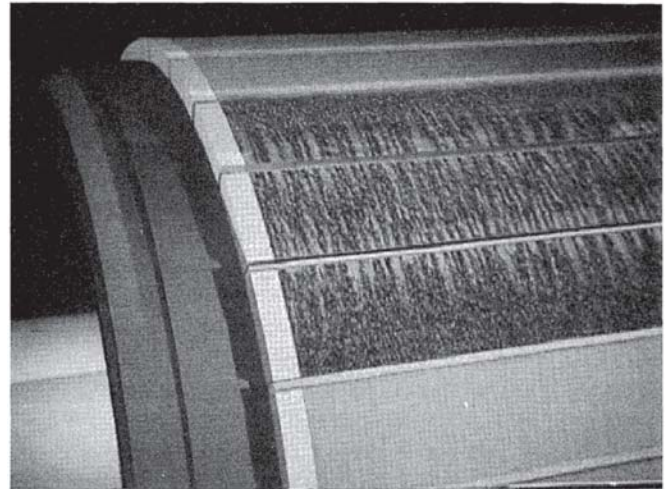


**Figure 13.8** Pitch bar burning. Commutator bar burning in a regular pattern caused by a cyclical mechanical or electrical disturbance. (Courtesy of National Electrical Carbon.)

to be considered. Insufficient brush pressure and poor riding brushes have a tendency to aggravate the overall problem.

#### 13.3.4.3 Threading

A threaded commutator is characterized by fine machined lines around the circumference that look similar to screw threads. Threading is caused by metal transfer from the commutator to the brush face. The metal particles lodge in a porous brush material and eventually become harder (through work hardening) than the original commutator surface. The brush then acts like a cutting tool on a lathe, machining the screw-like, threaded appearance shown in Fig. 13.9.

It is normal to experience some metal transfer to the brush face during current collection; however, most of the metal is vaporized at the higher energy levels produced when operating close to rated current loads. Operation at reduced loads lowers energy levels and allows for an excessive metal

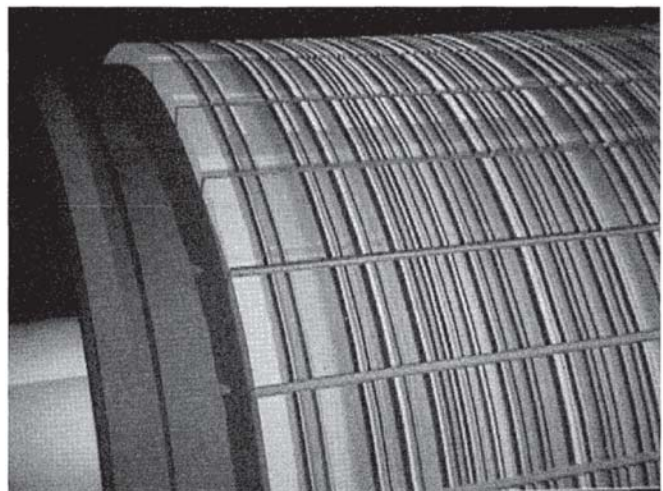


**Figure 13.9** Threading. Fine-machined lines in the commutator. (Courtesy of National Electrical Carbon.)

buildup in the brush face. Corrective measures that can be taken include the following.

1. Remove some brushes to increase current density to reasonable levels in the remaining brushes.
2. Use a graphite brush (which has fewer “holes” or “anchoring points”) instead of a porous electrographitic material.
3. Use a treated electrographitic material.
4. Maintain spring pressure within recommended limits.

Recommended safety and operational precautions must be followed when taking corrective action.

It is common to find a considerable amount of threading on commutators operating in the presence of acids, bases, and some oils. Metal accumulation in the brush face is accelerated by either (1) reduced vaporization of contaminated metal particles because of their protective outer coating, or (2) more metal being transferred because of the contaminant creating a better conductive path.

Use of some graphite brush materials and treated electrographitics can help reduce metal transfer by forming a protective coating on the commutator surface. Porosity is reduced in treated electrographitic materials, but they are still prone to threading at current densities less than  $45 \text{ A/in}^2$  ( $7 \text{ A/mm}^2$ ).

It is important to note that while threading is unsightly, it usually does not prohibit equipment operation since substantial operating time is normally required before detrimental limits are reached. It is beneficial to reduce threading levels as much as possible; however, be careful that a more serious problem, such as copper drag, does not develop when brush grades are changed.

#### 13.3.4.4 Copper Drag

Copper drag is a buildup of conductive material between commutator bars that can cause sparking and lead to flashovers when bar-to-bar voltages are significant. Copper drag is quite often associated with a combination of excessive metal transfer to the brush and environmental contamination that reduces metal vaporization. Excessive metal transfer can occur when electrical or mechanical disturbances stimulate increased sparking at the brush-commutator contact. The molten metal is formed into thin sheets by commutator rotation and brush pressure, eventually forcing the flattened particles into the commutator slots. They normally adhere to the trailing edge of the commutator bar, where they build up in layers similar to that shown in Fig. 13.10.

Some brush materials can operate satisfactorily in the presence of atmospheric contamination, such as oxygen-inhibiting lubricants, while other brushes will promote the growth of copper drag. Simply changing the treatment in an electrographitic brush material has eliminated copper drag on excavator shovel generators operating near lubricated cables. This is also true in oily steel mill atmospheres and contaminated papermill areas.

In general, reducing the causes for sparking and removing the contaminant will alleviate copper drag, but this is not practical in all cases and the simplest solution is to periodically

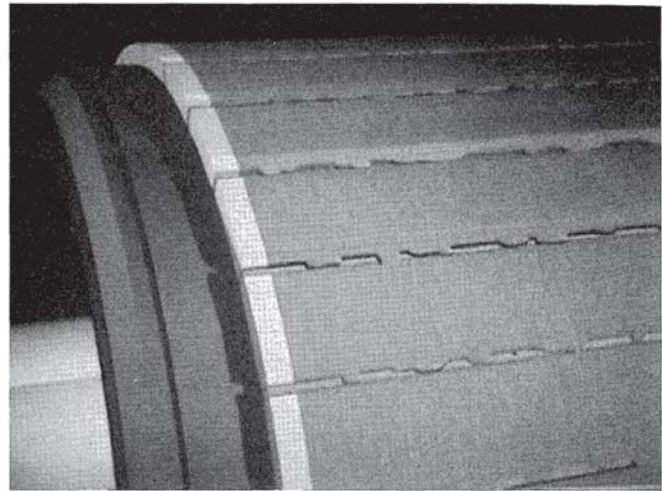


**Figure 13.10** Copper drag. Accumulation of conductive material on the trailing edges. (Courtesy of National Electrical Carbon.)

clean slots. Fortunately, copper drag is not tightly bonded to the bar edges and can easily be removed if there is sufficient access to the commutator.

Copper drag has also been known to occur on machines that are not normally heavily loaded and where contamination does not appear to be a major factor. Selective copper drag, or copper drag that may not develop on all brush paths, is common in these types of applications. Commutator grooving and rapid brush wear has also been observed on the brush path(s) experiencing copper drag. A considerable amount of copper has been found in brush faces removed from the grooved paths, indicating that the brush face copper is acting like a cutting tool to machine the commutator. Changing brush grade has been found to minimize or eliminate this problem since some grades have a tendency to be more selective than others.

#### 13.3.4.5 Grooving

Commutator grooving usually occurs completely across the brush paths, as shown in Fig. 13.11. Groove depth may vary

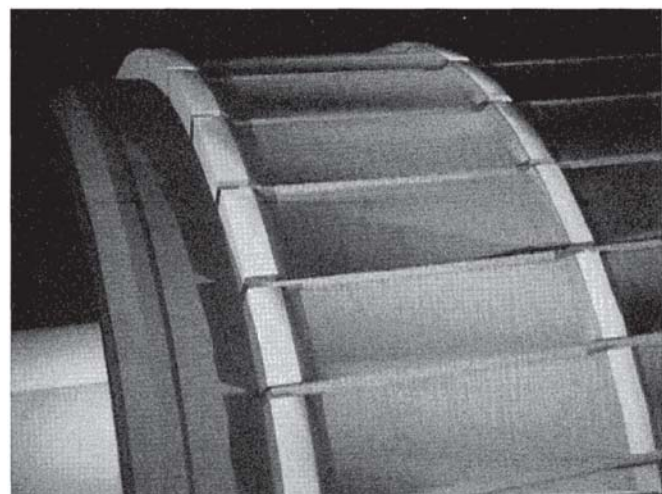


**Figure 13.11** Grooving. Metal machined from across the brush paths. (Courtesy of National Electrical Carbon.)

from path to path; however, depth in a particular path is fairly uniform around the commutator. This type of grooving is caused either by an abrasive brush or by abrasives in the atmosphere. A brush that is hard will not necessarily cause more grooving than a softer brush.

Usually the opposite is true, for many softer brushes are made from natural graphites that inherently contain ash. Sometimes ash is added to artificial graphite brushes to control filming properties in contaminated atmospheres. Both of these natural and artificial graphite materials are soft and have a tendency toward commutator grooving. Many harder brushes (electrographitics) are baked at temperatures well over 2000°C, which removes most of the abrasives that would cause commutator grooving. These electrographitic brush materials are often treated with additives that protect the commutator by promoting the establishment of a film that reduces the chemical reactions between the contaminants and commutator copper. Much of the grooving and costly periodic maintenance is thereby eliminated by the use of treated electrographitic brushes instead of the softer graphite variety that contains ash.

On some applications, grooving caused by atmospheric abrasives can be controlled with filters or by changing equipment ventilation systems to receive cleaner air. Brush wear is usually also greater in the presence of atmospheric abrasives since both members of the rotating contact are exposed.

#### 13.3.4.6 Selectivity, Film Stripping, and Grooving

Selectivity, film stripping, and grooving are three interrelated distress signals that have plagued a number of applications. Little is known about the exact physical phenomenon that triggers these events; however, certain environmental and/or operating conditions are usually present that suggest possible reasons for their occurrence.

Selectivity is the unequal distribution of current between brushes operating in parallel. Heavily loaded machines with numerous brush paths are more prone to be selective since there are more opportunities for variations in resistance between brushes. Resistance variations can be caused by a number of factors, including mixed grades on the same machine, poor electrical connections between the brush shunts and brush, inadequate fastening of brush terminals to the holder, paint on the holder-brush terminal connection, differences in spring pressures, variations in commutator film thickness between brush paths, temperature differences across the commutator, and sparking caused by mechanical or electrical disturbance.

Selectivity is a condition that usually continues once initiated since carbon electrical resistance decreases as temperature increases. Excessive brush currents, temperatures, and sparking can develop to the point of burning brush shunt connections and even flashing over. Brushes carrying the extra current usually wear much faster than other brushes on the same support arm.

Some brush materials have a tendency to be more selective than others. This is true for graphite brush materials that produce commutator films of varying thickness, creating major differences in path-to-path resistivity. Therefore, graphite materials are not normally used on commutators that have more

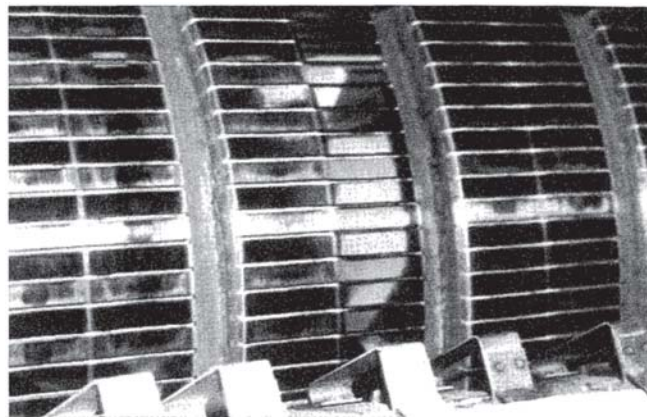


**Figure 13.12** Stripping. Less film on the fourth brush path is a destructive condition. The slot bar pattern is acceptable since the bars are not etched. (Courtesy of Carbon National Electrical.)

than four brush paths. Certain electrographitic brush treatments can also contribute to the formation of unequal current distributions between adjacent brushes of the same polarity. It is important to recognize the symptoms of potentially destructive conditions and to take appropriate action if problems arise. Reducing the causes of resistance variations mentioned earlier should be initiated as a first step. Sometimes removing a contaminant, such as oil, can correct the problem. A change of brush grades to a more compatible material can be made if the problem persists. Spiral grooving of the commutator surface to reduce brush “hot spots” is a technique that has proven worthwhile on a number of applications.

Commutator film stripping, as shown on the fourth brush path from the left in Fig. 13.12, is quite often associated with selectivity on machines that are subjected to heavy transient loads. Film stripping promotes additional selectivity since the contact drop between brush and commutator is less on the stripped paths, resulting in a further decrease in resistivity. Brush temperatures, currents, and sparking can then reach extremely high levels on the stripped paths. For example, excavator generator brush temperatures of over 260°C were recorded on stripped paths while adjacent brushes on filmed paths were operating at less than 150°C. Sparking levels had reached the “streamer” stage on stripped path brushes. Cold air flow on the commutator and low humidity can further aggravate an already poor situation.

Selective grooving can result if film stripping is not corrected. Very high current and sparking levels on heavily loaded machines are thought to vaporize the commutator copper during periods of excessive metal transfer. This differs from the selective grooving caused by machining on lighter-loaded machines described in Section 13.3.4.4.

#### 13.3.4.7 Nonconductive Filming

Nonconductive filming is an expression that is synonymous with the “overfilming” phrase heard quite often. Sparking and bar burning usually accompany this condition since high-resistance areas in the film can be found when the commutator is probed. Nonconductive films can be formed from

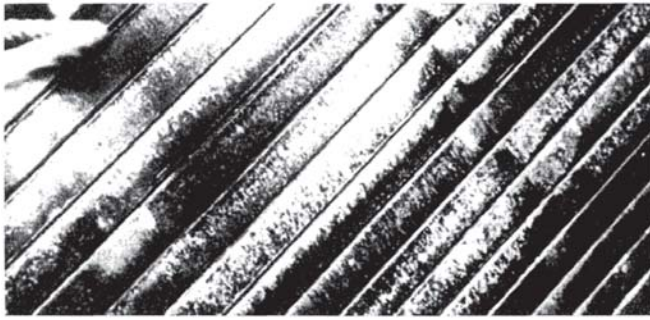


**Figure 13.13** Nonconductive filming. Brush sparking usually results from this condition. (Courtesy of Carbon National Electrical.)

contamination, certain types of brush materials, and sparking. Sometimes a combination of these three factors creates the unattractive commutator appearance shown in Fig. 13.13.

It is important to note that commutator film color should not be used to determine whether the film is nonconductive. It is not uncommon to see very dark films on papermill commutators that are performing quite well. This applies to other industries as well. The correct brush grade in the presence of contaminants can help provide for a successful application without costly maintenance.

### 13.3.5 Conclusion

Satisfactory brush and commutator performance is characterized by

1. Nondestructive sparking
2. Satisfactory brush life
3. Acceptable commutator life

These three interrelated criteria can occur on attractive commutators as well as on those considered not pleasing to the eye.

There are times when machine problems develop that emerge as distress signals at the brushes or commutator. The collector system acts like a thermometer in revealing equipment problems even if the cause originated elsewhere. It is important to locate the problem source and take corrective action quickly to prevent additional machine damage. The destructive commutator conditions discussed in this section should help engineering and maintenance personnel determine whether the source of a particular problem is machine or brush related.

### 13.3.6 Reference Note

The subject matter presented in this section was acquired by the author through years of experience as an electrical design engineer in the motor/generator field and through years of investigating and resolving commutator- and brush-related problems. Much of the information presented is based on the combined experiences of other experts in this field in addition to those of the author himself. Therefore, it is difficult to designate specific individuals, books, or periodicals for detailed references. A general reference is Bruni [13].

## 13.4 MONITORING FOR SIGNS OF WEAROUT

### 13.4.1 Introduction

Historically, electric motors have not been a major cause of downtime in plants. However, with enlightened maintenance strategies of paying increased attention to identifying, tracking, repairing, and eventually predicting mechanical problems, and with the aging of plants, operators typically find an increasing percentage of “electrical” problems in plant equipment. A number of techniques have become available for determining the health of electric motors. These techniques vary from smarter use of traditional measuring equipment to sophisticated instruments with embedded computers.

Most faults found in motors are mechanical in nature. A 1987 IEEE study of failure initiators, contributors, and underlying causes in over 300 motors [3] showed that when “other” (presumably unknown) reasons were not considered, mechanical breakage, stalling, and overheating constituted 70% of failure initiators, with the remainder being various types of electrical faults. In these cases, inadequate maintenance was listed as by far the largest single underlying cause. Defective components, poor installation and testing, and inadequate electrical protection were other underlying causes. Normal deterioration or aging was listed as the largest single contributing cause.

The point is that all machines eventually wear out, but that machine life can almost always be extended by operating the maintenance department in a proactive manner, paying attention to the machines, and understanding what easily detectable symptoms are saying about the machine condition. No great capital expenditure is required, only a will to change perspective, and a strategy.

Developing a strategy requires knowledge of what symptoms are observable, how these symptoms relate to impending failures, and what test equipment is available. Some techniques that have proven themselves commercially are examined below.

### 13.4.2 On-Line Tests

#### 13.4.2.1 On-Line Insulation Test

Vacuum impregnation and resin-rich epoxies are used to minimize the occurrence of minute, gas-filled voids in motor winding insulation. In high-voltage (over 4 kV) ac motors and generators the normal sinusoidal voltage gradient across these voids causes partial discharges in the voids. As the winding ages, the arcing deteriorates local regions of the insulation, eventually reaching the point where arcing occurs between adjacent conductors, or a conductor and ground, at which point it is referred to as a phase-to-phase fault or ground fault. In a darkened room, a bluish haze appears around the running motor. Occasionally the failures are spectacular, especially in machines operating in hazardous environments.

In addition to the visible effect described above, partial discharge produces effects measurable in the line current at very high frequencies. A special nonferrous, air-core current transformer, called a Rogowski coil, is installed on each phase near the motor line end, usually at the terminal box. (The

high-frequency effects are attenuated by distance, so that the coils must be placed at the motor end.) An oscilloscope is used to observe both a line voltage and the coil signal. Spikes seen in the current traces are produced by discharges. The winding condition is analyzed [14] by counting the number and amplitude of discharges, to establish the largest repetitive discharge that indicates specific faults. These observations are made every 6 to 12 months, and trended.

The major advantage of this technique over offline dielectric loss analysis is in the condition of the winding during the test. In service, the machine has a voltage gradient from the line end to the star point. In an offline test, the entire winding or phase is raised to line potential, a condition different from that seen in service. Also, with this on-line method, widespread low-level discharge activity, present in all motors under normal conditions, can be separated from localized high-energy discharges. Finally, the dynamic effects of vibration and thermal movement are included in the on-line test.

#### 13.4.2.2 On-Line Induction Rotor Test

Die-cast rotors are notorious for having porosities in the end ring or inconsistently shaped bar cross sections. Fabricated rotors can have poor brazing joints or material defects. Usually none of these manufactured-in defects are easily detectable by static resistance or even x-ray tests. Wound-rotor circuits can have poor connections. During operation, these defects form obstacles to the flow of current in the rotor, causing hot spots. Over time, mainly during start-up when the inrush current is several times normal, but especially in applications with severe torsional transients, these regions deteriorate into actual bar fractures, or burn spots. Die-cast rotors may eventually fling off molten material. Copper rotor bars may lift due to centrifugal force and contact the stator.

Analysis of the frequency spectra from a motor's electrical supply current or axial flux can detect rotor-related electrical faults in squirrel-cage induction motors. Such faults are broken rotor bars, high-resistance joints in copper rotors, voids in aluminum cast rotors, and cracked rotor end rings [15, 16]. The frequency spectrum reflects the influence of the motor's load and response on the supply current. During each turn of the rotor, electrical signals associated with the rotor induce currents in the stator. These currents appear as sidebands about the supply line frequency peak. These sidebands appear at a frequency equal to the number of poles times the slip frequency. The slip frequency is defined as the synchronous speed of the motor minus the running speed at which the data is acquired.

#### 13.4.2.3 On-Line Air Gap Tests

The clearance between the rotor and stator in synchronous and induction motors is critical. Designed to be typically several tens of thousandths of an inch, a static offset can develop due to misalignment, bearing and stator bores being nonconcentric, and so forth. In addition, a bent or out-of-round shaft can produce dynamic eccentricity, or a reduced air gap that rotates with the shaft. When the air gap is offset by about 60%, rotor-to-stator contact during start-up is almost guaranteed.

Eventually, air gap problems will show up as an apparent increase in the vibration level at two times line frequency that disappears immediately when power to the motor is removed.

It is also possible to monitor the change in air gap by examining slot-pass frequencies found in vibration, electric current, and flux signature analysis. These frequencies can be thought of as a family of frequencies. In vibration, the slot-pass family of frequencies consists of twice line frequency modulating about the number of rotor bar or stator slots times running speed (principal slot-pass peaks). Increased amplitude in this family of peaks indicates potential static eccentricity-related problems. Dynamic eccentricity will cause running speed sidebands to modulate about each family of frequencies produced by static eccentricity. When evaluating electric current and flux signatures, the slot-pass family of peaks will occur as in vibration. However, all frequencies will be offset by line frequency.

#### 13.4.2.4 On-Line Supply Test

An increasingly popular method of controlling motor speed is to use an induction motor with a variable-frequency supply in place of a dc motor. Varying the supply frequency involves a circuit with several SCRs.\* Firing at controlled times to produce a waveform that is approximately sinusoidal. The supply for a dc motor also involves SCRs. Whenever a fault develops in the supply, most commonly a failed SCR, the result is an increase in the "ripple" in the waveform produced. In the ac supply, the harmonic content increases. In the dc supply, a strong ac component appears. The change is also observable in motor vibration because of the abnormal magnetic forces produced in the motor.

This change is easily detectable with a spectrum analyzer, and can be diagnosed in both the vibration spectrum and in a spectrum of line current.

#### 13.4.2.5 Online Vibration

Vibration measurements on motors are discussed in detail in [Chapters 11](#) and [14](#). Note, however, specific electrical faults are typically not easily distinguished in vibration. For diagnosis of electrical faults, other techniques described in this section, are better suited.

### 13.4.3 Off-Line Tests

All off-line tests suffer from the problem of having to simulate the actual operating voltage in some manner that involves compromises. For example, in service, the voltage applied to a winding is a gradient from line voltage at the terminal to zero at the common connection of a wye-connected machine. When testing, however, the winding must be brought up to uniform potential, thus imposing a different condition than that seen in service. Thus, on-line tests are always more valuable when possible. However, an off-line test is sometimes

\*SCR is the abbreviation for silicon-controlled rectifier. This device is also referred to by the name thyristor. See [Sections 9.4](#) and [9.5](#) for further details.

the only test capable of predicting the needed results. Some commonly used off-line tests are described below.

#### 13.4.3.1 Megger Test and Polarization Index

The Megger test is simply a measure of the insulation resistance in megohms. This is the first test that will be applied to a winding before the application of ac voltage to the winding. It is necessary to establish that the winding is neither too damp nor contaminated, and safe to test. A badly contaminated or moist winding can result in high leakage current, localized instability, surface discharge, and tracking.

Insulation resistance should be measured phase to phase and phase to ground, checking for balance between phases. Stator winding insulation resistance should be related to voltage, and as an approximate rule should not be less than (rated voltage/1000) megohms. For low-voltage motors (rated less than 1000 V), the insulation resistance should be greater than 0.5 megohm. Motors testing less than this should be dried out using conventional methods, and a curve should be plotted of insulation resistance vs. time.

The polarization index (PI) is the ratio of the insulation resistance measured 10 minutes after application of the test voltage to the resistance measured after 1 minute. Due to absorbed moisture, contamination, and other degrading factors, the ratio changes as the insulation degrades. Generally, if the 10-minute value is less than 1.5 times the 1-minute value, the winding is considered contaminated. It is possible to have a good initial insulation resistance value with a poor PI (less than 1.5), in which case it is often quite safe to proceed with the tests.

The major limitation of this test (dc resistance and PI index) used by itself is that it normally indicates only the surface condition of the insulation.

#### 13.4.3.2 AC High Potential

An ac high-potential (hi-pot) test is commonly applied by manufacturers as a proof test because it provides a quick pass/fail indication for integrity of the winding's insulation to ground. However, it is generally considered to be a destructive test, causing winding degradation. There is no way of determining that failure is imminent so that the test can be aborted; the motor either passes the test or fails.

#### 13.4.3.3 DC High Potential

A dc hi-pot test also tests for quality of insulation to ground. However, this test does not degrade insulation. Moreover, rather than being a pass/fail test, it is a quantitative test. It provides an indication that winding failure is about to occur if the test is continued, so that the test can be aborted and the motor returned to service while arrangements are made to correct the problem.

The motor is disconnected from the supply, and the dc voltage (typically a few kilovolts) is applied to each phase in turn. Test voltage is increased in uniform increments up to the maximum prescribed for the motor. Leakage current is read on a microammeter and plotted versus applied test voltage. Healthy insulation results in a uniform increase in leakage current with test voltage early in the test, after which the increase in current

tapers off. An erratic increase in leakage current indicates impending failure if the test is continued, and that the failure is likely to occur in service in the near future.

Although it is better than no test, the main disadvantage of the dc hi-pot test is that the stator winding is not in its natural state of energization during the test.

#### 13.4.3.4 Growler and Single-Phase Induction Rotor Tests

These tests are designed to find cracked or broken bars and end rings in three-phase motors.

The growler is an iron-core test coil energized with the rotor cradled in its pole faces. A growler functions as a transformer having no secondary winding, only the primary and an open magnetic circuit. Placing the rotor on the growler pole faces closes that circuit through the rotor itself. This sends a strong magnetic field through the rotor. A steel blade, such as a common hacksaw blade, is laid parallel with and across each rotor slot in turn, as the rotor is revolved by hand through a full circle. Normally, the blade will vibrate to the touch while audibly buzzing or "growling." When the blade encounters a slot with a broken bar, it will not lie flat against the rotor, due to the abnormal magnetic field.

Theoretically, growlers can be made in almost any size. In practice, however, most are small, suited to rotors 1 or 2 feet in diameter.

In a single-phase test the motor is left installed but disconnected from the mechanical load and the supply. A temporary voltage source of about 1/4 (25%) of the normal line voltage is applied to one phase. While using a meter to monitor the current in the reduced voltage supply, the rotor is turned *slowly* by hand. A dip in the meter will occur if there is cage damage.

Both of these tests may be inconclusive because hairline cracks in bars and end rings tend to close up when the rotor is cold. When possible, heating until the cage is quite warm sometimes gives more reliable results.

#### 13.4.3.5 Surge Test

The most effective off-line winding test developed to date is probably the surge comparison tester. Two high-voltage pulses are discharged into two windings simultaneously, and the reflections of both signals are overlaid on an oscilloscope. Any faults prevent the traces from overlapping.

The surge test suffers from one major drawback. The position of the rotor can affect the results. The effect noticed is that the character of the reflected pulses changes slightly with rotor position in a manner that is difficult to distinguish from a fault. If the rotor can be removed before the test, potential ambiguities are eliminated. Some users report that, despite this phenomenon, useful trends can be obtained if extreme care is taken to validate the results. For most everyday users, however, removal of the rotor is advised.

A second, lesser problem is that, since the surge test instrument has a high-voltage source, it is possible to damage the winding under test. Strict adherence to the test procedure minimizes this potential problem.



DC hi-pot test capability is built into most commercially available surge testers.

#### 13.4.4 Continuous (On-Line) or Periodic (Off-Line)?

The majority of plant equipment does not usually experience rapid deterioration unless there is a serious flaw in the application or construction. Degradation usually proceeds at a fairly slow rate until an advanced stage is reached. Because of this, periodic (manual) inspection and monitoring will usually suffice for detecting symptoms. Online monitoring for electrically related faults is usually installed for protection. They are useful in minimizing domino failure effects by automatically taking quick action on unmanned or high-speed machines.

Commitment by management is the single most important ingredient when initiating a predictive maintenance program. Development of a successful predictive maintenance program requires agreement in advance on the plant equipment to be monitored, what constitutes “savings” obtained from adopting a predictive maintenance philosophy, and how the predictive maintenance team’s effectiveness will be measured. Planning for the annual performance review of the predictive maintenance project is as important as the technical and implementation planning.

Finally, in addition to the references cited above, the reader may wish to consult Refs. 17–20.

### 13.5 Reliability Impact of Adjustable Speed Drives (ASDs) on Bearings

#### 13.5.1 Introduction

Advances in bearing technology have raised industrial bearing life to 20,000 to 40,000 hours, with theoretical life from 40,000 to 60,000 hours. Among the causes for reduced bearing life are misapplications, inadequate maintenance, excessive load and/or speed and power quality. Recent surveys suggest 30% of all motor failures operated with 60-Hz sine wave voltage are bearing failures resulting from current conduction through the bearing [21]. All rotating machines dc and ac are susceptible to bearing currents regardless of size. Shaft voltage is a reliable indicator of bearing currents. Rotating machines have three basic sources of shaft voltage-to-drive bearing currents: electromagnetic induction, electrostatic coupled from internal sources or electrostatic coupled from external sources [22].

Shaft voltage may be due to small asymmetries in the air gap magnetic field, inherent in any practical machine design. Asymmetries may be caused by rotor eccentricity, stator-rotor slotting or slot combinations, rotor misalignment, inadequate manufacturing tolerances, air-gap variation, excessive lamination-to-lamination variance, slot punching irregularities, cooling ducts, keys and key ways, and variations in permeability. Design-induced shaft voltage are classified into two main categories. Homopolar flux-induced shaft voltages result from axial flux created by unbalanced amp-

Kliman figs

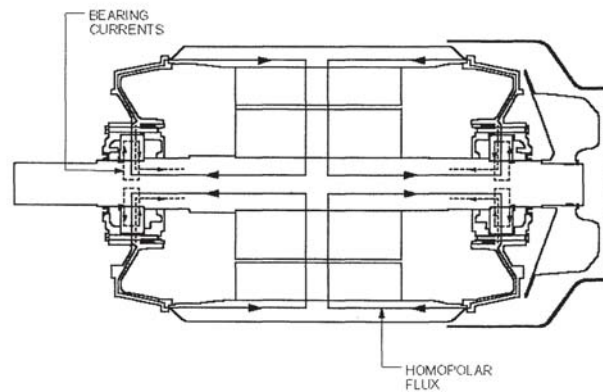


**Figure 13.14** Homopolar fluxes around stator, rotor, and shaft. (Courtesy of GAMBICA/REMA [22].)

turns encircling the shaft caused by broken rotor bar, residual magnetization or perhaps an eccentric air gap (Fig. 13.14). Basically a condition wherein the line integral of the field on a path enclosing the rotor is non-zero, thus having an equivalent encircling non-zero current and axial flux [22].

A second and more common source of shaft voltage results from an alternating flux linking the motor shaft. This radial flux and associated bearing current as depicted in Fig. 13.15a may be caused by asymmetries in the magnetic field as depicted in Fig. 13.15b. A net alternating flux links the circuit formed by the rotor shaft, bearings, and frame producing an end-to-end shaft voltage. The shaft voltage can be sufficient to raise the voltage across the bearing lubricant film beyond its withstand voltage-producing arcing and bearing damage [22].

Despite the numerous contributors to motor asymmetries, most induction motors are designed not to exceed a specific and tolerable maximum shaft voltage to frame ground. In those instances where excessive shaft voltages persist corrective measures including nonmagnetic shafts and insulated nondrive end bearings may be incorporated. This does not mitigate shaft voltage but rather the resulting bearing current.

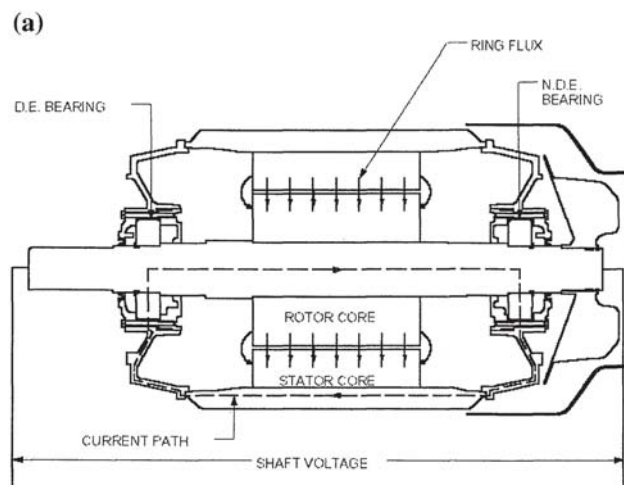


**Figure 13.15a** Showing shaft voltage due to asymmetric magnetic field. (Courtesy of GAMBICA/REMA [22].)

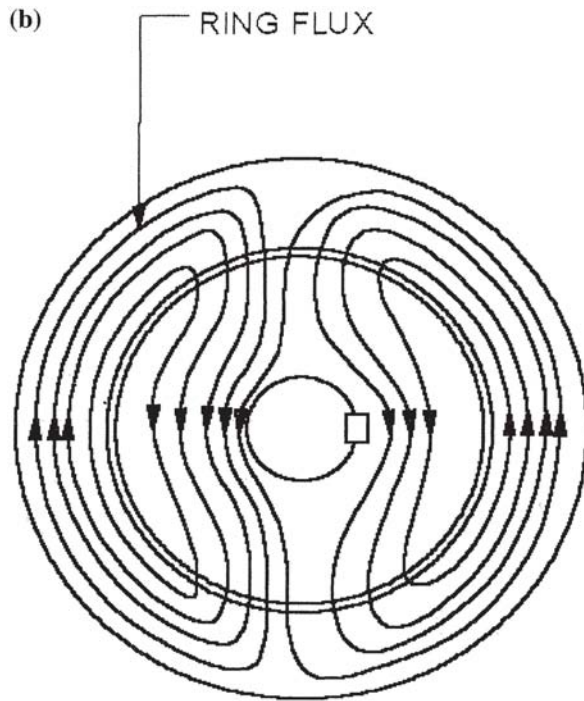


**Figure 13.15b** End view depicting asymmetric field. (Courtesy of GAMBICA/REMA [22].)

Non-design—induced shaft voltages may be internally induced by electrostatic buildup or associated with the quality of the supply. Electrostatic induced shaft voltage may be present with belt driven couplings, ionized air passing over rotor fan blades or high velocity air passing over rotor fan blades as in steam turbine [23]. Installing a shaft grounding brush to suppress shaft voltage to less than 1 V rms relative to ground prevents damaging bearing current [24].

Electrostatic-coupled shaft voltage from external rotor sources, such as a static exciter in a turbine generator, is possible and historically solved with the application of a shaft grounding brush [23]. Supply induced shaft voltages may be electromagnetic or electrostatic [24] and the contribution to bearing failure dependent on the source, its frequency spectrum and impedance of the electrical system.

### 13.5.2 Bearing Current Induced by Supply Voltage

Shaft voltage is an accepted indicator of the potential for bearing current. The combination of shaft voltage, its spectrum, and the electrical impedance of the bearing circuit determines the electrical current through the bearing and ultimately bearing damage [25]. Bearing damage from electrical current begins with pitting. Electrical pitting continues and in combination with mechanical action produces severe fluting, whereupon friction increases, further increasing losses and destruction of the bearing surface. Figure 13.16 shows typical fluting on a bearing race. One standard for roller bearings is the permissible peak current before appearance of pitting. However, contact area is

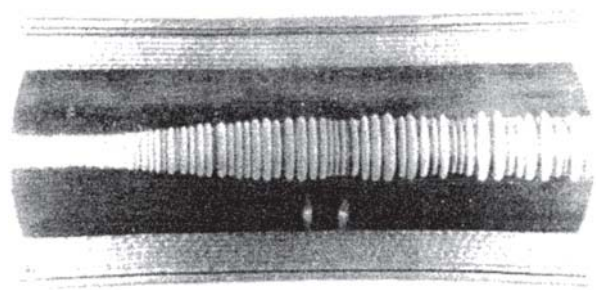


**Figure 13.16** Bearing race fluting. (Courtesy of SKF Corporation [25].)

nondeterministic being a function of bearing speed and load, vibration, method of installation, viscosity and temperature of the lubricant. Effective contact area increases with the bearing load raised to approximately the 1/2 power [24, 26].

#### 13.5.2.1 Bearing Current with Low-Frequency Supply

Clearly, bearing impedance as a function of loading is an important parameter to determine the severity of the problem. Surface contact by metal to metal, quasi-metallic surface contacts or metal point contact through electrically insulating surfaces between ball surface roughness and race roughness each presents unique electrical characteristics.

Nonrotating bearing contact area is large and consists mostly of quasi-metallic surfaces. The lubricant film is only 50 Angstroms ( $1 \text{ \AA} = 10^{-10} \text{ m}$ ) while quasi-metallic surfaces have metallic oxides of 100–120 Å. Quantum mechanical tunneling effects enable the current to pass through the contact zone with series resistances less than  $0.5 \Omega$ . This is evidenced by the low bearing resistance measurement made at low speeds in Fig. 13.17. Ref. 26 suggests that large current may

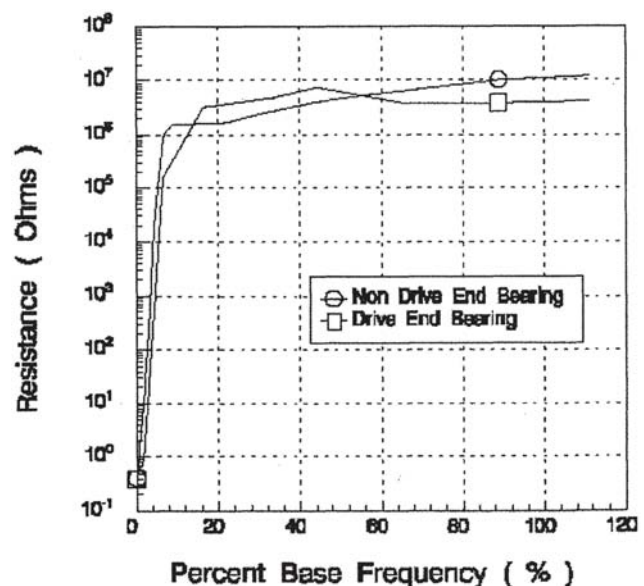


**Figure 13.17** Bearing resistance measurement.

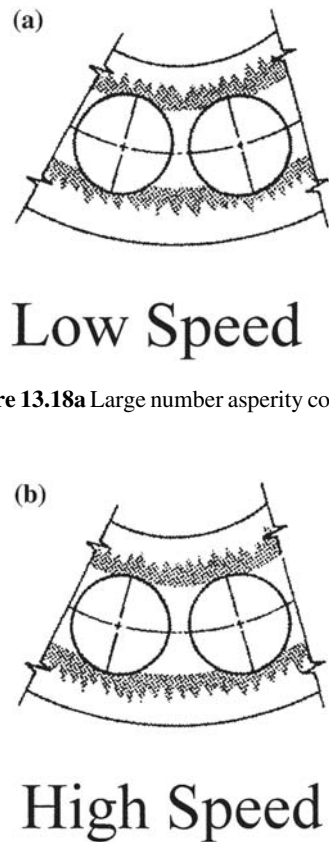


**Figure 13.18a** Large number asperity contacts.

**Figure 13.18b** Small number asperity contacts.

pass through nonrotating bearings without damage because of the large contact area [24].

Rotating bearings have a smaller contact area, which depends on bearing surface roughness. The contact area primarily comprises asperity point-like contact of ball metal to race metal as shown in Fig. 13.18a for low-speed operation. High-speed operation in Fig. 13.18b has fewer asperity contact points. Asperity contact duration is typically 100  $\mu\text{sec}$  at low speed and 33  $\mu\text{sec}$  at high speed. The increased bearing resistance with rotation shown in Fig. 13.17 suggests that the lubricant is introducing a *partially* insulating film between ball and race at speeds greater than 10% of rated. Typical surface roughness of the race and ball from Fig. 13.19 is seen to be in the 1–10  $\mu\text{m}$  range while the typical lubricating film of 0.1–2  $\mu\text{m}$  depends on speed, lubricant characteristics, and to a lesser extent on load [25]. Figure 13.20 shows the relationship between oil film and surface roughness in a bearing [26]. Percent film is the time percentage during which the “contacting” surfaces are fully separated by an oil or lubricant film while  $\gamma$  is the relationship of lubricant film thickness to rms value of contacting surface roughness. Most bearing applications operate in the  $\gamma=1$  to 2 region. This implies high-quality bearings are high impedance 80% of the time with the lubricant behaving capacitive. While lower quality bearings appear resistive due to metal-to-metal contact a majority of the time and only capacitive when race and ball are separated by a non-conducting lubricant [24].

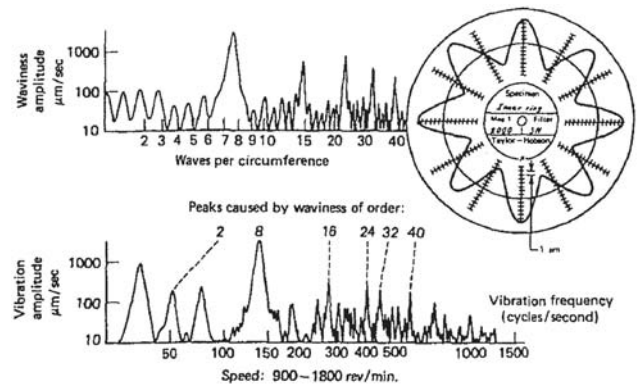


**Figure 13.19** Surface roughness, waviness and vibration. (Courtesy of SKF Corporation [25].)

Rotating bearings that appear resistive either because they are low quality or use low-resistive lubricants will be subjected to current in direct proportion to the magnitude of the shaft voltage. A high shaft voltage with increased current cause localized heating at the points of contact. Heating can become excessive at point contact areas, melt material and create craters, thus liberating wearing metal particles into the lubricant. A low shaft voltage has lower current amplitudes but decompose the lubricant into corrosive elements causing pitting [24].

In high-quality bearings with high-impedance grease, the junction bearing capacitor may discharge into a low-impedance circuit when the electric field exceeds the breakdown strength in the lubricant asperity points. As an example, the bearing breakdown voltage threshold for mineral oil is 0.4 V since mineral oil field strength is  $10^6$  V/m, a typical oil film is 0.2  $\mu\text{m}$  and there are two films in series. On occasion the bearing capacitor voltage, charged by the shaft voltage present, becomes high enough ( $>0.4$  V) to break down the grease and a short (nanoseconds) high-current impulse flows from the charged oil film capacitor within the bearing. This discharge current pulse, if it occurs, is a prime source of bearing

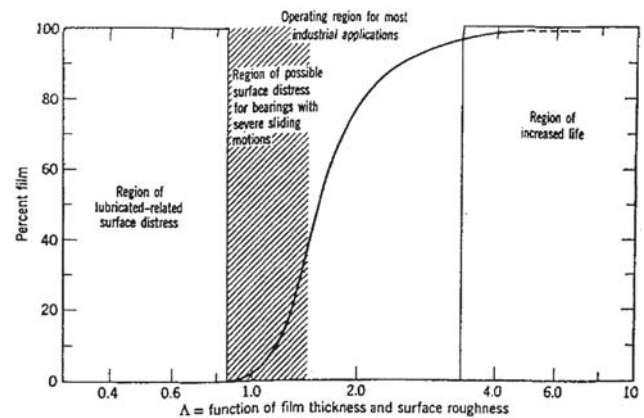


**Figure 13.20** Percent film vs.  $\gamma$  for a bearing. (Courtesy of Wiley Press [26].)

erosion and is commonly referred to as fluting or electric discharge machining (EDM). The washboard craters of Fig. 13.16 are formed from the microscopic pits that soften under repetitive heating of the race to its melting temperature [24].

A shaft voltage threshold above which EDMs and bearing damage occurs does not exist. Generally less than 0.3 V is considered safe, while 0.5–1.0 V may develop harmful bearing currents, and shaft voltages greater than 2 V may destroy the bearing. The rotating bearing break-over threshold voltage (when bearing current starts to flow) has been measured under dc source voltage to be 700 mV peak.

13.5.2.1.1 Sine Wave Operation of the Induction Motor

Stator neutral to ground, rotor to ground, and bearing current to ground signals are shown in Fig. 13.21 for a 15-hp, 480-V, 8-pole test induction motor on a 60-Hz 480-V sine wave supply at no-load. Figure 13.22 shows the physical construction of the test motor. Both the drive and nondrive ends of the rotor were outfitted with an insulated bearing support sleeve, which isolated the rotor bearings from the motor frame. This provided a measurement of the rotor open circuit voltage, and when shorted by the grounding strap, simulates an actual bearing mounting. In addition, the grounding strap provides a mechanism for measuring the bearing to ground current. Figure 13.22 shows a carbon brush for measuring the rotor voltage. The 60-V stator neutral voltage induced a less than 1 V rotor voltage, a 60 to 1 reduction. This rotor shaft voltage level is at the upper end of the standards. The bearing to ground current amplitude is in milliamps indicating the bearing is electrically capacitive and of high quality. No detectable low frequency end-to-end voltages were observed, nor is there EDMs present. *Thus even though the common mode shaft voltage is in the upper end of the acceptable range bearing damage from electrical current is not likely.*

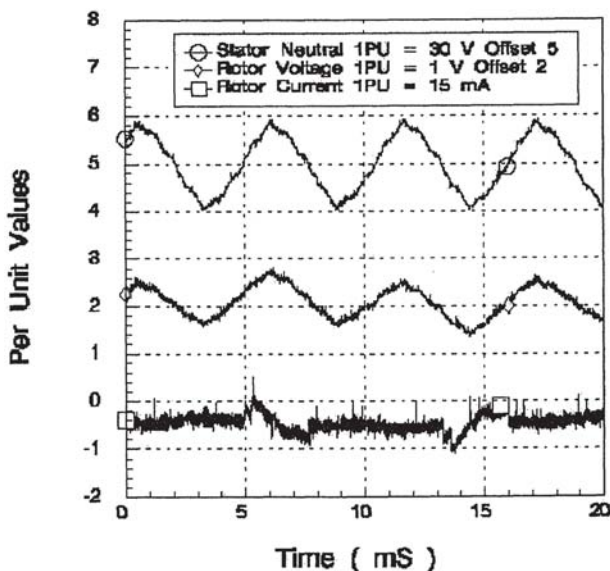


Figure 13.21 Alternating current (ac) line operation.

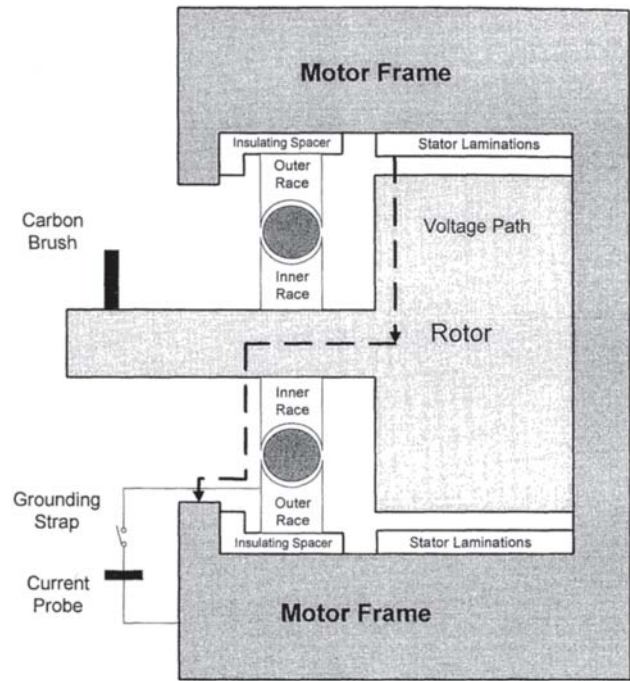


Figure 13.22 Physical construction of test motor.

13.5.2.1.2 Bearing Current with PWM Voltage Source Inverters

The preceding analysis was based on steady-state, low-frequency, and low  $dv/dt$  shaft voltage sources. However, PWM voltage source inverters are rich in frequency content and produce a non-zero common mode voltage. Depending on the modulation utilized and nonlinearities of the inverter, intermediate frequencies may contain unbalanced differential mode components. These unbalanced intermediate frequency voltages can produce the same effect on bearings as the low-frequency voltages discussed earlier. Suggested mitigation techniques follow those for low-frequency supply operation [24].

Because PWM voltage source inverters produce high frequency step-like voltage waveforms with high  $dv/dt$  the sum of the three-phase motor currents is non-zero as a result of the motor winding's stray capacitance. A consequence is a net alternating high-frequency flux linking the circuit formed by the shaft, bearings, and frame, not unlike that discussed earlier, with a consequent end-to-end shaft voltage. The subsequent circulating current can be a source of bearing damage [27].

PWM common mode voltages are also impressed across the stator neutral to frame ground. A portion of this waveform is also capacitively coupled to the rotor as a rotor shaft voltage to ground. The magnitude of the rotor shaft voltage can under certain conditions be established through simple voltage divider action and can be elevated by a synchronous rectifier or active front end in addition to the interaction of passive system elements, for example, common mode chokes.

The preceding sine wave analysis applies to PWM operation but with the change that the experimental static

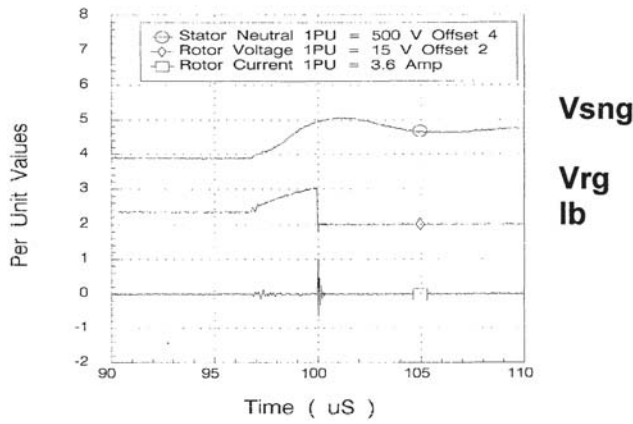


**Figure 13.23** Electric discharge machining (EDM) capacitive charging characteristics.

breakdown threshold voltage on the rotor shaft appears to increase to 8–15 volts (Fig. 13.23) vs. 700 mV for the same bearing monitored under 60 Hz sine wave operation (Fig. 13.21). This increase is explained using dielectric breakdown theory for pulsed sources [28]. Figure 13.24 shows the impulse breakdown strength of hexane ( $1.1 \times 10^6$  V/m) increases dramatically over the static value for short step-like pulse durations. The bearing voltage breakdown threshold also increases as a function of shaft voltage rate of change [29]. This increased breakdown level under PWM operation is undesirable since during bearing discharge the resulting EDM bearing currents are much higher than with sinewave operation. Furthermore, rough surfaces typically seen in bearings will have a statistical time lag of 3 ~sec prior to breakdown (Fig. 13.25), which agrees with measured value of Fig. 13.23 [24].

13.5.2.2 Evidence of Electric Discharge Machining (EDM)

EDM and its presence can be determined by suitable testing. Limiting the number of variables is essential in preventing

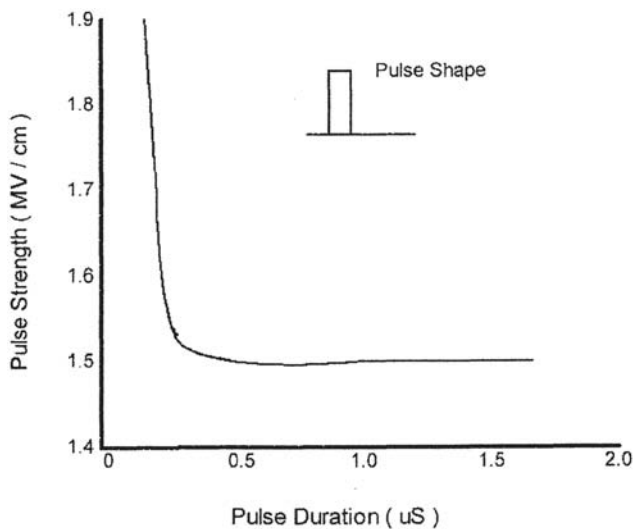


**Figure 13.24** Increased dielectric strength with impulse sources. (Courtesy of Oxford Press [28].)

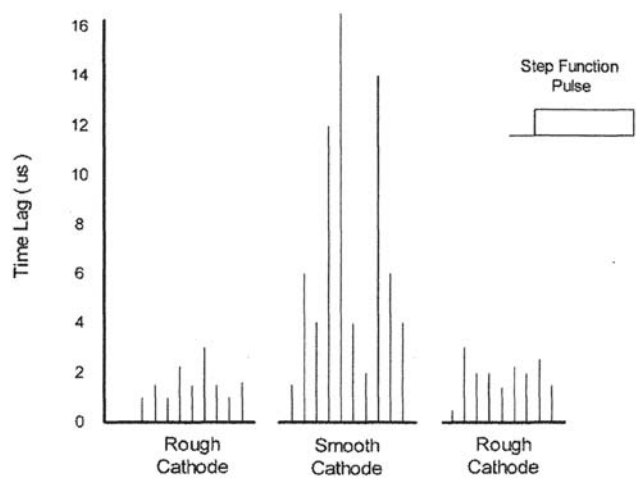


**Figure 13.25** Time lag to breakdown as a function of surface roughness. (© 1996 IEEE. Reprinted, with permission, from Transactions on Industry Applications, Vol. 32, No. 2, March/April 1996 [24].)

unjustifiable conclusions from experimental results, especially when investigating the effects of high-frequency IGBT inverters. A four-conductor, braided shield, grounded at drive end 2-m cable connected an IGBT voltage source inverter and test motor as shown in Fig. 13.26. Common mode chokes were not inserted in the input or output of the drive. Space

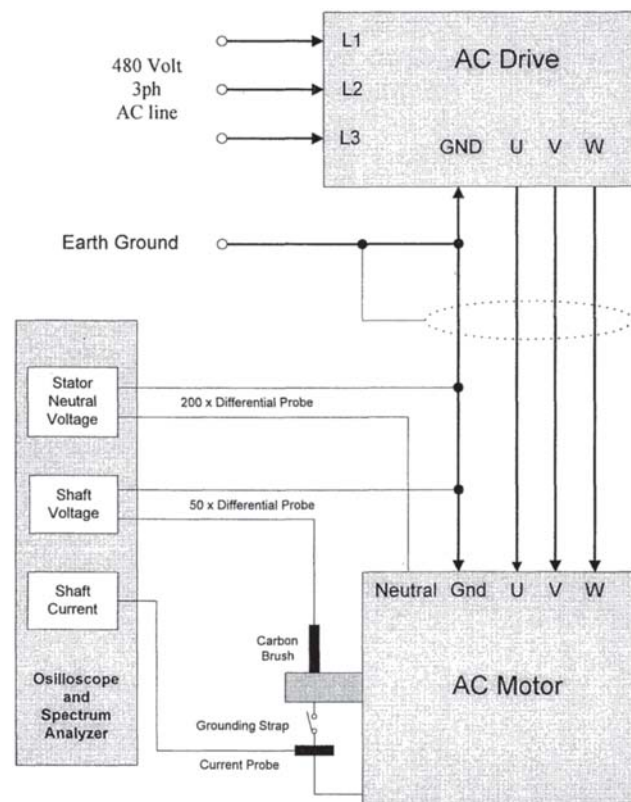


**Figure 13.26** Test fixture and instrumentation. (© 1996 IEEE. Reprinted, with permission, from Transactions on Industry Applications, Vol. 32, No.2, March/April 1996 [24].)

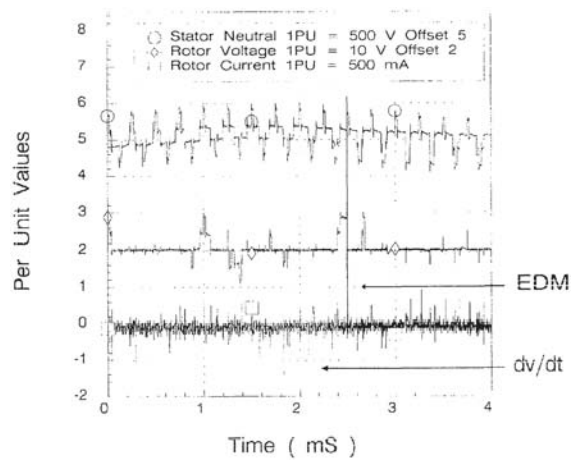


**Figure 13.27** Bearing EDM and  $dv/dt$  current with alternating current (ac) drive. (© 1996 IEEE. Reprinted, with permission, from Transactions on Industry Applications, Vol. 32, No. 2, March/April 1996 [24].)

vector modulation at 4-kHz carrier frequency provided a constant V/F voltage [24].

The stator neutral-to-ground voltage, rotor shaft-to-ground voltage, and bearing-strap current were monitored. Figure 13.27 shows experimental results when operating the ac drive at 48 Hz. The stator neutral-to-ground voltage displays the typical per carrier cycle waveform associated with PWM voltage source inverters. The rotor voltage, however, shows a quite different profile. For a majority of the time, the rotor is grounded, but occasionally the rotor tracks the stator neutral to ground voltage. Then quite suddenly, the rotor voltage collapses, producing a current pulse. Figure 13.23 is an expanded plot of an EDM discharge. As the stator to neutral voltage increases, the rotor voltage responds with a capacitive charging characteristic. In fact, the rotor voltage rises to a value 15 times larger than the measured value when operating on sine waves. At the instant of discharge an impulse of current occurs with the rotor voltage simultaneously collapsing [24].

Figure 13.28 is a sectionalized view of bearings from a motor operated on an ac drive. The fluting is quite pronounced. The outer bearing race on the left shows a random EDM discharge. The outer race on the right shows a continuous etching of the race surface [24].

The normal bearing  $dv/dt$  switching current of a properly grounded motor is in the hundreds of milliamp range and occurs with the rise in rotor potential. A review of the technical literature suggests the effect of this relatively small current on bearing life appear insignificant. However, the large current following the rapid collapse of the larger rotor voltage is believed to cause EDM. The value of the EDM shown is limited by the inserted grounding strap and its surge impedance. A standard drive's bearing current consists of the internal shorted bearing capacitance current and bearing short circuit current [24].

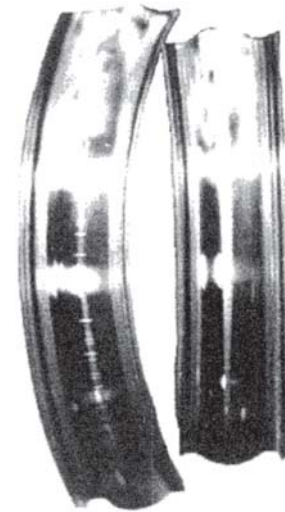


**Figure 13.28** Sectionalized bearing revealing electric discharge machining (EDM) induced fluting. (© 1996 IEEE. Reprinted, with permission, from Transactions on Industry Applications, Vol. 32, No. 2, March/April 1996 [24].)

### 13.5.3 An Equivalent Circuit for Bearing Displacement and EDM Currents

Bearing EDM discharges caused by electrostatic coupling result from a fundamentally different mechanism than discharges caused by electromagnetic coupling. Electromagnetic-induced discharges are a consequence of magnetic field coupling to a closed circuit that includes the bearing assembly. Common mode voltages from PWM voltage source inverters have a frequency spectrum broad enough to excite the common mode electrical circuit formed by the drive, cable, motor and mechanical system. Although the electrical system is inherently distributed a lumped parameter circuit model has been found acceptable for purposes of analysis and application of mitigation strategies.

#### 13.5.3.1 Bearing Impedance Model

Figure 13.29 depicts a motor's capacitive components. The stator-to-frame capacitance ( $C_{sf}$ ) is a distributed element representing the capacitive coupling to frame along the length of the stator conductors. For most investigations, magnetic coupling of the stator and rotor is sufficient. But with the high  $dv/dt$  present with modern power devices, capacitive coupling considerations cannot be ignored. Therefore, the stator to rotor capacitance ( $C_{sr}$ ) and the rotor to frame capacitance ( $C_{rf}$ ) are included [24].

The bearings, lubricating film, and insulating sleeve present a combination of capacitances, resistances, and a non-linear impedance (Fig. 13.30). First, there exists an inner and outer race resistance. Then, depending on the physical construction, the bearing consists of  $n$  balls in parallel; each ball having an effective resistance ( $R_{ball,i}$ ). In addition, each ball is immersed in the lubricating film; thus, each ball develops two capacitances ( $C_{ball,i}$ ) linking the ball to the inner and outer races. The ball portion of the bearing model,

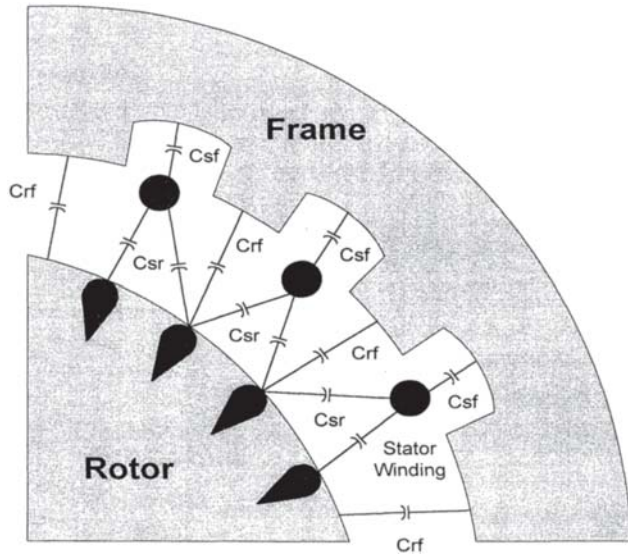


**Figure 13.29** Motor capacitance. (© 1996 IEEE. Reprinted, with permission, from Transactions on Industry Applications, Vol. 32, No. 2, March/April 1996 [24].)

therefore, consists of  $n$  parallel combinations of ( $C_{ball,i}$ ) and ( $R_{ball,i}$ ). Between balls, the inner and outer races are separated by the lubricant, which forms a dielectric barrier. Therefore, a capacitance ( $C_{gap,i}$ ) is formed between each pair of balls, resulting in  $n$  parallel capacitors. The nonlinear impedance ( $Z_{l,i}$ ) accounts for the mechanical and electrical abnormalities and randomness of the bearing [24].

Combining the individual components results in a reduced order bearing model, which is compatible with the motor drive models used in simulations and analyses. The reduced order model consists of a resistance ( $R_b$ ) in series with the parallel combination of an effective capacitance ( $C_b$ ) and a nonlinear impedance ( $Z_l$ ). Finally, the test motor's insulating sleeve adds a series capacitance ( $C_{sleeve}$ ) that is shorted when the grounding strap is used (Fig. 13.30) [24].

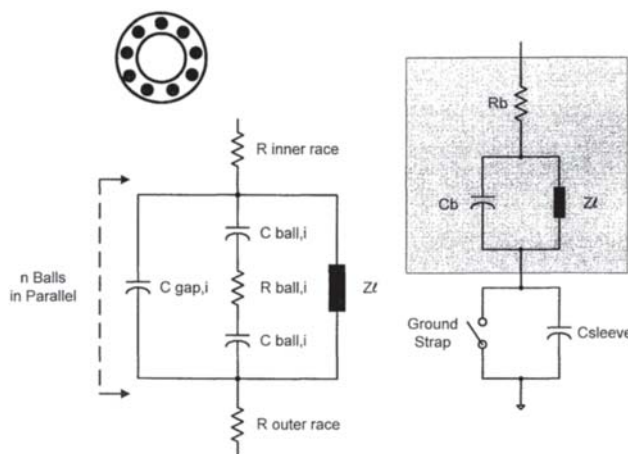


**Figure 13.30** Ball bearing electrical model. (© 1996 IEEE. Reprinted, with permission, from Transactions on Industry Applications, Vol. 32, No. 2, March/April 1996 [24].)

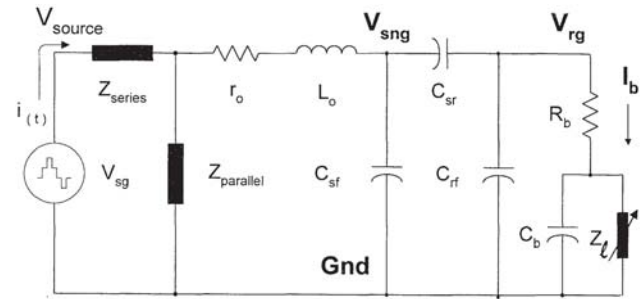


**Figure 13.31** Common mode model. (© 1996 IEEE. Reprinted, with permission, from Transactions on Industry Applications, Vol. 32, No. 2, March/April 1996 [24].)

Combining the above motor model with simple inverter and cable common mode models yields Fig. 13.31. Here, the inverter is modeled by a zero sequence source. Cables are represented by their common mode equivalent representation ( $Z_{series}$ ,  $Z_{parallel}$ ). The motor is modeled by a stator's zero sequence resistance and inductance ( $r_0$ ,  $L_0$ ), the capacitive coupling from stator to frame is lumped at the neutral of the stator winding and the capacitive coupling between the stator and rotor connects the stator and rotor zero sequence networks. Finally, the rotor to frame capacitance and bearing provide the paths to ground from the rotor shaft, here represented by the neutral of the rotor ( $V_{rg}$ ) [24].

From Fig. 13.31, it is clear  $dv/dt$  and EDM capacitive coupled bearing currents from PWM VSI drives depend on the following three conditions: (1) a source of excitation ( $V_{sg}$ ), which is transferred by the zero sequence or common mode components to the stator neutral-to-ground voltage ( $V_{sng}$ ), (2) a capacitive coupling mechanism, accomplished by the stator-to-rotor capacitance ( $C_{sr}$ ), and (3) sufficient  $V_{rg}$  buildup, a random occurrence depending on the existence of  $C_b$ . All three of these conditions must simultaneously exist for EDM currents to occur.

### 13.5.3.2 Explanation of the Cause of Bearing Displacement and EDM Currents

Examining the bearing model in the context of Fig. 13.27 the significance of the nonlinear impedance  $Z_l$  is apparent. Because the bearing capacitor normally exhibits a  $dv/dt$  or displacement current when the stator voltage changes, the nominal  $dv/dt$  current is limited by the impedance given by the model of Fig. 13.31 with  $Z_l$  equal to a low non-zero value. This corresponds to the bearing in a position of low impedance between outer and inner race. However, occasionally the bearing rides the lubricating film, which allows the rotor to track the source voltage with a random duration. This condition corresponds to a substantial increase in  $Z_l$ . When  $Z_l$  collapses, reflecting the preferred bearing position or the breakdown of the film, the capacitor  $C_b$  is discharged and an EDM current occurs, with the current through the bearing limited by the zero sequence or common mode impedance. Thus, the bearing's impedance is statistical in nature and depends on the position of the balls, the condition of the bearing and its lubricant. Approximate circuit parameter values may be obtained using classical formulations and appropriate tests [24, 30].

### 13.5.3.3 Mechanical Characteristics of Rolling Bearings Affecting Electrical Parameters, Bearing Current and Bearing Life

Bearing failures are attributed to traditional mechanical and thermal failure mechanisms or induced  $I_b$ . Mechanical failure mechanisms are produced by excessive vibration, while thermal failure results from overloads, which increase bearing temperature and decrease mechanical life. Induced  $I_b$  results from machine design or application.

Machines contain magnetic asymmetries inducing end-to-end axial voltage resulting in a circulating bearing current. Induced mechanical wear from circulating bearing current does not exist if end to end shaft voltage produces a bearing capacitance voltage less than a critical bearing Threshold voltage ( $V_{th}$ ) required to break down the insulating grease [31].  $V_{th}$  is 0.2 to 1 V under 60 Hz sine wave operation [25, 32]. This threshold, as pointed out earlier, depends on the form of the excitation and in the case of *PWM ASDs* may increase to approximately 30 V. Low  $I_b$  is a result of  $V_{rg}$  being less than  $V_{th}$ , which induces a chemical change of low resistivity lubricants, ultimately reducing life by raceway corrosion [33].  $V_{rg}$  exceeding  $V_{th}$  can produce damaging *EDM* currents caused by the bearing oil film acting as a capacitor in high resistivity lubricants and charging to open circuit  $V_{rg}$  levels [30, 34, 35]. When race-to-ball asperity contacts come close, the oil film electric field increases leading to breakdown with high discharge currents that create a localized elevated temperature of the race and molten pits (Fig. 13.32) [36]. The pits eventually lead to fluting (Fig. 13.16) and reduced mechanical life [36]. Small machines use inexpensive bearings and therefore ride upon the film less often; thus on average maintaining a  $V_{rg}$  less than  $V_{th}$ . Large machines or servo motors may employ lubricants with increased  $V_{th}$  thus reducing the occurrences of EDM current [37].

Establishing a maximum allowable  $I_b$  magnitude is difficult without knowing surface contact area of the passing current and grease composition. A nonrotating bearing, with its large contact area, may pass large sine wave currents without damage [25]. Also,  $I_b$  magnitude failure mechanisms are sensitive to the type of grease. High resistivity mineral oil greases act as capacitors with high  $V_{th}$  and produce EDM currents and arcing

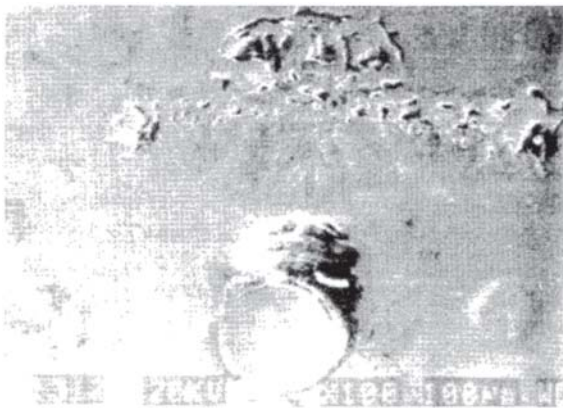


**Figure 13.32** Microscopic pits on bearing race due to electric discharge machining (EDM) current. (Courtesy of University of Wisconsin [36].)

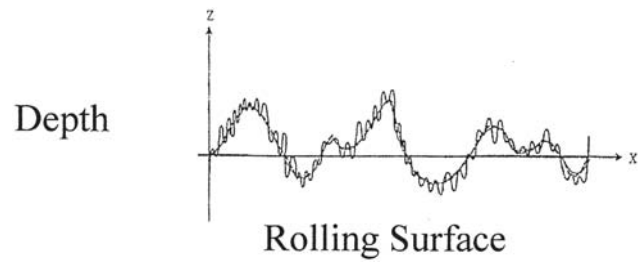


**Figure 13.33** Bearing surface waviness and roughness (15). (Courtesy of University of Wisconsin [36].)

on discharge. This failure is best analyzed using  $I_b$  density. High resistivity greases with low  $I_b$  do not produce arcing but may produce fritting. Fritting tempers the steel, which lowers surface hardness. Low resistivity lithium grease does not exhibit a  $V_{th}$  but acts as a resistor. Currents of 189 mA rms (267 mA peak) cause grease decomposition into lithium iron oxide, leading to increased wear and bearing failure [33]. Values of 0.5 A rms accelerate corrosion and fritting [33]. Thus, EDM currents and  $dv/dt$  currents should be analyzed for allowable  $I_b$  density and peak currents less than 267 mA peak for corrosive effects and fritting [37].

#### 13.5.3.3.1 Characteristics of the Bearing Surfaces and Contact Area

Accurate calculation of actual contact surface area in a rotating bearing is difficult, since it depends on surface roughness, “asperity contacts,” and the oil film thickness, which itself is a function of grease composition and temperature, motor speed and motor load. Each race and ball surface, viewed at the microscopic level, is composed of a waviness with a surface roughness riding the waviness. This is shown in Fig. 13.33 [36]. The Hertzian contact area results from the plastic and elastic deformation of two mating surfaces creating an elliptical shaped contact area. Typical Hertzian contact areas are demonstrated in Fig. 13.34 through macroscopic and microscopic scaled drawings [26, 37].

#### 13.5.3.3.2 Asperity Contact Area

Equations based on Hertzian point contact theory as provided by Harris generate curves relating contact area to load [26]. A single row radial ball bearing satisfies the assumptions of the

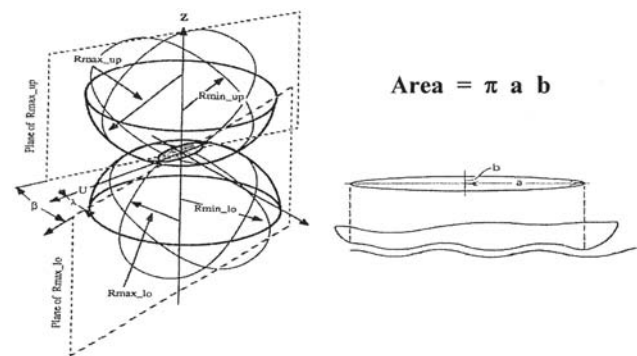


**Figure 13.34** Hertzian ellipse contact area—macroscopic and microscopic (10). (Courtesy of ASLE [31].)



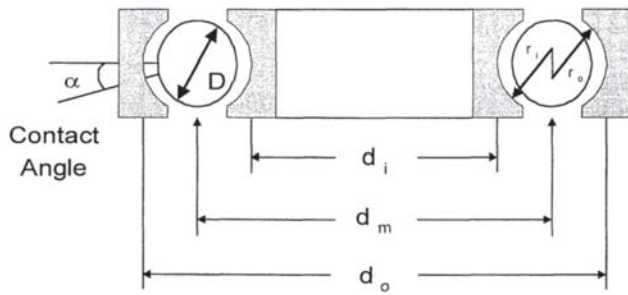


**Figure 13.35** Dimensions for bearing asperity point contact calculations (10). (Courtesy of ASLE [31].)

Hertzian equations. The necessary mechanical parameters obtained from bearing manufacturers include: the inner raceway diameter ( $d_i$ ) in millimeters, outer diameter ( $d_o$ ) in millimeters, ball diameter ( $D$ ) in millimeters, two ratios, the inner raceway curvature ( $r_i\_curve$ ) and the outer raceway curvature ( $r_o\_curve$ ), and the free contact angle ( $\alpha$ ) in degrees. Figure 13.35 identifies some of these mechanical dimensions [37].

Using equations from Harris, the elliptical contact area can be calculated for the inner and outer bearing race surfaces. Point contact areas were computed for the bearing of a 15-hp induction machine [34] as a function of load and the results plotted in Fig. 13.36. Consultation with bearing designers confirmed the reasonableness of the calculations [37].

**13.5.3.3.3 Bearing Current Density and Related Life Factors**

Bearing failure is best analyzed using  $Ib$  density. Establishing a maximum allowable  $Ib$  magnitude can be accomplished by knowing the surface contact area, magnitude of the passing current, and grease composition. Literature indicates a  $Ib$  density of less than 0.56 Arms/mm<sup>2</sup> as a safe condition,

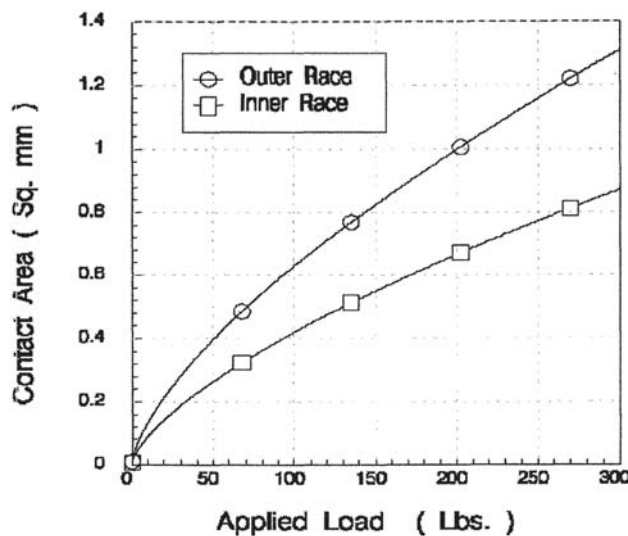


**Figure 13.36** Bearing asperity point contact as a function of load. (© 1995 IEEE. Reprinted, with permission, from Tenth Annual Applied Power Electronics Conference and Exposition, March 5–9, 1995, Vol. 1 [34].)

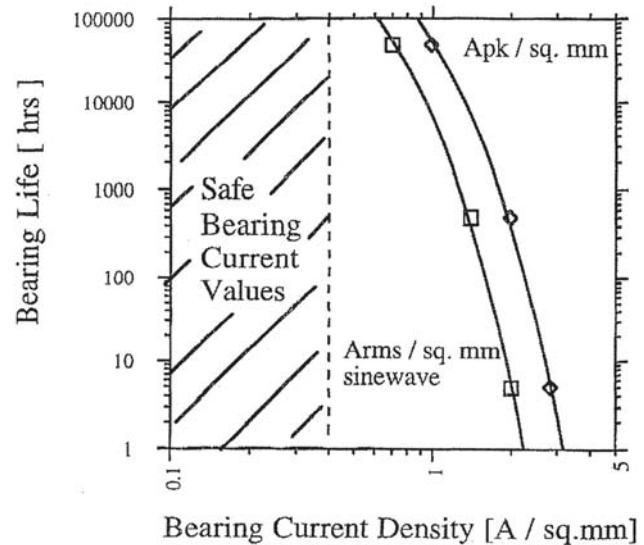


**Figure 13.37** Bearing life as a function of current density. (© 1997 IEEE. Reprinted, with permission, from Transactions on Industry Applications, Vol. IA-33, No. 2, March/April 1997 [37].)

allowing bearing life of 50,000 hours without electrically influenced damage [35, 37].

The main contributors to electrically based bearing damage are fluting and corrosion. Fluting of the outer race surface is caused by  $Vrg$ , charging followed by EDM discharge. This occurs when the  $Vrg$  exceeds  $Vth$  of the oil film, breaking down the film layer. Evidence of EDM damage can be seen in Fig. 13.32, as viewed through a scanning electron microscope. Low resistivity grease does not exhibit a  $Vth$  but acts as a resistor. Corrosion is caused by an electrochemical reaction between the metal surfaces and the resistivity of the grease. Data presently do not exist for this long-term failure mode [37].

Bearing current testing is historically based on 60 Hz, sine wave, rms amperes with a bearing rotating at rated base speed and using high resistivity grease. Bearing life is therefore based on destructive EDM currents occurring due to capacitive discharge breakdowns in high resistivity grease rather than corrosive degradation effects with low resistivity greases. Historical current density (Arms/mm<sup>2</sup>) is converted to estimate life as shown in Fig. 13.37 with EDM and  $dv/dt Ib$  under PWM operation. Equation 13.1 describes electrical bearing life using data from Fig. 13.37 [37].

$$Elec\ Life[hrs] = 7,867,204 * 10^{-2.17 \left(\frac{Apk}{mm^2}\right)} \tag{13.1}$$

$L_{10}$  is the standardized life calculation method for determining mechanical life of a rolling element bearings. It is defined as the number of operating hours at which a bearing can withstand before the first signs of fatigue failure are apparent. This refers to a statistical nature of which 10% of the bearings fail in the mode of operation. Typical mechanical life is then defined as 5 times the  $L_{10}$  life. The basic  $I_{10}$  life calculation is given in Eq. 13.2. In Eq. 13.2,  $C$  is the basic dynamic load rating,  $P$  is the equivalent dynamic load rating,  $n$  is the speed in rpm, and  $a$  the exponent of life equation—a value of three for ball bearings [35, 37, 38].

$$\text{Mechanical } L_{10} \text{ Life [hrs]} = \frac{10^6}{60n} \left( \frac{C}{P} \right)^a \quad (13.2)$$

The minimum load on a bearing is also related to ultimate bearing life. Additional factors contributing to failures of properly installed bearings include the duty cycles of the applied load and speed, and the lubrication method, selection, maintenance interval, and contamination. An additional method of determining life of mechanical bearings for ac motors, standardized by the International Standards Organization (ISO), is provided in Eq. 13.3. In Eq. 13.3,  $a1$  is the reliability factor,  $a2$  is the material factor to account for material differences, and  $a3$  is the lubrication factor. The lubrication factor refers to the lubricant film separation of the rolling elements [37, 39].

$$\text{ISO Refined Life} = a1 * a2 * a3 * L_{10} \text{ Life} \quad (13.3)$$

The  $L_{10}$  life establishes a lower limit for bearing life, and for industrial applications is typically 20,000 to 40,000 hours [33], with useful mechanical life approaching 40,000 to 60,000 hours. In comparison, Eq. 13.1 describes bearing life with  $Ib$  present. Based on this analysis, the maximum  $Ib$  density with PWM drives to be less than 0.8 (Apk/mm<sup>2</sup>) to ensure  $IB$  does not limit the mechanical life of the bearing [37].

The test motor's bearing (NTN #6208) contact area was calculated as a function of applied load (Fig. 13.36). Values were extrapolated for applications with no shaft load, so that rotor weight alone is the acting force  $Q$  and for applications with shaft force load three times rotor weight.  $Ib$  density is determined using measured peak EDM and  $dv/dt$  currents and calculated contact area. Estimated bearing life is found using Fig. 13.37 or Eq. 13.1 [37].

Table 13.17 shows a properly grounded motor's  $dv/dt$  currents do not degrade bearing life. Unloaded motors are more susceptible to EDM  $Ib$  damage than loaded motors. The magnitude of calculated bearing life must be tempered by realizing the difficulty of determining contact area and that worst case contact area with one ball bearing was assumed. In real life, the force may be distributed over 1 to 3 ball bearings, increasing contact area, while distributing EDM current pulses. How Fig. 13.37, the 60-Hz bearing current density vs. life curve, correlates to life with PWM pulsed EDM currents remains unknown. However, EDM  $Ib$  densities less than 0.6 to 0.8 Apk/mm<sup>2</sup> probably do not degrade bearing life. Accurate life predictions are difficult due to the steepness of the life curve, e.g., from 0.8 to 2.0 Apk/mm<sup>2</sup> life is greatly decreased [37].

**Table 13.17** Calculated Bearing Life for EDM and  $dv/dt$  Currents

Parameter	Units	Rotor weight	3 times rotor weight
Contact Area	mm <sup>2</sup>	0.62	1.29
<b>EDM Current</b>	Apk	2.2	2.2
Current density	Apk/mm <sup>2</sup>	3.5	1.7
Calculated life	hr	< 10	1570
<b>dv/dt current</b>	Apk	0.2–0.5	0.2–0.5
Current Density	Apk/mm <sup>2</sup>	0.32–0.8	0.15–0.38
Calculated life	hr	> 100,000	> 100,000

### 13.5.3.4 Capacitance Calculations for the Shaft Voltage and Bearing Current Model

#### 13.5.3.4.1 Mechanical Components— $Cb$

The occurrence of  $Vrg$  and bearing currents depends on the existence of  $Cb$ . Furthermore, the bearing impedance becomes capacitive only when a lubricant film occurs in the contact regions between the balls or rollers and the raceways [35]. The minimum film thickness is given by:

$$H^0 = 2.65 \bar{U}^{0.7} g^{0.54} / \bar{Q}_z^{0.13} \quad (13.4)$$

where  $U$  is a function of the fluid velocity and viscosity,  $g$  a function of the pressure coefficient of viscosity and modulus of elasticity, and  $Q$  the force or load acting on the ball or roller [26]. Other factors influencing the  $Cb$  include the temperature ( $T$ ), viscosity ( $\eta$ ), additives ( $\lambda$ ), lubricant film thickness relationship to the rms value of the contact surface ( $\Lambda$ ), and dielectric strength of the lubricant ( $\epsilon_r$ ) [30, 35].

The dielectric strength of lubricants is determined by static tests [28]. Data provided by lubricant vendors indicate dielectric strengths range from 1 to 30 kV/mm. These values reflect dielectric strengths of films on the order of millimeters. However, typical bearing loads together with Eq. 13.1 and measured data indicate lubricant film thickness ranges from 0.2 to 2.0  $\mu$ m. These values are significantly lower than those used by the static tests. Based on tests, the authors conclude that 15 Vpk/ $\mu$ m dielectric strength is reasonable. This suggests shaft voltages from 3–30 V can produce EDM currents [34]. Furthermore, tests performed on the 15-Hp induction motor of Ref. 34 showed a maximum withstand voltage of 30-V peak at pulse duration of 10  $\mu$ sec. Thus,  $Cb$  becomes a complicated function of all the above variables ( $Cb(Q, \epsilon_r, U, T, \eta, \lambda, \Lambda)$ ) [30,35].

#### 13.5.3.4.1.1 Mechanical and Lubricant Characteristics and Their Effects on Bearing Capacitance

With the bearing contact area established, bearing mechanical variables—load, speed, temperature, and lubricant viscosity and additives—and their effect on the bearing's electrical capacitance are now examined. This capacitance,  $Cb$ , is the critical mechanical component influencing the magnitude of  $Vrg$ , EDM, and  $dv/dt$  currents. First, operating point parameters—load, speed, temperature, and film thickness—are discussed and their influence on  $Cb$  established. This is followed by a review of lubricants and their dielectric characteristics. Finally, this section will close with the development of a more detailed model of  $Cb$ ; a model incorporating the above mechanical parameters [25].

#### 13.5.3.4.1.2 Operating Point Dependencies

The potential for  $Vrg$  and  $Ib$  depend on the existence of  $Cb$ . Furthermore, the bearing impedance becomes capacitive only when a lubricant film occurs in the contact regions between the balls or rollers and the raceways. The minimum film thickness is given by Eq. 13.4 [37].

**Mechanical Load:** As discussed in the previous section, bearing contact area establishes the current density at the point of contact between bearing and race. Furthermore, the Hertzian contact size increases with the load raised to  $1/n$  where  $n$

depends on the geometries involved [26]. For example,  $n=3$  for identical spheres in contact. Thus, with increasing bearing load, the current density through the bearing decreases, reducing the intensity of EDM current. Equation 13.11 also indicates the film thickness decreases with increasing load, although raised to a very low power ( $C_b(Q)$ ) [37].

Figure 13.23 shows a typical example of the development of  $V_{rg}$ . The fact that  $V_{rg}$  tracks the stator neutral  $V$  ( $V_{sng}$ ) establishes the existence of a film upon which the bearing rides, therefore, developing capacitance  $C_b$ . Field measurements, however, indicate a mitigating effect occurs with the addition of a mechanical load. The additional capacitance provided by the mechanical load increases the effective  $C_b$ . However, an evaluation of typical laboratory arrangements, wherein a load dynamometer is connected to the ac drive motor, showed  $V_{rg}$  was of sufficient magnitude to cause significant EDM current. Generalities about the presence or absence of  $V_{rg}$  should therefore be avoided and every application presents a unique capacitive load in parallel with the load motor  $C_b$ . Finally, the occurrence of  $V_{rg}$  proved independent of torque load; thus, confirming bearing or lateral load determines contact area and not load torque and vibration due to inverter harmonics [37]. **Motor Speed:** The existence of  $V_{rg}$  depends on the velocity of the lubricant and motor mechanical speed [29]. At low speed, the balls randomly make quasi-contact with the races and prevent  $V_{rg}$  buildup. With increasing speed, the balls ride a thin layer of lubricant, the thickness of which is a function of the lubricant's velocity  $U$  ( $C_b(Q, U)$ ) [37].

**Temperature:** The temperature ( $T$ ) of the bearing depends on the load, speed, mechanical alignment, and lubricant characteristics. The temperature rise due to localized heating from EDM and  $dv/dt$  currents creates craters and pits. With the contact time between the ball and outer race larger than the contact time between ball and inner race, bearing wear from EDM and  $dv/dt$  currents is greater in the outer race [40]. The lubricant temperature also affects the film thickness; thus  $C_b$  is temperature dependent ( $C_b(Q, U, T)$ ) [37].

**Lubricant Viscosity:** A bearing's capacitance depends on the thickness of the lubricant. However, a lubricant's viscosity ( $\eta$ ) determines its flow characteristics and influences  $C_b$ . As temperature increases, the viscosity decreases, ultimately reducing the film layer thickness. The viscosity index relates a lubricant's viscosity to its temperature. Furthermore, a lubricant's viscosity partially determines the heat transfer characteristics. An increase in base viscosity will lower the heat transfer coefficient and accelerate oxidation. A decrease in base viscosity reduces oil film thickness and oil circulation, which may accelerate bearing wear. Thus,  $C_b$  is a function of the viscosity  $\eta$  ( $C_b(Q, U, T, \eta)$ ) [37].

**Lubricant Additives:** Commercial lubricants are complex blends, with individual additives chosen for their relative abilities to combat corrosion, friction, wear, load, or other degradation processes. Most bearings are lubricated with grease, which is typically a mineral oil retained within a soap carrier. Mineral oil is a blend of paraffinic, naphthenic, and aromatic petroleum oils. Calcium, sodium, lithium, aluminum complex, and urea based soap carriers are available, each with unique applications. Wang and Tung conducted an

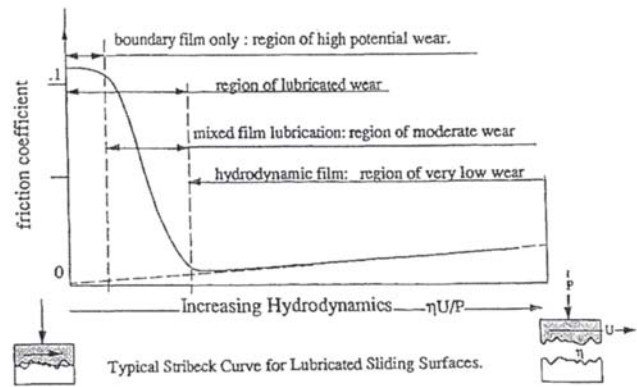


Figure 13.38 Stribeck curve for lubrication analysis (15). (Courtesy of University of Wisconsin [36].)

investigation on the effects of additives on metal. They discuss a specific case where an oleic acid blended with mineral oil produced a capacitance that is inversely proportional to additive concentration [41]. Thus,  $C_b$  is a function of the additive composition  $A$ , ( $C_b(Q, U, T, \eta, \lambda)$ ) [37].

#### 13.5.3.4.1.3 Oil Film Thickness

In a stationary bearing or bearing rotating at low speed, a large contact area exists between race and ball mainly consisting of quasi-metallic surfaces puncturing through the oil film. These mating surfaces result in the low bearing resistance of Fig. 13.17 and corresponds to the high friction region of the Stribeck curve of Fig. 13.38 [36, 37].

The Stribeck curve describes friction vs. ( $\eta U/P$ ), with  $\eta$  the oil viscosity,  $U$  the velocity, and  $P$  the pressure. Three regimes—boundary film, mixed film, and hydrodynamic film—are shown on the Stribeck curve. At startup or low sliding speeds within the boundary film region ( $<15$  rpm) asperity contacts result in high wear and friction. As the speed increases and the bearing enters the mixed film region, the load between the two surfaces is supported partly by the asperities and partly by a lubricating film, resulting in moderate amounts of wear. Finally the bearing enters the hydrodynamic film region ( $>90$  rpm), the two surfaces are separated by a full lubricant film, resulting in minimal wear [42]. Literature indicates a oil film thickness of  $50 \text{ \AA}$  to  $2 \text{ \mu m}$  at normal operating regimes [25, 37, 43].

The Stribeck curve, which is inversely related to the percent film vs.  $\gamma$  curve shown in Fig. 13.39, demonstrates the mechanical wear relationship of the bearing [30, 34]. Figure 13.39 converts this to a percent film, which is the amount of time the contacting surfaces are fully separated by an oil or lubricating film, while  $\lambda$  ( $\Lambda$ ) is the relationship of lubricant film thickness to rms value of contact surface roughness. Thus  $C_b$  is a function of the asperity contact area and the lubricant film thickness  $\Lambda$ , ( $C_b(Q, U, T, \eta, \lambda, \Lambda)$ ) [37].

#### 13.5.3.4.1 A Dielectric Properties of Lubricants

Traditionally, dielectric strength is associated with transformer oils and capacitor films. The insulating properties of any material are dependent on its dielectric strength and ability to withstand high voltage without breakdown. The dielectric strength of lubricants as measured by the American Society of Testing and Measurement (ASTM) standard D 877 is a static

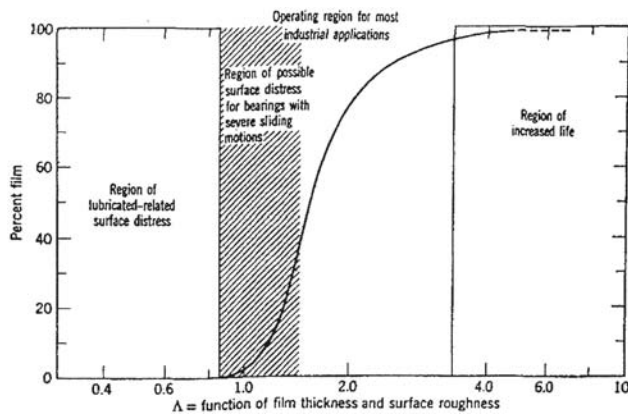


**Figure 13.39** Percent film vs. gamma for a bearing (10). (Courtesy of ASLE [31].)

test with conductive plates 2.5 mm apart. A sinusoidal voltage is applied across the plates and ramped at a rate of 3 kV per second until a leakage current is sensed. Data provided by lubricant vendors indicate a dielectric strength of roughly 15 kV/mm. With high resistance oil and high potentials, a spark can jump across the oil film and cause pitting of the race surface, similar to that caused by EDM in Fig. 13.32. With low-resistance oil and sufficient voltage, corrosion can form on the race surfaces, similar to  $dv/dt$  corrosion [37, 44].

Given the typical lubricant film thickness of 0.2–2.0  $\mu\text{m}$ , shaft voltages in excess of 2 Vpk under sine wave excitation cause EDM currents [30]. However, as discussed earlier as well as in [30], the pulsed excitation and rate of change of voltage extends the withstand voltage of dielectric materials. Tests reported on in [35] showed a maximum withstand voltage of 30 V peak at pulse duration's of 10  $\mu\text{sec}$ . Given the typical lubricant film thickness of 0.2–2.0  $\mu\text{m}$ , this is equal to a dielectric strength of 15 Vpk/ $\mu\text{m}$ . The debris within the lubricant alters the conductivity and dielectric withstand voltage [42]. As the bearing ages, mechanical contaminants arising from EDM and mechanical wear can significantly alter the lubricants electrical properties. In the extreme, the lubricant becomes a conducting grease, shorting the  $C_b$  and preventing  $V_{rg}$  buildup. In fact, one solution to  $V_{rg}$  buildup and  $I_b$  is to replace the conventional lubricant with a conductive grease; however, experience with conductive grease indicates the bearing life decreases by a factor of three. Thus  $C_b$  is a function of the lubricant film's relative dielectric constant  $\epsilon(C_b(Q, U, T, \eta, \lambda, \Lambda, \epsilon_r))$  [37, 45].

13.5.3.4.1.5 An Expanded Bearing Model

A per ball model for a general ball bearing is shown in Fig. 13.30. The model consists of an inner and outer race resistance ( $R_{in}$  and  $R_{out}$ ) in series with capacitors  $C_{ball,i}$  representing the film capacitances from outer and inner races to the ball and ball resistance  $R_{ball,i}$ . These series elements are then in parallel with a capacitance from the outer to inner races and a nonlinear element, which functions to randomly short the bearing outer and inner races replicating the balls penetrating the film layer [37].

Based on extensive conversations with bearing manufacturers and researchers, and further analysis by the

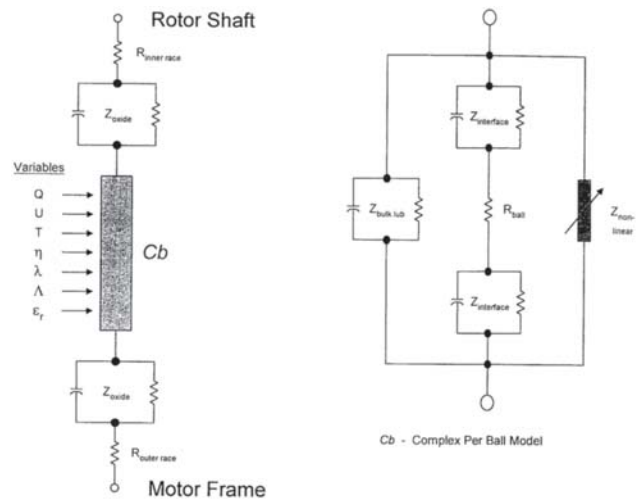


**Figure 13.40** Expanded ball bearing model. (© 1997 IEEE. Reprinted, with permission, from Transactions on Industry Applications, Vol. IA-33, No. 2, March/April 1997 [37].)

authors, a new per ball electrical model is proposed. This new model incorporates the findings presented above and is presented in Fig. 13.40. The major differences with the previous model are the division of the lubricant into three regions (outer race oxide, bulk layer, inner race oxide) and the parametric input channels ( $Q, U, T, \eta, \lambda, \Lambda, \epsilon_r$ ). The model now incorporates the effects of the mechanical parameters through the nonlinear capacitance and resistance elements. With this model, researchers across a broad range of disciplines have the opportunity of examining the problem of EDM and  $dv/dt$  bearing damage [37].

13.5.3.5 Electrical Components— $L_o, R_o, C_{sf}, C_{sr}, C_{rf}$

Although a distributed parameter system, lumped parameters adequately model the system as shown in Fig. 13.31. This system consists of the stator winding zero sequence impedance ( $L_o$  and  $R_o$ ), the stator winding to frame capacitance ( $C_{sf}$ ,  $C_{sr}$ , the rotor to frame capacitance ( $C_{rf}$ ), and  $C_b$ . A formula for each capacitance follows, together with calculations for machines from 5–1000 hp. These formulas assume the geometrical shapes depicted in Fig. 13.41. A comparison with experimental values for the 15-Hp machine of [34] is presented later [30].

**Calculation of  $C_{sf}$ :** The  $C_{sf}$  model consisted of  $N_s$  parallel capacitors, where  $N_s$  is the number of stator slots. Each slot consisted of a conductor  $L_s$  meters long,  $W_d$  meters deep, and  $W_s$  meters wide centered within a rectangular conduit with all sides at the same potential. A dielectric material separates the conductor and conduit by  $d$  meters with a relative permittivity of  $\epsilon_r$  (slot paper). Equation 13.5 provides the  $C_{sf}$  for  $N_s$  slots [46]. Figure 13.42 shows calculated values of  $C_{sf}$  for induction machines from 5–1000 Hp [30].

$$C_{sf} = K_{sf} N_s \epsilon_r \epsilon_0 (W_d + W_s) L_s / d \tag{13.5}$$

**Calculation of  $C_{sr}$ :** The stator to rotor coupling capacitance, shown in Fig. 13.41, consists of  $N_r$  sets of parallel conducting plates. The area of each plate equals the product of the length

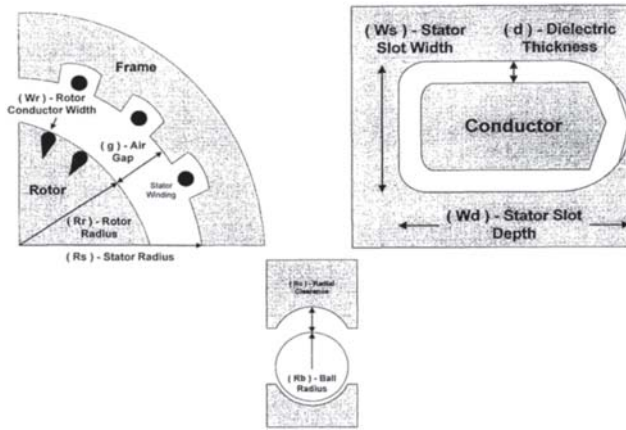


**Figure 13.41** System capacitance models. (© 1997 IEEE. Reprinted, with permission, from Transactions on Industry Applications, Vol. IA-33, No. 2, March/April 1997 [30].)

of the rotor ( $L_r$ ) and the width of the rotor conductor near the rotor surface ( $W_r$ ). This capacitance is given by Eq. 13.6; where the distance between the parallel plates ( $g$ ) is the air gap of the machine [46]. Figure 13.42 shows calculated  $C_{sr}$  for induction machines from 5 to 1000 Hp [30].

$$C_{sr} = K_{sr} N_r \epsilon_0 W_r L_r / g \tag{13.6}$$

**Calculation of  $C_{rf}$ :** The capacitive coupling between the rotor and frame, shown in Fig. 13.41, is determined as the capacitance of two concentric cylinders or a coaxial capacitor. In this case, the effective gap between the cylinders must compensate for the effect of the stator slot widths. If the inside radius of the outer cylinder (stator) is  $R_s$  and the outer radius of the inner cylinder (rotor)  $R_r$ , then the capacitance is given by Eq. 13.7 [46]. Figure 13.41 shows calculated  $C_{rf}$  for induction machines from 5 to 1000 Hp [30].

$$C_{rf} = K_{rf} \pi \epsilon_0 L_r / \ln(R_s / R_r) \tag{13.7}$$

**Calculation of  $C_b$ :** The bearing capacitance depends on the geometrical configuration of the bearing, load, speed, temperature, and characteristics of the lubricant. Each bearing type—ball, roller, journal, etc.—yields a capacitance model, with the capacitance value a function of physical and operating parameters. For example, a journal bearing’s capacitance increases with increasing eccentricity and length/diameter ratio [45]. The capacitance of all bearings depends on the load angle and relative permittivity of the lubricant.

The model selected for ball bearings, shown in Fig. 13.41, assumes a set of  $N_b$  pairs of concentric spheres, where  $N_b$  is the number of balls. Each capacitor pair includes an inner sphere (modeling the balls) within an outer sphere (modeling the raceways). Equation 13.5 provides the mathematical formula for this capacitance [46]. The radius of the inner sphere ( $R_b$ ) corresponds to the radius of the ball; the radius of the equivalent outer sphere equals the radius of the inner sphere plus the radial clearance ( $R_b + R_c$ ), the distance to the outer raceway. The bearing capacitance varies with the shaft diameter and radial clearance and is plotted in Fig. 13.42.

$$C_b = N_b 4 \pi \epsilon_0 \epsilon_{rl} \left( \frac{1}{R_b} - \frac{1}{(R_b + R_c)} \right) \tag{13.8}$$

Figure 13.42 shows with increasing machine size  $C_b$  decreases; the machine capacitances, however, increase with increasing horsepower [35]. These calculations are based on design data for 4-pole, 460-V ac induction machines and associated bearing dimensions [30].

*13.5.3.6 Experimentally Determined System Capacitances*

The machine zero sequence inductance and parasitic capacitances were measured on the induction machine of [34]. Measurement results and methodology for each element of the system model follow. Table 13.18 lists measured and calculated capacitance values for the machine of [34]. The measured capacitance values were made with the rotor externally driven at controlled speeds when appropriate [30].

**$L_o$  and  $R_o$ :** The common mode or zero sequence impedance of the machine equals one third of the stator resistance in series with one third of the stator leakage inductance. They were obtained by connecting the three stator lines and measuring the impedance line-to-neutral with a Hewlett-Packard 4284A LCR meter. A value of 300  $\mu$ H and 59.8  $\Omega$  was measured at 100 KHz [30].

**$C_{sf}$ :** For the 15-hp machine of [34], the  $C_{sf}$  obtained by LCR measurement with the rotor removed was 11.1 nF. By removing the rotor, the effects of  $C_{sr}$ ,  $C_{rf}$ , and  $C_b$  are eliminated. The 11.1 nF compares well with the calculated value 7.7 nF in

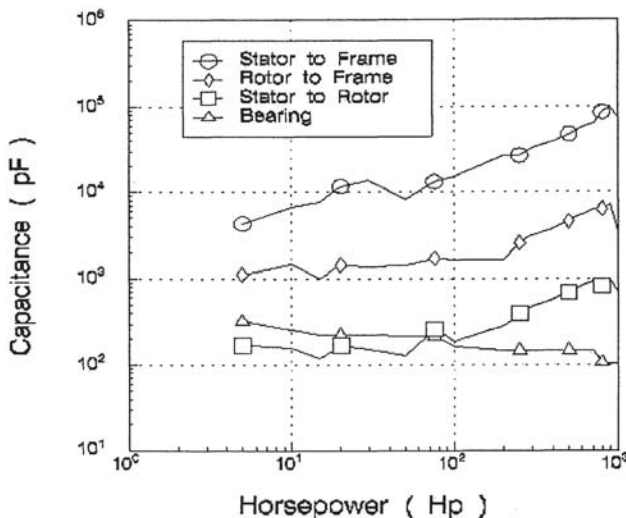


**Figure 13.42** Calculated motor and bearing capacitance values. (© 1997 IEEE. Reprinted, with permission, from Transactions on Industry Applications, Vol. IA-33, No. 2, March/April 1997 [30].)

**Table 13.18** Machine Bearing Capacitances—Calculated and Measured

	15-hp machine [34]	Calculated 15-hp machine
$C_{sf}$	11 nF	7.7 nF
$C_{rf}$	1.1 nF	1.0 nF
$C_{sr}$	100 pF	123 pF
$C_b$	200 pF	225 pF

Fig. 13.42, which is based on a different stack length than the motor of [30, 34].

*C<sub>sr</sub>*: Measurement of *C<sub>sr</sub>* was achieved by shorting the rotor shaft to frame and connecting a LCR meter to the three commonly connected stator terminals and the machine frame. To obtain *C<sub>sr</sub>*, the value of *C<sub>sf</sub>* is subtracted from the capacitance reading of the LCR meter. For the 15-hp machine of [34], the measured value was 100 pF; Fig. 13.42 shows a value of 123 pF. Fig. 13.42 suggests an increasing *C<sub>sr</sub>* with increasing horsepower, which is consistent with the increasing machine size [30].

*C<sub>b</sub>*: The bearing capacitance is a function of dielectric characteristics, resistivity, and temperature of the lubricant, geometrical construction, dynamics of the asperity contact of the balls with the race, and speed of the rotor. The *C<sub>b</sub>*, therefore, is dynamic and dependent on the operating conditions of the machine. Tests were performed with a segmented bearing and a pressure contact between the race, film, a known insulator, and the ball. For the 15-hp machine of [34], a *C<sub>b</sub>* of 200 pF was measured. This compares favorably with the calculated value of 225 pF of Fig. 13.42, predicted by the bearing model [30]. *C<sub>rf</sub>*: An indirect measurement of *C<sub>rf</sub>* is possible once *C<sub>sf</sub>*, *C<sub>sr</sub>*, and *C<sub>b</sub>* are known. By placing a LCR meter to measure the impedance from rotor to frame, the dominance of *C<sub>sf</sub>* can be reduced. The value obtained for the the 15-hp induction machine of [34] was 1.1 nF; Fig. 13.42 indicates 1.0 nF for a 15-hp machine, which compares favorably with the measurement [30].

### 13.5.3.7 System Model and Analysis

With the common mode model for the drive established, an analysis of the effects of system parameters on *V<sub>rg</sub>* and bearing currents is possible. Figure 13.31 allows for the investigation of common mode chokes or transformers, line reactors, and long cables through the modification of the series and parallel impedance elements; it provides a model capable of examining PWM modulation techniques and power device rise times; and it allows for an investigation of source to ground voltage levels [30].

*Steady-State Shaft Voltage Level*: With PWM frequencies much less than the natural frequency of the system zero sequence network impedance, the capacitors divide *V<sub>sng</sub>* and yield the following algebraic relationship for the *BVR* [30].

$$BVR = V_{rg} / V_{sng} = C_{sr} / (C_{sr} + C_b + C_{rf}) \tag{13.9}$$

This relationship, although simple, provides substantial information about bearing charge and discharge phenomena and potential improvements. For example, a value of *V<sub>rg</sub>*, the bearing threshold voltage (*V<sub>th</sub>*), exists for each value of film thickness below which dielectric breakdown EDM does not occur. This threshold depends on pulse duration and characteristics of the lubricant. However, Eq. 13.9 provides an estimate of *V<sub>rg</sub>*. This estimate when compared to *V<sub>th</sub>* determines the likelihood of EDM discharge. For example, with a dielectric strength of 15 Vpk/μm and lubricant film thickness varying between 0.2 and 2 μm *V<sub>th</sub>* ranges from 3–30 Vpk. With a *BVR* of 0.1 (Fig. 13.43), *V<sub>rg</sub>* is in the neighborhood of 35 Vpk for a 460-V system having a *V<sub>sng</sub>* equal to one half bus voltage or 350 Vdc. A *V<sub>rg</sub>* of this magnitude is sufficient to cause EDM discharge [30].

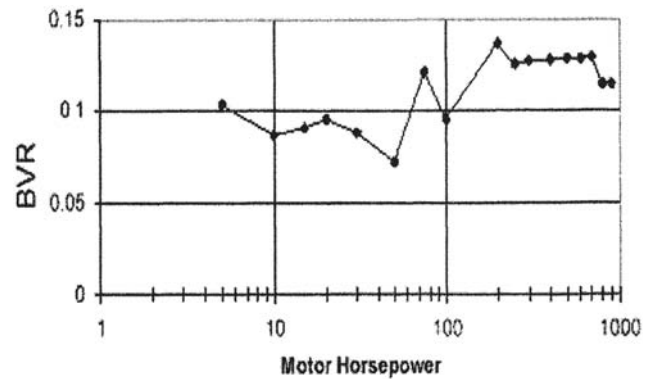


Figure 13.43 Bearing voltage ratio. (© 1997 IEEE. Reprinted, with permission, from Transactions on Industry Applications, Vol. IA-33, No. 2, March/April 1997 [30].)

Equation 13.9 also suggests a large *C<sub>b</sub>* reduces the bearing voltage; thus, to maintain bearing or shaft voltage below *V<sub>th</sub>*—the maximum sustainable voltage without dielectric breakdown EDM—increase the relative permittivity of the lubricant. *BVR* also explains why nonrotating bearings are less susceptible to shaft voltage buildup and EDM. Nonrotating bearings have large surface areas and small effective film thickness both aiding in increasing *C<sub>b</sub>*. In addition, the capacitive voltage divider indicates inserting an insulating sleeve or barrier may exacerbate the bearing charging since this reduces the effective *C<sub>b</sub>* [30].

Using Eq. 13.9 and combining it with results of the capacitance curves of the previous section, *BVR* as a function of horsepower was derived with the results shown in Fig. 13.43. From Fig. 13.43, the machine of [34] has a predicted *BVR* of 0.074. Figure 13.44 shows a typical sequence of *V<sub>sng</sub>*, bearing current, and *V<sub>rg</sub>* traces. It shows three different shaft voltage

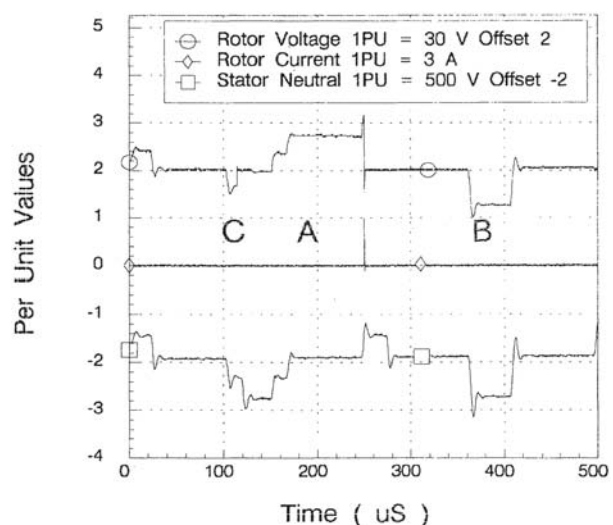
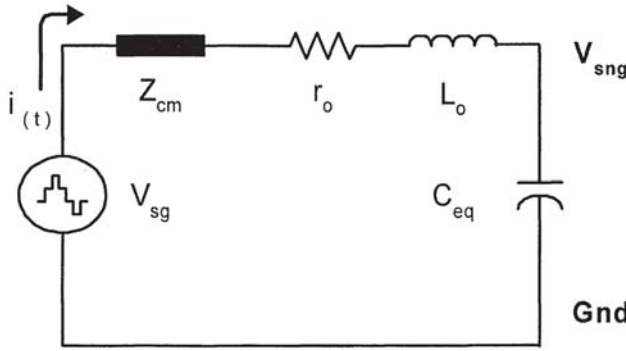


Figure 13.44 Examples of bearing breakdown mechanisms: Film breakdown, *dv/dt* currents, asperity contacts. (© 1995 IEEE. Reprinted, with permission, IEEE 21<sup>st</sup> Annual Industrial Electronics Conference, November 6–10, 1995, Vol. 1 [35].)



**Figure 13.45** Second-order bearing model. (© 1997 IEEE. Reprinted, with permission, from Transactions on Industry Applications, Vol. IA-33, No. 2, March/April 1997 [30].)

phenomena occurring in the bearing. Region A depicts the shaft and bearing charging according to the capacitor divider action of Eq. 13.9 followed by an EDM discharge. Region B represents a charging and discharging of the bearing without EDM current. Finally, region C shows the rotor and bearing charging, but to a much lower voltage level before EDM discharge [35]. The *BVR* is obtained by dividing *Vrg* by the *Vsng* at a point where the machine’s rotor rides the lubricant, region A for example. The experimental value (0.064) is in good agreement with the theoretical calculation of 0.074 [30].

*A Second-Order Model Approximation:* The common mode model of Fig. 13.31 adequately describes most of the observed phenomena associated with shaft voltages and common mode currents. However, the complexity of this model often obscures the cause and effect of PWM voltage source inverters on shaft voltages and bearing currents. A reduced order model, if applied correctly, would have a distinct advantage to the circuit of Fig. 13.31. Common mode chokes, line reactors, and output filters, for example, often are employed to reduce electromagnetic interference (EMI) from PWM voltage source inverters. Also, many applications require long cable lengths between the inverter and load. The reduced order model of Fig. 13.45, therefore, provides a simple model retaining the important effects of these elements on the *Vsng* of the machine [30, 47, 48].

The second order system of Fig. 13.45 has the following general solution for a step input:

$$V_{sng} = V_{sg} \left( 1 - \frac{1}{\sqrt{1-\zeta^2}} e^{-\zeta\omega_n t} \sin(\omega_n \sqrt{1-\zeta^2} t + \psi) \right) \tag{13.10}$$

$$i(t) = \frac{V_{sg}}{\sqrt{1-\zeta^2} Z_0} e^{-\zeta\omega_n t} \sin(\omega_n \sqrt{1-\zeta^2} t) \tag{13.11}$$

where:

$$\omega_n = \frac{1}{\sqrt{L_{eq} C_{eq}}} \quad \zeta = \frac{r_{eq}}{2} \sqrt{\frac{C_{eq}}{L_{eq}}} \quad Z_0 = \sqrt{\frac{L_{eq}}{C_{eq}}}$$

$$\psi = \tan^{-1} \left( \frac{\sqrt{1-\zeta^2}}{\zeta} \right)$$

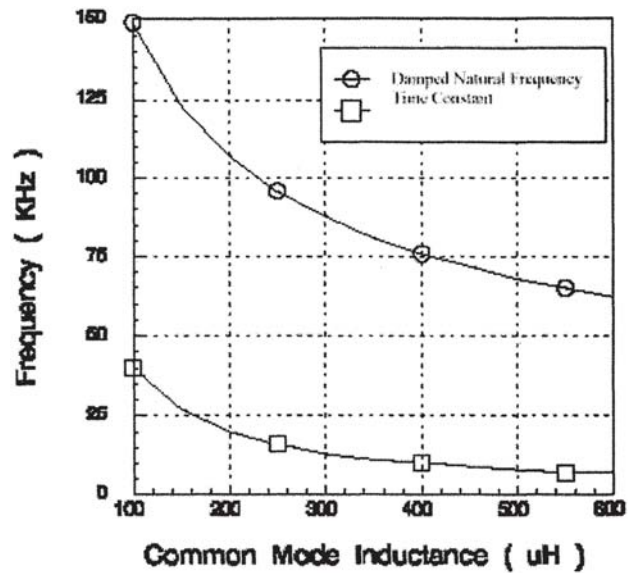


**Figure 13.46** System time constant and damped natural frequency vs. common mode inductance. (© 1997 IEEE. Reprinted, with permission, from Transactions on Industry Applications, Vol. IA-33, No. 2, March/April 1997 [30].)

and  $\omega_n$  is the undamped natural frequency,  $\zeta$  is the damping ratio,  $Z_0$  is the characteristic impedance, and  $\psi$  is the phase angle of *Vsng*. The equivalent capacitance, (*Ceq*), equals [*Csf* / (*Csr*+*Crf*//*Cb*)]—the *Csf* in parallel with the series combination of the *Csr* and the parallel combination of the *Crf* and *Cb* [30].

This formulation of the system equations also allows for an easy analysis of the rise time of the forcing function *Vsg*, the effect of the PWM frequency, and influence of the system parameters on damping, natural frequency, and overshoot. If the rise time of the stepped *Vsng* is longer than one half of the oscillation period, the zero sequence current is reduced substantially; thus reducing the *dv/dt* current through the bearing and frame. Furthermore, increasing the common mode inductance—with common mode chokes and line reactors—without considering the effect on the damping factor can raise the Q of the circuit. The higher Q and lower natural frequency may result in a near resonance condition with the stepped waveform of the forcing function’s PWM carrier [30].

Figure 13.46 shows system time constant ( $\zeta\omega_n$ ) and damped natural frequency ( $\omega_n\sqrt{1-\zeta^2}$ ) as functions of common mode inductance (*Lcm*) for the 15-hp induction motor of [34]. Both quantities have been converted into hertz or 1/seconds for easy comparison with typical carrier frequencies employed by IGBT inverters. IGBT VSIs often incorporate common mode chokes to reduce the *dv/dt* current. Figure 13.46 indicates damped natural frequency and time constant decrease with increasing common mode inductance. For typical common mode inductances, the damping in the system decreases and the damped natural frequency is well within the dominant frequencies of the common mode voltage source of IGBT inverters, setting up a potential resonance condition [30].

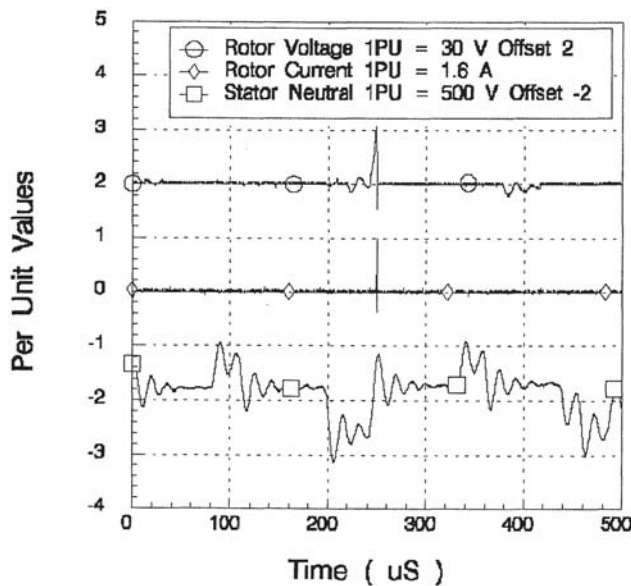


**Figure 13.47** Response with common mode choke. (© 1997 IEEE. Reprinted, with permission, from Transactions on Industry Applications, Vol. IA-33, No. 2, March/April 1997 [30].)

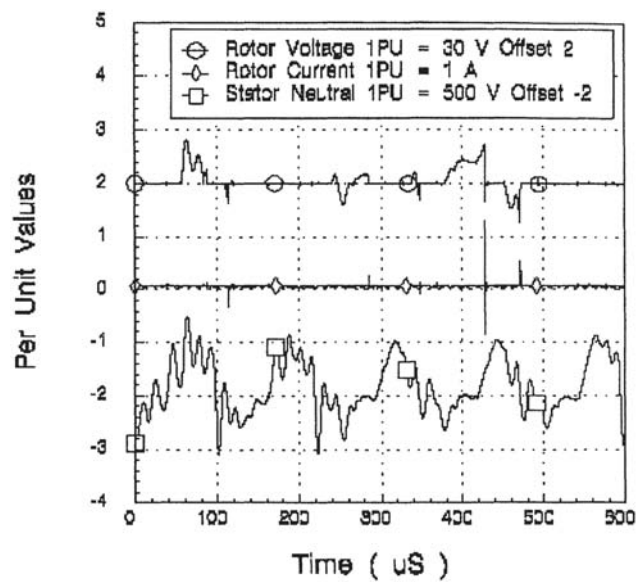


**Figure 13.48** Response with series reactor. (© 1997 IEEE. Reprinted, with permission, from Transactions on Industry Applications, Vol. IA-33, No. 2, March/April 1997 [30].)

### 13.5.3.8 Model Evaluation and Component Analysis

Evaluation of the second-order model requires experimental results that allow a comparison of the natural frequency and damping factors with the predicted values based on Fig. 13.45. The response of the stator neutral voltage, rotor shaft voltage, and bearing current to a PWM VSI with various system components inserted between the inverter and motor provides data for model evaluation and demonstrates the effect of system components on bearing currents [30].

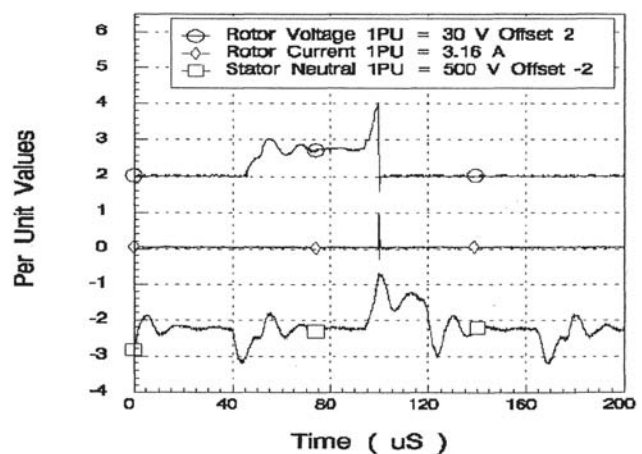
*Effects of Common Mode Components, Line Reactors, and Cable Lengths:* With the appearance of IGBT inverter drives, common mode noise presents a significant challenge to drive design. Common mode chokes and transformers, inserted between the inverter output and load motor, provide additional impedance to common mode current without affecting the fundamental component. Another approach inserts a three phase line reactor, but at the price of reduced fundamental voltage at the terminals of the machine [30].

Figure 13.47 shows the response of  $V_{sng}$ ,  $V_{rg}$ , and bearing current with a common mode choke of  $270 \mu\text{H}$  and  $2.6 \Omega$  inserted between inverter output and load motor. The  $V_{sng}$  oscillates at 60 kHz with a damping ratio of 0.12. Using the model of Fig. 13.45, the calculated values are 62.7 kHz and a damping factor of 0.12. Adding the common mode choke to reduce  $dv/dt$  current also affects the response of  $V_{sng}$  and  $V_{rg}$ . The reduced damping causes the machine's  $V_{sng}$  to overshoot considerably the nominal steady state value for each switching instant. The decreased damping also provides the rotor the opportunity to charge once the bearing rides the lubricant film [30].

To examine the effects of reduced damping in more detail, a three-phase series reactor with a common mode reactance of  $600 \mu\text{H}$  was inserted between the inverter output and load motor. The theoretical frequency and damping factor were 50.3 kHz

and 0.0158, respectively. Experimental results for a 15-hp induction machine (Fig. 13.48) show a lightly damped 50-kHz oscillation. The decrease in damping increases the probability of  $C_b$  charging. This is because the system capacitance never achieves the steady-state charge associated with the forcing function. Each time the bearing rides the film, the presence of  $C_b$  alters the system topology and the voltage distribution must change to reflect the change in impedance. Thus with relatively light damping,  $V_{sng}$  is excited and rings to an excessively large value. In the case of Fig. 13.48,  $V_{sng}$  exceeds 590 Vpk, which is 280 Vpk larger than one half  $V_{bus}$  [30].

A cable's length also affects  $dv/dt$  current, shaft voltage buildup, and bearing current discharge. Figure 13.49 shows



**Figure 13.49** Response with long cable. (© 1997 IEEE. Reprinted, with permission, from Transactions on Industry Applications, Vol. IA-33, No. 2, March/April 1997 [30].)



the  $V_{sng}$ ,  $V_{rg}$ , and bearing current with a 600-foot cable. At the frequencies of interest, the cable presented an equivalent series impedance of  $3.2 \Omega$  and  $80 \mu\text{H}$ , and a parallel resistance of  $3.0 \Omega$  in series with  $22 \text{ nF}$  of capacitance. The Thévenin equivalent equals a resistance of  $10.9 \Omega$  in series with  $129 \mu\text{H}$ . The calculated damped natural frequency and damping ratio for the model of Fig. 13.45 are  $71.7 \text{ kHz}$  and  $0.18$ . These compare well with the experimental values of  $76.0 \text{ kHz}$  and  $0.19$ , respectively [30].

The transient response of the long cable system shows the  $V_{sng}$  rings up to over  $600 \text{ Vpk}$ , with a nominal  $630 \text{ Vdc}$  bus. The bearing rides the lubricant film and charges to  $25 \text{ Vpk}$  just before the ring up of  $V_{sng}$ . Once the stator begins to ring up to the  $600 \text{ Vpk}$  level,  $V_{rg}$  responds with a slight delay and achieves almost  $65 \text{ Vpk}$  before an EDM of  $3.2 \text{ Apk}$  occurs. Experimental results similar to these confirm excessive  $V_{sng}$  and  $V_{rg}$  are possible with long cable lengths. The resulting current densities— $2.48$  to  $5.16 \text{ Apk/mm}^2$ —are in the region to reduce bearing life [30].

### 13.5.4 Methods to Mitigate Bearing Currents and Their Cost

The previous sections examine the fundamentals of bearing damage from high frequency voltages impressed by adjustable speed drives (ASDs). New coupling mechanisms were discussed and the adverse effects on bearing life presented. However, it must be remembered most ASD applications experience no discernible loss of bearing life. Bearing failures associated with ASD operation are often the result of inadequate grounding of the motor and drive load. If high frequency grounding procedures are neglected, the path of least impedance back to the inverter may pass through the bearing (Fig. 13.50) [48]. This diversion of common mode current in addition to the bearing's  $dv/dt$  current can degrade the lubricant and result in bearing pitting. This section will present standard procedures for mitigating the known electrical contributors to bearing damage and where known a cost estimate for the correction.

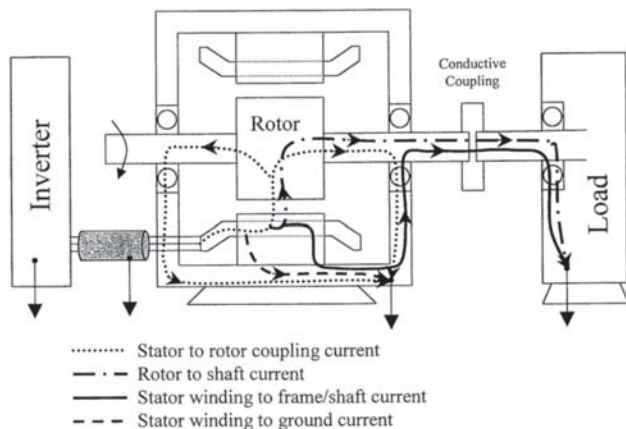


**Figure 13.50** Return paths for common mode current 0. (Courtesy of Rockwell Automation [48].)

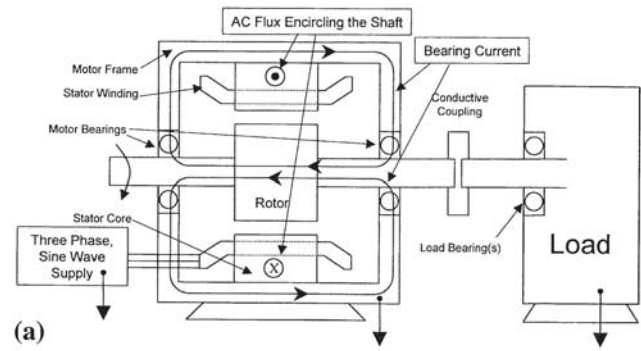


**Figure 13.51a** Sine wave excitation with flux induced bearing current. (Courtesy of Rockwell Automation [48].)

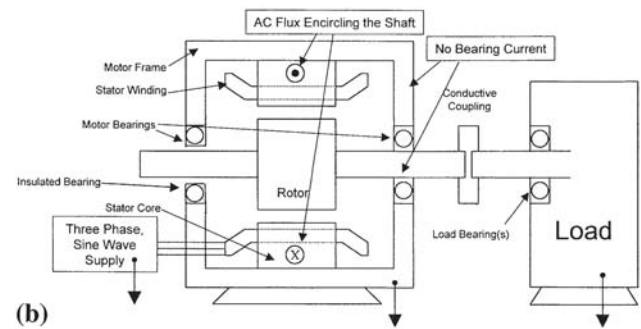


**Figure 13.51b** Sine wave excitation with insulated bearing. (Courtesy of Rockwell Automation [48].)

#### 13.5.4.1 One/Two Insulated Bearings on Motor (Except for Homopolar Flux)

Low frequency circulating bearing currents induced by flux coupling circuit formed by the rotor shaft (Fig. 13.51a) [48], bearings and motor frame are historically controlled by inserting an insulating ring between the rotor shaft and inner race on the non-drive end (Fig. 13.51b) [48]. This approach is very effective provided the flux is not in the frequency range associated with ASD common mode voltages. Under these conditions the insulator thickness can become excessive ultimately interfering with proper heat transfer. (NDEIB 14% motor cost 90 kW, 7% 250 kW, 3% 500 kW).

#### 13.5.4.2 Shaft Grounding Brush Without Insulated Bearings

Provides an alternate path around drive end bearing diverting common mode current and shorts shaft voltage to motor frame (Fig. 13.52) [48]. Does not mitigate flux induced circulating currents or prevent shaft conduction currents through the mechanical load (at 75 kW approximately \$125).

#### 13.5.4.3 Proper Grounding Between Motor and Drive

Providing a low impedance return from motor to drive establishes a preferred path for common mode current (Fig. 13.53) [48]. Although incapable of preventing circulating or shaft to ground bearing currents, by establishing a preferred

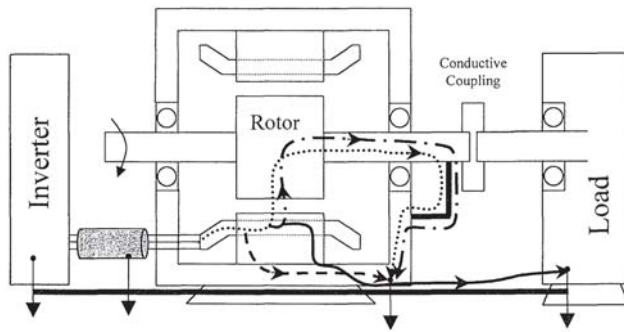


**Figure 13.52** Shaft grounding brush mitigates common mode voltage bearing current. (Courtesy of Rockwell Automation [48].)

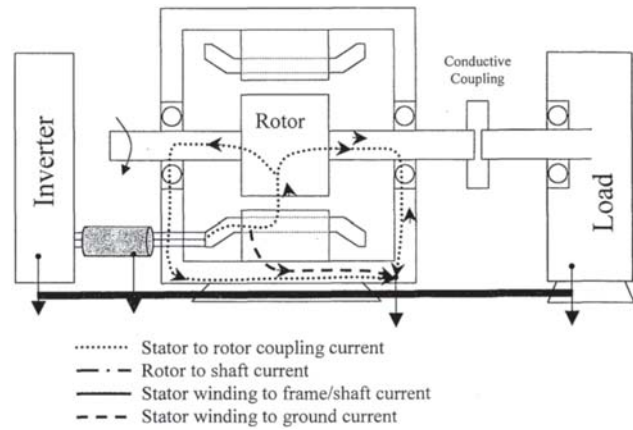


**Figure 13.54** Properly grounded drive/motor/mechanical system. (Courtesy of Rockwell Automation [48].)

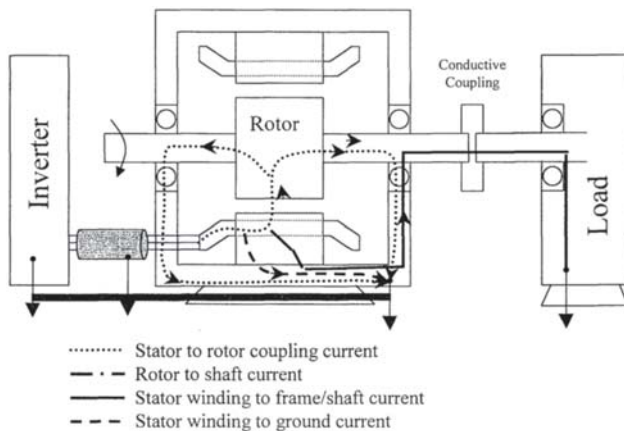


**Figure 13.53** Properly grounded drive/motor system. (Courtesy of Rockwell Automation [48].)

return path the mechanical load is less likely to serve as a return path for common mode current and succumb to damaging current levels.

#### 13.5.4.4 Proper Grounding from Motor to Driven Load/ Equipment

Maintaining common potential between motor frame and mechanical load prevents back feeding common mode frame current through motor bearings and returning via the mechanical load (Fig. 13.54) [48]. However, it does not prevent  $dv/dt$  or EDM motor or load currents since the shaft voltage is not reduced.

#### 13.5.4.5 Isolate Coupled Load from Motor (Fig. 13.55) [48]

1. Insulated coupling between motor and driven equipment including encoders.
2. Reduce the likelihood of common mode current conduction through the driven load use an insulated coupling. This raises the impedance between the motor shaft and the mechanical load impeding common mode current conduction.

3. Requires insulator with sufficient high frequency impedance to divert current through preferred path.

#### 13.5.4.6 Passive Filter (82% Drive Cost 90 kW, 30% 250 kW)

1. Provides differential and/or common mode filtering attenuating the high frequency voltage spectrum to acceptable levels.
2. Reduces both carrier frequency and high frequency flux induced circulating currents.
3. Reduces common mode  $dv/dt$  currents and reduces shaft voltage levels below EDMs.
4. Can be difficult to apply because of resonance.
5. If incorrectly applied can amplify EDMs and  $dv/dt$  current.

#### 13.5.4.7 Common Mode Core (3% Drive Cost >500 V)

1. Attenuates shaft voltage and common mode current flux induced circulating currents.
2. Can cause resonance and amplify EDM potential and  $dv/dt$  current amplitudes.

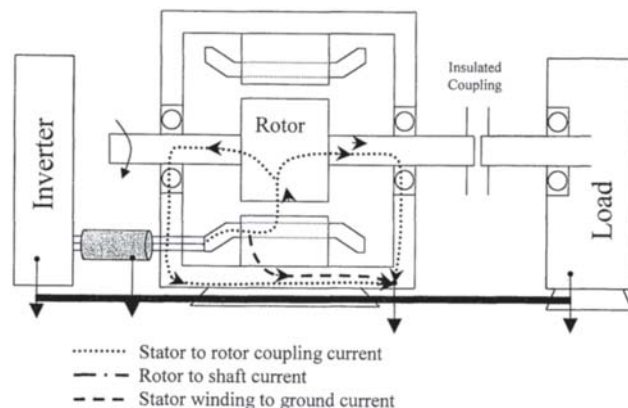


**Figure 13.55** Insulated coupling between motor and driven load. (Courtesy of Rockwell Automation [48].)

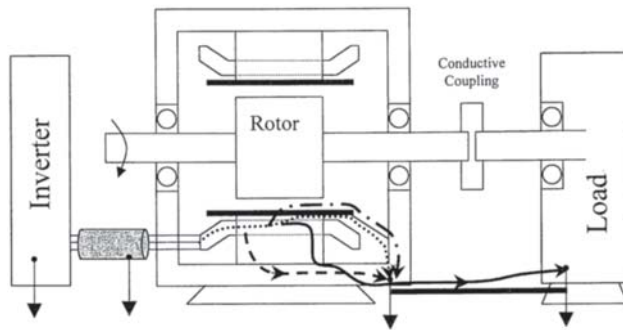


Figure 13.56 ESIM motor with motor to load ground strap [46].

#### 13.5.4.8 Inline Reactors

1. Must handle drive rated current.
2. Reduces circulating currents from carrier frequency flux.
3. If no common mode impedance no reduction in common mode voltage.
4. Cost?

#### 13.5.4.9 Electrostatically Shielded Motor (Fig. 13.56)

1. Grounded shield interrupts charging of  $C_{sr}$  reducing the shaft voltage.
2. Reduces probability of EDMs from common mode voltage.
3. Reduces  $dv/dt$  currents through bearing.
4. Cost adder at 75 hp is approximately 25% of basic motor cost.

#### 13.5.4.10 Conductive Lubricants (Abrasive and Used with Care)

1. Provides a low impedance path to frame.
2. Added conductive elements cause abrasion and shorten bearing life.
3. Inexpensive.

#### 13.5.4.11 Ceramic Bearings

Ceramic bearings prevent pitting. Shaft voltage is present thus jeopardizing the mechanical load. Cost is coming down.

#### 13.5.4.12 ASD Settings

Select lowest carrier setting allowed by application. This reduces the number of common mode transitions and therefore  $dv/dt$  and EDM discharges. No additional cost.

### 13.6 RELIABILITY IMPACT OF ADJUSTABLE SPEED DRIVES (ASDs) ON INSULATION

The harmonic-rich, fast risetime waveform of the inverters used in ASDs have other deleterious effects on motors such as vibration, noise, and insulation deterioration. The most serious of these is insulation deterioration. This has led to the development and increasing use of corona resistant insulation for motor windings. A more detailed examination of the effects of ASDs on motor insulation may be found in Section 8.4.

### REFERENCES

Note: In the following listing, abbreviations have the following meanings:

- AIEE American Institute of Electrical Engineers (predecessor to IEEE)  
 ASM American Society for Metals  
 EPRI Electric Power Research Institute  
 IEEE Institute of Electrical and Electronics Engineers  
 IEEE Institute of Electrical and Electronics Engineers

1. IEEE Committee Report, P.O'Donnell, Coordinating Author, "Report of Large Motor Reliability Survey of Industrial and Commercial Installations—Part 1," *IEEE Transactions on Industry Applications*, vol. IA-21, no. 4, July/Aug. 1985, pp. 853–864.
2. IEEE Committee Report, P.O'Donnell, Coordinating Author, "Report of Large Motor Reliability Survey of Industrial and Commercial Installations—Part 2," *IEEE Transactions on Industry Applications*, vol. IA-21, no. 4, July/Aug. 1985, pp. 865–872.
3. IEEE Committee Report, P.O'Donnell, Coordinating Author, "Report of Large Motor Reliability Survey of Industrial and Commercial Installations—Part 3," *IEEE Transactions on Industry Applications*, vol. IA-23, nos. 1, Jan./Feb. 1987, pp. 153–158.
4. IEEE Committee Report, "Report on Reliability Survey of Industrial Plants, Parts I, II and III," *IEEE Transaction, on Industry Applications*, vol. IA-10, no. 2, Mar./Apr. 1974, pp. 213–252; "Parts IV, V, and VI," vol. IA-10, no. 4, July/Aug. 1974, pp. 456–476; "Correction to Part VI," vol. IA-10, no. 5, Sept./Oct. 1974, p. 681.
5. Dickinson, W.H., "Report of Reliability of Electrical Equipment in Industrial Plants," *Transactions of the AIEE, Part II*, July 1962, pp. 132–151.
6. Albrecht, P.F., J.C.Appiarius, E.P.Cornell, D.W.Houghtaling, R.M.McCoy, E.L.Owen, and D.K.Sharma, "Assessment of the Reliability of Motors in Utility Applications—Part 1," *IEEE Transactions on Energy Conversion*, vol. EC-2, no. 3, Sept. 1987, pp. 396–406.
7. Albrecht, P.F., et al., "Assessment of the Reliability of Motors in Utility Applications—Part 2," *IEEE Transactions on Energy Conversion*, vol. EC-1, no. 1, Mar. 1986, pp. 39–46.
8. Widner, R.L., and W.E.Littmann, "Bearing Damage Analysis," National Bureau of Standards Special Publication 423, *Definition of the Problem*, Proceedings of the Mechanical Failures Prevention Group, May 1974, published April 1976.
9. Widner, R.L., "Failures of Rolling-Element Bearings," *Metals Handbook*, 9th edn., vol. 11, *Failure Analysis and Prevention*, American Society for Metals, Metals Park, Ohio, 1986.
10. Sibley, L.B., "Rolling Bearings," *Wear Control Handbook*, American Society of Mechanical Engineers, 1980, pp. 699–726.
11. Harris, Tedric A., "Friction and Wear of Rolling-Element Bearings," *ASM Handbook*, vol. 18, *Friction, Lubrication, and Wear Technology*, American Society for Metals, pp. 499–514.
12. Littmann, W.E. (with R.L.Widner, et al.), "The Role of Lubrication in the Propagation of Contact Fatigue," *Journal of Lubrication Technology*, American Society of Mechanical Engineers Transactions, 1968, pp. 89–100.
13. Bruni, K.A., *Guidelines for Successful Commutator and Brush Operation*, Carbon Products Operation Inc., East Stroudsburg, PA, pp. 1–7.
14. Edwards, D.G., "On-Line Monitoring of Stator Winding Insulation in High Voltage Motors," Society of Petroleum Engineers, 1989, No. 19272.
15. Nailen, R.L., "Detecting and Correcting Open Rotor Bars," *Electrical Apparatus Magazine*, July 1986.
16. Motor View for RBM wave Reference Manual, Revision 3, Computational Systems, Incorporated Knoxville, Tennessee, 2002.
17. Rowan, S., "Non-Invasive On-Line Diagnostics for Electrical Systems," *Mining Technology Magazine*, July 1988.

18. Maxwell, J.H., "Induction Motor Magnetic Vibration," Arizona Public Service Co., Palo Verde Nuclear Generating Station, Phoenix, Arizona 85036.
19. Bonnett, A.H., and G.C.Soukop, "Rotor Failures in Squirrel Cage Induction Motors," IEEE Paper No. PCIC-85-24.
20. Kochensparger, J., "Minimize Motor Failure Downtime (Surge Testing)," *Plant Engineering Magazine*, Dec. 17, 1987.
21. Prashad, H., "Theoretical analysis of Capacitive Effect of Roller Bearings on repeated Starts and Stops of a Machine Under the Influence of shaft Voltages," *Journal of Tribology*, Jan. 1991.
22. Report prepared for GAMBICA (The Association for Instrumentation, Control and Automation) and REMA (The Rotating Electrical Machines Association).
23. Ammann, C., Reichert, K., Joho, r., Posedel, Z., "Shaft Voltages in Generators with Static Excitation Systems-Problems and solutions," 1987 IEEE Power Eng. Society summer Mtg.
24. "Effect of PWM Inverters on AC Motor Bearing Currents and Shaft Voltages," Jay Erdman, Russel J.Kerkman, Dave Schlegel, and Gary Skibinski, *IEEE Transactions on Industry Applications*, Vol. 32, No. 2, March/April 1996, pp. 250-259.
25. Andreason, S. "Passage of Electrical Current thru Rolling Bearings," SKF Gothenberg.
26. Harris, T. *Rolling Bearing Analysis*, Wiley, 1984.
27. S. Chen, T.A. Lipo, and D.W.Novotny, "Circulating Type Motor Bearing Current in PWM Inverter Drives," Conference Record of the IEEE IAS Annual Meeting, 1996, Vol. 1, pp. 162-167.
28. Alston, L., *High Voltage Technology*, Oxford Press, 1968.
29. Prashad, H., "Theoretical Evaluation of Capacitance, Resistance and their Effects on Performance of Hydrodynamic Journal Bearings," *Journal of Tribology*, Oct. 1990.
30. "System Electrical Parameters and Their Effects on Bearing Currents," Doyle Busse, Jay Erdman, Russel J.Kerkman, Dave Schlegel, and Gary Skibinski, *IEEE Transactions on Industry Applications*, Vol. IA-33, No. 2, March/April 1997, pp. 577-584.
31. Kaufman, H., Boyd, J., "The Conduction of Current in Bearings," ASLE Conf, 1958.
32. NEMA MG-1 Specification Part 31, Section IV, 1993.
33. Murray, S., Lewis, P., "Effect of Electrical Currents on Ball Bearing Damage in Vacuum and Air," 22nd ALSE annual meeting May 1, 1967.
34. Erdman, Jay, Kerkman, Russel J., Schlegel, Dave, and Skibinski, Gary, "Effect of PWM Inverters on AC Motor Bearing Currents and Shaft Voltages," APEC '95, Tenth Annual Applied Power Electronics Conference and Exposition, March 5-9, 1995, Vol. 1, pp. 24-33.
35. Busse, Doyle, Erdman, Jay, Kerkman, Russel J., Schlegel, Dave, and Skibinski, Gary, "Bearing Currents and Their Relationship to PWM Drives," IECON '95, IEEE 21<sup>st</sup> Annual Industrial Electronics Conference, November 6-10, 1995, Vol. 1, pp. 698-705.
36. Tevaarwerk, J.L. and Glaeser, W.A., "Tribology," University of Wisconsin-Milwaukee, College of Engineering & Applied Science, Center for Continuing Engineering Education, May 15-16, 1995.
37. "The Effects of PWM Voltage Source Inverters on the Mechanical Characteristics of Rolling Bearings," Doyle Busse, Jay Erdman, Russel J. Kerkman, Dave Schlegel, and Gary Skibinski, *IEEE Transactions on Industry Applications*, Vol. IA-33, No. 2, March/April 1997, pp. 567-576.
38. Bonnet, A., "Cause and Analysis of Anti-Friction Bearing Failures in AC Induction-Motors," US Electrical Motors Inc.
39. Perrin, Martin C., "Large Induction Motor Anti-Friction Bearing Selection," 41st Annual IEEE Petroleum and Chemical Industry Conference, Vancouver, British Columbia, Canada, September, 1994.
40. Prashad, H., "Theoretical Analysis of the Effects of Instantaneous Charge Leakage on Roller Tracks of Roller Bearings Lubricated with High Resistivity Lubricants Under the Influence of Electric Current," *Journal of Tribology*, Jan 1990, Vol. 112, pp. 37-43.
41. Wang, Simon S., Tung, Simon C., "Using Electrochemical and Spectroscopic Techniques as Probes for Investigating Metal-Lubricant Interactions," *STLE Transactions*, Vol. 33, pp. 563-572, 1990.
42. Tung, Simon C., Wang, Simon S., "Friction Reduction From Electrochemically Deposited Films," *STLE Transactions*, Vol. 34, pp. 23-34, 1991.
43. Prashad, H. "Effect of Operating Parameters on the Threshold Voltages and Impedance Response of Non-Insulated Rolling Element Bearings Under the Action of Electrical Currents," *Wear*, Vol. 117, 1987, pp. 223-240.
44. Godfrey, Douglas, Herguth, William R., "Physical and Chemical Properties of Industrial Mineral Oils Affecting Lubrication," *Lubrication Engineering*, October, 1995, pp. 825-828.
45. Prashad, H., "Theoretical Evaluation of Capacitance, Capacitive Reactance, Resistance and Their Effects on Performance of Hydrodynamic Journal Bearings," *Trans. of the ASME*, Oct. 1991, Vol. 113, pp. 762-767.
46. Hayt, William H., *Engineering Electromagnetics*, McGraw-Hill, 5<sup>th</sup> edition, 1989.
47. Melsa, James L., Schultz, Donald G., *Linear Control Systems*, McGraw-Hill, 1969.
48. *Inverter-Driven Induction Motors Shaft and Bearing Current Solutions*, Rockwell Automation Industry White Paper.

# 14

## Maintenance

**Paul L.Cochran** (Section 14.1.1)/**Walter E.Littmann** (Section 14.1.2)/**Stewart Bowers** (Section 14.2)/**Glenn Goebel and Phil Packard** (Section 14.3)/**Carbon Products Operation Group\*** (Section 14.4)/**J.Edward Jenkins, Jr.** (Section 14.5)/ **Nils E.Nilsson** (Sections 14.6.1–14.6.4)/**Mladen Sasic, Dereck Paley, and David Bertenshan** (Section 14.6.5)

<b>14.1 LUBRICATION</b>	<b>694</b>
14.1.1 Lubrication and Maintenance of Sleeve Bearings	694
14.1.2 Lubrication and Maintenance of Antifriction Bearings	694
<b>14.2 IMPLEMENTATION OF A RELIABILITY BASED MAINTENANCE PROGRAM</b>	<b>698</b>
<b>14.3 MAINTENANCE AND REPAIR OF COMMUTATORS</b>	<b>700</b>
14.3.1 Causes of Poor Commutation	701
14.3.2 Ordering New Parts	702
<b>14.4 BRUSH REPLACEMENT</b>	<b>702</b>
14.4.1 Introduction	702
14.4.2 When to Replace Brushes	702
14.4.3 Installation of Brushes	702
14.4.4 Summary	704
<b>14.5 MAINTENANCE AND REPAIR OF WINDINGS</b>	<b>704</b>
14.5.1 Installation of New Equipment	704
14.5.2 Establishing a Maintenance Schedule	705
14.5.3 Choosing Test Equipment	705
14.5.4 Performing Preventative Maintenance	707
14.5.5 Evaluating Winding Failures	711
14.5.6 Choosing Repair Facilities	715
14.5.7 Selecting Repair Methods	716
14.5.8 Testing Repaired Windings	718
14.5.9 Evaluating Repaired Equipment	718
14.5.10 General References on Maintenance and Repair of Windings	719
<b>14.6 CORE TESTING</b>	<b>719</b>
14.6.1 Loop Test Physical Arrangement	719
14.6.2 Thermovision Monitoring During the Loop Test	720
14.6.3 Other Core Test Factors	721
14.6.4 Core Hot Spot Repairs	721
14.6.5 EL CID Test	721
<b>REFERENCES</b>	<b>727</b>

---

\* The Carbon Products Operation Group includes Kenneth A.Bruni, Richard D.Hall, George G.Kalinovich, and Roland Roberge.

## 14.1 LUBRICATION

### 14.1.1 Lubrication and Maintenance of Sleeve Bearings

Sleeve bearings have a very long to theoretically infinite life if they are correctly designed and manufactured. Since it can be expected that the manufacturer has correctly designed and manufactured them, a failure will nearly always result from extraneous causes, such as oil-supply failure, contaminated oil, foreign matter entering the bearing housing, misapplication (such as a coupled-drive motor being subsequently used as a belted-drive motor, with lateral belt pull, for which it was not designed), and mechanical abuse. Thus, a well-designed sleeve bearing that has been properly manufactured and applied and that has not been subjected to any of the extraneous causes of failure mentioned above will probably never require replacement. However, it is necessary that the design of the bearing and bearing housing be such that bearings may be easily inspected at regularly scheduled maintenance periods and that a bearing may be easily replaced if necessary. This is because some of the extraneous causes of failure mentioned above do arise in the field from time to time.

To enhance ease of inspection and removal, most large sleeve bearings are split about the horizontal centerline. [Figure 11.22](#) (p. 598) shows the two halves of such a bearing, and [Fig. 11.23](#) shows the same bearing assembled. Such a horizontal split does not affect the performance because the logical location of the side grooves is also on the horizontal centerline. In general, access to the bearing for inspection or replacement is obtained in the following manner. The bearing cap is first removed, exposing the upper half of the bearing. After removing the bolts or screws securing the two halves of the bearing together, the top half may be removed for inspection. To relieve the rotor weight from the bottom half of the bearing, a jack may be placed under the coupling on the shaft-extension end or under a stud placed in a centered hole on the opposite end of the shaft; the journal may then be raised a few mils. The bottom half of the bearing may then be rolled 180 degrees around the journal and removed for inspection. Reassembly of the bearing and bearing housing is accomplished by performing the previous steps in reverse sequence. Bearing-cap disassembly, bearing removal and replacement, and bearing-cap reassembly may be accomplished in most cases without disturbing the alignment with the driven equipment or without breaking the coupling.

Although it may never be needed, it is good insurance to have a spare bearing in stock for an important, large motor drive. With a well-designed bearing and bearing housing, it is possible even in the case of an unexpected bearing failure to shut down the unit, replace the bearing, and restart the unit in less than 1 hour. Although a sleeve bearing can be repaired with limited facilities by “puddling in” babbitt, it will not have the dependability of a bearing manufactured in the manufacturer’s factory or in a regional repair shop.

With few exceptions, mineral-base lubricating oil is used for lubricating sleeve bearings of electric drive motors. Although some synthetic or other special types of lubricants may be recommended for some unusual applications, this occurs so infrequently as not to be discussed here, except to recommend that the motor manufacturer’s instruction book be followed.

The mineral-base oil that is normally recommended for motor bearings is either a light turbine oil having a kinematic viscosity of about 150 SSU (Saybolt Seconds Universal) at 100°F and about 44 SUS at 210°F or a medium turbine oil with a kinematic viscosity of about 300 SUS at 100°F and about 55 SUS at 210°F. Most motor manufacturers recommend a lubricating oil with a rust inhibitor and an oxidation inhibitor. Also, a load-carrying “oiliness” agent and an antifoaming agent may be recommended.

The frequency of oil change depends upon such considerations as the method by which oil is supplied to the bearing, ambient temperature, bearing total temperature, cleanliness of the motor environment, and the presence of various gases in the air. Oil may be supplied by rings or disks from a small reservoir or by an external lubricating system, which may also include a filter. The presence of any discoloration, as well as of dirt, sludge, or other contaminants in the oil, indicates that the oil should be changed. Periodic inspection of the bearings, as discussed earlier, provides an opportunity for changing the oil. Certainly it is safe to err on the conservative side and to change the lubricating oil too frequently instead of too infrequently. Finally, the motor manufacturer’s instruction book should be consulted and followed concerning the frequency of oil change.

### 14.1.2 Lubrication and Maintenance of Antifriction Bearings

#### 14.1.2.1 Lubricant Selection

The critical functions of the lubricant are to reduce friction and wear within the bearing, to transfer heat generated in the bearing, to minimize the damage from solid debris particles and other contaminants, and to prevent corrosion of the bearing surfaces. Oil (or oil from the grease) provides lubrication for the sliding contacts between the rolling elements and the cage (retainer), for the contacts with roller guidance surfaces, and for the elastohydrodynamic lubrication (EHL) of the rolling contacts (described in Section 11.4.2.4). The lubricant material in most electric motor bearings is oil or grease.

Since most rolling bearings can be used with oil or grease lubrication, the decision whether to use oil or grease is often related to design and maintenance considerations rather than the application conditions. Simplicity and initial cost favor “sealed-for-life grease lubrication.” Oil lubrication provides more effective transfer of the heat generated in the bearing, is easier to drain and refill, lends itself to lubrication of adjacent parts of a machine, and is more readily used at high temperatures. Grease requires less maintenance, addition of new lubricant can be less frequent, and it aids in sealing the bearing enclosure. The final choice between grease versus oil and of a specific lubricant should be reviewed with the manufacturers of the bearings and the lubricant.

#### 14.1.2.2 Effect of Lubrication on Bearing Life and Expected Failure Modes

The physical and chemical properties of the lubricant have an important influence on bearing life and the failure modes to be

expected. Generally, petroleum oils of higher viscosity allow rolling bearings to have the maximum useful life, comprising the life to initial contact fatigue damage plus propagation life.

#### 14.1.2.3 Sealed Grease Lubrication

Grease lubricants are a mechanical mixture of oil with a thickener such that the grease has the desired mechanical and chemical properties. The grease provides a supply of oil for lubrication within the bearing and heat transfer from the rolling and sliding contacts in the bearing to the outer ring and housing, and aids in sealing the bearing to prevent ingress of solid or liquid contaminants. As the transferred oil from the grease degrades or is lost by oxidation, migration, or centrifugal force, the grease provides a supply of additional oil as needed. However, oxidation of the oil and shearing of the grease within the bearing causes a progressive breakdown of the grease structure, so provisions for periodic grease additions or relubrication may be required. When application conditions allow adequate heat flow to avoid overheating, grease lubrication with an appropriate closure (seal) is often the favored lubrication system because of simplicity and low cost.

##### 14.1.2.3.1 Grease Type

Considerations that influence the selection of the specific grease for a given application are listed in Table 14.1. Figure 14.1 illustrates the temperature range of use for various lubricant fluids in military specification greases [1]. Because of the variety of grease types that are available and proprietary differences in terminology among grease suppliers,

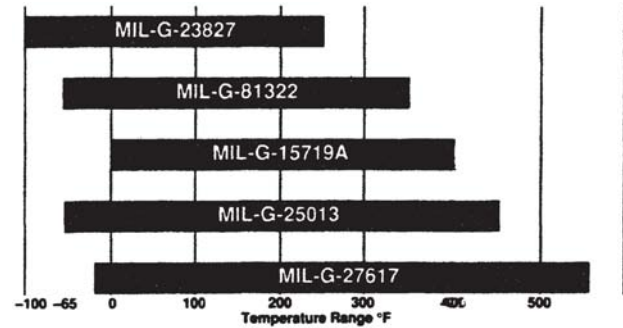


**Figure 14.1** Lubrication grease temperature ranges. (Courtesy of the Fafnir Division of The Torrington Company [1].)

recommendations from the bearing and grease supplier should be compared in making a specific grease selection.

##### 14.1.2.3.2 Grease Relubrication Intervals

Thermal decomposition and oxidation of the lubricant fluid and breakdown due to shearing of the thickener are the principal causes of grease degradation. The recommendations for relubrication intervals with grease are found in bearing suppliers' literature, for example, Refs. 2 and 3. Figure 14.2 is an example of how the relubrication interval is based on bearing size and rotational speed at temperatures up to about 70°C. Grease life from Fig. 14.2 is halved for every 25°F (14°C) increase of temperature over 158°F (70°C).

**Table 14.1** Grease Selection Criteria

Operating conditions	Grease characteristics	Grease type
Low speed, low load	General purpose	Calcium, sodium, lithium thickeners
Low speed, high load	High viscosity, EP <sup>a</sup> or solid lubricant additives	
High speed, low load	Good adhesive properties, shear stability	
High speed, higher load	Good adhesive properties, shear stability, EP <sup>a</sup> or solid lubricant additives	Lithium soap, barium complex soap, or organic synthetic thickeners with synthetic base oil of low viscosity
Low friction		Low viscosity synthetic base oil, penetration NLGI #2 <sup>b</sup> , lithium soap
Low noise level		Filtered grease with high viscosity oil
Inclined or vertical axis	Penetration NLGI #3 <sup>b</sup> , thermal stability must exceed maximum operating temperature	
Lubrication for life	Good shear, thermal, and oxidation stability at maximum operating temperature	Depends on application conditions
Scheduled relubrication	Penetration NLGI #2	
Environmental conditions		
Ambient temperature	See example of test requirements in Reference 3	See Fig. 14.1
Water resistance		
Splash or washing	Water wash resistance	Calcium (150°F maximum), lithium, barium, calcium complex and aluminum complex types
Condensation	Emulsifies water, corrosion resistance	
Solid particle contaminants	Stiff grease, NLGI #3 <sup>b</sup>	

<sup>a</sup>EP, extreme pressure additives react to form protective films on rolling/sliding surfaces.

<sup>b</sup>NLGI, National Lubricating Grease Institute penetration numbers indicate grease consistency as indicated by penetration of a conical indenter under specified conditions, American Society for Testing and Materials, ASTM Designation D 217-60T.

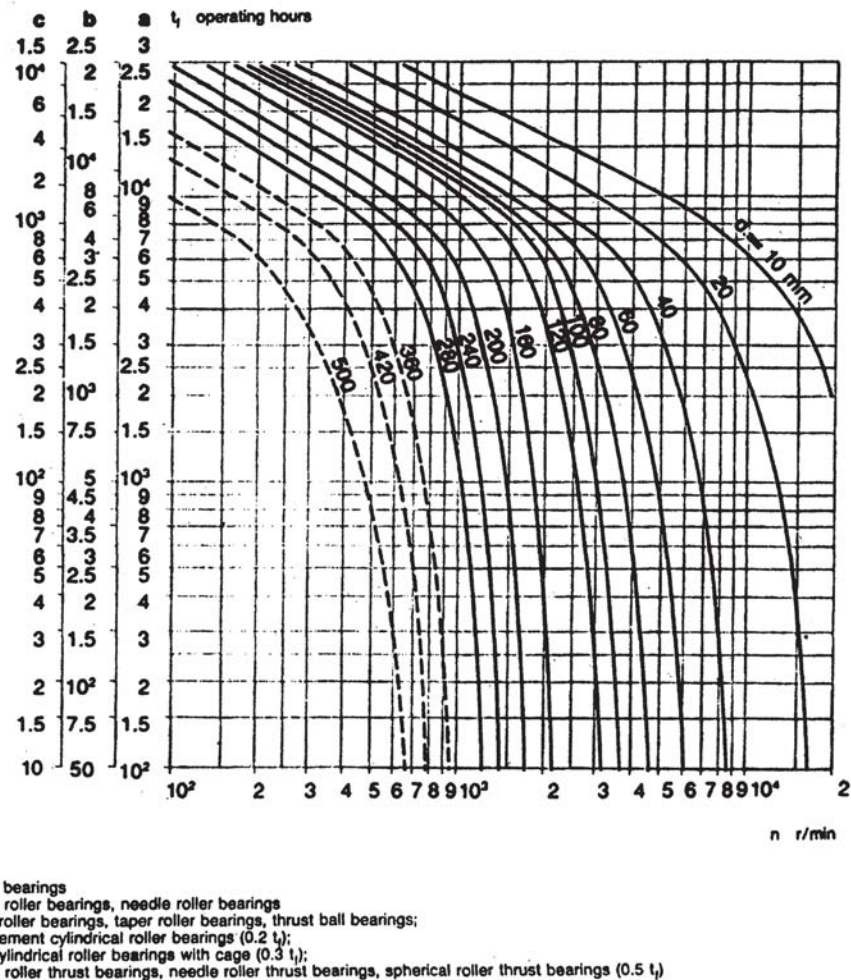


**Figure 14.2** Grease relubrication intervals for rolling bearings. This chart applies to good-quality lithium type greases at temperatures not exceeding 158°F (70°C). Grease life will be halved for every 15°C above 70°C. (Courtesy of SKF USA, Inc. [2].)

#### 14.1.2.3.3 Precautions with Grease Lubrication

- With sealed bearings that are “lubed for life,” do not provide a grease fitting because adding grease may damage seals and allow subsequent leakage loss of lubricant and bearing failure.
- Never mix greases of different base oil, soap, or thickener types.
- Check compatibility of grease with seal materials.
- Initial grease fill and operating grease level should not exceed 1/3 to 1/2 of the bearing volume or housing space, and a path must be provided for the escape of excess grease in the event of overfilling without leakage past the grease seals.
- Do not use high pressure for initial filling or relubrication of sealed bearings in order to avoid damage to seals.

#### 14.1.2.4 Oil Lubrication

##### 14.1.2.4.1 Oil Bath

The simplest oil lubrication systems are a wick feed to sliding bearings in fractional horsepower motors or a static level in

an oil sump for rolling bearings. The maximum oil level should be at the center of the lowest rolling element in the bearing when it is not rotating, and may not be allowed to fall below the lowest rolling contact in the bearing in order to assure that oil will be picked up by the balls or rollers and carried through the bearing. If the maximum oil level should be exceeded, the heat generated by the churning oil will contribute to degradation of the oil and may lead to an overheat failure of the bearing. Drip-feed lubrication may be used to provide a controlled flow of oil through the bearing, with a drain location that will avoid accumulation of oil above the center of the lowest ball or roller under no rotation.

For circulating oil systems, the oil inlet should be at the top of the bearing; drains should be below the bottom of the bearing with an opening that is larger than the inlet so as to avoid oil accumulation in the bearing cavity, and located to maintain a minimum oil level that wets the lowest contact surface. In higher speed motors, pressurized jets should be aimed at the loaded portion of the bearing at the center of the bottom ball or roller and the cage guide surface. In high-speed motors, the jet velocity should be more than 20% of the inner ring



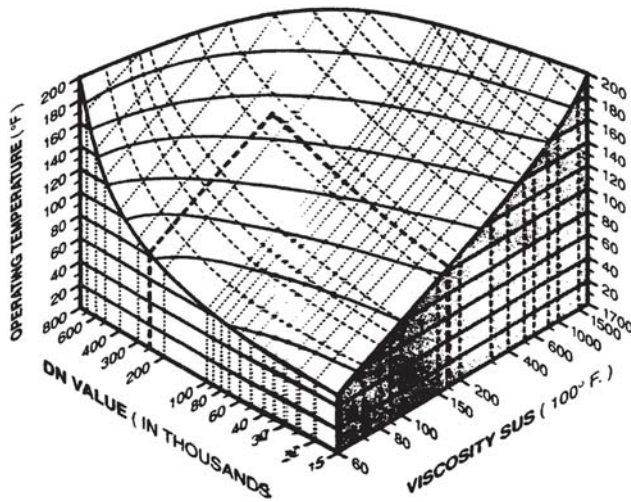


**Figure 14.3** Oil viscosity selection for ball bearings. To use this chart, proceed as follows:

1. Determine the DN value: Multiply the bore diameter in mm by the shaft rpm.
2. Select the expected operating temperature of the bearing, usually higher than the ambient temperature.
3. At the DN value move vertically along or parallel to the nearest dotted line to intersect the solid temperature-DN curve.
4. Move along or parallel to the nearest dashed line downward on the curved surface and vertically to read the appropriate viscosity of the oil in Saybolt Universal Seconds (SUS).

*Example:* With a bore (D) of 140 mm and shaft speed (N) of 1800 rpm,  $DN=252,000$ . If operating temperature is to be  $150^{\circ}\text{F}$ , the heavy dashed line will be followed to a viscosity of 175 SUS. (Courtesy of Fafnir Division of The Torrington Company [4].)

outer surface velocity so as to penetrate the air film rotating with the bearing.

Oil mist may be used in high-speed bearings, for example, in motorized machine tool spindles, to provide minimum heat generation from oil churning with effective cooling by a constant supply of fresh oil.

#### 14.1.2.4.2 Oil Viscosity

The base oil type, additive package, and viscosity grade must be matched with the bearing geometry and expected operating conditions of bearing speed, ambient temperature, and heat flow conditions. Figure 14.3 illustrates how the bearing speed and expected operating temperature can be used to select the appropriate viscosity for oil lubrication of ball bearings.

Since the inlet viscosity that governs the EHL film thickness depends on the viscosity at the contact surface temperature, the heat generation within the bearing, heat flow to the environment, and oil cooling must be considered in specific oil selection. If the motor is connected to a heat source, for example, a pump for high-temperature fluid, soak-back temperatures that may be encountered should also be considered in the design of the lubrication system and the lubricant selection. Synthetic fluids or special petroleum oils are available for extreme temperature conditions or to minimize viscosity variation over a wide range of operating temperatures.

Oxidation, thermal decomposition, and accumulation of water, wear debris, or other contaminants are the principal reasons for periodic draining, flushing, and refilling of an oil lubrication system. Analysis of oil samples at regular intervals can be used to determine when oil should be changed.

#### 14.1.2.4.3 Oil Selection for Sliding Bearings

Section 14.1.1 contains general information on the selection and application of lubricant materials for sliding bearings. Detailed criteria for electric motors can be found in Refs. 5 and 6.

#### 14.1.2.5 Condition Monitoring and Predictive Maintenance

Because of the degradation of rolling bearings and the lubricants with continuous or intermittent operation, condition monitoring should be used to determine whether failure is imminent or the bearing or lubricant has lost its ability to perform its function reliably.

##### 14.1.2.5.1 Incipient Damage/Failure Detection

The principal tools for condition monitoring are temperature and vibration measurements and periodic analysis of lubricant samples. Disassembly and inspection of bearings can also be used as a preventative maintenance tool. Touch thermocouple or infrared thermography can be used to plot bearing temperature trends, based on housing temperatures. For critical applications, a thermocouple may be installed in contact with the bearing outer diameter (OD) to obtain continuous or periodic temperature data. After the normal temperature data are known, any significant temperature rise may indicate the onset of bearing damage. In conjunction with vibration measurements and oil sample analysis, such data can be used to predict when the machine should be shut down for bearing inspection or replacement. Vibration monitoring may be performed with hand-held detector/analyzers or utilizing threaded locations for attachment of vibration transducers. A growing number of organizations offer limited or comprehensive condition monitoring services, including trend analysis of temperature, vibration, and oil analysis data.

The analysis of lubricant samples taken from the scavenge line ahead of the filter in a circulating oil system or from a static sump can provide valuable information on the bearing and lubricant condition. Analysis should include physical and chemical properties of the oil, that is, viscosity, acid number, water, coolant, fuel and solids contamination, and wear particle analysis. The results of oil sample analysis should be plotted versus time; the trend analysis provides advance warning of bearing damage before failure occurs. Considerable savings in maintenance costs can be achieved by scheduling inspections and replacement of damaged bearings before failure occurs, with possible damage to related components beyond the bearing. In new machinery, oil analysis can be used to prevent costly premature failures by detection of damage due to errors in design, manufacture, and assembly of components.

##### 14.1.2.5.2 Inspection Methods

Where machine configuration allows access, the condition of a bearing may be assessed by visual inspection, using an

optical borescope or a fiber-optic video probe. In larger bearings and where the cage does not interfere, a probe can be inserted between the balls or rollers to look for evidence of bearing damage. Metal particles and/or debris denting of the raceways are indicative of contact fatigue damage. Excessive wear or fatigue cracking of the cage can also be detected.

14.1.2.6 Bearing Failure Analysis

When a bearing failure does occur, especially if it appears to be premature, failure analysis may be justified to assure that the replacement bearing will give satisfactory performance and life. After removal and cleaning with solvent, the cage should be cut to allow visual examination of the rolling contact surfaces and the cage pockets. The observed damage can be compared with photographic examples found in the manufacturer’s literature or among the references listed in the bibliography of bearing failure analysis publications [7].

14.1.2.7 Bearing Replacement

If a used bearing is found to be free of damage and is to be reused, it should be carefully cleaned and oiled to prevent fingerprint corrosion. Installation can be done as with a new bearing. It is important to inspect the shaft and housing for dimensional changes due to fretting damage to ensure that internal clearance control is maintained. Check to be sure that the preservative oil on the new or used bearing is

compatible with the machine lubricant. Follow the manufacturer’s recommendations for details of installation and grease fill, if any. Avoid any application of force that might cause brinelling or other mechanical damage to the bearing, for example, dropping the bearing on the floor or forcing a cocked bearing on a shaft during press fitting. Where possible, the bearing or housing should be heated to obtain the desired interference fit without using a hydraulic press.

14.2 IMPLEMENTATION OF A RELIABILITY BASED MAINTENANCE PROGRAM

Reliability-based maintenance (RBM) is a strategy to improve plant productivity by integrating preventive maintenance (PM), predictive maintenance (PDM), and proactive maintenance (PAM) in a balanced approach to modify the normal failure profile of plant machinery. PM is time-or intervalbased; PDM is machinery condition-based; and PAM is rootcause/failure analysis-based. PDM is the pivot point in this balance, possessing the tools to monitor machinery condition. This condition monitoring provides the information needed to optimize PM job tasks and frequencies, and to identify proactive and root-cause analysis candidates. Benchmark RBM facilities have been able to significantly modify the “bathtub” curve or normal failure profile of plant machinery through the use of RBM. The white curved line in Fig. 14.4 represents this modification.

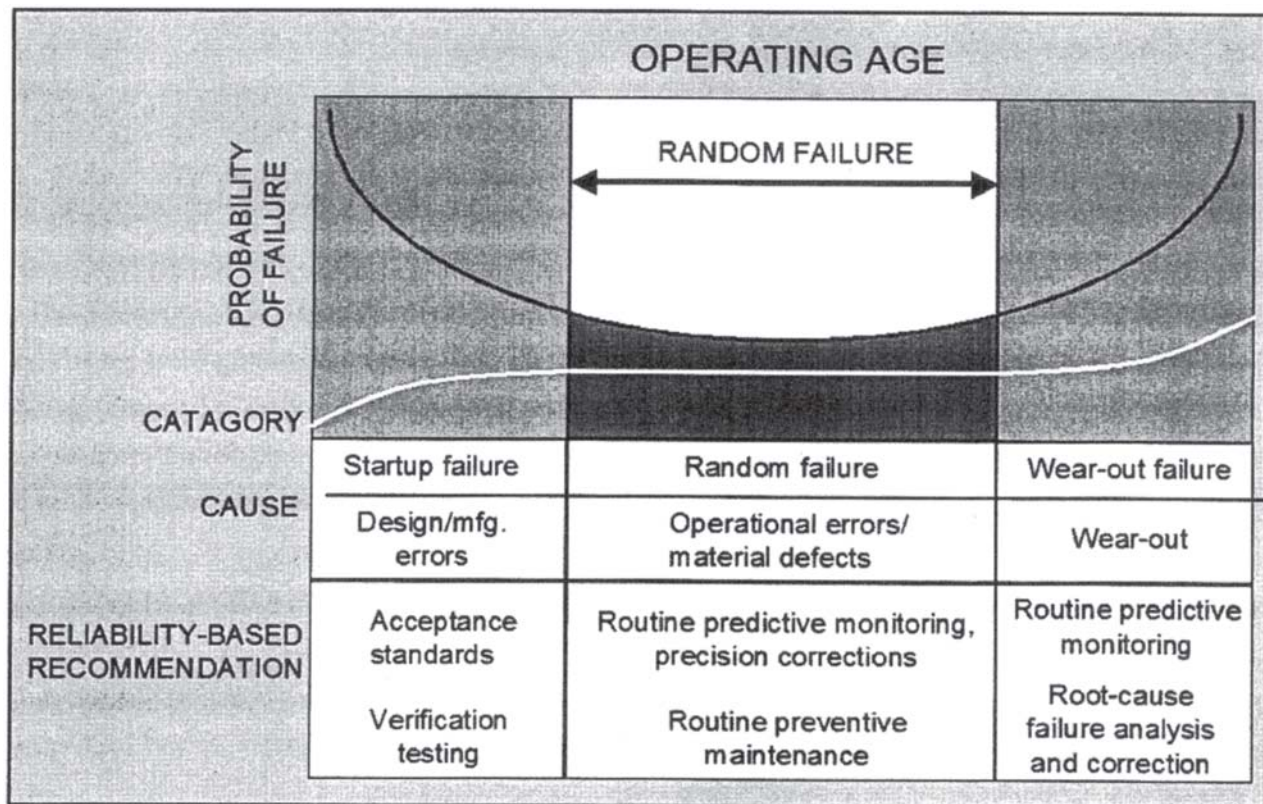


Figure 14.4 Operating age or failure mode for motors and other plant machinery. The dark (black) “bathtub” curve represents the normal failure mode of plant machinery. The white curve represents a modified failure mode expected when an effective reliability-based approach to maintenance is practiced. (Courtesy of Computational Systems, Inc., an Emerson Process Management Company, Knoxville, TN.)

A major reduction in the number of start-up or “infant mortality” failures has been achieved with the development of acceptance standards on vendors’ products for new and rebuilt equipment. Studies by many industries have shown that a high incidence of machinery problems are brought into plants via suppliers’ equipment or components, and can be eliminated by the use of tighter acceptance standards. This is an extremely easy and no-cost improvement that any plant can implement. Random failures during the normal service life of plant machinery are reduced by improving reliability through the use of condition monitoring and by the optimization of preventive maintenance, with the elimination of unnecessary invasive maintenance activities. The extension of the useful service life of plant machinery is achieved by the use of predictive maintenance condition monitoring for the identification of candidates for proactive maintenance or root-cause failure analysis.

The balanced approach of an integrated RBM program requires a functional preventive maintenance program. The best of these PM programs are performed through a dedicated PM module of a computerized maintenance management system (CMMS) software package.

Initially, the implementation of a structured PM program results in a marked increase in manpower requirements because of increased maintenance procedures or PM “job tasks.” The condition monitoring capabilities of PDM are required to streamline and optimize the PM process, eliminating invasive maintenance activities and arbitrary interval-based replacements of bearings, belts, etc. PDM programs can typically reduce preventive maintenance requirements by 50%, with additional reductions in spare parts usage and inventory. It should be noted that the use of a PDM software system that can integrate and communicate with the facility CMMS system is very important in maximizing these savings.

What is to be achieved, and what are the goals of an RBM program? While the rewards of an RBM program are numerous, the most important returns can be outlined as:

- Increased plant capacity/production through the elimination of downtime.
- Reliable knowledge of machinery condition providing status of overall plant capacity.
- Extension of the useful service life of plant machinery through the identification and elimination of failure modes at the source.
- Development of work teams responsible for the combination of maintenance and capacity.
- Maintenance, production, and engineering function as partners in maximizing plant capacity.
- Maintenance provides credible machine information to assist in crucial decision-making on plant operations.
- Creation of a learning organization where mistakes are not repeated.
- Development of a systematic approach for each maintenance situation (reactive, preventive, and predictive) based on logic and history.
- Continued and increased management support for RBM: In general, the goal is to gain control of plant machinery, significantly reducing maintenance costs, increasing productivity, improving product quality, and thereby increasing plant profitability.

To achieve these goals, a team must be selected to perform the functions in the RBM program. The two teams, for purposes in this book, will be called the Maintenance Planning Group and the Reliability Improvement Group.

The Maintenance Planning Group performs all the standard maintenance planning functions and may already exist in the facility, perhaps as the PM group. Its focus and direction must go beyond work-order generation and job tracking to full-scope maintenance planning. Maintenance must move “out of its shell” and think globally, interacting with all plant groups involved with productivity.

The reliability improvement group focuses on the implementation of predictive maintenance technologies and performance record keeping, adding technologies as support and budgets allow, advancing toward proactive maintenance as the program matures. Initially, these two core group functions may be performed by one small team, or even one individual, which can develop into the two distinct groups as the program expands. The key here is remembering the importance of the core responsibility of each group.

In order to implement a success RBM program, the facility’s needs must be identified. An understanding of the production and maintenance needs is required to categorize the facility equipment as critical, essential, support, or nonessential. This identification process determines the most suitable RBM technology based on critically. It is vital for RBM program success that critical plant machinery and processes are brought under control first. This ensures the greatest initial successes, or “bang for the buck,” allowing for the expansion to additional equipment as these results bring the confidence and support of other departments and management.

The identification of facility needs leads to the selection of predictive maintenance technologies. For many years, the primary tool of PDM has been vibration analysis. While vibration analysis still remains the foundation for most PDM programs, today’s predictive maintenance covers a wide range, integrating many advanced technologies such as:

- On-line vibration analysis
- Oil and wear particle analysis
- Infrared thermography
- Precision alignment and balancing
- Motor stator analysis
- Motor current signature analysis
- Ultrasonics

Technology selection should be based on equipment criticality. It must be remembered that plant machinery condition monitoring is a process. Within this process it is possible to detect, diagnose, confirm, perform root-cause analysis, and ultimately correct an equipment problem. The goal is to complete this process in a rapid and cost-efficient manner.

It is very important to have the proper mix of field and office tools that will support this process of plant machinery condition monitoring—the detection to correction process—for critical plant equipment.

While the PDM program will be initiated with the one technology that best suits critical equipment needs, the goal should always be the implementation and integration of additional technologies to support the process of plant

machinery condition monitoring. For motors, combining vibration, oil, infrared, electric current, flux, ultrasonic and corrective technologies will ensure the detection, diagnosis, and ultimately root cause of problems. The total value of a fully integrated RBM program is greater than the sum of its individual components. While, individually, each RBM technology can offer significant returns on investment (ROI), the use of multiple technologies compounds these returns.

The typical RBM program goes through three stages of progression. The initial successes achieved after the start-up of a program are simple, single event analysis issues that are used to gain acceptance and build confidence for the program with management and other departments. It is easy to show these “saves” with the associated cost avoidance.

In the expansion phase, the performance measurement begins to shift away from single event analysis to plant bottom line improvement with the introduction of the PAM component. The focus is on the reduction in breakdowns through the prediction and elimination of problem sources. This phase will produce reduction in downtime, labor savings in the optimization of preventive maintenance, the elimination of “emergency” work orders, and reduced overtime labor hours.

In the mature RBM program, the performance measurement is totally based on concrete bottom line improvements, which are required to sustain RBM program growth. Improvements include:

- Overall reductions in maintenance costs;
- Increased plant productivity;
- Reduced spare part inventories;
- Improved product quality; and
- Reduced energy consumption.

As has been shown, implementation of an RBM program on motors is essential in today’s market. While the vibration analysis technology is the backbone to a successful program [8–11], other technologies are necessary. When a successful program is in place, the following can be expected:

- Uptime increased productivity
- Reduced maintenance costs (manpower, parts, overtime, etc.)
- Reduction in PM costs (optimize component life through condition monitoring)
- Reduced energy consumption
- Increased product quality
- Reduced spare parts inventory
- Extended equipment life for capital assets
- Increased safety and environmental protection

The savings that are available in each of these combine to reduce the total cost of plant maintenance. Such savings will definitely have a positive impact on plant profitability.

### 14.3 MAINTENANCE AND REPAIR OF COMMUTATORS

The first and oldest known type of commutator is the steel and mica design. It is also known as a steel-core or cap-and-cone commutator. This type of commutator consists of a

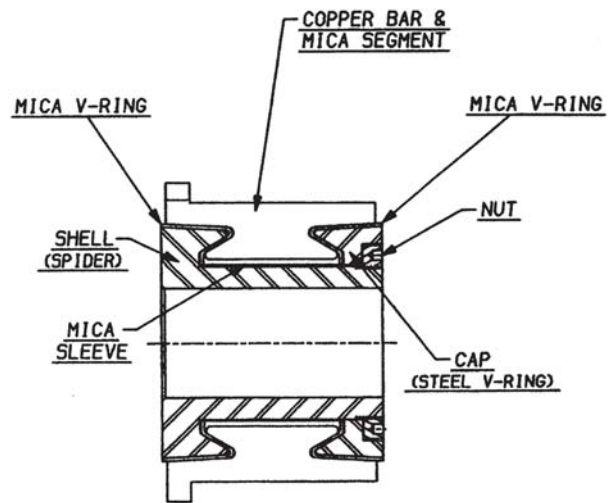


Figure 14.5 Cross section through a typical commutator.

number of wedge-shaped copper bars separated by mica segments. These are stacked to form a cylindrical assembly that is mechanically held together with insulated steel clamping parts (see Fig. 14.5).

Some commutators were originally designed without dovetails. The copper and mica assembly is held in place with either glass bands or steel shrink rings. Glass-banded commutators derive the radial squeeze by controlled shrink of the “B” stage polyester tape during its cure cycle. Shrink ring commutators obtain the radial squeeze by contraction of a heated steel ring, which contracts after the commutator is assembled.

Mica-molded commutators, as the name implies, consist of the copper bar and mica assembly mechanically held with a molding compound. Typically, a reinforced phenolic compound, either mineral- or glass-filled, is used in this type of commutator construction. These are made both with and without a bushing. A new design interlocks the anchoring dovetail of each copper bar with the steel core bushing. A relatively narrow band of molding compound separates and insulates the copper bars from the steel core. Another variation of mica molded designs incorporates steel or fiberglass rings embedded in the molding compound, which helps to lock the copper bars in place. Another type of construction is a molded air gap commutator. In this construction, the mica insulation is eliminated and only an air gap space separates the copper bars. The copper bar is normally a thin shell anchored in the molding compound. This type is primarily used for appliance and small tool applications.

This discussion will encompass two aspects of the maintenance and repair of commutators: basic maintenance, typically performed by the user, and more advanced maintenance and repair, which is done by the repair shop.

The periodic preventative maintenance that should be performed by the user comprises turning, undercutting, and stoning or dressing of the commutator. This should be done whenever the brushes are changed. There is a minimum safe diameter to which a commutator may be turned. If the commutator is turned too much, the copper bars may no longer have enough mechanical strength. The manufacturer of the

motor may have published this minimum commutator diameter information.

Prior to turning the brush surface, the commutator should be observed to determine if any anomalies in the brush track are apparent that should be addressed at this time. Streaking, threading, grooving, and so forth of the brush surface area may suggest use of a different brush grade, brush tension modification, or improper brush alignment.

When turning a commutator with subflush mica (undercut), a synthetic diamond tool is recommended, with a surface speed of approximately 750 ft/min. The approximate depth of metal removed per cut should be about 0.007 to 0.010 inch. Alternately, a carbide tool can be used satisfactorily at speeds of about 500 ft/min with the same amount of metal removed.

The commutator should then be undercut. The depth is typically the same as the thickness of the mica segment. The mica segment thickness of the typical motor or generator is from 0.025 to 0.045 inch. Special applications can, of course, vary higher or lower as the design engineer of the original manufacturer may specify.

Undercutting saws are available in two designs, one being the “U” shaped and the other “V” shaped. They both do a good job. The “V” slots are self-cleaning, but do require more frequent undercutting than the “U” slots to avoid mica fins. If there is insufficient centrifugal force, the “U” slots will trap contaminants that can cause short circuits.

In the service shop, after the turning and undercutting have been performed, rebanding of the armature may be required. This may take the form of wire banding or glass banding with “B” stage glass tape. The service shop may also elect to do a vacuum-pressure impregnation (VPI). This is a method of applying electrical varnish. There are two types of varnish commonly used today. The first and oldest is air drying and the second is thermal setting. Thermal setting is the preferred method in use today.

After the steps above have been accomplished, balancing should be performed. Dynamic balancing is preferred to eliminate vibrations at the bearings supporting the armature. The unit of measurement most commonly used is ounce-inches.

Tightening of nut- or bolt-type commutator should be performed every time the armature is removed from the frame. Protecting the commutator V-ring extension as it protrudes beyond the commutator bar is an essential part of assuring the commutator’s longevity. This is typically accomplished by string banding or glass taping with a “B” stage glass tape. Glass tape banding is the preferred method as it has a smoother surface than string banding. When string banding is used, it should be covered with an air-drying varnish or Glyptol to further seal this surface. Teflon creepage bands are also used, but traction applications are their only current use.

The following repairs are generally part of service shop activity and not that of the user. The first is replacement of mica V rings. To replace mica rings, the copper bars must be banded to retain as much radial pressure as possible. The old mica rings must be thoroughly cleaned off of the steel retaining members. When the new mica rings are installed, a heat seasoning and torquing operation must be done. The temperature and duration vary according to the binder in the mica rings, size, and application of the motor. Failure to perform

this seasoning operation can result in unstable commutator bars. Patching of mica rings should only be considered as an emergency measure. Loose pieces of mica can be laid over a damaged area with a shellac binder for a temporary fix.

Rewinding of the armature is another repair that is typically performed by the service shop rather than the user. Care should be exercised when soldering or tungsten inert gas (TIG) welding the lead connections to the risers so there is not an excessive heat buildup. Rather than welding the bars consecutively, it is recommended rather strongly that the bars be welded in a random order.

For a long commutator and brush life, commutator film must have a lubricating characteristic. On request, any brush manufacturer or supplier can usually provide an illustrated copy of the various brush filming patterns. The reader is also directed to Section 13.3.

There are also specialty commutators made of gold, silver, or platinum. These are normally required for applications associated with long inactivity before the motor is placed in operation. In other words, no oxidation can be present to inhibit commutation or cause voltage drop between brush and commutator. Gold-plated commutators, due to their high cost, are used on small motors for military or space hardware. Silver is used where low voltage drop and low noise are essential. Applications include computers, tachometer-generators, and some small motors in applications where low noise levels must be maintained.

Platinum is used to improve the trackability of the brush with the commutator to minimize noise and to increase effective brush life. The platinum commutator is made by a selective plating process that can be applied, theoretically at least, to any size of commutator. The plating is applied to the commutator brush surface on a finished wound armature. The chemicals that comprise the plating processes contain acids and other potentially toxic substances. Follow instructions for use exactly as printed on their labels.

### 14.3.1 Causes of Poor Commutation

1. High commutator bars will cause sparking and noisy operation. They will also chip brushes and cause excessive wear.
2. Streaking or threading of the commutator surface will cause sparking. The source of the problem may be
  - a. Low current density in brushes.
  - b. Oil or other contaminants in the atmosphere.
  - c. Improper brush grade.
  - d. Low humidity.
3. Burning and etching of the commutator surface is a result of
  - a. High mica or mica fins.
  - b. Dirty commutator.
  - c. Operating with brushes off neutral.
  - d. Incorrect tension on springs.
4. A rough commutator at the pole pitch spacing can cause flashover.
5. Burning is caused by shorted commutator bars or coils. Open armature or field circuits and vibration can also cause this condition.

### 14.3.2 Ordering New Parts

When ordering parts for any motor or generator, all the nameplate data should be available. This includes model, serial number, frame size, and voltage. This will assist in supplying the correct parts. Some independent suppliers will require physical dimensions or a sample. This is very common and this information should be available when ordering.

Every user should aggressively pursue commutator maintenance to assure longevity of the motor/generator. If there are any doubts as to the practice or procedure, a repair shop should be contacted.

## 14.4 BRUSH REPLACEMENT

### 14.4.1 Introduction

Brushes are a replaceable component in rotating machines that use them. When the brushes are properly maintained, they provide many years of successful machine operation. It is important to understand when they should be replaced. Correct installation of the new brushes is essential for successful machine operation. In this section brush replacement and installation are described in detail.

### 14.4.2 When to Replace Brushes

Different manufacturers of brushes use different methods to indicate the usable wear length of the brush. Different types of wear markers include wear band indicators on the shunts, wear lines stamped on the side of the brush, and wear grooves machined into the sides of the brush. These forms of indication are used in various ways. When the wear band on the shunt comes into contact with the top of the brush box, the brush needs to be replaced. As a wear line approaches the commutator or collector ring surface, the brush needs to be replaced. As the wear groove advances, usually from right to left, the brushes need to be replaced. The type of wear indicator is determined by the machine designer but can be altered by the end user if requested.

Two criteria are involved in determining where a wear marker should be positioned. The brush wear marker should be positioned so that the proper wear indication is reached

1. Before the hardware of the brush comes in contact with the commutator or collector ring surface.
2. Before the spring force is below recommended values.

The results of the brush hardware coming into contact with the rotating surface include damage to the rotating surface and a possible short circuit between the positive and negative brushes. Loss of spring pressure can cause rapid brush wear through excessive sparking. Both of these conditions can result in excessive damage to the rotating surface, requiring expensive repair work.

A third important criterion used to determine when to replace brushes is the length of time between machine inspections. This criterion is not used as a control when a wear marker is applied to a brush. However, it is very important to insure the minimum length of the brush is not reached before the brush is

replaced. For example, if the usable wear length of the brush is 1 inch, and the brushes are inspected every 6 months, then if during the inspection some brushes are found to have worn 3/4 inch those brushes should be replaced.

### 14.4.3 Installation of Brushes

Brushes provide a sliding electrical contact that passes current from the stationary components to the rotating windings of various direct current (dc) and alternating current (ac) machines. To provide good contact, it is important that the faces of the brushes match the radius of the commutator or collector ring. This is accomplished by “seating” the brushes. Brush fit is important for two reasons:

1. Adequate contact area of the brush face is needed to carry the required brush current. This is true for both ac and dc machines. If an adequate contact area is not provided, localized heating of the carbon can result in burning of the brush carbon or decomposition of organic treatment in the brush. Arcing can be associated with the heating, causing damage to the commutator or collector ring surface.
2. In dc motors contact must be made from the leading to the trailing edges of the brush face. Commutation (current reversal in the armature coils) is going on as the commutator bars connected to those coils pass under the brushes. If there is not full face contact in the circumferential direction, contact is made too late or broken too soon. This will result in arcing and damage to the brushes and commutator and could possibly cause a “flashover.” In addition, lack of brush face contact can affect output characteristics of the motor or generator such as speed or voltage regulation.

#### *Brush Face Designs*

Although brushes generally run on round surfaces, many brush designs have flat faces. Motor manufacturers may use the same design of brush on a variety of motors with various commutator or slip ring diameters and slightly varying face angles. In order to avoid having many different brush designs, the motor manufacturers do not request a face radius but instead seat the brushes in the machine in which they will be used. Brush seating contours the brush face to the diameter of the commutator or collector ring and compensates for variations of alignment of the brush holders in the motors. Flat brush faces are the most common brush design and they are easiest to manufacture.

An additional machining process can be applied to the brush to form a radius that closely fits the commutator or collector ring surface. If the commutator or collector ring diameter is known, pre-radiusing the brush allows for quicker seating of the brush face. On small-diameter surfaces, preradiused brushes can be a great benefit, especially if the brush thickness (the dimension measured in the circumferential sense) is large relative to the collector radius. Small dc motors and many collector ring applications fall into this category. Motor manufacturers sometimes request pre-radiused brushes in these cases, so the standard brush will be of this design. Pre-radiused

brush faces are much less beneficial on larger diameter commutators or collectors with relatively thin brushes. On these machines, the face angle tolerances, holder alignment tolerances, and slight variations in holder angle designs are much more of a factor in brush fit than is the face radius.

An alternate brush type used to provide quicker seating is the fluted brush. Fluting is accomplished by machining a series of diagonal grooves in the brush face. The reduction in material increases per-unit pressure and decreases the amount of material that must be worn away to get full seating of the brush. Fluted brushes also increase the current density at the brush face, which will assist in forming a film on the commutator or slip ring. Pre-radiused and fluted brushes make seating faster and easier but they do not eliminate the need for seating.

### *Seating Brushes*

Seating of the brushes is most critical when a full set of brushes is installed in a machine. Flat faces and fluted faces (which are machined on a specified angle) obviously do not match a round surface. Pre-radiused brushes do not match the surface well enough for many machines because of brush holder size and angle tolerances. To improve the brush fit to the rotating surface, the brush faces should be sanded.

Sanding brushes to the contour of the commutator can be accomplished by various methods. One method is to obtain sandpaper in rolls that can be as wide as the commutator, or at least as wide as one or two brush paths. The recommended grade of sandpaper is 100 to 150 grit. This fairly coarse sandpaper does not get clogged up with carbon, allowing the sanding process to be accomplished in a reasonable time and leaving some roughness in the brush face that allows it to wear in faster.

*Warning:* All power should be off and the motor should be locked out before any work is performed on the machine. Refer to OSHA 29 CFR Sub-Part J 1910.147, “The Control of Hazardous Energy” concerning Lockout/Tagout procedures.

*Caution:* Never use emery cloth to sand in brushes. The particles are conductive and quite abrasive and will cause problems in the motor or wear of the commutator from particles that become embedded in the brush faces.

The commutator surface should be near room temperature so the masking tape used to hold the sandpaper will stick to the commutator and not leave any residual adhesive. The sandpaper should be long enough to wrap completely around the commutator or collector ring and overlap. Place the paper on the commutator or collector ring, rough side out. Tape the leading end of the paper securely to the commutator surface using masking tape. Place the brushes down in the brush boxes with the springs installed. Turn the rotor by hand in the direction of normal rotation until the brush face is formed to the contour of the commutator or collector ring. It may not be possible to sand all of the brushes at once due to the torque required to turn the armature, or because the forces on the paper will tear loose the masking tape. In those cases, partial sets of brushes can be sanded at one time. The brushes should be sanded in the brush holders in which they will be used. A minimum of three or four turns of the armature is necessary to completely fit the brushes. When sanding is completed, the brush face fit will not be exact since the sandpaper will slightly increase the effective diameter of the surface.

In some cases large sandpaper may not be available or it may not be possible to turn the armature of the machine. In these situations the “shoeshine method” can be used to sand the brushes. This procedure is accomplished by placing a piece of sandpaper under one brush at a time. The brush spring is installed and the sandpaper is pulled back and forth to sand the brush. Again the fit will not be exact due to the differences between the diameter of the commutator or ring and the diameter with the sandpaper installed. It is preferred that the paper be pulled only in the direction of rotation to avoid rocking the brush back and forth in the holder, but this is not always practical. It is critical that the ends of the sandpaper be held in contact with the surface of the commutator or ring and not lifted away. If the sandpaper is lifted, the leading and trailing edges of the brushes will be rounded off and the brush face will not be properly seated. This method is more difficult but may be the only method available. Fluted brushes and pre-radiused brushes make this job easier.

As previously mentioned, the brush face will not exactly match the contour of the commutator after sanding. To improve the brush fit further, a brush seater stone should be used. Brush seater is a white, chalky material that is used to seat brush faces without damaging the commutator or ring material.

Use of brush seater may or may not be allowed in your facility or industry. Contact your facility safety personnel concerning the use of brush seater and note the warnings below. Brush seating is a job that requires specific skills and qualifications. You should not attempt to perform brush seating unless you are qualified to do so and use all required safety apparatus and protective gear. Specific instructions for the proper use of each product should be obtained from its manufacturer.

### *Warning:*

1. All power should be off and the motor should be locked out before any work is performed on the machine. Refer to your facility’s Lock-out/Tagout procedures or OSHA 29 CFR Sub-Part J 1910.147, “The Control of Hazardous Energy.”
2. Safety glasses, a face shield, and a dust mask must be worn to provide protection from flying dust and particles. Insulated rubber gloves must be worn to protect from electrical shock. Care must be taken to avoid entanglement with rotating machinery. Do not wear rings, watches, or jewelry of any kind, or loose-fitting clothing. Long hair must be restrained. In some cases, using holders supplied by the brush seater manufacturers or taping the brush seater to an insulated stick can help reduce electrical and rotating machinery contact hazards. Contact equipment vendors, manufacturers, and the safety or maintenance personnel at your facility to determine if the use of brush seater or other products is allowed and for the proper procedures for their use.

These safety warnings are not all-inclusive and are not intended to supersede your company’s or the manufacturer’s requirements, but are intended to reinforce the observation of safety rules. This author assumes no liability for injury or accident.

With the motor or generator running, place the brush seater in contact with the commutator or ring, at the leading edge of

each brush. The brush seater will wear and particles will be carried under the brush to complete the seating. The machine should be vacuumed and/or blown out with clean, dry compressed air to remove any remaining particles. The cleanup process should be accomplished with the machine deenergized and locked or tagged out.

Pre-radiused or fluted brushes may require only the use of seater stone without sanding. This depends on the brush grade and the brush geometry. Seater stone will remove the film on the commutator or ring. The film will rebuild as the motor is operated.

#### *Installing Partial Sets of Brushes*

If partial sets of brushes are installed, it may not be necessary to seat these brushes. On large machines, if 20% or less of the brushes (per arm on dc machines or per collector on ac machines) are installed at one time, the remaining brushes will handle the load and commutation until the new brushes seat in. On dc machines with only two brushes per arm or ac machines with only two brushes per ring, one brush can be installed without seating.

The discussion above sets forth general guidelines for seating brushes. For a particular machine, you may discover that more or fewer brushes may be installed without seating, depending on the design and operation of that machine. Of course, if there is only one brush per arm or ring, it must be fitted prior to operating the machine.

#### **14.4.4 Summary**

Proper brush maintenance can save costly motor repair work. Though brush wear is not always predictable, regular maintenance will establish a good indication of brush life. When short brushes are found, they should be replaced. It is better to replace a few short brushes than to have the machine down for costly repair work. Good maintenance practices and routine inspections will keep machines running and the associated manufacturing process operational.

### **14.5 MAINTENANCE AND REPAIR OF WINDINGS**

Maintenance procedures on windings should begin when the motor is received and continue throughout its operation, failure, and repair or replacement. Testing, routine maintenance procedures, and record-keeping are suggested in this section under the assumption that the motor's function is important. Since these procedures require instruments, records, and time, many motors in industry are installed and forgotten. These "forgotten" motors may run satisfactorily for the economic life of the equipment with no maintenance performed. Managers responsible for motor operation and maintenance must balance the costs of performing routine maintenance with the value of the reliability gained in their own plant.

#### **14.5.1 Installation of New Equipment**

Maintenance is "maintaining" the equipment for operation under design conditions specified or accepted by the motor

manufacturer. These conditions (supply, ambient, and load) should be verified at the time of installation. The physical condition of the motor should be also checked.

##### *14.5.1.1 Inspection of New Windings*

The condition of the motor windings on a new motor should be observed and felt if the motor has viewing ports or openings in the end bells. The windings should be clean and dry, with no evidence of mechanical impact or damage in transit. No packing material, insect or animal nests, or similar foreign matter should be present.

If the motor is totally enclosed, the end bell flanges and weep holes should be examined for rust or other indications of moisture. If the motor has been damp, it may need to be disassembled and dried out before being placed in service.

The leads should be smooth and clean, with no evidence of cracking or of being mashed in handling. The connection numbers or letters should be clearly visible on all leads.

If the motor windings pass the visual (and feel) test, the ground insulation should be checked using a megohmmeter. New equipment insulation test results should be near infinity (1000 megohms). Larger windings reading as low as 100 megohms may also be satisfactory if the humidity is high.

Small motors or noncritical motors can then be connected for operation without further tests. Before motors above 100 hp are connected, they may be acceptance tested with a high potential of 75% of the proof test value used by the motor manufacturer. High-potential tests are described in Section 14.5.3.1 below.

Hamer [12] gives extensive test and inspection suggestions for purchasers of large motors. Some of these tests may be conducted at the motor manufacturer's own plant.

##### *14.5.1.2 Winding Inspection Records*

The motor record should include the vendor, the maintenance information supplied by the manufacturer, the invoice date, and the date placed in service. Many manufacturers will warranty motors placed in service after their warranty period has expired if the motor has been stored suitably and checked carefully before installation. Manufacturers may also recommend the renewal parts and spare windings that should be stocked to insure quick correction of likely faults. Many manufacturers now place maintenance instructions and spare parts suggestions on their websites. *Renewal Parts for Motors and Generators*, NEMA RP 1-1981 (R1987) [13], also provides general suggestions. Also see NFPA 70-B [39].

The operating conditions expected should also be recorded: Starting duration and frequency, load parameters, running time, and ambient conditions. Finally, the ground insulation test data, no-load current, full-load current, line voltages, and operating temperature of the winding and motor housing should be included in the motor records. If winding temperature is to be measured by the resistance/temperature method, a cold resistance reading should be made on all separate windings, and these readings should be recorded along with the ambient temperature.



**Table 14.2** Insulation Test Table: High-Potential Test Voltages for Ground Test of Winding Insulation in AC and DC Machines

Rated voltage of motor (Volts)	Test potential and condition of winding under test					
	New winding test at motor manufacturer or rewind shop		Acceptance test of new winding at user's location		In service test of used winding, clean and dry	
	V ac	V dc	V ac	V dc	V ac	V dc
250	1000	1700	750	1280	400	600
600	2200	3740	1650	2800	900	1500
2400	5400	9200	4350	7400	3480	5900
4160	9300	15,800	7000	11,900	5600	9500
5000 and above:	Consult manufacturer for recommendations					

All tests for 1-minute duration

Caution: After a dc high-potential test, the winding must be grounded to the core until the charge has dissipated.

Table compiled from References [13] and [23].

In larger equipment, it is particularly useful to mark all supply leads and motor leads. The test data should then show exactly which circuit is being tested. These markings are also useful in reconnecting equipment removed for test.

#### 14.5.1.3 Reinspection After Start-Up

Within a few days of start-up, motor operating conditions should be verified again to be sure that the new windings are functioning satisfactorily and that the load is in the range predicted for this motor. Smeaton [14], in his chapter on preventive maintenance, notes that motor failure rates in the first several months after installation are much higher than the failure rates for years thereafter.

### 14.5.2 Establishing a Maintenance Schedule

Owner experience, judgment, motor size, function, and operating conditions must be used in setting maintenance schedules. Winding maintenance will usually be less frequent than mechanical maintenance, lubrication, and brush replacement. However, temperature readings and cleanliness observations at times when mechanical checks are made also contribute to winding maintenance records.

Specific winding inspection is rarely justified more than twice a year, and annual records are more usual. Single-phase motors and three-phase induction motors below 20 hp do not justify more than the annual megohm reading and visual inspection. Larger frame three-phase motors, dc motors, and wound-rotor ac motors should have their windings checked every 6 months. Motors above 500 hp may justify observation monthly if their function is critical. Occasional inspections by a conscientious, observant person are much more valuable than frequent, routine inspections done by a careless person.

### 14.5.3 Choosing Test Equipment

Every maintenance employee should have adequate tools for removing conduit box covers and observation ports and for disconnecting leads from the power lines. All motors undergoing winding maintenance should be locked out and the circuit interrupter tagged to provide electrically safe

working conditions. Once the leads and windings are accessible, an observation light and a long-handled mirror are likely to be useful in viewing the back of the winding. In addition, instruments are needed to perform the various tests. The instruments required are described with the various tests below. The reader is also referred to [Chapter 8](#) for further discussion on insulation tests.

#### 14.5.3.1 Tests for Ground Insulation

If the megohm reading is over 10 megohms, an overpotential test may be performed on the ground insulation. Either a 500 V or a 1000 V megohmmeter is satisfactory for this purpose. If a winding reads less than 10 megohms at normal ambient temperatures (10–30°C), no further tests should be performed. The integrity of the insulation is questionable in the range of 1 to 10 megohms. If the reading is below 1 megohm, the motor should be removed from service and repaired. Prevention of an arc to ground is much better than correcting the burned and welded laminations after an arc has occurred.

If the megohm reading is satisfactory, an overpotential test may be performed on the ground insulation. Overpotential test values for various voltage motor windings are illustrated in Table 14.2. This table refers to maintenance values, and does *not* include the proof test values used by the motor manufacturer.

Ground test or high-potential (hi-pot) testers are available in many types, voltages, and power ratings. A multipurpose unit is illustrated in [Fig. 14.6](#). This particular unit includes a megohmmeter, a 4 kV ac source, and a 5 kV dc source for ground testing. It requires a 115-V or 230-V source, either 50 Hz or 60 Hz.

#### 14.5.3.2 Circuit Tests

A good volt-ohm-milliammeter, with automatic overload protection, is basic to all electrical circuit checks. A digital version is suggested to reduce reading errors. A multimeter should not be used to measure energized circuits rated above 600 V. The ohmmeter scales can be used in locked-out circuits of any voltage rating for simple circuit continuity tests and for



**Figure 14.6** Portable dielectric strength tester, Biddle Model 230 425, 0 to 4000 V ac, 0 to 5000 V dc, 12 mA. (Courtesy of AVO International, Dallas, TX.)

field resistance measurements in dc and synchronous motors. Winding resistance checks require a Kelvin bridge or similar instrument that can measure resistances below 100 microhms. For large motors, the bridge should be capable of providing at least 10 A to test the integrity of connections in the winding.

#### 14.5.3.3 Temperature Tests

Although glass thermometers can be used satisfactorily, they are subject to breakage. A hand-held digital-reading temperature sensing device with a thin, flexible probe is recommended. This probe can be placed on the motor laminations and on the external frame. A minimum range of 0–150°C is required.

On larger motors, winding resistance at operating temperature is often used to calculate winding temperature. A Kelvin bridge or similar low-resistance reading instrument is needed to measure winding resistance at ambient temperature and at operating temperature. This bridge may use a low test current, but should permit readings down to 100 microhms.

#### 14.5.3.4 Voltage, Current, and Power Tests

The multimeter mentioned above for circuit tests will also verify motor voltage. Some digital multimeters also have a clamp-on current probe that can be used to measure motor current. Otherwise, a separate clamp-on ammeter should be used. Clamp-on ammeters can be obtained to measure both ac and dc current. However, they cannot be used to read the ac current in wound rotors, since the rotor current frequency is too low to register accurately.

Power tests of ac motors require wattmeters or testers incorporating wattmeters. The instrument illustrated in Fig. 14.7



**Figure 14.7** AC power monitor, Dranetz Power Platform pp1. (Courtesy of Dranetz-BMI, Edison, NJ.)

will read voltage, current, power, and power factor in ac motors and print the results. This type of instrument is useful in verifying motor load and efficiency. It is also useful in studying load and line transients.

#### 14.5.3.5 On-Line Monitoring and Spectral Analysis

Computer-controlled test instruments are available that will monitor motor operation over a period of time and indicate potential failures in both mechanical and electrical systems. The instrument most useful for winding analysis monitors line currents and uses a spectrum analysis of the current to predict the presence of partial discharges in the winding insulation and arcing in broken squirrel-cage rotor bars. To be good failure predictors, these tests should first be run on the winding when it is new and operating satisfactorily. Periodic repetition of the tests will indicate when changes occur in the winding's condition.

**Figure 14.8** from Thomson et al. [15] illustrates a spectral analysis of the current in one supply line to an induction motor. A normal frequency spectrum is shown above a second supply current spectrum recorded after one bar was broken in the rotor. Broken bars and high-resistance sections create sidebands on the fundamental current which increase in size as the failure progresses.

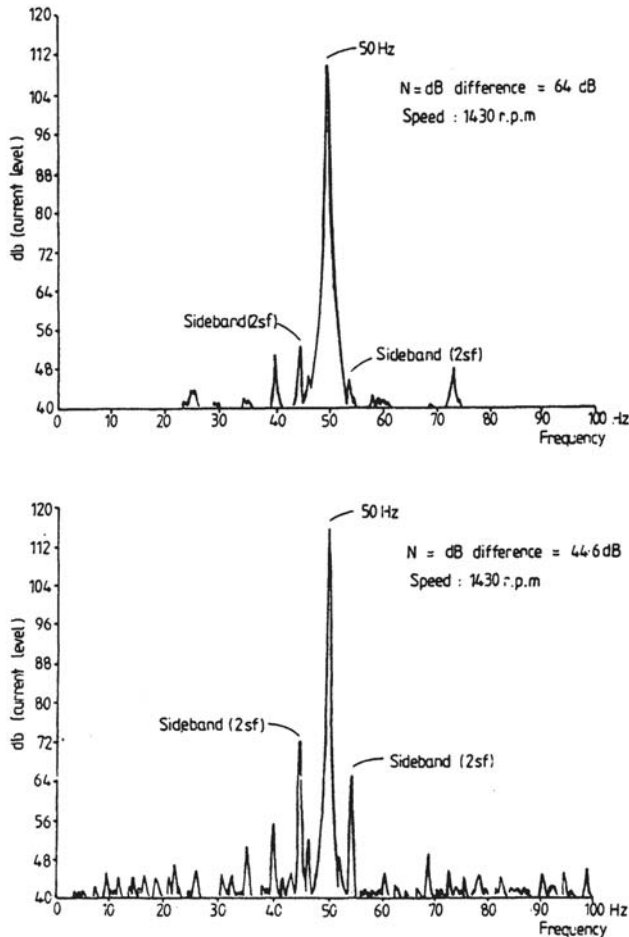


**Figure 14.8** Phase current spectra for squirrel-cage rotor. (Courtesy of Entek Scientific Corporation, Cincinnati, OH.)

In very large electrical equipment, gas chromatography is used to examine the cooling stream for insulation failure traces. This is rarely justified in motor maintenance. Other monitoring references are given by Thomson, Nailen, and Trutt [39].

#### 14.5.3.6 Test Equipment Calibration

Test equipment should be calibrated annually by a laboratory traceable to the National Institute of Science and Technology (NIST) or an equivalent, government-approved standards laboratory. An instrument record should be kept of calibration dates, and the instrument should bear a dated inspection sticker. Calibration information is helpful in substantiating test results, particularly when warranty claims arise.

### 14.5.4 Performing Preventative Maintenance

The preceding sections all referred to performing maintenance, but did not actually say what is to be done. This section suggests appropriate procedures to check, clean, and maintain windings in safe operating condition. Before approaching the motor for tests, the power supply to the motor should be

cut off and the switch locked out and tagged. Control and sensing circuits should also be cut off. Further safety procedures are suggested by Gill [16]

#### 14.5.4.1 Observation

Contamination and excessive ambient temperature are problems external to the winding that maintenance should detect. The maintenance person should check the surroundings of the motor for dripping water, condensate, or similar leaking fluids. The frame surface should be carefully wiped to determine the degree of dirt buildup, and the inside should be examined for any material that might obstruct ventilation or provide a conducting path from windings to ground. Boards, covers, and canvas should never be left around motors in operation.

Immediately after turning off the power to the motor, the frame should be touched carefully to estimate the motor temperature. If the motor feels hotter than hot tap water (typically 60°C or 140°F), readings should be taken of frame and lamination temperatures. Frame temperatures below 60°C do not need to be measured.

The person who regularly visits a motor location, listens to the noise it makes, feels the frame temperature and vibration, and observes its cleanliness can provide the most information about the motor condition. This person may be the machine operator or an area foreman, rather than a “maintenance” person. The operator is also more likely to know if the operating schedule has been changed, if the material process has changed, or if other equipment has been connected to the same circuit. It is important to capture observer information and comments on the maintenance records as well as the test records of the routine maintenance person.

If the motor must be disassembled to replace bearings or for any other reason, the insulation should be examined for evidence of deterioration or damage, as suggested by IEEE Std. 432–1992 [17].

The motor windings should be examined for the following.

- Puffiness, cracking, or separation indicating thermal aging.
- Contamination of coil or connection surfaces.
- Loose main field poles or interpoles, or loose coils.
- Abrasion or other mechanical stresses.
- Evidence of corona discharges.
- Loose wedges, fillers, or ties.
- Cracks or breaks in bands or surge rings.
- Cracks or splits in lead insulation.
- Corrosion of frame or laminations.

Once bearings have been replaced, care should be taken to insure that the air gap is concentric because off-center rotors may rub and quickly damage insulation.

#### 14.5.4.2 Cleaning Windings

Cleaning of an installed motor is at best difficult, since dust packs tightly in air passages and seeps below windings and commutators into voids in the frame and rotor. This hidden contamination provides a conducting path that can be reduced

but not eliminated. However, cleaning the passages by suction or by blowing with compressed air and by wiping observable surfaces will help the motor to cool. These cleaning procedures are worthwhile if the motor is large enough for the windings to be accessible. IEEE Std. 432–1992, Section 10 “Cleaning Instructions” [17], gives useful suggestions on cleaning techniques.

Wiping with a dry cloth is safe on all insulations. The cloth should be free of lint, which might adhere to rough surfaces and trap more contaminants. Dirt may also be removed using a brush and a vacuum source. This technique has the advantage of removing the dirt directly from the windings. Compressed air may be used to reach channels that cannot be wiped, brushed, or vacuum cleaned. Several warnings are appropriate. The cleaner should:

- Clear the air line of all moisture and contaminants before blowing on insulation.
- Set the pressure regulator not to exceed 30 psi to limit operator hazard and to avoid damage to insulation.
- Wear goggles and other protection needed for eyes and skin.
- Blow dirt out from the windings rather than toward crevices and recesses where it may be trapped.

A soft abrasive such as ground corncobs or ground walnut shells may be added to the compressed-air stream to remove hardened dirt. This procedure requires collecting the spent debris to avoid contaminating nearby equipment.

If grease and similar sticky contaminants are present on the winding, a solvent will be needed along with the wiping cloths and air stream. A safety type petroleum-based solvent (flash point above 100°F, 37.8°C) is recommended. These solvents are less likely to attack fully cured insulation varnish than the chlorinated solvents. However, Traister [18] says petroleum spirits may not be satisfactory on silicone-based insulations.

Whenever solvents are used, worker protection is required:

- Adequate ventilation is needed for breathing and to prevent fires or explosions.
- Metal nozzles used with solvent sprays should be grounded.
- Goggles and/or a face mask, neoprene gloves, and protective aprons are desirable for skin and eye protection.

If the petroleum-based solvent is not satisfactory, water in combination with steam, detergent, or alkaline cleaning compounds may be used. The winding should be thoroughly rinsed with clean water after detergents or alkaline cleaners are used. After exposure to water, any insulation must be dried before voltage can be reapplied to the winding.

Where windings have already been contaminated by dripping water or flooding, immediate washing with copious amounts of clean water is recommended, followed by drying.

Figure 14.9 illustrates motor parts on the turntable of a large mechanical washing machine. The cycle involves wet steam, water, and a mild detergent. A separate rinsing hose is provided for manually flushing the windings with clean water after the wash cycle is completed.

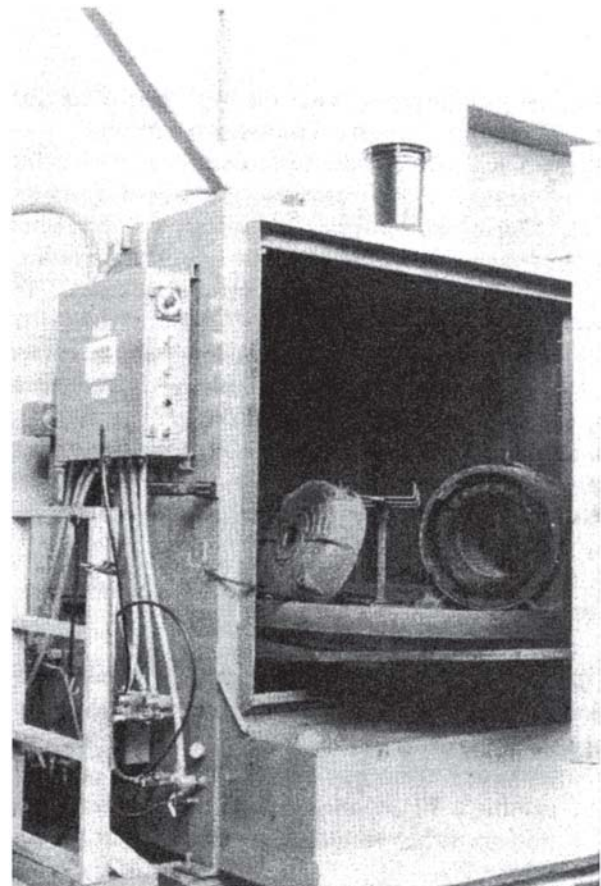


**Figure 14.9** Equipment washing machine with motor parts on the turntable. (Courtesy of The Mart Corporation, Maryland Heights, MO.)

#### 14.5.4.3 Drying Wet Windings

Electric motor windings must be dried out after cleaning with water or steam. They may also need to be dried out if they have been shipped in damp weather or have been stored where they could pick up moisture.

Motors may be dried in place by hot-air blowers or radiant heaters. Approximately 100 watts per square foot of surface area should be sufficient to warm the motor. Winding temperatures should be kept below 90°C during drying to prevent buildup of vapor pressure in damp pockets in the insulation.

Nailen [19] describes circuits that keep windings dry by exciting the windings with low voltage ac or dc. The goal is to keep the windings at least 5°C warmer than their ambient by keeping approximately 25% of full load amps flowing through the winding when the motor is not running. Trickle heating with single-phase ac at 5–15% of nameplate voltage will produce this current. If dc is used, only a few percent of nameplate voltage will be required to produce the same current. Because dc will not induce any current in the rotor or adjacent windings, it is safe for use with multiwinding motors and dc field coils.

**Table 14.3** Space Heater Application in AC Motors

Motor frame number		Motor frame diameter		Heater power (W)	Typical rating (4-pole)	
NEMA	IEC	(in)	(mm)		(hp)	(kW)
140	90	7	180	25	2	1
180	112	9	224	25	5	3
210	132	10 <sup>1</sup> / <sub>2</sub>	264	50	10	7
250	160	12 <sup>1</sup> / <sub>2</sub>	320	75	20	15
280	180	14	360	100	30	22
320	200	16	400	125	50	37
360	225	18	450	150	75	55
400	250	20	500	150	125	93
440	280	22	560	200	200	150
500	315	25	630	300	500	350

Source: Typical data courtesy of Jenkins Electric Company, Charlotte, NC.

Space heaters are also used in motors to maintain the windings above the dew point (5–10°C above ambient) whenever the windings are not excited. Table 14.3 lists typical heater values for use in NEMA and IEC frame ac motors. DC motors may require 50–100% more wattage than the values given in this table to prevent condensation in the armature and around the field poles.

Explosion-proof motors use low-intensity space heaters to limit potential hot spots on the external frame. This effect can be obtained by putting only half the rated voltage on each heater. At half voltage, the heater produces only 25% of its rated power output.

Space heaters may be installed by the motor manufacturer or installed later during maintenance. Figure 14.10 illustrates flexible space heaters that may be tied to winding end-turns to provide heat directly on the windings. Other manufacturers bolt heaters to the bottom of the motor frame or inside the end bells.

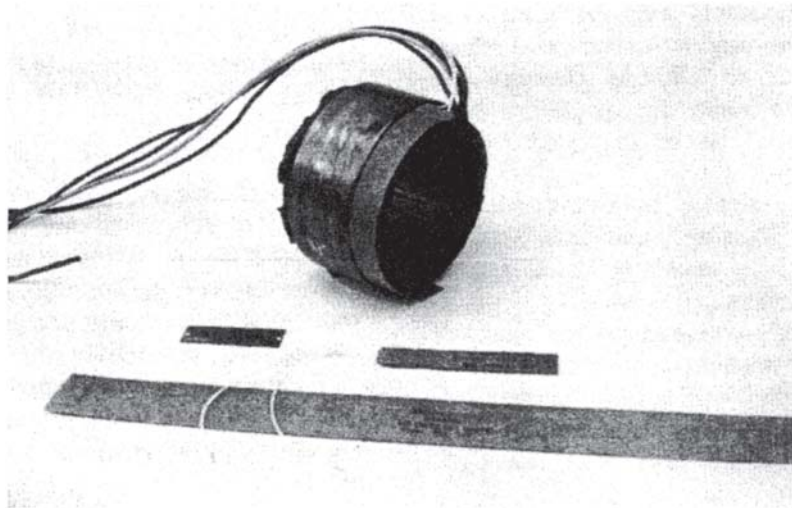


**Figure 14.10** Heaters mounted on windings to reduce condensation. (Heaters made by Watlow Electric Manufacturing Company, St. Louis, MO.)

#### 14.5.4.4 Insulation Tests

Two insulation tests were mentioned earlier, an insulation resistance test using a megohmmeter and a high-potential ground test using an ac or dc source. Polarization tests, surge tests, and tip-up tests are also used on critical windings. These will be described below. The reader is also directed to Chapter 8, Sections 8.2.2 and 8.3.3.

##### 14.5.4.4.1 Polarization Index

Ground insulation is the dielectric material placed between windings and between windings and the frame of the motor. Hence there is interwinding capacitance and winding to frame capacitance. The polarization index (PI) is a measure of the integrity of the dielectric. Once an ideal capacitor is charged (or polarized) by a dc potential, no further current flows in the circuit. Any remaining current must be due to flaws in the dielectric allowing leakage or breakdown current. The polarization process takes time, during which the charging current declines exponentially. The PI is a ratio that represents the slope of the charging current decay over a standard time interval. See IEEE Std. 43–1974 [20] for a more detailed description.

Typically, a PI test involves connecting the winding in question to one terminal of a dc hi-pot tester. The other terminal of the tester is connected to the frame of the motor and to all other windings in that frame except the winding being tested. The dc potential is raised slowly to 1000 V and held for 1 minute. A reading is taken of the leakage current at the 1-minute interval. This reading is divided by the reading of leakage current taken at the end of 10 minutes of excitation. The 1000 V potential (or any other convenient, constant test voltage) is maintained at all times. The ratio of the two readings is the winding PI:

$$PI = \frac{\text{leakage current at 1 minute}}{\text{leakage current at 10 minutes}}$$

New form-wound windings, with VPI insulation, should have a PI of 3 or higher. Clean and dry windings should have a PI of

2 or higher. Some random-wound motor windings may be in good condition and exhibit a PI of only 1.5. PI values lower than this indicate either winding contamination or insulation failure.

New windings on smaller motors in good condition may have such low charging currents that reading is difficult with a high-potential tester. An insulation resistance reading near 1000 megohms is enough verification of satisfactory insulation condition for these windings; a PI test is not needed.

The operator should be careful during hi-pot testing to discharge the winding capacitance after the test is completed. All winding terminals should be grounded for several minutes for smaller motors, several hours for very large motors.

#### 14.5.4.4.2 Surge Testing

Surge testers operate by discharging a capacitor into the motor windings under test. (The surge test capacitor should not be charged any higher than the relevant dc potential given in Table 14.2.) This capacitor discharge results in a pulse of current through the winding. The current amplitude versus time characteristic is observed on an oscilloscope, and the trace is compared with the trace in other phases of the motor, or with previous traces from that same winding or similar windings. See Fig. 8.4 in Chapter 8 for example waveforms. With experience using this technique, the operator can diagnose turn-to-turn shorts and other winding failures by examining the shape of the current trace. Modern surge test instruments have internal data storage as well as serial ports that permit transfer of test data to computer record and analysis systems. See Schump [21] and IEEE Std. 522–1992 [22] for details on surge testing.

#### 14.5.4.4.3 Step Voltage Test (Tip-Up Test)

Winding insulation condition can also be tested by determining the dc leakage current at various voltage levels. The leakage current should increase linearly with voltage if no breakdown is occurring. A controlled overvoltage test usually begins by running a polarization index test on the

**Table 14.4** Winding Resistance of AC Induction Machines, Measured Line-to-Line (ohms)

Horsepower rating	Typical winding resistance for standard efficiency NEMA B design motors at various rater voltages			
	230 V	460 V	2300 V	4000 V
1	4.5	18		
5	0.88	3.5		
25	0.14	0.55		
50	0.06	0.24		
100	0.02	0.09	2.2	
200	0.01	0.04	1.0	3.0
400		0.02	0.5	1.5
1000			0.2	0.6
2000			0.1	0.3
5000			0.04	0.012
10,000			0.02	0.060

Note: These values are for a typical four-pole motor in a NEMA frame, given by Andea in Ref. [39] for 1 to 200 hp. Higher horsepower and voltage values are extrapolated, assuming winding resistance varies directly with voltage squared, and inversely with horsepower.

winding at a voltage equal to one-third of the maximum dc test potential suggested for the winding rating and condition. After the initial 10 minutes, the test potential should be raised each minute by 3% (or less) of the maximum suggested test potential. The leakage current should be read at the end of each 1-minute period. If this current value jumps substantially, the test should be stopped. The “tip-up” in the current curve is a warning of impending failure. IEEE Std 95–1977 (p. 14) [23] describes this procedure in detail.

#### 14.5.4.5 Circuit Tests

##### 14.5.4.5.1 Circuit Resistance and Turn Insulation

Typical winding resistance values, measured line-to-line, are shown in Table 14.4 for three-phase ac induction motors. This table illustrates how winding resistance decreases as horsepower increases. High-efficiency windings will have resistance values lower than those listed in the table. Regardless of the absolute value, the resistance measurements from phase A to phase B, B to C, and C to A, should be within 1% of each other [Ref. 43, Donner, et al.—“A Motor Primer—Part I,” p. 1461.

An ordinary ohmmeter can be used to check the resistance of field windings. A low-resistance reading bridge will be needed to check armature, rotor, and stator winding resistance. In the case of high-current windings, two types of faults can occur. An open in one of the parallel circuits of the winding will cause an increase in the apparent resistance of that phase. A poor connection internally or at the terminals will also cause an increase in resistance. However, connection resistance shows up only if a significant test current is used. To detect this type of fault, the bridge should be capable of establishing a current of 10 A or more through each winding circuit.

A surge tester can be used to compare winding circuits with previous tests (and phase-to-phase, in the case of ac). A change in this test result also indicates a likely circuit fault.

Winding insulation resistance measurements in ohms are normally specified at 40°C. Readings taken on very cold or very hot equipment should be corrected to a common base. It is not necessary to correct all readings to 40°C if the equipment test temperature is relatively constant.

If insulation resistance readings must be corrected to a common temperature, the most accurate method is to plot the resistance for that winding as the temperature rises from ambient during motor start-up. If this effort is not justifiable, an estimated correction is possible by assuming that resistance will decrease by half for every 10°C rise in temperature. For instance, an actual reading of 4 megohms taken at 20°C would correct to 2 megohms at 30°C and 1 megohm at 40°C. See page 9 of IEEE Std. 43–1974 [20] for a plot of the resistance correction coefficient ( $K_r$ ) versus temperature.

##### 14.5.4.5.2 Voltage Drop Tests

In the case of field and interpole windings, voltage drop tests are useful in determining turn insulation failure. Rated dc current is applied to all coils in series and the voltage drops across the individual coils are compared. If dc excitation is used, a variation of 5% or more in the voltage drops across individual coils indicates questionable turn insulation.

If ac excitation is used for a voltage drop test, higher voltages can be applied to series windings and interpoles than is possible with the dc test. Therefore, an ac drop test is more likely to find faults. However, the ac test is more susceptible to variation from adjacent coil structures, so the allowable voltage variation per coil is 10% of the maximum voltage drop in one coil. In some dc machines, the final turns of a field coil may be shorted together to provide a firm anchor for the lead. These coils cannot be tested with ac voltage drop.

#### 14.5.4.5.3 Field Polarity Tests

Polarity is important in synchronous and dc motor fields. The opposite polarity of adjacent field poles will be assured if a soft iron bar is attracted to the poles when the coils are energized. A compass is also useful for checking polarity of the energized windings. The needle should reverse direction as the compass is moved from one pole face to an adjacent pole face.

#### 14.5.4.5.4 Induction Rotor Tests

Defective cast-aluminum squirrel-cage rotors are difficult to diagnose. The phase current spectra in Fig. 14.8 show one test result which indicates open circuits in the rotor winding. Serious defects may be revealed by a single-phase test. Two leads of a three-phase motor are excited by a single-phase voltage of about 25% of the motor rating. The rotor is then turned by hand, and the exciting current is monitored. A change of 1 % or less in the single-phase exciting current indicates that the rotor is good. A change of 5% or more in the exciting current indicates that the rotor is defective [42]. A repair shop may perform a similar test using a growler or a core-loss tester. None of these tests is fool-proof.

#### 14.5.4.6 Repairs to Insulation

Motor insulation deteriorates with age and must eventually be replaced. Its life can be prolonged by limiting the ambient and operating temperatures, by preventing incursion of contaminants and water, and by limiting vibration and other mechanical damage mechanisms. IEEE Std. 432–1992 [17] addresses these specific problems.

The first steps in repair have been discussed above; the winding should be clean and dry. The next step is the repair of mechanical damage that may have occurred due to starting surges, vibration, or overload. Broken coil ties, loose wedges, distorted surge rings, missing support blocks, and broken rotor or armature bands should be repaired or replaced. Finally, the skin of the insulation can be painted, pasted, or dipped to seal it against further contamination. Where particles have cut or abraded the insulation, an epoxy paste is often useful to cover the bare spots. Air-drying varnish or insulating paint can be used over the entire surface.

Dipping the windings in varnish may or may not help. If the cleaning process is successful and all contaminants have been removed, then the winding insulation system benefits from a dip-and-bake treatment. If there are carbon-containing contaminants still trapped in the winding, they will eventually form a coke-like conducting material and cause winding failure. The dip treatment in that instance has only added a little more thermal insulation to the conductors and caused

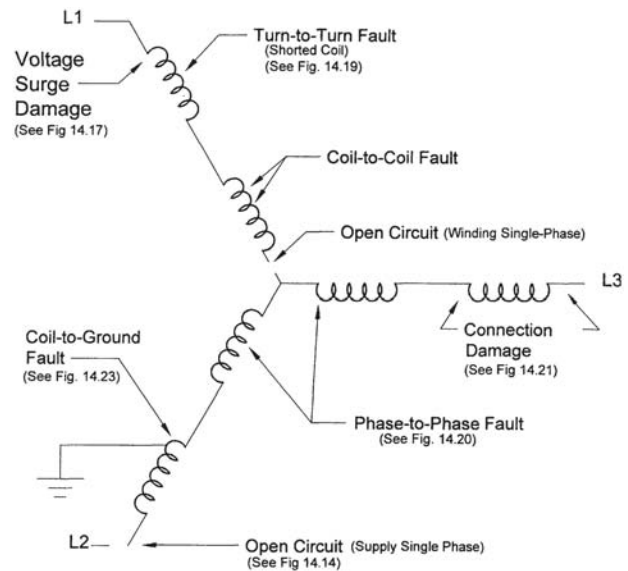


**Figure 14.11** Wye-connected stator winding diagram showing possible failure locations.

the winding to run slightly hotter. An extra dip and bake in that instance accelerates failure.

#### 14.5.4.7 Maintenance Records

A written record of winding repairs is useful in determining the benefits obtained from insulation maintenance. In the case of larger motors, photographs are also valuable in training maintenance personnel in repair procedures. The record should include the damage noted, the cleaning material used, the repairs made, and the test results taken before and after the repair.

### 14.5.5 Evaluating Winding Failures

“Winding failure” may occur in conductors, turn insulation, ground insulation, laminations, or leads. Figure 14.11 shows where winding failures may occur in a three-phase, wye-connected ac stator. Bonnett [24] notes that it is possible to have single failures or any combination of these failure modes. The cause may be normal insulation breakdown or premature breakdown caused by excess load, starting surge, excess voltage, high ambient temperature, vibration, or mechanical damage. O’Donnell et al. [25] concluded that the majority of electrical failures occur because of mechanical damage. These mechanically caused failures are discussed first.

#### 14.5.5.1 Mechanical Causes of Failure

Mechanical rubbing of rotating and stationary laminations occurs when bearings fail, when shafts bend or break, or when foreign matter enters the air gap. The heat generated by the ensuing friction and vibration, as well as the displacement of laminations, is likely to damage the insulation on both laminations and winding conductors.

Core laminations have a thin layer of insulation on at least one side of each sheet of steel. This insulating layer limits the eddy current path length in the core to the thickness of one sheet, typically 0.6 mm (0.025 inches). When the rotor rubs,



**Figure 14.12** Winding damage due to overload. (Courtesy of the Electrical Apparatus Service Association, St. Louis, MO.)

the edges of these laminations may be welded together, creating a conducting path and hot spot in the laminations.

The hot spot may cause the insulation system to fail immediately or the failure may occur over time. The rubbing may also damage the winding insulation by causing small cracks to appear or varnish to flake off the conductors.

#### 14.5.5.2 Load-Related Failures

A typical motor will pull 150–200% of its rating without stalling. Overload generates heat in the windings and causes uniform overheating and deterioration of the insulating materials. The entire winding will be dark or charred. The ac motor stator in Fig. 14.12 illustrates this type of failure. A similar pattern would occur in an overloaded dc armature. This type of failure also occurs when balanced overvoltage is applied to an ac winding. The overexcited ac motor may run and pull its load satisfactorily, but it will have a pronounced electrical hum and draw excess current. Similarly, if the supply voltage is too low, line current will rise and cause thermal deterioration of the winding.

If the load torque exceeds the stall torque, the rotor will not turn, but the motor will draw a balanced, high current. If the stator winding remains intact long enough, the rotor winding will fail. In Fig. 14.13 the aluminum end turns of the rotor winding have begun to melt and run over the stator winding. This failure is typical in stall conditions or when excessive numbers of starts or reversals are required.

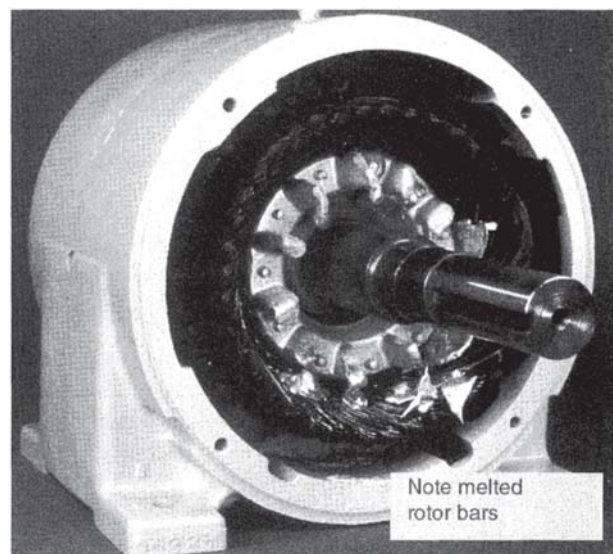
#### 14.5.5.3 Power Supply-Related Failures

The most common failure in a three-phase power supply is the loss of one conductor. This leaves a single-phase supply circuit for the motor. Figure 14.14 illustrates the failure pattern in a wye-connected winding when one supply conductor breaks, a contact in the motor starter burns open, a fuse blows, a lead

connection opens in the winding, or the winding is improperly connected. Two-thirds of the coils try to carry the motor load and are blackened by the heat.

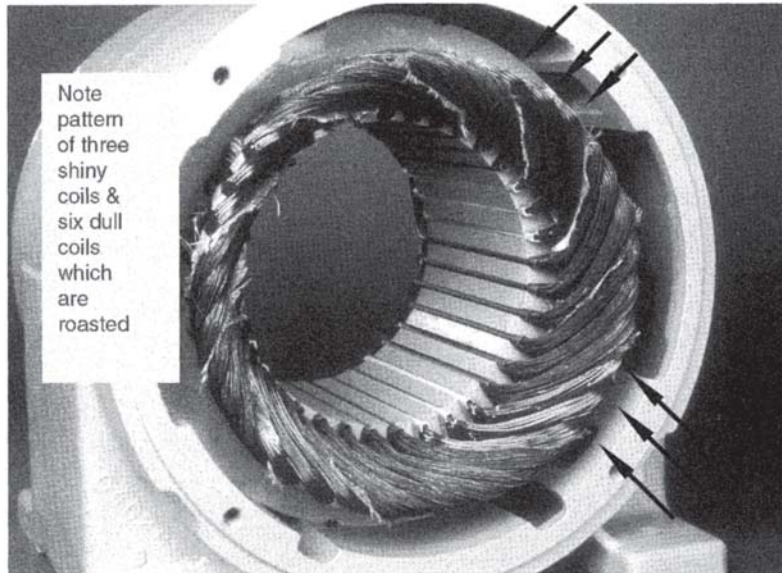
Figure 14.15 illustrates the failure pattern when the winding is delta-connected. In this picture, only one-third of the coils carried excess current and overheated.

Figure 14.16 illustrates the stator winding appearance when the supply voltage is unbalanced due to a poor connection, an unbalanced circuit load, or a faulty supply transformer. The failure pattern caused by unbalance is not as pronounced as in the single-phase case, and varies with winding connection.



**Figure 14.13** Damage caused by locked rotor. (Courtesy of the Electrical Apparatus Service Association, St. Louis, MO.)





**Figure 14.14** Damage due to single-phasing (loss of one power phase) with the winding wye-connected. (Courtesy of the Electrical Apparatus Service Association, St. Louis, MO.)

Voltage surges from lightning or from heavy-current switching cause conductor failure near a lead if the transient waveform has a fast rise time. [Figure 14.17](#) illustrates one such failure. Surge-related failures may also occur further inside the windings at the weakest point. It is usually difficult to prove that a particular winding failure was caused by a surge in the power supply lines.

#### 14.5.5.4 Winding Insulation Failures

Surges, abraded insulation, contaminants, mechanical damage, and voltage and thermal aging eventually cause all windings

to fail. Some failures may not show up in a ground test. One such failure is the shorted coil shown in [Fig. 14.18](#). A shorted coil occurs when two or more bare conductors touch one another. The “bare” situation may occur because of faulty conductor insulation or inadequate varnish treatment, or because the insulation is damaged, abraded, or flakes away. Thermal aging of insulation breaks the bond to the wire and allows the flaking process to begin. Dakin [26] describes similar erosion effects due to aging by continuous applied voltage, or by partial discharge. The motor may run for a short time with conductors shorted in one coil, but it will have a pronounced hum, particularly on start-up.

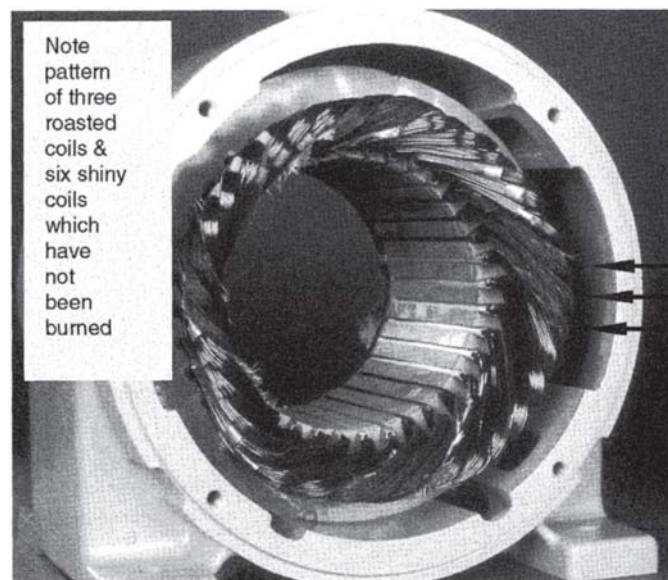


**Figure 14.15** Damage due to single-phasing (loss of one power phase) with the winding delta-connected. (Courtesy of the Electrical Apparatus Service Association, St. Louis, MO.)

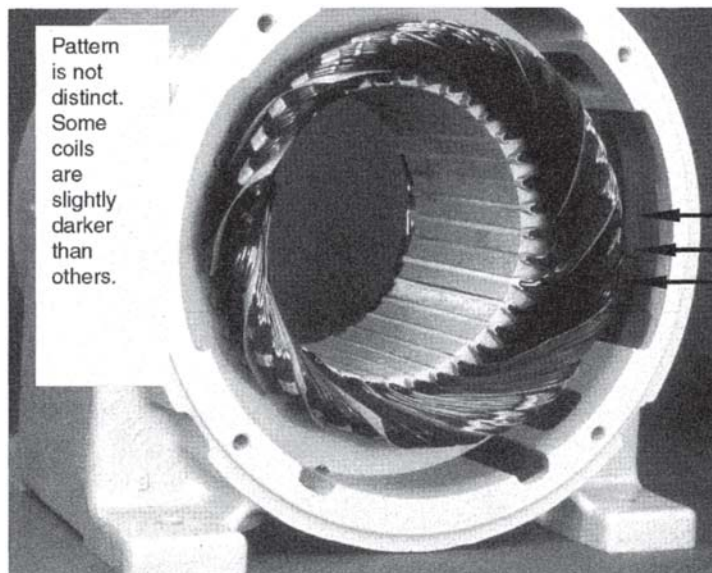


**Figure 14.16** Phase damage due to unbalanced voltage. (Courtesy of the Electrical Apparatus Service Association, St. Louis, MO.)

**Figure 14.19** illustrates a failure that occurred when the conductors from two adjacent coils touched or at least arcing began between them. Poor varnish treatment allows end turns to move and rub together. This failure may start within one coil and spread, or it may occur initially between two coils. Modern design practice for large motors permits up to 200 V between adjacent random-wound coils in the same phase group.

**Figure 14.20** illustrates a failure between coils of two phases. The fault current may be high in this instance if the coils are near a supply lead. The shorted connection failure is very obvious in **Fig. 14.21**.

Ground insulation failures may burn themselves clear and not show up in a low-megohm reading. **Figure 14.22** illustrates a hole blown in the winding due to an arc at the end of a slot cell. The sharp edge at the end of the slot produces electrical

and mechanical stress on the winding. A weakness or break in the edge of the slot cell is a prime source of electrical insulation breakdown. The slot cell or coil wrapper may initially be weakened by movement of the coil in the slot. Windings, should be checked for tightness to be sure movement is not occurring.

**Figure 14.23** illustrates the most damaging failure in a motor. When a coil shorts in the slot and begins to arc, it will burn through the slot cell and arc to ground. Alternately, a coil conductor turn may first short to ground, and then the ground arcs spread to adjacent conductors. No matter what causes the initial arc in the slot, the result is damage to the laminations in that slot, as well as failure of the winding. A color brochure containing all of the failures illustrated in **Figs. 14.12** through **14.23** can be obtained from electric motor repair shops who are members of the Electrical Apparatus Service Association.

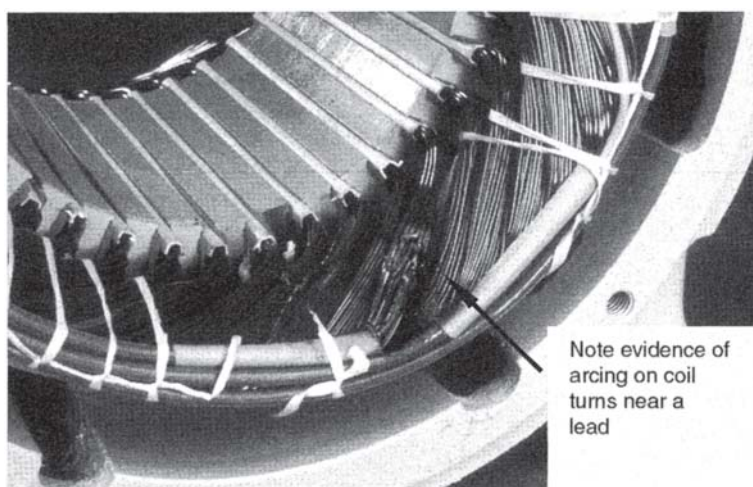


**Figure 14.17** Winding damage from voltage surge. (Courtesy of the Electrical Apparatus Service Association, St. Louis, MO.)

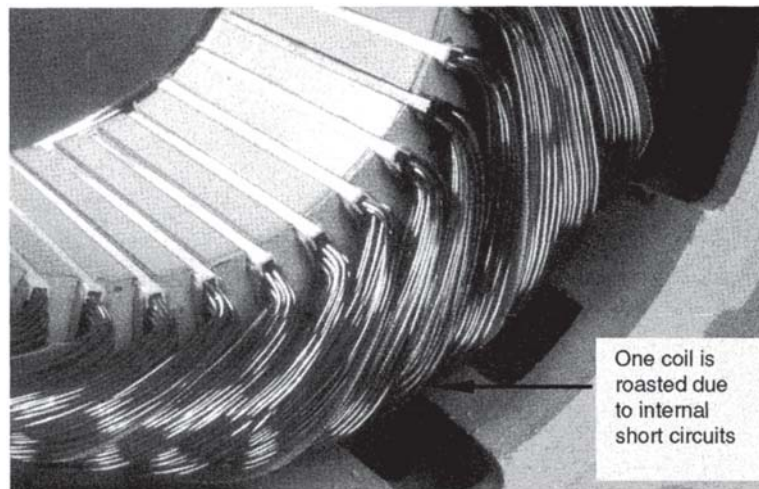


**Figure 14.18** Winding with shorted coil. (Courtesy of the Electrical Apparatus Service Association, St. Louis, MO.)

### 14.5.6 Choosing Repair Facilities

There are many sorts of electrical repair shops available. Nailen [27] suggests a procedure for evaluating shops as to capability, stability, and reliability.

Smaller independent shops are generally competent to repair standard three-phase motors up to about 50 hp unless redesign or special problems are involved. These shops may also repair single-phase motors, but replacement is generally cheaper and quicker than repair. The low overhead in small shops generally allows them to do a good job at a lower price, and they are likely to be available within a few miles of most businesses. Those that belong to a trade association can obtain and verify rewind data from the association engineers.

Several electrical manufacturers have their own service shop organizations. These shops are usually large and well equipped, with good supervision. They are financially

responsible, with ample capital to conduct their business. They have access to the original design information of the products their organization manufactures. These capabilities make them a good source of repairs on large, specialized equipment of that brand name. However, they may have limited access to data from their competitors, and their procedures and processes may be generated by staff engineers at a distant headquarters office. This may limit their service flexibility.

Between these extremes there are a number of larger independent repair shops. These shops are often authorized to repair equipment for a number of manufacturers. Their selection by the manufacturer is an assurance of their reliability and competence to do the work for which they are authorized. These shops are usually members of a trade association, and share rewind data and specifications on a wide variety of equipment.

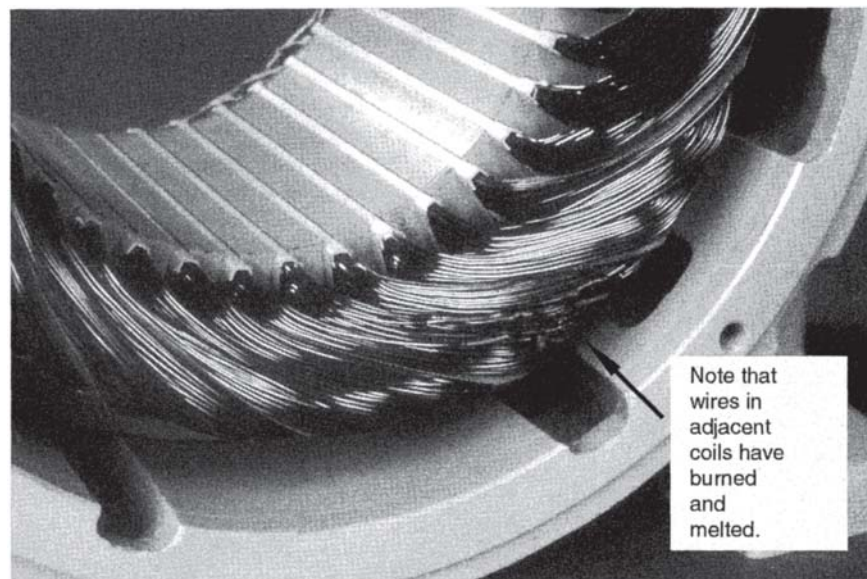


**Figure 14.19** Winding shorted turn-to-turn. (Courtesy of the Electrical Apparatus Service Association, St. Louis, MO.)

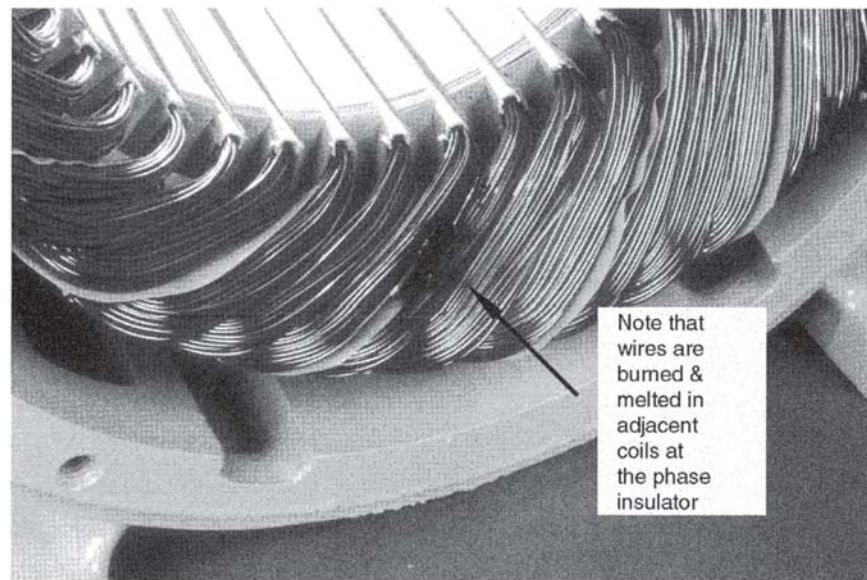


**Figure 14.20** Winding shorted phase-to-phase. (Courtesy of the Electrical Apparatus Service Association, St. Louis, MO.)

Shops repairing motors for special applications may be able to refer to procedures such as the guideline prepared by Bilanin [28] at EPRI for nuclear power plant motors. A similar standard is available for oil and chemical industry motors, IEEE Std. 1068–1996 [29].

High-performance servomotors, stepper motors, and other control motors cannot be tested without special equipment. The original equipment manufacturers and a few independent repair shops have the procedures and equipment to repair these special motors.

To summarize, it appears advisable to send large, specialized equipment to the service shop of the manufacturer who made it. Other large motors, direct-current motors, and smaller specialized equipment could be handled by selecting

a larger independent shop. The remainder could be well served by a small, nearby independent shop.

Repair costs are difficult to predict before the exact scope of work is known. Once a repair procedure is agreed, there are industrial cost guides (Lammers [30]) that indicate the likely cost of repairs at normal rates, without overtime. Standard ac motors below 20 hp are usually as cheap to replace as to rewind. Direct-current motors below 5 hp are also good candidates for replacement if both armature and field windings need replacement. In an overtime (rush) situation, replacement may be the best economic choice up to 100 hp ac and 25 hp dc.

#### 14.5.7 Selecting Repair Methods

A well-qualified repair shop, given knowledge of the motor's operating conditions, is able to provide an appropriate rewind and insulation system. However, if the user or manufacturer has developed techniques for special motors, this information should be passed on to the repair shop. With these provisos, comments are offered below on repair methods.

##### 14.5.7.1 Removal of Old Windings

Before repairs can begin, the old windings must be measured, the turns and span calculated, and the wires and insulation removed from the slots. One end of the winding may be cut off to simplify coil removal. The remainder of the winding is softened or degraded by heat or chemical solvents, and then mechanical force is used to pull or strip the wires from the slots. A high-pressure (10,000 psi) water jet may also be used to break the insulation and loosen the wires in the slots. This technique is hazardous unless it is closely controlled by a skilled operator.

If the heat and mechanical force used to remove windings are excessive, the frame and laminations may be distorted or broken, and the interlaminar insulation may be damaged.

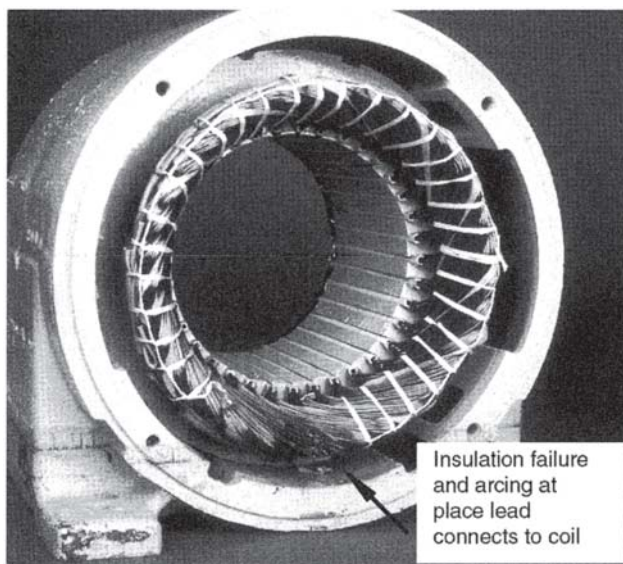


**Figure 14.21** Winding with shorted connection. (Courtesy of the Electrical Apparatus Service Association, St. Louis, MO.)

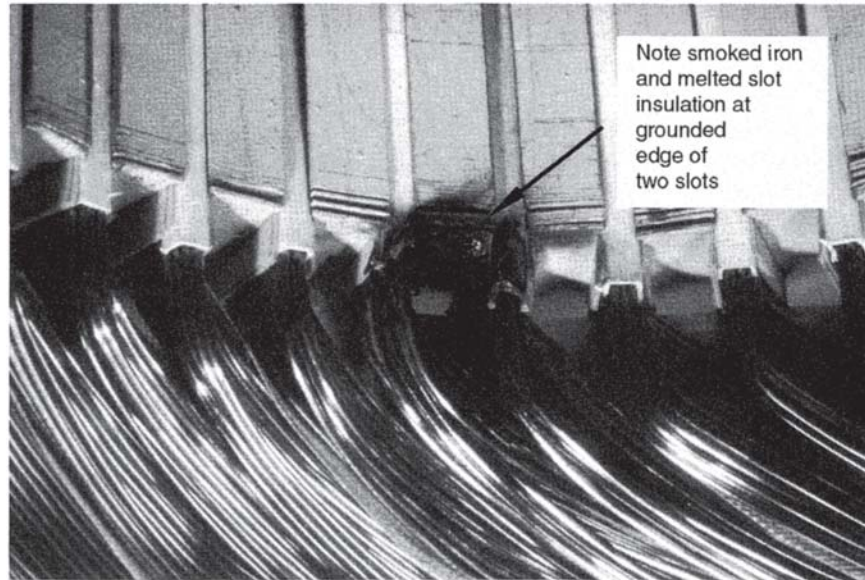


**Figure 14.22** Winding grounded at edge of slot. (Courtesy of the Electrical Apparatus Service Association, St. Louis, MO.)

Controversy over winding burnout techniques resulted in a core damage study (Zeller et al. [31]) that indicated that use of heat to strip motors did not result in core damage if the oven temperature was maintained at 650°F (340°C) or below during the stripping cycle. Oxygen starvation and water injection can be used to limit the heat rise in ovens used to degrade insulation.

Damage has occurred to some motors where a heavy epoxy encapsulation has been burned off. The fuel value of this epoxy was so high that the temperature was difficult to hold down.

#### 14.5.7.2 Lamination Repair

Modern shops generally check the core before and after removing the winding to detect changes in the magnetic

characteristics and to find localized hot spots. Hot spots can often be removed by grinding or chemical etching.

If lamination damage is extensive, the laminations may be separated, straightened, and lightly varnished. The core is then restacked to spread the damaged slot sections throughout the stack. Replacement laminations can also be purchased if some layers are damaged beyond use.

Section 14.6 discusses core testing methods in detail.

#### 14.5.7.3 Insulation Systems

Modern electric motors are usually designed for operation up to class B temperatures (135°C). However, most insulation systems are at least Class F (155°C), and many components are rated Class H (180°C) or Class N (200°C). The higher

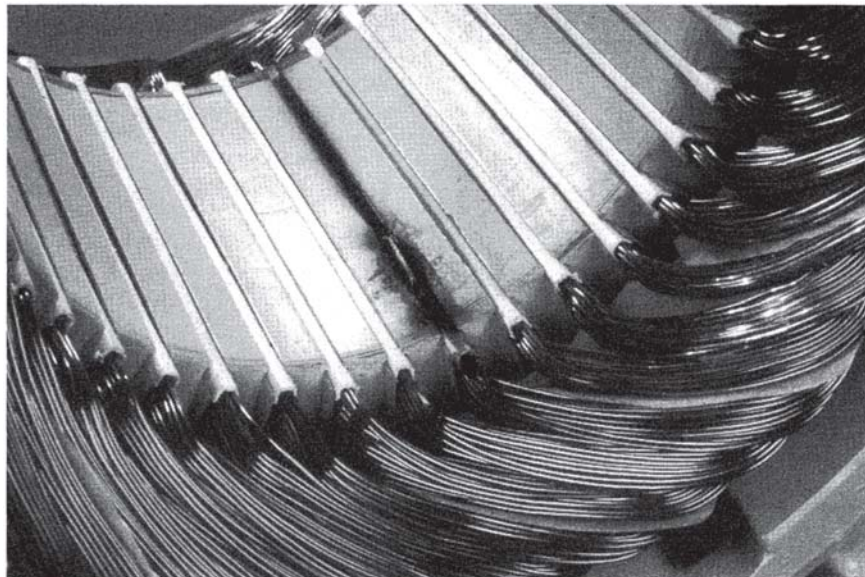


**Figure 14.23** Winding grounded in the slot. (Courtesy of the Electrical Apparatus Service Association, St. Louis, MO.)

classes may be desirable in traction armatures or similar duty. For normal duty, Class F insulation applied in a workmanlike manner is satisfactory. Higher-temperature lead wires may be stiff, or the glass braid may be objectionable.

Varnish treatment is usually applied to all windings after they are placed in the slots and connected. Original equipment manufacturers now typically use polyester varnishes on smaller motors and epoxy varnish on larger machines. The smaller motors are dipped once or twice in the varnish and baked after each dip to cure the film. Larger machines are typically treated by vacuum-pressure impregnation (VPI). This treatment insures complete penetration and wetting of all the insulation surfaces. Motors designed for VPI treatment may not perform within their heat rise and environmental ratings unless they are repaired using the VPI technique.

A qualified repair shop should be able to explain the insulation system they use, and verify their experience with it. The major choices involved are slot cell material, wire coating, lead wire insulation, and varnish treatment. Repair records should indicate the choices made for these major insulating materials.

#### 14.5.7.4 Winding Replacement

A repair shop normally rewinds a motor using the same design as the winding that has failed. The shop should be told if the motor has been rewound elsewhere, or if particular problems have occurred with these rewinds.

Some motors can carry increased load if aluminum conductors are replaced by copper or if the size of the conductor is increased. It is often possible to get larger wire into the slot by hand winding than by machine winding (as in the OEM manufacturing process). However, these changes have little effect on load capacity (perhaps 10%) and are more useful in keeping the operating temperature down than in increasing load capacity.

AC windings can be redesigned to change speed, but the available torque is limited by the dimensions of the air gap surface, which cannot be changed. In addition, the torque is also limited by the flux path in the back portion (back-iron) of the lamination. Torque capability will usually be reduced if the rated speed is increased.

Aluminum squirrel-cage windings can also be replaced by copper windings, but this changes the speed-torque characteristic of the motor. In most applications, the change is acceptable. However, the higher operating speed of a copper rotor may overload a motor driving a speed sensitive load such as a fan or pump. Large or specialized rotors should be rebuilt with bars and end rings having the same conductivity as in the original design.

DC motor windings can rarely be redesigned, since commutator, armature, and fields are all designed to work together.

### 14.5.8 Testing Repaired Windings

No matter what type of winding is contemplated, Montgomery [32] strongly recommends that the user should “demand high quality and high value for all motor rewind expenditures and insist that the quality be verified by test.”

#### 14.5.8.1 Insulation Tests

New windings should be tested at the repair shop according to NEMA Standard MG 1 [33] and other tests chosen by the user for the specific application (see [Table 14.2](#)). Water immersion tests at a lower potential are also used to qualify special-duty motors. This water test is described in section 20.49 of NEMA Standard MG 1 [34].

Many repair shops use a surge test on their windings to check for winding faults. This test is often done before the winding is dipped and baked. Faults are much easier to repair before the insulating varnish locks the conductors in place.

All motors should be run at full voltage unless the repair facility does not have this capability. The exciting current level and balance are good indicators of the winding design and flux density in that specific magnetic core.

#### 14.5.8.2 Performance Tests

The repair shop may run a load test on a repaired motor, particularly if its performance is in question. The load test can reveal ac rotor faults and dc commutation problems. No-load running is usually a sufficient test on a standard ac motor.

DC motor design has become more compact, with finer setting required of the brush neutral. One common test, to be sure the neutral is set properly, involves running the motor at full load in both directions. The forward and reverse full-load speeds will not differ by more than 1% if the brush position is set properly.

Where energy efficiency is a significant factor in motor selection, a full-load test at rated operating temperature is often desired. However, it is difficult to obtain a load test with results that are accurate within  $\pm 1\%$ .

Performance test procedures are outlined in IEEE Std. 112–1996 [34] for induction motors and IEEE Std. 115–1995 [37] for synchronous machines. Standards for dc machines [35] and single-phase motors [36] have been withdrawn.

#### 14.5.8.3 Test Records

Load test records provide important reference information. If the motor current is known at 25%, 50%, 75%, 100%, and 125% of rated load, later operating current readings can be directly correlated with shaft load. The repair shop should provide the current-versus-load results if a load test is requested.

### 14.5.9 Evaluating Repaired Equipment

The new windings should be even in appearance, indicating good workmanship in their insertion into the slots and in the forming of the end-turns. The varnish treatment should be apparent, but the thickness of the coating does not have much electrical significance, nor does the presence or absence of paint.

Historically, good rewinds have been laced, tied, and blocked. These factors matter less with modern varnishes. VPI treatment provides blocking by saturating and hardening felts inserted between coils. Leads should be securely tied to the end-turns, since starting surges can cause movement. The free portion of the leads should be flexible and adequately marked,

and the terminals should be securely affixed. Some shops use pressure-crimped terminals alone. Others solder after crimping, or use solder alone. No matter what method is used, care must be taken in making good connections, since poor joints are a significant source of problems.

The acceptance tests specified in Section 14.5.1 are relevant for all rewound motors: megohm, high-potential, and no-load running. The same records are also suggested: the name and warranty of the shop making the repairs, and the new operating conditions and supply readings.

Stevenson [38] has concluded that properly rewound motors maintain their original energy efficiency. Provided there is no damage to the core iron and the lamination insulation, there is no physical limit to the number of times a motor can be rewound satisfactorily. However, proper maintenance and overload control should limit the need for repeated rewinds.

#### 14.5.10 General References on Maintenance and Repair of Windings

In addition to the references cited above, a selected list of other sources of information appears as Ref. 39. Useful information is also available on most motor manufacturers' websites.

### 14.6 CORE TESTING

The stator and rotor cores of large induction motors and the stator cores of synchronous generators comprise thin sheets of laminated steel. As discussed in Section 4.7.3, a typical lamination might be 24 standard gauge, or 0.0635'-cm (0.025-inches) thick. During normal operation, the flux is carried circumferentially in the lamination until it exits the core and enters the air gap between the stator and rotor (or crosses to a slot containing an electrical conductor). Eddy currents form a loop around the flux but are constrained such that they must reside within the lamination. These loops can be mapped across the back-iron region, along the side of the lamination, across the tooth (or the slot bottom) region and then along the other side of the lamination.

Eddy currents are a component of core loss that the design engineer attempts to minimize by making the laminations as thin as possible. Problems begin to develop when laminations become shorted electrically. High-magnitude eddy currents result that can cause excessive localized heating. A core test,

**Table 14.5** Reasons Why Laminated Cores Develop Hot Spots

1. Rotor to stator rubbing because of bearing wear or failure
2. Lamination insulation damage due to coil removal in a burnout oven in which the temperature was not adequately controlled
3. Welding together of stator laminations during a stator winding short-circuit fault that results in high winding temperatures and coil failure
4. Lamination punching burrs that were not removed prior to core stacking and that have shorted together as the core wears during in-service operation
5. Foreign object in the motor air gap that nicks the laminations, shorting two or more together

known as a loop test, can be performed to identify eddy current problems in cores. Table 14.5 lists a few events that can initiate core overheating.

#### 14.6.1 Loop Test Physical Arrangement

An unshielded power cable is looped around the core in order to couple flux into the core. The loop is supported so that generally there is a clearance between the loop and the core. Some distance away from the power loop, a search coil is also installed around the core and connected to a voltmeter to permit the monitoring of flux in the core. *Westinghouse Electrical Maintenance Hints* [40] provides information on how to size the power cable for a flux density that corresponds to 105% of rated voltage. Table 14.6 summarizes the ampacities.

Additional guidance is given by IEEE Std. 56-1977 [41]. The total core flux in lines can be computed as follows:

$$\phi = B L_{\text{eff}}(D_1 - D_2)/2 \quad (14.1)$$

where:

- $B$  = design core peak flux density in lines/inches<sup>2</sup>
- $L_{\text{eff}}$  = effective length of the core (inches)
- $D_1$  = outside diameter of the core (inches)
- $D_2$  = diameter of the slot bottoms (inches)

The effective length of the core can be computed as follows:

$$L_{\text{eff}} = (L - N_v b_v) F_s \quad (14.2)$$

where:

- $L$  = gross length (in)
- $N_v$  = number of ventilation ducts
- $b_v$  = width of ventilation ducts (in)
- $F_s$  = core stacking factor

If the core stacking factor is not available, an approximate value of 0.93 can be utilized.

The volts per turn (VPT) across each of the loop coils and across the search coil can be computed as follows:

$$\text{VPT} = 4.44f\phi \times 10^{-8} \quad (14.3)$$

Also, the anticipated loop current can be computed as follows:

$$I = \frac{\pi(ATPI)(D_1 + D_2)}{2N_t} \quad (14.4)$$

where:

- $ATPI$  = ampere turns per inch of mean core periphery
- $N_t$  = number of turns

**Table 14.6** Loop Test Flux and Current Parameters

Core flux density (kilolines/inches <sup>2</sup> )	Loop current (Ampere-turns/inch of mean core periphery)
85	9
90	18
95	37
106	145

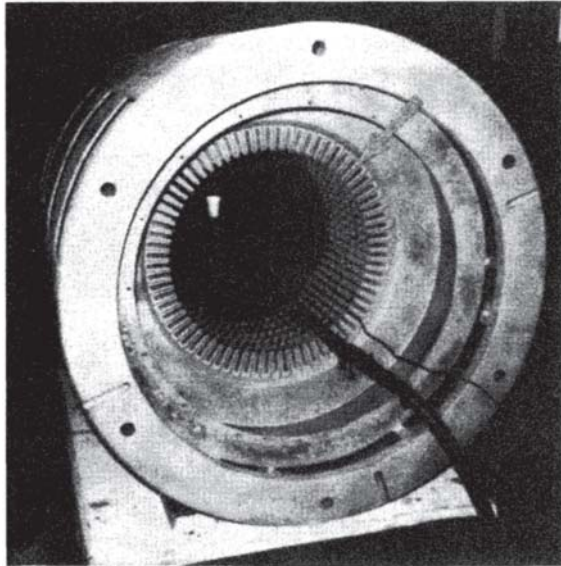


**Figure 14.24** Induction motor stator core test. (Courtesy of Ohio Edison Company, Akron, Ohio.)

The number of turns  $N_t$  that must be looped around the core given the voltage limit of the test set rheostat (or a single-valued voltage source) is:

$$N_t = \frac{V_{set}}{VPT} \quad (14.5)$$

Once the physical setup has been completed, the test set is energized and the search coil voltmeter is checked to verify that the proper core flux has been established.

Prior to the development of more sophisticated detection means, hot spots were located by touch. If a spot in the core was too hot to permit the tester to keep his hand on it shortly after energizing the loop, then core repair work was necessary. Next, contact thermometers were used for this purpose. This was an improvement. Nevertheless, this measuring technique does not allow for monitoring the entire core at once. Presently, the method used to identify hot spots requires the use of infrared thermovision equipment. Thermography is described in the next section.

#### 14.6.2 Thermovision Monitoring During the Loop Test

Heat energy moves from hot locations by three different mechanisms: conduction, convection, and radiation. The thermal radiation has a spectrum in the infrared zone. Radiation depends on the fourth power of absolute temperature. For objects that are black bodies (that is, good radiators) net heat flow is described by:

$$Q = \sigma k (T_1^4 - T_2^4) \quad (14.6)$$

where:

$$\sigma = \text{Stefan-Boltzmann constant} = 1.714 \times 10^{-9} \text{ BTU}/(\text{h}\cdot\text{ft}^2\cdot\text{R}^4)$$

$k$  = geometric factor accounting for the difference in the black body locations

$T_1$  = temperature of the hotter black body on the Rankine scale

$T_2$  = temperature of the colder black body on the Rankine scale

Objects that are not black bodies do not radiate as well as black bodies. A correction factor  $\epsilon$ , called emissivity, is used to account for the reduction in emissive power of the radiating body.

Infrared cameras are available that can display a picture on a cathode ray tube (CRT) screen showing the temperature differences on the surface of an object. Early thermovision sets, as these infrared cameras have come to be known, required a low-temperature reference. Liquid nitrogen poured from a Dewar flask cools the thermovision set and establishes the required low-temperature reference. Some of the newer electronic thermovision sets do not require this low-temperature reference.

Figure 14.24 illustrates the test setup for an induction motor stator test. Note the large power conductor that carries the loop current and the small search coil wire. The arrow marks the location of lamination shorting that has penetrated deep into the stator core iron as can be seen in Fig. 14.25. The lighter the area in the thermovision photograph, the hotter the surface area as compared to the surrounding core surface. Repair facilities use specific levels of hot spot temperature differentials to identify stator cores that require repair work. A typical value is  $10^\circ\text{C}$ .

The thermovision set has adjustments that permit the tester to determine the temperature differential. Figure 14.26 shows an induction motor rotor thermovision photograph in which the hot spot temperature differential is  $108^\circ\text{C}$ . A much higher core test temperature differential can be tolerated in an induction motor rotor before core repair work is necessary. The reasons for this are as follows.



**Figure 14.25** Thermal hot spot near the end of the stator core. (Courtesy of the Ohio Edison Company, Akron, Ohio.)



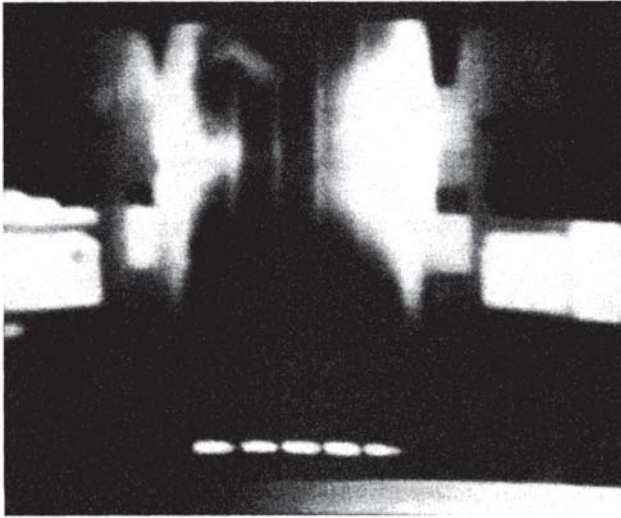


**Figure 14.26** Induction motor rotor with 108°C core test hot spots. (Courtesy of the Ohio Edison Company, Akron, OH.)

1. There is no electrical conductor insulation that is subject to thermal damage between the rotor bars and the rotor slots.
2. The rotor normally experiences locked-rotor current levels and locked-rotor current slip frequency only during startup. At steady-state, the rotor cools down from the temperature reached during acceleration.

### 14.6.3 Other Core Test Factors

With modern core testers, sufficient information is available to determine the power factor of the kilovolt-ampere during the test and the core loss per pound of core material. These factors become important when there has been a general deterioration of the interlamination electrical insulation but there are no significant hot spots. Various shops have different values for these parameters that can be used to determine whether or not a core is in poor condition. Almost all shops will agree that if core loss reaches or exceeds 10 watts per pound of core iron, the core is in poor condition.

Likewise, the power factor of a sound core generally falls within a standard range when performing a core test. If the power factor falls outside a range of 0.2 to 0.8, there could be a core problem. Values at the low end of the standard range are indicative of a better core. If this test range is exceeded but other test parameters are normal, the grade of core steel may be different than that normally encountered.

### 14.6.4 Core Hot Spot Repairs

If the core tests well except for a few hot spots, it can usually be repaired. Minor core surface damage can be corrected by using a chisel-like tool to separate the laminations. More serious damage may require grinding or etching. If the hot spot damage extends into the core between the laminations, an insulating varnish will have to be applied during the lamination spreading process. Mica paper insulation will

occasionally have to be inserted between laminations if the hot spot damage is severe.

Once in a while a shop will have to work on an apparatus that has experienced a hard stator-to-rotor rub. When the core tests poorly and lamination material has been scraped away, causing a nonuniform air gap, it will usually be necessary to scrap the core. If the core is to be reused in this situation, it is usually necessary to restack it, staggering the location of the damaged core surface.

### 14.6.5 EL CID Test

The construction of a motor stator core from many thin sheets of laminated steel was discussed earlier in this section. It described how failure of the insulation between laminations provides short-circuit paths with resultant, potentially damaging, high-magnitude eddy currents. These currents can cause excessive local heating and hot spots that may not be dissipated adequately by local cooling, causing more interlaminar failure or damage to the stator windings.

Section 14.6.1 describes a thermal loop test method to identify hot spots, typically by means of thermovision monitoring as described in Section 14.6.2. This conventional test uses a supply sufficient to provide the relatively high power levels for the excitation winding in order to induce rated flux in the core. Although loop testing is an effective tool, there are often disadvantages in exciting the stator core to operating flux levels, particularly with larger high-voltage machines. These disadvantages include:

- Access to high-voltage, high VA power supply and provision of a high voltage winding cables.
- Possibility of further damage to core or windings during the test because of 100% or over 100% flux without normal cooling.
- Significant safety considerations during test excitation, with cessation of other work requiring access to the bore or vicinity.
- Considerable time to run test and evaluate severity of hot spots, especially on larger machines with long thermal time constants.
- Possible failure to detect faults located on the walls or base of a slot if windings still in place, and similarly for faults buried in the core.

For an alternative method to be advantageous, it would ideally be quicker and easier to use at a safe, low-power excitation level. Although heat produced by faults at low-level excitation is not readily discernible, the presence of these low-level currents gives rise to electromagnetic fields that can be detected by electromagnetic sensors. A further advantage of electromagnetic detection is that the fields are not affected by the presence of windings in the slots.

A system has been devised to sense these fault currents by electronic means and to separate them from other magnetic fields present due to the excitation winding, giving rise to the now familiar EL CID, an acronym derived from electromagnetic core imperfection detector.

#### 14.6.5.1 Theoretical Background of EL CID Testing

Experimental work has verified that the magnitude and other parameters of fault currents flowing at low excitation levels may be used to provide an indication of the severity of hot spots that would result from corresponding fault currents flowing at normal operational excitation levels.

Although the exact level of low excitation used is not critical, provided the level is recorded for scaling purposes, the standard EL CID test uses a core excitation level of 4% of operating flux and the induced voltage along the bore of the core is therefore also 4% of the operating voltage. Figure 14.27 shows a section of a core with a typical fault on the lamination surface at the base of a slot. The current flows along the surface fault and in this instance finds a return path via the building bars at the back of the core, although other return paths (such as other faults) are possible and the fault could also be subsurface. The fault current produces a local flux pattern, which adds to the circumferential flux in the core produced by the excitation winding.

Figure 14.28 shows a vector diagram of the relative excitation current and flux, together with the quadrature voltage generated along an energized core. Any fault current flowing in phase with this voltage because of imperfections in the interlamination insulation will produce heat. As a result of the inductive nature of the core material, fault current may not be in phase with the generated voltage, but the element of the current flowing through fault resistance will be, and this will be the source of any heating effect. Figure 14.28 shows the heat producing vector of the fault current in quadrature with the excitation flux.

A more complete overview of this work and other fundamental considerations is provided by Sutton in [47].

#### 14.6.5.2 Practical Considerations for Low-Power Testing

For low-power testing the system will need to make provision to acquire and process the additional electrical signals. Also, as the stator core is energized in a manner similar to that with a high-power test, but at an excitation level of 4% (voltage and resultant current), the required VA will be reduced to 1/625 of that for 100% excitation. At only a few volts per meter along the bore length, operators may safely work inside the bore while energized, and even carry out non-EL CID test or maintenance activities concurrently. Accurate adjustment of the excitation level may be carried out by means of a variable autotransformer, although it is often possible to arrange the number of excitation turns to match the available voltage supply adequately.

Care is required on positioning the excitation winding to prevent near-field effects on the electrical sensors and excessive field distortions. The ideal positioning of the excitation winding is along the central axis of the core and at least 1 m beyond the core before commencing the outer return path. This may not always be feasible within the confines of the available space, particularly with tests with the rotor fully or partly in position, and distortions of the test result background levels will normally result.

The theory to calculate the correct excitation level for the test is the same as that for a loop test although of course the full operational flux level must be scaled down to 4%. The normal method to determine the correct EL CID test excitation level is to ascertain the voltage normally induced along a

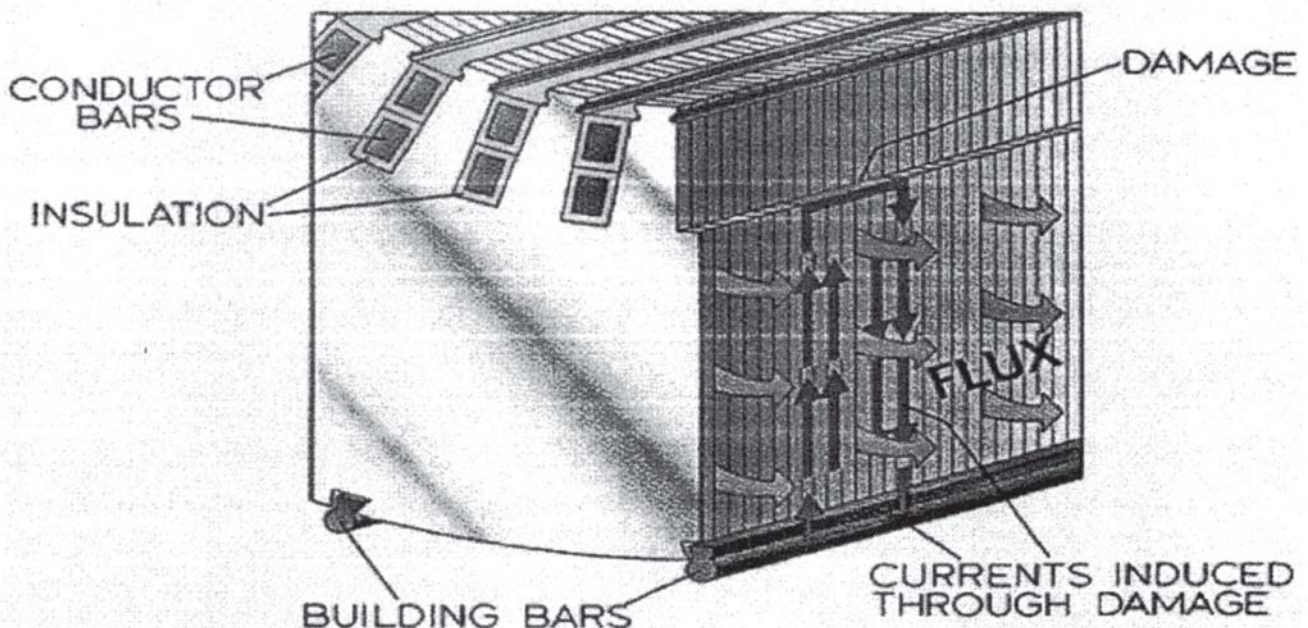
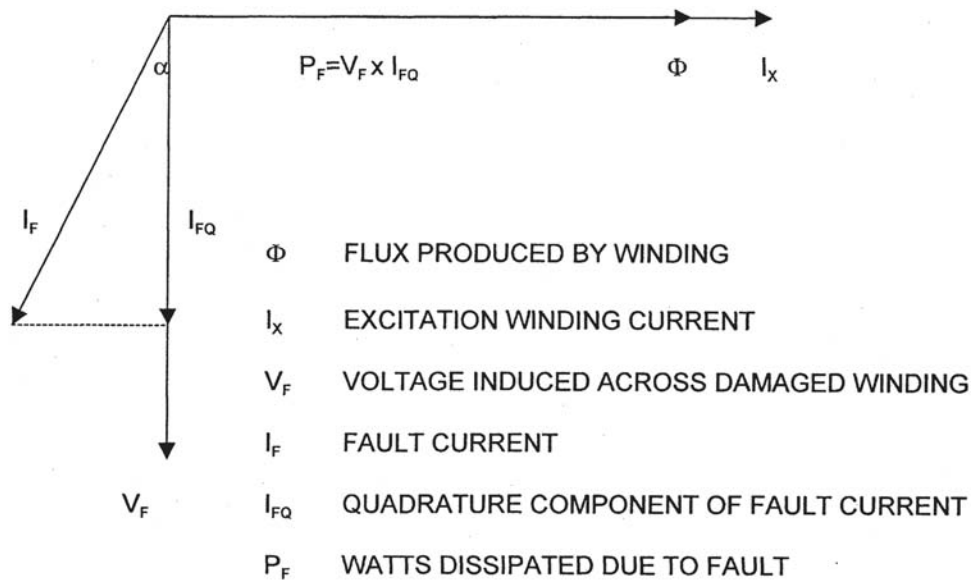


Figure 14.27 Typical fault current paths resulting from damage.



**Figure 14.28** Vector diagram of excitation flux with induced voltage and fault current.

single conductor bar (effectively the same as the single length of the stator core), and then to scale this to the required 4% test value. The supply to the test excitation winding should then be adjusted to produce this voltage on a single-turn voltage monitoring winding.

To determine the single conductor bar voltage it is necessary to ascertain the number of machine turns connected in series to make up a winding for one phase. Each turn of the machine is normally made up of two conductor bars in series, with the voltages of the bars being additive because of their positions in the stator with respect to the rotor poles. Although machine windings may also consist of turns in parallel, these are not relevant to the calculation as they only share the current and do not affect the total voltage.

Hence, the calculation for the standard EL CID test excitation level is given for 4% excitation by:

$$V_{\text{test}} = V_{\text{ph-ph}} \times 1/\sqrt{3} \times 1/2tp \times 1/k \times 4/100$$

Where  $tp$  is turns in series per phase,  $k$  is the combined form and pitch factor (usually assumed to be 0.92). In some instances information on construction of the core windings is not available and core excitation may need to be calculated from consideration of the core dimensions and operating flux level.

EL CID fault current signals are detected by a sensor in the form of a Chattock coil, a long flexible solenoid of fine wire [47] providing an output proportional to the magnetic potential between its two ends in contact with the core surface. A fault current will give rise to magnetic potentials within the core in the vicinity of the fault and may therefore be located by the coil.

To scan a complete core for faults (a global test) the core is divided into a number of strips along its length. Each of the strips is scanned in turn to cover the whole core internal surface. A suitable strip for this purpose is conveniently

defined by each slot. By scanning each slot including the width of both adjacent teeth, a degree of overlap between scans is achieved which is useful in providing additional information on fault location. Figure 14.29 shows the location of a Chattock sense coil across a slot and tooth pair.

The magnetic potential across each tooth pair will be comprised of the in-phase excitation field (the PHASE signal) together with any phase quadrature (the QUAD signal) produced by a fault current. The QUAD signal is separated from the PHASE signal by a phase discriminator in the EL CID signal processor unit. The phase discriminator requires a phase angle reference for the in-phase component, and this is provided by a phase pickup coil, which may be derived in a number of ways including from the excitation current, as shown in Fig. 14.30b, or background excitation field within the bore.

The stator bore may be scanned by various manual or automatic means dependent on the size and orientation of the core and whether the rotor is removed, as is currently more normal. Figure 14.31 shows a typical manual scan in progress on a core, and Fig. 14.32 a typical test in progress (except the operator has stepped aside for the photo!)

Test results are best displayed in the form of a test trace of the amplitude of the QUAD signal against distance along the bore, normally displayed on a computer screen and stored on PC media. Similar traces for the PHASE signal vector may yield additional information for test result interpretation.

Figure 14.30a shows a standard EL CID test configuration. Apart from any large excitation winding and any associated autotransformer, the system parts will normally fit within a large portable case. The configuration shown is for a full system with provision for recording of all PHASE and QUAD test results on a computer or chart recorder which is normally used for large motors and generators. Less complex systems (normally known as motor core testers or MCT, but still utilizing

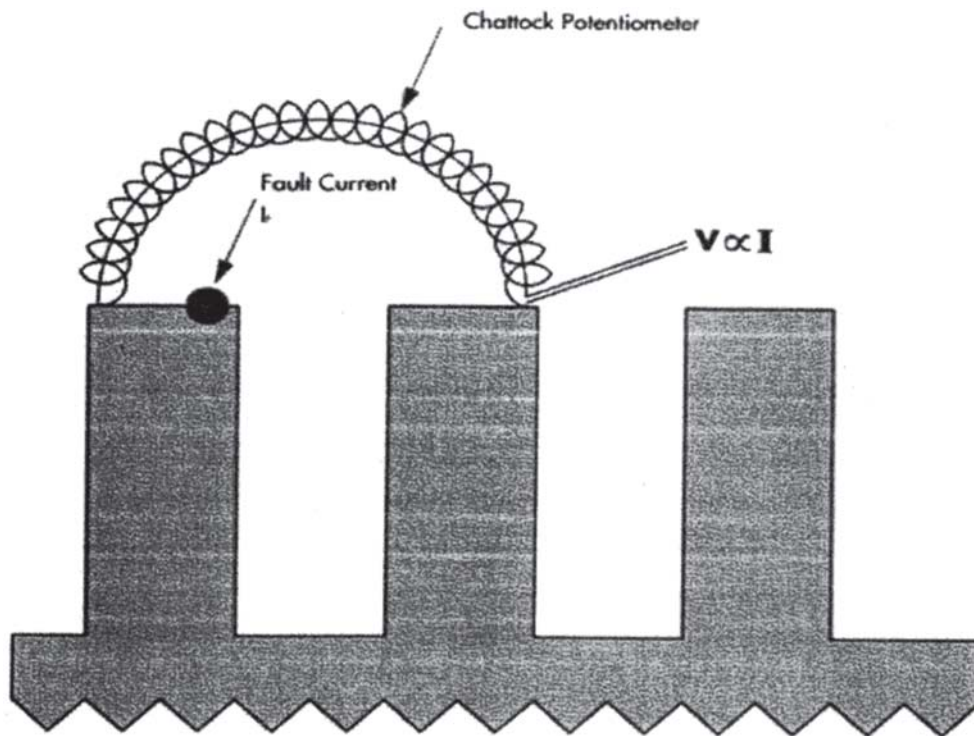


Figure 14.29 EL CID sense coil positioning on stator teeth for global test scanning.

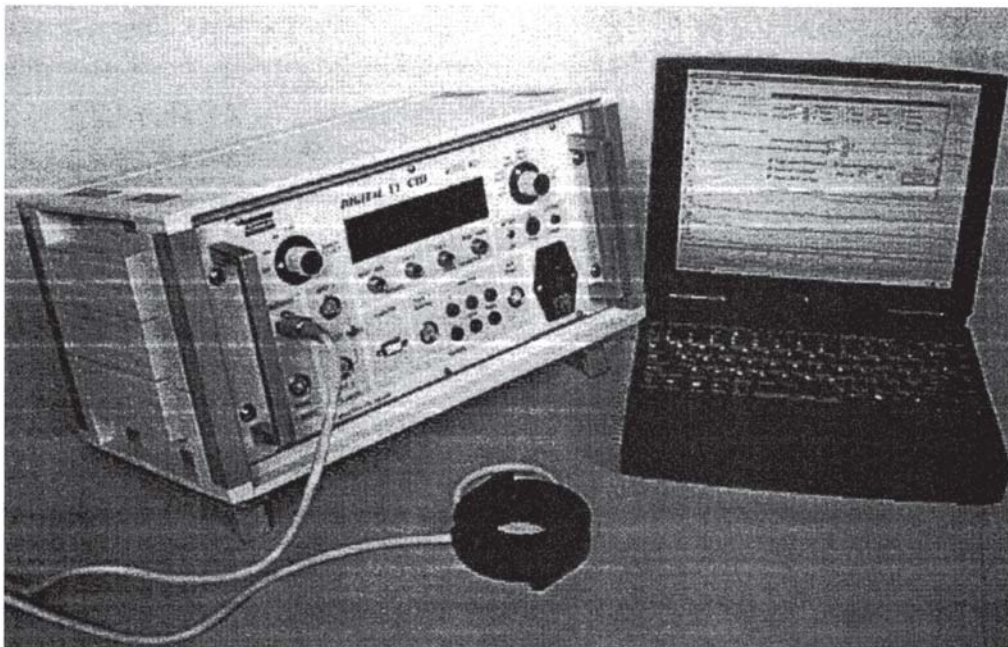


Figure 14.30a Typical EL CID test configuration.

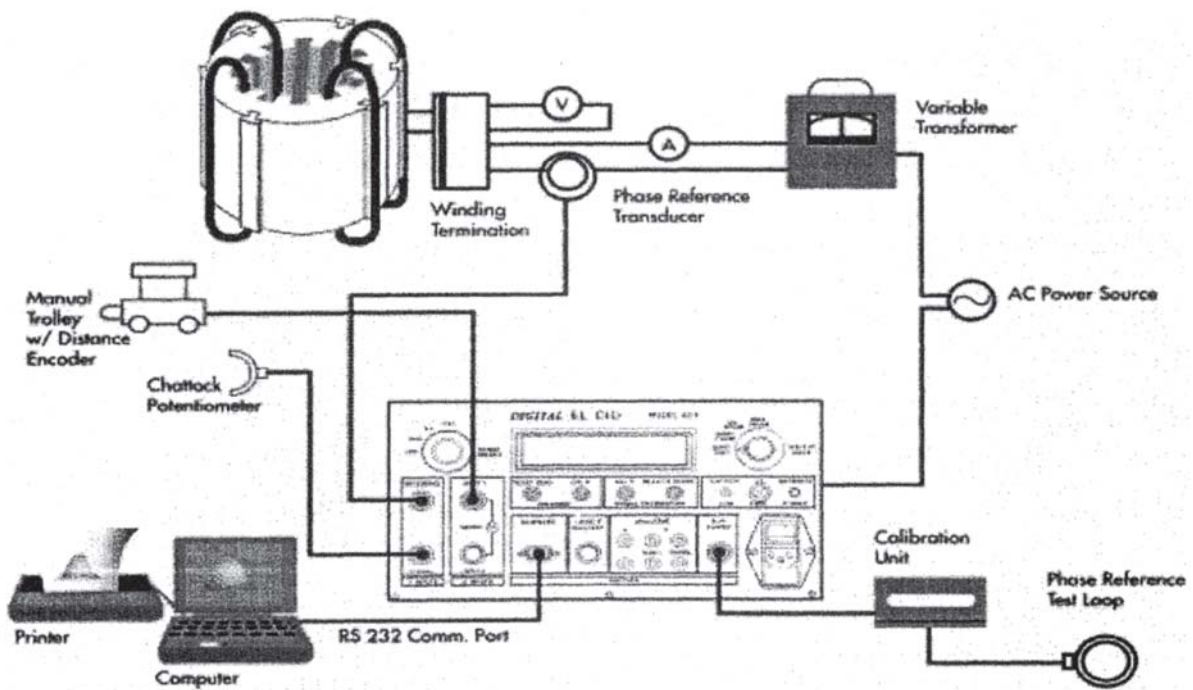


Figure 14.30b Typical EL CID connections for core test.

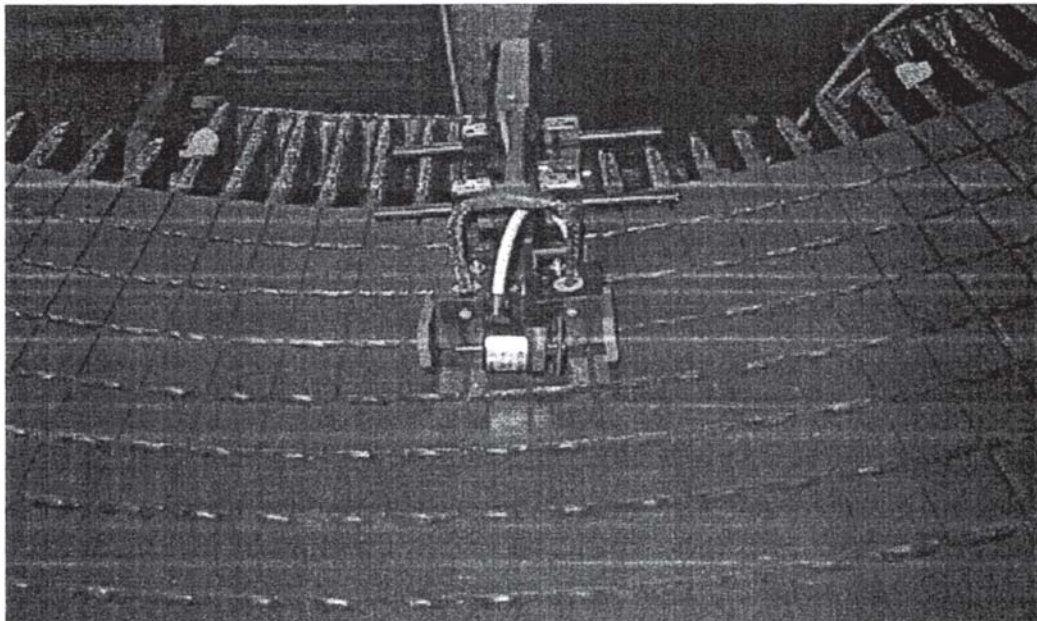
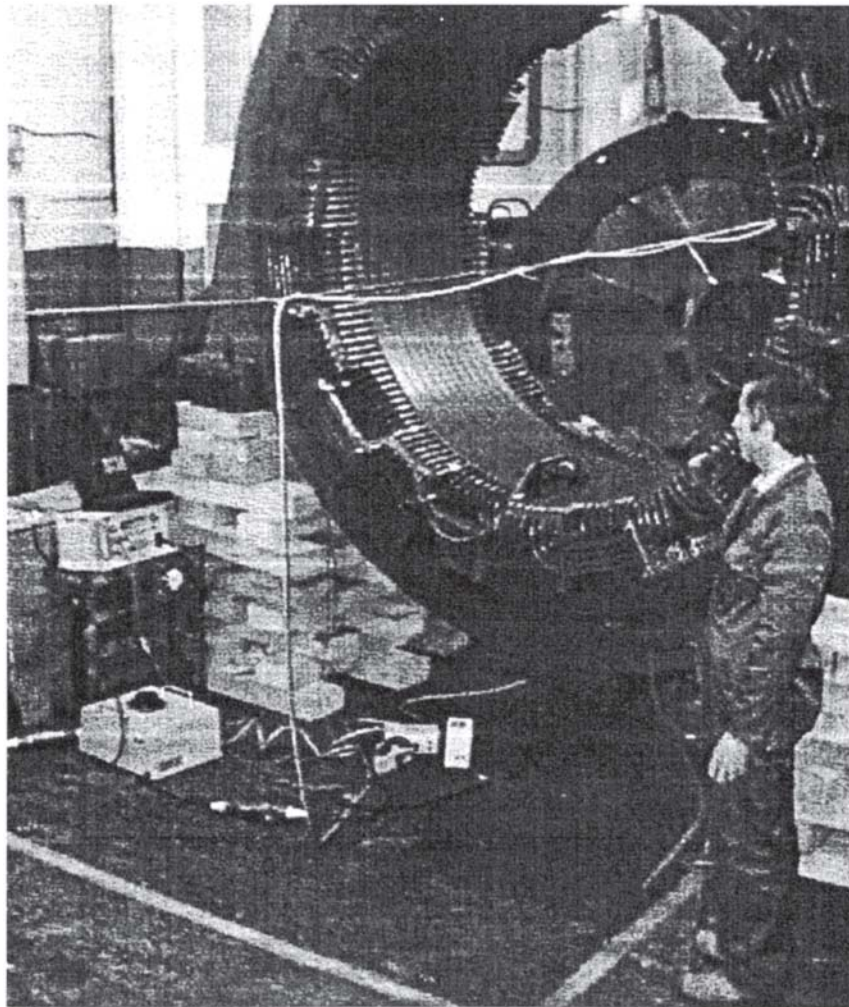


Figure 14.31 Manual scanning of slots using a magnetically attached guided trolley carrying the Chattock sensor.



**Figure 14.32** EL CID test in progress on 6.6-kV, 3000-hp motor.

EL CID technology) enable the same tests to be performed on smaller machines without the automatic test result recording facilities [49]. However, manual records of significant fault parameters may be made from the instrument display indicators.

In a fault-free uniformly constructed generator, a slot QUAD trace (or QUAD indication on an MCT) will theoretically be a straight line along the zero axis and the PHASE trace will be a line corresponding to the level of excitation. However, in practice a number of effects may give rise to offsets and perturbations in the QUAD trace, and faults will normally be indicated by deviations from a mean level. At the standard excitation level of 4%, a threshold of 100 mA fault signal is normally taken as a level above which more detailed examination is required. Although correlation with thermal tests will be dependent on a number of factors, this threshold level has been shown to correspond to approximately a 5°–10° C rise in temperature. The correlation for a number of different faults is given in [45] and [46].

#### 14.6.5.3 Fault Interpretation

The Chattock potentiometer test coil senses both the amplitude and polarity of magnetic potentials around the core. Therefore, the position of any fault relative to the ends of the coil, including whether the fault is within the span of the coil, will affect the signal produced. Fault interpretation also makes use of adjacent slot trace information and a guide to recognition of common faults and locations is provided in [44, 48], which also covers the possibility of improved detection of faults deeper in the core body by means of scanning across multiple slots. Polarity of the magnetic potential difference sensed by the Chattock potentiometer may be used to determine whether the source of the signal is within the span of the coil.

The low voltages used in EL CID testing permit an operator to enter the excited core to perform local tests with small hand-held coils to obtain precise location of faults detected in the global scan. [Figure 14.33](#) shows a traditional guide to fault location using this principle. [Figure 14.34](#) shows an actual test

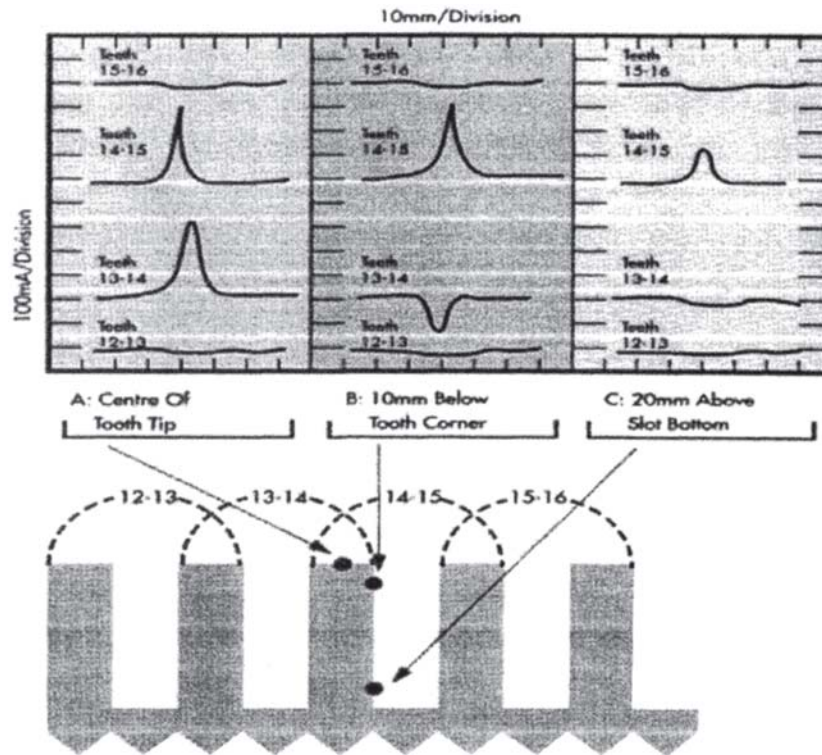


Figure 14.33 Fault signal interpretation.

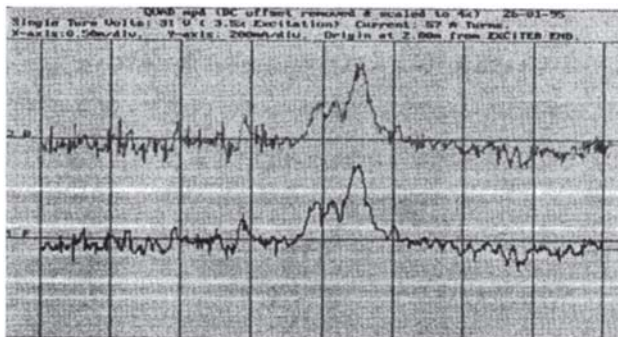


Figure 14.34 Tooth surface fault within two slot scans.

typical response for a fault on the surface of a tooth within the span of two adjacent slot scans.

## REFERENCES

Note: In the following listing, the abbreviations have the following meanings:

ANSI American National Standards Institute  
 EASA Electrical Apparatus Service Association  
 IEEE Institute of Electrical and Electronics Engineers  
 ISO International Organization for Standardization  
 NEMA National Electrical Manufacturers Association  
 Sources for standards are listed in [Appendix B](#).

1. The Torrington Company Service Catalog, Form No. 100–292–75M, 4th printing, The Torrington Company, Torrington CT, p. E58.
2. SKF General Catalog, Catalog 400 US Reg. 47.50 000. 1991–01 SKF Group, King of Prussia PA, pp. 114–121.
3. “Duplex Bearings and Preloading,” The Torrington Company Service Catalog, Form No. 100–292–75M, 4th printing, The Torrington Company, Torrington CT, pp. E59–60.
4. The Torrington Company Lubrication Guide, Form No. 640–15M193, 2d printing, The Torrington Company, Torrington CT. 0000.
5. Beebe, Theodore J., “Industrial Electric Motors,” *CRC Handbook of Lubrication (Theory and Practice of Tribology)*, vol. I, *Application and Maintenance*, E.Richard Booser, Editor, CRC Press, Inc., Boca Raton FL, 0000, p. 181.
6. Cheng, Herbert S., “Elastohydrodynamic Lubrication,” *CRC Handbook of Lubrication (Theory and Practice of Tribology)*, Vol. II, *Theory and Design*, E.Richard Booser, Editor, CRC Press, Inc., Boca Raton FL, 0000, p. 140.
7. Bibliography of Bearing Failure Analysis Publications:  
 Tallian, T.E., G.H.Baile, H.Dalal, and O.G.Gustafsson, *Rolling Bearing Damage—A Morphological Atlas*, SKF Industries, King of Prussia PA, 1974.  
*How to Recognize and Prevent Tapered Roller Bearing Damage*, 5M-04–88 Order No. 5011, The Timken Company, Canton OH, 1987.  
*Bearing Failure Prevention Guide*, Form No. 639–25M-693, 3d printing. The Torrington Company, Torrington CT.  
*Bearing Failures and Their Causes*, 30M.2.3.3 CI, Reg. No. 770, 148–110, SKF Industries, Inc., King of Prussia PA, Feb. 1983.  
 Tallian, T.E., *Failure Atlas for Hertz Contact Machine Elements*, American Society of Mechanical Engineers, New York, 1992.
8. ISO 2372, Mechanical Vibration of Machines with Operating Speeds from 10 to 200 rev/s. (Basic for specifying evaluation standards.)

9. ISO 2373, Mechanical Vibration of Certain Rotating Electrical Machines with Shaft Heights Between 80 and 400 mm. (Measurement and evaluation of vibration severity.)
  10. ISO 3945, Mechanical Vibration of Large Rotating Machines with Speed Range from 10 to 200 rev/s. (Measurement and evaluation of vibration severity *in situ*.)
  11. ISO/DIS 7919/1, Mechanical Vibration of Nonreciprocating Machines. (Measurements on rotating shafts and evaluation of results.)
  12. Hamer, P.S., "Acceptance Testing of Electric Motors and Generators," *IEEE Transactions on Industry Applications*, vol. IA-24, no. 6, 1988, pp. 1138–1152.
  13. NEMA RP 1–1981 (R1987), Renewal Parts for Motors and Generators (Performance, Selection, and Maintenance). (Withdrawn.)
  14. Smeaton, R.W., *Motor Application and Maintenance Handbook*, 2d edn., McGraw-Hill, New York, 1987, p. 17–7.
  15. Thomson, W.T., S.J.Chalmers, and D.Rankin, "An On-Line Computer-Based Current Monitoring System for Rotor Fault Diagnosis in Three-Phase Induction Motors," *Turbomachinery International (UK)*, Nov./Dec. 1987, pp. 17–24.
  16. Gill, A.S., *Electrical Equipment Testing and Maintenance*, Reston (Prentice-Hall), Reston VA, 1982, pp. 398–404.
  17. ANSI/IEEE Std. 432–1992, IEEE Guide for Insulation Maintenance for Rotating Electrical Machinery.
  18. Traister, J.E., "Insulation Cleaning and Drying," *Handbook of Polyphase Electric Motors*, Prentice-Hall, Englewood Cliffs NJ, 1988, pp. 175–184.
  19. Nailen, R.L., *Managing Motors*, Barks Publications, Chicago IL, 1991, pp. 5–22–5-28.
  20. ANSI/IEEE Std. 43–1974 (Reaffirmed 1991), IEEE Recommended Practice for Testing Insulation Resistance of Rotating Machinery.
  21. Schump, D.E., "Reliability Testing of Electric Motors," *IEEE Transactions on Industry Applications*, vol. IA-25, no. 3, 1989, pp. 386–390.
  22. IEEE Std. 522–1992, IEEE Guide for Testing Turn-to-Turn Insulation on Form-Wound Stator Coils for Alternating-Current Rotating Electric Machines.
  23. ANSI/IEEE Std. 95–1977 (Reaffirmed 1991), IEEE Recommended Practice for Insulation Testing of Large AC Rotating Machinery with High Direct Voltage.
  24. Bonnett, A.H., "Analysis of Winding Failures in Three-Phase Squirrel Cage Induction Motors," *IEEE Transactions on Industry Applications*, vol. IA-14, no. 3, 1978, pp. 223–226.
  25. O'Donnell, P., R.N.Bell, D.W.McWilliams, C.Singh, and S.J. Wells, "Report of Large Motor Reliability Survey of Industrial and Commercial Installations, Parts I and II," *IEEE Transactions on Industry Applications*, vol. IA-21, no. 4, 1985, pp. 853–872.
  26. Dakin, T.W., "Electric Machine Insulation," *Handbook of Electric Motors*, S.A. Nasar, Editor, McGraw-Hill, New York, 1987, pp. 13–1–13–15.
  27. Nailen, R.L., "A User's View of Motor Repair Standards and Specifications," *IEEE Transactions on Industry Applications*, vol. IA-24, no. 6, 1988, pp. 1131–1137.
  28. Bilanin, W.J., "Guidelines for the Repair of Nuclear Power Plant Safety-Related Motors (NCIG-12)," NP-6407, Electric Power Research Institute, Palo Alto CA, 1990.
  29. IEEE Std. 1068–1996, IEEE Recommended Practice for Repair and Rewinding of Motors for the Petroleum and Chemical Industry.
  30. Lammers, D.M., *Vaughen's Electric Motor Price Guide*, Vaughen's Price Publishing Company, Pittsburgh PA. (Issued annually.)
  31. Zeller, E., F.S. Stephens, and D.L. Gebhart, "Core Iron Study by EASA Core Testing Committee," Electrical Apparatus Service Association, St. Louis. MO., 1983, 14 pages.
  32. Montgomery, D.C., "The Motor Rewind Issue—A New Look," *IEEE Transactions on Industry Applications*, vol. IA-20, no. 5, 1984, pp. 1330–1336.
  33. NEMA Standard Publication MG 1–1998, Motors and Generators.
  34. ANSI/IEEE Std. 112–1996, IEEE Standard Test Procedure for Polyphase Induction Motors and Generators.
  35. ANSI/IEEE Std. 113–1985, IEEE Guide on Test Procedures for DC Machines. (Withdrawn.)
  36. IEEE Std. 114–1982, IEEE Standard Test Procedure for SinglePhase Induction Motors. (Withdrawn.)
  37. ANSI/IEEE Std. 115–1995, IEEE Test Procedures for Synchronous Machines.
  38. Stevenson, J.E., "Repairability of Energy-Efficient Motors," *IEEE Transactions on Industry Applications*, vol. IA-20, no. 2, 1984, pp. 364–366.
  39. Bibliography of other references on motor maintenance and repair: Armintor, K., R.W.Mills, and W.G.Stiffler, "Repair, Restoration, and Revitalization of Large Induction Motors," *IEEE Transactions on Industry Applications*, vol. IA-17, no. 6, 1981, pp. 581–586. (This reference contains a useful motor failure troubleshooting chart.)
- Bonnett, A.H., and G.C.Soukop, "Rotor Failures in Squirrel Cage Induction Motors," *IEEE Transactions on Industry Applications*, vol. IA-22, no. 6, 1986, pp. 1165–1173. (This reference discusses causes of failures.)
- ANSI/IEEE Std. 4–1978, IEEE Standard Techniques for High Voltage Testing.
- ANSI/EASA Std. AR100–1998, Recommended Practice for the Repair of Rotating Electrical Apparatus.
- Jenkins, J.E., Sr., "How to Perform Electrical Maintenance on Induction Motors," *Currents*, vol. 24, no. 7, 1990, Electrical Apparatus Service Association, St. Louis, MO.
- NEMA Standards Publication MG 2–1989, Safety Standard for Construction and Guide for Selection, Installation, and Use of Electric Motor and Generators.
- Soukop, G.C., "Determination of Motor Quality Through Routine Electrical Tests," *IEEE Transactions on Industry Applications*, vol. IA-25, no. 5, 1989, pp. 873–880. (This reference suggests user acceptance tests on new motors from 100 to 3000 hp.)
- Bonnett, A.H., and G.C.Soukop, "Cause and Analysis of Stator and Rotor Failures in Three-Phase Squirrel-Cage Induction Motors," *IEEE Transactions on Industry Applications*, vol. 28, no. 4, 1992, pp. 921–937.
- Thomson, W.T., and Mark Fenger, "Current Signature Analysis to Detect Induction Motor Faults," *IEEE Industry Applications Magazine*, vol. 7, no. 4, 2001, pp. 26–34.
- NFPA 70-B, "Recommended Practice for Electrical Equipment Maintenance," National Fire Protection Association, (173 pp., 1998).
- Krause, P.C., and O.Wasynczuk, *Analysis of Electric Machinery*, 2<sup>nd</sup> Ed, Purdue University, 2001.
- IEEE Std. 841–2001, IEEE Standard for the Petroleum and Chemical Industry-Severe Duty Totally Enclosed Fan-Cooled (TEFC) Squirrel Cage Induction Motors-Up to and Including 500 hp.
- Nailen, R.L., "Making the Right Choices When Buying Equipment and Services," *Electrical Apparatus*, vol. 53, no. 8, 2000, pp. 31–33.
- Nailen, R.L., "What burnoff temperature is right?" *Electrical Apparatus*, vol. 51, no. 12, 1998, pp. 39–40.
- Nailen, R.L. "Are the New Motor Maintenance Tests Really That Great?" *Electrical Apparatus*, Part 1, vol. 52, no. 12, 1999, pp. 29–33, Part 2, vol. 53, no. 1, 2000, pp. 31–35.
- Trutt, F.C., J.Sottile, and J.L.Kohler, "Detection of AC Machine Winding Deterioration Using Electrically Excited Vibrations," *IEEE Transactions on Industry Applications* vol. 37., no. 1, 2001, pp. 10–13.



- Andreas, John C., *Energy-Efficient Electric Motors*, Marcel Dekker, NYC, 1992.
40. *Westinghouse Electrical Maintenance Hints*, 2d printing, Westinghouse Electric Corporation, Trafford PA 15085, 1974, pp. 19–25.
  41. ANSI/IEEE Std. 56–1977 (Reaffirmed 1991), IEEE Guide for Insulation Maintenance of Large AC Rotating Machinery (10,000 kVA and Larger).
  42. EA Staff, “What current variation indicates a bad rotor?” *Electrical Apparatus*, vol. 54, no. 9, 2001, p. 6.
  43. Thorsen, O.V., and M.Dalva, “A Survey of Faults on Induction Motors in Offshore Oil Industry, Petrochemical Industry, Gas Terminals, and Oil Refineries,” *IEEE Transactions in Industry Applications*, vol. 31, no. 5, 1995, pp. 1186–1196.
  - Nyberg, C., “Internet Provides Access to World of Knowledge; Use Online Technology to Find Answers, Information,” *Currents*, vol. 34, no. 10, 2000, Electrical Apparatus Service Association, St. Louis, MO.
  - Campbell, B.H., “Failed Motors: Rewind or Replace?” *IEEE Industry Applications Magazine*, vol. 3, no. 1, 1997, pp. 45–50.
  - EPRI TR-103585, “Guidelines for the Selection, Procurement, and Acceptance of Nuclear Safety-Related Mild Environment Motor Insulation for Rewinds,” Electric Power Research Institute, Charlotte, NC, 1994.
  44. J.Sutton “History of EL CID and Fundamentals” EPRI Motor & Generator Predictive Maintenance & Refurbishment Conference November 1995.
  45. J.W.Shelton & B.M.Reichman “A comparative analysis of turbo-generator core inspection techniques”. 47<sup>th</sup> Annual Meeting of the American Power Conference April 1985.
  46. D.Paley, B.McNamara & G.Mottershead “Verification of the effectiveness of EL CID on a hydrogenerator stator core” Hydrovision Conference July 1998.
  47. A.P.Chattock “On a magnetic potentiometer” *Phil. Mag.*, 24 1887.
  48. G.K.Ridley “Hydrogenerator stator core condition monitoring by EL CID” EPRI Motor & Generator Predictive Maintenance & Refurbishment Conference November 1995.
  49. D.Bertenshaw “Improvements in Testing Stator Core Condition of Medium to Large Motors” CWIEME Conference, Berlin, July 2000.

# 15

## Electronic Motors

Thomas A.Lipo and Karel Jezernik (*Section 15.1*)/T.J.E.Miller (*Section 15.2*)/Edward J.Woods (*Section 5.3*)

<b>15.1 ALTERNATING CURRENT MOTOR SPEED CONTROL</b>	<b>732</b>
15.1.1 Introduction	732
15.1.2 Thyristor-Based Voltage-Controlled Drives	733
15.1.3 Thyristor-Based Load-Commutated Inverter Synchronous Motor Drives	736
15.1.4 Transistor-Based Variable-Frequency Induction Motor Drives	740
15.1.5 Field Orientation	746
15.1.6 Induction Motor Observer	752
15.1.7 Permanent Magnet Alternating Current Machine Control	754
<b>15.2 SWITCHED-RELUCTANCE MACHINES</b>	<b>759</b>
15.2.1 Definition, History, and Properties	759
15.2.2 Theory of Operation	760
15.2.3 Controller Architecture	763
15.2.4 Applications	763
<b>15.3 BRUSHLESS DC MOTORS</b>	<b>763</b>
15.3.1 Introduction	763
15.3.2 Rotor Construction	764
15.3.3 Magnets and the Magnetic Circuit	765
15.3.4 Armature Windings	768
15.3.5 Torque Analysis	769
15.3.6 Voltage Analysis	770
15.3.7 Equivalent Circuit	770
15.3.8 Motor Drive Circuit	770
15.3.9 Performance	771
<b>REFERENCES</b>	<b>772</b>

## 15.1 ALTERNATING CURRENT MOTOR SPEED CONTROL

### 15.1.1 Introduction

An important factor in industrial progress during the past five decades has been the increasing sophistication of factory automation that has improved productivity many-fold. Manufacturing lines typically involve a variety of variable speed motor drives that serve to power conveyor belts, robot arms, overhead cranes, steel process lines, paper mills, and plastic and fiber processing lines to name only a few. Prior to the 1950s all such applications required the use of a direct current (dc) motor drive because alternating current (ac) motors were not capable of smoothly varying speed because they inherently operated synchronously or nearly synchronously with the frequency of electrical input. To a large extent, these applications are now serviced by what can be called general-purpose ac drives. In general, such ac drives often feature a cost advantage over their dc counterparts and, in addition, offer lower maintenance, smaller motor size, and improved reliability. However, the control flexibility available with these drives is limited and their application is mainly restricted to fan, pump, and compressor types of applications where the speed need be regulated only roughly and where transient response and low-speed performance are not critical.

More demanding drives used in machine tools, spindles, high-speed elevators, dynamometers, mine winders, rolling mills, glass float lines, and the like have much more sophisticated requirements and must afford the flexibility to allow for regulation of a number of variables, such as speed, position, acceleration, and torque. Such high-performance applications typically require a high-speed holding accuracy better than 0.25%, a wide speed range of at least 20:1, and fast transient response, typically better than 50 rad/sec, for the speed loop. Until recently, such drives were almost exclusively the

domain of dc motors combined with various configurations of ac-to-dc converters depending on the application. With suitable control, however, induction motor drives have been shown to be more than a match for dc drives in high-performance applications. While control of the induction machine is considerably more complicated than its dc motor counterpart, with continual advancement of microelectronics, these control complexities have essentially been overcome. Although induction motors drives have already overtaken dc drives during the next decade it is still too early to determine if dc drives will eventually be relegated to the history book. However, the future decade will surely witness a continued increase in the use of ac motor drives for all variable speed applications.

AC motor drives can be broadly categorized into two types, thyristor-based and transistor-based drives. Thyristors possess the capability of self-turn-off by means of an associated gate signal but must rely on circuit conditions to turn off whereas transistor devices are capable of both turn on and turn off. Because of their turn-off limitations, thyristor-based drives must utilize an alternating electromotive force (emf) to provide switching of the devices (commutation) which requires reactive volt-amperes from the emf source to accomplish.

A brief list of the available drive types is given in Fig. 15.1. The drives are categorized according to switching nature (natural or force commutated), converter type, and motor type. Naturally commutated devices require external voltage across the power terminals (anode-cathode) to accomplish turn off of the switch whereas a force commutated device uses a low-power gate or base voltage signal that initiates a turn-off mechanism in the switch itself. In this figure the category of transistor based drives is intended to also include other hard switched turn-off devices such as gate turn-offs (GTOs), MOS Controlled Thyristors (MCTs), and insulated gate bipolar transistor (IGBTs) that are, in reality, avalanche turn-on (four-layer) devices.

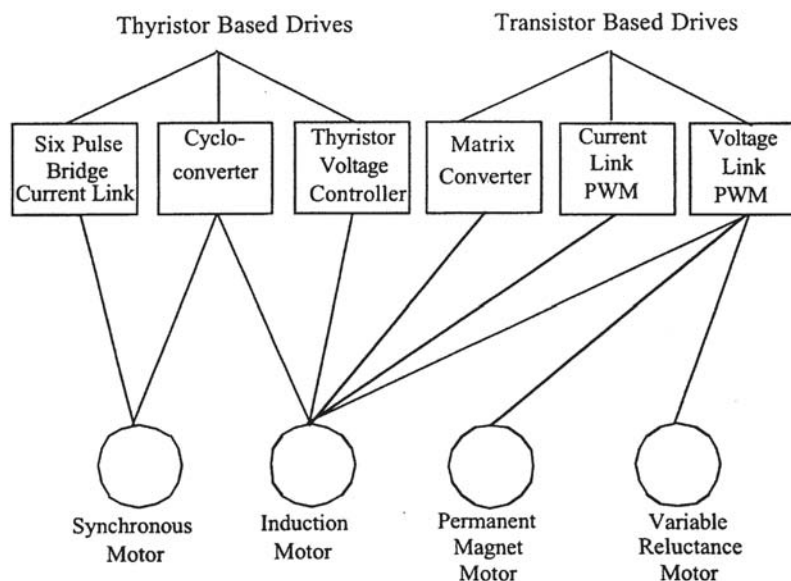
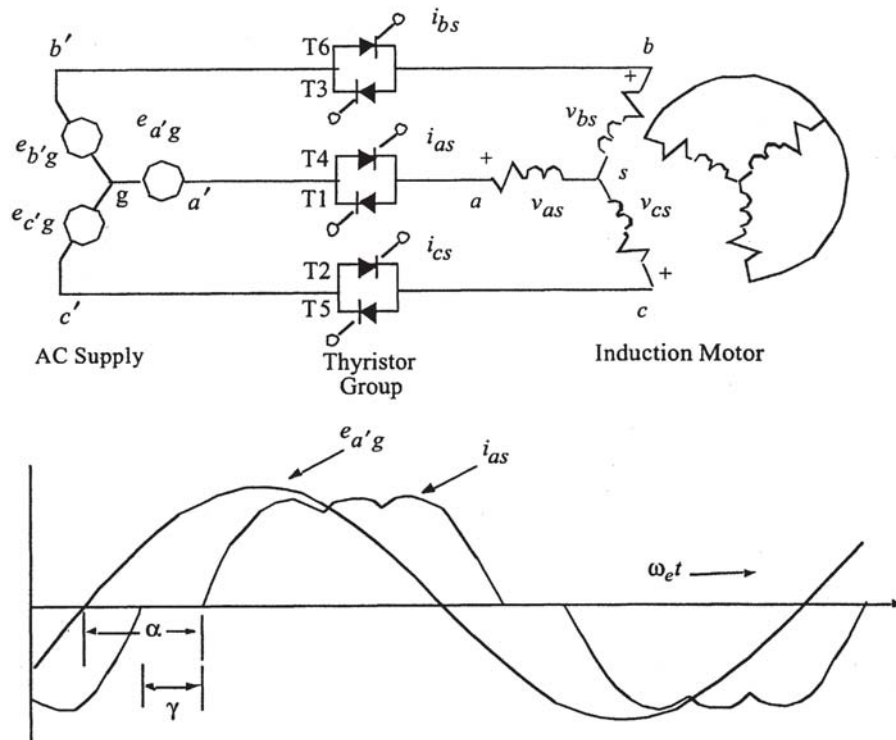


Figure 15.1 Major drive type categories.



**Figure 15.2** Induction motor voltage controller using inverse-parallel thyristors and typical current waveform.

The numerous drive types associated with each category is clearly extensive and cannot be treated in complete detail here. However, the speed control of the four major drive types having differing control principles will be considered, namely: (1) voltage-controlled induction motor drives, (2) load commutated synchronous motor drives, (3) volts per hertz and vector-controlled induction motor drives, and (4) vectorcontrolled permanent magnet motor drives. The control principles of the remaining drives of Fig. 15.1 are generally straightforward variations of one of these four drive types.

### 15.1.2 Thyristor-Based Voltage-Controlled Drives

#### 15.1.2.1 Introduction

During the middle of the last century, limitations in solid-state switch technology hindered the performance of variable

frequency drives. In what was essentially a stop-gap measure, variable speed was frequently obtained by simply varying the voltage to an induction motor while keeping the frequency constant. The switching elements used were generally back-to-back connected thyristors as shown in Fig. 15.2. These devices were exceptionally rugged compared to the fragile transistor devices of this era.

#### 15.1.2.2 Basic Principles of Voltage Control

The basic principles of voltage control can be obtained readily from the conventional induction motor equivalent circuit shown in Fig. 15.3 and the associated constant voltage speedtorque curves illustrated in Fig. 15.4. The torque produced by the machine is equal to the power transferred across the airgap divided by synchronous speed:

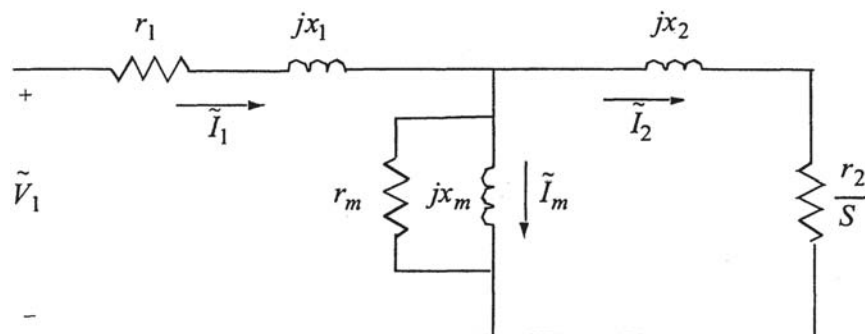


**Figure 15.3** Per-phase equivalent circuit of a squirrel-cage induction machine.

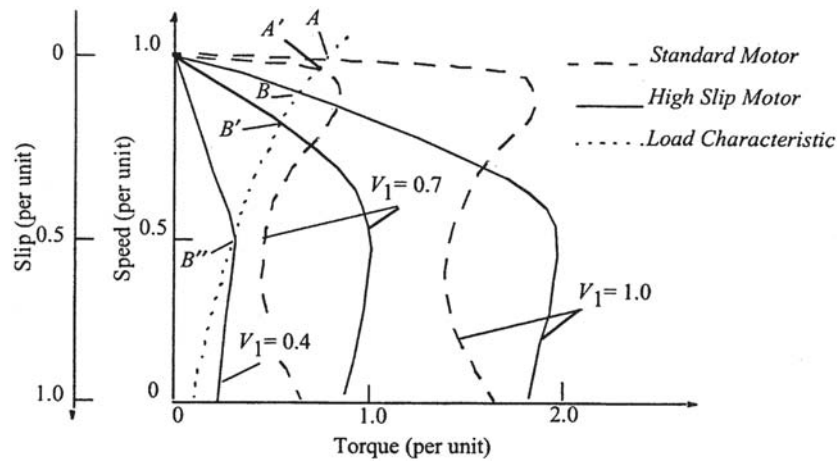


Figure 15.4 Torque vs. speed curves for standard and high slip induction machines.

$$T_e = \frac{3}{2} P \left( \frac{I_2^2 r_2}{S \omega_e} \right) \quad (15.1)$$

where  $P$ =number of poles,  $S$  is the per unit slip,  $\omega_e$  is line frequency and  $I_2$ ,  $r_2$  are the rotor rms current and rotor resistance respectively.

The peak torque points on the curves in Fig. 15.4 occur when maximum power is transferred across the airgap and are easily shown to take place at a slip:

$$S_{MaxT} \approx \frac{r_2}{x_1 + x_2} \quad (15.2)$$

where  $x_1$  and  $x_2$  are the stator and rotor leakage reactances. From these results and the equivalent circuit, the following principles of voltage control are evident:

1. For any fixed slip or speed, the current varies directly with voltage and the torque and power with voltage squared.
2. As a result of (1) the torque-speed curve for a reduced voltage maintains its shape exactly but has reduced torque at all speeds (see Fig. 15.4).
3. For a given load characteristic, a reduction in voltage will produce an increase in slip (from A to A' for the conventional machine in Fig. 15.4, for example).
4. A high-slip machine has relatively higher rotor resistance and results in a larger speed change for a given voltage reduction and load characteristic (compare A to A' with B to B' in Fig. 15.4).
5. At small values of torque, the slip is small and the major power loss is the core loss in  $r_m$ . Reducing the voltage will reduce the core loss at the expense of higher slip and increased rotor and stator  $Pr$  loss. Thus there is an optimal slip that maximizes the efficiency and varying the voltage can maintain high efficiency even at low torque loads.

### 15.1.2.3 Converter Model of Voltage Controller

It has been shown that a very accurate fundamental component model for a voltage converter comprised of inverse parallel thyristors (or Triacs) is a series reactance given by [1]:

$$x_{eq} = x'_s f(\gamma) \quad (15.3)$$

where  $x'_s = x_1 + x_2 x_m / (x_2 + x_m)$  and  $x_1$ ,  $x_2$ ,  $x_m$  are the induction motor stator leakage, rotor leakage, and magnetizing reactances respectively and  $\gamma$  is the thyristor *hold-off angle* identified in Fig. 15.2 and:

$$f(\gamma) = \left( \frac{3}{\pi} \right) \frac{(\gamma + \sin\gamma)}{1 - \frac{3}{\pi}(\gamma + \sin\gamma)} \quad (15.4)$$

This reactance can be added in series with the motor equivalent circuit to model a voltage-controlled system. For typical machines the accuracy is well within acceptable limits although the approximation is better in larger machines and for smaller values of  $\gamma$ . In most cases of interest, the error is quite small. However, the harmonic power losses and torque ripple produced by the current harmonics implied in Fig. 15.2 are entirely neglected. A plot of typical torque vs. speed characteristics as a function of  $\gamma$  is shown in Fig. 15.5 for a 0.4-horsepower (hp) squirrel-cage induction machine [2].

### 15.1.2.4 Speed Control of Voltage-Controlled Drive

Variable-voltage speed controllers must contend with the problem of greatly increased slip losses at speeds far from synchronous and the resulting low efficiency. In addition, only speeds below synchronous speed are attainable and speed stability may be a problem unless some form of feedback is used.

An appreciation of the efficiency and motor heating problem is available from Eq. 15.1 rewritten to focus on the rotor  $I^2 r$  loss:

$$3I_2^2 r_2 = SP_{gap} = S \frac{2}{P} \omega_e T_e \quad (15.5)$$

Thus the rotor copper loss is proportional not only to the torque but also to the slip (deviation from synchronous speed). The inherent problem of slip variation for speed control is clearly indicated.

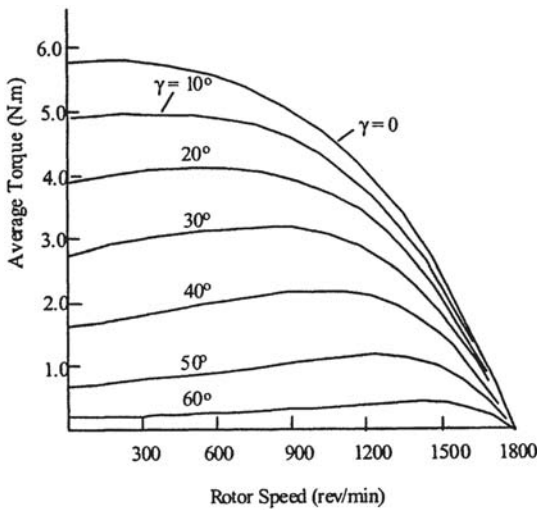


Figure 15.5 Torque speed curves for changes in hold off angle  $\gamma$ .

As a result of the large rotor losses to be expected at high slip, voltage control is only applicable to loads in which the torque drops off rapidly as the speed is reduced. The most important practical case is fan speed control in which the torque required varies as the speed squared. For this case, equating the motor torque to the load torque results in:

$$\frac{3}{2} P \frac{I_2^2 r_2}{S \omega_e} = K_L \omega_e (1 - S)^2 \tag{15.6}$$

Solving for  $I_2^2$  as a function of S and differentiating yields the result that the maximum value of  $I_2^2$  (and hence of rotor loss) occurs at:

$$S = 1/3 \tag{15.7}$$

or at a speed of two-thirds of synchronous speed. If this worst case value is substituted back to find the maximum required

value of  $I_2^2$  and the result used to relate the maximum rotor loss to the rotor loss at rated slip, the result is:

$$\frac{\text{Maximum rotor } I^2 r \text{ loss}}{\text{Rated rotor } I^2 r \text{ loss}} = \frac{(4/27)}{S_{Rated}(1 - S_{Rated})} \tag{15.8}$$

where  $S_{Rated}$  equals rated slip. Figure 15.6 illustrates this result and from this curve it is clear that to avoid excessive rotor heating at reduced speed with a fan load, it is essential that the rated slip be in the range 0.25–0.35 to avoid overheating. While the use of such high-slip machines will avoid rotor overheating, it does not improve the efficiency. The low efficiency associated with high slip operation is inherent in all induction machines and the high-slip losses implies that these machine will generally be large and bulky.

As noted previously, speed stability is an inherent problem in voltage-controlled induction motor drives at low speeds. This is a result of the near coincidence of the motor torque characteristic and the load characteristic at low speed. The problem occurs primarily when the intersection of the motor torque characteristic and the load characteristic occurs near or below the speed of maximum motor torque (see point B in Fig. 15.5).

Reduced voltage operation of an induction machine will result in lower speed but this requires increased slip and the rotor  $I^2 r$  losses are accordingly increased. This type of high-slip drive is therefore limited in application to situations where the high losses and low efficiency are acceptable and, generally, where the speed range is not large. Such drives are today generally limited to relatively low power ratings because of cooling problems.

The voltage controller of Fig. 15.2, however, remains popular for motor starting applications. Motor starters are intended to provide a reduction in starting current. Inverse parallel thyristor starters reduce the current by the voltage ratio and the torque by the square of the ratio. Unlike autotransformer or reactance starters that have only one or two steps available, an inverse parallel thyristor starter can provide step-less and continuous

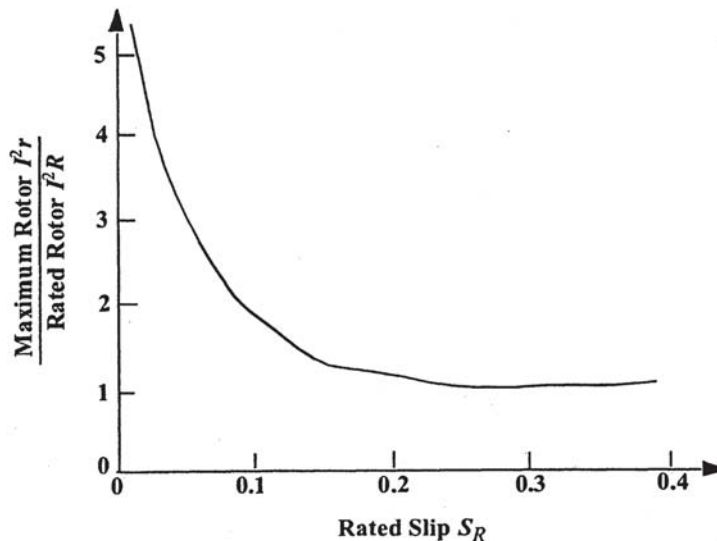


Figure 15.6 Worst case rotor heating for induction motor with a fan load.

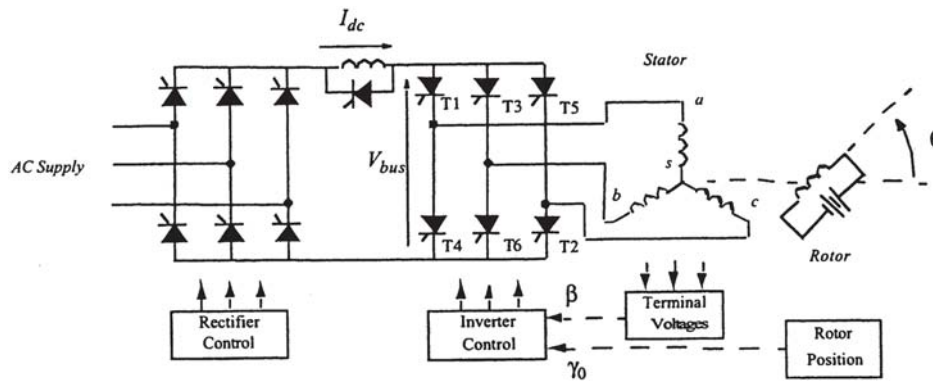


Figure 15.7 Load commutated inverter synchronous motor drive.

“reactance” control. These electronic starters are often fitted with feedback controllers that allow starting at a preset constant current, although simple timed starts are also available. Some electronic starters are equipped to short-out the inverse parallel thyristor at the end of the starting period to eliminate the losses caused by forward voltage drop during running. Other applications include “energy savers” that vary the voltage during variable-load running conditions to improve efficiency.

### 15.1.3 Thyristor-Based Load-Commutated Inverter Synchronous Motor Drives

The basic thyristor-based load-commutated inverter synchronous motor drive system is shown in Fig. 15.7. In this drive, two static converter bridges are connected on their dc side by means of a so-called dc link having only an inductor on the dc side. The line side converter ordinarily takes power from a constant frequency bus and produces a controlled dc voltage at its end of the dc link inductor. The dc link inductor effectively turns the line-side converter into a current source as seen by the machine side converter. Current flow in the line side converter is controlled by adjusting the firing angle of the bridge and by natural commutation of the ac line.

The machine-side converter normally operates in the inversion mode. Since the polarity of the machine voltage must be instantaneously positive as the current flows into the motor to commutate the bridge thyristors, the synchronous machine must operate at a sufficiently leading power factor to provide the volt-seconds necessary to overcome the internal reactance opposing the transfer of current from phase to phase (commutating reactance). Such load emf-dependent commutation is called *load commutation*. As a result of the action of the link inductor, such an inverter is frequently termed a *naturally commutated current source inverter*.

Figure 15.8 illustrates typical circuit operation. Inverter thyristors 1–6 fire in sequence, one every 60 electrical degrees of operation, and the motor currents form balanced three-phase quasi-rectangular waves. The electrical angles shown in Fig. 15.8 pertain to commutation from thyristor 1–3. The instant of commutation of this thyristor pair is defined by the *phase advance angle*  $\beta$  relative to the machine terminal voltage  $V_{ab}$ . Once thyristor 3 is switched on, the machine voltage  $V_{ab}$  forces current from phase  $a$  to phase  $b$ . The rate of rise of current in thyristor 3 is limited by

the commutating reactance, which is approximately equal to the subtransient reactance of the machine.

During the interval defined by the *commutation overlap angle*  $\mu$  the current in thyristor 3 rises to the dc link current  $I_{dc}$  while the current in thyristor 1 falls to zero. At this instant,  $V_{ab}$  appears as a negative voltage across thyristor 1 for a period defined as the *commutation margin angle*  $\Delta$ . The angle  $\Delta$  defines, in effect, the time available to the thyristor to recover its blocking ability before it must again support forward voltage. The corresponding time  $T_r = \Delta/\omega_e$  is called the *recovery time* of the thyristor. The phase advance angle  $\beta$  is equal to the sum of  $\mu$  plus  $\Delta$ . The angle  $\beta$  is defined with respect to the motor terminal voltage. In practice it is useful to define a different angle  $\gamma_0$ , measured with respect to the internal emf of the machine. This angle is called the *firing angle*. Because the internal emfs are simply equal to the time rate of change of the rotor flux linking the stator windings, the firing angle  $\gamma_0$  can be located physically as the instantaneous position of the salient poles of the machine, i.e., the  $d$ -axis of the machine relative to the magnetic axis of the outgoing phase that is undergoing commutation (in case phase  $a$ ). Hence, in general, the system is typically operated in a self-synchronous mode where the output shaft position (or a derived position-dependent signal) is used to determine the applied stator frequency and phase angle of current.

A fundamental component per-phase phasor diagram of Fig. 15.9 illustrates this requirement. In this figure the electrical angle  $\gamma$  is the equivalent of  $\gamma_0$  but corresponds to the phase displacement of the fundamental component of stator current with respect to the EMF. Spatially,  $\gamma$  corresponds to 90 degrees minus the angle between the stator and rotor magnetomotive forces (mmfs) and may be called the *mmf angle*. A large leading mmf angle  $\gamma$  is clearly necessary to obtain a leading terminal power factor angle  $\phi$ .

#### 15.1.3.1 Torque Production in a Load-Commutated Inverter Synchronous Motor Drive

The average torque developed by the machine is related to the power delivered to the internal emf  $E$ , and, from Fig. 15.9, can be written as:

$$T_e = \frac{3E I_s \cos \gamma}{\omega_{rm}} \quad (15.9)$$

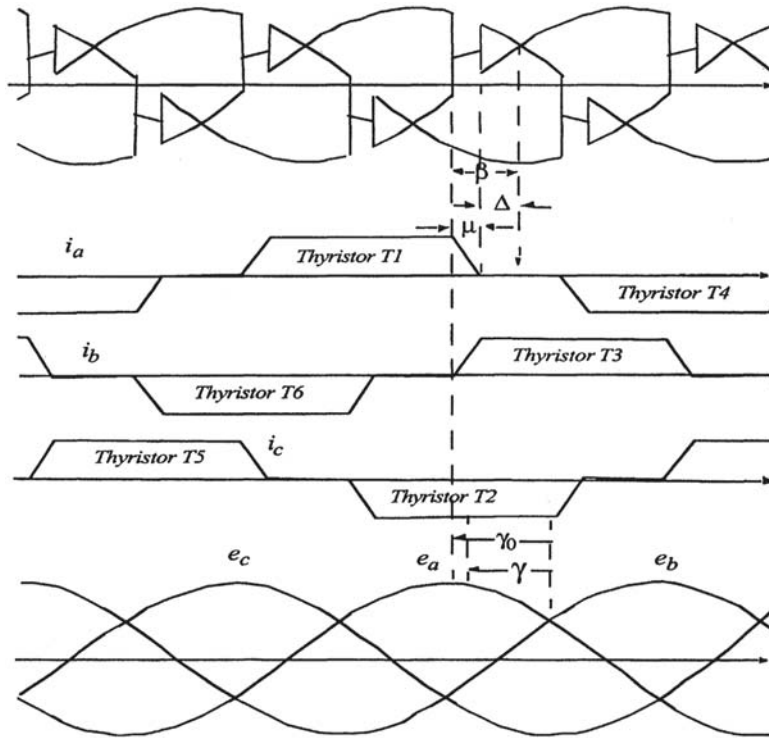


Figure 15.8 Load commutated synchronous motor waveforms and control variables.

where  $\omega_m$  is the mechanical speed (i.e.,  $\omega_m=2\omega_e/P$  for steady-state conditions). The angle  $\gamma$  is the electrical angle between the internal emf and the fundamental component of the corresponding phase current and is located in Fig. 15.8 for the  $c$  phase. It should be noted that this angle is very close to the angle  $\gamma_0$  that corresponds to a physical angle that can be set by means of a suitably located position sensor.

In general,  $E_i$  is speed-dependent:

$$E_i = \frac{P}{2} \omega_m \lambda_{af} \tag{15.10}$$

and the apparent speed dependence vanishes whereupon Eq. 15.9 takes the form:

$$T_e = \frac{3}{2} P \lambda_{af} I_s \cos \gamma \tag{15.11}$$

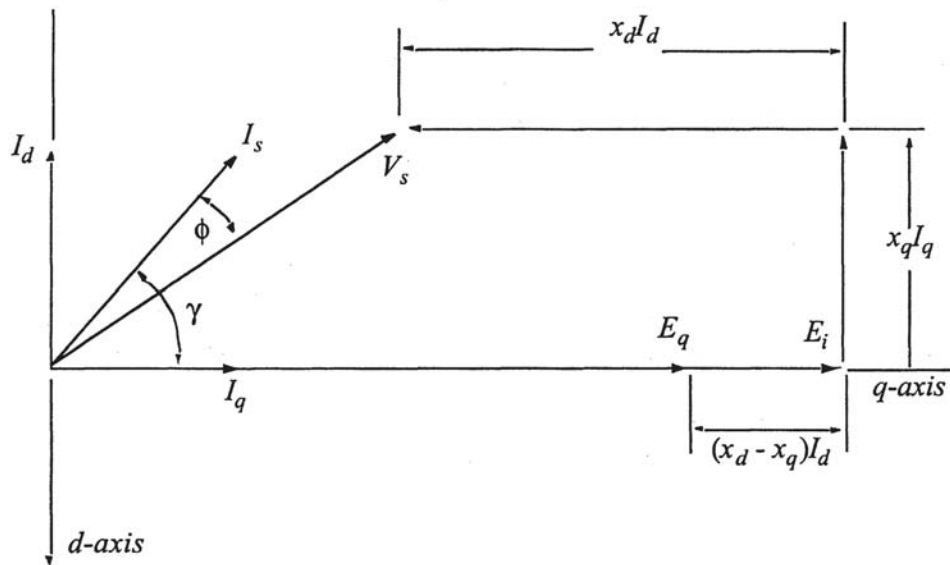


Figure 15.9 Phasor diagram for load-commutated inverter synchronous motor drive.



where  $\lambda_{af}$  is rms value of the field flux linking a stator phase winding. Thus, for a fixed value of the internal angle  $\gamma$ , the system behaves very much like a dc machine and its steady-state torque control principles are possible.

### 15.1.3.2 Torque Capability Curves

One useful measure of drive performance is a curve showing the maximum torque available over its entire speed range. A synchronous motor supplied from a variable-voltage, variable-frequency supply will exhibit a torque-speed characteristic similar to that of a dc shunt motor. If field excitation control is provided, operation above base speed in a field-weakened mode is possible and is used widely. The upper speed limit is dictated by the required commutation margin time of the inverter thyristors.

Figure 15.10 is a typical capability curve assuming operation at constant-rated dc link current, at rated (maximum) converter dc voltage above rated speed and with a commutation margin time  $\Delta/\omega_c$  of 26.5 ms corresponding to  $\Delta=12$  degrees at 50 Hz. At very low speeds, where the commutation time is of the order of the motor transient time constants, the machine resistances make up a significant part of the commutation impedance. The firing angle must subsequently be increased to provide sufficient volt-seconds for commutation as shown by the companion curves of Fig. 15.11. The resulting increase in internal power factor angle reduces the torque capability. At intermediate speeds the margin angle can be reduced to values less than 12 degrees to maintain 26.5-ms margin time and slightly greater than rated torque can be produced.

Above rated speed the inverter voltage is maintained con

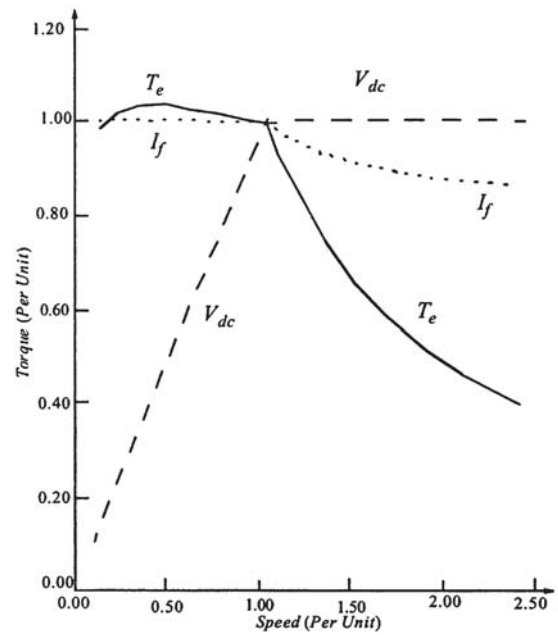


**Figure 15.10** Capability curve of a load-commutated inverter synchronous motor drive with constant dc link current and fixed commutation margin time, field weakening operation above one per unit. Speed assumes operation at constant dc link voltage.

stant and the drive, in effect, operates in the constant kilovoltampere mode. The dc inverter voltage reaches the maximum value allowed by the device ratings and the maximum output of the rectifier. Although Fig. 15.10 shows a weakening of the field in the high-speed condition, the

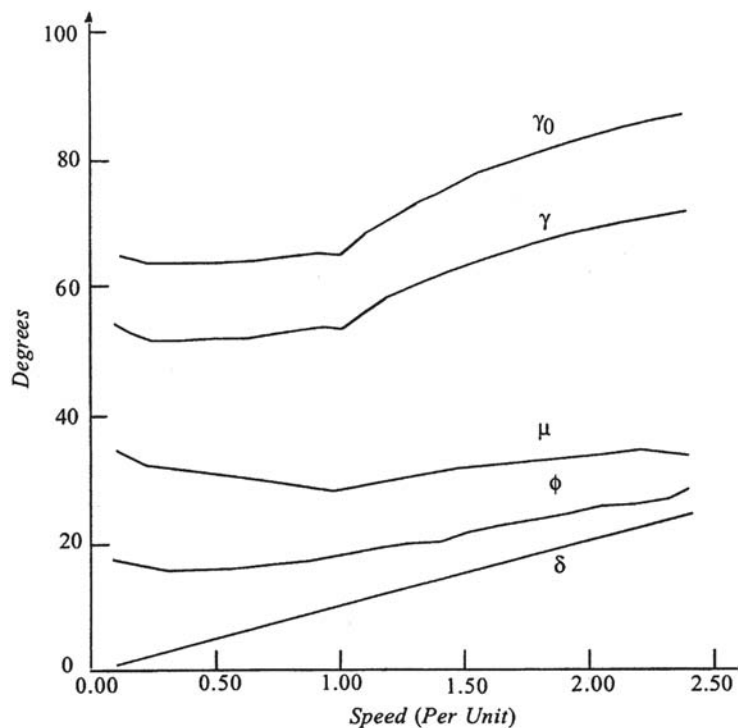


**Figure 15.11** Characteristic electrical control angles for load-commutated synchronous motor drive.

reduction is not as great as the inverse speed relationship required for constant horsepower operation. This again is a consequence of the constant commutation margin angle control. Because the margin angle increases with speed, i.e., frequency, to maintain the same margin time, the corresponding increase in power factor angle results in a greater demagnetizing component of stator mmf. This offsets partly the need to weaken the field in the highspeed region.

### 15.1.3.3 Constant Speed Performance

When the dc link current is limited to its rated value, the maximum torque can be obtained from the capability curve (Fig. 15.10). However, operation below maximum torque requires a reduction in the dc link current. When the field current is adjusted to keep the margin angle  $\Delta$  at its limiting value, the curves of Fig. 15.12 result. It can be noted that the torque is now essentially a linear function of dc link current so that the dc link current command becomes, in effect, the torque command.

### 15.1.3.4 Control Considerations

Direct control of  $\gamma_0$  by use of a rotor position sensor has traditionally been applied in load-commutated inverter drives but has largely been replaced by schemes using terminal voltage and current sensing to indirectly control  $\gamma$ . The basic principle is to use Eq. 15.11 as the control equation. If terminal voltage across the machine and the dc link current are

measured, then if  $\gamma$  is held constant the dc link current required for given torque is:

$$I_s = \frac{T_e \omega_{rm}}{3E_i \cos\gamma} \quad (15.12)$$

The dc link current that must be supplied can be determined from the current  $I_s$  by relating the fundamental component of a quasi-rectangular motor phase current (see Fig. 15.8) to its peak value  $I_{dc}$ . The result is, with reasonable approximation:

$$I_{dc} = \frac{\pi}{\sqrt{6}} I_s \quad (15.13)$$

The internal rms phase voltage  $E_i$  can be calculated by considering the reactive drop and is obtained from Fig. 15.9. Control is implemented such that the machine side converter is controlled to maintain either  $\gamma$  or  $\beta$  constant while the line-side converter is controlled to provide the correct dc link current to satisfy Eq. 15.12.

Direct control of the commutation margin angle  $\Delta$  (more correctly, the margin time  $\Delta/\omega_e$  where  $\omega_e$  is the motor angular frequency) has the advantage of causing operation at the highest possible power factor and hence gives the best utilization of the machine windings. The waveforms in Fig. 15.11 also demonstrate that changes in the commutation overlap angle  $\mu$  resulting from current or speed changes produce significant differences between the actual value of  $\gamma$  and the ideal value  $\gamma_0$ . For this reason, compensators are required in direct  $\gamma$  controllers. This compensation is automatic in systems based on controlling the margin angle  $\Delta$ .

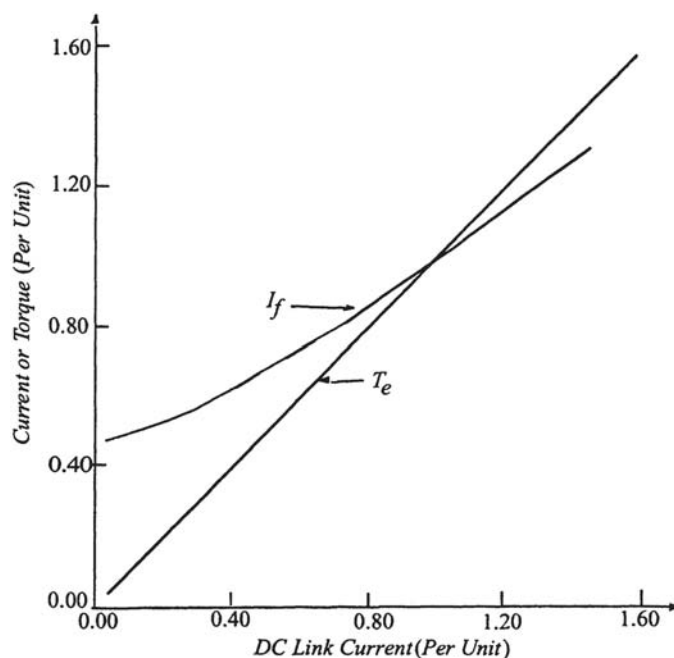


**Figure 15.12** DC field current required to produce a linear variation of torque with dc link current, operation at rated speed, margin angle  $\Delta=10$  degrees.

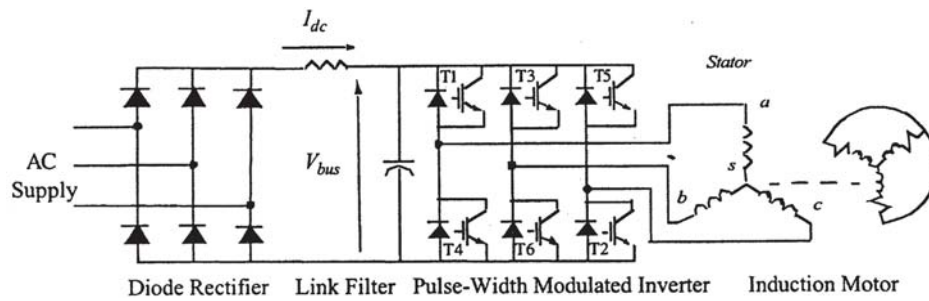


Figure 15.13 Basic circuit topology of pulse-width modulated inverter drive.

### 15.1.4 Transistor-Based Variable-Frequency Induction Motor Drives

#### 15.1.4.1 Introduction

Variable-frequency ac drives are now available from fractional kilowatts to very large sizes, e.g., to 15,000 kW for use in electric generating stations. In large sizes, naturally commutated converters are more common, usually driving synchronous motors. However, in low to medium sizes (up to approximately 750 kW) transistor-based pulse-width modulation (PWM) voltage source converters driving induction motors are almost exclusively used. Figure 15.13 illustrates the basic power circuit topology of the voltage source inverter. Only the main power-handling devices are shown; auxiliary circuitry such as snubbers or commutation elements are excluded.

The modern strategy for controlling the ac output of such a power electronic converters is the technique known as PWM, which varies the *duty cycle* (or *mark-space* ratio) of the converter switch(es) at a high switching frequency to achieve a target average low-frequency output voltage or current. In principle, all modulation schemes aim to create trains of switched pulses that have the same fundamental volt-second average (i.e., the integral of the waveform over time) as a target reference waveform at any instant. The major difficulty with these trains of switched pulses is that they also contain unwanted harmonic components which should be minimized.

Three main techniques for PWM exist. These alternatives are:

1. Switching at the intersection of a target reference waveform and a high frequency triangular carrier (*double-edged naturally sampled sine-triangle PWM*).

2. Switching at the intersection between a regularly sampled reference waveform and a high frequency triangular carrier (*double-edged regular sampled sine-triangle PWM*).
3. Switching so that the amplitude and phase of the target reference expressed as a vector is the same as the integrated area of the converter switched output over the carrier interval (*space vector PWM*).

Many variations of these three alternatives have been published, and it sometimes can be quite difficult to see their underlying commonality. For example, the space vector modulation strategy, which is often claimed to be a completely different approach to modulation, is really only a variation of regular sampled PWM, which specifies the same switched pulse widths but only places them a little differently in each carrier interval.

#### 15.1.4.2 Double-Edged Naturally Sampled Sine-Triangle PWM

The most common form of PWM is the naturally sampled method in which a sine wave command is compared with a high-frequency triangle as shown for one of three phases in Fig. 15.14. Intersections of the commanded sine wave and the triangle produce switching in the inverter as shown in Fig. 15.15. The triangle wave is common to all three phases. Figure 15.15(b) shows the modulation process in detail, expanded over a time interval of two subcycles,  $\Delta T/2$ . Note that because of switching action the potentials of all three phases are all equal making the three line to line voltages (and thus the motor phase voltages) zero. The width of these zero voltage

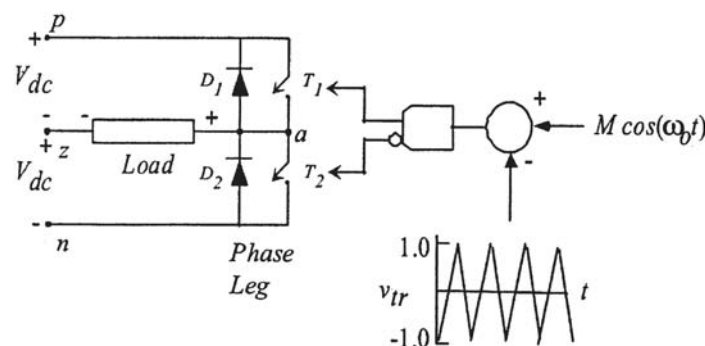
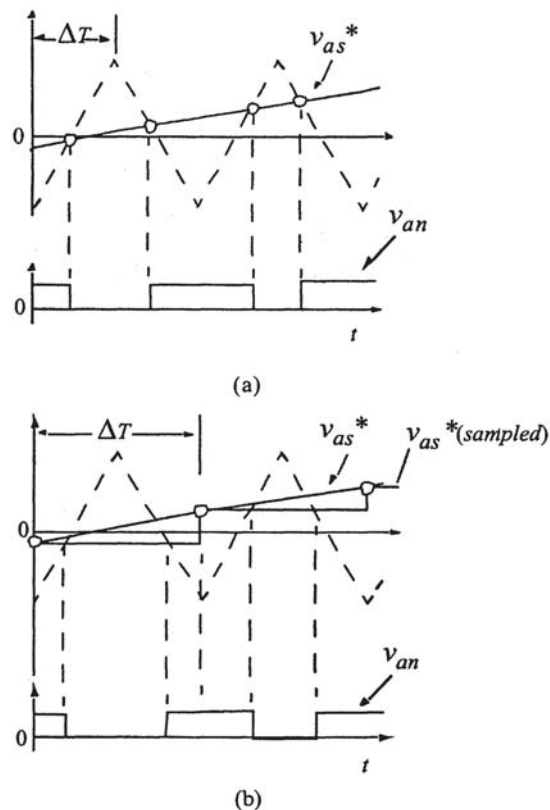


Figure 15.14 Control principle of naturally sampled pulse-width modulation (PWM) showing one of three phase legs.



**Figure 15.15** (a) Naturally sampled pulse-width modulation (PWM) and (b) symmetrically sampled PWM.

intervals essentially provides the means to vary the fundamental component of voltage when the frequency is adjusted so as to realize constant volts per hertz (nearly constant stator flux) operation. A close inspection of Fig. 15.14 indicates that this method does not fully utilize the available dc voltage because the sine wave command amplitude reaches the peak of the triangle wave only when the output line voltage is  $2/\pi$  or 0.785 of the maximum possible value of  $V_{bus}$ . This deficiency can be reduced by introducing a zero-sequence third harmonic component command into each of the controllers. With a third harmonic amplitude of 1/6 that of the sine wave command, the output can be shown to be increased to  $(\sqrt{3})/2$  or  $0.866V_{bus}$ . Additional zero sequence

harmonics can be introduced to further increase the output to  $(\sqrt{3}\pi)/6$  or  $0.907V_{bus}$ . Further increase in voltage can only be obtained by introducing a low-frequency odd harmonic into the output waveform.

#### 15.1.4.3 Double-Edged Regular Sampled Sine-Triangle PWM

One major limitation with naturally sampled PWM is the difficulty of its implementation in a digital modulation system, because the intersection between the reference sinusoid and the triangular or sawtooth carrier is defined by a transcendental equation and is complex to calculate. To overcome this limitation the modern alternative is to implement the modulation system using a regular sampled PWM strategy, where the low-frequency reference waveforms are sampled and then held constant during each carrier interval. These sampled values are then compared against the triangular carrier waveform to control the switching process of each phase leg, instead of the sinusoidally varying reference.

The sampled reference waveform must change value at either the positive or positive/negative peaks of the carrier waveform, depending on the sampling strategy. This change is required to avoid instantaneously changing the reference during the ramping period of the carrier, which may cause multiple switch transitions if it was allowed to occur. For a triangular carrier, sampling can be *symmetrical*, where the sampled reference is taken at either the positive or negative peak of the carrier and held constant for the entire carrier interval, or *asymmetrical*, where the reference is resampled every half carrier interval at both the positive and the negative carrier peak. The asymmetrical sampling is preferred because the update rate of the sampled waveform is doubled resulting in a doubling in the harmonic spectrum from the PWM process (Fig. 15.16). The phase delay in the sampled waveform can be corrected by phase advancing the reference waveform.

#### 15.1.4.4 Space Vector PWM

In the mid 1980s a form of PWM called space vector modulation (SVM) was proposed, which was claimed to offer significant advantages over natural and regular sampled PWM in terms of

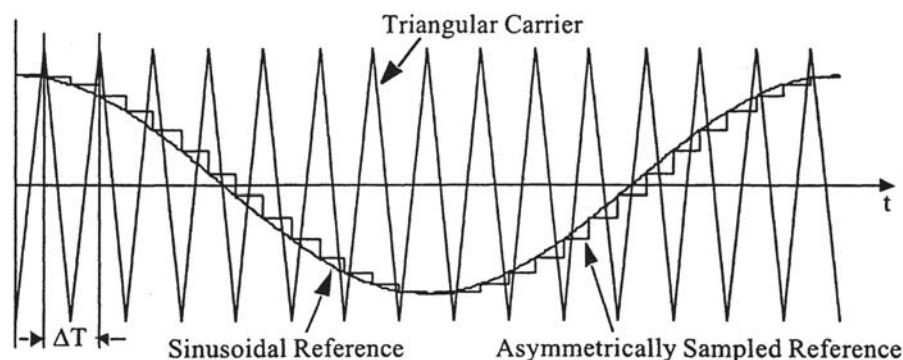


**Figure 15.16** Regular asymmetrically sampled pulse-width modulation (PWM).

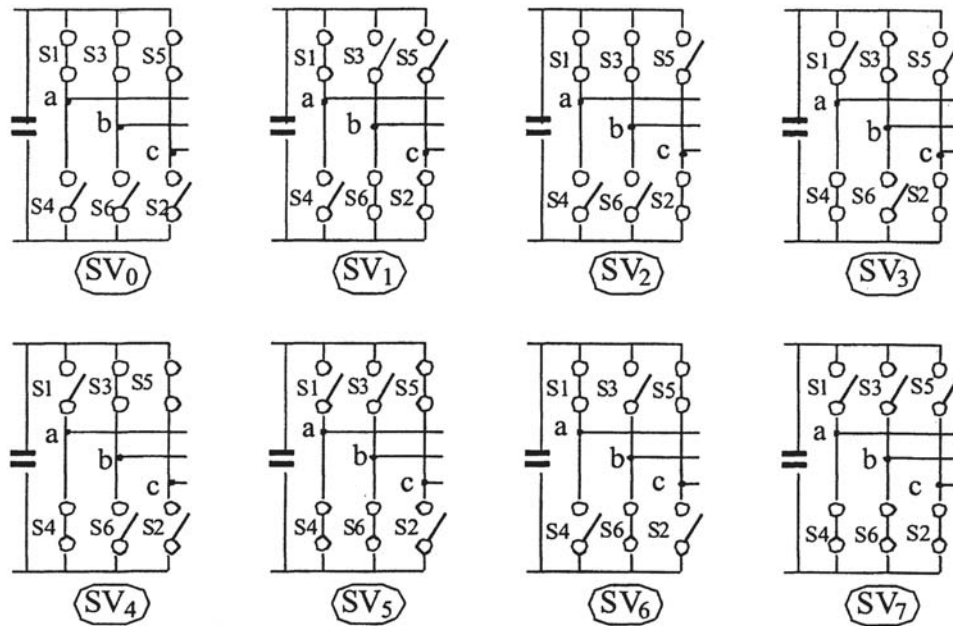


Figure 15.17 Eight possible phase leg switch combinations for a VSI.

performance, ease of implementation, and maximum transfer ratio [4, 5]. The principle of SVM is based on the fact that there are only eight possible switch combinations for a three-phase inverter. The basic inverter switch states are shown in Fig. 15.17. Two of these states (SV<sub>0</sub> and SV<sub>7</sub>) correspond to the short circuit discussed previously, while the other six can be considered to form stationary vectors in the *d-q* plane as shown in Fig. 15.18. The magnitude of each of the six active vectors is:

$$V_m = \frac{2}{3}V_{bus} \tag{15.14}$$

corresponding to the maximum possible phase voltage. Having identified the stationary vectors, at any point in time, an arbitrary target output voltage vector  $V_o$  can then be made up by the summation (averaging) of the adjacent *space vectors* within one switching period  $\Delta T$ , as shown in Fig. 15.19 for a target vector in the first 60-degree segment of the plane. Target vectors in the other five segments of the hexagon are clearly obtained in a similar manner.

For ease in notation, the *d-q* plane can be considered as being complex. The geometric summation shown in Fig. 15.19 can then be expressed mathematically as:

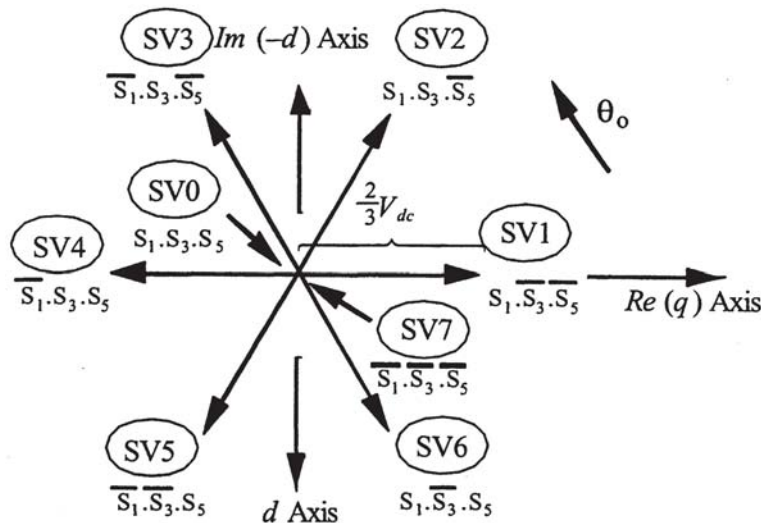
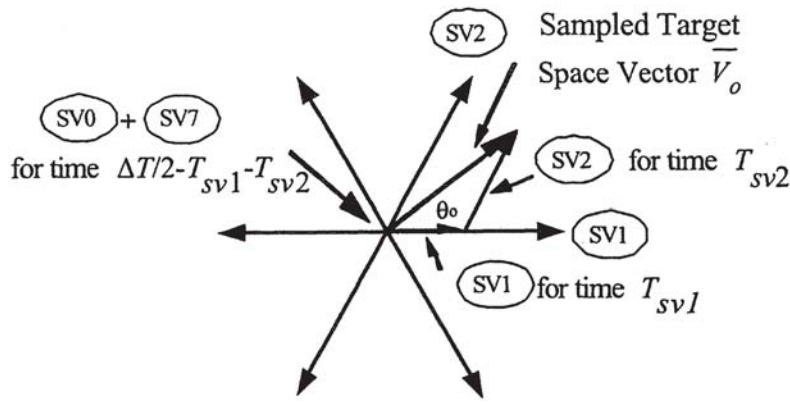


Figure 15.18 Location of the eight possible stationary voltage vectors for a VSI in the *d-q* (*Re-Im*) plane. Each vector has a length  $(2/3)V_{bus}$ .



**Figure 15.19** Creation of an arbitrary output target phasor by the geometrical summation of the two nearest space vectors.

$$\frac{T_{SV1}}{(\Delta T/2)} \overline{SV1} + \frac{T_{SV2}}{(\Delta T/2)} \overline{SV2} = \overline{V_0} \quad (15.15)$$

for each switching period of  $\Delta T/2$ . That is, each active space vector is selected for some interval of time that is less than the one-half carrier period. It can be noted that SVM is an intrinsically a regular sampled process, because in essence it matches the sum of two space vector volt-second averages over a half carrier period to a sampled target volt-second average over  $\Delta T$ . In phasor form:

$$T_{SV1} V_m \angle 0 + T_{SV2} V_m \angle \pi/3 = \left(\frac{\Delta T}{2}\right) V_0 \angle \theta_0 \quad (15.16)$$

or in Cartesian form:

$$T_{SV1} V_m + T_{SV2} V_m \left(\cos \frac{\pi}{3} + j \sin \frac{\pi}{3}\right) = V_0 (\cos \theta_0 + j \sin \theta_0) \frac{\Delta T}{2} \quad (15.17)$$

Equating real and imaginary components yields the solution:

$$T_{SV1} = \frac{V_0}{V_m} \frac{\sin\left(\frac{\pi}{3} - \theta_0\right)}{\sin \frac{\pi}{3}} \frac{\Delta T}{2} \quad (\text{active time for SV1}) \quad (15.18)$$

$$T_{SV2} = \frac{V_0}{V_m} \frac{\sin(\theta_0)}{\sin \frac{\pi}{3}} \frac{\Delta T}{2} \quad (\text{active time for SV2}) \quad (15.19)$$

Because  $0 \leq T_{SV1}, T_{SV2} \leq \Delta T/2$ , the maximum possible magnitude for  $V_0$  is  $V_m$ , which can occur at  $\theta_0 = 0$  or  $\pi/3$  radians.

In addition a further constraint is that the sum of the active times for the two space vectors obviously cannot exceed the half carrier period, i.e.,  $T_{SV1} + T_{SV2} \leq \Delta T/2$ . From simple geometry, the limiting case for this occurs at  $\theta_0 = \pi/6$ , which means:

$$\frac{T_{SV1} + T_{SV2}}{\left(\frac{\Delta T}{2}\right)} = \left(\frac{V_0}{V_m}\right) \frac{2 \sin \frac{\pi}{6}}{\sin \frac{\pi}{3}} \leq 1 \quad (15.20)$$

and this relationship constrains the maximum possible magnitude of  $V_0$  to:

$$V_0 = V_m \sin\left(\frac{\pi}{3}\right) = \frac{1}{\sqrt{3}} V_{bus} \quad (15.21)$$

Because  $V_0$  is the magnitude of the output *phase* voltage, the maximum possible *l-l* output voltage using SVM must equal:

$$V_{0(l-l)} = \sqrt{3} V_0 = V_{bus} \quad (15.22)$$

This result represents an increase of  $2/(\sqrt{3})$  or 1.1547 compared to regular sampled PWM (Section 15.4.2) but is essentially the same when zero sequence harmonics are added to the voltage command as was previously discussed.

#### 15.1.4.5 Constant Volts/Hertz Induction Motor Drives

The operation of induction machines in a constant volts per hertz mode back to the late 1950s and early 1960s but were limited in their low-speed range [6]. Today constant volt per hertz drives are built using PWM-IGBT-based inverters of the types discussed in Sections 15.4.2 to 15.4.4 and the speed range has widened to include very low speeds [7] although operation very near zero speed (less than 1 Hz) remains as a challenge mainly due to inverter nonlinearities at low output voltages.

Ideally, by keeping a constant *V/f* ratio for all frequencies the nominal torque-speed curve of the induction motor can be reproduced at any frequency as discussed in Section 15.2.2. Specifically if stator resistance is neglected and keeping a constant slip frequency the steady-state behavior of the induction machine can be characterized as an impedance proportional to frequency. Therefore, if the *V/f* ratio is kept constant the stator flux, stator current, and torque will be constant at any frequency. This feature suggests that to control the torque one needs to simply apply the correct amount of volts per hertz to stator windings. This simple, straightforward approach, however, does not work well in reality for several factors, the most important ones being:

1. Effect of supply voltage variations.
2. Influence of stator resistance.
3. Nonideal torque/speed characteristic (effects of slip).
4. Nonlinearities introduced by the PWM inverter.

Low-frequency operation is particularly difficult to achieve because these effects are most important at low voltages. Also, the nonlinearities within the inverter, if not adequately compensated, yield highly distorted output voltages which, in turn, produces pulsating torques that lead to vibrations and increased acoustic noise.

In addition to these considerations, a general purpose inverter must accommodate a variety of motors from different manufacturers. Hence it must compensate for the abovementioned effects regardless of machine parameters. The control strategy must also be capable of handling parameter variations caused by temperature and/or saturation effects. This fact indicates that in a true “general purpose” inverter it is necessary to include some means to estimate and/or measure some of the machine parameters. Another aspect that must be considered in any practical implementation deals with the dc bus voltage regulation, which, if not taken into account, may lead to large errors in the output voltage.

Because general purpose drives are cost sensitive it is also necessary to reduce the number of sensing devices within the inverter. Generally speaking only the dc link inverter voltage and current are measured, hence the stator current and voltage must be estimated based only on these measurements. Speed encoders or tachometers are not used because they add cost as well as reduce system reliability.

Other aspects that must be considered in the implementation of an “ideal constant  $V/f$  drive” relate to:

1. Current measurement and regulation.
2. Changes in gain caused by pulse dropping in the PWM inverter.
3. Instabilities as a result of poor volt-second compensation that result in lower damping. This problem is more important in high efficiency motors.
4. Quantization effects in the measured variables.

Another aspect that must be carefully taken into account is the quantization effect introduced by the A/D converters used for signal acquisition. A good cost to resolution compromise seems to be the use of 10-bit converters. However, a high performance drive is likely to require 12-bit accuracy.

#### 15.1.4.6 Required Performance of Control Algorithms

The key features of a typical control algorithm, is defined as follows:

1. Open loop speed accuracy: 0.3–0.5% (5.4–8.2 rpm).
2. Speed control region: 1–30 to 1:50 (60–1.2 Hz to 60–2 Hz).
3. Torque range: 0–150%.
4. Output voltage accuracy: 1–2% (1.15–2.3 V).
5. Speed response with respect to load changes: less than 2 seconds.
6. Self-commissioning capabilities: parameter estimation error less than 10%.
7. Torque-slip linearity: within 10–15%.
8. Energy saving mode: for no-load operation the power consumed by the motor must be reduced by 20% with respect to the power consumed at full flux and no load.

Current sensors are normally of the open-loop type and their output needs to be compensated for offset and linearity. In addition the dc link bus voltage is typically measured. The switching frequency for the PWM is fixed at typically 10–12 kHz.

It is frequently also required to measure or estimate the machine parameters used to implement the control algorithms. In such cases it is assumed that the number of poles, rated power, rated voltage, rated current, and rated frequency are known.

#### 15.1.4.7 Compensation for Supply Voltage Variations

In an industrial environment, a motor drive is frequently subjected to supply voltage fluctuations that, in turn, imposed voltage fluctuations on the dc link of the inverter. If these variations are not compensated for, the motor will be impressed with either an under or an overvoltage which produces excessive  $I^2R$  loss or excessive iron loss respectively. The problem can be avoided if the dc link voltage is measured and the voltage command  $V_1^*$  adjusted to produce a modified command  $V_1^{**}$  such that:

$$V_1^{**} = \frac{V_{busR}}{V_{bus}} V_1^* \quad (15.23)$$

where  $V_{busR}$  is the rated value of bus voltage.

#### 15.1.4.8 $I_r$ Compensation

A simple means to compensate for the resistive drop is to boost the stator voltage by  $I_1^* r_1$  (voltage proportional to the current magnitude) and neglect the effect of the current phase angle. To avoid the direct measurement of the stator current this quantity can be estimated from the magnitude of the dc link current [8]. In this paper a good ac current estimate was demonstrated at frequencies as low as 2 Hz but the system requires high accuracy in the dc link current measurement making it impractical for low cost applications. A robust  $I_r$  boost method must include both magnitude and phase angle compensation. Typically currents of two phases must be measured with the third current inferred because the currents sum to zero. In either case the value of the stator resistance must be known.

The value of the stator resistance can be estimated by using any one of several known techniques [9–11]. Unfortunately these parameter estimation techniques require knowing the rotor position or velocity and the stator current. An alternate method of boosting the stator voltage at low frequencies is presented in [12]. Here the  $V/f$  ratio is adjusted by using the change in the sine of the phase angle of motor impedance. This approach also requires knowing the rotor speed and it is also dependent on the variation of the other machine parameters. Its practical usefulness is questionable because of the technical difficulty of measuring phase angles at frequencies below 2 Hz.

Constant volts per hertz control strategy is typically based on keeping the stator flux-linkage magnitude constant and equal to its rated value. Using the steady-state equivalent circuit of the induction motor, shown in Fig. 15.3, an expression for stator voltage compensation for resistive drop can be shown to be:

$$V_1 = \frac{\sqrt{2}}{3} I_{1(Re)} \cdot \hat{R}_1 + \sqrt{\frac{V_{1R} f_e}{f_R} + \frac{2}{9} (I_{1(Re)} \cdot \hat{R}_1)^2 - (I_1 \hat{R}_1)^2} \quad (15.24)$$

where  $V_{1R}$  is the base (rated) rms phase voltage at base frequency,  $f_R$  is the rated frequency in hertz,  $\hat{R}_1$  is the estimated value of resistance,  $I_1$  is the rms current obtained as a instantaneous basis by:

$$I_1 = \sqrt{\frac{2}{3} \sqrt{i_a(i_a + i_c) + i_c^2}} \quad (15.25)$$

and  $I_{1(Re)}$  is the real component of rms stator current obtained from:

$$I_{1(Re)} = i_a \left[ \cos \theta_e - \cos \left( \theta_e - 2\frac{\pi}{3} \right) \right] + i_c \left[ \cos \left( \theta_e + 2\frac{\pi}{3} \right) - \cos \left( \theta_e - 2\frac{\pi}{3} \right) \right] \quad (15.26)$$

where  $i_a$  and  $i_c$  are two of the instantaneous three-phase stator currents  $\theta_e = \omega_e t$  and the cosine terms are obtained from the voltage command signals. The estimated value of resistance can be obtained either by a simple dc current measurement corrected for temperature rise or by a variety of known methods [13–15]. Derivation details of these equations are found in [16]. Given the inherently positive feedback characteristic of an  $I_r$  boost algorithm it is necessary to stabilize the system by introducing a first order lag in the feedback loop (low-pass filter).

#### 15.1.4.9 Slip Compensation

By its nature, the induction motor develops its torque as a rotor speed slightly lower than synchronous speed (effects of slip). In order to achieve a desired speed, the applied frequency must therefore be increased by an amount equal to the slip frequency. The usual method of correction is to assume a linear relationship exists between torque and speed in the range of interest. Hence, the slip can be compensated by knowing this relationship. This approximation gives good results as long as the breakdown torque is not approached. However, for high loads the relationship becomes nonlinear. Reference 16 describes a correction that can be used for high slip:

$$f_{slip} = \frac{1}{2 - A \cdot P_{gap}} \times \left\{ \sqrt{(f_e^*)^2 + \frac{S_m S_{linear}}{2 \left( \frac{T_{bd}}{T_R} \right)} \cdot P_{gap} - B \cdot P_{gap}^2 - f_e^*} \right\} \quad (15.27)$$

where  $f_e^*$  is the external command frequency and:

$$A = \frac{P}{4\pi S_{bd} T_{bd} f_R} \quad (15.28)$$

and:

$$B = \left( \frac{P}{4\pi T_{bd}} \right)^2 \quad (15.29)$$

and  $P$  is the number of poles. The slope of the linear portion of the torque-speed curve is given by:

$$S_{linear} = \left( \frac{P}{\pi} \right) \frac{S_R f_R}{T_R} \quad (15.30)$$

Finally, the air gap power is:

$$P_{gap} = 3V_1 I_1 (\text{pf}) - 3I_1^2 \hat{R}_1 - P_{core} \quad (15.31)$$

where  $P_{core}$  at rated frequency can be obtained from:

$$P_{coreR} = P_{inR} \left( 1 - \frac{\eta_R}{1 - S_R} \right) - 3I_{1R}^2 \hat{R}_1 \quad (15.32)$$

where the caret “^” denotes an estimate of the quantity. The quantities  $S_R$ ,  $f_R$ ,  $\eta_R$ ,  $I_{1R}$ ,  $P_{inR}$ , and  $T_R$  are the rated values of slip frequency, line frequency, efficiency, stator current, input power and torque, respectively. All of these quantities can be inferred from the nameplate data.

#### 15.1.4.10 Volt-Second Compensation

One of the main problems in open-loop controlled PWM-VSI drives is the nonlinearity caused by the nonideal characteristics of the power switches. The most important nonlinearity is introduced by the necessary blanking time to avoid short circuiting the DC link during the commutations. To guarantee that both switches are never on simultaneously a small time delay is added to the gate signal of the turning-on device. This delay, added to the device’s inherent turn-on and turn-off delay times, introduces a magnitude and phase error in the output voltage [17]. Because the delay is added in every PWM carrier cycle the magnitude of the error grows in proportion to the switching frequency, introducing large errors when the switching frequency is high and the total output voltage is small.

The second main non-linear effect is due to the finite voltage drop across the switch during the on-state [18]. This introduces an additional error in the magnitude of the output voltage, although somewhat smaller, which needs to be compensated.

To compensate for the dead-time in the inverter it is necessary to know the direction of the current and then change the reference voltage by adding or subtracting the required volt-seconds. Although in principle this is simple, the dead time also depends on the magnitude and phase of the current and the type of device used in the inverter. The dead-time introduced by the inverter causes serious waveform distortion and fundamental voltage drop when the switching frequency is high compared to the fundamental output frequency. Several papers have been written on techniques to compensate for the dead time [17, 19–21].

Regardless of the method used, all dead-time compensation techniques are based on the polarity of the current, hence current detection becomes an important issue. This is specially true around the zero-crossings where an accurate measurement is needed to correctly compensate for the dead time. Current detection becomes more difficult because of the PWM noise and because the use of filters introduces phase delays that needed to be taken into account.

The name “dead-time compensation” is often misleading because the actual dead time, which is intentionally intro



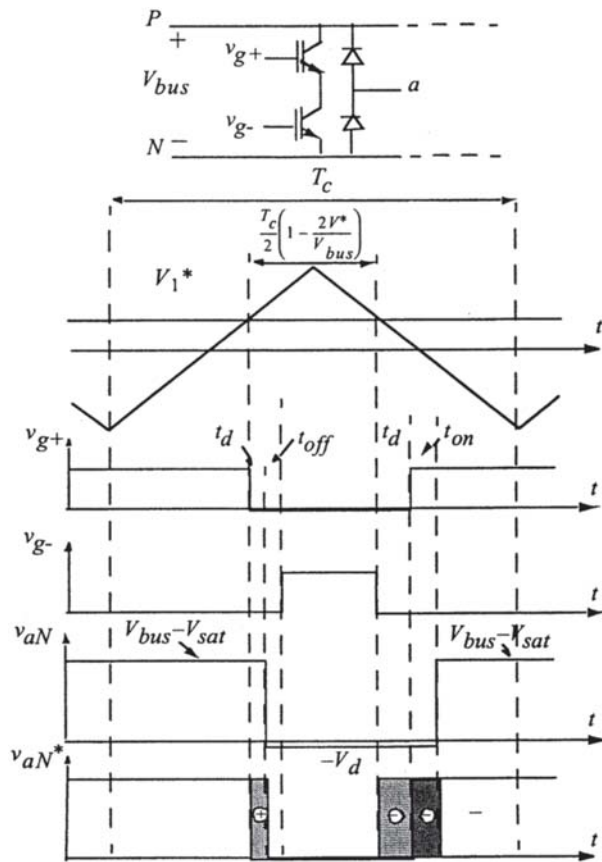


**Figure 15.20** Pulse-width modulation (PWM) voltage waveforms for positive current.

duced, is only one of the elements accounting for the error in the output voltage, for this reason here it is referred as volt-second compensation. The volt-second compensation algorithm developed is based on the average voltage method. Although this technique is not the most accurate method available it gives good results for steady state operation. Figure 15.20 shows idealized waveforms of the triangular and reference voltages over one carrier period. It also shows the gate signals, ideal output voltage, and pole voltage for positive current. For this condition, the average pole voltage over one period can be expressed by:

$$\begin{aligned} \langle v_{an} \rangle &= V_{bus} \left( \frac{1}{2} + \frac{V^* \cos \theta}{V_{bus}} \right) - \left( \frac{t_d + t_{on} - t_{off}}{T_c} \right) \\ &\quad \times (V_{bus} - V_{sat} + V_d) - \left( \frac{V_{sat} - V_d}{V_{bus}} \right) V^* \\ &\quad - \left( \frac{V_{sat} + V_d}{2} \right) \end{aligned} \tag{15.33}$$

where:

- $\langle v_{an} \rangle$ : average output phase voltage with respect to negative dc bus over one switching interval,
- $V_{sat}$ : device saturation voltage,
- $T_c$ : carrier period,
- $V_{bus}$ : DC link bus voltage,
- $t_d$ : dead time,

- $t_{on}$ : turn-on delay time,
- $t_{off}$ : turn-off delay time,
- $V_d$ : diode forward voltage drop.

The first term in Eq. 15.33 represents the ideal output voltage and the remainder of the terms are the errors caused by the nonideal behavior of the inverter. A close examination of the error terms shows that the first and last terms will be rather large with the middle term being much smaller. Hence one can approximate the voltage error by:

$$\Delta V \approx \frac{t_d + t_{on} - t_{off}}{T_c} (V_{bus} - V_{sat} + V_d) + \frac{V_{sat} + V_d}{2} \tag{15.34}$$

and the output voltage can be expressed as:

$$v_{an} \approx V_{bus} \left( \frac{1}{2} + \frac{V^* \cos \theta}{V_{bus}} \right) - \Delta V \tag{15.35}$$

if the current is positive and:

$$v_{an} \approx V_{bus} \left( \frac{1}{2} + \frac{V^* \cos \theta}{V_{bus}} \right) + \Delta V \tag{15.36}$$

if the current is negative. Since the three motor phase voltage must add to zero the voltage of phase *a* with respect to the motor stator neutral *s* is therefore:

$$v_{as} = \frac{2}{3} v_{an} - \frac{1}{3} v_{bn} - \frac{1}{3} v_{cn} \tag{15.37}$$

The voltages of the remaining two phase voltage are obtain in similar manner.

As shown in Fig. 15.20, the voltage error corresponds to the difference in areas between the commanded voltage and the actual voltage. The (+) and (-) signs in the bottom trace indicate in which part of the cycle there is a gain or loss of voltage. The algebraic sum of these areas gives the average error over a pulse period. The voltage error can be corrected either on a per pulse basis or, less accurately, on a per cycle basis. The compensation algorithm is thus based on commanding a voltage modified by  $\pm \Delta V$  depending on the polarity of the current. An overall volts per hertz control scheme including *IR*, slip and volt-second compensation is shown in Fig. 15.21 [16].

### 15.1.5 Field Orientation

#### 15.1.5.1 Complex Vector Representation of Field Variables

Although the large majority of variable speed applications require only speed control in which the torque response is only of secondary interest, more challenging applications such a traction applications, servomotors and the like depend critically upon the ability of the drive to provide a prescribed torque whereupon the speed becomes the variable of secondary interest. The method of torque control in ac machines is called either *vector control* or, alternatively *field orientation*. Vector control refers to the manipulation of terminal currents, flux linkages and voltages to affect the motor torque, while field orientation refers to the manipulation of the field quantities within the motor itself. Because it is common for machine designers to visualize motor torque production in terms of the

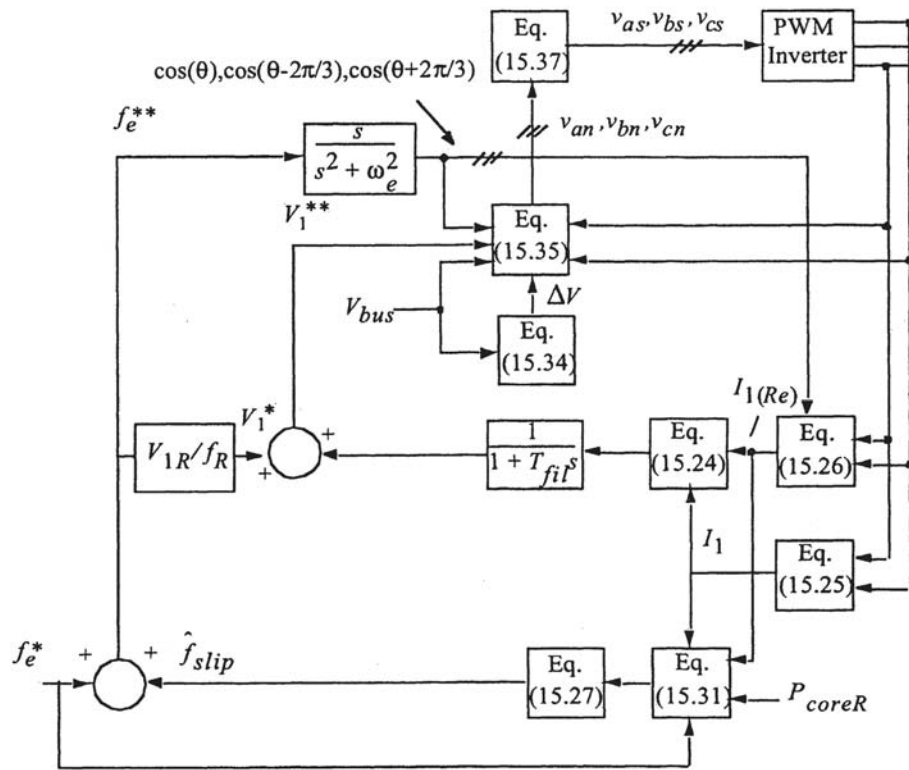


Figure 15.21 Complete volts per hertz induction motor speed controller incorporating IR, slip, dc bus, and volt-second compensation.

air-gap flux densities and mmfs instead of currents and fluxes that relate to terminal quantities, it is useful to begin first with a discussion of the relationship between the two viewpoints.

Consider, first of all, the equation describing the instantaneous position of the stator air-gap mmf for a simple two pole machine. If phase *as* is sinusoidally distributed then the mmf in the gap resulting from current flowing in phase *a* is:

$$F_{as} = \frac{N_s}{2} i_{as} \cos \beta. \quad 0 \leq \beta \leq 2\pi \quad (15.38)$$

where  $N_s$  is the effective number of stator turns and  $\beta$  is the angle measured in the counterclockwise direction from the magnetic axis of phase *as*. Similarly, if currents flow in phases *bs* or *cs* which are spatially displaced from phase *as* by 120 electrical degrees, then the respective air gap mmfs are:

$$F_{bs} = \frac{N_s}{2} i_{bs} \cos \left( \beta - \frac{2\pi}{3} \right) \quad (15.39)$$

$$F_{cs} = \frac{N_s}{2} i_{cs} \cos \left( \beta + \frac{2\pi}{3} \right) \quad (15.40)$$

As written Eqs. 15.38 to 15.40 are real quantities. They would be more physically insightful if these equations were given spatial properties such that their maximum values were directed along their magnetic axes which are clearly spatially oriented  $\pm 120$  degrees with respect to the magnetic axis of phase *as*. This can be done by introducing a complex plane in which the unit amplitude operator  $\bar{a} = e^{j2\pi/3}$  provides the necessary spatial orientation. Specifically spatial quantities  $\bar{F}_{bs}$  and  $\bar{F}_{cs}$  can now be defined where:

$$\bar{F}_{bs} = \bar{a} F_{bs} = \bar{a} \frac{N_s}{2} i_{bs} \cos \left( \beta - \frac{2\pi}{3} \right) \quad (15.41)$$

$$\bar{F}_{cs} = \bar{a}^2 F_{cs} = \bar{a}^2 \frac{N_s}{2} i_{cs} \cos \left( \beta - \frac{2\pi}{3} \right) \quad (15.42)$$

where † denotes the complex conjugate.

The net (total) stator air-gap mmf expressed as a space vector is simply the sum of the three components or:

$$\bar{F}_{abcs} = F_{as} + \bar{a} F_{bs} + \bar{a}^2 F_{cs} \quad (15.43)$$

Introducing the Euler equation:

$$e^{j\beta} = \cos \beta + j \sin \beta \quad (15.44)$$

Eq. 15.43 can be manipulated to the form:

$$\bar{F}_{abcs} = \left( \frac{3}{2} \right) \left( \frac{N_s}{2} \right) (\bar{i}_{abcs} e^{-j\beta} + \bar{i}_{abcs}^\dagger e^{j\beta}) \quad (15.45)$$

where, if the three-phase current sum to zero:

$$\bar{i}_{abcs} = i_{as} + \bar{a} i_{bs} + \bar{a}^2 i_{cs} \quad (15.46)$$

$$= i_{as} + j \frac{1}{\sqrt{3}} (i_{bs} - i_{cs}) \quad (15.47)$$

Equation 15.45 is general in the sense that the three stator currents are arbitrary functions of time (but must sum to zero). Consider now the special case when the currents are balanced sinusoidal and have a positive sequence. In this case it can be shown that:

$$\bar{i}_{abc s} = I_s e^{j\theta} \quad (15.48)$$

$$\text{and } \bar{i}_{abc s}^\dagger = 0$$

where  $I_s$  is the amplitude of each of the phase currents and  $\theta = \omega t$ . The corresponding mmf is:

$$\bar{F}_{abc s} = \left(\frac{3}{2}\right) \left(\frac{N_s}{2}\right) I_s e^{j(\theta - \beta)} \quad (15.49)$$

The stator current  $\bar{i}_{abc s}$  in complex form can be clearly visualized as a “vector” having a length  $I_s$  making an angle  $\theta$  with respect to the real axis. On the other hand, the complex mmf quantity  $\bar{F}_{abc s}$  is not strictly a vector because it has spatial as well as temporal attributes. In particular  $\bar{F}_{abc s}$  varies as a sinusoidal function of the spatial variable  $\beta$ . However at a particular time instant  $t = \theta/\omega$  the maximum positive value of the MMF is, from Eq. 15.49, clearly located spatially at  $\beta = \theta$ . Hence, the *temporal (time) position of the current vector also locates the instantaneous spatial position of the corresponding mmf amplitude*. This basic tenet is essential for the understanding of ac motor control.

It can be further shown that the temporal position of the air gap flux linkage can be related to the position of the corresponding flux density by:

$$\bar{B}_{abc(ag)} = \frac{1}{\left(\frac{2}{\pi} \tau_p l_e N_s\right)} \lambda_{(ag)} e^{j(\theta - \gamma)} \quad (15.50)$$

where  $\lambda_{(ag)}$  is the length of the vector  $\bar{\lambda}_{abc(ag)}$ . Thus the *location of a flux linkage vector in the complex plane uniquely locates the position of the amplitude of the corresponding flux density along the air gap of the machine*. While not strictly correct in terms of having spatial properties along the air gap, the flux linkage corresponding to leakage flux is also given an spatial interpretation in which case, for example, the total rotor flux linkage can be defined as:

$$\bar{\lambda}_{abcr} = L_2 \bar{i}_{abcr} + L_m (\bar{i}_{abc s} + \bar{i}_{abcr}) \quad (15.51)$$

where  $\bar{i}_{abc s}$  and  $\bar{i}_{abcr}$  are the three phase motor stator and rotor currents treated a complex quantities as in Eq. 15.46.

It should now be clear that while torque production in an ac machine is physically produced by the interaction (alignment) of the stator mmf relative to the air-gap flux density, it is completely equivalent to view torque production as the interaction (alignment) of the stator current vector with respect to the air gap flux linkage vector. This is the principle of control methods that concentrates on instantaneous positioning of the stator current vector with respect to a presumed positioning of the rotor flux vector. The fact that these temporal based vectors produce spatial positioning of field quantities which are in simple proportion to these vectors has prompted the use of the term *space vectors* for such quantities and the control method termed *field orientation*.

### 15.1.5.2 The $d$ - $q$ Equations of a Squirrel-Cage Induction Motor

Motion control system requirements are typically realized by using torque control concepts in the induction machine that

are patterned after dc machine torque control. The action of the commutator of a dc machine in holding a fixed, orthogonal spatial angle between the field flux density and the armature mmf is emulated in induction machines by orienting the stator current with respect to the rotor flux linkages (i.e., the stator mmf with respect to the rotor flux density as explained above) so as to attain independently controlled flux and torque. Such controllers are called *field-oriented controllers* and require independent control of both magnitude and phase of the ac quantities and are, therefore, also referred to as *vector controllers*. The terms “field orientation” and “vector control” are today used virtually interchangeably.

It can be noted from Eq. 15.47 that the current vector describing behavior of the three-phase currents reduces to a complex two phase quantity if one defines:

$$\bar{i}_{qs}^s = i_{as} \quad (15.52)$$

and:

$$\bar{i}_{ds}^s = \frac{1}{\sqrt{3}} (i_{cs} - i_{bs}) \quad (15.53)$$

The symbols  $d$ - $q$  and the polarity of the current  $\bar{i}_{ds}^s$  are specifically selected to be consistent with conventions set up for the synchronous machine. The superscript “s” is used to indicate that the reference axes used to define the  $d$ - $q$  currents are *stationary*, i.e., non-rotating or fixed to the stator. The differential equations of the squirrel cage machine employing the complex  $d$ - $q$  notation of Eqs. 15.47, 15.52, and 15.53 are [22]:

$$\bar{v}_{qds}^s = r_1 \bar{i}_{qds}^s + p \lambda_{qds}^s \quad (15.54)$$

$$0 = r_2 \bar{i}_{qdr}^s + p \lambda_{qdr}^s - j \omega_r \bar{\lambda}_{qdr}^s \quad (15.55)$$

$$T_e = \frac{3}{2} \cdot \frac{P}{2} \cdot \frac{L_m}{L_r} (\lambda_{dr}^s i_{qs}^s - \lambda_{qr}^s i_{ds}^s) \quad (15.56)$$

A basic understanding of the decoupled flux and torque control resulting from field orientation can now be attained from the  $d$ - $q$  axis model of an induction machine with the reference axes rotating at synchronous speed  $\omega_e$  [22].

$$\bar{v}_{qds}^e = r_1 \bar{i}_{qds}^e + p \lambda_{qds}^e + j \omega_e \bar{\lambda}_{qds}^e \quad (15.57)$$

$$0 = r_2 \bar{i}_{qdr}^e + p \lambda_{qdr}^e + j (\omega_e - \omega_r) \bar{\lambda}_{qdr}^e \quad (15.58)$$

$$T_e = \frac{3}{2} \cdot \frac{P}{2} \cdot \frac{L_m}{L_r} (\lambda_{dr}^e i_{qs}^e - \lambda_{qr}^e i_{ds}^e) \quad (15.59)$$

where:

$$\bar{v}_{qds}^e = v_{qs}^e - j v_{ds}^e, \bar{i}_{qds}^e = i_{qs}^e - j i_{ds}^e, \bar{i}_{qdr}^e = i_{qr}^e - j i_{dr}^e \quad (15.60)$$

$$\bar{\lambda}_{qds}^e = \lambda_{qs}^e - j \lambda_{ds}^e = L_1 \bar{i}_{qds}^e + L_m (\bar{i}_{qds}^e + \bar{i}_{qdr}^e) \quad (15.61)$$

$$\bar{\lambda}_{qdr}^e = \lambda_{qr}^e - j \lambda_{dr}^e = L_2 \bar{i}_{qdr}^e + L_m (\bar{i}_{qds}^e + \bar{i}_{qdr}^e) \quad (15.62)$$

and  $L_r = L_2 + L_m$ , and  $r_1, r_2, L_1, L_2$ , and  $L_m$  are the per-phase stator and rotor resistance, leakage inductances and magnetizing inductance respectively for a star connected machine. Also  $P$  denotes the number of poles and  $p$  is the time derivative

operator  $d/dt$ . In these equations the superscript “ $e$ ” is intended to indicate that the reference axes are rotating with the *electrical* frequency. The effect of iron loss is typically neglected in these equations but can be easily incorporated if necessary.

Because the  $d$ - $q$  representation may be unfamiliar to the reader it is instructive to consider the form of these equations when steady state is reached. From Eq. 15.48 it is apparent that when the phase currents are balanced, the space vector associated with stator current  $\bar{i}_{qds}$  rotates with constant angular velocity  $\omega_e$  with a constant amplitude  $I_s$ . If this same vector is portrayed in a reference which rotates with the vector itself, the synchronous frame representation is simply a complex constant. Similar statements apply for the stator voltage and rotor current vectors and thus for the flux linkage vectors. Because all of the vectors are constant in the steady state the terms of Eqs. 15.57 and 15.58 are zero. These equations become, for the steady state:

$$\bar{V}_{qds} = r_1 \bar{I}_{qds} + j\omega_e \bar{\Lambda}_{qds} \quad (15.63)$$

$$0 = r_2 \bar{I}_{qdr} + j(\omega_e - \omega_r) \bar{\Lambda}_{qdr} \quad (15.64)$$

where the use of capitals denote steady state values (constants). Utilizing Eqs. 15.60, and 15.61 it is not difficult to show that these two equations can be manipulated to the form:

$$\bar{V}_{qds} = r_1 \bar{I}_{qds} + j\omega_e [L_1 \bar{I}_{qds} + L_m (\bar{I}_{qds} + \bar{I}_{qdr})] \quad (15.65)$$

$$0 = \frac{\omega_e r_2}{(\omega_e - \omega_r)} \bar{I}_{qdr} + j\omega_e [L_2 \bar{I}_{qdr} + L_m (\bar{I}_{qds} + \bar{I}_{qdr})] \quad (15.66)$$

which are nothing more than the conventional per phase phasor equations for an induction motor in the steady state wherein the variables are expressed in terms of their peak rather than rms values. Thus the induction motor  $d$ - $q$  equations in the synchronous frame are simply an extension of the conventional phasor equations to account for transient conditions.

### 15.1.5.3 The Field Orientation Principle

The field orientation concept implies that the current components supplied to the machine should be oriented in such a manner as to isolate the component of stator current magnetizing the machine (flux component) from the torque-producing component. This can be accomplished by choosing the reference frame speed  $\omega_e$  to be the instantaneous speed of the rotor flux linkage vector  $\bar{\lambda}_{qdr}^e$  and locking its phase such that the rotor flux is entirely in the  $d$ -axis (now equivalent to the flux or magnetizing axis), resulting in the mathematical constraint:

$$\lambda_{qr}^e = 0 \quad (15.67)$$

Assuming the machine is supplied from a current regulated source so the stator equations can be omitted, the  $d$ - $q$  equations in a rotor flux-oriented (field-oriented) frame become:

$$0 = r_2 i_{qr}^e - (\omega_e - \omega_r) \lambda_{dr}^e \quad (15.68)$$

$$0 = r_2 i_{dr}^e + p \lambda_{dr}^e \quad (15.69)$$

$$\lambda_{dr}^e = L_m i_{ds}^e + L_r i_{dr}^e \quad (15.70)$$

$$\lambda_{qr}^e = 0 = L_m i_{qs}^e + L_r i_{qr}^e \quad (15.71)$$

$$T_e = \frac{3}{2} \cdot \frac{P}{2} \cdot \frac{L_m}{L_r} \lambda_{dr}^e i_{qs}^e \quad (15.72)$$

The torque equation (Eq. 15.72) clearly shows the desirable torque control property of a dc machine, that of providing a torque proportional to the armature current component  $i_{qs}^e$ . A direct (ampere-turn or mmf) equilibrium relation between the torque command current  $i_{qs}^e$  and the rotor current  $i_{qr}^e$  follows immediately from Eq. 15.71:

$$i_{qr}^e = \frac{-L_m}{L_r} i_{qs}^e \quad (15.73)$$

so that this component of stator current does not contribute to the rotor flux component producing torque, i.e., the flux linkage  $\lambda_{dr}^e$ .

Combining Eq. 15.68 and Eq. 15.73 yields another algebraic constraint that is commonly called the *slip relation*:

$$S\omega_e = -r_2 \frac{L_m}{L_r} \frac{i_{qs}^e}{\lambda_{dr}^e} \quad (15.74)$$

that must always be satisfied by means of control if the constraint of Eq. 15.71 is to be satisfied.

Eq. 15.69 shows that in the steady state when  $\lambda_{dr}^e$  is constant, the rotor current component  $i_{dr}^e$  is zero. However, whenever the flux changes,  $i_{dr}^e$  is not zero but is given by:

$$i_{dr}^e = \frac{-1}{r_2} p \lambda_{dr}^e \quad (15.75)$$

Combining Eq. 15.75 and Eq. 15.70 to eliminate  $i_{dr}^e$  yields the equation relating  $i_{ds}^e$  and  $\lambda_{dr}^e$  (flux producing component of stator current and resulting rotor flux)

$$\lambda_{dr}^e = \frac{r_2 L_m}{r_2 + L_r p} i_{ds}^e \quad (15.76)$$

where the operator  $p$  can now be interpreted as equivalent to the Laplace operator  $s$ .

The close parallel to the dc machine now becomes clear. Eq. 15.72 emphasizes this correspondence in terms of torque production. The relation between the flux command current  $i_{ds}^e$ , and the rotor flux  $\lambda_{dr}^e$  is a first-order linear transfer function with a time constant  $T_r$ , where:

$$T_r = \frac{L_r}{r_2} \quad (15.77)$$

This resistance corresponds to the open circuit field winding time constant of a dc machine, where the time constant  $T_r$  is that associated with the field winding time constant. The slip relation expresses the slip frequency that is inherently associated with the division of the input stator current into the desired flux and torque components. It is useful to also note that, in contrast to a dc motor, the ampere turn balance expressed in Eq. 15.73 implies there is no “armature reaction” in a field-oriented controlled induction machine. The cross-magnetizing

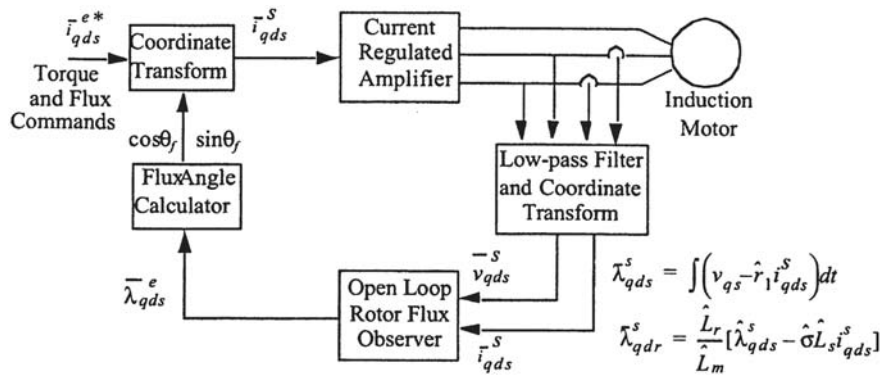


**Figure 15.22** Direct field orientation with rotor field angle  $\theta_f$  determined from terminal voltage and current, “^” denotes estimate of a motor parameter, “\*” a commanded quantity, and  $\sigma=1-L_m^2/(L_r L_s)$ .

component  $i_{qs}^e$  that produces the torque is cancelled by  $i_{qr}^e$ , and thus there is no effect on rotor flux even under saturated conditions.

Field orientation with respect to fluxes other than the rotor flux is also possible [23] with the stator and air gap fluxes being the most important alternatives. Only the rotor flux yields complete decoupling, however, for some purposes (wide range field weakening operation for example) the advantages of choosing stator flux orientation can outweigh the lack of complete decoupling [24].

15.1.5.4 Direct Field Orientation

In direct field orientation the position of the flux to which orientation is desired is directly measured using sensing coils or estimated from terminal measurements. Because it is not possible to directly sense the rotor flux, a rotor flux-oriented system must employ some type of computation to obtain the desired information from a directly sensed signal. Figure 15.22 illustrates the nature of these computations for terminal voltage and current sensing; the most frequently used technique for direct field orientation.

In cases where flux amplitude information is available, a flux regulator can be employed to improve the flux response. A variety of flux observers can be employed to obtain improved response and less sensitivity to machine parameters. Some of these are discussed in a later section. A major problem with most direct orientation schemes is their inherent problems at very low speeds where the machine  $Ir$  drops are dominant and/or the required integration of signals becomes problematic.

15.1.5.5 Indirect (Feed-forward) Field Orientation

An alternative to direct sensing of flux position is to use the slip relation, Eq. 15.74, to estimate the flux position relative to the rotor. Figure 15.23 illustrates this concept and shows how the rotor flux position can be obtained by adding the integral of the slip frequency calculated from the flux and torque commands to the sensed rotor position to produce an angular estimate of the rotor flux position. In the steady state this approach corresponds to setting the slip to the specific value that correctly divides the input stator current into the desired magnetizing (flux producing) and secondary (torque producing) currents. Indirect field orientation does not have

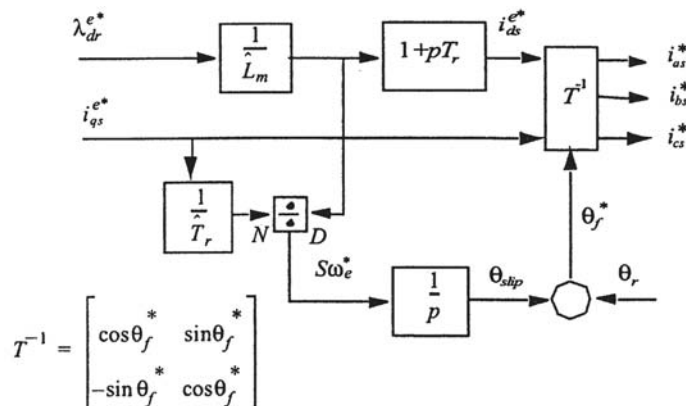


**Figure 15.23** Indirect field orientation controller using rotor flux and torque producing current commands.

inherent low-speed problems and is thus preferred in most systems that must operate near zero speed.

15.1.5.6 Influence of Parameter Errors

Because knowledge of the machine parameters is a part of the feedback or feed-forward controllers, both basic types of field orientation have some sensitivity to machine parameters and provide nonideal torque control characteristics when control parameters differ from the actual machine parameters. In general, both steady-state torque control and dynamic response differ from the ideal instantaneous torque control achieved by a correctly tuned controller.

The major problem in the use of indirect control is the required knowledge of the rotor open circuit time constant  $T_r$ , which is sensitive to both temperature and flux level [25]. When this parameter is incorrect in the controller the calculated slip frequency is incorrect and the flux angle is no longer appropriate for field orientation. This results in an instantaneous error in both flux and torque that can be shown to excite a second order transient characterized by eigen-values having a real part equal to  $-1/T_r$  and an oscillation frequency related to the (incorrect) commanded slip frequency. Because  $T_r$  is an open circuit time constant and therefore rather large, these oscillations can be poorly damped. There is also a steady-state torque amplitude error because the steady-state slip is also incorrect. Steady-state slip errors also cause additional motor heating and reduced efficiency.

Direct field orientation systems are generally sensitive to stator resistance and total leakage inductance, but the various

systems have individual detuning properties. Typically, parameter sensitivity is less than in indirect control, especially when a flux regulator is used. In all cases, both direct and indirect, parameter sensitivity depends on the ratio  $\sigma L_s/r_1$  with larger values giving greater sensitivity. In the steady state the quantity determines the location of the peak torque and thus the shape of the torque versus slip frequency characteristic. Thus, large, high efficiency machines tend to have high sensitivity to parameter errors, and field weakened operation further aggravates this sensitivity.

15.1.5.7 Current Regulation

It has gradually been recognized that field oriented control allows speed loop bandwidths far exceeding that of the dc motor (100 Hz or more) making induction motor servos the device favored for demanding applications. However such a bandwidth can only be achieved with careful tuning of the current regulator which serves to overcome the stator transient time constant. Current regulators remain a rich area of research. However, the present methods can be categorized generally as follows:

- Sine-triangle current regulation
- Hysteresis current regulation
- Predictive (dead-beat) current regulation

The three types of regulators are illustrated in Fig. 15.24.

The sine-triangle intersection method uses the same basic principles as sine-triangle PWM except that the input command to the comparator is the error between a desired current value and the actual instantaneous value. Hence, the controller

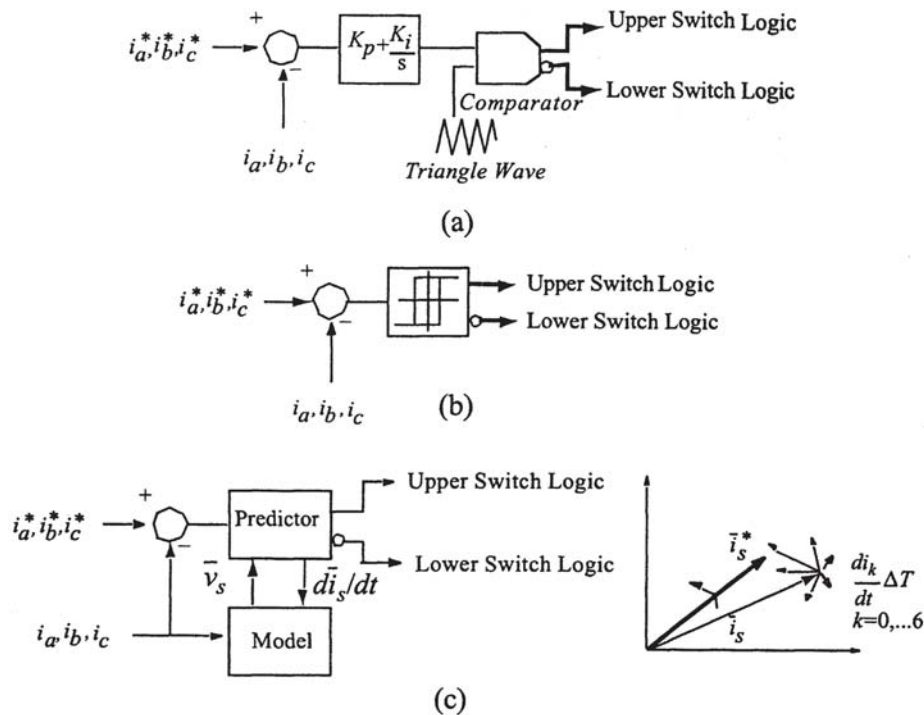


Figure 15.24 Basic current regulation schemes, (a) Three-phase sine-triangle comparison, (b) Three-phase hysteresis control, (c) Predictive regulation.

attempts to control the input current error to zero. The current error in Fig. 15.24(a) can be interpreted as the equivalent to an instantaneous voltage command  $V_1^*$  of zero in Fig. 15.14. An advantage of this controller is that the switching frequency is set by the triangle wave frequency so that the harmonic structure is not appreciably altered compared with voltage PWM. Care must be taken however not to introduce excessive proportional gain or added intersections command and triangle wave could occur as a result of the harmonics introduced by the current feedback. Excessive integrator gain, however, can cause oscillatory behavior. Because of the phase shift introduced by the integrator, the current error of this regulator can not be reduced to zero if the input command is sinusoidal (as is usually the case). Hence, the regulation is usually accomplished in the synchronous frame, operating on current commands which becomes constant in the steady state (see Section 15.5.2) [26].

The hysteresis regulator of Fig. 15.24(b) produces switching whenever the sign of the current error plus the hysteresis band changes polarity. The proper setting of the hysteresis band is critical for this type of controller because the band essentially sets the switching frequency. However, the frequency of switching is not constant because the voltage producing a current change is equal to the difference between the applied inverter voltage and the internal emf of the machine. Because the emf varies sinusoidally throughout a cycle, the pulse (switching) frequency varies throughout the cycle. Since the switching frequency becomes a variable dependant upon the instantaneous value of back-emf, the spectrum produced by the switching events are spread over a continuous band of frequency and becomes difficult to predict. Thus, computation of motor losses produced by this type of input becomes very difficult. Means for reducing the switching frequency variation have been reported [27–29] and work is ongoing.

The third type of current regulator is the predictive regulator of Fig. 15.24(c). It can be recalled from Section 15.4.4 that switching of a three-phase inverter is characterized by only eight states including two with zero voltage output. Hence, only seven unique switching states exist as shown in Fig. 15.17. If the future trajectory of the current is calculated just before each switching event for all seven unique switch states, then the trajectory that directs the current space vector in the best direction for tracking the commanded current can be determined or predicted. Clearly the accuracy of the method is critically dependant on the motor model that is used to predict the current trajectory. Many variations on this theme exist with Refs. 29 and 30 being a good starting point.

#### 15.1.5.8 Sensorless Speed Control

As ac motor drives have gradually matured, the cost and unreliability of the speed/position encoder required for field oriented control has gradually been recognized. Beginning with Joetten and Maeder [31], work has continued on a myriad of alternatives to eliminate the speed/position sensor, many of which have appeared in manufacturer's equipment. In reality, of course, these sensorless methods refer only to the fact that speed is not explicitly measured but, rather, is inferred from electrical measurements and the machine model.

As an introduction to the approach, the  $d$ -axis components of the squirrel cage induction machine in a fixed, nonrotating frame "s" can be written, from Section 15.5.2:

$$v_{ds}^s = r_1 i_{ds}^s + \frac{d\lambda_{ds}^s}{dt} \quad (15.78)$$

$$0 = r_2 i_{dr}^s + \omega_r \lambda_{qr}^s + \frac{d\lambda_{dr}^s}{dt} \quad (15.79)$$

$$\lambda_{ds}^s = L_s i_{ds}^s + L_m i_{dr}^s \quad (15.80)$$

$$\lambda_{dr}^s = L_r i_{dr}^s + L_m i_{ds}^s \quad (15.81)$$

where  $L_s = L_1 + L_m$  and  $L_r = L_2 + L_m$ . Solving Eq. 15.81 for  $i_{dr}^s$  and substituting the result into Eq. 15.80:

$$\lambda_{ds}^s = \frac{L_m}{L_r} \lambda_{dr}^s + \sigma L_s i_{ds}^s \quad (15.82)$$

where  $\sigma = 1 - L_m^2 / (L_s L_r)$ , or

$$\lambda_{dr}^s = \frac{L_r}{L_m} \lambda_{ds}^s - \frac{\sigma L_r L_s}{L_m} i_{ds}^s \quad (15.83)$$

The back-emf of the  $d$ -axis rotor circuit is therefore:

$$e_{dr}^s = \frac{d\lambda_{dr}^s}{dt} = \frac{L_r}{L_m} \frac{d\lambda_{ds}^s}{dt} - \sigma \frac{L_s L_r}{L_m} \frac{di_{ds}^s}{dt} \quad (15.84)$$

or from Eq. 15.78:

$$e_{dr}^s = \frac{L_r}{L_m} (v_{ds}^s - r_1 i_{ds}^s) - \sigma \frac{L_s L_r}{L_m} \frac{di_{ds}^s}{dt} \quad (15.85)$$

In the same manner, for the  $q$ -axis emf:

$$\lambda_{qr}^s = \frac{L_r}{L_m} \lambda_{qs}^s - \frac{\sigma L_r L_s}{L_m} i_{qs}^s \quad (15.86)$$

$$e_{qr}^s = \frac{L_r}{L_m} (v_{qs}^s - r_1 i_{qs}^s) - \sigma \frac{L_s L_r}{L_m} \frac{di_{qs}^s}{dt} \quad (15.87)$$

Finally, from Eq. 15.79, the rotor speed can now be expressed as:

$$\omega_r = \frac{1}{\lambda_{qr}^s} \left[ r_2 \left( \frac{\lambda_{dr}^s}{L_r} - \frac{L_m i_{ds}^s}{L_r} \right) - e_{dr}^s \right] \quad (15.88)$$

where,  $\lambda_{qr}^s$  is obtained from Eq. 15.86, and  $e_{dr}^s$  from Eq. 15.85. A block diagram of the complete speed sensor, developed previously in [32], is shown in Fig. 15.25. Clearly, perfect knowledge of all the machine parameters are needed to implement the approach, which is rarely the case. However, a reasonable estimate of the parameters provide a speed estimate that is adequate for moderate response speed control that does not include lengthy operation near zero speed. A multitude of variations of this principle have appeared in the literature, which is summarized in Ref. 32.

#### 15.1.6 Induction Motor Observer

After 50 years of ac drive development the design of a sensorless induction motor drive is still an engineering challenge. The basic problem is the need for speed estimation, which becomes especially difficult at low speed and under a light load condition. The majority of speed identification methods rely

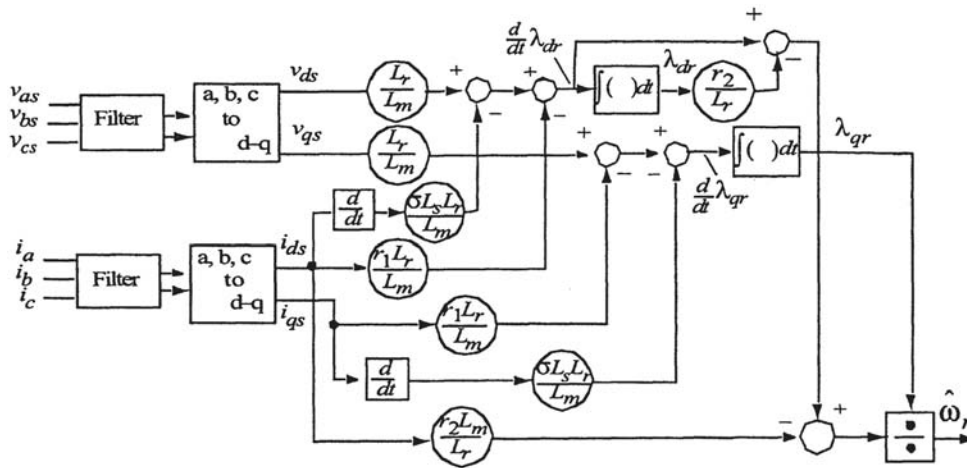


**Figure 15.25** Sensorless sensing of rotor speed; mechanical speed in rad/sec.  $\omega_m = \omega_r / (P/2)$  where  $P$  is the number of poles.

on an approximate fundamental component model of the machine. The use of the stator equation, particularly the integration of the stator voltage vector, is common for all methods. Its solution is fairly accurate when the switched stator voltage waveform is measured at high bandwidth and when the parameters that determine the contributions of the resistive and the leakage voltage components are well known. As the influence of these parameters dominates the estimation at low speed, the steady state accuracy of speed sensorless operation tends to be poor in during low or zero speeds.

One promising approach to solving this barrier is the *sliding mode* approach to rotor flux and speed estimation of an induction machine. The sliding mode method is a nonlinear method for feedback control, state estimation, and parameter identification [33]. The property of the sliding mode approach is due to use of straightforward fixed nonlinear feedback control functions that operate effectively over a specified magnitude range of system parameter variations and disturbances.

From Eqs. 15.84 and 15.85 one can note that the rotor flux is related to the stator voltage by:

$$\frac{L_m}{L_r} \frac{d\lambda_{dr}^s}{dt} = v_{ds}^s - i_{ds}^s r_1 - \sigma L_s \frac{di_{ds}^s}{dt} \quad (15.89)$$

where the second two terms ( $I_r$  and leakage  $L di/dt$  drop) can be considered as corrections to the major term, the applied  $d$ -axis voltage. This equation defines what is called the *voltage model*. A similar equation applies for the  $q$ -axis circuit.

Alternatively the  $d$ -axis rotor flux can be calculated by combining Eqs. 15.79 and 15.82, whereupon:

$$\frac{d\lambda_{dr}^s}{dt} = -\omega_r \lambda_{qr}^s - \frac{r_2}{L_r} \lambda_{dr}^s + r_2 \frac{L_m}{L_r} i_{ds}^s \quad (15.90)$$

In this case the input to the equation is the stator current and thus forms the *current model*. Similar expressions for the  $q$ -axis rotor flux components can be readily obtained.

In the interests of compactness it is convenient to cast these equations in complex form, similar to Eqs. 15.54 and 15.55, as:

$$\frac{L_m}{L_r} \frac{d\bar{\lambda}_{qdr}^s}{dt} = \bar{v}_{qds}^s - \bar{i}_{qds}^s r_1 - \sigma L_s \frac{d\bar{i}_{qds}^s}{dt} \quad (\text{voltage model}) \quad (15.91)$$

and:

$$\frac{d\bar{\lambda}_{qdr}^s}{dt} = \left( j\omega_r - \frac{r_2}{L_r} \right) \bar{\lambda}_{qdr}^s + r_2 \frac{L_m}{L_r} \bar{i}_{qds}^s \quad (\text{current model}) \quad (15.92)$$

The most significant limitation of the rotor flux observer based on voltage model is that it does not function at zero speed. At zero speed and low speed the amplitude of the electromotive force is too small to determine accurately and reliably the rotor flux angle necessary for both field orientation and speed estimation. At low speed the flux estimation given by voltage model deteriorates as a result of the effect of an inaccurate value of the stator resistance  $r_1$ , which causes a slight deviation of the rotor flux space vector. The current model requires information about speed, so in a speed sensorless control one needs to estimate both the rotor flux and mechanical speed.

To achieve a current-based observer suitable for a sensorless drive, the observer control input should be a known function of motor speed so that after establishing a sliding mode in a torque tracking loop, the speed can be determined as unique solution [34]. Combining the voltage and current model:

$$\frac{d\bar{i}_{qds}^s}{dt} = \frac{1}{\sigma L_s} \left[ \bar{v}_{qds}^s - r_1 \bar{i}_{qds}^s - \frac{L_m}{L_r} \left( \bar{e}_{qdr}^s + r_2 \frac{L_m}{L_r} \bar{i}_{qds}^s \right) \right] \quad (15.93)$$

where, the emf:

$$\bar{e}_{qdr}^s = \left( j\omega_r - \frac{r_2}{L_r} \right) \bar{\lambda}_{qdr}^s \quad (15.94)$$

A current estimation error can be defined as:

$$\frac{d\bar{\epsilon}_i}{dt} = \frac{d(\bar{i}_{qds}^s - \hat{i}_{qds}^s)}{dt} = \frac{1}{\hat{\sigma} L_s}$$



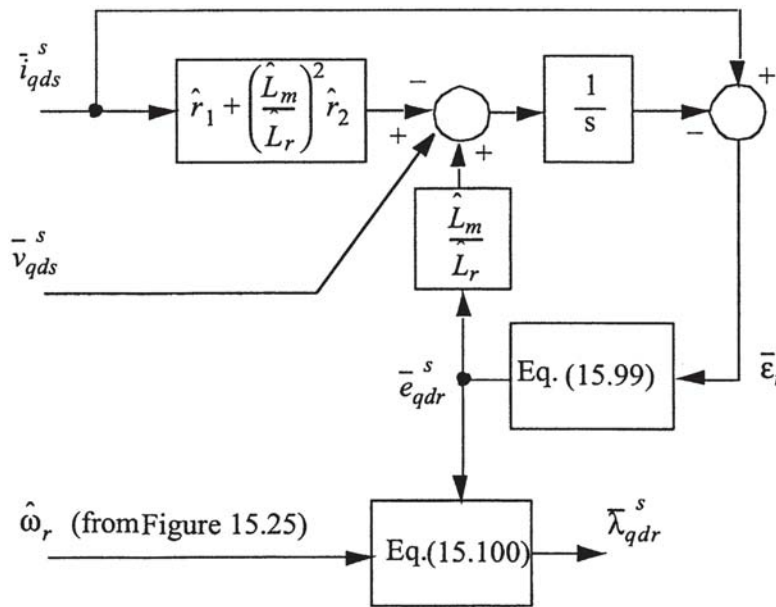


Figure 15.26 Closed-loop rotor flux observer.

$$\times \left\{ \frac{L_m}{L_r} (\bar{e}_{qdr}^s - \hat{e}_{qdr}^s) - \left[ \hat{r}_1 + \hat{r}_2 \left( \frac{\hat{L}_m}{\hat{L}_r} \right)^2 \right] \cdot \bar{e}_i \right\} \quad (15.95)$$

$$\hat{e}_{qdr}(k) = \hat{e}_{qdr}(k-1) + \frac{\hat{\sigma} \hat{L}_s}{T} \frac{\hat{L}_r}{\hat{L}_m} \times [(1 + TD_i) \bar{e}_i(k) - \bar{e}_i(k-1)] \quad (15.99)$$

and the caret “^” again denotes an estimate.

If the derivative in Eq. 15.95 is written in discretized form:

$$\frac{d\bar{e}_i}{dt} = \frac{1}{T} [\bar{e}_i(k) - \bar{e}_i(k-1)] \quad (15.96)$$

Equation 15.95 can be rewritten as:

$$\begin{aligned} \bar{e}_i(k) - \bar{e}_i(k-1) &= \frac{T}{\hat{\sigma} \hat{L}_s} \\ &\times \left\{ \frac{\hat{L}_m}{\hat{L}_r} [\bar{e}_{qdr}(k) - \hat{e}_{qdr}(k)] \right. \\ &\left. - \left[ \hat{r}_1 + \hat{r}_2 \left( \frac{\hat{L}_m}{\hat{L}_r} \right)^2 \right] \cdot \bar{e}_i \right\} \end{aligned} \quad (15.97)$$

which can be rearranged to the form:

$$\begin{aligned} \bar{e}_{qdr}(k) - \hat{e}_{qdr}(k) &= \frac{\hat{\sigma} \hat{L}_s}{T} \frac{\hat{L}_m}{L_r} \\ &\times \left( \left[ 1 + \frac{T}{\hat{\sigma} \hat{L}_s} \left[ \hat{r}_1 + \hat{r}_2 \left( \frac{\hat{L}_m}{\hat{L}_r} \right)^2 \right] \right] \right. \\ &\left. \bar{e}_i(k) - \bar{e}_i(k-1) \right) \end{aligned} \quad (15.98)$$

On examining Eq. 15.98 it is clear that if the current error  $\bar{e}_i(k)$  is driven to zero then the error in the estimate of the emf is driven to zero. This observation can be used to implement a controller which, by utilization of a current regulated PWM algorithm (Fig. 15.24) the current error can be driven to zero. Hence, an estimate of the rotor back-emf can be obtained.

A new updated value of emf at time step  $k$  based on the previous value at time step  $k-1$  plus the current estimation error can now be expressed as:

where  $T$  is the length of the time step (sampling time) and  $D_i = (r_1 + r_2(L_m/L_r)^2)/(\hat{\sigma}L_s)$ . The process of zeroing the error utilizing current regulated PWM is the essence of *sliding mode control*.

A rotor flux observer can now be selected by utilizing Eq. 15.94, whereupon, solving for the flux linkage

$$\bar{\lambda}_{qdr}^s = \frac{\left( j\omega_r + \frac{r_2}{L_r} \right) \bar{e}_{qdr}^s}{\omega_r^2 + \left( \frac{r_2}{L_r} \right)^2} \quad (15.100)$$

The speed estimate needed in Eq. 15.100 can be obtained from Fig. 15.25. A block diagram of the rotor flux algorithm is given in Fig. 15.26. By manipulation of the  $d-q$  machine equations other expressions for rotor linkage and rotor speed are possible. For example one could use a simple integration of Eq. 15.91, the voltage model, which performs well for speeds sufficiently far from zero or Eq. 15.92, the current model, which is frequently used for low speeds. The reader is referred to the literature [32–34] for further information.

### 15.1.7 Permanent Magnet Alternating Current Machine Control

#### 15.1.7.1 Machine Characteristics

In contrast to induction machines that are overwhelmingly of the squirrel-cage construction, permanent magnet alternating current (PMAC) machines have been realized in a variety of practical implementations depending upon stator winding pat

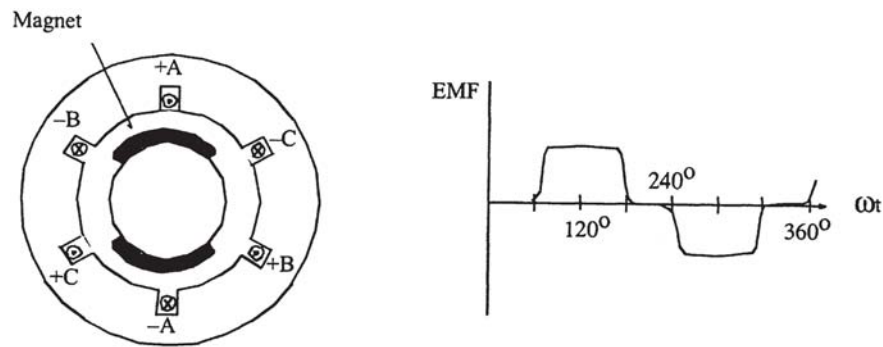


Figure 15.27 Rectangular emf permanent magnet machine utilizing surface magnets.

tern, magnet disposition, air gap flux direction (radial, axial or a combination-transverse flux) and presence or absence of a rotor cage. However, two broad categories can be identified: (1) trapezoidal emf machines and (2) sinusoidal emf machines. The trapezoidal emf machine is equipped with windings concentrated into only one or at most a few full-pitch slots per pole. The magnet disposition of these machines are usually located on the rotor surface and generate a trapezoidal or rectangular emf in the stator phase windings. The span of the magnets are chosen so as to produce a 120 degree quasirectangular waveform as shown in Fig. 15.27. Because the emf is rectangular, the optimal stator current waveform is also quasi-rectangular. Rectangular currents are easily obtained by using only a single dc link current sensor and a relatively crude position sensor which requires only a  $3P$  pulses per revolution, where  $P$  denotes the number of poles. However, these machine are plagued with torque pulsation issues which are very complicated due to the effects of armature reaction and are slowly being phased out in favor of sinusoidal emf machines.

While the stator windings of trapezoidal PMAC machines are concentrated into narrow phase belts, the windings of a sinusoidal machine are typically distributed over multiple slots in order to approximate a sinusoidal distribution. Whereas trapezoidal excitation strongly favors PMAC machines with nonsalient rotor designs (surface magnets) so that the phase inductances remain constant as the rotor rotates so as to minimize the effects of armature reaction. In contrast, PMAC machines with salient rotor poles can offer useful performance characteristics when excited with sinusoidal emf, providing flexibility for adopting a variety of rotor

geometries including a variety of inset or buried magnet as alternatives to the baseline surface magnet design as shown in Fig. 15.28.

The most convenient manner of analyzing a sinusoidal emf PMAC machine again uses instantaneous current, voltage, and flux linkage space vectors in a reference frame fixed to the rotor flux presented in Section 15.5.2. In this case the reference frame rotates synchronously with the applied stator field so that the rotor speed in electrical radians per second  $\omega_r = \omega_e$ . Referring to Eqs. 15.57 to 15.62, these equations can be adapted to characterize a PMAC machine by assuming that the flux produced by the  $d$ -axis rotor current is constant. That is, an equivalent permanent magnet field is modeled when:

$$L_m i_{dr} = \lambda_m = \text{constant}, \quad L_m i_{qr} = 0 \quad (15.101)$$

Since no time-varying currents flow in the rotor, the rotor equation, Eq. 15.58, is not necessary when the rotor does not have a starting cage as is usually the case in a drive application. Combining Eqs. 15.57, 15.61, and 15.101 and separating the complex stator equation into its two components becomes, in scalar form, neglecting iron loss:

$$v_{qs}^e = r_1 i_{qs}^e + p(L_1 + L_m) i_{qs}^e + \omega_e (L_1 + L_m) i_{ds}^e + \omega_e \lambda_m \quad (15.102)$$

$$v_{ds}^e = r_1 i_{ds}^e + p(L_1 + L_m) i_{ds}^e - \omega_e (L_1 + L_m) i_{qs}^e \quad (15.103)$$

In cases in which the magnets are buried below the rotor surface as in Fig. 15.28, the air-gap inductances of the two axes must be modified to account for the effect of saliency. With this modification, the equations for a buried magnet machine in

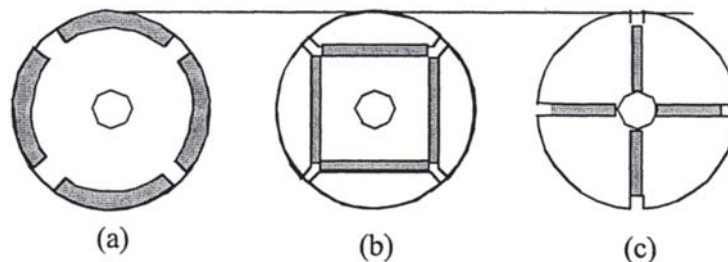
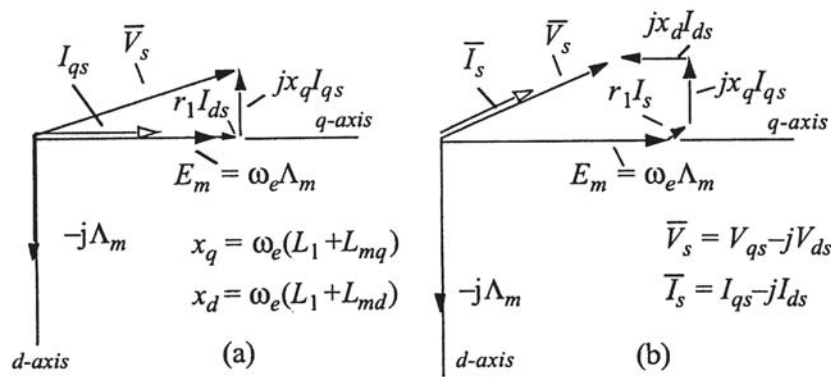


Figure 15.28 Rotor configurations for four-pole permanent magnet alternating current (PMAC) machines, (a) inset, (b) interior radial flux, and (c) interior circumferential flux magnet orientation.



**Figure 15.29** Basic steady-state relationships for sinusoidal permanent magnet alternating current (PMAC) machine in synchronously rotating reference frame using  $d$ -axis alignment with rotor magnet flux linkage  $\bar{\lambda}_m$ , (a) maximum torque per ampere, (b) unity power factor.

the steady state, wherein the  $p=d/dt$  terms are set to zero, become:

$$V_{qs}^e = r_1 I_{qs}^e + \omega_e(L_1 + L_{md})I_{ds}^e + \omega_e \Lambda_m \tag{15.104}$$

$$V_{ds}^e = r_1 I_{ds}^e - \omega_e(L_1 + L_{mq})I_{qs}^e \tag{15.105}$$

Capital letters are used here to denote steady-state conditions. As demonstrated previously, the space vector equations and phasor equations are identical in the steady state except that space vector representation is usually interpreted in terms of peak values whereas the phasor form is interpreted in terms of rms quantities. A plot of the basic space vector (phasor) relationships for the sinusoidal emf PMAC machine is shown in Fig. 15.29. The use of the superscript “ $e$ ” has been dropped for simplicity.

As indicated in Fig. 15.29, the direct or  $d$ -axis has been aligned with the permanent magnet flux linkage vector  $\bar{\lambda}_m$ , so that the orthogonal quadrature or  $q$ -axis is aligned with its time-rate-of-change, the resulting back-emf  $E_m$ . The amplitude of the back-emf phasor  $E_m$  can be expressed very simply as:

$$E_m = \omega_e \Lambda_m = \frac{P}{2} \omega_{rm} \Lambda_m \tag{15.106}$$

where  $P$  is the number of poles  $\omega_m$  is the mechanical speed in rad/sec and  $\Lambda_m$  is the magnet flux linkage amplitude. The

sinusoidal three-phase current excitation is expressed in Fig. 15.29 as an instantaneous current vector  $\bar{I}_s$  made up of  $d$ - and  $q$ -axis scalar components  $i_{ds}$  and  $i_{qs}$ , respectively, and the applied stator voltage phasor  $\bar{V}_s$  can be similarly depicted.

The value of magnetizing inductances  $L_{md}$  will be smaller than  $L_{mq}$  in salient-pole PMAC machines using buried or inset magnets because the total magnet thickness appears as an incremental air gap length in the  $d$ -axis magnetic circuit (i.e.,  $\mu_r \cong 1$  for ceramic and rare earth magnet materials). Interior PMAC machine designs of the type shown in Fig. 15.28 with a single magnet barrier typically provide  $L_{mq}/L_{md}$  ratios in the vicinity of 3, while novel laminated designs have been reported with saliency ratios of 7 or higher.

This  $d$ - $q$  phasor representation leads to the following general expression for the instantaneous torque developed in a sinusoidal PMAC machine:

$$T_e = \frac{3}{2} \cdot \frac{P}{2} \cdot [\lambda_m i_{qs} + (L_d - L_q) i_{ds} i_{qs}] \tag{15.107}$$

where  $L_d$  and  $L_q$  are the  $d$ - and  $q$ -axis stator phase inductances, corresponding to  $(L_{md} + L_1)$  and  $(L_{mq} + L_1)$ , respectively, in the Fig. 15.30 equivalent circuits. Since  $L_q$  is typically larger than  $L_d$  in salient-pole PMAC machines, it is worth noting that  $i_{ds}$  and  $i_{qs}$  must have opposite polarities for the second term to contribute a positive torque component. The first “magnet”

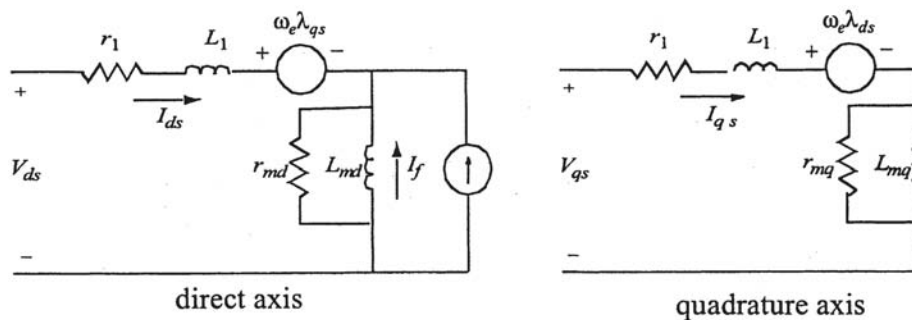


**Figure 15.30** Coupled  $d$ - $q$  equivalent circuits for a sinusoidal permanent magnet alternating current (PMAC) machine in the synchronously rotating reference frame as defined in Fig. 6.22.

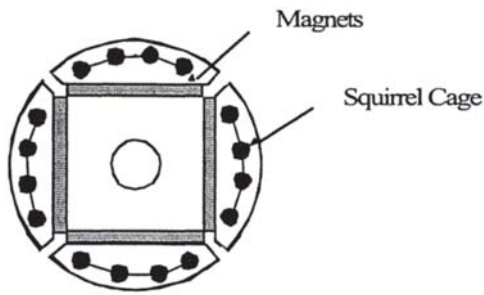


**Figure 15.31** Cross section of a four pole permanent magnet/induction machine, showing simplified block diagram of open loop volts-per-hertz control scheme.

torque term is independent of  $i_{ds}$  but is directly proportional to stator current component  $i_{qs}$  which is in phase with the backemf  $E_m$ . In contrast, the second “reluctance” torque term is proportional to the  $i_{ds}i_{qs}$  current component product and to the difference in the inductance values ( $L_d-L_q$ ) along the two axes. This interpretation emphasizes the hybrid nature of the salient pole PMAC machine. Note that the torque is no longer linearly proportional to the stator current amplitude in the presence of magnetic circuit saliency.

#### 15.1.7.2 Open-Loop Volts-per-Hertz Control

As discussed briefly in Section 6.1.1, buried-magnet PMAC machines can be designed with an induction motor squirrelcage winding embedded along the surface of the rotor as shown in Fig. 15.31. This hybridization adds a component of asynchronous torque production so that the PMAC machine can be operated stably from an inverter without position sensors. This simplification makes it practical to use a simple constant volts-per-hertz (V/Hz) control algorithm in much the same manner as for the induction machine. According to this approach, a sinusoidal voltage PWM algorithm is implemented that linearly increases the amplitude of the applied fundamental voltage amplitude in proportion to the speed command to hold the stator magnetic flux approximately constant. Compensation is again required for  $IR$  drop and for dc bus voltage changes, but clearly, no compensation is needed for rotor slip.

The open-loop nature of this control scheme makes it necessary to avoid sudden large changes in the speed command or the applied load to avoid undesired loss of synchronization (pull-out) of the PMAC machine. However, an appealing aspect of this drive configuration is that the same constant volts-per-hertz control approach can be used in many packaged induction motor drives for general-purpose industrial speed control applications. Thus, cage-type PMAC motors can be selected to replace induction motors in some adjustable speed drive applications to improve system operating efficiency without changing the drive control electronics.

#### 15.1.7.3 High-Performance Closed-Loop Control

In contrast to open-loop operation, a rotor position sensor is typically required to achieve high-performance motion control with the sinusoidal emf PMAC machine. The rotor position feedback needed to continuously perform the self-synchronization function is essentially the same as an induction motor. However, cogging torque (torque pulsations) caused by interaction of the magnets with the stator slot harmonics places a heavier burden on the encoder to smooth out these effects. As result, an absolute encoder or resolver requiring a high resolution is frequently needed. In addition, in contrast to the induction machine, special provision is frequently needed to provide smooth, controlled starting performance since inappropriate energization at start can produce a brief negative rather than positive rotation.

One baseline approach for implementing this type of high-performance torque control for sinusoidal PMAC machines is shown in Fig. 15.32 [35]. According to this approach, the incoming torque command  $T_e^*$  (asterisk designates command) is mapped into commands for  $d-q$  axis current components  $i_a^*$  and  $i_q^*$  that are extracted from torque equation, Eq. 15.107. These current commands in the rotor  $d-q$  reference frame (essentially dc quantities) are then transformed into the instantaneous sinusoidal current commands for the individual stator phases ( $i_a^*$ ,  $i_b^*$ , and  $i_c^*$ ) using the rotor angle feedback  $\theta_r$ , and the inverse vector rotation equations included as part of Fig. 15.23.

The most common means of defining  $d-q$  current component commands  $i_{ds}^*$  and  $i_{qs}^*$  as a function of the torque

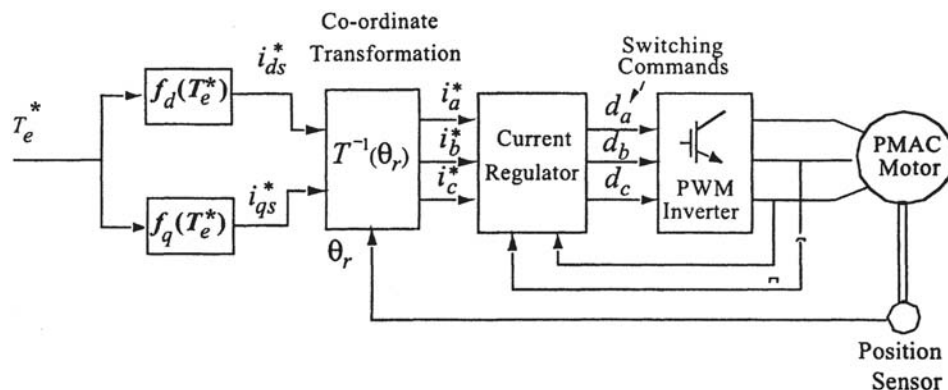


**Figure 15.32** Torque control scheme for sinusoidal permanent magnet alternating current (PMAC) motor.

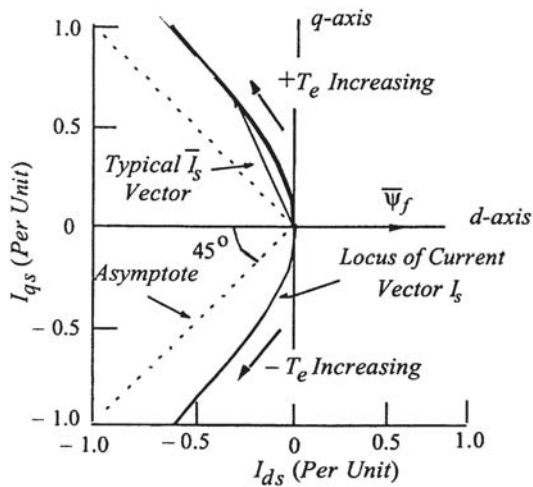


**Figure 15.33** Trajectory of stator current vector  $\bar{I}_s$  in the synchronous reference frame as torque increases.

command  $T_e^*$  into is to set a constraint of maximum torque-per-ampere operation that is nearly equivalent to maximizing operating efficiency (see Fig. 15.29). Trajectories of the stator current vectors  $\bar{i}_{qds}$  the rotor  $d$ - $q$  reference frame that obey this maximum torque-per-amp constraint are plotted in Fig. 15.33 for a typical salient-type PMAC machine. The trajectories are plotted over a range of torque amplitudes ranging from negative (generating/braking) to positive (motoring) values [36].

It can be noted that the maximum torque-per-amp trajectory initially moves along the  $q$ -axis for low values of torque before swinging symmetrically into the second and third quadrant towards 45 degrees asymptotes. For motoring operation, this behavior means that maximum torque for a given amount of stator current is developed by advancing the phase angle of the stator phase currents so that they lead their respective back-emf waveforms by angles between 0 and 45 degrees (electrical). The maximum torque-per-amp trajectory reflects the hybrid nature of the permanent magnet machine having the capability of producing reluctance torque as well as magnet torque. The corresponding currents  $i_{ds}$  and  $i_{qs}$ , which define the maximum torque-per-amp trajectory for the salient pole PMAC machine are plotted in Fig. 15.34 [35].

Alternative field-oriented formulations of the sinusoidal PMAC machine control algorithm have been reported that are also capable of achieving high performance by aligning the rotating reference frame with the stator flux vector rather than with the rotor magnet flux [37, 38]. Although the performance characteristics of these two control formulations are quite similar at low speeds, their differences may become more apparent at higher speeds during the transition from constant torque to constant horsepower operation.

#### 15.1.7.4 Regenerative Braking Operation

Figure 15.34 shows that the maximum torque-per-amp trajectories are mirror images in the second and third quadrants. Stated in a different way, the  $I_{qs}$  function plotted in Fig. 15.34

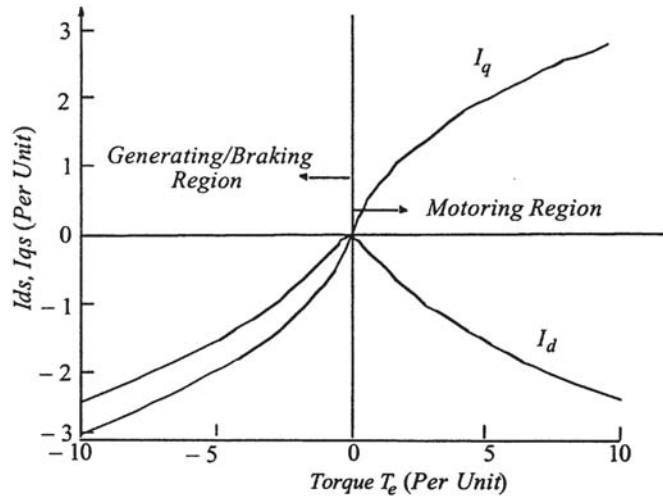


**Figure 15.34** Direct and quadrature axis stator currents required to produce maximum torque per ampere for a salient-pole permanent magnet machine.

is sensitive to the polarity of the torque command, while the  $I_{ds}$  function depends only on its absolute value.

#### 15.1.7.5 Field Weakening

The load torque limits in the speed range from zero to rated speed is set by the maximum current that can be supplied from the inverter, that is:

$$\sqrt{I_{qs}^2 + I_{ds}^2} \leq I_{max} \quad (15.108)$$

The limiting value of Eq. 15.108 can be visualized as a circle in the  $i_{ds}$ - $i_{qs}$  plane centered at the origin with radius  $I_{max}$ .

Beyond rated speed another constraint is imposed because the inverter pulse width modulator saturates and the output voltage becomes a constant. In this case, clearly:

$$\sqrt{V_{qs}^2 + V_{ds}^2} \leq V_{max} = \frac{2}{\pi} V_{bus} \quad (15.109)$$

Using Eqs. 15.104 and 15.105 and rearranging the result, Eq. (15.109) can be expressed as:

$$\frac{2}{\pi} \frac{V_{bus}}{\omega_e} = i_{qs}^2 + \left( \frac{L_{ds}}{L_{qs}} \right)^2 \left( i_{ds} + \frac{\lambda_m}{L_{ds}} \right)^2 \quad (15.110)$$

Equation 15.110 can be visualized as a second ellipse in the  $i_{ds}$ - $i_{qs}$  plane with a focal point at  $i_{qs}=0$  and  $i_{ds}=-\lambda_m/L_{ds}$ . The size of the ellipse continues to decrease as the speed ( $\omega_r=\omega_e$ ) increases.

Control of the  $d$ - $q$  currents in the field weakening range must be such that the current remains in the circle of Eq. 15.108 and tracks along the shrinking elliptical boundary as shown in Fig. 15.35. It can be noted that the  $d$ -axis current is driven negative implying a stator mmf component acting to reduce the magnet flux (demagnetize the magnet). When  $I_{ds}$  becomes equal to  $\lambda_m/L_{ds}$ , the flux in the magnet has been driven to zero. Further negative increases in  $I_{ds}$  must now be prevented. As a result the torque producing component  $I_{qs}$

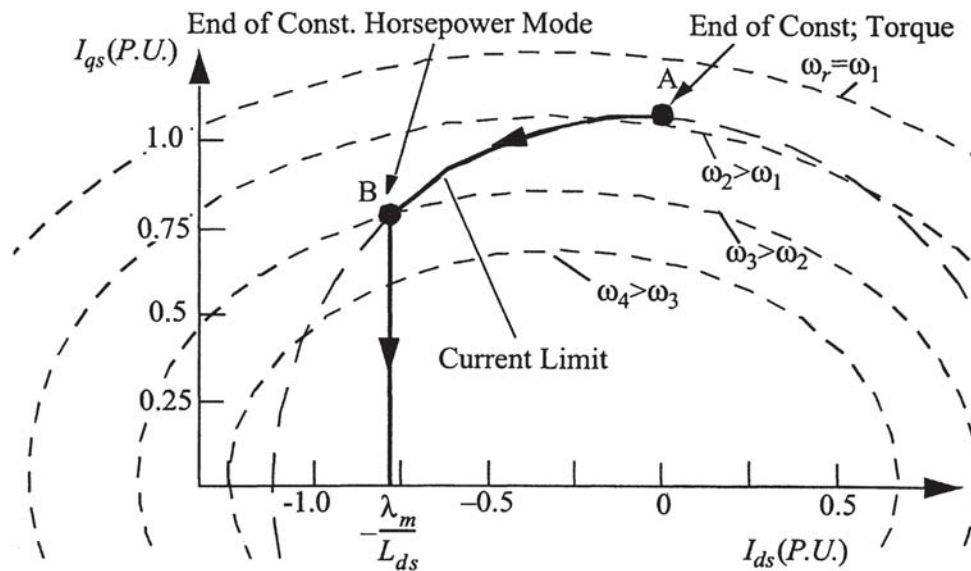


**Figure 15.35** Locus of current vector in the  $d$ - $q$  plane during operation above rated speed (constant horsepower region is A–B).

now begins to decrease rapidly and constant horsepower operation can no longer be maintained. The field weakening region in Fig. 15.35 corresponds to the segment from point A to point B.

## 15.2 SWITCHED-RELUCTANCE MACHINES

### 15.2.1 Definition, History, and Properties

A *reluctance machine* is one in which torque is produced by the tendency of its moveable part to move to a position where the inductance of the excited winding is maximized [39]. Because there are no magnets or field windings, the reluctance motor is said to be *singly excited*. The motion may be rotary or linear, and the rotor may be interior (as in Fig. 15.36) or exterior. The moveable part is a simple component usually made of laminations of soft magnetic iron, shaped in such a way as to maximize the variation of inductance with position. The absence of rotor windings or permanent magnets suggests low manufacturing cost with improved reliability and robustness. However, the degree to which this promise has been translated into commercial reality is so far limited to no more 20–30 practical products.

The rotor and stator both have salient poles, and the magnetic field is switched between groups of poles in synchronism with the rotation of the rotor, by commutating the currents electronically between different *phases* of the winding. The flux must be established directly by the phase current, and therefore, it is not constant but arises in pulses along with the pulses of current. The magnetic field does not rotate smoothly as it does in true ac machines, but is commutated from phase to phase at discrete rotor positions in much the same way as in the brushless dc permanent magnet motor with “square-wave” drive. The magnetic field suffers considerable distortion as the poles pass one another. Torque is also produced in pulses by the associated changes in

electromagnetic stored energy as the rotor poles pass the stator poles. Its variation with respect to rotor position and current is highly nonlinear, so that the production of smooth ripple-free torque is not inherent and requires a somewhat complex optimization of the current waveform according to the speed and load.

The switched-reluctance machine is distinct from the *synchronous*-reluctance motor, which is a true ac rotating-field machine with salient poles only on the rotor. The synchronous-reluctance machine operates with three-phase ac current flowing in a stator that is similar to that of an induction motor, and it can therefore be designed to run from a sine wave voltage source without an electronic drive,

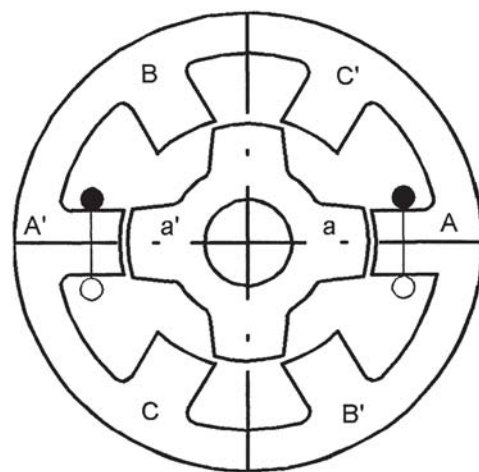


**Figure 15.36** Cross-section of typical switched reluctance motor with six stator poles and four rotor poles. This motor has three phases.

provided that it has some means of starting (such as a cage winding on the rotor). Apart from a few specialty machines mainly developed in the 1960s and 1970s to operate from voltage-source inverters, most of the current research interest in synchronous reluctance machines is in connection with variable-speed ac drives using current-regulated PWM inverters, one for each motor.

The switched reluctance motor is topologically and electromagnetically similar to the variable-reluctance stepper motor [39]. But there are significant differences in the engineering design, in the control method, and in performance and application characteristics. The switched-reluctance motor is normally operated with shaft-position feedback to synchronize the commutation of the phase currents with precise rotor positions, whereas the stepper motor is normally run *open-loop*, i.e., without shaft-position feedback. Whereas switched-reluctance motors are normally designed for efficient conversion of significant amounts of power, stepper motors are more usually designed to maintain *step-integrity* in position controls. Switched reluctance motors are usually larger than stepper motors, with far fewer poles or teeth, and the airgap length is generally larger, being comparable with the airgap in an induction motor.

Nasar appears to have been the first to coin the term *switched reluctance* in describing a rudimentary dc switched-reluctance motor [39, 40]. The switching is really a process of *commutation*, so a more precise name might be *doubly salient singly excited electronically commutated brushless reluctance motor*. The history of the switched reluctance-motor concept goes back to the 1830s but it was not until the advent of modern power semiconductor switching devices that industrial development really started in earnest. A thorough review of the history is given by Anderson [40], including a summary of key patent milestones since approximately 1965.

In its simplest form, the switched-reluctance machine has no magnets or windings on the rotor. This makes the rotor construction simple and avoids the costs and problems associated with permanent magnets (such as magnetization and demagnetization). On the other hand, the excitation provided by magnets is very considerable in small motors, and this leaves the switched reluctance machine at a disadvantage in small sizes. In ratings typically above 10 kW the switched-reluctance motor often has to compete with induction motors the performance of which improves with size, leaving a decreasing margin for performance improvement (especially efficiency). Moreover, the ac drive technology developed for induction motors is now so advanced and so mature that the specialty controllers needed with switched-reluctance machines are handicapped by high development cost and low production volumes. For these reasons switched-reluctance machines are relatively rare and are most often used for their special advantages, which include high overload capacity, freedom from magnets and rotor windings, and the possibility of cost reduction in large production volumes.

The switched-reluctance motor has many of the features that are known to cause high acoustic noise in electric machines, including relatively compliant lamination geometry, concentrated magnetic force vectors, intense local

saturation, high windage loss (at high speed), and pulsed excitation. Because every switched-reluctance motor (and its drive) has to be designed more or less from scratch, noise reduction is often an integral component of the development process. Even after all the general rules have been followed [40], measures such as current wave-shaping may be necessary.

The reliance on a single excitation source, coupled with the effects of fringing fields and magnetic saturation, renders the reluctance motor nonlinear in its control characteristics. At the very least it is necessary to control the amplitude of the current and two commutation angles (switch-on and switch-off in each phase). To achieve performance competitive with that of other modern motor types, it is generally necessary to control the entire current waveform electronically. This requires a digital controller, the sophistication of which will depend on the performance requirements and on the type of shaft position sensor, if any. Sensorless drives for switched-reluctance motors have been under development for approximately 20 years, and are only now beginning to appear in commercial production.

### 15.2.2 Theory of Operation

Figure 15.37 shows the waveforms of the current  $i$ , instantaneous torque  $T$ , and flux-linkage  $\psi$  associated with one phase, such as the winding AA' comprising two opposite stator coils in a motor such as the one shown in Fig. 15.36. The traces cover one *stroke*, that is, the entire pulse of current applied while the rotor poles aa' are approaching alignment with the stator poles AA'. At the right is plotted the locus of the point  $(i, \psi)$ , which is closed at the origin because both  $i$  and  $\psi$  start and end at zero. Both  $i$  and  $\psi$  are unidirectional. The torque is substantially unidirectional, but this depends on the firing angles, as we shall see later. The  $(i, \psi)$  loop lies between two bounding curves, the *unaligned* magnetization curve U and the *aligned* magnetization curve A. The aligned curve corresponds to the positions of the rotor poles aa' and AA' in Fig. 15.36. It is characterized by a steep slope (the *unsaturated aligned inductance*  $L_{au}$ ) at low current, which saturates at relatively low current. The unaligned curve has a much smaller slope  $L_u$ , typically of the order 10–30% of  $L_{au}$ . It corresponds to a rotor position that is displaced  $\pi/N_r$  from the aligned position,  $N_r$  being the number of rotor poles. In this position there is a large air gap surrounding the stator poles and consequently the unaligned curve does not saturate until the current reaches much higher values (usually beyond the thermal rating of the machine). At positions intermediate between U and A, the magnetization curve takes up an intermediate value.

The area  $W$  enclosed within the  $(i, \psi)$  loop is equal to the energy converted from electrical to mechanical in one stroke, so that the average electromagnetic torque is  $SW/2\pi$ , where  $S$  is the number of strokes per revolution. Evidently a design objective is to maximize the product  $SW$  in order to maximize the torque.  $S$  is generally equal to  $mN_p$ , where  $m$  is the number of phases. A simple rule for relating the numbers of stator and rotor poles is  $N_s = q(N_r \pm 2)$ , where  $q$  is an integer, and the number of phases is indicated as  $m = N_s/2q$ . From this it might appear desirable to maximize the number of phases, which clearly involves an increase in  $N_r$  and  $N_s$ . Unfortunately this tends to

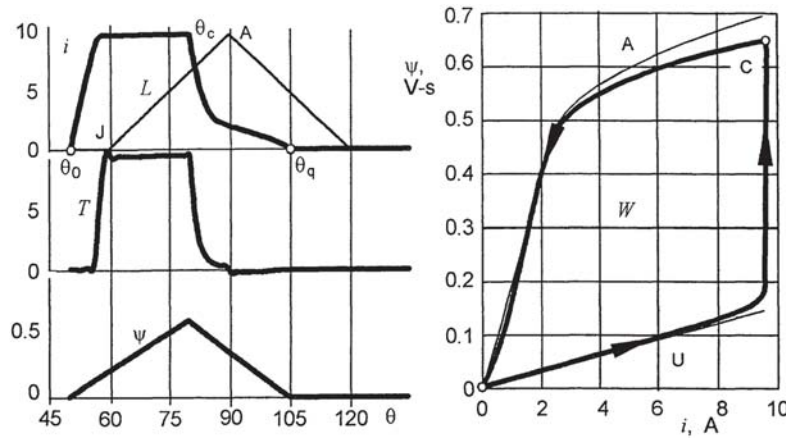


**Figure 15.37** Waveforms of current  $i$ , torque  $T$ , flux-linkage  $\psi$ , vs. rotor position  $\theta$ , shown with reference to the normalized graph of pole overlap  $L$  between the active stator and rotor poles. At right is the locus of the point  $(i, \psi)$  bounded by the unaligned and aligned magnetization curves. The condition shown here is at such a speed with such firing angles that the current waveform has a substantially flat top.

reduce both the inductance ratio  $\delta=L_{av}/L_a$  and the maximum (saturated) flux-linkage per phase, so that not only is  $W$  reduced, but the current required to achieve it is increased. For this reason switched-reluctance motors are rarely designed with more poles than the popular configurations  $N_s=12, N_r=8, m=3$  or  $N_s=8, N_r=6, m=4$ .

In Fig. 15.37 the current waveform is a flat-topped pulse that starts at  $\theta_0$  when the transistors are turned on. A typical drive circuit for one phase is shown in Fig. 15.38, with the current path highlighted in (a) immediately after turn-on. The transistors are switched off at  $\theta_c$ , the commutation angle, causing the current to freewheel through the diodes as shown in (c), eventually extinguishing at  $\theta_q$ . During the interval

between  $\theta_0$  and  $\theta_c$  the flux-linkage  $\psi$  increases because the supply voltage is connected forwards across the winding. Between  $\theta_c$  and  $\theta_q$  it decreases because the diodes connect the reverse of the supply voltage across the winding. The rise and fall are almost linear: this follows naturally from Faraday's law, which states that the back-emf  $e$  is equal to the rate of change of flux-linkage,  $e=d\psi/dt$ , so if the resistance  $r$  is small the volt-drop  $ri$  will be small and  $e=V_s$ , the supply voltage.

Torque is produced in the positive (motoring) direction as long as the phase inductance is increasing. This corresponds to the rising slope of the line marked  $L$  in Fig. 15.37, which represents the overlap between the stator and rotor poles. Although the relationship between torque and current is

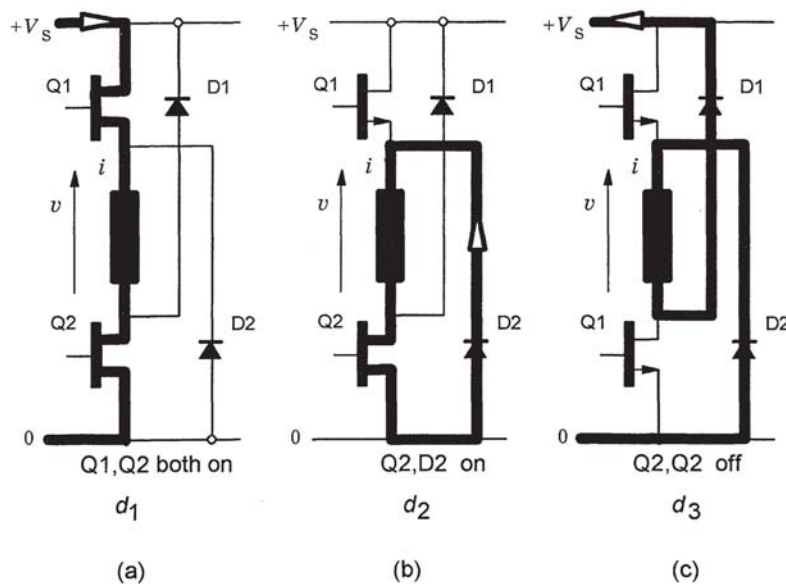


**Figure 15.38** A typical drive circuit has two transistors and two diodes per phase, (a) Both transistors conducting, (b) One transistor and one diode conducting, (c) Both diodes conducting.



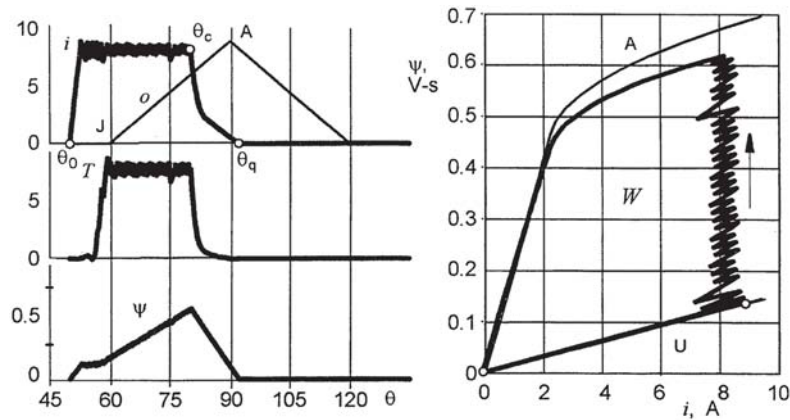


**Figure 15.39** Waveforms of current  $i$ , torque  $T$ , flux-linkage  $\psi$ , at low speed, controlled by chopping.

nonlinear, it can always be said that the higher the rate of change of inductance with rotor position, the greater the torque per ampere. Evidently the torque reverses sign and becomes a braking torque after the rotor passes the aligned position at  $90^\circ$ , but by that time the current is small, and the rate of change of inductance also small, so the braking effect is negligible. The aligned position is reached when the current is approximately 2A and the flux-linkage approximately 0.4 V-s, and from this point onwards the  $(i, \psi)$  loop begins to bulge inwards, reducing the total energy-conversion area. But the effect in this example is very small.

With a fixed supply voltage, the flat-topped current waveform in Fig. 15.37 occurs naturally only in a narrow range of speed and firing angles. At lower speeds, the current waveform must be regulated by chopping or pulse-width modulation of the transistor switching, as shown in Fig. 15.39. The need for this arises because the back-emf  $e$  is proportional to speed, so at low speed it has less effect in limiting the current. “Chopping” entails switching one or both transistors on and off at high frequency, with a duty-cycle (ratio of on-time to switching period) that is controlled in a suitable way to achieve the desired current waveform. The “defluxing”

interval  $\theta_c$  to  $\theta_q$  is now much shorter than the “fluxing” interval  $\theta_0$  to  $\theta_c$ : in fact the ratio of these periods is approximately equal to the duty-cycle  $d$  if “soft” chopping is used (i.e., switching only one of the two transistors, as shown in Fig. 15.38(b)). Because the “tail” or defluxing part of the current and torque waveforms is relatively short, there is more freedom at low speed to control the current waveform to have the desired shape, and it is possible to take advantage of this to reduce torque ripple and even acoustic noise.

At high speed the back-emf increases and may even exceed the supply voltage, as shown in Fig. 15.40. Here the turnon angle  $\theta_0$  has been advanced well ahead of the start of overlap, to permit the current to build-up during an interval where the inductance is low and not changing, and accordingly the back-emf is negligible. When the poles start to overlap, the back-emf  $e$  suddenly appears with a value sufficient to reverse the  $di/dt$  and cause the current to decrease. The energy conversion loop can be seen to be diminishing in area, indicating a falling-off of torque as the speed increases. By phase advance it is possible to maintain constant power by sustaining the torque to be no less than inversely proportional to speed, but eventually the firing angles reach a limit imposed by continuous conduction,

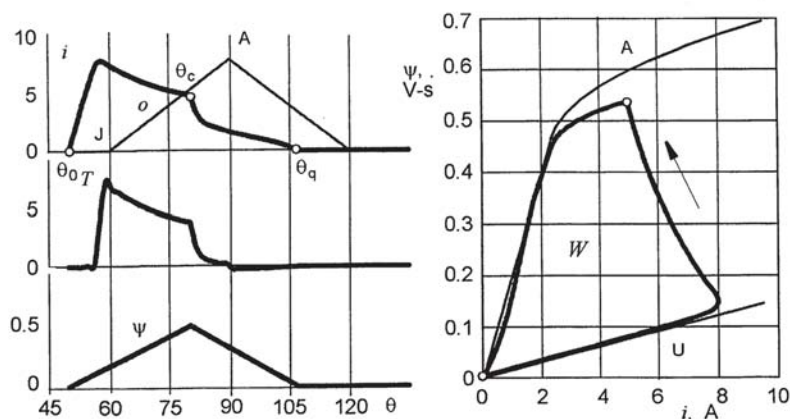


**Figure 15.40** Waveforms of current  $i$ , torque  $T$ , flux-linkage  $\psi$ , at high speed. There is no chopping, and control is possible only by adjusting the firing angles.

and the torque falls more rapidly as the speed increases still further. Constant-power operation can be sustained over a speed range of perhaps 2 or 3:1, but of course this value depends on the design and the ratings of the power semiconductors, and it may be higher or lower than these values.

The switched-reluctance machine can work as a generator or as a controlled brake, by delaying the firing angles  $\theta_0$  and  $\theta_c$  so that the current pulse coincides with an interval of falling inductance, rather than rising inductance. If the power circuit of Fig. 15.28 is used, the excitation power and the output power share the same port; but variants are possible in which the diodes freewheel into a separate circuit, thus separating the excitation port from the output port. The voltampere requirements in the excitation (transistor) part of the circuit can be a sizeable fraction (30–50%) of the output voltamperes, so a separate excitation circuit may need to be quite large.

The output impedance of the system as a generator is that of a capacitor charged to the dc output voltage, usually with a control system that tries to maintain this voltage constant. Protection against short-circuit faults therefore requires some means of indicating to the controller that there is a fault, so that appropriate action may be taken. Notwithstanding its unconventional features, the switched reluctance machine has been extensively studied for applications such as aircraft generators and starter/generators, because of its relative immunity to the worst effects of electrical failures. Because there are no magnets, the effect of a short-circuited turn, for example, is evidently less severe than it would be in a permanent-magnet machine.

### 15.2.3 Controller Architecture

The architecture of the drive controller depends on the performance requirements. A comprehensive review of switched reluctance controller technology is given in [40]. The most sophisticated controllers achieve the equivalent of vector control or direct torque control used in ac drives, principally by regulating the current waveform electronically to give instantaneous torque control. Because of the nonlinearity of the switched-reluctance machine, and the fact that it is never in a steady state but is always undergoing some kind of transient, the algorithms used in such controllers have to be programmed for specific motors and applications. With sufficient attention to these details it is possible to achieve not only high dynamic response, but also high-bandwidth torque control adequate to reduce torque ripple to very low levels, especially at low speeds.

### 15.2.4 Applications

The switched-reluctance machine has appeared in several commercial products including washing machines, centrifuges, compressors, door openers, weaving machinery, automotive cruise-control mechanisms, and many others, [40, 41]. In the early days (beginning in the 1970s and continuing into the 1980s) the expectations were high because of the obvious shift in the balance of cost away from “copper and

iron” in the direction of “silicon.” It took time to overcome the engineering problems of acoustic noise and to devise suitable controller architectures, during which time the competing technologies of brushless permanent-magnet motors (in smaller sizes) and induction motors (in larger sizes) made significant gains, so that the number of applications that turned out to be well served by switched-reluctance drives has so far proven to be relatively small. The unfamiliarity of the necessary design procedures for the motor and the control are undoubtedly another reason that switched-reluctance motors are not developed more often. The design procedures for induction motors and inverters are just as complex, but much more familiar to a wider school of design engineers; moreover, it is supported by the infrastructure of component supplies and working practices. Although the mathematical design theory of the switched-reluctance motor is simple on paper, it is difficult to implement in practice and requires computer methods for even the simplest design calculations.

It therefore seems likely that future applications will follow existing ones. Most of these are highly engineered specialty drives the development cost of which is borne by a single application, whose unique features render it the best choice, and whose development is not hindered by prior investment in manufacturing plant and infrastructure for another type of motor that could do the job equally well (or nearly so). Development requires a combination of intensive computation including electromagnetic, mechanical, and electronic design; then a significant phase of laboratory testing, and finally a suitable investment in tooling. The controller will be specific for each application and its design cannot rely on traditional thinking about sinewaves, space vectors, field-orientation, and so on; instead, one must work with computed numerical data whose structure is not easily discernible. Possibly the computer age will resolve these issues.

## 15.3 BRUSHLESS DC MOTORS

### 15.3.1 Introduction

Brushless dc motors are typically configured as permanent magnet synchronous motors with electronics to supply power to each of the stator winding phases in synchronism with the rotor angular position. The motor drive electronics usually derive power from a dc power bus and the field is supplied by a rotating permanent magnet configuration without a wound field or brushes (hence the term brushless dc). In many applications, a front-end rectifier is built into the same electronics package as the motor control to take power from an ac source. The advantage of brushless dc motors lies in the absence of rotating contacts such as slip ring brushes in the case of conventional wound-field synchronous motors, or commutating brushes in the case of conventional commutator-type dc motors. The lack of brushes eliminates the periodic inspection and maintenance required for brush-type motors. The brushless dc motor, however, requires rotor position sensing, requires that the magnets be firmly restrained on the rotor structure, and lacks field control (motor back-emf is a function of speed only, and is affected by magnet temperature

and an mature winding mmf). In spite of these disadvantages, the brushless permanent magnet motor is gaining increasing use because of its low maintenance and the availability of inexpensive and robust power electronics for motor control.

### 15.3.2 Rotor Construction

#### 15.3.2.1 Surface Mounted Magnets

The simplest form of brushless dc motor rotor construction uses a cylindrical shaft and a ferromagnetic rotating structure with a surface on which magnets are affixed. The magnets are radially magnetized and the magnet outer surfaces are ground or preformed to be concentric with the stator inside diameter. The magnets are held in place by a structural adhesive to prevent radial movement during operation. The inner magnetic structure is machined round or with an even number of flat surfaces around the periphery to accept magnets with matching inner surfaces. This structure may suffice for many applications where the motor is small (usually fractional horsepower ratings) and the maximum operating or overspeed rating is low enough to prevent structural failure of the rotor. This simple surface-mount construction helps to keep motor costs down, but the cost of rotor failure can be high when the stator or connected shaft load is damaged, or an unsafe condition results from rotor failure. Figures 15.41 and 15.42 show two 6-pole brushless dc rotor cross sections with two different magnet mounting surface configurations. The magnet polarity, designated by N or S, alternates around the periphery. The figures also show a magnet containment band on each rotor surface.

#### 15.3.2.2 Rotor Failure

Rotor failure can result from structural adhesive failure or magnet material failure. Structural adhesives such as epoxies may be very good at their normal designated operating temperatures, but their tensile strength decreases as the temperature increases.

Operation of a permanent magnet rotor at extreme elevated temperatures may cause the adhesive to weaken to the point where the magnets cannot be held onto the rotor surface. In addition, thermal cycling of the rotor structure can cause fatigue

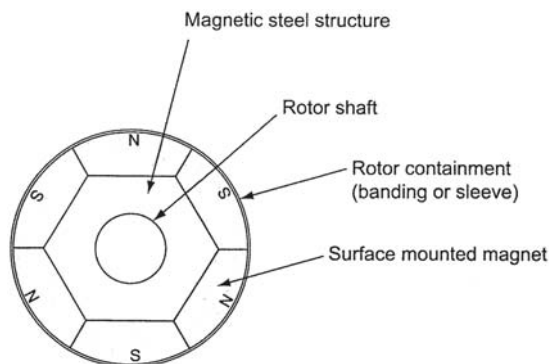


**Figure 15.41** Rotor cross-section of six-pole brushless direct current (dc) motor with magnets mounted on rotor flats.

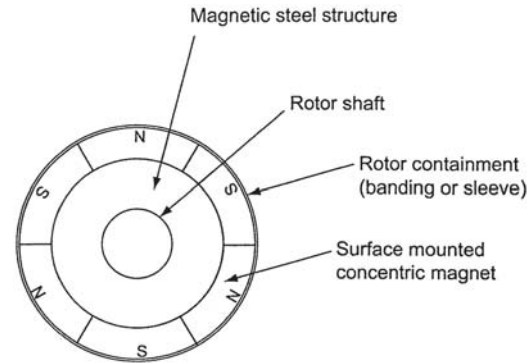


**Figure 15.42** Rotor cross-section of six-pole brushless direct current (dc) motor with magnets mounted on cylindrical rotor structure.

of the adhesive where differential expansion of the rotor structure and the permanent magnet material occur. Some magnet materials (for example, ferrites and samarium cobalt) are brittle, and can be easily cracked by rough handling during manufacture and assembly. These cracks may show up as magnet chips being detached from the magnet, or may result in total magnet structural failure as a result of the centrifugal forces of high operating speeds. Most magnet material tensile strength is relatively low compared to high-strength steel, and cannot always be relied on for the structural integrity required for a high-speed, high-power motor design. Some of the Alnico materials have high tensile strength, even though their magnetic properties are considerably poorer than samariumcobalt or neodymium-iron-boron magnets, and are used for rotating applications other than brushless dc motors.

#### 15.3.2.3 Sleeved Rotors

In high-speed integral horsepower motors, there are several ways to retain the permanent magnets without significant loss of motor performance. One of the most popular is a thin steel sleeve shrunk on the rotor surface over the magnet outside diameter (see Figs. 15.41 and 15.42). The steel is high strength and can be stainless non-magnetic or magnetic steel. For a magnetic steel sleeve the sleeve will divert a very small portion of the magnetic flux away from the air gap to the adjacent opposite-polarity magnet, but the performance loss is small because of the steel saturation and small radial dimension of the sleeve. In this construction method, the hoop strength of the sleeve is relied on to prevent the magnets from lifting off the rotor structure at the maximum rotor overspeed condition.

#### 15.3.2.4 Banded Rotors

Another method is adhesive-impregnated glass tape, carbon fiber, or other high-strength fiber banding. The banding is wound around the rotor under tension after the magnets have been assembled on the rotor surface. The tension is calculated to be enough to prevent the magnets from lifting off the mounting surface at the highest overspeed condition. The adhesive is cured in an oven and relied on to hold the fibers together during all modes of operating temperature and speed. This method works well where there are no sharp magnet

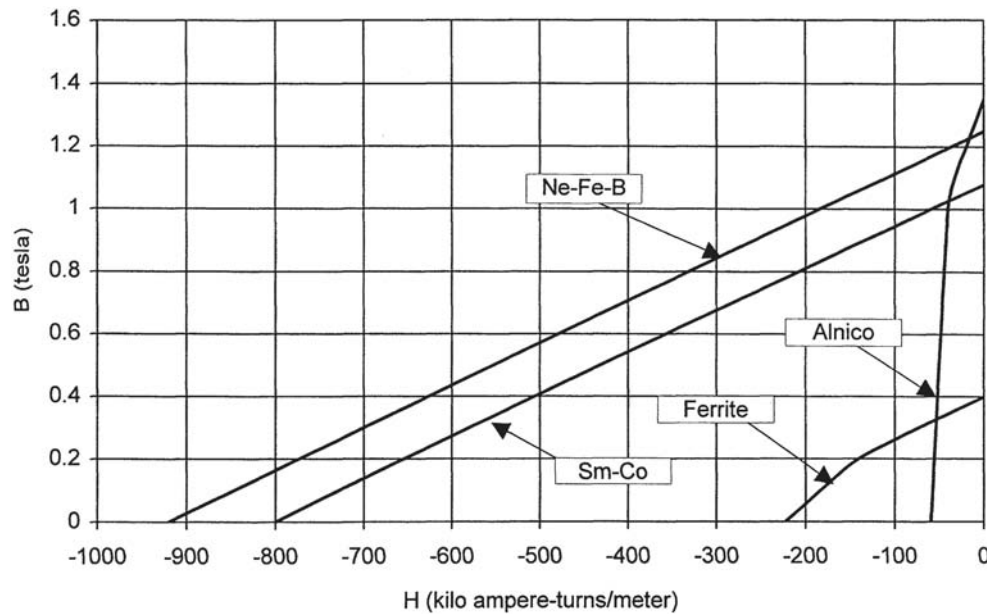


Figure 15.43 Typical  $B$ - $H$  curves for several magnet types.

corners or edges on the rotor surface to cause a stress concentration in the high-strength fiber banding.

#### 15.3.2.5 Buried Permanent Magnets

An additional means of construction to ensure rotor integrity is the buried magnet configuration in which the magnets are inserted into axial slots in a laminated rotor structure. Small saturable bridges are used to provide a continuous outer cylinder for tensile strength, while various nonmagnetic openings are punched in the laminations to provide tangential flux baffles. In some designs, these rotor configurations have aluminum cast into the rotor for line starting from an ac supply, and are not used as brushless dc motors.

#### 15.3.2.6 Rotor Position Sensing

Rotor position sensors are necessary for precision brushless dc motor control, and these sensors must be mechanically and electrically sound for all operating conditions to provide a highly reliable drive system. Rotor position sensing may be performed optically, magnetically, or by some other means to send rotor position information to a stationary controller without brushes or other rotating contacts. These types of sensing devices tend to reduce motor reliability, and care must be taken to provide a robust rotor position sensing method.

### 15.3.3 Magnets and the Magnetic Circuit

#### 15.3.3.1 Magnet Material

A variety of magnet materials are available to provide the required rotating magnetic field in a brushless dc motor. The most popular are ceramic ferrite, samarium-cobalt, and neodymium-iron-boron magnets. Alnico magnets, once very

popular, are not used extensively in brushless dc motors because of their poor demagnetization resistance. Ferrites are the least expensive, but have a low  $B$ - $H$  characteristic, and require a thick magnet to obtain a reasonable air-gap magnetic flux density. Samarium-cobalt magnets are expensive, but have a high  $B$ - $H$  characteristic and a high Curie temperature and thus a high operating temperature capability. Neodymium-iron-boron magnets are expensive but have the highest  $B$ - $H$  characteristic. The Curie and operating temperatures are lower than for samarium-cobalt magnets.

The magnetic properties are characterized by a  $B$ - $H$  curve showing the basic demagnetization properties of the material independent of the magnetic circuit in which it will be used. This  $B$ - $H$  curve is a second-quadrant plot of magnet flux density ( $B$ ) vs. magneto-motive force per unit length ( $H$ ). Figure 15.43 shows a  $B$ - $H$  plot for several magnet material types. Because of the large number of magnet characteristics available within each of the four family types shown in Fig. 15.43, the curves show only gross characteristics for each magnet family, and not for a specific member of the family. The units used on the two axes are teslas (webers per square meter) for flux density and kiloampere-turns per meter for magnetomotive force per unit length.

#### 15.3.3.2 Magnet Flux-MMF Curves

While a magnet material  $B$ - $H$  curve is a second-quadrant plot of the intrinsic magnet material properties of flux density and ampere-turns per unit length, the actual magnet capability for a given configuration is represented by a second-quadrant plot of the magnet flux vs. magnet ampere-turns. The magnet flux is obtained by multiplying flux density  $B$  by magnet area, and the magnet ampere-turns obtained by multiplying magnetizing force  $H$  by the magnet length.

Magnet flux and mmf are given by:

$$\Phi_m = B A_m = \text{magnet total flux per pole in webers} \quad (15.111)$$

$$F_m = H t_m = \text{magnet total mmf in ampere-turns} \quad (15.112)$$

where:

$B$  = magnet flux density in tesla

$A_m$  = magnet area per pole in square meters

$H$  = magnet strength in ampere-turns per meter

$t_m$  = magnet radial thickness in meters

The complete magnetic circuit comprises magnet, air gap, magnetic steel, and stator winding mmf. The effect on the magnet operation is shown in Fig. 15.44 with a samarium-cobalt magnet of approximately 0.01 m thick and approximately 0.1 m<sup>2</sup> area. The vertical axis shows the magnetic flux and the horizontal axis shows the ampere-turns available to force the magnetic flux through the magnetic circuit. A load line drawn from the origin represents the magnetic circuit without any iron saturation or demagnetizing ampere-turns because of stator winding mmf. The intersection of the load line with the magnet curve defines the no-load operating point of a given magnet in terms of magnet total flux and ampere-turns. This load line is also the airgap line, because it represents the mmf consumed by the air gap for the given flux density (and is of course linear.)

The air-gap or load line mmf is:

$$F_g = L_{ge} B_{gm} / \mu_0 = \text{air gap mmf in ampere-turns} \quad (15.113)$$

where:

$B_{gm}$  = maximum air gap flux density in tesla

$L_{ge}$  = air gap effective radial length in meters

$\mu_0$  =  $4\pi \cdot 10^{-7}$  = permeability of air in wb/amp-m

An additional load line parallel to the first load line represents the addition of demagnetizing armature reaction ampere turns. A curve diverging away from the straight line represents magnetic saturation of the iron circuit (mostly in the stator lamination core and teeth) as shown in Fig. 15.44. The resultant

operating point is shown as the intersection of the load line and the magnet characteristic.

### 15.3.3.3 Optimum Design

The optimum design for a brushless dc motor depends on the importance of motor cost versus size, heating, and efficiency. The most important factors in the design optimization are the type of magnet material and the acceptable current loading level a designer is willing to build into a motor. Typically, a high-performance motor would utilize a high-energy-product magnet material such as samarium-cobalt or neodymium-iron-boron. It is not enough to simply employ these magnet types to achieve a high power-to-weight ratio. It is also critical to select the operating point of the magnet such that the armature current loading is not excessive. For example, choosing the operating point of the magnet to be at the maximum energy product of the magnet material will result in minimum magnet volume and magnet cost. However, the resultant average air gap flux density will be low (about one-half of the magnet  $B_r$ ), and therefore the armature winding will take a larger portion of the stator volume (thinner stator teeth and larger stator slots) to provide the same torque (the product of flux and armature ampere turns). Using a somewhat thicker magnet results in a more expensive magnet, but increases the air-gap flux density, reduces the armature current loading, and results in a better balance of stator lamination iron and stator copper. The design with the thicker magnet is more efficient and easier to cool, with a stator that is easier to wind because of less copper to insert in the slots, and with smaller end turns.

### 15.3.3.4 Temperature Effects

In general, magnet  $B_r$ , the residual induction at zero magnetizing force, will decrease with increasing temperature, and increase with decreasing temperature relative to room temperature. For ferrites, the value of  $H_c$ , the coercive force required to bring the magnet to a zero flux condition, decreases substantially with

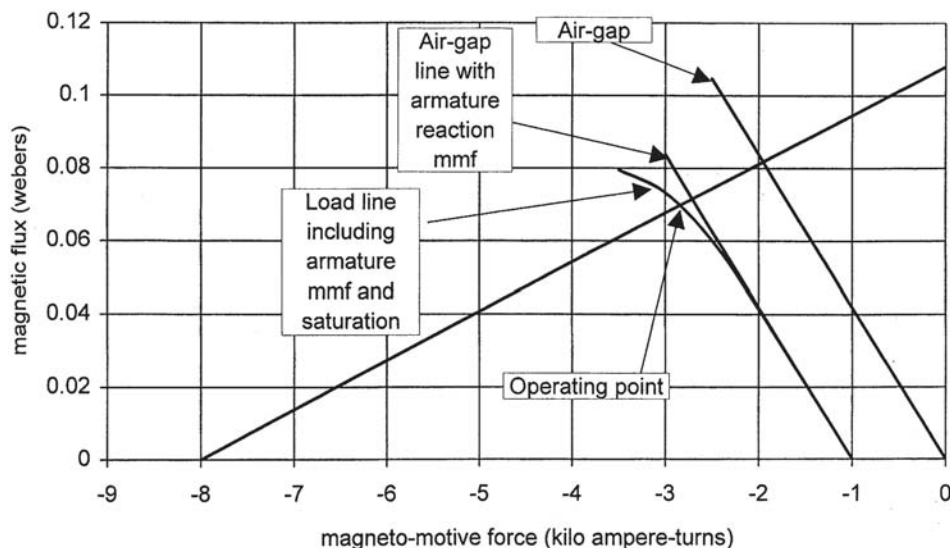


Figure 15.44 Load lines superimposed on magnet characteristics.

decreasing temperature. For neodymium-iron-boron, the effect is opposite, with a dramatic decrease in  $H_c$  with increasing temperature. These temperature effects are reversible as long as the magnet operating point does not go below the “knee” of the demagnetization curve and suffer permanent demagnetization. This relationship between temperature and  $B_r$ , and the relationship between temperature and  $H_c$  requires the motor designer to account for temperature extremes in sizing the magnets so that the motor has sufficient torque per ampere and the magnets do not suffer permanent loss of magnetic capability during extreme temperature conditions.

An additional temperature effect is the loss of all permanent magnetism by exceeding the Curie temperature. The Curie temperature is different for each of the permanent magnet types, and determines the maximum magnet operating temperature. For ferrite, Alnico, and samarium-cobalt magnets, the Curie temperatures are approximately 450°C, 900°C, and 700°C, respectively. For neodymium-iron-boron magnets, the Curie temperature is considerably lower at just over 300°C. As the magnet materials approach the Curie temperature, some irreversible loss in magnetism takes place, so the magnet working temperature should be kept well below the Curie temperature. Typical working temperature limits are approximately 500°C for Alnico, 400°C for ferrite, 250–300°C for samarium-cobalt, and only 150–200°C for neodymium-iron-boron.

### 15.3.3.5 Magnet Shape and Flux Density Distribution

Two different magnet shapes are shown in Figs. 15.41 and 15.42. Each of these shapes will produce a slightly different air-gap magnetic flux density distribution. Other magnet shapes, such as a magnet that does not span a full pole pitch of 180 electrical degrees, will produce a different air gap flux density distribution. The air-gap flux is the flux that crosses the air gap and interacts with the stator winding to produce a generated voltage or back-emf in the stator winding. The magnet leakage flux is that which does not cross the air gap, but travels peripherally to the adjacent magnets. The portion of the magnet adjacent to the next magnet of opposite magnetic polarity will produce leakage flux, and actually be on a different demagnetization curve than the total average magnet curve shown in Fig. 15.44. To determine the exact shape of the air gap flux density distribution, a detailed flux plot performed by hand or preferably from a finite-element magnetic field analysis computer program, should be used. A computer analysis that uses the finite-element method (FEM) can include the effects of saturation and armature reaction demagnetization on the magnet operating point for each load condition and rotor position relative to the current-carrying stator windings.

A simplified method to determine the no-load radial air gap magnetic flux, for an initial design effort, is to assume that the radial air gap flux density distribution is trapezoidal along the periphery, with the total radial air gap flux being the area under the trapezoid. The magnet total flux is the sum of the radial gap flux and the tangential leakage flux. An approximation is made to account for the fact that thicker magnets have proportionately more magnetic flux leakage to adjacent magnets than thinner

magnets. The trapezoid of flux density starts with a zero value at the interpolar boundary and rises to a maximum at a distance along the periphery equal to one half of the magnet thickness. This method is illustrated in Fig. 15.45 for constant-thickness radial magnets. The maximum value of air gap flux density is constant along the trapezoid and equal to the value obtained from solving Eq. 15.113 for  $B_{gm}$ .

$$B_{gm} = \mu_0 F_g / L_{ge} \quad (15.114)$$

where:

$L_{ge}$  equals the effective radial air gap taking into consideration the stator slotting.

The solution of this will require iteration to determine the intersection of the air gap line with the actual magnet demagnetization curve. This iteration can be performed by graphically plotting a point on the magnet demagnetization curve and drawing a line from the origin. Remember that the leakage flux must be added to the air gap flux before plotting total magnet flux vs. magnet mmf at the magnet average area (magnet axial length multiplied by tangential length at the magnet radial midpoint).

After performing the integration of the trapezoidal flux density distribution over one pole pitch from Fig. 15.45, the air gap flux per pole is:

$$\Phi_g = B_{gm} (\pi D_r / P - t_m) (L_m + L_s) / 2 + B_{gm} t_m / 2 (L_m + L_s) / 2$$

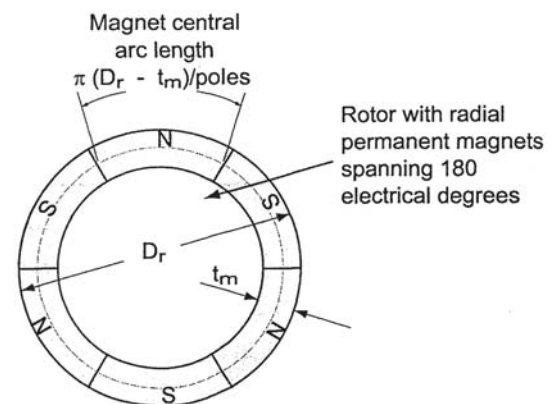
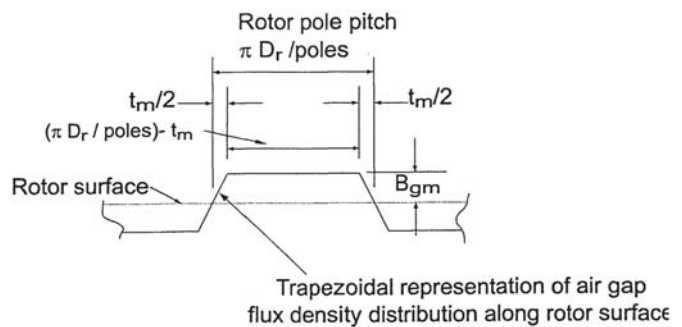


**Figure 15.45** Trapezoidal air-gap flux density distribution for a radial magnet configuration.

which can be simplified to:

$$\Phi_g = B_{gm} (\pi D_r / P - t_m / 2) (L_m + L_s) / 2 \text{ webers} \quad (15.115)$$

where

$L_m$  = magnet axial length in meters

$L_s$  = stator axial length in meters

$D_r$  = rotor diameter over magnets in meters

$t_m$  = radial magnet thickness in meters

$$\Phi_1 = L_m B_{gm} t_m / 2 \text{ leakage flux per pole in webers} \quad (15.116)$$

$$\Phi_m = \Phi_g + \Phi_1 \text{ total magnet flux per pole in webers} \quad (15.117)$$

$$B_m = \Phi_m / A_m = \Phi_m / (L_m \pi (D_r - t_m) P) \text{ teslas} \quad (15.118)$$

The air gap load line crosses the magnet demagnetization characteristic where the mmfs are equal:

$$F_g = F_m \quad (15.119)$$

To solve for the point where the two mmfs are equal, the following procedure can be used:

1. Assume a value for  $B_{gm}$
2. Calculate  $\Phi_g$ ,  $\Phi_1$ , and  $\Phi_m$  from above Eq. 15.116, 15.117, 15.118
3. Calculate  $F_g$  from Eq. 15.113
4. Locate  $\Phi_m$  on the magnet curve
5. If the corresponding value of  $F_m$  is not equal to  $F_g$  select a new value of  $B_g$  and repeat steps 2 through 4 or go to step 6.
6. For a graphical solution, plot the point  $F_g$ ,  $\Phi_m$  on the magnet mmf-flux plot and draw a straight line through the point from the origin.

For other magnet configurations, such as a magnet arc that does not span a full pole pitch or the case in Fig. 15.41 where the magnet has non-uniform radial thickness, other approximations can be made. It is best to perform a detailed FEM analysis to obtain at least a verification of a particular approximating calculation such as the one presented above.

### 15.3.4 Armature Windings

A number of stationary winding types may be used for brushless dc motors, including two-phase and three-phase concentric and distributed windings that are supplied with power from electronic controllers. The electronic controllers require some form of rotor position feedback for switching power among the phase windings so that the stator (armature) currents follow the rotor to produce a torque in synchronism with the rotor speed. Most large brushless dc motors utilize a three-phase distributed stator winding that is wound in 60-degree phase belts with two coil sides per slot. This section covers, the characteristics of this conventional three-phase

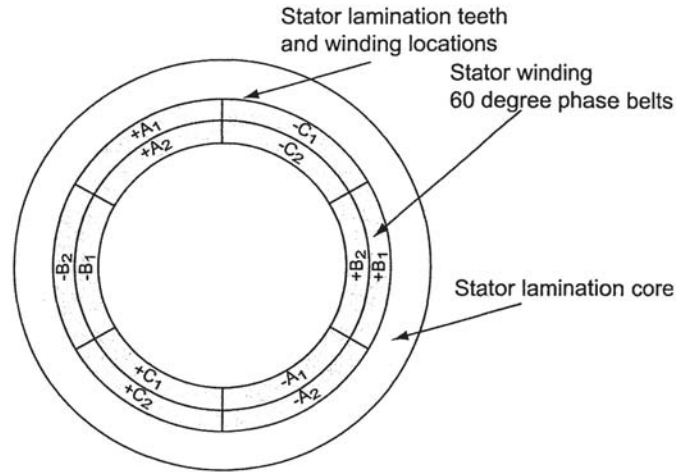


**Figure 15.46** Phase locations for three-phase, two-pole, full-pitch, two-layer stator winding.

winding type and its associated effects on the magnet and torque production.

Figure 15.46 shows a representation of the phase belt locations inside the stator core where the stator slots are located for a two-pole, three-phase, two-layer, full-pitch winding.

In this winding for a two-pole motor, there are two coil sides per slot and each coil spans 180 degrees, mechanical as well as electrical. This winding, with the current-carrying conductors located directly in the magnetic flux created by the rotor magnets, produces an mmf that adds to one-half of the rotor magnet mmf and subtracts from the other half of the rotor magnet mmf. On average, without saturation, the total demagnetization effect is near zero. However, in the portion of the magnetic field enhanced by the stator mmf, stator tooth density may be driven further into saturation, and the total ampere-turns required to drive the magnetic flux into the stator is increased in a nonlinear fashion that changes the operating point of the magnet as shown in Fig. 15.44. Because this effect is difficult to determine without a magnetic field analysis, the usual value of 10% of the total stator (armature) mmf for conventional dc machines can be assumed as the additional amount of ampere turns required to be supplied by the magnet under load conditions.

The approximate value to use for armature mmf demagnetization is:

$$AMMF_m = 0.1 I_{dc} N_c / (2 P) \text{ ampere-turns per pole} \quad (15.120)$$

where:

$P$  = number of motor poles

$N_c$  = Total number of current-carrying conductors  
= 2/3 (Slots) (coil sides per slot)

$$\text{(turns per coil)/circuits} \quad (15.121)$$

The 2/3 in the equation for  $N_c$  is for the fact that only 2 of the 3 phases are conducting current at a time for 120-degree conduction.

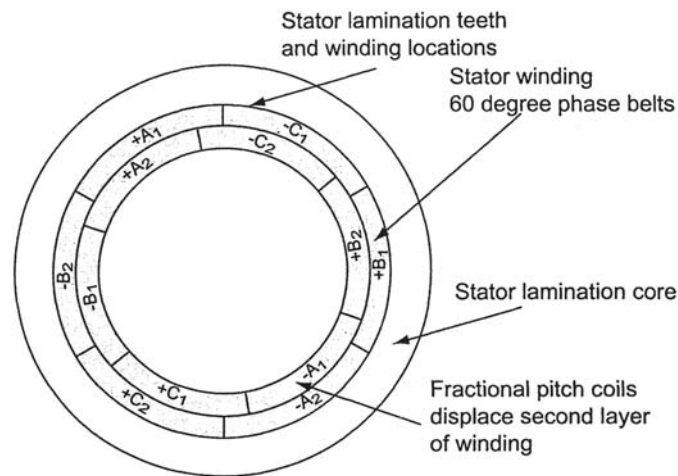


**Figure 15.47** Phase locations for three-phase, two-pole, fractional-pitch, two-layer, stator winding.

Figure 15.47 shows the phase belt locations for a fractional-pitch winding. In this winding for a two-pole motor, each coil side spans less than 180 degrees, and while producing slightly less back-emf, results in smaller end turns and a more distributed mmf. A short-pitched winding is more typical of ac synchronous and induction machines to produce a more sinusoidal stator mmf. For the brushless dc motor, the use of a short-pitched winding reduces some of the torque pulsations resulting from the electronic commutation of the stator phases.

The stator winding mmf is concentrated at the coil sides carrying current, and the rotor torque is developed from the interaction of the rotor magnetic flux and the stator currents. In a conventional dc motor, the load angle is approximately 90 electrical degrees because the stator coils are commutated one at a time, and the brush position is such that the armature coils carrying current are in the maximum dc field flux virtually all the time. A brushless dc motor controller, however, switches a large portion of the winding every 60 electrical degrees and the current carrying stator conductors are not always centered with respect to the rotor magnetic flux. For this reason, some reduction of the winding effectiveness results, and must be considered in the design process.

### 15.3.5 Torque Analysis

For a motor controller that applies current to two phases at a time, the current (and thus the stator mmf) spans 120 electrical degrees at any one time (except during the brief period of commutation when the controller is changing from one phase to another). This commutation takes place when the rotor has traveled around the stator periphery approximately 30 degrees toward the next phase to start conducting. Each phase will conduct for approximately 120 electrical degrees at a time with one polarity and then be commutated off for approximately 60 degrees before being turned back on with the opposite polarity current. For this mode of operation, the two conducting phases are carrying equal and opposite current (assuming a wye-connected motor). The peak torque is obtained when a magnetic pole centerline is aligned with the

center of the stator current-carrying coil sides. This peak occurs for all rotor poles simultaneously, and the torque is summed for all poles.

For example, if phases A and B were each carrying equal and opposite current in Fig. 15.46, the maximum rotor torque would occur when the magnet centerline lines up with the line denoting the boundary between phases +A and -B. Because the region of constant air-gap flux density produced by the rotor may extend somewhat beyond the 120-degree central region (see Fig. 15.45), the region of maximum torque will carry beyond the point where the coil sides are lined up with the magnet center. As the rotor approaches the 30-degree commutation point, the coil sides carrying current are starting to leave the air gap maximum flux density region, and the torque falls off until after the new conducting phase sees a higher flux region.

For a machine with controlled dc current in the current-carrying stator phases, the torque calculation can be approximated using the conventional dc machine torque equation:

$$T_{gap} = K_a \Phi_t I_{dc} \text{ newton-meters} \quad (15.122)$$

where:

$$K_a = \text{armature winding constant} = p N_c / (2\pi) \quad (15.123)$$

$P$  = number of motor poles

$N_c$  = total number of current-carrying conductors

$\Phi_t$  = total effective flux per pole in webers (found by integrating the flux density trapezoidal waveshape along the air gap periphery for the maximum gap density portion of the waveshape only)

$I_{dc}$  = average dc bus current in amps

Note that the value of  $\Phi_t$  is different from the conventional dc machine equation that uses the total magnetic flux per pole. This torque calculation gives approximately the peak torque, but must be reduced somewhat for the torque pulsations during commutation to determine the average torque. The reduction factor will vary with the effective amount of air gap



flux density produced by the magnet, and must be determined from testing, a detailed FEM analysis, or experience with similar machines.

Another type of motor control utilizes 180-degree electrical conduction of the phase windings. For 180-degree conduction, one phase conducts full current for 120 degrees, and half current for the other 60 degrees, resulting in a somewhat higher efficiency and torque per amp, but more complicated motor controller operation and commutation.

Some brushless dc motors are fed with a sinusoidal voltage waveshape. This is accomplished by using a rotor encoder or resolver that gives much more accurate rotor position information than that required for commutation every 60 degrees. For this type of motor drive the accurate rotor position information is utilized to apply a sine wave of voltage that subsequently produces a sine wave of current to develop a requested torque value. For this configuration the motor acts more like a pm synchronous motor and the torque can be analyzed as the interaction between the fundamental stator mmf and the fundamental of the rotor flux density waveshape.

### 15.3.6 Voltage Analysis

Because the stator current and the rotor flux are constant over some distance of rotor travel before commutating to the next stator phase, a conventional dc machine equation can be used to calculate the stator generated emf:

$$E_a = K_a \Phi_r \text{ rpm } 2\pi/60 \text{ volts} \quad (15.124)$$

where:

- $K_a$  = armature winding constant = Poles  $N_c / (2\pi)$
- $P$  = number of motor poles
- $N_c$  = Total number of current-carrying conductors in series
- $\Phi_r$  = total effective flux per pole in webers (found by integrating the flux density trapezoidal waveshape along the air gap periphery for the maximum gap density portion of the waveshape only)
- $\text{rpm}$  = rotor speed in revolutions per minute

The 2/3 is again used here for  $N_c$  because only two of the three phases are active in generating voltage at a time for 120-degree conduction.

The voltage equation shows an identical winding constant  $K_a$  being used for both torque and voltage. Some motor manufacturers provide a motor torque constant as the product of  $K_a \Phi_r$ , and a conversion factor depending on torque units, and a voltage constant as the product of  $K_a \Phi_r$ , and  $2\pi/60$  which gives a numerically different value.

### 15.3.7 Equivalent Circuit

The dc machine equivalent circuit for a brushless dc motor consists of a dc source, a series resistance, and a generated voltage that opposes the source voltage. Because the brushless dc motor is a variable speed device, the input voltage must be controlled to match current and voltage to the desired load and speed. The applied motor terminal voltage is given by:

$$V_T = E_a + I_{dc} 2R_a \quad \text{volts} \quad (15.125)$$

where:

- $E_a$  = stator generated voltage volts
- $I_{dc}$  = stator (armature) current  
(same as dc bus current) amps
- $r_a$  = stator resistance per phase ohms

The voltage  $V_T$  is the steady-state voltage applied directly to the motor terminals by the electronic motor controller, and is controlled to give the desired torque and speed in response to some desired steady-state motor performance point. For transient performance, a series inductance should be included in the equivalent series circuit. The inductance would be the modified leakage inductance for two stator phases in series. A standard leakage inductance calculation for a three-phase stator is given in Section 4.5. Because the typical brushless dc motor has magnets only on the rotor, and no surface iron structure, the zig-zag component of leakage inductance should be eliminated from the calculation, and the peripheral component should be included since the equivalent total air gap includes the magnet thickness. The resultant equation for the equivalent stator leakage inductance per phase is:

$$L_{le} = L_1 L_{zz} + L_p \text{ henrys per phase} \quad (15.126)$$

where:

- $L_1$  = the conventional leakage inductance per phase with zig-zag but not including peripheral air gap leakage inductance
- $L_{zz}$  = the normal zig-zag leakage inductance
- $L_p$  = the peripheral air gap leakage inductance

The modified equation for transient conditions is:

$$V_T = E_a + I_{dc} 2r_a + 2 L_{le} d(I_{dc})/dt \text{ volts} \quad (15.127)$$

The brushless dc motor circuit is shown in Fig. 15.48.

### 15.3.8 Motor Drive Circuit

Brushless dc motor operation and control requires an electronic circuit with the capability to apply the required voltage to the motor terminals to produce a pattern of current in the stator windings in synchronism with the rotor movement. The electronic control circuit must respond to rotor position sensors, input voltage source variations, and input commands for rotor shaft position, rotor speed or acceleration. For high performance servo operation, a feedback control is incorporated. The feedback control is active in controlling and limiting current to achieve a certain performance with the correct amount of damping to limit overshoot of current, position, and speed. A simplified motor controller is shown in Fig. 15.49 where various capacitors, snubbers, and inductors used for filtering and spike suppression are not shown.

In Fig. 15.49, the voltage control is accomplished by high speed switching of the motor input transistors and voltage is controlled in response to the input command and various feedback signals such as current, rotor speed and rotor or load position. In a braking mode the rectifier output is disconnected, the generated current is fed back through the inverter diodes, and the controller uses the braking transistor and resistor to

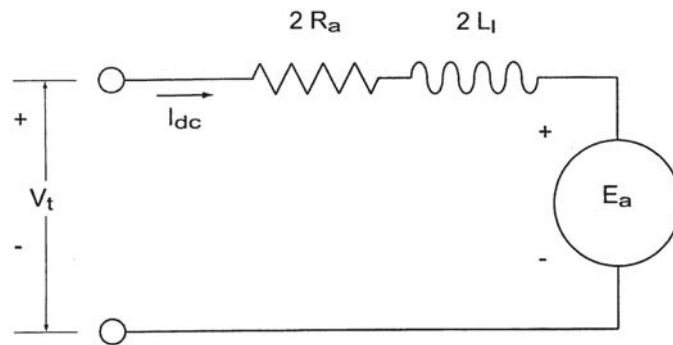


**Figure 15.48** Brushless direct current (dc) motor equivalent circuit including stator inductance.

dissipate the load energy. In addition, the converter shown allows the motor to reverse direction of rotation by reversing the sequence of current applied to the three-phase stator windings. The motor input transistors also direct input current to the proper winding in response to the rotor position sensors to assure synchronism of the rotor and stator mmfs. The rotor position sensing can be accomplished by Hall-effect devices sensing magnetic field variations as the rotor turns or by light-emitting diode LED photodetectors that sense an interruption of light by an encoded wheel or cylinder. An alternative method is to use a signal from the unexcited stator winding phase for controllers that use 120-degree conduction with only two phases conducting at a time. These methods work well for commutation every 60 degrees. For brushless dc motors fed with a sinusoidal voltage waveshape, the rotor

encoder is more accurate and more complicated than the sensors described above. Other motor controller types use controlled rectifier inputs to control the dc bus voltage or chopper control at the input to the inverter section. In addition to the simple dynamic braking shown, a more complicated input section can be added to allow regenerative braking to return energy to the source and produce what is known as four-quadrant converter operation. A four-quadrant converter allows the motor to rotate in either direction and act as a motor or generator.

### 15.3.9 Performance

Performance for a brushless dc motor and drive system is measured by how well the motor drives the load to meet the load requirements. Many small brushless dc motors are used

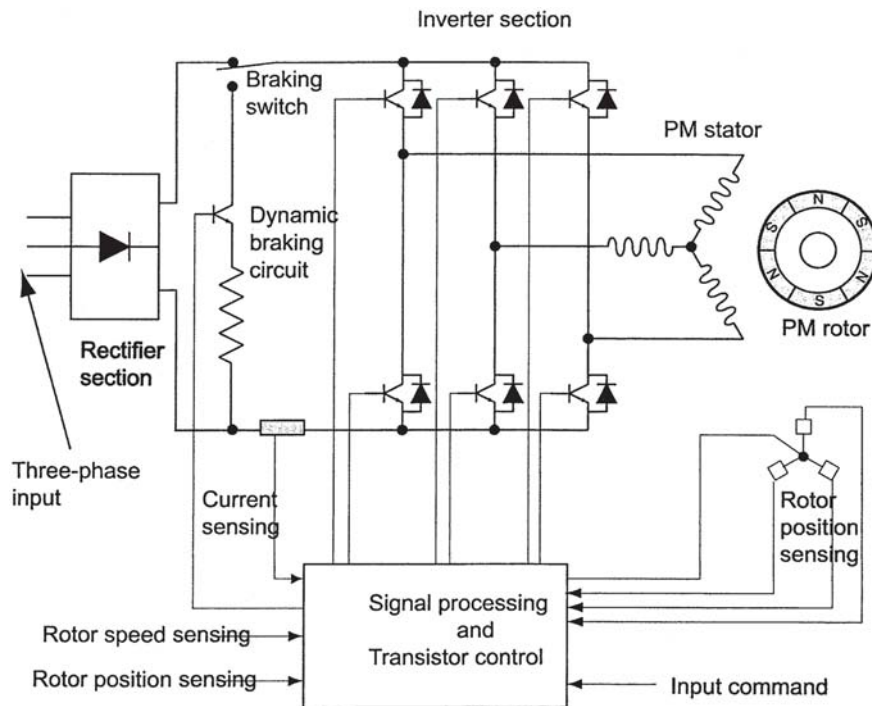


**Figure 15.49** Simplified motor controller circuit diagram.

to drive computer peripherals such as disk and hard drives. These applications require rapid acceleration up to a constant speed with very little in the way of torque pulsations due to intermittent loads. Other brushless dc motors are required to drive machine tools or industrial processing equipment that may have high acceleration and deceleration rates, accurate speed requirements, and nonuniform load profiles. Still other applications such as robotics and aerospace flight-control actuation have requirements for acceleration and deceleration rates under varying load conditions, and position holding at zero speed and varying load conditions.

### 15.3.9.1 Acceleration

Angular acceleration is defined by the torque available to increase the speed of the load as follows (the load values here are referred to the motor shaft):

$$\alpha_m = (T_{gap} - T_{load} - T_{loss}) / (J_{motor} + J_{load}) \text{ rad/sec}^2 \quad (15.128)$$

where:

$T_{gap}$  = motor torque from Eq. 15.122 in newton-meters

$T_{load}$  = load torque referred to the motor shaft in newton-meters

$T_{loss}$  = motor torque loss due to friction, windage, magnetic hysteresis loss, or magnetic eddy-current loss in newton-meters

$J_{motor}$  = motor inertia in kg/m<sup>2</sup>

$J_{load}$  = load inertia referred to motor shaft in kg/m<sup>2</sup>

Acceleration is of course limited by the amount of current the motor controller can apply to the motor. The current is in turn limited by the rating of the transistors in the motor drive, the motor heating due to stator winding losses, and the voltage available to overcome the  $I r$  drop and generated back-emf in Eq. 15.124.

Deceleration or braking is limited by the current that can be drawn from the motor acting as a generator. If the application requires no specific deceleration, then turning off the power to the stator windings will produce a negative acceleration given by Eq. 15.128 with  $T_{gap}$  set equal to zero. Utilizing the dynamic braking circuit of Fig. 15.49, the braking circuit can cycle off and on, or stay on until the braking effort is complete. The term  $T_{gap}$  is negative in Eq. 15.128 for dynamic braking.

### 15.3.9.2 Control

Typically, a feedback controller is used to control the desired motor output quantity such as speed or rotor position. This quantity is usually sensed at the load and subtracted from the desired value to produce an error signal. The error signal may then be fed through a proportional controller that acts to control motor current (and thus motor torque). An integral control is usually added in the feedback loop to eliminate steady-state errors. To assist in reducing overshoot of the desired control quantity, a derivative component is also added to the control algorithm. This is known as a proportional-integral-differential (PID) controller. Computer simulation of the entire system of motor and load equations along with the PID control can aid

in the system design and predict performance in advance of the actual hardware buildup.

### 15.3.9.3 Torque Pulsations

Torque pulsations in the developed motor torque due to motor phase winding commutation, cogging of magnets aligning with stator teeth, and pulsations in the rectified dc bus voltage can be troublesome in some applications where the speed or output position must have extreme accuracy. For many applications, the rotor and load inertias are sufficient to dampen the torque pulsations to a low level. Torque pulsation magnitudes can be further reduced in varying degrees by short-pitching the stator winding, skewing the stator slots or rotor magnets, using 180-degree conduction, and applying sinusoidal waveshapes of current to the stator phases.

### 15.3.9.4 Power Quality

Power quality degradation in the form of current harmonics on the supply side of the motor controller is mainly caused by the rectification of the three-phase input to create an internal dc bus. In addition, however, high-frequency switching in the inverter section to achieve motor current and waveshape control can cause conducted and radiated high-frequency problems at the motor controller input. As more motor controllers are used for a variety of applications on electric utility systems, these power quality issues need to be addressed. In many cases, passive filtering has been used to suppress high-frequency emissions as well as low-frequency current harmonics. Some systems have gone to active filtering where an attempt is made to actively suppress the offending harmonics.

### 15.3.9.5 Design Margins

The operating capability of a brushless dc motor and control depends on a number of assumptions including  $B-H$  magnet characteristics, operating temperature, flux density distributions, stator winding effectiveness, electronic commutation, and torque pulsations. Because of the assumptions and approximations presented above, it is important to allow design margins to account for any deficiencies introduced by analysis, material quality, or manufacturing processes. A reasonable margin can be obtained by reducing the magnet  $B-H$  curves by 10–20% of the published values. As experience is gained through actual design, manufacturing and testing, proper design margins can be determined. As stressed previously, for magnetic circuit analysis, a finite-element magnetic-field analysis is recommended. For the operation and control of the motor, a complete dynamic computer simulation is recommended.

With proper design and application, the use of brushless permanent magnet dc motors will increase dramatically over time, and replace other motor types now in use for specific applications.

## REFERENCES

1. F.M.H.Khater and D.W.Novotny, "An equivalent circuit model for phase back voltage control of AC machines, *IEEE Transactions*

- on *Industry Applic.*, vol. 22, no. 5, Sept./Oct., pp. 835–841.
2. T.A.Lipo, “The analysis of induction motors with voltage control by symmetrically triggered thyristors”, *IEEE Trans, on Power Apparatus and Systems*, vol. PAS-90, no. 2, March/April 1971, pp. 515–525.
  3. J.Davoine, R.Perret and H.Le-Huy, “Operation of a self-controlled synchronous motor without a shaft position sensor”, in *Conf. Rec. IEEE IAS Annual Meeting*, 1981, pp. 696–701.
  4. J.Holtz and S.Stadtfield, “A predictive controller for the stator current vector of ac machines fed from a switched voltage source”, in *Conf. Rec. IPEC Conf*, Tokyo, 1983, pp. 1665–1675.
  5. H.W.Van der Broeck, H.Skudelny and G.Stanke, “Analysis and realization of a pulse width modulator based on voltage space vectors”, *IEEE Trans, on Industry Applications*, vol. 24, no. 1, Jan./Feb., 1988, pp. 142–150.
  6. B. Mokrytzki, “The controlled slip static inverter drive,” *IEEE Trans. On Industry and General Applications*, vol. IGA-4, May/June 1968, pp. 312–317.
  7. K.Koga, R.Ueda and T.Sonoda, “Achievement of high performances for general purpose inverter drive induction motor system”, in *Conf. Rec. IEEE IAS Annual Meeting*, 1989, pp. 415–425.
  8. F.Blaabjerg and J.K.Pedersen, “Ideal PWM—VSI inverter using only one current sensor in the DC-link”, in *Conf. Rec. IEE 5th Power Electronics and Variable—Speed Drives Conf.*, 1994, pp. 458–464.
  9. S.I.Moon and A.Keyhani, “Estimation of induction machine parameters from standstill time-domain data”, *IEEE Trans, on Industry Applic*, vol. 30, no. 6, 1994, pp. 1609–1615.
  10. J.Stephan, M.Bodson and J.Chaisson, “Real-time estimation of the parameters and fluxes of induction motors”, *IEEE Trans, on Industry Applic.*, vol. 30, no. 3, 1994, pp. 746–758.
  11. J.A.Capolino, “Identification of induction machine parameters”, in *Conf. Rec. of the Int. Aegean Conf. on Electric Machines and Power Electronics*, vol. 2, 1995, pp. 627–637.
  12. Y.Kishimoto, S.Asaba, K.Nakata and S.Kawatsu, “Control device for induction motor,” U.S. Patent 5,231,339, July 27, 1993.
  13. S.I.Moon and A.Keyhani, “Estimation of induction machine parameters from standstill time-domain data”, *IEEE Trans, on Industry Applications*, vol. 30, no. 6, 1994, pp. 1609–1615.
  14. J.Stephan, M.Bodson and J.Chaisson, “Real-time estimation of the parameters and fluxes of induction motors”, *IEEE Trans, on Industry Applications*, vol. 30, no. 3, 1994, pp. 746–758.
  15. J.A.Capolino, “Identification of induction machine parameters”, *Proc. of the Int. Aegean Conf. on Electrical Machines and Power Electronics*, vol. 2, 1995, pp. 627–637.
  16. A.Munoz-Garcia, T.A.Lipo and D.W.Novotny, “A new induction motor open-loop speed control capable of low frequency operation”, *IEEE Trans, on Industry Applications*, vol. 34, no. 5, July/August, pp. 813–821.
  17. D.Leggate and R.Kerkman, “Pulse based time compensator for PWM voltage inverters”, in *Conf. Record of IEEE IEC ON*, 1995, pp. 474–481.
  18. J.W.Choi, S.I.Yong and S.K.Sul, “Inverter output voltage synthesis using novel dead time compensation”, *IEEE Trans, on Industrial Applic.*, vol. 31, no. 5, 1995, pp. 1001–1008.
  19. Y.Murai, T.Watanabe and H.Iwasaki, “Waveform distortion and correction circuit for PWM inverters with switching lag-times”, *IEEE Trans, on Industrial Applic.*, vol. 23, no. 5, 1987, pp. 881–886.
  20. T.Sukegawa, K.Kamiyama, T.Matsui, and T.Okuyama, “Fully digital, vector controlled PWM-VSI fed AC drives with an inverter dead-time compensation strategy”, in *Conf. Rec. IEEE IAS Annual Mtg.*, 1988, pp. 463–469.
  21. J.W.Choi, S.I.Yong and S.K.Sul, “Inverter output voltage synthesis using novel dead time compensation”, in *Conf. Rec. IEEE IAS Annual Mtg.*, 1994, pp. 100–106.
  22. D.W.Novotny and T.A.Lipo, “Vector control and dynamics of AC drives”, (book) Oxford Press, Oxford England, 1996.
  23. R.de Doncker and D.W.Novotny, “The universal field oriented controller”, in *Conf. Rec. IEEE IAS Annual Meeting*, Oct. 1988, p. 450–456.
  24. X.Xu and D.W.Novotny, “Selection of the flux reference for induction machines in the field weakening region”, *IEEE Trans, on Industry Applic.*, vol. 28, no. 6, November/December 1992, pp. 1353–1358.
  25. K.B.Nordin, D.W.Novotny and D.S.Zinger, “The influence of motor parameter deviations in feedforward field orientation drives systems”, *IEEE Trans, in Industry Applic.*, vol. IA-21, no. 4, July/August 1985, pp. 1009–1015.
  26. T.Rowan and R.Kerkman, “A new synchronous current regulator and an analysis of current-regulated PWM inverters”, *IEEE Trans, on Industry Applic.*, vol. IA-22, no. 4, July/August 1986, pp. 163–171.
  27. L.Malesani and P.Tenti, “A novel hysteresis control method for current controlled VSI PWM with constant switching frequency”, *IEEE Treans. onm Industry Applic.*, vol. IA-26, no. 1, Jan/Feb, 1990, pp. 88–92.
  28. Q.Yao and D.G.Holmes, “A simple, novel method for variable-hysteresis-band current control of a three phase inverter with constant switching frequency”, in *Conf. Rec. IEEE IAS Annual Meeting*, 1993, pp. 1122–1129.
  29. J.Holtz and S.Stadtfield, “A predictive controller for the stator current vector of AC machines fed from a switched voltage source”, in *Conf. Rec. IPEC*, Tokyo, 1983, pp. 1665–1675.
  30. A.Nabae, S.Ogasawara and H.Akagi, “A novel control scheme for current-controlled PWM inverters”, *IEEE Trans, on Industry Applic.*, vol. 22, no. 4, July/August, 1986, pp. 697–701.
  31. R.Joetten and G.Maeder, “Control methods for good dynamic performance induction motor drives based on current and voltage as measured quantities”, *IEEE Transactions on Industry Applic.*, vol. IA-19, no. 3, May/June 1983, pp. 356–363.
  32. K.Rajashckara, A.Kawamura and K.Matsuse (editors), “Sensorless control of AC motor drives”, (book) IEEE Press, 1996.
  33. V.I.Utkin, “Sliding mode control design principles and applications to electric drives”, *IEEE Trans, on Ind. Elec.*, Vol. 40, 1993, pp. 23–36.
  34. M.Rodic, K.Jezernik, A.Sabanovic, “Speed sensorless sliding mode torque control of induction motor”, in *Conf. Rec. IEEE-IAS Ann. Meeting*, 2000, pp. 1820–1827.
  35. T.M.Jahns, G.B.Kliman and T.W.Neumann, “Interior PM synchronous motors for adjustable-speed drives”, *IEEE Trans, on Industrial Applic.*, vol. 22, no. 4, July/August 1986, pp. 738–747.
  36. S.Morimoto, Y.Takeda, T.Hirasa and K.Taniguchi, “Expansion of operating limits for PM motor by optimum flux weakening”, *IEEE Trans, on Industrial Applic.*, vol. 26, no. 5, Sept./Oct. 1990, pp. 866–871.
  37. B.K.Bose, “A high-performance inverter-fed drive system of an interior PM synchronous machine”, *IEEE Trans, on Industrial Applic.*, vol. 24, no. 6, Nov./Dec. 1988, pp. 987–998.
  38. M.A.Bilewski, A.Fratta, L.Giordano, A.Vagati and F.Villata, “Control of high performance interior PM synchronous drives”, in *Conf. Rec. IEEE-IAS Annual Meeting*, 1990, pp. 531–538.
  39. T.J.E.Miller, “Switched reluctance motors and their control”, Magna Physics Publishing/Oxford University Press, 1993 [ISBN 1-881855-02-3; [Motorsoft@worldnet.att.net](mailto:Motorsoft@worldnet.att.net)]
  40. T.J.E.Miller [Ed.], “Electronic control of switched reluctance motors”, Newnes Power Engineering Series, ISBN 0750650737, May 2001.
  41. R.Furmanek, A.French and G.E.Horst, Horizontal axis washers, Appliance Manufacturer, March 1997, pp. 52–53.
  42. T.J.E.Miller (ed.), Optimal design of switched reluctance motors, invited paper for Special Section Papers of IEEE Transactions on Industrial Electronics, Vol. 49, No. 1, February 2002, pp. 15–27.

# Appendix A

## EQUIVALENT UNITS

The following abbreviations are used in this table:

A	ampere	m	meter
cm	centimeter	N	newton
ft	foot	Oe	oersted
G	gauss	oz	ounce
hp	horsepower	rad	radian
h	hour	rev	revolution
in	inch	s	second
J	joule	T	tesla
kg	kilogram	W	watt
km	kilometer	Wb	weber
lb	pound		

---

Length	1 m	3.281 ft	39.37 in
Linear velocity	1 m/s	3.600 km/h	3.281 ft/s
Angular velocity	1 rad/s	0.1592 rev/s	57.30°/s
	1 rev/s	2 $\pi$ rad/s	
Mass	1 kg	2.205 lb (mass)	0.06852 slug
Force	1 N	0.2248 lb	7.233 poundals
Torque	1 N m	0.7376 lb-ft	141.6 oz-in
Energy	1 J	1 W s	0.7376 lb-ft
Power	1 W	1.341 $\times 10^{-3}$ hp	
	1 hp	550 ft-lb/s	745.7 W
Moment of inertia	1 kg m <sup>2</sup>	23.73 lb-ft <sup>2</sup>	0.7376 slug-ft <sup>2</sup>
Magnetic flux	1 Wb	10 <sup>8</sup> maxwells (lines)	
Magnetic flux density	1 Wb/m <sup>2</sup> = 1 T	10,000 G	64.52 kilolines/in <sup>2</sup>
Magnetizing force	1 A-turn/m	0.02540 A-turn/in	0.01257 Oe
	1 Oe	1 gilbert/cm	

---

## Appendix B

### ASSOCIATION AND INSTITUTE ADDRESSES

ANSI  
American National Standards Institute  
[www.ansi.org](http://www.ansi.org)  
25 West 43<sup>rd</sup> Street  
New York, NY, 10036, USA  
212-642-4909  
212-302-1286 fax

ANSI publications, publications of the International Organization for Standardization (ISO), and publications of the International Electrotechnical Commission (IEC) may be ordered from the address above or from:

American Technical Publishers, Inc  
[www.ameritech.co.uk](http://www.ameritech.co.uk)  
27/29 Knowl Piece, Wilbury Way  
Hitchin, Hertfordshire, SG4 OSX, UK

Japanese Standards Association  
[www.jsa.or.jp](http://www.jsa.or.jp)  
4-1-24 Akasaka Minato-ku  
Tokyo 107, Japan, 107-8440  
81-3-3583-8005  
81-3-3586-2014 fax

SCC  
Standards Council of Canada  
[www.scc.ca](http://www.scc.ca)  
270 Albert Street, Suite 200  
Ottawa, ON, K1P 6N7, Canada  
613-238-3222  
613-564-7800 fax

For ANSI standards in microfilm/microfiche format:

IHS  
Information Handling Services, Inc.  
IHS Enterprise Solutions  
[www.ihs.com](http://www.ihs.com)

15 Inverness Way East  
Englewood, CO, 80150, USA  
800-525-7053 ext.6359  
363-858-6359  
363-858-6836 fax

ASME  
American Society of Mechanical Engineers  
[www.asme.org](http://www.asme.org)  
POB 2300  
Fairfield, NJ, 67037-2300  
800-843-2763  
973-882-1107  
973-882-5717 fax

ASTM  
American Society for Testing Materials  
[www.astm.org](http://www.astm.org)  
100 Bar Harbor Drive  
West Conshocken, PA, 19428-2959  
610-872-9585  
610-872-9555 fax

CSA  
Canadian Standards Association  
[www.csa.ca](http://www.csa.ca)  
5060 Spectrum Way  
Mississauga, ON, L4W 5N6 Canada  
800-463-6727  
416-747-4000  
416-747-2500 fax

EPRI  
Electric Power Research Institute  
[www.epri.com](http://www.epri.com)  
POB 10412  
3412 Hillside Avenue  
Palo Alto, CA, 94304, USA  
800-313-3774

IEEE publications may be ordered from:

IEEE  
Institute of Electrical and Electronic Engineers

[www.ieee.org](http://www.ieee.org)

Service Center

445 Hoes Lane

Piscataway, NY, 08855-1331. USA

800-678-4333

908-981-1392

908-562-9667 fax

COMM 2000

[www.comm-2000.com](http://www.comm-2000.com)

ILI

Infonorme-London Information

[www.ili-info.com](http://www.ili-info.com)

Index House

Ascot Berkshire, SL5 7EU, UK

42-1344-636400

42-1344-291194 fax

Global Engineering Documents

[www.global.chs.com](http://www.global.chs.com)

15 Inverness Way

Englewood, CO, 80112, USA

800-854-7179

303-797-7956

303-792-2181 ext 1950

303-792-2192 fax

IEC

International Electrotechnical Commission

[www.iec.ch](http://www.iec.ch)

3 Rue de Varembe

POB 131

CH-1211 Geneva 20, Switzerland

41-22-9190211

41-22-9190300 fax

NEMA

National Electrical Manufacturers Association

[www.nema.org](http://www.nema.org)

1300 North 17<sup>th</sup> Street, Suite 1647

Rosslyn, VA, 22209, USA

703-841-3200

703-841-5900 fax

NFPA

National Fire Protection Association

[www.nfpa.org](http://www.nfpa.org)

1 Battery march Park

Quincy, MA, 02369-9101, USA

613-770-3004

613-770-0700

*(Note: The NFPA is the sponsoring organization for the National Electrical Code (NEC), which is ANSI approved. The NEC may be ordered directly from the NFPA or from ANSI and it is frequently available from other sources (e.g., electrical supply houses) at the time a new edition is published.)*

UL

Underwriters Laboratories Inc.

[www.ul.com](http://www.ul.com)

333 Pfingsten Road

Northwood, IL, 60062-2090, USA

847-272-8800

847-272-8129 fax

*(Note: UL Standards may also be ordered from ANSI.)*